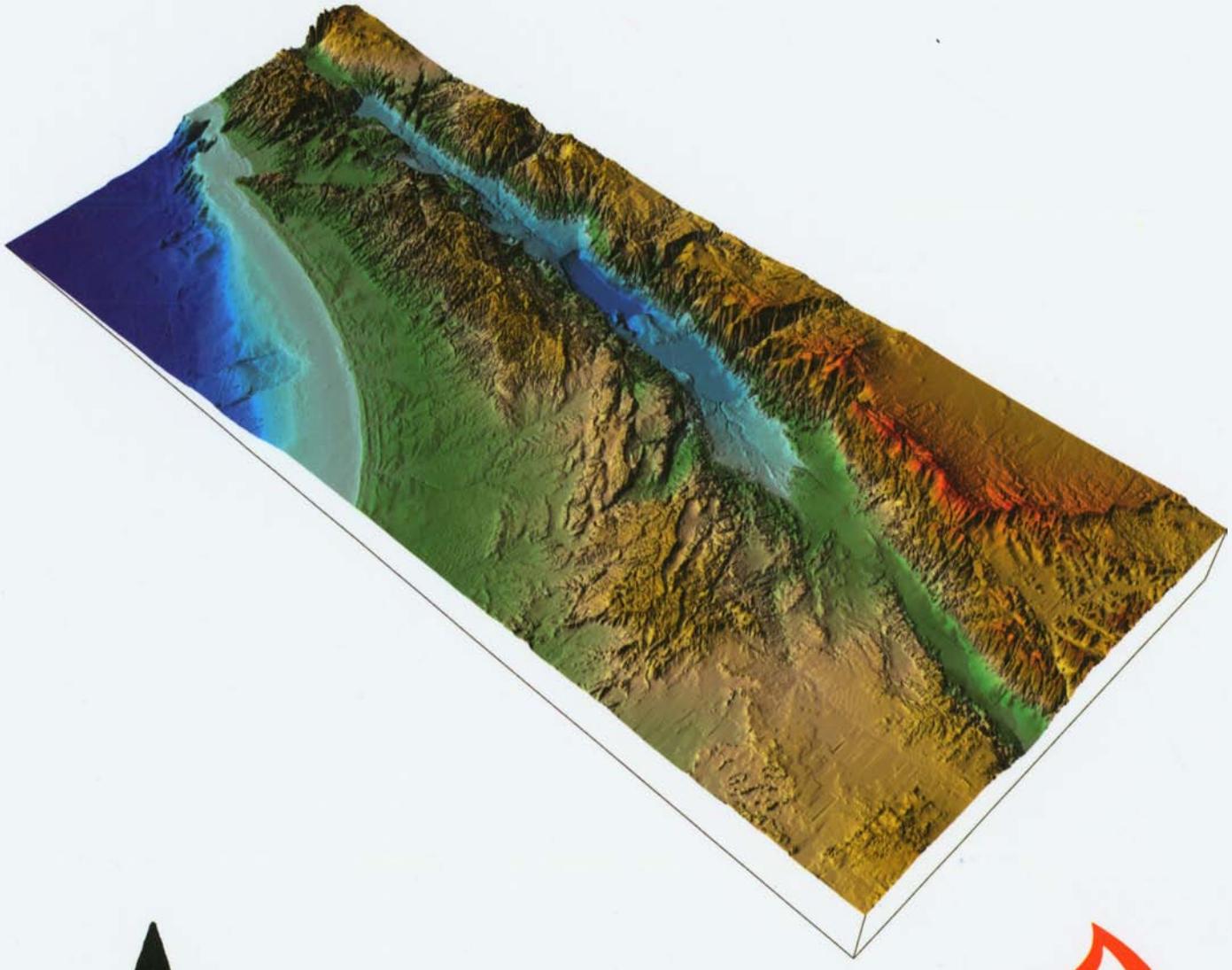
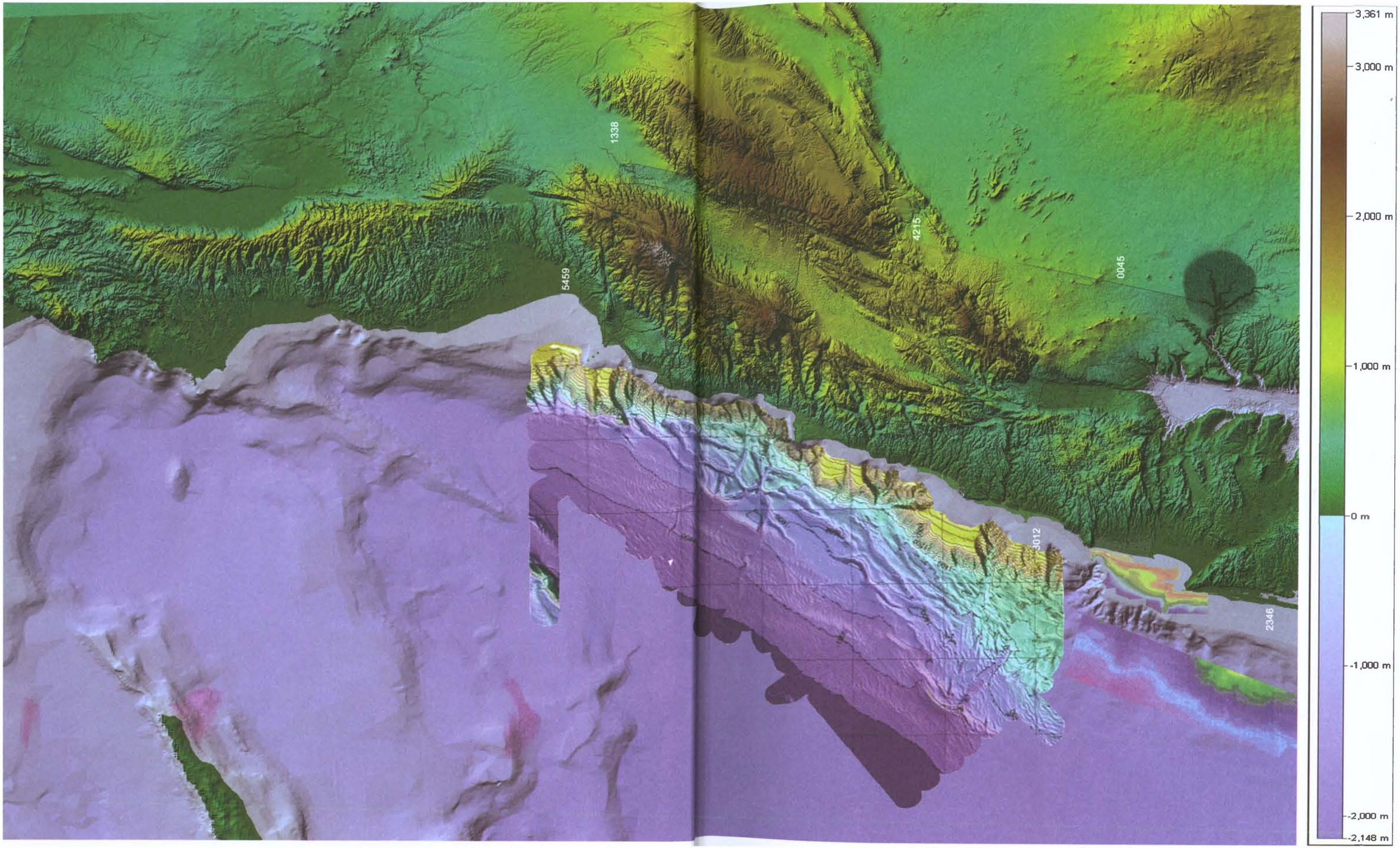
GEOLOGICAL FRAMEWORK of the LEVANT

VOLUME II: The LEVANTINE BASIN and ISRAEL




1338
5459
4215
0045
3012
2346
3,361 m
3,000 m
2,000 m
1,000 m
0 m
-1,000 m
-2,000 m
-2,148 m

Geological Framework of the Levant

Volume II: The Levantine Basin and Israel

Edited by

John K. Hall
Geological Survey of Israel
Marine Geology, Mapping & Tectonics Division
30 Malchei Israel Street,
Jerusalem 95 501, Israel

Valery A. Krasheninnikov
Geological Institute of the Russian Academy of Sciences
Pyzhevsky Pereulok 7,
109017 Moscow, Russia

Francis Hirsch
Geological Survey of Israel
30 Malchei Israel Street,
Jerusalem 95 501, Israel

Chaim Benjamini
Department of Geological and Environmental Sciences
Ben-Gurion University of the Negev
P.O.B. 653, Beersheva 84 105, Israel

Akiva Flexer
Department of Geophysics and Planetary Sciences,
Tel-Aviv University, Tel-Aviv 69978, Israel

Jerusalem, April 2005

Front Cover: Surfer® 8 3-D representation of the Digital Terrain Map (DTM) of Israel. This DTM was prepared by J. K. Hall in 1987-1993 on a 25 m grid from the 1:50,000 scale topographic maps of the Survey of Israel (SOI), as well as bathymetric maps prepared by the Geological Survey of Israel (GSI).

Inside Front Cover: The eastern margin of the Levantine Basin. This composite image shows the datasets available at present for visualizing the complex topography accompanying the Yammouneh bend in the Dead Sea Fault. The background bathymetry is from the 50 m contours of the bathymetric chart of Hall (1994). The land topography is the 90 m data from the SRTM, overlain by 8 ASTER scenes with 30 m grids. Offshore the schematic results of three multibeam surveys have been superimposed. These are, from north to south, the Ifremer SHALIMAR campaign of the N/O Le Suroît from 27 September to 26 October 2003, which used a Simrad EM300 system, and is described on the web at (http://www.ifremer.fr:582/sismer/catal/campagne/campagne.htql?Cmo=3020120), the northern end of a three day survey for the Israeli Navy by the Turkish survey vessel TCG Çeşme (A-599 - formerly the USNS Silas Bent – TAGS 26) using a SeaBeam 1050 multibeam, and the northern part of the Israel National Bathymetric Survey (see Figure 16.6), carried out with a shallow water Simrad EM1002 multibean. The results from the Ifremer BLAC and SHAL-LIBAN campaigns (October-November 2003) farther north are not yet released, and a number of reconnaissance tracks of the F/S Meteor off Haifa Bay during Cruise 52/2/ in 2002 are omitted as they do not constitute a complete mapped polygon.

Inside Back Cover: Two views of Israel with the relief added using topography on a 100 m grid derived from the 25 m DTM of Israel (Hall, 1997). Global Mapper® 6.06 software was used to georeference the map sheets, and then to 'texture map' the topography at 20x vertical exaggeration onto the map as shaded relief. Sun illumination is from the northwest (N315°E) at an elevation of 45°. The area below sea-level has been shaded light blue using another useful feature of the software.
Top: A location map, first published in English in 1961 by the Survey of Israel (SOI - today the Israel Mapping Center), and reprinted some 38 years ago as the 'Map of the Cease-Fire Lines' following the Six-Day War in 1967. The map consists of the standard 1:250,000 scale North and South Israel sheets joined together. The grid is the Old Israel Grid, between 300 and -120N, and 80 and 240E. The main roads are shown in red, with the hydrological network in blue.
Bottom: Map of Potentially Active Faults in Israel. Compiled by Y. Bartov, A. Sneh, L. Fleischer, V. Arad, and M. Rosensaft, and published as Geological Survey of Israel Report GSI/23/2000. Green circles are epicenters of historical earthquakes with Richter magnitude between 2 and 6.5. Formations that are Pliocene to recent are shaded orange. Reproduced with permission, courtesy of the Geological Survey of Israel.

Back Cover: The world centered on the Levant. This image was prepared using Interactive Visualization Systems® (IVS) Fledermaus software, wrapping the 2' worldwide ETOPO2 dataset onto a sphere. With this software it is possible to zoom into and pan across every part of the Earth's surface.

©2005 Historical Productions-Hall
All rights reserved
©British Crown Copyright [1919-1993], on materials on pages 8-9, 141-142, 144, 150-151, and 172-173.
Published by permission of the Controller of Her Magesty's Stationery Office and the UK Hydrographic Office (www.ukho. gov.uk).

All materials subject to this copyright and included in this volume may be photocopied for the non-commercial purpose of scientific and educational advancement. This does not apply to the materials covered by British Crown Copyright.

Copyright is not claimed on any material prepared by government employees within the scope of their employment.

Typeset using Adobe® InDesign® CS ME for Macintosh from original Microsoft® Word 2000 files.

Prepress, layout, color separations, plates and printing by Art-Plus
Harashei Barzel 19, Talpiot Industrial Zone, Jerusalem 93420, Israel. Tel: +972-2-648-2228.

Printed and bound in Israel
ISBN 965-7297-03-6

Contents of Volume II

PART III - THE LEVANTINE BASIN

0. Introduction 1
J. K. Hall

9. Reflection Seismic Processing and Images of the Eastern Mediterranean from Cruise 5 of the R/V "Akademik Nikolay Strakhov" 21
D. Klaeschen, N. Vidal, A. Kopf, R. von Huene, and V A. Krasheninnikov

10. Seismic Images from South-East of Cyprus to the Syrian Coast 41
N. Vidal, D. Klaeschen, A. Kopf, R. von Huene, and V. A. Krasheninnikov

11. Multi-Channel Seismic Profiles across Eratosthenes Seamount and the Florence Rise reflecting the incipient collision between Africa and Eurasia near the island of Cyprus, Eastern Mediterranean 57
A. Kopf, N. Vidal, D. Klaeschen, R. von Huene, and V. A. Krasheninnikov

12. The Deep Structure of Eratosthenes Seamount from Seismic Refraction Data 73
S. M. Zverev, and D. A. Ilinsky

13. Peculiarities of sediments and basement structure in the Frontal Zone of the Cyprus Arc (based on seismic refraction data) 113
S. M. Zverev

14. Gravity field of the northeastern part of the Mediterranean Sea (to the south and west of Cyprus) 127
V. A. Toulin

15. Digital terrain model (DTM) of Cyprus: The island, its continental shelf, and the surrounding sea 135
J. K. Hall

16. Bathymetry of the Syria-Lebanon continental margin 149
J. K. Hall

17. Explanatory Notes to the IBCM-SED Map Series Unconsolidated Sediments of the Meditearranean Sea (Scale 1:1,000,000)and the Black Sea (Scale 1:2,000,000) 183
E. M. Emelyanov, K. M. Shimkus†, and P. N. Kuprin

PART IV - ISRAEL

Introduction **215**
A. Flexer, F. Hirsch, and J. K. Hall

18. Stratigraphy **269**
F. Hirsch, T. Weissbrod, C. Benjamini, Y. Eshet, A. Rosenfeld, and O. Orlova

18A Introduction to the Stratigraphy of Israel **269**
F. Hirsch

18B The Paleozoic in Israel and Environs **283**
T. Weissbrod

18C The Permian Fusulinids of Israel **317**
O. Orlova and F. Hirsch

18D The Triassic of Israel **331**
C. Benjamini, F. Hirsch, and Y. Eshet

18E The Jurassic of Israel **361**
F. Hirsch

18F The Cretaceous of Israel **393**
A. Rosenfeld, and F. Hirsch

18G The Paleocene – Eocene of Israel **437**
A. Rosenfeld and F. Hirsch

18H The Oligocene – Pliocene of Israel **459**
F. Hirsch

18I The Late Pliocene to Quaternary **489**
F. Hirsch

18J Strike-slip faulting west of the Dead Sea Escarpment **515**
A. Gilat

19 Bouguer Gravity Map of the Levant – A New Compilation **539**
M. Rybakov and A. Al-Zoubi

20 Depth to Crystalline Basement in the Middle East with Emphasis on Israel and Jordan **543**
M. Rybakov and A. Segev

21 **Magmatic Rocks** 553
A. Segev

22 **Whole Mantle Convection as the Cause of the Spiraling Global System of Lithospheric Geosutures: with Special Attention to the Central Plate (Between the Pelusium Line and the Lut Vortex)** 577
D. Neev and J. K. Hall

Epilogue 700
V. A. Krashenninikov, J. K. Hall, F. Hirsch, V. G. Kazmin, N. Bragin, D. Klaeschen, A. Kopf, S. A. Silantyev, N. Vidal, R. von Huene, and S. Zverev

APPENDICES

A **Regional Bibliographies on CDROM: Geology, Geophysics, Oceanology, and Related Subjects** 733
J. K. Hall

B **The NES Academik Nikolaj Strakhov and its Eastern Mediterranean Multi-Beam Swath Sounding Data on CDROM** 739
J. K. Hall

C **Top Judea Group – Digital Structural Map of Israel** 745
L. Fleischer and R. Gafsou

D **Geological Map Inventory for some Middle east Countries (Israel, Jordan, Syria, and Lebanon)** 755
R. Calvo and J. K. Hall

E **Merged Geological Map Sets for Syria, Jordan, Lebanon, and Israel** 769
R. Calvo and J. K. Hall

F **The RAS Marine Gravity Data from the Levantine Basin** 773
V. A. Toulin and J. K. Hall

G **Shaded Relief Images of the IBCM Bathymetry and Geological-Geophysical Overlays** 807
J. K. Hall

Plates

(In separate plate box)

I. Geomorphological Map of Syria (1963) Scale 1:1,000,000.

II. Tectonic Units of Syria (Kazmin, 2005, Chapter 8, Figure 1).

III. Structural Map of Syria (Kazmin, 2005, Chapter 8, Figure 2).

IV. Mediterranean and Black Sea Recent Sediments, Scale 1:5,000,000. (Emelyanov et al., 2005, Chapter 17).

V. Top Judea Group, Digital Structural Map of Israel, North Sheet 1:200,000 scale – Oversize. Shaded colored relief on one side, Contours on back.

VI. Top Judea Group, Digital Structural Map of Israel, South Sheet 1:200,000 scale – Oversize. Shaded colored relief on one side, Contours on back.

VII. Top Judea Group, Digital Structural Map of Israel, Color at 1:500,000 scale.

VIII. Stratigraphic Table of Israel, L. Fleischer, 2002.

IX. Tectonic Map of the Mediterranean Sea, 1:5,000,000 scale. (Bogdonov et al., 1994).

X. Digital Shaded Relief of the Island of Cyprus, 1:250,000 scale. Grayscale and color.

XI. Landforms of Israel, Digital shaded relief map, 1:500,000 scale. Grayscale and color.

Part III – The Levantine Basin

Introduction

John K. Hall
Geological Survey of Israel, 30 Malchei Israel Street, Jerusalem 95501, Israel

The Levantine Basin is traditionally the deep basin at the eastern end of the Mediterranean. Since its physiography was first described in the seminal work of Emery, Heezen and Allan (1966) based upon a reconnaissance cruise of the R/V Aragonese in the very early sixties, the Levantine Basin has piqued the interest of earth scientists. The region hosts the junction of three plates, whose interaction has produced complex structures. Because of its relative remoteness, and the uneasy relationships between the seven national entities along its littoral, the area was not easy to investigate. However, the probing since the 1970s has shown that the basin is filled with a great quantity of sediments (12 km or more), and that the nature of its underpinnings is not simple.

Many investigators have studied the area. Some have returned again and again to this problematic place. Most propose models for its origin and history based on the findings of the particular tools employed, whether they be bathymetry, gravity, magnetics, seismic reflection, seismic refraction, teleseismic investigations, or submarine geology based on coring, drilling, and dredging. The region's recent history also seems to beckon. From the pioneering study of our colleague Ya'akov Petrovitch Malovitskiy (1978) who proposed on the basis of seismic investigations that the Levantine Basin was a sunken continent, we advance to recent extrapolations (www.discoveryofatlantis.com - Sarmast, 2003) regarding the 'finding' of Atlantis at depths of ~1500 m between the West Tartus Ridge and the Gelendzhik Rise, based upon a computer analysis of the Strakhov's multibeam soundings.

PART III LAYOUT

Six of the nine chapters in this section deal with the continuing study of geophysical data collected during Cruise 5 of the NES Strakhov. Multi-channel seismics collected on eight profiles have undergone detailed analysis and reanalysis at GEOMAR by Dirk Klaeschen, Achim Kopf, Neus Vidal, and Roland von Huene (Chapters 9-11). 'Tweaking' of the data has resulted in new looks to depths of 14 km, presumably into the crystalline basement.

Working with seismic refraction data from Strakhov Cruises 5 and 10, and Boris Petrov Cruise 19, Sergey Zverev and Dmitry Illinsky (Chapters 12-13) have attempted to wring out additional information on the deep layering, acoustic velocities and therefore composition, and seismic signatures. This data, with magnetics and gravity from the compilations of Makris and Wang (1994) have suggested that Eratosthenes Seamount is atop an ancient volcano.

This conclusion recalls a similar analysis of the Mount Carmel structure in Israel, just 250 km to the ESE, where Gvirtzman, Klang and Rotstein (1990) postulate the existence of a shield volcano. Their conclusions are based on gravity and magnetic anomalies plus the penetration of 2,499 m of the Early Jurassic Asher Volcanics in the Atlit-1 well. The modeled diameter of the shield volcano is about 40 km, which is similar to the core of Eratosthenes Seamount.

Another similar buried intrusive structure was recently reported some 90 km off the shores of Israel by Folkman and Ben Gai (2004). It appears to be some 20 km in diameter, with its summit 8 km below the sea surface. And reinterpretation by Rybakov and Gardosh (2004) of the gravity data presented below suggests a fourth possible buried volcanic body beyond the one beneath Eratosthenes Seamount. Chapter 23 by Rybakov, Gardosh, and Ben-Avraham presents the results of that reinterpretation.

A new gravity compilation is offered by Vladimir Toulin (Chapter 14) based upon measurements from NES Boris Petrov (**Fig. III.1**) in 1989, and the NES Strakhov in 1990. These data supplement the piecemeal coverage that previously existed. The Russian Academy of Sciences, via World Data Center B in Moscow, kindly consented to make this dataset available for distribution on the CDROM which is described in Appendix F. Similar new compilations are in the offing as oil and gas exploration proceeds, among them the recent 8043 km of coverage by the M/V Northern Access in the Israeli EEZ (ARK Geophysics Ltd., 2002), as well as 3-D surveys by ISRAMCO, SAMEDAN, the British Gas Group, and others in the southeastern Mediterranean, and by companies working off the Lebanese and Syrian offshore that are mentioned in Chapter 16.

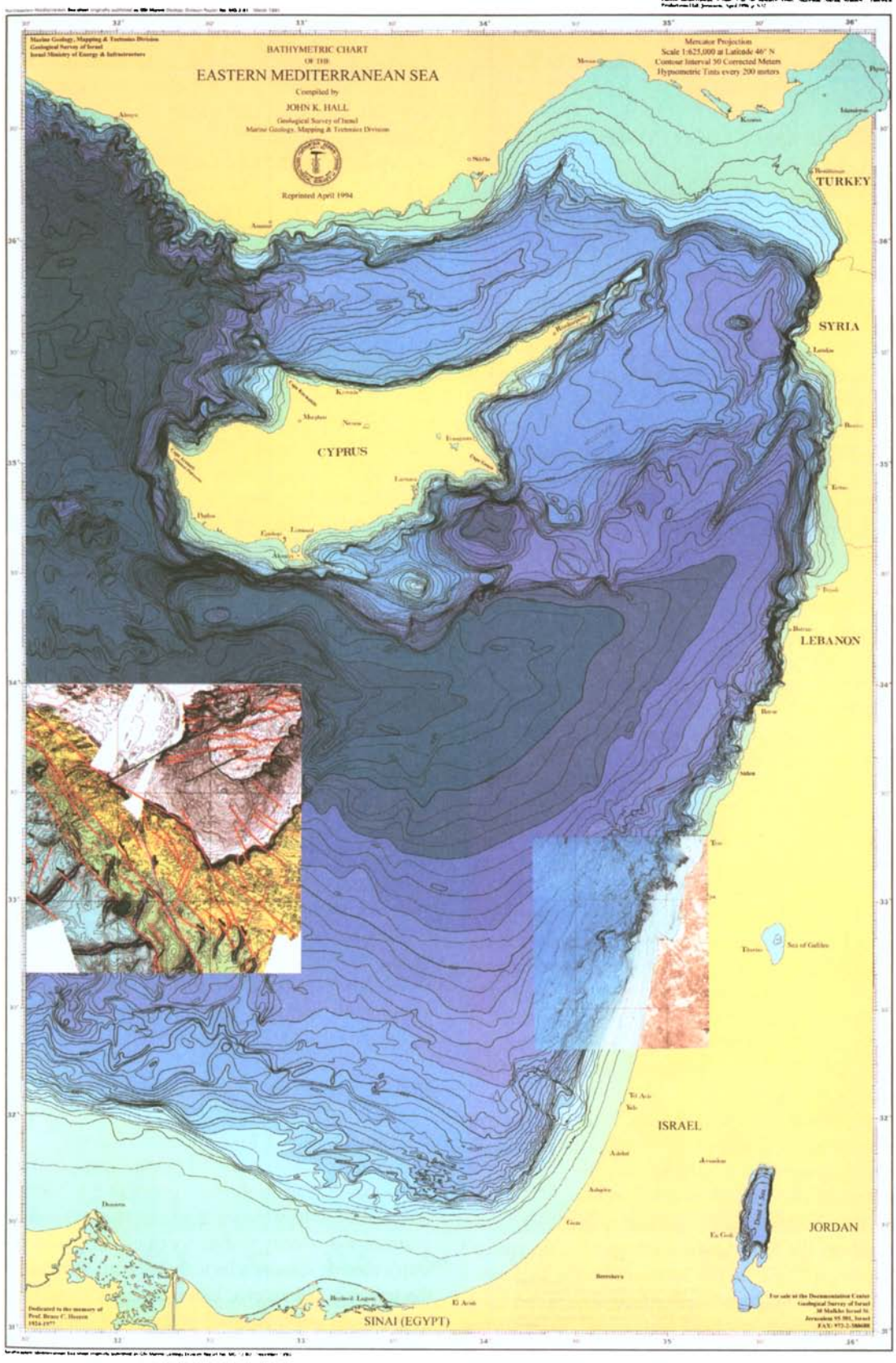
Chapters 15 and 16 deal with the author's activities in compiling bathymetric charts as part of the GEBCO and IBCM projects (see below), as well as preparation of digital terrain models (DTM) for Israel and its neighbors, including the island of Cyprus. Chapter 16 also delves into the various DTMs available for the specific area as well as worldwide.

The explanatory notes to the IBCM-SED recent sediment map of the Mediterranean and Black Seas are presented in Chapter 17. This immense undertaking by our Russian colleagues Emelyanov, Shimkus, and Kuprin, is one of the five geological/ geophysical overlays to the International Bathymetric Chart of the Mediterranean (IBCM - see below). It is being published here in lieu of publication like the other four explanatory notes to the IBCM overlays, the IBCM-G with Bouguer gravity anomalies (Makris et al., 1998), instrumental seismicity IBCM-S



Figure III.1. Photograph of the NES Akademik Boris Petrov. The ship is one of three research vessels built in Finland in the mid-1980s for the Russian Academy of Sciences. The NES Akademik Nikolaj Strakhov is a sister-ship, along with the NES M. A. Lavrentyev. The ships are 75.5 m (248') in length, and displace 2600 tons. Additional details on this class may be found in Appendix B of this volume.

Figure III.2. Bathymetric chart of the Eastern Mediterranean (Hall, 1994) with an overlay of the contours from the PRISMED-II survey over Eratosthenes Seamount from Mascle et al. (2001), and an update of the contours of the Dor Disturbance off Haifa from Hall and Almagor (1984). The original 50 m contours have been digitized, with corrections added for improvements in the bathymetry off northern Israel. Merged with land topography and presented as a colored shaded relief image (Fig. III.3), it presents a fair representation of the 'real' Levantine Basin, (but without the fascinating fabric which 100% swath mapping will reveal).


BATHYMETRIC CHART
OF THE
EASTERN MEDITERRANEAN SEA
Compiled by
JOHN K. HALL
Geological Survey of Israel
Marine Geology, Mapping & Technics Division
Reprinted April 1994
Mercator Projection
Scale 1:625,000 at Latitude 46° N
Contour Interval 50 Corrected Meters
Hypsometric Tints every 200 meters
TURKEY
SYRIA
CYPRUS
LEBANON
ISRAEL
JORDAN
SINAI (EGYPT)
Sea of Galilee

(Legros and Bonnin, 1996, 1999), Plio-Quaternary isopach and structural contours IBCM-PQ (Gennesseaux et al., 1999), and magnetic anomalies IBCM-M (Zanolla et al., 1998, 2000), in the geophysically-oriented Bollettino di Geofisica Teorica ed Applicata of the University of Trieste in Italy.

THE IBCM, IBCM-II, AND GEBCO COMPILATIONS

In our first book on the work of the NES Strakhov (Krashennikov and Hall, 1994), we published a bathymetric chart from 1978 of the eastern Mediterranean (Hall, 1994a). For reference purposes this chart is reproduced in **Fig. III.2**, overlain by the contours from the PRISMED-II survey over Eratosthenes Seamount from Mascle et al. (2001), and an update of the contours of the Dor Disturbance off Haifa from Hall and Almagor (1984). The original 50 m contours have been digitized, with corrections added for improvements in the bathymetry off northern Israel. Merged with land topography and presented as a colored shaded relief image (**Fig. III.3**), it presents a fair representation of the 'real' Levantine Basin, (but without the fascinating and detailed fabric which 100% swath mapping would reveal).

My compilational efforts in the 1970s were followed in the 1980s by an ongoing involvement in two joint Intergovernmental Oceanographic Commission of UNESCO (IOC) and International Hydrographic Organization (IHO) projects called GEBCO (General Bathymetric Chart of the Oceans) and IBCM (International Bathymetric Chart of the Oceans). In April 2003 GEBCO celebrated its Centenary (Carpine-Lancre et al., 2003). Founded in 1903 by HSH Prince Albert I of Monaco (1848-1922), GEBCO took on the task of compiling bathymetric contours for all the world's oceans in a series of 16 Mercator charts at 1:10,000,000 scale and two Polar Stereographic charts at 1:6,000,000 scale. Five editions were published, the last in 1982 by the Canadian Hydrographic Service. These editions used 500 m depth contours, with a 200 m contour inshore, compiled from echo-sounding profiles and spot soundings.

In the early 1980s GEBCO's emphasis slowly changed to the compilation of a gridded digital dataset, originally planned for a grid spacing of 2.5' (≤ 4630 m) and ultimately refined and completed at 1' (≤ 1852 m). This new grid was finally published in April 2003 in conjunction with the GEBCO Centenary celebrations in Monaco as two CDROMs (BDOC, 2003), with the land data taken from the 0.5' GLOBE land grid (Hastings and Dunbar, 1999; Verdin and Greenlee, 1996).

Much earlier, in the late 1970s, the IOC and IHO spun off another series of seven regional projects called the IBCs (for International Bathymetric Charts). IBCM was the first, for the Mediterranean and Black Sea. This was followed by IBCCA for the Caribbean, IBCEA for the Eastern Atlantic, IBCWIO for the Western Indian Ocean, IBCSWP for the Southwest Pacific, IBCAO for the Arctic Ocean, IBCSEP for the Southeast Pacific, and now a proposed IBCSO for the Southern Ocean (circum-Antarctica).

Each of the IBCs work at a local scale of 1:1,000,000, with 200 m contours and 20 m contours inshore. As the pioneer, IBCM concluded its 10 sheet bathymetric chart by 1983 (Morelli and Val'chuk, 1988), and then proceeded to prepare overlays of the Bouguer gravity anomalies (IBCM-G), seismicity (IBCM-S), Plio-Quaternary structural/isopach map based on the Messinian salt deposits (IBCM-PQ), recent bottom sediments (IBCM-SED), and magnetic anomalies (IBCM-M). To date none of the other IBCs have compiled such overlays. **Fig. III.4** shows postcards with the reductions of the original IBCM, IBCM-G, IBCM-S, and IBCM-PQ compilations.

In the early 1990s the Editorial Board of the IBCM decided to produce a gridded IBCM-II, which would be at 0.25' spacing. By 1995 this spacing had shrunk to 0.1' due to the increasing capability of multibeam sonars, the ongoing 'digitalization' of the local hydrographic offices, and a new feeling of confidence that it was possible. While IBCM-II was confined to the Mediterranean and Black Seas, my personal area of interest was considerably larger, *i.e.* the seas surrounding the Arabian Plate. To this end over 1700 navigational charts and hydrographic survey fairsheets for the Mediterranean, Black, Caspian, Red, and Arabian Seas were digitized, along with those for the Persian Gulf. The charts were scanned and then the techniques outlined in Chapters 15 and 16 used to extract the soundings. **Fig. III.5** gives an example of the wealth of data available in these historical surveys. These soundings were then used to interpolate grids using a number of numerical schemes.

Fig. III.6 shows the colored shaded relief in the expanded area including the Mediterranean and the seas surrounding the Arabian Plate. This was the first try at producing a 1' gridded dataset for this expanded area of interest. A DTM of the rapidly shrinking Aral Sea has been prepared from a contour map produced by DLR, the German Space Agency, but is not included. A discussion of the DTM compilation for the Black and Caspian Seas is given in Hall (2002). **Fig. III.7** shows the initial gridding for the Mediterranean Sea using the digitized Russian soundings plus the digitized IBCM contours.

Hence my search for newer and better datasets naturally led to my involvement with the Strakhov cruise, and our distinguished chief editor V. A. Krashenninikov. However the experience of joining the Strakhov for six weeks during Cruise 11 in 1990 with Dr. Gleb B. Udintsev also introduced me to the world of multibeam bathymetry, and the quantum leap in understanding bottom topography that the technique offers.

ROLE OF POST-STRAKHOV SWATH BATHYMETRY

The Strakhov Cruises 5 and 10 were the first systematic multibeam surveys in the Levantine Basin. However in present terms the 15 beam Hollming system of the 1980s was a dinosaur. Swath soundings were taken without accurate navigation, without *in situ* sound velocity profiles for calculating refraction, and without ship's motion sensors which allow beam-forming to always direct the transmit and receive lobes downward and place each arrival in its proper place. Because of these error sources, the full dataset was seldom used. In fact, users of early 15 beam systems usually

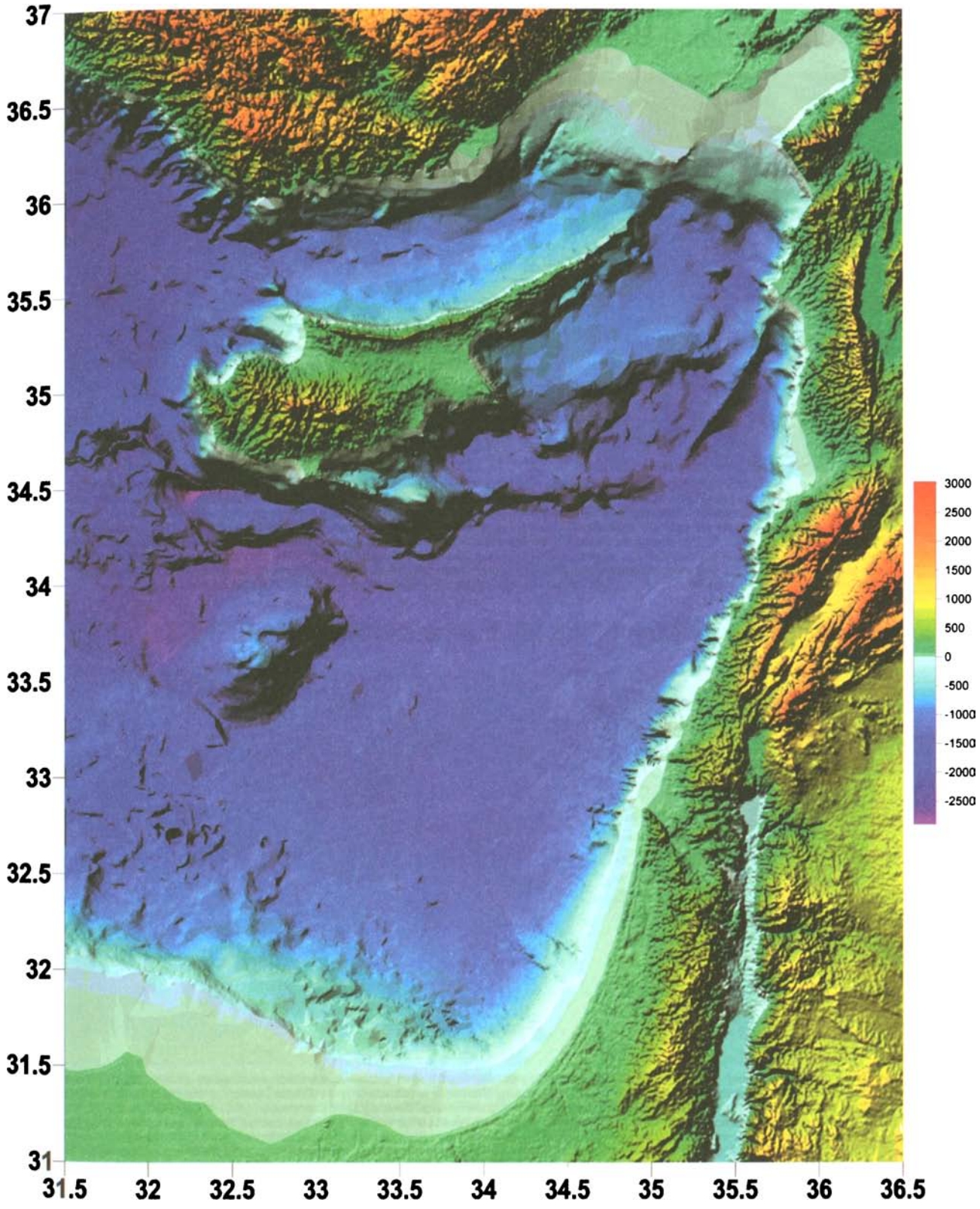
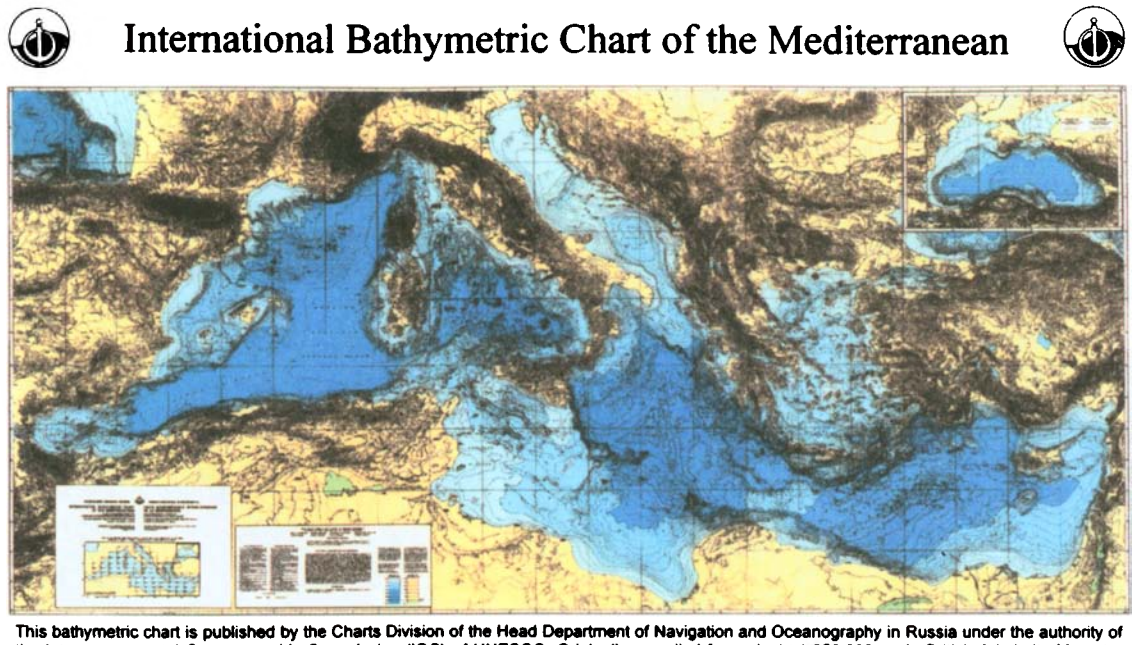


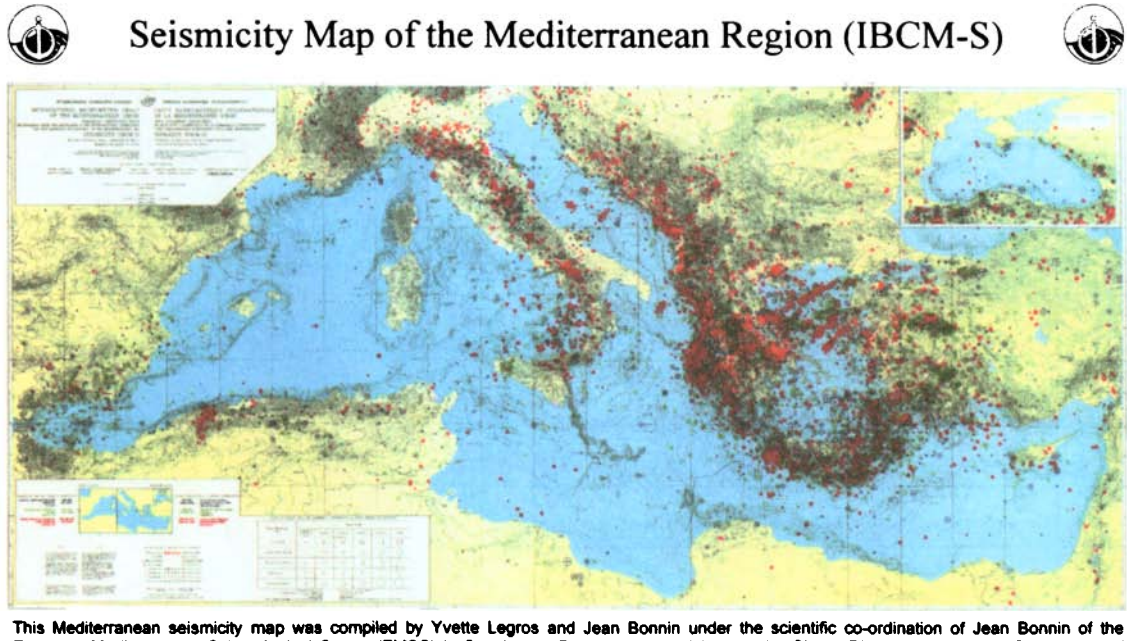
Figure III.3. Hysometrically colored bathymetric and topographic shaded relief of the Eastern Mediterranean. The original 50 m contours in Fig. III.2 were digitized and merged with land topography to produce a fair representation of the 'real' Levantine Basin, but without the fascinating fabric which 100% swath mapping and the latest SRTM topography would reveal.

(a)



This bathymetric chart is published by the Charts Division of the Head Department of Navigation and Oceanography in Russia under the authority of the Intergovernmental Oceanographic Commission (IOC) of UNESCO. Originally compiled from ninety 1:250,000 scale British Admiralty Mercator plotting sheets for oceanic soundings, it presents the bathymetry and land topography as 200 m contours with supplemental 20 m, 50 m, and 100 m contours at sea. Several versions are available; a 10 sheet set (each 74 x 90 cm) at 1:1,000,000 scale at 38°N, and a photo-reduction to 1:5,000,000 scale (the source of this postcard). This chart, with an inset of the entire Black Sea at half scale, is also the basemap for a Geological/Geophysical series with Bouguer gravity anomalies (IBCM-G), seismicity (IBCM-S), thickness of Plio-Quaternary sediments (IBCM-PQ), unconsolidated bottom surface sediments (IBCM-SED), and magnetic anomalies (IBCM-M). Digital variants and explanatory brochures for these series are in preparation. The digitized marine contours are available on CD-ROM as part of the British Oceanographic Data Centre's GEBCO Digital Atlas.

(c)

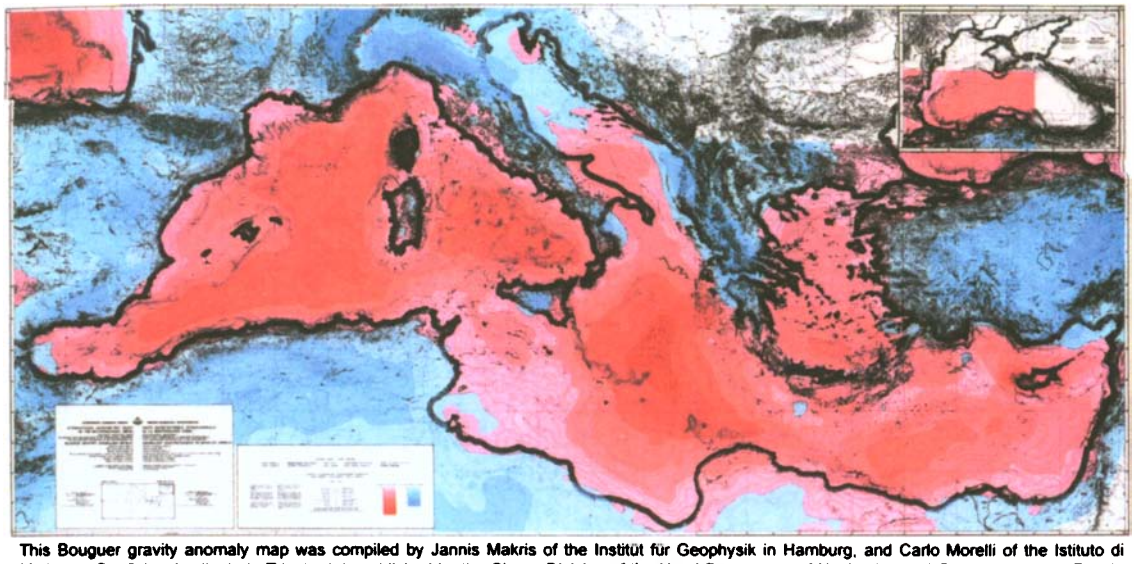


This Mediterranean seismicity map was compiled by Yvette Legros and Jean Bonnin under the scientific co-ordination of Jean Bonnin of the European-Mediterranean Seismological Centre (EMSC) in Strasbourg, France. It is published by the Charts Division of the Head Department of Navigation and Oceanography in Russia under the authority of the Intergovernmental Oceanographic Commission (IOC) of UNESCO. Some 33,000 separate seismic earthquake epicenters in the Mediterranean region were recalculated and are plotted as colored symbols, with shape denoting depth of focus, size reflecting magnitude, and color (blue, green, red) showing the historical catalog (1904-1963; 1964-1975; 1976-1988) from which the events are taken. Explanations are in English and French. The bathymetry is from the 200 m contours of the original IBCM with supplemental 20 m, 50 m, and 100 m contours at sea. Two versions are available; a 10 sheet set (each 74 x 90 cm) at 1:1,000,000 scale at 38°N, and a photo-reduction to 1:5,000,000 scale (the source of this postcard). An expanded explanatory brochure and printed earthquake catalog are in preparation.

Figure III.4. Reproductions of four postcards prepared by the author to illustrate (a) the original IBCM bathymetric chart, (b) the IBCM-G Bouguer gravity anomalies, (c) the IBCM-S seismicity map showing earthquake epicenters, and (d) the IBCM-PQ with the isopachs and structural contours

(b)

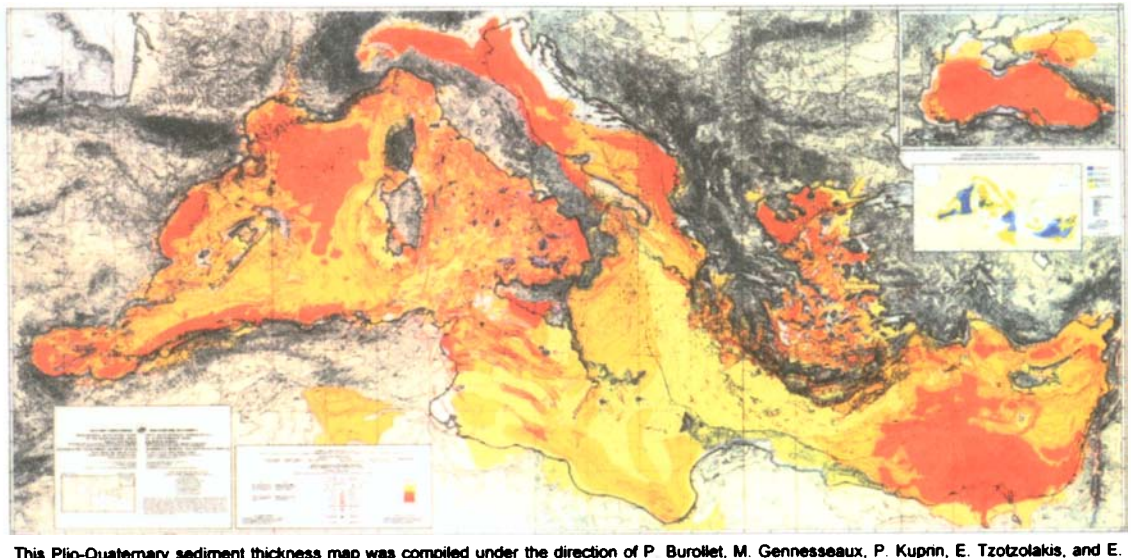
Mediterranean Bouguer Gravity Anomalies (IBCM-G)



This Bouguer gravity anomaly map was compiled by Jannis Makris of the Institüt für Geophysik in Hamburg, and Carlo Morelli of the Istituto di Miniere e Geofisica Applicata in Trieste. It is published by the Charts Division of the Head Department of Navigation and Oceanography in Russia under the authority of the Intergovernmental Oceanographic Commission (IOC) of UNESCO. The primary data are from over 114,000 nm of marine survey carried out in 1965-1972 by OGS in Trieste, and in 1973-1974 by the Dept. of Geodesy and Geophysics of Cambridge University, together with land compilations. It presents the anomalies in milligals, based upon the 1967 normal gravity formula, a 2.67 g/cm³ Bouguer density, and topographic corrections to 167 km for the land area in the easternmost four sheets. Contours are every 10 mGal with changes in tint every 50 mGal. Red tints are positive. The bathymetry is from the 200 m contours of the original IBCM with supplemental 20 m, 50 m, and 100 m contours at sea. Two versions are available; a 10 sheet set (each 74 x 90 cm) at 1:1,000,000 scale at 38°N, and a photo-reduction to 1:5,000,000 scale.

(d)

Plio-Quaternary Sediment Thickness Map (IBCM-PQ)

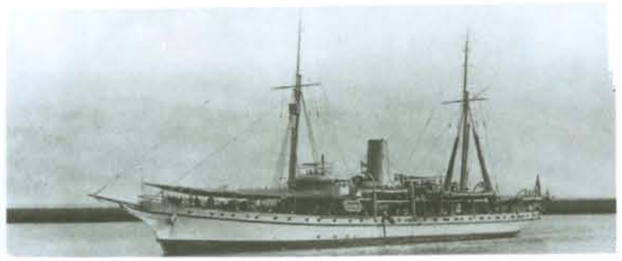


This Plio-Quaternary sediment thickness map was compiled under the direction of P. Burollet, M. Gennesseaux, P. Kuprin, E. Tzotzolakis, and E. Winnock. It is published by the Charts Division of the Head Department of Navigation and Oceanography in Russia under the authority of the Intergovernmental Oceanographic Commission (IOC) of UNESCO. The primary data derive from numerous marine seismic surveys of the depth to the top of the Messinian salt layer, together with land compilations. Contours are in increments of 0.2 sec two-way travel time, with changes in tint at 0.2, 1.0, 2.0, and >3.0 sec. The bathymetry is from the 200 m contours of the original IBCM with supplemental 20 m, 50 m, and 100 m contours at sea. Explanations are in English and French, and tectonic, diapiric, and volcanic features are indicated. Inset is a sketch map showing the Messinian evaporite deposits in the Mediterranean. Two versions are available; a 10 sheet set (each 74 x 90 cm) at 1:1,000,000 scale at 38°N, and a photo-reduction to 1:5,000,000 scale (the source of this postcard). An expanded explanatory brochure is in preparation.

of the Plio-Quaternary sediments laid down following the Messinian Salinity Crisis. This occurred in the late Miocene (between 5.96 and 5.33 myBP) when the Mediterranean mostly dried up..

UKHD Nile Cone Surveys

HMS Endeavour 1919-1922



6 The yacht-like *Endeavour*, designed specially for surveying and built by Fairfield in 1912, seen here in the Suez Canal about 1925. (Swan Hunter)

Figure III.5. Composite of five of the plotting sheets prepared by officers of the HMS Endeavour during summer surveys off the Nile Delta in 1919-1922. Altogether about a quarter million spot soundings were made using a steam powered wire sounding machine. For the inset in Abu Kir (Aboukir) Bay some 64,000 soundings were recorded on a single fairsheet. This is the area in which archeologists have recently uncovered the remains of the sunken cities of Herakleion and Menouthis (which occurred sometime after 740 CE), as well as French shipwrecks from the Battle of Aboukir Bay when on 1 August 1798 Admiral Horatio Nelson defeated the fleet of Napoleon Bonaparte.

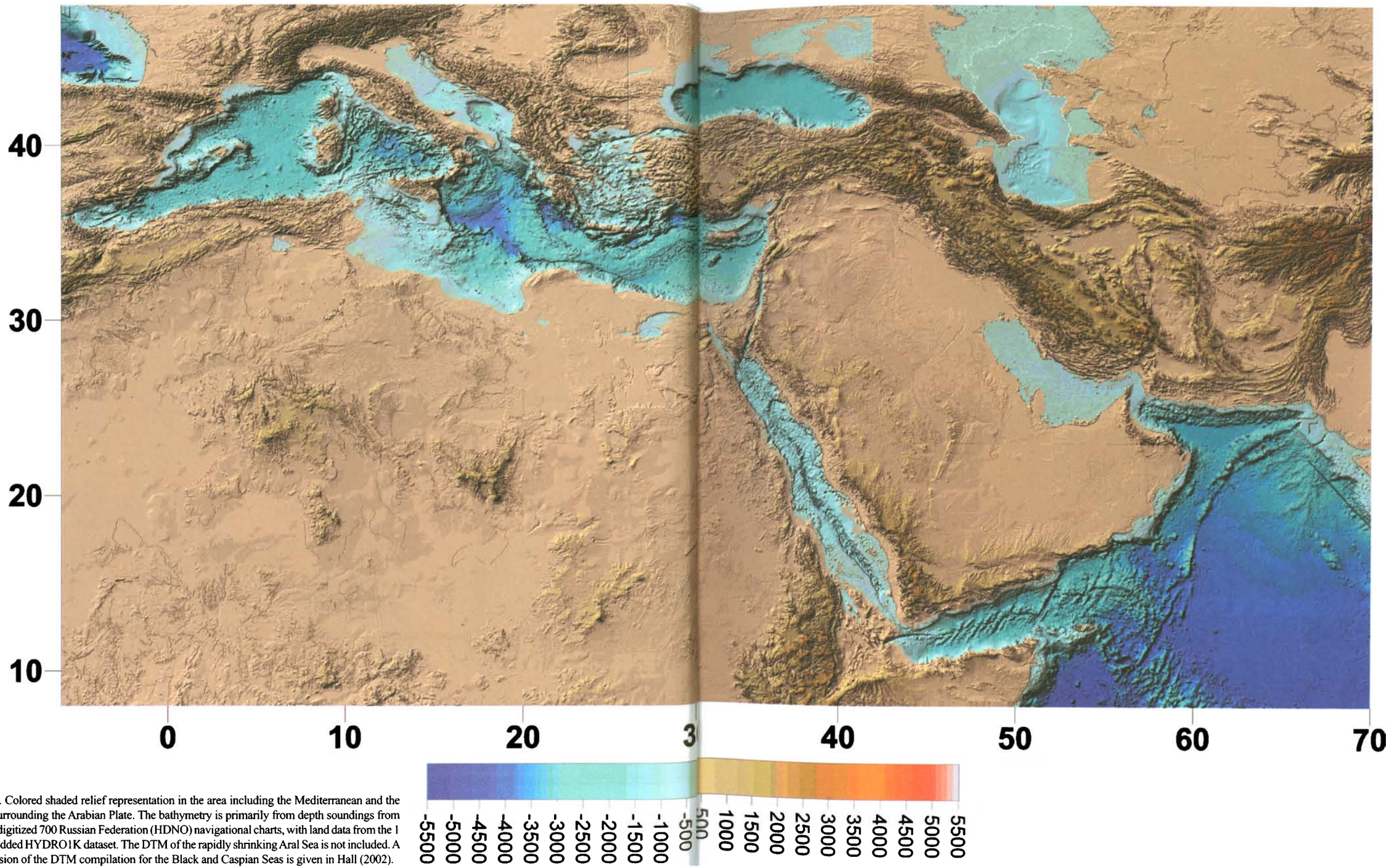


Figure III.6. Colored shaded relief representation in the area including the Mediterranean and the seas surrounding the Arabian Plate. The bathymetry is primarily from depth soundings from some digitized 700 Russian Federation (HDNO) navigational charts, with land data from the 1 km gridded HYDRO1K dataset. The DTM of the rapidly shrinking Aral Sea is not included. A discussion of the DTM compilation for the Black and Caspian Seas is given in Hall (2002).

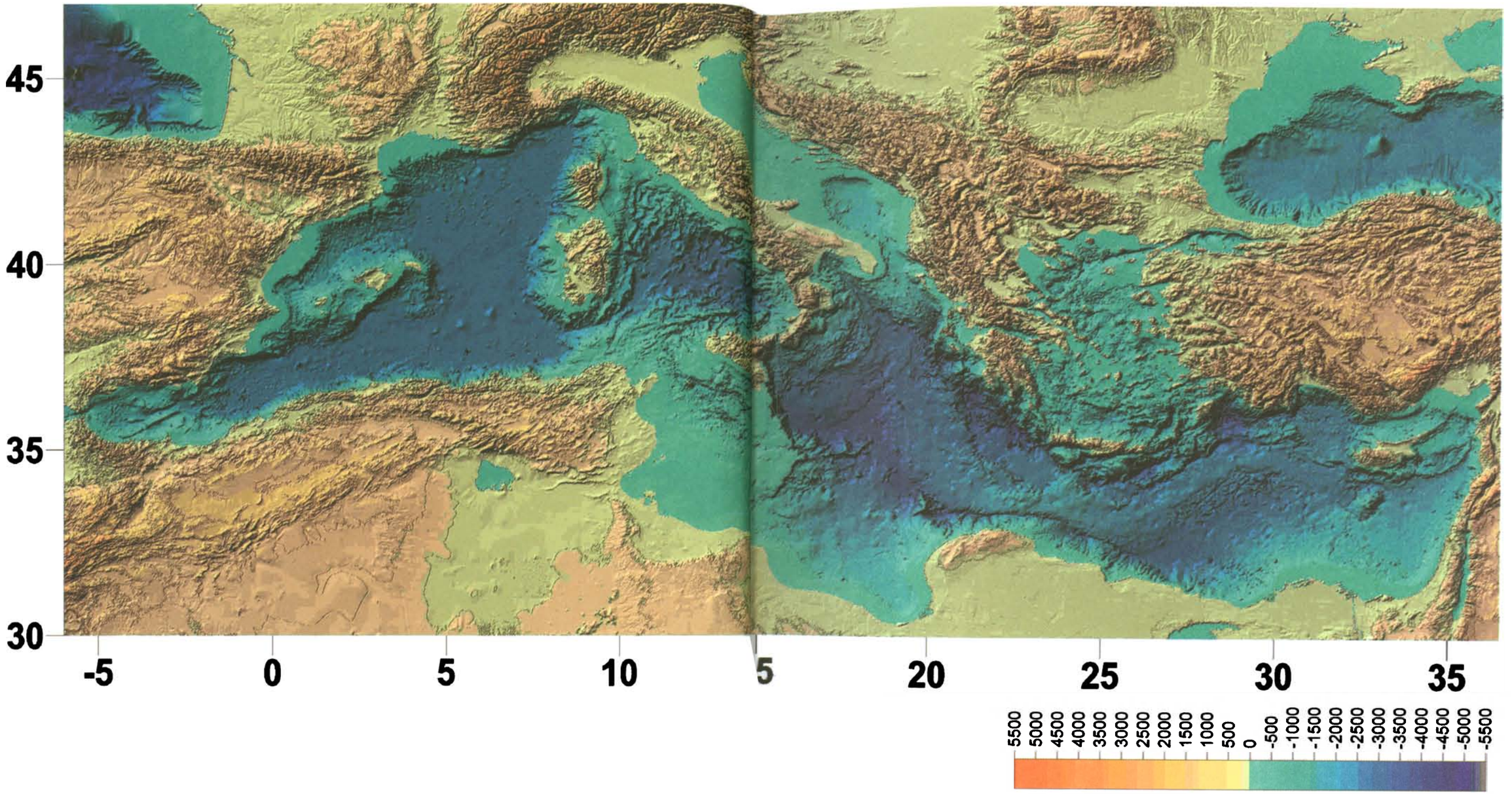


Figure III.7. Colored shaded relief representation of the IBCM coverage of the Mediterranean and Black Sea. This is a first try at producing a 1' gridded dataset from digitized Russian Federation soundings merged with the older 200 m IBCM contours from the GEBCO Digital Atlas. A discussion of the much higher resolution DTM compilation for the Black Sea is given in Hall (2002). The IBCM-II compilation will be a gridded 0.1' dataset based upon spot soundings and inshore contours plus deeper water multibeam data, merged with 0.1' onshore topography from the Shuttle Radar Topographic Mission (SRTM) of February 2000.

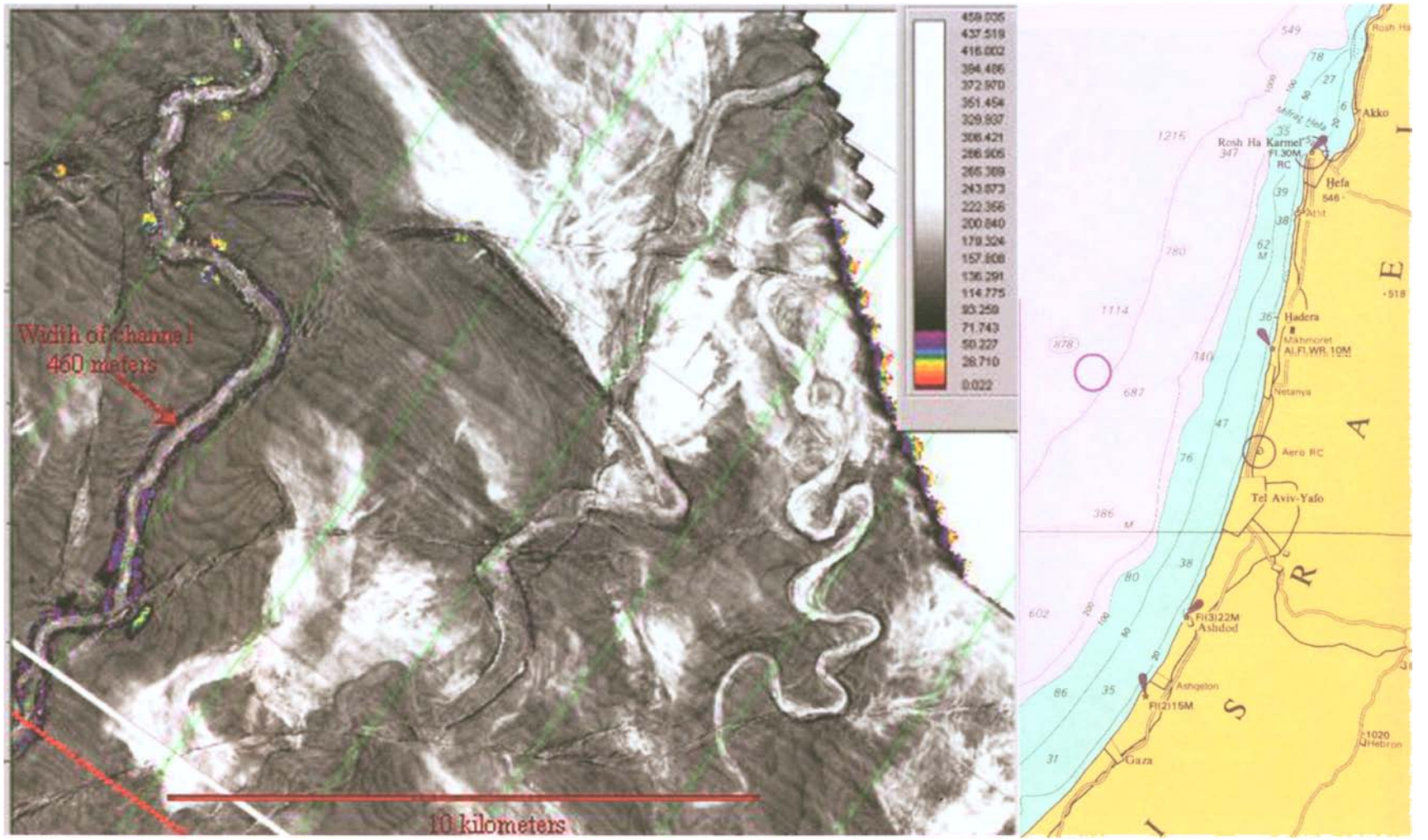


Figure III.8. Meandering deep sea channels observed at depths of 1100-1350 m in imagery based upon the first arrival amplitude from 3-D seismic mapping by the British Gas Group (Hall and Canning, 2001). This area is located west of Netanya in central Israel. Three such channels, 200-600 m wide and 18 m deep are observed. Folkman (2003) attributes them to a northern network of channels emanating out from the Nile distal fan, like those reported off the Damietta and Rosetta branches of the Nile by Wescott and Boucher (2000) and Bellaiche et al. (2002), which probably continue downslope into the moat east of Eratosthenes Seamount. At depth the 3-D seismic datasets show similar older buried channel-levee networks in the underlying Plio-Pleistocene sequence (Wescott and Boucher, 2000; Folkman, 2003). Image courtesy of Dr. Yehoshua Folkman.



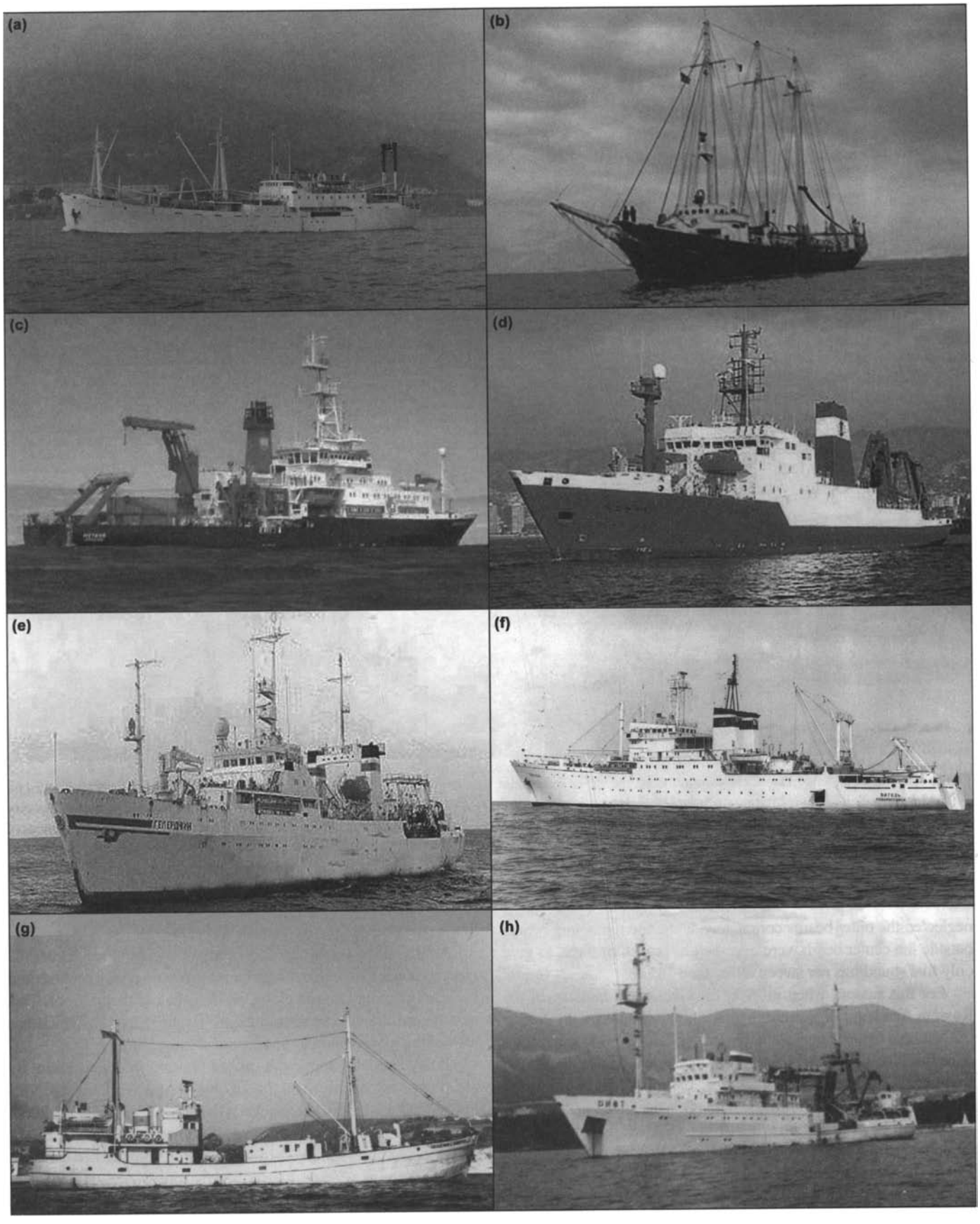
Figure III.9. Independence Day Celebration aboard the drillship Glomar Challenger, July 4, 1969, DSDP Leg 6, Hawaii-Guam. From left to right, Alexander P. Lisitzin (Shirshov Institute, Academy of Sciences of the USSR), Alfred G. Fischer (Princeton), Bruce C. Heezen (Lamont-Doherty Geological Observatory), Lloyd Dill (Captain of the Glomar Challenger), Valery A. Krasheninnikov (Geological Institute, Academy of Sciences of the USSR), and Anthony C. Pimm (Scripps Institution of Oceanography). Photo courtesy of V. A. Krasheninnikov, identifications by Dr. James V. Gardner.

neglected the outer beams completely, while the remaining beams outside the center beam were averaged in groups of three, to give only five soundings per sweep rather than 15.

For this reason, when in 1995 the Geological Institute of the Russian Academy of Sciences requested that I transfer the data to the National Geophysical Data Center (NGDC - World Data Center A in Boulder, Colorado, USA), only the center-beam dataset was supplied. For the sake of completeness, the full Strakhov Hollming dataset with some 4.65 million soundings is discussed in Appendix B, and will be available on request on CDROM. Appendix A has an update of the extensive bibliography which was printed (Hall, 1994b) in the original book. This bibliography, also on CDROM, includes much new information gathered in the Mediterranean area in the past decade.

Nearly forty years ago, my Lamont mentor Prof. Bruce C. Heezen noted that with detailed bathymetric mapping, much could be learned about what is going on deep below the seafloor. This was before the advent of multibeam swath mapping, which has proved that observation to be particularly cogent.

It is certainly borne out in the eastern Mediterranean by the pioneering swath mapping of the French IFREMER/CNES PRISMED, PRISMED II, and FANIL studies (Mascle et al., 2000, 2001; Loubrieu, Satra, and Cagna, 2001; Bellaiche et al., 2002). These new surveys were carried out using Simrad EM12D and EM300 systems with up to 162 beams spread over an arc of up to 150°, differential GPS navigation, ship's motion sensing, and


(a)
(b)
(c)
(d)
(e)
(f)
(g)
(h)

sound velocity profiles. Our French colleagues (Jean Mascle, pers. comm. 2003) intend in the coming years to continue the deep water multi-beam surveys in the far eastern Mediterranean and the Cilicia Basin, and ultimately throughout the remainder of the unmapped deep Mediterranean. This was exemplified by the recent SHALIMAR and BLAC surveys carried out by the N/O Le Suroît in October-November 2003 off Syria and Lebanon.

Around Israel, recent multi-beam work has convinced us that our understanding of the eastern Mediterranean was severely limited. In 2001 the author and the Geological Survey of Israel (GSI), together with the Israel Oceanographic & Limnological Research Ltd. (IOLR) and the Survey of Israel (SOI) began a comprehensive mapping of the Israel Mediterranean offshore with a Simrad EM1002 95 kHz system installed on the IOLR's vessel R/V Etziona (Hall et al., 2002). Results to date have shown numerous unknown geologic features. These include extensive scour indicating sediment transport directions, carbonate-cemented quartz sandstone ('kurkar') ridges and eolian-like bedform platforms, pockmarks and gas vent craters, recent faulting, erosional channels etc. Because most of the work has been inshore where progress is slow, the mapping of the deeper features to 1000 m depth will come later. An example of these findings appears in Chapter 16.

However a brief look at what awaits us was afforded in 2002 during F/S METEOR Cruise 52/2 off Israel. In addition to gravity, magnetics, CDP reflection, and OBS refraction, METEOR made continuous swath mapping with a 90° (61 beams, coverage of 2 times the depth) Atlas Hydrosweep system, with narrow beam Parasound sub-bottom profiler (Grant and Schreiber, 1990). Off southern Israel, in water depths over 1 km, meandering relict deep-sea channels were observed in areas of very low gradient, generally flowing north. The channels curve by up to 300° inside a circle of about 1.5 km diameter. The channel beds were up to 300 m across, and incised some 30 m into the regional slope. They exhibited all the features associated with deep-sea fan channels, such as levee deposits and side slumps. These features are relict, as all the area is blanketed with ~12 m of sticky yellow Holocene mud.

Farther north, in an area of some 900 km² 130 km west of Netanya, Folkman (2003) observed similar features in water depths of 1100-1350 m in imagery based upon the first arrival amplitude from 3-D seismic mapping by the British Gas Group (Hall and Canning, 2001). In this imagery (**Fig. III.8**) three such meandering channels, 200-600 m wide and 18 m deep are observed. Folkman attributes them to a northern network of channels emanating out of the Nile distal fan like those reported off the Damietta and Rosetta branches of the Nile by Wescott and Boucher (2000) and Bellaiche et al. (2002), which probably continue downslope into the moat east of Eratosthenes Seamount. The 3-D seismic datasets show similar older buried channel-levee networks in the underlying Plio-Pleistocene sequence (Wescott and Boucher, 2000; Folkman, 2003).

The Hydrosweep/Parasound recordings and the 3-D seismic imagery also show numerous sharp ridges and faults, one of which Folkman (2003) correlates with the onshore Or Akiva fault. It is highly likely that within a few years, as complete swath mapping becomes available in the deeper waters offshore, the detailed pattern of faulting and associated halokinetic deformation will cast light on what transpired in the recent geological past.

CONCLUDING REMARKS

Our previous book on Cruise 5 of the NES Akademik Nikolaj Strakhov (Krashenninikov and Hall, 1994) was apparently quite instrumental in bringing about ODP Leg 160 which drilled four holes (Nos. 965-968) in a S-N transect across Eratosthenes Seamount. This provided interesting insights into the geological history and sequence of vertical movements (Kempler, 1998; Mart and Robertson 1998; Robertson, 1998a, b). The following eight chapters in the present book add to this body of knowledge. However many aspects of the history remain unanswered, such as the oceanic, continental, or mixed nature of the underlying crust throughout the basin, the age and distribution of the oldest sediments, and the sequences of compression, rifting, deformation and faulting within the tectonic framework. Several new refraction profiles associated with the DESERT 2000 program and the METEOR 52/2 GEMME work off northern and southern Israel have been carried out with much improved recording and OBS spacings. These will undoubtedly add new data and constraints.

My own feeling is that at this point future deep probes should be based upon the findings of the upcoming detailed bathymetric picture and the deep seismics, which will result from the oil prospection programs which are or will shortly be underway. Until this new generation of swath mapping is completed, the nearly quarter century old compilation in Fig. III.1 will continue to be among the best representations available for the easternmost Mediterranean.

ACKNOWLEDGEMENTS

The compilation business cannot proceed in a vacuum. I gratefully acknowledge the support and understanding given me over many years by the Geological Survey of Israel, which was somehow convinced that some good would come out of these efforts. As I took part in very few of the cruises which were used in these compilations I am particularly grateful to the various chief scientists, data archivists, hydrographers, and fellow compilers



Figure III.10. Photographs of various ships that carried out geophysical work in the Mediterranean. a) Maria Paolina, NATO SACLANT Centre, La Spezia; b) R/V Vema, LDEO. c) F/S Meteor, DFG, Germany; d) F/S Sonne, BMBF Germany; e) R/V Gelendjik, Southern Branch, Shirshov Institute of Oceanology of the RAS; f) R/V Vityaz, Southern Branch, Shirshov Institute of Oceanology of the RAS; g) R/V Sergei Vavilov, Southern Branch, Shirshov Institute of Oceanology of the RAS; h) R/V Rift, Southern Branch, Shirshov Institute of Oceanology of the RAS.

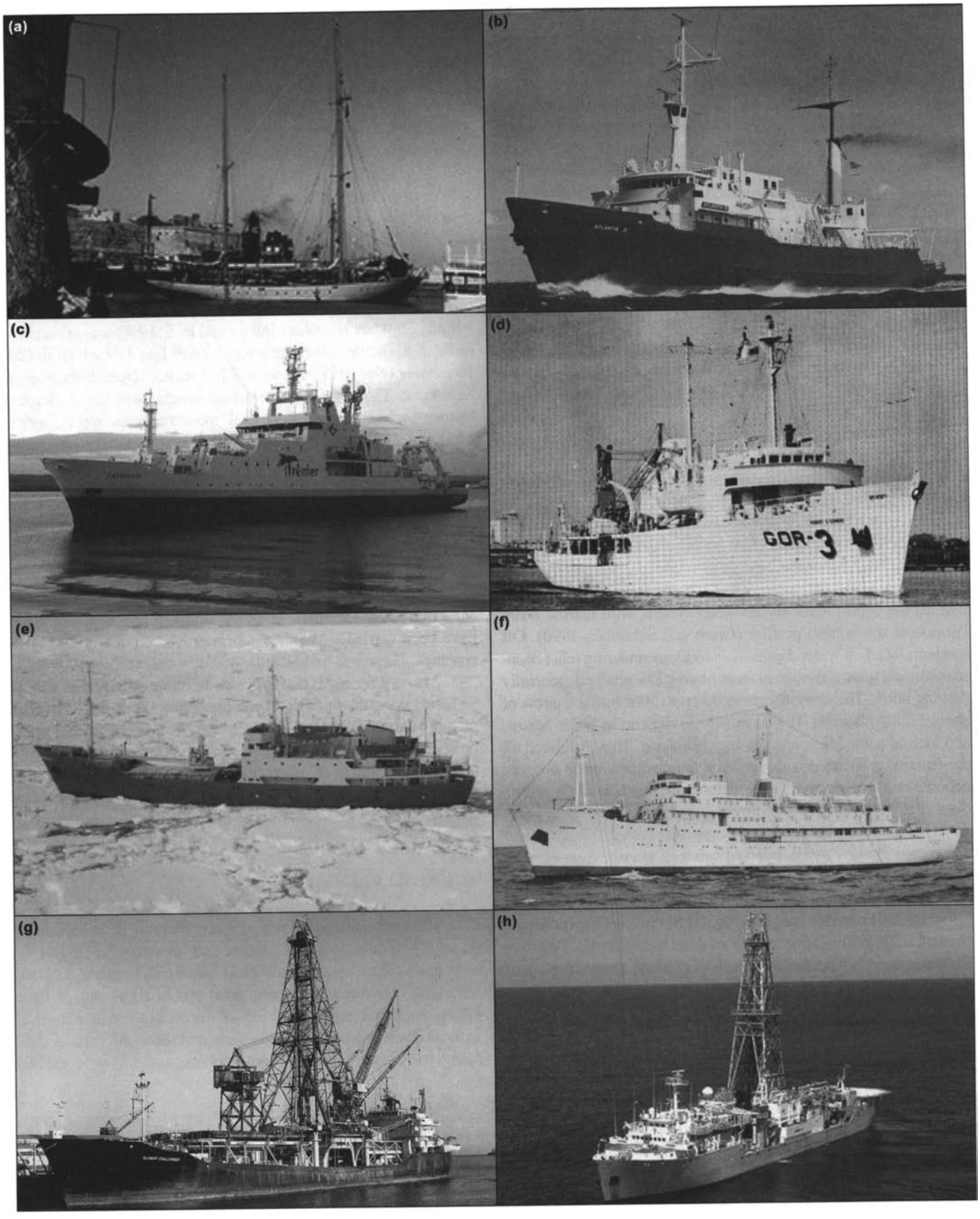

(a)
(b)
(c)
Thetis
(d)
GOR-3
(e)
(f)
(g)
(h)

Figure III.11. Photographs of additional ships that carried out geophysical work in the Mediterranean. a) R/V Atlantis, in Valleta, Malta, WHOI; b) R/V Atlantis II, WHOI; c) N/O L'Atalante, Ifremer. d) R/V Robert D. Conrad (GOR-3), LDEO; e) RRS Shackleton, IOS Wormley, Godalming, UK; f) RRS Discovery, IOS Wormley, Godalming, UK; g) Glomar Challenger, DSDP; h) JOIDES Resolution, JOIDES. Photos of additional ships can be seen in Chapters 15 and 16.



and data scroungers who suffered my visits and enquiries, and who ultimately delivered. In particular I wish to thank Bill Watson and Gordon Taylor at the United Kingdom Hydrographic Office (UKHO) in Taunton, former UKHO hydrographers Desmond P. D. Scott and Brian Harper who were longtime members of GEBCO and IBCM, the IBCM Chairman Prof. Carlo Morelli, former GEBCO Chairman Sir Anthony Laughton, former and present IHB Presidents Admirals Guiseppe Angrisano and Alexandros Maratos, and especially my long term colleague and friend, Norman Z. Cherkis.

And finally, in recognition of the part played by our chief editor and my mentor Bruce C. Heezen in the study of the Mediterranean, as well as by the many ships which did the work and do not appear in other chapter figures, I offer **Figs. III-9, III.10** and **III.11**, with my sincere thanks to the many scientists, officers, and crew members who manned these ships throughout the years.

REFERENCES CITED

ARK Geophysics Ltd., 2002. Offshore Israel 2001: East Mediterranean Sea Phase I, 2D Gravity and Magnetic Survey, Processing Report, prepared for TGS-NOPEC Geophysical Company. ARK Project No. ARK01051, March 2002, 43 p.

Bellaiche, G., Loncke, L., Gaullier, V., Droz, L., Mascle, J., Courp, T., Moreau, A., Radan, S., and Sardou, O., 2002. The Nile deep-sea fan and its channel-levees system: results from the PRISMED II and FANIL cruises. In: CIESM, 2002. Turbidite systems and deep-sea fans of the Mediterranean and the Black Seas. CIESM Workshop Series, N°17, 120 pages, Monaco. p. 49-53. <www.ciesm.org/publications/ Bucharest02.pdf>,

Bogdanov, N. A., Khain, V. E., Koronovsky, N. V., Lomize, M. G., and Chekhovich, V. D., 1994. Tectonic Map of the Mediterranean Sea. Scale 1:5,000,000. Institute of the Lithosphere of the Russian Academy of Sciences, and Moscow State University, 1 sheet.

British Oceanographic Data Centre, 2003. Centenary Edition of the IHO/IOC General Bathymetric Chart of the Oceans. 2 CDROMs and brief printed explanation.

Carpine-Lancre, J., Fisher, R., Harper, B., Hunter, P., Jones, M., Kerr, A., Laughton, A., Ritchie, S., Scott, D. P. D., Whitmarsh, M., and others, 2003. The History of GEBCO 1903-2003. GITC bv., Lemmer, The Netherlands, 140 p.

Emery, K. O., Heezen, B. C., and Allan, T. D., 1966. Bathymetry of the Eastern Mediterranean Sea. Deep-Sea Res., 12(2), p. 173-192.

Folkman, Y., 2003. The Nile Deep - Sea Fan Channels Offshore Israel. Israel Geological Society Annual Meeting, Abstracts, Ein Boqeq, 25-27 March 2003, p. 33.

Folkman, Y., and Ben Gai, Y., 2004. The "Jonah" buried seamount: Intrusive structure in the southeastern Levant Basin offshore Israel. In: B. Schilman, Y. Harlavan, Y. Haiel, and R. Calvo (eds.), Abstracts, Ann. Meet. .Isr. Geol. Soc., Hagoshrim, 23-25 Mar. 2004, p. 29.

Gennesseaux, M. Burollet P. and Winnock E., 1999. Thickness of the Plio-Quaternary sediments (IBCM-PQ). Boll. Geof. Teor. ed Appl., 39(4), p. 243-284.

Grant, J. A., and Schreiber, R., 1990. Modern swathe sounding and sub-bottom profiling technology for research applications: The Atlas Hydrosweep and Parasound systems. Mar. Geophys. Res., 12(1-2), p. 9-19.

Gvirtzman, G., Klang, A. and Rotstein, Y. (1990). Early Jurassic shield volcano below Mount Carmel: new interpretation of the magnetic and gravity anomalies and implication for Early Jurassic rifting. Isr. J. Earth Sci., 39(2-4), p. 149-159.

Hall, B, and Canning, J., 2001. British Gas Group internal report on offshore 3-D seismic surveys.

Hall, J. K., 1994. Bathymetric Chart of the Eastern Mediterranean Sea, Scale 1: 625,000. 1 Map sheet (Plate I, Fig. 1.13) accompanying Hall, J. K., Udintsev, G. B. and Odinokov, Yu. Yu., (1994). The bottom relief of the Levantine Sea. In: Krasheninnikov, V., and Hall, J. K. (eds.), Geological structure of the North-eastern Mediterranean (Cruise 5 of the Research Vessel 'Akademik Nikolaj Strakhov'), pp. 5-31. Historical Productions-Hall, Jerusalem, April 1994.

Hall, J. K., Sade, R., Avrahamov, L., Amit, G., and Golan, A., 2002. The National Bathymetric Survey: Highlights from the first year of operation. Israel Mediterranean Continental Margin- 14th Yohai Bin-Nun Conference, Haifa, 21 May 2002, Collected Abstracts, p. 42-46,

Hall, J. K., 2002. Bathymetric compilations of the seas around Israel. I: The Caspian and Black Seas. In: R. Bogoch (ed.), GSI Current Research, Vol. 13, Jerusalem, December 2002, p. 105-108.

Hall, J. K., 2003. GOMap, GEBCO, IBCM, and the Israeli NBS. Isr. Geol. Soc., Ann. Meet., Ein Boqeq, 25-27 March 2003, Abstr., p. 50.

Hastings, D. A., and Dunbar, P. K., (Editors), 1999. Global Land One-kilometer Base Elevation (GLOBE). Digital Elevation Model, v. 1.0, Documentation v. 1.0, U. S. Dept. of Commerce, NOAA, National Geophysical Data Center, Boulder, CO, 138 p.

Loubrieu, B., C. Satra, and R. Cagna, 2001. Morpho-bathymetry of the Mediterranean Ridge and surrounding areas. Acoustic image of the Mediterranean Ridge and surrounding areas. Two sheets, Mercator Projection, at scale 1:1,500,000 at 35°°N, Ifremer, Plouzane.

Kempler, D., 1998. Eratosthenes Seamount: the possible spearhead of incipient continental collision in the Eastern Mediterranean, Chap. 53, In: Robertson, A. H. F., Emeis, K. -C., Richter, C., and Camerlenghi, A. (Eds.), Proceedings of the Ocean Drilling Program, Scientific Results, Vol. 160, p. 709-722.

Krasheninnikov, V. A., and Hall, J. K., (Editors), 1994. Geological Structure of the North-Eastern Mediterranean (Cruise 5 of the Research Vessel 'Akademik Nikolaj Strakhov'), Historical Productions-Hall, Jerusalem, 396 p. + viii.

Legros, Y., and Bonnin, J., 1996. Seismicity (IBCM-S) Explanatory booklet. European-Mediterranean Seismological Centre, International Bathymetric Chart of the Meditarranean (IBCM). 52 p.

Legros, Y., and Bonnin, J., 1999. Investigating instrumental seismicity data sources for the Mediterranean Region (IBCM-S). Boll. Geof. Teor. ed Appl., 40(2), p. 79-146.

Makris J., Morelli C., and Zanolla C., 1998. The Bouguer gravity map of the Mediterranean Sea (IBCM-G). Boll. Geof. Teor. ed Appl., 39(1), p. 79-98.

Makris, J.,Wang, J., Odintsov, S. D., and Udintsev, G., 1994. The magnetic field of the Eastern Mediterranean Sea. In: V. A. Krasheninnikov and J. K. Hall (eds.), Geological Structure of the North-Eastern Mediterranean Sea (Cruise 5 of the Research Vessel 'Akademik Nikolaj Strakhov'), Historical Productions-Hall, Jerusalem, p. 75-85.

Makris, J., and Wang, J., 1994. Bouguer gravity anomalies of the Eastern Mediterranean Sea. In: V. A. Krasheninnikov and J. K. Hall (eds.), Geological Structure of the North-Eastern Mediterranean Sea (Cruise 5 of the Research Vessel 'Akademik Nikolaj Strakhov'), Historical Productions-Hall, Jerusalem, p. 87-98.

Malovitsky, Y. P., Emelyanov, E. M., Kazakov, O. V., Moskalenko, V. N., Osipov, Shimkus, K. M., and Chumakov, I. S., 1975. Geological structure of the Mediterranean sea floor (based on geological and geophysical data). Mar. Geol., 18(4), p. 231-261.

Mart, Y., and Robertson, A.H.F., 1998. Eratosthenes Seamount: an oceanographic yardstick recording the Late Mesozoic-Tertiary geological history of the Eastern Mediterranean. Chap. 52. In: Robertson, A. H. F., Emeis, K. –C., Richter, C., and Camerlenghi, A. (Eds.), Proceedings of the Ocean Drilling Program, Scientific Results, Vol. 160, p. 701-708.

Mascle, J., Benkhelil, J., Bellaiche, G., Zitter, T., Woodside, J., Loncke, L., and the Prismed II Scientific Party, 2000. Marine geologic evidence for the Levantine-Sinai plate, a new piece of the Mediterranean puzzle. Geology, 28(9), p. 779-782.

Morelli, C., and S. Val'chuk, 1988. The International Bathymetric Chart of the Mediterranean (I.B.C.M.) published under the authority of the Intergovernmental Oceanographic Commission of UNESCO. In: J. K. Hall (ed.), Preprint of Chapter 1 in the IBCM Supporting Volume, Jerusalem, Israel, 10 p.

Robertson, A.H.F., 1998a. Formation and destruction of the Eratosthenes Seamount, Eastern Mediterranean Sea, and implications for collisional processes. Chap. 51 In: Robertson, A. H. F., Emeis, K. –C., Richter, C., and Camerlenghi, A. (Eds.), Proceedings of the Ocean Drilling Program, Scientific Results, Vol. 160, p. 681-700.

Robertson, A. H. F., 1998b. Mesozoic-Tertiary tectonic evolution of the easternmost Mediterranean area: integration of marine and land evidence, Chap. 54 In: Robertson, A. H. F., Emeis, K. – C., Richter, C., and Camerlenghi, A. (Eds.), Proceedings of the Ocean Drilling Program, Scientific Results, Vol. 160, p. 723-782

Rybakov, M., and Gardosh, M., 2004. Eratosthenes Magnetic Anomaly - Integrated interpretation. In: B. Schilman, Y. Harlavan, Y. Haiel, and R. Calvo (eds.), Abstracts, Ann. Meet. .Isr. Geol. Soc., Hagoshrim, 23-25 Mar. 2004, p. 94.

Sade, R., Hall, J. K., and Gur-Arieh-Avrahamov, L., 2003. Israel's National Bathymetric Survey. Kongsberg-Simrad FEMME 2003, Cadiz, Spain, April 1-4.

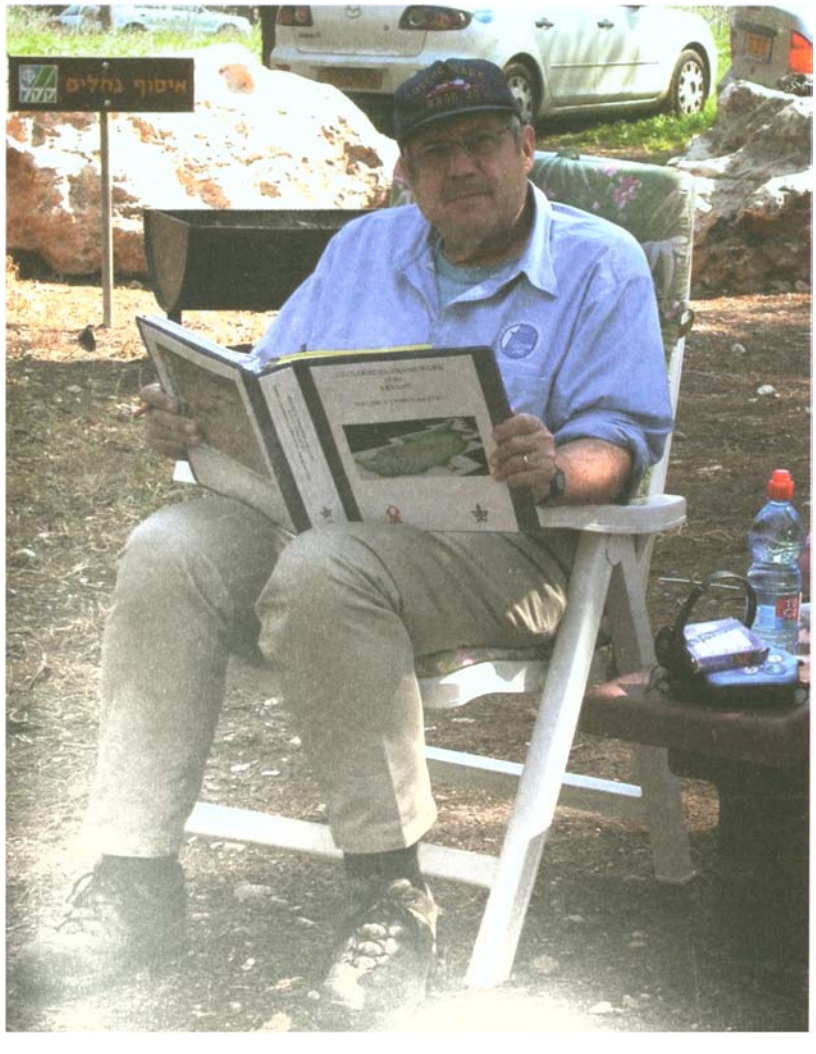
Sarmast, R., 2003. Discovery of Atlantis: The Startling Case for the Island of Cyprus. Origin Press, 190 p. 67 illustrations.

Verdin, K. L., and Greenlee, S. K., 1996. Development of continental scale digital elevation models and extraction of hydrographic features. In: Proceedings, Third International Conference/Workshop on Integrating GIS and Environmental Modeling, Santa Fe, New Mexico, January 21-26, 1996. National Center for Geographic Information and Analysis, Santa Barbara, California.

Wescott, W. A., and Boucher, P. J., 2000. Imaging submarine channels in the western Nile Delta and interpreting their paleohydraulic characteristics from 3-D seismic. The Leading Edge, 19(6), 580, 582, 584, 586, 588, 590-591.

Zanolla C., Morelli C. and Marson, I.; 1998. The magnetic anomalies of the Mediterranean Sea (IBCM-M). Boll. Geof. Teor. ed Appl., 39(1), p. 1-36.

Zanolla C., Morelli C., and Marson, I., 2000. The magnetic anomalies of the Eastern Mediterranean revisited and the Black Sea ones presented. Boll. Geof. Teor. ed Appl., 41(1), p. 79-83.



The author checking the galleys of Volume I of the **Geological Framework of the Levant**. Photo taken February 26, 2005 during a family outing at the Keren Kayemet Leisrael (KKL) Forest in Mitzpe Modi'in, Israel, near the graves of the Maccabeans. Note the signs connecting the author with the sea — the shirt bearing the logo of the Center for Coastal and Ocean Mapping (CCOM) at the University of New Hampshire (UNH), and the ball cap from the USCGC Healy (WAGB-20), a 19,000 ton U. S. Coast Guard icebreaker that took the author back to the southern part of his Arctic thesis area over the Chukchi Borderland in 2003 and 2004 during his sabbatical a UNH. Photo by Naomi Y. Hall (age 10¾).

Chapter 9

Reflection Seismic Processing and Images of the Eastern Mediterranean from Cruise 5 of the Research Vessel 'Akademik Nikolaj Strakhov'

Dirk Klaeschen
GEOMAR Research Centre, Wischofstrasse 1-3, D-24148 Kiel, Germany
Neus Vidal
Escola Universitaria Salesiana de Sarria, Rafael Battle 7, 08017 Barcelona, Spain
Achim J. Kopf
Geosciences Azur, B. P. 48, 06230 Villefranche-sur-Mer Cedex, France
Roland von Huene
GEOMAR Research Centre, Wischofstrasse 1-3, D-24148 Kiel, Germany
Valery A. Krasheninnikov
Geological Institute of the Russian Academy of Sciences, Pyzhevskiy pereulok 7, 109017 Moscow, Russia

ABSTRACT

We present the results of ~1700 line km of reprocessed multichannel deep seismic reflection data recorded in the eastern Mediterranean Sea, extending from south-west of Cyprus to the coast of Syria. The data required careful processing, including individual deconvolution operators to remove the effects of ghost and bubble pulses inherited from the streamer and airgun configurations, and to improve the temporal resolution. The primary reflections were masked by multiple energy from the seafloor and the uppermost sedimentary layers which required *f-k* and wave-equation demultiple procedures. Pre-stack depth migration provided a first insight into both the subsurface and deep velocity information for the area, which revealed from west to east a complex pattern of crustal blocks and sedimentary-tectonic units. These reflect the various stages of the incipient collision between Africa and Eurasia.

1. INTRODUCTION

The geometry and precise location of the plate boundary between Africa and Eurasia in the eastern Mediterranean Sea has been a matter of debate, and its evolution is still unclear (*e.g.* Kempler, 1994; Woodside et al., 1997). Seismicity, high resolution bathymetry, gravity, magnetics as well as several shallow seismic surveys and some wide-angle data indicate that there are different tectonic segments (*e.g.* Hall et al., 1994; Makris and Wang, 1994; Makris et al., 1994; Udintsev et al., 1994; Makris et al., 1983). The multichannel seismic data acquired during Cruise 5 of the Research Vessel 'Akademik Nikolaj Strakhov' provided the opportunity to illustrate the deeper structures and the deformational pattern of the area. A set of profiles from south-east of Cyprus to the coast of Syria were oriented subparallel to the presumed direction of plate convergence and are tied by a crosscutting SW-NE-striking line (**Fig. 9.1**). The most prominent topographic high in the area, Eratosthenes Seamount south of Cyprus, is crossed by two profiles (Lines 8 and 10, Fig. 9.1). Another topographic high, the Florence Rise west of Cyprus, is traversed by Line 9 (Fig. 9.1). The three seismic lines in the west provide useful information on the deformational patterns resulting from the collision of tectonic fragments (both from the north and the south) in a convergent regime, and its affect on the vertical tectonics of the Cyprus area.

2. DATA ACQUISITION

In 1987, Strakhov Cruise 5 yielded more than 1700 km of multichannel seismic (MCS) data along ten profiles between the Herodotus abyssal plain in the west and the Syrian coast in the east (Fig. 9.1). The first images of CMP-stacked sections were processed at the computer center of SOYUZMORGEO in Krasnodar (near Gelendzhik), and were presented by Kogan and Stenin (1994). For the seismic acquisition an airgun array sound source with a total volume of 12 liters and a chamber pressure of 15 MPa (150 bar) was used. The source airgun array consisted of 4 chambers, each displacing 3 liters, which was towed at a depth of 12 m. The shot point interval was approximately 100 meters for all the seismic lines. The hydrophone array had 48 channels, each group consisting of 21 receivers spread along 45 meters. The centers of each hydrophone array group were separated by 50 m, resulting in a total active array length of 2350 meters. The minimum and maximum offset from the source was 375 m and 2725 m, respectively. For more details, see Kogan and Stenin (1994). The seismic data from the survey were stored digitally on 130 magnetic tapes at 1600 bpi in SEG-B format, with a sampling rate of 4 ms and a trace length of 12 s.

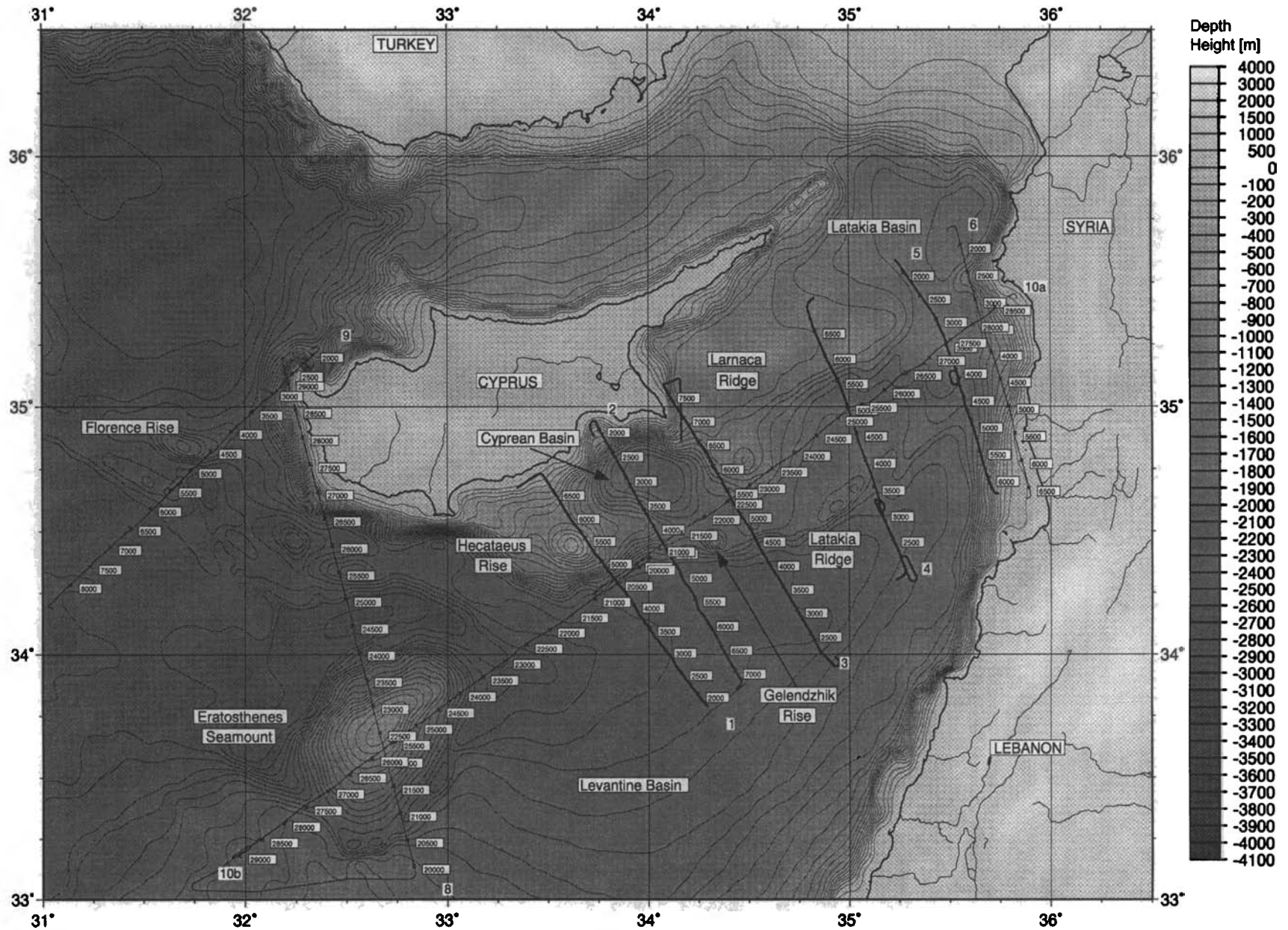
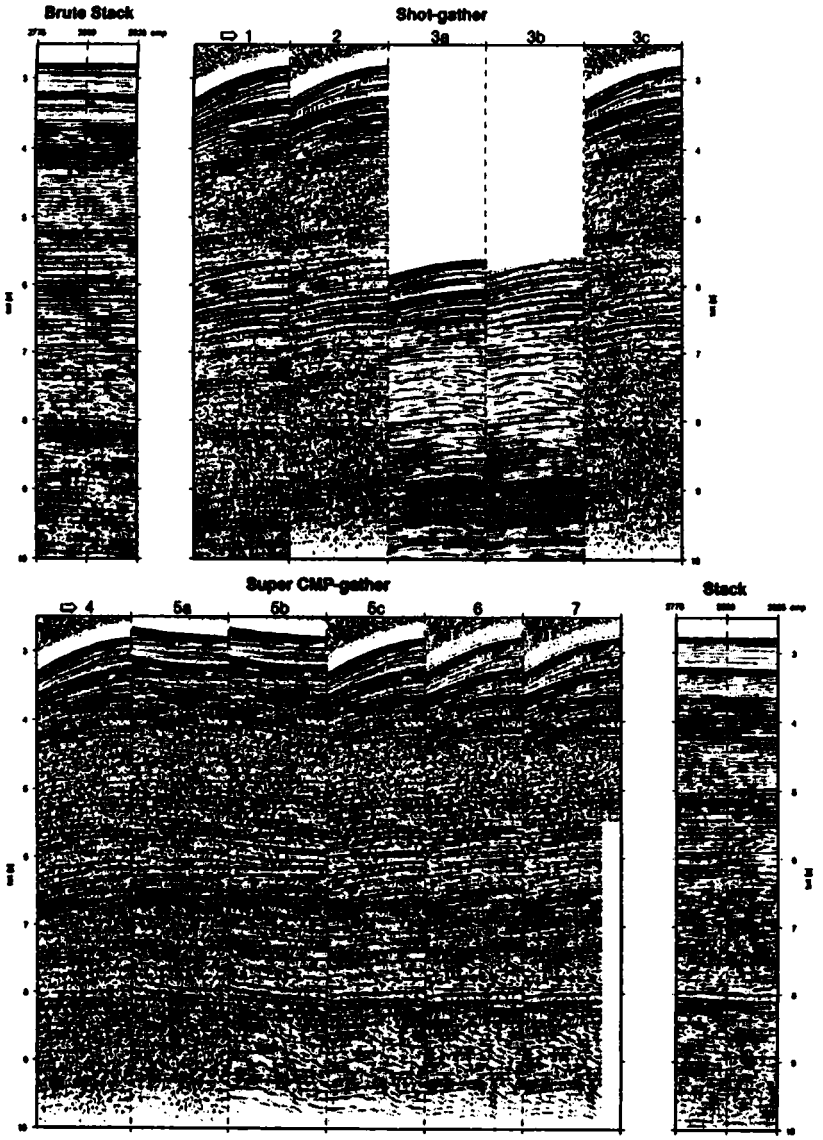


Fig. 9.1. Bathymetric map of the Eastern Mediterranean Sea, including the locations of Lines 1-10 collected during Cruise 5 of ' Strakhov'.



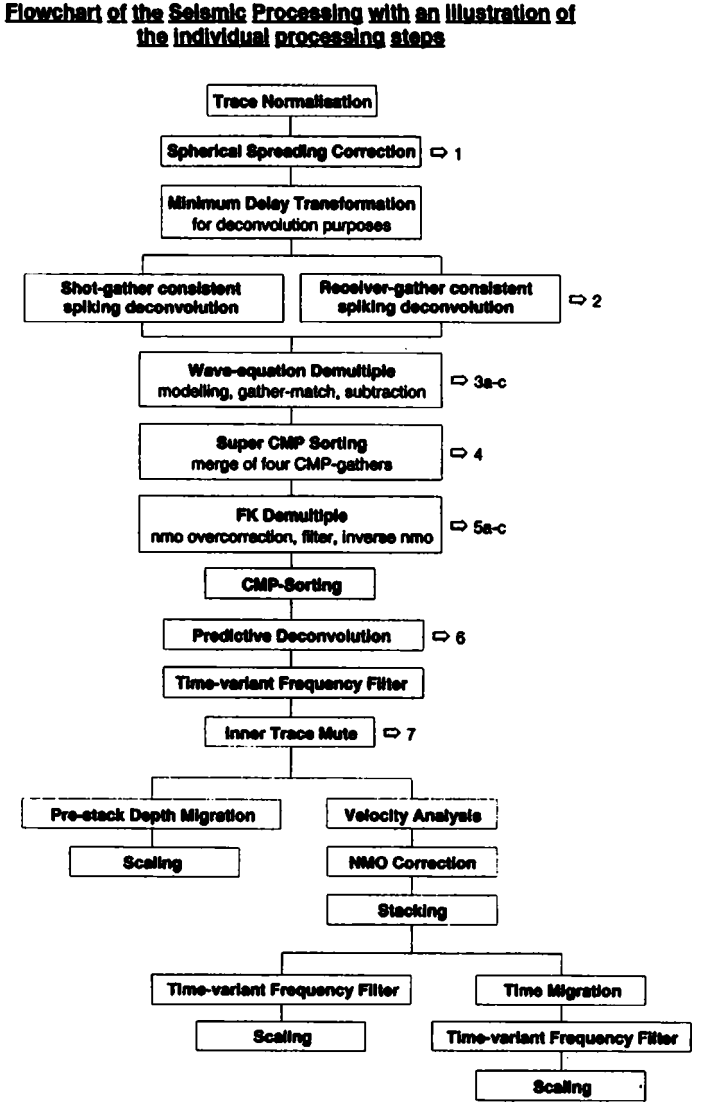


Fig. 9.2. Flowchart of the seismic processing sequence illustrating the individual processing steps. The data example is of the brute stack before preprocessing and the stack after preprocessing from Line 1, CMP 2775-2825. The shot gather and super CMP gather shown approximately correspond to the location of CMP 2800.

Table 9.1. The seismic lines acquired during Cruise 5 of 'Strakhov'. Line 7 and Line 10c are not shown here as they did not undergo the full reprocessing cycle to depth migration.

Profile No.	Record No.	CMP No.	Length (km)
1	998-2224	1942-6893	123.8
2	998-2253	1942-7009	126.7
3	989-2430	1924-7735	145.3
4	990-2188	1926-6765	121.0
5	990-2518	1926-6189	106.6
6	996-2144	1938-6577	116.0
7	996-2180	1938-6721	119.6
8	10001-12312	19948-29239	232.3
9	998-2831	1942-8317	159.4
10a	9996-12219	19938-28830	222.3
10b	9998-12300	19942-29197	231.4
10c	9998-10266	19942-21014	26.8
		Total Length in km	1731.2

3. SEISMIC DATA ANALYSIS AND PROCESSING

First of all, the magnetic tapes on which the raw seismic data were archived had to be physically cleaned. They were then temporarily copied onto a different magnetic media in order to avoid read errors for the following procedures. The cleaned tapes were then demultiplexed and rewritten in SEG-Y tape format. To simplify the acquisition geometry, a constant shot point distance of 100 meters was assumed. For CMP-binning, a bin width of 25 meters was defined, resulting in a 12 fold coverage (**Table 9.1**). As the raw data were recorded with spatially varying time delays, a near trace section was used to define the time shifts along the seismic lines. To determine the geographical locations of the MCS lines, the seismic data were time-migrated with water velocity and the resulting seafloor topography compared to the time converted seafloor depths acquired simultaneously by the Hollming multibeam echo-sounder. The geographical coordinates were then interpolated from the TRANSIT navigational satellite system fixes acquired during the seismic survey. The processing sequence applied to the data is displayed in a flow chart (**Fig. 9.2**) which illustrates each processing step.

All the preprocessing algorithms, which were applied to improve the quality of the subsurface information, are part of the commercial GEOSYS® software package from PRAKLA-SEISMOS GmbH. From the initial check on the data quality using the shot gathers it became apparent that the individual channels of the streamer had different amplitude levels, which sometimes changed along the line. A long window trace normalization followed by a spherical spreading correction was used to compensate for these spatial and temporal variations in amplitude. As the source contained an oscillating bubble and the streamer depth continuously varied along its active length, a complex interference of the bubble pulse and the streamer ghost was superimposed on the main arrivals.

Thus, a special signal processing procedure became necessary. Firstly, a deterministic minimum delay transformation was applied, to fulfill the requirements for the deconvolution processes. A shotgather-consistent spiking deconvolution was followed by a bandpass filtering in minimum delay characteristic, so that most of the source bubble energy was removed. After sorting the data into common receiver gathers, a receiver gather-consistent spiking deconvolution and subsequent bandpass filtering in minimum delay characteristic of the 48 neighboring shots were applied. In this domain, the receiver ghost appears most coherent in the autocorrelation function assuming that the streamer depth for one receiver varies only slightly along the seismic profile. To remove all multiple reflection events created between the free surface and the seafloor, a Kirchhoff-based wave equation demultiple procedure was applied (Wiggins, 1988). No assumptions were made concerning the complexity of the seafloor topography.

From the knowledge of the seafloor topography a multiple model was calculated from the shot gathers by wave-field extrapolation. Thus, a primary reflection produces the first multiple. From the location of the first multiple, the second order multiple can be predicted, and so on. By this procedure, all multiples created between the free surface and the seafloor can be simulated. Next, the predicted multiples have to be matched in phase and amplitude to the original data before they can be subtracted from the real shot gather. After subtraction, most of the multiple energy is removed from the original data (even from those multiples having a complex geometry).

To remove the remaining multiple energy in the data, a multiple suppression procedure, which is based on the apparent velocities between primary and multiple events in the common mid-point (CMP) domain, was applied. To reduce the spatial aliasing in the CMP-domain, four neighboring CMP gathers were merged together to create a super CMP-gather. After a normal moveout (NMO) correction and an additional time correction, the primary events dip upward whereas the remaining multiple energy still dips downward. Based on these differences in the apparent velocity, a frequency-wave number (*i.e. f-k*) filter was designed to remove only the downward dipping events. After filtering, these additional time and normal-moveout corrections are removed from the filtered gather.

To improve the temporal resolution of the seismic data, a two-window-predictive single trace deconvolution was applied, which is a compromise between temporal resolution and signal-to-noise ratio. The two windows were designed to accommodate the uppermost 2-3 s of the sedimentary layers and the remaining time samples in the lower part of the data respectively. As a final step in the preprocessing sequence for the data, a time variant frequency filter and an inner trace mute were applied, because the multiple energy mostly remains on the near offset traces.

The unstacked preprocessed data were then either used for input into the pre-stack depth migration procedure, or to produce a stack and time migrated section. To produce a stack, the velocity function was determined from conventional velocity analysis by constant velocity CMP stacks and NMO-corrected CMP gathers along the seismic profiles. As the stacked data do not represent the geological cross section when the subsurface structure is complex, a post-stack time migration was applied. To define the velocity information necessary for the migration, the stacking velocities

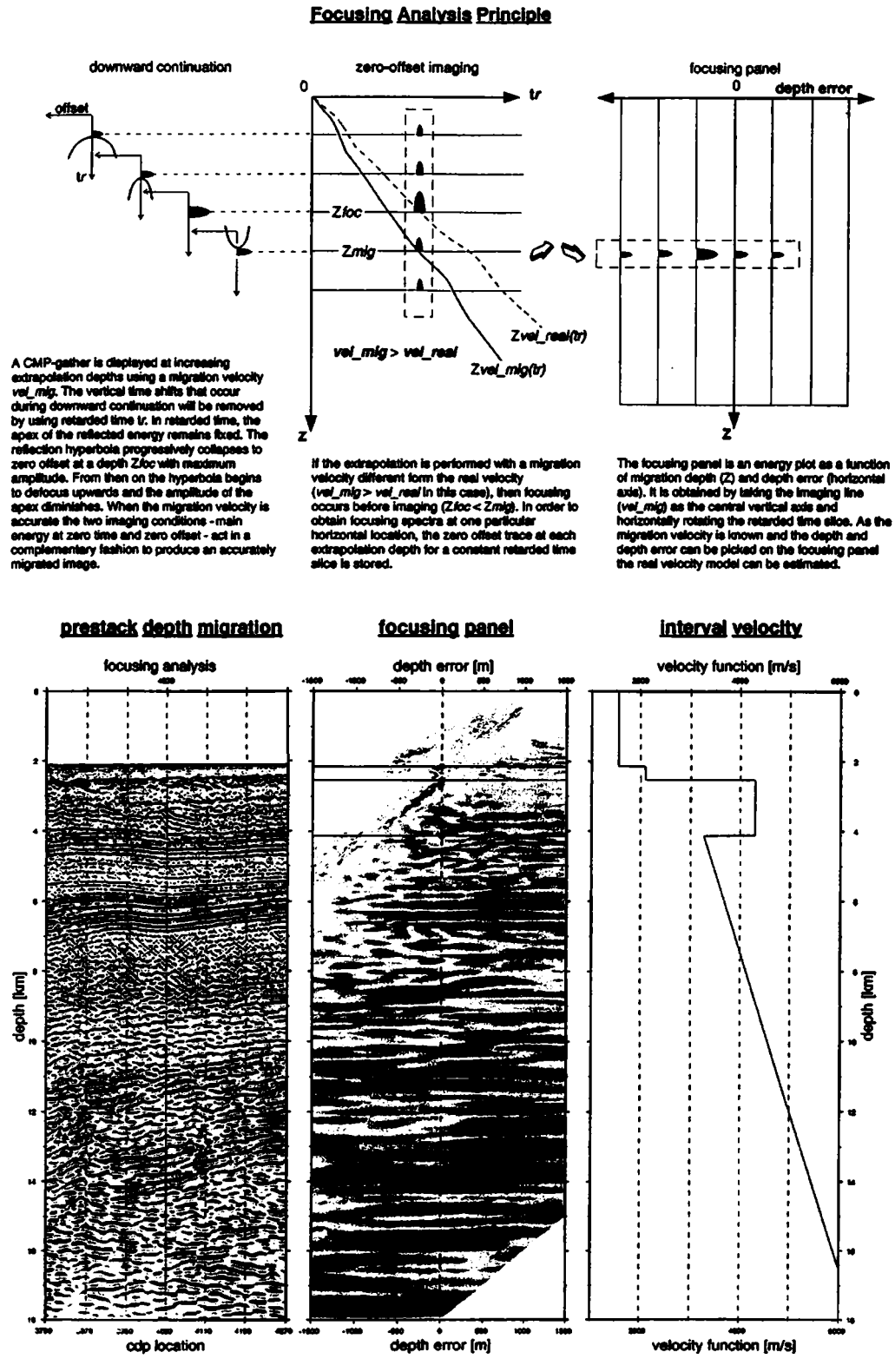


Fig. 9.3. Focusing Analysis Principle to determine the velocity model for the pre-stack depth migration. Top: the principle of focusing analysis in combination with depth migration (downward continuation), zero-offset imaging, and the focusing depth-error panel. Bottom: a real data example of the pre-stack depth migration from Line 1 CMP 3790-4270. The focusing panel together with the interval velocity shown correspond to the location of CMP 4030.

were converted into interval velocities, and were then manually smoothed. The time migration algorithm used is based on recursive downward extrapolation and is performed in the *f*-x (frequency, spatial coordinate) domain with a 45 degree operator. This migration algorithm allows vertical and lateral velocity variations.

Given that the seismic images consist of predominantly gently dipping reflectors and moderate lateral velocity gradients, conventional CMP velocity analyses of MCS data often provide good regional estimates of seismic velocity and the subsurface image. Traditional analyses fail in regions of dipping horizons or strong lateral velocity variations. To avoid problems resulting from variable data sets with inclined structures, we used a combination of iterative pre-stack depth migration and focusing analyses to determine a geologically plausible velocity model resulting in a true depth subsurface image for detailed structural interpretation.

Depth migration does not only produce a section in depth, but (in contrast to conventional processing and imaging) it also corrects for refraction due to bending of the rays at velocity gradients and interfaces (Hubral, 1977) according to Snell's law. Such effects may become particularly important when features like high-velocity salt structures abut low-velocity sediments. Overall depth migration produces an image that is geometrically more correct than the best possible time-migrated or depth-converted section.

The pre-stack depth migration algorithm, which was used to image and analyze reflective boundaries, is part of the commercial KirPack Kirchhoff migration package (SIRIUS® from GX Technology), and includes focusing depth error analysis. The focusing analysis principle – main energy at zero offset and zero time - is shown at the top of **Fig. 9.3**. Pre-stack depth migration uses two imaging conditions, zero time and zero offset, during downward continuation to form a migrated depth section. When the migration velocities are precisely defined, the two imaging conditions interact in a complementary fashion to yield a focused image. When the migration velocities are inconsistent, the reflected energy collapses to zero offset at a depth incompatible with the zero-time imaging condition. However, by interpreting the non-zero times at which focusing actually occurs, the migration velocities can be updated iteratively in a process called depth-focusing analysis (MacKay and Abma, 1992).

Here, it is necessary to create a velocity model on a 'one layer at the time' basis, as the overburden velocities affect those velocities determined for deeper levels. First the water velocity is estimated for the area, and an iteration is run. Thus, we first checked the estimated water velocity, then incorporated the determined velocity into the second iteration together with the velocity of the topmost sedimentary layer estimated, and so on. As some uncertainty exists concerning the assumed velocity for every following iteration (*i.e.* the next deeper layer), depth-focusing error analysis was used for quality control of the estimates at intervals of every 80 CMP locations.

The procedure described above was repeated five to ten times on each profile (depending upon the complexity of the cross section) until the entire section had been analyzed for velocity. As the quality of the focusing analysis changed significantly along a seismic line and between the lines, a special model building procedure was needed. At distinct locations on the profiles a very detailed model was determined based on several reflecting boundaries.

To build a consistent velocity model for the whole region, especially in the areas of the crosscutting tie points and those with poor reflective energy of the returns, a vertical and horizontal velocity gradient was estimated which:

a) satisfied the detailed velocity function determined from several reflecting boundaries;

b) was consistent at the crossing points between the profiles;

c) followed the lateral changes in the geological units;

d) was consistent with the mean interval velocity for the existing wide-angle data models; and

e) was consistent with the observations from drillholes and the sampling results along the Eratosthenes Seamount.

The upper limit for the velocity values was chosen to be 6 km/s. From wide-angle data obtained by Makris et al. (1983) and Makris et al. (1994), a mean crustal velocity of 6.7 km/s was assumed for depths greater than 12-14 km below the Levantine Basin, and a mean velocity of 6 km/s at depths greater than ~6 km for Eratosthenes Seamount. However, even if the assumed migration velocity differs from the velocity of the rocks, the error in the migrated energy is not significant at depths greater than 10 km. The reason for this is the relatively short streamer length of ~2.4 km, as velocity errors only affect the depth positioning of reflected migrated events. As a result, an optimized depth migration image and velocity model, both detailed and geologically meaningful, were obtained for each line. However, reflectors at crustal depths have to be treated with caution.

An example of depth imaging and focusing depth-error analysis on the real data is shown at the bottom of Fig. 9.3. The vertical velocity gradient underneath the salt layers was determined from several sediment reflectors along the profiles. The mean interval velocity, without the velocity gradient from 4 km depth down to the interpreted basement reflection at ~11 km, corresponds to an average of 4 km/s.

4. SEISMIC IMAGES

Figs. 9.4 through **9.14** show the processed seismic sections which contain the stacks, the depth migrated image, and the interval velocity model derived by depth focusing analysis overlaid by the line drawing of the depth migration. At several locations, the velocity function is shown with a deflection corresponding to the velocity grayscale bar. Because weak signals may sometimes have been lost at greater depth as a result of the depth migration, interpretation of the deeper section was carried out on the stacked section. The interpretation was then depth-converted and integrated into the line drawing.

Figs. 9.4 through 9.10 show the images of seismic lines 1, 2, 3, 4, 5, 6, and 10a in the eastern part (see also Fig. 9.1). A structural interpretation of these lines crossing the Levantine Basin, Hecataeus Rise, the Cyprean Basin, and the Larnaca and Latakia

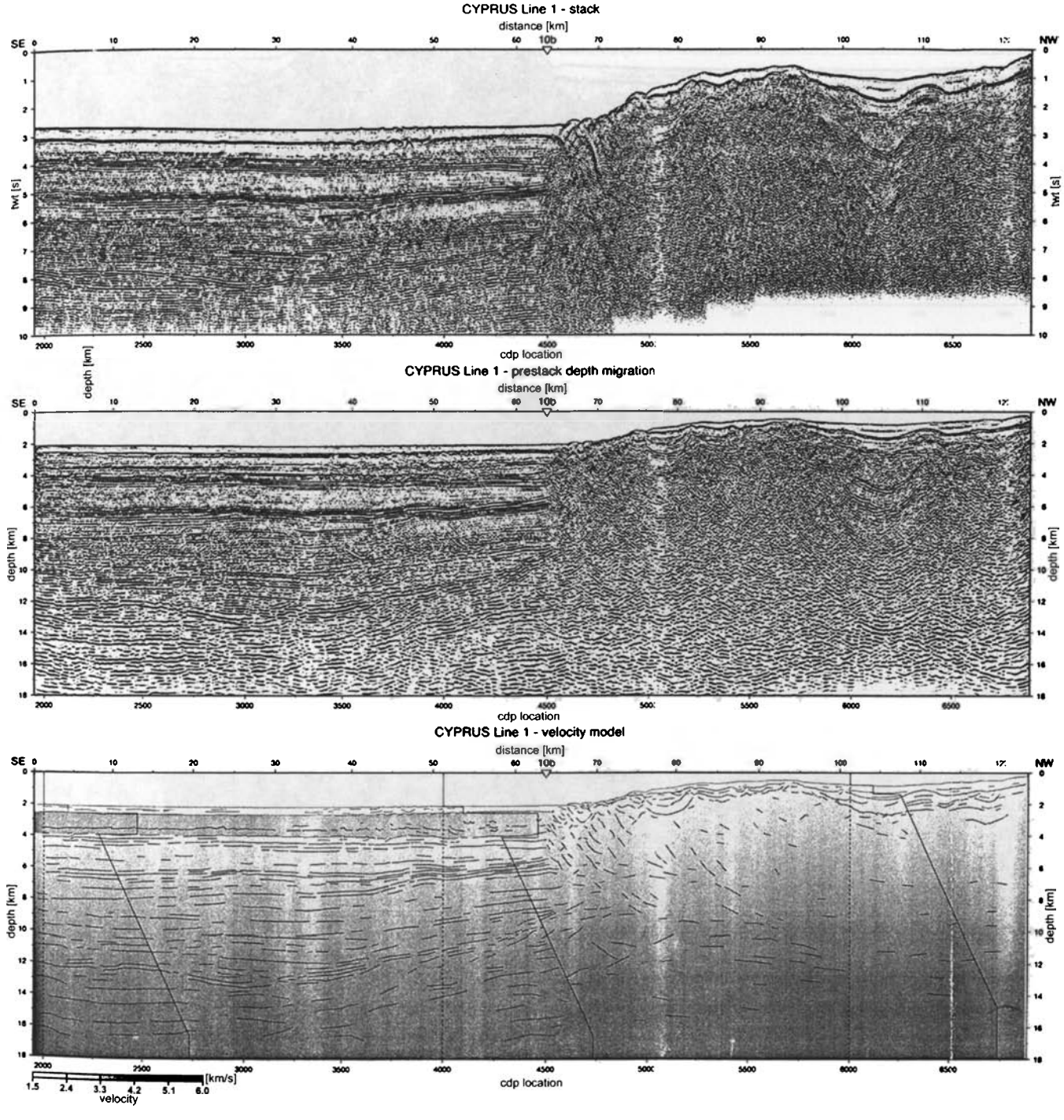


Fig. 9.4. Line 1: stack, pre-stack depth migration, and the interval velocity model overlaid by the line drawing of the depth migration image. At several locations, the velocity function is shown with a deflection corresponding to the velocity grayscale bar.

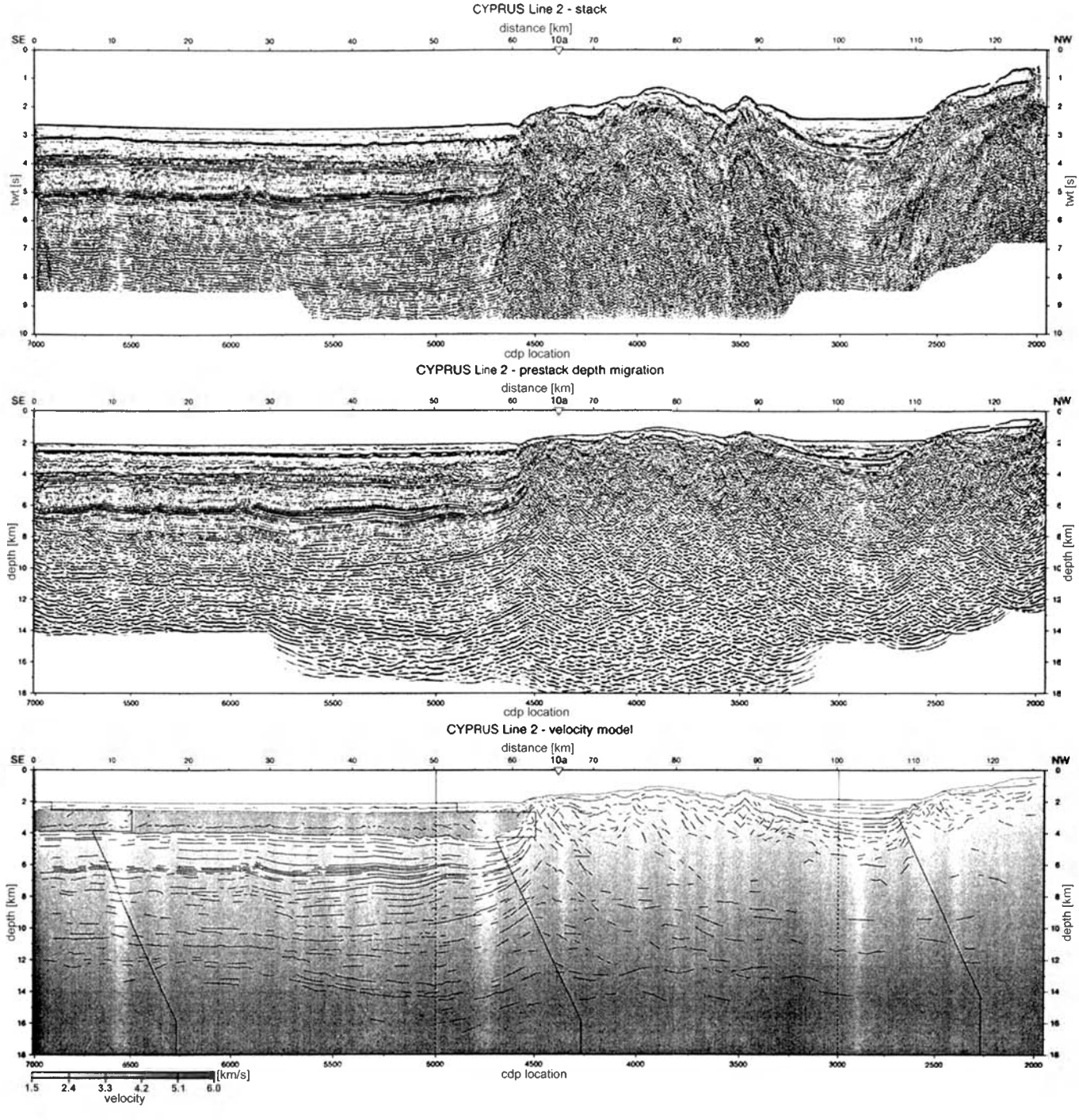


Fig. 9.5. Line 2: stack, pre-stack depth migration, and the interval velocity model overlaid by the line drawing of the depth migration image. At several locations, the velocity function is shown with a deflection corresponding to the velocity grayscale bar.

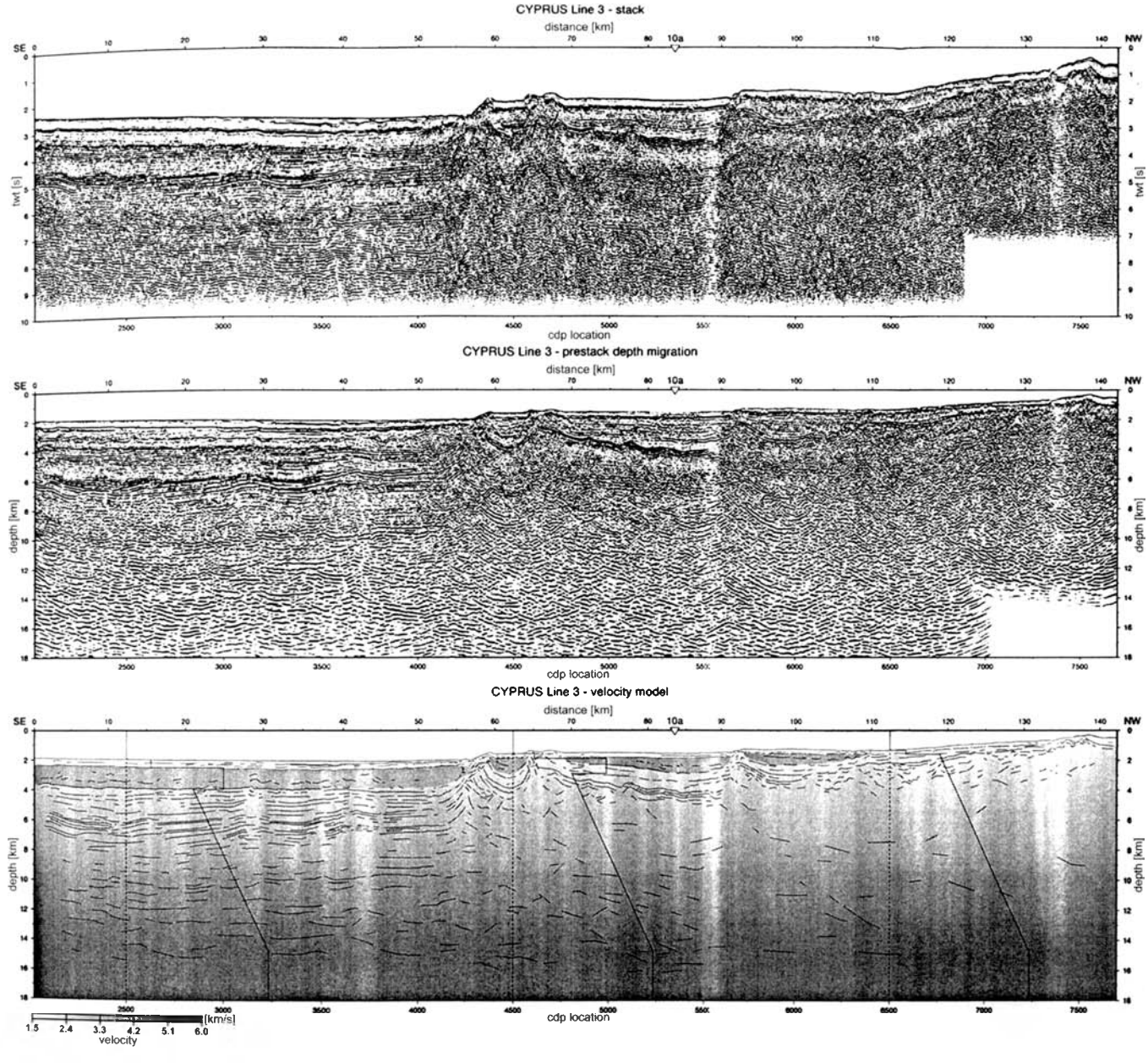


Fig. 9.6. Line 3: stack, pre-stack depth migration, and the interval velocity model overlaid by the line drawing of the depth migration image. At several locations, the velocity function is shown with a deflection corresponding to the velocity grayscale bar.

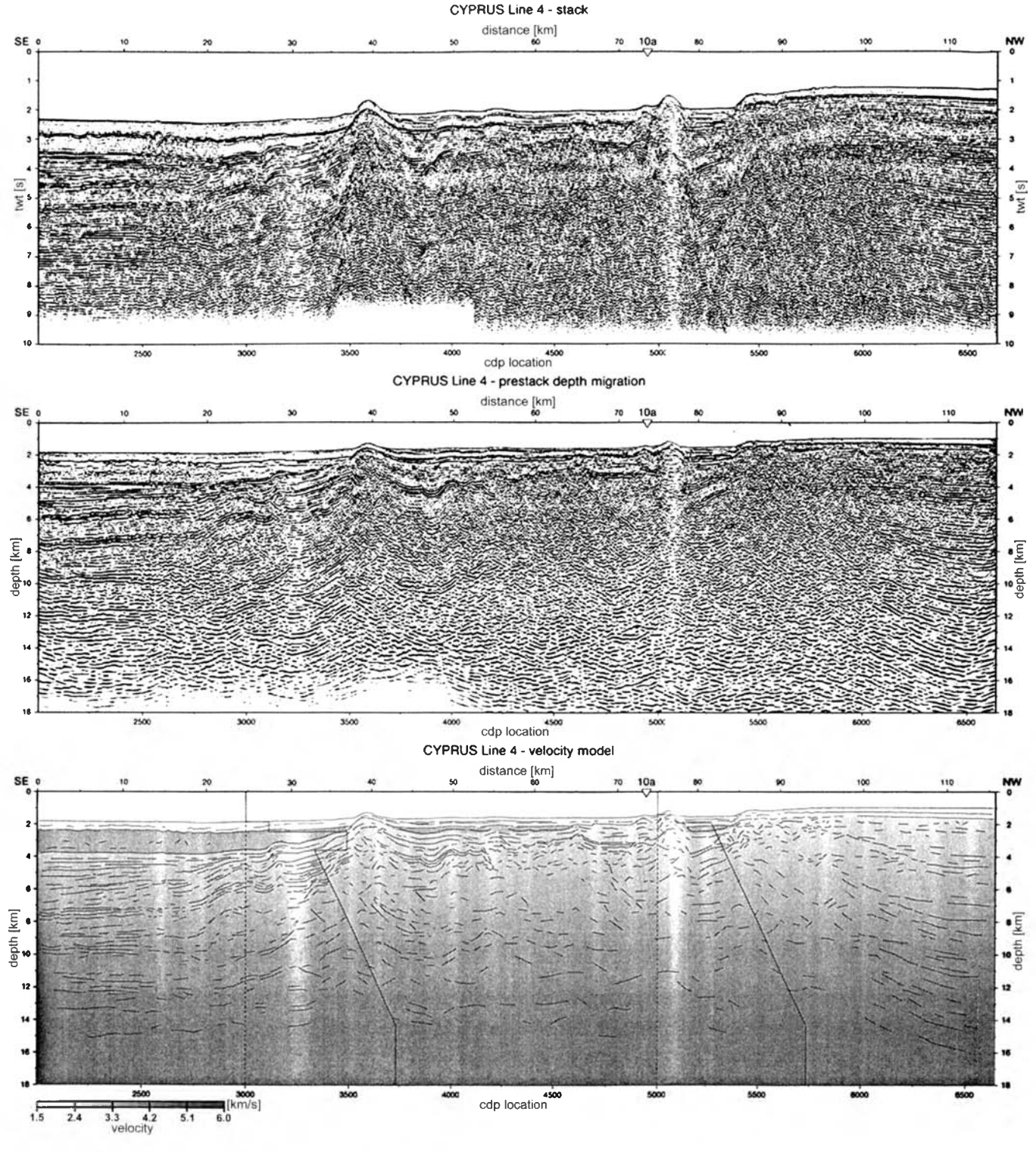


Fig. 9.7. Line 4: stack, pre-stack depth migration, and the interval velocity model overlaid by the line drawing of the depth migration image. At several locations, the velocity function is shown with a deflection corresponding to the velocity grayscale bar.

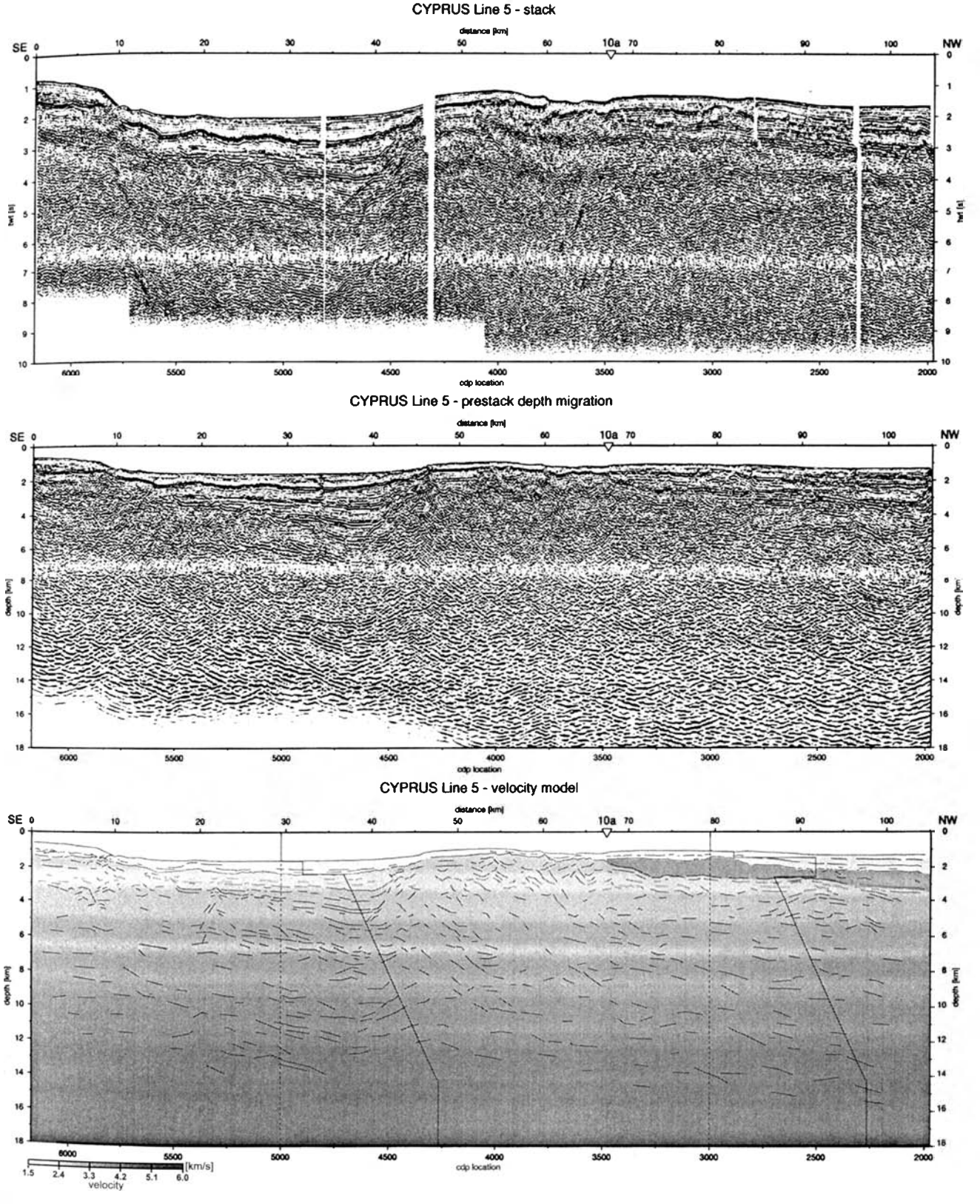


Fig. 9.8. Line 5: stack, pre-stack depth migration, and the interval velocity model overlaid by the line drawing of the depth migration image. At several locations, the velocity function is shown with a deflection corresponding to the velocity grayscale bar.

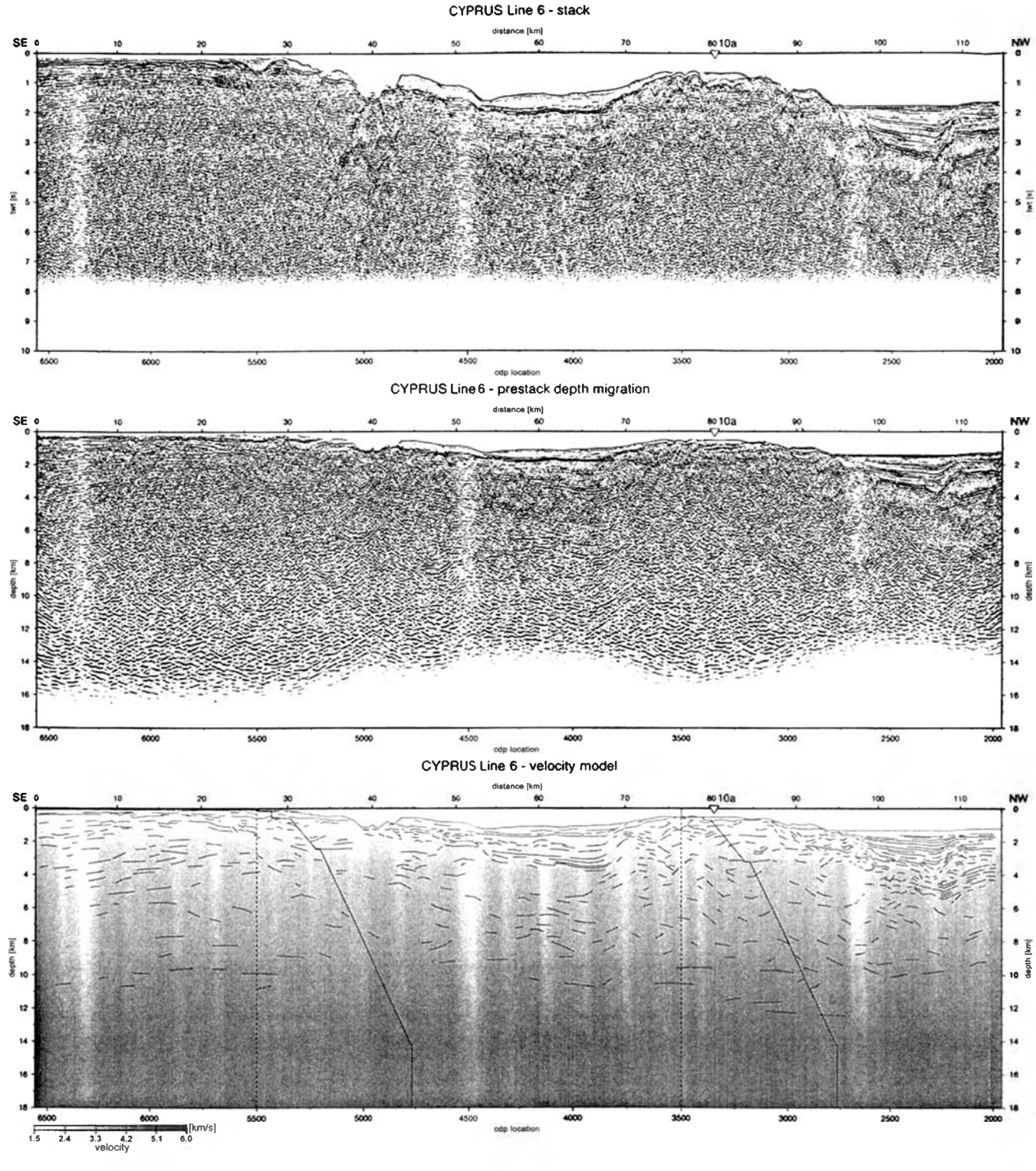


Fig. 9.9. Line 6: stack, pre-stack depth migration, and the interval velocity model overlaid by the line drawing of the depth migration image. At several locations, the velocity function is shown with a deflection corresponding to the velocity grayscale bar.

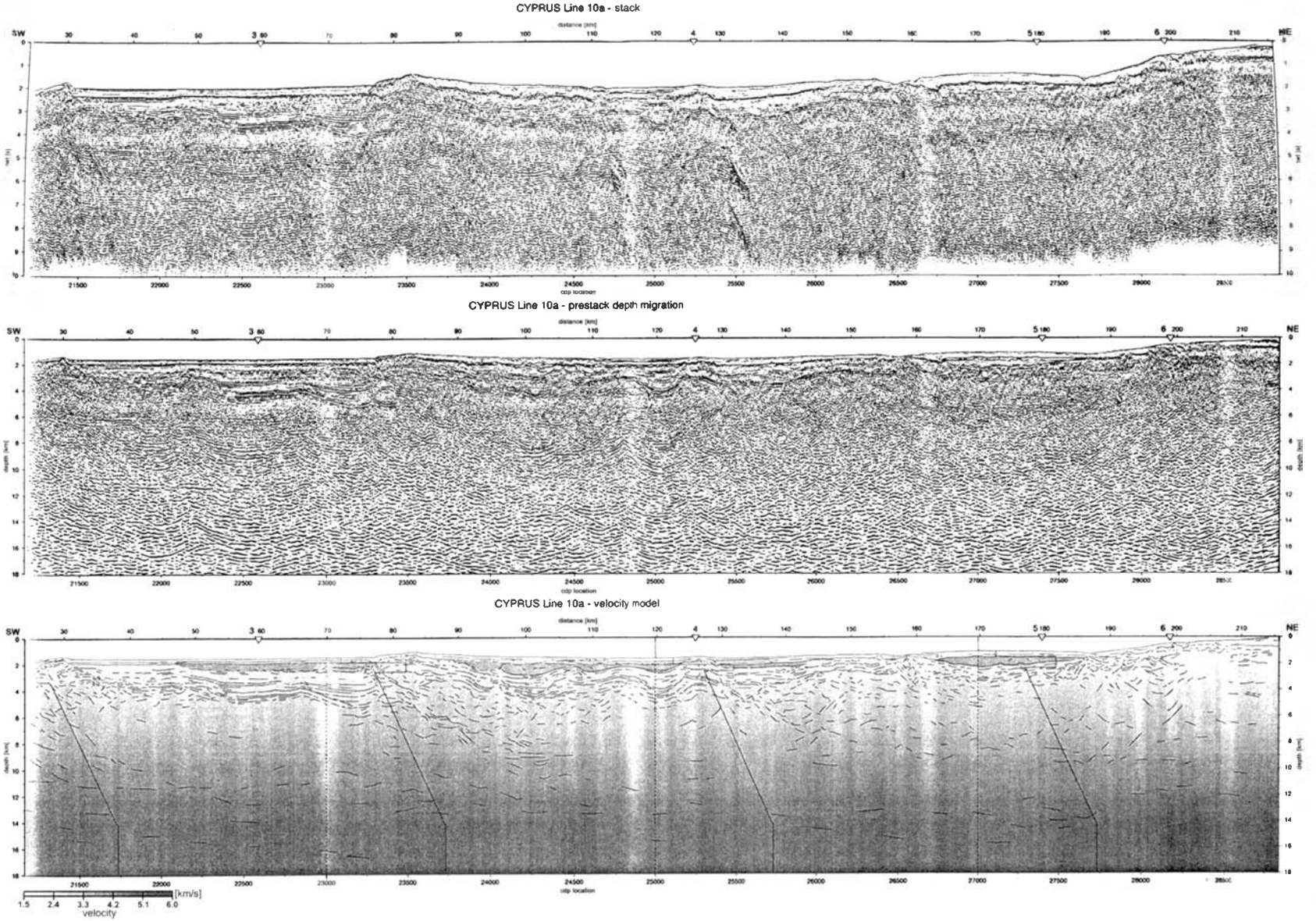


Fig. 9.10. Line 10a: stack, pre-stack depth migration, and the interval velocity model overlaid by the line drawing of the depth migration image. At several locations, the velocity function is shown with a deflection corresponding to the velocity grayscale bar.

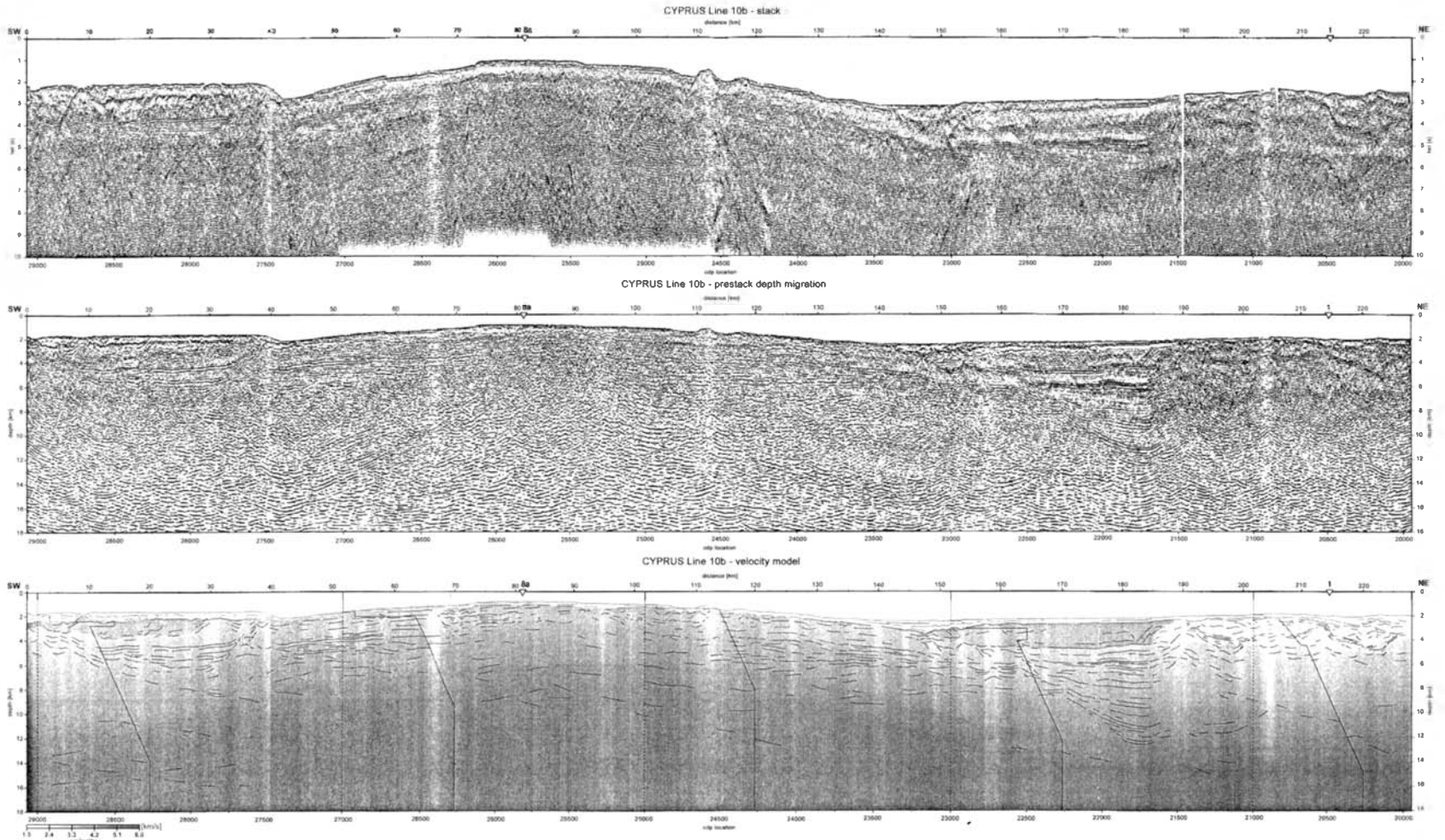


Fig. 9.11. Line 10b: stack, pre-stack depth migration, and the interval velocity model overlaid by the line drawing of the depth migration image. At several locations, the velocity function is shown with a deflection corresponding to the velocity grayscale bar.

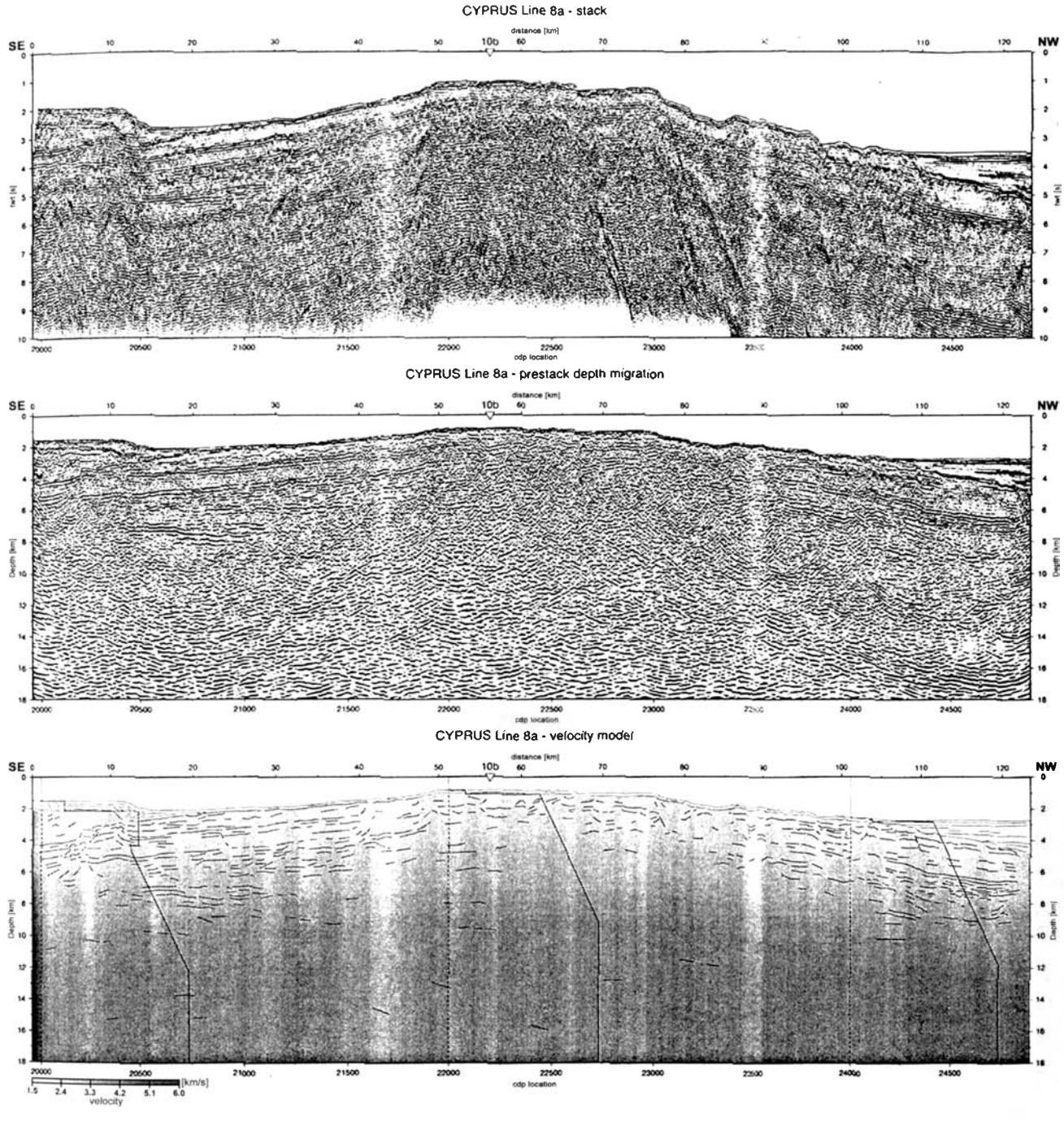


Fig. 9.12. Line 8a: stack, pre-stack depth migration, and the interval velocity model overlaid by the line drawing of the depth migration image. At several locations the velocity function is shown with a deflection corresponding to the velocity grayscale bar.

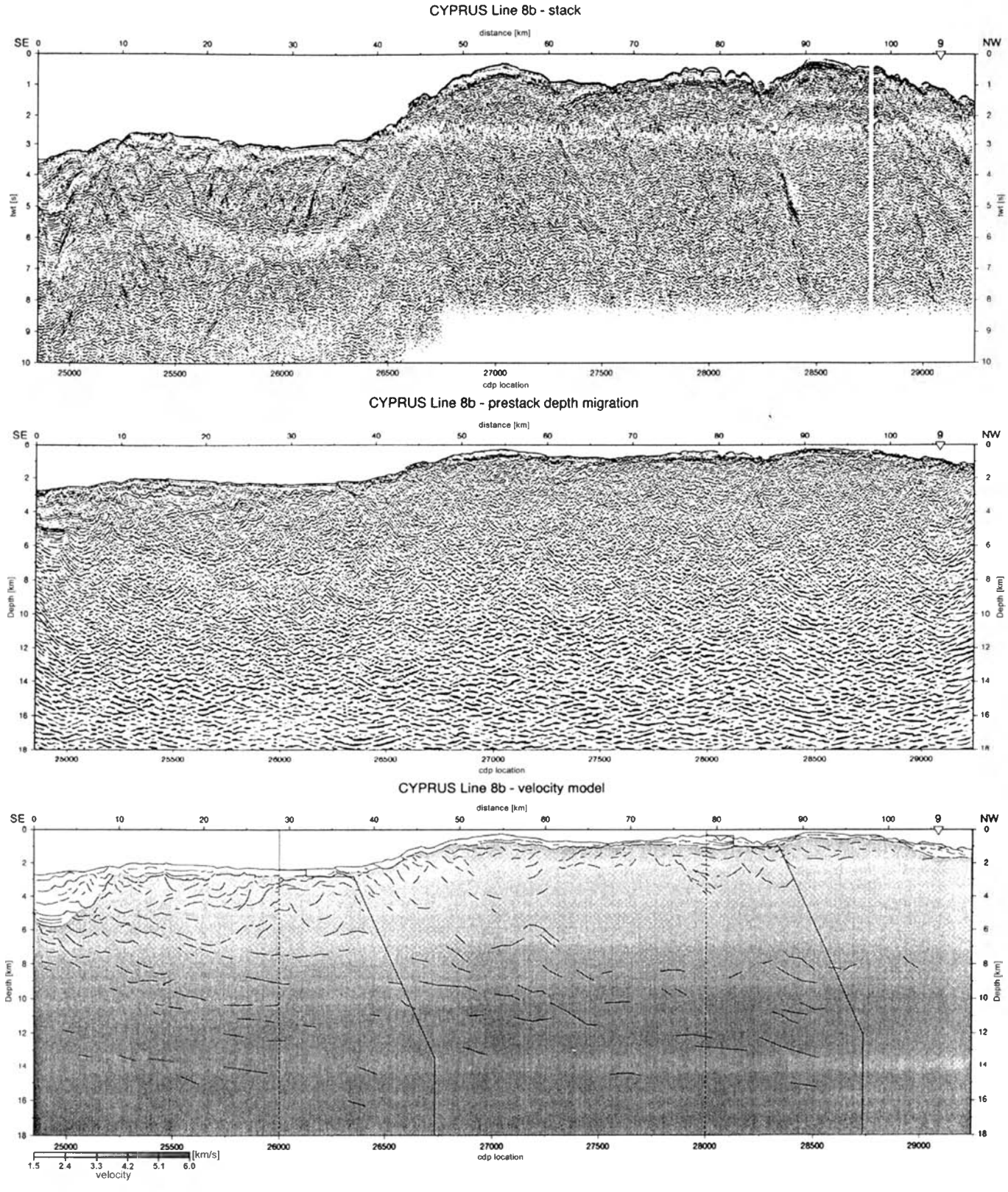


Fig. 9.13. Line 8b: stack, pre-stack depth migration, and the interval velocity model overlaid by the line drawing of the depth migration image. At several locations, the velocity function is shown with a deflection corresponding to the velocity grayscale bar.

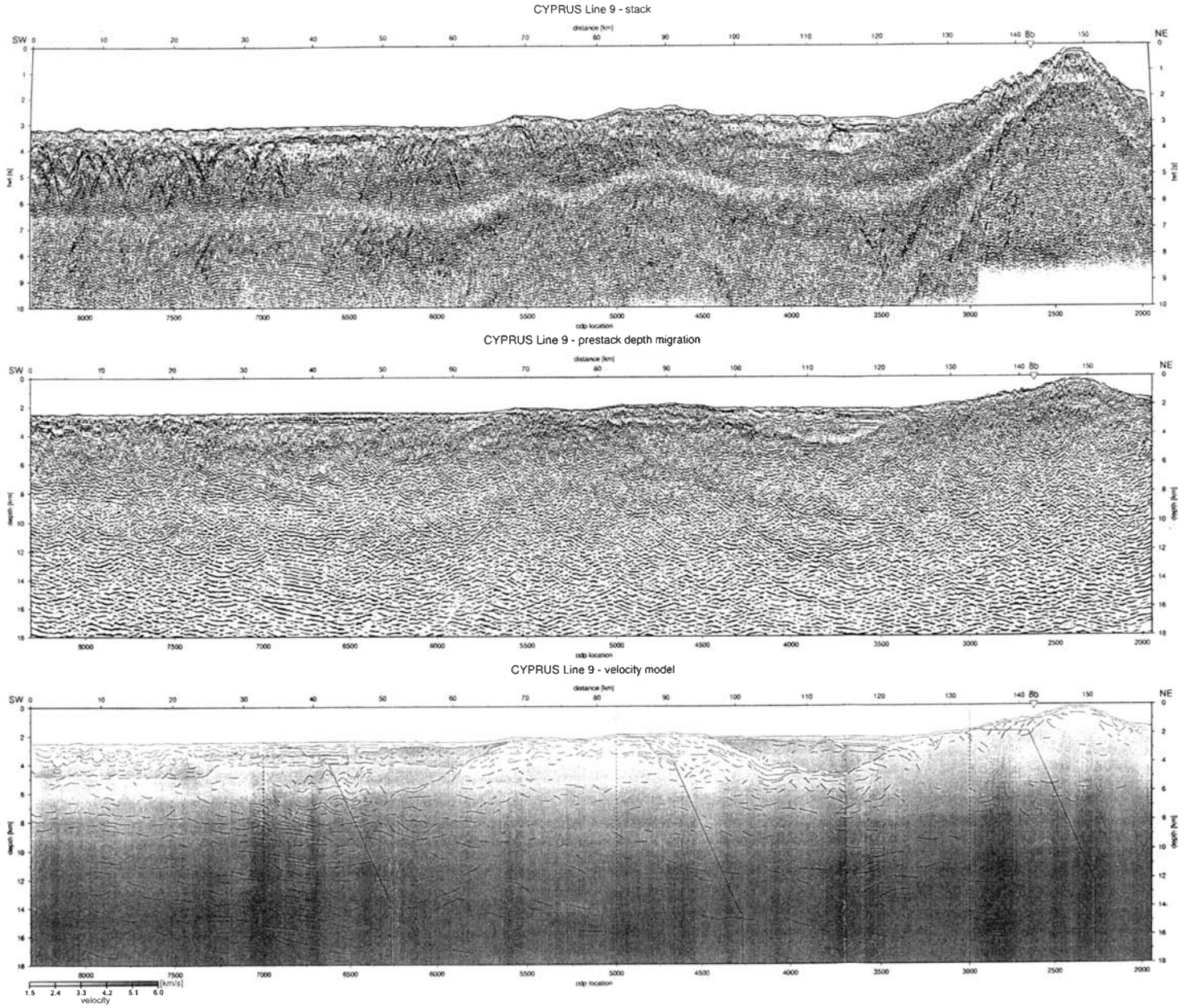
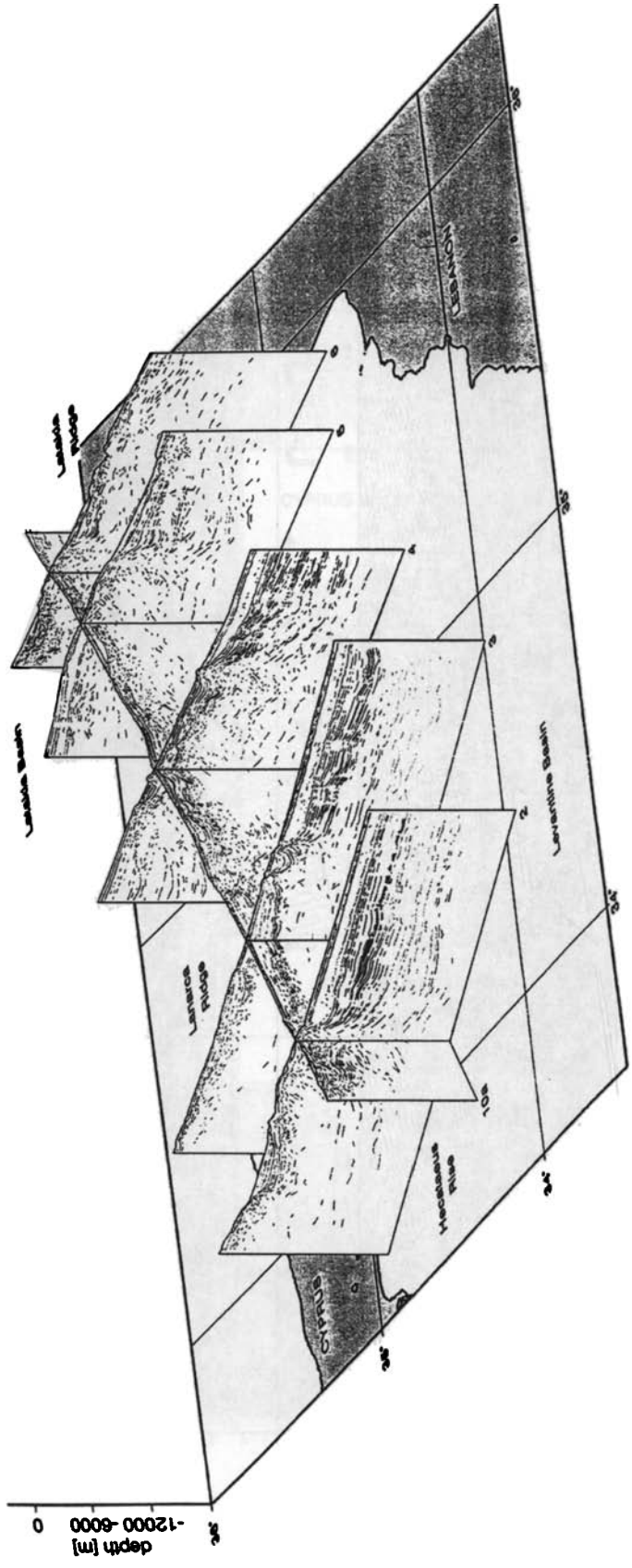


Fig. 9.14. Line 9: stack, pre-stack depth migration, and the interval velocity model overlaid by the line drawing of the depth migration image. At several locations, the velocity function is shown with a deflection corresponding to the velocity grayscale bar.


depth [m]
0
-12000 -8000
Lesser Antilles Ridge
Lesser Antilles Ridge
Lesser Antilles Ridge
Hispaniola Ridge
Caribbean Basin
Caribbean Basin
Caribbean Basin

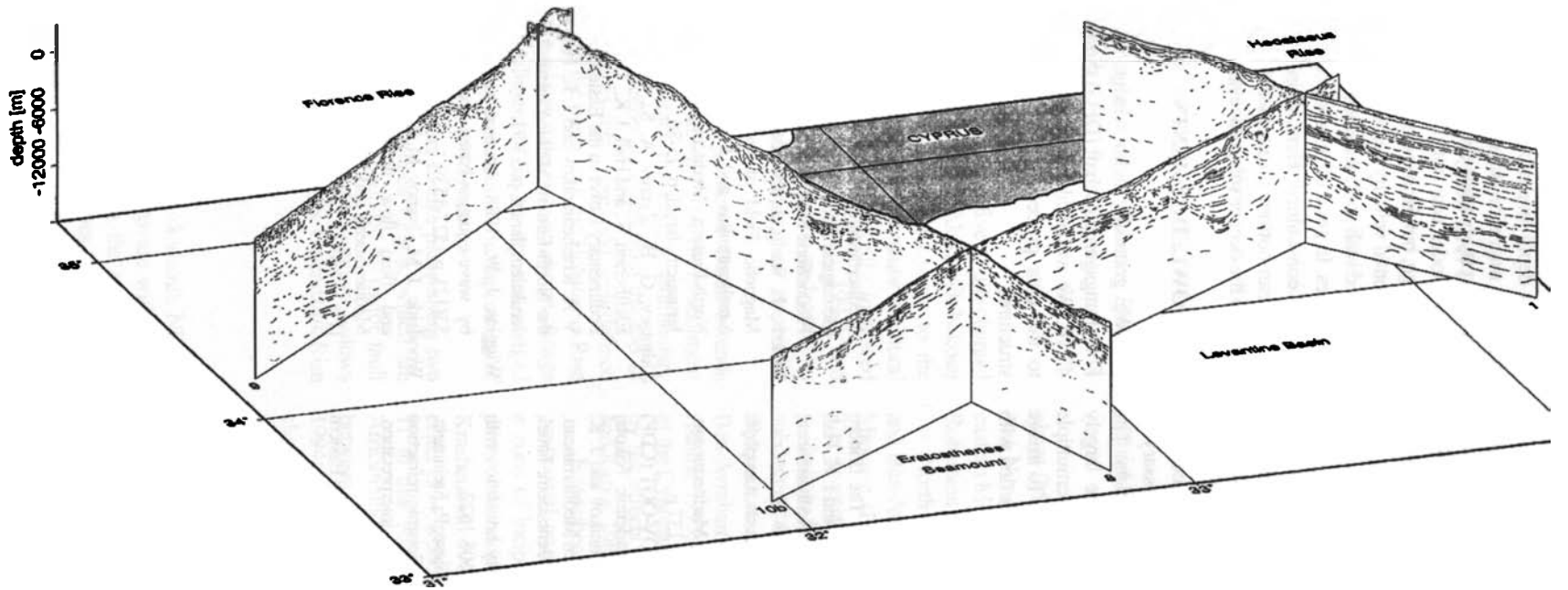


Fig. 9.16. 3-D view looking from a south-west direction of the western part of the study area, including interpretative line drawings of seismic lines 10b, 1, 8, and 9.

Ridges is presented by Vidal et al., this volume. Figs. 9.11 through 9.14 show the seismic images of seismic lines 8a, 8b, 9, and 10b, in the western part (see also Fig. 9.1). A structural interpretation of these lines which cross Eratosthenes Seamount and the Florence Rise is presented by Kopf et al., this volume. Three-dimensional views of the lines of the eastern and western part are shown in **Fig. 9.15** and **Fig. 9.16**, respectively.

5. CONCLUSIONS

The processing of the multichannel seismic lines collected during Cruise 5 of the R/V 'Akademik Nikolaj Strakhov' has provided the first images at depth of the collision zone between the African and Eurasian plates. To image the shallow sediment structures in detail, special signal processing was necessary to optimize the temporal resolution of the recorded wavelets. The multiple events created within the water column were largely removed by a cascaded application of a wave equation demultiple procedure followed by a velocity filter in the *f-k* domain. To image subsurface structures in detail beneath a complex overburden with strong lateral velocity variation (including *e.g.* salt structures), a pre-stack depth migration was applied to each line. By performing the depth migration iteratively before stacking, it was possible to create velocity models through depth focusing error analysis. The velocity model was not only necessary to produce an optimum depth image, but further constrained the interpretation. The vertical and horizontal velocity variations in the deeper subsurface could be determined with good accuracy in areas containing strong reflecting boundaries. In areas of poor reflectivity the velocity information is not well constrained. Here, closely spaced wide-angle data (*e.g.* from ocean bottom seismometers or hydrophones) are needed to improve the deeper subsurface structure.

ACKNOWLEDGEMENTS

We gratefully acknowledge the support of the Deutsche Forschungsgemeinschaft (DFG) through grants HU 470/3 and HU 470/6. We would like to thank C. Docherty for his contributions to the data processing and for discussions of the subsurface structures.

REFERENCES

Hall, J. K., Udintsev, G. B., and Odinokov, Yu. Yu., 1994. The Bottom Relief of the Levantine Sea. In: V. A. Krasheninnikov and J. K. Hall (eds.), Geological Structure of the North-Eastern Mediterranean, Historical Productions-Hall Ltd., Jerusalem, Israel, p. 5-28.

Hubral, P., 1977. Time migration: some ray theoretical aspects. Geophys. Prospect., v. 25, p. 738-745.

Kempler, D., 1994. Tectonic patterns in the easterNMOst Mediterranean. Unpublished Ph.D. thesis, Hebrew Univ., Jerusalem, 137 p.

Kogan, L. E., and Stenin, A. M., 1994. Multichannel MOV-OGT (CDP) Seismic Profiling during Cruise 5 of R/V 'Akademik Nikolaj Strakhov' (Preliminary results). In: V. A. Krasheninnikov and J. K. Hall (eds.), Geological Structure of the North-Eastern Mediterranean, Krasheninnikov, Historical Productions-Hall Ltd., Jerusalem, Israel, p. 99-112.

MacKay, S., and Abma, R., 1992. Imaging and velocity estimation with depth-focusing analysis. Geophysics, 57(12), p. 1608-1622.

Makris, J., Ben Avraham, Z., Behle, A., Ginzburg, A., Giese, P., Steinmetz, L., Whitmarsh, R. B., and Eleftheriou, S., 1983. Seismic refraction profiles between Cyprus and Israel and their interpretation. - Geophys. J. Roy. Astron. Soc., v. 75, p. 575-591.

Makris, J., and Wang, J., 1994. Bouguer Gravity Anomalies of the Eastern Mediterranean Sea. In: V. A. Krasheninnikov and J. K. Hall (eds.), Geological Structure of the North-Eastern Mediterranean, Historical Productions-Hall Ltd., Jerusalem, Israel, p. 87-98.

Makris, J., Wang, J., Odintsov, S. D., and Udintsev, G. B., 1994. The Magnetic Field of the Eastern Mediterranean Sea. In: V. A. Krasheninnikov and J. K. Hall (eds.), Geological Structure of the North-Eastern Mediterranean, Historical Productions-Hall Ltd., Jerusalem, Israel, p. 75-86.

Udintsev, G. B., Zverev, A. S., Odinokov, Yu. Yu., Efremov, V. N., Eleftheriou, S., and Hall, J. K., 1994. Structure of the Post-Messinian Sedimentary Cover in the Eastern Part of the Mediterranean Sea. In: V. A. Krasheninnikov and J. K. Hall (eds.), Geological Structure of the North-Eastern Mediterranean, Historical Productions-Hall Ltd., Jerusalem, Israel, p. 33-73.

Wiggins, J. W., 1988. Attenuation of complex water-bottom multiples by wave-equation-based prediction and subtraction. Geophysics, 53(12), p.1527-1539.

Woodside, J. M., Ivanov, M. K., and Limonov, A. F., 1997. Neotectonics and fluid flow through seafloor sediments in the Eastern Mediterranean and Black Seas. IOC Reports, Technical Series, 48 (Pts. 1 and 2), 226 p.

Chapter 10

Seismic Images from South-East of Cyprus to the Syrian Coast

Neus Vidal
Escola Universitaria Salesiana de Sarria, Rafael Battle 7, 08017 Barcelona, Spain
Dirk Klaeschen
GEOMAR Research Centre, Wischofstrasse 1-3, D-24148 Kiel, Germany
Achim J. Kopf
Geosciences Azur, B. P. 48, 06230 Villefranche-sur-Mer Cedex, France
Roland von Huene
GEOMAR Research Centre, Wischofstrasse 1-3, D-24148 Kiel, Germany
Valery A. Krasheninnikov
Geological Institute of the Russian Academy of Sciences, Pyzhevskiy pereulok 7, 109017 Moscow, Russia

ABSTRACT

We present the results of reprocessing five multi-channel seismic (MSC) profiles from Cruise 5 of R/V 'Akademik Nikolaj Strakhov'. The lines extend from the south of Cyprus to the Syrian coast and are oriented perpendicular to the major structural elements in the area. Reprocessing has substantially improved the previously published images (Kogan and Stenin, 1994), and now reveals the complete sedimentary succession and provides geometric constraints on the structural complexities associated with the plate boundary.

The sedimentary sequence in the Levantine Basin extends down to 8-9 s, which corresponds to about 12-14 km of sediment thickness. The salient features within the basin's sedimentary sequence include the strong reflection signature from the top of the Messinian deposits, as well as their base, and well-defined unconformities. The junction of the basin with the Hecataeus Rise lies within a complex region, and coincides with an abrupt change in the reflection character. Sedimentary layers are not imaged beneath the rise. This junction may represent the juxtaposition of the African and Anatolian plates south of Cyprus.

To the east, the deformation appears to take place along two separate segments, the Latakia and Larnaca Ridges, which are joined by the Gelendzhik Rise. They are bounded by major fault systems. We suggest that the most active plate boundary follows the southernmost deformation front (*i.e.* along the Gelendzhik Rise and Latakia Ridge).

1. INTRODUCTION

MSC profiles from Cruise 5 of the R/V 'Akademik Nikolaj Strakhov' (Krasheninnikov and Hall, 1994) provide widespread coverage to the south and east of Cyprus, in the easternmost Mediterranean. Five NW-SE trending seismic lines, shown in **Fig. 10.1**, cross an area of active continental collision. The Cyprean Arc forms the plate boundary between the African and Anatolian plates (McKenzie, 1970, 1972; Smith, 1971; Dewey et al., 1973; and Nur and Ben-Avraham, 1978). Its Late Tertiary-Quaternary eastern Mediterranean tectonic evolution is reviewed in a paper by Robertson and Grasso (1995).

Northward subduction along this active margin (Kempler and Ben-Avraham, 1987) is considered to have begun in the early Miocene (Eaton and Robertson, 1993; Robertson et al., 1990). The geometry of the plate is a matter of debate, and its evolution is likely to have varied laterally. West of Cyprus, north-eastward subduction of the eastern Mediterranean crust is well established (Rotstein and Kafka, 1982; Kempler and Ben-Avraham, 1987; Ben-Avraham et al., 1988; Woodside, 1976, 1977; Ambraseys and Adams, 1993; Oral et al., 1995). South of Cyprus, in the central part of the Cyprean Arc, the present northward subduction is influenced by the effects of the collision of continental fragments (Rotstein and Kafka, 1982).

Eratosthenes Seamount is considered to be a fragment of continental crust that is undergoing subsidence and break-up in a zone of incipient collision between the African and Eurasian plates (Woodside, 1977, 1991; Ben-Avraham and Nur, 1986; Krasheninnikov and Hall, 1994; Makris and Wang, 1994; Limonov et al., 1994; Robertson et al., 1990, 1994, 1995; Kopf et al., Chapter 11 in this volume), thus establishing the junction between the African and Anatolian plates. East of Cyprus, differential motion between the African, Arabian and Anatolian plates (Westaway, 1994; Oral et al., 1995; Reilinger et al., 1997) is responsible for a change in the mode of convergence and in the type of deformation in this area. Sinistral strike-slip motion with some component of shortening is proposed east of Cyprus (Kempler and Ben-Avraham, 1987; Kempler and Garfunkel, 1994). According to many authors, the main area of active convergence extends from southern Cyprus to Iskenderun Bay, towards the junction of the East Anatolian fault with the extension of the Dead Sea rift system (McKenzie, 1970, 1972; Dewey and engör 1979; engör, 1979; Rotstein and Kafka, 1982; Girdler, 1990). Ben-Avraham (1978), however, suggested that there is no well defined plate boundary in this area, and Le

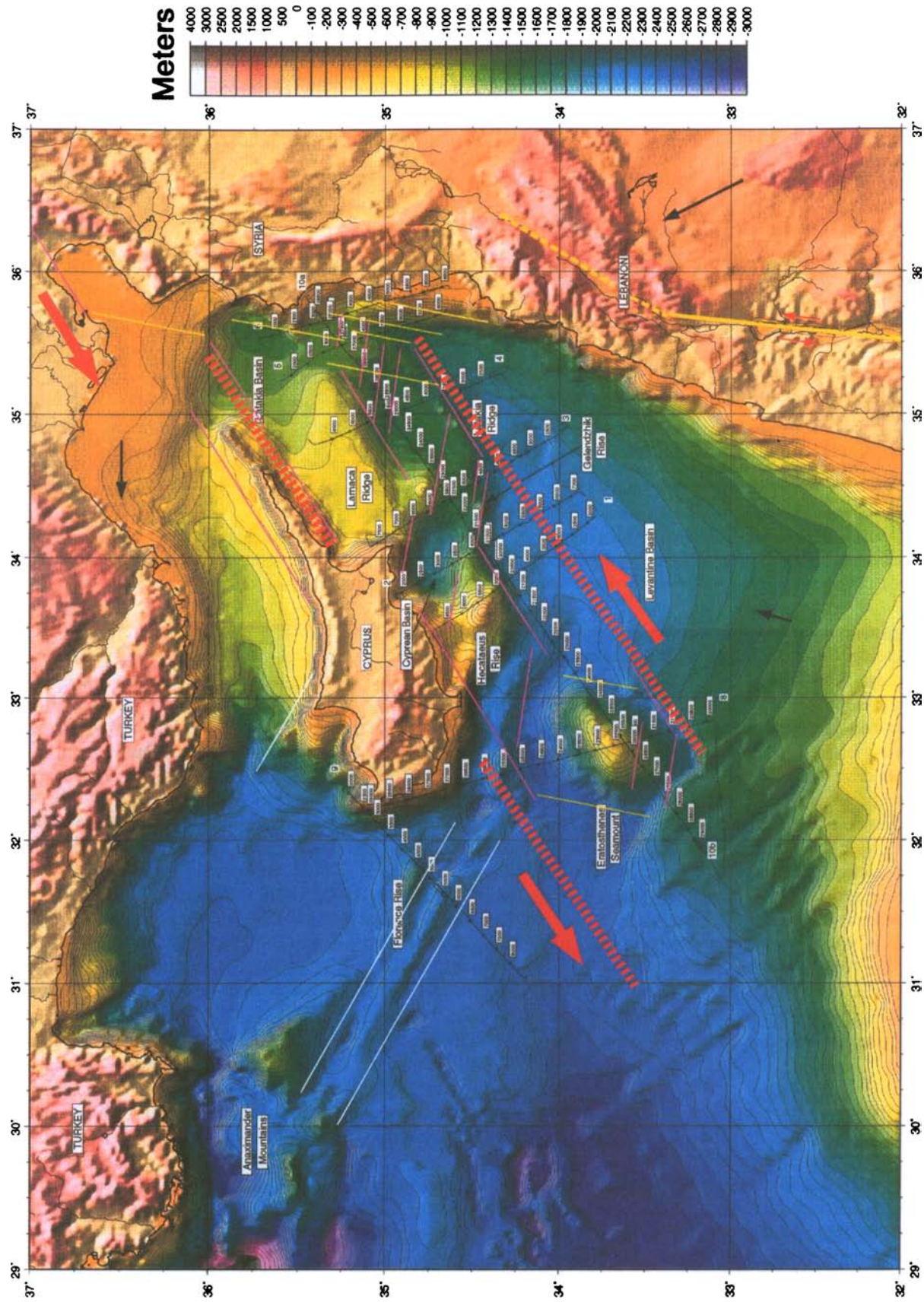


Fig. 10.1. Location map of profiles of 'Strakhov' Cruise 5.

Pichon and Angelier (1979) considered it to consist of a broad zone of thrusting rather than a discrete plate boundary.

The latest results incorporating bathymetry and shallow seismic reflection lines (Ben-Avraham et al., 1995) suggest that the present plate boundary lies at the Eastern Cyprean Arc and extends along the Gelendzhik Rise and Latakia Ridge to the continental margin of Syria. The dataset of Strakhov Cruise 5 provides the first deep seismic reflection images of the area. These images suffered from multiples and diffracted energy, which to a large extent masked the sedimentary succession and structure. In this paper, we present and discuss the principal results obtained after the reprocessing of five lines from this survey, located southeast of Cyprus (Fig. 10.1). Multiple energy and diffraction tails were largely eliminated to reveal a very thick sedimentary succession within the Levantine basin, and the structural complexities at the plate boundary. Here we focus on the lateral west-to-east structural variations.

2. SEISMIC DATA DESCRIPTION

In 1987, Cruise 5 of 'Strakhov' acquired 1700 km of marine multi-channel seismic reflection data at the convergence zone from southwest of Cyprus to the coast of Syria. A 12-liter airgun seismic source and a 48 channel streamer were used on all lines. The shotpoint spacing was 100 m and the hydrophone array had an active length of 2350 m. The recording length with variant time delays was 10 s two-way travel time (TWT). The results of the preliminary processing were presented by Kogan and Stenin (1994). The data required careful reprocessing due to the low fold (12 traces by a common midpoint (cmp) spacing of 25 m) and poor signal quality. The reprocessing is described in detail by Klaeschen et al. (Chapter 9 in this volume). In this paper, we present the post-stacked time-migrated seismic results for five of the lines.

Selected parts of the data are displayed at a larger scale to enhance the details and amplitude information.

2.1 Lines 1 and 2

From SE to NW, Line 1 passes over the Levantine Basin, crosses the Hecataeus Rise, and terminates near the coast of Cyprus (Fig. 10.1). The post-stack time-migrated section is shown in **Fig. 10.2**. From the southeast, the first 60 km traverse the thick fill sequence of the Levantine Basin. Reprocessing has attenuated the strong multiples to reveal the stratigraphy of the Tertiary-Mesozoic sequence. A set of horizontal reflections is observed to the maximum 10 s TWT depth of the record. The nomenclature and interpretation of the principal structural units are taken from Kogan and Stenin (1994).

Based on the regional geology and the seismic data previously available, the main depositional sequences correspond to Pliocene-Holocene, Upper Miocene-Messinian, Paleogene-Neogene, and Cretaceous-Jurassic. The Pliocene-Quaternary and Miocene units are clearly deformed from km 35 up to the Hecataeus Rise (Fig. 10.2 and **Fig. 10.3**). Small folds are present in these units and the irregular sea-floor topography attests to the recent activity associated with these structures. Another remarkable feature is the marked unconformity at 5 s (km 40-65), as well as the pronounced upward bend of the proposed Mesozoic units towards the Hecataeus Rise. Kogan and Stenin (1994) interpreted the reflector at 7.8-8.0 s (Fig. 10.2) to be the base of the Mesozoic-Paleozoic sedimentary unit corresponding to the top of the crystalline basement. Reprocessing of this line substantially enhanced the resolution of this reflector, which rises from 8 s (km 30) to 6.5 s (km 65) upon approaching the rise. Unfortunately the 10 s recording precludes our seeing any change in the reflective character below. The basin is assumed to terminate approximately at the junction with the Hecataeus Rise to the north, where the layered character of the entire sedimentary sequence ends abruptly (at km 65 in Figs. 10.2 and 10.3). There is no northward continuity of the sediment reflectivity associated with the Levantine Basin even though weak reflections below the rise are visible. Northward, from km 65 to the end of the profile, the strong signature of the Messinian unconformity (M reflector) on the rise is the most prominent feature.

Beneath the M reflector, two weak sub-horizontal reflections are distinguished and can also be traced. They are interpreted as the base of the Upper-Miocene and the Paleogene-Neogene units. Unfortunately, the presence of strong remnant multiple energy from the sea bed/water interface and uppermost sediment masks the imaging of the deep structure. Nevertheless, there is no evidence of any continuous reflectivity across the area. Line 2 lies about 25 km to the northeast and is sub-parallel to Line 1 (Fig. 10.1). It extends from the Levantine Basin to the eastern flank of the Hecataeus Rise, and then across the Cyprean Basin up to the coast of Cyprus. Its post-stacked time migrated seismic section is displayed in **Fig. 10.4**.

The structure below the Levantine Basin is similar to that described for Line 1. Although main depositional units appear similar for both lines, there are some differences. Deformation affecting the Pliocene-Quaternary and Miocene units extends for some 15 km south of the rise, in front of a 35 km wide zone of deformation that is broader than that observed in Line 1. Towards the rise the upward bend of the reflectors associated with the Mesozoic-Paleozoic units is also evident here (between km 40-60), but appears to be concentrated in the junction area between the basins. At this point, the entire sedimentary sequence terminates abruptly (**Fig. 10.5**). To the north of the Levantine Basin, beneath the Pliocene-Quaternary sediments, the Messinian sedimentary layer is again the most prominent event. It appears faulted and deformed, with some faults reaching the seafloor in places. Between the Hecataeus Rise and the continental slope, the Cyprean Basin is clearly imaged with its 1.8 s thick Pliocene-Quaternary, Miocene, and Paleogene sedimentary sequence (**Fig. 10.6**). The sedimentary layers thin towards the north and the south. In accordance with Line 1, the observed weak reflectors underneath the basin fill may be interpreted as the top of the Mesozoic unit. There is little evidence of prominent 'real' reflections, but only of remnant multiple energy imaged at deeper levels.

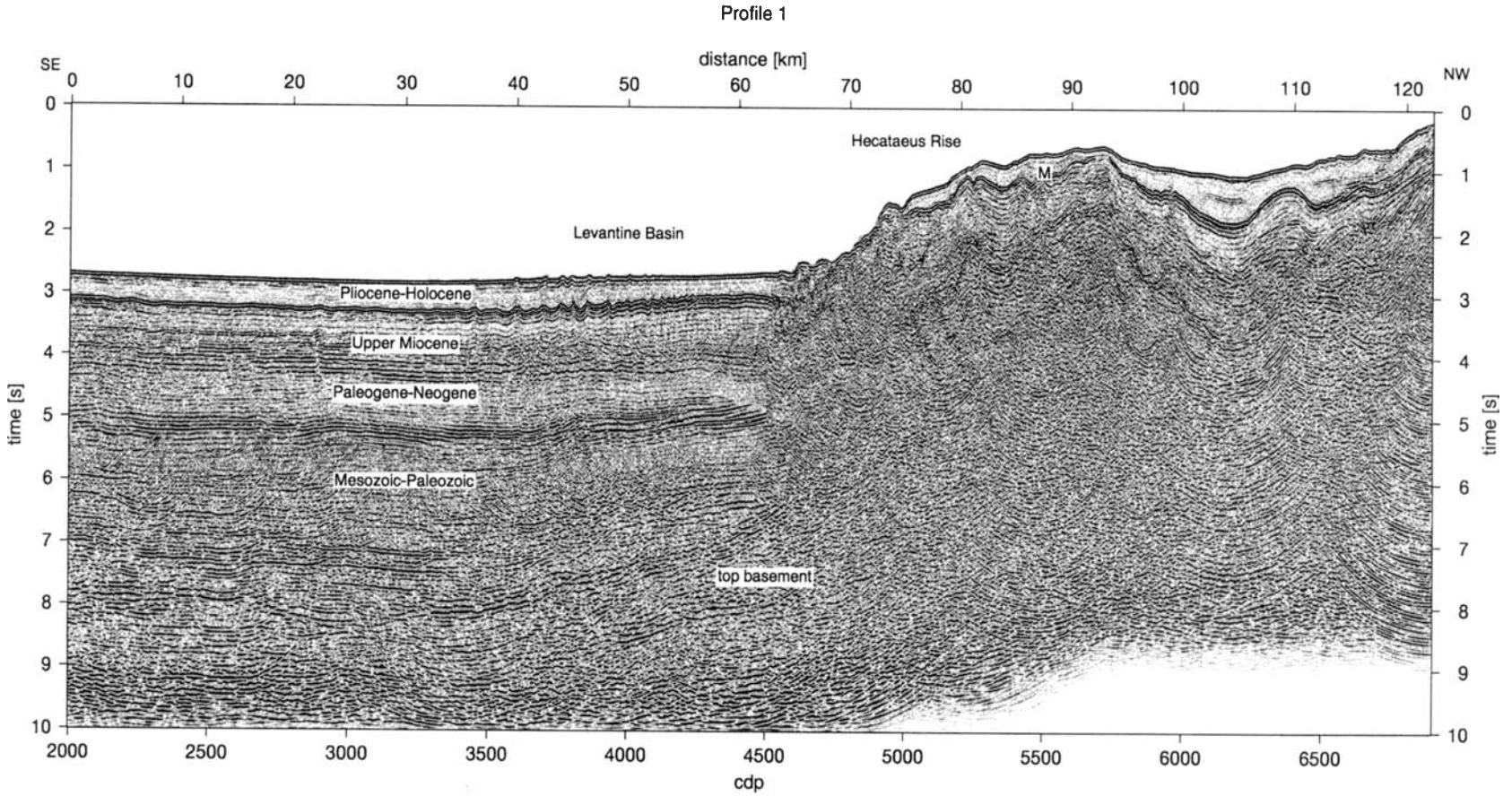


Fig. 10.2. Post-stacked time-migrated section of Profile 1.

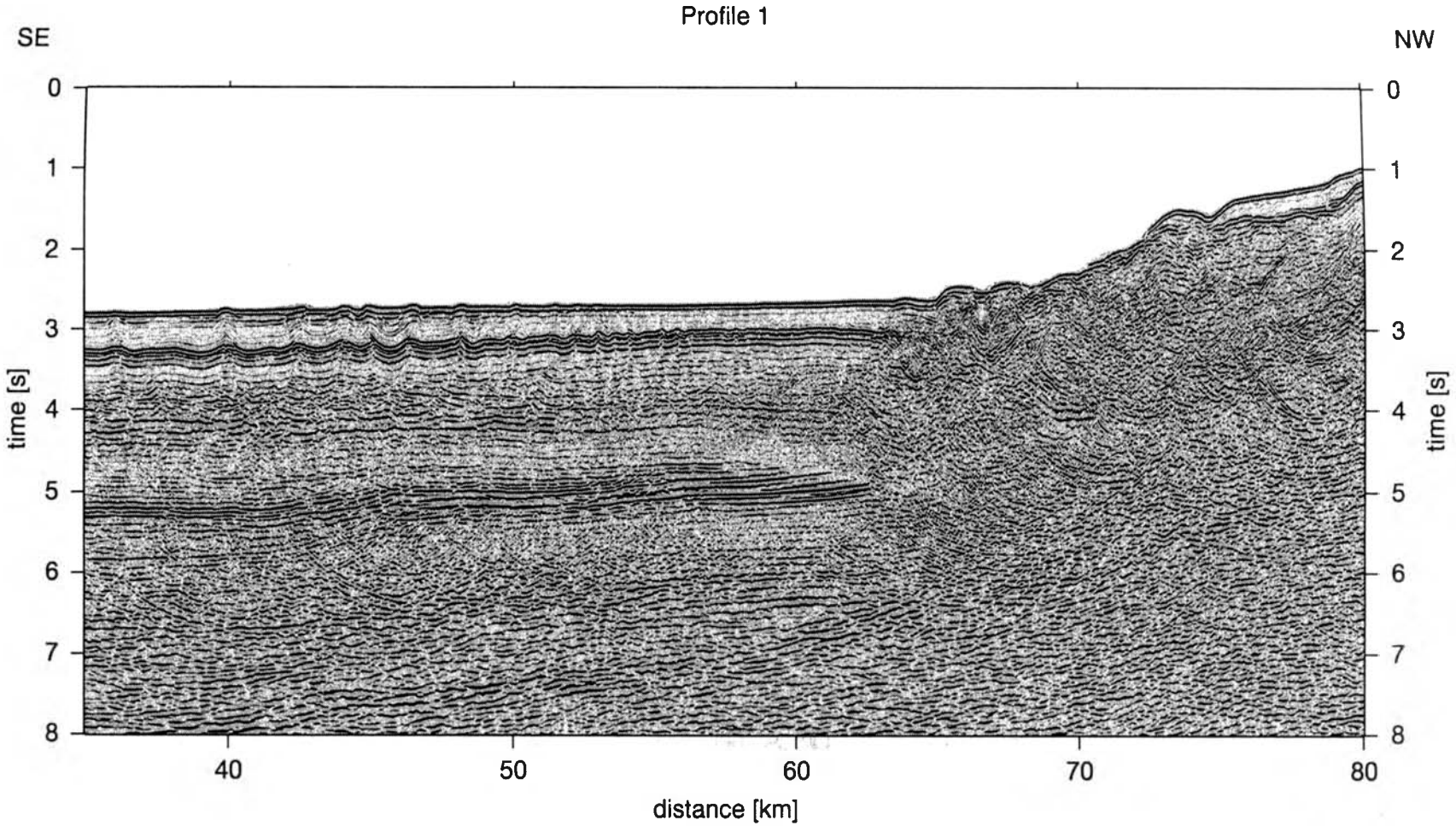


Fig. 10.3. Blow up of Profile 1: junction of the Levantine basin-Hecataeus Rise.

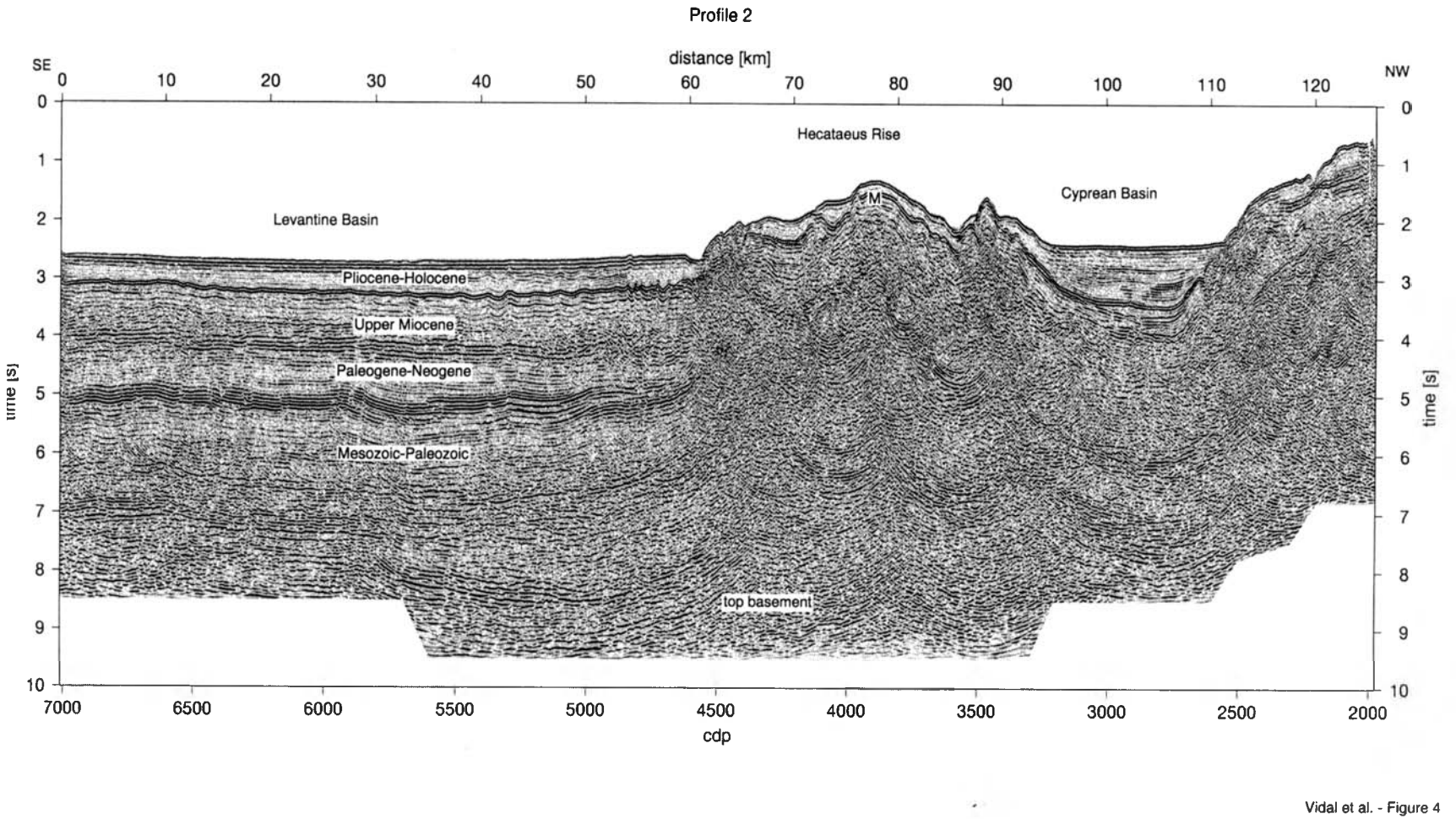


Fig. 10.4. Post-stacked time-migrated section of Profile 2.

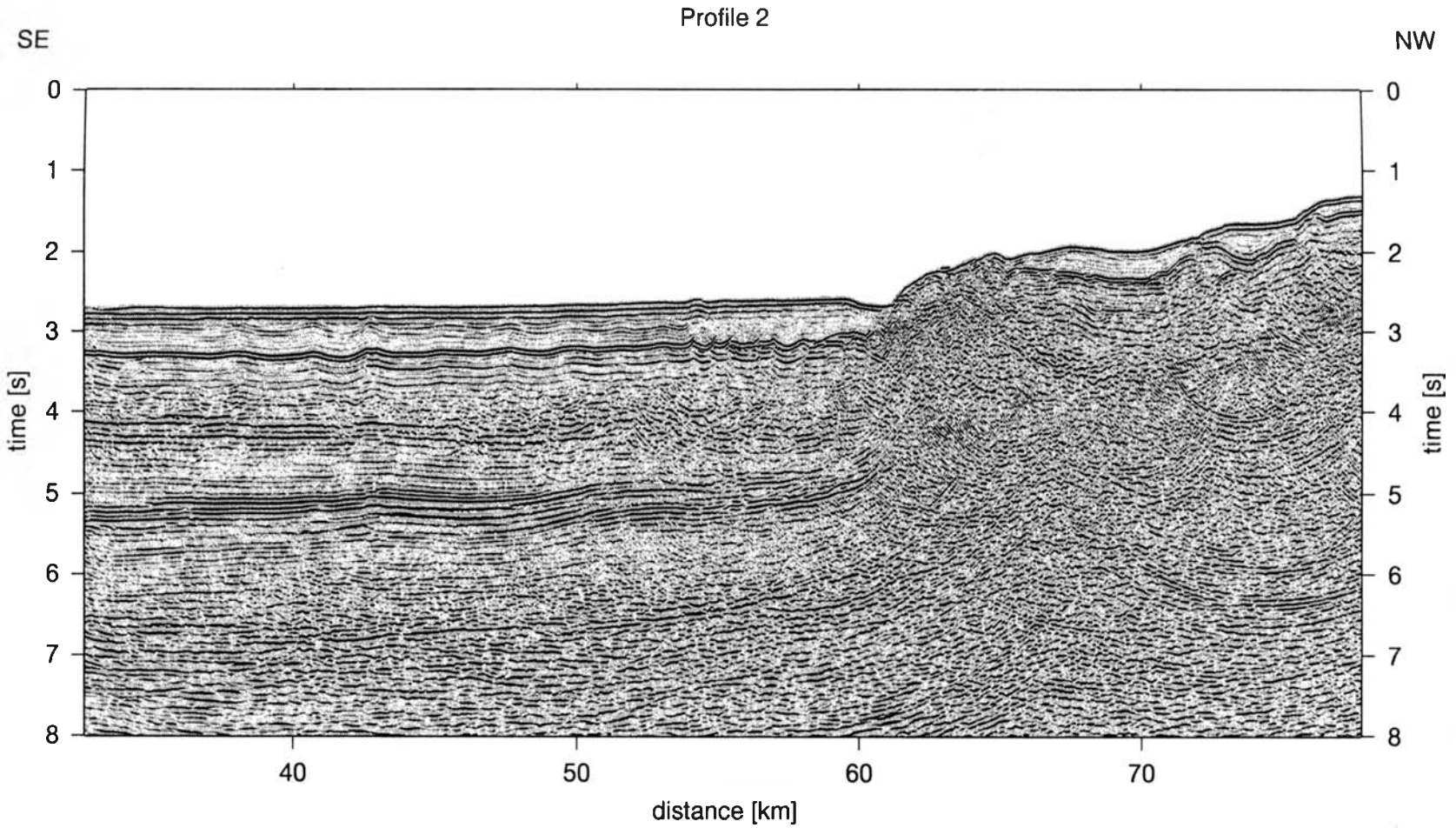


Fig. 10.5. Blow up of Profile 2: junction of the Levantine basin-Hecataeus Rise.

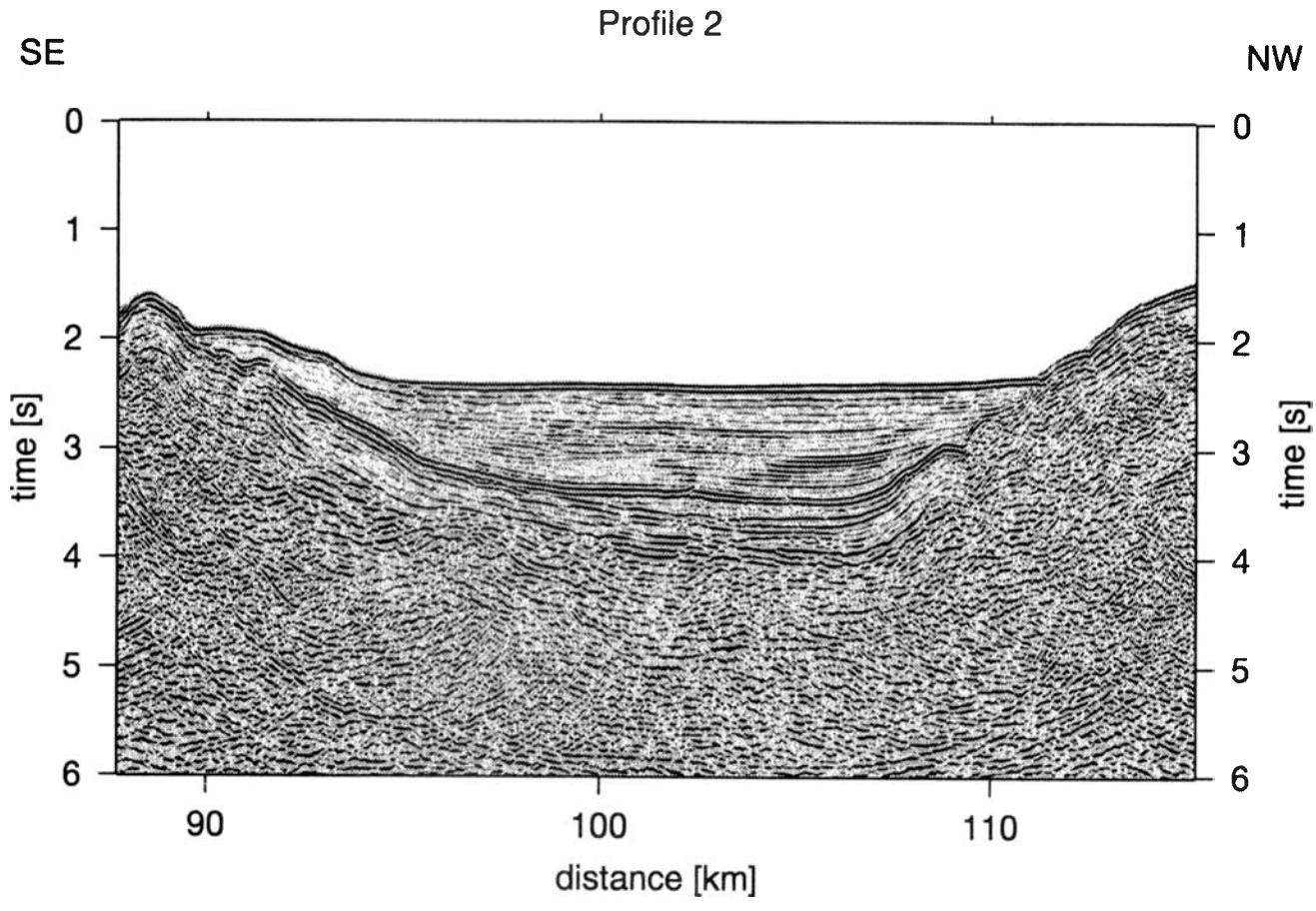


Fig. 10.6. Blow up of Profile 2: Cyprean Basin.

2.2 Lines 3, 4, and 5

Profiles 3 and 4 extend along the eastern segment of the Cyprean Arc (Fig. 10.1). Their post-stacked time-migrated sections are displayed in **Fig. 10.7** and **Fig. 10.8**. This complex area is composed of several basins and ridges that are clearly seen in the bathymetric data (Fig. 10.1; Hall et al., 1994). The northern ridge is the Kyrenia Ridge, considered to be the north-eastern extension of the Kyrenia Range in Cyprus (Robertson and Woodcock, 1986). It separates the Adana Basin (between Cyprus and Turkey) from the Latakia Basin and continues as a structure into Iskenderun Bay. To the south, the Larnaca Ridge extends from southeast of Cyprus up to Antakya Bay. South of Larnaca are located the Cyprean Basin and its prolongation to the east. Finally, the Latakia Ridge is the lowermost step in the Cyprean Arc, north of the Levantine Basin. The junction between the Larnaca and Latakia Ridges is marked by the NE-SW trending Gelendzhik Rise. The 'Strakhov' lines do not reach the Kyrenia Ridge, but they extend across the Larnaca and Latakia Ridges, and the Latakia, Cyprean and Levantine Basins.

The structure of the sedimentary sequence in the Levantine Basin for Lines 3 and 4 (Figs. 10.7 and 10.8) is similar to that described for Lines 1 and 2 (Figs. 10.2 and 10.4). Although the same units are observed in both lines, they display clear differences associated with a change in the intensity of sediment deformation towards the Latakia Ridge (**Fig. 10.9** and **Fig. 10.10**). Below the Pliocene-Quaternary units, more deformation is observed to the east, with a pronounced upward bending of the pre-Messinian sedimentary sequence. This upward pull is also observed along Line 3 but it is less gradual and concentrated at the end of the Levantine Basin. As with Lines 1 and 2, there is deep reflectivity between 6-8 s which may be associated with the Mesozoic-Paleozoic unit. The basin terminates abruptly at the southern border of the ridge (Fig. 10.9), where the sedimentary sequence pinches out. A clear onlap is observed along the evaporitic unit (Fig. 10.10, km 25-35 at 3.5 s). This infers that the deformation affecting the area is Upper Miocene in age.

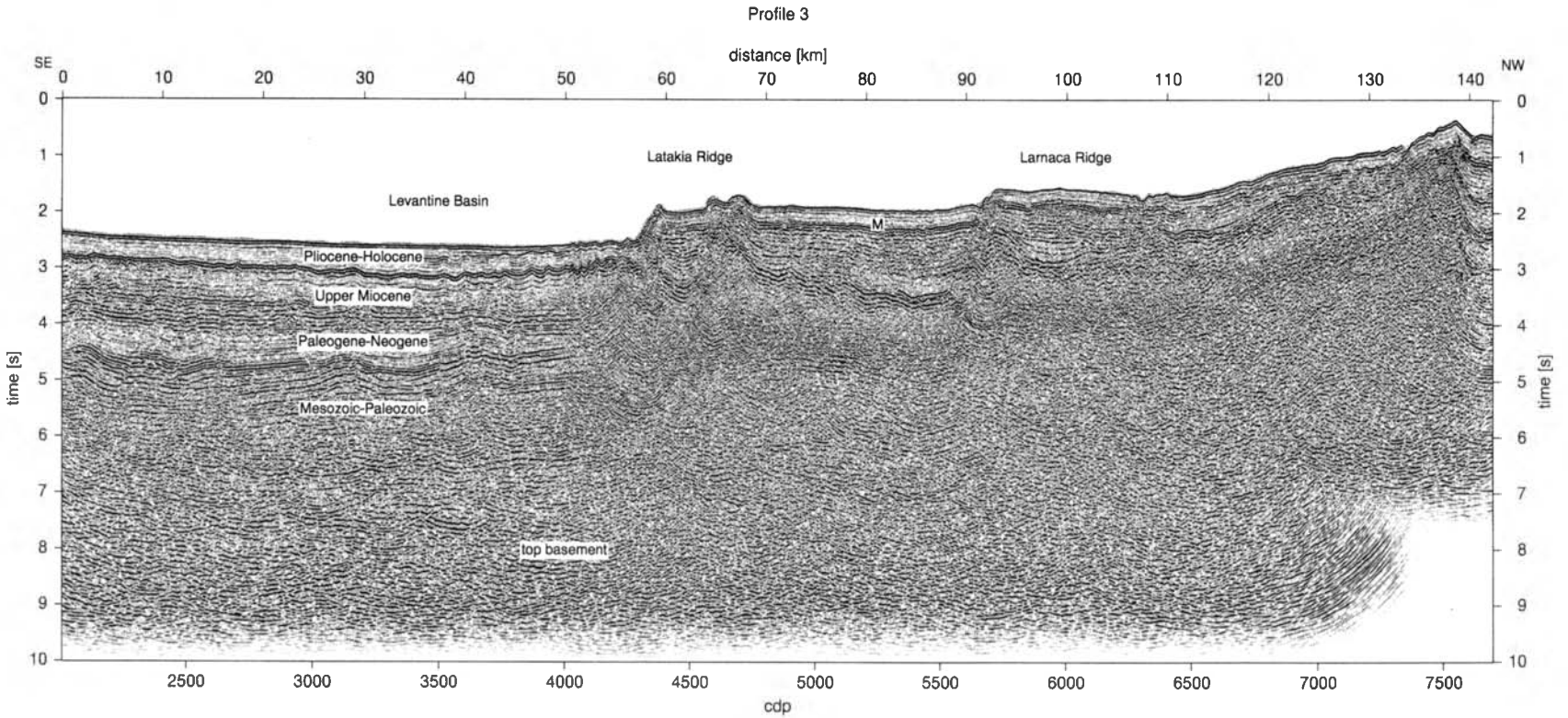


Fig. 10.7. Post-stacked time-migrated section of Profile 3.

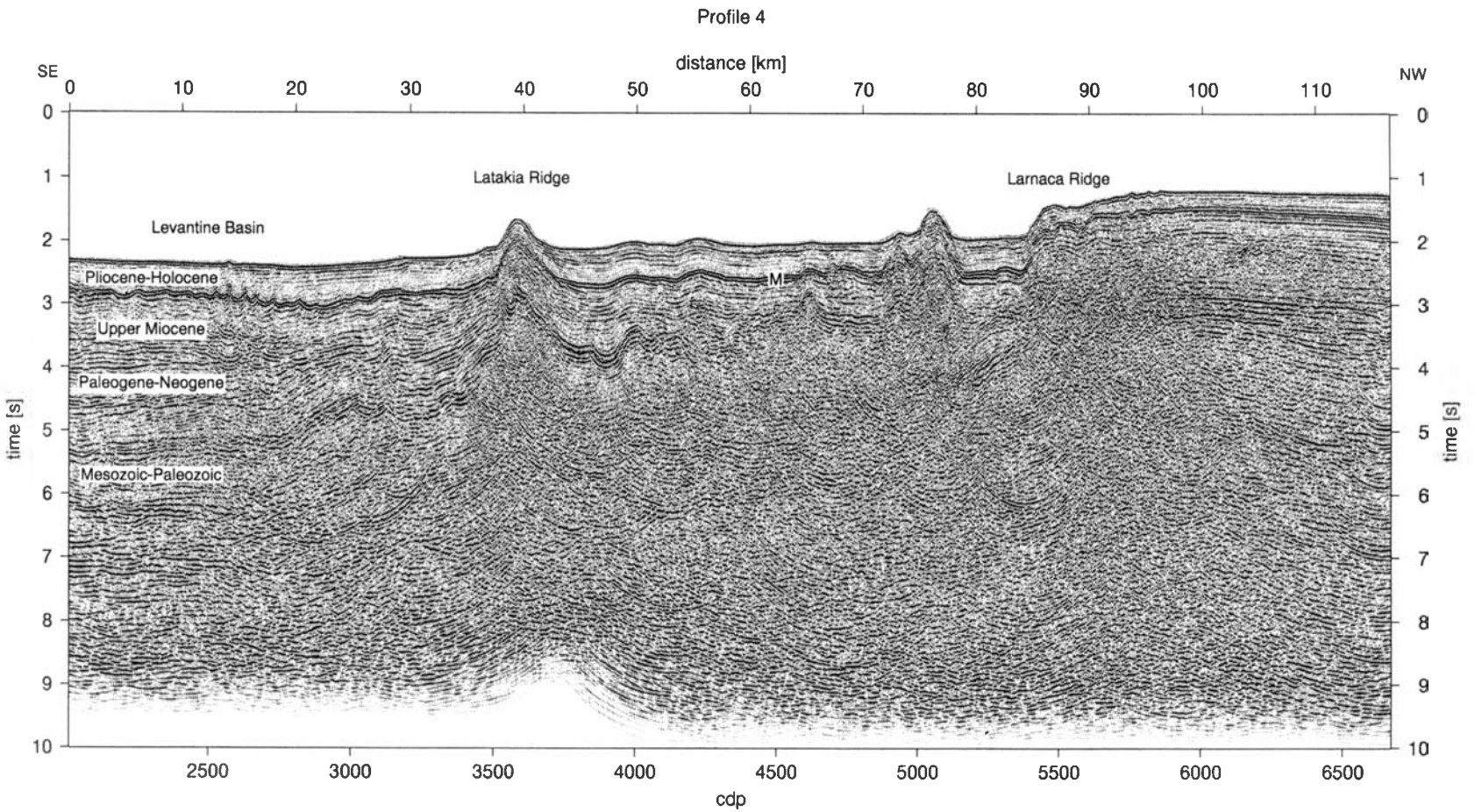


Fig. 10.8. Post-stacked time migrated section of Profile 4.

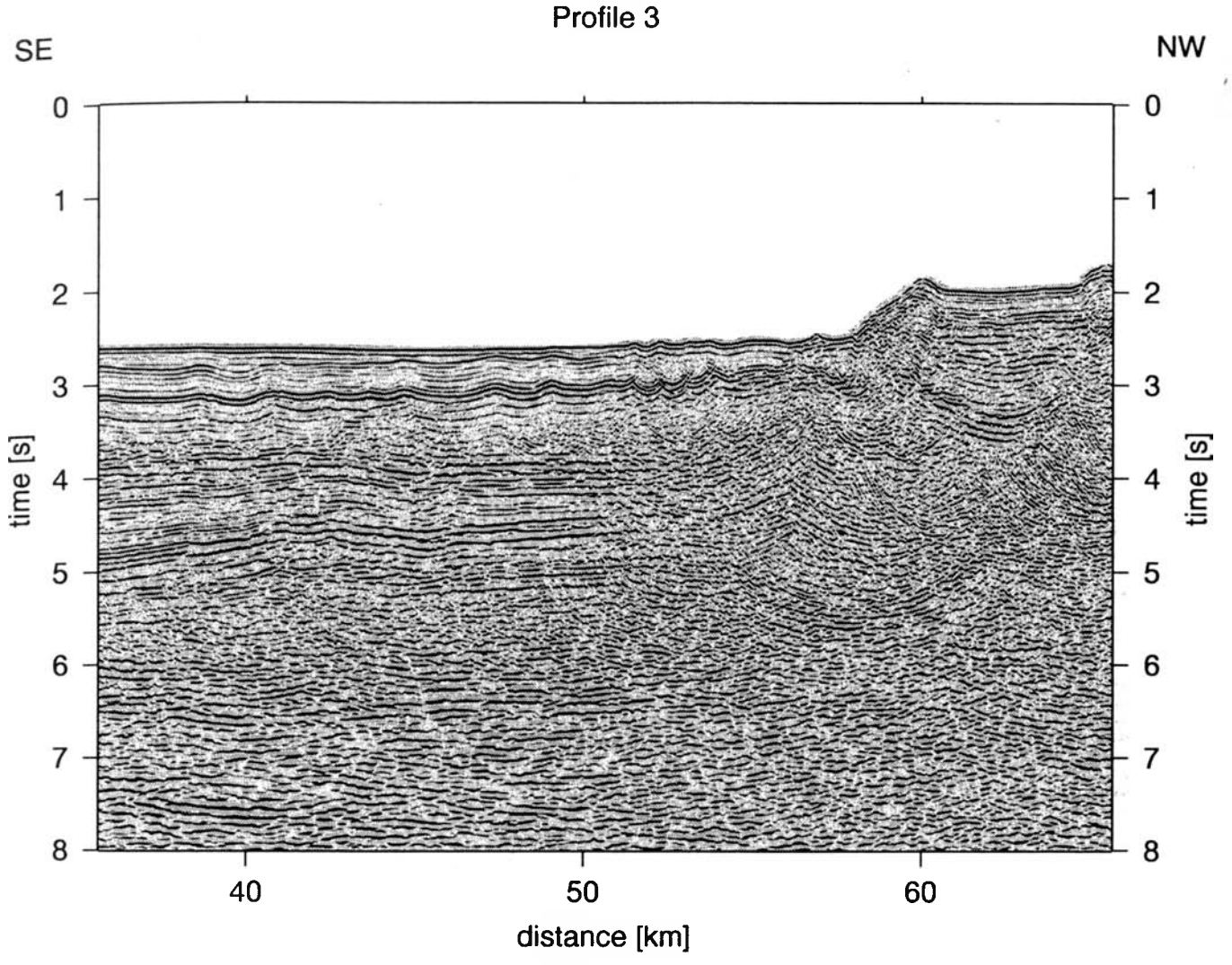


Fig. 10.9. Blow up of Profile 3: junction of the Levantine basin-Latakia Ridge.

To the north, the deformation associated with the Latakia and Larnaca Ridges and the Latakia and Cyprean Basins controls the tectonic structure of the Eastern Cyprean Arc (Figs. 10.7 and 10.8). The basins show some similarities, both being inclined to the south and clearly deformed in their southern parts towards the two ridges. The Pliocene-Quaternary layer is cut by faults in some areas and protruded by evaporite diapirs. In some areas, especially in the ridges, the post-Messinian sediments are pulled up, attesting for its recent activity. Below this upper sedimentary sequence, the M horizon is the most pronounced reflector. The evaporitic sequence is thinner for the Latakia and Cyprean Basins than the one observed in the Levantine Basin. Well beneath the evaporites a clear discontinuity can be traced and has been interpreted as possibly the top of the Mesozoic-Paleozoic sequence. Despite the similarities between the two basins and the tilting of the sedimentary units towards the adjacent ridges, the images of Lines 3, 4, and 5 differ substantially and suggest a change in the character of deformation of the arc to the northwest.

Another important feature is the existence of some deep reflections, observed mainly between the Larnaca and Latakia Ridges (Figs. 10.7 and 10.8). The easternmost area of the Cyprean arc (Line 5, **Fig. 10.11**) is influenced by the proximity of the Syrian coast (Fig. 10.1). The sedimentary fill south of the Larnaca Ridge is thicker than that seen on Lines 3 and 4. As the ridge is approached the nature of the reflectivity changes (**Fig. 10.12**), with a sharp boundary observed immediately on its southern flank.

3. DISCUSSION AND CONCLUSION

Interpretion of the seismic images along Lines 1-5 show

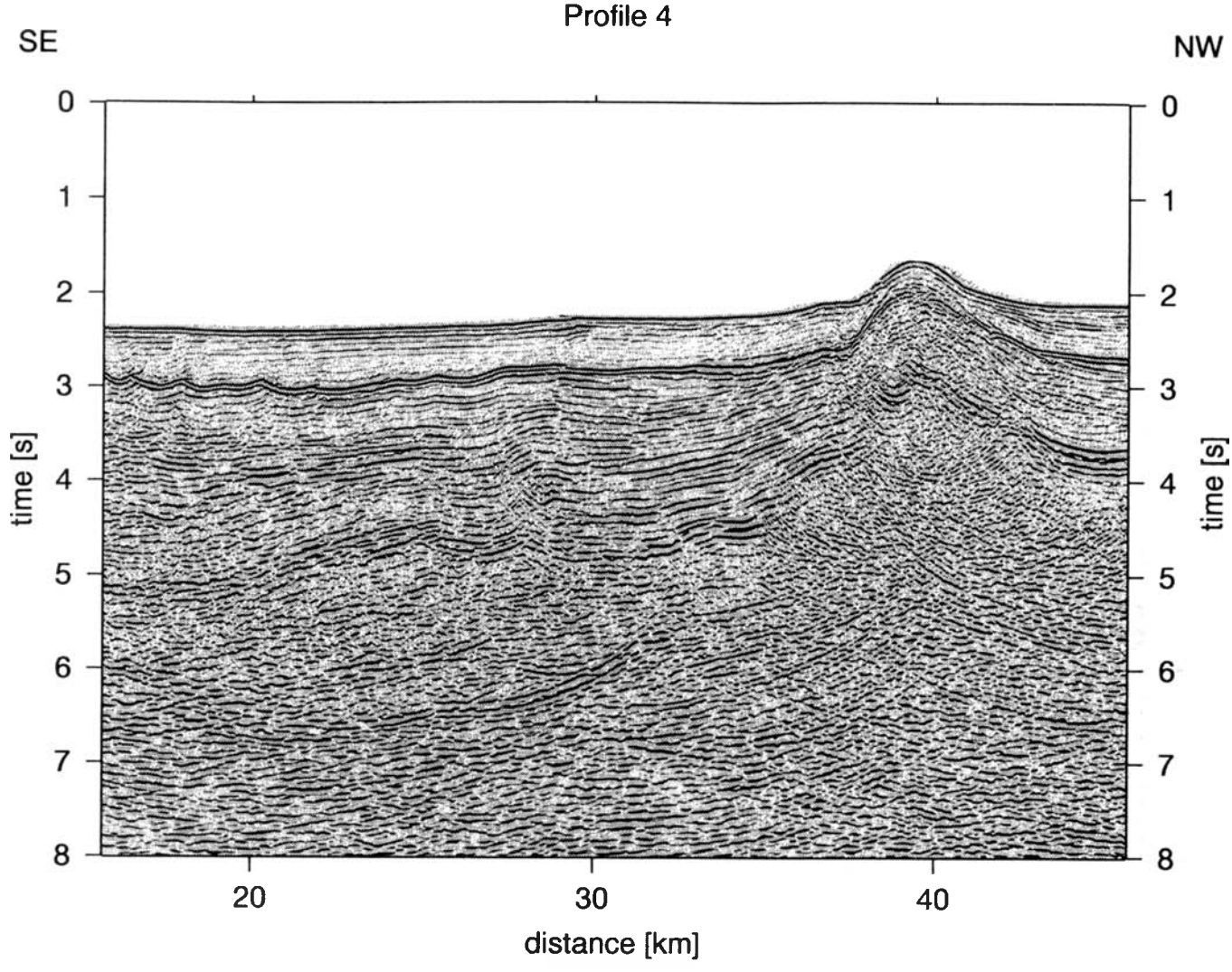


Fig. 10.10. Blow up of Profile 4: junction of the Levantine basin-Latakia Ridge.

a regular sedimentary pattern throughout the Levantine Basin fill (Figs. 10.2, 10.4, 10.7, and 10.8). A detailed velocity-depth profile down to 6-7 km is provided by the pre-stack depth-migration of Klaeschen et al. (Chapter 9 in this volume). The Pliocene-Quaternary sedimentary cover is between 400 to 600 m thick. Beneath a 100 m thick unit with a seismic velocity of 2 km/s, a 2.5 km/s velocity is observed. At about 2.5 km depth, the top of the Upper Miocene-Messinian unit is seen. It has an average thickness of 1.3 km and its velocity is 4.3-4.5 km/s. These interval velocity values are consistent with a salt layer. Its base is at a depth of approximately 4 km. The underlying Paleogene-Neogene layer marks a decrease in the interval velocity to 3.2-3.8 km/s that extends to a highly reflective package at 6 km depth. The horizon around 6 km is interpreted as the top of the Mesozoic-(?)Paleozoic sedimentary unit. The velocity control beneath this depth is not reliable.

Although an increase in velocity is suggested, no precise values are derived from the data. The velocity of 4.5 km/s obtained from the previous wide-angle study in the area (Makris et al., 1983) has been used as a reference velocity to migrate the deep levels. Even though some remnant multiple energy exists, the real reflections can be followed along the lines down to the end of the 10 s recording. Energy at 8 s is interpreted as the lowermost reflector, indicating a depth of 12-14 km. This reflector could represent the top of the crystalline basement in the area. It agrees with the depth suggested from the wide-angle interpretations (Makris et al., 1983).

Nevertheless, we do not observe a fundamental change in reflectivity and the 10 s recording does not allow the deeper structure to be imaged. Processing has revealed the complex junction between the Levantine Basin and the Hecataeus Rise

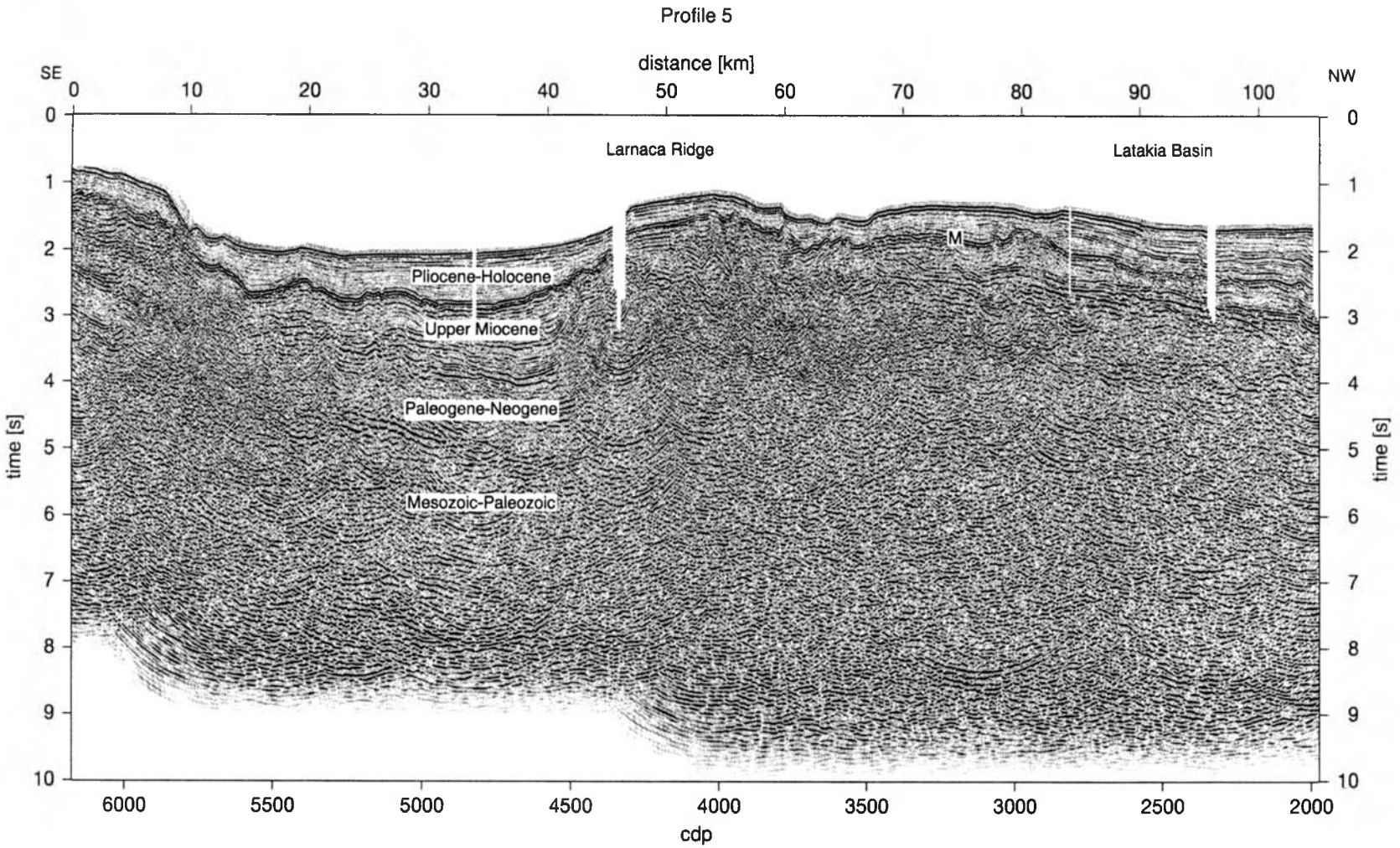


Fig. 10.11. Post-stacked time-migrated section of Profile 5.

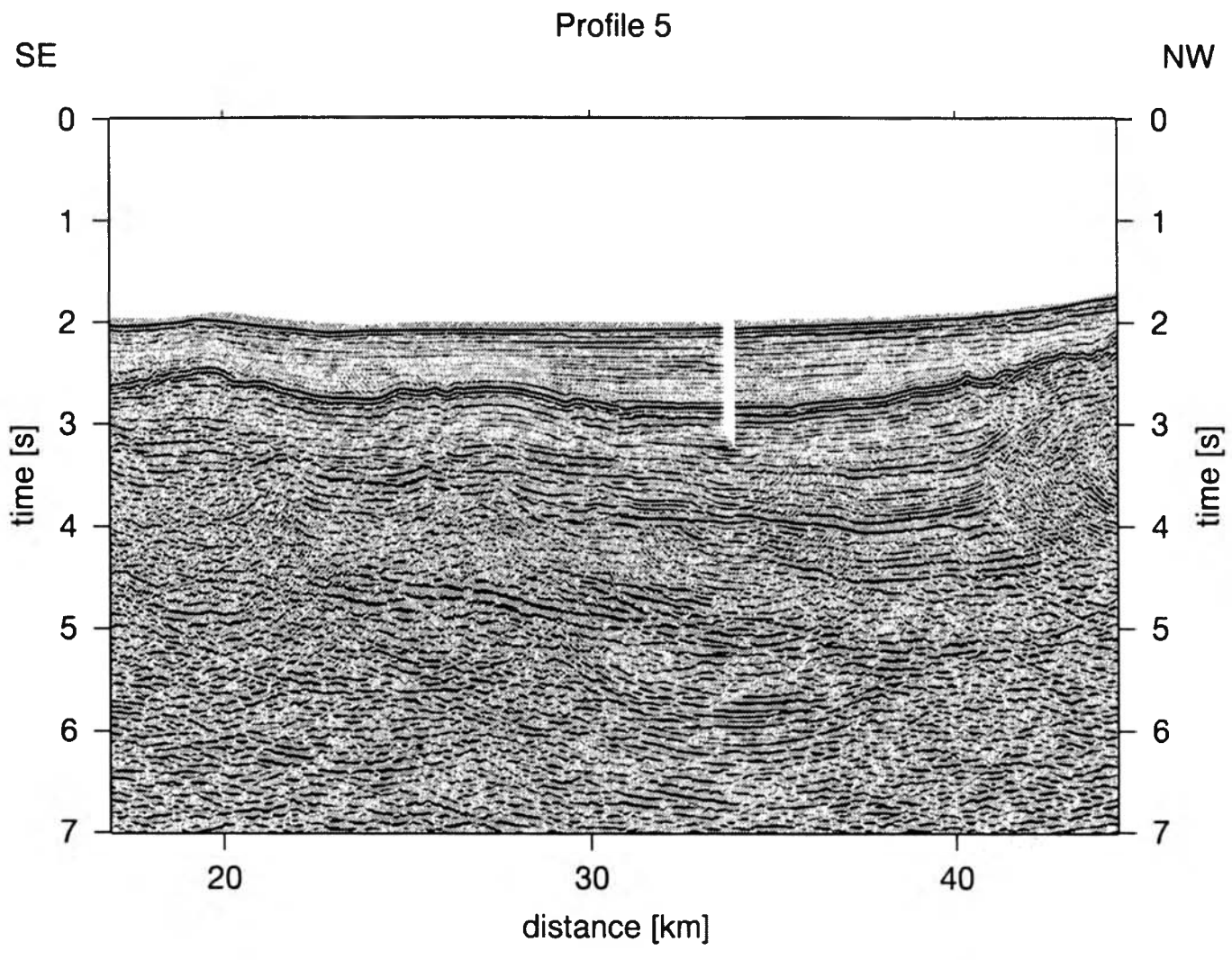


Fig. 10.10. Blow up of Profile 4: junction of the Levantine basin-Latakia Ridge.

(Figs. 10.3 and 10.5). The results suggest the existence of an important west to east variation in the deformation character of the area. South of Cyprus, present-day northward subduction is well established (Robertson et al., 1990, 1995) influenced by the effect of the collision of Eratosthenes Seamount. A comparison of the results obtained there by Kopf et al. (Chapter 11 in this volume), with the structure found at the junction with the Hecataeus Rise, shows there is no evidence for subduction to the east. No trench is observed, and no dipping and no increase in the sedimentary thickness either approaching or below the rise (Fig. 10.4).

However, from south to north an important discontinuity is imaged. There is an abrupt change in the reflective character, and the sedimentary layers are not imaged beneath the rise. This vertical and abrupt discontinuity infers the presence of a strike-slip fault system at the southern boundary of the rise. We interpret the junction area as the plate boundary for Lines 1 and 2. We consider the Hecataeus Rise to be the southern border of the Anatolian plate, south-east of Cyprus. Active faulting and deformation are observed along the Hecataeus Rise with the evaporite unit protruding through the younger sediments and rising to the seafloor in places. Evidence of subsidence was pointed out by Udintsev et al. (1994) who carried out a detailed analysis of the post-Messinian sedimentary cover. A young, well-stratified regressive sedimentary sequence occurs in the Cyprean Basin (Fig. 10. 5), offlapping the Hecataeus Rise slope and onlapping the fault scarp of the Cyprean slope. It may suggest recent subsidence of a block of the Hecataeus Rise relative to the Cyprean Massif, and would therefore suggest a young age for the Cyprean Basin.

The eastern part of the Cyprean Arc is marked by two main structural lineaments: the Latakia and Larnaca Ridges (Fig. 10.1). The Latakia Ridge defines an abrupt N-S-change in reflectivity of the structures and in the type of deformation. The boundary is

characterized by the existence of a steep fault that can be traced on both Lines 3 and 4 (Figs. 10.9 and 10.10). The seismic images display occasional flower structures along these profiles suggesting strike-slip movement on this fault. The transpressional tectonic movements in the area suggest that lateral slip dominates fault displacement south of the Hecataeus Rise, while only a minor component of downward subduction occurs. There are no indications that support accretion.

The eastern extension of this boundary close to the Syrian coast can also be seen along Line 5 (Figs. 10.7, 10.8, and 10.11). The image obtained here suggests that the fault has deviated to the north, *i.e.* to the area of the Larnaca Ridge. This change in the location of the boundary could be attributed to its proximity to the Syrian coast and to the influence of the Arabian plate moving in a north-west direction.

The Larnaca Ridge also constitutes a major lineament in this area. It is characterized by a second fault system marked on Lines 3, 4 and 5 (Figs. 10.7, 10.8, and 10.11). Evidence of extension is inferred by the configuration of the two basins between the ridges, as well as by normal faulting along their margins. These features, however, are of minor significance as compared to the overall compressional deformation resulting from a scenario of ridges with thrusts and reverse faults. The MCS profiles show that the location of the plate boundary for the Eastern Cyprean Arc follows the prolongation to the east of the Anatolian-African plate boundary located between southern Cyprus and Eratosthenes Seamount, and runs east-west at the junction of the Hecataeus Rise and the Levantine Basin. From there, it follows the Gelendzhik Rise to Latakia Ridge and is displaced east-northeastward upon approaching the Syrian coast. This plate boundary is marked by two NE-trending structural lineaments, which follow the Latakia and Larnaca Ridges and are governed by the transpressional fault system.

The seismic images appear to support a northeastward bending of the plate boundary towards Syria (*i.e.* into the direction of the East Anatolian fault zone). The Anatolian plate moves to the west with a major component of counterclockwise rotation versus translation (McKenzie, 1970; Dewey and engör, 1979; Jackson and McKenzie, 1988; Westaway, 1994; Oral et al., 1995). The important differential motion of 15 mm/yr (Oral et al., 1995) between the Arabian and African plates is accommodated by left lateral motion along the Dead Sea transform fault.

ACKNOWLEDGEMENTS

We gratefully acknowledge the long-term support for this study from the Deutsche Forschungsgemeinschaft (DFG) through grants HU 470/3 and HU 470/6. We would like to thank C. Docherty for his contribution to the data processing and discussions on the subsurface structures.

REFERENCES CITED

Ambraseys, N. N., and Adams, R. D., 1993. Seismicity of the Cyprus region. Terra Nova, No 5, p. 85-94.

Ben-Avraham, Z., 1978. The structure and tectonic setting of the Levant continental margin, eastern Mediterranean. Tectonophysics, 46(3-4), p. 313-331.

Ben-Avraham, Z., Kempler, D., and Ginzburg, A., 1988. Plate convergence in the Cyprean arc. Tectonophysics, 146(1-4), p. 231-240.

Ben-Avraham, Z., and Nur, A., 1986. Collisional processes in the Eastern Mediterranean. Geol. Rundsch., 75(1), p. 209-217.

Ben-Avraham, Z., Tibor, G., Limonov, A. F., Leybov, M. B., Ivanov, M. K., Tokarev, M. Y., and Woodside, J. M., 1995. Structure and tectonics of the eastern Cyprean Arc. Mar. Petrol. Geol., 12(3), p. 263-271.

Dewey, J. F., Pitman W. C. III, Ryan, W. B. F., and Bonnin, J., 1973. Plate tectonics and the evolution of the Alpine system. Geol. Soc. Am., 84(10), p. 3137-3180.

Dewey, J. F., and engör, A. M. C., 1979. Aegean and surrounding regions: Complex multiplate and continuum tectonics in a convergent zone. Geol. Soc. Am. Bull., 90(1), p. 84-92.

Eaton, S., and Robertson, A. H. F., 1993. The Miocene Pakhour Formation, southern Cyprus, and its relationship to the Neogene tectonic evolution of the Eastern Mediterranean. Sedim. Geol., 86(3-4), p. 273-292.

Girdler, R. W., 1990. The Dead Sea transform fault system. Tectonophysics, 180(1), p. 1-13.

Hall, J. K., Udintsev, G. B., and Odinokov, Yu. Yu., 1994. The bottom relief of the Levantine Sea. In: V. A. Krasheninnikov, and J. K. Hall (eds.). Geological Structure of the Northeastern Mediterranean, Jerusalem, Historical Productions-Hall Ltd., Jerusalem, p. 5-32.

Jackson, J., and McKenzie, D. P., 1988. The relationship between plate motions and seismic moment tensors, and the rates of active deformation in the Mediterranean and Middle East. Geophys. J. Roy. Astron. Soc., 93(1), p. 45-73.

Kempler, D., and Garfunkel, Z., 1994. Structures and kinematics in the northeastern Mediterranean: A study of an irregular plate boundary. Tectonophysics, 234(1-2), p. 19-32.

Kempler, D., and Ben-Avraham, Z., 1987. The tectonic evolution of the Cyprean Arc. Annales Tectonicae, 1(1), p. 58-71.

Kogan, L. E., and Stenin, A. M., 1994. Multichannel MOV-OGT (CDP Seismic Profiling during Cruise 5 of R/V 'Akademik Nikolaj Strakhov' (Preliminary results). In: V. A. Krasheninnikov, and J. K. Hall (eds.). Geological Structure of the Northeastern Mediterranean, Jerusalem, Historical Productions-Hall Ltd., Jerusalem, p. 99-112.

Krasheninnikov, V. A., and Hall, J. K. (Eds.), 1994. Geological Structure of the Northeastern Mediterranean (Cruise 5 of the Research Vessel 'Akademik Nikolaj Strakhov'), Historical Productions-Hall Ltd., Jerusalem, 396 p.

Limonov, A. F., Woodside, J. M., and Ivanov, M. K., (Eds.). 1994. Mud Volcanism in the Mediterranean and Black Seas and Shallow Structure of the Eratosthenes Seamount. Initial Results of the Geological and Geophysical Investigations during the Third 'Training-through-Research' Cruise of the R/V Gelendzhik (June-July 1993). UNESCO Rep. Mar. Sci., No 64.

Le Pichon, X., and Angelier, J., 1979. The Hellenic Arc and Trench System: a key to the neotectonic evolution of the Eastern Mediterranean area. Tectonophysics, 60(1-2), p. 1-42.

Makris, J., and Wang, J., 1994. Bouguer gravity anomalies of the Eastern

Mediterranean Sea. In: V. A. Krasheninnikov, and J. K. Hall (eds.). Geological Structure of the Northeastern Mediterranean, Jerusalem, Historical Productions-Hall Ltd., Jerusalem, p. 87-98.

Makris, J., Ben-Avraham, Z., Behle, A., Ginzburg, A., Gieze, P., Steinmetz, L., Whitmarsh, R. B., and Eleftheriou, S., 1983. Seismic refraction profiles between Cyprus and Israel and their interpretation. Geophys. J. Roy. Astron. Soc., 75(3), p. 575-591.

McKenzie, D. P., 1970. Plate tectonics of the Mediterranean Region. Nature, 226(5242), p. 239-343.

McKenzie, D. P., 1972. Active tectonics of the Mediterranean Region. Geophys. J. Roy. Astron. Soc., 30(1), p. 109-185.

Nur, A., and Ben-Avraham, Z., 1978. The Eastern Mediterranean and the Levant: tectonics of continental collision. Tectonophysics, 46(3-4), p. 297-311.

Oral, M. B., Reilinger R. E., Toksvz M. N., King R. W., Barka A. A., Kinik I., and Lenk O., 1995. Global positioning system offers evidence of plate motions in eastern Mediterranean. EOS, Trans. AGU, 76(1), p. 9-12.

Reilinger, R. E., McClusky, S. C., Oral, M. B., King, R. W., Toksöz, M. N., Barka, A. A., Kinik, I., Lenk, O., Sanli, I., 1997. Global Positioning System measurements of present-day crustal movements in the Arabia-Africa-Eurasia plate collision zone. J. Geophys. Res., 102(B5), p. 9983-10,000.

Robertson, A. H. F., Eaton, S., Follows, E. J., and McCallum, J. E., 1990. The role of local tectonics versus global sea-level changes in the Neogene evolution of the Cyprus active margin. In: D. I. M. MacDonald (ed.), Sea-level Change at Active Margins, Spec. Publ., Inst. Assoc. Sedimentol., v. 12, p. 331-369.

Robertson, A. H. F., Emeis, K. -C., Richter, C., Blanc-Valleron, M. M., Bouloubassi, I., Brumsack, H. J., Cramp, A., De Lange, G. J., Di Stefano, E., Flecker, R., Frankel, E., Howell, M. W., Janecek, T. R., Jurado, M. J., Kemp, A. E. S., Koizumi, I., Kopf, A., Major, C. O., Mart, Y., Pribnow, D. F. C., Rabaute, A., Roberts, A. P., Rillkotter, J. H., Sakamoto, T., Spezzaferri, S., Starker, T. S., Stoner, J. S., Whiting, B. M., and Woodside, J. M., 1995. Evidence of collisional processes associated with ophiolite obduction in the eastern Mediterranean. Results from Ocean Drilling Program Leg 160. GSA 5, 11.

Robertson, A. H. F., and Grasso, M., 1995. Overview of the Late Tertiary-Recent tectonic and paleo-environmental development of the Mediterranean region. Terra Nova, 7(2), p. 114-127.

Robertson, A. H. F., Kidd, R. B., Ivanov, M. K., Limonov, A. F., Woodside, J. M., Galindo-Zaldivar, J., Nieto, L., and the Scientific Party of the 1993 TTR-3 Cruise. 1994. Probing Continental collision in the Mediterranean Sea. EOS, 75(21), p. 233-238.

Robertson, A. H. F., and Woodcock, N. H., 1986. The role of the Kyrenia Range Lineament, Cyprus in the geological evolution of the eastern Mediterranean area. Phil. Trans. Roy. Soc. London, A 317, p. 141-177.

Rotstein, Y., and Ben-Avraham, Z., 1985. Accretionary processes at subduction zones in the Eastern Mediterranean. Tectonophysics, 112(1-4), p. 551-561.

Rotstein, Y. and Kafka, A. L., 1982. Seismotectonics of the southern boundary of Anatolia, eastern Mediterranean region: subduction, collision and arc jumping. J. Geophys. Res., 87(B9), p. 7694-7706.

Şengör, A. M. C., 1979. Mid-Mesozoic closure of Permo-Triassic Tethys and its implications. Nature, No 5714, p. 590-593.

Smith, A. G., 1971. Alpine deformation and the oceanic areas of the Tethys, Mediterranean and Atlantic. Bull. Geol. Soc. Am.. 82(8), p. 2039-2070.

Udintsev, G. B., Zverev, A. A., Odinokov, Yu. Yu., Efremov, V. N., Eleftheriou, S., and Hall, J. K., 1994. Structure of the Post-Messinian Sedimentary Cover in the Eastern Part of the Mediterranean Sea. In: V. A. Krasheninnikov, and J. K. Hall (eds.). Geological Structure of the Northeastern Mediterranean, Jerusalem, Historical Productions-Hall Ltd., Jerusalem, p. 33-73.

Westaway, R., 1994. Present-day kinematics of the Middle East and eastern Mediterranean. J. Geophys. Res., v. 86, p.12,071-12,090.

Woodside, J. M., 1991. Disruption of the African Plate margin in the eastern Mediterranean. - In: M. J. Salem, A. M. Sbeta, M. Bakbak, and M. Rida, (eds.), The Geology of Libya: Symp. Geol. Libya, 3, p. 2319-2329.

Woodside, J. M., 1977. Tectonic elements and crust of the Eastern Mediterranean sea. Mar. Geophys. Res., 3(3), p. 317-354.

Woodside, J. M., 1976. Regional vertical tectonics in the eastern Mediterranean. Geophys. J. Roy. Astron. Soc., 47(3), p. 493-514.

Chapter 11

Multi-Channel Seismic Profiles across Eratosthenes Seamount and the Florence Rise Reflecting the Incipient Collision between Africa and Eurasia near the Island of Cyprus, Eastern Mediterranean

Achim Kopf
Géosciences Azur, B.P. 48, 06230 Villefranche-sur-Mer Cédex, France
Neus Vidal
Escola Universitaria Salesiana de Sarria, Rafael Battle 7, 08017 Barcelona, Spain
Dirk Klaeschen
GEOMAR Research Centre, Wischhofstrasse 1-3, D-24148 Kiel, Germany
Roland von Huene
GEOMAR Research Centre, Wischhofstrasse 1-3, D-24148 Kiel, Germany
Valery A. Krasheninnikov
Geological Institute of the Russian Academy of Sciences, Pyzhevskiy pereulok 7, 109017 Moscow, Russia

ABSTRACT

Multichannel seismic reflection lines across the collision zone between the African and Eurasian plates provide insight into the deformational pattern of microplate tectonics. Three lines were acquired across Eratosthenes Seamount and the Florence Rise during Cruise 5 of the R/V 'Akademik Nikolaj Strakhov'. They reveal the complex deformational patterns related to the collision of continental fragments with the subduction system west and southwest of Cyprus.

Careful reprocessing of the original data (*i.e.* deconvolution, *fk*, and wave-equation demultiple operators etc. - see Klaeschen et al, Chapter 9, this volume) removed artifacts and improved the temporal resolution to provide detailed images. Prominent reflections in depth-migrated sections were traced down to depths of 12-14 km.

Eratosthenes Seamount is a continental fragment, detached from the North African margin, that is now causing tectonic uplift of Cyprus as its northern flank undergoes subduction. As the trench sediments north of the seamount appear undeformed on seismic lines, it is assumed that the down-going slab undergoes extensional deformation at its top, possibly due to flexural effects. This is also mirrored by normal block faulting, and the horst-and-graben topography of the carbonates on top of Eratosthenes. Nevertheless, the breakup of the seamount is illustrated by northeastward-dipping faults which are believed to mark the northward migration of the present plate boundary between Africa and Eurasia. On its southwestern and southern flanks, the seamount is overridden by sediment from the Herodotus abyssal plain which may be viewed as undergoing back-thrusting. North of Eratosthenes, accreted material, which was supposedly scraped off the Levantine seafloor before the initial collision of the seamount, forms an odd-shaped wedge immediately south of the backstop (*i.e.* the Cyprus margin).

Although of proposed northern (*i.e.* Anatolian) origin, the Florence Rise shows similarities to Eratosthenes Seamount. It is a topographically less elevated area with a partly chaotic seismic pattern, indicating a considerable amount of compressional tectonic deformation. The southern boundary of the rise is imbricated, attracting the northernmost sediments of the Herodotus abyssal plain into this deformation. Although a thrust fault which was previously interpreted to be the plate boundary may still be active, our data indicate outward (*i.e.* southwestward) migration of the westernmost Cyprean Arc. Both the Messinian evaporites and low-velocity sediments of unknown age are involved in the thrust faulting.

In summary, the collision of Eratosthenes Seamount with Cyprus has caused tectonic uplift of the hanging wall. The ongoing convergent movement is reflected by thrusting, imbrication, and outward migration of the frontal thrust. With time, as considerable amounts of Messinian evaporites from the Herodotus abyssal plain get involved in this faulting, the incipient collision may lead to another topographic high, like the Mediterranean Ridge farther to the west.

INTRODUCTION

The eastern Mediterranean has long been known as an area where several microplates and crustal fragments are undergoing subduction between the converging African and Eurasian Plates (Ryan et al., 1973). As a result, plate fragments whose crustal characteristics are poorly understood are separated by numerous faults and fault systems in the zone of deformation. The major disruption in this area of the eastern Mediterranean lies between 31° and 32°N (*i.e.* from the Florence Rise to Egypt). Its eastern margin is on the western slope of Eratosthenes Seamount (**Fig. 11.1**). Therefore, the structural features observed on Lines 8, 9, and

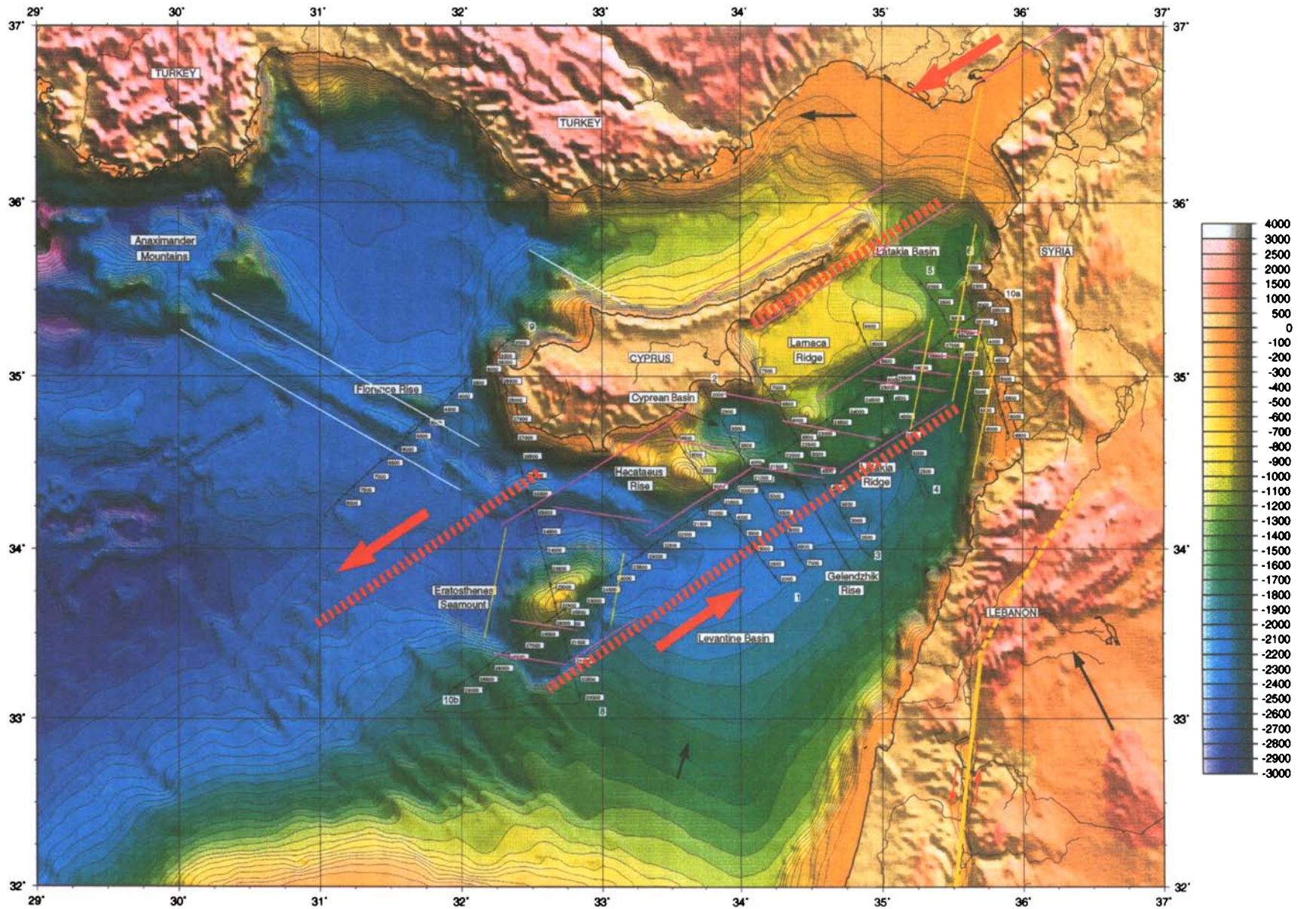


Fig. 11.1. Bathymetric map of the study area including seismic reflection lines 1-10 obtained from Cruise 5 of 'Strakhov'. Highlighted profiles 8, 9, and 10 (western part) are shown in Figs. 11.2-11.4.

10 have to be seen in the context of the tectonic framework of the area, namely the zone of deformation between Africa and Eurasia.

At present, the African Plate is migrating nearly orthogonally northward at a rate of 10 mm/yr (McKenzie, 1978; Le Pichon, 1982; Reilinger et al., 1997). At the line of transition from subduction to collision, prominent submarine topographic highs occur along the plate boundary, *e.g.* the Mediterranean Ridge accretionary complex or Eratosthenes Seamount.

Near Cyprus, the incipient collision is reflected by two prominent topographic highs, the Florence Rise west of Cyprus, and Eratosthenes Seamount south-southwest of Cyprus (Fig. 11.1). A combined study of the on land geology of Cyprus and the deep sea drilling results from Eratosthenes Seamount has shown that the collision of the seamount with Cyprus has led to ~2 km of tectonic uplift since the early Pliocene (Robertson, 1992; Krasheninnikov and Hall, 1994; Robertson et al., 1995a). Eratosthenes Seamount has been thrusting beneath both Cyprus in the north and the Levantine Basin in the south. The northward thrusting appears to post-date the Messinian (Robertson et al., 1995b).

The African plate is separated from the Arabian plate by the left-lateral Dead Sea transform fault in the east, and undergoes subduction in the north along a strike-slip fault of variable geometry, which coincides with the trend of the Cyprean Arc (Vidal et al., Chapter 10, this volume). The main reason for this is the sinistral motion due to counter-clockwise rotation of the Anatolian microplate, which is a part of the Eurasian plate behaving as a separate unit. The main trends of the structural features of Eratosthenes Seamount coincide with E-W and SE-NW-trends in Egypt (*i.e.* west of 30°E), and the predominant direction in the Syrian Arc which is ENE-WSW in Northern Sinai and the Levant (*i.e.* east of 30°E). Moreover, the direction of the break between the Cyprean Arc and the Florence Rise is subparallel to the northern boundary of Eratosthenes Seamount adjacent to the plate boundary between Africa and Eurasia (Fig. 11.1). Eratosthenes Seamount itself is suggested to have rotated counter-clockwise since its time of detachment (Ben-Avraham et al., 1976).

The nature of the structural lineaments observed across the Florence Rise, as well as the potpourri of different rocks recovered from sampling of the seafloor, provide an incomplete and poorly understood picture of this topographic high (Woodside et al., 1997). Nevertheless, parts of the Florence Rise and the Anaximander Mountains can be correlated with outcrops in Turkey to indicate a northern origin for these features, and translation along a set of subparallel shear zones trending NNW-SSE (Woodside et al., 1997). Moreover, northeastward subduction is indicated by earthquake data (Rotstein and Kafka, 1982; Kempler and Ben-Avraham, 1987) and crustal shortening along the Florence Rise and Antalya Basin indicated by observations of folding, thrusting, and NE-tilting (*e.g.* Woodside, 1977). South and southeast of Cyprus, strike-slip motion apparently predominates in the zone of convergence (Kempler, 1994).

This chapter concerns the deep structure of the Florence Rise and Eratosthenes Seamount as observed in extensively reprocessed seismic data. Types of faulting, structural relationships, and their consequences for the geometry of the plate boundary between Africa and Eurasia will be discussed below. Fortunately, the pre-stack depth migrations allow us to trace and interpret the geometry of these structures to subbottom depths of ~12 km below sea level.

DATA ACQUISITION AND PROCESSING

The Multi-Channel Seismic (MCS) data presented here were acquired in 1987 during Cruise 5 of R/V 'Akademik Nikolaj Strakhov' which investigated the eastern Mediterranean south and east of Cyprus (Krasheninnikov and Hall, 1994). The western parts of some ten profiles, *i.e.* Lines 8-south (8a), 8-north (8b), 9, and 10-west (10b), crossed Eratosthenes Seamount and the Florence Rise adjacent to the south-west coast of Cyprus (Fig. 11.1).

Data were collected using a 12-liter airgun and a 48-channel streamer. The shotpoint spacing was 100 m, the active length of the hydrophone array was 2350 m, and the recording length was 12 s two-way travel time (TWT). After the initial processing (see Kogan and Stenin, 1994), which lacked resolution due to diffractions, multiple reflections, and bubble pulse interference, the data were carefully reprocessed at the GEOMAR research center in Kiel, Germany. A detailed description of the treatment of the seismic data is given by Klaeschen et al., (Chapter 9, this volume). In summary, ghost and bubble inherited effects, as well as strong multiple arrivals could be removed so that the overall temporal resolution has considerably improved. As a consequence, structural trends in the deep part of the profiles can now be observed down to subbottom depths of more than 10 km in the pre-stack, depth-migrated lines (**Fig. 11.2A**).

ERATOSTHENES SEAMOUNT - A CONTINENTAL FRAGMENT FROM THE SOUTH

Eratosthenes Seamount is a distinct topographic feature which rises about 2 km above its surroundings, from a depth of 2700 m on its southern flank by the Levantine (or Phoenician) abyssal plain to ~750 m at its peak (Fig. 11.2 and **Fig. 11.3**). Its shape is elliptical (120 km N-S by 80 km E-W) with its major axis oriented NW-SE. It has been the subject of numerous marine geological investigations for a long time span, as outlined in detail by Mart and Robertson (1998) or Krasheninnikov and Hall (1994, see their bibliography).

Reconstruction of the tectonic history can now be based on the results of geophysical surveys (Krasheninnikov and Hall, 1994) as well as dredging and drilling efforts (Limonov et al., 1994; Emeis et al., 1996; Robertson et al., 1998). These suggest Eratosthenes Seamount to have been located at the northern slope of the African margin. The detachment occurred in pre- to syn-Cretaceous time (Robertson et al., 1995a). Both the southern margin of the Levant Basin and Eratosthenes Seamount subsided to bathyal depths during the Late Cretaceous-Early Palaeogene (Mart and Robertson, 1998). Evidence for a southern origin is provided by the distinct differences between the Cretaceous carbonates recovered from Eratosthenes Seamount (Emeis et al., 1996; Robertson et al., 1998) and the contemporaneous ophiolitic rocks and deep sea sedimentary

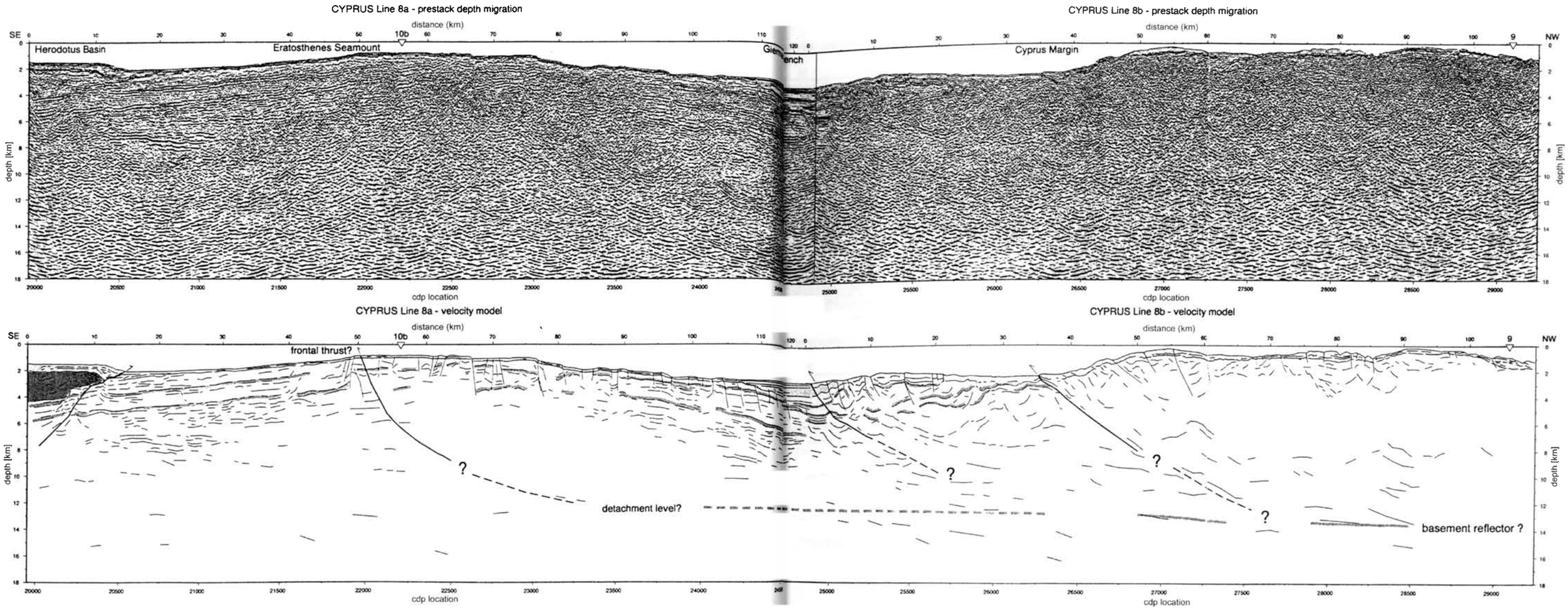
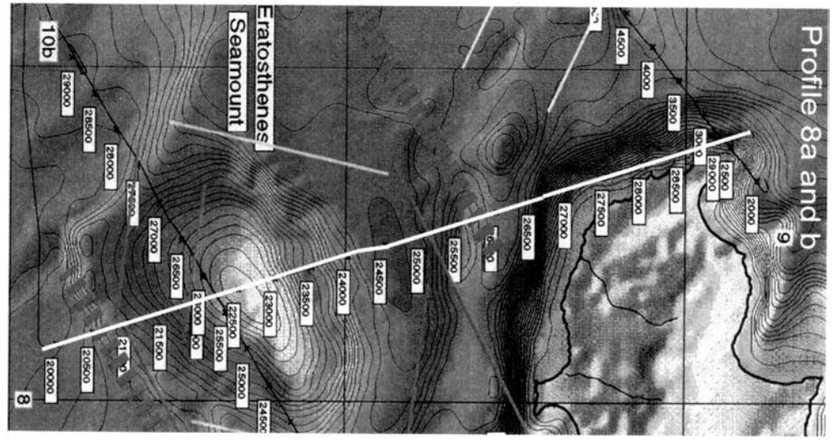


Fig. 11.2: Pre-stack depth migration (A) and interpreted line drawing underlain by the interpreted tectono-stratigraphic units (B) for MCS Line 8 across the Eratosthenes Seamount and the Cyprus margin. Note the northward-dipping flank of the African plate underneath the undisturbed 'trench fill' south of the island of Cyprus. Pliocene-Quaternary sediments show light gray shading; Messinian evaporites dark gray. Prominent reflectors are underlain by gray colors. See Fig. 11.1 for location.



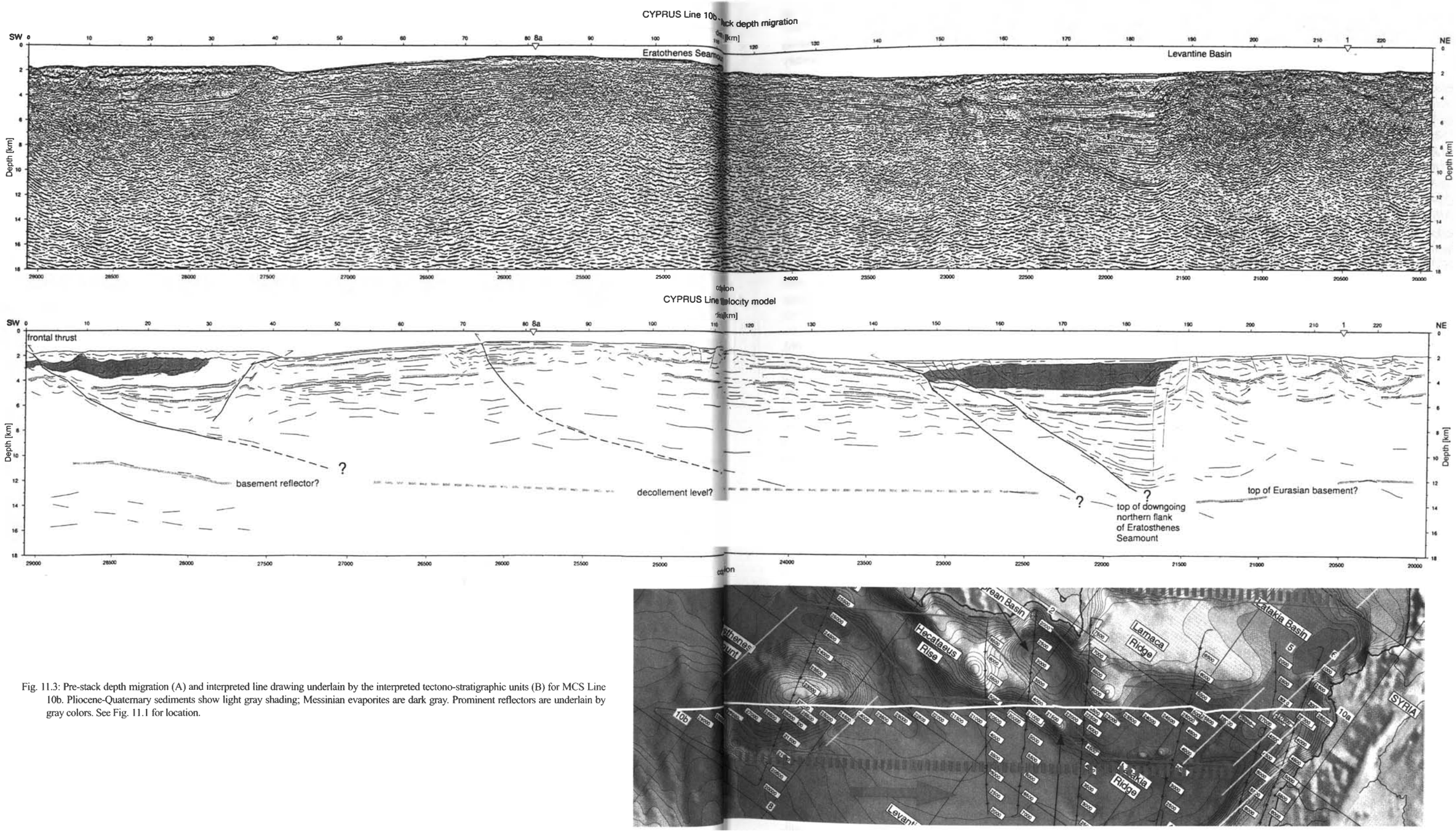


Fig. 11.3: Pre-stack depth migration (A) and interpreted line drawing underlain by the interpreted tectono-stratigraphic units (B) for MCS Line 10b. Pliocene-Quaternary sediments show light gray shading; Messinian evaporites are dark gray. Prominent reflectors are underlain by gray colors. See Fig. 11.1 for location.

cover found in the Troodos Massif on the island of Cyprus. On Eratosthenes Seamount, the presence of shallow water carbonates of Miocene age beneath deeper-water hemipelagic sediments of Pliocene-Quaternary age allows us to date the initiation of subsidence. The vertical tectonics have been complex, as suggested by the location of sedimentary hiatuses within the succession recovered from ODP drilling (Flecker et al., 1998).

Eratosthenes Seamount appears to have been thrusted beneath both Cyprus in the north and the Levant Basin in the south. Northward thrusting is suggested to post-date the Messinian (Robertson et al., 1995a). It has been found that the main structural style of deformation of the crestal area (down to a depth of ~800 m) is normal block faulting (Emeis et al., 1996; Robertson et al., 1998). This is similar to adjacent features such as the Hecataeus Rise (Vidal et al., Chapter 10, this volume) or the Anaximander Mountains farther to the north-west (Woodside et al., 1997). As interpreted from Formation MicroScanner images in ODP deep sea Sites 965-967 (Emeis et al., 1996; Robertson et al., 1998), the orientation of the faults and fractures is highly variable, reflecting different tectonic influences with time, instead of showing a consistent trend (Flecker et al., 1998). Both the steep (60° and steeper) normal faults which separated the different blocks and the fractures within the deposits of different age have undergone a complex tectonic history, especially regarding their vertical component. As can be seen from seismic images (Figs. 11.2 and 11.3) and seafloor mapping (Mascle et al., 1998; Loubrieu et al., 2001), the main trend of the faulting is E-W. The different units, however, have fracture and fault orientations varying between NE-SW and NW-SE for the Eocene, Oligocene, and Cretaceous, and both N-S and E-W for the Miocene deposits (Flecker et al., 1998).

Seismic profile 8 is oriented NNE-SSW and runs towards the western margin of Cyprus (Fig. 11.1). The section across Eratosthenes Seamount (*i.e.* the southern part of Line 8) reveals dominant reflectors as deep as 8-9 km, especially in the south where Eratosthenes Seamount is overthrust by the sediments of the Levantine Basin. The seamount itself lacks characteristic features in its deepest part. The shallow sets of reflectors, which are oriented subparallel to the seafloor, disappear at a depth of about ~5 s TWT (or 5 km depth below the seafloor; Fig. 11.2A). On top of the seamount, a succession of Pliocene-Quaternary sediments can be observed. These hemipelagic oozes (Emeis et al., 1996; Robertson et al., 1998) have velocities between 1650 and 2050 m/s (see Klaeschen et al., Chapter 9, this volume) and locally reach thicknesses of up to 1 km. Nevertheless, their cover on Eratosthenes Seamount itself rarely exceeds a couple of hundreds of meters.

Structurally, Eratosthenes Seamount appears to be a homogeneous structure with a rough surface, at least at first sight. However, the seafloor topography is the result of dominantly meso-scale normal block faulting. One can distinguish between two characteristic structural patterns that result from this:

i) the horst-and-graben-type separation of small units (*i.e.* hundreds of meters wide in cross-section, referred to as meso-scale deformation), and

ii) downslope movement of faulted blocks. These apparently dominate the northern flank of the seamount (Fig. 11.2A).

A fragment which had undergone mass wasting was drilled during ODP Leg 160 (site 967; Robertson et al., 1995a; 1998). It could be shown to have been at a shallower water depth in Miocene-Early Pliocene time. A summary of both the sedimentary and vertical tectonic history of Eratosthenes Seamount is given in Robertson et al. (1995a; 1998) and Flecker et al. (1998).

On a macro-scale, two northerly dipping faults dominate Eratosthenes Seamount, cutting across almost the entire feature (Fig. 11.2A). In addition, the continuation of its northern flank reflects the active present-day plate boundary. This gently (~15°) northward-dipping structure underlies the trench sequence in the middle of Line 8, but can be traced on the northern part of the profile as well (Fig. 11.2A - noting the 2x vertical exaggeration). The main fault trace, which crops out on the seafloor at approximately common mid-point (cmp) 21900 (Fig. 11.2B), shows a minor reverse offset and is presumed to represent the active frontal thrust at the present time. This separation may result from the incipient friction due to the collision, forcing the seamount to break up. This breakup may cause a set of faults at angles of around 50° (Fig. 11.2A) which may act as thrust faults in a scenario involving outward migration of the deformation front/plate boundary (see discussion below).

The western part of the longest seismic profile (Line 10b), which crosses the majority of the other profiles, trends approximately SW-NE. It also covers the Eratosthenes area (Fig. 11.1). Along Line 10b, the northeastern flank of Eratosthenes Seamount can be traced down to a subbottom depth of about 12 km (~21000-21400 cmp; Figs. 11.3A and 11.3B) underneath the sediments of the northernmost Levantine Basin. On its southwestern flank, another northeastward-dipping fault is observed as well as a backthrust fault, as indicated by Messinian and Pliocene-Quaternary sediments having been pushed onto the seamount (Fig. 11.3B). On either side, the seamount is bounded by a pile of Messinian evaporites with a velocity of ~4500 m/s. Both the carbonates of Eratosthenes (Robertson et al., 1995a; 1998) and the evaporites are overlain by a Pliocene-Quaternary succession several hundreds of meters in thickness. The velocity of these hemipelagic sediments was found to be between ~1850 and 2100 m/s. The velocities for the Pliocene-Quaternary sediments, as well as for the upper part of the carbonate platform forming Eratosthenes Seamount (see velocity models in Klaeschen et al., Chapter 9, this volume), are in good agreement with the measurements on cores and from the downhole ODP logging (Emeis et al., 1996; Robertson et al., 1998).

The evaporitic body east of the seamount was apparently deposited in a depression between the eastern flank of Eratosthenes Seamount and a small zone of deformed sediments which is now slightly elevated relative to its surrounding (19940–~21600 cmp in Fig. 11.3A). These sediments have rather low to moderate velocities, gradually increasing with depth. The deformed state of the series suggests that a compressional (*i.e.* subducting) component exists, along with the strike-slip motion inferred from flower structures seen in the seismic profiles (Fig. 11.3A; Harding, 1985). Only few structures are observed in the uppermost deposits, simply because the beginning of intense deformation apparently

predates the Messinian (note that the salt was precipitated on top of the western flank of this unit, and appears not to have undergone significant deformation; Fig. 11.3B). Also, the base of this unit cannot be seismically differentiated from the deeper rocks, although at around 5 km depth, the velocities increase with a lower gradient (see below).

Structurally, the western part of Line 10b shows a lot of similarities with the southern part of Line 8 (Figs. 11.2A and 11.3A). Parts of the crestal area as well as the entire northeastern flank are ruptured by block faulting. Also, thrusting of the Levantine Basin sediments over the base of the seamount flank can be seen both in the west and south of Eratosthenes. These observations indicate that only part of the convergent motion between Africa and Eurasia can be taken up by Eratosthenes. Most likely, the rate of convergence of the seamount has slowed temporarily since it hit the Cyprus margin, so that

i) the deformation front started to migrate outward, and

ii) the evaporite-bearing sediments from the Levantine Basin are thrusted north, presently overriding the base of Eratosthenes' flanks (see backthrust in Fig. 11.3B).

The velocity analyses were found to be very consistent in the perpendicular cross sections of Lines 8 and 10b (Klaeschen et al., Chapter 9, this volume). As indicated by wide-angle seismic data (Makris et al., 1983; Makris and Stobbe, 1984) and magnetic and gravimetric studies in the area (Woodside, 1977; Makris et al., 1994; Makris and Wang, 1994), elevated velocities underneath the seamount suggest a change in the physical properties of the rock, and most likely in its composition. Velocities of around 6 km/s are consistently found at a subbottom depth of ~5 km beneath the seamount, an observation which can be explained most easily by the crustal nature of the material. Although the updoming of high-velocity rock cannot provide evidence for crust at this shallower level, it indicates that a sliver of crust may have been detached along with the carbonate platform which now forms Eratosthenes Seamount, when it separated from North Africa.

The northern part of Line 8 is oriented NNE-SSW (Fig. 11.1). It reveals some interesting features about the boundary between the sediments in the Giermann Trench and the Cyprus margin (Fig. 11.2). The trace of the basal reflector of the succession can be followed to around 26600 cmp in the north (Fig. 11.2A), which corresponds to a subbottom depth of ~14 km, before it disappears at this location (Fig. 11.2A). This presumed fault, which was suggested to represent the plate boundary (Robertson et al., 1995a), turns out to be the frontal thrust of a more complex fault system to the north. If we look at the seafloor topography, it is different as compared to the southern part. While the southern part is characterized almost everywhere by either normal block faulting or horst-and-graben-type structures with normal offsets, the Cyprus margin shows characteristic features of imbricate thrusting. Although perhaps to be expected, this has aroused controversy in the past.

One of the main outcomes of the drilling at ODP Site 968 on the Eurasian plate (somewhere around 25000 cmp, if projected to line 8b, Fig. 11.2A) was the dominant extensional regime with so signs of reverse faulting. This, however, can be shown to be a local phenomenon, since the seismic data are distinctly overprinted by shortening and thrusting. Among a variety of moderately to steeply dipping thrusts within the stack, a prominent thrust crops out on the sea floor at 35 km or 26240 cmp (Fig. 11.2A and 11.2B) and then cuts the strata down to a subbottom depth of at least 8 or 9 km where it may even originate in a detachment (at ~70 km, 27700 cmp; Fig. 11.2A and 11.2B).

An interpretation of the Cyprus margin deposits as part of a subduction system is supported by McCallum et al. (1993) who interpreted seismic profiles of the British Geological Survey and Shell. In a study combining marine data with geological observations on the island of Cyprus, McCallum et al. (1993) suggested that the age of the undeformed Giermann Trench sediments and the accreted material north of the trench is pre-Messinian. Nevertheless, their interpretation of the underlying reflectors being a 'basement ridge' contradicts the reprocessed 'Strakhov' data. Fig. 11.2A clearly illustrates that the strong reflector at the base of the trench can be traced down to a subbottom depth of approximately 6-7 km. This distinct signal is interpreted to be the top of the down-going slab.

Thrusting due to convergence is also reinforced by the dominant northward dip, not only of the faults, but also the other reflectors as well (most likely remnants of sedimentary layering). Unfortunately, no information is available regarding the rocks which form the western margin of Cyprus. The reprocessed 'Strakhov' data lack evidence as to its nature, mainly as a result of the loss of resolution due to suppression and removal of multiples (*e.g.* the pale area between 25300 and 26400 cmp at ~8 km below the seafloor in Fig. 11.2A). The basement reflector, if interpreted correctly, coincides with the frontal thrust and roughly dips beneath Cyprus at an angle of ~10°, *i.e.* slightly less steep than the slope of Eratosthenes (Fig. 11.2). The most intense deformation seems to occur between the frontal thrust and the second prominent thrust fault, *i.e.* within the southernmost 40 km of the northern part of Line 8, (Fig. 11.2A).

Surprisingly enough, all the stress appears to be taken up by this area while the under-consolidated trench sediments further south are undeformed (*i.e.* those adjacent to the overthrusted slope of Eratosthenes Seamount; Fig. 11.2A, right end of the profile). It is therefore suggested that, in this shallower area of the Cyprus margin (as compared to the more elevated part starting northwards at 40 km, or 26400 cmp), evaporites may decrease friction along fault planes. The evaporites, which exhibit ductile behavior under these circumstances, may have thinned out significantly, and may not have been resolvable on the seismic images. The presence of evaporites is supported by the ODP drilling, where a thin layer of Messinian sediment (less than 20 meters thick), presumably gypsum, was recognised at Site 968 (Emeis et al., 1996; Robertson et al., 1998).

The velocity field for the northern part of Line 8 only distinguishes between the youngest sediments (mainly Pliocene-Quaternary) and an underlying unknown rock which does not seem to be too different from the continental fragment of Eratosthenes Seamount further south. Consequently, the gradient of velocity increase versus depth, which was used for Lines 8 (southern part

across Eratosthenes Seamount) and 10b, was applied here, and on the basis of the velocity analyses carried out by the reprocessing program (see above), showed satisfactory results. A velocity of 6 km/s, corresponding to a crustal composition, was reached at a subbottom depth of about 12 km beneath the Cyprus margin north of the Giermann Trench (see Klaeschen et al., Chapter 9, this volume, for the detailed velocity structure).

THE FLORENCE RISE - A CONTINENTAL FRAGMENT FROM THE NORTH

The Florence Rise must have been a topographic high since Late Miocene (Messinian) time as the salt bodies on its north, with thicknesses up to more than 1.5 s TWT, pinch out towards it (Woodside, 1977, Fig. 8). Evidence for Messinian evaporites also exists south of the Florence Rise in the Herodotus Basin (see below). Whether the Florence Rise may be an eastward continuation of the Mediterranean Ridge (connected via the Strabo Trench system), or whether it links the nappes and ophiolites of Cyprus in the east with the Antalyan Nappes of Turkey in the northwest (Biju-Dival et al., 1974), remains a subject of ongoing debate. However several lines of evidence propose the latter possibility to be the case. Magnetic anomalies suggest that the Florence Rise contains ophiolites, which may be related to the Troodos ophiolites on Cyprus (Woodside, 1977).

Detailed seafloor mapping of the Florence Rise area has been carried out during the TTR-1 Cruise with the R/V Gelendzhik (Ivanov et al., 1992; Woodside et al., 1992), and later on during the Anaxiprobe-95 Cruise with R/V L'Atalante (Woodside, 1995). In order to avoid repetition in the discussion below, we will always be referring to these earlier studies as well as to the bathymetric map presented in Fig. 11.1.

The southern province of the Anaximander Mountains area includes Anaximenes and Anaxagoras Seamounts, the northern slopes of the Mediterranean Ridge, and the Florence Rise. Here, the bathymetry shows a more or less constant water depth of 2500 m, with low amplitude relief, and without strong morphological trends (Woodside, 1995). Anaxagoras Seamount is the southeasternmost; its slope merges with the Florence Rise. A comparison of the Florence Rise with its adjacent features shows that it is less elevated than Eratosthenes Seamount or the Anaximander Mountains.

The Florence Rise was once considered to be an old trench slope break (Dickinson, 1973), developed during pre-Miocene time, and now underthrust beneath Cyprus as the leading edge of the African plate. Its basal structures might have been inherited from the gravity slides which occurred along the arc during the Late Cretaceous. Continuing with this hypothesis, its present topography suggests that its collision with Cyprus must have been initiated much earlier than that of Eratosthenes Seamount, and that the Florence Rise must have contributed considerably to the uplift of the island.

Other theories regarding the nature of the basal rocks of the rise consider that they are fragments of Africa which collided with Turkey (Rotstein and Ben-Avraham, 1985), or upthrusted blocks of seafloor (Woodside, 1977). There is little evidence to support any of these hypotheses.

The results of the scientific cruises during the early 1990s provide some evidence that the Anaximander Mountains are foundered parts of the Southern Turkish microplate (Ivanov et al., 1992). More recently, dredging of the Anaximander Mountains recovered a variety of rocks which show remarkable similarities to material in southern Turkey, and, therefore, support this hypothesis (Woodside et al., 1997). The fault pattern on the seafloor, as imaged recently by Mascle et al. (1998), is complex in the Florence Rise area, with a couple of distinct scarps. Most prominently, a set of NNE-SSW trending faults traversing the rise seems to be related to structural lineaments on land in Turkey (Limonov et al., 1994; Woodside et al., 1997). Several of the sedimentary and tectonic units in southern Turkey (see Gutnic et al., 1979, for details) have been shown to extend some distance to the south, beneath the Mediterranean Sea, probably since prior to Miocene time. Uplift and block faulting of the units of the Taurus belt may have led to graben basins and massifs which were then affected by erosion and/or gravitational tectonics which resulted in the development of the orogenic system of the Hellenic and Cyprean Arcs (and the area of the Florence Rise in between).

Perpendicular to the main NNE-SSW structural trends in southern Turkey, and their continuations on the Mediterranean seafloor, the southern trench slope break represents the present-day plate boundary in the Florence Rise area. A northwestward-dipping fault, as well as thrusting and imbrication, can be seen on single-channel seismic lines across the rise (Mascle et al., 1998). The rise itself does not reveal many structures on its crest, which suggests that it is comprised of repetitively deformed older rock rather than younger marine strata. A fault scarp along the southern edge of the Florence Rise is primarily observed in the western and eastern ends of the feature. But to the east, it continues as a distinct fault at the southern edge of the continental slope of Cyprus (which dips 6° to the south). The eastern branch of this fault may continue in the east as the Amanos fault on land (*i.e.* towards the Cyprean Arc). South of Hecataeus Seamount, a fault scarp is also seen (with normal faulting on the seamount slope). Its continuation towards Syria was interpreted by Mulder et al. (1975) to have a predominant component of underthrusting dipping to the north.

The continuation of the eastern fault scarp from the Hecataeus Rise towards Syria is observed on the 'Strakhov' Cruise 5 seismic Lines 1-6, but are discussed separately byVidal et al. (Chapter 10, this volume). The variable geometry of the plate boundary is discussed below in the context of seismicity, sense of movement within the microplate framework, and previous work.

'Strakhov' seismic Line 9 shows the most complex structural patterns. Trending roughly SW-NE, it crosses the northern Herodotus abyssal plain, the topographically elevated area of the Florence Rise, and runs up to the north-westernmost edge of the continental margin of Cyprus (Fig. 11.1 and **Fig. 11.4**).

The sediments of the Herodotus Basin can be divided into four major units. The Pliocene-Quaternary sediments, with velocities between 1750-2000 m/s, are underlain by a thin succession of

moderate velocities (see velocity model of Klaeschen et al., Chapter 9, this volume). These rocks were deposited on an series of Messinian evaporites up to ~2-km thick. As mentioned briefly above, at between 4000-6000 cmp this series is interrupted by a low-velocity unit of assumed sedimentary origin. Within the fourth (deepest) unit, there are no distinct reflectors that can be traced throughout the profile. Therefore, a gradual increase in velocity with depth was assumed to represent the physical properties of this rock unit until either basement (or basement velocities) are reached.

The Pliocene-Quaternary sediment cover varies widely in thickness, reaching up to 1.5 km in the Herodotus Basin to the southwest, but less than 200 m on the Florence Rise and near north-western Cyprus (Fig. 11.4A). Underneath these deposits, Messinian evaporites are found in the Herodotus Basin (Fig. 11.4A and Fig. 11.4B up to 65 km, *i.e.* ~5600-~8350 cmp;) as well as in the depression between the Florence Rise and the Cyprus margin (97-122 km, *i.e.* 3420-~4400 cmp; Fig. 11.4). Velocities of 4500 m/s (see below) indicate that these sediments are predominantly halite. In the deepest parts, they are up to 2.5 km thick, but thin towards the topographic highs.

The northeastern part of the profile does not reveal many structures underneath the Pliocene-Quaternary succession (Fig.8.4A, right end). However, the Florence Rise, appearing as a smooth topographic feature in the central part of Line 9, has a complicated internal structure. Its central crestal area is overlain by a thin sedimentary cover. Underneath this, the upper 2-km-thick part of the Florence Rise (Fig. 11.4A and 11.4B) shows low velocities (~2300-~3300 m/s; see velocity data in Klaeschen et al., Chapter 9, this volume). Continuous layering can rarely be observed in this part of the profile, suggesting that it has undergone a great deal of deformation. Low velocities may be due to fracturing or underconsolidation (due to increased quantities of pore water since the flanks of the rise are capped by Messinian evaporites). Beneath the low velocity rocks, the majority of the reflectors are seen to mirror either the seafloor topography, orto dip gently northwards. By contrast, the Herodotus Basin sediments appear more or less undeformed and sub-horizontally layered beneath the evaporites (Fig. 11.4A, left end).

Regarding the velocity field across the Florence Rise, the most unexpected feature is a series of low-velocity sediments and rocks forming the minor topographic high southwest of the Rise (Fig. 11.4, ~4000-6000 cmp). Its shape and position indicate that during the Middle Miocene or earlier, this body must have undergone vertical uplift. At the end of the Miocene, during desiccation of the Mediterranean, Messinian evaporites were precipitated on top of its flanks. Moreover, the contact between this low-velocity unit and its underlying rock appears to be discontinuous.

Although clearly visible over the Herodotus Basin in the southern part of Line 9 (Fig. 11.4), the Messinian evaporites pinch out both towards the low-velocity unit and the Florence Rise. The most prominent northward dipping fault plane which undercuts the Florence Rise can be traced to a subbottom depth of 12 km and deeper. The layered succession on the Herodotus abyssal plain, which is of proposed Cretaceous to Miocene age (Ben-Avraham et al., 1995), is bounded on the NW by a series of faults which generally dip northwards (Figs. 11.4A and 11.4B at around 55 km or 6250 cmp and further north of this location). The sediment underneath the evaporites is affected by shortening (both folding and faulting), while the salt has been faulted and partly dissolved (Figs. 11.4A and 11.4B, south-west of the rise). In addition, two northward-dipping reverse faults intersect the rise at its northern end, reaching the seafloor at 4440 and 4950 cmp (Figs. 11.4A and 11.4B). These have been interpreted as the present-day plate boundary (Mascle et al., 1998), but it can also be argued that the faulting observed further south (~47 km to the south at 6400 cmp) indicates an outward migration of the deformation front.

The bathymetry of the area suggests that the location of the plate boundary is at the base of the southern flank of the Florence Rise, with the ductile evaporites of the Herodotus Basin overthrusting the Rise in the process. As is the case for Eratosthenes Seamount, imbrication is indicated by the dominant trend of the northward-dipping reflectors within the Rise, but in a less clear manner.

DISCUSSION AND CONCLUSIONS

Regional as well as local evidence (*i.e.* on the islands of Crete and Cyprus) suggests that the present day plate boundary existed in the eastern Mediterranean as early as the Miocene (Dewey and engör, 1979; Meulenkamp et al., 1994). Despite this, the distribution of earthquake epicenters provides no direct clues to the presence or location of the subduction between the plates. The seismicity is particularly low in the Pliny/Strabo trench system and, further towards Cyprus, in the Pytheus and Giermann Trenches, but comparitively high along the Hellenic Arc and East Anatolian fault zone (Woodside et al., 1997). The seismicity of the region indicates a broad Benioff zone with northward dip (Rotstein and Kafka, 1982), reaching down to ~100 km. The Florence Rise, as well as the Anaximander Mountains, lie within and near the southern edge of this zone. A northward-dipping subduction zone can be observed on all Cruise 5 'Strakhov'-seismic lines shown here, and elsewhere (Vidal et al., Chapter 10, this volume).

Further east, this fault again steepens in Syria (A. H. F. Robertson, personal communication, 1998), joining the Dead Sea fault zone in the process. Evidence from seismic activity and the geometry of the plate boundary suggests that for the Florence Rise/ Eratosthenes Seamount area, the kinematics along the fault are normal with only a minor strike-slip component. After a subtle jump towards the south, considerable lateral movement occurs along the almost vertical fault at the southern boundary of the Hecataeus Rise (see Fig. 11.1). After having acquired a shallower dip again in the north-easternmost Levantine Basin, the fault develops into a nearly vertical transform fault on land. Some uncertainty exists regarding the location of the plate boundary near the Florence Rise, especially as imbricate stacking and southward migration of the frontal thrust can be inferred from the seismic data. The Florence Rise appears to be mechanically blocked by Herodotus abyssal plain sediments between the island of Cyprus and the downgoing plate. As a consequence, both faulting and folding can be observed

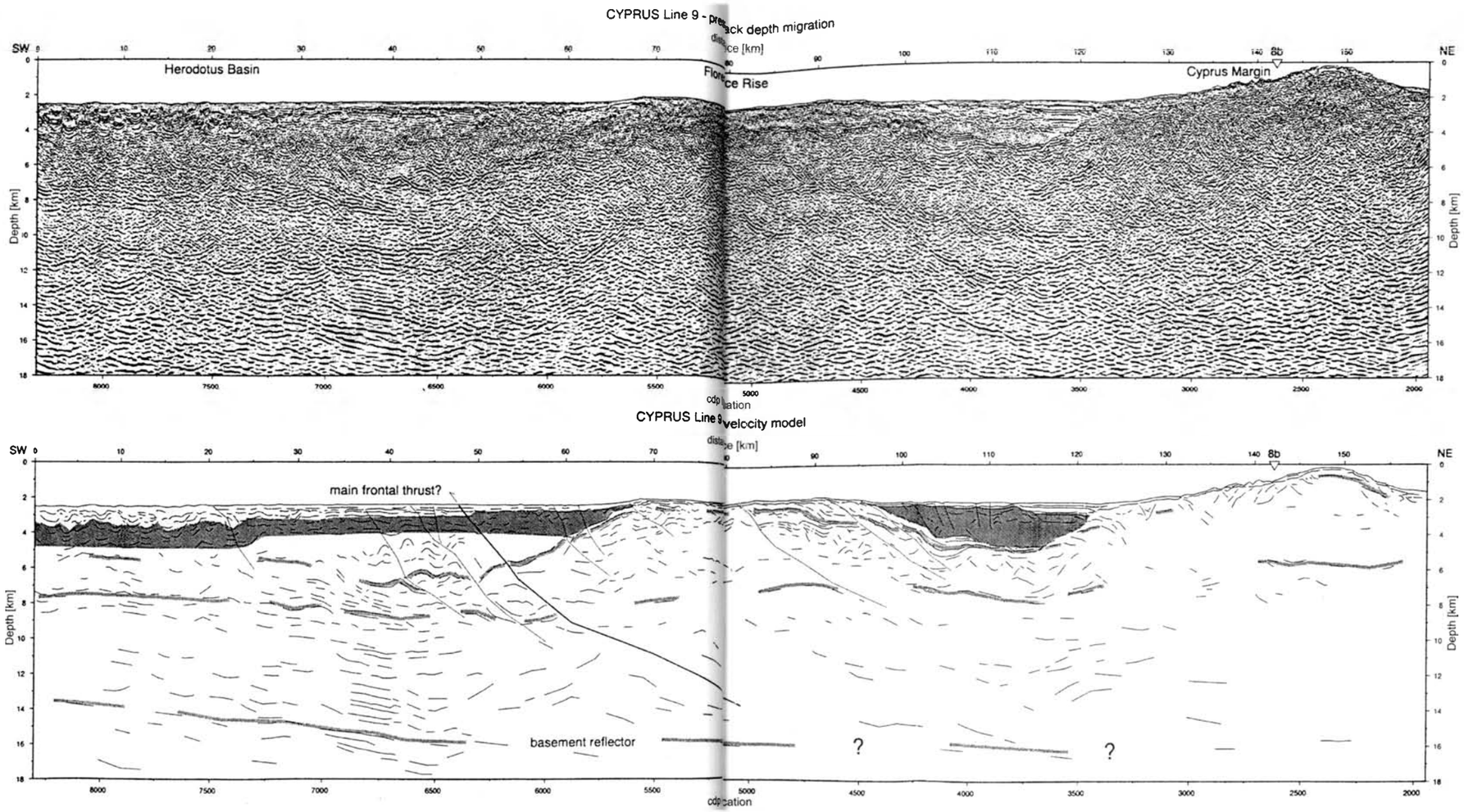
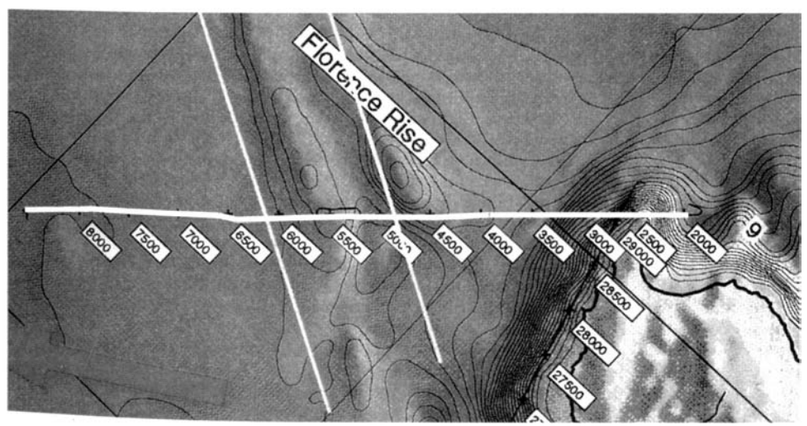


Fig. 11.4. Pre-stack depth migration (A) and interpreted line drawing underlain by the interpreted tectono-stratigraphic units (B) for MCS Line 9 across the northwestern part of the Phoenician Basin and Florence Rise. Pliocene-Quaternary sediments show light gray shading; Messinian evaporites are dark gray. Prominent reflectors are underlain by gray colors. See Fig. 11.1 for location.



on its southern margin, and compression of the sediment fill to the northeast (Fig. 11.4).

Further to the east, an even earlier stage of collision can be seen as the topographically high Eratosthenes Seamount halted after hitting Cyprus. This is illustrated by the virtually undeformed trench sediments north of it, which may have been shielded by a deeper root of the seamount already being stuck. It this were the case, it would also explain the following:

i) the incipient breakup of the feature, as indicated by the deeply penetrating, northward dipping crestal faults (Fig. 11.2), and

ii) the overthrusted Levantine/Herodotus Basin sediments at its western and southern flanks (Figs. 11.2 and 11.4).

However, the breakup and normal block faulting at the seamount crest may also be explained by a flexure of the downgoing plate, causing extension at its very top. If this tendency of southward migration of the frontal thrust is assumed to continue for some time, the consequence may be a geological scenario with the Cyprean Arc and the Hellenic Arc coalescing. The process of imbrication may be triggered as soon as evaporitic deposits from the Herodotus Basin became involved.

Regarding the deeper structure of these new profiles, it is apparent that underneath Eratosthenes Seamount, as inferred from seismic reflectors and the velocity field, there is material with velocities of ~6km/s. These findings are in agreement with the results from seismic refraction studies carried out earlier (Makris et al., 1983, their Figs. 10-12; Makris and Wang, 1994). It cannot yet be determined from our data if this material is a consequence of updoming (being the result of a discontinuity further below), or a mantle sliver which was detached when the northward drift of the seamount began. Moreover, it remains unclear which type of crust underlies Eratosthenes Seamount.

For the Levantine Basin, oceanic-type crust of ~16 km thickness is inferred from geophysical data, while further to the north, about 35 km of crustal thickness exist beneath the island of Cyprus (Makris and Stobbe, 1984). A transition within the crustal structure was detected beneath Eratosthenes Seamount, and has been interpreted as a structural boundary of unknown type (Makris et al., 1983). Nevertheless, one should treat these interpretations with caution as quite a considerable part of the tectonic history of the Mediterranean was poorly understood at the time.

The Eratosthenes Seamount gravity anomaly is thought to be a topographic effect (Woodside, 1991), although it has been suggested (see above) that the feature is a crustal discontinuity, with possible westward-tilting of the crust underneath the seamount, and depression of the crust on both sides.

The major magnetic anomaly (>400 nT) over Eratosthenes Seamount (Woodside, 1977) is possibly due to ophiolitic (or, generally speaking, basic or ultrabasic) material. The main trends of the structural features of the seamount coincide with the E-W and SE-NW-trends in Egypt (*i.e.* west of 30°E), as well as the predominant direction of the Syrian Arc which is ENE-WSW in Northern Sinai and the Levant (*i.e.* east of 30°E). The bend within the Cyprean Arc in the Florence Rise area seems to correspond to the strike of the northern boundary of Eratosthenes Seamount, while the structural lineaments further west on the Florence Rise coincide with tectonic structures in southern Turkey (Woodside et al., 1997). At present the seismicity is elevated here, with many strong earthquakes.

Despite all the new details revealed in these reprocessed profiles, the deep reflection and velocity data reveal no new evidence regarding the nature of the crust involved in the deformational processes. In this area of the eastern Mediterranean, it will remain difficult to distinguish deformation related to regional neotectonic plate interactions (inferred from faulting and folding) from local effects caused by mud volcanism/diapirism and halokinetics.

ACKNOWLEDGEMENTS

We thank C. Ranero and Y. Mart for discussions. Funding for this study was provided by Deutsche Forschungsgemeinschaft grants (DFG) HU 470/3-2 and HU 470/6-1 to Roland von Huene.

REFERENCES CITED

Ben-Avraham, Z., Shoham, Y., and Ginzburg, A., 1976. Magnetic anomalies in the Eastern Mediterranean and the tectonic setting of the Eratosthenes Seamount. Geophys. J. R. Astr. Soc., 45(1), p. 105-123.

Ben-Avraham, Z., Tibor, G., Limonov, A. F., Leybov, M. B., Ivanov, M. K., Tokarev, M. Yu., and Woodside, J. M., 1995. Structure and tectonics of the eastern Cyprean Arc. Mar. Petrol. Geol., 12(3), p. 263-271.

Biju-Dival, B., Letouzey, J., Montadert, L., Courrier, P., Mugniot, F., and Sancho, J., 1974. Geology of the Mediterranean Sea Basins. In: C. A. Burk and C. L. Drake, (eds.), The Geology of Continental Margins, Springer Verlag, Berlin, 1009 p.

Dewey, J. F., and Şengör, A. M. C., 1979. Aegean and surrounding areas: Complex multiplate and continuous tectonics in a convergent zone. Geol. Soc. Am. Bull., 90(1), p. 84-92.

Dickinson, W. R., 1973. Widths of modern Arc-Trench gaps proportional to past duration of igneous activity in associated magmatic arcs. J. Geophys. Res., v. 78(17), p. 3376-3389.

Emeis, K.-C., Robertson, A. H. F., Richter, C., et al., 1996. Proceedings ODP, Initial Reports 160. College Station, TX (Ocean Drilling Program), 972 p.

Flecker, R., Kopf, A., and Jurado-Rodriguez, M. J., 1998. Structural evidence for the nature of hiatal gaps in the Upper Cretaceous to Holocene succession recovered from the Eratosthenes. In: A. H. F. Robertson, K. -C. Emeis, C. Richter, et al. 1998. Proc. ODP, Sci. Results., v. 160, College Station, TX (Ocean Drilling Program). p. 517-526.

Gutnic, M., Monod, O., Poisson, A., and Dumont, J. -F., 1979. Géologie des Taurides occidentales (Turquie). Mem. Soc. Géol. France, v. LVIII, p. 1-112.

Harding, T. P., 1985. Seismic characteristics and identification of negative flower structures, positive flower structures, and positive structural inversion. Am. Assoc. Petrol. Geol. Bull., 69(4), p. 582-600.

Ivanov, M. K., Limonov, A. F., and Woodside, J. M., 1992. Geological and geophysical investigations in the Mediterranean and Black Seas. Initial Results of the TTR Cruise of R/V Gelendzhik (June/July 1991). UNESCO reports in marine science, v. 56, 206 p.

Kempler, D., and Ben-Avraham, Z., 1987. The tectonic evolution of the Cyprean Arc. Ann. Tect., 1(1), p. 58-71.

Kempler, D., 1994. Tectonic patterns in the easternmost Mediterranean. Unpubl. Ph.D. thesis, Hebrew Univ., Jerusalem, 137 p.

Kogan, L. E., and Stenin, A. M., 1994. Multichannel MOV-OGT (CDP) Seismic Profiling during Cruise 5 of R/V 'Akademik Nikolaj Strakhov' (Preliminary results). In: V. A. Krashenninikov and J. K. Hall, (eds.), Geological structure of the northeastern Mediterranean (Cruise 5 of R/V 'Akademik Nikolaj Strakhov'). Historical Productions-Hall Ltd., Jerusalem, Israel, p. 99-112.

Krashenninikov, V. A., and Hall, J. K., (eds.). 1994. Geological structure of the northeastern Mediterranean (Cruise 5 of R/V 'Akademik Nikolaj Strakhov'). Historical Productions-Hall Ltd., Jerusalem, Israel, 395 p.

Le Pichon, X., 1982. Land-locked oceanic basins and continental collision. the Eastern Mediterranean as a case example. In: K. J. Hsü, (ed.), Mountain Building Processes, Academic Press, New York, p. 201-211.

Limonov, A. F., Woodside, J. M., and Ivanov, M. K., (eds.). 1994. Mud volcanism in the Mediterranean and Black Seas and shallow structure of the Eratosthenes Seamount. Initial results of the geological and geophysical investigations during the Third 'Training-through-Research' Cruise of the R/V Gelendzhik (June-July, 1993). UNESCO Report in Marine Sciences, v. 64, 173 p.

Loubrieu, B., Satra, C., and Cagna, R., 2001. Cartographie par sondeur multifasceaux de la Ride Méditeranéenne et des domaines voisins: Morpho-Bathymetry and Acoustic Image of the Mediterranean Ridge and surrounding areas. Scale 1:500,000 at 35°N. Ifremer, Brest.

Makris, J., Ben-Avraham, Z., Behle, A., Ginzburg, A., Giese, P., Steinmetz, L., Whitmarsh, R. B., and Eleftheriou, S., 1983. Seismic refraction profiles between Cyprus and Israel and their interpretation. Geophys. J. R. Astron. Soc., 75(3), p. 575-591.

Makris, J., and Stobbe, C., 1984. Physical properties and state of the crust and upper mantle of the Eastern Mediterranean Sea as deduced from geophysical data. Mar. Geol., 55(3-4), p. 347-363.

Makris, J., and Wang, J., 1994. Bouguer gravity anomalies in the eastern Mediterranean Sea. In: V. A. Krashenninikov and J. K. Hall, (eds.), Geological structure of the northeastern Mediterranean (Cruise 5 of R/V 'Akademik Nikolaj Strakhov'). Historical Productions-Hall Ltd., Jerusalem, Israel, p. 87-98.

Makris, J., Wang, J., Odintsov, S. D., and Udintsev, G. B., 1994. The magnetic field of the Eastern Mediterranean Sea. In: V. A. Krashenninikov and J. K. Hall, (eds.), Geological structure of the northeastern Mediterranean (Cruise 5 of R/V 'Akademik Nikolaj Strakhov'). Historical Productions-Hall Ltd., Jerusalem, Israel, p. 75-86.

Mart, Y., and Robertson, A. H. F., 1998. Eratosthenes Seamount: an oceanographic yardstick recording the Late Mesozoic-Tertiary geological history of the Eastern Mediterranean. In: A. H. F. Robertson, K. -C. Emeis, C. Richter, et al., (eds.). Proc. ODP, Sci. Results., v. 160, College Station, TX (Ocean Drilling Program), p. 701-708.

Mascle, J., and shipboard scientists of PRISMED-2, 1998. New data in the Eastern Mediterranean from the Prismed-2 survey (R/V L'Atalante). EGS abstract volume.

McCallum, J. E., Scrutton, R. A., Robertson, A. H. F., and Ferrari, W., 1993. Seismostratigraphy and Neogene: recent depositional history of the south-central continental margin of Cyprus. Mar. Petrol Geol., v. 10(5), p. 426-438.

McKenzie, D. P., 1978. Active tectonism in the Alpine-Himalayan belt: the Aegean Sea and the surrounding regions. Geophys. J. Roy. Astron. Soc., 55(1), p. 217-254.

Meulenkamp, J. E., van der Zwaan, G. J., and Van Wamel, W. A., 1994. On Late Miocene to Recent vertical movements in the Cretan segment of the Hellenic Arc. Tectonophysics, 234(1-2), p. 53-72.

Mulder, C. J., Lehner, P., and Allen, D. C. K., 1975. Structural evolution of the Neogene salt basins in the Eastern Mediterranean and the Red Sea. Geologie en Mijnbouw, 54(3-4), p. 208-221.

Reilinger, R. E., McClusky, S. C., Oral, M. B., King, R. W., Toksöz, M. N., Barka, A. A., Kinik, I., Lenk, O., Sanli, I., 1997. Global Positioning System measurements of present-day crustal movements in the Arabia-Africa-Eurasia plate collision zone. J. Geophys. Res., 102(B5), p. 9983-10,000.

Robertson, A. H. F., 1992. Drilling the Eratosthenes Seamount: Mediterranean collision tectonics and Plio-Quaternary palaeo-oceanography in the light of the geology of Cyprus. Rapp. Comm. Mer Médit., v. 33, p. 393.

Robertson, A. H. F., and shipboard scientists ODP Leg 160, 1995a. Evidence of collisional processes associated with ophiolite obduction in the Eastern Mediterranean: Results from Ocean Drilling Program Leg 160. GSA Today, 5(1), p. 215-221.

Robertson, A. H. F., Kidd, R. B., Ivanov, M. K., Limonov, A. F., Woodside, J. M., Galindo-Zalvidar, J., Nieto, L., and Scientific Party of the TTR-3 Cruise.1995b. Eratosthenes Seamount: collisional processes in the easternmost Mediterranean in relation to the Plio-Quarternary uplift of southern Cyprus. Terra Nova, v. 7(2), p. 254-264.

Robertson, A. H. F., Emeis, K. - C., Richter, C., Camerlenghi, A., et al., 1998. Proceedings ODP, Scientific Results, Vol. 160. College Station, TX (Ocean Drilling Program), 817 p.

Rotstein, Y., and Ben-Avraham, Z., 1985. Accretionary processes at subduction zones in the Eastern Mediterranean. Tectonophysics, 112(1-4), p. 551-561.

Rotstein, Y., and Kafka, A. L., 1982. Seismotectonics of the southern boundary of Anatolia, eastern Mediterranean region: subduction, collision, and arc jumping. J. Geophys. Res., 87(B9), p. 7694-7706.

Ryan, W. B. F., Hsü, K. J., et al. 1973. Init. Repts DSDP, 13, U. S. Govt. Printing Office, Washington, 1447 p.

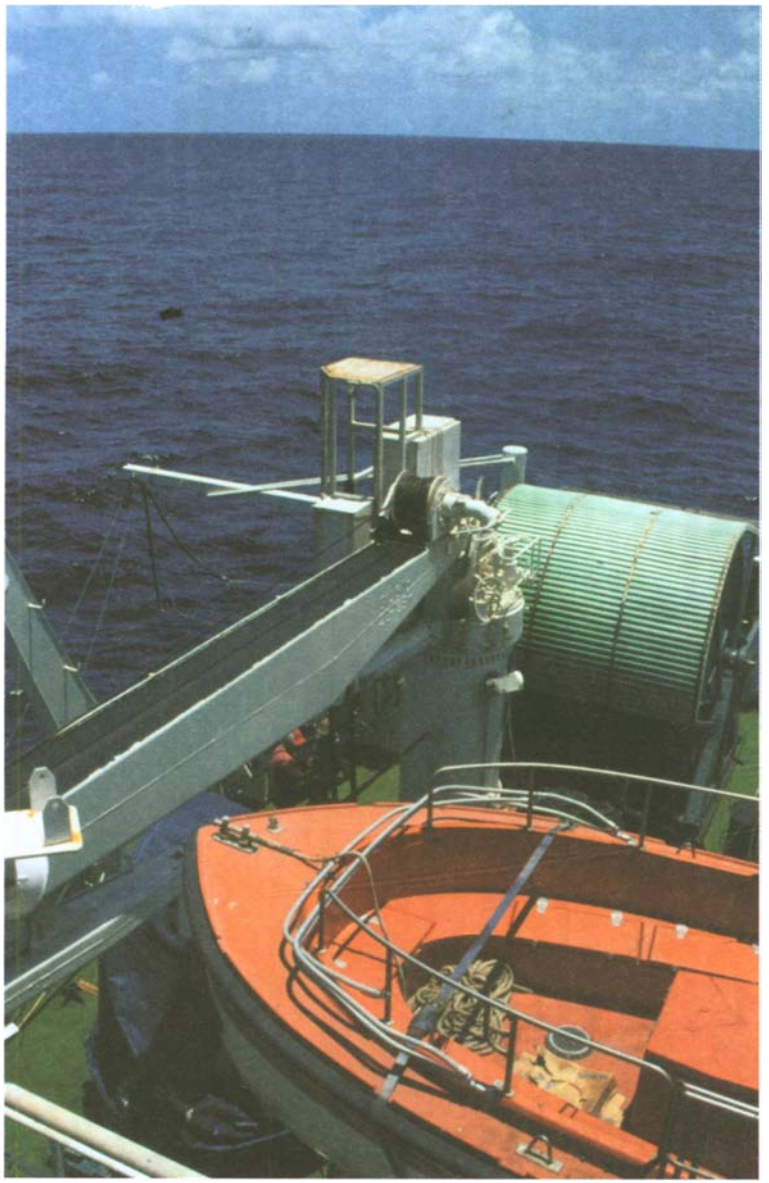
Woodside, J. M., 1977. Tectonic elements and crust of the Eastern Mediterranean Sea. Mar. Geophys. Res., 3(3), p. 317-354.

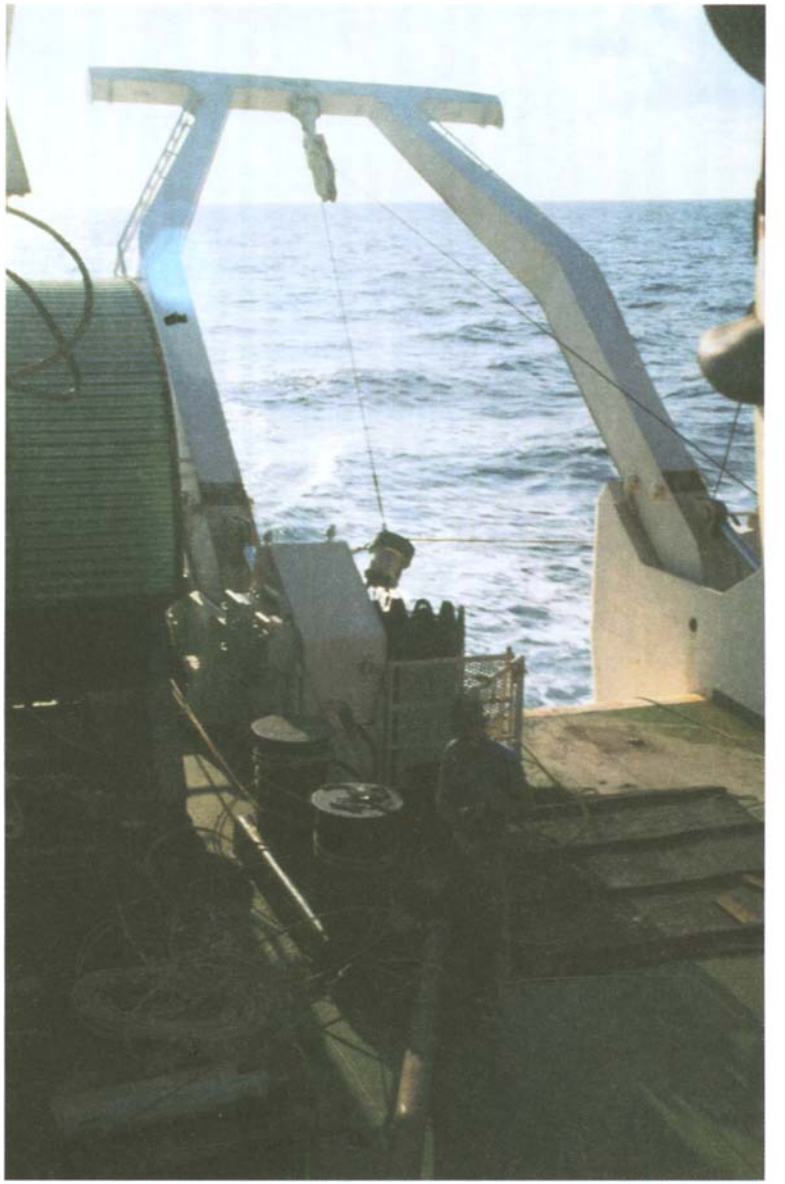
Woodside, J. M., 1991. Disruption of the African Plate margin in the Eastern Mediterranean. In: M. J. Salem, A. M. Sbeta, and M. R. Bakbak, (eds.), The Geology of Libya, vol. VI, Elsevier, Amsterdam, p. 2319-2329.

Woodside, J. M., 1995. ANAXIPROBE-95. Report of the 'L'Atalante' expedition, 4-11 August 1995, Heraklion, Crete to Port Said, Egypt. - Unpubl. Report, Vrije Universiteit, Amsterdam, Netherlands.

Woodside, J. M., Ivanov M. K., and Shipboard Scientific Party, 1992. The Anaximander Mountains: linking the Hellenic and Cyprus arcs; and an introduction to Kuznetsov's poster. Special session on TREDMAR Results, XXIIIeme Congress and Plenary Assembly of CIESM, Trieste 12-17 October 1992. Also as: Rapp. et Proc.-Verb. des Réunions, Monaco, v. 33, 155 p.

Woodside, J. M., Ivanov, M. K., and Limonov, A. F., 1997. Neotectonics and fluid flow through seafloor sediments in the Eastern Mediterranean and Black Seas. IOC Reports, Technical Series, v. 48 (Pts. 1 and 2), 226 p.





Photos of seismic equipment aboard the R/V Strakhov – Cruise 11, October-November 1990.
Left: View of the starboard quarter of the NES Academik Nikolaj Strakhov, with the marine seismic hydrophone cable winch beneath the greenish corrugated cover. This is the hydrophone used with a standard airgun for MCS (Multichannel Seismic) work.
Right: The large volume airgun being lowered for seismic shooting to OBSs of the Institut für Geophysik (Hamburg) in the area of the Strakhov Fracture Zone in the Equatorial mid-Atlantic. Photos taken by J. K. Hall during Leg 2 of Cruise 11 of the Strakhov - Southhampton, England to Recife, Brazil, October-November 1990.

Chapter 12

The Deep Structure of Eratosthenes Seamount from Seismic Refraction Data

Sergey M. Zverev and Dmitry A. Ilinsky
Institute of Physics of the Earth of the Russian Academy of Sciences, Bolshaya Grusinskaja Str. 10, 123810 Moscow, Russia

INTRODUCTION

In 1987, 1989 and 1990 the Schmidt Institute of Physics of the Earth (IPhE) of the Russian Academy of Sciences participated in the International Tethys Project, a series of large-scale multidisciplinary geological and geophysical investigations on the island of Cyprus and in the adjacent areas of the eastern Mediterranean.

An extensive Tethys research program was implemented during two cruises of the R/V 'Akademik Nikolaj Strakhov' (Cruise 5 in 1987 and Cruise 10 in 1989) and one cruise of R/V 'Akademik Boris Petrov' (Cruise 19 in 1989). This program saw the application of a wide range of scientific methods, and the combination of land and marine investigations. The broad coverage of the region by detailed observations provided important new data with great potential for yielding clues to the geological structure of the eastern Mediterranean.

The IPhE team, in cooperation with specialists from the Geological Survey of Cyprus, performed seismic refraction investigations. The materials obtained consisted of seismic data recorded along two land-marine profiles across Cyprus, and several profiles in the adjacent marine areas (**Fig. 12.1**).

For both onshore and offshore seismic experiments, we used autonomous seismic analog magnetic recording stations to digitize the primary records obtained. The IPhE did not possess digital equipment at that time, so the first digitizing and processing were performed using the facilities of the Geological Survey of Cyprus and St. Johns University in Canada. The preliminary stage of interpretation was completed in 1993. A report for the Geological Survey of Cyprus was submitted (Deep seismic sounding..., 1993), and a brief summary of the results was published (Zverev et al., 1993).

In 1996, D. A. Ilinsky designed a hardware-software combination for the digitizing, processing and interpretation of seismic refraction data (Deep Seismic Sounding - DSS) utilizing the vast experience which the IPhE had accumulated during its many years of DSS studies. We used digitized records for the optimum recognition of seismic waves from various parts of the deep sections, taking into account the complex and non-homogeneous nature of real geological sections. Our major objective was to obtain the most realistic geological model of a seismic section possible. It was necessary to find those waves with close affinity to the deep boundaries and to trace them along the profile, while analyzing variations in their kinematic and dynamic parameters. We avoided extending these waves through those segments in which they were not present.

Using this approach, we chose the data set collected along the profile crossing Eratosthenes Seamount for our first attempt at analyzing wave fields using digitized records. The seamount is located south of Cyprus (Fig. 12.1). It is separated from the island by a depression with slightly deformed relief on the seafloor. This seamount has attracted the attention of scientists for a long time.

We tested various approaches to the digital analysis of seismic data collected in the area of Eratosthenes Seamount, *e.g.* the best method of presenting record sections, usage of reverse and overlapping observations, and studying the peculiarities of time and amplitude. These methods were employed in the preparation of a starting model which more closely described the real geological structure, and which was then used later for the 2-D mathematical modeling corrections.

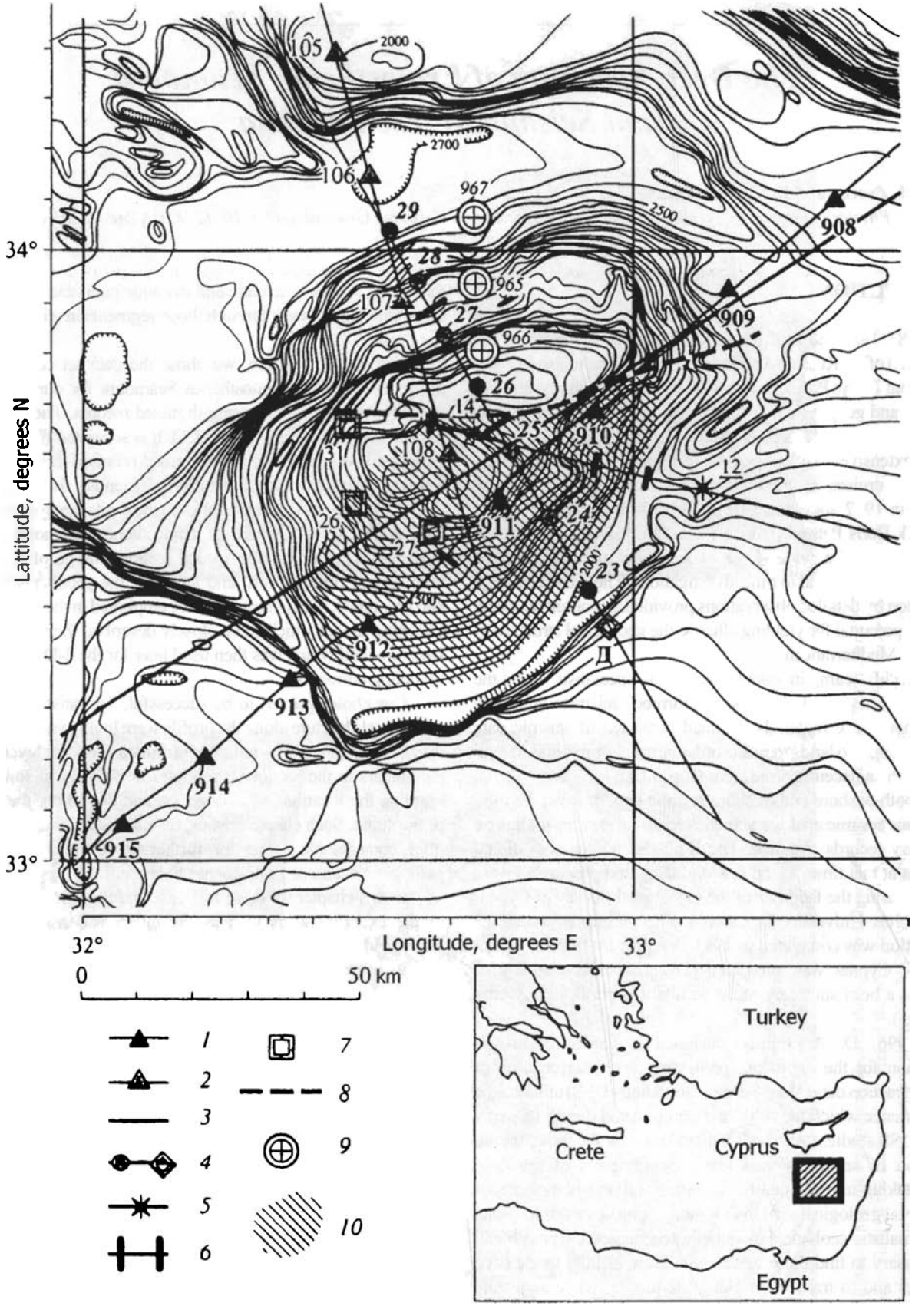
Our choice proved to be successful. The seismic wave field and crustal structure along the profile were highly variable. Seismic refraction data gave us reliable information on the layer velocity parameters in the sections, showing low velocity in some layers, marking the locations of fault zones, and describing the behavior of the strata. Such characteristics, together with other information, offer considerable scope for furthering our knowledge of the geological nature of Eratosthenes Seamount.

In this chapter we describe the seismic equipment and details of the experiment, as well as the interpretation of the seismic wave field. We also discuss our results in light of other data. Some aspects of the interpretation have already been published (Zverev and Ilinsky, 1998, 2000).

DESCRIPTION OF THE EXPERIMENT

Seafloor Topography of Eratosthenes Seamount

In addition to the general bathymetric maps of the eastern Mediterranean, we used the detailed bathymetric maps prepared by Hall (1980, 1981, 1994). New bathymetric measurements were made along profiles with a Hollming multibeam echosounder during Cruises 5 and 10 of the R/V 'Akademik Nikolaj Strakhov', and the results published in a book on these cruises edited by Krasheninnikov and Hall (1994). A comprehensive analysis of the topography was given by Hall et al. (1994). Another multibeam


105
2000
2700
106
967
29
2500
908
34°
28
965
107
27
909
966
26
14
25
910
31
108
12
26
911
24
27
2000
23
2500
912
Д
913
914
915
33°
Lattitude, degrees N
32°
Longitude, degrees E
33°
0
50 km
1
2
3
4
5
6
7
8
9
10
Turkey
Crete
Cyprus
Egypt

survey, the French PRISMED2 expedition carried out in 1998, mapped the entire area with similar but much higher resolution coverage (Loubrieu, Satra and Cagna, 2001). Below we discuss the bathymetric data as it relates to the geophysical results.

Eratosthenes Seamount has an oval outline with a diameter at its base of about 70 km. It has a flat top, with steep slopes on its upper part and more gentle slopes on the lower part (Fig. 12.1). The depths above the flat top range from 800 to 1100 m, with 1500 m in the southwest, about 2000 m in the east and northeast, and more than 2000 m in the north and northwest The deepest sector is associated with a depression and zone of slightly deformed seafloor, which separates the Cyprean Arc from Eratosthenes Seamount itself. A distinctive feature is a local depression around the seamount with depths greater than the depth of the adjacent areas. This depression looks like a near rectangular trough bounding the seamount. The repeated deepening of this depression suggests a continuation of the subsidence. The oval shape of the seamount originates from extensive linear and curvilinear topographic features indicating faults. They are demonstrated most clearly on the western, northern and southeastern slopes of the seamount. The flat top is intersected by a rough ENE-WSW fault with a pronounced topographic expression. Many indications of faulting on the flat top of the seamount were described by Krasheninnikov et al. (1994). It is important to note that the topography of the northern part of the seamount differs substantially from that of its southern part (Fig. 12.1). The slopes of the southern part are more even, while those of the northern part are highly dissected and deformed. The base of the seamount is 1000 m deeper on the north than on the south. This suggests that the northern part of the seamount continues to subside significantly.

Profile Locations

In the text below the IPhE profiles are generally numbered by PR and a number. In referring to the results obtained from a given Ocean Bottom Seismograph or OBS on that profile, the profile number precedes the OBS number (*i.e.* OBS 606 for instrument 6 on Profile 6).

The seismic refraction profile crossing Eratosthenes Seamount is oriented SW-NE. It starts on the plain, passes along the western border of the South Levantine Basin, and crosses the southern slope, the flat top and the northern slope of Eratosthenes Seamount. From there it continues across the front of the Cyprus Basin, passes a complicated zone of structures near the right-angled intersection of the Hecataeous submerged ridge and the Cyprean depression, and then runs along the western side of the North Levantine Basin (Fig. 12.1 and Fig. 13.1). The DSS on Profile 9 consisted of three independent arrays of Ocean Bottom Seismograph (OBS) stations, overlapping by 40 km, and using airgun sound sources on every segment of the profile. The southern array of Profile 9 (PR 9-3) covers Eratosthenes Seamount.

The seismic refraction profile begins in the area to the southwest of Eratosthenes Seamount, where the depths range between 1550 and 1600 m, and the complex pattern of depth contours suggests structural inhomogeneities. OBSs 915, 914, and 913 were located there (Fig. 12.1). Further on, the profile continues across the foredeep, the southern slope of the seamount and comes to the southern edge of the flat-topped seamount. OBS 912 was located on the slope, and OBS 911 on the top. Before coming up to the northern edge of the flat top, the profile runs above the northeastern slope of the seamount (OBS 910) and further on to its foot (OBS 909). Then the profile crosses the depression and runs across the front of Cyprean Arc.

Equipment and OBS Observation Techniques

For the DSS measurements we used autonomous bottom seismic stations (OBS) designed at the IPhE in the 1970s (Zverev et al., 1978). The problems inherent in OBS construction and their application to DSS work have been discussed in a number of papers (*e.g.* Zverev, 1988).

Analog data were collected by direct magnetic recording at a low magnetic tape speed (0.5 mm/s). Two levels of recording provide a dynamic range up to 70 dB. They allow undistorted recording of the weak deep seismic refraction waves and regional background noise, as well as strong reflections from sediments and water waves. The OBS tape recorder runs continuously for up to 14 days, and provides recording of all events in the frequency range of 3-25 Hz. This gives enough time to arrange the deployment of the many OBS units, and perform the complicated seismic refraction experiments, recording the seismic pulses from either explosive or airgun sources along a line up to several hundreds of kilometers in length. A quartz clock in the OBS maintains exact timing with an instrumental error of not more than 0.03-0.05 s for all the recorded events.

Each OBS was equipped with either a one-component 4 Hz or a three-component 5 Hz seismometer. In order to fix the position of the OBS we used a special recording channel for measuring the water wave arrivals. This channel records the envelope of high frequency components of the arriving waves (more than 20 Hz).



Fig. 12.1. Schematic map of Eratosthenes Seamount. The seamount topography is given after Hall (1980, 1981, 1994). The hatched area on the southeastern side of the seamount defines the high-velocity layer on the seamount. The map also shows the locations of seismic profiles, DSDP holes, and dredging sites (Zverev and Ilinsky, 2000). Legend: (1-2) refraction profiles surveyed by the Institute of Physics of the Earth in 1987-1990 and locations of the OBSs: (1) Profile 9-3, 1990; (2) Profile 1-2, 1987 (Zverev et al., 1993); (3) line of CDP profile shot from R/V 'Akademik Nikolaj Strakhov' in 1987 (Kogan, and Stenin, 1994); (4) refraction profile surveyed by J. Makris et al. in 1978 (Makris et al., 1983): OBS locations are shown by squares, seismic shots by circles with numbers; (5) refraction profile shot by Z. Ben-Avraham and others in 1989, and the location of OBS sites (Ben-Avraham et al., 2002); (6) limits of a high-velocity layer at the top of the crust (on profiles 1, 2, 4, and 5); (7) dredging sites (Mouraviev et al., 1994); (8) crustal fault separating the southern and northern parts of Eratosthenes Seamount; (9) sites of DSDP holes (Emeis et al., 1995); (10) high-velocity region. The inset map shows the map location.

Seismic waves are not registered on this channel due to their lower natural frequency, but the water wave arrivals are clearly seen.

The instrument suite, including seismometers, electronics, a clock and batteries, is mounted in a cylindrical housing which can withstand pressure depths of more than 6 km. The whole OBS consists of a floating buoy, a nylon rope, the OBS package in its housing, and a bottom anchor. The OBS package sinks into the soft bottom sediments, and thus flow noises do not affect the data. A special length of buoyant rope insulates the housing from movements of the anchor.

The level of recorded background noise is often close to that of the regional noise level. A special study showed that the minimal background noise on the ocean floor in the 3-25 Hz frequency range is about 40-60 nanometers per second. Its value is independent of sea depth, bottom sediment type, and the region of experiments. In the region of our study, the Mediterranean bottom background noise is often comparable to the noise measured in the abyssal basins of the South Atlantic Ocean (Zverev, 1996). We observed some increase in noise during storms, or from passing ships. Bottom currents generate the most significant component of OBS noise, especially in places with coarse bottom relief. In general, noise levels depend on the local environment of the sea bottom at the OBS location. Depressions and troughs provide usually better conditions. The worst places are on the tops of hills and on steep slopes, *i.e.* in areas with bottom currents.

The above characteristics apply to all OBSs, regardless of design, including the buoy-equipped OBS. For these types of OBS, the attached buoy allows more accurate OBS positioning and a better signal-to-noise ratio. However, a disadvantage of using such a buoy is the difficulty in deploying more than 10 such OBS systems from one small ship.

The simple and reliable IPhE OBS equipment and deployment techniques were previously used for a series of DSS experiments at different scales, ranging from lithospheric study with big explosions over long distance profiles along the Angola-Brazil geotraverse (Zverev et al., 1996) to the detailed upper crust investigations described here for the eastern Mediterranean. Losses or damage to instruments rarely occurred. During the Angola transect only 5 OBSs were lost from the 104 that were used. In the Mediterranean we lost only one out of the 50 OBSs that were deployed.

Six OBS were deployed on the 140 km long PR 9-3 profile in the Eratosthenes region, separated by distances of 17 to 35 km. OBS 910 had to be sited on the steep slope near the top of the seamount, and its records were more affected by bottom noise than the other OBSs.

The total experimental time accuracy can be estimated from the time discrepancies on the reverse time-distance curves, and it did not exceed 0.05 seconds.

Seismic Shooting

We used a powerful pneumatic airgun with single chamber volumes of either 120 or 240 liters. At a tow depth of 42 meters and with an air pressure of 150 megapascals, the frequency of the maximum energy for the 120 liter chamber was 8.5 Hz, and 7.5 Hz for 240 liters. The spectral energy level for the bigger chamber was 36% higher then that for the smaller one. The time intervals between shots depended on the capacity of the air compressor and was about 4 min for the 120 liter source and 8 min for the 240 liter source. The ship's speed during the airgun shooting was 3 knots, and thus the distance interval between shots was approximately 400 m and 800 m respectively.

PROCESSING OF SEISMIC DATA

a) Digitizing of analog data and preparation of record sections

The signals from the seismographs were continuously recorded during the experiment on an analog magnetic tape recorder in the OBS unit. Time code signals were recorded from a stabilized quartz clock of IPhE design. A special hardware-software system was developed for inputting the analog seismic information into the computer. We recorded the times of shots and assembled record sections of common receiving points for every OBS.

The hardware includes an analog play-back magnetic tape recorder device for transferring information from the tape into the computer. Its reading speed is 100 times greater than the original recording speed of the OBS. This decreases the effect of electronic noise through the increase in the amplitude of the signal brought about by the increase in speed.

The analog play-back signals come to the input port of a multichannel analog-digital converter printed circuit card (designed by L-CARD, Moscow). It can be installed into the early IBM PC models with Intel 80386 or higher processor. All the data processing programs were written at IPhE in TURBO PASCAL.

In order to start the data processing, the operator must first input the schedule of airgun shooting times and then switch the tape recorder to play-back mode. The program analyzes the time codes and writes the appropriate segments of the records to its hard disk. Then it transforms the record sections to common recording points in SEG-Y format, and appends a header containing all the information about the experiment for every trace. Any tape speed deviations from the recording and play-back procedures will have been corrected, and the sampling intervals of the seismic channels have been reduced to 10 milliseconds, with 40 seconds of readings from the instant of the shot on each channel. Data input is fully automatic. It takes little time and requires minimal effort. For example, input of data from one OBS with 600 airgun shots and 4 min between shots requires only 24 min.

b) Determination of distances between OBS and airgun shots

For the experiments in 1989-90 our ships were equipped with the AN/SRN-9 TRANSIT Doppler satellite navigation system. At that time the more modern Global Positioning System (GPS) was not installed. The interval between TRANSIT satellite fixes was about one hour. The accuracy of the satellite fixes was not less than 500 m. The ship's track between satellite fixes was estimated by using the ship's speed and direction. The 'real' ship's track was interpolated between fixes assuming a constant current set and drift. The tracks with fixed shot positions are shown in Fig. 12.1.

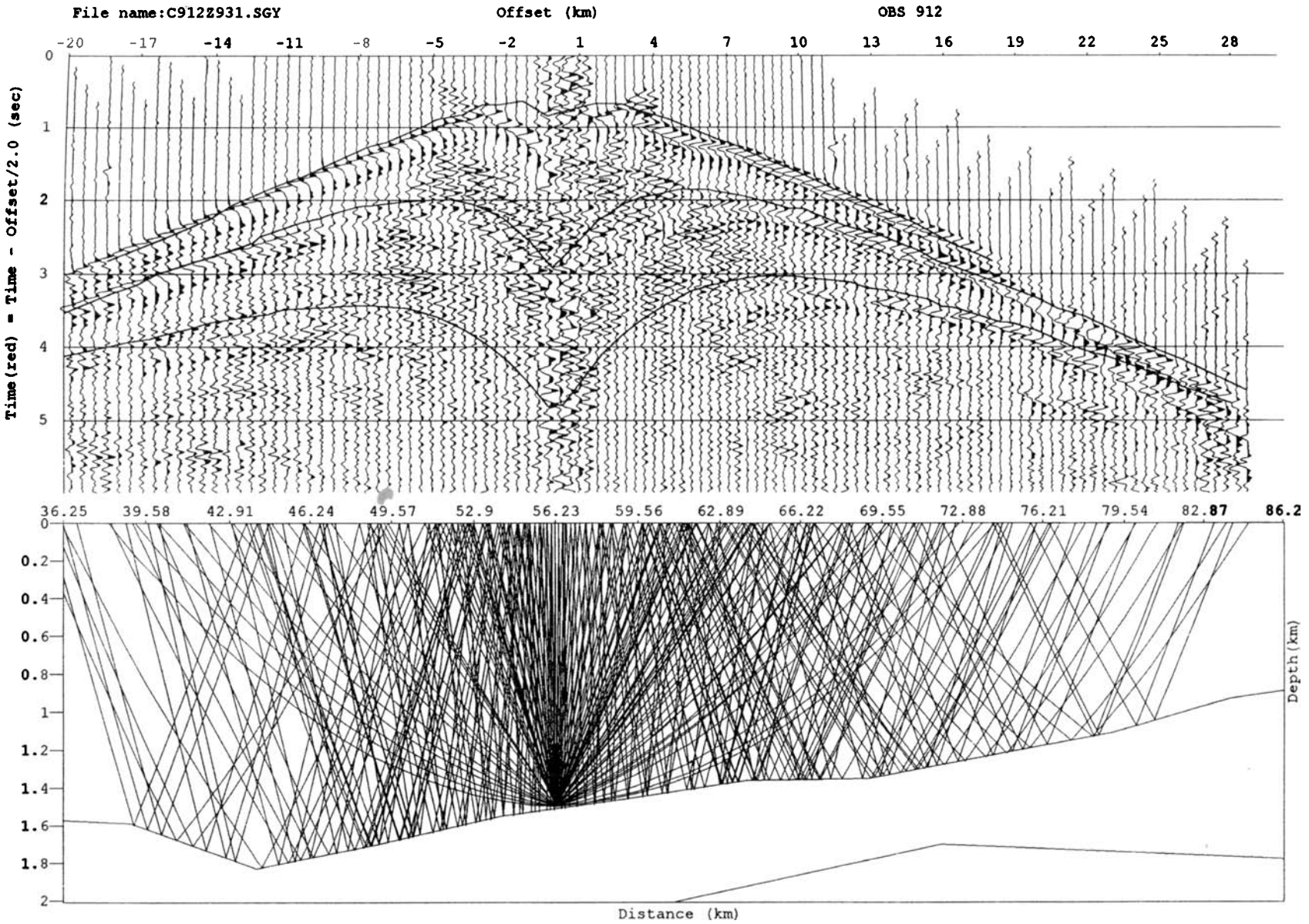


Fig. 12.2. Record section of the OBS 912 special water wave channel showing the direct and multiple water waves. These waves were used for distance fixing between the OBS and the airgun source. The lower ray tracing diagram was used to determine the theoretical arrival time curve superimposed on the experimental record section.

The determination of true position for the OBSs was more difficult. The OBS package was lowered to the sea floor with a nylon rope. This operation takes some time (about 40 min. to a depth of 2 km), and the ship can drift away from the initial point by up to 1-2 km.

In order to minimize the movements of the anchor holding the buoy, the length of the rope to the OBS was usually 100 m more than the water depth. Therefore the buoy could be displaced from the real OBS position by up to 0.64 km in water 2 km deep. For the precise OBS location to be determined we used the water wave arrivals.

A special channel was designed to study these water wave arrivals. It records the envelope of high frequency components (more than 40 Hz) of the arriving signals (Zverev, 1988). Seismic waves are not recorded on this channel, and separate arrivals of direct and multiple water waves can be clearly seen. The computer program using the data on this channel for OBS-shot distance corrections was prepared at IPhE by D. A. Ilinsky. **Fig. 12.2** gives an example in which the theoretical ray-tracing curves of the time arrivals (below) are superimposed on the experimental record (above).

c) Search for parameters for the best tracing of seismic waves

A special interactive program was developed for analyzing the seismic data using a PC with Microsoft Windows 3x or Windows 95 operating system. The program is designed for processing the DSS refraction wave section results. All the record sections for DSS PR 9-3 are presented in **Fig. 12.3a, b, and c**.

The seismic signals were filtered by a band-pass filter with optimal bandpass of 4-12 Hz. Seismic data can be represented in terms of an absolute amplitude scale (on limited segments of a profile), or on a relative amplitude scale normalized to the maximum amplitude on each separate trace. High amplitude waves (direct or reflected) can be extracted by normalization. Automatic gain control can be used with a variable time window (from 300 to 1000 ms), but this would not improve the wave tracing for large distances (>60 km). In some cases a compromise can be found if the trace normalization is made in two windows: before and after arrival of the direct and multiple water waves. The boundary between the two windows is determined as the parabolic function $d = (t^2 - h^2/v^2)^{0.5}$, where d is distance, t is arrival time, h is the depth, and v is the sound velocity in the water (Fig. 12.3, OBSs 910, 913, and 915). The OBS 911 records show a combined section with a big airgun source (volume 240 liters, shot spacing 800 m) for distances from -90 to -32 km, and a small airgun source (120 liters, shot spacing 400 m) for distances from -32 to 52 km. The big airgun shots allow an increase in the reception range of the first waves up to 90 km for this OBS, while the small airgun gives only 40 km. The big airgun was used for OBSs 915-912 only at relatively small distances, and the data do not show an advantage over that of the small airgun.

SEISMIC WAVE FIELD AND SEISMIC CROSS SECTIONS

General Remarks

A series of reversed and overlapping time-distance curves were derived from the seismic refraction investigation on Eratosthenes Seamount by means of the many OBSs deployed, powerful airgun shots, and the high accuracy of determining positions, depths, and times. High quality data were collected and the OBS records were digitized. We then chose the best techniques for presentation and analysis of the data obtained in order to investigate the nature of the seismic waves within the framework of the classical DSS refraction methods using digital records.

The following approaches were used for the analysis and interpretation of the wave field.

a) We primarily used real observed wave arrivals, thoroughly confirmed by the mutual reverse points. Priorities were given to those waves with amplitudes exceeding the background wave noise. We did not use time-distance curves prolonged by a combination of overlapping branches, or stretched through the segments where these waves were not observed.

b) Overlapping systems present valuable information for the decoding of the seismic wave field. Parallel time-distance curves correspond to the same boundary. Time and amplitude variations related to the same portions of a profile indicate horizontal inhomogeneity of the section. Such features help us to understand the wave field in complex zones and to define inversion methods for preparing the sections.

c) The equality of times for mutual reverse points does not prove the existence of a common seismic boundary between these points. It shows only that the waves pass through in the same manner, while the media in that section could be rather complicated either by horizontal inhomogeneity, or by vertical layering.

d) Breaks and delays in the time-distance curves were studied with particular care in order to search for low velocity zones. In such cases, layer velocities were not taken as being equal to those at the boundary.

e) Independent information about possible regional structure was taken into consideration during the seismic interpretation and preparation of the sections. We have focused our attention on those portions of the profiles where the seismic wave field shows considerable variation.

The analysis and interpretation of the seismic wave field was carried out using large scale record sections, far greater than those shown in the examples of Fig. 12.3. A unified scale was used for all sets of data. A reduction velocity of 7 km/s was chosen with a horizontal scale of 1 cm=2 km and a vertical scale of 1 cm=0.5 s. A correction for the water layer was applied. All possible pairs of reverse records were used for calculating t_o and V_b by means of the 'differences of time-distance curves (t_o)' method and plotting of the boundaries (Gamburtsev et al., 1952; Gurvitch, 1960; Seismic Prospecting..., 1966; Sheriff and Geldart, 1987). An analysis of overlapping records allows plotting of time curves for complicated portions of the profile. All the operations mentioned above were

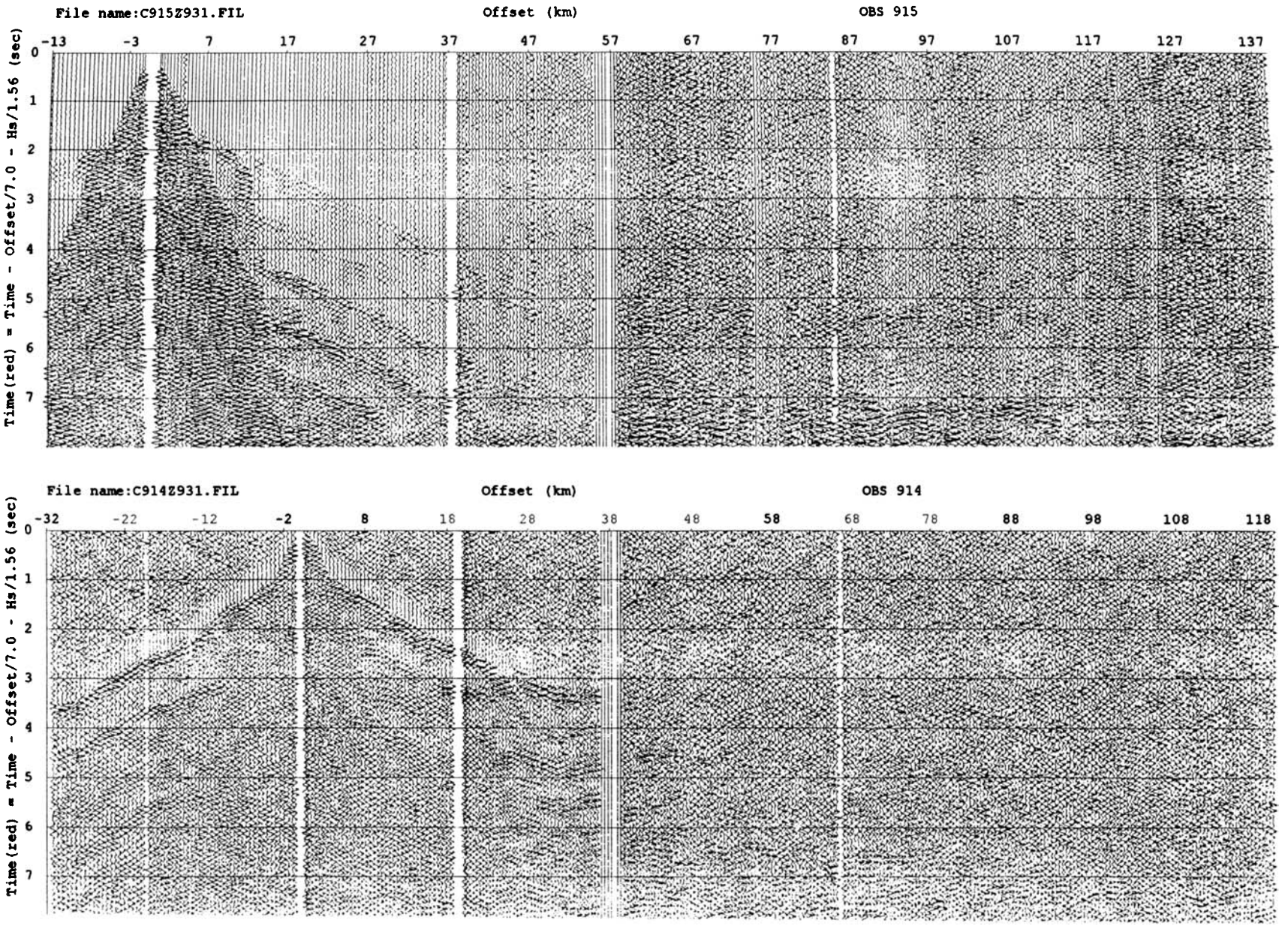


Fig. 12.3(a) Record sections of OBS 915 and 914 with reduction velocity 7.0 km/s and applied water layer static correction.

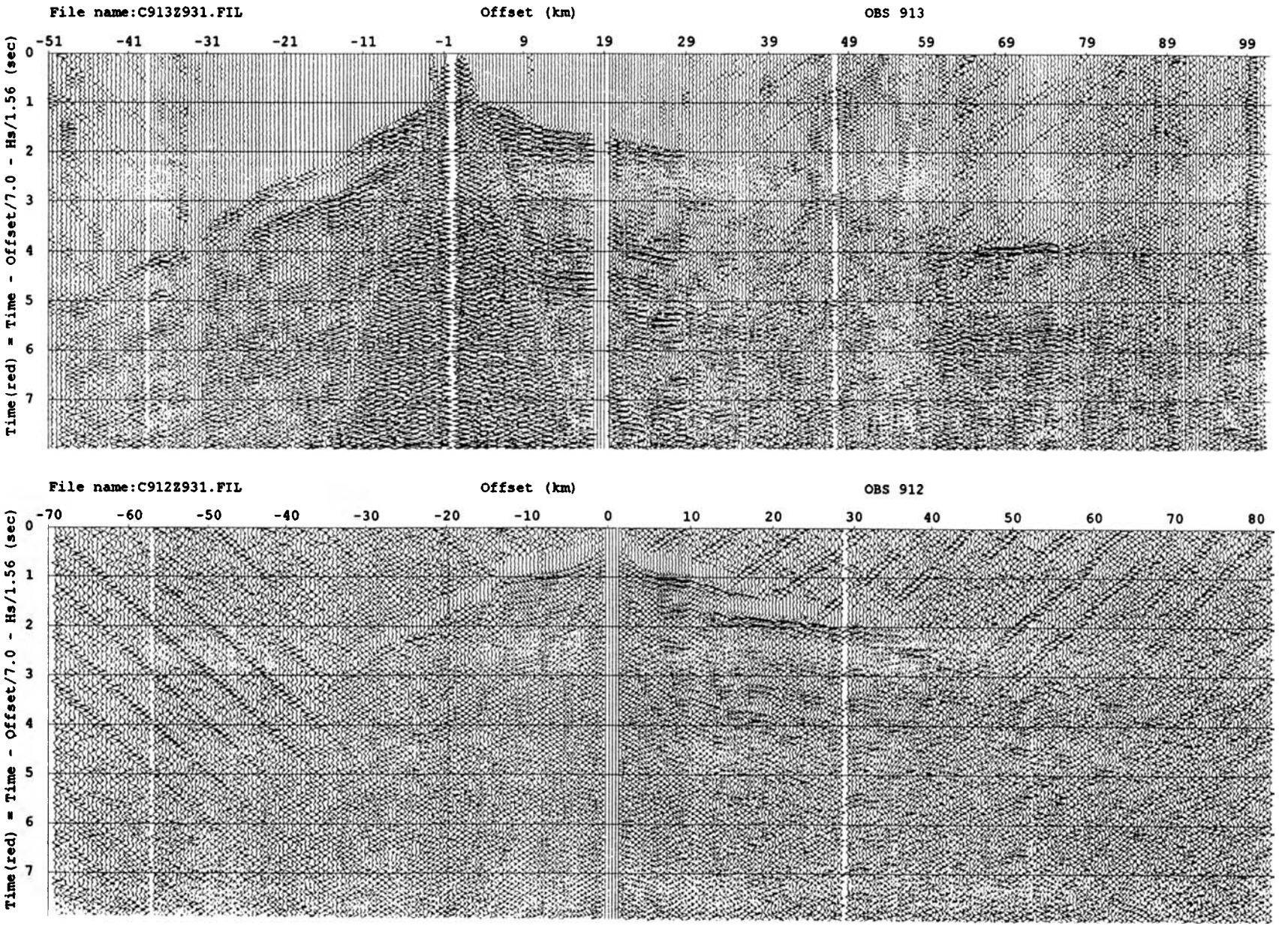


Fig. 12.3(b) Record sections of OBS 913 and 912 with reduction velocity 7.0 km/s and applied water layer static correction.

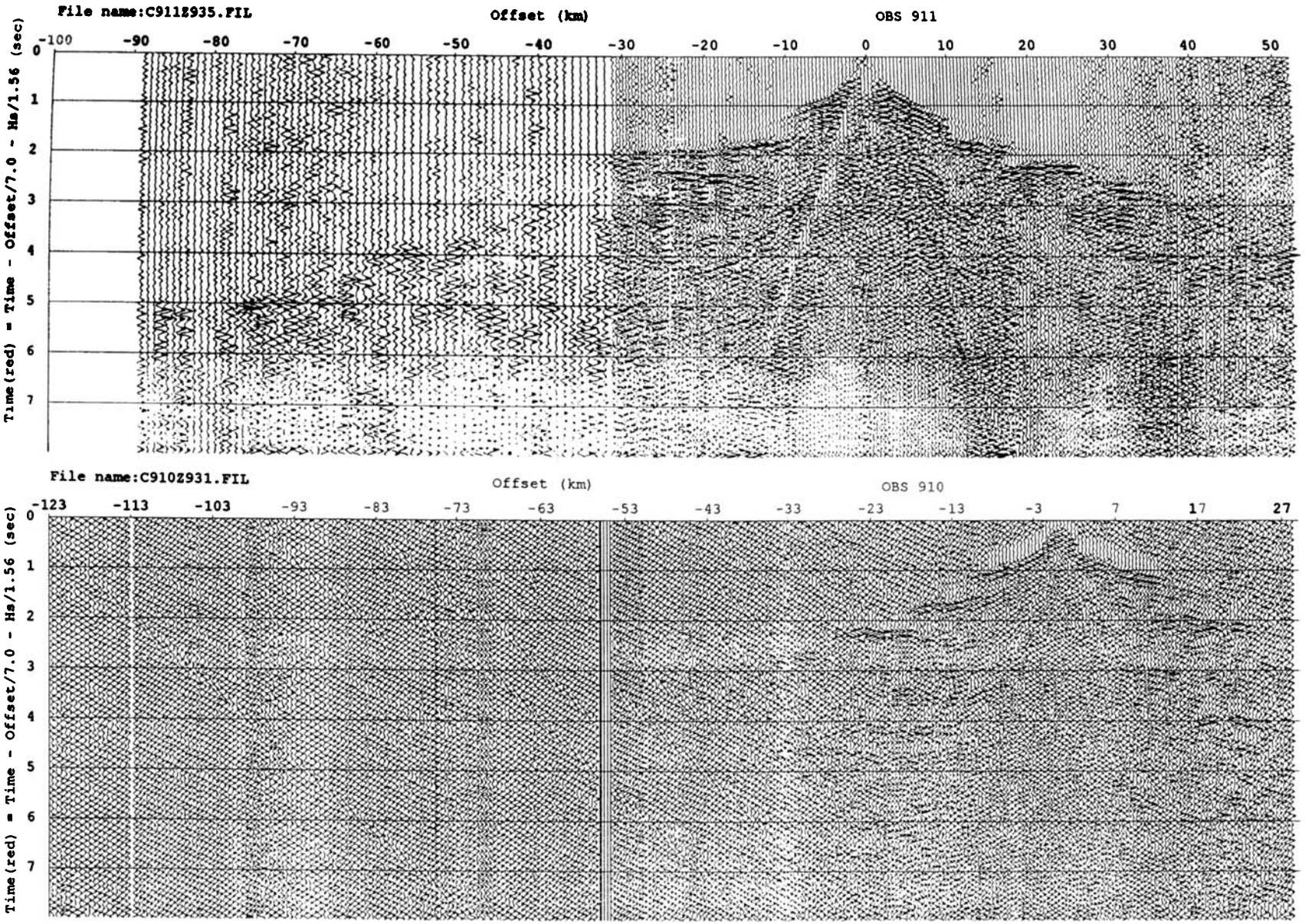


Fig. 12.3(c) Record sections of OBS 911 and 910 with reduction velocity 7.0 km/s and applied water layer static correction.

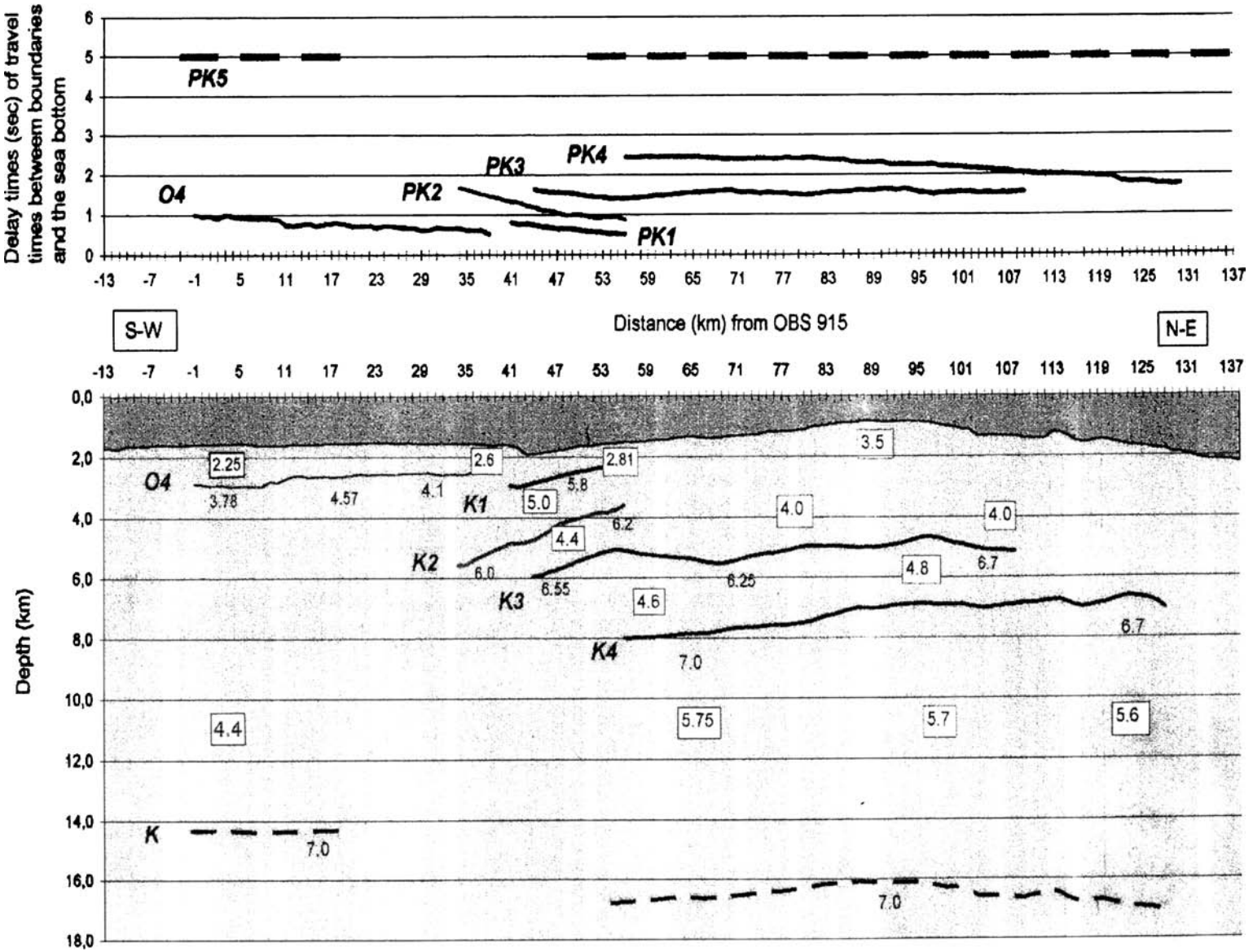


Fig. 12.4. Preliminary velocity cross-section received from analysis of the wave field and application of method 'differences of time-distance curves (to)' (Seismic prospecting..., 1966). Upper section shows time-delay values for different model layers. Lower section shows preliminary velocity model with superimposed P-phase velocity values (km/s). The velocities in white rectangles are average layer velocities and the other digits show the values of boundary velocities.

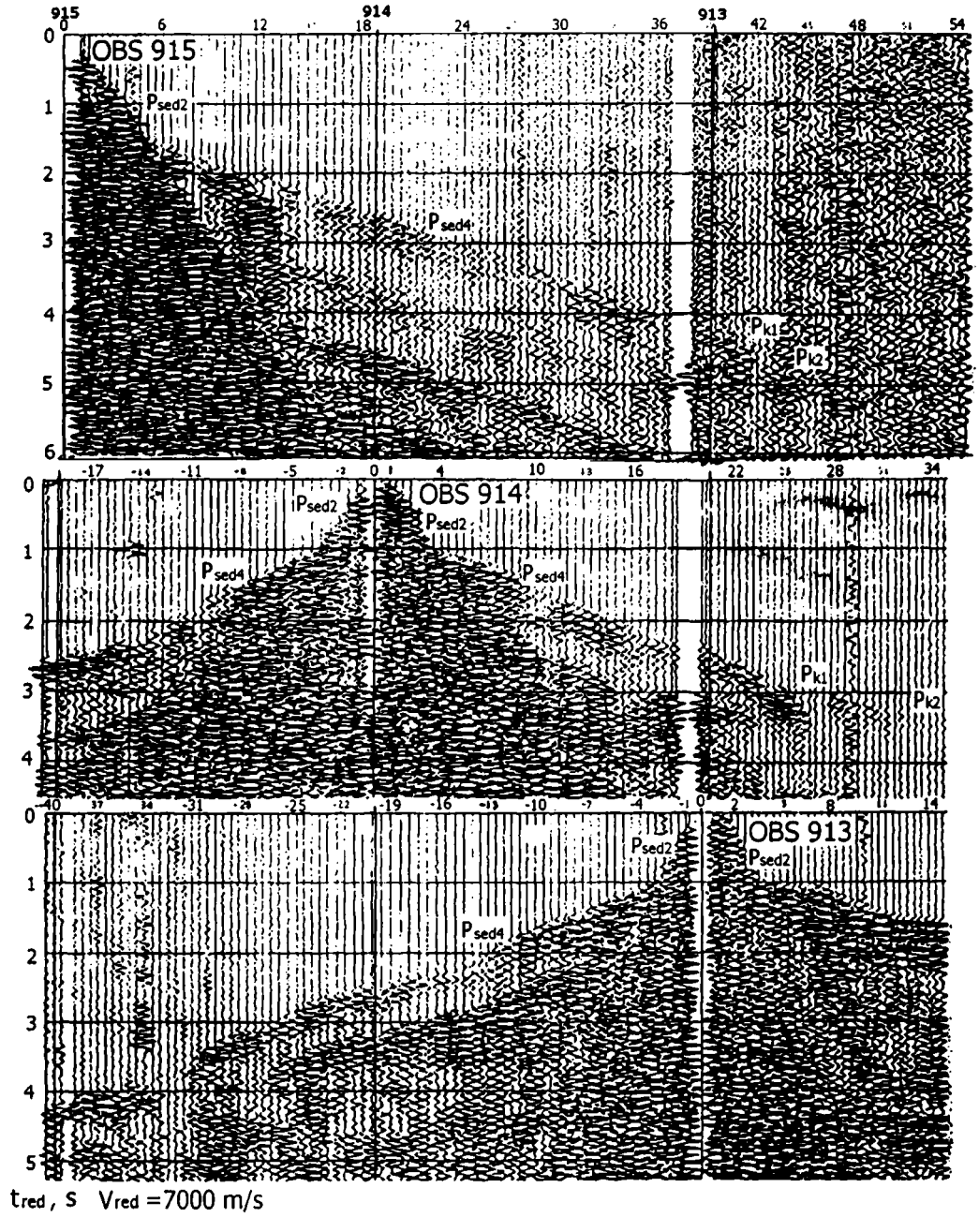


Fig. 12.5. Systems for OBS 915, 914 and 913 illustrating the behavior of the seismic field at the plain to southwest of Eratosthenes Seamount.

performed graphically. Primary waves were identified for all data sequences. Average velocities were estimated at the intersection points of the time curve branches.

In the discussion below a number of conventions are used which require explanation. Characteristic waves from specific boundaries are given name indices such as P_{sed2} and P_{sed4}, which are related to sedimentary waves with appropriate velocities. An apparent velocity is indicated by V*. The left or right (SW or NE) branches of the time curves of an OBS are indicated by suffixes l or r, so for instance OBS 914l and OBS 914r denote respectively the left or right branches of the time curves for the OBS 914 records. The term PK denotes the 'picket' or trace of a profile at a given distance, hence PK 45 is at a distance of 45 km from the beginning of the observation line taken at the OBS position.

The good quality data collected shows large variations in the seismic wave field along the profile. We will discuss separately

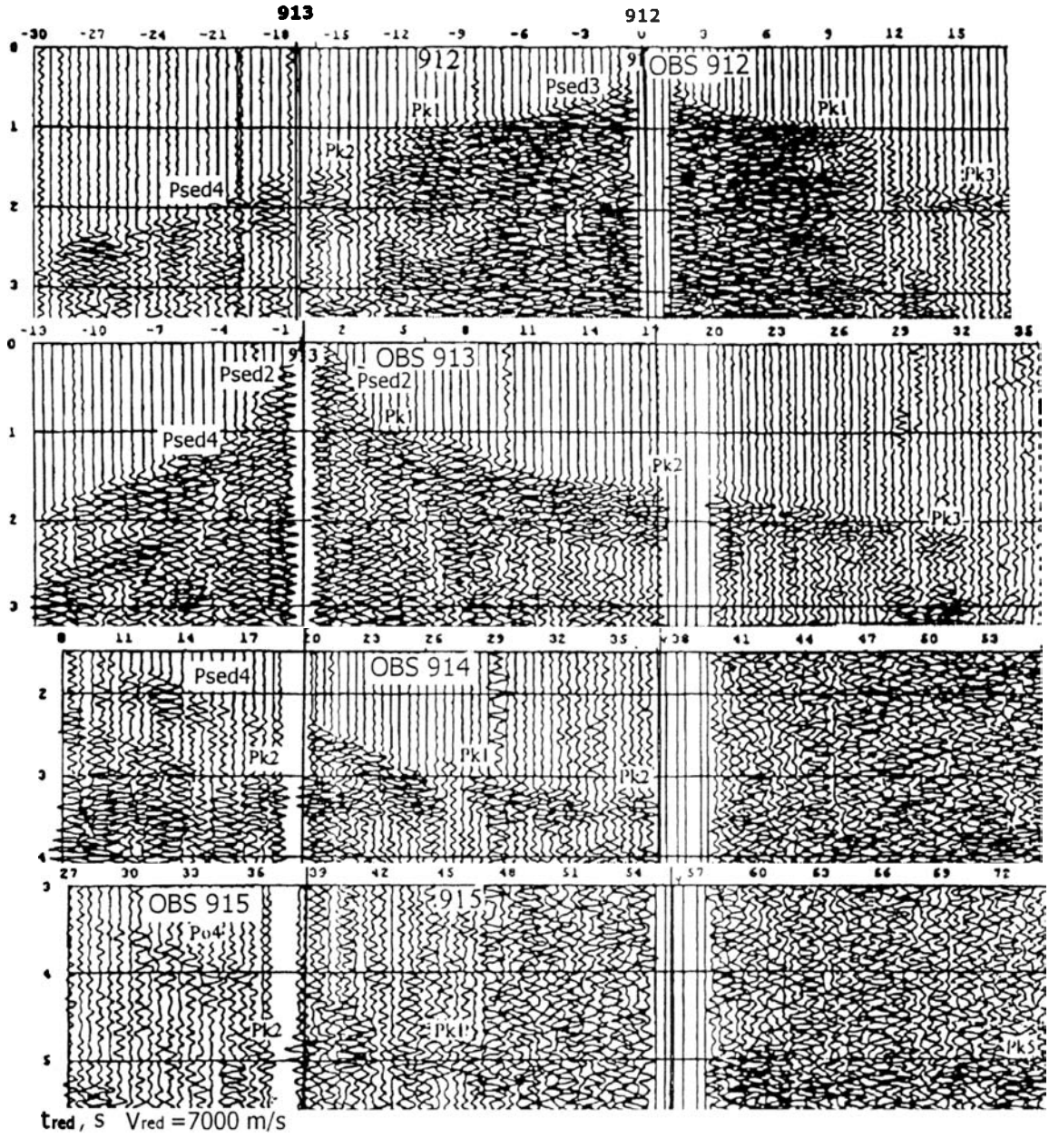


Fig. 12.6. Seismic records illustrating the behavior of the seismic field at the transition from the Levantine Sea plain to the SW slope of Eratosthenes Seamount. The locations of the OBS units are shown in Fig. 12.1. The records are given in the time scale reduced to velocity of 7 km/s and to the bottom of the sea. The seismograms of different OBS units are arranged in accordance with their locations on the profile. The first arrivals show a change from the P_{sed4} phase (4.2 km/s) to the Pk1 phase (5.8 km/s) at the transition from the plain to the slope. Continuous transitions on the record of one wave arrival into another (OBS 914, OBS 913 to the left) are easily seen as well as transitions with sudden time changes on the slope (OBS 912) indicating layers of low velocity. All OBS records show that a change in the wave pattern occurred at a distance of 45 km from OBS 915 where a crustal fault emerges to the sea bottom at the base of the seamount. Key: (1). Record of OBS 912; (2). Record of OBS 913; (3). Record of OBS 914; (4). Record of OBS 915; (5). Distance from OBS, km; (6). Tred = T-Distance - 7.0-H of water/1.52 s.

several segments of this profile.

The Plain Southwest of Eratosthenes Seamount

OBSs 915, 914 and 913 (Fig. 12.1) were deployed on the plain southwest of Eratosthenes Seamount. Water depths varied from 1550 to 1600 m, but the complexity of the depth contours in the map in Fig. 12.1 suggests a complex deep structure.

Fig. 12.4 shows the plot of t_o and the starting model of the deep section which was then prepared for the data from OBS 915. The V* for P_{sed4} waves is essentially variable along the profile. These

variations are repeated on overlapping curves and confirmed on reversed sections, *i.e.* they are related to variations in the boundary velocity. Overlapping curves are parallel to within ±0.02-0.03 s. This justifies referring these waves to the same boundary. We chose those pairs of reverse branches, confirmed in mutual points, and calculated V_b and t_o. V_b variations were assessed to be in the range of 3.8 to 4.5 km/s with a median value of 4.3 km/s. The t_o-line shows an increase of t_o from 1.0 s below OBS 915 and 0.5 s below OBS 913, *i.e.* a decrease of the sedimentary layer thickness towards Eratosthenes Seamount. The average velocity for the uppermost soft sediments with velocities ranging from 2.02 to 2.80 km/s is 2.5 km/s.

A similar wave picture was observed on records from OBSs 915-913 which are shown in **Fig. 12.5**. Intensive P_{sed2} phases with an apparent velocity of V* = 2.0-2.5 km/s at distances of 3-5 km change into weak P_{sed2} phases with V* = 4.2-4.5 km/s.

The Southwestern Foot and Slope of Eratosthenes Seamount

A shallow depression is situated at the foot of the slope bordering the seamount, which separates it from the adjacent structures. OBS 913 was deployed on the lower slope of the depression, and OBS 912 on the side slope of the seamount, a third of the way up to its summit (Fig. 12.1).

We observed a sharp change in seismic wave properties in the vicinity of OBS 913. The V* of the first waves increases to 5.8-6.2 km/s instead of the 4.4-4.5 km/s observed between OBS 915 and OBS 913 (Fig. 12.5 and **Fig. 12.6**). The shape of the time-distance curve is still more complicated. The transformation of first waves into second waves is observed by delays in the first arrivals.

The series of reversed time-distance curves for OBSs 913 and 912 and overlapping time-distance curves from OBSs 914 and 915 allow an analysis of the wave picture. The reversed records from OBSs 913r and 912l are reliably confirmed at their mutual points. The OBS 912l curve consists of four branches. Near the OBS, a P_{sed3} phase is seen with V* close to 3 km/s. This wave is replaced at a distance of about 3 km by a P_K1 phase with velocity 5.8 km/s. The latter disappears at a distance of 13 km from the OBS. The next P_K2 phase is traced with a delay of 0.4 s. This wave continues out to 22 km, where we observe a decrease of V*. Some P_K2 phases can be traced as second arrivals near the OBS out to a distance of more than 6 km.

OBS 913r recorded a short branch of the wave that can be seen after the P_{sed3} phase with velocity near 7 km/s, similar to that of the P_K1 branch. Its time-distance curve comes to the branch of the P_K2 phase at 13 km after passing through the segment with decreased velocity. This wave abruptly disappears beyond a mutual point at a distance of more than 20 km.

The overlapping curves from OBSs 914r and 915r show (Fig. 12.6) that the P_{sed4} phase pattern becomes more complicated at PK 43 km, where short high velocity branches can be seen parallel to the P_K1 branch on the OBS 913r records. At PK 51 km it merges with a high velocity branch which parallels the P_K2 on the OBS 912 records. The P_K2 phase exists as an oscillation with dominant amplitude on the OBS 912, 913, 914 and 915 records only over a short segment of the profile. It is limited at PK 35 in the south-west where the oscillation disappears on the OBS 914r and 915l records, and it changes the slope of the curve on OBS 912l. In the north-east it is limited by PK 59-61 where oscillations on the OBS 913r records disappear. On the OBS 915r records some oscillation can be traced a bit longer, but they are delayed at larger times and belong to the next phase P_K3.

Both branches of OBS 912 were used to prepare the deep section of the P_K1 phase. The OBS 912l and 913r branches were prolonged to mutual points (considering overlapping branches). We limited the wave at PK 42 (from OBS 913-915 data) on the left and at PK 67 (from the end of the OBS 912r record) on the right. For the P_K2 phase a branch of the OBS 913r curve was prolonged to the left, parallel to branches of OBS 914 (and 915), and its existence was verified between PK 35 and 63. Fig. 12.4 shows the plots of $t_o(x)$ and V_b that were calculated. The boundary velocity for the P_K1 phase is V_b = 5.9 km/s, and 6.0-6.2 km/s for P_K2.

Examination of various aspects of the P_K1 phase behavior shows that while it decreases quickly on the OBS 912l record, and it exists for only a short segment of the profile on the OBS 913r records, on OBS 912r records its amplitudes become more intensive. We can assume that on the segment between OBSs 912 and 913 the P_K1 phase is derived from a thin layer, which is inclined towards the OBS 913 position. Under this assumption we processed the data for OBSs 915 and 913. The resulting t_o and V_b values conform to the data for the OBS 913 and 912 combination, as well as for OBSs 915 and 913. It also makes it possible to depict on the deep section the interrelation of the seismic boundaries in the transition from the foot to the slope of Eratosthenes Seamount.

The average velocity data ($\bar{V}$) give us the following results. For the P_{sed4} phase below OBS 913l, $\bar{V}$ = 2.8 km/s. For the P_K2 phase from the OBS 913r, 912r and 912l branches, $\bar{V}$ = 2.5-2.8 km/s, and for the first arrivals the value $\bar{V}$ = 2.5 km/s was taken. For the P_K2 phase on the records of OBS 913r, $\bar{V}$ = 3.7 km/s; for OBS 914r, 3.9 km/s; for OBS 915r, 4.4 km/s. An average value of $\bar{V}$ = 3.8 km/s was taken for the first arrivals.

The Top of Eratosthenes Seamount

The steep south-west slope of the seamount comes to a flat cap with coarse surface relief. The refraction profile crosses the southern side of the flat cap, comes to the steep eastern slope and continues on down the northeastern slope (Fig. 12.1). OBS 911 was located on the flat top, OBS 910 on the eastern slope close to the top, and OBS 909 on the lower part of the northeastern slope (OBS 909 belongs to the next OBS array PR 9-2).

Certain features characterize the seismic wave field for the records from OBS 912r, 911, 910, and 909l (**Fig. 12.7**). At small distances from the OBS, the wave velocities are typical of non-consolidated sediments, *i.e.* velocities of 2.5-2.8 km/s, and for OBS 911, 3.5 km/s. As the distances increase, the slopes of the time-distance curves change and more high velocity waves appear as first arrivals. These velocities are estimated at approximately 6 km/s for OBS 912r, and 4.6-4.8 km/s for the other OBSs. Such waves are abruptly attenuated at a distance of about 8-10 km from

the OBS. High velocity waves remain as first arrivals with delays of 0.5-1.0 s, *i.e.* we observe a break in the time-distance curve. It indicates a low velocity layer below the boundary and the point at which the wave ceases to exist. A similar scenario can occur as a result of horizontal inhomogeneity, or disappearance of the seismic boundary. An analysis of overlapping and reversed time-distance curves allows us to differentiate between these two cases. Disappearance of the boundary should be expressed by the absence of proper waves starting from certain places along the profile, regardless of the distance. If a lowering of the velocity with depth is assumed, then the limit point should be located at a more or less constant distance from the OBS.

For the OBS 912l records we can assume that both reasons affect the right limit of the PK2 phase. Two lines of evidence support this hypothesis: a limited region of PK2 existence (determined by the OBS 914-913-912 pairing, see above) and the high velocity PK2 phase that is close to 6 km/s. For OBSs 911 and 910 these values are 4.6-4.8 km/s, so we can define these as sedimentary phases P_{sed5}. The time curves for these waves do not reach the mutual points, and we can approximately estimate V_b by V* values along both directions. Branches are confirmed exactly at the zero distance (t_o), and for OBSs 911 and 910 V* toward the southwest (left) are 4.59 and 4.66 km/s, and toward the right are 4.85 and 4.87 km/s. The value of t_o under OBS 910 is less than that under OBS 911, *i.e.* there is some evidence about the rise of the boundary toward the north beneath the sea floor. However here the sea floor is much more steeply inclined to the north, and the dense sediment boundary essentially dips to the northeast.

The velocity values for consolidated sediments on top of Eratosthenes Seamount are 4.7 km/s instead of the 4.3 km/s found beneath the plain to the southwest of the seamount. We can assume that the origin of the sediments in this place was somewhat different.

The values of the velocity below the seismic boundary should be estimated approximately because of the existence of low velocity zones, and they will be partly corrected by the modeling.

The next phases PK3 are observed after the break of the time-distance curves of the first phases. They are found on branches of OBSs 912r, 911l, 911r, and 910l (Fig. 12.7). Such waves are reliably traced by phase correlation over long intervals (sometimes up to 30 km). They confirm well at mutual points. The V* are close to 6.5 km/s, *i.e.* less than the reducing velocity. Recording times (using a reducing velocity of 7.0 km/s) vary from 1.9 to 2.1 s to the south from OBS 912 position, and around 0.6 s in the vicinity of OBS 910. PK3 is observed about 0.25-0.30 s later than PK2 in the region of its reappearance.

The most exciting tracing of the PK3 phase using phase correlation is found between PK 44 and PK 108. The clearest picture is observed on the OBS 911 records from the big airgun source. The southern limit of this wave can be estimated from the OBS 912-913 pairing (Fig. 12.6). The wave is observed in late arrivals on the OBS 912r branch, and it merges with P_{sed4} phase at a point located to the south of the OBS 913 position in the fault zone on PK 35. A rise of the boundary is indicated by values of V* on the left and right branches of the OBS 912 records. The value at the left (south) is less than that at the right, *i.e.* the boundary inclines toward the south. The northern limit of the PK3 phase can be noted at PK 108, where it finishes on the OBS 911r records at a distance of 18 km from the OBS and arises on the opposite (left) branch of OBS 910l at a distance of 8 km.

The t_o and V_b curves were calculated with confidence for the pairs of time-distance curves by an interpolation of the branches to zero distances. The maximum t_o (near 2.0 s) was found on the southern side (in the fault zone at PK 35). Then t_o drops to 1.4 s beneath OBS 912 and varies between 1.4 and 1.6 s toward the north. The boundary velocity is V_b = 6.5 km/s in the southern part, 6.2 km/s between OBSs 912 and 911, and 6.8 km/s between OBSs 911 and 910. Average velocities were only approximately estimated at 4.0 km/s. Deviations from this value by ± 0.2 km/s give depth variations of ± 8%.

The next phase PK4 replaces PK3 after it vanishes at PK108 km. Its time curve is shifted later by 0.5 s, and the (reduced) arrival times vary from 2.0 to 2.8 s in the segment between OBSs 912 and 910. The time curves are almost parallel to the distance axes, *i.e.* V_b is close to 7.0 km/s. (Fig. 12.7).

The PK4 phase can be traced southward from OBS 911 to the location of OBS 912 by phase correlation and there are high amplitudes at the mutual points for the OBS pairs 912r and 911l. Some indications can be traced further south, but we consider that the beginning of this wave can only be reliably taken near OBS 912 at PK 58 km. Northward from OBS 911 the PK4 phase is easily traced and conforms at mutual points to the OBS 910 data. Farther to the north, the tracing becomes difficult, and the shape of the time-distance curve varies. Time control at mutual points is possible, but it requires a prolongation of the OBS 910r branch due to the cessation of shooting 5 km before the position of OBS 909. We observed the disappearance of the wave phases and a sharp increase in the times of first arrivals on the OBS 909l branch 5 km before the location of OBS 910 (PK 116-120 km). Other specific features of the wave field disturbances can also be observed at this place. The PK4 phase (that replaces the P_{sed5} phase on the OBS 909l branch of first arrivals) is traced well at times of 2.2-2.4 s up to PK 117, but then its amplitude decreases below the background noise level, and low velocity phases appear. Here we also observe variations in the PK6 phase behavior (the PK6 phase with velocity near 7 km/s belongs to a deeper boundary) on the records of OBS 915 (at a distance of 107 km), OBS 914 (at 96 km), and OBS 913 (at 75 km). This allows us to presume that a deep fault exists near PK 117, which crosses all the seismic boundaries. The bathymetric map shows such a fault bordering the flat cap of Eratosthenes Seamount on the north and crossing the whole structure of the seamount.

The North-Eastern Slope and Foot of the Seamount

The fault going across the top of the seamount traverses this segment. It marks the transition zone from Eratosthenes Seamount to the folded structure of the Cyprean Arc. The sea floor deformation zone (the Giermann Fault) is situated here. OBSs 909, 908 and 907

cover this segment called Profile PR 9-2, comprising the second OBS array of the three.

The PK4 phase, as was mentioned above, can be traced for OBSs 910r and 909l via a fault according to the formal parameters of wave phase correlation and mutual point time control. However the boundary velocity V_b is essentially decreased in comparison to the adjacent seamount cap. The thickness of sediments changes too. A break in the time-distance curves (which was seen clearly on the OBS 910r records), disappears on the OBS 909 and 908 records, *i.e.* a low velocity layer disappears below the upper boundary of the dense sediments. Below OBS 909 a thin sedimentary layer with velocity 3.1-3.6 km/s comes into view (the P_{sed3} phase), blanketed by a thickness of unconsolidated (Recent?) sediments (the P_{sed2} phase, 2.5 km/s). The velocity at the base of this layer decreases toward the north from OBS 909 (up to 4.0 km/s instead of 4.8 km/s southward from OBS 909). The thickness of Recent subbottom sediments decreases, and below OBS 909 a boundary with velocity greater than 3.5 km/s (P_{sed3} phase) reaches the seafloor. For the OBS 909r and 909l pairing to was calculated as 0.3-0.7 s, and $V_b = 4.0$ km/s. A careful analysis shows the complexity of the wave pattern and a gradual transition from the P_{sed3} phase to the Psed4 phase; the to value increases from 1.1 to 1.3 s, toward the north for the PK4 phase, and $V_b = 6.1$ km/s.

Large disturbances of the wave field are observed between OBSs 908 and 907 at PK 182 km. Data from OBS 908 show that the waves are similar on both the northern and southern branches at small distances from the OBS (from the uppermost parts of the section) up to PK 182 (12 km to the north of OBS 908). Farther to the north a difference arises, and on the right branch wave amplitudes decrease, and arrival times increase, *i.e.* V* changes. The overlapping branch of OBS 909r shows strong amplitude attenuation for the PK4 phase just beyond OBS 908. Reversed OBS 907l records show a quite different picture. The most intensive first phase has V* = 1.7 km/s. Weak waves of decreasing amplitude with velocity 4.0 km/s spread outward from the strong first wave. Its time at the position of OBS 908 is 2.3 s, and the time at the mutual point of the OBS 907l branch can be found by extrapolation of the Psed4 phase after its attenuation. A reversed section was used for calculation of t_o (which varies from 0.3 to 0.6 s) and $V_b = 4.5$ km/s (Fig. 12.4).

The time-distance curves for the OBS 908l and OBS 909r pairing was used to study the PK4 phase. Its t_o value varies from 2.1 to 2.5, and $V_b = 6.1$ km/s, with an average velocity of 3.7 km/s. The boundary dips to the north and disappears at PK 183 km, where a big fault borders the Cyprean Arc.

Phases from Deep Boundaries

The previous paragraphs discussed seismic waves which propagate through and thus help clarify the structure of the upper 10-12 km of the earth's crust. The high intensity of such waves and the complete coverage with reverse and overlapping observations provide detailed and reliable data on the section, which shows its complicated horizontally inhomogeneous structureThe waves from deeper boundaries provide less reliable information about the deep structure. There are two reasons for this:

1) The first is that deep waves appear at large distances from the source (many tens of km) and require a long array in order to be studied. In our experiment the shooting line was 63 km with a big airgun, and 145 km with a small airgun, and this determined a maximum length of the time-distance curves. All profiles were covered by three separate arrays of OBSs (9-3, 9-2 and 9-1), with 9-3 and 9-2 arrays overlapping by 50 km. Eratosthenes Seamount was covered by array 9-3. OBSs 909, 908 and 907 were deployed on the adjacent 9-2 array. Its data helped us to understand the wave picture for the upper part of the section, but it did not contain information about the deep waves.

2) The second reason is that waves from deep boundaries were found as weak oscillations due to the properties of the deep section in the region. On seismograms obtained with the small airgun, the deep waves can be picked out as synphase arrivals with amplitudes not exceeding the background noise level. Multiple arrivals of deep waves sometimes help to control the wave pattern. When we used the big airgun (records OBS 911 and OBS 912; Fig. 12.3), we could see that the amplitudes of the deep waves sometimes exceeded the noise level, but in this case the length of the shooting line was only about 60 km, and the interval over which the deep waves could be traced did not exceed 30 km.

The most extended branch of the time-distance curve for the PK5 phase was recorded by OBS 915 (Fig. 12.3a). The wave begins at a distance of 44-47 km and is observed a little later than the PK2 phase. Then the wave is traced only as short pieces of synphase arrivals. But at distances of more then 60 km it can be better seen, through the presence of attendant intensive multiple waves. The multiple arrivals are delayed by 2 seconds, and this corresponds to double arrival times in the water layer near the location of OBS 915. This wave is observed up to distances of 110-112 km (a little beyond the location of OBS 910) and cannot be picked out further on. Its V_b is close to 7 km/s; the arrival times are almost constant and are about 5.0-5.2 s (reduced). However the wave pattern is complex, the synphase axes are short, and the amplitudes vary. All these features indicate a complexity of the boundary. We observe some weak waves with a low V* and linear shape on the time curves coming out of the PK5 phase at PK 80-85 and 105-110.

We did not find regular arrivals of PK5 phases on reversed records of OBS 911l with small airgun impulses. Intense waves can be seen at big airgun shots, starting at 65 km distance with times 4.8-5.0 s. These waves are confirmed at mutual points of the OBS 915 data. On the OBS 912l branch the waves can be seen with times of 5.0-5.1 s, starting from 43-45 km and moving up to the end of the shooting line (at 59 km). The waves are confirmed at mutual points of the OBS 915 data. Records of OBS 914r are similar to those of OBS 915r, but they are less informative. The PK5 phase on OBS 914r can be found initially with the arrival of multiples at distances of 55-60 km (PK 75-80 km) and at times of 4.7-4.8 s. Then it can barely be traced up to the location of OBS 910 (PK 110 km). We observe some branching off, likewise on OBS 915r. The PK5 phase is linked to the OBS 911l data. On the OBS 913r records the PK5 phase is traced over distances of 60-75

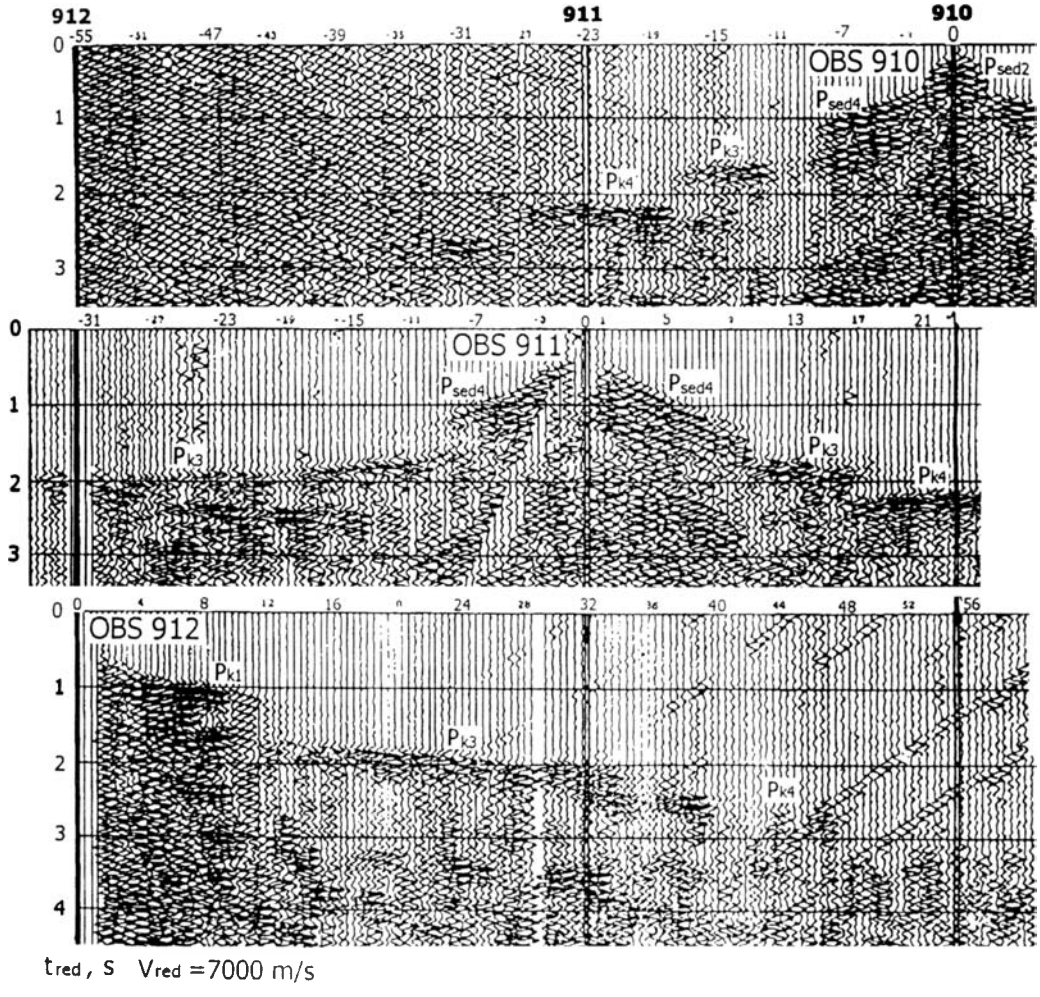


Fig. 12.7. OBS 912 to OBS 909 system illustrating the behavior of the seismic field at the top and on the northeastern slope of the seamount.

km at times 5.1-5.3 s, but do not extend to mutual points.

Hence the P_{K5} phase with velocity 7.0 km/s is traced from the beginning of the profile to PK 110 km. Beyond this range we do not see the wave on any OBS records up to the end of the shooting line (at PK 140 km). The P_{K5} phase is also not observed on PK 30-45 km, *i.e.* the location of this wave on the OBS records is somehow related to the position of the faults, previously and reliably marked on the upper parts of the section. The time-distance curves for the P_{K5} phase do not form a real system of long reversed and overlapping curves. But its branches are concordant at mutual points, and are recorded inside a narrow time interval from 4.8 to 5.2 s. These time deviations are dependant on the properties of each OBS. For example, all times of OBS 914 are 0.3 s less than for OBS 915. In preparing the section for the starting model we can neglect variations in time and velocity and take time to be equal to 5 s and V_b=7.0 km/s. For this approximation the depth variations in the section can be determined by average velocity values.

Available data for average velocity $\bar{V}$ estimations are rare. We have a crossing point of the P_{sed4} and P_{K4} phases for OBS 915. It gives $\bar{V}$ = 4.3 km/s for the region of the plain to the south of Eratosthenes Seamount. There are no crossing points within the limits of the seamount, but the P_{K5} phase emerges on the records of OBSs 912r, 911l and 913r. We assumed that this is an initial point of a refracted (head) wave and found $\bar{V}$= 5.3 km/s (from OBS 912l) and $\bar{V}$ = 5.6 km/s (from OBSs 911l and 913r). These values are attributed to the section below the body of the seamount.

The boundary where the P_{K5} phase begins extends from the south end of the profile up to the fault at PK 116, and is interrupted by another fault at PK 30-35. Waves pass across these fault zones, but do not exit to the surface. This can be explained by high absorption of the energy of the seismic waves due to distortions in the rocks within the boundaries of the fault zone.

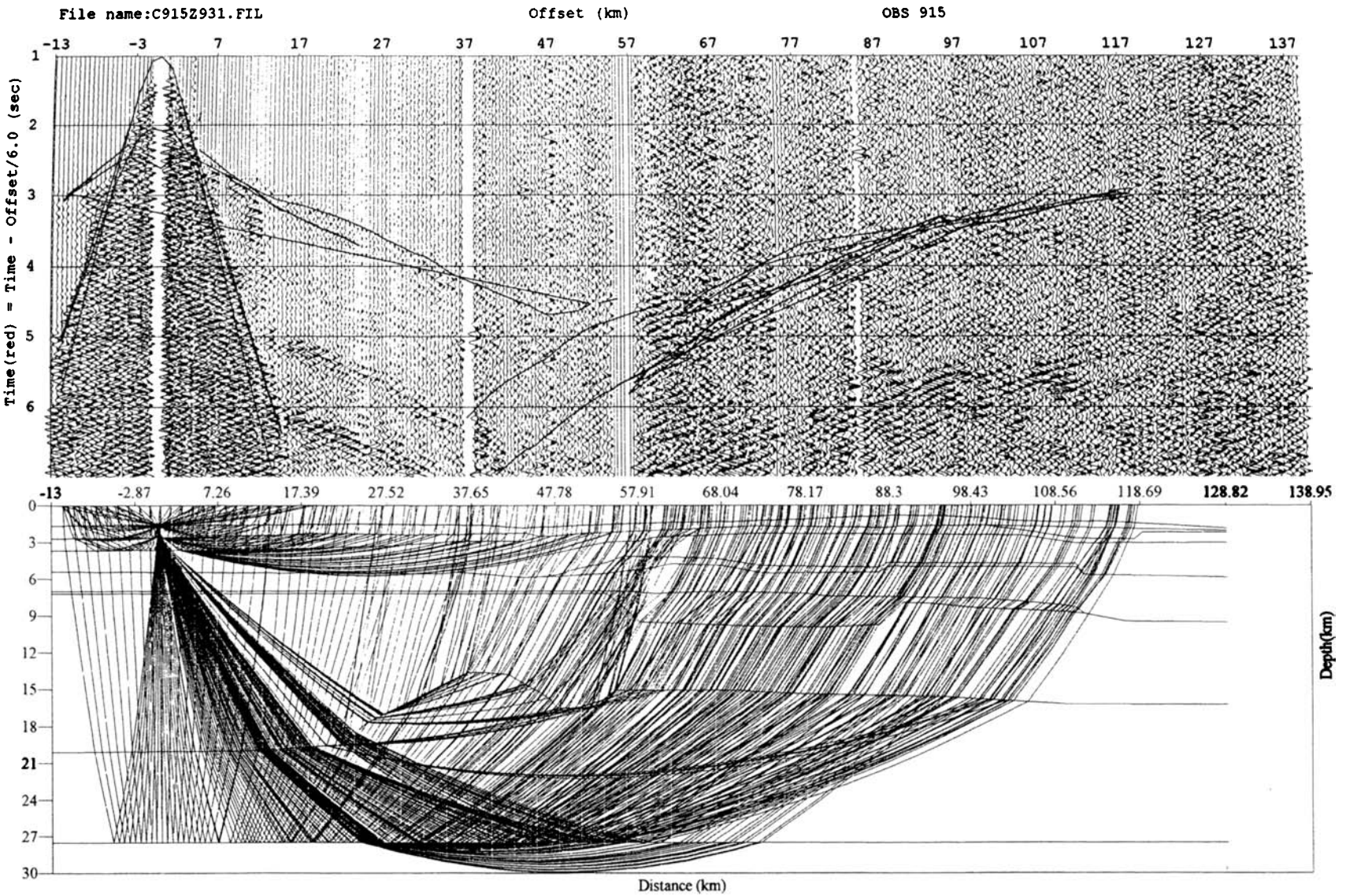


Fig. 12.8. Record section of OBS 915 with calculated travel times superimposed.

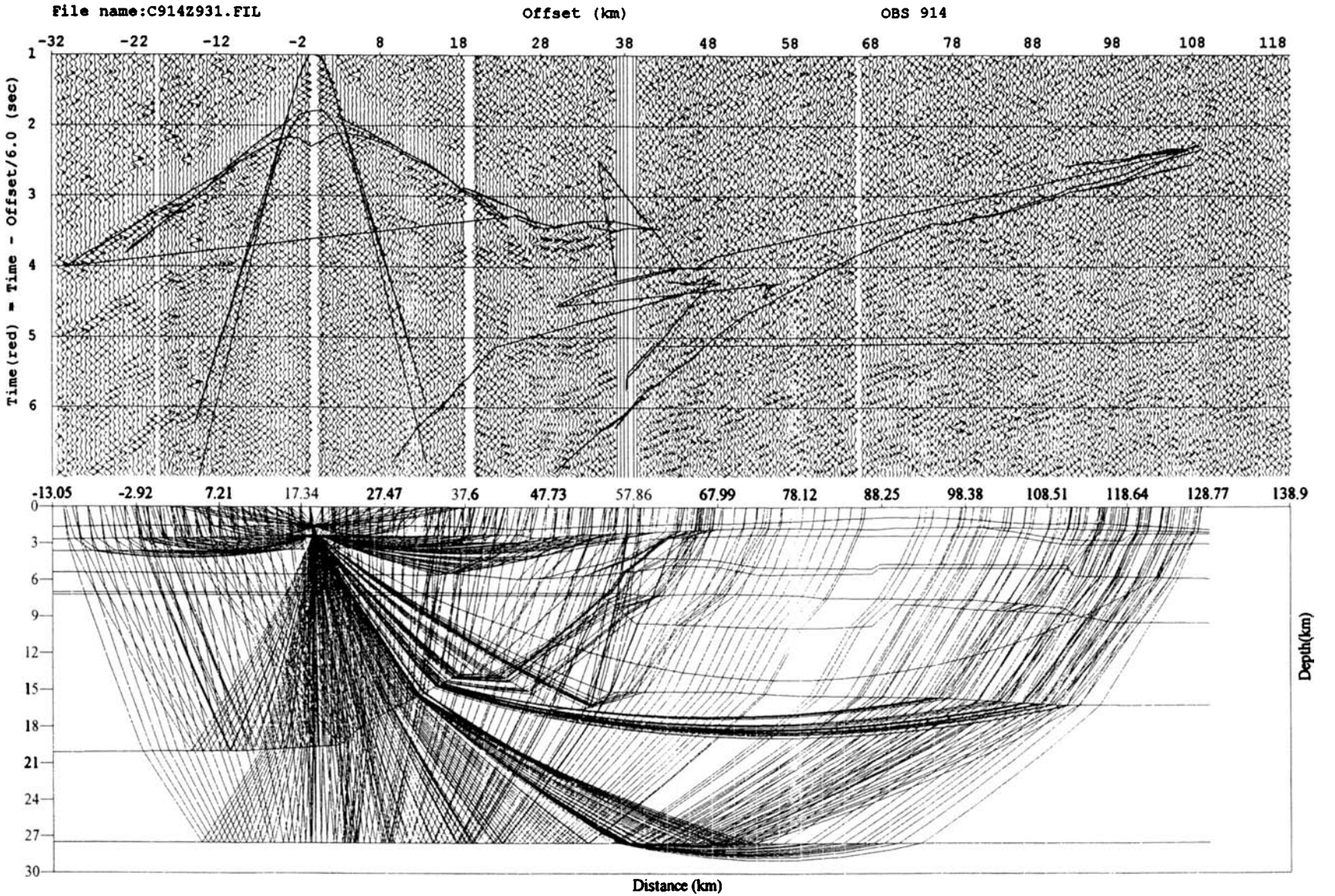


Fig. 12.9. Record section of OBS 914 with calculated travel times superimposed.

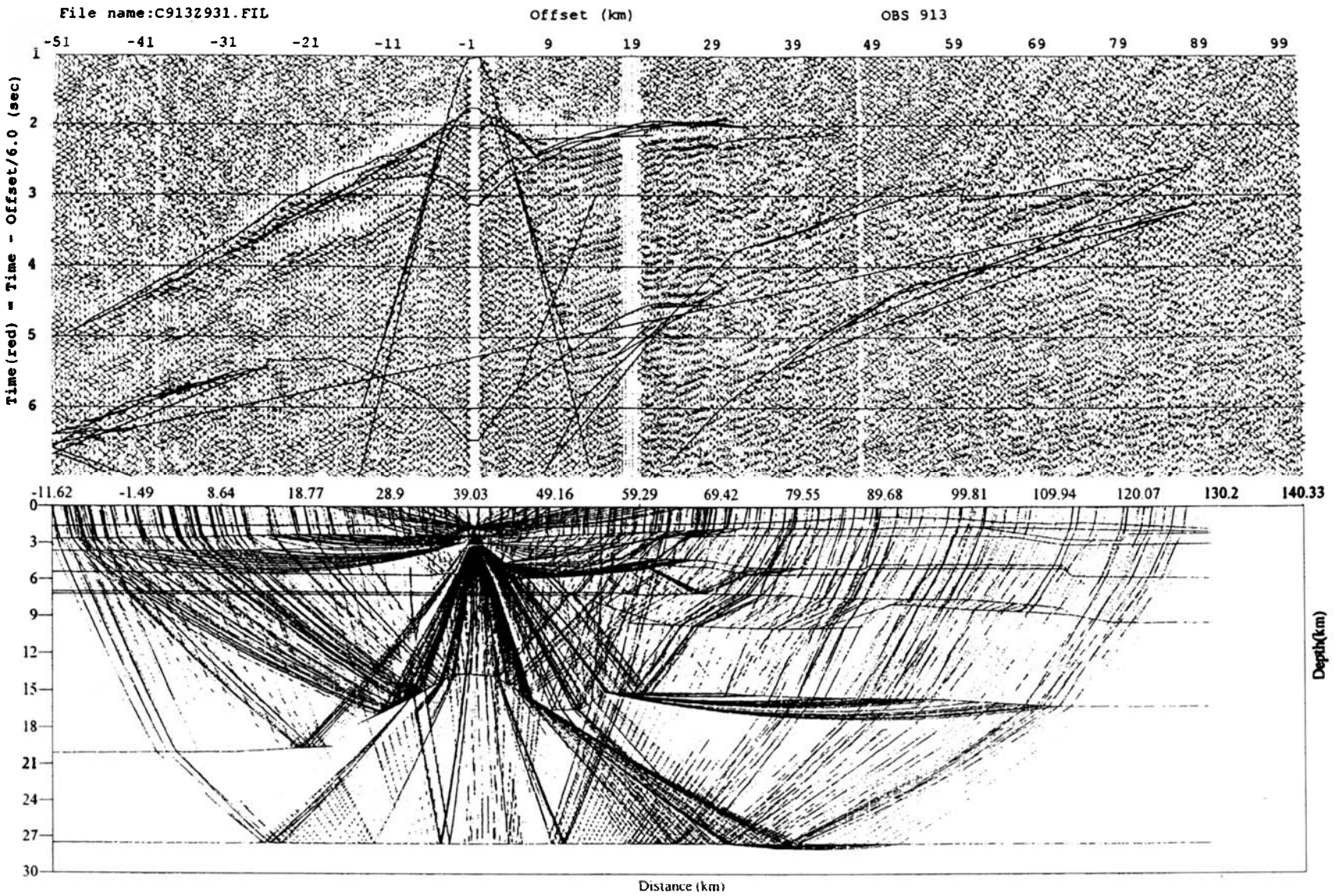


Fig. 12.10. Record section of OBS 913 with calculated travel times superimposed.

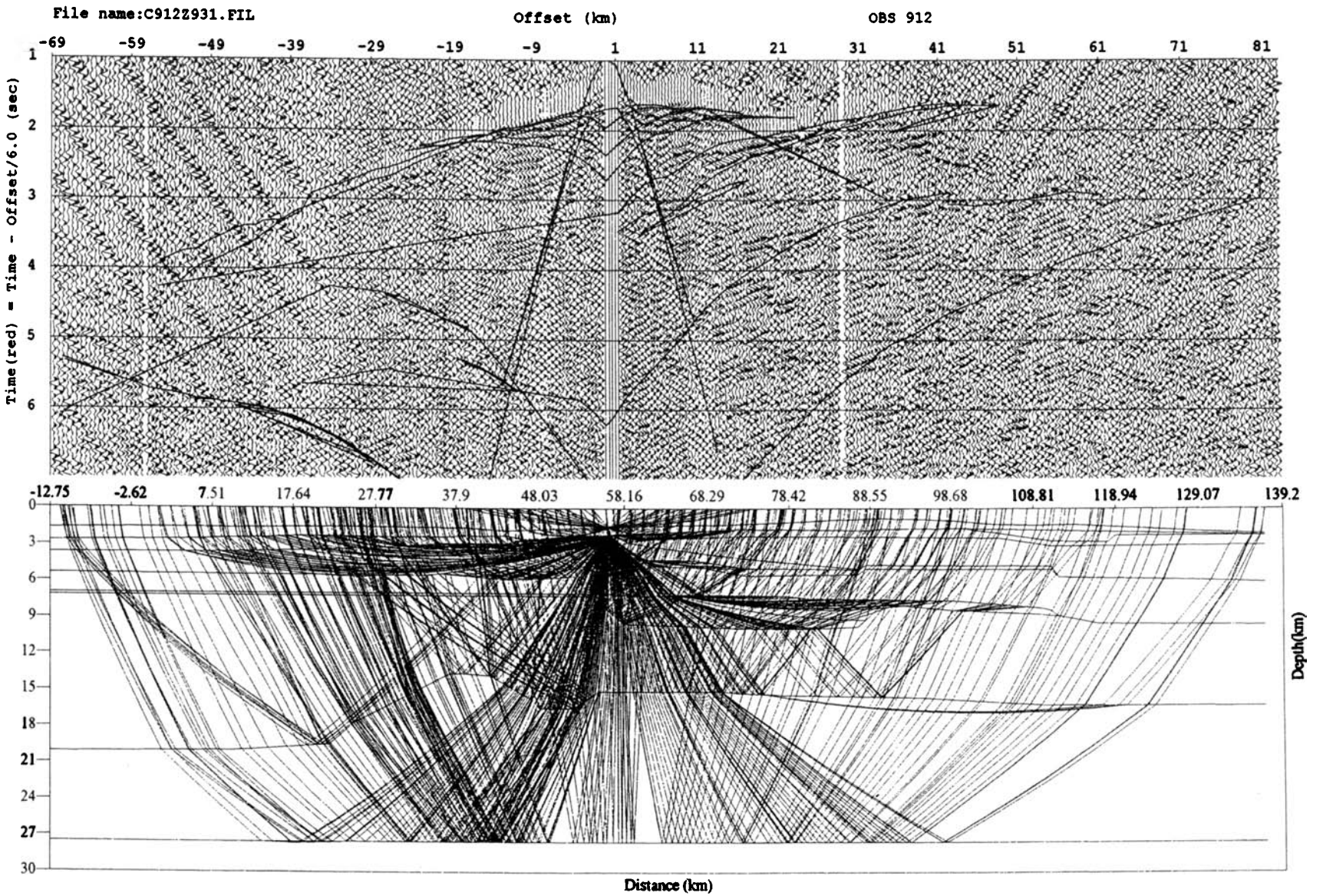


Fig. 12.11. Record section of OBS 912 with calculated travel times superimposed.

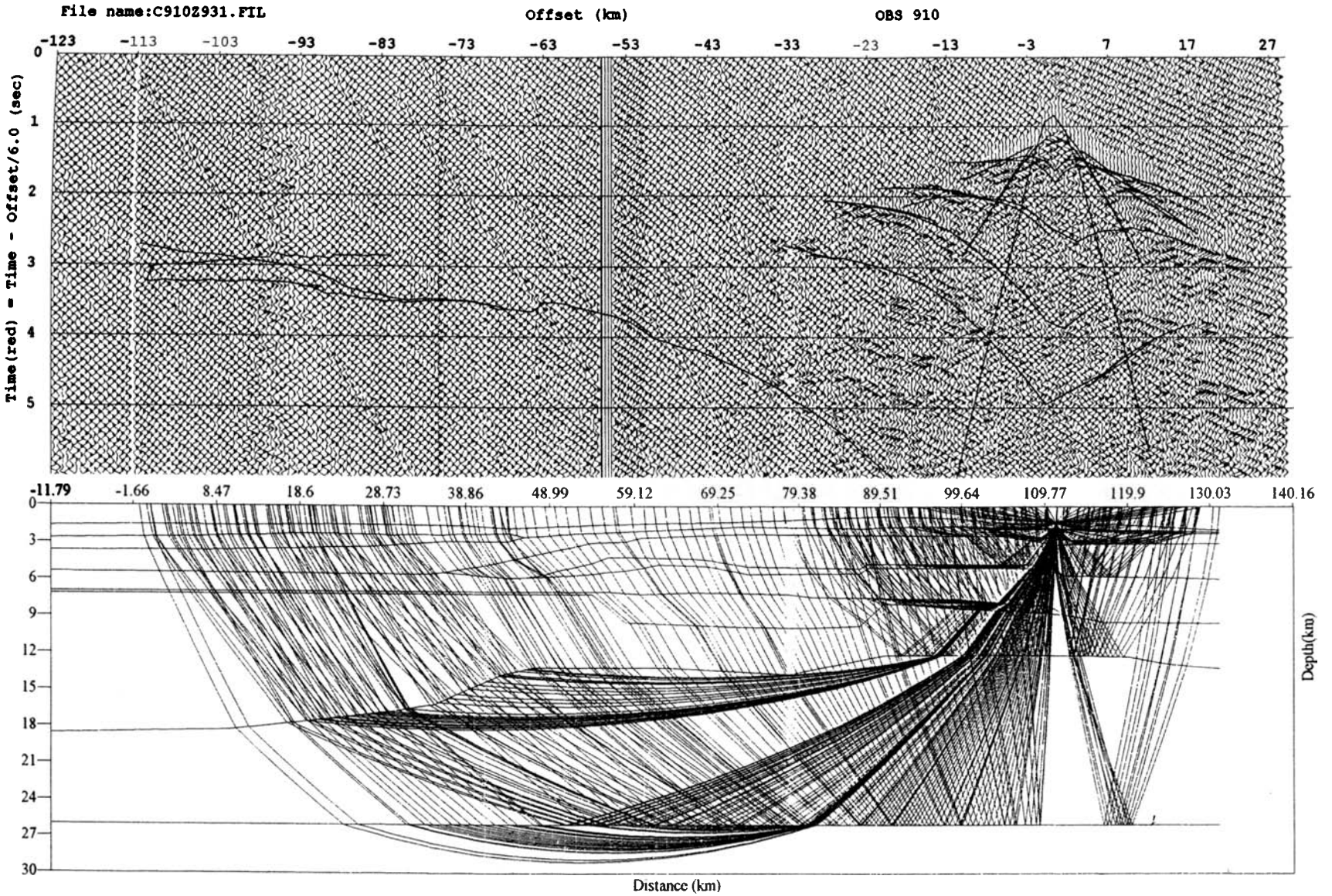


Fig. 12.12. Record section of OBS 910 with calculated travel times superimposed.

The depths of this boundary can be approximately estimated as 14 km below the plain at the south of the profile, and 20 km under Eratosthenes Seamount.

We carefully searched for waves reflected from the Moho boundary. For a continental crust some 30-40 km thick such waves appear in second arrivals as strong amplitude waves at distances of more than 60 km and at times of 6-7 s. On our records here we can sometimes observe groups of synphase oscillations, but they are only traced briefly and cannot be considered as typical of continental crust.

Deep Section for a Starting Model

Using the common approaches to interpretation we prepared a deep section as a starting model. The data of reversed profiles were used as a base. The values of t_o and V_b were obtained graphically by means of the 'Differences of time-distance curves (t_o)' method (Seismic prospecting..., 1966). Breaks and delays in the time-distance curves implied the presence of low velocity layers; therefore we used average velocities. We prepared the cross sections by considering all variations of velocities related to the segments of the profile. Fig. 12.4 demonstrates t_o lines, V_b and $\bar{V}$ values and the section for the starting model.

The peculiarities and reliability of the positioning of a boundary depend upon experimental conditions and they are not identical for different parts of the section. Within depths ranging from 2 to 15 km the waves are linked according to systems and are observed clearly against the background noise. For the upper 1-2 km our data are quite schematic due to the large OBS spacing. For depths between 15 and 20 km the data are less reliable due to the small amplitude of the waves being comparable with that of the background noise and insufficient for tracing of deep waves along large portions of the profile.

Velocity Model Resulting from the Modeling

We prepared a starting model in order to solve the direct 2-D problem for the seismic section by means of the classical refraction method. It was an informal but important part of the interpretation process that significantly influenced our final results. Under those conditions when the wave field is complicated and the crust ('среда' or 'media' in Russian, implying some sort of a volume, with all of its particularities) is also complicated with inhomogeneous layering, the known part of the section that was covered by seismic rays from reversed profiles only occupies a small portion of the whole plane of the sections.

We had to make extra assumptions to convert the wave information into a section if it was not adequately covered by the time-distance curves. In order to fill the gaps in the plane of the section with values for the velocity function, we have to advance arguments which are not formally supported by the real wave field properties. This is why the starting model, and the model as corrected by fitting to a certain crustal type, cannot be considered as the final and irrevocable version of the crustal structure. Schematic and rough models are simpler to apply, but much information about the characteristics of the crust which are important for geological interpretation can be lost. There are several possible model versions that more or less reflect the properties of the seismic wave field.

The initial sections for a crust were discussed above, and they were prepared by means of the 'Differences of time-distance curves (t_o)' method. These sections were applied to the starting models and checked by the SEIS-83 program which is designed to calculate the wave field by ray approximation (Cerveny and Psencik, 1983). Calculated times of wave arrivals were applied to the observed records and were accompanied by ray diagrams (**Figs. 12.8-9.12**).

The SEIS-83 program was designed to interactively model the media for DSS refraction data. This allowed one to quickly and effectively choose the 2-D velocity section for a crust which fits the observed data. The first steps in the calculation show a significant disagreement of the starting model with the observed data. The velocity section was prepared as a result of a lengthy fitting procedure (**Figs. 12.13 and 12.14**).

The first sediment layer below the sea floor has a velocity of 1.8-2.0 km/s in the southern Levantine Basin on the southwestern part of the profile at a depth of 1.5 km, and a velocity of 3.0 km/s on the top of Eratosthenes Seamount at a depth of 800 m, where its thickness is 1 km. The parameters for this layer were determined separately for every OBS unit (multiple systems of OBSs are absent), under the assumption that there is a continuous lateral variation in velocity between the OBSs. Multiple waves in this layer are clearly seen on records as strong second arrivals which parallel the first arrivals. The time delay is 1 s for OBSs 915, 914, and 913 (**Fig. 12.15**).

The second sediment layer, with velocities of 3.5-4.2 km/s, is about 1 km thick in the southern part of the Levantine Basin. Then it disappears near the foot of the seamount, is nonexistent below the top of the seamount, and is seen again on its northeastern slope. Multiple waves in this layer are delayed by 0.5 s relative to the first waves, and they are visible on the OBS 914l branch.

The third layer has a complex structure. It is very thick in the southern portion of the profile (up to 14 km). The velocities vary from 4.4 to 5.1 km/s, which gives some indication of its composition. The velocity rises abruptly up to 5.7 km/s near the southwestern foot of Eratosthenes Seamount, which shows a transition in the layer toward crystalline rocks. Such rocks are observed below the entire slope over a length of 30 km. The velocity drops to 4.7 km/s near the top of the seamount (again indicating sediments). Some gaps in the wave tracing and time delays are interpreted as low velocity layers. The value of the velocity in the low velocity layer and its thickness are controlled by the position of the initial point of arrival of the wave from the bedded layer (**Fig. 12.16**).

The thicknesses of the high velocity interlayers below the seamount were calculated using two types of waves: refracted waves, passing along the upper part of the layer, and reflected waves, from the bottom of the interlayer. The limited observation range of the refracted waves and the small vertical velocity gradient (almost straight reversed and overlapping time-distance curves) indicate a small thickness for the high velocity (5.5 km/s) interlayer at a depth of 6 km below the seamount crest (according to data for the pairings of OBSs 912-911 and OBSs 910-911). In addition, the

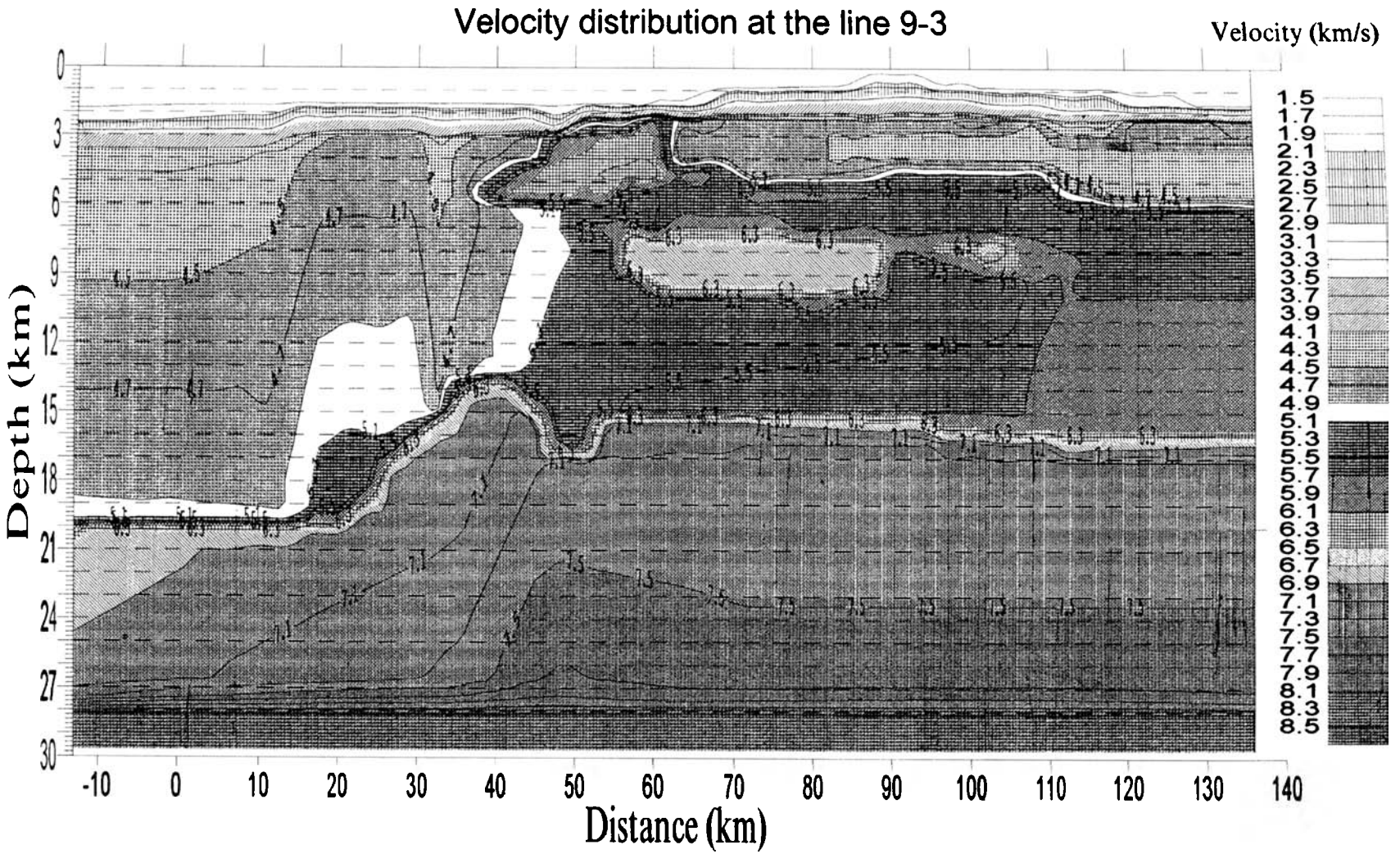


Fig. 12.13. Deep seismic section in velocity contour lines, plotted by the methods of fitting and mathematical modeling using refraction data from the profile shot across Eratosthenes Seamount. The most reliable data were obtained for the depth interval of 3-15 km, data on the M discontinuity are given after (Makris et al., 1983). Key: (1) P-phase velocity distribution on Profile 9-3; (2) Depth, km; (3) Distance from OBS 915, km; (4) P-wave velocity, km/s.

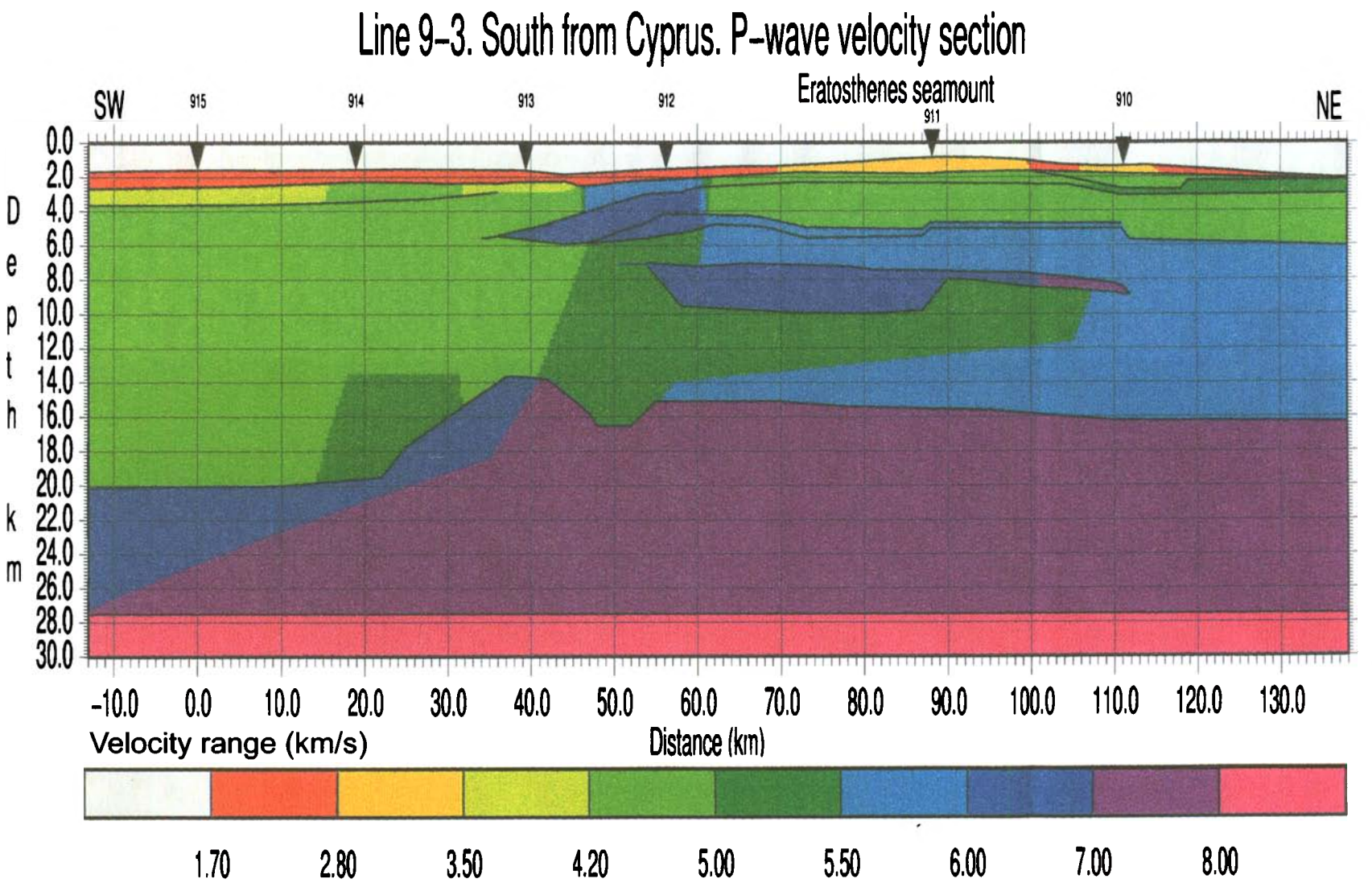


Fig. 12.14. Velocity depth model in color.

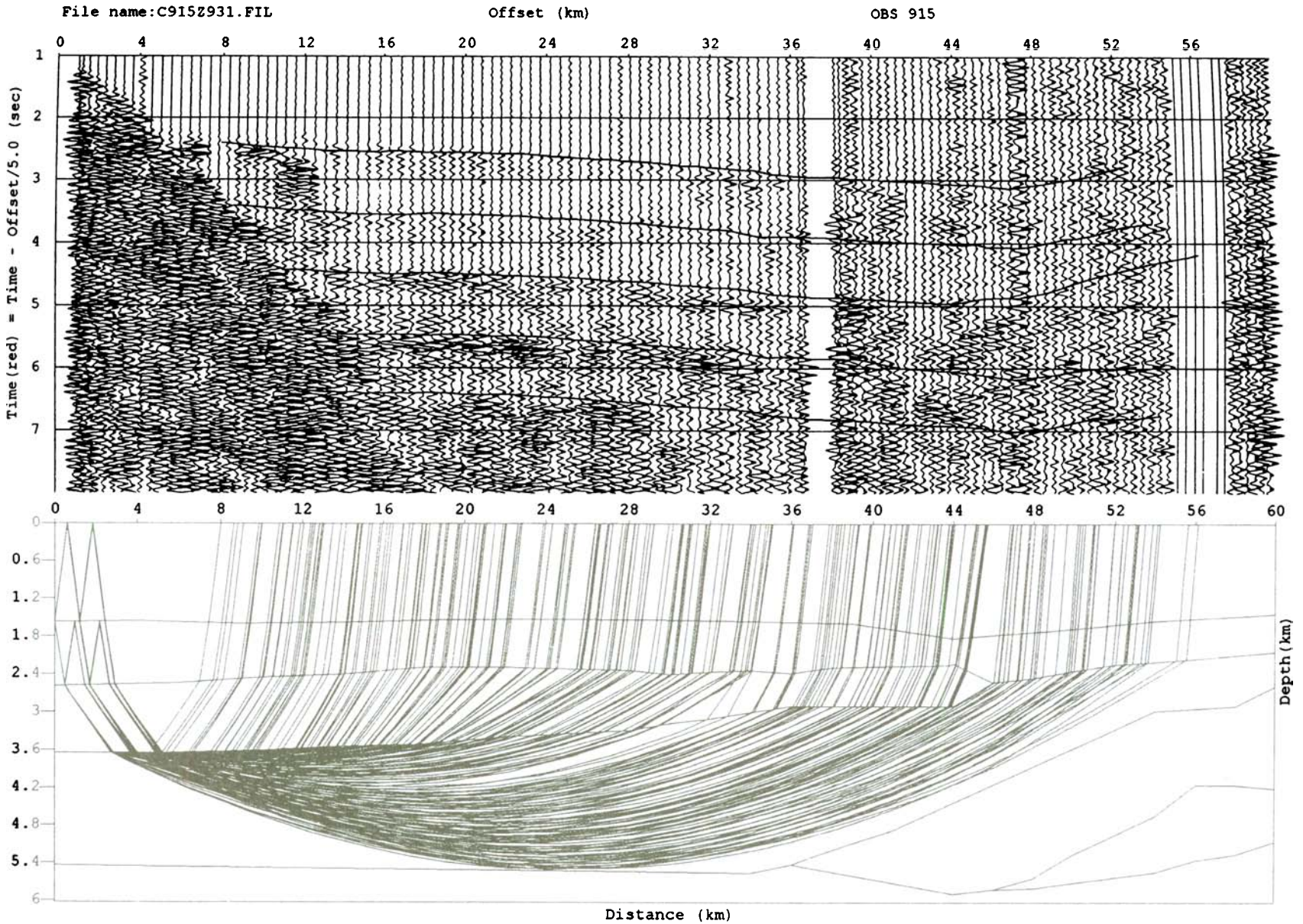


Fig. 12.15. Evidence of water and sediment multiples for OBS 915. Calculated travel times were superimposed over the recorded section. The first arrivals are refracted waves in layer S4 under sediments, the second arrivals with 0.5 s delay are multiple in layer S2 (the first sediment layer with P velocity about 1.9 km/s). The arrivals #3 with 1 s delay are water multiples to the first arrivals and arrivals S4 are water multiples to the arrivals S2. Note the good agreement between the calculated travel times and the observed data section.

reflections from the bottom of the interlayer arrive simultaneously with refracted waves from its topside. This also confirms the small thickness of the interlayers. The only exception is a deep-seated high velocity interlayer with velocity 6.6 km/s observed at PK 57 to PK 88 km. The thickness of this interlayer is up to 3 km. A good reflection from its base is seen on the OBS 911 records.

A crystalline basement surface (velocity 6.9-7.1 km/s) occurs deep in the Southern Levantine Basin (19 km). It rises quickly near the southwestern foot of Eratosthenes Seamount and then is buried almost horizontally at the depth of 15 km. The velocity values and the behavior of the boundaries are well controlled by the data of OBSs 915, 913 and 911.

The depth of the Moho M surface was taken as 27.5 km from the published section of Makris et al. (1983) on the Israel-Cyprus refraction profile. The modeling shows that the M position does not contradict our data. This fact explains why we do not see M phases at distances of up to 110-120 km. Only two events can be identified with M phases. They might be 4 s arrivals on the OBS 9111 records at distances of 80-90 km, and very weak 2.8-3.0 s arrivals on OBS 915 at distances of 107-117 km.

DISCUSSION OF THE RESULTS

The eastern Mediterranean is a complex assemblage of geologic structures concentrated in the area of contact between the African and the Eurasian plates. The Phoenician and Levantine Basins of the Mediterranean Sea are filled with a very thick 10-12 km pile of sediments (Malovitsky, Emelyanov et al., 1975; Ben-Avraham et al., 1976; Lort, 1977; Woodside, 1977; Malovitsky, 1978; Makris and Stobbe, 1984; Tanner and Williams, 1984; Sage and Letouzey, 1990; Krasheninnikov et al., 1994 and others). They resemble the basins of the landlocked Black and Caspian seas. The southern part of the Levantine Sea is a continuation of the African platform. To the south and west of Cyprus the Cyprean Arc represents the convergence front between the African and Eurasian plates. Eratosthenes Seamount stands near the outer edge of the Cyprean Arc. The seamount is surrounded by foredeeps and differs in morphology from the adjacent area of the Phoenician Sea and from the other seamounts and islands.

Most aspects of the nature of the earth's crust under, and the relationships between the large morphostructures of the eastern Mediterranean Sea are still a matter of heated debate among geologists (*i.e.* continental or oceanic crust?) (Malovitsky et al., 1982; Makris et al., 1983; Hirsch et al., 1995). This can largely be attributed to the fact that the eastern part of the Mediterranean Sea was studied by geophysical methods at a later time than many other regions, and that there is insufficient factual data.

The results of investigations carried out 5-15 years ago have only recently begun to be published (Emeis, Robertson and Richter, 1995; Hall, Udintsev. and Odinokov, 1994; and this volume). Hopefully, our knowledge of the tectonics of the eastern Mediterranean will be improved significantly in the near future, closing the gap between the data of the well known surrounding lands and the poorly known seas. Some results have already been published (Ben-Avraham et al., 1998; Hall, Aksu and Calon, 1998; Kopf et al., 1998).

Eratosthenes Seamount is among the key structures of the region. It has long attracted the attention of geologists and geophysicists. There is a fairly extensive literature which represents individual efforts at collecting and generalizing the various experimental data (Ben-Avraham, Shoham and Ginzburg, 1976; Ben-Avraham et al., 1998; Tanner and Williams, 1984; Woodside, 1977). Following publication of the paper by Makris et al. (1983), the popular view was that Eratosthenes Seamount had a continental crust.

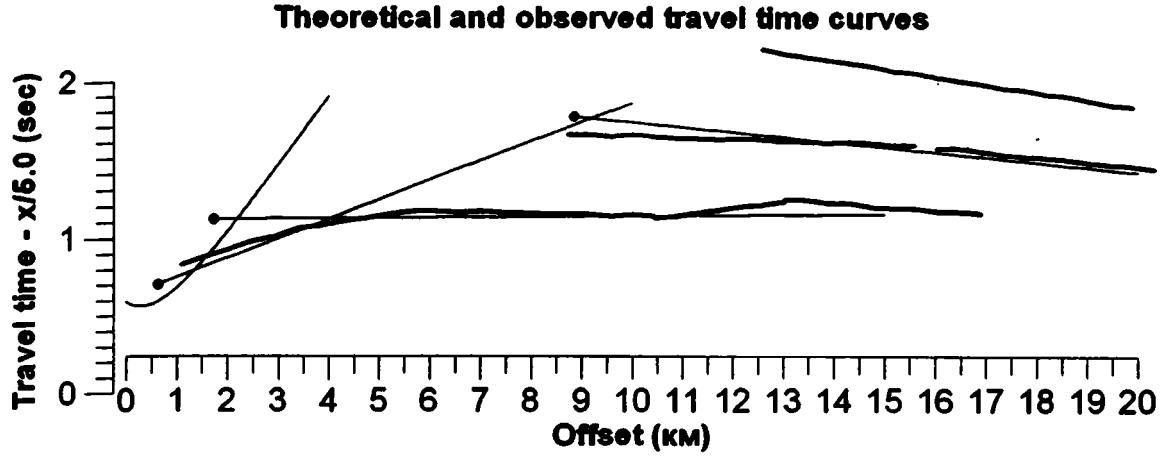
Russian geoscientists have made a considerable contribution to the study of the Mediterranean Sea. The papers and books published by Ya. P. Malovitsky and his coauthors (Malovitsky, 1978; Malovitsky et al., 1982; Moskalenko, 1974) described their investigations in the 1960s and 1970s. Some years ago a new tectonic map of the Mediterranean was published (Bogdanov et al., 1994), which is reproduced in the accompanying plates. In 1987-1991 various geological and geophysical investigations were performed in Cyprus and in the adjacent seas in the framework of the Tethys Project (Zverev et al., 1993; Krasheninnikov and Hall, 1994). Although the seismic interpretation process has taken a very long time, it is at long last bearing fruits (*e.g.* Zverev and Ilinsky,1998, 2000; this chapter).

Deep Geologic Section from Seismic Refraction Data

The deep structure of Eratosthenes Seamount is markedly different from the structure of the adjacent areas. The OBS 915, 914, 913, and 912 records, shown in Fig. 12.3 and Fig. 12.5, illustrate a change in the structure at the transition from the relatively level seafloor to the southwestern slope of the seamount. In the OBS 915-913 segment, the rock sequence is characterized by a gradual increase in velocity with depth, the upper 10 km of rocks having velocities lower than 4.6 km/s. Refracted waves with higher velocities (6.0 and later 6.5 and 7.0 km/s) arrive at this transition to the seamount (OBS 912). Breaks and delays in the travel time curves appear, indicating the alternation of layers with higher and lower velocities. The change in the section type is fairly abrupt and is confined to the axis of the piedmont depression, where a deep crustal fault seems to be located. The fact that layers of higher velocity were restricted to certain segments of the profile gives evidence as to the lateral variation of the rocks.

The depth section was plotted using the conventional method of refraction travel time curves and refined further using mathematical modeling. The seismic section in the form of a velocity distribution with depth is presented in Fig. 12.13, and in a schematic form, along with other data, in **Fig. 12.17** and **Fig. 12.18**.

The experimental conditions (the relative distances between the OBS locations and the shot points, the total lengths of the OBS arrays and shooting lines, and the characteristics of the wave field) required a different level of accuracy for plotting the various parts of the section. The best studied depth interval was from 2 to15 km. The sediments at depths less than 2 km were incompletely studied, mainly around the OBS sites. The waves



Model

# of layer	1	2	3	4	5
P-wave velocity (km/s)	1.52	3.10	4.94	4.425	5.925
layer thickness (km)	1.10	0.85	0.70	2.400	

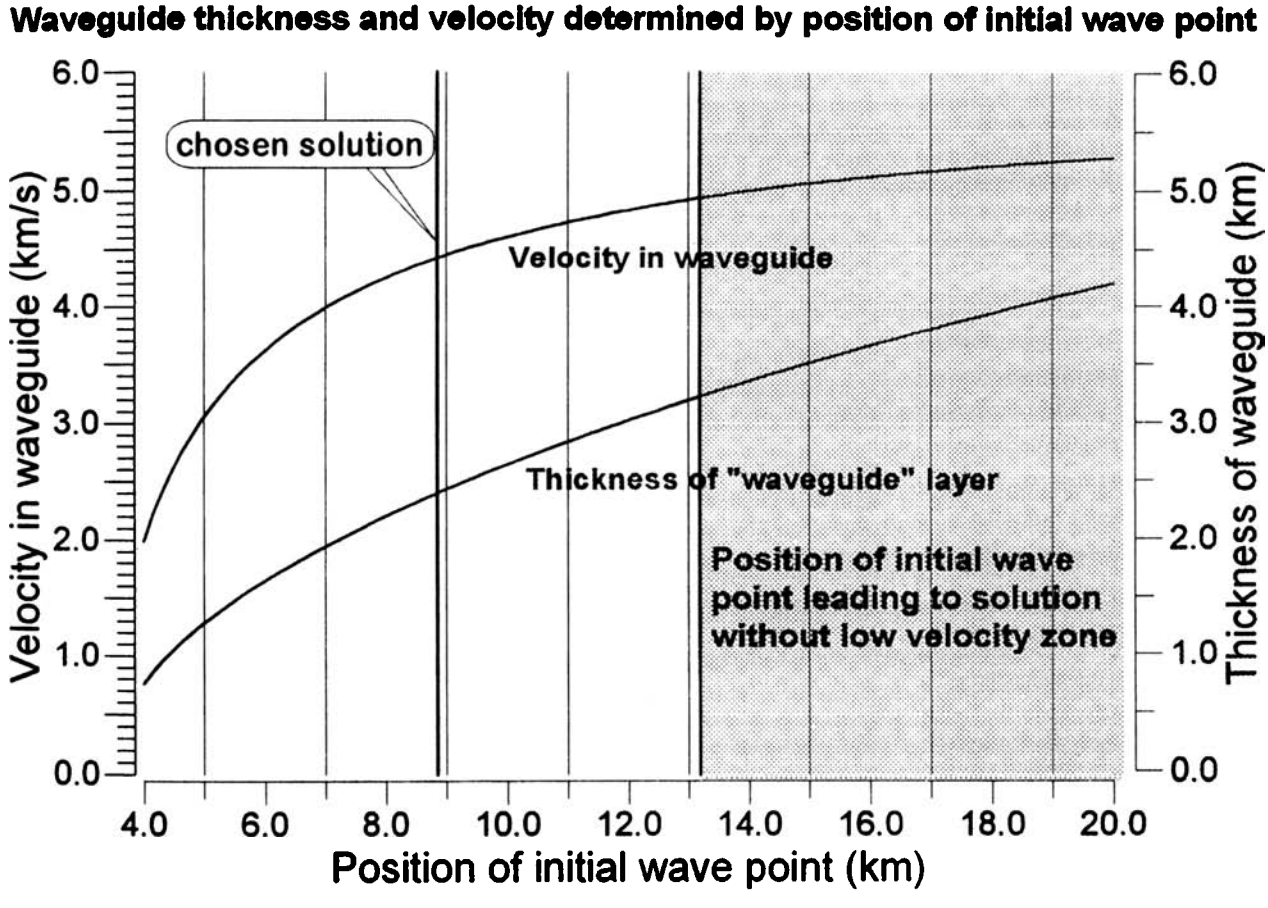
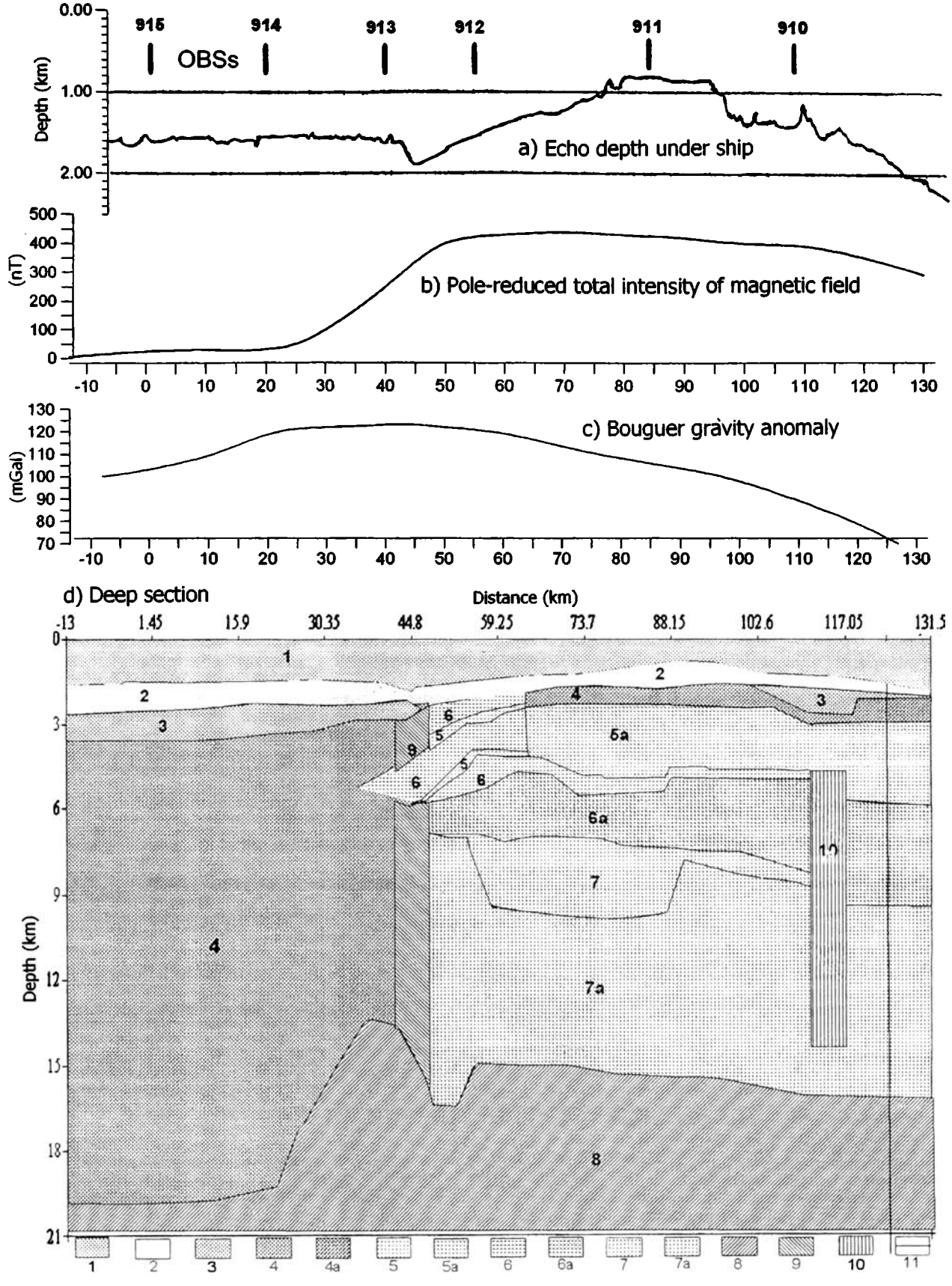


Fig. 12.16. Evidence of the low-velocity layer and determination of its thickness and velocity based on refraction wave initial point location in the layer # 5 (Figs. 12.13 and 12.14 with final model). Theoretical and measured travel times curves with the velocity model are shown at the upper section. Thick solid lines mark travel times for OBS 911 in the northeastern direction. Thin lines represent calculated travel times for the model located below. The small black circles mark the calculated initial points of the refracted waves. Lower section show the curves of waveguide velocity and thickness versus initial wave point position (for layer #5). Initial refraction wave point for layer #5 moves along the travel times curves for this layer. Solid vertical lines mark the chosen solution for parameters of the waveguide. Note the good agreement between the calculated and observed travel times.


915
914
913
912
911
910
OBSs
Depth (km)
a) Echo depth under ship
(nT)
b) Pole-reduced total intensity of magnetic field
(mGal)
c) Bouguer gravity anomaly
d) Deep section
Distance (km)
Depth (km)
1
2
3
4
4a
5
5a
6
6a
7
7a
8
9
10
11

refracted from deep interfaces turned out to be sufficiently weak so that the sections plotted for depths greater than 15 km were less reliable. In the intervals of alternating layers with higher and lower velocities, the velocity at and the depth to the top of the higher velocity layer were the more reliable. These parameters were only approximately determined in those rock sequences with relatively lower velocities.

In terms of the upper crustal structure the profile can be subdivided into three segments. The southwestern segment, adjoining the southern Levantine Basin, is characterized by the presence of a layer of unconsolidated sediments, labeled S2, with a thickness of 1.0-1.5 km and a velocity of ~2.0 km/s. This is underlain by a 1-km thick layer of Messinian evaporates, labeled S3, with a velocity of ~3.5 km/s. Below follows a thick (~10 km) sequence of rocks apparently of sedimentary origin, with a velocity of ~4.5 km/s (layer S4). The underlying boundary is nearly horizontal, and lies at depths of 17-18 km with a velocity of ~7 km/s.

The next, and middle segment of the profile, covers the southwest slope and top of Eratosthenes Seamount. The seismic section changes considerably starting from the nearly rectangular seafloor depression at the base of the seamount. The upper boundaries of the high velocity layers, equal to those of the basement (5.8 to 6.6 and 7.0 km/s), appear under a thin layer of unconsolidated sediments. The layers below this boundary rise toward the top of the seamount. The upper two layers, K1 and K2, pinch out within the slope and are overlain by a flat layer of sediments with velocities of 4.5-4.8 km/s. The lower layers, K3 and K4, grow flatter and are almost parallel to the seamount topography. This structure, close to being horizontally layered, was recorded over a length of almost 40 km.

The wedging out of the high-velocity layers is accompanied by changes in the seafloor topography, which can be seen in the bathymetric map and in the echo-sounding profile (Figs. 12.1 and 12.17). The disappearance of the K1 and K2 layers is accompanied by slope scarps, and the wedging out of layer K3 takes place on the northern cliff of the summit of the seamount. These topographic features have intricate outlines in plan and their trends are usually directed at oblique angles to the seismic profile (Fig. 12.1). K5, the lower boundary in the crust, rises toward the seamount base to depths of less than 15 km and plunges gently, after some undulations, northward to depths of 16-17 km.

An important feature of the seismic section in this segment is the occurrence of low-velocity layers under the seismic boundaries. This affects all of the mapped boundaries which have the velocities of sedimentary and crystalline rocks. The occurrence of low-velocity layers in the seismic section of the seamount might have been caused by various factors. As far as the sedimentary sandy-clayey or carbonate rocks are concerned, this might have been associated with differences in the degree of rock compaction, changes in the facies composition, the occurrence of individual layers in the sequence, or with some other factors. Low-velocity layers were reported (Finetti and Morelli, 1973; Montadert, Letouzey and Mauffret, 1978) from the Messinian Formation of the Mediterranean Sea.

As regards the crystalline rocks with seismic velocities characteristic of the basement, relative velocity decreases can be attributed to serpentinization, as well as to crumpling, crushing, and other processes of dynamic metamorphism. Another group of factors might be the effects of contact metamorphism, *i.e.* by the heating and transformation of rocks during the emplacement of intrusive bodies. It cannot be ruled out that decreases in velocity might have been caused by various processes associated with weathering. Velocity variations in the volcanic rocks can be explained by differences in their facies, varying from dense basalts to loose tuffs. Eventually, the presence of low-velocity layers is indicative of some peculiar events during the geologic history of the southwestern slope and top of the seamount, which are different from the conditions prevailing in the adjacent areas.

The third, seismically different segment of the profile, was located on the northern slope and base of the seamount and on their continuations toward the Cyprean Arc. Here the sedimentary sequence includes layers inclined away from the seamount top, where folds were recorded. There is no low-velocity layer at the base of the sedimentary sequence. The K3 basement layer wedges out, and the boundary velocities in the underlying K4 layer are found to be much lowered (7.0 to 6.6 and even down to 6.1 km/s). Changes in the velocity structure were found to be especially great toward the zone of folded deformations at the front of the Cyprean Arc, located beyond the discussed segment of the seismic line.

The zones marked by changes in the seismic section types, as considered above, occupy short lengths (a few kilometers) of the profile. They are accompanied by linear elements in the seafloor topography, and by changes in the velocity structure which extend to great depth. For these reasons they can be interpreted as deep faults. We located three major fault zones: at the southwestern base of the seamount, at the northern edge of its flat top, and in



Fig. 12.17. Possible geological cross-section across Eratosthenes Seamount with magnetic, gravity and sea bottom curves along this line. Legend to geological section: (1) Water (V_p = 1.5 km/s); (2) Upper unconsolidated marine sediments (Vp=1.9-2.0 km/s); (3) evaporite sediments (Vp=3.3 km/s); (4) consolidated sediments (Vp=4.4-5.1 km/s); (4a) the same with thin low velocity layers; (5) volcanic sediment layers (Vp = 5.3-5.6 km/s); (5a) the same with thin low velocity layers; (6) lava layers (Vp = 5.8-6.7 km/s); (6a) the same with thin low velocity layers; (7) magmatic basic rocks (Vp=7.0-7.1 km/s); (7a)- the same with thin low velocity layers;)8) lower crust (Vp = 7.2-7.7 km/s); (9) faults around Eratosthenes Seamount; (10) faults inside the Eratosthenes block; (11) northeastern boundary of reliable seismic reconstruction of the velocity model. Key: (1) (a) echosounder curve; (2) depth, km; (3) (b) magnetic intensity corrected for the pole; (4) magnetic intensity, nT; (5) (c) Bouguer gravity anomaly; (6) Bouguer anomaly, mgal; (7) (d) geological section; (8) distance, km; (9) depth, km.

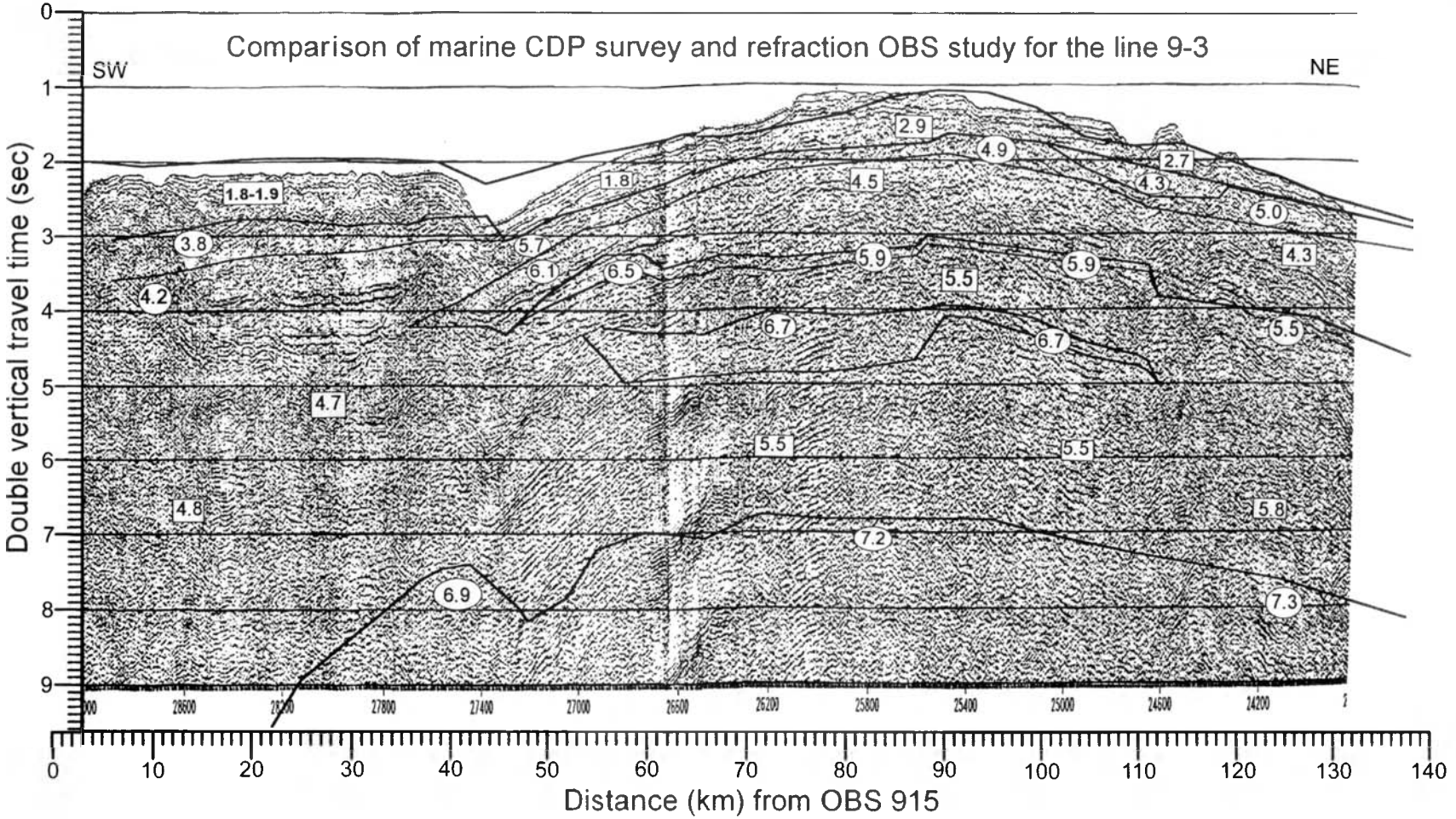


Fig. 12.18. Comparison of the marine CDP survey and the refraction OBS study of Eratosthenes Seamount. The background is the final CDP stack obtained from D. Klaeschen and I. Belykh (Geological structure..., 1994). The thick black lines are boundaries from velocity model (Fig. 12.13) recalculated to the double vertical travel times. Digits in the circles are the value of P-phase velocity (km/s) under the marked boundaries. Digits in rectangles show average layer P-phase velocity (km/s). The southwestern part of the refraction line was about 20 km to the south of the CDP line, so the seafloor profiles do not coincide with one another over this part of the profile. The crossing point of the CDP and refraction lines is located at the northeastern part of Eratosthenes Seamount. Note that: (1) there is good agreement between the CDP reflectors and the three upper refraction model boundaries for this part; (2) the CDP section is affected by strong interference from multiples, especially between the 2700 and 2620 CDP bins, which is produced by uplifting of the high velocity layer. Multiple noise was not completely removed from the CDP section and thus the profile is less reliable; (3) the limited depth penetration of CDP study (less then 5 sec) as compared with the refraction results.

the area of folded deformations. Each of these zones has its own characteristic features.

In the first zone, restricted to the seafloor depression at the base of the seamount, a 5-8 km segment of the profile is marked by a change from a low-velocity sedimentary sequence, more than 10 km thick, to the high-velocity layers of crystalline rock, rising toward the top and overlain unconformably by sedimentary layers.

The second zone on the northern edge of the top of the seamount is marked by notable displacements in the seafloor topography and in the offsets of the seismic boundaries. These displacements are accompanied by: the wedging out of the K4 layer, the gradual disappearance of the low-velocity zones under the sedimentary and crystalline rocks, the beginning of a decrease in the boundary velocity, inclination of the boundary away from the top, and by the inability to trace a deep boundary with a velocity of 7 km/s.

The third fault zone, at the front of the Cyprean Arc, is marked by a drastic change in the properties of the sequence to a depth of at least 10 km, and by the replacement of the rocks by loose sediments with low velocities.

Structure of Sediments and Basement from Reflection Data

The Mediterranean Sea has been covered by a fairly dense network of seismic reflection profiles. The eastern Mediterranean Sea south and east of Cyprus was surveyed by reflection shooting later than the western and central parts of the sea. Apart from investigations by research institutions and universities, much seismic reflection work was done by oil companies which sometimes allowed the results to be used for scientific purposes (Finetti and Morelli, 1973; Hall, Aksu and Calon, 1998; Kopf et al., 1998; Montadert, Letouzey and Mauffret, 1978).

Here we will briefly review the available evidence for the sediments in the Eratosthenes area. High-resolution reflection work by continuous seismic profiling (CSP) showed (Krasheninnikov et al., 1994; Udintsev et al., 1994) that the typical reflections from the Late Miocene evaporites, observed almost everywhere around this seamount, were not recorded on its slopes or top. The cover of young loose sediments is thin on the steep upper slopes (a few dozens of meters) and is as thick as 50-70 m on the more gentle lower slopes. The thickness of loose sediments is also small on the top. Here, they cover the eroded surface of the acoustic basement. Both the basement and the sediments are cut by normal faults. The loose sediments are as thick as 100-150 m in the depression surrounding the base of Eratosthenes Seamount. They are thicker (200 m) in the Levantine Basin and attain a thickness of 300 m and more in the depressions west and north of Eratosthenes Seamount.

The deeper part of the section was studied using multichannel common depth point (CDP) methods. The seamount was intersected by two CDP profiles during Cruise 5 of the R/V 'Akademik Nikolaj Strakhov' (Kogan and Stenin, 1994). Profile 10b crossed the seamount along a line close to our refraction profile, and Profile 8a was shot along a roughly N-S line across the top of the seamount. Preliminary time sections were studied by Kogan and Stenin (1994), and the first results of the digital processing of these data, obtained by D. Klaeschen and I. Belykh at GEOMAR, were reported in a 'Note added in proof' and reproduced (*op. cit.*, p. 112, and Plate 4). Both profiles revealed a similar geological structure. The nearly rectangular seafloor depression separates quite different areas and is complicated by a complex (fault?) zone. The southern slope of the seamount has bedding parallel to the slope (PR 10c) or slightly steeper. Bedding is less distinct under the flat top than on the slopes, the boundaries being almost horizontal. Beginning from the northern edge of the flat top the bedding is more distinct, the boundaries are inclined away from the top (northward) and dip steeper than the slope of the seamount. Differences in the structure along the SW and SSE directions on the southern slope of the seamount are expressed in the 0.3-0.5 s differences in the arrival times of stable reflections (from the basement?). Accordingly, the thickness of the sediments was found to be 30% smaller on the southern slope than on the southwestern.

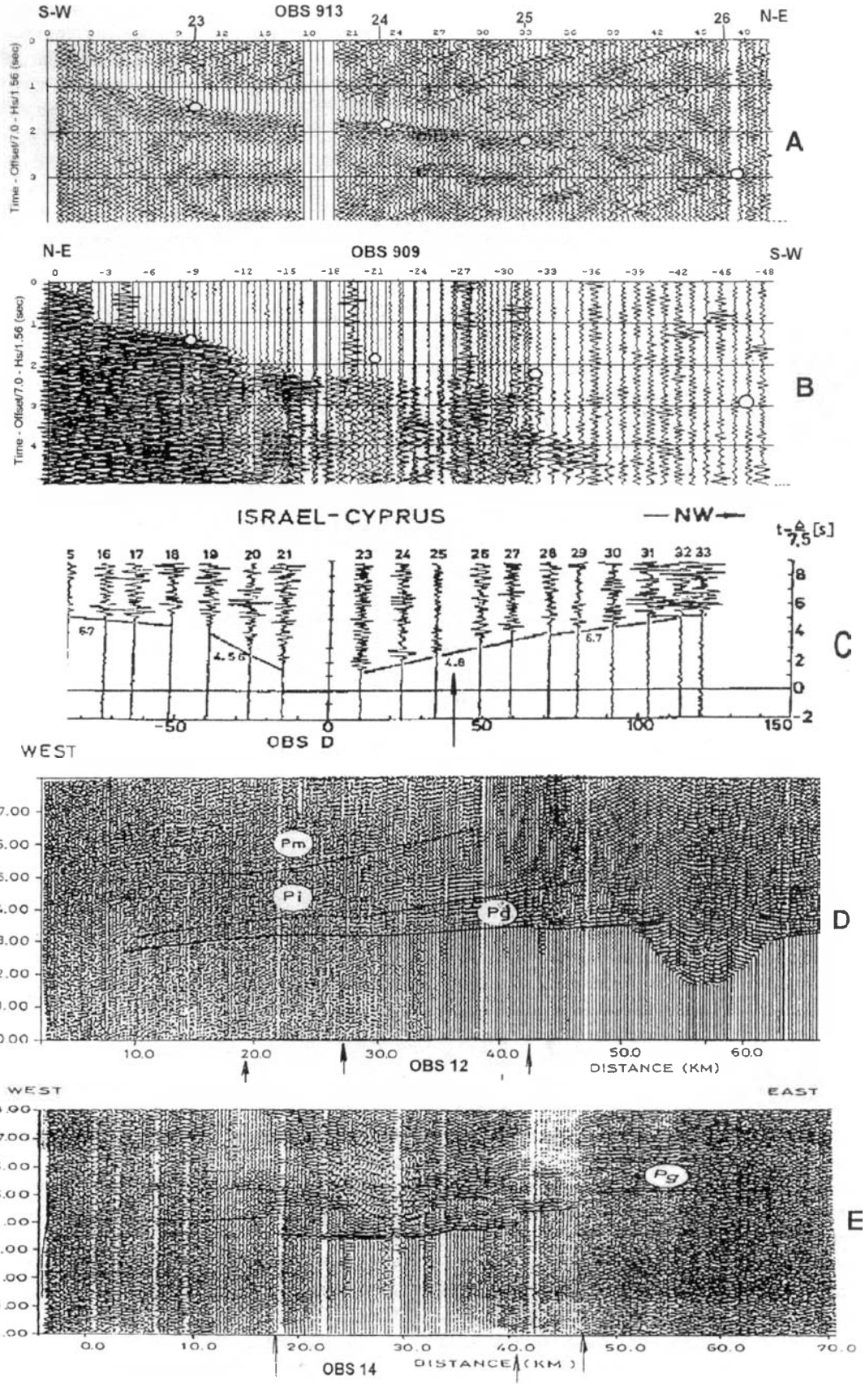
The results of the CDP profiling are suitable for comparison with the refraction data because the DSS refraction and CDP profile lines are nearly coincident (Fig. 12.1). A comparison was done and discussed in the paper of Zverev and Ilinsky (1998). The final refraction section, derived after 2-D modeling (Fig. 12.13), was transformed into times of vertical reflections and superimposed on the CDP section (**Fig. 12.19**). The modeling of the refraction section was done for the entire sequence of the section, including the water layer. Some discrepancy in the seafloor topography in the left-hand part of the section was caused by the non-coincidence of the profiles lines there.

The refraction and CDP data showed a good correlation for the upper part of the section. Below, under the top of the seamount, the CDP data did not show distinct boundaries, whereas the refraction data revealed an obvious layering. Good refractors were recorded at times of 4-5 s and 7-8 s, where the CDP data were unreliable. The CDP section often showed many details which were smoothed on the refraction section. Naturally, the data on refractor and layer velocities plotted on the refraction section were not expressed on the CDP section. The refraction records and section showed a change in the sequence at the southern foot of the seamount. The site of this change was located via the refraction data to an accuracy of a few kilometers (Figs. 12.6 and 12.13). The CDP shooting yielded an obscure, complex (diffraction?) zone more than 10 km wide on this segment of the profile.

To sum up, the CDP shooting yielded comprehensive information only for the upper 2-3 km of the sequence. The refraction method has a greater depth of investigation compared with the CDP method, providing data on velocities at the boundaries and inside the layers, which is important for understanding the nature of the deep layers, and specifying particular features of the fault zones.

Comparison of the DSS with the Israel-Cyprus and Israel-Eratosthenes Profiles and Elements of the Eratosthenes 3-D Structure

A DSS profile was made along an Israel to Cyprus transect in 1978 for the purpose of investigating the crustal structure there


S-W
OBS 913
N-E
23
24
25
26
Time - Offset/7.0 - Hs/1.56 (sec)
A
N-E
OBS 909
S-W
B
ISRAEL-CYPRUS
—NW—
$t=\frac{\Delta}{7.5}$ [s]
5 16 17 18 19 20 21 23 24 25 26 27 28 29 30 31 32 33
6.7
4.56
4.8
6.7
C
OBS D
WEST
Pm
Pi
Pg
T-X/6.0 S
D
OBS 12
DISTANCE (KM)
WEST
EAST
Pg
E
OBS 14
DISTANCE (KM)

(Makris et al., 1983). Explosive charges of 800 kg were used. Seismic waves were recorded by land-based systems located at the ends of the profile and by three OBS units located on the seafloor in between. The distance between the shots was 10 km, and that between the OBS units, 100 km. The travel time curves were as long as 400 km. The layout and procedure of the experiment, as well as the seismic records and the results of their interpretation, were described by Makris et al. (1983).

The profile was shot in a NNW direction across Eratosthenes Seamount. One of the OBS units (D) was located at the base of the southern slope of the seamount near the nearly rectangular seafloor depression in an environment similar to that of our OBS 913 (Fig. 12.1). The intersection point with our profile was in the vicinity of our OBS 911. Seven shots (23-29) were made, spaced 10 km apart, within the seamount area from its SE to NW base. The record section showed distinct first arrivals and sometimes subsequent strong phases (Fig. 12.19c).

We made an attempt to compare the DSS records with our records (Fig. 12.19). The OBS D records from shots 23, 24, and 25 showed the first arrivals of phases P_{K3} and P_{K4} and yielded an apparent velocity V* of about 6 km/s similar to the records of our OBS 913 (Fig. 12.19a). In the case of the next shots, 26 and 27, the first arrivals were delayed approximately 1 s relative to a straight line from the model of Makris et al. (1983, Fig. 4). At the same time it should be noted that the record of our OBS 909 was principally different from that of OBS D (Fig. 12.19b).

The land-based seismic systems located on Cyprus and in Israel at distances of 100-160 km and 270-360 km from Eratosthenes Seamount recorded the first waves from the M discontinuity 1-2 s later for the shots in the seamount area. Larger first-arrival times were recorded by the seismic systems on Cyprus for shot points SP 25, 24, 23, and 21 and for the systems in Israel for SP 27-33 (Figs. 5, 6, 10, and 11 in Makris et al., 1983). Taking into account reverse migration, the profile segment where the first waves were delayed on arrival at the remote observation sites was located between SP 25 and SP 27, that is, north of the high-velocity region on our profile PR 9-3.

This proves that the results of the 1978 DSS experiment agree with our data. On this basis, we presume that the high-velocity layer underlying the sediments in the southwestern part of the seamount, from the base of the slope toward OBS 912 and farther on to OBS 911, continues on to the southeastern slope under OBS D and under shots 23, 24, and 25. The profile segment with lower velocity for the waves from deep boundaries is located in the northern half of Eratosthenes Seamount (Fig. 12.1).

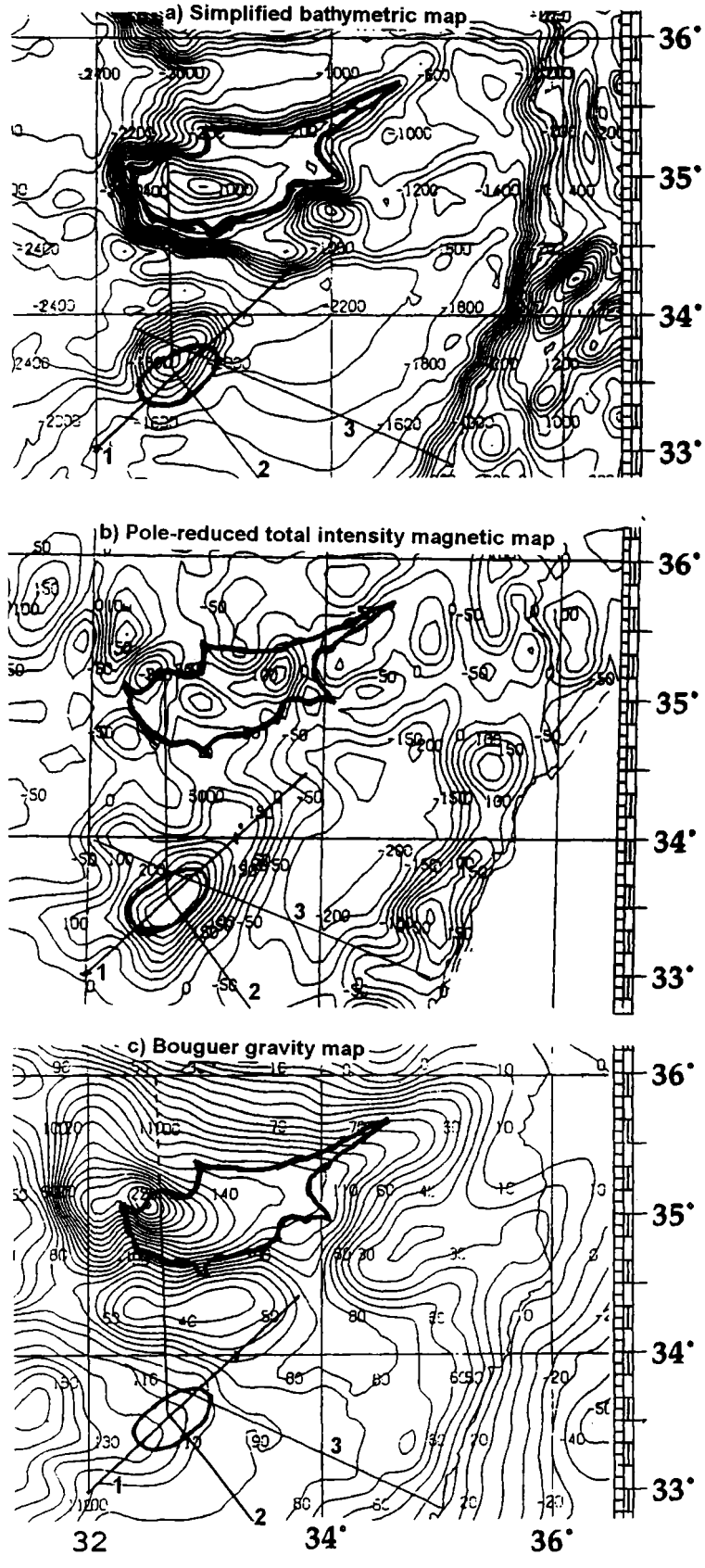
A refraction experiment using OBS units and airguns was performed in 1989 along a roughly W-E profile from Eratosthenes to Israel (Ben-Avraham et al., 1996). The authors of this paper presented the records of three OBS units, two of which were located in the Eratosthenes area: OBS 12 at the eastern base of the seamount, and OBS 14 on its top. The location of OBS 12 was similar to the location of our OBS 913. OBS 14 at the top of the seamount was located west of the profile PR 9-3 at approximately equal distances from OBS 911 and OBS 910. The records of OBS 12 and 14 are presented in Figs. 12.19d and 12.19e. Unfortunately, both of these OBS units were located away from the profile shooting line: OBS 14 at a great distance (the wave from the basement was the first to arrive at the smallest distances); OBS 12 was located at a smaller distance, however the arrival time of the sound wave was notably greater than the time of reflection from the bottom. For this reason we cannot compare the arrival times of the waves, and will thus restrict ourselves to the qualitative comparison of the records.

The first wave that arrived at OBS 14 (Fig. 12.19e) was a wave with V* of ~6 km/s (in a westward direction) and with a slightly lower velocity (in an eastward direction). This wave was recorded only at distances of ±10 km from the point of projection of OBS 14 onto the shooting line. In the west, this wave ceased to be recorded approximately in the middle of the seamount top, and was not recorded further on. In the eastward direction from OBS 14 (toward the slope and basin) the waves were observed with time intervals of 0.5 s and 1 s. In the case of OBS 12 an obvious asymmetry was observed. The travel time curve was continuous, and the V* values were significantly lower than 6 km/s eastward toward the basin. Westward, the V* values were close to 6 km/s in a segment coinciding with the lower part of the seamount's slope. The next wave arrived 0.3 s later and had a V* value greater than 6 km/s. It started to attenuate where the slope changed to the flat top. The next wave was shifted in time by 0.2-0.3 s and disappeared without reaching the middle of the flat top. No distinct arrivals were observed farther westward (Fig. 12.19d). This pattern was similar in many respects to that observed for OBS 913 and OBS 912.

The Eratosthenes slope and top were crossed by the southern end of Profile 1 surveyed by the Schmidt Institute of Physics of the Earth in 1987 by refraction using an OBS unit (108) and a small (15-liter) airgun. The OBS unit was located in the northern part of the seamount's flat top (Fig. 12.1) and yielded an asymmetric wave pattern with high velocities (7.2 km/s) southward and low velocities (<5 km/s) northward. The arrival times for the southern branch coincided exactly with those recorded by our OBS 913 in the northeast E direction.



Fig. 12.19.Comparison of seismic records obtained during different refraction experiments in the Eratosthenes area (Fig. 12.1). (A, B) Comparison of arrival times from explosions to OBS-D (circles on the records and SP numbers 23-26 above them); (C) OBS-D record (Makris et. al., 1983); (D, E) OBS 12 and OBS 14 records on the profile shot in 1989 (Ben-Avraham et al., 1996). Arrows in the C, D, and E records indicate regions with no records or changes of waves with breaks in travel time curves plotted on lines 1, 4, 5 in Fig. 12.1. Key: (1) SW; (2) OBS 913; (3) Distance from OBS, km; (4) NE; (5). T_{red} = T-X/7.0-H water/1.56, s; (6). OBS 909; (7) Israel-Cyprus profile, OBS-D; (8) Shot numbers; (9) NW; (10) W; (11) Israel-Eratosthenes profile, OBS 12; (12) E; (13). T_{red} = T--X/6.0, s; (14) Distance, km; (15) Israel-Eratosthenes profile, OBS 14; A B C D E.


a) Simplified bathymetric map
b) Pole-reduced total intensity magnetic map
c) Bouguer gravity map
36°
35°
34°
33°
32
34°
36°
1
2
3

All the data available were sufficient to visualize the qualitative 3-D structure of the seamount. For this purpose we used the available bathymetric maps to plot the sites where the high-velocity layer had been located under the sediments, the points of sudden changes in the travel time curves, the no-record sites, and the low-velocity regions recorded by remote seismic systems (Fig. 12.1). A high-velocity layer was recorded under the southeastern and southern slopes of the seamount. It begins in the vicinity of the nearly rectangular piedmont seafloor depression and rises toward the seamount's top. In the middle of the slope this layer is occasionally interrupted by interlayers of lower velocity and then again replaced by another high-velocity layer. The underlying sequence is also characterized by the interbedding of low- and high-velocity interlayers. All data points that occur in the region with high-velocity layers were mapped south of the line separating the seamount into two parts. This line coincides with a roughly E-W fault that intersects the flat top and is well expressed in the seafloor topography. The low-velocity region was mapped under that part of the flat top north of the fault. No experimental seismic data are available for the western sector of the seamount.

Of interest in this respect is the character of the seafloor topography on the seamount's slopes south and north of the fault. The bathymetric map and a 3-D model for the seafloor topography (Krasheninnikov and Hall, 1994) show that the southern part of the seamount has an even seafloor relief for the slope, whereas the northern part has a rough, folded topography. This suggests that:

1) the existence of a high-velocity (high-density?) layer under the sediments has favored the preservation of an even seafloor topography;

2) the northern and western limits of the high-velocity layer follow the E-W fault on the top of the seamount and the landward slope of the piedmont seafloor depression, respectively. In this case the region of high-velocity layers under the sediments must be elongated in a NE direction and have a narrower northern end, its southern end being broader (Fig. 12.1).

Although this reconstruction of the 3-D structure of the seamount was based on a set of reliable experimental data, its representation in Fig. 12.1 is merely qualitative and approximate. More exact conclusions can be derived on the basis of other observations that were made, but which have not yet been adequately reported in the literature

Comparison of Refraction Data with Magnetic and Gravity Maps

It has long been known that Eratosthenes Seamount is marked by a significant positive magnetic anomaly. In terms of its size and magnitude, this is the most prominent feature in the magnetic field of the eastern Mediterranean. This peculiarity attracted the attention of investigators from various countries. Different assumptions were proposed as to the possible sources of this anomaly (Ben-Avraham, Shoham and Ginzburg, 1976; Tanner and Williams, 1984; Ben-Avraham et al., 2002).

The map of magnetic anomalies published by Makris et al. (1994) shows that the anomaly is elongated in a NE-SW direction, and that it has a flat top and variously dipping steep slopes. The anomaly is not restricted to the top of the seamount but marks its southeastern slope. For our comparison we used the topographic, magnetic, and gravity maps made at the same scale (Makris et al., 1994; Makris and Wang, 1994) **(Fig. 12.20)**. Apart from the seismic profiles discussed in these papers, Fig. 12.20 shows the position of our profile, and also the zone of high-velocity layers under the sediments. One can see that the contours of the high-velocity zone and of the significant positive magnetic anomalies almost coincide.

Our attempt to correlate the refraction section with the magnetic anomaly was based on the high seismic velocities (as high as 7 km/s) in the basement which were found to be comparatively shallow in the southern part of the seamount. It follows from the map of magnetic anomalies reduced to the pole (Makris et al., 1994) that the positive anomaly in the south of the seamount has an intensity of >400 nT. The anomaly is almost isometric in map view and is surrounded by regions of low magnetic values. Our calculations showed that this anomaly could be explained by the assumption that the seismic layers with velocities ~7 km/s, lying in the depth interval of 7-10 km (K4 in Fig. 12.17d), have a magnetization of 5 A/m. A magnetization of this order is known for oceanic basalt samples raised from deep-sea drilling holes, and also follows from modeling results (Gorodnitsky, 1993, 1995, 1996). The high-velocity layers observed above (under the sediments) do not possess high magnetization. Therefore the high-velocity layers lying under the seamount at depths below 7 km are likely to be basic igneous rocks.

It is worth mentioning that the pattern of the magnetic anomaly under the seamount is substantially different from the anomalies



Fig. 12.20. A high-velocity region in the top of the crust on Eratosthenes Seamount (Fig. 12.1) plotted in the schematic maps of bathymetry (a), total magnetic intensity reduced to the pole (b), and Bouguer gravity anomalies (c). The maps are given after Makris et al. (1994), Makris and Wang (1994). Key: 1. (a) Simplified bathymetric map; (b). Map of magnetic intensity corrected for the pole; (c) Map of Bouguer anomalies. Fig. 12.1. Schematic map of Eratosthenes Seamount. The seamount topography is given after Hall (1980, 1981, 1994). The hatched area on the southeastern side of the seamount defines the high-velocity layer on the seamount. The map also shows the locations of seismic profiles, DSDP holes, and dredging sites (Zverev and Ilinsky, 2000). Legend: (1-2) refraction profiles surveyed by the Institute of Physics of the Earth in 1987-1990 and locations of the OBSs: (1) Profile 9-3, 1990; (2) Profile 1-2, 1987 (Zverev et al., 1993); (3) line of CDP profile shot from R/V 'Akademik Nikolaj Strakhov' in 1987 (Kogan, and Stenin, 1994); (4) refraction profile surveyed by J. Makris et al. in 1978 (Makris et al., 1983): OBS locations are shown by squares, seismic shots by circles with numbers; (5) refraction profile shot by Z. Ben-Avraham and others in 1989, and the location of OBS sites (Ben-Avraham et al., 1996); (6) limits of a high-velocity layer in the top of the crust (on profiles 1, 2, 4, and 5); (7) dredging sites (Mouraviev et al., 1994); (8) crustal fault separating the southern and northern parts of Eratosthenes Seamount; (9) sites of DSDP holes (Emeis et al., 1995); (10) high-velocity region. The inset map shows the map location.

observed above the Troodos ophiolite on Cyprus and above the Baer-Bassit ophiolite in Syria. At the same time there is a magnetic maximum on the coast of Israel near Haifa (Ben-Avraham and Hall, 1977), in an area of Cretaceous basalts, which resembles the maximum above Eratosthenes. The magnetic and gravity anomalies of this area have even been reinterpreted to suggest the existence of a Early Jurassic shield volcano under Mount Carmel (Gvirtzman et al., 1990). No similar maxima were reported for areas of younger basalts (Rybakov et al., 1994). It would be useful to study the land maximum in Israel to possibly gain an understanding of the nature of the maximum above Eratosthenes.

Turning to the map of gravity anomalies, we emphasize that Eratosthenes Seamount has no distinct expression in the Bouguer gravity map. This suggests that the average density of the rocks in the seamount rising above the surrounding seafloor can be close to the density of 2.67 g/cm^3 used to calculate Bouguer anomalies. One can see on the map of Fig. 12.20 that the gravity minimum dominating the area around Eratosthenes is observed between Eratosthenes and Cyprus. It is associated with a deep trough filled with sediments, and a gravity maximum was discovered to the west of the seamount. The effect of the high-velocity zone, recorded under the southern part of the seamount, expresses itself as a local distortion of the gravity contour lines on the eastern slope of this gravity maximum. It is represented by a relative high in the Bouguer gravity curve on the southwestern slope and at the base of the seamount (Fig. 12.17c). Our estimates suggest that this high can be explained by a rise of 13-16 km in the lower crust surface (with velocity of 7 km/s - Fig. 12.17d).

Dredging and Drilling Results

The material raised by dredging during Cruise 5 of R/V 'Akademik Nikolaj Strakhov' generally consisted of Quaternary and Miocene sedimentary rocks, except for two dredges which contained one granite fragment, one basalt fragment (Site 26), and many serpentinite fragments (Site 27) (Krasheninnikov et al., 1994; Mouraviov, Kaleda and Boiko, 1994). These findings were quite unexpected. These authors advanced the suggestion that the granite fragment might have been derived from the crystalline basement in the course of its destruction and faulting. However they did not rule out its accidental nature (p. 128, in Krasheninnikov et al., 1994). The map of Fig. 12.1 shows the location of the dredging sites. In the seismic section they are restricted to the place where the layers with velocities of 5.8-6.2 km/s disappear. There is reason to believe that the dredged rocks were the broken remnants of the upper layer of crystalline rocks. During the dredging operations at Site 31, located on the southern side of a roughly WSW-ESE fault intersecting the top of the seamount, a fragment (35x25 cm) of Cenomanian(?) massive limestone plate was raised from a depth of 1300 m (Krasheninnikov et al., 1994). We believe that these are rocks from the layer with a velocity of ~4.8 km/s, which replaces, near the top of the seamount, a layer with velocities of 5.8-6.2 km/s which is supposedly of crystalline composition.

Within the framework of DSDP Leg 160, drilling was performed in the Eratosthenes area (Emeis, Robertson and Richter, 1995; Robertson et al., 1998). Four holes were drilled along a N-S line passing from the northern edge of Eratosthenes' flat top (Hole 966), to the northern slope of the seamount (Hole 965), to its northern base (Hole 967), and to the southern slope of the Hecataeus Ridge (Hole 968) (Fig. 12.1). The drilling depths ranged between 200 and 500 m below the seafloor. Holes 965-967, drilled in the seamount, encountered a small thickness of Messinian deposits. Also found there were Miocene and Eocene deposits (Holes 966 and 965), as well as Maestrichtian and Santonian limestones as thick as 500 m (Hole 967). A drill core 300 m long raised from Hole 968 consisted of Messinian deposits.

The Upper Cretaceous limestone struck at the bottom of Hole 967 was found to be of nearly the same Upper Cretaceous age as the dredge sample raised at Site 31. Note that at Site 31 Cretaceous limestones were found at a depth of 1300 m below sea level, whereas in Hole 967 they were found at a depth of 2900 m. This indicates that the northern edge of the seamount has been dropped down some 1,600 m by a normal fault (Krasheninnikov et al., 1994).

GEOLOGICAL INTERPRETATION

The majority of investigators consider Eratosthenes Seamount to be a part of the African platform. Sage and Letouzey (1990) offered two possibilities for its genesis. According to the first, the seamount is a sea cape detached from the continent, and according to the second, this is a young structure, which developed as a result of bending of beds at the front of a thrust. Malovitsky et al. (1982) believe that the seamount is a horst belonging to a low velocity layer of the Precambrian African platform. Krasheninnikov et al. (1994) suggest the seamount is the northern rim of the Precambrian African-Arabian platform.

After the seismic refraction survey between Cyprus and Israel (Makris et al., 1983) it was suggested that Eratosthenes Seamount was a part of continental crust extending to Cyprus. This concept is still popular (Ben-Avraham et al., 1998; Hirsch et al., 1995). In fact, instead of a thick sedimentary sequence filling the Levantine Sea, the uplifted layers are characterized by velocities as high as 6 km/s.

Our study confirmed the uplifting of high-velocity rocks and, at the same time, establishes a very complex layering pattern in the upper 15 km of the crustal sequence, *i.e.* layers with velocities as high as 6.2-7.0 km/s alternating with layers of lower velocity.

Generally the possibility of assigning the crust to one major type or another is determined by its particular set of characteristics. However, apart from the major crustal types there are some transitional ones. And each of the basic types includes its own subtypes. Accordingly, six models of the crust are known (Beloussov and Pavlenkova, 1985).

One of the fundamental characteristics of the continental crust is monotonous variation of crustal rock properties and an increase of velocity with depth. Usually stable Pg phases are traceable as first arrivals at distances of > 200 km from the source. The results of our shooting, as well as the records of other investigators (Ben-

Avraham et al., 2000; Makris et al., 1983), indicate that no waves of this type have been recorded on Eratosthenes Seamount; therefore its crust cannot be interpreted as typically continental. The region where high-velocity layers are raised closer to the surface is located in the southern half of the seamount.

Undoubtedly Eratosthenes Seamount is a basement high. However, we believe that it cannot be interpreted as a structure with a typical continental crust that differs from the crust of the adjacent basins, which some investigators consider to be oceanic (Ben-Avraham et al., 2000; Makris et al., 1983).

There are reasons to interpret Eratosthenes Seamount as an ancient long-lived volcanic edifice. The accumulation of volcanic rocks could cause the development of ring faults, the subsidence of the cone, and the formation of a nearly rectangular depression in the seafloor topography. Keeping this in mind, consider the following evidence and possible explanations.

The northern and southern parts of the structure have experienced different geological histories. Lava flows in the southern part produced gently dipping slopes whose geometries are expressed in the modern topography of the seamount. The uppermost lava flow (having a velocity of 5.8 km/s on the PR 9-3 profile) is of minor thickness and thins out at the base of the slope. It was subjected to destruction on the upper part of the slope, where fragments of crystalline rocks have been found. This lava flow ran over the destroyed surface of the older lava flows which consist of stronger rocks with velocities of 6.0-6.2 km/s. The older lava flows are 30 km long and have a total thickness of more than 1.5 km. They flowed over and beneath the ring fault and are traceable under the sediments for another 5 km. Near the flat top of the seamount the loose sediments are underlain by a dense sedimentary layer (4.8 km/s) instead of a volcanic layer (5.8 km/s). This sedimentary layer is underlain by a sequence of low-velocity rocks 2 km thick. We interpret this locality as the summit of the volcano, where the weathered volcanic rocks are covered by marine sediments.

Starting from the ring fault, layers with high velocities (6.5-6.7 and 7.0 km/s) were observed at depth intervals of 5-6 km and 7-9 km under all of the seamount. Rocks with relatively lower velocities underlie these layers. The layers can be interpreted as the upper rims of a magma chamber and/or intrusive bodies which originally served as magma feeders. At greater depths these bodies are made up of highly magnetic basic rocks and produce a positive magnetic anomaly.

The northern part of the seamount is separated from the southern by a fault striking roughly in a WSW-ENE direction. The fault serves as an obstacle for the propagation of seismic waves arriving from different directions. The waves arriving from deep-seated interfaces have lower velocities to the north of the fault. The seafloor topography to the north of the fault differs from that in the south. The slopes of the seamount are dissected by valleys, having scarps and varying in steepness. The seismic boundaries are inclined away from the top. There are folds at the base of the slope.

We believe that this structure was formed as a result of the substantial sagging of the upper crust in the zone bordering the volcanic seamount to the north. It grades from an initial region of recent deformations into the subduction zone which surrounds the Cyprean Arc in the south. The evidence supporting the idea that the sagging process continued north of the seamount is the deep seafloor depression (> 2700 m), filled with 1.5 km of Pliocene-Quaternary sediments, within which the deep DSDP borehole met limestones at a depth 1.3 km greater than on the top of the seamount. Reflection shooting clearly showed that, contrary to the southern part, the northern part of the seamount had not been protected from disintegration of the solid rock. In the course of sagging, the northern segment of the ring depression and slope was destroyed, and part of the old volcanic edifice was buried.

When volcanic activity ceased, the edifice subsided, to be followed by the accumulation of a roughly horizontal sequence of sediments. The sedimentation conditions on the top were different from those in the adjacent basins, *i.e.* there are no Messinian deposits, and the flat-lying compact sediments show velocities of 4.8 km/s instead of the 4.3 km/s seen in the basins.

In concluding this discussion on the possible volcanic origin of Eratosthenes Seamount, it is worthwhile noting some of the latest investigations of underwater volcanoes in the Tyrrhenian Sea (Gorodnitsky, 1993). Despite some similarity in topography, a recent Tyrrhenian seamount shows a more complex pattern of magnetic anomalies that that for Eratosthenes. Besides, the layer of recent sediments covering the volcanic rocks of the young seamounts is very thin.

It should again be mentioned that the map of magnetic anomalies of Israel and the eastern Mediterranean (Rybakov et al., 1994) demonstrates a long magnetic anomaly comparable to that of Eratosthenes. Such an anomaly was mapped in the vicinity of Mount Carmel, an area of Cretaceous volcanic rocks, and suspected of covering an older shield volcano. We believe that a comprehensive comparative study of these two areas may clarify the origin of Eratosthenes Seamount.

Judging by the age of the limestones on the top of the seamount (Upper Cretaceous, probably Cenomanian), it was formed during pre-Cretaceous time. It is difficult to imagine that the ancient volcano could preserve the structural features similar to those of recent volcanoes. Hirsch et al. (1995) advanced the idea that the thick (12 km) sedimentary sequence in the eastern Mediterranean accumulated under platform conditions on the Precambrian basement. Such an idea seems to admit this possibility. It is also logical to propose the alternative that the high-velocity and highly magnetic layers recorded in the interior of Eratosthenes are protrusions and slices and slabs of igneous rock similar to those known to be abundant in the ophiolite belts of Cyprus and Syria.

It is advisable to redefine the deep structure of Eratosthenes on the basis of the various available seismic data. They indicate the existence of deep roots for this structure and provide further grounds for discussing ideas about the magnitude of horizontal movements. These new data that were accumulated for the eastern Mediterranean are sufficient to progress, from hypotheses on the nature and mechanism of tectonic processes, to real models based on knowledge of the geological structure of the land and on

geophysical data relevant to the deep structure at various levels in the crust.

ACKNOWLEDGEMENTS

The seismic refraction investigations on Eratosthenes Seamount were a part of the extensive multidisciplinary Tethys Project. We gratefully acknowledge the support of Prof. L. V. Dmitriev of the Vernadsky Institute of Geochemistry and Analytical Chemistry of the Russian Academy of Sciences, who was the main initiator of the project. He suggested the deep seismic refraction study and invited us to carry it out. We appreciate the help of G. Constantinou, A. Panajotou, and S. Eleftheriou of the Cyprus Geological Survey. Our thanks go to the IPhE team that carried out marine seismic observations with ocean bottom seismographs under the supervision of Dr. N. M. Nardov, and to the airgun crew under the guidance of Dr. Ju. V. Sapsovitch. The scientific teams from the Geological Institute and the Vernadsky Institute of Geochemistry and Analytical Chemistry, as well as the crews of the R/V 'Akademik Boris Petrov' and R/V 'Akademik Nikolaj Strakhov', helped us with marine operations.

The initial interpretation of the seismic refraction data was undertaken at the IPhE under the guidance of Dr. G. A. Yaroshevskaya. We acknowledge the support of Prof. J. Makris from the University of Hamburg, who placed his data and facilities at our disposal, as well as for his productive discussions of the results. Prof. Jeremy Hall from Saint Johns University, Canada, helped us to process the records. Problems of the geological interpretation were discussed with Prof. V. A. Krasheninnikov, Prof. V. G. Kazmin, and Prof. S. A. Silantyev. Only the great efforts of Prof. V. A. Krasheninnikov made this chapter possible. We are grateful to all those mentioned above.

REFERENCES CITED

Beloussov, V. V., and Pavlenkova, N. I., 1985. Types of the Earth's crust. Geotektonika, N 1, p. 3-14. (In Russian).

Ben-Avraham, Z., Shoham, Y., and Ginzburg, A., 1976. Magnetic anomalies in the Eastern Mediterranean and the tectonic setting of the Eratosthenes Seamount. Geophys. J. Roy. Astron. Soc., 45(1), p. 105-123.

Ben-Avraham, Z., Ginzburg, A., Makris, J., and Eppelbaum, L., 2002. Crustal structure of the Levant Basin, eastern Mediterranean. Tectonophysics, 346(1-2), p. 23-43.

Ben-Avraham, Z., and Hall, J. K., 1977. Geophysical survey of Mount Carmel structure and its extension into the Eastern Mediterranean. J. Geophys. Res., 82(5), p. 793-802.

Ben-Avraham, Z., Wdowinski, S., Arvidson, R., and Ekstrom, G., 1998. Segmentation and seismicity of the Cyprean Arc. Nice, Annales Geophysical Supplement, EGS Abstracts, Part 1. p. 304.

Bogdanov, N. A., Koronovskiy, N. V., Lomize, M. G., et al., 1994. Tectonic Map of the Mediterranean Sea, Scale 1:5,000,000. Moscow, PKO Kartografiya, 1 sheet, Explanatory Notes, 78 p. (In Russian).

Cerveny, V., and Psencik, I., 1983. SEIS-83 – numerical modeling of seismic wave fields in two-dimensional laterally varying layered structure by ray tracing method. In: E. R. Engdahl (ed.), Documentation of earthquake algorithms, World Data Center (A) for Solid Earth Geophysics, Report SE-35, p. 36-40.

Emeis, K. -Ch., Robertson, A. H. F., and Richter, C., 1995. Mediterranean Sea: Science Operator Report, DSDP Leg 160, p. 11-20.

Finetti, I., and Morelli, C., 1973. Geophysical exploration of the Mediterranean Sea. Bull. Geophys. Teor. e Appl., 15(60), p. 263-341.

Gamburtsev G. A., Riznitchenko, Ju. V., Berzon, I. S., Epinatieva, A. M., Pasetchnik, I. P., Kosminskaya, I. P., and Karus, E. V., 1952. Correlating method of the refracted waves. Publishing House of the USSR Academy of Sciences, Moscow, 239 p. (In Russian).

Deep seismic sounding on Cyprus Island and adjacent sea areas. 1993. Final report about seismic investigations submitted to the Geological Survey Dept. of Cyprus. Institute of Physics of the Earth, Russian Academy of Sciences, Moscow, 130 p.

Gorodnitsky, A. M., (Ed.), 1993. Magnetic Field of the Ocean. Moscow, Nauka, 304 p. (In Russian).

Gorodnitsky, A. M., (Ed.), 1995. Anomalous Magnetic Field of the World Ocean. CRC Press, Boca Raton,, Ann Arbor, London, Tokyo, 253 p.

Gorodnitsky, A. M., (Ed.), 1996. Origin of magnetic anomalies and oceanic crust structure. Moscow, VNIRO, -- p. (In Russian).

Gurvitch, I. I., 1960. Seismic prospecting. Gostoptechisdat, Moscow, 504 p. (In Russian).

Gvirtzman, G., Klang, A., and Rotstein, Y., 1990. Early Jurassic shield volcano below Mount Carmel: a new interpretation of the magnetic and gravity anomalies and implications for early Jurassic rifting. Isr. J. Earth Sci., 39(2-4), p. 149-159.

Hall, J. K., 1980. Bathymetric Chart of the Southeastern Mediterranean Sea. Geological Survey of Israel, Jerusalem

Hall, J. K., 1981. Bathymetric Chart of the Northeastern Mediterranean Sea. Geological Survey of Israel, Jerusalem.

Hall, J. K., 1994. Bathymetric Chart of the Southeastern and Northeastern Mediterranean Sea. - Geological Survey of Israel, Jerusalem

Hall, J. K., Udintsev, G. B., and Odinokov, Yu. Yu., 1994. The Bottom relief of the Levantine Sea. In: V. A. Krasheninnikov and J. K. Hall (eds.), Geological Structure of the Northeastern Mediterranean, Historical Productions-Hall Ltd., Jerusalem, p. 5-32.

Hall, Jeremy, Aksu, A., and Calon, T., 1998. Neogene tectonics of the Cyprean Arc region. Nice, Annales Geophysical Supplement, EGS Abstracts, Part 1, p. 304.

Hirsch, F., Flexer, A., Rosenfeld, A., and Yellin-Dror, A., 1995. Palinspastic and crustal setting of the Eastern Mediterranean. J. Petrol. Geol., 18(2), p. 149-170.

Kogan, L. I., and Stenin, A. M., 1994. Multichannel MOV-OGT (CDP) seismic profiling during Cruise 5 of NES Akademik N. Strakhov (Preliminary Results). In: V. A. Krasheninnikov and J. K. Hall (eds.), Geological Structure of the Northeastern Mediterranean, Historical Productions-Hall Ltd., Jerusalem, p. 99-112.

Kopf, A., Vidal, N., Klaeschen, D., and von Huene, R., 1998. MCS Profiles in a zone of incipient collision between Africa and Eurasia, Eastern Mediterranean, Nice, Annales Geophysical Supplement. EGS abstracts, Part. 1, p. 304.

Krasheninnikov, V. A., and Hall, J. K., (Eds.), 1994. Geological Structure of the North-Eastern Mediterranean (Cruise 5 of NES 'Akademik Nikolaj Strakhov'). Historical Productions-Hal, Ltd., Jerusalem, 408 p.

Krasheninnikov, V. A., Udintsev, G. B., Mouraviev, V. I., and Hall, J. K., 1994. Geological structure of Eratosthenes Seamount. In: V. A. Krasheninnikov and J. K. Hall (eds.), Geological Structure of the Northeastern Mediterranean, Historical Productions-Hall Ltd., Jerusalem, p. 113-130.

Lort, J. M., 1977. Geophysics of the Mediterranean Sea basins. Chapter 4 in A. E. M. Nairn, W. H. Kanes, and F. G. Stehli (eds.), The Ocean Basins and Margins, Volume 4A, The Eastern Mediterranean, Plenum, New York, p. 151-213.

Loubrieu, B., Satra, C., and Cagna, R., 2001. Morpho-bathymetry of the Mediterranean Ridge and surrounding areas. Acoustic image of the Mediterranean Ridge and surrounding areas. Two sheets, Mercator Projection, at scale 1:1,500,000 at 35°°N, Ifremer, Plouzane.

Makris, J., Ben-Avraham, Z., Behle, A., Ginzburg, A., Giese, P., Steinmetz, L., Whitmarsh, R. B., and Eleftheriou, S., 1983. Seismic refraction profiles

between Cyprus and Israel and their interpretation. Geophys. J. Roy. Astr. Soc., v. 75, p. 575-591.

Makris, J., and Stobbe, C., 1984. Physical properties and state of the crust and upper mantle of the Eastern Mediterranean Sea deduced from geophysical data. Mar. Geol., 55(3-4), p. 347-363.

Makris, J., Wang, J., Odintsov, S. D., and Udintsev, G. B., 1994. The magnetic field of the Eastern Mediterranean Sea. In: V. A. Krasheninnikov and J. K. Hall (eds.), Geological Structure of the Northeastern Mediterranean, Historical Productions-Hall Ltd., Jerusalem, p. 75-85.

Makris, J., and Wang, J., 1994. Bouguer gravity anomalies of the Eastern Mediterranean Sea. In: V. A. Krasheninnikov and J. K. Hall (eds.), Geological Structure of the Northeastern Mediterranean, Historical Productions-Hall Ltd., Jerusalem, p. 87-98.

Malovitsky, Ya. P., 1978. Mediterranean Seafloor Tectonics. Moscow, Nauka. (In Russian).

Malovitsky, Ya. P., Chumakov, I. S., Shimkus, K. M., Esina, L. A., and Moskalenko, V. N., 1982. The earth's crust and the geological history of the Mediterranean Sea. Moscow, Nauka (In Russian).

Malovitsky, Ya. P., Emelyanov, E. M., Kazakov, O. V., Moskalenko, V. N., Osipov, G. V., Shimkus, K. M., and Chumakov, I. S., 1975. Geological structure of the Mediterranean sea floor (based on geological-geophysical data). Mar. Geol., 18(4), p. 231-261.

Moskalenko, V. N., 1974. The structure of the earth's crust in the deep sea basin of the Levantine Sea. Geotektonika, No. 4, p. 58-65 (In Russian).Montadert, L., Letouzey, J., and Mauffret, A., 1978. Messinian Event: seismic evidence. In: Init. Rep. DSDP, v. 42, part. 1, p. 1037-1050.

Mouraviov, V. I., Kaleda, K. G., and Boiko, N. I., 1994. Lithology of Late Quaternary sediments of the Eastern Mediterranean. In: V. A. Krasheninnikov and J. K. Hall (eds.), Geological Structure of the Northeastern Mediterranean, Historical Productions-Hall Ltd., Jerusalem, p. 131-140.

Robertson, A. H. F., Emeis, K. -C., Richter, C., Camerlenghi, A. et al., 1998. Proceedings ODP, Scientific Results, Vol. 160. College Station, TX (Ocean Drilling Program), 817 p.

Seismic prospecting, 1966. Handbook of Geophysics. V.4., Nedra Publ. House, Moscow, 749 p. (In Russian).

Sheriff, R. E., and Geldart, L. P., 1987. Exploration Seismology. V.2. Cambridge University Press. (Translation into Russian). Moscow, 'Mir' Publ. House.

Rybakov, M., Goldshmidt, V., Folkman, Y., Rotstein, Y., Ben-Avraham, Z., and Hall, J. K., 1994. Israel Magnetic Anomaly Map, Scale on 1:500,000. Geological Survey of Israel, Institute for Petroleum Research and Geophysics.

Sage, L., and Letouzey, J., 1990. Convergence of the African and Eurasian Plates in the Eastern Mediterranean. In: J. Letouzey (ed.), Petroleum and Tectonics in Mobile Belts, Paris, p. 49-68.

Tanner, S. J., and Williams, C. A., 1984. A detailed survey near Mount Eratosthenes, Eastern Mediterranean. Mar. Geophys. Res., 6(2), p. 205-222.

Udintsev, G. B., Zverev, A. S., Odinokov, Yu. Yu., Efimov, V. N., Eleftheriou, S., and Hall, J. K., 1994. Structure of the Post-Messinian sedimentary cover in the eastern part of the Mediterranean Sea. In: V. A. Krasheninnikov and J. K. Hall (eds.), Geological Structure of the Northeastern Mediterranean, Historical Productions-Hall Ltd., Jerusalem, p. 33-73.

Woodside, J. M., 1977. Tectonic elements and crust of the Eastern Mediterranean Sea. - Mar. Geophys. Res., 3(3), p. 317-354.

Zverev, S. M., (Ed.), 1988. Autonomous bottom seismic apparatus. Institute Physics of the Earth of the USSR Academy of Sciences, Moscow, Dep. VINITI 6857-V88, 174 p. (In Russian).

Zverev, S. M., 1996. Ocean floor seismic noise monitoring in the South Atlantic. Vulkanol. Seismol., No. 6, p. 62-85. (In Russian).

Zverev, S. M., 2004. Peculiarities of sediments and basements structure in Cyprus Arc Frontal Zone based on seismic refraction data. Chapter 13, this volume.

Zverev, S. M., Akimov, G. N., Novikov, B. N. et al., 1978. Apparatus for deep seismic sounding and local earthquakes study on land and at sea. Seismicheskie pribori, No. 11, Moscow, p. 75-77. (In Russian).

Zverev, S. M., Kosminskaya, I. P., and Tulina, Yu. V. (Eds.), 1996. Deep seismic sounding of the lithosphere on the Angola-Brazil Geotraverse, 1996. Trans. Institute of Physics of the Earth, Russian Academy of Sciences, Moscow (OFIZ RAN), Inst. Planet. Geofiziki, p. 88-99.

Zverev, S. M., Nardov, N. M., Yaroshevskaya, G. A. et al., 1993. Deep seismic sounding of Cyprus Island and adjacent sea areas. Trans. Institute of Physics of the Earth, (OFIZ RAN), and Nat. Geophys. Comm., Russian Academy of Sciences, Moscow, 150 p. (In Russian).

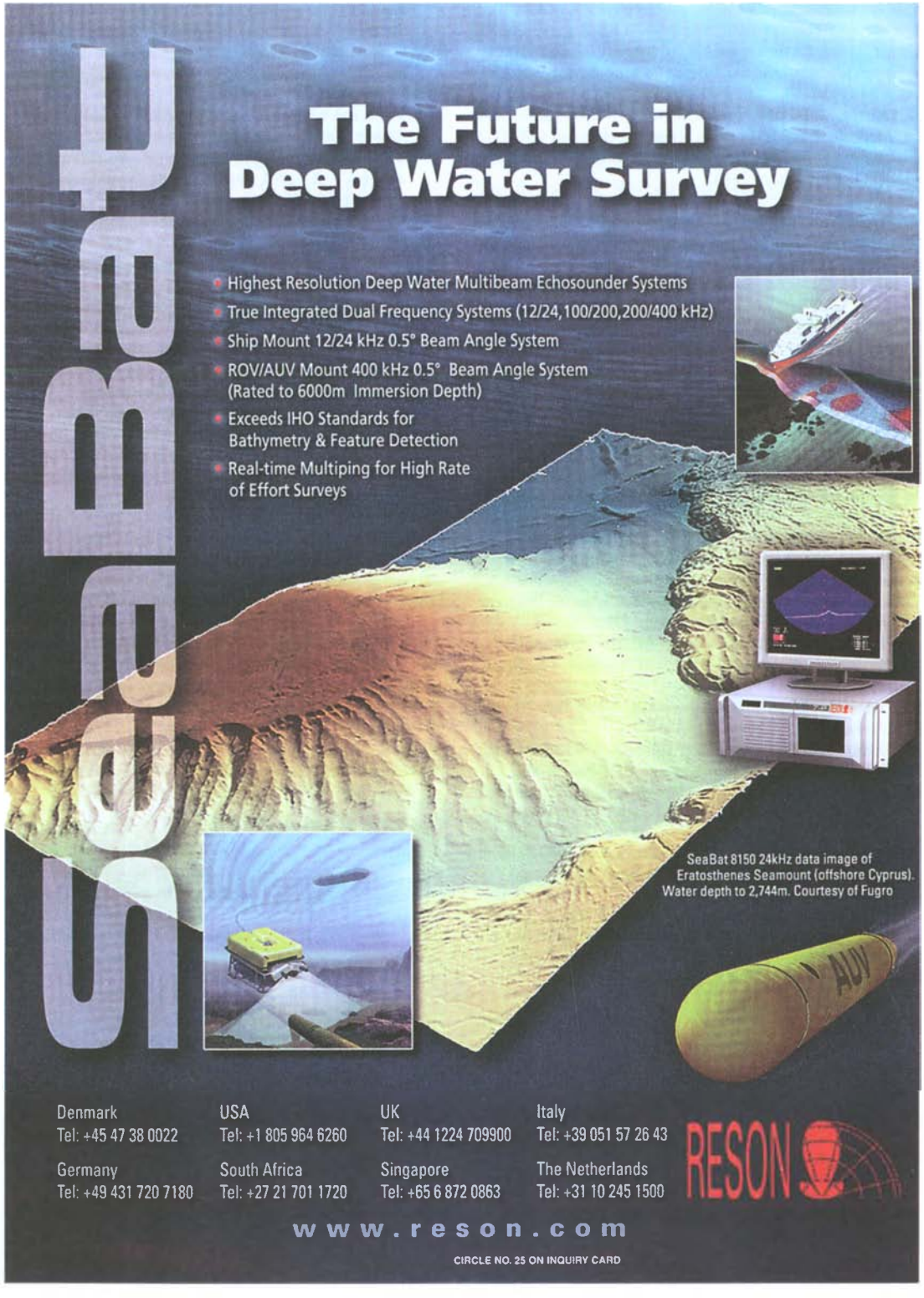
Zverev, S. M., and Ilinsky, D. A., 1998. Regional seismic refraction and reflection shooting in the Eastern Mediterranean. Geofizika, No. 6, p. 31-41. (In Russian).

Zverev, S. M., and Ilinsky, D. A., 2000. Deep structure and inferred origin of Eratosthenes seamount (Eastern Mediterranean). Geotektonika, No. 4, p. 67- 84.





Fore and aft views of the R/V Strahov in Recife, Brazil, November 1990.
Left: Prof. Gleb B. Udintsev, Cruise 11 chief scientist and veteran of over 100 expeditions and over 25 years at sea. Photos taken by J. K. Hall during Leg 2 of Cruise 11 of the Strakhov - Southhampton, England to Recife, Brazil, October-November 1990.



Most recent imaging of Eratosthenes Seamount. Advertisement appearing in the December 2004 issue of Sea Technology magazine, featuring a Reson SeaBat 8150 24 kHz multibeam echosounder image of Eratosthenes Seamount obtained in a survey by Fugro. This is probably the highest resolution look to date at this feature, as the system has very narrow 0.5° beams. The look direction is from the southwest in the direction of underthrusting. The moat surrounding Eratosthenes on two sides is clearly seen, as is a small slump or slide scar on the flank of the seamount. Complete coverage of the Mediterranean using such techniques will reveal many details about the underlying geology and ongoing processes.

Chapter 13

Peculiarities of Sediments and Basement Structure in the Frontal Zone of the Cyprean Arc (Based on Seismic Refraction Data)

Sergey M. Zverev
Institute of Physics of the Earth of the Russian Academy of Sciences, Bolshaya Grusinskaya Str. 10, 123 810 Moscow, Russia

INTRODUCTION

The frontal zone of convergence of the African and Eurasian plates crosses the northern part of the eastern Mediterranean. It is expressed as steps, depressions, and deformations of the seafloor as well as the specific geological structure of the Troodos Ophiolite Massif of Southern Cyprus. This structure is known as the Cyprean Arc.

This region has attracted considerable interest, and numerous marine geological and geophysical investigations have been carried out (Malovitskiy, 1978; Malovitskiy et al., 1982; Finetti, and Morelli, 1973; Hirsch et al., 1995; Makris et al., 1983; Makris and Stobbe, 1984; Montadert, Letouzey, and Mauffret, 1978; Sage and Letouzey, 1990; Ben-Avraham et al., 2002). However, up to now these investigations have been rather isolated, not very detailed and, on a whole, not very conclusive.

In 1987-1990 studies of a more comprehensive and multidisciplinary nature were carried out during three cruises of the research vessels 'Akademik Nikolaj Strakhov' and 'Akademik Boris Petrov' of the USSR Academy of Sciences (Krasheninnikov and Hall, 1994). Multidisciplinary geological and geophysical observations, including marine and land-marine seismic refraction (DSS), were performed with a number of profiles located on Cyprus and the adjacent marine areas. The preliminary results of the initial analysis of the seismic refraction data were published by Zverev et al. (1993). The comprehensive processing and interpretation of all the complex seismic refraction data was delayed for a number of reasons, and more thorough analyses were only made for certain sections of the profiles (Zverev and Ilinsky, 1998, 2000).

We employed a powerful airgun sound source to make strong impulses along fixed seismic refraction profiles in the eastern Mediterranean. These explosions provide good-quality seismic data at a number of Ocean Bottom Seismograph (OBS) stations emplaced along the profile. The analyses show that the seismic wave field is strongly variable. Reversed and overlapped OBS data obtained during the experiment show that many of the existing features of the seismic wave field recur in overlapping records, *i.e.* they come from horizontal inhomogenieties of the geological section. The precise analysis of the records gives us, as a first approximation, an insight into the nature of the seismic waves, and allows us to pick the different arrivals along the profiles and thus plot out the time-distance curves of the system. However, for a structure with complicated strata, the conversion of time-distance curves into deep velocity sections is extremely difficult. During the first attempted seismic refraction processing many scientists used the popular technique of horizontal-homogeneous (1-D) media structure. As a result they transformed all horizontal inhomogenieties of the sections into deep inhomogenieties, and the real sections become distorted and erroneous. After a formal correction of the sections, by means of mathematical modelling, they received distorted sections for a given incorrect starting model.

We tried to construct a correct starting model by using the classic approach for the analysis and processing of seismic wave fields developed for seismic refraction prospecting (Gamburtsev et al., 1952). Moreover, the digital recording technique makes it possible to obtain a more detailed and accurate analysis. Attention was primarily focused on the investigation of the kinematical and dynamical parameters of the waves. They reveal differences between wave properties along the profile, which correspond to lateral variations in the geological section. These variations in the wave parameters were considered in defining the initial models for the seismic sections. This is the major difference between our approach to interpretation and the traditional way. In the traditional approach the emphasis is placed on searching for, and separating out, those waves with similar kinematic parameters, and then tracing them along the whole profile, but not taking into consideration the strong attenuation, and sometimes even extinction, of the waves along the profile. A new approach was used to interpret the data for the profile that crosses Eratosthenes Seamount. There we detected layers with velocities appropriate to sedimentary and crystalline rocks, which were often overlain by a low velocity layer, and fault zones which we also noted. The features we discovered in this area correspond well to the seafloor relief, geological data, seismicity, and other measured geophysical fields, and thus allow a consistent geological interpretation (Zverev and Ilinsky, 2000).

In this chapter we discuss the properties of the sedimentary units and crystalline basement obtained from the refraction deep seismic sounding (DSS) studies. We present important new information about the geological section with several examples from three profiles, located to the south and east of Cyprus. We also consider a starting model of seismic cross section; to give a comprehensive analysis of the extended south-western Profile 6. We will also carry out comparative studies of the other two lines.

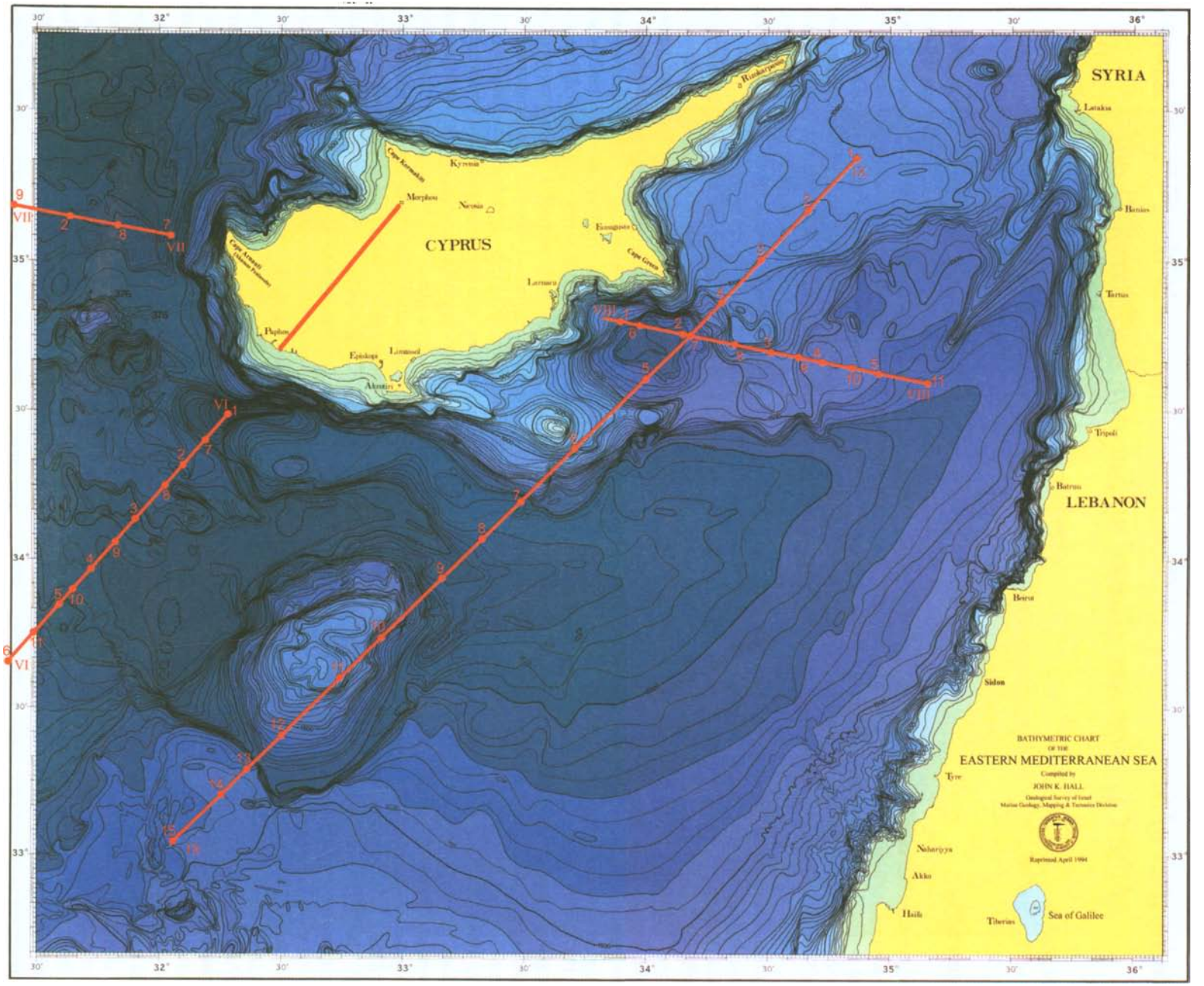


Fig. 13.1. Location of seismic refraction profiles on the bathymetry map of Hall (1980-1981). Locations and identity numbers of the up to 15 OBSs used are shown on the shooting lines.

The data in this study were collected under the guidance of the author during his participation within the framework of the Tethys Project. Scientists of three institutes of the Russian Academy of Sciences (the Geological Institute, the Vernadsky Institute of Geochemistry and Analytical Chemistry, and the Schmidt Institute of Physics of the Earth) worked together with their colleagues from the Geological Survey of Cyprus. Together we performed the seismic DSS investigations, including the fieldwork with the OBS and the airgun runs, followed by digitization of the records, data processing, and initial interpretation.

AREA STUDIED AND GENERAL RESULTS OF THE SEISMIC REFRACTION INVESTIGATION

Below is a discussion of the data collected on DSS Profiles 6, 8 and 9, to the south and east of Cyprus (**Fig. 13.1**). In this part of the eastern Mediterranean we observe a complex seafloor relief. The transition to stepwise relief is located to the east where the sea depths in the southern part of the Levantine Basin are more than 2000 m and in the northern part less than 1500 m. Three structural elements are located to the east of Cyprus. They are the Hecataeus Ridge, with depths less than 500 m, which extends along the island's continental slope to the south-east; the oval Cyprus Basin (with depths >1000 m); and farther north, the step down to the level seafloor of the northern Levantine basin. A steep slope stretches to the south of Cyprus down to the deep Giermann Trench (> 2500 m), a broad depression which separates Cyprus from Eratosthenes Seamount. Here the known deformation zone goes from east to west. The arcuate shape of the main bottom structures of the Cyprean Arc can be observed on the bathymetric maps published by Hall (1980; 1981; 1994) and Loubrieu et al. (2001), but it is distorted by the straight and wavy elements of differing orientation reflecting the complicated three-dimensional deep structures of the region. Generally the seafloor relief of the study area is much more distorted then that of the adjacent areas.

The locations of the airgun shooting lines and positions of the ocean bottom stations (OBS) are shown on the map in Fig. 13.1. The detailed description of the techniques used in the refraction experiment is given in Zverev and Ilinsky (1998; 2000; and Chapter 12, this volume). In the following discussion the profile number will precede the OBS number (*i.e.* OBS 606 for instrument 6 on Profile 6) when describing the results obtained from a given bottom seismograph.

Below we will investigate some aspects of the seismic waves which present the peculiarities of the most important features of the deep geological structure. These can be used to prepare the starting model for the seismic sections which will then be corrected by mathematic modelling. We will not describe all the details of the seismic wave properties, and the procedure for preparing the section, but will demonstrate the geological significance of well-established properties of seismic waves.

Figure 13.2 shows different data from Profile 6 which extended to the south-west of Cyprus. Eleven OBSs and several land seismic recording stations (LS) were deployed along this line. The bathymetric map and echogram in Figs. 13.2a and 13.2b show the complex deformations of the seafloor. The reversed and overlapping arrivals were used for seismic wave studies. We were able to discriminate between refracted waves from unconsolidated sediments (P_{sed2} - velocity V<3 km/s), from dense sediments (P_{sed4} - 3.5<V<4.7), from crystalline layers (P_{K4} - 6.6<V<7.0), and from the basement (P_{K5} - V>6.8). The waves with velocity 7.5 km/s we associate with the basement. They can be distinctly traced all along Profile 6. The P_{K4} waves were detected in some parts of the profile, ahead of the P_{K5} waves with velocities less than 7 km/s.

Fig. 13.2c shows the boundary velocities for the consolidated sediment layers, and Fig. 13.2d shows the time section for the main refracted waves as distribution times and boundary velocities V_b, calculated from the reverse time-distance curves by the difference method. The level of reliability of the data is also noted.

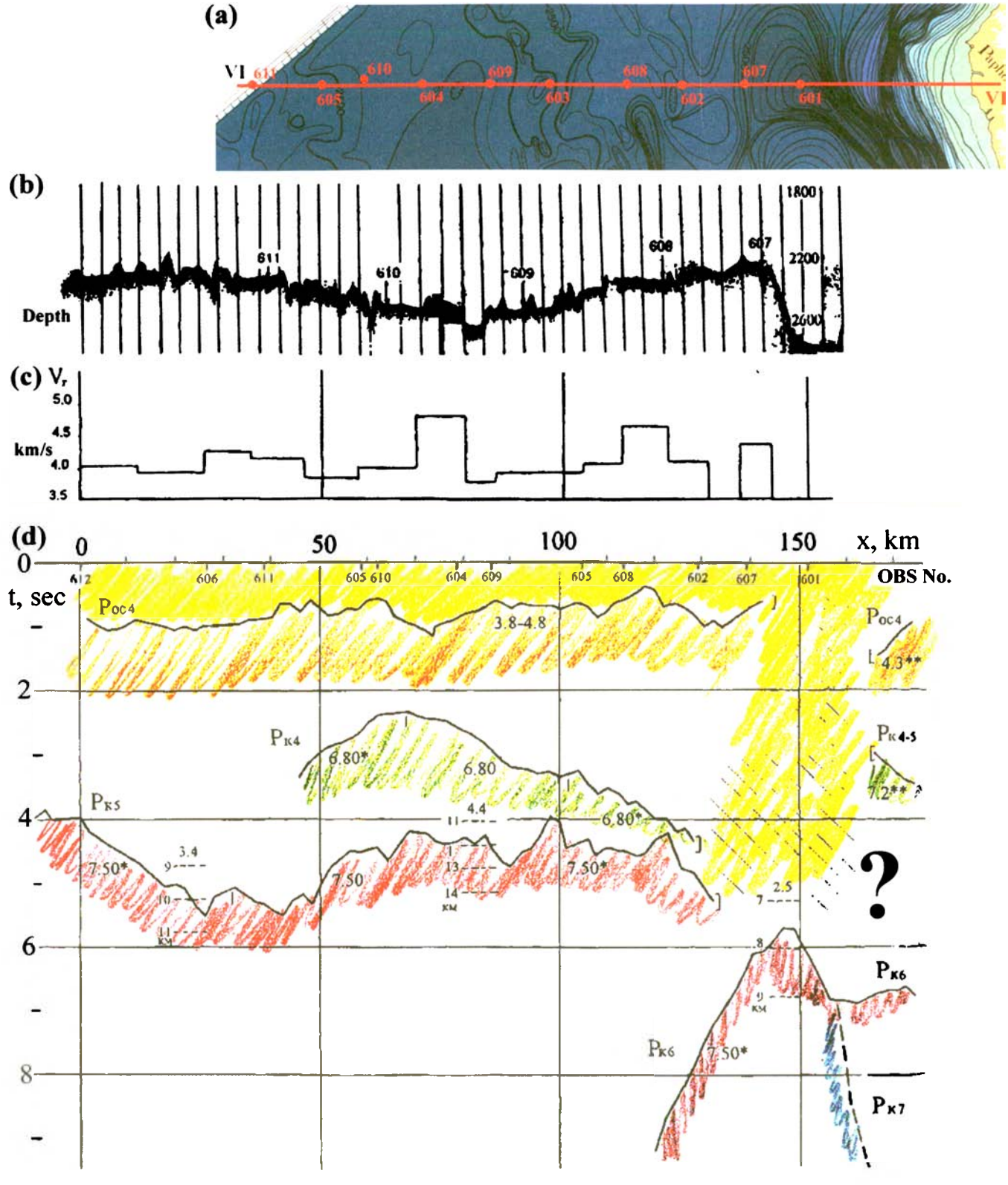
In order to convert time sections into deep sections, we must determine a velocity distribution over the whole plane of the section. The real data on velocities is derived only for a part of the plane of the section, *i.e.* that covered by the seismic rays. The general picture is improved during the mathematical modelling. The approximations for the deeper section are shown in some parts of Profile 6 in Fig 13.2d as depth scales based upon estimated velocities. The section is very complicated, especially in the north-east where the profile probably crosses the convergence front. The section will be discussed below.

Sedimentary thickness properties

Seismic velocities from reflection and refraction studies of the sedimentary cover of the Mediterranean Sea have been discussed in general publications (Malovitskiy, 1978 and others). In general, the seismic propagation velocity in the uppermost layers of Recent soft sediments are near 1.8 km/s, the Pliocene–Quaternary sediment layer is up to 2.0-2.5 km/s, and the Messinian and pre-Messinian layers of dense sediments are 3.5-4.7 km/s. The solid evaporite layers (salt and gypsum) of the uppermost part of the Messinian strata are often observed to have velocities of about 4.5 km/s. The interlayers sometimes found below salt horizons can have relatively low velocity, and the decrease can reach 1 km/s (Montadert et al., 1978).

Seismic reflection studies are mostly limited to depths of less than 6 km. The latest CDP reflection observations gave better results and in some places penetrated a total thickness of sediments of up to 10-12 km. Some publications (Montadert et al., 1978; Udintsev et al., 1994 and others) present the distribution schemes for the Messinian deposits and possible existence of other sedimentary formations.

Previous publications on seismic refraction studies mostly presented only the schematic sections. Seismic refraction records connected with sedimentary thickness were neither revealed nor discussed. The distribution of seismic properties of sediments was not examined. This is especially true of the eastern Mediterranean, where seismic studies were carried out much later than for other seas.


(a)
VI
611
610
609
608
607
605
604
603
602
601
VI
(b)
Depth
611
610
609
608
607
1800
2200
2600
(c) V_r
5.0
4.5
km/s
4.0
3.5
(d)
0
50
100
150
x, km
t, sec
OBS No.
612
606
611
605 610
604
609
605
608
602
607
601
P_{OC4}
3.8-4.8
P_{OC4}
4.3**
P_{K4}
6.80*
6.80
P_{K4-5}
7.2**
P_{K5}
4.4
6.80*
3.4
7.50*
7.50
7.50*
2.5
?
P_{K6}
P_{K6}
7.50*
P_{K7}

Our high quality refraction studies show the variation in sedimentary layer properties in some areas of the region. The uppermost several tens of meters (successfully studied by the high resolution single channel reflection method) are given a velocity of 1800 m/s. These layers are beyond of resolution of our refraction techniques, where we can establish the average properties of soft sediments not less than 200-300 meters in thickness. The observed velocities are 2.0-2.5 km/s, and the thickness varies from 0.3 to 1 km and more in this region. We stand a good chance of effectively studying the underlying consolidated sediments by our experimental setup with closely spaced airgun shots and OBSs located at intervals of 10-20 km along the profile. The sediment velocity parameters are relatively stable. Reversed data show the boundary velocities for Psed4 in Profile 6 to vary from 3.8 to 4.8 km/s. These values suggest Messinian deposits. Some local variations derive from changes in velocity, wave record patterns, range dependent variation in the high amplitude first arrivals and even their disappearance through interactions with other wave trains. These parameters reflect the properties (thicknesses) of the whole sedimentary cover with upper boundary velocity of 3.8 to 4.8 km/s.

Some examples from Profile 9 are shown in **Fig. 13.3** which presents data collected by OBS 901 deployed in the shallow northern part of the Levantine Sea on the plain to the north-east of Cyprus. There is a small thickness of soft sediment, and waves with velocity 2 km/s can be observed only close to the OBS. The waves with velocity 4.5 km/s are characterised by sharp high amplitude arrivals with an abrupt decrease and subsequent extinction at distances of more than 7-9 km from the source. The next regular packet of first arrivals comes following a delay of about 1 s. Such a pattern suggests a high velocity contrast at the top of the dense sediment layer, and the limited effect of the uppermost interlayer with velocity 4.5 km/s (salt?). A relative decrease in seismic velocities exists in the underlying layers.

Elsewhere a different pattern is observed. Fig. 13.3b shows data collected by OBS 908 deployed in the trough separating Eratosthenes Seamount from Hecataeus Ridge. Elements of strong low velocity waves can be seen at small distances, associated with unconsolidated sediments in the first few hundreds of meters. At distances of more than 1 km. the observed wave has a velocity of about 4.5 km/s. The velocity and pattern of the wave varies slightly. It can be traced continuously up to a distance of 20 km from the OBS and ends as a basement wave. Such a wave can be attributed to the total thickness of sediments, extending from the top through the Messinian layers. The duration of the traced wave can be explained by a positive velocity gradient in all the sedimentary section below and by the absence of a considerably higher velocity interlayer (salt?) at the top of this pile.

Figure 13.3c shows the velocity depth curve for sediments for the whole Mediterranean, from Montadert et al. (1978), based on reflection records and the geological column. The solid lines of the velocity curve fit well to a section with a thick evaporite layer imbedded within low velocity sediments. This pattern matches the refraction record in Fig. 13.3a.

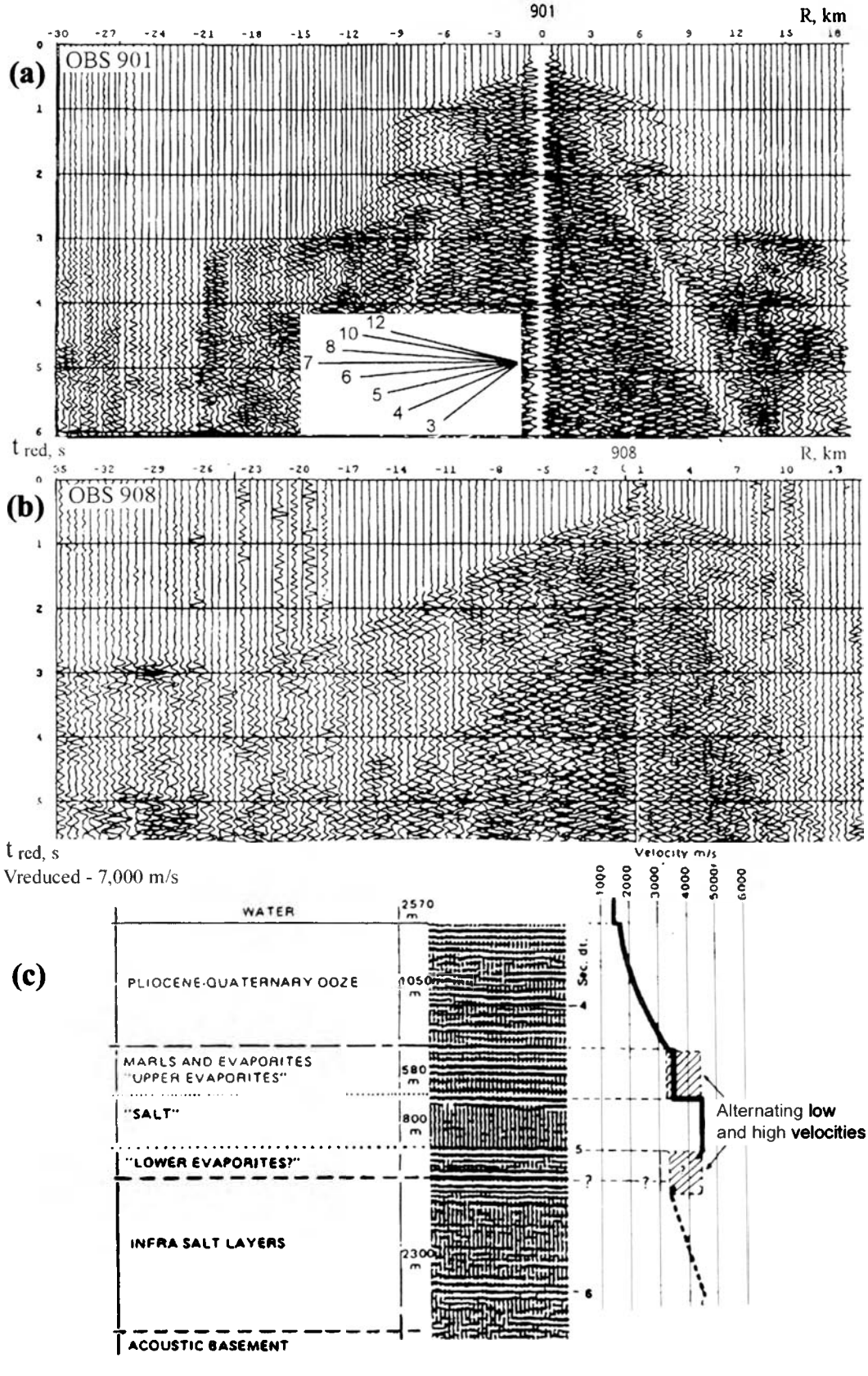
Refraction records similar to the first or second examples and their combinations, are observed in some places within our study area. By analysing seismic refractions, we can determine the sediment properties of the region. For Profile 6 the picture is more complicated than for the other examples shown. The breaks of the time curves for the first arrivals of the 4.5 km/s waves are often insignificant, but velocity variations are more typical. Reversed records allow calculation of the boundary velocity, which ranges from 3.8 to 4.8 km/s (Fig. 13.2c).

Some special features of the sediments are observed in some localities. Examples of recorded data from both OBS and land stations (LS) are shown in **Fig. 13.4**. It shows data for the northern part of Profile 6, close to the shore of Cyprus. OBSs 602 and 601 were deployed in the deep water trough near the base of the island slope (601) and on the upper edge of the rise south of the trough (602) (see Figs. 13.1, 13.2a, and 13.2b). LS c616 was deployed at a distance of 20 km from the northern end of the shooting lines. In the OBS 602 records (Fig. 13.4a) we can see the Psed4 wave traced northward with a velocity of about 4.5 km/s up to 145 km (16 km to OBS 602 position). Here we can see a sharp decrease in velocity down to 2.5 km/s. In the reverse records of OBS 601 southwards (Fig. 13.4b), the first sediment wave Psed2 has a velocity of 2.5 km/s; it is traced up to 139 km (10 km. from OBS 601) where it is transformed into the weak wave Psed4 (4.5 km/s).

A similar picture can be seen on the records of the LS c616 (Fig. 13.4c). We can detect a change of velocity in the same place as in the records of OBS 601. For the points with drastic velocity changes, the difference in distance is 6 km between the observations as made from the south and from the north,. This coincides with double the length of deviation for seismic rays leaving the seismic



Fig. 13.2. Dataset for Profile 6, extending to the south-west of Cyprus. (a) OBS positions plotted on a large scale bathymetric map; (b) echosounder records along the profile; (c) distribution of the boundary velocities Vb for the upper part of consolidated (Messinian?) sediments, calculated by using many pairs of reversed refraction records; (d) Time-distance section to OBS 606 and OBS 603 for main observing waves, calculated by means of the 'differences of time distance curves (to)' method, using reversed and overlapping curves. Relative distances (X - in km) are shown on the horizontal axis along with OBS numbers, travel times relative to seafloor on the vertical axis. Wave indices are written above the lines: Psed4 is for consolidated (Messinian?) deposits, Pк4, Pк5, Pк6 and Pк7 are for crystalline layers. Index numbers are chosen on the basis of velocity value and position of the layer in the section. Boundary velocities Vb (km/s) are shown below the lines: calculated values are indicated by a vertical stroke under the horizon; extrapolated values are marked by a star, and assumed values by two stars. Hatched lines indicate areas with less reliable data. Approximate depths in km are plotted in columns with rows of dashes, and the average velocity used is noted on top. The Pк5 surface underlies sediments in the left (southern) part of profile, and the Pк4 surface appears in the middle. A sharp discontinuity is seen in the section between 130 and 160 km, near the coast of Cyprus, where the in the place of base of steep submerged slope near island shore.


901
R, km
(a)
OBS 901
12
10
8
7
6
5
4
3
t red, s
908
R, km
(b)
OBS 908
t red, s
Vreduced - 7,000 m/s
Velocity m/s
(c)
WATER
2570 m
PLIOCENE-QUATERNARY OOZE
1050 m
MARLS AND EVAPORITES "UPPER EVAPORITES"
580 m
"SALT"
800 m
"LOWER EVAPORITES?"
INFRA SALT LAYERS
2300 m
ACOUSTIC BASEMENT
Sec. dt.
Alternating low and high velocities

boundary. Hence many seismic records show that the sedimentary layer, with velocity about 4.5 km/s, does not exist on Profile 6 in the narrow 14 km wide zone beneath the axial part of the deep trough south of Cyprus (Fig. 13.2).

One can see a similar picture in Profile 9 in the sector situated south-east of Cyprus at the base of the steep southern slope of the Hecataeus Ridge. Reverse records from OBS 907 and OBS 908 allow us to precisely identify the place where the extended sedimentary layer with velocity 4.5 km/s (built up on the northern side) was replaced by soft sediments with velocity 2.5 km/s. Unlike the previous examples, here the low velocity sediments extend north up to several tens of kilometers and underlie all of the cataeus Ridge.

A similar narrow trough filled with unconsolidated sediments is also found on Profile 8 when approaching the Cyprus depression from the east. It is located at the junction of this depression with the northern plain of the Levantine Sea. As OBS 802 and 808 records demonstrate, here the width of this trench is approximately 10 km. The positions of the narrow depressions filled with unconsolidated sediments are marked by dots on the respective records (**Figs. 13.5** and **13.6**).

The soft sediments filling the narrow depressions absorb seismic energy. This is manifested by strong attenuation of the seismic waves propagating through the body of soft sediments. Hence OBS 601 and OBS 602, deployed close to the depression, do not record waves from sound sources beyond the depression. Below we will provide other examples of this.

Properties of the basement wave arrivals

Prior to our investigation, information on the bedding of sedimentary layers in this region was only known from some aspects of DSS experiments (Moskalenko, 1974; Makris et al., 1983; Makris and Stobbe 1984). In general, for DSS experiments, basement waves are considered as regular waves with velocities more than 5 km/s, which at some distance become first arrivals. Essentially basement wave properties vary from place to place in the areas that were studied due to the complexity of the geological structure. Figure 13.2c provides an example with the time section model for Profile 6. A layer with velocity 6.8 km/s was detected in the middle of the profile beneath sediments, but in the southern part we can only see the 7.5 km/s layer. This layer can be reliably traced under the 6.8 km/s layer to the north. The waves with velocities of 7.0-7.6 km/s with reversed and overlapping recordings can also be observed on all the profiles studied around Cyprus. Such waves are traced for long distances as first arrivals and account for the big thickness of the consolidated crust. They compare well with each other on the three different profiles. The deep section parameters provide representative data on these waves. That is why we take waves with velocities of about 7 km/s as a standard for the basement in this region. The presence of the above high velocity layers (7.0>V>5.5) will in each case be specifically addressed.

The basement wave records for OBS 606 are plotted in Fig. 13.5. The basement wave P_{K5} moving from OBS 606 north-eastwards starts at 25 km and goes up to 100 km. A complex pattern of arrivals can be seen occurring at intervals of 10-15 km, with the reduced arrival times decreasing south to north. The general slope of the time-distance curve is approximated by a velocity of 7.5 km/s up to distance of 100 km. The seismic records shown in Fig. 13.5 offer a clear view of the basement surface relief (assuming a constant average velocity above the basement).

An abrupt distortion of the pattern of the records takes place at 125 km (at a distance of 104 km from the OBS). A new wave P_{K6} arises. It is accompanied by a time delay of 1 s. at first arrivals and an increase of apparent velocity to more than 8 km/s. We can assume the P_{K6} wave is a second arrival, for it appears as a first arrival some 18-20 km before. The P_{K6} wave is easily traced further northwards up to the end of the shooting line. Data from several stations with reversed and overlapping time-distance curves are shown in Fig. 13.6. First wave records of the LS c616 (Fig. 13.6a) show a good correspondence with the P_{K5} wave (OBS 606) at distances of less than 125 km. However, a correspondence with the P_{K6} wave is not that clear. We assume that a new wave P_{K7} arises in the OBS 606 records at distances of 104, 116, and 124 km as weak regular long period waves appearing after the first waves (Figs. 13.5 and 13.6). We can also see such waves in the OBS 603 records (Fig. 13.6c). They can possibly be attributed to the steeply sloping seismic horizons dipping under Cyprus.

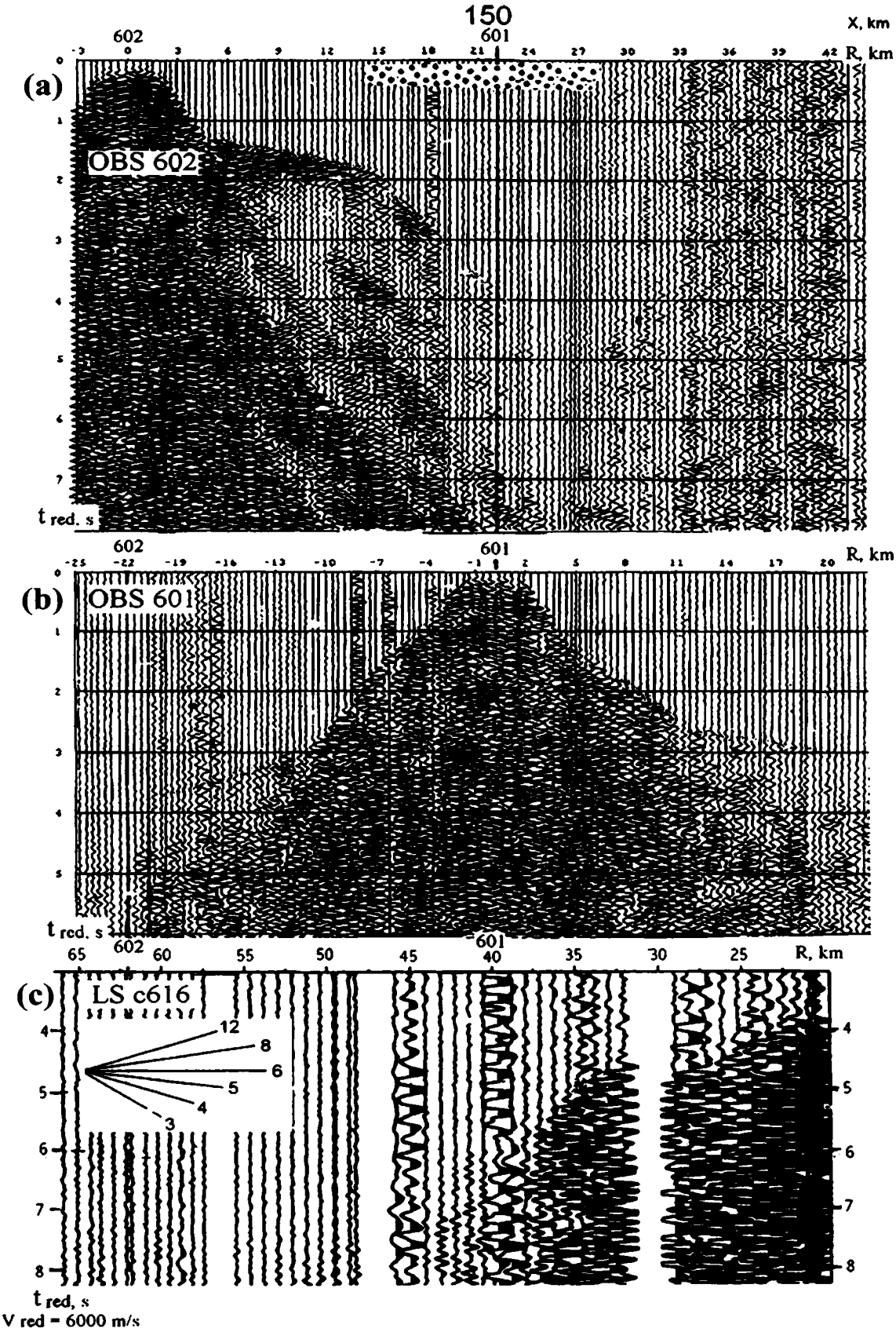
Figures 13.5 and 13.6 also show the amplitude attenuation of those basement waves crossing the narrow soft sediment-filled depression.

Hence the basement in Profile 6 is broken into many blocks. Adjacent to Cyprus a big flat basement block (slab) rises up steeply up toward the shore. It is accompanied by indications of seismic horizons dipping steeply under the island.

On Profiles 8 and 9 we can observe many similar features in the basement. The arrival times of basement waves for Profile 8 are greater than those for Profiles 6 and 9 (7-8 s versus 5-6 s, when using the 7000 m/s reduction velocity).This might be explained by differences in depths and average velocities. The OBS 805 records are shown in **Fig. 13.7**. The broken arrival times represent a faulted basement surface with blocks ranging from 6 to 10 km in size.



Fig. 13.3. Typical records of refracted seismic waves from consolidated (Messinian?) sediments and summary section for Mediterranean Sea basin sediments. (a) Recordings of OBS 901, located on the northern Levantine Sea plain to the north-east of Cyprus; b) Data from OBS 908, in the trough between Eratosthenes Seamount and Hecataeus Ridge; c) velocity-depth curve for sediments, related to seismic reflection records and geological section of sediment thickness (from Montadert et al., 1978). A solid line on the velocity-depth curve shows the high velocity salt layer within the section, which corresponds approximately to refraction records on Fig. 13.3a. Distances from OBS and reduced times are noted on the records, also the apparent velocity diagram for a reduction velocity of 7000 m/s (on a). Times are related to the seafloor.


150
602
601
X, km
R, km
(a)
OBS 602
t red. s
602
601
R, km
(b)
OBS 601
t red. s
602
601
R, km
(c)
LS c616
12
8
6
5
4
3
t red, s
V red = 6000 m/s

Arrival times show the rising of the basement towards the west and the Cyprus depression (where the time is about 6 s). We can see the broken basement of the Levantine Sea changing toward the west into a big uniform slab which rises towards the island beneath the Cyprus depression and flattens near the shore. This picture is similar to that seen in Profile 6.

A more complex case is observed in Profile 9. The records of OBSs 909 and OBS 908, which orthogonally cross the Hecataeus Ridge, show a large thickness of low-velocity sediment starting at the base of the southern slope and continuing under the whole of the Hecataeus Ridge up to the Cyprus basin. The basement here is broken into blocks ranging between 7 and 12 km in size. These waves have a velocity of 7 km/s.

Data on the above-mentioned basement waves are derived from reversed and overlapping observations and closely spaced shooting between the many OBSs on Profiles 8 and 9. Profile crossings provide 3-D coverage for this complicated area, but the realization of a more exact configuration will be very difficult.

AREAL DISTRIBUTION OF THE SEDIMENTARY AND BASEMENT FEATURES

Figure 13.8 gives a schematic view of the distinguishing features discussed above, together with the generalized seafloor relief and the geological data for Cyprus. We can offer the following suppositions about their correlation. The rise of the basement within the Cyprus depression possibly extends up to the Troodos Ophiolite Massif. The whole body of the Hecataeus Ridge is composed of soft sediments. They evidently continue into the depression adjacent to the island which is filled with Tertiary sediments. Narrow depressions filled by Recent sediments border the base of the island of Cyprus. These depressions mark a strip where the basement surface is influenced by strong faulting and formation of a slab which rises towards the centre of the island, accompanied by steeply dipping layers and their broken remnants. This coincides with a zone of local seismicity.

Hence, a close correlation can be seen between the seismic parameters, bottom relief, and the geological structure, expressed as a complicated picture of crustal structure in the frontal zone of the Cyprean Arc. The strict linkage of seismic data to geologic reality gives us an accurate picture of the tectonic structure, instead of just tentative estimates of some seismic parameters at this stage of the seismic interpretation.

For many reasons we can suggest that the above picture is a complicated manifestation of tectonic activity in a convergence zone related to subduction processes. Low velocity non-layered sediments on the submerged Hecataeus Ridge and the adjacent depression by Cyprus can represent accretionary prism deposits. The narrow bands of gaps in the consolidated sediment, filled by soft Recent sediments, mark precisely the real position of the convergence front. This depression may have originated from the subsidence of the unconsolidated sediments and their underlying layers through subduction. The first evidence of a subduction process (looking at the convergence front from the south) is seen in a sharp distortion of the basement surface and by a big block or slab rising toward the land. The accompanying steeply dipping layers and their broken remnants can be attributed to the slide surfaces incurred by subsidence of some layers during subduction. The high seismic velocity of the masses of crystalline rocks rising through the basement surface can probably be traced up to the Troodos Ophiolite Massif, which outcrops in the middle of the island.

Seismic data present the deep structure in a definite and exact manner. For example, the narrow depressions filled by low velocity sediments to the south and east of Cyprus are characteristically 10-14 km in width. The position of their edges (as marked by the emergence of the appropriate seismic waves) can be determined to within 1 km. The seismic wave field reflects even small and diverse details of the structure. They follow the changes in the seafloor relief. The first attempt at comparison allows us to clearly see a correlation between the deep structure and the seismicity and other geophysical fields. The common data set shows a real and extremely complicated picture of the deep structure. But here we come up against some problems in the inversion of the seismic wave field into a deep cross-section with laterally complicated inhomogeneous media, including steep slopes and vertical boundaries, and low velocity layers.

Some other general comments can be made in relation to the data discussed in this chapter and in Zverev and Ilinsky (2000). The study area is now viewed as a couple of blocks with crust of both continental and oceanic types (Makris et al., 1983; Sage and Letouzey, 1990, and others). Our seismic data now show that this approach is too simplified. Extensive and stable waves with a seismic velocity near 6 km/s (typical for the basement of continents) are not observed in this region. We also found no evidence for a real oceanic crust. Oceanic crust is characterised by a total thickness of less than 10 km, thin sedimentary cover, and a variable second layer which is not thick. A third layer comprises the main part of the oceanic crust. Its seismic wave velocities are stable in the ocean basins at about 6.7±±0.1 km/s. Layers with 7.2 km/s velocity are rare in occurrence.



Fig. 13.4. Records from Profile 6 expose a gap in the consolidated sediment layers and identify it as a narrow depression, filled with unconsolidated deposits. See Fig. 13.1 and 13.2 for Profile and OBS locations. Reverse records of (a) OBS 602 and (c) LS c616 show clearly the sharp change in velocity from 4.3-4.5 to 2.3-2.5 km/s on both sides of the depression at distances of 142 and 158 km, or from Index Psed4 into Psed2. The OBS 601 records (Fig. 13.4b) present the opposite picture of changes in the waves. The position of the depression is marked by dots on the record of Fig. 13.4a, taking into account deviations of the seismic rays. The strong attenuation in amplitude of the waves, which pass thorough the depression, can be seen. Records are reduced using a velocity of 6000 m/s and times are related to the seafloor.

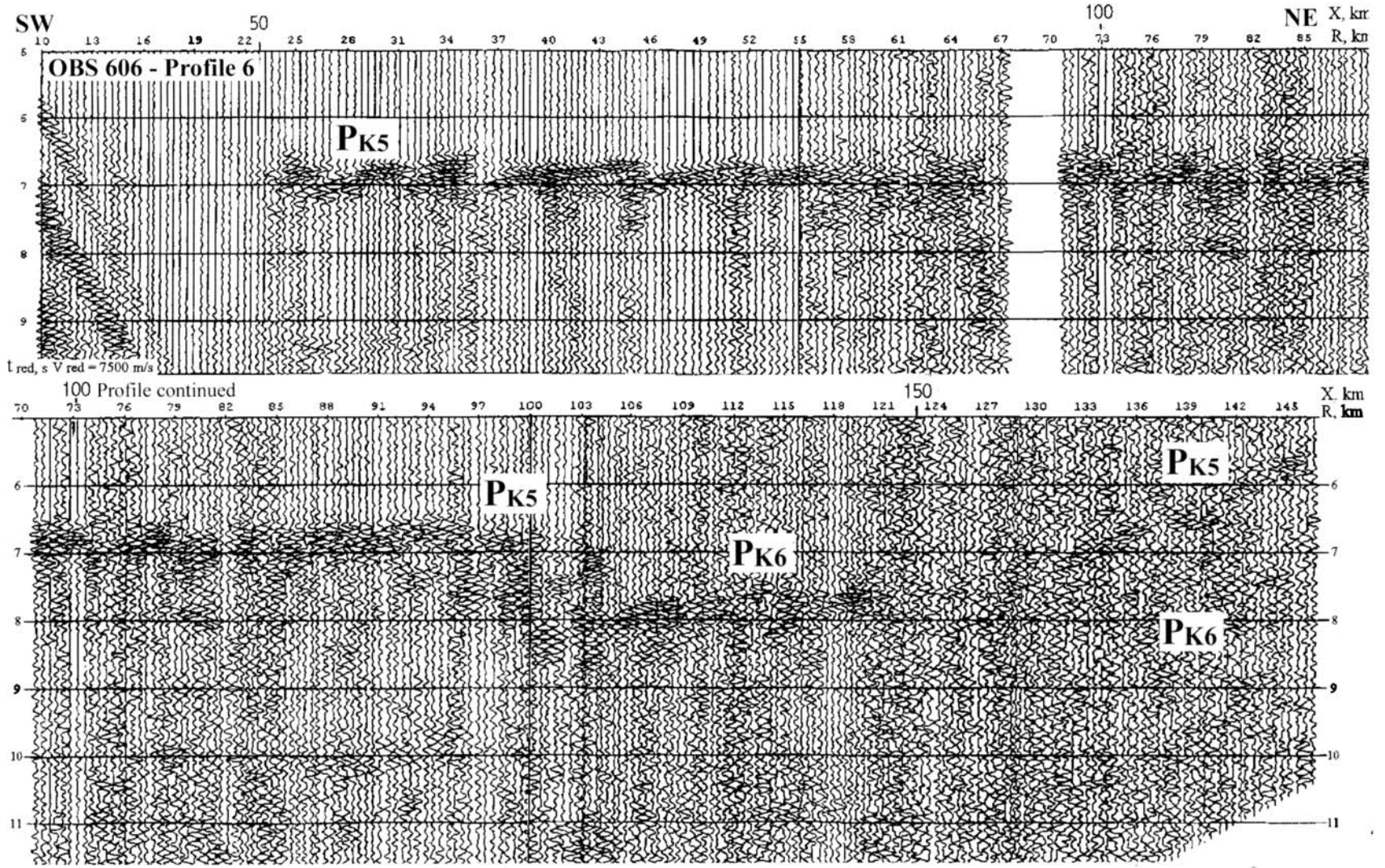


Fig. 13.5. Basement refracted waves recorded by OBS 606. The records are reduced using a velocity of 7500 m/s, close to the apparent velocity of the first arrivals. The **arrival** variations can be interpreted as the basement surface if it assumed that the boundary velocities are equal to the reduction value, and that the average velocities are constant. The basement surface is broken into blocks. A great fault can be seen at 130 km (100 km from OBS 606), where new waves appear, raised and lowered toward the coast of Cyprus. Times are relative to the sea surface. The wave indices (PK5, PK6) are discussed in the **text.**

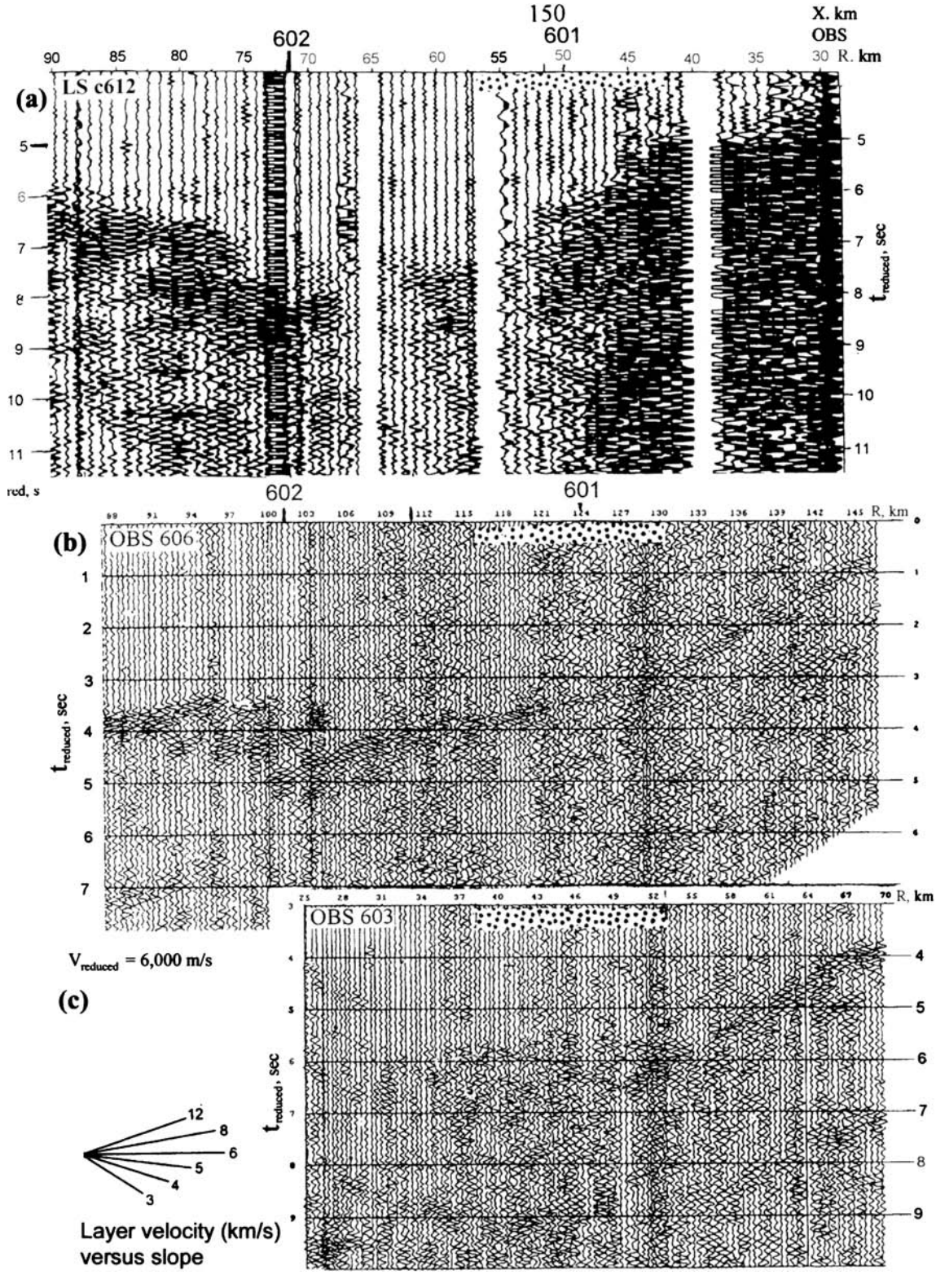


Fig. 13.6. Set of records for the more complicated northern part of Profile 6 close to the Cyprus shore. Reverse records for LS c616 (a) and OBS 606 (b) are coordinated appropriately for wave Pк5, but its interrelation with the Pк6 wave is extremely complicated and not yet understood completely. The overlapping records for OBS 606 and 603 (c) show the parallelism of the time curves for Pк6 and Pк7 waves. Records are presented by reduction velocity 6000 m/s and related to the seafloor.

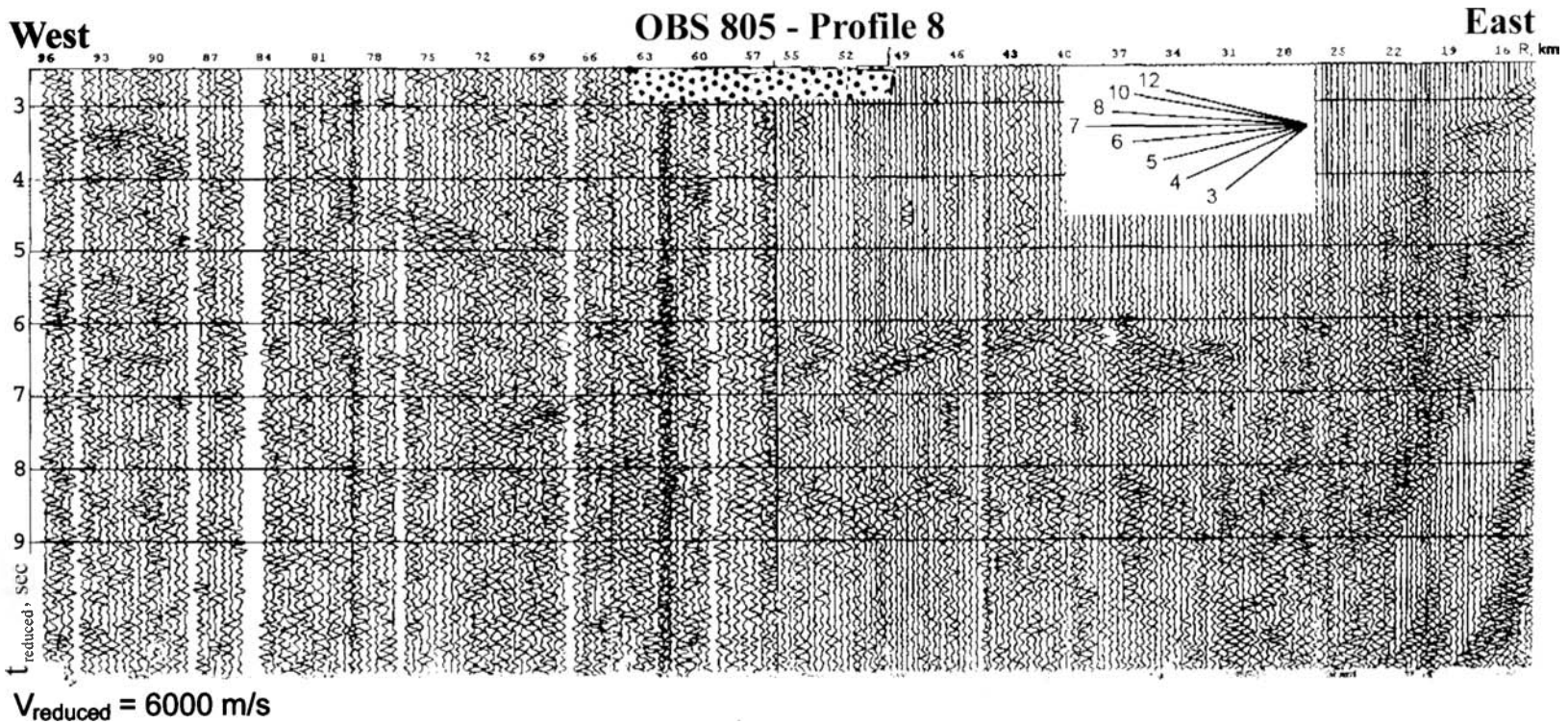


Fig. 13.7. Basement wave records on Profile 8, coming into the Cyprus depression (see Fig. 13.1). A block-like basement relief can be seen, rising toward the island, as well as arrivals from steeply dipping seismic horizons, dropping beneath the island. The seafloor of the Cyprus depression coincides with the rise in the basement. A subbottom depression filled with soft sediments is marked by dots. The records are reduced with an assumed velocity of 6000 m/s and times are relative to the seafloor.

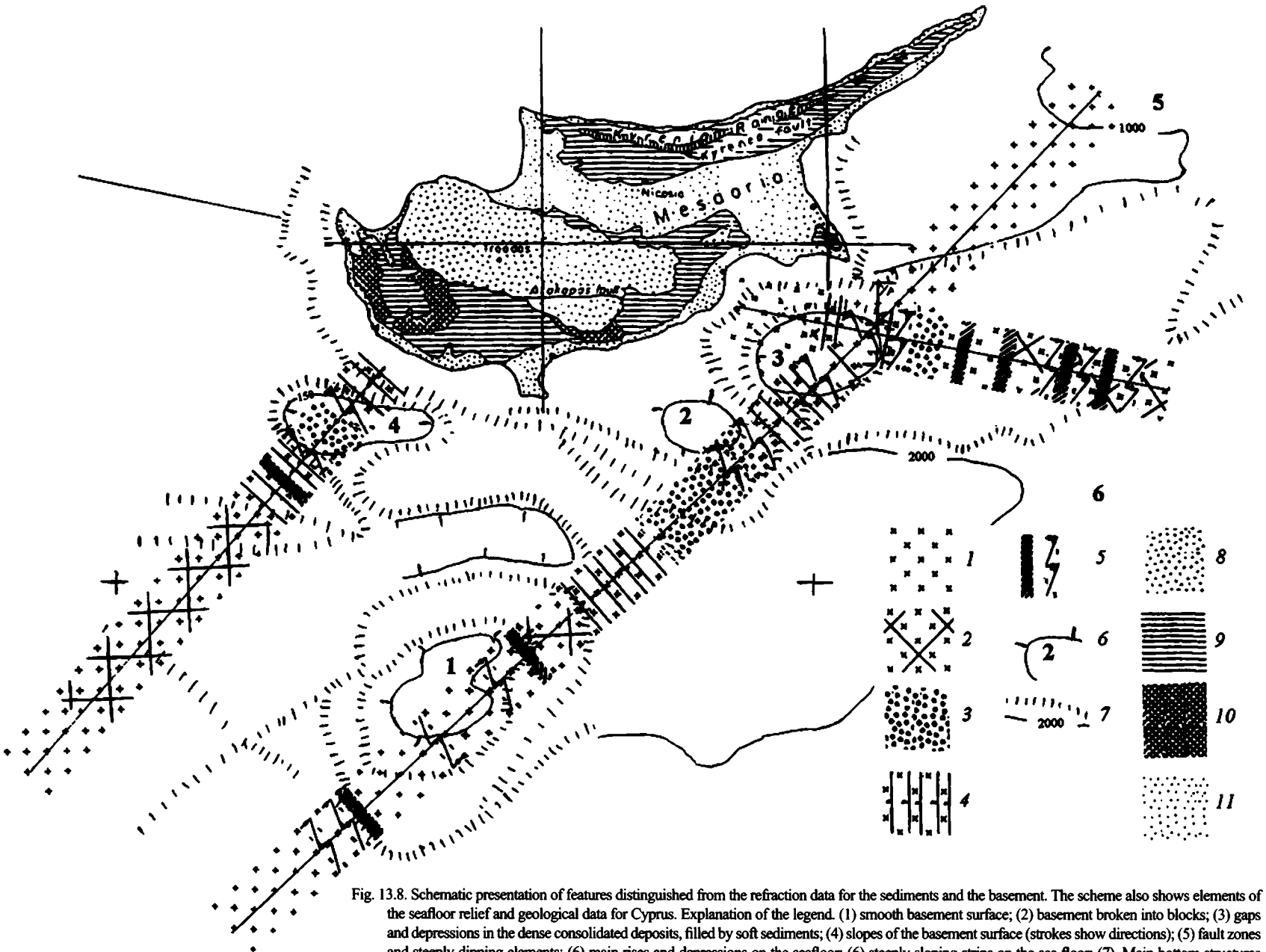


Fig. 13.8. Schematic presentation of features distinguished from the refraction data for the sediments and the basement. The scheme also shows elements of the seafloor relief and geological data for Cyprus. Explanation of the legend. (1) smooth basement surface; (2) basement broken into blocks; (3) gaps and depressions in the dense consolidated deposits, filled by soft sediments; (4) slopes of the basement surface (strokes show directions); (5) fault zones and steeply dipping elements; (6) main rises and depressions on the seafloor; (6) steeply sloping strips on the sea floor; (7). Main bottom structures numbered as follows: 1 - Eratosthenes Seamount, 2 - Hecataeus Ridge, 3 - Cyprus depression, 4 - local deep water trough to the south of Cyprus, 5 - the northern basin of the Levantine Sea, 6 - the southern basin of the Levantine Sea; (8-11) Data on Cyprus geology: (8) Troodos Ophiolite Massif; (9) Tertiary sediments; (10) Mammonia complex; (11) Recent sediments

Only some features of the oceanic crust are observed in our region, namely the absence of a 6 km/s layer beneath the sediments. The basement wave velocities (7.0-7.6 km/s) significantly exceed the typical values for the third layer of the oceanic crust. Reliable data on the crustal structure close to the continent (thickness near 30 km) are only observed on the Israel to Cyprus profile of Makris et al. (1983), and all those results belong to the southern basin of the Levantine Sea. The estimates of crustal thickness based on the fragments of seismic waves recorded within the second arrivals are not very reliable. The existence of continental crust under Cyprus and Eratosthenes Seamount is similarly not established. After detailed and careful investigations the real picture of the deep structure looks very complicated, non-standard, variable in both the vertical and horizontal directions, and requiring an appropriate approach for its elucidation.

CONCLUSIONS

We observed many specific features of the recorded seismic waves from sedimentary layers and basement in the frontal zone of the Cyprean Arc. They represent different aspects of the deep geological structure.

The well-known zone of seafloor deformation is accompanied by variations in boundary velocities (from 3.7 to 4.7 km/s) for the Messinian evaporite layers (bedded unconsolidated sediments) which demonstrate its complicated structure. Messinian deposits were not found in some localities. The sedimentary thickness below the Hecataeus Ridge consists of low velocity (<3 km/s) deposits. Narrow depressions were observed at the base of the steep slopes of the submerged base of Cyprus where dense sediments are replaced by unconsolidated non-layered sediments which extend to depth. Their velocities are around 2.2-2.4 km/s, and these values are close to those of Pliocene–Quaternary deposits. The crystalline basement is characterised by greater velocities (7.0-7.6 km/s) and its surface is broken into big blocks with differing characteristics from place to place. Beneath the depression a large uniform crystalline block or slab starts to rise toward the island. We also found some evidence of seismic horizons dipping steeply below the island.

These newly discovered features are precisely linked to the relief of the seafloor, the geological structure of Cyprus, and the seismicity and other geophysical fields. They give an insight into the nature of these features and provide evidence of active deep-seated tectonic processes. An analysis of the distribution of these features somewhat clarifies the tectonic setting in this complex zone of plate convergence. We have progressed from general conclusions to a real reconstruction of the separate profile localities and a common picture of the regional tectonic structure.

The challenge now is to convert these indications from seismic waves into a detailed deep geological section. It is an extremely complicated problem. All existing methods of processing refraction data and calculation of deep velocity sections are based on very simple interpretative models and leave out important information collected by high-performance DSS observations with OBS, closely spaced shots, and reversed and overlapping recordings.

REFERENCES CITED

Ben-Avraham, Z., Ginzburg, A., Makris, J., and Eppelbaum, L., 2002. Crustal structure of the Levant Basin, Eastern Mediterranean. Tectonophysics, 346 (1-2), p. 23-43.

Finetti, I., and Morelli, C., 1973. Geophysical Exploration of the Mediterranean Sea. Bull. Geophys. Theor. Appl., v. 15 (60), p. 263-340.

Gamburtsev, G. A., Riznitshenko, Ju. V., Berzon, I. S., et al., 1952. Correlation method of the refracted waves. Publ. House of the USSR Academy of Sciences. Moscow, 239 p. (In Russian).

Hall, J. K., Bathymetric Chart of the Southeastern and Northeastern Mediterranean Sea. 1980-1981. Geological Survey of Israel.

Hirsch, F., Flexer, A., Rosenfeld, A., and Yellin-Dror, A., 1995. Palinspastic and crustal setting of the Eastern Mediterranean. J. Petrol. Geol., 18(2), p. 149-170.

Krasheninnikov, V. A., and Hall, J. K., (Editors), 1994. Geological Structure of the North-Eastern Mediterranean (Cruise 5, R/V 'Akademik Nikolaj Strakhov'). Historical Productions-Hall, Jerusalem, 396 p.

Loubrieu, B., Satra, C., and Cagna, R., 2001. Morpho-bathymetry of the Mediterranean Ridge and surrounding areas. Acoustic image of the Mediterranean Ridge and surrounding areas. Two sheets, Mercator Projection, at scale 1:1,500,000 at 35°N, Ifremer, Plouzane.

Makris, J., Ben-Avraham, Z., Behle, A., Ginzburg, A., Giese, P., Steinmetz, L., Whitmarsh, R. B., and Eleftheriou, S., 1983. Seismic refraction profiles between Cyprus and Israel and their interpretation. Geophys. J. R. Astr. Soc., v. 75(3), p. 575-591.

Makris, J., and Stobbe, C., 1984. Physical properties and state of the crust and upper mantle of the Eastern Mediterranean Sea deduced from geophysical data. Mar. Geol., v. 55 (3-4), p. 345-361.

Malovitskiy, Ya. P., 1978. Mediterranean seafloor tectonics. Moscow, Nauka, 95 p. (In Russian).

Malovitskiy, Ya. P., Chumakov, I. S., Shimkus, K. M., Esina, L. A., and Moskalenko, V. N., 1982. The Earth's crust and the geological history of the Mediterranean Sea. Moscow, Nauka, 207 p. (In Russian).

Montadert, L., Letouzey, J., and Mauffret, A., 1978. Messinian event: seismic evidence. In: Init. Rep. DSDP, v. 42, part. 1; p. 1037-1050.

Moskalenko, V. N., 1974. The structure of the Earth's crust in the deep sea basin of the Levantine Sea. Geotektonics, Vol. 4, p. 225-229 (In Russian).

Sage, L., and Letouzey, J., 1990. Convergence of the African and Eurasian plates in the Eastern Mediterranean. In: J. Letouzey (ed.), Petroleum and tectonics in mobile belts, Paris, p. 49-68.

Udintsev, G. B., Zverev, A. S., Odinokov, Yu. Yu., Efremov, V. N., Elefteriou, S., and Hall, J. K., 1994. Structure of the Post-Messinean cover in the eastern part of the Mediterranean Sea. In: V. A. Krasheninnikov and J. K. Hall (eds.), Geological Structure of the North-Eastern Mediterranean, Historical Productions-Hall, Jerusalem, p. 33-73.

Zverev, S. M., Nardov, N. M., Yaroshevskaya, G. A., et al., 1993. Deep seismic sounding on Cyprus Island and adjacent sea areas. Moscow, Inst. of Physics of the Earth, p. 88-90 (In Russian).

Zverev, S. M., and Ilinsky, D. A., 1998. Regional seismic refraction and reflection shooting in the Eastern Mediterranean. Geofizika, N 6, p. 31-41 (In Russian).

Zverev, S. M., and Ilinsky, D. A., 2000. Deep structure and inferred origin of Eratosthenes Seamount (Eastern Mediterranean). Geotectonics, 34 (4), p.315-331. (In Russian).

Zverev, S. M., and Ilinsky, D. A., 2004. The deep structure of the Eratosthenes Seamount from seismic refraction data. Chapter 12, this volume.

Chapter 14

Gravity Field of the Northeastern Part of the Mediterranean Sea (South and West of Cyprus)

Vladimir A. Toulin
Institute of Physics of the Earth of the Russian Academy of Sciences, Bolshaya Grusinskaya Str. 10, 123810 Moscow, Russia

INTRODUCTION

Gravity field investigations in the eastern Mediterranean (to the south and west of Cyprus) were carried out by scientists of the Schmidt Institute of Physics of the Earth (IPhE) of the Russian Academy of Sciences during Cruise 12 of R/V 'Akademik Boris Petrov' in 1989 (Fig. III.1) and Cruise 10 of R/V 'Akademik Nikolaj Strakhov' in 1990.

The observations of 1989 only followed the lines of deep seismic sounding (DSS), but the limited reconnaissance data which were collected were used for planning the network for 1990. The gravity observation program for 1990 aimed to investigate in detail the gravity field in those areas to the south and west of Cyprus where the deep seismic sounding lines were situated.

This chapter discusses mostly the methods behind the observations and the accuracy of the 5 mGal contours plotted on the final gravity anomaly maps. Interpretation of these results can only be made in conjunction with the analysis of all the geophysical data.

The preparation of the equipment, the carrying out of the measurements at sea, and the analysis of the data were made by the author with the able assistance of L. V. Afanasieva, C. M. Baranova, E. A. Bojarsky, A. A. Efremov, D. A. Illinsky, O. D. Nikiforova, T. K. Nikiforov, and V. A. Juzvenko.

Previous regional study

We had very little information about the study area before beginning our expedition. The best information on previous work was available at the National Geophysical Data Center (NGDC) in Boulder, Colorado, USA. In the area east of 30°E, according to the NGDC, data only existed for some eight cruises, five of them for the years 1964 to 1966, and three from 1977 to 1984. We estimated that in our study area approximately 1000 miles of previous track had been measured. As the data from these last three cruises comprised only 20% of the total, and as we felt that the measurements from 1964-66 were too inaccurate to include in our compilation, we were then left with only a few hundreds of miles of track with reliable data.

Because the production of an accurate and quality gravity anomaly map requires an accurate dataset acquired on a regular grid of lines, it was decided that a completely new survey would be carried out, and that the earlier results would be used just for planning and interpretative purposes. For this reason, we will forego a detailed discussion of the results of earlier works. Suffice it to say that the earlier semi-systematic surveys provided the basis for the production of the IBCM-G Bouguer Gravity Map of the Mediterranean (Morelli et al., 1988), and for the gravity modelling studies of Makris and Wang (1994). It is highly unlikely that inclusion of these data would add more information, and indeed they would probably disturb the accuracy of estimation of our survey, and make correction of the data which are at our disposal more difficult.

Equipment and treatment procedure

Observations were made with AMG broad band gravimeters, developed by the IPhE for global oceanic investigations (Toulin and Osinskaya, 1970). The gravimeters were installed on a passive type of gyroscopic stabilizer, developed by the IPhE and the Tula Polytechnic Institute (Kireev et al., 1978). As is the usual practice in Russia, several identical gravimeters were used aboard the vessel to carry out simultaneous measurements. This allows a check on the data collected, to identify malfunctions, and it increases the measurement accuracy. Four instruments were used aboard each vessel, three in operation and one kept as a spare.

Prior to each cruise, the gravimeters passed laboratory tests on land, including calibration, and trials on a platform for imitating the accelerations aboard ship. The most important step is adjusting the stabilization to minimize errors generated by the ship's vertical and horizontal accelerations. Some numerical corrections should be including after trials, and accelerometers are mounted for this purpose on one of the stabilizer sets. Cross-coupling errors are low for the AMG due to the use of a pair of oppositely oriented pendulums in the sensor of a gravimeter, and its influence is negligible.

The AMG's measurement counts are recorded on a magnetic tape. The scanning frequency is 10 cps, 30 adjoining counts are averaged and written on the tape. Original data are thus presented as a sequence of averaged data at 3 sec intervals. The tapes are read into a computer at the end of measurement intervals of up to 12 hours duration. The analysis showed that no corrections for horizontal accelerations were necessary.

Shipboard analysis included calculation of average counts for standard time intervals (usually 5 min), including accuracy

estimation from the redundant gravimeter counts, and without making corrections for zero-point deviation, and Eötvös-effect. This was sufficient to guarantee proper performance and control of the observations.

The 3 sec measuring interval and the average of the last 5 min of observations were available for cleaning the gravity signal by filtering out the influence of vertical accelerations. The last analysis procedure is the calculation of weighted averages by Cosine weighting techniques, applied to the ends of the averaging interval. Such a simple method is very effective, reducing the remaining errors to less than 0.1 mGal.

Computing Equipment on the Ship

The ship's main computer was of the ES-1011 type, connected to the basic ship's equipment. An additional KAMAK computer was used for inserting the gravity data into it, with the results of the shipboard treatment then stored on floppy disks.

Positioning and Navigational Coordinates

Position fixing for the cruises was carried out with the U. S. Navy's AN/SRN-9 TRANSIT satellite Doppler navigation system. The time interval between observations was usually 40-60 minutes, but sometimes increased to 2 hours. Observational data from a MAGNAVOX navigation receiver were operated on by the KOKOS navigation survey program (Boyarsky and Afanasieva, 1992) for navigating the profiles and repetition of the measurements if necessary.

This program operates on the principle that the real track of a ship on a profile is not a series of lines (as shown by linear interpolation between fix points), but by some smooth curve, resulting from the influence of winds and currents on the ship. A search of the best fitting curve was made by using bicubic spline interpolation. Experiments show that such a technique increases the accuracy of the gravity measurements. A good computer and some effort is necessary to carry out this procedure, but the navigation data can be post-processed at home. The final 'smoothed' coordinates probably lie within 0.1 miles of the correct position. On gravity tracks we used 'coursographics' for defining the course changes between tracks.

Depths

The two ships were equipped with Hollming multibeam (15 beams) swath echosounders. According to the instructions issued for gravity survey we used only the depths directly under the ship as determined by the center beam.

The depths collected for the gravity reductions are different from those used for geomorphological observations. When traditional and approximate methods are used, the various methods for processing navigational information can give variations in the ship's position of up to 1 mile at the very same time. Thus in the bathymetric mapping of areas of complicated relief some mistakes can occur. This is the reason that the bathymetric maps drawn by our methods can differ in details from the traditional maps. These errors are probably negligible in geological-geophysical interpretation, but are very important to the accuracy evaluation by track crossings in a gravity survey. The depths are thus used as a very well determined third coordinate and any misties at the crossing points are an indication of positional error.

Depths were digitally recorded on magnetic tape on the ES-1011 computer, and for backup insurance in analog form on echograms. Depths were sampled every minute, and the average value was calculated from 5 adjacent samples. The resulting depth is associated with the center of the gravity observation interval, which is also the gravity value. To control errors, these were plotted out, and echograms were used if necessary. In practice, depth data was always available.

Gravity Base Station Observations

The gravity observations at sea were tied to the world gravity base network in Limassol Harbor. The base network on the island of Cyprus was set up in 1958 by the British Geological Survey (Gass and Masson-Smith, 1960). Two points from the 46 in the base network are located in Limassol, but, unfortunately, we had no possibility of reaching these points. At our request, Dr. C. Xenophontos of the Geological Survey of Cyprus made the connection between the Malounda base point and a local site in the harbor. We then tied the gravity value from this place to the ship's position. The ships measured several positions for Limassol Harbor, with the main position data as follows: g=979,791.7 mGal, latitude 34°39'35"N, longitude 33°01'03"E. These coordinates were taken from the TRANSIT satellite observations (which were based on the WGS-72 datum).

Some doubts exist about the magnitude of the errors for basic gravity determinations. The random error for ties is estimated at around 0.10-0.15 mGal, but we do not know the accuracy of the base point in Nicosia, from which the Cyprus base network evolved. According to the last recommendation of Gass and Masson-Smith (1960) we have to take into account a value for systematic error of -11.1 mGal. This contradicts the widely known correction to the IGSN-71system of 14.0 mGal.
However, this uncertainty in the base value does not distort the results of our sea survey, as the primary and final ties were occupied at the same point. Only a small variation (2-3 mGal) in the general level of the results is possible.

Gravity Observations at Sea

The gravimeters were mounted in the place closest to the pitch/roll center of each ship. The instruments (including the stabilizer) were switched on some days before observations began and were not switched off until the end of the survey. The survey was made along tracks planned in advance, and its positioning was checked by the gravity men on duty. The course and speed of the ships were held constant (on log and gyrocompass), and in the case of changes appropriate remarks were made in an observation log, which was later used for reduction of the navigational data.

The work at sea lasted a total of 23 days, and took place over three periods of time:

1) 1.5 days prior to initial arrival in Limassol;

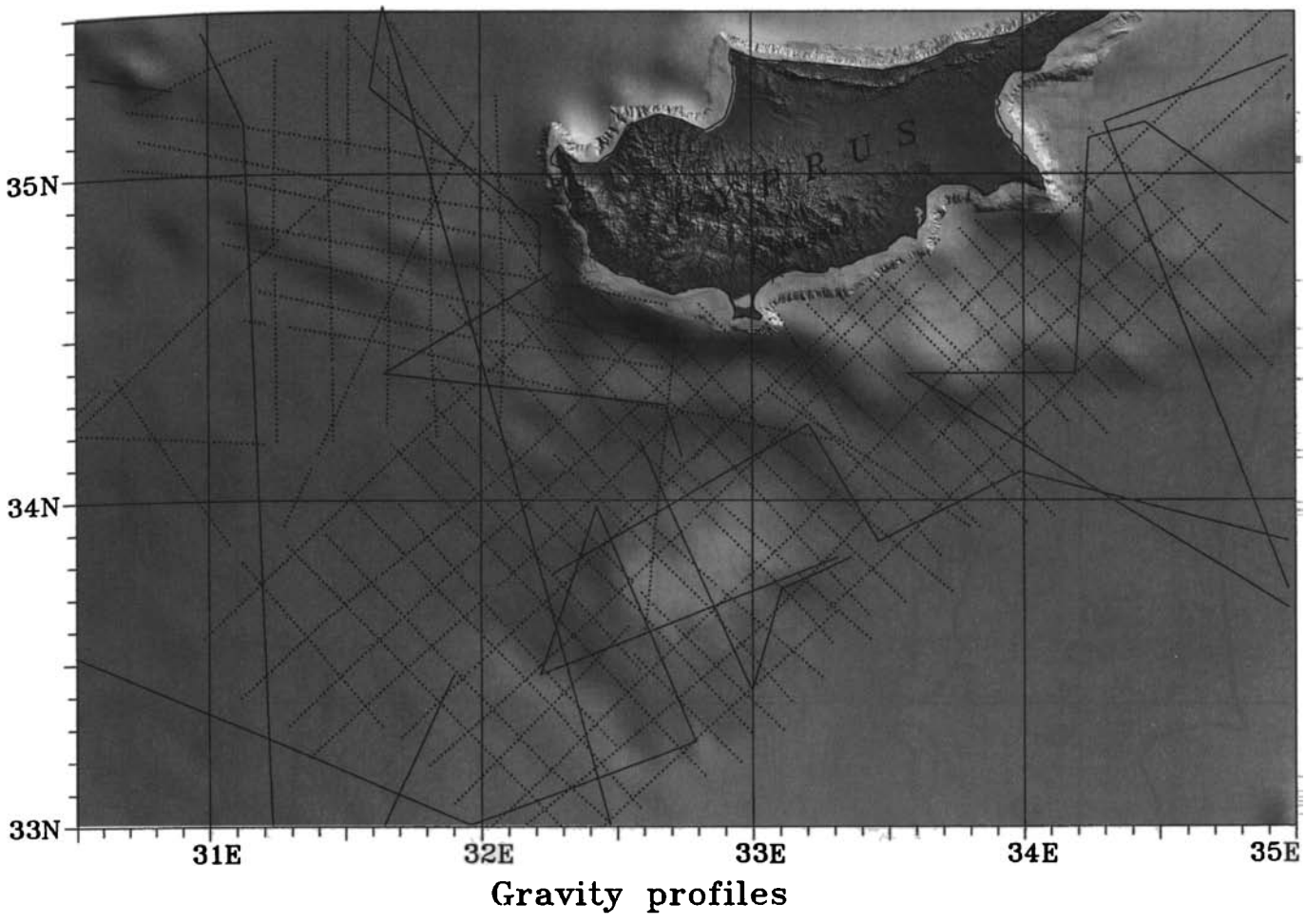


Fig. 14.1. Network of gravity tracks in the area to the west and south of Cyprus. Dotted lines are the tracks made by R/V 'Akademik Nikolaj Strakhov' in Cruise 10, 1990; solid lines are the tracks of other expeditions. Each dot marks one of the 5149 gravity observations made in these surveys.

2) 18.5 days between Limassol-2 berthing and Limassol-3 berthing;

3) 3 days after departure from Limassol.

The 1st and 3rd periods were not closed by gravity tie calibrations, but we do not expect significant errors due to the null-point extrapolation, so the time interval for them was very close to the basic observations.

Ninety-nine gravity tracks were run, but two of them were useless due to stormy weather. The 97 good tracks covered a total length of 4839 nautical miles, and 5149 gravity points were determined. The spacing between tracks was around 7 miles. The survey was made on a grid of orthogonal tracks, and controlled by the values at the crossing points. The positions of the tracks are shown on **Fig. 14.1**. The tracks are marked by the locations of the gravity observations. The total area surveyed is about 53,000 km^2. The main aim of the survey was a more precise observation, depending not only on the gravimeter measurement accuracy, but also on the ship displacement, instrument mounting place, an area of study, and sea state. The survey errors depended equally on gravimeters and on the quality of the navigation. In the process of planning sea work more attention should be given to the arrangement of precise (inside and outside) measurement control.

Final treatment of data

The Magellan-PC software package (Boyarsky and Afanasieva, 1992) was used to analyze the data. The package contains (as of December 1990) 14 programs for treatment of laboratory and marine gravity measurements at catalog level in the Russian MVF-77 format (which practically coincides with the international MGD-77 format), including accuracy of estimation. The package provides the possibility of using the Golden Software Inc. GRAPHER® programs to visualize the results.

The error of measurement for one point was estimated from its similarity to mutual results of the group of gravimeters, and

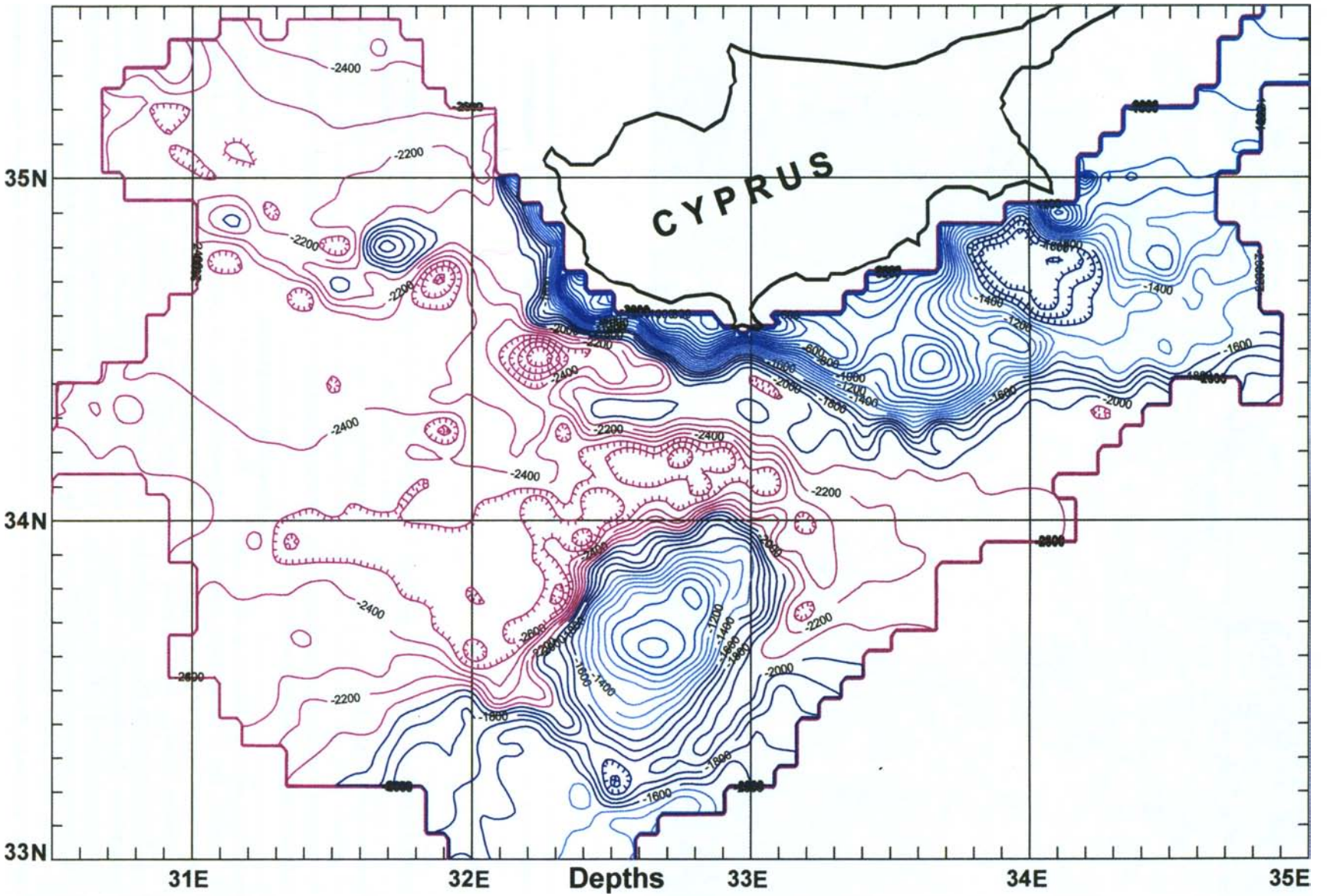


Fig. 14.2. Bathymetric map of the area to the west and south of Cyprus. The map was drawn by using the depths measured during the gravity survey aboard the 1990 Cruise 10 of R/V 'Akademik Nikolaj Strakhov'. Depth contour interval is 100 m. Mercator projection, scale 1:2,000,000 at latitude 34°N.

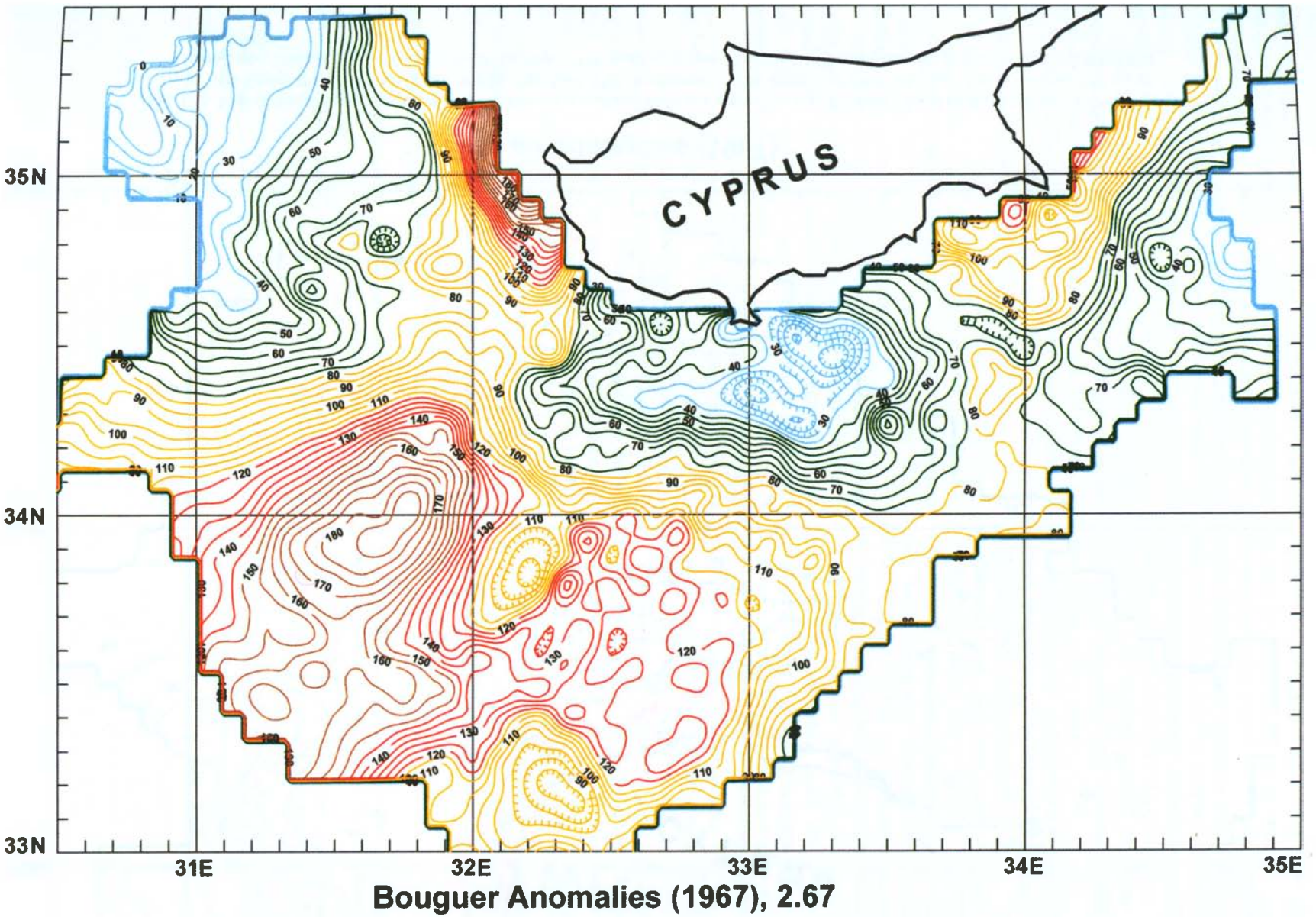


Fig. 14.3. Map of Free air gravity anomalies of the area to the west and south of Cyprus. The map was drawn based upon results of gravity survey from the 1990 Cruise 10 of R/V 'Akademik Nikolaj Strakhov'. The international gravity formula of 1967 was used. The isoanomaly contour interval is 10 mGal. Mercator projection, scale 1:2,000,000 at latitude 34°N.

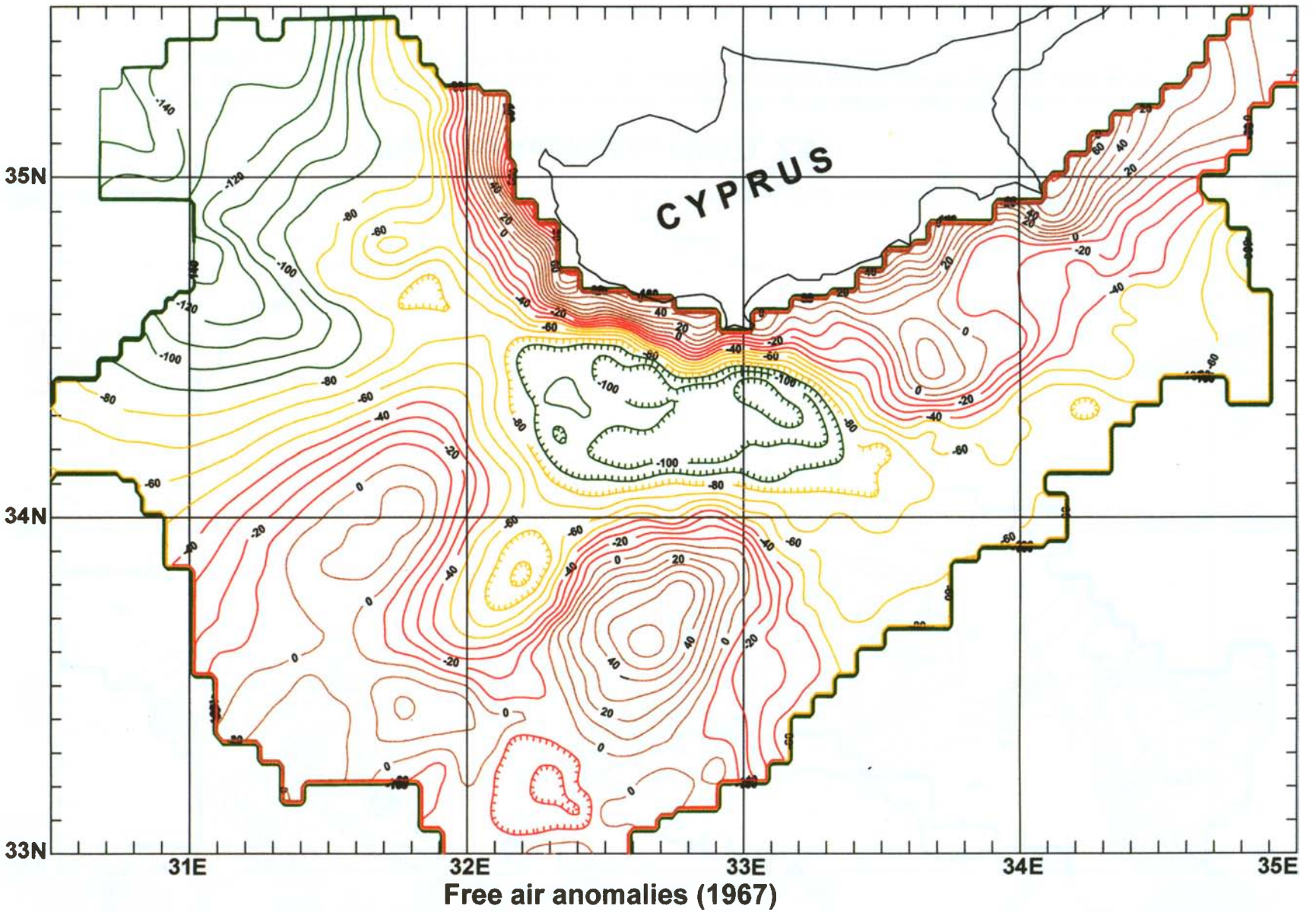


Fig. 14.4. Map of Bouguer gravity anomalies of the area to the west and south of Cyprus. The map was drawn based on the results of gravity survey in 1990 Cruise 10 of R/V 'Akademik Nikolay Strakhov'. The international gravity formula of 1967 was used, density value is 2.67 g/cm³. Topographic corrections were used out to 100 km radius. The isoanomaly contour interval is 10 mgal. Mercator projection, scale 1:2,000,000 at latitude 34°N.

totals 1.01 mGal. The overall error, estimated by the misties at 318 crossing points, is equal to 1.98 mGal. This allows us to draw gravity maps with contours of 5 mGal. The accuracy of the data in our cruises depended not only on errors from longitude smoothing (Eötvös correction calculation) but also from latitude smoothing, because there are large areas with high gravity gradients in the region studied.

The new Global Positioning System (GPS) would give the best navigational results in a gravity survey. The GPS system permits continuous observations with insignificant errors. As a result, the level of navigation mistakes can be lowered to below 1 mGal.

RESULTS OF GRAVITY OBSERVATIONS

Anomalies were calculated by the international 1967 formula, and Bouguer anomalies were calculated according to topographic reduction estimated for a 100 km radius. The density of the intermediate layer was taken as 2.67 g/cm^3.

Maps of the bathymetry and free air anomalies are presented in **Fig. 14.2 and Fig. 14.3**. Drawing contours near the seashore is mostly a formality, as the survey coverage is insufficient for the high gradients in the gravity field. Similar problems apply to the periphery of the area surveyed.

For a discussion of these maps let us briefly consider the map as a trapezoid between the 33° and 34° North parallels and the 33° and 35° East meridians.

The main features of the region studied are as follows. Eratosthenes Seamount is a great morphological structure whose top is located at 33°06' N and 32°06' E. The behaviour of the field shows that as a rule free air anomalies followed the submerged bottom relief. It is observed in the following one degree squares: 34°-35°N, 32°-33°E; 33°-34°N, 32°-33°E; 33°-34°N, 33°-34°E; and 34°-35°N, 33°-34°E. In other places such a relationship is not observed. On the trapezoids (34°-35°N, 34°-35°E) and (35°-35°5'N, 34°-35°E) the seafloor contours are oriented E-W, but the isoanomaly trends are SW-NE. The disagreement between the depths and the free air anomaly map can be seen on the trapezium to the west of 32° E. On the flat bottom to the north-west of Eratosthenes Seamount an area with a large anomaly exists (centered at 33.9°N, 31.7°E), comparable in amplitude (but not by level) to that of Eratosthenes. This north-oriented anomaly does not coincide with the bottom relief. An exception can be seen only on the N-E corner of the trapezoid at 34°-35°N, 31°-32°E.

The main features of the Bouguer anomaly (Fig. 14.4) are seen near the shore of the island:

1) an anomaly with gradient near 6 mGal/km to the west;
2) an anomaly near 3 mGal/km to the east; and
3) some depressions on the south.

Features 1) and 2) generally coincide to those seen in Fig. 14.3, but feature 3) differs greatly from it. This picture illustrates the extremely nonhomogenous densities of the rocks in the coastal area. An interesting set of anomalies can be seen in the 33°-34°N, 32°-33°E and 33°-35°N, 31°-32°E trapezoids in Fig. 14.4. Here the anomaly associated with Eratosthenes Seamount is practically absent. But the anomaly centered at 33.9°N, 31.7°E is seen very clearly, and its amplitude is nearly 100 mGal (with an absolute level of +190 mGal and a gradient approaching 2 mGal/km). Such behaviour of the anomalies allows us to suppose that:

1) the density of the rocks of Eratosthenes Seamount is compatible to the densities of the rocks below the seafloor; and
2) a similar submerged high density structure exists to the northwest of Eratosthenes Seamount.

Comparison of our data to the previous Bouguer gravity map of Morelli et al. (1988, see overleaf) shows that the general features of both data sets are in agreement. Differences can be seen concerning the position of the anomaly maximum in the 33°-35°N, 31°-32°E trapezium, in the position of a depression to the south of Cyprus and, especially, in the details of the anomalies. These differences in the positions and the amplitudes of the anomalies derive from the dense coverage of the latest survey.

REFERENCES CITED

Boyarsky, E. A., and Afanasieva L. V., 1992. The software for treatment of gravity measurements. In: International science-technical conference "Marine Gravimetry-92", St. Petersburg, p. 26-27. (In Russian).

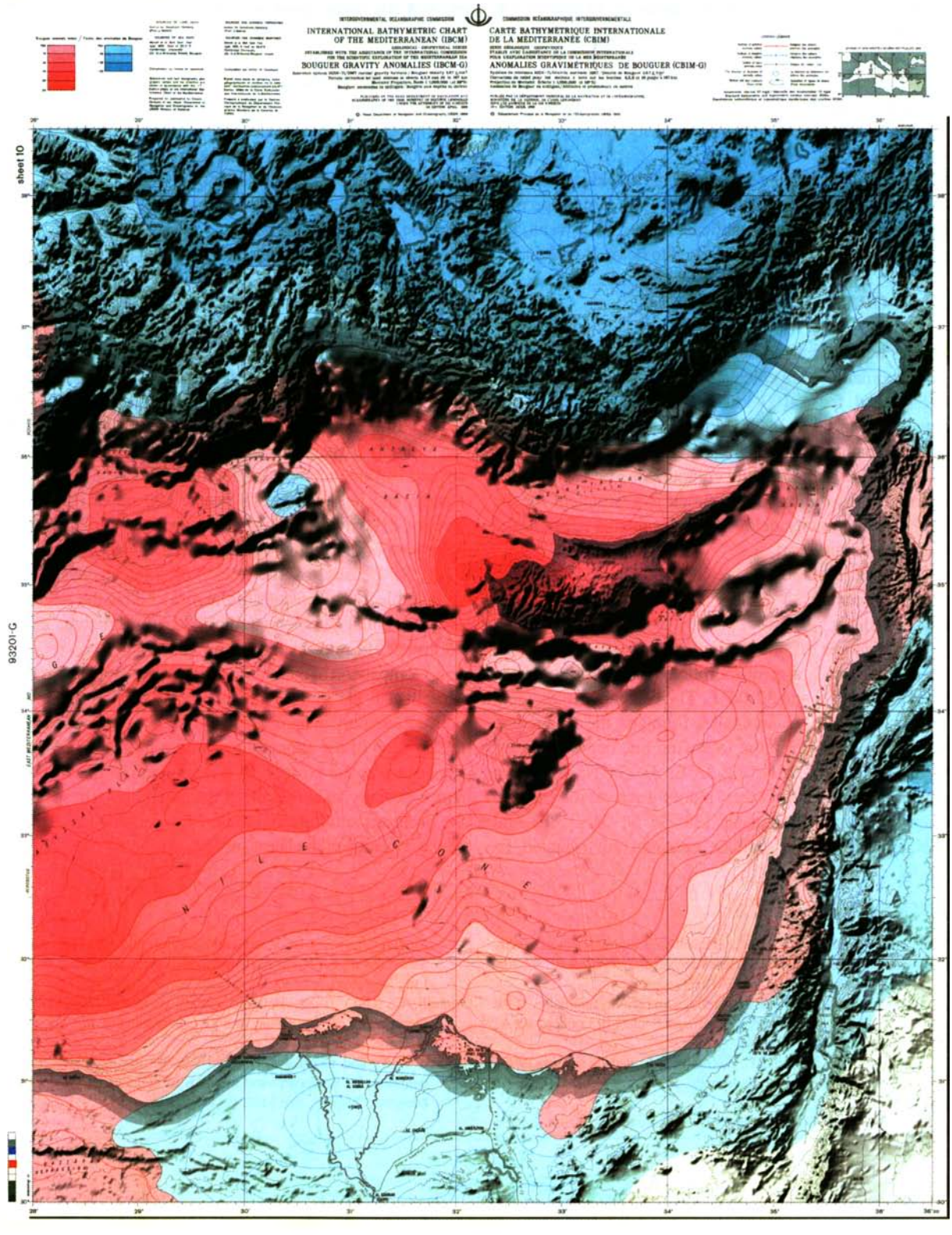
Gass, I. G., and Masson-Smith, D., 1960. The geology and gravity anomalies of the Troodos massif, Cyprus. Phil. Trans. of the Royal Society of London, ser. A., N. 1060, v. 255, p. 417-467.

Kireev, K. N., Koutepov, V. S., Poushina, L. V., Toulin, V. A., and Cheremisin, V. G., 1978. Stabilization of the marine gravimeter. Moscow, "Nauka", 79 p. (In Russian).

Makris, J., and Wang J., 1994. Bouguer gravity anomalies of the Eastern Mediterranean Sea. In: V. A. Krasheninnikov and J. K. Hall (eds.), Geological Sstructure of the North-Eastern Mediterranean, Historical Productions Hall Ltd., Jerusalem, p. 87-98.

Morelli, C., (Ed.). 1988. Bouguer gravity anomalies (IBCM-G). The Head Department of Navigation and Oceanography of the USSR Ministry of Defence, Leningrad.

Toulin, V. A., and Osinskaya, S. V., 1970. Marine gravimeter with automatic counting. In: Equipment and methods of counting of gravity figures at sea, Moscow, "Nauka", p. 93-101. (In Russian).



IBCM-G Bouguer Gravity Anomaly Sheet 10 of the eastern Mediterranean Sea. Complete description of this IBCM Geological-Geophysical Overlay Series can be found in Appendix G. This compilation, published in 1988, is primarily based upon east-west tracks of cruises of Cambridge University in the UK. Contours are every 10 mGal, with changes in tint every 50 mGal. Red tints are positive and blue tints are negative. The map has been shaded by Global Mapper® using the 2' ETOPO2 topographic/bathymetric dataset.

Chapter 15

Digital Terrain Model (DTM) of Cyprus: The Island, its Continental Shelf, and the Surrounding Sea

John K. Hall
Geological Survey of Israel, Marine Geology, Mapping & Tectonics Division, 30 Malchei Israel Street, Jerusalem 95 501, Israel

INTRODUCTION

The construction of digital terrain models (DTMs) is basically a time-consuming and masochistic undertaking. Because the methods for making DTMs of land and sea are so completely different, the two will be divided into separate sections below. The section for the land DTM is excerpted from an article in GSI Current Research Vol. 11 (Hall, 1998a). This article describes the method accompanying the preparation of the 25 m DTM of Cyprus, and the publication of the 1:250,000 scale shaded relief poster of Cyprus (Hall, 1998b), which is reprinted to accompany these volumes.

INTRODUCTION – THE LAND DTM

Topography represents one basic layer within a geographic information system (GIS). The construction of a detailed DTM is usually an expensive and time consuming undertaking. During 1993-96 a digital terrain model (DTM) of Cyprus was produced, within the Geological Survey of Israel project 'DTM of the Middle East', to support the preparation of a geophysical GIS for the eastern Mediterranean (Krasheninnikov and Hall, 1994; Morelli and Val'chuk, 1988). The work was carried out in collaboration with the Cyprus Geological Survey Department, and Rohr Productions Ltd., a company interested in the illustrated physical geography and history of the island. This DTM required more than 2,000 hours of interactive computer analysis of the 10 and 20 m elevation contours in the 1:50,000 scale topocadastral mapping. The digital DTM will provide a detailed topographic basis for future GIS work on the island. When visualized as shaded relief or in colored hypsometric format, the DTM graphically shows the overall morphology and the many features of this geologically very complex island. These include the central protrusion of the Troodos, the sinuous northern Kyrenia ridge, the intervening valley and all the associated drainage, faults and lineaments.

The new 25 m DTM of the island of Cyprus is among the highest resolution DTM datasets in the world (Wolf and Wingham, 1992).

EXISTING TOPOGRAPHIC MAPPING

The modern 1:50,000 scale topocadastral coverage of Cyprus consists of the K717 series of 24 sheets (**Table 15.1**). These were produced under the direction of the UK Directorate of Military Survey, Ministry of Defence, London. They were compiled by photogrammetric methods and drawn by Fairey Surveys Ltd. from aerial photographs taken in 1970. Individual sheets used here indicate revisions up to the third edition, and were printed between 1973 and 1988 by the United Kingdom Mapping and Charting Establishment RE (Royal Engineers). The maps are on the Universal Transverse Mercator Projection (UTM), International Spheroid, with the European Datum for the horizontal datum, and Mean Sea Level for the vertical datum. Elevations are all in meters, with contour interval 20 in and supplementary contours at 10 in intervals.

MAKING THE DTM

The DTM was produced using the same methods used for making the DTM of Israel and vicinity (Hall, 1993). The original color maps were joined into a seamless sheet which was then cut into 42 separate 20 by 20 km map tiles (**Fig. 15.1**; **Table 15.2**). The four quadrants of each tile were then scanned at 300 dpi on a grayscale scanner. A variable threshhold was manually applied to each quadrant to generate a bitmap with maximum definition of the originally brown contours, and minimum interference of the various color screens showing vegetative cover and cultural information. The four quadrants for each tile were then reassembled and edited using the innovative raster analysis software developed for the Israeli DTM (Hall et al., 1990; Hall, 1995).

The resulting DTM is on a 25 m grid locked into the UTM grid used in the K717 map series. Thus there is an elevation value for every 0.25 mm^2 of map, and each square kilometer is represented by a 40 by 40 array of elevations, or 1600 separate heights. The vertical resolution for the DTM is a decimeter (10 cm). The DTM agrees exactly with all the contour data and for nodes between contours represents a weighted average of the E-W and N-S bicubic spline profiles passing through the adjacent contours. Constraints on the bicubic splines required that they not range more than 5 m above or below an E-W or N-S straight line joining any two adjacent contours.

The DTM is stored as 42 separate binary files, each representing its own tile and each occupying less than one 3.5" diskette. Each file gives the 641,601 elevations for that 20 by 20 km tile. The elevations in decimeters are written as signed two-byte integers. The file begins with the northwest corner and proceeds to the southeast corner as a series of west to east lines, each with 801 elevations. This is the same format used in the DTM for Israel and vicinity.

It should be noted that in parallel, the mostly 1:50,000, 1:

Table 15.1. Listing of Series K717 1:50,000 UTM topocadastral map sheets for Cyprus. From the Map legend: Produced under the direction of the Directorate of Military Survey, Ministry of Defence, London. Compiled by photogrammetric methods and drawn by Fairey Surveys Ltd. from air photographs dated 1970. Printed by Mapping and Charting Establishment RE (Royal Engineers). Universal Transverse Mercator Projection. International Spheroid. Horizontal Datum: - European Datum. Vertical Datum: - Mean Sea Level. Elevations in meters, contour interval 20 in with supplementary contours at 20 m intervals.

No	Sheet Name	Edition	Year	No	Sheet Name	Edition	Year	No	Sheet Name	Edition	Year
1.	Ayia Irini	1-GSGS	1973	9.	Kambos	1-GSGS	1973	17.	Pano Panayia	1-GSGS	1973
2.	Lapithos	1-GSGS	1973	10.	Morphou	1-GSGS	1973	18.	Troodos	1-GSGS	1973
3.	Kyrenia	2-GSGS	1988	11.	Paleometokho	2-GSGS	1988	19.	Pelekhori	1-GSGS	1973
4.	Lefkoniko	2-GSGS	1988	12.	Nicosia	2-GSGS	1988	20.	Pano Lefkara	1-GSGS	1973
5.	Trikomo	2-GSGS	1988	13.	Athienou	1-GSGS	1973	21.	Larnaca	2-GSGS	1982
6.	Yialousa	1-GSGS	1973?	14.	Famagusta			22.	Pissouri	2-GSGS	1981
7.	Rizokarpaso	1-GSGS	1973?	15.	Cape Greco	1-GSGS	1977	23.	Limassol	3-GSGS	1980
8.	Polis	1-GSGS	1973	16.	Paphos	1-GSGS	1973	24.	Zyyi	1-GSGS	1973

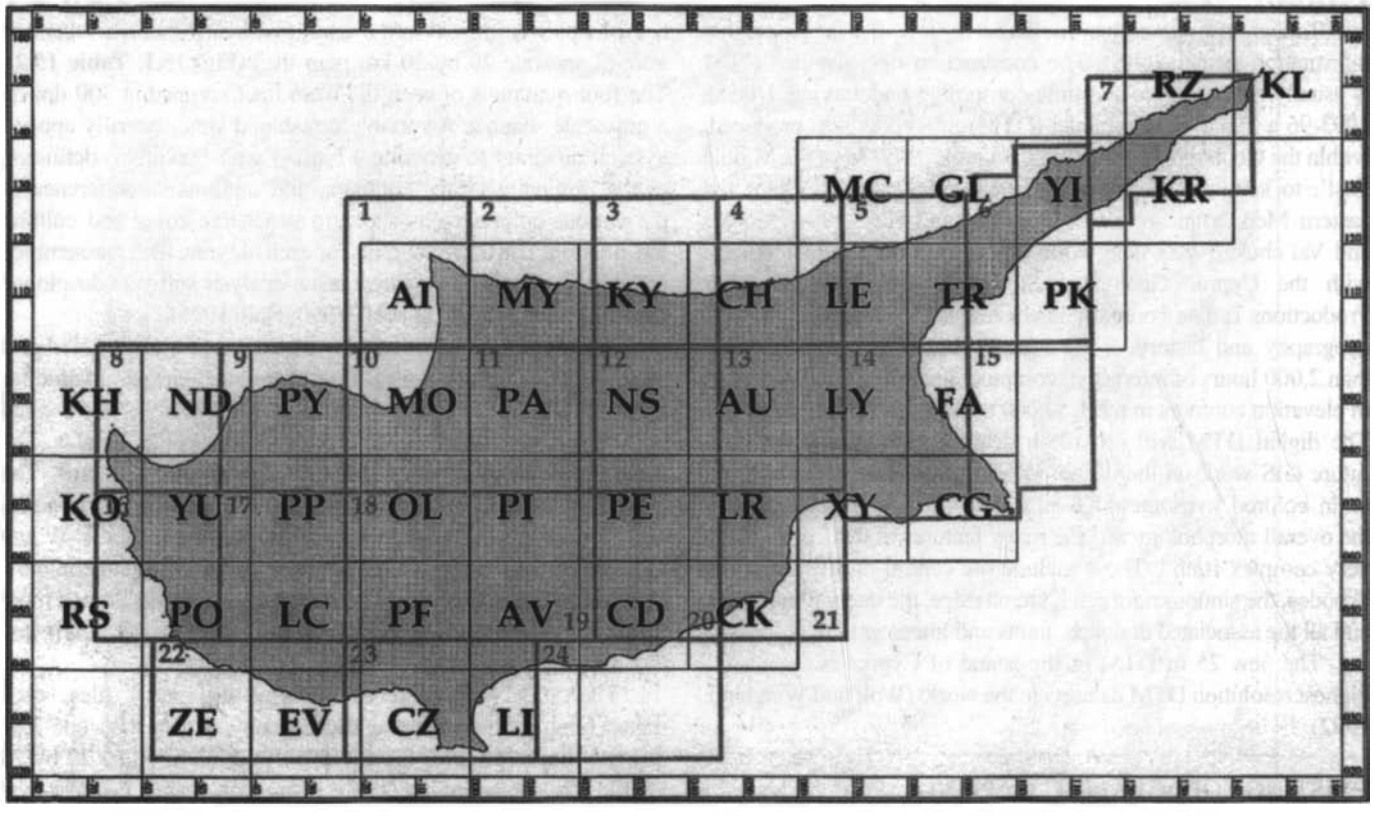


Figure 15.1. Schematic diagram showing the subdivision of the island of Cyprus into the forty-two 20 by 20 km 'tiles' which are analyzed separately to generate the DTM. The exterior grid (in km) is modified from that of the original UTM Grid Zone Designation 36S by the subtraction of 500 km from the easting (x coordinate) and 3,800 km from the northing (y coordinate).

Table 15.2. Listing of map sheet tiles used in the DTM of Cyprus (Sorted by the arbitrarily defined Quadrangles in Fig. 15.1),

Quad	Tile	Tile Name	Quad	Tile	Tile Name	Quad	Tile	Tile Name
1-IV	RZ	Rizokarpaso	7-IV	KO	Koppo Island	11-II	FA	Famagusta
2-III	KL	Klidhes Islands	8-I	ND	Nea Dhimmata	11-III	XY	Xylophaghou
3-III	AI	Ayia Irini	8-II	PY	Kato Pyrgos	11-IV	CG	Cape Greco
3-IV	MY	Myrtou	8-III	YU	Yiolou Sheet	12-II	RS	Rouskia
4-III	KY	Kyrenia	8-IV	PP	Paho Panaya	13-I	PO	Polis
4-IV	CH	Chatos	9-I	MO	Morphou	13-II	LC	Lagouda Chiftlik
5-I	MC	Missing Corner	9-II	PA	Peristerona	13-III	ZE	Cape Zephyros
5-II	GL	Galatia	9-III	OL	Mount Olympus	13-IV	EV	Evdhimou Bay
5-III	LE	Lefkoniko	9-IV	PI	Pitsilia	14-I	PF	Perapedhi Forest
5-IV	TR	Trikomo	10-I	NS	Nicosia	14-II	AV	Ayia Varvara
6-I	YI	Yialousa	10-II	AU	Athienou	14-III	CZ	Cape Zevgari
6-II	KR	Karpasia	10-III	PE	Perakhorio	14-IV	LI	Limassol
6-III	PK	Pano Koronia Forest	10-IV	LR	Larnaca	15-I	CD	Cape Dolos
7-II	KH	Khamilis Island	11-I	LY	Lysi	15-II	CK	Cape Kiti

25,000, and 1:12,500 scale fairsheets of hydrographic surveys carried out in the 1930s and 1950s by the British Admiralty Hydrographic Department around Cyprus were digitized (Hall, 1996). Approximately 183,000 depth soundings have been extracted and will be used to generate a continuation of the 25 m land DTM out to depths of about 100 m.

TOPOGRAPHIC VISUALIZATION

The high resolution DTM allows us to visualize the topography in a number of ways. Figure 15.2 is a shaded relief representation of the island, as if it were illuminated by a light source in the northwest at 30° elevation. Because illumination of the surface from different azimuths and elevations serves to accentuate its morphology, this format is very useful for identifying topographic texture or fabric, subtle expressions of slope such as those exhibited by drainage systems, and linear fractures and lineaments which have topographic expression that is not parallel to the light source. This northwest illumination has long been the standard for shaded relief presentations.

Figure 15.3 shows the topography as colored hypsometry. In this format, similar to the well-known contour maps, seventy-two different colors are used to identify the heights, in bands of 20 m, at each point on the grid. This format is very useful for identifying relative as well as absolute heights, and especially flat areas and the continuation of linear features through drainage patterns, subtle ridges, or congruence of height color patterns.

GEOGRAPHICAL DATA

The DTM allows computation of the island's physical characteristics. By examining the average elevation of each of the 25 by 25 m DTM facets (each 625 m² in area) it is possible to calculate the hypsometric curve (**Fig. 15.4**). This shows the area above various elevations in 10 m increments. A separate calculation, determining the volume under each facet, allows calculation of the total volume of the island. The DTM gives an area of facets with elevation greater or equal to zero (the offshore was set at -1 m) of 9,214 km², and a volume of 2,750 km³. Dividing the two gives an average height for a tabular Cyprus of 335 m.

The coastline was also digitized from the 1:50,000 UTM map sheets using a digitizer with 0.001" resolution (theoretically 1.27 m on the map). The area within the digitized coastline using the method of Hall (1976) is 9,248.4 km², while the perimeter is 801.6 km, and the center of mass is located at UTM coordinates 20.524N, 70.885E.

Some 130 islands lie offshore, and were also digitized. Altogether these have an aggregate area of 0.6 km² and total perimeter of 31.5 km. Many of these were mere specks, and the digitization of their coastline is only approximate.

DISCUSSION OF THE LAND DTM

An analysis of the faults, fractures, and other linear features observed in Figure 15.2 is obviously beyond the scope of this brief note. What is clear however is that the shaded relief imagery shows many additional features which will definitely augment the structures indicated on the revised 1:250,000 Geological Map of Cyprus (Geological Survey Department, 1995).

It is curious to note the discrepancy in area given by various sources. The area calculated here within the 130 islands and the main island is 0.5654 km² plus 9,248.373 km², or 9,248.938 km². This is in close agreement with the area of 9,251 km² given by the

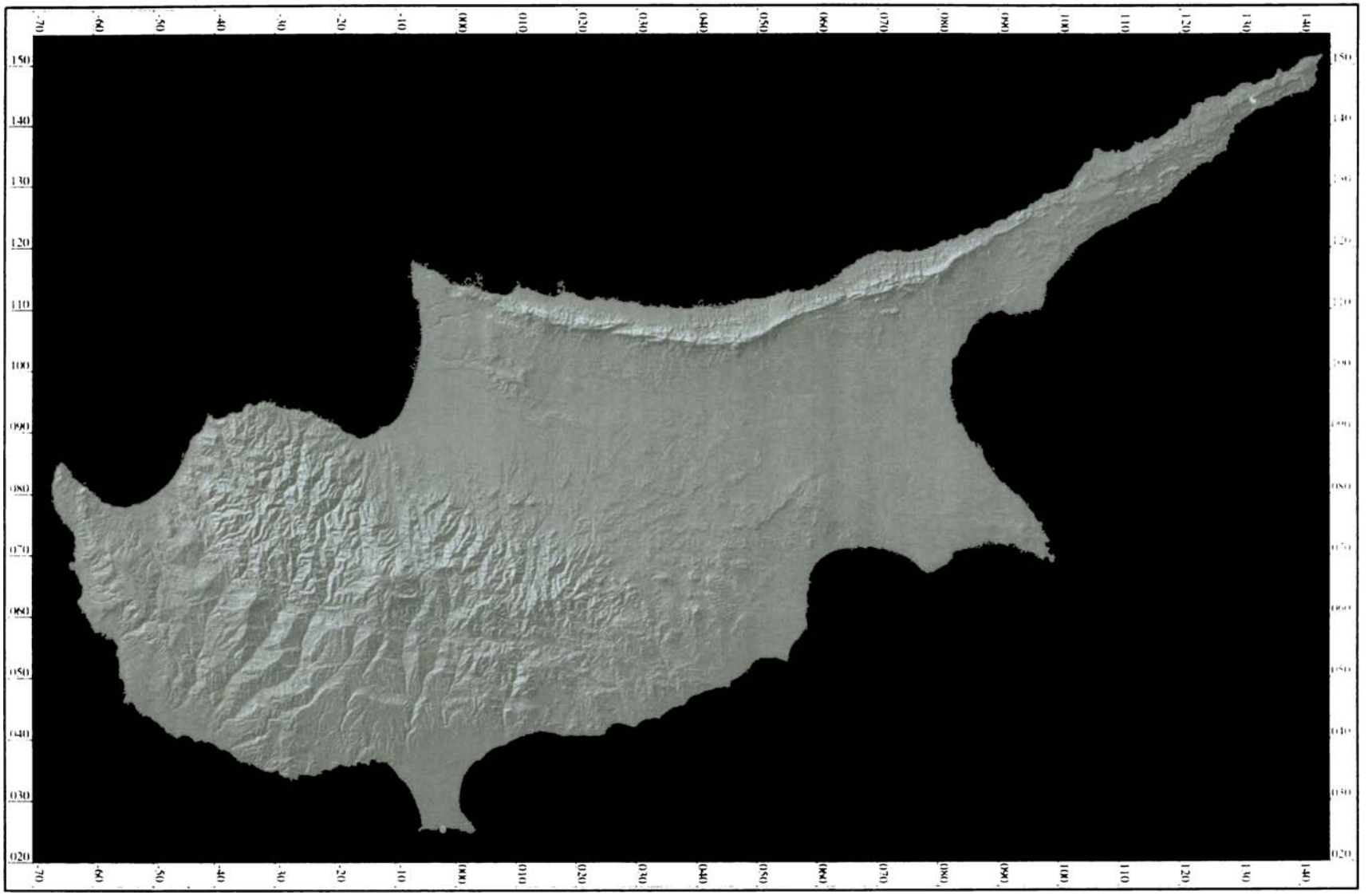


Figure 15.2. Shaded relief image of the island of Cyprus prepared by computer from the gridded 25 m DTM of Cyprus. The relief is shown by analytic hillshading, in which the surface is illuminated by a light source in the northwest at an elevation of 30 degrees. This is the best way in which to see the fabric of the physiography. This is included as a 1:250,000 scale poster in the maps section. The exterior grid (in km) is modified from that of the original UTM Grid Zone Designation 36S by the subtraction of 500 km from the easting (x coordinate) and 3,800 km from the northing (y coordinate).

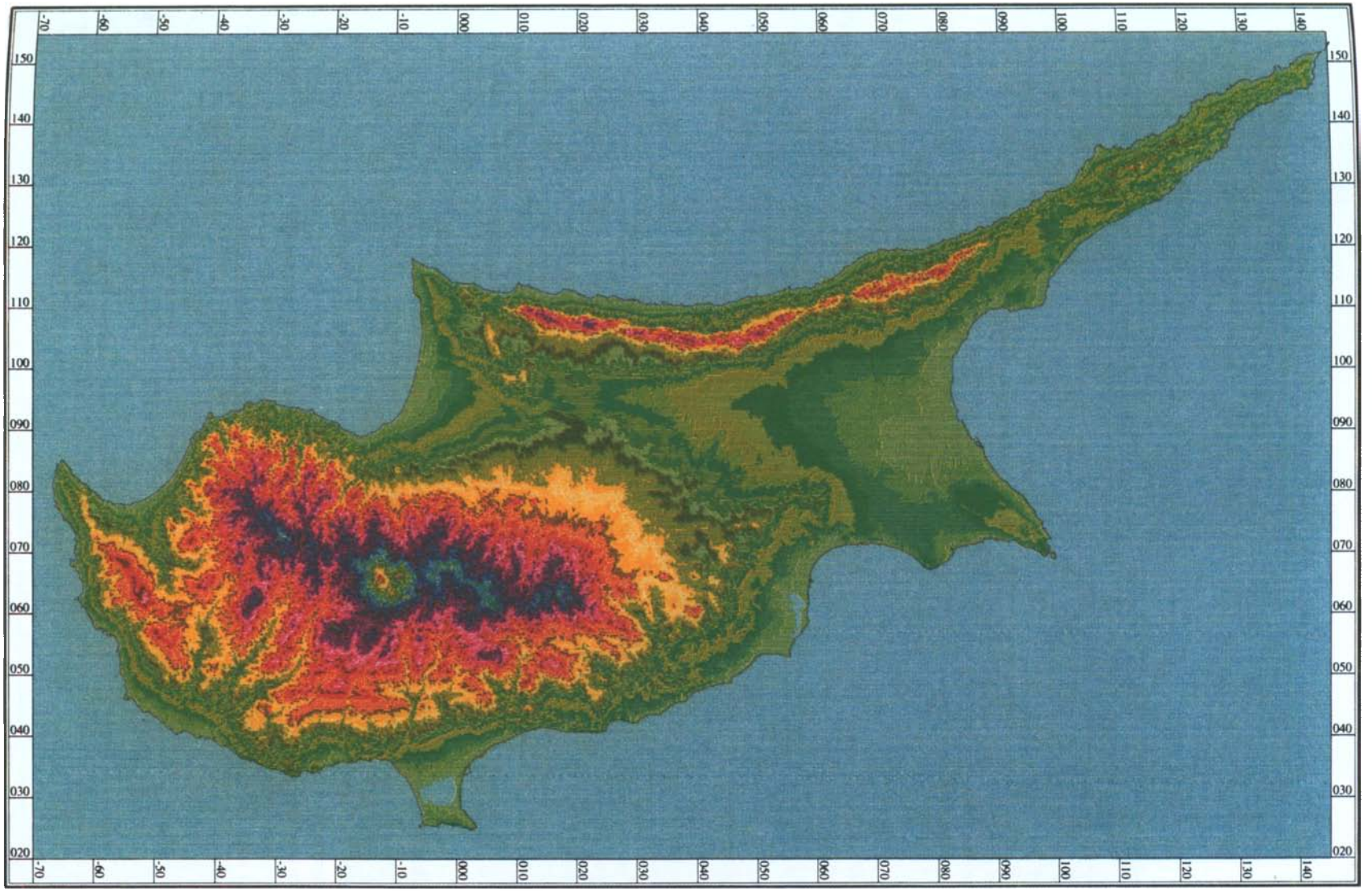


Figure 15.3. Colored hypsometric map of Cyprus. A seventy-two color palette indicates the height intervals every 20 m. The four geological zones of Cyprus are evident: The elevated Kyrenia Terane along the northern coast; the elevated Troodos (Ophiolite) Terrane with 1951 m high Mount Olympus in the southern part; the horseshoe shaped circum-Troodos sedimentrary succession wrapping around the Troodos on the east; and the smaller isolated Mamonia Terrane in the southwest. UTM projection, scale 1:1,000,000. The exterior grid (in km) is modified from that of the original UTM Grid Zone Designation 36S by the subtraction of 500 km from the easting (x coordinate) and 3,800 km from the northing (y coordinate).

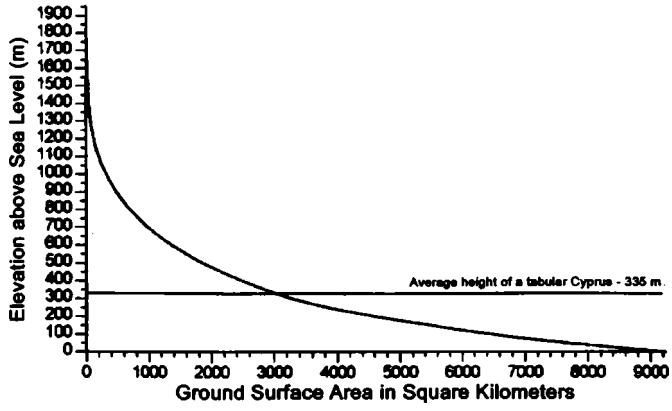


Figure 15.4. Hypsometric curve or hypsometric integral for the new 25 m grid DTM of the island of Cyprus. Maximum height of the island is 1951 m at Mount Olympus. Volume calculations indicate that the average height of a tabular island would be 335 m.

Royal Geographical Society (1983) Atlas, and the 9,250 km^2 of the more recent George Philip's (1996) Atlas, but some 250 km^2 greater than the 8,995 km^2 given in the Hammond (1994) Odyssey Atlas of the World.

INTRODUCTION – THE MARINE DTM

As part of an active program to map their colonial areas, the British Admiralty Hydrographic Department maintained survey vessels that worked in the Mediterranean Sea, off West Africa, and in the Arabian Sea and the Persian Gulf in the 1930s (Ritchie, 1994, 1995; Morris, 1995). In the winter months HMS Ormonde would carry out surveys in the Red Sea and Indian Ocean, and then move to the cooler Mediterranean in the summer months for surveys of Cyprus. HMS Endeavour divided her time between surveys in West Africa and along the coasts of Mandatory Palestine (Morris, 1995).

THE EARLY HYDROGRAPHIC VESSELS

At present, much of the information on the charts around Cyprus is derived from surveys carried out over long months by a small flotilla of specialized hydrographic vessels or warships pressed into hydrographic service. A brief rundown of the vessels whose survey data have been used in this compilation is given here, in order of launch date. The vessels are shown in **Figure 15.5.**

HMS Endeavour was built by Fairfields, Govan, in 1912. Her displacement was 1280 tons, maximum speed was 13 kts and dimensions were 241 by 34 by 11.25 ft. She was a purpose built surveying ship with a handsome yacht-like profile. She was well equipped, but with only one screw, her manoeuverability was limited. She was reduced to an accomodation hulk in 1943, after carrying out the surveys of the Israeli port of Elat in the Gulf of Aqaba/Elat in possible preparation of an alternative supply port should Egypt by occupied by Rommel's Africa Corps. HMS Endeavour never actually surveyed Cyprus, but is included here because of her extensive work off the Nile Delta in Egypt and of Mandatory Palestine.

HMS Ormonde was one of the 24 patrol sloops of the so-called '24' or 'Racehorse' class, na Company in 1918, converted for surveying in 1923, and used until 1936. She displaced 1320 tons, had a maximum speed of 17 kts, and was 276.5 by 35 by 12 feet.

HMS Challenger, named after a very famous predecessor, was a surveying ship built at Chatham Dockyard. She was launched 1 June 1931 and used until 1953. Her displacement was 1140 tons and dimensions were 220 by 36 by 12.5 ft.

HMS Dalrymple was a Bay Class frigate, built by Pickersgill She was originally christened the Loch Class, and then renamed the Luce Bay. Launched on April 12 1945, she displaced 1600 tons, had a maximum speed of 18 kts, and was 307.33 by 38.5 by 12.75 ft HMS Dalrymple was outfitted for surveying in 1947, and worked until 1965, when she became the Portuguese ship Afonso de Albequerque. She was named after Alexander Dalrymple, the Scot (1737-1808) who outfitted the HMS Endeavour for the expedition of Capt. James Cook, and was later the first Hydrographer of the Royal Navy in 1795.

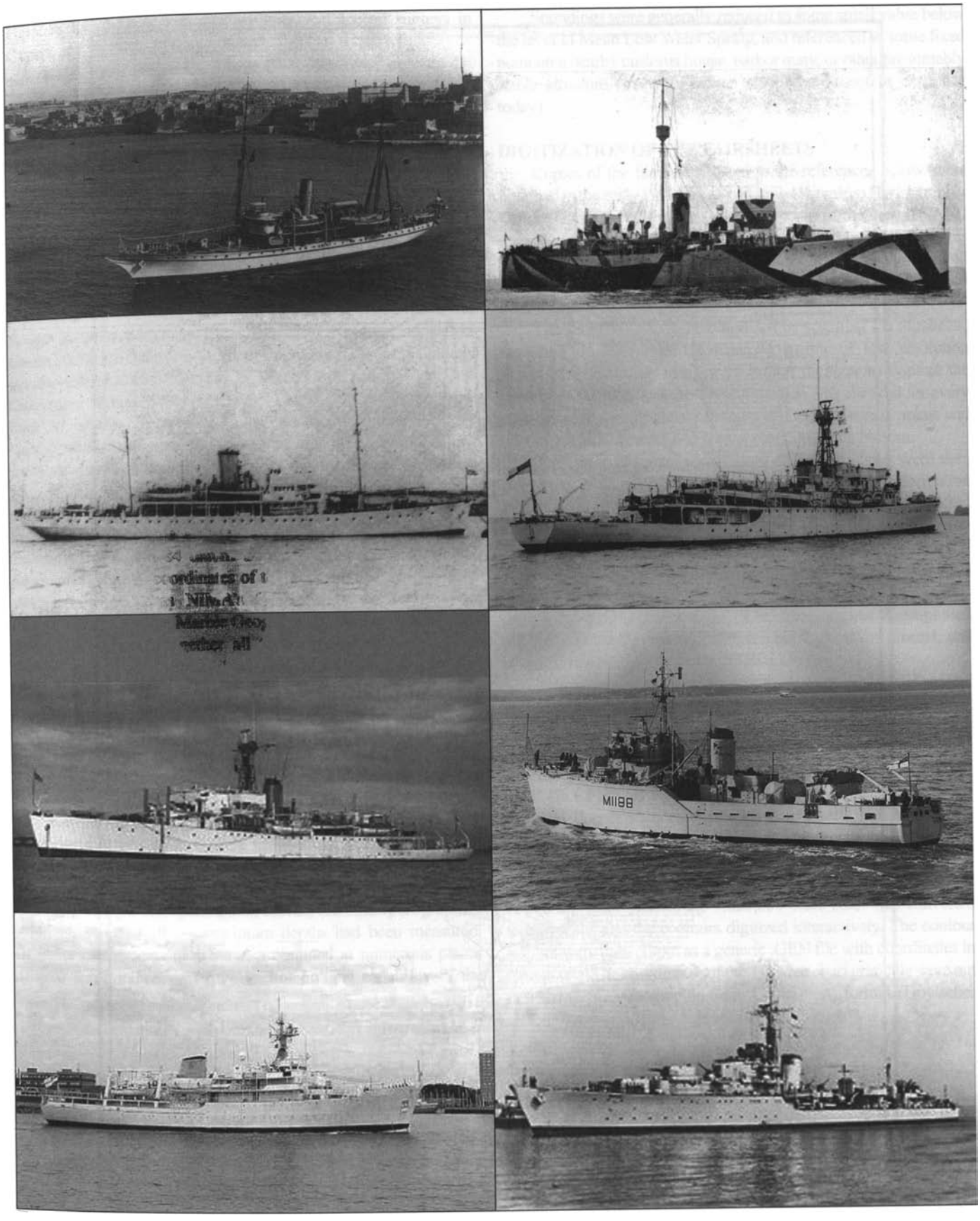
HMS Owen is a sister ship of HMS Dalrymple. She was built by Hall Russell in Aberdeen. Originally named the Loch Muick, then the Thurso Bay, she was launched 19 October 1945 and outfitted for surveying in 1949. She carried out hydrographic surveys until 1965, and was scrapped in 1970.

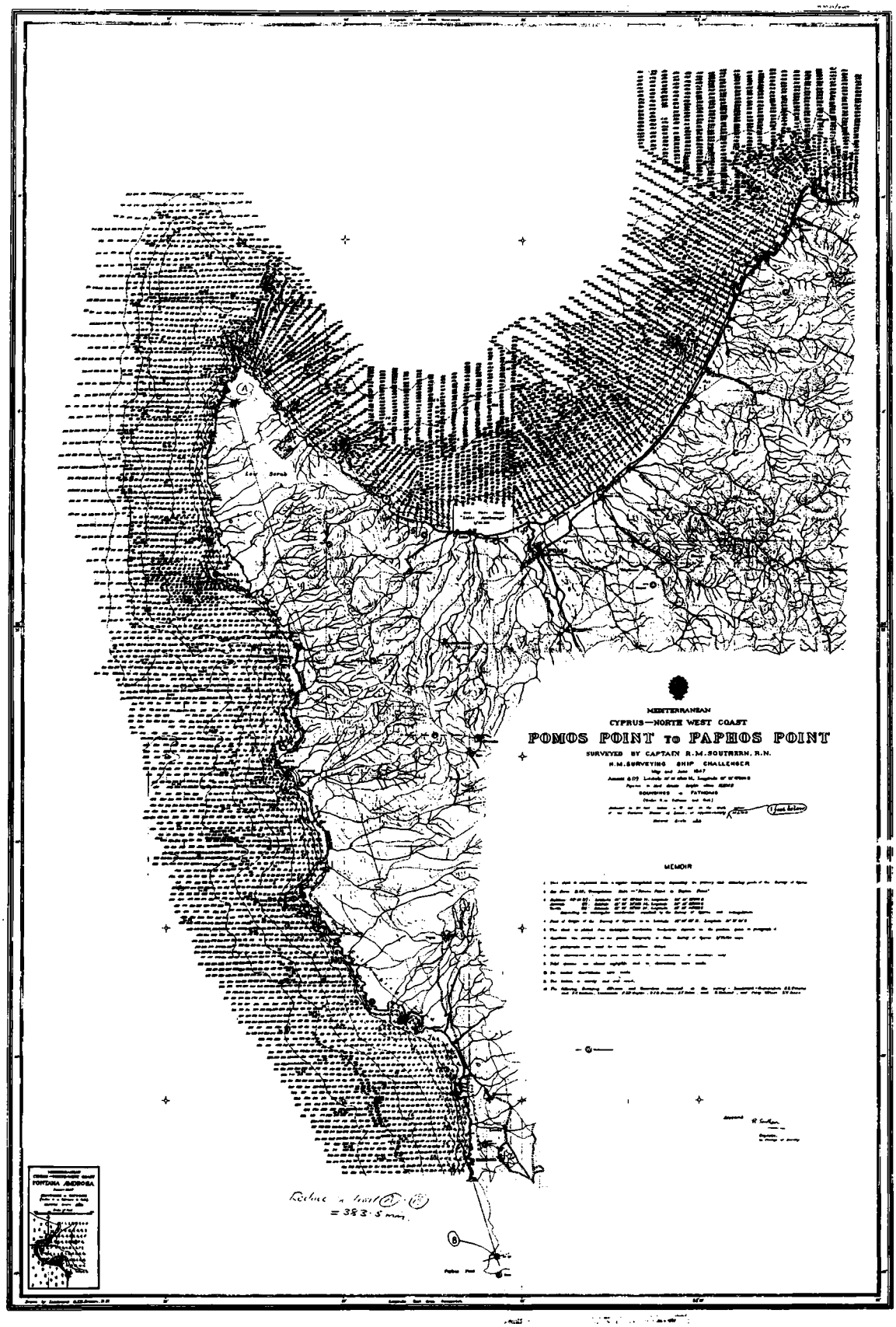
HMS Walkerton, pennant M1188, was a Coniston-Ton Class minesweeper, launched by Thornycroft on 21 November 1956. Her displacement was 425 tons, and dimensions 152 by 28 by 8 ft. In January 1970 she was converted for duties with the Royal Navy College in Dartmouth.

HMS Herald, an improved Hecla Class Ocean Survey Ship pennant H138, was built by Robb Caledon, Leith. Launched on 4 October 1973, she was in service until her decommissioning in May 2001. Her dimensions were 250 by 60 by 16 ft, with 2700 tons displacement and 14 kts maximum speed. Interestingly, HMS



Figure 15.5. Photographs of the British Admiralty Hydrographic Department (BAHD - now UKHO) survey vessels that carried out the hydrographic surveys around the island of Cyprus. a) HMS Endeavour, the surveying workhorse of the Nile Delta and Mandatory Palestine, shown here in Grand Harbour, Malta, circa 1934 (from Ritchie, 1994); b) HMS Ormonde in her World War I camouflage (photo courtesy of Blyth Ship Building Company); c) HMS Challenger (photo from IOC, 2003); d) HMS Dalrymple; e) HMS Owen in a photo supplied by Carl Procter; f) HMS Walkerton g) HMS Herald; h) HMS Trafalgar.


M1198


MEDITERRANEAN
CYPRUS—NORTH WEST COAST
POMOS POINT to PAPHOS POINT
SURVEYED BY CAPTAIN R.M.SOUTHERN, R.N.
H.M.SURVEYING SHIP CHALLENGER
SOUNDINGS in FATHOMS
MEMOIR
PONTOYA AMBROSA

Herald's last deployment was for additional coastal surveys in Cyprus and an official visit to Beirut.

HMS Trafalgar was a Battle Class destroyer, pennant D-77. Built by Swan Hunter in Walsend, she was laid out in 1943, launched in 1944, and commissioned July 23, 1945. She was deployed in the Mediterranean in 1960-61. Displacement was 2325 tons, and dimensions 379 by 40.25 by 17.5 ft.

INSHORE HYDROGRAPHIC SURVEYS 1930-1937; 1948-1954; 1960-1963.

A series of systematic surveys around Cyprus began in the summer of 1930 when HMS Ormonde made hydrographic survey fairsheets at scales of 1:10,000 to 1:50,000. These were interrupted for more than a decade by the advent of World War II and its aftermath. After the war, HMS Challenger and HMS Owen continued the work, and then following another break likely occasioned by the Suez crisis in 1956, HMS Owen and HMS Dalrymple completed the mapping. The references for the more than 30 surveys and deeper water circum-navigations by other survey vessels are given in a separate reference section below, together with the number of soundings and annotations recovered. **Figure 15.6** shows one such fairsheet for the area around Cape Arnauti, the northwestward protrusion of Cyprus extending from Pomos Point in the northeast to Paphos Point in the south.

From the 1930s to the 1960s hydrographic surveying progressed from primarily wire soundings with a steam-powered sounding engine, to acoustic echo-soundings calibrated by 'bar checks'. These consisted of lowering a target plate to fixed depths below the sounder and noting the depth indication, an effective way to empirically calibrate the sounder without knowing the exact speed of sound in the seawater. Navigation also steadily improved, from the determination of the sounding's location by use of ship based horizontal sextant angle observations of three or more landmarks on shore, or shore-based theodolites, to electronic distance or phase-measuring systems which allowed location relative to elaborate grids.

The layout of the survey lines was primarily controlled by concerns about SOLAS (Safety Of Life At Sea), which meant delineating the underwater features that a prudent navigator must avoid. As the soundings showed the bottom becoming more complex, then the line spacing was halved, until the hydrographers were assured that all the minimum depths had been measured. Samples of the seafloor were also obtained at numerous places to give some indication of the anchor holding capability of the bottom.

Soundings were generally reduced to some small value below the level of Mean Low Water Spring, and referenced to some fixed point on a nearby customs house, harbor quay, or other presumably stable structure (many of which are probably not in existence today).

DIGITIZATION OF THE FAIRSHEETS

Copies of the fairsheets, listed in the references below, were obtained in the early 1990s from the United Kingdom Hydrographic Office (UKHO) in Taunton, for the purposes of the new IBCM-II compilation in the former 'British Zone of Responsibility'. This was accomplished through the assistance of Brian Harper and Desmond P. D. Scott, both very active in IBCM and GEBCO, and both formerly with the UKHO.

The soundings were then digitized by scanning the fairsheets, breaking the raster scan files into a matrix of low resolution PC screens, and then using a 16 button digitizer to digitize the soundings on every screen. The digitization was checked for every such screen by immediately fitting a surface to the data points and displaying an isometric 3-D fishnet diagram of the bottom.

The raster file pixel coordinates of the soundings were then converted to actual geographic coordinates via a transformation based upon the digitized map graticule. This transformation was specifically designed for this purpose, and combines finite difference techniques with a rubber-sheeting factor (Doytscher and Hall, 1997). The methods are described in fuller detail in Chapter 16. The digitization was done by the author, and most soundings should be well within 2-3 pixels of their original hand-plotted position. At 1:10,000 scale this is within 2 m on the ground, and about 10 m at 1:50,000.

A total of about 183,000 soundings were digitized, together with additional attributes such as bottom type, obstructions, wrecks, and foul areas. **Figure 15.7** shows the distribution of these soundings around the island of Cyprus.

THE DEEPER OFFSHORE

The deeper waters are comparatively poorly sounded. For the purposes of this compilation, the 50 m contours of the bathymetric chart of the Eastern Mediterranean (Hall, 1980, 1981, 1994) were digitized using Able Software Corporation's R2V for Windows. A 300 dpi color scan of the 1:625,000 scale chart was converted to grayscale, and the contours digitized interactively. The contour vectors were then output as a generic .GEN file with coordinates in scan pixels. The coordinates of the 1 degree chart graticule were put into the .GSC (Geographic Scan Calibration) format (Doytscher



Figure 15.6. Reproduction of the E-8226-1 fairsheet for Pomos Point to Paphos Point (BAHD, 1948). This fairsheet was surveyed by Capt. R. M. Southern, R.N., and the officers of H. M. Surveying Ship "Challenger" in May and June 1947. Bears Hydrographic Department stamp dated 14 January 1948. Includes an inset map of Fontana Amorosa from June 1947 at scale 1:1250. Soundings in fathoms (fathoms and feet in less than 11 fathoms). Mercator projection at natural scale 1:50,060, 1 sheet. IBCM Code PT, 9,023 soundings and 203 attributes digitized. The map states that the soundings are "reduced to 8.1 feet below a a cut on the south corner of the Customs House at Latzi, or approximately 1 foot below M.L.W.S."

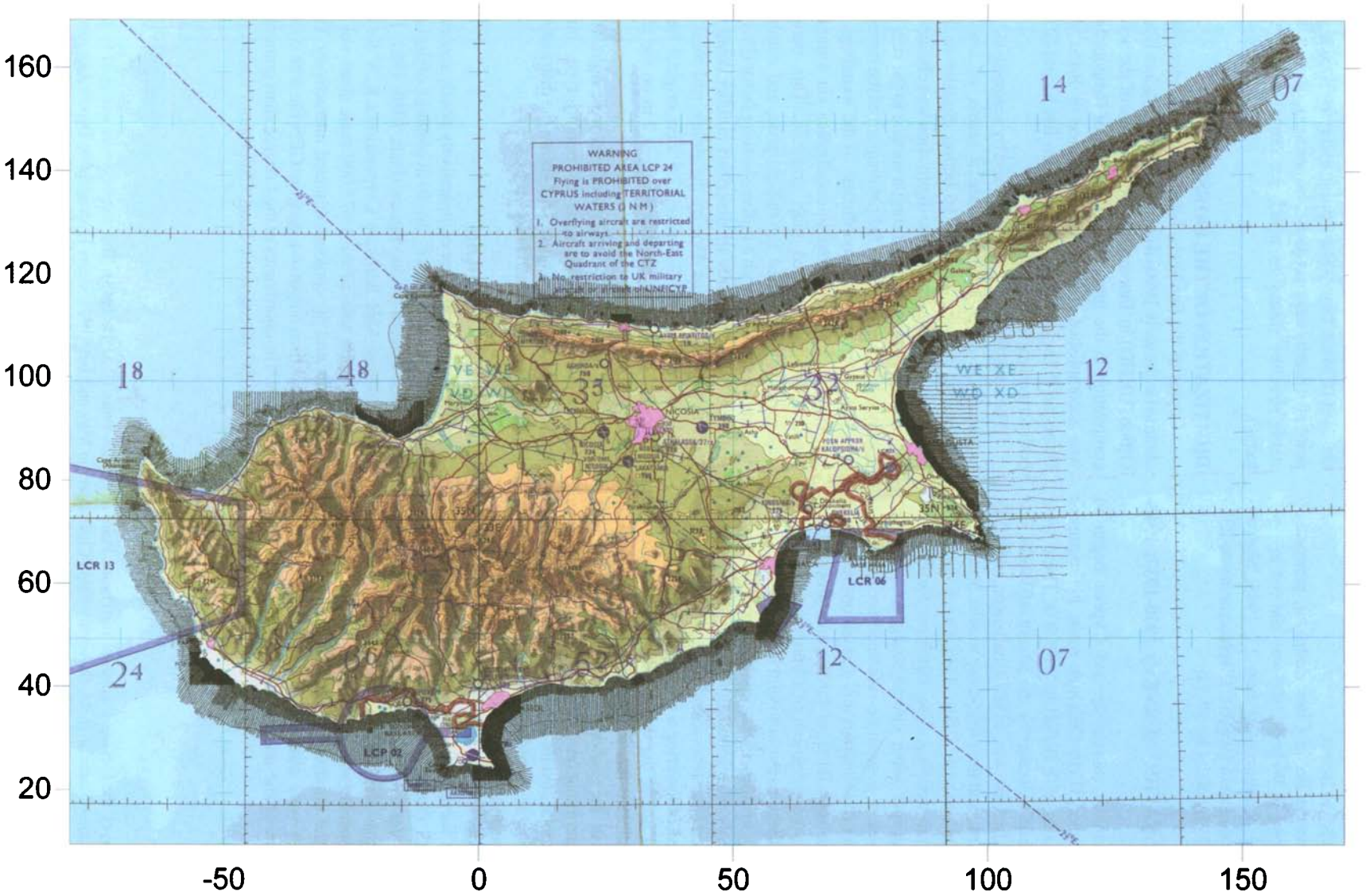


Figure 15.7. Plot of the 183,000 soundings around Cyprus overlaid on the 1:500,000 scale Tactical Piloting Chart (U. K. Ministry of Defence, 1975). The exterior grid (in km) is modified from that of the original UTM Grid Zone Designation 36S by the subtraction of 500 km from the easting (x coordinate) and 3,800 km from the northing (y coordinate).

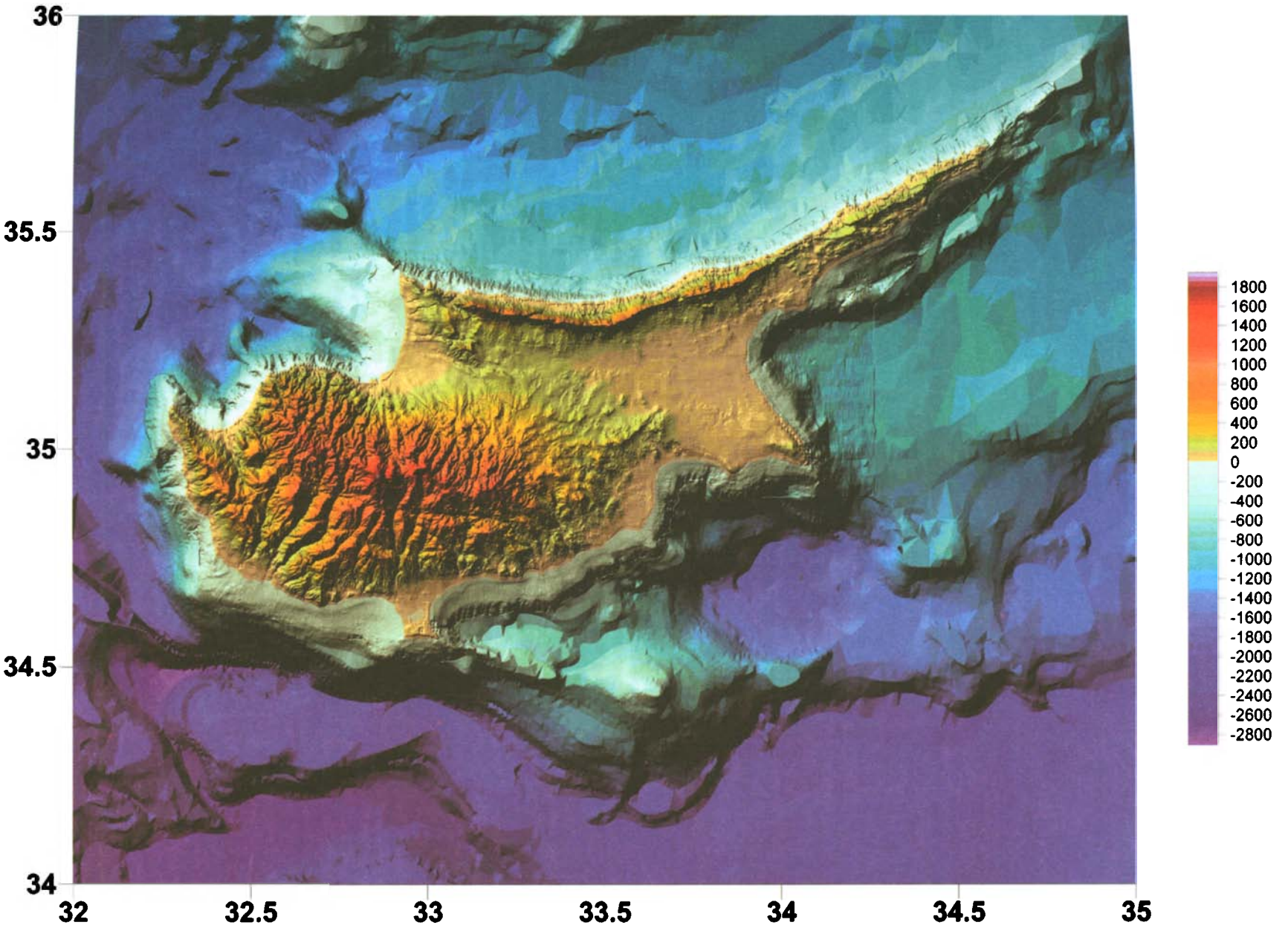


Figure 15.8. Color plot of Cyprus within its continental shelf and the surrounding deep water bathymetry. Coordinates are in degrees latitude and longitude.

and Hall, 1997) and then used to convert the vectors to x,y,z triads in latitude, longitude and depth (*i.e.* negative elevation). These triads were merged with the land elevations every 0.5' from the USGS GTOPO30 dataset, and then interpolated to a 0.25' and 0.5' grid. A simple TIN (Triangular Irregular Network) scheme was used within Golden Software Incorporated's Surfer 8®. The resulting colored shaded relief image, also rendered from Surfer 8®, can be seen in the Introductory Remarks to Part III of the book.

CONSTRUCTION OF THE DTM (Figure 15.8)

The DTM for the land was originally in UTM coordinates. These were converted to geographic coordinates, and then a Triangular Irregular Network (TIN) interpolation performed to obtain a 0.1' (≤185.2 m) grid. Due to datum differences between the land mapping and the hydrographic surveys, a shift of 50 m in easting and 500 m in northing was introduced based on fit of the hydrographic data to the land shoreline. The land DTM was then clipped at sea level within the Surfer 8 program, and merged with a TIN interpolation of the hydrographic surveys. These two were then clipped at the maximum extent of the hydrographic surveys, and again merged with a TIN of the digitized 50 m contours from the Bathymetric Chart of the Eastern Mediterranean at 1:625,000 scale (Hall, 1994, Fig. 1.13 and Plate 1).

ACKNOWLEDGEMENTS

Financial support for production of the land DTM of Cyprus was provided by Dr. Richard L. W. Cleave of Rohr Productions Inc. in Nicosia. The editing of the forty-two map tiles was carried out by Bracha Moalem, Miguel Calvente Chazanoff, and the author during his 1994-96 sabbatical at the Ocean Mapping Development Center of the University of Rhode Island (URI). Some of the original topocadastral sheets were provided by Dr. George Constantinou, Director of the Geological Survey Department, Ministry of Agriculture, Natural Resources and Environment, Nicosia, Cyprus.

The marine part of the DTM was also carried out in part during the 1994-96 sabbatical at URI. I am indebted to Brian Harper and Desmond P. D. Scott for acquiring the fairsheets from the archives of the UKHO for the IBCM-II compilation, and to Gordon J. Taylor of the UKHO for technical assistance. Other materials were kindly supplied by Norman Z. Cherkis of the Naval Research Laboratory in Washington DC.

This work was carried out as part of Project 20743 (MEDMAP-DTM), under the aegis of the project 'DTM of the Middle East' of the Geological Survey of Israel, Ministry of National Infrastructures.

REFERENCES

Doytsher, Y. and Hall, J. K., 1997. Gridded affine transformation and rubber-sheeting algorithm with FORTRAN program for calibrating scanned hydrographic survey maps. Computers & Geosciences. 23(7), p. 785-791.

Geological Survey Department, Cyprus, 1995. Geological Map of Cyprus, scale 1:250,000. 1 sheet at 1:250,000 scale, revised 1995.

George Philip Ltd., 1996. Philip's World Atlas and Gazetteer. George Philip Ltd., Reed Books, London, 176 p.

Hall, J. K., 1976. Algorithms and programs for rapid computation of area and center of mass; Computers and Geosci., 1(3), p. 203-205.

Hall, J. K., 1993. The GSI Digital Terrain Model (DTM) Project completed. Isr. Geol. Surv., Curr. Res. 8, p. 47-50.

Hall, J. K., 1995. Israeli DTM and STM (SPOT-TM MERGE) satellite imagery databases: Results, applications, and observations. In: E. Shlomi and N. Kadmon (eds.), Cartography in Israel 1995, Survey of Israel Cartographic Papers, No. 13, p. 116-130.

Hall, J. K., 1996. Historical bathymetric surveys of the inner continental shelf of the southeastern Levant. Isr. Geol. Surv., Curr. Res. 10, p. 40-45.

Hall, J. K., 1998a. Digital terrain model of the island of Cyprus. In: T. Weissbrod (ed.), Isr. Geol. Surv., Current Research, Vol. 11, p. 45-50.

Hall, J. K., 1998b. Three-dimensional map of the Island of Cyprus. Grayscale sheet of land topography at 1:250,000 scale, Geological Survey of Israel and Cyprus, Jerusalem, one sheet. Sheet prepared for ICGEM-3, Third International Conference on the Geology of the Eastern Mediterranean, Nicosia, Cyprus, September 23-26, 1998.

Hall, J. K., Schwartz, E., and Cleave, R. L. W., 1990. The Israeli DTM (Digital Terrain Map) Project. In: J. Thomas Hanley and Daniel F. Merriam (eds.), Microcomputer Applications in Geology, Volume 11, p. 1 11-1 18, Pergamon Press. Hammond, 1994. Hammond's Odyssey Atlas of the World, Hammond Incorporated, USA, 72 p.

Hall, J. K., Udintsev, G. B. and Odinokov, Yu. Yu., 1994. The bottom relief of the Levantine Sea. In: Geological structure of the North-eastern Mediterranean (Cruise 5 of the Research Vessel 'Akademik Nikolaj Strakhov'). (V. Krasheninnikov and J. K. Hall, eds.), pp. 5-31. Historical Productions-Hall, Jerusalem, April 1994.

Intergovernmental Oceanographic Commission, 2003. International Geological-Geophysical Atlas of the Pacific Ocean. Moscow-Sankt Petersburg, 192 p., 3 maps.

Krasheninnikov, V., and Hall, J. K. (eds.), 1994. Geological structure of the North-eastern Mediterranean (Cruise 5 of the Research Vessel 'Akademik Nikolaj Strakhov'), Historical Productions-Hall, Jerusalem, 396 + vii p, April 1994

Morelli, C., and Val'chuk, S., 1988. The International Bathymetric Chart of the Mediterranean (I.B.C.M.). Intergovernmental Oceanographic Commission of UNESCO. Chapter 1 in Hall, J. K., (ed.), IBCM Supporting Volume, Jerusalem, reprinted June 1997, 12 p.

Morris, R. O., 1995. Charts and surveys in Peace and War: The History of the RN Hydrographic Service 1919-1970. Ministry of Defence, H. M. Stationary Office, 280 p.

Ritchie, G. S., 1994. No day too long – An Hydrographer's Tale. Second Edition, The Pentland Press Ltd., 250 p.

Ritchie, G. S., 1995. The Admiralty Chart: British Naval Hydrography in the Nineteenth Century. Second Edition, The Pentland Press Ltd., 444 p.

Royal Geographical Society, 1983. Atlas of the World. Special edition of the Times Atlas of the World, John Bartholomew & Son Ltd., Edinburgh, 225 p., and 123 plates.

U. K. Ministry of Defence, 1975. Tactical Piloting Chart TPC G-4D (Cyprus, Iraq, Israel, Jordan, Lebanon, Saudi Arabia, Syria, Turkey). 1st Edition. Scale 1:500,000. Lambert Conformal Conic Projection, UTM and geographic grids superimposed. Contour interval 500 ft (152.4 m).

Wolf, M., and Wingham, D., 1992. The status of the world's public-domain digital topography of the land and ice. Geophys. Res. Lett., 19(23), p. 2325-2328.

LISTING OF BAHD-UKHO CYPRUS FAIRSHEETS AND CHARTS

British Admiralty Hydrographic Department, 1930. Chart E3272 - Mediterranean - Cyprus - East Coast – Famagusta Harbour. Hydrographic fairsheet surveyed by Cdr. A. G. N. Wyatt, R.N., and the officers of H. M. Surveying Ship "Ormonde" in June and July 1930. Soundings in feet. Mercator projection at natural scale 1:10,000, 1 sheet. IBCM Code FH, 7,647 soundings and 128 attributes digitized.

British Admiralty Hydrographic Department, 1931. Chart E3383 - Mediterranean - Cyprus - East Coast – Famagusta Bay – Southern Portion. Hydrographic fairsheet surveyed by Cdr. A. G. N. Wyatt, R.N., and the officers of H. M. Surveying Ship "Ormonde" in 1930-1931. Soundings in fathoms and feet (in less than 11 fathoms). Mercator projection at natural scale 1:24,540, 1 sheet. IBCM Code FB, 11,901 soundings and 221 attributes digitized.

British Admiralty Hydrographic Department, 1933. Chart E3582 - Mediterranean - Cyprus - East Coast - Approaches to Famagusta. Hydrographic fairsheet surveyed by Cdr. A. G. N. Wyatt, R.N., and the officers of H. M. Surveying Ship "Ormonde" in May-June 1931. Bears Hydrographic Department stamp November 25, 1933. Returned from HMS Ormonde with additional work to 1933. Includes an inset map of Boghaz Trading Station at scale 1:1200. Soundings in fathoms and feet (in less than 11 fathoms). Mercator projection at natural scale 1:50,100, 1 sheet. IBCM Code FM, 12,023 soundings and 365 attributes digitized.

British Admiralty Hydrographic Department, 1934. Chart E4469 - Mediterranean - Cyprus - North Coast - Karavostasi. Hydrographic fairsheet surveyed by Cdr. A. Day, R.N., and the officers of H. M. Surveying Ship "Ormonde" in June and July 1934. Bears illegible Hydrographic Department stamp. Soundings in fathoms (fathoms and feet in less than 11 fathoms). Mercator projection at natural scale 1:24,580, 1 sheet. IBCM Code KI, 5,571 soundings and 97 attributes digitized.

British Admiralty Hydrographic Department, 1935. Chart E4465 - Cyprus - South Coast - Approaches to Larnaca. Hydrographic fairsheet for bathymetric survey carried out by H. M. Surveying Ship "Ormonde" under the command of Cdr. A. Day R.N. from July to October 1934. Mercator projection at a scale of 1:49,930, soundings in fathoms, 1 sheet. IBCM Code LN, 12,900 soundings and 266 attributes digitized.

British Admiralty Hydrographic Department, 1934. Chart E4466 - Mediterranean - Cyprus - South Coast – Larnaca. Hydrographic fairsheet surveyed by Cdr. A. Day, R.N., and the officers of H. M. Surveying Ship "Ormonde" in July to September 1934. Bears Hydrographic Department stamp dated 26 April 1934. Soundings in fathoms (fathoms and feet in less than 11 fathoms). Mercator projection at natural scale 1:25,030, 1 sheet. IBCM Code LA, 9,015 soundings and 161 attributes digitized.

British Admiralty Hydrographic Department, 1934. Chart E4295 - Cyprus - Dhekelia. Hydrographic fairsheet surveyed by Cdr. A. Day, R.N., H. M. Surveying Ship "Ormonde" in 1934. Bears Hydrographic Department stamp September 21, 1934. Soundings in fathoms and feet (in less than 11 fathoms). Mercator projection at natural scale 1:25,000, 1 sheet. IBCM Code DK, 1,663 soundings and 91 attributes digitized.

British Admiralty Hydrographic Department, 1935. Chart E4468 - Mediterranean - Cyprus - North Coast - Kyrenia. Hydrographic fairsheet surveyed by Cdr. A. Day, R.N., and the officers of H. M. Surveying Ship "Ormonde" in May and June 1934. Bears Hydrographic Department stamp dated 26 April 1935. Soundings in fathoms and feet (in less than 11 fathoms). Mercator projection at natural scale 1:12,500, 1 sheet. IBCM Code KQ, 3,362 soundings and 73 attributes digitized.

British Admiralty Hydrographic Department, 1935. Chart E4879 - Mediterranean - Cyprus - South Coast – Paphos. Hydrographic fairsheet surveyed by Cdr. A. Day, R. N., and the officers of H. M. Surveying Ship "Ormonde" in April and May 1935. Bears illegible Hydrographic Department stamp. Soundings in fathoms (fathoms and feet in less than 11 fathoms). Mercator projection at natural scale 1:12,550, 1 sheet. IBCM Code OS, 2,404 soundings and 44 attributes digitized.

British Admiralty Hydrographic Department, 1935. Chart E4877 - Mediterranean - Cyprus - South Coast - Limassol. Hydrographic fairsheet surveyed by Cdr. A. Day, R.N., and the officers of H. M. Surveying Ship "Ormonde" in June and July 1935. Bears illegible Hydrographic Department stamp. Soundings in fathoms and feet (in less than 11 fathoms). Mercator projection at natural scale 1:25,100, 1 sheet. IBCM Code LM, 5,944 soundings and 84 attributes digitized.

British Admiralty Hydrographic Department, 1935. Chart E4878 - Mediterranean - Cyprus - South Coast - Approaches to Limassol. Hydrographic fairsheet surveyed by Cdr. A. Day, R.N., and the officers of H. M. Surveying Ship "Ormonde" in June and July 1935. Bears illegible Hydrographic Department stamp. Soundings in fathoms and feet (in less than 11 fathoms). Mercator projection at natural scale 1:50,190, 1 sheet. IBCM Code LL, 8,538 soundings and 121 attributes digitized.

British Admiralty Hydrographic Department, 1935. Chart E4465 - Mediterranean - Cyprus - South Coast - Approaches to Larnaca. Hydrographic fairsheet surveyed by Cdr. A. Day, R.N., and the officers of H. M. Surveying Ship "Ormonde" in July to October 1934. Bears Hydrographic Department stamp May? 25, 1935. Soundings in fathoms and feet (in less than 11 fathoms). Mercator projection at natural scale 1:49,930, 1 sheet. IBCM Code LN, 12,900 soundings and 266 attributes digitized.

British Admiralty Hydrographic Department, 1937. Chart E4876 - Mediterranean - Cyprus - North Coast – Cap Kormakiti to Vavilas Point. Hydrographic fairsheet surveyed by Cdr. A. Day, R.N., and the officers of H. M. Surveying Ship "Ormonde" in August 1935. Bears Hydrographic Department stamp Illegible, 1937. Soundings in fathoms and feet (in less than 11 fathoms). Mercator projection at natural scale 1:50,320, 1 sheet. IBCM Code VP, 4,329 soundings and 79 attributes digitized.

British Admiralty Hydrographic Department, 1937. Chart E4880 - Mediterranean - Cyprus - South Coast - Approaches to Paphos. Hydrographic fairsheet surveyed by Cdr. A. Day, R.N., and the officers of H. M. Surveying Ship "Ormonde" in April and May 1935. Bears Hydrographic Department stamp dated 31 April 1937. Soundings in fathoms and feet (in less than 11 fathoms). Mercator projection at natural scale 1:50,060, 1 sheet. IBCM Code AP, 7,510 soundings and 106 attributes digitized.

British Admiralty Hydrographic Department, 1948. Chart E8226 - Mediterranean - Cyprus - North West Coast – Pomos Point to Paphos Point. Hydrographic fairsheet surveyed by Capt. R. M. Southern, R.N., and the officers of H. M. Surveying Ship "Challenger" in May and June 1947. Bears Hydrographic Department stamp dated 14 January 1948. Includes an inset map of Fontana Amorosa from June 1947 at scale 1:1250. Soundings in fathoms (fathoms and feet in less than 11 fathoms). Mercator projection at natural scale 1:50,060, 1 sheet. IBCM Code PT, 9,023 soundings and 203 attributes digitized.

British Admiralty Hydrographic Department, 1948. Chart E8393 - Cyprus - North Coast – Pomos Point to Cape Limniti. Hydrographic fairsheet surveyed by Capt. R. M. Southern, R.N., and the officers of H. M. Surveying Ship "Challenger" in May 1948. Bears Hydrographic Department stamp November 17, 1948. Soundings in fathoms and feet (in less than 11 fathoms). Mercator projection at natural scale 1:50,000, 1 sheet. IBCM Code CL, 1,574 soundings and 33 attributes digitized.

British Admiralty Hydrographic Department, 1950. Chart E8806 - Mediterranean - Cyprus - North Coast – Vavilas Point to Phourni Rock. Hydrographic fairsheet surveyed by Capt. H. Menzies, R.N., and the officers of H. M. Surveying Ship "Owen" in June-July 1950. Bears Hydrographic Department stamp November 24, 1950. .Soundings in fathoms and feet (in less than 11 fathoms). Mercator projection at natural scale 1:50,080, 1 sheet. IBCM Code VV, 10,908 soundings and 26 attributes digitized.

British Admiralty Hydrographic Department, 1953. Chart E8805-1 - Mediterranean - Cyprus - North Coast – Morphou Bay. Hydrographic fairsheet surveyed by Capt. H. Menzies, R.N., and the officers of H. M. Surveying Ship "Owen" in May and June 1953. Bears Hydrographic Department stamp November 24, 1953. Soundings in fathoms and feet (in less than 11 fathoms). Mercator projection at natural scale 1:50,080, 1 sheet. IBCM Code MU, 5,229 soundings and 85 attributes digitized.

British Admiralty Hydrographic Department, 1953. Chart E8805-2 - Mediterranean - Cyprus - North Coast – Morphou Bay. Hydrographic fairsheet surveyed by the officers of H. M. Surveying Ship "Owen" in May 1953. Bears Hydrographic Department stamp October 9, 1953. Soundings in fathoms and feet (in less than 11 fathoms). Mercator projection at natural scale 1:50,000, 1 sheet. IBCM

Code MY, 359 soundings and 2 attributes digitized.

British Admiralty Hydrographic Department, 1953. Chart E9466 - Mediterranean - Cyprus - North Coast – Phourni Rock to Cape Plakoti. Hydrographic fairsheet surveyed by Cdr. C. R. K. Roe, R.N., and the officers of H. M. Surveying Ship "Owen" in May and June 1953. Soundings in fathoms and feet (in less than 11 fathoms). Mercator projection at natural scale 1:48,000, 1 sheet. IBCM Code PH, 6,736 soundings and 73 attributes digitized.

British Admiralty Hydrographic Department, 1953. Chart E9467 - Mediterranean - Cyprus - North Coast – Akanthou Trading Station. Hydrographic fairsheet surveyed by Lt.Cdr. J. S. N. Pryor, R.N., and the officers of H. M. Surveying Ship "Owen" in May 1953. Bears Hydrographic Department stamp July 22, 1953. Soundings in fathoms and feet (in less than 11 fathoms). Mercator projection at natural scale 1:12,000, 1 sheet. IBCM Code AH, 2,231 soundings and 10 attributes digitized.

British Admiralty Hydrographic Department, 1953. Chart E9468 - Mediterranean - Cyprus - North Coast – Galounia Trading Station. Hydrographic fairsheet surveyed by Cdr. C. R. K. Roe, R.N., and the officers of H. M. Surveying Ship "Owen" in 1953. Bears Hydrographic Department stamp July 22, 1953. Soundings in fathoms and feet (in less than 11 fathoms). Mercator projection at natural scale 1:12,000, 1 sheet. IBCM Code GN, 2,599 soundings and 11 attributes digitized.

British Admiralty Hydrographic Department, 1954. Chart E9769 - Mediterranean - Cyprus - North Coast – Cape Plakoti to Exarchos Bay. Hydrographic fairsheet surveyed by Lt.Cdr. H. R. Hatfield, R.N., and the officers of H. M. Surveying Ship "Owen" in May-June 1954. Bears Hydrographic Department stamp dated 15 December 1954. Soundings in fathoms (fathoms and feet in less than 11 fathoms). Mercator projection at natural scale 1:48,000, 1 sheet. IBCM Code EX, 6,620 soundings and 133 attributes digitized.

British Admiralty Hydrographic Department, 1954. Chart E9678 - Cyprus – Cape Andreas. Hydrographic fairsheet surveyed by H. M. Surveying Ship "Owen" on 17 June 1954. Bears Hydrographic Department stamp dated 15 July 1954. Soundings in fathoms. Mercator projection at natural scale 1:48,000, 1 sheet. IBCM Code CD, 275 soundings digitized.

British Admiralty Hydrographic Department, 1959. Chart K2229 - Cyprus - North East Coast - Track south of Cape Andreas. Sounding line carried out by H. M. Ship "Walkerton". Mercator projection at a scale of 1:100,000, soundings in fathoms to sounder's limit of 60 fm, 1 sheet. IBCM Code CF.

British Admiralty Hydrographic Department, 1959. Chart K2229. Sounding lines carried out from H.M.S. Walkerton from 26th December 1958 to 22nd January 1959 by Lt. N.D.(N) I. B. James R.A.N. plotted on Chart 796 (1956) of Cyprus - North East Coast - Stazouza Point to Cape Eloea. Mercator projection at a scale of 1:100,000, soundings in fathoms, 1 sheet. IBCM Code CE.

British Admiralty Hydrographic Department, 1959. Chart K2233. Sounding lines carried out from H.M.S. Walkerton(?) plotted on Chart 796 (1956) of Cyprus - North East Coast - Stazouza Point to Cape Elœa. Mercator projection at a scale of 1:100,000, soundings in fathoms, 1 sheet. IBCM Code CC.

British Admiralty Hydrographic Department, 1960. Chart K2597 - Mediterranean - Cyprus – Cape Andreas. Hydrographic chart overlay of track soundings by H.M.S. "Trafalgar" in 1960. Bears Hydrographic Department stamp dated 15 June 1960. Soundings in fathoms. Mercator projection at natural scale ~1:100,000, 1 sheet. IBCM Code CB, 98 soundings digitized.

British Admiralty Hydrographic Department, 1961. Chart K3141/1– Mediterranean Sea – Cyprus – West Coast – Cape Limniti to Cape Aspro. Hydrographic chart overlay on UKHD Chart 775 with transit soundings of H. M. Surveying Ship "Owen" on 27th-28th October 1961. Bears Hydrographic Department stamp dated 1 December 1961. Soundings in fathoms. Mercator projection 1:100,000, 1 sheet. IBCM Code CN.

British Admiralty Hydrographic Department, 1961. Chart K3141/2 – Mediterranean Sea – Cyprus. Hydrographic chart overlay on UKHD Chart 2074 with transit soundings of H. M. Surveying Ship "Owen" on 27th-28th October 1961. Bears Hydrographic Department stamp dated 1 December 1961. Soundings in fathoms. Mercator projection 1:300,000, 1 sheet. IBCM Code CL, 948 soundings and 55 attributes digitized.

British Admiralty Hydrographic Department, 1961. Chart K3141/3 – Mediterranean Sea - Cyprus – South East Coast – Stazousa Point to Cape Elœa. Hydrographic chart overlay on UKHD Chart 796 with transit soundings of H. M. Surveying Ship "Owen" on 27th and 28th October 1961. Bears Hydrographic Department stamp dated 1 December 1961. Soundings in fathoms. Mercator projection 1:100,000, 1 sheet. IBCM Code CO, 529 soundings and 34 attributes digitized.

British Admiralty Hydrographic Department, 1961. Chart K3141/4 – Cyprus – South East Coat – Cape Kiti to Cape Elea. Hydrographic chart overlay on UKHD Chart 851 with transit soundings of H. M. Surveying Ship "Owen" on 28th October 1961. Bears Hydrographic Department stamp dated 1 December 1961. Soundings in fathoms. Mercator projection 1:100,000, 1 sheet. IBCM Code KE, 294 soundings and 33 attributes digitized.

British Admiralty Hydrographic Department, 1962. Chart K3478 - Mediterranean - Cyprus - Cape Andreas. Hydrographic fairsheet surveyed by Cdr. H. R. Hatfield, R.N., and the officers of H. M. Surveying Ship "Dalrymple" on 28th March to 14th May 1962. Bears illegible Hydrographic Department stamp. Soundings in fathoms (fathoms and feet in less than 11 fathoms). Mercator projection at natural scale 1:48,000, 1 sheet. IBCM Code CP, 12,997 soundings and 201 attributes digitized.

British Admiralty Hydrographic Department, 1963. Chart K3734 - Mediterranean - Cyprus – Melissakros Point to Cape Elœa. Hydrographic fairsheet surveyed by Cdr. H. R. Hatfield, R.N., and the officers of H. M. Surveying Ship "Dalrymple" on 15th April to 10th May 1963. Soundings in fathoms (fathoms and feet in less than 11 fathoms). Mercator projection at natural scale 1:48,000, 1 sheet. IBCM Code MP, 9,135 soundings and 89 attributes digitized.

British Admiralty Hydrographic Department, 1989. Chart M1325 - Cyprus – Akrotiri Bay. Hydrographic fairsheet surveyed by Cdr. R. A. Cotton, R.N., and the officers of H. M. Surveying Ship "Herald" on 12th to 16th March 1989. Bears Hydrographic Department stamp April 11, 1989. Soundings in meters (and meters and decimeters under 31 m). UTM projection, Zone 36, European Datum (1950), at scale 1:10,000, 1 sheet. IBCM Code KB, 1,759 soundings digitized.

U. K. Hydrographic Office, 1992. Chart 775 markup. Cyprus - West Coast - Cape Limniti to Cape Aspro. Mercator projection at a scale of 1:100,000, depths in meters, 1 sheet. IBCM Code WC.

U. K. Hydrographic Office, 1992. Chart 776 markup. Cyprus - North Coast - Cape Limniti to Stazousa Point. Mercator projection at a scale of 1:100,000, depths in meters, 1 sheet. IBCM Code NW.

U. K. Hydrographic Office, 1992. Chart 850 markup. Cyprus - South Coast - Cape Aspro to Cape Pyla. Mercator projection at a scale of 1:100,000, depths in meters, 1 sheet. IBCM Code CS.

U. K. Hydrographic Office, 1993. Chart 851 markup. Cyprus - South East Coast - Cape Kiti to Cape Elœa. Mercator projection at a scale of 1:100,000, depths in meters, 1 sheet. IBCM Code SQ.

Chapter 16

Bathymetry and Topography of the Syria-Lebanon Continental Margin

John K. Hall
Geological Survey of Israel, Marine Geology, Mapping & Tectonics Division, 30 Malchei Israel Street, Jerusalem 95501, Israel

INTRODUCTION

Up until late in 2003 the Syria-Lebanese continental margin was probably the least surveyed margin in the Mediterranean Sea. It is among the narrowest, most likely reflecting its origins in the shearing of the adjacent landmass. Because it lies off the mountainous chains of the Lebanon and Anti-Lebanon, it is deeply incised by submarine canyons, many apparently controlled by the extensions of onshore faults. A careful mapping of this margin will probably hold the key to a number of questions related to the structure of the Dead Sea Transform in Lebanon and Syria. In the south, difficulties in modeling the bend in the transform's Yammouneh Fault segment in Lebanon have led to ideas concerning a possible branching-off Roum Fault which presumably heads offshore, northward from the Beirut headland (Butler et al., 1997; Khair, 2001). Farther north, the details of the West Tartus Ridge (Hall et al., 1994), which constitutes the SSW-trending end of the Hecataetus-Latakia structural lineament of Kempler (1994), is similarly little understood. Off northern Syria the Heraclitus Seamount (Hall et al., 1994), rising some 300-400 m above the Latakia Basin, is based upon very little data.

In this chapter the physical relief data presently available for this coastal segment will be described both offshore and onshore. The analysis of this historical data is far from complete, and at the time of writing the big changes that have taken place may render them obsolete. These seminal events consist of the French swath mapping program in the offshore with the N/O Le Suroît, which took place in October-November 2003, and the recent release of the more detailed land topography from the 2000 space shuttle Endeavour radar mapping mission (SRTM – see below).

What has been done to date will be presented, and a prescription given for a more detailed analysis of whatever older data may complement these new findings.

HYDROGRAPHIC DATA SOURCES

First Hydrographic Survey - HMS Firefly 1859-1861

The earliest reconnaissance survey appears to be that of HMS Firefly in 1859-61. She was a steam paddlewheel sloop/gunvessel, launched in 1832, with 5 guns and 677 ton displacement. She was one of six survey vessels acquired in 1841 in a burst of activity within the Hydrographic Department of the Admiralty (Morris, 1995). Despite cutbacks in surveys of local waters, the British continued foreign surveys in the service of defence and trade, and the officers of HMS Firefly surveyed over 300 km of coast from southern Lebanon to southern Turkey and from depths of a few fathoms to well beyond the shelf-break.

The thousands of soundings from the 1860-1861 HMS Firefly surveys were presented on a series of five fairsheets (BAHO, 1861-62), one of which is reproduced in **Fig. 16.1**. For the most part these soundings still appear on the modern navigational charts for the Syrian and Lebanese coasts.

Lebanese Fisherman's Sediment Charts

Two sediment maps for fisherman were published by the Ministry of Agriculture in Lebanon (Boulos, 1962a, b). They show representative soundings in meters which are sparse in comparison with those of the 1859-61 survey, and which possibly may include a sampling of the original soundings in fathoms converted to meters.

French and Oil Pipeline Support Surveys

The 'modern' American and British charts refer to French hydrographic surveys carried out in 1921 for Jazirat Arwad (Tartus) in Syria and Saida (Sidon) in Lebanon.

In the 1940s the Trans-Arabian Pipeline (Tapline) was laid down to bring up to 500,000 bbl/d of Saudi oil to Haifa via Jordan. Following the establishment of Israel in 1948, the Tapline was diverted to Sidon in Lebanon (Feld, 2002a). To support the new oil terminal, surveys were carried out by Kelvin & Hughes (Marine) Ltd. in 1950 and 1961 (BAHO, 1951, 1952). The author tried to find some of these original survey records in London, but learned that they had been destroyed in a warehouse fire. Oil exports via the Tapline ceased in 1975 for economic reasons, coupled with the turmoil of the Lebanese civil war; the Lebanese portion of the Tapline was closed altogether in 1983.

In Banias, Syria, the Iraq Petroleum Company (IPC) carried out a hydrographic survey in 1950 (BAHD, 1952) of the terminus built for the IPC pipeline bringing oil from the Kirkuk oil fields in northern Iraq. This pipeline was closed in 1982 following a break in diplomatic ties, and suffered severe damage in the Gulf War in 1991. The pipeline was reopened in March 2000 (Feld, 2002b).

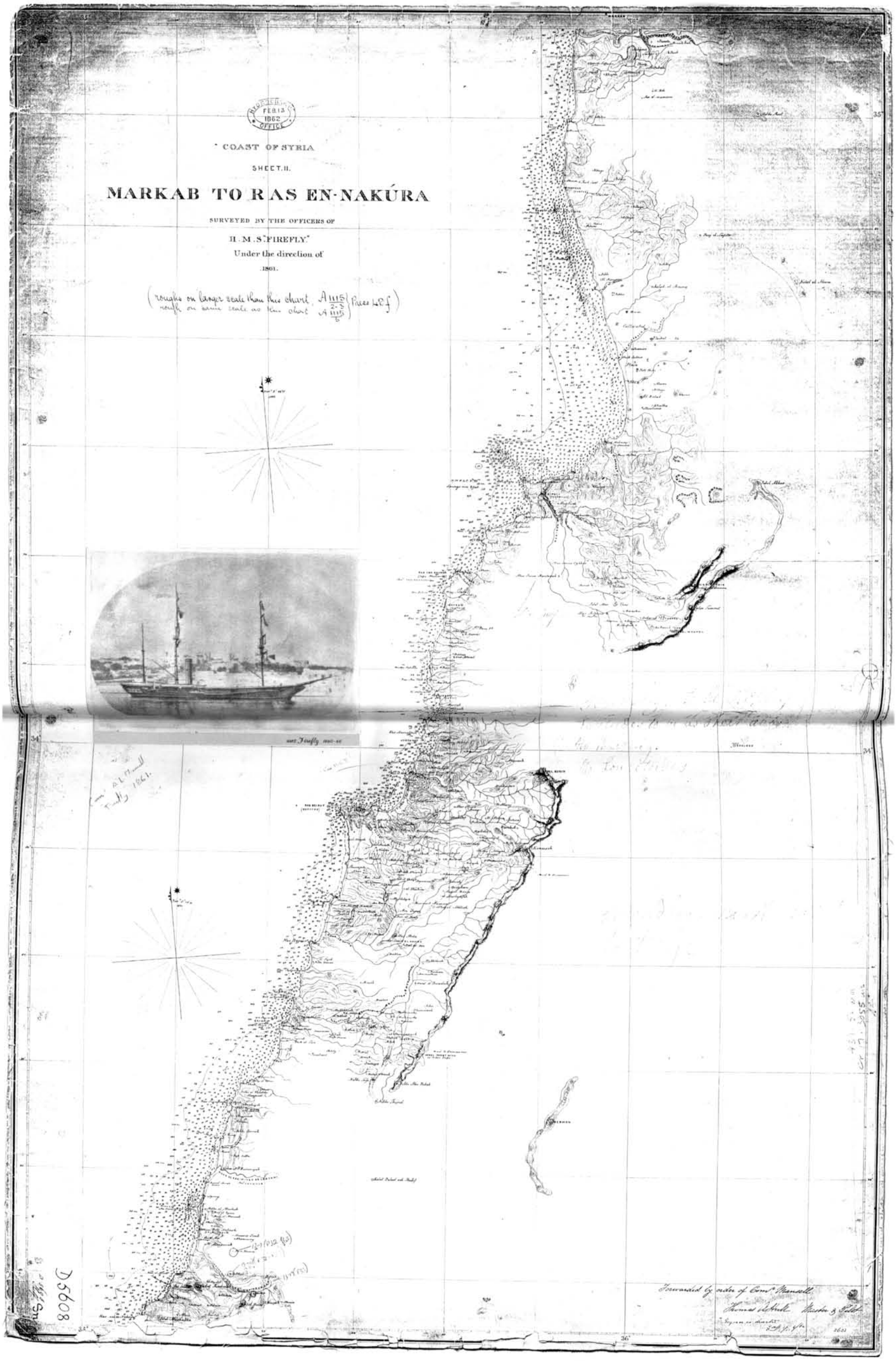


Fig. 16.1. Reproduction of the first systematic survey of the coast of Lebanon and Syria by HMS Firefly in 1861 (BAHO, 1861). The data from this survey and Chart D5608 - Coast of Syria - Sheet II - Markab to Ras En-Nakura still provide many of the offshore soundings for the modern nautical navigational charts for the area. A sketch of the HMS Firefly from the archives of the UKHO is inset. Reproduced with permission, courtesy of the United Kingdom Hydrographic Office, Taunton, UK.

Modern Reconnaissance Geophysical Surveys

In 1961 the NATO research vessel R/V Aragonese carried out a survey of the eastern half of the Mediterranean, which was the basis of the physiographic subdivision of the eastern basins (Emery et al., 1966). Bathymetry, magnetics, and gravity were measured continuously over an extensive grid. The echo-sounding records proved to be excellent for observing the physiography, but were not used for bathymetric compilations at the time because the Loran-C navigation was not considered to be sufficiently accurate. The author spent more than a decade trying to locate the original records in order to digitize them. They were finally located in a remote storage hut behind the labs at the NATO SACLANT Centre in La Spezia. Digitization of the records yielded over 120,000 'significant soundings' taken at changes in bottom slope.

In 1961, 1964, and 1966, Beirut was a port of call for three cruises of the research vessel R/V Chain of the Woods Hole Oceanographic Institution (WHOI - Woods Hole, MA, USA). Chain Cruise 21, one of the first trials of a sparker for continuous seismic profiling, made sounding lines in and out of Beirut between 6 and 11 November 1961, during which she also rendezvoused with the R/V Aragonese during its survey.

Between 11 and 19 June 1964, on its way home from the International Indian Ocean Expedition, Chain Cruise 43 carried out a brief reconnaisance survey off much of Lebanon. The seismic reflection profiles and bathymetry formed the basis of the M.Sc. thesis of D. H. Carlisle (1965). The survey consisted of two shore-parallel profiles on the outer slope (1050 to 1550 m depth) north of Beirut almost to Tarabulus, and about a dozen shore-parallel to north-south profiles off Beirut and as far south as Tyre (Sour) in depths of 200 to 1600 m. The navigation was primarily radar fixes off coastal landmarks, and while significant errors occur, the profiles did much to define the trend and magnitude of the numerous offshore canyons.

In early October 1966 Chain Cruise 61 circum-navigated Cyprus and from October 2-5 made seismic profiles off Lebanon and Syria and out into the Levantine Basin.

All these WHOI soundings, in fathoms assuming a constant 800 fm/sec sound velocity, have been digitized from the track and sounding reports, and are included in this compilation.

Farther offshore, a complementary survey at right angles to that of the R/V Aragonese was carried out in 1968 over all the eastern Mediterranean by the U. S. Naval Oceanographic Office ship USNS Sgt. Curtis F. Shoup (T-AG-175). In the 1970s sparse reconnaissance surveys were carried out in the easternmost Mediterranean by Cambridge University with the RRS Discovery and RRS Shackleton. Other inshore data was obtained by Tom Goedicke (1972, 1977; Goedicke and Sagebiel, 1976) in surveys along the coast from a small yacht. Photos of some of these vessels are shown in **Fig. 16.2a-h**.

Israeli Survey of Southern Lebanon - November 1982

Following the June 1982 Israeli invasion of southern Lebanon, a marine geophysical survey was carried out between Rosh Haniqra and Beirut during the period 7-18 November 1982 (Hall et al., 1983). The survey was a joint undertaking of the Geological Survey of Israel, the Israel Oceanographic and Limnological Research Ltd. (I.O.L.R.), and the Hydrographic Branch of the Israeli Navy.

Fig. 16.3a shows a track map with the more than 2,000 km of track that was surveyed during two cruise legs. The first leg during 7-12 November consisted of depth soundings and magnetics along some 35 profiles oriented perpendicular to shore. The profiles extended to depths of 1,500 m, and in accordance with the regional morphology were about 30 km long in the south and 15 km in the north. Six additional profiles were made in mid-depths parallel to shore for the purpose of better delineating the submarine canyons.

For the first leg navigation was available from a computerized Motorola Miniranger system using two shore-based radar transponders to give continuous precision position data. Depth soundings were made with a Gifft GDR-T-19 facsimile recorder and transceiver driving an EDO 12 kHz transducer mounted at a depth of 2.3 m on a leg hung outboard of the ship's port side. An ELAC (Model LAZ 17 Superior, Atair Type) sounder lent by the Steinitz Marine Laboratory of the Hebrew University provided data in very shallow water and acted as a backup when the Gifft was inoperable. Approximately 25,000 significant soundings, *i.e.* taken at changes in the bottom slope and therefore providing the best approximation to the bottom profile when joined, were digitized from the 19" paper records.

Until such time as multibeam work is carried out on the shallow shelf and slope of southern Lebanon, these soundings from the first week should have value of a reconnaissance nature.

Total field magnetic measurements were made with a Geometrics G-801 Marine Magnetometer with ¼γ (0.25 nT) sensitivity. Simultaneous base station measurements were made during the second leg at Tel Shikmona with a Geometrics G-855 Magnetometer. During the first leg the weather was quite stormy, with waves reaching 4-5 m.

The second leg, during 14-18 November, was about 1,000 km in length. Bathymetry and magnetics were taken as before, and continuous seismic reflection measurements were made with a 300 in^3 airgun source, with the signals being received on a SECO tapered array, conditioned on a Del Norte Model 502 Seismic Amplifier, and recorded on an EPC Model 4100 19" graphic

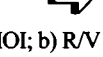
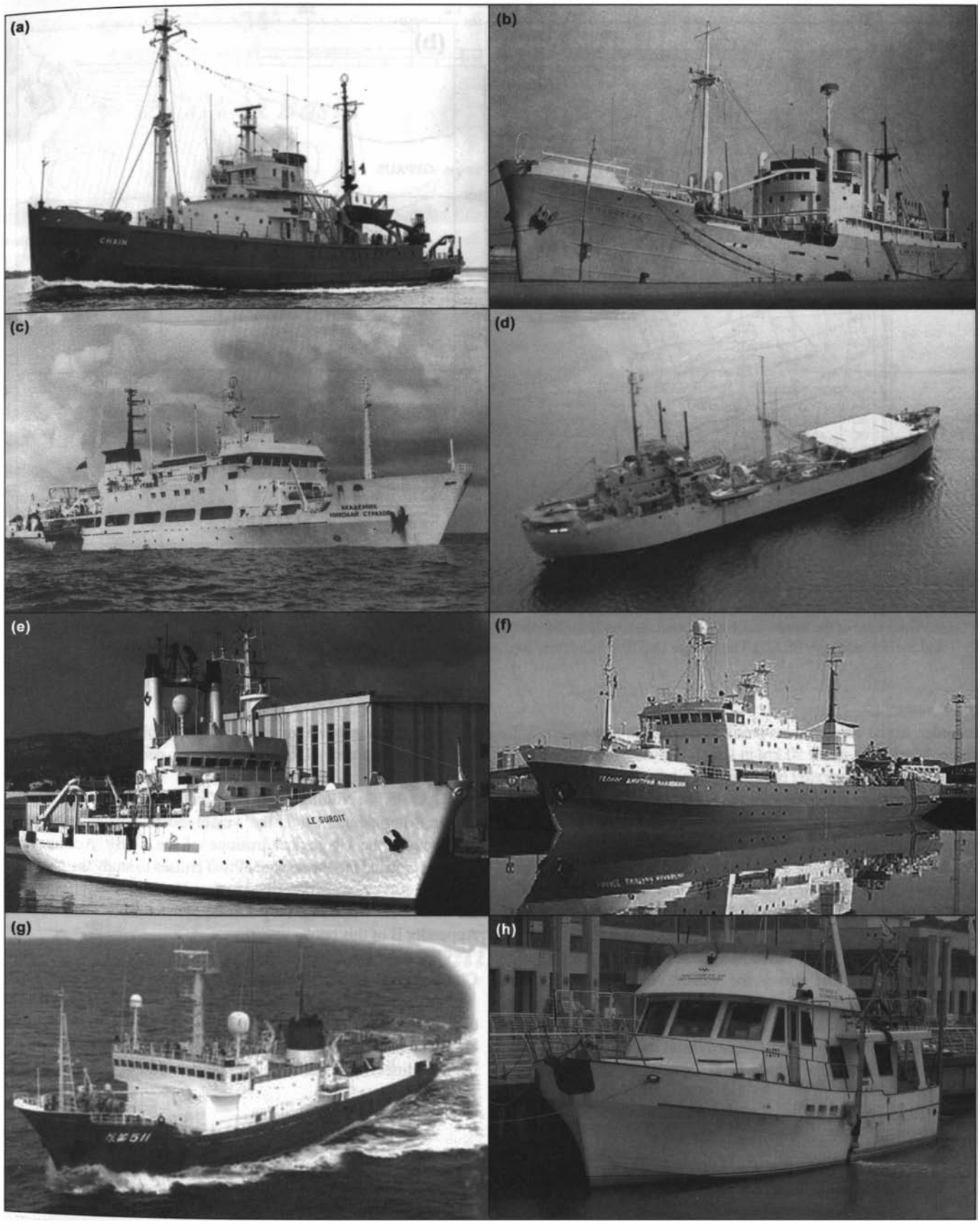


Fig. 16.2. Photographs of most of the vessels involved in systematic surveys off the coasts of Syria, Lebanon and Israel. a) R/V Chain, of WHOI; b) R/V Aragonese, NATO SACLANT Centre; c) NES Akademik Nikolaj Strakhov, Geological Institute, Russian Academy of Sciences; d) USNS Sgt. Curtis F. Shoup, U. S. Naval Oceanographic Office; e) N/O Le Suroît, Ifremer; f) S/V Geolog Dmitriy Nalivkin, Fugro-Geoteam; g) M/V Bin Hai 511, GECO-PRAKLA; h) R/V Etziona, Israel Oceanographic & Limnological Research Ltd.


(a)
(b)
(c)
(d)
(e)
LE SURCIT
(f)
(g)
(h)

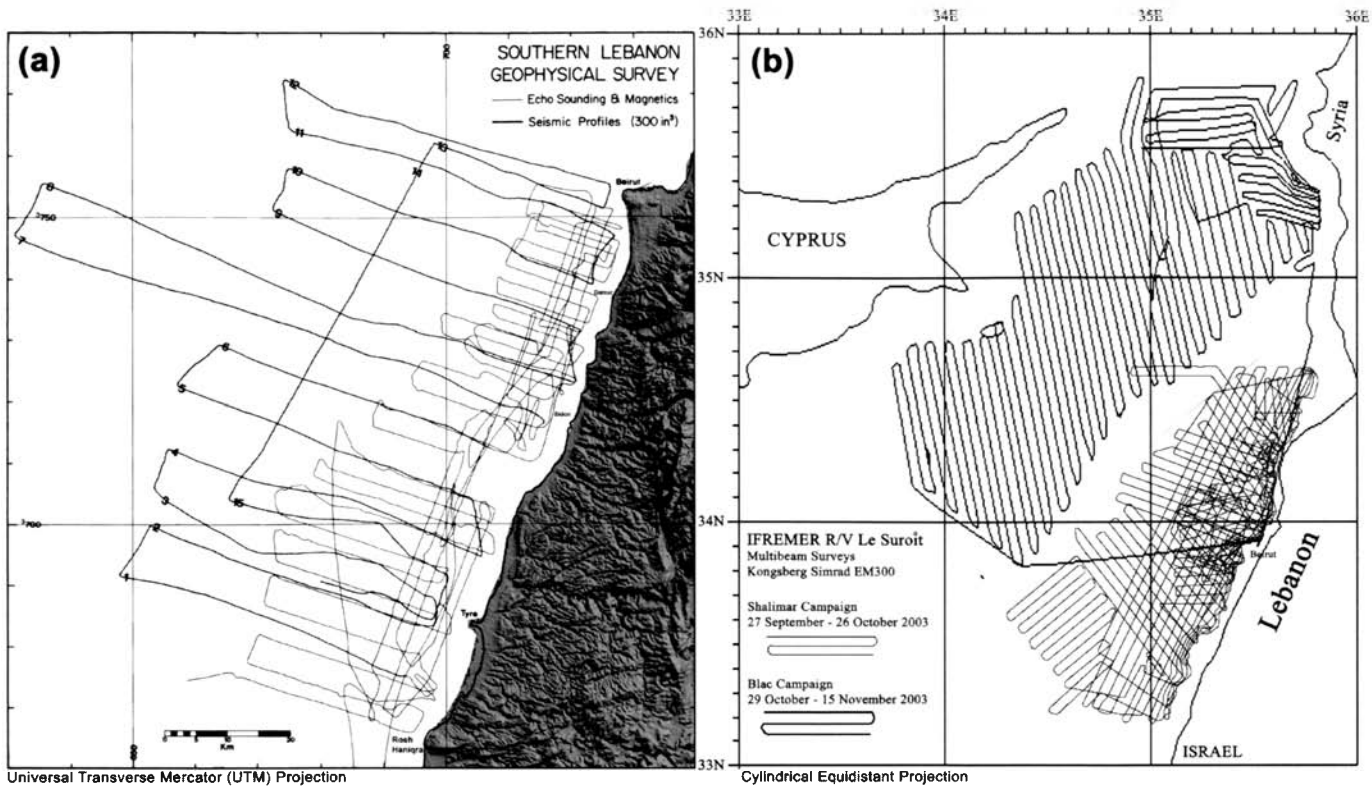


Fig. 16.3. (a) Track map of the marine geophysical survey off southern Lebanon. Continuous depth and magnetic field observations were made on all the lines, which total over 2,000 km. The lighter lines were navigated with a high precision Motorola Miniranger positioning system.
(b) Track map of the latest French multibeam surveys in the Mediterranean off Lebanon during October-November, 2003 (Campaign SHALIMAR) and Syria (Campaign BLAC). The Ifremer ship N/O Suroît was used with its Kongsberg-Simrad EM-300 multibeam system.

recorder. Some 13½ seismic profiles were made perpendicular to shore. Most were about 50 km in length but two were extended to 90 km. One shore-parallel profile was made.

The weather conditions for the second leg were ideal, so that the seismic results were excellent. For this leg the Miniranger system was unavailable. Navigation was therefore achieved by deduced reckoning using gyrocompass and speed-log inputs to a Magnavox MX-1105 Navigator, which was updated by periodic single channel TRANSIT/NAVSAT satellite fixes and infrequent Omega fixes. Radar fixing on prominent landmarks was used for inshore navigation. Some 2,570 MX-1105 positions were logged.

A week after the survey the survey vessel returned to the vicinity of Ras Beirut to check on shoal soundings marked on the 1:25,000 scale UKHO Chart 1563 in seemingly deep waters exceeding 1200 m. These soundings were all found to be erroneous, most likely the result of echoes from the acoustic deep scattering layer resulting from congregations of fish (probably lemon sharks, prized for their livers – Dr. Shmuel Pisanty, pers. comm. 1983).

NES Akademik Nikolaj Strakhov Cruise 10

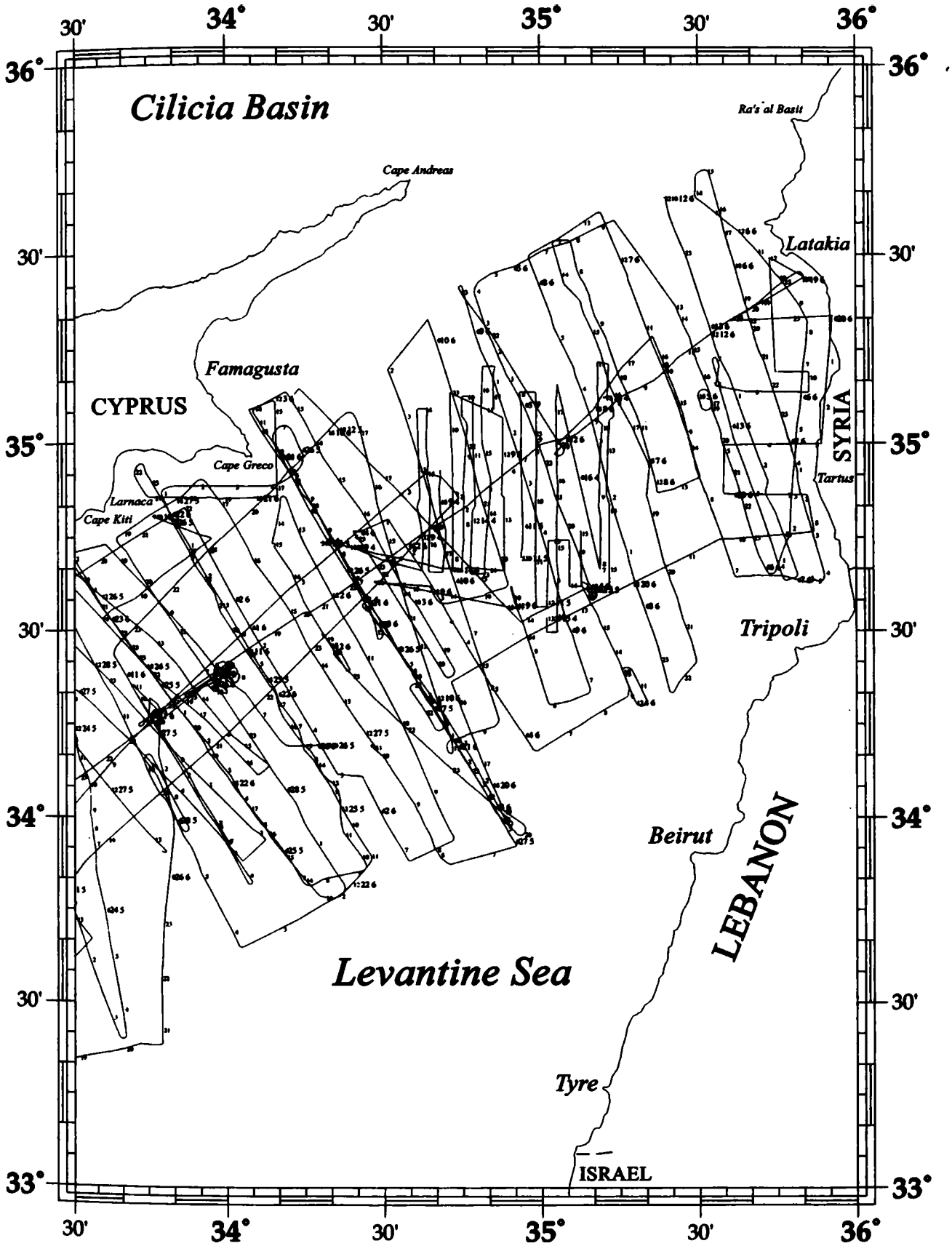
In March-June 1990, the vessel NES Akademik Nikolaj Strakhov of the Geological Institute of the USSR Academy of Sciences carried out the second of two cruises to study the Cyprean Arc. The surveys were described in detail by Hall et al. (1994), and the track is shown in **Fig. 16.4**. The equipment used is described in Appendix B of this book.

Commercial Seismic Prospection Surveys

In the mid-1970s the first speculative commercial work was done by GOEL/BEICIP/ROBERTSON (1975, 1976) with 7,400 km of seismic profiling in the eastern Mediterranean, which included lines off the easternmost margins. Part of the bathymetric



Fig. 16.4. Track chart of the R/V Akademik Nikolaj Strakhov off Lebanon and Syria from Cruise 5 - May-July 1987 and Cruise 10, March-June 1990. Mercator projection, tracks are annotated every hour, with day and month at the beginning of each line and every 6 hours. Adapted from the frontispiece of Krashenninikov and Hall (1994).


Cilicia Basin
Ra's al Basit
Cape Andreas
Latakia
Famagusta
CYPRUS
SYRIA
Cape Greco
Tartus
Larnaca
Cape Kiti
Tripoli
Beirut
LEBANON
Levantine Sea
Tyre
ISRAEL
30'
34°
35°
36°
33°

data for this work was obtained from Sefel Geophysical Ltd. in Calgary. However many of the original echo-sounding records were lost when the ship later sank following this survey.

Then, for a number of reasons, both political and economic, nothing was done for nearly 20 years. In 1993, hints began appearing of renewed marine seismic exploration activity within the EEZ (Exclusive Economic Zone) of Lebanon. Geophysical magazines carried reports (Anonymous, 1993, 1994) that GECO-PRAKLA's survey vessel M/V Bin-Hai 511 (Fig. 16.2g), in association with the Lebanese Ministry of Industry and Petroleum, had carried out a survey off northern Lebanon. The 500 km of 2D marine seismic data from that survey would be used to promote the interest of international oil companies in obtaining offshore exploration licenses.

Jumping forward some 10 years, a recent advertisement (Spectrum-Fugro, 2002) shows the relatively dense coverage obtained off Lebanon in 1976 by the British Spectrum Energy and Information Technology Ltd., and later surveys in partnership with Fugro in 2000 and 2002. Over 5000 km of seismic data were obtained off Lebanon. The advertisement also indicates over 22,000 km available east of 30°E and north of 33°N, in the Spectrum/Fugro East Med Data library.

And more recently, Oil and Gas International (2003) carried an announcement dated 29 January 2003 that Spectrum Energy had completed an inshore 2D survey for the Lebanese Ministry of Energy and Water that was merged with the earlier surveys of the EEZ. The survey consisted of 2000 km of 2D seismic, magnetics, and gravity in Lebanon's shallow water coastal zone. The survey was carried out by Fugro-Geoteam's vessel, the S/V Geolog Dmitriy Nalivkin (Fugro-Geoteam, 2003) (Fig. 16.2f). Spectrum reported more favorable indications of hydrocarbon potential in the northern part of the country.

THE COMPILATIONAL METHOD

Acquisition of passage soundings

Compiling a map is no easy task. Years ago, we were convinced that digitizing track charts of passage soundings was sufficient. If we could interpolate from fixes where the ship was at any time, and if we knew the time at which soundings were made, then we could either plot the soundings, or interpolate where the various depth contours were crossed, and then contour the map according to these crossings. Once we had collected data for about one hundred scientific cruises, we began to realize that most areas were without coverage. These first steps were in concert with the computer support then available. There were large digitizers, large and weighty plotters, and mainframe computers.

With the advent of the personal computer, new capabilities opened up. Now nineteen years into that revolution, I have somehow progressed through some 44 computers, 12 digitizers, two large plotters and myriad inkjets. Computing capacity has gone from a 8 MHz PC-AT to an Intel 3.06 GHz Xeon processor with 2 Gbyte of memory and nearly 1 Tbyte of disk space, and gridding capability from 300 to many millions of points.

In parallel, raster scanners became available, and beginning in 1987 large charts could be rendered into raster images, which could be worked on with heads-up digitizing. In my operation alone, over 1700 charts and fairsheets for the surrounding seas have been scanned and the soundings extracted.

In order to conveniently digitize material from these images, programs were written to allow proper registration of the data being extracted. My generation lived and breathed FORTRAN, hence all software was written in FORTRAN IV for the 16 color 350 by 640 pixel EGA graphics mode. The graphics package chosen for the Ryan-McFarlin IBCM Professional Fortran was Media Cybernetics' HALO, which had drivers for getting digitizer coordinates from GTCO 0.001" digitizers with 16 button cursors. These FORTRAN IV programs are still in use today.

Extraction of Spot Soundings

The methodology involves scanning the charts at 200 dpi in grayscale, usually in uncompressed TIFF format. A program such as Adobe PhotoShop® is used to rectify the scan, adjust the brightness and contrast to clean up the scan, and then convert it to a bitmap (black and white pixels). These bitmap images are then converted into a matrix of EGA screens, each 640 pixels wide and 350 pixels high, stored in the HALO semi-compressed .PIC format. The names, following the DOS convention of 8 characters with a three character extension, are a two or three character mnemonic for the chart, followed by the row of the matrix (2 digits) and the column (2 digits). Hence British Chart 2633 of the Syrian and Lebanese coasts (BAHO, 1974) is made up of files LF0101.PIC to LF2314.PIC. This method, even within the restrictions imposed by DOS, allows scans up to 64,000 pixels wide by 35,000 pixels high.

This matrix of screens is then worked on, one screen at a time. The soundings in each screen are digitized. The cross of the cursor is put over the sounding (usually the center of the imaginary rectangle encompassing the number) and the number is entered using the 16 buttons. When the cursor is moved off this point, the point is plotted as a small blue cross, and the number over-written in red. Screens seldom have more than 200 points. When all points are digitized the soundings from that screen, together with those from the eight surrounding screens, are used to calculate a multi-quadric (radial basis function) surface (Hardy, 1971). For example, a surface based on 200 points, represents the solution of 200 equations in 200 unknowns. It honors every data point, and the results are very similar to real topographic surfaces.

A grid for the area of the screen is computed from the results of this solution, and presented as an isometric 3-D 'fish-net' plot, with ten colors representing hypsometric intervals according a preset figure (usually 10 meters). Today only a few seconds are required for fitting up to 300 points. This system allows bad points to be immediately recognized by the fact that the surface looks unnatural. Corrections can then be immediately applied. At any time all the digitized points can be plotted together, with 10 colors again being used to differentiate between specific hypsometric intervals. This is useful for finding undigitized screens, and

blunders. This method has worked very successfully for several hundreds of thousands of screens, representing well over 20,000 hours of heads-up digitizing.

Once all the soundings (and other attributes which can be represented as text strings, such a bottom types, wrecks etc.) have been digitized, another program is used to digitize all the points on the graticule of the chart (lines of latitudes and longitudes). A small .GSC (Geographic-Screen-Calibration) file is constructed, along with the appropriate latitudes and longitudes, and an affine transformation procedure, together with a rubber-sheeting factor, is used to convert from digitized pixels to actual geographic position (Doytscher and Hall, 1997). The digitized graticule is first tested graphically to see that this very sensitive procedure is properly followed.

Finally, the digitized points and attributes from all the screens are converted and written into four separate ASCII files for each chart, as *x,y,z* triads in decimal degrees, and as latitudes and longitudes in degrees and minutes for manual comparison with a chart.

Gridding of the *x,y,z* Datapoints

These *x,y,z* triads can be plotted or gridded using versatile programs such as Surfer® from Golden Software. Since a large variety of chart datums are used, it is necessary to convert these datums to the WGS-84 datum used by the Global Positioning System (GPS). The coordinates of these files can be transformed by programs such as NIMA's Geotrans, or the Geographic Calculator® from Blue Marble Geographics.

Having merged together all the sounding data, it is then a straight-forward procedure to enter a program like Surfer® 8, and request a grid. However, for many reasons this automated result is seldom satisfactory, no matter what the gridding technique used. The same sounding, digitized from several charts with minor displacements, or errors like incorrect sound velocity corrections, or mixing fathoms with meters, or an overabundance of data in some places and a dearth of data in others, can play havoc with the gridding. Hence it is necessary to painstakingly go over the data, as outlined below.

INTERNATIONAL COMPILATIONS – IBCM & GEBCO

There are two main ocean mapping programs within the Intergovernmental Oceanographic Commission (IOC) of UNESCO, which are cooperative efforts with the International Hydrographic Organization (IHO). The first is called GEBCO, for the 'General Bathymetric Chart of the Oceans'. GEBCO has just completed 101 years of work preparing compilations for all the world oceans. Since 1903 it has produced five separate editions of charts with depth contours every 500 m, and for its Centenary in 2003 it completed a multi-year effort to produce the first 1' (≤1852 m) grid for the world, on both land and sea.

The second series of programs are called the IBCs, for International Bathymetric Charts of various regional seas. These are more detailed local undertakings. I am heavily involved in the Editorial Board of the IBCM, the International Bathymetric Chart of the Mediterranean (and Black Sea) and its Geophysical/Geological Overlay Sheets. Since 1981 charts at scale of 1:1 million and 1:5 million have been prepared for the IBCM bathymetry (Morelli and Val'chuk, 1988), Bouguer gravity anomalies (IBCM-G – Makris et al., 1998), seismicity (IBCM-S - Legros and Bonnin, 1999), Plio-Quaternary isopachs and structural contours (IBCM-PQ – Gennesseaux et al., 1998), recent bottom sediments (IBCM-SED see Chapter 17 of this volume), and magnetic anomalies (IBCM-M – Zanolla et al., 1998; 2000). Four of these geophysical/geological overlays can be seen in Fig. III.4 on pages 6 and 7. For the past ten years I have been working on the new IBCM-II, which will be a bathymetric and topographic grid for the Mediterranean and Black Sea at 0.1' (≤185.2 m) spacing.

As a first attempt to obtain a homogeneous dataset for the IBCM-II, almost all the charts published by the Head Department of Navigation and Oceanography (HDNO) of the Russian Federation were purchased, scanned, and their soundings digitized. This choice was mandated by the inclusion within these charts of published soundings of other hydrographic organizations that had been 'validated' by the hundreds of ships routinely reporting to the HDNO, and by the addition of many new soundings.

This effort has recently been completed, and grids prepared at 1' (Fig. III.7). Now begins the more difficult task to produce a 0.1' grid without the artifacts, blunders, and beauty marks that commonly sprout out from the grids. The ultimate objective is to prepare the grid from seamless coverage of the ocean floor by swath mapping using multibeam sonar. However until this is available, the trick will be to make the best approximation of the seafloor from what is available, and then to replace it with multibeam coverage as that becomes available, either from swath transit tracks, or from polygonal 'postage stamp surveys'.

The method to be used will be a fusion of the now available SRTM 30" (≤90 m) data on land (see below) with the inshore bathymetry taken from published navigational charts. This will be a labor intensive task, which will involve merging the two data sets in such a way that a valid shoreline separates them. Until now such a shoreline has only been available at roughly 1:200,000 scale, except in areas where detailed inshore maps are available at scales of 1:20,000 to 1:5,000. However in the near future a new shoreline, based upon LANDSAT imagery and applicable to scales of 1: 50,000, is expected to be released by the National Geo-Spatial-Intelligence Agency (NGA).

For the shallow waters of the continental shelf and the upper continental slope, the historical data outlined above will probably have to suffice for the foreseeable future. Swath mapping with 100% coverage of the bottom using multibeam sonar is generally not cost effective for reconnaissance work in shallow water. The geometry of the beams makes it necessary to run on very closely spaced tracks.

Thus the initial compilations for the inshore areas of the IBCM-II for the Mediterranean and Black Sea will be based upon shoal-biased soundings from hydrographic charts, unless data is made available from original hydrographic surveys like those shown in

Figs. III.5 or Fig. 15.6. For the deeper areas offshore, there is a good chance that within a few years swath mapping will be available due in great part to the foresight of scientists convinced that efforts in this direction will bear fruit even if the funding agencies place low priority on the need.

MULTIBEAM MAPPING OF THE LEVANT MERGIN

The French Surveys of the Eastern Mediterranean

For the past decade our French colleagues have made steady progress in mapping the deep seafloor of the eastern Mediterranean. Initially cruises of the Ifremer vessel N/O l'Atalante (Fig. III.11c) mapped the Mediterranean Ridge over as far as Eratosthenes Seamount (Loubrieu et al., 2000, Fig. 16.5). These campaigns consisted of MÉDÉE in 1992, HERALIS and ANAXIPROBE in 1995, and PRISMED II in 1998 which vastly improved the Strakhov coverage in the Eratosthenes Seamount area through the use of L'Atalante's Kongsberg Simrad EM12D system. This consists of dual 12 kHz heads producing 162 sonar beams spread over an arc of 150°, capable of mapping a swath up to 7.3 times the water depth.

In 1999 this work was interrupted by the need to survey the faults in the Sea of Marmara, following the disasterous Turkish Izmit earthquake of August 17, 1999 that registered 7.8 on the Richter scale. In 2000 the Ifremer vessel N/O Le Suroît (Fig. 16.2e) continued the systematic work with the FANIL campaign, filling in some of the gaps in the earlier coverage and surveying the lower reaches of the Nile Cone.

In October and November 2003 the Le Suroît carried out two massive surveys of the continental margins of Syria and Lebanon using a Simrad EM300 multibeam. This 30 kHz sonar swath mapping system is capable of mapping the seafloor at depths between 10 and 4000 m. Each ping sends out 135 1° by 2° beams out over an arc of up to 140°, covering a swath up to a maximum of 5.4 times the water depth. **Fig. 16.3b** shows the tracks covered by the two surveys, named SHALIMAR and BLAC. When the results from these two surveys are published they will completely supplant all the previous bathymetry, and should answer many questions related to the offshore physiography of this area.

Beyond the scientific interest in studying the Mediterranean seafloor, the SHALIMAR survey appears to have been carried out to augment the ongoing commercial assessment of the hydrocarbon potential of the margins, and especially to evaluate earthquake risk associated with the adjacent Dead Sea Transform of the Syrian-African rift (as evidenced by structures in the deep sea). Several years earlier the Lebanese had already evinced an interest in the existing bathymetry by establishing, with the help of UNEP a Coastal Information System for monitoring environmental pollution (GRID-Geneva, 2000). Although not acknowledged, in 1999, in order to further this project, the author supplied a 0.1' grid for the Lebanon offshore based upon the available data discussed above.

The BLAC campaign off Syria also appears to be related to tectonic concerns, and in particular to an announcement in 2001 of an interest in collaborating with the Greek Cypriot government in exploring potential offshore oil and gas reserves. This was apparently in response to declining onshore oil reserves.

Up to now such exploration has been minimal. For while Syria, unlike Lebanon and Israel, is a full member of the International Hydrographic Organization in Monaco, and while Syrian naval hydrographic representatives periodically attend the bi-annual meetings of the Mediterranean – Black Sea Hydrographic Commission (MBSHC), the author is unaware of any coastal surveys published by Syria. Despite claiming a 35 nmi territorial sea and 41 nmi contiguous zone, far wider than the almost universally accepted 12 nmi, Syrian hydrographic activity appears to be restricted to updating the detailed port charts, marking hazards to navigation, listing lights and beacons etc.

Israeli National Bathymetric Survey

In the case of Israel, a National Bathymetric Survey (NBS) led by the author and involving a cooperative effort by the Geological Survey of Israel, the Israel Oceanographic and Limnological Research Ltd. (the Israel National Oceanographic Institute), and the Survey of Israel has been in operation since 2001. The IOLR's 48' yacht trawler R/V Etziona (Fig. 16.2h) is equipped with a Kongsberg Simrad EM1002 system operating at 95 kHz. Its 111 2° by 2° beams cover an arc of up to 150° that can map a swath up to 7.3 times the water depth, in depths between 8 and 1000 m. As of this writing approximately 30% of the Israeli offshore has been covered, ultimately producing a DTM at 2 m spacing on the continental shelf. **Fig. 16.6** shows the coverage immediately adjacent to the border with Lebanon in northern Israel. Several features can be immediately noted, which should also pertain to similar shallow results once they are obtained off Lebanon:

1) Up to 15 carbonate or carbonate-cemented sandstone ('kurkar') ridges can be observed running parallel to the coast. These rise from 5-15 m above the surrounding seafloor.

2) North of Acre, off the western Galilee, several E-W faults can be observed. These are continuations of known onshore faults. Detailed examination in the future will determine their activity.

3) The Mount Carmel structure protrudes offshore as the Carmel Nose.

4) In the north, Achziv Canyon has steeply incised the continental shelf, whose shelfbreak is generally at about 125 m depth. Farther south the edge of the less pronounced Carmel Canyon can be seen.

5) Beyond the shore-parallel ridges the shelf shows some segmentation, with a deepening over a 5 km distance north of Acre, and a similar deepening over another five km stretch just south of Rosh Na-Niqra at the border with Lebanon.

6) Bedforms reminiscent of dunes and other nearshore features can be seen on the southwestern part of the Carmel Nose, and at water depths of over 30 m northwest of Acre.

It would appear from these preliminary results that the morphology of the shallow shelf arises from a complex interaction of several sedimentary processes (currents, the post-glacial transgression etc.) and neotectonic activity.

LAND TOPOGRAPHIC DATA - 5' to 0.5' COVERAGE

ETOPO5, GTOPO30, and HYDRO1K

Digital terrain models (DTMs) exist for Lebanon and Syria. The first was ETOPO5, produced by the U.S. Naval Oceanographic Office (USNOO) in the 1980s, with grid point elevations or depths every 5' or about every 9 km. This evolved into a better dataset on CDROM from the National Geophysical Data Center (NGDC) of NOAA called TerrainBase (Row et al., 1995). This was followed by DBDBV (V for variable), another U. S. Navy product, which for the Mediterranean was on a 1' grid (or ≤1.852 km). Then came several datasets primarily produced by NGDC and the U. S. Geological Survey (USGS) which were land-only and on a 0.5' grid or a little less than 1 km. These were GTOPO30 (Anonymous, 1997; USGS, 1997), GLOBE (Hastings and Dunbar, 1999), and HYDRO1K (Verdin and Greenlee, 1996). GTOPO30 was a collaborative effort by the staff of the USGS's EROS Data Center to produce a worldwide dataset to support satellite data acquisition. GLOBE, from the GLOBE Task Team of the Committee on Earth Observation Satellites, was an improved version of GTOPO30. HYDRO1K was a hydrologic derivative of GTOPO30 in which elevation anomalies were removed so that water would flow downhill. The HYDRO1K dataset was also different in that it was on a 1 km grid on Lambert Azimuthal Equal Area projections for each of the continents.

For the purposes of the GEBCO 1' compilations (see Hall, Introduction to Part III of this volume and Fig. III.6, p. 9-10), I used the HYDRO1K dataset. This was done by converting the digital files from big-ended to little-ended binary (Motorola to Intel byte order), and then out of the Lambert projection to geographic latitude and longitude, and then reinterpolating onto the desired grid in geographic coordinates. All these datasets are problematic as they were based upon different sources, different datums, different contour intervals etc.

In 2002 a new worldwide ETOPO2 land and marine 2' grid was released by NGDC, and this was followed in April 2003, at the GEBCO Centenary, by a quantum jump to the new GEBCO Digital Atlas on a 1' grid.

ACE – Altimetry Corrected Elevations

A new 1' gridded dataset (Berry et al., 2002) recently became available, based upon worldwide altimetric measurements from the European Space Agency's ERS-1 Geodetic Mission (Berry et al., 2000). A CDROM with the ACE data was tested and was used for land cover in early drafts of some of this chapter's figures. But in final drafts it was superceded by the SRTM data (see below), which was 100 times as dense. However, for the broad expanses of continent discussed in Chapter 22, the ACE dataset was widely used for background (*viz.* Figs. 22.7, 22.9, 22.10a, 22.11, 22.12, 22.15a, b, 22.21, and 22.23).

LAND TOPOGRAPHIC DATA - 0.5' to 0.05' COVERAGE

Shuttle Radar Topographic Mission (SRTM)

The datasets described above were completely supplanted by the release of the 3" DTM resulting from NASA's Shuttle Radar Topographic Mission, flown February 11-22, 2000 aboard the space shuttle Endeavour on STS-99. After deploying a 60 m mast the crew of the Endeavour (Fig. E.12 in the Epilogue) used C-band Interferometric Synthetic Aperture Radar (INSAR) techniques to make 220 km wide swaths from which a 1" or 30 m DTM for some 82% of Earth's landmass was determined. An X-band radar supplied by the German Space Agency (DLR) derived even finer resolution 10 m data along a narrower 40 m swath.

The SRTM datasets for this part of the world were released during the final stages of preparation of these volumes. As a result the backgrounds for various figures consist of a mixture of datasets. Data on a 3" (90 m) grid for North America was the first to be released, on 5 March 2003. This was followed by South America on 15 May 2003, Eurasia on 5 December 2003, and Africa on 1 April 2004. The data can be downloaded in 1° by 1° tiles from ftp://e0mss21u.ecs.nasa.gov/srtm/.

With 3" SRTM coverage for Eurasia and Africa now available for the three continents bordering the Mediterranean, making the land cover for the 0.1' IBCM-II grids becomes a reality. The raw 3" SRTM data tiles have small gaps in the coverage, due to shadowing by topography, lack of coherence due to water on the ground, and other effects. A number of schemes are freely available for patching these holes, the easiest being overlay of the 3" data over the 30" SRTM data in Global Mapper® (www.globalmapper.com), and then output of a new 3" grid.

The new 3" SRTM dataset is used in **Fig. 16.7** to give an overview of the area to be discussed below. Contrasting this image with that in Fig. III.3 (HYDRO1K on land - p. 5) shows the tremendous improvement in delineation of the land features possible with the SRTM data.

Advanced Spaceborne Thermal Emission and Reflection (ASTER)

Somewhat finer DTMs exist for Lebanon, either prepared from the contours of topographic maps, or from photogrammetric techniques on aerial photography or satellite imagery. For instance the 25 m DTM of Israel which I prepared in 1987-1993 from topographic map sheets at 1:50,000 scale had coastal coverage as far north as Sidon, just south of Beirut.

However equivalent DTMs farther north were derived from multiple coverage of areas by the ASTER (Advanced Spaceborne Thermal Emission and Reflection) sensor aboard the Terra satellite. Terra was launched in December 1999 as part of NASA's Earth Observing System. From December 2000 DTMs from some ASTER image pairs are available to the public from a USGS website (http:/edcimswww.cr.usgs.gov). The ASTER images are 67 km on a side, with resolutions between 15 and 90 m. Although they may be ordered against payment for specific needs, other scenes for different areas of the world are routinely processed and made available without charge.

All the freely available ASTER files in our immediate area have been downloaded. The extraction of the DTM from the

Figs. III.5 or Fig. 15.6. For the deeper areas offshore, there is a good chance that within a few years swath mapping will be available due in great part to the foresight of scientists convinced that efforts in this direction will bear fruit even if the funding agencies place low priority on the need.

MULTIBEAM MAPPING OF THE LEVANT MERGIN

The French Surveys of the Eastern Mediterranean

For the past decade our French colleagues have made steady progress in mapping the deep seafloor of the eastern Mediterranean. Initially cruises of the Ifremer vessel N/O l'Atalante (Fig. III.11c) mapped the Mediterranean Ridge over as far as Eratosthenes Seamount (Loubrieu et al., 2000, Fig. 16.5). These campaigns consisted of MÉDÉE in 1992, HERALIS and ANAXIPROBE in 1995, and PRISMED II in 1998 which vastly improved the Strakhov coverage in the Eratosthenes Seamount area through the use of L'Atalante's Kongsberg Simrad EM12D system. This consists of dual 12 kHz heads producing 162 sonar beams spread over an arc of 150°, capable of mapping a swath up to 7.3 times the water depth.

In 1999 this work was interrupted by the need to survey the faults in the Sea of Marmara, following the disasterous Turkish Izmit earthquake of August 17, 1999 that registered 7.8 on the Richter scale. In 2000 the Ifremer vessel N/O Le Suroît (Fig. 16.2e) continued the systematic work with the FANIL campaign, filling in some of the gaps in the earlier coverage and surveying the lower reaches of the Nile Cone.

In October and November 2003 the Le Suroît carried out two massive surveys of the continental margins of Syria and Lebanon using a Simrad EM300 multibeam. This 30 kHz sonar swath mapping system is capable of mapping the seafloor at depths between 10 and 4000 m. Each ping sends out 135 1° by 2° beams out over an arc of up to 140°, covering a swath up to a maximum of 5.4 times the water depth. **Fig. 16.3b** shows the tracks covered by the two surveys, named SHALIMAR and BLAC. When the results from these two surveys are published they will completely supplant all the previous bathymetry, and should answer many questions related to the offshore physiography of this area.

Beyond the scientific interest in studying the Mediterranean seafloor, the SHALIMAR survey appears to have been carried out to augment the ongoing commercial assessment of the hydrocarbon potential of the margins, and especially to evaluate earthquake risk associated with the adjacent Dead Sea Transform of the Syrian-African rift (as evidenced by structures in the deep sea). Several years earlier the Lebanese had already evinced an interest in the existing bathymetry by establishing, with the help of UNEP a Coastal Information System for monitoring environmental pollution (GRID-Geneva, 2000). Although not acknowledged, in 1999, in order to further this project, the author supplied a 0.1' grid for the Lebanon offshore based upon the available data discussed above.

The BLAC campaign off Syria also appears to be related to tectonic concerns, and in particular to an announcement in 2001 of an interest in collaborating with the Greek Cypriot government in exploring potential offshore oil and gas reserves. This was apparently in response to declining onshore oil reserves.

Up to now such exploration has been minimal. For while Syria, unlike Lebanon and Israel, is a full member of the International Hydrographic Organization in Monaco, and while Syrian naval hydrographic representatives periodically attend the bi-annual meetings of the Mediterranean – Black Sea Hydrographic Commission (MBSHC), the author is unaware of any coastal surveys published by Syria. Despite claiming a 35 nmi territorial sea and 41 nmi contiguous zone, far wider than the almost universally accepted 12 nmi, Syrian hydrographic activity appears to be restricted to updating the detailed port charts, marking hazards to navigation, listing lights and beacons etc.

Israeli National Bathymetric Survey

In the case of Israel, a National Bathymetric Survey (NBS) led by the author and involving a cooperative effort by the Geological Survey of Israel, the Israel Oceanographic and Limnological Research Ltd. (the Israel National Oceanographic Institute), and the Survey of Israel has been in operation since 2001. The IOLR's 48' yacht trawler R/V Etziona (Fig. 16.2h) is equipped with a Kongsberg Simrad EM1002 system operating at 95 kHz. Its 111 2° by 2° beams cover an arc of up to 150° that can map a swath up to 7.3 times the water depth, in depths between 8 and 1000 m. As of this writing approximately 30% of the Israeli offshore has been covered, ultimately producing a DTM at 2 m spacing on the continental shelf. **Fig. 16.6** shows the coverage immediately adjacent to the border with Lebanon in northern Israel. Several features can be immediately noted, which should also pertain to similar shallow results once they are obtained off Lebanon:

1) Up to 15 carbonate or carbonate-cemented sandstone ('kurkar') ridges can be observed running parallel to the coast. These rise from 5-15 m above the surrounding seafloor.

2) North of Acre, off the western Galilee, several E-W faults can be observed. These are continuations of known onshore faults. Detailed examination in the future will determine their activity.

3) The Mount Carmel structure protrudes offshore as the Carmel Nose.

4) In the north, Achziv Canyon has steeply incised the continental shelf, whose shelfbreak is generally at about 125 m depth. Farther south the edge of the less pronounced Carmel Canyon can be seen.

5) Beyond the shore-parallel ridges the shelf shows some segmentation, with a deepening over a 5 km distance north of Acre, and a similar deepening over another five km stretch just south of Rosh Na-Niqra at the border with Lebanon.

6) Bedforms reminiscent of dunes and other nearshore features can be seen on the southwestern part of the Carmel Nose, and at water depths of over 30 m northwest of Acre.

It would appear from these preliminary results that the morphology of the shallow shelf arises from a complex interaction of several sedimentary processes (currents, the post-glacial transgression etc.) and neotectonic activity.

LAND TOPOGRAPHIC DATA - 5' to 0.5' COVERAGE

ETOPO5, GTOPO30, and HYDRO1K

Digital terrain models (DTMs) exist for Lebanon and Syria. The first was ETOPO5, produced by the U.S. Naval Oceanographic Office (USNOO) in the 1980s, with grid point elevations or depths every 5' or about every 9 km. This evolved into a better dataset on CDROM from the National Geophysical Data Center (NGDC) of NOAA called TerrainBase (Row et al., 1995). This was followed by DBDBV (V for variable), another U. S. Navy product, which for the Mediterranean was on a 1' grid (or ≤1.852 km). Then came several datasets primarily produced by NGDC and the U. S. Geological Survey (USGS) which were land-only and on a 0.5' grid or a little less than 1 km. These were GTOPO30 (Anonymous, 1997; USGS, 1997), GLOBE (Hastings and Dunbar, 1999), and HYDRO1K (Verdin and Greenlee, 1996). GTOPO30 was a collaborative effort by the staff of the USGS's EROS Data Center to produce a worldwide dataset to support satellite data acquisition. GLOBE, from the GLOBE Task Team of the Committee on Earth Observation Satellites, was an improved version of GTOPO30. HYDRO1K was a hydrologic derivative of GTOPO30 in which elevation anomalies were removed so that water would flow downhill. The HYDRO1K dataset was also different in that it was on a 1 km grid on Lambert Azimuthal Equal Area projections for each of the continents.

For the purposes of the GEBCO 1' compilations (see Hall, Introduction to Part III of this volume and Fig. III.6, p. 9-10), I used the HYDRO1K dataset. This was done by converting the digital files from big-ended to little-ended binary (Motorola to Intel byte order), and then out of the Lambert projection to geographic latitude and longitude, and then reinterpolating onto the desired grid in geographic coordinates. All these datasets are problematic as they were based upon different sources, different datums, different contour intervals etc.

In 2002 a new worldwide ETOPO2 land and marine 2' grid was released by NGDC, and this was followed in April 2003, at the GEBCO Centenary, by a quantum jump to the new GEBCO Digital Atlas on a 1' grid.

ACE – Altimetry Corrected Elevations

A new 1' gridded dataset (Berry et al., 2002) recently became available, based upon worldwide altimetric measurements from the European Space Agency's ERS-1 Geodetic Mission (Berry et al., 2000). A CDROM with the ACE data was tested and was used for land cover in early drafts of some of this chapter's figures. But in final drafts it was superceded by the SRTM data (see below), which was 100 times as dense. However, for the broad expanses of continent discussed in Chapter 22, the ACE dataset was widely used for background (*viz.* Figs. 22.7, 22.9, 22.10a, 22.11, 22.12, 22.15a, b, 22.21, and 22.23).

LAND TOPOGRAPHIC DATA - 0.5' to 0.05' COVERAGE

Shuttle Radar Topographic Mission (SRTM)

The datasets described above were completely supplanted by the release of the 3" DTM resulting from NASA's Shuttle Radar Topographic Mission, flown February 11-22, 2000 aboard the space shuttle Endeavour on STS-99. After deploying a 60 m mast the crew of the Endeavour (Fig. E.12 in the Epilogue) used C-band Interferometric Synthetic Aperture Radar (INSAR) techniques to make 220 km wide swaths from which a 1" or 30 m DTM for some 82% of Earth's landmass was determined. An X-band radar supplied by the German Space Agency (DLR) derived even finer resolution 10 m data along a narrower 40 m swath.

The SRTM datasets for this part of the world were released during the final stages of preparation of these volumes. As a result the backgrounds for various figures consist of a mixture of datasets. Data on a 3" (90 m) grid for North America was the first to be released, on 5 March 2003. This was followed by South America on 15 May 2003, Eurasia on 5 December 2003, and Africa on 1 April 2004. The data can be downloaded in 1° by 1° tiles from ftp://e0mss21u.ecs.nasa.gov/srtm/.

With 3" SRTM coverage for Eurasia and Africa now available for the three continents bordering the Mediterranean, making the land cover for the 0.1' IBCM-II grids becomes a reality. The raw 3" SRTM data tiles have small gaps in the coverage, due to shadowing by topography, lack of coherence due to water on the ground, and other effects. A number of schemes are freely available for patching these holes, the easiest being overlay of the 3" data over the 30" SRTM data in Global Mapper® (www.globalmapper.com), and then output of a new 3" grid.

The new 3" SRTM dataset is used in **Fig. 16.7** to give an overview of the area to be discussed below. Contrasting this image with that in Fig. III.3 (HYDRO1K on land - p. 5) shows the tremendous improvement in delineation of the land features possible with the SRTM data.

Advanced Spaceborne Thermal Emission and Reflection (ASTER)

Somewhat finer DTMs exist for Lebanon, either prepared from the contours of topographic maps, or from photogrammetric techniques on aerial photography or satellite imagery. For instance the 25 m DTM of Israel which I prepared in 1987-1993 from topographic map sheets at 1:50,000 scale had coastal coverage as far north as Sidon, just south of Beirut.

However equivalent DTMs farther north were derived from multiple coverage of areas by the ASTER (Advanced Spaceborne Thermal Emission and Reflection) sensor aboard the Terra satellite. Terra was launched in December 1999 as part of NASA's Earth Observing System. From December 2000 DTMs from some ASTER image pairs are available to the public from a USGS website (http:/edcimswww.cr.usgs.gov). The ASTER images are 67 km on a side, with resolutions between 15 and 90 m. Although they may be ordered against payment for specific needs, other scenes for different areas of the world are routinely processed and made available without charge.

All the freely available ASTER files in our immediate area have been downloaded. The extraction of the DTM from the

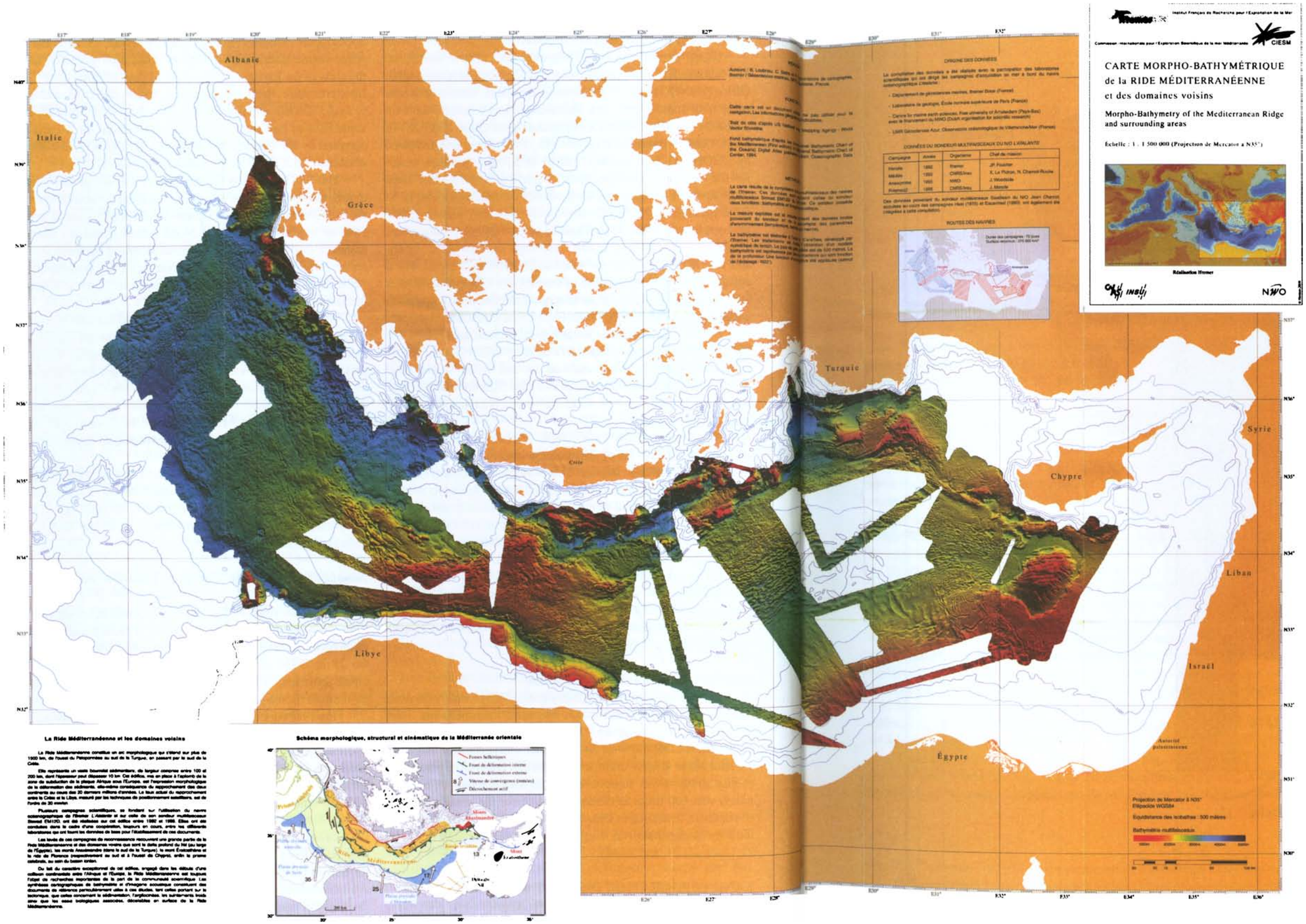


Fig. 16.5. Reproduction of the poster of Loubrieu, Satra, and Cagna (2000) showing the Morpho-Bathymetry of the Mediterranean Ridge and Surrounding Areas. The map is based on four campaigns of the Ifremer vessel N/O L'Atalante - Médée, Heralis, Anaxiprobe, and Prismed2. The ship used a dual head Simrad EM12D system with 162 beams. These campaigns, over a total of 70 days between 1992 and 1998, surveyed some 375,000 km². Additional work has filled in areas around the Nile Cone (FANIL) and recently along the margins of Syria and Lebanon. A description of the map is given below in the section entitled 'A Multibeam Bathymetric Map of the Deep Eastern Mediterranean Sea Basin' by B. Loubrieu et al.

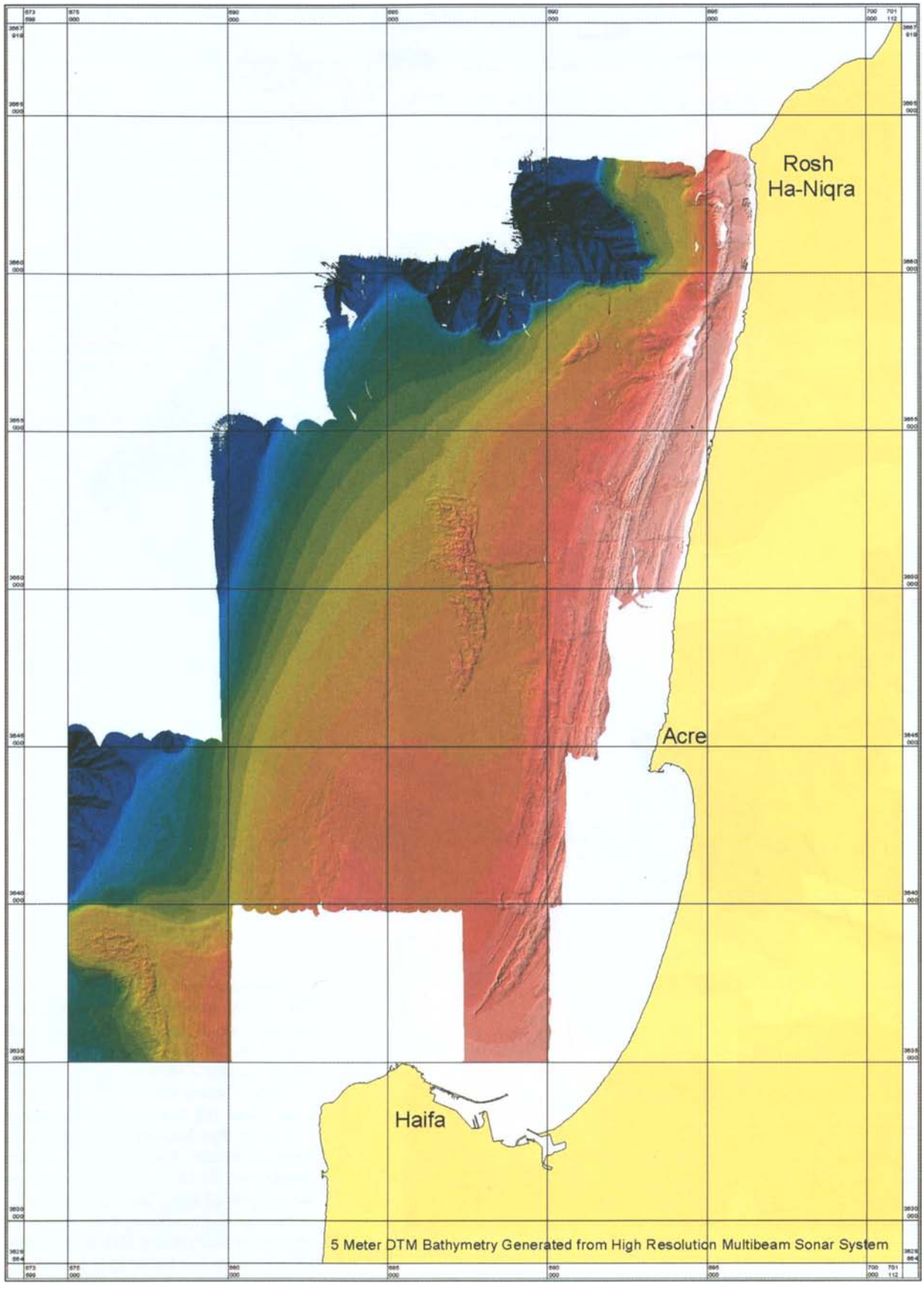

Rosh
Ha-Niqra
Acre
Haifa
5 Meter DTM Bathymetry Generated from High Resolution Multibeam Sonar System

Table 16.1: Files downloaded in order to make the DTM in Fig. 16.8.

ASTER_DEM20011120155459.hdf ASTER_DEM20011120155459_hdf_met.htm	**Tripoli**	5459
ASTER_DEM20020220131418.hdf ASTER_DEM20020220131418_hdf_met.htm	**Beirut**	1418
ASTER_DEM20020220141338.hdf ASTER_DEM20020220141338_hdf_met.htm	**AntiLebanon**	1338
ASTER_DEM20020220144215.hdf ASTER_DEM20020220144215_hdf_met.htm	**Bekaa**	4215
ASTER_DEM20020221093012.hdf ASTER_DEM20020221093012_hdf_met.htm	**Tyre**	3012
ASTER_DEM20020221105511.hdf ASTER_DEM20020221105511_hdf_met.htm	**Batrun**	5511
ASTER_DEM20020222132346.hdf ASTER_DEM20020222132346_hdf_met.htm	**Haifa**	2346
ASTER_DEM20020417120045.hdf ASTER_DEM20020417120045_hdf_met.htm	**Golan**	0045

downloaded files is not a trivial process. The process requires first to get the scene corner, so using something like Notepad, one enters the _hdf_met.htm file for the scene, and extracts the last latitude and longitude values from the GRingPointLatitude and GRingPointLongitude section. These are then converted from decimal degrees to UTM coordinates via something like the free web applet at http://www.cellspark.com/UTM.html.

Using a program called GEOTIFF4 available from www.terrainmap.com which is run by John Childs, an RPI graduate student of remote sensing, the Aster FP32 HDF format files can be processed and converted to DEM format files, which Global Mapper® can convert to Surfer® binary GRD files. These can then be mosaicked and manipulated by Surfer®. However, while the *x,y* precision of the ASTER files isn't bad, the regional *z* values fluctuate considerably, so that the coast can vary more than a hundred meters above or below sea level. Initial attempts to correct this for preparation of this chapter were not rewarding; but following the release of the 30" and 3" SRTM data, and improvements in the Global Mapper® software, it became possible to overlay 3" SRTM on the 30" SRTM, and then output an exact 30 m grid overlay to the ASTER files. Surfer® was then used to subtract this overlay grid from the original ASTER data, and then again subtract this difference grid from the original ASTER grid to obtain a new grid without these large errors in height.

As an introduction to the discussion below, **Fig. 16.8** shows the eight uncorrected ASTER 30 m DTM files overlain on the 90 m SRTM on the coast of Lebanon and Syria. The last four digits for each of the grids, given in **Table 16.1**, are noted in white on the figure. SRTM-corrected ASTER DTM files were used in the figures presented in the discussion of the coastal morphology below.

Two other examples demonstrating the high quality of the ASTER datasets are shown in Figs. 16.9 and 16.10. In **Fig. 16.9** of the northern Gulf of Aqaba (Elat) the 30 m ASTER data on the left is contrasted with the 90 m SRTM data on the right. The bathymetry for the gulf is shown as multibeam data from the F/S METEOR during Cruise 44/2 overlain on the bathymetric chart of Hall and Ben-Avraham (1979). In **Fig. 16.10**, from Wadi as Sirhan on the border between Jordan and Saudi Arabia, the ASTER data in the southwestern and northeastern quadrants show very clearly the fabric and texture of the topography. In the northwestern and southeastern quadrants the slightly less detail of the SRTM dataset is evident.

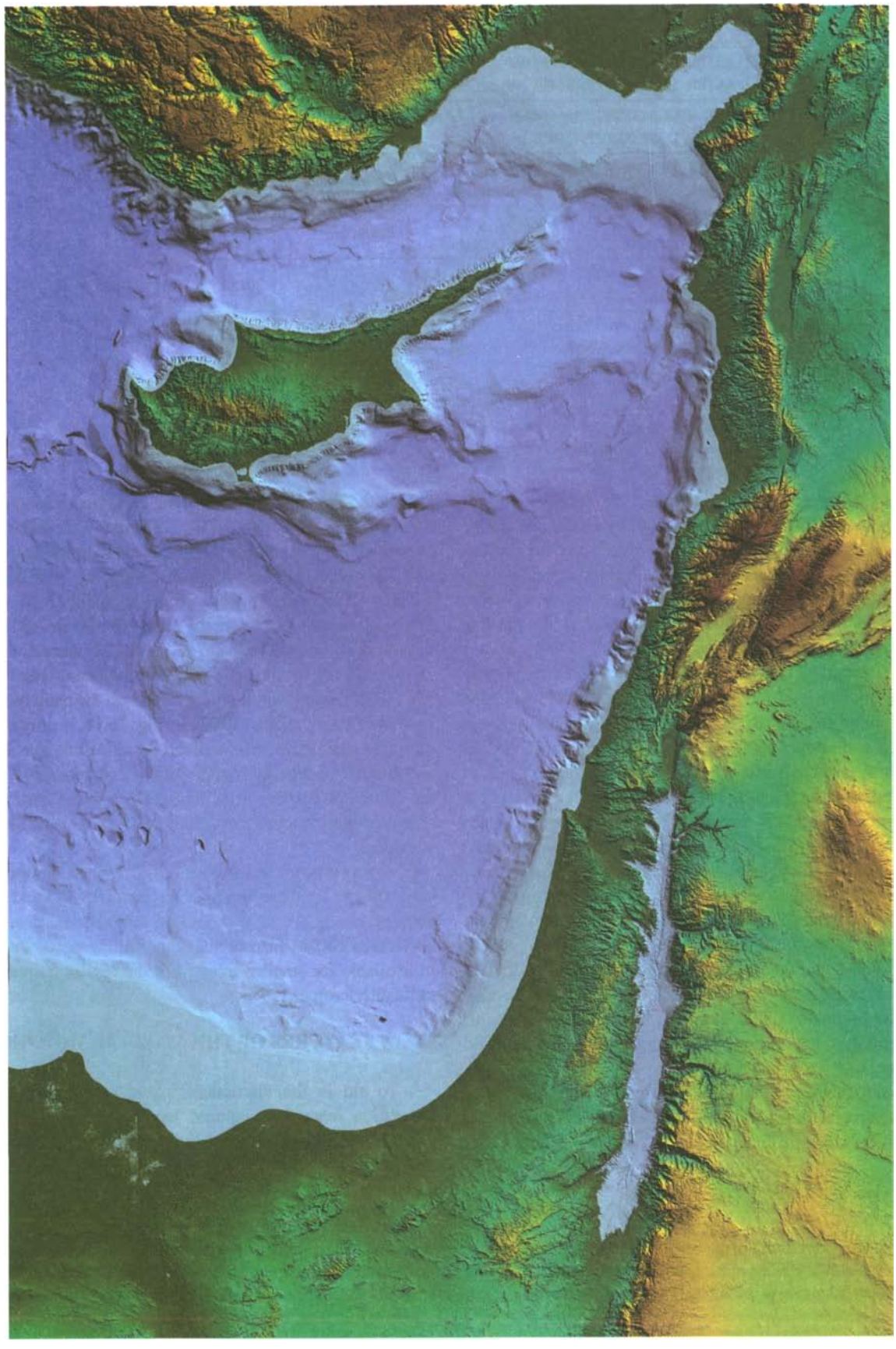
To my knowledge these are the highest resolution images yet available for these areas, which cover 19,473 and 36,218 km² respectively. However it should be remembered that the original unreleased SRTM measurements are at 30 m resolution with 10 m available for smaller areas from the higher frequency X-band rader interferometry.

MAIN FEATURES OF THE COASTAL MORPHOLOGY

To aid in the discussion below, and for the purposes of navigation relative to cultural landmarks, the Tactical Piloting Chart of the Lebanese-Syrian coast has been superimposed on the



Fig. 16.6. Preliminary 5 m DTM of the continental shelf off northern Israel from the multibeam surveys of the Israel National Bathymetric Survey. The research vessel R/V Etziona of the Israel Oceanographic & Limnological Research Ltd. is equipped with a Kongsberg-Simrad EM1002 multibeam sonar system belonging to the author. The system operates at 95 kHz, and has 111 2° by 2° beams capable of mapping a swath 7.3 times the water depth.



digitized bathymetry in **Fig. 16.11.** The area covered is the same as in Fig. 16.8. Two features of this coast are immediately evident:

a) The exceedingly narrow continental shelf from northern Israel up to Turkey, with the exception of the bay between Tripoli and Tartus and the triangular block widening out to sea off As Sarafand in southern Lebanon.

b) The increased density of offshore submarine canyons incising the shelf off the areas with coastal mountains.

The Offshore Faults

Fig. 16.12, simplified after Quennell (1984, Fig. 1, p. 277), shows the major faults along the coast between northern Israel and southern Turkey. The majority of the faults, around twenty in number, are found in the southern half south of Tripoli. They appear related to the offset in the Dead Sea Transform along the Yammouneh Fault, and for the most part are nearly perpendicular to the coast. North of Tripoli only five faults are indicated, and they are generally parallel to the adjacent coast.

Much has been written on the faulting in Lebanon (Beydoun, 1977; Arthaud et al., 1978; Walley, 1988; Ambraseys and Barazangi, 1989; Khair et al., 1997) and in particular on the Yammouneh Fault (Butler and Spencer, 1999; Daëron et al., 2001, 2003). The kinematics of the Dead Sea fault system cannot reconcile the fact that of the predicted 80 km of crustal shortening that should be accommodated by the Palmyride system in Syria, only 20 km can be accounted for (Chaimov et al., 1990). These difficulties have led to ideas concerning possible accommodation via the branching-off Roum Fault which presumably heads offshore, northward from the Beirut headland (Butler et al., 1997; Khair, 2001; Elias et al., 2001, 2003). **Fig. 16.13** shows the most detailed topographic representation published to date for this complex area.

Between Haifa and Saida the Roum Fault is seen to head NNW from the Hula Valley in northern Israel. Its exact trace is unknown, and most authors show it to exist for only half the distance between the Hula Valley and Beirut. However the fault has been the subject of great interest and speculation in that it could explain the above kinematic discrepancy, and because recent earthquakes have been attributed to the fault. Quoting from Darawcheh et al. (2000), "Analysis of the Byzantine primary and secondary sources for identifying the historical earthquakes in Syria and Lebanon reveals that a large earthquake ($Ms = 7.2$) occurred in July 9, 551 AD along the Lebanese littoral and was felt over a very large area in the eastern Mediterranean region. It was a shallow-focus earthquake, associated with a regional tsunami along the Lebanese coast, a local landslide near Al-Batron town, and a large fire in Beirut. It caused heavy destruction with great loss of lives to several Lebanese cities, mainly Beirut, with a maximum intensity between IX-X (EMS-92). The proposed epicenter of the event is offshore of Beirut at about 34.00°N, 35.50°E, indicating that the earthquake appears to be the result of movement along the strike-slip left-lateral Roum fault in southern Lebanon."

In addition, Khair (2001, p. 4240, Fig. 1, Table 1) relates that the three strongest seismic events in the past century (four events in June-July 1907, March 16, 1956, and March 26, 1997) "are located in the Roum fault zone including the Chouf region and its offshore area". These events, so close to the metropolis of Beirut, have raised great concern. The day after the 1997 quake, News@Lebanon.com reported "The Roum fault, east of Sidon, was the epicenter of Lebanon's last earthquake – the strongest earthquake since 1956. No casualties were reported, though there were some broken glasses and cracks in the walls. Additional 8 aftershocks were reported between 6:20 a.m. and 3:20 p.m. time. The one at 3.20 p.m. registered 4.3 on the Richter scale, and the 8 aftershocks registered between 2.5 and 3.5 Richter scale."

A recent new analysis of the seismic profiles (*e.g.* Fig. 16.14) obtained during our November 1982 survey off southern Lebanon has highlighted the existence of the 'Damur Disturbance', off Damur some 20 km south of Beirut (Ben-Avraham et al., 2004). It is similar to the 'Palmachim' and 'Dor Disturbances' studied in some detail off Israel (Almagor and Hall, 1984). The seismic data shows the presence of dominant growth faults associated with movements of the Messinian salts, as well as less evident deep-rooted faults. The bathymetric data in hand presents no clear picture of a NNW trending fault in the sea, although the new swath mapping is likely to clearly discern its trace if it exists.

The Offshore Canyons

The density of canyons along the southern sector of the coast closely follows the pattern of faults shown in Fig. 16.12. North of Tripoli the continental margin is smoother, with a short seaward extension opposite the ENE-WSW trending Tripoli thrust implicated in the disastrous 551 AD earthquake (Elias et al., 2001, 2003). Another series of canyons is clustered opposite the branching off of the Gharb Fault, and then extending southwest from Latakia is the 100 km long West Tartus Ridge. Its relation to the more northerly Amanos fault is unclear.



Fig. 16.7. Shaded relief bathymetry of the eastern Mediterranean from the 50 m contours of Hall (1994) merged with the 3" (≤90 m) Shuttle Radar Topographic Mission (SRTM) data for the land. Note the tremendous improvement in visualization of the bathymetry over the depth contours in Fig. III.2 (p. 3 of this volume), and the 30" (≤900 m) HYDRO1K land topography in Fig. III.3 (p. 5). It should be noted that the data density has been considerably decreased in order to make this figure. Of note are the several bends in the Dead Sea Transform (DST), the asymmetry of the Jordan Rift, the heights of the mountains of Lebanon and the Anti-Lebanon, Jebel Druze, and the Göksu River Valley in Turkey and its alignment with the shelf margin southwest of Iskenderun Bay. Note also how the deep margins of the easternmost Mediterranean are aligned with the general trends of the DST.

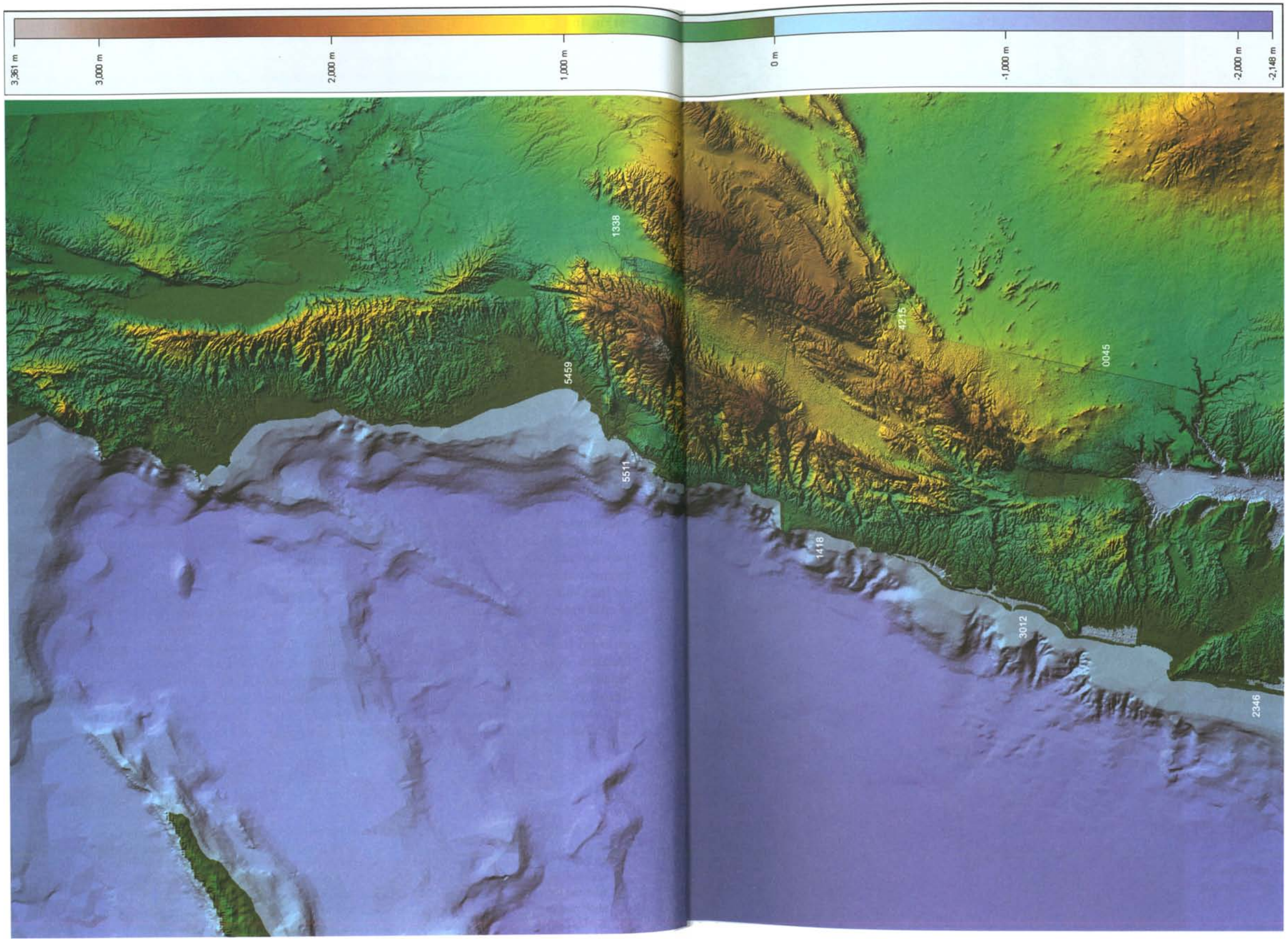


Fig. 16.8. Hypsometrically colored shaded relief plots of eight ASTER image scenes between Haifa and Tripoli, overlain on the 90 m SRTM land coverage and the digitized bathymetry from Fig. 16.7. The original file names are shown in Table 16.1. The last four digits for each ASTER scene are noted. The 30 m grid spacing of elevations from photogrammetric analysis of the scenes gives an excellent indication of the local physiography. Unfortunately the overall vertical precision is not well-constrained and the absolute elevations may be in error by tens to hundreds of meters. Holes in the data are primarily due to clouds which obscured the ground.

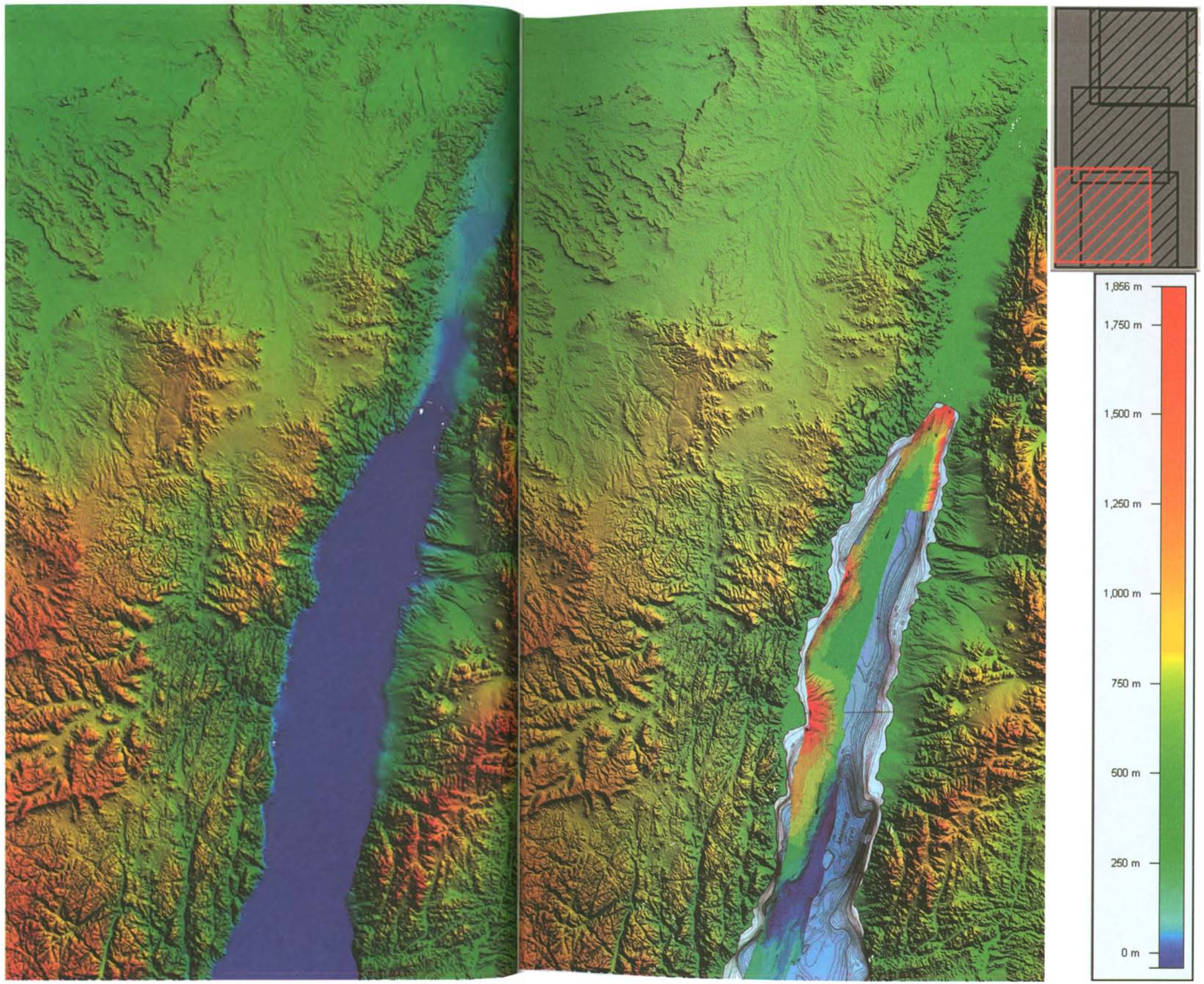


Fig. 16.9. Comparison of ASTER 30 m and SRTM 3" (≤90 m) data for the northern Gulf of Elat (Aqaba) in southern Israel, Jordan, and Egyptian Sinai. The projection is UTM for Zone 36 (30° to 36°E). On the left side is the ASTER data, corrected against the SRTM, overlaid on reinterpolated 30 m SRTM data. On the right side is the original 3" SRTM data reinterpolated to 90 m on the UTM projection. The area shown includes five ASTER 67 by 67 km tiles, whose location is shown in the upper right hand side inset. The comparison is surprisingly good. The color scale applies only to the left hand image. The area covered is 102 km wide and 191 km high, for an area of 19,473 km². This is almost the size of pre-1967 Israel.

In the right hand image, the bathymetry of the Gulf of Aqaba (Elat), taken from the map of Hall and Ben-Avraham (1979), has been superimposed., overlain by the preliminary swath data from the DS-2 Hydrosweep multibeam sonar system used aboard the German research vessel F/S METEOR during her cruise 44 Leg 2 (12 March - 7 April 1999) in the gulf. The swath grid is 30 m.

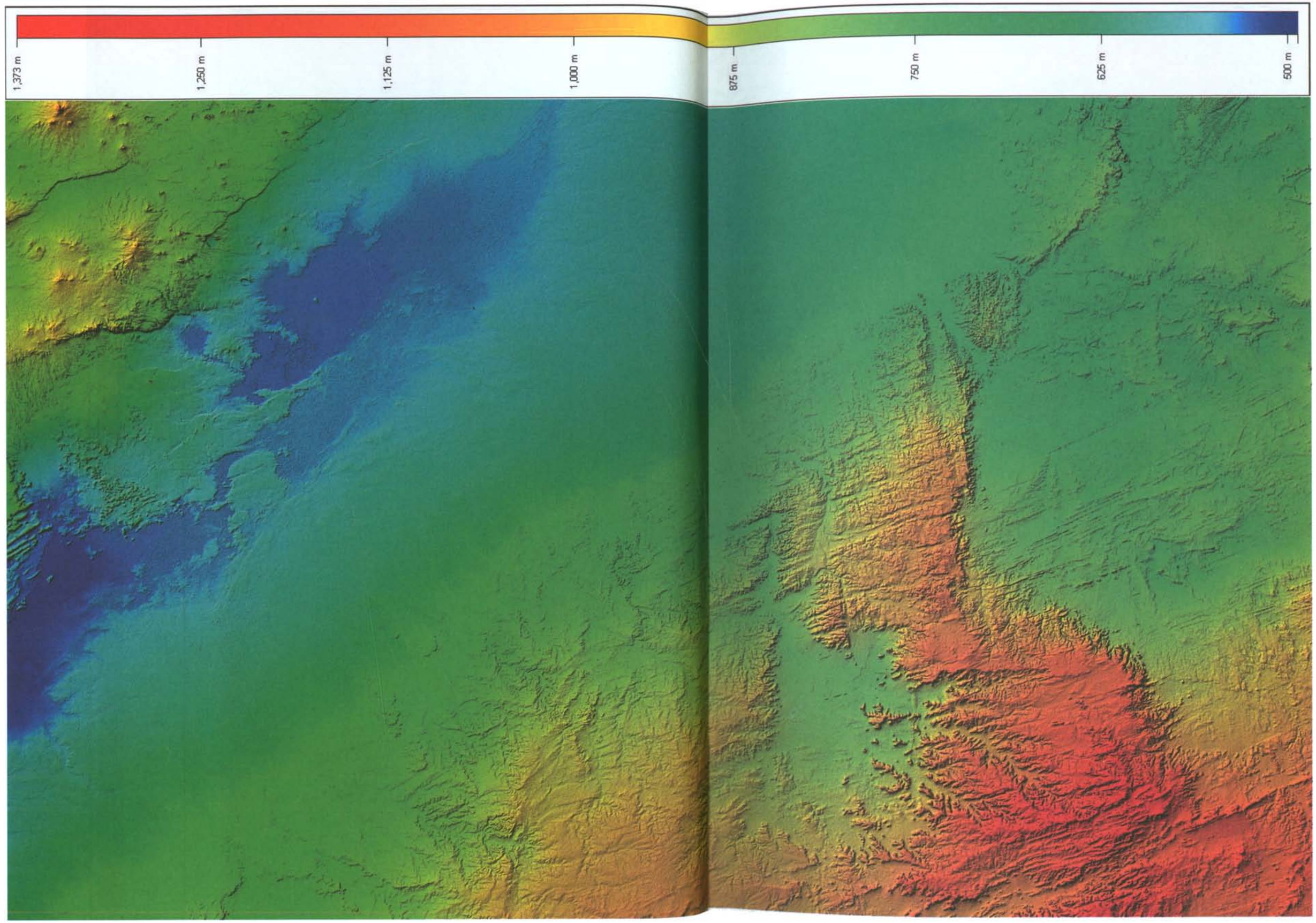
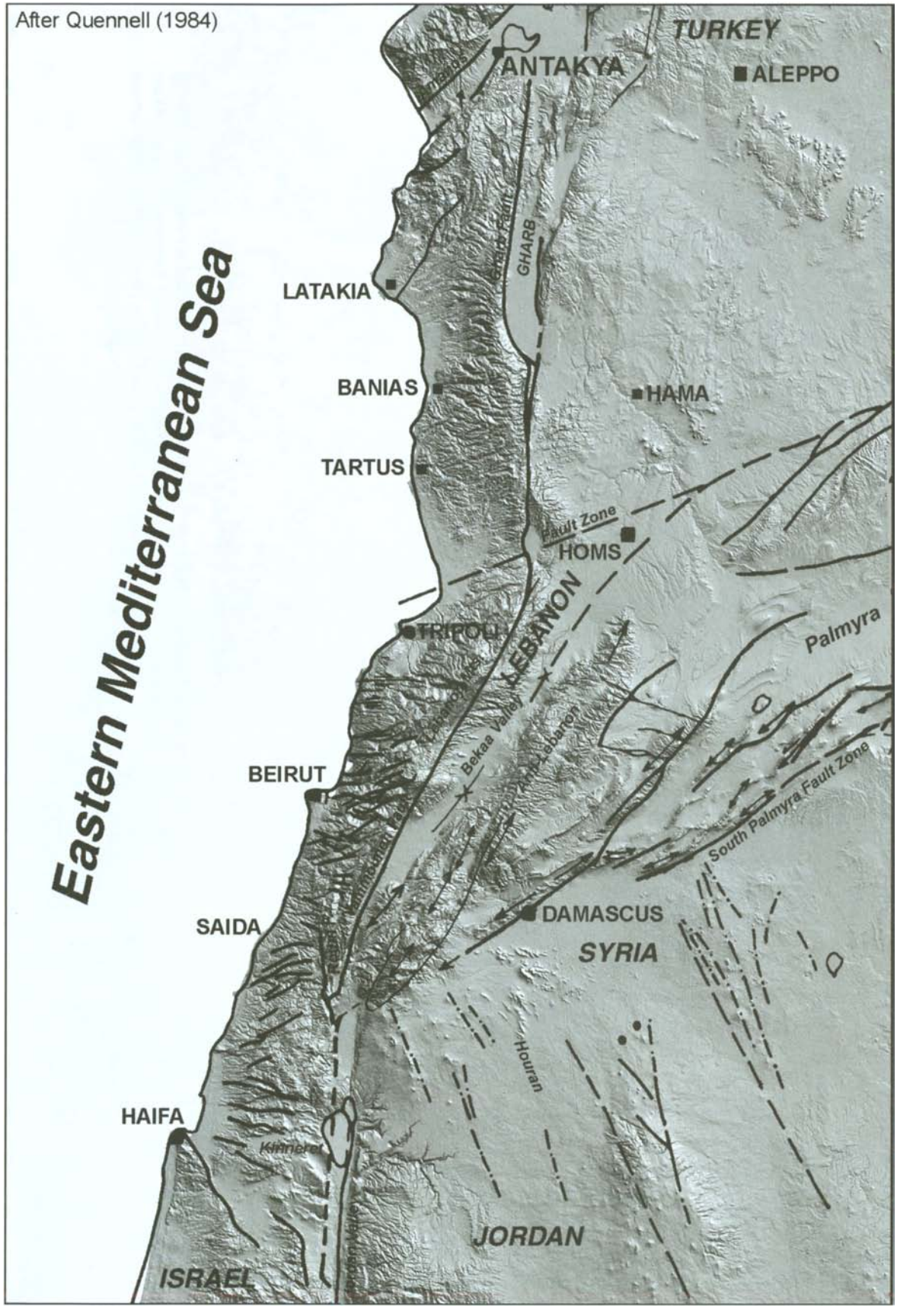


Fig. 16.10. Example of 30 m ASTER imagery for the area of Wadi as Sirhan, where the southern part of Jordan protrudes into Saudi Arabia. See figure on page 824 for location. The projection is UTM for Zone 37 (36° to 42°E), and the limits are approximately 29°-07' to 31°-17'N and 37° to 38°-20'E. Almost 900 m of topography is represented in this area of approximately 150 by 212 km, covering 36,218 km². Three ASTER images (2006, 2920, and 5924) are used here, in the southwestern and northeastern quadrants. They show very clearly the fabric and texture of the topography. In the northwestern and southeastern quadrants the slightly lesser detail of the SRTM dataset is evident.



Fig. 16.11. Shaded relief bathymetry of the eastern Mediterranean from the 50 m contours of Hall (1994) merged with the shaded relief Tactical Piloting Charts of Israel, Lebanon, Syria, and Turkey (UKMOD, 1975; DMAAC, 1984). While the area covered is the same as in Fig. 16.8 the Tactical Piloting Chart gives cultural information on the names, roads, borders, lakes etc. Note the higher density of submarine canyons in the south opposite the bend in the Dead Sea Transform. While all the canyons are a result of the scouring effects from the erosional products from the nearby high mountain chains, these are also clearly impacted by the local faulting.


After Quennell (1984)
TURKEY
ANTAKYA
ALEPPO
Eastern Mediterranean Sea
Ghab Fault
GHARB
LATAKIA
BANIAS
HAMA
TARTUS
Fault Zone
HOMS
TRIPOLI
LEBANON
Palmyra
Lebanon
Bekaa Valley
Anti-Lebanon
BEIRUT
South Palmyra Fault Zone
DAMASCUS
SAIDA
SYRIA
Hauran
HAIFA
Kinneret
JORDAN
ISRAEL

DISCUSSION

This chapter has attempted to describe in somewhat general terms the state of knowledge of the continental margin of the eastern Mediterranean. This is perhaps an unenviable task given that in the not too distant future there should be a few orders of magnitude improvement in visualization, expected from the acquisition of detailed seismic and swath bathymetry in the offshore. However, as it is unlikely that the swath mapping will concentrate soon on the shallower parts of the rise, slope, and shelf due to the concomitant increase in survey time required, the inshore data described here will have some value in guiding future work on the shelf, following its more detailed analysis.

ACKNOWLEDGEMENTS

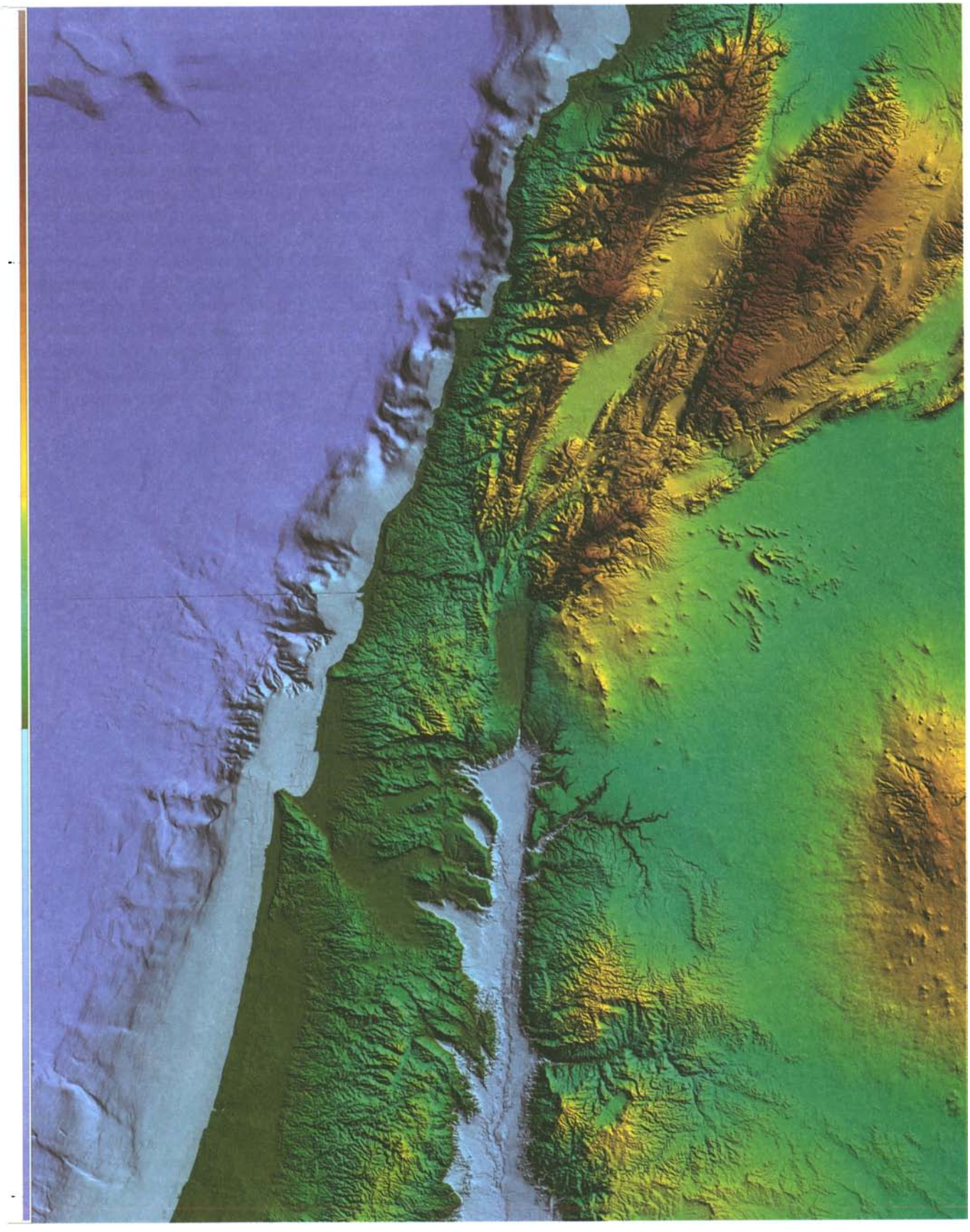
I am grateful to the Geological Survey of Israel and the Israel Ministry of National Infrastructures for giving me the freedom to pursue compilational activities within the Mediterranean on behalf of the International Bathymetric Chart of the Mediterranean (IBCM) on whose Editorial Board I serve as Vice Chairman.

Thanks are also due to all who have contributed data, trackmaps, echo soundings etc. For this I am obliged to my colleagues at Lamont-Doherty Geological Observatory (now L-DEO), and William 'Bill' Dunkle at Woods Hole Oceanographic Institution. I am especially grateful to Desmond P. D. Scott and Brian Harper, former GEBCO Permanent Secretaries, and Gordon J. Taylor of the United Kingdom Hydrographic Office, for making available the hydrographic fairsheets of the historical surveys of HMS Tartarus, Firefly, Endeavour, Ormonde, Owen, Dalrymple, and others in eastern Mediterranean waters for the purposes of the IBCM and GEBCO. Jerome Benvenisti of the European Space Agency alerted me to the ACE dataset, and James Garlick at De Montfort University (Leicester, UK) helped me to obtain the data.

And finally I salute my colleagues Aharon (Ronnie) Sade, Arik Golan, Limor Avrahami Gur-Arieh, and Gideon Amit for their outstanding work in carrying out the swath mapping of the Israeli Mediterranean offshore.



Fig. 16.12. Map simplified from Quennel (1984 Fig. 1, p. 277) showing the scheme of faults between northern Israel and southern Turkey. Over twenty faults occur in the southern half, south of Tripoli. These are primarily east-west faults, continuing into the sea, and probably related to the offset in the Dead Sea Transform along the Yammouneh Fault. North of Tripoli only five faults are indicated, generally parallel to the coast. The plot is overlain on Global Mapper® daylight shaded relief from a UTM projection (Zone 37) of the 90 m SRTM.



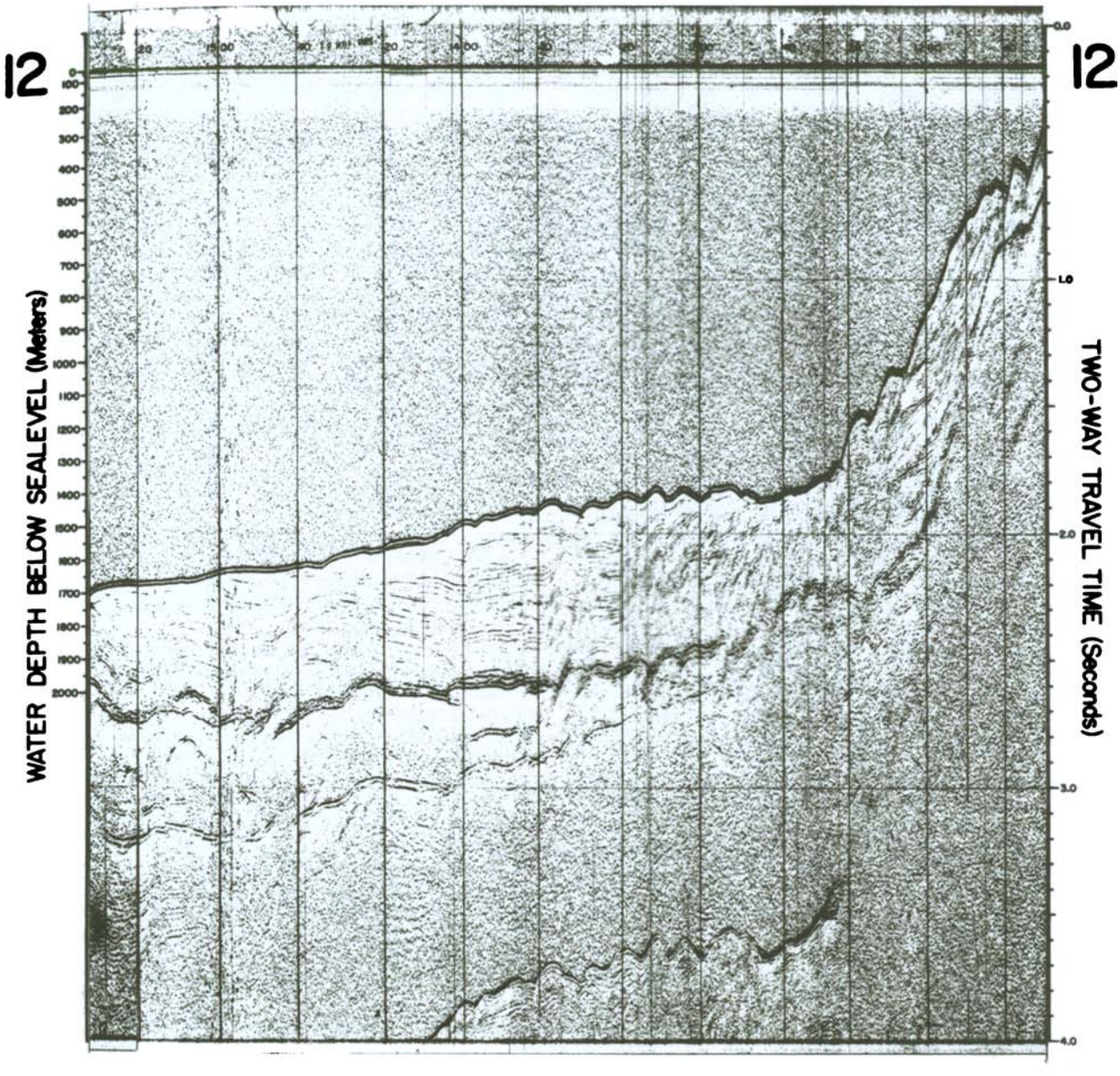


Fig. 16.14. Continuous single channel seismic profile No. 12 obtained mid-November 1982 off Ras Beirut. See Fig. 16.3a for location. Source was a 300 in^3 airgun with the signals received on a SECO tapered array, conditioned by a Del Norte Model 502 Seismic Amplifier, and recorded on an EPC Model 4100 19" graphic recorder. Note the very steep nature of the continental margin, and the strong reflector at depth marking the top of the Messinian salt reflector.



Fig. 16.13. More detailed shaded relief topography of the area between Tel Aviv and Tripoli. The 25 m DTM of Israel is overlain on the (SRTM corrected) 30 m ASTER data of Fig. 16.8, which overlies the 90 m SRTM data, together with the corrected bathymetry of the eastern Mediterranean from the 50 m contours of Hall (1994). The projection is UTM for Zone 36, and the pixel size is 50 m. This image shows, perhaps better than ever before, the configuration of the bend in the Dead Sea Transform and the myriad E-W trending canyons and faults. The trace of the Roum Fault is clearly seen, apparently entering the Mediterranean along the western flank of Ras Beirut.

REFERENCES CITED

Almagor, G. and Hall, J. K., 1980. Morphology of the continental margin off northern Israel and southern Lebanon. Isr. J. Earth Sci., 29(4), p. 245-252.

Almagor, G., and Hall, J. K., 1984. Morphology of the Mediterranean continental margin of Israel (A compilative summary and a bathymetric chart). Geological Survey of Israel, Bulletin No. 77. Jerusalem, May 1984, 31 p. and a 70 x 100 cm colored bathymetric chart.

Ambraseys, N. N., and Barazangi, M., 1998. The 1759 earthquake in the Bekaa Valley: Implications for earthquake hazard assessment in the eastern Mediterranean region. J. Geophys. Res., 94(B4), p. 4007-4013.

Ambraseys, N. N., and Jackson, J. A., 1998. Faulting associated with historical and recent earthquakes in the eastern Mediterranean region. Geophys. Jour. Int., 133(2), p. 390-406.

Arthaud, F., Dubertret, L., Masson, P., and Mercier, J, L., 1978. Etats de constraintes successifs post-eocènes les long des failles libano-syriennes au nord de Beyrouth. 6ème Réunion Annales Science de la Terre, Orsay (en depôt à la Societé Géologique de France).

Anonymous, 1993. Lebanon's new offshore survey. Europ. Assoc. Explor. Geophys. First Break, 11(11), p. 470.

Anonymous, 1994. News Briefs - New data sets. SEG, The Leading Edge, 13(1), p. 52.

Anonymous, 1997. New EROS datasets available to the public. Geotimes, 42(11), p. 10.

Ben-Avraham, Z., Hall, J. K., Schattner, U., Ben-Gai, Y., Neev, D., and Reshef, M., 2004. New insights into the tectonic and sedimentary processes in the northeastern Levant. In: B. Schilman, Y. Harlavan, Y. Haiel, and R. Calvo (eds.), Abstracts, Ann. Meet. .Isr. Geol. Soc., Hagoshrim, 23-25 Mar. 2004, p. 14. Also presented as the poster 'New seismic insights into the tectonic and sedimentary processes in the northeastern Levant' at the Fifth International Symposium on Eastern Mediterranean Geology, Thessaloniki, Greece, 14-20 April, 2004.

Berry, P. A. M., Hilton, R. D., Johnson, C. P. D., 2002. ACE: First full release of the new 30" GDEM incorporating satellite altimeter derived heights. XXVI General Assembly of the European Geophysical Society (EGS), Nice, France, April 2002.

Berry, P. A. M., Pinnock, R. A., Hilton, R. D., and Johnson, C. P. D., 2000. ACE: A new global Digital Elevation Model incorporating satellite altimeter derived heights. In: H. Sawaya (ed.), ERS-Envisat Symposium Proceedings, SP-461 (CD-ROM), ESA Publications Division, Noordwijk, The Netherlands, 10 p.

Beydoun, Z. R., 1977. The Levantine countries: the geology of Syria and Lebanon (maritime regions). In: A. E. M. Nairn, W. H. Kanes, and F. G. Stehli (eds.), The Oceans Basins and Margins, 4A, the eastern Mediterranean. Plenum Press, New York, p. 319-353.

Butler, R. W. H., and Spencer, S., 1999. Landscape evolution and the preservation of tectonic landforms along the northern Yammouneh Fault, Lebanon. In: B. J. Smith, W. B. Whalley, and P. A. Warke, (eds.), Uplift, erosion and stability: geological and morphological perspectives on landscape evolution, Geol. Soc.Lond. Spec. Publ. 162, p. 148-156.

Butler, R. W. H., Spencer, S., and Griffiths, H. M., 1997. Transcurrent fault activity on the Dead Sea Transform in Lebanon and its implications for plate tectonics and seismic hazard. J. Geol. Soc. London, Vol. 154, Part 5, p. 757-760.

Carlisle, D. H., 1965. A continuous seismic profiling survey off the coast of Lebanon. Unpublished M.Sc. thesis, M.I.T., Cambridge, Mass., 138 p.

Chaimov, T. A., Barazangi, M., Al-Saad, D., Sawaf, T., and Gebran, A., 1990. Crustal shortening in the Palmyride fold belt, Syria, and implications for movement along the Dead Sea fault system. Tectonics, 9(6), p. 1369-1386.

Daëron, M., Tapponier, P., Jacques, E., Elias, A., King, G., Sursock, A., Gèze, R., and Charbel, A., 2001. Evidence for Holocene slip and large earthquakes on the Yammouneh Fault (Lebanon). EOS Trans. AGU, 82(47), Fall Meeting Suppl. Abstr. S52D-0666, p. F932, Poster.

Darawcheh, R., Reda Sbeinati, M., Margottini, C., and Paolini, S., 2000. The 9 July 551 AD Beirut earthquake, eastern Mediterranean region. Jour. Earthquake Engineering, 4(4), p. 403-414.

Defense Mapping Agency Aerospace Center, 1984. Tactical Piloting Chart TPC G-4A (Syria, Turkey), 5th Edition. Scale 1:500,000, Lambert Conformal Conic Projection. Contour interval 500 ft (152.4 m). Compiled March 1976, Revised Sept. 1983.

Doytsher, Y., and Hall, J. K., 1997. Gridded affine transformation and rubber-sheeting algorithm with FORTRAN program for calibrating scanned hydrographic survey maps. Computers & Geosciences. 23(7): 785-791.

Elias, A., Tapponier, P., Daëron, M., Jacques, E., Sursock, A., and King, G., 2001. The Tripoli-Roum Thrust: source of the Beirut 551 AD earthquake and cause of the rise of Mount-Lebanon. EOS Trans. AGU, 82(47), Fall Meeting Suppl. Abstr. S12D-0636, p. F825, Poster.

Elias, A., Tapponier, P., Jacques, E., Daëron, M., Klinger, Y., and Sursock, A., 2003. Quaternary deformation associated with the Tripoli-Roum Thrust, and the rise of the Lebanese coast. Europ. Geophys. Soc., Geophys. Res. Abstracts, Vol. 5, 10137, EGS-AGU-EUG Joint Assembly, Nice, France, April 2003, 1 p.

Emery, K. O., Heezen, B. C., and Allan, T. D., 1966. Bathymetry of the eastern Mediterranean Sea. Deep-Sea Research, 13(2), p. 173-192.

Feld, L., 2002a. Israel Country Analysis Brief. US First Gov, Department of Energy (http://wwww.eia.doe.gov/eneu/cabs/israel.html).

Feld, L., 2002b. Syria Country Analysis Brief. US First Gov, Department of Energy (http://wwww.eia.doe.gov/eneu/cabs/syria.html).

Fugro-Geoteam, 2003. Lebanon 2D completed. Available from the internet at: http: //www.fugro.geoteam.no/newsarchives/Lebanon.htm.

Gennesseaux, M., Burollet, P., and Winnock, E., 1998. Thickness of the Plio-Quaternary sediments (IBCM-PQ). Bollettino di Geofisica Teorica ed Applicata, 39(4), p. 243-284.

Goedicke, T. R., 1972. Submarine canyons on the central continental shelf of Lebanon. In: D. J. Stanley (ed.), The Mediterranean Sea, Dowden, Hutchinson and Ross, Inc., Stroudsburg, Pa., p. 655-670.

Goedicke, T. R., 1977. The Pelusium Line and structures of western Lebanon. Rapp Comm. int. Mer Medit., 24(7a), p. 179-180.

Goedicke, T. R., and S. Sagabiel, 1976. Sediment movement in Lebanese submarine canyons. In: N. Hulings (ed.), Symposium on the eastern Mediterranean, Acta Adriatica, Split, 18(8), p. 117-128.

GOEL/BEICIP/ROBERTSON, 1975. Eastern Mediterranean Geophysical/ Geological Project, Proposal for a non-confidential regional study involving 7,400 kms marine seismic. 9 p., November 1972.

GOEL/BEICIP/ROBERTSON, 1976. Regional geological and geophysical synthesis of the eastern Mediterranean. October 1976, 97 p. plus Stratigraphic appendix of 46 p. Copyrighted and Proprietary.

GRID-Geneva, 2000. Remote Sensing Training for Lebanon's Environment Observatory. GRID-Geneva Quarterly Bulletin No. 2, p. 3.

Hall, J. K., and Ben-Avraham, Z., 1979. Bathymetric Chart of the Gulf of Elat. Three-color chart of the Gulf of Elat, with tracks on reverse side. Prepared for the International Symposium on Rift Zones of the Earth: The Dead Sea Rift, Jerusalem, September 10-20, 1979: One Sheet, Contour interval 50 m, overprinted on land with LANDSAT MSS imagery, Scale 1:250,000, Israel Grid.

Hall, J. K., Ben-Avraham, Z., and Shamai, E., 1983. A Marine Geophysical Survey off Southern Lebanon. Brief Research Report, In: A. Ehrlich and A. Sneh (eds.), G.S.I., Current Research 1982, p. 88-89.

Hall, J. K., Udintsev, G. B. and Odinokov, Yu. Yu. (1994). The bottom relief of the Levantine Sea. In: Geological structure of the North-eastern Mediterranean (Cruise 5 of the Research Vessel 'Akademik Nikolaj Strakhov'). (V. Krasheninnikov and J. K. Hall, eds.), Historical Productions-Hall, Jerusalem, April 1994. p. 5-31.

Hall, J. K., 1994. Bathymetric Chart of the Eastern Mediterranean Sea. Scale 1:625,000 at Latitude 46°N, 50 m corrected contours, three color, blue shade hypsometric gradations every 200 m. Included in map packet with Krasheninnikov, V. A. and Hall, J. K. (eds.), Geological structure of the North-eastern Mediterranean (Cruise 5 of the Research Vessel 'Akademik Nikolaj Strakhov'), Historical Productions-Hall, Jerusalem, 396 + vii p, April 1994.

Hastings, D. A., and Dunbar, P. K., (editors), 1999. Global Land One-kilometer Base Elevation (GLOBE). Digital Elevation Model, Version 1.0, Documentation Version 1.0, NGDC Key to Geophysical Records Documentation No. 34, May, 1999. National Geophysical Data Center, Boulder, CO, USA, 138 p.

Khair, K., 2001. The geomorphology and seismicity of the Roum fault as one of the active branches of the Dead Sea fault in Lebanon. J. Geophys. Res. 106(B3),

p. 4233–4245.

Khair, K., Tsokas, G. N., and Sawaf, T., 1997. Crustal structure of the northern Levant region: multiple source Werner deconvolution estimates for Bouguer gravity anomalies. Geophys. Jour. Int., 128(3), p. 605-616.

Legros, Y., and Bonnin, J., 1999. Investigating instrumental seismicity data sources for the Mediterranean region (IBCM-S). Bollettino di Geofisica Teorica ed Applicata, 40(2), p. 79-146.

Loubrieu, B., Satra, C., and Cagna, R., 2000. Cartography by multibeam echo-sounder of the Mediterranean Ridge and surrounding areas. Two maps, Mercator projection at 1:1,500,000 scale. 1. Morpho-Bathymetry of the Mediterranean Ridge and surrounding areas. 2. Acoustic Image of the Mediterranean Rdige and surrounding areas.

Makris, J., Morelli, C., and Zanolla, C., 1998. The Bouguer gravity map of the Mediterranean Sea (IBCM-G). Bollettino di Geofisica Teorica ed Applicata, 39(1), p. 79-98.

Morelli, C., and Val'chuk, S., 1988. The International Bathymetric Map of the Mediterranean (I.B.C.M.), published under the Authority of the Intergovernmental Oceanographic Commission of UNESCO. In: J. K. Hall, (ed.), Preprint with 1:10,000,000 color reduction of the IBCM., September 1988, 10 p.

Morris, R. O., 1995. Charts and Surveys in Peace and War: The History of the Royal Navy's Hydrographic Service 1919-1970. H. M. Stationary Office, Ministry of Defence, London, 280 p.

Oil and Gas International, 2003. Spectrum's Lebanon survey shows offshore hydrocarbons. On the internet at http://www.oilgasinternational.com/departments/geosciences/jan03_spectrum.html.

Quennell, A. M., 1984. The western Arabia rift system. In. J. E. Dixon and A. H. F. Robertson, (eds.), The Geological Evolution of the Eastern Mediterranean. Geol. Soc. Lond. Spec. Publ. No. 17, Blackwell Scientific, Oxford, p. 775-788.

Ron, H., 1987. Deformation along the Yammuneh, the restraining bend of the Dead Sea transform: paleomagnetic data and kinematic implications. Tectonics 6(5), p. 653-666.

Row, L. W. III., Hastings, D. A., and Dunbar, P. K., 1995. TerrainBase: Worldwide digital terrain data. Documentation Manual, CD-ROM Release 1.0. NGDC Key to Geophysical Records Documentation No. 30, April, 1995. National Geophysical Data Center, Boulder CO, USA, 186 p.

Spectrum-Fugro, 2002. Offshore Lebanon. Advertisement in AAPG Explorer, 23(11), p. 33.

U. K. Ministry of Defence, 1975. Tactical Piloting Chart TPC G-4D (Cyprus, Iraq, Israel, Jordan, Lebanon, Saudi Arabia, Syria, Turkey). 1st Edition. Scale 1: 500,000. Lambert Conformal Conic Projection. Contour interval 500 ft (152.4 m).

U.S.G.S., 1997. GTOPO30 Digital Elevation Model. U. S. Geological Survey, EROS Data Center, Sioux Falls, SD, USA.

Verdin, K. L., and Greenlee, S. K., 1996. Development of continental scale digital elevation models and extraction of hydrographic features. In: Proceedings, third International Conference/Workshop on Integrating GIS and Environmental Modelling, Sante Fe, New Mexico, January 21-26, 1996. National Center for Geographic Analysis, Santa Barbara, CA.

Walley, C. D., 1988. A braided strike-slip model for the northern continuation of the Dead Sea Fault and its implications for Levantine tectonics. Tectonophysics, 145(1-2), p. 63-72.

Zanolla, C., Morelli, C., and Marson, I., 1998. The magnetic anomalies of the Mediterranean Sea (IBCM-M). Bollettino di Geofisica Teorica ed Applicata, 39(1), p. 1-36.

Zanolla, C., Morelli, C., and Marson, I., 2000. The magnetic anomalies of the Eastern Mediterranean revisited and the Black Sea ones presented. Bollettino di Geofisica Teorica ed Applicata, 41(1), p. 79-83.

FAIRSHEETS AND NAUTICAL CHARTS ALONG THE LEBANESE AND SYRIAN COASTS

Boulos, I., 1962. Carte de Reconnaissance des Côtes du Liban, Beyrouth to Tripoli Sheet, Scale 1:150,000. Imprimerie Bassile Frères, Beyrouth, 1 sheet. IBCM Code IA, 401 soundings digitized.

Boulos, I., 1962. Carte de Reconnaissance des Côtes du Liban, Naqoura to Beyrouth Sheet, Scale 1:150,000. Imprimerie Bassile Frères, Beyrouth, 1 sheet. IBCM Code IB, 400 soundings digitized.

British Admiralty Hydrographic Office, 1861. Chart D5426 Part 1 of 2 - Coast of Syria - Ras-El-Khanzir to Markab (including Banias and Latakiyah). Hydrographic fairsheet surveyed by Lt. E. W. Brooker and Messrs. F. Skead, F. Christian, and Mr. Gray of H. M. Surveying Ship 'Firefly' in 1861. Bears Hydrographic Office stamp August 3 1861. Includes several inland topographic surveys. Soundings in fathoms. Mercator projection (?) at approximately 1:90,000, 1 sheet. IBCM Code 0N.

British Admiralty Hydrographic Office, 1861. Chart D5426 Part 2 of 2 - Coast of Syria - Ras-El-Khanzir to Markab. Hydrographic fairsheet surveyed by Lt. E. W. Brooker and Messrs. F. Skead, F. Christian, and Mr. Gray of H. M. Surveying Ship 'Firefly' in 1861. Bears Hydrographic Office stamp August 3 1861. Includes several inland topographic surveys. Soundings in fathoms. Mercator projection (?) at approximately 1:90,000, 1 sheet. IBCM Code 1N.

British Admiralty Hydrographic Office, 1861. Chart D5608 - Coast of Syria - Sheet II - Markab to Ras En-Nakura. Hydrographic fairsheet for bathymetric survey carried out by the officers of H. M. Surveying Ship 'Firefly' in 1861. Bears Hydrographic Office stamp February 13 1862. Includes several inland topographic surveys. Soundings in fathoms. Mercator projection (?) at approximately 1:230,000, 1 sheet. IBCM Code 2N.

British Admiralty Hydrographic Office, 1862. Chart D5353 - Coast of Syria - El-Hamam to Latakia. Preliminary hydrographic fairsheet for bathymetric survey carried out by the officers of H. M. Surveying Ship 'Firefly' in 1861. Bears Hydrographic Office stamp June 15 1862. Includes an inland topographic surveys south of Merkab. Soundings in fathoms. Mercator projection (?) at approximately 1:85,000, 1 sheet. IBCM Code Z0.

British Admiralty Hydrographic Office, 1862. Chart D5888 - Syria - Sheet II - Topography between Markab and Ras-Nakura. Topographic sketch map with place names surveyed by A. L. Mansell, commanding H. M. Surveying Ship 'Firefly' in 1862. Bears Hydrographic Office stamp July 29, 1862. Mercator projection (?) at approximately 1:187,000, 1 sheet.

British Admiralty Hydrographic Office, 1946. Chart E7906 - Lebanon - Beirut Approaches. Hydrographic fairsheet surveyed by Lt.Cdr. J. H. Hawkey R.N.V.R of H.M.M.L. 1254, Mediterranean Survey Unit No. 1, In June 1946. Soundings in fathoms. Mercator projection at scale 1:25,000, 1 sheet. IBCM Code ??

British Admiralty Hydrographic Office, 1951. Chart 2794 - Mediterranean - Lebanon - Cap Sahare to Ras Ech Chaq. Soundings in fathoms. Gnonomic projection, scale 1:25,000, from surveys by Kelvin & Hughes (Marine) Ltd. for the Trans-Arabian Pipeline Co. in 1950 & 1961, 1 sheet. IBCM Code SM, 1,151 soundings and 157 attributes digitized.

British Admiralty Hydrographic Office, 1952. Chart 1563 - Mediterranean Sea - Lebanon - Beirut. Soundings in fathoms. Gnonomic projection, scale 1:25,000, from French Government charts to 1950, with additional soundings from Admiralty Surveys of 1946, 1 sheet. Inset of Port of Beirut at scale 1:10,000.

British Admiralty Hydrographic Office, 1952. Chart 2796 - Mediterranean - Syria - Tel Soukas to Ras El Burj. Preliminary chart, Gnomonic projection at scale 1: 24,000, based upon a survey of the Iraq Petroleum Company 1950. Soundings in fathoms. 1 sheet. IBCM Code 0O. Inset charts at scale 1:6,000 of Hareissoun Bay and Boat Harbour (Nahr Hareissoun).

British Admiralty Hydrographic Office, 1970. Chart 2632 - Mediterranean Sea - Turkey and Syria - Anamur Burnu to Latakia including Iskenderun Korfezi. Soundings in fathoms. Mercator projection, scale 1:300,000, 1 sheet. IBCM Code BN, 2,540 soundings and 143 attributes digitized.

British Admiralty Hydrographic Office, 1974. Chart 2633 - Mediterranean Sea - Syria and Lebanon - Latakia to Sour. Soundings in fathoms. Mercator projection, scale 1:300,000, 1 sheet. IBCM Code LF, 1,171 soundings and 87 attributes digitized.

DMAHTC, 1925. Chart 56042 - Mediterranean Sea - Plans on the Coasts of Syria and Lebanon - Tarabulus and Roadstead. Soundings in fathoms. Mercator projection, scale 1:32,000, from a French survey in 1920 with additions from

a British survey in 1861, 1 sheet. IBCM Code TL, 1,305 soundings and 122 attributes digitized.

DMAHTC, 1950. Chart 56042 - Mediterranean Sea - Plans on the Coasts of Syria and Lebanon - Syria - Jazirat Arwad and Anchorage. Soundings in fathoms. Mercator projection, scale 1:29,000, from a French survey in 1921, 1 sheet. IBCM Code JC, 899 soundings and 10 attributes digitized.

DMAHTC, 1950. Chart 56045 - Mediterranean Sea - Lebanon - Sidon Terminal Port. Soundings in fathoms. Mercator projection, scale 1:12,500, from latest surveys to 1950, 1 sheet. IBCM Code SL, 1,175 soundings and 36 attributes digitized.

DMAHTC, 1975. Chart 54480 - Turkey-Syria - Mersin to Baniyas. Soundings in fathoms. Mercator projection, scale 1:256,600, from surveys between 1954 and 1956, with additions from a British chart of 1955, 1 sheet. IBCM Code MB, 734 soundings and 17 attributes digitized.

USNOO, 1945. Chart 4252 (46044) - Anchorages on the Lebanon Coast? Saida Anchorage. Soundings in fathoms. Mercator projection, scale 1:12,520, from French charts 5614, 5620, and French surveys in 1921, 1 sheet. IBCM Code SS, 1,102 soundings and 445 attributes digitized.

USNOO, 1945. Chart 4252 (46044) - Anchorages on the Lebanon Coast? Saida Anchorage. Soundings in fathoms. Mercator projection, scale 1:19,900, from French survey in 1921, 1 sheet. IBCM Code TA, 1,333 soundings and 507 attributes digitized.

USNOO, 1970. Chart 3973 (56040) - Mediterranean Sea - Syria-Lebanon - Markhab to Sur. Soundings in fathoms. Mercator projection, scale 1:242,490, from a British survey in 1860 with additions from various sources to 1950, 1 sheet. IBCM Code LS, 1,183 soundings and 68 attributes digitized.

A Multibeam Bathymetric Map of the Deep Eastern Mediterranean Sea Basin

Benoit Loubrieu
Ocean Research Division (DRO), Ifremer, BP 70 Brest, Plouzané, F-29280, France.
Jean Mascle
UMR Géosciences-Azur, Observatoire Océanologique de Villefranche, BO 48, Villefranche sur Mer, F-06235, France.
Nicolas Chamot-Rooke
Chargé de recherches CNRS, Laboratoire de Géologie, École Normale Supérieure (ENS), Paris, France.
Jean Paul Foucher
Ocean Research Division (DRO), Ifremer, BP 70 Brest, Plouzané, F-29280, France.
John Woodside
Center for Marine Earth Sciences, Free University, De Boelelaan 1085, 1081 HV Amsterdam, The Netherlands.

Based on a compilation of swath data collected between 1992 and 1998 in the Eastern Mediterranean Sea, we present (**Fig. 16.5**) and briefly discuss below a shaded color morpho-bathymetric map of the entire area from the Ionian abyssal plain in the west to the continental margin off Cyprus in the east (Loubrieu et al., 2000). This compilation has been promoted by J. Mascle, chairman of the CIESM Marine Geosciences Committee, and jointly published in 2000 by CIESM and IFREMER.

The various multibeam bathymetric datasets have been collected using the same Simrad EM12 Dual system, operated by Ifremer technical teams on board the R/V L'Atalante, during four successive surveys. The data have kindly been provided by:

1) The Geosciences Departement from Ifremer-Brest (HERALIS survey across part of the Ionian sea in 1992; Chief scientist J. -P. Foucher);

2) Laboratoire de Géologie, École Normale Supérieure de Paris (MÉDÉE survey in 1995; Chief scientists X. LePichon and N. Chamot-Rooke);

3) The Center for Marine Earth Science, Free University, Amsterdam (ANAXIPROBE survey, Chief scientist J. Woodside); and

4) Géosciences-Azur, Observatoire Océanologique, Villefranche sur Mer (PRISMED 2 survey, Chief scientist J. Mascle).

Data processing was undertaken by each individual laboratory for its own scientific research using the Caraibes software developed by IFREMER. A global DTM, with a grid spacing of 500 meters, has later on been created by the Ifremer Geosciences Cartographic office under the supervision of B. Loubrieu.

The resulting map, at a scale of 1/1,500,000 (Mercator projection at 35°N), for the first time illustrates at this level of detail a brand new picture of the deep Eastern Mediterranean sea basins. The results of multibeam echosounding have changed our knowledge of the different geological processes (sedimentary, tectonic, geochemical) shaping the deep sea basins

The main morphologic features seen on this map consist of the following:

a) A wide (about 200 km on average) and elongated (about 1500 km) bulge, called the **Mediterranean Ridge,** runs from west to east between the European and African continental margins. This ridge, whose depths vary between 3000 meters (in the Ionian basin; Nielsen, 2003) and less than 1300 meters (just north of Libya; Huguen, 2001), is the bathymetric expression of an actively deforming sedimentary wedge, which itself results from the stages of convergence/subduction/early collision between the African lithosphere and the southern border of the European Plate. The ridge is stongly deformed by a dense system of folds (particularly well developed south-east of Crete), a complex network of active faults, and by thusts. Moreover, the feature being strongly squeezed between the two bordering and rigid African and Aegean continental margins, is releasing important quantities of fluids escaping on the seabed, together with massive undercompacted mud emissions. As a consequence, wide mud flows, numerous scattered mud volcanoes,

and other mud/fluid/brine releasing features can be detected on the ridge sea floor.

b) Eastward, south of the island of Rhodes and south of Turkey, the Mediterranean Ridge connects through a series of faulted blocks, recently detached from southern Turkey. These are known as the **Anaximander mountains**; (Zitter, 2004), with another, smaller and arcuate line of relief, the **Florence Rise**. This rise, partly inherited from previous subduction processes, now constitutes a structurally active transcurrent relay with the ongoing starting collision between the African margin and the island of Cyprus; mud volcanoes, indicating also msasive fluid expulsions, characterize the whole area between southern Turkey and western Cyprus.

c) The flat-topped **Erathostenes Seamount** can be seen south of the island of Cyprus. Less than 1 km deep, it was once part of the African mainland. This feature, in collision with the island, bounds the northeastern domain of the Egyptian continental margin.

d) The **Nile Deep Sea Fan** is the submarine extension of the Nile terrigenous construction. It results from the progressive piling up of erosional sediments transported to the sea by the Nile River, and constitutes the most prominent sedimentary construction along the African continental margin of the entire Mediterranean Sea (Loncke, 2002). A map of the Nile Deep Sea Fan shows (Sardou and Mascle, 2003) a rather complex morphology. In its western area, off Alexandria, this is mainly from the interaction of important active terrigenous transports. In the central domain there are giant sedimentary collapses, well-expressed by large failures, while mostly in the eastern sector there are active gravity tectonics due to progressive gliding of the underlying salt-rich layers. And finally mud volcanoes express abundant release of subbottom fluids.

e) Off of **Libya** the continental slope appears quite narrow (averaging only 30 km); this can be considered as a geological artifact since most of the original continental margin is now tectonically overthrusted by the southward growing Mediterranean Ridge.

f) The continental margin off **Pelopponesus and Crete** consists of a series of massive faulted blocks and deep tectonic troughs reflecting the intense cutting by active faults related to extensional activity in the Aegean Sea.

The shaded hypsometrically colored bathymetric map shown here is now under revision. New multibeam data collected since 1998, particularly along the Egyptian margin, the Levantine margin, and in several restricted areas of the Aegean Sea, are being addedd. A new upgraded version will soon be published by **IFREMER** and **CIESM** within the series «Maps and Atlas» (knowledge and exploration of the Deep Mediterranean Sea).

REFERENCES

Huguen, C., 2001. Tectonique active et volcanisme boueux associé au sein de la Ride Méditerranéenne. Thése de Doctorat de l'Université P. M. Curie de Paris, 260 p.

Loubrieu, B., Satra, C., and Cagna, R., 2000. Cartographie par sondeur multifaisceaux de la Ride Méditerranéenne et des domaines voisins, éditions Ifremer/CIESM 2001, échelle 1/1,500,000ème. Deux cartes (Morphobathymétrie et mosaiques d'images acoustiques).

Loncke, L. 2002. Structure et évolution du delta profond du Nil. Thése de Doctorat de l'Université P. M. Curie de Paris, 180 p.

Nielsen, C., 2003. Étude de zones de subduction en convergence hyper-oblique: Ride Méditerranéenne et Marge Indo-Birmane. Thése Université Paris XI-Orsay, 172 p.

Sardou, O. and Mascle, J., 2003. Cartographie par sondeur multifaisceaux du delta sous marin profond du Nil et des domaines voisins. Deux cartes (Morphobathymétrie et mosaiques d'images acoustiques), *special publication CIESM/Géosciences-Azur*

Zitter, T., 2004. Mud volcanism and fluid emissions in Eastern Mediterranean neotectonic zones, Ph.D. academic thesis, Vrije Universiteit, Amsterdam, 99 p.



HMS Lightning, the first of the wooden paddle gunboats, launched in 1823. It had a 100 hp steam engine, 3 guns and a draft of 7 feet (Ritchie, 1967). This 1:96 scale model was built by Captain John Roe, DSO, OBE, RN around 1979, at Mary Tavy, Devon, England. This is the same design as that of HMS Firefly (see inset, Figure 16.1). Image (copyright holder unknown) downloaded from the National Maritime Museum (Greenwich, England) website at http://www.nmm.ac.uk/collections/collectionsDetail.cfm?ID=SLR0709.



Group photo of the attendees at the Eighth Session of the IOC Editorial Board for the International Bathymetric Chart of the Mediterranean (IBCM-EB) and its Geological-Geophysical Series in Kaliningrad, Russian Federation in September 1999. Front row, right to left: Prof. Emelyan M. Emelyanov (ABIORAS), Prof. Carlo Morelli (Chairman, IBCM), Capt. Andrei Popov (HDNO), Dr. Kazimeras M. Shimkus (SBIORAS), Mr. Dmitri Travin (IOC), and Dr. Pavel N. Kuprin (MSU). Back Row, right to left: Mr. Giannis K. Papaioannou (HNHS), Ing. General Patrick Souquiere (SHOM), Ing. en Chef Michel Huet (IHB), and Dr. Troy L. Holcombe (NGDC). The meeting was held 1-4 September aboard the historic research vessel Vitiaz. Information on the Vitiaz, then celebrating her 60th birthday on display at the Museum of the World Ocean in Kaliningrad, may be found at www.vitiaz.ru/engish/vitiaz.html.
Drs. Emelyanov, Shimkus, and Kuprin are the authors of the IBCM-SED bottom sediment compilation in Chapter 17.

Chapter 17

Explanatory Notes to the IBCM-SED Map Series Unconsolidated Sediments of the Mediterranean Sea (Scale 1:1,000,000) and the Black Sea (Scale 1:2,000,000)

Emelyan M. Emelyanov,
Atlantic Branch of the Shirshov Institute of Oceanology, Russian Academy of Sciences, 1 Prospekt Mira, 236000 Kaliningrad, Russia
Kazimiras M. Shimkus †
Southern Branch of the Shirshov Institute of Oceanology, Russian Academy of Sciences, Golubaya Buchta, Gelendzhik 7, Krasnodar region, 353470 Russia
Pavel N. Kuprin
Geological Faculty of the M. V. Lomonosov Moscow State University, Leninskaya Gory, 119899 Moscow, Russia

PREFACE

The IBCM-SED map (**Figure 17.1**) was compiled within the cooperative international program supported by the Intergovernmental Oceanographic Commission (IOC) of UNESCO. The map is a part of a series of geological/geophysical overlay sheets for the International Bathymetric Chart of the Mediterranean (and Black) Sea (IBCM) at 1,000,000 scale (Morelli and Val'chuk, 1988), which also included Bouguer Gravity (IBCM-G), Magnetics (IBCM-M), Seismicity (IBCM-S), and Plio-Quaternary isopachs/structural contours (IBCM-PQ). The compiling of the map consisted not only of generalization of existing studies but also involved collecting new data including the analysis of unconsolidated sediments (**Tables 17.1, 17.2, and 17.3**). The primary set consists of ten sheets at scale 1:1,000,000 for the Mediterranean (with the Black Sea on Sheet 5 at a scale of 1:2,000,000). All ten sheets were photographically combined without generalization into a single sheet at scale 1:5,000,000 for the Mediterranean (Emelyanov and Shimkus, 1990), and this is reproduced in Plate IV.

Compilation of the map was entrusted to scientists Dr. Prof. E. M. Emelyanov and Dr. K. M. Shimkus of the USSR (later Russia) by the IBCM Editorial Board, with participation of Dr. I. S. Chumakov (1980-1982) and later Dr. Prof. P. N. Kuprin. Work on the map began in 1980 with requests to scientists in other countries for contributions of sedimentary data. Collection of this data progressed very slowly, due in large part to the isolation of the principal investigators. A considerable amount of time was devoted to adopting a legend for the map, especially the choice of a classification for the bottom sediments according to their grain-size composition. Eventually the legend suggested by Emelyanov, Kuprin and Shimkus (1986) was accepted. Granulometric types were shown in accordance with Folk's triangle (Folk, 1974), while genetic types were indicated according to the scheme suggested by the authors.

We appreciate the contribution of the many scientists who participated in our joint work on this map. They provided a considerable amount of analytical data as well as overlay sheets for a number of regions on the shelves of the Mediterranean Sea.

Many published works (Table 17.2) were used for compiling the map. However, because they were often based on different principles and classifications, this caused certain difficulties in the transfer of the data in accordance with our adopted legend, due to the absence of precise analytical data. We realize that the relatively small scale (1:1M) for the maps requires more detailed material for all areas, and primarily for the dissected slopes and morphologically complex central and peripheral ridges of the eastern Mediterranean, Tyrrhenian, and Alboran Seas and the Aegean archipelago.

Below we present the new bottom sediments compilation for the Mediterranean and Black Seas. We would value constructive criticism from readers, and would hope that scientists would contribute additional data to improve any future compilations.

THE BASIS FOR THE IBCM-SED MAP

The Methodological Basis for Compiling the Map

The map gives, in a general way, a maximum amount of information about the genetic and granulometric types of sediments. It was very important to arrive at a common classification for both the shallow water and deep sea sediments. In the past, and at present, both types have been mapped according to different principles of classification. Our first priority was to eliminate these differences in interpreting the sediments of the Mediterranean and Black Seas. The authors' new legend helps to solve these problems and ease the difficult and in some cases impossible task of comparing the rapidly increasing volumes of new data, especially for the near shore areas.

The IBCM Editorial Board recommended the use of Folk's triangle (Folk, 1974, Fig. 1) for classifiying sediments according to grain-size composition. It was chosen because it best reflects the natural transitions and granulometric differentiation of sedimentary material, and has an advantage over the granulometric classification developed by Bezrukov and Lisitzin (1960) of the P. P. Shirshov

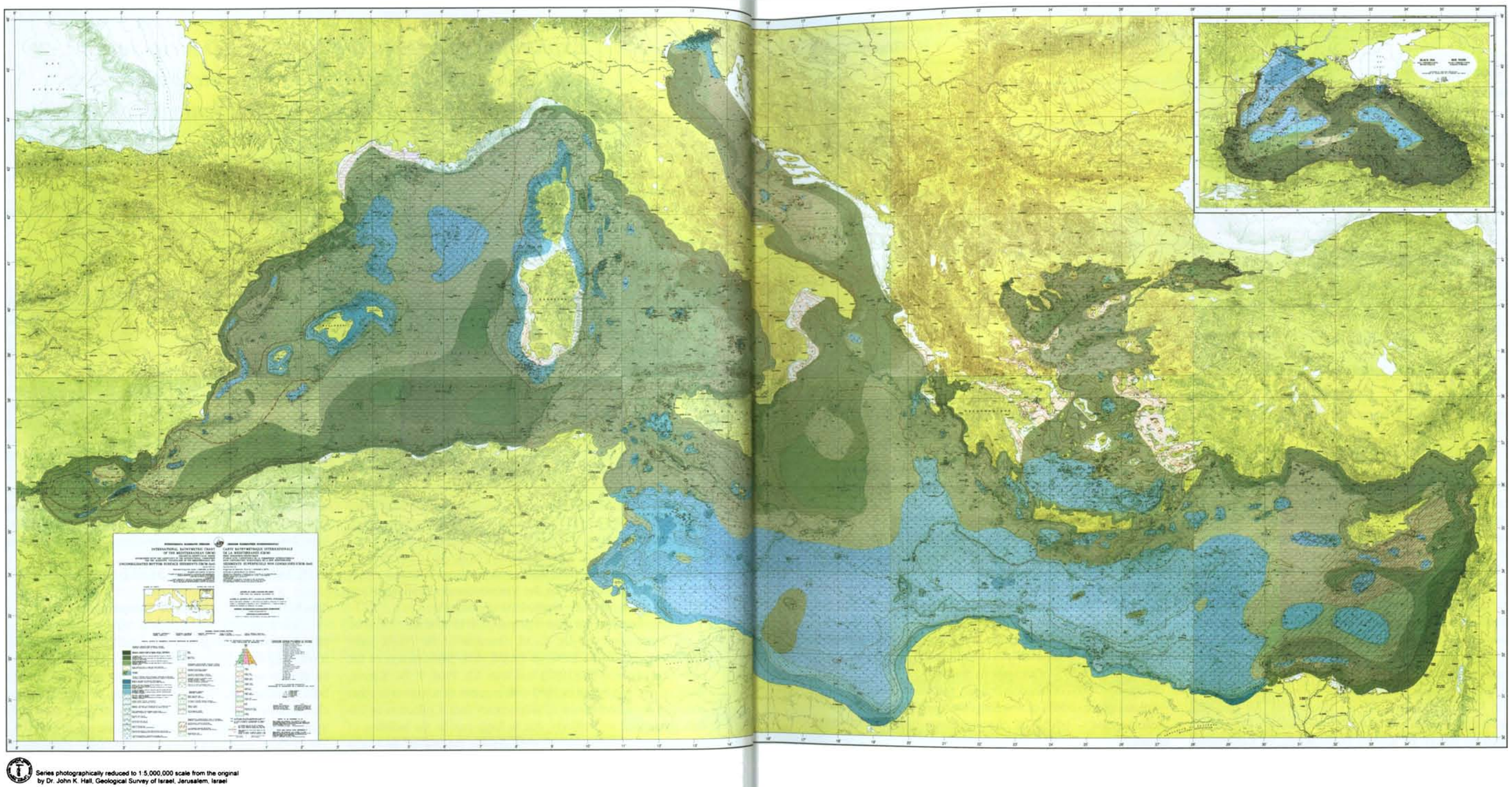


Figure 17.1: IBCM-SED. The Unconsolidated Bottom Surface Sediments Map of the Mediterranean and Black Seas. Reduction to 1:10,000,000. The legend is reproduced in greater detail in Figure 17.8.

Table 17.1: A list of main expeditions of the USSR (or Russia) in the Mediterranean Sea

Vessel	Vessel's index as on a map	Vessel's index as in data base	Year	Region
Akademik S.Vavilov	Va	ASV	1959-1961	M.S.
Akademik S. Kovalevska	K	AK		M.S.
Rift	R	R		
Vytyaz (I)	Vy	V(I)	1979	M.S.
Vytyaz (II)	Vy	V(II)	1986	T.S.
Akademik Mstislav Keldysh	AMK	AMK	1988-1990	T.S.
Akademik Nikolaj Strakhov	ANS	ANS		L.S.
Moskowsky Universitet	MU	MU	1973:1991	M.S.
Michail Lomonosov	ML	ML		E.M.
Akademik Petrovsky	P	AP		M.S.
Akademik Orbeli	ORB	ORB		
Choumakov	Chu	Chu		
Miklucho Maklay	MM	MM		
	ING	ING		
	Ak	Ah		
	Sh	Sh		

Note: M.S. – all Mediterranean Sea; T.S. – Tyrrhenian Sea; L.S. – Levantine Sea; E.M. – Eastern Mediterranean.

Institute of Oceanology of the Rusian Academy of Sciences (IORAS), since it better defines the granulometric profile.

Figure 17.2 clearly shows that some sectors of Folk's triangle include different granulometric types, which can be distinguished according to the IORAS classification. Because some types are confined to certain sectors of the triangle it is possible to graphically transfer between these classifications. The same applies with Shepard's (1954) triangle. We made such transfers in cases where analytical data were absent. If enough analytical data existed, the contents of various fractions were determined by making cumulative curves and then placed in the proper position within Folk's triangle.

A special 'Fraction' program was written to convert the Wentworth (1922) grain size classification (with steps of ½ and 2) used in Russian sediment analysis laboratories. All analytical results were kept in a data base in the Atlantic Geology Department of the Atlantic Branch of IORAS (ABIORAS), in Kaliningrad, Russia. After determination of the fractions the Md histogram and coefficient of sediment sorting (So) are automatically calculated.

The 'Fraction' program classifies the sediments according to Folk's triangle which differentiates between: 1) sand, 2) silty sand, 3) clayey sand, 4) sandy silt (aleurite), 5) sandy mud, 6) sandy clay, 7) silt (aleurite), 8) mud (silt and clay), and 10) clay (Fig. 17.2). The genetic sediment types were quantitatively distinguished on the basis of $CaCO_3$, C_{org}, Fe, and Mn contents using the accepted gradations in the legend (**Table 17.4**). In addition semi-quantitative microscopic examination estimated the content of volcanogenic, foraminiferal, and coccolithic material, shell detritus of malacofauna, and authigenic minerals, concretions, and nodules.

The well-known ore-manifestations in the Black Sea connected with Fe-Mn nodules were not specially defined for their mineral peculiarities. That is why this specific type is not identified on the map. The legend also does not include the different types of hydrothermal ore-manifestations in the Mediterranean Sea, since the results of the detailed investigations on some Tyrrhenian Sea seamounts were not then available.

The authors distinguish the following types of sediments according to the updated IORAS classification:

terrigenous - >50% of terrigenous material;

biogenic - >50% of biogenic (mainly carbonate) material;

volcanogenic - >50% of volcanogenic (mainly ash) material;

chemogenic - >50% of chemogeneous (mainly carbonate) material.

In the presence of >90% of genetically homogeneous material the sediments are called 'pure' terrigenous, 'pure' biogenic etc.

If calcareous biogenic remains predominate, then the following types of sediments are distinguished: shelly, foraminiferal, coccolithic (nanno-), foraminiferal-coccotithic, pteropodal, pteropodal-foraminiferal, etc.

Genetically nonhomogeneous (mixed) sediments get more complex names *e.g.*: biogenic-terrigenous (>>50% of terrigenous, 10-40% biogenic material); terrigenous-biogenic (>>50% of

Table 17.2: List of the data used in compiling the map

Polygon (see Fig. 17.4)	Kind of Material	Author
M-48, M-56, M-35, M-41, M-42, M-42E, M-84, M-85.	Spain (A. Maldonado) - Sediment Types and $CaCO_3$ of the Continental margins of Spain.	A. Maldonado et al., 1982-1992
Vr-1 - Saronikos Bay	Greece (S.P. Varnavas) - Sediment Types, C_{org}, Fe	Hopkins, Grimanis et al., 1983.
Vr-II - Zakynthos Strait	Sediment types	Ferentinos, Collins et al., 1985
Vr-III - Karinthiakos Bay	Stations, sediment types, $CaCO_3$, Fe, Mn.	Varnavas, Ferentinos, Collins, 1986
Vr-IV - Navarino Bay	Map of the stations. Fe, Mn, Ca, C_{org}	Varnavas et al., 1984
Vr-V - Kalamata Bay	Map of the stations. Mn, Fe, Ca	Varnavas et al., 1984
Vr-VI - Patraikos Bay	Station, Sediment types. Fe, Mn, Ca, C_{org}	Varnavas, 1981, 1984, 1989; Varnavas and Ferentinos, 1983
Vr-VII - Gulf of Amvrakia	Sediment types.	Piper, Kontopoulos, Panagos, 1983
Vr-VIII - Thermaikos Bay	Sediment types. Fe, Mn, $CaCO_3$, C_{org}	Baseline, 1983; Lykousis et al., 1981.
Vr-IX - Strimonikos Bay	Coordinates. Sediment types. Fe, Mn, Ca, C_{org}	Konispolitatis, 1984
Vr-X - Pagasitikos Bay	Map of sediment. Fe, Mn, C_{org}	Voutsinou-Taliadouri, Satsmadjis, 1982
Eastern Mediterranean	R/V 'Bannock', 1983; Cruise 'Mediba, 83' Coordinates, $CaCO_3$, C_{org}	Varnavas and Papaioannou
P-1	Sediment types, $CaCO_3$	C. Papavasiliou
Br-1 - Northern Adriatic Sea	Italy (A. Brambati) - Sediment Types, Stations, $CaCO_3$, Sediment Maps	A. Brambati
Adriatic Sea	Stations, $CaCO_3$, C_{org}	A. Brambati
Br-II - Southern Sardinia	Stations	A. Brambati
Cretean Sea	Stations	A. Brambati
C-I - Gulf of Oran	France (A. Monaco) - Sediment Types	Caulet, 1972
C-I - Gulf of Oran	Sediment Types	Caulet, 1972
C-III	Sediment Types	Caulet, 1972
L-2 - Gulf of Gigeli		Leclaire, 1968, 1972
MB-I - Pyrenean Continental Margin (Languedos, Gulf of Lion)	Sediment Types (map)	(A. Monaco) (Got et al., 1971) H. Got, 1973.
B-I - Sea of Pelagienne	Sediment Types	Burollet et al., 1979
K-S-I	USA - Sediment Types	Kelling, Stanley, 1972a, b
N-I - Shelf of Israel	Israel - Sediment Types. $CaCO_3$	Nir, 1973, 1984

biogenic, 10-40% of terrigenous); volcanogenic-biogenic-terrigenous; pyroclastic-hydrothermal; hydrothermal-pyroclastic etc.

Sources of the Data in the IBCM-SED Map

Mediterranean Sea.

The Southern Branch of the Institute of Oceanology (SBIORAS) in Gelendjik began carrying out geological-geochemical research in the deep areas of the Mediterranean Sea in 1959 (Emelyanov, 1961), and have continued until the present together with the Atlantic Branch of the Institute of Oceanology (ABIORAS). These investigations constitute the backbone of this project (Emelyanov et al., 1979; Emelyanov and Shimkus, 1986).

Data about the deep-sea sediments in all basins of the Mediterranean Sea came from the expeditions of R/V 'Akademik S. Vavilov'. During the past decade the IORAS ships R/V 'Vityaz', 'Rift', and 'Akademik Mstislav Keldysh' carried out detailed geological work in the regions of the seamounts and volcanoes in the Tyrrhenian Sea. R/V 'Rift' performed similar research on the positive structures of the African-Sicilian Sill. Some regions in the Mediterranean Sea were studied by expeditions of Moscow State University, and the Geological Institute and Vernadsky Institute of Geochemistry and Analytical Chemistry of the Russian Academy of Sciences. Material was also collected during dives of the submersibles 'Argus' and 'Mir' on the ridges and mountains (Baroni, Marsili, Palinuro, Verchelli) of the Tyrrhenian Sea (Table 17.1).

Table 17.3: List of Authors who contributed data for compiling the map.

Country	Authors	Material Sent
Turkey	M. Ergün, K.E. Izdar	Papers, analysis, maps
France	A. Monaco, G. Bellaiche, P. F. Burollet, P. Clairefond, E. Winnock, C. Duboul-Razavet	Papers, maps of Lion Gulf, Lasur shore, Gulf of Gabes, the Pelagian Sea (the book)
Germany	F. Fabricius, W. Heike, U. Von Ro, H. Oektzchener, R. Hesse, W. Sige	Papers (Otranto strait, Manfredonija Gulf, Eastern part of Ionian Sea)
Greece	S. Varnavas, C. Perissoratis, G. Ferentinos, V. Lykousis, G. Chronis, S. Stavrakakis, Chr. Anagnastou, C. Papavasiliou	Maps of the harbors, papers of the north part of Aegean Sea
England	G. Evans	Papers
Russia	P. N. Kuprin, V. M. Sorokin, V. L. Luksha, A. S. Polyakov, V. G. Shlikov.	Original data
Israel	D. Neev, Y. Nir	"Technical Report", 1965. Shelf of Israel. Grain-size distribution map, PhD. Thesis, 1973, 1984. The same map (as D. Neev). Tables of sediment types: $CaCO_3$, silicate analysis
Egypt	M. A. Mohamed (1968), A. A. Khafagy	M.Sc. thesis. $CaCO_3$ in the Nile delta sediments, map of the sediment types. Tables of grain-size distribution of the Nile delta.
Italy	A. Brambatti	Tables of sediment types: $CaCO_3$, C_{org}, $MgCO_3$, K, Na, Fe, Cu, Zn, etc. (Adriatic, Cretan Basin).
Spain	A. Maldonado	Shelf of Spain. Scheme of sedimentological parameters. Some publications. 3 sediment maps

Regional and detailed lithological-geochemical investigations in the Mediterranean Sea were also carried out by research vessels from a number of countries *e.g.* USA (R/V 'Atlantis', 'Chain', 'Pillsbury', 'Vema', 'Robert D. Conrad'), Italy (R/V 'Bannock'); Germany (R/V 'Meteor'), United Kingdom (R/V 'Shackleton', 'Discovery'), etc. (see 1:5M scale map on Plate IV). 'The Atlas of Studies of the Mediterranean Sea' (1990), published in Russian and English, gives an overview of the status of these lithological-geochemical studies by 1980, when the major portion of the regional data was obtained.

The Russian expeditions obtained very little data in the shallow areas of the Mediterranean. These areas were mapped mainly with the aid of published materials, which included D. J. Stanley's (1972) book 'The Mediterranean Sea', as well as other reports. We also used the results of special geological surveys in the shallow waters of Spain, Italy, Greece, and Israel thanks to the participation of our colleagues A. Maldonado, A. Monaco, A. Brambati, S. Varnavas, C. Papavassiliou, Y. Nir and others in compiling the corresponding sheets of the maps (Tables 17.2 and 17.3; **Figs. 17.3 and 17.4**). A very limited amount of American and German data were used in compiling the bottom sediment map, since neither American nor German scientists participated in the compilation.

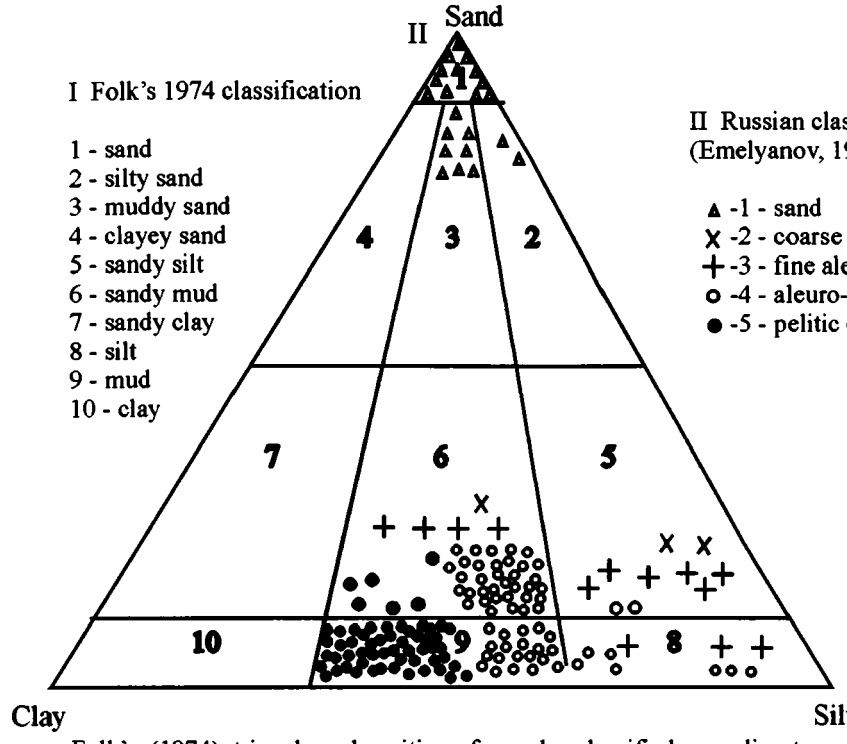
The Black Sea.

The map of Black Sea bottom sediments was mostly compiled according to data obtained by the SBIORAS in numerous regional surveys aboard R/V 'Akademik S. Vavilov' in collaboration with the Geological Faculty of the Moscow State University. In some areas we have also used the results of detailed investigations obtained during expeditions of the old 'Vityaz' and the new 'Vityaz II'. For the Bulgarian shelf we mostly used published data of Russian-Bulgarian investigations (Kuprin, 1980, 1988; Shtcherbakov et al., 1978; Sorokin and Shevchenko, 1980). Published data from American surveys aboard R/V 'Atlantis II' (Ryan and Heezen, 1965), and from Ukrainian and Turkish expeditions (Yaramar et al., 1992) have also been taken into account (Melnik and Demediuk, 1984; Demediuk, 1984).

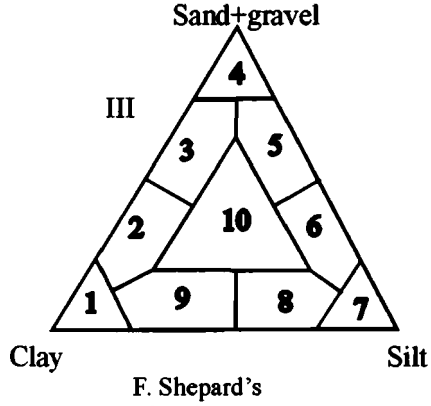
The contribution of the different countries and authors to the map are listed in Tables 17.2 and 17.3 as well as on the map itself. The different maps published by these authors were reworked by us and converted to the necessary classification and scale.

LABORATORY INVESTIGATIONS

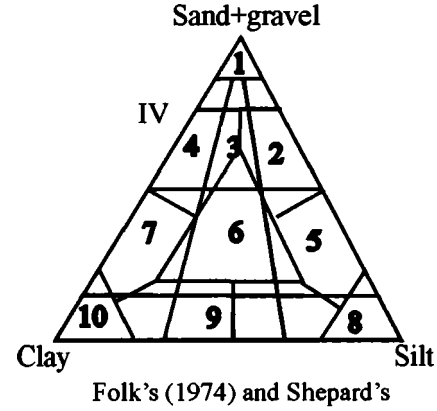
Wet samples of the sediments were packed in glass or plastic containers (or core-liners) for grain-size analysis. The analyses were made under hydro-mechanical conditions. The >0.05 mm fractions were dried (Temp ~100-110°C) and were sieved, while the <0.05 mm fractions were added to water, the density of the suspension being measured with the help of a float and special weights and the fractional content calculated according to a nomograph (Prokoptsev, 1964; Emelyanov, 1975). Thus the fractions are in a decimal classification system which was used throughout the USSR *i.e.* >1; 1-0.5; 0.5-0.25; 0.25-0.1; 0.1-0.05; 0.05-0.01; 0.01-0.005; 0.005-



Folk's (1974) triangle and position of samples classified according to Russian classification (Emelyanov, 1975)



F. Shepard's triangle



Folk's (1974) and Shepard's triangles

Figure 17.2: Folk's (1974) triangle, used in the present classification of granulometric sediment types in the Mediterranean and Black Seas. The granulometric sediment types, according to the Russian classification (II), are shown inside Folk's triangle (I). All previous Russian sediment maps were compiled according to classification II. Below is Shepard's triangle (III) and an overlay of Folk's triangle on that of Shepard (IV). These last triangles helped to convert all the maps of Maldonado et al. (1982-1992) compiled according to Shepard's classification, to Folk's classification.

0.001; and < 0.001 mm.

CHARACTERISTICS OF THE IBCM-SED MAP

The age of the surface sediments

The Mediterranean Sea.

The basic characteristics of the bottom sediments were obtained from samples collected from the surface layer of the sediments, which was usually 3, 5, 10, and rarely 25 cm in thickness. The age of samples in most cases is not older than Upper or Middle Holocene, *i.e.* 3-7 thousand years. One could obtain more precise data on the age of samples using the Holocene sedimentation rate scheme of Shimkus (1981) or via ^{14}C age determinations (Kuptsov et al., 1981). From the above, one could conclude that in the sedimentary basins where terrigenous or heterogeneous low-calcareous muds

Table 17.4: Genetic sediment types of the Mediterranean and Black Seas

Content of Component	Type of Sediments
<10% of $CaCO_3$	Non-calcareous
10-30% of $CaCO_3$	Low calcareous
30-50% of $CaCO_3$	Calcareous
50-70% of $CaCO_3$	Carbonate
70-90% of $CaCO_3$	High carbonate
>90% of $CaCO_3$	Pure carbonate
3-5% of C_{org}	Low sapropelic (or sapropelitic)
5-10% of C_{org}	Sapropelic
>10% of C_{org}	Sapropels
6-10% of Fe	Low ferruginous
10-20% of Fe	Ferruginous
0.2-5% of Mn	Low manganese
>5% of Mn	Manganese

predominate (the Alboran, Algerian-Provence, Tyrrhenian, and Marmara Basins, the northern area of the Central Basin, Pre-Nile and Pre-Anatolian areas of the eastern Mediterranean Basin etc.) the age of the studied samples is about 1000 years or less.

In the areas of calcareous and high-calcareous oozes (central and near-African zones of the Central and Eastern Basins) the age can be 3-5,000 and more rarely 7,000 years. Among the analyzed samples collected by the Russian expeditions, several hundred were selected from the cores, on which biostratigraphic investigations or absolute age dating were performed. The approximate age of the sediment samples was determined using age marker horizons such as volcanic ash, pteropod ooze, and sapropelitic mud.

Biostratigraphic (foraminiferal) analysis and geochemical (^{14}C) studies of cores of the upper Quaternary sediments showed that in some cases the surface layer was represented by neither Recent nor Holocene sediments. On the bottom various sections of the Upper Pleistocene are exposed and in some places more ancient sedimentary or volcanic rocks are found. This is true for shelves (for example, near the coast of Spain), slopes of underwater highs, tops of some seamounts, walls of submarine valleys, continental slopes, and the East Mediterranean Ridge. The steepest slopes of these areas are often deprived of loose sediments and hence bedrock of different ages from the Neogene to Mesozoic periods are exposed. This was revealed by dredging and deep-sea drilling. However, the area of the exposed bedrock is relatively small and random dredge sampling is insufficient to delineate all such exposures. However the real picture of the almost ubiquitous areal distribution of recent sediments should not be distorted by such chance findings of bedrock.

Along the periphery of large abyssal basins (the Algero-Provence, Tyrrhenian, Central, Herodotus) and in the bathyal deeps, the sedimentary layer is almost constantly increasing due to turbidites. Thus, within the valleys the surface sediments are not coeval, though their age differences over the area are less significant then in morphologically dissected regions. Absolute dating and biostratigraphic research carried out in a number of shallow water areas (Aloisi et al., 1975) of the marginal shelf zone *(i.e.* Bay of Lion, Catalonian, Algerian, Pre-Nile regions) has revealed relict sediments, coastal remnants of the last glacial regression.

The Black Sea.

The authors mostly used the results of analyses of samples collected from the top 0-5 cm horizon. Rarely did the thickness of the studied horizon reach 10 cm, and up to 25 cm only in those cases where the sediments seemed lithologically homogeneous, as initially described.

Over the total area of deep accumulation continuous stratigraphic sections of Holocene sediments are revealed by biostratigraphic subdivision of sediments (performed according to palynological analysis - Shimkus et al., 1973, 1979; Kuprin, 1980, 1988), absolute dating by ^{14}C (Shimkus et al., 1975; Ross and Degens, 1974), and lithological horizon markers. Nevertheless gaps exist throughout the entire Holocene in many areas on the Anatolian and Caucasian continental slopes (Shimkus, Komarov et al., 1979, Emelyanov and Shimkus, 1962). Vast exposures of Early Cenozoic and Mesozoic rocks are found over the Crimean, Anatolian, and Caucasian slopes (Shimkus et al., 1978, 1979; Shtcherbakov et al., 1977).

The minimum late Holocene sedimentation rates were estimated in the deep-sea chalystatic areas [abyssal areas without strong deep-sea currents], in which high-calcareous biogenic oozes enriched in organic matter are accumulated. A considerable increase in sedimentation rate (ten times) is observed around them, and in the vicinity of the continental slope. Thus, if in chalystatic areas the age of sediments (0-5 cm layer) can reach one thousand years it can only be several hundred years on the periphery. Hence, the age of the 0-5 cm layer in chalystatic areas will correspond to the age of the 10-25 cm (and more) layer near the continental slope.

Shallow water Holocene sediments occurring below 40 m depth over the vast shelf area have well marked lithological horizons, the stratigraphic meaning of which was defined according to mussel complexes, palynological data, and ^{14}C datings on the shelf of Bulgaria, Ukraine, and Russia (Shimkus et al., 1979; Shtcherbakov et al., 1978; Kuprin, 1980). Stratigraphically, the studied samples from this vast area can thus be confidently related to the Upper Holocene period, as seen in their lithological and faunistic features. It is difficult to determine the age for the shelf area shallower than 30-40 m without special studies. Here the bottom surface is mostly covered by Recent (late Holocene) sediments. More ancient deposits are present in some banks and underwater continuations of spits. In some places relict sediments outcrop at the edge of the Crimean, Bulgarian, and Turkish shelves. They correspond to the last glacial epoch and are of Chaudian age (0.7 million years).

Reliability of the spatial distribution for various types of recent

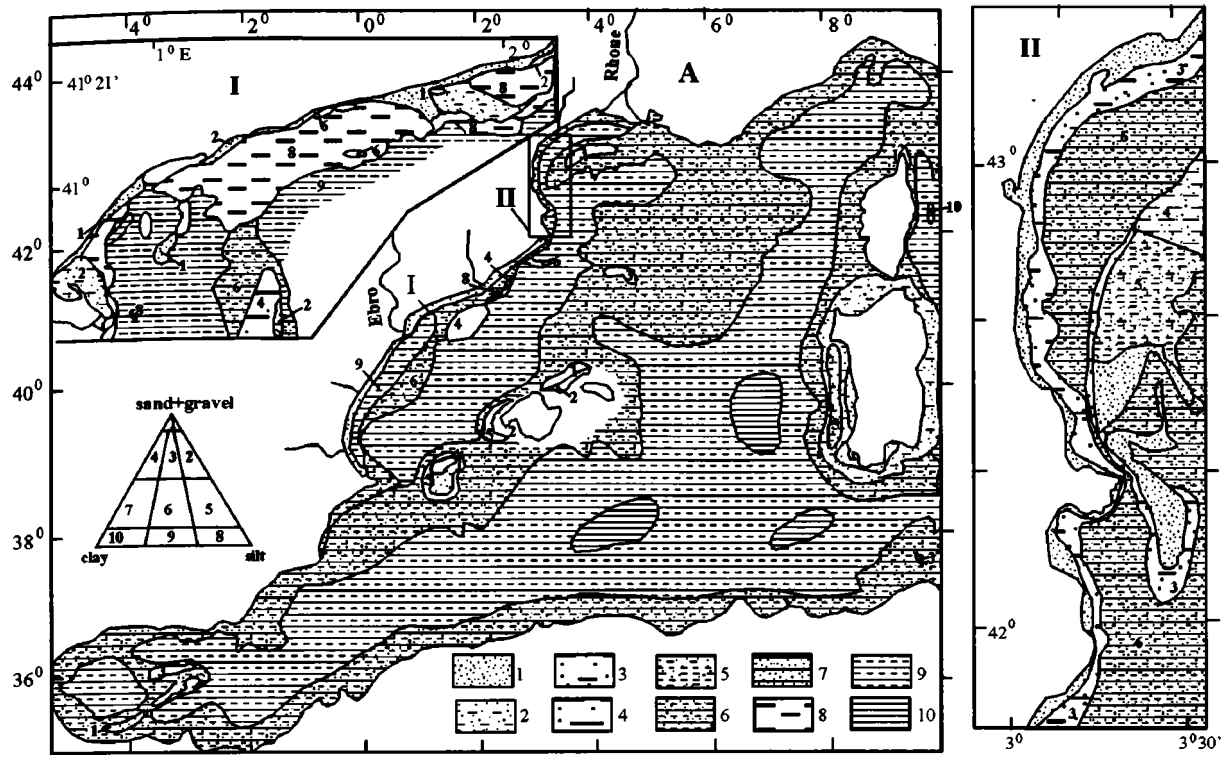


Figure 17.3: An example of two detailed sediment maps based on Shepard's triangle converted to the Folk's classification (the larger map) at two locations in the Alboran Sea.(Fig. 17.4 shows the overall locations of polygons MB-I and M-42). The legend is given according to Folk's triangle.

sediments

The Mediterranean Sea.

The spatial distribution of the various types of surface sediments on the deep abyssal plains is relatively simple due to the nature of their deposition. Detailed investigations have been carried out on a number of polygons on the Calabrian slope, East Mediterranean Ridge, and the Hellenic trenches which revealed a variety of types of surface sediments, connected with erosion, turbidites, and exposures of more ancient rocks. Thus these results have been used to give a general picture of the most likely distribution of these sediments on such morphologically dissected areas. In addition, small deeps were also discovered on the East Mediterranean Ridge. They are filled with highly saline waters due to Messinian salt dissolution *(e.g.* Bannock, Tyro Basins and others). Recent sedimentation in these small deeps occurs under anoxic conditions, caused by water stratification in the near-bottom layer (Cita et al., 1989; Emelyanov, 1992).

In the Tyrrhenian Sea, our detailed investigations, using the submersibles 'Argus' and 'Mir' and other devices for undersea observations, testify as to the complicated distribution of the surface sediments, including barren bedrock outcrops on the surface of underwater volcanoes and seamounts of non-volcanic origin. Though the amount of data available for the Aegean Sea (IBCM-SED Sheet 9) was considerably greater, we will require much more data to compile a detailed map. This archipelagic sea demands additional attention for the areas around the many islands, and between them, and the straits with differing widths and depths.

As far as the shallow water areas are concerned, we can only be confident about those regions mapped using detailed data. The fact is that the real picture of the spatial distribution of the bottom deposits over the shelf is very complex and changes from one region to another, which is demonstrated by the large inset maps. The Pre-African shelf in the Central and Eastern Mediterranean and the regions near the islands in the Aegean Sea appeared to be the least studied.

The Black Sea.

The map of bottom sediments (at scale 1:2,000,000) is good enough for both the deep-sea area and for the western, north-west, and northern areas of the shelf. The Anatolian shelf is characterized by numerous gaps as no detailed data were available to the compilers. For the Anatolian slope, we used the results of thorough lithological investigations carried out by IORAS, SBIORAS and by Ukrainian scientists (Demediuk, 1984; Melnik and Demediuk,

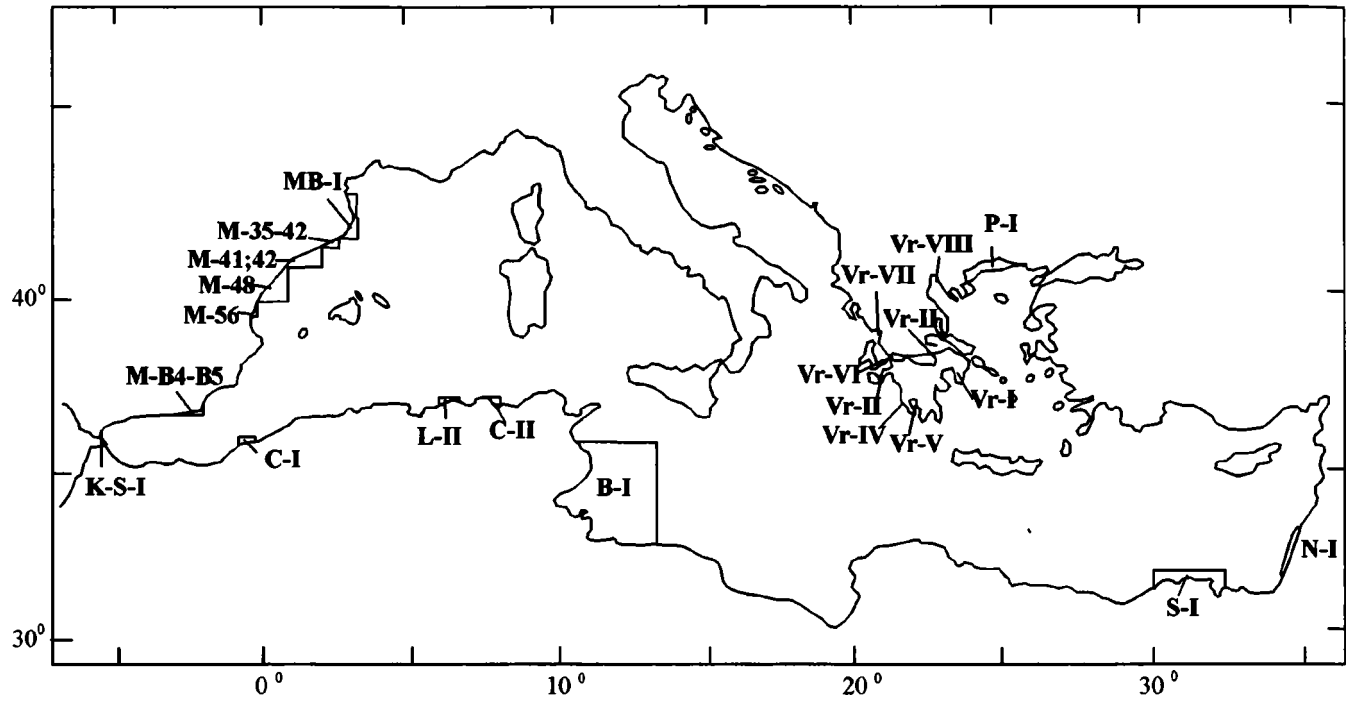


Figure 17.4: The location of the Polygons studied in detail (see Table 17.2).

1984), and Moscow State University (Kuprin, 1980; Kuprin et al., 1988; Shlykov and Luksha, 1980).

THE MAIN SEDIMENTATION FEATURES

The Mediterranean Sea

The main features of the recent sedimentation in the Mediterranean Sea are a product of its tectonic and morphological structure, climatic conditions, characteristics of water exchange with the ocean, and hydrological and hydrochemical structure.

Tectonics. The Mediterranean Sea includes the submerged edge of the African Platform and a complex region of Alpine folding, characterized by active neotectonic movements and recent volcanism. The south-eastern part of the Tyrrhenian Sea and the South Aegean region is typical. Here great volumes of pyroclastic material were erupted in pre-historic and historic time from powerful centers of recent subaerial volcanism at the Apennine coast of the Tyrrhenian Sea. These pyroclastics were also dispersed beyond the Tyrrhenian Basins. Underwater volcanoes within the deep basin, such as those of Marsili, Palinuro, and the Lipari group, display hydrothermal activity which constructs sedimentary formations. The eruption of Santorini volcano 3,300 years ago has revealed hydrothermal sedimentary ore in the sunken caldera.

Underwater volcanoes bring chemical elements into the deep-water basins of the Tyrrhenian Sea. They are mainly introduced by active creep of sedimentary material formed over a great range of depths and its accumulation at the base of the mountains. Clastic substrate materials are also produced. Almost the entire Mediterranean Sea is affected by neotectonic movements but they are most intensive in the Tyrrhenian and Aegean Basins and also in the deep-sea basins adjacent to the East Mediterranean Ridge. These movements rejuvenate ancient abyssal fractures, fissuring the bottom, producing new bedrock outcrops, and increasing hydrothermal activity. Anoxic basins are formed where these movements squeeze out brines from the Messinian salt, thus producing anomalies in what is otherwise a normally aerated sea basin.

Earthquakes connected with neotectonic processes break loose great masses of sedimentary material which slump downhill and are redeposited as turbidites. Tsunamis resulting from these earthquakes and slumps also play a great part in redeposition of bottom material. Tsunamis have also been held responsible for the accumulation of thick 'homogenite' layers at different hypsometric levels in the Central and Eastern Mediterranean deep sea basins (Cita et al., 1989).

Morphology. The Mediterranean Sea is divided into several sedimentological basins, characterized by different morphological bottom structures, and to some extent morphologically isolated. Shallow sills divide the Algerian-Provence Basin from the Central Mediterranean, the Aegean from the Eastern Mediterranean, and the Marmara from the Aegean.

The Algerian-Provence Basin has the largest abyssal plain

in the Mediterranean, followed by the Central Mediterranean Basin. The bottom is mostly uneven in the Eastern Mediterranean Basin, with the East Mediterranean Ridge and the Hellenic zone comprising the greater part of the small deep sea basins.

The Tyrrhenian, Alboran, and Aegean Basins are characterized by small flat areas. In most cases flat leveled areas are created by turbidite sedimentation, with pelagic sedimentation playing a minor role in the total input of sedimentary material. The turbididites consist mainly of heterogeneous river material transported to the deep-sea region via underwater valleys in the Algerian-Provence Basin, and in the Herodotus Basin. Turbidites are mainly triggered by earthquakes which break loose great blocks of accumulated material (volcanogenic, biogenic, terrigenous) at different depths in the Tyrrhenian and Cretean Basins. In small deeps turbidites cover the whole bottom surface while in large deep basins they are more concentrated in the peripheral parts of the abyssal plains.

Climate. The Mediterranean Sea is situated in different climatic zones: the southern region of the eastern Mediterranean is located in the arid subtropical zone, while the remainder is in a semiarid and a moderate humid zone. This explains the more intensive supply of river material from the areas draining into the Algerian-Provence, Tyrrhenian, Adriatic, and Aegean Basins.

The eastern Mediterranean is peculiar in that mainly eolian material is supplied from almost the whole of the southern arid drainage system, which also hosts the biggest river flowing into the Mediterranean (the Nile), whose source and water resources lie in the equatorial zone. Its detrital deposits control the terrigenous sedimentation in the south-eastern part of the Levantine Sea and to some extent even beyond (Emelyanov, 1994). This river creates a peculiar oasis of intensive terrigenous sedimentation in the 'desert' zone of the eastern Mediterranean. The terrigenous sedimentation is much weakened beyond this oasis, especially along the African coast to the west and the central regions of the eastern Mediterranean. On account of this a favorable situation for pelagic sedimentation appears, as the sediments are extremely poor in terrigenous material.

The terrigenous sedimentation in the Mediterranean Sea is mainly controlled by supply and spreading of the shore drifts of some of the biggest rivers: Rhone (100,543 km² watershed), Ebro (Spain, 82,587 km²), Chéliff (Algeria, 43,750 km²), Tiber (Italy, 16,545 km²), Po (Italy, 76,997 km²), and Nile (Egypt, 3,254,853 km²). Their influence over extensive areas of the sedimentary basins is clearly visible on maps showing the spreading of clayey minerals (Rateev et al., 1966; Shimkus, 1981). Thus, spreading of the shore-drifts of the Rona-Ebro River produces a large illite province in the northern part of the Algerian-Provence Basin. An illite-montmorillonite province in the Adriatic Sea and in the northern part of the Central Basin in influenced by drifts from the Po River, and the montmorillonite province in the south-eastern Mediterranean is a result of the Nile drifts. In the Hellenic zone a chlorite province of clayey minerals results from the combined effect of the many rivers in its northern drainage system on terrigenous sedimentation.

The presence of palygorskite emphasizes the primary role of eolian transport.

Numerous mineralogical provinces may result from the small amounts of sandy-aleuritic material emanating from a number of rivers (Fig. 17.5) and converging into the basin (Emelyanov, 1968, 1972).

Water exchange. The Mediterranean Sea communicates with the Atlantic Ocean through the narrow and shallow Straits of Gibraltar which prevent the entry of deep Atlantic water. Incoming Atlantic surface waters are depleted in carbonates and poor in nutrients. This explains why high productivity is usually directly connected with nutrients supplied from local terrestrial drainage systems.

The Mediterranean Sea belongs to the group of basins with low productivity. Intensive vertical mixing of the water masses precludes the accumulation of biogenic components. A good supply of oxygen brings about rapid oxidation and destruction of organic remains as they sink through the water column. Intensive decay continues on the bottom, so that organic matter is weakly fossilized and the sediments are generally not enriched in organic matter. This is typical for the southern part of the eastern Mediterranean where biological productivity is lowest. An increased organic matter content mainly occurs in the sediments of the fore-delta and debris cone of the big rivers in which organic allochthonous matter plays a significant role.

Hydrological and hydrochemical characteristics.

The Mediterranean Sea.

The waters of the Mediterranean Sea are a little more saline than in the ocean, especially in the eastern Mediterranean. The entrance of surface Atlantic waters and the outflow of deep Mediterranean water create an estuarine type of water circulation. At some sills these currents cause washout of the sediments in shallow as well as deep areas.

Dissolution of carbonates in the abyssal layers does not occur in the Mediterranean or at the same (0 to 4 km) depths in the ocean. The whole water column is oversaturated in carbonates thus creating favorable conditions for accumulation of chemical carbonate, primarily in the basins of the eastern Mediterranean, where the water temperatures are highest.

Only on the African shelf, where oolitic sands are formed over large areas, is there significant chemical precipitation of the carbonates. In other areas homogeneous carbonates are precipitated, but do not form significant deposits.

The normal salinity and high temperatures in the Mediterranean stimulate the growth of plankton and benthos, whose skeletons are made of carbonate material. For this reason the majority of the carbonates in sediments are biogenic. Their quantitative distribution is not only controlled by the volume of carbonate material produced by the plankton and benthos, but also by the degree of dilution by terrigenous silicate. The largest areas of high calcareous (foraminiferal-coccolithic) oozes are formed in the African offshore of the eastern Mediterranean, where most of the terrigenous material is eolian. Accumulation of these

oozes is obviously a passive process because biological carbonate formation here is at a minimum in comparison with other areas. This is shown in the amount of deposited carbonate calculated for the upper layer of the sediments (Shimkus, 1981; Emelyanov and Shimkus, 1986).

Paradoxically, sediments low in calcareous content are formed in areas of heightened or maximum biological productivity. The reason lies in the high rates of accumulation of terrigenous silicate matter which are much higher than the rates of sedimentation of the biogenic carbonates, which results in dilution of the carbonates (Shimkus, 1981).

Multilayer water circulation in the Mediterranean Sea promotes the appearance and long-term preservation of washout areas at different depths. These become sites for homogeneous accumulation of iron and manganese oxides as ore crusts on the hard ground. Carbonate crusts also occur in some places. These processes are intensified in regions of underwater volcanism.

As noted above, the big washout areas with no sedimentation are connected with the multilayer circulation in straits and over sills. As a result, large areas of rewashed shelly deposits and underwater meadows can be formed (*e.g.* in the African-Sicilian Strait).

The Black Sea

The principal differences in the recent sedimentation in the Black Sea as compared with the Mediterranean are due to hydrogen sulfide contamination of the water bodies. This H_2S provides the main condition for the accumulation here of abyssal sediments, rich in organic matter (sapropelitic nanno-oozes). At present these types of sediments are not being formed anywhere in the Mediterranean. This hydrogen sulfide is connected with the exchange of Mediterranean and the Black Sea waters as a result of very high runoff of fresh water from the surrounding lands. This forms a stable low-salinity upper layer with strong density stratification, which precludes significant vertical water exchange with the up to two kilometers of stagnant water below.

The lower stagnant water mass creates an environment for the accumulation of large volumes of biogenic material. The biggest rivers, *e.g.* the Dnieper (Ukraine, 533,966 km² watershed), Dniester (Ukraine, 68,627 km²), Don (Russia, 458,703 km²), and to some extent the Danube (Romania, 795,656 km²) provide an intensive supply of nutrients to the upper layer. These are derived mainly from the drainage system of the surrounding plains, stimulated by the high biogenic productivity in the humid Black Sea Basin. These nutrients cause a powerful increase in biological productivity in the upper photic layer. The organic matter thus produced returns to the lower layer, where it is mostly accumulated on the bottom with very little oxidation on the way because of the reducing conditions in the absence of oxygen.

As might be expected, our data show that the accumulation of organic matter in the Black Sea is far more intensive than in the Mediterranean. The increase in the organic matter in the recent sediments in the Black Sea is directly related to the increasing supply of organic planktonic matter. This sharp increase in the organic matter in the sediments (with the formation of sapropels) is happening in these areas of heightened biological productivity against a background of slow non-organic sedimentation. The large scale cyclonic surface water circulation has created large areas of these muds. These circulation centers are characterized by heightened biological productivity, along with small accumulations of terrigenous material.

The Black Sea abyssal sediments lack benthic fauna and consist of just plankton remains because of the H_2S contamination. The low salinity of the Black Sea surface waters caused taxonomic impoverishment of coccolithophorids and complete absence of planktonic foraminifera. The euryhaline coccolithophorid *Emiliania huxleyi* is widely distributed and its skeletons form coccolithic (nanno-) oozes.

THE DISTRIBUTION AND THE COMPOSITION OF THE SEDIMENTS

Peculiarities of the distribution of main types of the sediments

The Mediterranean Sea

Shelves. The shelves of the Mediterranean Sea are mainly covered by heterogeneous deposits which are mostly terrigenous-biogenic off the platform areas, and biogenic-terrigenous off submountainous areas. Terrigenous sediments are more characteristic of the coastal zone, and biogenic in the shallows and out to the edge of the shelf, where they mainly represent relict formations. The usual granulometric scheme for the gradation of sediment types from the shore to the edge of the shelf is: sands - silty-sands - silts - muddy sands, etc. Such a scheme is only typical for flat areas of the shelf. A spotty distribution of the sediment types is mainly typical for shelves off submountainous areas. In big gulfs, the distribution of granulometric sediment types is very spotty, *e.g.* in the Gulf of Gabes off Tunisia.

A peculiar feature of some shelf sediments is the existence of underwater meadows which occupy large areas on the African-Sicilian Sill (*e.g.* the Gulf of Gabes) and in some bays close to the Algerian coast (Burrollet et al., 1979). In particular, sapropelitic deposits are not formed here despite the intensive production of benthic organic matter in the near bottom layer. Shallow biogenic sediments are characterized by their concentration of benthic fauna, consisting mainly of mollusks and to a lesser degree benthic foraminifera. Here planktonic organisms such as pteropods and planktonic foraminifera are obviously subordinate. Relict deposits, usually formed of oyster shells and heterogeneous terrigenous material of different sizes, are found in zones of recent non-sedimentation or in regions of bottom washout stretching along or at an angle to the shelf. The terrigenous deposits off the submountainous areas are typified by shallow water granulometric variation. These heterogeneous sediments are also found in archipelagic seas, where the shelf width is highly variable and the shore line is punctuated by alternating bays and capes reflecting deep dissection of the land. In these areas the above progression in sediment grain-size is mainly the exception rather than the rule.

In some places a large part of the shelf, if not all the shelf,

is covered by sandy deposits with various admixtures of coarse-grained material, which can also form wide bands across the shelf. Examples are found in the Aegean Sea, off the Pyrenean shelf, and in the Algerian-Provence Basin near Provence. Strips of relict coarse-grained and rough-grained deposits are not rare, and they stretch for various distances along the edge of the shelf *e.g.* the Gulf of Lion, some bays on the Algerian shelf, the shelf off the Nile etc.

The Mediterranean straits each have their own granulometric compositions which are dependant on the width and depth of the strait and the bottom morphology. The Tunisian and Malta straits on the African-Sicilian Sill are unique and have extensive shallows side by side with numerous banks and considerably deeper sublatitudinal basins. The shallow water areas are characterized by a complex granulometric spectrum of sandy-aleuritic deposits containing an admixture of coarser material. Here the mosaic of granulometric types was predetermined by the development of patches of relict detritus, subject to wash-out and reaccumulation by recent bottom currents. This region is characterized by 'zero recent sedimentation'. In the coastal zones the recent sediments are represented by terrigenous sands, and aleurites. 'Normal' abyssal sediments, accumulated in the deeps of the African-Sicilian Sill, are in some places relatively enriched in shelly detritus, washed off from shallow water by near-bottom currents.

Deep basins. Terrigenous, biogenic (carbonate), and volcanogenic sediments are well-developed in the sedimentary basins in the Mediterranean Sea. They show the heterogeneous nature of the sedimentary cover. Chemogenic sediments, consisting of calcareous oolites and iron hydrothermal deposits and ores, are found in limited areas. In most cases the biogenic materials in the recent sediments are carbonates.

In abyssal sediments carbonates are represented by coccoliths, planktonic and benthic foraminifera, and pteropods. The quantity of coccolithophorids and planktonic foraminifera in the sediments is dependent upon the biological productivity in the active water layer (0-100 m). But the accumulation of pteropods is controlled by the depth, because of the depth-dependent processes of dissolution. Thus they almost don't exist in the sediments deeper than 2500-3000 m. The ratio of benthic to planktonic foraminifera is less than one and decreases even more with increasing depth.

Pure biogenic abyssal sediments consist of thin interlayers of coccolithic or foraminiferal-coccolithic oozes or foraminiferal aleurite and fine sands. The distribution of such deposits on the bottom has not been mapped. A new method of geological sampling is needed to investigate this thin uppermost sediment layer.

The discovery of interlayers in Quaternary sediments with abyssal-like provenance suggests the possibility that almost pure nanno-oozes are being accumulated on the seafloor in significant parts of the eastern Mediterranean and in some parts of other basins (Shimkus, 1981). High carbonate foraminiferal-coccolithic oozes, with different terrigenous admixtures, are widely spread in the abyssal parts of the central and eastern basins of the Mediterranean, and near Africa (Kuprin et al., 1977). They do not result for the high productivity of biogenic carbonates, but mainly from their weak dilution by terrigenous silicate material. Here the rate of accumulation is very low (Shimkus, 1981) because of the extremely small amounts of terrigenous material (mainly eolian) being supplied from Africa.

All kinds of mixed terrigenous-biogenic muds were produced by variations in the input of the biogenic and especially terrigenous material. The rates of sedimentation of terrigenous material are larger and far more variable than those of the biogenic. Biogenic oozes are not formed in regions with high rates of sedimentation of carbonate material because the rates of accumulation of the terrigenous silicate material are even higher *e.g.* the northern part of the eastern Mediterranean, the Algerian-Provence, Tyrrhenian, Adriatic, and Alboran Basins (Shimkus, 1981). Muds with different admixtures of biogenic material are being accumulated there.

Siliceous biogenic sediments do not exist in the Mediterranean Sea. Because of a lack of silicic acid in the Mediterranean waters, the siliceous skeletons of diatoms, radiolarians, and silicoflagellates are quickly dissolved in the upper water layer (Emelyanov, 1966), with very little reaching the bottom. Biogenic sediments enriched in organic matter are also not being formed in the Mediterranean Sea. This is the result of:

1) Low biological productivity in most of the sedimentary basins and

2) Intensive decomposition of the organic matter as it sinks through a water column enriched in oxygen. The relative organic enrichment of the sediments in the sea off the Nile is mainly connected with the accumulation there of great volumes of terrigenous organic matter produced in the Nile Valley and on the delta itself.

Recent volcanogenic sediments are located in the eastern and southern parts of the Tyrrhenian Sea and in the northern region of the Cretan deep. The volcanoes produce mainly eruptive (and lesser amounts of volcanoclastic) material which occurs as an admixture in the terrigenous and terrigenous-biogenic sediments and also in turbidites.

The main feature of the river-free African shelf is the widespread distribution of oolitic sands with shelly material.

The presence of wide areas off the Nile delta with low-ferruginous and low-manganese muds is a result of the Fe and Mn in the basic effusives from the Abyssinian plateau being leached out of the river and deposited in the onshore Nile delta sediments.

Metal-bearing sediments have a hydrothermal-sedimentary origin and are associated with Pleistocene, Holocene, and recent hydrothermal activity in areas of underwater volcanism like the Tyrrhenian Basin (Marsili and Palinuro Seamounts). In the shallow sediments of some subaerial volcanoes which are now inactive, such as the Lipari Islands, hydrothermal-sedimentary processes have produced important ore deposits. In some areas mineralization processes have occurred within recent tectonic fractures. Manganese films of hydrothermal origin, enriched in some other elements, are widespread on bedrock outcrops in the Mediterranean Sea.

The bottom deposits in abyssal areas show considerably less granulometric variability than those in shallow areas. Most areas of the Alboran, Algerian-Provence, Tyrrhenian, and Adriatic

Basins, as well as the northern part of the Central Basin, the Hellenic, Pliny, and Strabo Trenches, and the easternmost part of the Levantine Sea, where terrigenous deposits predominate, are covered by 'mud'. 'Clays' only occupy small areas within these 'muds', and minor areas of 'sandy clays' occur as well, where foraminiferal nanno-oozes are developed. They prefer the crestal areas of various hills or areas whose waters are iron-rich, where the accumulation of terrigenous material is weakest. These locations don't depend on bottom morphology, but are determined by the spatial distribution of cyclonically circulating surface waters. The purest carbonate deposits (>70% $CaCO_3$) are represented by the 'sandy muds' covering large areas off the African coast in the eastern Mediterranean. When the carbonate content drops to 50-70%, the 'mud' begins to predominate.

'Sandy muds' are developed among volcanogenic deposits, and especially near pyroclastic or volcanoclastic sources.

Recent turbidites are mainly developed below canyons cut into the continental slopes of the Algerian-Morocco, Apenninian, Cretan-Rhodes, and Peloponnesian margins. They are also deposited in some of the abyssal basins of the Hellenic trenches (Ferentinos et al., 1985).

Terrigenous sediments. About 75% of the Mediterranean Sea is covered by terrigenous sediments.

The shallow-water and deep-water coastal regions of the geosynclinal portions of the sea (northern and western parts of the Mediterranean) are characterized by non-calcareous (<10% $CaCO_3$) and low-calcareous (10-30% $CaCO_3$) terrigenous sediments with highly variable grain-size and physical properties (Emelyanov, 1965, 1975). They are usually colored gray and their moisture content ranges from 24-81%. They show marked differences in mineral composition, as they originate from different source areas.

The simplest terrigenous sediment distribution scheme is observed in places where the structure of the adjoining land and shelf is linear and level. One example is polygon N-I near Israel (Fig. 17.4). Non-calcareous terrigenous sediments are deposited here as follows:

1) Sands - from water's-edge up to 20-30 m,

2) Silt or mud - from 20-30 m depth up to 100 m,

3) Mud and clay - from 100 m and deeper up to 500-800 m (Neev, 1964, 1965; Nir, 1973, 1984). Approximately the same succession of sediments was found in the M-35-42. M-41-42 and M-84-85 polygons close to the Pyrenean peninsula (Fig. 17.3, Maldonado et al., 1982-1992), but they are remarkably spotty. It is a result of both tectonic (geomorphological) structure and hydrodynamic regime, producing either muddy areas or a considerable admixture of muddy material in the sands on the shelf (silts, sandy muds, or clayey sands).

The most complex distribution of granulometric types of sediments is observed on the shelves of mountainous coasts. Polygon P-I in the northern part of the Aegean Sea (Fig. 17.4) is an example of such a distribution (Lykousis et al., 1981). In the Northern Adriatic changes in the granulometric sediment types occur abruptly and rapidly within 2 to 3 miles; it is either silt, or mud. In the bay of Venice the spotty sediment distribution is related both to the tectonic (geomorphological) structure, and to the presence of a number of river mouths; usually muddy patches are among the sandy areas near river mouths. It is typical that in the bay of Venice there are many rock outcrops (Brambati, Ciabatti et al., 1988, Carta Sedimentologica).

Abyssal terrigenous (non-calcareous and low-calcareous) muds are either semi-fluid or soft sediments. They are gray with yellowish or brownish shades near fore-deltas. Moisture content varies between 45-63% (average is 54%). The density of fresh mud from Station ASV-601 (horizon 0-2 cm) is 1.43 g/cm^3 (Table 17.5). Under dry conditions terrigenous low-calcareous muds are brown-gray, very dense, and so solid they can hardly be broken with a hammer. The density of absolutely dry mud from Station ASV-562 (horizon 0-20 cm) is 1.896 g/cm^3, Baumé gravity is 2.580 g/cm^3, and porosity is 66.78%. Sandy mud is widespread in the Aegean Sea (Lykousis et al., 1981), on the African-Sicilian Sill, and in the northwestern Provence Basin. In all these cases the granulometry is mainly caused by a noticeable admixture of foraminiferal material. That fraction which is coarser than 0.01 mm consists of 80-50% of foraminifera and pteropod fragments.

Biogenic-terrigenous muds (30-50% $CaCO_3$) are light brownish-yellow in color under fresh conditions (brighter than low-calcareous muds). They are soft, plastic, and viscous. The moisture content ranges from 32 to 57% and averages 46%. It is considerably less than that of muds poorer in carbonate. The density of fresh wet mud is 1.448-1.580 g/cm^3 (Station ASV-582, Table 17.5). The muds are rather dense when dry. But in contrast to terrigenous non-carbonate muds they can be ground up with the fingers. They are whitish or pale-yellow. Average densities for Mediterranean sediments range from 1.918 to 2.216 g/cm^3, Baumé gravity from 2.552 to 2.617 g/cm^3, and porosity between 62.69 and 63.13%.

The median diameter of biogenic-terrigenous mud varies between wide limits (0.002-0.014 mm), and sorting is mainly poor. Remnants of *Clio pyramidata* predominate among the shelly material of pteropods. Its triangular, very fragile shells reach up to 3-10 mm. Consequently, the complete shells are in the >0.1 mm fraction while its numerous fragments are only in the most fine (<0.1 mm) fraction.

Representatives of globigerinids, especially *Globigerina bulloides, G. eggeri, G. pachyderma, G. quinqueloba, Globigerinoides ruber, G. tenellus, Globorotalia scitula, G. inflata,* and *Orbulina universa* (Parker, 1958; Blanc, 1958; Todd, 1958; Olausson, 1960, 1961) are predominant among planktonic foraminifers.

Coccolihic material is concentrated in the fine pelitic fraction (<3-5 μm). This material only exists in quantity in the sediments of the eastern Mediterranean. Predominant forms are usually *Coccolithus huxleyi* (Lohm.) Kampt., *C. atlanticus* Coh., *Cyclococcolithus leptoporus* (Murr., Blanc et Kampt.), and *Braarudosphaera bigelovi* Gran., and *Coccolithus variosus* Cohen are typical too. Sometimes reworked neogenic forms of coccoliths *(Discoaster challengeri* Bramlette et Riedel, *D. surculus* Bramlette et Martini) are found in the muds off the Turkish, Cretean-Peloponnesus, Sicilian, and

Table 17.5: Physical properties of recent sediments of the Mediterranean Sea

Station	Depth, m	Horizon, cm	Percentage in sediments			Specific weight, g/cm³		Volumetric weight of absolutely dry soil. g/cm³	Calculated porosity, %
			Fraction <0.01 mm, %	$CaCO_3$ %	Moisture Content, %	Naturally wet	Absolutely dry		
Terrigenous sand									
ASV-313	1833	0-3	6.02	3.20	32.11	1.716	2.579	2.317	54.95
Low calcareous terrigenous mud									
ASV-562	891	0-20	71.72	29.10	43.80	1.525	2.580	1.896	66.78
ASV-584	1104	0-20	67.39	29.56	48.40	1.475	2.605	1.770	70.96
ASV-601	2115	0-2	77.89	21.83	46.08	-	-	1.43*)	-
Calcareous-terrigenous mud									
ASV-391	94	0-7	63.20	42.93	40.14	1.580	2.552	2.216	63.13
ASV-359	297	0-9	35.97	44.80	23.55	1.897	2.620	2.144	44.66
ASV-602	648	0-2	70.24	30.70	44.10	-	-	-	-
ASV-412	698	0-21	73.13	35.93	66.56	1.448	2.530	1.917	83.41
ASV-578-1	700	0-12	62.00	45.57	39.10	1.621	2.617	1.919	62.69
ASV-406	820	0-20	69.08	35.47	39.64	1.577	2.576	1.918	62.85
ASV-381	1551	0-12	85.20	37.29	44.49	1.487	2.542	1.816	67.05
ASV-599	2197	0-10	70.73	31.61	50.40	1.483	2.592	1.702	72.48
ASV-325	3169	0-5	88.34	35.50	48.92	1.461	2.626	1.510	71.55
Foraminiferal ooze									
ASV-417	306	0-5	47.95	68.22	36.87	1.672	2.640	2.280	60.65
ASV-576-1	350	0-6	46.75	63.70	30.60	1.755	2.699	1.619	54.34
ASV-538	1531	0-7	66.04	50.30	36.20	1.664	2.674	2.226	60.41
ASV-582	1639	0-15	47.98	63.44	39.00	1.626	2.664	1.982	63.60
ASV-536-3	2156	0-20	67.13	55.26	38.70	1.618	2.654	1.720	62.63
ASV-396	2295	0-5	83.43	54.58	47.48	1.490	2.488	1.973	69.22

*) In natural wet samples

Table 17.6: Chemical composition of the sediments of Marsili Seamount area, Tyrrhenian Sea, $CaCO_3$ - Mg – in %, Cu - Co in 10^{-4}%

Station	Depth, m	Horizon, m	Sediment type	CaCO3	C_{org}	Fe	Mn	P	Ti	K	Na	Ca	Mg	Cu	Zn	Cr	Ni	Rb	Li	Co	CC% (x-ray data)
Vy-1659	484	0-3	B-V-1*), CLMnMcal	33.4	0.44	2.36	0.22	0.10	0.36	1.26	1.58	14.60	1.44	491	86	62	72	34	42	24	22
Vy-1666	520	0-5	B-V-T, CM	44.9	0.41	2.56	0.10	0.06	0.28	0.94	1.49	18.40	1.77	35	60	60	47	22	40	28	37
Vy-1643	934	0-3	V-T, LCM	29.7	0.47	3.84	0.11	0.06	0.35	0.88	1.66	11.70	1.38	41	274	77	12	27	48	34	-
Vy-1660	1050	0-3	B-V-T, CM	35.8	0.50	2.96	0.10	0.06	0.33	1.20	1.45	14.80	1.44	41	86	74	66	34	46	30	29
Vy-1639	1270	0-3	B-V-T, CM	37.0	0.62	3.00	0.07	0.07	0.29	0.98	1.09	15.30	1.38	50	88	73	84	30	44	24	21
Vy-1644	1580	0-3	B-V-T, CM	35.8	0.41	3.04	0.10	0.06	0.31	1.38	1.68	13.80	1.38	38	86	77	180	32	50	20	17
Vy-1662	2010	0-3	B-T, CM	34.2	0.52	3.64	0.10	0.06	0.2	1.2	1.45	15.10	1.44	46	230	84	86	36	46	24	32
Vy-1645	2280	0-3	B-T, CM	32.0	0.45	3.52	0.11	0.06	0.35	1.22	1.28	13.40	1.32	48	90	77	86	34	46	34	20
Vy-1647	2850	0-9	T, LCM	27.0	0.46	4.08	0.10	0.07	0.34	1.66	1.83	12.30	1.42	52	100	84	62	51	48	30	19
Vy-1663	3150	0-5	T, LCM	30.0	0.53	4.00	0.11	0.16	0.35	1.22	4.17	12.70	1.32	49	84	74	94	36	48	18	29
Vy-1669	3290	0-5	T, LCM	24.3	0.43	2.72	0.10	0.04	0.32	1.74	1.70	11.60	1.26	76	62	88	82	41	48	28	24
Vy-1633	3400	0-3	T, LCM	15.8	0.60	5.08	0.10	0.07	0.45	2.00	1.64	7.10	1.44	59	242	112	58	76	66	34	10
Vy-1673	3420	0-3	B-T, CLFeM	38.3	0.50	10.00	0.08	0.06	0.29	3.00	2.94	17.00	1.48	59	64	62	120	30	33	24	32

L = low; C = calcareous; M = mud; Mn = manganese; Fe = ferruginous; CC% = Carbonate Content in % (from bulk sediment sample). Note: *) B – biogenic, V – volcanoclastic, T – terrigenous

Tunisian coasts. Calcite of homogenous origin is in the mud as crystals and irregular grains. 5-7 μm in size, and it comprises a considerable part of the pelite (Emelyanov, 1972; Emelyanov and Shimkus, 1986).

Biogenic-terrigenous muds (30-50% $CaCO_3$) are the most widespread kinds of terrigenous sediments. According to their granulometric composition they are typical muds consisting of clay with silt admixture. With the aim of classifying the mud into two sub-types we divided them by their content of grains in the <0.01 mm fraction. According to the Russian (IORAS) classification, fine, pelitic, or clayey mud consists of more than 70% of this fraction, and it occurs in the deep pelagic zone. Less than 70% of this fine fraction defines inshore aleuro-pelitic mud or typical mud.

The bottom sediments, especially the terrigenous ones, were found to contain a large variety of minerals (Emelyanov, 1968, 1972, 1975, 1979). The quartz-to-feldspar ratio in terrigenous sediments is usually less than 1. For example we shall describe some mineralogical provinces from the Levantine Sea, especially the Nile province.

The Nile transports large quantities of sediment, mostly derived from the erosion of basic rocks and basalts. Within the 0.1-0.5 mm subfraction, quartz comprises from 18 to 46%, feldspars from 9 to 33%, micas from 1 to 12%, and weathered particles and basalt fragments 18-55% (Emelyanov, 1994). Dominant among the heavy minerals are clinopyroxenes (22-41%), common hornblende (9-14%), epidote-clinozoisite (5-10%), and the ore minerals ilmenite, chromite, and leucoxene (5-15%). The concentration of basaltic fragments in the heavy subfraction is also very high: 12-43%. The <0.001 mm fraction is dominated by montmorillonite. Precipitations of ore minerals and basaltic fragments occur closest to the Nile promontory; farther off are quartz, feldspars, clinopyroxenes, common hornblende, and biotite.

Since the Nile load is mostly products of basalt denudation, the sediments have similarly high concentrations of the basalt elements Fe, Ti, and Mn, and high contents of Na, Cr, Zn, and V. Areas with high concentrations of these elements, together with C_{org} and $CaCO_3$, are more prevalent around the Nile Cone than the areas of high clinopyroxenes. Thus, the sediments north and northeast of the Nile fore-delta belong to the unique Nile litho-geochemical province, which is specific to the eastern Mediterranean (Emelyanov and Shimkus, 1986, p. 487; Emelyanov, 1994).

The island of Cyprus is an independent source province. Around the island, the clastic minerals deposited are mostly typical of the onshore sedimentary and metamorphic rocks and peridotites (Emelyanov, 1994). The heavy fraction of 0.1-0.05 mm is dominated by black ore minerals, ordinary hornblende, epidote-clinozoisite, clinopyroxene, and disthene (kyanite) which is common (Emelyanov, 1975); in the light fraction are quartz and plagioclase, K-feldspars, volcanic glass, and calcite. Characteristically, no products of denudation of the serpentinites (serpentine, etc.) were found in the >0.05 mm fraction. These products might have been crushed to a size smaller than 0.01 mm, and could not be detected under an optical microscope. Peridotites (serpentinites) are enriched in Ni, Cr, Co, and Fe, and slightly in Mn. High concentrations of these elements were detected in the sea south of Cyprus. These results suggest that the sediments rich in Ni, Cr, Co, and Fe near Cyprus accumulate denudation products not only from sedimentary and metamorphic rocks, but also from ultramafics. Cr, Ni, and Fe- rich sediments are also found on Florence Seamount west of Cyprus, and Eratosthenes Seamount south of Cyprus. Hence, these seamounts also accommodate the erosional products of the ultramafic rocks. The mountains along the Syrian coast also appear to be a rich source of fine products of ultramafic denudation. There are four such sources on Cyprus and the Syrian coast, giving high concentrations of Ni and Cr (over 0.02%) in the offshore sediments.

The Rhodes terrigenous-mineralogical province (**see Figure 17.5**) stretches as far as Crete and south up to the East Mediterranean Ridge. The most typical minerals in the sediments of this province are garnets, yellow and brown biotite, black ore minerals, clinopyroxenes, rhombic pyroxenes, and fibrous amphiboles, with colored micas in the light subfraction. There is practically no serpentine or olivine. However, east of Rhodes high concentrations have been recorded of Cr and Ni and sometimes Fe. Apparently, this province accumulated the denudation products of sedimentary, metamorphic, and ultramafic rocks.

The Taurus terrigenous-mineralogical province is east of the Rhodes province and extends as far as Iskenderun. It is characterized by black ore minerals, clinopyroxenes, epidote-zoisite, rutile-anatase, and colored micas in the light subfraction.

The Levantine province embraces the deep-water areas of the Levantine Sea (west of the Cyprian and Nile provinces). Most typical are eolian quartz, feldspars, the black and red ore minerals ilmenite, hydrogoethite, and hematite, as well as common hornblende, epidote-clinozoisite, and yellow and brown biotites. The sediments in the province are largely represented by coccolith-pteropod-foraminiferal and pteropod-foraminiferal oozes. Biogenic carbonates dominate.

The terrigenous sediments can be characterized by the average composition of their main chemical constituents. The carbonate content and the content of the main and other elements in the sediments vary widely. The average content of $CaCO_3$ in the surface sediments is 40.32%. The highest average content (57.54%) of this constituent is in the sands, the lowest (32.01%) in the fine silty mud.

The average contents of all the main constituents correlate well with their grain-size distribution.

Biogenic carbonate sediments. Biogenic sediments occur from the shore out to depths of 3500-4000 m, and contain from 50 to 98% of $CaCO_3$ (Emelyanov, 1965, 1972, 1973, 1975).

Biogenic sediments are separated from the shore by terrigenous sediments and are found at a great distance away from the coastline in the northern regions, except where they often accrue near the mouths of rivers. These sediments are mainly relict.

Biogenic sediments mainly consist of shelly and coral material, and foraminifera, pteropods, and coccoliths. Shelly sediments are present at depths of 100-200 m; foraminiferal sediments are found at depths of 2.0-2.5 km, while pteropod-foraminiferal ooze

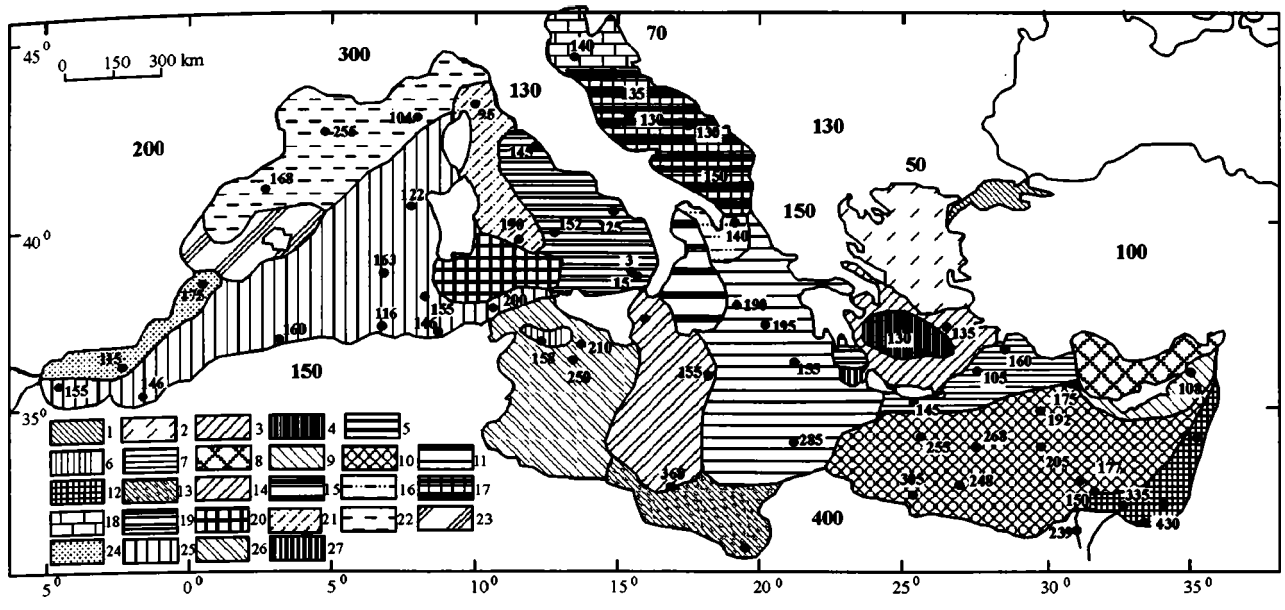


Figure 17.5: The terrigenous-volcanogenic mineralogical provinces of the coarse-aleuritic (0.1-0.05 mm) fraction from the upper sediment layers in the Mediterranean Sea (after Emelyanov, 1968) and the absolute ages of terrigenous-volcanogenic minerals (after Emelyanov et al., 1973). 1 - Sea of Marmara; 2 - Northern Aegean; 3 - Sea of Crete; 4 - Santorini; 5 - Southern Peleponnesus; 6 - Kythere; 7 - Rhodes (Nesos); 8 - Taurus; 9 - Cyprus; 10 - Levant; 11 - Ionian; 12 - Nile offshore; 13 - Sirte (Surt, Sidra); 14 - Eastern Sicilian; 15 - Calabrian; 16 - Apulian; 17 - Southern Adriatic; 18 - Northern Adriadic; 19 - Eastern Tyrrhenian; 20 - Southern Sardinian; 21 - Corsican; 22 - Provencal; 23 - Valencian-Balearic; 24 - Southern Spanish; 25 - Algerian; 26 - Tunisian-Sicilian; 27 - Pantellerian. Figures within the sea area are age of minerals (in Ma), figures (in large print) within adjacent land regions are absolute age of the most widespread rocks and soils (in Ma).

occurs at depths of 0.5-3.0 km, being succeeded at greater depths by coccolith-pteropod-foraminiferal and foraminiferal-coccolithic oozes. *Venus, Turritella, Nassa, Spondylus*, and *Chenopus pelicani*, etc. are commonly the dominant constituent of the shelly sediment. The remains of urchins, corals, and bryozoans as well as calcareous algae are also present in large quantities.

In the southern part of the African-Sicilian Sill (in the so- called Pelagian Sea) between the high carbonate coral-shelly sediments (coquina, sands, muddy sands, sandy muds and so on) there are widespread so-called meadows (Blanpied et al., 1979): in the near-shore areas *Cymodocea nodosa* meadow banks are colonized by Posidoniae, and slopes by *Caulerpa prolifera*. At a depth of 15-20 m the *Posidonia* meadow disappears and *Caulerpa* becomes more dominant. In the Gulf of Gabes the bottom is a muddy plain: this gulf is a trap for fine sediment.

In the Tunisian plateau there are different biogenic carbonate facies. The sandy-clayey bioclastic facies (up to 50-90 m) consists of pyritized vegetal remains, algae, mollusks, etc.

In the deep troughs of the African-Sicilian Sill bioclastic sandy mud and foraminiferal oxidized (ocre color) oozes are widespread. The rates of sedimentation are 10-12 cm/1000 years (Blanpied et al., 1979).

The carbonate content of the sediments of the African-Sicilian Sill and the Pelagian Sea range from 50.0 to 92.3%, including 2.0 to 6.2% $MgCO_3$. Carbonates are mainly present as Mg-calcite, and sometimes aragonite. Dolomite grains are often found. The terrigenous material is mainly represented by stable minerals such as quartz, magnetite, ilmenite, zircon, and rutile. Clastic matter is mostly delivered by winds from the deserts of Africa. The shelly sediments of the African-Sicilian Sill are mainly relict.

Coral-algal and coral-shelly sediments in the Mediterranean Sea are more or less widespread in shallow-water areas, especially near the Provencal coast, in the Tunisia Strait area, and the Sea of Crete. The authors have never encountered typical coralline sediments.

In the Aegean and Cretan Seas carbonate sediments are represented by foraminiferal and coccolith-foraminiferal oozes. Globigerina is noticeably more abundant than other foraminifera. The muds of the Sea of Crete showed a large number of the coccoliths *Syracosphaera pulchra* (Lohman), and *Helicosphaera carteri* (Wallich, etc.). Encrustations of Lithothamnia are often found in shallow water sediments and in areas of calcareous oozes. Magnesian-calcareous nodules of irregular shape 5-10 cm in diameter have been found in the Santorini area in the Sea of Crete. The sediments of the Sea of Crete contain up to 6.94% $MgCO_3$. Carbonates are represented mainly by Mg-calcite ($MgCO_3$ reaching more than 8.0%). Crystals of chemogenic (diagenetic) calcite, Fe-carbonates, and dolomite are also found (Emelyanov, 1965, 1972, 1975).

The mineral composition is rather variable in the central part of the Aegean and Cretan Seas and belongs to five mineralogical provinces (Fig. 17.5) (Emelyanov, 1968). Some of them are

characterized by volcanic glasses and clino- and orthorhombic pyroxenes, and others by basaltic hornblende, and by alkaline amphiboles (riebeckite, arfvedsonite etc.). Illite (30-90%) and kaolinite (10-30%) are the most common clay minerals. Montmorillonite is encountered in quantity only in the area of the Milos-Santorini-Nisiros volcanic isles. The absolute age of the terrigenous-volcanogenic minerals is 30-145 Ma (Emelyanov et al., 1973).

In the arid zone there is a trend which is evident in the distribution of the calcareous sandy mud: the lesser the $CaCO_3$ content, the finer-grained the sediment, and the larger the areas of occurrence. Biogenic sediments occurring in the deep water between Cyrenaica, Crete, and Alexandria contain from 50 to 60% $CaCO_3$. These are coccolith-pteropod-foraminiferal oozes. They are very compact (the moisture content ranges from 30.9 to 48.6%). The oozes are sticky and viscous, and are light-brown in color (Emelyanov, 1975). The density of the moist (fresh) oozes at Stations ASV-536-1 and ASV-538 was 1.618 and 1.664 g/cm^3 respectively (Table 17.5). In a dry condition, calcareous oozes are light grayish-yellow in color, and one can grind up the dry sediment with the fingers. The density is 1.720-2.226 g/cm^3, Baumé gravity 2.654-2.674 g/cm^3, and porosity 60.41-62.63%. Dry ooze is so light that for some seconds it won't sink in water.

There are a lot of delicate transparent shells of the pteropods *Clio pyramidata* in the oozes. The foraminiferal assemblage consists of planktonic *Globigerina bulloides* (d'Orb), *G. dubia* (d'Orb.), *Globigerinoides ruber, Globorotalia inflata*, and *Orbulina universa* (d'Orb.). There are 5,000-45,000 planktonic foraminifera shells in 1 gram of ooze. The shells of benthonic foraminifera are also found in abundance, with 10 to 2,000 shells in 1 gram of sediment (Korneva, 1966); *Gyroidina neosoldanii* (Brotzen), *Articulina tubulosa* Sequenza, and *Usbekistania charoides* (Jones and Parker) are common (Korneva and Saidovas, 1969). Coccolithic debris consists mainly of *Coccolithus huxleyi* (Lohm.) (Kampt.), *C. atlanticus* Coh., *C. variosus* Coh., *Cyclococcolithus leptoporus* (Murr. et Blac.) (Kampt.), and *Syracosphaera pulchra* (Lohm.). The most characteristic peculiarity of the coccolith-pteropod-foraminiferal oozes in this area is that almost everywhere they contain calcareous-clayey magnesian concretions of diagenetic origin (Emelyanov, 1961, 1965, 1972; Müller and Fabricius, 1971). These are 5-10 cm in diameter and have an irregular form. The concretions cover 40% of the bottom at Station ASV-536 (between Crete and Africa, in depths of 2130-2167 m). They are also found very often in the Aegean Sea and the Gulf of Sidra.

The tops of the undersea mountains and ridges are covered by 'carbonate caps'. The top of the Baroni Ridge (480-700 m) in the Tyrrhenian Sea is covered by foraminiferal or shelly-foraminiferal sands, silty sands, muddy sands, or sandy silt (**Figure 17.6**). There are a lot of dead Madreporaria corals (up to 8-10 cm in length) in the surface sediments. Fragments of urchins, Polychaeta tubes, and mollusks shells are also present. Below the 600 m isobath nanno-foraminiferal oozes prevail. They are light grayish-brown in color, soft and very viscous: they lie on the steep slopes (up to 25-30°) without slumping. The oozes contain 48-55% $CaCO_3$, 0.6%

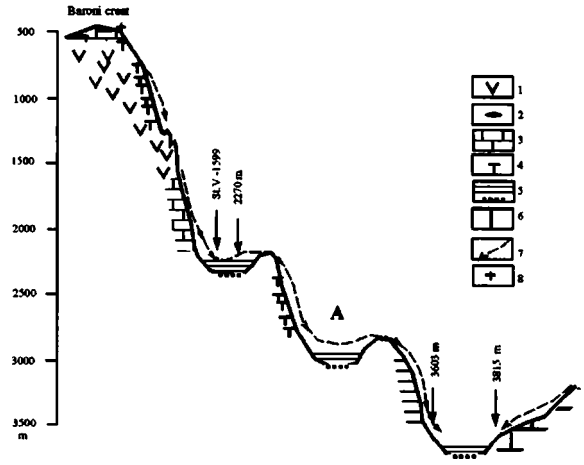


Figure 17.6: So-called 'hanging' sedimentary basins in the Tyrrhenian Sea east of the northern part of the Baroni crest (after Emelyanov, 1998). 1 - basalts; 2 - basaltic breccias; 3 - hard limestone (K_2?, nannofossils *Parhabdolithus* sp., *Lithraphidites* sp., *Micula* sp. and others); 4 - Foraminiferal oozes with remnants of dead corals (at 400-500 m depths); 5 - 'graded beddings' (microlaminated turbidites in the 'hanging' sedimentary basins (terrigenous matter, forams, and coccolothophorids), the thickness of layers is 0.2-2 mm (in one turbidite there are 10-15 microlayers); 6 - terrigenous low calcareous mud; 7 - the flows of the surface liquid mud (microturbidites); 8 - calcareous crusts (hard ground). A - 'hanging' sedimentary basin. The surface of all the sedimentary basins is ideally horizontal (numbers indicate the depths).

SiO_{2am}, 0.40% C_{org}, 1.90% Fe, 0.04% Mn, and 0.14% Ti. In some places on the Baroni Ridge there are outcrops of serpentinites, basaltic breccias, Late Cretaceous limestones, and hard Quaternary carbonate crusts ('hard ground'). They consist of biogenic detritus with calcite cement. 'Hard ground' was drilled by E. M. Emelyanov during a dive in the submersible 'Argus'.

In some places the surface oozes are Late Pleistocene in age - they belong to the *Gephyrocapsa oceanica* Zone.

Biogenic detrital (shelly) sands with coral remains are widespread on Verchelli Seamount. The sediments are actively being reworked by benthic organisms and by waves and currents at a depth of 200-250 m - the Late Glacial shore line. A lot of coral remains and rounded gravel and boulders occur at this depth. There is a steep cliff. On the flat bottom foraminiferal oozes are widespread.

Among the clastic minerals, quartz, feldspars, biotite, calcite, clinopyroxenes, and ilmenite-magnetite prevail. Olivine is also present.

In some ponds of the East Mediterranean Ridge there are stagnant conditions (Jongsma et al., 1982). These anoxic basins (Bannock, Tyro, Poseidon) are filled with brines, whose salinity is approximately ten times that of sea water. In the Bannock Basin the surface of the brines lies at the depth of about 3273 m, and the bottom at 3500 m. The bottom is covered by gray terrigenous-calcareous (nanno-foraminiferal) pelitic oozes. They contain 53-60% of $CaCO_3$, less than 1% SiO_{2am}, 0.3-0.8% C_{org},

and an average 0.3% Sr (Emelyanov, 1992). All other elements are present according to their standard abundance ratios. There are many crystals of gypsum, pyrite, magnesian calcite, and dolomite in the sediments, and strontianite is present. The thickness of the Holocene oozes is about 40 cm. The processes of sedimentation in the anoxic basins were described earlier by Cita et al. (1989), Erba (1989), and Emelyanov (1992).

Volcanogenic sediments. These include pyroclastic and volcanoclastic sediments. Volcanoclastic sediments of the Santorini Lagoon are present as sands, muddy sands, silty sands and mud (Butuzova, 1969). They consist of fragments of andesite-dacites, as well as volcanic glass, feldspars, hypersthene, and magnetite. The sediments are enriched in Fe and Mn and to a lesser degree in P, V and Cu. Cr, Ni, and Co concentrations are lower in the volcanoclastic sediments of the Santorini Lagoon than in the carbonate sediments of the marine areas beyond the caldera. These data show that volcanoclastic matter and hydrothermal action promote an increase in the concentrations of Fe, Mn and to a lesser degree P, V, and Cu in the sediments. They are not enriched in Cr, Ni, and Co.

Pyroclastic sediments are found down to 1797 m depths (Station ASV-316) in the area of the submarine cone of Stromboli Volcano (Emelyanov and Shimkus, 1986). These are yellow-gray sandy muds containing great quantities of black opaque particles of volcanic ash (43.3%), colorless glass (15.2%), and acid plagioclase (28.9%) in the light coarse-silt (0.1-0.05 mm) subfraction. The heavy subfraction also contains fragments of those and different opaque aggregates (38.9%) and clinopyroxenes (43.0%). They contain slightly higher amounts of K, Na, Mn, and Zn.

Pyroclastic and volcanoclastic sediments in which a prevalent component is black ash and volcanic glass have been retrieved from the Gulf of Naples where they occur at depths of 0-800 m (Müller, 1964). They were found at greater depths in the Tyrrhenian Sea (Emelyanov, 1972, 1973, 1975). These sediments are formed by the destruction of volcanogenic rocks of the adjacent coastal areas, as well as by the activity of the Vesuvius, Stromboli, and Etna volcanoes.

On the eastern slope of the Tyrrhenian Sea mixed calcareous-pyroclastic-terrigenous muds are widespread. They contain 10-30% $CaCO_3$ and 10-50% of pyroclastic (volcanoclastic) material. The clastic components of these muds belong to three mineralogical provinces (Fig. 17.5): the eastern part is characterized by a considerable admixture of ash, colorless glass, and clinopyroxenes; the northwestern part is characterized by minerals derived from metamorphic rocks developed on Corsica (alkaline and fibrous amphiboles, basaltic hornblende, disthene, micas, common hornblende, and epidote). There are a lot of minerals of the epidote group and zircon, but pyroclastic matter is almost entirely absent. Montmorillonite (10-30%) and illite (50-70%) prevail over the other clay minerals. Kaolinite is found only in the marginal parts of the basin. The absolute age of the clastic minerals ranges from 152 to 190 Ma (Emelyanov et al., 1973).

There are a lot of outcrops with lava, basalts, and volcanic breccias on the tops and slopes of the seamounts of the Tyrrhenian Sea. The soft sediments around these outcrops consist of mixed material: volcanoclastic particles, terrigenous material, and foraminifera. On the top and slopes of Marsili Seamount (480-1000 m) (**Figure 17.7**) there is unsorted muddy-sand and sandy-mud (Table 17.6) with many fragments of the lavas and basalts (Shimkus, Emelyanov and Yastrebov, 1998). The sediments are dirty grayish-brown in color. The mud is soft, sticky and viscous: it lies on the steep (10-30°) slopes of the seamount. Hydrothermal ferruginous deposits are found on the top of Marsili Seamount (Emelyanov, 1989).

The pyroclastic sediments of the Tyrrhenian Sea are somewhat enriched in K, Na, P, Mn, Fe, Cu, and SiO_{2am} (Table 17.6).

Sediments in which pyroclastic matter amounts to more than 10% of the total sediment are found nowhere in the Mediterranean Sea, including the Tyrrhenian Sea. Thus the role of volcanism in the contemporary sedimentation is significantly less than it was some thousands of years ago in earlier stages of the development of this basin. During the Late Pleistocene volcanic ash formed beds 10-22 cm in thickness, not only near the volcanoes, but in some areas of the Tyrrhenian Sea abyssal plain, in the Ionian Sea, and the northern part of the Levantine Sea (Mellis, 1948; Norin, 1958; Duplaix, 1958; Ryan and Heezen, 1965; Ninkovich and Heezen, 1965; Emelyanov, 1968, 1975; Shimkus, 1981; Emelyanov and Shimkus, 1986).

The same outcrops of hard volcanogenic rocks and soft Holocene and Late Quaternary mixed sediments are widespread on Vavilov, Magnaghi, and other seamounts. On all these mountains there are many tuff outcrops.

Magnaghi Seamount and its slopes (at depths of 1500 to 3420 m) are covered by hemipelagic nanno-foraminifer oozes. Thin layers of pteropod ooze were often found at Station AMK-2028 (depth 3380 m). Pteropod-foraminifer-coccolith oozes with intercalations of pteropod ooze (horizon - 20-25 cm) were found at Station AMK-2029 at a depth of 1780 m. The surface of the ooze is uneven, with furrows, and there are many shells of pteropods carried in by near-bottom currents.

Numerous pieces of effusive rocks (basalts), limestones and carbonate crusts covered by manganese film were detected during a dive (H2-6/17) with the 'Mir-2' submersible at Station AMK-2026 in depths from 2817 to 1888 m. The inner part of the crusts is softer and more friable than the external part; it contains calcareous nannofossils and foraminifera (probably Late-Quaternary). The summit of Magnaghi Seamount is a complicated morphological structure, with rock outcrops and tectonic fractures (transverse and dip-slip). In places the types of crater structures were studied with the help of a side-scan sonar (Shimkus et al., 1998).

The surface of Vavilov Seamount is uneven and its crestal ponds are covered by Upper-Quaternary sediments. A small ledge represents an outcrop of effusive rocks (usually olivine basalt). Carbonate crusts and the remains of coral are frequently seen.

The friable shelly-foraminifer and foraminifer oozes lie in ponds. On the summit parts of the seamount at depths of 1172, 1330, and 746 m, the crusts and hard limestones are covered by iron manganese-oxide film. The highest place on Vavilov

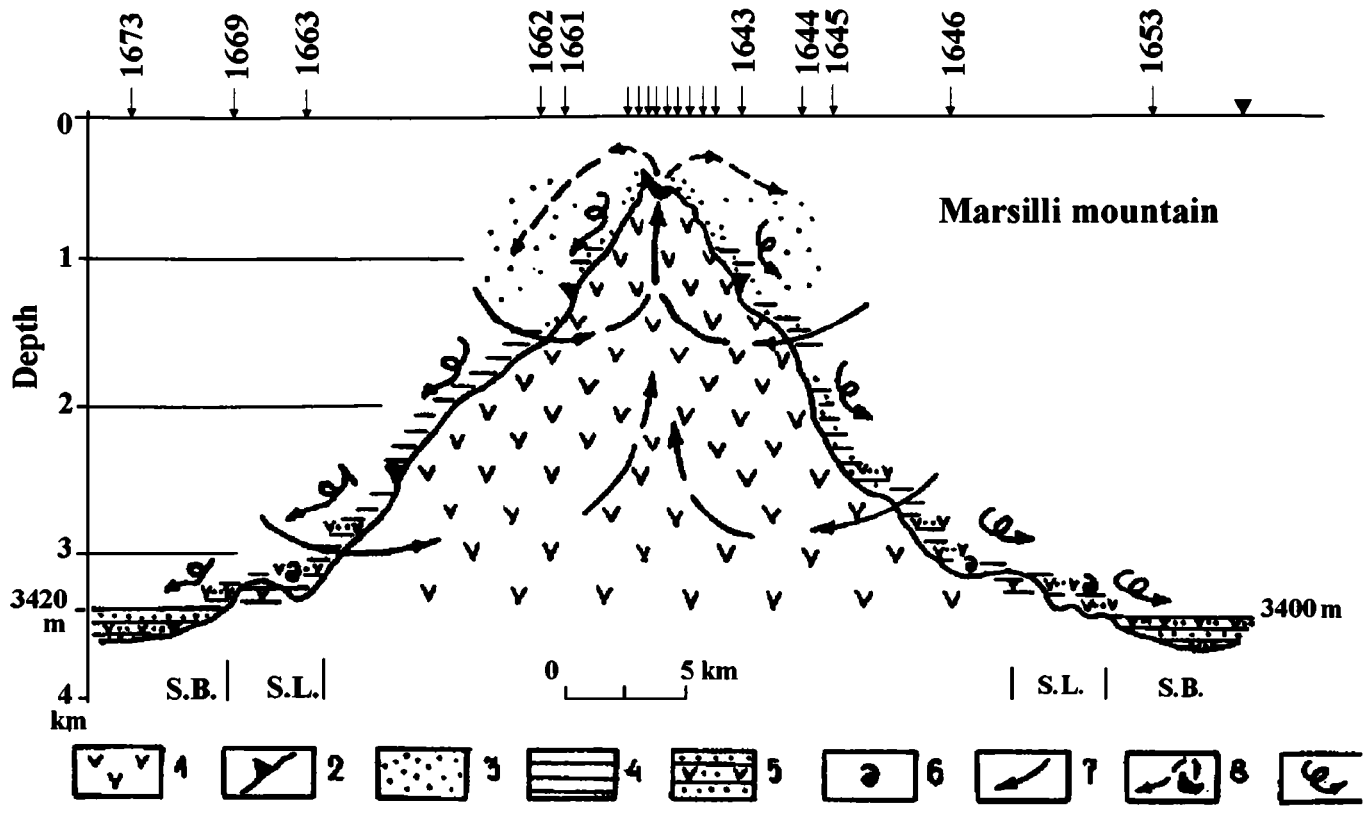


Figure 17.7: Sedimentation on Marsili Seamount. Adter Emelyanov, 1998. 1 - basalts and lavas; 2 - blocks of lava (outcrops); 3 - redistribution of hydrothermal iron and anganese hydroxides in the Holocene; 4 - mixed volcanoclastic-terrigenous low calcareous and calcareous (foraminiferal) mud; 5 - volcanoclastic-terrigenous and oraminiferal turbidites; 6 - foraminiferal ooze; 7 - circulation of seawater and hydrothermal waters; 8 - hydrothermal iron deposits (the cap is about 1 km²) and main irections of distribution of hydrothermal material in the Late Pleistocene; 9 - slumps and turbidites; The numbers and arrows on the top of the figure are geological stations (grabs, gravity corers, dredges, and dives with the submersibles 'Argus' and 'Mir'). S.B. is the 'hanging' sedimentary basins with ideally horizontal surfaces. Sl. - hills of slump origin.

Seamount (Goncharov's Peak) is crowned by branching corals, and also covered by a black manganese-oxide film. The presence of this film tells us that these formations are not recent. In the Vy-673 core at a depth of 1740 m, the Holocene sediments are nearly 20 cm thick. The rest of the core was formed during the last glaciation. Bright brown volcanic glass, long-prismatic clinopyroxenes (aegirine-augite), dark-brown biotite, plagioclase, apatite, and quartz were detected in the bottom sediments.

Lavas were detected on the slopes of the summit area of Vavilov Seamount. They form layered volcanoclastic deposits (tuffs, tuffs and lavas). Thanks to the 'coagulation' these formations were able to remain on the steep slopes, maintaining their primary bedded structure. There are thin turbidites at the foot of Vavilov Seamount.

Around the undersea seamounts there are depressions or ponds filled by volcanoclastic, mixed biogenic (calcareous-volcanoclastic-terrigenous) turbidites and 'normal' deep-sea muds. In a core 5-6 m long there are more than 100-200 turbidite layers (with graded bedding). They are especially well-expressed around Marsili Seamount. The number of turbidite cycles in the core indicates how many strong or weak earthquakes occurred. These sediment bodies are up to a hundred meters in thickness. Ideally they have flat horizontal surfaces. This surface occurs at different depths. Thus the ponds (or depressions) on the slopes are forming so-called 'hanging' sedimentary basins (Fig. 17.6; Figure 17.7).

Chemogenic sediments. Chemogenic and mixed chemogenic-biogenic sediments occur in a very limited number of areas. Oolitic-shelly high-calcareous sediments are found in the Gulf of Gabes, near Jerba Island, in the Gulf of Sirte (Sidra, Surt), and near the Egyptian coast (the Arabs Gulf). They also possibly cover all the coastal parts of the African shelf from Alexandria to Tunis (Lucas, 1955). The sand consists of about 80% of sand-size oolitic grains. Some of the grains had nuclei (quartz or shelly detritus), others were without. The accretion onto the nucleus is thick and concentric. The sands consist of oolite grains with a small admixture of pseudo-oolites representing well-rounded fragments

of shelly detritus or calcareous grains transported from the African deserts. Some of the pseudo-oolites may have been transported into the sea following the erosion of ancient coastal sedimentary rocks (Wood, 1964). Heavy minerals (ores and hornblende) are often observed as nuclei of oolites in the Gulf of Sirte. Oolitic sands near Jerba Island are found at up to 13 m depth. Oolitic sands contain from 90.05% to 91.70% $CaCO_3$, however they are impoverished in Fe, Mn, Ti, P, and SiO_{2am}.

Typical oolitic sands pass seaward into shelly sediments at depths of 30-100 m, with only a small admixture of oolites. The oolite grains are transported to greater depths either by winds or by currents from the beach. Single grains of oolites are found at depths down to 190 m.

Manganese sands occur on the top of a volcanic seamount in the southeastern Tyrrhenian Sea at Station ASV-7.9.3. These sediments contain 9.11% Mn, and they are low in Fe, Ti, and P. The following Mn contents have been determined in the different fractions: 7.66% in the 1.0-2.0 mm fraction; 6.47% in the 2.0-3.0 mm fraction; and 5.79% in the >3.0 mm fraction. The manganese is present as a black crust of irregular form or as oval grains whose size ranges from fractions of a millimeter to 10 mm. In addition to manganese crusts and micronodules, there is also a large amount of detrital mollusk shells, corals, and volcanic ash covered with a film of manganese in the sandy-gravel sediments.

Ferruginous and manganese sediments. These sediments are terrigenous, diagenetic, or hydrothermal.

The biggest area of low ferruginous and low manganese terrigenous sediment is located in the eastern part of the Levantine Sea and is forming under the influence of the Nile drift and the supply of volcanoclastic material from the coasts of Cyprus and Syria (Emelyanov, 1994).

Hydrothermal ferruginous and manganese deposits are discovered in some volcanic provinces:

1) Santorini lagoon (Behrend, 1936; Butuzova, 1969);

2) The shelf of Volcano Island (Valette, 1969; Honorez et al., 1973; Martini et al., 1980);

3) On the seamounts of Enarete, Eolo and Lametino (Rossi et al., 1980), Palinuro (Minitti and Bonavia, 1984), and Strombolichio (Bonatti et al., 1972);

4) On the eastern slope of the Tyrrhenian Sea at a depth of 900 m (Castelarin and Sartori, 1978);

5) On Eratosthenes Seamount at a depth of 1800 m (Varnavas et al., 1988);

6) In the Strabo Trench (Nesteroff, 1980);

7) And in some other places (Emelyanov and Shimkus, 1986; Shimkus et al., 1998).

In most cases they are ferruginous, and only manganese deposits on Lametino (Table 17.7).

A large field of ferruginous deposits (about 1 km^2) lies on the top of Marsili Seamount (488-600 m) (Emelyanov, 1988, 1989). They are covering (enveloping) blocks of lava and basalts, and the bottom of the small ponds. The maximum iron content is 54.3%. The Mn content is not high, only 0.5-1%. Only in the black band of the ore deposits does its content reach 9.19%. The main part of the ferruginous substance is amorphous (iron hydroxides) There is vernadite and barnesite with an admixture of proto-ferrihydrite, ferrihydrite, goethite, and crystobalite (Gorshkov, Emelyanov and Sivtsov, 1992). There are also some Fe-Mn microconcretions.

The presence of sulfate and sulfide sulfur (SO_4^{-2}- 2.34%, S - 0.77%) shows that the deposits contain an admixture of erosite or gypsum.

At Station AMK-2021 (1570 m) Fe-vernadite, Mn-ferroxide, goethite, Fe-x-mineral were found in the Fe-Mn crust on the basaltic block. Asbolane-buserite was found in the basalt block.

Outside of the hydrothermal field lie mixed biogenic-volcanoclastic-terrigenous sediments with slightly increased content of Mn (Table 17.6). Only in the sediments of Station Vy-1673 (3420 m) is the content of Fe 10.0%.

Diagenetic manganese sediments were found in some cores, where they form thin (1-5 cm) brown layers (Emelyanov and Shimkus, 1986). Surface sediments are enriched in Fe and Mn in some places in the eastern part of the Levantine Sea.

LITHOLOGICAL-GEOCHEMICAL ZONES OF SEDIMENTATION AND FACIES OF THE SEDIMENTS

Sedimentary material passes through a number of zones where its composition or quantity suffers marked changes during the course of mobilization, transportation, and existence within the basin itself. These so-called barrier-zones determine both the areal distribution of the bottom sediments and their lithological-geochemical features (Emelyanov, 1979, 1982, 1988).

Different lithological, faunal and geochemical characteristics were taken as the basis for defining zonation within the Mediterranean Sea (Emelyanov and Shimkus, 1986).

THE REGULATION OF RIVER DRAINAGE

During the past 40 years construction of hydroelectric power stations, irrigation systems, and dams has brought about a sharp decrease in the run-off of the largest rivers draining into the Black and Mediterranean Seas. These include the Danube, Dnieper, Don, Nile, Po, Rhone, and Ebro. For instance, nowadays the Ebro run-off is only 5% of its volume 50 to 60 years ago (Palanques et al., 1990). This has resulted in an extreme slowing down and even reversal of the progradational accretion of land on many fore-deltas. Degradation is observed in some cases, as for example the Nile fore-delta where the coast is predicted to recede many kilometers to the south by the year 2015 (Stanley, 1992). Active erosion is also happening in the Po fore-delta (Drake et al., 1992).

Limited run-off promotes an increase in erosional and abrasional processes on the shelves and decreases the rate of terrigenous sedimentation in the abyssal regions of the adjacent seas. There will probably be a concomitant decrease in biological productivity because of the decreasing volume of nutrients supplied by the drainage system. In comparison with sediments which were accumulated tens of years ago the changes in rates of terrigenous

Table 17.7: Chemical composition of iron and manganous deposits of the Mediterranean Sea and Atlantic Ocean

	Mediterranean Sea												Atlantic Ocean		
	M		St.	E.E.	San		St.	E.sl.	P		E	S	TAG	BM	NS
	1	2			1	2			M	S					
Fe	32.40	29.50	14.30	4.0	31.38	32.60	0.26	31.82	1.29	32.0	4.97	6.51	0.13	9.99	12.92
Mn	2.52	0.42	22.40	<8.3	0.05	0.03	48.02	3.26	-	-	9.10	2.08	41.00	2.31	17.36
Al	-	-	-	-	0.30	1.10	0.41	-	-	-	7.43	8.47	0.07	-	-
Ca	-	-	0.50	-	0.91	1.09	2.33	-	-	-	22.24	4.62	-	-	-
Mg	-	-	0.74	-	0.63	0.95	1.52	-	-	-	3.25	2.65	-	-	-
K	0.30	0.89	0.78	-	0.58	0.69	0.38	-	-	-	1.34	1.12	-	1.50	-
Na	3.53	2.20	2.20	-	4.30	-	2.61	-	-	-	3.13	2.82	-	2.95	-
Ti	0.09	0.18	0.006	-	-	0.04	0.02	-	-	-	0.59	0.60	-	0.25	0.50
P	0.62	0.70	0.30	-	0.06	-	-	-	-	-	-	-	-	0.72	0.16
$CaCO_3$	3.55	15.51	-	-	2.64	-	-	-	-	-	47.64	-	-	5.91	0.00
C_{org}	0.18	1.07	-	-	1.22	-	-	-	-	-	0.001	-	-	0.47	0.00
SiO_{2am}	-	-	-	-	-	-	-	-	-	-	-	-	1.26	-	-
Fe/Mn	12.50	70.00	0.60	-	628	1087	0.01	-	-	-	0.55	3.13	315	4.30	0.70
Cu	42	30	42-	400-900	27	34	8200	40	2700	22400	167	37	104	308	440
Zn	54	56	-	<1000	139	63	83	-	1400	-	157	115	-	320	525
Cr	10	10	5	-	-	5	-	-	-	-	-	-	-	-	31
Ni	115	130	15	<3000	-	5	249	230	-	-	135	82	440	314	208
Co	66	80	30	-	-	1	223	250	-	-	52	43	6	124	338
V	78	84	55	-	-	66	84	-	-	-	180	-	-	538	230
Mo	7	9	-	-	-	29	557	-	-	-	89	17	-	730	100
Ba	200	200	1070	-	-	103	3200	-	-	6	7862	226	400	-	660
Li	147	139	-	-	-	3	-	-	-	-	178	-	-	-	-
Rb	93	92	-	-	-	-	22	-	-	-	54	-	-	-	-
Sr	-	-	-	-	-	400	600	-	-	-	1384	168	-	-	-
Cd	-	-	-	-	-	-	-	-	-	-	2.4	-	-	-	-
Age	Plt	Plt	Plt(?)	-	Hl	Hl	Plt(?)	Plt	-	-	Hl-Plt_3	Plt(?)	Plt(?)	Plt	Mio

M – Marsili; St – Strombolichio (Bonatti et al., 1972); E.E. – Enarete and Eolo (Rossi et al., 1980); San – Santorini Lagoon (1- Butuzova, 1969; 2 – Smith and Cronan, 1975); ST – Southern Tyrrhenian (Lametino) (Rossi et al., 1980); E.sl. – Eastern slope of the Tyrrhenian Sea (Castelarin and. Sartoni, 1978); P – Palinuro (M – ore deposits, Sb – 1000, Bi – 500, As – 860 ppm; S – sulfides from the deposits, Sb – 9100, As – 2400, Ag – 220, Hg – 400 ppm (Minniti and Bonavia, 1984); E – Eratosthenes Seamount (Varnavas et al., 1988); S – Strabo Trench (Nesteroff, 1981); TAG - TAG area (Toth, 1980); BM – Brazilian Basin Seamount (Emelyanov and Trimonis, 1983); NS – Norwegian Sea (Emelyanov et al., 1978).

and biogenic sedimentation will inevitably lead to accumulation of different bottom sediments. Now is the time for a thorough study of all these processes. The newly compiled maps of bottom sediments will undoubtedly be useful for providing a baseline for such studies.

In some parts the expansion of existing sedimentary areas and the formation of new biogenic sedimentary areas due to the decrease in the diluting terrigenous silicate input has already begun. This process is most probable for the area near the Danube (northwestern Black Sea), the area off the Nile Delta, and the northern Algero-Provence and Central Basins.

TECHNOGENIC POLLUTION

The Black Sea.

The latest investigations have discovered great areas of technogenic pollution in the Black Sea. Technogenic processes affect and influence all components of the environment (Shimkus and Komarov, 1993; Konsulova, 1992). Intensive accumulation of pollutants occurs in bottom sediments. They are mainly washed out from the coastal zone by waves and currents along with pelitic material, but they reside for a rather long time in semi-closed bays and especially in their narrower parts.

A huge volume of pollutants (oil products, pesticides, heavy metals, radionuclides etc.) are supplied by the big rivers which traverse and drain numerous industrial centers and areas with intensive agriculture. These persistent pollutants are spread over the whole basin in accordance with the processes of terrigenous sedimentation. They are dispersed over large areas by surface currents and they are concentrated close to slopes by subbottom currents. This modern debris cone is very stable and becomes a powerful source of secondary pollution. One should emphasize the considerable polluting role played by small rivers (especially in their shallow parts) which drain mountainous catchments with resorts, agricultural complexes, and ports developed in the Black Sea near the Caucasus. Monitoring of the Black Sea off the Caucasus and in Burgas Bay (Bulgaria) as well as other areas is crucial (Shimkus and Komarov, 1993).

The Mediterranean Sea.

The scale of pollution within the whole Mediterranean basin has not yet been determined. We can just presume that pollution is less than in the Black Sea, mainly because of the far greater extent of the Mediterranean Sea and of the more intensive exchange with the Atlantic Ocean. In addition extensive areas of the drainage system in Africa are both sparsely populated and filtered by the meandering river networks. The vast areas of the Central and Eastern Mediterranean Basins off Africa, characterized by very slow rates of terrigenous accumulation, are not greatly threatened by pollution.

Nevertheless, the eastern part of this zone is under the influence of the Nile drifts, which despite the vast volumes of accumulation in the submerged parts of the Nile fore-delta (Shimkus, 1981; Emelyanov and Shimkus, 1986), were found to have considerable technogenic pollution. The main part of the finely dispersed material is supplied from the fore-delta and mainly distributed to the southeast where it passes along the Levant coast. It is deposited on the continental slope as a debris cone and in the adjacent abyssal deeps.

Waters of the Ebro (and Po) Rivers, polluted by technogenic wastes, form coarse sedimentary bodies in the fore-delta with heightened concentrations of heavy metals, radionuclides, and other dangerous pollutants. In the Alboran Sea the debris cone from the Ebro River forms close to the Pyrenean and Catalonian continental slopes. It is associated with the intensive transport of terrigenous material by near-bottom currents along submerged valleys. The Rhone River supplies vast quantities of drift into the intensively subsiding central part of the Gulf of Lyon, which is marked by high rates of accumulation of terrigenous material (Shimkus, 1981). Extensive volumes of finely dispersed material are also supplied to the slope and its base by surface currents. The drift distribution of other big rivers is similar.

Thus, the process of technogenic pollution accompanies the recent sedimentation which has occurred over vast areas of the Mediterranean Sea. The principal way that pollutants are distributed among the bottom sediments, and the influence of both large and small sources of pollution, can be determined from the terrigenous-mineralogical provinces of sandy-aleuritic and clayey materials within the Mediterranean. However, the consequences of further reductions in runoff have to be considered.

The open sea also suffers from extensive ship traffic which contributes its share of oil pollution and jettisoned garbage. Manned dives from the R/V 'Vityaz' and 'Akademik Mstislav Keldysh' found bottom pollution by bottles and other trash.

Data obtained in the coastal areas (Piper et al., 1983; Baseline, 1983; Pellegrini et al., 1992; Yaramar et al., 1992; Odzak and Zvonaric, 1992; Minganti et al., 1992; Jureti et al., 1992; Hanna, 1992; Balci, 1992; Ergin and Yücesoy, 1992; Rifaat et al., 1992) show that the most polluted areas are intensively subsiding fore-deltas, and large and small bays.

Organic carbon content increases up to 11.01% due to drainage in Patraikos Bay near Patras, but it is only 5.84% near an industrial zone while the quantities of Fe and Mn in the sediments decrease to <3 and 0.10% respectively (Varnavas and Ferentinos, 1982; Varnavas, 1981, 1984, 1989). A high content of C_{org} (6.38%) was discovered in subcoastal sediments in Polygon Vr-IV near the town of Piles on Navarino Bay (Varnavas et al., 1984) and 4.20% Fe and 0.19% of Mn.

High concentrations of nitrates and some other kinds of nutrients are also found in many subcoastal parts of the Mediterranean Sea, *e.g.* in eastern part of Adriatic Sea (Vukadin and Stojanovski, 1992).

Sediments of some subcoastal parts, especially in the gulfs, are very polluted by heavy and other metals. Thus, for example, the dry sediments in the Bay of Venice reach concentrations of: Zn - up to 5930 ppm, Cu - up to 463 ppm, Pb - up to 278 ppm, Cd - up to 25.4 ppm (Pavoni et al., 1987); and in dry sediments in Izmir (Turkey) they reach: Zn - up to 819 ppm, Cu - up to 213 ppm, Pb - up to 305

ppm, Cd - up to 6.6 ppm (Gey and Mordogan, 1988).

The level of technogenic pollution is higher in lagoon deposits than those in bays, with the highest pollution in Venice lagoon. Thus, pollutants are stopped on their way to the sea by lagoons, lakes and by other sedimentation traps

TECHNOGENIC POLLUTION BY RADIOACTIVE MATERIALS

Many technogenic pollutants from drainage systems migrate together. To some extend they are separated in sedimentary basins by the processes of geochemical and granulometric differentiation of the sedimentary material. Only radioactive materials remain aloof. They not only occur as solid and liquid industrial wastes, as radioactive materials and fertilizer byproducts (Georgescu et al., 1992a, b; Gasco Leonarte and Anton Mateos, 1992 etc.), but also as byproducts of nuclear explosions, atomic power stations, etc. Data obtained (Kendi, 1992; Tassi Pelati et al., 1992; Shimkus, 1993; Topcuoglu and Bulut, 1992; Georgescu et al., 1992a, b) show extensive distribution of radionuclides, some connected with the Chernobyl catastrophe.

PRACTICAL SIGNIFICANCE OF THE MAP

The map syntheses our knowledge about the distribution and composition of the sediments. It provides graphical information on the location of the various types of sediment, sedimentary rocks, and mineral resources. It may be used for:

1) Further scientific studies into the present sedimentary structure and history of the Mediterranean Sea,
2) Planning of scientific expeditions and
3) Educational purposes. In addition the map may be used for
4) Navigation,
5) Fishing grounds,
6) Ocean dumping,
7) Pollution studies - defining centers of pollution and protecting nature,
8) Technical tasks such as laying out cable routes or pipelines (*e.g.* the Black Sea segment of a pipeline from Gelendjik to Turkey and from Turkey to the Central Asian oil fields), or
9) To serve as an example for compiling similar maps of other marine basins or oceans, as part of the IOC-IHO program of making geological overlays to other series of International Bathymetric Charts.

THE MAP LEGEND (FIGURE 17.8)

How to read the maps.
Explanatory Notes by E. M. Emelyanov.

The IBCM-SED map (Emelyanov, Shimkus and Kuprin, 1996) contains a great deal of sedimentological information in the form of three overlays consisting of colors, symbols, and hatching. The legend for this map was the topic of several years of experimentation by the authors, with annual discussions with the members of the Editorial Board of the IBCM. The 1:5M reduction that accompanies this volume is an exact mosaicked reproduction of the ten sheets of the original 1:1M scale map. The smaller size of this reduction makes the legend very difficult to read, much less to understand. For this reason the legend on Sheet 6 of the IBCM-SED series is reproduced here in Fig. 17.8. The explanation below endeavors to explain this legend and thus facilitate the use of the map.

Colors.

Two colors, gray and blue, form the background of the map. Areas with no data are shown in white. The gray denotes areas with primarily terrigenous sedimentation, *i.e.* more than 50% terrigenous material. There are three shades of gray; dark gray is >90% terrigenous, medium-gray is 70-90% terrigenous, and light gray is 50-70%. Most of the map is shades of gray, reflecting the dominant terrigenous sedimentation of this internal sea. The blue color denotes areas of primarily carbonate sediments. Again there are three shades; dark blue is >90% $CaCO_3$, medium blue is 70-90% $CaCO_3$, and light blue is 50-70% $CaCO_3$. The blue shades are found mostly in the southeastern parts of the map.

Previous works on the subject made us think that biogenic carbonate sediments predominate in those parts of the ocean basins where they are not diluted by terrigenous material. In arid areas where river runoff is absent, there is a minor terrigenous contribution to the bottom sediments, which mostly explains the blue areas between Tunisia and the western Nile Cone. Gray areas along this margin mostly reflect a dominant eolian component from the deserts to the south.

East of about 30°E, notwithstanding the arid climate, the river-borne load of terrigenous sediments from the Nile predominates.

In the north the gray areas reflect the major terrigenous contribution from the Rona, Po, and Ebro Rivers. Dark gray strips off the mouths of these rivers are the major pathways whereby suspended material is transported from these rivers to the ocean, where they are often disbursed by the cyclonic multiscale surface current gyres. This is evident off the Nile where the drift is transported from the continental shelf down the continental slope, following the submarine topography.

Upon reaching about 34°N, one portion of suspended matter (seemingly a deep-sea turbidity layer) turns to the west looping around Eratosthenes Seamount from the north. The second portion of terrigenous suspended matter continues along the coasts of Israel, Lebanon, and Syria to Iskenderun Bay, and then heads west to 33°E. North of Cyprus the characteristic Nile deposits are predominantly allochthonous, consisting of monoclinic pyroxene, montmorillonite, organic carbon, Fe, Ti, and other chemical elements (Emelyanov, 1994).

The distribution of river-borne sediments in the Adriatic along the east coast of Italy is marked as a dark gray band.

Several dark gray strips stretch along the continental slope in deep water. An example is the northward pointing promontory

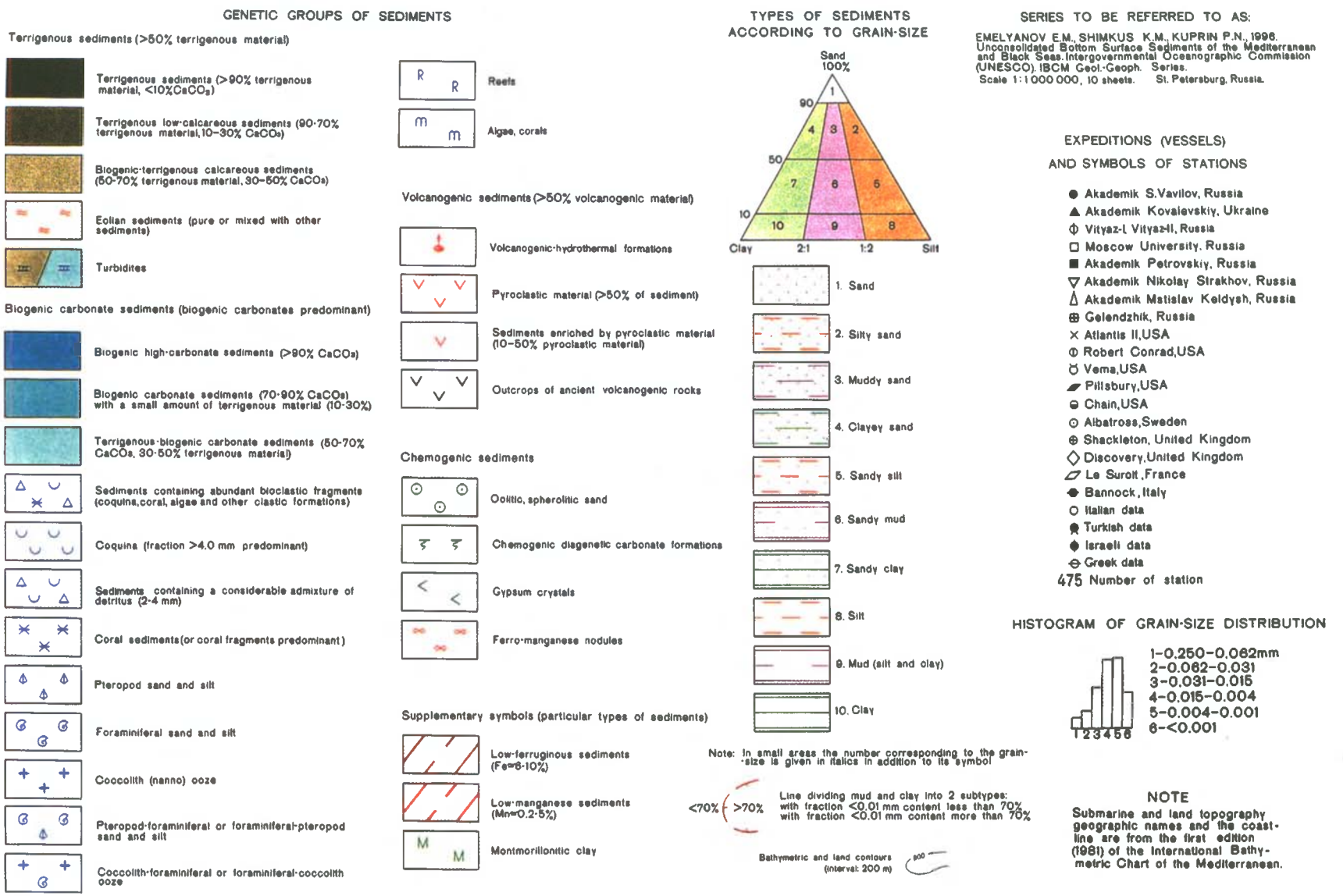


Figure 17.8: Legend of the IBCM-SED, modified after Emelyanov, Shimkus, and Kuprin, 1996. Note that on the map the legend appears in both English and French.

extending 400 km into the Algerian-Provencal Basin from the foot of the slope off Algeria. This strip comprises terrigenous muds formed as a result of denudation of the Atlas Mountains in North Africa.

A second dark gray strip extends 300 km southward from the Straits of Messina. The sedimentary pattern closely follows the deep-sea and bottom current flows, which we recognized earlier from the distribution of mica in bottom sediments (mica is evacuated from Sicily to Ras es Sider Bay in Libya - Emelyanov, 1972). This strip stretches from Otranto Strait to the deepest part of the Central Basin, marking the route of this terrigenous material from the strait.

Two important inferences can be drawn from the gray terrigenous sedimentary patterns:

1) The dark-gray strips mark deep-sea and bottom currents, indicating their existence, direction, and strength.

2) These strips reveal source areas, tracks, and transport distances of possible pollutants. Of primary interest should be nuclear wastes from atomic power stations, if their grain-size is commensurate with the clay fraction.

In the deep areas off the mouths of the Nile and Rona Rivers are twinned blue areas with carbonaceous sediments. They appear to be related to two cyclonic deep-sea gyres. In the Provencal Basin they indicate that large quantities of suspended river run-off load do not penetrate far beyond the edge of the continental slope.

Small blue areas in the deeps, *e.g.* west of Cyprus, in the vicinity of Hellenic Trenchs, and the Tyrrhenian Sea, are related to isolated highs like submarine ridges or seamounts. This would suggest that near-bottom currents are the primary movers of suspended terrigenous material in the deep-sea and the 'biogenic calcareous caps' on the highs are not significantly diluted by terrigenous material.

Blue areas around Sardinia, Corsica, and the Balearic Islands reflect the fact that:

1) There are no large rivers on these islands, and the total amount of sediment delivered by small rivers is very small;

2) The climate in this region is very warm and hospitable to benthos and plankton with calcareous skeletons or shells.

The blue color of the Sea of Crete reflects that the climate in the area is rather warm, there are no rivers on the nearby islands, and that suspended flows are weak or absent.

The two blue areas in the deep parts of the Black Sea indicate that:

1) Terrigenous material from mountainous drainage basins only accumulates on the shelves, slope, and the base of the slope;

2) There are two powerful cyclonic gyres and the biogenic sediments form at their centers. These blue areas are oblong owing to the irregular influx of terrigenous material to the basin center.

In the northwestern Black Sea the shallows are primarily blue and calcareous despite of the presence of the large Danube, Dnieper, and Dniester Rivers. The narrow dark-gray strip stretching southward along the coast from the Danube indicates the path of most of the river load, including pollutants. The absence of gray strips near the Dnieper and Dniester mouths shows that the total sediment load delivered to the Black Sea is insignificant. Both rivers enter brackish lagoons, which serve as effective sediment traps.

Comparison of the IBCM-SED with the IBCM-PQ (Pliocene-Quaternary) sediment isopach maps indicates that a dramatic rearrangement occurred in the river-born terrigenous sediment delivery systems. The Nile drift changed from a NNW direction to the present ENE, the Po River sediments moved SE, and the Danube River to the SSE as far as the central part of the sea. This happened for a variety of reasons, the most important being that:

1) Relatively low sea levels, especially during glacial periods, delivered the river load directly on the continental slope.

2) Straits shallowed by 100-200 m, and even closed.

Sea level lowering decreased exchange between ocean and sea and between basins, and altered the circulation pattern of surface and deep-sea currents. The Pliocene-Quaternary sediments were notably thicker. Owing to climatic factors the deltaic cones of the Po, Danube, and Rona Rivers were rather indistinct.

The melting of the glaciers in the Alps, Pyrenees, and northern Europe provided great volumes of sediments, even more than in the Holocene transgression. This formed thick Pliocene-Quaternary debris cones where the Dnieper, Dniester, and Danube Rivers enter the western Black Sea. The same happened off the Po River, and elsewhere. Now the input of river-borne sediments to the deep-sea is considerably less.

Although volcanogenic sediments are commonly denoted by red-shaded areas, this color is essentially non-existent on the map. Despite the large number of active volcanoes in the area, there are practically no accumulations of volcanogenic sediments on the seafloor. Volcanogenic material is sparsely dispersed over wide areas and can be found mainly in the Tyrrhenian Sea in the terrigenous sediments in trace amounts.

Symbols.

Symbols are printed on the background colors to indicate various admixtures to the terrigenous or calcareous sediments, or other peculiarities. Twenty-four such symbols appear on the legend. As shown on the legend (Fig. 17.8) which appears on Sheet 6 of the IBCM-SED series, they are:

1) A gray-brown (desert) symbol consisting of two wavy lines like a flapping = sign shows the presence of notable amounts of eolian material from the African deserts in the sediments.

Biogenic carbonaceous sediments (blue) contain relatively small amounts of this non-biogenic component. If the sediment contains up to 50-70% biogenic and chemogenic carbonates, then eolian and river-borne terrigenous inputs contribute the remainder, half of which is estimated to be eolian, with the amount decreasing with distance offshore from Africa. This estimate is borne out by the sediments' high wind-blown quartz content (Emelyanov and Shimkus, 1986) and the higher absolute age of debris minerals (> 200 Ma), which is only characteristic of those in African desert soils.

The great number of these yellow-brownish wavy symbols within a light-gray site just north of the Gulf of Sidra indicates that the eolian accumulation exceeds that of the carbonates.

2) Turbidites are indicated by a black equality symbol (=) with dots between the lines. They are generally terrigenous materials transported to the deep sea by turbidity currents. The same symbol in blue marks biogenic carbonaceous turbidites, again brought by turbidity currents.

3) The lower half of a circle denotes half a mollusk shell, and denotes coquina with the >4.0 mm fraction predominant.

4) An X with a dash through it denotes coral sediments, with coral fragments predominant, and possibly remains of corals, algae, and other bottom organisms like stars and sea-urchins.

5) A combination of the above two with triangles, which represent fragments of mollusk shells, indicates sediments containing abundant bioclastic fragments, such as coquina, coral, algae and other clastics.

A narrow dark-blue strip stretching along the eastern North African coast indicates highly carbonaceous sediments. It is interspersed with the three symbols described above.

6) Half circles and triangles are sediments containing a considerable admixture of 2-4 mm detritus. The proportion of one symbol or the other indicates the appropriate predominance.

7) A symbol consisting of two lobes resembling boat sails or a cone snail on its nose denotes pteropod sand or silt, marking an abundance of fragile and transparent mollusk shells in the sediments.

8) Spiral-shaped symbols resembling mollusk shells denote foraminiferal sand and silt. A blue area littered with such symbols indicates the occurrence of carbonaceous foraminiferal sediments,

9) A blue '+' symbol indicates a coccolith (nanno-) ooze, *i.e.* the sediments contain a considerable amount of calcareous remnants of the smallest algae-coccolith (nannoplankton).

10) A combination of the spiral and sail-shaped symbols against a blue background indicates a pteropod-foraminiferal or foraminiferal-pteropod sand or silt, depending upon which symbol predominates. Such sediments are abundant in areas with depths of not more than 2000-2500 m, or on isolated elevations.

11) A combination of the spiral and '+' symbols against a blue background indicates a coccolith-foraminiferal or foraminiferal-coccolith sand or silt, depending upon which symbol predominates. These sediments occur at depths of more than 2500-3000 m. They are at maximum depths and large distances from the shelf. Pure nanno-muds haven't been found, but this type of sediment is present locally in the Tyrrhenian Sea, but can't be identified because of the small-scale of this map.

12) Reefs are indicated by an 'R' symbol.

13) Algae and corals are indicated by an 'm' symbol.

14) A symbol showing a red arrow pointing upward from a horizontal ellipse marks volcanogenic-hydrothermal formations. Only four locations with present (Holocene) hydrothermal activity are known in the Mediterranean Sea, they are found near Ischia Island, by Stromboli Volcano, on the crest of Marsili Seamount in the Tyrrhenian Sea, and in the Santorini Island lagoon in the Aegean. Despite the high seismicity in the collision zone along the northern Mediterranean, its contribution to the formation of volcanogenic and hydrothermal ores is fairly insignificant.

15) Reddish-brown 'V' symbols indicate more than 50% of pyroclastic material. These areas are small and located in the Tyrrhenian and Aegean Seas. Volcanism has little influence beyond the Bay of Naples, the Aeolian Islands, the volcanic Marsili Seamount, and some other areas.

18) Round green circles with a central dot indicate oolitic and spherolitic sands. These symbols can be found against a deep blue background on the continental shelf of eastern North Africa. In these regions, characterized by an arid climate and seawater oversaturated with carbonates, limestone ooliths (consisting of a nucleus with a round calcareous covering) are formed by chemical processes. The terrigenous sediments also contain comparatively small amounts of calcareous biogenic remains of shells, skeletons, and debris. These components gradually decrease so that the (pale gray) calcareous terrigenous sediments grade into (darker-gray) purely terrigenous ones.

19) A horizontal green dash symbol with 'down-ward tail' indicates chemogenic diagenetic carbonate formations. It is preferentially located against a blue background in the eastern Mediterranean. These symbols show locations on the seafloor where magnesium-calcareous hemogene-diagenetic concretions are preferentially formed and are present.

These concretions on the sediment surface are cemented crusts of calcareous muds, but their 'roots' penetrate up to 10-15 cm into the sediment. The roots often consist of very sharp spines (needles) of aragonite and calcite. These green symbols appear in arid zone regions, where the sedimentation rate is fairly low so the concretions are not buried by terrigenous or biogenic particles. The temperature of the near-bottom water is anomalously high relative to the 'normal' ocean bottom temperature, and both the near-bottom and interstitial-waters are over-saturated with calcite.

20) A green '<' symbol indicates gypsum crystals. In areas where salt brines are found in small hollows on the seafloor, a great many large (up to 3-5cm) crystals of authigenic gypsum and microscopically small crystals of strontianite and ferrous sulfide can be found *e.g.* the stagnant Bannock Basin at 34°-20'N, 20°E. The same features are also seen at several other locations, mainly on the northern flank of the East Mediterranean Ridge, and at sites too small to plot at this scale near the Hellenic Trenches.

21) A red '∞' symbol indicates the presence of ferro-mangenese nodules (FMN), small and flat in shape, in the sediments. They are only found within small areas of the Black Sea, east of Crimea. These nodules are not found in the Mediterranean Sea, despite its diverse facies and areas enriched in Fe and Mn, which contribute to their formation. The reasons for this are apparently as follows:

a) Input of Fe and Mn to the sea is relatively small compared with other seas; their concentrations in seawater are low; and their participation in the biological cycle is minimal, owing to the low rates of biological productivity.

b) The lysocline and CCD are not present, with the result that these metals aren't derived from dissolution of calcareous shells and added to the sediments in the form of Mn and Fe hydroxides.

c) The bottom sediment rates of accumulation are relatively high, thus any slowly growing nodules on the surface would be quickly

buried and then dissolved while still in an embryonic state.

22) Brown slanted lines indicate low-ferruginous sediments with 6-10% Fe. This is mainly supplied as pyroclastic material below the Apennines slope, as it can be seen from increased contents of Fe, Zn and Rb in the sediments (Emelyanov, 1972, 1998).

The eastern part of the Levantine Sea is crowded with these diagonal brown lines indicating the weakly ferruginous sediments of the Nile province which is easily distinguishable by its increased Fe content (Emelyanov, 1966, 1994). Iron, titanium, and some trace elements are transported into the Levantine Sea from the Abyssinian Plateau, where basal weathering crusts are exposed on the drainage basin surface. Thus there is a 4500 km genetic connection between northern Equatorial Africa and the Levantine Sea.

23) Red slanted lines indicate low-manganese sediments with 0.2-5% Mn. This is supplied in the form of solutions in deep-sea muds of the Tyrrhenian Sea which increase the Mn content (as well as phosphorus) to a value about 2 times larger than that of sediments in the Algerian-Provence Basin. Unfortunately, this enrichment in these elements cannot be reflected on the map because of limitations in the scale and scope of the legend. More details are available in the earlier publications of Emelyanov (1998) and Emelyanov and Shimkus (1986).

Other areas lie in the Levantine Sea south of Cyprus and off Port Said on the Nile Delta. A notable proportion of manganese and iron is supposedly brought to the Levantine Sea by the Nile, inferring that there is a depositional system, which in terms of the marine chemistry, displays considerable differentiation of the elements iron and manganese. As the element of lesser mobility, iron mostly precipitates near the Nile's mouths, while both iron and manganese are precipitated a long distance away. Nevertheless, sediments enriched in manganese are found in the deep-sea part (200-1500 m depths) of the SE Nile Province as well, indicating partial precipitation of fine Fe and Mn-enriched Nile River sediments.

In this region, the major current transporting suspended matter away from the Nile River mouths changes from an easterly to northerly direction. The current speed evidently decreases, facilitating the precipitation of very fine clayey particles as slightly manganous clays on the seafloor.

Slanted brown and red dashed lines also indicate that a certain amount of ferruginous and manganous material is supplied to the Tyrrhenian Sea from volcanoes.

24) A green 'M' symbol indicates montmorillonite clay. Montmorillonite is the main (and practically the only) component of muddy Nile alluvium (Rateev et al., 1966). It is found from the Nile delta up to the passage between Cyprus and Syria (at 36°N), suggesting that the fine (clayey) Nile sediment load does reach this area.

If muds are not labeled with the 'M' symbol they are either dominated by kaolinite, montmorillonite and illite, or clean illite.

Hatching patterns.

Ten hatching patterns consisting of colored horizontal solid lines, dashed lines, and dots indicate the different granulometric types of bottom sediments, according to their place in the Folk's triangle, *i.e.* whether they are coarse or fine-grained. The grain-size composition of sediments influences their main physical characteristics and properties. It is of primary interest to engineers involved in any type of underwater construction activities.

The Folk's triangle (Fig. 17.2) consists of an equilateral triangle with ten compartments. Three colors, grayish-green, violet-mauve (lilac), and orange-brown define the grain-sizes grading from the sand to clay fraction, the sand to clay-silt fraction, and the sand to silt fraction respectively. The ten compartments, and their hatch patterns are as follows:

1) Sand; brown dots.
2) Silty-sand; brown dots with orange-brown dashes.
3) Muddy-sand; brown dots and violet-mauve dashes.
4) Clayey-sand; brown dots and grayish-green dashes.
5) Sandy-silt; brown dots and orange-brown dashes.
6) Sandy-mud; brown dots and violet-mauve solid and dashed lines.
7) Sandy-clay; brown dots and grayish-green solid line.
8) Silt; orange-brown dashes.
9) Mud (silt and clay); violet-mauve solid and dashed lines.
10) Clay; grayish-green solid lines.

We believe that the pattern of colored dots and horizontal lines makes it possible to determine at first glance what types of sediments - aleuritic, muddy, or clayey in terms of grain-size, are where.

Areas with only brown dots are pure sands, they are mostly found on the African and other shelves. The addition of solid and dashed lines indicate the fining of the granulometry. Dashed areas are sediments with several grain-size types. Dotted and lined areas are sediments having large content of sand material (50-90%), including muddy sand, sandy silt, and clayey silt (types 2, 3, 4). A combination of dashed and solid lines with brown dots indicates sediments containing large amounts of silt material (50-90%). These are sandy silt, muddy sand and clayey silt (types 5, 6, 7).

Finally, lined areas with no dots (types 8, 9 and 10) are sediments, in which sand is absent. These sediments contain small amounts of sand (<10%), if any. Such sediments are abundant in the Levantine Sea, the Hellenic Trenches, the Central Basin, the Algerian-Provencal Basin, and some other places. Horizontally lined areas free of dots are silt (8), mud (9), and clay (10). All these types are situated at the bottom of the triangle.

Large black numbers in italics indicate small areas of seafloor where sediments are dominated by a particular grain-size type whose pattern would be hardly distinguishable on the map. The numbers (from 2 to 9) indicate the appropriate compartment in Folk's triangle.

Histograms from Geological Sampling Stations.

Twenty-two different black symbols (Figure 17.8) are used to identify the locations of geological sampling stations occupied by research vessels of nine countries. Each station has an identifying number. At some stations histograms are plotted for the grain-size composition of the uppermost 0-5 cm of the bottom sediments. The histograms have six columns, representing from left to right the

0.250-0.062 mm, 0.062-0.031 mm, 0.031-0.015 mm, 0.015-0.004 mm, 0.004-0.001 mm, and <0.001 mm fractions. The total height of the columns on the histogram is 100%. To calculate contents of any grain-size fractions, one only needs to measure that column relative to the cumulative length.

Pelagic Mud Subdivision.

Pelagic muds consisting of varying proportions of <0.01 mm fraction are separated from each other by a dashed line which is easily distinguishable by its brown color. Hachures along the dashed line indicate that in the first area this fraction contributes >70% of the mud, while in the second one it is responsible for less than 70%. This brown dashed-line is used in the legend to facilitate the subdivision of pelagic sediment called 'mud', covering more than 50% of deep-sea area, into finer and coarser muds. Such a subdivision of muds makes our classification scheme close to that one increasingly popular in Eastern Europe and Russia (Bezrukov and Lisitzin, 1960). According to this classification, if the sediment (mud) contains more than 70% of the <0.01 mm fraction, it is called pelitic (clayey) mud; if it contains less than 70% (50-70%), it is an aleuro-pelitic mud. Such a subdivision of mud into finer and coarser types is a good way for marine sedimentologists to understand the mechanism of differentiation of sedimentary material, and to also give ideas about mud sources and routes of transportation.

There are a number of white seafloor locations on the map, especially in the outermost areas of the Aegean and Adriatic Seas, and also near the coast of France. In these regions there was either a lack of data, or the information was unavailable at the time of compilation.

Map Background - IBCM Base-Map.

The map in the background is the standard bathymetric base map for the International Bathymetric Chart of the Mediterranean (IBCM - Morelli and Val'chuk, 1988). Land and marine contours are drawn every 200 m, with additional 100 m, 50 m, and 20 m contours on wide shelves. Maximum depths are 5,000 m. This base map is from the original 1983 IBCM (Morelli and Val'chuk, 1988).

It can be seen that in many cases the bounds of the various sediment types are in reasonably good agreement with depth contours. Indeed, the types and varieties of sediments change as the depth increases (*i.e.* bathymetric zonation can be traced). For example, sands and silty sands are abundant mainly within the limits of the 0-200-m depth contours; sandy silts and silts – within the 200-1000 m depth contours; clays – at depths of 2000-4000 m, and so on. Thus analysis of the sediment map enables various aspects of the bottom topography to be deduced (and *vice versa).*

Availability of the IBCM-SED map sets.

The IBCM-SED map sets were printed by the Head Department of Navigation and Oceanography (Russian Federation Navy) in Saint Petersburg, Russia. The legends are printed in both English and French. The 1:1,000,000 scale map sets may be purchased from Geopubs, 4 Gliebe Crescent, Minehead, Somerset, TA24 5SN, England. Tel: +44-1643-709001. E-mail: accounts@geopubs.co.uk

ACKNOWLEDGEMENTS

The authors gratefully acknowledge the long drawn out effort and extreme patience of their colleagues J. K. Hall and V. A. Krashennikov in preparing this manuscript for publication. Because of its non-geophysical content, the paper was not included with the other explanatory brochures of the IBCM-G, IBCM-S, IBCM-PQ, and IBCM-M that were published in the Bollettino di Geofisica teorica ed applicata of the Istituto Nazionale di Oceanografia e di Geofisica Sperimentale - OGS Trieste (Italy). Instead, the editors agreed to include it with the other papers in Part III on the Levantine Basin, to prepare additional reprints that would accompany sales of the IBCM-SED map sets, and to reprint the photographic reduction to scale 1:5,000,000 as Plate IV.

The original manuscript, prepared upon completion of the IBCM-SED nearly a decade ago, contained a number of mistakes, mistranslations, missing references etc. Owing to the isolation of the authors, and the untimely death of Kasimeras M. Shimkus, the editors made valiant efforts to bring the manuscript up to its present form, with a final checking by E. M. Emelyanov.

The authors and editors hope that this paper will provide a sound basis for understanding the bottom sediments of the Mediterranean and Black Seas, as well as an appreciation for the tremendous amount of work that went into the data collection, compilation, and preparation of the maps. They apologize in advance for any errors of omission or commission that might cause offense to any of those who contributed.

And in conclusion, the Editorial Board of the IOC-IHO International Bathymetric Chart of the Mediterranean and Black Seas and its Geological-Geophysical Overlay Sheets has also expressed its heartfelt thanks to the authors and the editors for ensuring that this monumental work is finally published.

REFERENCES CITED

Aloisi, J. Cl., Monaco, A., Thommeret, J., and Thoromeret, Y., 1975. Evolution paleogéographique du plateau continental Langue-docien dans le carde du Golf du Lion: analyse comparée des données sismique, sédimentologiques et radiometrique concernant le Quaternaire recent. Rev. Géogr. Phys. et Geol. Dyn., 17(2), 1, p. 13-22.

Balci, A., 1992. Dissolved dispersed petroleum hydrocarbons in Eastern Aegean Sea. Rapp. Comm. Int. mer Médit., v. 33, p. 64.

Baseline, 1983. Metals in Polluted sediments from Thermaikos Gulf, Greece. Marine Pollution Bulletin, 14(6), p. 234-236.

Behrend, F., 1936. Eisen und Schwefel fordernde Gasquellen auf den Kameni Inseln. In: H. Reck (ed.), Santorin der Werdegang eines Inselvulkans und sein Ausbruch 1925-1928, Bd. 2 Kapitel 12, Berlin.

Bezrukov, P. L., and Lisitzin, A. P., 1960. Classification of sediments in recent basins. - Trudy IOAN, 32, p. 3-15.

Blanc, J. J., 1958. Recherches géologiques et sédimentologiques. Compagne de la Calypso (Sept.-Oct., 1955). Ann. Inst. Oceanograph., 34(3), Paris, p. 157-211.

Blanpied, C., Burollet, P. F., Clairefond, P., and Shimi, M., 1979. Sédiments actuels et Holocènes (Present and Holocene sediments). In: P. F. Burollet, P. Clairefond and E. Winnock (eds.), Géologie Méditerraneane. La Mer Pelagienne. Ann. Univ. Provence, 6(1), p. 61-82.

Bonatti, E., Honnorez, J., Joensuu, O., and Rydell, H., 1972. Submarine iron deposits from the Mediterranean Sea. In: D. J. Stanley (ed.), The Mediterranean Sea: a natural sedimentation laboratory, Dowden, Hutchinson and Ross, Inc., Stroudsburg PA, p. 701-710.

Brambati, A., Ciabatti, M., Fanzutti, G. P., Marabini, F., and Marocco, R., 1988. Carta Sedimentologica dell'Adriatico Centrale. Consiglio Nazionale delle Ricerche, Progetto Finalizzato 'Oceanografia e Fondi Marini'.

Burollet, P. F., Clairefond, P., and Winnock, E., (eds.), 1979. The Pelagian Sea; sedimentological and ecological study of the Tunisian continental shelf and the Gulf of Gabes. Géologie Méditerranéenne, Annales de l'Université de Provence, 6(1), 345 p.

Butuzova, G. Yu., 1969. Recent volcanogenic-sedimentary iron-ore process in the Santorini Volcano caldera (the Aegean Sea) and its influence on sediment geochemistry. Trudy Geol. Inst., 194. Moscow, Nauka, 109 p.

Castellarin, A., and Sartori, R., 1978. Quaternary iron-manganese deposits and associated pelagic sediments (radiolarian clay and chert, gypsiferous mud) from the Tyrrhenian Sea. Sedimentology, 25(6), p. 801-821.

Caulet, J. P., 1972. Les sédiments organogènes du précontinent algérien, Thèse d'Etat, Mém. Muséum Nat. Histoire Natur., Paris, XX, p. 1-289.

Cita, M. B., Camerlenghi, A., and Corselli, C., (eds), 1989. Anoxic basins of the Eastern Mediterranean, Universita degli studi di Milano, 104 p.

Demediuk, Yu. N., 1984. Structural-geomorphological zonation of Bosfor-Anatolian part of the Black Sea. In: E. E. Shnyukov (ed.), Studies of geological processes of recent sedimentation. Trudy, Intern. Symp., Kiev, Naukova Dumka, L. 2, p. 44-50.

Drake, D. E., Cacchione, D. A., Frascari, F., et al.. 1992. Erosion and transport of suspended sediment near the Po river delta, northern Adriatic Sea. Rapp. Comm. Int. mer Médit., v. 33, p. 128.

Duplaix, S., 1972. Les mineraux lourds de sables de plages et de canyons sous-marine de la Méditerranee Francaise. In: D. J. Stanley, (ed.), The Mediterranean Sea: a natural sedimentation laboratory Dowden, Hutchinson, Ross Inc., Stroudsbourg, Pensylvania, p. 293-304.

Emelyanov, E. M., 1961. New data on the Mediterranean Sea sediments. Dokl. AN SSR. 137. No. 6, p. 1437-1440.

Emelyanov, E. M., 1965. The grain-size composition of recent sediments and some features of their formation in the Mediterranean Sea. In: The main features of geological structure, hydrological regime and biology of the Mediterranean Sea. Moscow, Nauka, p. 42-67.

Emelyanov, E. M., 1966. Distribution of authigeneous silica in suspended matter and sediments of the Mediterranean Sea. In: Geochemistry of silica. Moscow, Nauka, p. 284-294.

Emelyanov, E. M., 1968. Mineralogy of sandy-aleuritic fractions of recent sediments of the Mediterranean Sea. Litologia i Poleznye iskopaemye, 2. p. 2-21.

Emelyanov, E. M., 1972. Principal types of recent bottom sediments in the Mediterranean Sea, their mineralogy and geochemistry. In: D. J. Stanley (ed.), The Mediterranean Sea: a natural sedimentation laboratory, Dowden, Hutchinson and Ross, Inc. Stroudsburg, PA, p. 355-386.

Emelyanov, E. M., 1973. The main types of recent bottom sediments in the Mediterranean Sea, their mineralogy and geochemistry. Litologia i Poleznye Iskopaemye, 1, p. 29-46.

Emelyanov, E. M., 1975. Bottom sediments of the Mediterranean Sea. In: Sedimentation in the Atlantic Ocean. Kaliningrad, Kaliningradskya Pravda, p. 309-426.

Emelyanov, E. M., 1979. Mineral composition of the Mediterranean Sea sediments. In: Oceanological investigations, 26. Results of Studies (Intern. Geoph. Projects). Moscow, Sov. Radio, p. 61-108.

Emelyanov, E. M., 1982. Sedimentalogenesis in the Atlantic Ocean Basin. Moscow, Nauka, 205 p.

Emelyanov, E. M., 1988. Iron hydrothermal deposits on the Marsili mountain (Tyrrhenian Sea). In: Geology of the oceans and seas. Abstracts of 8th All-Union Marine Geological School, vol. 3, Moscow, p. 26-27.

Emelyanov, E. M., 1989. 'Iron cap' on Marslli mountain. Science news. Priroda, p. 119.

Emelyanov, E. M., 1992. The sediments of the anoxic basins of the Mediterranean Sea. Okeanologiya, 32(3), p. 567-575.

Emelyanov, E. M., 1994. Recent Bottom Sediments of the Levantine Sea: their Composition and Processes of Formation. In: V. A. Krasheninnikov and J. K. Hall (eds). Geological Structure of the North-Eastern Mediterranean, Historical Productions-Hall Ltd., Jerusalem, p.141-158.

Emelyanov, E. M., Blazchishin, A. I., Kharin, G. S., Lozovaya, N, G., Zangalis, K, P., 1978. Mineral and chemical composition of sediments of the Voring Plateau, DSDP Leg 38. In: White, S. M., Supko, P. R., Natland, J., Gardner, J., Herring, J., (eds.), Initial reports of the Deep Sea Drilling Project; Supplement to volumes XXXVIII, XXXIX, XL, and XLI, Initial Reports of the Deep Sea Drilling Project, vol.38-41, Supplement, pp.31-44.

Emelyanov, E. M., Krylov, A. Ya., Silin, Yu. I., Shimkus, K. M., and Tsovbun, Ya. N., 1973. Age provinces of terrigeneous-volcanogenic material in the Mediterranean Sea. Litologia I Poleznye Iskopaemye, 4, p. 28-43.

Emelyanov, E. M., Kuprin, P. N., and Shimkus, K. M., 1986. Recent sedimentation map of the Mediterranean Sea. IOC Editorial Board for the International Bathymetric Chart of the Mediterranean and overlay sheets, UNESCO 1986, Second Session. Paris, 13-15, March. 1986, p. 1-3.

Emelyanov, E. M., Mitropolsky, A. Yu., Shimkus, K. M., and Moussa, A. A., 1979. Geochemistry of the Mediterranean Sea. Kiev, Naukova Dumka, 132 p.

Emelyanov, E. M., and Shimkus, K. M., 1962. On the question about variability of the deep-sea sediments of the Mediterranean Sea. Okeanologiya, 2(6), p. 1040-1049.

Emelyanov, E. M., and Shimkus, K. M., 1986. Geochemistry and Sedimentology of the Mediterranean Sea. D. Reidel Publ. Co., Dordrecht, Holland, 553 p.

Emelyanov, E. M., and Shimkus, K. M., 1990. Unconsolidated bottom surface sediments of the Mediterranean and Black Seas. The map. Scale 1:5,000,000, Head Dept. Navig. and Oceanogr. USSR, Leningrad.

Emelyanov, E. M., Shimkus, K. M., and Kuprin, P. N., 1996. Unconsolidated Bottom Surface Sediments of the Mediterranean and Black Seas. Intergovernmental Oceanographic Commission (UNESCO), IBCM Geol.-Geophys. Series, Scale 1:1,000,000, 10 sheets, Head Dept. Navigation and Oceanography, St. Petersburg, Russia.

Emelyanov, E. M., and Trimonis, E. S., 1983. Geochemical investigation of sediments from the Brazil Basin and the Rio Grande Rise. In: Barker, P. F., Johnson, D. A., et al., (eds.), Initial reports of the Deep Sea Drilling Project covering Leg 72 of the cruises of the drilling vessel Glomar Challenger, Santos, Brazil to Santos, Brazil, February-April, 1980, In: Whalen, Elizabeth (ed.), Initial Reports of the Deep Sea Drilling Project, vol.72, p.421-442.

Erba, E., 1989. Stratigraphy of cruise Tyro-87 cores from the Bannock, Tyro and Kretheus Basins. In: M. B. Cita et al. (eds.), Anoxic basins of the Eastern Mediterranean, Milano, Universita degli studi di Milano, p. 20-23.

Ergin, M., and Yücesoy, F., 1992. Reconnaissance study of heavy metals in surface sediments from the Southern Black Sea shelf and upper slope. Rapp. Comm. Int. mer Médit., v. 33, p.71

Ferentinos, G., Collins, M B.., Pattiaratchi, C. B., and Taylor, P. G., 1985. Mechanisms of sediment transport and dispersion in a tectonically active submarine valley canyon-system: Zakynthos Straits, N. W. Hellenic trench. Mar. Geol., 65(3-4), p. 234-269.

Folk, R. L., 1974. Petrology of sedimentary rocks. Hemphill's Book Store, Austin, TX, 184 p.

Gasco Leonarte, C., and Anton Mateos, M. P., 1992. Distribution of transuranics along the Palomares submarine canyon. Rapp. Comm. Int. mer Médit., v. 33, p. 274.

Georgescu, I. I., Dumitru, Cl., and Pincovscki, E., 1992a. Uranium as a pollutant from Fertilizer industries located on the Black Sea shore and upstream. From Danube Delta. Rapp. Comm. Int. mer Médit., v. 33, p. 275.

Georgescu, I. I., Pantelica, A., and Salagean, M., 1992b. Man-made and natural radionuclydes measured in the Danube River during. Rapp. Comm. Int. mer Médit., v. 33, p. 275.

Gey, H., and Mordogan, H., 1988. Concentrations of various heavy metals in near shore sediments of inner Bay and in some marine organisms in the Bay of Izmir. Doga TU Zoologie DC 12, 5.3. p. 216-224.

Gorshkov, A. I., Emelyanov, E. M., and Sivtsov, A. V., 1992. Comparative study of

Fe-Mn hydroxides from different sea deposits. In: A. P. Lisitzin (ed.), Geology of the oceans and seas. Abstracts of Marine Geological School, v. 1, Moscow, Institute of Ocean., p. 142-143.

Got, H., 1973. Étude des corrélations tectonique-sédimentation au cours de l'histoire quaternaire du précontinent pyrénéo-catalan. [Study of tectonic-sedimentation correlations during the Quaternary of the Pyrenees-Catalan precontinent]. C.N.R.S., Thèse doct. Sci. nat., Univ. Sci. Tech. Languedoc, 385 p.

Got, H., Monaco, A., Leenhardt, O., 1971. Grands traits structuraux et sédimentaires du précontinent pyréneen au large du Roussillon et de l'Ampurdan. [Structural and sedimentological features off the Pyrenean precontinent of Roussillon and Ampurdan]. Révue de l'Institut Français du Pétrôle et Annales des Combustibles Liquides, 26(4), p.355-368.

Hanna, R. G. M., 1992. Dissolved trace metals in Ligurian, Tyrrhenian, Ionian and East Atlantic deep waters. Rapp. Comm. Int. mer Médit., v. 33, p. 72.

Honnorez, J., Honnorez-Querstein B. M., Valette J. and Wausckuln, A., 1973. Recent day formation of an exhalative sulphide deposit at Vulcano (Tyrrhenian Sea). In: C. C. Ametuts and A. J. Bernard (eds.). Ores and sediments. Springer, Berlin, p. 139-166.

Hopkins, T. S., Grimanis, A., Papacostides, G., and Papadopoulos, T., 1973. Neutron activation techniques in the determination of pollutants in the bottom sediments of Saronikos. In: Report of the Working Conference on a Systems Approach to Eutrophication Problems in the Eastern Mediterranean, University of Washington, Dept. of Oceanography Special Report 53, p. 115-133.

Jongsma, D., Fortuin, A. R., Huson W., et al., 1983. Discovery of an anoxic basin within the Strabo Trench, Eastern Mediterranean. Nature, No 305, p. 735-797.

Jureti, I., Odzak, N., Zvonaric, T., and Baric A., 1992. Cadmium, Chromium, Lead and Manganese content in sediment of the Cruz Bay. Rapp. Comm. Int. mer Médit., v. 33, p. 73.

Kelling, G., and Stanley, D. J., 1972a. Sedimentation in the vicinity of the Strait of Gibraltar. In: D. J. Stanley, (ed.), The Mediterranean Sea, A Natural Sedimentation Laboratory, Dowden, Hutchinson and Ross. Inc., Stroudsburg, PA, p. 489-515.

Kelling, G., and Stanley, D. J., 1972b. Sedimentary evidence of bottom current activity, Strait of Gibraltar region. Marine Geol., 13(3), p. M51-M60.

Kendi, M., 1992. Radioactivity in sediments along the coast of Albania. Rapp. Comm. Int. mer Médit., v. 33, p. 338.

Konispoliatis, N., 1984. A study of the Strimonikos bay sediments. Unpublished Ph.D. Thesis, National Technical University of Athens, – p.

Konsulova, Ts., 1992. Seasonal structure and ecological status of Varna Bay (Black Sea) sandy and muddy macrozoobenthic coenoses. Rapp. Comm. Int. mer Médit., v. 33, p. 42.

Korneva, P. R., 1966. Distribution of foraminifera in a surface sediment layer of the Eastern Mediterranean. Okeanologiya, 5, p. 817-822.

Korneva, P. R., and Saidovas, Kh. M., 1969. Stratigraphy of sediments of the Eastern Mediterranean Sea on the benthic foraminifer basin: The main problems of micropaleontology and organogeneous sedimentation in oceans and seas. Moscow, Nauka, p. 188-189.

Kuprin, P. N., (ed.), 1980. Geological-geophysical researches of the Bulgarian part of the Black Sea. Bulgarian Acad. Sci. Publ. House, Sofia, 319 p.

Kuprin, P. N. (ed.), 1988. The history of geological development of continental margin of the western part of the Black Sea. Moscow, Moscow State Univ., 312 p.

Kuprin, P. N., Lilinnov, A. V., Mayer, E. G., Mirgunov, Yu. G., Kristev, I. L., and Perlitchev, D. G., 1988. The history of geological development of continental margin of the western part of the Black Sea. In: P. N. Kuprin (ed.). Trudy Inst. Ocean, Moscow, 210 p.

Kuprin, P. N., Shtcherbakov, F. A., Kurenkova, V. G., and Afanasieva, M. S., 1977. Stratigraphy note Quaternary sediments of the Central Basin of the Mediterranean. Vestnik Moscow Univ., No 2, p. 72-79.

Kuptsov, V. M., Emelyanov, E. M., Shimkus, K. M., Grakova, I. I., and Chabashvili, S. V., 1981. New radio-carbon datings of the Mediterranean bottom sediments and sedimentation rates. Okeanologiya, 21(3), p. 507-515.

Leclaire, L.. 1968. Contribution à l'étude géomorphologique de la marge continentale algérienne, Cah. Océano., XX, 6, 451-521.

Leclaire, L., 1972. La sédimentation holocène sur le versant méridional du bassin algéro-baléare, Thèse d'Etat, Paris, 391 pp.

Lucas, G., 1955. Oolithes marines actuelles et calcaires oolithiques récents sur le rivage Africain de la Méditerranée orientale (Egypte et Sud Tunisien). Stat. Océanogr. Tunis. Bull., 52, p. 266-278.

Lykousis, V., Collins, M. B., and Ferentinos, G., 1981. Modern sedimentation in the N. W. Aegean Sea. Mar. Geol., 43(1-2), p. 111-130.

Maldonado Lopez, A., Diaz Guerro, J. I., Parran Vert, M,, Giro Molner, S., Ecutia Dotti, C., and Serra Diez, M., 1982-1992. Mapa de sedimentos superficiales de la plataforma continental, mapa textural de superficie y mapa de relacion textura-carbonato 35, 41, 42, 42E, 84, 85. - In: Mapa geologico de la Plataforma continental Española y zonas adyacentes. Escala 1:200,000. IGME.

Martini, M., Piccardi, G., Cellini Legittimo, P., 1980. Geochemical surveillance of active volcanoes data on the fumaroles of Vulcano (Aeolian Islands, Italy). Bull. Volcanol., 43(1), p. 255-263.

Mellis, O., 1948. The coarse-grained horizons in the deep-sea sediments from Tyrrhenian Sea. Goteborgs Kgl. Vetoch. Vetterherts-samhall. Hande, 6, Ser. B, 5, No 13, p. 45-72.

Melnik, V. I., and Demediuk, Yu. N., 1984. Conditions of the sedimentogenesis and the types of bottom sediment of the southern part of the Black Sea. In: E. F. Shnyukov (ed). Studies of geological history and processes of recent sedimentation. Trudy Intern Symp., Kijev, Naukova Dumka, p. 2, p. 51-58.

Minganti, V., Fiorentino, P., De Pellegrini, R., and Capelli, R., 1992. Reactive and total Mercury in offshore waters of the Ligurian Sea. Rapp. Comm. Int. mer Médit., v. 33, p. 78.

Minniti, M., and Bonavia, F. F., 1984. Copper-ore grade hydrothermal mineralization discovered in a seamount in the Tyrrhenian Sea (Mediterranean): Is the mineralization related to porphyry-coppers or to base metal lodes? Mar. Geol. 59(1-4), p. 271-282.

Mohamed, M. A., 1968. Continental shelf sediments of the Mediterranean Sea north of the delta in the U.A.R. M.Sc. Thesis, Alexandria Univ., 90 p.

Morelli, C., and Val'chuk, S., 1988. The International Bathymetric Chart of the Mediterranean (I.B.C.M.) published under the authority of the Intergovernmental Oceanographic Commission of UNESCO. Jerusalem, Israel, p. 1-10.

Müller, G., 1964. Die Körngrossenverteilung in der rezenten Sedimenten des Golfes von Neapel. Deltaic and Shallow Marine Deposits, Amsterdam, London, N. Y., p. 282-292.

Müller, J., and Fabricius, F., 1971. Magnesian calcite nodules in the Ionian deep Sea. An actualistic model for the formation of some nodular limestones. In: Pelagic sediments: Land and Sea. Blackwell Scientific Publications. Oxford, p. 235-247.

Neev, D., 1964. Study of the shelf and slope of the Mediterranean coast of Israel. Based on analysis of piston and gravity core samples; Interim Report. Isr. Geol. Surv., Rep., 7 p. Submitted to N. S. F.

Neev, D., 1965. Submarine geological studies in the continental shelf and slope off the Mediterranean coast of Israel; Final Technical Report. Israel Ministry of Development, Israel Geol. Surv., Rep. QRG/1/65, 30 p. Submitted to the N. S. F., May, 1965. Incl. abstracts by Y. Nir, M. Pomerancblum, M. Rossignol, and G. Almagor.

Nesteroff, W. D., 1980. Recent metallogenesis of the pelagic sediments south of Crete. In: A. Panayiotou (ed.), Ophiolites; Proceedings, International ophiolite symposium, Cyprus, Minist. Agric. Nat. Resour., Geol. Surv. Dep., Nicosia, Cyprus, p. 774-780.

Ninkovich, D., and Heezen, B. C., 1965. Santorini tephra. Proc. 17th Symp. Colston. Res. Soc.. 17, p. 413-453.

Nir, Y., 1973. Geological history of the recent and sub recent sediments of the Israel Mediterranean shelf and slope. Geol. Survey Israel Marine Geol. Div.Rep. No, MG/10/73, 135 p.

Nir, Y., 1984. Recent sediments of the Israel Mediterranean continental shelf and slope. Ph. D. Thesis, Sweden, Univ. Of Goteborg, 181 p.

Norin, E., 1958. The sediments of the Central Tyrrhenian Sea. Rep. Swed. Deep-Sea Exp., 8, fasc. 1, Goteborgs. p. 1-136.

Odzak, N., and Zvonaric, T., 1992. Effects of weight and age on Cadmium and Lead levels in foot giles and the rest of soft tissue of Mussel *Mytilus galloprovincialis*. Rapp. Comm. Int. mer Médit., v. 33, p. 81.

Olausson, E., 1960. Description of sediment cores from the Medi-terranean and the Red Sea. Rep. Swed. Deep-Sea Exp. 1947-1948, 8, fasc, 3, p. 286-334.

Olausson, E., 1961. Studies of deep-sea cores. Sediment cores from the Mediterranean

snd the Red Sea. Rept. Swed. Deep-Sea Exp., 8, fasc. 3, p. 336-391.

Palanques, A., Plana, F., and Maldonado, A., 1990. Recent influence of man on the Ebro margin sedimentation system northwestern Mediterranean Sea. Mar. Geol., 95(3/4), p. 247-264.

Parker, F. L., 1958. Eastern Mediterranean foraminifera. Rep. Swed. Deep-Sea Exped. 8, fasc. 2, p. 217-283.

Pavoni, D., Donazzolo, R., Marcomini, A., Depretis, D., and Orio, A., 1987. Marine Pollution Bulletin, 18(1), p. 18-24.

Pellegrini, D., Giani, M., and Coppolelli, P., 1992. Mercury and Chromium in organisms of the coastal marine area between Po Delta and Rawena Harbour. Rapp. Comm. Int. mer Médit., v. 33, p. 81.

Piper, D. J. W., Kontopoulos, N., and Panagos, A. G., 1983. Some observations on surficial sediments and physical oceanography of the Gulf of Amvrakia. Thalassographia, 5(2), p. 63-80.

Prokoptsev, N. G., 1964. On the technology of grain-size analysis of pelitic fraction of marine sediments (suspended balance). Okeanologiya, 4(4), p. 699-706.

Rateev, M. A., Emelyanov, E. M., and Kheirov, M. B., 1966. Conditions for the formation of clay minerals in contemporaneous sediments of the Mediterranean Sea. Lithology and Mineral Resources (Eng. Translation), 4, p. 418.

Rifaat, A. E., El-Sayed, M. Kh., Beltagy, A., Morsy, M. A., and Nawar, A., 1992. Geochemical predictive models of manganese, zinc, nickel, cooper and cadmium in Nile shelf sediments. Mar. Geol., 108(1). p. 59-72.

Ross, D. A., and Degens, E. T., 1974. Recent sediments of the Black Sea. In: E. T. Degens and D. A. Ross (eds.), The Black Sea – Geology, chemistry and biology Amer. Assoc. Petrol. Geol., Memoir 20, Tulsa, OK, p. 183-199.

Rossi, P. L., Bocdu, G., Lucchini, P., and Valers, R., 1980. A manganese deposit from the Tyrrhenian region. Oceanologica Acta, 3(1), p. 107-113.

Ryan, W. B. F., and Heezen, B. C., 1965. Ionian Sea submarine canyons and the 1908 Messina Turbidity Current. Geol. Soc. Amer. Bull., 76(8), p. 915-932.

Shepard, F. P., 1954. Nomenclature based on sand-silt-clay ratios. J. Sed. Petrol., 24(3), p. 151-158.

Shimkus, K. M., 1981. Sedimentation of the Mediterranean Sea during Late Quaternary time. Moscow, Nauka, 240 p.

Shimkus, K. M., 1993. Modern fluxes of suspended matter in the Caucasian Black Sea coastal zone. In: O. Magoon and R. Kosyan (eds.), Coastlines of the Black Sea: Coastlines of the World, ASCE, New York, p. 368-392.

Shimkus, K. M., Emelyanov, E. M., and Trimonis, E. S., 1975. Bottom sediments and the features of late Quaternary history of the Black Sea. In: The Earth's Crust and the History of the Black Sea Basin development. Moscow, Nauka, p. 138-161.

Shimkus, K. M., Emelyanov, E. M., and Yastrebov, V. S., 1998. Geological structure and bottom sediments of the seamounts in the Tyrrhenian Sea. Commission Internationale pour l'Exploration Scientifique de la mer Méditerranée, Rapport du 35e Congrès de la CIESM, Dubrovnik (Croatia), 35(1), p. 98-99.

Shimkus, K. M., and Komarov, A. V., 1993. Technogenic pollution of the Caucasian Black Sea coastal zone and specific features of shelf purification. In: O. Magoon and R. Kosyan (eds.), Coastlines of the Black Sea: Coastlines of the World, ASCE, New York, p. 125-155.

Shimkus, K. M., Komarov, A. V., Vayshvilene, B., Savukinene, N., 1979. Stratigraphy of Black Sea deep-water sediments according to palynological data, and some paleogeographic conclusions. In: Malovitskiy, Ya. P. Shimkus, K. M., (eds.), Geologic and geophysical studies of the Mediterranean and Black Seas. Akad. Nauk SSSR, Moscow, USSR (SUN), p. 53-70. [In Russian].

Shimkus, K. M., Malovitskiy, Ya. P., and Shumenko, S. I., 1978. The bedrocks from the Black Sea bottom and some features of the deep sea basin structure. In: D. A. Ross, Yu. P. Neprochnov et al., (eds.), Init. Rep. Deep Sea Drilling Project, v. 42, part 2. Washington, p. 469-482.

Shimkus, K. M., Mukhina, V. V., and Trimonis, E. S., 1973. On the role of diatoms in Late Quaternary sedimentation of the Black Sea. Okeanologia, 13(6), p. 1066-1071.

Shimkus, K. M., Tchabasvili, S. V., and Dmitrov, P. S., 1979. Recent sediments. In: Geology of and Hydrology of the Western Section of the Black Sea. Publ. House of Bulgarian, Sofia, p. 114-126.

Shlykov, V. G., and Luksha, B. L., 1980. The distribution of clay minerals in the bottom layer of modern sediment of continental terrace. In: Geological-geophysical researches of the Bulgarian sector of the Black Sea, Sofia, Bulgaria, Acad. Publ. House, p. 257-264.

Shtcherbakov, F. A., Kuprin, P. N., and Shatov, A. S., 1977. Stratigraphy of the Late Quaternary deposits on the continental terrace and some paleogeographical questions of Black and Caspian Seas. In: Geology of Quaternary Period (Pleistocene), Yerevan, p. 208-218.

Shtcherbakov, F. A., Kuprin, P. N., Potapova, L. I., Poliakov, A. S., Zabelina, E. K., and Sorokin, V. M., 1978. Sedimentation on the continental margin of the Black Sea. Moscow, Nauka, 212 p.

Smith, P. A., and Cronan, D. S., 1975. Chemical composition of Aegean Sea sediments. Mar. Geol., 18(1), p. M7-M11.

Sorokin, V. I., and Shevchenko, A. Ya., 1980. The accumulation of carbonates and silica on the continental terrace in the Late Quaternary. In: Geological-geophysical Researches of the Bulgarian Sector of the Black Sea, Sofia, Bulgaria, Acad. Publ. House, p. 266-275.

Stanley, D. J., (Editor) 1972. The Mediterranean Sea: a natural sedimentation laboratory. Dowden, Hutchinson and Ross. Inc., Stroudsburg, PA, 765 p. 355-386.

Stanley, D. J., 1992. Nile, Delta, Egypt: effects of sea level climate, tectonic subsidence and man. Rapp. Comm. Int. mer Médit., v.33, p. 151.

Tassi Pelati, L., et al., 1992. Transfer of ortitical radionuclides through the Adriatic food-web. Rapp. Comm. Int. mer Médit., v. 33. p. 338.

Todd, R., 1958. Foraminifera from Western Mediterranean deep-sea cores. Rept. Swed. Deep-Sea Exp., 1947-1948, 8, fasc. 2.

Topcuoglu, S., and Bulut, A. M., 1992. Natural depuration rate of Chernobyl-derived ^{137}Cs in mussels (*Mytlius galloprovincialis*) from the Bosphorus. Rapp. Rapp. Comm. Int. mer Médit., v. 33, p. 278.

Toth, J. R., 1980. Deposition of submarine crusts rich in manganese and iron. Geol. Soc. Am. Bull., 91(1), p. 44-54.

Valette, J. N., 1969. Étude sédimentologique et géochimique de dépôts littoraux entourant l'île Vulcano (Sicile): Thèse 3eme cycle, Paris, 175 p.

Varnavas, S. P., 1981. Metals in polluted sediments from the Thermaikos Gulf, Greece, Baseline. Marine Pollution Bulletin, 14(6), p. 234-236.

Varnavas, S. P., 1984. Anthropogenic input of C_{org}., Zn, Cu, Cr and Pb in the Patraikos Bay, Greece. Marine Environmental Research.

Varnavas, S. P., 1989. The geochemistry of the sediments from the southern Aegean Sea. Athens, -- p.

Varnavas, S. P., and Ferentinos, G., 1982. Heavy metal distribution in the surface sediments of Patraikos Bay, Greece. VIeme Journées d'Étud. Pollutions en Méditeranee, Cannes, Comm. Int. Explor. Sci. Mer Mediterr., Monaco, p. 405-409.

Varnavas, S., Ferentinos, G., and Collins, M., 1986. Dispersion of bauxitic red mud in the Gulf of Corinth, Greece. Marine Geology 70(3-4), p. 211-222.

Varnavas, S. P., Panagos, G., and Lalos, G., 1984. Distribution of trace metals in Navarino bay, Greece. Environmental geology (unpublished).

Varnavas, S. P., Papaioannou, J., and Catani, J., 1988. A hydrothermal manganese deposit from the Eratosthenes Seamount, eastern Mediterranean Sea. Mar. Geol., 81(1-4), p. 205-214.

Voutsinou-Taliadouri, F., and Satsmadjis, J., 1982. Concentration of some heavy metals in east Aegean sediments. Rev. Int. Oceanogr. Med., 66/67, p. 71-76.

Vukadin, I., and Stojanovski, L., 1992. Distribution of nutrients in the Eastern Adriatic coastal sea. Past Algal Bloom, Rapports et Procès-verbaux des réeunions, v. 33, XXXIII Congrés CIESM. Trieste, p. 86.

Wentworth, C. K., 1922. A scale of grade and class terms of clastic sediments. J. Geol., 30(5), p. 377-392.

Wood, L. E., 1964. Pseudo-oolites of northern Libya: their occurrence and origin. J. Sed. Petrol., 34(3), p. 661-663.

Yaramar, O., Mordogan, H., Sunlu, U., and Onen, M., 1992. A comparative study on some heavy metal concentrations (Zn, Cu, Pb, Cd, Ni, Cr) in the sediments from Homa (Ismir) and Karine (Ayd in-Turkiye) Fisheries Lagoons. Rapp. Comm. Int. mer Médit., v. 33, p. 87.

PART IV

Israel
Introduction

Akiva Flexer
Department of Geophysics and Planetary Sciences, Tel-Aviv University, Tel-Aviv 69978, Israel
Francis Hirsch and John K. Hall
Geological Survey of Israel, 30 Malchei Israel Street, Jerusalem 95 501, Israel

MAIN FEATURES

Israel stretches along the southeastern Mediterranean coast. It is a part of the southern Levant and within the heart of the Middle Eastern Fertile Crescent. It is bordered by the wilderness of Sinai in the west and by the Jordan-Dead Sea-Arava Rift in the east.

This small land of merely 27,000 km² exhibits a fascinating geology, only matched by its archeology and history.

It comprises several morphotectonic regions. To the west, bordering the Mediterranean coast, extends the Coastal Plain of Israel, rising eastward to the peneplain of the Shefela. The valleys of Yizre'el, Beersheva, and the southern Negev plateau separate between the mountainous backbones. These are the mountains of the Galilee and the Carmel, Judea, the Negev Highlands and the Elat Mountains. To the east, the Rift encompasses the Jordan River, the Dead Sea Basin and the Arava Depression. Further east, the plateau of Jordan and the Golan Heights rise northward to the Anti-Lebanon. Each of these regions has its particular geological characteristics.

Main Physiographic features of the Israeli landscape

Israel is distinguished by its variegated landscape **(Figs. IV.1 to IV.18).** Deserts expose wild steep granitic hills and wide barren limestone plateaus, whereas the mountainous areas are often covered with vegetation. The world's lowest point is now at 413 m below sea level at the Dead Sea (Fig. IV.16), not far from the 2814 m high summit of Mount Hermon (Fig. IV.12) just across the border in Syria. It is also bound by the Mediterranean Sea to its west and the Red Sea at its southern tip (Fig. IV.18).

In order to illustrate the breadth of physiography available in this little wedge-shaped country between three continents, a series of posters published in recent years (Hall, 1994, 1997, 2000a, b, c, 2002) are reproduced herein. **Figure IV.1** shows the topography derived from the gridded 25 m digital terrain model (DTM) of Israel based upon digitization of the 10 m contours in the 1:50,000 topographical maps. **Fig. IV.2** shows the geological map of the country overlain on this topography (Sneh et al., 2000), a useful reference for the chapters to come. **Figs. IV.4 through Fig. IV.16** are originally posters at 1:100,000 scale showing the country as of 1987, based upon an orthophoto derived from merged LANDSAT and SPOT satellite image with 10 m pixels. This dataset is available for interactive visualization via the website www.rohrproductions.com. **Figs. IV.16 to IV.18** show the bathymetric contours of the Dead Sea, the Sea of Galilee (Kinneret) and the Gulf of Elat, set into the satellite imagery. **Fig. IV.19** is a satellite image (Hall, 2000c) of the area to the north of Israel, discussed in Part II of Volume I.

The region can be subdivided into four north-south tectonically-controlled physiographic belts.

PHYSIOGRAPHY

The characteristic variegated landscape of the southern Levantine part of the Fertile Crescent can be subdivided into longitudinal morphotectonic belts stretching between Sea and Desert:

1) The Coastal Plain and Shefela;
2) The Mountainous Backbones: the Galilee-Judea-Negev;
3) The Jordan and Arava Valleys - the depression of the Dead Sea Rift;
4) The Golan Heights;

(1) The Coastal Plain and Shefela

The Coastal Plain is a long wedge-like belt, some 50 km wide in the south, and totally pinching out at the protrusion of Mount Carmel. The Coastal Plain widens again to about 10 km beside Haifa Bay, and then disappears as a transversal fault system brings the western Galilee and Lebanese Hills down to the Mediterranean.

The offshore region includes the shelf, the slope. and the deep sea floor. Emery and Bentor (1960), Nir (1973), Neev et al. (1973, 1976) and Almagor (1976, 2002) present recent summaries of the submarine topography and geology along the coast of the southeastern Mediterranean. Almagor and Hall (1978) published a detailed bathymetric map of the sea adjacent to Israel, and Hall et al. (1994) give the bathymetry for all the eastern Mediterranean.

The continental shelf extends approximately to depths of 80-90 m, some 40 km offshore of El Arish. It becomes narrower toward the north, and near Tel Aviv is about 15 km wide. Opposite Mount Carmel it is reduced to about 5 km. The shelf is generally smooth with numerous ridgeline or irregular protrusions of 'kurkar', platforms of eolian-like structures, and gas-produced pockmarks (Sade et al., 2003). In the north it is deeply incised by Achziv Canyon.

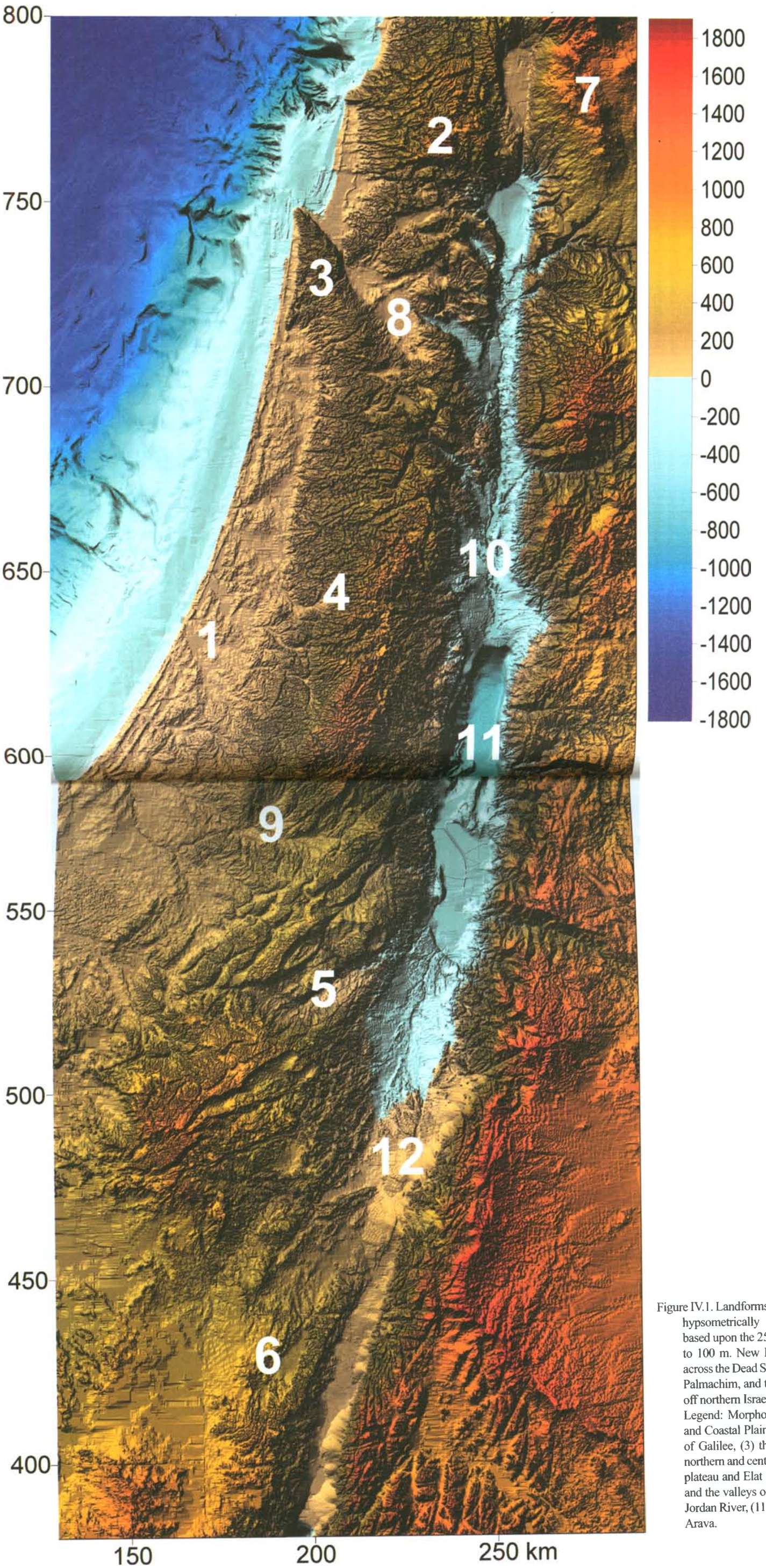


Figure IV.1. Landforms of Israel and adjacent areas. This hypsometrically colored shaded relief image is based upon the 25 m DTM of Israel, reinterpolated to 100 m. New Israel Grid. Note the asymmetry across the Dead Sea Rift, the 17 by 40 km slump off Palmachim, and the numerous submarine canyons off northern Israel.

Legend: Morphotectonic regions: (1) the Shefela and Coastal Plain, (2) the mountainous backbones of Galilee, (3) the Carmel, (4) Judea and (5) the northern and central Negev, (6) the southern Negev plateau and Elat Mountains, (7) the Golan plateau and the valleys of (8) Yizre'el, (9) Beersheva, (10) Jordan River, (11) the Dead Sea Basin, and (12) the Arava.



The Coastal Plain is a rolling terrain of low elevation, gently inclined from the mountainous area in the east to the Mediterranean coast in the west. The relief consists mainly of a belt of coastal dunes and several ridges of ancient (Pleistocene) indurated dunes known as 'kurkar ridges'. These rise up to 30-50 m above the adjoining valleys and lowlands.

The surface of the Coastal Plain is built up entirely of Quaternary sediments. These include sand dunes, indurated 'kurkar' dunes, red-brown 'hamra' soils, alluvial and colluvial deposits, and loess. The distribution of these deposits serves as a basis for the subdivision of the province into units.

Narrow sandy beaches border the Mediterranean shoreline, a few tens of meters wide. From south to north, the broader, gently sloping beaches of the Sinai coastal plain gradually give way to beaches limited by coastal cliffs developed in calcareous sandstones, and topped by recent sand dunes. In places, an almost continuous belt of dunes rises gently from the beach to elevations of up to 70 m and extends several kilometers inland (Figs. IV.5, IV.8). The sands are carried from the Nile Delta by longshore currents and blown inland by the prevailing westerly winds.

During the Quaternary diagenesis of loose sands proceeded in two directions:

1) Production of kurkar (a non-specific local name for calcareous sandstone), mainly an eolianite distinguished by a very high carbonate content;

2) Production of red sandy clay loam soil called 'hamra' and its associated catenas (Yaalon and Dan, 1992).

A belt of alluvial-colluvial soil associations covers the eastern parts of the province, east of the kurkar ridges. These also extend into the lower parts of the valleys of the mountain foothills, and in the west along the lower tracts of the stream valleys into the longitudinal troughs between the dunes and kurkar ridges.

(2) The Mountainous Backbone of Israel

This physiographic province is sharply bounded to the east by the Jordan-Dead Sea Rift Valley and to the west by the Coastal Plain. The highlands extend from Lebanon in the north to the high Sinai plateaus in the south. The mountainous belt comprises high mountains and vast plateaus exceeding 1000-1200 m in elevation.

Lithologically the rocks are mainly limestone, dolomite, and marls. Minor constituents are sandstone and crystalline rocks. The mountainous backbone is dissected by two conspicuous depressions, the Yizre'el Valley in the north, and the Beersheva-Arad Depression in the south. These divide it into into three sub-regions (from south to north in Fig. IV.1): The Negev, the Judean Mountains, and the Galilee.

By and large there is a good agreement between morphology and structure, although in several places inverse morphology is recorded.

Figure IV.2. Geological Shaded Relief Map of Israel and Environs, reduced from Sneh et al. (2000). Computer generated geological map on the digital shaded relief shown in Fig. IV.1.

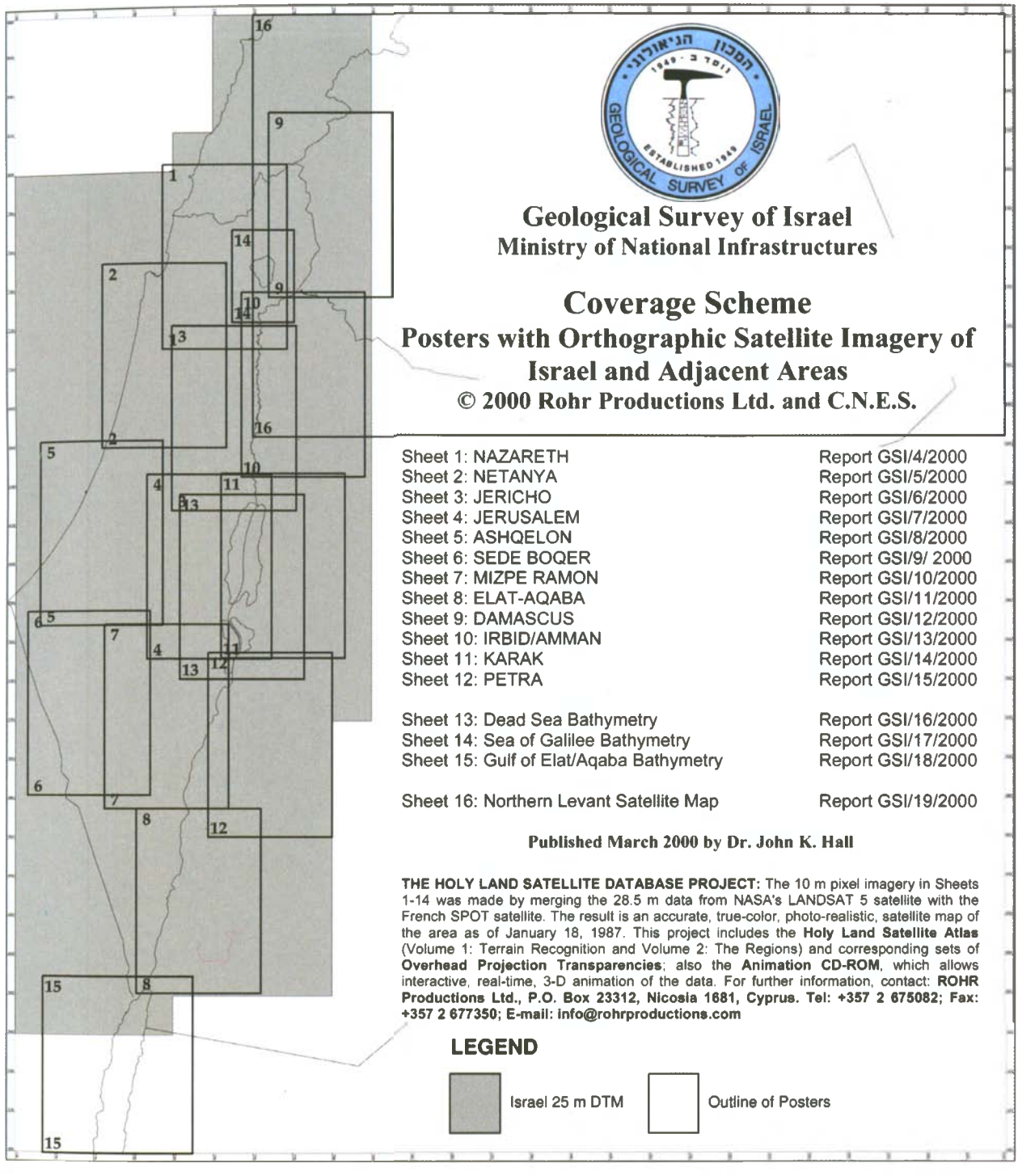


Figure IV.3. Coverage scheme for the poster reductions in Figs. IV.4 through IV.19. The projection is New Israel Grid, with a 20 km graticule. The shaded area is that covered by the 25 DTM of Israel. The imagery in Figs. IV.4 through IV.17 is from the **THE HOLY LAND SATELLITE DATABASE PROJECT**: This 10 m pixel imagery was made by merging the 28.5 m data from NASA's LANDSAT 5 satellite with the French SPOT satellite. The result is an accurate, true-color, photo-realistic, satellite map of the area as of January 18, 1987. This project includes the **Holy Land Satellite Atlas** (Volume 1: Terrain Recognition and Volume 2: The Regions) and corresponding sets of **Overhead Projection Transparencies**; also the **Animation CD-ROM**, which allows interactive, real-time, 3-D animation of the data. For further information, contact: **ROHR Productions Ltd., P.O. Box 23312, Nicosia 1681, Cyprus**. Tel: +357 2 675082; Fax: +357 2 677350; E-mail: info@rohrproductions.com. The STM data are copyright 2000 by Rohr Productions Ltd. and C.N.E.S.

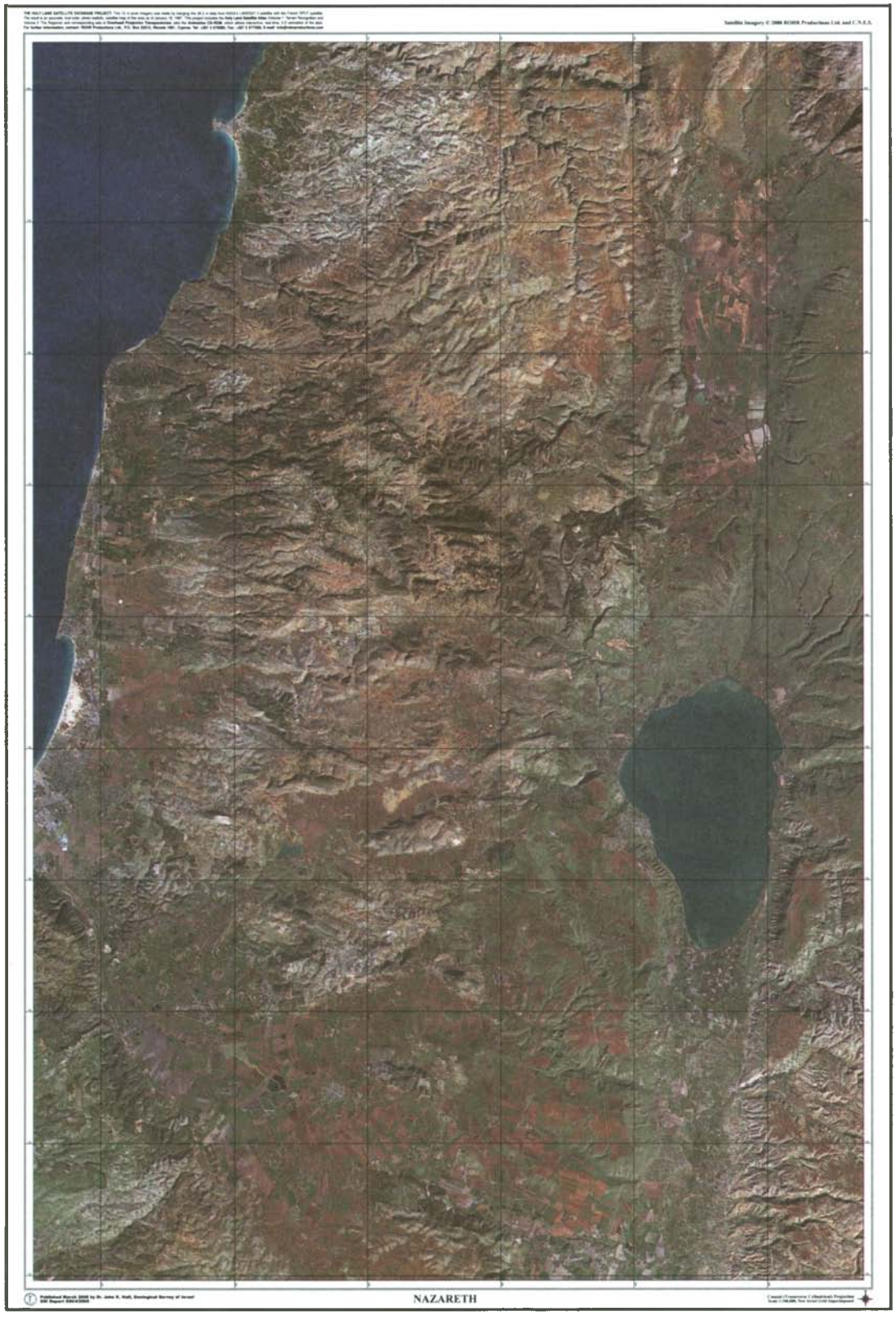


Figure IV.4. Nazareth. Sheet 1 of Hall (2000a). Reduction of Orthographic Satellite Imagery Coverage, Israel and Adjacent Areas. Scale 1:100,000. New Israel Grid, STM (LANDSAT TM and SPOT Panchromatic Merged) Imagery. Geol. Survey Israel Rept. GSI/4/2000.



Figure IV.5. Netanya. Sheet 2 of Hall (2000a). Reduction of Orthographic Satellite Imagery Coverage, Israel and Adjacent Areas. Scale 1:100,000. New Israel Grid, STM (LANDSAT TM and SPOT Panchromatic Merged) Imagery. Geol. Survey Israel Rept. GSI/5/2000.

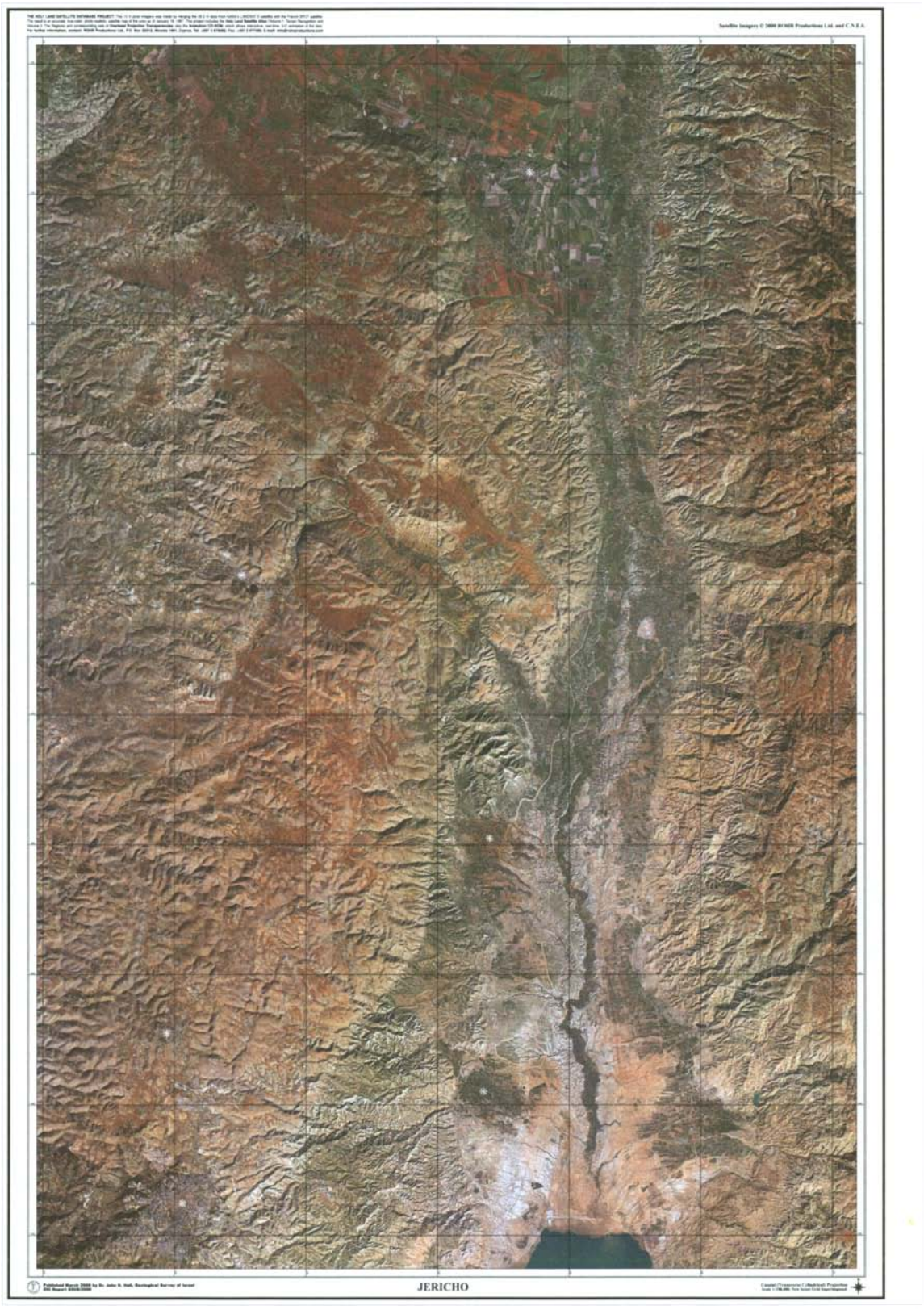


Figure IV.6. Jericho. Sheet 3 of Hall (2000a). Reduction of Orthographic Satellite Imagery Coverage, Israel and Adjacent Areas. Scale 1:100,000. New Israel Grid, STM (LANDSAT TM and SPOT Panchromatic Merged) Imagery. Geol. Survey Israel Rept. GSI/6/2000.

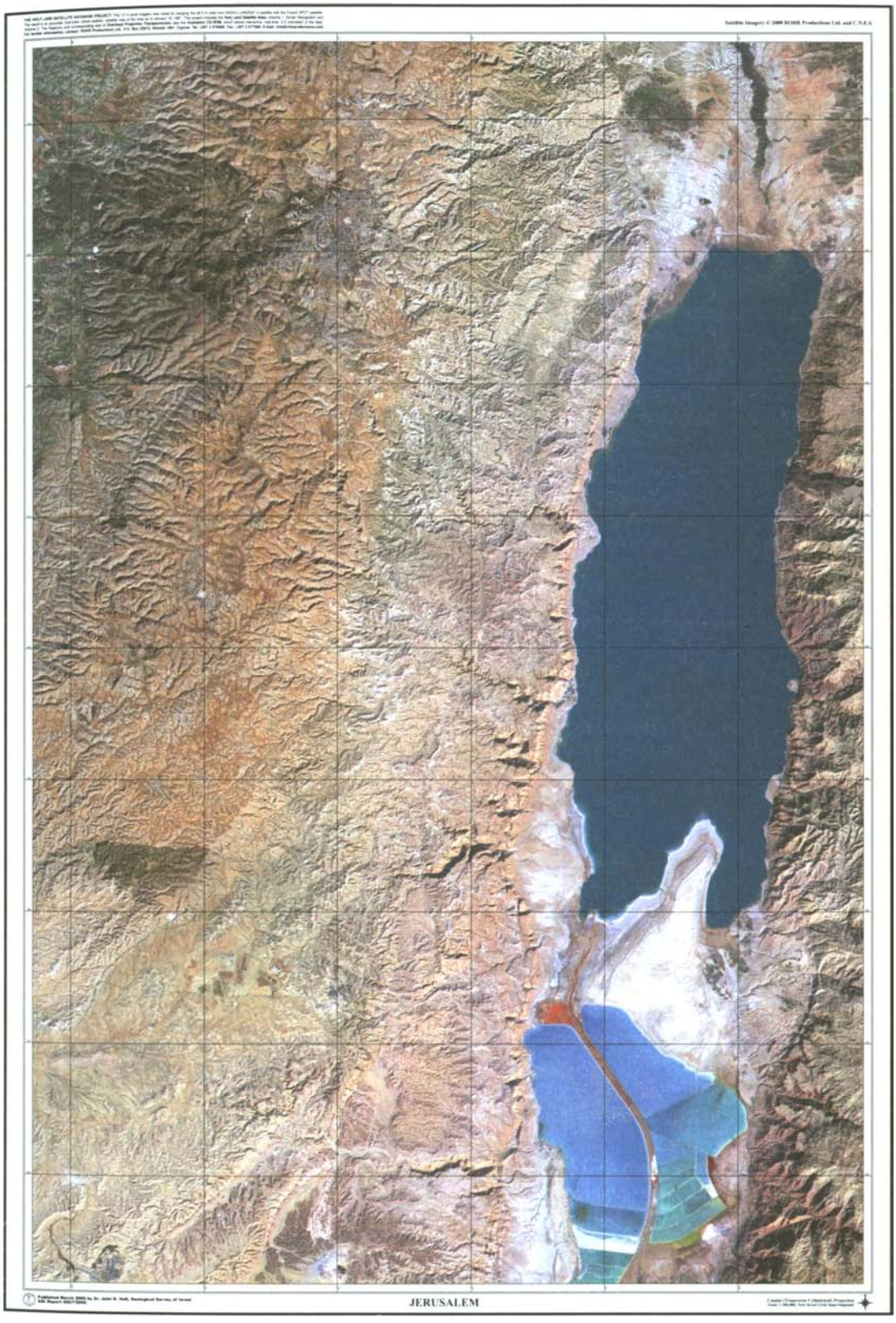


Figure IV.7. Jerusalem. Sheet 4 of Hall (2000a). Reduction of Orthographic Satellite Imagery Coverage, Israel and Adjacent Areas. Scale 1:100,000. New Israel Grid, STM (LANDSAT TM and SPOT Panchromatic Merged) Imagery. Geol. Survey Israel Rept. GSI/7/2000.

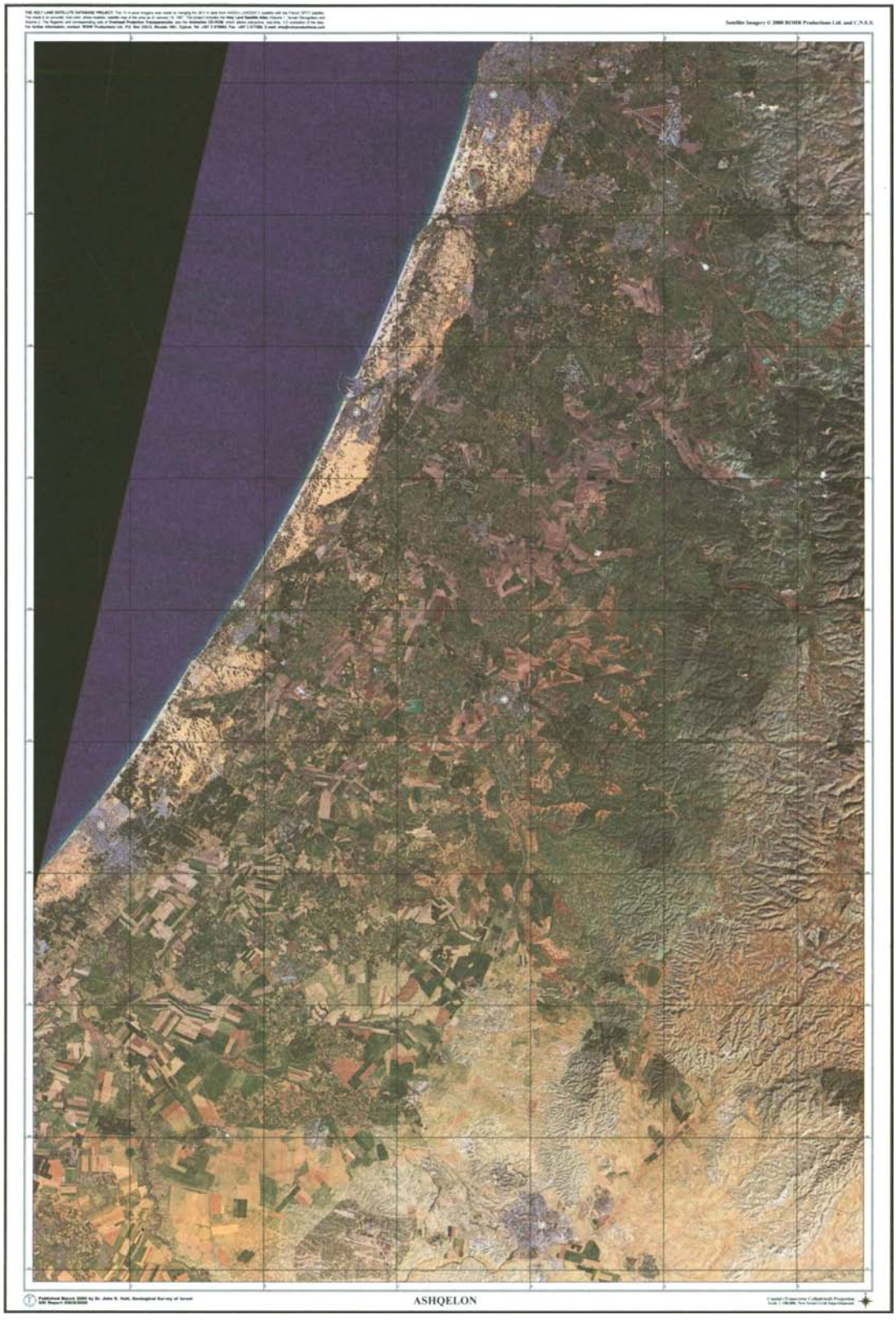


Figure IV.8. Ashqelon. Sheet 5 of Hall (2000a). Reduction of Orthographic Satellite Imagery Coverage, Israel and Adjacent Areas. Scale 1:100,000. New Israel Grid, STM (LANDSAT TM and SPOT Panchromatic Merged) Imagery. Geol. Survey Israel Rept. GSI/8/2000.

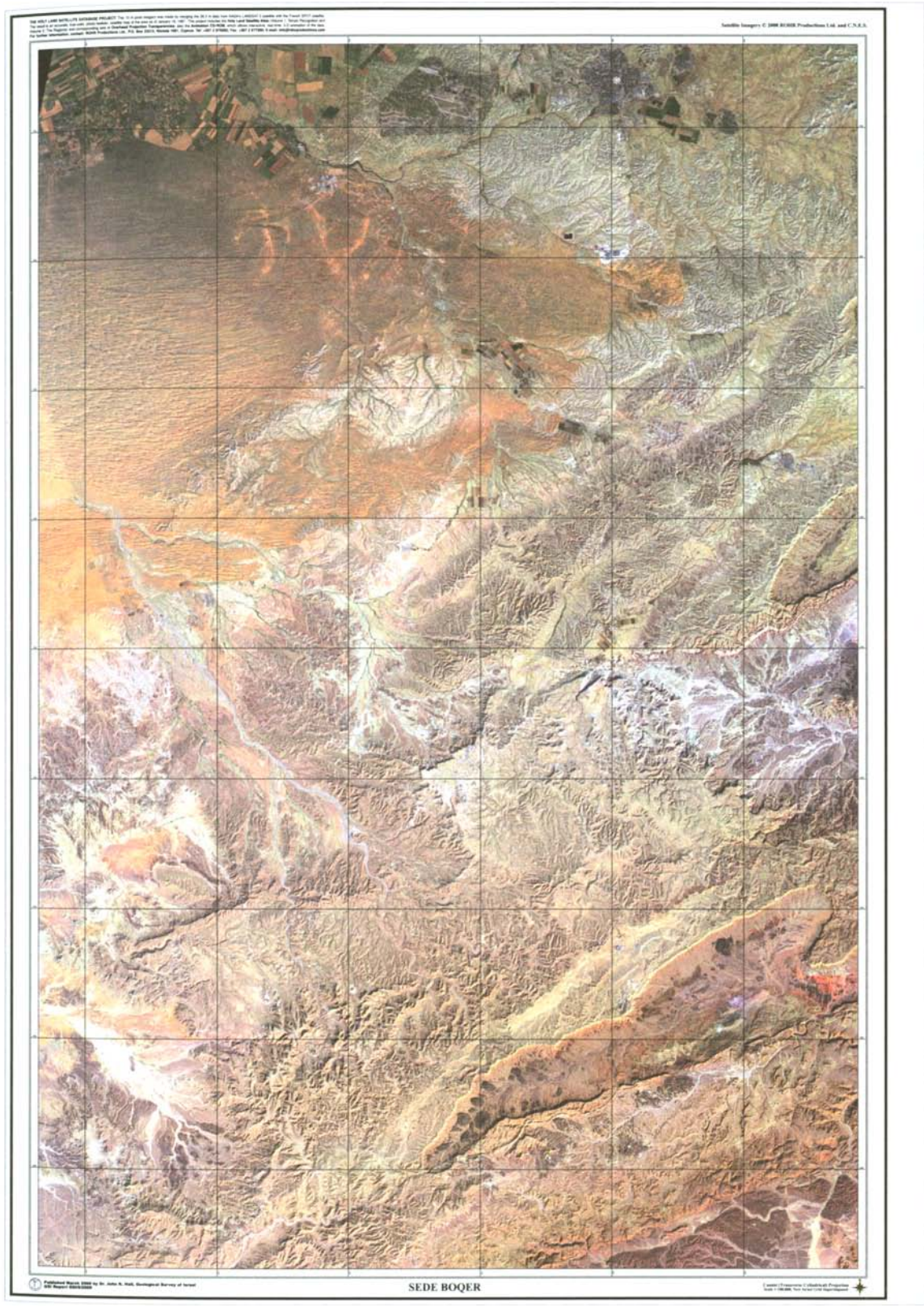


Figure IV.9. Sede Boqer. Sheet 6 of Hall (2000a). Reduction of Orthographic Satellite Imagery Coverage, Israel and Adjacent Areas. Scale 1:100,000. New Israel Grid, STM (LANDSAT TM and SPOT Panchromatic Merged) Imagery. Geol. Survey Israel Rept. GSI/9/2000.

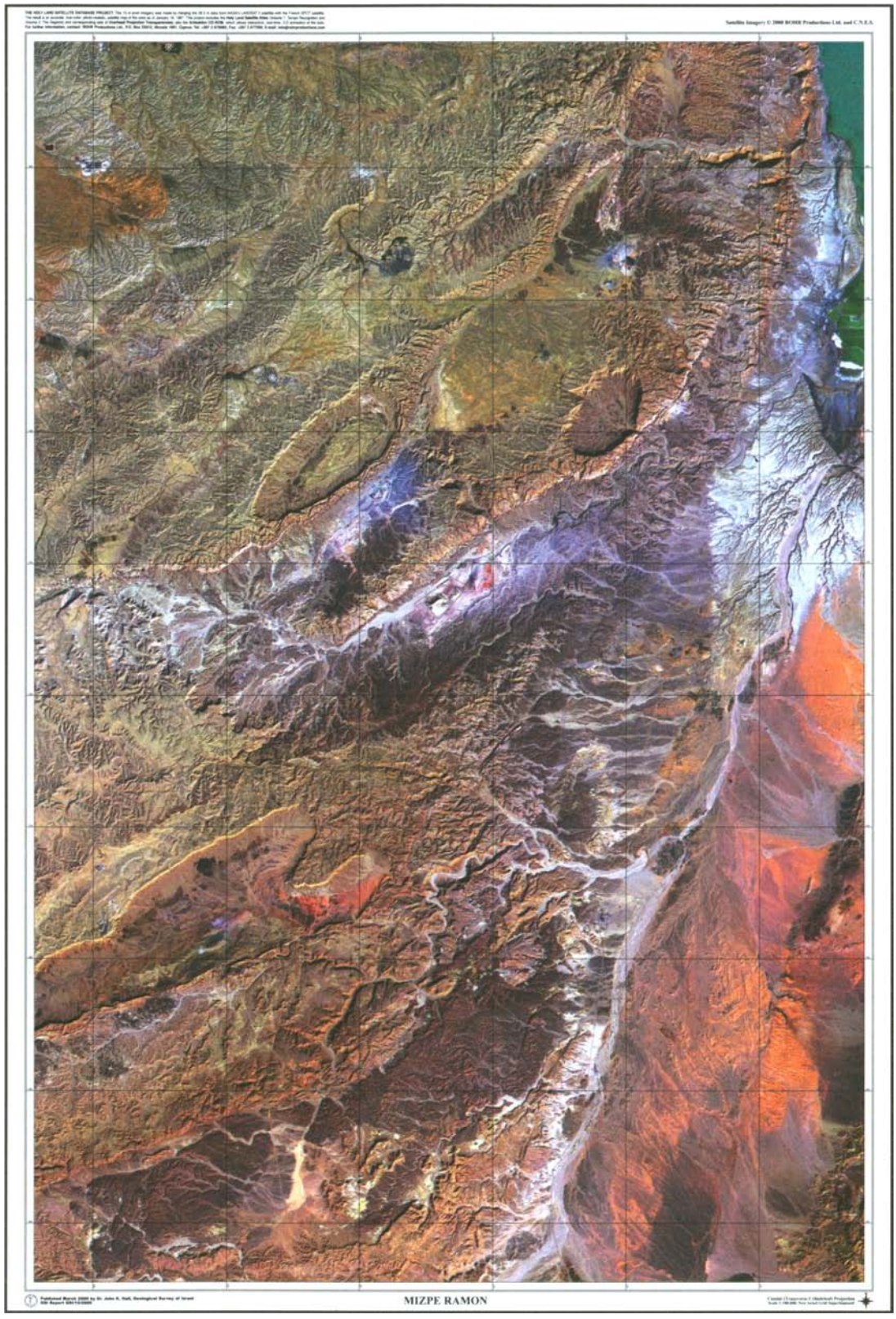


Figure IV.10. Mizpe Ramon. Sheet 7 of Hall (2000a). Reduction of Orthographic Satellite Imagery Coverage, Israel and Adjacent Areas. Scale 1:100,000. New Israel Grid, STM (LANDSAT TM and SPOT Panchromatic Merged) Imagery. Geol. Survey Israel Rept. GSI/10/2000.

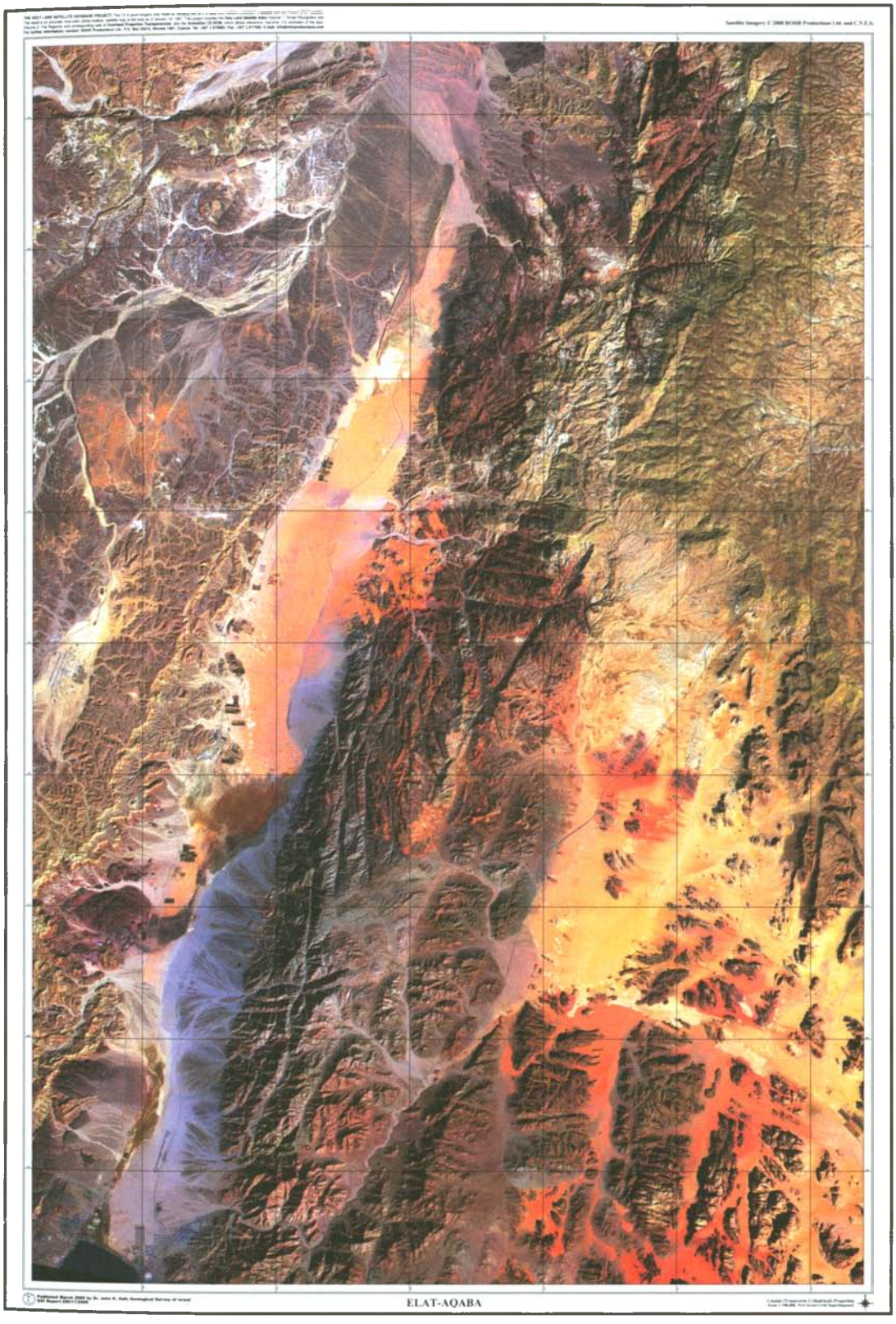


Figure IV.11. Elat-Aqaba, Jordan. Sheet 8 of Hall (2000a). Reduction of Orthographic Satellite Imagery Coverage, Israel and Adjacent Areas. Scale 1:100,000. New Israel Grid, STM (LANDSAT TM and SPOT Panchromatic Merged) Imagery. Geol. Survey Israel Rept. GSI/11/2000.

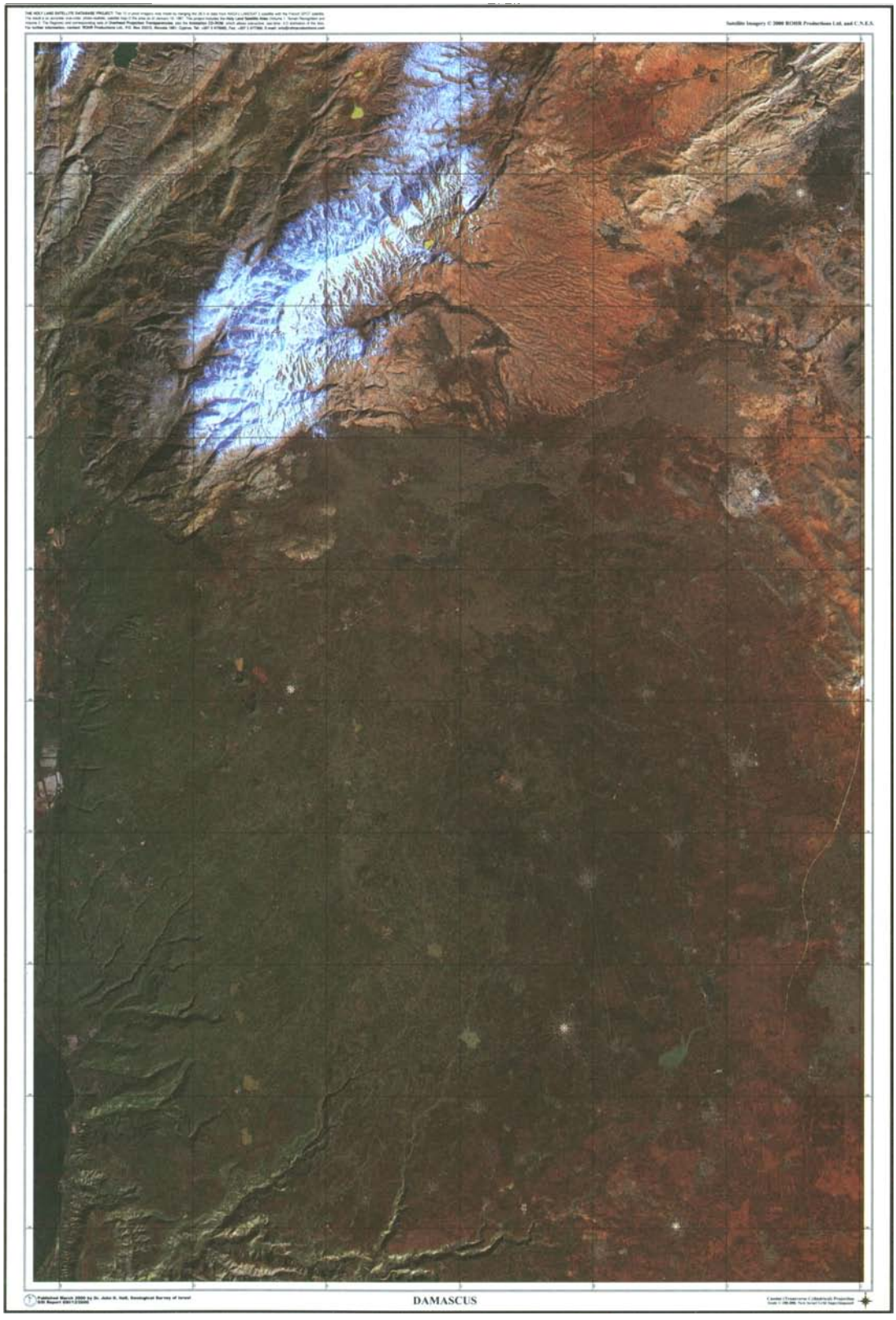


Figure IV.12. Damascus, Syria. Sheet 9 of Hall (2000a). Reduction of Orthographic Satellite Imagery Coverage, Israel and Adjacent Areas. Scale 1:100,000. New Israel Grid, STM (LANDSAT TM and SPOT Panchromatic Merged) Imagery. Geol. Survey Israel Rept. GSI/12/2000.



Figure IV.13. Irbid-Amman, Jordan. Sheet 10 of Hall (2000a). Reduction of Orthographic Satellite Imagery Coverage, Israel and Adjacent Areas. Scale 1:100,000. New Israel Grid, STM (LANDSAT TM and SPOT Panchromatic Merged) Imagery. Geol. Survey Israel Rept. GSI/13/2000.

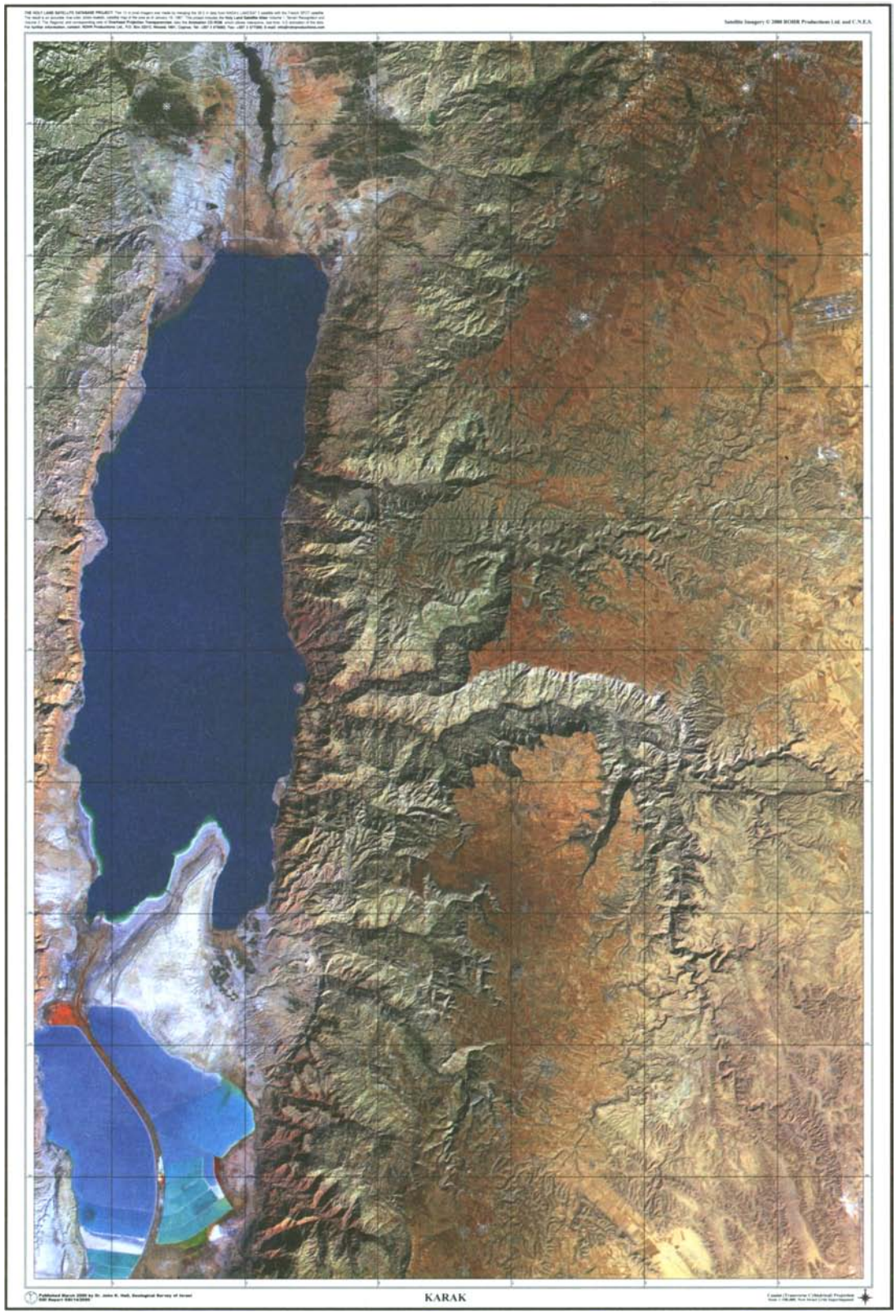


Figure IV.14. Karak, Jordan. Sheet 11 of Hall (2000a). Reduction of Orthographic Satellite Imagery Coverage, Israel and Adjacent Areas. Scale 1:100,000. New Israel Grid, STM (LANDSAT TM and SPOT Panchromatic Merged) Imagery. Geol. Survey Israel Rept. GSI/14/2000.

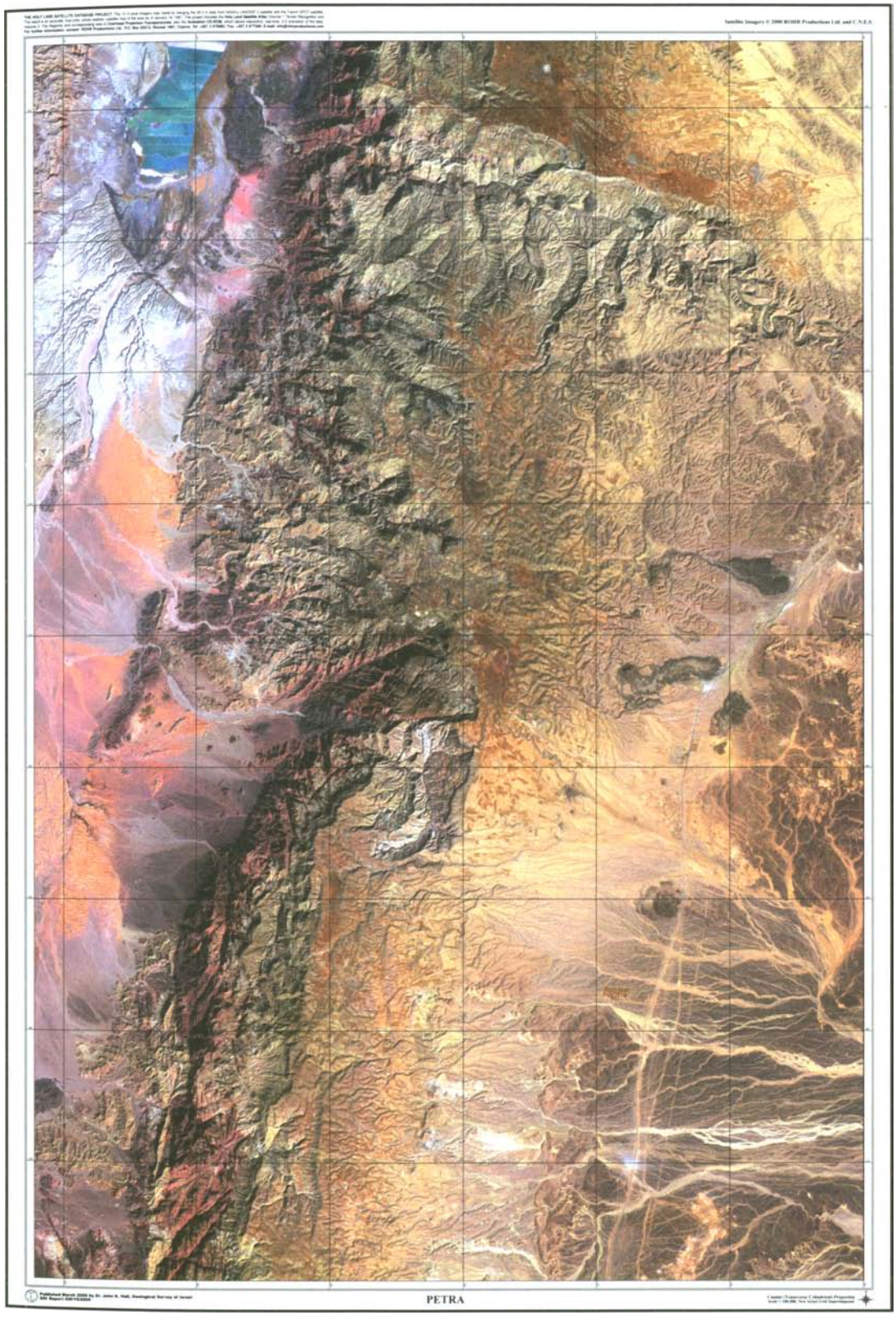


Figure IV.15. Petra, Jordan. Sheet 12 of Hall (2000a). Reduction of Orthographic Satellite Imagery Coverage, Israel and Adjacent Areas. Scale 1:100,000. New Israel Grid, STM (LANDSAT TM and SPOT Panchromatic Merged) Imagery. Geol. Survey Israel Rept. GSI/15/2000.

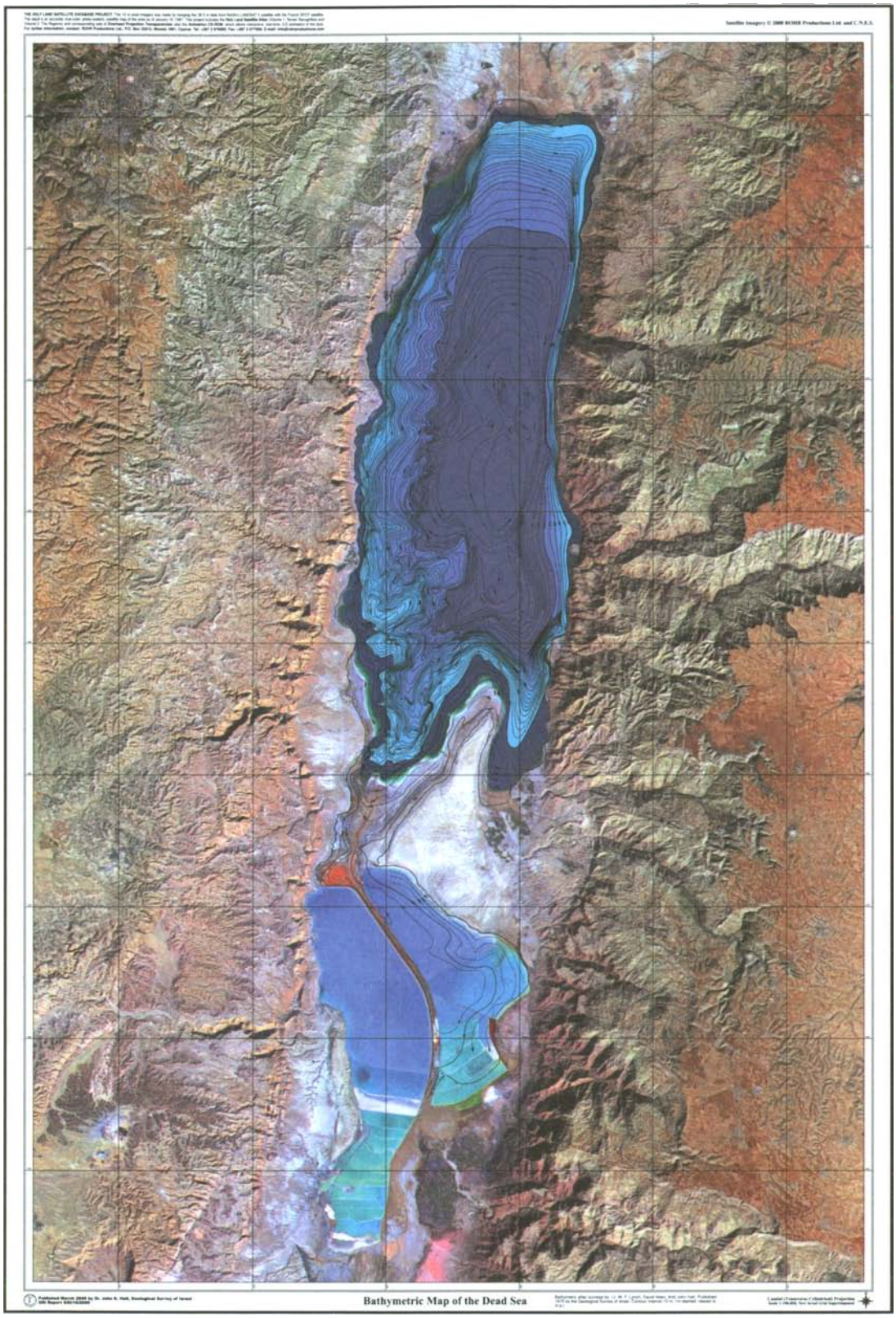


Figure IV.16. Dead Sea. Sheet 13 of Hall (2000b). Reduction of 1:100,000 scale Dead Sea bathymetric chart inset into Orthographic Satellite Imagery Coverage. New Israel Grid, STM (LANDSAT TM and SPOT Panchromatic Merged) Imagery. Geol. Survey Israel Rept. GSI/16/2000.

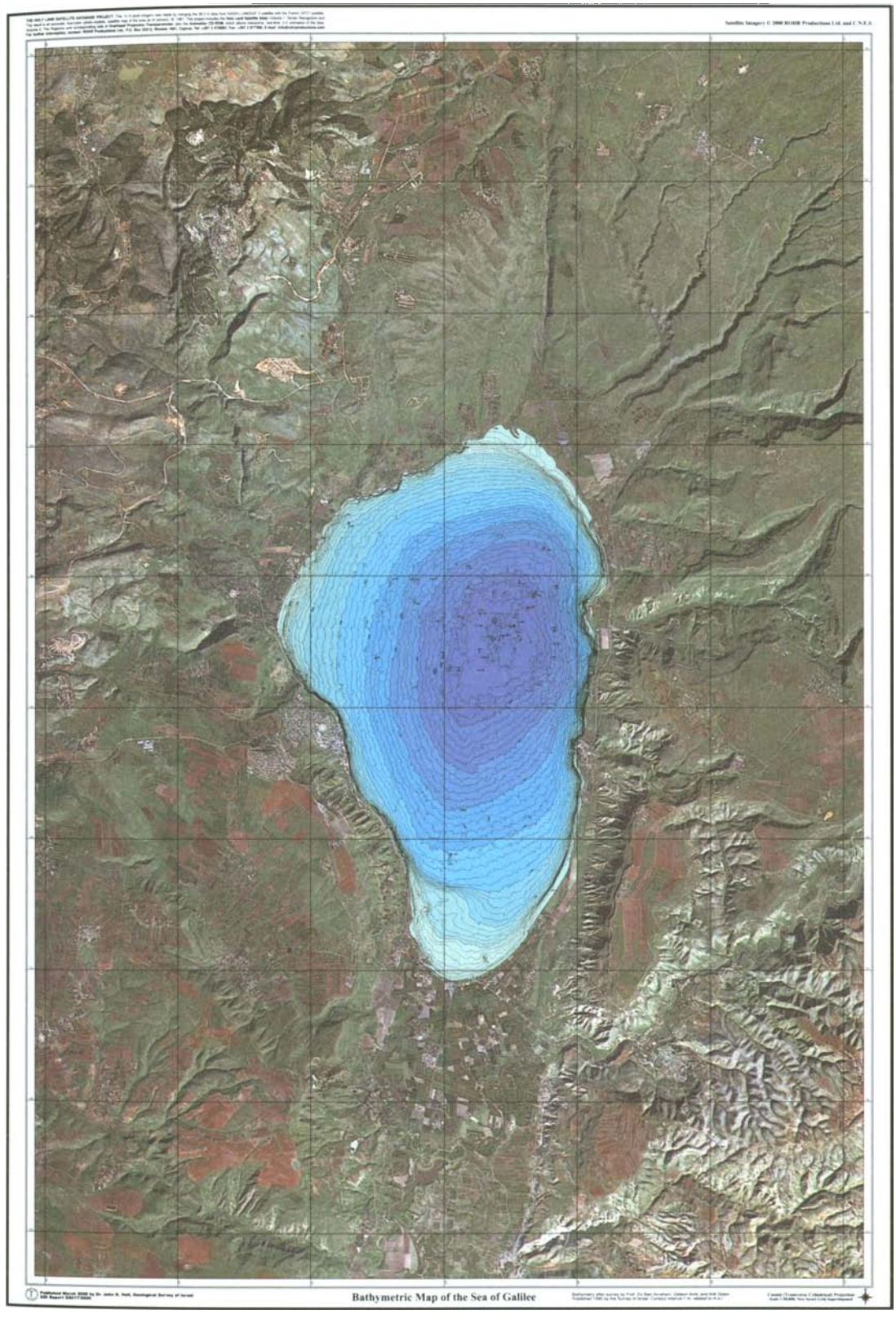


Figure IV.17. Sea of Galilee (Kinneret). Sheet 14 of Hall (2000b). Reduction of 1:50,000 scale Kinneret bathymetric chart inset into Orthographic Satellite Imagery Coverage. New Israel Grid, STM (LANDSAT TM and SPOT Panchromatic Merged) Imagery. Geol. Survey Israel Rept. GSI/17/2000.

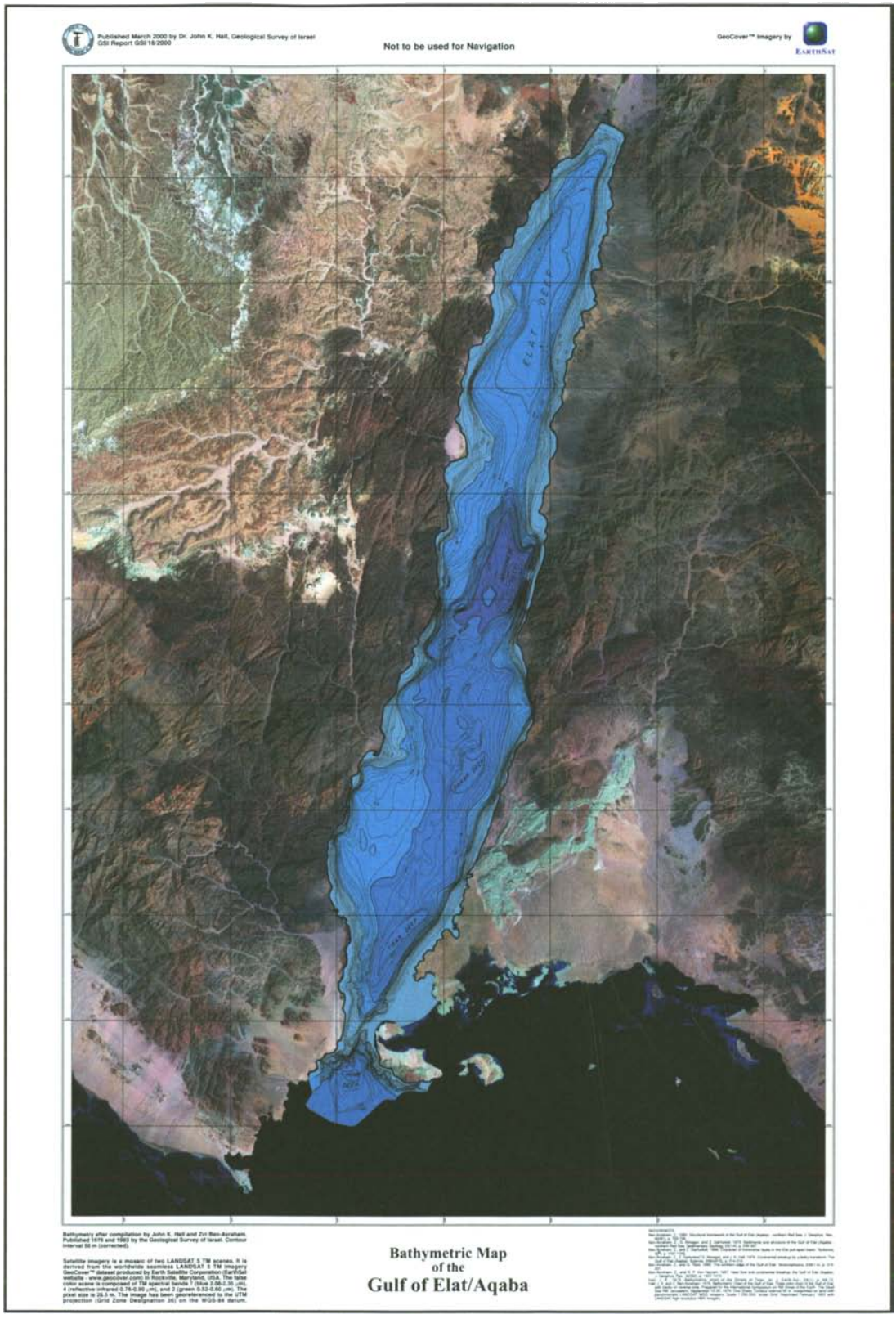


Figure IV.18. Gulf of Elat/Aqaba. Sheet 15 of Hall (2000b). Reduction of 1:250,000 scale bathymetric chart inset into Orthographic Satellite Imagery Coverage. New Israel Grid, STM (LANDSAT TM and SPOT Panchromatic Merged) Imagery. Geol. Survey Israel Rept. GSI/18/2000.

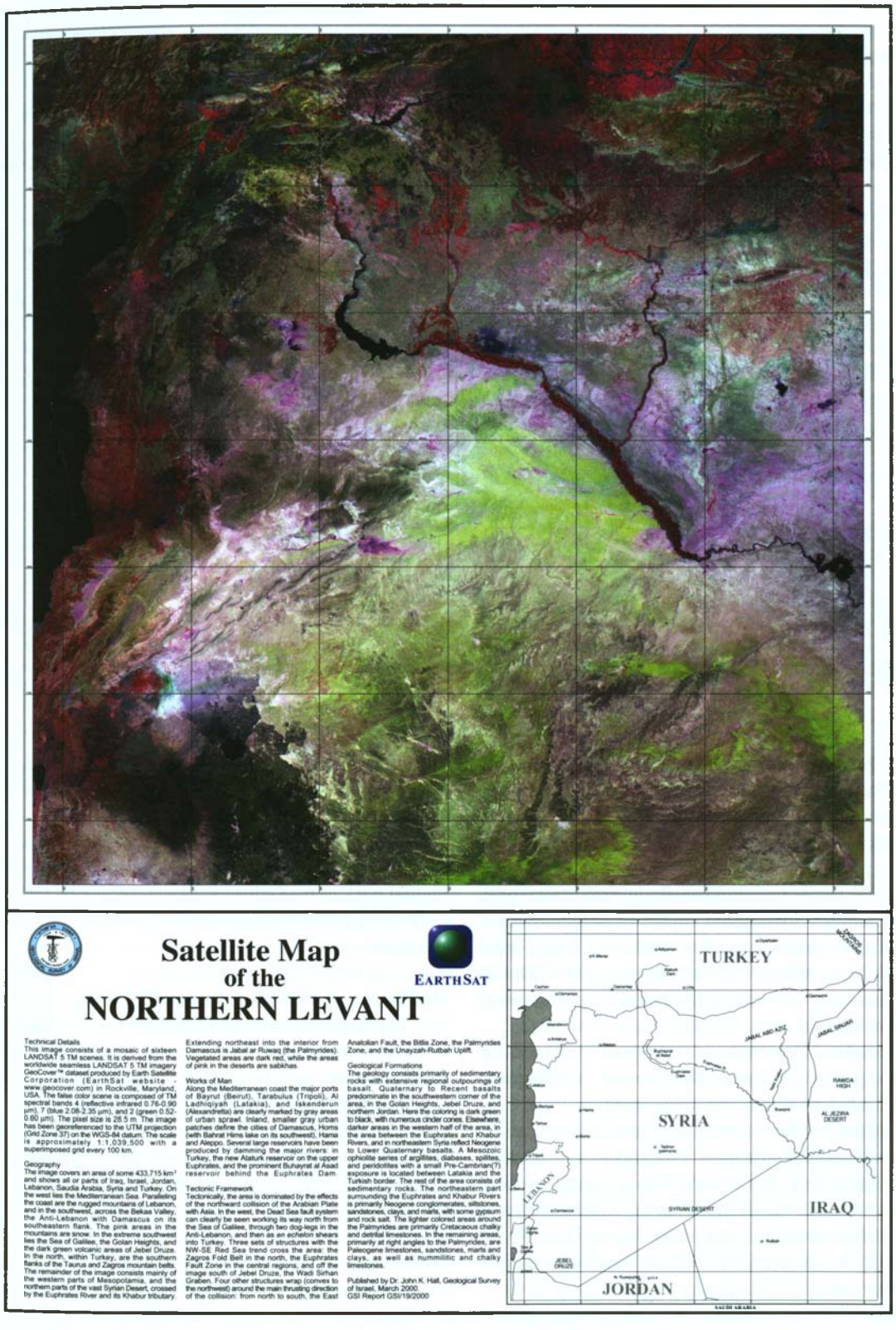


Figure IV.19. Northern Levant Satellite Map (Hall, 2000c), Reduction of 1:1,039,500 scale mosaic of sixteen LANDSAT 5 TM scenes covering all of Syria and parts of Turkey, Lebanon, Israel, Jordan, Iraq, and Saudi Arabia. Bands 2, 4, and 7. With text and location map. Sheet 16 of Orthographic Satellite Imagery Coverage Israel and Adjacent Areas, Geological Survey of Israel Rept. GSI/19/2000.

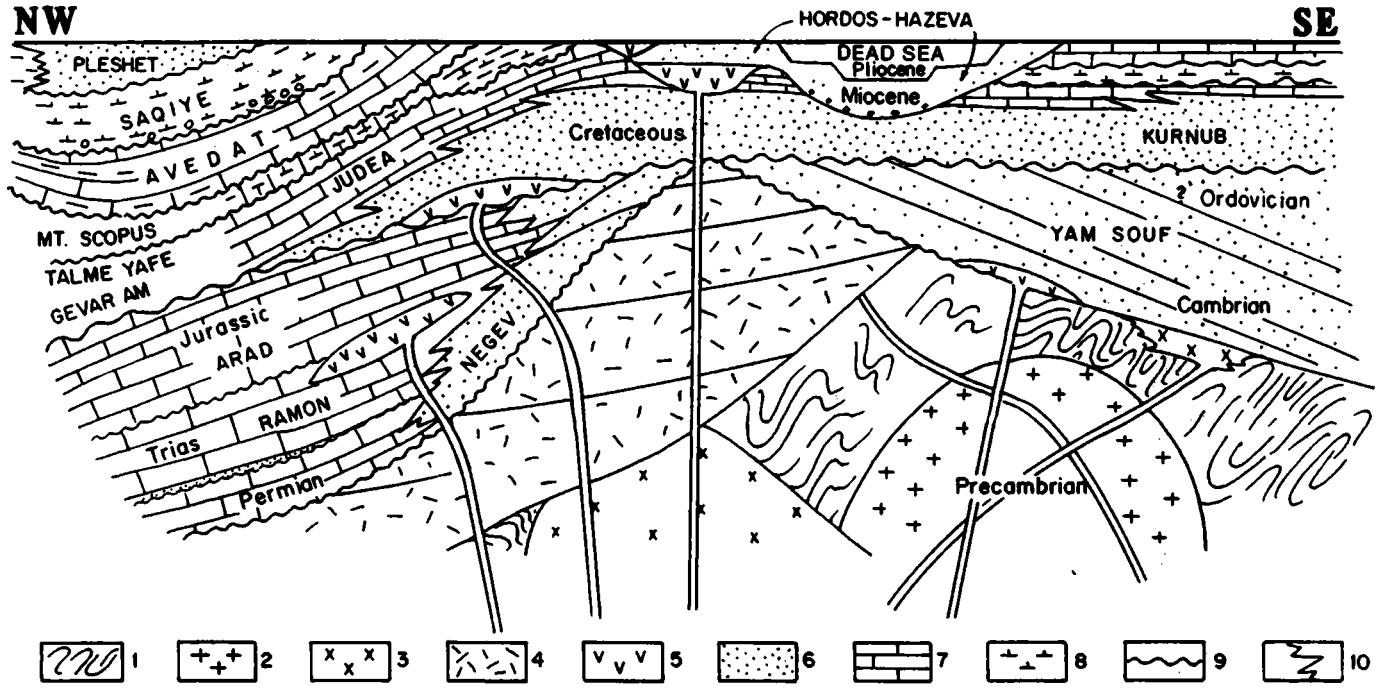


Figure IV.20. General Stratigraphic Scheme of Israel (after Freund, 1965 and Hirsch, 1990, p. 181, Fig. 3).
Legend: 1. Precambrian metamorphic complex: Eilat Shists and Gneiss; 2. Pan-African batholite; 3. Late Pan-African granites, rhyolites and volcanites; 4. Infracambrian Zenifim-molasses; 5. Paleozoic- Cenozoic volcanics; 6. Paleozoic- Cenozoic detritic formations; 7. Late Permian – Mesozoic and Eocene Carbonate Platform deposits; 8. Late Cretaceous – Neogene Pelagic formations; 9. Unconformities; 10. Lateral facies changes.

The Negev is built of three morpho-tectonic units:

1) The northwestern tip of the Arabian-Nubian crystalline rocks, forming steep dissected morphology;

2) High plateaus with horizontal to sub-horizontal sedimentary rocks and;

3) A chain of folds (some morphologically inverted anticlines), extending to the northern sub-regions of the mountainous area, which are part of the Syrian Arc or Levantide fold belt. Picard (1937) delineated the morphotectonic subdivision of the Middle East (**Fig. IV.20**) and based his units on the tectonic organization of the Arabian-Nubian Massif.

The Beersheva-Arad Depression is a morpho-tectonic valley formed by the axial plunging of the anticlinal zones of the Negev to the north, and of the Judean Mountains to the south.

The Judean Mountains form a broad anticlinorium built mainly of three *en-echelon* anticlinal structures. From south to north they are the Hebron, Judea, and Fari'a folds. Three broad synclinal terrains flank them: Bet Guvrin in the west, the Judean Desert in the east, and the Nablus syncline in the north (Figure IV.1). To the north the Judean Mountains reach into the Samarian Hills and their Mount Carmel extension.

Jerusalem (Fig. IV.7) is located in the structural saddle between the Hebron and Judea anticlines. The Yizre'el Valley (Fig. IV.4 and IV.5) is essentially a prominent deep graben separating the Samaria region in the south from the Galilee in the north. During Neogene times a number of ingressions advanced from the Mediterranean all through the Yizre'el Valley and into the Jordan-Dead Sea Rift Valley.

The Galilee (Fig. IV.4) is mainly a series of east-west trending horsts and grabens forming ridges and valleys respectively. The highest peak in the Galilee is Mount Meron (1208 m). Northward the Galilee plunges topographically into the lowlands of southern Lebanon.

(3) The Arava-Dead Sea-Jordan Rift Valley

The Arava-Dead Sea-Jordan Rift (Fig. IV.1) is one of the most striking physiographic features in the Middle East. It is a major rift system, extending from the Red Sea to the Syrian-Turkish border.

The Rift Valley is subdivided transversely into the following tectono-morphologic units (from south to north): The Elat (Aqaba) Gulf (Fig. IV.18), the Arava Valley (meaning steppe or dryland) (Figs. IV.10, IV.11, IV.15), the Dead Sea Valley (Fig. IV.15), the Jordan Valley (Figs. IV.4, IV.6, and IV.13), the Sea of the Galilee (Fig. IV.17), and the Hula Valley (Figs. IV.4 and IV.12). The width of the depression varies between 10 and 20 km. Elevations rise from about -413 m at the Dead Sea shore to +200 m near the water divide in the Arava Valley, +64 m at the water divide towards the Mediterranean in the Yizre'el Valley by Afula, and up to +400 m at the northern tip of the Hula Valley (the foothills of Mount Hermon) (Hall, 1996). The Arava-Dead Sea Rift in its present form owes

its origin to a major tectonic phase that affected the entire region, probably from the Late Pliocene to Early Pleistocene. Whether the origin of the Rift can be traced back to older geotectonic processes remains an open question. Tectonic activity along the Rift continues today, as shown by the seismicity and distribution of epicenters (Arieh, 1967; Shapira, 1979).

The diversity of geological formations and the interaction of tectonic, depositional, and erosional processes have created a considerable variety of landscapes within the Rift. Its southern part, the Arava Valley, is composed mainly of sediments of the Neogene continental Hazeva Formation, covered extensively by alluvial fans and plains, often transformed into reg surfaces. Mesa and butte-shaped hills rise above these plains displaying on their slopes the characteristic red and white coloring of the Hazeva sediments. The southern margins of the Dead Sea lie to the north of the Arava Valley. Physiographically they are badlands, cut out of the glaring white soft beds of the Lisan Formation. This formation consists of finely laminated varve-like gypsum, anhydrite, and aragonite (white laminae), alternating with layers of small rock fragments of quartz, dolomite, and clay minerals (dark laminae), and interfingering laterally with coarser clastics. More resistant beds of gypsum often form the flat tops of mesa-like hills.

Along the Rift border and the shores of the ancient lake, outcrops of the Lisan Formation reach elevations not exceeding 160 m below sea level. This is the highest level attained by Lake Lisan, which once extended north up to the Sea of Galilee.

Lava flows filled part of the northern segment of the Rift, between the Sea of Galilee and the Hula Valley, which is rich in peat deposits.

(4) The Golan Heights

The dark volcanic Golan Heights (Figs. IV.12, IV.17, and IV.19) lie above and east of the Sea of Galilee and the Jordan Valley. To their north rises the Anti-Lebanon mountain range, culminating in the often snow-capped Mount Hermon (2814 m – Fig. IV.12). The Golan Heights are bounded on the south by the Yarmouk River that separates them from the Jordan Highlands. These highlands consist of the mountains of Edom, Moab, and Gilead that reach up to +1500-1700 m. They drain towards the Rift via short deeply incised obsequent gorges or ravines cut into the escarpment (Fig. IV.17).

HISTORY OF GEOLOGICAL RESEARCH IN ISRAEL

The history of geological research in the Near East in general, and the Land of Israel in particular, depended much on local and international politics. Scientific observations were first made during the 18th century. Paraphrasing Horowitz (2001, p. 28), whose Chapter 2 contains a wealth of data (mostly centered on the Jordan Valley and some of which is used herein), it was always the Dead Sea that attracted the most attention from researchers, then as well as today. For example, visiting the region in 1738, the naturalist **Pococke** (1754) mentioned fossil mollusks in the vicinity of the Dead Sea. He also took the sample of Dead-Sea water on which Macquer, Lavoisier, and Sage (1778) conducted their analysis.

The 19th century saw travelers swarming into Palestine, which was then under Ottoman rule. Research activities were carried out by Austrian, British, American, French and German investigators, on invitation of the Turkish authorities. This period saw the pioneering geological investigations.

It was probably **Russegger** (1847) who made the first geological observations in the region, producing a map of the Sinaitic Peninsula and its surroundings.

In 1847, as head of a British team, Molyneux (1848) visited the Jordan River and the Dead Sea. In 1848, the American Navy expedition of Lieutenant Lynch (1849) visited the region with a geologist, H. J. **Anderson** (1852).

It was the interest aroused by the French expeditions of 1850-1851, headed by F. de Saulcy (1854), which soon prompted another in 1864, led by the Duc de Luynes, which brought us Louis **Lartet** (1865-1877). Giving detailed accounts on the geology and paleontology of the region, he presented the basics of a theory on the origin of the 'sillon' (furrow) of the Dead Sea Rift, confirming to a wider audience the facts which Leopold von Buch (1841) and Hitchcock (1843) had recognized.

The British 'Palestine Exploration Fund', founded in 1865, dispatched the geologist **Hull** (1886) who observed that the general outlines of the region were roughly determined during the Miocene epoch, after being submerged by an ocean for most of Mesozoic and Tertiary times. The German Society for the Study of Palestine was founded in 1877. **Noetling** contributed to the knowledge of the Cretaceous in Syria and Palestine (1886), and of the Jurassic of Mount Hermon (1887).

Towards the end of the 19th century the Sultan Abdul Hamid II invited the German geologist and paleontologist Max **Blanckenhorn**, resulting in the publication of nearly 80 papers, books, and geological maps on Syria and Palestine (1889 to 1940). Blanckenhorn's contribution was immense, ranging from the Jurassic, Cretaceous, Eocene, and marine Miocene and Pliocene in Syria, to the Cretaceous paleontology of Palestine. Paul **Oppenheim** assisted him in his 1926 and 1927 publications. The Oppenheim collections, mainly of fossils, still represent the crown jewels of the Geological Department of the Hebrew University in Jerusalem.

After WWI the region fell under French (Lebanon, Syria) and British (Palestine, Egypt) influence. This period brought British directed companies like the Iraq Petroleum Co (IPC, Palestine) as well as a mandatory geologist. At the same time, the implementation of the Balfour Declaration (1917) saw the establishment on Mount Scopus of the Hebrew University in Jerusalem.

In 1924, while still on the ship that brought him to Palestine, Leo **Picard** told Arthur Ruppin that he came to find water. He kept his promise and gave the impetus to groundwater geology. In 1932, he started a Geological Laboratory, later to become the Hebrew University's Geology Department. Picard also paid much attention to mapping, *e.g.* the western Nazareth Mountains.

Anecdotally, in 1935-1936 this triggered the young Heinz **Lowenstam**, later to become the 'father of biomineralization', to study the area east of Nazareth to see its continuation into the Dead

Sea Rift. All his notes ended up in an American oil company, which secretly financed his research through the courtesy of his friendly landlord back in Munich!

In 1935-1938, Paul **Solomonica** became Picard's assistant and together they surveyed the Beersheba-Gaza district (Picard and Solomonica, 1936).

The government geologist G. S. **Blake** dealt with mineral resources (1930, 1937), stratigraphy, and building stones (1935). The Survey of Palestine published geological maps at a scale of 1:250,000 (1939) and towards the end of the British mandate, when air photographs became available, the geological map of southern Palestine at 1:250,000. The map and explanatory notes of S. H. **Shaw** (1947), also using Petroleum Development (Palestine) Ltd. geologists' reports, summarizes well the geological knowledge of that region at the time. Geology and water resources were dealt with as well, by **Ionides and Blake** 1940, and **Blake and Goldschmidt**, 1947.

Researchers who contributed to the stratigraphic nomenclature and geology of the region are mentioned in Chapters 18 through 21 of Part IV.

The French geologist Louis **Dubertret** (1929-1976), mainly active in Lebanon and Syria, laid the foundations for the stratigraphy of the Galilee. In 1932 he was the first to suggest the idea of strike-slip along the Dead Sea Rift, but later changed his mind. Revived by **Quennell** (1959), with the help of Raphael **Freund** et al. (1970) it became the leading theory, although it still has its opponents (see Horowitz 1979, 2001).

The establishment of the State of Israel in 1948 brought the era of colonial research to an end, and opened the way for the development of modern scientific investigation. The universities and state agencies flourished. Leo **Picard** founded the Geological Survey of Israel (GSI) in 1949, and the Institute of Ground Water of the Hebrew University in 1966. As a team Yaakov **Bentor** and Akiva **Vroman** surveyed the Negev at a scale of 1:100,000.

Around 1950 the onset of deep drilling and geophysical measurements marked a significant turning point in the geological investigations. The first director of the Geological Survey was Fritz **Brotzen**, a paleontologist from Sweden. He and his wife Pnina laid the foundations of biostratrigraphy in Israel. Zeev **Reiss**, also assisted by his wife Pnina, further developed micro-paleontology. Moshe **Avnimelech** (1950) put in evidence a Late Turonian unconformity, now recognized as a major sea-level drop

In the meanwhile, Abraham **Parnes**, a former geography teacher in Yiddish and Hebrew seminars on the shores of the Baltic Sea, was a librarian at the Hebrew University. Parnes had developed an early interest in fossils, and had heard **Diener** lecturing in Vienna on his studies of the Hula Valley and southern Lebanon (1885). Discovering his skills, Prof. Moshe Avnimelech gave Parnes fossils to study. After earning a Ph.D. (1958) on Triassic ammonites, he spent most of his scientific carrier, although already retired, at the GSI. He died in 1989 while on a geological field excursion in the Golan, at the age of 97.

At the Hebrew University Zoology Department, Georg **Haas** was active in the study of vertebrate fossils. Most important to us are his contributions on Triassic reptiles (1959-1970).

Biographies and the bibliographies of Professors Picard and Reiss and Dr. Parnes, are given at the end of this Introduction.

If immigrant scientists had led much of the early research, most of their pupils were 'sabras' born in the country. This 'zabar' generation wrote M.Sc. and Ph.D. theses and research reports, mostly in the Hebrew language, but frequently followed by publication in international journals. Today departments of Earth Sciences are active at the Hebrew University, Jerusalem; Tel Aviv University; the Weizmann Institute of Science, Rehovot; the Ben Gurion University of the Negev, Beersheva; and at both the Israel Institute of Technology (the Haifa Technion), and the University of Haifa.

The GSI was later joined by two sister institutes, both government companies, within the same government ministry. Geophysical exploration in Israel is now the task of the Lod-based Geophysical Institute of Israel (GII), formerly the Institute for Petroleum Research and Geophysics (IPRG), and at Tel Shikmona in Haifa the Institute for Oceanographic and Limnological Rsearch Ltd. (IOLR) is the national oceanographic center. In Israel applied water exploration is now conducted by TAHAL (Water Planning for Israel).

OTHER REFERENCE MATERIALS

Books on the geology of Israel are still scarce. Material on the geology of Israel is to be found in the Bulletins, Reports, Technical Reports, Maps, and periodic GSI Current Research volumes of the Geological Survey of Israel. The Israel Journal of Earth Science, formerly the Bulletin of the Research Council of Israel (Section G), publishes peer-reviewed articles, usually with four issues annually. It is now an independent publication in its 54th year, sponsored in part by the Geological Society of Israel. The Israel Academy of Sciences and Humanities also occasionally publishes monographs.

Short geological overviews include Picard's 'Structure and Evolution' (1943) and 'Geology and Oil Exploration' (1959). to Excursion guide introductions for international geological congresses, like the 'Clay Conference' by Bentor (1966), and the Xth International Symposium of Sedimentology (Freund, Garfunkel et al., 1978) are also useful. A short 'Aperçu de l'histoire phanérozoique d'Israël' (Hirsch 1990) summarizes the stratigraphy of Israel. A number of special issues of the Israel Journal of Earth Sciences, like the 1980 issue in honor of Prof. Bentor and the 1991 issue in honor of Prof. Picard, encompass basic review papers summarizing much of the individual research of their authors. So does the 2000 festive issue of 'Current Research' for the 50th anniversary of the Geological Survey of Israel. Aharon Horowitz's books on the Quaternary of Israel (1979) and the Jordan Rift Valley (2001) both have introductions to the general geology of the country. Publication in 1994 of 'Geological Structure of the North Eastern Mediterranean (Cruise 5 of the Research Vessel 'Akademik Nikolaj Strakhov')' (Krasheninnikov and Hall, Eds., 1994) supplied the motivation for the present book.

THE STRATIGRAPHY OF ISRAEL

A Brief Outline (Fig. IV.20)

A 7000 m thick stack of layered rocks reveals the Precambrian and Phanerozoic cycles of deposition, cut by unconformities and gaps.

I: PRECAMBRIAN: 600 MILLION YEARS AGO

The Oldest Land - In the South

Volcanic-Sedimentary Island Arc Phase; Metamorphic-Kinematic Phase; Batholitic-Orogenic Phase and Final Phase of Crustal Stabilization; Crustal Structure and Composition of the subsurface Precambrian Basement, geophysical data, continental composition, transition zone, and question of oceanic crust.

The stratigraphic column in the Levant starts with Precambrian rocks in the basement. These are exposed in the Sinaitic peninsula and the Elat Region, west of the Dead Sea-Arava Graben as well as in Saudi-Arabia and Jordan as far north as the Dead Sea east of the Graben. These series are strongly metamorphosed, as they underwent a number of Precambrian orogenies. Since the end of the Precambrian a relative tectonic quiet dominated the Levant until the Early Senonian Alpine orogenic movements. The stratigraphic column is further characterized by a series of unconformities that reflect on happenings at the northern edge of the Gondwanian Plates, the global eustatic level changes, as well as major tectonic events. Expressing the lithostratigraphic development of the Levant, the stratigraphic column of Israel is subdivided into a number of groups, each separated from the others by such unconformities.

In the southern region of Elat, the stratigraphic column starts with the basement complex of Late Precambrian age. This large time span (from 800-600 Ma) witnessed the opening of an ocean and then its closure. The sediment fill of this opening ancestral ocean basin is represented by a complex of metamorphic series (Elat schists) and its closing by syn-orogenic granites and volcanics; rocks that penetrated and traversed the outer crust as it was folded, shortened, and uplifted. This pan-African orogeny sealed the landmass known as the Arabian-Nubian Craton. Its mountains were largely abraded, a process that ended with the development of a regional peneplain.

II: THE PALEOZOIC (540-250 Ma)

Cambrian with trilobites; Devono-Carboniferous wearing down; most of the country is out of the water; the Permian Paleo-Tethys

The Early Paleozoic of the Yam Suf Group (after the Hebrew name for the Red Sea) overlies an end-Precambrian peneplain in the south. In the Elat region it consists of an Early Cambrian marine inundation with trilobites, covered by a continental facies. The major unconformity and hiatus separating this lower group from the following Late Paleozoic Negev Group, is due to uplift and erosion of the Levant *i.e.* the Late Devonian and Late Carboniferous events of Gvirtzman and Weissbrod (1984).

This was followed by a long span of time out of the water, which caused intensive and extensive wearing down (the Ordovician-Carboniferous hiatus).

North of the Paran-line, the Late Paleozoic in the subsurface consists of the mixed Permian continental and marine phases of the Negev Group. Deposits of this age are exposed along the eastern coast of the Dead Sea. The Permian Negev Group is not exposed west of the Graben, but is widely recognized in drillings extending from the central Negev to central Israel and sporadically to northern Israel. East of the Dead Sea, the Negev Group is well-exposed at Humrat Main and Wadi Zarqa Main (Jordan) (Fig. IV.20).

III: THE DISTENSIONAL MESOZOIC (230-80 Ma) (Fig. IV.21)

Marine belts between the Nubian land (Gondwana) and Tethys Ocean; Triassic, Jurassic and Early-Middle Cretaceous, ammonites and dinosaurs;

A distentional phase (230-80 Ma) of marine belts between the Nubian land of Gondwana and the oceanic Tethys include its Triassic opening and Jurassic to Middle Cretaceous expansion. It is followed by the collision phase (80-50 Ma) of closure, generating our mountainous backbone of the Syrian Arc, in the shadow of the alpine mountain structure in Asia Minor.

North of the Paran-line, marine Early Triassic sets in. These strata are exposed only along the eastern coast of the Dead Sea.

Marine Middle-Late Triassic (Ramon Group), fluvio-deltaic and marine Early-Middle Jurassic, and marine Late Jurassic (Arad Group) are partly exposed in the erosional cirques of Ramon, Hathira, Kurnub, and Arif (in the Negev), the Malih gorge (in Samaria) and Mount Hermon (in the Anti-Lebanon).

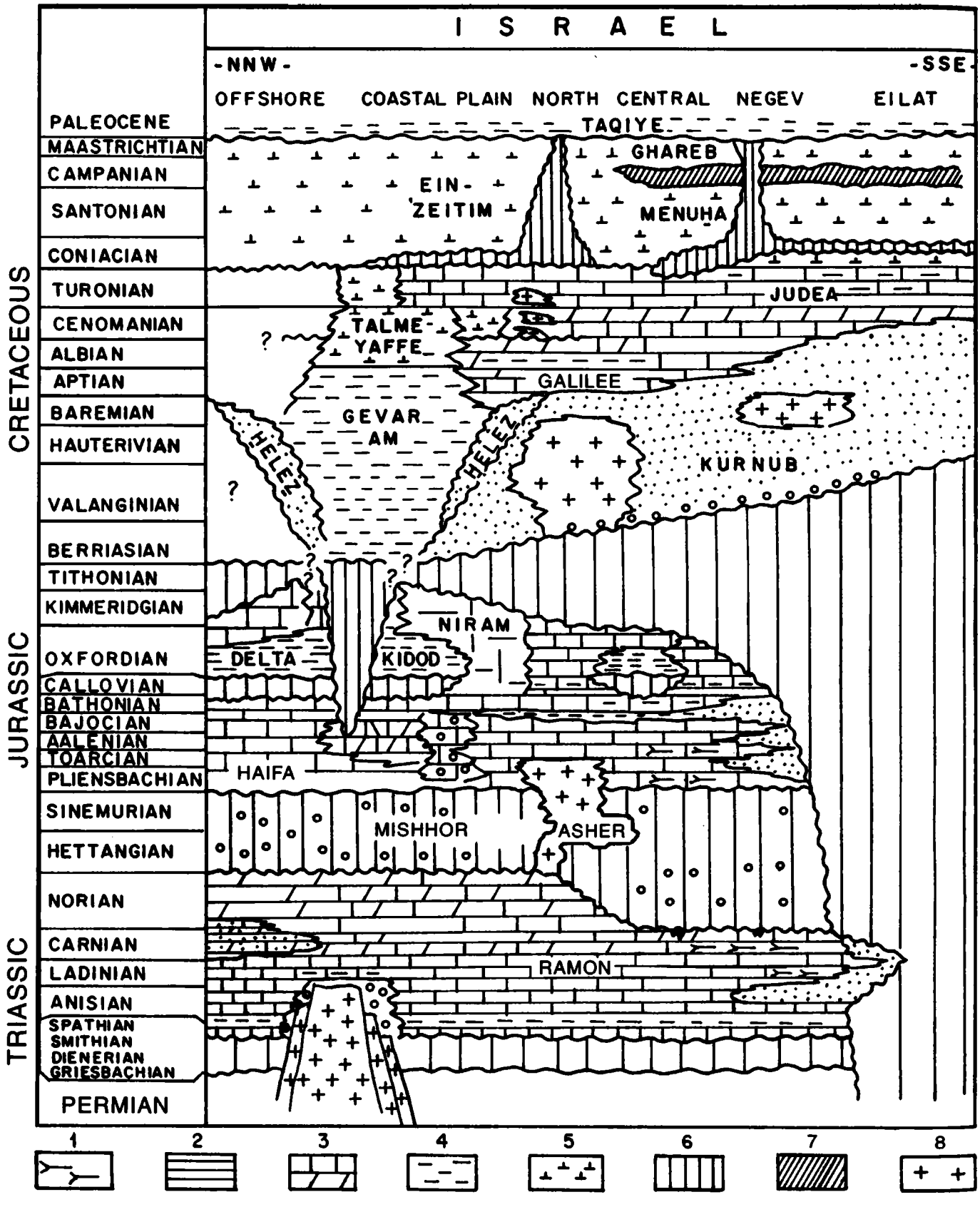
The Triassic-Jurassic and Jurassic-Cretaceous boundaries are both characterized by an angular unconformity, accompanied by erosional hiatus and volcanics, truncating edgewise the subjacent Mesozoic and Paleozoic deposits.

The unconformity separating the Negev Group from the overlying Ramon Group was originally thought to be a hiatus of the entire Early Triassic close to the top of the Zafir Formation. It seems however to be restricted to the Induan stage of the Lower Triassic, lower in the section, at the boundary of the 'Arqov and Yamin Formations.

An earliest Anisian hiatus, based on palynomorphs (Horowitz, 1971), may possibly correspond to the early Mesozoic reopening of the Tethys (Marcoux, 1978).

The Ramon Group is exposed only in the erosional cirques of Araif e Naqa (Sinai), Makhtesh Ramon, and Har Arif. East of the Graben, outcrops between Wadi Hisban and Wadi Zarqa expose rocks that belong to the Ramon Group. The Middle Triassic (Late Anisian and Ladinian) is characterized by the typical 'Muschelkalk' facies of the sephardic province (Hirsch, 1972). Early Late Triassic deposits consist of evaporites of the Carnian Tethyan salinity crisis. The Ramon Group, drilled in the Galilee and in the Coastal Plain, also includes Late Triassic (Norian- Rhaethian) platform type sediments.

The major unconformity separating the Triassic Ramon Group from the Jurassic Arad Group may be related to the early Cimmerian phase. It is characterized by a Hettangian-Sinemurian


ISRAEL
-NNW-
-SSE-
OFFSHORE
COASTAL PLAIN
NORTH CENTRAL NEGEV
EILAT
PALEOCENE
MAASTRICHTIAN
CAMPANIAN
SANTONIAN
CONIACIAN
TURONIAN
CENOMANIAN
ALBIAN
APTIAN
BAREMIAN
HAUTERIVIAN
VALANGINIAN
BERRIASIAN
TITHONIAN
KIMMERIDGIAN
OXFORDIAN
CALLOVIAN
BATHONIAN
BAJOCIAN
AALENIAN
TOARCIAN
PLIENSBACHIAN
SINEMURIAN
HETTANGIAN
NORIAN
CARNIAN
LADINIAN
ANISIAN
SPATHIAN
SMITHIAN
DIENERIAN
GRIESBACHIAN
PERMIAN
CRETACEOUS
JURASSIC
TRIASSIC
TAQIYE
GHAREB
EIN-ZEITIM
MENUHA
JUDEA
TALME YAFFE
GALILEE
GEVAR AM
HELEZ
KURNUB
NIRAM
DELTA
KIDOD
HAIFA
MISHHOR
ASHER
RAMON
1
2
3
4
5
6
7
8

emersion and lateritization process of regional extent.

The Arad Group includes the Jurassic stages from Pliensbachian to Kimmeridgian. It is exposed in northern Sinai at Gebel Maghara and Gebel Minshera (Egypt), in the Negev at Makhtesh Ramon, Makhtesh Hagadol, and Makhtesh Haqatan, and at Wadi Malih in Samaria. It exists east of the Rift as well, building up Mount Hermon, and exposed in the Wadi Yabbok (Nahr Zarqa) vicinity (Jordan). The Jurassic rocks are also well-known from more than 200 deep drillings all over Israel (Picard and Hirsch, 1987).

The Late Jurassic-Early Cretaceous denudation process, related to the late Cimmerian phase, truncated the underlying Mesozoic and Paleozoic Arad, Ramon, and Negev Groups in the form of a prograding unconformity plane from NW to SE. The Early Cretaceous Kurnub Group overlies Cambrian rocks in southern Israel and Precambrian metamorphics in Sinai.

The Cretaceous rocks, that cover an appreciable extent of the territory of Israel and adjacent regions, are subdivided into tectono-environmental groups.

Starting with volcanics ranging from Berriasian to Hauterivian, and clastics ranging from Aptian to Cenomanian in age, the rocks of the Kurnub Group account for a part of the so-called Nubian Sandstone. This sequence represents the top-sequence of Ball and Ball's (1950) Paleozoic-Early Cretaceous 'Lower Clastic Division'.

Onlapping Barremo-Aptian to early Albian and late Albian to early Coniacian platform carbonates built up the Galilee Group and the Judea Group respectively, representing Ball and Ball's Lower Carbonatic Division.

In the Coastal Plain Tithonian-Aptian marine deposits represent the Gevar'Am Group, followed by the pelagic Albian Talme Yafe Group. The boundaries between these groups are laterally defined by relatively gradual facies links. They are topped by the Coniacian unconformity of regional extent and related with the early 'mise en place' of thrust-sheets in the alpine Tauro-Zagrid range, expressed here by the embryonic folding of the Syrian Arc.

III(1): TRIASSIC

Permian-Triassic gap at base; Lower Triassic of paleotethyan alpine heritage; Sephardic identity of the Middle Triassic; Shallow Neo-Tethyan Late Triassic.

The marine Lower Triassic of the Mediterranean region inherited the Upper Permian Paleotethyan paleogeography. It is developed in the 'Werfen' type facies that extended without any marked differentiation from its Eurasian to its Gondwanian margins. This facies can be studied along the Dead Sea shore in Jordan, not far from Humrat Main. With the late Lower Triassic initiation of the Mesozoic Neotethys, in the form of a discrete seaway of Hallstatt-type facies in the Aegean region, a Middle Triassic rifting and narrow pelagic sea-ways reached as far as the Tyrhenian region, leaving the southern Tethyan 'Sephardic' margin an epicontinental shelf of Muschelkalk facies extending from the Levant to the western Mediterranean areas of Spain, Apulia, and the Sardo-Provencal regions. This facies can be seen in the outcrops of Har Arif and Makhtesh Ramon.

During the early Upper Triassic, increased shallowing of both sephardic and tethyan realms facilitated, in the first stage, the extent of sephardic faunal elements, followed in the second stage by the Carnian salinity crisis, which put an end to the sephardic realm. The gypsum quarried at Makhtesh Ramon is a product of this stage. The Upper Carnian restoration of normal marine conditions (at the very top of the Triassic outcrop in Makhtesh Ramon) is of alpino-type nature. The Norian Hauptdolomite-Dachstein type of platform with appropriate faunas is only found in the Coastal Plain subsurface (Ga'ash borehole), and in the cirque of Aarne (Hermon).

The Middle Triassic transgression started in the Levant in the Early Upper Anisian (Pelsonian) as a result of spreading of the Neo-Tethys. The slight hypersalinity of the huge shallow epicontinental water body of the southern Tethys generated the conditions for the development of the endemic taxa that characterize the **sephardic** realm.

Tornquist and Fallot (in Gignoux, 1960) considered the Middle Triassic of the western Mediterranean as the equivalent of that in the Germanic Basin, with which it was believed to communicate through the hypothetical gate of Burgundy. It was admitted that alpine faunas migrated into this basin, mixing with typical germanotype faunas of Muschelkalk facies type, following the discovery of entirely different invertebrate faunas in the Germanic and Mediterranean Basins. Identical ammonoids, conodonts and bivalves are not only found in Spain and Israel, but also in North Africa and Turkey (Lerman, 1960; Parnes, 1962; Hirsch, 1972). The realm extended as far north as the northern edge of the Apulian Plate, around which the growing Neo-tethys reached into the Toscanian Rift. Therefore the western Mediterranean Muschelkalk and their North African, Apulian, and Levantine equivalents were part of one and the same marine shelf, for which the name *sephardic* was adopted (Hirsch, 1972). In Israel (Ramon, Arif), Egypt (Arif E Naqa), Jordan (Hisban), southern Turkey (Tarasci-Seydisehir), and Slovenia, sephardic faunal elements occur: *i.e.* the ammonoids *Israelites, Gevanites* and *Iberites* and the conodonts *Sephardiella* and *Pseudofurnishius*.

The Late Triassic starts with the dramatic salinity crisis of the Early Carnian, affecting the entire Mediterranean region with gypsum and salt deposition (the Saharan event). The Late Carnian transgression restored marine conditions in the eastern Mediterranean region with the development of the Hauptdolomite



Figure IV.21. Mesozoic of Israel - General Stratigraphic Scheme (modified from Hirsch, 1984).
Legend: 1. Gypsum and anhydrite; 2. Sandstone; 3. Limestone and dolomite; 4. Marl and shale; 5. Chalk; 6. Hiatus; 7. Chert; 8. Intrusive, basement and eruptives.

facies, passing to the western Tethys margins to the Keuper Facies. Reefs (Dachstein) separated this shelf-lagoon area of the Tethys from the pelagic Hallstatt facies to the north. This 'alpinotype' regime lasted to the end-Triassic Early Cymmerian phase of emersion, denudation, and lateritization that terminated the Triassic proto-oceanic stage of the Mesozoic Neotethys.

In sequential terms four major ingression-regression cycles characterize the Olenekian, Late Anisian, Ladinian to Early Carnian, and Late Carnian-Rhaetian. Regional emergence and laterization terminated the Triassic sedimentary sequence.

The first cycle, including the Yamin and Zafir Formations (defined in boreholes in southern Israel) consists of shallow marine carbonates and sand bodies, near-shore and lagoonal mudstones and sandstones as well as possible deltaic complexes. The second sedimentary cycle, including the Ra'af and Gevanim Formations (defined in the Negev outcrops of Arif and Ramon) consists of shallow marine carbonates (Ra'af Formation), fluvial, fluvio-deltaic, and tidal nearshore sandstones, siltstones, and mudstones (Gevanim Formation.). The third cycle is the most extensive both in time and areal extent, and includes the Saharonim and Mohilla Formations (defined at Ramon). The sedimentary sequence of these cycles consists of shallow marine carbonates, tidal flat and lagoonal carbonates, and evaporites. The fourth cycle of shallow marine carbonates (Uppermost Mohilla-Shefayim Formation) is truncated by a regional emergence of low relief that has exposed the entire Triassic terrain to karst solution and laterization.

These marginal deposits gradually change southward, as more landward conditions of continental clastic deposits, known from the Sinai and Arabia, prevail. Northward (seawards) the marginal sequences interfinger with shallow marine carbonate and lagoonal and tidal flat evaporite sequence platform deposits (Druckman and Kashai, 1981).

III(2): JURASSIC

Early Jurassic tropical soils (laterites), rivers and carbonatic platforms; Middle Jurassic sea-level oscillations: Bajocian rise, Bathonian coals, and Callovian coral sea; Upper Jurassic anoxic deep water shales and spiculites (Lower-Middle Oxfordian) and shallow sea urchin limestone, oolites and marls (Upper Oxfordian-Kimmeridgian).

The Triassic-Jurassic boundary in the Levant is a distinct sedimentary break manifested by lateritic paleosols (Mishhor) and volcanics in the north (Asher Volcanics).

The central Negev Makhtesh Ramon, carved out in a NE-SW orientated asymmetric anticline, reveals Liassic-Early Bathonian strata. Molluscs including ammonoidea are described by Parnes (1981) in his monograph of the Liassic-Dogger Ardon-Inmar-Mahmal Formations. The fossil flora of the Inmar Formation was studied by Lorch (1967).

A marine platform carbonatic regime began with the ?Pliensbachian-Toarcian (Ardon) and continued in the Toarcian (Qeren). It was interrupted by Toarcian-Aalenian clastics in the Negev, adjacent Sinai, and along a belt crossing central Israel (Inmar-Rosh Pinna). In northern Israel, Lebanon, and the northern Anti-Lebanon, overlying basalts and tuffs of the Asher Volcanics and monotonous platform-carbonates represent most of the Jurassic sequence. This consists of the Liassic-Oxfordian sequence of the Haifa (=Kesroaune) Formation, west of the Rift, and of the Liassic-Callovian sequence of the Aarne, Beqassem, and Hermon Formations east of the Rift.

The Bajocian lithofacies varies from mixed clastic-carbonatic in the Negev Daya Formation. to largely marly in the Sinai Bir Maghara Formation, and to exclusively platform-carbonates in the Galilee. The Bajocian-Oxfordian Haifa Formation is a monotonous sequence of carbonates, that in the Coastal Plain becomes interwedged by Bajocian-Bathonian oolitic shoals (Sederot) and spiculitic limestones (Barnea).

The paralic clastics that dominate the Early Bathonian in the Sinai and the Negev (Safa-Sherif) are replaced by Middle-Late Bathonian micrites and marls (Sherif) while a shale-belt that straddles the Bathonian-Callovian boundary extends along the Coastal Plain and penetrates eastward into the Judean Desert (Karmon Formation).

The Early Callovian in the Coastal Plain consists of calcarenites (Brur), unconformably covered by the Oxfordian Kidod shales. The limestones and marls of the Zohar Formation extend from the Negev to Sinai, passing into the massive limestones of the Haifa Formation in the north. A thin condensed ammonite-rich hard-ground limestone tops the Callovian at Gebel Maghara (Sinai) and Majdal Shams (Hermon). From Hamakhtesh Hagadol in the northern Negev to the borehole of Gebel Hillal (Sinai) thick Late Callovian limestones and marls build up the Matmor Formation.

The northern Negev Hamakhtesh Hagadol (Kurnub Anticline) reveals about 200 m of Callovian-Oxfordian beds. Hudson's (1958) ammonoids (identified by Spath), molluscs (determined by Cox), and brachiopods (determination by Muir-Wood) led to his Middle Callovian-Sequanian subdivisions, now complemented by the paleontological contributions of Reiner (1968), Gill and Tintant (1975), Hirsch (1979), and Lewy (1983).

The Early Oxfordian consists of limestones in the Haifa facies in the Galilee. A shale basin extends from northern Sinai, through central Israel to Mount Hermon, known as the Majdal Shams Formation. (=Kidod). These interfinger in the Coastal Plain area with bioherms and reefs of the Nir'Am Formation. In the northern Negev Qeren-Halutza area, the Lower Oxfordian is absent.

Late Oxfordian-Kimmeridgian limestones, oolites, shales and sands, and algal limestones extend from the Galilee and the Anti-Lebanon (Nahal Sa'ar Formation) to the northwest Negev Qeren-Haluza area.

The Wadi el Malih (eastern Samaria Wadi Faria anticline) exposes some 200 m of Late Jurassic.

From Mount Hermon's southeast flank (Arneh) to its southern plunge at Majdal Shams Jurassic formations are well-exposed. Razvalyaev's survey (1966) has put Haas's (1955) ammonoids in stratigraphic sequence, while recently Mouty (2000) has cleared the stratigraphy within the cirque of Aarneh, putting into evidence the presence of the Asher volcanics, covering Late Triassic strata.

The period straddling the Jurassic-Cretaceous boundary

(Tithonian-Neocomian) in the Levant and eastern Mediterranean is characterized by intensive uplift, rifting and volcanism. The regional uplift put an end to Jurassic marine sedimentation, except for the Tithonian turbidites filling submarine canyons. The Tithonian-Hauterivian Tayasir- volcanics cover the Jurassic truncation surface (Fig. IV.21). The Jurassic paleogeographic pattern of the Negev High, the Judean Embayment and the Galilee High was replaced (Hirsch et al., 1995), by the pattern of the Pleshet Paleobasin (Cohen et al., 1988), divided into Western Platform and Eastern Platform provinces, followed by large-scale transgression. The development of the Pleshet Paleobasin was initiated by the opening of the north-south oriented Gevar'Am Trough, straddling the present Levant-shores (Fig.1). During this time interval (Tithonian-Barremian) the clastic deposition in the Gevar'Am Trough suggests sources from land-masses in the south-east as well as from a western basement high, ~50 km offshore from the present coastline. The eastern border of the Trough consists of a belt of reefoid upbuildings initiated in the Jurassic (Callovian-Oxfordian), recurring in the Lower Cretaceous (Aptian and Albian) times. Eastward of this belt, wide carbonatic shelf-lagoons were formed (Bein, 1976; Bein and Weiler, 1976; Sass and Bein, 1982; Rosenfeld and Raab, 1984).

During the Jurassic, the Levant was part of the Gondwanian Tethys shelf-platform. The paleotectonic setting of the Levant consisted in relative lows and highs, controlled by differential rates of subsidence.

Prior to the Infracretaceous truncation the paleotectonic setting of the Jurassic deposits in Israel and adjacent Sinai consisted of:

a) The Negev High, separating

b) The northern Sinai Maghara Basin from

c) The central Israel-Hermon Trough.

d) The platform of the Galilee, Lebanon, and the northern Anti-Lebanon.

The shallow Negev High accumulated 900-2000 m of Jurassic sediments, while in the Maghara Basin and the central Israel-Hermon Judea Embayment a 3000 m thick sequnce is found. The rather shallow northern platform of the Galilee accumulated an up to 2000 m thick sequence, thinning to the north in Lebanon and coastal Syria. The clastics of the Liassic-Bathonian part of the sequence are connected with the wearing down of the Arabian Massif in the south and southeast. Yet thickening of the Early Oxfordian shales in the offshore wells points to derivation from some landmass in the west, now hidden below the Mediterranean. (Hirsch et al., 1995).

The Gevar'Am Trough, alongside the present Levant-coast, formed during the Tithonian, initiating a separation between an Eastern Levant platform extending toward the Arabian-Nubian Massif and a western shallow marine platform and adjacent landmass. Volcanics witness a number of aborted Mesozoic intracratonic rifts at the beginning and end of the Jurassic. The Late Triassic-Liassic Asher basalts reach a thickness of 2000 m in the western part of a trough that crossed the Galilee at right angles to the present coast. The Kimmeridgian-Hauterivian Tayasir basalts, up to 500 m thick, extend from Samaria to the Galilee, Lebanon, and the Golan Heights. (**Fig. IV.1**)

III(3): LOWER-MIDDLE CRETACEOUS

Infracretaceous uplift, denudation and volcanism; The continental Kurnub sandstone; The submarine Gevar'Am canyon deep under the Coastal Plain; The deep sea Talme Yafe calcilutites from Sinai to Mount Carmel and deep under the Coastal Plain; The shallow marine Galilee gastropod calcarenite, limestone-cliff, Orbitolina-shale, iron-oolite and Knemiceras marl; The Judea dolomite, limestone and sand; The Mount Scopus syn-orogenic chalks and chert.

The Cretaceous period commenced with rifting, divergence and volcanism over the Levant countries and the eastern Mediterranean. It witnessed a large-scale transgression and sea level rise, known all over the world (Vail et al., 1977), and terminated with alpidic convergence and folding processes (Syrian Arc).

The Early Cretaceous consists primarily of continental clastics and volcanics (Kurnub Group), passing laterally into Tithonian-Barremian marine shales in the Coastal Plain (Gevar'Am Group). Aptian-Albian (Galilee Group) and Cenomanian and Turonian-Early Coniacian platform-carbonates (Judea Group) extend progressively from Lebanon and the Galilee to the Elat region and the Sinai Peninsula, passing laterally into the basinal facies of the Coastal Plain (Talme Yafe Group).

The Cretaceous period in Israel and the adjacent areas of the Levant is distinctive by the wide carbonate platform that extended to the west and the Arabian-Nubian Massif in the east (ESE). A graben-like basin extends to the west of the present Coastal Plain, bordered by a belt of reefoid upbuildings initiated during Jurassic times (**Fig. IV.21**) (Bein, 1976; Bein and Weiler, 1976; Sass and Bein, 1982).

The northern edge of the platform, situated in Turkey was emerged during a time span extending from Albian through Turonian (Monod, 1977).

Similar interruptions in the sedimentation (marked by bauxites) are also known fron Saudi Arabia (Harris et al., 1987), leaving the Levantine platform open only to the west.

The Cretaceous platform sediments consist of up to 1500 m of thick carbonates, sandstones and shales. Planktonic and benthonic foraminifera, ostracodes and calcareous nannoplankton as well as ammonites, bivalves and gastropodes allow a fair biostratigraphy. Among bivalves, the occurrence of colonial and isolated rudists as well as oysters is particularly abundant.

The Cretaceous System in the Levant is divided horizontally into three facies-belts: Terrigenous to the southeast, shallow marine in most of northern Sinai, Israel and Lebanon, and pelagic in the Coastal Plain and the nearest offshore (Pleshet Basin). Vertically three sedimentary megacycles are identified:

1) ?Tithonian-Aptian;

2) Albian-Early Coniacian;

3) Senonian.

The latter is mainly a uniform, plankton-rich marly chalk passing to the southeast to chert and phosphorite.

The begining of the first megacycle (Berriasian- Hauterivian)

is marked by a tectonic volcanic and erosional phase. Most of the Levant (namely, the Sinai, Trans-Jordan, Israel, Syria, and Lebanon) emerged and a considerable thickness of eolian-fluviatile sands, silts, and shales (the Nubian Sandstone of the Kurnub Group) accumulated on the platform. Westwards, the over 1 km thick sequence of monotonous detrital black shales of the Gevar'Am Group was deposited, filling up the deeply incised erosional relief (Cohen, 1971, 1976).

The differentiation of a carbonatic shelf-platform characterizes Barremian and Aptian times. The first megacycle ends with the Late Aptian-Early Albian regression (Yavne event).

During the second megacycle a belt of rudistid barrier reefs provides much of the calcilutite-calcisiltite detritus to the sedimentary prism-shaped contourites of the Talme Yafe Group (Bein and Weiler, 1976). Simultaneously, the platform accumulated shallow marine limestones and dolomites of the Judea Group (Sass and Bein, 1982).

The evidence for the Infra-Cretaceous tectonic phase, enhanced by a rather extensive global sealevel drop, consists of angular unconformities between Nubian Sandstone units in Sinai (Weissbrod, 1969b), erosional disconformity in the Hazera cirque (Gill, 1965), extensive occurrences of conglomerates and laterites in the Negev, Trans-Jordan and the Sinai (Goldberg and Friedman, 1974; Wetzel and Morton, 1959), the development of extensive sabkhaic evaporites in the eastern Arabian Peninsula (Murris, 1980) and the incision of the Gevar'Am Canyon in the continental shelf of Israel (Fig. 5; Cohen, 1976). The relative depth of this channel with respect to its shoulders, about 930 m exceeds the eustatic sea level drop very significantly (*cf.* Vail et al., 1977). Such a denudation necessitates, therefore, a considerable uplift in addition to the drop in sea level.

Distensional diastrophism is further evidenced by the extensive occurrence of basic-alkaline volcanism in northern Israel and in Lebanon (Lower Kimmeridgian to Hauterivian; Dubertret, 1954; Renouard, 1955; Mimran, 1972; Mimran et al., 1984, 1989; Bonen, 1980), by fault-induced thickness variations of basic flows and pyroclastics in Samaria, and of Kimmeridgian carbonates in the Haifa Bay-Carmel area (Derin, 1974). Both the southward increasing depth of truncation in Israel and in Trans-Jordan (Bender, 1974; Bandel, 1981; Druckman, 1982), and the decreasing age of the lowermost onlapping units in the same direction (Freund et al., 1975), suggest that the uplift was asymmetrical, with a hinge located somewhere in Saudi Arabia.

The transgressive-regressive Cretaceous record in Israel is in good agreement with global eustatic trends. The early Neocomian eustatic low is represented by the development of Wealden facies in Israel, Trans-Jordan and Lebanon (Aharoni, 1964; Bender, 1974; Beydoun, 1977). The extensive Aptian transgression is well-recorded by an extensive blanket of carbonates almost entirely replacing terrigenous deposits in the Coastal Plain of Israel.

The eustatic low at the Aptian-Albian boundary is represented in Israel both on the shelf-platform and in the basin. In the former, there is a prominent phase of arenaceous and shaly intercalations between carbonate units in the Mount Hermon area, Samaria, Judea and the Coastal Plain - the 'Main Shale Break' (Bein, 1974), while west of the hinge-line, thick pelitic sequences of semi-pelagic facies (the Gevaram and Talme-Yafe Formations) are separated by an unconformity (Bein and Gvirtzman, 1977).

A similar regressive phase is also reported from Saudi Arabia, where a clastic blanket covers the whole platform (Murris, 1980).

A poorly documented Albian distensional phase is inferred from some recently dated hypabyssal intrusions of peralkaline basalt and syenite in the Timna and Ramon areas (107 Ma; Starinsky et al., 1980; Beyth and Segev, 1983), northern Lebanon (Terbol-1 well; Beydoun, 1977) and in the southern Ansariyeh Mountains of Syria (Dubertret, 1937, in Wolfart, 1967).

The Albian to Early Coniacian stratigraphic record of the platform carbonates in Israel matches fairly well the details of the eustatic global sea level curve of the corresponding time interval (Haq et al., 1987). The five sedimentation sub-cycles of the Albian to Turonian (Bein and Gvirtzman, 1977, with chronostratigraphy after Lewy and Raab, 1976) involve alternating phases of shallowing and deepening.

In the Levant and eastern Mediterranean the period straddling the Jurassic-Cretaceous boundary (Tithonian-Neocomian) is characterized by intensive uplift, rifting and volcanism. The Jurassic paleogeographic pattern of the Negev High, the Judean Embayment, and the Galilee High was replaced (Hirsch et al., 1995) by the pattern of the Pleshet Paleobasin (Cohen et al., 1988), divided into Western Platform and Eastern Platform provinces, and followed by large-scale transgression. The development of the Pleshet Paleobasin was initiated by the opening of the north-south oriented Gevar'Am Trough, straddling the present Levant-shores **(Fig. IV.23)**. During this Tithonian-Barremian time interval the clastic deposition in the Gevar'Am Trough suggests sources from land-masses in the south-east as well as from a western basement high, ~50 km offshore from the present coast. The eastern border of the Trough consists of a belt of reefoid upbuildings initiated in the Jurassic (Callovian-Oxfordian), and recurring in Lower Cretaceous (Aptian and Albian) times. Eastward of this belt, wide carbonatic shelf-lagoons were formed (Bein, 1976; Bein and Weiler, 1976; Sass and Bein, 1982; Rosenfeld and Raab, 1984).

The southern edge of the Gevar'Am Trough is found in the exposures of Risan Aneize (Talme Yafe Formation, Sinai, Egypt).

The northern edge of the Gevar'Am Trough may reach as far as the Pisidian Taurus autochtonous Akkuyu Basin (Hirsch, 1984), an area of similar sedimentation, including the large sedimentary gaps due to emersion in Albian-Turonian times (Monod, 1977). Such interruptions in sedimentation, witnessed by bauxites, occur in the eastern Mediterranean offshore drillings (Hirsch et al., 1995).

The Gevar'Am Trough is thus genetically related to the origin of the Pleshet Paleobasin, a concept which encompasses the entire area of sagging or subsidence along and off the present Levant coast line. The narrow trough zone in the middle, and approximately located under the present Levant coastline, is bound by *en echelon* downfaulted edges (hinges), by both the Arabian-Nubian Massif (Eastern Province) and the Western Province of continental platform type situated offshore the present Mediterranean Sea (Rosenfeld

and Raab, 1981; Hirsch et al., 1995; Rosenfeld et al., 1995).

The thickness distribution of the Lower Cretaceous deposits varies from about 300 m in the northern Negev (Eastern Platform, vicinity of Nubian Craton) to more than 3,000 m under the Coastal Plain (Gevar'Am Trough).

The Lower Cretaceous tectono-environmental pattern of the Levant is dominated by SW-NE isopes. In a NW-SE cross-section from the Mediterranean offshore toward the Arabian-Nubian Massif four facies-belts can be distinguished:

1) Western Province platform facies (offshore, the Bravo-1 borehole on its margin);

2) Gevar'Am pelagic basin facies (Coastal Plain boreholes *e.g.* Shimon-1);

3) Eastern Province platform facies, clastic influx from the Arabian-Nubian Massif (Gebel Lugama, Helez, Judea);

4) Arabian-Nubian mixed marine platform and fluviatile/ continental facies (the Galilee, Golan, and the Negev).

The Cretaceous comprises the Gevar'Am, Kurnub, Galilee, Talme Yaffe, Judea, and Mount Scopus Groups.

III(4): MESOZOIC–PALEOGENE (Fig. IV.21):
Senonian-Eocene phase of collision and uplift

Our mountainous backbone - the Syrian Arc - in the shadow of the Alpine orogeny

The Alpine orogeny was echoed by the Levantid inversion of Early Mesozoic faults, producing the asymmetrical folds of the S-shaped Syrian Arc. This Arc extends from northern Sinai to the Negev, the southern coastal Plain of Israel, Judea and the Galilee, shaping a paleogeography of basins and islands that controlled the Senonian, Paleocene and Eocene (Mount Scopus and Avedat Groups) carbonatic and silicious sediments. The third Cretaceous sedimentary megacycle (Senonian) is characterized by open sea conditions with both thickness and facies of chalks, marls, phosphorites and chert being controlled by the incipient folding of the Syrian Arc (Flexer, 1968, 1971; Flexer and Honigstein, 1984).

The Senonian starts with a remarkable high-stand, which established an environmental pattern entirely different from that of the preceding Cenomanian-Turonian and changed the platform into a ramp (Sass and Bein, 1982). A radical change in the sedimentary regime marks the beginning of the Senonian. The paleo-topography of anticlines and synclines of the Syrian Arc controls facies and thickness of the predominantly chalky Coniacian, Santonian, and Campanian Menuha Formation. The deposition of the thick cherts, porcelanite, chalk, marls, and phosphorites of the Campanian Mishash Formation in the basinal synclinal channels contrasts with the thinning toward the anticlinal ridges that formed strings of islands. Continuous tectonic movements constantly renewed the paleogeographical pattern during the deposition of chalks and bituminous shales of the Maastrichtian Ghareb Formation. The chert ratio increases in the southern Negev (the Sayarim Facies), and decreases toward the Galilee and the Coastal Plain (Ein Zeitim). The Senonian carbonatic and silicious sedimentation of the Mount Scopus Group occurs in two different facies, thick synclinal versus reduced anticlinal deposits.

The pelagic chalk deposition persisted over the previous platform and basin areas (the Mount Scopus and Hashefela Groups respectively).

The new regime of Senonian-Eocene syntectonic sedimentation in the typically asymmetric Levantid folds of the Negev and Judea is composed of two groups:

1) Chalks with pelagic faunas and cherts, phosphorites and bituminous marls that characterize the Senonian-Paleocene Mount Scopus Group;

2) Marls, limestones and chalks of the Eocene Avedat Group.

The Senonian is often separated from the Paleocene by an unconformity, accompanied by iron crust and paleosol. The Cretaceous and Eocene share the largest surface extent in the Levant.

The C/T boundary is well-documented in the basinal facies. High iridium concentration at the base of the *G. eugubina* Zone and trace elements and microspherules occur between the *A.mayorensis* and *M. pseudobulloides* zones (Rosenfeld et al., 1989). Elsewhere the upper strata of the Maastrichtian are missing and the Paleocene-Early Eocene Taqiye shales onlap a paleorelief with paleosoil.

IV: CENOZOIC

Deposition of syn-orogenic Paleocene Taqiye shales and Eocene Avedat limestones and chalks; After the deposition of Oligocene Lakhish chalks and Sussita limestone, most of Israel is out of the water again; wearing down of the land to the Neogene sea in the west; our home-plate breaks up as it slips under the Cypryan Arc, Arabia slipping faster northward under the Eastern Taurid ophiolite belt; uplifting Mount Hermon; The Rift gapes apart, making space for Mio-Pliocene salt-deposits (Sedom) and a Pleistocene string-shaped lake (Lisan); The process is accompanied by basalts, tuffs and scoria.

The Holocene witnesses the making of the desert and the shrinking of the waters of the Rift to the Sea of Galilee and the Dead Sea.

The Paleocene-lowermost Eocene Taqiye Formation or Taqiye marls (= Esna shale in Egypt) are by definition a part of the Mount Scopus Group. Their inclusion in the Avedat Group would be justified due to the typical C/T boundary features and by local erosional events (Hirsch, 1990).

The Avedat Group encompasses siliciferous limestones and chalks that, like the Mount Scopus Group, may directly onlap the Levantid anticlines. The facies of the Avedat Group varies strongly. It comprises the five litho-stratigraphic and tectono-environmental subdivisions I-V (modified after Hatzor et al., 1994). Regional facies variations within the Avedat Group are expressed by numerous formations.

Lower Eocene: (I) Chalks with thin bands or nodules of chert (Zora Formation of the Shefela, Mor Formation of the Negev and Adulam Formation of the Galilee, Shefela, and the Jordan Valley); (II) Nummulitic limestone with chalk bands, chalky limestones, and chalks (Zora/Adulam Formation of central Israel, Nizzana Formation of the Negev and the Jordan Valley, the Meroz Formation of Mount Gilboa);

Lower-Middle Eocene: (III) Chalks and limestones with changing amounts of chert bands or nodules (Maresha Formations of northern and central Israel, Horsha and Paran Formations of the Negev, Masua and Sartaba Formations of the Jordan Valley, Yizreel Formation of Mount Gilboa);

Middle Eocene: (IV) Limestones and chalks (Matred Formation of the Negev, Bar Kochba Formation of Mount Gilboa, the Argaman Formation of the Jordan Valley);

Upper Eocene: (V) Chalks and limestones, (Bet Guvrin Formation in the Coastal Plain subsurface, Nahal Yeter, the Qeziot and Har Aqrav Formations of the Negev).

The inclusion of these Upper Eocene strata, originally part of the overlying Saqiye Group, into the Avedat Group was proposed by Cohen et al. (1987).

IV(1): OLIGOCENE-MIOCENE

Out of the water again, wearing down of the land to the sea in the west; our African homeplate breaks-up and Arabia slips north

At the end of the Avedat and lower Saqiye Group times most of the surface of Israel emerged from the sea.

In the Coastal Plain (Shefela) a regime of channel and canyon sedimentation contrasts with wide continental regimes of internal basins with lakes and fluviatile deposits. This regime, recognized within the Saqiye Group, culminated during the Miocene which ended with the Messinian events. The post-Eocene uncomformity separates the Avedat Group from the lower part of the Saqiye Group, which encompasses marine sediments of Oligocene age.

The Late Eocene-Oligocene sediments were widely destroyed by the regional uplift that ended the present phase, leaving only a few marine outcrops in the northern Negev, the Coastal Plain and Golan Heights.

The Paleogene part of the Saqiye Group consists of the Lower Oligocene ingressions of the Lakhish Formation in northern and central Israel, and of the Fiq and Sussita Formations east of the Sea of Galilee. After the mid-Oligocene unconformity, marine sedimentation resumed as the upper part of the Saqiye Group of Miocene age. To the east, during this span of time, the continental deposits of the Tiberias Group, consisting of the allochthonous drainage products from the mountains of the huge plateaus further to the south-east, and of autochtonous lake deposits, embraced the morphology generated by the mid-Oligocene regression.

Restricted to the strip of the Coastal Plain and Shefela, the marine deposition of the Saqiye Group was only scarcely exposed in the Coastal Plain rise (Beersheva), ingressing eastward the fluviatile deposits of the Tiberias Group.

Since the latest Oligocene-Early Miocene, a sinistral strike-slip along the Jordan-Gulf of Aqaba line took place. The Neogene-Quaternary sinistral wrench movement of over 100 km displacement, first put in evidence by Lartet (1869), was the result of the opening of the Red Sea, which created a chain of rhombs. East of this line, forming the limit between the African and Arabian Plates, crustal shortening generated the folding and thrusting of the Palmyrids. This regime ends with the opening of the Rift, leading to the final severance of the African and Arabian Plates.

The Saqiye Group encompasses all the Oligocene-Neogene marine sediments. The Paleogene part of the Saqiye Group consist of the marine Oligocene part of the Bet Guvrin Formation and Lakhish Formation in the Shefela and of the Fiq and Sussita Formations east of the Sea of Galilee.

The Oligocene regression resulted in regional emergence and erosion. Marine Neogene (Saqiye Group) in the Coastal Plain of Israel interfingered with continental deposits in the east. Since the Miocene, a sinistral strike-slip along the Jordan-Gulf of Aqaba line opened a chain of rhomb-shaped grabens. Neotectonic isostatic readjustments produced the sinking of the eastern Mediterranean Basin and the differential uplift of portions of the African, Levantine, and Arabian sub-plates, generating a new orography *e.g.* the Yizre'el Graben and the Jordan-Dead Sea-Arava Rift, accompanied by basalts that extended from the Golan Heights to the eastern Galilee, filling large parts of the Rift. A marine ingression in the Yizre'el Valley also reached the Rift, leaving thick evaporites.

The Lower-Middle Miocene part of the Saqiye Group consists of the marine deposits of the Ziqim and Ziqlag Formations and interfinger in the Beersheva and Yizre'el Embayments with the continental deposits of the Tiberias Group, prior to the opening of the Dead Sea Rift.

The Upper Miocene part of the Saqiye Group consists of the Patish, Mavqiim, and Afiq Formations. These formations are mostly buried under the Coastal Plain and in the Beersheva Embayment. They are partly exposed in the foothills along the Shefela.

The Pliocene strata of the Saqiye Group consist of the marine Yaffo Formation.

The Tiberias Group (Kefar Gilad Group of Flexer et al., 1981) encompasses the ?Late Oligocene-Early Miocene continental sedimentation in the Negev and the Jordan-Dead Sea-Arava depression. It is mainly of fluviatile and lacustrine nature. It encompasses the Hazeva, Ein Gev and Hordos Formations. A marine ingression into the Beersheva Embayment reached as far east as Yeroham and Dimona, where 'end of gulf' oysters encrusted along the sandy Hazeva shore.

IV(2): MIO-PLIOCENE TO PLEISTOCENE

The Rift gapes apart, generating a new hydrographic pattern; Salt deposits and a fresh water string-shaped lake.

After the Late Miocene, the opening of the Rift was accompanied by the deposition of the sediments of the Dead Sea Group, and the Pleshet Group in the Shefela (or Coastal Plain). The continental deposition of the Dead Sea Group in the intra-cratonic basin was compartmentalized as the rifting collapsed the string of rhomb-shaped grabens that formed along the Jordan-Dead Sea-Arava line. Uplift and erosion of most of the territory of Israel created a new water-shed, to the west of which extended the marine deposition of the Kurkar Group. The neo-tectonic activity was accompanied by the basalt, scoria and tuff eruptions of the Bashan Group.

This subdivision comprises the deposition since the Middle Miocene opening of the Rift. Neotectonic isostatic readjustments

produced the reshaping of the eastern Mediterranean and the Levant. The eastern Mediterranean portion of the African Plate underwent uplift and deepening of its basins, echoing the differential uplift of the adjacent Levant-Sinai portion of the African Plate, dissected into Negev, Judean, and Galilee blocks. The sinking of the Dead Sea Rift, echoed by the uplifted Transjordan portion of the Arabian Plate, generated a totally new orography, affecting the mountainous backbone of the Sinai-Levant Sub-plate.

These tectonic events were further accompanied by volcanism on the Golan Heights and the eastern Galilee, filling also parts of the Yizre'el Valley and the Jordan-Dead Sea-Arava Rift.

The continuous deepening of this Rift (Jordan and Arava Valleys) was echoed by the deposition of the Dead Sea Group, representing an independant province.

Late Miocene, presumably Tortonian, marine ingression into the Rift through the Yizre'el Valley left behind the thick evaporites of Zemah, south of the Sea of Galilee, and of Sedom, in the Dead Sea area. These marine ingressions that found their way into the young Rift, filling the freshly formed rhombs with thick evaporites, preceded the Messinian evaporites in the Mediterranean.

The Dead Sea Group encompasses the Late Miocene and Pliocene clastic sediments of the Rift extending from the Jordan to Arava Valleys, including the Arava Conglomerates and the Amora Formation. The marine ingressions into the Yizre'el Valley (Bira, Zemach, Gesher) reached the Dead Sea area (Sedom) leaving thick evaporites.

The Pleistocene Lake Lisan filled parts of the Jordan and Arava Valleys, associated with the ascent of man, and preceded the Holocene - present Dead Sea.

The Pleistocene deposits of the Coastal Plain of Israel reflect the oscillations of the Mediterranean Sea during the Glacial periods and the isostatic movements of the Levant Platform.

IV(3): HOLOCENE

The making of the desert and the shrinking of the Dead Sea. Includes the present Dead Sea, alluvium and Loess deposits.

SUMMING UP THE STRATIGRAPHY

The geology of Israel deals with the nature and evolution of an epicontinental platform between a craton and an orogenic belt. Its stratigraphic column or 7 km thick stack of sedimentary layers subdivides into four main phases of development:

Phase I:. The oldest rocks, exposed in the southern part of the Negev (Timna Park and Elat), consist of Late Precambrian syn-orogenic volcanics and metamorphics, consolidated by the pan-African orogeny. They build up the Arabian-Nubian Craton and are a part of the Gondwanian Plate agglomerate. This phase was ended by a regional peneplain.

Phase II. Comprises the rocks deposited during the time-span that lies between the pan-African and Alpine orogenies. It encompasses groups, separated by uplifts and volcanic events.

The Early Paleozoic Yam Suf Group, that consists of marine Early Cambrian arkoses, carbonates with trilobites, and Cambro-?Ordovician continental quartzites. Rocks of this phase are also exposed in the southern part of the Negev (Timna Park).

The sandstones and limestones of the Late Permian Negev Group and Early Triassic part of the Ramon Group are known from boreholes north of the Paran-line and from exposures along the eastern Dead Sea shore.

In Har Arif the Middle-Late Triassic part of the Ramon Group comprises Anisian limestones and sandstones and at Makhtesh Ramon, Anisian sandstones, Ladinian limestones, and Carnian dolomites and gypsum. The Ramon Group is covered by a regional lateritic event that represents the base of the Jurassic Arad Group. Furthermore in Makhtesh Ramon the latter consists of alternating fluvio-deltaic and marine clastic to carbonatic strata, representing the Liassic, Aalenian, and Bajocian stages. The Callovian stage is partly represented in the Hamakhtesh Hagadol, also known as the Hatira or Kurnub cirque. More comprehensive sections are exposed in Gebel Maghara (Sinai, Egypt) and Mount Hermon (the Anti-Lebanon). The Jurassic in the Negev is truncated by an angular unconformity.

The Early Cretaceous Kurnub Group consists of continental variegated sandstones and marls, with volcanics, exposed in the Ramon cirque. Particularly well-exposed in Hatira (Kurnub) are marine marly intercalations, witnessing ingressions into the Negev of the Barremo-Aptian and Early Albian sea, that formed the carbonates of the Galilee Group in the north of Israel. Late Albian-Early Coniacian platform-carbonates build up the Judea Group, well-exposed in the Judean Mountains and Negev anticlines, as the result of the next phase.

Phase III. The Alpine orogeny was echoed by the Levantinid inversion of Early Mesozoic faults, producing the asymmetrical folds of the S-shaped Syrian Arc. This extends from northern Sinai to the Palmyrids. Folds in the Negev and Judea are typically asymmetric.

The Syrian Arc shaped a paleogeography of basins and highs, sometimes islands, that controlled the carbonatic and silicious sedimentation of the Senonian-Paleocene Mount Scopus Group, the Eocene Avedat Group. and the Oligocene lower part of the Saqiye Group.

A regional uplift ended this phase, resulting in denudation and erosion.

Phase IV. After the Middle Oligocene regression, the marine Neogene of the middle part of the Saqiye Group was only slightly exposed in the Coastal Plain rise (Beersheva).

Marine deposition passes eastward into the continental deposits of the Tiberias Group.

Since the Late Oligocene or Early Miocene a sinistral strike-slip along the Jordan-Gulf of Aqaba line opened a chain of rhomb-shaped grabens, accompanied by basalt eruptions. The presumably Tortonian ingression in the Yizre'el Valley found its way into the Rift, depositing thick evaporites in the freshly collapsed rhombs south of the Sea of Galilee and in the Dead Sea, preceding to the Messinian evaporites in the nearby Mediterranean.

Pliocene isostatic readjustments produced the downwarp of the eastern Mediterranean Basin, echoed by the differential uplift

of portions of the African, Levantine and Arabian sub-plates. A Late Pleistocene Lake Lisan filled parts of the Jordan and Arava Valleys, associated with the ascent of man, preceding the Holocene formation of the present Dead Sea.

SHORT OUTLINE OF THE TECTONICS IN ISRAEL

- *Collisions and uplift, slipping and faulting;*
- *The interplay between the African-Arabian Cratons and the Alpine Orogenic Belt*
- *Nature and structure of our crust*
- *The twisting, slipping and colliding of plates*
- *The folding of the mountains*
- *The fracturation of the crust*

The tectonic setting of the eastern Mediterranean and the Levant consists of the triple junction of the African, Arabian and Anatolian Plates, bounded by the Cyprian Arc, Peri-Arabian Ophiolitic crescent, and Dead Sea Transform **(Fig. IV.22)**

The eastern Mediterranean Levantine Basin is possibly paved by a thinned ancient crust and filled by thick phanerozoic sediments of epicontinental nature. Geophysical and geological data suggest that paleotectonic structures cross the present Levant coast and that a number of highs and paleo-landmasses encircle the Mesozoic Pleshet aulacogen, a basin extending from the present Mediterranean offshore to the Coastal Plain subsurface and into the Judean Embayment.

The strongly interwoven geological and tectonic history of the Levant is punctuated by periods of subsidence and uplift, subdivided into phases:

1) The early geological history of the Levant is Gondwanian. A basement of accreted terranes, consisting of plutonics, volcanics, ophiolites and metasediments was consolidated by the Late Precambrian Pan-African orogeny, including the Menderes, Eratosthenes, and Arabian-Nubian Massifs, prior to regional peneplanisation.

2) The Paleozoic history of the Levant is one of End-Devonian, Permian, and post Permian domal uplifts, which resulted in the erosion of much of the Paleozoic deposition. Hardly anything is left of the Ordovician-Devonian sedimentation and the earliest Triassic is missing. A paleo-geological subcrop map of the Near East suggests that the post-Devonian high encompasses a large area of the eastern Mediterranean (See Chapter 18K: Tectonic Evolution, Fig. 18K.4).

3) The Early Triassic opening of Neotethys across Gondwana was echoed by Mesozoic epicontinental sedimentary cycles of the Ramon Group (Olenekian-Rhaetian), Arad Group (Pliensbachian-Tithonian), the Galilee Group (Berriasian-Aptian), and Judea Group (Albian-Coniacian), well-developed in the depocenters of respectively the Galilee, Palmyra, and Judea Embayments. These cycles are interrupted by intracratonic rifting, uplifts, volcanics, and/or eustatic sea level changes, possibly echoing the neoTethyan island arc and mid-oceanic volcanism and spreading.

4) Reflecting the alpidic Neotethys-Gondwana collision, the Levantid deformation of the Negev-Palmyrid belts is the result of the inversion of Early Mesozoic faults, producing the asymmetrical folds of the S-shaped Syrian Arc. These extend from northern Sinai to the Palmyrids. Folds in the Negev and Judea are typically asymmetric. As noted above, the carbonatic and silicious sedimentation of the Senonian-Paleocene Mount Scopus Group and of the Eocene Avedat Group were controlled by the basin and high paleogeography of the Syrian Arc. The Oligocene lower part of the Saqiye Group represents the last period of this phase. Sediments of this age were widely destroyed by the regional uplift that started the next phase, leaving only a few marine outcrops in the northern Negev, the Coastal Plain and Golan Heights.

5) A possible mid-Oligocene tectonic rebound coincides with a drop in sea level, enhancing regional regression, emergence, and erosion. Since the Late Oligocene, the opening of the Red Sea split the Gondwanian foreland into separate African and Arabian Plates. The continued collision at differing speeds with the neo-Tethyan Anatolian Plate, that generated the Dead Sea Transform, also resulted in the Miocene deformation of the Palmyrid belt, absorbing a part of the pressure. The sinistral strike-slip also opened a chain of rhomb-shaped grabens along the Jordan-Gulf of Aqaba line, accompanied by basalt eruptions at its northern end. Pliocene isostatic readjustments produced the downwarp of the eastern Mediterranean Basin, echoed by the differential uplift of portions of the African, Levantine, and Arabian sub-plates.

THE LEVANTID FOLDING BELT

The Levantid folding belt is a segment of the peri-Arabian foreland folding-arc, extending from the Pelusium transform in the west to the Euphrates graben in the east. (Fig. IV.23). This Levantid belt is split into the segments of the Negev-folds and of the Palmyrids by the Dead-Sea Transform, giving it an apparently S-shape. These folding arcs share northeast trending axes, asymmetry due to presence of basement-controlled reverse faults, and a multiphase history of deformation. The Senonian-Early Miocene W-WNW trend is actually referred to as the 'Syrian Arc' stress field, followed by the Late Miocene-Pleistocene 'Dead Sea' stress field (Eyal and Reches, 1983).

Starting in the Coniacian, the Levantid compression decomposes into transversal faulting with strike-slip components and vertical displacements, and in reverse faulting with asymmetric folding. These compressional pulses recurred until the Early Miocene. Post Oligocene deformation decomposed into folding and sinistral strike-slip movements, possibly in combination. In the Hermon the compressional deformation, though present from the Senonian, reached its peak only after the Oligocene, as happened to the Palmyrides (Chaimov et al., 1990).

The ultimate Levantide deformation is related to Late Neogene-Quaternery rifting, arching, and volcanism.

In summary, after consolidation of the Precambrian (Pan-African) basement, the Phanerozoic history of the Levant can be subdivided into a Cambrian-Devonian period of sedimentation and subsidence, ended by end-Devonian/pre-Carboniferous uplift

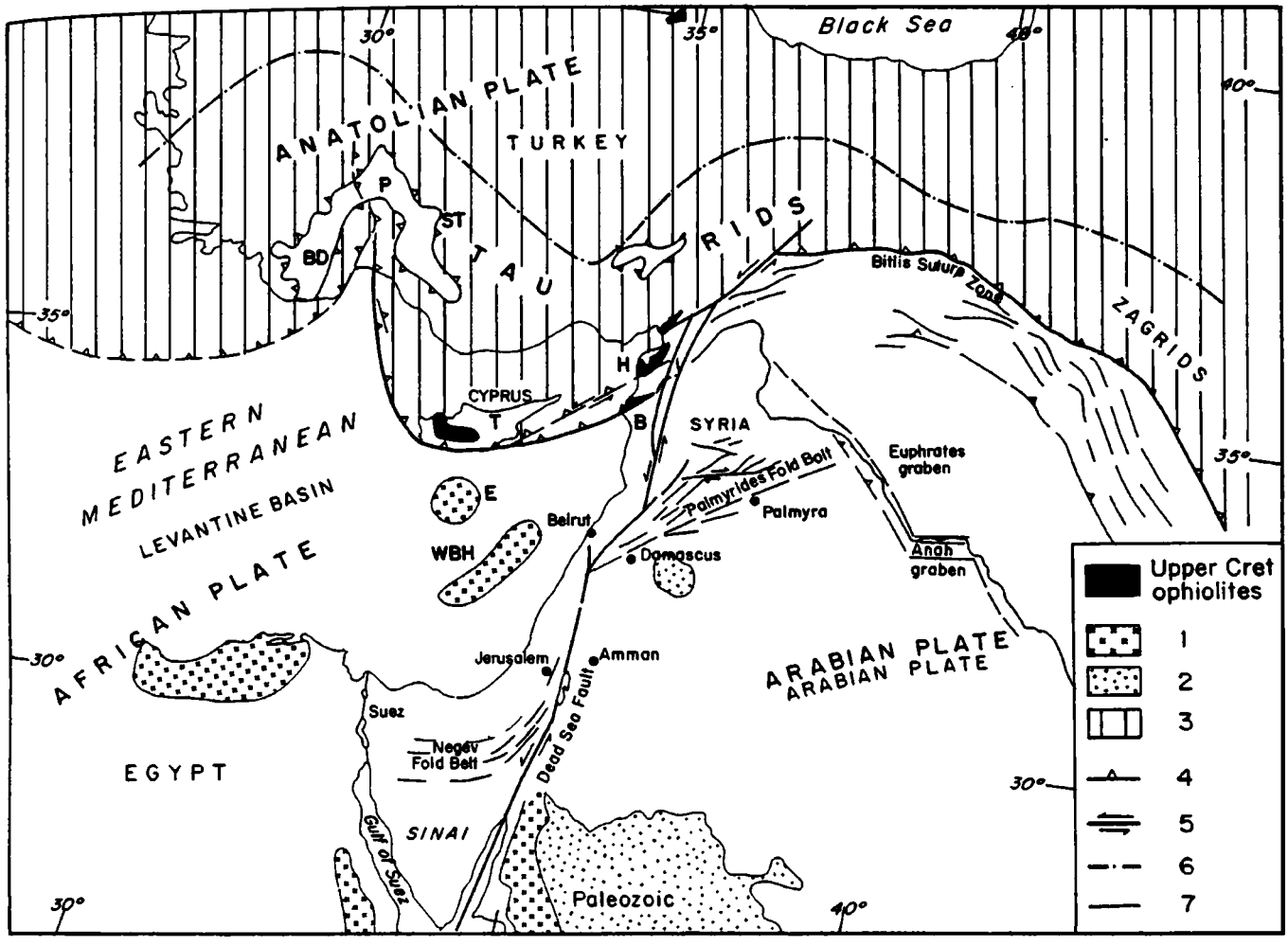


Figure IV. 22. Plate tectonic pattern of the eastern Mediterranean Levant with main Levantid features (modified after Hirsch et al., 1995 and Searle, 1994). Gondwanian elements: African and Arabian plates in white; 1. Precambrian basement exposed or geophysically signaled; 2. Paleozoic sediments; BD Bey Daglari; P Pisidia, ST Seydisehir-Tarasci; E Eratosthenes, WBH Western Basement high, PB Pleshet Paleobasin. Neotethyan elements: 3. Anatolian Plate. Ophiolites in black, B Baer-Bassit; H Hatay, T Troodos. Boundaries: 4. Tauro-Zagrid thrust-front; 5. Dead Sea transform; 6. Neotethyan suture; 7. Present coastlines. This figure also appears as Fig. 18K.2 in Volume II.

and erosion, recurring in Late Carboniferous/Early Permian and Late Permian/Early Triassic times. The Mesozoic depocenters are Neotethyan: the Triassic Galilee (Devorah) Embayment, the Jurassic Judea Embayment, and the Cretaceous Pleshet Paleobasin, prior to Alpine-Levantinid deformation and its subsequent syntectonic deposition.

Israel is located along the northwestern margins of the Arabo-Nubian continental Craton which is a part of the African-Arabian plates made up of rigid blocks composed of a complex assemblage of Precambrian igneous, metamorphic, and sedimentary rocks. During Cambrian to Holocene time, regional geologic conditions were dominated by interaction between this rigid continental mass and the oceanic areas to the north and northwest. This produced the stratigraphic sequences that have so far been observed in the surface and subsurface geologic record of Israel and surrounding areas. This interaction between the Arabian Craton and adjacent oceanic areas is further controlled by structural features and the interplay of four basic modes as follows:

1) Alternating advance and retreat of shallow epicontinental seas on the Arabian Craton, in response to cratonic subsidence/emergence and eustatic sea level changes.

2) Opening and closing of the Tethys, accompanied by faulting and volcanism.

3) Convergence and development of a alpidic folding system: the Levantide folds or the Syrian Arc (Senonian-Eocene).

4) Regional uplift and fracturation of the Arabian Craton margin as a part of the dismantling of the Arabian-African Plate and isostatic readjustments (Oligocene through Holocene time).

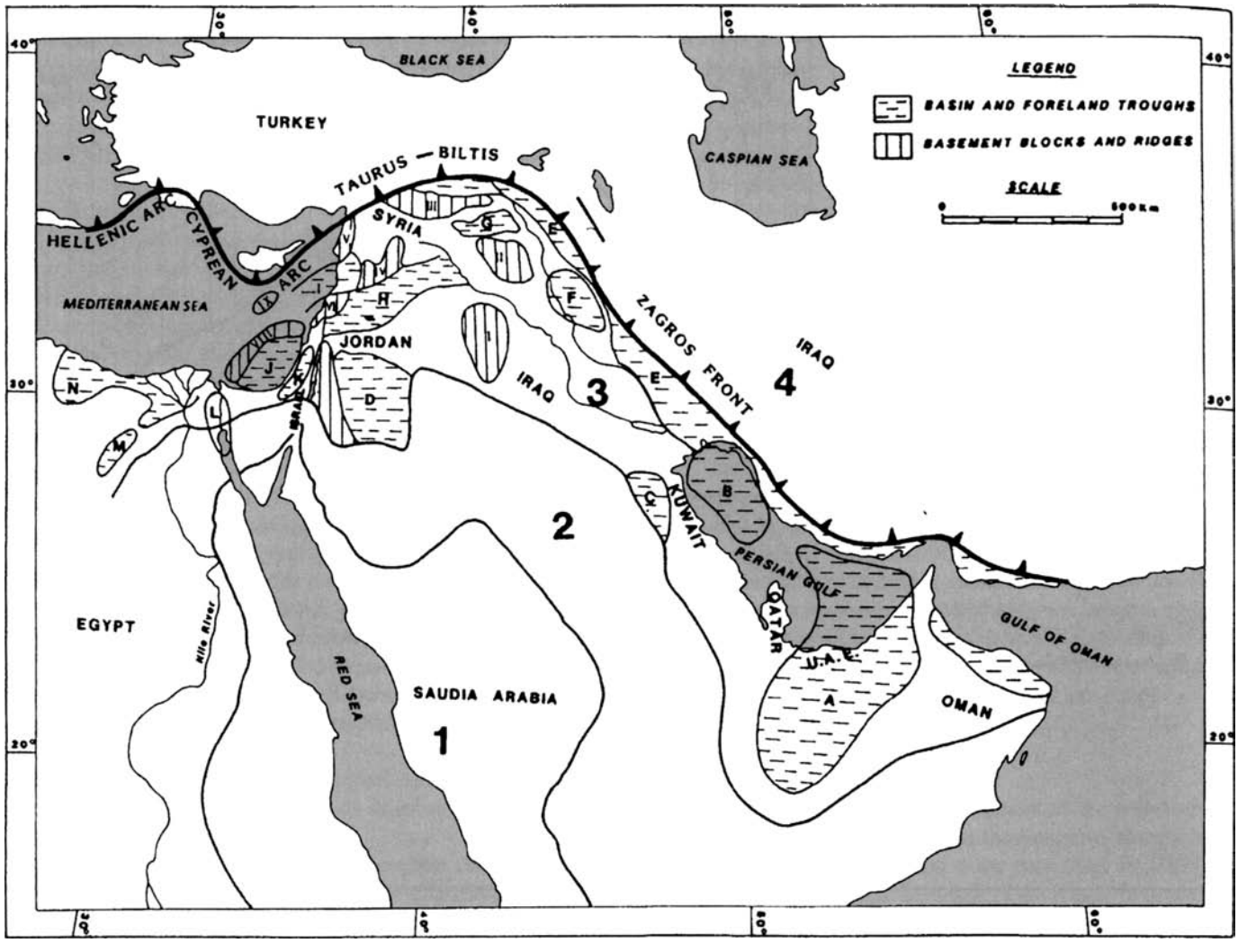


Figure IV.23. Middle East tectono-sedimentary framework. 1. Arabo-Nubian Shield; 2. Stable Shelf (continental beds and thin marine intercalations); 3. Unstable Shelf (mainly marine sediments); 4. Mobile Belt - the Alpine thrust zone.

Basins and Foreland Troughs. A. Rub al Khali; B. North Persian Gulf; C. Dibbdibba; D. Sirhan -Turajf; E. Oman and Zagros Mountains forelands; F. Kirkuk; G. Sinjar; H. Palmyra; I. Phoenician; J. Pleshet; K. Judea; L. Suez; M. Western Desert; N. Matruh and Natrun.

Basement Blocks and Ridges: I. Rutbah; II. Khleisia; III. Mardin; IV. Haleb; V. Amanos; VI. Beirut; VII. Jordan; VIII. Pleshet Western Flank; IC. Eratosthenes.

From Cohen, Z., Flexer, A., and Kapstan, V., 1988, which is modified after Picard (1937), Henson (1951), Said (1962), Powers et al. (1966), Ponikarov et al. (1967), Salem (1976), Druckman et al. (1982), Alsharhan and Nairn (1986), and Ben-Avraham and Ginzburg (1986). This figure also appears as Fig. 18K.1 in Volume II.

1. CRUSTAL STRUCTURE

The crustal structure is an important factor affecting the tectonic processes discerned in the sedimentary epidermis. Ginzburg et al. (1978.) point out that a relatively thick cratonic continental crust which occurs beneath southern and central Israel becomes thinner both to the west and northwest (towards the Mediterranean Sea) and to the north across an E-W zone in central Israel. These zones of crustal thinning have been interpreted as representing the ancient margins of the Arabian Craton now buried beneath a Phanerozoic sedimentary cover that thickens westward (Ginzburg and Gvirtzman, 1979; Ginzburg and Folkman, 1980, 1981). Differences in the composition of the crust might also occur in central and northern Israel.

For Ginzburg and Gvirtzman (1979) the crust beneath the sedimentary prism under the present Mediterranean shelf of Israel might represent a transition zone of oceanic type crust.

A thinning of the crust also takes place under the Rift Valley to a distance of 20 km west of the Rift. This is interpreted by Ginzburg et al. (1978) as a zone of upwelling where upper mantle material is intruded into the lower crust along a narrow active

zone. This process probably commenced in the south close to the geodynamically active area of the Red Sea, and gradually proceeded to the north.

To sum up it seems that the region of Israel can be divided into four crustal provinces:

1) Southern (and central?) Israel with a thick continental crust;

2) Northern (and central?) Israel with thinned continental crust;

3) The Dead Sea Rift with a thin continental crust and possible mantle upwelling;

4) The eastern Mediterranean with a thinned crust of oceanic character.

The boundaries between the various crustal provinces are poorly defined.

2. PLATE TECTONICS

The Middle Eastern portion of the African-Arabian Plate can be subdivided into the Arabian sub-plate, comprising Saudi Arabia, Jordan, Iraq and parts of Syria; the Sinai-Levant sub-plate comprising the Sinai Peninsula, Israel, Lebanon and parts of Syria; and the eastern Mediterranean sub-plate comprising the Levantine Basin.

The Arava-Dead Sea-Jordan Rift Valley is a plate boundary separating the Arabian sub-plate from the African Plate. It should be pointed out that this boundary has been developed since Miocene time as a major left-lateral transform fault zone in response to the culmination of a major collision of the African and Eurasian Plates. Previously during most of the Phanerozoic era the two plates were united into one tectonic unit under the local name of the Arabian-Nubian Massif or Craton.

The boundary separating the Sinai Levant Plate from the Levantine Basin has been defined in different ways by various authors. For Neev (1977) the plate boundary is the Pelusium Line (see Chapter 22), a left-lateral shear accompanied by geophysical discontinuities and sedimentary facies and thickness changes. Ben-Avraham et al. (1978) interpret the zone as a transition of continental crust to an oceanic-type crust and the present-day toe of the continental slope.

3. MOUNTAIN FOLDING

Israel subdivides into a number of tectonic provinces. Such provinces are defined in the geological sense, as zones having common geophysical, seismological, structural, sedimentary and historic characteristics. A tectonic province is separated from its adjacent provinces by a clearly defined zone or boundary. In most cases a tectonic province is expressed by a typical morphological character. Picard (1937) coined the five classical morpho-tectonic units of the Middle East. In the sense of Picard the Sinai-Levant Plate can be largely divided, into the following tectonic provinces (**Fig. IV.23**):

1) The Arabian-Nubian Massif, consisting of a Precambrian terrain devoid of sedimentary cover;

2) The Tabular zone, consisting of a thin sedimentary cover on a relatively thick continental crust, which has been relatively stable during and since the Paleozoic. It has only been subjected to slow, epeirogenic, long-wave length oscillations that brought about rhythmic advances and retreats of the sea over its margins. During the Paleozoic and the greater part of the Mesozoic, these generated a typical platform sedimentary cover of mature clastics (primarily sandstones) on a flat continental landscape, or carbonate-shale sequences in shallow epeiric seas. An accentuation of earth movements took place in Late Triassic and in Late Jurassic-Early Cretaceous times. The rate of historical seismicity in this tectonic province appears to have been very low.

3) The simple folding zone, consists of the Levantides Fold Belt or folds of the 'Syrian Arc'. It is a flat S-shaped band of folds that extends from north-western Sinai, through Israel and Lebanon, into Syria. The common characteristic of this tectonic province is the presence of generally normal concentric folds developed in the sedimentary cover. Most of the folds are strongly asymmetric, a feature generally attributed today to the presence of reverse faults at depth. Picard's complex folding zone and intermediate mountain mass are located beyond the area of the present work, mainly in southern Turkey and the Persian Gulf Area (Tauro-Zagrid ranges) and the central Turkish plateau.

4) The Levantine Basin represents a tectonic province that comprises the eastern part of the eastern Mediterranean. It extends from the Levant Continental Margin provinces westward beyond our study area. The crustal and tectonic structure in this province is poorly understood. Some workers believe that the crust is continental (*e.g.* Woodside, 1977), others claim that it is oceanic (*e.g.* Ryan et al., 1973). Recent crustal investigations between Israel and Cyprus (Makris et al., 1983) suggest that the Levant Basin is underlain by a normal oceanic crust overlain by a thick sedimentary sequence of over 12 km thickness. Recently Flexer et al., (1988) have placed most of this area into the offshore Pleshet Basin.

The physiography of the eastern Mediterranean is closely related to the tectonic processes in this region. The floor of the Levantine Basin is quite smooth due to the large accumulation of sediments, most of them are derived from the River Nile. Along the eastern and southern province boundaries with the continental margins of Israel and Sinai there are some indications that active faults occur in association with seismicity (Folkman, 2003).

4. TRANSVERSAL FAULTING

Transversal faults crossing the Sinai-Levant Plate are observed in the north (the Carmel-Gilboa fault) as well as in the south. A series of east-west trending tectonic lineaments transverse the Sinai Plate and extend from the Thamad fault northwards to the Zin Line. Each lineament consists of a system of faults accompanied by many small folds and fault-controlled depressions that form a conspicuous morphotectonic belt. Collectively, this series of east-west trending lines are referred to as the central Sinai-Negev Shear Zone.

A WNW fault system is discerned in central and northern Israel by field work, air photos, and geophysical methods.

ACKNOWLEDGEMENTS

Part IV of this book is due in great part to the outstanding public

relations activity of our GSI colleague Dov (Dovele) Ginzburg. At some International Geological Congress Dovele had the chance to meet Eric Neshan Tiratsoo (1915-2000), co-founder of the Journal of Petroleum Geology (see obituary in J. Petrol. Geol., Vol. 24, Nos. 1-4, 2001), and an old hand at the petroleum geology of Palestine. Dovele persuaded Tiratsoo to visit Israel to meet his old friend Leo Y. Picard. During this visit Tiratsoo proposed to Picard to write a book and publish it in his publishing house (among others he had published the Lebanese petroleum geologist Ziad Beydoun - 1925-1998). Picard replied that he was too old, but F. Hirsch, present at that meeting, told Tiratsoo later that he was intriqued by the suggestion and that he might do this together with A. Flexer. Tiratsoo agreed, and Hirsch and Flexer began on the project.

With the approval and encouragement of Dr. Gideon Steinitz, then Director of the GSI, the project to prepare a new Lexique Stratigraphique got underway, with the additional assistance in the computerization of Reuven (Robi) Roded. When it appeared that the present book would have a section on the Geology of Israel, much material had already been prepared by Hirsch and Flexer. Additional massive support came from Aharon Horowitz, who provided files containing the Neogene and Pleistocene definitions and descriptions of most formations of that age.

The Lexique thus became the driving force as well as the basis for some of the sub-chapters in Part IV. The credit for converting the tight and dry format of the Lexique to mostly readable English goes to J. K. Hall, who also hunted down the multitude of obscure references.

It is the hope of the authors that the following sections will provide a much-needed overview of the geology of this fascinating wedge between three continents.

REFERENCES CITED

Aharoni, E. 1964. Litho-electric correlation of the 'Kurnub Group' (Lower Cretaceous) in the northern Negev. Isr. J. Earth Sci., 13(2), p. 63-81.

Almagor, G., 1976. Physical properties, consolidation processes and slumping in recent marine sediments in the Mediterranean continental slope off southern Israel. Isr. Geol. Surv., Rep. MG/76/4, 2 vols., 132+50 p. (In Hebrew).

Almagor, G., 2002. The Mediterranean coast of Israel. Ministry of National Infrastructures, Geological Survey of Israel, 250 p. (In Hebrew).

Almagor, G., and Hall, J. K., 1978. Morphology of the continental margin off NE Sinai and southern Israel. Isr. J. Earth Sci., 27(3/4), p. 128-132.

Alsharhan, A. S., and Nairn, A. E. M., 1986. A review of the Cretaceous formations in the Arabian Peninsula and Gulf, Part 1, Lower Cretaceous (Thamama Group) stratigraphy and paleogeography. J. Petrol. Geol., 9(4), p. 365-392.

Anderson, H. J., 1852. Geological reconnaissance of part of the Holy Land. In W. F. Lynch (ed.), Official report of the United States' expedition to explore the Dead Sea and the River Jordan, p. 75-206. Baltimore: Murphy.

Arieh, E. J., 1967. Seismicity of Israel and adjacent areas. Isr. Geol. Surv. Bull. 43, 14 p.

Avnimelech, M., 1950. Sur les lacunes de la sédimentation Crètacée dans les environs de Jerusalem. Acad. Sci. Paris.

Ball, M. W., and Ball. D., 1953. Oil prospects of Israel. Am. Assoc. Petrol. Geol. Bull., 37(1), p. 1-113.

Bandel, K., 1981. New stratigraphical and structural evidence for lateral dislocation in the Jordan Valley connected with description of the Jurassic rock column in Jordan. - N. Jb. Geol. Paleont. Abh. 161, p. 271-308, 12 figs., Stuttgart.

Bein, A., 1974. Reef Development in the Judea Group from the Carmel and the Coastal Plain, Israel. Unpub. Ph.D. Thesis, Hebrew University of Jerusalem, 154 p. (In Hebrew).

Bein, A., 1976. Rudistid fringing reefs of Cretaceous shallow platform of Israel. Am.. Assoc. Petrol. Geol., Bull., 60(2), p. 258-272.

Bein, A., and Gvirtzman, G., 1976. A Mesozoic fossil edge of the Arabian Plate along the Levant coastline and its bearing on the evolution of the Eastern Mediterranean. - In: Structural History of the Mediterranean Basins, Int. Symp. Split, Yugoslavia. - Technip, Paris, p. 95-109.

Bein, A., and Weiler, Y., 1976. The Cretaceous Talme Yafe Formation: a contour current shaped sedimentary prism of calcareous detritus at the continental margin of the Arabian Craton. Sedimentology, 23(4), p. 511-532.

Ben-Avraham, Z., 1978. Structure and tectonics of the eastern Mediterranean. Tectonophysics, 46(3-4), p. 313-331

Ben-Avraham, Z., and Ginzburg, A., 1986. Magnetic anomalies over the central Levant continental margin. Mar. Petrol. Geol., 3(3), p. 220-233.

Bender, F., 1974. Geology of Jordan. Borntraeger, Berlin, 196 p.

Beydoun, Z. R., 1977. The Levantine countries: the geology of Syria and Lebanon (Maritime Regions), Chap. 7A in A. E. M. Nairn, W. H. Kanes, and F. G. Stehli (eds.), The Ocean Basins and Margins, Vol. 4A, The Eastern Mediterranean, Plenum, New York, p. 319-353.

Beyth, M., and Segev, A., 1983. Lower Cretaceous basaltic plug in the Timna Valley. Isr. J. Earth Sci., 32(4), p. 165-166.

Blake, G. S., 1930. The mineral resources of Palestine and Transjordan. Jerusalem, Printing & Stationery Office, 41 p., Maps.

Blake, G. S., 1935. The stratigraphy of Palestine and its building stones: 138 p. Jerusalem: Govt. Palestine Print. Stationary Office.

Blake, G. S., 1937. Mineral deposits of Palestine and Transjordan. Palestine News 3, p. 137-141.

Blake, G. S., and Goldschmidt, M. J., 1947. Geology and water resources of Palestine: 413 p. Jerusalem: Govt. Palestine.

Blanckenhorn, M., and Oppenheim, P., 1927. Neue Beitrdge zur Kenntnis des Neogens in Syrien and Palästina. Geol. Paläont. Abh., Neue Folge, 15(4), p. 321-358.

Bonen, D., 1980. The Mesozoic basalts in Israel. Unpubl. Ph.D. Dissertation, Hebrew University of Jerusalem, 158 p. (In Hebrew, summary in English).

Buch, L. von, 1841. Letter. In E. Robinson and E. Smith 1841. Palistina and die sudlich angrenzenden lander; Tagebuch einer reise im jahre 1838 in bezug auf die Biblische Geographie Unternommen. Vol. 2, 673 p., Halle: Weisenhaus.

Chaimov, T. A., Baranzangi, M., Al-Saad D., Sawaf T., and Gebran A., 1990. Crustal shortening in the Palmyride fold belt, Syria, and implications for movement along the Dead Sea fault system. Tectonics, 9(6), p. 1369-1386.

Cohen, Z., 1971. The Subsurface Geology of the southern Coastal Plain and Petroleum Research. Unpub. Ph.D. thesis, Hebrew University of Jerusalem, 67 p. (In Hebrew).

Cohen, Z., 1976. Early Cretaceous buried canyon: influence on accumulation of hydrocarbons in Helez oilfield, Israel. Am. Assoc. Petrol. Geol., Bull., 60(1), p. 108-114.

Cohen, Z., and the O.E.I.L.Exploration Department, 1988. Hydrocarbon potential of Israel. Highlights of Basin Analysis, 1988, Oil Exploration (Investments) Ltd., 148 p., Maps.

Cohen, Z., Kapstan, V., and Flexer, A., 1988. The Pleshet Basin: a newly-discovered link in the peripheral chain of basins of the Arabian Craton. J. Petrol. Geol., 11(4), p. 403-414.

Cohen, Z., Kapstan, V., Muravinski, E., Salhov, S., Shilo, A., and Wolff, O., 1987. Stratigraphic Table of Israel Outcrops and subsurface. Oil Exploration (Investment) Ltd.

Derin, B., 1974. The Jurassic of central and northern Israel. Ph.D.Thesis, HebrewUniv. Jerusalem, 70 p. (In Hebrew, English summary).

Diener, C., 1885. Die struktur des Jordanquellgebietes. Sitzungsber Akad. Kaiser. Wiss. Wien 92(1), p. 633-642.

Druckman, Y., 1982. Evidence for Early-Middle Triassic faulting and possible rifting from the Helez Deep borehole in the coastal plain of Israel. Geol. Soc. Lond., Int. Meet., Edinburgh, The Geological Evolution of the Eastern Mediterranean,

Abstr., p. 36.

Druckman, Y., Hirsch, F., and Weissbrod, T., 1982. The Triassic of the southern margin of the Tethys in the Levant and its correlation across the Jordan rift valley. Geol. Runds., 71(3), p. 919-936.

Druckman, Y., and Kashai, E., 1981. The Helez-Deep and Devorah-2A boreholes and their implication to oil prospects in pre-Jurassic strata in Israel. Isr. Geol. Surv. Rep. OD/1/81, 23 p.

Dubertret, L., 1937. Le Cretace. 1. Le Massif Alaouite Ou Djebel Ansariyeh. Notes et Memoires, Vol. 2, p. 9-42.

Dubertret, L., 1954. Carte Géologique au 200,000, Feuille de Beyrouth. Beirut, Ministere des Travaux Publics, 107 p., Plates., Map.

Emery, K. O., and Bentor, Y. K., 1960. The continental shelf of Israel. Geol. Surv. Israel Bull., 26, p. 25-40.

Eyal, Y. and Reches, Z., 1983. Tectonic analysis of the Dead Sea Rift region since the Late-Cretaceous based on mesostructures. Tectonics 2(2), p. 167-185.

Flexer, A. and Honigstein, A., 1984. The Senonian succession in Israel; lithostratigraphy, biostratigraphy and sea level changes. Cretaceous Research, 5(4), p. 303-312.

Flexer, A., 1968. Stratigraphy and facies development of the Mount Scopus Group (Senonian-Paleocene) in Israel and adjacent countries. Isr. J. Earth Sci., 17(3), p. 85-114.

Flexer, A., 1971. Late Cretaceous palaeogeography of northern Israel and its significance for the Levant geology. Paleogegr., Palaeoclimatol., Palaeoecol., 10(4), p. 293-316.

Flexer, A., Livnat, A., Sharfman, N. and Gill, D., 1981. Stratigraphic table of Israel. Atlas of Israel. Dept. Geophys. Planet. Sci., Tel Aviv. Univ.

Folkman, Y., 2003. The Nile deep-sea fan channels offshore Israel. Israel Geological Society Annual Meeting, Abstracts, Ein Boqeq, 25-27 March 2003, p. 33.

Freund, R., 1965. A model of the structural development of Israel and adjacent areas since upper Cretaceous times. Geol. Mag., 102(3), p. 189-205.

Freund, R., Goldberg, M., Weissbrod, T., Druckman, Y. and Derin, B., 1975. The Triassic-Jurassic structure of Israel and its relation to the origin of the eastern Mediterranean. Geol. Surv. Isr. Bull., 65, 26 p.

Gignoux, M., 1960. Géologie Stratigraphique. 5th. Edit. Masson, Paris 759 p.

Gill, D., 1965. Petrographic study of some carbonate rocks from the Jurassic outcrops in Maktesh Qatan, southern Israel. Isr. J. Earth Sci., 14(3-4), p. 122-138.

Gill, G. A., and Tintant, H., 1975. Les Ammonites Calloviennes du sud d'Israel. Stratigraphie et rélations paleogéographiques. Séances Soc. Géol. Fr., Comptes Rendu. Somm. No. 4, p. 103-106.

Ginzburg, A., and Folkman, Y., 1980. The crustal structure between the Dead Sea Rift and the Mediterranean Sea. Earth Planet. Sci. Lett., 51(1), p. 181-188.

Ginzburg, A., and Folkman, Y., 1981. Geophysical investigation of crystalline basement between the Dead Sea Rift and Mediterranean Sea. Am. Assoc. Pet. Geol., Bull., 65(3), p. 490-500.

Ginzburg, A., and Gvirtzman, G., 1979. Changes in the crust and in the sedimentary cover across the transition from the Arabian Platform to the Mediterranean Basin; evidence from seismic refraction and sedimentary studies in Israel and in Sinai. In: D. A. Ross and G. Gvirtzman (eds.), New aspects of sedimentation in small ocean basins. Sediment. Geol., 23(1-4), p. 19-36. (Abstract In: Rapp. Comm. Int. Mer Medit., Vol. 25/26, No. 2a, p. 115).

Ginzburg, A., Makris, J., Fuchs, K., Prodehl, C., Kaminski, W., and Amitai, U., 1978. Seismic study of the crust and upper mantle of the Jordan-Dead Sea Rift and their transition towards the Mediterranean Sea. IPRG Rep., Hamburg Univ. and Karlsrhue Univ.

Goldberg, M. and Friedman, G. M., 1974. Paleoenvironments and paleogeographic evolution of the Jurassic system in southern Israel. Isr. Geol. Surv., Bull. 61, 44 p.

Gvirtzman, G., and Weissbrod, T., 1984. The Hercynian Geanticline of Helez and the Late Palaeozoic history of the Levant. In: J. E. Dixon and A. H. F. Robertson (eds.), The Geological Evolution of the Eastern Mediterranean, Geol. Soc. Spec. Publ. No. 17, Blackwell Scientific, Oxford, p. 177-186.

Gvirtzman, G., Weissbrod, T., and Ginzburg, A., 1988. The Paleozoic Riyadh Geanticline in central Saudi Arabia: A structure similar to the Helez Geanticline. Isr. Geol. Soc., Annu. Meet., Abstr., p. 46-47.

Gvirtzman, G., Weissbrod, T., Baer, G., and Brenner, G. J., 1996. The age of the Aptian Stage and its magnetic events: New Ar-Ar ages and palaeomagnetic data from the Negev, Israel. Cretaceous Res., 17(3), p. 293-310.

Haas, O., 1955. Revision of the Jurassic ammonites fauna of Mt. Hermon, Syria. Am. Mus. Nat. Hist. Bull., vol. 108, article 1, 210 p.

Hall, J. K., 1994. Digital shaded-relief map of Israel and environs. Grayscale sheet at 1:500,000 scale with bathymetry. Location map printed on the reverse. Geological Survey of Israel, Jerusalem, August 1994 (reprinted February 1997).

Hall, J. K., 1996 Topography and bathymetry of the Dead Sea Depression. Tectonophysics, 266(1-4): 177-185.

Hall, J. K., 1997. Landforms of Israel and Adjacent Areas. Grayscale sheet of land topography at 1:500,000 scale with physiographic provinces by E. Zilberman and R. Bogoch (English Edition, Hebrew edition published in 1995). Geological Survey of Israel, Jerusalem, April 1997.

Hall, J. K., 2000a. Orthographic Satellite Imagery Coverage, Israel and Adjacent Areas. Scale 1:100,000. New Israel Grid, STM (LANDSAT TM and SPOT Panchromatic Merged) Imagery. 70 by 90 cm laminated posters and post cards. Sheet 1 Nazareth. Geol. Survey Israel Rept. GSI/4/2000; Sheet 2 Netanya. Geol. Survey Israel Rept. GSI/5/2000; Sheet 3 Jericho. Geol. Survey Israel Rept. GSI/6/2000; Sheet 4 Jerusalem. Geol. Survey Israel Rept. GSI/7/2000; Sheet 5 Ashqelon. Geol. Survey Israel Rept. GSI/8/2000; Sheet 6 Sede Boqer. Geol. Survey Israel Rept. GSI/9/2000; Sheet 7 Mizpe Ramon. Geol. Survey Israel Rept. GSI/10/2000; Sheet 8 Elat-Aqaba, Jordan. Geol. Survey Israel Rept. GSI/11/2000; Sheet 9 Damascus. Geol. Survey Israel Rept. GSI/12/2000; Sheet 10 Irbid-Amman, Jordan. Geol. Survey Israel Rept. GSI/13/2000; Sheet 11 Karak, Jordan. Geol. Survey Israel Rept. GSI/14/2000; Sheet 12 Petra, Jordan. Geol. Survey Israel Rept. GSI/15/2000;

Hall, J. K., 2000b. Bathymetric charts inset into Orthographic Satellite Imagery Coverage. New Israel Grid, STM (LANDSAT TM and SPOT Panchromatic Merged) Imagery. 70 by 90 cm laminated posters and post cards. Sheet 13 Dead Sea, 1:100,000. Geol. Survey Israel Rept. GSI/16/2000; Sheet 14 Sea of Galilee, 1:50,000. Geol. Survey Israel Rept. GSI/17/2000; Sheet 15 Gulf of Elat/Aqaba, 1:250,000. Geol. Survey Israel Rept. GSI/18/2000.

Hall, J. K., 2000c. Northern Levant Satellite Map, Scale 1:1,039,500. Mosaic of sixteen LANDSAT 5 TM scenes covering all of Syria and parts of Turkey, Lebanon, Israel, Jordan, Iraq, and Saudi Arabia. Bands 2, 4, and 7. With text and location map. Sheet 16 of Orthographic Satellite Imagery Coverage Israel and Adjacent Areas, Geological Survey of Israel Rept. GSI/19/2000, 70 by 90 cm laminated poster and post card.

Hall, J. K., Udintsev, G. B. and Odinokov, Yu. Yu., 1994. The bottom relief of the Levantine Sea. In: Geological structure of the North-eastern Mediterranean (Cruise 5 of the Research Vessel 'Akademik Nikolaj Strakhov'). (V. Krasheninnikov and J. K. Hall, eds.), p. 5-31. Historical Productions-Hall, Jerusalem, April 1994. Plate 1 (Figure 13.1) is a 1:625,000 scale (at 46°N) bathymetric chart of the eastern Mediterranean Sea).

Haq, B. H., Hardenbol, J., and Vail P. R., 1987. Chronology of fluctuating sea levels since the Triassic. Science, 235(4793), p. 1156-1166.

Harris, P. M., Frost, G. H., Seiglie, G. A., and Schneidermann, N., 1987. Regional Unconformities and Depositional Cycles, Cretaceous of the Arabian Peninsula. In: J. S. Schlee, (ed.), Interregional Unconformities and Hydrocarbon Accumulation, Am. Assoc. Petrol. Geol. Mem., 36, p. 67-79.

Hatzor, Y., Benjamini, C., Mimran, Y., and Grossowicz, L., 1994. The Eocene stratigraphy of Mt. Gilboa and northern Samaria, Israel. Isr. J. Earth Sci., 43(1), p. 1-20.

Henson, F. R. S., 1951. Observations on the geology and petroleum occurrences of the Middle East. Proc. Third World Petroleum Congress, The Hague.Section 1, p. 118-140.

Hirsch, F., 1972. Middle Triassic conodonts from Israel, southern France and Spain. Mitt. Ges. Geol. Bergbaustud., 21(2), p. 811-828.

Hirsch, F., 1979. Jurassic bivalves and gastropods from northern Sinai and southern Israel. Isr. J. Earth Sci., 28(4), p. 128-163.

Hirsch, F., 1984. The Arabian sub plate during the Mesozoic. In: J. E. Dixon and A. H. F. Robertson, (eds.), The Geological Evolution of the Eastern Mediterranean, Oxford, Blackwell, p. 217-223.

Hirsch, F., 1990. Aperçu de l'histoire phanérozoique d'Israël. Journal of African Earth Sciences, 11(1/2), p. 177-196.

Hirsch, F., Flexer, A., Rosenfeld, A. and Yellin-Dror, A., 1995. Palinspastic and crustal setting of the eastern Mediterranean. Jour. Petrol. Geol., 18(2), p. 149-170.

Hirsch, F., Rosenfeld, A. and Honigstein, A., 1994. Early Cretaceous ostracodes from

the southeastern slopes of Mount Hermon. Isr. Geol. Surv. Current Research, 9, p. 90-91.

Hitchcock, E., 1843. Notes on the geology of several parts of western Asia, founded chiefly on specimens and descriptions from American missionaries. Trans. Am. Geol. Assoc. 1840/1842, p. 348-421.

Horowitz, 2001. The Jordan Rift Valley. Balkema, Lisse, 730 p.

Horowitz, A., 1971. Climatic and vegetational developments in northeastern Israel during Upper Pleistocene - Holocene times. Pollen et Spores, 13(2), p. 255-278.

Hudson, R. G. S., 1958, The Upper Jurassic faunas of southern Israel. Geol. Mag. 95(5), p. 415-425.

Hull, E., 1886. The survey of western Palestine, memoir on the geology and geography of Arabia Petraea, Palestine and adjoining districts, with special reference to the mode of formation of the Jordan Arabah Depression and the Dead Sea. London: Palestine Exploration Fund, 145 p.

Ionides, M. G., and Blake, G. S., 1940. Report on the water resources of Transjordan and their development: 372 pp. London: Crown Agents.

Krasheninnikov, V. A., and Hall, J. K., (Editors), 1994. Geological structure of the North-eastern Mediterranean (Cruise 5 of the Research Vessel 'Akademik Nikolaj Strakhov'), Historical Productions-Hall, Jerusalem, 396 + vii p, April 1994.

Lartet, L. 1869. Essai sur la géologie de la Palestine et des contrées avoisinantes, telles que l'Égypte et l'Arabie, comprenant les observations recueillies dans le cour de l'Expédition du Duc de Luynes a la Mer Morte, Masson, Paris, 292 p.

Lerman, A., 1960. Triassic pelecypods from southern Israel and Sinai. Bull. Res. Counc. Israel, 9G(1), p. 1-51.

Lewy, Z., 1983. Upper Callovian ammonites and Middle Jurassic geological history of the Middle East. Israel Geol.Surv., Bull. 76, p 1-56.

Lewy, Z., Raab, M., 1976. Mid Cretaceous Stratigraphy Of The Middle East. Mus. Hist. Nat. Nice, Ann., 4, p. 1-20.

Lorch, J., 1967.- A Jurassic flora of Makhtesh Ramon, Israel. Isr. J. Botany, 16, p. 177-188

Lynch, W. E., 1849. Narrative of the United States' expedition to the River Jordan and the Dead Sea: 508 p. Philadelphia and London: Bentley.

Macquer, P. J., Lavoisier, A. L., and Sage, B. G., 1778 (Publ. 1781). Analysis of water from the Asphaltite Lake. Mem. Acad. R. Sci. Paris, 69.

Makris, J., Ben-Abraham, Z. Behle, A., Ginzburg, A., Giese, P., Steinmetz, L., Whitmarsh, R. B., and Eleftheriou, S., 1983. Seismic refraction profiles between Cyprus and Israel and their interpretation. Geophys. J. R. Astr. Soc., 75(3), p. 575-591.

Marcoux, J., 1978. A scenario for the birth of a new oceanic realm: The Alpine Neotethys. Jerusalem: Abst. 10th Intl. Cong. Sedimentol., p. 419-420.

Mimran, Y., 1972. The Tayasir Volcanics, a Lower Cretaceous Formation in the Shomeron, central Israel. Isr. Geol. Surv., Bull. 52, 9 p.

Mimran, Y., Lang, B., and Steinitz, G., 1984. K-Ar dating of the Tayasir volcanics and its geologic implications. Isr. Geol. Soc. Ann. Meet., Arad, April 1984, p. 70-71.

Mimran, Y., Shaliv, G., Hatzor, Y. and Lang, B., 1989. The margins of the Rift Valley south of Bet Shean and eastern Gilboa. Isr. Geol. Soc., Annu. Meet., Guidebook, p. 47-65. (In Hebrew).

Molyneux, A., 1848. Expedition to the Jordan and the Dead Sea. J. Roy. Geogr Soc. London, 18(2), p. 104-130.

Monod, O., 1977. Recherches geologiques dans le Taurus Occidental au Sud de Beysehir (Turquie). - Thèse, Univ. Paris Sud, 1839, 442 p.

Mouty, M. 2000. The Jurassic in Syria: an overview. Lithostratigraphic and biostratigraphic correlations with adjacent areas. In: S. Crasquin-Soleau and E. Barrier (Eds.), Peri-Tethys Mém. 5, Mém. Mus. natn. Hist. nat., v. 182, p. 159-168.

Murris, R. J., 1980. Middle East: stratigraphic evolution and oil habitat. Am. Assoc. Petrol. Geol. Bull., 64(5), p. 597-618.

Neev, D., 1977. The Pelusium Line – a major transcontinental shear. Tectonophysics, 38(3-4), p. T1-T8.

Neev, D., Almagor, G., Arad, A., Ginzburg, A., and Hall, J. K., 1976. The geology of the southeastern Mediterranean Sea. (Including a note on seismicity by E. Arieh). Isr. Geol. Surv., Bull. 68, 51 p.

Neev, D., Bakler, N., Moshkovitz, S., Kaufman, A., Magaritz, M., and Gofna, R., 1973. Recent faulting along the Mediterranean coast of Israel. Nature, 245(5423), p. 254-256.

Nir, Y., 1973. Geological history of the recent and subrecent sediments of the Israel Mediterranean shelf and slope. Isr. Geol. Surv. Rep. MG/2/73, 179 p.

Nötling, F., 1886. Das Tote Meer and der untergang von Sodom and Gomorraha. Deutsch. Montagsblatt Berlin 27, p. 31 and 33.

Nötling, F., 1887. Geologische skizze der umgebung von El-Hammi. Ztschr Dtsch. Paläst. Ver. 10, p. 59-88.

Parnes, A., 1958. Triassic Ammonites from Israel. (In Hebrew). Ph.D. Thesis, Hebrew Univ. Jerusalem, 57 p.

Parnes, A., 1962. The geology of Makhtesh Ramon (Negev, Israel). Part 3a: Triassic Ammonites from Israel. Isr. Geol. Surv., Bull. 33, 76 p.

Parnes, A., 1981. Biostratigraphy of the Mahmal Formation (Middle and Upper Bajocian) in Makhtesh Ramon (Negev, southern Israel). Isr. Geol. Surv., Bull. 74, 55 p.

Picard, L., 1931.Geological Researches in the Judean Desert. 'Mizi Akhdar', 'Arad Marble'. Goldberg Press, Jerusalem, 108 p.

Picard, L., 1932. Zur Geologie des mittleres Jordantales.

Picard, L., 1937. On the structure of the Arabian Peninsula. Bull. Geol. Dept. Hebrew Univ., 1, 9 p..

Picard, L., and Hirsch, F., 1987. The Jurassic stratigraphy in Israel and the adjacent countries. Jerusalem, Isr. Acad. Sci. Human., 106 p.

Picard, L., and Solomonica, P., 1936. On the geology of the Gaza - Beer Sheba District. Palest. Orient. Soc., Vol. 16, p. 180-223, Map (Heb. Univ. Jerusalem, Geol. Dept., Bull. 1, No. 2, 44 p.).

Pococke, R., 1754. Beschreibung des Morgenlandes and einiger anderer Lander Vol. II: Palestina, Syrien, Mesopotamien, Cypern: 374 p. Erlangen: Verlag der Stifthauses.

Ponikarov, V. P., Kazmin, V. G., Dolginov, Ye. A., Sulidi-Kondrat'yev, Ye. D., 1967. The character of the contact between the Arabian Platform and the Alpine geosynclinal region. Sovietskaya Geologiya, Vol. 2, p. 54-66. [In Russian].

Powers, R. W., Ramirez, L. F., Redmond, C. D., and Elberg, E. L. Jr., 1966. Geology of the Arabian Peninsula - Sedimentary geology of Saudi Arabia. USGS, Prof. Pap., No. 560-D, 147 p.

Razvalyaev, A.V., 1966. Explanatory notes to the Geological Map of Syria, 1:200,000. Syrian Arab Report of the Ministry of Industry, Department of Geological and Mineral Research, Damascus, 122 p.

Reiner, W., 1968. Callovian gastropods from Hamaktesh Hagadol (southern Israel). Isr. J. Earth Sci., 17(4), p. 171-198.

Renouard, G., 1955. Oil prospects of Lebanon. Amer. Assoc. Petrol. Geol. Bull., 39(11), p. 2125-2169.

Rosenfeld, A., Flexer, A., Honigstein, A., Almogi-Labin, A. and Dvorachek, M., 1989. First report on a Cretaceous/Tertiary section at Makhtesh Gadol, southern Israel. N. Jahr. Geol. Pal. Monatsh., Vol. 1989, No. 6, p. 474-488..

Rosenfeld, A., Hirsch, F., and Honigstein, A., 1995. Early Cretaceous ostracodes from the Levant. In: Riha, J. (ed.), Ostracoda and Biostratigraphy. Balkema, Rotterdam, p. 111-121.

Rosenfeld, A., Raab, M., 1981. Lower Cretaceous Ostracodes from Israel. Isr. Geol. Surv., Current Res., 1980, p. 62-65.

Rosenfeld, A., Raab, M., 1984. Lower Cretaceous Ostracodes from Israel and Sinai. Isr. J. Earth Sci., 33(3), p. 85-134. (Also: Isr. Geol. Surv., Spec. Publ. 4).

Russeger, J., 1847. Reisen in Unter-Agypten, auf der Halbinsel des Sinai and im gelobten Lande. 292 p. Stuttgart: Schweizerbart.

Ryan, W. B. F., Hsü, K. J., et al., (Editors), 1973. Initial Reports of the Deep Sea Drilling Project, 13 (Parts 1 and 2). U. S. Government Printing Office.

Sade, R., Hall, J. K., Gur-Arieh, L., Amit, G., and Golan, A., (2003). The National Bathymetric Survey (NBS): Second year of operation. Geological Society of Israel, Annual Meeting Abstracts, March 25-27, En Bokek, Dead Sea, Poster.50a.

Said, R., 1962. The geology of Egypt. Elsevier, Amsterdam-New York, 377 p.

Salem, R., 1976. Evolution of Eocene-Miocene sedimentation patterns in parts of northern Egypt. Am. Assoc. Petrol. Geol. Bull., 60(1), p. 34-64.

Sass, E., and Bein, A., 1982. The Cretaceous carbonate platform in Israel. Cretaceous Res., 3(1/2), p. 135-144.

Saulcy, F. de, 1854. Narrative of a journey round the Dead Sea and in the Bible lands in 1850 and 1851: Vol. 1: 560 p.; Vol. 2: 604 pp. London: Bentley.

Searle, M. P., 1994. Structure of the intraplate eastern Palmyride Fold Belt, Syria. Geol. Soc. Am., Bull., 106(11), p. 1332-1350.

Shapira, A., 1979. Redetermined magnitudes of earthquakes in the Afro-Eurasian Junction. Isr. J. Earth Sci., 28(4), p. 107-109.

Shaw, S. H., 1948. The geology and mineral resources of Palestine. Bull. Imper Inst., 46(1), p. 87-103.

Sneh, A., Bartov, Y., Weissbrod, T., Rosenhaft, M., and Hall, J. K. (2000). Geological Shaded Relief Map of Israel and Environs. Computer generated geological map on a Digital Shaded Relief Map by J. K. Hall. Scale 1:500,000, Geological Survey of Israel, December 2000. Printed in English and Hebrew.

Starinsky, A., Bielski, M., Bonen, D., and Steinitz, G., 1980. Rb-Sr whole rock age of the syenitic intrusions (Shen Ramon and Gevanim) in the Ramon area, southern Israel. Isr. J. Earth Sci., 29(3), p. 177-181.

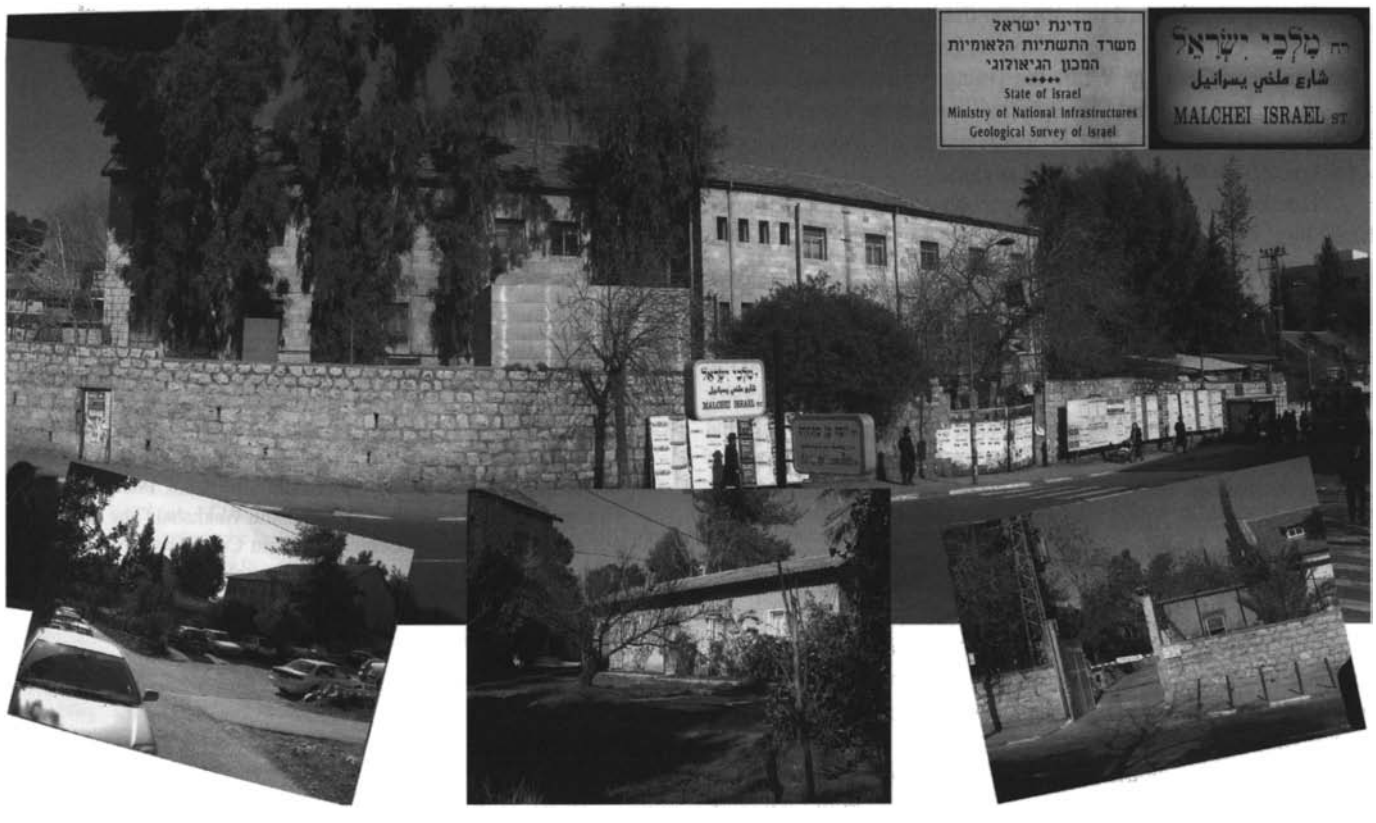
Vail, P. R., Mitchum, R. M., Jr. and Thompson, S., 1977. Seismic stratigraphy and global changes of sea level, Part 4: global cycles of relative changes of sea level. Seismic stratigraphy - application to hydrocarbon exploration. Am. Assoc. Pet. Geol., Mem. 26, p. 83-97.

Weissbrod, T., 1969. The Paleozoic of Israel and adjacent countries. Part II. The Paleozoic outcrops in southwestern Sinai and their correlation with those of southern Israel. Isr. Geol. Surv. Bull. 48, 32 p.

Wetzel, R., and Morton, D. M., 1959. Contribution à la géologie de la Transjordanie. Notes et Mém. Moyen Orient, 7, p. 95-191.

Wolfart, R., 1967. Geologie von Syrien und dem Libanon. Berlin, Gebrueder Borntraeger, 326 P., Maps.

Yaalon, D. H., and Dan, J., 1992. Factors controlling soil formation and distribution in the Mediterranean coastal plain of Israel during the Quaternary. In: Morison, R. B., and Wright, H. E., (eds.), Proceedings, Quaternary Soils – 7th Congress, International Association for Quaternary Research, Reno, NV, 9, p. 321-338.



The Geological Survey of Israel in Jerusalem. Collage of photos acquired in early 2005. Above, the survey as seen from across Malchei Israel (Kings of Israel) Street, in the Geulim quarter of Jerusalem, at the beginning of the religious quarter of Mea Shearim. The survey occupies about 2 acres at the edge of the Schneller military camp. Buildings date back to the British Mandate. The site is dominated by the Geochemistry Division, occupying most of the large building in the foreground. The Documentation Center (library) occupies the ground floor at the left behind the giant eucalyptus trees. The smaller images show, from left to right, the internal parking and the Geochemistry building, the Graphics Division in a Mandate-era shed, and the front gate and guardhouse. The Survey will be moving to new quarters within the near future.

PROFESSOR LEO YEHUDA PICARD

3 June 1900 -4 April 1997

Francis Hirsch
Geological Survey of Israel, Jerusalem, Israel

Leo Picard was born on the shores of Lake Constance, Germany. From his early youth he cultivated a love for nature. His interest in geology in particular developed thanks to a teacher who took his students on field-excursions in the nearby Table Jura and Hegau volcanoes. In addition to a secular modern education, he also manifested a strong interest in the Zionist cause, being an active member of the Blau-Weiss youth organisation.

He studied geology at the University of Freiburg/Breisgau, from which he graduated in 1923 having obtained a Ph.D. After another year at the university of Florence in Italy, he embarked for Palestine in 1924.

To people questioning him during the voyage about what brought him to Palestine, the young Picard simply answered "to find water".

And this is exactly what the 'Doktor von der Erd' (as his landlady called him) did, in the Yizre'el Valley, at Ginegar along the border fault that runs below the mountains of Nazareth.

The career of Picard did not stop there. After the opening of the Hebrew University in Jerusalem, he became the founder of its Department of Geology. While the young professor was forming his school, he also started his systematic study of the geology of Palestine and the Levant. In 1931 he obtained the degree of Doctor of Science from the University of London.

Thanks to his work as a geological consultant in Latin America and China, his vision became global. In 1937, with 'Structure of the Arabian Peninsula', he laid the basis for a new structural conception of the Arabian Peninsula, a scheme still widely in use today (Fig. IV.22).

With the founding of the State of Israel, Picard established the Geological Survey of Israel (1949), and the Hebrew University Center for Underground Water Research (1965). These institutions allowed the further systematic research and exploration of natural ressources and opened the country to young students of hydrogeology from Africa and Latin America.

Next to his activity as an advisor to the government, Picard was also a Board Member of several oil exploration companies.

Towards the end of his geological career, Leo Picard started his compilative study of the Triassic (1974) and Jurassic (1987) regional stratigraphy. Soon after, his last scientific paper (1989) again dealt with the Dead Sea Rift, a subject close to the Rhine-graben of his student years.

Picard also contributed to the understanding of the morphology of the Levant. He was fascinated by both prehistory and archeology. A great lover of classical music and close friend of Ardon, the painter, he also had a fine ethnographic collection. He read abundantly, especially biographies. The latter probably led him to write his own memoirs, based on his abundant letters with scholars around the world, as well as the many letters to and from his mother.

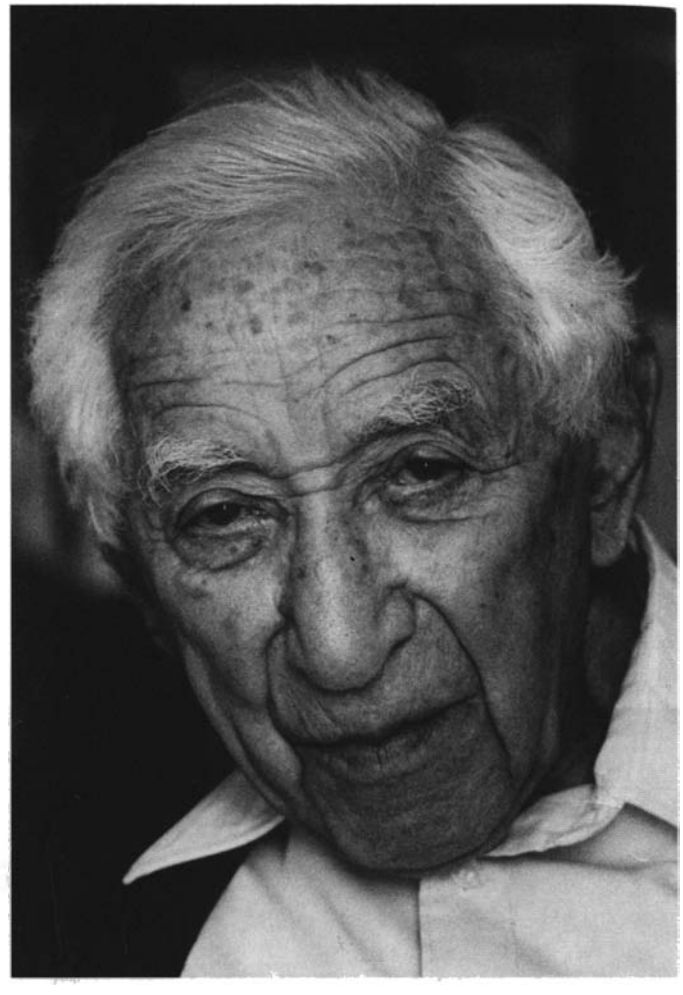


Figure IV.24. Prof. Leo Picard (1900-1997), Geologist, Israel. Prof. Picard founded the Geological Department of the Hebrew University in Jerusalem, the Geological Survey of Israel, and the Institute for Groundwater Research of the Hebrew University in Jerusalem. His contribution to the discovery of water earned him wide recognition and fame in the country. Academically he established the concepts of the structure and geological evolution of Israel. Photo by Hayim Goldgraber (1993) courtesy of Dr. Eliahu Wakhshal (The Leo Picard Groundwater Research Center, Seagram Center for Soil and Water Sciences, The Hebrew University of Jerusalem, Rehovot 76100).

Picard enjoyed life and did not lack a sense of humor. He loved to tell how in 1982, after a 'Penrose' conference in Capri, Italy, thanks to a physical ressemblance, he was mistaken for the famous pianist Rubinstein. The already closed airport restaurant was especially re-opened for him, and he enjoyed a very good meal, playing the 'maestro' to the end!

He was a member of many geological societies. He received honors, like the Israel Prize, and several Doctor Honoris Causa.

Having no children, his most dedicated students filled this gap with joy and pride.

His memoirs represent a history of the geologic research of Israel.

Leo Yehuda Picard, a pioneer of Levant geology, was laid to rest in Kibbutz Ginegar, not far from where he spudded in his first water well.

PUBLICATIONS OF L. Y. PICARD (Chronological Order)

Picard, L., 1923. Die Fraenkische Alb von Weissenburg I. B. und Umgebung. Ph. D. Thesis, Albert Ludwigs Univ., Freiburg I. B., 80 p.

Picard, L., 1926. Sur le Cenomanien du Carmel (Sud-Est d'Haifa). C. R. Acad. Sci. Paris, Vol. 183, p. 895-898.

Picard, L., 1927. Springs and groundwater in the Esdrelon Valley and the Coastal Plain. (In Hebrew & English). Construction & Industry; J. Assoc. Eng. Architects in Palestine, 6(5-6), p. 7-9 (In Hebrew); p. 8-10 (In English).

Picard, L., and Soyer, R., 1927. Sur la presence du Jurassique, du Cretace Inferieur et Moyen sur le versant ouest de l'Antiliban. C. R. Acad. Sci. Paris, Vol. 185, p. 656-658.

Picard, L., 1928. Ein Eocaenprofil des Gilboas in Palaestina. Centralbl. Mineral., Abt. B, p. 578-582.

Picard, L., 1928. Recherches nouvelles en Palestine. Bull. Soc. Géol. Fr., Ser. 4, Vol. 28, p. 79-83.

Picard, L., 1928. Ueber Die Verbreitung Des Pliocaens Im Noerdlichen Palaestina. Centralbl. Min., Abt. B, No. 5, p. 326-335.

Picard, L., 1928. Zur Geologie Der Kischonebene. Z. Dtsch. Palaestina Vereins, Vol. 51, p. 5-72, 2 Maps.

Picard, L., 1929. On Upper Cretaceous (Chiefly Maestrichtian) Ammonoidea From Palestine. Ann. Mag. Nat. Hist., Ser. 10, Vol. 3, p. 433-456.

Picard, L., 1929. Zur Geologie Der Besan-Ebene. Z. Dtsch. Palaestina Vereins, Vol. 52, p. 24-90, Figs., Map.

Picard, L., 1930. Report Einer Untersuchung Der Schwefellagerstaetten Bei Gaza. Report (Typewritten), 14 p.

Picard, L., 1930. Upper Cretaceous (Chiefly Campanian And Maestrichtian) Gastropoda And Pelecypoda From Palestine. Ann. & Mag. Nat. Hist., Ser. 10, No. 5, p. 513-543.

Picard, L., 1931. Geological Researches In The Judean Desert, With Geological Map And Illustrations. Jerusalem, 108 p., Plates., Map. (D. Sc. Thesis Approved For The Degree Of Doctor Of Sci. In The Univ. Of London).

Picard, L., 1931. Geologie De La Grotte D'oumm Qatafa. J. Palest. Orient. Soc., Vol. 11, p. 164-171.

Picard, L., 1931. Tektonische Entwicklungsphasen Im Noerdlichen Palaestina. Dtsch. Geol. Ges., Z., Vol. 83, No. 3, p. 164-184, Fig.

Picard, L., 1932. Geologische Probleme Am Suedrand Des Tiberias Sees. J. Palest. Orient. Soc., Vol. 12, 6 p.

Picard, L., 1932. Grabenstrukturen Im Jordantal. Fortschr. Geol. & Palaeontol., Berlin ("Deecke Festschr."), Vol. 11, p. 88-98.

Picard, L., 1932. Zur Geologie Des Mittleren Jordantales. Z. Dtsch. Palaestina Vereins, Vol. 55, p. 169-236, Map.

Willis, B., and Picard, L., 1932. The Jordan Valley And Judean Highlands. Geol. Mag., Vol. 69, p. 97-107.

Picard, L., 1933. On Problems Related To The Occurrence Of Asphalt Etc. Along The Eastern Shore Of The Dead Sea. Palestine Mining Syndicate Rep.

Picard, L., 1933. Zur Postmiocaenen Entwicklungsgeschichte Der Kontinentalbecken Nord Palaestinas. Neues Jahrb. Mineral., Beil-Bd., Vol. 70b, p. 93-115.

Picard, L., 1934. Les Depots De Mineraux Et D'eaux Souterraines En Palestine. La Bourse Egyptienne, 1.5.1934, p. 14.

Picard, L., 1934. Mollusken Der Levantinischen Stufe Nord Palaestinas (Jordantal). Arch. Molluskenk., Vol. 66, No. 3, p. 105-139.

Picard, L., 1934. Zur Geologie Des Gebietes Zwischen Gilboa Und Wadi Fara. Sdr. Centralbl. F. Miner., Abt. B, No. 1, p. 27-33.

Picard, L., 1935. Considerations On Water Resources In Kefar Ezyon Area. (In Hebrew). Jerusalem, 3 p.

Picard, L., 1935. Das Wasserproblem Palaestinas. Palaestina, Vol. 18, No. 3, p. 113-129.

Picard, L., 1935. The Geology Of Tel Aviv. (In Hebrew). Jubilee Book Of Tel Aviv, Vol. 1, p. 3-15.

Picard, L., 1935. Water Problems Of Palestine. (In Hebrew). Hassadeh, Vol. 15, No. 5-8, p. 1-8.

Avnimelech, M., Doncieux, L., and Picard, L., 1936. Sur la decouverte d'une serie Nummulitique au S.E. du Mont Carmel en Palestine. C. R. Soc. Geol. Fr., No. 3, p. 41-43.

Picard, L., 1936. Conditions Of Underground Water In The Western Emek. Jerusalem, Heb. Univ., Geol. Dept. Bull. No. 1, 24 P., Figs., Tabs. (Also In Hebrew).

Picard, L., 1936. Ueber Fauna, Flora Und Klima Des Pleistozaens Palaestina - Syriens. Int. Quart. Konfer., 3rd, Wien 1936; Verh., Vol. 2, p. 1-4.

Picard, L., and Solomonica, P., 1936. On The Geology Of The Gaza - Beer Sheba District. Palest. Orient. Soc., Vol. 16, p. 180-223, Map (Heb. Univ. Jerusalem, Geol. Dept., Bull. 1, No. 2, 44 P.).

Stekelis, M., and Picard, L., 1936. Jisr Banat Yaqub. Antiquities Dept. Palestine, Quart., Vol. 6, p. 214-215 & Vol. 7, p. 45.

Picard, L., 1937. Inferences On The Problem Of The Pleistocene Climate Of Palestine And Syria Drawn From Flora, Fauna And Stratigraphy. Prehistoric Soc., Proc., Vol. 3, Pt. 1, Paper 5, p. 58-70.

Picard, L., 1937. On The Structure Of The Arabian Peninsula. Heb. Univ. Jerusalem, Geol. Dept., Bull. 3, 12 p.

Picard, L., and Avnimelech, M., 1937. On The Geology Of The Central Coastal Plain. J. Palest. Orient. Soc., Vol. 17, p. 255-299. (Heb. Univ. Jerusalem, Geol. Dept. Bull. 4, 45 P.).

Picard, L., and Doncieux, L., 1937. Sur La Presence De L'eocene Superieur - Oligocene Inferieur Avec Nummulites Incrassatus De La Harpe En Palestine. C.R. Soc. Geol. Fr., No. 5, p. 62-63.

Picard, L., Doncieux, L., and Avnimelech, M., 1937. Sur L'existence D'un Etage Libyen Dans Les Environs De Maan (Transjordanie). C.R. Soc. Geol. Fr., No. 6, p. 74-75.

Picard, L., 1938. Economic Deposits And Groundwater In Erez Israel. (In Hebrew). Technica u'Mada, Vol. 2, No. 11, 2 p.

Picard, L., 1938. Synopsis of stratigraphic terms in Palestinian Geology. Heb. Univ. Jerusalem, Geol. Dept., Bull., 2(2), 24 p.

Picard, L., 1938. The Geology of New Jerusalem. (In Hebrew & English). Jerusalem, Heb. Univ., Geol. Dept., Bull., 2(1), 12 p.

Picard, L., 1938. The water problem in Palestine. (In Hebrew). Hassadeh, Vol. 16, No. 5-8.

Picard, L., 1939. On the structure of the Arabian Peninsula (With Discussion). Int. Geol. Congr., 17th, Ussr, Rep., Vol. 2, p. 415-423.

Picard, L., 1939. Outline on the tectonics of the Earth; with special Emphasis Upon Africa. Heb. Univ. Jerusalem, Geol. Dept., Vol. 2, No. 3-4, 66 p.

Picard, L., 1940. Groundwater In Palestine. Heb. Univ. Jerusalem, Geol. Dept., Bull., Vol. 3, No. 1, 24 p.

Picard, L., 1940. Report On Groundwater In Mekorot Water Wells Around Kefar Hasidim. (In Hebrew). Report, 16 P., Appen.

Picard, L., 1940. Underground Water In Palestine. (In Hebrew). Jewish Palestine Explor. Soc., Bull., Vol. 7, No. 2, p. 52-59.

Picard, L., 1941. Report On Water Supply Possibilities In The High Carmel. (In Hebrew). N.P., 32 P., Figs.

Picard, L., 1941. The Precambrian Of The North Arabian - Nubian Massif. Jerusalem, Heb. Univ., Geol. Dept., Bull., Vol. 3, No. 3-4, 30 p.
Picard, L., 1942. Coast Of The Dead Sea. Jerusalem, 5 p.
Picard, L., 1942. New Cambrian Fossils And Paleozoic Problematica From The Dead Sea And Arabia. Jerusalem, Heb. Univ., Geol. Dept. Bull., Vol. 4, No. 1, 19 p.
Picard, L., and Bentor, Y.K., 1942. Groundwater In The Qiryat Anavim - Ma'ale Ha'hamisha Area. (In Hebrew). Jerusalem, 22 P., Appen. (Typewritten).
Picard, L., 1943. Report Ueber Die Luftemanation Der Thermen Von Tiberias. 14 p. (Typewritten).
Picard, L., 1943. Structure And Evolution Of Palestine; With Comparative Notes On Neighbouring Countries. Heb. Univ. Jerusalem, Geol. Dept., Bull., Vol. 4, No. 2-3-4, 187 p.
Picard, L., 1947. Considerations On Water Resources In Kefar Ezyon Area. (In Hebrew). Jerusalem, Geol. Dept., 4 P., Figs., Maps.
Picard, L., 1948. Le Petrole En Palestine. Moniteur Du Petrole Roumain, Vol. I-Ii, p. 13-14.
Picard, L., 1949. Preliminary Geological Report On Sahl El Battauf. Jerusalem, 9 P., 1 Map. (Typewritten).
Picard, L., 1950. Geologic Report Of Jordan Exploration Company Concession, Dead Sea, Israel. Oil Prospects Of The Jordan Exploration Comp., By L. Franklin. Houston, Tx, 48 p.
Picard, L., 1951. Geomorphogeny Of Israel. Part I: The Negev. Isr. Geol. Surv., Publ. (Bull.) 1, 28 p. (Reprinted From: Isr. Res. Counc. Bull., 1951, Vol. 1, No. 1-2, p. 5-32).
Picard, L., 1952. The Geology Of Kefar Giladi Area. (In Hebrew). Eretz Israel, No. 2, p. 73-77.
Picard, L., 1952. The Pleistocene Peat Of Lake Hula. Isr. Res. Counc., Bull., Vol. 2, No. 2, p. 147-156. (Also Published As: Isr. Geol. Surv., Bull. 3, p. 1-10).
Picard, L., 1953. A. Outline On Groundwater Geology In Arid Regions. Isr. Geol. Surv., Bull. 4, p. 1-15. (Also In: Isr. Res. Counc., Bull., Vol. 2, No. 4, p. 358-371).
Picard, L., 1953. Disharmonic Faulting, A Tectonic Concept. Isr. Geol. Surv., Bull. 5, p. 132-135 (Reprinted From Isr. Res. Counc., Bull., Vol. 3, No. 1-2).
Picard, L., 1953. Disharmonic Faulting, A Tectonic Concept. Isr. Res. Counc., Bull., Vol. 3, No. 1-2, p. 132-135.
Picard, L., 1953. Outline Of Groundwater Geology In Arid Regions. Int. Geol. Congr., 19th, Alger 1952, Sect. 8, Fasc. 8, p. 117-136.
Picard, L., 1953. Outline Of The Hydrogeology Of The Area Covered By The Kishon Valley Scheme. Report On The Kishon Valley Project, By Tahal. Vol. 2 - Appen. A, p. 44-45.
Picard, L., 1953. Silurian In The Negeb (Israel). Int. Geol. Congr., 19th, Alger 1952, C.R., Sect. 2, Fasc. 2, p. 179-183.
Picard, L., 1953. The History Of Groundwater Exploration In Israel. Desert Res.; Proc. Int. Symp., Jerusalem 1952, p. 583-591. (Isr. Res. Counc., Spec. Publ. No. 2). (Also Published In: Isr. Geol. Surv., Bull. 4).
Picard, L., 1954. Disharmonic Faulting In The Jordan - Araba Graben. Int. Geol. Congr., 19th, Alger 1952; Assoc. Serv. Geol. Afr., Vol. 2, Fasc. 21, p. 213-214.
Picard, L., 1954. Geological Reasoning For Pontiac's Drilling Of Israel Continental's South Carmel Area. Montreal, Pamphlet Issued By Maine Investig. Co.).
Picard, L., 1954. History Of Mineral Research In Israel. Isr. Econ. Forum, Vol. 6, No. 3, p. 10-38 & Appen. p. 146-150.
Picard, L., 1954. The Structural Pattern Of Palestine (Israel & Cis Jordan). Isr. Res. Counc., Bull., Vol. 4, No. 1, p. 48-50.
Picard, L., 1954. The Structural Pattern Of Palestine (Israel & Jordan). Int. Geol. Congr., 19th, Alger 1952, C.R., Sect. 14, p. 301-305.
Picard, L., 1955. Geological Map Of Israel, 1:100,000. Sheet 2: Haifa. Isr. Geol. Surv., 1 Map, Colored.
Picard, L., 1955. Geological Map Of Palestine, 1:100,000, Sheet 9: Ramle. Isr. Geol. Surv., 1 Map.
Picard, L., 1955. Report On A Visit To Al Kandula Proposed Tunnel Site (11.7.55). Jerusalem, 1 P., Fig., Logs.
Picard, L., 1956. Geological Background For Petroleum Drilling At Zikhron Yaaqov (Southern Carmel). (In Hebrew). Isr. Explor. Soc., Bull., Vol. 20, No. 3-4, p. 121-128.
Picard, L., 1956. Geological Map Of Israel 1:100,000. Sheet 4: Zikhron Yaaqov. Isr. Geol. Surv., 1 Map, Colored.
Picard, L., 1956. The Geological Map Of Israel, 1:100,000. Sheet 1: Metulla. Isr. Geol. Surv., 1 Map.
Picard, L., 1956. The Geological Map Of Israel, 1:100,000. Sheet 3: Safad. Isr. Geol. Surv., 1 Map.
Picard, L., 1956. The Geological Map Of Israel, 1:100,000. Sheet 5: Nazareth. Isr. Geol. Surv., 1 Map.
Picard, L., 1956. The Geological Map Of Palestine, 1:100,000. Sheet 8: Yibna. Isr. Geol. Surv., 1 Map.
Picard, L., 1956. The Geological Map Of Palestine, 1:100,000. Sheet 11: Gaza. Isr. Geol. Surv., 1 Map.
Picard, L., 1956. The Geological Situation Of Jerusalem. (In Hebrew). The Jerusalem Book, Ed By M. Avi Yonah. Jerusalem & Tel Aviv, Bialik Inst. & Devir, p. 35-44.
Picard, L., 1958. Geological Background On Petroleum Drilling In Zikhron Yaaqov (S. Carmel). Isr. Res. Counc., Bull., Vol. 7g, No. 1, p. 20-26.
Picard, L., and Kashai, E., 1958. On The Lithostratigraphy & Tectonics Of The Carmel. Isr. Res. Counc., Bull., Vol. 7g, No. 1, p. 1-19, Figs., Map.
Picard, L., 1959. Geological Map Of Israel And Adjoining Territories, 1:500,000. Tel Aviv, Survey Of Israel, 1 Map.
Picard, L., 1959. Geology And Oil Exploration Of Israel. Isr. Res. Counc., Bull., Vol. 8g, No. 1, p. 1-30.
Picard, L., 1959. Geology And Oil Exploration Of Israel. World Pet. Congr., 5th, New York; Proc., Sect. 1, p. 311-336.
Picard, L., 1959. Problem Of Water Supply In Arid Regions. (In Hebrew). Mada, Vol. 3, No. 3-4, p. 21-25.
Picard, L., 1960. Groundwater Exploration In Israel. Lecture Delivered At The Int. Conf. On Sci. In The Advancement Of New States, Weizmann Inst. Sci., Rehovot, Aug. 1960, 12 p.
Picard, L., 1960. Memorial Meeting: G.S. Blake, 1876-1940. Isr. Res. Counc., Vol. 9g, p. 167.
Stekelis, M., Picard, L., Schulman, N., and Haas, G., 1960. Villafranchian Deposits Near Ubeidiya In The Central Jordan Valley; Preliminary Report. Isr. Res. Counc., Bull., Vol. 9g, No. 4, p. 175-184.
Picard, L., 1962. George Stanfield Blake, His Work In Palestine 1922-1940. Isr. Res. Counc., Bull., Vol. 11g, No. 2, p. 49-57.
Picard, L., 1963. The Quaternary In The Northern Jordan Valley. Jerusalem, Isr. Acad. Sci. Humanities; Proc., Vol. 1, No. 4, 34 P., 1 Map, Scale 1:125,000.
Picard, L., and Gilboa, Y., 1963. Structural Map Of Israel, 1:500,000. Atlas Of Israel, Sheet 3/Iii. Surv. Of Israel (2nd Ed., 1970, Sheet Iii/3, Text & Map).
Picard, L., and Eliezri, I., 1964. Oil Exploration In Israel. Beolam Hadelek, No. 9-10, p. 77-104.
Picard, L., 1965. Stones Of Iron And Hills Of Brass. Ariel, No. 12, p. 47-56.
Picard, L., 1965. The Geological Evolution Of The Quaternary In The Central - Northern Jordan Graben, Israel. Geol. Soc. Am., Spec. Pap. 84, p. 337-366.
Picard, L., Golani, U., Bentor, Y.K., Vroman, A.J., and Zak, I., 1965. The Geological Map Of Israel, Scale 1:250,000. Northern Sheet - By L. Picard & U. Golani; Southern Sheet - By Y.K. Bentor, A.J. Vroman & I. Zak. Tel Aviv, Survey Of Israel, 2 Sheets.
Picard, L., 1966. L'evolution Des Sciences Geologiques En Israel. Ariel, No. 12, p. 47-57.
Picard, L., 1966. Thoughts On The Graben System In The Levant. Canada, Geol. Surv., Pap. 66-14, p. 22-32.
Picard, L., and Baida, U., 1966. Geological Report On The Lower Pleistocene Deposits Of The Ubeidiya Excavations. Jerusalem, Isr. Acad. Sci. Humanities, 39 P., Figs., Plates.
Picard, L., and Baida, U., 1966. Stratigraphic Position Of The Ubeidiya Formation. Jerusalem, Isr. Acad. Sci. Humanities; Proc. Sect. Of Sci., No. 4, 8 p.
Picard, L., and Eliezri, I., 1967. Oil Exploration In Israel. U.N. Miner. Resour. Dev. Ser. No. 26 (1), p. 303.
Picard, L., 1968. On The Structure Of The Rhinegraben, With Comparative Notes On Levantgraben Features. Isr. Acad. Sci. Human.; Proc. Section Of Sci., No. 9, 34 p.
Issar, A., and Picard, L., 1969. On the correlation of the Tyrrhenian on the Israel - Lebanon. Inqua, 8eme Congr. Int., Paris, p. 210.
Issar, A., and Picard, L., 1969. Sur le Tyrrhenien des côtes d'Israel et du Liban. Bull. Assoc. Fr. pour l'Étude du Quaternaire, No. 18, p. 35-41.
Picard, L., 1970. Further Reflections On Graben Tectonics In The Levant.

Graben Problems; Int. Rift Symp., Karlsruhe, Oct. 1968; Proc. Stuttgart, E. Schweizerbart'sche Verlag., p. 249-267. {Int. Upper Mantle Project, Sci. Rep. No. 27}.

Picard, L., 1970. Geological Map, 1:500,000.; Geological Cross-Sections. Atlas Of Israel. Tel Aviv, Survey Of Israel & Amsterdam, Elsevier, 2nd Ed. Sheet III, Text & Map; Sheet Iii/2, Figs.

Picard, L., 1970. Lithological Map, 1:1,000,000. Atlas Of Israel. Tel Aviv, Survey Of Israel & Amsterdam, Elsevier, 2nd Ed., Sheet III, Text & Map.

Picard, L., 1970. On Afro-Arabian Graben Tectonics. Geol. Rundsch., Vol. 59, No. 2, p. 337-381.

Picard, L., and Issar, A., 1970. The Stratigraphy Of The Pleistocene In The Jordan Valley And The Coastal Plain. (In Hebrew). The Stratigraphy Of The Pleistocene In Israel, p. 2-4.

Picard, L., and Kadmon, N., 1970. Watercourse Gradients. Atlas Of Israel. Tel Aviv, Survey Of Israel & Amsterdam, Elsevier, 2nd Ed., Sheet V/2, Text & Map.

Bloch, M., and Picard, L., 1970. The Dead Sea - a sinkhole? Dtsch. Geol. Ges., Z., Sonderh. Hydrogeol. Hydrogeochem., p. 119-128.

Issar, A., and Picard, L., 1971. On Pleistocene shorelines in the Coastal Plain of Israel. Quaternaria, No. 15, p. 267-272.

Picard, L., 1972. Israel. Land Of- Geology. Encycl. Judaica, Vol.—, p. 193-220.

Picard, L., 1973. General Aspects Of Israel's Oil Search. N.P., 7 p.

Ginzburg, A., Picard, L., Hanreck, R. G .S., Kashai, E., Gvirtzman, G., Aharoni, E., and Derin, B., 1973. A plan for oil exploration in Israel and Northern Sinai. (In Hebrew). Prepared for Isr. Inst. Pet. Energy, 22 p.

Picard, L., 1974. The Geological Evolution Of The Quaternary In The Central - Northern Jordan Graben, Israel. Int. Symp. On Geomorphic Processes In Arid Environ.; Field Study Program, Comp. By R. Gerson & M. Inbar. Heb. Univ. Jerusalem, Geogr. Dept., p. 128-129.

Picard, L., and Flexer, A., 1974. Studies On The Stratigraphy Of Israel: The Triassic. (Negev; Sinai; Jordan; Saudi Arabia; Syria). Isr. Inst. Pet. Energy, 62 p.

Picard, L., and Wakshal, E., 1975. Evolution Of Fossil Karst Aquifer In Israel. 12th Int. Congr., Int. Assoc. Hydrogeol. Karst Hydrogeol., Abstr. Progr., Huntsville, Gulf Shores. Alabama, Geol. Surv., p. 78.

Picard, L., and Wakshal, E., 1977. Evolution Of Fossil Karst Aquifers In Israel. Karst Hydrogeol., Ed By J.S. Tolson & F.L. Doyle. Huntsville, Univ. Of Alabama, p. 21-22.

Issar, A., and Picard, L., 1978. A correlation between the marine and continental Pleistocene of Israel. Ben Gurion Univ., Inst. For Desert Res., Sede Boqer Campus; 1st Annu. Sci. Rep., Ed. by S. Dover, p. 56-57.

Picard, L. Y., and Freund, R., 1979. International symposium on Rift zones of the Earth, the Dead Sea Rift, program and abstracts. Hebrew Univ. Jerusalem.

Picard, L., 1987. The Elat (Aqaba) - Dead Sea - Jordan subgraben system. Tectonophysics, 141(1-3), p. 23-32.

Picard, L., and Hirsch, F., 1987. The Jurassic Of Israel And Adjacent Countries. Int. Symp. Jurassic Stratigr., 2nd, Lisbon; Abstr., p. 96.

Picard, L., and Hirsch, F., 1987. The Jurassic Stratigraphy In Israel And The Adjacent Countries. Jerusalem, Isr. Acad. Sci. Human., 106 p.

Hirsch, F., and Picard, L., 1988. The Jurassic Facies in the Levant. J. Pet. Geol., 11(3), p. 277-308.

Picard, L., 1990. In Memoriam - Zeev Shiftan. (In Hebrew). Isr. Geol. Soc., Annu. Meet.; Abstr., p. Tet-Yod.

Picard, L., 1996. Pioneering Geology Of Erez Israel; Benchmarks In The Exploration Of Groundwater And Natural Resources. (In Hebrew). Jerusalem, Isr. Acad. Sci. Human., 155 p. & 51 p.

Picard, L., 1996. Vom Bodensee Nach Erez Israel Germany, Kinstanz, Hartung-Gorre Verlan, 290 p.



Prof. Leo Y. Picard at work in his office in 1951, probably at the Geological Survey of Israel, which he founded in 1949. Photo by Edgar Hirshbain, Jerusalem, provided courtesy of Dr. Eliahu Wakhshal (The Leo Picard Groundwater Research Center, Seagram Center for Soil and Water Sciences, The Hebrew University of Jerusalem, Rehovot 76100).

PROFESSOR ZEEV REISS (1917-1996)

Zeev Lewy
Geological Survey of Israel, Jerusalem, Israel
Jonathan Erez
Institute of Earth Sciences, The Hebrew University of Jerusalem

Zeev Reiss, Professor Emeritus of Geology at The Hebrew University of Jerusalem, micropaleontologist, stratigrapher, teacher of several generations of students, died on 11th of July 1996 after a short illness. He was 79 years old.

Zeev Reiss was born in Czerniowitz, Rumania in 1917. His sense of esthetics attracted him to the study of natural life and the beauty of plants, animals, and landscapes. In 1937 he began to study natural sciences, majoring in biology, at the University of Czerniowitz. His studies were interrupted by World War II, which he survived in Nazi labor camps. After the war he managed the Health Department for displaced persons of the American Joint Distribution Committee in Munich, Germany. He immigrated to Israel in 1949 where he started work as a scientific-technical assistant at the Geology Department of The Hebrew University, Jerusalem, while pursuing a degree in Geology and Paleontology.

Introduced to micropaleontology by Professor M. Avnimelech, Zeev became greatly interested in microfossils, especially foraminifera. He rapidly learned the systematics of the foraminifera and observed the wide distribution of planktic foraminifera and their usage in biostratigraphic correlations. When the necessity arose, in 1950, to establish a micropaleontology-stratigraphy laboratory at the Geological Survey of Israel mainly for the purpose of groundwater exploration, Zeev took the task upon himself. Later he became chief micropaleontologist and director of the survey's Paleontology Division, a position he held until 1966. Subsequently he compiled the first biostratigraphic distribution charts for Israel. His routine work on thousands of analyses provided the updated biostratigraphic control for surface mapping and subsurface geological reconstructions. He was the first to introduce the modern concepts and nomenclature of stratigraphy, correlation, and facies changes – a major contribution to the geological mapping of Israel.

Because of his experience in micropaleontology he was appointed guest lecturer at the Department of Geology of the Hebrew University in 1953 while he was still completing his official geological education in the department. Years of routine research and the study of the available literature stimulated his curiosity to understand how alleged "primitive" unicellular organisms construct such complex endoskeletons, and to learn the function of each morphological feature. In 1954 he began to study the internal features of foraminiferal shells with special emphasis on their wall-structure. His publications were the basis for a fundamental reappraisal of the taxonomy and the phylogenetic relationships within foraminifera. His Ph.D. thesis in 1962 (which he completed *summa cum laude*) was a breakthrough in the understanding of foraminiferal shell structures. In 1960, while analyzing the foraminiferal assemblages of the Upper Cretaceous phosphorite deposits of Israel, he suggested for the first time the probability

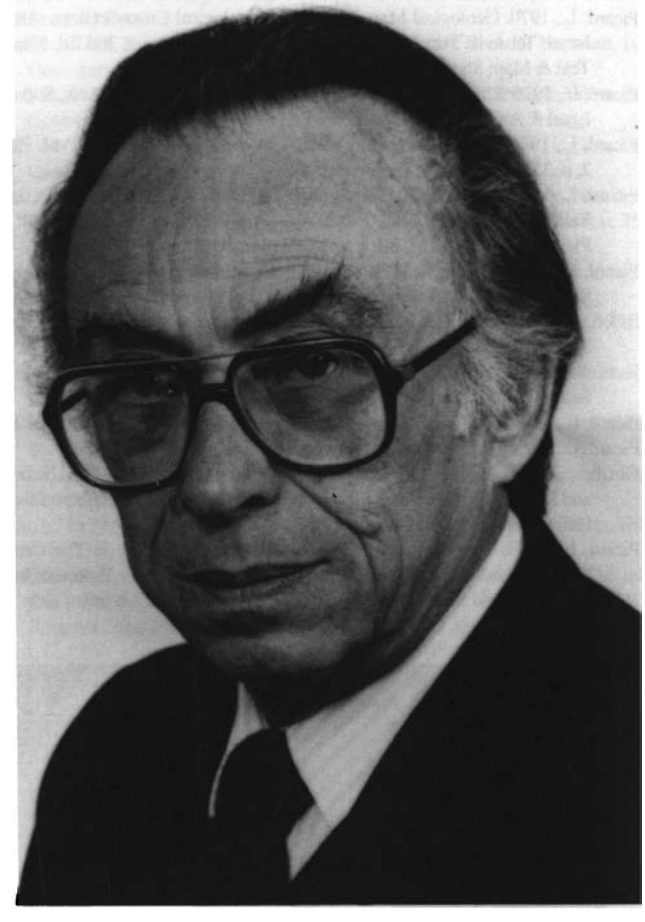


Figure IV.25. Prof. Zeev Reiss (1917-1996) Paleontologist, Israel. As the founder of micropaleontological studies in Israel, he organized laboratories at the Geological Survey and the Hebrew University and took part in the study of the Red Sea. For his life work he earned the medal of the Cushman Foundation. Photo courtesy of Pnina Merling Reiss, Prof. Reiss' widow.

that certain species were adapted to low-oxygen and high-water-fertility conditions. These theories, corroborated widely during the later years, became important tools in paleoceanographic research.

In 1966, Zeev was appointed Senior Lecturer in Geology at The Hebrew University of Jerusalem. A year later he was promoted to Associate Professor, and in 1971, to Full Professor. In 1969 he started investigating the living foraminiferal faunas of the Gulf of Aqaba. Recognizing the necessity to study these faunas within the framework of oceanographic settings of the gulf (then largely unknown), he initiated and directed a three-year program for the study of physical, chemical, and biological oceanography of this region. This program attracted many foreign scientists and students, resulting in a large number of publications, many of them authored or co-authored by Reiss. With his students he studied the foraminifera, pteropod, and coccolithophorid populations in the gulf, as well as the ecology and population dynamics of these groups. At this time, Reiss also obtained the cooperation of Woods Hole Oceanographic Institution whose research vessel took the first deep sea cores in the Gulf of Aqaba. These cores were studied by Reiss and his co-workers, and provided the basis for a paleoceanographic and paleoclimatic reconstruction of the gulf during the last 150,000 years. In 1984, together with L. Hottinger, Reiss published the results of these studies in the widely acclaimed book, "The Gulf of Aqaba," for which he received the annual award of the Israel Geological Society. The publication of Recent Foraminiferida from the Gulf of Aqaba, Red Sea by Hottinger, Halicz, and Reiss in 1993, was the culmination of an extensive study by SEM, X-ray, and light microscopy of the taxonomy and internal structure of more than 360 foraminifera species in the gulf.

Zeev Reiss served his profession on many national and international scientific committees. He was head of the Department of Geology of The Hebrew University of Jerusalem, as well as Director of its Institute of Earth Sciences, and Director of the H. Steinitz Marine Biology Laboratory in Eilat. He was elected vice-president and president of the Israel Geological Society, of which he later became an honorary member. He served on the editorial boards of the Israel Journal of Earth Sciences, Revista Española de Micropaleontologia (Spain), and Marine Micropaleontology (USA). For his significant scientific achievements he was elected Foreign Member of the Royal Netherlands Academy of Arts and Sciences (1983), received the J. A. Cushman Award for 1989 for Excellence in Foraminiferal Research of the Cushman Foundation for Foraminiferal Research, and an honorary doctorate from the University of Munich, Germany (1992).

Zeev Reiss will be remembered by his colleagues as a devoted teacher and mentor. He was elected "Distinguished Lecturer" of the Faculty of Sciences (1983) for his outstanding lectures. He devoted much of his time to students of geology in general, and particularly to students of micropaleontology, microfacies and paleoceanography. He closely followed the progress of his former students, many of whom work today as professors and senior scientists in various universities and scientific institutions in Israel and in other countries. After he retired from active teaching, Zeev continued his scientific work and advised graduate students. Recently he proposed some stimulating ideas on the paleo-ecological significance of foraminifera in the Eastern Mediterranean.

For nearly half a year he bravely struggled with his illness. It has put an end to a long period of remarkable scientific achievements that greatly contributed towards geological research in Israel, and that promoted modern approaches to paleoceanography, ecology, and functional morphology.

His dedication as a scientist and devoted teacher will be remembered and will serve as an example for his colleagues and students. He will be greatly missed by all.

PUBLICATIONS OF ZEEV REISS (Chronological Order)

Reiss, Z., 1952. On the occurrence of *Globotruncana Calcarata* Cushman 1927 in the Upper Cretaceous of Israel. Isr. Res. Counc., Bull., 2(3), p. 270-272.

Reiss, Z., 1952. On the Upper Cretaceous aAnd Lower Tertiary microfaunas of Israel. Isr. Res. Counc., Bull., 2(1), p. 37-50.

Reiss, Z., 1952. Two new species of foraminifera from Israel. Isr. Res. Counc., Bull., 2(3), p. 269-270.

Avnimelech, M., and Reiss, Z., 1953. On the Upper Cretaceous and Tertiary stratigraphy of a boring near Beth Govrin (Israel). Isr. Res. Counc., Bull., 3(3), p. 171-176. (Also: Isr. Geol. Surv., Publ. 6, 1954).

Reiss, Z., 1953. On the so-called Danian of Israel. Isr. Geol. Surv., Rep., 8 p.

Avnimelech, M., Parnes, A., and Reiss, Z., 1954. Mollusca and foraminifera from the Lower Albian of the Negev (Southern Israel). J. Paleontol., 28(6), p. 835-839.

Reiss, Z., 1954. Upper Cretaceous and Lower Tertiary Bolivinoides from Israel. Cushman Found. for Foraminiferal Res., Contrib., 5(4), p. 154-164, Plates.

Shadmon, A., and Reiss, Z., 1954. Report on the Anhydrite - Gypsum of the Beer Ora and Yotvata area (With a report on the micropaleontology of the area by Z. Reiss). Isr. Geol. Surv., 25 p.

Reiss, Z., 1955. A. Micropaleontology and Cretaceous-Tertiary boundary in Israel. B. Remarks on the age of some Late Cretaceous and Early Tertiary stratigraphic units in Israel. Isr. Geol. Surv., Bull. 8, 22 p. (Reprinted From: Isr. Res. Counc., Bull., 5B(1), p. 105-120 & 121-125).

Reiss, Z., 1957. Notes on foraminifera from Israel. 1. Remarks on *Truncorotalia Aragonesis* Caucasica (Glaessner). 2. Loxostomoides, A new Late Cretaceous and Early Tertiary genus of foraminifera. 3. Sigalia, A new genus of foraminifera. Isr. Geol. Surv., Bull. 9, 7 p. (Reprinted From: Isr. Res. Counc., Bull., Vol. 6B, p. 239-244).

Reiss, Z., 1957. Notes on foraminifera from Israel. 4. Occurrence and stratigraphical significance of *Cuvillierina Eocenica* Debourle. Isr. Geol. Surv., Bull. 10, 12 p.

Reiss, Z., 1957. Notes on foraminifera from Israel. 5. Studies on Victoriellidae. 6. Stratigraphical distribution of some Mesozoic and Cainozoic foraminifera from Israel. Isr. Geol. Surv., Bull. 11, 15 p.

Reiss, Z., 1957. Occurrence of Nezzazata in Israel. Micropaleontology, 3(3), p. 259-262.

Reiss, Z., 1957. The Bilamellidea, nov. Superfam., and Remarks on Cretaceous Globorotaliids. Cushman Found. for Foraminiferal Res., Contributions, Vol. 8, Pt. 4, No. 174, p. 127-145.

Grader, P., and Reiss, Z., 1958. On the Lower Cretaceous of Heletz area. Isr. Geol. Surv., Bull. 16, 14 p.

Reiss, Z., 1958. Classification of lamellar foraminifera. Micropaleontology, 4(1), p. 51-70.

Reiss, Z., 1958. Notes on foraminifera from Israel. 7. Remarks on the age of the so-called Dalia Marls in Northern Israel. 9. *Protopeneroplis Striata* Weynschenk from the Jurassic of Israel. Isr. Geol. Surv., Bull. 17, p. 3-4 & 8-10.

Reiss, Z., and Reiss (Merling), P., 1958. Structure of some Rotaliidea. Isr. Geol. Surv., Bull. 21, 19 p.

Vroman, A. J., and Reiss, Z., 1958. A. The Cenomanian-Turonian boundary in northern Israel. B. 7. Remarks on the age of the so-called "Dalia Marls" in N. Israel. 8. The systematic position of Sigalia and Bolivinoides. 9. *Protopeneroplis Striata* Weynschenk from the Jurassic of Israel. Isr. Geol. Surv., Bull. 17, 10 p.

Reiss, Z., 1959. Note Sur Pseudolituonella. Rev. Micropaleontol., 2(2), p. 95-98.

Reiss, Z., 1959. Notes on foraminifera from the Gulf of Eylath, Ras Muhamed and Tiran. Isr. Sea Fish. Res. Station, Bull., No. 20, p. 1-3.

Reiss, Z., 1959. The wall structure of Cibicides, Planulina, Gyroidinoides and Globorotalites. Micropaleontology, 5(3), p. 355-356.

Ben Tuvia, A., Bograd-Zismann, L., Gottlieb, E., Kimor, B., Neev, D., Neumann, J., Oren, O. H., Reiss, Z., and Steinitz, H., 1960. A programme for the oceanographic study of the Red Sea. N.P., 12 p. (Isr. National Plan, submitted to Indian Ocean Expedition - SCOR).

Bentor, Y. K., Grader, P., Parnes, A., Reiss, Z., Shiftan, Z., Vroman, A. J., Shadmon, A., Issar, A., Itzhaki, Y., Neev, D., Shalem, N., and Yaalon, D. H., 1960. Lexique Stratigraphique International. Vol. III: Asie. Fasc. 10 C 2: Israel. Paris, C.N.R.S., 151 p., Maps.

Grader, P., Reiss, Z., and Klug, K., 1960. Correlation of subsurface Lower Cretaceous units in the southern Coastal Plain of Israel. Isr. Geol. Surv., Bull. 28, 7 p.

Reiss, Z., 1960. Structure of so-called Eponides and some other Rotaliiform Foraminifera. Isr. Geol. Surv., Bull. 29, 29 p.

Reiss, Z., and Issar, A., 1960. Subsurface Quaternary correlations in the Tel Aviv Region. Isr. Geol. Surv., Rep., 35 p.

Reiss, Z., 1961. Lower Cretaceous microfacies and microfossils from Galilee. Isr. Res. Counc., Bull., Vol. 10G(1-2), p. 223-242.

Reiss, Z., 1961. Microfossils and microfacies of the Kudeifi Formation (Coniacian). Isr. Geol. Surv., Rep. PAL/4/61, 8 p., Plates.

Reiss, Z., 1961. Note on Revaha No. 1 and the Tithonian-Berriasian of the Coastal Plain, Israel. Isr. Geol. Surv., Rep. 1961/3, 8 p.

Reiss, Z., and Issar, A., 1961. Environmental analysis for stratigraphic correlation. Isr. Sci. Soc., Soil Sci. Soc. IV Congr.; Proc., p. 175-176 (In English); p. 128 (In Hebrew).

Reiss, Z., and Issar, A., 1961. Subsurface Quaternary correlations in the Tel Aviv region. Isr. Geol. Surv., Bull. 32, p. 10-26.

Reiss, Z., Klug, K., and Reiss (Merling), P., 1961. Recent foraminifera from the Mediterranean and Red Sea coasts of Israel. Isr. Geol. Surv., Bull. 32, p. 27-28.

Pomerancblum, M., Neev, D., and Reiss, Z., 1962. Sedimentological analysis of "Sakiebeds" in Beeri Core Hole No. 1 ("Sulphur"). Isr. Geol. Surv., Rep. REC/1/62, 39 p., Figs.

Reiss, Z., 1962. Negba - Core No. 26. Isr. Geol. Surv., 2 p. (A Letter to W. Randall, Lapidoth Chief Geologist).

Reiss, Z., 1962. Stratigraphy of phosphate deposits in Israel. Isr. Geol. Surv., Bull. 34, p. 1-23.

Reiss, Z., and Gvirtzman, G., 1962. Subsurface Neogene stratigraphy of the Israel Coastal Plain. Isr. Geol. Surv., Rep. PAL/4/62, 30 p.

Hamaoui, M., and Reiss, Z., 1963. Microfaunas of the Taqiya Formation and of the Hafir Member. Isr. Geol. Surv., Rep. PAL/3/63, 6 p., Figs.

Reiss, Z., 1963. Comments on wall structure of foraminifera. Micropaleontology, 9(1), p. 50-52.

Reiss, Z., 1963. Gan Yavne 3. Isr. Geol. Surv., Paleontol. Div. (Letter to G. J. Clair, Isr. Natl. Oil Co. Chief Geologist, 4 Plates.).

Reiss, Z., 1963. Note sur la structure des foraminiferes planctoniques. Rev. Micropaleontol., 6(3), p. 127-129.

Reiss, Z., 1963. Reclassification of perforate foraminifera. Isr. Geol. Surv., Bull. 35, 111 p. (Ph.D. Thesis, Hebrew Univ. Jerusalem, 1962).

Reiss, Z., 1964. Bibliography of foraminifera from Israel. Isr. Geol. Surv., Rep. PAL/5/64, 10 p.

Reiss, Z., 1964. Microbiostratigraphy of the Gan Yavne 2 Well. Isr. Geol. Surv., Rep. PAL/7/64, 8 p.

Reiss, Z., 1964. Microfaunas of the Jaffa 1 Well. Part 1: Planktonic Foraminifera. Isr. Geol. Surv., Rep. PAL/1/64, 23 p., Plates.

Reiss, Z., 1964. Paleontology and petroleum exploration In Israel - A Review. Isr. Geol. Surv., Rep. PAL/8/64, 8 p.

Reiss, Z., 1964. Range charts of Israel foraminifera. Isr. Geol. Surv., Rep. PAL/6/64, 9 P., Plates.

Reiss, Z., and Gvirtzman, G., 1964. Subsurface Neogene stratigraphy of Israel. Proc. 3rd Session in Berne, Committee on Mediterranean Neogene stratigraphy, p. 312-346.

Reiss, Z., Hamaoui, M., and Ecker, A., 1964. Pseudedomia from Israel. Micropaleontology, 10(4), p. 431-437.

Sohn, I. G., and Reiss, Z., 1964. Conodonts and foraminifera from the Triassic of Israel. Nature, 201(4925), p. 1209.

Derin, B., and Reiss, Z., 1965. Note on some Jurassic and Early Cretaceous Trocholina (Foraminiferida) from Israel. Jerusalem, Oil Companies, Micropaleontol. Lab. Rep. OS/1/65, 11 p., Figs., Plates.

Gvirtzman, G., and Reiss, Z., 1965. Stratigraphic nomenclature in the Coastal Plain and Hashephela regions. Isr. Geol. Surv., Rep. OD/1/65, 13 p.

Reiss, Z., 1965. Recent advances in marine Late Paleogene and Neogene stratigraphy of Israel. Isr. Geol. Surv., Rep. PAL/2/65, 14 p.

Derin, B., and Reiss, Z., 1966. Jurassic microfacies of Israel. Isr. Inst. Pet. Energy, Spec. Publ., 43 p., Plates.

Reiss, Z., 1966. Bibliography of foraminifera from Israel. Isr. Geol. Surv., Rep. PAL/2/66, 12 p. (2nd. Edition),

Reiss, Z., 1966. Recent advances in marine Late Paleogene and Neogene stratigraphy of Israel. Isr. J. Earth Sci., 15(1), p. 8-26.

Reiss, Z., and Gvirtzman, G., 1966. Borelis from Israel. Eclogae Geol. Helv., 59(1), p. 437-447.

Reiss, Z., Derin, B., and Gerry, E., 1966. On the so-called "Calcitic Eyes" in the shell walls of agglutinated foraminifera. Akad. Nauk SSSR, Otd. Nauk O Zemlie, Geol. Inst., Vopr. Micropal. 16, p. 234-242.

Sakal, E., Raab, M., and Reiss, Z., 1966. Upper Eocene in the South Eastern Negev, Israel. Isr. J. Earth Sci., 15(1), p. 42-45.

Shahar, Y., Reiss, Z., and Gerry, E., 1966. A new outcrop of marine Neogene in the Negev. Isr. J. Earth Sci., 15(2), p. 82-84.

Reiss, Z., 1967. Victoriella (Foraminiferida) from Israel. Isr. J. Earth Sci., 16(3), p. 111-119.

Reiss, Z., and Raab, M., 1967. Paleontological codes. (Incl. Index of Stratigraphical Units, compiled by M. Braun & E. Rosenthal). Isr. Geol. Surv., Rep. T/3/67 & Inst. Pet. Res. Geophys. Rep., 55 p., Index.

Reiss, Z., 1968. Foraminiferida. Hebrew Univ. Jerusalem, Geol. Dept., Summaries of lectures in Paleontology, 49 p. (2nd Revised Ed., 1971).

Reiss, Z., 1968. Planktonic Foraminiferids, stratotypes, and a reappraisal of Neogene chronostratigraphy in Israel. Isr. J. Earth Sci., 17(4), p. 153-169.

Reiss, Z., 1969. Recent Foraminiferida from the Gulf of Elat. Biota of the Red Sea and the Eastern Mediterranean. Hebrew Univ. Jerusalem, Zool. Dept. & Smithsonian Inst., Washington, D.C., p. 131-132.

Reiss, Z., and Schneidermann, N., 1969. Ultramicrostructure of Hoeglundina. Micropaleontology, 15(2), p. 135-144.

Flexer, A., Freund, R., Reiss, Z., and Buchbinder, B., 1970. Santonian paleostructure of the Galilee. Isr. J. Earth Sci., 19(3-4), p. 141-146.

Reiss, Z., and Luz, B., 1970. Test formation pattern in planktonic foraminiferids. Rev. Espan. Micropaleontol., 2(1), p. 85-96.

Derin, B., and Reiss, Z., 1971. Remarks on the Middle Miocene-Lower Pliocene stratigraphy of the Coastal Plain. Isr. Inst. Pet. Energy, Micropaleontol. Lab., Rep. 4/71, 8 p.

Reiss, Z., 1971. Progress and problems of foraminiferal systematics. Micropaleontology of Oceans, In: B. M. Funnell, et al., (eds.), London, Cambridge Univ. Press, p. 633-638.

Reiss, Z., Reiss (Merling), P., and Moshkovitz, S., 1971. Quaternary planktonic foraminiferida and nannoplankton from the Mediterranean continental shelf and slope of Israel. Isr. J. Earth Sci., 20(4), p. 141-177.

Hansen, H. J., and Reiss, Z., 1972. Scanning slectron microscopy of some Asterigerinid Foraminiferida. J. Foraminiferal Res., 2(4), p. 191-199.

Derin, B., and Reiss, Z., 1973. Revision of marine Neogene stratigraphy in Israel. Isr. J. Earth Sci., 22(4), p. 199-210.

Reiss, Z., Halicz, E., and Perelis-Grossowicz, L., 1974. Planktonic foraminiferida from Recent sediments in the Gulf of Elat. Isr. J. Earth Sci., 23(3), p. 69-105.

Zmiri, A., Kahan, D., Hochstein, S., and Reiss, Z., 1974. Phototaxis and thermotaxis in some species of Amphistegina (Foraminifera). J. Protozool., 21(1), p. 133-138.

Klinker, J., Kropach, C., Harpaz, H., Levanon, I., and Reiss, Z., 1975. DCPE - Data Collecting Program in the Gulf of Elat. (Physico-chemical and biological water mass properties and geological features - A multidisciplinary project). Report

No. 1. Elat, H. Steinitz Mar. Biol. Lab., 4th Rep., p. 46-54, Figs.

Perelis-Grossowicz, L., and Reiss, Z., 1975. Cibicididae in Recent sediments from the Gulf of Elat. Isr. J. Earth Sci., 24(3-4), p. 73-96.

Reiss, Z., 1975. Planktonic foraminiferida in the Gulf of Elat - A clue to extreme oceanic paleoenvironments. Elat, H. Steinitz Mar. Biol. Lab., 4th Rep., p. 35-37.

Zweig-Strykowski, M., and Reiss, Z., 1975. Bolivinitidae from the Gulf of Elat. Isr. J. Earth Sci., 24(3-4), p. 97-111.

Bein, A., and Reiss, Z., 1976. Cretaceous Pithonella from Israel. Micropaleontology, 22(1), p. 83-91.

Klinker, J., Reiss, Z., Kropach, C., Levanon, I., Harpaz, H., Halicz, E., and Assaf, G., 1976. Observations on the circulation pattern in the Gulf of Elat (Aqaba), Red Sea. Isr. J. Earth Sci., 25(3-4), p. 85-103. (Abstract In: Elat; H. Steinitz Mar. Biol. Lab., 5th Rep., 1976, p. 15-16).

Reiss, Z., and Halicz, E., 1976. Phenotypy in planktonic foraminiferida from the Gulf of Elat. Isr. J. Earth Sci., 25(1), p. 27-39.

Reiss, Z., Kropach, C., Levanon, I., Klinker, J., Harpaz, H., Shapiro, Y., and Ben Avraham, Z., 1976. DCPE - Data Collecting Program in the Gulf of Elat. Report No. 2. Elat, H. Steinitz Mar. Biol. Lab., 5th Rep., p. 22-68.

Almogi-Labin, A., and Reiss, Z., 1977. Quaternary pteropods from Israel: Pteropods from Recent sediments in the Gulf of Elat. Rev. Españ. Micropaleontol., 9(1), p. 22-48.

Reiss, Z., 1977. Foraminiferal research in the Gulf of Elat-Aqaba, Red Sea - A review. Utrecht Micropal. Bull., No. 15, p. 7-25.

Reiss, Z., Levanon, I., Raz, G., Harpaz, A., Ben Avraham, Z., and Padan, E., 1977. DCPE - Data Collecting Program in the Gulf of Elat. Elat, H. Steinitz Mar. Biol. Lab., 6th Rep., p. 31-54.

Klinker, J., Reiss, Z., Kropach, C., Levanon, I., Harpaz, H., and Shapiro, Y., 1978. Nutrients and biomass distribution in the Gulf of Aqaba (Elat), Red Sea. Mar. Biol., 45(1), p. 53-64.

Reiss, Z., Hottinger, L., Hansen, H. J., Drooger, C. W., Leutenegger, S., Larsen, A. R., Buchardt, B., Fermont, W. J. J., Thomas, E., Meulenkamp, J. E., Luz, B., Halicz, E., Erez, J., Perelis-Grossowicz, L., and Zweig-Strykowski, M., 1978. Sedimentological significance of foraminiferal ecology in a desert enclosed sea: the Gulf of Aqaba (Elat). Int. Congr. Sedimentol., 10th, Jerusalem; Abstr., Vol. 2, p. 541-542.

Winter, A., Reiss, Z., and Luz, B., 1978. Living *Gephyrocapsa Protohuxleyi* Mcintyre in the Gulf of Elat (Aqaba). Mar. Micropaleontol., 3(3), p. 295-298.

Halicz, E., and Reiss, Z., 1979. Recent Textulariidae from the Gulf of Elat (Aqaba), Red Sea. Rev. Españ. Micropaleontol., 11(2), p. 295-320.

Lee, J. J., McEnery, M. E., Shilo, M., and Reiss, Z., 1979. Isolation and cultivation of diatom symbionts from larger foraminifera (Protozoa). Nature, 280(5717), p. 57-58.

Levanon-Spanier, I., Padan, E., and Reiss, Z., 1979. Primary production in a desert enclosed sea - the Gulf of Elat (Aqaba), Red Sea. Deep Sea Res., 26(6A), p. 673-685.

Winter, A., Reiss, Z., and Luz, B., 1979. Distribution of living Coccolithophore assemblages in the Gulf of Elat (Aqaba). Mar. Micropaleontol., 4(3), p. 197-223.

Luz, B., Reiss, Z., Almogi-Labin, A., Halicz, E., Winter, A., Wolf, M., and Ross, D.A., 1980. Late Quaternary paleoceanography of the Gulf of Aqaba (Elat), Red Sea. Isr. Geol. Soc., Annu. Meet., Ophira, Progr. Abstr., p. 25.

Luz, B., Reiss, Z., Almogi-Labin, A., Halicz, E., Winter, A., Wolf, M., and Ross, D. A., 1980. Late Quaternary paleoceanography of the Gulf of Aqaba (Elat), Red Sea. Isr. Geol. Soc., Annu. Meet.; Abstr., p. 25.

Reiss, Z., Almogi-Labin, A., Halicz, E., Luz, B., and Winter, A., 1980. Ecological relations in desert enclosed seas: A key to the interpretation of past proxy climate indicators. Bat Sheva Seminar, Jerusalem & Rehovot, Oct. 1980; Progr. Abstr., p. 59-61.

Reiss, Z., Luz, B., Almogi-Labin, A., Halicz, E., Winter, A., Wolf, M., and Ross, D. A., 1980. Late Quaternary paleoceanography of the Gulf of Aqaba (Elat), Red Sea. Quaternary Res., 14(3), p. 294-308.

Zohary, T., Reiss, Z., and Hottinger, L., 1980. Population dynamics of *Amphisorus Hemprichii* (Foraminifera) in the Gulf of Elat (Aqaba), Red Sea. Eclogae Geol. Helv., 73(3), p. 1071-1094.

Halicz, E., and Reiss, Z., 1981. Paleoecological relations of foraminifera in a desert enclosed sea - Gulf of Aqaba (Elat), Red Sea. Mar. Ecol., 2(1), p. 15-34.

Reiss, Z., 1982. The importance of the Gulf of Elat for reconstructions of ancient environments. (In Hebrew). Sinai Summary Conference; Abstr. Isr. Minist. of Energy & Infrastructure, p. 34-35.

Reiss, Z., and Luz, B., 1982. Pleistocene paleoceanography of the Gulf of Elat and the Levant Basin. (In Hebrew). Hebrew Univ. Jerusalem, 3 p. (Report, Submitted to the Minist. of Energy & Infrastructure).

Reiss, Z., Luz, B., Almogi-Labin, A., Halicz, E., Winter, A., and Erez, J., 1982. Red Sea environments during the last 150,000 years - the Gulf of Aqaba. Int. Conf. on Mar. Sci. in the Red Sea, Al Ghardaqa, Apr. 1982; Abstr., p. 21.

Luz, B., and Reiss, Z., 1983. Stable carbon isotopes in Quaternary foraminifera from the Gulf of Aqaba (Elat), Red Sea. Utrecht Micropal. Bull., No. 30, p. 129-140.

Luz, B., Reiss, Z., and Zohary-Segev, T., 1983. Seasonal Variation of stable isotopes in Amphisorus from the Gulf of Aqaba (Elat), Red Sea. Utrecht Micropal. Bull., No. 30, p. 229-238.

Winter, A., Almogi-Labin, A., Erez, Y., Halicz, E., Luz, B., and Reiss, Z., 1983. Salinity tolerance of marine organisms deduced from Red Sea Quaternary record. Mar. Geol., 53(1/2), p. 17-22.

Halicz, E., Noy, N., and Reiss, Z., 1984. Foraminifera from Shura Arwashie Mangrove (Sinai). In: F. D. Por & I. Dor, (eds.), Hydrobiology of the Mangal: The Ecosystem of the Mangal, The Hague, W. Junk, p. 145-149. (Dev. in Hydrobiol., 20).

Reiss, Z., and Hottinger, L., 1984. The Gulf of Aqaba; Ecological micro paleontology. Berlin, Springer, 354 p. (Ecol. Stud. 50).

Reiss, Z., Luz, B., Almogi-Labin, A., Halicz, E., Winter, A., and Erez, J., 1984. Paleoceanography of the Gulf of Aqaba during the last 150,000 years. In: J. A. Coetzee and E. M. Van Zinderen, (eds.), Palaeoecology of Africa and the surrounding islands, Rotterdam, A. A. Balkema, Vol. 16, p. 55-64.

Gvirtzman, G., Moshkovitz, S., and Reiss, Z., 1985. Senonian to Early Eocene Mount Scopus Group in the Hashefela region, Central Israel: Stratigraphy and basin evolution. Isr. J. Earth Sci., 34(4), p. 172-192.

Haas, Y., Reiss, Z., and Honig, G., 1985. Note on Senonian radiolaria from Israel. Isr. J. Earth Sci., 34(4), p. 167-171.

Reiss, Z., Almogi-Labin, A., Honigstein, A., Lewy, Z., Lipson, S., Moshkovitz, S., and Zaks, Y., 1985. Late Cretaceous multiple stratigraphic framework of Israel. Isr. J. Earth Sci., 34(4), p. 147-166.

Almogi-Labin, A., Reiss, Z., and Caron, M., 1986. Senonian Globotruncanidae from Israel. Eclogae Geol. Helv., 79(3), p. 849-895.

Reiss, Z., Almogi-Labin, A., Lewy, Z., and Moshkovitz, S., 1986. Biostratigraphic datums in the Senonian of Israel. Proc. K. Ned. Akad. Wet., Ser. B, Vol. 89, No. 1, p. 95-104.

Gvirtzman, G., Moshkovitz, S., Almogi-Labin, A., Lewy, Z., Honigstein, A., and Reiss, Z., 1987. Upper Cretaceous correlations from Central Israel: Datum levels and their ages. Isr. Geol. Soc., Annu. Meet., p. 50-51.

Reiss, Z., 1988. Assemblages from a Senonian high productivity sea. Rev. Paleobiol., Vol. Spec. 2 (Benthos 86), Pt. 1, p. 323-332.

Gvirtzman, G., Almogi-Labin, A., Moshkovitz, S., Lewy, Z., Honigstein, A., and Reiss, Z., 1989. Upper Cretaceous high resolution multiple stratigraphy, northern margin of the Arabian Platform, Central Israel. Cretaceous Res., 10(2), p. 107-135.

Luz, B., Reiss, Z., and Almogi-Labin, A., 1989. Chemical changes in the deep Red Sea during the Late Pleistocene. Int. Conf. Paleo-Oceanogr., 3rd, Cambridge, Sept. 1989; Abstr., p. 6-7.

Moshkovitz, S., Gvirtzman, G., Almogi-Labin, A., Lewy, Z., Honigstein, A., and Reiss, Z., 1989. Upper Cretaceous high resolution stratigraphy in the pelagic sequence of the Judean Mts. and the Shephela region, Central Israel. INA (=Int. Nannoplankton Assoc.) Newsl., 11(2), p. 80-82. (Ina. Nannoplankton Assoc. Meet., Firenze, Sept. 1989; Abstr.).

Hottinger, L., Halicz, E., and Reiss, Z., 1990. Partitions and fistulose chamberlets in Textulariia (examples from Gulf of Elat). In: C. Hemleben, et al., (eds.), Paleoecology, biostratigraphy, paleoceanography and taxonomy of agglutinate foraminifera, Netherlands, Kluwer Acad. Publ., p. 37-49.

Hottinger, L., Halicz, E., and Reiss, Z., 1990. Wall texture of Spirorutilus. J. Foraminiferal Res., 20(1), p. 65-70.

Hottinger, L., Reiss, Z., and Halicz, E., 1990. Comments on Neoeponides (Foraminifera). (incl. samples from Gulf of Elat). Rev. Paleobiol., 9(2), p. 335-340.

Hottinger, L., Halicz, E., and Reiss, Z., 1991. Architecture of Eponides and Poroeponides (Foraminifera) reexamined. Micropaleontology, 37(1), p. 60-75.

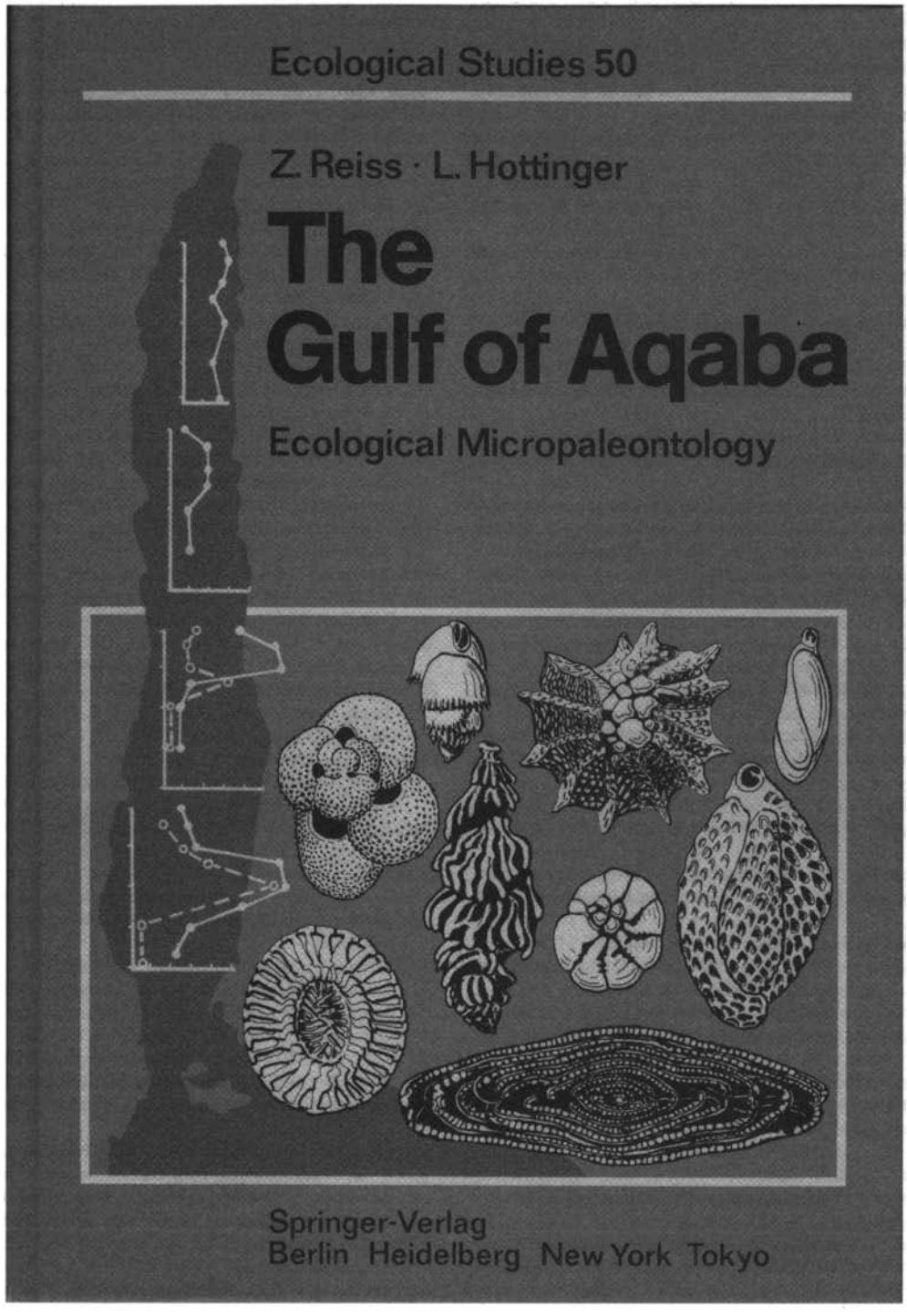
Hottinger, L., Halicz, E., and Reiss, Z., 1993. Recent foraminiferida from the Gulf of Aqaba, Red Sea. Ljubliana, Acad. Sci. et Art. Slovenica, Vol. 33, 179 p., 230 Plates.

Almogi-Labin, A., Reiss, Z., and Edelman, Y., 1994. Late Holocene paleoceanographic events in the Red Sea. Report submitted to the Minist. of Energy & Infrastructure, 9 p., Figs., Tables.

Furstenberg (Edelman), Y., Almogi-Labin, A., and Reiss, Z., 1995. Late Holocene paleoceanographic events in the Red Sea. Report submitted to the Minist. of Energy & Infrastructure, 19 p., Figs.

Reiss, Z., Halicz, E., and Luz, B., 1999. Late Holocene foraminifera from the SE Levantine Basin. Isr. J. Earth Sci., 48(1), p. 1-27.

Hottinger, L., Reiss, Z., and Langer, M., 2001. Spiral canals of some Elphidiidae. Micropaleontology, Vol. 47, Suppl. 2, p. 5-34.



Grayscale image of the cover of Reiss and Hottinger's (1984) seminal work on the Gulf of Aqaba.

AVRAHAM PARNES (1892-1989)

Moshe A. Avnimelech
Hebrew University of Jerusalem
Israel Journal of the Earth Sciences, Vol. 16, No. 2, p. 107-110.

As far as I can recall, my first meeting with Avraham Parnes was in 1934 or 1935. I had received a visit from a friend, a doctor, whom I conducted through the then small premises of the Hebrew University on Mount Scopus. We visited among other places, the National and University Library, where A. Parnes was working with the late Dr. Avraham Sharon (Schwadron), founder and organizer of the Authograph Collection of famous Jewish men. Parnes showed us the collection and explained its importance. Among the collection we found the authograph of Einstein's Relativity Theory. When my friend jokingly remarked: "Who can understand it?" Parnes earnestly retorted "Everyone can understand it". In retrospect after 30 years, this answer seems to characterize him: he can, or at least, he does not hesitate to attempt to understand everything. I have heard it said more than once that he is a "living encyclopedia". He belongs to the class of those broad-minded people who look upon details from a perspective of the widest horizons.

I don't know much about A. Parnes' early life history. He was born 75 years ago, December 4, 1892, in the famous Jewish-Galician town of Brody. He obviously received a very profound Jewish education, as well as a broad, general education in a classical "gymnasium" of the old, Austro-Hungarian style. In fact Dr. Parnes has retained a most adequate knowledge of Latin and Greek. In 1911 he entered the University of Lvov (Lemberg) where he studied law and sociology, and in addition, history, philosophy, pedagogics and even geography – this last subject, in the geography department under the directorship of the well known Prof. S. Romer. Presumably these studies were interrupted by the events of the First World War, when eastern Galicia was temporarily occupied by the Russian army. Nevertheless Parnes managed to complete his examinations and in 1916 received a certificate of "absolutorum", (attesting to the fact that he had completed his studies). In 1917, he registered at the University of Vienna in order to continue his studies in the fields of economics and political science, but shortly after he returned to Poland, this time not to the old Austro-Hungarian Galicia but to "Congress-Poland", former Russian territory. There, in 1919, he began a ten year long career as a teacher in Jewish gymnasiums and teacher-seminaries, a career which took him to Lodz, Rovno, Kalish, Lady, Vilno and Warsaw, all towns with large Jewish populations well known in the history of Polish Jewry. Parnes chiefly taught Hebrew language and literature, and Jewish history as well as geography. No doubt, his pedagogical activities harvested valuable crops, and many of his pupils who have survived, continue his work in various fields of social and cultural activity of the Hebrew national renaissance.

In 1926 he arrived in Palestine. Here he continued with his teaching career, at first in the rural schools of Nahalal, Beer-Tuviah and Petah-Tiqva, and later in Jerusalem. For a short period he assisted Dr. A. Sharon (Schwadron), in arranging and maintaining his priceless collection of Jewish authographs. At all times and

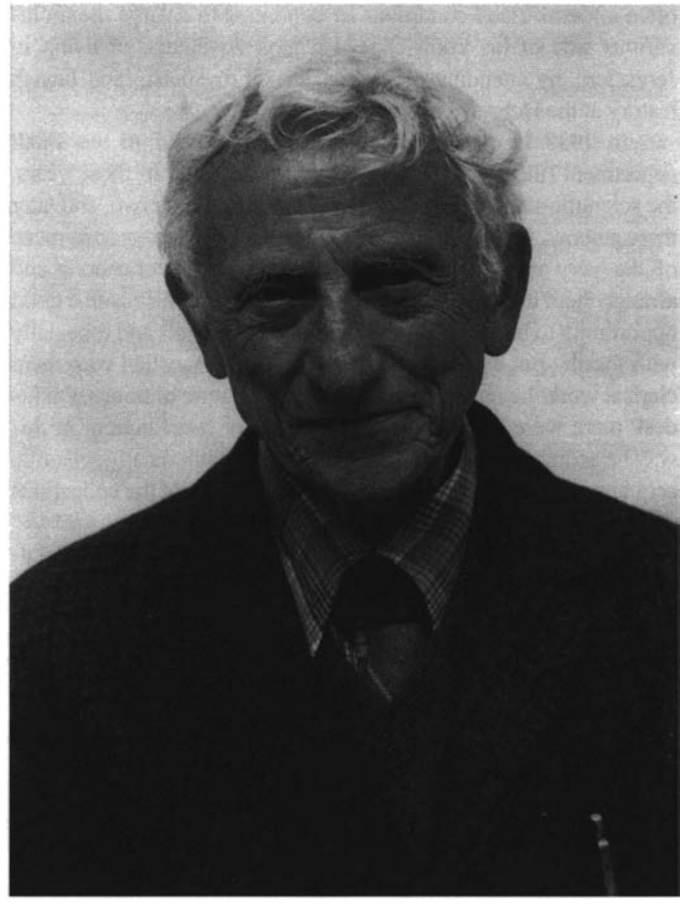


Figure IV.26. Dr. Avraham Parnes (1892-1989), Paleontologist, Israel. Nearing retirement in his non-geological profession, Dr. Parnes became an accomplished paleontologist, whose nearly half century long contributions to macro-fossil paleontology laid the foundations for biostratigraphy in Israel. Photo courtesy of Dr. Eliahu Wakhshal (The Leo Picard Groundwater Research Center, Seagram Center for Soil and Water Sciences, The Hebrew University of Jerusalem, Rehovot 76100).

often under difficult conditions he continued to enlarge the multivarious side of his knowledge. He took advantage of living in Jerusalem, by attending courses in Jewish mysticism and Jewish history at the Hebrew University.

In 1938 he began working as technical aid in the small department (then called "laboratory") of geology. In those years, the scientific staff of the department comprised only two, and later three persons. Parnes' duty was to register the numerous specimens of the very valuable geological-paleontological collections and arrange them in proper order. This work provided him with a good opportunity to become familiar with rocks, minerals and especially with fossils. But a man like Parnes can not be satisfied with mere clerical work; he must also be aware of the nature of things. On his desk there were always books necessary for consultation. In this way he acquired not only a visual but also a methodically scientific acquaintance of fossils. The present arrangement of the collections owe much to the work of Parnes.

On another occasion a relative of Haim Taubenhaus, a Zefat-born author of a small monograph on Palestinian Cretaceous ammonites, asked Parnes to translate his paper from German into Hebrew. The material of this monography forms part of Blanckenhorn's collections already in the possession of the department. Besides giving Parnes an opportunity to coin a number of Hebrew paleontological terms, the translation also developed his love for ammonites. Although the Hebrew version of Taubenhaus' paper has never been published, it did result some years later, in the publication of several valuable works by Parnes, dealing with Cretaceous, Jurassic and Triassic ammonites of the country.

During the War of Independence, Parnes was engaged in the geographical section of the young Israeli army, helping to prepare much needed maps.

At the end of the war, he returned to his work, devoting more time to the newly organized Geological Survey of Israel than to the Hebrew University. In 1952 he enlisted as a research student in order to prepare a Ph.D. thesis on the Triassic ammonites of the Negev. This thesis was presented six years later when the author was 63 years old. During these years Parnes was extremely busy; he accompanied most of the geological mapping parties of the Geological Survey, despite great physical inconveniences. No doubt he was greatly assisted by his late wife, Gusta, who found in his activity a source of great satisfaction. He helped young geologists in determining fossils they had collected and in this way he participated in making stratigraphical conclusions. The geological survey of the Negev and other parts of the country owe him much. At the University, he continued to initiate students into the knowledge of the fossils. More than one young geology master has quoted in his thesis long lists of fossils determined by Parnes.

Parnes' field of paleontological interest is broad. He had enough audacity to attack such difficult groups as Trilobites and Rudists. His young colleagues from the Geological Survey and the students of the University have supplied him richly with new material, but he himself was an able collector, with an experienced eye. In this manner he began in 1956 his study on the Trilobites of Timna area (Elat region), a study which helped to establish definitely the age of the formation as Upper Georgian Cambrian. During the later years he studied the ammonites of the Triassic for his Ph.D. title. As a result of this study, the connection of the Palestinian region in Trias times with the Alpine realm was well illustrated. Another fruit of his endeavour was the ammonites of the Coniacian (Lower Senonian) hitherto almost unknown in Palestine. The intensive phosphate quarrying in the Negev gave him the opportunity to investigate the fossils and the stratigraphy of phosphate deposits in Israel.

His work is characterized by a thorough and very detailed discussion and by the independence of his judgment, even in strong contradiction to well established authorities. His ability for concentration, and his memory for details are remarkable. In spite of his outstanding erudition, his way is modest, almost incognito-like. Sixteen years ago his brother-in-law, Prof. D. Sudan wrote: "We, his friends of bygone days, who are now his oldest pupils, are happy to see him richer in experience, acquired by hard learning and by accumulating knowledge, but at the same time we are not quite satisfied with his exaggerated modesty. Perhaps choosing a place in a hidden corner may do him good and suits his nature, but it doesn't please us, nor does it do us good...". (Translated from the Preface by D. Sudan to A. Parnes' "Mi'beyn hamaarkhoth".)

In spite of these claims Avraham Parnes has shown that in his quiet, modest way he has gained much for himself and has given much to others.

Editors' Note: Dr. Avraham Parnes passed away 'in harness', so to speak, while preparing for a field trip during the 1989 Annual Meeting of the Geological Society of Israel at Kibbutz Ramot on the Golan Heights overlooking the Sea of Galilee.

PUBLICATIONS OF A. PARNES (Chronological Order)

AVNIMELECH, M., PARNES, A. AND REISS, Z., 1954. Molluscs and Foraminifera from the Lower Albian of the Negev (Southern Israel), *J. Paleont.*, **28**(6), 835-839.

PARNES, A., 1956a. Upper Georgian of Timna, Israel Geol. Surv., Unpublished report.

PARNES, A., 1956b. Stratigraphy of the phosphatic belts in the Negev, *Bull. Israel Explor. Soc.*, **20**(3-4), 151-158 (in Hebrew).

PARNES, A., 1956c. The main features of the geomorphology of the Negev, *Ha-Negev*, "Adama", Ed. Jerusalem, 17-27 (in Hebrew).

PARNES, A., 1957. The Triassic in Makhtesh Arif, *Israel Geol. Soc. Bull.*, **4**, 9-12. (In Hebrew).

PARNES, A., 1958a. A Coniacian ammonite from the southern Negev (Israel), *Muniericeras lapparenti* Grossouvre var, *Bull. Res. Coun. Israel*, **7G**(4), 167-172.

PARNES, A., 1958b. The Triassic ammonites from Israel, Ph.D. thesis, Hebrew University, Jerusalem, 57 pp., 4 pls. (In Hebrew, English summary).

PARNES, A., 1959. N. Shalem - In Memoriam, *Bull. Israel Explor. Soc.*, **24**(l), 70. (In Hebrew).

BENTOR, Y. K., GRADER, P., PARNES, A., REISS, Z., SHIFTAN, Z., VROMAN, A. J., SHADMON, A., ISSAR, A., ITZHAKI, Y., NEEV, D., SHALEM, N., and YAALON, D. H., 1960. Lexique Stratigraphique International. Vol. **III**: Asie. Fasc. 10 C 2: Israel. Paris, C.N.R.S., 151 p., Maps.

PARNES, A., 1961a. Geological research of N. Shalem, *Israel Geol. Soc. Bull.*, **6**, 5-91 (in Hebrew).

PARNEs, A., 1961b. On the occurrence of *Pseudopygurus* Lambert in Southern Israel, *Bull. Res. Coun. Israel*, **10G**, 216-222.

PARNES, A., 1962. The geology of Makhtesh Ramon (Negev, Israel). Part 3a: Triassic ammonites from Israel, *Israel Bull. Geol. Surv.*, **33**, 2-76.

PARNES, A., 1963a. The Middle Jurassic fauna of Makhtesh Ramon, *Israel Geol. Soc. Bull., Makhtesh Ramon Symposium*, 13-14.

PARNES, A., 1963b. The Middle Jurassic fauna of Makhtesh Ramon, *Israel J. Earth-Sci.*, **12**(2), 91.

PARNES, A., 1964. Coniacian ammonites from the Negev (Southern Israel). *Israel Geol. Surv., Bull.*, **39**, 42 p.

PARNES, A., 1965. Note on Middle Triassic ammonites from Makhtesh Ramon (Southern Israel), *Israel J. Earth-Sci.*, **14**(1), 9-17.

PARNES, A., 1971. Late Lower Cambrian trilobites from the Timna Area and Har Amram (Southern Negev, Israel). *Israel J. Earth-Sci.*, **20**, 179-205.

PARNES, A., 1974. Biostratigraphic synchronization of the Middle Jurassic in Makhtesh Ramon, Gebel Maghara and Morocco. (In Hebrew and English). *Israel Geol. Soc., Annu. Meet., Abstr.*, 14-15.

PARNES, A., 1975. Middle Triassic ammonite biostratigraphy in Israel. *Israel Geol. Surv., Bull.*, **66**, 1-35, Plates.

PARNES, A., 1977. Middle Triassic ammonite biostratigraphy in Israel. *Israel Geol. Surv., Semin. 1974/76; Abstr. Pap.*, 28-29.

PARNES, A., 1977. On a binodose keeled Ceratitid from South Eastern Spain ("A representive of a line parallel to the Genus *Gevanites* Parnes 1975 from the Ladinian of Israel"). *Cuadernos Geol. Iberica*, **4**, 522-525.

PARNES, A., 1980. Lower Jurassic (Liassic) invertebrates from Makhtesh Ramon (Negev, Southern Israel). *Israel J. Earth Sci.*, **29**(1-2), 107-113.

PARNES, A., 1981. Biostratigraphy of the Mahmal Formation (Middle And Upper Bajocian) in Makhtesh Ramon. (Negev, Southern Israel). *Israel Geol. Surv., Bull.*, **74**, 55 p.

PARNES, A., 1984. Irregularly coiled *Stehanoceratidae* from the Upper Bajocian of Gebel Maghara, Sinai, Egypt. *Israel Geol. Surv., Current Res.*, **1983-84**, 29-32.

PARNES, A., BENJAMINI, C., and HIRSCH, F., 1985. New aspects of Triassic ammonoid biostratigraphy, paleoenvironments and paleobiogeography in Southern Israel (Sepharadic Province). *J. Paleontol.*, **59**(3), 656-666.

PARNES, A., 1986. Middle Triassic cephalopods from the Negev (Israel) and Sinai (Egypt), with an introduction on the Triassic in Israel, by I. Zak. *Israel Geol. Surv., Bull.*, **79**, 9-59, Plates.

PARNES, A., 1987. Radiation of species of the Genus Radiolites from the Upper Turonian at Gebel Er-Risha (NE Sinai, Egypt). *Israel J. Earth Sci.*, **36**(3), 133-153.

PARNES, A., 1988. Middle Jurassic (Middle Bajocian - Middle Bathonian) ammonites from Gebel Maghara, Sinai, Egypt, in the collection of the Geological Survey of Israel. *J. Afr. Earth Sci.*, **7**(4), 707-733.

Overleaf: Representative Triassic cephalopods studied and often discovered by Dr. Avraham Parnes (after GSI Bulletin 79, 1986).

PLATE 1 (All figures slightly less than half natural size)

1-3 *Gevanites cornutus* n. sp., Har Gevanim, Makhtesh Ramon, uppermost part of Fossiliferous Limestone Member, Saharonim Formation, Lower Ladinian; M-7094 (holotype), side and ventral views.

4 *Gevanites cornutus* n. sp., same locality and level as for Figs. 1-3; HU-34972, side view.

5-7 *Allogevanites crenatus* n. gen., n. sp., same locality and level as for Figs. 1-3; M-7903 (holotype), ventral view, apertural view of broken-off part and side view.

PLATE 2 (Figures slightly less than half natural size unless otherwise stated)

1 *Beneckeia* sp. cf. *B. wogauana posterior* Fritsch, Har Arif, Ra'af Formation, basal Upper Anisfan, *Balatonicus-Zone;* M-7901, side view, x 2.

2-4 *Negebites zaki* Parnes, Har Gevanim, Makhtesh Ramon, beds with *Israelites ramonensis* Lower Ladinian; M-7902 (paratype), apertural and ventral views.

5-7 *Israelites* sp. cf. *I. ramonensis compressus* Parnes, Areif en-Naga, Sinai, upper part of Fossiliferous Limestone Member, Saharonim Formation, Lower Ladinian; HU-16350 (SOLE no. 7692); side, ventral and apertural views.

8-10 *Israelites ramonensis gracilis* Parnes, same locality and level as for Figs. 5-7; HU-34986 ventral view of a neatly preserved small fragment.

PLATE 21 (All figures slightly less than half natural size)

1-4 *Pronoetlingites scaphoides* n. sp., Ramon-1 well, core 1, top Zafir Formation, upper part of Lower Anisian; M-5892, right side, ventral, axial section and left side views.

5, 6 *Protrachyceras wahrmani* Parnes, Makhtesh Ramon, uppermost part of Fossiliferous Limestone Member, Saharonim Formation, Lower Ladinian; M-7935, left side and ventral views.

7 *Protrachyceras* ***hispanicum hispanicum*** (Mojsisovics), Har Gevanim, Makhtesh Ramon, lower part of Limestone and Gypsum Member, Upper Ladinian; M-7944, right side view.

8,9 *Picardiceras picardi* n. gen., n. sp., Makhtesh Ramon, uppermost part of Fossiliferous Limestone Member, Saharonim Formation, Lower Ladinian; M-7960b, apertural and right side views, note similarity of apertural view to *Indonautilus awadi.*

PLATE 22 (Figures slightly less than half natural size unless otherwise stated)

1, *2* *Protrachyceras hispanicum attenuatum* n. ssp., Har Gevanim, Makhtesh Ramon, revised level: Upper Ladinian; HU-20868, left side and ventral views, x 4/5; (refigured from Parnes, 1962, p. 45, pl. 8, figs. 19, 20).

3 *Protrachyceras hispanicum attenuatum* n. ssp., Har Gevanim, Makhtesh Ramon, nodular limestone of upper part of Limestone and Gypsum Member, Saharonim Formation, Upper Ladinian, uppermost Longobardian; M-5768, right side view; (refigured from Parnes et al., 1985, p. 661, fig. 2.4).

4-6 *Protrachyceras ladinum amplum* n. ssp., Bar Gevanim, Makhtesh Ramon, nodular limestone of lower part of Limestone and Gypsum Member, Saharonim Formation, Upper Ladinian, Lower Longobardian; M-79389, left side, ventral and right side views.

7, 8 *Protrachyceras lermani* n. sp., Har Gevanim, Makhtesh Ramon, inferred level: Limestone and Gypsum Member, Saharonim Formation, Upper Ladinian, uppermost Longobardian; M-7935, left side and ventral views; (refigured from Parnes, 1962, p. 46, pl. 8, figs. 17, 18).

9, 10 *Gevanites epigonus epigonus* n. ssp., Areif en-Naga, Sinai, top Fossiliferous Limestone Member, Saharonim Formation, Lower Ladinian; M-7969, left side and ventral views.

PLATE 1



PLATE 2

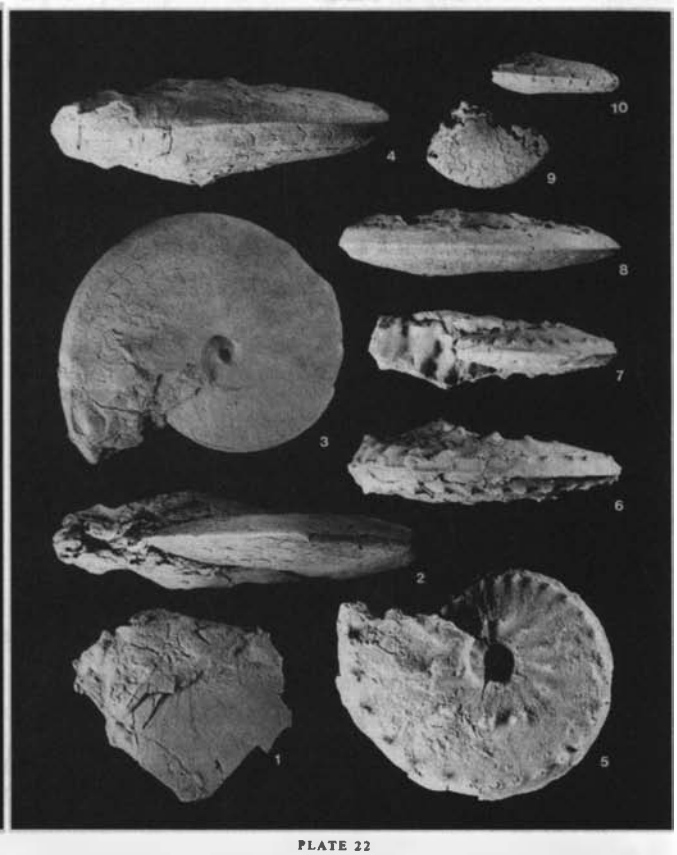


PLATE 21

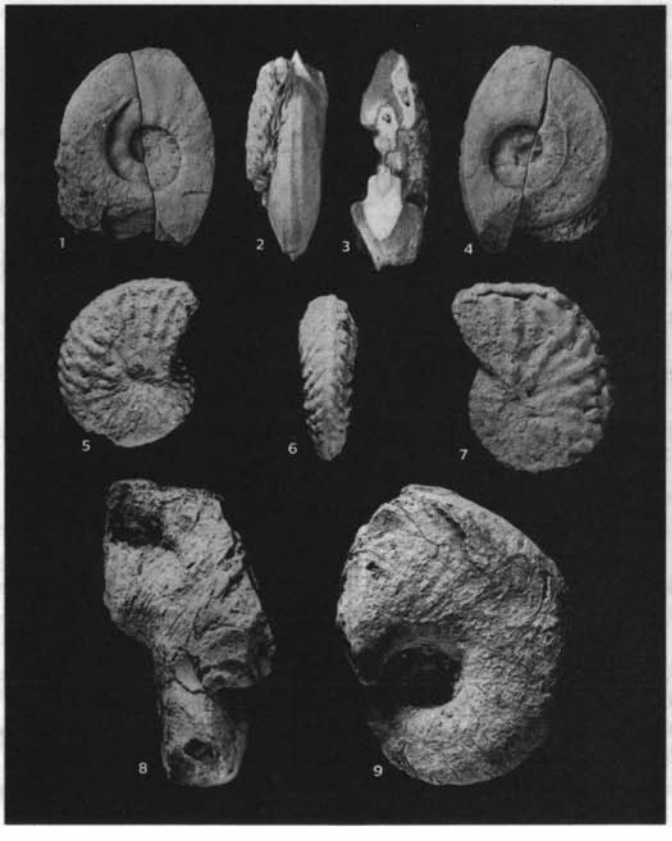
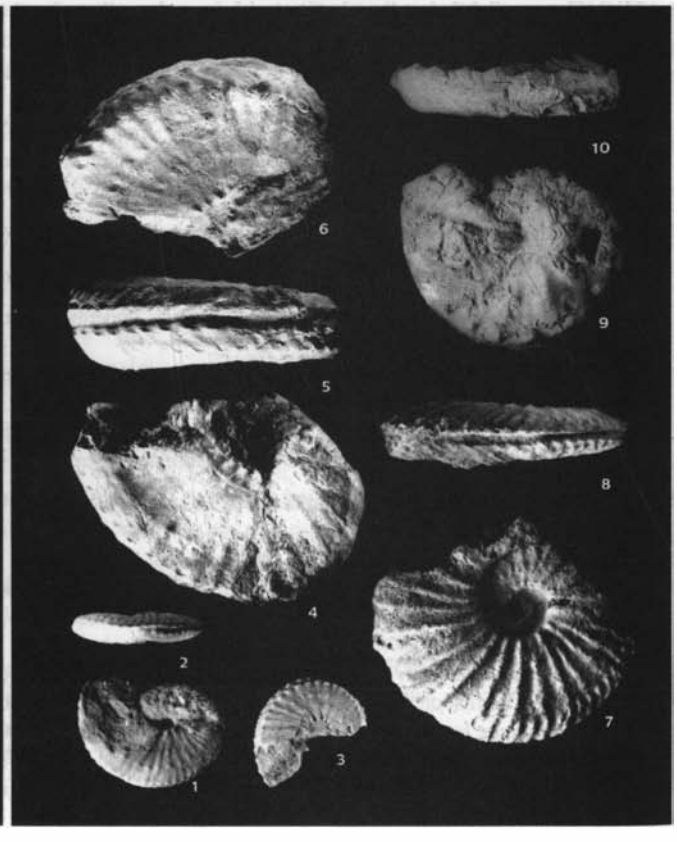


PLATE 22



Chapter 18A

Introduction to the Stratigraphy of Israel

Francis Hirsch
Geological Survey of Israel, 30 Malchei Israel Street, Jerusalem 95501, Israel

INTRODUCTION

The stratigraphic subdivision of Israel into groups is primarily based on a set of regional unconformities.

The Precambrian Basement Complex of the Sinaf Group is truncated by the *infra-Cambrian unconformity*, visible in southernmost Israel where it forms an impressive peneplain at the base of the Lower Paleozoic Yam Suf Group.

The Paleozoic consists of the Lower Paleozoic Yam Suf Group and the Upper Paleozoic Negev Group, separated from one another by the *pre-Permian unconformity*. This was the result of the 'Helez' uplift, which caused a substantial stack of Paleozoic sediments to be eroded from a large part of the Eastern Mediterranean and Levant Platforms (Gvirtzman and Weissbrod, 1984).

A *Permian-Triassic paraconformity* separates the Late Paleozoic Negev Group from the Triassic Ramon Group; it is expressed by the hiatus of the lower part of the Lower Triassic (Induan).

The *Triassic-Jurassic unconformity* forms the boundary between the Ramon Group and the overlying Jurassic Arad Group. The nature of this unconformity is two-fold:

1) It is tectonic, generating the angular unconformity;

2) It is also regressional, causing the progressive erosional truncation and karstification of the underlying Triassic substratum. The event is accompanied by volcanics (Asher Volcanics) in the Galilee and adjacent Anti-Lebanon, straddling the Triassic-Jurassic boundary. The angular unconformity is expressed by karstic pockets filled with laterites that penetrated deeply within the Upper Triassic substratum.

The *Infra-Cretaceous unconformity* truncates the Jurassic sequence as the result of the regional tilting and denudation of the Levant, accompanied by rifting and volcanism (Tayasir Volcanics).

A radical change of the sedimentary regime marks the beginning of the Senonian, with the beginning of alpidic folding. A regime of syntectonic deposition characterizes Senonian-Paleogene times.

In the course of the Late Oligocene, three events dominate the further geologic evolution of the southern Levant:

1) The Pre-Chattian global low-stand (Middle Oligocene);

2) The regional uplift that enhanced the late Oligocene regression, resulting in regional emergence and erosion of most of the territory of Israel. Late Eocene-Early Oligocene sediments were widely destroyed.

3) The latest Oligocene opening of the Red Sea that initiated the Dead Sea Transform. Since the latest Oligocene-Early Miocene, this sinistral strike-slip along the Jordan Valley-Arava and Gulf of Aqaba line amounts to a 105 km northward movement that separated Arabia from the African plate. A chain of rhomb-shaped grabens, formed by the shear, collapsed in Middle-Upper Miocene times, opening the Rift, and leading to the final severance of the African and Arabian Plates. The event was accompanied by basalt eruptions.

PRECAMBRIAN

The Precambrian Basement of the Arabo-Nubian Massif consists of the metamorphic complex of the Eilat Schist (600-800 Ma) and Roded Schist (Doroth Schist in the Helez Deep borehole, Druckman, 1984), and the magmatic Panafrican batholithic intrusives (600-580 Ma) of the Eilat and Roded Granites.

Truncating the Precambrian Basement, from which it is derived, the Sinaf Group (Cohen et al., 1987) or Late Precambrian Sedimentary Group of Weissbrod (1981), consists of conglomerates, arkoses, graywacke, and siltstones. Various intrusions and volcanic extrusions add to this oldest non-metamorphic rock sequence. This molassic deposition accumulated in shallow depressions and intramontane valleys of the Arabo-Nubian Massif, or was transported into a wide marginal basin to the north. In the most proximal zone of the fluvial environments of the southern Negev, the poorly sorted Eilat (=Saramuj) conglomerates reach a thickness of 250 m, truncated by the great regional unconformity of the sub-Cambrian peneplain. Forming a low-lying flat land, interrupted by tectonic humps and inselbergs of igneous rocks, it is covered by the Cambrian deposits of the Yam Suf Group. In the subsurface of the northern Negev basin, the Sinaf Group is represented by the Zenifim Formation and consists of poorly sorted arkoses and volcanics. The Negev Group unconformably overlies the Zenifim Formation.

Above the sub-Cambrian peneplain, that truncates the Precambrian in the southernmost part of Israel, follows the Lower Paleozoic (Cambrian-?Ordovician) Yam Suf Group (Weissbrod, 1981).

CAMBRIAN

The Amudei Shlomo Formation consists of coarse fluviatile arkoses and quartzitic conglomerates. The Timna Formation comprises sandstone, dolomite and dolomitic limestone, and shales. Mineralization (Cu, Mn) occurs in sandy dolomites. Copper-rich and phosphatic breccias are the result of erosion. The Trilobite age

of the Timna Formation is Georgian (Early Cambrian) (Parnes, 1971). Multicolored, white and variegated subarkosic sandstone, siltites and reddish shales characterize the Shehoret Formation. The base conglomerate and quartzite sandstone with no feldspars of the Netafim Formation discordantly truncate the Shehoret Formation. Burrows found in equivalent formations in Jordan and Arabia may date the Shehoret and Netafim Formations as Late Cambrian-Lower Ordovician. In the southern Negev the Netafim Formation is truncated by the Infracretaceous unconformity. Ordovician-Devonian strata, if deposited, have been eroded as the result of pre-Permian domal uplift. North of the Paran Line, the thin marine Late Permian Negev Group is known from boreholes, and similar deposits are exposed along the eastern coast of the Dead Sea.

PERMIAN

In the northern Negev, strata of Middle-Late Permian age, are identified as the Negev Group (Weissbrod, 1969; emend. Bartov et al., 1981a, b). In the type section of borehole Makhtesh Qatan-2, the Precambrian Zenifim Formation is overlain by the Middle Permian Sa'ad Formation and the Upper Permian 'Arqov Formation.

The Paleozoic Formations in the Levant are summarized in **Table 18A.1**.

The paraconformal nature of the Permian-Triassic boundary is characterized by a floral event (Eshet, 1990a, b), a depositional lacuna of the lowermost Triassic (Induan), and redeposition of pre-Triassic fragments (Hirsch, 1990; Zaslawskaya et al., 1995).

TRIASSIC

Early Triassic strata are found in the subsurface, but are exposed at Humrat Main along the eastern bank of the Dead Sea (Jordan). Most of the Induan is probably missing due to the hiatus of the earliest Triassic.

In the northern Negev, the Ramon Group consists of the Olenekian Yamin and Zafir Formations, well-defined by semi-clastic and carbonate strata. Its boundary with the Middle Triassic is marked by an Early Anisian hiatus. Upper Anisian is exposed in the erosional cirque of Har Arif, represented by the Ra'af and Gevanim Formations. The section in the Ramon crater consists of deltaic, open-marine and evaporitic strata belonging to the Late Anisian upper part of the Gevanim Formation, the Late Anisian, Ladinian and Early Carnian Saharonim Formation, and the Carnian Mohilla Formation. In the Galilee a very thick Olenekian- Carnian sequence of carbonates and evaporites is devoid of clastics.

In the subsurface of the Coastal Plain the apparently Early

Table 18A.1: Stratigraphic Table of Paleozoic Formations in the Levant

AGE	EASTERN DESERT	SINAI	SOUTHERN ISRAEL	SOUTHERN JORDAN	SYRIA	SAUDI ARABIA
Lower Cretaceous	Malha	Hatira	Hatira	Kurnub		
~~	~~~~~~~	~~~~~~~	~~~~~~~	~~~~~~~		
Lower Trias	Qiseib		Zafir Yamin		Amanous Shale	Sudair Shale
Upper Permian		? Amir Budra	Arqov	Umm Irna	Amanous	Khuff
Middle Permian	~~~~~~~~	~~~~~~~~	Sa'ad ~~~~~~~	Umm Irna ~~~~~~~~~~	Amanous	
Upper Carboniferous	Ataqa	Abu Thora			~~~~~~~~ Markada	
Lower Carboniferous	Um Bogma	Um Bogma			Markada	
Devonian					~~~~~~~~~~	Jauf
Silurian				Mudaw-wara	Tanf	Tawil Sharawra
Ordovician				Mudaw. Kherim Um Sahm Ram/ Disi	Affendi Swab Khanasser	Tabuk
Upper Cambrian		Netafim	Netafim	Qunaya/Ishrin	~~~~~~~ Sosink	Saq
Middle Cambrian		Shehoret	Shehoret	Burj	Burj	Saq
Lower Cambrian		Timna Amudei Shlomo	Timna Amudei Shlomo	Quweira / Saleb	Zabuk	Saq
Precambrian		Zenifim		Saramuj		

Triassic Karmia Shale is covered by the Late Triassic Or-Haner (=Erez) Conglomerate. The Carnian Sharon Formation covers it. Noro-Rhaetian strata, in carbonatic platform facies, are found only in the subsurface of the Coastal Plain, and are represented by the Shefayim Formation. Tectonic instability characterized a belt along the present Coastal Plain during the Triassic, which was accompanied by faulting.

JURASSIC

The Arad Group (Coates et al., 1964, emend. Goldberg, 1971) comprises all Jurassic strata. At Makhtesh Ramon, a section of alternating fluvio-deltaic and marine clastic to carbonatic strata represents the Pliensbachian, Toarcian, Aalenian, and Bajocian stages. At Hamakhtesh Hagadol, the Middle and Upper Callovian are well-exposed. Wadi Malih (Samaria) exposes Oxfordian-Kimmeridgian strata, topped by the Tayasir Volcanics. Boreholes have provided a wealth of data.

The Asher Volcanics in Galilee are replaced in central and southern Israel by Early Liassic Mish'hor laterites, covered by the Liassic carbonate Ardon Formation. The Toarcian-Oxfordian Haifa carbonates in Galilee are differentiated into the Toarcian-Aalenian Qeren, Bajocian Daya, Bathonian-Callovian Hermon, and Callovian carbonate Zohar and Matmor Formations in central Israel and Negev, intercalated by the Toarcian-Aalenian Inmar/Rosh Pinna, Bathonian Sherif/Karmon clastic formations, whose clastic ratio increases from north to south-east. The Oxfordian Majdal Shams shale (= Kidod, Delta) of the Judean Embayment (central Israel-Hermon) is overlain by the Late Oxfordian-Kimmeridgian Nahar Sa'ar echinid limestone (=Beersheba, Bloudane) and oolites with marl (Haluza, Batroun), passing laterally into the reefoid limestone Nir'Am Formation of the Coastal Plain. The Devorah Volcanics (=Bhannes) separate the Haifa and Nahar Sa'ar carbonates of Galilee.

The stratigraphic relations between Jurassic formations are summarized in **Table 18A.2**

CRETACEOUS

A Cretaceous subdivision into groups is not only based on regional unconformities but also on facies.

The Early Cretaceous Kurnub Group (Damesin, 1933) consists mostly of terrestrial deposits straddling the Jurassic-Cretaceous boundary in the Levant, resulting from tilting and taphrogenesis, accompanied by magmatism. In the southern part of the Negev, the group directly overlies Early Paleozoic Nubian Sandstone. In the north of the country the Kurnub Group consists of the Tayasir basalts at base, straddling the Jurassic-Cretaceous boundary, followed by variegated continental sandstones with interstratified plant remains, siltstones, some clays, basic intrusions, and lavas (140-110 Ma).

The Gevar'Am Group (Flexer et al., 1981a, b) represents the basinal to deltaic facies in the drillings of the Coastal Plain. Marine shale and sandstone of Beriassian-Hauterivian age represent the basinal facies. The 'glacis' facies of the eastern and western platforms that border the Gevar'Am Basin, consists of low-stand, transgressive/regressive, and high-stand deposits. Their deltaic to shallow marine facies is represented by the Beriassian-Barremian Helez Formation, topped by the high-stand carbonates of the Telamim Formation.

The Galilee Group (Kafri, 1972, emend. Rosenfeld et al., 1995) (=Kfar Blum Group, Sneh, 1974) includes the Barremian-Albian shallow marine platform sequence in the northern part of Israel, that borders the Gevar'Am Basin to the west and interfingers

Table 18A.2: Jurassic Stratigraphic Units in the Levant

	JORDAN	S. NEGEV	N. NEGEV	SINAI	SHEFELA	HERMON	GALILEE	LEBANON	J.AS SAHILYEH	MICROPALEONTOLOGY
BARR.-APT.	Kurnub	Hatira	Hatira	Hatira						
BERR.-HAUT.	////////////	////////////	////////////	////////////	Gevar'am	Tayasir	Tayasir	Tayasir		
TITHONIAN	////////////	////////////	////////////	////////////				Salima		*Hutsonia aduncа*
KIMMERIDGIAN	////////////	Haluza Beersheba	Haluza Beersheba	Haluza Rokba	Nir Am	Batroun Bloudane	Haifa Bay	Salima Bikfaya	Nasirah	*Alveosepta praelusitanica* *Alveosepta jaccardi Levantinella* G
OXFORDIAN	////////////	////////////	Kidod	Tauriat	Nir | Ki-Am | dod	Majdal Shams	Devorah Haifa	Bhamess Kesrouane	Nasirah	*Levantinella* F
CALLOVIAN	///// Mughanniyya	Matmor Zohar	Zohar	Arousiah	////////// Brur	Hermon	Haifa	Kesrouane	Wadi Al Ouyoun	*Steinekella steineki* E *Planikilianina hermonensis*
BATHONIAN	Hamam Ramla	Sherif	Sherif	Kehailia Safa	Karmon Haifa	Hermon	Haifa	Kesrouane	Machta	*Pfenderina salernitata* D
BAJOCIAN	Dhahab	Mahmal	Daya	Maghara Mahl	Haifa	Bqassem K.Jandal	Haifa	J3	Ouyoun	*Amijiella* C *Haurania* B
AALENIAN	Silal	Inmar	Inmar Qeren	Shusha Rajabiah	Rosh Pinna Haifa	Kalaat Jandal	Haifa	J2	Ouyoun	*Timidonella sarda* A
TOARCIAN	Silal	Inmar	Inmar	Mashabba	Haifa	Aame	Haifa	Chouane	Treize	A
PLIENSBACHIAN	Nimr	Ardon	Ardon	Ardon	Haifa	Aame	Haifa		Treize	*Orbitopsella primaeva*
SINEMURIAN HETTANGIAN	Hihi	Mishhor	Mishhor	Mishhor	Mishhor	Aame	Asher Volcanics		Treize	*Pseudocyclamina liassica*
RHETIAN-NORIAN	////////////	////////////	////////////	////////////	Shefayim	Rimeh	?	?	Jweikhate	*Aulotortus*
CARNIAN	Abu Ruweis	Mohilla	Mohilla	Mohilla	Sharon					

to the south with the Kurnub Group.

The Judea Group (Wellings, 1938, 1940; emend. Arkin et al., 1965a, b) is a marine plaform and ramp facies that dominates the Arabian Platform. It includes 'the fully marine sedimentation' above the Kurnub Group. The lower boundary of the Judea Group is at the lowermost appearance of Albian carbonates. The upper boundary corresponds with the unconformity marking the Senonian Levantid embryonic folding. The deposition of the Judea Group progrades in the direction of the Arabo-Nubian Craton, and is Late Albian in the Galilee and Coastal Plain to Early Cenomanian in the southern Negev.

The Talme Yafe Group interfingers with the Galilee and Judea groups. It encompasses the more basinal deposits, found in boreholes of the western Coastal Plain of Israel and the adjacent Mediterranean offshore Pleshet Basin. It consists of Aptian-Albian laminites and calcilutites, though the presence of Cenomanian and younger strata is inferred. Senonian sediments truncate the Talme Yafe Group, as the result of the Levantid folding.

The Mount Scopus Group (Coniacian-Paleocene) consists of carbonatic and silicious sedimentation. Its mode of deposition is syntectonic, controlled by the formation of the asymmetric Levantid anticlines of the Negev and Judea. As a result, two different facies occur with thick synclinal deposits versus reduced anticlinal deposits.

In the anticlinal facies, the Senonian Mount Scopus Group is clearly separated from the Paleogene Avedat Group by a Late Maastrichtian hiatus.

Table 18A.3: Time slice subdivision of the Eocene-Oligocene Avdat-Saqiye Groups

Early Eocene (Ypresian):
(I) [P6-8]: Chalks with thin bands or nodules of chert;
(II) [P8-9]: Nummulitic limestone with chalk bands, chalky limestones and chalks;
Middle Eocene (Lutetian):
(III) [P10] Chalks and limestones with changing amounts of chert bands or nodules;
(IV) [P11-12 partim]: Limestones and chalks;
---------hiatus----[P13]----------
(V) [P14 partim] (Biarritzian): chalks;
Upper Eocene (Priabonian):
(V) [P15]: chalks and limestones;
Early Oligocene (Rupelian)
(VI) [P18-21]: chalks and limestones;
Late Oligocene (Chattian)
(VII) [P21-22]: marine chalks/deltaic-fluviatile clastics (partim Tiberias Group).

In the synclinal facies, a high concentration of iridium and trace elements marks the passage from the Maastrichtian chalks to the overlying Paleocene shales, without any apparent hiatus.

The Cretaceous/Tertiary boundary is well-defined in the basinal facies. A high iridium concentration at the base of the *G. eugubina* Zone and trace elements and microspherules occur between the *A. mayorensis* and *M. pseudobulloides* zones (Rosenfeld et al., 1989). Elsewhere the upper strata of the Maastrichtian are missing and the Paleocene-Early Eocene Taqiye shales onlap a paleorelief with paleosoil.

PALEOCENE

The Paleogene portion of the Mount Scopus Group is represented by the Taqiye Formation, which in the basinal facies (synclines) conformably overlies the Ghareb Formation.

EOCENE

The Avedat Group comprises the Eocene strata, whose sedimentation is still controlled by folding of the Levantid system. The Ypresian-Lutetian sequence is composed of calcareous shales, chalk, limestones, and partly silicified limestones. Nummulitic limestones represent the reef facies. Toward the anticlines glauconitic, limonitic, and phosphatic layers occur. In some places gypsum occurs (Priabonian) and subsurface deposits are bituminous and pyritic. On the basis of its lithology and biostratigraphy, the Eocene Avedat Group and overlying lower part of the Saqiye Group subdivides into time-slices [Roman numbers] as outlined in **Table 18A.3**:

The Eocene strata in Israel span the zones P8-P12 and P14-P15. Strata of age P12 and younger are poorly represented in most of the Negev and appear to be mostly pelagic.

The thickness-figures of the Eocene deposits provide evidence of depo-centers in the Shehem (Nablus) Syncline and the Paran Basin. The more or less northeast strike of these features is conditioned by the Levantid structure. The basin of the Shehem Syncline may extend to the offshore Pleshet Basin, whereas the Paran Basin may be one of a string of basins, extending from Sinai (Egypt) to the Jordan Valley, and opposite the Dead Sea Transform to the Yarmuk Valley in Jordan.

The pelagic facies which predominate in the Jordan Valley are comparable with those in the Negev. A major unconformity occurs at the P10/P11 time (limit III/IV).

The Levantid structural ridges separate the basins. Although they do not show Eocene deposits, some may have been covered by thinner Eocene sediments before their removal in pre-latest Lutetian and certainly in Oligocene times. Relicts of Eocene chalk within karstic sinkholes in the northeast Negev bear witness to the presence of Eocene sediments on the flanks and possibly on top of the anticlines of the Levantids prior to erosion. In most of Israel the post-Middle Eocene (Early Bartonian) uncomformity (P13) represents the boundary between the Avedat Group and the Saqiye Group. In the Negev however, the late Eocene Qeziot and Har Aqrav Formations are also regarded as part of the Avedat Group.

OLIGOCENE-PLEISTOCENE

From the end of the Eocene, the Tethys retreated and the (apparently) mostly continuous marine Late Paleogene-Quaternary sedimentation is found along a rather narrow belt in the southern and central Coastal Plain. These sediments represent the Saqiye Group, widely buried under the Coastal Plain and in the Beersheva Embayment, and partly exposed in the foothills along the Shefela.

The Saqiye Group encompasses all Oligocene-Neogene marine sedimentation along the Coastal Plain of Israel. Marine incursions of the Saqiye Group penetrated into the wide canyon of the Afiq-Beersheva Valley, an incision that dates back to the Early Oligocene (P19). They are interwedged in the continental deposits of the Tiberias Group to the east. The Oligocene cycle, transgressing into an intricate drainage system formed toward retreating seas at the transition from the Eocene, mainly occupies structural lows of the Levantine folding belt (the Syrian Arc). The extent of the Oligocene transgression is manifested by marine sediments on the eastern shore of Lake Kinneret and farther south, and by infilling with fluviatile and lacustrine deposits of channels in the Dead Sea area. The occurence of the Indian Ocean foraminifer *Austrotrillina* in the Ein Gev suite (Lipson, 1971; Horowitz, 2000) has suggested ingression from the east.

Late Eocene-Early Oligocene sediments were widely destroyed by subsequent denudation and only a few marine outcrops survive in the northern Negev, the Coastal Plain [Lakhish-Gal'on and Ramleh (Shefela)] and the Golan Heights [En Gev (Sea of Galilee)].

Marine deposition of the Saqiye Group penetrated in two embayments: the wide canyon of the Afiq-Beersheva Valley, an incision that dates back to the Early Oligocene (P19), and the Yizre'el Valley, which became the gate for marine penetration into the Rift Valley. The Saqiye Group interwedges the continental deposits of the Tiberias Group in the east.

The Tiberias Group encompasses the Late Oligocene-Early Miocene continental sedimentation in the Negev and the Jordan-Dead Sea-Arava depression. It is mainly of fluviatile and lacustrine nature, filling the morphology generated by Late Oligocene erosion. They consist of the drainage-products from the mountains and huge plateaus further to the southeast. Oligocene river systems formed valleys and basins within which deposition resumed with the Hazeva Formation. Early Miocene mammals found their way out of Africa and made their home in the relatively humid Negev lake environments.

Since the late Miocene or latest part of the middle Miocene (Schulman, 1962; Horowitz, 1987; Steinitz and Bartov, 1991), a new drainage system appeared with the formation of the Dead Sea Rift. Plio-Pleistocene terraces, found above Holocene to Present thalwegs in Nahal Lot, witness the early graben drainage system.

The Dead Sea Group encompasses the Late Miocene, Pliocene and Pleistocene clastic and evaporitic sediments of the Rift extending from the Jordan to Arava Valleys. These include formations of marine origin, related to the Saqiye Group, and formations of terrestrial origin, forming the Dead Sea Group. Late Miocene marine ingressions of the Saqiye Group through the Yezreel Valley into the rift left huge masses of evaporites. The Pliocene sediments consist of similar formations.

The Kurkar Group represents the Pliocene and Pleistocene deposits of the Coastal Plain of Israel. They reflect the isostatic movements of the Levant platform and oscillations of the Mediterranean Sea during the glacial periods. It consists of sands and conglomerates.

REFERENCES CITED

Arkin, Y., and Braun, M., 1965a. Type sections of Upper Cretaceous formations in the northern Negev, southern Israel. Isr. Geol. Surv., Stratigr. Sec. 2a, 19 p.

Arkin, Y., Braun, M., Starinsky, A., Hamaoui, M., and Raab, M., 1965b. Type sections of Cretaceous formations in the Jerusalem-Bet Shemesh area. Isr. Geol. Surv., Stratigr. Sec. No. 1, 42 p., Figs., Pts.

Bartov, Y., Arkin, Y., Lewy, Z., and Mimran, Y., 1981a. Regional stratigraphy of Israel: A guide to geological mapping. Isr. Geol. Surv., Current Res. 1980, p. 38-41.

Bartov, Y., Arkin, Y., Lewy, Z., and Mimran, Y., 1981b. Regional stratigraphy of Israel; A guide for geological mapping. Isr. Geol. Surv., 1 colored chart.

Coates, J., Gottesman, E., Jacobs, M., and Rosenberg, E., 1964. Gas discoveries in the western Dead Sea region. Proc. Sixth World Petroleum Congress, Frankfort/ Main, p. 21-36.

Cohen, Z., Kapstan, V., Muravinski, E., Salhov, S., Shilo, A., and Wolff, O., 1987. Stratigraphic table of Israel: Outcrops and subsurface. Oil Exploration (Investments) Ltd. (OEIL), Enclosure 6, colored chart.

Damesin, 1933. Petroleum Development (Palestine) Ltd., unpublished geological report.

Druckman, Y., 1984. Evidence for Early-Middle Triassic faulting and possible rifting from the Helez Deep Borehole in the Coastal Plain of Israel. In: Dixon, J. E., and Robertson, A. H. F., (eds.), The Geological Evolution of the Eastern Mediterranean, Geol. Soc. Spec. Publ. 17, Oxford, Blackwell, p. 203-212.

Eshet, Y., 1990. Paleozoic-Mesozoic palynology of Israel. 1. Palynological aspects of the Permo-Triassic succession in the subsurface of Israel. Isr. Geol. Surv., Bull. 82, 57 p.

Eshet, Y., 1990. The palynostratigraphy of the Permian-Triassic boundary in Israel: Two approaches to biostratigraphy. Isr. J. Earth Sci., 39(1), p. 1-15.

Flexer, A., Gill, D., Livnat, A., Tamir, N., and Toister, A., 1981a. ATLAS Project (Israel Subsurface Geology Information Management System). Part A - Explanatory Notes, Oil Exploration (Investments) Ltd., Tel Aviv, 43 p., Figs. (In Hebrew).

Flexer, A., Gill, D., Livnat, A., Toister, A., Shafran, N., Tamir, N., 1981b. Computerized Information System in support of Oil and Gas Exploration in Israel. Oil Exploration in Israel; A Symp., Jerusalem, Dec. 1981; Abstr. Isr. Geol. Soc., Oil Exploration {Investments} & Isr. Geol. Surv., p. 16-20.

Goldberg, M., 1971. The Jurassic section in Gebel Maghara, northern Sinai. Isr. Geol. Soc., Ann. Meet., Abstracts, p. 9-12 (In Hebrew).

Goldberg, M., 1970. The lithostratigraphy of the Arad Group (Jurassic) in the northern Negev. Ph.D. Thesis Hebrew University Jerusalem, 136 p. (In Hebrew, English abstract).

Hirsch, F., 1990. The Cretaceous Judea Group in central Israel: Eustatic cycles. Cretaceous Field Conf., Jerusalem, Sept. 1990; Abstr. Progr., p. 12.

Horowitz, A., 1987. Palynological evidence for the age and rate of sedimentation along the Dead Sea Rift, and structural implications. Tectonophysics, 141(1-3), p. 107-115.

Horowitz, A., 2000. The Middle Oligocene of the Dead Sea and vicinity. Isr. Geol. Surv., Current Res., Vol. 12, p. 197-205.

Kafri, U., 1972. Geological map of Israel 1:50,000: Nahariyya, with Explanatory

Notes. (In Hebrew and English). Isr. Geol. Surv., 10 & 9 p., 2 Maps.
Kafri, U., 1972. Lithostratigraphy and environment of deposition, Judea Group, western and central Galilee, Israel. Isr. Geol. Surv. Bull. 54, 56 p.
Lipson, S., 1971. Micropaleontological study of some sections in the Golan Heights. Isr. Inst. Petroleum, Rep. 7/71, 7 p.
Parnes, A., 1971. Late Lower Cambrian trilobites from the Timna area and Har Amram (Southern Negev, Israel). Isr. J. Earth Sci., 20(4), p. 179-205.
Rosenfeld, A., Flexer, A., Honigstein, A., Almogi-Labin A., and Dvorachek, M., 1989. First report on a Cretaceous/Tertiary boundary section at Makhtesh Gadol, southern Israel. Neues Jahrb. Geol. Paleontol., Monatsh, 1989(6), p. 474-488.
Rosenfeld, A., Hirsch, F., and Honigstein, A., 1995. Early Cretaceous Ostracodes from the Levant. In: Riha, J., (ed.), Ostracoda & Biostratigraphy, Proc. 12th Intern. Symposium on Ostracoda, Prague, July 1994, Rotterdam, Balkema, p. 111-121.
Schulman, N., 1962. The geology of the central Jordan Valley. Unpubl. Ph.D. Thesis, Hebrew University of Jerusalem, 103 p. (In Hebrew; English Abstract).
Steinitz, G., and Bartov, Y., 1991. The Miocene-Pleistocene history of the Dead Sea segment of the Rift in light of K-Ar ages of basalts. Isr. J. Earth Sci., 40(1-4), p. 199-208.
Weissbrod, T., 1969a. The Paleozoic of Israel and adjacent countries. Part I: The subsurface Paleozoic stratigraphy of southern Israel. Isr. Geol. Surv., Bull. 47, & Inst. Pet. Res. Geophys., Rep. 1008, p. 1-23.
Weissbrod, T., 1969b. The Paleozoic of Israel and adjacent countries. Part II: The Paleozoic outcrops in southwestern Sinai and their correlation with those of southern Israel. Isr. Geol. Surv., Bull. 48, & Inst. Pet. Res. Geophys., Rep. 1033, 32 p.
Weissbrod, T. 1981. The Paleozoic of Israel and adjacent countries (lithostratigraphic study). Isr. Geol. Surv., Rep. MP 600/81, 276 p. (In Hebrew, English abstr.).
Wellings, F. E., 1938. Observations of Dead Sea structure. Geol. Soc. Am., Bull., 49(4), p. 659-667. (See also: Willis, B., 1938).
Wellings, F. E., 1941. Oil Prospects Of Palestine, Trans-Jordan, Syria And Cyprus. Iraq Pet. Co. Ltd., Geol. Dept., Geol. Rep. 181, 30 p.
Willis, B., 1938. Wellings' observations of Dead Sea structure (with discussion). Bull. Geol. Soc. Am., 49(4), p. 659-668.
Zaslavskaya, N., Eshet, Y., Hirsch, F., Weissbrod, T., and Gvirtzman, G., 1995. Recycled Lower Paleozoic microfossils (Chitinozoa) in the Carboniferous of Sinai (Egypt) and Permo-Triassic of the Negev (Israel): Paleogeographic considerations. Newsl. Stratign, 32(1), p. 57-72.

The Late Precambrian Basement Complex

Francis Hirsch
Geological Survey of Israel, 30 Malchei Israel Street, Jerusalem 95501, Israel
Akiva Flexer
Department of Geophysics and Planetary Sciences, Tel-Aviv University, Tel-Aviv 69978, Israel

INTRODUCTION

The Late Precambrian Basement Complex of the Levant is exposed in the Sinaitic peninsula (Egypt), the Elat region (Israel), east of the Dead Sea Rift in the Edom Mountains (Jordan), and south of Aqaba (Saudi-Arabia). These series are strongly metamorphosed as they underwent a number of Precambrian orogenies. (**Figure 18A.1**).

Early studies of the northern edge of the Arabo-Nubian Shield were summarized by Picard (1941). Detailed studies of the Elat area (Eyal, 1959; Weissbrod, 1961) were followed by the outline of the major Precambrian stages by Bentor (1961). Later, the studies of Garfunkel (1970), Shimron (1972) and Eyal (1975) led Garfunkel (1980) to delineate the comprehensive outline of the Precambrian igneous and metamorphic materials, on which this compilation is mainly based.

Simultaneously, Ginzburg et al. (1979) and Ginzburg and Gvirtzman (1979) have interpreted the seismic profiles that revealed the structure of the Precambrian crust. Ginzburg and Ben-Avraham (1991) summarized the gravitational properties of the crust.

The geochronology of the stages of the Arabian-Nubian Shield has been summarized in Eyal et al. (1992). These authors also introduced the concept of the Elat Terrain. (**Figure 18A.2**).

Shpitzer et al. (1992) studied the Timna Massif in detail and Peltz and Eyal (2000) gave an in depth account of the volcaniclastic complex.

In the south of Israel, the Late Precambrian basement complex covers a large time span (from 800 to 600 Ma) and was the theatre for the opening of an ocean and its subsequent closure. The sediment filling of this ancestral oceanic basin is witnessed by the complex of metamorphic series (*e.g.* Elat schists) and their closing by syn-orogenic granites and volcanics, rocks that penetrated and traversed the outer crust in the course of its folding, shortening and uplift. This pan-African orogeny sealed the landmass known as the Arabo-Nubian Craton. Its mountains were largely abraded, a process that ended with the development of a regional peneplain.

All Precambrian rocks were grouped together by Flexer et al. (1981) into the Shelomo Supergroup.

As a part of the Precambrian Arabo-Nubian Massif, the ***Igneous-Metamorphic Complex*** of southernmost Israel consists of schists and of Pan-African batholithic intrusives.

The ***Late Precambrian Sedimentary Group*** (Weissbrod, 1981) or Sinaf Group (Cohen et al., 1987) truncates the Igneous-Metamorphic Complex (See Chapter 18B in this volume). Various intrusions and volcanic extrusions add to this non-metamorphic sequence. This molassic deposition consists of conglomerates, arkoses, graywacke and siltstones, accumulated in shallow depressions and intramontane valleys of the massif. These consist in the most proximal zone, exposed in the southernmost Negev (Israel) and along the eastern Rift-escarpment (Jordan), of the **Eilat** and coeval **Saramuj Conglomerates**, respectively. It is truncated by the great regional unconformity of the sub-Cambrian. Forming a low-lying flat land, interrupted by tectonic humps and inselbergs

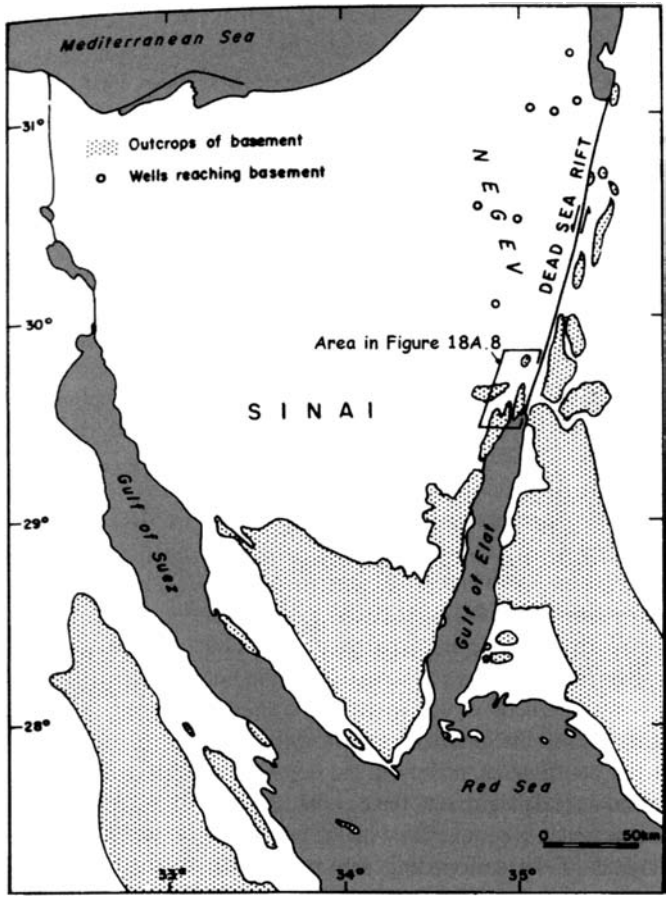


Figure 18A.1. Location Map of Precambrian Basement. From Garfunkel (1980, Fig. 1A, p. 26).

of igneous rocks, it is covered by the Cambrian deposits of the **Yam Suf Group**. In the Northern Negev subsurface basin, the Late Precambrian Sedimentary Group is represented by the arkoses and volcanics of the **Zenifim Formation**, unconformably overlain by the Late Paleozoic Negev Group.

The Precambrian Basement complex, exposed in the southern Israel Elat-Timna area, plunges northwards beneath a phanerozoic sedimentary cover. The nature of the basement in the northwestern Negev stems from geophysical and borehole data, briefly summarized below.

The seismic refraction study of Ginzburg et al. (1979) and interpreted by Ginzburg and Gvirtzman (1979) shows that the depth to the Moho-crust boundary changes gradually from 42 km in the central Negev to 30 km in the northwestern Negev, becoming reduced to some 20 km near the Mediterranean coast. (**Figure 18A.3**).

The isopach of the crystalline crust varies from 40 km, south of Makhtesh Ramon (Central Negev) to some 10 km beneath the coastline. (**Figure 18A.4**).

A change in the seismic velocities infers a different composition within the lower crust. Towards the northeast the crystalline crust is presumed to grade into thinner oceanic crust.

Gravity also reveals changing crustal thicknesses and compositions, indicating that the Negev has a genuine continental crust, whereas north of it, thinning is observed both in Judea-Samaria and Galilee-Lebanon, where crusts similar to that of the Levantine basin are observed. (**Figures 18A.5, 18A.6, and 18A7**).

Direct evidence on the nature of the basement in the northwestern Negev does not exist, but its composition may be inferred through the study of samples from the Helez 1 deep borehole. Rb-Sr and K-Ar age determinations on the Doroth chlorite schists demonstrate a good correlation of these rocks with those from the exposed Precambrian basement (Steinitz, 1980; Steinitz et al., 1981). Thus the extension of the igneous-metamorphic complex exposed in the south reaches at least as far to the northwest as the southern Coastal Plain of Israel.

THE IGNEOUS-METAMORPHIC COMPLEX (Fig. 18A.8).

The Igneous-Metamorphic ***Pan-African orogenic complex*** in the south of Israel (Timna, Elat) consists for Garfunkel (1980) of the **Elat** and **Roded** Associations. The latter Roded Association is characterized by migmas, indicating formation at great depth. Younger basement rocks including plutonic and volcanic-sedimentary sequences, constituting the transition to cratonic conditions, follow the orogenic complex. **Table 18A.4** summarizes the composition of this complex.

Eyal et al. (1992) distinguish four stages in the evolution of the Arabian-Nubian Shield, of which the last three are recognized in the Elat Terrain:

I) 950-850 Ma: tholeitic pillow basalts composing an oceanic crust;

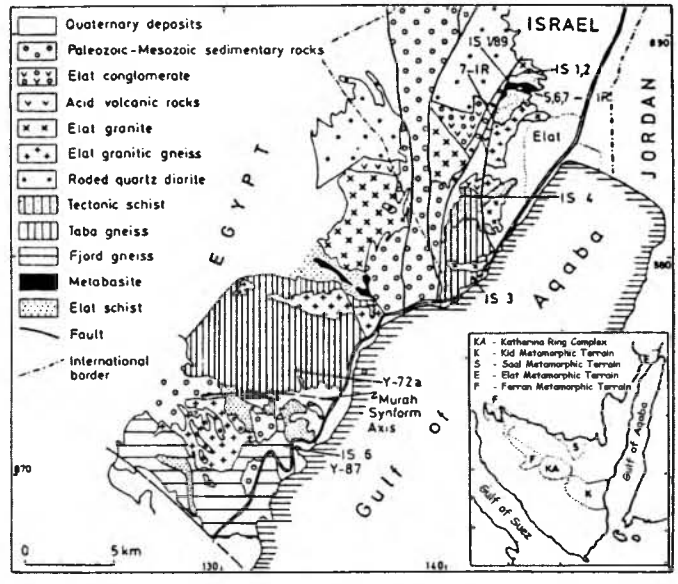


Figure 18A.2. Geological map of Elat terrain. From Eyal et al. (1992, Fig. 1, p. 6), modified after Kröner et al., 1990.

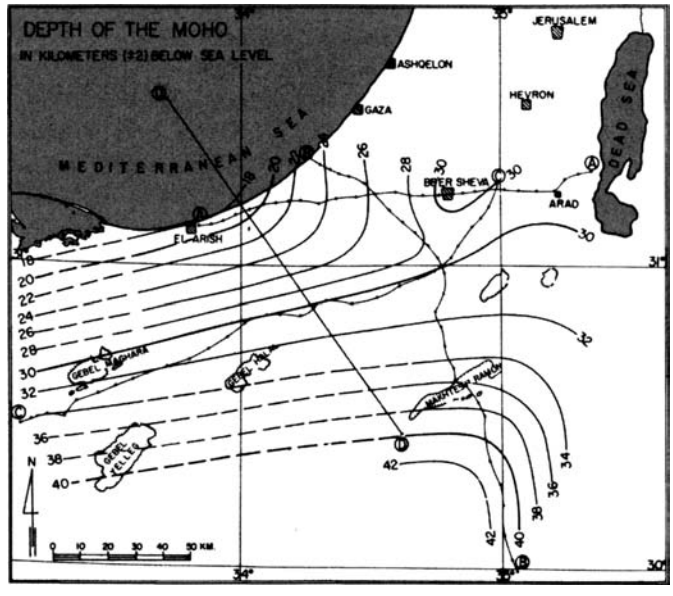


Figure 18A.3. Depth of upper mantle crust boundary (Moho) – 6.6-6.7 km/sec to 7.7-8.0 km/sec interface, in km below sea level. From Ginzburg and Gvirtzman (1979, Fig. **6,** p. 25).

II) 850-650 Ma: accreted andesitic-dacitic island arc **volcanism** and plutonism;

III) 650-580 Ma: cratonization of the shield, **characterized by** intermediate - acid, calc-alkaline magmatism;

IV) 600-580 Ma: intra-cratonic-taphrogenic magmatism, characterized by alkaline peralkaline granites and rhyolites.

Bentor (1961) recognized that the rocks, which he included in the metamorphic and intrusive complexes, record metamorphism, deformation and calc-alkaline magmatism which are typical and complementary aspects of orogenetic activity.

Within the ***orogenic complex,*** Garfunkel (1980) discriminates the two petrographically distinct **Elat** and **Roded** associations, which are separated by Late Precambrian E-W trending faults, their original distribution being further disrupted by Late Cenozoic left-lateral rift faults. (**Figure 18A.9**).

A. Pan-African orogenic complex

Elat Association (Garfunkel, 1980)

Pelitic schists. This oldest unit consists primarily of quartz, oligoclase-andesine and biotite and some muscovite. The lowest grade rocks, within the biotite isograd, *e.g.* biotite-muscovite-chlorite garnet bearing schists, occur in the north of the Elat Block. Most of the schists are within the garnet (almandine) isograd, and do not contain primary chlorite. The alumo-silicates form pophyroblasts up to a few centimeters in size. It is assumed that the protolith of the schists was a shaly-graywacke series.

Prograde metamorphism ranged well into the amphibolite facies and was of a low pressure (Abukuma) type. The cordierite-staurolite assemblage of the highest grade rocks indicates maximum temperatures in the range of 550-650°C, and pressures of 2-5 kbar, *i.e.* depth of about 7-15 km (Ganguly, 1972; Winkler, 1976).

Mica, concentrated into laminae produces a pronounced schistosity, sometimes parallel to the axial plane of tight mesoscopic folds. Mineral growth occurred after formation of this foliation. The schistosity outlines large scale and mesoscopic WNW-ENE to E-W trending folds, with local development of crenulations. In hinges of folds and in crenulations, the biotite forms polygonal arcs; other minerals bear little evidence of strain. A prominent lineation, roughly parallel to fold axes, is always developed.

Metamorphosed meta-diorite and gabbro. These rocks were referred to as **Elat Gabbro** (Bentor, 1961), amphibolites (Garfunkel, 1970) and metabasites (Shimron, 1972). They comprise a metamorphosed, layered and differentiated intrusion.

The most common petrography of this body is built of andesine-labradorite and amphiboles. Bands and layers vary in thickness from 1 cm to many meters. Layers consisting mainly of amphiboles, some biotite and very little plagioclase are prominent. A border zone, developed mainly on the north side of the intrusion in the Elat Block, consists of well layered rocks having a biotite- and quartz-dioritic composition. Near the borders the metabasites contain interbeds of schist. Biotite occurs mainly in the border rocks and in the ultramafic layers. Alkali feldspar and quartz are minor constituents, mainly in the border zone. The occurrence of actinolite and plagioclase, but no epidote, indicates low amphibolite facies, which is compatible with the position close to the almandine isograd of the surrounding schists. Widespread occurrences of

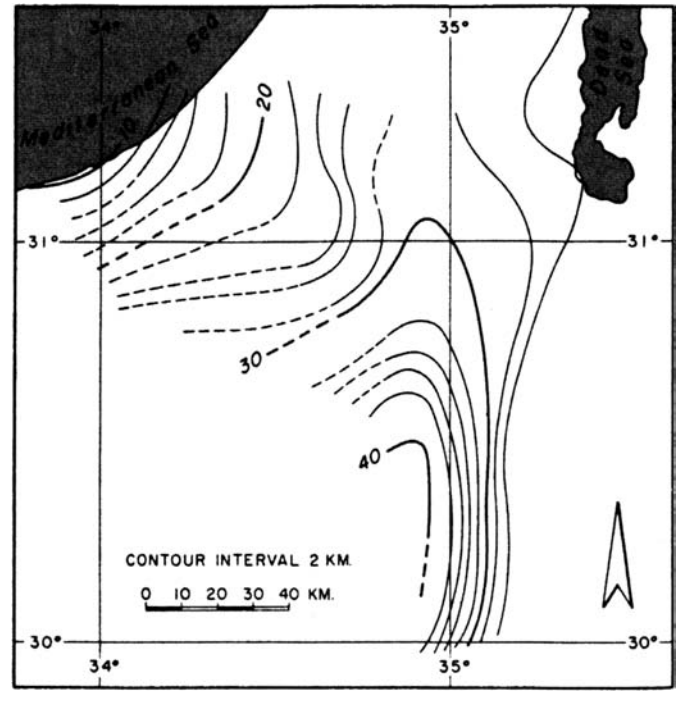


Figure **18A.4. Isopach map of the net crystalline crust with sediments removed. From Ginzburg et al. (1979, Fig. 11, p. 1581).**

Table 18A.4. Composition of the Pan-African Orogenic Complex - Pb ages are according to Eyal et al. (1992):

Association	Rock type	Derivation	Pb age
Elat	Schist	Island arc	813±7 Ma
Elat	Elat Gabbro		
Elat	Taba Gneiss	Tonalitic pluton	779±8 Ma
Elat	Granitic Gneiss		
Elat	Elat Granite		744±5 Ma
Roded	Gneiss	Quartz dioritic - Tonalitic pluton	
Roded	Migmatites		
Roded	Quartz diorite		
Roded	Granite porphyry		
Timna Block	Granite porphyry		625 Ma
Timna Block	Timna Granite	Alkali-granite	610 Ma
Timna Block	Porphyritic quartz syenite and syenite		
Amram Block	Amram Granite porphyry and quartz syenite		

secondary chlorite, and probably also the talc occurrences, signify retrograde metamorphism.

The strength of the regional deformation is proved by the abundance of shear zones and by the strong foliation developed in interbeds of hornblende schists and of granitic gneiss. Lineations are virtually absent.

Taba Gneiss. This gneiss consists primarily of intermediate plagioclase (50-60%), quartz (about 25%) and biotite. Occasionally some hornblende or microcline occurs. The rock is usually uniform, but occasionally has an indistinct coarse layering. Contacts with the schists are sharp. Eyal (1975) observed discordant contacts, apophyses and interbeds of Taba Gneiss in the schists as well as schist inclusions within the gneiss, interpreting this rather homogeneous gneiss as a metamorphosed tonalitic pluton.

Texture seems to indicate formation from a coarse-grained protolith and incomplete post-deformational recrystallization. The weak foliation and the prominent lineation in the Taba Gneiss are parallel to the structures developed in the adjacent schists. The gneiss was folded after formation of these fabrics. A part of this deformation occurred after emplacement of granitic and pegmatitic veins and dikes, which are offshoots of the Elat Granite. Deformation was especially intense in the Nahal Shelomo area where the gneiss was transformed into a very strongly linear rock. For Shimron (1972) the tectonized rocks are thrust over adjacent schists.

Granitic Gneiss was formed from granite plutons emplaced into the pelitic schists and Taba Gneiss, and also from small tabular bodies emplaced in the latter and into the metabasites. It consists of about equal amounts of oligoclase, alkali feldspar and quartz; biotite may amount to 5-15%. Migmatites are developed at the contact with the schists and in this region feldspathization aureoles are well developed. The oligoclase porphyroblasts in the aureole may contain oriented quartz and garnet inclusions, showing that the granite penetrated already metamorphosed pelites. Schist xenoliths occur in places.

The more deformed rocks are augen gneisses and flaser gneisses that form bands, especially along metamorphosed dikes. Small sheets of Granitic Gneiss within metabasites and Taba Gneiss are very deformed, having stronger lineations and foliations than their hosts.

The lineations and foliations of the gneiss are parallel to the contacts and to the structures in the enclosing rocks. North of Elat the Granitic Gneiss was strongly folded with the schists to form isoclinal to rather open E-W to ENE trending folds several meters to several hundred meters in size.

Metamorphosed dikes. Straight and rather steeply dipping bands of lineated hornblende bearing schistose rocks cross all rock types mentioned above. They are up to a few meters wide and a few hundred meters long, strike E-W to NE-SW, and tend to form swarms. Bentor (1961) interpreted these bands as metamorphosed dikes and called them 'schist dikes'.

The dikes were intruded after the development of schistosity, and after folding of the contact with the Granitic Gneiss. Subsequently a penetrative lineation was imposed on all rocks. Clearly this lineation was produced during metamorphism of the dikes, and is, thus, younger than the foliation of the pelitic schists. 'Schist dikes' cross the Taba and Granitic Gneiss and transgress their contact. There are several swarms having different directions: ESE to SE and NE. Lineation is mostly parallel to that of the host rock, like in the Elat Block.

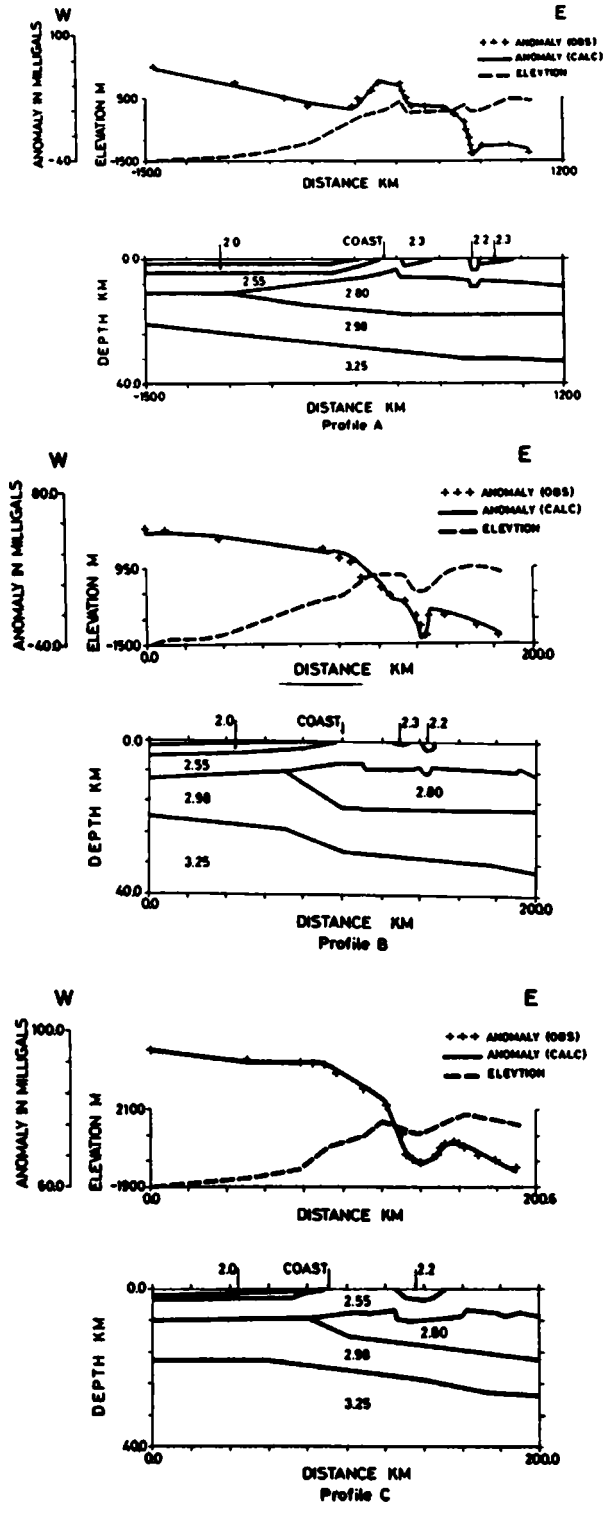


Figure 18A.5 Gravity profiles and computed models across Israel. Profile A is located south of Lake Kinneret, Profile B runs across Galilee, and Profile C runs across Lebanon near Beirut. Density values are in g/cm³ based on seismic velocities. From Ginzburg and Ben-Avraham (1991, Fig. 2, p. 126), after Ginzburg and Ben-Avraham, 1987.

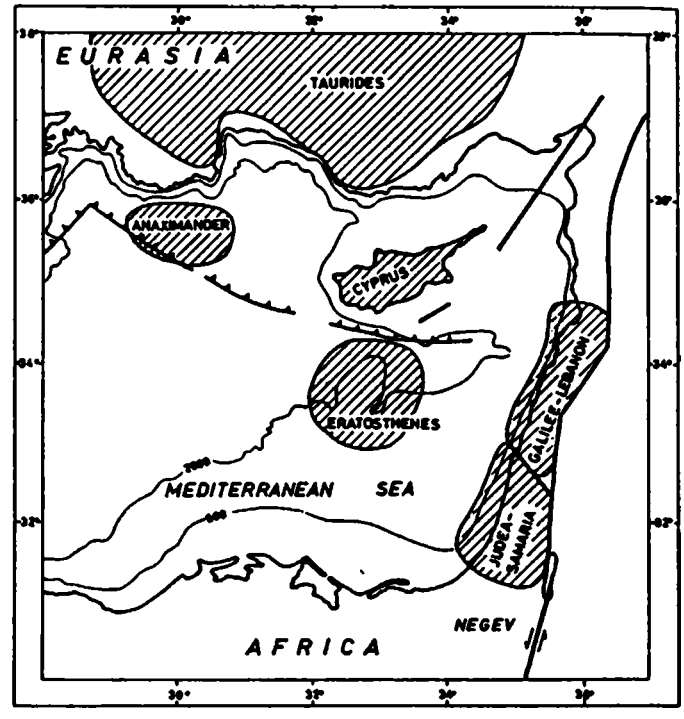


Figure 18A.6. Schematic distribution of terranes with distinct crustal structure in the Eastern Mediterranean. Plate boundaries are marked by heavy lines. From Ginzburg and Ben-Avraham (1991, Fig. 7, p. 130) after Ben-Avraham and Ginzburg, 1990.

Elat Granite Forming several plutons, it consists of very sodic plagioclase (up to 50%), microline (15-30%) which is predominantly non-perthitic, and quartz (ca. 25%). Biotite and some muscovite, often replaced by chlorite, occur in small quantities. Apatite, zircon and ore are minor accessories. This rock type belongs to a group of regionally very common calc-alkaline granites forming more than half of the northern part of the Arabo-Nubian Shield.

The texture is generally equigranular (2-7 mm). Plagioclase crystallized first, forming rectangular, generally hypidiomorphic crystals. Myrmekite and quartz drops in plagioclase are common.

The plutons of Elat Granite are grossly concordant with the regional structure of the enclosing rocks in spite of small scale complications of contacts. The metamorphics tend to dip away from the granite plutons. These relations suggest some shouldering aside of the country rock by the granite bodies.

Deformation continued during, or followed, the emplacement of Elat Granite, which is post-metamorphic, but still late-kinematic. This is proven by the strain of the granite, occurrence of weak foliation in satellite veins, and especially by their involvement in the late folding of the metamorphics of Nahal Shelomo area. Here the Elat Granite occupies the core of a WSW plunging antiform outlined by schists.

Roded Association (Garfunkel, 1980) This rock suite has hardly any rock types in common with the Elat association.

Furthermore, the structural trend in the Roded Block is close to N-S, almost perpendicular to that found in the rocks of the Elat Association. The following main rock types are present (Figs. 18A.2 and 18A.3):

Schists. The southern schists are metasediments (pelitic), somewhat similar to those of the Elat Association. They consist of sodic plagioclase, quartz, biotite and some muscovite, while hornblende is rare or absent. Garnet is often present. Some beds contain more than 5% quartz. Secondary epidote, chlorite and sericite are widespread. The texture consists of equigranular granoblastic mosaics, and there are no strained crystals.

Those of the northern area are quite different, and may be meta-volcanics. They consist essentially of andesine, biotite and hornblende. Some layers contain little or no biotite.

Gneisses of several types occur, mainly west of the aforementioned schist bodies. They generally have a quartz-dioritic or tonalitic composition, with up to 15% biotite, and frequently also some altered hornblende with quartz inclusions. Secondary chlorite, epidote and ore develop mainly at the expense of the mafic minerals. Larger rectangular plagioclase crystals may be relicts of an igneous protolith. However, most plagioclase crystals are polygonal and form granoblastic mosaics. The mafics produce the foliation and lineation. Locally the gneisses are folded on a scale of a centimeter to several meters.

In places the gneisses are banded, mainly close to migmatite areas. The gneisses were probably derived from rather homogeneous quartz-dioritic to tonalitic plutons.

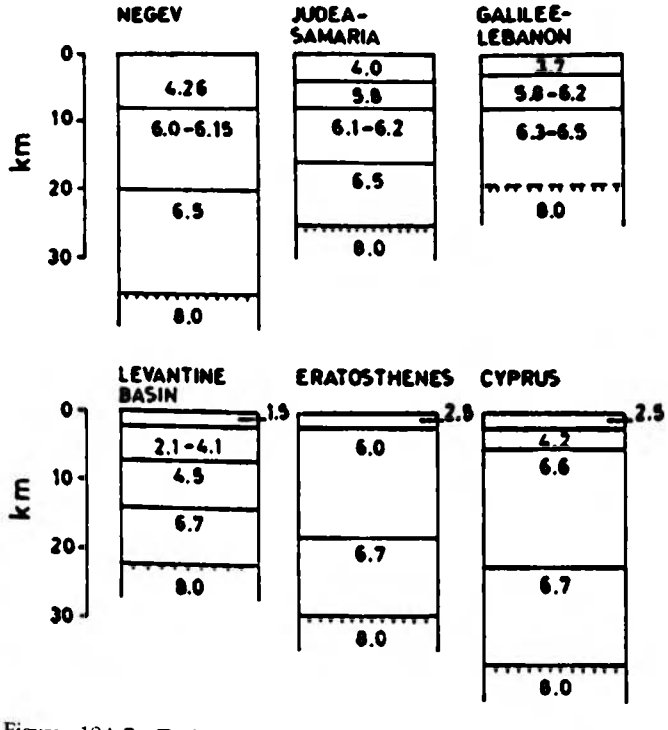


Figure 18A.7. Typical seismic refraction sections in the eastern Mediterranean. From Ginzburg and Ben-Avraham (1991, Fig. 8, p. 130), after Ben-Avraham and Ginzburg, 1990.

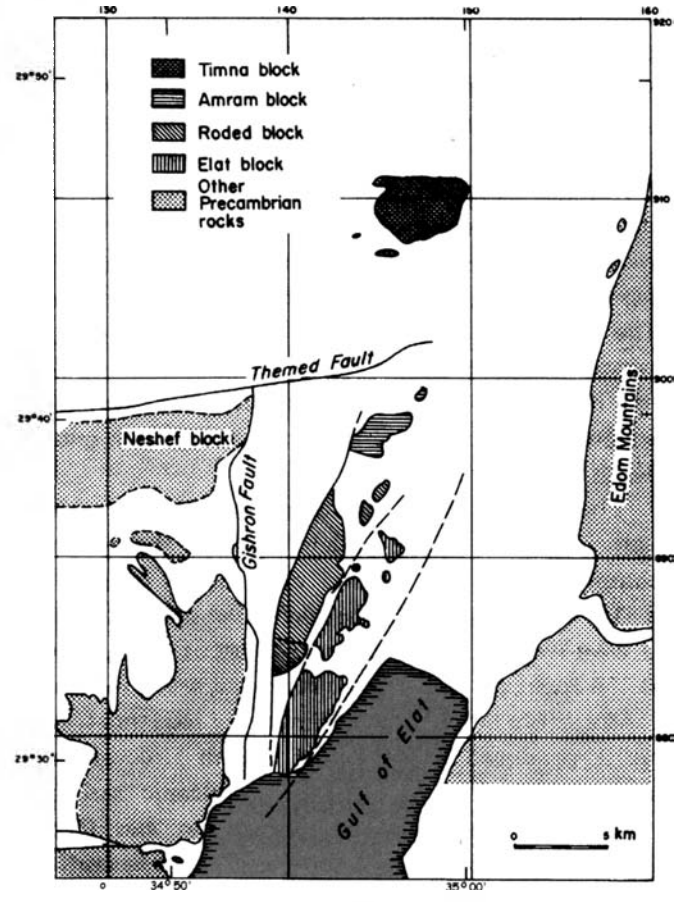


Figure 18A.8. Outcrops of Precambrian Basement and block structure in the Timna-Elat region. From Garfunkel (1980, Fig. 1B, p. 26).

Migmatites are widespread. In the periphery of the Roded quartz-diorite pluton they consist of often feldspathized schist layers and quartz-plagioclase layers. Biotite layers are common. These migmatites were probably formed by metamorphic differentiation.

Metamorphosed dikes. Regular bands of biotite-quartz-plagioclase schists, hornblende-quartz-plagioclase schists, hornblende-biotite schist and amphibolites crossing the gneisses are probably metamorphosed dikes. Their foliation and lineation are parallel to their walls. In addition the gneisses contain a variety of irregular schist inclusions which may range from mica schists through hornblende schists to amphibolites. They are often deformed. These may be in part xenoliths or metamorphosed and dismembered minor intrusions.

Roded Quartz Diorite. This rock type consists of variable amounts of oligoclase-andesine (50-70%), quartz (up to 20%), biotite (up to 25%) and hornblende (up to 15%) and minor microcline (up to 5%). Chlorite, ore, epidote, sericite and sometimes calcite replaces the mafics and plagioclase. The mafics often form elongated aggregates and tabular plagioclase crystals

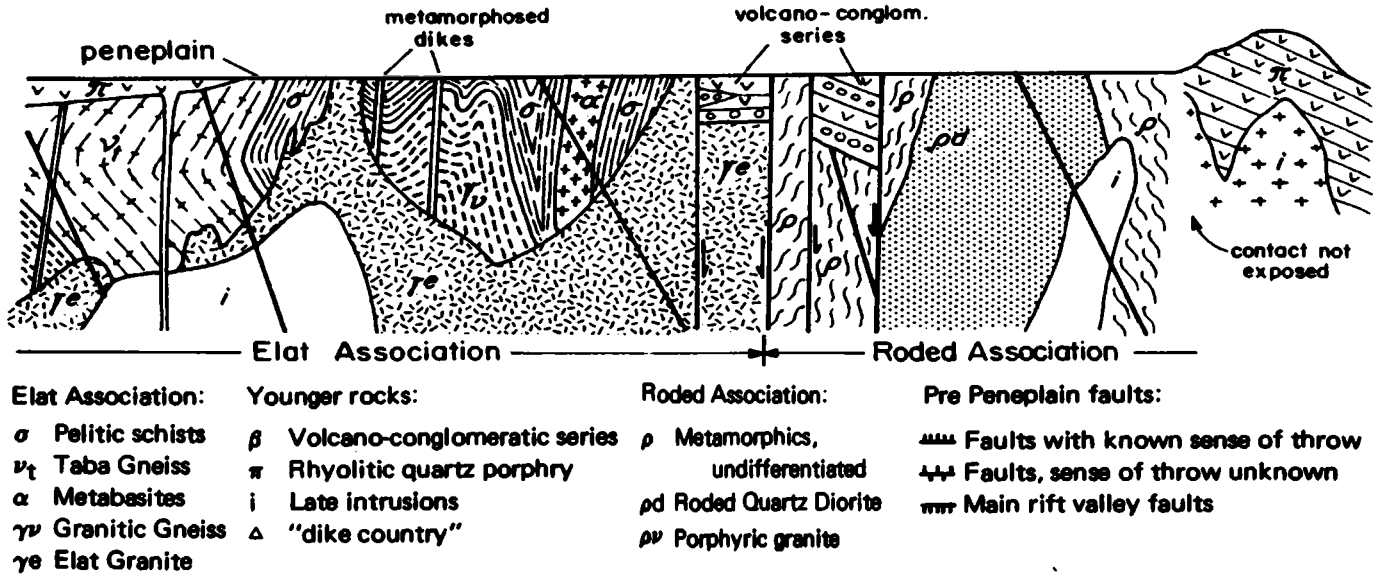


Figure 18.9. Schematic relation of Precambrian Basement of Elat. From Garfunkel (1980, Fig. 3, p. 32, Legend p. 31).

sometimes tend to be oriented. These features may produce a weak foliation which trends roughly N-S. Mafic stringers and elongated xenoliths, locally quite abundant, are arranged parallel to this foliation. The xenoliths have a meta-quartz dioritic to meta-dioritic composition. Alkali feldspar often replaces plagioclase. Myrmekite and drop-quartz in plagioclase are common.

The quartz-diorite body is interpreted as having been formed by anatexis, and did not move far from its place of origin. The mosaics of polygonal crystals and poikilitic hornblende crystals whose textures resemble those found in gneisses, and the stringers of mafics and the xenoliths, are probably relicts of the source rocks. The heterogeneity of the pluton suggests incomplete mixing and production of many batches of partial melt. It is also possible that a portion of the melt moved still farther up, so the present rock is a residue left behind. The bordering migmatites, most probably formed by metamorphic differentiation, must be genetically linked to the pluton, due to spatial relations.

The foliation of the quartz-diorite probably formed by flow during its emplacement. Post-emplacement deformation seems improbable in view of the absence of signs of strain.

Granite porphyry In the northern part of the Roded Block, this rock has many features resembling quartz diorite, being heterogeneous, rich in xenoliths and in bands of mafics. However the granite porphyry contains abundant microcline phenocrysts, often perthitic, enclosing plagioclase, quartz and mica crystals, also common in the matrix. The latter resembles that of quartz diorite, but is richer in quartz and microcline, has a lower color index and no hornblende. Mymekite and replacement of plagioclase by alkali-feldspar are common.

Migmatites are developed along the border of this rock type and contain alkali-feldspar in the leucosome, in contrast to the neighbouring migmatites developed on the northern periphery of the quartz diorite.

Leuco-granite intrudes with sharp contacts all the above mentioned rocks, forming small irregular stocks, dikes or veins. The composition is quite variable, and is characterized by the low color index and high content of alkali feldspar (25-50%). The plagioclase is albite-oligoclase.

The leuco-granites and the enclosing rocks are crossed by numerous fractures with displacements of less than a meter and by bands of cataclasis.

Doroth Schist (Helez Deep)

The ***Doroth Schist***, in the Helez Deep borehole (Derin, 1979; in Druckman, 1984, p. 204), is a dark muscovite-chlorite schist, which has undergone several phases of deformation. In addition to muscovite, chlorite and ore minerals, it consists of quartz and plagioclase. This rock type crystalized under low grade metamorphism of the greenschist facies (O. Amit, 1980, pers. comm., in Druckman, 1984). Rb-Sr age is Precambrian-Early Cambrian. Whole rock dating gave 636±107 Ma (Steinitz, 1980).

B. Younger Post-orogenic, Cratonic Plutonic rocks

Amram Block

North of the Roded Block, the Amram Block (Jebel Hindis) comprises the **Amram granite porphyry and quartz syenite**. They form an elongated body, composed of inequigranular varying amounts of orthoclase or perthite phenocrysts, sometimes with corroded plagioclase cores. Quartz may strongly be affected by hydrothermal alteration. Small amounts of ferro-magnesium minerals altered to chlorite and carries persistently hydrothermal calcite. The Amram igneous rocks are overlain unconformably by a thick sequence of acid volcanic flows.

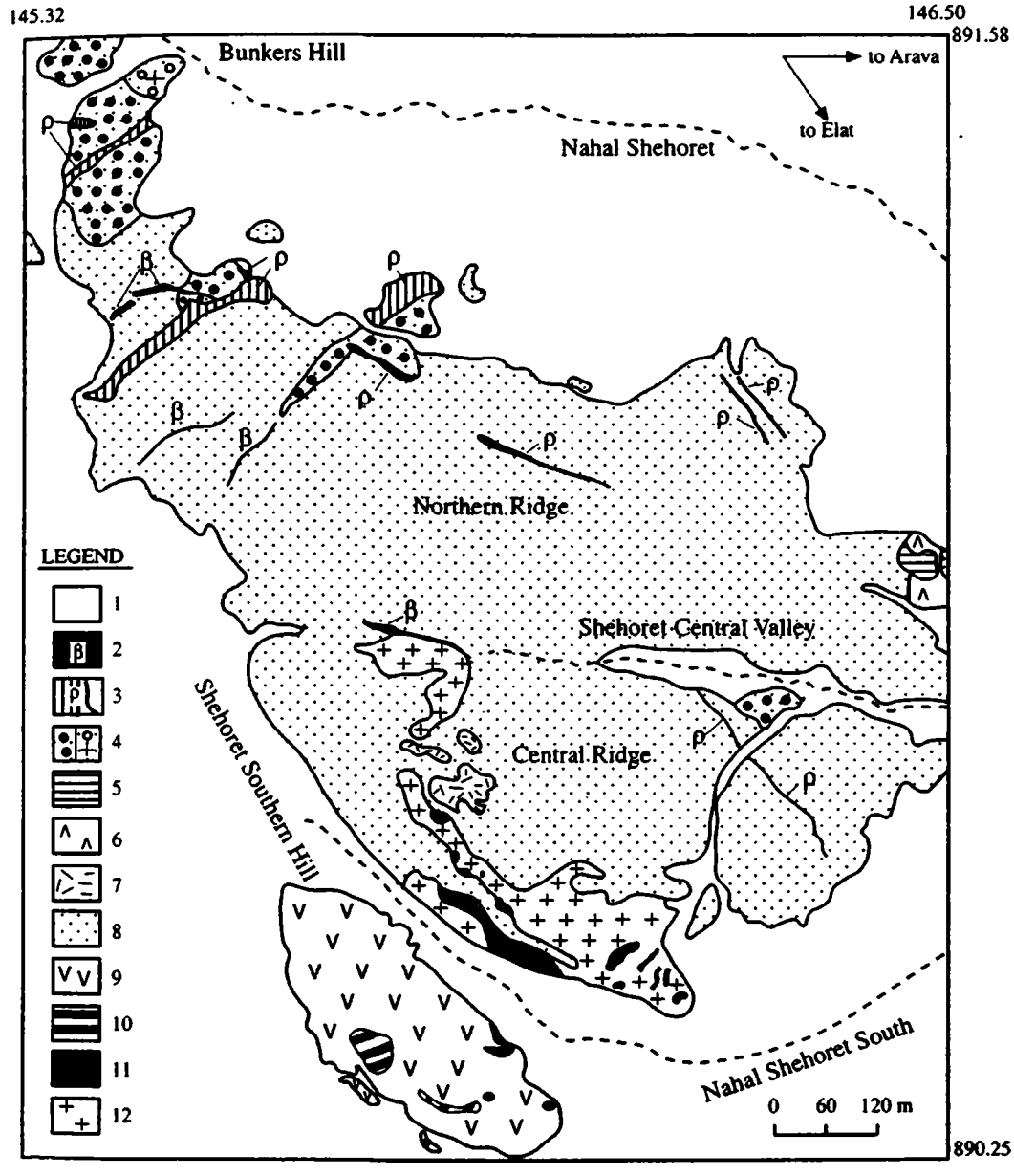


Figure 18A.10. Lithologic Map of Giv'ot Shehoret. From Peltz and Eyal (2000, Fig. 1, p. 105). Legend; 1. Quaternary deposits; 2. Doleritic dyke; 3. Rhyolitic dyke; 4. Elat Conglomerate Complex: a - conglomerate-sandstonic deposits; b - mixed, sedimentary-pyroclastic deposits; 5. Rhyolitic ignimbrite; 6. Rhyolitic lava flow; 7. Debris avalanche breccia; 7. Shehoret Tuff; 9. Trachyandesitic-trachytic lava flows; 10. Vitric pyroclastics; 11. Basalt trachyandesitic-trachybasaltic lava flows; 12. Elat Granite.

Timna Block

The igneous rocks of Mount Timna, located in the Timna valley, 25 km north of Elat, form an elongated E-W structural high, of an area of 15 km². They constitute the final stages of the Pan-African thermal event in the region (Bentor, 1985). Shpitzer et al. (1991) have put in evidence that the northern Timna igneous rocks, consisting of the peridodites, olivine norites, diorites and monzonites, were formed by differentiation of noritic magma and that a late quartz monzodiorite completes the plutonic sequence. These authors also indicate geothermobarometry of low pressure crystallization below 5 kbar and sub-solidus temperatures.

In his petrographic outline of the Precambrian in Israel, Bentor (1961) has described the **Timna Granite**, forming the largest part of the Timna Massif, as a rather fine-grained, reddish to pink granite composed of microcline-microperthite, subordinate oligoclase, quartz, some biotite and magnetite. The rock is cut by numerous dikes of andesite, rhyolite, rhyodacite, aplite, and dolorite, as well as by hydrothermal quartz veins. The more alkaline **Yehoshafat**

Granite intrudes the Timna Granite. The **porphyritic quartz syenite and syenite** intrudes the Timna Granite and consists of up to 50% of phenocrysts of perthite, embedded in a matrix of perthite, quartz and rare plagioclase and hornblende. The quartz forms intergrowths with feldspars. Some phenocrysts of sodic oligoclase occur, replaced by alkali feldspar.

Recently mapped by Beyth et al. (1999), the following radiometric ages were obtained: Quartz Monzonite, 600 Ma; Alkali Granite, 610 Ma; Monzodiorite, 610 Ma; Olivine Norite, 610 Ma, and Granite Porphyry, 625 Ma.

C. The Late Precambrian Elat Volcanic Field

The Late Precambrian Elat Volcanic Field, remnants of which are exposed on the Yotam heights directly overlooking Elat, the Roded Valley, Mount Amram and Mount Neshef, has been studied in detail in the Shehoret hills, 6 km northwest of Eilat (Peltz and Eyal, 2000).

The rocks range in composition from alkaline, subalkaline and calc-alkaline rhyolitic to basaltic magmas. The lithofacies varies from lava flows to ash flows and redeposited volcanic deposits. Representing the 'volcano-conglomerate complex' of Bentor (1961) they are part of the Ramat Yotam Caldera. In the Shehoret hills the basaltic-trachybasaltic lava flows of the Ramat Yotam volcano cover the Elat Granite. Effusive volcanism is represented by trachyandesitic to trachytic lava flows. The dynamics of the eruption column and dominance of the flow tuff indicate a Plinian type of volcanism. The fragments of dense vitric clasts flowed after landing as 'nuée ardente'. The Shehoret tuff consists of leuco-andesite ignimbrites from a satellite vent of the Ramat Yotam volcano. The final stage of the basaltic to rhyolitic magmatic activity in the Eilat Volcanic field is represented by minor intrusions of basaltic to rhyolitic dikes. **(Figure 18A.10)**.

Summing up: Starting with an ***orogenic phase*** of a duration of about 200 Ma, from 850 to 650 Ma, ***cratonization*** (650 to580 Ma) of the shield was achieved before the end of the Precambrian. The period of 600 to 580 Ma is characterized by the *intra-cratonic-taphrogenic magmatism* of alkaline peralkaline basaltic to rhyolitic nature.

REFERENCES

Ben-Avraham, Z., and Ginzburg, A., 1990. Displaced terranes and crustal evolution of the Levant and eastern Mediterranean. Tectonics, 9(4), p. 613-622.

Bentor, Y. K., 1985. The crustal evolution of the Arabo-Nubian massif with special reference to the Sinai Peninsula. Precambrian Res., 28(1), p. 1-74.

Bentor, Y. K., 1961. Petrographic Outline of the Precambrian in Israel Rep. No. 3, 9 p.

Beyth, M., and Heimann, A., 1999. The youngest igneous event in the crystalline basement of the Arabian - Nubian Shield, Timna igneous complex. Isr. J. Earth Sci., 48(2), p. 113-120.

Cohen, Z., Kapstan, V., Muravinski, E., Salhov, S., Shilo, A., and Wolff, O., 1987. Stratigraphic Table of Israel. Oil Exploration (Investment) Ltd. (OEIL).

Derin, B., 1979. Helez Deep 1A. Stratigraphic Log., scale 1:2000. Israel Inst. Petrol. Report 1/79.

Druckman, Y., 1984. Evidence for Early-Middle Triassic faulting and possible rifting from the Helez Deep Borehole in the Coastal Plain of Israel. In. J. E. Dixon and A. H. F. Robertson, (eds.), The Geological Evolution of the Eastern Mediterranean. Geol. Soc. Lond. Spec. Publ. No. 17, Blackwell Scientific, Oxford, p. 203-212.

Eyal, Y., Eyal, M., Kroener, A., 1992. Geochronology of the Elat terrain, metamorphic basement, and its implication for crustal evolution of the NE part of the Arabian-Nubian Shield. Isr. J. Earth Sci., (1992 for 1991), 40(1-4), p. 5-16.

Eyal, M., 1959. The geology and petrography of the Elat Massif, Southern Negev. Unpublished M.Sc. Thesis, Hebrew University Jerusalem. (Incl. Geol. Map, 1: 20,000). (In Hebrew).

Eyal, M., 1975. Stages in the magmatic history of the Precambrian in Sinai and Southern Negev. Unpubl. Ph.D. Thesis, Hebrew University Jerusalem, 155 p. Appendices. (In Hebrew; English Abstract).

Ganguly, J., 1972. Staurolite stability and related parageneses; Theory, experiments, and applications. . Petrology, 13(2), p. 335-365.

Garfunkel, Z., 1970. Tectonics of the western margins of the Southern Arava. Unpublished Ph.D. Thesis, Hebrew University Jerusalem, 204 p., Figs., Maps. (In Hebrew, English Abstract).

Garfunkel, Z., 1980. Contribution to the geology of the Precambrian of the Elat Area. Isr. J. Earth Sci., 29(1-2), p. 25-40.

Ginzburg, A, Makris, J., Fuchs, K., Prodehl, C., Kaminski, W., and Amitai, U, 1979. A seismic study of the crust and upper mantle of the Jordan-Dead Sea Rift and their transition toward the Mediterranean Sea. J. Geophys. Res., 84(B4), p. 1569-1582.

Ginzburg, A., and Ben-Avraham, Z., 1987. The deep structure of the central and southern Levant continental margin. Annales Tectonicae, 1(2), p. 105-115.

Ginzburg, A., and Ben-Avraham, Z., 1991. Crustal structure and tectonic processes in the Levant and the eastern Mediterranean, Isr. J. Earth Sci., 40(1-4), p. 125-133.

Ginzburg, A., and Gvirtzman, G., 1979. Changes in the crust and in the sedimentary cover across the transition from the Arabian Platform to the Mediterranean Basin: evidence from seismic refraction and sedimentary studies in Israel and in Sinai. Sediment. Geol., 23(1-4), p. 19-36.

Kröner, A., Eyal, M., and Eyal, Y., 1990. Early Pan-African evolution of the basement around Elat, Israel, and the Sinai Peninsula revealed by single-zircon evaporation dating, and implications for crustal accretion rates. Geology, 18(6), p.545-548.

Peltz, S., and Eyal, M., 2000. The Giv'ot Shehoret volcaniclastic complex, Elat, southern Israel. In: R. Bogoch (ed.), GSI Current Research, Vol. 12, Jerusalem, July 2000, p. 104-114.

Picard, L., 1941. The Precambrian of the North Arabian-Nubian Massif. Jerusalem, Hebrew University, Geol. Dept., Bull., 3(3-4), 30 p.

Shimron, A. E., 1972. The Precambrian structural and metamorphic history of the Elat Terrain. Unpublished Ph.D. thesis, Hebrew University, Jerusalem, 244 p.

Shpitzer, M., Beyth, M., and Matthews, A., 1992. Igneous differentiation in the Late Precambrian plutonic rocks of Mt. Timna. Isr. J. Earth Sci., (1992 for 1991), 40(1-4), p. 17-27.

Steinitz, G., 1980. Rb-Sr age determination on basement rocks from Helez Deep 1a Well. Isr. Geol. Surv., Rep. MM/1/80, 10 p.

Steinitz, G., Bielski, M., and Starinsky, A., 1981. The extension of the Arabian Shield beneath the Coastal Plain of Israel in light of Rb-Sr age determination. Ecog 7; 7th Eur. Collog. Geochron. Cosmochron. Isotope Geol., Jerusalem, Aug.-Sept. 1981, Abstr., 1 p.

Weissbrod, T., 1961. Mapping and petrography of the Roded Massif. Unpubl. M.Sc Thesis, Hebrew University, Jerusalem, 89 p.

Weissbrod, T., 1981. The Paleozoic of Israel and adjacent countries (lithographic study). Unpubl. Ph.D. thesis, Hebrew University, Jerusalem, also, Isr. Geol. Surv., Rep. M. P. 600/81, 276 p. (In Hebrew, English abstract).

Winkler, H. G. F., 1976. Petrogenesis of metamorphic rocks. Fourth Edition, Springer-Verlag, New York, N.Y., 334 p.

Chapter 18B

The Paleozoic in Israel and Environs

Tuvia Weissbrod
Geological Survey of Israel, 30 Malchei Israel Street, Jerusalem 95 501, Israel

GENERAL OUTLINE

Following the Pan-African orogenic event and the cratonization of the Gondwanan continental margin, Israel and its neighboring countries became part of a subsiding area, which faced a long period of pericratonic sedimentation. Beginning in the Neoproterozoic and throughout the Paleozoic, a thick pile of mostly siliciclastic sediments, displaying fluvio-deltaic to mid-shelf settings, were deposited on the Arabian Plate and adjacent areas, which were part of the long, wide, and stable northern passive margin of Gondwana bordering the Paleo-Tethys. They mostly accumulated in a broad basin, deepening gently northeastwards off the Arabo-Nubian Shield that extended over Arabia and across the Levant and Mesopotamia to the Taurus (Bitlis) and Zagros thrust belts (sutures) in Turkey and Iran. The southern part of the depositional basin covered the eastern and southeastern parts of the Arabian Peninsula, the Persian Gulf region and western Iran, whereas its western part extended over the North African Platform. Up to the Devonian the sediments were dominated by siliciclastic lithofacies with occasional intercalated carbonates, whereas from the Carboniferous onward the latter became increasingly abundant. Overall, mostly continental conditions (braided river pattern) prevailed close to the shield's area, while marine conditions repeatedly existed in the more northern and eastern parts of the basin.

In Late Precambrian (Vendian) the Arabian Plate was located close to the Equator and during the Early Paleozoic it moved southward, attaining its southernmost latitude of 55°S in the Late Ordovician. Only by the end of the Paleozoic did the plate leave the high latitudes. As it moved, the Arabian Plate changed orientation, rotating slightly anti-clockwise during the Cambrian and Ordovician, followed by a major clockwise rotation of over 90° from the Late Ordovician to Late Carboniferous, whereupon it achieved approximately its present position. Throughout most of the Paleozoic it was positioned in middle to high latitudes of the Southern Hemisphere, in temperate to cool-wet climatic belts (Konert et al., 2001). Nevertheless, occasional wandering of the paleomagnetic pole positioning the Arabian Plate in higher or in lower latitudes gave rise to relatively short periods of glaciogenic or to carbonate deposition.

The most southerly position of the Arabian Plate coincides with two episodes of glaciation affecting the landscape and deposition. During the Late Ordovician and Early Silurian, polar glaciers that advanced from African Gondwana covered the southern and western parts of the Arabian Peninsula (Vaslet, 1990), extending northward as far as northeastern Jordan (Andrews, 1992) and presumably over Israel. In the Late Carboniferous to Early Permian time interval a second glacial episode affected southern Arabia from Oman to Yemen. Intermittently, the lower latitude positions resulted in short periods of warmer climate and dominance of carbonate deposition over the platform during the Middle Cambrian, Early Devonian, Early Carboniferous, and Late Permian.

The siliciclastic section consists of coarse, immature, and poorly sorted, rift-related and intermontane molasse-type polymict conglomerates and arkoses, which are succeeded by medium- to fine-grained, platformal deposits, showing great lateral constancy and a distinct upward trend of maturation, evolving from arkoses and subarkoses to quartz-arenites with an ultrastable heavy-mineral suite and a kaolinite-dominated clay fraction.

The provenance area for these clastics was located south of the depositional basin, as indicated by the distribution of facies belts, isopachs, and paleocurrent dispersal trends. The molasse-type debris, however, originated from the weathering of the Pan-African igneous basement within the Arabo-Nubian Shield, with a minor contribution from more distant sources, whereas most of the detritus comprising the platformal sediments derived from Pan-African and earlier igneous crust further to the south and west, in interior Gondwana, and from recycled clastic material (conglomerate, arkose), and only a small part was derived from the shield's terrain.

The major shift of provenance probably occurred following the progressive denudation processes in Late Precambrian and the Early Cambrian, when the relief on much of the Arabo-Nubian Shield was levelled, and the landscape became mature and inactive, so it could not be a major source for the enormous quantities of Paleozoic detritus. Moreover, most of it was soon ubiquitously buried under the blanket of the basal platformal sediments (Yatib/Siq/Salib/Amudei Shelomo sandstones) and was only partly exposed following the uplift-and-erosion event ('Hercynian') in the Late Devonian. The thick sections of these units at the landward edge of the present exposures, indicate that originally they extended a considerable distance further inland. These considerations are supported by ion probe U-Pb dating study of detrital zircons from several exposures of Cambrian sandstones in southern Israel (Avigad et al., 2003). The analyses revealed that the age of most grains was concentrated between 650 and 550 Ma, apparently pointing to the Pan-African Arabo-Nubian Shield as the most likely provenance for the Cambrian detritus. Nevertheless, about 30% of the zircons yielded older, pre-Neoproterozoic ages (mostly 0.9-1.1 Ga), suggesting that they might originate from

more distant Kibaran and older rocks, which are not known from the juvenile Pan-African crust of the Arabian Shield and are currently exposed beyond the Arabian Peninsula, in central and south Africa, at least 3000 km away from Israel, and from other Gondwanan terranes that drifted away.

At the beginning of the Paleozoic, and less common at its termination, rifting and magmatism were prominently active in the evolution of the Arabo-Nubian Shield and its margins, but throughout this era region-wide epeirogenic arching set up the dominating structural pattern in the Gondwanan margins, marking turning points between deposition and erosion cycles and controlling the erosion rates and preservation of the sedimentary column. Otherwise it was tectonically quiescent, while block faulting was limited and compressive folding is practically unknown. Overall, the tectonic history shows an alternation of long periods of subsidence and short periods of basin inversion. The epeirogenic movements formed a series of uplifts that differentiated the area into region-wide swells, hundreds of kilometers in diameter, and their intervening basins. These swells were subsequently eroded, resulting in stratigraphic gaps, up to system-wide lacunae, while in the basins erosion was minor and the sediments accumulated without considerable breaks. The discontinuities within the section are generally the only indicators of the presence of the non-orogenic crustal swells.

Most investigators recognized the role of epeirogeny in the Paleozoic evolution of the region; however, opinions differ regarding the mechanism that produced these great structures, their spatial dimensions, and timing. At least three major uplift-and-erosion events occurred in the course of the Paleozoic: at the end-Silurian, in the Late Devonian to Early Carboniferous, and in the Late Carboniferous to Early Permian times. A previous event of uplift-and-erosion, though different in genesis, occurred at the Late Precambrian and developed eventually into a vast peneplain on the top of the Precambrian igneous basement. The latter and the Late Devonian-Early Carboniferous events display the most extensive rate of truncation, and separate between different depositional suites that are each characterized by a specific mineralogic signature and lithofacies.

The shifting in the locus of these structures and differences in their magnitude, and the rate of truncation resulted in an apparently chaotic spatial distribution of the time-rock sequences that has caused some correlation inconsistencies as well as misleading paleogeographies. Other prominent events that influenced the paleogeography and the sedimentary section involved glaciation and a drop in sea level, which occurred during the Late Ordovician to Early Silurian and the Late Carboniferous to Permian time intervals. The latter events are attested to by deep erosion that locally cut paleovalleys down to the Cambrian strata, and by fluvio-glacial and marine fill.

The Late Precambrian-Paleozoic sequence attains a cumulative thickness of more than 10,000 m, but due to truncation a complete time sequence is hardly found at any locality. About half of this sequence consists of Late Precambrian-Early Cambrian conglomerates and interbedded volcanic series, as well as evaporites and carbonates and of time-equivalent arkoses and graywackes, of which the thickest and the most complete sections are found in rift-related basins in the shield's terrain and within the peripheral basins. The other half are Paleozoic siliciclastic and some carbonatic sequences that are best preserved in almost persistently basinal areas, such as the Tabuk and Widyan Basins and the Ghawar oil field at the northern and eastern flanks of the Arabian Shield (Al Laboun, 1990), and in the Western Desert of Egypt (Keeley, 1989).

During the Permian and up to Jurassic times a different geodynamic pattern existed in the region, associated with extensional tectonics and sporadic magmatic activity that resulted in the opening of the Neo-Tethys. Several phases of block faulting and rifting took place along the Zagros-Taurus (Bitlis) Suture lines that separate the Iranian and Turkish Plates from Gondwana, and along the Mediterranean margin forming the passive continental margin of the Levantine Basin. The faulted blocks have placed plutonic/metamorphic basement, and Permian and Triassic sequences in the Mediterranean coastal area, in close stratigraphic proximity to one another.

Data on the paleogeographic setting of the Arabian Platform and the Paleo-Tethys deduced from paleomagnetic directions, facies distribution patterns, thickness changes, and paleocurrent trends, suggest that much of the Paleozoic platformal sediments once covered the entire region, but have been selectively truncated. In Israel the pre-Mesozoic section is stratigraphically very limited, and comprises only Late Precambrian (also ascribed to Infracambrian), Cambrian and Permian sequences. Ordovician to Devonian sediments, about 2500 m thick, similar to those which are today present in eastern and northern Saudi Arabia and further north in Jordan and Syria, were totally removed from Israel, Sinai, and the Eastern Desert of Egypt and partly from Jordan (northwest) and Syria (southwest) subsequent to the Upper Paleozoic uplift-and-erosion event. The Paleozoic of Israel is therefore described within a broader regional context.

THE PALEOZOIC SEDIMENTARY BLANKET

A thick blanket of clastic sediments covers the northern periphery of the Arabo-Nubian Shield, a relatively stable, passive continental margin which was consolidated and cratonized during the later stages of the Pan-African orogenic event, but deeply eroded already in Late Precambrian times. The greater part of the clastic sequence is of Late Precambrian (Vendian) and Paleozoic age. Today these clastics are exposed throughout Saudi Arabia, Egypt, Jordan and Israel (**Fig. 18B.1**), and have been encountered in numerous boreholes in these countries and in areas to the north. Distribution of the clastic series is discontinuous, provinces being separated by erosion gaps on the elevated igneous rocks of the Arabo-Nubian Shield in Saudi Arabia and Egypt, or by intercrustal depressions, such as the Red Sea and the Elat and Suez rifts.

The cratonic history of the region begins in the Late Precambrian during which the plutonic/metamorphic mountain belt was planed down and buried by its own debris. The earliest non-metamorphosed sedimentary succession, which was accompanied

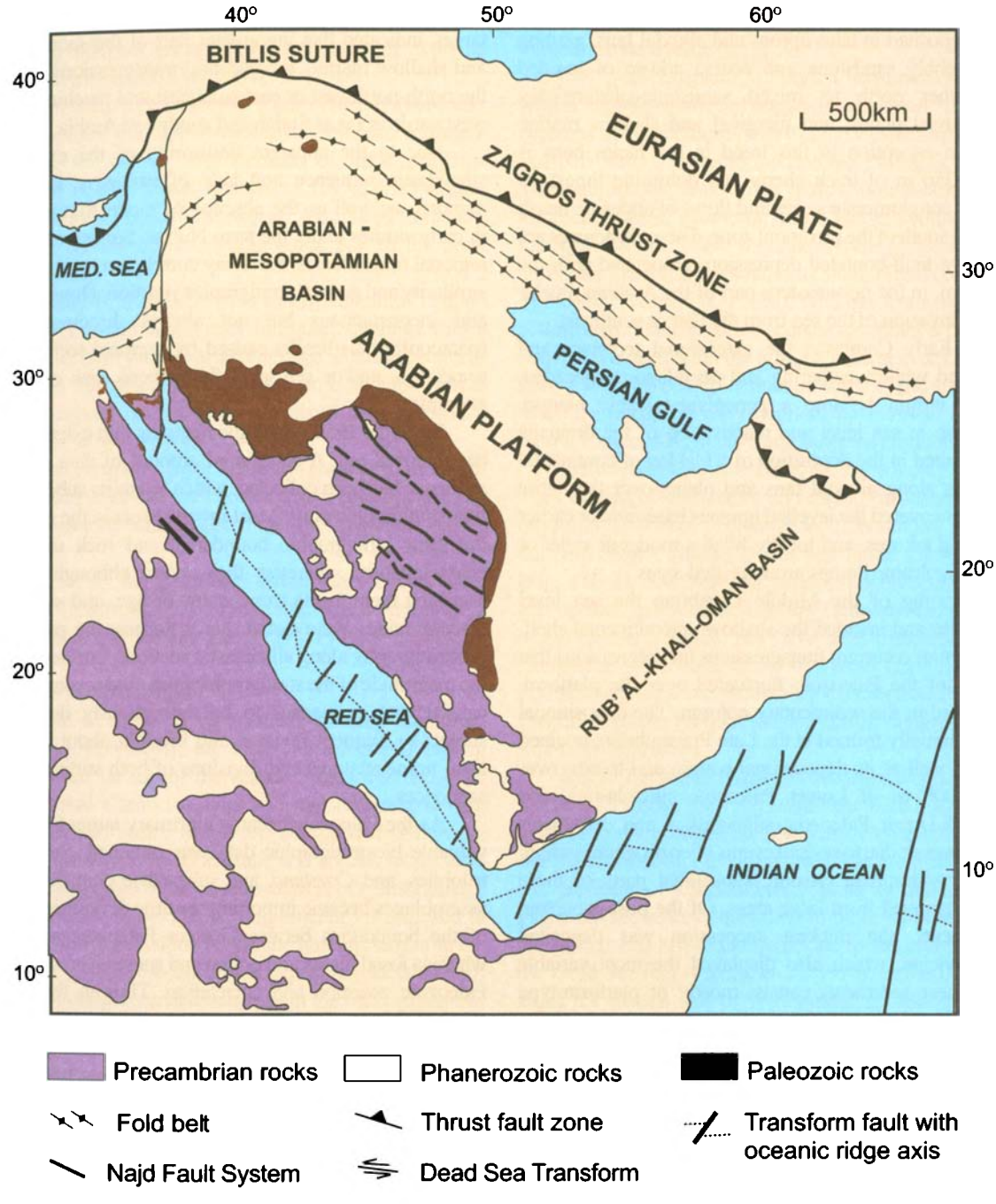


Figure 18B.1. The Arabian and adjacent plates showing the Pan-African igneous basement and Paleozoic outcrops and outlines of the main tectonic features.

by extensional tectonics and intra-continental magmatic activity, spans the Proterozoic-Phanerozoic boundary. It consists of coarse molasse-type immature sediments that were rapidly accumulated in intramontane valleys and syntectonic sags within the igneous terrain (conglomeratic facies), and in a broad pericratonic basin, which extended from the Arabo-Nubian Shield in the south to the passive margin and the Paleo-Tethys in the north and northeast (arkosic facies). The conglomerates are widely exposed in rift-related depressions in central and northern Arabia and the Eastern Desert of Egypt. They attain a thickness of up to 5000 m with several remnants along the Dead Sea Rift (up to 400 m thick), whereas the arkosic sediments are known from 19 deep boreholes in Israel and Jordan (penetrated thickness of 2500^{+} m) and from several exposures in southeastern Turkey.

Overall, the sedimentation involved boulder beds and conglomerates deposited in talus aprons and alluvial fans, grading northwards to pebbly sandstone and coarse arkose of braided plains, and further north to mixed sandstone-siltstone-clay sediments of alluvial plains, and marginal and shallow marine environments. An exception to this trend in the facies belts is the presence of 350 m of thick cherty and dolomitic limestone overlying a thick conglomerate series and flows of andesitic basalt (Jubaylah Group) south of the piedmont zone. These carbonates are restricted to active fault-bounded depressions associated with the Najd Fault System, in the northeastern part of the Arabian Shield, and represent an invasion of the sea from the east or southeast.

In the late Early Cambrian the extensional tectonics and magmatism abated while weathering and denudation proceeded, and the eroded terrain became a peneplaned stable margin. A subsequent drop in sea level and reactivation of the drainage systems have resulted in the deposition of a blanket of continental coarse subarkoses along alluvial fans and plains over the entire plate. This blanket covered the levelled igneous basement or earlier conglomerates and arkoses, and locally filled a moderate relief or surrounded small volcanic humps around rifted areas.

At the beginning of the Middle Cambrian the sea level again started to rise and invaded the shallow epicontinental shelf, setting up a pattern of recurrent transgressions and regressions that throughout most of the Paleozoic fluctuated over the platform, leaving their record in the sedimentary column. The depositional basin which was initially formed in the Late Precambrian, retained its dimensions as well as its depositional pattern and trends, over which almost 3000 m of Lower Paleozoic siliciclastics, and about 2000 m of Upper Paleozoic siliciclastics and carbonates accumulated. However, due to several events of epeirogenic arching accompanied by widespread erosion, substantial parts of these sediments were removed from large areas. Of the post-peneplain Paleozoic sediments, the thickest succession was deposited during the Ordovician, which also displayed the most variable environments. These sediments consist mostly of platform-type marine and continental siliciclastics, fairly homogeneous laterally, with only moderate changes in thickness over large distances and an upward trend of evolving maturation, better sorting and fining, all of which attest to a common geological history across the Arabian Platform and tectonic quiescence. Nevertheless, during certain transgressive events (i.e, Silurian and Carboniferous) several depocenters developed, apparently because of isostatic or tectonic subsidence.

Overall, the variations and changes of lithology and facies were controlled by the interplay of geographic position (latitudinal and elevation), sediment supply (provenance and transportation) and eustacy, whereas the presence of stratigraphic sequences, their thickness, rate of deposition and preservation were mainly controlled by isostasy (epeirogeny and subsidence) and local tectonic movements.

For a long time the Paleozoic sandy facies was considered to be mainly fluvial in origin, ranging from braided-stream to sinusoidal channel-type deposits. However research from the last 30 years, when the Paleozoic became a primary exploration target, indicated that the greater part of the sequence is marginal and shallow marine, representing transgressions that issued from the north-northwest or east-southeast and reaching southward and westwards as far as Sudan and southwest Arabia.

Due to the apparent uniformity of the exposed Paleozoic siliciclastic sequence and lack of extensive lateral lithological markers, as well as the absence of guide fossils, it was lumped in early studies under the term Nubian Sandstone and treated as a regional magnafacies. Far away correlation mostly relied on facies similarity and general stratigraphic position. However, the common and inconspicuous but not always discernable stratigraphic (paraconformal) breaks caused by regional tectonic movements, truncation, and/or sea level fluctuations, has complicated these attempts.

Since the 1950's geologic mapping and extensive studies have been carried out. A substantial amount of data on the Paleozoic sequence has been collected, which led to its subdivision into local lithostratigraphic units. Most investigators in the region recognized the same stratigraphic boundaries and rock units with similar characteristics, wherever they exist, although not necessarily ascribing them to the same status or age, and sooner or later the discontinuities were noted. Nevertheless, the paucity of reliable biostratigraphy along siliciclastic sections, erroneous evaluation of the magnitude of the stratigraphic gaps, and misleading correlations caused rock sequences to be ambiguously dated. These were subject to frequent revision and brought about a proliferation of local nomenclatures and divisions of both surface and subsurface sequences.

As the Paleozoic became a primary target for oil exploration, valuable biostratigraphic data was obtained. Surface graptolites, trilobites, and *Cruziana,* and subsurface chitinozoa and acritarch assemblages became important for time definitions and correlation of the boundaries between Lower Paleozoic series and stages, whereas fossil plants and pollen and spores were applied for Upper Paleozoic zonation and correlation. Thus in the later improved stratigraphic studies erroneous age assignments and misleading definitions or correlation of the past were eventually compensated for, and the extent of the stratigraphic gaps became evident. In addition, during the last decades many detailed and systematic sedimentological studies of the clastic sequence, and detailed analysis based on mineral diversity and other rock parameters demonstrated the close relationship of the Paleozoic over the entire region. These studies (*i.e.* Weissbrod and Perath, 1990; Amireh et al., 1994a) have provided refined criteria and better resolution for unit recognition and correlation. The ubiquity and lateral constancy of these criteria and the updated biostratigraphic inventory were applied to establish reliable local stratigraphies, and to weld them into a solidly current stratigraphic scheme of region-wide validity (**Fig. 18B.2**).

The Late Precambrian-Paleozoic sedimentary succession in the Arabian Platform is broadly divisible into major depositional cycles or packages, which are separated by unconformities and extensive erosion and are designated as groups or supergroups.

Each of these is divided into numerous formations. In Israel three groups displaying different mineralogical signatures of evolving maturation were distinguished (Weissbrod, 1980):

1) 'Precambrian Sedimentary Group' (Late Precambrian-Early Cambrian) - comprises the oldest non-metamorphosed sedimentary sequence in the region, and consists of thick polymict conglomerate and poorly sorted coarse- to fine-grained arkose with an unstable heavy-mineral assemblage. Associated intrusions and extrusions of mostly alkaline composition add to the great thickness of this group.

2) Yam Suf Group (Cambrian) - it is mostly medium- to fine-grained, moderately sorted subarkoses and quartz-arenites with a stable to ultrastable heavy-mineral assemblage. Extraformational conglomerates are restricted to the basal unit, though pebble layers occur throughout the sequence. A mixed carbonate-shale intercalation occurs at the lower part.

3) Negev Group (Permian-Lower Triassic) - consists of medium- to fine-grained, moderately to well sorted quartz arenites with an ultrastable heavy-mineral assemblage at the lower part overlain by carbonates.

Other divisions of the Paleozoic sedimentary cycles were applied in Egypt (Klitzsch, 1986, 1987) and Saudi Arabia (Al-Laboun, 1990; Stump and Van der Eem, 1994, 1995).

REGIONAL DISTRIBUTION

The Paleozoic in Israel is represented by only Cambrian and Permian strata. Previously, the rock unit directly overlying the peneplain surface on top of the igneous basement had been regarded as the basal Cambrian sequence, but radiometric data obtained from volcanic rocks which are interbedded within the pre-peneplain molasse-type conglomeratic and arkosic facies have revealed that the upper part of these sequences is of Cambrian age too. The conglomeratic facies (Elat Conglomerate) is exposed in several fault-bounded depressions within the igneous terrain in the Elat area. The rock sequence in the largest exposure (Har Shelomo) consists entirely of conglomerates, whereas in the other exposures the conglomerate is interbedded with rhyolitic quartz-porphyry and andesitic basalt flows or pyroclastics and large masses of ignimbrites (Katharina Group). The Elat Conglomerate is cut by a planar surface and is overlain by late Early Cambrian pebbly subarkose, though locally some of the associated acid volcanics form residual humps (inselbergs) above this surface. The most northward occurrence was encountered at the bottom of the Hameishar-1 borehole (central Negev) where the conglomeratic facies underlies or interfingers with the arkosic facies.

The arkosic facies (Zenifim Formation) is nowhere exposed in Israel and the bordering countries but has been penetrated in 11 boreholes in the subsurface of the Negev and the southern Coastal Plain (**Figs. 18B.3, 18B.4**). It is presumably present throughout Israel except for several limited areas along the Coastal Plain where tectonically interrupted stratigraphies have been encountered (Helez-1a; Gevim-1). The Zenifim Formation overlies the igneous basement and is bounded by unconformable boundaries. In the Sinaf-1 borehole it is overlain by late Early Cambrian subarkoses, whereas from the central Negev (Ramon-1) northwards Early Permian strata overlie it.

The post-peneplain Cambrian sequence is mostly arenitic with a middle shaly-carbonatic intercalation. It is known from outcrops in the southern Negev at the western margins of the Dead Sea Rift Valley, opposite the uplifted Paleozoic rocks of Jordan. The outcrops are limited to a narrow non-continuous strip, a few kilometers wide, extending from Timna southward to Elat and the Sinai border. These sediments were also encountered in two boreholes located in the southern (Sinaf-1) and central (Hameishar-1) Negev (Weissbrod, 1969a), whereas from there northwards it is truncated. The Cambrian sequence overlies a peneplain surface, which developed upon the igneous basement or Late Precambrian-Early Cambrian conglomerates (at surface) and arkose (subsurface). They are unconformably overlain by Permian (Hameishar-1) or Lower Cretaceous (Sinaf-1 and outcrops) formations.

Permian sediments in Israel are known only in the subsurface. They consist of siliciclastic and mixed carbonate/siliciclastic rock units and have been penetrated in 22 boreholes in the central and northern Negev, Judean Desert and in the southern Coastal Plain (Fig. 18B.3). The Permian strata probably extend to the central and northern parts of the country (Samaria and Galilee), whereas in the southern Negev they have been truncated. Apart from the Hameishar-1 borehole, where it overlies Cambrian subarkose, the Permian sequence unconformably overlies Late Precambrian-Early Cambrian arkose/igneous rocks and is disconformably overlain by Lower Triassic strata.

East of the Israeli Paleozoic occurrences juxtaposed Paleozoic sections in Jordan are represented by thick Cambrian to Silurian and Permian sequences, all of which are known from both outcrops and the subsurface. Devonian sediments are totally absent whereas the presence of Carboniferous strata is ambiguous. Wherever Paleozoic sequences equivalent to those of Israel are found, they are shifted 105 km to the north due to sinistral movements along the Dead Sea Rift (Freund et al., 1970). In the Dead Sea area and along the eastern side of Wadi Araba, several fault-bounded Late Precambrian-Early Cambrian conglomerates and interbedded pyroclastics are exposed, as well as numerous small stocks and large elongated masses of rhyolitic to andesitic lava flows and ignimbrites (Ahaymir Volcanic Suite). The Saramuj Conglomerate at the southeastern side of the Dead Sea is still of Precambrian age (pre-585 Ma), but a similarily termed conglomerate at Wadi Abu Barqa, which is overlain by a rhythmic sequence of thinly interlayered acid pyroclastics with siltstone and shale (Haiyala Volcaniclastic Formation), probably belongs to a later stage of deposition (up to Early Cambrian) corresponding to the Elat Conglomerate. It is cut by late Early Cambrian subarkoses, displaying an angular unconformity.

The Late Precambrian-Early Cambrian arkosic facies known from the subsurface of the Negev has also been penetrated in eight boreholes in the southern desert, Dead Sea, Azraq, and Northern Highlands areas of Jordan (Fig. 18B.3). The lower parts of this sequence were termed the Unassigned Clastic Unit and Unassigned Volcanic Unit (Andrews, 1991), whereas its upper part

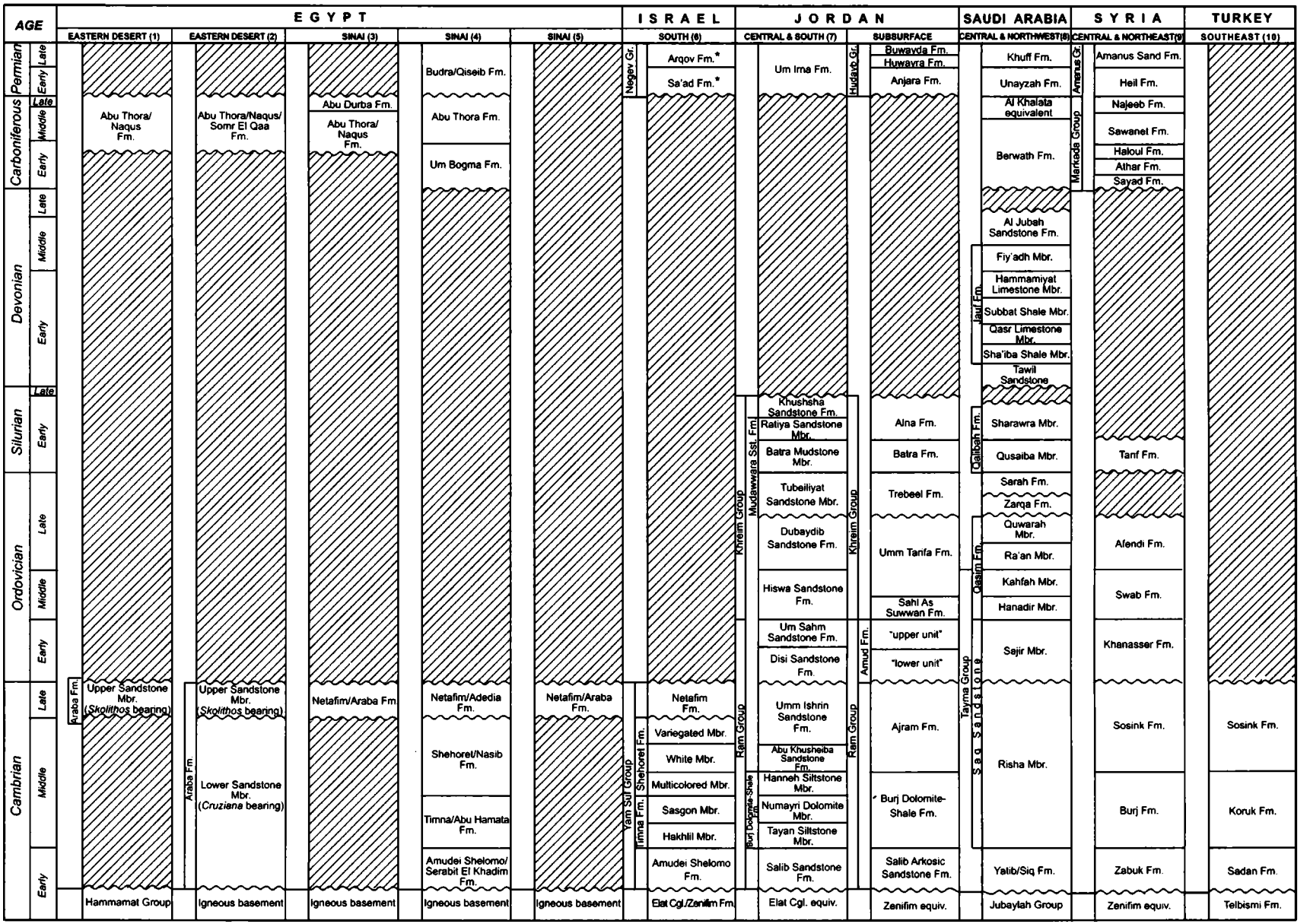


Figure 18B.2. Correlation chart of current Paleozoic rock sequences in Israel and adjacent areas (not to scale). Nomenclatures as given by the various authors. The juxtaposition of sections is according to the correlation and age (leftmost column) as proposed by the present author. Hatched areas represent stratigraphic gaps.

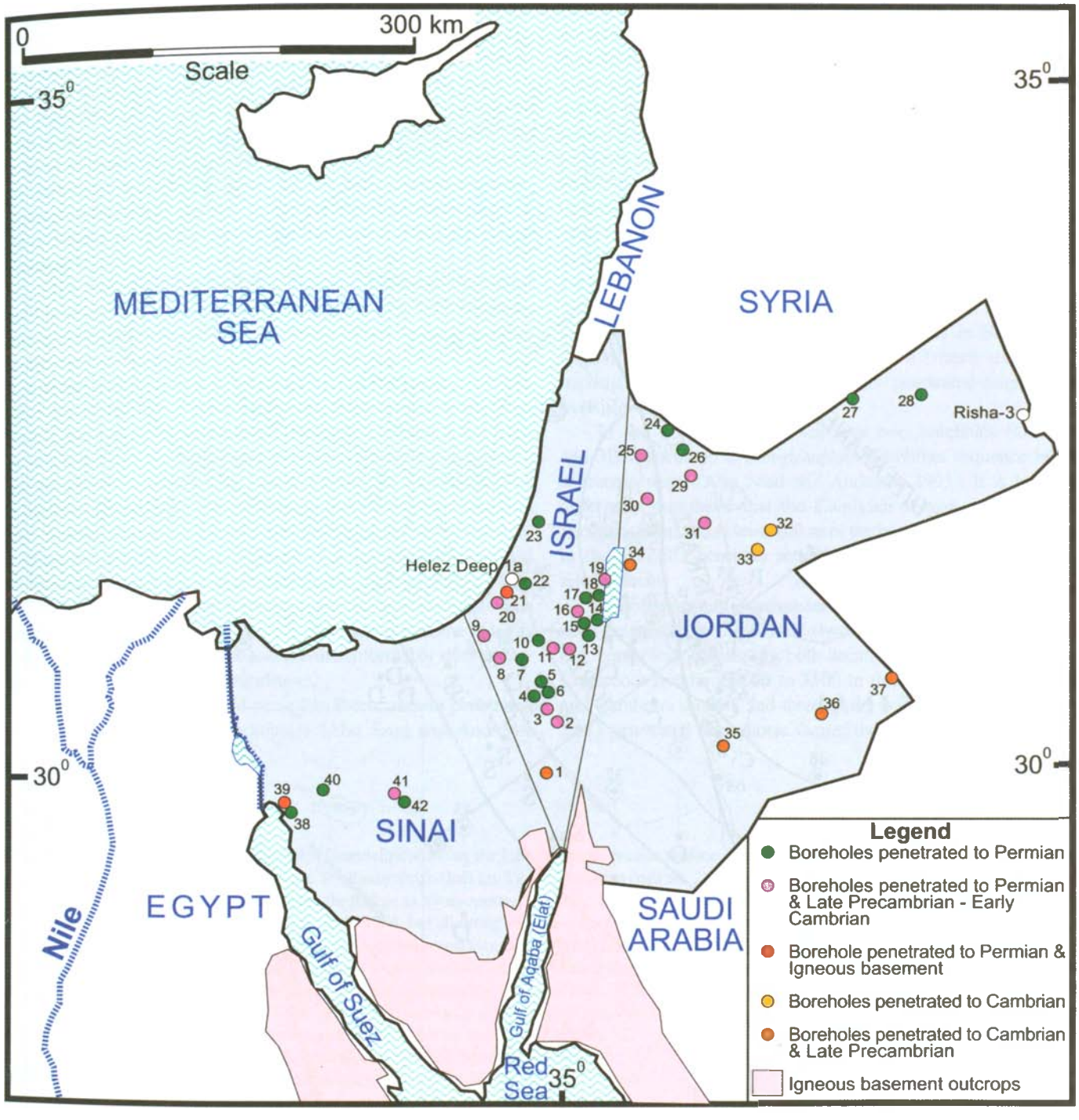
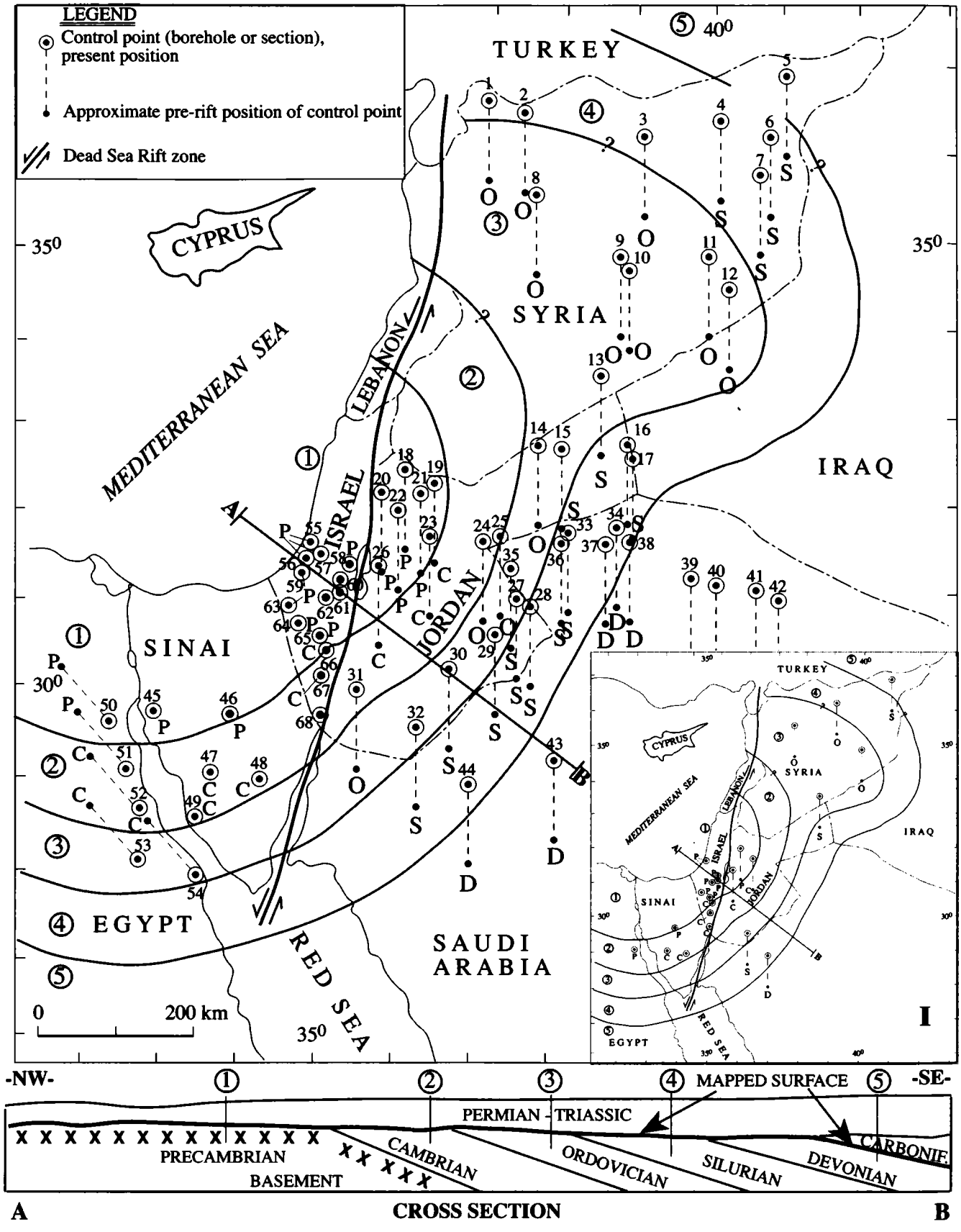


Figure 18B.3. Boreholes in Israel, Jordan and Sinai that penetrated Permian, Cambrian and Late Precambrian sequences (see legend).
Israel: 1=Sinaf-1; 2=Hameishar-1; 3=Ramon-1; 4=Avdat-1; 5-Nafha-1; 6=Nafha-2; 7=Boqer-1; 8=Shezaf-1; 9=Agur deep=1a; 10=Zavo'a-1; 11=Kurnub-1; 12=Makhtesh Qatan-2; 13=Heimar-1; 14=Lot-1; 15=Zuk Tamrur-1; 16=Zohar Deep-8; 17=Haqanaim-3; 18=Massada Deep-1; 19=Emunah-1; 20=Bessor-1; 21=Gevim-1; 22=Pleshet-1; 23=David-1a.
Jordan: 24=Northern Highlands-2; 25=Ajlun-1; 26=Er-Ramtha-1a; 27=Risha-2; 28=Risha-11; 29=Northern Highlands-1; 30=Suweileh-1; 31=Safra-1; 32=Fuluk-1; 33=Wadi Ghadaf-2; 34=Geothermal 3-D; 35=El Jafr-1; 36=Wadi Sirhan-3; 37=Wadi Sirhan-10.
Sinai: 38=Ayun Musa-1; 39=Ayun Musa-2; 40=Hamra-1; 41=Abu Hamth-1; 42=Nakhl-1.


LEGEND
Control point (borehole or section), present position
Approximate pre-rift position of control point
Dead Sea Rift zone
TURKEY
CYPRUS
SYRIA
LEBANON
MEDITERRANEAN SEA
ISRAEL
IRAQ
JORDAN
SINAI
EGYPT
SAUDI ARABIA
RED SEA
35⁰
30⁰
40⁰
0
200 km
A
B
I
-NW-
-SE-
MAPPED SURFACE
PERMIAN - TRIASSIC
CARBONIF.
DEVONIAN
SILURIAN
ORDOVICIAN
CAMBRIAN
PRECAMBRIAN BASEMENT
CROSS SECTION

was ascribed to Cambrian or Ordovician formations. However, the true stratigraphic nature of the entire sequence (equiv. Zenifim Formation) has been differently interpreted by Weissbrod and Sneh (2002), who evaluated its maximal penetrated thickness to be more than 2500 m. Three of the boreholes were reported to reach the granitic basement (Abu Saad and Andrews, 1993). The arkose sequence in the southern boreholes is cut by the Cambrian peneplain surface and is overlain by late Early Cambrian coarse-grained subarkoses, whereas in the northwestern boreholes it is unconformably overlain by a Permian section (Weissbrod and Sneh, 2002).

The post-peneplain Paleozoic sequence is exposed in central and southern Jordan in an almost continuous belt, 5-10 km wide, along the eastern side of the Dead Sea and Wadi Araba, extending southward to Ras en Naqb. From Zarqa Ma'in to Wadi Mujib the Cambrian rocks are directly overlain by Permian strata, which in turn are overlain by Triassic sediments; from there to Wadi Dana only Cambrian rocks are exposed, and farther to Jabal Ram in the south, Cambrian and Ordovician exposures are widely distributed, all of which are overlain by Lower Cretaceous formations. The Cambrian sequence is very similar to that in southern Israel on the western margin of the rift, and generally the same units are recognized, though bearing different local names. Ordovician and Silurian clastic sediments are exposed again from the Ras en Naqb - Batn el Ghul Escarpment extending continuously southeastwards and across the Saudi Arabian border. Formations become older as one moves from east to west and are unconformably overlain by Lower or Upper Cretaceous sandstone.

In the subsurface the post-peneplain Paleozoic was penetrated in approximately 60 deep boreholes (Abu Saad and Andrews, 1993) that encountered different straigraphic sections. In the northwest part of the country five boreholes (Ramtha-1a, Northern Highlands-2 and 1, Ajlun-1, Suweileh-1) encountered a Permian section, the latter three of them also penetrated the unconformably underlying Late Precambrian-Early Cambrian arkose. In north-central Jordan the Paleozoic was penetrated in 12 deep boreholes. In three of them the Permian overlies Cambrian (Safra-1) or Ordovician (Risha-2 and 11) sections, while in the others Lower Cretaceous (Wadi Ghadaf-1 and 2) or Triassic (Hamza 4 and 13, Wadi Hazim-1, Wadi Rajil-2 and 4, Fuluk-1, Dahikiyeh-1) sections overlie the Ordovician. Two of the boreholes (Wadi Ghadaf-2 and Fuluk-1) were bottomed in the Cambrian.

In northeastern Jordan, where most of the Risha field boreholes (24 of them) are located, a Silurian or Silurian and Ordovician sections were penetrated below a Triassic section. The maximal Silurian and Ordovician section penetrated attains 3800^{+} m (Risha-3).

In the northeast Dead Sea area two boreholes (GTZ-2D and 3D) penetrated a post-peneplain Cambrian sequence below a Triassic strata (Abu Saad and Andrews, 1993). It is herewith differently postulated that the Cambrian section is overlain by Permian strata, and at least 100 m of the basal Cambrian formation in the GTZ-3D borehole actually belongs to the pre-peneplain arkosic facies.

In southern and southeastern Jordan Paleozoic rocks have been penetrated in the El Jafr (two boreholes) and Wadi Sirhan (14 boreholes) Basins. At both localities the Lower or Upper Cretaceous overlie a 3000 to 3500 m thick Silurian, Ordovician, and Cambrian section, and three of the boreholes (WS-3 and 10; JF-1) penetrated the arkosic facies, the latter being bottomed in



Figure 18B.4. Model of the truncated Helez Geanticline showing the Late Paleozoic erosion surface and belts of the Lower Paleozoic subcrops. System units found below the erosion surface: P= Precambrian (belt no. 1); C= Cambrian (belt no. 2); O= Ordovician (belt no. 3); S= Silurian (belt no. 4); D= Devonian (belt no. 5). Inset I shows the feature as it was constructed, using 18 data points (Gvirtzman and Weissbrod, 1984). The present subcrop map includes 68 data points, unavailable in 1984, but all fitting into the subcrop belts predicted by the model. The data points (circled dots) east of the Dead Sea transform were shifted 105 km northward (see dashed lines) from their original Paleozoic position by the late Tertiary left-lateral movement of this block, whereas data points west of the Gulf of Suez were shifted some 80 km to the north (or northwest) to compensate for the post-Late Paleozoic displacement of this block (in accordance with Freund et al., 1970 and Rybakov et al., 1996, respectively). Numbered data points are name-listed in the appendix. Cross section A-B shows the (reconstructed) pre-Permian unconformity, which has in most localities superseded the Lower Carboniferous erosion surface, still visible in the SE data points (belt no. 5).
Names of the numbered data points (mostly boreholes) of the Helez Geanticline:
Syria: 1= Baflioun; 2=Aleppo; 3=Abba-1; 4=Afendi-1; 5= Qamishlye;
6= El Bowab; 7= Markada-101; 8= Khanasser-1; 9= Soukhne-1; 10= Doubayat-2
11= RV-101; 12= Swab-1; 13= Tanf-1.
Jordan: 14= Risha-2; 15= Risha-1; 16= Risha-6; 17= Risha-5; 18= Northern Highlands-2; 20= Ajlun-1; 21= Northern Highlands-1; 22= Suweileh-1; 23= Safra-1; 24= Wadi Rajil-1; 25= Wadi Hazim-1; 26= Zarqa Ma'in; 27= Wadi Sirhan-2; 28= Wadi Sirhan-1; 29= Wadi Sirhan-3;
30= El Jafr-1; 31= Jabal Arqa; 32= Mudawwara.
Saudi Arabia: 33= Jaraniyat; 34= Turaif; 35= S-432; 36= not exist in map; 37= S-223; 38= S-450; 39= S-459; 40= S-456; 41= S-254; 42= Badanah; 43= Al Huj; 44= Tabuk;
Sinai: 45= Ayun Musa-2; 46= Abu Hamth-1; 47= Um Bogma; 48= Gebel Dhalal; 49= Gebel Abu Durba.
Eastern Desert: 50= Ataka-1; 51= Wadi Araba; 52= Wadi el-Dakhl; 53= Wadi Qena (north); 54= Gebel el-Zeit.
Israel: 55= Helez Deep-1a; 56= Gevim-1; 57= Pleshet-1; 58= Emunah-1; 59= Bessor-1; 60= Zohar Deep-8; 61= Makhtesh Qatan-2; 62= Kumub-1; 63= Agur Deep-1a; 64= Shezaf-1; 65= Ramon-1; 66= Hameishar-1; 67= Sinaf-1; 68= Timna.

the igneous basement. The post-peneplain Paleozoic clastics in these basins in most respects resemble the Cambrian to Silurian sequences in northwestern Saudi Arabia.

Beyond the Saudi Arabian border the Paleozoic rocks are exposed in a wide arcuate belt in the northern, eastern, and southern flanks of the Arabian Shield, extending from the Jordanian border to Yemen (Fig. 18B.1). Paleozoic sediments, ranging from Cambrian to Permian, recline against the shield, either exposed or in the subsurface. The Paleozoic outcrops are often continuous over tens and hundreds of kilometers, and exhibit various stratigraphic relationships.

In northwestern Saudi Arabia the Paleozoic sediments are preserved in the Tabuk-Tayma and Widyan Basins, separated today by the Ha'il-Rutbah structural high. The outcrops curve around the northern margin of the Arabian Shield, disappearing under the mobile sands of the Great Nafud Basin in the east. In the Tabuk-Tayma Basin only Lower Paleozoic sediments are present. Those of Cambrian-Ordovician age appear in a wide zone closer to the igneous massif. Those of Silurian and Devonian age cover large areas more to the north. The widely distributed Devonian formations, which occur here but hardly anywhere else in the Near East, are partly carbonatic, thus relieving the clastic monotony of the sequence for the first time since the Middle Cambrian. In the Widyan Basin the extent of the exposures is much more limited, but numerous boreholes penetrated the Paleozoic sequence, including two of the few reported occurrences of Carboniferous strata in Saudi Arabia, which is supported by the presence of miospores and pollen (Clayton et al., 2000; Owens et al., 2000). The Lower Paleozoic sediments again crop out east and south of the Nafud Basin, in the Al Qasim province, where they form a longitudinal belt which curves around the eastern flank of the igneous basement in the west and is bounded on the east by Triassic or Jurassic strata. Along this outcrop belt the Lower Paleozoic sediments and the igneous basement are successively truncated southwards and onlapped by Permian beds (Khuff Formation), eventually wedging out completely near latitude 24°-20' N. Devonian rocks are exposed in the Ash Shu'aybah area as far as 27°-30'N, Silurian rocks extend until Buraydah at 26°-00'N, Ordovician rocks continue down to Al Uyun at 26°-30'N and the Cambrian sequence stretches out as far south as Ad Dawadimi at 24°-20'N. From there and southwards to Wadi Ad Dawasir at 20°-40'N only the igneous basement is exposed.

Continuing south Paleozoic rocks are quite abundant, occurring in the Jibal al-Wajid (as outcrops) and Rub al-Khali (subsurface) Basins, which are separated from the northern basins by the Central Arabian Arch (Powers et al., 1966). In these areas the Lower Paleozoic formations, which are equivalent to those exposed in central and northwestern Saudi Arabia, comprise most of the local sections. Carboniferous rocks (glacial-related) are limited in extent, whereas Permian sediments are only patchily preserved.

Paleozoic strata, both Lower and Upper, have also been encountered in numerous boreholes in the northern and eastern regions. In east-central Arabia significant oil and gas discoveries within the Paleozoic sediments have been made since the 1980s and the whole area is punctured by many exploration and production wells. The Paleozoic sequence is mostly siliciclastic consisting of alternating sandstones and shales, except for the Devonian and Permian systems, which include substantial carbonate sections.

The cumulative thickness of the Paleozoic sequence in the outcrops attains 2200 m, while more complete and much thicker sections, reaching up to 4000 m, have been encountered in the subsurface. Actually the Paleozoic in Saudi Arabia is even thicker, also encompassing part of the thick series of boulder conglomerate and sandstones interbedded with rhyolitic and andesitic volcanic rocks (which span the interval of 620-525 Ma) and littoral cherty and dolomitic limestone (Shammar and Jubaylah Groups). These pre-peneplain sequences fill rifts and grabens related to the Najd Fault System, and may by themselves reach as much as a 5000 m thickness. This prominent tectono-sedimentary element is widely exposed in the massif terrain of the central and northern parts of the Arabian Peninsula.

Bordering the Paleozoic of the Negev in the south and southwest are the Sinai occurrences. The Paleozoic sediments there are exposed over a belt, roughly 10 km wide, extending along the foot of the El Tih Escarpment across the peninsula, turning north of Dahab along the rift zone that forms the western shore of the Gulf of Elat and turning south along the rift zone that forms the eastern shore of the Gulf of Suez (Fig. 18B.1). They overlie the igneous basement which bulges up and becomes exposed southward, thus forming the fringing northern cuestas of the mountainous core of Sinai. They are overlain by younger Mesozoic sediments, which form the limestone plateaus of central and northern Sinai. The Paleozoic is exposed in four areas displaying different sections:

1) The area south of Elat (northeastern Sinai), between Wadi Taba and Wadi Quseib. Here the Paleozoic sequence is a southward extension of the units known from southern Israel, *i.e.* Early-Late Cambrian sandstone with an intercalated shale-carbonate unit overlain by Lower Cretaceous sandstone.

2) The triangle bordered by Wadi Quseib - Gebel Dhalal in the north and reaching Dahab in the south (east-central Sinai). The Paleozoic here is represented only by the Late Cambrian Netafim Formation, which is overlain by Lower Cretaceous sandstones. The thickness of this formation is up to 70 m.

3) The Um Bogma area (west-central Sinai), between Gebel Dhalal and Gebel Nukhul. Here Cambrian units correlative to those of southern Israel are overlain by Early Carboniferous, Permian - ?Triassic and by Lower Cretaceous sandstones.

4) The Abu Durba area, between Gebel Araba and the mouth of Wadi Feiran, east of the Gulf of Suez (southwestern Sinai). The Cambrian sequence includes only the Late Cambrian Formation overlain by Carboniferous units and these in turn, by Lower Cretaceous sandstones.

A different Paleozoic section has been encountered in the subsurface of Sinai, where only a Permian sequence was penetrated in five boreholes in the north-central part of the peninsula. It resembles the Permian sequence of the Negev in its lithofacies and stratigraphic relationships, overlying a Late Precambrian- Early

Cambrian dolerite (Zenifim Formation) or the igneous basement (Ayun Musa-2), and disconformably overlain by Early Triassic shales and carbonates (Weissbrod, 1980).

The Cambrian section in Sinai consists mostly of subarkoses and quartz-arenites resembling the Cambrian sequence of the southern Negev, and the same rock units have been distinguished. Even the shaly-carbonatic unit is largely present, though in reduced thickness and eventually wedging out southwards. Differently, Carboniferous siliciclastics are quite abundant in west-central and southwestern Sinai and in the juxtaposed Eastern Desert with a thick carbonate intercalation in the former area, whereas the overlying Permian in the same areas displays continental redbed lithofacies.

To the northeast of Israel are the Paleozoic sediments of Syria, which are known only in the subsurface, except for small, isolated structurally-slumped blocks of Carboniferous limestone within Cretaceous marls that are exposed at Jebel Abd el-Aziz in the northeastern part of the country. The subsurface Paleozoic section, which is up to 5000 m thick, consists of alternating sandstones and shales, with some massive Cambrian and Carboniferous carbonates. It was penetrated in more than 30 deep and rather widely spaced boreholes in central, north, and northeast Syria. None of the Syrian boreholes that penetrated the Paleozoic section reached the igneous basement. All Paleozoic systems are present in Syria with an extraordinary thick Carboniferous section. Positive proof for the Devonian strata (latest Famennian palynomorph taxa) in several boreholes in the northeastern part of the country was provided by Ravn et al. (1994), although the relationship of these Devonian to the underlying Silurian and overlying Carboniferous strata is still problematic.

The Lower Paleozoic formations are unconformably overlain, as the case may be, by Lower Carboniferous to Lower Permian formations with sub-Carboniferous truncation cutting progressively and stratigraphically deeper from the northeast, where an almost complete section is preserved (Devonian may be present in its uppermost part), to southwest where only Cambrian strata exist. In the central and southern parts of the country both Ordovician and Cambrian strata are widely distributed.

The Syrian Paleozoic sections display greater affinity with sections in northern Iraq and southeastern Turkey (Ala and Moss, 1979; Dean and Monod, 1990) rather than with contemporary rock units in countries to the south. Unlike neighboring countries, where the Upper Permian section is mostly carbonatic, in Syria it consists of fine clastics. Generally the Permian sequence is overlain by Triassic strata, but in the southeastern part (Rutbah High) it is unconformably overlain by Lower Cretaceous strata.

Seismic-refraction data across the country (Seber et al., 1993; Brew et al., 1997) delineated the deepest sedimentary layer which is bounded by the velocity interface of the igneous basement below and a prominent interface ('D reflector') representing the region-wide Middle Cambrian limestone (Burj Formation) above. This deep layer probably consists of the late Early Cambrian Zabuk Formation, and the underlying Late Precambrian-Early Cambrian arkose and/or associated volcanics. This layer is more than 2.5 km thick in the south (Rutbah High), similar to the thickness of this sequence that was penetrated in the Northern Highlands-1 borehole in northwest Jordan (Weissbrod and Sneh, 2002), and about 1 km in the north (Aleppo Plateau). The rock sequences that comprise this layer are exposed across the Turkish border in three regions along the Bitlis Suture. The pre-peneplain sequence consists of arkose, graywacke, and shales interbedded with volcanic rocks exceeding 2500 m, and the overlying post-peneplain Cambrian sequence comprises two clastic formations and a carbonate intercalation (Ketin, 1966; Dean et al., 1997).

The distribution of the Paleozoic sequences in the Arabian Platform demonstrates the great variety of different stratigraphic relationships across the area where sequences change from one location to another in an apparently chaotic and illogical pattern. Only in the last two decades has a geodynamic model for the evolution of the entire region been established (Gvirtzman and Weissbrod, 1984; Weissbrod and Gvirtzman, 1988). Earlier investigators were not aware of the overwhelming influence of structural control upon the regional preservation patterns of the Paleozoic, which has often led to erroneous concepts and discrepancies wherein investigators tend to invoke local block movements and non-deposition, and attempt to reconstruct paleogeographies that did not exist. Such misconceptions still persist.

STRUCTURAL PATTERN

Stratigraphic compilation of outcrop and subsurface sections throughout the Arabian Platform has made possible the correlation of the Israeli Paleozoic sequence with neighboring countries at the time-rock system level, and enabled modeling of the structural development and sedimentary evolution in the Gondwanan margin region (Gvirtzman and Weissbrod, 1984; Weissbrod and Gvirtzman, 1988). Accordingly, the Arabian and adjacent plates were structurally affected by a regional epeirogenesis during the Late Paleozoic that produced great symmetric swells or geanticlines with an area of culmination some 500 km in diameter, that were truncated as they rose, accumulating into a major stratigraphic gap. The erosion surface was subsequently covered by Carboniferous sediments, which were truncated by a later uplift-and-erosion, and eventually covered by Permian and Triassic sediments (**Fig. 18B.4**, cross section A-B). The evolution of this structure was accompanied by increasing heat flow (Weissbrod and Gvirtzman, 1988; Kohn *et al.*, 1992), possibly associated with a transient hot spot (Garfunkel and Derin, 1984).

The major phase of updoming started in the Late Devonian (Famennian), and by the Early Carboniferous (Late Tournaisian) it was already truncated. This age interval is indicated by paleontological evidence from the youngest sediments underlying the unconformity and the oldest sediments overlying it. The age is further supported by ages of fission-tracks in zircon grains obtained from Precambrian clastic host rocks in southern Israel (Kohn et al., 1992; Feinstein, 1985) which range from 328 to 373 Ma (Late Devonian to Early Carboniferous). Likewise, K/Ar and Rb/Sr reset ages of illite from the Cambrian Timna Formation fall on 374±4 and 373±2 Ma isochrons (Segev, 1986), which indicates a thermal

event that predated Late Devonian times.

The shape and boundaries of a Late Paleozoic swell that today underlies the countries of the Levant and Egypt, the so-called Helez Geanticline (Gvirtzman and Weissbrod, 1984) becomes apparent from a generalized subcrop map on the erosion surface at the base of the Lower Carboniferous strata. Only the eastern half of this structure can be reconstucted. The western part apparently drifted away following rifting and the formation of the passive continental margin of the Levantine Basin in Early Mesozoic times (Şengör, 1979; Gvirtzman and Weissbrod, 1984; Garfunkel, 1998). The pre-Carboniferous eroded surface of the Helez Geanticline is mostly superseded by Lower Permian erosion, with relicts mostly in Syria, northwest Saudi Arabia (Widyan Basin) and the Gulf of Suez area. Today it is mostly a virtual surface, as reconstructed for the areas of Israel, Jordan, and northern Sinai.

Depth of erosion increases toward the center of the structure, and has removed all Devonian, Silurian, and Ordovician sediments from the regions of Israel, Sinai and the Eastern Desert of Egypt and parts of Jordan. Overall, a sedimentary section of more than 2500 m was removed from these areas. Lower Paleozoic sequences reappear in roughly concentric belts toward the flanks, where they subcrop in successive horizontal belts, 100-150 km wide (Fig. 18B.4).

The Helez Geanticline borders on the southeast with the Riyadh Geanticline (**Fig. 18B.5**), another truncated Paleozoic structure that occupies large parts of the Arabian Peninsula (Gvirtzman et al., 1988; Weissbrod and Gvirtzman, 1988). The link between the two structures is found in northern Saudi Arabia, where the northwestern flank of the Riyadh structure mirrors the southeastern flank of the Helez structure, with the intervening Widyan and Tabuk Basins and with their thick, almost continuous Lower Paleozoic sequence. In this structure too, only the eastern half can be reconstructed due to widespread erosion in the west.

These swells are two of a whole series of similar contemporaneous structures that separated the northern Gondwanan shelf into swells and basins (Weissbrod et al., 1989). Some of the structures in North Africa (Sirte Basin in Libya and Hassi Messaoud in Algeria) resemble those of the Near East both in shape and in dimensions and can be similarly interpreted (Weissbrod et al., 1989). It appears that the initiation of the movements was simultaneous, and not scattered in time from place to place as suggested by some authors (*e.g.*, Al-Laboun, 1990).

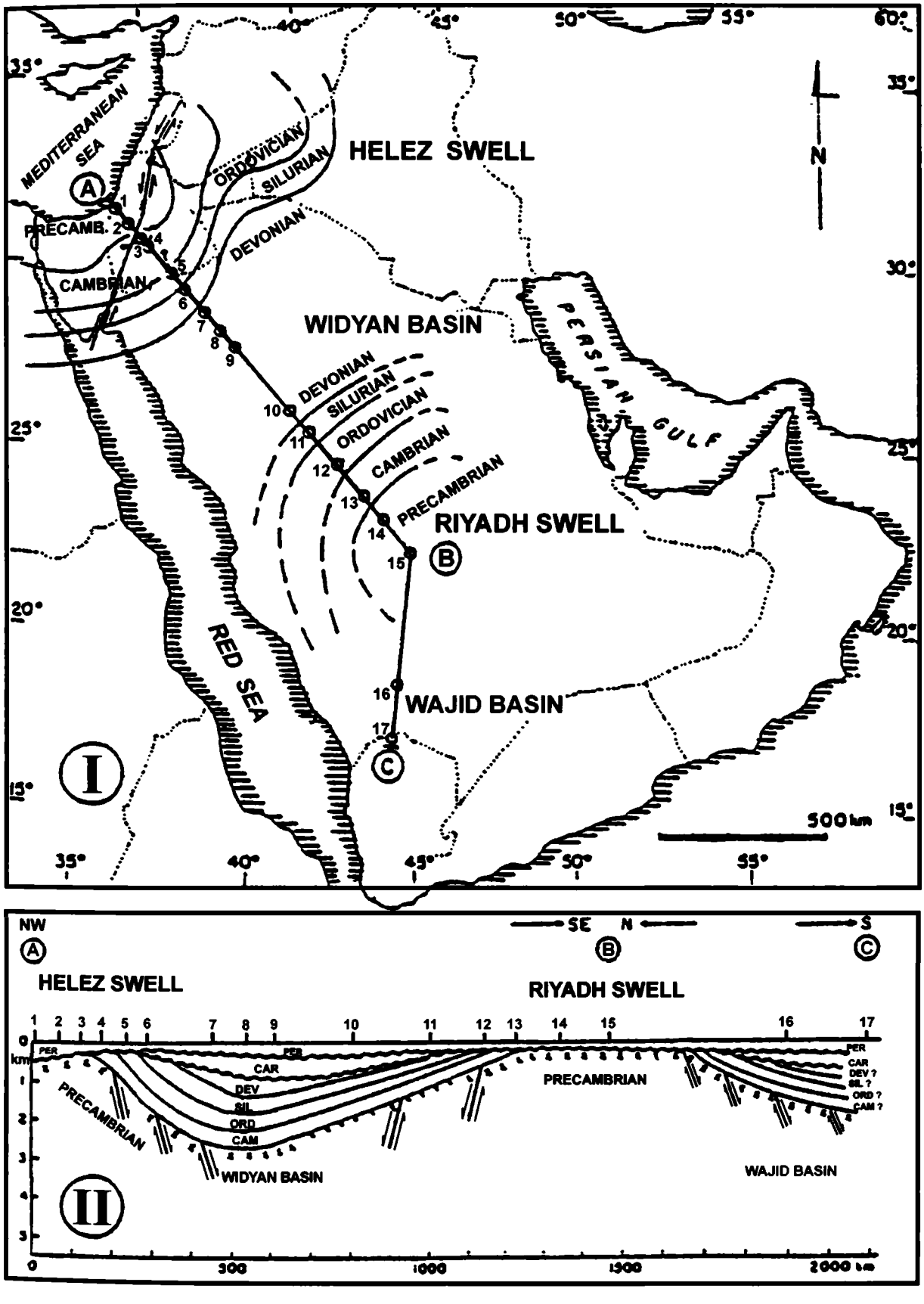
The Riyadh Geanticline has dimensions and characteristics similar to those described for the Helez structure. It shows concentric outcrop belts organized in accordance with their stratigraphical order, testifying to a stratigraphic gap which decreases gradually from the inner to the outer belt, from the center of the structure where Permian strata directly overlie the Precambrian igneous basement to its margins where the Paleozoic sequence is thick and almost complete (Fig. 18B.5).

Various opinions have been expressed regarding the formation of the Late Paleozoic swells, and the ideas differ regarding the chronology, spatial dimensions, and tectonic mechanisms. The progressive segmentation of the northern Gondwanan shelf into intracratonic swells and basins was assumed to be a consequence of the Late Devonian to Late Carboniferous collision of the northern margin of Gondwana with Laurasia along Turkey and Iran (Klitzsch, 1986; Husseini, 1992; Boote et al., 1998). Similarly, McGillivray (1995) argued that the uplift was initiated due to compression of the Arabian Plate, which resulted from subduction of Paleo-Tethyan oceanic crust beneath Gondwana and its associated magmatic arc as evidenced by Late-Middle Devonian-Late Permian ages for magmatic and metamorphic rocks in Iran (Berberian and King, 1981). Differently, Cohen et al. (1990) raised the idea that these structures are superimposed on inherited basement fabrics and attributed them to the motions of several basement highs, particularly active during the Late Paleozoic and Early Mesozoic. Weissbrod et al. (1989) raised the possibility that geophysical models and mechanisms suggested for continental rifting, which involve crustal extension and thinning, uprising of asthenospheric material and increased heat flow (Neugebauer, 1983; Turcotte and Emerman, 1983), could in part be applied to explain the formation of large swells and basins in the Arabian-African craton.

The Paleozoic epeirogenic events have been given 'orogenic' names such as 'Caledonian' or 'Hercynian' (Klitzsch, 1970; Gvirtzmann and Weissbrod, 1984) because their contemporaneity with mountain building events in convergence areas might imply some genetic relationship with these major tectonic events. They have also been referred to as Acadian or Ardennian, Bretonian, and the Sudetic compressional events (Sander, 1968; Guiraud et al., 2001).

The so-called 'Hercynian' epeirogeny, which formed the Helez and Riyadh Geanticlines and gave rise to a variety of stratigraphic situations in the Arabian Platform, is the best known. Evidence for a possible earlier ('Caledonian') deformation phase in the Near East is more difficult to trace and demarcate because the Silurian and earlier uplifts and their patterns and distributions were largely overprinted by subsequent events and have been obliterated due to later erosional phases. Nevertheless, there are frequent gaps within the Silurian sequence and hardly any remnants of Late Silurian sediments, which may point to regional uplifting and erosion at that time. The upper Silurian is missing from Arabia

Figure 18B.5. I. Schematic outline of the Helez and Riyadh Geanticlines on the reconstructed sub-Permian erosion surface (after Gvirtzman et al., 1988).
II. Schematic stratigraphic section across the Helez and Riyadh Geanticlines (some of the data points are projected).
Data points: 1=Pleshet-1; 2=Zohar Deep-8; 3=Hameishar-1; 4=Safra-1; 5=Jabal Arqa; 6=Mudawwara; 7=Al Huj; 8=Badanah (Ar'ar); 9=As-Sulaimaniyah (NW-44); 10=Turrabah; 11=Qusayba; 12=Ash Shamasiyah; 13=Shaqra-1; 14=Quway'iyah; 15=Umm Athul; 16=Jabal Al-Kaukab; 17=Sa'dah.


MEDITERRANEAN SEA
HELEZ SWELL
ORDOVICIAN
SILURIAN
DEVONIAN
CAMBRIAN
PRECAMB.
WIDYAN BASIN
PERSIAN GULF
RIYADH SWELL
PRECAMBRIAN
WAJID BASIN
RED SEA
500 km
I
NW
SE
N
S
HELEZ SWELL
RIYADH SWELL
PRECAMBRIAN
WIDYAN BASIN
WAJID BASIN
PER
CAR
DEV
SIL
ORD
CAM
II

and the Lower Devonian Tawil Formation rests on Early Silurian, Llandovery sediments. This regional hiatus represents a period of Paleozoic uplift-and-erosion event in Arabia, probably related to the 'Caledonian' movement (Al-Laboun, 1986).

When first presented in 1984, the Helez Geanticline was configured on the basis of 18 data points (Fig. 18B.4, I). Since then numerous new borehole and outcrop sections have been published, adding many more data points. When an additional 50 data points are plotted on the Lower Carboniferous subcrop map (Fig. 18B.4) it becomes apparent that the new data match the original boundaries of the subcrop belts, leaving them practically unchanged. This attests to the validity and precision of this geanticline model. The concentric belt pattern imposes certain probabilities and excludes others, and provides a means of checking on loosely established stratigraphies, especially where paleontological data are poor or lacking.

Evidently the model gives a logical explanation to the apparently chaotic distribution of the Lower Paleozoic sequences and can also be used as a tool for stratigraphic discrimination. Moreover, once the regional pattern of updoming and erosion is recognized, the Lower Paleozoic stratigraphy at a given structural locality becomes roughly predictable.

Overall, it can be concluded that the distribution of the Lower Paleozoic sequences in the region is a function of their position in relation to the 'Caledonian' or 'Hercynian' structures, which affected and controlled their preservation rather than their deposition.

Apart from the regional epeirogenetic uplift, local block movements, with different vertical magnitudes and rates of truncation that appear to be active along rejuvenated Precambrian faults, marginally influenced the preservation pattern. These motions are known in several areas and are mostly associated with the Late Carboniferous-Early Permian uplift-and-erosion event. The Summan Platform and probably the Quway'iyah-Riyadh area in central Saudi Arabia are such blocks where most of the Paleozoic sequence is missing and the Late Permian Khuff Formation directly overlies Infracambrian/Precambrian redbed metasediments or the igneous basement (McGillivray, 1995). Likewise, block faulting and erosion in the Abu Jifan and Farhah fields, in central Arabia have resulted in a variety of stratigraphic relationships whereby the Khuff Formation overlies different Permian, Silurian, or Ordovician strata (King, 1994). Permian tectonic movements are also known from Israel, where several rifting phases related to the formation of the Eastern Mediterranean Basin and its margins (Garfunkel, 1998) are expressed by normal faulting and igneous activity that have placed Permian (Gevim-1) and also later Triassic sediments (Helez 1a borehole) against the metamorphic basement, whereas the Late Precambrian-Early Cambrian arkose sequence (Zenifim Formation) known from nearby boreholes is missing. Earlier block movements took place in the Late Cambrian (Sardinian) in Sinai and the Eastern Desert of Egypt. In the uplifted areas erosion cut down to the igneous basement, removing the Early and Middle Cambrian sediments while in the stucturally low areas the depth of the truncation was minor, leaving much of the Cambrian section intact (Weissbrod, 2003).

Originally, the geanticlinal model was described as a two-phased structure. Accordingly, the Arabian Platform was planed-off during the Late Devonian-Early Carboniferous uplift-and-erosion event and a little later (late Tournaisian) was followed by subsidence and renewal of deposition, covering the sub-Carboniferous eroded surface with several hundred to more than 1500 m of siliciclastic and carbonatic sediments. It is assumed that Carboniferous sediments were deposited over most of the platform, though they are actually present only in several areas on the northwestern (Syria and Iraq), southwestern (Sinai and the Eastern Desert of Egypt) and southeastern (northwestern Saudi Arabia) flanks of the Helez Geanticline. Elsewhere on the Helez Geanticline and over the entire Riyadh Geanticline the sub-Carboniferous surface is superseded by a later sub-Permian erosion surface, formed at the end of the Carboniferous or the earliest Permian by a second phase of uplift, apparently at the same locus, but of a smaller magnitude. Much of the just-deposited Carboniferous sediments were removed, especially on the culmination of the geanticlines, as were parts of the remaining underlying Lower Paleozoic deposits, whose belts of exposure might have been narrowed and driven farther downflank. Today the sub-Carboniferous surface is mostly a virtual surface, as reconstructed for the areas of Israel, Jordan, northern Sinai and central Saudi Arabia (Fig. 18B.4, cross section).

Further lowering of the platform at the outset of the Permian was followed by deposition of sandstones and interbedded shales along fluvial to marginal tracts, covering the sub-Carboniferous surface, locally filling relief (mainly formed due to block faulting). In the Late Permian the sea level rose and transgressed over the entire region, depositing a mixed carbonate-shale sequence. The Permian sequence is presently known in the subsurface of Israel (excluding the southern Negev), northern Sinai, northwest and west-central Jordan, and southwest and northeast Syria, and both in outcrops and the subsurface in central and eastern Saudi Arabia. Elsewhere in these countries the sub-Permian erosion surface and the whole Permian sequence were obliterated by later Triassic or more often Early Cretaceous erosion.

Evaluating the distribution of the Carboniferous occurrence in the region, it becomes evident that unlike the Lower Paleozoic sequences, which were apparently uniformly distributed over the entire platform with only gradual changes along the depositional setting, the Carboniferous rocks were deposited in several depocenters ('lows'), each of them displaying prominent changes of facies and thickness. Following the Late Carboniferous to Early Permian phase of uplift-and-erosion, these sediments are totally absent on the culmination of the geanticlinal structures, but are preserved on the flanks (Syria, southwestern Sinai and the Eastern Desert of Egypt) and in the intervening basinal areas (western Iraq; Western Desert of Egypt; Widyan Basin in northwestern Saudi Arabia; Jibal al-Wajid and Rub al-Khali Basins in southwestern Saudi Arabia). Nevertheless, the non-continuous preservation on the flanks is not clearly understood and does not conform to a truncated symmetric dome with continuous concentric erosion belts, which the geanticlinal model requires.

It can therefore be argued that the geanticlinal model can satisfactorily resolve the current distribution of the Lower Paleozoic sequences in the region, but the pattern of Carboniferous distribution and/or preservation is still unknown.

STRATIGRAPHY AND SEDIMENTOLOGY

The Cambrian and Permian sequences that occur in Israel are reviewed, presenting aspects of stratigraphy and sedimentology. Counterparts in neighboring countries are only referred to in brief, applying the current lithostratigraphy.

1. THE NEOPROTEROZOIC-PHANEROZOIC TRANSITION

Following the Pan-African orogenic event the lithospheric dynamics of the Arabo-Nubian Shield changed from compression to extensional with associated intrusion of alkali-rich granitoids, massive emplacement of dykes and volcanism. Concurrently, the uplifted orogenic edifice was denuded over a period of almost 100 million years (620-525 Ma), crossing the Neoproterozoic-Phanerozoic boundary. The mountainous relief was rapidly eroded and the coarse debris (conglomeratic facies) was deposited in intramontane basins and in graben systems (such as the Najd Fault System), and in the piedmont zone at the front of the mountain ranges, while the finer and better sorted clastics (arkosic facies) were transported farther to peripheral basins at the passive margin (the Arabian-Mesopotamian and Oman-Rub al-Khali Basins). Altogether, voluminous amounts of the metamorphic-plutonic rocks were removed, estimated at 8-12 km in Israel and Sinai, and even twice this in Saudi Arabia (where reworked older continental crust underlies the younger juvenile crust), as attested to by the kind of metamorphism grade (green schist to granulite facies) of the present-day exposed igneous basement (Garfunkel, 1999). The detrital sediments accumulated mostly during the Late Precambrian, and their thickness locally exceeds several thousand meters due to repeated subsidence along fault-scarps and tectonic depressions, while the thick interlayered volcanics, pyroclastics and volcaniclastics rocks locally multiplied the amount of fill.

The conglomeratic facies, which is mainly exposed in rift-related depressions in northern Arabia and the Eastern Desert of Egypt, is up to 5000 m thick, while in Israel and Jordan only remnants of this facies have been preserved. On the other hand the arkosic facies is known only from the subsurface in Israel and Jordan where a section of more than 2000 m has been penetrated. The conglomeratic exposures along the Dead Sea and Wadi Araba presumably represent two dated phases of deposition. The proper, or type Saramuj Conglomerate in the southeast Dead Sea area is intruded by the Qunai Monzodiorite, which yielded radiometric mineral ages of 596-585 Ma. This indicates an earlier Neoproterozoic age for this conglomerate, whereas alkaline volcanics (mostly rhyolitic quartz-porphyry) in the Elat and central Wadi Araba areas, which are associated or interlayered with the Elat Conglomerate, yielded radiometric whole-rock dates (Rb/Sr and K/Ar procedures) ranging between 560 to 525 Ma, attesting to an Early Cambrian age for the upper part of the Elat Conglomerate. These conglomeratic phases are correlative to the Shammar and Jubaylah Groups of Saudi Arabia and the upper part of the Hammamat Group of the Eastern Desert in Egypt. Similar Early Cambrian radiometric ages (~532 Ma) were also obtained from volcanic rocks which are interbedded within the upper part of the arkosic facies.

Most of the detritus that comprises the above-described clastic section was removed at the end of or during the batholithic stage, so that by the late stages of the Neoproterozoic the relief was much lowered and the surface was more levelled. At this stage, probably in consequence to the melting of glaciers, global sea level recovered from its major Infracambrian low-stand, and from the east and southeast a shallow sea invaded parts of the platformal areas and rift-related depressions in the Persian Gulf, Oman, and in southeastern Saudi Arabia (Oman-Rub al-Khali Basin), depositing evaporites and carbonates (Huqf Group; Hormuz Series). This transgression proceeded through seaways to the Najd Fault System depressions in the central and northern parts of the shield in Saudi Arabia, where stromatolitic cherty limestone was deposited (Jubaylah Group). Concurrently, the sea transgressed the northern margins of the shield (Arabian-Mesopotamian Basin) and marginal marine tidal flats covered the former belt of alluvial plains, mostly depositing fine-grained arkose and graywacke, mudstone and shales. The two marine domains were separated by an E-W-trending, possibly tectonically-controlled, continental threshold, that extended over northern Egypt, Sinai, the southern Negev, and the southern desert of Jordan. Its continuation eastwards across the Tabuk-Tayma and Wydian Basins in Saudi Arabia towards the Persian Gulf is constrained by seismic data on its thick Infracambrian sedimentary section (up to 5000 m) in northern Saudi Arabia (Al-Hajri and Owens, 2000).

The Late Precambrian-Early Cambrian clastic sediments consist of first-cycle, immature, polymictic and poorly sorted conglomerates and arkose that were mostly derived from the Pan-African metamorphic and plutonic terrain in the Arabo-Nubiab Shield. These partly Cambrian sediments display two distinct facies, which supposedly merge with each other. In Israel they were designated as the following formations:

Elat Conglomerate

Relicts of the Elat Conglomerate are mostly confined to a narrow zone along the margins of Wadi Araba. They are preserved in grabens and are locally exposed within the limits of a presumed Late Precambrian-Early Cambrian rift that grossly coincides with the late Tertiary Dead Sea Rift (Weissbrod and Sneh, 2002). Deposition was accompanied by alkaline igneous activity, and the conglomerates are associated with flows and pyroclastics of rhyolitic quartz-porphyry and andesitic basalt composition, and large masses of ignimbrites (Katharina Group/Ahaymir Volcanic Suite). Radiometric analyses of these volcanics and coeval granitic intrusions from both sides of the Dead Sea Rift yielded ages that range between 553 to 523 Ma, spanning the Neoroterozoic/ Phanerozoic transition. In southern Israel the conglomeratic facies is exposed at several localities in the igneous basement of the Elat

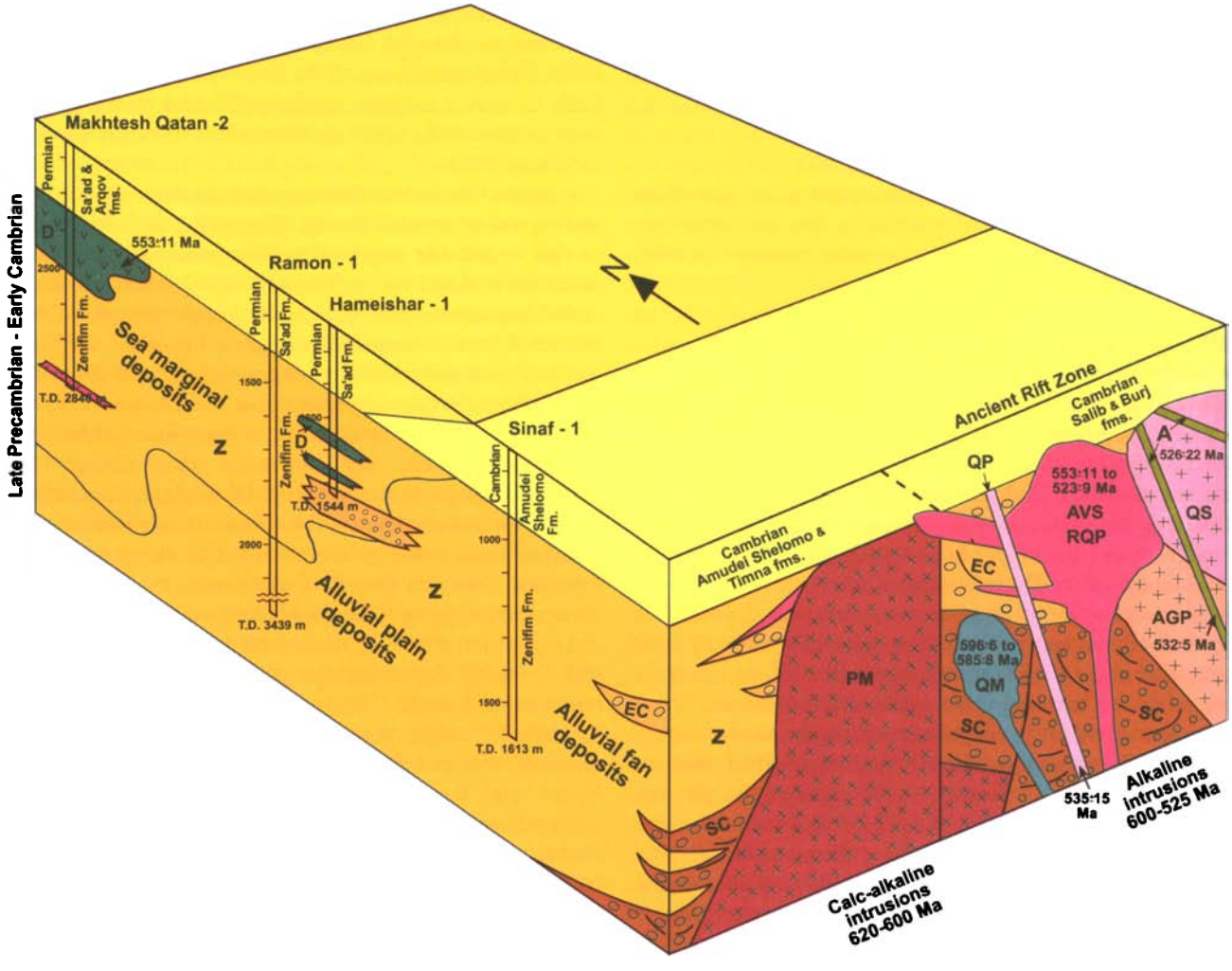


Figure 18B.6. Block diagram across the Late Precambrian-Early Cambrian sediments of the Negev displaying depositional setting and presumed relationships between the conglomeratic facies (Saramuj and Elat conglomerates) and the arkosic facies (Zenifim Formation) and magmatic rock units. Measured radiometric dates of igneous bodies are indicated. SC = Saramuj Conglomerate; EC = Elat Conglomerate; Z = Zenifim Formation (mostly arkose); PM = Plutonic and metamorphics; QM = Qunai Monzodiorite; AGP = Amram Granite Porphyry; AVS = Ahaymir Volcanic Suite; RQP = Rhyolitic Quartz-Porphyry; QS = Amram Quartz-Syenite; D = Dolerite; QP = Quartz-Porphyry (dike); A = Andesite (dike). North – south face of block diagram is approximately to scale; east – west face is schematic and not to scale (from Weissbrod and Sneh, 2002).

area. The largest exposures and thickest (~400 m) conglomeratic series occur in Har Shelomo and Har Asa. They consist of strongly cemented, red-brown to dark brown and gray, massive or thickly bedded, mostly clast-supported polymictic conglomerate. The pebbles are angular to rounded, generally 1-5 cm in size with boulders and blocks up to 1.5 m, which derived from plutonic and metamorphic country rocks, various dike material and rhyolitic quartz-porphyry volcanics. Locally the conglomerate is monomictic, consisting entirely of rhyolitic quartz-porphyry or ignimbrite. The matrix is usually arkose, or more rarely volcanic glass. Numerous quartz-porphyry and andesite dikes intruded the conglomerate. Other exposures are found in Nahal Mapalim at the northern slopes of Har Shelomo, where a 320 m thick sequence consists of eight volcanic units of vesicular or massive basalt and andesite lava flows and of agglomerate, tuff breccia and lapilli-tuff, and at Nahal Roded where the pebbly units are interbedded with indurated, mostly laminated tuff and ash sequences with some boulder layers of rhyolitic quartz-porphyry. Further north a 62^{+} m thick conglomerate section interbedded with fine- to coarse-grained arkose layers, up to several meters thick was penetrated at the bottom of the Hameishar-1 borehole. It is clast-supported with rounded to subrounded flat pebbles, dominated by quartz-porphyry, granite, and diorite. Though variously termed, these conglomerate occurrences represent a single stage and correspond in time to the conglomerates, which are exposed in Jordan on the eastern margins of the central Wadi Araba, at Wadi Dana, Wadi Zubda, Wadi Abu Khusheiba, and Wadi Abu Barqa. The latter is the largest of these exposures and displays a 40 m thick clast-supported conglomerate

with angular granitic and metamorphic pebbles. It is overlain by thinly bedded, fine- to coarse-grained acidic ash tuffs and lapilli tuff with dispersed metamorphic, plutonic and volcanic (rhyolite) clasts, interbedded with siltstone or shale and overlain by alkali-rhyolitic lava flows, together attaining a thickness of 200-250 m (Haiyala volcaniclastic Formation). The conglomerate at Wadi Abu Barqa has been previously correlated with the Saramuj Conglomerate exposed at the southeast corner of the Dead Sea and been similarly termed. However, the Saramuj Conglomerate at the type locality was deposited at an earlier stage, still in the Neoproterozoic (pre-585 Ma), whereas the Abu Barqa conglomerate and the overlying acidic tuffs and flows, like the Elat Conglomerate, are partly of Early Cambrian age (Weissbrod and Sneh, 2002). Conglomeratic sequences have been reported from the subsurface in Jordan (Safra-1, Ajlun-1 and Northern Highlands-1), but their true nature is ambiguous. Thicker, rift-related conglomeratic sequences are exposed in central and northern Saudi Arabia and in the Eastern Desert of Egypt. The upper part of the Shammar and the Jubaylah Groups of Saudi Arabia and the upper part of the Hammamat Group in Egypt temporally correspond to the Elat Conglomerate.

The conglomeratic facies, with clasts washed from an uplifted hinterland exposing mainly granitoid and gneissic rock types, was deposited in intramontane valleys, syntectonic depressions, and the piedmont zone, forming thick fault-scarp deposits and a braided alluvial fan system grading down the fan into an arkosic facies that was further transported to a marginal basin (Zenifim Formation). Much of the conglomeratic facies was removed from the Pan-African igneous terrain up to the Early Cambrian and during later stages of the basement exposure in the Late Paleozoic and Neogene times. Only a small portion of the syntectonic sediments and those that were downfaulted and sheltered are still preserved.

Zenifim Formation

The Zenifim Formation was deposited in a broad marginal basin, extending from the Arabo-Nubian Shield across Arabia, the Levant, and Mesopotamia to the edge of the Arabian Plate along the Bitlis and Zagros Sutures (the Arabian-Mesopotamian Basin –Weissbrod and Sneh, 2002). It consists of red to dark brown, massive, horizontally, or more often cross-stratified, fine- to coarse-grained and poorly sorted arkose with thin interlayers of siltstone and mudstone, and locally, stringers of pebbles and conglomerate lenses. The arkose is matrix-rich and well-cemented and contains up to 50% feldspar grains and a high proportion of lithic fragments. The arkosic sequence is associated with extrusive igneous rocks (dolerite, rhyo-dacite and andesite) varying in thickness from a few meters to more than 120 m. Radiometric ages (532±26 and 532±23 Ma; K/Ar procedure) obtained from dolerite bodies interlayered within the upper arkosic sequence have demonstrated that this part is already of Early Cambrian age. The Zenifim Formation has been penetrated in nine boreholes in the Negev (Sinaf-1, Ramon-1, Hameishar-1, Shezaf-1, Agur Deep-1a, Kurnub-1, Makhtesh Qatan-2, Zohar Deep-8, Emunah-1) and in three boreholes in the southern Coastal Plain of Israel (Bessor-1, Gevim-1, Pleshet-1) (Fig. 18B.3). It was also penetrated in three boreholes in southeast Jordan (El Jafr-1, Wadi Sirhan-3 and 10), one in central Jordan (Geothermal well, Ma'in-3D), four boreholes in northwest Jordan (Safra-1, Suweileh-1, Ajlun-1, Northern-Highlands-1), and in one borehole in north-central Sinai (Abu Hamth-1) (Fig. 18B.3). Formerly the arkosic facies in Jordan was designated the 'Unassigned Clastic Unit' and 'Unassigned Volcanic Unit' or as parts of the Salib and Ajram (Cambrian) or Amud (Ordovician) Formations. Al-Hajri and Owens (2000) reported that further south, in northern Saudi Arabia a thick sedimentary rock sequence (up to 5000 m) between the igneous basement and the known Cambrian units has been seismically documented. The most reasonable candidate for this sequence is the arkosic facies, though it is possible that it is made up partly or entirely of the conglomeratic facies. It is also postulated that most of the 1000-2,500 m thick interval between the velocity interfaces of the igneous basement and the Middle Cambrian Burj limestone ('D' reflector) that can be correlated across Syria probably represents the arkosic facies. Further northwards, in southeastern Turkey, arkose, graywacke, quartzite, and shale rock sequences that are interbedded with andesite and basalt flows, tuffs, and agglomerates (overall more than 2000 m thick) were described from three limited exposures along the Bitlis Suture (Ketin, 1966; Dean et al., 1997). These sequences form a lateral equivalent of the Zenifim arkose and are the only exposed sections of this facies.

The Zenifim Formation overlies the igneous basement. Its lower contact has not been reached in any of the Israeli boreholes, but three boreholes in Jordan (Ajlun-1, Safra-1, and El Jafr-1) in which an equivalent sequence was encountered, were reported to have reached the granitic basement. The thickest section of the arkosic facies (2500^{+} m, including magmatic intercalations) was penetrated in the Northern Highlands-1 borehole in northwestern Jordan, and 2014^{+} m of solely arkose was encountered in the Ramon-1 borehole (central Negev).

The arkosic rock sequence displays several lithofacies that overall indicate a transgressive succession of alluvial fans and alluvial plains dominated by sand flats of braided streams prevailing in the southern and central Negev, merging northwards to more distal tracts of marginal marine tidal flats and shallow marine environments (**Fig. 18B.6**). In the southern boreholes (Sinaf-1, Hameishar-1, and Ramon-1) the lithofacies is dominated by medium- to coarse-grained and poorly sorted arkose with rare pebbles and conglomerate layers, and in Hameishar-1 a thick conglomerate (presumably Conglomerate Elat) underlies the arkose sequence. These coarse clastics are regarded as alluvial outwash forming thick piedmont fans along the base of the mountain fronts. These merge to tabular sand bodies with massive or large scale cross-bedded layers of coarse-grained arkose with occasional patches of gravelly material in their lower part and small scale cross strata and ripple cross-lamination or rare thin lens-shaped shale interbeds at the top strata. These deposits form most of the Zenifim section in Ramon-1 and represent a network of bedload streams with no clearly defined overbank typical of braided alluvial plain. The upper part of the arkose sequence in the Ramon-1 borehole and the entire formation in Makhtesh Qatan-2 display different lithofacies, indicating a mostly intertidal environment.

The most prevalent lithofacies types are massive, horizontally-bedded or planar and trough cross-bedded arkose alternating with interlayered thick sand/silt and thin silt/clay horizons or massive clays, occasionally with burrowing structures, which represent alternating high- and low-energy conditions indicative of sand flat, mixed flat, and mudflat subenvironments.

The Zenifim Formation is everywhere truncated. In the southern Negev (Sinaf-1) and the southern Jordanian Desert (Jafr-1, Wadi Sirhan-3 and 10) it is overlain by late Early Cambrian strata and similar stratigraphic relations are assumed for central and northeast Jordan and most of Syria. From central Sinai and the central Negev in Israel and northwards, and in northwestern Jordan, it is unconformably overlain by Lower Permian sediments.

2. CAMBRIAN

The Cambrian System marks a major transition in the tectonic and sedimentary evolution of the Arabian and North African Plates, changing from an orogenic belt to a stable shelf, with a prominent shift in the composition and texture of the sediments and their mode of deposition, from local and short-distance, immature molasse-type deposits to far-transported mature and platformal clastics, and intermittent carbonates, evolving from arkose through subarkose to quartz-arenites, and becoming finer-grained and better sorted upwards. During this period the continent was positioned in temperate latitudes, closer to the Equator, with more intensive processes of weathering and alteration, and the shaping of the peripheral basins was established. Concurrently the global sea level recovered from a major Infracambrian low-stand, setting-up the pattern of the forthcoming Paleozoic transgressions.

A moderate drop in sea level during the Early Cambrian led to a short episode of regression, when the sea retreated from the entire Arabian and North African shelf. At this stage most of the extensional movements and volcanic activity abated, while denudation proceeded, filling-up the depressions and levelling the surface and eventually a vast peneplain was achieved. Most of the intramontane sediments in the metamorphic-plutonic terrain were already removed so that only part of the down-faulted sediments and associated magmatic rocks (conglomeratic facies) and the peripheral sediments (arkosic facies) were preserved. Nevertheless, some weak crustal movements accompanied by alkaline volcanism and shallow intrusions were still active along some of the filled rifts, which led to a local renewal of relief and the formation of volcanic/pyroclastic hills over the surrounding peneplain. Such features are seen along the present-day Dead Sea Rift, the location and boundaries of which grossly coincide with the former Late Precambrian-Early Cambrian longitudinal rift (Weissbrod and Sneh, 2002).

By the late Early Cambrian the sedimentary processes were accelerated, probably in response to tectonic uplifting in the interior Gondwanan continent and tilting of the platform margin. Consequently sandstone sheets, which were derived from new provenances and deposited in a system of alluvial fans grading to braided plains and deltas, began to accumulate and uniformly covered the peneplain surface.

At the beginning of the Middle Cambrian sea level started to rise consistently and transgressed over the continental shelf, depositing carbonate and mixed carbonate and siliciclastic facies over the basal blanket. Much of the Arabian Platform was covered by a shallow epicontinental sea, displaying changes in facies belts in response to eustatic developments. Subtidal carbonates dominated basinwards, while craton-wise they graded into mostly clastic facies consisting of sandstones interbedded with mudstones and low-energy carbonates in a marginal tidal flats setting. Though carbonates can be traced along the depositional strike as far south as southern Jordan and across Sinai to northeast Egypt, the sea inundated farther inland where the marine effects are recorded in the arenitic section by sedimentary structures and sequences, and by the presence of ichnofossils, mainly of the *Cruziana* and *Skolithos* types (Seilacher, 1990) and acritarch assemblages (Al-Hajri and Owens, 2000). In more marginal areas, however, braided and meandering rivers prograded over the wedge of marine sediments, and due to periodic fluctuations of the sea level and shifting of the active part of the fluviatile system, the section consists of braidplain deposits interrupted by tidal conditions. Along the basin margins the pattern of deposition even returned to proximal alluvial fan deposits. Apart from the short episode of carbonate deposition, the Cambrian sequence is dominated by clastic sediments, reflecting marine environments that prevailed in the north and mostly continental conditions in the south that continued during the Middle and Late Cambrian and into the Ordovician.

The Cambrian clastics consist mostly of first-cycle subarkoses and quartz-arenites and only partly of reworked earlier sediments. Unlike the Neoproterozoic and Early Cambrian conglomerates and arkoses, the mature clastics originated mostly from interior Gondwana, more to the south and west, which partly could have been a Pan-African terrain. The shift in sediment supply becomes evident since at this turn most of the shield's landscape has been matured (peneplain) and hardly active, so it could not be the major source for the basal cover. There is no indication for any rejuvenation of relief (except for limited areas, such as the longitudinal rift along the present-day Dead Sea Rift), and wherever Cambrian sediments cover the metamorphic-plutonic basement it displays a spectacular peneplain. Moreover, the Arabo-Nubian Shield, or at least most of its Asian part, was covered by the post-peneplain basal sequence (Amudei Shelomo-Salib-Yatib/Siq Formations), that today fringe the shield's area. These sequences do not show wedging-out relations at their limits, but are rather truncated, indicating that they extended inland to the south and west, far away from the present exposures. The same considerations are also applicable for the overlying Middle and Late Cambrian sequences.

The post-peneplain Cambrian sequence is up to 500 to 700 m thick. It generally thickens toward the north, but locally varies considerably depending on the relief beneath or due to truncation. The Cambrian sediments were deposited over most of the Arabian and North African Plates, but later were totally removed from northwestern Jordan and southwestern Syria, most of Israel (excluding the southern Negev), north-central Sinai, and from east-central Saudi Arabia following the crustal deformation

connected with the Late Paleozoic 'Hercynian' uplift-and-erosion event (Helez and Riyadh Geanticlines), and from the Arabo-Nubian Shield following uplift and rifting connected with the opening of the Red Sea in Tertiary times. Even earlier, during the Middle/Late Cambrian transition, part of the Cambrian sequence was truncated in Sinai and the Eastern Desert following differential block movements (Weissbrod, 2003). Three uplifted areas in northeastern and east-central Sinai (Wadi Quseib-Gebel El-Gunna-Wadi Gharba block), southwestern Sinai (Gebel Abu Durba-Gebel Huswa block) and in the Eastern Desert (north Wadi Qena - Gebel el-Zeit block) were subsequently eroded down to the igneous basement, removing the former Cambrian sediments, whereas in the intervening submerged areas they have been preserved. The entire basin was soon covered by Late Cambrian sandstones (Netafim Formation). This intra-Cambrian tectonic activity is also suggested by an abrupt shift in the provenance of the sands, when recycled quartz-arenites replaced the arkoses and subarkoses of the earlier deposition stages.

The remaining Cambrian sequences are exposed in southern Israel along the western margins of the Dead Sea Rift, extending from the Timna Valley to Elat and proceeding along the western shores of the Gulf of Elat in northeastern Sinai as far as Dahab. From there the belt of exposures turns westwards and crosses the peninsula along Gebel el-Gunna and the El Tih Escarpment to Gebel Nukhul (Um Bogma), and curves southwards to Wadi Feiran, continuing along the eastern shore of the Gulf of Suez from Gebel Abu Durba to Gebel Huswa. It is exposed again on the western side of the Gulf of Suez, from Wadi el-Dakhl southwards to north Wadi Qena. The most northern occurrence of Cambrian in the Sinai sub-plate was penetrated in the Sinaf-1 borehole (southern Negev). In Jordan the Cambrian exposures extend along the eastern margin of the rift from the Dead Sea (Wadi Zarqa Ma'in) to Jabal Ram in the southern desert and further southwards beyond the Saudi Arabian border. Away from the rift the Cambrian sequence has been penetrated in deep boreholes in the Azraq Basin (Wadi Ghadaf-2, Fuluk-1, and Safra-1) and in the southern desert (Wadi Sirhan-3 & 10 and El Jafr-1) (Fig. 18B.3). Farther southwards the Cambrian is extensively exposed in a belt fringing the Arabian Shield. The outcrops extend from the Tabuk Basin eastwards to the Great Nafud where they turn to the south and continue along the eastern flank of the igneous core (Qasim District) to Jabal Saq. It appears again in southwest Arabia in the Jibal al-Wajid Basin. The Cambrian section has been penetrated in several boreholes located to the north (Widyan Basin) and east (Ghawar oil field) of the exposure belt. In Syria the Cambrian is nowhere exposed and has been penetrated only in two boreholes (Khanasser-1 and Swab-1); however, a seismic interface ('D' reflector) that can be correlated across the country is attributed to the Cambrian limestone (Seber et al., 1993; Brew et al., 1997). This becomes more evident since a very developed Cambrian sequence including a thick dolomitic formation is exposed in several regions along the Bitlis Suture. The whole Cambrian sequence resembles those of Israel and Jordan both lithologically and stratigraphically.

The post-peneplain Cambrian rocks generally overlie unconformably the Precambrian crystalline basement or volcano-sedimentary series, but locally along the margins of the Dead Sea Rift, in southern Israel and southern Jordan, different rock units of Early or Middle Cambrian onlap a rejuvenated relief of the igneous basement, while in some areas in Sinai and the Eastern Desert, Late Cambrian sandstones directly overlie the igneous basement. The upper contact is more variable. In most of its occurences in Saudi Arabia, Syria, and Jordan it is conformably or disconformably overlain by Ordovician sequences, but in certain parts of these countries and in the Sinai sub-plate the entire Ordovician and overlying sections have been truncated and the Cambrian sequence is unconformably overlain by Carboniferous, Permian, or Lower Cretaceous strata, as the case may be. Thus in west-central (Um Bogma) and southwestern (Abu Durba) Sinai and in the Eastern Desert of Egypt (Wadi el-Dakhl) it is overlain by Carboniferous strata; in southwestern Syria it is overlain by either Carboniferous or Permian rocks; in east-central Saudi Arabia, central Jordan (from Wadi Zarqa Ma'in to Wadi Mujib) and in the central Negev (Hameishar-1 borehole) it is overlain by a Permian sequence and in the southern Negev (Sinaf-1 borehole and exposures), in central Jordan (from Wadi Mujib to Wadi Dana), and in northeastern and east-central Sinai (Taba-Dahab-Gebel Dhalal triangle) the Cambrian is overlain by Lower Cretaceous sandstones.

The post-peneplain Cambrian section is ascribed to four depositional sequences displaying different lithologic/mineralogic characteristics that were designated as the following formations:

Amudei Shelomo Formation

The Amudei Shelomo Formation overlies the peneplain surface on the igneous basement or on sediments and/or volcanic flows of the Late Precambrian-Early Cambrian arkosic and conglomeratic facies, and at the time covered most of the Arabian Plate with a veneer of continental pebbly sandstones. It consists of reddish-brown to pink and yellowish large-scale trough cross-stratified pebbly subarkose, arranged in thick tabular sheets. These are mostly medium- to very coarse-grained (occasionally grit-size) sandstones and rare laminated siltstone layers, and stringers of vein-quartz pebbles and a basal conglomerate, with no apparent regular vertical arrangement of grain-size and structures, which infill shallow channels that can be followed laterally for several hundred meters. They were deposited from the bed load of very powerful currents flowing to the north or northwestwards (Karcz and Key, 1966) in braided river channel systems on the slopes of piedmont and distal fans and outwash plains. The pebbly sandstone facies have sheet geometries with little regional thickness variations. They covered a vast peneplain that developed on the Pan-African igneous basement, or locally on the Late Precambrian-Early Cambrian conglomeratic facies, or on the arkosic facies (Zenifim Formation and equivalent rock units) in marginal areas to the north. Locally, along old rift structures, as observed at the margins of the present-day Dead Sea Rift, it fills a moderate relief of 100 to 200 m on the igneous basement (as in Har Timna) with an irregular contact. At Wadi Abu Barqa, on the eastern side of central Wadi Araba, the basal sandstones overlie the Hiyala Volcaniclastic

Formation with an angular unconformity (Bender, 1974). The Amudei Shelomo Formation is missing on the acid volcanic and ignimbrite inselbergs that protrude above their surroundings on both sides of the rift in Israel (Hare Shani and Har Amram) and Jordan (Jabal Taiyiba and Um Amed block). It is generally overlain by the Middle Cambrian Timna Formation (or the equivalent Burj Dolomite-Shale Formation), but where the latter wedges out, as in southern Jordan and Saudi Arabia, it is disconformably overlain by the Middle Cambrian Shehoret Formation or equivalent rock units. Only at Gebel Nukhul in west-central Sinai is it unconformably overlain by the Lower Carboniferous Um Bogma Formation (Weissbrod, 1969b, 1980).

Except for some non-diagnostic *Skolithos* burrows and sparse *Cruziana* trails that were reported from the upper part of the Salib Arkosic Sandstone Formation (which may actually belong to the overlying Umm Ishrin Sandstone Formation) the formation is barren and is estimated to be of late Early Cambrian age.

The Amudei Shelomo Formation and equivalent rock units are widely distributed, displaying similar rock characteristics. They have been recognized as a formal rock unit over the entire Arabian Platform, though they were variously named. The current nomenclature is presented in the correlation chart (Fig. 18B.2). Paleocurrent data indicate that unidirectional currents flowing in a general northerly direction in low sinuosity channels deposited this formation and the overlying Cambrian fluviatile sequences.

The maximal thickness of the Amudei Shelomo Formation and equivalent rock units is 300 m. It generally increases northwards along the depositional trend, or locally thins or thickens depending on the relief of the igneous basement, but in southeast Jordan and Saudi Arabia it changes in a different manner. The thickness in the outcrops in southern Jordan, southern Israel, and west-central Sinai (Um Bogma area) varies from 20 to 50 m and increases gradually northwards to almost 250 m in the Sinaf-1 borehole (Negev) and Wadi Numeira (Dead Sea), and to 293^{+} m in the Fuluk-1 borehole in the Azraq Basin (Abu Saad and Andrews, 1993). Similar thickness values have been measured in the Turkish exposures (Ketin, 1966). The much thicker sections attributed to the Salib Arkosic Sandstone Formation in Ajlun-1 (580 m), Northern Highlands-1 (571 m) and Suweileh-1 (931^{+} m) boreholes in northwest Jordan have been misinterpreted since the post-peneplain Cambrian sequence in this area has been totally truncated during the 'Hercynian' uplift-and-erosion event (Weissbrod and Sneh, 2002). Actually, these sections represent the earlier arkosic facies (equiv. Zenifim Formation). Other thick sections of the Salib sandstones were reported from the southern desert of Jordan in El Jafr-1 (289 m) and Wadi Sirhan-3 and 10 (750 and 260^{+} m) boreholes. These figures too are not in accordance with the regional depositional trend, and they apparently may be exaggerated because the boundary between the Salib Arkosic Sandstone Formation and the underlying Zenifim Formation has not been correctly differentiated (this explanation definitely applies to the section in the Wadi Sirhan-3 borehole). On the other hand, the Yatib/Siq equivalent rock units which are exposed in northwest and east-central Saudi Arabia also display great thicknesses (up to 130 m) that oppose the regional trend, which may indicate that the penetrated sections in the El Jafr-1 and Wadi Sirhan-3 boreholes (289 m and 260^{+} m) are indeed part of the Salib sandstones, and the change in the regional trend may perhaps be related to a differently oriented base level and a separate drainage system (to the east rather than to the north).

Timna Formation

The Timna Formation marks a transgressive sequence and displays three sedimentary suites of mixed siliciclastic-carbonate, carbonatic and siliciclastic lithofacies. The lower suite (Hakhlil Member) consists of a mixed siliciclastic-carbonate facies, up to 28 m thick, of rippled fine- to grit-size brown or pink subarkose alternating with greenish gray to reddish-brown finely laminated micaceous siltstone and shale layers, occasionally bioturbated, and a few intercalated massive or cross-bedded and desiccated sandy dolomite layers. It displays flaser, wavy, and lenticular bedding and contains a variety of ichnofossils (mostly *Cruziana* and *Skolithos*) and fragments of trilobites and brachiopods, pointing to a shallow flat system of subtidal to intertidal environments. In places a polymict conglomerate containing rounded vein-quartz pebbles and angular volcanic components, up to 20 cm in diameter, fills erosion channels at the base. In Har Amram and Hare Shani the Timna Formation onlaps the slopes of the acid volcanic hills, and rhyolitic quartz-porphyry monomictic breccia occur as talus aprons at the base of the formation.

The overlying suites (Sasgon Member) consist of three lithofacies of which the carbonatic (Nimra) and shaly (Mikhrot) are of sedimentary origin, whereas most of the sandy lithofacies (Nehushtan) is residual, resulting from the dissolution of the sandy carbonates by acid solutions (Segev, 1986). These lithofacies and the underlying rock unit (Hakhlil Member) were originally designated as formations (Bartura, 1966), but were later amended to lithofacies suites (Segev, 1984). In Jordan they (excluding the sandy lithofacies) were designated as the Tayan Sandstone, Numayri Dolomite Member, and the Hanneh Siltstone Members of the Burj Dolomite-Shale Formation (Powell, 1988). The lithofacies variations and epigenetic processes in the Timna Valley played a major role in the copper and manganese distribution, mineralization, and ore genesis and were thoroughly discussed by Segev and Sass (1989a, b).

The carbonatic lithofacies is the thickest (up to 30 m) rock sequence and consists of dark gray to brown, well-bedded, finely crystalline, peloid- and ooid-rich dolostone, limestone, and dolomitic limestone with cryptalgal to stromatolitic fenestral lamination and cyanobacterial mats (Soudry and Weissbrod, 1995) and bands and nodules of chert, up to 15 cm thick. The carbonates contain detrital quartz ranging between 10 and 50% and sandstone lenses, and infrequent disarticulated small brachiopods and trilobite fragments. The absence of scour together with the absence of bioturbation and the lack of subaerial exposure features in most of the carbonatic section indicates quiescence to moderate wave energy and suggests subtidal deposition. However, the presence of desiccation cracks and a poorly developed paleosol and laterally linked stromatolites indicate emergence conditions and an intertidal

to probably supratidal environment near the top of this unit.

The sandy lithofacies is residual resulted from the deposition of the detrital quartz grains within the sandy carbonates following its dissolution (Segev, 1986). This lithofacies consists of sandstone 5 to 7 m thick (locally up to 21 m), generally coarse- to medium-grained in the lower part becoming finer upwards, and displays alternating black (impregnated by manganese oxides) and white (manganese-free) laminations. Relicts of the dolomite are often found in the sandstone as well as chert relicts and phosphate-rich lenses, which randomly occur in the upper part. The contacts between the carbonatic (Nimra) and the sandy (Nehushtan) lithofacies are irregular and are attributed to secondary deformation, differential compaction and collapse. The dissolution processes were connected with the evolution of the rift valley in Neogene times and were accompanied by copper and manganese enrichment and ore genesis that were most effective in the Timna Valley and in the Feinan-Wadi Dana across the Dead Sea Rift and less effective or absent in other places along the rift.

The shaly lithofacies represents a regressive phase, resulting in increased influx of siliciclastics into the shallow carbonate basin. A thin part of this rock sequence (up to 6 m thick) is included in the Timna Formation whereas most of it comprises the lower member of the overlying Shehoret Formation. It consists of greenish gray to reddish-brown, lenticular and rippled cross-laminated micaceous siltstone and mudstone layers, occasionally bioturbated, with rare trilobite remains. This lithofacies is locally enriched in disseminated copper and manganese minerals as well as vein filling and as nodules of manganese oxides grading up to economic ores.

Fossils include mainly trilobites and brachiopods that were mostly obtained from exposures on the eastern side of the Dead Sea. Blanckenhorn (1912, 1914) studied carbonatic sections at Wadi Saramuj and Khirbet el-Burj, which yielded brachiopods (*Siphonotreta* sp.), trilobites (*Paradoxides* sp. and *Ptychoparia* sp.), and molluscs (*Hyolithes* sp.= *Hyolithus*), which he determined as Middle Cambrian. Based on these fossils and additonal trilobite species or re-defined ones (*Redlichia* [*Redlichops*] *blanckenhorni, Hesa problematica, Protelenus orientalis, Paleolenus campbelli, Anomocare campbelli* and *Kingaspis campbelli*), on new brachiopods (*Obolus radifer, Trematobolus palestinensis, Micrometra [Paterina] alata, Siphonotreta unguiculata*?, *S. verrucosa*?), and on tubes of *Hyolithes* (Orthotheca) *kingi,* or *H. fuchouensis* var. *moabiticus*, a Cambrian age for the carbonatic unit was confirmed by King (1923), Richter and Richter (1941, 1948), and Picard (1942), though they differ on the exact stratigraphic position. The first author assigned it a Middle Cambrian age, whereas the others attributed a late Early to early Middle Cambrian age. Parnes (1971) studied trilobites from the Timna Valley and Har Amram in southern Israel, and compared them with the Jordanian forms, assigning all of them a late Early Cambrian (Upper Georgian) age. He attributed Picard's *Protelenus orientalis* to *Resserops (Richterops) orientalis*, which together with Richter's *Redlichops blanckenhorni,* both from the SE Dead Sea exposures, are the oldest trilobites in the region, whereas King's *Kingaspis campbelli* from the NE Dead Sea is the youngest. The trilobites from southern Israel occupy an interim position. His dating was based on comparison with the biostratigraphical subdivision of the Cambrian in south Morocco, which has lately been re-dated by Geyer (1990) and Geyer and Palmer (1995).who assigned Hupe's zone VIII containing *Hamatolenus (Myopsolenus)* to lower Middle Cambrian. Accordingly, the trilobite faunas from both sides of the Dead Sea Rift may range from late Early to early Middle Cambrian age.

Lately, Rushton and Powell (1998) examined new material from the Dead Sea area and reviewd the older studies. They presented systematic descriptions of the redefined trilobites *Kingaspis campelli, Palaeolenus antiquus, Onaraspis palmeri, Realaspis?* and *Kingaspidoides* cf. *obliquoculatus*, considering them to be earliest Middle Cambrian close to the Lower/Middle Cambrian boundary (as recognised by Geyer, 1990 and Geyer and Palmer, 1995), rather than Lower Cambrian, as previously recorded. They also reported on ichnofauna characteristic of shallow water environment (*Rusophycus, Cruziana*, and *Skolithos*) in the Tayan and Hanneh siltstone members. Additional trace fossils (*Diplocraterion* and *Tigillites*) in the Hanneh Siltstone Member were identified by Amireh et al. (1994a). Other paleontological contributions have been made by Cooper (1976) who examined and revised brachiopods from the southeastern Dead Sea describing *Trematosia radifer, Psiloria alata*, and *P. dayi*, while Bandel (1986) and Yochelson (1988) discussed the taxonomic position of *Hyolithes kingi*. Various types of ichnofossils, including *Cruziana aegyptica, C.* cf. *nabatica, C. solomonis, Rusophycus, Tigillites*, and possibly *Scolicia*, characterize the interbedded mudstones within this facies.

The Timna Formation and equivalent rock units conformably overlie the Amudei Shelomo Formation, and wherever present it is overlain by the Shehoret Formation and equivalents. Only on the volcanic rhyolitic and ignimbritic hills that rose above sea level (*i.e.*, Har Amram and Hare Neshef in Israel; Jabal Taiyiba and Um El Amad in Jordan), does it onlap the high relief. The lower layers around these hills are interbedded with aprons of volcanic gravels.

The Timna Formation was widely distributed over the Arabian and North African Plates, but has been partly removed from large areas in Saudi Arabia and Egypt, and in central and northern Israel, northwestern Jordan, and southwestern Syria following the uplift-and-erosion events in the Middle/Late Cambrian, Late Devonian/ Early Carboniferous, and Late Carbon-iferous/Early Permian transitions, and during Late Tertiary and Neogene times.

The formation is most developed at the edge of the platform in Turkey and western Iran, where it is entirely carbonatic, and thins gradually southwards, wedging out at the shield's margin. In the exposures along the Bitlis Suture in southeastern Turkey it consists of gray, massive, finely-crystalline sandy dolomite and nodular limestone, with thin chert layers (Koruk Formation) attaining a thickness of 200-250 m (Ketin, 1966). Further inland it was penetrated in one borehole (Khanasser-1) in Syria and two boreholes in northern Jordan (Wadi Ghadaf-2 and Fuluk-1), but deep seismic refraction techniques have indicated the presence of the dolomitic layer (Burj Dolomite-Shale Formation) across

these countries (Brew et al., 1997; Teimeh and Taani, 1995). The thickness of the formation in these boreholes decreases from 160 to 135 m (Yankauskas and Talli, 1978; Andrews, 1992). Further south it is exposed along the eastern margins of the Dead Sea Rift from Wadi Zarqa Ma'in to Jabal Malaqa and thins shortly from 120 to 17-21 m and disappears completely south of Wadi Museimer. Nevertheless, thick sections of the shaly-carbonatic formation, apparently contrary to the conventional trend of thinning, have been reported in three deep boreholes located in the southern desert, 100-200 km east of the rift zone. The thickness increases eastwards from 61 m (El Jafr-1) through 96 m (Wadi Sirhan-3) to 113 m (Wadi Sirhan-10). These figures may be partly erroneous due to misinterpretation, but it could indicate that the sea invaded this area from the eastern (Pacific) side of the Paleo-Tethys.

On the western margin of the Dead Sea Rift the Timna Formation was penetrated in the southern Negev (Sinaf-1 borehole) and is exposed from the Timna Valley southwards as far as Wadi Quseib in northeastern Sinai where it is truncated. The thickness of the formation along these exposures decreases southwards from 60 m (Sinaf-1) to 45 m in the Timna Valley and to 10 m in northeastern Sinai (Taba area).

Segev (1984) reconstructed the paleogeography of the Cambrian marine intercalation along the Dead Sea Rift and differentiated two basins (Timna-Feinan and Elat-Abu Khusheiba) that were separated by an E-W-trending high volcanic ridge (Har Neshef - Har Amram - Jabal Taiyiba). Actually the dividing ridge was not continuous and the volcanic hills rose above the sea level as islands and at the time were encircled by onlapping marine sediments. Furthermore, the formation does not show any distinct lithological or facies change between the two basins and the varying thicknesses are in accordance with the regional depositional trend; however, the concept of two basins becomes evident in a later stage of the Middle Cambrian transgression and is reflected by the white fine-grained sandstones (White Member of the Shehoret Formation in Israel or the Abu Khusheiba Sandstone Formation in Jordan), which were deposited only in the southern (Elat-Abu Khusheiba) basin.

The Timna Formation (named differently as the Abu Hamata Formation) is exposed again in west-central Sinai (Um Bogma area), and consists mostly of fine-grained arkosic sandstone and micaceous shales with thin layers of sandy dolomite (0.2-1 m thick). It contains *Cruziana* specimens such as *Cruziana aegyptica, C. salomonis, C.* cf. *nabataeica, Bergaueria sucta, Dimorphichnus quadrifidus, D.* cf. *obliquus*, and other trace fossils within this sequence, proving its Cambrian age (Seilacher, 1990). As in Israel and Jordan, it is enriched in disseminated copper. The formation in this area is 21 m thick and thins out rapidly to the east and south. A similar marine intercalation, without any dolomite, is present across the Gulf of Suez in the Eastern Desert where Seilacher (1990) has described *Cruziana* traces.

The southern limits of this Cambrian transgression can be traced from southern Jordan, across Sinai to the Eastern Desert of Egypt, beyond which the shaly-carbonatic intercalation is apparently not known. Nevertheless, in the Tabuk outcrops of northwest Saudi Arabia, Helal (1968) described the presence of distinctive sandy shaly layers with abundant tracks, trails, and burrows which he called 'Spoor Zone' and which are located in a stratigraphic level (between the Yatib/Siq and Risha/Quweira Members of the Saq Sandstone) equivalent of the Timna Formation. Though carbonates are missing, the ichnofossil traces record a marine influence within the siliciclastic facies. This stratigraphic level is probably present in part of the Cambrian exposure belt fringing the Arabian Massif, and extending from northwest Saudi Arabia and curving southwards to the central part of the peninsula. This may also be supported by the presence of an Early to Middle Cambrian acritarch assemblage (Al-Hajri and Owens, 2000).

The presence of the Timna Formation or lateral equivalents in certain areas has been misinterpreted, as follows:

1) The thick sections attributed to the Burj Dolomite-Shale Formation in the Northern Highlands-1 (201 m) and Suweileh-1 (252 m) boreholes in northwestern Jordan have been misinterpreted since the post-peneplain Cambrian sequence in this area has been totally truncated during the 'Hercynian' uplift-and-erosion event. It is postulated here that the carbonate and shale interval assigned erroneously to the Cambrian is actually the Permian Hudayb Group, which in this area directly overlies the Late-Precambrian-Early Cambrian arkosic facies of the Zenifim Formation (Weissbrod and Sneh, 2002).

2) An Early Cambrian limestone ledge (4 m thick) containing stromatolites and archaeocyathids has been reported by Omara (1972) near the base of the clastic section in the Gebel Abu Durba area, southwestern Sinai. This is the only reference to the presence of Cambrian limestone in this area, but subsequent investigators could not verify it. Later, Weissbrod (1984, 2003) argued that the nature of this ledge and the taxonomy of the organic structures were misinterpreted. It is more likely a faulted block of Miocene age with Dacicladecae algal stromatolites, which resemble the sections figured in Omara's article and are highly distributed in the vicinity. Moreover, this finding is incompatible with the local stratigraphic setting since the Early-Middle Cambrian formations had been removed from this area and the Late Cambrian Netafim/Araba Formation directly overlies the Precambrian igneous basement.

Shehoret Formation

The Shehoret Formation was deposited in a tidal-dominated shoreline belt, although fluviatile progradation took place during short-lived regressions. In the lower part siltstone and mudstone layers alternate with cross-stratified subarkose and grit, that are succeeded by a dominantly sandy sequence displaying mostly small sets of trough, planar and wavy structures and less frequent ripple cross-lamination, with *Skolithos* burrows and other unidentified trace fossils.

The distribution of the Shehoret Formation is identical to that of the underlying formations; it is exposed along both sides of the Dead Sea Rift in Israel and Jordan, continuing southward and fringing the igneous basement in southern Sinai and northwestern and central Saudi Arabia. Northwards it has been penetrated in several boreholes in the southern desert and the Azraq Basin in

Jordan and in two boreholes in Syria. Further north, in southeastern Turkey it is exposed in three regions along the Bitlis Suture. The formation has been removed from most of Israel and Sinai (except for the Timna-Elat, northeastern and west-central Sinai exposure belts), northwestern Jordan, and the exposed Arabian Shield due to intra-Cambrian, Late Paleozoic, and Neogene uplift-and-erosion events.

In Israel and Sinai (northeastern and west-central areas) the Shehoret Formation overlies the Timna Formation just as it does in the Jordanian exposures from Wadi Zarqa Ma'in southwards to Jabal Malaqa, but from there to the southern desert and further south to central Saudi Arabia the dolomite-shale intercalation (Burj equivalent) is missing and the Umm Ishrin (its white or variegated parts) and Risha equivalents overlie the Salib or Siq/Yatib sandstones. Only on the acid volcanic hills that rose above their surroundings during the Early to Middle Cambrian members of the Shehoret Formation (or equivalent rock units) gradually onlap the high relief. In the lower part of these sandstones tongues of volcanic gravels are common. The upper contact is invariably unconformable. In most of its occurrences the Shehoret Formation is overlain by the Netafim Formation, but in the Sinaf-1 borehole and the Timna Valley Lower Cretaceous sandstones overlie it. There the section of the Shehoret Formation corresponds only to its lower part (Multicolored Member). In the Jordanian exposures the two formations were not differentiated and both comprise the Umm Ishrin Sandstone Formation. However, there are many indications that in most exposures the Netafim correlative part of the Um Ishrin Formation overlies the Shehoret equivalent. It is also postulated that similar relationships exist in Saudi Arabia, Syria and Turkey.

The maximum thickness of the Shehoret Formation in Israel (150 m) was measured at the type section (Nahal Shehoret), decreasing to 30 m in west-central Sinai (Um Bogma area). A thicker section has been reported from exposures in the southern desert of Jordan where the Umm Ishrin Sandstone Formation attains a thickness of up to 350 m (Bender, 1968). Farther to the southeast sections ranging between 290 and 370 m were encountered in the Wadi Sirhan-3 and 10 and El Jafr-1 boreholes, whereas only 196 to 226 m were penetrated in the Azraq Basin (Fuluk-1 and Wadi Ghadaf-2) in the north (Abu Saad and Andrews, 1993). These data apparently indicate that the Umm Ishrin sandstones in Jordan display an opposite trend of thicknening as compared to older Cambrian sequences, however, since the contact with the underlying formations is conformable and the paleocurrent data show that the transport direction remained unchanged (NW to NE), a shift in the depositional trend does not seem plausible. It is postulated that some of the thickness figures reported from Jordan are exaggerated due to stratigraphical misinterpretation. In any case, data on an equivalent rock sequence (the Sosink Formation) that was penetrated in the Swab-1 and Khanasser-1 boreholes in Syria show a northerly thickening trend that reaches a thickness of 750 to 1000 m (Yankauskas and Talli, 1976). Similar thick sections have been described from exposures along the Bitlis Suture where relevant rock units (Sosink, Yerlikaş and Tiyek Formations) are up to 1000 m thick. These formations consist of dolomite or nodular limestone in the lower part and yielded Middle Cambrian trilobites of the *Paradoxides* genus.

The Shehoret Formation yielded no index fossils and its age is deduced from stratigraphic relations of the sections in Jordan. There the age of the Umm Ishrin Sandstone Formation (equivalent to the Shehoret and Netafim Formations) is within the range of Middle Cambrian to Early Ordovician, as it is intercalated between the underlying trilobite-bearing Middle Cambrian Burj dolomite-Shale Formation and the overlying *Cruziana*-bearing Early Ordovician (Tremadocian-Skiddavian) Disi Sandstone Formation. The age can be further constrained since the upper boundary of the Shehoret Formation is erosive and manifests a certain stratigraphic gap. Based on these data and regional considerations the age of the Shehoret Formation is presumably Middle Cambrian, whereas the Netafim Formation is of Late Cambrian age.

Three members were differentiated in Israel based on lithological characteristics and on the common color, and were termed as the Multicolored, White, and Variegated Members. Correlative rock units have been distinguished on the eastern side of the rift (Fig. 18B.2).

Multicolored Member

The sedimentology of the Multicolored Member is similar to the upper shaly lithofacies of the Timna Formation and forms a continuation of it. In Jordan this rock sequence was designated as the Hanneh Siltstone Member and has been included within the Burj Dolomite-Shale Formation. It comprises several fining-upward sequences consisting of gray, brown and reddish-brown, coarse-grained, moderately sorted, planar and trough cross-stratified subarkose and grit units, 1 to 5 m thick, with scattered pebbles and mud clasts at erosive bases, alternating with thinly interlayered horizontal and ripple cross-laminated, locally desiccated, greenish-gray to reddish-brown mudstones, siltstones, and fine- to coarse-grained micaceous subarkose, 0.7-1.5 m thick, occasionally bioturbated and burrowed by *Skolithos*. In the upper part of the sequence, trilobite tracks are occasionally found and more rarely columnar siliciclastic arenaceous stromatolites (Soudry and Weissbrod, 1995). This suite displays alternations of migrated sand shoals and heterolitic facies which are interpreted as turbulent deposition of sand flats in an upper shoreface environment dissected by tidal channels.

The thickness of the Multicolored Member is generally 30 to 40 m, decreasing southwards to a few meters beyond the Egyptian border. At Har Amram it locally onlaps the high relief of volcanic rocks.

White Member

The White Member is white, light gray to greenish-gray, very fine- to fine-grained, locally coarse-grained, moderately well sorted and cross-stratified subarkose with several red and gray lenticular siltstone layers up to 1 m thick. Armoured mud balls and mud clasts occur at the base of the lower sets, whereas pebbles are generally absent except for tongues of quartz-porphyry gravels where it

onlaps volcanic hills. In Nahal Gishron and northeastern Sinai silty layers are more common. The sandy sets display trough and planar cross strata alternating with horizontal and ripple cross lamination and occasionally bipolar current flow directions. They are 10-20 cm thick in the lower part, 30-60 cm in the upper part, and up to 1 m thick in the middle part. *Skolithos* burrows occur throughout but they are more abundant in the lower part.

The White Member is exposed along the western margin of the Dead Sea Rift between Har Amram and Elat and further into northeastern Sinai down to Wadi Abiad, south of which it was truncated by the intra-Cambrian uplift-and-erosion. It is absent in the Timna Valley and in the Sinaf-1 borehole due to truncation. On the eastern side of the rift this facies has been termed the Abu Khusheiba Sandstone Formation (Powell, 1989) and extends from Wadi El Jariya in the north to Wadi Quseib in the south. Unlike the other Cambrian rock units which extend over much of the platform, the White Member is a local facies which is restricted to a basin that extended on both sides of the rift and is therefore most developed in the center of the basin (115 m at Wadi Abu Khusheiba) decreasing in thickness in the margins and eventually wedging out. In Israel the maximal thickness (52 m) was measured in the Nahal Shehoret-Nahal Gishron area decreasing to the south and northwards.

Variegated Member

The Variegated Member shows frequent alternations of reddish-brown and white sets of very fine to medium-grained and moderately to well-sorted, laminated or thinly cross-stratified subarkose and subordinate micaceous siltstone layers. The sandy units are frequently ripple cross-laminated, displaying also lenticular, wavy and flaser bedding, occasionally with bipolar flow directions, and are characterized by an abundance of *Skolithos*. More to the south the dominant bedforms, mostly in the lower part, are large-scale trough cross-stratification, whereas *Skolithos* burrows are rare. These sediments represent an overall intertidal setting, grading southwards to fluvial braided-stream environment. This member is up to 60 m in southern Israel, decreasing to 23 m in west-central Sinai.

In Jordan this rock sequence comprises the Umm Ishrin Sandstone Formation, and includes also the Netafim Formation, as the two rock units were not differentiated. According to Makhlouf and Abed (1991) and Amireh et al. (1994b) the depositional facies displays a northward gradation from proximal alluvial fans into sand flats facies of a braided stream, which in turn change laterally into fluvial- and tide-dominated deltas and finally into subtidal or upper shoreface facies. The braidplain facies and even the alluvial fan facies were many times inundated by the Paleo-Tethys, which reached the southern part of Jordan in response to periodic shifting of the active part of the braidplain system.

Netafim Formation

The Netafim Formation displays a prominent shift in compostion, changing from subarkose to quartz arenite. It consists of dark brown to red, fine-grained, moderately to well sorted and, for the most part, trough and planar cross-stratified sandstone units ranging from 0.5 to 3.5 m in thickness. In the lower part medium- to large-scale trough and planar cross stratification is prevalent, with occasional wedges or lenses of grit and bases filled with vein-quartz and quartz-porphyry pebbles or small mud clasts, followed by smaller scale structures, and in the upper part horizontal bedding alternates with small scale planar stratification, with occasional *Skolithos* burrows. The sandy units alternate with layers (0.2 to 1.5 m thick) of red and brown laminated micaceous siltstone and claystone, displaying several upward fining successions. These sediments were deposited in an intertidal environment where the laterally migrating tidal channels contributed extensive sequences. In east-central Sinai this sequence (Adedia Formation equivalent) was deposited as a series of sand bars, partly burrowed by *Skolithos*, which overall display transgressive conditions evolving from intertidal foreshore to inner offshore environments. (Morsy et al., 1994). Sections in Gebel El-Gunna, Gebel Shiti and Gebel Dhalal revealed that the lower part was deposited under intertidal foreshore conditions under the influence of NW-SE ebb-flood tidal currents. The middle part accumulated as medium to large-scale dune forms deposited by longshore currents in an upper shoreface environment, while the upper part was deposited under less energetic conditions than those of the underlying sediments (*i.e.* deeper marine). Storm-waves may have had an appreciable role in the suggested lower shoreface - inner offshore zone where these hummocky cross-stratified clayey sandstones were laid down. Similar tidal sandy and silty sequences strongly burrowed by *Skolithos* and *Diplocraterion* in the lower and middle parts of the Netafim Formation have been described from the same region in En Umm Ahmad and Wadi Umm Mara (Weissbrod and Sneh, 1983). A marginal marine environment was also attributed to the Araba Formation equivalent in southwestern Sinai (Abu Durba area) on the basis of sedimentological characteristics and the presence of *Skolithos* and *Cruziana* traces (Issawi and Jux, 1982; Bhattacharyya and Dunn, 1986).

The distribution of the Netafim Formation is similar to that of the underlying Cambrian strata, being exposed along both sides of the Dead Sea Rift in Israel and Jordan, continuing southward and fringing the igneous basement in Sinai and Saudi Arabia. In east-central and southwestern Sinai it is the only Cambrian rock unit present, directly overlying the igneous basement. Northwards the Netafim Formation (as part of the Umm Ishrin sandstones and equivalent rock units) was penetrated in several boreholes in the southern desert of Jordan and in the Azraq Basin and in two boreholes in Syria. Farther north in southeastern Turkey it is exposed in three regions along the Bitlis Suture. The Netafim Formation and correlative rock units have been removed from most of Israel (except for the Elat area), northern Sinai, northwestern Jordan, and the exposed Arabian Shield due to intra-Cambrian, Late Paleozoic, and Neogene uplift-and-erosion events. As already mentioned, the age of the formation is probably Late Cambrian since it overlies an erosional hiatus at the top of the Middle Cambrian strata and is overlain by *Cruziana*-bearing Lower Ordovician (Tremadocian-Skiddavian) sandstones (in southern Jordan).

The thickness of the Netafim Formation in outcrops ranges

from 20 to 130 m, though at several locations along the exposure belts, as in the Timna Valley and Nahal Gishron in southern Israel and in the Gebel Nukhul area in west-central Sinai, the formation has been entirely removed. The thinnest section is found in southern Israel, whereas the thickest was reported *from* southwestern Sinai near Gebel Abu Durba, on the eastern shore of the Gulf of Suez. In Jordan and Saudi Arabia the thickness may reach up to 100 m. Since the thickness is dependent on the level of erosion it is difficult to define any trend of thickening/thinning, but there is no reason to suspect any change from the general scheme as indicated for most clastic formations by paleocurrent dispersal.

The Netafim Formation is bounded by unconformities. In southern Israel, northeastern, and west-central Sinai it overlies the Shehoret Formation, sometimes displaying an irregular contact and an abrupt change in the sediment composition. Similar relationships probably exist in the Jordanian and Saudi Arabian sections as well as in Syria and southeastern Turkey, although the two formations have not been differentiated and the distinction between them is not always discernible. A different contact is observed in east-central and southwestern Sinai (and across the Gulf of Suez in the Eastern Desert) where the Netafim Formation directly overlies the igneous basement. The upper boundary is variable. In southern Israel, northeastern, and east-central Sinai the Netafim Formation is overlain by the Lower Cretaceous Amir Formation. This Lower Cretaceous unconformity is superimposed on a Late Paleozoic unconformity, which is still observed in west-central and southwestern Sinai and in the Eastern Desert of Egypt where Lower Carboniferous sediments (mostly sandstones but locally dolomite) overlie the Netafim Formation. In most of the Jordanian occurrences, as in the belt of exposures that extends from Wadi Dana southwards to the Saudi Arabian border, and in the boreholes that were drilled in the southern desert and the Azraq Basin, the Netafim equivalent is overlain by Lower Ordovician strata, whereas from Wadi Dana northwards to Wadi Mujib it is overlain by Lower Cretaceous strata, and from there to Wadi Zarqa Ma'in the Netafim equivalent is overlain by Permian sediments. In Saudi Arabia, Syria, and southeastern Turkey Lower Ordovician strata presumably overlie it.

Of special significance is the unconformity between the Shehoret and Netafim Formations, which enables the delineation of intra-Cambrian vertical movements in Sinai and the Eastern Desert of Egypt. Accordingly, the Cambrian sequence consists of a lower, subarkosic part (15-25% feldspar), with a shaly-carbonatic intercalation, and overlying it is an upper quartz-arenitic (feldspar-free) part (Weissbrod 1969b, 1980). In Israel and Sinai three rock units were distinguished in the lower part (Amudei Shelomo, Timna, and Shehoret Formations), whereas the upper part consists of only one rock unit (the Netafim Formation). The boundary between these two parts, which also differentiates between the Shehoret and Netafim Formations, is unconformable. This indicates an uplift-and-erosion event during which, in some areas of Sinai and the Eastern Desert, the three lower formations were entirely removed. The event is also manifested by an overall shift in the composition of the upper formation. The area that has been uplifted and eroded at the Middle/Late Cambrian transition can be variously constructed. It could have been a continuous ridge located south of a SW-NE line crossing the peninsula into the Eastern Desert. However such a ridge, though agreeing with the distribution of the Cambrian exposures in Sinai, is improbable when considering outcrop positions before rifting along the Gulf of Aqaba (Elat) and the Gulf of Suez. The presence of three mutually discontinuous displaced intra-Cambrian blocks is therefore considered more in agreement with the outcrop distribution (Weissbrod, 2003). The largest block area occurs in east-central Sinai, extending from the vicinity of Wadi Quseib to Gebel El-Gunna and westwards along Wadi Zalaqa to Gebel Dhalal. Another area is situated in southwestern Sinai, extending from Wadi Firan southwards to Gebel Huswa and a third block area appears on the western side of the Gulf of Suez, from Gebel Somr El-Qaa to Gebel el-Zeit. In the uplifted areas erosion cut down to the igneous basement, removing all the Lower and Middle Cambrian sediments, whereas in the stucturally low areas the depth of the truncation was minor, leaving much of the Cambrian section intact. By the Late Cambrian sea level rose and marine deposition returned to the region, covering it ubiquitously. Thus in the uplifted areas in Sinai and the Eastern Desert the Netafim Formation directly overlies the igneous basement, whereas in the rest of the region it overlies the Shehoret Formation.

In Jordan the intra-Cambrian unconformity has not been discerned and the Netafim Formation equivalent was not differentiated from the underlying Cambrian sandstones, and both rock sequences were designated as the Umm Ishrin Sandstone Formation. Although rift-associated solutions have altered part of the feldspars that distinguishes the two parts, and extensive iron mineralization has often obscured other rock characteristics, still some of these diagnostic features were observed in the Jordanian sections, but they have not been studied in detail. In this regard Lloyd (1969) and Abdelhamid (1990) reported that in the southern desert (Wadi Ram area) the lower part of the Umm Ishrin Formation is feldspathic, whereas the upper part is devoid of feldspars. A similar division was noticed by Weissbrod (1980) who examined samples from the Cambrian section in the Dead Sea area that was described by Wetzel and Morton (1959). The present data reveal that the two parts of the Umm Ishrin Sandstone Formation are present throughout Jordan. These two parts were also designated as a single formation in Saudi Arabia, Syria, and Turkey (Fig. 18B.2). It should be noted however, that within the Cambrian Sosink Formation in the Derik region in southeastern Turkey, Ketin (1966) distinguished between a Middle Cambrian part of up to 800 m of limestone, shales, siltstones, and sandstones, and a 250-300 m thick part of Late Cambrian quartzite, which is overlain by Ordovician black shales. The latter is apparently the equivalent of the Netafim Formation.

3. PERMIAN

At the outset of the Permian the uplifted structures (geanticlines) in the region were planed-down, while subsidence

of the platform was followed by deposition of sandstones and interbedded shales in an alluvial and swampy delta plain with some shallow marine incursions that blankated the eroded surface and filled the relief. This unconformable surface is well documented in the Levant (Helez Geanticline) and Arabia (Riyadh Geanticline). At the culmination of these structures basement rocks or arkoses are overlain by Early Permian sandstones (Unayzah or Saad Formations, respectively), whereas away from the center of the structures these formations or equivalent siliciclastics overlie progressively younger truncated sequences from Precambrian to Carboniferous (Figs. 18B.4 and 18B.5). Concurrently, extensional tectonics associated with the opening of the Neo-Tethys Ocean and the formation of the passive continental margin were active along northern and eastern Arabia and the coastal Mediterranean area, involving several rifting phases, block faulting, and sporadic igneous activity. At the initiative stages some local changes in the thickness of the Permian basal sandstones occurred (*i.e.*, Gevim-1 borehole), but with the acceleration of these movements, which lasted until the Jurassic, faulting became more prominent, resulting in interrupted sequences and chaotic stratigraphic contacts (Helez Deep-1a).

The Late Permian signals the recovery of the global sea level due to the melting of the Early Permian continental glaciers and the invasion of a shallow sea over the margins of the Arabian Platform. The sea moved back and forth over the platform, depositing cyclic transgressive-regressive sequences in an inland thinning sedimentary wedge, which developed upward into mixed sand/shale sediments, eventually becoming dominated by limestone. As a consequence of these changes in sea level and climatic conditions accompanying a shift in the latitudinal position, this transgressive event also records a change in the overall composition of the sediments, from dominantly siliciclastics to carbonates.

The Permian in Israel is known only from the subsurface (Fig. 18B.3). It was encountered in 22 boreholes: Ramon-1, Hameishar-1, Shezaf-1, Agur Deep-1a, Avdat-1, Nafha-1 and 2, Boqer-1, Zavoa-1, Kurnub-1, Makhtesh Qatan-2, Zohar Deep-8, Lot-1, Heimar-1, Massada Deep-1, Haqana' im-3, Zuk Tamrur-1 and Emunah-1 in the central and northern Negev and Bessor-1, Gevim-1, Pleshet-1 and David-1a in the southern Coastal Plain, and has been fully penetrated in 11 of them. The Permian succession consists of a massive basal sandstone overlain by alternating sandstones, shales, and carbonates, comprising two formations which display the transition from a fluviatile to marine facies (Weissbrod, 1969a, 1980). The thickness of the Permian sequence in the Negev ranges between 300 and 500 m, becoming thicker and displaying a reduction of the sand/shale ratio toward the northwest and an opposite trend in the clastic ratio. Carbonates are dominant in the transgressive units (lower Arqov Formation), while shales are abundant in the regressive ones (upper Arqov Formation).

The Permian sediments generally overlie Late Precambrian-Early Cambrian arkose and/or igneous rocks (Zenifim Formation), or Cambrian subarkose (Hameishar-1 borehole) and are overlain by marine Triassic strata, with no apparent unconformity. In the southern Negev it is completely truncated due to Lower Cretaceous erosion.

Permian sections displaying similar lithology and thickness have been penetrated in five boreholes in north-central Sinai (Ayun Musa-1 and 2, Nakhl-1, Abu Hamth-1, Hamra-1) and in seven boreholes in the Northern Highlands and the Azraq Basin (Northern Highlands-1 and 2, Er Ramtha-1a, Ajlun-1, Suweileh-1 Safra-1, Risha-2) in northwest Jordan (Fig. 18B.3) (Weissbrod, 1980; Andrews, 1992; Weissbrod and Sneh, 2002). As in the Negev boreholes, most of the Lower Paleozoic (except for the Cambrian) is missing below the Permian in this region, and the entire configuration is analogous to that in Israel, taking into account the post-Cretaceous 105 km sinistral displacement along the Dead Sea Rift (Freund et al., 1970).

The shallow marine platform was bounded to the east and south by a high continental domain that extended over most of Syria and Jordan, the southern Negev, northwestern Saudi Arabia, southern Sinai, and the Eastern Desert. The backbone of this domain coincides with the structurally controlled Al Jawf-Mardin axis, which acted as a barrier during the Late Paleozoic, separating the eastern part of the Arabian Platform from the western part (Robertson Research International Ltd., 1986). This domain has been characterized by deposition of fluviatile siliciclastics, though most of them were removed during Triassic and Early Cretaceous times. In Jordan the Permian siliciclastic sequence (Umm Irna Formation) is exposed east of the Dead Sea, between Wadi Mukheiris and Wadi Mujib, overlying a Cambrian section (Weissbrod, 1976; Bandel and Khoury, 1981). Some of these exposures are located within grabens, thus being preserved from the Lower Cretaceous erosion (Powell and Mohamed, 1993). In west-central Sinai and the Eastern Desert of Egypt the Permian continental sediments are represented by the Budra/Qiseib Formation, a redbed series with a thin marine intercalation (Abdallah et al., 1965; Druckman, 1974), whereas in Syria a relative thick section (up to 700 m thick) of syntectonic Permian siliciclastics (Heil and Amanus Sand Formations) is mostly preserved in the Palmyride Trough in central Syria, which began to subside during the Early Permian (Al Youssef and Ayed, 1992). The Aleppo Plateau to the north, the Rutbah High in the south, and the area east of the Euphrates Depression remained high with no record of Early Permian sediments, although they may be present, since in many boreholes the Permian has not been distinguished from the underlying Late Carboniferous due to similar lithologies and lack of fossils. On the other hand, the Late Permian sequence, which displays similar sedimentological characteristics and averages 125 m, has been encountered in many boreholes located in the elevated regions, while in others it has been removed.

Farther to the southeast and beyond the continental domain, another subsiding platform was established in the Permian over much of the Persian Gulf region and eastern Arabia and extending northward into western Iran, Iraq, and Turkey. This much broader platform was bounded to the west by the Arabian Shield and partly covered it. The Permian sediments there are similar to those in the western platform, displaying basal fluviatile to marginal siliciclastics that are succeeded by transgressive-regressive cycles

of shallow water evaporitic carbonate shelf facies. This Permian sequence is extensively exposed in northwestern and central Saudi Arabia, extending almost continuously in an arcute belt of cuestas that line the eastern flank of the Arabian Shield, stretching for 1200 km from the region of Bani Khatmah in the south (lat. 18°-00'N) to the Great Nafud in the north (lat. 28°-10'N) (Powers et al., 1966). It has been penetrated in many boreholes, most of them located in east-central Saudi Arabia and the Gulf states. The thickness of the Permian sequence is generally 400-500 m, increasing to the east, northeast and southeast (Rub al-Khali) where the thickest section (1000-1300 m) is found.

The Permian sequence in the Negev has been subdivided on the basis of lithology and E-log patterns into two formations, which together with the two overlying Triassic rock units and Carboniferous formations that are exposed in west-central Sinai, constitute the Negev Group depositional cycle (Weissbrod, 1969a). The Permian-Triassic transition does not coincide with the upper formation boundary, and is located in the lower part of the overlying, mostly Triassic Yamin Formation.

Saad Formation

The Saad Formation consists of white, poorly sorted, fine- to medium-grained, anhydrite-cemented sandstone with occasional floating granules and pebbles, alternating with beds of carbonaceous shales and clayey siltstone and a few layers of dolomite or limestone. The sandy units are several meters thick. They are massive or thinly cross-bedded and include small lenses and thin horizons of carbonaceous siltstone (containing plant remains), occasionally displaying upward-fining sequences. The shaly units are tens of centimeters to 4 m thick, massive or laminated, containing streaks of bituminous coal and small lenses of coarse sand. The Saad Formation was deposited in a marginal fluvio-deltaic setting. The sandstones with the carbonized plants were deposited in the distal part of the fluviatile system, possibly as point bars in moderate to high-sinuosity meandering channels, whereas the carbonaceous shales with its occasional coal seams suggest deposition in a littoral swamp, either in a delta or in a coastal barrier zone or even in lagoons. The presence of carbonate layers between the sandy units point to a lagoonar environment too. The thickness of the Saad Formation varies between 73 and 176 m. Other than the depositional trend, changes in thickness are attributed to local relief on the 'Hercynian' eroded surface (Makhtesh Qatan-2), contemporaneous tectonics (Gevim-1) or misidentification of the formation's upper boundary (Ramon-1?).

Equivalent rock sequences, displaying similar sedimentological characteristics and stratigraphic relationships, have been described in the neighboring countries. In northwest Jordan this siliciclastic sequence was penetrated in five boreholes (Suweileh-1, Northern Highlands-1 and 2, Ajlun-1, and probably Safra-1) and has been termed the Anjara Formation (Andrews, 1992), whereas in outcrops at the eastern side of the Dead Sea it comprises the lower part of the Umm Irna Formation (Bandel and Khouri, 1981; Makhlouf et al., 1991). In Saudi Arabia a correlative sandy unit is termed the Unayzah Formation (Al-Laboun, 1987) and is exposed along the shield's eastern flank, mainly in the Al Qasim District, and has been penetrated in numerous boreholes more to the east, in the east-central (Ghawar Field and Summan Platform) and northern (Widyan Basin) regions of the Kingdom. The Unayzah Formation has been thoroughly studied since it forms the main reservoir rock of Paleozoic oil in Saudi Arabia. In many of its occurrences an unconformable contact with the overlying Khuff Formation is evident. Other siliciclastic sections considered to be time equivalents, though differing in sedimentological details, are the lower part of the Budra/Qiseib Formation which is exposed in west-central Sinai and the Eastern Desert (Lejal-Nicol, 1987; Kora and Mansour, 1992), and the Heil Formation in central Syria that was encountered in the Doubayat-2, Sawanet-2, and Dolaa-1 boreholes (Al Youssef and Ayed, 1992).

Arqov Formation

The Arqov Formation consists of sandstone, shale and limestone units, which were deposited in the littoral zone, in lagoons, and coastal sand barriers. It displays three lithofacies types:

1) mixed units consisting of alternated calcareous shales, several tens of cm thick, massive or rippled and graded bedded sandstones and sandy layers with coaly horizons, several tens of centimeters thick;

2) fine- to medium-grained, cross-stratified sandstone units with gypsiferous or dolomitic cement, up to 10 m thick, and

3) carbonate units, generally gray to black, massive or thinnly bedded, finely crystalline, displaying biomicrite, micrite, intrabiomicrite, pelbiomicrite and biosparite types, quartz and glauconite grains, pellets and mud- or grain-supported intraclasts of skeletal fragments of pelycypods, ostracods, echinoids, foraminifers, and calcareous algae. These lithological associations and the sheet geometry of the sands indicate a nearshore marine environment - the mixed shaly units were deposited in coastal lagoons whereas the sand bodies are coastal regressive barriers that spread out over long distances. The carbonates are also indicative of coastal marine environments with high or low energy types characteristic of specific environments.

The traces of flora within the sands originated from the vegetation in marshes that bordered the barriers. In places the mixed sandy-shale facies indicates a transition between the sandy coastal zone and the lagoons. In most of the Negev boreholes, the formation can be differentiated into a lower, mostly transgressive carbonatic part, and an upper, more regressive clastic unit, but in the Coastal Plain the entire section is carbonatic. Such a distinction is also applicable in the subsurface in northwest Jordan, where the lower carbonatic part has been termed the Huwaira Formation and the upper clastic section was called the Suwayda Formation (Andrews, 1992). Southwards, in west-central Jordan the Late Permian sequence is clastic (upper Umm Irna Formation), representing a fluvial depositional setting (Makhlouf et al. 1991). A similar environment is also ascribed to the fine siliciclastics of the Late Permian Amanus Sand in Syria, which was encountered in several boreholes within and outside the Palmyride Trough (Al

Youssef and Ayed, 1992).

In the eastern Arabian Platform the Late Permian marine sequence comprising the Khuff Formation is extensively distributed in Saudi Arabia and the Gulf states. It represents shallow water evaporitic carbonate shelf facies with restricted marine fauna displaying four shallowing-upward peritidal cycles during which the depositional environment fluctuated between transgressive subtidal and open-marine carbonate sand shoals and lagoons and intertidal and regressive supratidal muddy and evaporitic deposits (Al-Jallal, 1994). The transgressive phase represents the deepening of the depositional environment, associated with a relative rise in sea level, whereas the regressive phase represents shallowing and the progradation of the supratidal facies over intertidal, subtidal, and open marine facies. The whole sequence has been subdivided into five members which coincide with the depositional cycles. The presence of subtidal oolitic facies (barriers) within the Khuff deposits may indicate that open marine (non-restricted) conditions prevailed in the outer shelf, which was located basinward (eastward) of the barrier, and restricted conditions dominated in the inner shelf, located landward (to the west). Most of the Khuff sediments were deposited in the inner shelf, in shallow waters within the euphotic zone, as indicated by the widespread occurrence of algae.

The age of the Permian strata in Israel is based on palynomorphs and is partly supported by ostracod and foraminifer taxa. Systematic and comprehensive studies on core and cutting materials were carried out by Horowitz (1970, 1973, 1974), Dunay (1974), Eshet (1983, 1990, 1992), and Eshet and Cousminer (1986), and by the 1990's these studies encompassed most of the Negev and Coastal Plain boreholes, establishing the current palynostratigraphy framework. The Permian sequence has been divided into two assemblage zones that grossly coincide with formation boundaries. However, different taxa were described by the various investigators and opinions differ on the age of the lower zone (Westphalian *sensu* Horowitz; Autunian according to Eshet and Dunay) and the position of the Permian-Triassic transition (upper part of the Zafir Formation *sensu* Horowitz; lower part of the Yamin Formation according to Dunay and Eshet). The following zones have been established by Eshet (1990):

Potoniesporites novicus Zone - This zone coincides with the Saad and lower Arqov Formations and with the *Punctatosporites minutus zone* of Horowitz (1973). It is generally dominated by striate bisaccate pollen grains and is characterized by abundance of *Distriatites insolitus, Vittatina ovalis, V. costabilis, Laevigatospiretes callosus, Pretricolpipollenites bharadwaji, Hamiapollenites insolitus, Protohaploxypinus microcorpus, Falcisporites nuthallensis, Punctatosporites minutus* and *Guttulapollenites hannonicus*. It is assigned to the Early Permian (Autunian stage) and resembles assemblages in Gondwana more than those of Laurasia. No age-significant fauna was found.

Protohaploxypinus spp. - *Lueckisporites virkkiae* Zone - This zone coincides with the Arqov and lower Yamin Formations with striate bisaccate pollen grains still abundant. It is characterized by the distribution and last appearance of *Protohaploxypinus diagonalis, P. richteri, P. limpidus, Klausipollenites shaubergeri, Falcisporites zapfei, Striatopodocarpites rarus, Luckisporites virkkiae, Striatopodocarpites rarus,* and *Limitisporites moerensis*. Other abundant taxa in this zone, which also appear in the underlying zone but do not extend upwards, include *Protohaploxypinus varius, P. microcorpus, P. jacobii, P. hartii, P. rugatus, Plicatipollenites indicus, Guthoerlisporites cancellosus, Striatoabeietes* sp., *Hamiapollenites karorooensis*, and *Vitreisporites pallidus*. This zone is assigned to the Late Permian (Thuringian stage) on the basis of equivalent ammonoid-controlled strata in Europe and the occurrence of the *L. virkkiae, K. shaubergeri*, and *P. varius* in Europe and Gondwana. The flora has a Cathaysian affinity (Lemoigne, 1981; Mustafa, 2003), as do most of the Late Permian palynomorph assemblages of the Middle East (Horowitz, 1972). A Cathaysian affinity of the microflora was concluded because the assemblage is rich in spores, somewhat poor in bisaccates, with only rare striatiti.

The Permian assemblages are similar to those reported from Gondwanan localities. Other paleontological evidence supports this age assignment. It includes the *Italogeisina transita-Hungarogeisina* cf. *H. permiana* ostracod assemblage zone known from Europe and Asia (Gerry and Honigstein, 1984; Gerry et al., 1987) and coexisting fusulinid-foraminifers and algae. Lately a rich fauna assemblage was found in the upper part of the Arqov Formation in the Gevim-1 borehole (Buchbinder et al., 1998), some species of which were noted earlier by Hamaoui (1966) and Derin and Gerry (1972) in other boreholes. The following foraminifers were listed: *Tuberitina* sp., *T. callosa, Fusiella* sp., *Frondina permica, Geinitzina* sp., *G. araxensis, Reichelina* sp., *Langella* sp., *Pachyphloya* sp., *Baisalina* sp., *Hemigordius*, sp., *H. ovatus, Glomospirella* sp., *Archaeodiscus* sp., *Paraglobivalvulina* sp., *Calvezina* sp., *Ichthyolaria* sp., *Aeolisaccus* sp., *Nankinella* sp., *Rectoglandulina* sp., *Alpinoschwagerina* sp., *Tubiphytes* sp. *Multidiscus* sp., *Neoschwagerina* sp., *Dunbarula* sp., *Cribrogenerina* sp., *C. sumatrana, Fusulina* sp., *Codonofusiella* sp., *Lunucammina* sp., and *Climacammina* sp. In addition the following algae have been recorded: *Pseudovermiporella* sp., *P. niponica, Permocalaculus* sp., *Gymnocodium* sp., *G. nodosum, Epimastopora* sp., and *Mizzia* sp.

The Khuff Formation in Saudi Arabia yielded a similar fossil inventory, supporting the Late Permian age assignment. Biostratigraphical data has been presented in numerous studies, those of the last decade are Al-Aswad and Kamel (1992), Warrington (1992), Broutin et al. (2002) and Stephenson and Filatoff (2000a, b).

The transition from the Permian to the Triassic in Israel is apparently continuous, with no obvious lithological break (Weissbrod 1980), though a red clay layer at the boundary suggests that local subaerial conditions related to regression effects may have occurred. Eshet (1989), who made a thorough study of the Permian and Triassic palynoflora in the Negev boreholes, reported on a drastic change in palynological assemblages across the P/Tr boundary, even where no unconformity is discerned. It involves a mass extinction of the Late Permian land flora followed by a proliferation of fungi (*Tympanicysta*) associated with reworked

carbonized terrestrial organic detritus and tintinnides (Eshet, 1992; Eshet et al., 1995 and Visscher et al., 1996) typical of the uppermost horizons of the Permian succession. This latest Permian proliferation of fungi ('fungal spike') is recognizable worldwide. The change is associated with the extinction of most Permian gymnosperm-dominated palynoflora and the later introduction of a new suite of palynomorphs of an Early Triassic age characterized by the dominance of marine acritarchs, followed by the appearance of lycopode spores such as *Endosporites pappilatus* and *Kraeuselisporites* spp. which characterize the overlying Scythian assemblage zone and eventual reappearance of bisaccate gymnosperm pollen.

4. FURTHER NOTES

The Paleozoic clastic series in the Arabian (and North African) Plate were considered in the past as a monotonous and azoic sequence of terrestrial origin ('Nubian Sandstone'). Upon closer view, however, besides carbonate rock intercalations, vertical and lateral changes became apparent in the composition, depositional setting, and thickness within the clastic rocks. The prominent vertical changes and turning points within the clastic facies are generally accompanied by major unconformities. The most drastic changes occurred across the late Early Cambrian regional peneplain, which separates two genetically different clastic packages. Other significant changes of various kinds within the clastic facies occurred in the Late Ordovician, Early Silurian, Late Devonian, Late Carboniferous, and in Late Permian, whereas clastic-carbonate alternations have been deposited in the Late Precambrian-Early Cambrian, Middle Cambrian, Early Devonian, Early Carboniferous, and in the Late Permian. Some of these changes and important events and/or their effects are observed in the stratigraphically limited local section and are indicated herewith, as well as changes within sequences that have been removed from Israel but are present in neighboring countries.

4.1) Until the late 1970s the peneplain surface on the igneous basement complex in the Arabian (and North African) Plate was regarded as the boundary between the Precambrian and Paleozoic. However, radiometric dates that were then carried out on samples from extrusive rocks that are intercalated within the sub-peneplain conglomerate and arkose sequences (partly listed and discussed by Weissbrod and Sneh, 2002) revealed that the upper part of these sequences is of Early Cambrian age, attesting to continuous sedimentation across the Precambrian-Paleozoic boundary, and the latest shaping of the peneplain surface before being buried was in the late Early Cambrian.

The changes in the sediments' composition across the peneplain were connected with shifting of latitudinal position and climate, different provenance and physiography, and the termination of tectonic and magmatic activities. The sediments evolved from first-cycle immature, very coarse and poorly sorted conglomerates, arkose and graywacke to mature, medium- to fine-grained, and moderately to well-sorted subarkose and quartz-arenite, some of which are recycled. The provenance shifted from local Pan-African plutonic-metamorphic rocks to faraway terranes of similar rocks and older crust, and partly of recycled sediments. The high topography and prominent relief were moderated and the mechanically eroded debris that was washed and deposited rapidly in nearby intramontane depressions and rift-related valleys changed to far-traveled detritus over moderate gradient subjected to chemical weathering through many stages of transport, storage, and reworking. Still another difference between pre- and post-peneplain sequences is the great thickness of the former due to repeated faulting along escarpments and associated volcanic flows and volcaniclastic series, and the relatively moderate thickness of the sediments proper in the basin that was controlled by regional subsidence.

4.2) Glacial deposits and 'hot' shale units display a conspicuous vertical change, forming also region-wide lithological markers throughout Arabia and North Africa.

Late Ordovician glacial deposits are exposed in northwestern, central, and southern Saudi Arabia and have been penetrated in boreholes in eastern Arabia, south of the Summan Platform. The continental glaciation is recorded by sedimentary facies and by pavements scoured into underlying rocks. The glacially influenced depositional processes led to the development of a strong paleorelief on the northern Gondwanan shelf. Characteristic features include thick sandstones and diamictites and glacial-related paleovalleys and channel-fill structures. In the Al Qasim area the glacial and periglacial deposits comprise two formations, which consist of tillite and sandstone, partly reworked or slumped, and boulder clay of continental, fluvial, lacustrine, and marine origin. Some of the deposits fill channels that in places cut down to the Cambrian strata (Vaslet, 1987; Halawani, 1994).

Related Late Ordovician fluvioglacial sediments were also reported from exposures in southeastern Jordan (Abed et al., 1993; Powell et al., 1994), where some paleovalleys which are incised down to 70 m in the Mudawwara Formation were distinguished. These valleys contain clastic fill with reworked faceted and striated exotic pebbles and cobbles of a probably nearby glacial till and vague traces of a striated pavement, while laterally equivalent beds with glaciomarine dropstones, laminites, and diamictites were reported within the Trebeel Formation in boreholes located in southeast (Wadi Sirhan) and northeast (Risha Field) Jordan (Andrews, 1991).

Contemporaneous fluvioglacial pebbly sandstones and several distinct striated pavements were reported 2000 km farther south in Jabal al-Qahr of the Jibal al-Wajid area (Evans et al., 1991). However, the glacial input is controversial. According to Stump and Van der Eem (1994, 1995), the glaciers did not reside in Arabia, and the striated boulders and faceted pebbles found within the channel fill originated from glaciers which were located in central Africa and were transported to Saudi Arabia in the fluvial drainage system.

A later glaciation event of Late Carboniferous-Early Permian age with boulder-bearing sandstones and tillite lenses has been reported from southwest Arabia (Khashm Khatmah and Jabal Umm Ghiran). McClure (1980) and McClure *et al.* (1988) regarded these polymict boulders, many of which are faceted and

striated, as glacial in origin, as did Helal (1964) already more than a decade earlier. Other glaciofluvial sediments of this event include glacial pavement and faceted pebbles that occur at Jabal Khurb al Ahmar and Bani Ruhaiya, some 150 km north of Jabal Umm Ghiran (Evans *et al.*, 1991).

4.3) Overlying the Late Ordovician glacial deposits are black, fissile, micaceous and organic-rich ('hot') shales of lowermost Silurian (Rhuddanian) age. The 'hot' shales unit was deposited during a far-reaching southward transgression, following ice melting and sea level rise. The 'hot' shales represent a short anoxic event and are rarely thicker than 25 m out of the thick Silurian sequence, which reaches as much as 1200 m (Keegan et al., 1990). The 'hot' shale unit is widely distributed throughout the northern shelf of Gondwana, though occurrences are discontinuous and its presence and thickness were controlled by the Late Ordovician paleorelief, or was due to the Late Devonian uplift-and-erosion event. This has led to its preservation within the basins and erodion from the intervening arches. The 'hot' shale unit is very abundant in north and central Saudi Arabia, Jordan, and Syria but is missing in Egypt, Sinai, and Israel. It is the main source of Paleozoic hydrocarbons for the generation of petroleum throughout Arabia and North Africa. Graptolite and palynomorph assemblage zones within the 'hot' shales provide accurate and high resolution biostratigraphic markers (Lüning et al., 2000).

4.4) The Paleozoic sequence displays many vertical changes that did not originate initially but resulted from later truncations that have placed various stratigraphies and lithologies of the eroded sequences and cover rocks in close contact. Such relationships formed mainly during the Late Paleozoic when the northern Gondwanan margin was affected by two episodes of arching that produced regional swells, apparently as a consequence of its collision with Laurasia. These swells were eroded as they rose, eventually resulting in stratigraphic gaps that decrease from the center of the structures, where erosion cut down to the Precambrian, to their flanks, where it gradually reached Cambrian to Devonian levels. The overlying strata thus covered different stratigraphic levels and different lithologies, though due to the dominance of clastic sedimentation in many cases the contact is between sandstone units. The variety of stratigraphic (and lithological) contacts is even greater since each of these structures was affected by two episodes of uplift, truncation, and reburial and the Lower Paleozoic sequences in the Helez and Riyadh swells (geanticlines) are covered by either Carboniferous or Permian sediments. The extension of the various stratigraphic contacts, which are apparently chaotic, becomes evident and logical by the demarcation of the erosion belts, as presented by the model of the Helez Geanticline (Fig. 18B.4).

The scene is even more complicated since local block faulting with different vertical magnitudes has brought various interrupted rock sequences against each other. Such faults are known in several areas and are mostly associated with the Late Carboniferous-Early Permian uplift-and-erosion event.

A particular benefit of these relations is that in many parts of the Near East that overlie the Helez Geanticline, and in particular the Riyadh Geanticline, the organic-rich Silurian 'hot' shales source rocks (Qusaiba Member of the Qalibah Formation) that have generated enormous quantities of oil and gas, were placed in direct or close contact with Permian sandstones (Unayzah Formation and/or 'Pre-Khuff Clastics') and carbonates (Khuff Formation) with good reservoir properties (Mahmoud et al., 1992; McGillivray and Husseini, 1992). In the faulted areas these source rocks were displaced against other rock sequences with good reservoir qualities.

4.5) The most conspicuous vertical changes are the contacts of carbonate sequences that are intercalated or interbedded within the clastic series. They were deposited under temperate to humid climate conditions, when northern Gondwana drifted to low latitudes, and are in many cases associated with evaporites, displaying transgressive-regressive cycles. Carbonate deposition was quite dominant during the Late Precambrian-Early Cambrian as part of evaporitic basins and intervening carbonate platforms that were developed along several belts in the Oman, the Persian Gulf, and the Zagros regions (Gorin et al., 1982). These carbonates may reach up to 1000 m in thickness and are coeval with the cherty and dolomitic limestone of the Muraykhah Formation (Jubaylah Group) that was deposited in faulted depressions along the Najd Fault System in central Saudi Arabia. During most of the Paleozoic clastic sediments prevailed with intermittent short episodes of carbonate deposition in the Middle Cambrian (Timna Formation in Israel/Burj Formation in Jordan and Syria), Early Devonian (Jauf Formation in Saudi Arabia) and Early Carboniferous (Haloul Formation in Syria/Um Bogma Formation in Sinai), attaining a thickness of several tens of meters. Only in the Late Permian did carbonates become dominant again, deposited over the newly formed eastern, northern, and western passive margins, following the break-up tectonics in the Early Permian. The thickness of the mostly carbonatic Late Permian in Israel (Arqov Formation) ranges between 150 and 250 m, whereas in eastern Saudi Arabia, the Gulf countries and the Zagros region the Late Permian sequence is up to 1650 m thick. In these regions the Late Permian carbonates (Khuff Formation) yield enormous quantities of gas within structural traps that are sealed by shales or by tight carbonates and evaporites. These hydrocarbons were also sourced by the Silurian 'hot' shales. Unfortunately, these source rocks were removed from Israel, Sinai and western Jordan following the uplift-and-erosion event during the Late Devonian-Early Carboniferous times.

ACKNOWLEDGEMENTS

The author gratefuly acknowledges the work of Bat-Sheva Cohen and Chana Netzer-Cohen in the preparation of the figures. Ms. Bevi Katz greatly improved the English in the text.

REFERENCES

Abdallah, A. M., El Adindani, A., and Fahmy N., 1965. Stratigraphy of the Lower Mesozoic rocks western side of the Gulf of Suez. Egypt. Geol. Surv. Min. Res. Dept., Pap. No. 27, 23 p.

Abdelhamid, G., 1990. The geology of the Jabal Umm Ishrin area (Wadi Ram). Map sheet 1:50,000 No. 3049 II (1986). NRA Geol. Bull., No. 14, 76 p.

Abed, A. M., Makhlouf, I. M., Amireh, B. S., and Khalil, B., 1993. Upper Ordovician glacial deposits in southern Jordan. Episodes, 16(1&2), p. 316-328.

Abu Saad, L., and Andrews, I. J., 1993. A database of stratigraphic information from deep boreholes in Jordan. NRA Subsurface Geol. Bull., No. 6, 182 p.

Al Youssef, W., and Ayed, H., 1992. Evolution of Upper Paleozoic sequences and the application of stratigraphy as a tool for hydrocarbons exploration in Syria. Egypt Gen. Petrol. Corp., 11th Petrol. Produc. Conf., Cairo 1992, Vol. 2, p. 636-657.

Ala, M. A., and Moss, B. J., 1979. Comparative petroleum geology of southeast Turkey and northeast Syria. J. Petrol. Geol., 1(1), p. 3-27.

Al-Aswad, A. A., and Kamel, S. M., 1992. Late Permian microfossils from the Khuff Formation, southern Saudi Arabia. Proc. 1st Int. Conf. Geol. Arab World, Cairo 1992, Vol. 2, p. 345-365.

Al-Hajri, S., and Owens, B., 2000. Sub-surface palynostratigraphy of the Paleozoic of Saudi Arabia. In: Al-Hajri, S., and Owens, B. (eds.), Stratigraphic Palynology of the Paleozoic of Saudi Arabia. GeoArabia, Spec. Publ., No. 1, Gulf PetroLink, Bahrain, p. 10-17.

Al-Jallal, 1995. The Khuff Formation: Its regional reservoir potential in Saudi Arabia and other Gulf countries; depositional and stratigraphic approach. In: Al-Husseini, M. I. (ed.), GEO 94 - The Middle East Petroleum Geosciences, Vol. 1, p. 103-119.

Al-Laboun, A. A., 1986. Stratigraphy and hydrocarbon potential of the Paleozoic succession in both Tabuk and Widyan Basins, Arabia. In: Halbouty, M. T. (ed.), Future Petroleum Provinces of the World. Am. Assoc. Petrol. Geol. Mem., No. 40, p. 373-397.

Al-Laboun, A. A., 1987. Unayzah Formation: A new Permian-Carboniferous unit in Saudi Arabia. Am. Assoc. Petrol. Geol. Bull., 71(1), p. 29-38.

Al-Laboun, A. A., 1990. The Paleozoic succession and the influence of the Hercynian equivalent movements in the greater Arabian Basin. Bull. Fac. Earth Sci., King Abdulaziz Univ., Jeddah, Vol. 3, p. 201-215.

Amireh, B. S., Schneider, W., and Abed, A. M., 1994a. Diagenesis and burial history of the Cambrian-Cretaceous sandstone series in Jordan. N. Jahrb. Geol. Paläontol. Abh., Vol. 192, p. 151-181

Amireh, B. S., Schneider, W., and Abed, A. M., 1994b. Evolving fluvial- transitional-marine deposition through the Cambrian sequence of Jordan. Sediment. Geol., 89(1-2), p. 65-90.

Andrews, I. J., 1991. Paleozoic lithostratigraphy in the subsurface of Jordan. NRA Subsurface Geol. Bull., No. 2, 75 p.

Andrews, I. J., 1992. Permian, Triassic and Jurassic lithostratigraphy in the subsurface of Jordan. NRA Subsurface Geol. Bull., No. 4, 60 p.

Avigad, D., Kolodner, K., McWilliams, M., Persing, H., and Weissbrod, T., 2003. Origin of northern Gondwana Cambrian sandstone revealed by detrital zircon SHRIMP dating. Geology, 31(3), p. 227-230.

Bandel, K., 1986. The reconstruction of Hyolithes Kingi as annelid worm from the Cambrian of Jordan. Mitt. Geol. Paläontol. Inst. Univ. Hamburg, No. 61, p. 35-101.

Bandel, K., and Khoury, H., 1981. Lithostratigraphy of the Triassic in Jordan. Facies, Vol. 4, p. 1-26.

Bartura, Y., 1966. Type sections of Paleozoic formations in the Timna area. Isr. Geol. Surv., Stratigr. Sect., No. 3, 12 p.

Bender, F., 1968. Geologie von Jordanien. Gebrueder Borntraeger, Berlin, 230 p.

Bender, F., 1974. Geology of Jordan. supplementary edition in English with minor revisions. Gebrueder Borntraeger, Berlin, 196 p.

Berberian, M., and King, G. C., 1981. Towards a paleogeography and tectonic evolution of Iran. Can. J. Earth Sci., 18(2), p. 210-265.

Bhattacharyya, D. P., and Dunn, L. G., 1986. Sedimentologic evidence for repeated pre-Cenozoic vertical movements along the northeast margin of the Nubian craton. J. Afr. Earth Sci., 5(2), p. 147-153.

Blanckenhorn, M., 1912. Naturwissenschaftliche Studien am Toten Meer und im Jordantal. Friedländer u. Sohn, Berlin, 478 p.

Blanckenhorn, M., 1914. Syrien, Arabien und Mesopotamien. Handb. region. Geol., Heidelberg, Vol. 5, p. 1-159.

Boote, D. R. D, Clark-Lowes, D., and Traut, M. W., 1998. Palaeozoic petroleum systems of North Africa. In: Macgregor, D. S, Moody, R. T. J., and Clark-Lowes, D. D. (eds.), Petroleum Geology of North Africa. Geol. Soc. London, Spec. Publ., No. 132, p. 7-68.

Brew, G. E., Litak, R. K., Seber, D., Barazangi, M., Al-Imam, A., and Sawaf, T., 1997. Basement depth and sedimentary velocity structure in the northern Arabian Platform, eastern Syria. Geophys. J. Int., 128(3), p. 617-631.

Broutin, J., Berthelin, M., Halawani, M., Vaslet, D., and Le Nindre, Y. -M., 2002. Mixed Late Permian floras and related paleoenvironments in the upper Khuff Formation of central Saudi Arabia. GEO 2002, 5th Middle East Geosci. & Exhib., Bahrain 2002; GeoArabia, Vol. 7, p. 219 (Abst.).

Buchbinder, B., Grossowicz, L., Peri, M., Eshet, Y., Rosenfeld, A., Siman-Tov, R., and Druckman, Y. 1998. Stratigraphy of the Gevim-1 borehole. Isr. Geol. Surv., Rep. GSI/18/98, 16 p.

Clayton, G., Owens, B., Al-Hajri, S., and Filatoff, J., 2000. Latest Devonian and Early Carboniferous miospore assemblages from Saudi Arabia. In: Al-Hajri, S., and Owens, B. (eds.), Stratigraphic Palynology of the Paleozoic of Saudi Arabia, Gulf PetroLink, Bahrain, p. 146-153.

Cohen, Z., Flexer, A., and Kaptsan, V., 1988. The Pleshet Basin: A newly discovered link in the peripheral chain of basins of the Arabian craton. J. Petrol. Geol., 11(4) p. 403-414.

Cooper, G. A., 1976. Lower Cambrian brachiopods from the rift valley (Israel and Jordan). J. Paleontol., 50(2), p. 269-289.

Dean, W. T., and Monod, O., 1990. Revised stratigraphy and relationships of Lower Paleozoic rocks, eastern Taurus Mountains, south central Turkey. Geol. Mag., 127(4), p. 333-347.

Dean, W. T., Martin, F., Monod, O., Gunay, Y., Kozlu, H., and Bozdogan, N., 1997. Precambrian? and Cambrian stratigraphy of the Penbegli-Tut inlier, southeastern Turkey. Geol. Mag., 134(1), p. 37-53.

Derin, B., and Gerry, E., 1972. Micropaleontological report - Zavoa 1 well. Isr. Inst. Petrol., Rep. No. 3/72, 3 p.

Druckman, Y., 1974. Triassic paleogeograpohy of southern Israel and the Sinai Peninsula. Proc. Int. Symp. Stratig. Alpin-Medit. Trias. Wien, Vol. 2, p. 79-86.

Dunay, R.E., 1974. Triassic and Permain palynostratigraphy from southern Israel. Isr. Geol. Surv., Rep., 8 p.

Eshet, Y., 1983. Palynostratigraphy, thermal alteration index and kerogen analysis of the Permo-Triassic succession in Makhtesh Katan 2 well, Negev, Israel. Isr. Geol. Surv. Rep. No. S/12/83, 172 p.

Eshet, Y., 1990. Paleozoic-Mesozoic palynology of Israel. 1. Palynological aspects of the Permo-Triassic succession in the subsurface of Israel. Isr. Geol. Surv. Bull., No. 81, 42 p.

Eshet, Y., 1992. The palynofloral succession and palynological events in the Permo-Triassic boundary interval in Israel. In: Sweet, W. C., Zunyi, Y., Dickins, J. M., and Hongfu, Y. (eds.), Permo-Triassic Events in the Eastern Tethys, World and Regional Geology, No. 2, Cambridge Univ. Press, p. 134-145.

Eshet, Y., and Cousminer, H. L., 1986. Palynozonation and correlation of the Permo-Triassic succession in the Negev, Israel. Micropaleontol., 32(3), p. 193-214.

Eshet, Y., Rampino, M. R., and Visscher, H., 1995. Fungal event and palynological record of ecological crisis and recovery across the Permian-Triassic boundary. Geology, 23(11), p. 967-970.

Evans, D.S., Lathon, R.B. Senalp, M., and Connally, T.C., 1991. Stratigraphy of the Wajid Sandstone of southwestern Saudi Arabia. Proc. 7th SPE Middle East Oil Shows Conf., Bahrain 1991, p. 947-960.

Feinstein, S., 1985. Coal rank and the thermal history of the sedimentary section in southern Israel. Unpublished Ph.D. Thesis, Ben Gurion University of the Negev, Beer Sheva, 138 p. (In Hebrew, English Abstract).

Freund, R., Garfunkel, Z., Zak, I., Goldberg, M., Weissbrod, T., and Derin, B., 1970. The shear along the Dead Sea rift. Phil. Trans. Roy. Soc. London, Ser. A, 267(1181), p. 107-130.

Garfunkel, Z., and Derin, B., 1984. Permian - early Mesozoic tectonism and continental margin formation in Israel and its implications for the history of the Eastern Mediterranean. In: Dixon J. E., and Robertson A. H. F. (eds.), The Geological Evolution of the Eastern Mediterranean, Geol. Soc. London, Spec. Publ., No. 17, p. 187-201.

Garfunkel, Z., 1998. Constraints on the origin and history of the Eastern Mediterranean Basin. Tectonophysics, 298(1-3), p. 5-35.

Garfunkel, Z., 1999. History and paleogeography during the Pan-African orogen to stable platform transition: Reappraisal of the evidence from the Elat area and the northern Arabian-Nubian Shield. Isr. J. Earth Sci., 48(3-4), p. 135-157.

Gerry, E., and Honigstein, A., 1984. Permian ostracodes of Israel. Isr. Inst. Petrol., Rep. No. 3/84, 10 p.

Gerry, E., Honigstein, A., Derin, B., and Flexer, A., 1987. Late Permian ostracodes of Israel; Taxonomy, distribution, and paleogeographical implications. Senckenb. Lethaea, 68(1-4), p. 197-223.

Geyer, G., and Palmer, A. R., 1995. Neltneriidae and holmiidae (Trilobita) from Morocco and the problem of Early Cambrian intercontinental correlation, J. Paleontol., 69(3), p. 459-474.

Geyer, G., 1990. Revised Lower to lower Middle Cambrian biostratigraphy of Morocco. Newsl. Stratigr., 22(2-3), p. 53-70.

Gorin, G. E., Racz, L. G., and Walter, M. R., 1982. Late Precambrian-Cambrian sediments of Huqf Group, Sultanate of Oman. Am. Assoc. Petrol. Geol. Bull., 66(12), p. 2609-2627.

Guiraud, R., Issawi, B., and Bosworth, W., 2001. Phanerozoic history of Egypt and surrounding areas. In: Ziegler, P. A., Cavazza, W., Robertson, A H. F., and Cransquin-Soleau, S. (eds.), Peri-Tethys Memoir 6: Peri-Tethyan Rift/Wrench Basins and Passive Margins. Mem. Mus. Nat. Hist. Natur., Vol. 186, p. 469-509

Gvirtzman, G., and Weissbrod, T., 1984. The Hercynian geanticline of Helez and the Late Palaeozoic history of the Levant. In: Dixon, J. E., and Robertson, A. H. F. (eds.), The Geological Evolution of the Eastern Mediterranean, Geol. Soc. London, Spec. Publ., No. 17, Blackwell Scientific, Oxford, p. 177-186.

Gvirtzman, G., Weissbrod, T., and Ginzburg, A., 1988. The Paleozoic Riyadh Geanticline in central Saudi Arabia: A structure similar to the Helez Geanticline. Isr. Geol. Soc. Ann. Meet., En Boqeq 1988, p. 46-47 (Abst.).

Halawani, M. A., 1994. Late Ordovician glacial sediments in northwest Saudi Arabia. 2nd Int. Conf. Geol. Arab World, Cairo 1994, p. 1311-1321.

Hamaoui, M., 1969. Note on Upper Paleozoic microfossils from southern Israel. Isr. Geol. Surv. Bull., No. 47, p. 25-35.

Helal, A. H., 1964. On the occurrence and stratigraphic position of Permo-Carboniferous tillites in Saudi Arabia. Geol. Rundsch., 54(1), p. 193-207.

Helal, A. H., 1968. Stratigraphy of outcropping Paleozoic rocks around the northern edge of the Arabian Shield (within Saudi Arabia). Z. Deutsch. Geol. Ges., 117(2-3), p. 506-543.

Horowitz, A., 1970. Palynostratigraphy of the Upper Paleozoic-Lower Mesozoic sequence in Zohar 8 borehole (southern Israel). Isr. Geol. Surv., Rep. No. P/1/70, 9 p.

Horowitz, A., 1972. Probable palaeogeographic implications of the global distribution of the Late Permian Cathaysian microflora. Ann. Acad. brasil. Cienc., Suppl., Vol. 44, p. 173-177.

Horowitz, A., 1973. Late Permian palynomorphs from southern Israel. Pollen et Spores, 15(2), p. 315-341.

Horowitz, A., 1974. Palynostratigraphy of the subsurface Carboniferous, Permian and Triassic in southern Israel. Geosci. Man, Vol. 9, p. 63-70.

Husseini, M. I., 1992. Upper Paleozoic tectono-sedimentary evolution of the Arabian and adjoining plates. J. Geol. Soc., London, 149(3), p. 412-429.

Karcz, I., and Key, C. A., 1966. Note on the pre-Paleozoic morphology of the basement in the Timna area (southern Israel). Isr. J. Earth Sci., 15(2), p. 47-56.

Keegan, J. B., Rasul, S. M., and Shaheen, Y., 1990. Palynostratigraphy of the Lower Paleozoic, Cambrian to Silurian, sediments of the Hashemite Kingdom of Jordan. Rev. Palaeobot. Palynol., 66(3-4), p. 167-180.

Keeley, M. L., 1989. The Palaeozoic history of the Western Desert of Egypt. Basin Res., 2(1), p. 35-48.

Ketin, I., 1966. Cambrian outcrops in southeastern Turkey and their comparison with the Cambrian of east Iran. Bull. Min. Res. Explor. Inst. Turkey, Vol. 66, p. 77-89.

King, A. W., 1994. Geology of the Permian to Ordovician clastic reservoirs of Abu Jifan/Farhah oilfields, Saudi Arabia. In: Al-Husseini, M. I. (ed.), GEO 94 - The Middle East Petroleum Geosciences, Vol. 2, p. 593-604.

King, W. B. R., 1923. Cambrian fossils from the Dead Sea. Geol. Mag., Vol. 60, p. 507-514.

Klitzsch, E., 1970. Die Strukturgeschichte der Zentral-Sahara: Neue erkenntisse zum Bau und zur Paleogeographie eines Taffellandes. [Structural history of the central Sahara; new data on the formation and paleogeography of a platform area]. Geol. Rundsch., 59(2), p. 459-527.

Klitzsch, E., 1986. Plate tectonics and cratonal geology in Northeast Africa (Egypt/Sudan). Geol. Rundsch., 75(3), p. 755-768.

Klitzsch, E., 1987. The paleogeographic development of NE Africa. In: Matheis, G., and Schandelmeier, H. (eds.), Current Research in African Earth Sciences, Balkema, Rotterdam, p. 159-164.

Klitzsch, E., 1990. Paleozoic. In: Said, R. (ed.), The Geology of Egypt, Chap. 21, p. 393-406. Balkema, Rotterdam.

Kohn, B. P., Eyal, M., and Feinstein, S., 1992. A major Late Devonian-Early Carboniferous (Hercynian) thermotectonic event at the NW margin of the Arabian-Nubian Shield: Evidence from zircon fission track dating. Tectonics, 11(5), p. 1018-1027.

Konert, G., Al-Afifi, A. M., Al-Hajri, S. A., and Droste, H. J., 2001. Paleozoic stratigraphy and hydrocarbon habitat of the Arabian Plate. GeoArabia, 6(3), p. 407-442.

Kora, M., and Mansour, Y., 1992. Stratigraphy of some Permo-Carboniferous successions in the Northern Galala, Gulf of Suez region, Egypt. N. Jahrb. Geol. Paläontol. Abh., 185(3), p. 377-394.

Lejal-Nicol, A., 1987. Flores nouvelles du Paleozoique et du Mesozoique d'Egypte et du Soudan septentrional. [New Paleozoic and Mesozoic floras from Egypt and northern Sudan]. Berliner Geowiss. Abh. (A), 75(1), p. 151-248.

Lemoigne, Y., 1981. Presence dune flore comprenant des elements cathaysiens, dans le centre de l'Arabie Saoudite au Permien superieur. [An Upper Permian flora, containing Cathaysian elements, from central Saudi Arabia]. C.R. Acad. Sci., Paris, 292(17), p. 1231-1233.

Lloyd, J.W., 1969. The hydrogeology of the southern desert of Jordan. UNDP/FAO 212, Tech. Rep. No. 1, 207 p.

Lüning, S., Craig, J., Loydell, D. K., Storch, P., and Fitches, B., 2000. Lower Silurian hot shale in North Africa and Arabia: regional distribution and depositional model. Earth-Sci. Rev., 49(1-4), p. 121-200.

Mahmoud, M. D., Vaslet, D., and Husseini, M. I., 1992. The Lower Silurian Qalibah Formation of Saudi Arabia: An important hydrocarbon source rock. Am. Assoc. Petrol. Geol. Bull., 76(10), p. 1491-1506.

Makhlouf, I. M., and Abed, A. M., 1991. Depositional facies and environments in the Umm Ishrin Sandstone Formation, Dead Sea area, Jordan. Sediment. Geol., 71(3-4), p. 177-187.

Makhlouf, I. M., Turner, B. R., and Abed, A. M., 1991. Depositional facies and environments in the Permian Umm Ima Formation, Dead Sea area, Jordan. Sediment. Geol., 73(1-2), p. 117-139.

McClure, H. A., 1980. Permian-Carboniferous glaciation in the Arabian Peninsula. Bull. Geol. Soc. Am., 91(12), p. 707-712.

McClure, H. A., Hussey, E. M., and Kaill, I. J., 1988. Permian-Carboniferous glacial deposits in southern Arabia. Geol. Jahrb. Reihe B, Vol. 68, p. 3-31.

McGillivray, J. G., and Husseini, M. I., 1992. The Paleozoic petroleum geology of central Arabia. Am. Assoc. Petrol. Geol. Bull., 76(10), p. 1473-1490.

McGillivray, J. G., 1995. Late Carboniferous and Early Permian petroleum geology, central Saudi Arabia. In: Global Environments and Resources, Can. Soc. Petrol. Geol. Mem., 17, p. 383-396.

Morsy, A. M., Kelling, G., El-Ghawaby, M. A., and El-Fawal, F. M., 1993. Sedimentology of the pre-Cenomanian succession, east-central Sinai, Egypt. Annal. Geol. Surv. Egypt, Vol. 19, p. 301-325.

Mustafa, H., 2003. A late Permian Cathaysian flora from the Dead Sea area, Jordan. N. Jahrb. Geol. Palaontol. Mh., No. 1, p. 35-49.

Neugebauer, H. J., 1983. Mechanical aspects of continental rifting. Tectonophysics, 94(1-4), p. 91-108.

Omara, S., 1972. An Early Cambrian outcrop in southwestern Sinai, Egypt. N. Jahrb. Geol. Paläontol. Mh., No. 5, p. 306-314.

Owens, B., Filatoff, J., Clayton, G., and Al-Hajri, S., 2000. Evidence of Mid-Carboniferous miospore assemblages from central Saudi Arabia. In: Al-Hajri, S., and Owens, B. (eds.), Stratigraphic Palynology of the Paleozoic of Saudi

Arabia, Gulf PetroLink, Bahrain, p. 154-167.

Parnes, A., 1971. Late Lower Cambrian trilobites from the Timna area and Har Amram (southern Negev, Israel). Isr. J. Earth Sci., 20(4), p. 179-205.

Picard, L., 1942. New Cambrian fossils and Paleozoic problematica from the Dead Sea and Arabia. Hebrew Univ. Geol. Dept. Jerusalem Bull., Vol. 4, p. 1-20.

Powell, J. H., and Mohamed, B. K., 1993. Structure and sedimentation of Permo-Triassic and Triassic rocks exposed in small-scale horsts and grabens of pre-Cretaceous age: Dead Sea margin, Jordan. J. Afr. Earth Sci., 17(2), p. 131-143.

Powell, J. H., 1988. The geology of the Karak area. Map sheet (1:50,000) No. 3152 III (1987). NRA Geol. Bull., No. 8, 172 p.

Powell, J. H., 1989. Stratigraphy and sedimentation of the Phanerozoic rocks in central and south Jordan. Part A: Ram and Khreim Groups. NRA Geol. Bull., No. 11, 72 p.

Powell, J. H., Mohamed, B. K., and Masri, A., 1994. Late Ordovician-Early Silurian glaciofluvial deposits preserved in palaeovalleys in south Jordan. Sediment. Geol., 89(3-4), p. 303-314.

Powers, R. W., Ramirez, L. F., Redmond, C. D., and Elberg, E. L. Jr., 1966. Geology of the Arabian Peninsula - Sedimentary geology of Saudi Arabia. USGS, Prof. Pap., No. 560-D, 147 p.

Ravn, R. L., McPhilemy, B., Rutherford, M., Talli, S., and Bahra, G., 1994. Late Devonian and Early Carboniferous palynostratigraphy and its applications in northeastern Syria. In: Simmons, M. D. (ed.), Micropalaeontology and Hydrocarbon Exploration in the Middle East, Chapman and Hall, London, p. 5-21.

Richter, R., and Richter, E., 1941. Das Kambrium am Toten Meer und die älteste Tethys. Abh. Senckenb. Naturf., Ges., Vol. 460, p. 1-48.

Richter, R., and Richter, E., 1948. Zur Frage des Unter-Kambrium in Nordost-Spanien. Senckenbergiana, Vol. 29, p. 23-29.

Robertson Research International Ltd., 1986. The Petroleum Geology of Syria. 2 parts.

Rushton, A. W. A., and Powell, J. H., 1998. A review of the stratigraphy and trilobite faunas from Cambrian Burj Formation in Jordan. Bull. nat. Hist. Mus. London (Geol.), 54(2), p. 131-146.

Sander, N. J., 1968. The preMesozoic structural evolution of the Mediterranean region. In: Barr, F.T. (ed.), Geology and Archaeology of Northern Cyrenaica, Libya, Petrol. Explor. Soc. Libya, 10th Ann. Field Conf., p. 47-70.

Seber, D., Barazangi, M., Chaimov, T. A., Al Saad, D., Sawaf, T., and Khaddour, M. 1993. Upper crustal velocity structure and basement morphology beneath the intracontinental Palmyride fold-thrust belt and north Arabian Platform in Syria. Geophys. J. Inter., 113(3), p. 752-766.

Segev, A., 1984. Lithostratigraphy and paleogeography of the marine Cambrian sequence in southern Israel and southwestern Jordan. Isr. J. Earth Sci., 33(1-2), p. 26-33.

Segev, A., 1986. Lithofacies relations and mineralization occurrences in the Timna Formation, Timna Valley. Unpublished Ph.D. Thesis, Hebrew University Jerusalem, 131 p. (In Hebrew, English Abstract).

Segev, A., and Sass, E., 1989a. Lithofacies and thickness control by epigenetic dissolution - The dolomitic Timna Formation, Cambrian, southern Israel. Sediment. Geol., 63(1-2), p. 109-126.

Segev, A., and Sass, E., 1989b. Copper-enriched syngenetic dolostones as a source for epigenetic copper mineralization in sandstones and shales (Timna, Israel). In: Boyle, R. W., Brown, A. C., Jefferson, C. W, Jowett, E. C., and Kirkham, R. V. (eds.), Sediment-hosted Stratiform Copper Deposits, Geol. Assoc. Can., Spec. Pap., No. 36, p. 647-658.

Seilacher, A., 1990. Paleozoic trace fossils. In: Said, R. (ed.), The Geology of Egypt, Chap. 32, Balkema, Rotterdam, p. 649-670.

Şengör, A. M. C., 1979. Mid-Mesozoic closure of Permo-Triassic Tethys and its implication. Nature, 279(5714), p. 590-593.

Shinaq, R., 1990. Mikrofazielle Untersuchungen Kambrischer, Triassischer und Jurassischer Karbonatgesteine Jordaniens. Unpublished Ph.D. Thesis, Geol. Palaontol. Inst. Univ. Hamburg, 196 p

Soudry D., and Weissbrod, T., 1995. Morphogenesis and facies relationships of thrombolites and quartzose stromatolites in a Cambrian tidal sequence - Elat area, southern Israel. Palaeo. Palaeo. Palaeo., 114(2-4), p. 339-355.

Stephenson, M., and Filatoff J., 2000a. Correlation of Carboniferous-Permian palynological assemblages from Oman and Saudi Arabia. In: Al-Hajri S., and Owen, B. (eds.), Stratigraphic palynology of the Paleozoic of Saudi Arabia, GeoArabia, Spec. Publ., No. 1, Gulf PetroLink, Bahrain, p. 168-191.

Stephenson, M., and Filatoff, J., 2000b. Description and correlation of Late Permian palynological assemblages from the Khuff Formation, Saudi Arabia and evidence for the duration of the pre-Khuff hiatus. In: Al-Hajri S., and Owen, B. (eds.), Stratigraphic palynology of the Paleozoic of Saudi Arabia,. GeoArabia, Spec. Publ., No. 1, Gulf PetroLink, Bahrain, p. 192-215.

Stump, T. E., and Van der Eem, J. G., 1994. Overview of the stratigraphy,. depositional environments and periods of deformation of the Wajid outcrop belt, southwestern Saudi Arabia. In: Al-Husseini, M. I. (ed.), GEO 94 - The Middle East Petroleum Geosciences, Vol. 2, p. 867-876.

Stump, T. E., and Van der Eem, J. G., 1995. The stratigraphy, depositional environments and periods of deformation of the Wajid outcrop belt, southwestern Saudi Arabia. J. Afr. Earth Sci., 21(3), p. 421-441.

Teimeh, M., and Taani, Y., 1995. A study of the Burj and Abu Khusheba Formations at outcrop and in the subsurface. NRA, Subsurface Geology Division, Rep. No. 12, 55 p.

Turcotte, D. L., and Emerman, S. H., 1983. Mechanisms of active and passive rifting. In: Morgan, P., and Baker, B. H. (eds.), Processes of Continental Rifting, Tectonophysics, 94(1-4), p. 39-50.

Vaslet, D., 1987. Early Paleozoic glacial deposits in Saudi Arabia: A lithostratigraphic revision. DMMR, Jeddah, BRGM, Tech. Rec. No. TR-07-1, 24 p.

Vaslet, D., 1990. Upper Ordovician glacial deposits in Saudi Arabia. Episodes, 13(3), p. 147-161.

Visscher, H., Brinkhuis, H., Dilcher, D. L., Elsik, W. C., Eshet, Y., Looy, C. V., Rampino, M. R., and Traverse, A., 1996. The terminal Paleozoic fungal event: Evidence of terrestrial ecosystem destabilization and collapse. Proc. Nat. Acad. Sci., U.S.A., Vol. 93, p. 2155-2158.

Warrington, G., 1992. Late Permian palynomorphs from Saudi Arabia. 8th Int. Palynol. Congr., Aix-en-Provence 1992, p. 158 (Abstr.).

Weissbrod, 1969a. The Paleozoic of Israel and adjacent countries: Part I - The subsurface Paleozoic stratigraphy of southern Israel. Isr. Geol. Surv. Bull., No. 47, p. 1-23.

Weissbrod, T., 1969b. The Paleozoic of Israel and adjacent countries: Part II - The Paleozoic outcrops in southwestern Sinai and their correlation with those of southern Israel. Isr. Geol. Surv. Bull., No. 48, 32 p.

Weissbrod, T., 1976. The Permian in the Near East. In: Falke, H. (ed.), The Continental Permian in Central, West and South Europe. Reidel Publ. Co., Dordrecht, p. 200-214.

Weissbrod, T., 1980. The Paleozoic of Israel and adjacent countries (lithostratigraphic study). Unpublished Ph.D. Thesis, Hebrew University Jerusalem, 275 p. (In Hebrew, English Abstract).

Weissbrod, T., 2003. Middle to Late Cambrian vertical movements in Sinai and the Eastern Desert of Egypt; lithostratigraphic consequences. Isr. J. Earth Sci., 52(2), p. 97-111.

Weissbrod, T., and Gvirtzman, G., 1988. The Late Devonian event in the Near East. Cour. Forsch.-Inst. Senckenb., Vol. 100, p. 221-233.

Weissbrod, T., Gvirtzman, G., and Perath, I., 1989. The Late Paleozoic geanticlines in the Near East and North Africa. C.R. 11th Congr. Int. Stratigr. Geol. Carbonifere, Beijing 1987, Vol. 4, p. 334-343.

Weissbrod, T., and Perath, I., 1990. Criteria for the recognition and correlation of sandstone units in the Precambrian and Paleo-Mesozoic clastic sequence in the Near East. In: Kogbe, C.A., and Lang, J. (eds.), Major African Continental Phanerozoic Complexes and Dynamics of the Sedimentation, J. Afr. Earth Sci., 10(1-2), p. 253-270.

Weissbrod, T., and Sneh, A., 2002. Sedimentology and paleogeography of the Late Precambrian-Early Cambrian arkosic and conglomeratic facies in the northern margins of the Arabo-Nubian Shield. Isr. Geol. Surv. Bull., No. 87, 44 p.

Wetzel, R., and Morton, D. M., 1959. Contribution à la géologie de la Transjordanie. Notes Mém. Moyen Orient, Vol. 7, p. 95-191.

Yankauskas, T. V., and Talli, S., 1978. The Paleozoic of the Arab Republic of Syria (ARS). Proc. Acad. Sci. USSR, Ser. 2, p. 92-97. (in Russian).

Yochelson, E. L., 1988. Comments and criticisms concerning Bandel's reconstruction of *Hyolithes kingi* as annelid worm from the Cambrian of Jordan. Mitt. Geol. Palaeontol. Inst., Univ. Hamburg, No. 67, p. 135-144.



Ras en-Naqb: the descent to Wadi Arabah (Arava) and the Gulf of Aqabah (Aqaba). Color image from The Holy Land Satellite Atlas, Volume II (1999, p. 214). ©Røhr Productions Ltd., Nicosia, Cyprus. Reproduced with permission. View towards the southeast.



Aerial view of Watiye Pass and the route to Mount Sinai, Sinai Peninsula. Color image from The Holy Land Satellite Atlas, Volume II (1999, p. 223). ©Røhr Productions Ltd., Nicosia, Cyprus. Reproduced with permission. View towards the south.

Chapter 18C

The Permian Fusulinids in Israel

Olga Orlova
Department of Zoology, Tel Aviv University, Ramat Aviv 69 978, Israel
Francis Hirsch
Geological Survey of Israel, 30 Malchei Israel Street, Jerusalem 95 501, Israel

INTRODUCTION

The Permian stage encompasses the youngest strata of the Paleozoic (285-245 Ma). Characterized by the final phases of the Hercynian orogeny and by dramatic shifts in climate, the Permian underwent a strong reduction of its marine extent and a large increase in its terrestrial domain. The extreme conditions varied from the formation of an austral ice-cap to the development of deserts and the build-up of tropical reefs. The constant changes in eustacy and the general drop of the world sea level are partly responsible for the extinction of much of Paleozoic life.

The paleogeographic evolution of the Permian ends in the establishment of Pangea, which was achieved after the Kungurian closing of the Ural seaway. The Permian deposits of the World Ocean (Panthalassa) are preserved in the circum-Pacific terranes and in its Tethyan branch. Low-latitude deposits are well-developed on the southwestern American midcontinent and in the Paleo-Tethys.

The extreme variety of conditions during the Permian resulted in the establishment of multiple time-scales (**Table 18C.1**), according to the type of sediments, faunas, and floras that define the facies of the deposits in each area. Standard stages have not yet been well-established from the marine sequences in the Urals, southwestern North America, and Tethyan southwestern Asia. As far as the Upper Permian is concerned, the correlation within the tropical Tethyan zone of southwestern Asia, to which the Levant belongs, is still tentative. Further research, among which Foraminifera represent a very important tool, is necessary in order to correlate the different Stages *e.g.* Murgabian, Djulfian, and Dorashamian, presently established by authors working in the Tethyan zone, with the Kazanian and Tatarian stages of authors working in the Urals.

Permian Stratigraphy of the Levant

The stratigraphic subdivision of the Levant is primarily based on regional unconformities that separate the stratigraphic column into periods of tectonically controlled sedimentation. Permian strata are represented by the Negev Group (Weissbrod, 1969; emend. Bartov et al., 1981), between the **pre-Permian unconformity** and the **Permian-Triassic paraconformity**. The **pre-Permian unconformity** was the result of a Hercynian uplift that caused a large part of the Paleozoic sediment to be eroded from the Levant (Gvirtzman and Weissbrod, 1984) and from a huge landmass, now buried under the eastern Mediterranean. The **Permian-Triassic paraconformity** was caused by regression and resulted in a hiatus during part of the Lower Triassic.

Paleogeography of the Levantine Permian

The Permian of the Levant (**Figure 18C.1**) consists of a depocenter crossing Israel in a northeasterly direction, from northern Sinai in Egypt to the Palmyrian Basin in Syria. This depocenter was a relatively narrow basin, between the Arabian-Nubian landmass to the southeast, and the Hercynian uplift of the Heletz landmass to the northwest (Gvirtzman and Weissbrod, 1984). The deposits include the carbonates (Fusulinid-limestones) of the 'Arqov Formation and a lining of clastics (Sa'ad, Umm Irna) of the equivalent Amanous Formation in Syria. The 'Arqov Formation, so far only detected in the Coastal Plain of Israel and in the northern Negev, is thus part of a much larger basin fill. Thickness figures and lithology (Weissbrod, 1969) suggest that this basin extends to the NNE into the subsurface of the Galilee and Lebanon and to the SSW to the subsurface of northern Sinai and farther to the west. From surface observations it can be stated that the carbonates wedge out towards the southeast, where they are replaced by clastics. The Permian carbonates in Israel compare well with the Khuff Formation of the circum-Arabian belt.

Lithology

In the subsurface of Israel the Permian consists of the Negev Group, unconformably overlying the Precambrian Zenifim Formation. **Permian** strata were encountered in the Negev boreholes Boqer-1, Zavoa-1, Makhtesh Qatan-2, Zohar-8, Haqanaim-3, Zuq Tamrur-1, Massada-1, and the southern Coastal Plain Pleshet-1 and Gevim-1 boreholes.

The type section of the Lower Permian Sa'ad Formation and Upper Permian 'Arqov Formation consists of fluviatile and shallow marine sediments in the Makhtesh Qatan-2 borehole (**Figure 18C.2**). The clastic sand to shale ratio increases to the southeast, whereas the carbonate ratio increases towards the northwest. As

| PERMIAN | | |

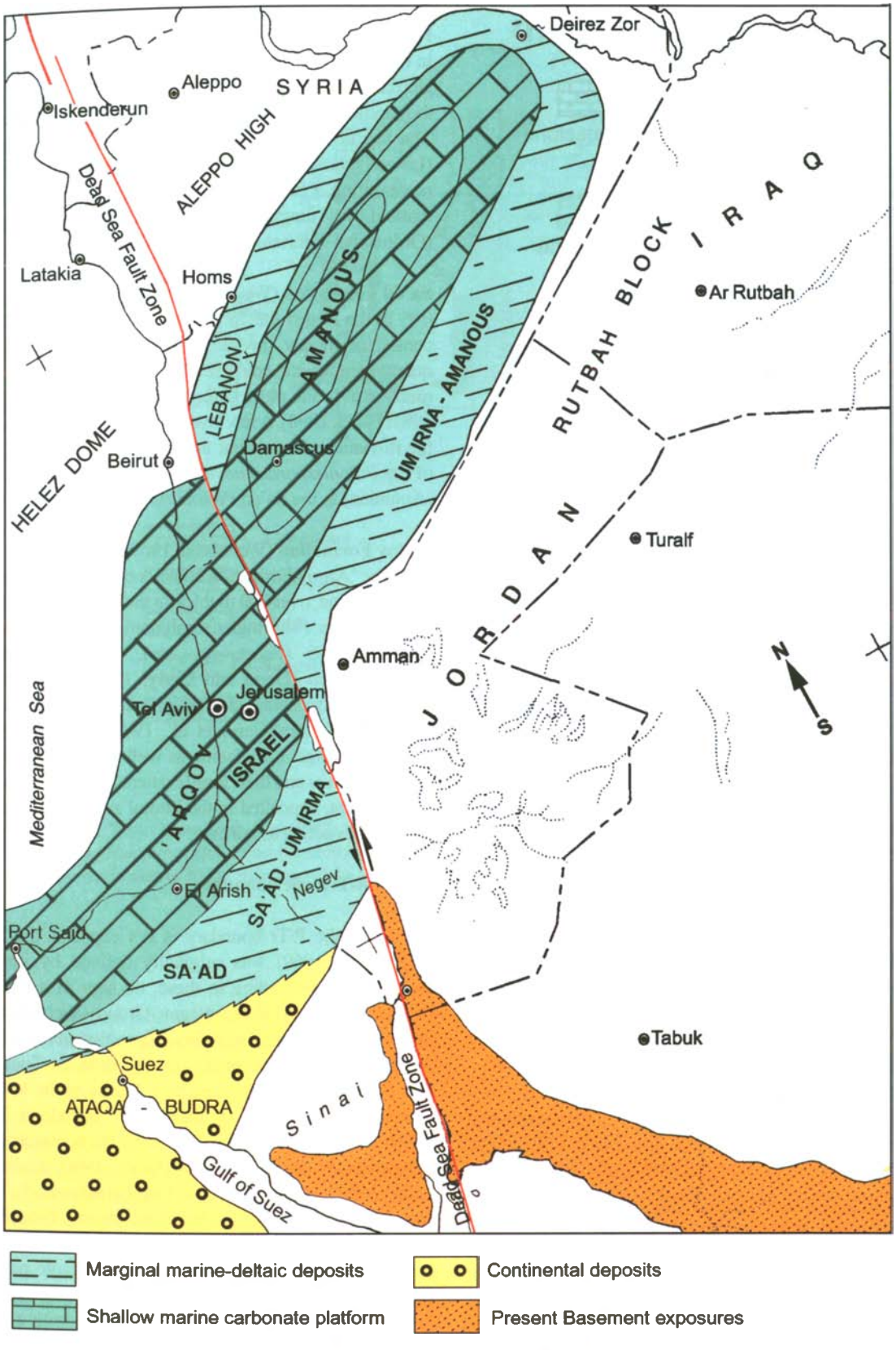


Figure 18C.1. The marine Permian in the Levant (modified after M. A. Ziegler, 2001).

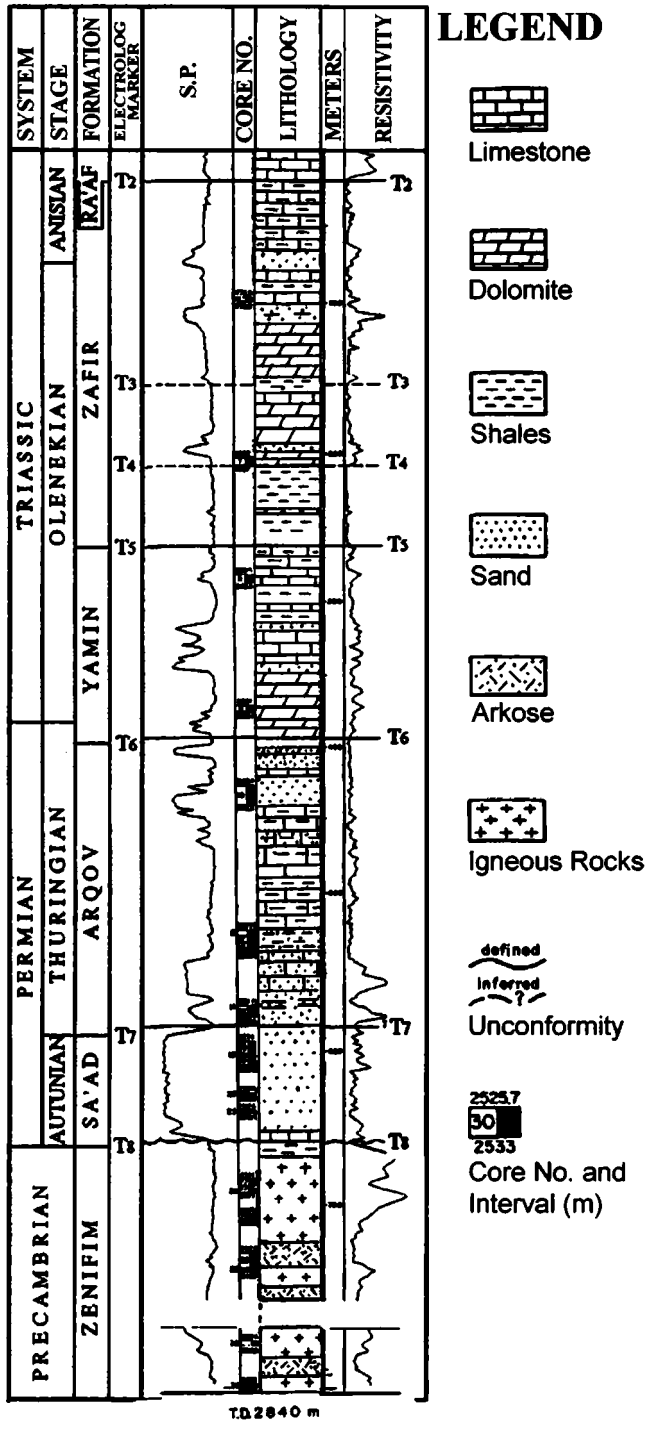


Figure 18C.2. Type section of the Permian-Triassic Sa'ad, 'Arqov, Yamin, and Zafir Formations, Makhtesh Qatan-2 borehole, northern Negev, Israel (from Zaslavskaya et al., 1995).

a result the stack of carbonate sediments represents a wedge-like body of strata which reaches a thickness of approximately 400 m in the Coastal Plain, versus the average 250 m of the 'Arqov Formation in the northern Negev. Practically no carbonates occur in the Umm Irna Formation in the exposed section of Zarqa Main (Jordan), across the Dead Sea Rift. The 'Arqov Formation overlies the sandstones and shales of the Lower Permian Sa'ad Formation. The top of the 'Arqov Formation is covered by the Olenekian (Lower Triassic) Yamin Formation, the boundary between them representing a hiatus of ?latest Permian and Induan strata, well-marked by a 'fungal spike' (Eshet, 1990) and recycled chitonozoa (Ordovician-Silurian) (Zaslavskaya et al., 1995).

Sa'ad Formation (Weissbrod, 1969)

In the Negev the 75 m thick deposits of the Sa'ad Formation consist of mostly fluviatile to deltaic sandstones, composed of quartz-arenites and coaly shales with plant remains. They are very much akin to the older Paleozoic deposits in the area (Weissbrod, 1981; Eshet, 1990). A few layers of limestone and dolomite interrupt the fluviatile environment that dominates the unit. Palynomorphs of the *Potoniesporites novicus* Zone confer an Early Permian age (Autunian) to the Sa'ad Formation (Eshet, *op. cit.*).

Arqov Formation (Weissbrod, 1969)

The 'Arqov Formation consists of alternating sandstone, shale and limestone, over 200 m thick in the Negev. The formation yields Late Permian (Thuringian) palynomorphs of the *Lueckisporites virkkiae* Zone (Eshet, *op. cit.*). The fusulinid foraminifer *Codonofusiella* (Derin and Gerry, 1981; Garfunkel and Derin, 1985) and the ostracodes of the *Italogeisina- Hungarogeisina* Assemblage zone (Gerry et al., 1987) indicate a Late Permian (Abadehian) age. Lithofacies, as well as the sheet geometry of the sandstone units and their fossil content, indicate a nearshore marine environment, deposited in the littoral zone or in lagoons, with the sand bodies acting as barriers.

Permian-Triassic boundary

Since the P/Tr boundary is not exposed, the Negev Group (Weissbrod, 1969) was originally defined by interpretation of electric logs. According to these, no sign of a marked break in the sedimentation of the Negev Group (Weissbrod, 1969) was detected, suggesting continuous deposition into the Early Triassic Yamin Formation. A hiatus at the Permian-Triassic boundary was postulated, characterized by a lacuna of the lowermost Early Triassic (Induan) stage, on the basis of conodonts (Hirsch, 1976, 1990). This view was strengthened by the occurrence of reworked palynomorphs and Chitinozoa (Eshet, 1990; Zaslavskaya et al., 1995) within a large interval of Late Permian-Early Triassic strata, suggesting major erosion processes during Late Paleozoic and Early Mesozoic times. Within these boundary horizons there is a characteristic abundance of terrestrial organic particles such as inertinites, pollen, spores and fungal spores (Eshet 1990). In several boreholes this fungal spore event coincides with a horizon of red clay (Eshet 1990), which marks the P/Tr boundary.

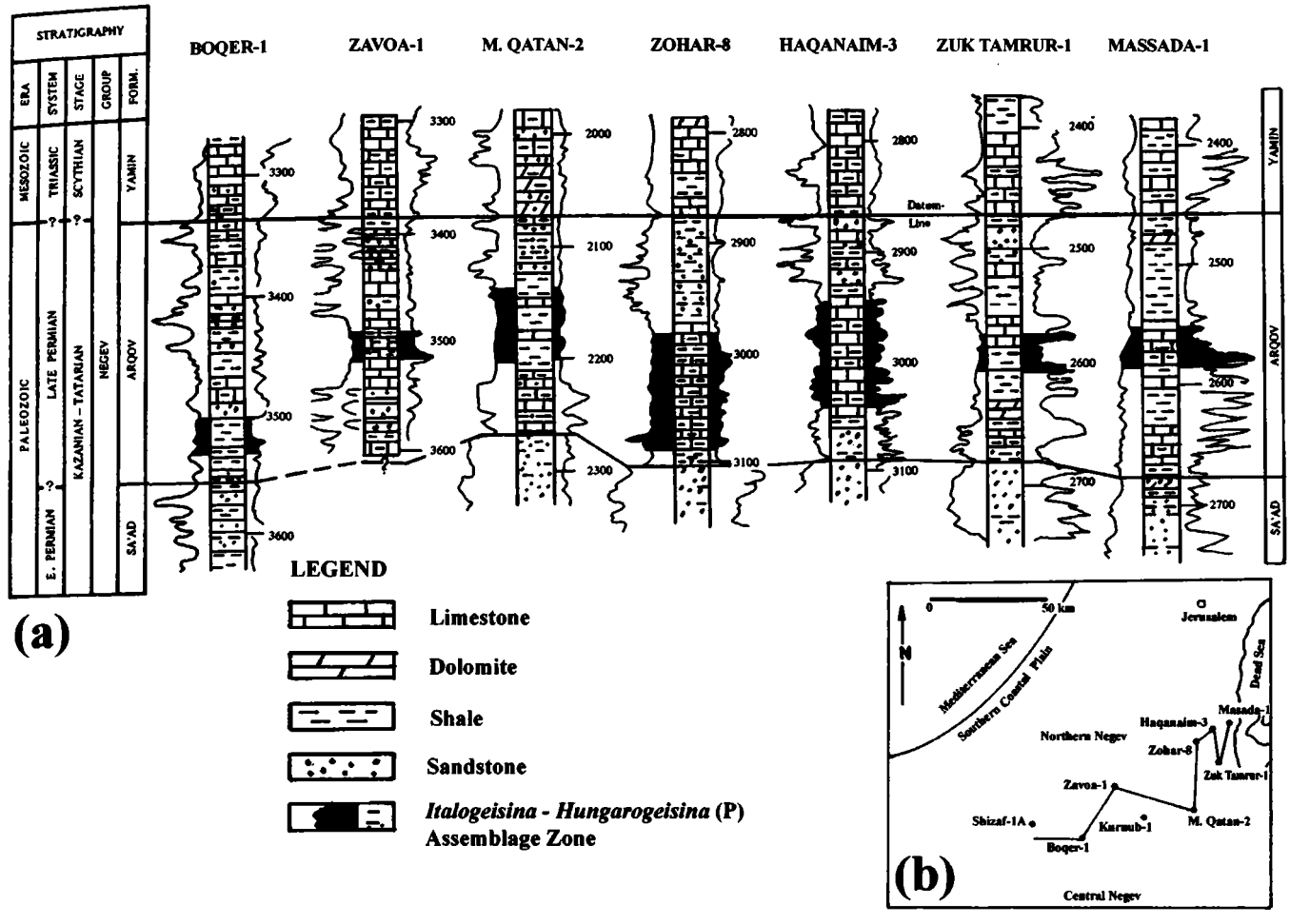


Figure 18C.3. Permian of the Negev (from Gerry et al., 1987). Occurrences of the Late Permian *Italogeisina-Hungarogeisina* Zone in Israel. a) Correlation chart of the *Italogeisina-Hungarogeisina* Zone (P) sections -Lithology, electric logs, and formation boundaries modified after well reports and Weissbrod (1981). Depths in meters. b) Location map of the wells.

Biostratigraphy

The Permian standard biostratigraphy which applies to our region is based on Fusulinids. In ascending order the Late Permian Fusulinid Faunal associations consist of the following faunal groups.

Early Murgabian

Cancellina-Armenina: The lower part of the Wordian stage is defined by the association of *Cancellina-Armenina*. It is closely related to the fusulinid associations of the zone of *Neochwagerina*. It is widely distributed within the Tethyan region, from Tunis to Timor (and New Zealand) and extends to the Cathaysian region of Eastern Asia and to the Japanese islands. Ross (1967) has singled out the Verbeekinid association from the three biofacies or sub-associations in the Tethyan realm. The sub-association that characterizes the eastern Mediterranean and parts of Iraq, Iran, and Western China, is composed of *Rugososchwagerina* and primitive species of *Polydiexodina* in a calcarenitic and sandy facies.

Late Murgabian -Early Midian

Neoschwagerina: The *Neoshwagerina* Zone defines the lower part of the Capitanian stage and the upper part of the Wordian stage. It is equivalent in age to the middle part of the Verbeekinid association and is widespread in a relatively narrow belt extending from the Mediterranean area of southern Europe across Asia to Japan. *Neoshwagerina* is characterized by the many genera of the family Verbeekinidae and by nearly all the new genera in the families Schubertellidae, Staffelidae, Fusulinidae, and Ozawainellidae. Conventionally, the Tethys association of *Neoshwagerina* is considered to be, at least in part, equivalent in age to the zone of *Polydiexodina* in North America. *Polydiexodina* occurs in association with *Verbeekina* in Afghanistan and Southern Turkey.

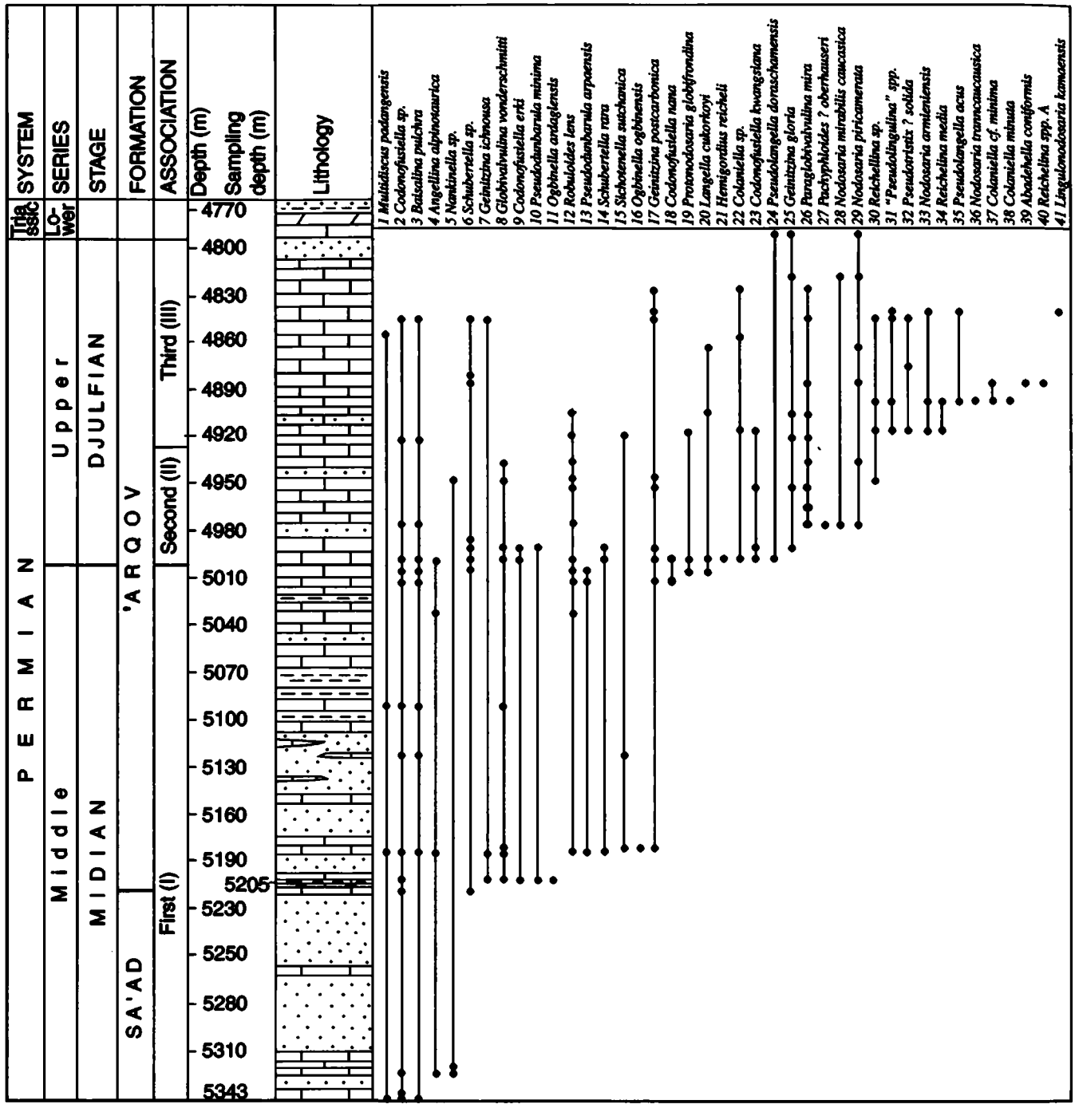


Figure 18C.4. Permian stratigraphy and distribution of the main foraminifers in Pleshet-1 borehole.

Late Midian

Lepidollina-Yabeina: The *Lepidolina-Yabeina* Zone defines the upper part of the Capitanian stage. It has been identified at numerous localites in the Eastern Hemisphere (including South-eastern Asia, Eastern Asia, Central Asia, Southern Europe, North Africa, Japan) and has been found in the Western Hemisphere (in British Columbia, Washington, and Oregon). At several places the *Lepidolina-Yabeina* association is known to occur stratigraph-ically above faunas of the Verbeekinid association. It includes *Lepidolina, Yabeina, Pseudodoilina, Codonofusiella, Schwa-gerina,* and *Dunbarella* (Ross, 1967, 1987, Thompson, 1964).

The *Palaeofusulina-Paradunbarula* and *Lepidollina-Yabeina* faunal associations represent the youngest fusulinacean-bearing rocks in the Tethys of the Eastern Hemisphere. The fusulinaceans became extinct in the narrow belt that extended from Oregon in North America, westward across the northern Pacific region to southern Asiá, and farther west at least to Tunisia in the Mediterranean area (Thompson, 1964).

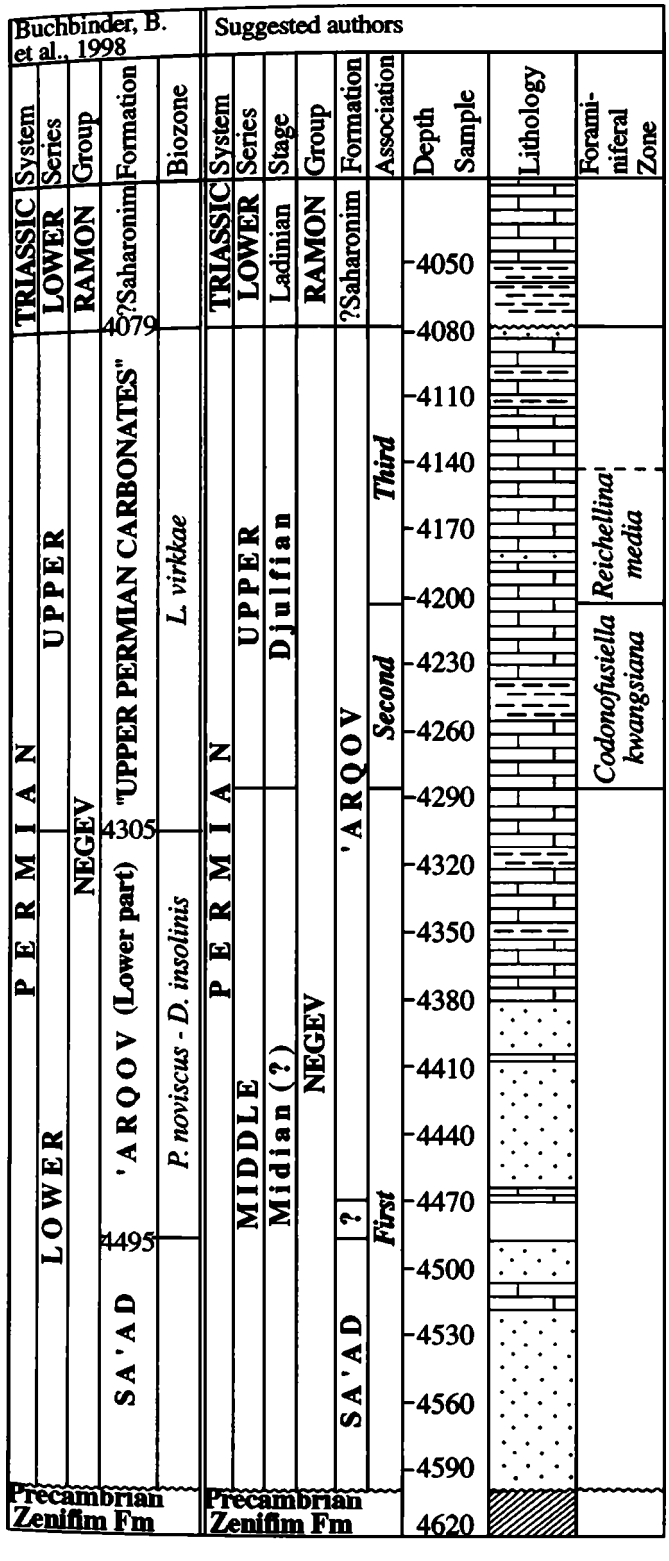


Figure 18C.5. Permian stratigraphy in Gevim-1 borehole.

Djulfian

Palaeofusulina-Paradunbarula: The youngest Permian fusulind zone includes *Paleofusulina* and *Parareichelina* and surviving genera from the zone of *Lepidolina-Yabeina*, such as *Reichelina, Dunbarella, Codonofusiella*, and several staffellid genera. *Palaeofusulina* is known only from the Tethyan region of southern Europe, northern Africa, central Asia, southwestern China, and southeast Asia, so that its biographic boundaries correspond closely to those of the Mesozoic Tethys. The Western Hemisphere (Ochoan) fusulinids are absent (Ross, 1967).

Israel (Plates 18C.1, 18C.2, and 18C.3)

Among the data for the local boreholes, the most comprehensive list of fossils is provided in the Gevim-1 Report (Buchbinder et al., 1998). The nearest studies deal with Turkey (Altiner et al., 1980; Zaninetti et al., 1981) and Iran (Zaninetti et al., 1979; Iranian-Japanese Research Group, 1981; Leven, 1999), and most recently Oman (Vachard et al., 2001) and Bahrain (Ziegler, 2001). The following levels were identified which according to three foraminiferal associations (Orlov-Labkovsky, 2002):

Level 1.	Pleshet-1	5343-5001 m
	Gevim-1	4500-4284 m

The interval can be dated as Upper Guadalupian (Upper Capitanian or Midian, possibly Lower Midian). Although the fusulinids listed do not include the genera *Yabeina* and *Lepidolina*, other fusulinids are characteristic of this age. Possibly the assemblage of smaller Foraminifers characterizes this interval as equivalent with the upper part of the Arpa Formation and lower part of the Khachic Formation of Transcaucasia; as well as with Unit 3 and 4(?) - Abadeh Formation, Central Iran; Unit 4 being analogous to the lower part of Khachic Formation in Transcaucasia. This is confirmed in Gevim 1 (4293-4299 m) by the occurrence of *Yangchienia cf. hainanica* Sheng.

Level 2.	Pleshet-1	5001-4926 m
	Gevim-1	4284-4203 m

This level is correlated with the *Codonofusiella kwangsiana* Zone, found in Unit 5 of the Abadeh Formation, as well as with the *Codonofusiella* beds in the upper part of Khachik Formation in Transcaucasia. This interval represents the transition between the Capitanian Stage (Middle Permian) and the Wuchiapigian Stage (Upper Permian) or that between the Midian and Djulfian stages. This interval would thus represent the transition between the Guadelupian Series in Texas, USA, which represents the strato-type of the Middle Permian, and the Lopingian series in South China, which represents the stratotype of the Upper Permian. One has to emphasize that nowhere is there a common

First Association

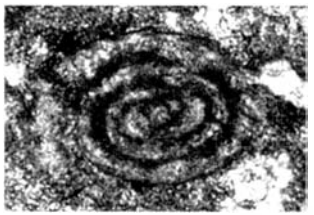
All x 50



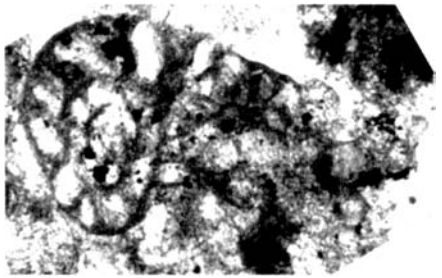
Nankinella sp.
Gevim 1,
4271-78 m



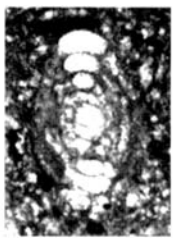
Schubertella paramelonica minor Suleimanov
Pleshet 1, 5181 –5187 m



Yangahienia cf. hainanica Sheng.
Gevim 1, 4293 - 4299 m



Codonofusiella sp.
Gevim 1, 4271 - 4278 m



Hemigordius ovatus Grozdilova
Pleshet 1 5338 – 43 m



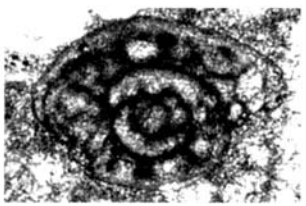
Ogbinella ogbinensis (Chedija).
Pleshet 1, 5181 -5187 m



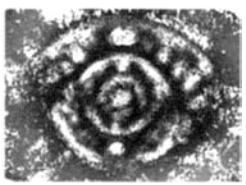
Multidiscus padangensis (Lange)



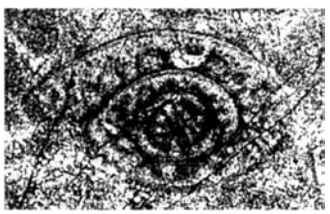
Sichotenella maichensis Sosnina
Pleshet 1
5181-5187 m



Pseudodunbarula aff. *arpaensis* Chedija
Gevim 1, 4293 - 4299 m



Pleshet 1, 5338 - 5343 m



Pseudodunbarula dzhagahzurensis Chedija,
Pleshet 1, 5193 -5203 m

Plate 18C.1. First Association fossils from the Pleshet-1 and Gevim-1 boreholes in Israel.

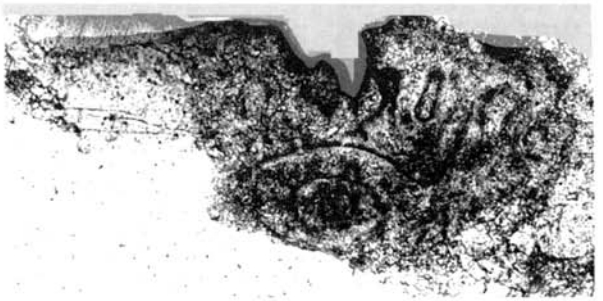
Second Association

All x 50

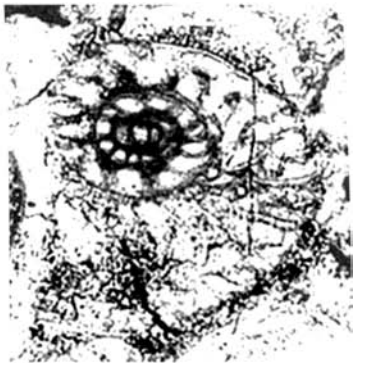
Codonofusiella kwangsiana Sheng.



Pleshet 1 4983 - 4992 m

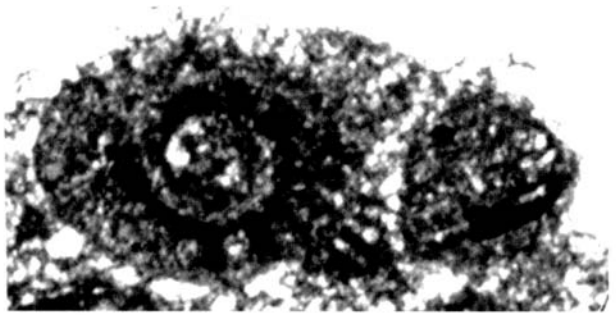


Gevim 1 4278 - 4284 m



Pleshet 1, P4983-92 (1),

Codonofusiella kwangsiana Sheng.



Gevim 1 4271 - 4278 m



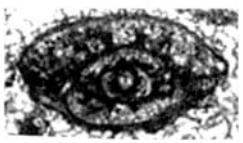
Gevim 1 4278-84(3)



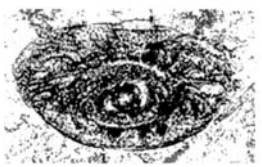
Nodosaria sp.

Codonofusiella sp.

Ogbinella aff. *ardaglensis (Chedija)*



Pleshet 1,
4992 - 5001 m



Pleshet 1,
4983 - 4992 m



Pleshet 1,
4992 - 5001 m

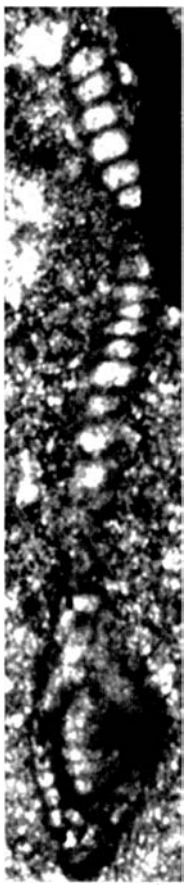


Pleshet 1, 4992 - 5001 m

Plate 18C.2. Second Association fossils from the Pleshet-1 and Gevim-1 boreholes in Israel.

Third Association

All x 50



Reichellina sp.
Gevim 1,
4203-4209 m



Reichelina media
K.Miklukho-Maclay
Gevim 1,
4203-4209 m



Reichellina spp. A
Pleshet 1, 4881-4890 m



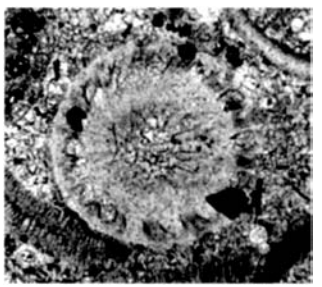
Codonofusiella erki Rauser,
Gevim 1, 4197 – 4203 m



Robuloides lens
Reichel
Pleshet 1,
4812-21



Frondina permica
Sellier et Dessauvagie
Pleshet 1,
4812-21



Colaniella sp.
Pleshet 1,
4812-21



Hemigordius sp.
Pleshet 1,
4839-45(2)-09



Schubertella rara Sheng
Gevim 1, 4131-4137 m



Paraglobivalvulina mira
Reitlinger
Pleshet 1, 4839-45(2)

Plate 18C.3. Third Association fossils from the Pleshet-1 and Gevim-1 boreholes in Israel.

boundary of the Guadelupian with the Lopingian Series

Level 3.	Pleshet-1	4926-4863; 4863-4791
	Gevim-1	4209-4090

In their lower part these strata are correlated with the *Reichelina media* Zone (the unit 6, possibly 2/3 of its volume) of the Hambast Formation, central Iran. This may represent the ammonoid *Vediocerас* Zone or higher, which are Wuchiapingian (or Djulfian) to Changsingian (or Dorashamian).

It is possible that in Pleshet-1 the 4863-4791 m interval is of early Dorashamian age.

REFERENCES CITED

Altiner, D., Baud, A., Guex, J., and Stampfli, G., 1980. La limite Permian-Trias dans quelques localites du Moyen-Orient: recherches stratigraphiques et micropaleontologiques. Riv. Ital. Paleont. Milan, 85 (1979)/3-4, p. 683-714.

Bartov, Y., Arkin, Y., Lewy, Z., and Mimran, Y., 1981. Regional Stratigraphy of Israel: a guide to geological mapping. Geol. Surv. Isr., Curr. Res., p. 38-41.

Buchbinder, B., Grossowicz, L., Peri, M., Eshet, Y., Rosenfeld, A., Siman-Tov, R., and Druckman, Y., 1998. Stratigraphy of the Gevim-1 Borehole. Geol. Surv. Isr., Report GSI/18/98, 16 p.

Derin, B., and Gerry, E., 1981. Late Permian – Late Triassic stratigraphy in Israel and its significance to oil exploration in Israel. Oil Exploration in Israel Symp. (abstracts). Isr. Acad. Sci. Human, p. 9-11.

Eshet, Y., 1990. Paleozoic-Mesozoic palynology of Israel. 1. Palynological aspects of the Permo-Triassic succession in the subsurface of Israel. Israel Geol. Surv. Bull., 81, 42 p.

Garfunkel, Z., and Derin, B., 1985. Permian-Early Mesozoic tectonism and continental margin formation in Israel and its implications for the history of the Eastern Mediterranean. In: J. E. Dixon and A. H. F. Robertson (eds.), The Geological Evolution of the Eastern Mediterranean, Geol. Soc. London, Spec. Publ., 17, Blackwell Scientific, Oxford, p. 187-201.

Gerry, E., Honigstein, A., Derin, B., and Flexer, A., 1987. Late Permian ostracodes of Israel; taxonomy, distribution, and paleogeographical implications. Senckenb. Lethaea, 68(1-4), p. 197-223.

Gvirztman, G., and Weissbrod, T., 1984. The Hercynian geanticline of Helez and the Late Palaeozoic history of the Levant. In: J. E. Dixon and A. H. F. Robertson (eds.), The Geological Evolution of the Eastern Mediterranean, Geol. Soc. London, Spec. Pub., 17, Blackwell Scientific, Oxford, p. 177-186.

Hirsch, F., 1976. Sur l'origine des particularismes fauniques du Trias et du Jurassique de la Plateforme Africano-arabe. [The origin of faunal peculiarities during the Triassic and Jurassic of the African-Arabian Platform]. Bull. Soc. Géol. France, 18(2), p. 543-552.

Hirsch, F., 1990. Aperçu de l'histoire phanérozoique d'Israël. [A sketch of the Phanerozoic history of Israel]. J. Afr. Earth Sci., 11(1-2), p. 177-196.

Iranian-Japanese Research Group, 1981. The Permian and lower Triassic systems in Abaden region, Central Iran. Mem. Fac. Sci. Kyoto Univ., ser. Geol and Miner., 47(2), p. 61-133

Jin, Y. G., Wardlaw, B. R., Glenister, B. F., and Kotlyar, G. V., 1997. Permian chronostratigraphic subdivisions, Episodes, 20(1), p. 10-15.

Kotlyar, G. V., Zakharov, Yu. D., Kochurkevich, B. V., Kropacheva, G. S., Rostovcev, K. O., Chedia, I. O., Vuks, G. P., and Guseva, E. A., 1983. The Upper Permian stage of the evolution of the organic world. Leningrad, Nauka, 157 p., 16 tables. (In Russian).

Leven, E. Ja., 1999. Permian fusulinids assemblages and stratigraphy of the Trancaucasia. Riv. Ital. Palaeont. Strat., 104(3), p. 299-328.

Orlov-Labkovsky, O., 2002. Associations of Permian Foraminifera from the subsurface of Israel. Abstract to Annual Meeting of the Geological Society of Israel. Kfar Nofesh Maagen, p. 88.

Ross, C. A., 1967. Development of fusulinid (Foraminiferida) Faunal Realms. J. Paleont. 41(6), p. 1341-1354.

Ross, C. A., 1987. Late Paleozoic sea levels and depositional sequences. In C. A. Ross and A. Haman (eds), Timing and Depositional History of Eustatic Sequences: Constraints on Seismic Stratigraphy, p. 137-149.

Thompson, M. I., 1964. Fusulinacea. In: Treatise on invertebrate paleontology. Lawrence, Pt. C, Protista 2, v. 1, p. c358-c436.

Vachard, D., Hauser, M., Martini, R., Zaninetti, L., Matter, A., and Peters, T., 2001. New Algae and problematica of algal affinity from the Permian of the Aseelah Unit of the Batain Plain (East Oman). Geobios, 34(4), p. 375-404.

Weissbrod, T., 1969. The Paleozoic of Israel and adjacent countries: Pt 1. The subsurface Paleozoic stratigraphy of southern Israel. Israel Geol.Surv. Bull., 47, p. 1-23.

Weissbrod T., 1981. The Paleozoic of Israel and adjacent countries: (Lithostratigraphic Study). Unpublished Ph.D. Thesis, Hebrew University Jerusalem. 275 p. (In Hebrew, extended English abstract).

Zaninetti, L., Altiner, D., and Catal, E., 1981. Foraminiferes et biostratigraphie dans le Permien superieur du Taurus oriental, Turquie. Notes Lab. Paleont. Université Genève, 7(1-2), p. 1-38.

Zaninetti, L., Broennimann, P., Huber, H., and Moshtaghian, A., 1979. Microfacies et microfaunes du Permian au Jurassique au Kuh-e Gahkum, Sud Zagros, Iran. Riv. Ital. Paleont. Milan, 84(4), p. 865-882.

Zaslavskaya; N., Eshet, Y., Hirsch, F., Weissbrod, T., and Gvirtzman, G., 1995. Recycled Lower Paleozoic microfossils (Chitinozoa) in the Carboniferous of Sinai (Egypt) and Permo-Triassic of the Negev (Israel): Paleogeographic considerations. Newsl. Stratigr., 32(1), p. 57-72.

Ziegler, M., A., 2001. Late Permian to Holocene paleofacies evolution of the Arabian Plate and its hydrocarbon occurrences. Gulf PetroLink, Bahrein, GeoArabia, 6(3), p. 445-504.

Note: The following bibliography, while not referenced in the text, is germane to the subject and is included for its possible utility.

Altiner, D., 1978. Trois nouvelles especes du genre Hemigordius (Foraminiferes) du Permian supérieur de Turquie (Taurus oriental). Notes. Lab. Paleont. Univ. Geneve, Genève, 2/5, p. 27-31.

Altiner, D., 1988. *Pseudovidalinidae* n. fam., and *Angelina* n. gen. From the Upper Permian of South and Southeast Turkey. Revue de Paleobiologie. Vol. Spec. No 2, Benthos '86, p. 25-36.

Altiner, D., and Zaninetti, L., 1977. *Kamurana bronnimanni*, n.gen., n.sp., un nouveau Foraminifere porcelane perfore du Permian superieur du Taurus oriental (Turquie). Notes. Lab. Paleont. Univ. Genève, Genève, 1/6, p. 1-5.

Altiner, D., and Bronnimann, P., 1980. *Louisettita elegantissima*, n. gen., n. sp., un nouveau Foraminifere du Permien superieur du Taurus oriental (Turquie). Notes. Lab. Paleont. Univ. Genève, Genève, 6/3, p. 39-43.

Arakeljan, R. A., Rauser-Chernousova, D. M., Reitlinger E. A., et al., 1964. Importance of Permian foraminifers of Transcaucasus for Permian correlation in Tethys. In: Upper Paleozoic and Mezozoic stratigraphy of the South biogeographic provinces. Rep. Soviet Geolog. At XXII Sess. IGC., Problem 16a., M., p. 63-75. (In Russian).

Baghbani, D., 1984. Upper Permian Foraminiferal Biostratigraphy of South-West Iran (Zagros Basin). Abst. 27 IGCC., M., 1(2), p. 8.

Bozorgnia, F., 1973. Paleozoic foraminiferal biostratigraphy of Central and Alborz Mountains, Iran. Nat. Iran Oil Company, Geol. Lab., Publ. No. 4, p. 1-167.

Bronnimann. P., Whittaker, J. E., and Zaninetti, L., 1978. Shanita, a new pillared Miliolacean Foraminifer from the Late Permian of Burma and Thailand. Riv. Ital. Paleont. Milan, 84/1, p. 63-92.

Canuti, P., Marcucci, M., and Pirini Radsizzani, C., 1970. Microfacies e microfaune nelle formazioni paleozoiche dell'anticlinale di Harzo (Anatolia sud-orientale, Turchia). [Microfacies and microfauna in the Paleozoic formations of the Hazro anticline, southeastern Anatolia, Turkey]. Boll. Soc. Geol. Ital., Rome, 89(1), p. 21-40.

Chedya, I. O., 1981. Some criteria for the subdivision of the species of *Lepidolina*, Neoschwagerinidae. Questions of. Micropaleontol, 24, p. 60-75. (In Russian).

Chen, S., 1956. The fusulinidae of South China. Pt. 2. Paleonto. Sinica. 6(5), p. 1-71

Ciry, R., 1942-43. Les fusulinides de Turquie. Ann.Paleont.,Vol. 30, p. 17-43

Derin, B., and Gerry, E., 1972. Micropaleontological report, Zavo'a 1 well. Israel Inst. Petrol., Rep. 3/72, 3 p.

Douglas, R. C., 1970. Morphologic studies of fuzulinides from the lower Permian of West Pakistan. Geol. Surv. Prof. Paper 643-G, Washington, p. G1-G11, plates I-VII.

Efimova, N. A., 1974. Triassic foraminifera of the Northwestern Fore-Caucasian area. Questions of Micropaleontol., 17, p. 54-83. (In Russian).

Efimova, N. A., 1979. The Early Triassic assemblages of foraminifera and their links with Paleozoic foraminifera on the example of the Caucasus. Questions of Micropaleantol, 22, p. 43-50. (In Russian).

Eshet, Y., 1990. The palynostratigraphy of the Permian-Triassic boundary in Israel: Two approaches to biostratigraphy.Isr. J. Earth Sci., 39(1), p. 1-15.

Gibshmann N. B., and Sipko, T. A., 1985. The new genus of the early Permian Staffellidae. Questions of Micropaleontol, 27, p. 24-32. (In Russian).

Gupta, V. J., and Kahler, F., 1973. Permische fuzuliniden aus dem Himalaya. [Parmian fusilinids from the Himalayas]. Neues Jahrb. Geol und Paleont., Vol. 4, p. 207-215.

Johnson, B., 1980. Microfaunal biostratigraphy of the Dalan Formation (Permian) Zagros Basin; South-West Iran. In: Permian Microfaunal Biostratigraphy of South-West Iran, Ch. 5, p. 52-60.

Kahler, F., 1974. Fuzuliniden aus Tien-Shan un Tibet. Mit Gedanken zur Geschichte der Fuzuliniden meere in Perm. The Sven Foundation (Publ. 52), Stockholm, p. 1-148.

Kahler, F., and Kahler, G., 1969. Einige permische Fuzuliniden aus dem Irak. [Permian fusilinids from Iraq]. Neues Jahrb. Geol Paleontol., Monat., 4, p. 232-241.

Kahler, F., 1974. Iranishe Fuzuliniden. Jahrb. Geol. Bund., Bd. 117, Wien, p. 75-107.

Khvorova, I. V., 1958. Atlas of the calcareous rocks of the Middle and Upper Carboniferous of the Russian Platform. Moscow, Publ. House of AN-USSR, 98 p., Tabl. 67. (In Russian).

Kotlyar, I. V., 1978. Correlation of the Upper Permian deposits with coeval deposits of the Tethys area and Boreal province. In: The Upper Paleozoic of North-eastern Asia, Vladivostok, p. 5-23. (In Russian)

Kummel, B., and Teichert, C., 1970. Stratigraphy and paleontology of the Permian-Triassic boundary beds, salt range and Trans-Indus range, West Pakistan. In: Stratigraphic Boundary Problems: Permian and Triassic of Pakistan, p. 62-110.

Lapparent, A. F., Blaise, J., and Lavigne Sainte-Suzanne, J., 1965. Sur les gisements a Fuzulines de L'Afganistan centrale. C. R., Acad. Sci., Paris, 260(19), p. 5073-5326.

Leven, E. Ya., 1967. Stratigraphia i fuzulinidy permskih otlozheniy Pamira. M., Nauka, 223 p., tab. 3.

Leven, E. Ya., 1971. Les gisements Permiens et les fusulinides de l'Afganistan du Nord. [The Permian beds and fusilinids of northern Afghanistan]. Notes et Memoirs Moyen-Orient, Paris, 12(1), p. 1-32, Plates 6.

Leven, E. Ya., 1977. On the question of the stage subdivision of the Tethyan Permian deposits. XXV Intl. Geol. Cong., Trasn. Soc. Geol., Stratigraphy and Sedimentology, Moscow, p. 82-95. (In Russian).

Leven, E. Ya., Pashkov, B. R., Mirzod, S. Kh., 1975. The Permian sedimentary rocks of Afghanistan. Bull. Moscow Society of Researchers in Nature, 50(5), p. 8-27. (In Russian)

Lys, M., 1987-1988. Biostratigraphie du Carbonifere et du Permien en Mesogee (Espagne, Afrique du Nord, regions Egeennes, Proche-Orient) Etudes micro paleontol.(Foraminiferes) Paleobiogeographie. Documents du B.R.G.M., Vol. 147, 315 p. (Universite de Paris-Sud, Orsay, France, 241 p., 21 plates).

Lys, M., and Lapparent, A. F., 1971. Foraminiferes et microfacies du Permiende L'Afganistan central. [Foraminifera and microfacies from the Permian of central Afghanistan]. Notes et Memoires sur le Moyen-Orient, 12(1), p. 47-133, Plates 22.

Lys, M., Stampfli, G., and Jenny, J., 1978. Biostratigraphie du Carbonifere et du Permian de l'Elbourz oriental (Iran du NE). [Carboniferous and Permian biostratigraphy of the eastern Elburz, northeastern Iran]. Notes Lab. Paleont. Univ. Geneve, 2(1-13), p. 63-100.

Maslov, V. P., 1956. Fossil algae of the USSR. Moscow, Publ. House of the AN/USSR, 300 p. (In Russian).

Maslov, V. P., 1973. Atlas of deposits formed by organic remains. Moscow, Nauka, 264 p.

Mehrnush, M., and Partoazar, H., 1977. Selected microfauna of Iran. Geol. Surv. of Iran, Report No. 33, p. 396, Part I Microfauna et biofacies of the late Devonian to late Permian PartII Microfauna et biofacies of the Triassic-Jurassic.

Micluho-Maklay, A. D., 1963. The Middle Paleozoic of Middle Asia. Leningrad, 327 p. (In Russian).

Montenat C., Lapparent, A., Lys, M., Termier, G., and Vachard, D., 1976. La transgression Permienne et son substatum dans le Jebel Akhdar (Montagnes d'Oman, Peninsule Arabique). [The Permian transgression and its substratum in Jebel Akhdar, Oman Mountains, Arabian Peninsula]. Annales, Soc. Geol. du Nord, 96(3), p. 239-258.

Nakazawa, K., and Kapoor, H. M., 1977. Correlation of the marine Permian in the Tethys and Gondwana. Sec.VI: Fourth Gondwana Symposium, Calcutta, India. Geol. Surv. India, p. 1-18.

Noe, S., 1988. Foraminiferal ecology and biostratigraphy of the marine Upper Permian and of the Permian-Triassic boundary in the Southern Alps (Bellerophon Formation, Tesero Horizon). Benthos '86, Revue de Paleobiologie. Spec. Issue 2, p. 75-88.

Ozawa, T., 1975. Evolution of *Lepidolina multiseptata* (Permian foraminifera) in East Asia. Mem. Fac. Kyushu Univ., 23(2), p. 117-164.

Pakistan-Japanese Research Group, 1985. Stratigraphy and correlation of the marine Permian-lower Triassic in the Surghar Range and Salt range. 25 p. Apparently in: Nakazawa, K., and Dickens, J. M. (eds.), 1985. The Tethys; her paleogeography and paleobiogeography from Paleozoic to Mesozoic, Tokai Univ. Press, Tokyo.

Permian System, International Congress, Perm, 1991. The Permian System of the World. Intl. Geol. Congress, 5-10 August 1991, Permian, Report Summaries, Sverdlovsk, 261 p. (In Russian).

Pronina, G., 1988. The Late Permian Smaller Foraminifers of Transcaucasus. Revue de Paleobiologie. Vol. Spec. No. 2, Benthos '86, p. 89-99.

Ross, C. A., 1986. Paleozoic evolution of southern margin of Permian Basin, Geol. Soc. Am. Bull., 97(5), p. 536-554.

Ross, C. A., and Ross, J. R. P., 1979. "Permian". In Treatise on Invertebrate Paleontology, Part A, Introduction. Fossilization (Taphonomy), Biogeography and Biostratigraphy, p. 291-350.

Sheng, J. C., 1963. Permian fusulinides of Kwangsi, Kueichow and Szechuan. Paleonto. Sinica, New. ser. B, 10, p. 1-247.

Skinner, I. W., 1969. Permian foraminifera from Turkey. Univ. Kansas Paleont. Contrib. Paper, no. 36, p. 1-14.

Stepanov, D. I., Golshani, F., and Stocklin, I., 1969. Upper Permian and Permian-Triassic boundary in north Iran. Geol. Surv. Iran, Rep. v. 12, p. 1-68.

Stepanov, D. L., Kotlyar, I. V., Leven, E., et al., 1980. The problem of straigraphy of the Permian system. Trans. of Soviet Geologists at XXVI Intl. Geol. Congr., Book V, Paleontology and Stratigraphy, Moscow, p. 172-180. (In Russian).

Taraz, H., 1971. Uppermost Permian and Permo-Triassic transition beds in Central Iran. Bull. Am.Assoc. Petrol. Geol., 55(8), p. 1280-1294.

Taraz, H., 1973. Correlation of uppermost Permian in Iran,Central Asia, and South China. Bull. Am.Assoc. Petrol. Geol., 57(6). p. 1117-1133.

Teichert, C., Kummel, B., and Sweet, E., 1973. Permian Triassic strata Kuh-e-bashi, Northwestern Iran. Bull. Mus. Comp. Zool., 145(8), p. 359-472.

Thompson, M. I., 1946. Permian fuzulinids from Afganistan. J. Paleontol., 20(2), p. 140-157.

Weissbrod, T., and Gvirtzman, G., 1988. The Late Devonian event in the Near East. Cour. Forsch. Inst. Senckenberg, Frankfurt/Main, 100, p. 221-233.

Weissbrod, T., and Perath, I., 1990. Criteria for the recognition and correlation of Sandstone units in the Precambrian and Paleo-Mesozoic clastic sequence in the Near East. In: C. A. Kogbe and J. Lang (eds.), Major African Continental Phanerozoic Complexes and Dynamics of the Sedimentation, J. Afr. Earth Sci., 10(1-2), p. 253-270.

Whittaker, J. E., Zaninetti, L., and Altiner, D., 1979. Further remarks on the micropaleontology of the late Permian of eastern Burma. Notes. Lab. Paleont. Univ. Geneve, Geneve, 5(1-7), p. 11-23.

Yankauskas, T. V., and Talli, S., 1979. The Paleozoic of the Arab Republic of Syria (ARS). Proc. Acad. Sci. USSR, Ser. 2, p. 92-97. (In Russian).

Zaninetti, L., and Altiner, D., 1981. Les Biseriamminidae (Foraminiferes) dans le Permien supérieur mésogéen: évolution et biostratigraphie. [Biseriamminidae

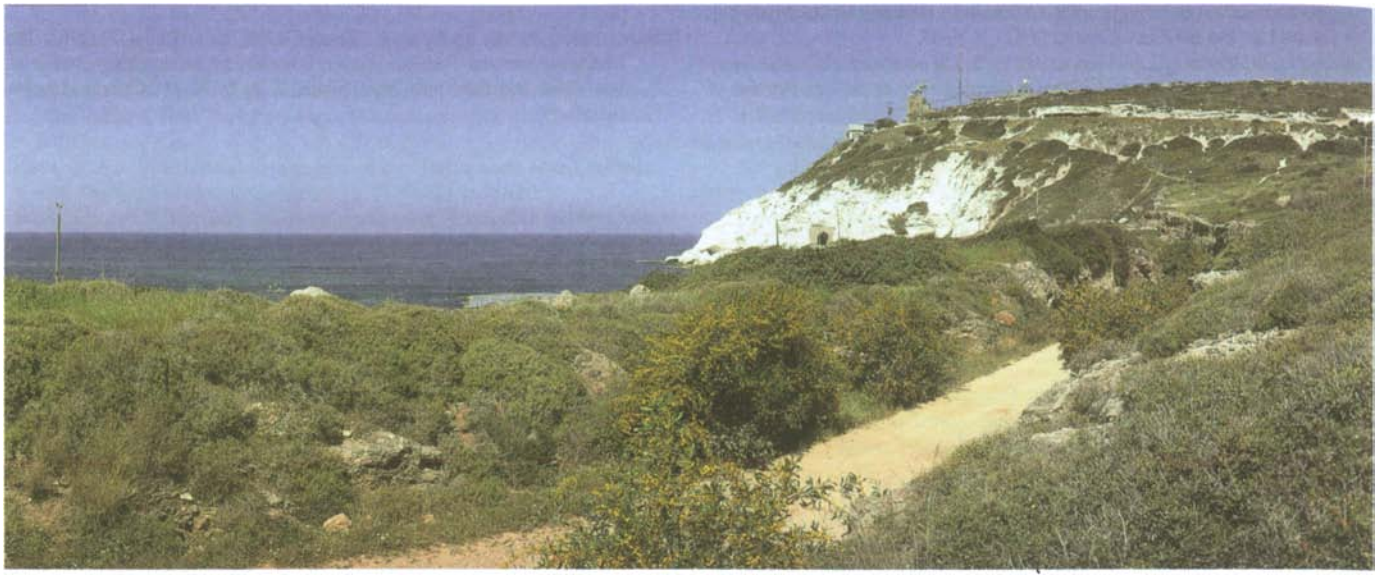
(foraminifera) in the Mésogaean Upper Permian; evolution and biostratigraphy]. Notes Lab. Paleont. Univ. Genève, 7(1-2), p. 39-47.

Zaninetti, L., Whittaker, J. E., and Altiner, D., 1979. The occurence of *Shanita amosi* Bronnimann, Whittaker et Zaninetti (Foraminiferida) in the Late Permian of the Tethyan region. Notes. Lab. Paleont. Univ. Genève, Genève, 5(1-7), p. 1-9.

Zhao J., Sheng, J., Yao Z., Liang, X., Chen, C., Rui, L., and Liao, Z., 1981. The Changhsingian and Permian-Triassic boundary in South China. Bull. Nat. Inst. Geol. and Palaeont., Acad. Sinica, 2, p. 1-112. (In Chinese, English summary).



The Central Plateau of the Upper Galilee.
Color image from The Holy Land Satellite Atlas, Volume II (1999, p. 50). ©Røhr Productions Ltd., Nicosia, Cyprus. Reproduced with permission. View towards the northwest.



The white chalk cliffs of Rosh Ha-Niqra at the border with Lebanon.
Color image from The Holy Land Satellite Atlas, Volume II (1999, p. 57). ©Røhr Productions Ltd., Nicosia, Cyprus. Reproduced with permission. View towards the northwest.



The Jezreel (Yizre'el) Valley and Mount Tabor.
Color image from The Holy Land Satellite Atlas, Volume II (1999, p. 47). ©Røhr Productions Ltd., Nicosia, Cyprus. Reproduced with permission. View towards the southeast.

Chapter 18D

The Triassic of Israel

Chaim Benjamini
Ben Gurion University of the Negev, Department of Geology, POB 653, Beersheva 84 105, Israel
Francis Hirsch and Yoram Eshet
Geological Survey of Israel, 30 Malchei Israel Street, Jerusalem 95 501, Israel

PREFACE

The Triassic of the region between the Levant coastal region and central Arabia was deposited along a series of peri-cratonic belts ranging in facies from continental to oceanic (**Fig. 18D.1**). A small number of outcrops located west of Suez, in southwestern and eastern Sinai, the Negev, and just east of the Dead Sea Rift, allow detailed inspection of much of the sequence in the field, but most of the regional distribution patterns are derived from borehole data.

First reports on lower and middle Triassic were by Cox (1924, 1932), from east of the Rift Valley. These exposures of Upper Permian-Middle Triassic strata are described from the gorges of Zarqa Main, Himara, Dardun, and Mukheiris, and the wadis of Ain Musa, Naur, Es Salt, Um Tina, and Zarqa, all of which empty into the Dead Sea Rift (Wetzel and Morton, 1959; Bandel and Khoury, 1981). Middle Triassic strata were recognized at Areif en Naqa (Sinai) by Awad (1945) and further described by Bartov et al. (1980). Shaw (1947) first described the Triassic sequence of Ramon, followed by Zak (1964) and Druckman (1969, 1974, 1976). The exposure at Har 'Arif (Negev) was first described by Zemel et al. (1956). Eicher (1947) discovered the first unquestionable conodonts of clearly Triassic age from these Sinai and Negev outcrops, although a detailed description of this fauna was published only much later by Eicher and Mosher (1974).

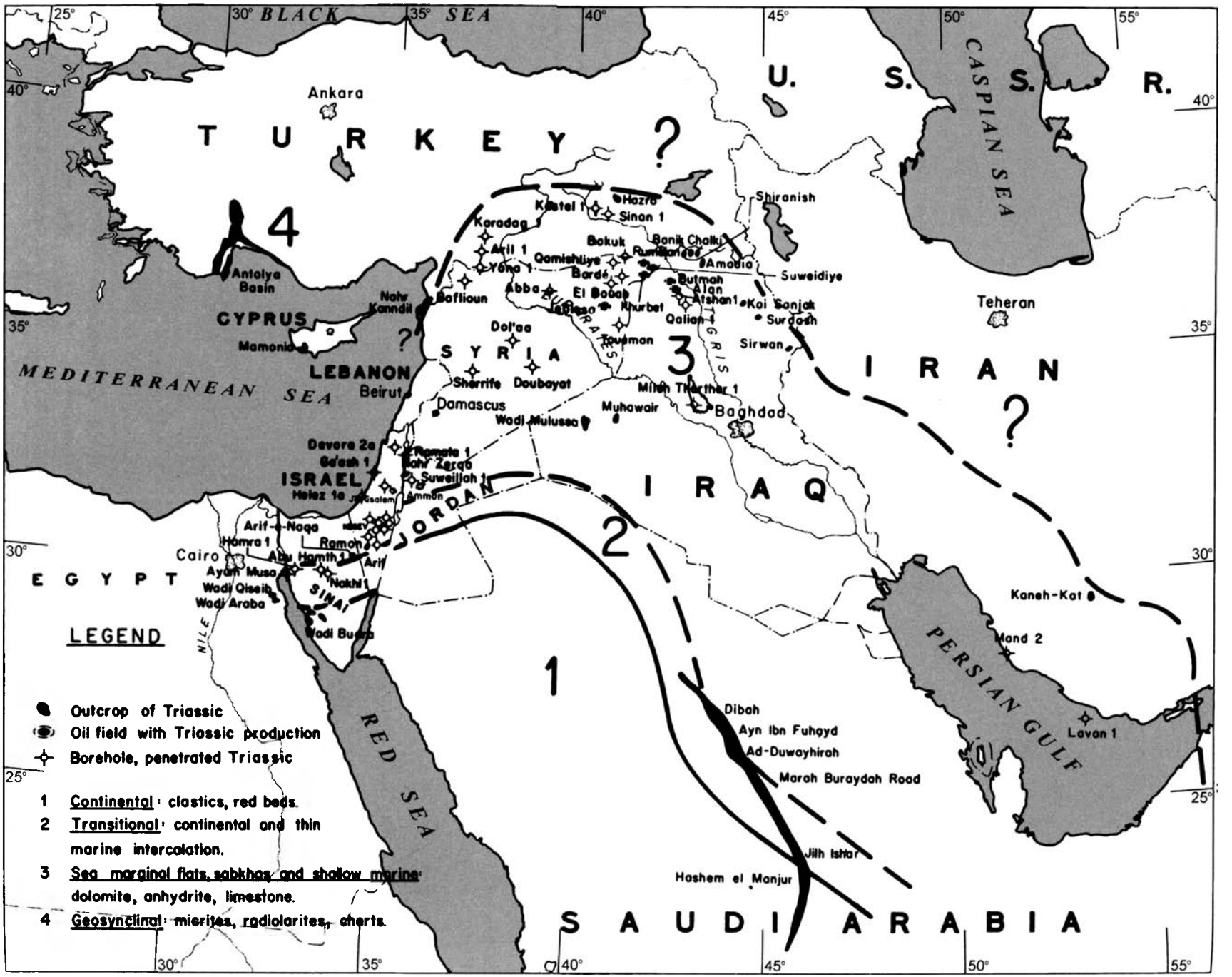
In Israel, the northern Negev region was penetrated by more than 20 boreholes (**Fig. 18D.2**), but in central and northern Israel by only 6 boreholes. Numerous seismic sections of varying quality provide additional data.

The Ramon sequence is best exposed, most accessible, and has been the most studied. Brotzen (1956) first published on the paleontological and biostratigraphical features of the outcrop, while Zak (1957, 1968) made an initial lithostratigraphic subdivision. Druckman (1969, 1974, 1976) extended the sedimentological and lithostratigraphical studies and applied them to the subsurface of the Negev. Picard and Flexer (1974) published a compilation and synthesis of Triassic stratigraphic data. Benjamini et al. (1993) presented an updated interpretation on the stratigraphy and environments of deposition of the Ramon outcrop.

Lerman (1960) studied the bivalve faunas of the Ramon outcrop, reporting for the first time on the presence of Carnian strata. He reported also the initial ammonoid determinations of Parnes, which were subsequently described in three monographs (Parnes, 1962, 1975, 1986). Nautilids were studied by Kummel (1960) and vertebrates by Haas (1959, 1963, 1969, 1970). Micropaleontological studies began with an initial report on foraminifers and conodonts by Sohn and Reiss (1964), and ostracodes (Sohn, 1968; Huddle, 1970; Hirsch, 1972; Hirsch and Gerry, 1973). Palynomorphs were first studied by Glikson

Table 18D.1: Lithostratigraphic units described for the Triassic of Israel.

STAGE	FORMATION	FACIES BELT & SOURCE	DOMINANT LITHOFACIES
Rhaeto-Norian	Asher Volcanics (partim)	II (Asher-Atlit borehole)	reefal carbonates interbedded with volcanics
Rhaeto-Norian	Shefayim Fm	II, III (Ga'ash borehole)	dolomite; limestone
Carnian	Mohilla (equiv)	II, III (Ga'ash borehole)	limestone; shale
Carnian	Mohilla Fm	I, II, III (Ramon, Devorah)	evaporites; carbonates
Carnian	Erez 'Conglomerate'	II (Helez, Ga'ash)	carbonate breccia
Anisian-Carnian	Saharonim Fm	I, II, III (Ramon, Devorah)	fossiliferous carbonates
Anisian	Gevanim Fm	I (Ramon, Negev)	sandstone; shale; marl
Anisian	Ra'af Fm	I, II (Har 'Arif; boreholes)	fossiliferous limestone
Olenekian	Zafir Fm	I (boreholes)	shale; sandstone; carbonates
Olenekian	Yamin Fm	I (boreholes)	carbonates; marl; sandstone


BLACK SEA
U. S. S. R.
CASPIAN SEA
Ankara
TURKEY
Antalya Basin
CYPRUS
Mamonia
Nahr Kannoit
Baflioun
MEDITERRANEAN SEA
LEBANON
Beirut
SYRIA
Damascus
Dol'aa
Sherrife
Doubayat
Wadi Mulussa
Muhawair
Baghdad
Mlish Thirthar 1
Teheran
IRAN
IRAQ
JORDAN
ISRAEL
Devora 2a
Ga'ash 1
Helez 1a
Jerusalem
Ammon
Ramote 1
Bahr Zarqa
Suweilah 1
Arif-el-Naqa
Homra 1
Ramon
Abu Hamth 1
Arif
Cairo
EGYPT
Ayun Musa
Wadi Qiseib
Wadi Araba
Nakhl 1
SINAI
Wadi Bucra
NILE
RED SEA
Karadag
Kastel 1
Hazro
Sinan 1
Arll 1
Qamishliye
Yoha 1
Bakuk
Bonik Chalki
Amodia
Shiranish
Suweidiye
Bardé
El Bosab
Abba
Jauseso
Khurbet
Butmah
Alan
Atshan 1
Qalian 1
Koi Sanjak
Surdash
Sirwan
Tawman
TIGRIS
EUPHRATES
Kaneh-Kat
Mand 2
PERSIAN GULF
Lavan 1
Dibah
Ayn Ibn Fuhayd
Ad-Duwayhirah
Marah Buraydah Road
Jilh Ishtar
Hashem el Manjur
SAUDI ARABIA
LEGEND
Outcrop of Triassic
Oil field with Triassic production
Borehole, penetrated Triassic
1 Continental: clastics, red beds.
2 Transitional: continental and thin marine intercalation.
3 Sea marginal flats, sabkhas and shallow marine: dolomite, anhydrite, limestone.
4 Geosynclinal: micrites, radiolarites, cherts.
1
2
3
4
?
25°
30°
35°
40°
45°
50°
55°

(1964) and Horowitz (1970). More recently, progress was made in updating the biostratigraphy using ammonites (Parnes et al., 1985), conodonts (Hirsch, 1975; Benjamini and Chepstow-Lusty, 1986), palynomorphs (Eshet, 1990a, b), foraminifers (Benjamini, 1983) and application of a sequence stratigraphic framework (Hirsch, 1992; Druckman et al., 1997).

I. TRIASSIC LITHOLOGICAL UNITS

The depositional patterns and main events characterizing the Triassic of Israel echo the history of the Triassic Neotethys: Commencement of spreading early in the Triassic; establishment of the Anisian-Early Carnian Sephardic faunal Province as faunas and carbonate depositional environments evolved; renewed rifting in the Carnian, followed by development of Neo-Tethyan (alpine-type) facies. The most important of the local findings include:

1) The P/Tr boundary is marked by a late Paleozoic algal spike, reworked early Paleozoic microfossils, and a hiatus marked by absence of the Induan.

2) A Werfen-like shallow clastic marine facies prevailed from the Olenekian to earliest Anisian, dated by conodonts and palynomorphs.

3) The development of carbonate-dominated facies from the Anisian to the Early Carnian was characterized by biofacies of the Sephardic Province, interfingering southwards with continental-derived clastics.

4) Carnian evaporite deposition on continental margins was the result of combined tectonic movements and global sea-level fall on a margin undergoing renewed rifting.

5) Late Carnian to Rhaetian restoration of shelf and offshore marine conditions were developed in Hauptdolomite/Dachstein-like lithofacies.

6) Truncation beneath the Jurassic was the result of tectonic uplift and associated volcanism.

In Israel, the local representation of the regional facies belts is as three types, differently positioned on the continental margin (Fig. 18D.2). Lithostratigraphic units of **Table 18D.1** reflect the difference in depositional patterns.

I. NEGEV-TYPE:

Continental deposits, sea marginal flats, and neritic marine sediments up to 1000 m thick are exemplified by the Negev outcrops and numerous boreholes. This facies type developed upon the stable shelf between the Arabo-Nubian continent and a Neotethyan embayment. The Negev-type facies is observed as far north as the Pleshet-1 borehole (**Figs. 18D.3, 18D.4, 18D.5, and 18D.9**).

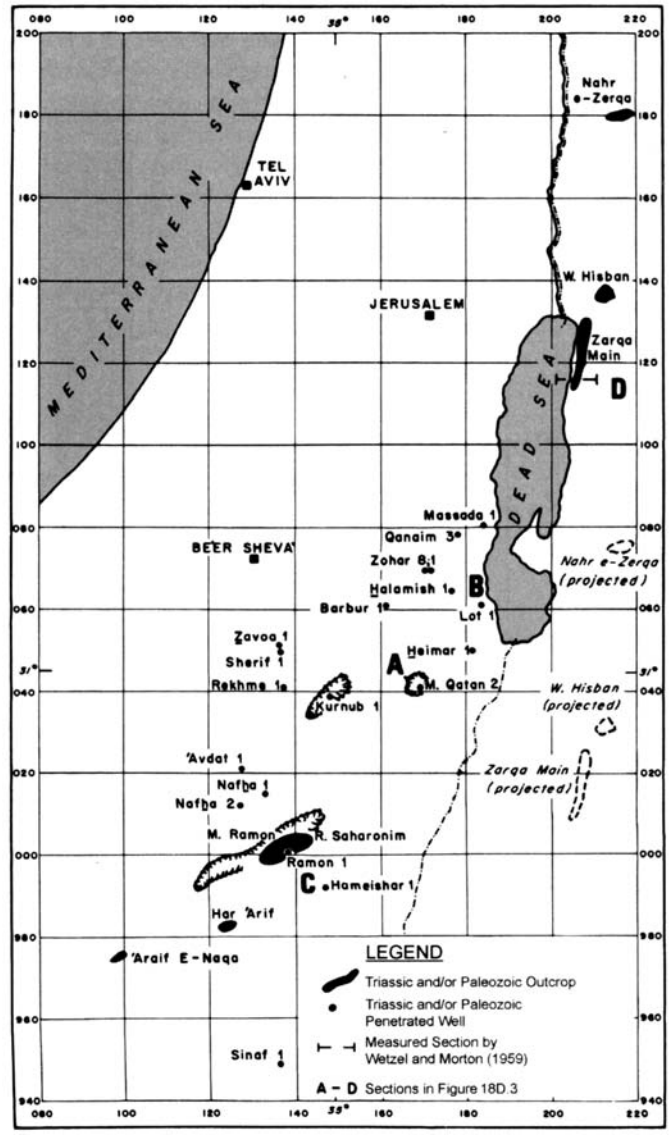


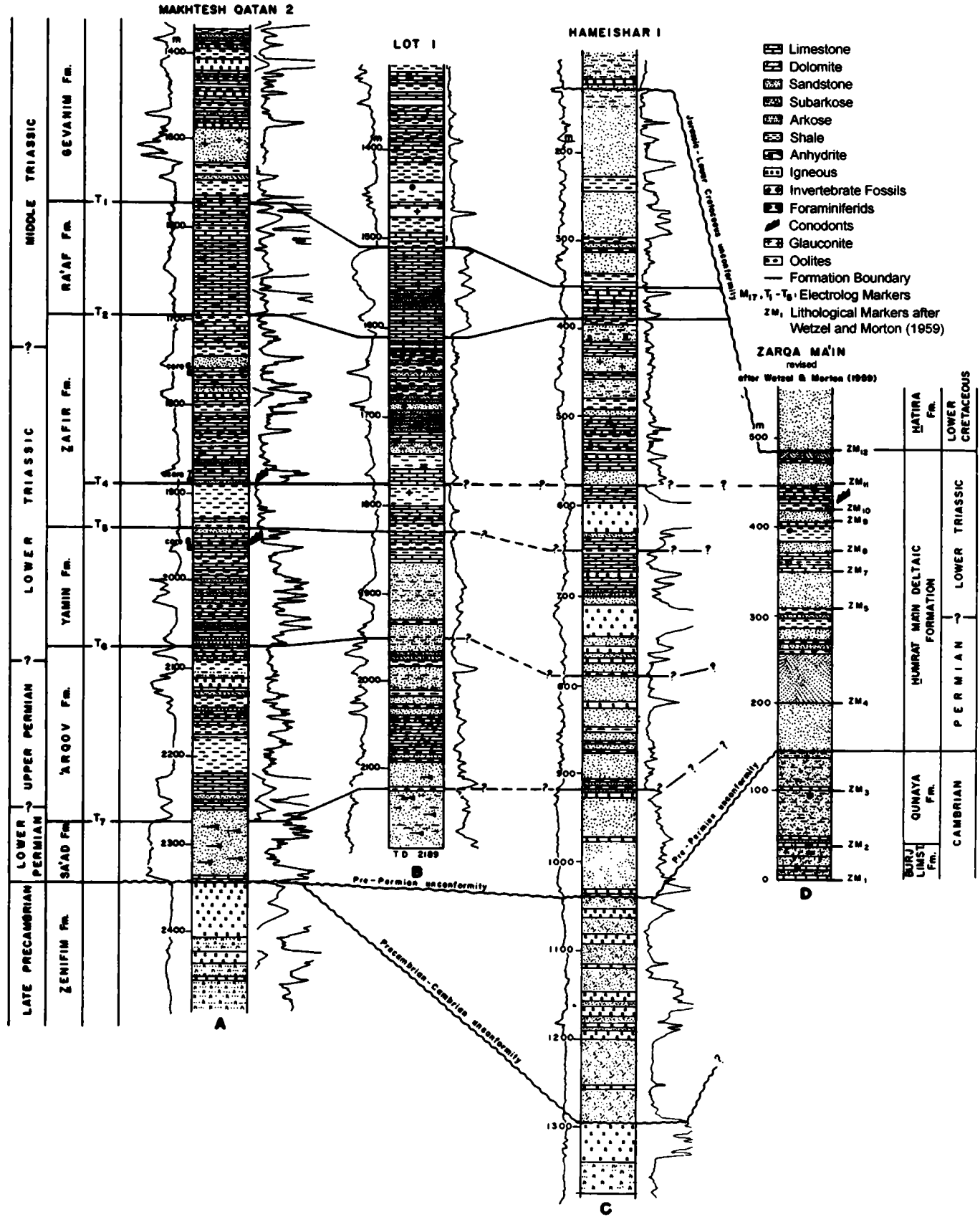
Figure 18D.2. Location map of Triassic and Upper Paleozoic exposures and boreholes of the Negev belt (modified, after Druckman et al., 1982, Fig. 1, p. 921).

II. HELEZ-TYPE:

A more rapidly subsiding zone distal to the Negev type shelf underlies the Coastal Plain region. The depositional pattern is known from only a small number of Coastal Plain boreholes, *e.g.*, the Helez-deep (850 m), Ga'ash (1000+ m) and Asher-Atlit (1000+ m) (**Figs. 18D.6, 18D.7, and 18D.8**)



Figure 18D.1. The Triassic exposures between the Levantine coast and Central Arabia. (Modified from Druckman et al., 1982, Fig. 2, p. 922-3, entitled 'Distribution of Upper Triassic facies along the margins of the Arabian Shield (after Druckman, Gvirtzman, and Kashai, 1975)' (rotated).


MAKHTESH QATAN 2
LOT 1
HAMEISHAR 1
ZARQA MA'IN
revised
after Wetzel & Morton (1959)
Limestone
Dolomite
Sandstone
Subarkose
Arkose
Shale
Anhydrite
Igneous
Invertebrate Fossils
Foraminiferids
Conodonts
Glauconite
Oolites
Formation Boundary
Electrolog Markers
Lithological Markers after Wetzel and Morton (1959)
LATE PRECAMBRIAN
LOWER PERMIAN
UPPER PERMIAN
LOWER TRIASSIC
MIDDLE TRIASSIC
ZENIFIM Fm.
SA'AD Fm.
'ARQOV Fm.
YAMIN Fm.
ZAFIR Fm.
RA'AF Fm.
GEVANIM Fm.
HATIRA Fm.
HUMRAT MAIN DELTAIC FORMATION
QUNAYA Fm.
BURJ LIMST Fm.
LOWER CRETACEOUS
LOWER TRIASSIC
PERMIAN
CAMBRIAN
Pre-Permian unconformity
Precambrian-Cambrian unconformity
TD 2189
A
B
C
D

III. DEVORAH-TYPE:

The Devorah subsiding deep, located in Judea and Galilee (central and northern Israel), is represented by shallow marine marginal flat sediments up to 3000 m thick. This facies type was encountered in only a few boreholes, namely, Ramallah-1 (1200$^+$ m) in central Israel and Devorah-1 (2600$^+$) in the north (Fig. 18D.6).

Triassic sediments were truncated by basal Jurassic and basal Cretaceous erosional episodes, and no Triassic section is preserved in the Negev south of the Paran lineament (Fig. 18D.5). In the Coastal Plain (*e.g.*, Ga'ash borehole) the Triassic sequence is most complete and Early Jurassic laterites (Mishhor Formation) overlie Rhaeto-Norian carbonates of the Shefayim Formation. In the Ramon, Har 'Arif (Negev), and Nahr Zarqa (Yabbok, Jordan) outcrops, the Jurassic variously overlies the Carnian, Ladinian, or even Anisian.

1. THE BASE OF THE TRIASSIC IN ISRAEL

At the dawn of the Mesozoic, the Precambrian crystalline basement of the African-Arabian continent was only exposed well to the south of the Sinai-Negev continental margin, with generally thin Paleozoic cover of various ages intervening. Around the P/Tr transition, the average position of the E-W striking coastline separating continental and marine facies was located in the mid-Sinai-Negev region. This line passed somewhat to the south of the Nahkl-1 borehole of central Sinai and the Meishar borehole in the central Negev (Fig. 18D.5) (Druckman, 1974a).

The P/Tr transition was encountered in a number of boreholes from the Negev and Coastal Plain regions (Hirsch and Weissbrod, 1986). Late Permian ages based on foraminifera (*Codonofusiella*) and ostracods (*e.g.*, *Sargentina*) in marine strata are recorded from the 'Arqov Formation (Derin and Gerry, 1981). The position of the P/Tr transition was originally placed in a variety of lithostratigraphic units, using electric-log stratigraphy criteria in each borehole (Weissbrod, 1968; Eshet, 1990). The Permian-Triassic boundary has now been definitively placed by several authors (Hirsch, 1976, 1990; Druckman et al., 1982) at a red clay horizon which lies between the 'Arqov and Yamin Formations. Eshet (1990b) showed in several boreholes that the uppermost occurrence of the Permian palynomorph *Lueckisporites virkiae* coincides with the red clay and a characteristic fungal spike, and therefore that is the local position of the P/Tr boundary (see also Eshet et al., 1995; Visscher et al., 1996). This red clay was previously placed according to the e-log stratigraphy in the uppermost part of the 'Arqov Formation in the Shezaf-1 and Zuq-Tamrur-1 boreholes, within the lower half of the Yamin Formation in Pleshet-1, Masada-1, Heimar-1, Makhtesh Qatan-2, and Avedat-1, near the top in Zohar-8, or at the 'Arqov-Yamin boundary in Ramon-1. These e-log definitions for the 'Arqov/Yamin Formation boundary are thus no longer tenable, and both the formation boundary and the P/Tr transition should be consistently placed at the red clay horizon.

Above the fungal spike, which appears to occur in continental facies, Induan strata are absent. In other Tethyan sections (*e.g.*, the southern Alps, Italy, Dinarids; Hirsch, 1975, 1992) the Induan stage is represented by the *Hindeodus parvus* and *H. isarcicus* conodont zones, which are absent in Israel. Recycled Lower Paleozoic chitinozoans and other Paleozoic palynomorphs and acritarchs were recovered from strata in this position (Eshet, 1990; Zaslavskaya et al., 1995) indicating a subaerially eroded Paleozoic substratum. The earliest Triassic conodont zone in Israel is the Olenekian *Hadrodontina anceps* conodont zone, in a Werfen-type clastic marine facies.

2. THE NEGEV-TYPE TRIASSIC

a) THE LOWER TRIASSIC IN THE NEGEV: BOREHOLE DATA (Figs. 18D.3, 18D.4, 18D.5).

The Yamin and Zafir Formations

The lowermost Triassic formations of the Negev, the Yamin and Zafir Formations, are together 400-500 m in thickness. Three lithofacies are present: sandstone, limestone/dolomite, and mixed clastics ranging from shale to fine-grained sandstone. The sandstone lithofacies consists of marine glauconitic sandstone interbedded with coquina-like carbonates, rarely amalgamated into dolomitized limestone. The tabular geometry of the sandstone horizons and the fossils in these units indicate an oscillating marginal marine environmental suite including lagoonal, barrier, foreshore or shoreface subenvironments, alternating with finer clastics and carbonates of more offshore conditions.

The Yamin Formation (Weissbrod, 1969) consists predominantly of thickly-bedded dolomitic sandstones, with a few carbonate-free sandstone layers in the lower part. Glauconite and pyrite are present, and shales are rare. Carbonate content varies from 75% in Kurnub-1 to 25% in Ramon-1, where sandstone represents 40% of the rocks. The thickness of the formation varies from 118-154 m.

The Zafir Formation (Weissbrod, 1969; Druckman, 1974; Picard and Flexer, 1974) consists of calcareous and pyritic shales, alternating with sandy, glauconitic, or dolomitic limestone. Layers of glauconitic sandstone with dolomitic and siliceous cement appear in the upper part of the formation. The proportion of sandstone increases southward. The thickness of the formation varies from 270 to 192 m.

Eshet and Cousminer (1986) and Eshet (1990a) report on the occurrence of the palynomorph taxa *Endosporites papillatus* and *Densoisporites nejburgii* in the Yamin and Zafir Formations. These



Figure 18D.3. The Early Triassic from the Negev Boreholes (Israel) across the Jordan Rift Valley (after 'Stratigraphic cross section of the Permian-Lower Triassic interval across the Jordan Rift Valley' of Druckman et al., 1982, Fig. 5, p. 928-929, itself modified after Weissbrod, 1976).

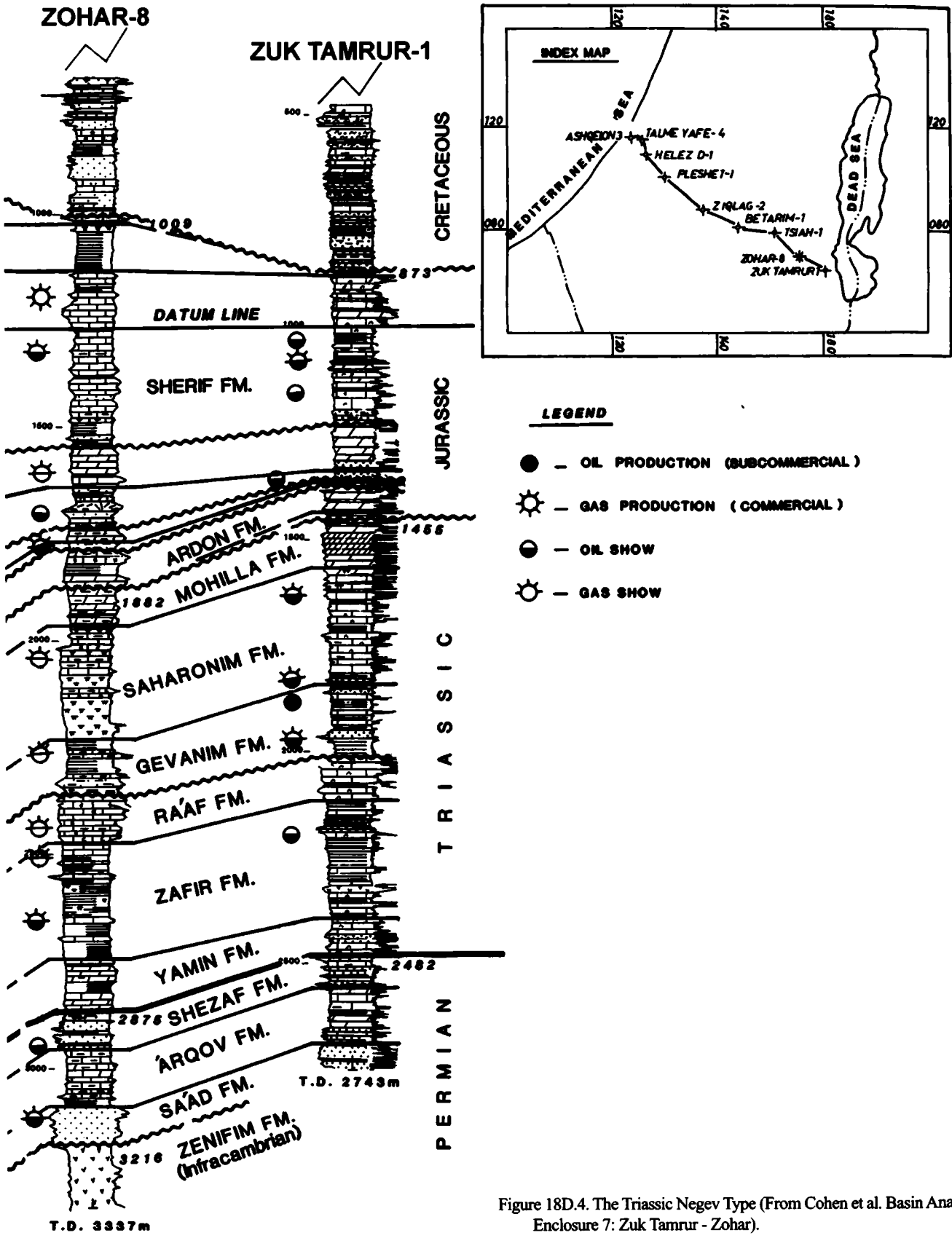


Figure 18D.4. The Triassic Negev Type (From Cohen et al. Basin Analysis Enclosure 7: Zuk Tamrur - Zohar).

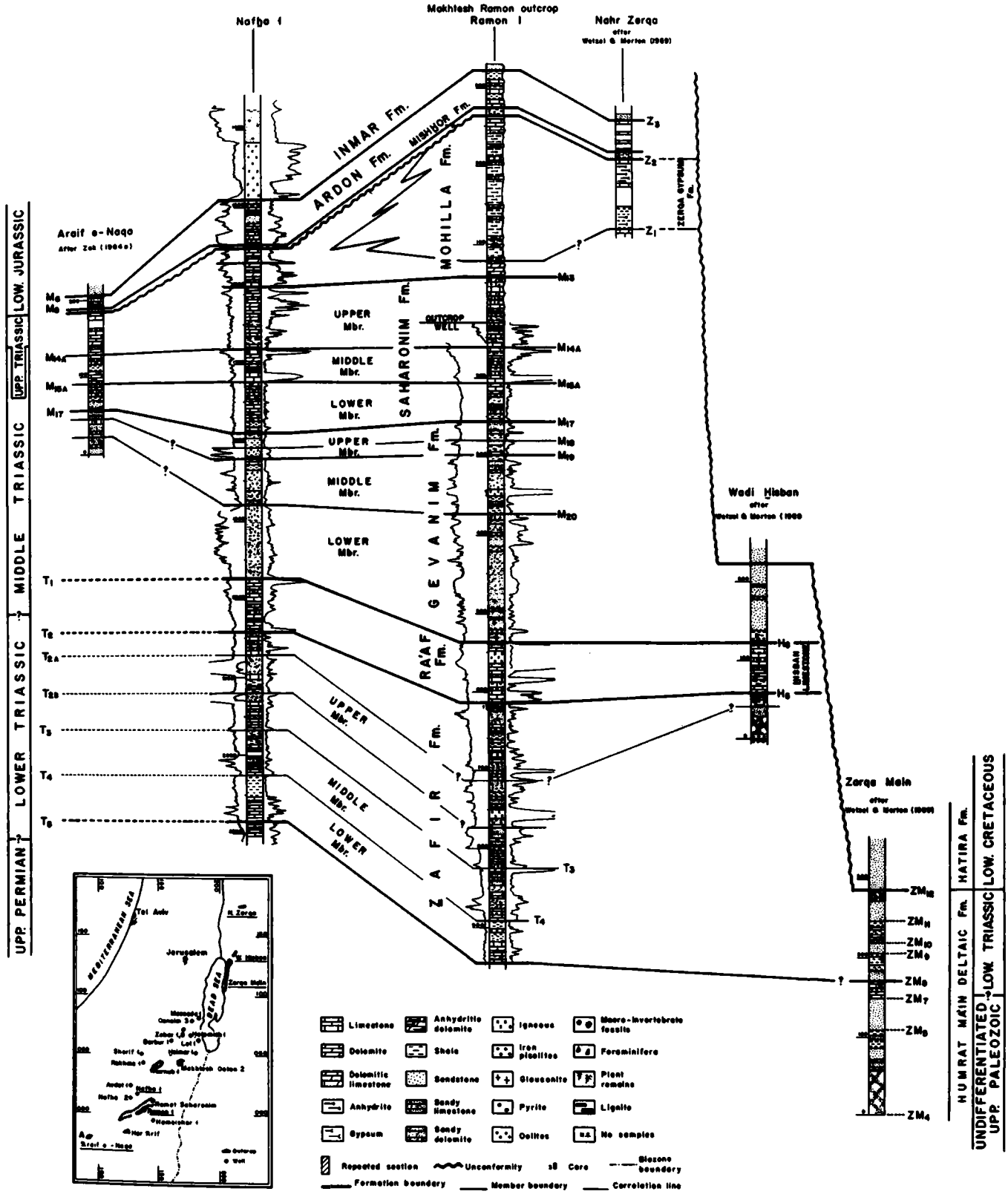


Figure 18D.5. The Middle-Late Triassic in the Negev (Israel) and Jordan (after Druckman, 1974a, p. 83, Fig. 2).

taxa characterize the *nejburgii-heteromorphus* 'phase' of Brugman (1986), and indicate an Olenekian age. *Endosporites papillatus* occurs from the lower part of the Yamin Formation in the Ramon-1 and Makhtesh Qatan-2 boreholes (Eshet, 1990), whereas in other boreholes, *e.g.* 'Avedat-1, Zohar-8, this assemblage occurs not lower than the upper part of the Yamin Formation (Dunay, 1973). The Olenekian conodont multi-elements *Hadrodontina anceps* and *Pachycladina obliqua* occur in the upper part of the Yamin Formation and in the lower part of the Zafir Formation in the Makhtesh Qatan-2 and Zavoa-1 boreholes (Hirsch and Gerry, 1974; Hirsch, 1975).

Anisian palynomorphs occur in the uppermost part of the Zafir Formation (Horowitz, 1973; Eshet and Cousminer, 1986; Eshet, 1990a). Late Anisian ammonoid and conodont faunas were reported from the top of the Zafir Formation in the Ramon-1 borehole (Hirsch, 1977).

In summary, the base of the Yamin Formation unconformably overlies the 'fungal spike' which defines the P/Tr transition. An Olenekian age can be assigned to the Yamin Formation and most of the Zafir Formation, with the Olenekian-Anisian boundary occuring in the upper part of the Zafir Formation.

b) THE MIDDLE-UPPER TRIASSIC IN THE NEGEV: BOREHOLES AND OUTCROPS (Fig. 18D.5).

The Anisian marine facies, encountered at the top of the Zafir Formation in numerous boreholes, continues upwards through the Ra'af and Gevanim Formations to the lower part of the Saharonim Formation. Outcrops of the Ra'af Formation occur at Har 'Arif, overlain by Gevanim Formation clastics. At the Ramon outcrop, a 500 m thick section of the Gevanim, Saharonim, and Mohilla Formations is exposed, representing the Late Anisian to Carnian. This is the thickest continuously exposed Triassic sequence in the Levant region.

Ra'af Formation (Zak, 1968)

The type section of the Ra'af Formation is from the Ramon-1 borehole. It has also been described from numerous deep boreholes, with its subsurface thickness averaging 100 m. The main lithologies are coquina-like bioclastic limestone and dolomite, oncolitic and pyritic shales, fine-grained limestones with foraminifera, molluscs, echinoid fragments, and brachiopods, minor oolites, and dolomite. The carbonates were considered by Druckman (1974) as indicative of deposition in a shallow marine environment, with oolitic shoals developed in the Sherif-Zavoa' area of the northwestern Negev. The dolomite/limestone ratio increases to the south, while thickness generally increases northwards. The exposure of the upper 38 m at Har 'Arif (Druckman, 1974) is described below.

1) Base is 10 m of coarsely crystalline dolomitized limestone, intruded by magmatics.

2) 14.5 m of reddish-yellow argillaceous, sometimes crinoidal limestone, with *Encrinus* sp., *Coenothyris vulgaris*, and the following ammonoids (det. Parnes, 1986): *Pronoetlingites arifensis*, *Beneckeia* cf. *wogauana posterior, Balatonites* close to *B. balatonicus, B.* cf. *jovis* and *B.* cf. *zimmeri*. Foraminifera include *Tolypammina gregaria, Planiinvoluta? mesotriassica, Meandrospira deformata, Glomospira negevi, Glomospirella raa* , and *Earlandia tintinniformis* (Benjamini, 1984).

3) 4.3 m of shallow marine sandstones.

4) 8.5 m of shales, sandstones and limestone with *Encrinus* sp., *Coenothyris vulgaris*, *Myalina* sp., *Pseudoplacunopsis fissistrata*, *Lima striata*, *Costatoria* cf. *costata*, *Enantiostreon difforme*, *Schafhautlia* cf. *mellingi*, and *Naticopsis* sp.

5) Top is overlain by Gevanim Formation sandstones.

The Ra'af Formation is assigned to the Pelsonian substage of the Late Anisian on the basis of the ammonoids *Pronoetlingites arifensis* and *Balatonites balatonicus* of Ammonite Level I of Parnes et al. (1985) (Table 18D.1), found at Har 'Arif and also in core 1 of the Ramon-1 borehole, together with the conodont *Nicoraella kockeli*. The foraminiferal assemblage containing *Glomospira densa* is common in the subsurface Ra'af Formation (Zaninetti, in Druckman, 1974).

Gevanim Formation (Zak, 1963)

The Gevanim Formation at Har 'Arif overlies the Ra'af Formation, and 145 m of section is exposed below the Lower Cretaceous truncation surface. At the type locality at Ramon only the upper 120 m is exposed, overlain by the Saharonim Formation. The Gevanim Formation was penetrated by many deep boreholes.

The lower part of the Gevanim Formation, exposed at Har 'Arif (Druckman, 1974, paleontological determinations by Parnes, 1962), is as follows (from base to top):

1) Base is 0-8.6 m of sandstone; wood-bearing.

2) 8.6-18 m of cross-bedded sandstone with a thin dolomite horizon at base. At the top is a coquina horizon yielding *Pachycardia* sp., *Trigonodus* aff. *costatus* or *carniolicus*, *Trigonodus tenuidentatus*.

3) 18-28 m of sandy shales.

4) 28-65 m of cross-bedded ferruginous sandstone with plant remains.

5) 65-82 m of sandstone and sandy shales.

6) 82-130 m of cross-bedded and laminated ferruginous sandstone with plant remains.

7) 130- 135 m of sandstone with shales and rare sandy limestones, containing *Lingula tenuissima*, *Trigonodus* sp., *Myophori-cardium* cf. *lineatum*, *Myophoriopis* sp., *Megalodon* cf. *carinthiacus*.

8) 135-145 m of sandstone.

9) 145-166 m of talus cover on contact with the Arod Conglomerate (Cretaceous).

The upper part of the Gevanim Formation exposed at Makhtesh Ramon was first described and subdivided into members by Zak (1964). No marker horizon occurs to enable identification of overlap or gap between the Ramon and Har 'Arif sections. The following horizons are determined, from base to top:

1) 0-27.5 m Quartzite Member: Cross-bedded fluviatile sandstone section terminating in a red silt horizon. Abundant plant remains.

2) 27.5-68 m Sandstone-Clay Member: Channelled fluviatile sandstones and overbank shales and siltstones, passing upwards

to tidal sandstones with *Lingula*; lagoonal silts and shales, and shoreface sands. The continental/sublittoral alternations represented by these strata are evidenced by the presence of wood *(Cedroxylon)* and other plant remains, together with intertidal brachiopods (*Lingula*) and gastropods, and *Placodus* teeth.

3) 68-92 m Sandstone-Limestone-Shale Member: Offshore to marginal marine shales, sandstones and thin limestones. The lower horizons of this member yield marine bivalves, and the brachiopods *Lingula tenuissima* Bronn, *Coenothyris vulgaris* (Schloth), and *Dielasma julicum*. The 'Beneckeia bed' (Brotzen, 1956) at the top is a marly limestone with rich faunas described by Parnes (1962). The ammonoid *Beneckeia levantina* Parnes was recovered from Ammonite Level II of Parnes et al. (1985), along with a rich marine fauna including nautilids, marine ostracods, the vertebrates *Nothosaurus* sp., *Psephosaurus mosis* Brotzen, *Placodus* (teeth), *Hybodus* sp., and *Tanystrophaeus* sp., the brachiopods *Lingula tenuissima* Bronn and *Dielasma julicum* (Bittner), the bivalves *Myophoria vulgaris* (Schloth.), *Lyriomyophoria intermedia* Schauroth, *Neoschizodus orbicularis* (Bronn), *Trigonodus tenuidentatus* Lerman, *Pseudoplacunopsis fissistriata* (Winkler), *Enantiostreon difforme* (Schloth.), *Myalina beneckei* Brotzen, *Gervillia joleaudi* Schmidt, *Pecten discites* (Schloth.), and the gastropod *Zygopleura* sp.

4) 92-126 m (Top) Sandstone-Reef Limestone Member: Littoral and marginal marine sandstones and shales, with some limestone and dolomite horizons. Faunas include *Lingula,* the reptiles *Nothosaurus* and *Psephosaurus*, and 'reef beds' of Brotzen (1956). The latter is a 5 m thick lenticular accumulation of shells of *Myalina ramanensis* in a black limy matrix. Lerman (1960) described this as a lumachelle "formed in nearshore, quiet waters". Benjamini et al. (1993) considered this accumulation to be estuarine, considering the near absence of associated, fully marine macro- or microfaunas, in contrast with highly diverse, fully marine horizons elsewhere in the Gevanim or Saharonim Formations.

The Gevanim Formation represents a short interval in which thick continental and marginal marine deposits accumulated across the northern Negev, during a Late Anisian low-stand. Continental lithofacies consist mainly of coarse to medium fluviatile sandstone with abundant plant remains, passing into marine lithofacies of dark gray shale with sandstone and sandy coquina intercalations to the north and west. Marginal marine faunas at Har 'Arif and Ramon, with small scale ripple cross lamination, horizontal bedding, flaser [streak] bedding, and burrows, in part also observed in the Zohar and Heimar wells, indicate tidal conditions. At Ramon, molluscan banks and an ammonite-rich horizon indicate more offshore marine environments. A fluviatile and deltaic model overprinted by sea level change, proximal in the Ramon region and extending distally to the north and northwest, was proposed for the Gevanim Formation by Druckman (1974, 1976) and Benjamini et al. (1993).

Saharonim Formation (Zak, 1963)

The Saharonim Formation is a primarily carbonate sequence with shale, marl, and evaporite interbeds, attaining a thickness of 174 m at Ramon. It represents the main transgressive phase of the Middle Triassic, which began towards the end of the Late Anisian, lasting until the Early Carnian. The Saharonim Formation at Ramon was subdivided into members by Druckman (1969, 1974) utilising a series of prominant limestone cliffs as dividing elements, as follows:

1) 0-37 m. Fossiliferous Limestone Member: Meter-thick clay and marly shale horizons with limestone terminations, overlain by mollusc limestone horizons with undulating bedding planes, and again by shale/limestone alternations. The unit is topped by a prominent limestone ledge, called by Awad (1946) the 'Mottled Scar'.

The lower part of this member contains Ammonoid Level III of Parnes et al. (1985) (Table 18D.1), the *Paraceratitoides brotzeni* horizon, belonging to the uppermost Anisian. The upper part of the member contains Ammonoid Level IV (Parnes et al., *ibid.*), the *Protrachyceras curionii* var. *ramonenesis* horizon. considered lowermost Ladinian. The *-shagami* conodont horizon described by Benjamini and Chepstow-Lusty (1986) is found in the middle part of the section. Near the top the conodont *Pseudofurnishius murcianus* was recovered, which occurs no earlier than the early Ladinian.

In all, this subunit is extremely rich in marine fossils. An extraordinarily rich bivalve and gastropod fauna was identified (Lerman, 1960; Parnes, 1962): *Leda* cf. *fibula* Mansuy, *Palaeoneilo elliptica* (Goldf.), *Lyriomyphoria elegans* (Dunker), *L. germanica* Hohenst., *Costatoria coxi* Awad, *C. multicostata* Lerman, *Neoschizodus laevigatus** (Ziethen), *Myophoriopis* cf. *subundata** (Schauroth), *Pseudoplacunopsis fissistriata** (Winkler), *P.* cf. *ostracina* (Schloth.), *Placunopsis* cf. *flabellum* Schmidt, *Ostrea montiscaprilis** Klipst., *Modiola* cf. *raibliana* Bittner, *M.* cf. *salzstettensis* Hohenstein, *Cassianella* cf. *decussata* (Munst.), *Cassianella* sp., *Gervillia joleaudi* Schmidt, *G.* aff. *alberti* (Goldf.), *G.* cf. *bouei* (Hauer), *Lima striata* (Schloth.), *Lima* sp., *Mysidioptera* cf. *vixcostata* (Stoppani), *Pecten discites** (Schloth.), *P. albertii* (Goldf.), *Schafhautlia* aff. *mellingi* (Hauer), *Anodontophora munsteri* (Wissm.), *Pleuromya* cf. *mactroides* (Schloth.), *Naticopsis* sp., *Zygopleura* sp., and *Omphaloptycha* sp. Crinoids, brachiopods, ammonoids, nautiloids, ophiuroids, vertebrates (mostly reptiles), ostracods, and conodonts are also abundant. This fauna contains many endemic ammonoids belonging to *Paraceratites, Israelites, Negebites, Gevanites*, and *Protrachyceras* (Parnes, 1962, 1975, 1986). These are defining forms of the Sephardic realm, the faunal realm that extended across the south Neotethyan shelf from the Near East to the western Mediterranean.

Foraminiferal faunas were rare and non-indicative, but in the 'Mottled Scar', in some localities, a diverse trocholinid-involutinid fauna is developed including *Lamelliconus procerus* var. *multispiroides*, and *Mesodiscus eomesozoicus* were found. These are primarily Ladinian forms.

The Fossiliferous Limestone Member of the Saharonim Formation was deposited under a low energy regime in an offshore marine environment, with a supply of continent-derived clays rhythmically interrupted by carbonate horizons, possibly storm concentrations. The 'Mottled Scar' represents a relatively distal

starved offshore facies.

2) 37-87 m. Limestone and Marl Member: This member consists at the base of 9 m of dark, nodular, bioturbated micrites, reminiscent of the 'calcaires vermicules' in Europe. This facies is overlain by fossiliferous limestones and marls with oolites, stromatolites, small molluscan mounds, flat pebble conglomerates, and several evaporite/dolomite/shale horizons, indicating a range of marine environments ranging from offshore to intertidal. A brief offshore episode in indicated by Ammonoid Level V of Parnes et al. (1985) (Table 18D.1), the *-epigonus* horizon of the Late Ladinian. The fauna occuring here consists of the ammonoids *Gevanites epigonus* and *G. cornutus*. The conodont *Pseudofurnishius murcianus* occur here as well. Bivalves marked above with an asterisk (*) in the underlying member occur here as well, with addition of *Lima telleri* Bittner.

The uppermost part again is transitional to more marine facies, with foraminiferal limestones (*Lamelliconus cordevolicus*, *L. procerus*, *Lamellidiscus sinuosus*, and large nodosariids). A prominant dark gray limestone ledge, dolomitized in its upper part labeled the 'Reddish Brown Scar A' by Awad (1946), is the termination of this unit. It represents a distal, clastic-free facies, similar to the 'Mottled Scar' limestone underlying this member.

3) 87-144 m. Limestone and Gypsum Member: This unit is composed of a variety of lithofacies, including fine-grained dolomite, foraminiferal and oncoidal limestones, algal stromatolites, and shale, marlstone, and gypsum intercalations. These fully marine limestones are characterized by their conodont, ostracod, bivalve, and cephalopod faunas. In the lower part of this unit, above the first gypsum horizon, Ammonoid Level VI, the *Protrachyceras hispanicum* horizon of Parnes et al. (1985) (Table 18D.1) is found, indicating the *-archelaus* Zone of the Longobardian (Late Ladinian), with *Protrachyceras ladinum* Mojs. and *P. hispanicum* Mojs. To this level also belong the conodonts *Sephardiella mungoensis* and *Pseudofurnishius murcianus*. Ostracods of the *Simeonella brotzenorum* Zone occur here in floods. At the top of this unit is Ammonoid Level VII of Parnes et al. (1985), indicating the latest Ladinian *-regoledanus* Zone, with *Protrachyceras sirenitiforme* Parnes, *P. rectangulare*, and *Clionites rarecostatus* Parnes. This is the uppermost Triassic ammonoid horizon identified in Israel.

The upper part of this member is characterized by a number of prominant ledges. 'Reddish Brown Scar B' of Awad (1946), within the unit, differs from the 'Mottled Scar' and other similar ledges, in that petrographic inspection shows it to be a dolomitized oolite facies, unlike the gray bioturbated micritic limestones of the other named cliff units. The top of the member is 'Reddish Brown Scar C' of that series.

4) 144-171 m. The Limestone Member: The uppermost member of the Saharonim Formation is represented by several morphological cuestas developed on a variety of lithofacies. Gray bioturbated limestones form ledges, with gypsiferous shales, dolomicrite, and algal stromatolites intervening. Rare bivalves, floods of ostracods, and foraminiferal limestones point to open marine facies shallowing to intertidal hypersaline to brackish environments, in several oscillations. 'Reddish Brown Scar D' occurs somewhat above the base, indicating offshore, starved conditions, as do a number of similar but less prominent ledges ('helminthoid limestones' of Zak, 1964) near the top.

The Saharonim Formation lithofacies indicate rapid deepening at first, commencing at the end of the Anisian, and then an oscillating pattern of facies, with each oscillation ranging from deeper marine environments with ammonoid faunas, shallowing progressively through shelf and marginal marine facies. A concomitant general climatic change can be traced as the fluviatile delta of the Gevanim Formation is replaced in the low-stands by relatively clastic-poor evaporitic lagoons in the Ladinian and early Carnian. In the subsurface, the Saharonim Formation thickens gradually to the northwest. Local thinning at the Lot-1 borehole is attributed to differential subsidence.

Mohilla Formation (Zak, 1963)

The Mohilla Formation in its type locality at Makhtesh Ramon represents most of the Carnian phase of deposition. It demonstrates considerable variations in thickness (110 to >200 m) and lithofacies, which include dolomite, shale and either a massive gypsum evaporitic facies, or laterally, a cellular limestone facies. A tripartite subdivision can be made:

1) 0-25 m. Dolomite Member: This part consists primarily of crinkly laminated saccharoidal dolomite, with clay- and marlstone interlayers, some oolites, algal stromatolites, and thin gypsum interbeds. An oolitic horizon with the foraminifera *Lamelliconus procerus* and *Aulotortus gaschei* is found in this unit.

2) 25-175 m. Gypsum and Dolomite Member: Two main facies were identified in the middle member of the Mohilla Formation, an evaporitic facies and a dolomitic facies, which are accompanied by thickness changes, with the evaporitic facies varying from 131 m to 206 m, and the dolomitic facies from 52 m to 123 m. In the central Makhtesh Ramon over 150 m of evaporitic gypsum occurs, consisting of cyclic alternations of varied gypsum lithofacies, with interbeds of laminated dolomites and dolomitic or bituminous shales. A peculiar nodular chert marker horizon occurs in the lower part. Rare fossiliferous horizons occur, including one with the brachiopod *Spiriferina lipoldi*, and beds with calcareous algae, stromatolites, rare bivalves, and floods of ostracods. At Ramat Saharonim in the east of Makhtesh Ramon, the dolomitic lithofacies occurs, consisting of a reduced section of thin-bedded dolomite, dolomitic limestone and gypsiferous marls, with oolites, algal stromatolites, and solution breccia. The thick gypsum is reduced here to two small units, each about 10 m in thickness.

3) 175-200 m Limestone Calcarenite Member: A limestone unit of variable thickness, truncated at the top by sub-Jurassic erosion, caps the Triassic section. The lithofacies is of well-bedded wavy limestone, sometimes oolitic, with stromatolites and laminated dolomite. It is dark in color and foetid-smelling when freshly broken. A bioclastic horizon in the middle yielded the bivalves *Costatoria inequicostata* and *Trigonodus* cf. *sandbergi*, the Late Carnian conodont *Paragondolella polygnathiformis* (Eicher and Mosher, 1974), and some foraminiferans, ascribed to a new genus

Agathaminella (Benjamini, 1988).

The Mohilla Formation was deposited in subsiding basins during an evaporite-dominated low-stand phase, characterized by cyclic alternations of supratidal sabkhas and hypersaline lagoons, often stagnant. Rare fossils and algal stromatolites indicate occasional freshening. The highest beds bearing molluscs and conodonts indicate restoration of normal marine salinity and renewed transgression of the latest Carnian. The low-stand is apparently correlative with global sea level fall in the beginning of the Late Triassic, followed by end-Carnian transgression. The thick sections deposited during the low-stand indicate subsidence of tectonic origin at this time (Druckman, 1974, 1976). The limestones of the top of the Mohilla Formation were affected by karstic erosion and contain residual pockets of kaolinitic flint-clays with aluminous and ferrigenous pisolites of the overlying Mishhor Formation (Early Liassic, Goldberg, 1964).

'Saharonim Basalt'

Baer et al. (1995) have reported basalt intrusions into the Carnian Mohilla Formation at Ramat Saharonim in Makhtesh Ramon. This 'Saharonim Basalt' gave Triassic Ar-Ar ages ranging from 209-216 Ma, which is Late Carnian-Early Norian. These ages correlate with subaerial volcanics interbedded with the Late Triassic reef sections of northern Israel (Korngrin and Benjamini, 2001). K-Ar ages of additional samples range from 202-210 Ma (Norian).

3. THE COASTAL PLAIN: HELEZ-TYPE TRIASSIC (Fig. 18D.6)

The sedimentary cycles of the Negev Triassic apparently track eustatic sea level fluctuations on the ramp-margins of the Arabian craton. In the subsurface of the present-day Levant coastline of the Mediterranean, the sedimentary pattern of the Triassic becomes more complex. The boreholes of Heletz-Deep, Ga'ash-2 and Atlit-1 indicate sedimentation in a more active tectonic environment, with volcanic input. The cyclic sedimentation pattern of the Negev is not strongly marked in this region.

For many rock units, no formal lithostratigraphic nomenclature has been established. Names derived from the Negev for superficially similar units with assumed age equivalence are sometimes used.

(a) HELEZ

The Helez Deep borehole was studied by Druckman (1984). It bottomed in Proterozoic metamorphic basement (Dorot Schist, 636±107 Ma; Steinitz, 1981) at a depth of nearly 6 km. This basement complex is overlain by 180 m of magmatics called the Gevim Quartz Porphyry. (Rb/Sr age 275±47 Ma; Segev, 2001; after Steinitz, 1981). This broad Permian to Lower Triassic age is corroborated by the Lower Triassic biostratigraphic age of the overlying unit:

Karmia Shale (Druckman, 1984)

This unit is of dark gray calcareous shale, often silty and sandy, intercalated by several meters of fine to medium-grained angular to subangular quartzitic sandstones. The nature of the contact with the underlying magmatic body is unclear. It is 43 m thick and is the oldest sedimentary unit encountered in the Helez Deep borehole. Palynomorphs indicate the *Ðpapillatus* Zone of the Early Triassic (Eshet, 1990a). The fungal spike characteristic of the Permian/Triassic boundary was not found.

Erez Conglomerate (Druckman, 1984)

This conglomerate unit overlies the Karmia Shale, and is 636 m thick. It is the same as the 'Or Haner Conglomerate' of internal reports by Derin et al. (1981). The lithology consists of angular to subrounded packed carbonate clasts (breccia) ranging in diameter from 0.5 m to sub-mm. The lower 350 m is polymictic, composed of diverse lithologies including lumpy micrites with abundant stylolites, oosparites, bioclastic limestones, ostracod, gastropod or pelecypod-rich sparites, foraminiferal micrites, laminated silty micrites, and black calcareous silty shale in a matrix of argillaceous micrite. The upper part is monomictic, composed of a finely crystalline dolomite mosaic, sometimes peloidal, and rarely bio- and oodolomicrites. Matrix is a ferruginous argillaceous dolomicrite with floating skeletal debris of bivalves, gastropods, and algal material. Clasts range from Permian to Anisian, based on palynomorphs (zones 4, 5, *-saturni* and *-amicus* zones of Eshet, 1990a) and Anisian foraminifers (*Glomospira densa, Meandrospira cf. dinarica*). Palynomorphs in the matrix give a Carnian age (zone 6, *-densus* Zone; Eshet, 1990a) to this interval. Druckman (1984) attributed emplacement of this conglomerate to a rifting event, taking place during deposition of the upper part of the epicontinental section of the Negev. Druckman (1974) also attributed basin differentiation in the Carnian Mohilla Formation of the Negev to rifting at that time.

'Mohilla' equivalent

The Erez Conglomerate is overlain by a 100 m thick sequence of dolostones containing *Ðdensus* Zone (Carnian) palynomorphs. It is placed in equivalence with the Mohilla Formation of the Negev on the basis of its Carnian age and presence of the dolomitic lithofacies in the Negev; however the formation there is much more highly variable, and is in fact predominantly evaporitic. The unit is truncated by the sub-Jurassic unconformity.

(b) GA'ASH (Fig. 18D.7)

The Ga'ash 2 borehole penetrated approximately 900 m of Triassic strata as dated by palynomorphs (Cousminer, 1981) and foraminifera (Derin, in Garfunkel and Derin, 1984), but did not reach the Permian.

'Ra'af - Saharonim' equivalent (5161-5500 m).

This interval corresponds to the 'Zafir-Ra'af-Gevanim equivalent' *sensu* Derin et al. (1981) and to the 'Ra'af' *sensu* Cousminer (1981) and Eshet (1990b). The 350 m sequence of limestone and dolomite, with some clastic influx near the base, yields foraminifers and ostracods of Anisian and probably Ladinian

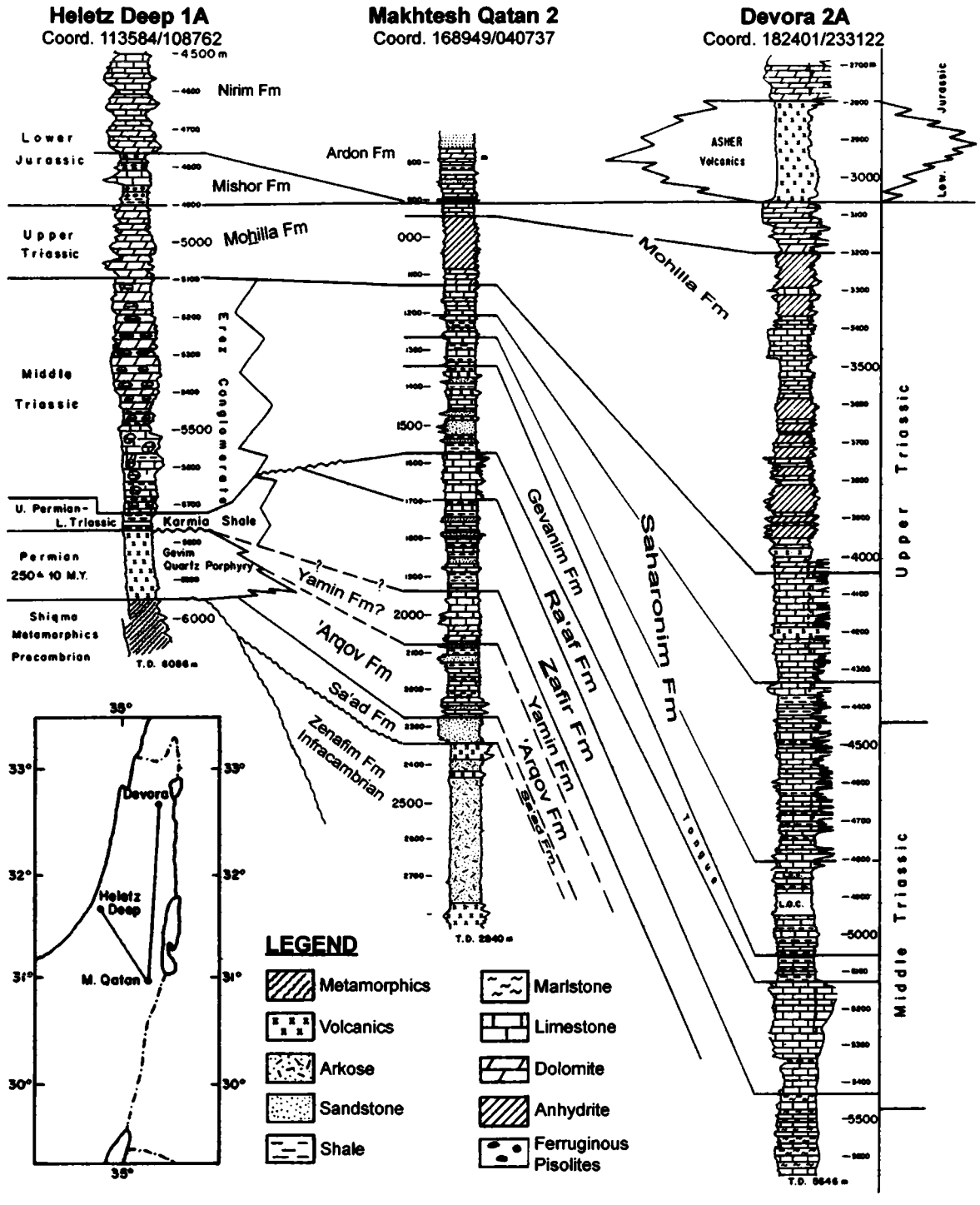


Figure 18D.6. The Triassic of the Heletz-Negev-Devorah boreholes (from Druckman and Kashai, 1981)

age: *Meandrospira* sp., *Glomospira densa, G. grandis, Trochammina* cf. *almtalensis, Turitellella* cf. *mesotriasica, Endothyra* sp., *Agathammina* sp., *Frondicularia* sp., and *Pseudomacrocypris* sp. A somewhat older age at the base is not ruled out. Palynomorphs (Cousminer, 1981; Eshet, 1990b) are Anisian (zone 4 *Dsaturni* Zone). There are many similarities with the Alpine Muschelkalk facies, and this part of the section differs from the Negev lithofacies by the absence of significant clastics, *e.g.*, the Gevanim Formation.

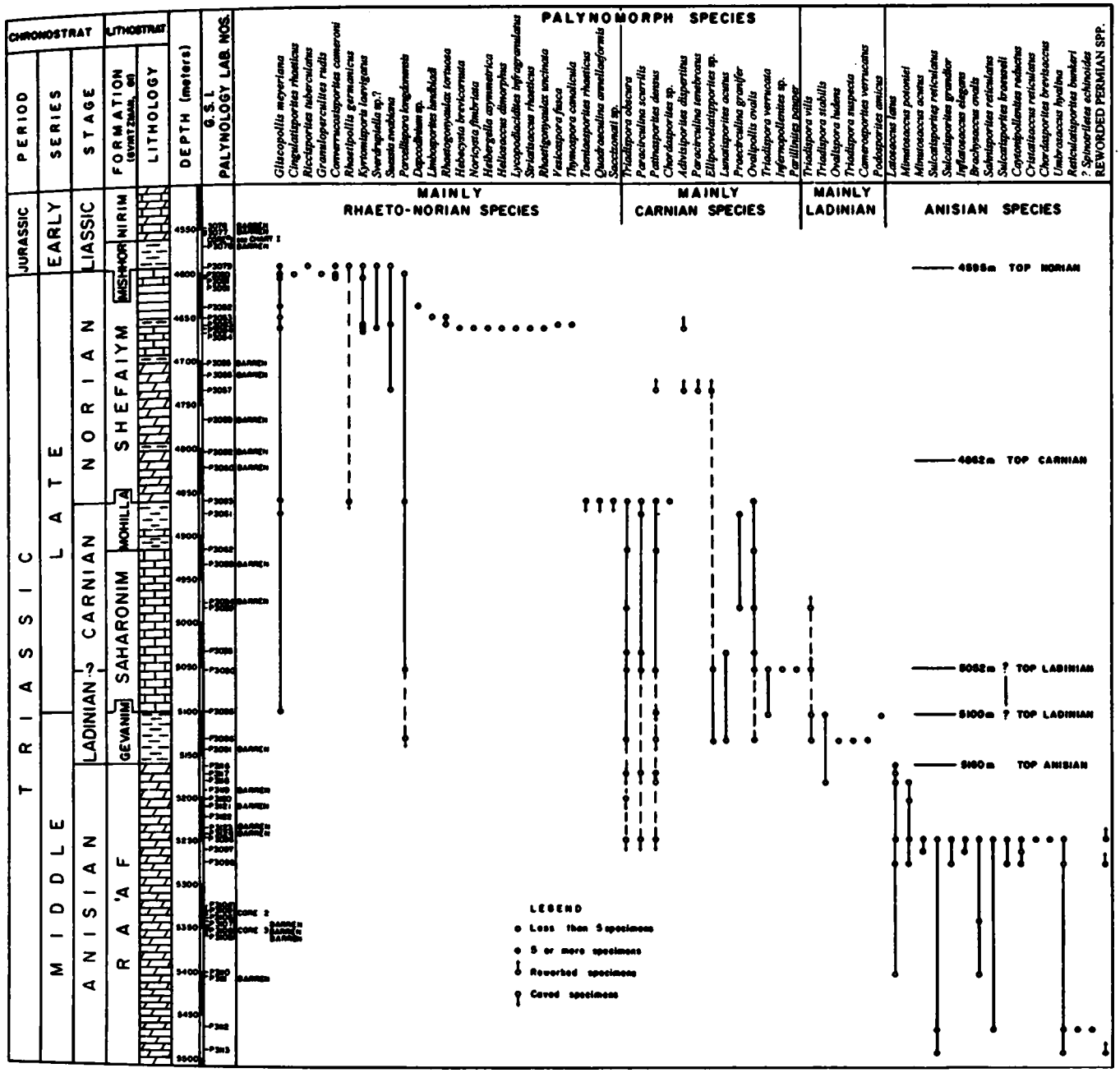
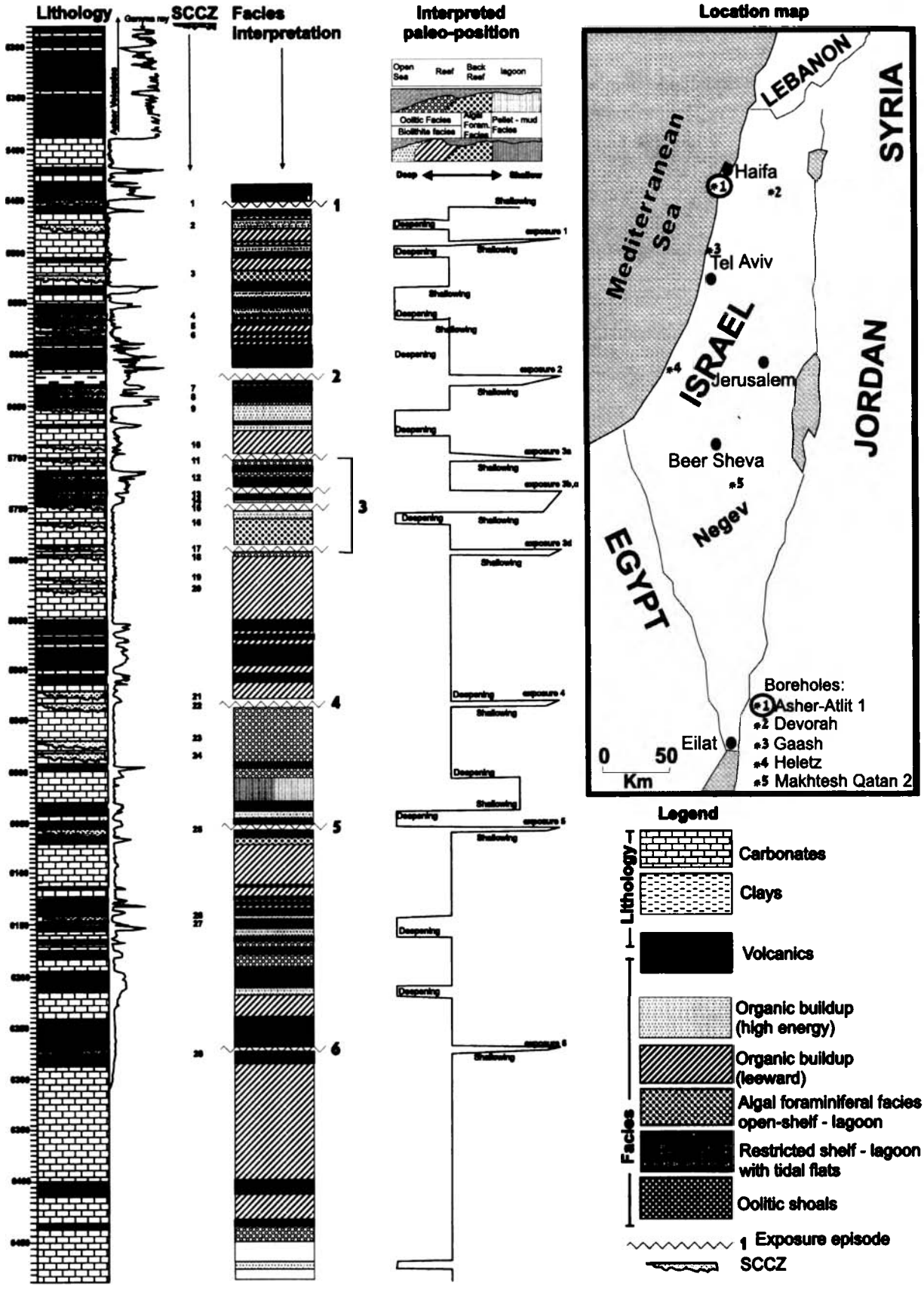


Figure 18D.7. The Trias of the Ga'ash borehole (from Cousminer, 1981, p. 23, Fig. 3).

Unconformity facies (Erez Conglomerate equivalent) (5100-5161 m).

This interval corresponds to the Sharon Formation *partim-sensu* Derin et al. (1981) and to the 'Gevanim equivalent' *sensu* Cousminer (1981) and Eshet (1990b). It consists of some 10 m of microconglomerate, concretionary dolomite, and coarse sandstone, with karstic weathering features, overlain by 50 m of variegated shale. The microconglomerate is barren of fossils. In the overlying shale, Cousminer (1981) found both Ladinian and Carnian palynomorphs. Carnian species appear in the middle of the shale unit, while the Ladinian marker species *P. amicus* appears in small numbers at its top. It therefore appears that the shale unit is Carnian in age, with most probably reworked Ladinian material near its top. The basal microconglomerate appears therefore to terminate an erosional event during which upper Anisian and Ladinian beds were removed, while the overlying shale is an *in-situ* depositional unit of the Carnian. This sequence of events is roughly equivalent to those recognized at Heletz, where Anisian and Ladinian strata


Lithology
SCCZ
Facies Interpretation
Interpreted paleo-position
Location map
Open Sea
Reef
Back Reef
lagoon
Oolitic Facies
Biolithite facies
Algal Foram. Facies
Pellet - mud Facies
Deep
Shallow
Deepening
Shallowing
exposure 1
exposure 2
exposure 3a
exposure 3b,c
exposure 3d
exposure 4
exposure 5
exposure 6
1
2
3
4
5
6
Mediterranean Sea
LEBANON
SYRIA
ISRAEL
JORDAN
EGYPT
Haifa
Tel Aviv
Jerusalem
Beer Sheva
Negev
Eilat
0
50
Km
Boreholes:
#1 Asher-Atlit 1
#2 Devorah
#3 Gaash
#4 Heletz
#5 Makhtesh Qatan 2
Legend
Lithology
Carbonates
Clays
Volcanics
Facies
Organic buildup (high energy)
Organic buildup (leeward)
Algal foraminiferal facies open-shelf - lagoon
Restricted shelf - lagoon with tidal flats
Oolitic shoals
1 Exposure episode
SCCZ

were removed during a significant erosional episode, followed by deposition of the thick Erez Conglomerate during the Carnian. In this respect, the subsidence event during which the Erez Conglomerate accumulated is represented at Ga'ash by deposition of variegated shale.

Mohilla equivalent (4862-5100 m).

This interval corresponds to the 'Saharonim-Mohilla' *sensu* Cousminer (1981) and Eshet (1990b) and 'Sharon Formation' *sensu* Gvirtzman (in Derin et al., 1981). Overlying the hiatus and 'Erez equivalent' shale, these 240 m of shale, marl and limestone with rare shallow marine faunas, are interbedded with terrigenous horizons with plant remains, and contain mostly Carnian palynomorph elements (Cousminer, 1981). This interval may be coeval in part with the Mohilla Formation of the Negev. However this marginal marine facies with some clastics is devoid of evaporites and in that respect also differs with the mostly dolomitic Mohilla Formation equivalent at Heletz deep. Aside from the lack of evaporites, there is similarity with the Alpine Raibl facies.

Shefayim Formation (4595 Ð4862 m) (Gvirtzman, 1981)

Gvirtzman (1981) established this unit for the uppermost 270 m of the Ga'ash-2 sequence. It consists of dolomitized carbonates of lagoonal and shallow marine origin, including reef facies and oolitic shoals. The foraminifers *Triasina hantkeni, Aulotortus friedli*, and *A.* cf. *gashei* (Derin et al., 1981) indicate a Norian-Rhaetian age, as does the palynomorph assemblage (Cousminer, *ibid.*; Eshet, 1990b). It is reminiscent of the 'Dachstein' alpino-dinaric platform facies.

In summary, the upper Triassic sequence of the Ga'ash borehole takes on some aspects of the rapidly subsiding shallow marine platform carbonates of the Alpine Tethyan realm.

(c) ASHER-ATLIT (Fig. 18D.8)

Asher Volcanics (partim)

The Asher Volcanics are found in the Asher-Atlit-1, Devorah-2, Haifa-1, and Yagur-1 boreholes.

At Asher-Atlit-1 (Dvorkin, 1988), a huge 2500 m thick sequence of basalts occurs in the Lower Jurassic and Late Triassic. Ar-Ar ages (Kohn et al., 1992, 1993) show age-clusters between 193 and 207 Ma. The Asher-Atlit-1 borehole in the Coastal Plain bottoms in the 2 km thick Asher Volcanics. Late Triassic carbonates occur within the lower 'Carbonate-Spilite Member' (6530-5390 m). It consists of a Rhaeto-Norian succession, mainly of reefal and associated facies, interbedded with volcanics.

The intercalated carbonates, only available as borehole-cuttings, are of Dachstein facies, found in a subsequently tectonically disturbed environment (Garfunkel and Derin, 1984). Reconstructing the sequence, Korngrin and Benjamini (2001) have discriminated six episodes of reef establishment, progradation, shallowing, and termination. The reef-building biota consist of sponges, encrusting organisms, and possibly corals. Reef-associated facies include fore-slope, central reef, ooid shoal, lagoonal, and intratidal conditions, terminated by supratidal environments, often sealed by pedogenetic overprints. Volcanic episodes tend to be associated with termination of carbonate sedimentation episodes, while volcanic quiescence and subsidence permit vertical accumulation and progradation of reefal and associated facies. The depositional and progradational environment belong to a regime well-known from the Neo-Tethys (Hirsch and Gerry, 1973; Druckman et al., 1982). The drilled Triassic succession was placed in the Norian-Rhaetian, based on the ostracod *Bisulcocypris-Darwinula* assemblage (Gerry and Derin, 1981), the palynomorph *Rhaetopollis germanicus* assemblage (Cousminer, 1981, 1982), and foraminifera, *e.g. Galeanella* sp. (Korngrin and Benjamini, 2001).

4. THE DEVORAH TYPE (Fig. 18D.6)

The Devorah-2A borehole in northern Israel penetrated more than 2,600 m of Triassic and represents the thickest Triassic section known to date in the Middle East. Despite this exceptional thickness, the base of the Triassic was not reached, and its top is truncated in the Carnian. It was described by Druckman and Kashai (1981), who subdivided it according to the lithostratigraphic units of the Negev. Biostratigraphic correlation, however, tends to show the irrelevance of this nomenclature. For example, the entire lower part of the section appears to be in a rather monotonous micrite and pelmicrite lithology, while the lower Triassic of the Negev, although frequently in marine facies, is predominantly clastic.

'Zafir Formation' equivalent (5428-5646 m) (Druckman and Kashai, 1981).

The lithology characteristic of the lower part of this borehole is almost entirely micrite and pelmicrite carbonates with Olenikian palynomorphs (*-papillatus* zone, Eshet, 1990) present in the basal 150 m to about 5500 m depth. Anisian palynomorphs (*-saturni* zone, Eshet, 1990, but not the nominate form) then appear and continue upwards into the overlying section. Therefore this section indeed correlates with part of the Zafir Formation of the Negev, but also to an unknown amount of the overlying section (Olenekian-Aegean?).



Figure 18D.8. The Triassic section in the Asher-Atlit-1 borehole (from Korngrin and Benjamini 2001, p. 3, Fig. 1). Lithology column shows carbonate, siliciclastic and volcanic horizons in adjusted position (within 3-6 m sampling interval), assisted by gamma-ray log (where available). First appearance of SCCZ's (sequential concentric cement zone) is shown in column 2. Facies interpretation columns show placement according to conceptual reef model based on microfacies interpretation, with exposure horizons (numbered 1-6) and interbedded volcanics shown. Facies shifts are related to a relative sea level change column (deepening-shallowing-exposure).

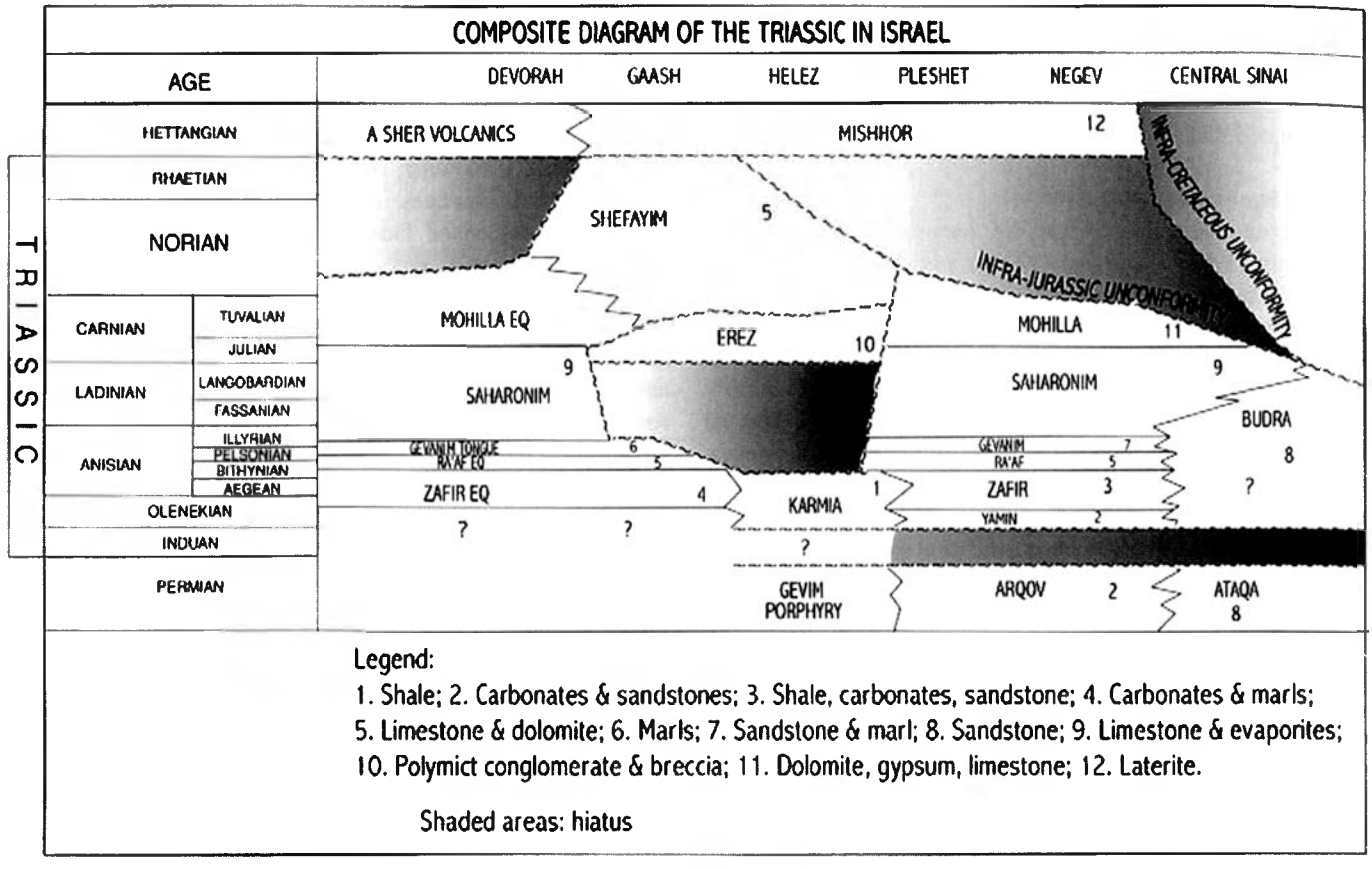


Figure 18D.9. Composite Diagram of the Triassic in Israel (from Lexique Stratigraphique, 2001).

'Uppermost Zafir-Lower Ra'af Formation' equivalent

This interval may be subdivided into two parts:

1) (5428-5120 m): The 308 m thick part of the section corresponds to the 'Ra'af Formation equivalent' of Druckman and Kashai (1981). It is lithologically similar to the limestones of the underlying unit but is somewhat more fossiliferous. The limestones consist mainly of micrites and pelmicrites and are sometimes slightly dolomitized. There are a few skeletal, ooid, algal, and foraminiferal biomicrites. Anisian foraminifera *Glomospira densa* and *Glomospirella grandis* indicate approximate age equivalence to the Ra'af Formation of the Negev. These forms occur above the base of the Anisian, and are present here in quantity only at the very top of this interval, from 5140 m; lower sporadic occurrences are probably cavings. Palynomorphs belong entirely to the Anisian *-saturni* Zone (Eshet, 1990), with the nominate species appearing in the upper part. This part of the section therefore is equivalent to the uppermost part of the Zafir Formation and lower part of the Ra'af Formation of the Negev, which is the position of the first appearance of the *G. densa* faunule (Aegean-?Bithynian).

2) (5120-5035 m): This 85 m interval is somewhat richer in shale but is poor in fossils, and was interpreted by Druckman and Kashai (1981) as a 'Gevanim tongue', equivalent to the clastic unit separating the Ra'af and Saharonim Formations in the Negev. However, intercalated limestones have foraminiferal and ostracod faunas predating appearance of the foraminifer *Meandrospira julia*, which occurs in the lower part of the Ra'af Formation in the Negev. Therefore correlation with the Negev is only to the lowermost part of the Ra'af Formation (?Bithynian-L. Pelsonian). Any comparison with the Gevanim Formation of the Negev is by lithologic similarity only, and the units are not correlative.

'Ra'af-Saharonim Formation' equivalent (5035-4038 m)

Druckman and Kashai (1981) compared this anomalously thick sequence (997 m) with the Saharonim Formation of the Negev. Its greater part is composed of limestones, with occasional shale and calcareous shale intervals. It can be subdivided into three parts:

1) Its lower part (5035-4775 m) is relatively fossiliferous. *M. julia* appears in the lower 60 m, indicating Early to early Late Anisian, and correlation with the lower part of the Ra'af Formation of the Negev. The uppermost limit of the *G. densa* faunule is at about 4775 m, which would indicate approximately the Lower Pelsonian and would be the equivalent of the upper part of the Ra'af Formation of the Negev.

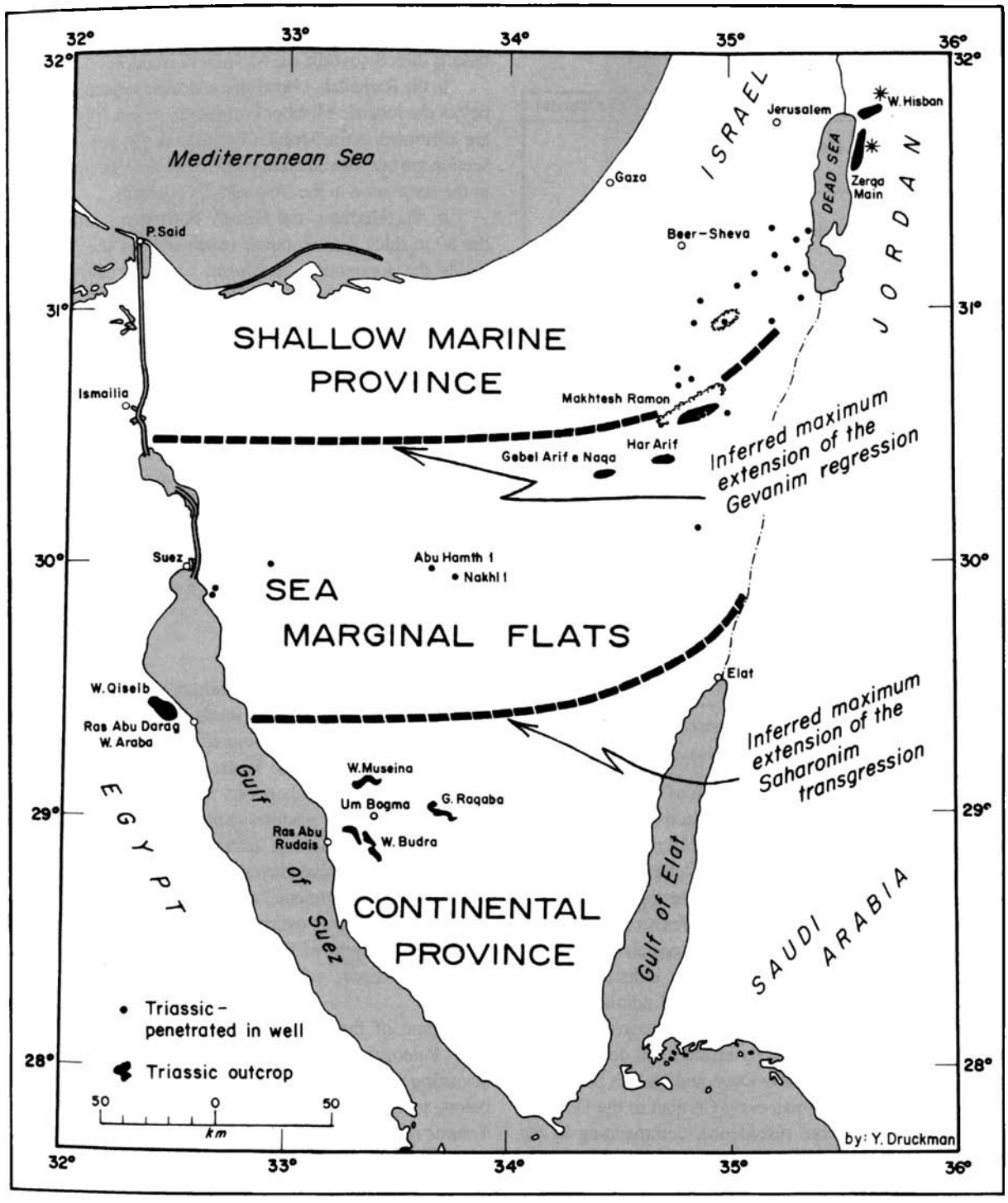


Figure 18D.10. Triassic of Eastern and Central Sinai (from Druckman et al., 1970).

2) The interval between 4775-4710 m represents the base of more concretional and stylolitized, occasionally laminated micrites. The Anisian *-saturni* palynomorph Zone is present in this sequence until 4710 m. This interval, late Pelsonian and Illyrian in age, would therefore correlate with the entire Gevanim Formation and the lowermost 10-15 m of the Saharonim Formation of the Negev.

3) The overlying interval (4710-4038 m) consists of the same

Table 18D.2: The correlation of Triassic formations in Jordan and the Negev, proposed by Bandel and Khoury (1981), is here modified on the basis of biostratigraphic data

Age	Jordan	Negev	Correlation basis (zones)
Carnian	Abu Ruweis	Mohilla	
	Um Tina	Saharonim	*-mungoensis* (Longobardian)
Ladinian	Iraq al Amir		*-murcianus* (Fassanian)
			-shagami (Illyrian)
Anisian	Mukheiris	Gevanim	
	Hisban	Ra'af	*-priscus* (Pelsonian) *-balatonicus/bulgarica* (Pelsonian) *-kockeli* (Pelsonian)
	Ain Musa	Zafir	
Olenekian	Dardun		*Pachycladina-Hadrodontina* (Olenekian)
	Ma'in	Yamin	
PERMIAN	Um 'Ima	Arqov	*Lueckisporites virkkiae*

stylolitized micrite lithology. The appearance of the palynomorph *P. amicus* at 4675 m indicates the Ladinian, and Ladinian species continue to be common up to 4405 m. This 270 m thick Ladinian interval is thus coeval to the major part of the Saharonim Formation of the Negev. The interval from 4290 m to the top of the unit is Carnian, supported by the appearance of the *-densus* palynomorph zone. The e-log marker that was mistakenly correlated with the M15A marker at the Lower/Middle Ladinian transition of the Negev, therefore marks approximately the Ladinian/Carnian transition. The position of the marker is therefore approximately at the break of tectonic origin, marked by erosion and deposition of the Erez Conglomerate, at the Heletz Deep and Ga'ash boreholes. The great thickness of the Ladinian-early Carnian in the Devorah borehole indicates considerable subsidence, commencing in the Ladinian.

Mohilla Formation (4038-3063 m)

This mainly evaporitic section, with dolomicritic carbonates at the base and top, is surprisingly thick, at 975 m. The bulk of the section consists of subparallel anhydrite laths intergrown and interlayered with dolomicrites. The evaporitic section is divided into a lower and upper unit by a carbonate subunit of massive pelmicrites and micrites, with some ostracode-bearing layers. The Mohilla Formation at Devorah-2A is dated to the Carnian by the ostracode *Renngartenella sanctaecrucis* and the *-densus* palynomorph zone (Gerry et al., 1990). Some 273 m of Asher basalts directly overlie the Mohilla Formation.

In the Ramallah-1 borehole, a similar sequence was penetrated below the Jurassic Mishhor Formation. About 1000 m of evaporites are attributed to the Mohilla Formation, whereas about 400+ m of section are considered comparable with the 'Saharonim Formation' in the sense used in the Devorah-2A borehole.

In the Hermon, the Rimeh Formation, immediately under the 60 m thick Aarneh basalt (equivalent of the Asher Volcanics) yields the foraminifer *Aulotortus sinuosus* and was considered Norian-Rhaetian (Mouty and Zaninetti, 1998; Mouty, 2000). These determinations are at odds with the findings of the Russian workers who considered these beds to be Jurassic (See Chapter 6, in Volume I).

5. TRIASSIC OF EASTERN AND CENTRAL SINAI (EGYPT) (Fig. 18D.10)

A thin intercalation of shelly Muschelkalk-like limestone, called the Qiseib Formation (Abdallah et al, 1965) occurs near Ras Abu Darag (Suez Gulf), and was also identified in the central Sinai Nakhl-1 and Abu Hamth boreholes (Schlatter, 1950a, b). Druckman et al. (1970) interpreted it as a tongue of the Saharonim Formation.

Budra Formation

The Budra Formation (Druckman et al., 1970), is a continental, fluviatile deposit occurring in south-western Sinai, and is truncated by the Early Cretaceous unconformity. Alternating variegated sand-, silt- and claystone layers with ferruginous and silicified tree trunks in several horizons represent channel and overbank deposits. Limonitic pisolites with concentric rims in a siltstone matrix may be pedogenic features. In the middle of the section thin carbonaceous shale layers are found. The Budra Formation is regarded as the continental equivalent of the Qiseib Formation. It is distinguished from overlying and underlying clastic formations by its high content of fine clastics, and is marked by variegated red, violet, brown, yellow, and ochreous siltstone layers close to the top.

Some of the Nubian-type sandstones intercalated between Late Paleozoic Ataqa and Lower Cretaceous Kurnub series occurring near Um Bogma, in the vicinity of the Gulf of Suez, may belong to the Budra Formation, and represent a clastic facies of the Triassic of central Sinai (Egypt)

6. THE TRIASSIC SEQUENCE IN JORDAN (Fig. 18D.11)

The relative positions of the isolated outcrops of Permian and Triassic rocks in Jordan (Cox, 1924, 1932; Blake, 1936; Wetzel and Morton, 1959; Daniel, 1963) was imprecise until it became possible to correlate with the more continuous outcrops of the Negev (Weissbrod, 1969, 1976; Druckman, 1974; Druckman et al., 1982; Bandel and Khoury, 1981; Bandel and Waksmundzki, 1985) (**Table 18D.2**). They also provide stratigraphic evidence for the debate concerning the evolution and nature of movement along the

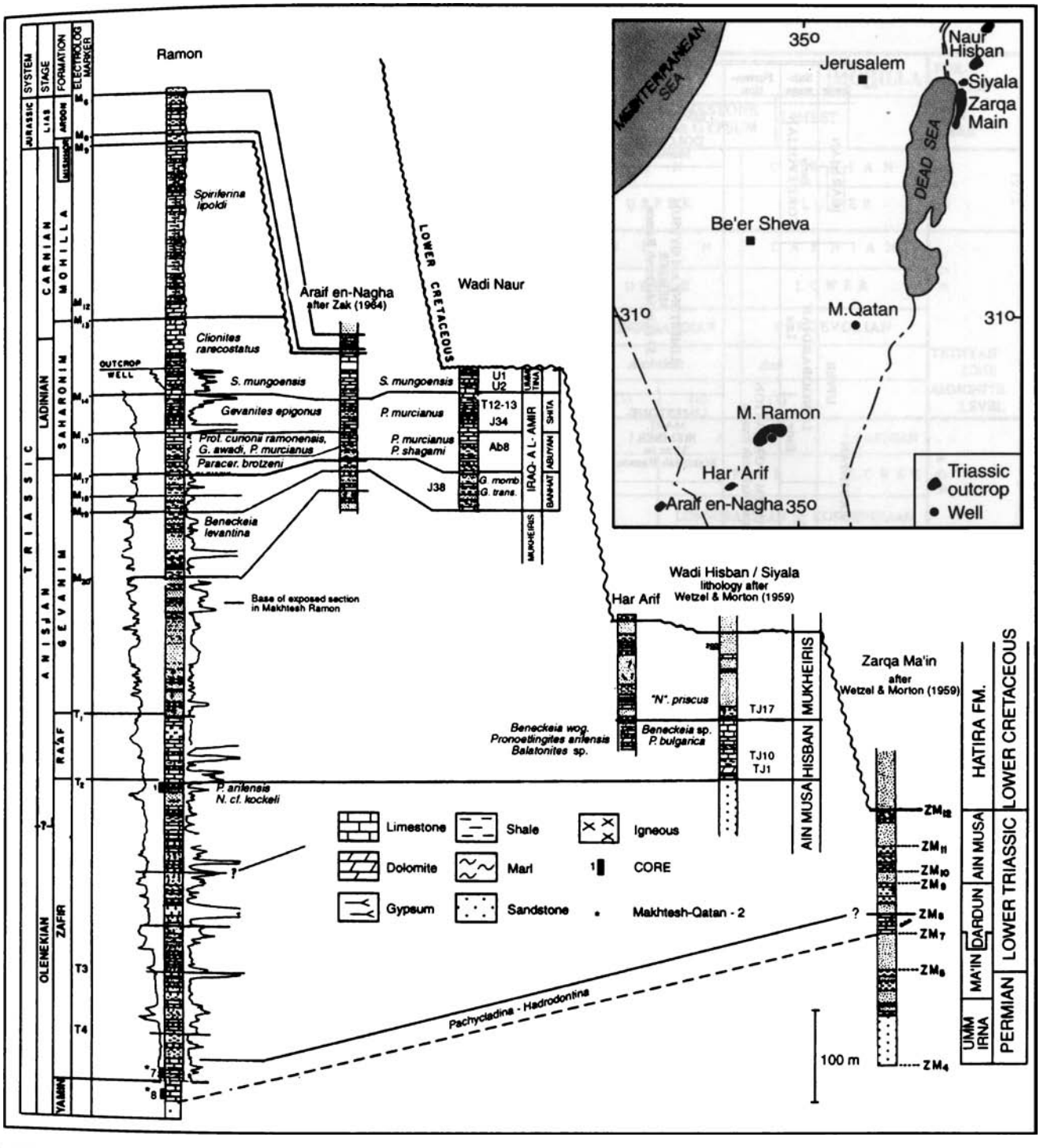


Figure 18D.11. Correlation of the Triassic across the Dead Sea Rift: Arif E Naqa (Sinai, Egypt), Makhtesh Ramon and Ramon-1 well, Har 'Arif (Negev, Israel), Wadi Siyala, Wadi Naur and Zarqa Ma'in (Jordan). (From Hirsch, 1997, Fig. 1, modified after Druckman 1974a, Bandel and Khoury, 1981, and Saddedin and Kozur, 1992).

Dead Sea Rift (Quennell, 1958; Bender, 1968; Freund et al., 1970), via thickness and clastic ratio trends and gradients across the rift valley. Recent paleontological data allows improved correlation: Conodonts from Wadi Siyala and Wadi Naur (Jordan) can be correlated by various authors with conodonts of the Negev and the ammonoid zonation of Parnes et al. (1985) and Parnes (1986).

Table 18D.3.Triassic ammonite Biostratigraphy (from Parnes et al., 1985, Table I, p. 658).

Stage	Sub-stage	Formation	Member (lithology)	Sub-unit	Fossils	Levels (Zone)
CARNIAN	Early CORDEVOLIAN	SAHARONIM FORMATION 153 m in Makhtesh Ramon	LIMESTONE and DOLOMITE Member		*Gruenwaldia woehrmanni* (Bittner)	
			LIMESTONE and GYPSUM MEMBER 53 m in Makhtesh Ramon	Upper part	*Clionites rarecostatus* Parnes *Clionites* spp. *Protrachyceras sirenitiforme* Parnes *Protrachyceras rectangulare* Parnes *Protrachyceras* spp.	Level VII (*Regoledanus* Zone)
LADINIAN UPPER	LONGOBARDIAN Late			Lower part	*P. hispanicum* (Mojs.), attenuate form *Protrachyceras ladinum* (Mojs.), wide form *Protrachyceras hispanicum* (Mojsisovics) *Judahella geryi* Sohn *Simeonella brotzenorum* Sohn *Carinella mungoensis* (Diebel) *Pseudofurnishius murcianus* Boogaard	Level VI (*Archelaus* Zone)
	LONGOBARDIAN Early		LIMESTONE-MARL MEMBER 35 m in Makhtesh Ramon		*Pseudofurnishius murcianus* Boogaard *Gevanites epigonus* Parnes *Pseudoplacunopsis fissistriata* (Winkler) Crinoidea	Level V
LOWER	FASSANIAN		FOSSILIFEROUS LIMESTONE MEMBER 38 m in Makhtesh Ramon LIMESTONE-SHALE Alternation	Upper part	*Indonautilus awadi* Kummel *Protrachyceras curionii* (Mojs.) var. *ramonensis* Parnes *Protrachyceras wahrmani* Parnes *Monophyllites* sp. *Sturia* sp. *Proarcestes* spp. *Gevanites awadi* Parnes *Israelites ramonensis* Parnes *Pseudofurnishius murcianus* Boogaard *Negebites zaki* Parnes	Level IV (*Curionii* Zone)
UPPER ANISIAN	ILLYRIAN			Middle part	*Coenothyris* bank *Reubenella avnimelchi* Sohn *Gevanites inflatus* Parnes *Psephosaurus picardi* Brotzen *Mojsvaroceras* cf. *morloti* (Mojsisovics) *Paraceratitoides brotzeni* Avn. (compressed form)	Level III (*Trinodosus* Zone)
				Lower part	*Mojsvaroceras* cf. *augusti* (Mojsisovics) *Paraceratitoides brotzeni* Avnimelech (typus) *Discoptychites* sp.	
	PELSONIAN	GEVANIM FORMATION 270 m in Makhtesh Ramon (exposed 130 m)	SANDSTONE-LIMESTONE Member	40 m at Makhtesh Ramon	Wood *Myalina ramonensis* Brotzen *Neoschizodus orbicularis* (Bronn.)	Level II (*Binodosus* Zone)
			SANDSTONE-SHALE-LIMESTONE Member	45 m at Makhtesh Ramon	*Frechites* sp. *Beneckeia levantina* Parnes *Psephosaurus mosis* Brotzen *Myalina beneckei* Brotzen *Trigonodus tenuidentatus* Lerman	
			QUARZITE Member	30 m at Makhtesh Ramon	Wood	
			SANDSTONE-SHALE Member	110 m at Har'Arif	*Trigonodus-Pachycardia* beds	
		RAAF FORMATION 70 m in Ramon-1 well 27 m exposed in Har'Arif	SHALE		Crinoidea *Costatoria costata*	Level I (*Balatonicus* Zone)
			LIMESTONE-SHALE Alternation		*Beneckeia wogauana* (Meyer) var. *posterior* Fritsch *Pronoetlingites arifensis* (Parnes) *Balatonites* gr. *balatonicus* (Mojs.) *Balatonites* cf. *jovis* Arthaber *Balatonites* cf. *zimmeri* Rassmuss	
			DOLOMITE BOSTONITE Sills		*Costatoria costata* (Zenker) Crinoidea *Neospathodus kockeli* (Tatge)	
? LOWER ANISIAN		ZAFIR FORMATION	UPPER Member 130 m (subsurface)		*Triebacythere* sp.	

Table 18D.4. Revision of Triassic Ammonite Zonation (From Parnes, 1986, p. 11, Table 1, courtesy of Dr. Aline Ehrlich).

ZAFIR	RA'AF	GEVANIM			SAHARONIM				MOHILLA	LITHOLOG. UNITS: FOR-MATION / MEM-BER
UPPER	LOW. UPP.	LOW.	MID.	UPP.	FOSSILIFEROUS LIMESTONE	LIMEST. & MARL	LIMESTONE & GYPSUM	LIMEST.		

						PARNES, 1975
ANISIAN			LADINIAN		CARNIAN	AGE
LATE LOWER	UPPER	LOWER		UPPER	LOWER	

							PARNES ET AL., 1985
ANISIAN			LADINIAN		CARNIAN		AGE
LOWER	UPPER		LOWER	UPPER	LOWER		
	PELSONIAN	ILLYRIAN	FASSANIAN	LONGOBARDIAN	CORDEVOLIAN		
	Balatonicus	*Binodosus*	*Trinodosus*	*Curionii*	*Archelaus*	*Aon*	TETHYAN ZONE
	(1)	(2)	(3)	(4)	(5) (6)	(7)	AMMONITE LEVEL

									PRESENT WORK (PARNES, 1996)
ANISIAN			LADINIAN					CARNIAN	AGE
LOWER	UPPER		LOWER		UPPER			LOWER	
BITHY-NIAN	PELSONIAN	ILLYRIAN	FASSANIAN		LONGOBARDIAN		CORDEVOLIAN		
	Balatonicus	*Binodosus*	*Trinodosus / Avisianus*	*"Reitzi"*	*Curionii*		*Archelaus*	*Aon*	TETHYAN ZONE
Scaphoi-des (1)	Arifensis (2)	Levantina (3)	Salina-rius(4)	Brotzeni (5)	Curionii ramonensis (6)	Epigo-nus (7)	Hispanicum (8)	Sireniti-forme(9)	CEPHALOPOD LEVEL

The Triassic section in Jordan may be subdivided by a conodont zonation useful throughout the Levant:

1. OLENEKIAN (*-pachycladina* Zone):

The Dardun Formation (Bender, 1968), in the Lower Triassic of Wadi Zarqa Main along the eastern shore of the Dead Sea (Jordan), yields the same Ellisoniid assemblage as found in the upper Yamin-lower Zafir Formations in the Negev subsurface (Hirsch and Gerry, 1973; Druckman et al., 1985).

2. PELSONIAN (*-kockeli* Zone):

At the base of the Ra'af Formation (Core 1, Ramon-1 borehole) occurs the Bithynian/Pelsonian neospathid morph '*N.*' cf. *kockeli* (Hirsch, 1977) accompanied by the ammonoid *Pronoetlingites scaphoides* (Parnes, 1986). At Wadi Siyala (Jordan), in the lower part of the Hisban Formation, the equivalent to the Ra'af Formation of the Negev, *Paragondolella bifurcata* occurs (sample TJ 1, Saddedin and Kozur, 1992) and in the upper part of the Hisban Formation, an alleged specimen of *Beneckeia levantina* occurs with *Paragondolella hanbulogi (*sample TJ 10, Saddedin and Kozur, 1992). At a slightly higher level, in the exposed upper part of the Ra'af Formation at Har 'Arif (Negev), the ammonoids *Beneckeia* cf. *wogauana, Pronoetlingites arifensis* and above all *Balatonites balatonicus* confer a Pelsonian age (*-balatonicus* Zone) to this interval (Parnes, 1986).

The lowermost part of the Mukheiris Formation, overlying the Hisban Formation at Wadi Siyala, yields the conodonts '*Pseudofurnishius*' *priscus* and *'P' siyalaensis* (sample TJ 17, Saddedin and Kozur, 1992) near the *Trigonodus*-bearing horizon. This level correlates to the lower part of the Gevanim Formation, which at Har 'Arif also bears *Trigonodus* sp. The Gevanim Formation has a total thickness of 270 m at Ramon, and the Pelsonian level of *Beneckeia levantina* Parnes (*-binodosus* Zone, according to Parnes, 1986) occurs 220 m above the base. The level of '*Pseudofurnishius' siyalaensis* (Saddedin and Kozur, 1992) and of '*P'. priscus* (Sadeddin, 1990) in Wadi Siyala is thus no younger than Pelsonian, and not Ladinian. This part of the sequence predates the exposed section of Wadi Naur (Jordan).

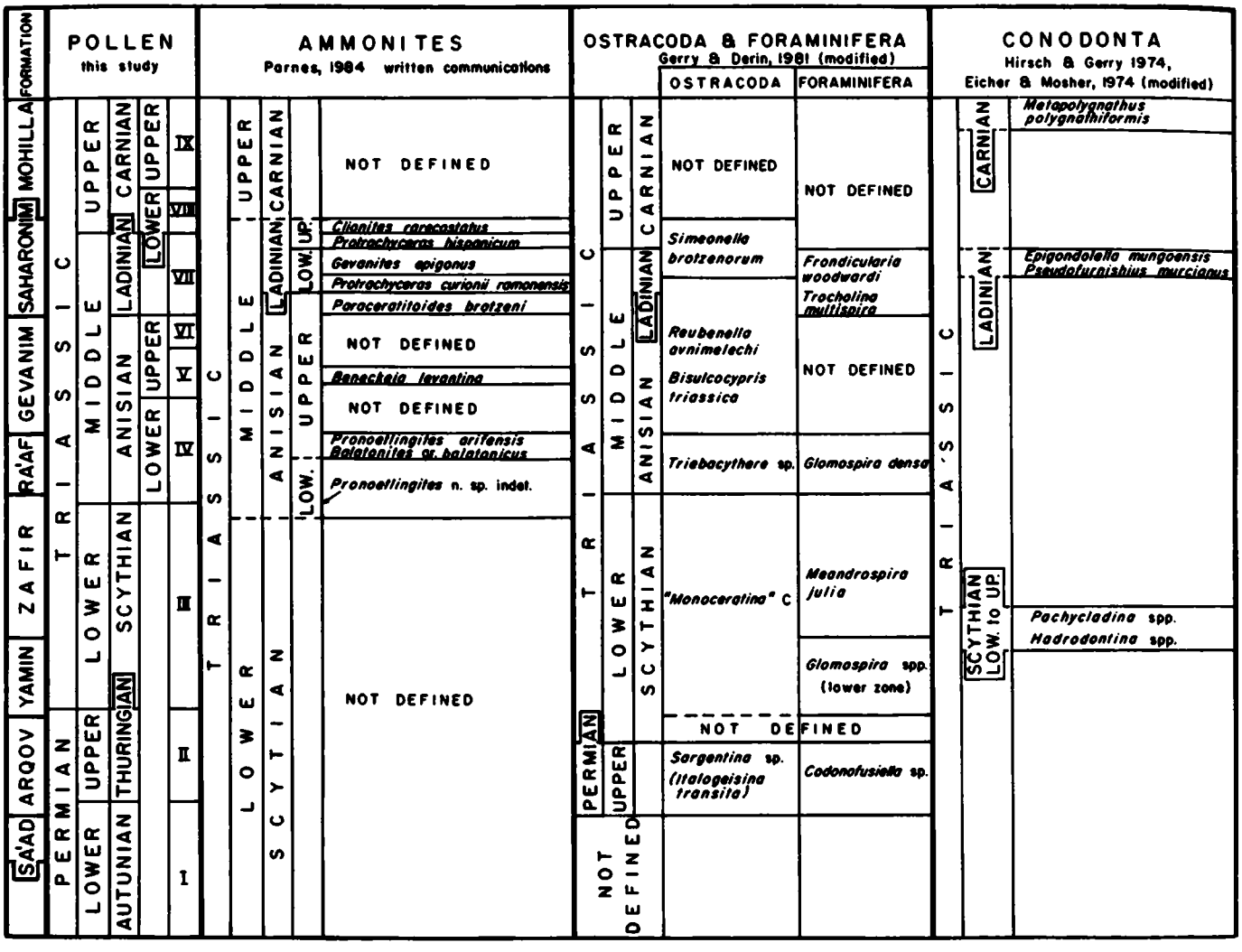
3. ILLYRIAN (*-constricta* Zone equivalent):

The section of Wadi Naur encompasses the Iraq-al-Amir Formation and the lower member of the Um-Tina Formation. The Bahhath Member at the base of the Iraq-al-Amir Formation yields ammonites and the conodonts *Neogondolella transita* and *N. mombergensis* (Sample J 38, Bandel and Waksmundzki, 1985) in a rather sandy facies. The Fossiliferous Limestone Member of the Saharonim Formation at Makhtesh Ramon (Israel) yields the ammonoid *Paraceratites brotzeni* Parnes in its lower part (Parnes, 1986), for which a Late Anisian (Illyrian) age is assumed. While *N. transita* is thought to indicate the Lower Ladinian, '*N. mombergensis'* occurs also in the Illyrian *-constricta* Zone.

4. FASSANIAN (*-shagami* Zone):

At Ramon the Fossiliferous Limestone Member of the

Table 18D.5. Comparison of the major biozones in the Permo-Triassic sequence in Israel (from Eshet, and Cousminer, 1986, Fig. 6).



Saharonim Formation yields in its upper part the ammonoids *Gevanites inflatus, G. altecarinatus, Israelites ramonensis* Parnes and *Protrachyceras curionii ramonensis* (Parnes 1986). The upper part of this interval yields the neospathid or primitive neogondolellid morph *'N.' shagami* (Benjamini and Chepstow-Lusty, 1986). At 55 m above the base of the section at Wadi Naur, in the Abu Yan Member, middle part of the Iraq-al-Amir Formation, an allegedly juvenile conodont-element was recovered, attributed to *'P.' priscus* (sample Ab 8 of Sadeddin, 1990), which is probably a specimen belonging to *'N.' shagami*.

5. FASSANIAN- LANGOBARDIAN (-*murcianus* Zone):

Toward the top of the Fossiliferous Limestone Member of the Saharonim Formation, *Pseudofurnishius murcianus* Van den Boogard occurs (samples 39 and 42, Hirsch, 1972). The Limestone-Marl Member of the Saharonim Formation yields the endemic ammonoid *Gevanites epigonus* Parnes and the conodont *P. murcianus* (sample 50, Hirsch, 1972; sample 29779, Huddle, 1970; samples 50134-50143, Eicher and Mosher, 1974). This interval corresponds apparently to the Shita Member of the Iraq-al-Amir Formation in Jordan, in which *P. murcianus* was also found (sample J 34, Bandel and Waksmundzki, 1985).

6. LANGOBARDIAN (-*mungoensis* Zone):

In the Limestone-Gypsum Member of the Saharonim Formation, *P. murcianus* is found together with *Sephardiella mungoensis* (Diebel), just below the bed of *Protrachyceras ladinum* (Mojs.) of the Longobardian *-archelaus* Zone (Parnes, 1986). These conodonts, repeatedly found in Makhtesh Ramon (Israel) and Arif en-Naqa (Egypt) (sample 29777, Huddle, 1970; sample 50148, Eicher and Mosher, 1974), occur also in Jordan at the top of the Shita Member of the Iraq-al-Amir Formation (samples T 12-13, Bandel and Waksmundzki, 1985) and possibly within the lower member of Um-Tina Formation (sample U2, Saddedin, 1990). No Carnian conodonts were recovered from these outcrops.

Table 18D.6. Palynological Zonation (from Eshet, 1990, p. 19, Fig.6).

AGE	PALYNOZONE	FORMATION	LITHOLOGY (Generalized)
Rhaeto-Norian ???	*Rhaetogonyaulax rhaetica* Spp. (Zone VII)	Shefayim (in Ga'ash-2 well only)	Carbonates with some shales
Carnian	*Patinasporites densus* (Zone VI)	Mohilla	Mostly gypsum, dolomite and anhydrite; Some marl and limestone
Ladinian	*Podosporites amicus* (Zone V)	Saharonim	Mostly limestone; some marl; Dolomite and gypsum at top.
Aniisian	*Aratrisporites salurni* (Zone IV)	Gevanim	Sandstone; siltstone; Clay and shale.
		Ra'af	Limestone and shale.
Scythian	*Endosporites papillatus* (Zone III)	Zafir	Carbonate and shale; More clastics in upper part.
		Yamin	Mostly limestone.
Thuringian	*Lueckisporites virkkiae* (Zone II)	Arqov	Limestone, dolomite and shale; Some sandstone horizons.
Autunian	*Potoniesporites novicus* (Zone I)	Sa'ad	Mostly sandstone; Some shale

II. ZONAL BIOSTRATIGRAPHY

Ammonoids range from Middle to early Late Triassic (**Tables 18D.3, 18D.4**). The palynostratigraphic zonation scheme (Eshet and Cousminer, 1986; Eshet, 1990) encompasses the entire Triassic sequence (**Table 18D.6**). Ostracoda, Foraminifera and Conodonta provide an important biostratigraphic complement (**Table 18D.5**).

a) Lower Triassic (Olenekian) palynostratigraphy with two conodont horizons. The Early Triassic *Endosporites papilatus* Zone III (Eshet, 1990) has been recognized in several boreholes (Ramon, Makhtesh Qatan, Zohar, Zuk Tamrur, Pleshet, and partially in Ramallah and Devorah). According to Brugman (1986) the assemblage found in Israel is characteristic for the Spathian substage (upper Olenekian), a fact confirmed by the presence of the conodont genera *Hadrodontina* and *Pachycladina* in the lower part of the Early Triassic interval.

b) Middle Triassic (Anisian-Ladinian) ammonoid biostratigraphy, established by Parnes (1962, 1975, 1986) and Parnes et al. (1985). Seven levels of ammonoids and one nautiloid level can be correlated with corresponding standard zones in the Mediterranean region (Tables 18D.3, 18D.4):

I *-arifensis* level - *-balatonicus* Zone (Assereto, 1974) with *Pronoetlingites arifensis* (Parnes) and several forms of the genus *Balatonites,* including *B.* gr. *balatonicus* (Mojs.). This level also contains the conodont *'Nicoraella' kockeli* (Tage), a Pelsonian marker.

II *-levantina* level - *-binodosus* Zone (level 3 of Assereto, 1971) with *Beneckeia levantina* Parnes.

III *-salinarius - brotzeni* levels - *-trinodosus* Zone (level 4 of Assereto, 1971) with *Germanonautilus salinarius* Mojs. and *Paraceratites brotzeni* Avnimelech.

IV *-curionii-ramonensis* level - *-curionii* Zone, consisting of beds yielding *Eoprotrachyceras curionii* (Mojs.), *Israelites ramonensis* Parnes and *Protrachyceras wahrmani* Parnes.

V *-epigonus* level - Beds containing *Gevanites epigonus* Parnes

are regarded as representing the base of the Upper Ladinian (Parnes, 1975).

VI *-hispanicum* level - *-archelaus* Zone, yielding *Protrachyceras ladinum* (Mojs.) and *P. hispanicum* (Mojs.), as well as the charactistic conodont-marker *Sephardiella mungoensis* (Diebel).

VII *-sirenitiforme* level - *-regoledanus* Zone, yielding *Protrachyceras sirenitiforme* and *Clionites rarecostatus,* belongs in the Ladinian as part of the former 'Cordevolian'.

c) Upper Triassic (Carnian-Rhaetian). In palynostratigraphic terms the Upper Triassic consists of two zones: the Carnian *Patinosporites densus* Zone (VI) and the Norian-Rhaetian *Rhaetogonyaulax rhaetica* (VII).

The first appearance of *Patinosporites densus* occurs at the base of the former 'Cordevolian'. The base of the Carnian (*-aon* ammonoid zone) starts higher, and consequently the base of the *P. densus* Zone (VI) straddles the Ladinian/Carnian boundary. The upper part of the Carnian is marked by the conodont *Paragondolella polygnathiformis*. The 'Cordevolian' is also marked by the appearance of the foraminifer assemblage of *Involutina gaschei* (Ladinian-Carnian). The interval of the dinoflagellate *Rhaetogonyaulax rhaetica* Zone corresponds to the range of post-Carnian sporomorphs, *e.g. Corolina torosa*. The Norian-Rhaetian interval (Shefayim Formation in the Coastal Plain) also bears the foraminifera *Triassina hantkeni* and *Aulotortus* sp.

The Triassic-Jurassic boundary can also been established on the basis of palynomorphs, at the appearance of Late Pliensbachian-Toarcian *Mancodinium, Deltoidospora toralis* and *Corolina torosa* above Norian-Rhaetian *Rhetaogonyaulax rhaetica* (Dunay, 1974, pers. comm.; Conway et al, 1990).

III. PALEOGEOGRAPHY (Fig. 18D.12)

The early Triassic of the Mediterranean region inherited Late Permian Palaeotethyan palaeogeography. The African-Arabian-Apulian platform represents the southern margin of the initial Tethys rift and its subsequent pelagic seaway (Fig. 18D.12, Hirsch, 1990, Fig. 6A). Carbonate platforms off the southern margin of the nascent Neotethys occur in the Dinarids, Taurids, Hellenids, and eastern and southern Alps. Mediterranean terrains directly attached to the Gondwana shelf during the Triassic and Early Jurassic extended from Spain to Arabia, until Tethyan rifting reached the Proto-Atlantic edge of the Mediterranean region.

The earliest Triassic is developed in the 'Werfen'-type facies, of alternating marine sandstones with plant remains, shales, marls and marly limestones. The Werfen facies extended from the Alpine region to the eastern Mediterranean without any marked differentiation between Eurasian and Gondwanian margins and consisted of a number of sea level oscillations. The presence of Induan through Olenekian in the southern Alpine region is established by conodonts (Huckriede, 1958). In the Levant however, only Olenekian is found, based on palynomorphs (Eshet, 1990a) and conodonts (Hirsch and Gerry, 1974).

The Mesozoic Neotethys was initiated by rifting in the early Triassic, in the form of a discrete seaway of Hallstatt-type facies in the Aegean region. Rifting is reported as far as the Tyrrhenian

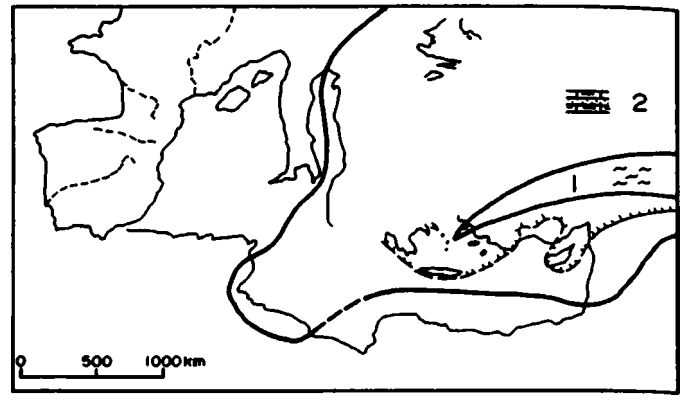


Figure 18D.12. Olenekian palaeogeography of the Mediterranean Triassic (from Hirsch, 1990, Fig. 6A). Legend: 1. Pelagic seaway of Hallstatt facies; 2. Werfen facies.

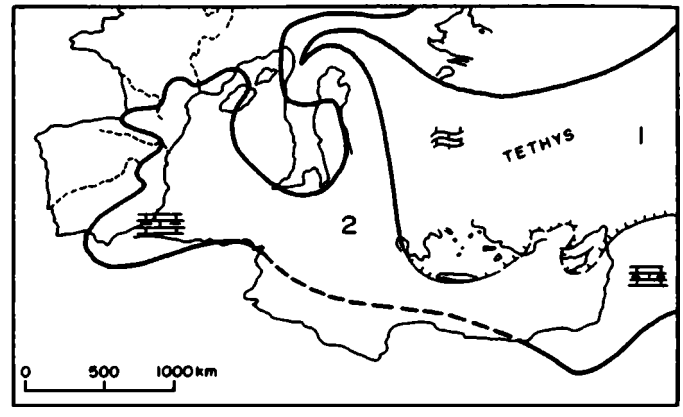


Figure 18D.13. Ladinian palaeogeography of the Mediterranean Triassic (from Hirsch, 1990, Fig. 6D). Legend: 1. Pelagic Tethys facies; 2. Sephardic Realm.

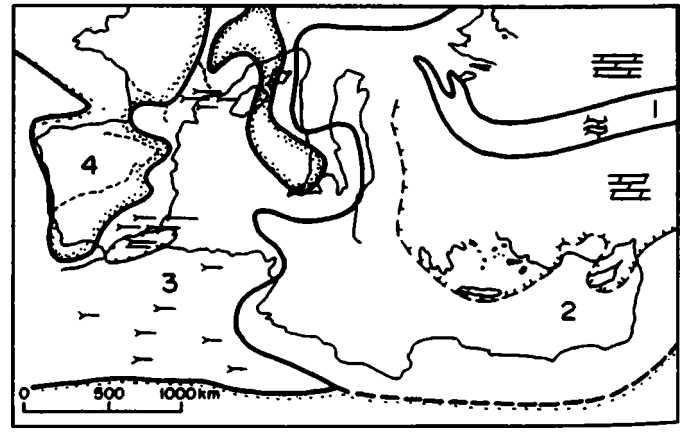


Figure 18D.14. Late Triassic palaeogeography of the Mediterranean Triassic (after Hirsch, 1990, Fig. 6F). Legend: 1. Pelagic Tethys facies; 2. Dolomitic and evaporitic facies; 3. Saharan salt-facies; 4. Continental facies.

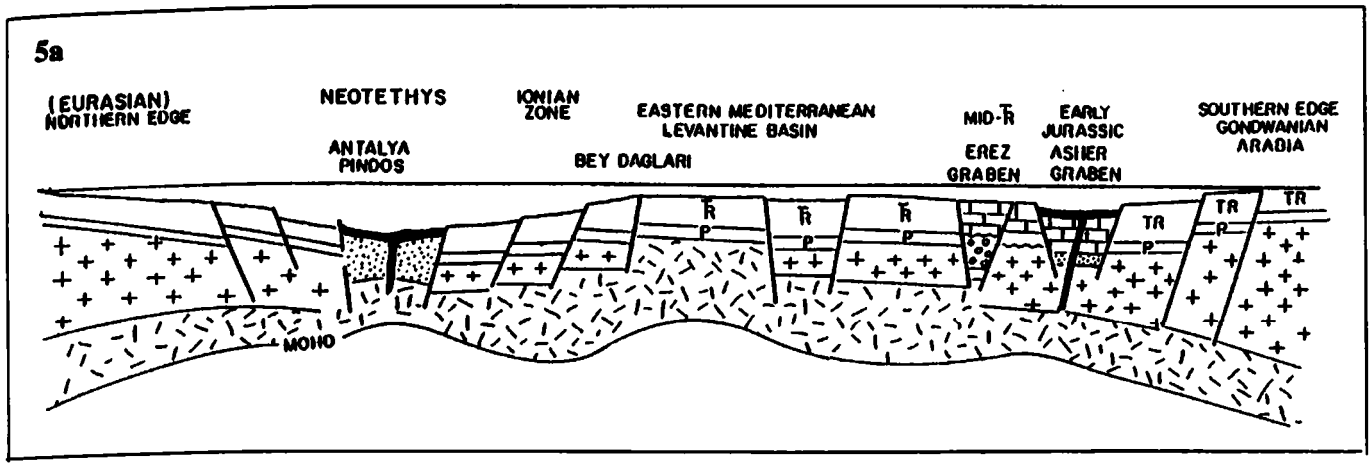


Figure 18D.15. Schematic Eastern Mediterranean palinspastic cross-section between Laurasia and Gondwana during Middle Triassic-Early Jurassic times (from Hirsch et al., 1995, p. 159, Fig. 5a).

region during the Middle Triassic, separating the southern Tethyan Sephardic margin from the Eurasian epicontinental Muschelkalk-type shelf facies (**Fig. 18D.13**). The Sephardic Neotethys margin of Gondwana extended from the Levant to the western Mediterranean, including the Betic terranes and North African, Iberic, Catalonian, Apulian, and Sardo-Provencal platforms.

The early part of the Late Triassic was characterized by shallowing of both Sephardic and Tethyan realms, and the first enhanced migration of Sephardic taxa into the shallow Tethys. Somewhat later in the early Carnian, a salinity crisis put an end to the entire distinct Sephardic realm. From Late Carnian onward, facies and faunal distribution in the Mediterranean region consisted of Hauptdolomite-Dachstein platforms on both sides of the Hallstatt seaway of the Neotethys (**Fig. 18D.14**; Hirsch, 1990, Fig. 6F).

A schematic cross-section extending from Sinai to the Antalya Neotethyan seaway crosses the continental shelf of Sinai, the epicontinental ramp or platform of the Negev extending into Syria including the Helez structure, the offshore geanticline at Tarasci, and continental rise and talus, and thinned continental crust of Bey Daglari, with reef and backreef facies of the rifted seaway (**Fig. 18D.15**). Ophiolites resulting from Triassic spreading, mostly pillow lavas, are present in the Antalid units (Ricou, 1982) and in equivalent terranes of the Mammonia complex (Cyprus) and the Tamima Nappe (Syria) (Knipper and Sharaskin, 1994).

Thus Neotethys, as the seaway separating the Eurasian and Gondwanian landmasses, initially encompasses narrow rifting or spreading zones, later to become oceanic. The epicontinental shelf zones on either side were ecologically similar, but heterogeneity in regard to depth, salinity, and temperature across the nascent Neotethyan ocean environment seems to have restricted free migration of newly evolving post-Permian taxa. Some taxa communicated freely, whereas others were strictly isolated. For example, faunas of the German Muschelkalk and of the Sepharadic Saharonim Formation are superficially similar, but frequently differ at the species and often at the generic level. Faunas of the Hallstatt pelagic seaway facies are only rarely seen on either epicontinental platform. Boundaries based on distribution of particular taxa thus define the Tethyan, Germanic and Sephardic faunal realms. Ammonoids, halobiids and conodonts define the Hallstatt facies, while megalodonts, foraminifers, and algae define the Dachstein facies. A large array of bivalves and a smaller array of ammonoids, conodonts, crinoids, and reptiles define the distinct Germanic and Sephardic realms.

IV. TECTONISM AND EUSTATIC CYCLES (Fig. 18D.16 Burial curve)

The tectonic environment of the Levant during the Triassic was attached to a rather 'mature' Gondwanan hinterland, characterized by rather smooth relief, following long and steady denudation of the Precambrian Arabo-Nubian massif. The margin of this region experienced the tensional Tethyan spreading regime, with vertical movements underlying Triassic depositional patterns. Especially in the Early and Late Triassic, rifting is evident from sedimentation patterns, *e.g.* as indicated by thick deposits of the Anisian Gevanim Formation despite the low-stand, the evaporite-filled subsident basins of the Carnian, and the Erez Conglomerate adjacent to the Helez High. Late Triassic deposition is accompanied by volcanic activity of Asher-Atlit type increasing towards the north, and ophiolites indicate proximity to the spreading axis. In northern Israel, accelerated subsidence rates accompanied by sufficient bio- and chemo-productivity to keep up, resulted in accumulation of over 2500 m of mostly Upper Triassic evaporites and carbonates, centered along an approximately WSW-ENE axis traversing Galilee (Devorah) and continuing into the Palmyrides. This trough may be the continuation of late Paleozoic trends. Truncation of Late Triassic to the south may be attributed to regional tilting early in the Jurassic in the Negev and Sinai.

The epicontinental Triassic of the southern part of this

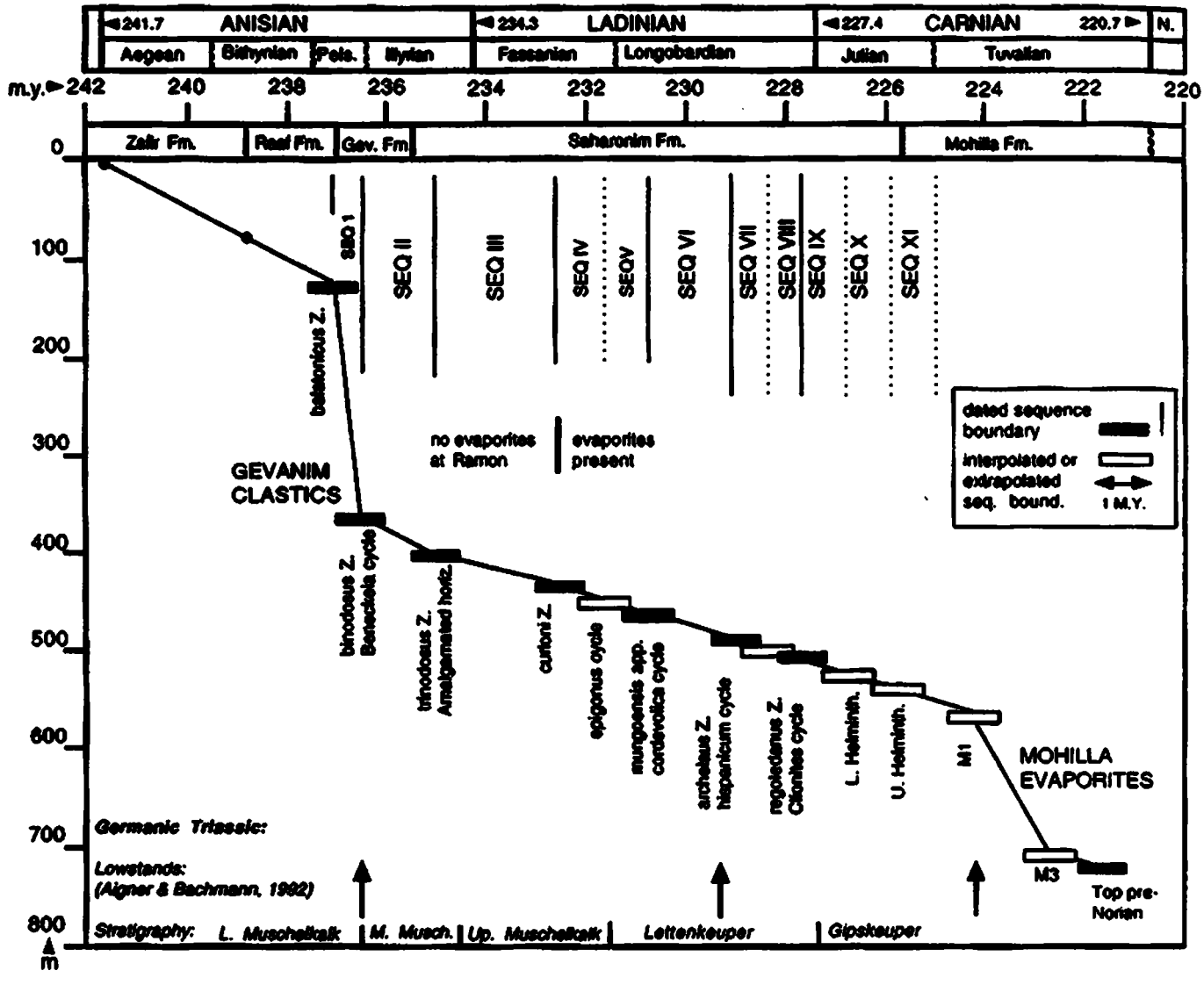
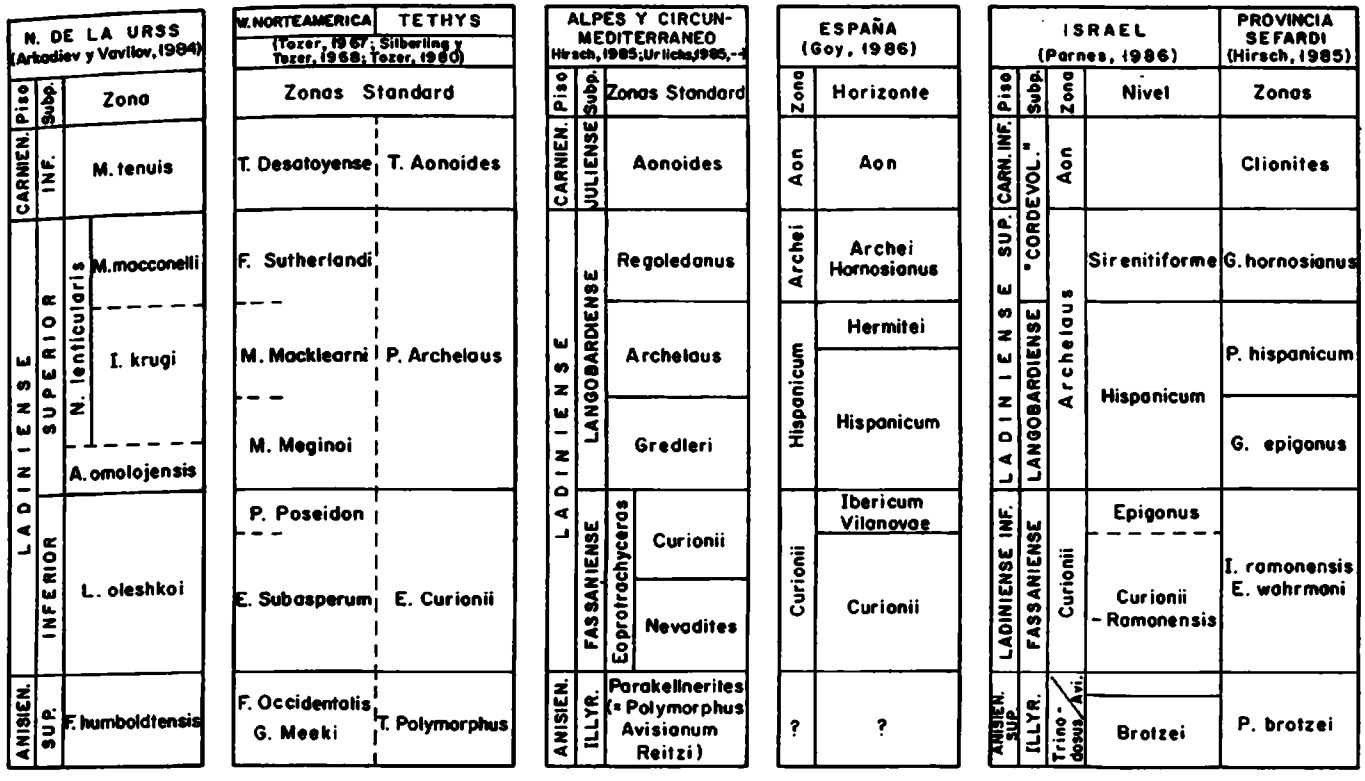


Figure 18D.16. Burial Curve and Cycles of the Ramon Triassic (from Druckman et al., 1997).

region displays shallow marine sedimentary oscillations, pacing the advance of Tethys over the Arabian craton. Epicontinental deposition appears to be characterised by low sedimentation rates and abundant lacunae and truncations, interrupted by at least one significant event of deltaic deposition, the 300 m thick Gevanim Formation, deposited over a very short time-span in the early Late Anisian. Druckman et al. (1982) pointed out that the belt of ingressions and regressions was relatively narrow, of not more than several tens of km. Four sedimentary cycles were proposed.

Hirsch (1991) attempted to identify the cycles of Haq et al. (1988) within the Triassic sequence in Israel. He suggested that the high-stands of the Yamin and Zafir Formations match global eustatic sea-level rises UAA 1.3 and 1.4; the Ra'af Formation may correspond to the Pelsonian-early Illyrian high-stand of cycle UAA 2.1, while the sedimentation rate within the Anisian clastic interval of the Gevanim Formation is mismatched as it is particularly high. Cycle 2.2, initiated in the Gevanim Formation fossiliferous shales and reaching its high-stand in the fossiliferous Saharonim Formation marine facies, is the most extensive in its southward geographic distribution. The long high-stand (HS) represented by the Saharonim Formation was split by Picard and Flexer (1974) in the middle by a 'lithostratigraphical break' marked by an evaporitic event. This large-scale cycle is terminated by a thick sequence of low-stand evaporites - the Mohilla Formation - of Early Carnian age. This low-stand (LS) is a manifestation of the global eustatic sea-level fall, perhaps the same that puts an end to the distinct Sephardic faunal realm. This pan-Mediterranean salinity crisis completely changed the circum-Mediterranean

Table 18D7. Worldwide Ladinian Ammonoid correlation (from Goy, 1995).



palaeobiogeography and represents the beginning of the regressive Keuper and Raibl facies of evaporites (halite, gypsum). Finally, in the Late Carnian, corresponding to UAA 3.2, shallow marine carbonate deposition was re-established above the evaporite sequence, extending to the Rhaetian. Most of the deposits of this cycle were truncated during regional emergence associated with volcanism, at the Triassic-Jurassic boundary.

A provisional burial curve based on Druckman et al. (1997) (Fig. 18D.16) divides the Triassic of southern Israel, in particular the sections exposed at Arif and Ramon, into 11 sequences. Using this curve, comparison of the Sephardic (NE Spain, Levant) and the Germanic Middle Triassic cycles (Aigner and Bachmann, 1992) show some heavily contrasting features: The Bithynian-Pelsonian Germanic Lower Muschelkalk represents an HS corresponding in late Pelsonian to the Sephardic HS of the Spanish M1 (Olesa) and Negev Ra'af HS, the short Gevanim LS precedes in time both the LS of the Germanic Middle Muschelkalk of Illyrian age and the Spanish Tramo Rojo intermedio (M2). The Late Illyrian transgression in the Levant slightly precedes both the Upper Muschelkalk of the German basin, mostly of Fassanian age and the Spanish M3. The Langobardian Germanic Lettenkohle LS is echoed by the Spanish M3 HS and by the Ramon cycles V-VIII (Saharonim 3).

V. SYNOPSIS OF THE LEVANT AND CIRCUM-MEDITERRANEAN TRIASSIC

Early Triassic

The nature of the Early Triassic transgression is characterized overall by clastics of a Werfen-type facies, though a significant carbonate intercalation occurs in the upper Yamin Formation and several carbonate layers are present in the lower part of the Zafir Formation. Minor regressions and shifting deltas further characterise the deposition of the Early Triassic in the eastern part of the Mediterranean region. Marine sandstones alternate with plant remains, shales, marls, and marly limestone with bivalves (*Claraia, Anodontophora* and *Costatoria*) and conodonts (*Hadrodontina, Pachycladina*). Palynomorphs include *Endosporites papilatus* and *E. nejburgi*. The deposition of Werfen-type facies in Israel persists into the Anisian. The embryonic Neotethys rifting possibly created an Early Anisian lacuna documented by a floral break in the Levantine region

Middle Triassic

Although Olenekian-Anisian sedimentation was continuous in the early Neotethys seaway (Chios; Kocaeli Peninsula), fully marine deposition resumed in the Levant in the Upper Anisian (Pelsonian) with the carbonates of the Ra'af Formation. The Middle Triassic transgression of the Saharonim Formation, commencing in the Late Anisian, and reaching its peak during the Late Ladinian or Earliest Carnian, submerged regions well within the African-Arabian platform, *e.g.* the Azizia Formation in Libya or the Jilh Formation in Central Arabia. The huge, shallow, slightly

hypersaline, epicontinental southern Neotethyan margin generated conditions for development of endemic taxa that characterized the Sephardic realm. Tornquist and Fallot (in Gignoux, 1960) had conceived the Middle Triassic of the Western Mediterranean to be similar to the Germanic basin, with alleged communication via a hypothetical gate of Burgundy. It was known that alpine faunas migrated into the Germanic basin, mixing with typical faunas of Muschelkalk facies type.

The observation that entirely different bivalve, ammonoid and conodont faunas occur in the Germanic and Mediterranean basins, and the similarity of faunas of Spain and Israel, led Lerman (1960), Parnes (1962, 1977), Parnes et al. (1985), and Hirsch (1972, 1977) to consider the Western Mediterranean Muschelkalk and their North African and Levantine equivalents to be part of a continuous platform or shelf, named the Sephardic realm (Hirsch, 1972). This realm extended along the south and west of the Tethyan seaway. Conodonts, *e.g. Pseudofurnishius murcianus*, found in Slovenia (Ramovs, 1997) indicate that the Sephardic realm extended to the northern edge of the Apulian plate. As one proceeds from Israel (Ramon, Arif) to Egypt (Arif en-Naqa), Jordan (Hisban) and the Pisidian Taurus (Tarasci, Turkey), the facies becomes less distinctive: Sephardic and Tethyan elements mix together (*Israelites, Iberites*, and *Sephardiella mungoensis* with *Protrachyceras pseudoarchelaus* and *Daonella lommeli*) toward the northern edge of the Sephardic shelf.

A similar feature can be observed in the Iberian Peninsula (Goy, 1995) where ammonoids of the genera *Negebites, Gevanites and Protrachyceras* of Sephardic and Tethyan affinity intermix. Elements of Sephardic biostratigraphy are summarized in **Table 18D.7** (from Goy, 1995, Fig. 3)

Late Triassic

The dramatic salinity crisis of the Early Carnian affected the entire Mediterranean region by gypsum and salt deposition (Saharan event). Marine conditions were restored in the Late Carnian in the Eastern Mediterranean region, with development of the Hauptdolomite facies, in contrast with the persistence of the Keuper facies further west. Dachstein-type reefs in places separated the Hauptdolomite shelf-lagoon from the open marine Hallstatt facies to the north. This 'alpinotype' regime lasted to the end of the Triassic. An early Cimmerian uplift phase brought about emersion and terminated Triassic deposition on the southern shelves of the Mesozoic Neotethys.

REFERENCES CITED

Abdallah, A. M., El Adindani, A. and Fahmy, N., 1965. Stratigraphy of the Lower Mesozoic rocks, western side of Gulf of Suez, Egypt. Geol. Surv., and Min. Res. Dept. Paper 27, p. 1-23.

Aigner, T., and Bachmann, G. H., 1992. Sequence-stratigraphic framework of the German Triassic. Sed. Geol., 80(1-2), p. 115-135.

Assereto, R., 1971. Aegean and Bithynian. Proposal for two new Anisian substages in: Zapfe, H. (ed.) Die Stratigraphie der alpin-mediterranen Trias. Schriftenreihe. Erdwiss. Komm. Oesterr. Akad. Wiss. p. 23-39.

Awad, G. H., 1945. On the occurrence of Marine Triassic (Muschelkalk) Deposits in Sinai. Bull. Inst. Egypte 27, p. 397-427.

Awad, G. H., 1946. On the occurrence of marine Triassic (Muschelkalk) deposits in Sinai. Bull. Inst. Egypt, XXVII, p. 397-427. Pts. I-III.

Bandel, K., and Khoury, H., 1981. Lithostratigraphy of the Triassic in Jordan. Facies, 4, p. 1-26.

Bandel, K., and Waksmundzki, B., 1985. Triassic Conodonts from Jordan. Acta Geologica pol., 35(3-4), p. 288-304.

Bartov, Y., Lewy, Z., Steinitz, G., Zak, I., 1980. Mesozoic and Tertiary stratigraphy, paleogeography and structural history of the Gebel Areif En Naqa area, eastern Sinai. Isr. J. Earth Sci., 29(1-2), p. 114-139.

Bender, F., 1968. Geologie von Jordanien, Beiträge zur Regionalen Geologie der Erde 7, Gebriider Borntraeger, Stuttgart, 230 p.

Benjamini, Ch., 1983. The stratigraphy of the Sartaba area. (In Hebrew). The geology of eastern Shomeron. Isr. Geol. Soc., Conf. and Field Trip, Nov. 1983, p. 2-5. (Also in: The Sartaba and the Samaria Desert, M. Rosenfeld (ed.), Isr. Soc. for the Protection of Nature, 1984, p. 8-11).

Benjamini, Ch., 1984a. Stratigraphy of the Eocene of the 'Arava Valley (eastern and southern Negev, southern Israel), Isr. J. Earth Sci., 33(4), p. 167-177.

Benjamini, Ch., 1984b. Foraminifera from the Ra'af Formation (Anisian), Har 'Areif, western Negev, Israel. In: Oertli, H. J. (ed.), Benthos '83; 2nd Intl. Symp. Benthic Foraminifera (Pau, April 1983), p. 35-40

Benjamini, Ch., 1988. Triassic foraminifera from Makhtesh Ramon, Central Negev, Southern Israel. Revue de Paleobiologie, Vol. Spec. Issue 2, p. 129-144.

Benjamini, Ch., and Chepstow-Lusty, A. 1986. *Neospathodus* and other Conodonta from the Saharonim Formation (Anisian-Ladinian) at Makhtesh Ramon. J. Micropalaeontol., 5(1), p. 67-75.

Benjamini, Ch., Weinbaum-Hefetz, M., and Moshkovitz, S., 1997. The biostratigraphy of calcareous nannoplankton across the Lower/ Middle Eocene boundary in the northern Negev of Israel. (In Hebrew; English. Abstr.). Report, submitted to the Minist. of Energy and Infrastructure, No Paging., Figs.

Benjamini, Ch., Druckman, Y., and Zak, I., 1993. Depositional cycles in the Ramon Group (Triassic), Makhtesh Ramon. Isr. J. Earth Sci. 42(3-4), p. 115-124.

Blake, G. S., 1936. The stratigraphy of Palestine and its building stones. Jerusalem, Printing and Stationery Office, 133 p.

Brotzen, F., 1956. Stratigraphical stdies on the Triassic vertebrate fossils from Wadi Raman, Israel. Arkiv for Mineralogi och Geologi, Kungl. Svenska Vetenskapakad, 2(9), p. 191-217.

Brugman. W. A., 1986. Palynological characterization of the Upper Scythhian and Anisian of the Trans-danubian Central Region (Hungary) and the Vicentinian Alps (Italy). Unpubl. Ph.D. thesis, State Univ. Utrecht, 95 p.

Cohen, Z., Kapstan, V., Muravinski, E., Salhov, S., Shilo, A., and Wolff, O., 1987. Stratigraphic table of Israel outcrops and subsurface. Oil Exploration (Investments) Ltd.

Conway, B., Cousminer, H. L., Eshet, Y., and Hirsch, F., 1990. Palynozones at the Triassic/Jurassic boundary in Israel. Working Group Limite Trias/Jurassique, Comm. Int. Stratigraphie, Lyon, 1988, Cah.Univ. Catholique, Lyon, p. 137-150.

Cousminer, H. L., 1981. Palynostratigraphy, thermal alteration index and Kerogen characteristics of the Ga'ash-2 well sequence. Isr. Geol. Surv. Rep. P/2/81, 20 p.

Cousminer, H.L., 1982. Palynology and thermal alteration index of samples from Atlit-1 well. Rep. Submitted to Oil Exploration (Investments) Tel Aviv, 3 p.

Cox, L. R., 1924. A Triassic fauna from the Jordan Valley. Ann. Mag. Nat. Hist. Ser. 9, XIV, p. 52-96, plates I-II.

Cox, L. R., 1932. Further notes on the Transjordan Trias. ibid, Ser. 10, X, p. 93-113, pl. VII.

Daniel, E., 1963. Lexique Stratigraphique International Jordanie, III, Fasc. 10C, Centre National de la Recherche Scientifique, Paris, p. 295-437.

Derin, B., and Gerry, E., 1981. Late Permian Late Triassic stratigraphy in Israel and its significance to oil exploration. Oil Exploration in Israel. Symp. Isr.Acad. Sci.and Human., p. 9-11.

Derin, B., Lipson, S., and Gerry, E., 1981. Ga'ash 2, stratigraphic log 1:2000. Isr. Inst. Petr. And Energy, Tel Aviv, Report 14/81, — p..

Derin, B., and Gerry, E., 1981. Late Permian-Late Triassic stratigraphy in Israel and its significance to oil exploration. Oil Exploration in Israel, Symposium,

Abstracts, Israel. Geol. Soc., Jerusalem, p. 9-10.

Druckman, Y., 1969. The petrography and environment of deposition of the Triassic Saharonim Formation and the Dolomite Member of the Mohilla Formation in Makhtesh Ramon, Central Negev (southern Israel). Isr. Geol. Surv. Bull., 49, 24 p.

Druckman, Y., 1976. The Triassic in southern Israel and Sinai: A sedimentological model of marginal epicontinental marine environments. Ph.D. Thesis, Hebrew Univ. Jerusalem, 188 p. Also: Isr. Geol. Surv., Rep. OD/1/76. (In Hebrew; Engl. Abstr.).

Druckman, Y., 1974a. The stratigraphy of the Triassic sequence in southern Israel. Isr. Geol. Surv. Bull., 64, 94 p.

Druckman, Y., 1974b. Triassic Paleogeogeography of Southern Israel and the Sinai Peninsula. Die Stratigr. Der Alpin-Mediterranen Trias, Symp. Wien, May 1973. Oesterreichische Akademie der Wissenschaften, Schriftenreihe der Erdwissenschaftliche Kommissionen, 2, p 79-86.

Druckman, Y., 1984. Evidence for early-Middle Triassic Faulting and possible rifting from the Helez-Deep borehole in the Coastal Plain of Israel. In: Dixon, J. E., and Robertson, A. H. F., (eds.), The Geological Evolution of the Eastern Mediterranean. Geol. Soc. Spec. Publ. 17, Oxford, Blackwell, p. 203-212.

Druckman, Y., Gvirtzman, G., and Kashai, E., 1975. Distribution and environments of deposition of Upper Triassic on the northern margins of the Arabian Shield and around the Mediterranean Sea. 9th Int. Geol. Cong., Proc., Theme 5, p. 183-192.

Druckman, Y., Hirsch, F., and Weissbrod, T., 1982. The Triassic of the southern margin of the Tethys in the Levant and its correlation across the Jordan Rift valley. Geol. Rundsch., 71(3), p. 919-936.

Druckman, Y., and Kashai, E., 1981. The Helez Deep and Devora-2A boreholes and their implication to oil prospects in pre-Jurassic strata in Israel. Isr. Geol. Surv., Rep. OD/1/81, 23 p.

Druckman, Y., Weissbrod, T., and Horowitz, A., 1970. The Budra Formation: A Triassic continental deposit in southwestern Sinai. Isr. Geol. Surv. Rep. OD/3/70, 20 p.

Dunay, R. E., 1973. Report on interval 1934-2157 m., Makhtesh Qatan 2 well (written communication).

Eicher, D. B., 1947. Micropaleontology of the Triassic of northern Sinai. Inst. Egypte Bull. 28, p. 87-92

Eicher, D. B., and Mosher, L. C., 1974. Triassic conodonts from Sinai and Palestine. J. Paleont., 48(4), p. 727-739.

Eshet, Y., Rampino, M. R., and Visscher, H., 1995. Fungal event and palynological record of ecological crisis and recovery across the Permian-Triassic boundary. Geology, 23(11), p. 967-970.

Eshet, Y. 1990a. Paleozoic-Mesozoic palynology of Israel, I. Palynological aspects of the Permian-Triassic succession in the subsurface of Israel. Isr. Geol. Surv. Bull., 81, 57 p. Plates.

Eshet, Y., 1990b. The Palynostratigraphy of the Permian-Triassic Boundary in Israel: Two approaches to Biostratigraphy. Isr. J. Earth Sci., 39(1), p. 1-15.

Eshet, Y., and Cousminer, H. L., 1986. Zonation and correlation of the Permo-Triassic succession in the Negev, Israel. Micropaleontology, 32(3), p. 193-214.

Freund, R., Garfunkel, Z., Zak, I., Goldberg, M., Weissbrod, T., and Derin, B., 1970. The shear along the Dead Sea Rift. Phil. Trans. Roy. Soc. London, A., 267(1181), p. 107-130.

Garfunkel, Z., and Derin, B., 1984. Permian - Early Mesozoic tectonism and continental margin formation in Israel and its implications for the history of the eastern Mediterranean. In: Dixon, J. E., and Robertson, A. H. F., (eds.), The Geological Evolution of the Eastern Mediterranean, Geol. Soc. Spec. Publ. 17, Oxford, Blackwell, p. 187-201.

Gerry, E., Honigstein, A., Rosenfeld, A., Hirsch, F., and Eshet, Y., 1990. The Carnian salinity crisis: ostracods and palynomorphs as indicators of paleoenvironment. In: R. Whatley and C. Maybury (eds.), Ostracoda and Global Events. London, Chapman and Hill, p. 87-99.

Gignoux, M., 1960. Geologie Stratigraphique. 5th. Edit. Masson, Paris 759 p.

Glikson, M. R., 1964. Palynological investigations in "Makhtesh Qatan 2", boring in the Negev, Israel. Isr. J. Earth Sci., 13(1), p. 16-26.

Goldberg, M., 1964. Problems of Jurassic Stratigraphy in Southern Israel. Isr. J. Earth Sci., 13(3-4), p. 169-171.

Goy, A., 1995. Ammonoideos Triassico Medio de España: Bioestratigrafia y correlaciones. Cuadernos Geol. Iberica, 19, p. 21-60.

Haas, G., 1959. On some fragments of the Dermal skeleton of Placodonta from the Triassic of Arayif en Naqa, Sinai Peninsula. Kungl. Sven. Vetenskapakad. Handlingor, Frarde Serien, 7, 4.

Haas, G., 1963. Micronothosaurus stensoi, Ein Neuer Nothosauride aus dem Oberen Muschelakl des Wadi Ramon, Israel. Palaont. Zeit., 37, p. 161-178.

Haas, G., 1969. The armour of Placodonts from the Muschelalk of Wadi Ramon, Israel. Isr. J. Zoology 18, p. 135-147.

Haas, G., 1970. Eine bemerkenswerte Interclavicula von (?) Tanystropheus aus dem Muschelkalk des Wadi Ramon, Israel. [An unusual interclavicle of Tanystropheus? from the Muschelkalk of Wadi Ramon, Israel]. Palaont. Zeit., 44(3-4), p. 207-214.

Hirsch, F., 1972. Middle Triassic conodonts from Israel, southern France, and Spain. Innsbruck Symp. Triass. Microfacies, Mitt. Ges. Geol. Bergbaustud., 21(2), p. 811-828.

Hirsch, F., 1975. Lower Triassic conodonts from Israel. Geol. Surv. Israel Bull., 66, p. 39-49.

Hirsch, F., 1976. Sur l'origine des particularismes de la fauna du Trias et du Jurassique de la platform Africano-Arabe. [The origin of faunal peculiarities during the Triassic and Jurassic of the African-Arabian Platform].Bull. Soc. Géol. France, 18(2), p. 543-552.

Hirsch, F., 1977. Note on *Neospathodus* cf. *N. kockeli (Tatge)* (Conodonta) from Ramon 1 well Central Negev. Isr. J. Earth Sci., 26(3-4), p. 94-96.

Hirsch, F., 1990. Aperçu de l'histoire phanérozoique d'Israël. [A sketch of the Phanerozoic history of Israel]. J. Afr. Earth Sci., 11(1-2), p. 177-196.

Hirsch, F., 1992. Circummediterranean Triassic eustatic cycles. Isr. J. Earth Sci., 40(1-4), p. 29-38.

Hirsch, F., 1997. The Triassic Conodont zonation across the Dead Sea Rift. Geol. Surv. Isr. Current Research 11, p. 62-64.

Hirsch, F., Flexer, A., Rosenfeld, A., and Yellin-Dror, A., 1995. Palinspastic and crustal setting of the Eastern Mediterranean. J. Petrol. Geol., 18(2), p. 149-170.

Hirsch, F., and Gerry, E., 1974. Conodont and ostracode biostratigraphy of the Triassic in Israel. Proc. Inter. Symposium of the Alpin-Mediterranean Triassic Stratigraphy, Vienna May 1973, Schriftenreihe Erdwiss, Komm. Osterr. Akad. Wiss. 2, p. 107-114.

Hirsch, F., and Roded, R., 2001. Lexique Stratigraphique for Israel in digital form. Diskette at the Documentation Center, Geological Survey of Israel.

Horowitz, A., 1970. Palynostratigraphy Of The Upper Paleozoic - Lower Mesozoic Sequence In Zohar 8 Borehole (Southern Israel). Isr. Geol. Surv., Rep. P/1/70, & Inst. Petrol. Res. Geophys. Rep. 1038, 9 p., Figs.

Horowitz, A., 1973. Late Permian palynomorphs from southern Israel. Pollen et Spores, 15(2), p. 315-341.

Huckriede, R., 1958. Die Conodonten der mediterranen Trias und ihr stratigraphisher Wert. Palaeont. Zeit., 32(3-4), p. 141-175.

Huddle, W., 1970. Triassic conodonts from Israel. U. S. G. S. Prof. Paper, 700B, p. B124-B130.

Karcz, I., and Braun, M., 1964. Sedimentary structures and paleocurrents in the Triassic sandstones of Makhtesh Ramon. Isr. Geol. Surv., Bull. 38, 18 p.

Knipper, A. L., and Sharaskin, A. Y., 1994. Tectonic evolution of the western part of the Peri-Arabian Ophiolite Arc. In: Krasheninnikov, V. A., and Hall, J. K., (eds.), Geological Structure of the North-eastern Mediterranean. Historical Publications-Hall, Jerusalem, p. 295-306.

Korngrin, D., and Benjamini, Ch., 2001. Upper Triassic reef facies in the Asher-Atlit 1 Borehole, northern Israel: Microfacies, cement stratigraphy and paleogeographic implications. Facies, 45, p. 1-24.

Kummel, B., 1960. Middle Triassic Nautiloids from Sinai, Egypt and Israel. Bull. Mus. Comp. Zool. Harvard College, 123(7), p. 285-302.

Lerman, A., 1960. Triassic pelecypods from southern Israel and Sinai. Bull. Res. Counc. Israel, 9G(1), p. 1-51.

Marquez-Aliaga, A., and Hirsch, F., 1988. Migration of Middle Triassic bivalves in the Sephardic Province. Congreso Geol. de España, Comm., 1, p. 301-304.

Mouty, M., 2000. The Jurassic in Syria: an overview. Lithostratigraphic and biostratigraphic correlations with adjacent areas. In: Crasquin-Soleau S., and Barrier, E., (eds.), New data on Peri-Tethyan sedimenatry basins, Peri-Tethys Memoir 5, Museum National d'Histoire Naturelle, Paris, p. 159-168.

Mouty, M., and Zaninetti, L., 1998. Le Jurassique du Mont Hermon (Anti-Liban). Decouverte de Trias et de Lias, Archs. Sci. Genève, 51(3), p. 295-304.

Parnes, A., 1987. Radiation of species of the Genus Radiolites from the Upper Turonian at Gebel Er-Risha (NE Sinai, Egypt). Isr. J. Earth Sci., 36(3), p. 133-153.

Parnes, A., 1962, Triassic ammonites from Israel. Isr. Geol. Surv. Bull. 33, 76 p., 9 plates, 12 figs.

Parnes, A., 1975, Middle Triassic ammonite biostratigraphy in Israel. Isr. Geol. Surv. Bull. 66, 35 p., 5 plates, 2 figs.

Parnes, A., 1986, Middle Triassic Cephalopods from the Negev (Israel) and Sinai (Egypt). Isr. Geol. Surv. Bull. 79, 59 p., 23 plates, 4 figs.

Parnes, A., Benjamini, Ch., and Hirsch, F., 1985. Some aspects of Triassic ammonite biostratigraphy, paleoenvironments and paleogeography in southern Israel. J. Paleont., 59(3), p. 656-666.

Picard, L., and Flexer, A., 1974. Studies on the stratigraphy of Israel: The Triassic. Negev; Sinai; Jordan; Saudi Arabia; Syria. Isr. Inst. Pet. Energy, 62 p.

Quennell, A. M., 1958. The structure and geomorphic evolution of the Dead Sea Rift. Quart. J. Geol. Soc. Lond., Vol. 114, Part 1, No. 453, p. 1-24.

Ramovs, A., 1997. Skelettapparat von *Pseudofurnishius murcianus* (Conodontophorida) im Mitteltrias Sloweniens (NW Yugoslawiens). N. Jb. Geol. Paleont. Abh., 153/3, p. 361-399.

Ricou, L. E., Marcoux, J., and Whitechurch, H., 1984. The Mesozoic organization of the Taurides: one or several ocean basins? In: Dixon, J. E., and Robertson, A. H. F., (eds.), The Geological Evolution of the Eastern Mediterranean. Geol. Soc. Spec. Publ. 17, Oxford, Blackwell, p. 349-359.

Sadeddin, W., and Kozur, H., 1992. *Pseudofurnishius siyalensis* n.sp. (Conodonta) from the Lower Ladinian of Wadi Siyala (Jordan). N. Jb. Geol. Palaeont., 1992(6), p. 359-368.

Schlatter, L. E., 1950a. Geological report on Well Abu Hamth-1. Unpubl. Rept. No. 889, Anglo-Egyptian Oil Com., 27 p.

Schlatter, L. E., 1950b. Geological report on Well Nakhl-1. Unpubl. Rept. No. 890, Anglo-Egyptian Oil Com., 16 p.

Segev, A. 2001. The Principal Phanerozoic Tectono-Magmatic Periods in the Levant and their Stratigraphic Record. GSI Current Research, 12, p. 115-124.

Shaw, S. H., 1947. Southern Palestine: Geological Map on a scale of 1:250,000 with Explanatory Notes. Government of Palestine, Government Printer, Jerusalem, 42 p. Map.

Sohn, I. G., 1968. Triassic ostracodes from Makhtesh Ramon, Israel. Geol. Surv. Israel Bull., 44, 71 p.

Sohn, I. G., and Reiss, Z., 1964. Conodonts and Foraminifera from the Triassic of Israel. Nature, 201(4925), p. 1209.

Visscher, H., Brinkhuis, H., Dilcher, D. L., Elsik, WC., Eshet, Y, Looy, C. Y., Rampino, M. R., and Traverse, A., 1996. The terminal Paleozoic fungal event: Evidence of terrestrial ecosystem destabilization and collapse. Proc. Natl. Acad. Sci. USA, Ecology, 93, p. 2155-2158.

Weissbrod, T., 1969. The Paleozoic of Israel and adjacent countries. Part I: The subsurface Paleozoic stratigraphy of southern Israel. Isr. Geol. Surv. Bull. 47, 35 p.

Weissbrod, T., 1976. The Permian in the Near East. In: H. Falke (ed.), The Continental Permian in Central West and South Europe, Netherlands, Reidel Publ. Co., p. 200-214.

Wetzel, R., and Morton, D. M., 1959. Contribution à la géologie de la Transjordanie, Muséum National d'Histoire Naturelle, Notes et Mémoirs Moyen-Orient, Paris, 7, p. 95-191.

Zak, I., 1957. The Triassic in Makhtesh Ramon. Unpublished M.Sc. Thesis, Hebrew University Jerusalem, 98 p. (In Hebrew).

Zak, I., 1963. Remarks on the stratigraphy and tectonics of the Triassic of Makhtesh Ramon. Isr. J. Earth Sci., 12(2), p. 87-89.

Zak, I., 1964. The Triassic in Arief en-Naqa, Sinai. Geol. Surv. Israel Rep, Geochem., 61/4, 28 p.

Zak, I., 1986. The Triassic period in southern Israel. Geol. Surv. Israel Bull., 79, p. 1-8.

Zaslavskaya, N., Eshet, Y., Hirsch, F., Weissbrod, T., and Gvirtzman, G., 1995. Recycled Lower Paleozoic microfossils (Chitinozoa) in the carboniferous of Sinai (Egypt) and Permo-Triassic of the Negev (Israel): Paleogeographic considerations. Newsl. Stratign, 32(1), p. 57-72.

Zemel, M., Wuerzburger, M., and Bartura, Y., 1956. Geological Map of Makhtesh Arif, scale 1:10000. Isr. Geol. Surv, Unpublished Rep. (In Hebrew).



Dr. Avraham Parnes at age 95 in the field (1987).
From GSI Current Research, Vol. 12, (2000, p. 279). Dr. Parnes was active right up to his death during the Annual Meeting of the Israel Geological Society at Kibbutz Ramot on the Golan Heights in the spring of 1989.

Chapter 18E

The Jurassic of Israel

Francis Hirsch
Geological Survey of Israel, 30 Malchei Israel Street, Jerusalem 95 501, Israel

PREFACE

The Jurassic in Israel is exposed at the Makhtesh Ramon, Hamakhtesh Hagadol (Negev, Israel), and at Wadi Malih (Samaria). Numerous exploration drillings provide an overview of the paleogeography and facies. The outcrops at Gebel Maghara (Sinai, Egypt), the Yabbok River (Jordan), and Mount Hermon (the Anti-Lebanon) provided additional information to understand the Jurassic of the southern Levant, described in the monograph of Picard and Hirsch (1987). The biostratigraphy of the Jurassic in the Levant is based on ammonites, calcareous nannoplankton, foraminifera, algae, bivalvia, gastropods, ostracodes, brachiopods, and palynomorphs (pollen, spores, dinocysts, and acritarchs), as recently compiled by Hirsch et al. (1998). The new contributions in the field of paleontology and biostratigraphy include palynomorphs (Conway, 1990), brachiopods (Feldman et al., 2001), ostracodes (Rosenfeld et al., 1987a, b, 1988, 1991), ammonites (Cariou et al., 1997), foraminifera, and algae (Bassoullet and Perelis Grossowicz, in press). Further data (Mouty and Zaninetti, 1998) have clarified the question of the Triassic-Jurassic boundary in the massif of Mount Hermon (the Anti-Lebanon).

Interpretation of seismic profiles offshore the Israel coast as well as the drilling of bore-holes offshore the Sinai coast have shed new light on the paleogeography in the Levant Basin (Hirsch et al., 1995). The presence of a thick sedimentary cover, including a Jurassic sequence in the Levant basin, suggests that the Jurassic facies of the Levant covered an undivided African-Apulian-Arabian shelf-platform, south of the Neotethys.

INTRODUCTION

Israel has few Jurassic outcrops, but a large number of bore-holes provide necessary links between the large outcropping sections of Northern Sinai (Egypt) and the Lebanon-Anti-Lebanon ranges, providing a good insight into the development of the Jurassic in the Levant.

The Northern Sinai sections of Gebel Maghara, Minshera, Um Mafrut, Ras Gihan, and Risan Aneiza expose over 2000 m of Late Liassic to Kimmeridgian strata. The Sinai Jurassic is very similar to the Negev sequence. The nearly 2200 m of Middle to Upper Jurassic strata, exposed in Mount Hermon, give a good insight into the sequence that is buried under Central Israel. The Jurassic of Lebanon is similar to the sequence in northern Israel.

As the few Jurassic outcrops in Israel expose only short intervals of the sequence that is mostly known from bore-holes, the Lower and Middle Jurassic sequence in Makhtesh Ramon (Central Negev) is of great importance, providing the stratotypes of the Mishhor, Ardon, Inmar, and Mahmal Formations. Only a tiny part of the Middle Jurassic Zohar Formation is exposed in Makhtesh Qatan (Northern Negev). Its stratotype was chosen in the nearby Hamakhtesh Hagadol, where a larger part of it is exposed, underlying the Late Callovian Matmor Formation. The latter represents a unique facies of the Latest Callovian in the Middle East.

The Late Jurassic exposed in Wadi el Malih (Eastern Samaria) belongs entirely to the Nahar Sa'ar Formation, unconformably covered by the Tayasir Volcanics. This section is similar to Upper Jurassic and Lower Cretaceous strata of Mount Hermon.

In the stratigraphic subdivision of Israel, Jurassic strata correspond to the Arad Group. The present review attempts to retain only formation names, duly based upon exposed stratotypes. A few subsurface names had to be retained (marked by *): Mishhor, Asher*, Ardon, Inmar, Qeren*, Mahmal, Daya*, Sherif*, Haifa*, Hermon, Zohar, Matmor, Nir'Am*, Majdal Shams, Nahar Sa'ar and Gevar'Am*.

SYNOPSIS

The Jurassic paleogeography of the Southern Levant subdivides into three provinces in Israel:

The Negev-type facies, around the Arabo-Nubian craton, the Judean Embayment, extending to the Anti-Lebanon and Palmyra chain, and the Galilee platform, that extends to Lebanon and Coastal Syria. Offshore, the Delta-Akkuyu trough (embryonic Gevar'Am trough) separates the onshore facies from an eastern Mediterranean paleoland.

Six major transgressions (second order cycles) characterize the Jurassic in our region: Pre-Toarcian, Aalenian, Late Bajocian, Middle Bathonian, Callovian-Oxfordian, and Kimmeridgian.

The Jurassic in Israel and adjacent countries (Syria and Lebanon) is framed by volcanic events: The Triassic-Jurassic boundary corresponds to the Asher/Yagur/Aarneh volcanics in Galilee-Anti-Lebanon and to the derived Mishhor laterite in the Negev and southern Coastal Plain.

A smaller event, the Oxfordian Devorah/Bahnnes Volcanics, occurs only in the Galilee and Lebanon. The Jurassic-Cretaceous boundary corresponds with the Tayasir Volcanics (Tithonian-Berriasian in Northern Israel and Mount Hermon, which overlie Kimmeridgian strata). Towards the south, this boundary is replaced by the angular unconformity between Lower Cretaceous

sandstones, overlying Upper Callovian in Kurnub and Upper Bajocian in the Ramon. In the Coastal Plain boreholes, shale or limestone of the Tithonian-Valanginian Gevar'Am Group overlie Upper Jurassic carbonates or shale. Where shale rests on shale or carbonate on carbonate, the recognition of the boundary depends on micropaleontology (foraminifera, palynomorphs, calcareous nannoplankton).

Tectonism is characterized by uplift at the Triassic-Jurassic boundary, uplift of the Coastal Plain area prior to the Oxfordian transgression, and regional uplift prior to Tithonian-Berriasian times. The Jurassic paleotectonic setting in Israel consists of relative lows and highs, controlled by differential rates of subsidence. To the north the Galilee-Lebanon platform (1500-2000 m Jurassic thickness) extends to Coastal Syria (300 m). The Judean embayment in Central Israel extends from Helez (3000 m) to the Hermon (2000 m), and the Palmyra basin (100 m), being part of the Permian-Jurassic Palmyra embayment (Dercourt et al., 2000). The latter is separated from the Sinaitic Maghara basin (3000 m) by the nose of the Negev high (900-2000 m). **(Figure 18E.1)**

The biostratigraphy of the Jurassic in the Levant often exhibits endemic character, related to the isolation of the southern Tethys shelf. Ammonite correlation of the Arabian Province with SESSS (Submediterranean European Standard Scale Stages) and the calibration of large Foraminifera and Palynomorphs with Ammonite scales, provide reliable biostratigraphic frames.

a) STRATIGRAPHY

Introduction

During the Jurassic the Levant was part of the Gondwanian Tethys platform-shelf. The paleotectonic setting of the Levant consisted of relative lows and highs, controlled by differential rates of subsidence. In southern Israel the shallow Negev high (900-2000 m) separated the Maghara basin (3000 m) from the Central Israel-Hermon trough (2000 m). The shallow northern platform of Galilee and Lebanon (2150-1200 m) extended far to the north into Syria, Lebanon, and southern Turkey).

Liassic through Bathonian clastics are the result of the wearing down of the Arabian Massif in the south and southeast. Yet thickening of the Early Oxfordian shales in the offshore wells points to derivation from some landmass in the west, now hidden below the Mediterranean (Hirsch et al., 1995). The Gevar'Am trough, alongside the present Levant coast, formed during the Tithonian. It initiated a separation between an Eastern Levant platform extending toward the Arabian-Nubian Massif and a Western Levant shallow marine platform and adjacent landmass. Volcanics witness a number of aborted Mesozoic intracratonic rifts at the beginning and end of the Jurassic.

The Triassic-Jurassic boundary in the Levant is marked by lateritic paleosols (Mishhor Formation). They are probably derived from the destruction of the Late Triassic-Liassic Asher basalt, which is 2000 m thick in the Yagur-Asher area in the western part of a trough that crossed the north and middle parts of the country from the present coast into the Galilee (Devorah, 280 m) and Anti-Lebanon (60 m).

The Jurassic-Cretaceous boundary consists of the Tithonian-Hauterivian Tayasir basalts, up to 500 m thick from Samaria to Galilee, Lebanon and the Golan Heights **(Figure 18E.2)**.

Marine platform carbonates started during Pliensbachian-Toarcian times (Ardon Formation), interrupted by fluviatile clastics (the Toarcian-Aalenian Inmar Formation) in the Negev and adjacent Sinai (Egypt). Crossing central Israel, a belt of shales (Rosh Pinna Formation) marks the Aalenian. To the north (Galilee, Lebanon, and the northern Anti-Lebanon) monotonous platform- carbonates persisted without interruption throughout the Oxfordian (Haifa Formation). The Bajocian lithofacies varies from mixed carbonatic and clastic in the Negev (Daya Formation) to largely marly in Sinai (Bir Maghara Formation) and carbonatic in the north. Oolitic shoals (Sederot Formation) and spiculitic limestones (Barnea Formation) are found in the Coastal Plain, recurring in the Bathonian. Early Bathonian paralic clastics invade the south, followed by marls (Sherif Formation) while a shale-belt extending along the Coastal Plain, reaches eastward into the Judean Desert (Karmon Formation) and straddles the Bathonian-Callovian boundary.

The lower part of the Callovian is a constant sequence of calcarenites (Brur) in the Coastal Plain and of micrites and marls (lower Zohar Formation). The Middle-Upper Callovian, largely not present and truncated in the central Coastal Plain, is represented by limestones and marls in the Negev (upper Zohar Formation) and massive limestones in the north. A thick Late Callovian limestone and marl sequence in the Negev (Matmor Formation) is coeval to thin condensed ammonite-rich limestones at Gebel Maghara and the South Anti-Lebanon. Early Oxfordian shales (Majdal Shams Formation) extend from northern Sinai, through Central Israel to the South Anti-Lebanon. Bioherms and reefs (Nir'Am Formation) represent the Oxfordian in the Coastal Plain area. Late Oxfordian-Tithonian limestones, oolites, shales and sands (Nahar Sa'ar Formation) are found from Galilee and the Golan to the Northwest Negev. Tithonian-Baremian turbidites (Gevar'Am) cover a truncation surface in the Coastal Plain of Israel (Fig. 18E.2).

A number of outcrops at Makhtesh Ramon, Hamakhtesh Hagadol, Gebel Maghara (Sinai, Egypt) and Mount Hermon (the Anti-Lebanon) provide insight into the Jurassic sequence. Over 200 drillings that penetrated the Jurassic of Northern Sinai (Egypt) and Israel include the Helez-Kokhav oil fields of the southern Coastal Plain and the gas field of Zohar-Kidod in the southern Judean Desert. Nearly every anticlinal structure in the Northern and Central Negev, the Judean Hills, the Dead Sea Graben, Galilee, and the Mediterranean offshore was drilled.

Representative outcrops are found in the Central Negev: Makhtesh Ramon (Lias-Bajocian) **(Figure 18E.3)**; in the Northeastern Negev Hamakhtesh Hagadol (Callovian) **(Figure 18E.4, Figure 18E.5)**. These are complemented by the Qeren, Boqer, and Kurnub boreholes **(Figure 18E.6, Figure 18E.7)**.

In Sinai (Egypt) the sequence of Gebel Maghara, complemented by the borehole of Gebel Hallal, correlates well with the northwestern Negev boreholes of Hazerim, Beersheva,

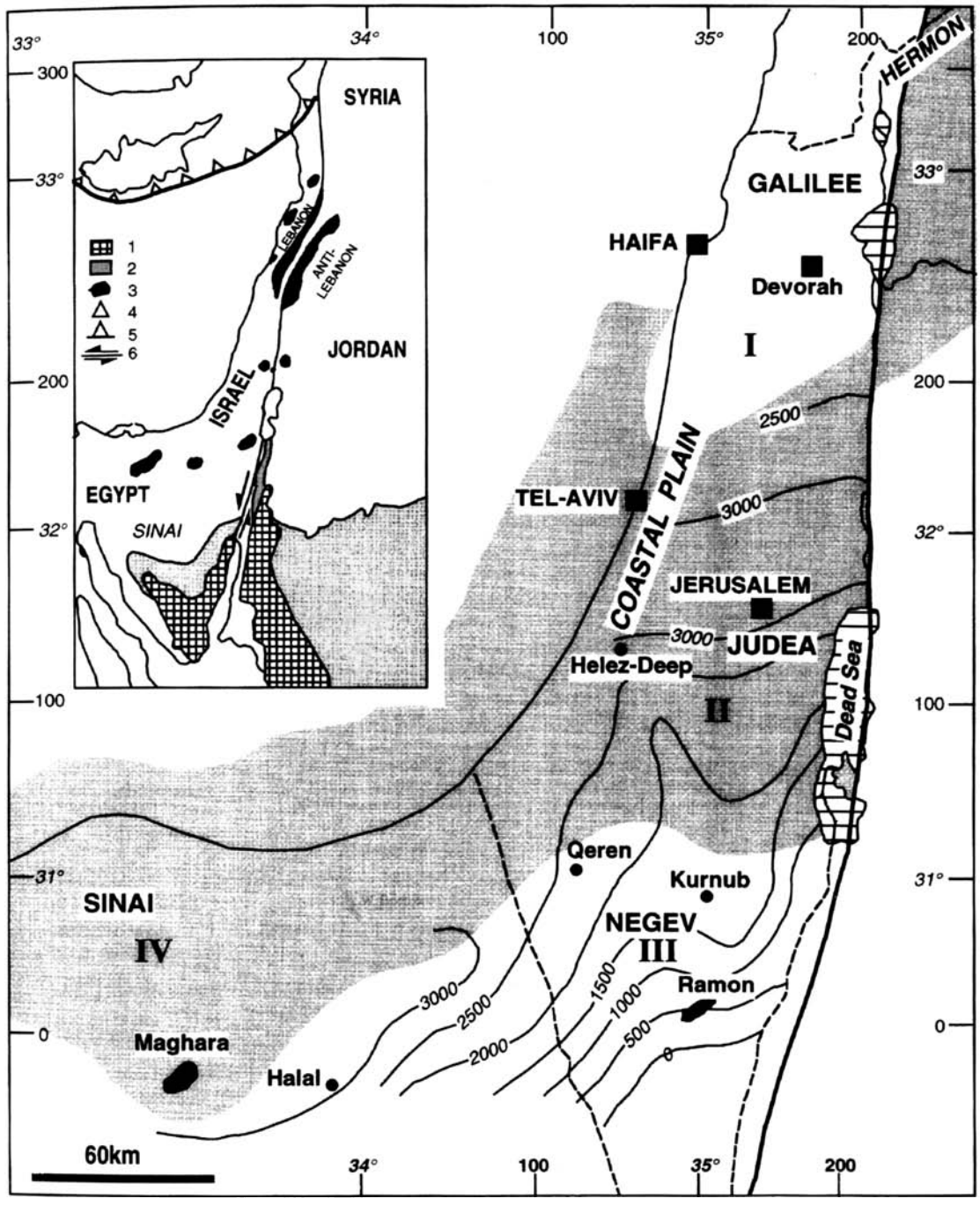


Figure 18E.1. Location map (From Hirsch et al., 1998).

and Betarim.

The Central Israel and Coastal Plain bore-holes of Helez, Talme Yaffe, Beeri, Gerar, Delta, Ramallah, Motza, and Halhul are best compared with the section of the Hermon. The Northern Israel bore-holes of Foxtrot, Haifa, Asher, Devorah, Rosh Pinna, Carmel, Ga'ash, and Petah Tiqva compare with the exposures of Lebanon.

First of all the Negev Region comprises the outcrop of Makhtesh Ramon. This large erosion-funnel exposes 430 m of Liassic to Late Bajocian beds. Jurassic strata in Makhtesh Ramon were first mentioned by Shaw (1947, p. 20-21). An informal subdivision was established by Bentor and Vroman (1951). The mineralogy and sedimentology of the Lower Liassic Mishhor Formation was studied by Slatkin and Heller (1961) and Wurzburger (1963) and its lateritic residual nature was established by Goldbery (1979).

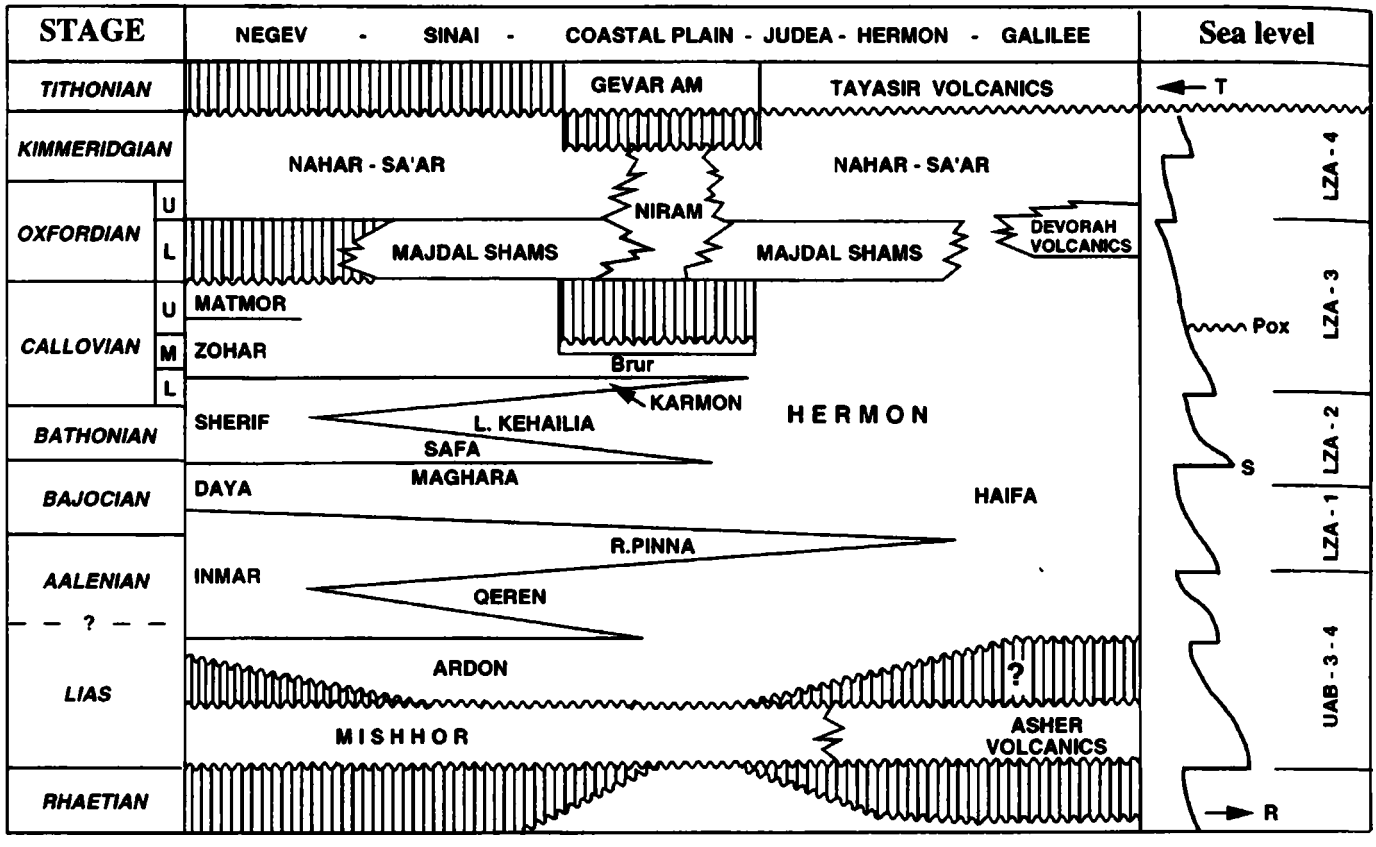


Figure 18E.2. Composite diagram of the Jurassic in Israel (From Hirsch et al., 1998).
Legend: S: Sherif-Safa Regression; Pox: Pre-Oxfordian tectonic event; R: Regression; T: Transgression.

The carbonatic Ardon Formation and the clastic Inmar Formation were established by Nevo (1963). A detailed study of the Bajocian Mahmal Formation was done by Katz (1968). Paleontological studies were carried out by Parnes (1961, 1967, 1974, 1980, 1981). The flora of the Mishhor Formation was determined by Chaloner and Lorch (1960) and that of the richer Inmar Formation by Lorch (1967).

The Jurassic sequence in Hamakhtesh Hagadol was discovered by I. P. C. geologists and surveyed by Shaw (1947) and Bentor and Vroman (1951). Hudson (1958) recognized Callovian, 'Divesian', 'Argovian' and 'Sequanian' stages. Goldberg (1963) subdivided the section, adopting the subsurface formations of Coates et al. (1963) *i.e.* Zohar, Kidod, and Be'er Sheba. Gill and Tintant (1975), Gill et al. (1985), and Lewy (1983) refined the biostratigraphy on the basis of ammonites.

The Jurassic sequence in Hamakhtesh Hagadol consists of 205 m of Middle-Late Callovian carbonates, marls, and shales. The exposed lower 55 m correlate with the upper part of the Zohar Formation. The overlying 150 m thick Late Callovian shales, marls and limestones correlate with a coeval subsurface sequence in the Qeren, Zavoa, Sherif, Rehkme, Boqer (Northern Negev), and Hallal (Northern Sinai, Egypt) boreholes. This rock sequence represents the most complete and uninterrupted sequence of Middle-Late Callovian strata exposed in the Levant. It is characterized by the absence of any Early Oxfordian shale, similar to the onlap of the Majdal Shams Formation.

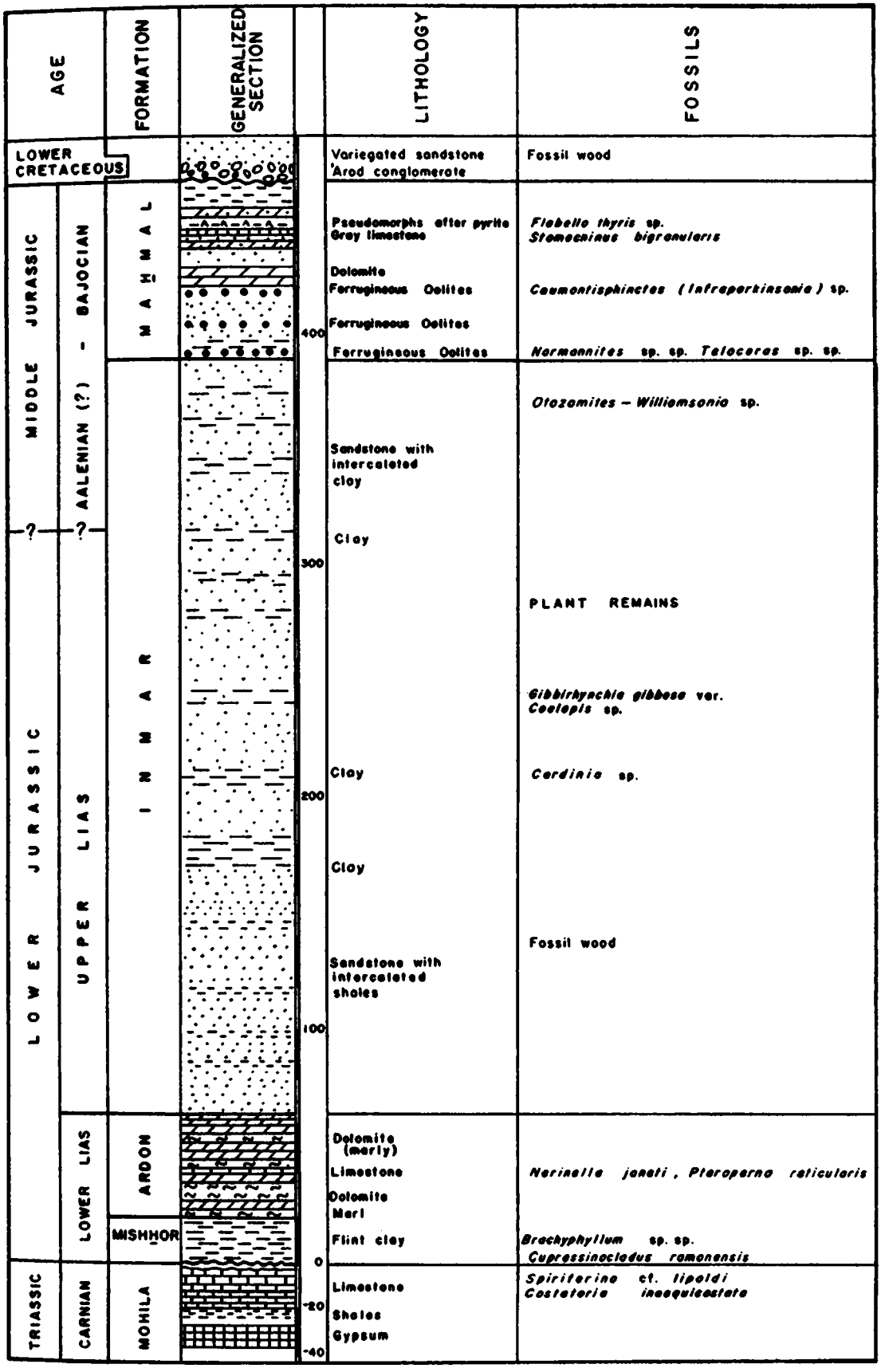
Only fragments of it occur at Hamakhtesh Haqatan, Gebel El Minshera (Sinai, Egypt), and Kasem El Galala (Suez Gulf, Egypt). The exposed Jurassic section in Hamakhtesh Haqatan consists of some 30 m of limestones alternating with shales and sandstones that correspond to the Halamish and Ziyya Members (Goldberg, 1963).

The Jurassic section of Gebel Maghara (Sinai, Egypt) exposes 2000 m of strata, ranging from Aalenian to Oxfordian. The facies still widely reflects the Negev conditions of mixed clastic and carbonatic sedimentation.

The bore-holes of Foxtrot, Haifa, Asher, Devorah, Rosh Pinna, Carmel, Ga'ash, and Petah Tiqva have a certain similarity with the



Figure 18E.3. Generalized columnar section of the Jurassic in Makhtesh Ramon (modified after Parnes, 1981, in Picard and Hirsch, 1987).


AGE
FORMATION
GENERALIZED SECTION
LITHOLOGY
FOSSILS
LOWER CRETACEOUS
Variegated sandstone
'Arod conglomerate
Fossil wood
MIDDLE JURASSIC
AALENIAN (?) - BAJOCIAN
MAHMAL
Pseudomorphs after pyrite
Grey limestone
Flabello thyris sp.
Stomechinus bigranularis
Dolomite
Ferruginous Oolites
Ferruginous Oolites
Ferruginous Oolites
Caumontisphinctes (Infraperkinsonia) sp.
Normannites sp. sp. Teloceras sp. sp.
400
LOWER JURASSIC
UPPER LIAS
INMAR
Otozamites – Williamsonia sp.
Sandstone with intercalated clay
Clay
300
PLANT REMAINS
Gibbirhynchia gibbosa var.
Coelepis sp.
Clay
Cardinia sp.
200
Clay
Fossil wood
Sandstone with intercalated shales
100
LOWER LIAS
ARDON
Dolomite (marly)
Limestone
Dolomite
Marl
Nerinella jonati, Pteroperna reticularis
MISHHOR
Flint clay
Brachyphyllum sp. sp.
Cupressinocladus ramonensis
0
TRIASSIC
CARNIAN
MOHILA
Limestone
Shales
Gypsum
Spiriterina cf. lipoldi
Costatoria inaequicostata
-20
-40

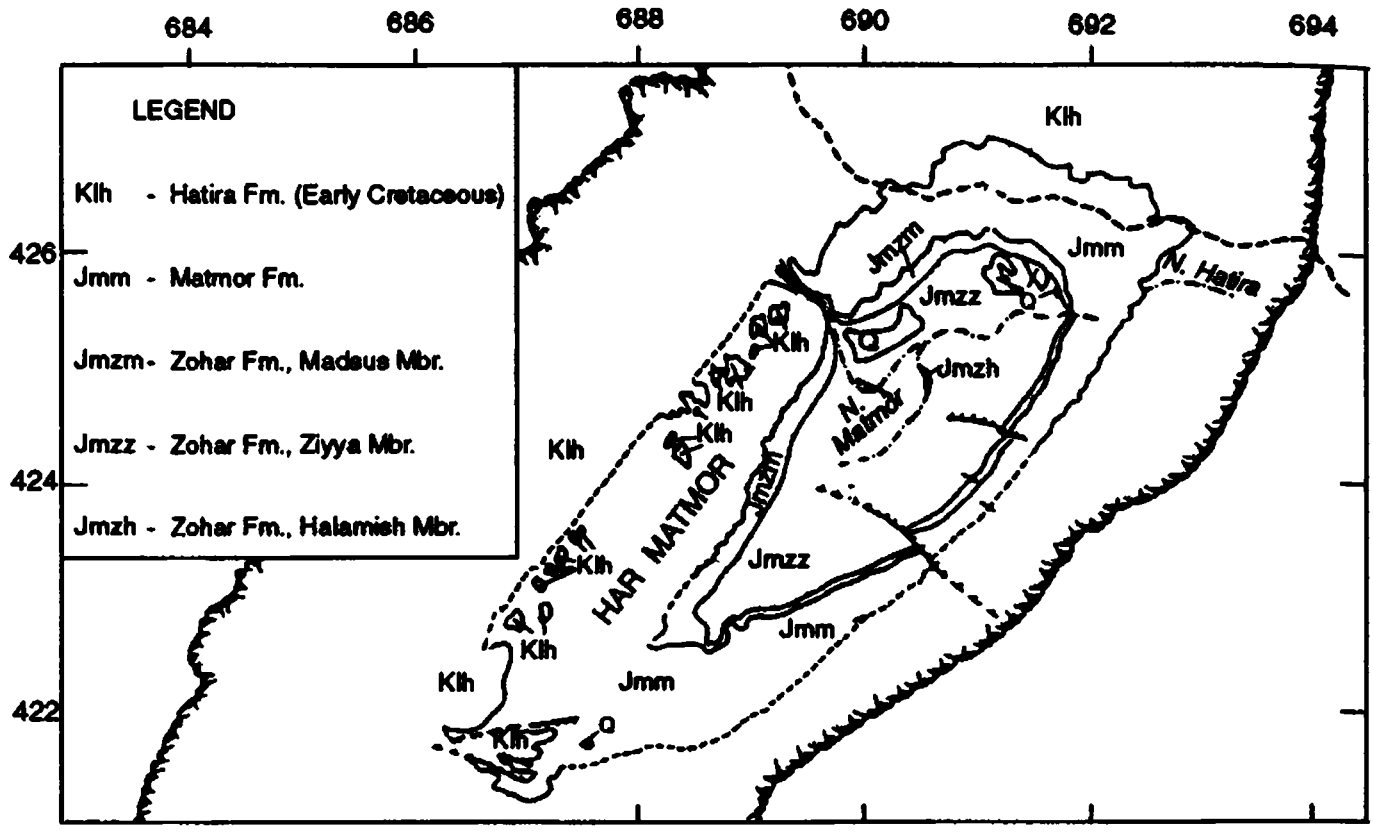


Figure 18E.4. Sketch Map of the Jurassic in Hamakhtesh Hagadol (Kurnub).

sequence in Lebanon, based on Renouard (1951) and Dubertret (1975) with the micropaleontological data of Bischoff (1990).

I. LOWER-MIDDLE JURASSIC

Mishhor Formation (Goldberg, 1964)

The Mishhor Formation consists of a bauxitic-lateritic paleosoil and flint clays, resting on an eroded Triassic land surface. Goldbery (1982) and Valeton et al. (1983) regarded the Mishhor Formation to be the result of leaching related to groundwater movement pene-contemporaneous to and after burial of the clastic lateritic suite.

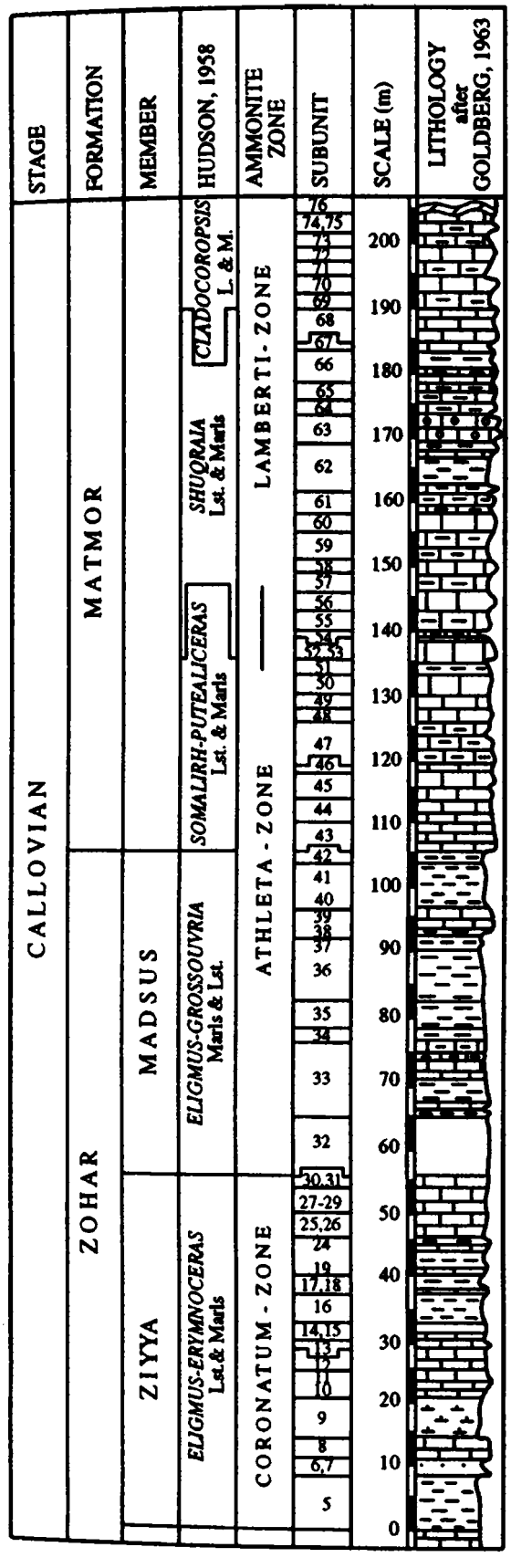
The Mishhor Formation has been reached by a number of drillings in the Negev and Central Israel, where its average thickness does not exceed 50 m. In the north of the country it is replaced by the Asher Volcanics. The most dramatic development of the Mishhor Formation occurs in the northern Sinai (Egypt) bore-hole of Gebel Halal, where a 500 m thick sequence of red marls, some dolomites and sands of Norian (*Granulo- perculatipollis rudis*) through Early Liassic (*Araucariasites australis*) age underlie the typical Mishhor pisolites and red clays. Normally the Mishhor Formation overlies a karstic surface leaching the Carnian Mohilla or Noro-Rhaetian Shefayim Formation

Asher Volcanics

In northern Israel bore-holes (Atlit, Haifa, Asher, and Devora) and the Hermon exposure (Aarne), the Mishhor laterites and the Ardon carbonates are replaced by the Asher-Volcanics (Garfunkel and Derin, 1985; Mouty, 2000). These consist of basalt, agglomerates, and tuffs (with a few thin dolomite and shale interbeds), ranging in age from 206 to 190 Ma (Lang and Steinitz, 1989). The unusually thick volcanic sequence in the Atlit bore-hole is interstratified by Norian (Late Triassic) and Early Jurassic limestones and shales. It suggests a Late Triassic-Early Jurassic graben-like trough over 4000 m deep. (**Figure 18E.8a**).

Ardon Formation (Nevo, 1963)

Overlying the Mishhor Formation are up to 50 m of marly sandstones, sandy shales, and sandy dolomites with algal mats and small molluscs. Among these a typical *Nerinella* fauna occurs. The Ramon section well-represents the shallowest known nearshore lithofacies of the Ardon Formation. To the north and west the formation develops into hundreds of meters of shallow carbonates with evaporites. This enormous thickening and the passage to open marine shelf carbonates, intermixed with evaporites, is observed in the numerous bore-holes of the Negev. In the Northern Sinai (Egypt) Hallal bore-hole, the Ardon Formation reaches a thickness of almost 800 m These carbonates, microfaunistically



poorly dated, may contain at their very base the Pliensbachian foraminifera *Orbitopsella primaeva* (Henson), mostly representing the Toarcian.

Inmar Formation (Nevo, 1963)

After the short marine incursion of the Ardon Formation, up to 300 m of thick clastics follow, represented mainly by cross- bedded sandstones, interbedded with kaolinitic clays, coally flint-clays, and alunite horizons (Goldbery, 1982). Lorch (1967) compares the sequence of the Inmar Formation with the Aalenian Lower Estuarine beds of Yorkshire. A thin marine intercalation yields Toarcian brachiopods (Parnes, 1980).

The cross-bedded sandstones of the Inmar Formation of Makhtesh Ramon can be identified in the Negev and northern Sinai bore-holes where they are separated into two clastic units by the marine intercalation known as the Qeren Formation, which is well-developed in Gebel Maghara's Rajabiah Formation. The Lower Inmar Formation thins out toward the north and west.

At Gebel Maghara, where the base of the Liassic section in Northern Sinai is not exposed, the **Mashaba Formation** (Al Far, 1966) is equivalent to the lower Inmar Formation and consists of reddish coarse- to medium-grained cross-bedded sandstone, sandstone with petrified trees and plant remains, intercalations of thin fossiliferous shale and limestone, mainly built of algal pelmicrites. The entire sequence points to very shallow littoral deposition.

Qeren Formation (Goldberg, 1964; *emend.* Cohen in O.E.I.L., 1988)

The Qeren Member of the Inmar Formation (Goldberg, 1964; Goldberg and Friedman, 1974) or *Qeren subfacies* (Picard and Hirsch, 1987) consists of carbonates that in the bore-holes west of Ramon, interwedge the fluvio-aeolian-deltaic Inmar clastics, gradually replace the clastic Lower Inmar Formation, and become united with the underlying Ardon carbonates. The pelbiomicrites, oosparites and dolomicrites yield the Aalenian-Lower Bajocian foraminifera *Timidonella sarda* (Bassoullet) accompanied in the oolitic shoals at Helez by *Gutniciella cayeuxi* (Lucas) of the same age. At Gebel Maghara the clastic Mashaba Formation is followed by the **Rajabiah Formation** (Al Far, 1966), which may serve as a stratotype for the Qeren Formation. It consists largely of organogenic oolitic limestones abundant in solitary corals, intercalated with sandstone and shale that yield brachiopods and bivalves. An ammonite fragment attributable either to *Grammoceras* or *Sonninia* confers a Toarcian-Aalenian age to this unit (Arkell, 1956).

Upper Inmar Formation

In the Negev bore-holes (Qeren, Makhtesh Qatan, Kurnub,

Figure 18E.5. Stratigraphic columnar section of the Jurassic in Hamakhtesh Hagadol (Kurnub).

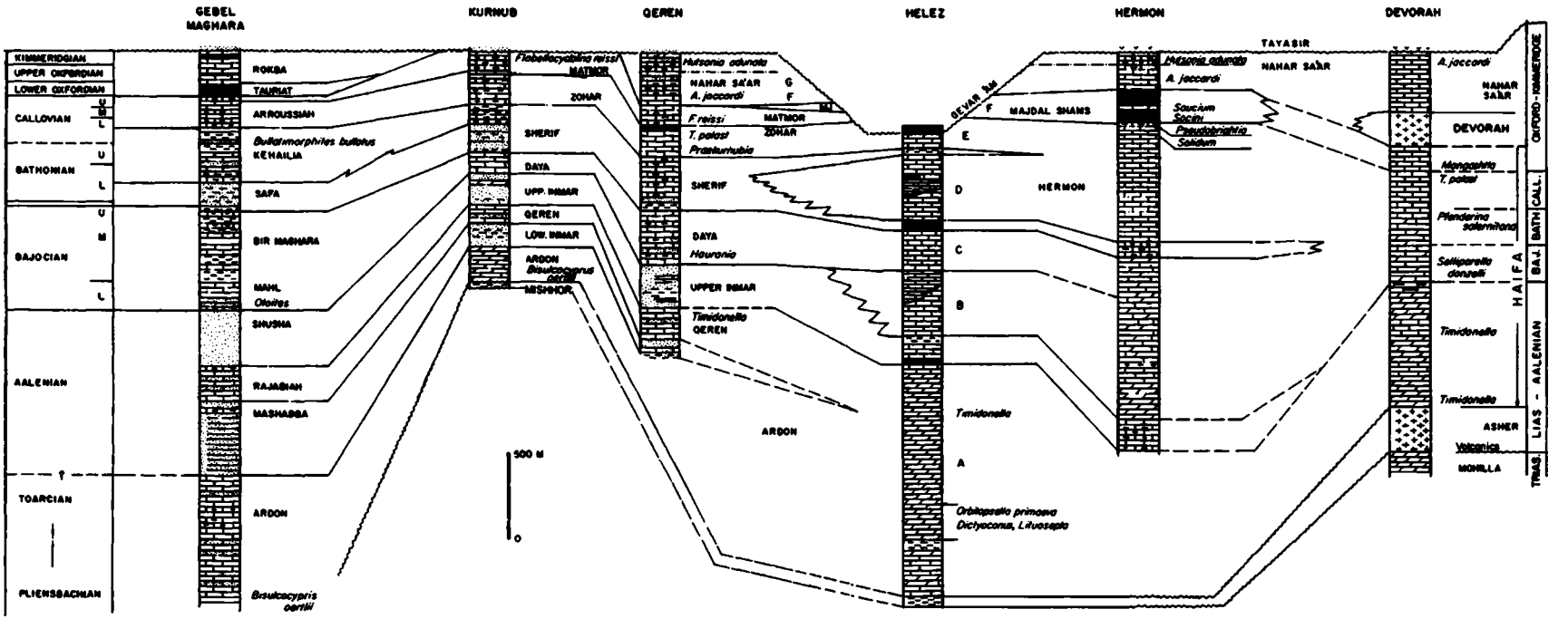


Figure 18E.6. Stratigraphic Sections including:

(I) Galilee High Devorah: the Liassic Asher Volcanics are covered by the Middle Jurassic carbonatic Haifa Formation, the volcanic Devorah tuffs, interstratified within the Oxfordian, followed by the Oxfordian - Kimmeridgan Nahar Sa'ar Formation.

(II) Judean embayment Helez - Hermon: in the Helez borehole, the Liassic Mishhor laterites are followed by Pliensbachian - Toarcian carbonates (Ardon). In the Ramallah borehole Aalenian carbonates (Qeren) directly overlie the Mishhor laterites. Middle Jurassic is primarily represented by carbonates of Haifa - Hermon type. The lower Oxfordian is characterized by the development of the Oxfordian Majdal Shams shales, which extend to the NW Negev and Sinai (Egypt).

(III) Negev High (Kurnub-Qeren): The Negev section is characterized by numerous elastics in the Kurnub borehole, becoming more carbonatic toward the Qeren borehole. The Liassic consists of the Mishhor and Ardon Formations. The Aalenian Inmar Formation is split by the Qeren carbonates. The Middle Jurassic is diversified, comprising the Daya, Sherif, Zohar and Matmor Formations. The Upper Jurassic is truncated in Kurnub, its development being well-represented at Qeren by the Nahar Sa'ar Formation.

(IV) Maghara Deep: Gebel Maghara exposure and Halal borehole: In the more clastic succession of the Maghara Deep, the Negev units are still well-represented, though the total thickness has more than doubled. A-G: palynozones (after Conway, 1990).

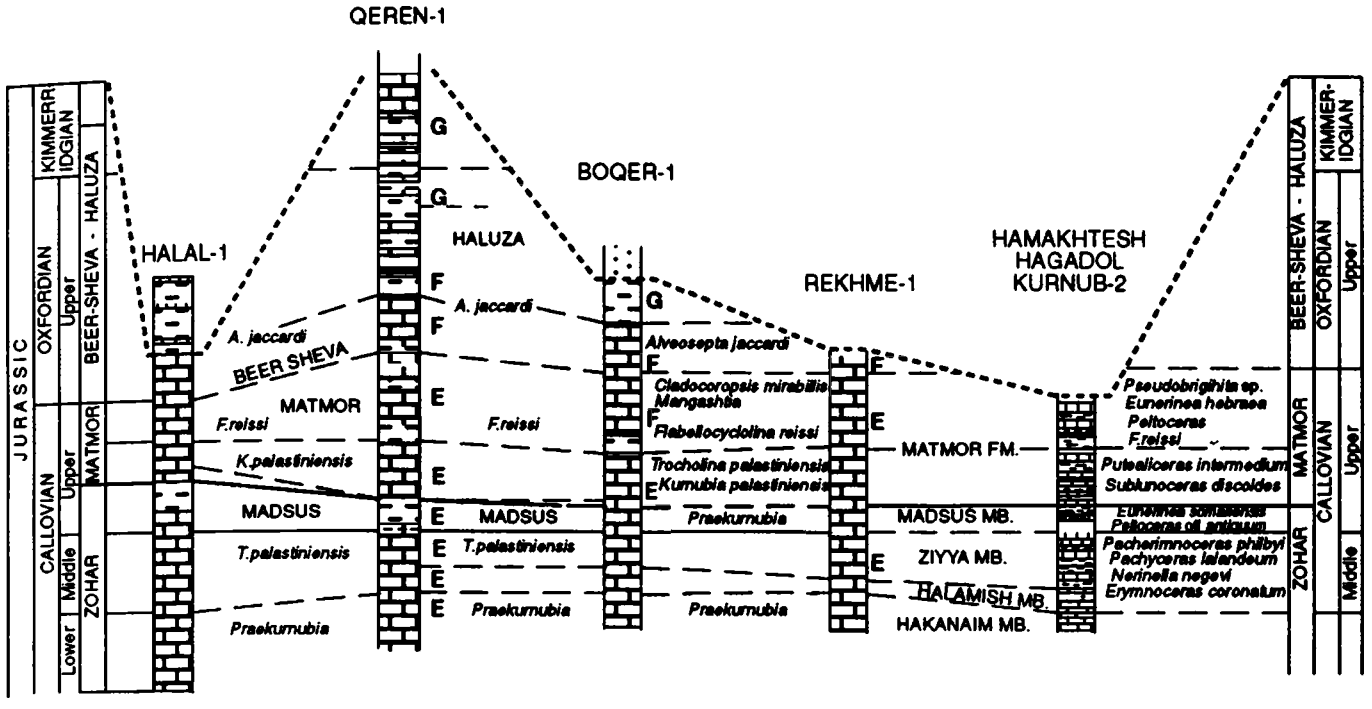


Figure 18E.7. Stratigraphic correlation of Callovian–Oxfordian sequence in Hamakhtesh Hagadol and boreholes in the Northern Negev (Israel) and adjacent Sinai (Egypt) with distribution of palynostratigraphic assemblages: F *Millioudodinium nuciformis* Zone; E *Palystephanosphorus calathus* Zone (modified after Picard and Hirsch, 1987 and Conway, 1990).

Daya, Barbur, Boqer, Rekhme) and Sinai (Halal) the upper part of the Inmar formation consists of sandstones and shales. At Gebel Maghara, the **Shusha Formation** (Al Far, 1966) overlies the Rajabiah Formation and consists predominantly of coarse-grained, often cross-bedded, limonitic sandstones interstratified with calcarenites and plantiferous shales. Coal seams and marine bivalves and gastropods of Aalenian affinity (Hirsch, 1979) suggest a paralic environment. The upper Inmar facies passes from predominantly continental in the Ramon subfacies to shallow marine to the west and north, replaced by shaley marls (Rosh Pinna facies of Derin, 1974).

Further west and north the upper Inmar (Rosh Pinna) facies wedges out, replaced by the carbonatic facies of Picard's (1959) over 3000 m thick Lebanon facies, Derin's (1974) Haifa Formation, or Dubertret's (1975) Kesrouane Formation.

Daya Formation (Eliezri, in Coates et al, 1963) - **Mahmal Formation** (Katz, 1968)

The Mahmal Formation, uniformly called the Brown Cuesta in Makhtesh Ramon, is a nearly 100 m thick marine sequence of cross-bedded sands with ripple marks, ferruginous oolitic dolomites and plantiferous shales, in which are found ammonites of Late Middle and Late Bajocian age (Parnes, 1981), recalling the fauna of Bir Maghara (Sinai). The top beds consist of clays and sands with a limestone interbed that holds small bivalves known from the Safa Formation of Gebel Maghara. Recently the equivalent of the Mahmal Formation was described in Jordan (Basha, 1995).

In the Negev, the mostly carbonatic sequence of the **Daya Formation** differs from the more arenaceous Mahmal Formation of Ramon and more marly Bir Maghara Formation (northern Sinai). It is defined by the foraminifera *Haurania*.

The 500 m thick **Bir Maghara Formation** (Al Far, 1966) starts with a plantiferous clastic sequence of shaly limestone, shales, shaley sandstone and coal streaks. Follow massive oolitic oncolitic coralline limestones, interstratified by thick marls and shales, rich in ammonoids (Douville, 1916; Arkell, 1952, 1956; Parnes, 1981), topped by a unit of black shales, from which the ammonite *Thambites planus* was determined (Parnes, 1981). This top unit was already assigned to the basal beds of the overlying Safa Formation (Al Far, 1966).

In the Hermon section Razvalyaev (1966) measured 950 m of thick carbonates with volcanic intercalations, equivalent to the 600 m thick **Qala'at Jendal Formation** (J2) of Dubertret (1975).

The 170 m of medium to fine-bedded oolitic organo-clastic, ochreous-stained limestones, that yielded Late Bajocian-Early Bathonian brachiopods and bivalves (Razvalyaev, 1966) represent the 'calcaires ocres' of Vautrin (1934), the **Bqassem Formation** (J3) of Dubertret, or the **Bet Jin Formation** of Goldberg et al. (1981).

Sherif Formation (Eliezri in Coates, 1963)

In the Negev boreholes, the Daya Formation is followed by

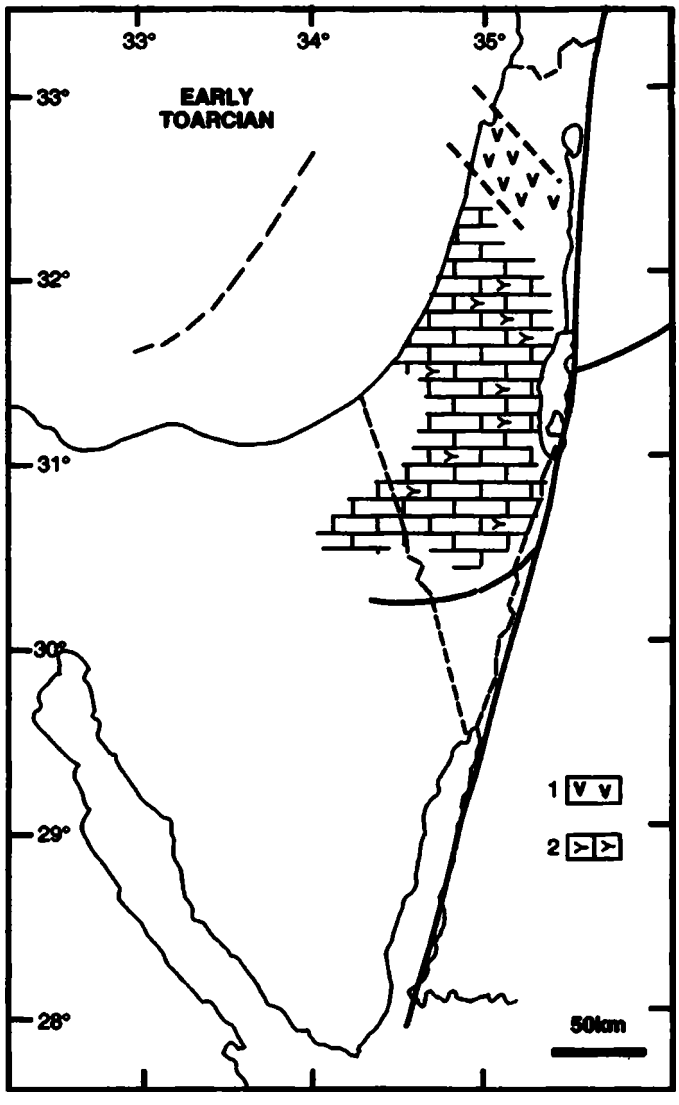


Figure 18E.8a. Early Toarcian Facies Map. The early Toarcian is represented by an interval within the huge mass of platform carbonates with evaporitic layers that build up the Ardon Formation. Its existence toward Lebanon is not clear and the interval may onlap directly the Asher Volcanics (VV) in the northern part of Israel. It is estimated to consist on the slope toward the Judean Embayment of over 200 m, thickening towards the central axis of the embayment to about 500 m. 1 - basalts; 2 - carbonates and evaporites.

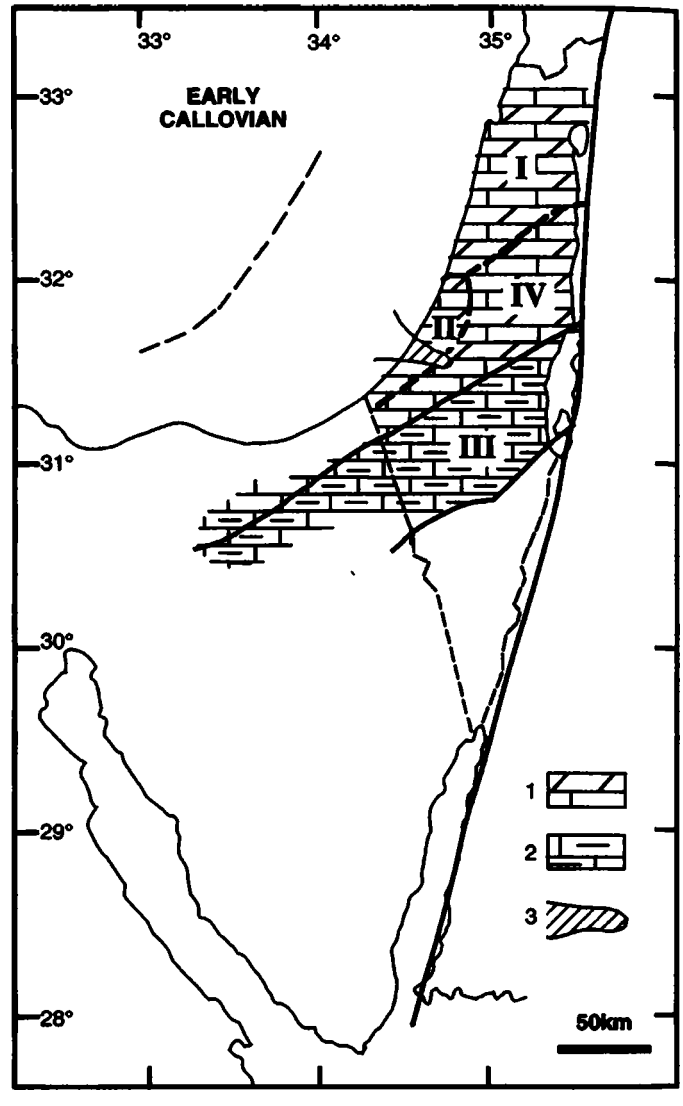


Figure 18E.8b. Early Callovian Facies Map. This ~100 m thick interval subdivides in tectono-sedimentary zones: I - calcarenites (Haifa); II - calcarenites (Brur) of the 'unstable zone', truncated by a karstic event; III - shales (Upper Sherif-Karmon), calcarenites and marls (lower Zohar); IV - massive calcarenites (Hermon), 1 - carbonates; 2 - limestones and marls; 3 - eroded.

a sequence of alternating sandstone, shales, pelmicritic and some sparitic limestone. The more sandy lower part corresponds to the **Safa Formation** at Gebel Maghara, while the more shaly upper part of the formation corresponds at Gebel Maghara to the **Kehailia Formation** (Hirsch, 1979).

In the Coastal Plain this interval becomes the so-called Karmon shale, rich in calcareous nannoplankton, ostracods and foraminifera. Northwest of Beer-Sheba the Sherif Formation is replaced by carbonates of the Hermon Formation.

The Safa Formation consists of cross-bedded hematitic stained sandstones alternating with limonitic shales with abundant plant remains and several coal-seams. The absence of fluvial sediments and the presence of thin oolitic limestone beds point to paralic depositional conditions.

The Kehailia Formation corresponds to the lower part of the Masajid Formation (Al Far, 1966). It is a 300 m thick sequence, consisting in oolitic limestones with frequent shale and occasional thin sandstone interstratified beds. The ammonite *Micromphalites*

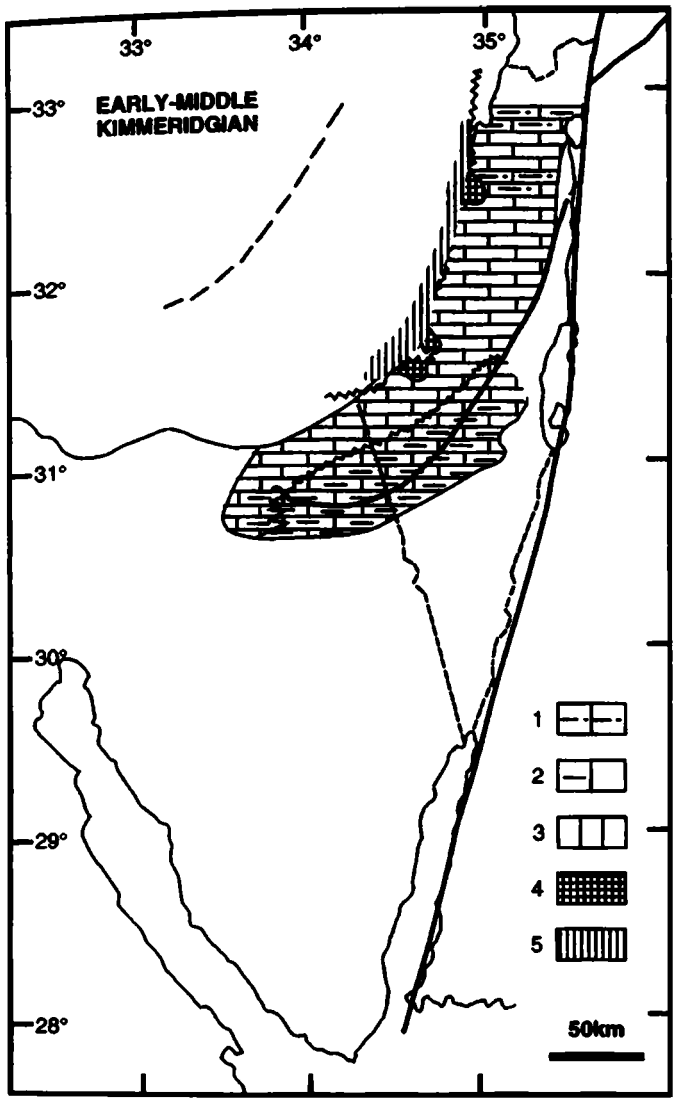


Figure 18E.8c. Early–Middle Kimmeridgian Facies Map. Consists of reefs, oolites, shales and sands (Nahar Sa'ar). Eroded by the infra-Cretaceous uplift along the present Levant coast and in the southeast Negev. 1 - oolites; 2 - marls; 3 - limestones; 4 - reef; 5 - eroded.

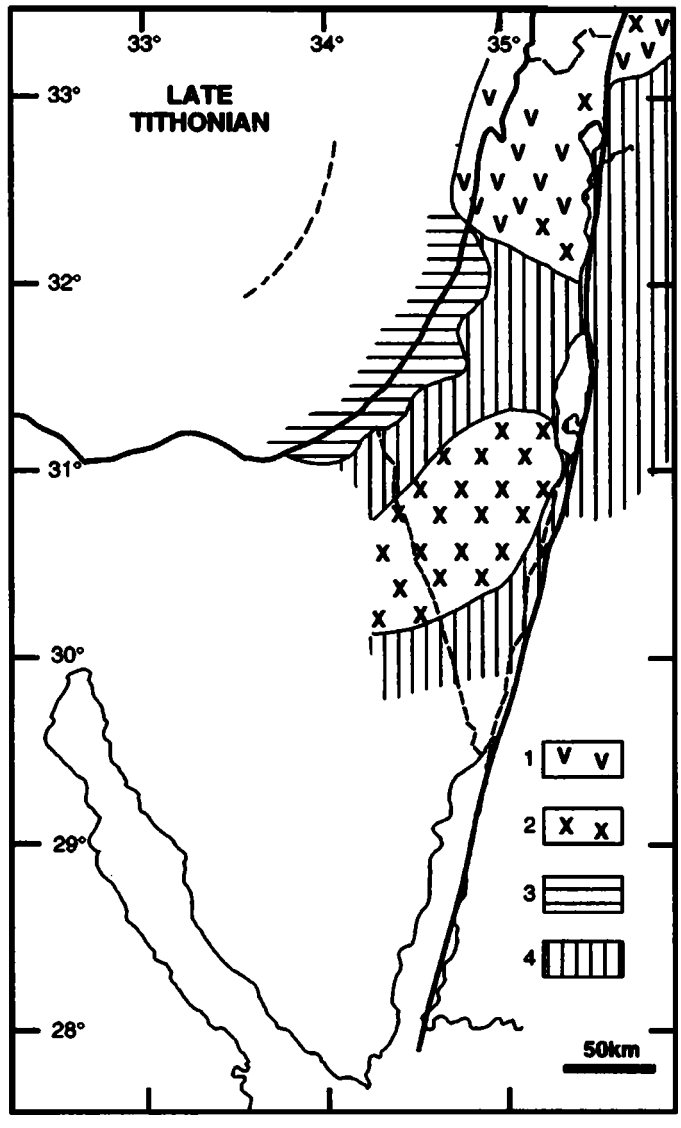


Figure 18E.8d. Late Tithonian Facies Map. This interval belongs virtually to the infra-Cretaceous tectono-environmental phase. It is marked by wide denudation, Tithonian-Hauterivian volcanics (Tayasir) and turbidites (Gevar'Am canyon). 1 - alkaline basalts; 2 - basic intrusion; 3 - shales; 4 - eroded.

pustuliferus (Douv.) confers a Lower Bathonian age to the lower part, and *Bullatimorphites bullatus* (d'Orb.) a Late Bathonian-Early Callovian age to the shaley-carbonatic upper part.

Zohar Formation (Rosenberg in Coates et al., 1963)

The **Zohar Formation** was established in the Negev Zohar-Kidod boreholes, for the alternating limestone-marl sequence that follows above the Sherif Formation. At Hamakhtesh Hagadol, its upper part is exposed. At base this consists of 55 m of marls and limestones with one sandstone intercalation (subunits 6, 7) corresponding to the *Eligmus-Erymnoceras* Beds of Hudson (1958). This interval is placed in the Middle Callovian *coronatum* Zone (Gill and Tintant, 1975; Gill et al., 1985). It correlates well to the Tsiyya member of the Zohar Formation of the Judean Desert and northern Negev bore-holes (Goldberg and Friedman, 1974).

The overlying sequence consists of 20 m thick sequence of alternating marls and limestones and 30 m of shales with a characteristic calcarenite intercalation. This 50 m interval corresponds to the *Eligmus-Grossouvria* Beds (Hudson, 1958), representing a part of the Late Callovian *athleta*-Zone (Gill and Tintant, *op. cit.*, and Lewy, 1983). This sequence represents the Madsus Member (Hirsch and Roded, 1996) and correlates with a

coeval interval in the boreholes of Qeren, Rekhme, Boqer (northern Negev), and Hallal (Sinai, Egypt).

Abundant bivalves and gastropods characterize the Zohar Formation, exposed in Hamakhtesh Hagadol. The fauna recalls the 'bathonian' taxa of Europe, and many taxa are found in Somalia.

Matmor Formation (Goldberg, 1963; *emend.* Hirsch and Roded, 1996)

At Hamakhtesh Hagadol, a thick sequence was recognized as the **Matmor Formation**, consisting of alternating fossiliferous limestones and marls. The lower 30 m thick interval of the Matmor Formation (subunits 43-52) corresponds to Hudson's (*op. cit.*) *Somalirhynchia-Putealiceras* beds, yielding ammonites of the Late Callovian *athleta* and *lamberti* Zones (Gill and Tintant, *op. cit.*; Lewy, *op. cit.*). The bivalve and gastropod fauna of this lower interval are still similar to those found in the Zohar Formation. The 70 m thick upper interval of the Matmor Formation consists of Hudson's Shuqraia (subunits 53-71) and *Cladocoropsis*-beds (subunits 72-74). The middle part of the Shuqraia beds contains a characteristic oolitic marker (subunit 63). The upper part of the Matmor Formation (subunits 59-74) consists of alternating yellow shales, white reefoid and lagoonal limestones with characteristic large bivalves and gastropods (Nerineids). Late Callovian ammonites as *Peltoceras solidum* (subunits 60) and *Pseudobrightia* sp. (subunit 72), assign this interval to the *lamberti* Zone (Cariou et al., 1997).

In the Negev Hamakhtesh Hagadol and the Hallal, Qeren, Rehkme, Boqer, and Zavoa wells (**Figure 18E.7**), these shallow water reefoidal white limestones, marls, and oolites yield the foraminifera *Kurnubia* ex gr. *palastiniensis* Henson in its lower half and *Flabellocyclolina reissi* Hottinger in its upper half. The large bivalves and gastropods of the genera *Purpuroidea* and *Eunerinea* (Hirsch, 1979) of the upper part of the Matmor Formation show affinities with European Oxfordian taxa.

The Zohar and Matmor formations of the Negev correspond at Gebel Maghara to the middle part of the Masajid Formation, that corresponds to the **Aroussieh Formation** (Hirsch, 1979). This 185 m thick carbonatic sequence yields in its lower part foraminifera of the group of *Planikilianina* sp., a new taxon (Bassoullet, pers. comm.) and the brachiopod *Septirhynchia hirschi* (Feldman, 1987). The particularly fossiliferous topmost part of the formation yields ammonites of the genus *Pachyerymnoceras*, assigned by Lewy (1983) to the Late Callovian. The Aroussieh Formation is topped by a compacted hard-ground. The Callovian age, adopted by Douville (1925) for the rock sequence in which Cossmann's fauna 'd'apparence bathonienne' occurs, was first proposed by Moon and Sadek (1921). This age attribution precedes the recognition that the Early Callovian fauna of Western Europe was the result of the boreal spread at the end of the Bathonian (Hallam, 1971). Callovian warm-water faunas (*e.g.* corals, nerineids) persisted only in the ecological shelter of the southern Tethys margin. This explains the absence in the Levant of boreal taxa, thought to be the only characteristic Early Callovian markers, thus mimicking a hiatus (Hirsch (1979).

Haifa Formation (Derin, 1974)

From the northern Coastal Plain (Ga'ash) to the north (Carmel, Galilee and Lebanon) over 1000 m of dolomicrites, occasionally anhydritic, build up a sequence ranging from Late Liassic to Oxfordian, called the Haifa Formation. The Late Liassic interval of the Haifa Formation is characterized by Aalenian-Bajocian foraminifera *Timidonella sarda* (ex *Orbitopsella* cf. *praecursor*), the Bajocian interval by *Haurania,* the Bathonian interval by *Pfenderina salernitana* Sartoni et Crescenti, whereas the Callovian interval is distinguished by assemblages of *Satorina apuliensis* and *Trocholina palasteniensis*.

The Middle Jurassic uniform sedimentary regime of the Haifa Formation, as a carbonatic platform, persists from the northern Coastal Plain to northern Israel (Galilee, Carmel) into the Late Jurassic. There the upper part of the Haifa Formation comprises micrites yielding the algae *Pseudoclypeina* and the foraminifera *'Mangashtia' egyptiensis* (Fourcade et al., 1983) indicating the presence of Early Oxfordian strata.

The Calcaires de **Kesrouane** (Dubertret, 1975), exposed at Nahr Ibrahimin in Lebanon reveals a 75 m thick dolomitic limestone with bivalves, put into the Bajocian and nearly 500 m of hard dolomites with platy dolomitic limestones and rare marly intercalations, including three fossiliferous horizons, ranging from Bathonian to Lower Oxfordian. This sequence corresponds to the Haifa Formation.

Hermon Formation (Dubertret, 1960)

For Razvalyaev (1966) the bright bluish-gray limestones and dolomites (J3C1) with corals and brachiopods, that attain a thickness of 700 m, are entirely of Callovian age. This sequence was termed by Dubertret (1960) as the **Hermon Limestone** Formation (J4) and Nimrod Formation by Saltzman (1968). For Derin (in Goldberg, 1969), the microfauna of the massive limestone in the lower 600 m of the Hermon Formation is equivalent to that of the Bathonian interval of the subsurface Haifa Formation (Derin, 1974). The upper 100 m of the Hermon Formation also consist of massive limestones and yield foraminifera of an assemblage of *Planikilianina* (Bassoullet and Perelis Grossowicz, in press) conferring an Early Callovian age to this sequence. Along the southeastern slopes of Mount Hermon, in a strip extending from the village of Majdal Shams toward the Newe Ativ Graben, the uppermost part of the Hermon Formation consists of alternating limestone and marl beds that yield abundant Late Callovian belemnites, bivalves and ammonites of the *athleta* Zone (*collotiformis* subzone) (Cariou et al., 1997).

Hermon Formation equivalent

In Central Israel from the Coastal Plain to Judea, the equivalent of the Hermon Formation is interwedged by up to 600 m of oosparites (**Sederot** facies) and by micrites repleted with poriferan spiculae (**Barnea** facies), that in Talme-Yafe reach 400 m.

In the southern Coastal Plain, around Helez, a shaly horizon, known as the **Hodaya** member (Derin, 1974) interwedges the oosparites and spiculites of the Sederot and Barnea facies, close to the Bajocian-Bathonian boundary. Shales of Late Bathonian-Early

Callovian age, known as the Karmon shale (Derin, 1974), interrupt the Hermon-type regime of the southern Coastal Plain, where the effect of the Negev facies (Sherif Formation) is still felt.

The Sederot shoals of the coastal plain appear again in the form of reefoidal patches in the Early Callovian around Ashdod as the sparitic 'Brur calcarenite' bearing the foraminifera assemblage of *Planikillianina*.

II. Upper Jurassic

Majdal Shams Formation (Dubertret, 1960; *emend.* Saltzman, 1968; Hirsch, 1996)

It consists of 200 m of Early to Middle Oxfordian fossiliferous shales at base, platy limestones and silicasites at top. The shales, with limonitic concretions, are interbedded by marls and occasional thin limestone or dolomitic beds. The basal beds are extremely rich in small pyritized ammonites, the age of which was established by Noetling as early as 1887. Noetling's Early Oxfordian *Brightia socini* Zone was put by Arkell (1956) into the *'Mariae'* Zone. In his monograph, Haas (1955) studied 7600 ammonites from Majdal Shams, the exact level of which, within the 43 m thick lower marls, was retrieved by the bed by bed collection reported by Razvalyaev (1966). The nuculide bivalve infaunal mobile detritus feeders confirm the statement of Haas that the paramount darkish shale facies with pyritic dwarf forms is intimate to a less aerated depositional environment - remarkably also occurring in the *Renggeri* Zone with equal lithofacies in Europe. Vautrin's (1934) overlying 'Lusitanian' Stage consists of argillaceous marls and yellow limestone intercalated by marls holding fossils that Arkell (1956) puts into the *Transversarium* Zone. Razvalyaev (1966) puts the upper pelitomorphic limestones and alternating dark marls 'most probably into the *Bimammatum* Zone'. The shale interval of the Majdal Shams Formation is present in the Israeli subsurface and in the Tauriat shales of Gebel Maghara (Sinai, Egypt). The spiculitic limestones at the top of the Majdal Shams Formation in the Hermon section consist of thin-bedded dark platy limestones with marl interbeds and a 'tripoli'-like yellow silicatic ledge towards the top.

At Gebel Maghara, the Early Oxfordian is well-represented by the **Tauriat Formation** (Hirsch, 1979), a nearly 70 m thick sequence of shale with abundant pyritized ammonites at its base that corresponds to the Majdal Shams Formation.

The dark highly pyritic shales with nodules and pyritized fossils, interbedded with few limestones or dolomites (Goldberg and Friedman, 1974) that overlie the Zohar carbonates in the Zohar-Kidod gas-field and the Brur calcarenites in the Coastal Plain Helez-Kokhav oil-field, were termed '**Kidod**' by Coates et al. (1963), a term largely followed by exploration geologists. Picard and Hirsch (1987) emphasized the Oxfordian age of these shales and put in evidence their onlapping nature on a Callovian reductional hard ground as well as the absence of a genuine 'Kidod' facies in the area that includes Hamakhtesh Hagadol and the bore-holes of Qeren, Rehkme, Boqer, and Gebel Hallal.

In many coastal plain wells Early Oxfordian shales rest directly on the thin Lower Callovian Brur calcarenite, showing karstification (Goldberg and Bogosh, 1978; Buchbinder, 1981).

The Majdal Shams Formation reaches over 200 m in Central Israel (from the Helez area eastwards to Judea and the Jordan Valley). In most of the northern Negev and northern Sinai, it is reduced to an average 100 m. In the offshore borehole of Delta-1, northwest of Caesarea, a 200 m thick sequence is still present, comprising a carbonitic upper and shaley lower section. The 80 m thick lower section consists mostly of black and green shales rich in dinoflagellates, spores, and coccoliths (Moshkovitz and Ehrlich, 1981; Conway and Cousminer, 1981), of Early Oxfordian age. Fragments of volcanics and of bio-intrasparites were interpreted by Friedman et al. (1971) as cobbles or pebbles deriving from the shelf edge and transported by turbitity currents into the depositional area of mudstone called 'Delta Facies'.

No trace of Oxfordian has been left in the larger and deep erosion funnel around the Helez wells (Barnea, Gevar'Am, Helez, Talme Yafe).

Nahar Sa'ar Formation (Saltzman, 1968)

This consists of two parts, totalling up to 180 m for which a Late Oxfordian-Early Kimmeridgian age is attributed by the foraminifera *Alveosepta jaccardi* (Derin, 1974). Ostracods (Hirsch et al., 1998) found in the uppermost part of the unit belong to the genus *Hutsonia*, of Kimmeridgian or Tithonian age (Bishoff, 1990). Razvalyaev (1966) reports the finding in dark-gray limestone and clayey limestone of the brachiopods *Septaliphoria jordanica* (Noetling), *Somalirhynchia africana* Weir, and *S. somalica* Daque.

1) The echinoid limestone at the base consists of ~40 m of massive limestones, yielding abundant spines as well as a few complete specimens of the echinoid *Balanocidaris glandifera*. It has been correlated at Gebel Maghara and Um Mafrut (Sinai, Egypt) with the **Rokba Formation** (Picard and Hirsch, 1987) representing the top beds of Al Far's Masajid Formation. It consists of flinty limestones in rather massive beds, interstratified with yellow marls that delivered to Bircher (1940) and Farag (1959) abundant echinoids and crinoids. At Ras Jeham (in Arkin et al., 1975) 110 m of gray, rarely dolomitic, biomicritic and sometimes oncolitic calcarenites and thin yellowish brownish shales are abundant in echinoid spines, silicified corals, stromatoporoids, *Alveosepta jaccardi* and *Clypeina jurassica* Favre.

Comparison of the Hermon biomicritic-biosparitic cliff-producing limestones with algae, oncolites, stromatoporoids, corals, sponge spicules, gastropods, brachiopods and echinid-radioles, with the nearest (110 km distant) outcrops of the section of Wadi El Malih (Samaria) shows lithological and faunistical affinities. Medium-bedded micritic-sparitic, oolitic limestones, marly limestones and a 25 m thick hard limestone, specked with quartzitic and cherty nodules yield *Alveosepta jaccardi, Iberina praelusitanica* and *Cladocoropsis mirabilis* Felix (Aizenberg, 1968; fossil determinations by Derin).

2) Then follow 140 m of well-bedded yellow oolites, fossiliferous marls, with a massive limestone in its upper part. In Wadi E Shatr shales and thin limestones overlie this limestone, representing the youngest strata below the Infra-Cretaceous unconformity.

The sequence of the Nahar Sa'ar Formation encompasses all the sediments deposited in the same time span as the equivalent *Glandaria* Limestone, 'Calcaires jaunes inferieures', of Aazour, Bikfaya, and Salima in Lebanon.

The surface sequence of the Nahar Sa'ar Formation at the Hermon, corresponds to a number of previously established subsurface formations. The lower massive limestone corresponds to the subsurface **Beersheba Formation**, whereas the upper, more shaley or sandy unit, with upper massive limestone intercalation corresponds respectively to the subsurface **Haluza** and **Haifa Bay Formations**.

The lower part of the Nahar Sa'ar Formation, characterized by the foraminifera *Alveosepta jaccardi*, is of Late Oxfordian-Early Kimmeridgian age. In the Devora bore-hole in the Galilee, volcanics occur in this interval. In northern Israel (Haifa Bay, Hazon, and Hula bore-holes) as well as in a narrow belt from northern Sinai (Risan Aneiza outcrop) to the northern Negev (Haluza and Qeren bore-holes), the carbonates are associated with *Vaginella striata* Carozzi and *Alveosepta personata*, besides *Clypeina jurassica* Favre, an algae found throughout the entire Late Jurassic, which represent the Kimmeridgian and Tithonian.

In Lebanon the 90 m thick massive limestone rich in echinoid radioles of the **Calcaire a *Cidaris glandaria*** and the 80 m of brown to yellow oolitic limestones and marls of the **Couches jaunes inferieures** is found. The latter yields *Kurnubia palastiniensis*, *Alveosepta jaccardi, A. personata, A. powersi, Anchispirocyclina lusitanica,* and *Everticycclamina virguliana.* The overlying 50 m thick **couches d'Azour** yield, besides the foraminifera *E. virguliana*, the ostracods *Hutsonia subsolana, H. aazourensis,* and *H. turgida,* which for Bischoff (1990) indicate Middle Kimmeridgian or Lower Tithonian.

The topmost Jurassic beds in Lebanon are the ~50 m thick limestone ledge of the **Falaise de Bikfaya** and the up to 150 m thick **Couches de Salima.** According to Bischoff (1964) the latter yield the ammonite *Berriasella richteri*, which for Arkell (1956) is an important Upper Tithonian guide fossil. This interval also yields the foraminifera *E. virguliana* and *Rectocycclamina chouberti* as well as the ostracods *Hutsonia adunca* and *H.salimaensis*. Close to the Jurassic-Cretaceous boundary, they become sandy and pass apparently without discordance into the Neocomian Grès de Base. Or they become truncated by the 180 m thick Volcanic Complex, consisting of basaltic sheets and weathered pillows, volcanic tuffs interfingered by lignites and marls alternating with thin limestones, inferring deposition in an aquatic milieu, equivalent to the Tayasir Volcanics in Israel. The Nahar Sa'ar Formation is coeval with the **Batroun** and **Bloudane Formations** in Syria (Mouty, 2000).

Nir'Am Formation (Derin, 1974)

A reefoidal facies of biolithites of stromatoporoidea, corals, porifers and bryozoans occurs under the Coastal Plain around Cesarea and in the Kokhav oil field. In the Beer Yaakov, Gerar, Kfar Darom, Nirim, and Kissufim wells it overlies thin Majdal Shams shales. The age of the Nir'Am Formation, estimated from its vertical relationship with other formations probably represents the Oxfordian. Thickness figures reach 400 m in the Carmel bore-hole.

Gevar'Am Group (partim) - (Derin and Reiss, 1966; *emend.* Flexer et al., 1981)

The Gevar'Am Group consists of Tithonian-Hauterivian gray dark sandy shales, that in borehole Negba-1 (from a core) yield ammonites of Late Jurassic (Tithonian) affinity (Raab, 1962). This assumption is strengthened by the finding by Moshkovitz and Ehrlich (1981) of *Conusphaera mexicana* in the Gevar'Am Group of the offshore Delta-1 well. Recently De Haan (1997) found Late Jurassic palynofloras in the Gevar'Am shales of a number of wells of the Coastal Plain.

b) BIOSTRATIGRAPHY

The biostratigraphy of the Jurassic of Israel has been reviewed by Picard and Hirsch (1987) and more recently by Hirsch et al. (1998). It is based on ammonites (Parnes, 1981; Lewy, 1983; Gill and Tintant, 1975; Gill et al., 1985; Cariou et al. 1997). Accordingly the Jurassic ammonite zonation for the Hermon, Negev, and Northern Sinai may be correlated with the zonation of Enay and Mangold (1994) for Arabia and with the submediterranean standard zonation (Cariou et al., 1997). (**Table 18E.1**).

The importance of other fossil groups is evident from the numerous studies that include calcareous nannoplankton (Moshkovitz and Ehrlich, 1976), foraminifera and algae (Maync, 1966; Derin, 1974; Frenkel, 1975; Perelis Grossowicz et al., 2000) (**Plates 18E.1-18E.5** and **Table 18E.2**), bivalvia and gastropods (Hirsch, 1979), ostracodes (Rosenfeld and Honigstein, in Hirsch et al., 1998), brachiopods (Feldman and Owen, in Hirsch et al., 1998; Owen et al., 2001) and palynomorphs (pollen, spores, dinocysts, and acritarchs) (Conway, 1982, 1990; Conway, in Hirsch et al., 1998).

Early Jurassic

No ammonites of that age occur. Palynomorphs found in strata from the continental Mishhor Formation, the marginally marine Ardon and Inmar Formations and in the marine Qeren (Nirim) Formations contain dinocysts of the *Applanopsis turbatus* Zone (including *Nannoceratopsis pellucidus* and *Dapsilidinium? deflandrei*) that correlate well with Aalenian to Middle Bajocian boreal suites. The Liassic dating, using foraminifera, remains challenged. The earliest forms are apparently not older than Pliensbachian. *Orbitopsella primaeva* does apparently appear in the lowermost parts of the section, in the Helez, Halal and Hazerim bore-holes, assigning to it a Pliensbachian age (Maync, 1966; Derin and Reiss, 1966; Derin, 1974; Perelis Grossowicz et al., 2000).

Ostracodes provide good markers, though their biostratigraphic value is limited to ecostratigraphic levels. In shales at Makhtesh Ramon (Southern Israel) a *Bisulcocypris oertlii* Assemblage Zone, that marks the base of the Ardon Formation, yielded the non-marine ostracodes *Bisulcocypris oertlii* Gerry, *Fabanella ramonensis* Rosenfeld and Honigstein, and *Laevicythere*

TABLE 18E.1: Distribution of Ammonites in the Jurassic Deposits of Israel (by E. Cariou, in Hirsch et al., 1998).

STAGE	EUROPE	LEVANT
Tithonian		*Virgatosphinctes?*
Middle Oxfordian	*Plicatilis* *Cordatum*	*Euaspidoceras perarmatum*
Early Oxfordian	*Mariae*	*Creniceras renggeri, Scaphitodites, scaphitoides*
Late Callovian	*Lamberti* *Athleta*	*Lunuloceras lunuloides Peltoceras solidum*
Middle Callovian	*Coronatum*	*Pachyerymnoceras Kurnubiella hatirae (LEWY)*
Late Bathonian- Early Callovian		*Bullatimorphites*
Early Bathonian	*Zigzag*	*Micromphalites*
Late Bajocian	*Parkinsoni* *Garantiana* *Subfurcatum* *Humphresianum*	*Thambites planus* *Thamboceras-Magharina* *Ermoceras mogharense* *Normannites egyptiacus*
Middle Bajocian		*Dorsetensia*
Early Bajocian	*Laeviuscula*	*Otoites*

sp. In drillings the marine *Ektyphocythere* cf. *vitilis* (Apotolescu, Magne and Malmoustier) may also exist, but not in the same layers as the nonmarine taxa, pointing to alternating environments of fresh/brackish water and shallow sea. The nonmarine fauna is endemic at the species level, whereas the marine form shows European affinity.

Aalenian-Bajocian

The Early Bajocian ammonite *Otoites* occurs at Gebel Maghara in the Mahl Formation, which is equivalent in the Negev with the lowermost part of the Daya Formation. Higher up, in the lower part of the Bir Maghara Formation, the Middle Bajocian ammonite *Dorsetensia* occurs.

The Late Bajocian is well-documented in the *Ermoceras* beds. The *Garantiana* and *Subfurcatus* Zones are represented here by *Thamboceras, Magharina* and *Ermoceras mogharense.*

A latest Bajocian age is ascertained by the occurrence of *Thambites planus* in the shales topping the Bir Maghara Formation, corresponding to the *Parkinsoni* Zone.

The foraminifera *Timidonella* cf. *sarda* Bassoullet indicates an Aalenian-Bajocian age. It is found in the Rajabiah Formation at Gebel Maghara (Hirsch, 1979), a unit corresponding to the Qeren Formation in the Negev. *Haurania* generally indicates the Bajocian, and *Selliporella donzelli* Sartoni et Crescenti appears in oosparitic interbeds.

Among calcareous nannofossils *Crepidolithus crassus* and *Schizosphaerella punctulata* occur.

Palynomorphs consist of the *Korystocysta kettonense* Zone (Late Bajocian) and *Dichadogonyaulax sellwoodii* Zone (Latest Bajocian).

Ostracods are frequent and are represented by *Cytherella ?toarcensis* (Bizon), rare to common *Ektyphocythere bucki* (Bizon), *Isobythocypris ovalis* (Bate and Coleman), *Praeschuleridea inmarensis* Rosenfeld and Gerry, and *Kinkelina kadeshensis* Rosenfeld and Gerry. These forms define the *Ektyphocythere bucki* Assemblage Zone.

At Gebel Maghara, the frequent *Glyptogatocythere magharaensis* Rosenfeld and Gerry and the common to rare *Cytherella bashai* Rosenfeld and Gerry, *Monoceratina striata* Triebel and Bartenstein, *Rutlandella transversiplicata* Bate and Coleman, and *Ektyphocythere zerqaensis* Basha are characteristic and restricted to this assemblage zone, whereas *Glyptocythere huniensis* Basha and *Bairdia* sp. proceeds higher. The environment of deposition was warm shallow marine, though *Monoceratina* indicates somewhat deepening of the facies. The assemblage still shows affinities with European forms, though more taxa and the dominant taxon are endemic (Israel, Jordan), an observation that is corroborated by ammonites and bivalves (Parnes, 1981; Hirsch, 1979).

Bathonian

At Gebel Maghara, the Early Bathonian age of the ammonite *Micromphalites* was proposed by Enay and Mangold (1994) and differs from Parnes's original Middle Bathonian assumption. Late Bathonian is indicated by *Bullatimorphites.*

Ostracodes are dominated at Gebel Maghara by *Progonocythere honigsteini* Rosenfeld and Gerry, *Fastigatocythere bakeri* (Basha), *Praeschuleridea hornei* Rosenfeld and Gerry,

TABLE 18E.2: Correlation of Jurassic Stratigraphic Units in the Levant, and Distribution of Different Groups of Fossils.

CORRELATION OF JURASSIC STRATIGRAPHIC UNITS IN THE LEVANT

	JORDAN	S. NEGEV	N. NEGEV	SINAI	SHEFELA	HERMON	GALILEE	LEBANON	J.AS SAHILYEH	MICRO-PALEONTOLOGY
BERRIASIAN					Gevar'am	Tayasir	Tayasir	Tayasir		
TITHONIAN								Salima	Nasirah	*Hutsonia adunca*
KIMMERIDGIAN		Haluza Beersheba	Haluza Beersheba	Rokba	Nir Am	Batroun Bloudane	Haifa Bay	Bikfaya	Nasirah	*Alveosepta praelusitanica* *Alveosepta jaccardi Levantinella* **G**
OXFORDIAN		////////////////////	Kidod	Tauriat	Kidod	Majdal Shams	Devorah Haifa	Bhanness Kesrouane		*Levantinella* **F**
CALLOVIAN	//////////////////// Mughanniyya	Matmor Zohar	Zohar	Arousiah	////////// Brur	Hermon	Haifa	Kesrouane	Wadi Al Ouyoun	*Steinekella steineki* **E** *Platykilianina*
BATHONIAN	Hamam Ramla	Sherif	Sherif	Kehailia Safa	Karmon Haifa	Hermon	Haifa	Kesrouane	Machta	*Pfenderina salernitata* **D**
BAJOCIAN	Dhahab	Mahmal	Daya	B.Maghara Mahl	Haifa	Bqassem K.Jandal	Haifa	J3	Ouyoun	*Amijiella* **C** *Haurania* **B**
AALENIAN	Silal	Inmar	Inmar Qeren	Shusha Rajabiah	Rosh Pinna Haifa	Kalaat Jandal	Haifa	J2	Ouyoun	*Timidonella sarda* **A**
TOARCIAN	Silal	Inmar	Inmar	Mashabba	Haifa	Aarne	Haifa	Chouane	Treize	
PLIENSBACHIAN	Nimr	Ardon	Ardon	Ardon	Haifa	Aarne	Haifa		Treize	*Orbitopsella primaeva*
SINEMURIAN	Hihi	Mishhor	Mishhor	Mishhor	Mishhor	Aarne	Asher Volcanics		Treize	*Pseudocyclamina liassica*
HETTANGIAN										

STAGE	PALYNOMORPHS	OSTRACODES	FORAMINIFERA
Kimmeridgian-Late Oxfordian		*Hutsonia adunata*	*Anchispirocyclina praelusitanica,* *Alveosepta jaccardi*
Middle-Late Oxfordian	*Epiplosphaera reticulospinosa* **G**		
Early-Middle Oxfordian	*Millioudodinium* **F** *nuciformis*	*Exophthalmocythere? kidodensis*	*Levantinella egyptiensis*
Late-Middle Callovian	*Polystephanephorus* **E** *calathus*	*Ektyphocythere zoharensis*	*Flabellocyclolina reissi Steinekella* cf. *steinekei* *Kurnubia palastiniensis*
Early-Middle Callovian	*Polystephanephorus* **E** *calathus*		*K.*cf *wellingsi,Kurnubia variabilis,* *Kilianina* sp *Praekurnubia crusei*
Bathonian	*Energlynia accolaris* **D**	*Progonocythere honigsteini -* *Fastigatocythere bakeri*	*Paleopfenderina salernitana*
Late Bajocian	*Dichadogonyaulax* **C** *sellwoodii* *Korystocysta kettonense* **B**	*Glyptogatocythere magharaensis*	*Selliporella donzellii*
Middle Bajocian	*Applanopsis turbatus* **A**		*Amijiella amiji*
Aaleno-Bajocian	*Applanopsis turbatus* **A**		*Timidonella* sp., *Gutnicella* gr. *cayeuxi*
Toarcian-Aalenian	*Applanopsis turbatus* **A**	*Ektyphocythere bucki*	
Pliensbachian			*Orbitopsella primaeva*
Low-Middle Liassic		*Bisulcocypris oertlii*	

TABLE 18E.2 Continued. Distribution of Different Groups of Fossils.

STAGE	AMMONITES	BIVALVES/GASTROPODS	CALCAREOUS NANNOPLANKTON
Tithonian	*Virgatosphinctes*		*Conisphaera mexicana*
Kimmeridgian			*Watznaueria manivitae*
Late Oxfordian			*Watznaueria manivitae*
Middle Oxfordian	*cordatum*		*Watznaueria manivitae*
Early Oxfordian	*mariae*		*Watznaueria manivitae*
Late Callovian	*lamberti athleta*	*Eunerinea hebraea, Bucardiomya somaliensis*	*Watznaueria manivitae*
Middle Callovian	*coronatum*	*Bucardiomya aubryi Eligmus aualites*	*Stephanilithion bigoti*
Early Callovian			*Stephanilithion bigoti*
Late Bathonian	*Bullatimorphites*	*Eligmus asiaticus*	*Stephanilithion speciosum*
Middle Bathonian	*Micromphalites*	*Africogryphaea costellata*	*Stephanilithion speciosum*
Early Bathonian	*Thambites*	*Nuculana decorata*	
Late Bajocian	*Ermoceras*	*Eligmus integer*	*H. magharaensis*
Middle Bajocian	*Dorsetensia*	*Pholadomya orientalis*	
Early Bajocian	*Otoites*		
Aalenian		*Trigonia costata*	*Schizosphaerella punctulata*
Toarcian		*Trigonia similis*	*Crepidolithus crassus*
Pliensbachian		*Nerinella janeti*	

Upper Bajocian			
Late Bajocian	*Dichadogonyaulax* **C** *sellwoodii Korystocysta kettonense* **B**	*Glyptogatocythere magharaensis*	*Selliporella donzellii*
Late Bajocian	*Ermoceras*	*Eligmus integer*	*H. magharaensis*

and *Zerqacythere subiehensis* Basha. The first occurrence of *Glyptogatocythere malzi* Basha, *Ektyphocythere shulamitae* Rosenfeld and Gerry, *E. aardaensis* Basha, and *Terquemula goldbergi* Rosenfeld and Gerry is also characteristic here.

In the drilled sequences, Bathonian is generally indicated by *Pfenderina salernitata* that appears in the upper part of the Bathonian facies.

Callovian

The Lower Callovian seems defined by the foraminifera *Planikilianina hermonensis* Bassoulet and Grossowicz (in press). The beds containing this taxon are now also dated as Early Callovian by Palynomorphs. This is in agreement with the Callovian age, assumed in Saudi Arabia by Le Nindre et al. (1987) for the concurrent form *Praekurnubia.*

Cariou (in Cariou et al., 1997; Hirsch et al., 1999) has clearly affirmed the presence of genuine Middle Callovian (*Coronatum* zone) and Late Callovian (*Athleta* and *Lamberti* Zones), the latter reaching the top of the exposed sequence in the Negev, at Hamakhtesh Hagadol.

The Middle and Upper Callovian is well-characterized by *Trocholina palastiniensis* and the appearance of the genus *Kurnubia.* The uppermost Callovian seems to be characterized by the taxon *Flabellocyclolina reissi* Hottinger.

The ostracods *Ektyphocythere zoharensis* Rosenfeld and Gerry and *Terquemula gublerae* (Bizon) are found throughout the Zohar and lower Matmor Formations at Hamakhtesh Hagadol (Negev, Israel). The assemblage comprises *E. zoharensis* Rosenfeld and Gerry, *Bairdia* aff. *hilda* Jones, *Afrocytheridea faveolata* Bate, *Progonocythere* aff. *parastilla* Whatley and *Micropneumatocythere laevireticulata* Rosenfeld and Honigstein.

In the upper part of the Matmor Formation at Hamakhtesh Hagadol *Exophthalmocythere? kidodensis, Mandelstamia hirschi* Rosenfeld and Honigstein, *Cytherella index* Oertli and *Oligocythereis* aff. *fullonica* (Jones and Sherborn) appear in the assemblage of *E. zoharensis.*

Palynomorphs are characterized by the *Polystephanephorus calathus* Zone.

Oxfordian-Kimmeridgian

The shaly facies of the Oxfordian is well documented by ammonites in the exposures of Anti-Lebanon and to a lesser extent at Gebel Maghara (See Table 18E.1).

The endemic foraminifera taxon *Levantinella egyptiensis* seems to indicate the lower half of the Oxfordian. Kimmeridgian Algae include *Pseudoclypeina* and *Clypeina jurassica.*

Palynomorphs of the *Millioudodinium nuciformis* Zone indicate the Early to Middle Oxfordian, whereas the *Epiplosphaera reticulospinosa* Zone has a Middle to Late Oxfordian range.

Ostracodes occur in the shales of the Majdal Shams (Kidod) Formation. At Gebel Maghara it yields *Exophthalmocythere? kidodensis* Rosenfeld and Gerry, *Progonocythere* aff. *parastilla* Whatley, and *Terquemula gublerae* (Bizon). At Majdal Shams (Golan Heights) an abundant assemblage comprises *E.? kidodensis* and *T. gublerae*, also *T.* cf. *martini* (Bizon), *Cytherella* cf. *umbilica* Bate, *Monoceratina stimulea* (Schwager), and *M.* cf. sp. B Bate, as well as *Cytherelloidea atlantolevantina* Rosenfeld and Honigstein, *Eucytherura oxfordiana* R. and H., *Acrocythere dubertreti* R. and H., *Homerocythere hermonensis* R. and H., and *Oligocythereis irregularis* R. and H. The environment of deposition of the Kidod Formation of Majdal Shams (Hermon) is definitely in deeper water with euxinic bottom conditions.

Kimmeridgian-Tithonian

This youngest Jurassic time interval seems to be defined by the *Hutsonia adunata* Assemblage Zone. It was found in several localities, from Ein Qunyia in the Hermon Massif (Nahar Sa'ar Formation) the bore-holes of Qeren, Haluza, Boqer, Kohal, Beersheva, and Hazon in the Negev. The taxon *Hutsonia adunata* is also known from the Kimmeridgian or Tithonian of Lebanon (Bishoff, 1990).

PALEOGEOGRAPHY, PROVINCIALISM, TECTONICS AND EUSTATIC CYCLES

Introduction

Regional correlation through interpretation of stratigraphic data in terms of unconformities, transgressions, regressions and dynamics of sedimentation, paleogeography, facies and thickness contours, tectonic uplifts, relative sea level change and event stratigraphy suggest the folowing:

The Jurassic paleotectonic setting consists of relative lows and highs, controlled by differential rates of subsidence (average thickness in parenthesis) (Fig. 18E.1):

I) Galilee-Lebanon platform (1500-2000 m), extending to the Coastal Ranges in Syria (300 m);

II) Central Israel-Hermon Judean Embayment (3000 m), extending into the Palmyran basin (100 m), and separated by

III) Negev high (900-2000 m) extending to Jordan, from the

IV) Maghara basin (3000 m) of Sinai. The dismantling of the Helez High, a paleoland extending from the Coastal Plain westward into the eastern Mediterranean, starts with rifting, initiating the Gevar'Am trough.

The Jurassic Paleogeography of the Levant consists thus of **(Figure 18E.10):**

A) The Negev-type facies around the Arabian-Nubian craton;

B) The Judean Embayment-Golan-Palmyra;

C) The Galilee-Lebanon-Coastal Syria;

D) The Late Jurassic Arabian evaporite basin;

E) Delta-Akkuyu trough;

F) Mediterranean paleoland.

Tentative Regional Jurassic Stratigraphic Scheme:

Correlation of Jurassic stratigraphic units in the Levant are proposed for Jordan, Negev, Sinai (Egypt), Central Israel, the Anti-Lebanon, Galilee, Lebanon, Syria and an extension of the Jurassic

Levant facies into the Pisidian Taurus may be postulated.

a) Unconformities

The Jurassic is framed by the Infra-Jurassic and Infra-Cretaceous unconformities. In the Judean 'Embayment' the Middle and Upper Jurassic are separated by the Infra-Oxfordian unconformity.

The Triassic-Liassic contact in the Levant is a distinct sedimentary break marked by lateritic paleosols (Mishhor) or volcanics (Asher).

The contact between the Early Cretaceous and the Jurassic is not solely unconformable. Prior to Early Cretaceous magmatic activity, the area was tilted, followed by a phase of denudation and subaerial erosion. Basaltic flows thus cover an erosional surface of the Jurassic substratum and can overlie levels as deep down as the Majdal Shams Formation (Shimron and Peltz, 1993; Mor, 1985). Infra-Cretaceous normal faulting most certainly accompanied the regional tilting, though the question remains whether this tectonic activity took place before or during Early Cretaceous magmatic activity. Collapse, subsequent to volcanism, has been inferred (Shimron and Peltz, 1993).

b) Dynamics of sedimentation

During the Middle-Late Liassic transgressions, a true marine platform carbonate regime quickly developed (Ardon). Between the Negev and adjacent Sinai, the Judean Embayment developed as a SW-NE trending depocenter across central Israel and the adjacent southern Anti-Lebanon. Regressive clastic interruptions mark the proximal sides of the basin (Aalenian Inmar facies). In the Central Israel Judean Embayment the Ardon and Qeren carbonates merge, being interspersed by oolites and evaporites. At the top, shales replace the sandstones of the Upper Inmar. In Northern Israel, Lebanon and the northern Anti-Lebanon platform all clastics have vanished and carbonates persist without interruption from the Liassic to the Upper Jurassic (Haifa).

In the Central Coastal Plain Middle Jurassic lithofacies of oolitic shoals (Sederot) and spiculites (Barnea) interwedge the Hermon Formation. In the Negev the mostly marine regime of mixed carbonatic and clastic strata of the Bajocian (Daya) are interrupted by regressive Early Bathonian paralic clastics and coal (Sherif), followed by micrites and marls. The Late Bathonian regression of shales and sandstone of the upper part of the Sherif Formation is represented in the Coastal Plain by the Karmon shales. These shales proceed to the Early Callovian, separating Bathonian (Sederot) from Callovian (Brur) calcarenites (**Figure 18E.8b**).

The interplay of continental arenaceous (Arabian Massif) with littoral-tidal shales and carbonates continues on into the Callovian Zohar Formation in southern Israel and the adjoining northern Sinai. Micrites with *Trocholina palastiniensis* and *Kurnubia palastiniensis* define the Middle-Upper Callovian in the Negev micritic limestone, abundant in shale interbeds and a few thin sandstones of subordinate non-fluviatile origin, that represent the Zohar Formation. In the Halal, Qeren, Sherif, Rekhme, and Boqer wells and Hamakhtesh Hagadol reefoidal carbonates add a thick Upper Callovian sequence.

The very top of the Hermon Limestone Formation, Razvalyaev's 17 m top beds (J3C1), consist of pelitomorphic limestone and clayey limestone that bear belemnites, brachiopods and the ammonoid *Hecticoceras (Sublunuloceras)* cf. *lunuloides* Kil., assigned to the Late Callovian.

The top of the Callovian limestone is coated by iron crusts in the Hermon and Maghara sections, pointing to starvation of the basin at the Callovian-Oxfordian boundary.

On the other hand, the karst phenomena described by Buchbinder et al. (1984), occurring at the top of the Lower or within the Middle Callovian in the Coastal Plain bore-holes, witness an emergence that might be related to a tectonic uplift chracterising this part of the basin. This could explain the missing Middle and Upper Callovian underneath the transgressive onlap of the Early Oxfordian Majdal Shams shales.

This infra-Oxfordian unconformity, where Early Oxfordian shales onlap a level lower in the Callovian carbonates, thus sometimes filling the karstic landscape (Brur), contrasts with the apparent continuous Callovian-Oxfordian carbonate platform regime of northern Israel.

South of the Judean Embayment, the Negev platform micrites, interwedged by marls and biostromes represent a continuous Callovian sequence (Zohar-Matmor).

The Early Oxfordian, represented in the Judean Embayment by the Majdal Shams Formation is, in contrast to older formations (*e.g.*, Sherif, Inmar), poor in arenaceous beds. Its thickness seems to be directly related to the extent of the hiatus or strong compaction of the Middle and Upper Callovian, progressively decreasing with the increase of Middle to Upper Callovian Haifa or Zohar carbonates. The absence of genuine Early Oxfordian markers south of the Judean Embayment, suggests a hiatus of this substage on the Negev platform.

A Late Oxfordian-Kimmeridgian shallowing restores platform conditions, characterized by oolites in northern Israel. Bioherms (Nir'Am) occur in the Upper Jurassic of the Coastal Plain. Shales and occasionally sandstones are found in southern Israel (Nahar Sa'ar).

A regional uplift has generated the Infra-Cretaceous unconformity, marked by subareal erosion and the formation of submarine canyons. Volcanic effusions may have started during the latest Jurassic (Tayasir). In the south the erosional gap between Jurassic and Cretaceous rapidly widens from a nearly complete sequence in the area of the northwest Negev (*e.g.* Qeren) to a deeply truncated sequence in the higher Negev (Ramon), south of which no Jurassic is left below the Cretaceous volcanics (Tayasir) or continental sandstones (Kurnub). In the wells drilled into the canyons of the 'Helez erosion embayment' nearly all Callovian and Upper Jurassic formations are missing, as they were removed by submarine erosion. The latter canyons are filled with thick marine shales of Latest Jurassic (Tithonian) and Early Cretaceous age (Gevar 'Am), pointing to a series of tectonically linked events before the end of the Jurassic.

c) Facies and Thickness Contours

The Jurassic paleotectonic setting of Israel is displayed in an isopach-map, providing a reconstruction of the paleogeographic configuration prior to Infra-Cretaceous truncation and to the ~100 km sinistral displacement of the Golan-Jordan side along the Levant-transform. (Fig. 18E.1).

The following paleogeographic domains are identified:

The **Negev High,** plunging to the northwest and forming the 'Negev Nose' that separates the two major depo-centers of **northern Sinai Deep** (Maghara-Halal) and of the Central Israel **Judean Embayment**. The latter is bound to the north by the shallow **Galilee Platform** that extends to Lebanon and the northern Anti-Lebanon.

The **Galilee High,** almost totally devoid of clastics, that extends to adjacent Lebanon and the northern Anti-Lebanon. The tectono-environmental evolution of the Jurassic in Israel consists of a Lower (Liassic-Callovian) and Upper (Oxfordian- Kimmeridgian) subdivision.

During the Liassic-Callovian timespan, the **Negev High** accumulated abundant clastics resulting from the wearing down of the Arabian Massif to the south and southeast. The clastic ratio of the sand and shale, littoral and paralic sediments (Inmar-Sherif Facies) increases in the eastern parts of the Negev. The Negev High subdivides into Avdat and Massada 'blocks' separated by the Kurnub 'basin' (Goldberg, 1970). The Massada block is a structural feature that probably was part of a wider Eastern Negev - Jordan High. The Negev High plunges towards the northwest. To the east, the Maghara-Hallal **Northern Sinai Deep** is still characterized by a high ratio of Early-Middle Jurassic clastics (Mashaba, Susha, Safa, and Kehailia) due to the vicinity of the Arabian-Nubian craton. To the north, due to the influence of the open Tethys Sea, a dominance of shallow platform carbonates prevails over most of central and northern Israel. In the central Israel trough of the Helez-Ramallah-Hermon **Judean Embayment** the carbonates account for a marked decrease of the clastic ratio (Hermon Facies). North of the Judean Embayment, in the overall thinner Early-Middle Jurassic column of the **Galilee High,** the uniform carbonates are mostly devoid of clastics (Haifa Facies).

The Late Jurassic bioherms and biostromes (Nir'Am) interfinger with the sudden Early Oxfordian shale deposition of the deeps, suggesting strong epeirogenic movements. The distribution of these shales (see facies map **Figure 18E.8c**) suggests a landmass to the west, now hidden below the Mediterranean (Picard and Hirsch, 1987).

d) Volcanism

The beginning and end of the Jurassic is characterized by truncation and denudation. Possibly even surpassing the Triassic-Liassic boundary events of volcanism, truncation and lateritization, the events that took place towards the outgoing Jurassic include the abrasional effect of the Tithonian(?) and Neocomian sea in the west with their Gevar'Am channelings as well as the coeval counteraction of subareal denudation documented in the east by the Lower Cretaceous Kurnub Facies with accompanying Tayasir volcanics. The marine and subareal elimination in the various areas is illustrated in a subcrop-map (**Figure 18E.8d**). The Tithonian-Hauterivian Gevar'Am shales reached down to the Dogger of the Coastal area, whereas the Kurnub clastics cut to the Triassic-Paleozoic in the southern Negev.

Magmatic and sedimentary facies are controlled by Early-, Middle and Late Jurassic epirogenetic uplift movements of the Arabian Massif that reacted on the Gondwanian borderland by cyclic transgressions and regressions, independant of the global eustatic sea-level fluctuations.

The volcanic rocks known from different Jurassic levels, in particular in the Carmel, Galilee-Lebanon (Atlit, Yagur, Devorah, Bhannes) but also as sills and dykes in the Negev, are of typical non-orogenic association. This concurs with the continental-epicontinental facies that reigned in the Levant region during the Jurassic (and generally during the Mesozoic).

e) Provinces

The Early Jurassic paleogeography in the Levant bears witness to an undivided Gondwanid shelf-platform. Mid-Late Jurassic continuous widening of the Neo-Tethys, and the progressive fragmentation of Gondwana into Ethiopian (African-Apulian-Arabian) and Indian plates prior to Atlantic and Indian oceanic rifting, enhanced biogeographic provincialism of neritic taxa and created new seaways for pelagic taxa. Neritic taxa shared a common habitat along the North-African and Levantine margins of a platform that comprised the Taurus calcareous backbone, and extended to the Arabian platform, edged by the peri-Arabian ophiolite belt of the Neo-Tethys.

Interpretation of seismic profiles in the Levantine Basin and the drilling activity offshore of the Sinai coast (Hirsch et al., 1995) have shed new light on the existence of an ancient (although modified) crust and the presence of a thick sedimentary cover, including a Jurassic sequence offshore of the present coast of Israel.

The paleogeographic relations of the Levant and Neotethys, interrupted during the Early Jurassic emergence (laterites) of the African-Arabian platform, were renewed by the marine inundation, characterized by bivalves (Trigonids) and a distinct fauna of ammonites (*Bouleiceras, Nejdia*) and foraminifera (*Orbitopsella, Timidonella*). The characterization of the African-Arabian-Ethiopean platform became more definite after the junction of the Middle Liassic Neotethys (*ammonitico rosso* seaway) with the Proto-Atlantic Rift. The contrast became even clearer in the Callovian, when following the North Atlantic boreal spread (Hallam, 1971), a distinct warmwater fauna of corals, nerineids, brachiopods (*Septirhynchia*) and foraminifera (*Satorina, Planikilianina*) occupied the Gondwanian (Ethiopian) side of Neotethys as an ecological shelter. Finally, by the end of the Jurassic (Tithonian) total isolation of the Ethiopian province from its Eurasian counterpart was achieved by the completion of the Neotethys-North Atlantic oceanic divide.

The Jurassic paleogeographic setting of the Levant appears, after geological and geophysical reevaluation, to fit well within a African-Apulian-Arabian plate model that includes the Levantine Basin, located south of a single Neo-Tethys ocean. Jurassic facies

of offshore wells also suggest the existence since Tithonian times of western (offshore) and eastern (onshore) paleo-highs, separated by a trough (Gevar'Am), located presently under the Levant Coast.

f) Global Cyclic Events

Biostratigraphic and global events are linked (Fig. 18E.2). Following the Hettangian-Sinemurian and possibly Pliensbachian emersion, endemic taxa became dominant. Low stand system tracks are related to the regressions of Inmar (Aalenian), Safa (Early Bathonian), Karmon (Late Bathonian), post-Brur (pre-Oxfordian), and in the Late Oxfordian and pre-Tithonian.

Six major transgression and high stand system tracks are found in the Ardon (Pliensbachian-Toacian), Daya (Bajocian), Kehailia (Early Bathonian), Zohar (Early-Middle Callovian), Matmor-Majdal Shams (Late-Callovian – Early-Oxfordian) and Nahar Sa'ar (Late Oxfordian-Kimmeridgian).

The question of the Oxfordian transgression

The Oxfordian transgression is well documented in the Majdal Shams shale (Hermon) and Tauriat shale (Maghara). It raises the question of the so-called 'Kidod' shales in the Coastal Plain of Israel, which represent apparently two events: one Late Callovian event in the Ashdod region, coeval with the Madsus of the Southern Negev, as well as with the marls of Wadi Al-Karn, northeast of Mount Hermon, along the Beirut-Damascus highway.

The Callovian age of the Madsus shale at Hamakhtesh Hagadol is established by ammonites and is matched by palynomorphs and/or foraminifera in the coeval bore-holes of Halal, Qeren, Rekhme, and Boqer (Figure18E.7). Brachiopods (det. Almeras) and foraminifera postulate the Callovian age of the yellow marl at Wadi al Karn (Mouty and Zaninetti, 1998).

In the boreholes of the Ashdod region, shales overlying an unconformity marked by subaerial erosion and karstification of the underlying Zohar carbonates, may yield Callovian palynomorphs (B. Conway, pers. comm.).

Oxfordian shales extend from Northern Sinai (Tauriat shales at Gebel Maghara) to the Hermon Massif (Majdal Shams Shales). The Oxfordian age of these shales is rigorously based upon ammonites and is matched by the Oxfordian *Milioudodinium nuciformis* Zone F in the 'Kidod' Formation of the Gerar, Hazerim, Motza, and Massada bore-holes, from the Coastal Plain, Judea and the northern Negev (Conway 1990).

The Late Callovian and Oxfordian harbor rather proximal high stand system tracks, characterized by tropical neritic faunas, whereas the more distal Late Callovian-Lower Oxfordian shows evidence for connection with the pelagic western Neo-Tethys.

The regional Jurassic cyclic evolution versus global events in the Levantine portion of Gondwana, starts with an Hettangian-Sinemurian and possibly Pliensbachian period of karst, filled with Mishhor laterites that deeply penetrate the underlying Late Triassic strata, as the result of the Early Liassic regional emersion of long term Upper Absaroka B (UAB) drop in sea level.

Pliensbachian-Toarcian Ardon-Nirim evaporites with shallow lagoon and reefoid carbonates, alternating with deltaic and paralic Lower Inmar sands, express the long term rise with minor short term oscillations, characterizing the end of the UAB.

Aalenian Upper Inmar-Rosh Pinna clastics abruptly set in with the onset of Lower Zuni-A (LZA-1) sea level drop and subsequent rise, reaching a significant high stand in the Bajocian Daya transgression (*Laeviscula-Otoites)* and following characteristic *Ermoceras* and *Eligmus* assemblages, ending in the *Parkinsoni-Thambites* low stand.

The Early Bathonian Safa - Lower Sherif sands and paralic coals seem to delineate a regression that characterizes the Levantine platform. Then follows the lower Kehailia (*Zigzag-Micromphalites)* LZA-2-2 transgression with endemic *Africogryphaea.*

The Late Bathonian regression of the Karmon shales, upper Kehailia or upper part of the Sherif Formation (LZA-2-4) precedes the Callovian rise (LZA-3) with *Bullatimorphites.*

The Callovian reaches a regional high, inundating most of the Arabian platform with typical 'Zohar-Matmor' type carbonates, yielding Nerineacea, foraminifera (*Kurnubia*-lineage, *Flabellocyclolina*), brachiopods (*Striithyris, Kutchthyris, Digonella*) and abundant bivalves (*Eligmus*), mostly related to Ethiopean-Somalian taxa. Epirogenic movements caused emersion along the Coastal Plain of Israel, causing karst phenomena and the hiatus of a significant part of the Callovian.

The Early Oxfordian (*mariae* Zone) Majdal Shams shale-onlap covered the previous hiatus. In the northern Sinai Deep and Judean Embayment, these shales conformably cover the 'starvation facies' of the Late Callovian (Gebel Maghara, Hermon) (**Figure 18E.9a, b**). It is unclear how these shales interfinger with the Galilee carbonatic type facies.

The Late Oxfordian-Kimmeridgian shallowing and progressive regression (*Alveosepta jaccardi*) occurred in contrast to the global trend of a general sea level rise (LZA-4), generating the emersion of the Syrian (Mardin) promontory, the development of thick evaporites in Central Arabia and the deposition of sands and shales from the Negev to northern Egypt (**Figure 18E.10**).

Epirogenic movements obscured the Late Jurassic global regression by juxtaposing 'Tithonian' graben-fillings with emersions, continental deposits, and basaltic flows.

Changing ecological and tectono-environmental conditions in the Middle Eastern Levantine Jurassic are echoed by the composition of floral and faunal assemblages, endemism and cosmopolitism. To a wide extent the paleogeographical and environmental evolution match the cycles of Haq et al. (1988), although it suggests that Levantine 'African-Arabian-Apulian' sea level anomalies, due to 'noises' generated by the Proto-Atlantic opening and southern Neo-Tethys rifting, perturb the global sea level record.

CONCLUSIONS

The Jurassic in Israel fits into a number of frames:

1) Volcanic: Asher Triassic/Jurassic, Devorah/Bahnnes (Oxfordian), Tayasir (Berriasian);

2) Tectonic: Early Liassic uplift, a Pre-Oxfordian Event, and

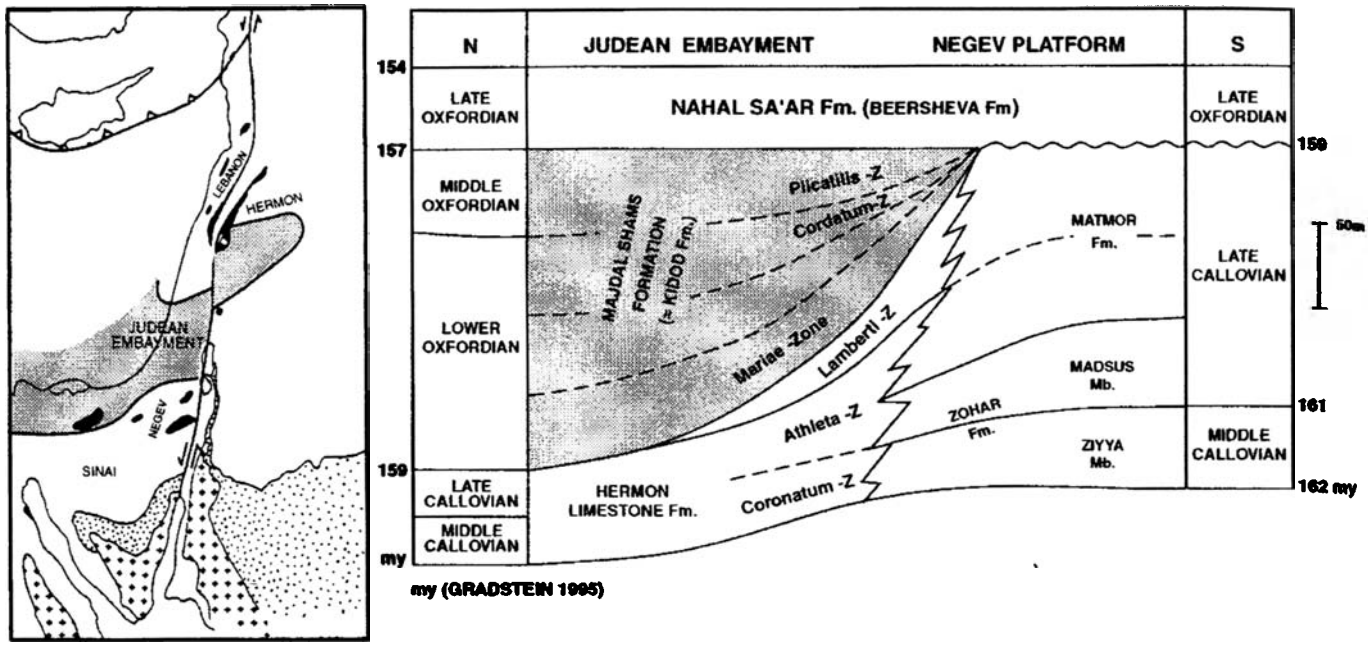


Figure 18E.9. Correlation of Callovo-Oxfordian strata of Judean Embayment and Negev Platform.

?Tithonian tilting and uplift;

3) Biostratigraphic: The Jurassic fauna in the Levant often exhibits endemic character, related to the southern Tethys shelf: Ammonite correlation of Arabian Province with the Submediterranean European Standard Scale Stages and calibration of large foraminifera and palynomorphs with ammonite scales are established.

Summing up: a series of cycles characterize the Jurassic deposition in the Levant. From the Triassic-Jurassic boundary in the Levant, marked by lateritic paleosols (Mishhor Formation) or volcanics in the north (Asher Volcanics), follows the development of marine platform carbonates, not before Pliensbachian times (Ardon). A number of oscillations bring Late Pliensbachian -Toarcian clastics (Lower Inmar) that invaded the Negev, followed by carbonates (Qeren). The Toarcian-Aalenian regression is marked by clastics in the Negev, adjacent Sinai, and along a belt crossing central Israel into the southern Anti-Lebanon (Upper Inmar). In northern Israel, Lebanon, and the northern Anti-Lebanon monotonous platform-carbonates persisted without interruption through the Oxfordian (Haifa). The Bajocian lithofacies varies from mixed carbonatic and clastic in the Negev (Daya Formation), to largely marly in Sinai (Egypt), or carbonatic in the north. The oolitic shoals and spiculitic limestones of the Coastal Plain recur in the Bathonian. Paralic clastics dominate the Lower Bathonian in the Negev and Sinai, followed by Late Bathonian marls (Sherif-Karmon).

The Callovian to Oxfordian calcarenites and bioherms (Brur-Nir'Am) of the Coastal Plain are replaced by micrites, wedged in between marls and biostromes (Zohar, Matmor). The Oxfordian transgressive shale-onlap (Majdal Shams) covers a Middle-Late Callovian hiatus in the Coastal Plain, wedging out toward Central Israel and the southern Anti-Lebanon (Judean Embayment). Late Oxfordian-Kimmeridgian biostromes, oolites, shales and sands from the Negev to northern Israel (Nahar Sa'ar-Haifa Bay) close the Jurassic cycle. Tithonian-Hauterivian volcanics (Tayasir) and turbidites (Gevar'Am canyon) cover an eroded surface.

During the Jurassic the Levant was part of the Gondwanian Tethys platform-shelf. The paleotectonic setting of the Levant consisted of relative lows and highs, controlled by differential rates of subsidence. In southern Israel the shallow Negev high (900-2000 m in thickness) separated the Maghara basin (3000 m) from the Central Israel-Hermon trough (3000-4000 m). The rather shallow northern platform of Galilee and Lebanon (2000-2500 m) extended far north (Syria, Lebanon, southern Turkey) and westward (Levantine Basin). Liassic through Bathonian clastics are the result of the wearing down of the Arabian Massif in the south and southeast. Yet thickening of the Early Oxfordian shales in the offshore wells point to derivation from some landmass in the west, now hidden below the Mediterranean (Hirsch and al., 1995). The Gevar'Am trough, alongside the present Levant-coast, formed during the Tithonian, initiating a separation between an Eastern Levant platform extending toward the Arabian-Nubian Massif and a western shallow marine platform and adjacent landmass. Volcanics indicate a number of aborted Mesozoic intracratonic rifts at the beginning and end of the Jurassic. The Late Triassic-Liassic Asher basalts reach a thickness of 2000 m in the western part of a trough that crossed the Galilee at right angles to the present coast. The Kimmeridgian-Hauterivian Tayasir basalts, up to 500 m thick, extend from Samaria to Galilee, Lebanon, and the Golan Heights.

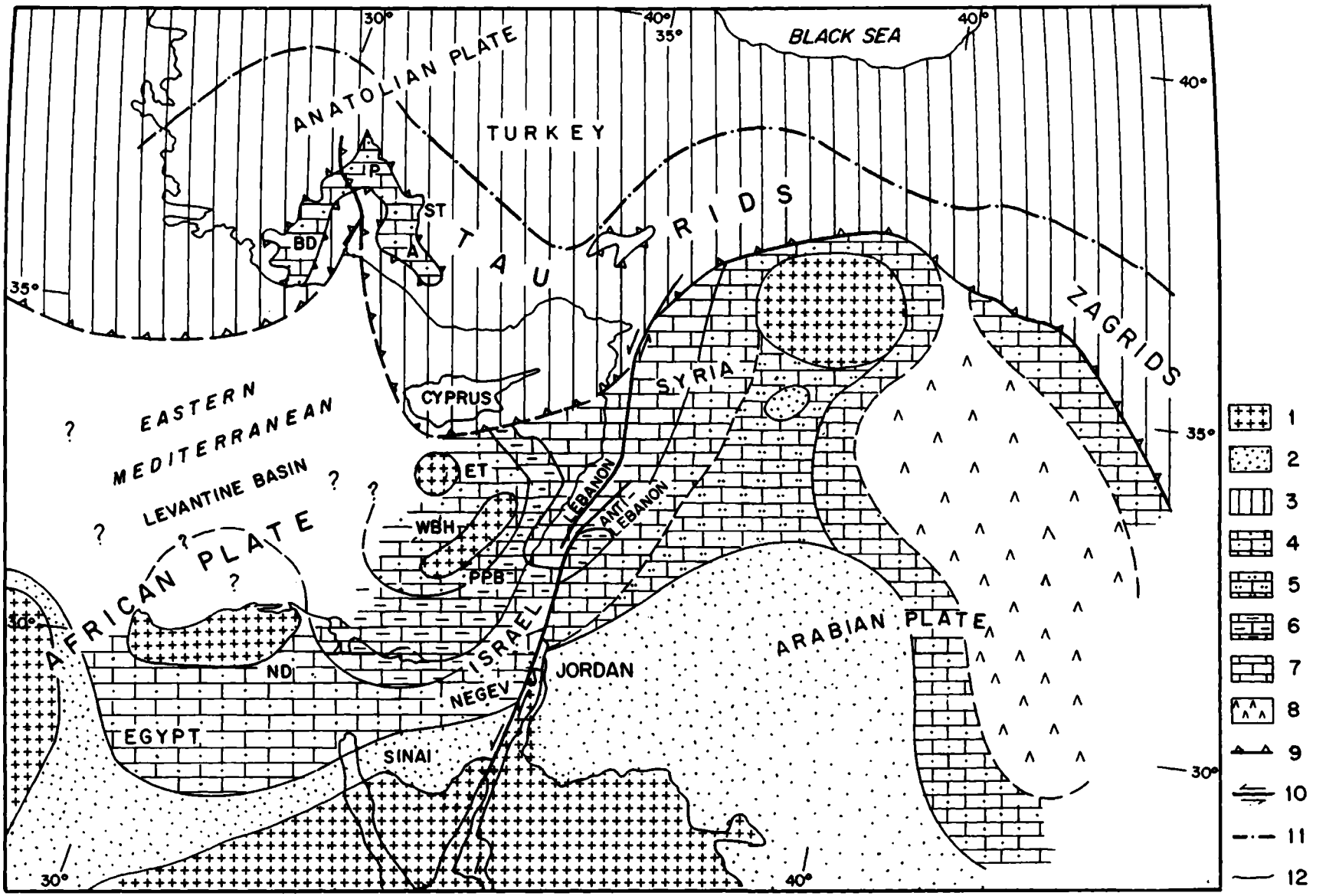


Figure 18E.10. Schematic Jurassic paleogeographic map of the Levant and adjacent areas.

Legend: 1 - Precambrian basement; 2 - predominantly sandstone; 3 - Tauro - Zagrid Tethyan terranes; 4 - Carbonatic Negev type facies; 5 - Semi-clastic facies of the Syrian promontory; 6 - Shales and carbonate facies of Delta and Judean Embayment; 7 - Bank and reef arbonate facies of Haifa and Lebanon type; 8 - Evaporites; 9 - Alpine thrust front; 10 - Dead Sea Transform; 11 - Approximate northern limit of African-Arabian Plates; 12 - Present coastlines.; BD - Bey Daglari; ST - Seydisehir-Tarasci; ET - Eratosthenes Seamount; WBH - Western Basement High; PPB - Pleshet Paleo Basin; ND - Nile Delta.

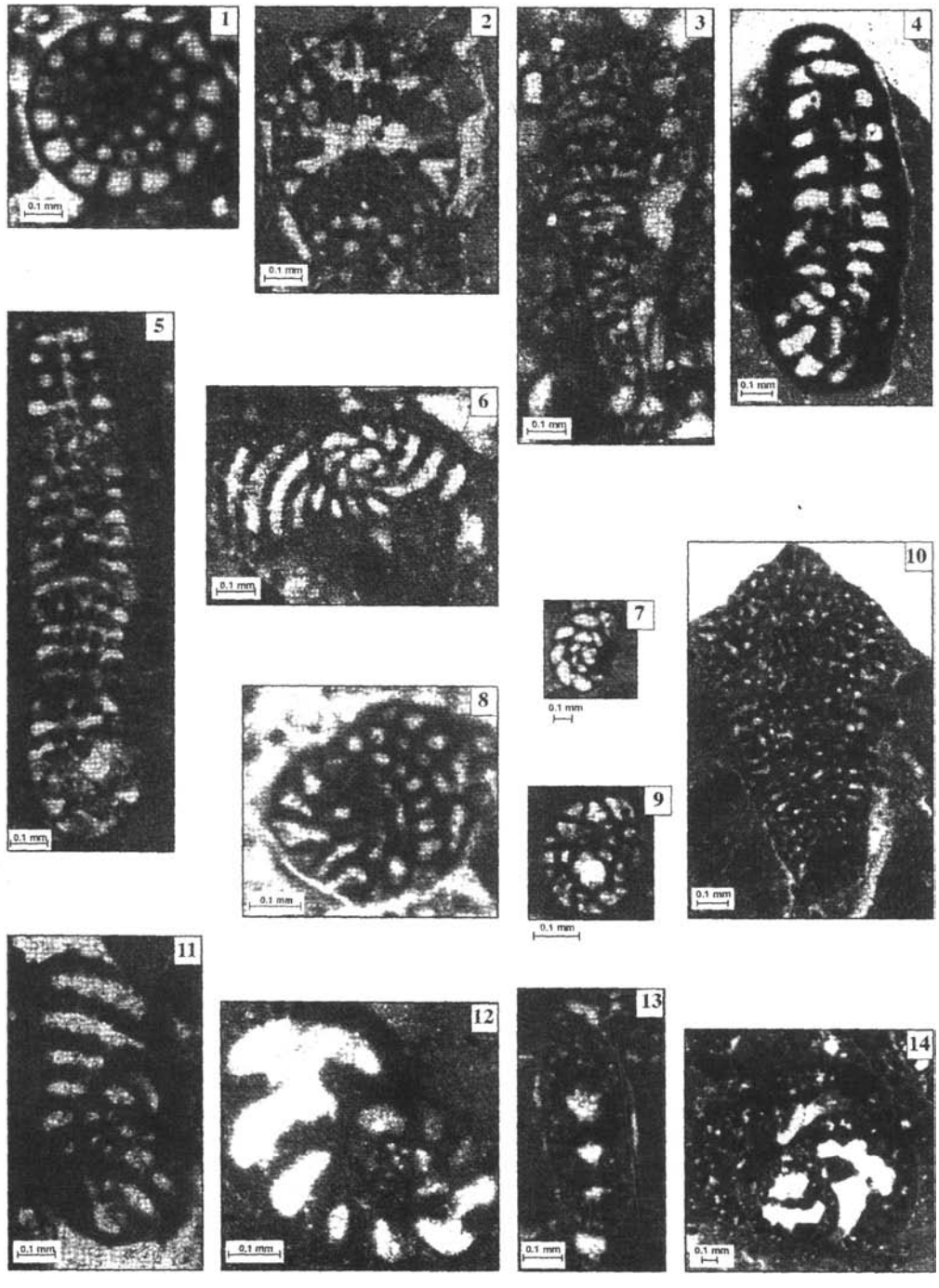


PLATE 18E.1: all plates from Perelis Grossowicz et al., 2000.

1. *Nautiloculina circularis* Said and Barakat, Middle-Upper Jurassic, Gevim-1, 2729-2732 m.
2. *Amijiella amiji* (Henson), Upper Sinemurian-Bathonian, Gevim-1, 2757-2760 m.
3. Hauraniidae / *Socotraina* sp., Upper Sinemurian-Bathonian, Boqer-1, 2116-2125 m.
4. *Planisepta compressa* (Hottinger), Pliensbachian, Boqer-1, 2116-2125 m.
5. *Orbitopsella primaeva* (Henson) or *Planisepta compressa* (Hottinger), Lower-Middle Liassic, Heletz-22, 4355-4364 m.
6. Transitional form between *Paleomayncina* sp. and *Planisepta compressa* (Hottinger), Boqer-1, 2116-2125 m.
7. "*Mesoendothyra*" sp., Toarcian-Lower Bajocian, Gevim-1, 2729-2732 m.
8,9,10. *Orbitopsella primaeva* (Henson), Lower Pliensbachian, (8) Besor-1, 3709 m., (9,10) Hazerim-1, 3460-3469 m.
11. *Paleomayncina termieri* (Hottinger), uppermost Sinemurian-Lower Pliensbachian, Ga'ash-2, 4251-4260 m.
12. "*Mesoendothyra*"sp., (Liassic taxa), uppermost Sinemurian-Lower Pliensbachian, Helez-22, 4378-4380 m.
13,14. *Pseudocyclammina liassica* Hottinger, uppermost Pliensbachian-Lower Toarcian, (13) Boqer-1, 2116-2125 m, (14) Gevim-1, 3027-3030 m.

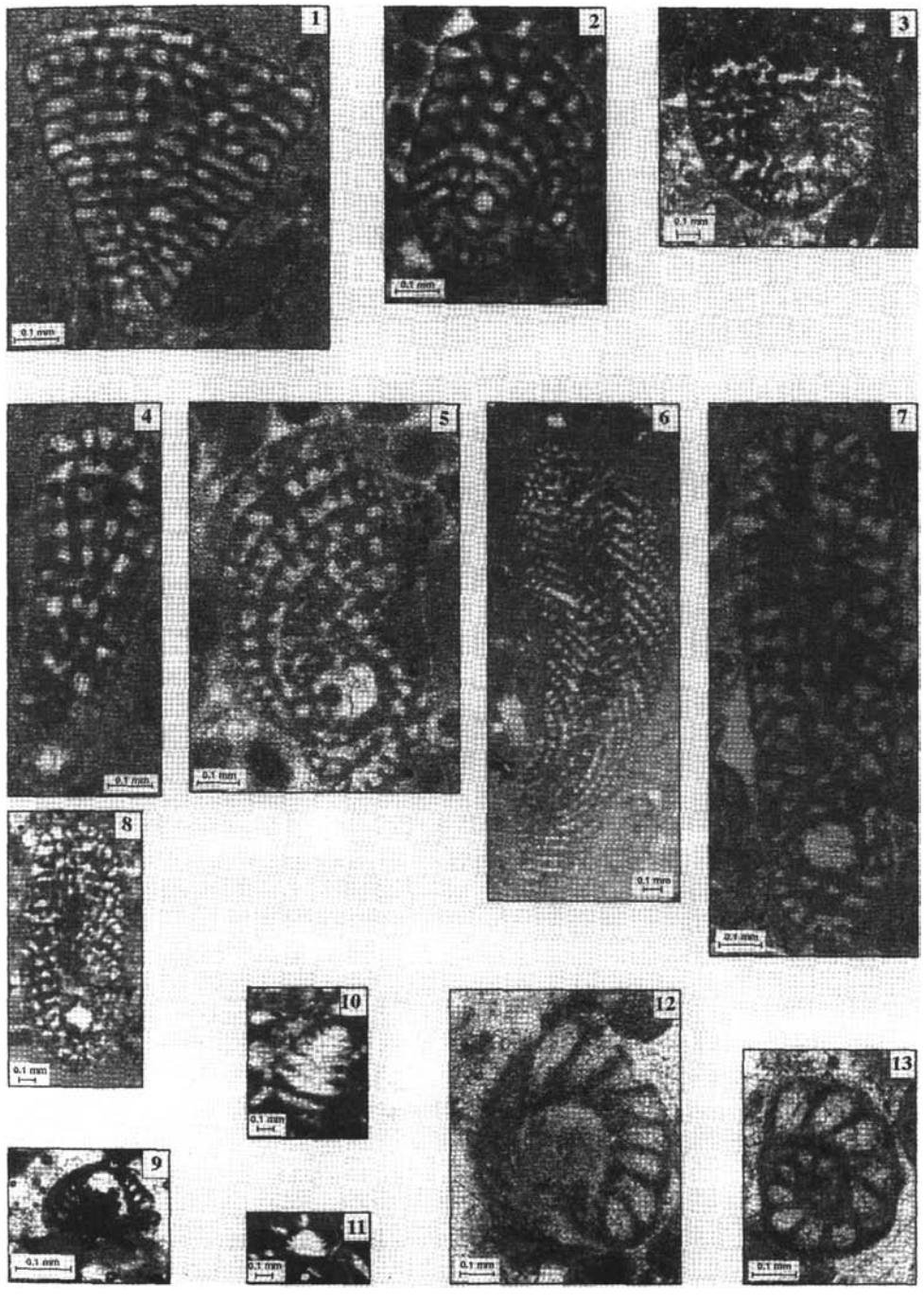


PLATE 18E.2:

1, 2. *Gutnicella cayeuxi* (Lucas), Aalenian-Bajocian, Heletz-22, core 18, B-2, B-1, 3610 m.

3. *Spiraloconulus perconigi* (Alleman and Schroeder), Aalenian-Bajocian, Heletz-22, core 16, 3515 m.

4,5,6,7,8. *Timidonella sarda* Bassoullet, Chabrier and Fourcade, Aalenian-Lower Bajocian, Heletz-22, core 16, 3515 m.

9,10,11. *Trocholina palastiniensis* Henson, Bathonian-Callovian, (9) Besor-1, 2677 m, (10) Har Amir-1, 1896 m, (11) Maanit-1, 2106-2109 m.

12,13. *Protopeneroplis striata* Weynschenk, Aalenian-Tithonian, (12) Caesarea-3, 2802 m., (13) Gevim-1, 2729-2732 m.

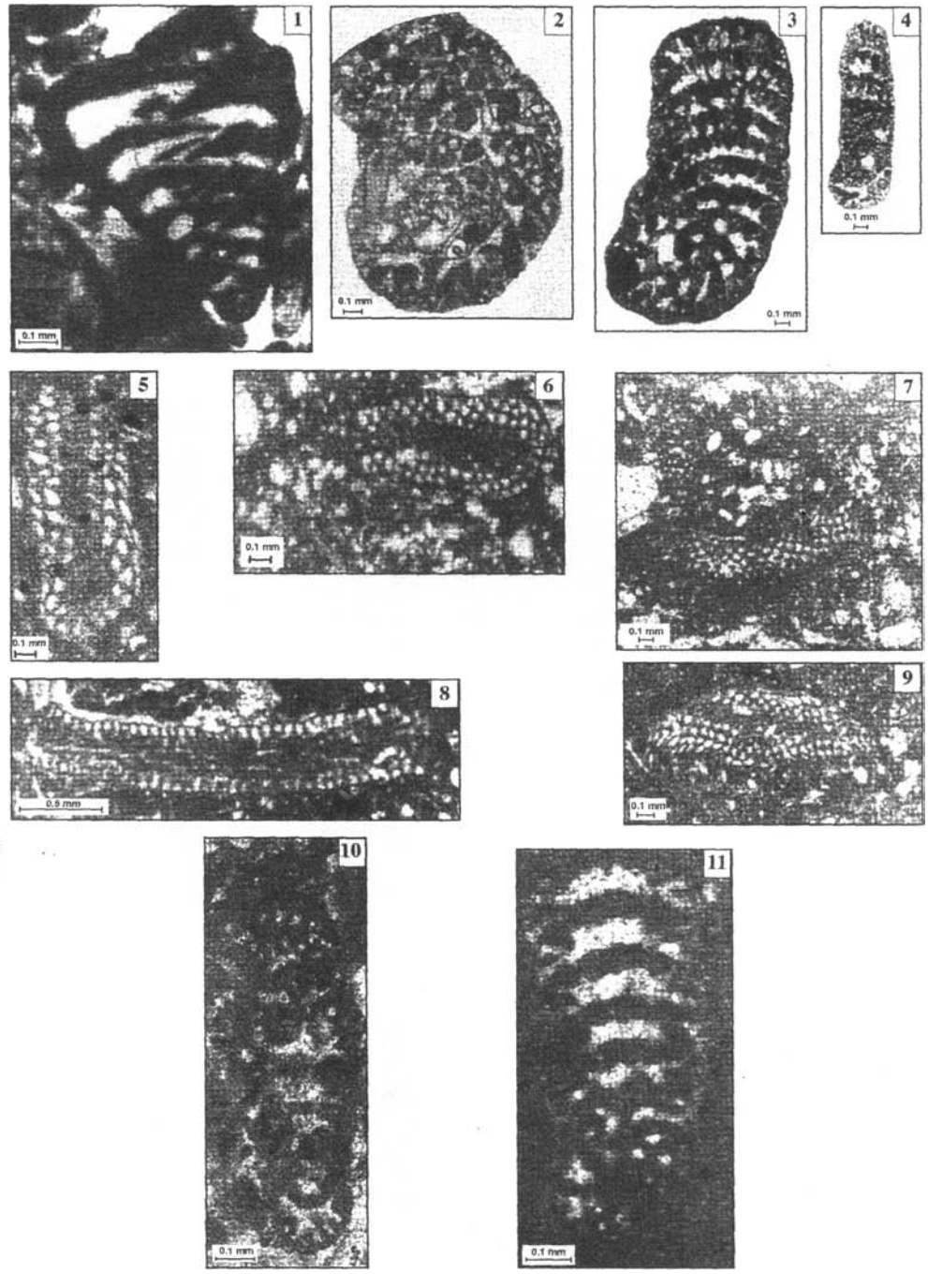


PLATE 18E.3:

1. *Redmondoides lugeoni* (Septfontaine), Bajocian-Lower Tithonian, Gevim-1, 2729-2732 m.

2,3,4. *Pseudocyclammina* (?), *P. smouti* Banner, Callovian-Lower Oxfordian, Gebel Maghara (Sinai), G.S.I. Field No. YM-1091-1092. These photographs were previously published by H. Frenkel, 1975.

5,6,7,8,9. "*Kilianina*" sp. The description of this new species, relative to *Kilianina* sp., is in publication. Uppermost Bathonian-lowermost Middle Callovian, Hermon Mt., G.S.I. Field Numbers: (5) H-107, (6) H-19, (7) H-110, (8,9) H-21.

10,11. *Pseudocyclammina maynci* Hottinger, Bathonian-Callovian, (11) Ga'ash-2, 3419 m, (12) Ga'ash-2, 3401-3410.

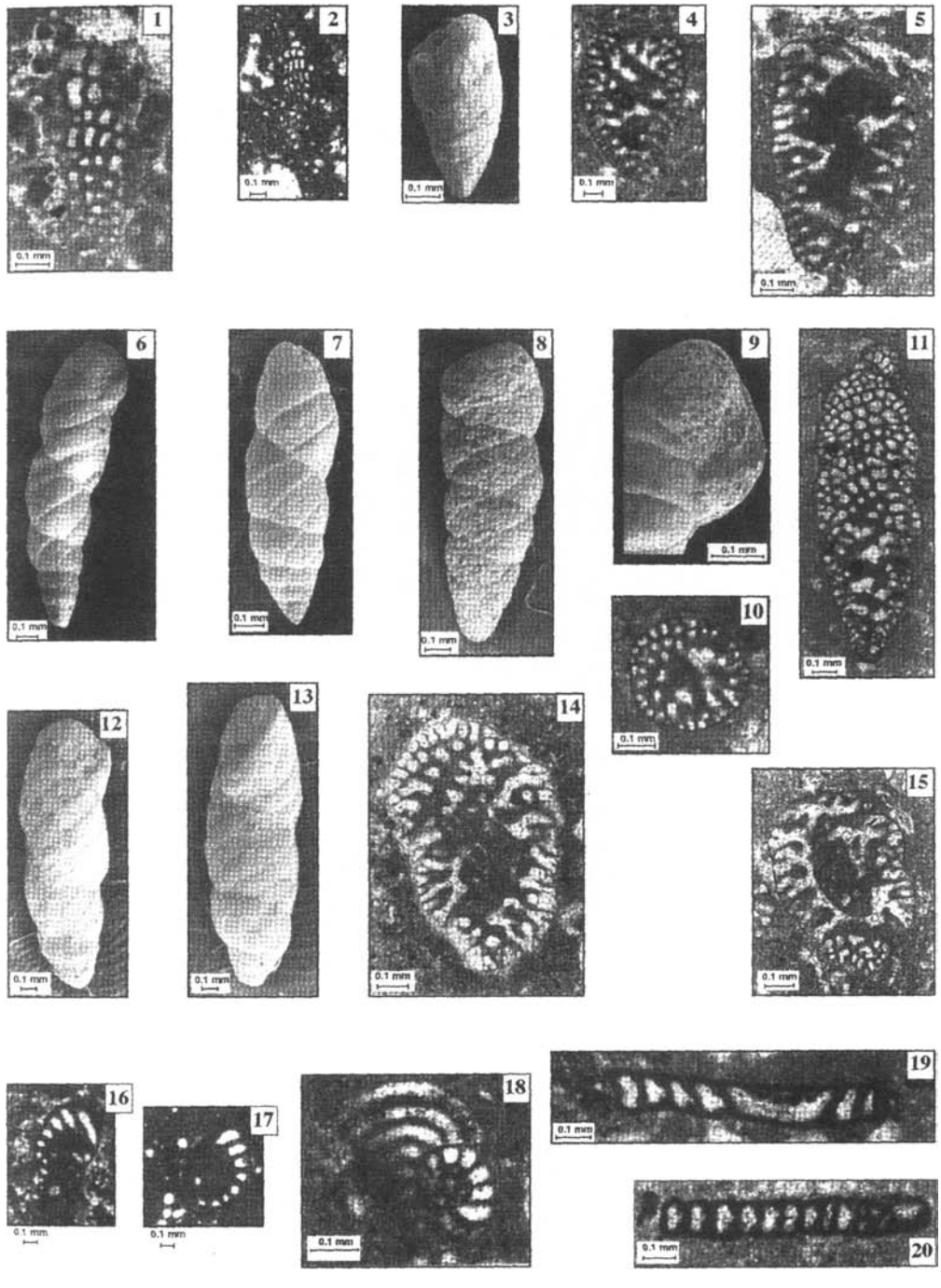


PLATE 18E.4:

1,2. *Praekurnubia crusei* Redmond, uppermost Bathonian-Middle Tithonian, (1) Yinnon-1, core 9, B-6, (2) Hermon Mt., G.S.I. Field No. H-110.

3,4,5. *Kurnubia variabilis* Redmond, Lower-Middle Callovian, (3) Kurnub, G.S.I. Field No. K-9, (4) Hulda-1, 7230-7250 m, (5) Hulda-1, 7250-7265 m.

6,7,8,9,10,11. *Kurnubia palastiniensis* Henson, Middle Callovian-Middle Tithonian , Kurnub, G.S.I. Field No. (6,7) K-18, (8) K-64, partially etched specimen showing subepidermal reticulation, (9) K-19, detail of apertural face, (10) K-64, transversal section, (11) K-60, longitudinal section.

12,13,14,15. *Kurnubia wellingsi* (Henson) Middle Callovian-Lower Kimmeridgian, Kurnub, G.S.I. Field No. (12,13) K-53, (14,15) K-64, longitudinal sections showing internal core delimited by an annular uncontinuous zone and subepidermal partitions.

16. *Paleopfenderina salernitana* (Sartoni and Crescenti), Upper Bathonian-Callovian, Har Amir-1, 2118 m.

17. *Paleopfenderina trochoidea* (Smout and Sugden), Upper Bathonian-Callovian, Har Amir-1, 2118 m.

18,19,20. *Flabellocyclolina reissi* Hottinger, Upper Callovian, Kurnub, G.S.I. Field No. (18) K-60, (19,20) K-69.

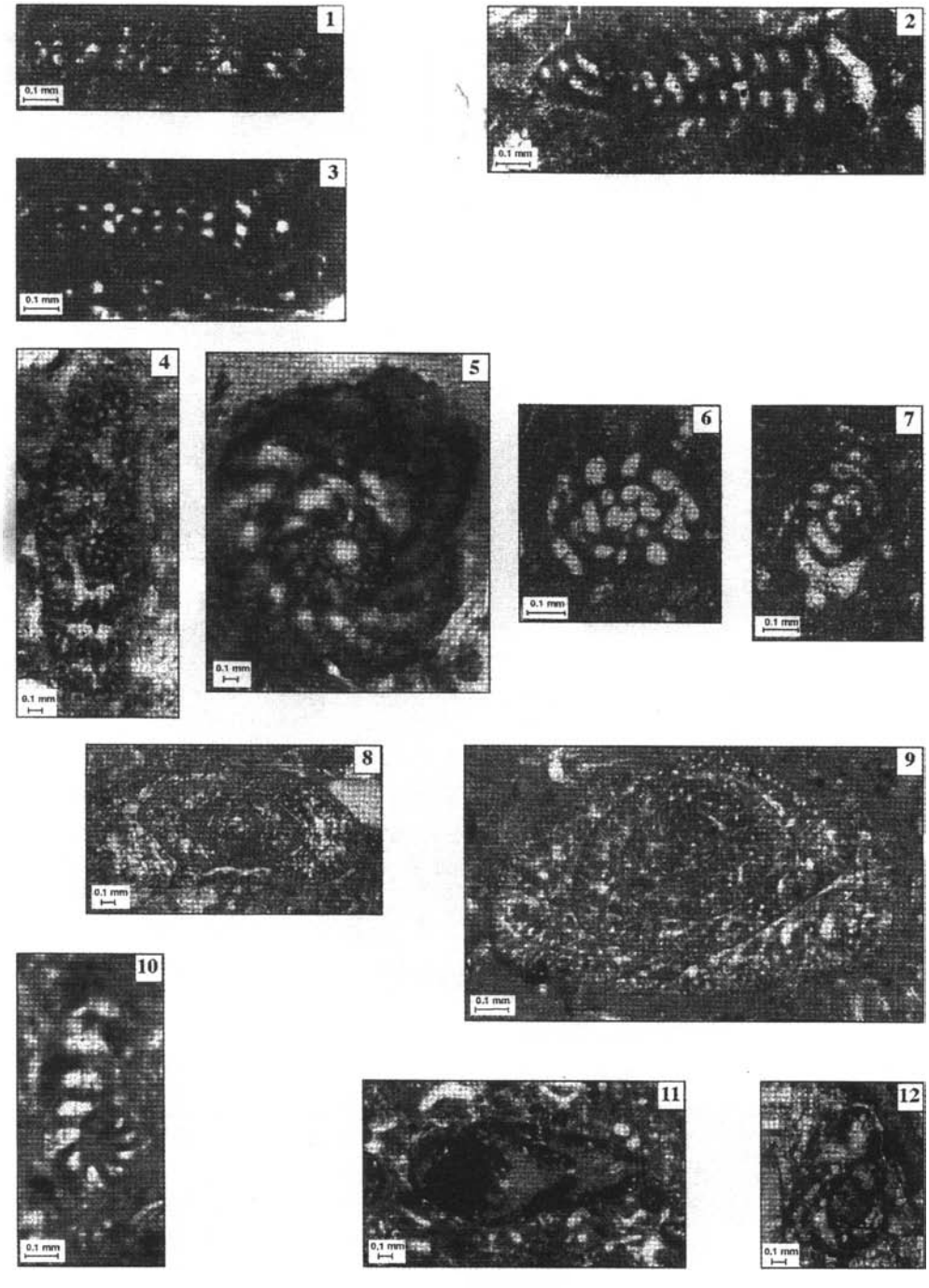


PLATE 18E.5:

1,2,3. *Levantinella egyptiensis* (Fourcade, Arafa and Sigal), Oxfordian, (1,3) Har Amir-1, 1690 m, (2) Sarid-1, 1809-1815 m.

4,5. *Alveosepta jaccardi* (Schrodt), Upper Oxfiordian-Kimmeridgian, (4) Ga'ash-2, 2606 m, (5) Qeren-1, core 4, 1344 m.

6,7. *Libyrinthina mirabilis* Weynschenk, uppermost Oxfordian-lowermost Tithonian, Har Amir-1, 1786 m.

8,9. *Alveosepta praelusitanica* (Maync), Upper Oxfordian-Kimmeridgian, Hermon Mt., G.S.I. Field No. H-162.

10. *Fuertilla frequens* Maync, uppermost Kimmeridgian-Lower Cretaceous, Har Amir-1, core 2, 1579-1582.5 m.

11,12. *Everticyclammina* gr. *E. virguliana* (Koechlin), uppermost Oxfordian-Lower Cretaceous, Har Amir-1, core 2, 1579-1582.5 m.

REFERENCES CITED

Al Far, D. M., 1966. Geology and coal deposits of Gabal El Maghara (N. Sinai). Egypt Geol. Surv. Pap. 37, p. 1-59.

Arkell, W. J., 1952. Jurassic Ammonites from Jebel Tuwaiq, Central Arabia. Phil. Trans. Roy. Soc. London, Ser. B, 236(633), p. 241-314.

Arkell, W. J., 1956. Jurassic Geology of the World. Olivier and Boyd, London, 808 p.

Aizenberg, E., 1968. Composite columnar section of the Jurassic in Hammam El Malih area. Report to Naphta Oil. Co.

Arkin , Y., Bartov, Y., and Goldberg, M., 1975. The Geology of Risan Aneiza. Isr. Geol. Surv., Report MM2/75, 19 p.

Basha, S. H., 1995. On the occurrence of the Liassic Stage in Jordan. Neues Jahrb. Geol. Palaeontol., Monatsh., 1995(7), p. 385-396.

Bassoullet, J. P., and Perelis Grossowicz, L., In Press. A new large foraminifera *Planikilianina hermonensis* gen.n., n.sp. (Textulariina), from the Middle Jurassic of the Levant. Rivista Italiana di Paleontologia e Stratigrafia. Milano

Bentor, Y. K., and Vroman, A., 1951 Geological Map of the Negev 1:100,000, Sheet 18: Ovdat. (explanatory notes in Hebrew)

Bircher, W., 1940. Paleontological report on collection of Jurassic fossils from the Maghara aere. (C.E. Thiebaud collection) Report 334, AEO, Cairo, 35 p.

Bischoff, G., 1964. Ostracoden-Studien im Lebanon; 3, Die Gattung Cytherelloidea im Oberen Jura und in der Unterkreide. Senck. Leth., 45(1-4), p. 1-27.

Bischoff, G. C. O., 1990. The Genus *Hutsonia* in the Late Jurassic. Senck. Leth., 70(4-6), p. 397-429.

Buchbinder, L., 1981. Dolomitization, porosity development and late mineralization in the Jurassic Zohar (Brur Calcarenite) and Sederot Formations in Ashdod-Gan Yavne. Isr. J. Earth Sci. 30(2-3), p. 64-80.

Buchbinder, L. G., Magaritz, M., and Goldberg, M., 1984. Stable isotope study of karstic related dolomitization: Jurassic rocks from the Coastal Plain, Israel. J. Sediment. Petrol., 54(1), p. 236-256.

Chaloner, W. G. and J. Lorch, 1960. An opposite leafed conifer from the Jurassic of Israel. Paleontology, 2(2), p 236-242.

Cariou, E., 1973. Ammonites of the Callovian and Oxfordian. In Atlas of Palaeobiogeography, A. Hallam (ed.); Elsevier Scientific Publishing Company, Amsterdam, p. 287-295.

Cariou, E., 1984. Biostratigraphic subdivisions of the Callovian stage in the Subtethyan province of ammonites, correlations with the Subboreal zonal scheme. In O. Michelsen and A. Zeiss eds; International Symposium on Jurassic Stratigraphy, Erlangen, 2, p. 315-326. Copenhagen, Geol. Surv. Denmark.

Cariou, E., Bassoullet J. P., Grossowicz L., and Hirsch F., 1997. Le Callovo-Oxfordien du Sud Levant: Données Biostratigraphiques nouvelles (Ammonites, Foraminifères) Endémisme et Corréations Stratigraphiques. Réunion Spécialisée APF-SGF 'De la Biostrastigraphie à la Paléobiogéographie", Lyon 27-28 Novembre 1997, Soc. Géol. France Edit. ISBN 2-85363-078-1, p. 21.

Cariou, E., Contini, D., Dommergues, J. L., Enay, R., Geyssant, J., Mangold, Ch., and Thierry, J., 1985. Biogéographie des ammonites et évolution structurale de la Téthys au cours du Jurassique. Bull. Soc. Géol. France, Ser. 8, 1(5), p. 679-697.

Coates, J., Gottesman, E., Jacobs, M. and Rosenberg, E., 1963. Gas discoveries in the western Dead Sea Region. Sixth WPC in Frankfort/Main.

Conway, B., 1982. Mesozoic palynomorphs from Hallal 1 bore-hole. Isr. Geol. Surv. Current Res. 1981, p 41-43.

Conway, B. 1990. Paleozoic-Mesozoic palynology of Israel. II. Palynostratigraphy of the Jurassic Succession in the Subsurface of Israel. Isr. Geol. Surv. Bull. 82. 39 p., 18 pl.

Conway, B. and Cousminer, H.L., 1981. Dinoflagellate age sequence and thermal maturity in Delta 1 well, offshore Natanya, Isr. Geol. Surv. Report P/1/81, p. 1-7.

De Haan, P. J., 1997. Early Cretaceous palynomorphs from the southern coastal plain of Israel and a study of striate spores of the fern family Schizaeaceae. Unpublished Ph.D. Thesis. University of California, Davis, 277 p.

Derin B., 1974. The Jurassic of Central and Northern Israel. Unpublished Ph.D. Thesis, Hebrew Univ. Jerusalem, 152 p. (In Hebrew, English summary),

Derin, B., and Gerry, E., 1972. Jurassic biostratigraphy and environments of deposition in Israel. 5th African Micropaleontological Colloquium, Addis Abeba, Abstract.

Derin, B., and Reiss, Z., 1966. Jurassic Microfacies of Israel. Israel Institute of Petroleum, Tel Aviv. Special Publ, 43 p.

Douville, H., 1916. Les terrains secondaires dans le Massif du Moghara à l'est de l'Isthme de Suez d'après les exploration de M. Couyat Barthoux; Paléontologie. Acad. Sci., Paris, Mém., ser. 2, vol. 54, 184 p.

Douville, H., 1925. Le Callovien dans le massif du Maghara. Bull. Soc. Geol. France, ser 4, Vol 25, p. 303-328 (avec description des fossiles par M. Cosmann).

Dubertret, L., 1960. Feuille Hermon, Notice explicative. Rep. Libanaise, Min. Trav. Publ., Beyrouth, p. 1-46.

Dubertret, L., 1975. Introduction à la carte géologique à 1/50000 du Liban. Notes et Mémoires sur le Moyen-Orient, vol. 13, p. 345-403.

Enay R., and Mangold, Ch., 1994. Première zonation par ammonites du Jurassique d'Arabie séoudite, une référence pour la province arabique. [First zonation by ammonites of Saudi Arabian Jurassic, a reference for the Arabian Province]. In E. Cariou and P. Hantzpergue (eds), 3rd International Symposium on Jurassic Stratigraphy, Poitiers 1991. Géobios, Mem. Spec., 17(2), p. 161-174.

Farag, I. A. M., 1959. Contribution to the study of the Jurassic formations in the Maghara massif (northern Sinai, Egypt). J. Geol. U.A.R. (1961 for 1959), 3(2), p. 175-199.

Feldman, H. R., 1987. A new species of the Jurassic (Callovian) Brachiopod *Septirynchia* from Northern Sinai. J. Palaeont., 61(6), p. 1156-1172.

Feldman, H. R., Hirsch F., and Owen E., 1982. A Comparison of Jurassic and Devonian Brachiopod Communities: Trophic Structure, Diversity, Substrate Relations and Niche Replacement. Third North American Paleontological Conv., Proc., vol. I, p. 169-174.

Feldman, H. R., Owen E., and Hirsch F., 1991. Brachiopods from the Jurassic of Gebel El-Maghara, Northern Sinai. Am. Museum Novitates, 3006, 28 p.

Feldman, H. R., Owen, E. F., and Hirsch, F.,. 2001. Brachiopods from Jorassic (Callovian) of Hamakhtesh Hagadol (Kurnub Anticline), Southern Israel Paleontology, 44 (4), p. 637-658, 2 plates.

Fourcade, E., Arafa, A. A., and Sigal, J., 1983. Description of a new species of foraminifera in the Malm of the Middle East: *Mangashtia? egyptiensis* n.sp., Revue Micropal., 27(1), p. 21-29.

Flexer, A., Gill, D., Livnat, A., Tamir, N., and Toister, A, 1981. ATLAS Project <Israel Subsurface Geology Information Management System>. Part A - Explanatory Notes, Oil Exploration (Investments) Ltd., Tel Aviv, 43 p., Figs. (In Hebrew).

Frenkel, H., 1975. *Pseudocyclammina (?) P. smouti* Banner from the Bathonian Sherif Formtion of Gebel Maghara (northern Sinai). Isr. J. Earth Sci., 23(3), p 63-67.

Friedman, G. M., Barzel, A., and Derin, B., 1971. Paleoenvironments of the Jurassic in the central coastal belt of northern and central Israel and their significance in the search for petroleum reservoirs. Isr. Geol. Surv., Report OD/1/71, 26 p.

Garfunkel, Z., and Derin, B., 1985. Permian-Early Mesozoic tectonism and continental margin formation in Israel and its implication for the history of the Eastern Mediterranean. Geol. Soc. London, Spec. Publ. 17, p. 187-207.

Gill, G. A., Thierry, J., and Tintant, H., 1985. Ammonites calloviennes du sud d'Israel: systematique, biostratigraphie et paleobiogéographie. [Callovian ammonites of southern Israel; systematics, biostratigraphy and paleobiogeography]. Géobios, 18(6), p. 705-768.

Gill, G. A., and Tintant, H., 1975. Les Ammonites Calloviennes du sud d'Israel. Stratigraphie et relations paleogéographiques. Soc. Géol. Fr., Suppl., 4, 17(4), p. 103-106.

Goldberg, M., 1963, Reference section of Jurassic sequence in Hamakhtesh Hagadol (Kurnub Anticline). Detailed binocular sample description, including field observations. Unpubl. Intern. Rep. Oil Division, Geol. Surv. Isr. Jerusalem, 50 p. 1 fig.

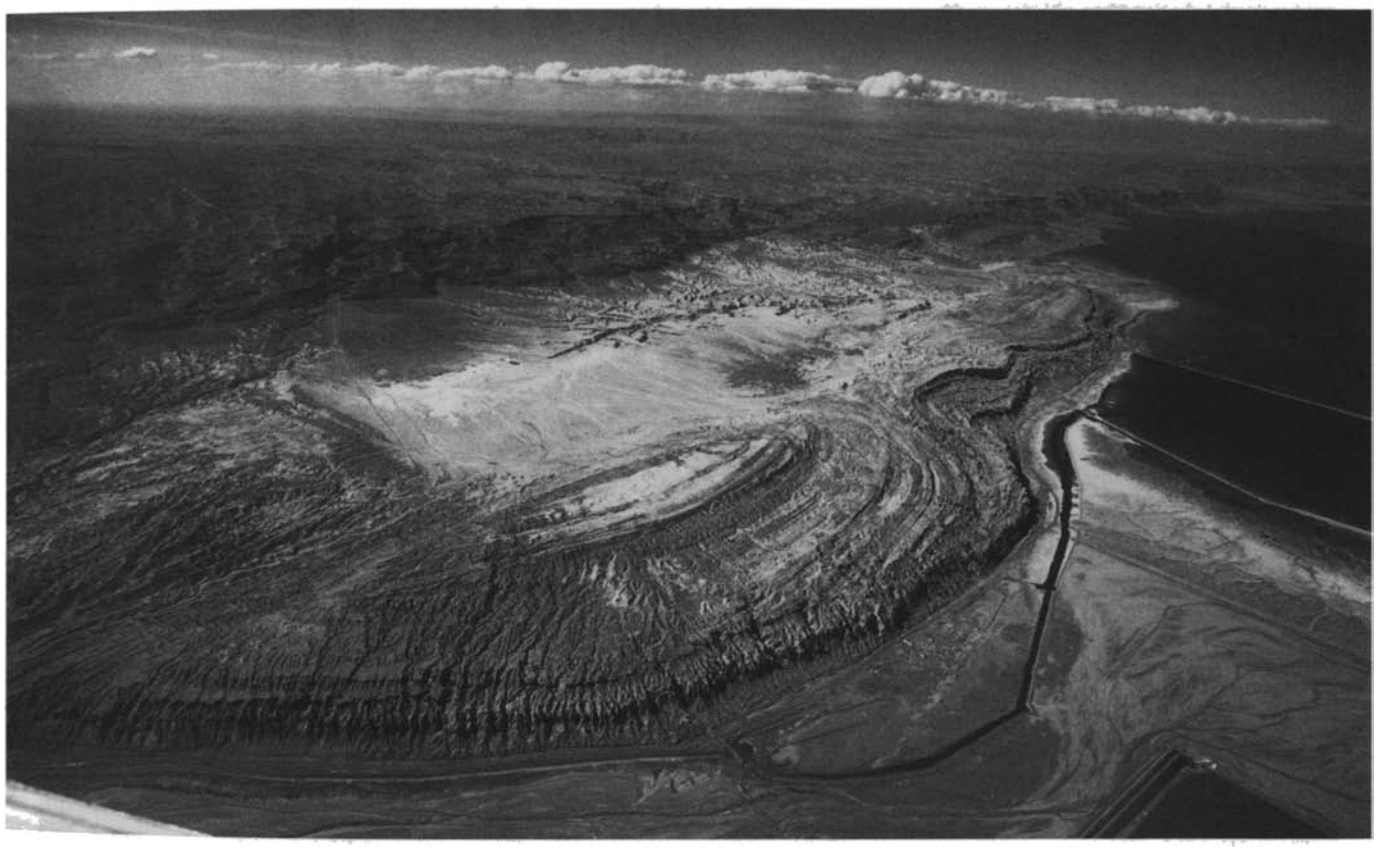
Goldberg, M., 1964. Problems in the Jurassic stratigraphy of Southern Israel. Isr. J. Earth Sci., 13(3-4), p. 169-171

Goldberg, M., 1969. The Jurassic of Majdal Shams area, Mt. Hermon. Measured and sampled by M. Goldberg, M. Braun, M. Raab, B. Derin. Israel Geological Society, Proceedings of Annual Meeting, Katzrin.

Goldberg, M., 1970. The lithostratigraphy of the Arad Group (Jurassic) in the northern Negev (In Hebrew, English abstr.) Unpublished Ph.D. Thesis, Hebrew Univ.

Jerusalem, 136 p.
Goldberg, M., and Bogoch, R., 1978. Dolomitization and hydrothermal mineralization in the Brur Calcarenite (Jurassic), southern coastal plain, Israel. Isr. J. Earth Sci., 27(1-2), p. 36-41.
Goldberg, M., and Friedman, G. M., 1974. Paleoenvironments and paleogeographic evolution of the Jurassic system in southern Israel. Isr. Geol. Surv. Bull., 61, p. 1-44.
Goldberg, M., Hirsch, F., and Mimran, Y., 1981. The Jurassic sequene of Mt. Hermon. Isr, Geol. Soc. Proc. Ann. Meet., p. 14-19.
Goldbery, R., 1979. Sedimentology of the Lower Jurassic flint clay bearing Mishhor Formation, Makhtesh Ramon. Israel. Sedimentology, 26(2), p. 229-251.
Goldbery, R., 1982. Paleosols of the Lower Jurassic Mishhor and Ardon Formations ("Laterite Derivative Facies"), Makhtesh Ramon, Israel. Sedimentology, 29(5), p. 669-690.
Haas, O., 1955. Revision of the Jurassic ammonite fauna of Mount Hermon, Syria. Bull. Am. Mus. Nat. Hist., 108, p. 1-210.
Hallam, A., 1971. Mesozoic geology and the opening of the North Atlantic. J. Geol., 79(2), p. 129-157.
Haq, B., Hardenbol, J., and Vail, P. R., 1988. Mesozoic and Cenozoic chronostratigraphy and cycles of sea-level change. SEPM Spec. Publ., 42, p. 71-108.
Hirsch, F., 1976. Lower Mesozoic disconformities in Israel as related to global tectonics. Isr. Geol. Soc., Ann. Meeting, Askelon (Abstracts) p. 21
Hirsch, F., 1976. Sur l'origine des particularismes de la faune du Trias et du Jurassique de la plate-forme africano-arabe. Bull. Soc. Géol. France, part 7, vol. XVIII, no. 2, p. 543-552.
Hirsch, F., 1978. Biological constituents in the Callovian - early Oxfordian (Jurassic) sediments of southern Israel and northern Sinai. 10th Int. Congr. Sedimentol., Jerusalem, July 1978, Abstr., vol. 1, p. 309.
Hirsch, F., 1979. Jurassic bivalves and gastropods from northern Sinai and southern Israel. Isr. J. Earth Sci., 28(4), p. 128-163.
Hirsch, F., 1985. The Arabian sub-plate during the Mesozoic. In: J. E. Dixon and A. H. F. Robertson (eds.), The Geological Evolution of the Eastern Mediterranean, Geological Society, Special Publication, 17, Blackwell Scientific Publications, Oxford, p. 217-223.
Hirsch, F., 1987. The Gondwanian Triassic and Jurassic Tethys shelf: Sephardic and Ephiopian faunal realms. Shallow Tethys 2, Balkema, p. 215-232.
Hirsch, F., 1988. Jurassic biofacies versus sea level changes in the Middle eastern Levant (Ethiopian province). 2nd Intern. Symp. Jurass. Stratigr., Lisbon, p. 963-981.
Hirsch, F., 1996. Geology of the Southeastern slopes of Mount Hermon. Geological Survey of Israel, Current Research, 10, p. 22-27.
Hirsch, F., Flexer, A., Rosenfeld A., and Yellin-Dror, A., 1994. Palinospastic and Crustal Setting of the Eastern Mediterranean. J. Petrol. Geol., 18(2), p. 149-170.
Hirsch, F. Bassoullet, J. -P., Cariou, E., Conway, B., Feldman, H. R., Grossowicz, L., Honigstein, A., Owen, E. F., and Rosenfeld, A., 1998. The Jurassic of the southern Levant. Biostratigraphy, palaeogeography and cyclic events. In: S. Crasquin-Soleau and E. Barrier (eds.), Peri-Tethys Memoir 4, p. Epicratonic Basins of Peri-Tethyan Platforms. Mem. Mus. Nat. Hist. Natur., Paris, 179, p. 213-235.
Hirsch, F., and Picard, L., 1988. The Jurassic Facies in the Levant. J. Petrol. Geol., 11(3), p. 277-308.
Hirsch F., and Roded, R., 1996. The Jurassic Stratigraphical Nomenclature in Hamakhtesh Hagadol. Geol. Surv. Isr. Current Research, 10, p. 10-14.
Hudson, R. G., S., 1958, The Upper Jurassic faunas of Southern Israel. Geol. Mag., 95(5), p. 415-425.
Katz, A., 1968. Petrological and geochemical problems in the Mahmal Formation (Southern Israel). Unpublished Ph.D. Thesis Hebrew Univ., Jerusalem. (In Hebrew, English summary).
Lang, B., and Steinitz, G., 1989. K-Ar dating of Mesozoic magmatic rocks in Israel: A review. Isr. J. Earth Sci., 38(2-4), p. 89-104.
Le Nindre, Y. M., J. Manivit, and Vaslet, D., 1987. Histoire gélogique de la bordure occidentale de la platforme Arabe du Paléozoique Inférieur au Jurassique Supérieur. Thèse Doct., Paris VI Univ. Sci. Naturelles, 4 vols. Also B.R.G.,M. 1990. Doc. 191, 192, 193, 194.
Lewy, Z., 1983. Upper Callovian ammonites and Middle Jurassic geological history of the Middle East. Israel Geol. Surv., Bull. 76, p 1-56.
Lorch, J., 1967. A Jurassic flora of Makhtesh Ramon, Israel .Israel J. Botany, 16, 177-188.
Maync, W., 1966. Microbiostratigraphy of the Jurassic of Israel. Geol. Survey of Israel, Bull. No. 40. and The Institute for Petroleum Research and Geophysics Report 1007, p. 1-56.
Moon, F. W., and Sadek, H., 1921. Topography and geology of northern Sinai. Petr. Res. Bull. Cairo, 10, 154 p.
Mor, D., 1985. The Geological Map of Israel. Sheet Har Odem. Preliminary Edition. Survey of Israel.
Moshkovitz, S., and Ehrlich, A., 1976. *Schizosphaerella punctulata* Deflandre et Dangeard and *Crepidolithus crassus* (Deflandre, Noel), Upper Liassic calcareous nannofossils from Israel and Northern Sinai. Isr. J. Earth Sci., 25(2), p. 51-57.
Moshkovitz, S., and Ehrlich, A., 1981. Late Jurassic Calcareous Nannofossils in Israel's offshore and onland areas. Isr. Geol. Surv. Curr. Res. (1980), p. 65-72
Mouty, M., 2000. The Jurassic in Syria: an overview. Lithostratigraphic and biostratigraphic correlations with adjacent areas. In: S. Crasquin-Soleau and E. Barrier (eds.), Peri-Tethys Mém. 5, Mém. Mus. Nat. Hist. Natur., Vol. 182, p. 159-168.
Mouty, M., and Zaninetti, L., 1998. Le Jurassique du Mont Hermon (Anti-Liban). Decouverte de Trias et de Lias. Arch. Sci. Genève, 51(3), p. 295-304.
Nevo, A., 1963. The Jurassic strata of Makhtesh Ramon. Isr. Geol. Soc. Summary of Lectures, Makhtesh Ramon Symposium, p. 11-12.
Noetling, F., 1887. Der Jura am Hermon. Schweizerbart'sche Verlagsbuchhandlung, Stuttgart, 46 p.
O.E.I.L., 1988. Hydrocarbon potential of Israel; Highlights of Basin Analysis. Prepared by O.E.I.L. Exploration Department, under guidance of Z. Cohen, Chief Geologist, Tel Aviv. 148 p., Figs., Maps.
Parnes, A., 1961.On the occurrence of *Pseudopygurus* Lambert in Southern Israel. Isr. Res. Council. Bull., 10G (1-2), p. 216-222.
Parnes, A., 1967. A report on the age of the flora, In: Lorch, J., 1967. A Jurassic flora of Makhtesh Ramon, Israel .Isr. J. Botany, 16, p. 177-188
Parnes, A., 1974. Biostratigraphic correlation of the middle Jurassic in Makhtesh Ramon, Gebel Maghara and in Morocco. Abstract of Lectures, Isr. Geol. Soc. Proc. Ann. Meet. Jerusalem.
Parnes, A., 1980. Lower Jurassic (Liassic) Invertebrates from Makhtesh Ramon (Negev, Southern Israel). Isr. J. Earth Sci., 29(1-2), p. 107-113.
Parnes, A., 1981. Biostratigraphy of the Mahmal Formation (Middle and Upper Bajocian) in Makhtesh Ramon (Negev, Southern Israel). Israel Geol. Survey, Bull. 74, p. 1-55.
Perelis Grossowicz, L., Bassoulet, J. -P., Hirsch, F., and Peri, M., 2000. Jurassic large foraminifera from Israel. GSI Current Research, Vol. 12, p. 132-144.
Picard, L., 1959. Geology and Oil Exploration of Israel. Hebrew University of Jerusalem, 216. Isr. Res. Council. Bull., 8G(1), p. 1-30; and in Proc. 5th. Intern. Petrol. Cong. New York.
Picard, L., and Hirsch, F., 1987. The Jurassic Stratigraphy in Israel and the Adjacent Countries. The Israel Academy of Sciences and Humanities, Jerusalem, 106 p.
Raab, M., 1962. Jurassic-Early Cretaceous Ammonites from the Southern Coastal Plain, Israel. Geol. Surv. Israel, Bull. 34, p. 24-30.
Razvalyaev, A. V., 1966. Explanatory Notes to the Geological Map of Syria, 1:200,000. Syrian Arab Report of the Ministry of Industry, Department of Geological and Mineral Research, 122 p., Damascus.
Reiner, W., 1968. Callovian Gastropods from Hamakhtesh Hagadol (southern Israel). Isr. J. Earth Sci., 17(4), p. 171-198.
Renouard, G., 1951. Sur la decouverte de Jurassique inferieur (?) et du Jurassique moyen au Liban. Acad. Sci. Paris, C. R., 232(10), p. 992-994.
Roded, R., 1978. The Geological Map of Israel 1:50,000, sheet Oron. Isr. Geol. Survey and Survey of Israel.
Roded, R., 1983. The Geological Map of Israel 1:50,000, sheet Oron. Isr. Geol. Survey. Explanatory notes. 20 p.
Rosenfeld, A., Gerry, E., and Honigstein, A., 1987a. Jurassic Ostracodes from Gebel Maghara, Sinai, Egypt. Rev. Españ. Micropaleont., 19(2), p. 251-280.
Rosenfeld, A., and Honigstein, A., 1991. Callovian-Oxfordian Ostracodes from the Hamakhtesh Hagadol Section, Southern Israel. Rev. Espan. Micropaleont., 23(3), p. 133-148.
Rosenfeld, A., Honigstein, A., Gerry, E., Oertli, H., and Flexer, A., 1988. Early Jurassic Ostracodes from the Ardon Formation in Israel and Sinai. Geol. Surv.

Isr. Current Research, 6, p. 50-56.
Rosenfeld, A., Oertli, H., Honigstein, A., and Gerry, E., 1987b. Oxfordian Ostracodes from the Kidod Formation of the Majdal Shams Area, Mount Hermon, Golan Heights. Bull. Centres Rech. Explor.-Prod. Elf-Aquitaine, 11(2), p. 233-248.
Saltzman, U., 1968. The geology of the southeatern Hermon slopes. Tahal, Internal Report., 46 p. (In Hebrew).
Saltzman U., Bartov, Y., Gottlib, G.., Magharitz, M., and Mimran, Y., 1968. Composite columnar section of sequences exposed at the SE flank of Mt. Hermon. TAHAL, Tel Aviv, 1 fig.
Shaw, S. H., 1947. Southern Palestine geological map on a scale of 1:250,000 with explanatory notes. Palestine, Govt. Printer, 42 p., map.
Slatkin, A., and Heller, L., 1961. A petrological study of the flint clay from Makhtesh Ramon, Israel. Int. Geol. Cong. XXI Session, Norden, 1960, p. 88-107.
Shimron, A., and Peltz, S., 1993. Early Cretaceous pyroclastic volcanism in the Hermon Range. Isr. Geol. Surv., Bull. 84, 43 p. 2 references
Valeton, I., Stuetze, B., and Goldbery, R., 1983. Geochemical and mineralogical investigations of the Lower Jurassic flint-clay bearing Mishhor and Ardon formations, Makhtesh Ramon, Israel. Sedimentary Geology, 35(2), p. 105-152.
Vautrin, H., 1934. Contribution à l'étude de la série jurassique dans la chaîne de l'Anti-Liban et plus particulièrement dans l'Hermon (Syrie). Acad. Sci., Fr., C. R., 198(16), p. 1438-1440.
Wurzburger, U., 1963. The flint clay of Makhtesh Ramon. Isr. Geol. Soc., Summary of lectures, Makhtesh Ramon Symposium.



Aerial view of Mount Sedom and the salt pans of the southern Dead Sea.
Grayscale rendition of color image in The Holy Land Satellite Atlas, Volume II (1999, p. 200). ©Røhr Productions Ltd., Nicosia, Cyprus. Reproduced with permission. View towards the northwest. Mount Sedom (or Sodom or Sdom) is a diapiric ridge some 200 m high above the salt pans, and with crestal heights of about 190 to 210 m below Mediterranean sea level. It occupies about 13 km². Recent INSAR and geodetic measurements indicate that it is rising at about 8 mm/yr.



Computer generated oblique satellite image of Israel looking south.
Grayscale rendition of color image in The Holy Land Satellite Atlas, Volume II (1999, p. i). For further information on this oblique satellite image see 'Biblical Archaeologist': Vol. 60, No. 3, September 1997. The image consists of the merged SPOT and LANDSAT TM satellite imagery described in the Introduction to Part IV of this volume, draped over the 25 m DTM of Israel.
©1999 C.N.E.S, EOSAT, and Røhr Productions Ltd., Nicosia, Cyprus. Reproduced with permission.

Chapter 18F

The Cretaceous of Israel

Amnon Rosenfeld and Francis Hirsch
Geological Survey of Israel, 30 Malchei Israel Street, Jerusalem 95 501, Israel

INTRODUCTION

The tectonic and depositional evolution of the Cretaceous rocks in Israel exhibits many lateral facies-changes and regional unconformities, which dictate a subdivision into groups (**Figure 18F.1**).

The Berriasian-Albian Kurnub Group (Damesin, 1933) consists of continental variegated sandstones and marine intercalations which accumulated unconformably above the Jurassic-Cretaceous boundary. Its base is associated with volcanism (*e.g.* the Tayasir Volcanics in Samaria), also occurring in the Galilee, the Golan, and the Negev.

The Kurnub Group interfingers laterally with the Barremian-Early Albian shallow marine Galilee Group (Kafri, 1972) in the north. To the west, in the Coastal Plain and offshore of Israel, the Tithonian-Barremian Gevar'Am and the Aptian-?Turonian Talme Yafe Groups (Flexer et al., 1981) represent deep trough sediments. The deeper marine shaly Talme Yaffe Group characterizes the Pleshet Basin, west of the so-called 'hinge belt'.

The Judea Group (Wellings, 1940) encompasses Late Albian-Early Coniacian limestones and dolomites, interbedded with marls. Onlapping the clastic Kurnub Group, sediments of the Judea Group dominate over most of the region. They were mostly deposited under a shallow platform regime, extending over a large area of the Arabian Platform.

The Alpine-type tectonics of the Syrian-Arc folding event in Israel controlled the sedimentary rock deposition during the Late Cretaceous. The deposition of the chalks and siliceous rocks of the Late Coniacian-Paleogene Mount Scopus Group (Flexer, 1968) coincided with the earlier phases of the Syrian-Arc folding event. The relative thickness of these units in Israel is controlled by their position with respect to the structural features which are mostly asymmetric Levantid anticlines. Synclinal facies are distinguished by thick sections of chalk, marl, and chert while anticlinal sections are much reduced in thickness and may contain glauconite. Significant biostratigraphic hiatuses characterize anticlinal sections.

The passage from the Maastrichtian into the Tertiary can only be discerned in synclinal sections by the presence of high iridium and concentrations of trace elements, and by the first occurrence of *Globigerina eugubina* (Rosenfeld et al., 1989). In anticlinal sectors the transition is unconformable with red-colored chalks at the boundary.

In the sections below, the locations, geographic names, and boreholes mentioned can be found in the Survey of Israel's North and South Israel maps at scale 1:250 000, and in the 'Wells of Israel' of Fleischer (2000).

HISTORY OF RESEARCH

The Cretaceous is well-exposed in our region and has been described by many authors since the 19th century. Many terms, coined in the past, are still used informally and appear in the first Lexique Stratigraphique International (Bentor, 1963). The following is a review of the older nomenclature:

Neocomian

The term Neocomian has been in use since Douville (1910) for part of the Early Cretaceous deposits of Lebanon. Later on, the term was used in the stratigraphy of the region to comprise all strata of 'post-Jurassic and pre-Aptian age' (Bischoff, 1964). They include the terrestrial fresh-brackish water deposits of the Wealden type, mainly sandstones of Nubian type, shales, clays, and marls up to 500 m thick.

Barremian-Aptian

The Lebanese nomenclature was used for exposures in the Galilee (Rosenberg, 1960). The term 'Couches à Gasteropodes' was coined by Heybroek (1942) for the sand, marls and oolitic limestones that are well-exposed in southern Lebanon.

The term 'Muraille de Blanche' was applied by Dubertret (1937) to a prominent marker ledge, first observed in Lebanon by Blanche as early as 1847. This ledge is overlain by the soft marls and sands of the so-called 'Couches a Orbitolines' in the Lebanon terminology of both Dubertret (1937) and Heybroek (1942).

Albian

Marine strata of Albian age were first described by Blake (1935) from various places in the mountains of Judea and Samaria, as well as from the Galilee (Ramallah, Wadi Farah, Biq'at Bet Netofa-Battauf, Jebel Arus, Wadi Sellamah south of Safad, and Menara-Hunin west of the Hula Depression). The gray or yellow, frequently ferruginous, thin-bedded or massive limestones, occasionally oolitic, alternate with clay and marl. Typical fossils are: *Knemiceras syriacum* v.d. Buch, *Epiaster blanckenhorni* Mant., *Enallaster* cf. *constrictus* Fourteau, *Pholadomya depacta* Hamlin, '*Ceromya*' cf. *sinuata* Hamlin, *Meretrix libanotica* (Fraas), *M.* cf. *obruta* (Conr.), *Cardium syriacum* Conr., *Trigonia distans* Conr., *Arca longa* Conr., *Pleurotomaria* cf. *perspectiva* (Mant), and *Nucula submucronata* Conr.

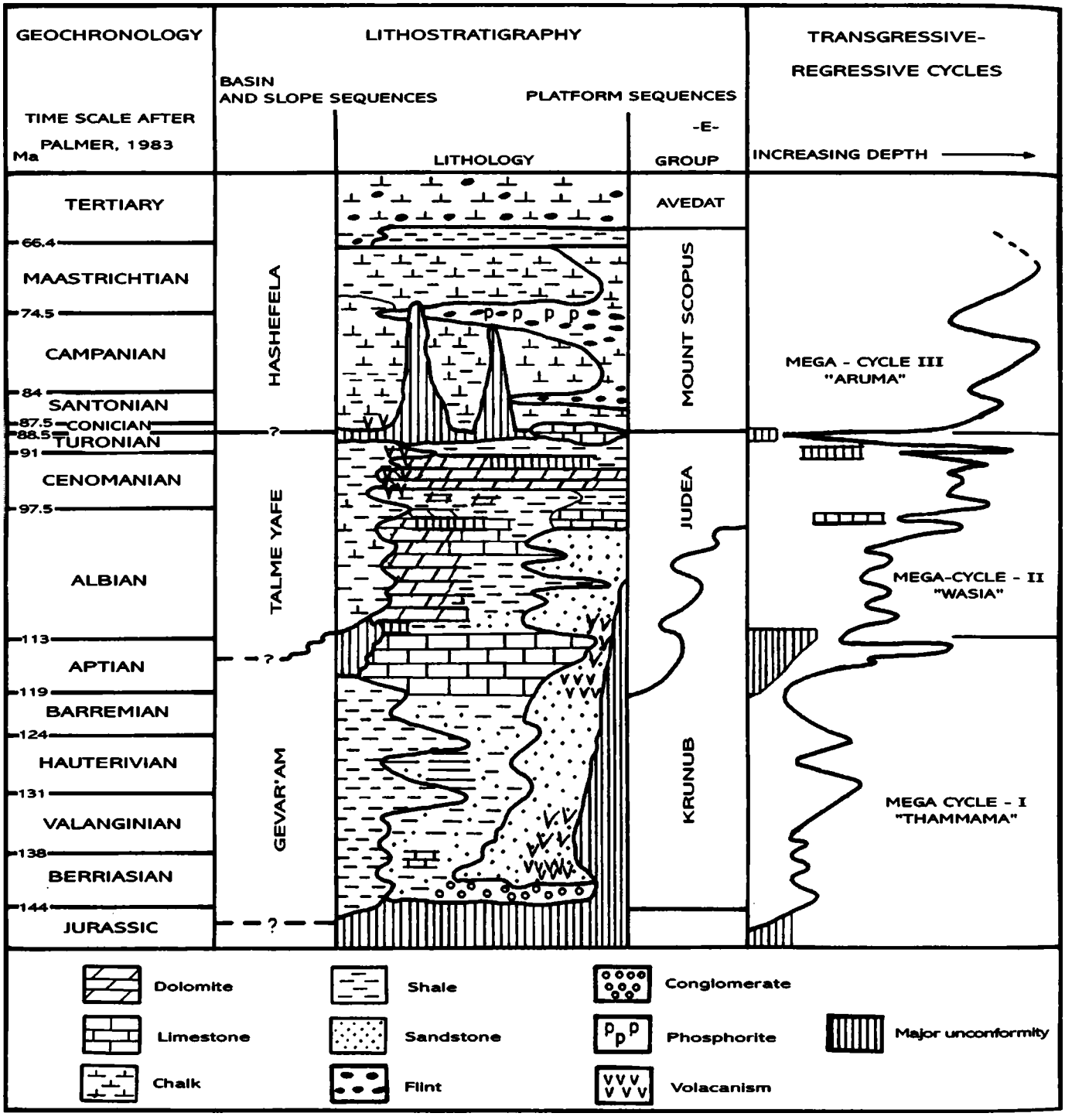


Figure 18F.1. Subdivision in Groups: The tectonic and depositional evolution of the Cretaceous rocks in Israel exhibits many lateral facies-changes and regional unconformities (after Flexer et al., 1981a).

Cenomanian of the Carmel and Galilee

Noetling (1886) established the name 'Feuerstein-Fuehrende Kalke Des Karmel Gebirges', originally regarded by him as belonging to the Upper Senonian, for the Cenomanian in the Mount Carmel and Galilee area. These rocks were later described as the Flint Limestone of Zikhron and Ijzim by Vroman (1938). Picard (1928b) placed these 'Feuersteinkalke' in the Upper Cenomanian (or Turonian?). They are a sequence of chalky limestones with nodular

flint, containing several beds rich in *Orbitolina concava* Lmk. on Mount Carmel. Blake (1935) placed these beds into the upper part of his *Chalk-Flint Series* of late Cenomanian age. The sequence is underlain by chalky limestone with *Acanthoceras newboldi* Kossmat, forming the lower part of the *Chalk-Flint Series;* and is overlain by the *Rudist-Meleke Series,* also of late Cenomanian age. Blake's (1935) Chalk-Flint Series were later called Flint Limestone (Vroman, 1938) or the Main Chalk Complex (Picard and Kashai, 1958). The latter represents the predominantly chalky marine rock sequence, about 250 m thick, found on Mount Carmel. The following sub-divisions were described, from bottom to top: *Isfiya Chalk, Meleke-Gryphaea Beds, Khureibe Chalk* and *Juneidiya Chalk.* The sequence also comprises layers of pyroclastics at various levels. It overlies the *Yagur Dolomite* and underlies the *Muhraqa Series.* This rock sequence extends to the Galilee where it is composed of chalk, chalky, argillaceous or flinty limestone, and hard, well-bedded, frequently yellow limestone and dolomite. Interlayered beds of submarine volcanic tuffs and agglomerates occur at various levels. Flint concretions are plentiful. The thickness of the sequence averages 250 m. Locally the sequence is very fossiliferous and contains *Acanthoceras newboldi* Kossmat, *Exogyra flabellata* Goldf., *Ostrea olisiponensis* Coq., *Pecten karmeliticus* Blanck., *Pecten shawi* Perv., *Liopistha (Psilomya) pervenquieri* Greco., *Liopistha alta* (Roemer), *Cardium (Trachycardium) productum* Sow., *Protocardia coquandi* Seg., *Trigonia* sp., *Strombus pervetus* Conr., *Nerinea* sp., and *Orbitolina concava* Lmk.

The sequence conformably overlies a thick dolomitic complex attributed to the Lower Cenomanian, and is overlain conformably on Mount Carmel by the *Rudist-Meleke Series* and in the Galilee by the Upper Cenomanian dolomite.

The name of the Fureidis Marl (Picard and Kashai, 1958) is derived from the village Fureidis, on the western slope of Mount Carmel, and stands for a local slightly marly development of the Khureibe Chalk (Vroman, 1960). The few meters thick yellow dolomitic marl, exposed in southern Carmel, was considered to overlie the *Daliya Series*, and consequently to be of late Cenomanian-early Turonian age.

Some terms are rather confusing as for instance the term 'Stufe des Radiolites syriacus Conrad', coined for the mainly Albian 'Cenomanian' of Noetling (1886). It accounts for the 'Radiolitenzone' (Fraas, 1878), the 'Libanon Kalkstein' (Diener 1886), and the 'Niveau a Radiolites' (Douville, 1910). These hard crystalline rudist limestones and dolomites of Lebanon, overlying the gray limestones and marls with *Knemiceras syriacum* (v. Buch) (see *Zone des Ammonites Syriacus v. Buch)* are overlain by the platy limestone with fish remains of Hakel. This sequence was later renamed by Noetling as his '*Stufe des Radiolites Syriacus* Conrad' [=*Eoradiolites lyratus* (Conrad)], regarded by both authors to be of late Turonian age. Douville (1910) however, showed that *Eoradiolites lyratus* (Conrad) occurs from the base of the Cenomanian sequence upward into strata of late Cenomanian age (*Niveau a Radiolites).* Picard (1938a) introduced the term into the geology of Palestine and correlated the sequence with the Lower Turonian *Meleke* of Jerusalem. Rudist Limestones carrying *Eoradiolites lyratus* (Conrad) are widely distributed in the Albian-Cenomanian strata of Israel, mainly in the Judean Mountains and Mount Carmel etc. Locally, such as in Wadi Mughara (Mount Carmel), *E. lyratus* is found in strata where it is associated with *Caprinula* sp. and *Sphaerulites* cf. *foliaceus* Lmk.

Albian-Cenomanian and Turonian of the Jerusalem area

Among the pioneers of Cretaceous stratigraphy in the Jerusalem area, Shalem's contribution may have been the most comprehensive. His subdivision encompasses, at base, the 'Calcari Inferiore A Radioliti' (Shalem, 1927). In the Jerusalem area it consists of dolomites and dolomitic limestones with quartz and flint concretions containing *Eoradiolites lyratus* Conr., *Hemiaster* sp., *Strombus* sp., *Echinoconus* sp., *Nerinea cochlaeformis*, and *Cerithium elias,* and referred to the Lower Cenomanian. The total thickness of these strata is about 450 m, of which the lower 350 m have been termed by Shalem (*op. cit.*) *Calcari a Cerithium elias* Boehm while the upper 100 m he called *Calcare a Nerinea cochlaeformis* Conr. The Calcari Inferiore A Radioliti overlie the *Marne argillose verdatre* and underlie the *Argille a Corbula eretzisraelensis,* which is the equivalent of the Moza Marl. For Shalem (1925) the Upper Cenomanian consists of the Calcari A Pterodonta Deffisi.

The name has been given by Shalem to limestones in the Jerusalem area carrying *Exogyra columba, E. flabellata, Pyconodonta capuloides, Pterodonta deffisi, Harpagodes heberti, Stombus* sp. *Heterodiadema libycum, Orbitolina* etc., and occurring between the *Marne e calcari ammonitiferi* above, and the *Argille e marne argillose* below. Their thickness is about 70 m.

Another pioneer was Blanckenhorn (1905). He first recognized the Der Jasini (now the Kfar Shaul Formation), Calcare deriassinico a l'astre (Shalem, 1926), or Der Jasin laminated limestone (Picard, 1938). The name of the sequence is derived from the village of Deir Jasin, west of Jerusalem. It was adopted by M. Blanckenhorn to designate a well-bedded sequence, 30 m thick, of yellow and pink, platy limestones rich in calcite geodes alternating with thin horizons of clay, occurring in the vicinity of Jerusalem. Blanckenhorn placed the Der Jasini in his *Unterer Mizzi* and correlated it, because of its numerous well-preserved fish remains, with the Cenomanian fish beds of Hakel in Syria. Shalem (1926) determined the exact stratigraphic position of the sequence; it overlies the *Zone of Acanthoceras rhotomagensis* and underlies the *Mizzi Yehudi.* He determined its age as late Cenomanian on the basis of a rich fauna which comprises, among others, fishes (mainly Teleostei), *Neolobites peroni* Hyatt, *Heterodiadema libycum* Desor., *Hemmiaster saulcyanus* d'Orb., *Pholodomya vignesi* Lart., and *Exogyra columba* Lmk, as well as marine and terrestrial plant remains.

Shalem (1925) gave the name Marne E Calcari Ammonitiferi to about 70 m of marls and chalks rich in *Acanthoceras (A. mantelli* Schl.), *Exogyra, Cardium, Hemiaster* and *Pecten,* exposed in the Jerusalem area. They overlie the *Calcari a Pterodonia deffisi* and are overlain by the Der Jasini. Shalem regards these strata as a 'rhotomagiano' and Picard (1938b) stated that they are

identical with the *Zone of Acanth. palestinense and rhotomagense* of Blanckenhorn (1905) and correlative with the Zone of the fossiliferous marly limestone of Picard (1938a).

The term Mizzi Yehudi (Jehudi, Yahudi), now part of the Middle Cenomanian Weradim Formation, was first used by Blanckenhorn (1905).

The Upper Cenomanian-Turonian strata consist of the Calcari Superiore A Radioliti (Shalem, 1927). Under this name Shalem included limestones known as *Mizzi Yehudi, Meleke and Mizzi Helu* of the Jerusalem area, containing *Eoradiolites* sp., *Nerinea cochlaeformis*, *Hastula fraasi* etc. Their combined thickness in the Jerusalem area is about 120 m and the strata overlie the *Der Jasini* and underlie Senonian chalks. The term is synonymous with the present Weradim and Bi'na Formations. Earlier, Fraas (1867) applied the name 'Hippuritenbanke' for crystalline to semicrystalline and lithographic limestones in the Jerusalem area. This sequence is underlain by reddish, hard, dolomitic limestones and dolomites (*Mizzi Ahmar*) and overlain by chalky limestones ('*Ka'akuhle*') with *Texanites* of Santonian age. Fraas (*op. cit.*) divided the sequence into:

1) *Meleke* or '*Untere Hippuritenbank*' with *Hippurites syriacus*.

2) '*Zweite Hippuritenbank*', composed of a 'light white marble' with *Radiolites mortoni (= Sphaerulites patera* Arnaud).

3) The *Nerineaen Marmor* with *Nerinea requieniana* and *Nummulites cretacea* Fraas, which together with Miliolidae and other foraminifera, build a dense hard limestone overlain by

4) The '*Dritte Rudistenzone*' or '*Obere Hippuritenbank*' with '*Hippurites sulcatus*' (most probably = *Bournonia judaica* Blanckenh.), *Nerinea* and *Actaeonella (Trochactaeon) salamonsis* Fraas. The stylolithic *Mizzi* is partly platy and lithographic (*Mizzi Helu*), and contains in the uppermost layers silicified fossils. These fossiliferous beds were called by Fraas: '*Kieselige Schneckenbank*' (see *Actaeonella Flint Beds).*

Picard (1938a) gave the following thicknesses of the sequence, from base to top:

1) *Meleke* of Turonian age 20 to 25 m;

2) *Mizzi Helu* and *Miliola* limestone 40 m;

3) *Actaeonella* flint beds 5 to 10 m;

4) *Mizzi Helu*, poor in fossils and siliceous *Ka'akuhle* 40 m.

The term Meleke (Arabic: Royal), originally a stone-masons' term, was introduced into geological literature by Fraas (1867) to denote a stratigraphic horizon of late Cenomanian or Turonian age. The term has since been used repeatedly to denote various stratigraphic horizons; thus Picard (1938a) called a horizon in the Jerusalem area 'Meleke of the Upper Cenomanian'. The term denotes a white, coarse-grained, granular to spathic partly re-crystallized rudist limestone, which is readily dolomitized and may appear at various stratigraphic horizons, particularly in strata of late Cenomanian and Turonian age. Both terms Mizzi Ahmar and Mizzi Helu were also introduced in the geological literature by Blanckenhorn and refer to rock types within the Bi'na Formation.

Senonian

The earliest account dates back to Russegger (1847) who used the name 'Obere Weisse Kreide voll Feuerstein und Feuerstein-strata' for sediments of Senonian age in the Middle East.

The existence of the Senonian in Israel and surrounding countries has been known since the first half of the 19th Century and Blanckenhorn (1914) subdivided it for the first time into Santonian, Campanian, and Danian. Picard (1931a), including the Coniacian in the Santonian, singled out the Maastrichtian as part of the Danian of Blanckenhorn. This concept of the Senonian was followed by most of the later authors. Reiss (1955a) pointed out that the Maastrichtian is a separate stage, equal in rank and younger than the Senonian, and that the Danian belongs to the Tertiary. At present, the Senonian is divided into three sub-stages: Coniacian, Santonian and Campanian. Its lower boundary is defined by the appearance of the first Senonian Ammonites (*e.g. Barroisiceras*) and its upper limit by the extinction of *Libycoceras* and the appearance of typically Maastrichtian foraminifera such as *Neoflabellina reticulata* (Reuss) and *Bolivinoides draco draco* (Marsson) etc.

Senonian strata in Israel attain a maximum thickness of about 600 m. The strata are composed of limestones, chalky limestones, chalks (often highly bituminous), flint layers, phosphate beds, argillaceous chalks, and occasionally dolomitic limestones and dolomites.

Almost everywhere the Senonian strata unconformably overlie the Turonian ones, while the upper contact is gradational.

The megafauna is rich in ammonites, ostreids, various lamellibranchs, and mainly pelagic foraminifera.

Volcanic tuffs of Senonian age occur in the Carmel region.

Coniacian: Bentor and Vroman (1957) discovered strata of Coniacian age in the southern Negev. Earlier, Coniacian strata were either unknown in the country or supposed to be within strata of Santonian age (Picard, 1931). Coniacian strata reach their maximum thickness of more than 70 m in the Tsenifim anticline in the southern Negev. Lithologically the strata are subject to great local variations. The dominant rock types are hard, brown, glauconitic and sandy detrital or oolitic limestone, frequently rich in silicified shells of *Alectryonia dichotoma* Bayle, yellow marl, white chalk, hard nodular limestone with flint concretions, and, more rarely, clays. Locally the strata are very fossiliferous and carry, in addition to the fauna mentioned above (Parnes, 1958), *Leiocidaris subvenulosa* (Per. and Gauth.), *Rachiosoma delamarrei* (Deshayes), *R. majus* (Coq.), *Holectypus serialis* Deshayes, *Clypeopygus waltheri* (Gauthier), *Pseudoholaster moabiticus* (Blanck.), *Avicula atra* Coq., *Plicatula ferryi* Coq., *Ostrea papieri* Thom and Per., *Muniericeras lapparenti* Grossouvre, as well as Barroisiceratidae such as *Reesidoceras gallicum* (Grossouvre) and *Forresteria allaudi* (B.L.T). Strata of Coniacian age overlie hard Turonian limestone and underlie Santonian chalk. Both contacts are conformable. In the northern Negev Coniacian strata wedge out, and the chalk of the *Menuha Formation* then overlies unconformably rocks of Turonian age.

Coniacian-Santonian: Limestones or chalky limestones at the base of the Senonian are often referred to as *Ka'akuhle.* This term was introduced by Fraas (1867) after an Arabic stone-masons' term for semi-hard, white, yellowish, or reddish-striped limestones.

Blanckenhorn (1905) subdivided the Ka'akuhle into two parts: a lower one, believed to be of Santonian age and an upper one, placed by him into the Campanian. Later the term Ka'akuhle has been used only for strata of Santonian age. The Ka'akuhle carries in many places *Texanites*, as well as rich foraminiferal assemblages, including among others *Globotruncana concavata* (Brotzen). Taubenhaus (1920) introduced the term of 'Emsherstufe' for certain ammonites examined by him, which, however, came from various localities and stratigraphic levels. Picard (1931) introduced the term 'Flammenkalk' for the reddish striped limestones and chalks of the *Ka'akuhle* and 'Emscherian' type. He included the Coniacian and the Santonian to the *Lower Senonian* or *Emscherian.*

Santonian: Blanckenhorn (1914) introduced the term Santonian in Palestinian stratigraphy for white, pink, reddish or brownish, chalky limestones, often fossiliferous (*Pecten, Gryphae, Texanites,* Selachii-remains etc.). Santonian strata composed of bituminous or limonitic marls, as well as a glauconitic, phosphatic and sandy limestones occur in the Negev and in the subsurface of various parts of the country. Some dolomitic limestones of Santonian age are also known. The Santonian strata are separated in most places of the country from Turonian ones by an unconformity (Coniacian rocks being mostly absent), while the upper contact is gradational into strata of Campanian age. Santonian strata are, however, absent in various places of the country, either because of non-deposition or erosion (Grader and Moser, 1957). Micropaleontologically, the Santonian strata are defined mainly by the occurrence of *Globotruncana concavata* (Brotzen), *Sigalia deflaensis* (Sigal), *Globorotalites subconica* (Morrow). Santonian strata in Israel are found in the lower part of the Menuha Formation.

Campanian: Lartet (1869) applied the name 'Couches a Leda' to soft chalks, exposed mainly in Judea, which are rich in bivalves, especially *Leda.* Koert (1924) used 'Phosphorit-truemmerkalke' for the phosphatic beds, described first by Blanckenhorn (1898) as 'Phosphatkalke' or 'Koprolithenkalke'. Blanckenhorn attributed a Campanian or Danian age to these beds, whereas Koert (*op. cit.*) placed them in the Danian. Picard (1931) suggested a Maastrichtian age for these 'Phosphatic limestones', on the basis of the occurrence of *Bostrychoceras, Libycoceras,* and *Ptychoceras,* which were later shown to be Campanian. The phosphate beds, which are widely distributed in Israel, are partly of brecciated nature, which led Krusch (1911) to name them 'Truemmergestein'.

Blanckenhorn (1914) introduced the term Campanian in Palestinian stratigraphy for the middle division of the Senonian as interpreted by him. As originally described by this author, the Campanian in Palestine is represented by chalks and marls, flint layers and lime-phosphates, often carrying rich megafaunas, including Ammonites (*Bosstrychoceras, Libycoceras, Baculites* etc.). Reiss (1952, 1955a, b), on the basis of microfaunas, and Parnes (1956b) the megafaunas, have corroborated the Campanian age of the flint and phosphate layers. The Campanian in Israel thus includes chalks, limestones, dolomitic limestones, bituminous chalks, flint layers, phosphate beds, and some calcareous shales carrying rich mega- and microfaunas such as *Leda, Nucula, Gryphaea, Scala, Turitella, Baculites, Hoplitoplacenticeras, Libycoceras, Bostrychoceras, Lamna, Enchodus, Corax, Neoflabellina, Globotruncana* etc. The Campanian strata of southern Israel are particularly rich in flint and phosphate layers, while those of central and northern Israel are poor in flint and phosphates; in the Galilee, no flint layers are known west of the Safed region. The total thickness of the Campanian strata is variable and attains a maximum of about 450 m (in subsurface sections, *e.g.* Judean foothills region). In some places the contact between the Campanian and Santonian strata is unconformable, and in others Campanian strata rest unconformably on strata of Turonian age. The upper contact of the Campanian formations is gradational in several places, while in others Campanian strata are overlain unconformably by Tertiary (Middle Eocene) strata.

Maastrichtian: The term Maastrichtian was introduced in Palestinian stratigraphy by Picard (1931) for strata Blanckenhorn (1914) included in the Campanian, *viz:* chalks, limestones, shales and marls, partly bituminous, as well as flint and phosphate beds, carrying *Libycoceras, Bostrychoceras, Baculites* etc. Reiss (1952, 1955a, b) and Parnes (1956b) have shown on the basis of micro- and mega-fauna that the strata, included by Picard (*op. cit.*) and later authors in the Maastrichtian, actually belong to the Campanian. The Maastrichtian stage is represented in Israel by calcareous shales, chalks, limestones, and rather rare dolomitic limestones and marls. These strata are sometimes strongly bituminous, often limonitic and glauconitic, as well as slightly phosphatic and gypsiferous in the Ghareb Formation. The Hajar Musa, which is approximately 20 m thick, overlies phosphatic limestones with *Bostrychoceras* (Campanian) and is unconform-ably overlain by late Tertiary-Quaternary oolitic limestones.

Much earlier, Seetzen (1810) mentions these Hajar Musa, a popular Arabic name meaning stone of Moses, applied to a black bituminous, partly shaly, limestone with some gypsum veins, and carrying *Pecten obrutus* Conr., exposed in the region of Nebi Musa in the Judean Desert. It includes a thin dolomitic limestone bed at the top. Later Lartet (1869) reported these as 'Calcaire asphaltique de Nebi Musa' or 'Pierre de la Mer Morte'. Blanckenhorn (1905, 1914) called it 'Stinkkalke', 'Asphaltkalke' or 'Bitumenkalke', first regarded as Campanian-Danian, but attributed later (1914) to the Maastrichtian.

Megafauna is rather rare in the Maastrichtian of Israel and includes *Terebratulina* and *Pecten* of the *obrutusfarafraensis* group. Some Maastrichtian strata are rich in Porifera (*Ventriculites* etc.). The rich microfaunal assemblages include *Neoflabellina reticulata* (Reuss), *Bolivinoides draco draco* (Marsson), *Bolivina incrassata* Reuss. The Maastrichtian strata attain a maximum thickness of about 120 m. The general facies scheme of the Cretaceous in Israel is shown in **Figure 18F.2**.

STRATIGRAPHY

I. THE KURNUB GROUP

Encompassing the Cretaceous part of the 'Nubian' series, the Kurnub Group subdivides in two heterochronic facies realms:

I) The northern facies realm extending from Lebanon to the Galilee, the Golan, and Samaria, comprises the Hauterivian-Aptian

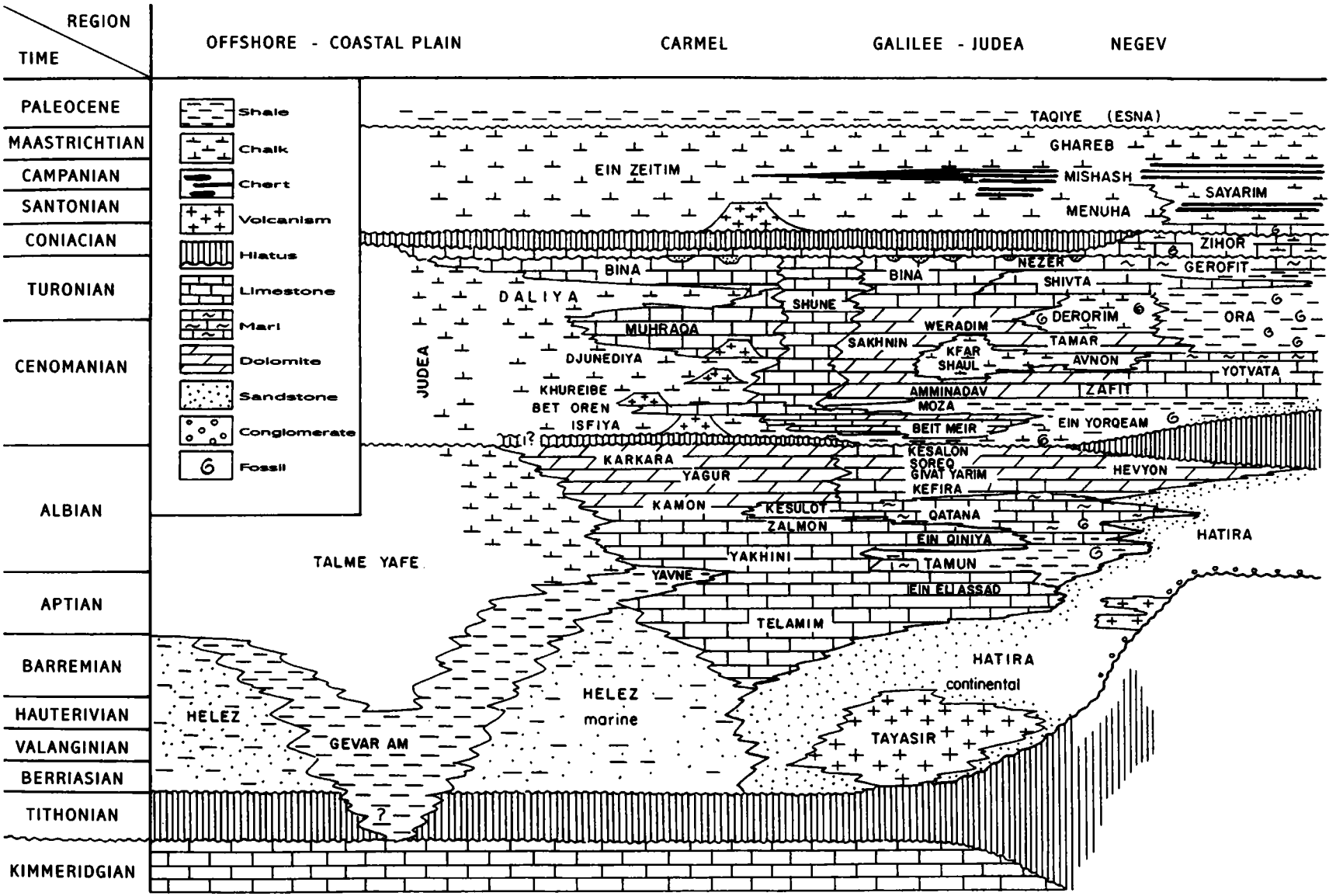


Figure 18F.2. General facies scheme of the Cretaceous in Israel. (Modified after Hirsch, 1990).

continental variegated sandstones and the shales of the 'Grès de Base' of Lebanon, deposited in a freshwater environment.

II) The southern facies realm that includes the Aptian-Albian continental variegated sandstones (Hatira Formation) with up to three marine intercalations reaching into the Negev, reflecting the transgressive units of the Galilee Group of central and northern Israel.

The Berriasian-Albian Kurnub Group (Damesin, 1933) consists mostly of terrestrial deposits, resulting from tilting and taphrogenesis, accompanied by magmatism (Tayasir Volcanics) that straddles the Jurassic-Cretaceous boundary in the Levant. The Kurnub Group includes all beds between the Jurassic marine Arad Group and the Middle Cretaceous marine Judea Group. In the southern part of the Negev, the Kurnub Group lies directly on the Early Paleozoic Nubian Sandstone of the Amir Formation, as part of the Kurnub Group dated to the Late Paleozoic. In the north of the country, the Kurnub Group comprises the Tayasir basalts (see Chapter 21) and consists of the variegated continental sandstones of the northern facies, with interstratified plant remains, siltstones, some clays, and further basic intrusions and lavas. Cohen et al. (1987) established the term Ramim Formation for the shales and sandstones underlying the Tayasir Volcanics in the Galilee. They established the term Kohal Formation for the clastic facies of the Hatira Formation in northern Israel.

In Makhtesh Ramon the Kurnub Group starts with the Arod Conglomerate. The Southern Facies of the Hatira Formation consists here of: 1) The Red Valley Member, wedged in by the Aptian Zeweira marine tongue; 2) The Avrona Member; 3) The Ramon basalt; and 4) The Samar Member, interfingered with the Albian Uza marine tongue.

The hard ferruginous crust of the 'Black Cuesta' marks the lower contact of the Kurnub Group in Hamakhtesh Hagadol (Shaw, 1947). The Hatira Formation consists of:

1) The 'Brown Cuesta' continental clastics with Zeweira marine tongue;

2) The 'Orange Cuesta' ferruginous oolite and Early Albian Deragot marine tongue;

3). The Malhata continental sandstones; and

4) The 'Yellow Cuesta' Early Albian Uza Member, consisting mainly of sandy limestones with some marls, shales and dolomites.

Ramim Formation (Cohen et al., 1987).

The Ramim Formation is 149 m thick in the Hula-2 well, in northern Israel, where it overlies Jurassic carbonates and underlies the Tayasir Volcanics. It consists of interbedded shales and sandstones with lignite and pyrites of the Wealden facies. A Berriasian age is attributed to this formation according to the absolute age determination of the Tayasir Volcanics in Samaria.

Tayasir Volcanics (Mimran, 1972).

These Late Jurassic-Early Cretaceous volcanics were first identified as 'Massive Basalt' (Blake, 1936); and 'Basaltic Neck' (Rofe and Raffety, 1965). The Tayasir Volcanics correspond to the basalts and tuffs of the 'Complexe volcanique de base'. In the Galilee, Golan, and Samaria the Tayasir Volcanics as well as the Younger Volcanics in the Negev (*e.g.* Ramon) intercalate at the base of the Kurnub Group

In the Wadi el-Malih area in northeastern Samaria, 5 km WNW from the village of Tayasir, a 232 m thick sequence of alkaline extrusives (tuffs and analcite-basanite basalt) was subdivided into three members: the Lower Flow, the Tuff Member, and the Upper Flow. The **Lower Flow** consists of 10.9 m of spheriodally weathered analcite-basanite, with pillow lava structures, which are intensely jointed. Primary minerals are altered to clay minerals, chlorite, and limonite. It has porphyritic texture with olivine phenocrysts and elongated plagioclase, sometimes with a poorly developed trachytic texture. The **Tuff Member** is 41 to 161 meters thick and consists mainly of green-gray, thinly-bedded tuff, interbedded in the lower part by laminated green-brown calcareous shales. The **Upper Flow** is up to 60 m thick and consists of analcite trachy-andesite. The rock is black, dense, intensely jointed, and shows a characteristic trachytic texture, forming a cliff at Ras Abu Shushe.

The carbonaceous intercalation in the volcanics near Ein Quniya (Golan) yields a Berriasian microflora (Conway, 1991).

The Tuff Member and the Upper Flow were deposited on a young morpho-tectonic relief which developed contemporaneously with their extrusions. The Lower Flow and the lower third of the Tuff Member were extruded and deposited in a rich ostracode system of lakes in a fresh-brackish water environment of deposition indicating a Wealden Facies affinity (=Late Jurassic to Barremian age; Rosenfeld and Raab, 1984; Rosenfeld et al., 1995). In general the volcanics unconformably overlie the Oxfordian-Kimmeridgian limestone and marl of the Upper Member of the Malih Formation (Rofe and Raffety, 1965; Aizenberg, 1968), and in one case the volcanics overlie a small exposure of the Lower Cretaceous Hatira sandstone (Shaw, 1947). The Tayasir tuffs and basalts cover a paleo-relief, carved deep within the Jurassic. Near the village of Majdal Shams, these volcanics rests directly on the Oxfordian Majdal Shams Formation (Mor, 1987). The entire sequence is overlain by sandstone of the Hatira Formation.

The Tayasir Volcanics are well-exposed in southern Lebanon (Heybroek, 1942). They were drilled in the Galilee (Hula, Hazon, Devorah, Amir, Carmel, Asher, and Haifa Bay boreholes) and a 480 m thick sequence was drilled in the eastern Galilee Hula-2 borehole. The Tayasir Volcanics of Wadi E'Shatr (Hermon) consist of 130 m thick basalts and tuffs, intercalated with lacustrine sediments (Shimron and Peltz, 1993). The Tayasir magmatic phase was active from the Late Jurassic (Tithonian) to Early Cretaceous (Early Albian) and comprises the following events: Tihonian-Hauterivian (Tayasir Sandstone, Hermon I), Barremian (Hermon II, Gavnunim), and Aptian-Early Albian (Hermon III, Ramon, Timna).

The Amir Formation (Weissbrod, 1969, 1970, 1993).

The Amir Formation corresponds to the Raqaba Formation in west-central Sinai (Barakat et al., 1986) and the Dhulal Formation

in eastern Sinai (Morsy et al., 1993). It consists of 20 to 70 m of super-mature quartz-arenite, with some siltstone and kaolinitic clay, and an ultra-stable heavy-mineral suite. Lithology consists mainly of white, fine- to medium-grained, or moderate to moderately well-sorted cross-stratified sandstones. Alternating with thin layers of gray and red siltstone, the sands, which in outcrop exhibit a characteristic yellow-beige weathering crust, are moderately consolidated to friable, cemented by well-ordered authigenic kaolinite, about 20% by weight. Syntaxial quartz overgrowths are quite common, while calcite, as cement, is sporadically present.

The uppermost 10-15 m of the Amir Formation consists of fine- to very fine-grained, either flat- or gently cross-bedded sandstones with accessory laminated sandstone and siltstone layers. Thin sets of ripple-laminated sands also occur. Irregular limestone lenses and mudclast breccia may also appear within the sandy mass.

The Amir Formation is exposed in southern Israel in a discontinuous narrow belt along the western margin of the Dead Sea Rift, extending from the Timna Valley, 30 km north of Elat, to the Sinai (Egyptian) border with intermittent outcrops in the riftward-draining canyons. Good exposures are known from Har Amir and from the Timna Valley, where a local dome has been half-sheared by the western faults of the Rift and breached by young erosion. It was encountered 40 km north of Timna in the Sinaf-1 borehole (Weissbrod et al., 1994). In Sinai the Amir Formation is exposed along the Gulf of Elat, swinging west halfway down the gulf, and forming a belt of outcrops along the foot of the El Tih Escarpment across the Sinai Peninsula. It is truncated west and south of Wadi el-Humur (Weissbrod, 1969) and is altogether missing across the Gulf of Suez in the Eastern Desert of Egypt. The Amir Formation has also a transgressive phase over the mature landscape of the Arabo-Nubian Massif. The age of the Amir Formation is at the Jurassic-Lower Cretaceous transition.

The Amir Formation was deposited in a marine nearshore arenitic environment of sand-silt cycles, mostly current-stratified. The top of the formation is a well-preserved surface of a fossil tidal channel system, with an associated ichnofossil (Skolithos facies) zone, which was buried almost synchronously beneath fluvial sand sheets of the Avrona Formation. Bioturbation activities of various tubular and U-shaped burrowers in the middle and upper parts of the formation is moderate. The channeled upper surface of the formation is locally marked by colony-like clusters of these ichnofossils. The Amir Formation unconformably overlies the Cambrian Netafim or Shehoret Formations in Israel and east Sinai, or the Permian Budra Formation in west-central Sinai, and it is always overlain by the Lower Cretaceous Avrona Formation (Weissbrod, 1969, 1970).

Arod Conglomerate (Nevo, 1963).

The base conglomerate of the Lower Cretaceous in the Makhtesh Ramon (Negev) and Areif En Naqa (Sinai, Egypt), is named after Mount Arod (Ramon), and ranges in thickness from 0-15 m. In a clear erosional unconformity, it overlies the Mahmal Formation (Bajocian) in Ramon and both the Inmar (Aalenian) and Ardon (Liassic) Formations in Areif En Naqa. In Har Arif it truncates the lower part of the Middle Triassic Gevanim Formation. The conglomerate is composed of various quartzites, limonites and calcareous pebbles that can reach sizes of 30 cm and more, embedded in friable sandstone.

Hatira Formation (Wetzel and Morton, 1959).

The Hatira Formation was defined at Wadi Hatira (Hamakhtesh Hagadol) by Shaw (1947). In the north of Israel and Golan, the unit represents an older sequence, deposited prior to the black or brown cuestas of the Hatira Formation in the Negev (Weissbrod et al., 1990). The Hatira Formation reaches 70-80 m near Ein Qinia and over 50 m at Ramim. It consists mostly of coarse reddish sandstones, cross-bedded in places.

In the south, the Hatira Formation has been subdivided into different units, including the continental sandstones (Avrona and Samar Members) and marine intercalations (Zuweira, Dragot, and Uza Members).

At Hamakhtesh Hagadol the Hatira Formation represents the entire Kurnub Group. Overlying the truncated top of the Jurassic, the 'Black Cuesta' is a hematitic sandstone crust about one meter thick, that at the Hamakhtesh Haqatan yields the bivalve *Protocardia judaica*. The bulk of the formation consists of some 400 m of dominantly white and variegated, friable continental sandstones, intercalated by four marine tongues of dolomite, limestone and marl, forming the 'Brown', 'Orange' and 'Yellow' Cuestas. The latter is characterized by several prominent carbonate ledges and yellow marly scree. (Lewy, 1990).

The sediments of the Hatira Formation are represented at their type locality by about 400 m of mostly continental quartz-arenites. Variations in vertical fining clearly reflect different point bar morphologies. These may be due to the changes of the position of the same meander bend (Weinberger, 1980, 1986). Conglomerates at the base of a sandstone unit may overlie a planar to uneven erosion surface with small local scours. Some of the pebbles are armoured mud balls. Intra-formational conglomerates ressemble those in the lower reaches of river systems, frequently concentrated at the base of point bars (channel lag deposits).

The sandstones range from very fine-grained to coarse, moderately to well-sorted. They are cross-bedded on a large-scale. Trough-shaped sets were probably formed by migrating dunes, similar to those found on many recent point-bars. Structures, similar to those observed in the Kurnub sandstones, are common in recent fluvial sediments where they may reflect rapid fluctuation in river stage. The siltstones display parallel lamination and small-scale cross lamination, but are otherwise extensively bioturbated. This section is regarded as a levee deposit. The complex of inter-tonguing lithologies is caused by repeated phases of erosion and deposition during the flood cycle.

The sediment load of the fluvial system that deposited the Hatira Formation appears to have been medium- to fine-grained, with coarse intraformational debris. The high proportion of mud in the sequence suggests that the rivers carried much suspended material.

The lower part of the Hatira Formation is of continental origin. It consists mostly of white, locally variegated, friable, medium to

coarse-grained quartz-arenites, some 48 m thick. Several upward fining sequences are discerned. Cross-bedded and horizontal sandstone units, 2-5 m thick, are overlain by siltstone layers, occasionally ferruginous. Plant remains (fragments of stems, leaves, and fruits) are locally abundant.

The ~16 m thick 'Brown Cuesta' of the lower marine ingression consists largely of fine-grained sandstone and siltstone, capped by thin banks of sandy dolomite and ferruginous crusts. Fossils are rare, though bivalves were found in this sequence at other parts of the Hatira cirque.

In the section of the Makhtesh Ramon the marine beds are much more fossiliferous and contain a rich assemblage of bivalves, as well as gastropods, arthropods, and brachiopods (*Lingula*). This marine ingression is assumed to be of Early Aptian age. It is followed by a 70 m thick, poorly exposed sequence, very similar to the continental unit below. Some siltstone layers are ferruginous, containing ferruginous plant fragments of *Weichselia reticulata*, with limonitic pseudomorphs of cubic pyrite. These siltstone layers are probably lacustrine, indicating a lake or a swamp in a fluviatile environment.

The middle marine intercalation, 48 m thick, of the 'Orange Cuesta' is characterized by a variety of lithofacies among which sandstone is a minor component. The sequence is chiefly composed of siltstone and mudstone, with abundant iron crusts in its lower part, and glauconitic mudstones in the upper part. In the middle part banks of limestone, dolomite, and marl occur, as well as an iron oolite layer less than 1 m thick. Fossils consist of burrowing and sessile bivalves, indicating non-turbulent, fairly aerated bottom conditions. Ammonites *Knemiceras syriacum* and *K. flexiloculosum* indicate an Early Albian age for this intercalation. Epifaunal bivalves (pectinids, trigonids and ostreids) are broken and often corroded by boring organisms, suggesting intermittent destructive currents and bioturbation, periodically turbated by gusts of high-energy that cause winnowing and sorting of the skeletal fragments into coquinous beds. At the top of the marl strata are many molts of the crab *Protocallianassa* which serve as centers of phosphatization. The upper third of the middle intercalation is dominantly clayey, with ostracods and prints of *Corbula* valves, pointing to a brackish environment.

Above the re-occurrence of continental deposits follows the Upper Marine Intercalation of the 'Yellow Cuesta'. It consists of very fine to fine-grained sand with three prominent limestone ledges. They contain remnants of terrestrial plants beside a marine fauna, and the intervening siltstones, mudstones, and sands are somewhat bioturbated. The sequence carries *Knemiceras dubertreti*, *Exogyra boussignaulti*, *Exogyra plexa*, *Trigonia distans*., *Anomia syriaca*, *Opis neocomiensis*, and *Fusus bhamdunensis*. The fossils in the white marly limestone include casts of burrowing bivalves, and well-preserved epifaunal bivalves (*Exogyra*, *Nayadina*), echinoids, and gastropods. The latter include very large *Strombus*. *Knemiceras dubertreti*, indicating an Albian age for this incursion. The relative density of fairly large-sized fossils on a small surface area points to calm conditions and to high productivity during the deposition of this bed. Glauconitic-ferruginous sands in the upper part of this interval contain a fauna of partly broken burrowing bivalves.

Above the final continental facies of the Hatira Formation, a change from continental to marine facies is marked by a transition zone, characterized by glauconite-rich layers, a well-known phenomenon accompanying unconformities. The glauconite typically occurs as pellets in a wide variety of shapes, including ovoid, spherical, botryoid, accordion-shaped, and intracrystalline. Weinberger and Flexer (1986) consider the glauconite a product of fecal pellets. The glauconite in Israel occurs at the base of all the Cretaceous marine transgressions, marking the moving shore of the inundating sea. It is well-recognized at the base of the widespread Albian transgression.

Avrona Formation (Weissbrod, 1966).

The Avrona Formation overlies the Amir Formation in the southern Negev. It is a 40 to 60 m thick sandstone sequence, consisting of gray-white, medium- to coarse-grained, cross-stratified sandstones and grits with stringers and lenses of pebbles and sandy siltstone. At the base of the formation a conglomerate comprising clast-supported, imbricated sandy intraclasts, and rounded quartz pebbles with a coarse sand matrix occurs locally as lenticular bodies. The Avrona sandstones are believed to have been deposited in braided alluvial channels with no clearly defined overbank terrain, consisting largely of channel lag gravels and channel bar sands.

II. THE GEVAR'AM GROUP

Representing the trough sedimentation of the Coastal Plain of Israel, the Gevar'Am Group (Flexer et al., 1981) or Yoav Group (Cohen et al., 1987), comprises gray to black sandy to silty shales. Carbonaceous interlayers are found at several intervals. The Gevar'Am Group passes laterally into units of the Kurnub and Galilee Groups and is overlain by the Talme Yafe Group.

The Gevar'Am Group consists of the basinal and shallow marine to deltaic facies of the Coastal Plain. The basinal facies is represented by marine shales and sandstones.

Ostracodes (Rosenfeld and Raab, 1984) and Dynocysts (De Haan, 1997) are useful in the reconstruction of the sequential history and palaeogeographic configuration of the Lower Cretaceous sediments of Israel and adjacent regions. The sedimentary sequence that started before the beginning of the Cretaceous overlies an erosional Jurassic relief. At the base, the angular unconformity between the Gevar'Am Shale and the underlying Jurassic strata reflects an Infra-Cretaceous tectonic phase, preceding the series of rather extensive global drop in sea level. Development of a carbonatic shelf-platform characterizes Valanginian, Hauterivian and Barremian-Aptian high-stands (HS).

Tithonian-Beriassian: The lower part of the Gevar'Am Group yields a poorly preserved ammonite, *Blanfordiceras* sp., found in the Helez-2 well, core 29 (Parnes et al., 1958), the nannoconus assemblage N-1 (Moskovitz, 1972), and the Tithonian-Late Berriassian dynocyst interval zone *Biorbifera johnewingii* (Leereveld, 1995).

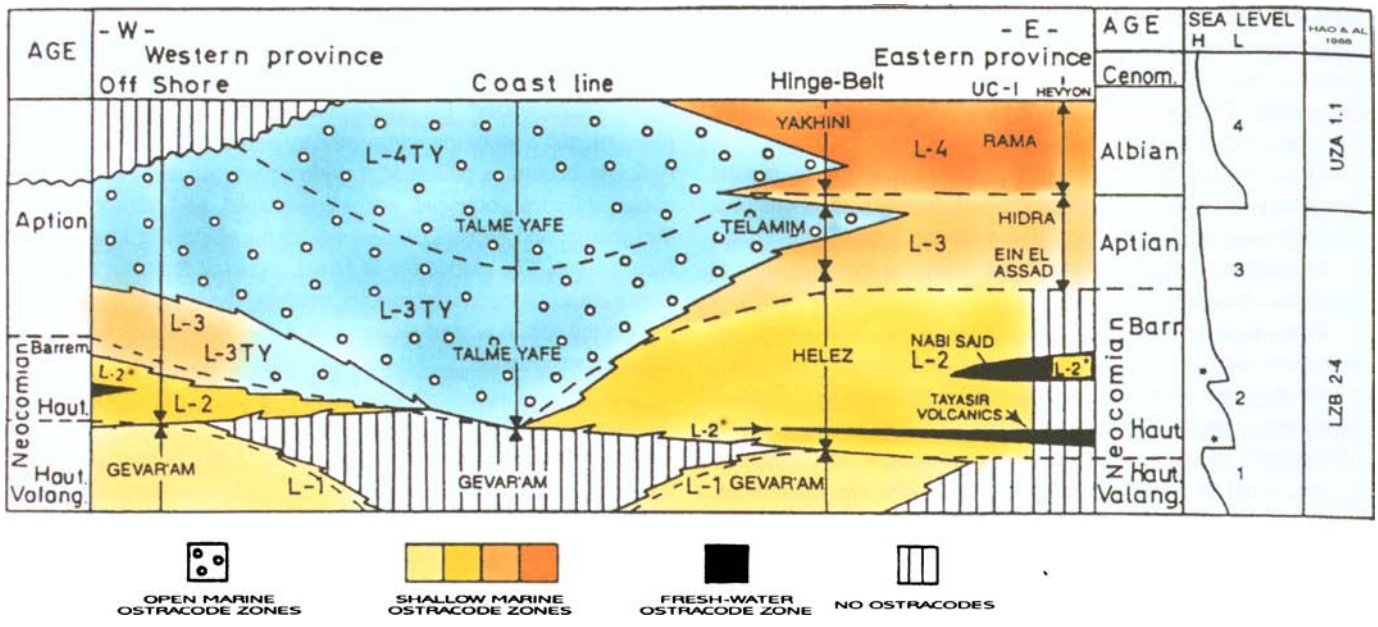


Figure 18F.3. Schematic distribution of Early Cretaceous facies types. (Modified after Rosenfeld et al., 1998, Fig. 9, p. 192).

Valanginian-Hauterivian: The upper part of the Gevar'Am Group consists of dark shales that contain the Valanginian Ostracode Zone L-1. It passes laterally into the base of the Helez Formation, which represents the deltaic to shallow marine facies of the Gevar'Am Group. Zone L-1 marks the Valanginian transgressive system track and high-stand, represented by the base of the Helez Formation (Mashen Limestone).

Helez Formation (Eliezri, 1963)

The Helez Formation was established in the Kokhav-Helez field of the Coastal Plain of Israel, describing a 300 m sequence of Hauterivian-Barremian (Rosenfeld et al., 1998).

The Helez Formation consists from bottom to top of the Mashen Limestone, Lower Sand, Nehora Shale, Kokhav Dolomite, Middle Sand, Rewaha Shale, Upper Sand, and Sederot Limestone. It is overlain by the Telamim Formation.

Hauterivian: This consists of the Lower Sand (L-2*) representing the Hauterivian low-stand wedge, followed by 'Nehora Shale' transgressive deposits (L-2) and Kokhav Dolomite high-stand.

Barremian: The low-stand iteration of the Middle Sand, transgressive Rewaha Shale, Upper Sand, and high-stand carbonatic sequence of the Sederot Limestone (uppermost Helez).

The sequence represents three cycles:

1) Mashen Limestone at the base, representing the high-stand of the lower cycle;

2) Lower Sand, Nehora Shale tongue, and Kokhav Dolomite, representing low-, transgressive and high-stand of the middle cycle;

3) Middle Sand, Rewaha Shale tongue, Sederot Sand; shale and limestone, representing low- and transgressive stands of the third cycle, topped by the carbonates of the Lower Aptian Telamim Formation, that represent the high-stand of that cycle and the Telamim Formation (L-3).

The Helez Formation is found in northern Sinai (Egypt), in a mainly detritic sequence, which yields Hauterivian-Aptian ammonoids and ostracodes (Rosenfeld and Raab, 1984; Rosenfeld, Hirsch and Honigstein, 1995).

The Helez Formation generally overlies various Jurassic formations. However, in the Helez, Brur, Gevar'Am, and Ashqelon wells, it conformably overlies the mainly black carbonaceous shales of the lower part of the Gevar'Am Group.

Laterally, to the west, the Helez Formation passes into the deeper facies of the Gevar'Am Shale.

Shenhav (1971) recognized littoral beach, tidal flat, lagoon and swampy lagoonal-type sediments in the lower Helez Formation. Cohen (1976) described a southeast to northwest trending river paleo-canyon, draining the Helez area into the Tethys at the end of the Jurassic.

The coexistence of both freshwater (L-2*) and marine ostracodes(L-2) in the same samples (*e.g.* Ramim section northern Galilee, Rosenfeld et al., 1995) supports the assumption that intense activity of the continental freshwater, rivers, lakes and lagoonal environments of deposition began to supply organic detritus, sand, and shales which accumulated in estuaries and deltas (Sohn, 1968; Rosenfeld et al., 1995). The combination of freshwater supply and sea water favors a high nutrient content in the water which could encourage the generation of a maximum number of

organisms. This, together with a high rate of sedimentation, could have created optimum conditions for oil accumulation. Similar palaeoenvironmental conditions prevailed also in the western province, in the Mediterranean offshore with mixed shallow marine and fresh-brackish water environment (L-2* ostracode zone) that prevailed during the Hauterivian-Barremian (Wealden) period.

Telamim Formation (Eliezri, 1963).

The Telamim Formation consists of carbonates dated as late Barremian-Early Aptian by Derin and Reiss (1965). The base consists of oolitic, shaly limestones and black calcareous shales to more sandy limestones. The upper part consists of oolitic and shaly limestones with intercalations of black calcareous shale (Cohen, 1983; Grader and Reiss, 1958).

The schematic distribution of Early Cretaceous environments in Israel is shown in **Figure 18F.3,** and the facies distribution map of the Lower Cretaceous is shown in **Figure 18F.4.**

III. THE GALILEE GROUP

The Galilee Group (Kafri, 1972) represents the marine sediments that overlie the Kurnub Group in northern Israel. They consist of the ferruginous oolites, sandy limestones, and sandstones (Netofa, Nabi Said, Couches à Gastéropodes), oolitic limestones (Ein-El-Assad, Falaise de Blanche), ferruginous oolites, shales, marls, sands and limestones (Hidra, Couches à Orbitolines), and mainly marls (Rama, Couches à Knemiceras, Zalmon). The shallow marine Galilee Group sequence is coeval with the marine intercalations within the sequence of the Kurnub Group in the Negev. It is also coeval with the upper part of the Gevar'Am Group and lower part of the Talme Yafe Group. For Rosenfeld et al. (1995) the Galilee Group comprises the Barremian-Aptian sediments of the platforms that border the Gevar'Am Basin. The Galilee Group is well-exposed in Lebanon where the informal nomenclature was coined (Heybroek, 1942). The rocks of the Galilee Group were first described from the central and upper Galilee near Safad and west of the Hula Depression by Blake (1935). Further localities are in the Galilee (Rami, Kiriat Shemona), Samaria (Faria, Malih), and the Golan (Ein Qunia, Massade). Nevo (1956, unpublished) described the marine Aptian sequence cropping out at Rami (central Galilee) as being 300 m thick, composed of greenish oolitic and dense white limestone, and shales rich in *Orbitolina*. The thickness of the Hunin sequence, near Margaliot in the Naftali Mountains, is 400 m. The fauna quoted by Blake (1935), determined for him by L. R. Cox, includes such characteristic species as *Neithea* cf. *morrisi* (Pict. and Camp.), *Trigonia undulatocostata* Blanck., *Trigonia* cf. *pseudocrenulata* Noetl., and *Amauropsis subcaniculata* Hamlin.

Netofa Formation (Golani, 1962) and **Nabi Said Formation** (Eliezri, 1965).

The Netofa Formation and Nabi Said Formations are synonymous. At Wadi Nabi Said, 30.8 m of ferruginous sands and 11.4 m of brown oolitic detrital sandy limestone with *Natica biconica* Blanc and *Ostrea* sp. represent a fairly inaccessible and poorly preserved section. The section at Har Netofa, along the northern flank of the Netofa Plain, exposes 77 m. It consists of interchanging shales, siltstones, sandstones, and detritic (calcarenitic) oolitic limestones (Golani, 1962). Its distribution stretches from central Lebanon to the Galilee and Samaria. In Lebanon, the Abeih Formation (Couches A Gasteropodes) varies from a thickness of 170 m at Abeih in the Chouf, to 65 m towards Jebel Barouk. A similar wedging out occurs between the Galilee (100 m) and Hermon areas (20 m). Its environment of deposition can be described as ranging from an estuarine shoreline to a storm-dominated shelf. A sequence of 78 m is exposed at Har Ramim (Rosenberg, 1966), 86 m at Ras Ramali in Samaria (Mimran, 1972), 77 m at Har Netofa, west of the Sea of Galilee, and over 42 m (base not exposed) at Rami in the Galilee (Eliezri, 1965). At the Hermon slope in the vicinity of Ein Qunia, it may represent the proximal end of the facies. A Late Barremian-earliest Aptian age is attributed to the formation, based on the occurrence of *Palorbitolina lenticularis* and *Chofatella decipiens* (Bachmann and Hirsch, in press).

The columnar section of the Lower Cretaceous on the Golan Heights is shown in **Figure 18F.5**.

Ein-El-Assad Formation (Eliezri, 1965).

The Ein-El-Assad Formation represents the 'Muraille de Blanche' of Dubertret (1937). In Lebanon this rock unit is now called the Mdairej Limestone Formation (Dubertret, 1963, emend. Walley, 1983, 1997). The Ein-El-Assad Formation averages a thickness of 50 m, consisting of uniform fine-grained sub-lithographic white to buff limestone. Its wide distribution extends from Lebanon to north-central Israel and Syria. The prominent cliff of the Ein-El-Assad Formation was first identified much earlier in Lebanon by Blanche (1847), hence 'Muraille de Blanche' (Dubertret, 1937; Heybroek, 1942). This clear landmark can be followed from the Druze village of Ein Qinia (also spelled Ein Qunia) into Syria, east of Majdal Shams. In the village of Ein Qinia and its vicinity, landslides have dislocated portions of the formation into slabs on which parts of the village are built. The 42 m thick cliff at Ramim, above Qiriat Shmona in the upper Galilee, also forms a landmark (Rosenberg, 1960). An Early Aptian age is assigned by the occurrence of *Palorbitolina lenticularis*, *Chofatella decipiens, Praeorbitolina cormyi* and *Orbitolina lotzei* (Bachmann and Hirsch, in press).

Hidra Formation (Eliezri, 1965).

The Hidra Formation was established at Rami in the Galilee, where it reaches 133 m in thickness. Named after the Hidra Spring in Wadi Nabi Said, it represents the 'Couches à Orbitolines', named the Tammun Formation in Samaria (Shachnai, 1968; Mimran, 1969), or the Katih Formation in the Golan (Saltzman, 1968; Sneh et al., 1985). The Hidra Formation consists of sandstones, iron-oolites, limestones with *Orbitolina*, and shale. In the Galilee sections of Menara and Har Ramim, well-known for their iron oolites, the formation measures 105 m (Rosenberg, 1960). Above the village of Ein Qunia (Golan), the sequence reaches 80 m. The Hidra Formation is equivalent to the lower part of the Kobar Formation

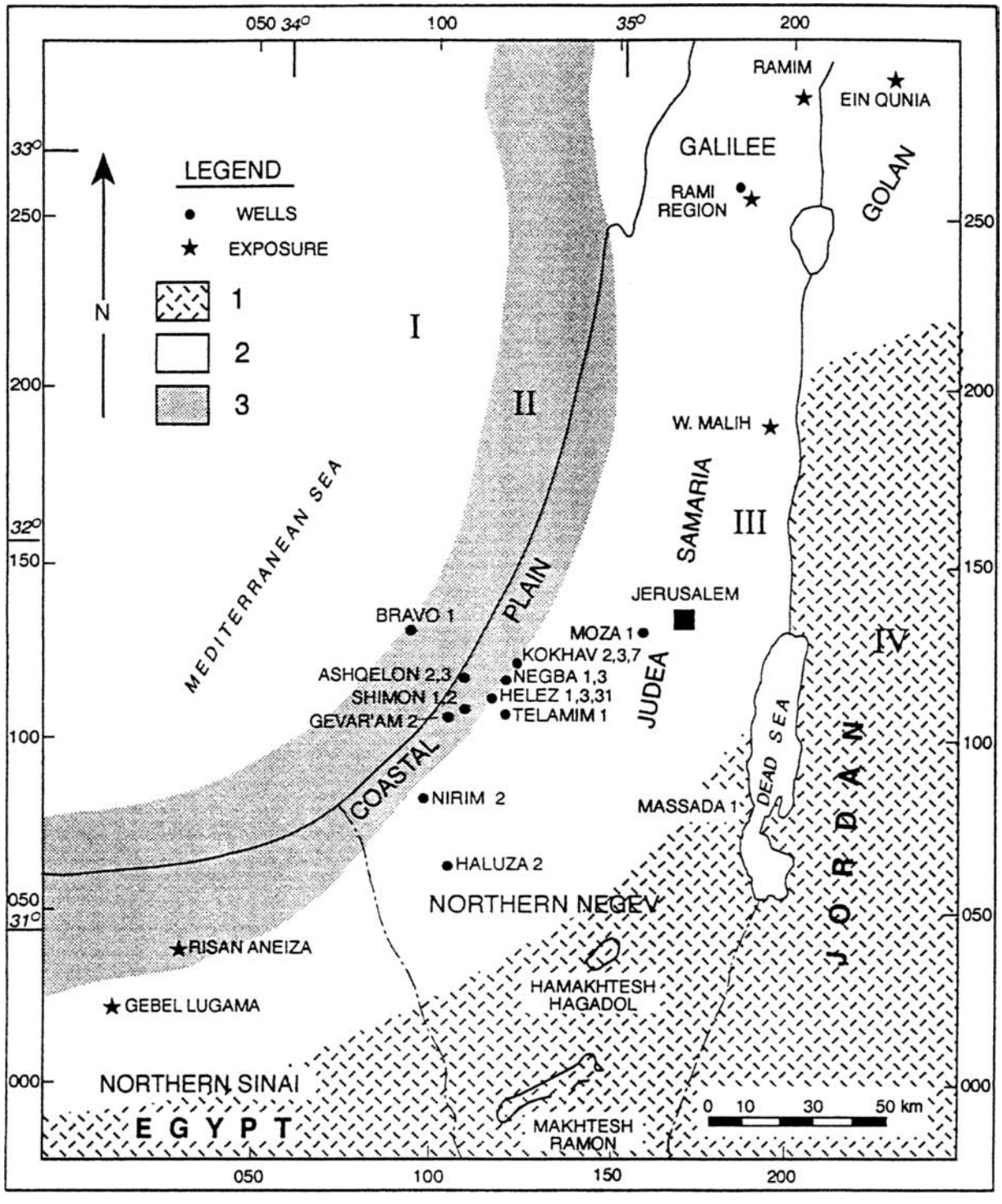
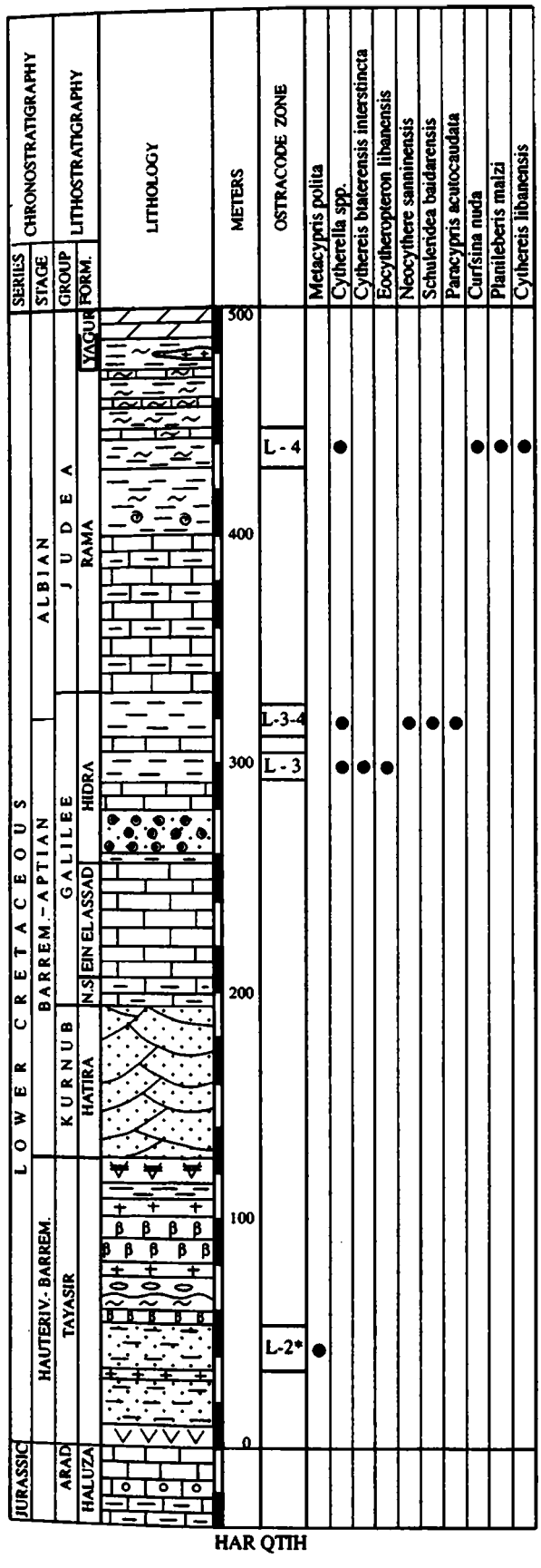


Figure 18F.4. Facies distribution of Lower Cretaceous in Israel (from Rosenfeld et al., 1998).
Legend: 1. Mostly continental; 2. Gevar'Am Trough; 3. Marine facies of Western and Eastern Platform.



(Burdon et al., in Rofe and Raffety, 1963). Ostracodes (L-3 zone) indicate an Aptian age (Hirsch et al., 1994) and a more precise age attribution is provided by the Orbitolinid zones *P. cormyi- O. lotzi* (Late Bedoulian) and *O. parva* (Early Gargasian) that correspond to the late Early and early Late Aptian (Bachmann and Hirsch, in press).

The *Asfuri* limestone, a 12 m thick ledge at Rami consisting of brown oolite, was identified above the Hidra Formation (Eliezri, 1965).

Rama Formation (Eliezri, 1965).

At Rami (Galilee), the total thickness of the Rama Formation is 204.9 m. It can be divided into three parts:

1) The lower 79 m thick part is composed of limestone and marl.

2) The middle 84.7 m thick part is composed of yellow fossiliferous marl.

3) The 41.2 m thick upper part is composed of alternating limestone and marl.

At Wadi Nabi Said it has the same thicknesses.

Fossils indicating an Albian age were found throughout and include: *Orbitolina cf. discoidea* Graas, *Anisocardia hermittei* Choffat, *Cardita* sp., *Cardium* sp., *Crassatella* sp., *Dosinia* sp., *Exogyra* cf. *boussingaulti* d'Orb., *Granocardium* sp., *Liopistha ligeriensis* (d'Orb.), *Meretrix* sp., *Neithea* sp., Nucula sp., *Ostrea dieneri* Blanck., *Pecten* sp., *Pholadomya* sp., *Trigonia* sp., *Cerithium* sp., *Leptomeria* sp., *Pleurotomaria* sp., *Strombus* sp., *Tylostoma* sp., *Diplopodia hermonensis* DeLor., *Heteraster delgadoi* DeLor., *Trochodiadema* sp., *Ophiura* sp., *Knemiceras dubertreti* Basse, and *Knemiceras* sp.

East of the Jordan River between Ein Qunia and Massada, the Rama Formation consists of up to 230 m of limestones and marls (Hirsch, 1996).

At base the lower *Limestone and Marl Member* consists of 80 m of nodular limestones with marly intercalations, forming a distinctive ledge. It may correspond to the Zumoffen Ledge at Ramim above Qiriat Shemona (Heybroek, 1942), which consists of 25 m of hard, fine-grained, partly oolitic limestone (Rosenberg, 1960). The top bed of the member is covered by a fossiliferous hard-ground. In the lower half of this interval Bachmann and Hirsch (in press) have recently identified the orbitolinid zone of *O. texana-O. parva*, conferring to it a late Gargasian-Clansayesian (Late Aptian) age. The upper part of the interval yields *Orbitolina subconcava*, which is uppermost Aptian to Albian.

The upper *Marl and Shale Member* consists of up to 150 m of soft marls and thin fossiliferous limestones. The member yields the ammonite *Knemiceras* sp. and abundant large bivalves. Ostracodes (Hirsch et al., 1994) and Orbitolines (Bachmann and Hirsch, in press) indicate an Albian age. On the Har Odem geological map



Figure 18F.5. Columnar section of the Lower Cretaceous on the Golan Heights (from Hirsch, 1996).

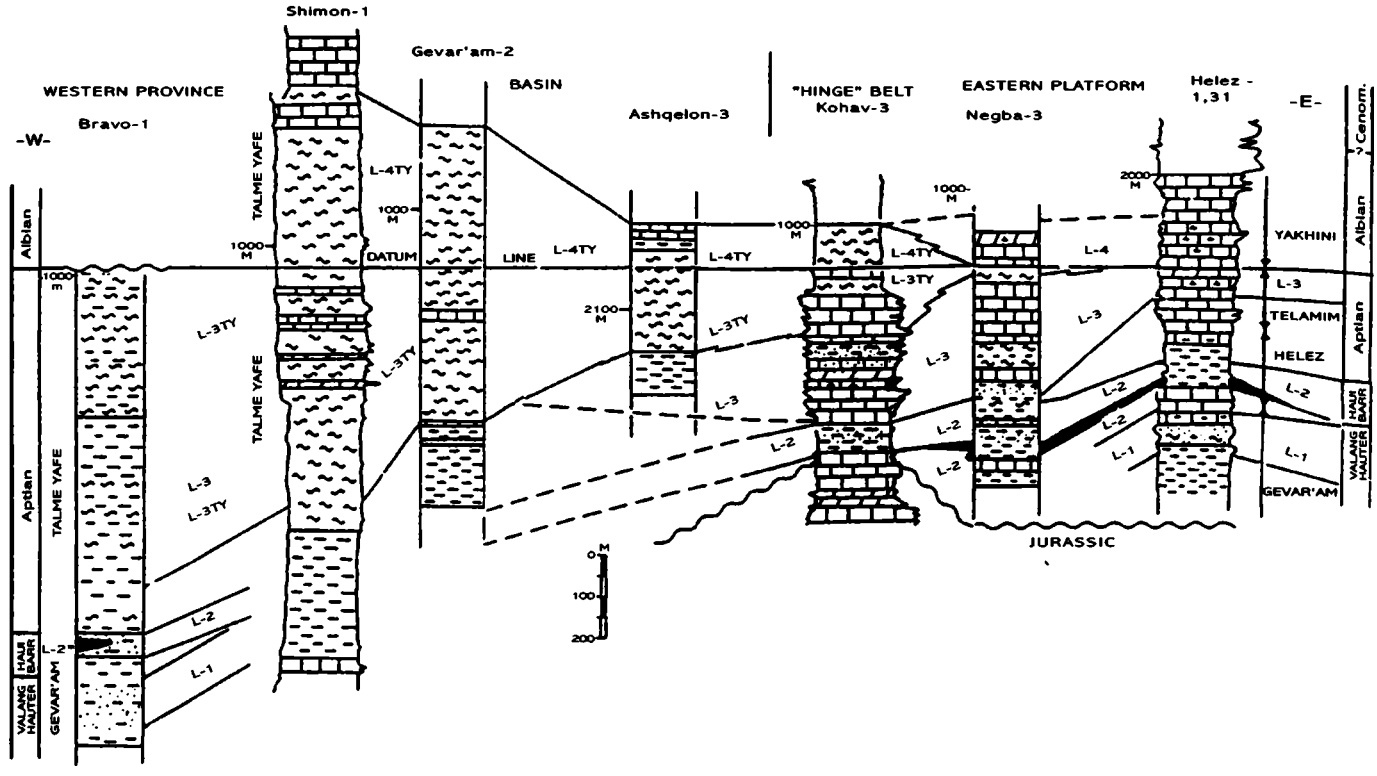


Figure 18F.6. Early Cretaceous correlation from Western Province into the Eastern Province (from Rosenfeld et al., 1998, Fig. 10, p. 193).

sheet (Mor, 1987) this sequence is termed as Mas'ada Formation (Saltzman, 1968). At Ramim the unit consists of 126 m of yellowish marl and argillaceous limestone (Rosenberg, 1960). This interval corresponds to the 'Couches à Knemiceras' (Heybroek, 1942) and is probably coeval to the Qatana Marls (Bentor, 1945) in the Jerusalem vicinity and to the Uza marine intercalation within the Hatira Formation of the Negev.

The Rama Formation is coeval to the middle and upper parts of the Kobar Formation, established in Samaria by Burdon (in Rofe and Raffety, 1963).

Zalmon Formation (Golani, 1961).

The Zalmon Formation was established in the Lower Galilee Zalmon area. Golani (1957) split Heybroek's (1942) 'Couches à Knemiceras' into a lower 'limestone and marl series with 'Knemiceras' and an 'Upper limestone series'. The latter was subsequently renamed as 'Tsalmon Formation' (Golani, 1961). The Zalmon Formation is thus equivalent to the third (upper) member of the Rama Formation (*sensu* Eliezri, 1965). It is not discriminated in the Naftali or Ramim Escarpment (Rosenberg, 1960).

The Zalmon Formation was recognized in Lower Galilee (Picard, 1955; Vroman, 1958) and Mount Carmel, below the Yagur Dolomite (Folkman et al., 1966). In the Nazareth Hills, along the southern slope of Har Devora, Weiler (1961) established the Devora Formation. It is also recognized on the western flank of Mount Tabor above the village of Dabburiya.

The ~45 m of well-bedded limestone and yellow marls is rich in macrofossils (Golani, 1957) and consists of hard biocalcarenites, rounded fragments of oysters, orbitolines, echinoids, and lithoclasts of older rocks. Glauconite pellets give the rock a greenish tint. Limonitic concretions and impregnation of joints with ferruginous matter are frequently observed. Greenish-gray to reddish-brown marl contains orbitolines and moulds of other fossils. Lumachelle banks occur as yellowish-brown biocalcirudites composed mainly of lamellibranch moulds, some echinids and gastropods being cemented by calcite. On the southern slopes of Har Devora occur subangular quartz grains (not *in situ*), ferruginous oolites, and fossil fragments (mainly oysters and orbitolines) cemented by calci-micrite.

The Zalmon Formation at Mount Devora and Mount Tabor yields: *Knemiceras syriacum* (Buch), *Heteraster delgadoi* de Loriol, *Orbitolina* sp., *Neithea* sp., *Pholadomya* sp., *Dosinia* sp., *Cardita* sp., *Protocardium* sp., *Venus* sp., *Ostrea* sp., *Cytherea* sp., *Chenopus* sp., *Strombus* sp., *Tylostoma* sp., *Neithea aff. duplicicosta* Roemer, *Neithea syriaca* (Conard), *Pholodomya* cf. *vignesi* Lartet, *P. decisa* Conard, *Eoradiolites* sp., and *Tylostoma* cf. *choffati* Douv. Lowenstam (1942) described also: *Orbitolina conica* d'Archiac, *Anisocardia orientalis* Conard, *Lima (Radula) naamensis* Whitfield, *Exogyra flabellata* Goldfuss. Blake (1936) also mentions *Pholadomya depacta* Hamlin.

Table 18F.1: Judea Group Level 1.

Coastal Plain	Galilee	Samaria	Judea	Negev
Yakhini	Rama*	Qatana*	Qatana*	Uza ingression**

*See Galilee Group **See Kurnub Group

Westwards, the shallow marine rocks of the Galilee Group pass laterally into the deep calcilutites of the mostly Aptian-Albian Talme Yafe Group.

IV. THE TALME YAFE GROUP (Figs. 18F.6 and 18F.7)

The more basinal deposition in the subsurface of the western Coastal Plain of Israel and the adjacent Mediterranean offshore was identified as the Talme Yafe Formation (Cohen, 1971), and later raised to the Talme Yafe Group by Flexer et al. (1981). A few exposures occur, as in the NW Carmel, and a Talme Yafe tongue was identified in the Risan Aneize 'inselbergs' of northern Sinai (Egypt).

The Talme Yafe Group succeeds the Gevar'Am Group and passes laterally into Albian carbonates of the Galilee and Judea Groups. The term Ga'ash Group was established by Cohen et al. (1987) for all strata comprised herein within the Judea and Talme Yafe Groups. The Talme Yafe Group consists of laminites and calcilutites, made of carbonatic (bio)-detritus with minor clays and represents the pelagic facies of the Pleshet Basin. The Talme Yafe Group is made up of open deep marine sediments (Rosenfeld and Raab, 1980), and turbidites suggest deposition near a slope (Bein, 1974). The Talme Yafe Group comprises the Talme Yafe Formation (Cohen, 1971), the Item Formation (Cohen et al., 1987), and the Ziv Formation (Flexer et al., 1981). The age of the Talme Yafe Group is Aptian-Albian, though the presence of Cenomanian and younger strata is inferred. The Talme Yafe Group is truncated by Senonian sediments, as the result of the Levantid folding.

Ziv Formation (Flexer et al., 1981).

The Ziv Formation in borehole Ziv-1 (offshore Sinai) is a 988 m thick sequence (bottom not reached) that consists of graded lithic arenites, alternating with dark gray and green shales with some limestone. It represents the lower part of the Talme Yafe Group. The Ziv Formation consists of deep-sea turbidity currents, as suggested by its unusual dips within the cores taken in the well. Age is assumed to be Albian to Upper Aptian.

Item Formation (Cohen et al., 1987; Shilo and Wolff, 1989).

The Item Formation consists of hard, dark, deep water, laminated calcisiltite and fine grainstone, found in the offshore Delta-1A and Item-1 drillings. It represents the upper part of the Talme Yafe Group with more abundant carbonates. These provide a higher resistivity than the usual Talme Yafe marlstone below or lateral to it. Its thickness in Delta-1A is 688 m. The Item Formation underlies the Negba Formation. Its lower contact is set by the marlstone of the lower Talme Yafe Group. Age is Albian.

V. THE JUDEA GROUP

The 'Judea Limestone Formation' (Wellings, (1940),

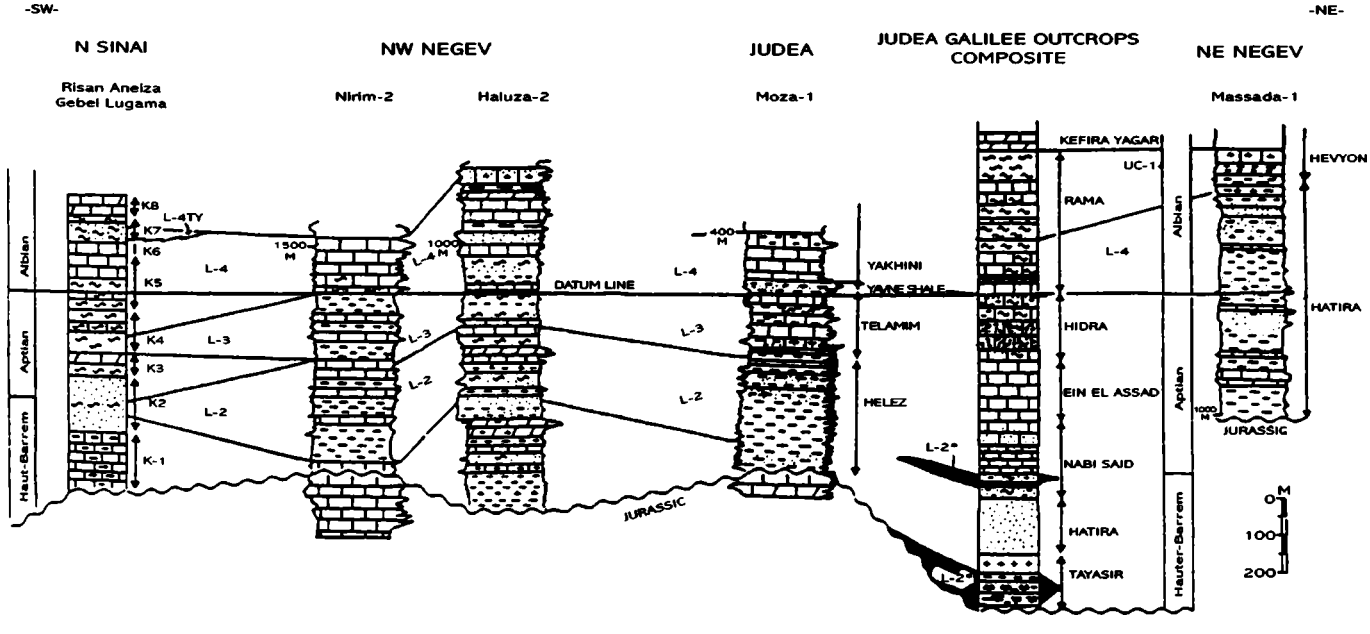


Figure 18F.7. Early Cretaceous correlation from N. Sinai into the Negev, Judea, Judea and Galilee (from Rosenfeld et al., 1998, Fig. 11, p. 193).

Table 18F.2: Judea Group Level 2.

Coastal Plain	Carmel	Galilee	Judea	Negev
Yagur	Yagur	Karkara	Kesalon	Hevyon
		Kamon	Soreq	
		Kesullot	Givat Yearim	
			Kefira	

emended to Judea Group (Arkin et al., 1965), includes 'the fully marine sedimentation' above the Kurnub Group. This is especially true in the Negev, where the transgressive Judea Group progrades toward the Arabo-Nubian Massif and the base of the Judea Group consists in the mainly dolomitic sequence of the Late Albian Hevyon Formation, overlying the sandstone sequence of the Hatira Formation of the Kurnub Group. However, outside the Negev, the clastic Hatira Formation is first overlain by the mixed sequence of the Galilee Group, consisting of several hundred meters of limestone and marls. Here the Judea Group starts at the base of the Kefira Formation, which overlies the Qatana Shale (Arkin and Hamaoui, 1967). Consequently, in Galilee, the base of the Judea Group is at the first appearance of the dolomites of the Kesullot Formation (Kafri, 1972).

In the Coastal Plain, the Late Aptian Yavne Shale, at the base of the Yakhini Formation, separates the carbonates of the Telamim Formation from those of the Yakhini Formation (the so-called 'Main Shale Break' of Gvirtzman et al., 1974). In their sequential stratigraphic approach, Rosenfeld et al. (1995) also place the initial lower limit of the 'fully marine' sedimentation of the Judea Group in the Coastal Plain of Israel, at the Infra-Albian regional low-stand of the Late Aptian Yavne-Hidra event. The Yakhini Formation thus represents the oldest unit of the Judea Group. Alternatively, Bartov et al. (1981) and Flexer et al. (1981) have considered that the Ein-El-Assad Formation represents the lowest unit of the Judea Group.

The upper limit of the Judea Group corresponds to the unconformity marking the Senonian Levantid embryonic folding.

The deposition of the Judea Group progrades in the direction of the Arabo-Nubian Craton. Age is Early Albian in the Galilee and Coastal Plain to Early Cenomanian in the southernmost Negev.

The Judea Group is subdivided into levels.

Early Albian level of the Yakhini Formation (Table 18F.1).

The carbonatic Yakhini Formation overlies the Aptian regressive Yavne Shale in the Coastal Plain subsurface. This lower subdivision of the Judea Group is only represented in the Coastal Plain. Its carbonatic facies interfingers eastward with the marly facies of the early Albian Rama Formation of the Galilee Group.

Yakhini Formation (Flexer et al., 1981; Cohen et al., 1987).

The Yakhini Formation is the carbonatic interval between the Telamim and Yagur Formations. A few planktonic foraminifers, such as *Ticinella roberti* and *Orbitolina* sp. occur with ostracoda of the L-4 assemblage zone (Rosenfeld and Raab, 1984), indicating a rather shallow warm marine environment of Early Albian age.

Late Albian level of the Yagur Formation (Table 18F.2).

The Yagur Formation was drilled in the subsurface of the Coastal Plain and is exposed in the Carmel and the Galilee. It consists of monotonous dolostones, further subdivided into Kesullot, Kamon, and Karkara (Kafri, 1972) or Sajur Members/ Formations (Freund, 1959). A differentiation within this subdivision of the Judea Group intensifies in Judea, with the distinction of the Kefira, Givat Yearim, Soreq, and Kesalon Formations (Itzhaki et al., 1964). The up to 350 m thick sequence consists of dolostones with relict gypsum, alternating with fine-grained laminated to skeletal limestones with yellow marl interbeds. Shallowing south-eastward, this Late Albian sequence passes into the more terrestrial Hevyon Formation of the Negev. It consists of limestone, dolomite and dolomitic limestone, alternating with marl and marly limestone beds, reaching a thickness of 120 m. In Jordan this facies corresponds to the lower part of the Naur Formation. A sedimentary break occurs at the top of this interval, respectively at the top of the Hevyon, Kesalon, and Yagur Formations (Hirsch, 1985; Kafri, 1987), witnessed by karstic fillings and conglomerates in the Galilee and by a typical oyster lummachelle (*Pycnodont*-bank) from the Galilee, through Judea, to the northern Negev.

COASTAL PLAIN AND CARMEL:

Yagur Formation (Picard and Kashai, 1958).

The name Yagur Dolomite was given by Picard (1956) to a sequence of dolomites, at least 350 m thick, which forms the steep cliffs of the eastern Carmel slope above Yagur. These strata are poor in well-preserved fossils. In Wadi Rushmia the Yagur Formation, whose base is not exposed, contains *Nerinea cochleaeformis* Conr., *Cerithium elias* Boehm, *Cerithium aciformis* Blanck., and rudists. Laterally the Yagur Formation diversifies into the Kesullot, Kamon, and Karkara Formations, previously considered as either members or formations. In the Galilee, these units should be considered as formations.

GALILEE:

Kesullot Formation (Weiler, 1961, 1968).

The Kesullot Formation, also called the Kesullot Member of the Kamon Dolomite (Bein, 1967; emend. Kafri, 1972) was named after Har Kesullot, on the southern slope of Har Devora and the western side of Mount Tabor. The Kesullot Formation consists

mainly of well-bedded saccharoidal dolomite, with dolomitic marl. The dolomite shows ghost texture. The Kesullot Formation overlies the alternating marls, shales, and limestones of the Albian Zalmon Formation, and is overlain by the Kamon Dolomite of the Yagur Formation. Lithologically the formation forms a passage zone between the detrital limestones of the Zalmon Formation and the dolomites of the Kamon Dolomite. The Lower Member is composed mainly of finely crystalline, marly dolomite with some marl alternations, forming a relatively rough morphology of prominent ledges. In the subsurface the member is gray-colored, and contains some pyrite. Outcrops are yellow, and somewhat limonitic.

The Upper Member consists of limonitic yellow marls with alternations of marly dolomites, forming a relatively soft morphology. In the subsurface the member is composed of gray, pyrite-bearing shales and marls with some alternations of marly dolomites. The Kesullot Formation is exposed in the central Galilee in the mounts of Hillel, Hazon, Devora, Tavor, and Kesullot. It was penetrated in the subsurface by several wells. The formation is continuous over most of the central and western Galilee, except for several wells in the north-western Galilee, where the Kamon Member directly overlies the Zalmon Formation. The average thickness varies between 40-80 m, being at Har Kesullot about 85 m. It wedges out to the north (Golani, 1957, 1961; Bein, 1967) and to the west. In Har Netofa, about 15 km north of Kesullot, only a few meters of it are detected; in Mount Carmel some 30 km west of Kesullot, about 5 m of this unit are known (Folkman et al., 1966). The formation, completely missing in parts of the northern Galilee (Ya'ara-4, Kabri-3 and Kabri-8), reaches 100 m in the Asher-1 borehole (Zevulun Plain).

Kamon Formation (Golani, 1961).

The Kamon Formation comprises the 'Sajur Dolomite' of Freund (1956), the Ha'ari Dolomite of Eliezri (1965), the Karkara Formation, Lower Member, of Baer (1962), and the Parod Member of Bein (1967). About 160 m are exposed on the eastern slope of Mount Kamon, north of the Netofa Valley. In the western Galilee, only 33 m in the 'Amqa-1 and 45 m in the Qeren-5 wells were drilled. It thickens in the western Galilee towards the west and northwest to a maximum known thickness of 195 m in the Kabri-15 well. The isopach lines form an elongate pattern with a general NW direction. In central Galilee, where data points are more widely spaced, a trend of thickening from east to west is also observed, with the smallest known thickness of 71 m in the Kadoorie-2 well, and the maximum 166 m thick sequence in Mount Kamon. It mainly occurs as a gray, saccharoidal well-bedded dolomite, in layers of 1.5 m. About one hundred meters above the base of the formation a few strata contain flint nodules, quartzolites, and small geodes of milky quartz. Quartzolitic replacement in overlying beds is common. Exposures are known mainly from the central Galilee, in the mounts of Kesullot, Tavor, Netofa, 'Azmon, Zalmon, Kamon, Hazon, Shazor, and Ha'ari. It is exposed in the western Galilee only in the Nahal Bezet River Valley. It was also penetrated by several wells, mainly in the western Galilee. The outcrops on Har Devora are situated on the dip-slope side of the hill.

Contacts: The Kamon Member of the Yagur Formation generally overlies the Kesullot Formation, except in the northwestern part of western Galilee, where it overlies the Zalmon Formation. In its upper part the Kamon Member grades into the somewhat chalky, chert-bearing dolomites of the Karkara Member of the Yagur Formation. In the eastern slope of Mount Kamon the Kamon dolomites are overlain by the Rosh Haniqra Member of the Deir Hanna Formation. The upper contact of the Kamon Member with the Karkara Member is gradational. The dolomites become gradually softer, and more interspersed with chert. In the subsurface, the Kamon Formation is sometimes distinguished from the Karkara Formation only by the presence or absence of cherts. The location of this contact, as obtained from well logs, may thus be misleading due to drillhole contamination.

Karkara Formation (Baer, 1962).

The Karkara Formation (Baer, 1962) represents a part of the Peqi'in Formation of Freund (1958), the Hamima Formation of Eliezri (1965), and the 'Lower Dolomite Member' of the Deir Hanna Formation (Golani, 1961). This interval was described by Golani (1961) as a sequence of 52 m of well-bedded, fine-grained, crystalline, dense, yellow dolomite with abundant nodules, lenses or irregular layers of brown chert, differing from the underlying Kamon Dolomite by the occurrence of chert. This sequence was regarded as the upper part of the Yagur Formation (Picard and Kashai, 1958; Kafri, 1969, 1972).

Its thickness varies greatly, in general inversely to the thickness of the underlying Kamon Formation, becoming thicker in the central Galilee from west to east. It is missing in eastern Mount Kamon.

The Karkara Formation consists of yellow to light gray, soft, chalky, dolomites or chalky limestones. Chert appears in the form of lenticular concretions or nodules and quartzolite with silicified gastropods is common. Chalk occurs in lenses or in thin horizons. In northwestern and central Galilee dolomite is dominant. The chert-bearing limestone contains forminifera and shell fragments.

From the Mount Zevul region Eliezri (1965) reports the following fauna: *Exogyra* sp., *Gryphaea* sp., *Pecten* sp., and *Protocardia* sp., (determ. Raab). In the Meron region were *Avicula* sp., *Chlamys* sp., *Corbula* sp., *Hemiaster* sp., *Nerinea* sp., *Pecten shawi* Pervinquiere, *Pinna* sp., and *Vola* sp. Microfossils: miliolids and ostracodes are abundant. Its age is Albian.

The lower boundary of the Karkara Formation is gradational to the Kamon Formation. The Karkara Formation is generally overlain by the chert-bearing chalks of the Deir Hanna Formation (Rosh Haniqra Member). In regions where the latter is missing it is overlain by dolomites of the Sakhnin Formation. The Karkara Formation is exposed over wide areas in central Galilee, in Mount Tur'an, and the Nazareth Hills, and is also known from a few exposures near Rosh Haniqra, in the eastern part of the Bezet Valley, in the Keziv Valley, in Mount Zevul, and near Jatt.

JUDEA:

Kefira Formation (Itzhaki et al., 1964).

The Kefira Formation stands for the lower part of the Calcari inferiori a Radioliti (Shalem, 1927). It is equivalent to the lowermost part of the Lower Bet Kahil Formation (Rofe and Raffety, 1965). The thickness varies from 100 to 180 m. It consists of predominantly well-bedded limestone alternating with limey dolomite. Oolitic limestone appears in the lower and middle parts of the formation. The formation has been nicknamed 'Emmenthal' for its characteristic and suggestive cavities. The Kefira Formation has been attributed to the Lower Cenomanian since Shalem (1927). Rudists (Blanckenhorn, 1934; Keller, 1933; Picard, 1938; Raab, 1965) are the principal fossils encountered. Hamaoui (1965) found *Orbitolina concava* and *O.* gr. *Discoidea* that point to the Late Albian to Cenomanian, and *Permocalculus* cf. *inopinatus* that has a Barremian-Albian range in the Middle East. The Kefira Formation is developed in Judea and Samaria. Its facies is also present in the lower part of the Yagur Formation in the Galilee. It overlies the Qatana Formation and is followed by the Givat Yearim Dolomite. Lateral passages are not visible, but apparently correspond to the more dolomitic facies in the Yagur Formation in the Galilee and with the sandy dolomites of the lower part of the Hevyon Formation in the Negev. In the Coastal Plain subsurface the Kefira Formation is replaced by the calcilutic Talme Yafe facies. A warm, normal saline, clear and shallow facies is suggested by rudists and foraminifera.

Givat Ye'arim Formation (Itzhaki et al., 1964).

The Givat Ye'arim Formation is a subdivision of the 'Calcari inferiori a Radioliti' of Shalem (1927), uniting the non-formal names Shoeva Dolomite of Flexer (1960), or Platy Quartzolite of Bentor (1959), and the Khirbet el Umur Quartzolite of Flexer (1960). In the Palestinian nomeclature it corresponds to the upper part of the Lower Bet Kahil Formation (Rofe and Raffety, 1965). The type locality at Khirbet al Umar exposes 82.7 m of well-bedded 0.5-1.5 m thick dolomite beds, mostly finely crystalline with coarse crystalline dolomite. Platy quartzolite, 0.9 m thick, with rudists and other bivalves is found in the upper part. Extending all over Judea-Samaria, the unit is very similar to the Yagur Dolomite in the Galilee. It overlies the Kefira Formation and underlies the Soreq Formation.

Soreq Formation (Itzhaki et al., 1964).

The Soreq Formation stands for a part of the 'Calcari Inferriore A Radioliti' of Shalem (1927) in the Jerusalem-Bet Shemesh area. The lower part of the Upper Bet Kahil Formation (Rofe and Raffety, 1965) corresponds to the Soreq Formation. In Nahal Soreq near Ya'ar Canada, a 7 m thick limestone is followed by 120 m of argillaceous dolomites. The limestone is a thin-bedded sequence of alternating limestones and marls. The argillaceous dolomites consist of well- and evenly-bedded (0.5-1 m thick) soft dolomite and interbedded marl, building a characteristic terraced morphology. South of Jerusalem, in the Halhul region, cyclic sequences can be recognized, including rudist biostromes. Quartz spherulites and flint concretions occur parallel to the bedding. In Judea/Samaria the Soreq Formation conformably overlies the Givat Ye'arim Formation and underlies the Kesalon Formation. The Soreq Formation is probably a lagoon facies, passing laterally into the massive dolomites of Yagur. The Dasycladacea and ophiurian remains, benthic imperforate foraminifera, and scarce planktonic foraminifera as well as dynosaur foot-prints point to a shallow marine environment of deposition.

Kesalon Formation (Itzhaki et al, 1964).

The Kesalon Formation stands for a part of the 'Calcare inferiore a Radioliti' of Shalem (1927), designated as 'Main Quartzolite' by Bentor (1945). The Kesalon Formation is equivalent with the upper part of the Upper Bet Kahil Formation (Rofe and Raffety, 1965). In the area of Jerusalem-Bet Shemesh, at Nahal Kesalon, 48 m consist of one of the three following facies types (Braun and Hirsch, 1994):

1) **Dolomite Cliff Unit**. Starting with porous dolomite with rudist and gastropod fragments and often intraformational conglomerate, it mainly consists of cliff-forming massive dolomite beds, as in the area of the Kesalon type section;

2) **Limestone Cliff Unit.** Building an almost vertical cliff, it is mostly devoid of bedding, except on top, where a characteristic oyster bed with occasional corals forms a pseudo-concretional limestone. It occurs mainly in a belt from En Karem (west of Jerusalem) to Tapuah (west of Hebron), known as the 'white hill' at Gush Etzion, as well as in an area NE of Ramallah;

3) **Cyclic Unit**. A lateral development consisting of well-bedded dolomites, varying from 20 to 10 m. It nearly wedges out between the underlying Soreq Formation and overlying Bet Meir Formation, in a belt from Salfit to Nebi Samuel, east of Halhul and southwest of Dura (Hebron Hills).

The Kesalon Formation can be traced over most of Judea and Samaria. It overlies the Soreq Formation and is followed by the overlying Bet Meir Formation.

Its age is top Albian-Earliest Cenomanian (Lewy and Raab, 1976).

NEGEV:

Hevyon Formation (Arkin and Braun, 1965, emend. Hirsch, 1988).

Established within unit C_1 of Bentor and Vroman (1960) at Hamakhtesh Hagadol, the 124 m thick Hevyon Formation consists of well-bedded limestone and dolomite with some marl. It overlies the friable variegated sands of the Hatira Formation (Kurnub Group) and contains quartz and glauconite grains in its lower 1-2 m. Quartz geodes and silicified fossils (mainly rudists) occur in its upper part. The basal beds are glauconitic-dolomitic sandstones which pass upwards into sandy dolomites and dolomites that form a very distinct yellowish cliff. The glauconite disappears about 10 m above the base. The sandstones are quartzose, the coarse grains (up to 0.2 mm) are finer than those of the uppermost beds of the underlying Hatira Formation and are corroded when embedded in dolomite.

Table 18F.3: Judea Group Level 3.

Coastal Plain	Carmel	Galilee	Judea	Negev
Negba	Junediya	Sakhnin	Weradim	Tamar
	Khureibe		Kfar Shaul	Avnon
	Bet Oren	Deir Hanna/Ya'ara	Amminadav	Zafit
	Isfiye	Deir Hanna/ Rosh Haniqra	Moza Bet Meir	'En Yorqe'am

The lower part (50 m) consists of limestone, glauconitic sandy and argillaceous at base, limey dolomite, dolomitic limestone and dolomite, interbedded with marl and marly limestone, with green clay lenses. Fossils comprise molluscs and echinoids. The limestones and dolomites are gray to yellow, very finely crystalline and contain abundant fossil fragments. The marls and marly limestones are yellow, fossiliferous, and contain minor green to gray clay lenses. The fossils are represented by gastropods, lamellibranchs anad echinoids. The base of the member is characterised by a glauconitic sandy argillaceous limestone which corresponds to part of the C_1 subunit. A yellow to green clay layer, 1.8 m thick, appears at the top of this unit.

The middle part of the member consists of 60 m of soft dolomite interlayered with thin beds of marls and clay. Three hard dolomite layers form small cliffs. The dolomite is gray to yellow, finely crystalline, and contains fossil fragments. Flint concretions appear in the lower beds.

The upper part consists of well-bedded limestones forming a cliff of about 13.5 m. The limestones are gray to yellow, fine to medium crystalline, and contain abundant, partly silicified fossil fragments. The fossils are represented by lamellibranchs, echinoid, gastropods, and ammonites. The top 0.5 m of the Hevyon Formation form the ostreid bank marker horizon of the Cenomanian sequence in the Negev. Gray dolomites, in places with brownish-gray chert nodules (up to 5 cm), form hard ledges at the top.

The top of the Hevyon Formation is made of a 10-20 cm thick ferruginous, highly fossiliferous marly limestone bed. This bed contains earliest Cenomanian ammonites and abundant *Pycnodonte vesiculosa* (Sowerby) filling vugs within the underlying rock. This bank at the top of the Hevyon Formation should therefore be regarded as the base of the 'En Yorqe'am Formation. The upper part of the Hevyon Formation corresponds well with the Kesalon Formation of the Judean Mountains. In Jordan, the lower part of the Naur Formation corresponds to the Hevyon Formation.

Fauna: Besides *Cerithium elias* Boehm, the Late Albian ammonite *Hypengonoceras* sp. occurs in the first third of the Hevyon Formation, indicating that the Albian-Cenomanian boundary probably occurs within the uppermost part of the Hevyon Formation (Lewy, 1981).

Age is Late Albian, with the top-bed possibly Cenomanian.

Early-Middle Cenomanian level of the Negba Formation of the subsurface of the Coastal Plain (**Table 18F.3**).

In Mount Carmel and the Galilee it subdivides into a complex facies system, the correlation between whose parts is often difficult due to intensive block faulting. In this subdivision vertical boundaries between chalk and limestone channels and dolomite ridges prevail. In the Carmel area the succession of the Isfiye Chalk, Bet Oren Limestone, and Khureibe and Junediya Chalks is bounded by the Carmel Reef Complex, intercalated by the Igzim, Fureidis, Umm-E-Tuss, and Shefeya volcanic Tuffs. The western and central Galilee Rosh Haniqra Chalk (Peqi'in/Tufaniya), and Ya'ara and Yanuh Limestones combine together into the Deir Hanna Formation, bounded by the dolomite Sahnin Formation (Rosh Tsurim). In the Judean Hills and Negev the lithostratigraphic subdivision comprises the Lower Cenomanian chalks, dolomites, marls, and dolomitic limestones of the 'En Yorqe'am, Bet Meir, Moza Marl, and Zafit/Amminadav Formations respectively. The Middle Cenomanian consists of the chalk/limestone channels of the Avnon/Kfar Shaul Formation, bounded by the dolomite flats of the Weradim/Tamar Formation. A distinct regression characterizes the end of the cycle, marked by hard-ground and a faunal break.

COASTAL PLAIN:

Negba Formation (Gvirtzman and Buchbinder, 1966).

The Negba Formation is defined at the Negba-1 well at a depth between 163 and 540 m. The lower third of the sequence comprises dolomites with marl intercalations (Lower Member). The upper two thirds encompasses more marls with dolomite and limestone interbeds (Upper Member). The lithology of the Upper Member may vary, becoming more limy in the Negba-SH8, Beeri-2, and Massuot Yizhak wells etc. The Negba Formation overlies the Yagur Formation. At its top it is overlain by the Daliyya Formation. The Lower Member and the lower marls of the Upper Member yield the Early Cenomanian planktonic foraminifer (*Favusella washitensis*). Most of the Upper Member yields Middle Cenomanian foraminifers.

CARMEL:

Isfiya Formation (Picard and Kashai, 1958).

The name of the Isfiya Formation is derived from the village of Isfiya on Mount Carmel. It was first identified as the Lower Chalk by Picard and Kashai (1958), within the *Main Chalk Complex* of Mount Carmel or the *Chalk-Flint Series* of Blake (1935). It is 70 m thick, overlying the *Yagur Dolomite* and is overlain by the *Meleke-Gryphaea Beds*. The Isfiya Formation consists of white or yellowish, slightly argillaceous chalk; it contains limonitic concretions and nodules of flint. Locally, the chalk passes laterally

into dolomites and crystalline limestones, and partly brecciated Rudist reef-limestones.

Bet Oren Limestone (Karcz, 1959).

The Bet Oren Limestone is a 30 m thick coarse crystalline 'meleke' limestone with rudistids passing to the northwest into the '*Gryphaea vesiculosa*' marly limestone. The unit intercalates the chalk series, overlying the Isfiye Chalk and being overlain by the Khureibe Chalk.

Khureibe Formation (Picard and Kashai, 1958).

The Khureibe Formation, the 'Khureibe Chalk'of Picard and Kashai (1958), stands for the Middle Chalk. The name is derived from the village of El Kureibe on Mount Carmel. This sequence, which is 120 m thick, forms one of the subdivisions of the *Main Chalk Complex* of Mount Carmel, referred to earlier by Blake (1935) as the *Chalk-Flint Series.* It overlies the *Meleke-Gryphaea Beds* and underlies the *Juneidiya Chalk.* It consists of white, slightly argillaceous chalk with flint nodules, overlain by hard limestones or dolomites. The sequence is very fossiliferous and yields *Acanthoceras* sp. *Mantelliceras* sp., *Euomphaloceras* sp., as well as *Orbitolina* sp.

Juneidya Formation (Picard and Kashai, 1958).

The Juneidya Formation corresponds to the Upper Chalk or uppermost subdivision of the *Main Chalk Complex* of Mount Carmel, referred to earlier by Blake (1935) as the *Chalk Flint Series.* The Juneidya Formation overlies the *Khureibe Formation* and underlies the *Mushraqa Formation.* Its thickness is 60 to 80 m and consists of chalky limestone - locally named *Sultaneh* - occasionally alternating with fine-bedded limestone. Flint concretions appear either in the lower or the upper part of the sequence. The fossiliferous unit carries *Eucomphaloceras meridionale.*

GALILEE:

A wealth of units have been described in the Galilee for the Early-Middle Cenomanian interval of the Judea Group. These encompass 'Middle Cenomanian' (Picard, 1956; Vroman, 1958), the Main Chalk Complex (Picard and Kashai, 1958), the Peqi'in and Tufania Formations (Freund, 1958), the Deir Hanna Formation (Golani, 1961), the Jermaq Formation (Eliezri, 1965), the Sulam Zor Formation (Baer, 1962), and the Balatun Chalk (Wolff, 1967).

Deir Hanna Formation (Golani, 1961).

At the type section on the southern slope of Mount Kamon, west of Wadi Kamana, the thickness of the Deir Hanna Formation is around 200 m. It reduces to 110 m in the region of Ramim and Misgav Am (Rosenberg, 1960). The Deir Hanna Formation consists of two main facies types.

Towards the west and north, the **chalk and limestone facies** is almost devoid of dolomite. It extends from Ramim/Manara to the Mediterranean coast. With transitions at Mount Meron, Bet Jann and Sasa, a **dolomitic facies** appears, that extends toward the east and south, into the central Galilee (Nazareth Hills, Mount Tir'an, Mount Netofa, Mount Kamon) and Mount Gilboa.

Golani (1961) subdivided the Deir Hanna Formation into three members:

1) The 'Lower dolomite member', a sequence of 52 m differing from the underlying Kamon Dolomite by the occurrence of chert. It is coeval with the Karkara Formation (Baer, 1962);

2) The 'Median chalk member', a 105 m thick chalk and limestone-rich chert, coeval with the Rosh Haniqra Member (Kafri, 1969);

3) The 'Upper dolomite member', 40 m of well-bedded dolomites with chert and some chalk, coeval with the Ya'ara Member (Kafri, 1969).

In the northwestern Galilee the *Rosh Haniqra Member* (Kafri, 1969) represents a thick morphologically soft unit of chert-bearing chalks alternating with limestone or dolomite beds. The chalks are biomicrites containing microfossils and megafossil debris of various sizes and degrees of sorting. Intraformational conglomerates, so-called 'Pseudobreccias' of limestone, dolomite, and chalk were derived from the same basin of sedimentation. The meter to decimeter thick limestone intercalations consist of mud-supported and sometimes grain-supported biomicrite and biosparite containing micro and megafossils. The soft white chalk with many brown chert nodules or layers, abundant quartz concretions, small black nodular chert, limestone built of Rudists debris and pink limestones at top, attains over 300 m in thickness in the region of Rosh Haniqra, on the Mediterranean coast (Grader, 1958). The chalky lithology of the Rosh Haniqra Member becomes marly in the subsurface. Pyrite and basalt cuttings were found in the Kabri-15 well at the base of the member. In northwestern Galilee, the Rosh Haniqra Member develops into three small 'basins' separated by 'ridges':

A) The Kabri-Rosh Haniqra Basin (A), elongated in a NW direction, reaches a thickness of 220-280 m in the Kabri and Ga'aton wells.

B) It is separated by the northwest trending Montfort-Shelomi ridge from the WNW elongated Rosh Hamabua'-Ya'ara Basin (B), which reaches a thickness of over 170 m in the Nahal Ukam Valley.

C) The WNW oriented Fassuta-Iribin ridge has almost no deposition of the Rosh Haniqra Member. The Biranit Basin (C) is also WNW-directed and is over 110 m thick at Mount Rahav.

In central Galilee the Rosh Haniqra Member becomes considerably thinner, composed of marly chalks alternating with clayey, soft, limonitic dolomites. Rudistid 'reef' zones (eastern Mount Kamon, Nahal Hilazon and Shazor area) contain intraformational conglomerates, adjacent to the reefs. Chert nodules and lenses, abundant in most of the area, decrease in the Ya'ara region. In central Galilee and in the southern part of western Galilee and the Zevulun Plain, the Rosh Haniqra Member is reduced to 20-40 m. Over wide areas it is laterally replaced by dolomites or rudistid reef dolomites with quartzolites. A NE-trending belt of such 'reefs' runs from western Mount Kamon through the Sakhnin Valley, Kaukab, and west of the Beit Netofa Valley. The chalky

formation of the Carmel has the same stratigraphical position. There is much similarity between the chalky Deir Hanna facies of the northern Galilee and that of the Carmel (Kashai, 1958). The Rosh Haniqra Member overlies the dolomites and limestones of the Karkara Formation (or Yagur Formation) except for one place in eastern Mount Kamon, where it directly overlies the Kamon Formation. It is overlain either by the Ya'ara Member dolomites of the Deir Hanna Formation, or where the Ya'ara Member is missing, by the Sakhnin Dolomite. The upper contact is generally irregular.

Fauna (described by Freund, Eliezri, Weiler and Gratch): *Acteonella* sp., *Cerithium* sp., *Exogyra columba* Lmk., *Exogyra flabellata* Goldfuss, *Gryphaea* cf. *vesicularis* Lmk., *Hemiaster* sp., *Neithea* sp., *Nerinea cochleaeformis* Conrad, *Nerinella* sp., *Pecten Shawi* Pervinquiere, *Protocardia* spp., *Sauvagesia* sp., *Trigonia ethra* Conquand, as well as (det. Raab): *Belemnites* sp., *Dunveganoceras* sp., *Cardium (Protocardium) coquandi* Seg., *Euomphaloceras africanum* (Pervinquiere), *Forbesiceras* sp., *Protacanthoceras aff. P. compressum* (Jukes-Browne) *P. judaicum* (Taubenhaus), *Scalaria philippii* Reuss. Planktonic foraminifera (det. Hamaoui): *Hedbergella* sp., *Hedbergella (Asterohedbergella) asterospinosa Hamaoui,* and *Praeglobotruncana* sp. Benthonic foraminifera include: *Gavelinellidae, Gavelinella aumalensis* (Sigal), *Gyroidynoides* sp., *Oligostegina* sp., and *Spiroplectammina* sp. Textulariidae, Lagenidae, Lituolidae, and Ostracodes are also present. Age is Cenomanian.

The *Ya'ara Member* (Kafri, 1969) is composed of well-bedded light-colored chalky dolomites or limestones, intercalated with some chalks and marls and containing chert. The limestones, often chalky, with limonitic staining, are mud-supported biomicrites. The limestone facies of the Ya'ara Member is restricted to the eastern part of the Kabri-Rosh Haniqra Basin (Keziv Valley, eastern Kabri wells, and the Jatt and 'Amqa-3 wells) and to the Mount Manor region. In all other places (Ya'ara, Zuriel, Beit Jann, Mount Shazor, the central Galilee, and the western Kabri and Qeren wells) the facies is dolomitic and is identical with the 'Upper Dolomite Member' of Golani (1961).

In the Ya'ara region of the western Galilee it reaches 109 m (Ya'ara-4 well), and 131 m in the Karkara section. Towards the east and west, the member decreases drastically and is completely missing in the Fassuta-Iribin and the Shelomi areas. In the Mount Manor section the Ya'ara Member is 53 m thick, while further east of this region it wedges out completely. In the central Galilee a thickness of 48 to130 m is found.

Contacts: The Ya'ara Member passes laterally into or overlies the chalks of the Rosh Haniqra Member and in one place, where the latter are absent (Eilon region), it directly overlies the Karkara Formation or Yagur Formation. The Ya'ara Member passes laterally into and is overlain by the dolomites of the Sakhnin Formation. The Ya'ara Member yields well-preserved megafossils in the Nahal Keziv Valley. Megafossils (det. Raab) are *?Cariophyllina Gen. aff. Trochocyathus* sp., *Douvilleaster vatonnae* (Coquand), *Protocardia* sp., *Trigonia ethra* (Coquand), *?Calycoceras harpax* (Stoliczka), *Protacanthoceras* sp., *P. angolaense* Spath, and *P. judaicum* (Taubenhaus). Rudist biostromes occur approximately 2-3 km west of Mount Kamon (Golani, 1961).

Planktonic foraminifera (det. Hamaoui) are: *Globigerinelloides* sp., *Hedbergella (Asterohedbergella) asterospinosa* Hamaoui, and benthonic microfossils: *Gavelinella aumalensis* (Sigal), and *Oligostegina* sp. Ophthalmidiidae, Textulariidae, and Ostracods are also present. Its age is Cenomanian.

Sakhnin Formation (Golani, 1961).

The Sakhnin Formation corresponds to the Rosh Tsurim Dolomite of Freund (1959), the Peqi'in Dolomite of Eliezri (1965), and the Eilon Formation of Baer (1962). Along the northern slope of Mount Kamon, near the village of Sakhnin, the 205.5 m thick section consists of hard, fairly well-bedded, thick to very thick dolomite. The Sakhnin Formation forms a dark gray rough rocky landscape distinct from any other formation in the Galilee. Calcitic dolomites often pass laterally into coarsely crystalline limestones of the 'meleke' type. Dolomite-types include aphanocrystalline to coarsely crystalline dolomites, rich in vugs which are partly filled by a drusy dolomitic mosaic; finely crystalline dolomites; grain-supported biomicrites, found in thin transition zones between the Sahknin and Yanuh Formations, associated with fossil-bearing quartzolites; and microbreccias of dolomites containing large intraclasts, known from the margins of the thick dolomite regions.

In some places the Sakhnin dolomites pass laterally into the Rosh Haniqra or the Ya'ara Member. Dedolomitization occurs. The lower, partly biohermal part of the Sakhnin Formation is characterized by its dark, massive appearance. Bedding develops towards the upper part. The massive Galilee dolomitic development of the Sakhnin Formation can be traced to the south into the Judean hills (Amminadav-Weradim Formations) and into the Negev (Zafit-Tamar Formations). The Sakhnin Formation sharply overlies the soft yellow dolomites and chalks with chert of the Deir Hanna Formation. The Sakhnin dolomites overlie the Ya'ara Member, and in places where the latter is absent, directly over the Rosh Haniqra Member. Where the Rosh Haniqra chalk is missing, the Sakhnin Formation overlies the Karkara Formation (Iribin, Montfort, the central Galilee). The upper contact of the Sakhnin Formation is either with the Yanuh Formation or transitional to the bedded lithographic limestone of the Bi'na Formation. This transition has been discussed by Golani (1961), Baer (1962), Kafri (1965), and Sass (1966). At Beit Netofa, the Sakhnin Formation is unconformably overlain by the Senonian Menuha Chalks.

The distribution of the Sakhnin Formation in the Galilee is controlled by the lateral development of the Khreibe/Junediya Formations of the Carmel or the Deir Hanna Formation of the Galilee. The lateral changes from the shallower platform facies of Sakhnin to the relatively deeper Deir Hanna facies, exposed in the Galilee (Kafri, 1972, 1991) are found in the Judean Mountains and in the Negev, in the lateral changes of the Kefar Shaul/Weradim and Avnon/Tamar Formations respectively. The Sakhnin Formation contains *Acteonella* sp. *Chondrodonta* sp., *Hemiaster* sp., *Nerinea* sp., *Nerinea requieni d'Orb. Sauvagesia* sp., *Trochalia* sp. and rudists: (det. A. Parnes) *Caprinula* sp., *Ichthyosarcolites* sp., and

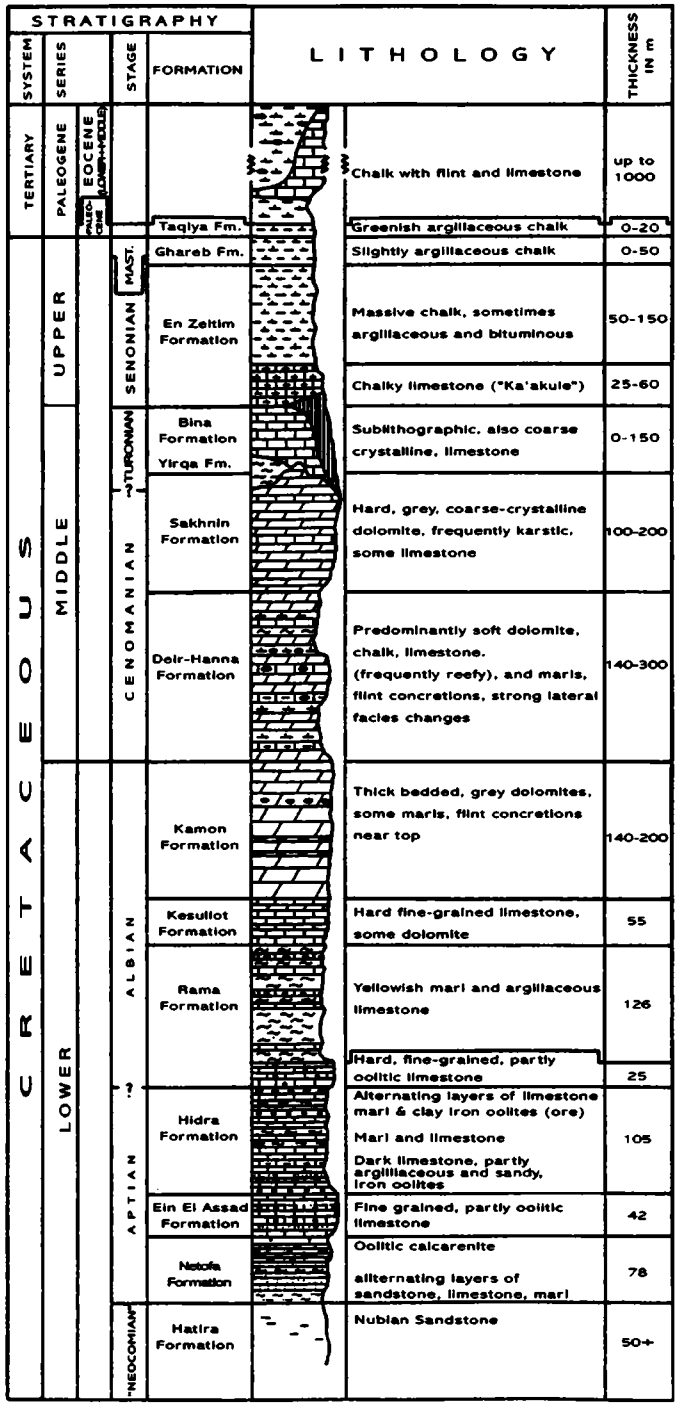


Figure 18F.8. The Cretaceous of Galilee (after Bentor, 1963 - Clay conference).

Radiolites sp. The age of the Sakhnin Formation, in regions where it is transitional to the overlying Bi'na Formation, is considered Cenomanian-Turonian. In those limited areas where it is overlain by the Upper Cenomanian Yanuh and the Lower Turonian Yirka Formations, its age is Upper Cenomanian.

JUDEA:

Bet Me'ir Formation (Itzhaki et al., 1964).

The Bet Me'ir Formation (Itzhaki et al., 1964) stands for the 'Calcare inferiore a radioliti' (partim) of Shalem (1927); and Yatta Formation (partim) of Rofe and Raffety (1965).

At Nahal Kesalon, Jerusalem, the formation consists of well-bedded dolomites, whereas south of Jerusalem, it may be represented by yellowish chalky marl (*e.g.* the so-called 'yellow hill' at Gush Etzion). The latter contains abundant ammonites of Early Cenomanian age. The well-terraced alternations of dolomite and marl contain abundant flint concretions, called 'Elias balls'. The uppermost part of the formation is often rich in large bivalves and gasteropods.

The lower contact of the Bet Me'ir Formation with the underlying Kesalon Formation is apparently conformable, although it is often characterised by infiltration into the underlying unit, in the form of neptunian dykes and conglomerate. It is conformably overlain by the Moza Formation.

Early Cenomanian ammonites occur at its base (Lewy and Raab, 1976). From Judea and Samaria the formation passes laterally into the 'En Yorqe'am Formation (partim) of the Negev and the Isifya (partim) or Deir Hanna (Rosh HaNiqra - partim) of northern Israel.

Moza Formation

The Moza Formation embraces the Early Cenomanian *Argille e marne argillose* of Shalem (1925), the 'Marne argillose di Motza' of Shalem (1926) emend. Moza Marl of Picard (1938), emend. Itzhaki et al. (1964), and uppermost part of the Yatta Formation of Rofe and Raffety (1965). At its type locality near Zova 15.1 m (5 m near Moza) it consists of yellowish-green marls and calcareous clays. According to Shalem (1928) it yields: *Cerithium tenouklense* Coq., *Nerinella subequalis* d'Orb., *Tylostoma syriacum* Conr., *T. induratum* Conr., *Pterodonta* sp., *Plicatula auressensis* Coq., *Exogyra columba* Lmk., *E. flabellata* Goldfuss, *Pecten dutrugei* Coq., *Septifer lineatus* Sow., *Cardita forgemoli* Coq., *Cardium* cf. *syriacum* Conr., *Protocardia combei* Lartet, *Dosinia delettrei* Coq., *Pholadomya vignesi* Lartet, *Corbula eretzisraelensis* Shalem *Heterodiadema libycum* Cott., *Goniopigus menardi* Des., *Holectypus larteti* Cott., *Exogyra columba, Cardita forgemoli, Dosinia delettrei, Pholadomya vignesi, Corbula eretzisraelensis, Turbo magnolfae, Scalaria grilli, Fusus, Chrysodomus, Helectypus larteti,* and Vermes etc. These strata have been subdivided by Shalem into a lower part, called by him *Argille a Corbula eretzisraelensis* Shalem and an upper part he refers to as *Marne argillose di Motza.*

The Early Cenomanian Moza Formation of the Judean Mountains conformably overlies the Bet Meir Formation and underlies the Amminadav Formation. The Moza Formation corresponds to the upper part of the 'En Yorqe'am Formation in the Negev, part of the Deir Hanna (Rosh Haniqra) and Isifiya Formations in northern Israel.

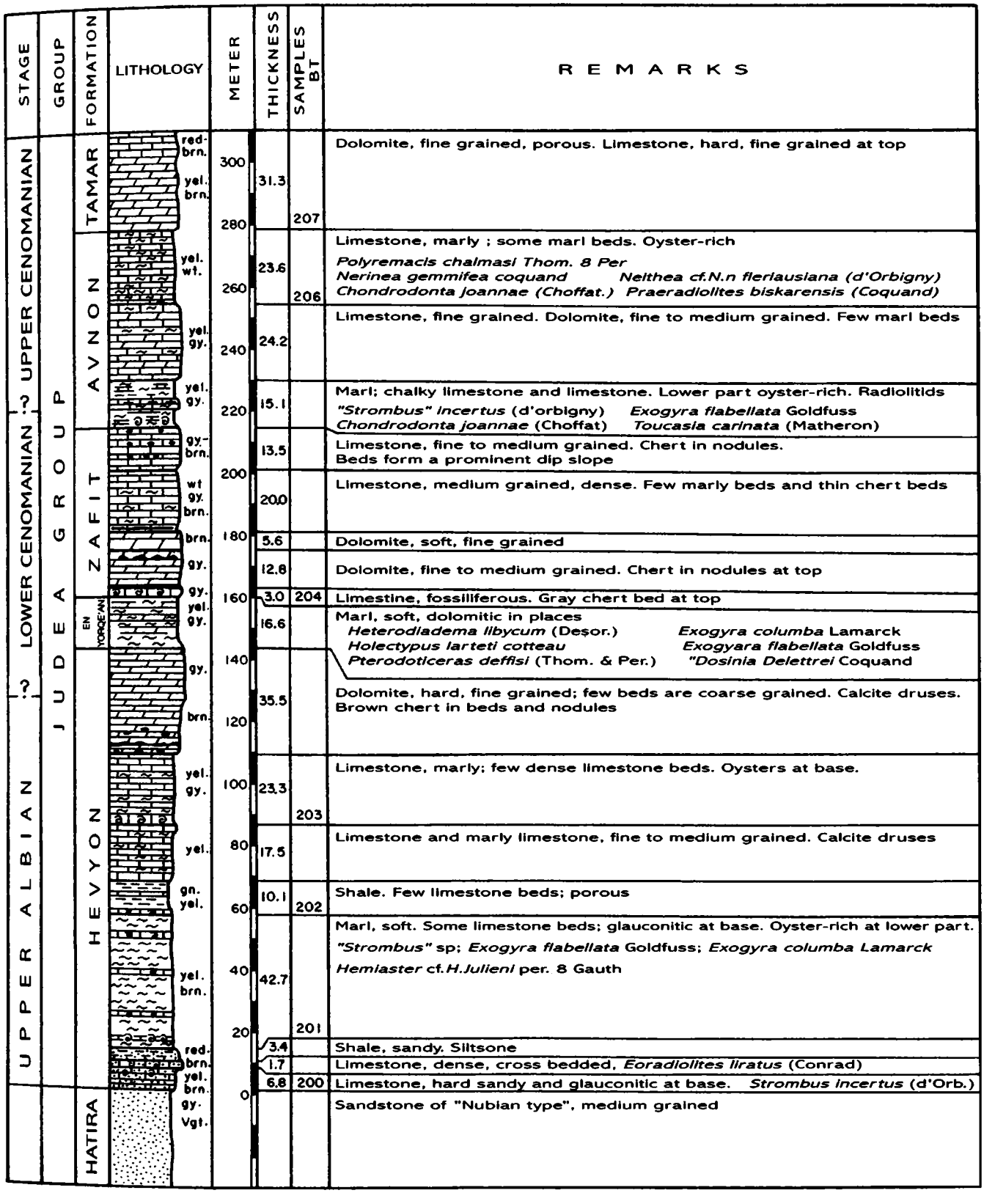


Figure 18F.9. Albian–Cenomanian columnar section in the Northern Negev (modified after Bartov et al., 1980, Fig. 6, p. 120).

The Marne argillose di Motza separates between the *Calcare a Pterodonta deffisi* and the *Calcare inferiore a radioliti* and thus corresponds entirely to the Moza-Marls of Picard (1938b).

Amminadav Formation (Itzhaki et al., 1964).

The Amminadav Formation stands in the Jerusalem-Bet Shemesh area for the 'Calcari a Pterodonta deffisi' of Shalem (1925) or the 'Dolomite and Meleke' of Picard (1938). Near the village of Amminadav, southwest of Jerusalem, 95 m of predominantly dolomites pass into limestones at the top. The dolomite and limestone often contains silicified inclusions called quartzolites.

The formation extends to Samaria in the north and passes into the Zafit Formation of the Negev towards the south. It is coeval with part of the Deir Hanna Formation in the Galilee.

Kefar Sha'ul Formation (Itzhaki et al., 1964).

The Kefar Sha'ul Formation includes the 'Deir Jassini' and 'Acanthoceras marly limestone'. Near Giv'at Sha'ul (Jerusalem) it consists of a lower argillaceous member of fossiliferous argillaceous limestone and marl and an upper laminated limestone member that yields fossil fishes. It is 75 m at the type locality but wedges out or passes laterally into bedded dolomites. The rich megafauna indicate a Middle Cenomanian age. The Kefar Sha'ul Formation is limited to certain corridors within the Judean Hills of Samaria and Judea. Sharp contacts with the underlying Amminadav Formation and overlying Weradim Formation contrast with lateral passages or changes in facies such as in the Judean Mountains between the Jerusalem and Hebron areas, where well-bedded dolomites may replace the formation.

In the Galilee the Kefar Sha'ul Formation corresponds to part of the Deir Hanna Formation. In the Carmel region it is replaced by the Khureibe Formation. The Negev Avnon Formation corresponds to the Kefar Sha'ul Formation. The Kefar Sha'ul Formation probably represents the deepest open marine facies of the Judea Group. It occurs as large channels, bounded by shallower carbonates.

Weradim Formation (Itzhaki et al., 1964).

The Weradim Formation stands for the 'Calcari superiore a Radioliti' (partim) of Shalem (1927), the Mizzi (Misi) Yahudi (Jehudi) of Blanckenhorn (1905), and the Bethlehem Formation of Rofe and Raffety (1965). It consists of 25-100 m of well-bedded to massive dolomites and limey dolomites with lenses of crystalline limestone. The Weradim Formation is equivalent to the Sahknin and Tamar Formations. Usually the Weradim Formation conformably overlies the Kfar Shaul Formation, however it may directly overlie the Amminadav Formation south of the Jerusalem-Bet Shemesh area, apparently replacing the Kefar Sha'ul Formation.

NEGEV:

'En Yorqe'am Formation (Arkin and Braun, 1965; emend. Begin, 1975).

The 'En Yorqe'am Formation is 57.5 m thick at Hamakhtesh Hagadol, where it consists of soft gray fossiliferous marls, argillaceous limestones, and dolomite. The lower 20 m consist of fossiliferous argillaceous limestone with quartz geodes and marl. The middle 11.5 m are white to yellow, thin-bedded silicious limestones, rich in echinoid spines in the upper beds.

The upper 26 m consists of fossiliferous limestone, argillaceous limestone, and clay interbeds. A glauconitic layer occurs 3.5 m below the top. Abundant bivalves, gastropods and echinoids occur throughout the formation. Orbitolinids and ostracodes are frequent. A light brown glauconitic sandstone layer 0.5 m thick appears near the top of the formation. South of Nahal Rehavam (*e.g.* at Sheikh Atiya) a sandstone tongue is well-developed. Fine-grained calcitic sandstones occur at the base of the formation, overlain by shales and marls. In the Be'er Ora region marly-shales occur in the lower part, followed in the middle and upper parts by fossiliferous argillaceous limestones, with spotted dolomites and limonitic concretions. The formation extends from the Negev into the Jordan Valley.

The 'En Yorqe'am Formation passes laterally into the Bet Meir and Moza Formations. It is coeval with the Isifiya and Rosh Haniqra Formations in northern Israel. In Jordan, the middle part of the Naur Formation corresponds to the 'En Yorqe'am Formation.

Fauna are: Corals, *Heterodiadema libycum* (Desor), *Holectypus larteti* Cott., *Holectypus subpentagonalis* Blanck., *Hemiaster batnensis* Coq., *Ostrea* sp., *Exogyra africana* (Lam.), *Exotyra flabellata* Goldfuss, *Neithea* sp., *Corbis rotundata* d'Orb, *Liopistha alta* Roemer, *Cardita forgemolli* Coq., *Cardium* sp., *Dosinia delettrei* Coq., *Pterodonta dutrugei* Coq., *Cerithium tenouklense* Coq., *Kingena umbaghensis* Shalem, *Exogyra flabellata* Goldf., *E. columba* Lmk., *E. africana* Lmk., *Pecten dutrugei* Coq., *P. (Neitha) Shawi* Perv., *Inoceramus* cf. *elevatus* Conr., *Cardita forgemoli* Coq., *C. beuquei* Coq., *Dosinia delettrei* Coq., *Protocardia hillana* Sow., *Cerithium tenouklense* Coq., *Architectonica* sp., *Pterodonta homarensis* Blanck., *Deltoido-nautilus triangularis* (Monfort), Nautilus sp., and Nerinella sp. The age is Early Cenomanian.

Zafit Formation (Arkin and Braun, 1965; emend. Hirsch, 1986).

The Zafit Formation is a 47 m thick sequence at the type section, located in Hamakhtesh Haqatan approximately 200 m east of the entrance to the Makhtesh Haqatan. The Zafit Formation is composed mainly of gray limestones forming a massive cliff. The lower part forms a distinct cliff with 25 m of massive-bedded limestone, dolomitic limestone and dolomite. The limestones are gray to brown, nodular, white-gray, hard, fine-grained limestones, well-bedded with soft marl interbeds, and contain fossil fragments of bivalves and rudists. The dolomite is gray, finely crystalline and contains flint concretions in places. Chert nodules are frequent, some have a brown concentric banding. The upper 22 m consists of thin well-bedded dolomite and calcitic dolomite with horizons of flint concretions and fossil fragments. The upper beds contain iron concretions and a pink phosphate mineral. *Nerinea* occurs sometimes in banks in the southern outcrops. The Zafit Formation occurs in the Negev and Dead Sea cliffs, it is equivalent to the Aminadav Formation in Judea and to the upper part of the Naur Formation in Jordan. Fauna consists of *Nerinea* sp. and *Eoradiolites* sp. *Neolobites* sp. was found in the lower part of the Formation near Be'er Ora.

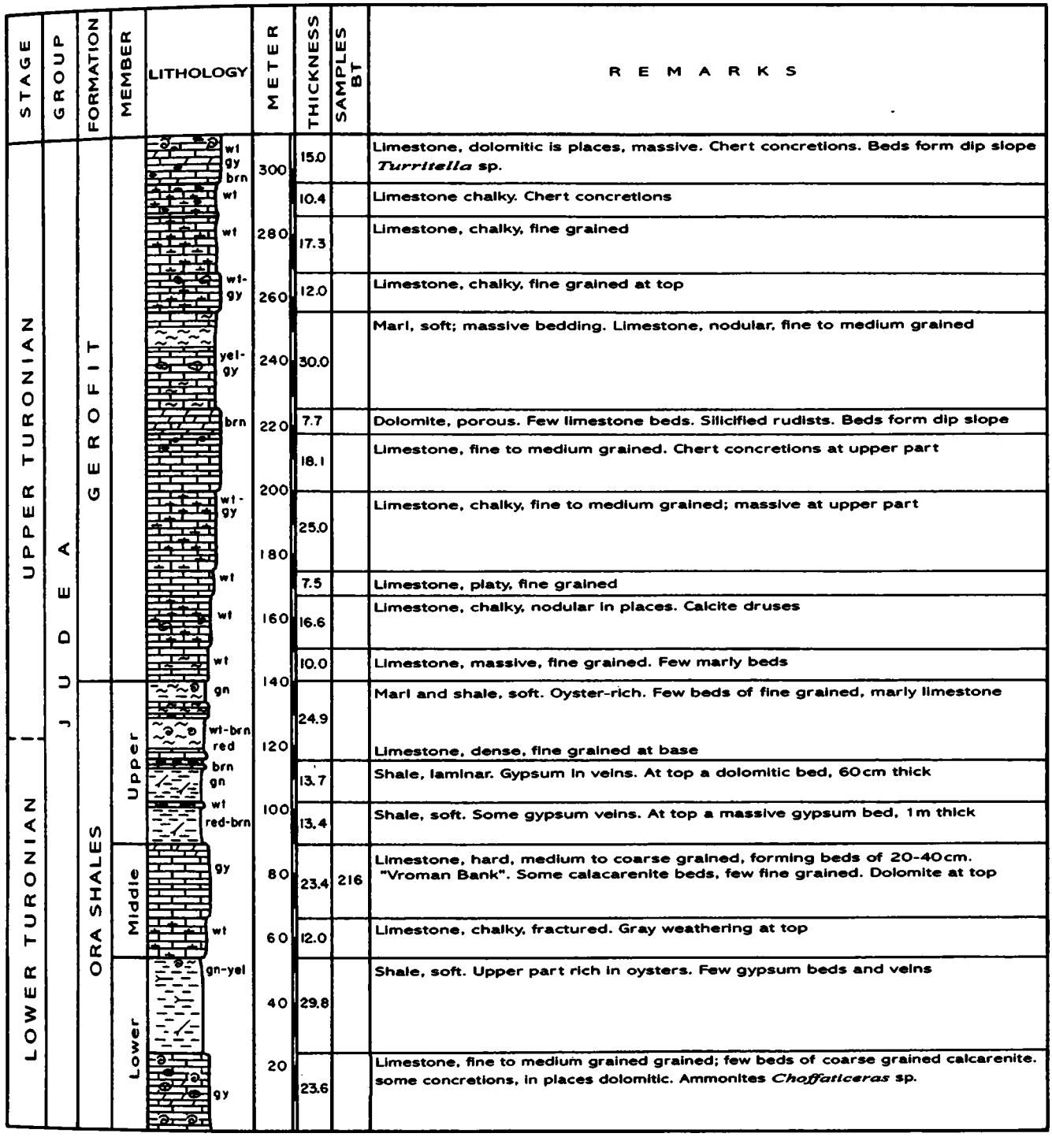


Figure 18F.10. Turonian columnar section of the Southern Negev (after Bartov et al., 1980, Fig. 8a, p. 122).

Avnon Formation (Arkin and Braun, 1965; emend. Begin, 1975).

Hamakhtesh Haqatan is the type section of the Avnon Formation where it reaches 104 m in thickness. In Nahal Hazera, at the entrance of Hamakhtesh Haqatan, the formation consists of three parts.

1) The lower 12 m consists of white to light yellow, microcrystalline limestone containing calcitized and limonitized fossil fragments. The limestone is interbedded with yellow to green marls containing *Gryphaea* and echinoids.

2) The middle 80 m consists of a lower section of 44 m of yellow-white limestone and dolomitic limestone, with fragments of rudists and other molluscs. A detrital fossiliferous limestone layer and a black bituminous limestone layer are characteristic of the top of this section. Above follows a section of 36 m of massive-bedded dolomite which forms two cliffs. The dolomite is gray to brown, fine to coarse crystalline and contains fragments of rudists, other bivalves, and gastropods. Both the limestone and dolomite form small cliffs separated by the softer layers.

3) The upper 12 m consists of soft limestone, marl, and dolomite. The limestone is gray to light brown, very finely crystalline and in places becomes limey and argillaceous.

The total thickness of the formation at its type section is 104 m. A Middle Cenomanian age can be attributed, based partly on ostracodes. Lateral passage into the overlying Tamar Formation is common. Such features also characterize the coeval Kfar Shaul/Weradim and Deir Hanna/Sahnin Formations. The formation extends from the Negev to the Dead Sea cliffs and the southern Jordan Valley. The Avnon Formation corresponds to the Kfar Shaul Formation in central Israel and the Fuheis Formation in Jordan.

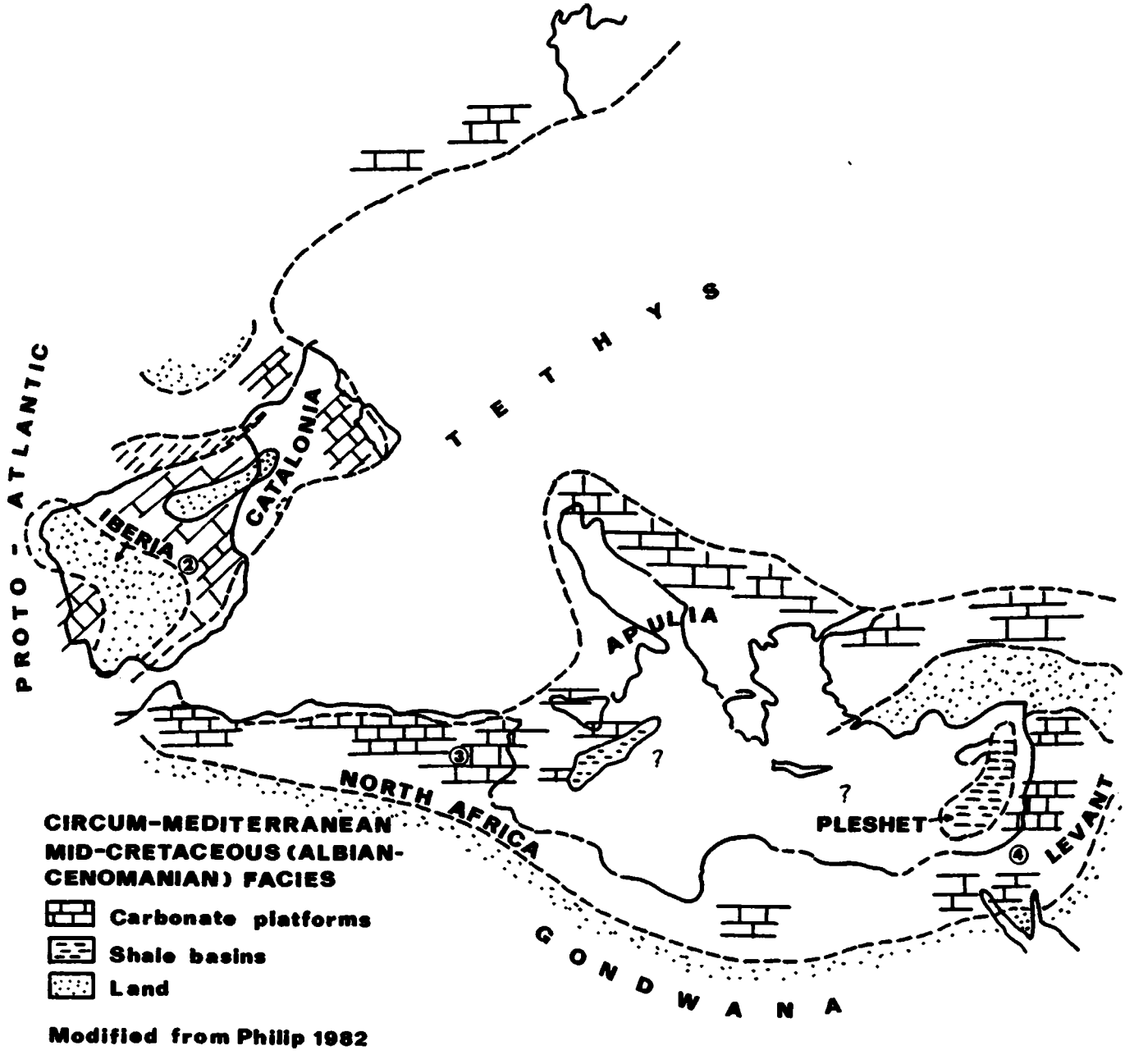


Figure 18F.11. Circummediterranean Albian–Cenomanian facies (modified after Philip, 1982).

Tamar Formation (Arkin and Braun, 1965; emend. Hirsch, 1986).

At Hamakhtesh Haqatan the Tamar Formation is 44 m thick, but elsewhere it varies considerably. It forms a hard, mainly dolomitic unit that consists of brown-yellow dolomite, dolomitic limestone and limestones alternating with marl. The lower part of the formation is harder and forms a prominent massive cliff. Its middle part contains some limestone and marl beds of a soft appearance separating a lower and an upper cliff. The upper part consists of well-bedded dolomite and dolomitic limestone. The top of the Tamar Formation locally shows hard-ground phenomena such as bivalve borings and ferruginous impregnation, thus representing a hiatus at the top (Lewy, 1990). The Tamar Formation is equivalent to the Weradim and Sakhnin Formations.

Lateral passages of the Avnon Formation into the overlying Tamar Formation are frequent. As a result, thickness variations compensate each other. The Avnon and Tamar Formations together maintain an average thickness of 150-160 m.

Hazera Formation (Arkin and Braun, 1965).

The Hazera Formation is a formation established in the northern Negev (southern Israel) for units C1-C5 of Bentor and Vroman (1960). The name is derived from Nahal Hazera, which drains the Makhtesh Hagadol. It was subdivided into five members which were later elevated to the Hevyon, 'En Yorqe'am, Zafit, Avnon, and Tamar Formations (emend. Begin, 1972; Hirsch, 1988).

The approximately 380-400 m thick rock sequence of the Makhtesh Hagadol and Makhtesh Haqatan is reduced to 110 m in the Elat region. This reduction, mostly at the expense of the lower units, is accompanied by facial changes of the upper units. The term Hazera Formation, as retained in the southernmost Negev, comprises in its lower part equivalents of the Hevyon, 'En Yorqe'am, and Zafit Formations. Its upper part is coeval with the Yotvata Member of the Ora Formation (*sensu* Sakal, 1967), but replaces the Avnon and Tamar Formations. The Hazera Formation onlaps the Hathira Formation and is covered by the Derorim or Ora Formations.

Yotvata Member (Eckstein and Rosenthal, in Hamaoui, 1966): The Yotvata Member is included in the Hazera Formation, although not developed at the type section. Sakal (1967) therefore set the lower boundary of the Ora Shales so as to include these beds. According to Bartov (1972), the unit is lithologically similar to the underlying sequence attributed to the Hazera Formation, while differing considerably from the overlying shaly strata. The Yotvata Member seems to be a lateral replacement for the Avnon and Tamar Formations. Its top, forming a morphologically broad shoulder, is a convenient boundary. In the Elat area, the lower part is composed of soft fossiliferous, well-bedded, white to gray, argillaceous limestones alternating with rarer marl and shale beds. Some beds are exceptionally rich in fossils, mainly ostreids. In the upper part, two gray-brown platy limestone beds ('paper limestones' of Freund, 1962) form prominent ledges. Limonite concretions, up to 5 cm in diameter, and a fine limonitic impregnation parallel to the bedding are common in these beds. Fish remains are sometimes present. Overlying the 'paper limestone' beds is a rather soft, white limestone, the so-called *Neolobites* beds, topped by a reddish-brown 1 m thick dolomite marker. These two beds define the top of the Yotvata Member (and of the Hazera Formation) in the area from Yotvata southwards.

Fauna: Stromatoporids are *Aspidiscus cristatus* Lam., *Holectypus larteti* Cott., *Archiacia palmata* Gauthier, *Archiacia* sp., *Neithea shawi* (Perv.), *Ostrea* sp., *Exogyra africana* (Lam.), *Exogyra luynesi* (Lartet), *Exogyra haliotidea* (d'Orb.), *Exogyra flabellata* Goldfuss, *Exogyra Columba sulcata* (Lam.), *Dosinia delettrei* Coq., *Cardium syraicum* Conrad, *Trachycardium productum* Sowerby, *Praeradiolites biskraensis* Coq., *Strombus incertus* d'Orb., *Pterodonta homarensis* Blanck., *Pterodonta germeri* Blanck., *Pterodonta dutrugei* Blanck., *Pterodonta* sp., and *Neolobites vibrayeanus* (d'Orb). Age: *Neolobites vibrayeanus* (d'Orbigny) is abundant in the uppermost beds and is indicative of the late Cenomanian.

Late Cenomanian-Early Turonian Lower Bi'na Level (=Bi'na I) **(Table 18F.4a)**.

The spatial facies differentiation reaches its peak during this subdivision of the Judea Group. The Shune, Muhraqa, and Umm-E-Zinat limestone reef complexes of the Carmel, behind which the Yirka Marl extends, binds the deep anoxic shales of the subsurface Daliyya Formation of the Talme Yafe Group. In Judea the platform of the lower part of the Bi'na limestone extends toward the northern Negev. This facies subdivides into the chalks and limestones of the Derorim/Shivta Formation, passing in the southern Negev to the shales of the Ora Formation. A regional sea-level drop, marked by a sand intercalation (Bani Naim clastic unit) interrupts the carbonate deposition for a short while, ending the cycle.

COASTAL PLAIN/CARMEL:

Daliyya Formation (Picard and Kashai, 1958, emend. Gvirtzman and Reiss, 1958).

At Daliyat el Karmil, the Daliyya Formation consisting of 60 to 90 m of marine chalk, somewhat argillaceous, with thin intercalations of lithographic or detrital limestone, yellow marls alternating with white limestones, and some flint nodules, can

Table 18F.4a: Judea Group Level 4.

Coastal Plain	Carmel	Galilee	Judea	N. Negev	S. Negev
Daliyya	Shune/U e Zinat	Yirqa/Bina	**Bi'na C Bi'na B**	Shivta	Ora 2
	Shune/Muhraqa	Yanuh	**Bi'na A**	Derorim	Ora 1

be subdivided into two units. At the base and in the lower 35 m, soft, yellow, chalky marls contain hippuritid and radiolitid patch reefs in places. Fragments of reef fossils are found together with micro-quartz grains imbedded in the marls and calcilutites. The 45 m upper part of alternating monotonous yellow-green marls and chalky limestone is characterized by an increase of the amount of limestone. Several detrital, pelletoidal, fine to coarse crystalline, hard gray limestone beds alternate with soft, yellow layers. Limestone intraclasts are found in the uppermost sediments of the section.

The Daliyya Formation is pinched between limestones of the Muhraqa Formation at its base, and limestones of the Umm ez Zinat Formation at the top.

Planktonic foraminifera of the *Helvetoglobotruncana helvetica* total range zone occur throughout the section (Lipson-Benitah et al., 1988) and have a range from Early to Middle Turonian. Ostracods of the marine *Cytheresis rawashenthis kenaanensis* (UC-6) assemblage zone (Rosenfeld and Raab, 1974) occur in the lower and middle part of the section. In the upper part, marine species are found together with brackish water species of the *Neocyprideis vandenboldi* (UC-5) assemblage zone (Rosenfeld and Raab, 1974).

Age is Late Cenomanian-Early Turonian (Vroman, 1958; Reiss, 1958), or Early Turonian, (Freund, 1961; Rosenfeld and Raab, 1974). The ammonite *Romaniceras deverianum,* at the top of the Daliyya marls (Kashai, 1966) defines the Early-Late Turonian boundary (Lewy and Raab, 1978). This ammonite may confer an early Late Turonian age to the uppermost part of the Daliyya Formation (Kashai, 1966). *H. praehelvetica* in the uppermost part of the Daliyya type section indicates a Middle Turonian age for the entire type section of the Daliyya Formation.

Environment of deposition: Planktonic foraminifera and ostracods indicate changes in environment and fluctuations in the depth of deposition between the lower and upper part of the type section of the Daliyya Formation. The marls accumulated in a local depression of the shelf, with a connection to the Talme Yafe open sea facies (Freund, 1961, 1965; Bein, 1977). Planktonic foraminifera and ostracods of the UC-6 zone indicate open marine, well-oxygenated waters above the oxygen-depleted layer of ~100-200 m water depth (Schlanger et al., 1987). Dominance of keeled spiroconvex foraminifera (*Marginotruncana)* suggests an intermediate environment (Zone 3 of Hart and Bailey, 1979) and temporary shallowing is signalled by the association of *Hedbergella* and *Herohelicidae* (Zone 1 of Hart and Bailey, 1979). *H. helvetica,* dominant in deeper waters (Zone 4 of Hart and Bailey, 1979), occurs here only in its shallow water form (Hart, 1982).

The typical deep water morphotype of *H. helvetica* is however encountered in the southern Coastal Plain of Israel. An increase in diversity and abundance of foraminifera is accompanied by the appearance of high salinity tolerance ostracods (*Neocyprideis vandenboldi* - UC-5 assemblage zone, Rosenfeld and Raab, 1974), reflecting transitional marine to brackish waters in the upper part of the Daliyat el Karmil section. Fauna in the bituminous marls of the Galame section (Kashai, 1966) indicate deeper water and anoxic conditions (Honigstein et al., 1989).

Picard and Kashai (1958) considered the *Fureidis Marl* to be the upper part of the *Daliya Series* which overlies the *Muhraqa Series* and underlies the *Umm ez Zinat Series.* Its age is early Turonian. Vroman (1958) has shown the *Fureidis Marl* to be part of the Cenomanian *Khureiba Chalk* and the *Daliya Series* to be overlain not by the *Umm ez Zinat Series,* but by the late Turonian *Qumbaza Series.* Kashai (1958) points out that the *Daliya Series* thins toward the south and locally disappears. Vroman (1958) and Gvirtzman and Reiss (1958) correlate the *Daliya Series* with the *Leoniceras Zone* of the Negev. (See also: *Helvetica-Zone*).

Shuna Formation (Picard and Kashai, 1958).

The Shuna Formation consists of a sequence of coarse Rudist-reef-limestone (*Meleke*) about 100 m thick, occasionally with dense dark dolomite in its middle part, exposed at Khirbet es-Shuna on the east flank of the southern Mount Carmel nose. It overlies the *Zikhron Marl* and underlies the *Umm-ez-Zinat Series.* According to Vroman it is identical with the *Muhraqa Series,* and therefore overlies *Juneidya Chalk* and underlies the *Daliya Series,* or, where the latter is lacking, the late Turonian *Qumbaza Series,* its age is thus late Cenomanian

Muhraqa Formation (Picard and Kashai, 1958).

The name of the sequence is derived from the monastery of Muhraqa on the southern Carmel. The Muhraqa Formation stands for the Rudist-Meleke Series (Blake, 1935), a sequence 70 to 80 m thick in the southern part of Mount Carmel. In its lower part it consists of crystalline reef limestone (*Meleke*) rich in rudists, and in its upper part of detritic micro-organogenic limestone. The highest strata are well-bedded and distinguished by their pseudo-oolitic microtexture. Quartz beds or lenses occur near the base of the sequence. Locally the limestones are replaced by dolomites. Blake (1935) cites the following fauna: *Eoradiolites* cf. *syriacus* Conr., *Ostrea olisiponensis* Coq., *Ostrea olisiponensis* Coq., *Durania* sp., and *Nerinea* sp. The Muhraqa Formation overlies the Juneidiya Formation and is overlain by the Daliya Formation. Both contacts are probably conformable.

GALILEE:

Yanuh Formation (Freund, 1958, 1959).

The Yanuh Formation is also called the Sabalan Formation (Eliezri, 1965), or the Balatun Chalk (Wolff, 1967). Freund (1958) includes three rock units in this formation. The lower and upper members are identical to the facies of the Bi'na Formation, whereas only the middle member corresponds to the Yanuh facies as found below the village of Yanuh (also spelled Yanuch). The facies and thickness of the Yanuh Formation varies from 80 m in the middle of the central section (facies 2-3) to 145 m on its flanks (facies 1). The Yanuh Formation is restricted to a few areas. It is exposed at Adamit (65 m), Mount Manor (54 m), the northern margin of the Fassuta

Valley (75 m), Mount Zevul, Ma'alot, Balatun, Yanuh, Yirka, and in the subsurface in the Asher-1 well (40 m). Small lenses of this unit are found within the Sakhnin Dolomite near Hardalit Spring and near the Ga'aton Springs. The Yanuh Formation consists of three rock-facies:

1) White porous coarse limestones with prominent reefs (bioherm) follow a line from Mugharat-Hamman (west of Majd-el-Kurum) to Kh. Tufaniya, framing

2) Chalks and fine white limestone with flint and

3) Yellow lithographic limestones. The limestones are well-bedded, partly chalky, passing laterally into chalk lenses and horizons. Typical yellow-brown soils cover the formation. The limestones are well-sorted with mud-supported biomicrites, and only a few are grain-supported. Some intrabiomicrites occur, with intraclasts composed of micrite and usually well-sorted small faunal debris.

The formation contains many horizons of chert nodules. In some places, *e.g.* Mount Manor, the chert forms flattened lenses up to 50 cm in length, with a typical kidney shape. Dolomites are rare in this formation. In the transition zones to the Sakhnin Formation the micrites are found to contain small idiomorphic dolomite crystals. Dedolomitization is known from a few places. In the Yanuh-Yirka region the Yanuh Formation overlies the Rosh Haniqra Member (Tufaniya Chalk) (Freund, 1958). In most other places it overlies the Sakhnin Formation, or in places where the latter thins to a few meters of medium to coarsely crystalline limestones (Adamit-Manor area), it overlies these limestones. The formation is generally overlain by the Yirka or the Bi'na Formations. In places of deep pre-Senonian erosion it may be unconformably overlain by Senonian chalks (Asher-1 well). Laterally the limestones are replaced by the coarse Rosh Tsurim Dolomite (Sachnin Formation). The fauna consists of *Prota-canthoceras* sp. and *Hemiaster* sp., found in the Mount Zevul and Zuriel areas. Microfossils (det. Hamaoui) include *Discorbiidae, Globotruncana* sp., *Hedbergella (Asterohedbergella) astero-spinosa* Hamaoui, and *Heterohelix* sp. An Upper Cenomanian age is based on *Protacanthoceras* sp.

Yirka Formation (Freund, 1959).

The Yirka Formation overlies the Yanuh Formation. The contact between them is very irregular, because of an angular discordance over the above-mentioned Yanuh reefs (rock facies I). According to its ammonite fauna, this formation is Lower Turonian in age. The Yirka Formation consists of reddish-laminated chalk and limestone in thin beds with flint attaining a thickness of 10-20 m and yielding *Leoniceras luciae* Pervinquiere and *Choffacticeras* cf. *quasi* Peron, followed by coarse detritic yellow limestone irregularly-bedded with yellow marl of a thickness of about 25 m, containing *Thomasites rollandi* Thomas and Peron, *Thomasites jordani* Pervinqere, *Neptychites cephalotus* Courtiller, *Neoptychites Xetriformis* Pervinquiere, *Leoniceras luciae* Pervinquiere, *Choffaticeras* cf. *quasi* Peron, *Mammites* sp., and *Nautilus* sp. Parnes (pers. comm.) regards the Yirka Formation to be stratigraphically equivalent to the 'Dalia' Marls of Mount Carmel, which suggests a Lower Turonian age.

GALILEE-JUDEA:

Bi'na Formation (Shadmon, 1959; emend. Itzhaki et al., 1964).

The rocks of the Bi'na Formation are well-known under the names Meleke, Calcaire Meleke (Reale), Calcare Misi Hilu (Dolce), and Misi Helu.

The name of the Actaeonella Flint Beds (Picard, 1938), goes back to the Kieselige Schneckenbank of Fraas (1867). Near its type locality the Bi'na Formation correponds to the Kisra Limestone of Freund (1959), and the Faht-e-Tabaqe Formation of Baer (1962).

Though the original type section is in the Galilee, a better reference section is at Nahal Dolev in the Bet Shemesh area. In the Judean Mountains, four members are distinguished:

A) The **dolomite and limestone member** or 'Mizzi Ahmar'. It consists of finely crystalline fossiliferous limestones with flint concretions, dolomites and dolomitic limestones, 23 m thick, at base. It is not found in the Galilee.

B) The **detrital limestone member** or 'Meleke', is 40 m thick;

C) The **limestone** and **nari member** or 'Actaeonella flint; lowermost part of Mizzi Hilu', is 40 m thick. This unit also encompasses the clastic unit of 'Bani Naim' (Scarpa and Hirsch, 1999), which represents the boundary between Bi'na levels I and II;

D) The **sublithographic limestone member** or 'Mizzi Hilu', is 56 m thick.

The total thickness of the Bi'na Formation in its reference section in the Judean Mountains is 160 m. Elsewhere it maintains thicknesses of ~100 m.

Units A and B define the Lower Bi'na Level I, separated from the Upper Bi'na Level II by the clastic unit of Bani Naim contained within unit C. Though the clastic unit is not recognized in all Bi'na sections, correlation with the Negev units suggests that part of unit C belongs into the Upper Bi'na Level II, best defined by unit D.

From the Judean Mountains to the Negev, the members of the Bi'na Formation pass laterally into the Derorim, Shivta and Nezer/Ora, and Gerofit Formations (Wdowinski, 1984).

The relations between the Level I members of the Bi'na

Table 18E4.b: Equivalence and subdivisions of the Bi'na I Level.

Judea (Jerusalem/Hebron)	Northern Negev (Zavoa/Boqer)	Central Negev (Ramon)
Limestone and Nari member of Bina Fm.	lowermost Nezer Formation	Ora Formation (upp.mb.)
'Clastic unit of Bani Naim'	Clastic unit	Clastic unit
Detrital Limestone member of Bina Fm	Shivta Formation	Ora Formation (middle mb. = 'Vroman Bank')
Dolomite and Limestone mb of Bina Fm.	Derorim Formation	Ora Formation (lower member).

Formation and their equivalents among formations in the Negev is shown in **Table 18F.4b**.

The Bi'na Formation extends from the Galilee to the southern edge of the Judean Mountains. In the Galilee the Sakhnin and Bi'na Formations pass vertically and laterally into each other through a transition zone. Where the Yanuh or Yirka Formations are present, the Bi'na Formation overlies one of them. In the Judean Mountains, the contact with the underlying Weradim Formation is conformable.

In the Judea-northern Negev area, the lower member of the Bi'na Formation possibly includes the Cenomanian-Turonian boundary. The age of the entire Bi'na Formation is Upper Cenomanian-Coniacian.

NORTHERN NEGEV:

Derorim Formation (Bentor and Vroman, 1963).

The Derorim Formation (Bentor and Vroman, 1963) was established for the so-called 'Leoniceras beds' of Bentor and Vroman (1953) after the type locality in Nahal Derorim (Ecker, 1962). The Upper Cenomanian-Lower Turonian from the northern Negev consists mainly of marls with some chalk and limestone and carries *Exogyra olisiponensis* Sharpe, *Pleuromya vignesi* Lartet, and *Pygnodonta vesiculosa* Sow. The so-called *Leoniceras* Zone is very fossiliferous and consists in part of shell breccias. The most important fossils are *Neoptychites cephalotus* Court., *Mamites nodosoides* Schloth., *Pseudaspidoceras armatus* Perv., *Thomasites* cf. *rollandi* Thom. and Per., *Leoniceras segne* Solger, *L. discoidale* Perv., and *L. quassi* Per. The sequence is 15 m thick in the south, increasing to 36 m in the north. Further north it is affected by dolomitization, and in the Ef'e as well as west of the Dead Sea, more littoral, shallow water reddish marls, with some coarse-grained, as well as smooth, fine-bedded hard limestone, form the '*Red Passage Beds*' of Bentor and Vroman (1951).

In the area of the Hazera Anticline the Derorim Formation reaches a thickness of 35 m. Its maximum thickness of 60 m is recorded at Beer Menuha. In the Sodom region, its thickness varies from 15 to 36.5 m. The sequence consists of light yellow to reddish, soft and very fossiliferous limestones alternating with marls. Ammonoids in the Derorim Formation range from Late Cenomanian to Early Turonian: *Neoptychites cephalotus* Court., *Mammites nodosoides* Schloth., *Pseudaspidoceras armatus* Perv., *Pseudoaspidoceras dubertreti* Basse, *Thomasites* sp., *Leoniceras segne* Solger, and *Leoniceras quaasi* Peron. Furthermore: *Exogera olisiponensis* Sharpe, *Pholadomya molli* Coq., and *Crassatella pusilla* Coq. The Derorim Formation occurs in the northern Negev and passes southward into the lower part of the Ora Formation (Ora shales). Northward it is replaced by the lower part of the Shivta and Bi'na Formations (Agnon, 1983). Vroman (1958) correlated the unit of the Negev with the *Daliya Series* of Mount Carmel (*Helvetica-Zone)*. In Jordan the lower part of the Shuayb Formation corresponds to the Derorim Formation.

Shivta Formation (Bentor and Vroman, 1964; Arkin and Braun, 1965).

The unit was named after the Nabatean town, now referred to as Horvot Shivta. In Nahal Nezer it is made up of nearly 30 m of a massively-bedded, oolitic calcarenite with rudist fragments, locally cross-bedded, containing megafossils (mainly molluscs). Silicified beds and flint concretions, as well as patches of fossils, are abundant in the upper half of the formation. This formation is correlative with the 'Vroman Bank' of the southern Negev Ora Formation, middle member. The Shivta Formation ranges in age from the Early Turonian (zone 4 of Freund, 1962) to the earliest Late Turonian. Mainly silicified rudists and gastropods occur throughout the formation. A significant bed, the so-called '*Actaeonella*' bed, occurs at the top of the formation.

From the northern Negev, it wedges out toward the south, where it is reduced to the so-called 'Vroman bank' within the Ora Formation. In central Israel it is equivalent to the middle member and part of the upper members of the Bi'na Formation. The Shivta Formation overlies the Derorim Formation, to which it passes laterally, until it may directly cover the Tamar Formation. The contact with the overlying Nezer Formationis is conformable.

SOUTHERN NEGEV:

Ora Formation (Freund, 1962).

The lower part of the Ora Formation includes the Leoniceras Zone of Bentor and Vroman (1951) At Nahal Netafim three members are recognized. Considerable lateral changes occur in the Middle Member between Nahal Netafim and Be'er Ora. The thickness is rather constant over the whole area (98-108 m).

The Ora Formation consists of thick soft shale beds with calcareous intercalations and gypsum layers which form steep and dissected slopes, often debris covered. The topmost beds are red shales associated with gypsum.

Lower Member: The Lower Member consists mainly of green-gray and brown soft shales with a few hard, yellow, nodular limestone beds. Numerous gypsum veins criss-cross the shales.

The clay minerals in the lower part of the member are mainly kaolinite and montmorillonite, accompanied by silt-sized quartz grains. Kaolinite, mixed layer clays, and illite compose the shales of the upper part, which are to a large extent calcareous. The nodular limestones are micritic; abundant fossil fragments consist of sparry calcite. Clastic quartz and glauconite are present in these limestones.

Age: Early Turonian ammonites (Freund, 1962; Freund and

Table 18F.5a: Judea Group Level 5.

Carmel		Galilee	Judea	N. Negev	S. Negev
		Kisra	**Bi'na D**	Nezer 2	Gerofit
Qumbaza	Daliyya	Kishk	**Bi'na C**	Nezer 1	Ora 3

Table 18F.5b: The three facies realms of Level 5 in the Galilee.

North-West Galilee	Central Galilee	South-East Galilee
Kisra Limestone	Kisra Limestone	Kisra Limestone
Rosh Tsurim Dolomite	Kishk Limestone	Rosh Tsurim Dolomite
Yanuh Limestone	Yirka Limestone	Yanuh Limestone
Yanuh Limestone	Yanuh Limestone	Yanuh Limestone

Raab, 1969) comprise: *Paramammites* sp., *Pseudaspidoceras* sp., *Vascoceras* sp., *Paravascoceras tavensi* (Faraud), *Paravascoceras cauvini* (Chudeau), *Paravascoceras crassus* (Furon), *Thomasites rollandi* (Thomas and Peron), *Thomasites* sp., *Choffaticeras meslei* (Peron), *Choffaticeras securiformi* (Eck.), *Choffaticeras segne* (Solger), *Choffaticeras pavillieri* Perv., *Choffaticeras quaasi* (Peron), and *Hoplitoides* sp. Additional fossils are: *Exogyra columba* (Lam.), *Exogyra africana* (Lam.), and *Exogyra olisiponensis* Sharpe.

Middle Member: The Middle Member is distinguished by frequent facies changes in contrast with the more constant lithology of the Lower and Upper Members. The main rock types are yellowish, nodular limestones, fossiliferous argillaceous limestones, oolitic limestones, dolomites, marls, and shales. The shales are composed of kaolinite, mixed layer clays and illite, with some dolomite and calcite. The limestones, partly dolomitic, are micrites with minor amounts of glauconite and angular quartz grains. Fossil vugs are often filled by drusy dolomite. The upper part of the member is composed of oolitic (up to 1.2 mm in diameter), and grain supported limestone whose cement is either micritic or dolomitic. Facies changes are clearly seen in the vicinity of Be'er Ora. To the south and west of Be'er Ora, limestone beds are well developed, but are absent in the Be'er Ora-Yotvata area, where soft shales and marls predominate. The Nahal Evrona sections (2 km south of Be'er Ora) are characterized by an oolitic limestone cliff, 7 m thick, which thins out northwards (to 1 m at Be'er Ora). It seems that this member is the lateral equivalent of the 'Vroman Bank', a very distinct cliff developed in the area between Ramon and Hameshar, as well as in the central Sinai. This correlation is based upon

1) Ammonites below the 'Vroman Bank' and

2) A red shale marker, characterized by gypsum beds and/or sandstones, immediately above these beds, *i.e.* at the base of the Upper Member in the Elat region.

Fauna: *Hemiaster syriacus* Conrad, *Hemiaster luynesi* Cott., *Hemiaster* sp., *Phymosoma* sp., *Pholadomya luynesi* Lartet, *Pholadomya* sp., and *Plicatula* sp.

Upper Member: The Upper Member is composed of red and green shales, massive gypsum beds, fossiliferous limestones, glauconitic dolomites, and sandstones. The clay minerals are mainly illite. The topmost layers (10 m) are mainly illite and kaolinite. More layers of montmorillonite occur at Ma'ale Gerofit (Bentor, 1966). Brown fossiliferous limestones (lamellibranch remains, intraclasts, glauconite and quartz grains) occur in the uppermost part of the member. Thin lenticular, soft, yellow sandstone beds occur in the Be'er Ora region, thickening at Ma'ale Gerofit to 4 m thick red-brown sandstones and passing laterally into gypsum beds (Eckstein, 1963). Fossil plants are present at the Ma'ale Shani junction and at 'En Netafim. Rare *Hoplitoides* sp. occur.

The Ora Formation overlies the Tamar or the Yotvata Members of the Hazera Formation and is overlain by the Gerofit Formation. According to Freund (1962), the ammonite zones represented in the Derorim Formation are also developed in the lower parts of the Ora Shales, suggesting that the Derorim Formation is contemporaneous to the Lower Member of the Ora Shales. The middle and upper parts of the Ora Shales pass northwards into the Shivta and the lower Nezer Formations.

Late Turonian-Early Coniacian Upper Bi'na Level (=Bi'na II) (**Table 18F.5a**).

A limestone platform extends with the Kishk and Kisra/Bi'na Formations from the Galilee to the Carmel as the Qumbeze Limestone. In Judea carbonatic sedimentation resumes in the upper Bi'na Formation, following the sandy break. This carbonatic facies is represented in the northern Negev by the Nezer Formation, which in the southern Negev passes laterally into the upper Ora and Gerofit Formations. The Judea Group generally ends with the regional unconformity, caused by the Levantid folding of the Syrian Arc.

CARMEL:

Qumbaza Formation (Picard and Kashai, 1958).

At Khirbet Qumbaza on the southern Carmel, a sequence of limestones, 40 to 80 m thick, occurs along the southeastern flank of Mount Carmel. In its lower part it consists of 20 to 30 m of lithographic limestone, followed by fine-grained crystalline limestone varying in thickness from 20 to 50 m. The main fossils are: *Nerinea* sp., and *Durania* sp., as well as Miliolidae (Vroman, 1936). For Picard and Kashai (*op. cit.*) it overlies the Shuna Formation but according to Vroman (*op. cit.*) it conformably overlies the Daliya

Table 18F.5c: Equivalence and subdivisions of the Bi'na Level II.

Judea (Jerusalem/Hebron)-	Northern Negev (Zavoa/Boqer)	Central Negev (Ramon)
Sublithographic limestone -	Nezer Formation	Gerofit Formation
Limestone and Nari member -	lowermost Nezer Formation	Ora Formation (upp.mb.)

Table 18F.6: Correlation across the Dead Sea Transform (Modified after Powell, 1989; Sneh, 1998; Lewy, pers. comm.)

ISRAEL		JORDAN
ZIHOR		KHUREIJ
GEROFIT	NEZER	WADI ES SIR
ORA 3		SHUAYB
ORA 2	SHIVTA	SHUAYB
ORA 1	DERORIM	SHUAYB
TAMAR-		HUMMAR (Karak Lmst)
AVNON		FUHEIS
ZAFIT		NAUR- D
EN YORQEAM		NAUR- C
HEVYON		NAUR- B
HEVYON		NAUR- A (Wadi Juheira Mb.)

Formation or, where the latter is missing, the Muhraqa Formation. The Qumbaza Formation is overlain, probably disconformably, by chalk of Senonian age.

GALILEE:

The three facies realms that can be recognized in the Galilee are shown in **Table 18F.5b**.

Kishk Formation (Freund, 1960).

In Wadi Kishk the Kishk Formation is a cliff-forming ledge some 20-60 m in thickness. It is a coarse detritic yellow limestone, containing *Nerinea requieni* d'Orbigny. *Acteonella sanctaecrucis* Futterer, *Sauvagesia* sp., and *Sphaerulites* sp. It overlies the Yirka Formation and is overlain by the lithographic limestone with stylolites (Mizzi Hilu) of the Kisra Formation.

Kisra Formation (Freund, 1959).

The name Kisra Formation was coined by Freund (1959) for the lithographic limestone with stylolites (Mizzi Hilu) overlying the Kishk Formation.

JUDEA:

Bi'na Formation (Shadmon, 1959; Emend. Itzhaki et al., 1964).

The Bi'na Formation, described under the former subdivision, comprises in the Bi'na Level I, the A, B and C members, the latter also known under the name 'Meleke'; whereas the strata of Bi'na Level II are mostly represented by the sublithographic limestone of member D, also known under the name Misi Helu.

In the Judean Mountains (Nahal Dolev, Bet Shemesh area), the upper part of the Bi'na Formation consists of:

C) The **limestone and nari member,** or lowermost part of 'Mizzi Hilu', is some 40 m thick, encompassing in some places the clastic unit of 'Bani Naim' (Scarpa and Hirsch, 1999) in its lower part, and placing most of the unit into the Bi'na level II.

D) The **sublithographic limestone member** or 'Mizzi Hilu', is some 56 m thick. The clastic unit of 'Bani Naim', which forms the limit between Bi'na Levels I and II, is not everywhere recognized. However it seems reasonable that part of member C as well as all of member D -'Mizzi Hilu'- Misi Helu- represents Level II.

The relation between the Level II members C and D of the Bi'na Formation and their equivalents within the formations in the Negev is as follows (**Table 18F.5c**):

The contact with the Mount Scopus Group consists generally of an unconformity. However, the top of the Bi'na Formation is not always as abrupt as one would expect, in general the lower beds of the Menuha Formation being represented by the so-called Ka'akuhle.

In the Galilee, where the Bi'na Formation is framed by the Lower Turonian Yirka Formation (Freund, 1958), it may pass gradually and undisturbed into the well-defined Santonian Har Zefat Formation, showing no evidence of the lacuna between the Turonian and the Santonian. (Flexer, 1964; Kafri, 1965).

NORTHERN NEGEV:

Nezer Formation (Bentor and Vroman, 1964; Arkin and Braun, 1965).

At the type locality in Nahal Zipporim the Nezer Formation is 36 m thick. It consists of well-bedded hard limestone, usually fine-grained (sublithographic) containing silicified patches and abundant fossil fragments. Quartz granules and crystals and flint concretions occur at the top of the formation. A few marl and soft chalky limestone beds may occur as well as dolomite beds in the eastern Negev. In places a layer of variegated sandstone occurs at the base of the Nezer Formation, as well as some quartz grains in the lower limestone beds. This early Late Turonian event of sandstone deposition is well-known from Sinai and the southern Negev up to central Israel (Judean Hills, Judean Desert, and Bet Naballa). At Har Zavo'a (Braun, 1964) another layer of variegated sandstone and clay occurs in the upper part of the Nezer Formation (Upper Turonian, Coniacian; Hamaoui and Raab, 1965). The sand and clay penetrate into older beds (Nezer and Shivta Formations) through karstic chimneys, suggesting intensive karstic activity as a result of exposure to meteoric waters before the deposition of the sand (Sandler and Zilberman, 1984).

This sandstone layer has been traced in boreholes in the northwestern Negev, as well as further north *e.g.* in the Hazerim-1 borehole. The nearest possible source of this sandstone must have been somewhere in southern Egypt or northwest Saudi Arabia because more northern areas were covered by Cenomanian and Turonian limestone according to sections in Sinai (Bartov and Steinitz, 1977). Rudists include *Sauvagesia* and *Praeradiolites*, conferring a Late Turonian to Coniacian age.

SOUTHERN NEGEV:

Gerofit Formation (Eckstein, 1963; Eckstein and Rosenthal, in Hamaoui, 1966).

The Gerofit Formation was described in the Yotvata area at Nahal 'Eteq. It reaches a thickness of 113 m. The Gerofit Formation is a uniform sequence of well-bedded massive limestones and

dolomites, with minor amounts of marls, shales, and nodular chert. The hard gray limestone beds up to 1 m thick alternate with thin argillaceous and shaly layers. The limestones are micrites with recrystallized fossil fragments. 'Reefs' of *Radiolites praesauvagesi* Toucas in vertical life position are common in the upper part of the section at Nahal Raham, Nahal 'Eteq, Gerofit, and Sheikh Atiya. Chalky limestones, massive, thick and fine-bedded, overlie the Rudist banks. The white chalky limestones are exceptionally rich in littoral foraminifera and ostracods. Half meter thick beds of montmorillonite with minor amounts of kaolinite and quartz are responsible for the mechanical deformations and the flow of shales into open cracks at Ma'ale Gerofit, Nahal Raham, Ma'ale Sayyarim, Nahal Yehoshafat, and Nahal Rehavam, as well as disharmonic folding of the limestones. The upper, cliff-forming part of the Gerofit Formation is rich in burrows and the topmost beds are often cross-bedded. The chert appears as small single spherical nodules (up to 20 cm) with concentric banding in the chalky limestones of the lower and upper parts of the section. Dark chert is associated with abundant silicified fossils in the thin (0.5 m thick) topmost bed of the Gerofit Formation. This chert is lenticular or irregularly-bedded with abundant rudists, hydrozoa, gastropods, and bivalve fragments. The hard limestones and dolomites of the Gerofit Formation form a prominent cliff that conformably overlies the Ora Shale in the southern Negev. It is conformably overlain by the softer Zihor Formation.

Fauna are Hydrozoa, *Nucleopygus pseudominimus* (Peron and Gauthier), *Nucleopygus* sp., *Phymosoma* sp., Echinoids, Rudists, *Radiolites praesauvagesi* Toucas, *Leda* sp., *Cardita* sp., *Turritella* sp., *Strombus* sp., *Coilopoceras* sp., and *Coilopoceras zihoricum* Parnes.

Age is Late Turonian, based upon the occurrence of *Radiolites preasauvagesi* Toucas. The lower part of the formation is Coniacian, based on the occurrence of *Coilopoceras zihoricum* Parnes at the top of the formation in the Zenifim area.

Late Coniacian (=Zihor).

Where the platform sedimentation was less affected by the Levantid folding process, the deposition of the Judea Group persisted into the Coniacian Zihor Formation. The Zihor Formation covers the southern part of the Negev and extends to Sinai (Egypt).

Across the Dead Sea Transform the Judea Group corresponds to the Ajlun Group. The correlation of the units of these groups is shown in **Table 18F.6**.

Zihor Formation (Sakal, 1966).

The Zihor Formation is also known as the 'Coniacian strata' of Bentor and Vroman (1954) and Bentor et al. (1960), the 'Upper Nezer' of Eckstein (1963), and the 'Eteq Formation of Bartov

Table 18F.7: Middle Cretaceous Ammonite, Foraminiferal and Ostracodes Biozones (After Lewy and Raab, 1976; Lewy, Kennedy and Chancelor, 1984; Lipson-Benitah, 1980; Rosenfeld and Raab, 1974).

STAGE	AMMONITES	FORAMINIFERS	OSTRACODES
EARLY CONIACIAN	CA3 *A. galoppei* *CA2 P.sinaitica* *CA1 P. kaffrarium*	*Marginotruncana angusticarinata*	*Oertliella dextrospinata* UC7
LATE TURONIAN	T9 *C. requienianum* T8 *Coilopoceras* sp.	*Helvetoglobotruncana helvetica*	*Cythereis rawashensis* UC6
MIDDLE TURONIAN	T7 *Romaniceras inerme* T6 *Choffatticeras luciae* T5 *Vascoceras harttiforme* T4 *Choffaticeras securif.*	*Helvetoglobotruncana helvetica*	*Cythereis rawashensis* UC6 *Neocythere vandenboldi* UC5
EARLY TURONIAN	T3 *Vascoceras pioti* T2 *Pseudoaspidoceras* sp. T1 *Vascoceras cauvini*	*Helvetoglobotruncana helvetica*	*Neocythere vandenboldi* UC5
LATE CENOMANIAN	CE5 *Metoiococeras gesslinianum*	*Rotalipora cushmani*	
MIDDLE CENOMANEAN	CE4 *Neolobites vibrayensis*	*Rotalipora globotruncanoides* *R. brotzeni*	*Amphicytherura distinta* UC2/ *Metacytheropteron berbericum* UC4
EARLY CENOMANIAN	CE 3 *Turriletes scheuchz.* CE2 *Metoicoceras besairei* CE1 *Graysonites wooldridgi*	*Rotalipora globotruncanoides* *R. brotzeni*	*Amphicytherura distinta* UC2/ *Veeniacythere jezzineense* UC3
LATE ALBIAN	*Mortoniceras Hypengonoceras*	*Rotalipora appeninica* *Planomalina buxtor* *Th. Ticininensis*	*Neocythere bissulcata* UC1 *Monoceratina shimonensis* L4TY
EARLY ALBIAN	*Engonoceras* sp. *Knemiceras syriacus*	*T. praeticinensis*	*C. talmeyafaensis* L3TY

(1967). At Nahal Zihor in southern Israel, it is 52 m thick but decreases to 30-35 m in the Elat region. A ***northern facies*** consists of a lower chalky limestone unit and an upper marly bioclastic limestone unit (type section, Nahal Zihor). A ***southern facies*** occurs in the Elat region, characterized by dolomite, clays, quartz, glauconite, and bioclastics. The major rock types of the Zihor Formation are dolomites, limestones, and argillaceous limestones, often fossiliferous. Detrital quartz is locally abundant. The gray and coarse-grained dolomites are sandy, especially towards the top of the formation (up to 10% quartz grains). Locally fine sandstone beds are also present. These clastic and dolomitic rocks often exhibit depositional structures such as planar cross-bedding and ripple marks. Some beds are rich in spherical to angular concretions of gray chert, in places with the long axis parallel to the cross beds. The topmost beds are fossiliferous, detrital limestones rich in large pellets (up to 4 mm), quartz grains, echinoid and ammonite fragments, as well as small quartz druses (5 cm).

The Zihor Formation is found only in the southern Negev and is absent in the north, either due to non-deposition or to early Santonian erosion. Strata with definite Coniacian fossils are not found north of Makhtesh Ramon (Bentor et al., 1960), where the Santonian-Campanian chalks of the Menuha Formation overlie the sparsely fossiliferous rocks of the mostly Turonian Nezer Formation. The soft basal beds of the Zihor Formation conformably overlie the hard limestones of the Gerofit Formation. Its top is defined as the highest beds below the first massive chalks of the Sayyarim Formation. Local unconformities at the base of the Zihor Formation are recorded from several structures in the central Negev, Makhtesh Ramon (Garfunkel, 1964), Rehkes Menuha (Sakal, 1967), and at Gebel Areif En Naq'a (Z. Lewy, pers. comm.), but are not known in the Elat area. The upper part of the Nezer Formation may partly be a coeval time equivalent of the Zihor Formation.

The Zihor Formation can be correlated south of the Elat area into the Sinai Peninsula (Egypt), where the sections at Sheikh Atiya and Bir Zafra comprise mainly sandstones and minor carbonates. The latter sandy lithofacies resembles the lower part of the Matulla Formation (Ghorab, 1961) in the central Gulf of Suez region. The rich fauna of this formation is Coniacian (Sakal, 1967). It consists of *Petalobrissus letebrei* (Fourteau), *Petalobrissus djelfensis* Gauthier, *Petalobrissus vorax* (Fourteau), *Petalobrissus waltheri* Fourteau, *Nucleopigus hierosolymitanus* (Blanck.), *Nucleopygus pseudominimus* (Peron and Gauthier), *Nucleopygus luynesi* (Cott.), *Hemiaster fournelli* Deshayes, *Hemiaster* sp., *Plicatula ferryi* Coq., *Plicatula fourneli* Coq., *Plicatula* sp., *Alectryonia dichotoma* Bayle, *Arca (Cucullaea) maresi* Coq., *Vaccinites praegiganteous* Toucas, *Coilopoceras zihoricum* Parnes, *Barroisiceras* fragments, *Tissotia (Metatissotia) robini* (Thioliere), and *Plesiotissotia* fragments. Shaw (1947) related these beds to the Santonian. Parnes (1964) and Sakal (1967) attributed a Coniacian age, based on the rich fossil assemblages.

Summing up: One can reach the conclusion that the present subdivision of the Judea Group into six elements, sometimes cutting lithological units (*e.g.* Bi'na), may represent sequential units. The sensitivity of ostracods is remarkable, as they present clues to the environment in almost every facies-type. In particular the distribution of elements in the UC-5 assemblage clearly shows high-stand as well as low-stand conditions, related to the famous drop in sea level towards the end of the Lower Turonian or beginning of the middle Turonian, the low-stand-peak of which is well-expressed lithologically by the clastic unit of Bani-Naim, that separates the Bi'na I and II levels.

The distribution of the Zihor Formation shows that the folding phase of the Negevid part of the Levantid folding did not reach the southern Negev and adjacent Sinai (Egypt), as witnessed by a conformable passage to the Mount Scopus Group.

Biostratigraphy: The Judea Group can be subdivided into ammonite, foraminifer, and ostracode biozones (see **Table 18F.7**).

The formations of the Judea Group correlate across the Dead Sea Transform with the formations of the Ajlun Group as shown in Table 18F.6.

VI. MOUNT SCOPUS GROUP

A radical change in sedimentary regime marks the beginning of the Senonian. The paleo-topography of anticlines and synclines of the Syrian Arc controls facies and thickness of the predominantly chalky Coniacian, Santonian, and Campanian Menuha Formation. The deposition of thick cherts, porcelanite, chalk, marls, and phosphorites of the Campanian Mishash Formation in the basinal synclinal channels contrasts with the thinning toward the anticlinal ridges that formed island strings. Continuous tectonic movements constantly renewed the pattern of the paleogeography during the deposition of the chalks and bituminous shales of the Maastrichtian Ghareb Formation. The chert ratio increases in the southern Negev (Sayarim Facies), and decreases toward the Galilee and the Coastal Plain (Ein Zeitim Facies). The C/T boundary is well-documented in the basinal facies. A high iridium concentration occurs at the base of the *G. eugubina* Zone, and trace elements and microspherules occur between the *A. mayorensis* and *M. pseudobulloides* zones (Rosenfeld et al., 1990). Elsewhere the upper strata of the Maastrichtian are missing and the Paleocene-Early Eocene Taqiye shales onlap a paleorelief with paleosoil.

The Senonian and Maastrichtian carbonatic and silicious sedimentation of the Mount Scopus Group truncates the Judea Group in a regional erosion event that took place during the Late Coniacian (Lewy, 1975). The Late Coniacian-Santonian transgression which followed is marked by the deposition of the chalk of the Menuha Formation over all of Israel. At its base the chalk contains clastic components, derived locally from reworked older rocks. A 1 m thick chalky white sandstone layer occurs at the base of the Menuha Formation at Har Zavo'a (about 5 m in the Hazerim-1 and Haluza-2 boreholes). This sand may have been derived from locally reworked Late Turonian quartz sands. The age of the lower part of the chalk sequence (Menuha Formation) in the northwestern Negev may be Late Coniacian (Upper Turonian-Coniacian) overlain by Santonian chalk (Shezaf-1 borehole).

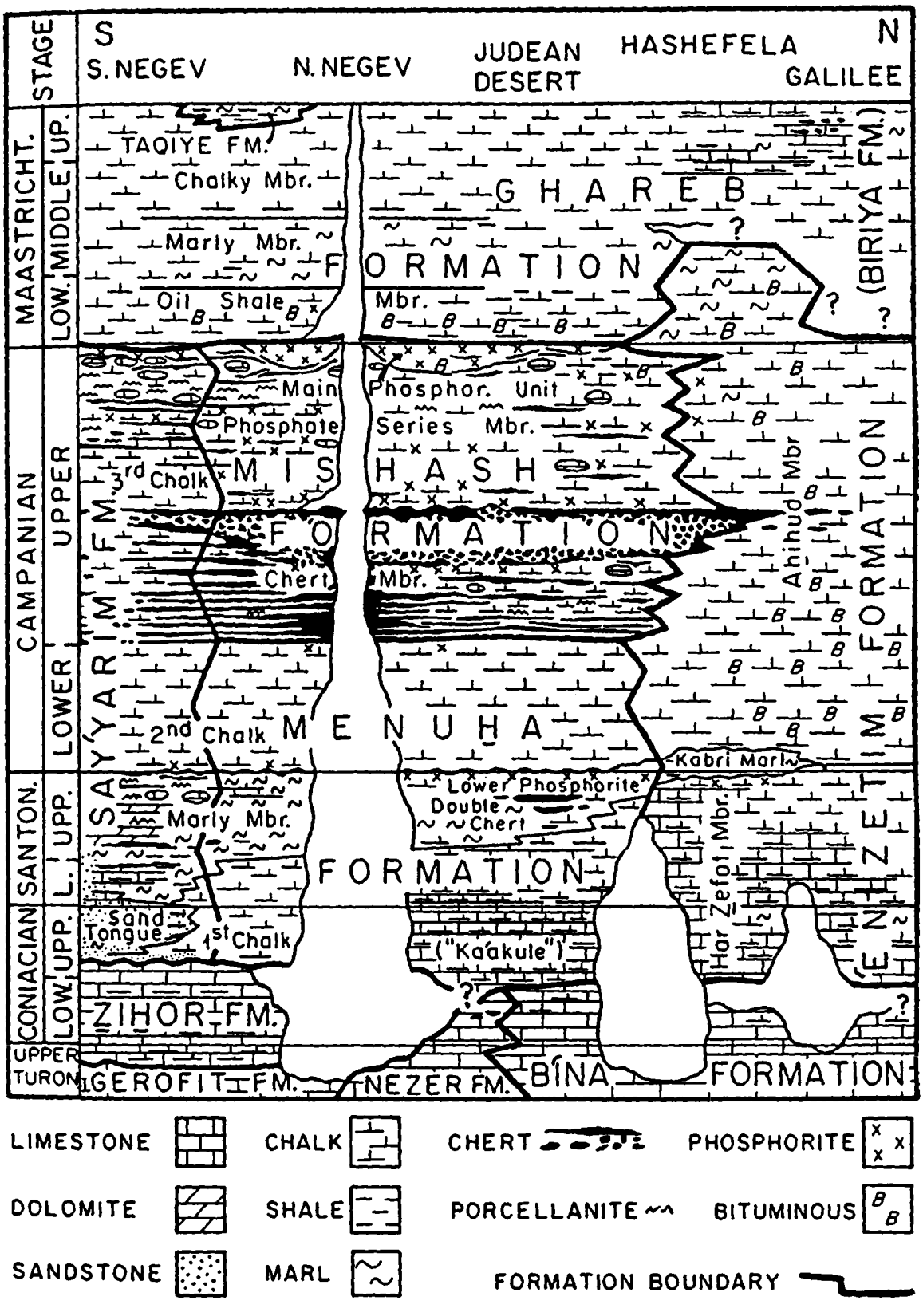
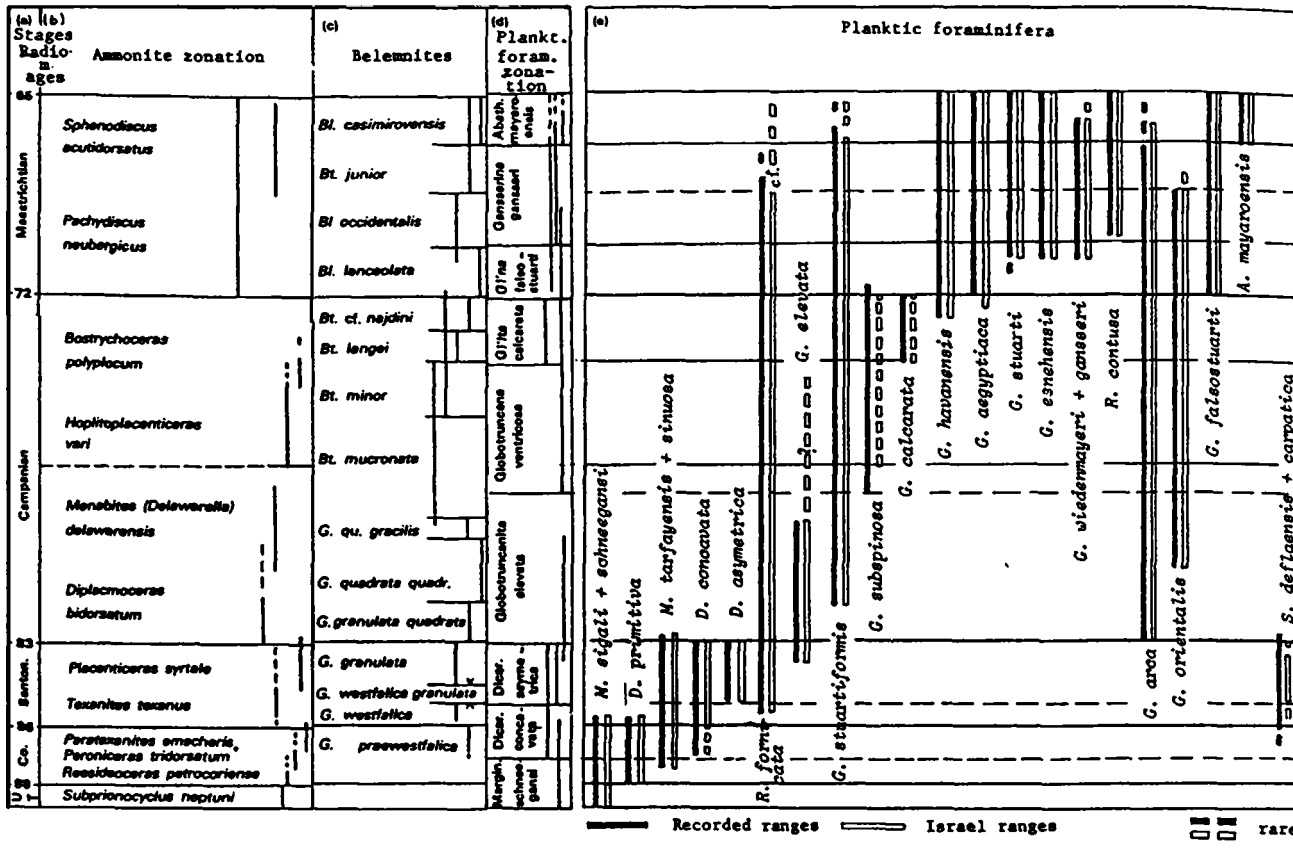
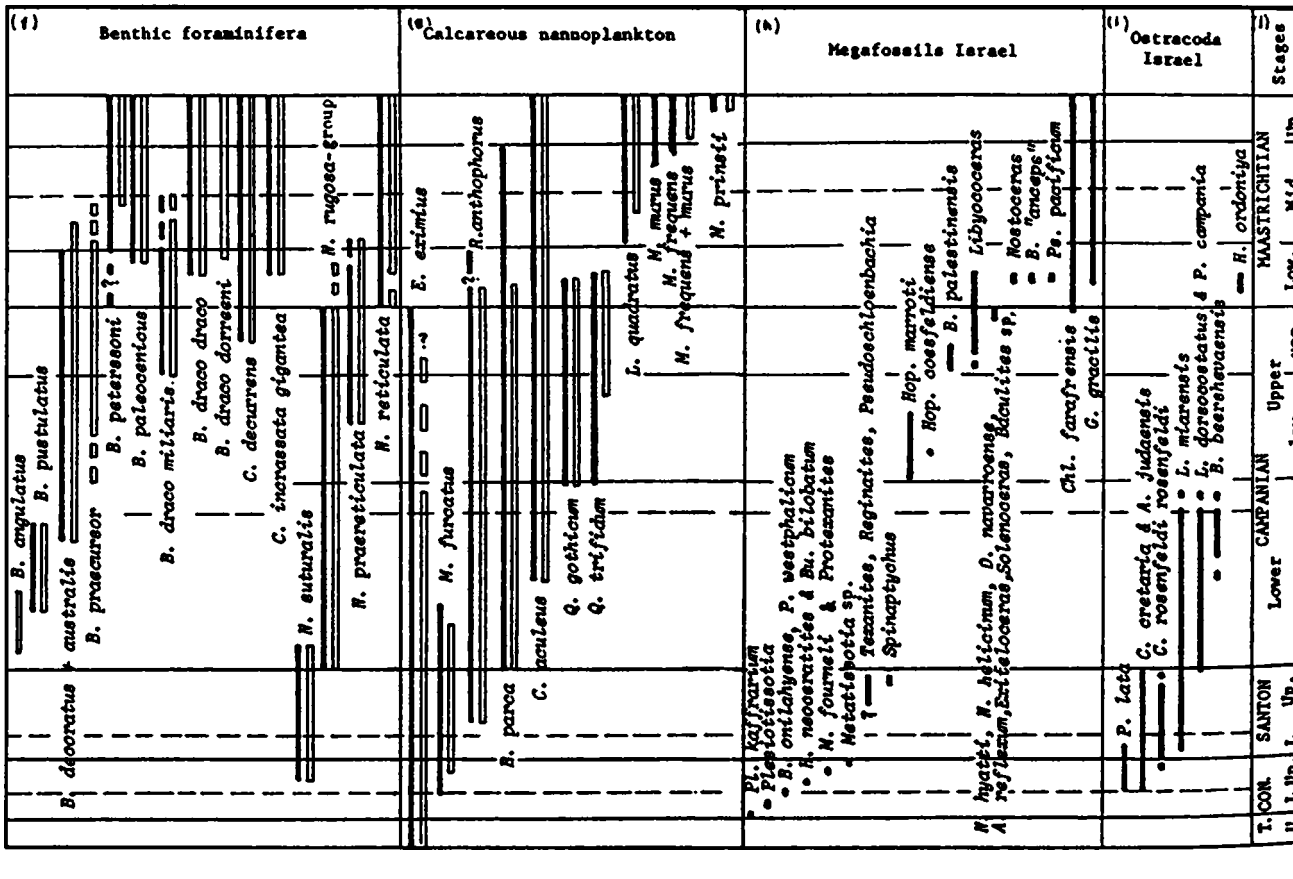


Figure 18F.12. Correlation chart of Late Cretaceous in Israel (after Reiss et al., 1985, Fig. 6, p. 158).


(a) (b) Stages Radiom. ages
Ammonite zonation
(c) Belemnites
(d) Plankt. foram. zonation
(e) Planktic foraminifera
Maastrichtian
Campanian
Santon.
Co.
Sphenodiscus acutidorsatus
Pachydiscus neubergicus
Bostrychoceras polyplocum
Hoplitoplacenticeras vari
Menabites (Delawarella) delawarensis
Diplacmoceras bidorsatum
Placenticeras syrtale
Texanites texanus
Peroniceras tridorsatum
Reesidoceras petrocoriense
Subprionocyclus neptuni
Bl. casimirovensis
Bt. junior
Bl occidentalis
Bl. lanceolata
Bt. cf. najdini
Bt. lengei
Bt. minor
Bt. mucronata
G. qu. gracilis
G. quadrata quadr.
G. granulata quadrata
G. granulata
G. westfelica granulata
G. westfelica
G. praewestfelica
Abath. mayaroensis
Gansserina gansseri
Gl'ta falsostuarti
Gl'ta calcarata
Globotruncana ventricosa
Globotruncanita elevata
Dicar. asymetrica
Dicar. concavata
Marginotruncana schneegansi
N. sigali + schneegansi
D. primitiva
M. tarfayensis + sinuosa
D. conoavata
D. asymetrica
R. formosa
G. stuartiformis
G. elevata
G. subspinosa
G. calcarata
G. havanensis
G. aegyptiaca
G. stuarti
G. esnehensis
G. wiedenmayeri + ganseri
R. contusa
G. arca
G. orientalis
G. falsostuarti
A. mayaroensis
S. deflaensis + carpatica
Recorded ranges
Israel ranges
rare


(f) Benthic foraminifera
(g) Calcareous nannoplankton
(h) Megafossils Israel
(i) Ostracoda Israel
Stages
T. COM.
U.
L.Up.
SANTON
L.
Up.
CAMPANIAN
Lower
Upper
low.
upp.
MAASTRICHTIAN
Low.
Mid.
Up.
B. anguliatus
B. pustulatus
B. australis
B. praecursor
B. petersoni
B. paleocenicus
B. draco miliaris
B. draco draco
B. draco dorreni
C. decurrens
C. inaequata gigantea
N. suturalis
N. rugosa-group
N. praereticulata
N. reticulata
B. decoratus
E. asimus
R. anthophorus
N. furcatus
B. parca
C. gothicum
Q. trifidum
L. quadratus
M. murus
M. frequens + murus
N. prinsii
Pl. kalfariense
Plabotisotia
B. omilahyense, P. westphalicum
R. neocretatica & Bu. biobatum
N. fourneti & Protexanites
Metatissotia sp.
Texanites, Reginaites, Pseudoschlönbachia
Spinaptychus
Hop. marroti
Hop. coesfeldiense
B. palestinensis
Libycoceras
Nostoceras
B. "ancepe"
Ps. pacificum
M. hyatti, N. helicinum, D. navarroense
A. reflexum, Exiteloceras, Solenoceras, Baculites sp.
Chl. farafrensis
G. gracilis
P. lata
C. cretaria & A. judaense
C. rosenfeldi rosenfeldi
L. miarensis
L. doroscostatus & P. campania
B. beershebaensis
H. ordoniya

In the Hazerim-1 borehole a sandstone bed at a depth of 327 m is overlain by a 42 m thick chalky sequence with *Baculites* at its base, which is herein assumed to represent the Coniacian-Santonian sequence. It is followed by 3 m of sandstone overlain by 7 m of marl and sandy chalk. This latter marly-sandy unit may be the lithostratigraphic equivalent of the 'Lower Phosphorite' or the Marl Member (see Bartov et al., 1972) which separates the Menuha Formation into two chalk units. The 'Lower Phosphorite' occurs at Har Zavo'a in the form of nearly 2 m of a phosphorite-rich chalk (some 7 m above the base of the Menuha Formation) containing at the base an ammonite fragment of *Texanites*, attributed to the Upper Santonian. The thickness of the chalky Menuha Formation (topped by the chert of the Mishash Formation) varies widely throughout the northwestern Negev; 10 to 63 m in the Imara-Sherif region (Braun, 1964), 24 m in the Be'er Sheva-1, 150(?) m in the Hazerim-1, and 160 m in the Shezaf-1 boreholes. Its age ranges from Late Coniacian to early Late Campanian.

The Menuha Formation in the Negev is overlain by the Mishash Formation. It is characterized by chert in the lower and phosphorite in the upper part, both associated with chalk, limestone, and porcellanite. The chert of the Mishash Formation wedges out westward within the northwestern Negev. It thins from 20-30 m near Makhtesh Hatira (Roded, 1982a), to nearly 30 m at Shezaf, 8 m near Har Zavo'a (Braun, 1964) and the Mash'abim borehole, 2 m in Be'er Sheva-1, and traces in the Hazerim-1 boreholes. To the north of these no chert occurs in the El-Khabra, Haluza-2, and Revivim-1 boreholes. This chert unit is made up of brecciated and pseudo-conglomeratic brown chert overlain (in the southern regions) by hard massive layered chert; therefore it may be correlated with the Main Chert Member (see Bartov et al., 1972). The chert is overlain by chalk with some chert, phosphate grains, limonite, and some clastics (quartz grains and clay).

Macrofauna (Shezaf-1 and Hazerim-1 boreholes) attributes this chalk unit to the Campanian and it is thus coeval to the carbonates and phosphate series (above the main chert member) of the northern Negev synclines. This correlation is corroborated by the Maastrichtian age attributed to the rather thin (19-20 m in Haluza-2 and Hazerim-1 boreholes; 43 m in the Shezaf-1 borehole) overlying marly chalk and chalky limestone (with chert in the Haluza-2 and Hazerim-1 boreholes), which is the time equivalent of the Ghareb Formation in the central and southern Negev. This Maastrichtian unit hardly resembles the typical Ghareb Formation, whereas the underlying chalky marly unit (locally with phosphate) is more similar to the typical Ghareb Formation, and is regarded as such in the Shezaf-1 borehole, where the Campanian part of it reaches a thickness of nearly 225 m. In the Be'er Sheva-1 borehole it has been designated as the 'En Zetim Formation, comprising 70 m of chalk with some phosphate in the upper part.

The total thickness of the Senonian sequence in the northwestern Negev ranges from nearly 440 m in Shezaf-1, 184 m in Haluza-2 (227(?) m in Hazerim-1), to 109 m in the Be'er Sheva-1 borehole. These remarkable thickness changes over short distances seem to be a function of intensive folding (and faulting?) before and during the Senonian (Bartov et al., 1976), as well as of differential rates of sediment accumulation. The latter, in general retains a low bottom gradient as reflected by the quite similar synchronous lithofacies changes throughout large areas of the country. According to the few microfaunal datings of borehole samples, the most intensive differential subsidence within this area occurred during the Late Campanian (267 m in Shezaf-1 relative to 50-60 m in the Hazerim-1 and Haluza-2 boreholes). These differential movements during the Senonian contrast with the gradually subsiding large shelf platform during Aptian-Late Turonian times.

Menuha Formation (Shaw, 1947).

The Menuha Formation is a marine, predominantly chalky, sequence sometimes resting conformably on strata of Coniacian age, but mostly discordantly on Turonian strata; its upper limit is defined by the first flint layer of the Mishash Formation. The unit may attain a maximum thickness of 150 m, but in most places its thickness is 40-50 m. Reiss (1955b) showed that the Menuha Formation ranges in age from Santonian to Middle Campanian. According to later microfossil work, a Late Coniacian to Early Campanian age was assigned to the Menuha Formation by the ostracode S-1, S-2, S-3, and part of the S-4 Assemblage Zones (Honigstein, 1984; Reiss et al., 1985).

Bentor and Vroman (1951) distinguished three different facies developments:

1) A *chalky facies* characterizing synclinal deposition, mainly composed of soft white unbedded chalk with some chalky limestone, carrying *Pycnodonta vesicularis* Lmk., and *Baculites* sp. The lower part is frequently formed by hard splintery chalk (see Ka'akuhle) carrying *Texanites quinquenodosus* Red. and *Texanites oliveti* Blanck. In a few places it contains phosphate beds ('Lower Phosphate') with *Lamna texana* F., *Othodus appendiculatus* Ag., *Dicrolum serotina* Chavan, and *Corax* sp. The central part frequently consists of gypsiferous marls and shales;

2) A *dolomitic facies*, found in the Dead Sea area, in which the chalks of the synclinal basins appear as hard well-bedded dolomite.

3) A thin only 1-20 m thick *detrital facies* ('Baqara' facies) characterizing deposition on anticlinal slopes, composed mainly of detrital, glauconitic, sandy and frequently salty chalk. In the Negev the Menuha Formation is widely distributed in all the synclines, but missing, owing to non-deposition, in the anticlinal areas. In



Figure 18F.13. Multiple stratigraphic framework for the Late Cretaceous of Israel (after Reiss et al., 1986, Fig. 5). Intercalibrated ranges of selected planktic and benthic foraminifera, calcareous nannofossils, molluscs, and ostracodes in Israel (derived from numerous surface and subsurface sections), as compared with their total ranges recorded in the literature and with the planktic foraminiferal zonation, juxtaposed to the cephalopod biostratigraphy of Europe, and as interpreted in terms of standard stages.

the northern parts of the country, it is difficult to distinguish it from younger Senonian strata.

The Menuha Formation is subdivided into two members. The Lower Member, which is known by the local name 'Ka'akule', consists of hard, slightly limonitic chalk. The Upper Member consists of soft, white chalks and marls. No distinction is made between the two members in the present geological maps. The formation is weathered to nari, especially the soft upper chalk. Usually, the formation unconformably overlies the Judea Group. It seems, however, that in some localities the contact is conformable and transitions from the Judea limestones into the Menuha chalks do occur. The formation is conformably overlain by the Mishash Formation. The formation thins toward the flanks of all major anticlines. It gains its greatest thickness toward the center of the Hashephela synclinorium. As it thickens, the formation passes laterally into the 'Ein Zeitim Formation, although this occurs only in the subsurface (Gvirtzman and Reiss, 1965).

Mishash Formation ('Meshash Flint', Fairbridge, Nasr and Tiratsoo, 1940, in Shaw, 1947).

The Mishash Formation is named after Be'er Mishash, in the Beersheba Valley, on the southwest plunge of the Quseife anticline. It includes the *Upper Campanian Phosphate Series* (Bentor and Vroman, 1957) or 'Phosphattrummer-gestein' of Koert (1924) that forms the upper part of the Mishash Formation. It is a marine, lagoonal sequence composed of calcareous, oolitic, phosphate layers alternating with phosphatic chalk, gray marl, and limestone. The sequence yields *Libycoceras ismaeli* Zittel, *Libycoceras chargense* Blanckenh., and *Serpula discoidea* Wanner. Corals are found and a rich fish fauna containing among others *Lamma biauriculata* Wanner, *Lamna appendiculata* Ag., *Otodus biauriculata* Zittel, *Corax pristodontus* Ag., *Corax kaupi* Ag., *Enchodus bursauxi* Arambourg, *Enchodus elegans* Dartev., *Stephanodus libycus* Dames, *Stephanodus splendens* Zittel, and *Ancistrodon* cf. *libycus* Dames.

The Mishash Formation attains a maximum thickness of 130 m and its average thickness is about 60 m.

It is widely developed in the synclinal areas of the Negev and reaches its maximum development in the north-central part of the region, where it is locally mined for its phosphates.

A marine sequence is composed mainly of alternating beds of flint and chalk, or of flint alone. Bentor and Vroman (1951, 1961) distinguished three different facies:

1) The flinty-chalky 'Ashosh' facies is a synclinal deposit. In this facies the sequence is thick and consists of many thin flint layers, separated by beds of chalk and occasionally of limestone and dolomite. In the upper part phosphate layers appear which in the Negev also form the uppermost 2 to 10 m of the sequence overlying the flint (*Main Phosphate Horizon*). The sequence contains elliptical concretions of hard foetid limestone up to 0.5 m across and is occasionally bituminous; locally it contains clastic limestone and flint breccias.

Fauna: The sequence carries *Hoplitoplacenticeras marroti* Coq., *Hoplitoplacenticeras coesfieldiense* Schluether, *Libycoceras ismaeli* Zittel, *Baculites asper* Morton, *Baculites syriacus* Conr. *Protocardia silicea* Blanck., *Nucula tenera* Rueller, *Lucina dachelenses* Wanner, *Leda perdita* Conr. *Natica (Euspira) judaica* Blanck., and *Scala goryi* (Lartet).

2) The Chalky 'Judean Mountain' facies is also synclinal. It is dominated by chalks with subordinate flint layers and widely developed in the southern Judean Desert.

3) The Flinty 'Haroz' facies is an anticlinal deposition, consisting only of thick flint beds, mostly topped by a flint breccia.

Roded et al. (1972a, b) put an end to a long polemic about the 'Ashosh' and 'Haroz' facies relations by subdividing the Mishash Formation into two members:

1) The **Main Chert Member** forms the base of the Mishash Formation. It consists of brecciated gray to reddish chert with occasionally partially silicified chalk and porcellanite with chert concretions at its base. The member forms a characteristic ledge. Its thickness in the Negev varies between 20 and 30 m.

2) The **Phosphate Series Member** (Roded et al., 1972a, b) is well-developed in synclinal areas, where it consists of an alternation of phosphorite beds, phosphatic chalk, porcellanite, clays, limestone beds, and limestone concretions, as well as narrow bands of chert. Most characteristic of the member are the phosphorite beds and the limestone concretions.The thickness of the member varies from approximately 40 m in the synclines to a few meters on the anticlines. The main decrease in the thickness of the section is due to the thinning out of the chalk, porcellanite, and clays which are found between the phosphorite beds, while the phosphorite beds themselve are little affected by this decrease (Roded, 1983).

Environment: More recently, Soudry and Natan (1980) paid much attention to the palaeo-environment of deposition of the Negev phosphorites. The most common components are phosphate peloids, which are found to be the result of convergent diagenetic processes. The most important are growth around a foreign grain (*e.g.* a foraminifer), phospho-micritization of bone fragments, fragmentation and abrasion of intraclasts, pelletization of aggregates and phosphatization, as well as fragmentaton of fecal pellets. These phenomena, not exclusive to phosphatic sediments, entail a combination of biological, chemical, and mechanical agents, like any other type of diagenetic sediment.

Age: The geologists of the Petroleum Development (Palestine) Ltd. (P.D.P.) considered the Mishash Formation to be mainly of Campanian and perhaps partly of Santonian and Maastrichtian age. Shaw (1947) placed it into the Campanian-Maastrichtian, while Reiss (1955b), on the basis of microfauna, and Parnes (1956b), on the basis of macrofauna, have shown it to range from the Middle to Upper Campanian. The Mishash Formation either conformably overlies the Menuha Formation or disconformably overlies rocks of Turonian or Cenomanian age. It is either conformably overlain by the Ghareb Formation or unconformably overlain by younger strata (up to Middle Eocene). Toward the center of the Hashephela synclinorium the formation is only represented by a tongue within the 'Ein Zeitim Formation (Gvirtzman and Reiss, 1965).

En Zeitim Formation (Shiftan, in Flexer, 1964).

The En Zeitim Formation is named after the village of 'Ein

Zeitim in the Galilee. The formation attains its greatest thickness (300 m) in the subsurface, toward the center of the Hashephela synclinorium (Gvirtzman, 1969). Towards the east the formation passes laterally into the Menuha Formation. Consisting of white chalk and marly chalk, it is sometimes highly bituminous. In the eastern and central Hashephela, it is intercalated by the flinty Mishash Tongue, that is exposed close to Sha'alavim near Gezer, and attains a thickness of 0 to 5 m. The Mishash Tongue wedges out towards the west. The formation is mostly weathered to nari. The formation unconformably overlies the Judea Group and is overlain by the Ghareb Formation. The formation is mostly exposed in the northern part of the Hashephela, in the Nahshon structure near Kefar Uriya, and in the vicinity of Sha'alavim and Modi'in (the Gezer-Lod area). The age is Upper Santonian-Campanian (Flexer, 1964). According to the ostracode biozonation within the En Zeitim Formation, the S-1, S-2, S-3, S-4 and S-5 Assemblage Zones indicate Late Coniacian to Late Campanian age, pointing to a warm marine moderately shallow shelf environment of deposition (Honigstein, 1984).

Kabri Marl (Baida, 1964).

The Kabri Marl is a 3-6 m thick grayish-green soft marl and clay unit with brown limonitic stains. The lower part is very phosphatic. An early Campanian age is provided by abundant foraminifera. Well-preserved fish teeth occur in the lower part. Megafauna also comprises *Gryphaea vesicularis* Lam., *Scala goryi* Lartet, and *Baculites* sp. Planktonic foraminifera become more frequent upwards. The 'Kabri Marl' separates the 'Chalky limestone Formation' from the 'Lower chalk'. It extends from Shefar'Am in the south to Nahal Ga'aton in the north, except in the area east and southeast of Julis, where it is missing. The 'Kabri Marl' sometimes directly overlies the Bi'na Formation.

Sayyarim Formation (Bartov, 1974).

In the Rekhes Menuha region, the Sayyarim Formation is part of the Menuha Formation or the Maliha Chalk (Shaw, 1947; Sakal, 1967). The Menuha-Mishash boundary is defined as the first appearance of massive chert. The lateral tracing of this boundary to the Elat area shows it to be located high above the first massive chert units there. Therefore, the chert bearing lateral equivalents of the Menuha and Mishash Formations of the north are united in the south into a single formation - the Sayyarim Formation, leaving only the lower chalk in the Menuha Formation. At the 'Eteq syncline near Ma'ale Sayyarim, alternating soft chalks and harder units of sandstones, shales, limestones, dolomites, cherts, porcellanites, and phosphorites some 160 m thick were subdivided into eight members.

The base is always a detrital chalk rich in quartz grains and chitinous remains (corresponding to the 'Baqara facies' of Bentor et al., 1960). Chert, forming small elongated nodules, is often concentrated in layers. Toward the south, the amount of sandstones increases markedly and some of them are variegated (Nubian type) due to an iron oxide cement. Well-rounded and spherical pebbles, mostly chert, are often dispersed in the sandy beds, or concentrated into a few layers. The chert pebbles contain relicts and ghosts of Upper Cenomanian-Turonian foraminifers. Well-bedded marls and shales compose the soft units, Shales (montmorillonitic) are very gypsiferous and variegated (purple, green, and red).

Large shells of *Gryphaea vesicularis* Lmk. are dispersed in the chalk or concentrated in beds. The so-called '*Main Chert Member*' forms the most prominent cliff of the Sayyarim Formation. It is followed by well-bedded chalk. A *Porcellanite Member* represents the top-most member of the Sayyarim Formation in the innermost parts of the 'Eteq, Shehoret, Rehavam and Taba synclines only.

Contacts: The Sayyarim Formation unconformably overlies the Zihor Formation and is overlain by the Ghareb Formation. The base is the first occurrence of white chalk, and its top is a phosphorite bed which underlies the pale yellowish marls and chalks of the Ghareb Formation. Fauna are *Protocardia silicea* Blanck., *Baculites aff. B. vagina* Forbes, *Baculites* sp. *Nostoceras (Planostoceras) rehavami* Lewy, *Nostoceras* sp., *Exiteloceras eteqense* Lewy, *Exciteloceras* sp, *Solenoceras humei* Douville, *Nostoceras hyatti* Stephanson, *Solenoceras humei densicostata* Lewy, *Scaphites (Hoploscaphites) elatensis* Lewy, *Libycoceras chargense* Blanck., and Vertebrata. Ammonites from the uppermost member, described by Lewy (1967, 1969) indicate a Late Campanian age.

Ghareb Formation (Browne, Gwin and Nasr, 1941 - 'Ghareb Chalk' in Shaw, 1947).

The Ghareb Formation has had many names: 'Senonian' (part) (Blake, 1928); 'Nebi Musa' (part) (Blake, 1930); 'Bituminous limestone' Ditto; 'Nebi Musa' (part) and 'Bituminous lime' (Picard, 1931); 'Maastrichtian' (part) (Avnimelech, 1936); 'Senonian' (part), Danian (part) (Picard and Avnimelech, 1936); 'Couches de Sar'a' (part), (Avnimelech, 1936); 'Upper Cretaceous' (part) (Henson, 1938); 'Medra chalk' (Glynn and Rogers, 1940; Gwin and Nasr, 1940); 'The White or Ghareb Chalk' (Wellings, 1944).

At Naqb el-Ghareb (Ma'avar Zin) on the southwest plunge of the Kurnub Anticline (Negev), the Ghareb Formation locally reaches 170 m, but its average thickness is about 30 m. It consists of yellow and pink, limonitic, marly chalk, with small pyrite and some phosphate nodules. Bentor et al. (Lexique, 1960) describes "A marine sequence, consisting mainly of white, yellow or reddish argillaceous, phosphatic, limonitic, occasionally sandy and glauconitic chalks; it also contains, especially in its lower part, gray-green gypsiferous shales. Rare dolomites appear in the upper part, and locally the sequence is highly bituminous. The occurrence of large marcasite concretions is characteristic. The sequence is normally unbedded, but may occasionally show excellent bedding."

In the Negev and the Judea Desert, the lower Oil-Shale Member appears black due to the high content of organic carbon (12%-20%; Minster et al., 1997). The upper part is more marly. Rod- or worm-like limonitic stains are locally characteristic. The formation is heavily weathered, with nari crusts attaining 1-3 m, and presenting lapies surfaces. The formation occurs over most of the Negev, usually confined to morpho-tectonic basinal regions. It seems to increase in thickness towards the southeast and reaches some 35 to 40 m in the Yamin Basin. West of Kuseife, it is some 9.5 m thick. Some 8 m of marl, red and pink, grades down to

black bituminous marl, and this in turn becomes limestone, black, nodular, and phosphatic with some flint nodules. Some *Ostrea* sp. and fish remains and teeth make up the fauna. It also occurs as a narrow strip immediately overlying the Mishash Flint, all along the western edge of the Judean Arch at least as far north as Bab el Wad. In the Negev the formation is regressive, being deposited in basinal areas while the anticlinal structures grew above sea level, or at least above depositional level. This is very different from conditions in the interior of Syria, where the equivalent sea appears to have been strongly transgressive.

The formation is widely distributed in the synclines of the Negev, but missing in the anticlinal areas owing to non-deposition. The Ghareb Formation overlies the Mishash and 'Ein Zeitim Formations and is overlain by the Taqiye Formation. At some localities the formation is affected by contact metamorphism known as the Hatrurim Facies. In the southern Negev it conformably overlies the Sayyarim Formation. The upper contact with the Taqiye Marl is conformable and gradational in basinal regions, but the upper beds of the Taqiye Marl transgress with marked overlap as structural highs are approached.

Fauna: Besides fish remains, including teeth, the Ghareb Formation yields *Pecten farafrensis* Zitt., *Terebratulina* sp. *Ventriculites poculum* Zitt., *Schizorhabdus libycus* Zitt., and *Lamna serrata* Ag.

On the basis of microfauna, Reiss (1955b) claimed a late Campanian to Maastrichtian age for the Ghareb Formation. Based on detailed biozonation using foraminifera and calcarous nannoplankton, a Maestrichtian age is now assigned to the sediments of the Ghateb Formation (Almogi-Labin et al., 1990).

ACKNOWLEDGEMENTS

This chapter is largely based upon the work of Francis Hirsch and Reuven Roded on the computerized Lexique of Israel (2001). The authors gratefully acknowledge the effort of John K. Hall to render the compact language of the Lexique into more readable English, and to assemble the appropriate references. Some early references are to proprietary works that are imbedded in earlier versions of the Lexique (*viz.* Damesin, 1933) and are thus unavailable.

REFERENCES CITED

Agnon, A., 1983. Development of sedimentary basins and morphotectonics in the southern sector of the Western Dead Sea Escarpment. Unpublished M.Sc. Thesis, Hebrew University Jerusalem, 61 p. (In Hebrew).

Aizenberg, E., 1968. Composite columnar section of the Jurassic in Hammam El Malih area. Report to Naphta Oil. Co.

Almogi-Labin, A., Flexer, A., Honigstein, A., Rosenfeld, A., and Rosenthal, E., 1990. Biostratigraphy and tectonically controlled sedimentation of the Maastrichtian in Israel and adjacent countries. Rev. Espafi. Paleontol., Vol. 5, p. 41-52.

Almogi-Labin , A., Eshet, Y., Flexer, A., Honigstein, A., Moskovitz, S., and Rosenfeld, A., 1991. Detailed biostratigraphy of the Santonian/Campanian boundary interval in northern Israel. J. Micropalaeontol, 10(1), p. 39-50.

Arkin, Y., and Braun, M., 1965. Type sections of the Upper Cretaceous formations in the northern Negev (southern Israel). Isr. Geol. Surv. Stratigraphic team, Section 2a., 19 p.

Arkin, Y., and Hamaoui, M., 1967. The Judea Group (Upper Cretaceous) in central and southern Israel. Isr. Geol. Surv. Bull. 42, 17 p.

Arkin, Y., Braun, M., Starinsky, A., Hamaoui, M., and Raab, M., 1965. Type sections of Cretaceous formations in the Jerusalem-Bet Shemesh area. Isr. Geol. Surv., Stratigr. Sec. No. 1, 42 p., Figs., Plates.

Avnimelech, M., 1936. Étude géologiques dans la region de la Shephela en Palestine. Ann. Univ. Grenoble, Trav. Lab. Geol. Grenoble, Allier Freres, 144 p., Figs.

Bachmann, M., and Hirsch, F., (in press). Lower Cretaceous carbonate platform of the Eastern Levant - Galilee and the Golan Heights- stratigraphy and 2nd order sea-level change. Cretaceous Research.

Baer, R., 1962. The geology of the Sulam Tsor region. Unpubl. M.Sc. Thesis, Hebrew University Jerusalem, -- p. (In Hebrew).

Baida, U., 1964. On the geology of the Ga'aton-Hillazon area, Western Galilee. Isr. J. Earth Sci., 13(1), p. 1-15.

Barakat, M. G., Darwish, M., and El-Barkooky, A. N., 1986. Lithostratigraphy of the post-Carboniferou pre-Cenomanian clastics in east central Sinai and Gulf of Suez, Egypt. Egypt. Gen. Petrol. Corp. 8th Expolor. Conf., Cairo, Nov. 1986, 15 p., Figs.

Bartov, Y., 1967. The geology of the Beer Ora region. (In Hebrew). Unpubl. M.Sc. Thesis, Hebrew University Jerusalem, 39 p., Appen.

Bartov, Y., 1974. A structural and paleogeographical study of the central Sinai faults and domes. Unpubl. Ph.D. Thesis, Hebrew University of Jerusalem, 143 p., Figs, Maps. (In Hebrew; English Abstract).

Bartov, Y., Arkin, Y., Lewy, Z., and Mimran, Y., 1981. Regional stratigraphy of Israel: A guide to geological mapping. Isr. Geol. Surv., Current Res. 1980, p. 38-41.

Bartov, Y., Arkin, Y., and Steinitz, G., 1976. The Zin Fault Zone. An example of Senonian faulting in the northern Negev of Israel. Isr. J. Earth Sci., 25(1), p. 40-44.

Bartov, Y., Eyal, Y., Garfunkel, Z., and Steinitz, G., 1972. Late Cretaceous and Tertiary stratigraphy and paleogeography of southern Israel. Isr. J. Earth Sci., 21(2), p. 69-97.

Bartov, Y., Lewy, Z., Steinitz, G., and Zak., I., 1980. Mesozoic and Tertiary stratigraphy, paleogeography and structural history of the Gebel Areif en Naqa area, eastern Sinai. Isr. J. Earth Sci., 29(1-2), p. 114-139.

Bartov, Y., and Steinitz, G., 1977. The Judea and Mount Scopus Groups in the Negev and Sinai with trend surface analysis of the thickness data. Isr. J. Earth Sci., 26(3-4), p. 119-148.

Begin, Z. B., 1972. Correlation between Judea Group formations in the Negev, Judean Mts. and Shomeron. (In Hebrew). Isr. Geol. Soc., Annu. Meet., Abstr., p. 33-36.

Begin, Z. B., 1975. The geology of the Jericho area. Isr. Geol. Surv., Bull. 67, 35 p., Plates.

Bein, A., 1967. Upper peat - Hula Valley; Summary Report. (In Hebrew). Isr. Geol. Surv., Rep., 6 p., Figs., Maps.

Bein, A., 1974. Reef development in the Judea Group from Carmel and the Coastal Plain, Israel. (In Hebrew; English Abstr.). Unpubl. Ph.D. Thesis, Hebrew University Jerusalem, 154 p., Plates.

Bein, A., 1977. Shelf basin sedimentation: Mixing and diagenesis of pelagic and clastic Turonian carbonates, Israel. J. Sediment. Petrol., 47(1), p. 382-391.

Bentor, Y. K., 1945. Petrographic investigations of the Upper Albian - Lower Cenomanian near Jerusalem and contribution to the problem of dolomitization and quartzification. Unpubl. Ph.D. Thesis, Hebrew University Jerusalem, 232 p.

Bentor, Y. K., 1966. The clays of Israel; Guide-book to the excursions. (Includes: An outline to the geology of Israel; The clays of Israel; Negev Excursion; Mount Carmel - Galilee Excursion). Int. Clay Conf., Jerusalem 1966. Isr. Progr. for Sci. Transl., 121 p.

Bentor, Y. K., Grader, P., Parnes, A., Reiss, Z., Shiftan, Z., Vroman, A. J., Shadmon, A., Issar, A., Itzhaki, Y., Neev, D., Shalem, N., and Yaalon, D. H., 1960. Lexique Stratigraphique International. Vol. III: Asie. Fasc. 10 C 2: Israel. Paris, C.N.R.S., 151 p., Maps.

Bentor, Y. K., and Vroman, A. J., 1951a. The geological map of the Negev 1:100,000, Sheet 18: Ovdat/Avedat. Tel Aviv (Explanatory notes in Hebrew). (In Hebrew). Israeli Army, Sci. Sect., 98 p., Maps, Figs.

Bentor, Y. K., and Vroman, A. J., 1951b. Decouverte de gres à facies Nubien dans le Turonien superieur du Neguev septentrional (sud d'Israel). Bull. Soc. Géol. Fr.,

Ser. 6, 1(7), p. 491-495.

Bentor, Y. K., and Vroman, A. J., 1954. The geological map of the Negev, Sheet 21: Mount Omer. Isr. Defence Forces, 1 Geol. Map and 1 Struct. Map, Scale 1: 100,000.

Bentor, Y. K., and Vroman, A. J., 1957. Geological map of Israel, 1:100,000, Series A - The Negev. Sheet 19: Arava Valley. Isr. Geol. Surv., 66 p., Maps. (Hebrew and English Editions).

Bentor, Y. K., and Vroman, A. J., 1960. Geological map of Israel, 1:100,000, Sheet 16: Mount Sdom. Isr. Geol. Surv., 117 p., Figs., Separate Folder With 19 Encl. (Hebrew and English Editions). 1st Edition - 1954; 2nd Edition - 1960.

Bentor, Y. K., and Vroman, A. J., 1961. Geological map of Israel, Ser. A: The Negev, Sheet 17: Nitsana (Cross Sections). Isr. Geol. Surv., 1 Sheet - Cross Sections.

Bentor, Y. K., and Vroman, A. J., 1964. The geological map of Israel, Ser. A - The Negev. Sheet 20: Mount Lots. (In Hebrew and English). Isr. Geol. Surv., 1 Map, Scale 1:100,000.

Bischoff, G., 1964. Ostracoden-Studien im Libanon, 3, Die Gattung Cytherelloidea im oberen Jura und in der Unterkreide. Senck.Leth. 45(1-4), p. 1-21.

Blake, G. S., 1928. Geology and water resources of Palestine. Jerusalem, Govt. Report, 51 p.

Blake, G. S., 1930. The mineral resources of Palestine and Transjordan. Jerusalem, Printing and Stationery Office, 41 p., Maps.

Blake, G. S., 1935. On the occurrence of marine Miocene in Palestine. Geol. Mag., 72(3), p. 140-142.

Blake, G. S., 1936. The stratigraphy of Palestine and its building stones. Jerusalem, Printing and Stationery Office, 133 p.

Blanche, Ch. I., 1847. Lettre du Liban: "Coupe d'une montagne sru laquelle est Abey, village du Liban, comprenant le terrain crétacé et une roche ignée". Bull. Soc. Géol. France, 5, p. 12-17, illus.

Blanckenhorn, M., 1905a. Geologie der naeheren Umgebung von Jerusalem: Ztschr. dtsch. Pal. ver., 28, p. 75-120. 1:10,000 scale map.

Blanckenhorn, M., 1905b. Ueber die Geologie die naeheren Umgebung von Jerusalem : Monatsber. d. dtsch. geol. Ges., (1), p. 35-43.

Blanckenhorn, M., 1905c. Ueber die letzten Erdbeben in Palaestina und die Erforschung etwaiger kuenftiger. Ztschr. dtsch. Palaest. Ver., 28, p. 206-221.

Blanckenhorn, M., 1905d. Ueber die Steinzeit und die Feuersteinartefakte in Syrien-Palaestina. Ztschr. f. Ethnologie, Berlin, 37, p. 447-471, illus.

Blanckenhorn, M., 1914. Syrien, Arabien, Mesopotamien. Heidelberg, Winter's Universitaetsbuchhanglung, Handbuch der Regionalen Geologie, 5(4), 159 p.

Blanckenhorn, M., 1934. Die Bivalven der Kreideformation von Syrien - Palaestina nebst einem Ergaenzendem Nachtrag ueber Brachiopoden, Gastropoden und Pteropoden und einem Ueberblick ueber die gesampe Molluskenfauna. - Palaeontographica, v. 81 A, N 4-6, p. 161-302.

Braun, M., 1964. The geology of Imara-Sherif area (Mt. Zavoa and Mt. Shahar). (In Hebrew). Isr. Geol. Surv., Rep. MM/1/64, 33 p., Figs., Maps.

Braun, M., and Hirsch, F., 1994. Mid-Cretaceous (Albian-Cenomanian) carbonate platforms in Israel. Cuadernos Geol. Iberica, No. 18, p. 59-81.

Browne, R. V., Gwin, J. W., and Nasr, S. N., 1941. Geological report on the Sinaf, Meliha, Urief and Taqiye areas. Petroleum Development (Palestine), Unpublished report, 31 p.

Cohen, A., 1983. Lithofacies and environments of deposition of the Lower Cretaceous Helez and Telamim Formations, Israel. Isr. Geol. Surv., Rep. S/5/83, 139 p.

Cohen, Z., 1971. The geology of the Lower Cretaceous of the Helez Field, Israel. Unpubl. Ph.D. Thesis, Hebrew University, Jerusalem, 98 p. (In Hebrew, English abstract).

Cohen, Z., 1976. Early Cretaceous buried canyon: influence on accumulation of hydrocarbons in Helez oilfield, Israel. Am. Assoc. Petrol. Geol., Bull., 60(1), p. 108-114.

Cohen, Z., Kapstan, V., Muravinski, E., Salhov, S., Shilo, A., and Wolff, O., 1987. Stratigraphic table of Israel outcrops and subsurface. Oil Exploration (Investment) Ltd.

Conway, B. H., 1991. Early Cretaceous (Berriassian) mocroflora on Mount Hermon. J. African Earth Sci., 13(3/4), p. 499-504.

Damesin, 1933. Unpublished P.D.P. Geological Report.

De Haan, P. J., 1997. Chronostratigraphic reinterpretation of the Early Cretaceous in the subsurface of the Israeli coastal Plain. Unpubl. Ph.D. Thesis, University of California, Davis, 277 p.

Derin, B., and Reiss, Z., 1965. Note on some Jurassic and Early Cretaceous Trocholina (Foraminiferida) from Israel. Jerusalem, Oil Companies, Micropaleontol. Lab. Rep. OS/1/65, 11 p., Figs., Plates.

Diener, C., 1886. Libanon, grundlinien physischen Geographie und Geologie von Mittel Syrien. - Wien, A. Hoelder, 412 p., map at scale 1:500 000.

Douville, H., 1910. Études sur les Rudistes. Mem. Soc. Géol. France, No. 41, Rudistes du Liban.

Dubertret, L., 1937. Le Cretace. 1. Le Massif Alaouite ou Djebel Ansariyeh. Notes et Mémoires, Vol. 2, p. 9-42.

Dubertret, L., 1963. Liban, Syrie: Lexique Stratigraphique International, Vol. 3, Asie, Fasc. 10 Cl. (Liban, Syrie, Jordanie) CNRS Paris, 155 p.

Ecker, A., 1962. The microfauna and microfacies of the type section of the Derorim Formation. (In Hebrew). M.Sc. Thesis, Hebrew University Jerusalem, 66 p., Figs. (Isr. Geol. Surv., Rep. Pal/2/62).

Eckstein, Y., 1963. The geology of the Gerofit area. (In Hebrew). Isr. Geol. Surv., Rep. Hydro/6/63, 41 p., Figs., Maps. (M.Sc. Thesis, Hebrew University Jerusalem).

Eckstein, Y., and Rosenthal, E., 1966. En Boqeq 1 well: Possibilities for exploitation. (In Hebrew). Isr. Geol. Surv., Rep. Hydro/1/66, 12 p., Figs.

Eliezri, I., 1963. The Jurassic-Cretaceous unconformity in the Coastal Plain and the Negev. Isr. J. Earth Sci., 12(2), p. 80.

Eliezri, I. Z., 1965. The geology of the Beit Jann region (Galilee, Israel). Isr. J. Earth. Sci. 14(2), p. 51-66.

Fairbridge, R. W., Nasr, S. N., and Tiratsoo, E. N., 1940. Unpublished P.D.P. (Palestine) reports.

Fleischer, L., 2000. Index of Oil and Gas wells drilled in Israel (updated, January 2000). Ministry of National Infrastructures, Earth Sciences Research Administration, Oil and Gas Unit Report OG/8/2000, and Geophys. Inst. Isr., Report 874/01/2000. 44 p. Map at 1:250,000 scale.

Flexer, A., 1961. The geology of Mount Gilboa. Isr. Res. Counc., Bull., 10G(1-2), p. 64-72, 1 Map.

Flexer, A., 1964. The paleogeography of the Senonian and Maestrichtian in northern Israel. (In Hebrew; English Abstr.). Unpubl. Ph.D. Thesis, Hebrew University Jerusalem, 157 p., Figs.

Flexer, A., Dimant, E., Dagan, G., and Vered-Weiss, J., 1981. Inground crude oil storage (the Kurkar Ridge of Atlit). (Geology: A. Flexer and E. Dimant; Hydrology: G. Dagan; Engineering: J. Vered-Weiss). Tel Aviv, Petroleum Services, Eng. Dept., 23 p.

Flexer, A., Gill, D., Livnat, A., Tamir, N., and Toister, A., 1981a. ATLAS Project (Israel Subsurface Geology Information Management System). Part A - Explanatory Notes. (In Hebrew). Tel Aviv, Oil Exploration {Investments}, 43 p., Figs.

Flexer, A., Gill, D., Livnat, A., Toister, A., Shafran, N., and Tamir, N., 1981b. Computerized information system in support of oil and gas exploration in Israel. Oil Exploration In Israel; A Symp., Jerusalem, Dec. 1981; Abstr. Isr. Geol. Soc., Oil Exploration {Investments} and Isr. Geol. Surv., p. 16-20.

Folkman, Y., Lasman, N., and Raab, M., 1966. Lower Cretaceous outcrops on Mount Carmel (northern Israel). Isr. J. Earth Sci., 15(1), p. 38-41.

Fraas, O., 1867. Aus dem Orient: Geologische Beobachtungen am Nil, auf der Sinai Halbinsel und Syrien. Stuttgart.

Fraas, O., 1878. Aus dem Orient. 2. Geologische Beobachtungen am Libanon. Jahrb. Verein. Natur., Wuerttemberg, p. 257-392.

Freund, R., 1958. The geology of the Yarqa-Peqiin Area (Western Galilee). (In Hebrew). Unpubl. M.Sc. Thesis, Hebrew University, Jerusalem, 39 p., Maps, Figs.

Freund, R., 1959. On the stratigraphy and tectonics of the Upper Cretaceous in western Galilee. Isr. Res. Counc., Bull., 8G(1), p. 43-50.

Freund, R., 1960. Type sections of three formations in western Galilee. Isr. Res. Counc., Bull., 9G(2-3), p. 159-164.

Freund, R., 1961. Distribution of Lower Turonian Ammonites in Israel and the neighbouring countries. Isr. Res. Counc., Bull., 10G(1-2), p. 79-100, Maps.

Freund, R., 1962. Problems in the stratigraphy of the Cenomanian-Turonian in Israel. (In Hebrew; English Abstr.). Unpubl. Ph.D. Thesis, Hebrew University Jerusalem, 189 p.

Freund, R., 1965. A model of the structural development of Israel and adjacent areas since Upper Cretaceous times. Geol. Mag., 102(3), p. 189-205.

Freund, R., and Raab, M., 1969. Lower Turonian Ammonites from Israel. London, Paleontological Assoc., Spec. Pap. 4, 83 p.

Ghorab, M. A., 1961. Abnormal stratigraphic features in Ras Gharib oilfield. 3rd Arab Petroleum Cong., Alexandria, 11 p.

Glynn, J., and Rogers, D. C., 1940. The Kurnub structure. Petroleum Development of Palestine (P.D.P.), Geol. Rept. No. 154, 19 p.

Golani, U., 1957. The geology of the Maghar area. (In Hebrew). Unpubl. M.Sc. Thesis, Hebrew University Jerusalem, 54 p., Figs.

Golani, U., 1961. On the Cenomanian-Turonian lithostratigraphy of central Galilee. Isr. Res. Counc., Bull., 10G(1-2), p. 115-146.

Golani, U., 1962. The geology of Lake Tiberias region and the geohydrology of the saline springs. Jerusalem, Tahal, 54 p.

Grader, P., 1958. Geological outline of the Sasa region, Galilee. Isr. Geol. Surv., Bull. 20, 10 p., Map.

Grader, P., and Moser, F., 1957. A type composite log of the Upper Cretaceous and Lower Tertiary formations. Isr. Geol. Surv., Bull. 15, 6 p.

Grader, P., and Reiss, Z., 1958. On the Lower Cretaceous of Heletz area. Isr. Geol. Surv., Bull. 16, 14 p.

Gvirtzman, G., 1969a. Subsurface data on the Saqiye Group (Late Eocene to Early Pleistocene) in the Coastal Plain and Hashephela regions, Israel. Isr. Geol. Surv., Rep. OD/1/69 and Inst. Pet. Res. Geophys., Rep. 1037, Various Pagings.

Gvirtzman, G., 1969b. The Saqiye Group (Late Eocene to Early Pleistocene) in the Coastal Plain and Hashephela regions. Vol. 2: Maps. (Vol. 1 was never published). Isr. Geol. Surv., Bull. 51 and Inst. Pet. Res. Geophys., Rep. 1022. 38 Maps.

Gvirtzman, G., and Buchbinder, B., 1966. Tertiary Project. Holon, Inst. Pet. Res. Geophys., Semi Annu. Progr. Rep., Apr. 1966 - Sept. 1966, p. 11-16.

Gvirtzman, G., and Reiss, Z., 1965. Stratigraphic nomenclature in the Coastal Plain and Hashephela regions. Isr. Geol. Surv., Rep. OD/1/65, 13 p.

Gwin, J. W., and Nasr, S. N., 1940. The Ramon Anticline. Petroleum Development (Palestine) Limited, Geological Report, 25 p.

Hamaoui, M., 1966. Microfossils from Cenomanian sections in the Negev. Isr. Geol. Surv. Report Pal./3/66, 12p.

Hamaoui, M., and Raab, M., 1965. Type sections of Cretaceous formations in the Jerusalem-Bet shemesh area. II. Biostratigraphy. Isr. Geol. Surv., stratigraphic sections, 1.

Hao, Y., Zeng, X., Guo, X., 1988. The marine Cretaceous in the western part of the Tarim Basin of Xinjiang and its depositional environments. Acta Geologica Sinica (Eng. Ed.), 1(1), p. 13-27.

Hart, M. B., 1982. Turonian foraminiferal biostratigraphy of southern England. In: Colloque su le Turonien. Mém. Res. du Muséum Nationale d'Histoire Naturelle, Ser. C, Vol. 49, p. 203-207.

Hart, M. B., and Bailey, H. W., 1979. The distribution of planktonic foraminifera in the mid-Cretaceous of N.W. Europe. Aspekte der Kreide Europas, I.U.G.S., A6, p. 527-542.

Henson, F. R. S., 1948. Foraminifera of the genus Trocholina in the Middle East. Ann. and Mag. Nat. Hist. Ser 11, XIV.

Heybroek, F. V., 1942. La géologie d'une partie du Liban sud. Leidsche Geol. Med., 12, p. 251-470. Leiden.

Hirsch, F., 1985. Geological and structural maps (1:50,000) of the Mazal Concession (Hamakhtesh Haqatan, Sheet 19-II). Tel Aviv, Eastern Medit. Oil and Gas Co.

Hirsch, F., 1986. Zoo-palaeogeographic evidences against an eastern Mediterranean Mesozoic Mesogean Ocean. Isr. Geol. Soc., Annu. Meet., Abstr., p. 66-67.

Hirsch, F., 1988. Geology of the northern plunge of the Hazera anticline, NE Negev, Israel.Isr. Geol. Surv., Current Res., 6, p. 41-46.

Hirsch, F., 1996. Geology of the southeastern slopes of Mount Hermon. Isr. Geol. Surv., Current Res., Vol. 10, p. 22-27.

Hirsch, F., Flexer, A., Rosenfeld, A. and Yellin-Dror, A., 1994. Palinospastic and crustal setting of the eastern Mediterranean. J. Petrol. Geol. 18(2), p. 149-170.

Hirsch, F., Rosenfeld, A. and Honigstein, A., 1994. Early Cretaceous ostracodes from the southeastern slopes of Mount Hermon. Isr. Geol. Surv., Curr. Res. 9, p. 90-91.

Honigstein, A., 1984. Senonian ostracodes from Israel. Isr. Geol. Surv. Bull. 78, 48 p.

Honigstein, A., Lipson, S., Conway, B. H., Flexer, A., and Rosenfeld, A., 1989. Mid-Turonian anoxic event in Israel - A multidisciplinary approach. Palaeogeogr. Palaeoclimatol. Palaeoecol., 69(1-2), p. 103-112.

Itzhaki, Y., Arkin, Y., Braun, M., and Lasman, N., 1964. Jerusalem-Bet Shemesh: Geological Map, 1:50,000. Isr. Geol. Surv., 1 Map.

Kafri, U., 1965. The geology of the Segev area (western Galilee, Israel). Isr. J. Earth Sci., 14(2), p. 67-75.

Kafri, U., 1969. Geology and groundwater of the Cenomanian formations in the Galilee, west of the watershed. (In Hebrew; English Abstr.). Unpubl. Ph.D. Thesis, Hebrew University Jerusalem, 188 p., Figs., Tabs.

Kafri, U., 1972. Lithostratigraphy and environment of deposition, Judea Group, western and central Galilee, Israel. Isr. Geol. Surv., Bull. 54, p. 1-56.

Karcz, Y., 1959. The structure of the northern Carmel. Bull. Res. Counc. Israel, 8G(2-3), 119-130.

Kashai, E., 1958. A note on the revision of the stratigraphy of the southern Carmel. Bull. Res. Councel Israel, 7G (2-3) 164-165.

Kashai, E., 1966. The Geology of the eastern and southwestern Carmel. Unpubl. Ph.D. Thesis, Hebrew University Jerusalem, 115 p. (In Hebrew).

Keller, A., 1933. Sur quelques rudistes du Djebel Ansarijeh et de l'Amanus (Syrie septentrionale). Notes et Mémoires, 1, p. 45-52.

Koert, W., 1924. Geologische Beobachtungen in Syrien und Palaestina wachrend des Feldzuges 1917/18. Zeitschr. dtsch. Geol. Ges., 76(1-2), p. 1-46.

Krusch, P., 1911. Die Phosphatlagerstaette bei Es-Salt im Ost-Jordanlande. Zeitschr. f. prakt. Geol., 19, p. 397-406.

Lartet, L., 1869. Essai sur la Geologie de la Palestine. Thesis, Fac. Sci., Paris, v. 316, Paris: Masson, 292 p.

Leereveld, H., 1995. Dinoflagellate cysts from the Lower Cretaceous Rio Argos succession (SE Spain). LPP Contribùtion Series 2, Ph.D. Thesis, University Utrecht, ---- p.

Lewy, Z., and Raab, M., 1976. Mid-Cretaceous stratigraphy of the Middle East. Annales du Museum d'Histoire Naturelle de Nice, IV, 32, p. 1-20.

Lewy, Z., 1975. The geological history of southern Israel and Sinai during the Coniacian. Isr. J. Earth Sci., 24(1-2), p. 19-43.

Lewy, Z., 1981. A late Albian *Hypengonoceras* (Ammonoidea) from the 'Bentonite-bed' at Makhtesh Ramon, southern Israel. Isr. J. Earth Sci., 30(1), p. 35-38.

Lewy, Z., 1990. Transgressions, regressions and relative sea level changes on the Cretaceous shelf of Israel and adjacent countries. A critical evaluation of Cretaceous global seal level correlations. Paleooceanography, 5(4), p. 619-637.

Lewy, Z., Kennedy, W. J., and Chancellor, G., 1984. Cooccurrence of *Metoicoceras geslinianum* (d'Orbigny) and *Vascoceras cauvini* Chudeau (Cretaceous Ammonoidea) in the southern Negev (Israel) and its stratigraphic implications. Newsl. Stratigr., 13(2), p. 67-76.

Lipson-Benitah, S., 1980. Albian to Coniacian zonation of the western Coastal Plain of Israel. Cretaceous Res., 1(1), p. 3-12.

Lipson-Benitah, S., Rosenfeld, A., Honigstein, A., Flexer, A. and Kashai, E., 1988. The Middle Turonian Daliyya type section in Israel: biostratigraphy, palaeoenvironment and sea-level changes. Cretaceous Res., 9(4), p. 321-336.

Lowenstam, H. A., 1942. Geology of the eastern Nazaret mountains, Palestein. I. Cretaceous stratigraphy. J. Geology, 50(7), p. 813-845.

Mimran, Y., 1969. The stratigraphy of the Lower Cretaceous of Wadi Malih. Isr. J. Earth Sci., 18(3-4), p. 166-167.

Mimran, Y., 1972. The Tayasir Volcanics. Isr. Geol. Surv. Bull. 52, 9 p.

Minster, T., Yoffe, O., Nathan, Y., and Flexer, A., 1997. Geochemistry, mineralogy, and paleoenvironments of deposition of the Oil Shale Member in the Negev. Isr. J. Earth Sci., 46(1), p. 41-59.

Mor, D., 1987. Geological Map of Israel, Sheet 2-II: Har Odem, Golan Heights, 1: 50,000, prelim. Edit. Isr. Geol. Surv.

Morsy, A. M., Kelling, G., El-Ghawaby, M. A., and El-Fawal, F. M., 1993. Sedimentology of the pre-Cenomanian succession, east-central Sinai, Egypt. Annal. Geol. Surv. Egypt, 19, p. 301-325.

Moshkovitz, S., 1972. Biostratigraphy of the genus *Nannoconus* in the Lower Cretaceous sediments of the subsurface: Ashqelon-Helez area, central Israel. Isr. J. Eart-Sci., 21(1), p. 1-28.

Nevo, E., 1956. Report on the Lower Cretaceous of the Rami area. Isr. Geol. Surv. Unpubl. Rep. (In Hebrew).

Nevo, E., 1963a. The Jurassic strata of Makhtesh Ramon. Isr. J. Earth Sci. 12(2), p. 90-91.

Nevo, E., 1963b. The Jurassic strata of Makhtesh Ramon. Isr. Geol. Soc., Summary Lect., Makhtesh Ramon Symp., Abst., p. 11-12.

Noetling, F. 1886. Entwurf einer Gliederung der Kreideformation in Syrien und Palaestina. Z. Deutsch. Geol. Ges., v. 38, p. 824-875, Berlin.

Palmer, A. R. (compiler), 1983. The Decade of North American Geology 1983 Geologic Time Scale. Geology, 11(9), p.503-504.

Parnes, A., 1956. Stratigraphy of the Phosphatic Belts in the Negev. (In Hebrew). Isr. Explor. Soc., Bull., 20(3-4), p. 151-158.

Parnes, A., 1958. A Coniacian Ammonite from the southern Negev (Israel): Muniericeras Lapparenti Grossouvre Var. Isr. Res. Counc., Bull., 7G(4), p. 167-172.

Parnes, A., 1964. Coniacian Ammonites from the Negev (southern Israel). Isr. Geol. Surv., Bull. 39, 42 p.

Philip, J., 1982. Paleogéographie des Rudistes et géodynamique des marges mésogeennes au Crétace supérieur. Bull. Soc. Géol. France. (7), 24(5-6), p. 995-1006.

Picard, L., 1928. Zur Geologie der Kischonebene. Zeitschr. Dtsch. Palaestina Vereins, Vol. 51, p. 5-72, 2 Maps.

Picard, L., 1931. Geological researches in the Judean Desert. 'Mizi Akhdar', 'Arad Marble'. Goldberg Press, Jerusalem. 108 p.

Picard, L., 1938a. Synopsis of stratigraphic terms in Palestinian geology. Hebrew University Jerusalem, Geol. Dept., Bull., 2(2), 24 p.

Picard, L., 1938b. The geology of New Jerusalem. (In Hebrew and English). Jerusalem, Hebrew University, Geol. Dept., Bull., 2(2). 1, 12 p.

Picard, L., 1955. Geological Map of Israel, 1:100,000. Sheet 2: Haifa. Isr. Geol. Surv., 1 Map, Colored.

Picard, L., 1956a. Geological background for petroleum drilling at Zikhron Yaaqov (southern Carmel). (In Hebrew). Isr. Explor. Soc., Bull., 20(3-4), p. 121-128.

Picard, L., 1956b. Geological Map of Israel 1:100,000. Sheet 4: Zikhron Yaaqov. Isr. Geol. Surv., 1 Map, Colored.

Picard, L., 1956c. The Geological Map of Israel, 1:100,000. Sheet 1: Metulla. Isr. Geol. Surv., 1 Map.

Picard, L., 1956d. The Geological Map of Israel, 1:100,000. Sheet 3: Safad. Isr. Geol. Surv., 1 Map.

Picard, L., 1956e. The Geological Map of Israel, 1:100,000. Sheet 5: Nazareth. Isr. Geol. Surv., 1 Map.

Picard, L., 1956f. The Geological Map of Palestine, 1:100,000. Sheet 8: Yibna. Isr. Geol. Surv., 1 Map.

Picard, L., 1956g. The Geological Map of Palestine, 1:100,000. Sheet 11: Gaza. Isr. Geol. Surv., 1 Map.

Picard, L., 1956h. The geological situation of Jerusalem. (In Hebrew). The Jerusalem Book, Ed by M. Avi Yonah. Jerusalem and Tel Aviv, Bialik Inst. and Devir, p. 35-44.

Picard, L., and Avnimelech, M., 1937. On the geology of the central Coastal Plain, Bull. Geol. Dep., Hebr. Univ., 1(4), p. 1-45.

Picard, L. and Kashai, E., 1958. On the lithostratigraphy and tectonics of the Carmel. Bull. Res. Coucil Israel, 7G(1), p. 1-26.

Powell, J. H., 1989. Stratigraphy and sedimentation of the Phanerozoic rocks in central and southern Jordan. Part B: Kurnub, Ajlun and Belqua Group. Natural Resources Authority, Jordan, Bull. 11, 130 p.

Raab, M., 1965. Megafossils of the "Ora Shale" (Part) and of the Nezer Formation in the Gerofit Area. Isr. Geol. Surv., Rep. Pal/7/63, 5 p., Figs.

Raab, M., 1965. Megafossils of the Shivta Formation. Isr. Geol. Surv., Rep. Pal/6/63, 3 p., Plates.

Reiss, Z., 1952. On the occurrence of *Globotruncana Calcarata* Cushman 1927 in the Upper Cretaceous of Israel. Isr. Res. Counc., Bull., 2(3), p. 270-272.

Reiss, Z., 1952. On the Upper Cretaceous and Lower Tertiary Microfaunas of Israel. Isr. Res. Counc., Bull., 2(1), p. 37-50.

Reiss, Z., 1955. A. Micropaleontology and Cretaceous-Tertiary boundary in Israel. B. Remarks on the age of some Late Cretaceous and Early Tertiary stratigraphic units in Israel. Isr. Geol. Surv., Bull. 8, 22 p. (Reprinted From: Isr. Res. Counc., Bull., 5B(1), p. 105-120 and 121-125).

Reiss, Z., 1958. Notes on Foraminifera from Israel. 7. Remarks on the age of the so called Dalia Marls in northern Israel. 9. *Protopeneroplis Striata* Weynschenk from the Jurassic of Israel. Isr. Geol. Surv., Bull. 17, p. 3-4 and 8-10.

Reiss, Z., Almogi-Labin, A., Honigstein, A., Lewy, Z., Lipson-Benitah, S, Moshkovitz, S., and Zaks, Y., 1985. Late Cretaceous multiple stratigraphic framework of Israel. Isr. J. Earth Sci., 34(4), p. 147-166.

Roded, R., 1983. The Geological Map of Israel 1:50,000, Sheet Oron. Isr. Geol. Survey. Map completed in 1978, published in 1982. Explanatory notes in Hebrew and English, 20 p and 14 p.

Roded, R., and Shiloni, Y., 1972a. Geological survey for phosphate at Sede Zinim. (In Hebrew). Isr. Geol. Surv., Rep. MPBK/385/72, 9 p., Figs.

Roded, R., Shiloni, Y., Cook, P., and Ginzburg, D., 1972b. The phosphate fields along Nahal Zin. (In Hebrew). Isr. Geol. Surv., Rep. MP/530/72, 45 p.

Rofe and Raffety Consulting Eng., 1963. Jerusalem And District - Water Supply; Geological And Hydrological Report. London, Rofe and Raffety, 79 p., Figs., Tabs., Appen.

Rofe and Raffety, 1965. (Burdon, D. J., Borthwick, Q. W. and Eccleston, B. L.) Geological map of Jerusalem and Nablus districts, 1:20,000, Rofe and Raffety, chartered civil engineers. (unpublished).

Rosenberg, E., 1960. Geologische Untersuchungen in den Naftali Bergen. Mitt. Geol. Inst. ETH and Univ. Zurich, ser. C, 80, 107 p.

Rosenfeld, A., Flexer, A., Honigstein, A., Almogi-Labin, A., and Dvorachek, M., 1989. First report on a Cretaceous/Tertiary section at Makhtesh Gadol, southern Israel. Neues Jahr. Geol. Pal. Monatsh., 1989(6), p. 474-488.

Rosenfeld, A., Hirsch, F., and Honigstein, A., 1995. Early Cretaceous Ostracodes from the Levant. In: J. Riha (ed.), Ostracoda and Biostratigraphy. Proc. 12th Int. Symp. on Ostracoda, Prague, July 1994, Rotterdam, Balkema, p. 111-121.

Rosenfeld, A., Hirsch, F., Honigstein, A., and Raab, M., 1998. The palaeoenvironment of Early Cretaceous Ostracodes in Israel. What about Ostracoda? Bull. Centre Rech. Elf Explor. Prod., Mém. 20, p. 179-195.

Rosenfeld, A., and Raab, M., 1974 Cenomanian-Turonian ostracodes from the Judea Group in Israel. Isr. Geol. Surv., Bull., 62, p. 1-64.

Rosenfeld, A., and Raab, M., 1981 Lower Cretaceous ostracodes from Israel. Isr. Geol. Surv., Current Res., 1980, p. 57-61.

Rosenfeld, A., and Raab, M., 1984 Lower Cretaceous Ostracodes from Israel and Sinai. Isr. J. Earth Sci., 33(3), p. 85-134.

Russegger, J., 1847. Reisen in Unter-Egypten, auf der Halbinsel des Sinai und im geloben Lande. Vol. III, p. 1-292, illust., maps.

Sakal, E., 1966. Upper Cretaceous Project: Geology of the Menuha Ridge. Holon, Inst. Pet. Res. Geophys., Semi Annu. Progr. Rep., Apr. 1966 - Sept. 1966, p. 18-25, Figs.

Sakal, E., 1967. The geology of the Menuha ridge. Unpubl. M.Sc. Thesis, Hebrew University Jerusalem., 115 p. (In Hebrew).

Saltzman, U., 1968. The geology of the southeastern Hermon slopes. Tahal, Internal Report., 46 p. (In Hebrew).

Sandler, A., and Zilberman, E., 1984. Sandstones in the Nezer Formation. Isr. Geol. Soc., Annu. Meet., Abstr., p. 84-85.

Sass, E., 1966. Geology and petrology of the Umm El Fahm Area. Unpubl. Ph.D. Thesis, Hebrew University Jerusalem, 174 p. (In Hebrew).

Scarpa, D., and Hirsch, F., 1999. The variegated sands of the Bani Naim Member within the Jerusalem Formation (Turonian) in the Bethlehem and Hebron Districts. Bethlehem Univ. J., Vol. 18, p. 105-110.

Schlanger, S. O., Arthur, M. A., Jenkyns, H. C. and Scholle, P. A., 1987, The Cenomanian-Turonian oceanic anoxic event, I. Stratigraphy and distribution of organic carbon-rich beds and the marine $\delta^{13}C$ excursion. In: J. Brooks and A. J. Fleet (eds.), Marine Petroleum Source Rocks, Geol. Soc. London, Spec. Publ. 26, p. 371-399.

Seetzen, U. J., 1810. Une courte description des pays autour du lac de Tibériade, du Jourdain et de la Mer Morte. Annal. de Voyages, Paris, Vol. 7, p. 137-191.

Shachnai, E., 1968. Composite section of the Lower Cretaceous at Ein Qinyia-Ein Arik (Ramallah Region) including type sections of Ein Qiniya Formation and Qatana Formation (In: Geological Map of Ramallah area). Geol. Surv. Israel, Interim Report, Jerusalem.

Shadmon, A., 1959. The Bina Limestone. Isr. Geol. Surv. Bull., 24, 4 p.

Shalem, N., 1925. Il Cenomaniano ad occidente di Gerusalemme. Bull. Soc. Geol. Ital., 44, 2, 1-18.

Shalem, N., 1926. Nuovo materiale per lo studio dell'eta Della pietra in Palestina. Arch. Antropol. e Etnol., 55(1-4), p. 1-17.

Shalem, N., 1927. La Creta Superiore nei Dintorni di Gerusalemme. Boll. Soc. Geol. Ital., 46(2), p. 171-192.

Shalem, N., 1928. Fauna Nuova Cenomaniana delle Argille Verdi di Gerusalemme. Boll. Soc. Geol. Ital., 47(1), p. 69-108.

Shaw, S. W., 1947. Southern Palestine, Geological Map on a Scale of 1/250,000 with Explanatory Notes. Govt. of Palestine, Jerusalem, 42 p.

Shenhav, H., 1971. Lower Cretaceous sandstone reservoirs, Israel: petrography, porosity, permeability. Am. Assoc. Petrol. Geol. Bull., 55(12), p. 2194-2224.

Shilo, A., and Wolff, O., 1989. Subsurface formations. O.E.I.L., Internal Rep.
Shimron, A., and Peltz, S., 1993. Early Cretaceous pyroclastic volcanism on the Hermon Range. Isr. Geol. Surv. Bull. 84, 43 p.
Sneh, A., Druckman, Y., and Mimran, Y., 1985. Complementary mapping of sedimentary units of northern Golan, 1:50,000 Sheet. Isr. Geol. Surv., Rep. GSI/21/85, 12 p.
Sohn, I. G., 1968.) Palaeogeographical implications of nonmarine Lower Cretaceous Cyprideina in Israel and *Metacytheropteron parnesi* n.sp. (Ostracoda, Crust.). Isr. J. Earth Sci., 16(3), 120-131.
Soudry, D., and Natan, Y., 1980. Phosphate peloids from Negev phosphorites. J. Geol. Soc. London, 137(6), p. 749-755.
Taubenhaus, H., 1920. Die Ammoneen der Kreideformation Palaestinas und Syrien. Zeitschr. D. deutsch. Palaestina-Vereins, XLIII, vol. 1-2.
Vroman, A. J., 1938. Geology of the region of south western Carmel (Palestine). Unpubl. Ph.D. Thesis, Utrecht Univ., 71 p., Maps.
Vroman, A. J., 1958a. The Cenomanian-Turonian boundary in northern Israel (preliminary note), Isr. Geol. Survey, Bull. 17, p. 1-2.
Vroman, A. J., 1958b. The Geological Map of Israel, 1:50,000. Serie 1: Galilee. Isr. Geol. Surv., 6 Maps. (Sheet 1: Tarshiha; 2-W: Safad; 2-E: Hula; 3-E: Nazareth; 4-W: Tabor; 4-E: Tiberias).
Vroman, A. J., 1960. Note on rock units of Mount Carmel, Israel. Isr. Geol. Surv., Bull. 27, 4 p., Maps.
Walley, C. D., 1983. A revision of the Lower Cretaceous stratigraphy of Lebanon. Geol. Rundschau, 72(1), p. 377-388.
Walley, C. D., 1997. The stratigraphy and geological history of Lebanon: An Outline. (Preprint).
Wdowinski, S., 1985. The geology of the southern Hebron Mountains. Unpubl. M.Sc. Thesis, Hebrew University Jerusalem, 68 p. (In Hebrew).
Weiler, Y., 1961. The geology of the Nazareth and Tabor Mountains. Unpubl. M.Sc. Thesis, Hebrew University, Jerusalem, 33 p. (In Hebrew).
Weiler, Y., 1968. Geology of Nazareth Hill and Mount Tabor (southern Galilee, Israel). Isr. J. Earth Sci., 17(2), p. 63-82.
Weinberger, G., and Flexer, A., 1984. Macro and micro facial analysis of Lower Cretaceous rocks, Makhtesh Katan. Isr. Geol. Soc., Annu. Meet., Abstr., p. 102-103.
Weinberger, G., and Flexer, A., 1985. Marine prograding sequences in the Lower Cretaceous Hatira Formation. Isr. Geol. Soc., Annu. Meet., p. 104.
Weinberger, G., and Flexer, A., 1989. A tectonic framework for the Hatira Formation of central and northern Negev. Isr. Geol. Soc., Annu. Meet., p. 164.
Weinberger, G., and Flexer, A., 1989. Styles of fluvial sedimentation in the Lower Cretaceous, Hatira Formation of central and northern Negev, Israel. Isr. Geol. Soc., Annu. Meet., p. 163.
Weissbrod, T., 1966. Paleozoic Project. Semi Annual Progress Report on the Geological Research Projects, Apr. 1966 - Sept. 1966. Holon, Inst. Pet. Res. Geophys., Rep. 1018, p. 45-51.
Weissbrod, T., 1969a. The petrography of the Shahmon Massif, southern Negev, Israel. Unpubl. M.Sc Thesis, Hebrew University, Jerusalem, 64 p. (In Hebrew).
Weissbrod, T., 1969b. The Paleozoic of Israel and adjacent countries, Part I, Geol. Surv. Isr. Bull. 47, 34 p.
Weissbrod, T., 1969c. The Paleozoic of Israel and adjacent countries, Part II, the Paleozoic outcrops in southwestern Sinai and their correlation with those of southern Israel. Geol. Surv. Isr. Bull. 48, 32 p.
Weissbrod, T., 1970a. 'Nubian Sandstone' [Discussion]. Am. Assoc. Petrol. Geol., Bull., 54(3), p. 526-529.
Weissbrod, T., 1970b. The stratigraphy of the Nubian Sandstone in southern Israel (Timna-Elat Area). Isr. Geol. Surv., Rep. OD/2/70 and Inst. Pet. Res. Geophys. Rep. 1047, 22 p.
Weissbrod, T., 1971. Reply to Discussions by by Prasas, Issawi, and Hassan. Am. Assoc. Petrol. Geol., Bull.,55(6), p. 890-891.
Weissbrod, T., 1993. Lithology and stratigraphy of Lower Cretaceous formations in the southern Negev (Elat Region). GSI Current Res. 8, p. 62-64.
Weissbrod, T., Gvirtzman, G., and Conway, B. H., 1994. The Early Cretaceous sequence of the Sinaf 1 Borehole (southern Negev) and its stratigraphic implications. Isr. Geol. Surv., Current Res., Vol. 9, p. 67-72.
Weissbrod, T., Gvirtzman, G., and Lewy, Z., 1990. Early Cretaceous marine ingressions in the Negev: New findings. Isr. Geol. Soc., Annu. Meet., p. 91-92.
Weissbrod, T., Gvirtzman, G., Weinberger, G., and Sandler, A., 1990. Interfingering of marine and non-marine Cretaceous in southern Israel. Cretaceous Field Conf., Jerusalem, Sept. 1990; Guidebook, p. 65-97.
Weissbrod, T., Sneh, A., and Gvirtzman, G., 1990. Tidal channels at the top of the Lower Cretaceous (Aptian) Amir Formation in southern Israel. Cretaceous Field Conf., Jerusalem, Sept. 1990; Abstr. Progr., p. 12.
Wellings, F. E., 1944. Revision of south Palestine stratigraphy. Petrol. Development (Palestine) Ltd., Geol. Dept. Rep., (unpublished).
Wetzel, R., and Morton, D. M., 1959. Contribution a la géologie de la Transjordanie. Notes et Mémoires Moyen Orient, 7, p. 95-191.
Wolff, O., 1967. The geology of the Kabri-Miilia area. Unpubl. M.Sc. Thesis, Hebrew University Jerusalem. (In Hebrew).



Arad and the southern foothills of Judea at sunrise.
Grayscale rendition of color image in The Holy Land Satellite Atlas, Volume II (1999, p. 196). ©Røhr Productions Ltd., Nicosia, Cyprus. Reproduced with permission. View towards the north.

Chapter 18G

The Paleocene – Eocene of Israel

Amnon Rosenfeld and Francis Hirsch
Geological Survey of Israel, 30 Malchei Israel Street, Jerusalem 95 501, Israel

INTRODUCTION

Paleocene and Eocene rocks are deposited over most of Israel (**Fig. 18G.1**). The Paleocene and lowermost Eocene are represented in the uppermost part of the Mt. Scopus Group (Taqiye Formation). Most of the Eocene is represented in the Avedat Group, though in the Coastal Plain the upper part of the Eocene is regarded as a part of the Saqiye Group.

The term Hashefela Group has been used by several authors for the Senonian to Eocene sequence in the Coastal Plain subsurface (**Fig. 18G.2**).

The shales, siliciferous limestones, and chalks of the Paleocene and Eocene onlap the Levantid anticlines.

In the following **Table 18G.1**, group names (italics upper case) and formation names (italics lower case) are listed according to regions and Eocene levels as adopted in this chapter (Roman numbers):

A. PALEOCENE

MOUNT SCOPUS GROUP (UPPER PART)

The Paleocene portion of the Mount Scopus Group is represented by the Taqiye Formation, which in its basinal facies conformably overlies the Ghareb Formation. The C/T boundary is well-documented in the basinal facies by a high iridium concentration at the base of the *G. eugubina* Zone, and trace elements and microspherules occur between the *A. mayorensis* and *M. pseudobulloides* zones (Rosenfeld et al., 1989).

Elsewhere, the upper strata of the Maastrichtian stage are missing and the Paleocene-Early Eocene Taqiye Formation onlaps a paleo-relief with paleosoil.

History of research:

The term Danian was introduced into Palestinian stratigraphy by M. Blanckenhorn (1915) for strata overlying the bone and phosphate beds with Ammonites (*Libycoceras)* in this region. In his view the Danian represented the uppermost division of the Senonian (in which he also included the Santonian and Campanian). Picard (1931) followed Blanckenhorn's concept of Danian, but placed the *Libycoceras* layers into the Maestrichtian. The term Paleocene is first mentioned in Picard's (1943) 'Structure and Evolution of Palestine' in his discussion of the Danian-Paleocene 'transition-

Table 18G.1 Paleocene and Eocene formations of the Mt. Scopus, Avedat and Saqiye Groups

AGE	FACIES	Negev/Arava	Jordan Valley	Shefela	Galilee/ N.Samaria	Samaria Nablus
Upper Eocene (V)	chalks and limestones	*AVEDAT Qeziot/Har Aqrav*		*SAQIYE Bet Guvrin*		
Middle Eocene (IV)	Limestones and chalks	*AVEDAT Matred/Nahal Yeter*	*AVEDAT Argaman*	*AVEDAT Maresha*	*AVEDAT Bar Kochba*	*AVEDAT Nablus*
Middle Eocene (III)	Chalks and limestones, chert	*AVEDAT Horsha/Paran/ Nahal Yeter*	*AVEDAT* Horsha	*AVEDAT Maresha*	*AVEDAT Yizre'el*	*AVEDAT Nablus*
Early Eocene (II)	Nummulitic limestone with chalk	*AVEDAT Nizzana/Paran*	*AVEDAT Nizzana*	*AVEDAT Adulam*	*AVEDAT Meroz*	*AVEDAT Nablus*
Early Eocene (I)	Chalks with chert nodules	*AVEDAT Mor*	*AVEDAT Zora*	*AVEDAT Adulam*		*AVEDAT Adulam*
Paleocene	Shales and limestone	*MT. SCOPUS Taqiye*				

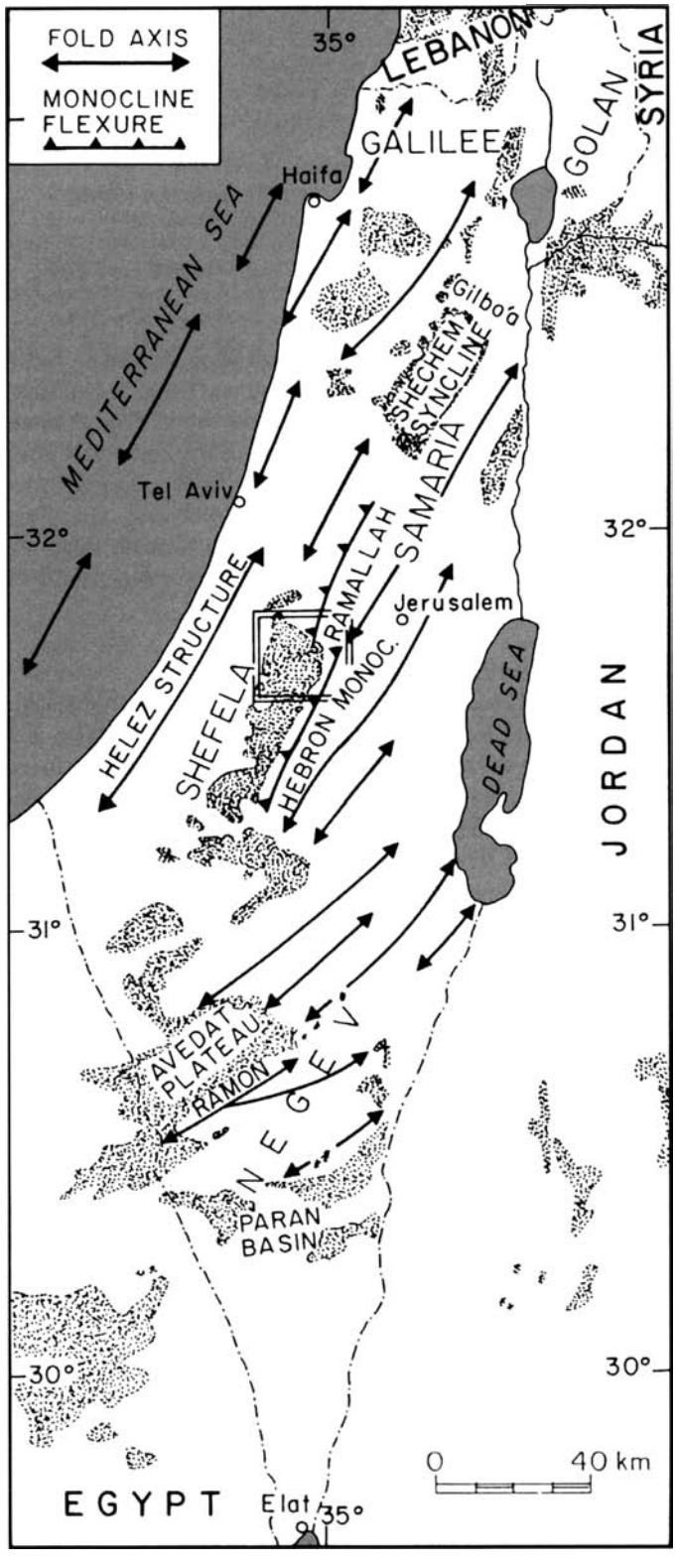


Figure 18G.1. Map of Eocene outcrop locations, named localities, and major structures of the Syrian Arc fold system, in Israel and adjacent countries. The boxed area is shown in detail in Fig. 18G.4 (after Buchbinder et al., 1988, p. 259, Fig. 2).

series' in Palestine and adjoining countries. Later authors preferred the names *Danian, so-called Danian, Dano-Montian,* or more generally *Cretaceous-Tertiary Transition series, Passage-beds,* and *Cretaceous-Eocene transition* for the deposits between the upper limit of the occurrence of ammonites and the lower limit of deposits of unquestionable Ypresian age. Reiss (1955a, b) has shown that the age of these strata ranges from Maestrichtian or uppermost Campanian to early Ypresian. He included, however, the Danian in his *Danian-Paleocene* unit. At present in Israel, the Paleocene comprises all strata between those of Maestrichtian and those of Ypresian age and comprises two parts: the Danian (*Globigerina*-zone) and the Landenian (*Globigerina-Truncorotalia*-zone).

R. V. Browne, J. W. Gwinn and S. N. Nasr (1941) established the term 'Taqiya Marls' at Jebel Abu-Taqiye (Har Kippa), later published by Shaw (1947). The term stands for the lowermost part of the 'Couches de Sar'a' of Avnimelech (1936).

Stratigraphy:

The Taqiye Formation consists of green shale at the base, passing gradually upwards into argillaceous chalks and chalky limestones. The sequence of blue-gray to gray-green or brown, partly calcareous shale is frequently gypsiferous, bituminous and limonitic, containing concretions of marcasite. In the upper part several beds of white and yellow, highly siliceous chalk with flint are always found. Controlled by the Levantid folding, the formation thins from a thickness of 150 m in the Hashephela synclinorium to an average thickness of about 50 m near the flanks of the Judea Mountains. When disconformably overlying pre-Paleocene deposits, the Danian may be absent. In a few places an erosional unconformity may however separate late Paleocene from late Eocene (Priabonian) strata. Elsewhere, the highest Paleocene strata, yielding *Truncorotalia velascoensis* (Cushman) grade upwards into Ypresian rocks. Except for some porifera and fish-teeth, pelagic foraminifera are abundant in Paleocene rocks. Paleocene ostracod assemblages were described by Honigstein and Rosenfeld (1995).

The Taqiye Formation is further subdivided into two members: A lower marly member and an upper member of chalk and marl known as the Hafir Member (Bentor and Vroman, 1960). The lower member exhibits a uniform lithological character with characteristic pyrite concretions, gypsum veins, and barite concretions. Its detrital clay assemblages are characterized by montmorillonite (40-80%), kaolinite (20-50%) and illite (0-20%). Toward the upper part of this member the amounts of carbonate and montmorillonite gradually increase while the detritic clay fraction decreases (Arkin et al., 1972).

The Hafir Member consists of a chalk bank with chert concretions in the base and marly beds at its top. Its thickness ranges between 0-30 m and decreases toward the structural highs. This member is characterized by an authigenic clay assemblage: sepiolite (0-20%), palygorskite (10-60%), and montmorillonite (40-90%). The transition between the detrital and authigenic facies occurs below the Hafir Member and is very sharp (Arkin et al., 1972). On the other hand, the transition from the marly facies of the Taqiye Formation to the chalky sequence of the Avedat Group

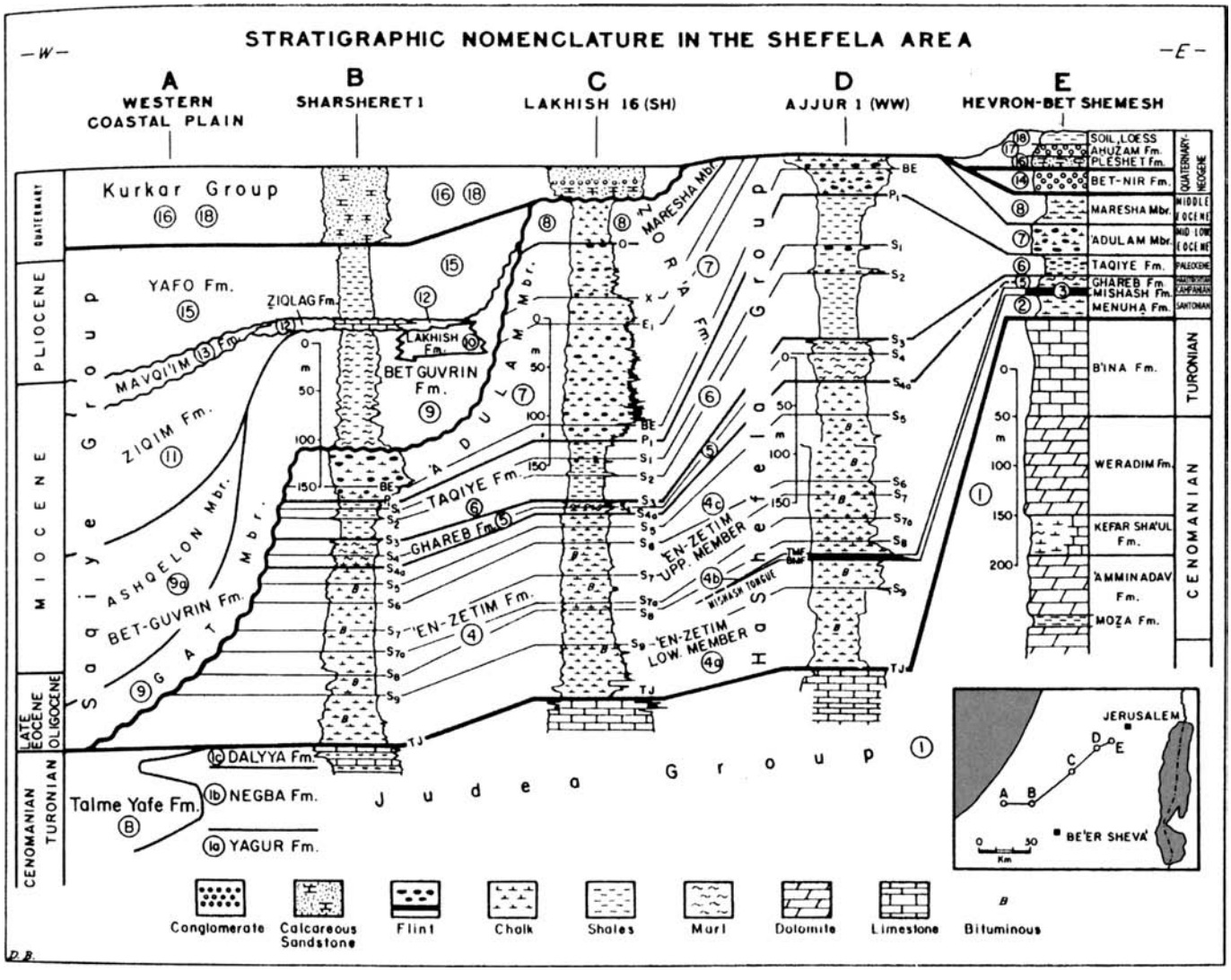


Figure 18G.2. Stratigraphic and electric log correlation in outcrops and boreholes from the Shefela and coastal plain areas (from Gvirtzman, Buchbinder **and Mimran, 1981,** p. 45, Fig. 1).

reflects a gradual change which started in the Landenian on the higher parts of the structures, and continued in the synclines during the Lower Eocene. This reflects a gradual change in the ecology of the sea, probably resulting from a reduced clay supply which deepened the photic zone and caused the increase of the planktonic biomass in the sea water. The reduction of the clay supply is linked to the Lower Eocene transgression, which covered most of the Syrian Arc in southern Israel and great parts of the Arabo-Nubian Massif. The thickness of the Taqiye Formation reflects the structural pattern of the central Negev during the Paleocene (Arkin et al., 1972). It conformably overlies the Ghareb Formation in the synclines but unconformably overlies older rock units on the higher parts of the folds. The Taqiye Formation is covered by the Lower Eocene Mor Formation in the synclines and by its equivalent limestone facies of the Nizzana Formation in the structurally higher areas. Its fauna is **poor** in macrofossils, but occasionally contains *Lamna* cf. *obliqua* Ag. in its upper part and extremely rare Neobelemnoids.

B. EOCENE

History of research:

The term Eocene has been used in this region since Bellardi (1885), who recorded the first *Nummulites* from the Megiddo region of Northern Israel. The first description of the Eocene deposits goes back to Blanckenhorn (1914). Eocene rocks in Israel are grouped within the Avedat Group (formerly Abda Limestone Formation, Browne, Gwinn and Nasr, 1941; emend. Braun, 1967). The name derives from the Nabatean city of Avedat, Negev, 50 km south of Beersheba.

Early nomenclature includes among others ('Lexique Stratigraphique, Israel', Bentor, 1960): 'Bancs a Nummulites' (Nablus) (Roman and Doncieux, 1927); 'Quseime limestone' (Daniel and Wellings, 1935); 'Nummulitic limestone of Mishrafa and Ain el Gederat' (Blake, 1935); 'Massive limestone of Nablus' (Blake, 1936); 'Couches de Sara' (Maastrichtian-Eocene) (Avnimelech, 1936). The latter was emended to Zor'a Formation (Itzhaki, Arkin, Braun, and Lasman, 1964) that encompasses only the Early-Middle Eocene part of the original 'Couches de Sara' and was subdivided into the Adulam and Maresha Members, later emended to the rank of formation (Begin and Druckman, 1987).

Reiss (1955) subdivided the Eocene into *Lower Eocene (I, II and III), Middle Eocene (lower and upper parts),* and *Upper Eocene.*

Stratigraphy:

The data presented herein are based on the studies of Benjamini (1979, 1980, 1984), Buchbinder et al. (1988), Hatzor et al. (1994), and Honigstein et al. (2002).

1. AVEDAT GROUP

The thickness of the group is controlled by the Levantid folding (Syrian Arc). In the area of Avedat it varies within the 250 m range, though the individual facies-controlled formations vary greatly in thickness. Elsewhere it reaches over 400 m but the maximum thickness of Eocene strata is less than 1000 m.

The sequence is composed of calcareous shales, chalks, limestones, and partly silicified limestones, often containing flint beds and flint concretions (Ypresian-Lutetian in basinal facies). Nummulitic limestones are described in part as pseudo-conglomeratic because of their 'conglomeratic' appearance (Ypresian-Lutetian in reef facies). There are also soft chalks and shales, partly glauconitic, limonitic, and slightly phosphatic, in some parts of the country rich in gypsum, and rather rare crystalline limestones (Priabonian). Subsurface deposits of Eocene age are bituminous and pyritic in some places.

Early Eocene strata rest either conformably on late Landenian strata, or are separated from older strata (as old as Turonian) by unconformities. As a result, the base of the Lower Eocene (Ypresian) is incomplete along the flanks of the Levantid structures. A major unconformity occurs within the upper part of the Middle Eocene (Lutetian), marked by a base conglomerate. The late Lutetian-early Priabonian marine strata occur only in the Negev and in the Hashefela subsurface.

While in some of the subsurface basins in Western Israel sedimentation was continuous from the late Eocene into the Oligocene (see also *Sakiebeds*), in other parts of the country strata of Oligocene (or later) age rest unconformably (often with conglomerates) on Eocene deposits.

Megafauna is rare in formations of Eocene age; *Pecten Propeamussium* in the late Ypresian - basal Lutetian, *Conoclypeus* in the Lutetian, *Aturia* in the Priabonian, while microfaunas are abundant. Pelagic Foraminifera and Radiolaria are found in basinal sediments, Nummulitidae, Discocyclinidae, and calcareous algae in the platform sediments.

The Eocene strata in Israel span the zones P8-P12 and P14-P15. Strata of age P12 and younger are poorly represented in most of the Negev and appear to be mostly pelagic.

On the base of its lithology and biostratigraphy, the Eocene Avedat Group can be subdivided into five main time-slices:

Early Eocene (Ypresian):

(I) [P6-8]: Chalks with thin bands or nodules of chert;

(II) [P8-9]: Nummulitic limestone with chalk bands, chalky limestones and chalks;

Middle Eocene (Lutetian):

(III) [P10] Chalks and limestones with changing amounts of chert bands or nodules;

(IV) [P11-12 partim]: Limestones and chalks;

--------hiatus--------

(V) [P14 partim]: chalks (in the Negev only);

Upper Eocene (Priabonian):

(V) [P15]: chalks and limestones (in the Negev only).

A hiatus separates the divisions IV and V.

The upper limit of the Avedat Group in general is a strong angular and erosional unconformity.

The Eocene deposits are subdivided into regional facies types:

1) Negev-type (Avedat Plateau 30°-46'N/34°-47'E - Ramat Matred 30°-46'N/34°-38'E and Arava 30°-37'N/35°-10'E): comprises the Mor Formation (I), Nizzana Formation (II), Horsha Formation (III), Paran Formation (II-III), Matred Formation (IV), Nahal Yeter Formation (III-IV); and following the hiatus, the Qeziot and Har Aqrav Formations (V) (**Fig. 18G.3**).

Mor Formation (Early Ypresian) (Bentor and Vroman, 1951, 1964); Synonym: 'Medra Chalk', Medra Chalk Formation (Browne, Gwinn, and Nasr, 1941); Consists of alternations of pelagic foraminiferal chalk with chert bands and nodules, occasionally filling burrows. Radiolarians are also present. Thickness: from a few meters up to more than 60 m.

Nizzana Formation (Late Ypresian) (Bentor and Vroman, 1964); Consists of chalk interbedded with limestone. Prominent are *Nummulites, Discocyclina, Atktinocyclina, Operculina* and *Paratalia.* Thickness: up to 90 m.

Horsha Formation (Lutetian) (Bentor and Vroman, 1964). Consists of chalk, chert being generally absent. Thickness up to 80 m.

Paran Formation (Ypresian-Lutetian) (Benjamini, 1984). This formation was established in the Arava Valley. It represents a lateral equivalent of the Nizzana Formation, Horsha Formation and lower part of the Matred Formation. Its thickness reaches 150 m.

Matred Formation (Lutetian) (Bentor and Vroman, 1964). Consists of limestone at the base, chalk with limestone in the middle and limestone at top. Large *Nummulites* and *Dyscocyclina* with calcareous algae are common in the limestone. Thickness may reach 40 m.

Nahal Yeter Formation (latest Ypresian-middle Lutetian) (Benjamini, 1979). Bedded chalky limestone in its lower part, followed by chalk with some quartz sand, subdivided by a limestone

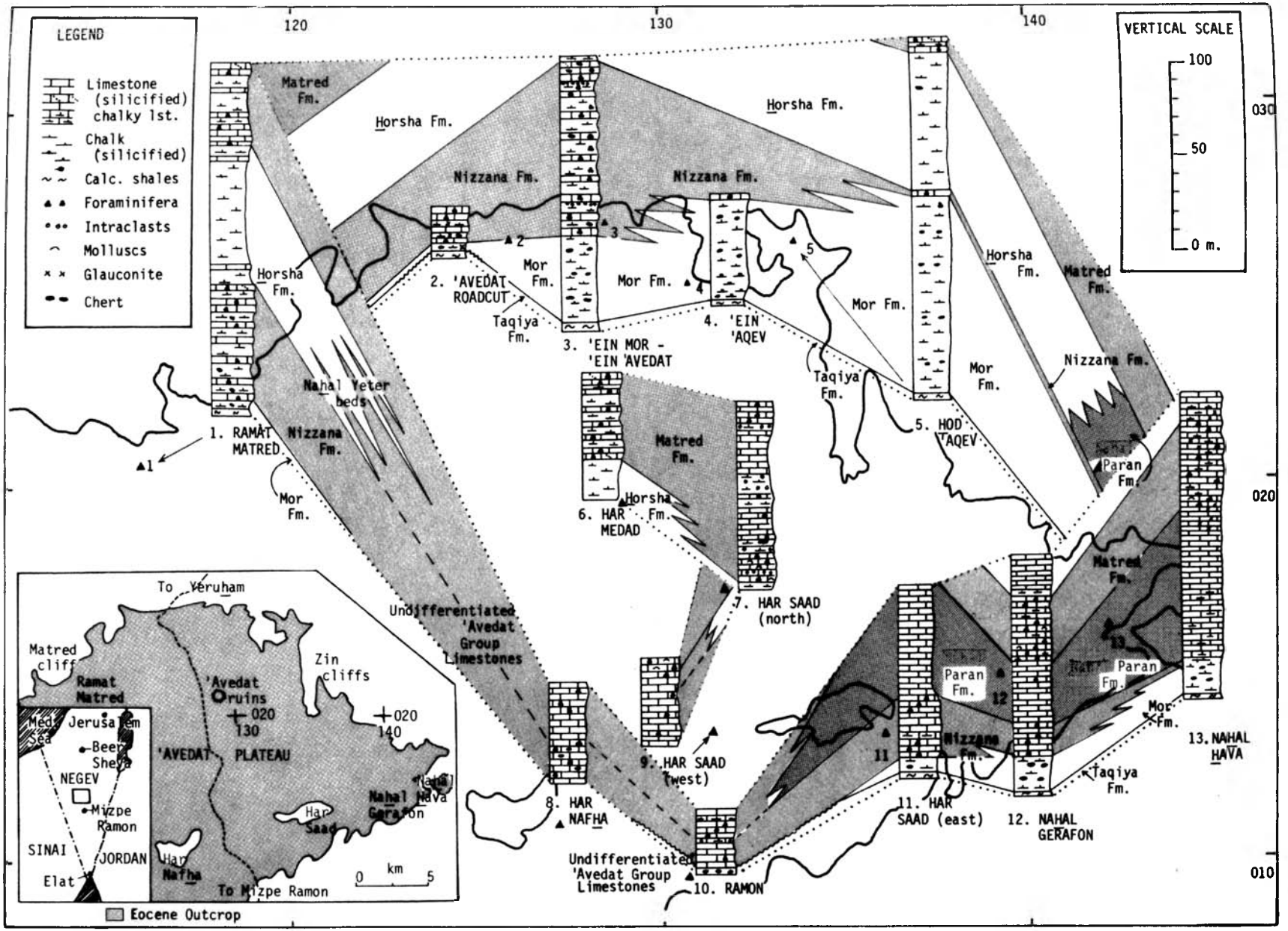
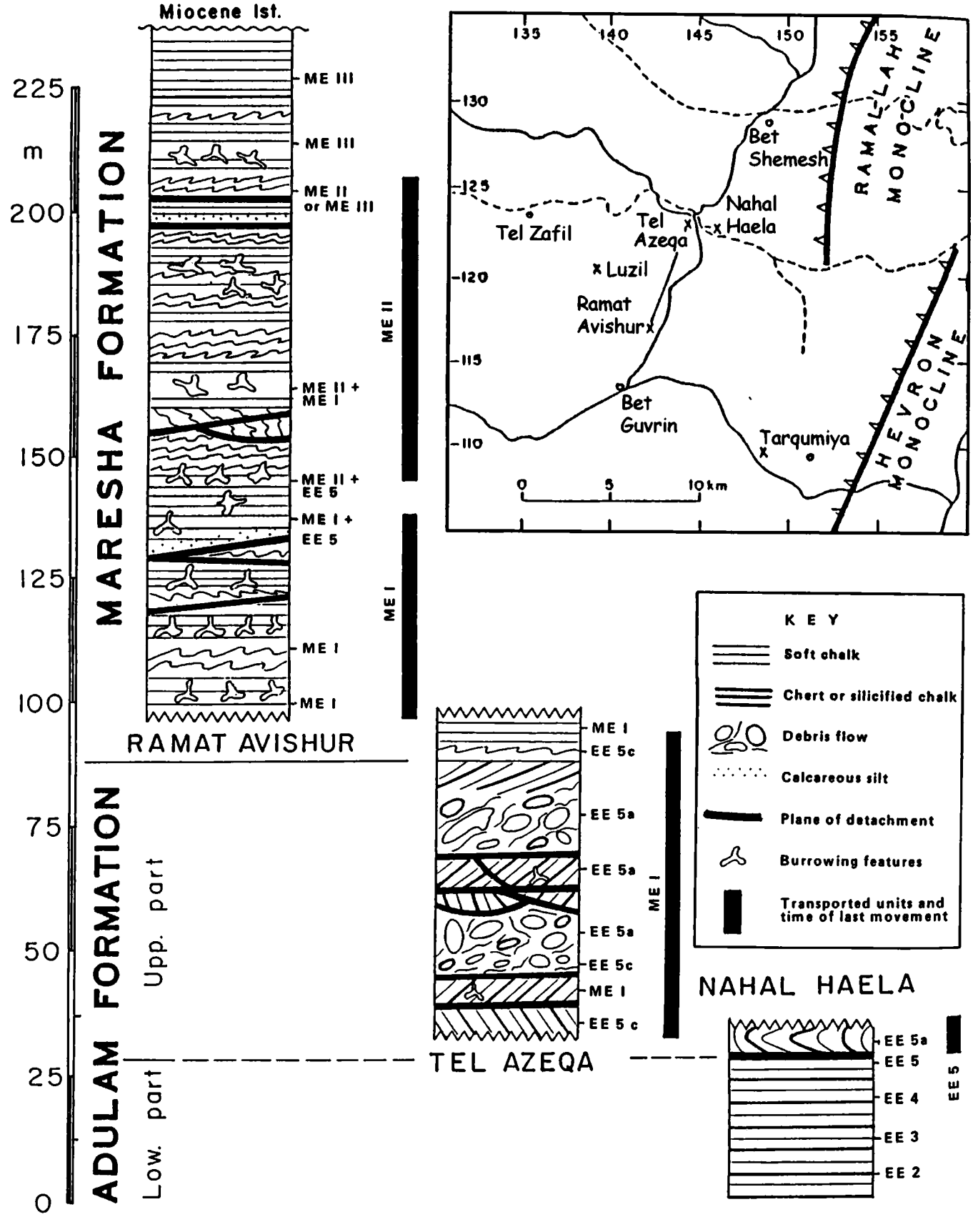


Figure 18G.3. The Eocene outcrops of the Avedat Plateau (Benjamini, 1979, p. 48, Fig. 1).

Lithostratigraphy of the Eocene sequence of the 'Avedat area. Darker coloring indicates limestone. Numbered triangles show geographical position of sections on the base map. Geological map after Bentor and Vroman (1951, 1963), and Bentor, Vroman and Zak (1965).


Miocene Ist.
225
m
200
175
150
125
100
75
50
25
0
MARESHA FORMATION
ADULAM FORMATION
Upp. part
Low. part
ME III
ME III
ME II or ME III
ME II + ME I
ME II + EE 5
ME I + EE 5
ME I
ME I
ME II
ME I
RAMAT AVISHUR
ME I
EE 5c
EE 5a
EE 5a
EE 5a
EE 5c
ME I
EE 5 c
ME I
TEL AZEQA
NAHAL HAELA
EE 5a
EE 5
EE 4
EE 3
EE 2
EE 5
135
140
145
150
155
130
125
120
115
110
Bet Shemesh
RAMAL-LAH MONOCLINE
Nahal Haela
Tel Azeqa
Tel Zafil
Luzil
Ramat Avishur
Bet Guvrin
Tarqumiya
HEVRON MONOCLINE
0
5
10km
KEY
Soft chalk
Chert or silicified chalk
Debris flow
Calcareous silt
Plane of detachment
Burrowing features
Transported units and time of last movement

bed passing laterally, and vertically to conglomerate with chalk matrix. The silicified limestone at top contains large foraminifers. Thickness is 40 m at type (102E/996N). The unit passes laterally into the Horsha and Matred Formations. It correlates with the Maresha Formation of the Shefela.

Qeziot Formation (Late Lutetian-Priabonian) (Bentor and Vroman, 1964). It consists of chalk and marl. The formation starts with a conglomerate and unconformably overlies the Nizzana Formation or Nahal Yeter Formation. Banks of *Nummulites* are intercalated, and the chalks are pelagic. Its thickness is at least 40 m but may reach 55 m.

Har Aqrav Formation (Priabonian) (Benjamini, 1980b). Consists of indurated chalk and limestone, conformably overlying the Qeziot Formation. Coral reefs of massive limestone occur in its lower part. At top occur molluscan remains. The thickness reaches 130 m.

2). Shefela-Galilee type (Nahal Haela-Tel Azeqa 31°-42'N/34°-57'E and Ramat Avishur 31°-38'N/34°-55'E): The original Zora Formation (I-IV), is now subdivided into Adulam (I-II), and Maresha (III-IV) Formations (**Figs. 18G.4 and 18G.5**).

Adulam Formation (Ypresian) (Gvirtzman and Buchbinder, 1966). The Adulam Formation reaches 100 m in the area of Tel Safit-Nahal Ha-Ela - Tel Azeqa (Buchbinder et al., 1980, Fig. 1, p. 47), but reaches 200 m thickness in the Lakhish-16 borehole (Gvirtzman et al., 1980, Fig. 1, p. 45). It consists of white chalk and silicified chalk. The lower part is bedded: thin chert horizons and chert nodules occur. The upper part comprises folded and distorted beds of silicified chalk with slump structures and angular unconformities. The unit wedges out towards the Judean Mountains. Exposed over wide areas in Hashefela, Beersheva Valley, Jordan Valley, Samaria, and Galilee, the upper part of the Adulam Formation corresponds to the Meroz Formation in the Gilboa area. It overlies the Paleocene Taqiye Formation at a sharply delineated contact and is overlain by the Maresha Formation. Extending into the Negev, its lower part is designated as the Mor Formation and its upper part as the Nizanna Formation

Maresha Formation (Lutetian) (Gvirtzman and Buchbinder, 1966). Consists of white globigerinid chalks, 30-100 m thick throughout the Shefela area.

Bet Guvrin Formation (partim) [See Oligocene Saqiye-Group]. The Late Eocene lower part of the Bet Guvrin Formation starts with a boulder conglomerate near Adorayim (31°-31'N/34°-49'E) unconformably overlying various older formations. In the Hashefela it mostly overlies the Maresha Formation. It ranges into the Oligocene. Its upper part is overlain by the Oligocene Lakhish

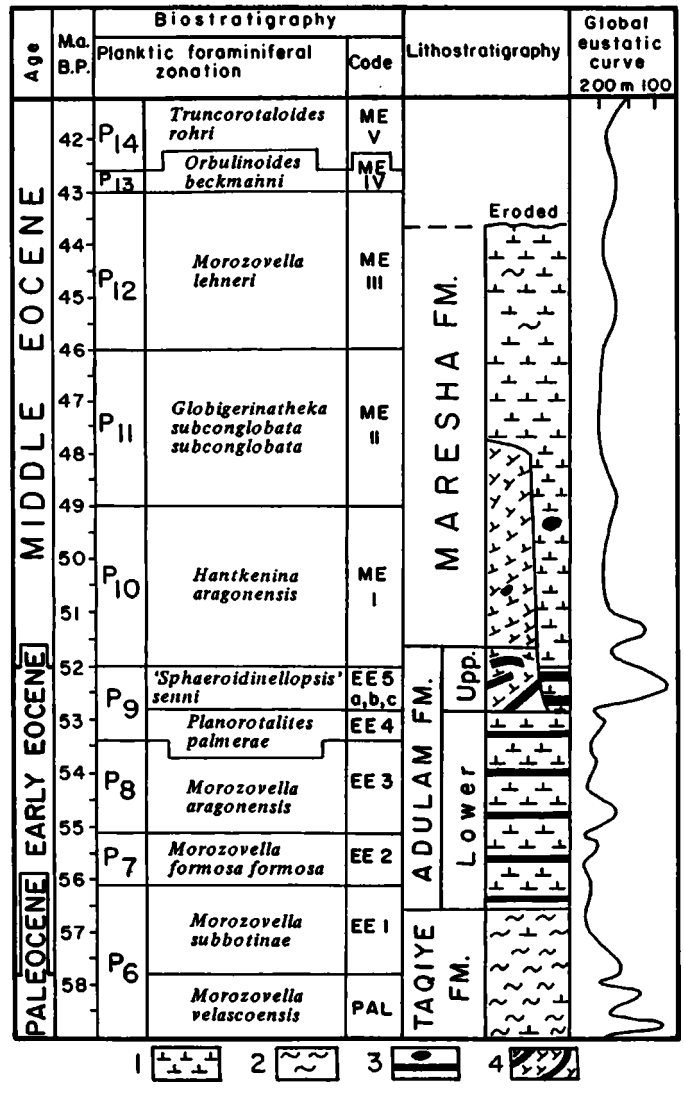


Figure 18G.5. Biostratigraphy of Adulam/Maresha Formations (from Buchbinder et al., 1988, p. 261, Fig. 4). Lithostratigraphy, biostratigraphy (Bolli, 1957a, b; Berggren, 1971, and Benjamini, 1980), time scale (Berggren et al., 1985), and eustatic sea-level curve (Haq et al., 1987, adjusted to time scale of Berggren, *ibid.*) of the early to middle Eocene with reference to the Shefela area. Laterally to the right, the disturbed sequence passes to undisturbed sediments. Patterns: 1 - chalk; 2 - marl; 3 - chert beds or nodules; 4 - mass-transported units of chalk and chert.



Figure 18G.4. Columnar section of Adulam/Maresha Formations (Buchbinder et al., 1988, p. 260, Fig. 3).
A composite section of the Eocene of the Shefala area (insert, including local Israel coordinate grid). Position of mass transport features is in the upper part of the Adulam Formation and in the Maresha Formation. Biostratigraphy is shown along the right side of the lithological columns, with zonation as in Fig. 18G.5. The Ramat Avishur section is from a borehole (coord. 1422/1173, elev. 385 m), while the Tel Azeqa (coord. 1442/1231) and Nahal HaEla (coord. 1450/1223) are outcrop sections. Vertical bars denote time of movement of mass-transported units, based on age of youngest participating material.

Formation, or by various younger formations *e.g.* the Middle Miocene Ziqlag Formation.

3) Shechem (Nablus) type (Burkaa/Zawata 168E/190N - Eval 177E/182N):

The Central Samaria facies consists of Adulam (I) at base, followed by the Nablus Formation (II- IV).

The Nablus Formation (Ypresian-Lutetian), that has never been formally established, encompasses the 'Nummulitic limestone of Mishrafa and Ain el Gederat' of Blake (1935), later called the 'Massive limestone of Nablus' (Blake, 1936). The unformal units e1-4 of Cook et al., 1970 (**Fig. 18G.6**) consist of:

1) The 'e1' unit that is equivalent to the Adulam Formation;

2) The 'e2' unit that is 100-180 m thick and consists of nummulitic limestones, starting with a conglomerate, that onlaps the underlying 'e1' unit; Laterally chalky limestones with slump structures recall the upper part of the Adulam Formation The 'e2' sequence is correlative with the Meroz and Yizre'el Formations at the Gilboa Mts. (Hatzor et al., 1994) (**Fig. 18G.7**) and covers zones P 9-10 (**Fig. 18G.8**);

3) The 'e3' unit: The 40-200 m thick overlying chalk is equivalent to that of the Maresha Formation A limestone inter-wedge starts with a conglomerate. Its age is zone P11.

4) The 'e4' unit: the sequence is a microcrystalline limestone passing laterally to limestone with chalk interbeds. The lower part of this unit is nummulitic with rare alveolinids, it corresponds to the upper part of the Bar Kochba Formation at Gilboa; this interval corresponds to zone P12 and younger.

5) Mt. Gilboa type (Northern Samaria, Nahal Bezeq 32°-24'N/ 35°-25'E): consists of the Meroz (II), Yizre'el (III), and Bar Kochba (IV) Formations (Figs. 18G.7, 18G.8, and **18G.9**);

Meroz Formation (late Ypresian) (Flexer, 1961). Consists of lithographic limestones bearing chert nodules, 200 m thick. Age Late Ypresian, zone P9.

Jezreel Formation (late Ypresian - early Lutetian) (Flexer, 1961). This so-called Jezreel marble consists of coarsely crystalline limestone with silicified *Nummulites*, 120 m thick. Age Late Ypresian - Early Lutetian, zones P 9 -10.

Bar Kochba Formation (Lutetian) (Flexer, 1961). The Bar Kochba Limestone consists mostly of lithographic limestone with interbedded flint nodules alternating with cliff forming nummulitic limestone, some 300-400 m thick.

6) Jordan Valley type (Qeren Sartaba 32°-05'N/35°-27'E) (Figs. 18G.8 and **18G.10**): consisting of the Zora Formation (I), Nizzana Formation (II), Horsha–Paran–Masua–Sartaba Formations (III), and Argaman Formation (IV). Despite the proximity to Gilboa, the pelagic facies is predominant in the Jordan Valley and calls for a comparison with the Negev. A major unconformity occurs at the P10/P11 time (limit III/IV).

The Masua Formation (P9) (Benjamini, 1973) represents possibly a tongue of the Yizre'el Formation.

The Sartaba Formation (P10-11) (Benjamini, 1973) is an equivalent of the upper part of the Horsha Formation.

The Argaman Formation (P11) (Benjamini, 1973) consists of approximately 40 m of shallow water sediments, mostly limestone.

Numerous unconformities indicate that in the later Middle Eocene the regions of the Negev (pelagic sediments with nummulitic intercalations of Matred) and Samaria have become decoupled (Hatzor et al., 1994).

The Avedat Group is subdivided into five levels or divisions, which according to their regional development consist of a great variety of formations.

(I) *Basal division* of chalks with thin bands or nodules of chert:

The Mor Formation consists of chalk with chert, which is well-developed in the Zin Syncline where it attains a thickness of 60-100 m. It is thinner toward the Ramon Anticline in the SE, and in Ramat Matred it is only 5 m thick. In Har Hamran the Nitzzana Formation directly overlies the Taqiye Formation and in the western part of the Qeren Anticline the Mor Formation is only several meters thick. The Mor Formation passes laterally and vertically into the Nizzana Formation (Bentor and Vroman, 1951), which consists of chalk with interbedded bioclastic limestone. The Early Eocene Mor Formation, exposed between the Ramon and the Qeren-Rogem anticlines, passes laterally to the Adulam Formation in the Shezaf-Revivim Syncline and in the Haluza area.

(I-II) The Lower Eocene 'Adulam Formation (Gvirtzman and Buchbinder, 1966; emend. Druckman and Begin, 1987) is the lateral equivalent of both the Mor and the Nizzana Formations and represents the lower part of the Zor'a Formation. In its lower part (I) it exhibits the same lithology as the Mor Formation, characterized by well-bedded chalk, chalky limestone and flint or silicified chalk beds. In the Shezaf-Revivim Syncline more than 150 m of the Adulam Formation have been penetrated by the Revivim-1 water well and a sequence 200 m thick was found in the Shephela area (Gvirtzman, 1970). In Hashefela, Beersheva Valley, Jordan Valley, Samaria, and the Galilee, the Adulam Formation consists of 30-200 m of white chalk and silicified chalk. The upper part compares to the Nizzana Formation (Division II) as it comprises folded and distorted beds of silicified chalk with slump structures and angular unconformities which are typical of the Nizzana Formation around the Ramon Anticline. The greatest thickness occurs in the center of the Hashephela synclinorium. The 'Adulam Formation reaches 100 m in the area of Tel Safit-Nahal Ha-Ela - Tel Azeqa (Buchbinder et al., 1980, Fig. 1, p. 47), but reaches 200 m thickness in the Lakhish 16 borehole (Gvirtzman et al., 1980, Fig.1, p. 45). The unit wedges out towards the Judean Mountains. The frequency of the flint beds decreases toward the upper parts of the formation. In a few places barite nodules and concretions were found. The 'nari' crust is thin in comparison to the crust on the Maresha or Ghareb Formation. The unaffected flint beds and nodules are clearly distinguished in the nari matrix. In the Hashefela, the 'Adulam Formation is exposed in the vicinity of Latrun, Eshta'ol, Zor'a, 'Adulam and Kefar Zekharya, Nahal Adorayim, Devira and Lahav. The silicified chalks of the 'Adulam Formation sharply overlie the marlstones of the Paleocene Taqiye Formation at a delineated contact ('Adulam). The upper contact with the Maresha Formation appears to be conformable.

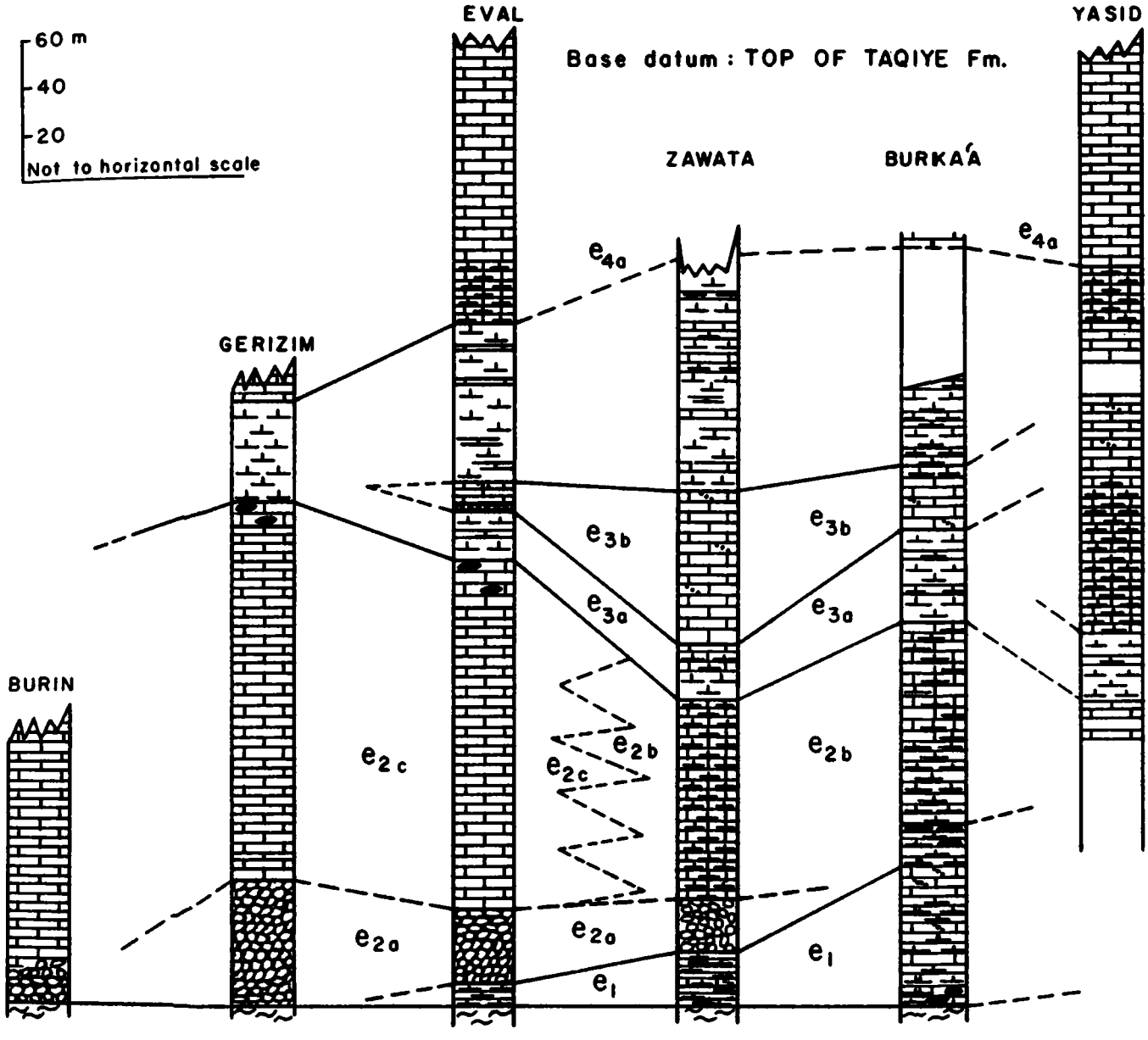


Figure 18G.6. Stratigraphic sections in the Shechem Syncline (from Cook et al., 1970).

(II) *Second division* of nummulitic limestone with chalk bands, chalky limestones and chalks:

The Nizzana Formation is a limestone-chalk sequence frequently disrupted by sedimentary structures such as folds, slumps, small faults, syn-sedimentary conglomerates (the result of slumps of semi-lithified limestone), and load structures. Most of the limestone beds are disturbed and it seems that the transition zone between the Mor and the Nizzana Formations was shaped by bioclastic units which were deposited on the higher parts of the Ramon area and dislocated down the anticline (Benjamini, 1979; Zilberman, 1981). The Nizzana Formation becomes thicker as the thickness of the Mor Formation decreases. The bioclastic limestone contains abundant benthonic fauna such as large foraminifera (*Asterocyclina, Discocyclina, Nummulites* and *Operculina*), calcareous algae, molluscan and echinoderm debris. The Nizzana Formation is more limy in the Har Hamran area where it directly overlies the Taqiye Formation. There it consists mainly of chalky limestone and limestone with several extensively silicified horizons. This facies appears also in the Qeren Anticline. To the north the Lower Eocene Nizzana Formations passes laterally into the chalk and chert facies of the 'Adulam Formation. In Nahal Zipporim the Nizzana Formation overlies Cretaceous formations.

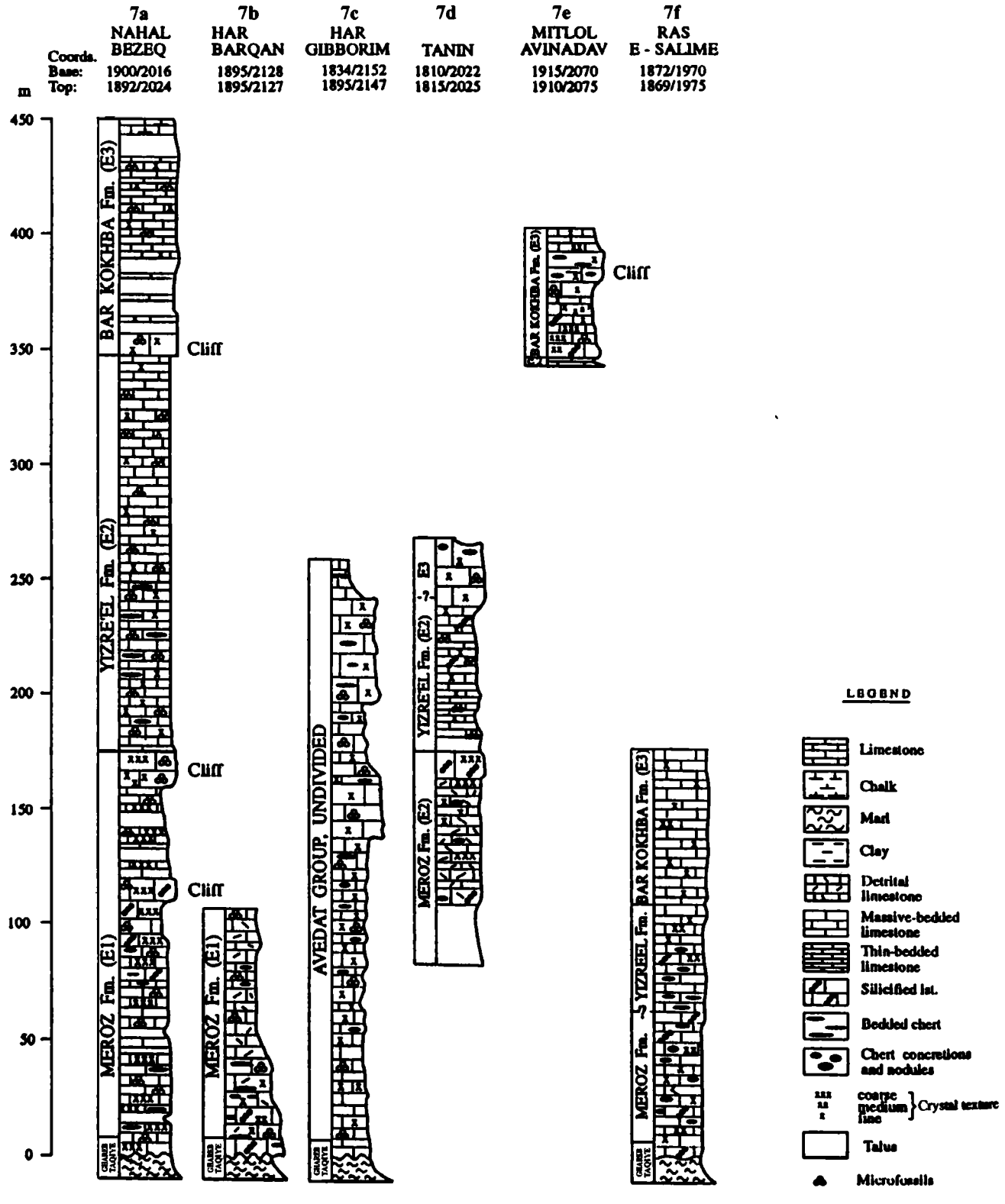


Figure 18G.7. Columnar sections of the Gilboa area (from Hatzor et al., 1994, p. 3, Fig. 3). Six columnar sections of the Eocene sequence in the study area. Section 7a is the type section of the Meroz Formation and Yizre'el Formation. Section 7e is the type section of the Bar Kochba Formation. Section 7f is from Cook et al., 1970.

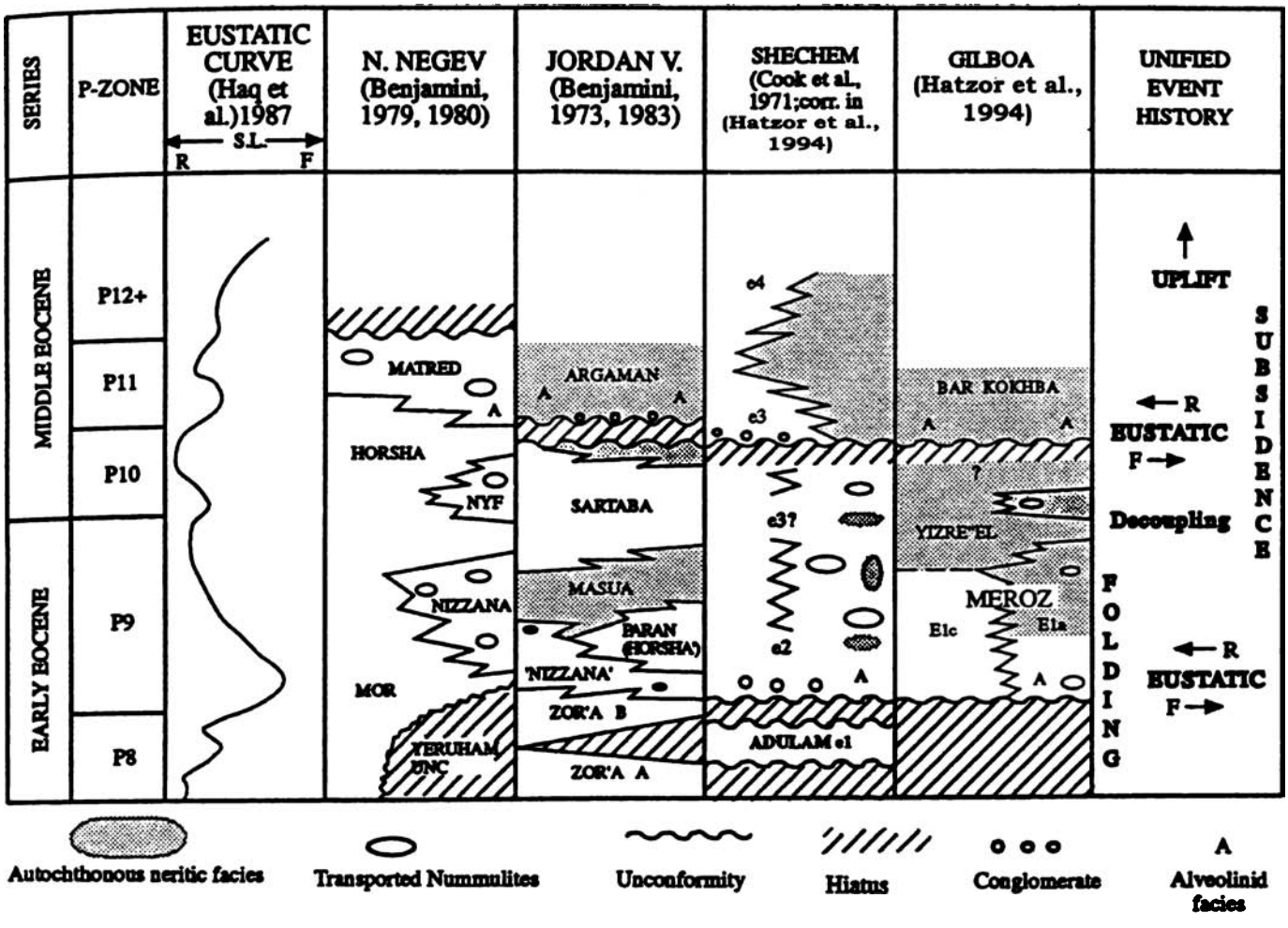


Figure 18G.8. Correlation diagram and unified event history (from Hatzor et al., 1994, p. 12, Fig. 6).

In the Gilboa area, the upper part of the Adulam Formation corresponds to the Meroz Formation. In the area of Shechem, the Central Samaria facies consists of Adulam (I) at base, followed by the Nablus Formation (II- IV).

(III) *Third division* of chalks and limestones with changing amounts of chert bands or nodules:

The Middle Eocene Horsha Formation (Bentor and Vroman, 1951) in Ramat Avedat and Ramat Matred is a thick extensive sedimentary lens of massive pelagic chalk, accumulated mainly in the Zin Syncline, and thinning gradually towards the Ramon Anticline and Har Hamran. The thickness of the Horesha Formation ranges from 80 m in the Zin Syncline to several meters in the Har Hamran area, where it interfingers with the Nahal Yeter Formation. Near Nahal Hava, in the eastern part of the Ramat Avedat, it passes into a chalky limestone which characterizes the Paran Formation in the southern Negev and the Arava area (Benjamini, 1979). The upper boundary of the Horsha Formation is determined by the first bioclastic lens which marks the overlying Matred Formation.

The Maresha Formation consists of chalk with some interbedded chalky limestone. In the Revivim Syncline it is 100-150 m thick and in the Shephela it attains a thickness of 200 m (Gvirtzman, 1970). The transition from the Nahal Yeter to the Maresha Formations occurs at the southwestern edge of the Revivim Syncline. In the area of Mt. Gilboa (Northern Samaria, Nahal Bezeq) this subdivision is represented in the Yizre'el Formation. A major unconformity occurs at the P10/P11 time (limit III/IV).

(IV) *Fourth division* of limestones and chalks:

The lithological character of the Matred Formation in Ramat Avedat and Ramat Matred is similar to that of the Nizzana Formation. It consists of bioclastic limestone lenses interbedded with chalk, which form a sequence 40-60 m thick. However, it represents a shallower environment as indicated by numerous local unconformities – marked by conglomerates and silicified horizons – and by a typical shallow-water faunistic assemblage of calcareous algae, very large *nummulites* (2-5 cm), *miliolids,* and

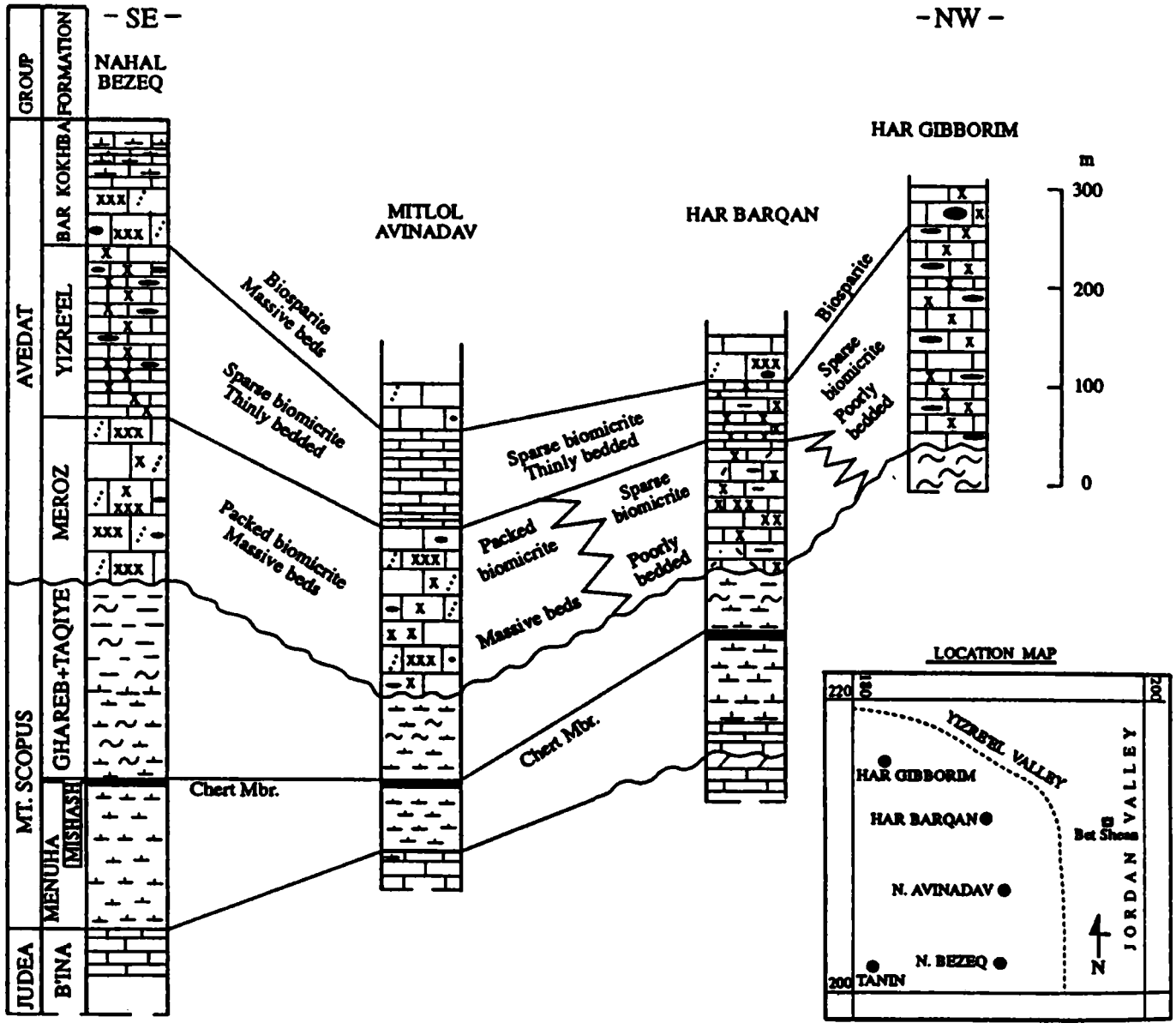


Figure 18G.9. Local correlation of Eocene units at Gilboa (Hatzor et al., 1994, p. 8, Fig. 4). Local correlation of Eocene mapping units at Gilboa. Note that towards western Gilboa the threefold subdivision wanes.

alveolina (Benjamini, 1979). This evidence for a shallow-water environment becomes widespread towards the upper part of the sequence, reflecting a regional regression event that is marked by an extensive erosional surface which developed on top of the Avedat Group. Sedimentary disturbances are widespread in the Matred Formation and these are of a longer scale than those of the Nizzana Formation. In the eastern part of Ramat Avedat the Matred Formation is overlain by the Upper Eocene Har 'Aqrav Formation (Benjamini, 1979). Toward the Ramon Structure, both the Horesha and Matred Formations change gradually into a bedded limestone sequence.

(III-IV) The Nahal Yeter Formation (Benjamini, 1979) is the lateral equivalent of the Horesha and Matred Formations. The massive chalk which accumulated in the Zin Syncline in the beginning of the Middle Eocene becomes thinner towards the western Negev where the sequence consists of alternations of chalk and limestone of shallow marine origin. The Nahal Yeter Formation reflects a very shallow environment of deposition similar to that of the Matred Formation, as evidenced by benthonic fauna and local unconformities. The Nahal Yeter Formation is found in Ramat

Barne'a, where its thickness is less than both the Horesha and Matred Formations in Ramat Avedat, and only 40 m occur south of Har Horesha. The sedimentary structures within the Nahal Yeter Formation are the most prominent in the northwestern Negev. Syn-sedimentary conglomerates 2-4 m thick can be traced for several kilometers reflecting a large scale slumped semi-liquified limestone transported a long distance from its original site of deposition (Zilberman, 1981). The upper part of the Nahal Yeter Formation, which forms the present day surface at Ramat Barne'a, consists of a thick limestone unit, which was detached into separate blocks several hundred meters across. These blocks sank into the underlying chalk, forming a very complicated sedimentary pattern. The top of the Nahal Yeter Formation is marked by an erosional relief on which the Upper Eocene Qeziot Formation was deposited. This unconformity is also characterized by a faunistic hiatus, as the biozones III-V of the middle part of the Middle Eocene to the Late Middle Eocene are missing (Benjamini, 1979). To the north, as the limestone units wedge out, the Nahal Yeter Formation passes gradually into the thick chalk unit of the Maresha Formation. At Gilboa, the subdivision is represented by the Bar Kochba Formation and at Qeren Saraba (JordanValley), it consists of the Argaman Formation (Benjamini, 1973). Despite the proximity to Gilboa, the pelagic facies which predominate in the Jordan Valley call for a comparison with the Negev.

(V) *Fifth division* of chalks and limestones in the Negev only:

The Late Eocene has been preserved on the highest parts of the plateau which surrounds the northwestern flank of the Ramon Anticline, on the eastern part of Ramat Avedat at an elevation of 600-650 m and in the western Negev, forming the erosional surface extending between Har Horesha and Har Harif (at 900-1000 m elevation). The Upper Eocene sequence unconformably overlies the Avedat Group. Two facies, separated by the structural high of Har Hamran, characterize the Upper Eocene sequence in the western Negev. The marly facies of the Qeziot Formation is dominant in the Shezaf Syncline while the chalk and limestone of

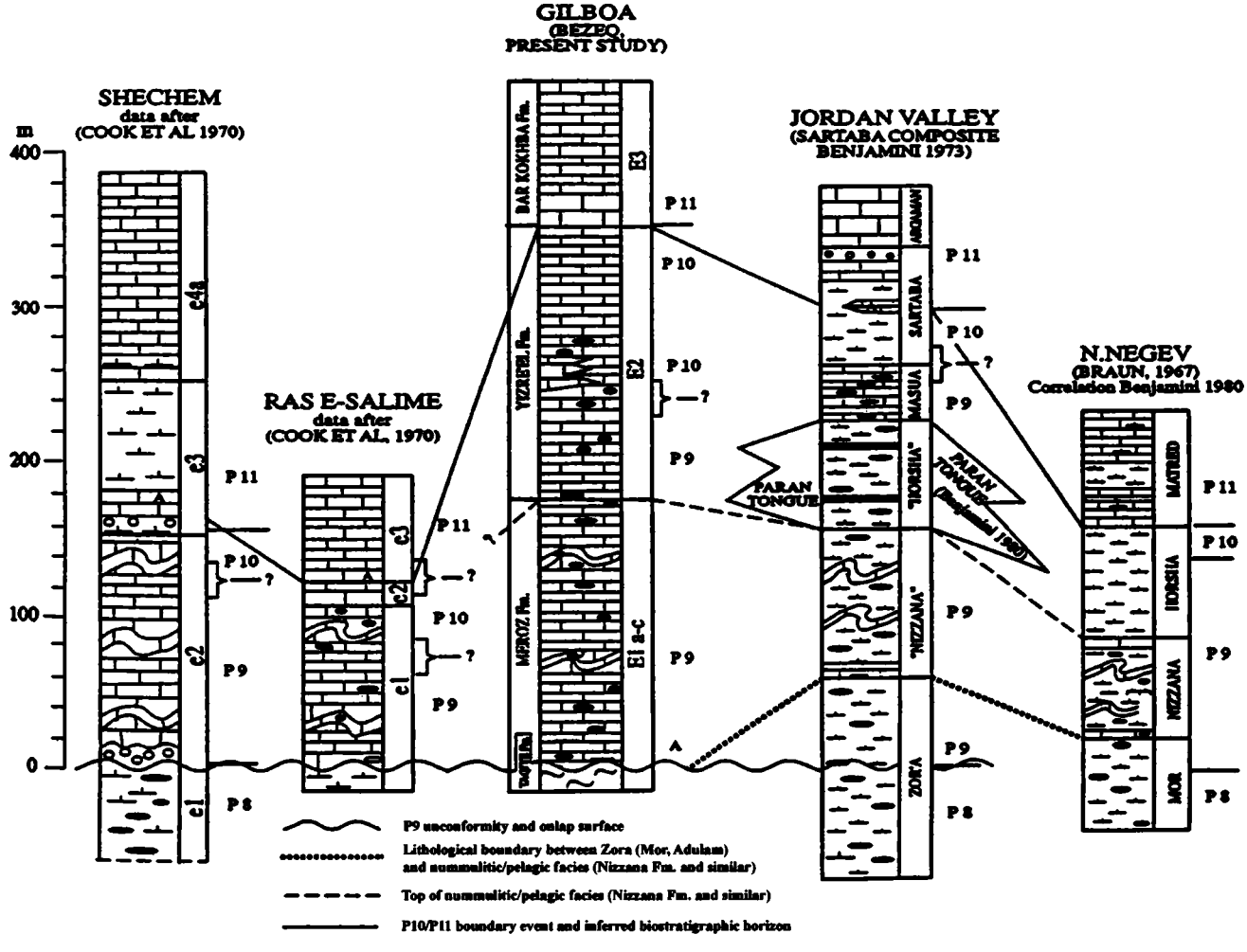


Figure 18G.10. Regional litho- and biostratigraphic correlation between Negev, Jordan Valley, Gilboa and Shehem (from Hatzor et al., 1994, p. 14, Fig. 7).

the Har 'Aqrav Formation are the main constituents of the sequence at Har Horesha. The gradual transition between the two facies toward the south reflects the control of the Ramon Structure on the distribution of facies.

The Qeziot Formation (Bentor and Vroman, 1961) in the western Negev unconformably overlies the Nahal Yeter Formation. In Har Horesha and Har 'Ayarim it is covered by the Har 'Aqrav Formation, while north of this high plateau it is overlain by Pliocene-Quaternary conglomerates.

In the Shezaf Syncline the Qeziot Formation consists of bituminous marl and chalk some 120 m thick in the 'Auja-el-Hafir well on the base of foraminifera and calcareous nannoplankton (Reiss, 1952; Moshkovitz, pers. comm., 1984). This basinal facies was preserved in a narrow N-S trending syncline, developed along the western margins of the Kevuda Anticlinorium. A bank of bioclastic limestone rich in coral fragments and shallow benthonic fauna appears at the lower part of the sequence in its southern outcrops (Benjamini, 1979). A few hermatypic corals were found within the bioclastic bank south of Qeziot. Further to the south, the lower chalk and marl disappear and the corals are found to unconformably overlie the top of the Avedat Group. The lower part of the Qeziot Formation rests with angular unconformity on the northern margins of the Har Hamran structure. This reduced sequence is slightly tilted to the north and is truncated by the horizontal Plio-Pleistocene conglomerate (Zilberman, 1981). South of Har Hamran, the Qeziot Formation appears in a chalky facies 30-40 m thick, which is widely distributed between Nahal Nizzana and Nahal Yeter in the east and Qadesh Barne'a in the west. It is also exposed at the base of the Har Horesha - Har 'Ayarim cliffs. Hermatypic coral of the patch-reef type are widespread in this area (Benjamini and Zilberman, 1979) forming prominent silicified limestone banks within the chalk sequence. They are most developed along the unconformity on the south-dipping flank of the Har Hamran Structure and are strongly tilted to the south (Zilberman, 1981). The faunal assemblage and the microfacies characterizing the Qeziot Formation indicate an open sea environment (Benjamini, 1979). To date the Qeziot Formation has not been found on the higher parts of the Ramon Anticline, although several building stones made up of a hermatypic coral reef were identified in the Nabatian-Byzantian ruins of Avedat town. The ancient town was built in Ramat Avedat on top of the Matred Formation, the building stones being quarried in the town's vicinity (I. Perath, personal communication). Since the only known Eocene coral limestone in the Negev is found within the Qeziot Formation it is possible that the Qeziot Formation once covered Ramat Avedat in a shallow reef facies.

The age of the Qeziot Formation ranges from late Middle Eocene (Late Lutetian) to Late Eocene. The Qeziot Formation at Har Horesha is correlative to the lower part of the Qeziot Formation at Qeziot, both having been deposited during the uppermost part of the Middle Eocene and the early Late Eocene. The age of the upper part of the basinal sequence in the Shezaf Syncline has not been determined, but the north-dipping sequence in this area suggests that younger parts of the sequence are exposed farther to the north.

The Har 'Aqrav Formation (Benjamini, 1979) represents the latest and most extensive stage of the Upper Eocene transgression. It has been preserved on the highest parts of the Eocene plateau (Ramat Avedat and Har Horesha). It consists of a well-bedded sequence of yellow chalky limestone and chalk which build the upper part of the EW trending cliffs of the Har Horesha and Har 'Ayarim, where it attains a thickness of 140 m. In the eastern part of Ramat Avedat it is only several meters thick, unconformably overlying the Matred Formation, and covered by the continental Hazeva Formation. In the western Negev, it generally overlies the Qeziot Formation, as well as interfingering laterally with it. Its top is eroded, forming an extensive flat surface which stretches along the NW flank of the Ramon Anticline. The age of the Har 'Aqrav Formation is not clear, due to the poor preservation of the indicative fauna, but it is assumed to be of Upper Eocene-Oligocene age (Benjamini, 1979).

In basinal areas, the lower contact of the Avedat Group with the Taqiye Formation is conformable and gradational. But over structural highs the Avedat Group progressively overlaps all older formations down to the Mishash Formation. At the type locality the Avedat Group is not covered by any younger unit, but occasionally the Hazeva Formation overlies it with strong angular unconformity.

Summing up, the Avedat Group, which for Cohen et al. (1987) encompasses all Eocene rocks in Israel, conformably overlies the Taqiye Formation in the synclines and unconformably overlies the Senonian to Lower Turonian rock units on the higher parts of the anticlines. An extensive erosion surface marks the top of this sequence around the Ramon Anticline, where it is reduced to several meters. The thickness of the Eocene sequence ranges between 200 m in Ramat Avedat and Ramat Matred, 300 m in Har Horesha, and more than 300 m in the Revivim syncline. The Lower to Middle Eocene sequence is separated from the Late Middle-Upper Eocene (Qeziot and Har 'Aqrav Formations) by a major unconformity. Though in the Negev, the late Eocene Qeziot and Har Aqrav Formations are regarded as a part of the Avedat Group. In most of Israel the post-Middle Eocene (Early Bartonian) uncomformity (P13) represents the boundary between the Avedat Group and the Saqiye Group.

2. THE SAQIYE GROUP (LATE EOCENE LOWER-MOST PART)

The Saqiye Group (Loewengart, 1927, 'Sakiebeds', emended by Gvirtzman and Reiss, 1965) consists of marly chalks, marls and bioclastic limestones that unconformably overlie the Avedat/ Hashephela Groups (Gvirtzman, 1969a, b; Gvirtzman and Buchbinder, 1969). The Saqiye Group is extensively developed only in western Hashephela and the formations of the Saqiye Group are widely buried under the Coastal Plain and in the Beersheva Embayment. They are partly exposed in the foothills along the Shefela. In the central and eastern Hashephela, the group displays its marginal facies in scattered outcrops (Fig. 18G.2).

In most of Israel the post-Middle Eocene (Early Bartonian) uncomformity (P13) represents the boundary between the Avedat

Group and the Saqiye Group, though in the Negev the Late Eocene is still regarded as part of the Avedat Group.

Apparently the most continuous marine sedimentation of Late Eocene-Quaternary age is found along a rather narrow belt in the Southern and Central Coastal Plain. These sediments represent the Saqiye Group and consist in their lower part of the Late Eocene-Early Miocene Bet Guvrin Formation (P15-N9).

The Late Eocene part of the Saqiye Group in the Coastal Plain and adjacent Shefela is coeval with subdivision (V) [P15]. The more basinal facies is comprised within the Bet Guvrin Formation.

Bet Guvrin Formation (Late Eocene-Oligocene). The term Bet-Jibrin Series (Picard and Solomonica, 1936) and its synonyms, Jibrin facies, Jibrin Series, Bet-Jibrin Chalk (Picard and Solomonica, 1936), 'Craie de Beit Jibrin' (Avnimelech, 1936), 'Beit Jibrin chalk Formation' (Fairbridge, Nasr and Tiratsoo, 1940). 'Units 6, 7 and 8(UE)' (Golik, 1960; Greitzer 1960) have apparently been used for any chalk without flint overlying the flinty limestones of Eocene age. Emended by Gvirtzman and Reiss (1965), with a reference section given by Gvirtzman (1969b), the Bet Guvrin Formation has a common thickness in the Lakhish area of about 50 m. Toward the west, the formation rapidly attains its greatest thickness of up to 300 m.

This compact, unstratified, fine-grained chalky limestone, poor in fossils, occurs in the foothills region of Bet Guvrin (Bet Jibrin) and was first described from the village of Deir Nakhas on the old Bet Guvrin-Hebron road.

The Bet Guvrin Formation consists of yellow brownish chalky marlstone, glauconitic in part, which in the Foothills region of Bet Guvrin appear as compact, unstratified, fine-grained chalky limestone, poor in fossils. The Late Eocene lower part of the Bet Guvrin Formation starts with a boulder conglomerate near Adorayim (coordinates 1306E/1040N and 1322E/1031N or 31°-31'N/34°-49'E) unconformably overlying various older formations (Golik, 1960; Greitzer, 1960). In a few places fine bioclastic limestone lenses were found. The formation is partly covered by a nari crust.

The Bet Guvrin Formation crops out at the center of the Hashephela synclinorium, in the Lakhish-Gal'on area. It is also exposed in Nahal Gerar and in Nahal Shiqma near Tel Hesi.

The Bet Guvrin Formation unconformably overlies various formations of the Hashephela Group. In Hashephela it is found mostly overlying the Maresha Member of the Zor'a Formation. It interfingers laterally with or is overlain unconformably by the Oligocene Lakhish Formation or by various younger formations *e.g.* the Middle Miocene Ziqlag Formation and Beit Nir Formations, or by various formations of the 'Kurkar' Group.

Reiss and Gvirtzman (1966a) attributed to it a Late Eocene-Oligocene age (P15-N9).

EOCENE BIOSTRATIGRAPHY

A detailed biostratigraphy of Eocene rocks was initiated by Reiss (1952, 1955a, b, 1957a,b,c,d) who divided the Eocene into six parts using ranges of common planktonic foraminifera. Benjamini (1980a) expanded this biostratigraphy to correlate with the zonation schemes of Bolli (1957, 1966). Honigstein et al. (1991) attempted to apply the P-zone biostratigraphy of Berggren et al. (1985) and Berggren and Miller (1988) to sections of the Jordan Valley. Schaub et al. (1995) presented a detailed multiple biostratigraphy of the Eocene of the Negev based on planktonic foraminifera, calcareous nannofossils and nummulites, based on planktonic P and NP zonation schemes following Berggren et al. (1985), Berggren and Miller (1988), Martini (1971), and Romein (1979).

The Eocene of the Negev is well-subdivided by a particularly detailed biostratigraphy (Honigstein et al., 2002) (**Fig. 18G.11**). Placing the ostracods within this framework, it is based on the planktonic foraminiferal zonation of Berggren and Miller (1988) and nannofossil zones of Martini (1971) and Okada and Bukry (1980), as elucidated by Benjamini (1980a, 1980b, 1995) and Benjamini et al. (1995), and correlated with the nummulite biostratigraphy of Schaub (1995). However, the P-zonation in the sense of Berggren et al. (1995) was used, taking note of minor changes over previous studies, *e.g.*, Berggren and Miller (1988).

The Paleocene/Eocene boundary in the Negev is generally conformable. Arkin et al. (1972) found it to vary in position with respect to the lithological transition between the marls of the Taqiye Formation and the cherty chalk of the Mor Formation. Benjamini (1992), using the benthic foraminiferal extinction and the boundary between the P6b/c transition of Berggren and Miller (1988) as the criterion, located this boundary consistently within the upper part of the hemipelagic Taqiye Formation. The Lower Eocene sequence also includes the overlying Mor Formation (chalk, chert nodules) and its lateral equivalent the Nizzana Formation (bedded chalk with nummulitic limestone), and also the lower part of the Horsha Formation (chalk).

The interval containing the Early/Middle Eocene boundary is apparently represented by a very expanded, albeit pelagic section, affording increased resolution of stratigraphic ranges of key species. Criteria for defining the boundary differ for planktonic foraminifera, calcarous nannofossils, and nummulites, and occur at different horizons here (Benjamini, 1980a). The calcareous nannofossil NP14a/b transition (Martini, 1971) occurs well within the Nizzana Formation, with foraminifera of zone P9 (Berggren and Miller 1988) and Cuisian nummulites of the *N. campesinus* Zone. Earliest Lutetian nummulites of the *N. gallensis* Zone appear higher, in the lower part of the Horsha Formation. The first appearance of *Hantkenina nuttalli*, marker for zone P10, occurs much higher in that formation, within calcareous nannozone NP15.

Using the latter criterion, the Middle Eocene then includes most of the Horsha Formation and the overlying Matred Formation (chalk with limestone intercalations), and their lateral equivalent in the western Negev, the Nahal Yeter Formation (chalk, limestone). These units contain Lutetian nummulites (Schaub, 1995).

Benjamini (1980b) found an erosional unconformity between the earlier Middle and latest Middle Eocene sedimentary episodes. A latest Middle to Late Eocene transgressive episode left a chalk and limestone lithofacies extending over most of the Negev (Sakal et al., 1966). This is the Qeziot Formation (chalk marl), which in part passes laterally into a limestone facies, called the Har 'Aqrav Formation, in the western Negev. The Middle/Late Eocene boundary,

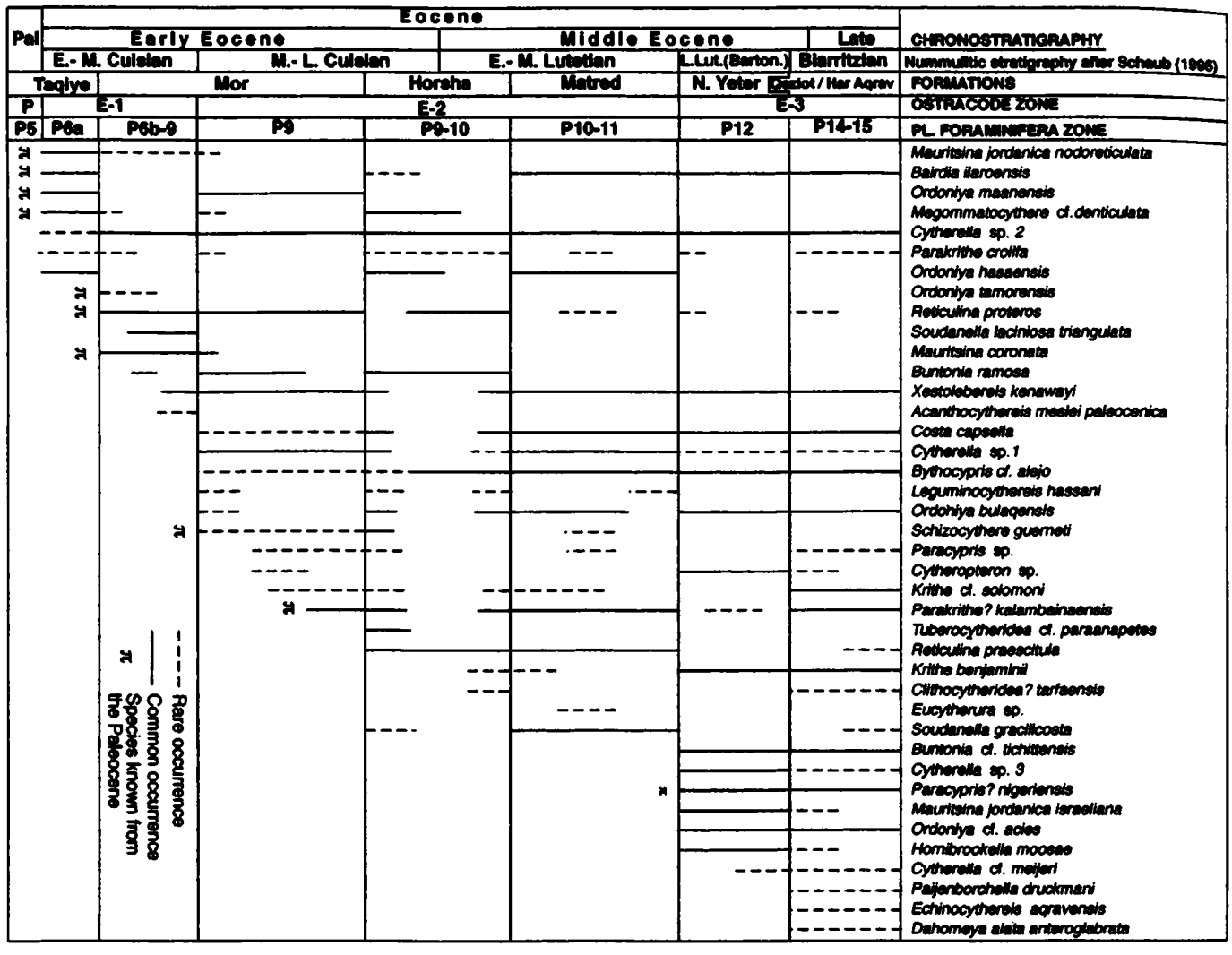


Figure 18G.11. Distribution chart of Eocene ostracodes in Southern Israel (Honigstein et al., 2002, p. 375, Fig. 4).

based on sequential extinction of muricate planktonic foraminifera, followed by first appearance of *Globigerinatheka semiinvoluta* (P14/15 of Berggren and Miller, 1988), is located within the lower part of the Qeziot Formation (Benjamini, 1980b). This horizon also yields Biarritzian nummulites (Schaub, 1995).

Mor Formation: (Section 1, **Fig. 18G.12**) In the nearly 100 m thick cliff section south of Wadi Zin near Hod Aqev, the marly Taqiye Formation is followed by the Mor Formation that forms most of the section. But the greater part of the Mor Formation here is laterally equivalent to the Nizzana Formation, which is characterized by nummulitic limestone intercalations, which wedge out eastwards (Benjamini, 1980a). The Hod Aqev section ranges from zone P5 to zone P9 of the updated planktonic foraminiferal biostratigraphic scheme of Berggren et al. (1995).

Samples 801 and possibly 802 contain morozovellids of the *Morozovella velascoensis* group including *M. acuta* and *M. occlusa*, *M. subbotinae*, *M. aequa* and *M. gracilis*, acarininas of the *Acarinina coalingensis* - *A. primitiva* group, and some *A soldadoensis*. Also present are early *Igorina*. These species are characteristic of the upper part of P5 ('*M. velascoensis* Zone' or P6a of earlier zonations). Thus the base of the section may be assigned to the Paleocene.

Samples 803 to 807 (about 5 m of section) postdate the LAD of *M. velascoensis* group species and belong to P6a ('*M. rex* zone' or P6b of earlier schemes), considered to be Early Eocene The earliest Eocene morozovellids *M. subbotinae, M. gracilis,* and *M. aequa* are present. The dominant acarininids are similar to those of the late Paleocene.

Samples 808 to around 818 (about 15 m of section) are from indurated rocks and relatively poorly preserved, but the lower samples contain low, biconvex, keeled morozovellids which are difficult to determine, but may be attributed to *M. formosa* and *M. lensiformis*, and therefore belong to zones P6b (P6c of earlier zonation) and P7. The upper samples contain *M. aragonensis* but

no low biconvex morozovellids, and are placed therefore in zone P8. Among the acarininids, species of the *A. coalingensis/primitiva* group become less common while *A. pseudotopilensis* and the *A. soldadoensis* group increase across this interval. A temporal interval of the Early Eocene (on the order of 4 Ma according to calibrations of Berggren et al., 1995) is represented by less than 15 m of section, and apparently the induration of the chalks here is associated with a reduced rate of sedimentation and possibly some condensation.

The boundary between P8 and P9 is unclear. At the transition there is a significant increase in variability in the genus *Igorina* centered about *I. broedermanni*, and in forms of *Planorotalites pseudoscitula*. The dominant acarininids are *A. pseudo-topilensis* and the *A. soldadoensis* group. Sample 823 and upwards are attributed to Zone P9, which is defined by the FAD of *P. palmerae*, which was rarely encountered in strata equivalent to sample 823 along the same cliff (Benjamini, 1980a). Other characteristic species occur gradually upwards in the section, such as *'S.' senni*, and gradual replacement among the acarininids of the *A. soldadoensis* group by 5 (or more) chambered forms, of the *A. pentacamerata/A. aspensis* group.

Morozovella aragonensis s.s. appears sporadically throughout zones P8 and P9 but is common only in P8. *M. aragonensis* var. *caucasica* has a short range in the middle part of Zone P9.

Zone P9 reaches exceptional thicknesses on the Avedat Plateau, with 70 m to the top of the sampled section at Hod Aqev, and continuing upwards well into the Horsha Formation. Berggren et al. (1995) indicate less than 2 Ma can be attributed to the interval represented here by 100 m of section.

Horsha Formation (Section 2, Fig. 18G.12). At Borot Ramalieh, west of the Avedat Archeological Park, massive white chalk begins near the base of the Horsha Formation. There is no chert, and few visible bedding planes. A prominent nummulitic limestone intercalation some 1 m thick, uncharacteristic of the Horsha Formation, is 10 m above the base, and a second, thinner zone somewhat above. Benjamini, (1979b) regards the limestone intercalation as a distal expression of the Nahal Yeter lithofacies, into which the Horsha Formation passes in the western Negev.

The Horsha Formation of the Borot Ramalieh section ranges

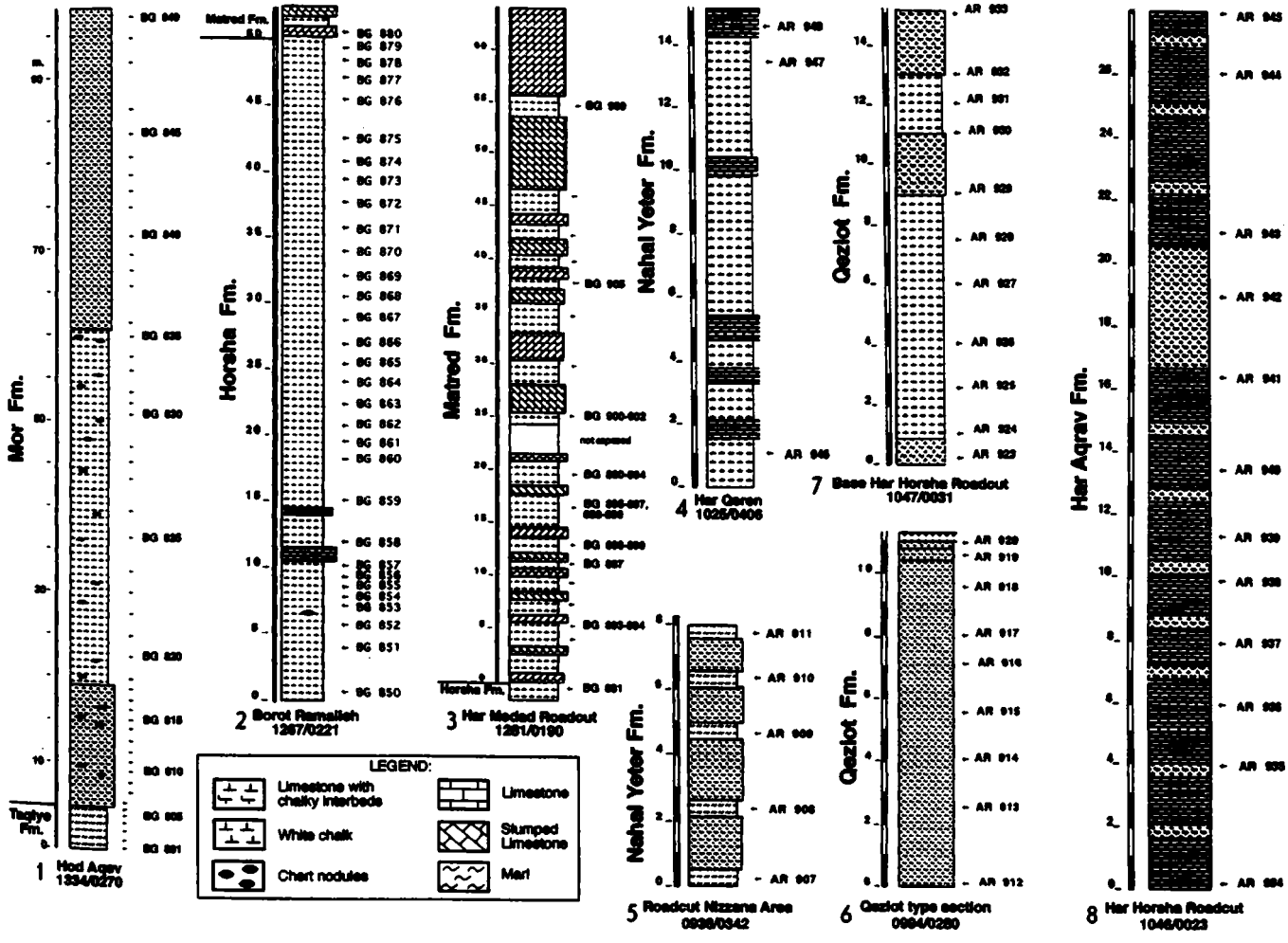


Figure 18G.12. Eocene sections of the Avedat Group on the Avedat Plateau (Honigstein et al., 2002, p. 371, Fig. 2).

from zone P9 to P10 of the planktonic foraminiferal biostratigraphic scheme of Berggren et al. (1995). Samples 850 to 870 (35+ m of section) contain planktonic foraminifera of the upper part of zone P9, with *Turborotalia cerroazulensis frontosa, Acarinina bullbrooki, Truncorotaloides rohri*, abundant *A. pentacamerata/ A. aspensis,* and *I. broedermanni.* Transitional forms from *A. bullbrooki* to *M. spinulosa* appear towards the top of the interval. *'S.' senni* is common. A varied subbotinid fauna culminates in appearance towards the top of *Clavigerinella* spp. and related forms (Benjamini, 1980a). The first appearance of *Hantkenina* in sample 871 represents the base of zone P10. Samples 872 to 880 (15+ m of section) contain *Hantkenina nuttalli, M. spinulosa, A. bullbrooki, A. matthewsae* and *A. pentacamerata*, and belong to zone P10.

Matred Formation: (Section 3, Fig. 18G.12). Along the Har Medad roadcut, the top of the Horsha Formation and the entire thickness of the Matred Formation are exposed. The lithofacies of the Matred Formation here is primarily chalk, but frequent nummulitic limestone intercalations occur especially near the base and top. The chalks are slightly glauconitic. The limestones are partially silicified but no chert is present in the chalk. The limestone lithofacies is associated with sedimentary deformations, with features such as troughs, shears, intraformational folds, and sedimentary breccias indicating lateral, presumably downslope transport. Of 40 m of cumulative thickness, only 10 m of chalks are autochthonous. Their biostratigraphy was nevertheless consistent, with the base belonging to P10, and the bulk of the formation belonging to P11. Samples 881 and 882 were characteristic of P10, containing *Hantkenina nuttalli* and *Turborotalia cerro-azulensis possagnoensis.* From Samples 884 to 909, *Globigerinatheka* spp. mostly *Gka. subconglobata subconglobata, Turborotalia cerroazulensis pomeroli*, and somewhat higher in the section, *Truncorotaloides topilensis* indicate zone P11. In all these samples the muricates *A. bullbrooki, T. rohri, M. spinulosa*, and (decreasing upwards) *A. pentacamerata* are the dominant species.

The top of the section of deformed sheets of limestone forms the surface of a plateau. Few undeformed chalk beds are preserved, and in the absence of demonstrably autochthonous chalks, zone P12 was not identified here. This zone was identified elsewhere in Matred Formation sections further to the north.

Nahal Yeter Formation: (Sections 4 and 5 in Fig. 18G.12). Situated on the flanks of the Har Qeren anticline, east of the road branching northward from the main Beersheva-Nizzana highway, the Nahal Yeter Formation (Zilberman, 1982) consists of white massive chalk with limestone intercalations, lacking chert, and overlain by a silicified limestone conglomerate, possibly indicating the position of the regional unconformity underlying the Qeziot Formation.

Samples 946 to 948 belong to zone P12, on the basis of the presence of *Morozovella lehneri, Globigerinatheka* spp. including *Gka index index, Turborotalia cerroazulensis pomeroli*, and large, inflated subbotinids transitional to *Globoquadrina galavisi.*

In the Nizzana roadcut, located on the new road to the Nizzana border crossing, only 8 m of thick chalk and marl beds

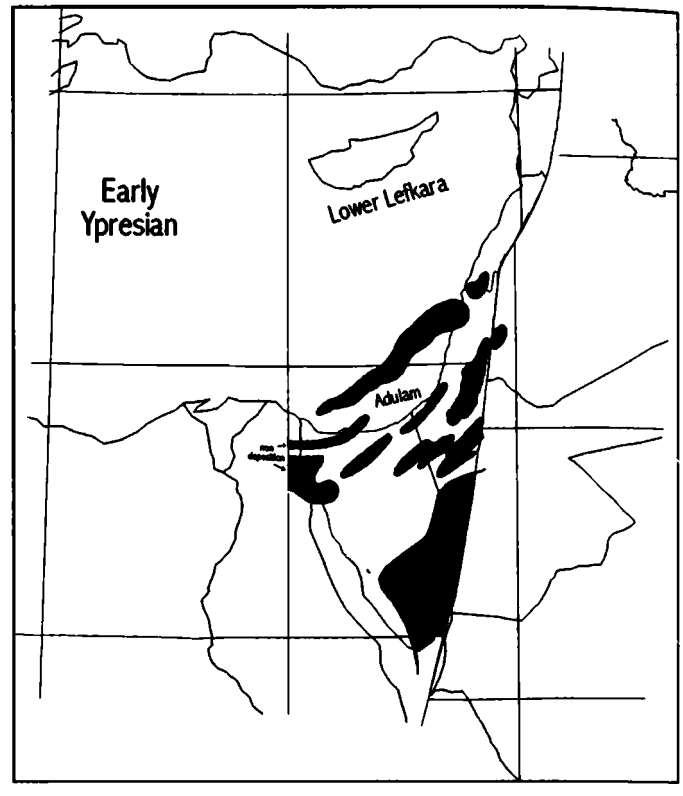


Figure 18G.13. Eastern Mediterranean Sketch-map showing the disposition of basins and high grounds (shaded) in Israel and Sinai during the Early Ypresian. Modified after Peritethys Program 2000 and Cohen et al., 1987.

belong to the Nahal Yeter Formation. Samples 907 to 911 are indicative of zone P12, similar to section 4, but muricate species are sparse, mostly *Truncorotaloides rohri*, some *A. bullbrooki*, and rare *M. spinulosa* are present, indicating a younger age than at Section 4. The lithology is slightly more marly and resembles the Qeziot Formation in its more southerly lithofacies. The thin section precludes identification of typical limestone intercalations characteristic of the Nahal Yeter Formation, into which it is placed in biostratigraphic and regional considerations

Qeziot Formation: (Sections 6 and 7 in Fig. 18G.12). The section in the bed of Nahal Nizzana, at the foot of a low ridge extending southwards from the settlement of Qeziot, was designated by Benjamini (1980b) as the type section of the Qeziot Formation as mapped by Bentor and Vroman (1964). The top of the section is truncated by a Neogene conglomerate.

Samples 913 to 918 (about 7 m) are indicative of the upper part of Zone P14, with *M. spinulosa* in the lower samples only and *T. rohri*, and *T. topilensis* continuing to Sample 918. Abundant *Globigerinatheka* of groups *Gka. subconglobata* and *Gka index* are common. *Turborotalia cerroazulensis pomeroli* and *T. c. cerroazulensis* are abundant, as are *T. pseudoampliapertura* and early *Globoquadrina* such as *Gq. tripartita*, and *Gq.*

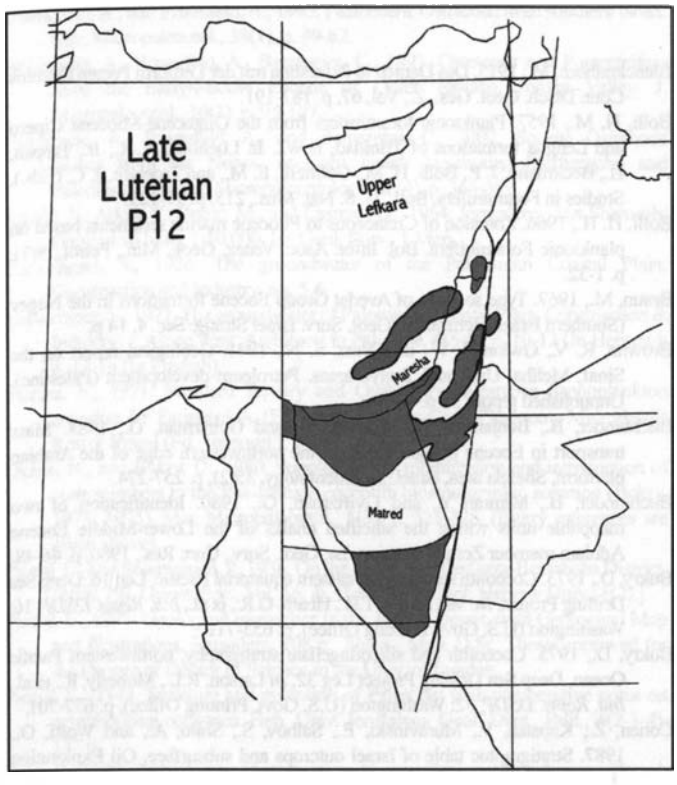


Figure 18G.14. Eastern Mediterranean Sketch-map showing the disposition of basins and high grounds (shaded) in Israel and Sinai during the Early Middle-Late Lutetian. Modified after Peritethys Program 2000 and Cohen et al., 1987.

pseudovenezuelana. From Sample 919 to the top of the section, Zone P15 is indicated, with extinction of the larger muricate forms and FAD of small, somewhat atypical *Gka. semiinvoluta*. Small muricates referable *to Acarinina rugoso-aculeata* persist well into Zone P 15. Hantkeninids are either rare or poorly preserved, and only broken chambers with spines were recovered. The Qeziot Formation is further represented in the lower part of the roadcut section of Har Horsha (samples 923-933).

Har 'Aqrav Formation: (Section 8 in Fig. 18G.12). Roadcuts on the north flank of Har Horsha, on the newly paved border road between Israel and Egypt, expose a sequence just above the unconformity between the Nahal Yeter and Qezi'ot Formations, mistakenly identified by Bentor and Vroman (1964) as equivalent to the Horsha and Matred Formations. Benjamini (1980b) established the Har 'Aqrav Formation for the bedded limestone lithofacies forming the top of the section. A single limestone intercalation rich in larger foraminifera, echinoderms, and molluscs, somewhat above the base of the Qeziot Formation and below the sampled section of the lower roadcut, contains the Biarritzian nummulitic fauna described by Schaub (1995).

Samples 923 through 945 all belong to Zone P15, though assemblages are poor when compared to the type section at Section 6. *Globigerinatheka* including *Gka semiinvoluta, Turborotalia cerroazulensis pomeroli* and *T. c. cerroazulensis, T. pseudo-ampliapertura* and the *Globoquadrina tripartita/pseudo-venezuelana* group are still recognized.

PALEOGEOGRAPHY

The Levantid structural ridges separate between the basins, as they do not show Eocene deposits, though some may have been covered by thinner Eocene sediments before their removal in pre-latest Lutetian and certainly in Oligocene times. Relicts of Eocene chalk within karstic sinkholes in the NE Negev witness the presence of Eocene sediments on the flanks and possibly on top of the anticlines of the Levantids prior to erosion.

The Eocene deposits consist predominantly of pelagic chalks, occasionally with chert, nearly free of clastics. Nummulitic limestone beds and intercalations are sporadic and controlled by features related to the Syrian Arc fold belt. Though Neritic lithofacies primarily developed on elevated parts of the Syrian Arc folds, much material was syn-depositionally transported into the adjoining basins. Further manifestations of the influence of syn-sedimentary structural relief were a reduced rate of sedimentation on paleohighs, and occasionally reduced connection to the open Tethys, especially in the southeastern Negev.

The thickness figures of the Eocene deposits put the depo-centers of the Shehem Syncline and the Paran Basin in evidence. The more or less NE strike of these features is conditioned by the Levantid structure. The basin of the Shehem Syncline may extend to the offshore Pleshet Basin, whereas the Paran Basin may be one within a string of basins, extending from Sinai (Egypt) to the Jordan Valley, and opposite the Dead Sea Transform to the Yarmuk Valley (Jordan).

The Levantid structural ridges separate between the basins (**Figs. 18G.13 and 18G.14**). These ridges do not show Eocene deposits, but some may have been covered by Eocene sediments before their removal in pre-latest Lutetian and certainly in Oligocene times. Relicts of Eocene chalk within karstic sinkholes in the NE Negev witness the presence of Eocene sediments on the flanks and possibly on top of the anticlines of the Levantids prior to erosion.

ACKNOWLEDGEMENTS

The authors gratefully acknowledge the effort of John K. Hall to render the compact language of the Lexique into more readable English, and to assemble the appropriate references.

EDITORIAL REMARK

This chapter was originally to be written by Prof. Chaim Benjamini. Unfortunately, due to a serious medical situation he was unable to undertake the task. This chapter is thus largely based upon the Paleocene-Eocene portions of the computerized Lexique of Israel (Hirsch and Roded, 2001).

REFERENCES CITED

Arkin, Y., Nathan, Y., and Starinsky, A., 1972. Paleocene-early Eocene environments of deposition in the northern Negev (southern Israel). Bull. Geol. Surv. Israel, 56, p. 1-17.

Avnimelech, M., 1936. Etude géologiques dans la region de la Shephela en Palestine. Ann. Univ. Grenoble, Trav. Lab. Géol. Grenoble, Allier Frères, 144 p., Figs.

Begin, B., and Druckman, Y., 1987. List of Formations (Internal GSI Mapping Recommendations).

Bellardi, L., 1885. Cataloge regionata fossili Nummulitici d'Egitto. Mem. de Reale Acad. Torino, 2 ser., vol., 15.

Benjamini, C. 1973. The stratigraphy and structural geology of the Sartaba area, Samaria. Unbublished M.Sc. thesis, Hebrew Univ., Jerusalem, 98 p., 2 p. plates (Hebrew abstract, 5 p.).

Benjamini, C., 1979. The geological history of central and southern Israel during the Eocene. Unpublished Ph.D. dissertation, Dept. Geol., Hebrew Univ. Jerusalem (In Hebrew). Vol. I: English summary 41 p., Vol. II, Appendices. App. 1-31 p.; App. 2-82 p.; App. 3-51 p.; App. 4-10 p.; App. 5-4 p.; App. 6-38 p.; App. 7-27 p.; App. 8-43 p.

Benjamini, C., 1979. Facies relationships in the Avedat Group Eocene in the northern Negev. Israel J. Earth Sci., 28(2-3), p. 47-69.

Benjamini, C., 1980a. Planktonic Foraminiferal Biostratigraphy of the Avedat Group Eocene in the Northern Negev. J. Palaeont., 54(2), p. 325-358.

Benjamini, C., 1980b. Stratigraphy and foraminifera of the Qezi'ot and Har Akrav Formations (latest middle to late Eocene) of the western Negev, Israel. Israel J. Earth Sci. 29(4), p. 227-244.

Benjamini, C., 1984. Stratigraphy of the Eocene of the Arava Valley (eastern and southern Negev, southern Israel). Israel J. Earth Sci. 33(4), p. 167-177.

Benjamini, C., 1992. The Paleocene - Eocene Boundary in Israel - A candidate for the boundary stratotype. Neues Jahrb. Geol. Palaeontol., Abh., 186(1-2), p. 49-61.

Benjamini, C., Weinbaum-Hefetz, M., and Moshkovitz, S., 1995. Calcareous nannofossil biostratigraphy of the Middle Eocene, Northern Negev, Israel. Report submitted to the Ministry of Energy & Infrastructure, 12 p.

Benjamini, C., and Zilberman, E., 1979. Late Eocene coral reefs of the Western Negev, Israel. Israel J. Earth Sci., 28(1), p. 42-46.

Bentor, Y. K., Grader, P., Parnes, A., Reiss, Z., Shiftan, Z., and Vroman, A., 1960. Lexique Stratigraphique International, vol. III, Asie, Fasc. 10C2, Israel. CNRS, Paris.

Bentor, Y. K., and Vroman, A. J., 1951. The Geological Map of the Negev, Sheet 18: Avedat, Scale 1:100,000. (In Hebrew). Israeli Army, Sci. Sect., 98 p., Maps, Figs.

Bentor, Y. K., and Vroman, A. J., 1960. Geological Map of Israel, 1:100,000, Sheet 16: Mount Sdom. Isr. Geol. Surv., 117 p., Figs., Separate folder with 19 Encl. (In Hebrew & Engl. Editions). 1st Edition - 1954; 2nd Edition - 1960.

Bentor, Y. K., and Vroman, A. J., 1961. Geological Map Of Israel, Ser. A: The Negev, Sheet 17: Nitsana (Cross Sections). Isr. Geol. Surv., 1 Sheet.

Bentor, Y. K., Vroman, A. J., 1964. The Geological Map of Israel, Ser. A - The Negev. Sheet 20: Mount Lots. (In Hebrew and English. Isr. Geol. Surv., 1 Map, Scale 1:100,000.

Berggren, W. A., Kent, D. V., Flynn, J. J., and Van Couvering, J. A., 1985. Cenozoic geochronology. Geol. Soc. Am. Bull., 96(11), p. 1407-1418.

Berggren, W. A., Kent, D. V., Swisher, C. C., III, and Aubry, M. -P., 1995, A revised Cenozoic geochronology and chronostratigraphy, In: Berggren, W. A., Kent, D. V., Aubrey, M. -P., and Hardenbol, J. (eds.), Geochronology, Time Scales and Global Stratigraphic Correlation: SEPM (Society for Sedimentary Geology) Special Publication No. 54, p. 129-212.

Berggren, W. A., and Miller, K. G., 1988. Paleogene tropical planktonic foraminiferal biostratigraphy and magnetobiochronology. Micropaleontology, 34(4), p. 362-380.

Blake, G. S., 1935. On the occurrence of marine Miocene in Palestine. Geol. Mag., 72(3), p. 140-142.

Blake, G. S., 1936. The stratigraphy of Palestine and its building stones. Jerusalem, Printing & Stationery Office, 133 p.

Blanckenhorn, M., 1914. Syrien, Arabien und Mesopotamien. Handb. Region. Geologie, Heidelberg 5(4), p. 1-159.

Blanckenhorn, M., 1915. Das Danien in Palaestina mit der Leitform Pecten Obrutus Conr. Dtsch. Geol. Ges., Z., Vol. 67, p. 187-191.

Bolli, H. M., 1957. Planktonic foraminifers from the Oligocene-Miocene Cipero and Lengua formations of Trinidad, B.W.I. In Loeblich, A. R., Jr., Tappan, H., Beckmann, J. P., Bolli, H. M., Gallitelli, E. M., and Troelsen, J. C. (Eds.), Studies in Foraminifers. Bull., U. S. Nat. Mus., 215, p. 97-123.

Bolli, H. H., 1966. Zonation of Cretaceous to Pliocene marine sediments based on planktonic Foraminifera. Bol. Infor. Asoc. Venez. Geol., Min., Petról., 9(1), p. 1-32.

Braun, M., 1967. Type sections of Avedat Group Eocene formations in the Negev (Southern Israel). Jerusalem: Geol. Surv. Israel Stratig. Sec. 4, 14 p.

Browne, R. V., Gwinn, J. W., and Nasr, S. N., 1941. Geological report on the Sinaf, Meliha, Ureif and Taqiye areas. Petroleum development (Palestine), Unpublished report, 31 p.

Buchbinder, B., Benjamini, C., Mimran, Y., and Gvirtzman, G., 1988. Mass transport in Eocene pelagic chalk on the northwestern edge of the Arabian platform, Shefela area, Israel. Sedimentology, 35(2), p. 257-274.

Buchbinder, B., Mimran Y., and Gvirtzman, G., 1980. Identification of two mappable units within the silicified chalks of the Lower-Middle Eocene Adulam member Zora Formation. Isr. Geol. Surv., Curr. Res., 1980, p. 46-48.

Bukry, D., 1973. Coccolith stratigraphy, eastern equatorial Pacific, Leg 16, Deep Sea Drilling Project. *In:* van Andel, T.H., Heath, G.R., et al., *Init. Repts. DSDP,* 16: Washington (U.S. Govt. Printing Office), p. 653-711.

Bukry, D., 1975. Coccolith and silicoflagellate stratigraphy, northwestern Pacific Ocean, Deep Sea Drilling Project Leg 32. *In* Larson, R.L., Moberly, R., et al., *Init. Repts. DSDP,* 32: Washington (U.S. Govt. Printing Office), p. 677-701.

Cohen, Z., Kapstan, V., Muravinski, E., Salhov, S., Shilo, A., and Wolff, O., 1987. Stratigraphic table of Israel outcrops and subsurface. Oil Exploration (Investment) Ltd.

Cook, P., Roth, I., Mimran, Y. 1970. The geology of the Shechem syncline. Geol. Surv. Isr. Rep. 102/70 MD, 20 p.

Daniel, E. J., and Wellings, F. E., 1935. Internal Report of IPC/PDP (unpublished).
Druckman, Y., and Begin, Z. B., 1985. Geological mapping units in Israel and their symbols. Isr. Geol. Surv., Rep. GSI/35/85, 17 p.

Fairbridge, R. W., Nasr, S. N., and Tiratsoo, E. N., 1940. Final geological report on Licences 10 And 11 in the Beersheba Sub District. Haifa, Iraq Pet. Co. Ltd., Geol. Dept. Rep., 24 p., Maps.

Flexer, A., 1961.The geology of Mount Gilboa. Isr. Res. Counc., Bull., 10G(1-2), p. 64-72, 1 Map.

Golik, A., 1960. On the geology of the Ziklag area, Israel. Isr. Res. Counc., Bull., 9G(2-3), p. 129-152.

Greitzer, Y., 1960. On the geology of the Lakhish area. Isr. Res. Counc., Bull., 9G(2-3), p. 109-128.

Gvirtzman, G., 1969a. Subsurface data on the Saqiye Group (Late Eocene to Early Pleistocene) in the Coastal Plain and Hashephela regions, Israel. Isr. Geol. Surv., Rep. OD/1/69 & Inst. Pet. Res. Geophys., Rep. 1037, Various pagings.

Gvirtzman, G., 1969b. The Saqiye Group (Late Eocene to Early Pleistocene) in the Coastal Plain and Hashephela regions. Vol. 2: Maps. (Vol. 1 was never published). Isr. Geol. Surv., Bull. 51 & Inst. Pet. Res. Geophys., Rep. 1022. 38 maps.

Gvirtzman, G., 1970. The Saqiye Group (Late Eocene To Early Pleistocene) in the Coastal Plain and Hashephela regions, Israel. /In Hebrew; Engl. Abstr./. Isr. Geol. Surv., Rep. OD/5/67 & Inst. Pet. Res. Geophys., Rep. 1022, 170 p., Figs., Maps. (Preprint of the maps - Rep. OD/1/67). (Unpublished Ph.D. Thesis, Hebrew Univ. Jerusalem).

Gvirtzman, G., and Buchbinder, B., 1966. Tertiary Project. Holon, Inst. Pet. Res. Geophys., Semi Ann. Progr. Rep., Apr. 1966 - Sept. 1966, p. 11-16.

Gvirtzman, G., Buchbinder, B. and Mimran, Y., 1981. Electric log correlation of the Shefela Group (Senonian to Middle Eocene). Isr. Geol. Surv., Current Res., 1980, p. 45-46.

Gvirtzman, G., and Reiss, Z., 1965. Stratigraphic nomenclature in the Coastal Plain and Hashephela regions. Isr. Geol. Surv., Rep. OD/1/65, 13 p.

Hatzor, Y., Benjamini, C., Mimran, Y., and Grossowicz, L., 1994. The Eocene stratigraphy of Mt. Gilboa and northern Samaria, Israel. Israel J. Earth Sci. 43(1), p. 1-20.

Honigstein, A., and Rosenfeld, A., 1995. Palaeocene Ostracods from southern Israel. Rev. Micropaleontol., 38(1), p. 49-62.

Honigstein, A., Rosenfeld, A., Benjamini, C., 1991. Ostracods and Foraminifera from the Early-Middle Eocene of Qeren Sartaba, Jordan Valley. J. Micropaleontol., 10(1), p. 95-107.

Honigstein, A., Rosenfeld, A., and Benjamini, C., 2002. Eocene Ostracode faunas from the Negev, southern Israel: Taxonomy, Stratigraphy and Paleobiogeography. Micropaleontology, 48(4), p. 365-389.

Itzhaki, Y., Arkin, Y., Braun, M., and Lasman, N., 1964. Jerusalem - Bet Shemesh: Geological Map, 1:50,000. Isr. Geol. Surv., 1 Map.

Loewengart, S., 1926. The groundwater of the Palestinian Coastal Plain. Construction and Industry, no. 5-6.

Loewengart, S., 1927. The groundwater of Palestinian Coastal Plain. Construction & Industry; J. Assoc. Eng. Architects in Palestine, 6(5-6), p. 10-12 (In Hebrew); p. 13-14 (In English).

Martini, E., 1971. Standard Tertiary and Quaternary calcareous nannoplankton zonation. In: Farinacci, A. (Ed.), Proc. 2nd Int. Conf. Planktonic Microfossils Roma: Rome (Ed. Tecnosci.), 2, p. 739-785.

Okada, H., and Bukry, D., 1980. Supplementary modification and introduction of code numbers to the low-latitude coccolith biostratigraphic zonation (Bukry, 1973; 1975). Mar. Micropaleontol., 5(3), p. 321-325. (Bukry references are given above).

Picard, L., and Solomonica, P., 1936. On the geology of the Gaza-Beersheba District. Journ. Pal. Orient. Soc., Vol. 16. &. Bull. Geol. Dept. Hebrew Univ., 1(2).]

Picard, L., 1931. Geological researches in the Judean Desert, with Geological Map and illustrations. Jerusalem, 108 p., Plates., Map. D.Sc. Thesis approved for the Degree of Doctor of Science in the Univ. of London.

Picard, L., 1943. Structure and evolution of Palestine; with comparative notes on neighbouring countries. Heb. Univ. Jerusalem, Geol. Dept., Bull., 4(2-3-4), 187 p.

Reiss, Z., 1952. On the Upper Cretaceous and Lower Tertiary Microfaunas of Israel. Isr. Res. Counc., Bull., 2(1), p. 37-50.

Reiss, Z., 1955a. A. Micropaleontology and Cretaceous-Tertiary boundary in Israel. B. Remarks on the age of some Late Cretaceous and Early Tertiary Stratigraphic Units in Israel. Isr. Res. Counc., Bull., 5B(1), p. 105-120 & 121-125.

Reiss, Z., 1955b. A. Micropaleontology and Cretaceous-Tertiary boundary in Israel. B. Remarks on the age of some Late Cretaceous and Early Tertiary stratigraphic units in Israel. Isr. Geol. Surv., Bull. 8, 22 p.

Reiss, Z., 1957a. Notes on foraminifera from Israel. 1. Remarks on Truncorotalia Aragonesis Caucasica (Glaessner). 2. Loxostomoides, A new Late Cretaceous and Early Tertiary genus of foraminifera. 3. Sigalia, A new genus of foraminifera. Isr. Geol. Surv., Bull. 9, 7 p. (Reprinted From: Isr. Res. Counc., Bull., Vol. 6B, p. 239-244).

Reiss, Z., 1957.b. Notes on foraminifera from Israel. 4. Occurrence and stratigraphical significance of Cuvillierina Eocenica Debourle. Isr. Geol. Surv., Bull., 10, 12 p.

Reiss, Z., 1957.c. Notes on foraminifera from Israel. 5. Studies on Victoriellidae. 6. Stratigraphical distribution of some Mesozoic and Cainozoic Foraminifera from Israel. Isr. Geol. Surv., Bull., 11, 15 p.

Reiss, Z., 1957d. Occurrence of Nezzazata in Israel. Micropaleontology, 3(3), p. 259-262.

Reiss, Z., and Gvirtzman, G., 1966. Borelis from Israel. Eclogae Geol. Helv., 59(1), p. 437-447.

Roman, F., and Doncieux, L. 1927. Observations sur l'Éocene de Syrie et de Palestine. C. R. Somm. Séances Soc. Géol. Fr. No. 14, p. 171-173

Romein, A. J. T., 1979. Lineages in Early Paleogene calcareous nanoplankton. Utrecht Micropaleontological Bulletins, 22, 231 p.

Rosenfeld, A., Flexer, A., Honigstein, A., Almogi-Labin, A., and Dvorachek, M., 1989. First report on a Cretaceous/Tertiary boundary section at Makhtesh Gadol, Southern Israel. Neues Jahrb. Geol. Palaeontol., Monatsh., 1989(8), p. 474-488.

Sakal, E., Raab, M., and Reiss, Z., 1966. Upper Eocene in the south eastern Negev, Israel. Israel J. Earth Sci., 15(1), p. 42-45.

Schaub, H., 1995. Nummulites of Israel. In: Schaub, H., Benjamini, C., Moshkovitz, S., (eds.), The biostratigraphy of the Eocene of Israel, Nummulites, planktic foraminifera and calcareous nannofossils. Schweizerische Paläontologische Abhandlungen, 117, p. 19-31, 12 pls.

Schaub, H., Benjamini, C., and Moshkovitz, S., (eds.), 1995. The bio-stratigraphy of the Eocene of Israel, Nummulites, planktic foraminifera and calcareous nannofossils. Schweizerische Paläontologische Abhandlungen, 117, 58 p.

Shaw, S. H., 1947. Southern Palestine Geological Map on a scale of 1:250,000 with Explanatory Notes. Palestine, Govt. Printer, 42 p., Map.

Zilberman, E., 1981. The Geology of the Central Sinai - Negev Shear Zone, Central Negev. Part A: The Saad-Nafha Lineament. Isr. Geol. Surv., Rep. Hydro/1/81, 59 p., 2 Maps.

Zilberman, E., 1982. The Geology of the Qeren - Haluza Area. (In Hebrew; Engl. Abstr.). Isr. Geol. Surv., Rep. GSI/4/82, 33 p., Maps.



The rocky promontories off Dor (or Dora), an ancient seaport with over two millennia of history.
Grayscale rendition of color image in The Holy Land Satellite Atlas, Volume II (1999, p. 68). ©Røhr Productions Ltd., Nicosia, Cyprus. Reproduced with permission. View towards the north.



Nahal Shiqma enters the Mediterranean, draining the southern Coastal Plain south of Ashkelon.
Grayscale rendition of color image in The Holy Land Satellite Atlas, Volume II (1999, p. 169). ©Røhr Productions Ltd., Nicosia, Cyprus. Reproduced with permission. View towards the northeast. Most of the coastline of Israel consists of sandy beaches such as this.

Chapter 18H

The Oligocene–Pliocene of Israel

Francis Hirsch
Geological Survey of Israel, 30 Malchei Israel Street, Jerusalem 95 501, Israel

INTRODUCTION

This chapter is widely based on the concepts of Benjamin Buchbinder, Ezra Zilberman, and Aharon Horowitz, and on the new edition of the 'Lexique Stratigraphique' of Israel (2001), compiled by Francis Hirsch and Reuven Roded. The historical background rests largely on Bentor's Lexique (1963) and on the proofs of the unpublished version by Daniel (1959).

This chapter encompasses the Late Eocene-Pliocene Saqiye Group, Oligocene-Miocene Tiberias Group, and the Late Miocene-Pliocene Dead-Sea Group. (**Table 18H.1**).

The dominantly marine Saqiye Group is sparsely exposed in the Coastal Plain, where it is mainly recognized in the subsurface **(Fig. 18H.1).** It passes eastward into the continental deposits of the successive Tiberias and Dead Sea Groups.

The Tiberias and Dead Sea Groups consist of fluviatile deposits, originating in a first phase from the mountainous areas to the south-east and being transported west in the direction of the Mediterranean. The Dead Sea Group consists of a later phase, the filling of an intra-montane basin, which also received sediments from the west.

Since the Late Oligocene (or earliest Miocene), the opening of the Red Sea caused the shear along the Jordan Valley, Arava, and Aqaba line. It was accompanied by basalt eruptions, leading to the subsequent severance of Arabia from the African plate. It also generated a totally new topography. Horowitz (2001) recognizes three phases of development of the Dead Sea Transform (also called the Levant Fault):

1) From its start in the latest Oligocene until the Middle Miocene, a sinistral strike-slip generated a chain of rhomb-shaped grabens. The drainage goes west, into the Para-Tethyal Mediterranean. The Saqiye Group represents marine deposition from the west, whereas fluviatile sediments from the east and south represent the upper part of the Tiberias Group.

2) Enhanced subsidence formed an Upper Miocene-Pliocene basin, developing an intracratonic drainage system, including the Negev, Moab, and Eastern Judea. As a result, the Tiberias Group gives way to the Dead Sea Group.

3) The collapse of the previously formed rhomb-grabens finalized the opening of the Rift, subsequently accumulating thick Plio-Pleistocene Rift deposits of the Upper Dead Sea, Central Jordan Valley, and Hula 'Groups' (Horowitz, 2001).

These neo-tectonic events, due to isostatic readjustments,

Table 18H.1. Oligocene–Pliocene Groups and main formations

AGE	Negev and Rift Valley	Shefela
Pliocene PIACENZIAN [N20-21] ZANCLEAN [N18-20]	DEAD SEA GROUP Amora Arava Sedom Gesher	SAQIYE GROUP Yafo
Upper Miocene MESSINIAN [N17] TORTONIAN [N14-17]	DEAD SEA GROUP Hula, Tanur Bira, Hufeira / Umm Sabune	SAQIYE GROUP Mavqiim Upper Ziqim/ Sheva/Pattish
Erythrean Faulting Event		
Middle Miocene SERRAVAGLIAN [N9-14] LANGHIAN [N 8]	TIBERIAS GROUP Hazeva / Hordos	SAQIYE GROUP Lower Ziqim Bet Guvrin / Ziqlag
Lower Miocene BURDIGALIAN [N 6-7] AQUITANIAN [N 4-5]	TIBERIAS GROUP Hazeva / Hordos	SAQIYE GROUP Bet Guvrin
Late Oligocene CHATTIAN [P21-22]	TIBERIAS GROUP Zefa / En Gev	SAQIYE GROUP Bet Guvrin
Early Oligocene RUPELIAN [P18- 21]	TIBERIAS GROUP Susita/Fiq	SAQIYE GROUP Lakhish / Bet Guvrin / Ashdod

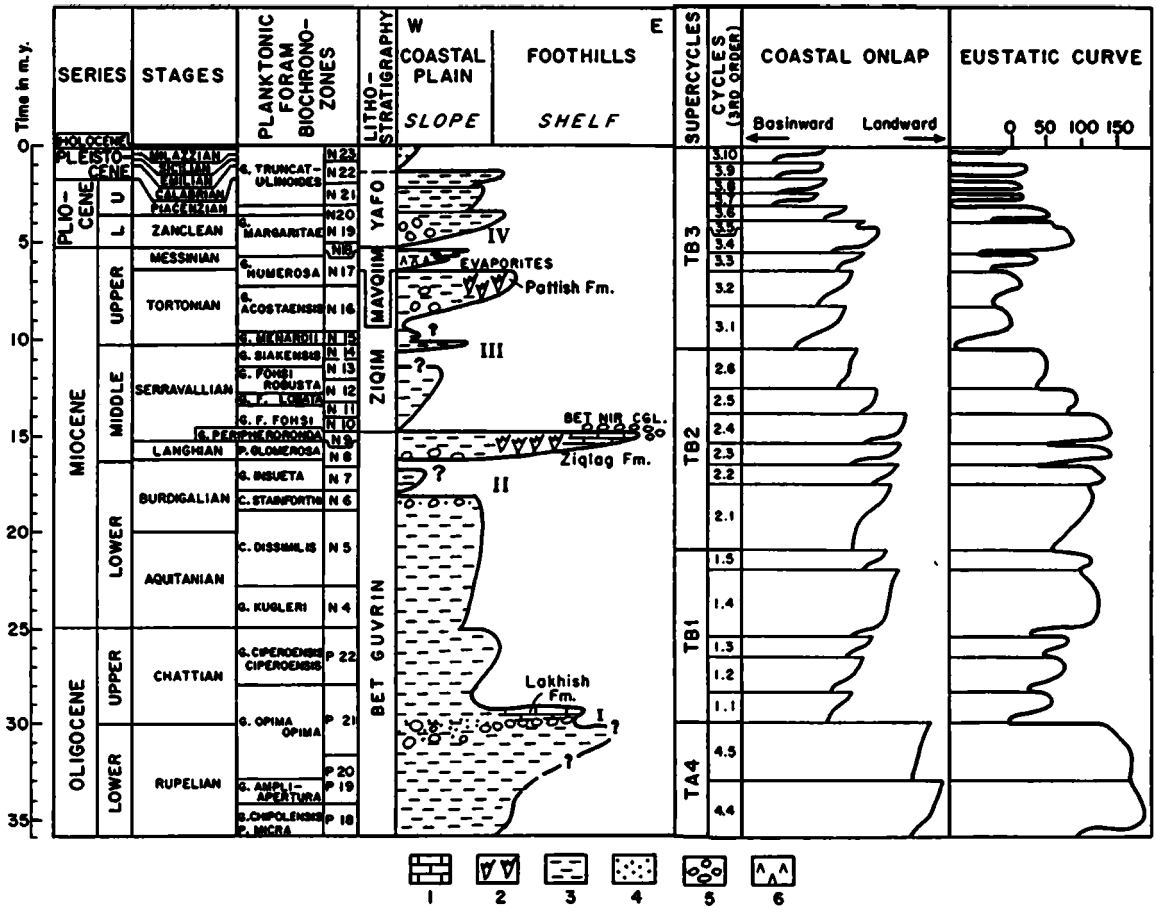


Figure 18H.1. Stratigraphic scheme of the Oligocene-Pliocene marine sequence in Israel (from Buchbinder et al., 1993, Fig. 5, p. 105). Oligocene-Neogene marine section in Israel correlated with Haq et al.'s (1977, 1978) chronostratigraphy, sequence stratigraphy, and eustatic curve. Roman numerals I-IV denote major erosion events. Lithology: 1. shelf platform limestones; 2. coral reefs; 3. claystones and marlstones; 4. sandstones; 5. conglomerates; 6. anhydrite or halite.

reshaped the tectono-environment of the eastern Mediterranean Levantine, and Sinaitic parts of the African plate. The continuous deepening of the basins of the eastern Mediterranean and Dead Sea Rift was echoed by the differential uplift of the adjacent Negev, Judea, and Galilee blocks west of the transform, as well as the Syro-Jordan blocks of the Arabian subplate to the east. The accompanying volcanism of the Bashan Group is characterized by basalt, scoria and tuff from the Golan Heights to Eastern Galilee, also filling parts of the Yizre'el-Jordan-Dead Sea-Arava basin and the subsequent Rift.

HISTORY OF RESEARCH

Oligocene:

Blake (1928) placed the Oligocene strata near Ramle in the southern Shefela, which Blanckenhorn (1931) held to be Eocene, into the Miocene. Cox (1934) established the Ramle outcrop as Chattian. Avnimelech (1936) recognized Rupelian-Chattian (or Stampian) and Aquitanian substages in the Bet Guvrin area. Avnimelech (1939) also recognized the marine Oligocene at Megiddo in the Yizre'el Valley.

These up to 50 m thick calcareous marls, sandy chalks, limestones, and conglomerates in the Shefela and at Megiddo yield mollusks, echinids, bryozoans, calcareous algae and the large foraminifers *Lepidocyclina* and *Operculina*. Among the bivalves are: *Pecten arcuatus* Brocchi, *Echinolampas angulatus* Merian, *Opisaster scillae, Nummulites bouillei* de la Harpe, *N. incrassatus* de la Harpe, *Amphistegina lessonii* d'Orb., *Nephrolepidina* sp., *Heterostegina* sp., *Operculina complanata* Defr. (Stampian) and *Ostrea fabellulaeformis* V. Schauroth, *Chlamys deleta* Michel., *C. praescabriusculus* Font., *Xancus episomus* Micht., *Spiroclypeus* sp., *Myogypsinoides dehaarti* VanderVlerk, *Nephrolepidina tournoueri* Lem. and Douv., *N. simplex* Douv., *Eulepidina dilatata* Michel., *E. raulini* Lem and Douv., and *Heterostegina praecursor* TanSinHok (Aquitanian). *Nautilus blakei* Avnimelech is Stampian-Aquitanian. This facies, under the name Ramle Member, is now part of the Lakhish Formation.

The Tall Duweir Formation of Daniel (1935), at Tall ad Duweir

(Arabic for ancient Lakhish) was considered Oligocene-Aquitanian, while the Zeita-Qubeibeh Facies of Picard and Solomonica (1936), in the Southern Judean foothills, yielding *Lepidocyclina, Nummulites, Operculina*, and *Orbitoides* was identified as Stampian.

At Bet Ras in the Ramot Menashe area (SE of Mt. Carmel), Avnimelech (1939) identified as Oligocene about 60 m of yellow glauconitic calcarenites, topped by hard bituminous chalks, which Arad (1965) later named the Bet Rosh Formation.

Marine Miocene:

Blake (1928) first gave a Miocene age to chalky limestones at El-Kubeiba, and Avnimelech (1936) attributed a Burdigalian age to the upper part of this formation at El-Kubeibe and Iraq el Manshiya (southern Shefela) leaving the remainder in the Oligocene as proposed earlier by Cox (1934).

Blake (1928) also attributed a probable Miocene age to the blue clays and marls, exposed between Artuf and Naaneh in the central Shefela, which are now considered to be part of the Sakiebeds.

Loewengart (1928), Picard and Solomonica (1936), Picard and Avnimelech (1937), and Grader (1958) described Miocene marine strata in boreholes from the Haifa Bay to the Gaza strip. They recognized three different facies, striking roughly parallel to the present coastline. These include sandy clays and marls with intercalations of white algal limestones in the lower part of the *Sakiebeds,* which thicken westward to more than 1400 m. Interbedded organogenic limestones, associated with marl and calcareous sandstone, carrying *Amphistegina* and other foraminifera were found in patches from Nahariya through Ramat Yohanan and at the top of the Carmel Mountain (Avnimelech, 1947; Picard and Kashai, 1958) as well as farther south at Tulkarm, Wadi Sarar, and El Yuheir (El Gherheir) (Blake 1935, 1936). Avnimelech (1935, 1936) identified these rocks as Vindobonian, while Picard and Solomonica (1936) called them Helvetian at Wadi Hesi (Tell Nejeile). The conglomeratic limestone, found in the more eastern zone of the Bab-el-Wad region through Bir Khweife to the Beersheva 'Great Quarry', contain *Pecten benedictus* Lmk., *Ostrea gryphoides* (Schloth, Dolfus and Dautz.), *Arca noe* Linn., *Cardium* sp. cf. *C. erinaceum* Lmk., and *Antigona miocenica,* identified as Tortonian by Blake (1935, 1936), Avnimelech (1935, 1936), and Picard and Solomonica (1936).

Blake (1935) regarded fossiliferous limestones at Bir Khweilfe as Tortonian, while Picard and Solomonica (1936) identified its fauna of *Callistotapes vetulus* Bost., *Divaricella divaricata* Linn., *Venus plicatus* Gmel. var. *dertonensis* Sacco., and *Ostrea gryphoides* Schloth. as Helvetian. They also attributed a Helvetian ('Schlier Stage') age to 5 m of marls from Tell en Nejile (Wadi Hesi) including *Pecten* cf. *demudatis* Reuss, *Nuculana* aff. *lecoentrea* Dolfus and Dautzenberg, and *Brissopsis* aff. *attrangensis. R.* Hoernes.

Daniel (1935) recognized the Beersheva Freestone Formation as being of Miocene age. This unit, named presently the Sheva Formation is synonymous with the 'Wadi al Jurrah series' also named by Daniel (*op. cit.*). In the Beersheva Great Quarry (2 km north of the Mosque at Beersheva) it consists of 25 m of finely granular to gritty, well and thickly-bedded, white to cream-colored chalky limestone. It is cleanly jointed vertically, and can be cut freely and easily with a saw as freestone, commonly used for building in Beersheva. The rock is largely made up of minute echinoid debris with some fragments of *Lithothamnium*. A strong angular unconformity separates these rocks from the overlying Mansura Marl Formation (Daniel, 1935) of Mio-Pliocene age. This unit, named after Mansura village, about 4 km NNW of the Wadi-as-Surar railway station, was included in the 'Sakieh beds' (Loewengart, 1927, 1928).

The Juheir Limestone Formation (Miocene) of Wellings (1944) was established at Al Juheir, 27 km southeast of Gaza. It is synonymous with the 'Lithothammenkalke' of Blanckenhorn (1914), and the 'Ifteis limestone' of Wellings (1941). Today this unit is known as the Ziqlag Formation.

Blake (1935) attributed a Helvetian age to the few meters thick coral reef limestones containing *Lucina columbella* Lmk., *Tellina (Acropagia) crassa* Penn. var. *lammelosa Dollfus*, and *Antigolna subrotunda* at Wadi Sarar. Overlying chalky limestones of late Eocene-Oligocene age it was placed by Picard and Avnimelech (1937) into the Vindobonian. Blake (*op. cit.*) also considered a Helvetian age for a limestone containing *Ventricula burdigalensis* Mayer at El-Juheir (El Ghirheir).

Continental Miocene:

Continental deposits of Miocene age, composed mainly of reddish sandstones, red and green shale, conglomerates and some chalk and limestone, were first described by Blake (1928) as 'calc-ferruginous sandstones and gypseous beds' from the vicinity of Kurnub and a 'red sandstone series' from Ain Hosb or Ein Hazeva in the Northern Arava. Blanckenhorn (1931) attributed an Upper Pliocene to this sequence. This Hosb Sandstone (Blake, 1935), Hosb Series or Kurnub Sands and Sandstones (Picard, 1943); Hasb Series (Shaw, 1947), Hatseva Series (Bentor and Vroman, 1954) also includes the 'Abu Treife Series' (Bentor and Vroman, 1951). In the area of Wadi Abu Treife on the Ovdat Plateau, Central Negev, these consist of over 150 m of variegated, partly calcareous sandstones, with flint splinters and subordinate amounts of red and green shales, gypsiferous marls, hard limestones and dolomites, with a base conglomerate normally being present. Picard (1943) considered the formation as Middle Miocene to possibly Pliocene. In reports of the Petroleum Development (Palestine) Co. Ltd. the formation is regarded as Mio-Oligocene or Plio-Pleistocene, or simply post-Eocene.

In the Dead Sea region, Picard (1943) attributed a Miocene age to the lower and middle parts of the Sdom Formation.

Picard and Vroman (1950) introduced the term 'Foothill Series' for a Neogene terrestrial sequence of more than 700 m of clays, marls, sandy marls, sands, sandstones, and conglomerates, which encircle the foothill region of Mount Sdom. Later Bentor and Vroman (1951, 1954, 1957) attributed Miocene ages to both the lower part of the Foothill Formation at Mt. Sdom and Base Conglomerate of the Hatseva Formation in the Negev. Consequently, Bentor and Vroman (1960) correlated the Foothill Formation at Mt. Sdom with the Hatseva Formation of the northern Negev.

In south-eastern Galilee, the Yizre'el and Jordan-Arava

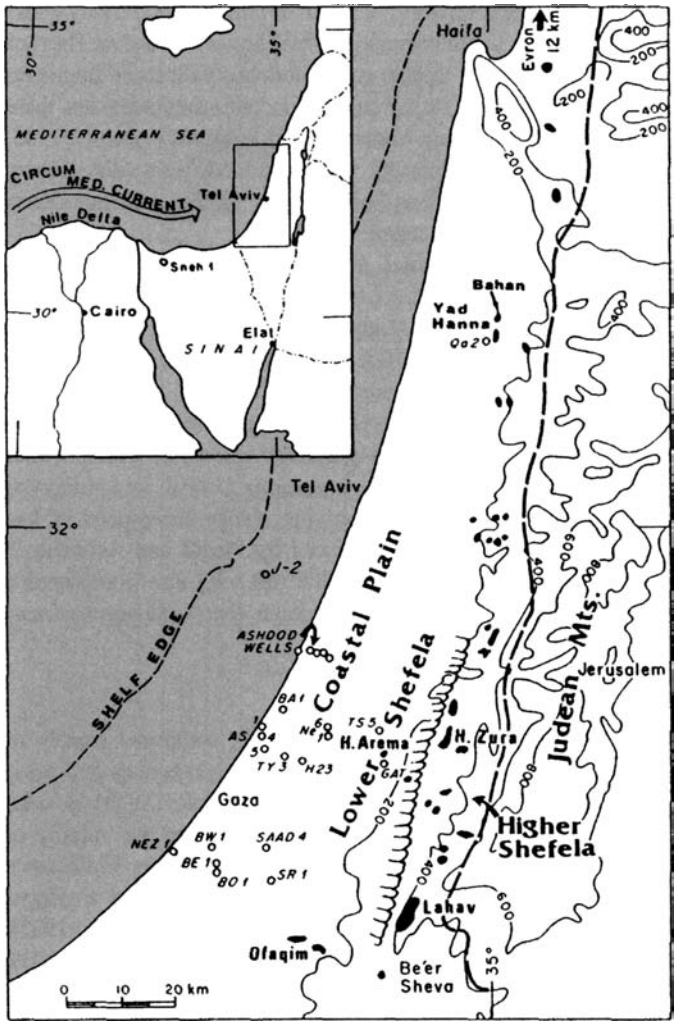


Figure 18H.2. Location map of the study area, showing physiographic units, topographic contours (in meters), outcrops of Miocene limestones (black patches), and drillholes (circles) (from Buchbinder, 1996, p. 334, Fig. 1). The thick dashed line marks the easternmost extension of the Miocene reef limestones. The jagged line marks the scarp separating the higher Shefela from the lower Shefela. Borehole abbreviations: AS - Ashqelon, BA - Barnea, BE - Beeri, BO - Beeri Old, BW Beeri West, H - Helez, J - Joshua, Ne - Negba, NEZ - Nezarim, SR - Sharsheret, TS - Tel Safit, TY - Talme Yafe, and Qa - Qaqun.

Valleys, as well as in the synclinal areas of the northern and central Negev, Picard (1943) identified the clastic series at Mount Herod, as the Middle-Upper Miocene 'Tiberias Series'. These beds, associated with marl and gypsum, contain fresh water fish remains (Avnimelech and Steinitz, 1951). The 'Tiberias Series' contains the Herod Formation in its lower, and the Poriya Formation in its middle and the Degania Formation in its upper part.

The name Poriya Formation (Bentor, 1960) designates the 'Brakish Series'. These brackish limestones, gypsiferous clays, and gypsum (now Bira Formation) include volcanic ash and tuffs. It gradually passes upward into the lacustrine Degania Formation.

Picard (1943) and Schulman (1957) described volcanics, widely distributed in eastern Galilee and the Yizre'el Valley as basaltic lava flows and tuffs, partly interfingering with lacustrine deposits. Avnimelech (1936) mentioned basalt components in Miocene conglomerates and tuff associated with Miocene marls in the central Shefela.

Pliocene:

Blanckenhorn and Oppenheim (1927) placed the soft chalks of Yagur (Yajur facies) into the Astian (Middle Pliocene). The faunal assemblage recorded by Picard (1928) includes: *Pecten flexuosus* Pol., *Pecten benedictus* Lmk., *Lucina* cf. *collumbella* Lmk., *Lucina* cf. *multilamellata, Lucina leucoma* Turt., *Elphidium* sp., *Gryphaea cochlear* Pol., *Leda pella* Linn., *Callistotapes vetulus* Basterot, *Tellina nitida* Poli, *Vernerupis irus irus* Linn., and *Trachicardium multicostatum* Brocchi. Blanckenhorn (1914) described from southeastern Galilee, along the western shore of the Sea of Galilee south of Tiberias. a predominantly calcareous sequence, also called

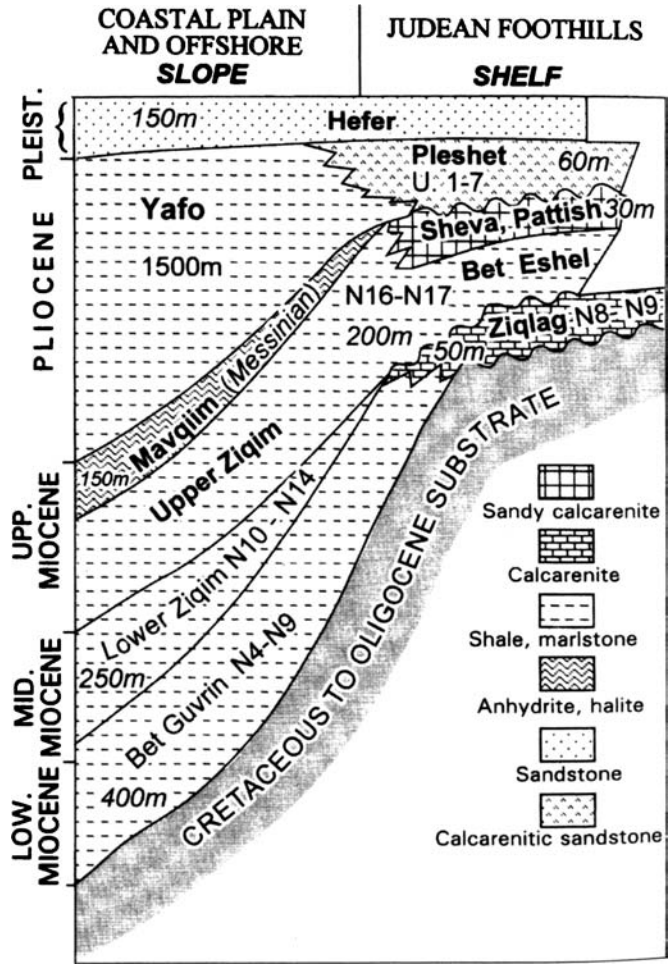


Figure 18H.3. A schematic E-W section across the Neogene shelf and slope showing lithostratigraphic units, N biozones and maximum thicknesses in m. (From Buchbinder and Zilberman, 1997, p.10, Fig. 4).

'Fresh Water Series', including the Main Oolite Series, Chalk Series and Hydrobia Series. Called the Degania Formation by Bentor (1960), from the nearby settlement of Degania in the Jordan Valley 10 km south of Tiberias, it designates a 130 m thick predominantly calcareous sequence that consists of three parts. A 35 m thick lower part composed of white or yellow limestone and marls, yields *Planorbis* sp., and *Hydrobia fraasi*. A middle part, 25 m thick, consists mainly of soft chalk. The 70 m thick upper part, also called the *Main Oolite Series*, is composed of hard, oolitic limestone passing into dense platy limestone, oolitic chalk, and some beds of conglomerate, Pyroclastic material, either ash or lapilli, occurs in various parts of the sequence. The unit either overlies conformably the Poriya Formation, or rests unconformably on basalt flows of Miocene age. It is unconformably overlain everywhere by tuffs or flood basalts of Pliocene age.

The name Degania Formation (now Gesher Formation) was given by Bentor (1946) to the 'Fresh Water Series' of Blanckenhorn (1914).

I. THE SAQIYE GROUP

The 'Sakiebeds' (Loewengart, 1927) were emended to Saqiye Group by Gvirtzman and. Reiss (1965). They consist of marly chalks, marls and bioclastic limestones that unconformably overlie the Avedat/Hashephela Groups (Gvirtzman, 1969a, b; Gvirtzman and Buchbinder, 1969a, b). The Saqiye Group is extensively developed only in western Hashephela where widely buried under the Coastal Plain and in the Beersheva embayment. Exposures are rare. In the central and eastern Hashephela, the group displays its marginal facies in scattered outcrops.

In most of Israel the post-Middle Eocene (Early Bartonian) uncomformity [P13] represents the boundary between the Avedat Group and the Saqiye Group, though in the Negev, the Late Eocene is still regarded as part of the Avedat Group.

The apparently mostly continuous Late Eocene-Quaternary marine sedimentation is found along a rather narrow belt in the Southern and Central Coastal Plain. These sediments represent the Saqiye Group, which in space and time are developed as follows.

1. Southern and Central Coastal Plain:

The apparently continuous Latest Eocene to Pleistocene marine sedimentation of the Saqiye Group encompasses up to 2500 m of marine sediments.

Late Eocene [P15]: The upper part of the Avedat Group passes laterally from the Negev into the more basinal facies of the Bet

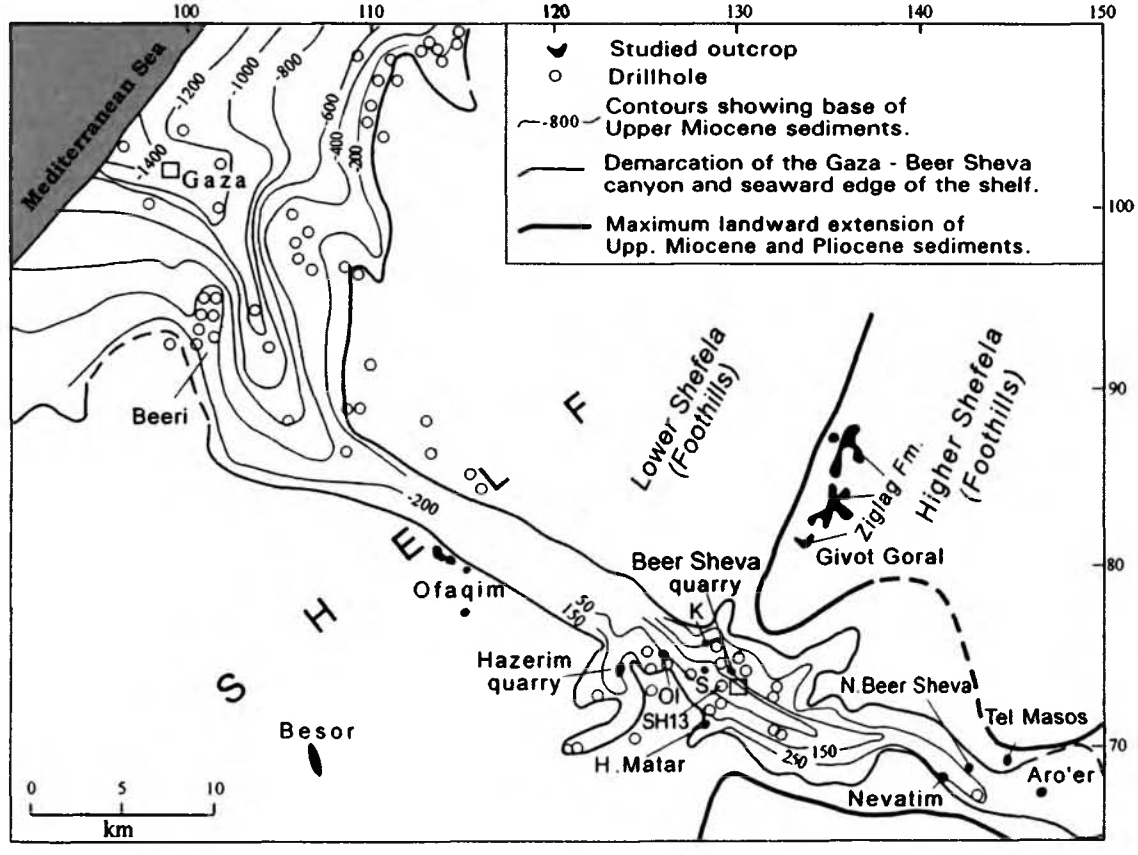


Figure 18H.4. The Gaza-Beer Sheva Canyon as expressed by contours at the base of the Upper Miocene sediments. (From Buchbinder and Zilberman, 1997, p. 11, Fig. 4).
Legend. K - Nahal Kovshim, Ol - Nahal Olim, S - Shaul Hamelekh.

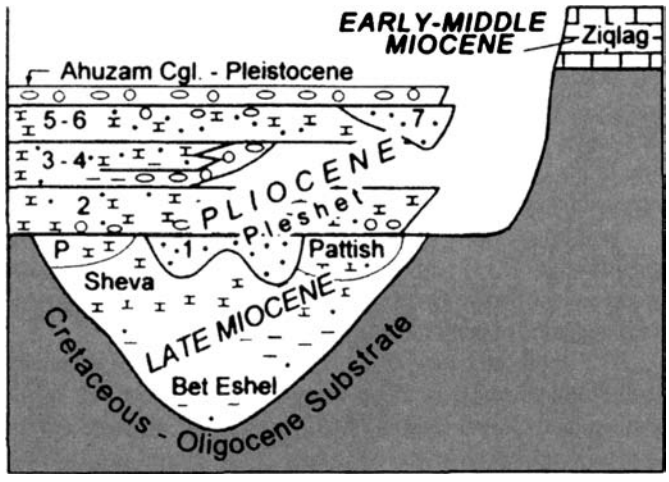


Figure 18H.5. Stratigraphic Scheme of Miocene and Pliocene sediments in the Beer Sheva area. (From Buchbinder and Zilberman, 1997, p.11, Fig. 5). Note that the Late Miocene sediments fill the canyon which postdates the early-Middle Miocene Ziqlag Formation. The Pliocene calcareous sandstone and **conglomerates** (Pleshet Formation) are subdivided into seven units.

Guvrin Formation of the Saqiye Group.

Early Oligocene (Rupelian) [P18-P21]: Chalks and limestones. The sedimentation of the marine Saqiye Group persisted and penetrated into the wide canyon of the Afiq-Beersheva Valley, an incision that dates back to the Early Oligocene [P19], creating the thalweg for the continental deposits of the Tiberias Group to the east. In the El Arish-Ashdod area the Bet Guvrin Formation is interwedged by the up to 600 m thick clastic Ashdod Formation. The Bet Guvrin Formation of the Coastal Plain and adjacent Shefela passes laterally into the shallow marine, reefoidal Lakhish Formation [P21]. A link between the Saqiye Group of the Shefela and the marine deposition of the Tiberias Group around the Sea of Galilee is assumed through the Yizre'el Valley. Regional uplift ended this phase. It generated a regional regression and emersion of most of the territory of Israel, widely destroying the Late Eocene-Early Oligocene sediments, and leaving only a few marine outcrops in the northern Negev, the Shefela (Lakhish-Gal'on, Ramleh) and the Sea of Galilee (En Gev).

Late Oligocene (Chattian) [P21-P22]: Marine chalk deposition persisted in the Coastal Plain of Israel only, However, marine ingressions penetrated during certain high-stands far into the Yizre'el Valley, where they interwedge the deltaic-fluviatile clastics of the Tiberias Group in the East. In the latest Oligocene, the Dead Sea Transform fault was initiated, the sinistral strike-slip along the Jordan-Gulf of Aqaba line of 105 km being the result of the opening of the Red Sea.

Miocene: The marine deposition persisted in the Coastal Plain of Israel and the Lower-Middle Miocene Bet Guvrin [N4-N9] and Ziqim [N10-N17] Formations. The Late Miocene (Messinian) evaporites of the Mavqiim Formation and their associated Afiq/Shiqma Formations close the Miocene. Clastics of the Gaza-Afridar Formations may occur at the Bet Guvrin-Ziqim boundary.

Pliocene: The Saqiye Group further consists of the marine Plio-Pleistocene Yafo Formation [N19-N23], which interfingers with the continental deposits of the Kurkar Group. Though the formations of the Saqiye Group are widely buried under the Coastal Plain and in the Beersheva Embayment, they are partly exposed in the foothills along the Shefela.

2. Shefela:

In the adjacent Shefela, the Saqiye Group is subdivided by end Burdigalian [limit N7-8], Middle Tortonian [N16] and Early Zanclian [N18] erosional unconformities. **(Figs. 18H.2 and 18H.3)**

The Neogene part of the Saqiye Group in the Shefela encompasses three subdivisions:

i) The Aquitanian-Langhian part of the Bet Guvrin Formation [N4-N9], passes laterally into the shallow marine Langhian-Early Serravalian Ziqlag Formation [N8-N9]; the latter being sealed by the pedogenetic and fluviatile interval of the Bet Nir Formation;

ii) The Middle-Late Miocene Ziqim Formation [N10-N17], Bet Eshel Formation [N16-N17], the shallow Sheva Formation and the fringing reef of the Pattish Formation, ending with the Messinian event, which is marked by the Mavqiim Formation and conglomerates of the Afiq/Shiqma Formations;

iii) The Plio-Pleistocene Yafo Formation [N19-N22] which interfingers laterally with the Pleistocene continental deposits of the Kurkar Group.

3. Afiq-Beersheva Valley:

The wide canyon, an incision that dates back to the Early Oligocene [P19], is the locus of marine penetrations of the Saqiye Group. The marine deposits interwedge the continental deposits of the Tiberias Group to the east. These fluviatile and lacustrine sediments fill the morphology generated by the mid-Oligocene regression and consist of the drainage products from the mountains and huge plateaus further to the southeast. In the Beersheva Embayment the Ziqlag, Bet Eshel, Sheva, Pattish, Mavqiim Formations and Afiq/Shiqma Members have been identified. An 'end of gulf' deposition with *Crassostrea gingensis* reaches 31°N, 35°E in the Dimona-Yeruham area, presumably during the Ziqlag ingression. **(Figs. 18H.4 and 18H.5).**

4. Med-Dead connection:

The Saqiye Group has twice penetrated into the Yizre'el Valley, north of the Carmel fracture, intermixing with the Tiberias Group by inundating portions of the then existing Rift Valley. The resulting Late Miocene (Tortonian) Bira and Zemah salt Formations are restricted to the area around the Sea of Galilee. The Messinian events severed the marine connection to the Rift. The Pliocene restoration of the Med-Dead Sea connection is again witnessed by carbonates and evaporates, consisting of the Gesher Formation and salt of the Sedom Formation. Alternatively it may be considered that the Gesher Formation is still part of the Tortonian.

Bet Guvrin Formation

Picard and Solomonica (1936) established the Bet Jibrin Series, later emended by Gvirtzman and Reiss (1965) to Bet Guvrin Formation. This 'Craie de Beit Jibrin' (Avnimelech, 1936) reaches about 50 m in the Lakhish area. Towards the west, the formation rapidly attains its greatest thickness. It was first described at Deir Nakhas along the old Bet-Guvrin-Hebron road.

The Bet Guvrin Formation consists of yellow brownish chalky marlstone, glauconitic in part, which in the Foothills region of Bet Guvrin appears as compact, unstratified, fine-grained chalky limestone, poor in fossils. The Late Eocene lower part of the Bet Guvrin Formation starts with a boulder conglomerate near Adorayim, unconformably overlying various older formations (Golik, 1960; Greitzer, 1960). In a few places fine bioclastic limestone lenses were found. The Beit Guvrin Formation crops out at the center of the Hashephela synclinorium, in the Lakhish-Gal'on area. It is also exposed in Nahal Gerar and in Nahal Shiqma near Tel Hesi.

The Beit Guvrin Formation is mostly found overlying the Eocene Maresha Formation. Its Oligocene part interfingers laterally with or is unconformably overlain by the Lakhish Formation. It is overlain by various younger formations as the Middle Miocene Ziqlag Formation or by the 'Kurkar' Group. Its age is Late Eocene-Miocene [P15-N9] (Reiss and Gvirtzman, 1966a).

Lakhish Formation Oligocene

Gvirtzman and Buchbinder (1967), established this unit near Tel Lakhish, for the 'Marine Oligocene' (Blake, 1928); the 'Tall Duweir Formation' (Daniel, 1959); the 'Zeita-Qubeiba Facies' or the 'Ramle Facies' (Picard and Solomonica, 1936); the 'Oligocene-Aquitanian' (Avnimelech, 1936); and Units 9 and 10, Oligocene (Greitzer, 1960).

The Lakhish Formation reaches up to 40 m in the type area and was subdivided into two members: The lower, Ramle Member is composed of chalky boulders of the underlying Zor'a and Bet Guvrin Formations in a marly-chalky matrix with abundant large foraminifera (*Operculina* spp. *Lepidocyclina* spp.) and various molluscal and echinoid bioclasts and calcareous algae. The upper Gal'on Member consists of hard, yellow, biosparites and biomicrites with the same fauna and bioclasts as in the Ramle Member. The Lakhish Formation is exposed in the Lakhish-Gal'on area, and near Ramle.

In the Lakhish area the Lakhish Formation unconformably overlies the Beit Guvrin Formation. Towards the north (Gal'on) and the west (Coastal Plain) the formation interfingers with the marlstones of the Beit Guvrin Formation. The Lakhish Formation is unconformably overlain by the Ziqlag and Beit Nir Formations. Age: Upper Eocene-Oligocene (Greitzer, 1960).

Ashdod Clastics

Cohen et al. (1987) recognized 350 m of conglomerates and sands in the Ashkelon-4 borehole, embedded in marl or chalk. In the Haruvit-1 borehole southwest of Gaza, over 600 m of sands and marl, and in Nahal Oz-1 borehole, next to Gaza, 250 m of conglomerate were found. The Ashdod Clastics interwedge the Bet Guvrin Formation These Oligocene hemipelagic sediments [P19-P20], interbedded by pebbles of Cretaceous limestones and dolostones, fill submarine canyons incised in the drowned shelf edge and slope of the early Oligocene Mediterranean margins [P19 zone] (Druckman et al., 1995).

Gaza Sands/Afridar Clastics Early Miocene

The Afridar conglomerate and shale in the Barnea-1 borehole (Cohen et al., 1987), and the Gaza sands in the Gaza-1 borehole, are identical Early Miocene clastic intercalations.

Ziqlag Formation Langhian

The term was coined by Gvirtzman and Reiss (1965) from the Ziqlag Hills, southern Hashephela (Gvirtzman and Buchbinder, 1969a). It stands for the 'Bir Khuweilfe Limestone' in reports of the Petroleum Development of Palestine Ltd. (1934-1947); the 'Helvetian' and 'Tortonian' of Blake (1935) and Picard and Solomonica (1936); the 'Vindobonian' of Avnimelech (1936); the 'El Juheir Limestone' of Daniel (1959), and 'Unit II (Miocene) of Greitzer (1960).

The Ziqlag Formation [N8-N9] is composed of up to 40 m of bioclastic limestones, coralline and algal reefs in the Ziqlag and Lahav hills. The level of the higher platform of the Ziqlag Formation is at the average high of 400-500 m (above present Mediterranean sea-level) and represents an important tectono-morphological marker. The lower platform of the Ziqlag Formation (at 120-150 m elevation) is coeval with that of the Bet Eshel and Sheva-Pattish [N16-N17] levels.

Scattered relict outcrops are widely distributed in the Hashephela region, from the Latrun area southwards down to the Beersheva Valley. The Ziqlag Formation unconformably overlies the Taqiye, Zor'a, Beit Guvrin, and Lakhish Formations.

Bet Nir Conglomerate post Langhian

Gvirtzman and Buchbinder (1967, 1969a) established the Beit Nir Conglomerate near the moshav of the same name, in the Hashephela region. It is synonymous with Unit 12 (Miocene) of Golik (1960) and Greitzer (1960). The 0-30 m thick polymict conglomerate is composed of pebbles of Judea limestones and dolomites, chalks of the Hashephela Group, flint of the Mishash Formation and the 'Adulam Member, and bioclastic limestones of the Ziqlag Formation. The conglomerate is strongly weathered and altered to nari. Only the flint pebbles are resistant to 'narization'. The fairly rounded pebbles are poorly sorted and diameters vary from a few millimeters up to 50 cm. The cement is marly or calcareous, but usually it is 'narified' and difficult to determine. In the Hashephela the Bet Nir Conglomerate forms the terrace left behind by the regression of the Ziqlag sea. Its age is therefore post-Langhian.

Ziqim Formation Middle-Late Miocene

Gvirtzman and Reiss (1965) established the Ziqim Formation [N10-N17] in the Ziqim-1 borehole, where its chalky marls and chalk reach over 350 m, subdivided into Serravaglian [N10-N14]

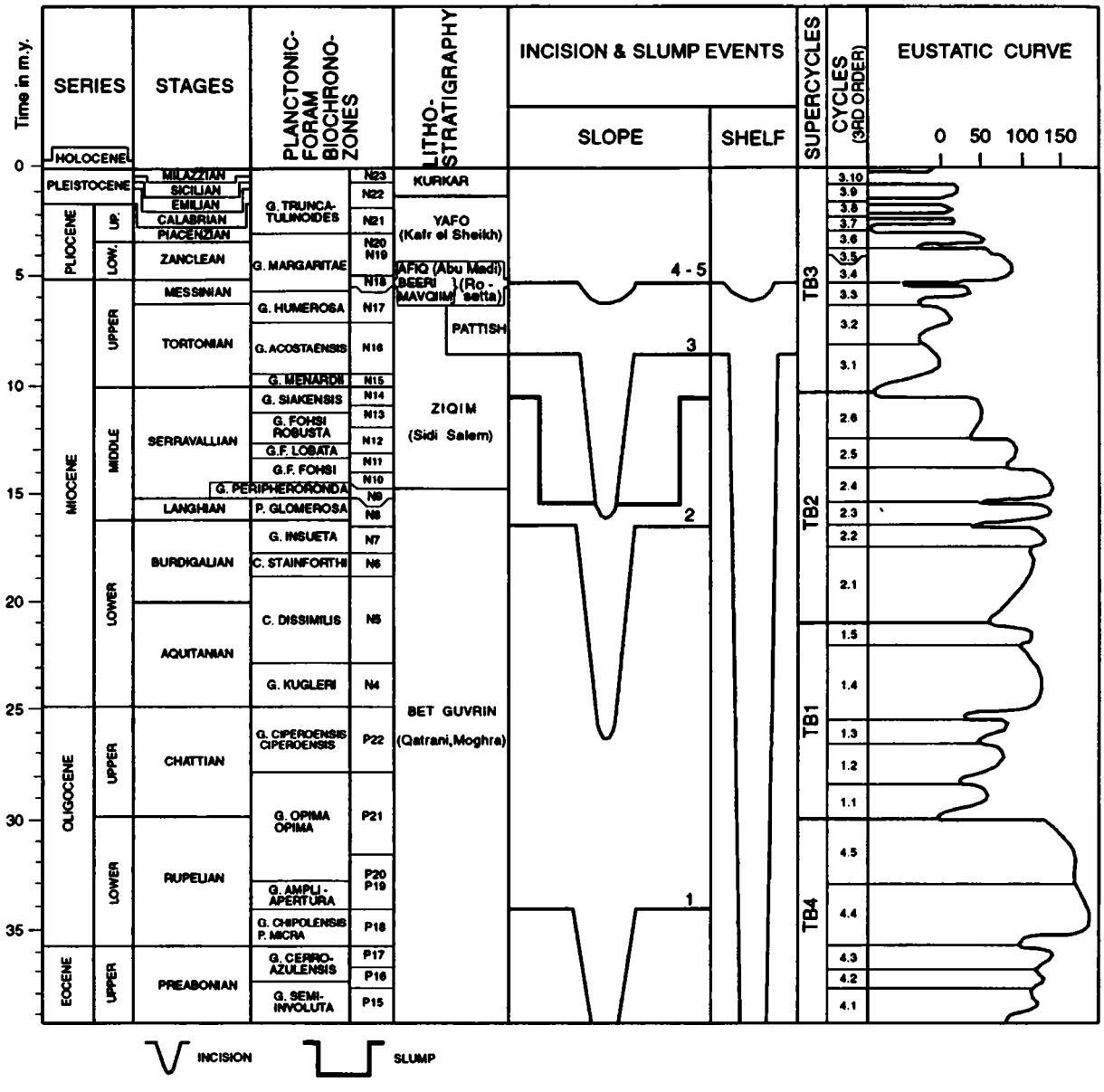


Figure 18H.6. Incision and slumping events recorded in the Afiq Canyon as related to Haq et al.'s (1988) biostratigraphy, chronostratigraphy, and eustatic curve. (From Druckman et al, 1995, p. 172, Fig. 4). The large-scale slumping event (box-shaped heavy line) took place in late Middle Miocene time. Note that the upstream (shelf) portion of the canyon was incised only in Late Miocene times (incision #3). The lithostratigraphic names in parenthesis refer to the equivalent formations in the Nile Delta (Egypt).

and Tortonian [N16-N17] subdivisions.

Bet Eshel Formation Upper Miocene

Established by Martinotti et al. (1978), after the canyon of the same name in the Beersheva area, the Bet Eshel Formation, a lateral deposition of the Upper Ziqim Formation, yields a fauna of the N16-N17 Zones. It represents a Late Miocene filling of the Beersheva Canyon cut into Late Cretaceous-Eocene strata. It consists of 200 m thick marls and some conglomerates, passing upwards into the Sheva-Pattish Formation. The shales and calcarenite of the Bet Eshel Formation subdivide into a 41 m thick lower part that contains Campanian-Maastrichtian elements and a 144 m thick upper part with Paleogene elements.

Pattish Formation Tortonian [N16-N17]

This formation was established by Buchbinder (1996) for clinoform beds of dolomitized rhodoliths alternating with marlstones and rare colonies of poritid corals. Once considered to

belong to the Langhian Ziqlag Formation, but younger in age, it is therefore part of the Tortonian.

Sheva Formation Tortonian

Established by Buchbinder and Gvirtzman (1969) in the Beersheva Great Quarry, the Sheva Formation is characterized by the appearance of abundant molluscan shell fragments and coarse bioclasts. The age of the Sheva Formation is Tortonian [N16-N17].

Mavqiim Formation Messinian (Late Miocene)

Gvirtzman and Buchbinder (1967) established the Mavqiim Formation. The subdivision into members comprises the Anhydrite Member (Gvirtzman and Reiss, 1966) at base, covered by the Afiq Member (Gvirtzman, 1966). The evaporites of the Mavqiim Formation [N17-N18], mostly anhydrite or gypsum, are synonymous with the Beeri Gypsum. In their stratigraphic table, Flexer et al. (1981) use the term Shiqma Member, which is equivalent to the Afiq Member of the Mavqiim Formation. The Afiq fluvio-lacustrine event (*lago mare*), consisting of sandstone and conglomerate, that follows the evaporitic and carbonate deposition of the Messinian Mavqiim Formation (Beeri Gypsum), can well be defined in the Afiq borehole, located in the canyon-like feature of the same name. The thalweg of the latter was successively cut in the Oligocene and Miocene channeling phases within a substratum of Eocene to Lower Cretaceous strata (Druckman et al., 1995). **Fig. 18H.6.**

National Park Volcanics Neogene

Grader and Gvirtzman (1961) described the Late Miocene National Park Volcanics. These occur mainly in the subsurface of the Coastal Plain, interwedged between the Mavqiim and Yafo Formations. Only a few relict outcrops occur in the Hulda-Yesodot area of the western Hashephela (Gvirtzman and Buchbinder, 1969a; Gvirtzman, 1969a, b). The National Park Volcanics are found in the Bat Yam-1 borehole, where they reach 300 m in thickness, and in the NP-1 borehole near Ramat Gan (Tel Aviv). They are Miocene-Pliocene (4.6-8.4Ma).

Yafo Formation Pliocene-Pleistocene

The Yafo Formaiton was established by Gvirtzman and Reiss (1965) at the Jaffa-1 borehole. It is part of the 'Sakiebeds' of Loewengart (1927); the 'Marne de Mansura, de Ouadi Malih et Tell Malat' (Avnimelech, 1936); the 'Plaisancian' (Picard, 1943); or the 'Niana Marls', 'Ramle Marls', and 'Mansura Marl Formation' (Petroleum Development of Palestine reports 1937-1947 - in Daniel, 1959); the 'Sharon Formation' (Issar, 1961); and the 'Ramat Gan Formation', partim (Grader and Gvirtzman, 1961). The Yafo Formation consists of typical gray, pyritic marls in the drill holes of the Coastal Plain. They are oxidized in outcrop into limonitic marls of yellow hue. Detailed descriptions of the outcrops and the stratigraphic relationships are given in Gvirtzman and Buchbinder (1969a). Only a few relict outcrops occur in Hashephela, near Yesodot-Hulda south of Beit Shemesh, near Har'el, and north of Gat. The Yafo Formation unconformably overlies the Shiqma, Afiq, and Mavqiim Formations in Hashephela. It interfingers and is overlain mainly by the Pleshet Formation of the Kurkar Group. The 1000 m thick formation found in the Yafo-1 borehole, reaches a thickness up to 1500 m in the western Hashephela (Gvirtzman, 1969a, b). Its age is Pliocene-Pleistocene [N19-N22].

II. THE TIBERIAS GROUP

Since the end of the Eocene, when the Tethys had retreated from the area now occupied by the endoreic Jordan Rift Valley, the Oligocene cycle, transgressed into an intricate drainage system formed toward the retreating seas at the transition from the Eocene. The extent of the Oligocene transgression is manifested by marine sediments on the eastern shore of Lake Kinneret (Fiq and Sussita) and further south, and in the Dead Sea area by the filling up of channels with fluviatile and lacustrine deposits.

Fossil-bearing Oligocene sediments are known from two localities in the Jordan Rift Valley: several outcrops at the eastern escarpment, near En Gev on the Lake Kinneret shore (Michelson, 1972), near Khirbet Shuna some 10 km south of the lake, and in Wadi Taiyiba, another 10 km farther south (Bender, 1974, p. 90). The other occurrence is only known from the subsurface, namely the deepest section, almost 100 m thick, of the Sedom Deep-1 borehole, drilled at the southern end of the Dead Sea (Horowitz, 1996).

During its **pre-rift** phase, the sedimentation within the Jordan-Dead Sea-Arava depression was represented by fluviatile and lacustrine deposits of the **Tiberias Group** in the area of the Sea of Galilee, Jordan Valley, Dead Sea, Arava and Negev, interfingered by Middle Miocene marine ingression, as in the Beersheva Canyon.

The Late Oligocene-end Middle Miocene pre-rift formations are somewhat thicker within the rift as compared with adjoining areas, though not due to any conspicuous faulting. They fill the morphology generated by the end-Early Oligocene regression, consisting of the drainage-products from the mountains and huge plateaus further to the southeast (Horowitz, *op. cit.*).

The Late Oligocene continental deposits of the Tiberias Group to the east, interwedge the marine deposits of the Saqiye Group to the west. These sediments consist of the fluviatile and lacustrine En Gev Formation in the area of the Sea of Galilee, and of the Zefa Formation in the Dead Sea-Arava and Negev area (Horowitz, 1979). The latter, though devoid of characteristic fossils, occurs outside the Rift and is intimately connected with one of its ancient drainage systems, located in the Ef'e syncline, west of the northern Arava (Shahar, 1973). Other occurrences of fossiliferous Oligocene beds are known from the Kingdom of Jordan from several boreholes and from outcrops in Wadi Sirhan (Wetzel and Morton, 1959; Daniel, 1963), quite far to the east.

The sequence near En Gev, described in detail by Michelson (1972), comprises three formations: Fiq, Susita and En Gev Sands. They are only known from limited outcrops east of Lake Kinneret, from the vicinity of En Gev down to some 20 km south of the lake, where the Taiyiba Beds and the lower part of the Usdom Group (Wetzel and Morton, 1959) seem to correlate with the Fiq and Susita Formations. The sequence unconformably overlies middle and upper Eocene limestones and chalks of the Zor'a Formation ('Sar'a Chalk and Flint Formation' in Jordan). As a result of the regression

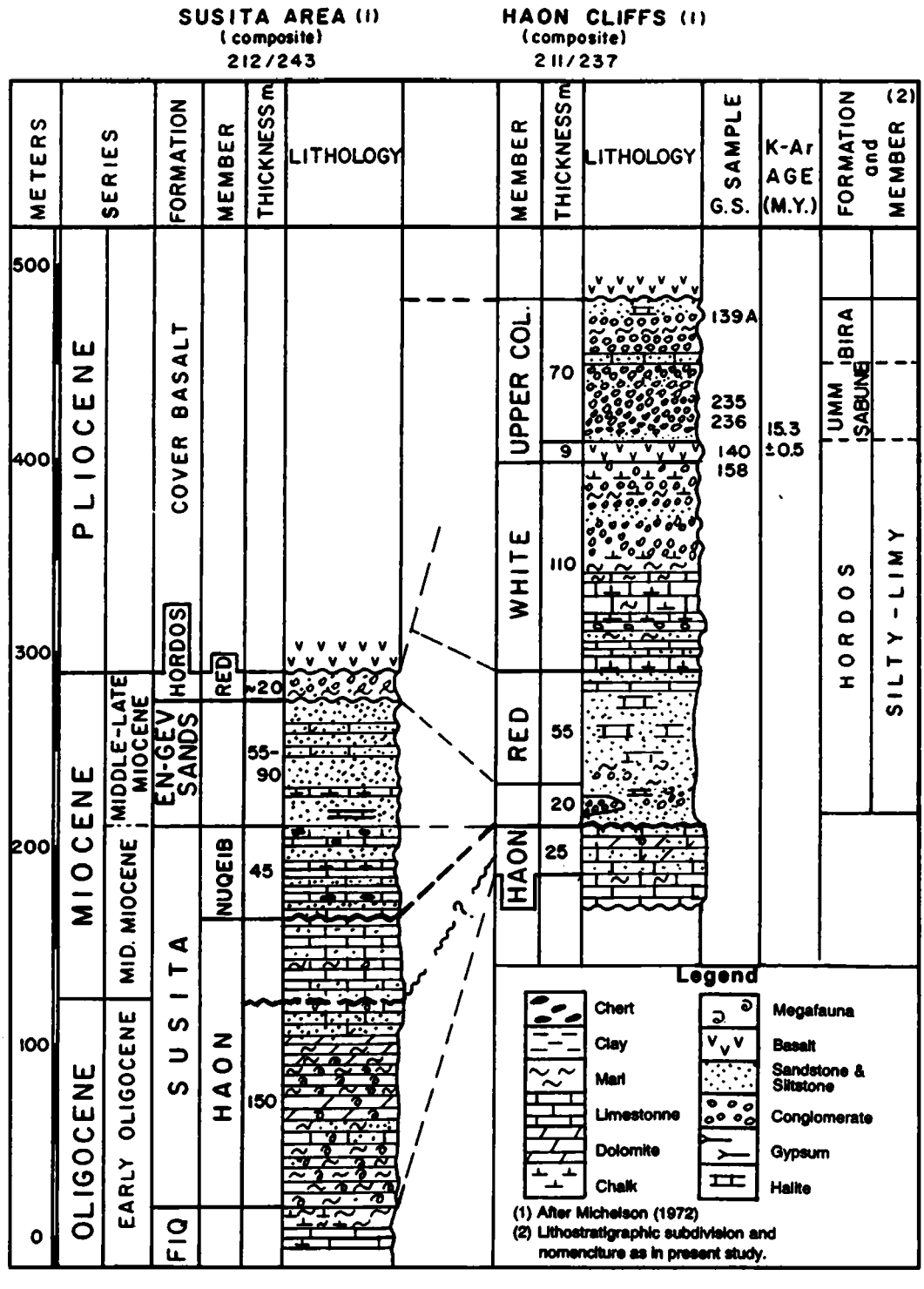


Figure 18H.7. Stratigraphy of the Susita area and Ha'on Cliffs (after Shaliv, 1991, Fig. 10, p. 20).

and renewed erosion at the late Oligocene, in approximately the same channels as before, the sequence is again unconformably overlain by the Miocene complex of transgressions, characterized by renewed filling up of these channels with mainly fluviatile and lacustrine sediments. The process rather abruptly ceased some time near the end of the Miocene, by initiation of the Erythrean faulting. Slight unconformities, both erosional and angular, are also quite common within the sequence.

The Late Oligocene-Early Miocene continental sedimentation, mainly of fluviatile and lacustrine nature, and evaporitic deposits of the Tiberias Group (= Kefar Giladi Group, Flexer et al., 1981a, b) are widespread in the Negev and in the Jordan-Dead Sea-Arava depression. The Early-Middle Miocene part of the group encompasses the Herod (or Hordos) Formation from Lake Kinneret to Wadi Fari'a and the Hazeva Formation from the southern Dead Sea to the boundary between the northern and southern Arava. The two domains are separated by a northeast trending structural high, crossing the Rift Valley some 60 km north of the Dead Sea (Bender, 1974). The Hazeva Formation is intercalated by the marine ingression of the Saqiye Group into the Beersheva Embayement, reaching as far east as Yeroham and Dimona in the northern central Negev, where 'end of gulf' oysters interwedge the sands of the Gidron Member (Hazeva Formation). These are the only true marine Miocene sediments, intercalating with the continental strata (Goldsmith et al., 1988). Westward, the marine sediments increase their share in the sequence. It is possible that the sea may have reached further inland in some areas *e.g.* the area now occupied by the Jordan Rift Valley, but none of its deposits remained due to erosion by the regressing sea, which followed the peak of transgression.

Middle Miocene sediments and volcanics are very abundant in the Jordan Rift Valley, extending over wide areas even outside its limits, but with somewhat lesser thicknesses. These are chiefly of fluviatile or fluvio-lacustrine origin, with the subsiding rift region acting as a series of intermediate basins, filled up with mainly clastic sediments. The marine regression during the Oligocene-Miocene boundary caused renewed incision of the channels leading to the sea, removing much of the Oligocene sediments. Sedimentation and filling up of these channels was initiated by the Miocene rise in sea level, which raised the erosion base level and lowered the energy of rivers. During the maximum of the Miocene transgression, as in the Oligocene, the energy of transporting agents was considerably diminished, so that lakes were formed in most of the inland basins.

The end of the Tiberias Group is related to the onset of the Erythrean faulting. As such the Top Conglomerate members of the Hazeva Formation are conceptually coeval with the base of the Dead Sea Group.

1. Jordan Valley-Lake Kinneret (Sea of Galilee):

Fiq Formation Early Oligocene

Michelson (1972) described the 45 m thick unit in Wadi Fiq (Nahal En Gev), on a hill north of Susita, near En Gev on the eastern shore of Lake Kinneret.

The Fiq Formation chiefly consists of detrital limestones that form a prominent ledge in the landscape. It consists of pel-biosparite, quite rich in foraminifers, with some chalk, marly limestones, and marl. The latter are slightly glauconitic, whitish-yellowish. The lower part of the Fiq is very rich in glauconite, up to 30% of the rock, diminishing upward. Burrows occur at base, where also large concentrations of barite occur. Burrows are occasionally present also in the upper part of the sequence, which is more chalky, containing some flint nodules.

The thickness at the type section is 45 m, and is usually maintained wherever this unit crops out. The base of the Fiq Formation overlies a regional unconformity developed on the Eocene Maresha Formation, and is quite significant in the landscape due to a typical light brown-greenish cliff of detrital limestone, standing in contrast to the soft underlying chalk. The upper contact is much less definitive, and the Fiq grades into the overlying Susita Formation rather conformably. There is a typical horizon rich in Pecten shells at the transition, which forms the base of the overlying Susita Formation. The unconformity plane at the base of the Fiq is wavy and casts filling burrows are common, as well as barite concretions and glauconite grains.

The typical fossils of the Fiq Formation consist of fragments of large benthonic foraminifera, such as *Discocyclina, Lepidocyclina, Nummulites*, Rotaliids, together with *Globigerina* (Lipson, 1971). Planktonic globigerinids become more frequent toward the middle part, but upward the benthonic elements again prevail. One of the more interesting components of the faunal assemblage in the Fiq Formation is *Austrotrillina*, a foraminifer not known from the Mediterranean, however very common in the Indian Ocean domain. Some ostracods and Lithothamnion algae are also found, as well as mollusks. The environment of deposition is littoral-neritic. The age, assigned by *Casssigerinella chipolensis* and *Globanomalina micra* at the base is early Oligocene. The planktonic globigerinids of the middle part led Lipson to assign this unit to the P19 Zone of Blow (1969). The Fiq Formation is only exposed over a very limited area in the En Gev-Ha'On region, approximately the southern half of Lake Kinneret eastern shore, somewhat more than 10 km long. The Fiq Formation extends into Jordan, where it is described as Taiyiba Beds (Horowitz, in Lexique 2001). These Tayebe beds (Nasr and Medaisco, 1947, in Daniel, 1963) are exposed at Wadi Taiyiba, some 20 km south of Lake Kinneret. They unconformably cover an erosional relief within the Eocene Chalk and Flint, and are overlain, again unconformably by sands of the Herod Formation. Deposited by a sea connected to the Mediterranean, not the Indian Ocean as the Wadi Sirhan sequence, the occurrences of *Austrotrillina* in the En Gev suite seem to corroborate Daniel's assumption of the transgression of the middle Oligocene sea from the southeast. Foraminifera include *Textularia, Uvigerina* and *Operculina*; and bivalves are *Pecten, Chlamis* (*Aequipecten*) *judaica* and oysters, accompanied by echinoids, Bryozoa, charophytes and Cichlid fish teeth (Bender, 1974).

Sussita Formation Early Oligocene.

Golani (1962) established the 'Susita Conglomerate', emended by Michelson (1972). **(Fig. 18H.7).**

The Susita Formation, near the archaeological site of Susita, conformably overlies the Fiq Formation, commencing with a 3-10 m thick marly horizon, particularly rich in Pecten shells, always appearing as a guide horizon at the base of this unit. The Susita Formation is unconformably overlain by the En Gev Sands, over a gentle erosional relief, occasionally with slight angular contact. In places where the En Gev Sands are missing, either due to non-deposition or erosion, the Herod Formation unconformably overlies

the Susita Formation.

The distribution of the Susita Formation extends to the same localities as the underlying Fiq Formation. At Nuqeh, the Sussita Formation attains 145 m, decreasing to the southeast of Lake Kinneret.

The Susita Formation comprises fossiliferous yellow marls and marly limestones, greenish sugary dolomite containing glauconite and fossils, some lumachel horizons and detritic sandy or bioclastic limestones, some quartzolite, flint and quartzite concretions, some chalky white limestones and yellowish quartz sands. The formation subdivides into two members, the lower Ha'On and the upper Nuqeb Member, named after settlements in the area. Lumachel, dolomites and marls characterize the Ha'On Member, forming small cliffs in the landscape. Detritic sandy limestones with thin layers of quartzolite and sands typify the overlying Nuqeb Member. A slight angular unconformity, 5-6°, separates the two members.

Fauna: Typical fossils include foraminifers such as *Archaias, Austrotrillina, Operculina*, miliolids and others, indicating an Oligocene age with clear affinity to the Indian Ocean province. Abundant planktonic foraminifera indicating the same age are *Globigerina ampliapertura* (Lipson, 1971). Megafossils include bryozoa, corals, echinids, gastropods such as *Turitella, Cerithium, Bithium* and *Conus*. Bivalves are plentiful, including *Pecten, Cardium, Arca, Lucina*, oysters and others. Lithothamnion and other unidentified algae are common.

According to Michelson (1972), the age of the Susita Formation is Oligocene to early Miocene. It seems however that the foraminifera (Lipson, 1971) justify an Oligocene age for both the Fiq and Susita Formations.

The environment of deposition of the Susita sediments is littoral-neritic, however mudcracks that were noticed in the upper part of Nuqeb Member indicate a coastal environment which occasionally dried up.

Correlation: At Wadi Taiyiba, the lowermost 49 m of the Usdom Group (Wetzel and Morton, 1959) seem to correlate with the Susita Formation. These are composed of 38 m of white-yellowish sands and fine-grained, hard calcareous sandstones containing oysters and reworked(?) foraminifers. Occasional Eocene limestone pebbles occur at the base, which rests unconformably over the Taiyiba Beds. The upper 11 m comprise hard, white and pink sandy limestone, with oysters and ostracods, overlain unconformably by the Herod Formation. [A.H.]

En Gev Sands Late Oligocene

Established by Golani (1962) as the 'En Gev Sandstone', it was emended by Michelson (1972). The type section of the En Gev Sands is in the vicinity of the settlement of En Gev, on a hill south of Susita. Golani (1962) had included the En Gev Sands in the overlying Herod Formation. Michelson (1972), following a much more detailed study, had shown the two to be separate units, considerably differing from one another. The En Gev Sands overlie unconformably the Nuqeb Member of the Susita Formation. The unit is unconformably overlain by the Herod Formation or by the Lower Basalt. Both unconformities are erosional, occasionally slightly angular. The En Gev Sands are sporadically exposed, between En Gev and Ha'On, east of Lake Kinneret, with a single small occurrence some 3 km north of En Gev. The thickness is 80 m at the type section, where the base is not exposed. Michelson (1972) estimates the maximum thickness as some 90 m.

The Sands comprise principally yellow quartz grains, unconsolidated or slightly cemented by carbonate, with thin laminar chalky or marly limestone horizons, 0.5-1.5 m thick, which may occasionally contain some quartz grains. Most of the sands are fine-grained, some 15-25% are medium, sometimes containing carbonate and glauconite particles.

The Sands are sterile of any fossils, so the problem of both their exact age and environment of deposition remains a matter of speculation. Michelson (1972) tends to regard the sand as of either fluviatile or lacustrine origin. It seems however that at least the limestone horizons were laid down in a shallow lake or a near shore lagoon. Granulometric analyses of the En Gev Sands led Giveon (1984) to suggest a continental alluvial fan as the principal environment of deposition, with occasional occurrences of shallow seasonal lakes and playas, under arid or semi-arid climates.

Traditionally the En Gev Sands were thought to be a part of the Miocene system, since sandstones are the most common sediment type in many inland Miocene formations (Horowitz, 1979). This led Golani to include them within the Herod. Michelson considered them as an independent Miocene unit. Another reason lies in the fauna of the underlying Susita Formation, most of the megafauna and benthonic foraminifera ranging through into the Miocene. Thus it was usually referred to as 'Oligo-Miocene' (Lipson, 1971; Michelson, 1972). Any overlying unit would thus logically be Miocene. However, apart from the two being sandstone formations, the En Gev Sands differ significantly from the Herod Formation. The nature of the En Gev Sands should be regarded as the final stage of the Oligocene transgressive cycle, that precedes the Late Oligocene regression (Horowitz, Lexique 2001).

Hordos (Herod) Formation Miocene
(Fig. 18H.8)

The name of the formation is derived from Mount Hordus (Herod, Mount Berenice) 1.5 km south of Tiberias. It was originally named 'Herod', which is the English name for this king, from the Latin 'Hordus' and Hebrew 'Hordos'. First mentioned by Blake (1928), the unit forms the lower part of the Tiberias Series, as defined by Picard (1943). The Herod Formation (Bentor, 1946) includes for Schulman and Rosenthal (1968) the lower part of the Beida Formation of Roffe and Raffety (1965). Michelson (1972) identified the Hordos Formation east of Lake Kinneret and Shaliv (1991) added several outcrops of the central Jordan Valley into the Hordos Formation. Shaliv (1991) also proposed a reference section west of Tiberias hot springs, being the thickest known sequence, interbedded with six basalt flows which enabled radiometric dating.

At base a 10 m thick 'Lower Conglomerate Member' is built up of local components, usually chalk pebbles, overlying with erosional and slight angular unconformity chalks of the Mount Scopus

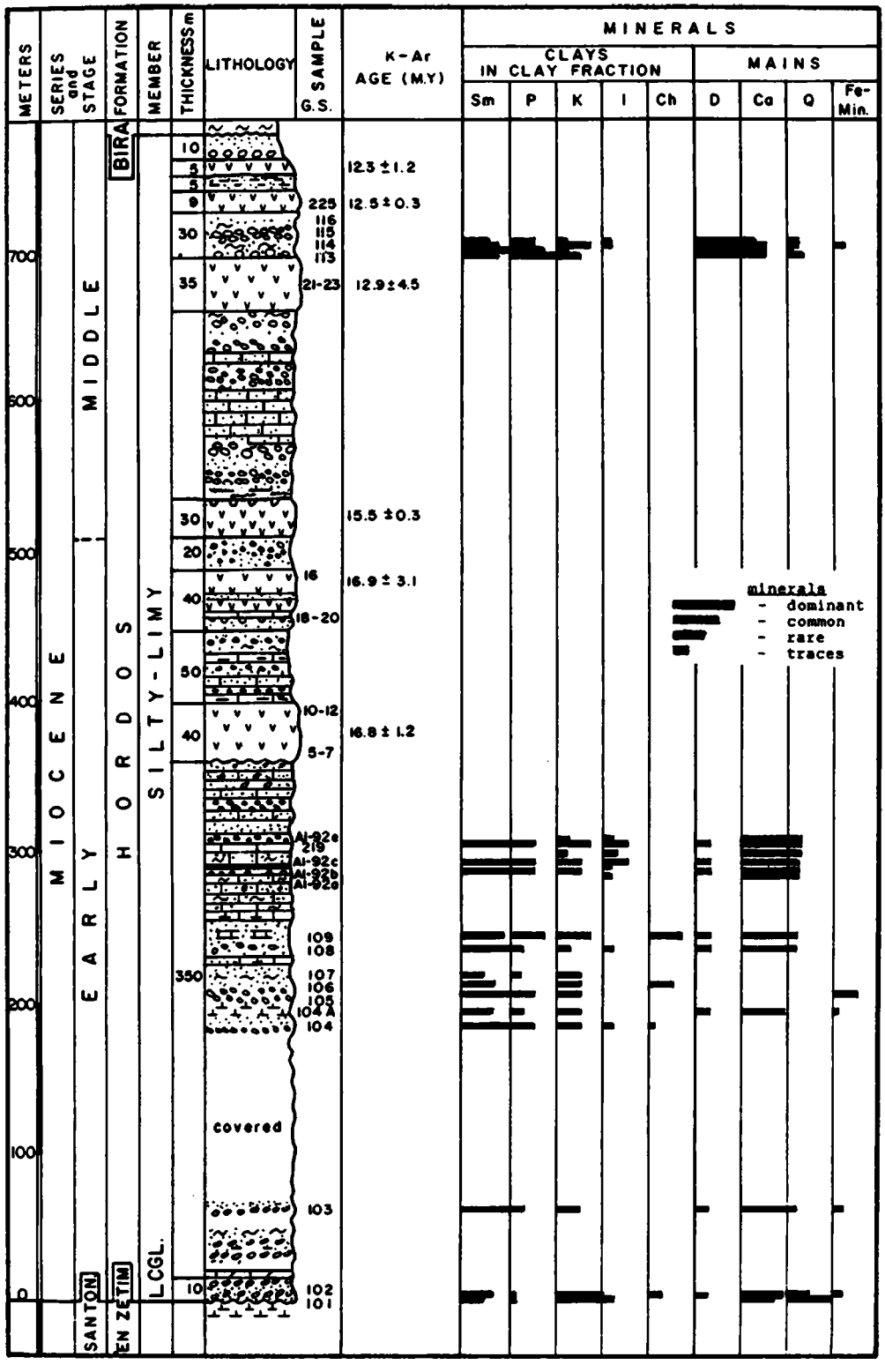


Figure 18H.8. Stratigraphy and Mineralogy of the Hordos (Herod) Formation (after Shaliv, 1991, Fig. 9, p.15).

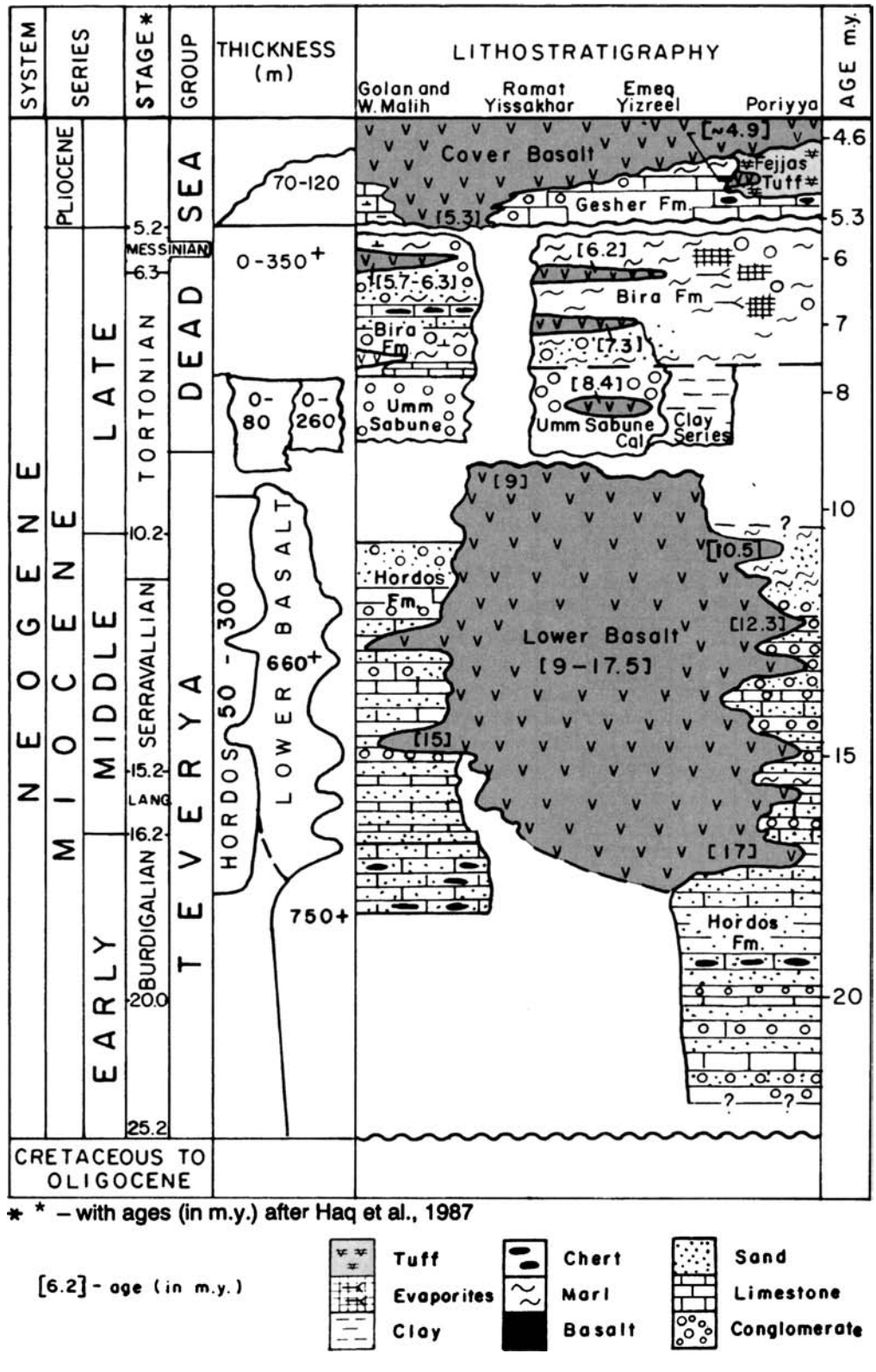


Figure 18H.9. Stratigraphic relations between Lower Basalt (9-17.5 Ma), Intermediary Basalts (8.4, 7.3 and 6.2 Ma) and Cover Basalt (5.3-4.9 Ma) and their 'host' formations (after Shaliv, 1991, p. 13, Fig. 7).

Group. Above the 'Silty-Limy' or 'Lacustrine' Member consist of alternations of reddish calcareous sands and silts, with lenses and layers of coarse and fine, very well cemented conglomerates, and horizons of hard limestones. The fine clastics and limestones are well-bedded, usually platy. The pebbles are mostly limestone and chalk, occasionally flint, very poorly sorted, 5-50 cm across. The sequence is interfingered by six basalt flows, the lowest of which overlies an irregular erosional relief of the underlying sediments. The pebbles above the lower basalt flows are from carbonate rocks of the Judea Group and weathered basalts, poorly sorted, medium rounded, 2-40 cm across. It seems that the roundness and sorting indicate a close by source for the pebbles, however somewhat more remote than the provenance of the base conglomerate components. Above the third and fourth basalt flows, the lower parts of the conglomerates are made solely of basalt pebbles. Resistant benches, up to five meters high, occur between the basalt flows, made of very well-cemented coarse conglomerates, with intercalations of carbonate silts bearing small pebbles, red clays and yellowish limestone. The pebbles building the upper benches are mainly derived from Eocene limestones.

South of the reference section basalt intercalations become considerably thicker, until the Lower Basalt completely replaces the Herod Formation at the Yavne'el escarpment. In several outcrops and boreholes, similar sediments of various thickness interfinger with dated Lower Basalt flows and can be attributed to the Herod Formation (Shaliv, 1991).

Contacts: The base is only exposed in the uplifted block of Mount Hordus near Tiberias, where it can be seen unconformably overlying Senonian chalk. The Herod Formation also unconformably overlies a variety of older rock units, tilted and eroded prior to its deposition (Schulman, 1962; Mimran, 1984). West of Lake Kinneret and the Jordan River, it mostly overlies late Cretaceous rocks, except to the south, where the Eocene Zor'a Formation underlies. Eastward, the Herod overlies late Cretaceous, Eocene and Oligocene formations, such as the Susita Formation or the En Gev Sands, with an angular unconformity. West of the Jordan River, the Cover Basalt, Umm Sabune Conglomerate, Bira and Gesher Formations cover or truncate the Herod Formation.

Distribution: The Herod Formation is known from outcrops and boreholes in the central Jordan Valley up to approximately midway along both sides of Lake Kinneret, (Michelson, 1972; Shaliv, 1991). South of Bet She'an Valley, in the Marma Feiyad-Wadi el-Malih region, Roffe and Raffety (1965) described the Beida Formation. Its lower part is correlated with the Herod (Schulman and Rosenthal, 1968) and the sequence was subdivided (Shaliv et al., 1988) in the same manner as near Tiberias, with the addition of a capping 'Upper Conglomerate', overlying the lower part with angular unconformity. Reconsidering, Shaliv (1991) attributed this unit to the overlying Umm Sabune Conglomerate. This brings us to the controversial opinions that have been raised about a 100 m thick sequence of conglomerates at the northwestern edge of Lake Kinneret, assigned by Saltzman (1964) to the Herod Formation. This sequence comprises, in addition to the usual late Cretaceous and Eocene components, also Jurassic and early Cretaceous pebbles, indicating provenance of at least some of the gravel from the north, perhaps Mount Hermon. Shaliv (1991) regards this sequence as a part of the Umm Sabune Conglomerate. Kafri (1997), who assigned various outcrops in Galilee to the Herod Formation, admits these to be probably closer in their stratigraphic position to the Umm Sabune Conglomerate (U. Kafri, Geological Survey of Israel, 1998, pers. comm.).

In Wadi Taiyiba, overlying unconformably Oligocene sediments, over 100 m of marls with fine gravel was described by Wetzel and Morton (1959). They are topped by thick brick red to pink conglomerates, some marl, flint and Eocene limestone pebbles, containing some glauconite and reworked microfossils, with no volcanics, including a bed of lacustrine sandy limestone in the middle of the sequence. This sequence was considered part of the Usdom Group (Daniel, 1963). Other outcrops occur along the eastern flank of the Jordan Valley, down to the area opposite Marma Feiyad (Bartov, 1994, Map).

Thickness: East of Lake Kinneret, Michelson (1972) reports a thickness of 242 m and west of Lake Kinneret, Shaliv (1991) reports more than 750 m. Since the top is always truncated, the original thickness must have even been larger. It is overlain either by the Gesher Formation or by flows of the Cover Basalt.

Environment of deposition: The Hordos Formation is a fluvio-lacustrine sequence that contains, unfortunately yet undetermined, fresh water mollusks (Avnimelech, 1937).

Age: The Hordos Formation is interwedged and covered by the Lower Basalt (9-17.5 Ma), conferring it a Early-Middle Miocene age. **(Fig. 18H.9).** The only fossils found in the Herod Formation are pollen grains, quite abundant in borehole samples. [A.H.].

2) Negev-Arava:

Zefa Formation Oligocene
(Fig. 18H.10)

Shahar (1973) defined the 'Zefa Member', emended by Horowitz (2001), as the lowermost member of the Hazeva Formation. Considering its unique nature, different lithology, and paleogeographic significance, it is suggested to regard it as an independent formation. It is named after Nahal (Wadi) Zefa (Hebrew for viper), where the type section is located. It is a tributary of Nahal Ef'e (Hebrew for another kind of viper), which drains the Rotem Valley through Nahal Heimar to the southern end of the Dead Sea, some 20 km distant.

The Zefa Formation is known from the Ef'e syncline, where it covers an area of some 2 km², and attains a thickness of up to 18 m. It unconformably overlies the Ghareb Formation (Late Cretaceous) and is in turn unconformably overlain by the Shahaq Member, the lowermost member of the Miocene Hazeva Formation, as defined by Sneh (1967, 1981). Both the underlying and overlying unconformities are erosional. A totally different concept has been proposed by Calvo et al. (1997), using the name Zefa for the unit at the base of the upper division of the Hazeva Formation. He disregards the stratigraphic relations at the type locality, as described by Shahar (1973).

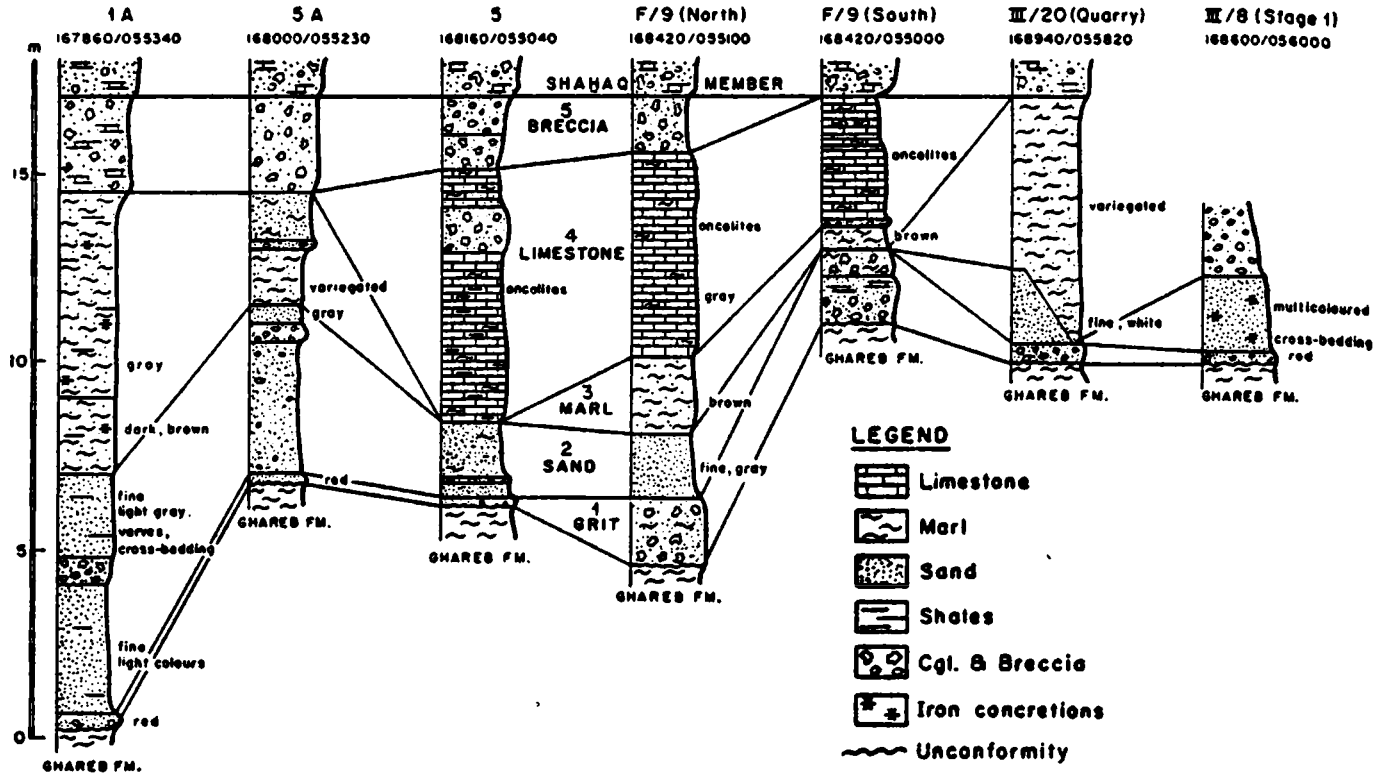


Figure 18H.10. Sections in the Zefa Formation in the Ef'e area (after Shahar, 1973, Fig. 3, p. 35).

The base of the Zefa Formation comprises coarse grit, gravel and breccia, which grade upward to sandy marls, oncolite-rich limestones, and back to clastics, similar in nature to those at the base. The base unit of coarse-grained grit is up to 2.5 m thick, reddish-black due to an abundance of iron oxides. Most of the pebbles are made of flint, with some of limestone and chalk, of Maastrichtian or Eocene age. The pebbles, which are more abundant at the base, are well-rounded, varying in size from a few up to 50 cm. This layer is overlain by gray-white fine-grained sand, up to 6 m thick, which occasionally contains flint, limestone or orthoquartzite pebbles, up to several cm across. Cross-bedding and limonite concretions are quite common.

Above this clastic unit follow slightly sandy variegated marls, up to 7 m thick, rich in limonite, barren of any fossils. In the center of the area occupied by the Zefa Formation a light gray limestone bed overlies or occasionally replaces the marls entirely. The limestone is slightly friable, containing unidentified plant remains and oncolites. The latter are several centimeters in size, oval in shape, probably originating from freshwater blue algae (Buchbinder, in Shahar, 1973). These marls and limestones represent a shallow lake or lagoon, while the top unit of the Zefa Formation comprises several meters of breccia. The breccia has fragments up to 10 cm across, most of them made of flint, some of limestone, embedded in a sandy or rarely carbonate matrix. This sequence, described and illustrated in columnar sections (Shahar, 1973) represents a complete transgressive cycle, prior to the Hazeva Formation.

The Eocene pebbles found within the Zefa define its post-Eocene age, whereas the Burdigalian (Early Miocene) age of the fauna found in the Hazeva Formation suggest the Zefa Formation to be pre-Miocene, hence an Oligocene age is most plausible. This puts the Zefa Formation, in terms of sequence stratigraphy, in a very similar situation to that observed at En Gev, where the Fiq, Susita and En Gev Sands sequence is dated by fauna. A correlation between the two sequences is thus suggested here, based on these similarities. It is suggested that deposition of both sequences was controlled by the Oligocene transgression. [A.H.]

***Crassostrea gingensis* (Yeruham) Bank**

This consists of an oyster-bank interwedging the sandstones of the Hazeva Formation, as far inland as the townships of Yeruham and Dimona. This presumably [N8-N9] Langhian-Serravallian Ziqlag equivalent was also dated by Sr^{87}/Sr^{86} at 17.9±0.16 Ma (Goldschmidt et al., 1988).

Hazeva Formation Early-Middle Miocene
(Figs. 18H.11 and 18H.12)

The Hazeva Formation is named after a settlement in the northern Arava. It was described by various authors from different localities in both Israel and Jordan, using names such as: 'Hasb' or 'Hosb' Sandstone (Arabic for Hazeva) or Series; 'Kurnub

Sands and Sandstones' (Bentor, 1960; Daniel, 1963). The 'Lower Syntectonical Conglomerates' in southwestern Jordan, and possibly also part of the 'Upper Syntectonical Conglomerates' (Bender, 1974) seem to refer to the Hazeva Formation as well, designated as the Dana Formation on Jordanian maps.

Bentor and Vroman (1954) recognized three parts to the Hazeva Formation: a base conglomerate, a sandy middle part, and a top conglomerate (the Arava Conglomerate). However, Bentor and Vroman (1957) pointed out that the Arava Conglomerate unconformably overlies the other parts of the Hazeva Formation and should therefore be considered a separate unit. The lower and upper contacts of the formation are unconformable. The thickness of the Hazeva Formation is subject to large variations; 60 m at Ein Yahav, to probably reach over 500 m in the Rotem-Arad area, and exceed 1000 m in the Paran Valley.

From the vicinity of Ein Hazeva in the northern Arava, to the Paran Basin, the formation is of lacustrine origin. The Hazeva Formation also extends to the mountains of the Northern Negev, where it unconformably overlies Cretaceous to Oligocene strata. In the eastern part of the mountain belt, the sequence is fluviatile and also eolian in origin. In some places it yields bones of *Hippopotamus*. It interfingers to the west with marine sandstones and shales carrying *Ostrea gingensis* Schloth., suggesting a Middle Miocene age for these strata.

In his revision of the Hazeva Formation in the Central and Northern Negev, Zilberman (1992) retained four members: Base Conglomerate, Fluvial Lacustrine, Top Conglomerate and Karkom.

Sneh (1981) subdivided the Hazeva Formation in the northern Arava into three members, the lowermost Shahaq Conglomerate, followed by the Mashaq and Gidron Members, for which he gave detailed columnar sections.

In the Yeroham-Dimona region 35-40 km west of the southern tip of the Dead Sea, Harash (1967) subdivided the Hazeva Formation into five members; the Shu'alim, Mingar, Yeroham, Aro'er, and Ashalon Members.

Shahar (1973) described the Zefa, Base Conglomerate, and Rotem Members in the Rotem Basin. The latter are high energy fluviatile sands with allochtonous quartzite and Eocene chert pebbles. A marine ingression with oysters coming from the west is interwedged into the Yeroham and Dimona basins.

The Shu'alim Member of Harash (1967) seems identical to Sneh's Shahaq Conglomerate; the overlying fluviatile Mingar Member is correlated with the Mashaq Member and part of the Gidron Member; no correlation with the Arava is suggested for the oyster bearing, littoral Yeroham, while the Aro'er Member is correlated by Harash (1967) with the upper part of the Gidron Member. The uppermost Ashalon Member does not occur in the Arava (Sneh, 1981). Calvo et al. (1997) subdivided the Hazeva in the Karkom Graben, some 20-40 km west of the central Arava, into a lower subdivision similar to Sneh's three members, and an upper subdivision comprising up to 2000 m of clastics, adding the Hufeira Member between the Rotem and Karkom Members.

A) The Base Conglomerate (Lower Miocene) is of fluvio-

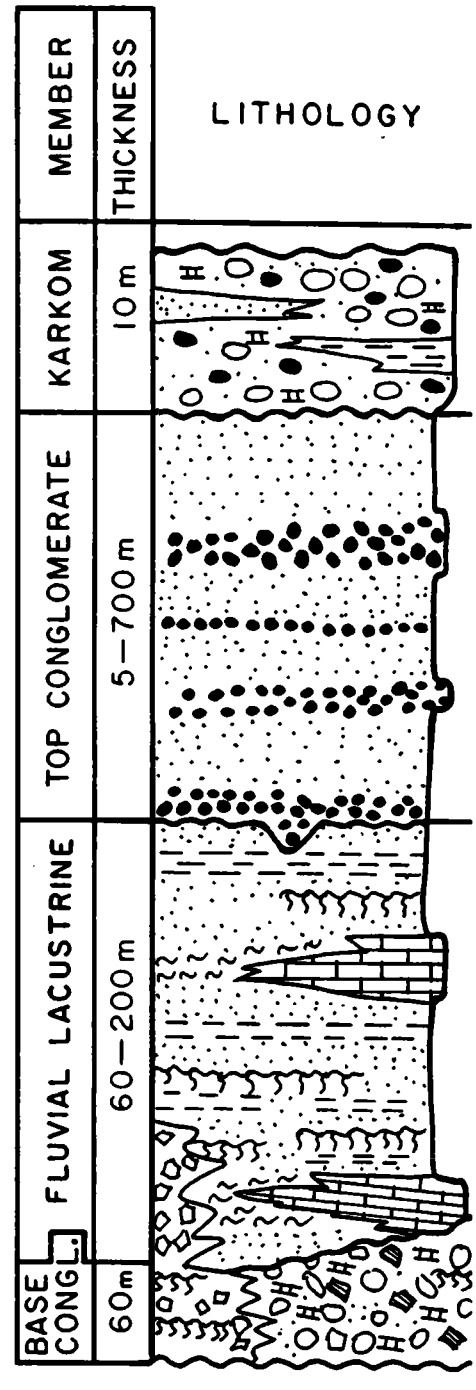


Figure 18H.11. Composite section of the Miocene Hazeva Formation in the Central and Northern Negev (after Zilberman, 1992, Fig. 2b, p. 7).

lacustrine origin, and consists of local lithologies of bajada, forming a lining of the basin (Roded and Hirsch, 1989). It contains no fossils. It overlies the Zefa Formation in the Rotem Basin, where it varies in thickness from only 0.5 m to 80 m. There it consists of large subangular pebbles, mainly of Eocene limestone and Mishash flint, strongly cemented by red, sandy argillaceous limestone. It

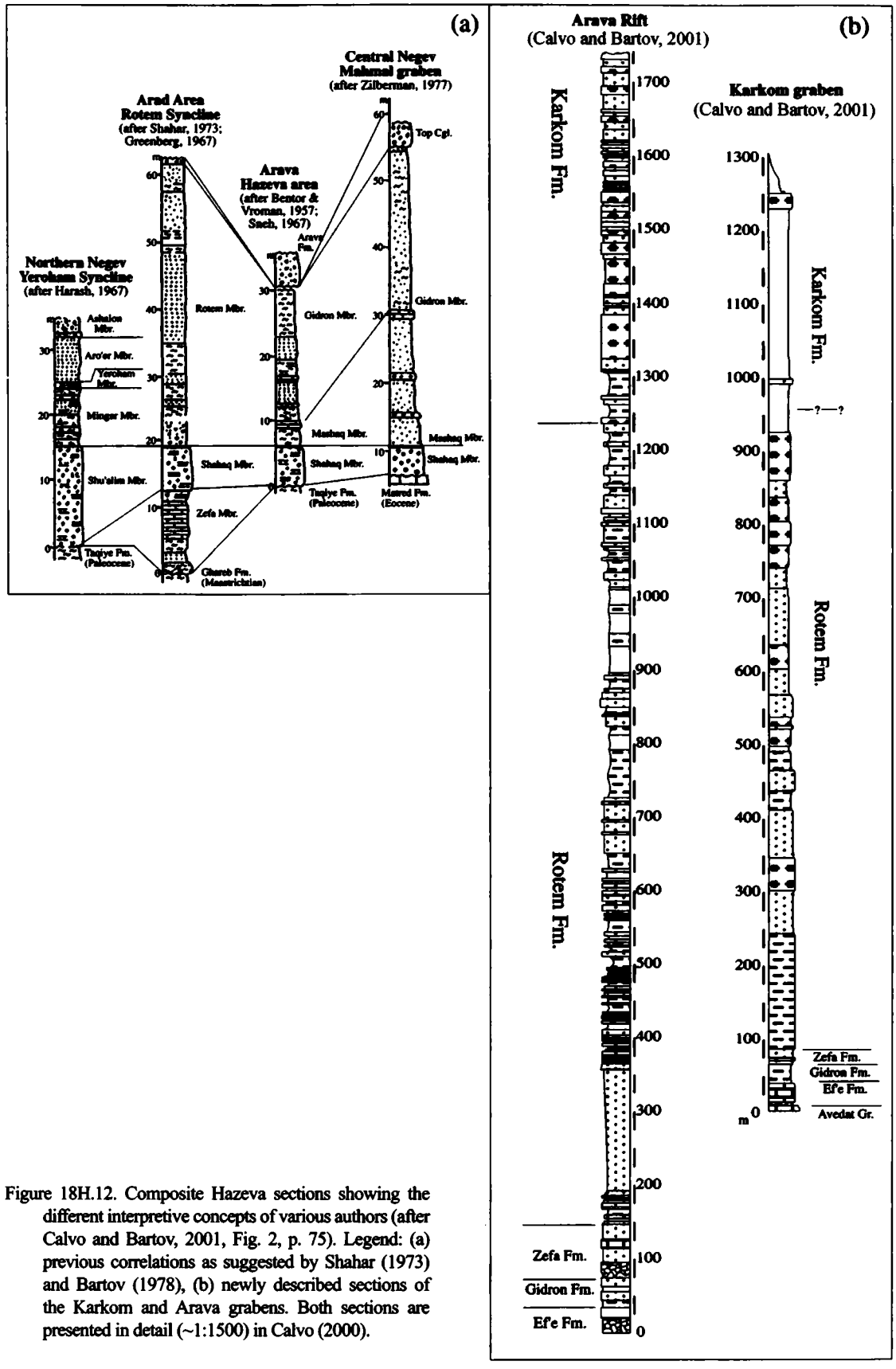


Figure 18H.12. Composite Hazeva sections showing the different interpretive concepts of various authors (after Calvo and Bartov, 2001, Fig. 2, p. 75). Legend: (a) previous correlations as suggested by Shahar (1973) and Bartov (1978), (b) newly described sections of the Karkom and Arava grabens. Both sections are presented in detail (~1:1500) in Calvo (2000).

is equivalent with the Shualim member of Harash (1967) in the Yeruham Basin. In the Northern Arava, the Shahaq Conglomerate of Sneh (1981) is usually several meters thick, attaining some 22 m at Nahal Shahaq, some 40 km south of the Dead Sea. It sometimes exhibits a fan-shaped geometry. The badly sorted sub-angular to sub-rounded pebbles, 1-40 cm across, are mostly limestone and flint derived from the Avedat and rarely from the Mount Scopus Group. The conglomerate is often well-cemented by calcite, forming small cliffs, while sometimes it can be rather loose. A local origin can be deduced from the size and composition of the pebbles. They vary in size with distance from the source rocks. The immediate vicinity seems to be the norm, with long distance transport being subordinate for the conglomerates. Though the conglomerate is usually massive, some crude bedding is occasionally observed. The upper part of the Base Conglomerate Member sometimes includes algal limestone and marls. It is overlain by the Mashaq Member.

B. The Fluviatile and Lacustrine Deposits (Lower-Middle Miocene) of the Hazeva Formation comprise a variety of facies, in a number of localities, under different names.

1) The Mashaq Member (Sneh, 1981) abruptly or occasionally gradually overlies the Shahaq conglomerate or older rocks in the northern Arava. The lacustrine Mashaq limestone comprises some sandy marls, clays, and gravels, forming prominent cliffs. It is overlain by the Gidron Member, or by younger units such as the Arava Formation and others.

2) The Gidron Member, at the type locality in Nahal Mashaq, close to Nahal Shahaq, where its base is not exposed, is 25.5 m thick (Yechieli, 1987). It varies in thickness over rather short distances. The low energy Gidron Member consists of mainly gray-pink, hard limestone, with sandstone lenses, forming small cliffs. Facies changes over very short distances are common. Limestone predominates to the west, while marls take the upper hand eastward and southward, indicating deepening of the basin (Sneh, 1981). The Gidron Member covers the widest areas in the northern Arava, conformably overlying the Mashaq Member, and occasionally overlapping earlier rocks. The transition from limestones to sandstones and red clays marks the boundary. Its typical red colors make it very prominent in the landscape. It is unconformably overlain by the Arava Formation or younger rocks. The thickness in the reference section is 35.5 m, but composite sections attain up to 80 m. The unit is considerably thicker in boreholes (Sneh, 1981), reaching more than 200 m. The Gidron Member comprises alternations of red clayey, calcareous mudstones, siltstones and fine to very fine quartz sandstones, unimodal, well-sorted, with subordinate mica, feldspar and occasionally redeposited glauconite grains. The sandstones display horizontal bedding or planar and trough cross-beds. The red clays are washed over the outcrops, giving the entire Hazeva Formation a typical reddish hue. Lateral changes in lithology over short distances are quite common, making exact correlations difficult.

3) In the Rotem Basin type area, the Rotem Member (Shahar, 1973) consists of alternations of coarse sandstones and red shales. Some of the sand layers are rich in well-rounded flint, quartz, some limestone, and 'imported' flint pebbles. The thickness of the unit may reach several hundred meters.

4) The Hufeira Member (Calvo et al., 1997) was established at Jebel el Hufeira, near En Yahav in the central northern Arava, some 50 km south of the Dead Sea. The Rotem and Hufeira Members, grade laterally into one another. Thicknesses, especially of the Rotem Member, vary considerably from the northern Negev where it attains only several tens of meters, to the Karkom Graben, where it exceeds a kilometer. They seem to pass conformably upwards into the Karkom Member.

C. Upper Conglomerate units (?Upper Miocene): The upper members of the Hazeva Formation postdate the onset of the Erythrean faulting.

These units are missing in the exposures of the Arava, but seem to reach substantial thicknesses in boreholes and down-faulted structures. They comprise the Ashalon Member (Harash, 1967), the Karkom Member (Zilberman, 1992), and possibly part of the 'Upper Syntectonical Conglomerates' in Jordan.

1) The Ashalon Member (Harash, 1967) was named after the Ashalon well east of Dimona, in the Dimona-Yeroham basin of the central northern Negev far away from the rift. The Ashalon Member consists of several meters of sandy conglomerates, most of the pebbles made from well-rounded and sorted flint. This flint is traditionally termed 'imported', since no known source could be located in the vicinity. The flint is very rich in foraminifers, which were at first thought to indicate a late Cretaceous age (Reiss, in Garfunkel and Horowitz, 1966). The rock is considerably different from late Cretaceous flints of the northern Negev, thus 'imported'. Later, detailed analyses of the microfauna yielded an Eocene age, and similar flints were found within sequences of this age in the central Negev (Horowitz, 1974). In any case the roundness and sorting seem to indicate, anyway, a long transport for these pebbles. Unidentified, silicified wood fragments are found within the otherwise barren sequence. The unit conformably overlies the Aro'er Member, which is correlative with the upper part of the Gidron Member in the northern Arava. The top is always truncated by erosion, and occasionally covered by a thin veneer of Quaternary sediments. The Ashalon Member is only known from regions outside the rift, such as Dimona-Yeroham and Arad to the west. A small outcrop on the western Dead Sea shore, near En Boqeq, may represent this member (Garfunkel, 1997).

2) The Karkom Member (Zilberman, 1992) is made of red sandstones and clays, rich in somewhat angular Eocene limestone pebbles, with subordinate flint gravels. Occasionally the conglomerates are very rich in 'imported' flint pebbles, appearing in a similar manner to the Ashalon Member, which may exceed, in some places, a hundred meters. It is overlain by various rock units, the oldest of which is the Arava Formation. These units are known from the northern Arava, and the northern and central Negev. No fossils are reported, but the stratigraphic and structural position seems to justify a late Miocene age (Calvo et al., 1997, 1998).

Distribution: The Hazeva Formation, abundant in the northern Arava, extends westward to the central Negev (Bentor and Vroman, 1954, 1957; Harash, 1967; Eidelman, 1979; Sneh, 1981; Eyal, 1984; Yechieli, 1987; Roded, 1996; Hirsch, 1996). There it is

mainly developed in synclines, where thick sequences have been accumulated, better protected from subsequent erosion. Occasional outcrops are also known from structurally high localities (Bartov, 1974; Zilberman, 1992). Farther west, the Hazeva interfingers with marine Miocene sediments of the Lower Member of the Sheva Formation, grading further westward into the Ziqim Formation (Horowitz, 1979). Southward, in down-faulted structures, outcrops of considerable thickness occur, more than 2000 m, mainly of the upper parts of the formation which are usually missing from most of the region (Calvo et al., 1997). Normally the southern sequences are very limited (Avni, 1997; Ginat, 1997), extending into southeastern Sinai (Garfunkel and Horowitz, 1966). The northernmost outcrops are in the vicinity of the town of Arad, west of the Dead Sea. To the east they are reported from Adh-Dhira, just east of the Lisan Peninsula. However outcrops of the Hazeva Formation are quite rare farther east of the northern Arava, except for subordinate occurrences (Bender, 1974).

In their study of the Negev and Arava using outcrops and seismic lines, Calvo, Frieslander and Bartov (1997) postulate erosional unconformities at the base of their 'Zefa', Rotem and Hufeira Members. Their less than 200 m thick *Lower Subdivision,* consisting of the conglomerates, lake sediments and soils of the Shahaq, Mashaq and Gidron Members, is separated from their *Upper Subdivision*, comprising thick fluviatile and lacustrine series such as the 'Zefa', Rotem, Hufeira, and Karkom Members, by an angular unconformity. This angular unconformity is "related to tectonic activity of the Syrian Arc", and isostatic oscillations of the hinterland controlling the energy and composition of the fluviatile components.

The sedimentation of the Hazeva Formation started after the Late Oligocene denudation. A fluviatile system draining the highs from across the present Rift Valley to the Paratethys (present Mediterranean) reached the oscillating seashore along a line running parallel to the Judean foothills (estimated at between the present 300-400 m elevation contours). The Beersheva Canyon (Neev, 1960) penetrated deep into the Northern Negev, enabling the marine ingression of the Yeroham Basin (oysters). The Top Conglomeratic units accumulated after severance from the link across the present Rift Valley.

Contacts: The Hazeva Formation overlies, with angular and erosional unconformities, a variety of pre-Miocene rocks. The youngest of these is the Oligocene Zefa Formation in Nahal Ef'e. It is overlain by a suite of Pliocene and younger formations, the oldest of which is the Arava Formation (Sneh, 1981), or the 'Upper Syntectonical Conglomerates' (or maybe only their upper parts) on the Jordanian side of the Arava (Bender, 1974). Slight unconformities are also quite common within the formation, causing the appearance of different parts of the formation in certain localities, due to channel fillings.

Age: The sedimentation of the Hazeva Formation started after the Late Oligocene denudation. The start of the Hazeva deposition may be estimated from the Ashosh Volcanics (23-21 Ma).

The Mashaq limestone contains only freshwater mollusks such as *Melanopsis*, *Melanoides*, and *Planorbis*, ostracods, stromatolites, oncolites, and algal debris, indicating a lacustrine environment in the Arava region. Its fluviatile system drained the highlands across the present Rift valley to the Paratethys (present Mediterranean), using the Beersheva Canyon (Neev, 1960). In the canyon it interfingers with the marine ingression of the Yeroham Member that contains oyster beds (*Crassostrea gingensis,* according to Tchernov et al., 1987, and possibly some *Ostrea edulis*, according to Harash, 1967), indicating a brackish estuary environment. However none of these fossils are truly age indicative. Yeroham oysters were dated at 17.9 Ma, approximately the deposition time of the Ziqlag Formation. Clays of the Gidron Member occasionally contain plant remains, among which J. Lorch (1998, pers. comm.) identified fruit and large leaves of *Lotus* sp.

Fossils of vertebrates, discovered by Neev (1960) are quite common in the Mingar Member at the Yeroham-Dimona basin, some 5-10 m below the oyster beds. Bones collected from the Rotem Basin, some 10 km eastward, may be somewhat younger since the bearing strata contain fragments of reworked oysters (Tchernov et al., 1987; Goldsmith et al., 1988). Bones are also found in the Arava, in the Gidron Member (Savage and Tchernov, 1968). The beds yielded 19 mammal taxa, mostly of African affinity, such as the proboscideans *Prodeinotherium* and *Gomphotherium*, the artiodactyls *Canthumeryx syrtensis*, two species of *Dorcatherium* and *Gazella negevensis*, rodents such as *Megapedetes*, the lagomorph *Kenyalagomys*, and the creodont *Anasinopa haasi*. Unidentified carnivores and primates also occur, along with numerous fish remains (among which only *Lates* and Clariidae were identified), unidentified amphibians, and reptiles such as the large water turtles Trionychidae, and the crocodile *C. pigotti*. The same outcrops also yielded numerous plant remains, usually silicified, particularly of a variety of palms (*Palmoxylon*) and *Leguminoxylon* (Lorch and Fahn, 1959; Zohary, 1959).

Tchernov et al. (1987) suggest an early Miocene, possibly Burdigalian age for the vertebrates, based on correlations with somewhat similar assemblages, mainly from Africa. The taxa indicate that the environment of the bone-bearing beds is mainly riverine, and partly lacustrine. The vegetation must have been lush, with forested and marshy habitats, but also with open, fairly dry country not too far away. The end of the Hazeva deposition coincides with the deepening of the Rift, an event sealed by the En Yahav dike, dated at 6 Ma (Bartov and Steinitz, 1990). [F.H./A.H.].

Correlation Into Jordan:

The Lower Syntectonical Conglomerates (Dana Formation) are intimately connected with the Rift Valley, leading Bender (1974) to apply a genetic name for the sequence. Common along the eastern escarpment of the northern Arava, known mostly from down-faulted blocks which were partially sheltered from subsequent erosion, they do not occur much further east of the Rift. Their lowermost beds in Gharandal contain internal molds of freshwater gastropods and charophytes. The upper part, at Dahal 25 km south of the Dead Sea, contains *Ammonia beccarii*, leading to the assumption that the Lower Syntectonical Conglomerates in the Arava had connections with marine environments (Bender, 1974). The latter can no longer

be considered as an indication of a near-shore marine depositional environment since this foraminifer was found living today in brackish spring waters near the Dead Sea (Almogi-Labin et al., 1991). Bender correlated the Lower Syntectonical Conglomerates with the Taiyiba Beds, assigning an Oligocene to Miocene age to the former. [A.H.]. It can logically be assumed that the Hazeva and coeval Hordos (Herod) Formations correlate with the Lower and Upper Syntectonical Conglomerates (Bender, 1968, 1974).

Tectonic implications:

The lower part of the sequence of the Hazeva and Hordos Formation belong in the pre-rift Tiberias Group, while the upper part, including the coeval 'Top Conglomerate', Ashalon, Karkom, and Umm Sabune are posterior to the Erythrean faulting. [A.H.].

III. THE DEAD-SEA GROUP

Introduced by Langotzki (1966), the Dead Sea Group encompasses the Late Miocene and Pliocene clastic sediments of the Rift extending from the Jordan Valley to the Arava.

The Late Miocene-Pliocene **proto-rift** phase resulted from the uplift of a mountainous backbone between the Mediterranean and the area of the Dead Sea Transform that created a new watershed, west of which extended the Late Miocene-Pliocene marine deposition of the Saqiye Group, and east of which extended the intramontane basin of the Dead Sea Group. Marine ingressions into the Yizre'el Valley reached the Dead Sea basin, leaving thick evaporites.

In the Jordan Valley the Late Miocene part of the Dead Sea Group encompasses the fluviatile conglomerates and clays of the Umm Sabune Conglomerate. These are coeval in the Dead-Sea and Negev areas with such 'Top Conglomerate units' as the Karkom and Ashalon Members of the Hazeva Formation. The presumably Tortonian marine ingression, that found its way through the Yizre'el Valley into the northern part of the Dead Sea basin, left behind evaporites and brackish deposits. These form the Bira Formation, which comprises the Zemach salt plug, at the south end of Lake Kinneret. This event precedes the low-stand that made possible the accumulation of Messinian evaporites in the Mediterranean.

The Pliocene part of the Dead Sea Group consists of the gypsum of the Gesher Formation in the Jordan Valley as well as the thick halite of the Sedom and Amora Formations, passing laterally into the clastic fluviatile and lacustrine Arava Formation. The evaporites witness an Early Pliocene, post-Messinian marine ingression.

Within the Rift, late Miocene sediments show considerable thickness, on the order of hundreds or thousands of meters, drilled in the Hula Valley south of Lake Kinneret, and in the southern Dead Sea (Horowitz and Horowitz, 1990a, b; Horowitz, 1996). Outside the Rift such sequences are only known from the Karkom graben in the central Negev (Calvo et al., 1997). The sections are limited to 200 m and less except in low lying terrains, however most regions surrounding the Jordan Valley were subject to erosion, removing large quantities of the older formations. This is the result of the considerable faulting and trough formation of the Erythrean system, which marked the transition from middle to late Miocene (Horowitz and Horowitz, 1990a, b; Calvo et al., 1997).

1. Kinneret (Sea of Galilee)-Central Jordan Valley Region

The Neogene Mediterranean reached the area of the Jordan Valley through the Yizre'el Valley, making the central Jordan Valley a meeting point of continental and marine environments of deposition.

Umm Sabune Conglomerate Miocene (Early Tortonian)

Schulman (1962) described these conglomerates. They are composed largely of basalt pebbles and clays, interwedged by basalt (8.4 Ma). They are named after Wadi Umm Sabune (Nahal Tzabun) near Belvoir, a subsidiary of Wadi Bira (Nahal Tavor) just west of the central Jordan Valley. Shaliv (1991) expanded Schulman's definition to include various conglomerate beds of local origin, not necessarily dominated by basalt pebbles, thus considerably enlarging the geographic extent of this unit, which represents the base of Dead Sea Group.

Lithology: The lowermost 50 m of the type section (Schulman, 1962) comprises very coarse conglomerates, with loosely cemented unsorted basalt pebbles up to 60 cm across. Above lie some 130 m of coarse to fine rudites, arenites, and siltites, with fine quartz grains. Upward, clear bedding is being gradually developed. This part is better-cemented than the lower one, with cement made of weathering products of basalt and some calcite. The uppermost 20 m are very finely-bedded or occasionally laminated, made of fine limestone and basalt clastics, with some unidentified plant remains.

Contacts: At the type locality, the Umm Sabune Conglomerate unconformably overlies the Lower Basalt over an erosional, faulted relief. In other localities this unit unconformably overlies a variety of older rocks and its upper part para- or disconformably grades into the overlying Bira Formation (Schulman, 1962). Shaliv (1991) indicates a gradual transition, both vertically and horizontally, into the Bira, which seems to be based on some similarity of the upper part of the Umm Sabune and the lower beds of the Bira, though in other localities Shaliv observed unconformable contacts.

Distribution: According to Shaliv (1991), Schulman (1962), and Schulman and Rosenthal (1968), the Umm Sabune Conglomerate covers wide areas beyond the extent of the Herod Formation. These are mainly in the central Jordan Valley, but extending northward on both sides of Lake Kinneret (Sea of Galilee) and possibly to southern Lebanon, southward down to Marma Feiyad, and westward to the Yizre'el Valley. In the deeper central parts of the Yizre'el Valley, known mainly from boreholes and only a few outcrops, the conglomerates seem to be replaced by brown to yellowish clays (the 'Clay Series' of Picard, 1943) resting on what appears to be like the Lower Basalt, overlain by the Bira Formation marls. Braun (1992) described similar beds near Tiberias as the 'Yachza'el Formation', agreeing to its correlation with the Umm Sabune Conglomerate.

Numerous units were assigned to the Umm Sabune Conglomerate such as the 'Clay Series'. The Umm Sabune can be firmly defined only when it is found overlying Miocene sediments with an angular unconformity, and is itself overlain by Pliocene rocks.

Such is the case near Marma Feiyad, where the Herod Formation (previously termed 'Beida Formation' in Rofe and Raffety, 1965) dips 60° SE, while its uppermost 40 m, assigned by Shaliv (1991) to the Umm Sabune, dips 15° SW and is covered by the Pliocene Gesher Formation (Schulman and Rosenthal, 1968).

The Umm Sabune Conglomerate reaches some 200 m at the type section area, in the central Jordan Valley (Schulman, 1962), where it fills a faulted, deeply incised relief, diminishing to nothing over short distances. Other outcrops and well sequences described in Shaliv (1991) are usually several meters to several tens of meters thick. The thickest seems to be the 'Clay Series' sequence, attaining up to 260 m in one of the boreholes in the Yizre'el Valley.

Environment: The Umm Sabune Conglomerate fills a continental relief system, usually river channels, with occasional small ponds or lakes, most likely formed following the regressing late Miocene sea. The erratic, rather rare outcrops and the problematic correlations make precise paleogeographic reconstructions somewhat questionable.

Age: No fossils except for plants are reported from the Umm Sabune Conglomerate, thus a direct age assignment is impossible. Most authors preferred an early Pliocene age, based on stratigraphic grounds (Schulman, 1962; Horowitz, 1979, p. 76; and many others). Based on radiometric ages obtained on basalts below and above the conglomerates, Shaliv (1991) suggests a late Miocene age, which also matches the morpho-structural considerations. [A.H].

Bira Formation Late Miocene (Tortonian)

The term Bira Series was coined by Picard (1943), following Blake, 1928), emended by Schulman (1962) to 'Bira Marl', after Wadi Bira (Nahal Tavor) which joins the central Jordan Valley in southeastern Galilee. Synonyms are 'Tonmergel' (Picard, 1932), 'Brackish Water Formation' (Bentor, 1946), 'Brackish-Lagoonal Series' or 'Brackwater Series' (Schulman, 1959), and 'Poriyya Formation' (Bentor, 1960). It stands for a sequence of brackish, yellow and gray marls, interspersed with gypsum beds, up to 20 m thick and overlain by fresh-water limestones, partly oolitic, which carry *Hydrobia fraasi* Blanck. Its base is nowhere exposed and it reaches a thickness of 350 m. Schulman (1962) gave the Bira Formation a type section in Wadi Umm as Sawalil, a small tributary of Wadi Bira, where only the basal member of the Bira Formation occurs, while for the rest only reference sections are available, in many localities in the central Jordan and Yizre'el Valleys (Schulman, 1959, 1962; Shaliv, 1991).

In places where the Umm Sabune Conglomerate occurs, such as Belvoir, the Bira Formation overlies it disconformably or paraconformably (Schulman, 1962). Otherwise, the Bira discordantly overlies a variety of older rocks, over a structural and erosional relief. The Bira Formation is conformably or paraconformably overlain by the Gesher Formation, and by the Cover Basalt in places where the Gesher does not occur, such as the Yizre'el Valley, where the entire Pliocene sequence is of lagoonal nature.

The Bira Formation is occasionally intercalated by volcanics of the Intermediate Basalt and Fajjas (Fejjas) Tuff, known from the entire central Jordan Valley, extending westward and covering large areas in the Yizre'el Valley and vicinity. North and eastward, in the Korazim, Hula Valley, and Golan Heights areas, the Bira Formation is replaced by a variety of freshwater and fluviatile sediments. Evaporites are progressively more common southward. Thickness varies considerably, from several hundred meters in the deeper basins such as the central Jordan Valley and the central parts of the Yizre'el Valley, to complete disappearance at the margins of the depositional basins. Average thickness figures are between several tens of meters and 200 m.

The lowermost 20 m comprise alternations of unsorted coarse and fine clastics composed of basalt pebbles and basalt in a variety of weathering stages. The fine-grained horizons bear small badly-preserved mollusks, grading in places to biocalcarenite. Toward the margins of the basin a lumachel is developed, built of hard limestone rich in oyster shells, which is also known from the eastern side of the central Jordan Valley (Wetzel and Morton, 1959) and the En Gev region (Michelson, 1972).

The main body of the Bira Formation comprises a complex of clayey, chalky, marly, and gypsiferous sediments, especially rich in pyrite and organic matter, both of which are oxidized at the outcrops. Irregular occurrences of gypsum are quite common. Occasionally, thin beds of hard, limonitic crystalline limestone occur, as do beds of black-brown clay or cryptocrystalline dolomite. These are finely stratified, very soft rocks, white to yellow at the outcrops, which are usually covered by slumps.

According to Schulman (1962) the top of the Bira Formation is sandy, limonitic, and brownish, indicating a paraconformable transition to the overlying Gesher Formation. In places, such as near the settlement of Gesher, the sands grade into gypsum up to 14 m thick. The lower main part is a massive pure gypsum, bearing some authigenic magnetite, overlain by a thin layer of clays rich in gypsum, iron minerals, and organic matter. Further up several thin, black gypsum layers occur, grading upward into shales with gypsum, iron, and some calcite. Calcite increases within a distance of several meters, until the rocks become the platy limestone forming the base of the Gesher Formation. Based mainly on geochemical grounds, Raab (1998) suggested uniting the gypsum and dolomite occurrences at the top of Bira with the platy limestone (f1) basal member of Gesher Formation, also rich in dolomite. This new unit is termed the 'Dolomite-Gypsum Member'. In the Zemach borehole at the southern end of Sea of Galilee, a Late Tortonian salt plug represents a lateral development of the Bira Formation.

Unidentified plant remains and redeposited Cretaceous and Eocene foraminifera are very common in the Bira Formation (Reiss, in Schulman, 1962). Foraminifers indicating a general Neogene age and brackish environment are *Ammonia beccarii* and a variety of benthonic miliolids (Weiler, 1961). Others indicating lagoonal or shallow marine environments are ostracods such as *Cyprideis torosa* (Rosenfeld, in Shaliv, 1991), clams, of which *Crassostrea* and *Ostrea* (possibly *edulis*) are common, accompanied by *Chama, Lucina, Cardium* (Bentor, 1946), *Lithophaga* and others, and gastropods such as *Cerithium*. Occasionally the environment of deposition becomes less saline, evidenced by occurrence of freshwater mollusks such as *Melanoides tuberculatus, Theodoxus*

jordani, and *Melanopsis praemorsa* (Lewy, in Shaliv, 1991). Clupeid fish remains are reported from the gypsum layers (Avnimelech and Steinitz, 1951). Unfortunately, none of these fossils are age indicative, since most of them range from the Miocene to the present day.

The age of the Bira Formation is considered Pliocene by most investigators. It contains the two flows of the Middle Basalt. Radiometric ages are 7.3 and 6.2 Ma, which led Shaliv (1991) and Heimann et al. (1996a, b) to suggest a late Miocene (Tortonian) age for the Bira Formation.

Gesher Formation Pliocene

Schulman (1962) named the formation after the settlement of Gesher, on the western rim of the central Jordan Valley. Type sections are at nearby Nahal Hemed and Nahal Ghareb. The formation represents the 'Pliozäne Süsswasserkalke' (Blanckenhorn, 1912); 'Plattenkalk' overlain by 'Oolithkalk' (Picard, 1932); '*Melania* Limestone' or *Hydrobia fraasi* Beds' (Blake, 1935); 'Limnic' or 'Freshwater Beds' (Picard, 1943); 'Freshwater Series' (Bentor, 1946) and the 'Degania Formation' (Bentor, 1960).

Schulman (1962) subdivided the section into three members.

a) 22 m of 'Plattenkalk' (Picard, 1932) conformably overlie the gypsum beds of the underlying Bira Formation. It is characterized by very fine bedding of mainly extremely white limestones. In places white chalk occurs, with some ostracods possibly indicating a hypersaline environment (Rosenfeld et al., 1981). Fish remains, most probably Cichlidae, are found at the base (Avnimelech and Steinitz, 1951), but no other fossils were found. Primary limonite and manganese nodules are quite common, some of the rocks are saline, some are silicified.

b) 17.5 m of 'Main Oolite' (Bentor, 1946), forming gray-white, hard cliffs, of medium to coarse bedding, consisting of detritic limestones, composed chiefly of oolites, accumulated around ostracod shells. Epigenetic silicification and dolomitization are quite common, forming very hard rocks. The abundant ostracods indicate a freshwater environment of deposition (Rosenfeld et al., 1981), as do the numerous shells of the gastropod *Hydrobia fraasi*.

c) 6 m of variegated clays are rich in freshwater fossils, organic matter, and plant remains.

The Gesher Formation does not show frequent facies changes, except when approaching the lakeshores, where the sediments may contain some clastic components. The Fajjas (Fejjas) Tuff is intercalated within the Gesher sediments. The Gesher Formation overlies the Bira Formation, mostly unconformably, but in several localities the latter grades conformably into the former (Schulman, 1962). In the Yizre'el Valley to the west the freshwater Gesher is replaced by a lagoonal environment, therefore termed 'Bira', closer to the sea. The Gesher Formation may unconformably overlie a variety of older rocks in different locations. The Gesher Formation is laterally bounded and unconformably overlain, over an erosional relief, by the Cover Basalt (5.3-4.9 Ma).

The Gesher Formation varies in thickness from 0-120 m, being usually 20-50 m all around the central Jordan Valley. It is somewhat thicker 100 km southward at Marma Feiyad (Schulman and Rosenthal, 1968), eastward in the Golan, and northward at the northwestern corner of Lake Kinneret, where it attains some 120 m (Saltzman, 1964).

Intense faulting and tilting along the west side of the Jordan Valley, from the Samarian structure to Gesher-Poriyya, affected the deposition of the Neogene beds. In the Marma Feiyad segment of the Jordan Valley, Neogene sediments are continuously exposed from the mountain border in the west, to the mountain border in the east. At Marma Feiyad the Bira Marl is missing altogether and the calcareous freshwater beds, which Schulman (1962) suggested to correlate with the Gesher Formation, overlie, with an angular unconformity, a 'conglomerate member'. The latter may belong to the Miocene Herod Formation, representing a stage of intensified tectonic activity in the adjacent uplifted blocks.

Ostracods and *Hydrobia* sp, ranging from Neogene to Recent, witness the freshwater environment of deposition of the Gesher Formation. At Marma Feiyad a 100 m thick section of freshwater-limestone, chalk, marl and travertine yields a freshwater fauna: *Dreissensia* sp.? gr. *D. rostiformis* Andrussov, *Pisidium* sp., *Theodoxus jordani* Sowerby, *Theodoxus jordani unicarinatus* Picard, *Melania tuberculata* Muller, and *Melanopsis* sp.? gr. *M. buccinoidea* Olivier (Schulman and Rosenthal, 1968, determ. M. Raab). The Gesher Formation is Early Pliocene, framed by volcanics of 5.3-4.9 Ma age.

2. Negev, Arava, and Dead Sea Region

Sedom Formation Pliocene

Established by Wyllie (1931), the Jebel Usdum Series were hebraized to Sdom Serie (Bentor and Vroman, 1954), emended by Bentor and Vroman (1960) to 'Sdom Formation'. The formation was well-investigated by Zak (1967). The correct spelling should be Sedom Formation (Langotzky, 1966), as it is named after Mount Sedom, at the southwestern tip of the Dead Sea ('Jebel Usdum or Khashm Usdum' in Arabic), where the legendary Biblical city of Sodom is thought to have been located. The type section is taken at this locality, which is the only outcrop of these rocks, however well-known from numerous boreholes. The formation consists of a thick sequence of chemical and subordinately detrital terrestrial sediments.

The base of Sedom Formation is not exposed at the type locality, but is known from several boreholes in the vicinity to overlie, most probably unconformably, late Miocene sediments which seem correlative to the uppermost member of the Hazeva Formation. The Sedom Formation is unconformably overlain by various types of cap-rock, or by the Amora and Lisan Formations. The outcrops at Mount Sedom cover an elongated north-south oriented strip, some 10 km long, and 1-1½ km wide. Zak (1967) estimated the thickness at 1500-2000 m. An almost similar occurrence is known from a borehole drilled in the Lisan Peninsula, and several others are suggested to cause and underlie diapirs in the northern Dead Sea basin (Neev and Hall, 1979) and in the Jordan Valley, north of the Dead Sea (Belitzky, 1996; Belitzky and Mimran, 1996).

The Sedom Formation comprises principally massive rock-

salt, alternating with thinner shale units. The salt units are mainly halite, accompanied by some anhydrite, dolomite, clay, and silt, as thin laminae or interspersed within the salt. The shale units consist of finely laminated dolomite, silt and clay, accompanied by fine to coarse-bedded red or white sandstones and white or gray gypsum, and anhydrite. The Sedom Formation is subdivided into five members, of which the lower two, the Karbolet (crest) salt and shale Member, and the Lot salt Member, comprise the major part, some 1400 m. They are overlain by the Benot (daughters of) Lot shale Member, the Mearat (cave of) Sedom salt Member, and the Hof (beach) shale and salt Member, attaining somewhat less than 500 m in thickness.

The Karbolet Member comprises mainly rock-salt, with intercalations of silt, clay, dolomite, sandstone, anhydrite and gypsum. The overlying Lot Member also consists chiefly of rock-salt, with subordinate dolomite, clay, and anhydrite. The Benot Lot Member is made of sandstones, anhydrite and shales, partly dolomitic, overlain by the massive, almost pure rock-salt of the Mearat Sedom Member. The sequence is topped by the Hof shale and salt Member, however always truncated, built of sandstones, clay, salt, and anhydrite.

Age: Except for the numerous pollen grains and occasionally quantities of unidentified plant debris, the Sedom Formation is poor in fossils. Notable are fish fossils of *Mugil priscus* (H. Steinitz in Bentor and Vroman, 1960), very common in some horizons of the formation. Footmarks of birds and a large mammal are reported in Zak (1967), as well as some insect remains, but were not identified. The Sedom Formation was assigned a variety of ages by different authors, from Cretaceous by Lartet (1869), who mis-correlated the fossil fish with others known at that time from the Lebanon, through Oligocene to Miocene (Bentor, 1960), Pliocene by most investigators, and Pliocene-Pleistocene(?) by Zak (1967). Based on K-Ar ages of basalts east of the Rift Valley, and their estimated rates of erosion, Steinitz and Bartov (1992) suggested an age for the base of the Sedom Formation younger than 7-9 Ma, maybe as young as 6 Ma, while the top was assigned an age of 4-3.4 Ma.

The environment of deposition is hypersaline lagoonal, with remote but clear connections with the Mediterranean Sea, as evidenced by the geochemistry of the evaporites (Zak, 1967; Raab, 1998).

Mount Sedom is probably a diapir, which continues its upward movement at rates of 7-8 mm/yr until the present day (Pe'eri et al., 1999; Pe'eri, 2003). In times when this process pushed the salt into lakes or sea (Raab, 1998), its upper part dissolved and the insoluble residue accumulated as caprock, noted already by Anderson (1852). Various such stages, attaining up to 40 m in thickness, are described in Zak (1967) and in Raab (1998), however dating these uplift and dissolution stages is far from certain. [A.H.].

Amora Formation Pliocene

Langotsky (1963) originally put into the Quaternary a unit first called 'Gypseous-Argillaceous Division' or 'Gypsum and Shale' by Wyllie and al. (1922), emended by Picard and Vroman (1950) into 'Foothill Series', and by Bentor and Vroman (1960) to 'Foothill Formation'. The Amora Formation is named after the lost Biblical city of Gomorra (Amora in Hebrew), and the type section is in Mount Sedom. The Amora Formation unconformably overlies the Sedom Formation and some of its caprock horizons. It is truncated by an erosional and structural relief and covered by the late Pleistocene Lisan Formation and younger lake terraces. The Amora beds may also be covered by the Samra Formation (Picard and Vroman, 1950; Zak, 1967). Patches of the Amora Formation encircle the foothills of Mount Sedom in an alternation of soft and hard rocks, described by Picard and Vroman (1950, p. 6) as "Opposing erosion, the gypsum beds form conspicuous cathedral-like peaks". The sequence was penetrated in many boreholes and reaches a thickness of more than 700 m. Zak (1967) placed the lower part of the 'Foothill' into the Sedom Formation, leaving for the Amora proper somewhat more than 400 m.

The Amora Formation comprises laminar or shaley chalky marls, anhydrite and gypsum, rock-salt, sandstones, and conglomerates of light colors, usually gray-yellowish, olive gray, brownish and whitish. It was subdivided by Zak into five members: the lowermost, the 'Amc' Member, comprised of marl, sand, and conglomerates more than 130 m thick, with the gravel made of flint, limestone, quartz porphyry, and a variety of other igneous rocks. This is overlain by 70 m of the 'Ama' Member composed mainly of marl and anhydrite with subordinate conglomerates, consisting of the same variety of gravel as below. The third 'As' Member, consists of 6 m of massive rock-salt, on which lies the 'Am' Member, 130-150 m of mainly marls, again with subordinate gravel of similar composition to those below. The top 'Ams' Member is built chiefly of marl, chalk, and sand, and attains more than 100 m in thickness.

The environment of deposition is considered terrestrial by Bentor and Vroman (1850), lagoonal by Zak (1967) and by Horowitz and Zak (1968), with a remote connection with the Mediterranean Sea.

No fossils are reported from the Amora Formation, except for plant debris and pollen grains. The age is believed to be Pliocene (Picard and Vroman, 1950; Horowitz and Horowitz, 1990a, b), Miocene-Pliocene (Bentor and Vroman, 1960), or Pleistocene (Zak, 1967). Based on the K-Ar ages of basalts east of the Rift Valley and their estimated rates of erosion, Steinitz and Bartov (1992) suggested an age for the base of Amora Formation of 4-3.4 Ma, while the top was placed at a little more than two million years.

Arava Formation Pliocene
(Fig. 18H.13)

Bentor and Vroman (1957) established the 'Arava Conglomerate'; emended by Garfunkel and Horowitz (1966), Horowitz (1974), Sneh (1982), Eyal (1984), and Avni (1997).

It was first considered part of the Hazeva Formation. For most authors, the Arava Formation represents river sediments of a hydrographic system leading to the Sedom embayment, whose terminal base level is the Mediterranean, during a short Pliocene

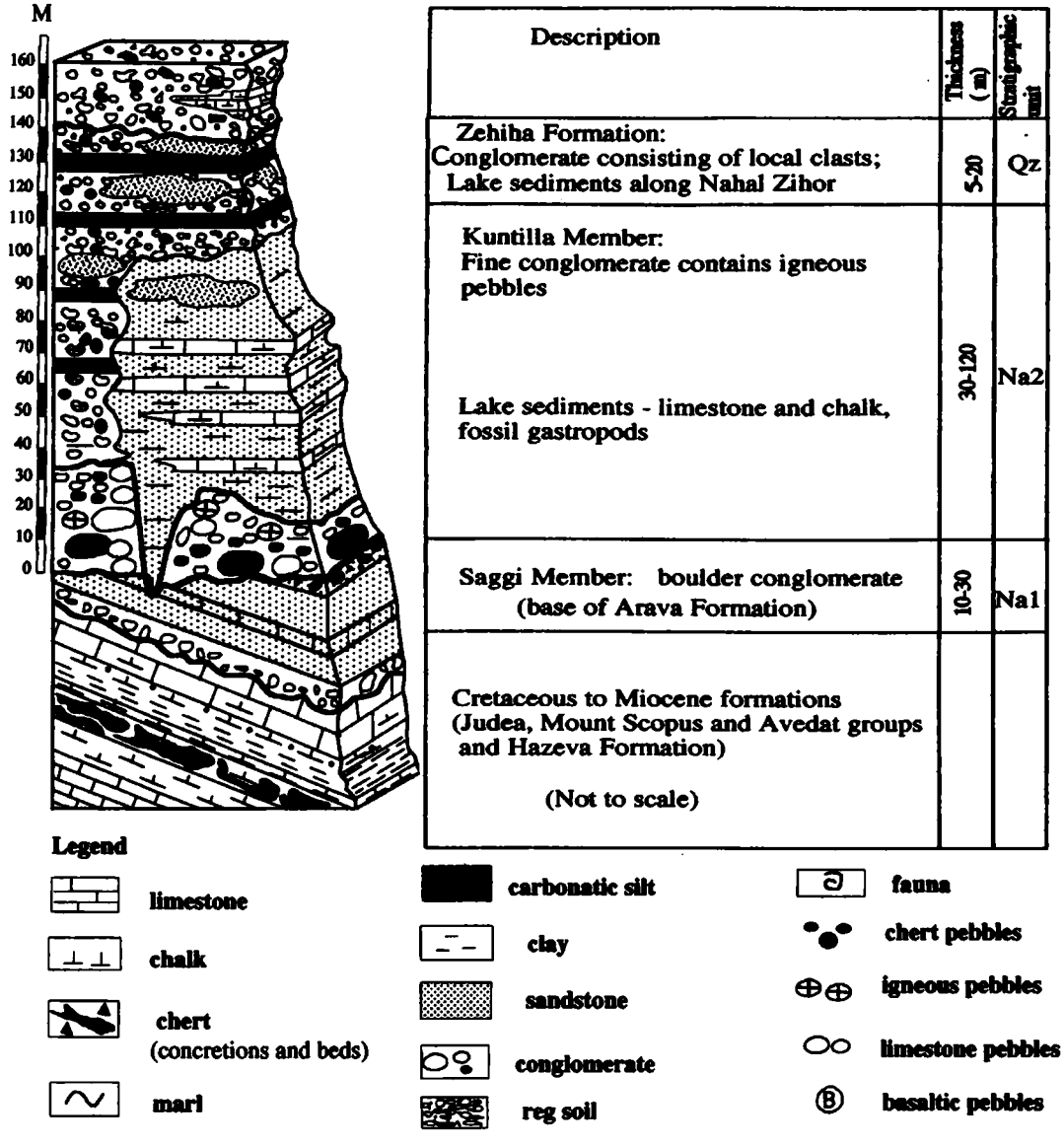


Figure 18H.13. The Arava Formation in the Paran Basin (after Avni et al., 2001, Fig. 5, p. 109).

time span (Bentor and Vroman, 1957; Garfunkel and Horowitz, 1966; Horowitz, 1974, 1979, 1992; Horowitz and Horowitz, 1990). However, an alternative view regards the Arava Formation as a large fluviatile system, draining a large hinterland into the Dead Sea from Late Miocene until nearly the present day (Sneh, 1982; Avni, 1997).

The thickness of the Arava Formation varies considerably, from just a few meters up to several tens in the deeper channels.

The Arava Formation is made of loosely cemented conglomerates, in a reddish sandstone matrix, occasionally with sand lenses. The pebbles vary in size, composition and sphericity according to their relative locations in the channels. The sequence is well-stratified, commonly with imbrications and cross-bedding. Two principal facies are distinguished (Eyal, 1984). The *En Yahav facies* is typified by perfectly rounded pebbles, and the *Dohan facies* much less so. The first is notable for its magmatic and metamorphic constituents, indicating far away provenance such as the Edom Mountains in southern Jordan, or the Neshef Hills close to Elat. The other facies, of a local nature, comprises less-rounded and sorted pebbles, derived from closeby sources. Another, of local significance only, is the *Nekarot facies* (Baer, 1981), which contains a suite of pebbles originating in the Makhtesh Ramon erosion cirque, indicating its drainage to the Arava. No fossils have ever been recovered from the Arava Formation, which was deposited in a large river system.

In the Paran Basin the Arava Formation subdivides into the

Saggi Member (boulder conglomerate, base of Arava Formation) and the Kuntilla Member (lake sediments - limestone and chalk with fossil gastropods and fine conglomerate including pebbles of magmatic and sedimentary rocks) (Avni, 2001).

The Arava Formation was established in the northern Arava, where it overlies, always unconformably, the Hazeva and older formations. The Arava Formation extends over vast areas in the southern and central Negev, and the northern Arava up to the Dead Sea, where its typical pebbles were found in the Amora Formation (Zak, 1967).

The top of the Arava Formation is cut and filled by younger gravel beds, of which the oldest is the Pleistocene Zehiha Formation (Avni, 1997) which is coeval to the HaMeshar Formation (Garfunkel and Horowitz, 1966). A number of units, closely related to the Arava Formation, were established as independent formations. One of them, the Mazar Formation, interfingers with the Arava conglomerates in several localities south of the Dead Sea. This unit (also spelled Mazzar) was established by Shahar et al. (1966) for a brackish-freshwater interval. It is named after Nahal Mazzar, near the erosion cirque of Makhtesh Qatan some 25 km southwest of the Dead Sea,. The Mazzar conformably interfingers within the Arava Formation (Elron, 1980; Eyal, 1984). Various similar occurrences of this facies having different fossil assemblages are spotted in the northern and central Arava (Livnat and Kronfeld, 1990). At Nahal Mazzar, the microfauna is brackish, while elsewhere freshwater fauna prevails. For Avni (1997) the entire string of outcrops was part of one large lake, occupying the whole of the northern Arava, while Horowitz (pers. comm.) views the Mazzar in its original context as a marginal marine intercalation within the Arava Formation. The 6 m thick section in Nahal Mazzar comprises alternations of a few cm thick well-bedded layers of light gray marls, with pink, reddish, yellow or gray sands cemented by carbonate (Eyal, 1984). Fine ripple marks and north-south oriented load structures, probably indicating a beach, are present. Numerous unidentified carbonized plant remains are reported. The foraminifera *Ammonia beccarii* and *Elphidium* sp., and the ostracod *Cyprideis littoralis* indicate a Neogene to recent marine brackish environment, similar to what was designated as the 'Lido facies' of the Bira Formation near Tiberias (Reiss, Gerry, in Eyal, 1984) and in Mount Sedom (Zak, 1967). Similar assemblages are reported from the En Gedi-2 and Arava-1 boreholes, at depths corresponding to Palynozone Pa (Neev and Emery, 1967; Bartov, in Elron, 1980; Horowitz and Horowitz, 1990). Zak (1967), Horowitz (1974), Elron (1980), and Eyal (1984) suggested a broad correlation of the Mazzar Formation with the Pliocene formations to the north.

Another unit is the Yeelim Conglomerate (Agnon, 1983) which describes exotic pebbles, found as terraces and hanging valley fillings, between elevations of 190-110 m in Nahal Lot, a canyon south of the Dead Sea. They are found to extend, as the highest terrace, to a much larger paleo-drainage area than that of the present Nahal Lot. In places the conglomerate underwent pre-Holocene pedogenesis (R. Gerson, pers. comm.). The pebbles presumably derive from sediments of the Hazeva Formation that were exposed higher to the northwest. They were transported in the direction of the Dead Sea Rift. Later the catchment of most of the Lot drainage basin by the present thalweg system of Nahal Heimar took place. The preservation of the ancient terraces in Nahal Lot is probably due to its relatively small Holocene-Present drainage basin. This conglomerate is probably contemporaneous with the deposition of the Arava Formation.

Age: The Arava Formation is Late Miocene-Pliocene for Sneh (1981) and Avni (1997). A Pliocene age was attributed by Horowitz and Horowitz (1990), after palynozones Pa and Pb in borehole Arava-1.

The tectono-environment of the Arava Formation is that of a new hydrographic system, draining the Negev into the Dead Sea. This followed the deepening of the Dead Sea Basin (Proto-Rift Phase) that generated the Mediterranean-Dead Sea water-divide. It comprises polymictic fluviatile rounded boulder-conglomerates and lacustrine limestone and chalks (Kuntilla Lake). The Sedom evaporites interwedge the Arava deposits.

In Jordan, the Upper Syntectonical Conglomerates are intimately connected with the Rift Valley, which led Bender (1968) to apply a genetic name for the sequence located 2 km ENE of Gharandal in the central Arava. They overlie the Lower Syntectonical Conglomerates without a visible, or only slight disconformity, or unconformably rest on a variety of older formations. The sequence is known from numerous outcrops in the Arava and eastward, its northernmost occurrence being Edh-Dhira, east of the Lisan Peninsula (Bender, 1974).

The Upper Syntectonical Conglomerates commence with a scarp, and consist of 1-8 m of coarse conglomerate beds, alternating with brown-ochre and pale yellow, fine conglomeratic sandstones. The coarse clastic constituents are late Cretaceous and Eocene, sub- to well-rounded rocks, cemented by a calcareous-sandy, hard matrix. No fossils are reported, thus, based solely on similarity in lithology, Bender (*op. cit.*) broadly correlated the sequence with the Hazeva Formation.

3. Hula Valley-Upper Galilee

Tel Hai Formation Neogene

Picard (1952) established the 'Lower Neogene Lacustrine Series', also named 'Süsswaser Mergel und Kalke' (Rosenberg, 1960), for which Glikson (1966) used the term 'Tel Hai Freshwater Limestone'.

The Tel Hai Formation is named after Tel Hai, a settlement at the northwestern corner of the Hula Valley, where its thickness attains some 400 m in the type section. It consists of lacustrine limestones unconformably overlying middle Eocene rocks, whose top is always truncated, which seem to grade laterally into the Tanur Conglomerate.

The main lithologies are interbedded detritic and fine-grained limestones, accompanied by marl, chalk, calcarenites, shales, and some conglomerate horizons. The limestones, usually fine, and occasionally medium to coarse-grained, are limonitic, hard, thinly-bedded, platy or laminated, and form small cliffs. Fossil gastropods are abundant, especially in the limestones and chalk,

and consist of freshwater taxa such as *Hydrobia fraasi, Chondrina jamina, Lymnaea, Planorbis*, and terrestrial *Helix*. They indicate a lacustrine environment, but are unfortunately not very helpful with age, since all range from early Miocene until today. Based mainly on paleogeographic considerations, Horowitz (1973) placed the Tel Hai Formation in the Pliocene. Sneh (1996) suggested a late Miocene age, correlative with the Umm Sabune Conglomerate.

Tanur Conglomerate

Picard (1952) established the 'Lower Neogene Pudding Conglomerate', emended by Rosenberg (1960) to 'Nummuliten-Marmor Konglomerate'; and Tanur Conglomerate by Glikson (1966). Sneh (1996) views both the Tel Hai Formation and Tanur Conglomerate as a single entity, which he termed the 'Kefar Gil'adi Formation'.

The Tanur Conglomerate is named after the Tanur (oven) waterfall, near Qiryat Shemona north of the Hula Valley. The Tanur Conglomerate unconformably overlies middle Eocene limestones, however in most of the outcrops the contacts with other rock units are along faults. It grades in some places into freshwater limestones of the Tel Hai Formation. The Tanur Conglomerate, as originally defined by Glikson, is confined to the northeastern corner of the Hula Valley and somewhat northward. Other conglomerates of similar nature are reported (Horowitz, 1973) from both flanks of the Valley, extending southward to areas close to Lake Kinneret. The thickness at the type section is on the order of 100 m, but since the base is not exposed and the top truncated, this is regarded as a minimum figure. Heavy faulting and subsequent erosion affect the Tanur Conglomerate, which, as Glikson (1966) maintains, may attain up to 400 m in thickness, based on the claim that the Tanur and Tel Hai Formations are correlative.

The Tanur Conglomerate is composed of sub-angular to well-rounded limestone pebbles and cobbles, well-cemented by calcarenite. The rock is stratified, hard, forming a landscape resembling the late Cretaceous rocks in the region. The pebbles comprise two main types of light-colored limestones, one microcrystalline, homogenous, dense with calcite veins, the other made largely of *Nummulites*, accompanied by other middle Eocene fossils. The environment of deposition is no doubt fluviatile, but no fossils are known from the matrix. When interfingering with the Tel Hai occurs, the typical fossils of the latter occur.

In the northern Hula Valley a gravel unit some 10-40 m thick, defined by Heimann (1985) as the 'Egel Gravel' and consisting of Jurassic, Cretaceous, and possibly Pliocene components, was considered by Horowitz (1973), Sneh (1996), and Kafri (1998, pers. comm.) to be correlative with the Tanur Conglomerate, the differences in pebble lithology being viewed as derivation from different sources. Based mainly on paleogeographic considerations, Horowitz (1973) placed the Tanur Conglomerate in the Pliocene. Sneh (1996) suggested a late Miocene age, correlative with the Umm Sabune Conglomerate.

TECTONIC IMPLICATIONS:

The late Miocene Erythrean faulting considerably changed the face of the southern Levant. The hydrographic connections with the east had terminated, the late Miocene troughs had been filled up with sediments, and the landscape became peneplaned. Consequently, the Pliocene transgression caused flooding of vast regions by shallow seas, lagoons and lakes, fed by a newly developed river system, which left its gravels as testimony (Garfunkel and Horowitz, 1966; Horowitz, 1973, 1979). This paleogeography resulted in lateral facies changes, so that lagoonal sediments grade into lacustrine, themselves gradually changing to fluviatile, all indeed synchronous. Despite this, different formation names, being termed according to lithologies, were given to time-correlative units over relatively short distances.

REFERENCES CITED

Agnon, A., 1983. An attempted revision of the Neogene stratigraphy in the Dead Sea Valley. Nazerat: Abst., Israel Geol. Soc. Ann. Mtg., p. 1.

Almogi-Labin, A., Hemleben, C., Meischner, D., and Erlenkeuser, H., 1991. Climatic fluctuation in the northernmost Red Sea region during the Late Quaternary (last 130,000 years) as inferred from the marine record. Isr. Geol. Soc., Ann. Meet., Abstr., p. 5.

Anderson, H. J., 1852. Geological reconnaissance of part of the Holy Land. In W. F. Lynch (ed.), Official report of the United States expedition to explore the Dead Sea and the river Jordan, p. 75-206. Baltimore: Murphy.

Arad, A., 1965. Geological outline of the Ramot Menashe Region. (Israel). Isr. J. Earth Sci., 14(1), p. 18-32, maps.

Avni, Y., 1997. Geological evolution of the central and southern Negev as an indicator of the evolution of the Dead Sea Transform western margin in the Late Neogene and Quaternary. Unpublished Ph.D. Thesis, Hebrew Univ. Jerusalem, Vol. 1, 91 p., plates; Vol. 2, Appendices. (In Hebrew, English Abstract).

Avni, Y., 2001. Geological map of Israel, 1:50,000, Sheet 21-III: Har Loz. Isr. Geol. Surv., 1 Map.

Avni, Y., Bartov, Y., Garfunkel, Z. and Ginat, H., 2001. The Arava Formation; a Pliocene sequence in the Arava Valley and its western margin, southern Israel. Isr J. Earth Sci., 50(2-4), p. 101-120.

Avnimelech, M., 1935. Notes sur les calcaires d'El Kubab en Palestine. Bull. Soc. Hist. Nat., Toulouse, No. 67, p. 74-75.

Avnimelech, M., 1936. Étude géologiques dans la region de la Shephela en Palestine. Ann. Univ. Grenoble, Trav. Lab. Geol. Grenoble, Allier Frères, 144 p., Figs.

Avnimelech, M., 1937. Sur les mollusques trouves dans les couches prehistoriques et protohistoriques de Palestine. J. Palest. Orient. Soc., Vol. 17, p. 81-92.

Avnimelech, M., 1939. On the geology and morphology of the Megiddo area. J. Palest. Orient. Soc., Vol. 19, p. 18-37.

Avnimelech, M., 1947. L'extension en Palestine du Miocene cotier Libanais. C. R. Soc. Géol. Fr., No. 16, p. 343-345.

Avnimelech, M., Steinitz, H., 1951. On fish remains in the continental Neogene of the Jordan Valley (Israel). Eclogae Geol. Helv., 44(2), p. 443-447.

Baer, G., 1981. The geology of the Arif-Batur lineament, Ma'ale HaMeshar area. MSc thesis, Dept. Geol., Hebrew Univ. Jerusalem, 56 p. (In Hebrew, English summary, unpubl.).

Bartov, Y., 1974. A structural and paleogeographical study of the central Sinai faults and domes. Unpublished PhD dissertation, Dept. Geol., Hebrew Univ. Jerusalem, 143 p. (In Hebrew, English summary, unpubl.).

Bartov, Y., 1978. Arava Rift Valley and the Dead Sea. 10th Int. Congr. Sedimentol., Jerusalem; Guidebook, Pt. 2, p. 37-48.

Bartov, Y., 1994. Geological photomap of Israel and adjacent areas, 1:750,000.

Jerusalem: Geol. Surv. Israel.

Bartov, Y., and Steinitz, G., 1990. The geology of the Beer Ora Area. (In Hebrew). Isr. Geol. Soc., Ann. Meet., Geol. Field Trips, Elat Area, p. 47-55, Maps.

Belitzky, S., 1996. Tectonic geomorphology of the Lower Jordan Valley - An active continental rift. (In Hebrew, English Abstract). Unpublished Ph.D. Thesis, Hebrew University Jerusalem, 98 p., Appen.

Belitzky, S., 1996. Tectonic Geomorphology Of The Lower Jordan Valley - An Active Continental Rift. (In Hebrew, English Abstract). Ph.D. Thesis, Hebrew University Jerusalem, 98 p., Appen.

Bender, F., 1968. Geologie von Jordanien. Gebr. Borntraeger, Berlin, Stuttgart, 230 p.

Bender, F., 1974. Geology of Jordan. Borntraeger, Berlin, 196 p.

Bentor, Y. K., 1946. The hydrogeological conditions of the area of Tiberias - Kinneret - Yavneel - Hadatha - Kefar Kama - Lubya (Lower Galilee). Hebrew University Jerusalem, 76 p., Figs. (Report for the Palestine Water Co.).

Bentor, Y. K., 1960. Mineral resources of Israel; Exploitation and development problems. Isr. Geol. Surv., Rep., 24 p. (In Hebrew).

Bentor, Y. K., 1963. Salt deposits of the Dead Sea area. Geol. Soc. Am., Spec. Pap. 73, 270. p.

Bentor, Y. K., and Vroman, A. J., 1951. Geological map of the Negev, Sheet 18: Avedat, Scale 1:100,000. Israeli Army, Sci. Sect., 98 p., Maps, Figs. (In Hebrew).

Bentor, Y. K., and Vroman, A. J., 1954. Geological map of the Negev, Sheet 21: Mount Omer. Isr. Defence Forces, 1 Geol. Map & 1 Struct. Map, Scale 1:100,000.

Bentor, Y. K., and Vroman, A. J., 1957. Geological map of Israel, 1:100,000, Series A - The Negev. Sheet 19: Arava Valley. Isr. Geol. Surv., 66 p., Maps. (Hebrew & English Editions).

Bentor, Y. K., and Vroman, A. J., 1960. Geological map of Israel, 1:100,000, Sheet 16: Mount Sdom. Isr. Geol. Surv., 117 p., Figs., Separate Folder With 19 Encl. (Hebrew & Engl. Editions). 1st Edition - 1954, 2nd Edition - 1960.

Blake, G. S., 1935. On the occurrence of marine Miocene in Palestine. Geol. Mag., 72(3), p. 140-142.

Blake, G. S., 1936. The stratigraphy of Palestine and its building stones. Printing & Stationery Office, Jerusalem, 133 p.

Blanckenhorn, M., 1912. Kurzer Abriss der Geologie Palaestinas. Begleitworte zu Einer Neuen Geologischen Karte von Palaestina. Z. Dtsch. Palaestina Vereins, Vol. 35, p. 113-139, 1 Map, 1:700,000.

Blanckenhorn, M., 1914. Syrien, Arabien und Mesopotamien. Heidelberg, Winter's Universitaetsbuch- Handlung, 159 p. (Handbuch Der Regionalen Geol., 5(4)).

Blanckenhorn, M., 1931. Geologie Palaestinas Nach Heutiger Auffassung. Leipzig, Hinrichs'sche Buchhandlung, 50 p. (Reprinted From Z. Dtsch. Palaestina Vereins, Vol. 54).

Blanckenhorn, M., and Oppenheim, P., 1927. Neue Beitraege zur Kenntnis des Neogens in Syrien und Palaestina. Geol. Palaeontol. Abh., N.F., Vol. 15, No. 4, p. 321-357.

Blow, W. H., 1969. Late middle Eocene to Recent planktonic foraminiferal biostratigraphy. In P. Bronnimann and H. H. Renz (eds), Proc. 1st Intl. Conf Planktonic Microfossils, Geneva 1967, Brill, Leiden, p. 199-475.

Braun, D., 1992. The geology of the Afigim region. Unpublished M.Sc. Thesis, Dept. Geol., Hebrew Univ. Jerusalem, 93 p. (In Hebrew).

Buchbinder, B., 1996. Middle and Upper Miocene reefs and carbonate platforms in Israel. S.E.P.M. Concepts in Sedimentol. Paleontol., No. 5, p. 333-345.

Buchbinder, B., and Gvirtzman, G., 1969. Outcrops of Neogene formation in the central and southern Coastal Plain, Hashefela and Beer Sheva regions, Israel. Isr. J. Earth Sci., 18(3-4), p. 158.

Buchbinder, B., Martinotti, G. M., Siman-Tov, R., and Zilberman, E., 1993. Temporal and spatial relationships in Miocene reef carbonates in Israel. Palaeogeogr., Palaeoclimatol., Palaeoecol., 101(1-2), p. 97-116.

Buchbinder, B., and Zilberman, E., 1997. Sequence stratigraphy of Miocene-Pliocene carbonate-siliciclastic shelf deposits in the eastern Mediterranean margin (Israel): Effects of eustasy and tectonics. Sediment. Geol., 112(1-2), p. 7-32.

Calvo, R., 2000. Stratigraphy and Petrology of the Hazeva Formation in the Arava and the Negev: Implications for the development of sedimentary basins and the morphotectonics of the Dead Sea Rift Valley. Ph.D. Thesis, Hebrew University, Jerusalem, Vol. 1 - 113 p.; Vol. 2 - 123 p. Figs., Plates., Tables. (In Hebrew; English Abstract).

Calvo, R., and Bartov, Y., 2001. Hazeva Group, southern Israel; new observations, and their implications for its stratigraphy, paleogeography, and tectono-sedimentary regime. Isr. J. Earth Sci., 50(2-4), p. 71-100.

Calvo, R., Bartov, Y., and Ayalon, A., 1997. New stratigraphic scheme for the Hazeva Formation as a basis for locating water boreholes in the Arava. Progress Report No. 1. (In Hebrew). Isr. Geol. Surv., Progr. Rept. TR-GSI/1/97, 33 p., Figs. (Prepared for the Water Commission).

Calvo, R., Bartov, Y., and Ayalon, A., 1998. New stratigraphic scheme for the Hazeva Formation as a basis for locating water boreholes in the Arava; Progress Report No. 3: Summary Report. Isr. Geol. Surv., Tech. Rept. TR-GSI/3/98, 67 p., Figs., Maps. (In Hebrew).

Calvo, R., Frieslander, U., and Bartov, Y., 1997. A new stratigraphic division of the Hazeva Formation in the Negev and the Arava. Isr. Geol. Soc., Ann. Meet., Abstr., p. 13.

Cohen, Z., Flexer, A., and Kaptsan, V., 1987. The Pleshet Basin - a newly discovered link in the peripheral chain of basins of the Arabian Craton. Tel Aviv, Oil Exploration {Investments} Rept. & Tel Aviv Univ., 17 p., Figs.

Cox, L. R., 1934. On the occurrence of the marine Oligocene in Palestine. Geol. Mag., 71(843), p. 431.

Daniel, E. J., 1935. Beersheba "Great Quarry", "Wadi al Jurrah Series", "Wadi Arara Series" I. P. C. Rep.

Daniel, E. J., 1959. Stratigraphic Lexicon of Palestine. 67 p., 1 Chart. (Unpublished draft sent to Y. K. Bentor by R. C. Van Bellen in June 1959).

Daniel, E. J., 1963. Jordanie (Ensemble). Lexique Stratigraphique Int.: Asie, 3(10), C1. Paris, C.N.R.S., p. 295-399.

Druckman, Y., and Begin, Z. B., 1985. Geological mapping units in Israel and their symbols. Isr. Geol. Surv., Rept. GSI/35/85, 17 p.

Druckman, Y., Buchbinder, B., Martinotti, G. M., Siman-Tov, R., and Aharon, P., 1995. The buried Afiq Canyon (eastern Mediteranean, Israel); a case study of a Tertiary submarine canyon exposed in late Messinian times. Marine Geology, 123(3-4), p. 167-185.

Eidelman, A., 1979. The geology of the Arava Rift margin in the En Yahav-Ramat Zofar region. Isr. Geol. Surv., Rept. MM/10/79, 66 p., Plates. (M.Sc. Thesis, Hebrew University Jerusalem). (In Hebrew, English Abstract).

Elron, E., 1980. The geology of the Nahal Zin area (northern Hazeva Sheet). Isr. Geol. Surv., Rept. MM/6/79, 54 p. (M.Sc. Thesis, Hebrew University Jerusalem). (In Hebrew, English Abstract).

Eyal, A., 1984. The geology of the northern Arava Valley and its western margins in the En Yahav-Hazeva region., Jerusalem: Geol. Surv. Israel Rept. GSI/10/91, 63 p. (In Hebrew, English Abst.).

Flexer, A., Gill, D., Livnat, A., Tamir, N., and Toister, A., 1981a. Atlas Project (Israel Subsurface Geology Information Management System). Part A - Explanatory Notes. (In Hebrew). Tel Aviv, Oil Exploration {Investments}, 43 p., Figs.

Flexer, A., Gill, D., Livnat, A., Toister, A., Shafran, N., and Tamir, N., 1981b. Computerized information system in support of oil and gas exploration in Israel. Oil exploration in Israel; A Symp., Jerusalem, Dec. 1981, Abstr. Isr. Geol. Soc., Oil Exploration {Investments} & Isr. Geol. Surv., p. 16-20.

Garfunkel, Z., 1997. The history and formation of the Dead Sea Basin. In: T. M. Niemi, Z. Ben-Avraham, and Y. Gat (eds.), The Dead Sea: The Lake and its setting, Oxford Univ. Press, p. 36-56.

Garfunkel, Z., and Horowitz, A., 1966. The Upper Tertiary and Quaternary morphology of the Negev, Israel. Isr. J. Earth Sci., 15(3), p. 101-117.

Ginat, H., 1997. Paleogeography and the landscape evolution of the Nahal Hiyyon and Nahal Zihor Basins (sedimentology, climatic and tectonic aspects). Unpublished Ph.D. Thesis, Hebrew University Jerusalem, 109 p. (In Hebrew, English Abstract).

Giveon, M., 1984. Paleogeographic studies: Hordos Formation and En Gev Sands in eastern Lake Kinneret. Unpublished M.Sc. Thesis, Dept. Geol., Hebrew University Jerusalem, 86 p. (In Hebrew).

Glikson, Y., 1966. The lacustrine Neogene in the Kefar Gil'adi area, northern Jordan Valley. Israel J. Earth Sci. 15(3), p. 85-100.

Golani, U., 1962. The geology of Lake Tiberias region and the geohydrology of the saline springs. Tahal, Jerusalem, 54 p.

Goldsmith, N. F., Hirsch, F., Friedman, G. M., Tchernov, E., Derin, B., Gerry, E., Horowitz, A., and Weinberger, G., 1988. Rotem mammals and Yeroham

Crassostreids: Stratigraphy of the Hazeva Formation (Israel) and the paleogeography of Miocene Africa. Newsl. Stratigr., 20(2), p. 73-90.

Golik, A., 1960. On the geology of the Ziklag area, Israel. Isr. Res. Counc., Bull., 9G(2-3), p. 129-152.

Grader, P., and Gvirtzman, G., 1961. Neogene gas prospects in the central Coastal Plain, Israel. Isr. Res. Counc. Bull., 10G(1-2), p. 147-172.

Greitzer, Y., 1960. Groundwater salinity in the Cenomanian-Turonian aquifer of central Israel. Tahal, Tel Aviv, 30 p., Figs., Maps. (In Hebrew).

Greitzer, Y., 1960. On the geology of the Lakhish area. Isr. Res. Counc., Bull., 9G(2-3), p. 109-128.

Gvirtzman, G., 1969a. Subsurface data on the Saqiye Group (Late Eocene to Early Pleistocene) in the Coastal Plain and Hashephela regions, Israel. Isr. Geol. Surv., Rept. OD/1/69 & Inst. Petrol. Res. Geophys., Rept. 1037, Various pagings.

Gvirtzman, G., 1969b. The Saqiye Group (late Eocene to early Pleistocene) in the Coastal Plain and Hashephela regions, Israel. Vol. 2: Maps. (Vol. 1 was never published). Isr. Geol. Surv., Bull. 51 & Inst. Petrol. Res. Geophys., Rept. 1022, 38 Maps.

Gvirtzman, G., and Buchbinder, B., 1967. Outcrops of Neogene Formations in the Coastal Plain, the Shephela and the Beer Sheba regions, Israel. Inst. Petrol. Res. Geophys., Holon, & Isr. Geol. Surv., Rept., 23 p., Figs.

Gvirtzman, G., and Buchbinder, B., 1969a. Outcrops of Neogene Formation in the Central and Southern Coastal Plain, Hashephela and Be'er Sheva regions, Israel. Isr. Geol. Surv., Bull., 50, & Inst. Petrol. Res. Geophys., Holon, Rept. 1040, 52 p.

Gvirtzman, G., and Buchbinder, B., 1969b. The stratigraphy of the Hashefela and Saqiye Groups in Hashefela Region. Isr. J. Earth Sci., 18(3-4), p. 161.

Gvirtzman, G., Reiss, Z., 1965. Stratigraphic Nomenclature In The Coastal Plain And Hashephela Regions. Isr. Geol. Surv., Rept. OD/1/65, 13 p.

Haq, B. U., and Berggren, W. A., 1978. Late Neogene calcareous plankton biochronology of the Rio Grande Rise (South Atlantic Ocean). J. Paleontology, 52(6), p.1167-1194

Haq, B. U., Berggren, W. A., and Van Couvering, J. A., 1977. Corrected age of the Pliocene-Pleistocene boundary. Nature, 269(5628), p.483-488.

Haq, B. U., Herdenbol, J., and Vail, P. R., 1988. Mesozoic and Cenozoic chronostratigraphy and cycles of sea-level change. In: C. K. Wilgus, B. S. Hastings, C. A. Ross, H. W. Posamentier, J. Van Wagoner, C. G. St. C. Kendall, (eds.), Sea-level changes; an integrated approach. SEPM Spec. Publ. 42, p. 72-108.

Harash, A., 1967. The Geology Of The Yeroham - Dimona Plain. (In Hebrew). M.Sc. Thesis, Hebrew University Jerusalem, 72 p.

Heimann, A., Steinitz, G., Mor, D., and Shaliv, G., 1996a. The geochronology of the Cover Basalt: revised K-Ar and new $^{40}Ar/^{39}Ar$ results. Isr. Geol. Surv., Rept. GSI/6/96, 35 p.

Heimann, A., Steinitz, G., Mor, D., and Shaliv, G., 1996b. The Cover Basalt Formation, its age and its regional and tectonic setting: implications from K-Ar and $^{40}Ar/^{39}Ar$ geochronology. Isr. J. Earth Sci., 45(2), p. 55-71.

Heimann, A., Zilberman, E., and Amit, R., 1996. Paleoseismic survey in the Dead Sea Rift, Northern Israel: geological background - preliminary investigations and work program. Isr. Geol. Surv., Tech. Rept. TR-GSI/11/96, 15 p. (In Hebrew).

Hirsch, F., 1996. Geological Map of Israel, scale 1:50,000, sheet 19-II, Hamakhtesh Haqatan, Jerusalem.

Hirsch, F., and Roded, R., 1998. Towards a new 'Lexique': A computerized stratigraphical data base for Israel. Isr. Geol. Surv., Current Res., Vol. 11, p. 23-26.

Horowitz, A., 1973. Development of the Hula Basin, Israel. Isr. J. Earth Sci., 22(2), p. 107-139.

Horowitz, A., 1979. The Quaternary of Israel. New York, Academic Press, 394 p.

Horowitz, A., 1974. The Late Cenozoic stratigraphy and paleogeography of Israel. Tel Aviv Univ., Inst. Archaeol., 174 p., Figs.

Horowitz, A., 1979. Tertiary. Encycl. Hebraica, Vol. 31, p. 978-979. (In Hebrew).

Horowitz, A., 1992. Palynology of Arid Lands. Elsevier Publishers, Amsterdam, 546 p.

Horowitz, A., 1996. The principal stages of subsidence along the Dead Sea Rift. Isr. Geol. Soc., Ann. Meet. Abstr., p. 45.

Horowitz, A., 2001. The Jordan Rift Valley. A.A. Balkema, Lisse, 730 p. (Includes contributions by A. Flexer, A. Ginzburg, Z. Ben-Avraham and Z. Garfunkel).

Horowitz, A., and Horowitz, M., 1990a. Palynostratigraphy of Admon 1 Borehole. Isr. Natl. Oil Co., Tel Aviv, 12 p.

Horowitz, A., and Horowitz, M., 1990b. Palynostratigraphy of En Gedi 2 Borehole. Isr. Natl. Oil Co., Tel Aviv, 15 p.

Horowitz, A., and Zak, I., 1968. Preliminary palynological analysis of an evaporitic sequence from Mount Sedom (Israel). Rev. Palaeobot. Palynol., 7(1), p. 25-30.

Issar, A., 1961. The geology of the groundwater resources in the Shefela and Sharon regions. Unpublished Ph.D. Thesis, Hebrew University Jerusalem, (In Hebrew, English Abstract). Also Isr. Geol. Surv. & Tahal, 143 p., Figs.

Kafri, U., 1997. Neogene to Quaternary drainage systems and their relationship to young tectonics: Lower Galilee, Israel. Isr. Geol. Surv., Rept. GSI/1/97, 50 p.

Langozky, Y., 1963. High level lacustrine sediments in the Rift Valley at Sdom. Isr. J. Earth Sci., 12(1), p. 17-25.

Lartet, L., 1869. Essai sur la géologie de la Palestine et des contrées avoisinantes telles aue l'Égypte et l'Arabie, comprenant les observations recueillies dans le cours de l'expedition du Duc de Luynes à la mer Morte. Ann. Sci. Geol., Paris, Vol. 1, p. 1-116 & 149-329. Also Bibl. École Hautes Étud. Sci. Natur., Paris, 2(1), p. 5-296 & Vol. 7(3), 1873, p. 48-73. (Also: Paris, Imprimerie de E. Martinet, 292 & 95 p.).

Lipson, S., 1971. Micropaleontological study of some sections in the Golan Heights. Isr. Inst. Petrol. Energy, Micropaleontol. Lab., Rept. 7/71, 5 p. (Also published in Michelson, 1972).

Livnat, A., Kronfeld, J., 1990. Pleistocene lakes in the Arava Rift of Israel (Sayif Formation): facies and paleoenvironmental setting. J. Afr. Earth Sci., 10(3), p. 409-420.

Loewengart, S., 1927. The groundwater of Palestinian Coastal Plain. Construction & Industry, J. Assoc. Eng. Architects in Palestine, 6(5-6), p. 10-12 (In Hebrew); p. 13-14 (In English).

Loewengart, S., 1928. Zur Geologie der Kuestenebene Palaestinas. Centralbl. Mineral. Geol. Palaeontol., Vol. 9B, p. 498-519.

Lorch, J., and Fahn, A., 1959. A new species of Leguminoxylon from the Mio-Pliocene of Israel. Bull. Res. Coun. Israel, 71(2), p. 65-70.

Martinotti, G. M., Gvirtzman, G., and Buchbinder, B., 1978. The Late Miocene marine transgression in the Beer Sheva area. Isr. J. Earth Sci., 27(1-2), p. 72-81.

Michelson, H., 1972. Hydrogeology of Southern Golan Heights. Tahal, Tel Aviv, Rept. HR/72/37, 89 p. (In Hebrew).

Mimran, Y., 1984. Unconformities on the eastern flank of the Fari'a Anticline, and their implications on the structural evolution of Samaria (Central Israel). Isr. J. Earth Sci., 33(1-2), p. 1-11.

Neev, D., 1960. A pre-Neogene erosion channel in the southern Coastal Plain of Israel. Isr. Geol. Surv., Bull. 25, 21 p., Maps.

Neev, D., and Emery, K. O., 1967. The Dead Sea, depositional processes and environments of evaporites. Isr. Geol. Surv., Bull. 41, 147 p.

Neev, D., and Hall, J. K., 1979. Geophysical investigations in the Dead Sea. Sediment. Geol., 23(1/4), p. 209-238.

Pe'eri, S., 2003. Calculating the uplift of Mount Sodom using INSAR. Unpublished Ph.D. thesis, Tel Aviv University, ~150 p. (Hebrew abstract).

Pe'eri, S., Wdowinski, S., Shtibelman, A., Bechor, N., and Bock, Y., 1999. Current deformation across the Dead Sea fault as observed from 18 months of continuous GPS monitoring. Isr. Geol. Soc. Ann. Mtg. Abst., En Boqeq, p. 65.

Picard, L., 1928. Ueber die Verbreitung des Pliocaens im Noerdlichen Palaestina. Centralbl. Min., Abt. B, No. 5, p. 326-335.

Picard, L., 1932. Geologische Probleme am Suedrand des Tiberias Sees. J. Palest. Orient. Soc., Vol. 12, 6 p.

Picard, L., 1943. Structure and evolution of Palestine, with comparative notes on neighbouring countries. Hebrew University Jerusalem, Geol. Dept., Bull., 4(2-3-4), 187 p.

Picard, L., 1952. The geology of Kefar Giladi area. Eretz Israel, No. 2, p. 73-77. (In Hebrew).

Picard, L., and Avnimelech, M., 1937. On the geology of the central Coastal Plain. J. Palest. Orient. Soc., Vol. 17, p. 255-299. (Also Hebrew University Jerusalem,

Geol. Dept. Bull. 4, 45 p.).
Picard, L., and Kashai, E., 1958. On the lithostratigraphy and tectonics of the Carmel. Isr. Res. Counc., Bull., 7G(1), p. 1-19, Figs., Map.
Picard, L., and Solomonica, P., 1936. On the geology of the Gaza-Beer Sheba District. Palest. Orient. Soc., Vol. 16, p. 180-223, Map (Also Hebrew University Jerusalem, Geol. Dept., Bull., 1(2), 44 p.).
Picard, L., and Vroman, A., in Franklin, L., 1950. Oil Prospects of the Jordan Exploration Co. Ltd. Concession at the south end of the Dead Sea, Israel. Unpublished Report, Jordan Exploration Co. Ltd. Israel.
Raab, M., 1998. The origin of the evaporites in the Jordan-Dead Sea Valley in view of the evolution of brines and evaporites during seawater evaporation. Isr. Geol. Surv., Rept. GSI/1/98, 138 p. (Ph.D. Thesis, Hebrew University Jerusalem, 1996). (In Hebrew, English Abstract).
Reiss, Z., and Gvirtzman, G., 1966. Borelis from Israel. Eclogae Geol. Helv., 59(1), p. 437-447.
Roded, R., 1996. Geological map of Israel, 1:50,000: Dimona. Isr. Geol. Surv., 1 Map.
Roded, R., and Hirsch, F., 1987. Geomorphological history of Rotem-Yamin Basin in Neogene "Hazeva" time. Ann. Meet., Israel Geol. Soc., Israel, p. 105.
Rofe & Raffety Consulting Eng., 1965. Nablus District water resources survey. London, Report For Jordan Govt., Central Water Authority, 120 p., Appen., Maps.
Rosenberg, E., 1960. Geologische Untersuchungen in den Naftalibergen. (Am Rande des Noerdlichsten Teiles der Jordansenke, Israel). Zuerich Univ., Mitt. Geol. Inst. Eidg. Tech. Hochsch., Ser. C, No. 80, 107 p., Figs., Maps. (Unpublished Ph.D. Thesis, Zurich University)
Rosenfeld, A., and Raab, M., 1981. Lower Cretaceous Ostracodes from Israel. Isr. Geol. Surv., Current Res. 1980, p. 62-65.
Saltzman, U., 1964. The geology of the Tabgha-Hukok-Migdal area. Unpublished MSc thesis, Dept. Geol., Hebrew Univ. Jerusalem, 55 p. (In Hebrew).
Savage, R. J. G., and Tchernov, E., 1968. Miocene mammals of Israel. Proc. Geol. Soc. Lond. 1648, p. 98-101.
Schulman, N., 1957. The geology of the central Jordan Valley from Wadi Fejas to Wadi Ishshe. Unpublished M.Sc. Thesis, Hebrew University Jerusalem, 40 p., Fig., Geol. Map. (In Hebrew).
Schulman, N., 1959. The geology of the central Jordan Valley. Isr. Res. Counc., Bull., 8G(2-3), p. 63-90.
Schulman, N., 1962. The geology of the central Jordan Valley. Unpublished Ph.D. Thesis, Hebrew University Jerusalem, 103 p. (In Hebrew, English Abstract).
Schulman, N., and Rosenthal, E., 1968. Neogene and Quaternary of the Marma Feiyad area, south of Bet Shean. Isr. J. Earth Sci., 17(2), p. 54-62.
Shahar, Y., 1973. The Hazeva Formation in the Oron-Ef'e Syncline, Israel. Isr. J. Earth Sci., 22(1), p. 31-49.
Shahar, Y., Reiss, Z., and Gerry, E., 1966. A new outcrop of marine Neogene in the Negev. Isr. J. Earth Sci., 15(2), p. 82-84.
Shaliv, G., 1991. Stages in the tectonic and volcanic history of the Neogene Basin in the Lower Galilee and the valleys. (In Hebrew, English Abstract). Isr. Geol. Surv., Rept. GSI/11/91, 94 p. (Report based on Ph.D. Thesis, Hebrew University Jerusalem, 1989).
Shaliv, G., and Steinitz, G., 1988. K-Ar ages of Lower Basalt, Intermediate Basalt and base of Cover Basalt in Northern Israel. Isr. Geol. Surv., Current Res., Vol. 6, p. 22-28.
Shaw, S. H., 1947. Southern Palestine geological map on a scale of 1:250,000 with explanatory notes. Palestine, Govt. Printer, 42 p., Map.
Sneh, A., 1967. The Hazeva Formation. Isr. Geol. Surv., Rept. OD/6/67 & Inst. Petrol. Res. Geophys. Rept. No. 1023, p. 7-10. (Semi-annual Progress. for the period Oct. 1966 - March 1967).
Sneh, A., 1981. The Hazeva Formation in the Northern Arava, Israel. Isr. J. Earth Sci., 30(2-3), p. 81-92.
Sneh, A., 1982. Quaternary of the Northwestern Arava, Israel. Isr. J. Earth Sci., 31(1), p. 9-16.
Sneh, A., 1996. The Dead Sea Rift: lateral displacement and downfaulting phases. Tectonophysics, 263(1-4), p. 277-292.
Steinitz, G., and Bartov, Y., 1992. The Miocene-Pleistocene history of the Dead Sea segment of the rift in light of K-Ar ages of basalts. Isr. J. Earth Sci., (1992 For 1991), 40(1-4), p. 199-208.
Tchernov, E., Ginsburg, L., Tassy, P., and Goldsmith, N. F., 1987. Miocene mammals of the Negev (Israel). J. Verteb. Paleontol., 7(3), p. 284-310.
Weiler, Y., 1961. The geology of Nazareth and Tavor mountains. Unpublished M.Sc. Thesis, Dept. Geol., Hebrew University Jerusalem, 33 p. (In Hebrew).
Wellings, F. E., 1941. Oil prospects of Palèstine, Trans-Jordan, Syria and Cyprus. Iraq Petrol. Co. Ltd., Geol. Dept., Geol. Rept. 181, 30 p.
Wellings, F. E., 1944. Revision of South Palestine stratigraphy. Petrol. Dev. (Palestina), Geol. Rept. 182.
Wetzel, R., and Morton, D. M., 1959. Contribution à la géologie de la Transjordanie. Nôtes et Mémoires sur le Moyen Orient, Vol. 7, p. 95-191.
Wyllie, B. K. N., 1931. The geology of Jebel Usdum, Dead Sea. Geol. Mag., 68(806), p. 366-372.
Wyllie, B. K. N., Campbell, A. K., and Lees, G. M., 1922. Preliminary notes on Jebel Usdum, Dead Sea Area, Palestine. Turkish Petroleum Co., Geol. Rep., 16 p.
Yechieli, Y., 1987. The geology of the northern Arava Valley and Mahmal Anticline, Hazeva region. M.Sc. Thesis, Hebrew University Jerusalem, 94 p., Appen. (In Hebrew, English Abstract). (Also Isr. Geol. Surv., Rept. GSI/30/87).
Zak, I., 1967. The geology of Mount Sedom. (In Hebrew, English Abstract). Unpublished Ph.D. Thesis, Hebrew University Jerusalem, 208 p., Appendices, Plates.
Zilberman, E., 1977. The geology of the Sa'ad-Nafha lineament in the Avedat plateau. M.Sc. Thesis, Hebrew University, Jerusalem, 70 p. Also published as: The geology of the Sa'ad Nafha Lineament, Avedat Plateau. Isr. Geol. Surv., Rep. MM/6/77, 70 p. (In Hebrew).
Zilberman, E., 1992. Remnants of Miocene landscape in the central and northern Negev and their paleogeographical implications. Isr. Geol. Surv., Bull. 83, 54 p.
Zohary, M., 1959. Geobotany. Merhavia (Israel), Sifriat Poalim, 589 p. (In Hebrew).

Chapter 18I

The Late Pliocene to Quaternary of Israel

Francis Hirsch
Geological Survey of Israel, 30 Malchei Israel Street, Jerusalem 95501, Israel

INTRODUCTION

The present compilation is primarily based on data from the new edition of 'Lexique Stratigraphique' (Hirsch and Roded, 2001), including materials on the youngest sediments in Israel which Prof. Aharon Horowitz of Tel Aviv University kindly provided for that project.

The Late Pliocene, Pleistocene, and Holocene deposition treated in this chapter belongs to the following groups:

a) The Uppermost Saqiye Group and Kurkar Group, related to the Mediterranean, and;

b) The Hula Group, Central Jordan Valley Group, and Upper Dead Sea Group, related to the Dead Sea Rift.

The limit between Neogene and Quaternary can only be established with palynomorphs.

The Pleistocene of Israel can be correlated with the Mediterranean interglacial terraces and glacial stratigraphy.

TECTONO-SEDIMENTARY BACKGROUND

The Plio-Pleistocene deposits of Israel comprise marine Mediterranean Deposits, continental sediments draining into the Mediterranean, and Rift Formations consisting of deposits which either drained into the Dead Sea Rift, or strictly In-Rift Formations without an outside connection.

Neotectonic isostatic readjustments produced a reshaping of the Eastern Mediterranean and the Levant. The Eastern Mediterranean portion of the African Plate underwent uplift and deepening of its basins, echoing the differential uplift of the adjacent Levant-Sinai portion of the African Plate, dissected into Negev, Judean, and Galilee blocks. The sinking of the Dead Sea Rift, echoed by the uplifted Transjordan portion of the Arabian Plate, generated a totally new orography affecting the mountainous backbone of the Sinai-Levant sub-plate.

These tectonic events were further accompanied by volcanism on the Golan Heights and Eastern Galilee, filling also parts of the Yizre'el Valley and Jordan-Dead Sea-Arava Rift.

Since the Late Miocene opening of the Rift Valley, as the result of the collapse of the rhomb-shaped grabens that formed along the Jordan-Dead Sea-Arava line and were active since the end of the Oligocene, individualized intra-cratonic basins were formed, filled with the continental deposition of the Hula, Central Jordan Valley, and Upper Dead Sea Groups. The ongoing uplift of most of the territory of Israel since the proto-rift phase created new drainage patterns, one to the west, which inter-fingers with the marine Mediterranean deposition of the Kurkar Group, and one eastern pattern, branching into the Rift-Valley (Dead Sea, Jordan Valley, and Hula Valley). The neotectonic events are accompanied by the basalt, scoria, and tuff eruptions of the Bashan Group.

Late Pliocene global sea level drop

The late Pliocene global sea level drop ceased the flooding of the Jordan Valley and its surrounding regions, where lagoons, lakes and rivers deposited the suite of Pliocene formations described above. The base level was lowered with the regression, causing westward channeling toward the retreating sea, accompanied by slight structural disturbances and volcanism. The early Pleistocene Calabrian and Sicilian transgressions again raised sea level by approximately 120 and 90 m respectively, compared to the present day. These rises could not even closely reach the Jordan Valley region, instead depositing marine sediments only on the Mediterranean coastal plain (Horowitz, 1979). However the higher erosion base levels caused silting up of the drainage systems, leaving behind predominantly fluviatile sediments, with several intermediate lakes occupying several basins within the slowly subsiding Jordan Rift Valley (Levin and Horowitz, 1987).

In contrast with the pre-rift deposits of the Saqiye-Tiberias Groups and proto-rift formations of the Dead Sea Group, which run extensively over the Rift-borders, the in-Rift rocks of the Upper Dead Sea, Central Jordan Valley and Hula Groups have been deposited only within the limits of the narrow Rift Valley depression. Following its formation as an endoreic or internal drainage system some time during the early Quaternary, distinct basins formed, in which extensive subsidence caused accumulations of thousands of meters of lacustrine and fluviatile sediments (Horowitz, 1987, 1989; Horowitz and Horowitz, 1990). In spite of the considerable subsidence, the Hula and Central Jordan Valley Groups also experienced some differential uplifts, resulting in partial exposures of lateral facies of the entire sequences (Horowitz, 1979). The Dead Sea Basin, being the terminal base level of this system, shows extended subsidence and very little uplifting, thus its in-rift formations are almost entirely known from the subsurface. The three basins have been penetrated by deep boreholes and studied palynologically, resulting in age assignments to the various rock units.

Climate

As a general rule, Quaternary wetter periods caused spreading

of lakes over considerable areas of the Jordan Rift Valley, while drier times were characterized by their shrinkage. Consequently most formations deposited during the latter periods are only known from the subsurface, while wetter periods are represented also in outcrops, depending also on structural behavior. The in-rift formations were referred to three groups: the Hula Group, the Jordan Group of the central Jordan Valley, and the Upper Dead Sea Group (Horowitz, 1979). The last term is used for rock units deposited in the Dead Sea region ever since it became a terminal basin; the term 'Dead Sea Group' (Zak, 1967) also includes the underlying Sedom and Amora Formations, laid down when the area was still connected with the Mediterranean Sea.

In their shape, terraces formed by wadis and rivers descending from all sides into the rift depression bear witness to both tectonics and changing climates. Some wadis leading to the Dead Sea basin became lakes, usually of short duration (Bentor, 1946; Ginat, 1997). Abundant springs, mainly due to faulting, line the Jordan Valley and deposited travertines (Horowitz, 1979; Heimann, 1985; Kronfeld et al., 1988; Enmar et al., 1998). The eastern flank of the Rift enjoys more rain than the western, which is in the rain shadow zone. During the entire Quaternary this most probably also resulted in a greater number of perennial rivers and springs, depositing larger volumes of gravels in comparison with the western side of the Jordan Valley. Some in-rift volcanism is also known. [AH].

Table 18I.1, after Horowitz (1979), summarizes the Quaternary stratigraphy in Israel.

I. MEDITERRANEAN DEPOSITS

The Pliocene and Pleistocene 'Mediterranean' deposits of the Coastal Plain of Israel reflect the isostatic movements of the Levant Platform and the oscillations of the Mediterranean Sea prior to and during the glacial periods. The marine part of these deposits belongs to the **Uppermost Saqiye Group**, which primarily consists of the Ga'ash and Yarkon Formations, whereas the continental deposits make up the **Kurkar Group,** consisting traditionally of the Pleshet Formation, and the Ahuzam and Nahshon Conglomerates. The upper part of the Kurkar Group in the Coastal Plain consists of a dozen 'kurkar' dune ridges and red 'hamra' paleosols. Horowitz (1979) integrated these into the Gaza Formation. Gvirtzman et al. (1984) grouped more or less the same units into their Hefer Formation. The fluviatile systems of the HaMeshar Formation (Higher Negev) and Amud Conglomerate (Galilee) are apparently Mediterranean tributaries (Horowitz 1979).

The 'mountain top', 'Villafranchian' or Bethlehem Conglomerate (Judea) correlates with the Pleistocene Ahuzam Formation of the Mediterranean.

A. UPPERMOST SAQIYE GROUP

1. Ga'ash Formation Calabro-Sicilian

Horowitz (1974, 1979) established the type section from the 159-195 m depth interval of the Ga'ash-1 borehole. The sequence

Table 18I.1. Quaternary Stratigraphy in Israel (after Horowitz, 1979).

STAGE	AGE in years	PALYNO ZONES Q	COASTAL PLAIN KURKAR / U. SAQIYE GAZA / YARKON		JORDAN - DEAD SEA RIFT VALLEY HULA VALLEY	CENTRAL JORDAN V	UPPER DEAD SEA
RECENT	4.5 K	X	HADERA	L4	MALLAHA	REHOV	
ATLANTIC	7.5 K	X	TA'ARUHA		ASHMURA	TABGHA	
VERSILIAN	11.5 K	X	TEL AVIV				
LATE WÜRM	17 K	IX	NETANYA				
EPIMONASTIRIAN	22 K	IX	DOR	M3		LISAN	LISAN
MID WÜRM	30 K	IX					
LATE MONASTIRIAN	40 K	IX					
EARLY WÜRM	70 K	IX	NAHSHOLIM				HAMARMAR
MONASTIRIAN	130 K	VIII	RAMAT GAN	M2a	HULATA		
RISS	300 K	VII	HOLON		BENOT Y	NAHARAYIM	SAYIF Traver.
TYRRHENIAN	700 K	VI	GEDERA	M2	AYYELET		
MINDEL	1.0 M	V	DOROT		MISHMAR	UBEIDIYA	
MILAZZIAN	1.4 M	IV	KHARUVIT	M1	NOTERA		
GUENZ	1.7 M	III	KHESI		GADOT-HAZ	E. E. AHMAR	IDAN
SICILIAN	2.0 K	II	GA'ASH	GA'ASH	GONEN		
DONAU	2.4 K	I C			MAHANAYIM	MELECH SEDOM	
CALABRIAN	2.7 M	I B					
BIBER		I A					

comprises alternations of shale and calcareous sandstone and the top-shale contains fossils. The Ga'ash Formation crops out in Nahal Besor, near Kibbutz Urim. It overlies the Ahuzam Conglomerate over a base conglomerate. Toward the east, the marls interfinger with coastal sediments and beachrock at elevations of 110-125 m above m.s.l. The malacofauna (Moshkovitz, 1963, 1968) indicates a Calabro-Sicilian age. Synonymy: 'CP Unit' (Shahnai, 1967); 'Q-9 Unit' (Bar Yosef, 1964); 'Lower Gravel Series' (Picard, 1943); 'Villafranchian' (Avnimelech, 1943). It overlies the Petah Tiqwa Coquina Member at Ga'ash-1, and the Pleshet Formation and Ahuzam Conglomerate in the northwestern Negev. The Ga'ash Formation is overlain by the Gaza Formation. It interfingers westwards with the lower part of the marine Quaternary.

*2. **Yarkon Formation*** Glacial Pleistocene

Horowitz (1974, 1979) described this unit from the type section at the Reading 33-0 borehole.

Synonyms are the 'Pleshet Formation of marine origin', (Issar, 1968) or Sharon Formation. Overlies the Ga'ash Formation. Consists of six members M1A, M2, M3, M2A, M3 and M3A, and L4 (Reiss and Issar, 1961) with a total thickness of 170 m. Its lithology encompasses shales and limestone (M1A, depth 145-111 m), calcareous sandstone with *Marginipora* (M2, 111-58 m), calcareous sandstone with *Marginipora* and *Planorbulina*, conglomeratic upwards (M2A, 58-37 m), loamy sands (M3, 37-18 m), topped by continental sandstone (M3A, 18-4.5 m) and continental sands (L4). Rossignol (1969) recognizes ingressions and regressions. From the west, the Yarkon Formation passes laterally eastward into the Gaza Formation.

B. KURKAR GROUP

Established by Loewengart (1928), the Kurkar Group is derived from the so-called 'kurkar', consisting of marine calcareous sandstone, bio-clastic limestone, beach-rocks, and eolianites.

The Kurkar Group also encompasses 'Hamra', comprised of clayey silts and reddish sandstone, as well as conglomerates and non-consolidated dune sands.

The 'Kurkar' Group includes the various sandy formations overlying the Saqiye Group in the Coastal Plain and Hashephela. The Kurkar Group interfingers laterally with the Uppermost Saqiye Group.

The term Kurdane Series of Picard (1928) was applied to a 17 m thick sequence of calcareous sandstones and red limestones from the Haifa Bay area. Blake and Goldshmidt (1947) state that it unconformably overlies chalks of Eocene age and is overlain by limestones of undetermined age. The faunal assemblage seems to indicate a late Pliocene age (Blanckenhorn, 1927). It contains Carallinicеae, Miliolides, *Cassidulina*, and *Operculina* (?). Picard (1943) considered the Kurdane Series to be Lower Pleistocene.

Issar (1961) established the Sharon Formation in a borehole at Kefar Shalem, where the term designates marine to lagoonal clays, shales, silts, and marls. It is developed in four deep marine, shallow open marine, shallow marine, and lagoonal and brackish facies. The age is Neogene to Holocene. Issar (1960, 1961) also established the Rehovoth Formation, after a well at Rehovot. It includes all the reddish to brown silts, clays, loams and sandy loams, locally called Hamra. The facies types consist of terrestrial soils, found as red sands and loams and of limnic black to brown clays (Swamp deposits). The thickness is about 50 m. The age of the Rehovoth Formation is Pleistocene to Recent.

COASTAL PLAIN AND HASHEFELA

*1. **Pleshet Formation*** Late Pliocene-Early Pleistocene

Hull (1886) established the 'Calcareous Sandstone of Philistaea'. Issar (1961) called these beds 'Pleshet Formation'. Known also as 'Lithothamniumkalk' (Blanckenhorn, 1914); 'Kurkar' (Loewengart, 1928); 'Shelly Oolitic Limestone' (Blake, 1935); 'Abu Hareira Sandstone' (Picard and Solomonica, 1936) and considered 'Astian' by these authors or 'Pliocene' by Avnimelech (1953). The type-section was studied in the Migdal (Ashqelon) well No. 5a. The maximum thickness of this formation is 160 m.

Lithology: The Pleshet Formation includes all the calcareous sandstones and sandy limestones - locally called Kurkar - of the Coastal Plain. Conglomeratic sandstone is more abundant at the bottom. Three main rock facies were found in this formation:

a.) Littoral facies: Calcareous sandstone to sandy limestone, with mainly angular quartz grains and rather abundant mica flakes, rich in well-preserved microfossils such as foraminifera, ostracodes, bryozoa, etc.;

b.) Sea shore environment facies: characterized by calcareous sandstone rich in broken and rounded micro and macro shells of marine origin;

c.) Continental facies: found mainly in the form of concretional platy friable sandstone containing small rounded shell-pieces, broken shells, and casts of continental snails.

The Pleshet Formation is exposed in the Lower Hashephela and Coastal Plain only, in the Kefar Menahem-Tel Zafit area, and in the Nahal Shiqma-Tel Qeshet area.

The Pleshet Formation conformably overlies the Sharon Formation, or unconformably the various formations of the Saqiye Group. It is overlain by the Ahuzam and Nahshon Conglomerates and by subrecent soils and gravels. *Glycimeris* beds are abundant in the Pleshet Formation.

The age of the Pleshet Formation is Late Pliocene-Early Pleistocene (Gvirtzman and Buchbinder, 1969a).

*2. **Ahuzam Conglomerate*** Early Pleistocene

Issar (1961) described the type in a section near Ahuzam Village. Synonyms are 'Les Terrasses de Ouadi Sarar, Vallée d'Ayalon et de Ouadi en-Natuf' (Avnimelech, 1936); 'Upper and Lower Gravel Horizons' (Picard, 1943); 'Villafranchian' (Avnimelech, 1950); 'Ancient River Terrace of Quaternary-Neogene' (Picard, 1955); 'Unit Q IX' (Bar Yosef, 1964); 'The High Conglomerate' (Feldman, 1964). It is also described by Gvirtzman and Buchbinder (1969). It is 0-20 m thick, shaping the present day topographic plain of the lower Shefela.

Its polymict composition consists of pebbles from the Judea, Hashephela and Saqiye Groups, as well as pebbles from the Pleshet Formation, partly cemented by calcrete. It contains several calcic-palaeosol horizons, especially in the Beer Sheva Valley. The index of roundness is usually high, and sorting poor. The pebbles vary in size from a few millimeters up to 50 cm and even more. The matrix is sandy, calcareous or marly, and usually altered to nari.

The Ahuzam Conglomerate is exposed along the main wadis of Hashephela, as a river terrace, 20-50 m above the present river channels. It is extensively developed in the Ayalon Valley, in Nahal Soreq, Nahal Ha'ela, and Nahal Adorayim.

Contacts: The Ahuzam Conglomerate overlies formations of the Hashephela and Saqiye Groups, as well as the Pleshet Formation. In Hashephela the conglomerate occurs as river terraces, but towards the Coastal Plain it dips below the surface and is overlain by the young (Tyrrhenian) formations of the 'Kurkar' Group. The fluvial deposits of migrating channels and overbank deposits were subjected to soil weathering. These continental deposits follow the retreat of the sea from the shelf, though it cannot be related to a specific eustatic low-stand. It represents a tectonic uplift or tilting phase which preceded further flooding of the shelf despite the repeating high-stands of the Pleistocene. Buchbinder and Zilberman (1997) attribute a Pleistocene age to the Ahuzam Conglomerate, inferred from its position between the overlying Hefer Formation and underlying Pleshet Formation.

*3. **Gaza Formation*** Glacial Pleistocene (**Table 18I.2**)

The Gaza Formation consists of fossil 'kurkar' dune ridges and of red 'hamra' paleosols. It is of terrestrial origin, influenced by sea level and pedogenetic processes. Recognized in boreholes in the Gaza area, the formation is never exposed in its entirety. The Gaza Formation corresponds almost entirely to its junior synonym, the Hefer Formation, which was defined in the Jaffa-1 borehole.

Overlying the Ahuzam Conglomerate, the thickness of the Gaza Formation varies considerably though; in the Gaza area it reaches 80-90 m. It may overlie many previous Mio-Pliocene or even Cenomanian rock units, as in the Carmel and Sharon. The Gaza Formation interfingers laterally with the Ga'ash and Yarkon Formations. In the Be'er Sheva Basin of the Northwestern Negev, thick loess accumulations were designated as the Ruhama Loess Member, Monastirian through Recent in age (Horowitz, 1979). The formation overlies the Jaffa Formation in the Jaffa-1 borehole at a depth of 215 m.

Along the Hasharon coastal cliff, from Shefayim to Ga'ash and Netanya, the upper beds of the Gaza Formation are exposed and define the Ga'ash type or Shefayim Member (units 2-7), consisting of (top to bottom):

7. Hadera (dune sands, Roman-Byzantine artifacts);
6. Ta'arukha (unconsolidated sands with land snails and plant remains, Early Bronze-Byzantine artifacts);
5. Tel Aviv (eolianite kurkar);
4. Netanya (reddish loose sand, hamra);
3. Dor Kurkar bed (eolianite kurkar);
2. Nahsholim Hamra bed (loosely bedded silty sand, land snails),'café au lait' (Avnimelech, 1952);
1. Ramat Gan Kurkar Member (eolianite, kurkar).

The lower members of the Gaza Formation comprise, from top to bottom:

5. Holon Hamra Member and Ga'aton Travertine;
4. Gedera Kurkar Member;
3. Dorot Hamra Member;
2. Kharuvit Kurkar Member;
1. Khesi Conglomerate (=Ahuzam).

This sequence overlies the Ga'ash Formation. The term Ruhama Loess Member (Horowitz, 1974) was coined for extensive 25-30 m thick loess accumulations within the Gaza Formation, between Ruhama and Dorot, displaying alternative layers of white and buff colors. In the western part of the Coastal Plain it is developed in the facies of the Hefer Formation, overlying the Petah Tiqva member of the Yafo Formation. Gvirtzman et al. (1984) recognized the following members (top-bottom):

12. Tel Aviv (kurkar-eolianite) (Horowitz, 1979);
11. Netanya (hamra) (Avnimelech, 1952);
10. Givat Olga (kurkar-eolianite);
9. Kefar Vitkin (hamra);
8. Herzliyya (kurkar, eolianite and marine sandstone);
7. Poleg (hamra);
6. Ashdod (kurkar, eolianite and marine *Marginopora* sandstone;
5. Caesarea (terrestrial shale with plant remains);
4. Upper Bat Yam (kurkar, marine sandstone);
3. Nizzanim Member (hamra);
2. Lower Bat Yam Member (kurkar);
1. Dan (silts, clays and marine calcareous sandstone), *Gephyrocapsa oceanica, Hyalinea balthica.*

*4. **Nahshon Conglomerate*** Pleistocene

Buchbinder (1969) established the term after a section at Nahal Nahshon near Latrun, for 'Les Terrasses de Ouadi Sarar, Vallée d'Ayalon et de Ouadi en-Natuf' (Avnimelech, 1936); 'Ancient river Terrace of Quaternary-Neogene' (Picard, 1955); 'The Low Conglomerate' (Feldman, 1964); and Baq'a Conglomerate (Horowitz, 1974).

The up to 30 m thick polymictic conglomerate consists of pebbles from the Judea, Hashephela, Saqiye, and 'Kurkar' Groups. Many of the conglomerate components are reworked pebbles of the Beit Nir and Ahuzam Conglomerates. The index of roundness is high, and the sorting poor. The Nahshon Conglomerate is usually unconsolidated, the matrix consisting of alluvial soil and marls. The conglomerate is only slightly altered to nari.

Distribution: The Nahshon Conglomerate is found as low terraces (5-15 m above the wadi channels) in the wadis of Hashephela. It is widely distributed in the valleys of Nahal Ayalon, Nahal Soreq, and Nahal Ha'ela. Horowitz (1974) has established the Baq'a Conglomerate in the Jerusalem area, for the second bench of the Nahshon Conglomerate. The terraces of the Baq'a Conglomerate, yielding rich Acheulian artifacts (Arensburg and Bar Yosef, 1966; Stekelis, 1948), extend to the Negev, the Carmel,

Table 18I.2. Gaza Formation (Horowitz, 1974, 1975, 1979, p. 109-115). The Gaza Formation consists of fossil 'kurkar' dune ridges and of red 'hamra' paleosols. It is of terrestrial origin, influenced by sea level and pedogenetic processes. Recognized in boreholes in the Gaza area, the formation is never exposed in its entirety. The Gaza Formation corresponds **almost entirely to its junior synonym, the Hefer Formation, which was defined in the Jaffa-1 borehole.**

Overlying the Ahuzam Conglomerate, it comprises the following members from top to bottom:

RECENT	HISTORIC	HADERA DUNES
ATLANTIC	NEOLITHIC	TA'ARUKHA HAMRA
VERSILIAN		TEL AVIV KURKAR
LATE WURM	EPI-PALEOLITHIC	NETANYA HAMRA
MIDDLE WURM	LATE PALEOLITHIC	DOR KURKAR & TEL BARUCKH HAMRA
EARLY WURM	MIDDLE PALEOLITHIC	NAHSHOLIM HAMRA
MONASTIRIAN		RAMAT GAN KURKAR
RISS	LATE ACHEULIAN	HOLON HAMRA
TYRRHENIAN		GEDERA KURKAR
MINDEL	MIDDLE ACHEULIAN	DOROT HAMRA
MILAZZIAN		TEL FARA KURKAR
GUNZ	EARLY ACHEULIAN	HASI MEMBER (gravels, marsh deposits, paleosol)
SICILIAN		GERAR KURKAR
DONAU		ZE'ELIM HAMRA
CALABRIAN		HARUVIT KURKAR

The thickness of the Gaza Formation varies considerably though; in the Gaza area it reaches 80-90 m. It may overlie many previous Mio-Pliocene or even Cenomanian rock units, as in the Carmel and Sharon. The Gaza Formation interfingers laterally with the Ga'ash and Yarkon Formations. In the Be'er Sheva Basin of the Northwestern Negev, thick loess accumulations were designated as the Ruhama Loess Member, Monastirian through Recent in age (Horowitz, 1979).

and Upper Galilee. The Nahshon Conglomerate correlates with the Hasa Formation (Vita-Finzi, 1966) east of the Jordan River.

5. Amud Conglomerate

Kafri and Heimann (1994) defined a unit after Nahal Amud, west of Lake Kinneret, unconformably overlying late Cretaceous or early Tertiary rocks, filling a channel system which cuts through the Miocene Herod Conglomerate. The top is exposed, in places turned into hard caliche crust (Nari), or covered by some soil. As a result of subsequent erosion the Amud Conglomerate occurs in a few localities along Nahal Amud as lens-shaped bodies several meters thick and tens of meters in length.

The Amud Conglomerate is made up of rounded to sub-angular polymictic pebbles, from a few cm up to 20 cm across, mostly derived from nearby Cenomanian-Turonian carbonate rocks. Weathered basalt pebbles also occur, diminishing in number as one goes WNW. They are derived from the Amud Basalt and yield K-Ar ages of 2.7-2.3 Ma. The matrix is a slightly reddish chalk, which forms the caliche crust on the surface.

The Amud Conglomerate fills a drainage system that once flowed in a general WNW direction toward the Mediterranean Sea, most probably at the same time as or slightly younger than the Amud Basalt. Other conglomerate horizons of similar appearance from which artifacts are reported, located some 15-20 km to the north, are covered by the Dalton Basalt which yielded an age of 2.4 Ma (Ronen, 1996).

*6. **Bethlehem Conglomerate*** Early Pleistocene

Established by Gardner and Bate (1937), 'Bone Bearing Beds of Bethlehem'; emend. Horowitz (1974).

The unit is named after the city of Bethlehem, south of Jerusalem, where during the 1930s Gardner, Bate, and Stekelis had excavated what they described as a 'solution pothole', finding numerous bones and questionable artifacts. Solomonica (1948) and Horowitz (1974) recognized that this was not a local unit but rather had a regional occurrence, left by a fluviatile system. The type section is at Bethlehem, where some 10-12 m of this unit had been excavated.

The fluviatile sediments usually fill erosion channels cut into the late Cretaceous rocks of the Judean hills, but in places are also

incised into early Tertiary rocks, or a late Neogene erosion surface (Horowitz, 1979). The top is hardly ever covered, except by soil. The Bethlehem Conglomerate is exposed in many localities on the crests of the Judean Hills, at elevations of approximately 800 m above sea level, but also on both flanks of the watershed, at lower altitudes (Horowitz, 1979). Eastward it extends down to the Dead Sea region, where it is designated 'Ghor el Qatar Series'. To the west it is encountered down to some 200 m above the present day Mediterranean, where the Conglomerate overlies the Pliocene Pleshet Formation and is termed the Ahuzam Formation (Buchbinder and Sneh, 1983-1984). Thicknesses in the centers of the channels may attain 15 to 20 m.

The sequence comprises conglomerates and gravel embedded in red and green clays, talus and flint agglomerates, with components ranging in size from small, well-rounded pebbles to angular blocks over one meter across. Some gravel horizons have a hard carbonate matrix cementation. The clayey matrix comprises chiefly kaolinite, with up to 1% titanium, indicating a rather long transport and partly basaltic provenance, most probably east of the present Jordan Valley. Mammal bones unearthed in the Bethlehem 'pit' (Hooijer, 1958) include *Archidiskodon planifrons, Leptobos, Hipparion, Giraffa* cf. *Camelopardalis, Felis, Hippopotamus, Bos, Hipparion, Rhinoceros* cf. *Etruscus, Stegodon*, and *Elephas*. Among others, turtle bones are known from Bethlehem, while crocodile remains were found at Mount Scopus, north of Jerusalem. These fossils led to the generally accepted view of a Villafranchian age for the Bethlehem Conglomerate.

Cave Travertines

Numerous caves occur in wadis leading to the Jordan Valley, and almost all contain some accumulations of travertine. Most of these are small and had never been inhabited, but several larger ones were used for human shelter over long periods of time. The most famous are in Nahal Amud, a few km west of Lake Kinneret, and in Wadi Hareitun near Bethlehem, less than 20 km west of the Dead Sea. Both were uranium series dated by Schwarcz et al. (1980).

Dates obtained from the Zuttiyeh Cave in Nahal Amud suggest that an Acheulo-Yabrudian industry accumulated there, beginning approximately 150 Ka ago, replaced by Mousterian some 95 Ka ago. The 'ante-Neanderthal' skull fragments predate 164 Ka. A single date from Umm Qatafa Cave, Bed E1, yielded an age of 115±18 Ka for the contained artifact assemblage of ovate and lanceolate hand-axes, with a few Levallois-like flakes and other flake tools of Middle Paleolithic aspect.

THE NEGEV (Table 18I.3)

1. Adarim Formation Pliocene-Pleistocene

This unit was established by Roded et al. (2001) for the Red Unit (Roded et al., 1993) in Nahal 'Adarim, along the NW flanks of the Daya anticline, west of Dimona, northern Negev. The lower part of the sequence consists of sand, silt and clay, highly modified by pedogenic processes, which give it a typical reddish color. It is 10-15 m thick, forming steep slopes. The upper part consists of coarse conglomerates and contains allochthonous chert clasts originating from the Hazeva Formation, limestone and dolomite fragments from the Judea Group, as well as Eocene chalk. The size of the clasts ranges between few cm to 10-15 cm, but occasionally larger blocks up to one meter in size are also found. A thick calcrete crust covers the conglomerate and forms a hard cap rock paving today's interfluves. The conglomerate extends from the 'Aroer area in the southeastern part of the Be'er Sheva Valley to the Nevatim area in the west.

The Adarim Formation overlies the Late Cretaceous or Late Miocene continental sequence of the Hazeva Formation near 'Aroer and the Late Miocene marine Sheva Formation in the west near Nevatim. The 'Adarim Formation correlates with the Ahuzam Formation in the western Be'er Sheva valley, where it occupies a similar stratigraphic position.

2. Hameshar Formation Early Pleistocene

Garfunkel and Horowitz (1966); emended by Avni (1998) named the sequence after the HaMeshar (flatland) Valley in the central Negev. It was previously known by various names encompassing several other gravel beds, such as 'Quaternary-Neogene hammada' (Bentor and Vroman, 1957; Picard, 1959) and 'Alluvium and undivided Neogene-Quaternary Series' (Shaw, 1948).

In the rather deep channel of the drainage system in which the HaMeshar Formation was deposited, the sequence attains a thickness of several tens of meters. It consists almost entirely of conglomerates, whose flint, limestone, and dolomite pebbles are derived from the close vicinity. Rare magmatic, metamorphic, and quartzite pebbles are only found close to outcrops of the Arava Formation, from which they are redeposited. The local character of HaMeshar is particularly conspicuous when compared with the underlying Arava and Hazeva Formations. The size of the constituents varies from sand up to several tens of cm. The sorting is poor, the pebbles are angular to sub-rounded, and the angular and sub-angular often predominate. The matrix is loose, comprising carbonaceous silts or clays, occasionally of a reddish hue. Sandy horizons within the gravel layers are made of medium to coarse flint and limestone grains, with subordinate quartz, loosely cemented by carbonate or clayey matrix. Clay and chalk horizons occur in places. Two facies types are recognized: that of ancient channel fillings comprise the better-rounded gravel, occasionally bearing fine-grained layers, indicating a transition to temporary lacustrine conditions (Avni, 1997), while the floodplain deposits are extensive, rather thin, sedimentary sheets, typified by angular to sub-angular components.

The HaMeshar Formation overlies the Pliocene Arava Formation with a slight unconformity and also a variety of older formations. Its upper surface is usually exposed and eroded by wadis, all leading to the Dead Sea (Garfunkel and Horowitz, 1966; Horowitz, 1974, 1979).

The HaMeshar Formation is found in the entire southern Negev, where it covers considerable areas, usually as a veneer

Table 18I.3. Late Miocene–Pliocene–Pleistocene Formations (after Avni, 1998).

AGE	Age in Years	Central Negev Avni 1998		Southern Negev Garfunkel & Horowitz, 1966	Northern Arava Bentor & Vroman, 1957	Dead Sea Basin S&B 1991, Zak 1967, Levin 1985	SE Judea Agnon, 1983/ Hirsch, 1988	Beer-sheba Valley Roded et al., 1993	Eastern Arava Rabba 1994; Bender 1974	Southern Arava Garfunkel 1970/ Ginat et al. 1994
PLEISTOCENE	17 K 2.7 M	Zehiha Fm.		Hameishar Fm.		Arava/ Mor/ Amora		Ahuzam		Garof/ Eilot
PLIOCENE	2.7 M	Arava Fm.	Kuntilla Mb. --------- Saggi Mb	Hameishar Fm. --------- Arava Conglomerate	**Arava Conglomerate**	Arava/ Amora/ Meleh Sedom --------- Sedom	Arava/ Mor / Yeelim / Lot	Pleshet / Red Unit	Pla2/q2 --------- Plg1/q2	Garof/ Eilot
	5 M									
LATE MIOCENE						Basalt East of Dead Sea 6-9 Ma		Sheva Fm.		

several meters thick.

Remarks: For Avni (1998) the lower part of the HaMeshar Formation is part of the upper part of the Arava Formation, while his Zehiha Formation represents its upper part. The latter is based on his correlation with the Nahal Zihor lake sediments, the drainage of which led to the Dead Sea. Reconstructing the drainage system, Garfunkel and Horowitz (1966) concluded that it led to the Mediterranean, without any notable depression in the Arava at that time (Horowitz, 1979).

Age: In the absence of fossils, the early Pleistocene age of the Hameshar Formation, assigned by Garfunkel and Horowitz (*op. cit.*), is based on its stratigraphic position, younger than the Arava Formation and cut by the wadis leading to the Dead Sea.

3. Zehiha Formation Palynozones QII -QIII

In Nahal Zihor, Southern Negev, Ginat (1997) described a wadi that ran through the northern Arava over a distance of some 90-100 km to the Dead Sea. Named after the closeby Zehiha (extremely arid) hills, the Zehiha Formation rests unconformably on Arava and older formations. In places, caliche horizons may underlie or interwedge a so-called 'Red unit', which replaces the lateral fluviatile facies of the lake sediments. Terrace Q1 covers the top gravel bed of the unit. (**Figure 18I.1**).

The lacustrine facies reaches a thickness up to 20 m, covering an area of approximately 20 km^2. The Zehiha Lake may have been larger, as witnessed by somewhat more detritic, possibly correlative outcrops, closer to the Arava, notably at Biq'at Demama (silence valley) some 10 km north of Gav Ha'Arava, where a section of 45 m is described in Ginat (1997).

At Nahal Zihor it comprises 10 m of alternating white and green limestones, the latter detritic, with several thin highly organic black clay beds. The sequence is made of three such cycles, separated by minor unconformities. It grades laterally into a fluviatile 'Red unit', made principally of sands and gravel, itself grading laterally into a suite of paleosols.

The Zehiha Formation is very rich in freshwater fossils, such as mollusks, ostracods, fish, and charophytes. Typical freshwater ostracods are *Candona angulata, Cypridopsis* sp., and *Cypris pubera* (Rosenfeld, in Ginat, 1997). (**Figure 18I.2 and Plate 18I. I**). These ostracods are also found in the Erk el Ahmar and Ubeidiya Formations (Rosenfeld et al., 1981). Of the variety of mollusks found in the Zehiha Formation, *Melanoides dadiana* and *M. jordanica* (Tchernov, in Ginat, 1997) are characteristic of the Erk el Ahmar Formation at the central Jordan Valley (Schütt and Ortal, 1993), while the rest occur along the entire Quaternary sequence. Pollen grains have also been recovered, indicating Palynozone QIII for the lake sediments, and QII for the Red unit underlying the lake sediments (Horowitz, in Ginat, 1997). Avni (1997) attempted to define a gravelly correlative of the Zehiha further north. However, this bed constitutes part of the HaMeshar Formation (Garfunkel and Horowitz, 1966), which is older than the lake sediments, of QI Palynozone (Horowitz, 1992). Large, crude, Lower Paleolithic artifacts and flakes (Ginat and Saragusti, 1996), found in intimate connections with the Zehiha Formation's lake shore sediments, are

however doubtfully *in situ* (Saragusti, pers. comm. - in Horowitz, 2001).

II. RIFT FORMATIONS

The Plio-Pleistocene 'In Rift formations' (Horowitz, 2001) consist of fluvial terraces and lake deposits. Conglomerates, sands and marls alternate with travertines. They subdivide into three groups.

1) The **Hula Group** comprises the Mahanayim Marl, Gonen, Gadot, Hazor, Notera, Mishmar HaYarden, Ayyelet HaShahar, Benot Ya'aqov, Hulata, Ashmura, Mallaha, and various gravel bed formations. Travertines include the Kefar Yuval, Dan, Fasayil, Sayif, and Mo'a sub-recent and cave-travertines.

2) The **Central Jordan Valley Group** comprises the Erk el Ahmar, Ubeidiya, Naharayim, Lisan, Tabgha, and Rehov Formations. Travertines include the Bet She'an Formation.

3) The **Upper Dead Sea Group** comprises the Idan Formation, Melekh Sedom Sands, Lisan Formation and 'Post-Lisan Deposits'. Travertines include the Nahal Zin and sub-recent travertines.

These formations, often known from boreholes, are almost always thicker within the Jordan-Dead Sea Basin than outside. Their nature and extent is controlled both by tectonics and by sea level changes, while climate played a subordinate role. The stratigraphic terms of these formations and erosion phases are therefore those defined by the late Cenozoic changes in sea level (Horowitz, 2001).

A. HULA GROUP

Horowitz (1973) and Horowitz and Horowitz (1985) applied this term to a suite of formations confined to the Hula Basin. Due to locally uplifted small blocks, their marginal facies is mostly exposed at the southern end of the valley, in the vicinity of the Benot Ya'aqov Bridge. However, the bulk of the Hula Group is buried within the basin itself, known from several boreholes such as Notera-3 and Emeq Hula-1. Picard (1952) referred to the upper part of the group, penetrated by boreholes down to 120 m below the surface, as the 'Hula Series'. The group only includes those formations laid down in the basin since the Dead Sea became an endoreic system, approximately two million years ago (Horowitz and Horowitz, 1985, 1990; Kafri and Heimann, 1994).

The question remains open whether the Hula drained to the north through the Litani River, or the Litani has flowed into the Hula (Heimann, 1985).

The majority of the Hula Group comprises lacustrine sediments, on the valley's rims all around, grading laterally into fluvio-lacustrine, fluviatile, and spring deposits and soils. Under certain conditions, mostly climatic, the Hula Lake shrank to give way to marshes, in which highly organic sediments, often peat, were accumulated, especially in the upper part of the sequence. Subordinate volcanism occasionally intercalates within the sedimentary column.

It seems (Horowitz, 1973) that most of the sediments accumulated in rather shallow lakes, the rates of subsidence of the substrate approximately coinciding with the rates of deposition. The Hula Basin always supported intermediate lakes, except for some short periods in which the sediments are barren of autochthonous fossils (such as the Gadot and the lower part of Ashmura Formation), possibly indicating increased salinity.

Pioneering studies of the Hula Group, both from outcrops and boreholes, were carried out by Picard (1952, 1963, 1965), Bein (1967) and others (unpublished) in connection with the possible exploitation of the abundant peat and natural gas. Detailed palynostratigraphic studies throughout the last 25 years enabled clarification of the stratigraphy and chronology of the basin's fill. The various formations of the Hula Group are named after localities in the Hula Valley. The entire Hula Group sequence was penetrated in the Notera-3 borehole, drilled at the center of the basin, where all the formations conformably overlie one another. A rich malacofauna (Tchernov, 1973, 1979; Schütt and Ortal, 1993) as well as diatoms (Ehrlich, 1973) contribute to many of the conclusions reached below. The suite of the Hula Group seems to start with the Mahanayim Marl

1. Mahanayim Marl

Heimann (1990) introduced the unit, named after a closeby settlement. The type section is at the Ayyelet HaShahar quarry, some 2 km to the north. The base is not exposed. The only 3 m thick marl is known in only one exposure in the Hula Valley, where it is overlain, probably conformably, by a basalt sheet. It comprises gray marl, chalk and clays, rich in *Melanopsis* shells. The overlying basalt yielded K-Ar ages of 2.3 Ma at the base, up to 1.6 Ma for its top. Based on these ages, Heimann correlated the Mahanayim and the basalt with a sequence drilled 11 km to the north, in the Notera-3 borehole, at depths of 1000-1600 m, which overlies Pliocene deposits.

2. Gonen Formation Palynozone QII

Horowitz and Horowitz (1985) report this formation only from the Notera-3 borehole, from depths of 1300 up to 1235 m. The base rests on Melekh Sedom Sands (Palynozone QI) and the Ruman Basalt. The formation is only encountered in a single borehole. The Gonen Formation seems to be time equivalent with the erosion surface over which the Gadot and Hazor Formations were laid down. Lithology comprises sandy, somewhat organic marls deposited in a shallow lake or marshes, in which several basalt flows interfinger. Abundant pollen grains assign the Gonen Formation to Palynozone QII.

3. Gadot and Hazor Formations Palynozone QIII

The Gadot Formation was established by Picard (1952), as 'Gadot Chalk'; emended by Horowitz (1973), after the nearby settlement of Gadot. The formation overlies the Ruman Basalt (Heimann, 1990), previously considered part of the Cover Basalt (Horowitz, 1979), over an erosional and taphrogenic unconformity. In the Notera-3 borehole the Gadot Formation conformably overlies the Gonen Formation, and is similarly overlain by the Notera

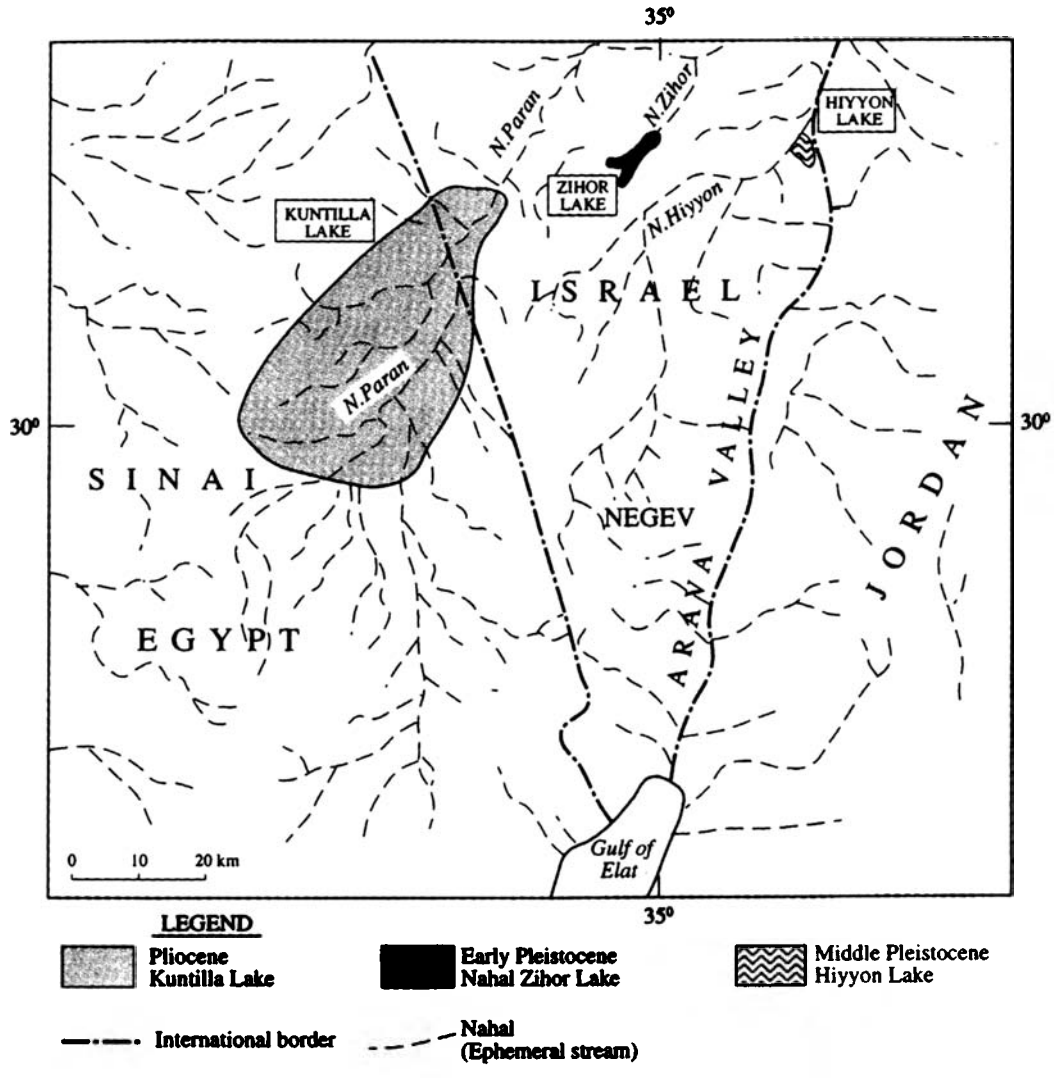


Figure 18I.1. Location map of Plio-Pleistocene lakes in southern Israel (from Rosenfeld et al., 2002, p. 87, Fig.1, modified after Ginat et al., 1996).

Formation. At Benot Ya'aqov, the Gadot Formation is overlain by a lateral equivalent of the Notera Formation and Mishmar HaYarden Formation. The Yarda Basalt fills ravines deeply cut into the Gadot Formation, which led Picard (1963) and Schulman (1967) to consider the volcanics older than the sediments. The Gadot Formation occurs in the southern part of the Hula Valley, north of the Korazim Block, covering an area of several square kilometers. In several localities the Gadot Formation interfingers with the Hazor Formation. On the order of 25-30 m thick at the outcrops, the Gadot Formation attains a thickness of up to a hundred meters in some boreholes (Heimann, 1990) and 145 m at Notera-3 (Horowitz and Horowitz, 1985). The Gadot Formation is made of white to buff, massive, rather dense lacustrine chalk, in which only rare *Melanopsis* shells were found. Westward, the chalk grades laterally into the gravel of the Hazor Formation. The Gadot Formation was deposited in a lake extending somewhat south of the present day Hula Valley. The chalk may indicate a rather saline lake, which did not favor life on its bottom. The lake was shallow, as can be seen from the interfingering gravel horizons, which hardly display any depositional dips.

The 'Hazor Gravel' of Picard (1952), emended by Horowitz (1973) is named after the nearby settlement of Tel Hazor. Like the Gadot Formation, the Hazor Formation overlies the Ruman Basalt (Heimann, 1990), over an erosional and taphrogenic unconformity. The Yarda Basalt overlies the Hazor Formation unconformably. Like the Gadot Formation, the Hazor Formation occurs in the southern part of the Hula Valley, north of the Korazim Block, often interfingering with the Gadot Formation. The 25-145 m thick Hazor Formation consists of coarse, polymictic, poorly sorted, rounded to sub-angular gravels, with boulders up to 20-30 cm in

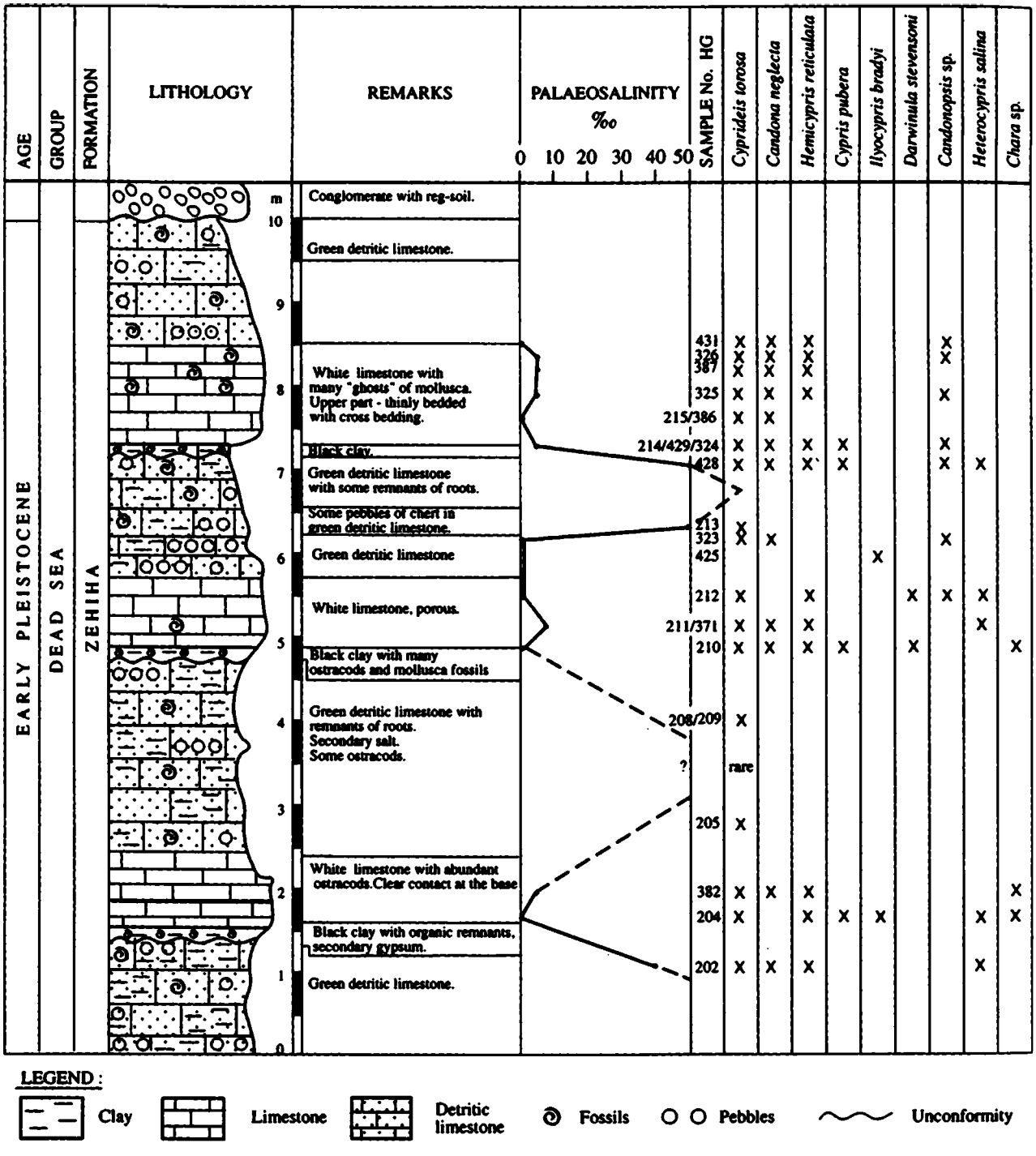


Figure 18I.2. The Early Pleistocene Zehiha Formation at Lake Zihor; salinity and ostracod distribution (from Rosenfeld et al., 2002, Fig. 3, p. 90). Ostracod distribution modified after Ginat et al., 1996, and paleosalinity changes are based on the sieve-pore shape method in *Cyprideis torosa* (Rosenfeld and Vesper, 1977).

diameter, mostly deriving from Eocene rocks, but some from late Cretaceous, and some are weathered basalt components.

The environment is one of rivers leading to the Gadot Lake. The Hazor Gravel extends eastward to the lower reaches of the eastern Galilee hills (Heimann, 1990), covered by caliche and soil, where it overlies late Cretaceous through Eocene rocks and also the Dalton Basalt.

Based on pollen assemblages, both the Gadot and Hazor Formations are assigned to Palynozone QIII. Radiometric datings of the underlying Ruman and overlying Yarda Basalts led Heimann to assign an interval of 1.6-0.9 Ma for the Gadot and Hazor Formations. Since the Yarda overlies also the Mishmar HaYarden Formation, the younger age limit seems too young. Heimann views the Egel and possibly Si'on gravels as correlative, at least partly, with the Hazor Formation.

*4. **Notera Formation*** Palynozone QIV.

Horowitz and Horowitz (1985) established the formation at the Notera-3 borehole, from a depth of 1090 up to 850 m. The sequence is mainly made of chalk, somewhat organic in the lower part, and sandy in the middle; the top is interfingered by several basalt flows. At the type section the Notera Formation conformably overlies the underlying Gadot Formation and is overlain by the Mishmar HaYarden Formation.

At the Benot Ya'aqov Bridge outcrop, a 2 m thick, grayish-brown paleosol separates the Gadot and Mishmar HaYarden Formations. The light color and high carbonate content, as opposed to more common red paleosols, indicates its formation under relatively dry conditions, supporting its correlation with the Notera Formation. The sediments indicate a shallow lacustrine environment, occasionally grading to a paludine or marsh-like environment. Pollen grains indicate Palynozone QIV.

*5. **Mishmar Hayarden Formation*** Palynozone QV

The 'Tilted Villafranchian Beds - *Melanopsis* Stage' of Picard (1963) were emended by Horowitz (1973).

The type section was taken at its only outcrop, at Benot Ya'aqov. It is however well developed in boreholes. At the outcrop, the Mishmar HaYarden Formation is separated from the underlying Gadot Formation by a paleosol, which is also a lateral equivalent of the Notera Formation. The Yarda Basalt covers it, probably unconformably. The thickness at Benot Ya'aqov is only a few meters, comprising white to buff lacustrine chalk and marl, very rich in mollusks and vertebrate bones. The top layer is made of 30-40 cm of peat. In the Notera-3 borehole the sequence attains 133 m of mainly lacustrine marls, somewhat organic, occasionally turning into limestone layers. The upper part contains several paleosol horizons, derived from weathered basalts.

Among the vertebrates, hippopotamus bones are the most common. Mollusks (Tchernov, 1973, 1987) include *Theodoxus jordani, Valvata saulcyi, Bulimus hawaderiana, Melanopsis praemorsa, Lymnaea lagotis, L. palustris, Planorbis planorbis, Gyraulus piscinarum, Anisus spirorbis, Segmentina nitidae, Ancylus fluviatilis, Succinea pfeifferi, Pisidium casertanum*, and *Unio terminalis*.

Several artifacts, mostly large flakes, had been found in the Mishmar HaYarden Formation, which bear a general resemblance to assemblages from Ubeidiya (Horowitz et al., 1973; Bar-Yosef in Horowitz, 1979). Horowitz and Horowitz (1985) attributed the Mishmar HaYarden Formation to Palynozone QV. Heimann (1990) considered the Mishmar HaYarden to be an upper member of the Gadot Formation; however this view is not acceptable, since at the Notera-3 borehole the two formations are separated by the 240 m of the Notera Formation.

*6. **Ayyelet Hashahar Formation*** Palynozone QVI

Horowitz (1973) established the Ayyelet HaShahar Formation at the Emeq Hula-1 borehole, from its bottom, at 455 m, up to depth of 340 m. It was further penetrated in the Notera-3 borehole from 345 down to 717 m, which represents a full section, conformably overlying the Mishmar HaYarden Formation. In both boreholes the Benot Ya'aqov Formation conformably overlies the Ayyelet HaShahar Formation. Consisting mainly of marls, several distinct peat layers as well as basalt tongues interfinger the sequence. Mollusk remains include *Melanopsis, Melanoides*, and *Theodoxus* recovered from the drill cuttings, while abundant pollen belong in Palynozone QVI. An unconformity which is both erosional and structural, separating the Mishmar HaYarden and Benot Ya'aqov Formations at the outcrop, is a time equivalent of the Ayyelet HaShahar Formation.

*7. **Benot Ya'akov Formation*** Palynozone QVII

Stekelis et al. (1937) named the 'Benat-Yaqub Gravel'; also named 'Lower Lacustrine' (Picard, 1952) and 'Jordan Terrace' (Picard, 1963); it was emended by Horowitz (1973).

The type section is near the Benot Ya'aqov Bridge. The Hebrew name 'Benot Ya'aqov' or Benat Yaqub in Arabic, was translated from 'Filles de Saint Jacques', an order whose nuns acquired concession for passage at this locality in the 19th Century. At base, a conglomerate overlies the faulted and eroded relief of the Mishmar HaYarden Formation and the Yarda Basalt. The overlying base conglomerate of the Ashmura Formation truncates the Benot Ya'akov beds. The outcrop stretches along the Jordan River gorge over a few km from south of the former Hula Lake to south of the bridge at Benot Ya'aqov. The emended type section is at the Emeq Hula-1 borehole, where it is fully developed between depths of 155 to 340 m. In many drillings in the Hula Valley it lies conformably between the Ayyelet HaShahar Formation below and the Hulata Formation above.

A single, very limited outcrop south of Lake Kinneret (Braun and Tchernov, 1991) appears lithologically and faunistically similar to the Benot Ya'aqov Formation, bearing plenty of *Viviparus apameae*. Mainly shallow lacustrine marls, organic to some degree in the lower and upper parts, much more so in the middle sector, are very rich in mollusks shells both at the outcrops and the boreholes. The lacustrine sediments grade into fluviatile gravels southward, westward and eastward toward the valley margins, and northward into extensive travertine sheets. The most abundant mollusk is *Viviparus apameae galileae*, typical only for this formation (Schütt and Ortal, 1993), as are also *Semisalsa longiscata, Melanopsis corrugata*, and *M. blanckenhorni*. Others include numerous *Valvata saulcyi, Bythinella* sp., *Bulimus hawaderiana, Melanpsis praemorsa*, and *Pisidium casertanum*. Less frequent are *Theodoxus jordani, Lymnaea lagotis, Gyraulus piscinarum*, and *Unio terminalis*. The outcrop at Benot Ya'aqov



EXPLANATION OF PLATE 1

1. *Candona neglecta* Sars, 1888, female right valve, Lake Zihor, sample HG 428.
2. *Candona neglecta* Sars, 1888, male right valve, Lake Kuntilla, sample YA 11.
3. *Eucypris stephanidesi* Petkovski, 1959, right valve, Lake Hiyyon, sample NH 2c.
4. *Darwinula stevensoni* (Brady and Robertson, 1870), left valve, Lake Zihor, sample HG 212.
5. *Hemicypris reticulata* (Klie, 1930), left valve, Lake Zihor, sample HG 428.
6. *Cyprideis torosa* (Jones, 1850), left valve, Lake Zihor, sample HG 428.
7. *Chara* sp., Lake Kuntilla, sample YA 13.
8. *Ilyocypris bradyi* Sars, 1890, right valve, Lake Zihor, sample HG 425.
9. *Cypris pubera* Mueller, 1776, left valve, Lake Zihor, sample HG 428.
10. *Candonopsis* sp., left valve, Lake Hiyyon, sample NH 2c.
11. *Heterocypris salina* (Brady, 1868), right valve, Lake Hiyyon, sample NH 3a.

PLATE 18I.1: Plio-Pleistocene Ostracods of the Negev lakes (Southern Israel) (from Rosenfeld et al., 2002, Plate 1, p. 88).

yielded abundant vertebrate fossils described in detail in Hooijer (1959, 1960), including *Equus* cf. *Caballus, Elephas trogontherii, Dicerorhinus merckii, Sus* cf. *Scrofa, Hippopotamus amphibius, Dama* cf. *mesopotamica, Cervus* cf. *elaphus,* cf. *Bison priscus*, and *Stegodon mediterraneus*.

At the same locality, rich flint and basalt artifact assemblages (Stekelis, 1960; Gilead, 1970; Goren-Inbar, 1995), as well as a human femur (Geraads and Tchernov, 1983) were found. Pollen assigns the Benot Ya'aqov Formation to Palynozone QVII. Diatoms are very abundant, with dominant planktonic species such as *Cyclotella kutzingiana, Melosira ambigua, Stephanodiscus astraea,* and *Fragilaria* spp. The sediments and diatoms indicate that the Benot Ya'aqov was deposited in a fairly deep alkaline lake, extending beyond the present day limits of the Hula Valley. The middle part was laid down in a smaller, rather shallow lake, or in marshes.

8. Hulata Formation Palynozone QVIII

The 'Main Peat' of Picard (1952) was defined in the No. Zero borehole at the northern border of the former Hula Lake and emended by Horowitz (1973) to Hulata Formation. It is conformably sandwiched between the Benot Ya'aqov and the overlying Ashmura Formation in the Emeq Hula-1 borehole. The formation was also penetrated by numerous drillings all around the Hula Valley, but is not known from outcrops, save for some lateral gravel horizons (Heimann, 1985). The sequence at the No. Zero borehole comprises 54 m, of which the lower 20 m and upper 19 m consist of massive peat. The 15 m thick middle part is mainly made of peat with several limnic chalk intercalations. The thickest 75 m sequence, somewhat more marly, was encountered in the Emeq Hula-1 borehole. Pollen assemblages assign the Hulata Formation to Palynozone QVIII. Diatoms include high percentages of epiphytic species such as *Epithemia,* which together with abundant Chrysostomaceae and phytoliths indicate a very shallow, alkaline, eutrophic water environment of deposition.

9. Ashmura Formation Palynozones QIX- QX

Horowitz (1973) emended the 'Upper Lacustrine' beds of Picard (1952) to Ashmura Formation. The type section consists of the uppermost 80 m in Emeq Hula-1 borehole and comprises white to gray lacustrine chalk, with several horizons rich in organic material. Northward, the Ashmura grades into gravel and paleosols, interfingering with extensive travertines (Heimann, 1985). The Ashmura Formation is found all over the Hula Valley, deposited in a lake that occupied the region until recently, when it was artificially drained. During the Holocene the lake gradually shrank, giving way to marshes to the north, where peat of the Mallaha Formation was deposited. Known in boreholes all around the Hula Valley, it is also exposed along the Jordan River to the south, down to the Benot Ya'aqov Bridge. It was deposited on the northern edge of the Korazim Block until about 4500 years ago, when this area was tectonically uplifted (Carmi, in Horowitz, 1979). It conformably overlies the Hulata Formation. In localities where the latter is present, the upper part of the Ashmura Formation grades laterally into the Mallaha Formation, passing from lake into marsh deposits. In places where the Hulata Formation is absent, the Ashmura Formation unconformably overlies older rocks, occasionally over a base conglomerate.

Fauna: A rich mollusk assemblage occurs in the uppermost meters, comprising *Theodoxus jordani, Valvata saulcyi, Bythinella* sp., *Bulimus hawaderiana, Melanpsis praemorsa, Melanoides tuberculata, Lymnaea lagotis, Gyraulus piscinarum, Ancylus fluviatilis, Succinea pfeifferi, Pisidium casertanum, Sphaerium* sp., *Corbicula fluminalis*, and *Unio terminalis.*

Diatoms are quite abundant, especially planktonic forms such as *Cyclotella* and *Melosira*. Benthonic diatoms are only accessories, while epiphytic are rare, indicating a fairly deep, alkaline, freshwater lake, similar to the lake in which the Benot Ya'aqov Formation was deposited. The Ashmura Formation diatoms compare well to those of the underlying Hulata Formation. The uppermost part is characterized by an abundance of epiphytic diatoms, indicating shallowing of the lake. Pollen assemblages of the Ashmura assign the major part of the sequence to Palynozone QIX, while the uppermost part is QX. The outcrops at Benot Ya'aqov yielded some artifacts, ranging from Mousterian at the lower part through to Chalcolithic and Early Bronze at the top (Bar-Yosef, in Horowitz, 1979).

10. Mallaha Formation

The 'Upper Peat' of Picard (1952); emended by Horowitz (1971). The type section is from the UP-15 borehole, drilled in the center of the marsh area north of the Hula Lake. It comprises 12.7 m of peat, conformably but diachronously overlying and grading laterally to the Ashmura Formation (see above). The peat is abundant in the northern part of the Hula Valley, occupied until recently by marshes which were then artificially drained. Fossils are quite rare in the Mallaha Formation. Abundant pollen grains indicate the upper part of Palynozone QX. Diatoms consist of a fairly poor epiphytic flora dominated by *Fragillaria* and some acidophilous forms such as *Eunotia*. Abundant sponge spicules, phytoliths, and Chrysostomaceae cysts indicate the somewhat more acid environment of a very shallow, eutrophic water body mixed with some acid waters, in comparison with the underlying Ashmura Formation. Eastward, westward and northward the Mallaha grades into soils, some gravel, and subordinate spring deposits. Radiocarbon dates indicate the Mallaha Formation deposition commenced some 4500 years ago at its deepest occurrence (Horowitz, 1971). The base is however diachronous, transgressive over the Ashmura, becoming progressively more so southward.

Gravels

'Gehaenge-Shutt'-type gravels, similar in their relation to time and conditions of deposition along steep mountain slopes, though different as to the source of their lithologies, have been described in the Hula Valley.

The 'Si'on Gravel' (Mor, 1986) in the northern Hula Valley, descending from the slopes of Mount Hermon, is a sequence of some 80+ m of gravels chiefly made up of Jurassic Mount Hermon

components. The Si'on is considered by Heimann (1985) to be the northern correlative of the Hazor Formation. However Heimann (1990) sees the Si'on Gravel as a marginal equivalent of most of the lacustrine Quaternary formations of the Hula Basin. The Si'on Gravel is 'equivalent' to another similar feature, termed the 'Dishon Gravel'.

The 'Dishon Gravel' (Heimann, 1990) occurs on the eastern slopes of the Galilee hills.

The 'Buteiha Gravel' (Mor, 1986) is made of basalt pebbles, and is found along the Golan Escarpment, down to Lake Kinneret.

The 'Egel Gravel' (Heimann, 1985) is 10-40 m thick, consisting of Jurassic, Cretaceous, and possibly Pliocene components, cemented by a reddish, hard calcareous matrix. It occurs at the northern end of the Hula Valley. Heimann suggests its correlation with the Hazor Formation and Si'on Gravel, from which it differs in its components, indicating a different hinterland. Heimann (1990) regarded the two gravels as separate entities. However, Horowitz (1973), Sneh (1996), and Kafri (1998, pers. comm.) consider these gravel beds as correlative with the Pliocene Tanur Conglomerate, viewing the differences in pebble lithology as due to different sources. Since nothing conclusive changes this view, it is still held here.

Travertines

The Kfar Yuval Travertine was named by Picard (1963) after a settlement in the northern Hula Valley, where it is unconformably sandwiched between volcanic flows. It overlies the Hasbani (as redefined in Heimann, 1985) and Dalwe Basalts, dated at around one million years (Heimann and Sass, 1989), and underlies the Ma'yan Barukh Basalt, previously termed 'Hasbani' (Horowitz, 1979) and dated at 73±14 Ka (Siedner and Horowitz, 1974), or some red, clayey paleosols. In places, the younger Dan Travertine directly overlies the Kefar Yuval; occasionally the two are quite difficult to differentiate. Middle to Upper Acheulian artifacts are found in intimate connection with the Travertine. Laterally, the spring deposits grade to clastics, designated the 'Si'on Gravel' by Heimann (1985).

The Kefar Yuval extends over approximately 18 km². In the northern Hula Valley its thickness varies from two up to 30 m. The carbonate rocks are porous to very porous and soft, occasionally hard, massive, with rare traces of bedding, and in most localities very rich in well-preserved plant molds. Stromatolite-like structures are quite common in places. Fossil plants recovered from the layers (Danin and Lev-Ari, in Heimann and Sass, 1989) include leaves of *Quercus ithaburensis, Platanus orientalis, Celtis australis, Salix acmophylla, Ficus carica*, and *Populus*, growing in the close vicinity. Water plants are very abundant, mainly reed and cattails, *Arundo donax*, and *Phragmites communis*. Mollusk shells, usually *Melanopsis*, are very rare, maybe due to dissolution of their aragonitic shells (Heimann and Sass, 1989). Several thousand Middle to Upper Acheulian artifacts were recovered from the paleosol cover of the Kefar Yuval Travertine (Stekelis and Gilead, 1966), however some of these are coated with travertine (Schwarcz et al., 1980).

Heimann and Sass (1989) assumed that the travertine began accumulating about one million years ago, which together with the overlying Dan Travertine continued until some 25 Ka ago, when deposition ceased due to structural disturbances that changed the paleogeography. Horowitz (1979) gave a much narrower interval for the Kefar Yuval, broadly correlating it with the Benot Ya'aqov Formation of Palynozone QVII.

Picard (1963) identified the 'Younger Travertines'; emended by Horowitz (1973) to Dan Travertine. Plant fossils are numerous; mollusks are rare and of the same types found in the underlying unit. Scarce artifacts of Middle through Upper Paleolithic cultures are occasionally found (Horowitz, 1973), which prompted their correlation with the lower part of Ashmura Formation and Palynozone QIX. Radiocarbon dates of the upper layers of the Dan Travertine (Kaufman, in Heimann, 1985) are 33,100±1600 and 25,300±800 years, confirming the correlation suggested above, as does the date for the underlying basalt.

Several fossil spring deposits are exposed along the walls of Wadi Fasayil (Fatza'el), interfingering with terrace gravels containing Middle Paleolithic (Levalloiso-Mousterian) artifacts. Two uranium series dates obtained from these travertines (Schwarcz et al., 1980) seem questionable: 136±9 and 63±4 Ka. The first was on a dense, impermeable calcitic travertine, which should be reliable but is considered too old for the artifacts; the second, in agreement with culture, was obtained from a highly porous, powdery sample, seemingly unreliable. Though the authors suggested no solution, it seems however that if more recent ages for Mousterian artifacts are accepted (Valladas et al., 1987), the older age may be within limits. [A.H.].

B. CENTRAL JORDAN VALLEY GROUP

Horowitz (1974) applied this term to include a suite of formations exposed in the central Jordan Valley; ranging from the time the Rift Valley became an endoreic system until the present day. The central Jordan Valley basin extends from the southern part of Lake Kinneret southward, most probably down to Marma Feiyad, or somewhat north of that locality. The Tabgha Formation, deposited in Lake Kinneret during the last 18,000 years or so, is also included in this group. Outcrops of the Central Jordan Valley Group have been studied in great detail, chiefly due to the abundance of artifacts, especially in its earlier parts, bearing witness to the antiquity of Man in this region. Subsurface information is much scantier, since only a single borehole, Zemah-1 just south of Lake Kinneret, was sunk deep enough.

The central Jordan Valley basin acted completely different as compared with the Hula and the Dead Sea sections of the Rift. Its major phase of subsidence is restricted to the Neogene and early Quaternary, attaining more than 4 km (Marcus and Slager, 1984; Horowitz and Horowitz, 1990; Horowitz, 1992). The Central Jordan Valley Group comprises mainly lacustrine formations, laid down under wetter climates, while erosion took place during the dry periods, with the exception of one (QIV) in the section of the Zemah-1 borehole. Holocene sediments are only partially eroded

or covered. The central Jordan Valley remained an intermediate basin on the way to the Dead Sea for the whole timespan of the group.

The youngest ages obtained for the volcanics underlying the Central Jordan Valley Group are in the range of 2.0-1.7 Ma (Siedner and Horowitz, 1974), marking a maximum limit to initiation of the group. At Zemah-1, the Central Jordan Valley Group unconformably overlies the Melekh Sedom Sands, with Palynozone QII missing (Horowitz and Horowitz, 1990).

1. Erk El Ahmar Formation Palynozone QIII

Horowitz (1974) established this unit, named after a north-facing cliff (the red cliff) of the Jordan gorge, close to the road from Gesher to Menahemya, some 10 km south of Lake Kinneret. Blanckenhorn (1914), Blanckenhorn and Oppenheim (1927), Picard (1932, 1943), Schulman (1959) and Picard and Baida (1966a) attributed the Erk El Ahmar outcrop to the Ubeidiya Formation and the only photograph of the 'Ubeidiya' in Picard and Baida (1966a) is the type locality of Erk el Ahmar. The first to note the difference between the two formations, suggesting that Erk el Ahmar may be older, was Baida in 1964, and later verified by Horowitz (1974) on the basis of field relations and palynostratigraphic considerations. Also Tchernov (1975) pointed out differences between the respective malacological assemblages.

Further outcrops of the Erk el Ahmar Formation occur south and west of the Jordan River down to Nahal Tavor (Horowitz, 1979). Near the type section, the Erk el Ahmar sediments overlie the Cover Basalt, on a faulted, erosional relief (Horowitz, 1979). In the subsurface it unconformably overlies the Melekh Sedom Sands in the Zemah-1 borehole, with Palynozone QII missing (Horowitz and Horowitz, 1990). The Erk el Ahmar Formation is almost everywhere truncated by the late Pleistocene Lisan Formation, over an angular unconformity. In some localities older formations, such as the Naharayim Formation and the Yarmouk Basalt, unconformably overlie the Erk el Ahmar (Tchernov, in Schütt and Ortal, 1993). The Yarmouk Basalt is K-Ar dated at 0.8 Ma (Mor and Steinitz, 1985). At the Zemah-1 borehole the Erk el Ahmar is overlain by sediments of Palynozone QIV, however it is difficult to assess the nature of the contact, which seems conformable. The thickness is 80-90 m, both at the type section and in the subsurface. It comprises clays and marls, occasionally varved, with rare occurrences of silts and sands, some gravel horizons of basalt, flint, and limestone components up to 20-25 cm across, with several thin lacustrine limestones.

Erk el Ahmar Formation sediments yielded extensive mollusk assemblages (Tchernov, 1975; Schütt and Ortal, 1993), some vertebrate bones such as from a giraffe or camel, and an impressive elephant skull and tusks, as yet unidentified. In addition, hominid artifacts such as chopping tools and flakes were unearthed from the upper part of the sequence (Horowitz, 1979; Braun et al., 1991; Eitan Tchernov, Department of Evolution, Systematics and Ecology, the Hebrew University of Jerusalem 1998, pers. Comm. - in Horowitz, 2001). Of the rich malacofauna recovered from the Erk el Ahmar, the following are unique to this Formation: *Theodoxus jordani pliocostulus, Viviparus unicolor, Bythinia multicostata, Limnidia hebraica, Staja Lycica, Falsipyrgula barroisi, Ginaia picardi, Chilopyrgula ahmara, Melanopsis aaronsohni, M. Praecursor, Melanoides dadiana, M. jordanica, Potomida subrectangularis,* and *Dreissena israelica.*

Paleomagnetic studies of the sequence (Verosub and Tchernov, 1991; Braun et al., 1991) revealed a reverse-normal-reverse alternation, the upper part of which is attributed in both studies either to the beginning of the Olduvai or the upper Reunion subchrone, which assigns the Erk el Ahmar Formation an age of approximately two million years. Based on the rich pollen flora, Horowitz and Horowitz (1990) assigned the formation to Palynozone QIII. The Erk el Ahmar Formation was laid down primarily in a shallow freshwater lake, with rivers supplying the gravel.

2. Ubeidiya Formation

Picard and Baida (1966) named the Ubeidiya Formation, known before as the '*Melanopsis* (or *Unio-Melanopsis*) Stufe' (Blanckenhorn (1897) and 'Levantinische Stufe' (Picard, 1932). The name is that of an abandoned settlement, which also gave its name to the prehistoric site some 3 km south of Lake Kinneret on the western bank of the Jordan River. The type section is located at the excavations of the site. The base is not exposed, however westward the Ubeidiya Formation overlies the Cover Basalt and Neogene rocks which are faulted and eroded. The top is always truncated, overlain with angular unconformity by the Naharayim and Lisan Formations, or else exposed. Some 30-40 m of the Ubeidiya Formation are known from the Zemah-1 borehole, overlying Palynozone QIV sediments with what seems to be a conformable contact. The top is most probably truncated, covered by Naharayim Formation sediments (Palynozone QVII).

The Ubeidiya Formation is typically known from the region south of Lake Kinneret, totally covering an area of a few square kilometers. Rosenthal (1980) suggested that several occurrences of conglomerates and marls, containing *Melanopsis*, known from outcrops and boreholes in Bet She'an region, should also be regarded as the Ubeidiya Formation. The type section attains a thickness of 190 m, however this only represents part of the original sequence, considering the nature of the lower and upper contacts. It was studied in artificial trenches dug during the excavations.

Picard and Baida (1966b) subdivided the Ubeidiya Formation into four members. The lowermost 'Clay, Silt and Limestone Member (Li)' is 52 m thick, comprising lacustrine clay and silt varves, hard oolitic limestone beds, soft chalk and marls and silty, rarely sandy layers. Except for the varves, all other horizons are rich in freshwater mollusks and vertebrates, primarily fish. Veins of secondary idiomorphic gypsum are abundant within the varves. Some well-preserved plant fossils were found in the uppermost varves (Lorch, 1966), such as *Rhus tripartita, Pistacia lentiscus, Myriophyllum,* and *Ranunculus. Melanopsis* shells are very abundant, however this Clay, Silt and Limestone Member is devoid of artifacts and land vertebrates.

The overlying 'Intraconglomerate and Clay Member (Fi)'

is 22-30 m thick, displaying different facies on each flank of a miniature anticline that was exposed at the site during excavations. The western flank consists entirely of clays and conglomerates, the latter comprising sub-angular components. The matrix varies between clay, chalk, marl, silt, and basaltic sand. Some beds yielded artifacts, among which choppers, flakes and cores are common (Stekelis, 1966b). The layers contain numerous freshwater gastropods and ostracods, together with well-preserved vertebrate bones. The clay beds of this member are sometimes reddish, unfossiliferous, and most probably paleosols. At the eastern flank of the minor fold the conglomerate horizons are thinner, made of smaller components, often very sandy or silty. Clays are predominant, intercalated by limestone and chalk beds, and very rich in mollusk fossils. Picard and Baida (1966b) concluded that to the west it was deposited mainly in a river, grading eastward over a rather short distance (see also Bar-Yosef and Tchernov, 1972) to swamp and lake environments.

This member was the first to be excavated (Stekelis et al., 1960), on the assumption that it was the provenance of *Homo erectus* remains (Tobias, 1966). Stekelis (1966b) classified the artifacts from the lower part of this member as 'The Israel Variant of Olduvan II Culture, Phase I', while those from the upper part are designated as 'Phase II'. The fauna comprises rich assemblages of vertebrates and mollusks (Haas, 1966; Tchernov, 1987). Abundant mammals include *Crocidura russula, Canis arnensis, Praemegaceros verticornis, Hippopotamus behemoth, Equus tabeti*, and numerous rodents. Mollusks typical for Ubeidiya are (Schütt and Ortal, 1993) *Theodoxus jordani unicarinatus, T. j. bicarinatus, T. j. tricarinatus, Bithynia phialensis syriaca, Melanopsis obediensis, M. turriformis, Potomila littoralis ubeidiyensis*, and *Sinanodonta tchernovi*, among many other taxa.

The third, 'Main Silt Member (Lu)', attains a thickness of 56 m. It consists of lacustrine, occasionally well-bedded white-grayish-yellow silts, with some silty marl and clay layers, very rich in ostracods. The rather well-bedded lower part consists of limnic clay, chalk and chalky marls, in which freshwater ostracods, gastropods, and fish remains are quite abundant. This is overlain by the uppermost 'Upper Conglomerate Member (Fu)', made up of 16 m of conglomerates, ranging in size from very fine micro-conglomerates to big boulders, with mainly basalt, some flint, and a few limestone constituents. The base displays fine clastics, interspersed in a 2 m thick marly chalk layer. The clastic layers reveal repeated cycles of graded, well-rounded and sorted pebbles, occasionally interrupted by less rounded, unsorted horizons. The uppermost layer contains big, fairly rounded basalt boulders, up to 80 cm across and small flat pebbles, up to 10 cm in diameter. Neither fossils nor artifacts are found in this Main Silt Member.

Early investigators suggested a late Pliocene or early Pleistocene age for the Ubeidiya Formation (including Erk el Ahmar). During the 1960s the term 'Villafranchian' was applied (Stekelis et al., 1960, followed by others), based on faunal comparisons with European sites. Bar-Yosef and Tchernov (1972) compared the lithic assemblages and suggested a Mindel age, which was followed by Horowitz (1974, 1979, 1988). Tchernov (1987), again based on faunal considerations but having collected many more fossils, suggested a Biharian age, approximately corresponding to 1.4 million years. K-Ar ages (Horowitz et al., 1973; Siedner and Horowitz, 1974; Mor and Steinitz, 1985) placed the Ubeidiya between the 2.0 Ma of the uppermost flows of basalts then considered Cover Basalt, and the Yarmouk Basalt, in the range of 0.8-0.6 Ma. The sequence is paleomagnetically reversed (Verosub and Tchernov, 1991), as might be expected for the Matuyama.

The Ubeidiya Formation was deposited in a wide shallow lake, which occupied the central Jordan Valley, changing its size, depth and shorelines several times during accumulation of the sequence. Rivers flowing into the lake brought gravel, common in the formation especially at times of lake shrinkage.

An outcrop comprising several meters of hard, conglomeratic, partly pisolitic limestones, unconformably overlying the Ghor el Qatar Series, was found near Abu Habil east of the Jordan River some 36 km south of Lake Kinneret. Bender (1974) and Tchernov (1987) correlated it with the Ubeidiya Formation, while Horowitz (1979) thought that its lower part may correlate with the underlying Erk el Ahmar Formation, while only the upper may correspond to the Ubeidiya. Huckriede (1966) defined pre-Abbevillian pebble tools of Olduvan and Münzenberger type, which bear the same nature as those recovered at Ubeidiya.

3. Naharayim Formation

Picard (1932, 1965) emended the 'Alt-Alluviale Jarmuq-Schotter' of Noetling (1887), to 'Naharaim-Schotterstufe'. The Naharayim Formation is named after the confluence of the Yarmouk and Jordan Rivers south of Lake Kinneret ('Naharayim' means two rivers), where the type locality was defined. The older definitions refer only to the gravel beds, conformably sandwiched between thick, brown paleosol horizons, termed by Picard (1932) 'Basislehme A' and 'Hangendlehme B'. Picard (1965) subsequently included these into the Naharayim Formation. It rests unconformably on the Yarmouk Basalt and older formations both in outcrops and boreholes. It underlies, again unconformably, the Raqqad Basalt and the Lisan Formation. The Naharayim *sensu strictu* is only known from the central Jordan Valley. However, stratigraphically similar occurrences of gravel horizons are known along the Jordan Valley down to the Dead Sea, and possibly also further south (Bender, 1974).

The sequence at the type locality comprises up to 20-30 m of mainly medium-sized basalt and limestone gravels, intermingled with red, occasionally sandy loams, most probably floodplain paleosols, and some thin sandy horizons. In a single locality, some 10 km south of Lake Kinneret, a thin bed very rich in *Viviparus apameae* shells (Braun and Tchernov, 1991; Braun, 1992) was found at the base of the Naharayim. It overlies the Yarmouk Basalt and could have been laid down in a small shallow lake. Only rare melanopsids occur. The thickness decreases gradually in all directions further away from the type area, to a few meters or less. Rare artifacts of Upper Acheulian affinity are reported from the Naharayim and its correlatives (Huckriede, 1966). It seems that the

Naharayim Formation was deposited in a large delta and floodplain complex of the Yarmouk and Jordan Rivers, in times of larger water supply. Radiogenic ages for the Naharayim are between the 600 and 70 Ka of the Yarmouk and Raqqad Basalts (Siedner and Horowitz, 1974).

For Braun (1994) the Naharayim Formation in the Central Jordan Valley comprises a lower unit of Conglomerates, the Yarmouk Basalt, a limestone tongue of the Benot Ya'akov Formation and an upper unit of Conglomerates. It unconformably overlies the Erk Al Ahmar or Ubeidiya Formations and underlies the Lisan Formation.

4. Lisan Formation (See Upper Dead Sea Group)

5. Tabgha Formation Palynozones QIX- QX

Horowitz (1971) defined the Tabgha Formation in a borehole drilled underwater near a locality of that name, at the northwestern corner of Lake Kinneret. The Tabgha Formation encompasses the sedimentary sequence laid down in Lake Kinneret ever since its formation some 18 Ka ago and up until the present day. As such, its lower part corresponds to the Fatza'el Member of the Lisan Formation. The Tabgha conformably overlies the Ami'az Member in the southern parts of Lake Kinneret, where the latter was deposited. Elsewhere it unconformably rests over older rocks. The Tabgha Formation is known from numerous boreholes in Lake Kinneret and also from several outcrops around the lake, particularly in the Buteiha area, where parts of the sequence had been deposited in times of greater extension of the lake, under more humid climates.

The type section comprises 22 m of loose dark brown to black clays, with subordinate sand-sized grains of quartz, chert, basalt, limestone, and dolomite. The unit thickens up to some 30 m at the lake's center (Ben-Avraham in Horowitz, 1979), but thins toward the margins, grading into gravel beds and soils. Bones of *Hippopotamus, Bos* and other vertebrates were recovered from exposures at the Buteiha; prehistoric sites were discovered around Lake Kinneret in littoral facies of the unit; and the rather rich mollusk fossils, also in the littoral facies, are those living today in the lake. The more common are *Melanopsis praemorsa, Theodoxus jordani, Bulimus hawaderiana, Melanoides tuberculata, Unio terminalis, U. semirugatus*, and *Corbicula fluminalis* (Tchernov, 1973). Pollen assemblages assign the lower part of Tabgha to the upper part of Palynozone QIX, while the rest is Palynozone QX, of Holocene age.

Travertines

Travertine of Bet She'an

Picard (1929) named the 'Kalksinter von Beisan'; emended by Shaliv et al. (1991), who adopted the term 'Bet She'an Travertine' suggested by Horowitz (1979), but also included within the Rehov Formation. It consists of spring deposits exposed in and around Bet She'an. The base of the travertines is nowhere exposed, except where they unconformably overlie considerably older rocks. It is overlain by the lake sediments of the Rehov Formation (Horowitz, 1979, p. 166). The travertines cover an area of some 100-150 km², comprising a sequence of up to about 60 m (Shaliv et al., 1991), with the uppermost 18 m exposed due to subsequent faulting.

It is made of yellowish-brown friable carbonates, massive with no discernible bedding, bearing numerous plant molds, algal stromatolites, and mollusks such as *Melanopsis* and *Melanoides tuberculata*. The upper 16 m has been both radiocarbon and uranium series dated (Kronfeld et al., 1988), indicating a continuous deposition between 41 and 22 Ka ago, broadly correlative with the Ami'az Member of the Lisan Formation, into which the Bet She'an most possibly interfingers eastward. If the sequence indeed comprises the 60 m reported in Shaliv et al. (1991), then the base could well predate the Lisan Lake.

Rehov Formation Holocene

Horowitz (1979) intended the establishment of the term 'Rehov Formation' to avoid confusion with the better known 'Bet She'an Lake Sediments' (Neev, 1967). The Rehov Formation is named after a settlement on top of these deposits, south of the city of Bet She'an. Shaliv et al. (1991) view the unit as an upper 'Marl Member' of the Bet She'an Travertine. A suite of shallow lake sediments is described by Neev (1967) from the area in and around Bet She'an, covering some 100 km² to the south and east of the city. These sediments lie over a paleosol, which in turn covers the Bet She'an Travertines. The top is either exposed or covered by a thin soil. The sequence comprises up to 30 m of white-brownish, occasionally black clays and marls, with very abundant pisolites and *Melanopsis* shells, which yielded radiocarbon ages of about 5,000 years. The sediments are rich in Chalcolithic potsherds and flint implements, while Early Bronze settlements are located on the surface.

The Bet She'an Lake existed during the humid Atlantic period (5,500-3,200 BCE), at the mid-Holocene. It came to an abrupt end by a structural disturbance some 4,500 years ago, which downfaulted its eastern side and today forms a conspicuous scarp (Horowitz, 1979).

C. UPPER DEAD SEA GROUP

The Late Pliocene-Holocene continental, mostly clastic, fluviatile and lacustrine sedimentation in the continuously deepening intra-cratonic Dead Sea Rift, is identified as the upper Dead Sea Group.

This term was suggested by Neev and Emery (1967) for the sedimentary suite deposited in the Dead Sea Basin, extending from the Northern Dead Sea to the Arava Valley, ever since it became a terminal inland base level. In places the Upper Dead Sea Group encompasses thousands of meters of Late Pliocene and Pleistocene clastic and evaporitic sediments, accumulated due to the considerable subsidence of this region (Horowitz, 1989, 1996, 1997). However, most of these sequences are only known from boreholes, drilled at the deeper parts of the basin; the margins, being continuously subject to erosion, display only very poor

correlative rocks.

The only exception is the late Pleistocene Lisan Formation, discussed above, which is not yet entirely gone by erosion, given the short time that has passed since its deposition. The Lisan is conformably overlain in the Dead Sea itself by a suite of sediments deposited ever since the lake was formed, some 15-18 Ka ago. This suite was termed 'Unnamed post Lisan sediments' by Neev and Emery (1967) and considered to be stratigraphically equal to the Tabgha Formation of Lake Kinneret by Horowitz (1979).

Limited exposures of lake sediments preceding the Lisan, termed the Sayif Formation by Sneh (1982), and uranium series dated to an interval spanning 275-150 Ka ago by Livnat and Kronfeld (1985), are known from the northern Arava, down to the area just north of the watershed at Gav Ha'Arava (Livnat and Kronfeld, 1990). The sequence is several meters thick and mainly composed of lacustrine limestones and marls, unconformably truncating a variety of older formations. They are disconformably overlain by the Lisan Lake sediments, in places grading laterally to spring deposits (the Sayif Travertine), or to gravels of the third lakeshore terrace. According to pollen (Horowitz, 1987; Weinstein-Evron, 1987) the age corresponds to Palynozone QVII.

The drilled sequences have been subject to detailed palynostratigraphic studies.

1. *Melekh Sedom Sands* Early Pleistocene

The 'Melekh Sedom Sands is a term coined by Clark et al. (1984) and used by oil companies operating in the Jordan Rift Valley to describe a sequence of clastics attaining a maximum thickness of 920 m, penetrated in the Melekh ('King of') Sedom-1 borehole drilled in the southern Dead Sea Basin. All numbers concerning this unit are assumed to be apparent since dips are known to exist but have never been accurately measured. The sequence rests on sediments of Palynozone Pb of late Pliocene age, and is covered by deposits of Palynozone QII of later early Pleistocene. The nature of both contacts, known only from drillings, is not clear. Melekh Sedom Sands are known from numerous boreholes in the Jordan Valley, from the Hula Basin where some 400 m were penetrated, down to the southern Dead Sea, with varying thicknesses, but always on the order of several hundred meters (Levin and Horowitz, 1987).

Levin (1985) subdivided the sequence at the type borehole into three units. The 'Lower shale unit' comprises 430 m of carbonaceous shales, partly silty or sandy, occasionally limonitic. The 'Sandy unit' is some 350 m thick, consisting mainly of sand, alternating with sandy or carbonaceous shales in the lower and upper parts, with almost pure sand in the middle 180 m. The sand is fine to medium, poorly sorted, and almost exclusively rounded to sub-angular quartz grains. This 'Sandy unit' is the only part of the sequence referred to by Levin as 'Melekh Sedom Sands'. In its composition the uppermost 320 m 'Upper shale unit' very much resembles the lower one. To the north, in the central Jordan Valley and the Hula, the clastics are mainly conglomerates, with interfingering basalt tongues and possibly some paleosols.

The Melekh Sedom Sands are very rich in palynomorphs, indicating an early Pleistocene (Palynozone QI) age and a fluvio-lacustrine environment of deposition.

2. Idan Formation

Eyal (1984) established the Idan Formation at Nahal Idan, in the northern Arava. It overlies the Hazeva Formation over an erosive surface and is unconformably overlain by the lake sediments of the Lisan Formation. The Idan Formation occurs widely in the northern Arava, its thickness is on the order of tens of meters. Although the type section is 23 m thick, Eyal (*op. cit.*) recognized 302 m of this formation in the Hazeva-5 borehole, near the settlement of Hazeva.

Eyal subdivides the Idan Formation into two members, an 8 m thick, mainly marly lower member, and an upper, chiefly sandy one which attains 15 m. The lower member comprises alternations of white and gray marls, calcareous sandstone and sandy marl, quite loose, topped by 3 m of somewhat harder, well-stratified white marl. The Sandy Member commences with a hard layer of cross-bedded calcareous sandstone, while the rest is made of gray, soft sand and grit, with several marl and gravel horizons. The latter may occasionally contain magmatic components derived from Transjordan (Bentor and Vroman, 1957). No fossils were ever found.

The Idan Formation was previously considered an early stage of the Lisan Formation (Bentor and Vroman, 1957). Based on its different and distinct sandy lithology, Eyal (1984) defined it as an independent unit, probably considerably older than the Lisan. Horowitz and Horowitz (1990) suggested, based on the lithological characteristics, a possible correlation of the Idan Formation with the Melekh Sedom Sands.

3. *Samra Formation*

Picard (1943) introduced the term 'Samra Series'; emended successively by Bentor and Vroman (1954, 1957, 1960) to 'Samra Beds' and 'Samra Stage'. Bender (1974) also mentions the term.

The Samra Formation is named after Khirbet Samra, 6 km NE of Jericho, where its gravels were quarried. The lower contact is not exposed in the type locality, where the unit underlies the late Pleistocene Lisan Formation with a slight angular unconformity, gently dipping to the east. Bentor and Vroman (1957) report the Samra as unconformably overlying the Arava Formation and older rocks, overlain by the Lisan in the same manner as described by Picard (1943). Picard reports a thickness of 10-12 m from the type locality, while Bentor and Vroman indicate up to 25 m from the northern Arava. Picard described the Samra from the southern Jordan Valley, while Bentor (1960) includes occurrences from the northern Arava, extending northward up to Beth She'an, as well as possibly also in the eastern Judean Desert.

Picard (1943) describes the Samra at the type area as comprising some 6-10 m of calcareous sandstones in the lower part, practically without quartz, but with fine flint particles, and with a thin intercalation of calcareous marl. These are topped by 1-2 m of hard loam, fine flint sand and flint conglomerate, with pebbles several centimeters across. Northward, in the Marma

Feiyad area, Picard describes the Samra as a lacustrine limestone with *Hydrobia, Bythinia, Planorbis*, and *Melanoides* shells. Schulman and Rosenthal (1968) assigned these beds to the Gesher Formation. Bentor and Vroman (1957) described the Samra Formation from the northern Arava as consisting of fine grained, partly calcareous sandstone and silt, oolitic chalk and limestone, finely bedded calcareous shales, green clays, conglomerates and breccias, with flint and limestone pebbles and fragments. They also report fossils similar to those described by Picard, however they are not indicative of any precise age. Both authors suggested a 'Lower Pleistocene' age and a fluvio-limnic environment of deposition for the Samra Formation. Picard further indicated that both the Samra and the Oolitic Formation are time-equivalent, different facies of the same system. Picard (1943) describes a sequence of well-cemented conglomerates sandwiched within the Samra in Wadi Malih, west of Marma Feiyad, which he designated the 'Wadi Malih Gompholites'. Schulman and Rosenthal (1968) maintain that these should be younger.

Daniel (1963) states that the Samra sequence rests with an angular unconformity on the Pliocene Usdom Series. He also included the late Pleistocene Naharayim Formation gravels (Picard, 1965) within the Samra Formation.

4. *Lisan Formation*

The name goes back to Lartet (1869), who described the 'Dépôt de la Liçan', 'Marnes de la Liçan', 'Anciens Dépôt de la Mer Morte'; and was emended by Bentor and Vroman (1954), Langotzky (1960), Begin et al. (1974), and Horowitz (1974).

The Lisan Formation was named after the Lisan (tongue) Peninsula, on the east side of the Dead Sea. Synonymy: 'Ancient Deposits of Salt Sea' (Hull 1886), 'Lisan Mergel' (Blanckenhorn, 1914), 'Lisan Stage' (Picard, 1937), 'Lisan Marl' (Picard, 1938), 'Lisan Series', 'Lisan Deposits' (Picard, 1943) etc.

Formally no type section of the Lisan Formation was established. A great number of reference sections were however described (*e.g.* Zak, 1967; Picard and Baida, 1966b; Neev and Emery, 1967; Begin et al., 1974; and others).

The thickness is some 60-80 m in the Dead Sea region, diminishing somewhat northward. Bentor and Vroman (1954, 1957) included the entire Upper Dead Sea Group within the Lisan (of which some 600 m were known at the time from drillings).

Volume: Langotzky (1960), Begin et al. (1974), and Horowitz (1979, p. 148) suggested a threefold subdivision of the Lisan Formation into members (from bottom to top):

1) Hamarmar Member (Langotzky, 1960);
2) Ami'az Member (Langotzky, 1960); and
3) Fatza'el Member (='Peza'el') (Horowitz, 1974).

Begin et al. (1974) further subdivided the Ami'az Member into ***'Laminated'*** and ***'White cliff'*** beds (emend. Horowitz, 1974).

Lithology: the lower and upper members are clastic, whereas the middle member is predominantly composed of alternating varves of aragonite and clay or silt, of lacustrine origin.

In the reference section near Deir Shaman (Begin et al., 1974), 15 km north of the Dead Sea in the middle of the basin, the Lisan Formation attains a thickness of 58+ m (base not exposed).

Hamarmar Member: comprises 17 m of predominantly sands and sandy silts, which grade outward at the basin's margins to gravel. The unit is diachronous, occasionally the entire Lisan sequence becomes clastic toward the shores of the lake. These gravels acquired several names, such as 'Sandy Member' (Bentor and Vroman, 1954) or 'Hamarmar' (Langotzky, 1960) at the southern Dead Sea region, and 'Samachschotter' (Picard, 1932) in the central Jordan Valley, or was (erroneously) thought to represent the Samra Formation (Begin et al., 1974; Bender, 1974).

Ami'az Member: conformably overlying, the 25 m of Laminated Bed is composed of finely laminated, whitish, soft varves of alternating aragonite and clays, occasionally silty or sandy, with several subordinate sand or gypsum layers. Sulfur concretions are quite common in this unit.

The overlying 6-7 m thick White Cliff Bed withstands erosion somewhat better; its lower part is made of varves, capped by a rather hard 1 to 2 m thick gypsum layer. The contact between the two beds may be somewhat unconformable. Close to the lake's shores, especially where wadis are present, the sequence becomes more detritic. This is particularly apparent in the northern Arava, where a vast area was drained into the Lisan Lake through a rather narrow outlet (Begin et al., 1980; Sneh, 1982). Close to the shores, in numerous localities, algal tufas were formed, probably where some freshwater influx entered the otherwise saline lake (Buchbinder et al., 1974).

Fatza'el Member: Chiefly clastic, it consists of fine clay, silt and sand at the center of the basin, grading to conglomerates intermingled with red clayey loams at the basin's margins. The Fatza'el member was referred to as 'Unnamed clastic unit' in Begin et al. (1974), or 'Damya Formation' by Abed (1985).

Distribution: Lake Lisan extended from the middle of the present Lake Kinneret continuously southward through the northern Arava to some 35 km south of the Dead Sea. In the central and southern Jordan Valley, the Lisan Formation consists mainly of its middle or Ami'az Member. The distribution of its upper or Fatza'el Member is much more restricted.

Contacts: The Lisan Formation overlies a multitude of older formations, but rests conformably only on sediments of Palynozone QVIII, a contact known solely from boreholes in the Dead Sea area. The youngest formation overlain, possibly quite conformably, by the Lisan in the central Jordan Valley is the Raqqad Basalt. Within the Lisan Formation contacts between members vary.

The Fatza'el Member conformably overlies the White Cliff Bed at Deir Shaman, and unconformably in many other localities.

Fossils: Quite rare in the Lisan Formation, except for diatoms, indicative of salinity and environment, and pollen grains. Begin et al. (1974) distinguished three euryhaline diatom zones within the Ami'az Member, while the Fatza'el Member is characterized by a freshwater flora. Freshwater diatoms are also more common in the entire sequence, both at the northern and southern reaches of the lake (Begin et al., 1980). Freshwater mollusks and ostracods are reported by Bender (1974) from the lower part of the Lisan

Formation, which according to his lithological description seems to correspond to the Hamarmar Member, south of the Damya Bridge. Various authors reported rare occurrences of mollusks, particularly *Melanopsis*, from the northern exposures of the Lisan Formation in the central Jordan Valley.

Age: Pollen assigns the Lisan to Palynozone QIX. No artifacts were found within the lacustrine sediments of the Lisan Formation. However, marginal fluviatile gravels yielded a sequence from Middle Paleolithic, corresponding more or less to the base of the sequence, through Epi-Paleolithic at the top. The Fatza'el Member is quite rich in sites yielding Neolithic artifacts (Bar-Yosef et al., 1974; Horowitz, 1988, 1989).

Environment: It seems that the lower Hamarmar Member represents the phase of expansion at the initial stages of Lake Lisan, while the upper Fatza'el Member documents the final shrinkage of the lake, due to structural disturbances creating the deep northern Dead Sea Basin and Lake Kinneret some 16,000 years ago, followed by drying up of the regional climate (Horowitz, 1979, p. 151). The middle, more conspicuous Ami'az Member was laid down in a rather saline lake, more so in its central parts, decreasing both north and southward (Begin et al., 1980).

Geochemistry: Numerous geochemical and isotopic studies were made, particularly on the Ami'az Member sediments (Stein et al., 1997, among others). These resulted in detailed information concerning changing salinities, provenance of water, etc. Radiogenic datings, especially radiocarbon and uranium series based, are again mainly concentrated on the Ami'az Member, whose chemical deposits are suitable for these methods. These studies commenced in the 1960s, when Neev and Emery (1967) gave a span of 70-18 Ka for the sequence. With only minor refinements, almost all investigators had arrived at similar figures (Kaufman, 1971; Vogel, in Horowitz, 1979, p. 151; Schramm et al., 1997, among others). Thus, the Hamarmar and Fatza'el Members are somewhat older and younger, respectively, than the termination of the Lisan Lake, attributed to the transition from the Pleistocene to the Holocene, some 11 Ka ago.

'Unnamed post-Lisan sediments'

Neev and Emery (1967) and Horowitz (1979) gave no name to a suite of sediments that conformably overlie the Lisan Formation, deposited ever since the Lisan Lake was formed, some 15-18 thousand years ago. Stratigraphically the suite equals the Tabgha Formation of Lake Kinneret.

Arava Terraces

The terraces of the northern Arava that are mainly cut into the Pliocene Arava Formation are considered a part of the Arava Formation by Sneh (1982), but represent a separate set of units (Horowitz, 1979) which are also considered part of the 'Arava Lake' (Avni,, 1997). These terraces, mostly built of gravel, occasionally grading to lacustrine limestones or marls, form a succession of four levels. The highest, apparently most ancient, is Sneh's 'Shezaf Hills Conglomerate'. It is cut by the 'Upper Dome Country Terraces', which are cut in turn by the 'Lower Dome Country Terraces'. Terraces of the Lisan Lake subsequently cut these terraces. The two highest terraces are chiefly of fluviatile origin, with no traces left of their corresponding lake deposits. However their connection with expanded lakes could be seen in sequences penetrated by boreholes in close vicinity (Horowitz and Horowitz, 1990). The two lower terraces are intimately connected with lacustrine chalks. The upper one with the Sayif (or 'Seif') Formation and travertines (Horowitz, 1979; Sneh, 1982; Livnat and Kronfeld, 1990; Avni, 1997), and the youngest with the Lisan (Sneh, 1982). Using uranium series, Livnat and Kronfeld (1985, 1990) dated the Sayif to isotope stage 7.

These four sets of terraces have been correlated (Horowitz, 1979) with the four known expansion phases of lakes in the Jordan Valley, ever since it became an internal drainage system.

Travertines

Sayif Travertine Palynozone QVII

Sneh (1982) named this sequence after a wadi in the northern Arava (previously transliterated 'Seif'), some 30-35 km south of the Dead Sea. The Sayif is termed 'Arava Travertine' in Enmar et al. (1998). The Travertine is unconformably sandwiched between a suite of older formations and the Lisan Formation sediments. Small outcrops of the Sayif are known from the entire northern Arava. Occasionally fossil *Melanopsis* and *Melanoides* shells are present, together with numerous unidentified plant molds. Pollen assemblages testify to Palynozone QVII.

The Mo'a Travertine Palynozone QIX

Enmar et al. (1998) named the sequence after ruins in Nahal Omer, some 65 km south of the Dead Sea. It was previously described by Sneh (1982), who had not named it. Morphologically, the Mo'a Travertine cuts and fills channels in the underlying Sayif Travertine and lake deposits, and is in turn cut and filled up by sub-recent wadis and travertines. The unit, never exceeding a few meters in thickness, is found in small isolated outcrops all along the northern Arava. It merges laterally with lacustrine sediments of the Lisan Formation.

The usual plant molds and rare mollusks also occur in this Travertine, but are useless as age indicators. Uranium series datings (Livnat and Kronfeld, 1985) are within the 60-120 Ka range. Pollen assemblages (Weinstein-Evron, 1987; Horowitz, 1987) assign the Travertine to Palynozone QIX. Mousterian artifacts (Bar-Yosef, in Livnat and Kronfeld, 1985) are reported from the top of the Mo'a Travertine.

Nahal Zin Travertines Sub-recent

Schwarcz et al. (1979) uranium series dated several travertine occurrences upstream Nahal Zin and its tributary Nahal Aqev, which leads to the Dead Sea some 75 km to the east-northeast. An older assemblage of samples yielded ages in the range of 150-300 Ka, which is correlated by Livnat and Kronfeld (1985) with ages obtained for the Sayif spring and lake sediments in the northern Arava.

Younger travertine occurrences, in which Mousterian artifacts

are embedded, represent the time interval of 50-40 Ka ago. These dates are somewhat younger than those obtained by Livnat and Kronfeld for the Mo'a Travertine, but are comparable to the lower part of the Lisan Formation. A sub-recent travertine was dated at 11.8±0.9 Ka.

ACKNOWLEDGEMENTS

The author gratefully acknowledges the efforts of John K. Hall to render the compact language of the Lexique into more readable English, and to assemble the appropriate references. Dr. Hall in turn gratefully acknowledges the great assistance in the bibliographic work rendered by the librarians at the Geological Survey of Israel, as well as the access provided to AGI's on-line bibliographic GeoRef database during his 2003-2004 sabbatical as Visiting Scholar at the University of New Hampshire's Center for Coastal and Ocean Mapping.

APPENDIX

METASEDIMENTS

Combustion phenomena have produced a series of metasediments from the Senonian–Plio-Pleistocene sediments in several areas of Israel and Jordan (**Figure 18I.3a**). In Israel these rocks are found in the Shefela, Maale Adumim-Jericho area, the Rift Valley, and especially Arad. The presumed age of the probably subareal combustion (or hydrothermal events as claimed by some) is Late Late Neogene-Early Pleistocene. These rocks were long known as the 'Mottled Zone' (Picard, 1931) and are also known as 'Mizi Akhdar' and 'Arad Marble'.

Gvirtzman and Buchbinder (1966) have established the name **Hatrurim** after the main development of these rocks in the Hatrurim Basin, southeast of the city of Arad (**Figure 18I.3b**).

Gross (1977) studied the mineralogy, and Burg (1990) and Burg et al. (1991) analyzed the genesis of these metasediments that form irregular bodies intermingled within the original sedimentary rocks (the protoliths) from which they were derived.

The principal distinction criterion is the metamorphic grade or the extent to which the metamorphic rock differs from the protolith, from slightly metamorphic (KuPh1) to high metamorphic grade (KuPh2-4). Metamorphic rocks never underlie non-metamorphic protoliths. Starting from the lowest unit upwards, several protoliths and their corresponding metamorphic units are recognized by Burg (1990). (**Figure 18I.4**).

The Mishash Formation - Phosphorite Member, forming the outer framework of the Hatrurim Basin is metamorphosed to different grades of higher metamorphism, by decarbonation of the original francolite (Matthews and Nathan, 1977) and recrystallization to high-grade metamorphic apatitic marble, known as 'Mizi Akhdar'.

The Ghareb Formation, consisting of bituminous marls at its base, containing up to 30% organic matter, and chalk, is followed by the Taqiye Formation, composed of marls and clays, sometimes dolomitic with conspicuous concretions of pyrite and sometimes barite. Bedded chalks and some marl represent the Hafir Member at the top. Carbonate content of Taqiye rocks ranges from 47% to 76%. The metamorphosis of these formations is classified into KuPh1-4 types.

KuPh1 - The carbonate unit. Low-grade metamorphic minerals, hydrogrossular, zeolites and apatite, are the result of weak metamorphism of carbonate protoliths.

Retrograde carbonates are the product of weathering, evidenced by hydration, recarbonation and sulfatization. Veins of gypsum, calcite and halite, volkonskoite and coarse calcite are abundant. The meta-chalk at the base of the formation contains halite. Dispersed mainly within the lower part of the KuPh1 unit are small bodies of higher grade melilite fels (gehlenite) and larnite, containing garnet, fluorapatite or nagelschmidtite and wollastonite, vesicles filled with white calcite, tobermorite, and hydrated minerals. Brownmillerite, mayenite, ye'elimite, and fluorapatite occur.

Weathering products of the retrocarbonates are mostly calcite,

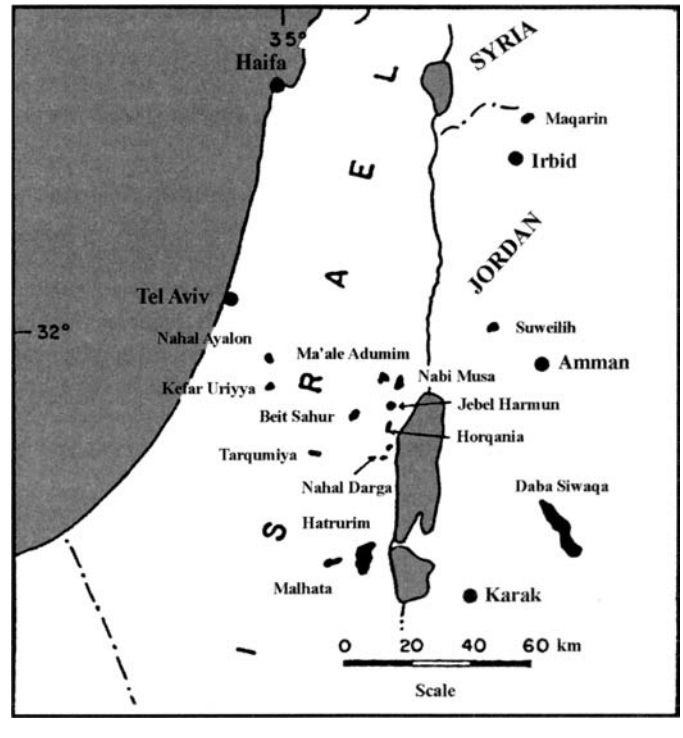


Figure 18I.3a. Location map of metasediments in Israel and Jordan (after **Burg et al., 1991, Fig. 1a, p. 108).**

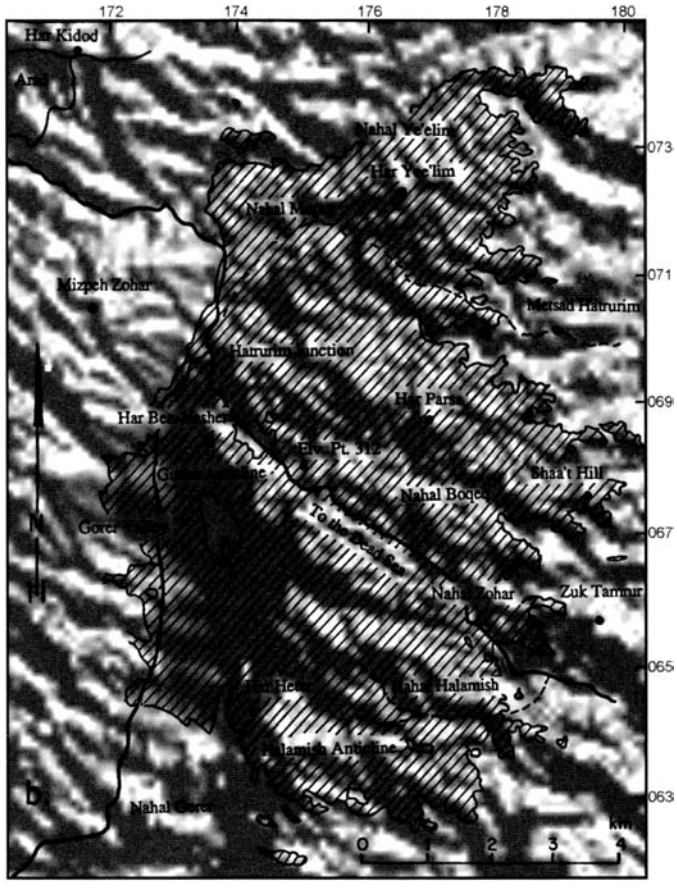


Figure 18I.3b. The Hatrurim Basin of Arad. (Modified from Burg et al., 1991, Fig. 1b, p. 108). The background is from the 100 m DTM of Israel, illuminated from the northwest. Old Israel Grid coordinates.

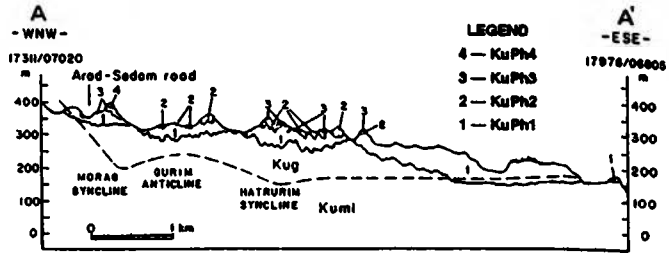


Figure 18I.4. Cross section across the Arad Hatrurim Basin. (From Burg et al., 1991, Fig. 7, p. 117).
Legend: Kumi = Mishash Formation; Kug = Ghareb Formation.

gypsum, aragonite, halite, and hydrates such as hydrogrossular, tobermorite, jennite, afwillite, ettringite, portlandite, iron oxides, and a few relict metamorphic minerals such as gehlenite, yankinite, and fluorapatite. Carbonate cooling-contraction prisms (Avnimelech, 1964) bear high-grade metamorphic minerals (spurrite). Some isolated outcrops of the KuPh1 unit are rich in zeolites and garnets. a 'lizardite rock' in the upper part of the KuPh1 consists of calcite, lizardite, hematite, gypsum, and some dolomite.

The transition from the carbonate unit to higher grade units is irregular and gradual.

KuPh2 - Spurrite rocks consist of calcite-spurrite marble that may form NW-SE oriented dike-like structures. Minerals like brownmillerite, mayenite, apatite and garnet occur, hematite concretions with pseudomorphs of fossils may contain brachiopods *e.g. Gyrosoria gracilis* (Schlotheim) and oysters *e.g. Chlamys farafrensis* (Zittel) both of Maastrichtian age. The spurrite-calcite marbles are commercially known as 'Arad Marble'. *Larnite rocks* consist of larnite-gehlenite and spurrite.

KuPh3 - Calcite-zeolite-garnet and anorthite-diopside fels. Several types of 'olive' rocks (Bentor, 1949) are distinguished:

1) Low-grade 'olive' - calcite-hydrogrossular rock, with aragonite, aluminous serpentine, vaterite, hematite, zeolites, andradite, grossular, and apatite as well as barite concretions;

2) Medium-grade 'porous olive' - a calcite-zeolite (thomsonite, gismondite, phillipsite, chabazite) - garnet (hydrogrossular or grossular) rock, dotted with maghemite or hematite. Calcite, diopside, maghemite, hematite, serpentine, aragonite, and vaterite occur. Barite concretions and heavy, black maghemite-hematite concretions are also abundant in the porous olive rocks;

3) High-grade 'dense olive' - anorthite-diopside fels - very hard, massive, containing hematite-maghemite concretions, dispersed magnetite, causing the black staining. Major minerals are diopside, anorthite, grossular, wollastonite and some calcite. Zeolites, serpentine, andradite, and gehlenite are accessory;

4) High-grade gehlenitic 'dense olive' - wollastonite fels. - A rare, very hard rock, containing small barite and maghemite-hematite concretions. Major minerals are gehlenite, wollastenite, garnet, and in some cases, diopside, as well as accessory thomsonite, calcite, and hydrogrossular. Weathered it contains hydrates such as jennite and tobermorite.

Unit KuPh4 - bedded larnite rocks. (a) Larnite rock that may also carry some bredigite, and (b) spurrite or spurrite-calcite marble. They may bear hematite concretions. Layers of retrograde rock contain hydrogrossular, tobermorite, jennite, and sometimes calcite.

The Metamorphic Conglomerates (Bentor and Vroman, 1960; Kolodny et al., 1973; Burg, 1990) relate to the Arava Formation (Ye'elim Member), found in the 'low terrace' that gradually descends from 312 to 220 m with a slope of 2° towards the SE, and in the 'high conglomerates' between 290 m and 370 m between Mount Ye'elim, Hatrurim Junction, and Mount Parsa, as well as south of the Gurim anticline, consisting of local polymictic chert and phosphorite pebbles (Mishash Formation), 'allochtonous chert' and sandstone (Hazeva Formation), limestone pebbles (Judea Group), and metamorphic pebbles (recycled Hatrurim fragments).

REFERENCES CITED

Abed, A. M., 1985. Geology of the Damya formation. Dirasat, 12(2), p. 99-108.

Arensburg, B., Bar Yosef, O., Chen, M., Goldberg, P., Laville, H., Meignen, L., Rak, Y., Tchernov, E., Tillier, A. M., and Vandermeersch, B., 1985. Une Sepulture Neandertalienne dans la Grotte de Kebara (Israel). C. R. Acad. Sci. Paris, Ser. 2, 300(6), p. 227-230.

Avni, Y., 1997. Geological evolution of the central and southern Negev as an indicator of the evolution of the Dead Sea Transform western margin in the Late Neogene and Quaternary. Unpubl. Ph.D. Thesis, Hebrew University Jerusalem, Vol. 1 - 91 p., plates., Vol. 2 - Appen. (In Hebrew; English Abstract).

Avni, Y., 1998. Paleogeography and tectonics of the central Negev and the Dead Sea Rift western margin during the late Neogene and Quaternary. Jerusalem: Geol. Surv. Israel Rep. GSI/24/98, 231 p. (In Hebrew, English Abst.).

Avnimelech, M., 1936. Étude géologiques dans la region de la Shephela en Palestine. Ann. Univ. Grenoble, Trav. Lab. Geol. Grenoble, Allier Freres, 144 p., Figs.

Avnimelech, M., 1943. Contribution to the geological history of the Palestinian Coastal Plain: The surroundings of Nahariyya. Bull. Jewish Explor. Soc., 10(2-3), p. 39-46. (In Hebrew).

Avnimelech, M., 1950. Contribution to the knowledge of the Quaternary oscillations of the shoreline in Palestine. Riv. Ital. Paleontol. (Inst. Paleontol. Univ. Firenze), p. 44-56.

Avnimelech, M., 1952a. Late Quaternary sediments of the Coastal Plain of Israel. Isr. Res. Counc., Bull., 2G(1), p. 51-57.

Avnimelech, M., 1952b. The history of soils in the Coastal Plain of Israel. Eretz Israel Book, Vol. 2, p. 67-71. (In Hebrew).

Avnimelech, M., 1953. A new Pliocene outcrop in the central Coastal Plain of Israel. Isr. Res. Counc., Bull., 2G(4), p. 422-424. (Also: Isr. Geol. Surv., Publ. 6, 1954).

Avnimelech, M., A., 1964. Remarks on the occurrence of unusual high-temperature minerals in the so-called "mottled zone" complex of Israel. Isr. J. Earth Sci., Vol. 3(4).

Bandel, K., 1981. New stratigraphical and structural evidence for lateral dislocation in the Jordan Valley connected with description of the Jurassic rock column in Jordan. N. Jb. Geol. Palaeont. Abh. 161, p. 271-308, 12 figs., Stuttgart.

Bar-Yosef, O., Goldberg, P., and Leveson, T., 1974. Kebaran and Natufian sites in Wadi Fatza'el, Jordan Valley, Israel. Paleorient, 2(2), p. 415-428.

Bar Yosef, O., Tchernov, E., 1972. On the palaeo ecological history of the site of Ubeidiya. Jerusalem, Isr. Acad. Sci. Humanities, 35 p., Plates.

Bar Yosef, O., Tchernov, E., 1974. Archaeology; Excavations, Ubeidiya. Isr. Explor. J., 24(3-4), p. 252-253.

Begin, Z. B., Ehrlich, A., and Nathan, Y., 1974. Lake Lisan; the Pleistocene precursor of the Dead Sea. Isr. Geol. Surv., Bull. 63, 30 p., Plates.

Begin, Z. B., Nathan, Y., and Ehrlich, A., 1980. Stratigraphy and facies distribution in the Lisan Formation, new evidence from the area south of the Dead Sea, Israel. Isr. J. Earth Sci., 29(3), p. 182-189.

Bein, A., 1967. Upper peat - Hula Valley; summary report. Jerusalem: Geol. Surv. Israel Rep., 6 p. (In Hebrew).

Bender, F., 1974. Geology of Jordan. Berlin: Gebruder Borntrager, 196 p. (English translation of above, with minor revisions).

Bentor, Y. K., 1946. The hydrogeological conditions of the area of Tiberias - Kinneret - Yavneel - Hadatha - Kefar Kama - Lubya (Lower Galilee). Hebrew University Jerusalem, 76 p., Figs. (Report for the Palestine Water Co.).

Bentor, Y. K., 1949. The Negev mapping, 1949. Field notes, vols. 1-2. Photoreproduction of hand-written notes. Geol. Surv. Isr. Rep. GSI/10/85. (In Hebrew).

Bentor, Y. K., Grader, P., Parnes, A., Reiss, Z., Shiftan, Z., Vroman, A. J., Shadmon, A., Issar, A., Itzhaki, Y., Neev, D., Shalem, N., and Yaalon, D. H., 1960. Lexique Stratigraphique International. Vol. III: Asie. Fasc. 10 C 2: Israel. Paris, C.N.R.S., 151 p., Maps.

Bentor, Y. K., and Vroman, A. J., 1954. A structural contour map of Israel (1:250,000) With remarks on its dynamical interpretation. Isr. Res. Counc., Bull., 4G(2), p. 125-135, Map. (Also as: Isr. Geol. Surv.,

Bentor, Y. K., and Vroman, A. J., 1957. Geological map of Israel, 1:100,000, Series A - The Negev. Sheet 19: Arava Valley. Isr. Geol. Surv., 66 p., Maps. (Hebrew and English Editions).

Bentor, Y. K., and Vroman, A., 1960. The geological map of Israel, 1:100,000 Sheet 16, Mount Sedom. Isr. Geol. Surv., 117 p.

Blake, G. S., 1935. On the occurrence of marine Miocene in Palestine. Geol. Mag., 72(3), p. 140-142.

Blake, G. S., and Goldschmidt, M. J., 1947. Geology and water resources of Palestine. Jerusalem, Dept. of Land Settlement & Water Commissioner, 412 p., Maps. (Draft Edition - 1941).

Blanckenhorn, M., 1897. Zur Kenntnis der Suesswasserablagerungen und Mollusken Syriens. Palaeontographica, No. 44, p. 71-144.

Blanckenhorn, M., 1914. Syrien, Arabien und Mesopotamien. Heidelberg, Winter's Universitaetsbuch- Handlung, 159 p. (Handbuch der Regionalen Geol., Vol. 5, No. 4).

Blanckenhorn, M., and Oppenheim, P., 1927. Neue Beitraege zur Kenntnis des Neogens in Syrien und Palaestina. Geol. Palaeontol. Abh., N. F., 15(4), p. 321-357.

Braun, D., Ron, H., and Marco, S., 1991. Magnetostratigraphy of the hominid tool bearing Erk el-Ahmar Formation in the northern Dead Sea Rift. Isr. J. Earth Sci., 40(1-4), p. 191-197.

Braun, D., and Tchernov, E., 1991. Viviparus beds from central Jordan Valley - the southern correlative of Gesher Benot-Ya'akov Formation. Akko: Abst., Israel Geol. Soc. Ann. Mtg., 18.

Buchbinder, B., 1969. Geological map of Hashephale Region, Israel, Scale 1:20,000, with Explanatory Notes. Isr. Geol. Surv., Rep. OD/1/68 & Inst. Pet. Res. Geophys. Rep. 1030, 13 p., 6 Maps.

Buchbinder, B., Begin, Z. B., and Friedman, G. M., 1974. Pleistocene algal tufa of Lake Lisan, Dead Sea area, Israel. Isr. J. Earth Sci., 23(4), p. 131-138.

Buchbinder, B., and Gvirtzman, G., 1966: Semi Annual Progress Report.

Buchbinder, B., and Sneh, A., 1984. Marine sandstones and terrestrial conglomerates and mudstones of Neogene - Pleistocene age in the Modi'in Area: A re-evaluation. Isr. Geol. Surv., Current Res. 1983-84, p. 65-69.

Buchbinder, B., and Zilberman, E., 1997. Sequence stratigraphy of Miocene - Pliocene carbonate-siliciclastic shelf deposits in the Eastern Mediterranean margin (Israel): Effects of eustasy and tectonics. Sediment. Geol., 112(1-2), p. 7-32.

Burg, A., 1990. The geology of the Hatrurim Formation. M.Sc. thesis, Hebrew Univ., Jerusalem, 118 p. (In Hebrew). Also issued as Isr. Geol. Surv. Rep. GSI/18/91, 118 p.

Burg, A., Starinsky, A., Bartov, Y., and Kolodny, Y., 1991. Geology of the Hatrurim Formation ("Mottled Zone") in the Hatrurim Basin. Isr. J. Earth Sci., 40(1-4), p. 107-124.

Carmi, I., Noter, Y., and Schlesinger, R., 1971. Rehovot radiocarbon measurements I. Radiocarbon, 13(2), p. 412-419.

Clark, S. A., Langozky, Y., Speight, A. G., 1984. Har Sedom 1: Recommendation for drilling. Tel Aviv, Sismica Oil Exploration, Rep. 84/113, 13 p., Appen.

Dubertret, L., 1952. Carte géologique au 1:50,000, feuille de Mardjayoun. Beirut: Min. des Travaux Publiques.

Dubertret, L., 1963. Liban et Syrie. Lexique Stratigraphique International, Vol. 10 cl, p. 7-154. Paris: CNRS.

Ehrlich, A., 1973. Quaternary diatoms of the Hula Basin (northern Israel). Bull. Geol. Surv. Israel, 58, p. 1-40.

Enmar, L., Katz, A., Starinsky, A., and Heimann, A., 1998. The geochemistry of the travertines and the paleohydrology of springs in the Arava Valley, southern Israel. Isr. Geol. Soc., Annu. Meet., Abstr., p. 24.

Eyal, A., 1984. The geology of the northern Arava Valley and its western margins in the En Yahav-Hazeva region., Jerusalem: Geol. Surv. Israel Rep. GSI/10/91, 63 p. (In Hebrew, English Abstract).

Feldman, U., 1964. The morphology of the catchment area of Nahal Zanoah. Unpubl. M.A. Thesis, Hebrew University Jerusalem, 92 p., 1 Map, 1:5,000. (In Hebrew).

Gardner, E. W., and Bate, D. M. A., 1937. The bone-bearing beds of Bethlehem: their fauna and industry. Nature, 140(3540), p. 431-433.

Garfunkel, Z., and Horowitz, A., 1966. The Upper Tertiary and Quaternary morphology of the Negev, Israel. Isr. J. Earth Sci., 15(3), p. 101-117.

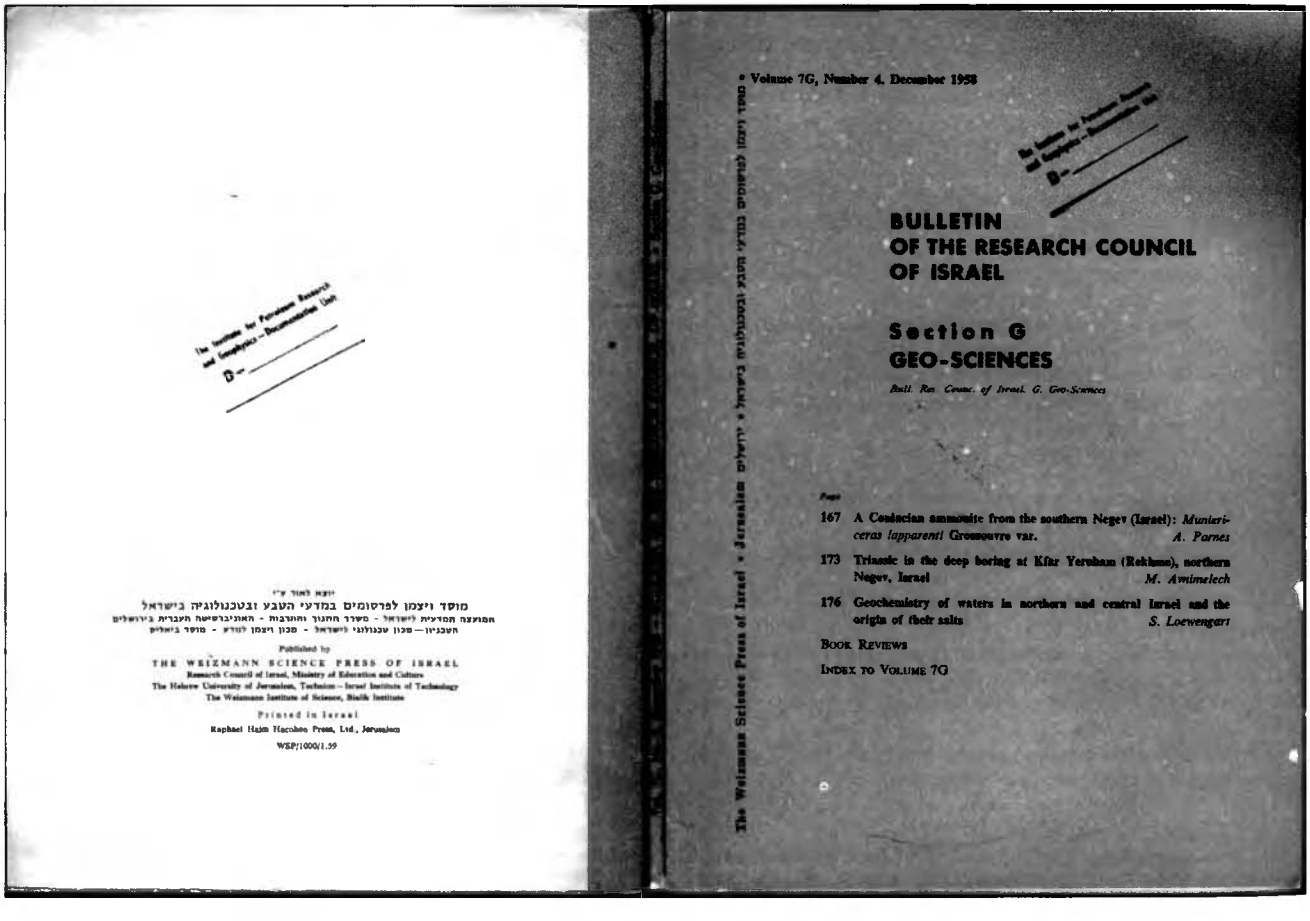
Geraads, D., and Tchernov, E., 1983. Femurs Humains du Pleistocene Moyen du Gesher Benoth Ya'acov (Israel). Anthropologie, 87(1), p. 138-141.

Gilead, D., 1970. Handaxe industries in Israel and the Near East. World Archaeol.

2(1), p. 1-11.
Gill, D., 1965. Subsurface geology of the Petah-Tigwa area (Upper Cretaceous - Pleistocene). Isr. Nat. Oil Comp., Tel Aviv, 61 p. (In Hebrew).
Ginat, H., 1997. Paleogeography and the landscape evolution of the Nahal Hiyyon and Nahal Zihor Basins (sedimentology, climatic and tectonic aspects). Unpubl. Ph.D. Thesis, Hebrew University Jerusalem, 109 p. (In Hebrew; English Abstract).
Ginat, H., and Saragusti, I., 1996. Lower Paleolithic finds from the region of Nahal Zihor, southern Negev. Isr. Geol. Soc., Annu. Meet., Abstr., p. 30.
Ginat, H., Zilberman, E., and Rosenfeld, A., 1996. New finding of early Pleistocene lake deposits in Nahal Zihor, southern Negev. GSI, Current Res., 10, p. 55-61.
Golik, A., 1960. On the geology of the Ziklag area, Israel. Isr. Res. Counc., Bull., 9G(2-3), p. 129-152.
Goren-Inbar, N., 1995. The Lower Paleolithic of Israel. In T. E. Levy (ed.), The Archaeology of Society in the Holy Land, London: Leicester Univ. Press, p. 93-109.
Greitzer, Y., 1960. On the geology of the Lakhish area. Isr. Res. Counc., Bull., 9G(2-3), p. 109-128.
Gross, S. 1977. The mineralogy of the Hatrurim Formation, Israel. Isr. Geol. Surv. Bull., 70, 80 p.
Gvirtzman, G., 1969a. Subsurface data on the Saqiye Group (Late Eocene to Early Pleistocene) in the Coastal Plain and Hashephela regions, Israel. Isr. Geol. Surv., Rep. OD/1/69 & Inst. Pet. Res. Geophys., Rep. 1037, Various Pagings.
Gvirtzman, G., 1969b. The Saqiye Group (Late Eocene to Early Pleistocene) in the Coastal Plain and Hashephela regions. Vol. 2: Maps. (Vol. 1 was never published). Isr. Geol. Surv., Bull. 51 & Inst. Pet. Res. Geophys., Rep. 1022. 38 Maps.
Gvirtzman, G., Buchbinder, B., 1966. Tertiary Project. Semi Annu. Progr. Rep., Apr. 1966 - Sept. 1966, Holon, Inst. Pet. Res. Geophys. Rep. 1018, p. 11-17.
Gvirtzman, G., and Buchbinder, B., 1969. Outcrops of Neogene formations in the central and southern Coastal Plain, Hashephela and Be'er Sheva regions, Israel. Isr. Geol. Surv., Bull. 50, & Inst. Pet. Res. Geophys. Rep. 1040, 52 p.
Gvirtzman, G., and Reiss, Z., 1965. Stratigraphic nomenclature in the Coastal Plain and Hashephela regions. Isr. Geol. Surv., Rep. OD/1/65, 13 p.
Gvirtzman, G., Shachnai, E., Bakler, N., and Ilani, S., 1984. Stratigraphy of the Kurkar Group (Quaternary) of the Coastal Plain of Israel. Isr. Geol. Surv., Current Res. 1983-84, p. 70-82.
Haas, G., 1966. On the vertebrate fauna of the Lower Pleistocene site of Ubeidiya. The Israel Academy of Sciences and Humanities, Jerusalem.
Heimann, A., 1990. K-Ar ages of basalt units in the Quneitra Valley, the Golan Heights, Israel. Qedem; Monographs of the Inst. Archaeol., Hebrew University Jerusalem, No. 31, p. 34-38.
Heimann, A., and Sass, E., 1989. Travertines in the northern Hula Valley, Israel. Sedimentology, 36(1), p. 95-108.
Hooijer, D. A., 1958. An early Pleistocene mammalian fauna from Bethlehem. Bull. Brit. Mus. (Nat. Hist. Geol.), 3(8), p. 267-292.
Hooijer, D. A., 1959. Fossil mammals from Jisr Banat Yaqub, south of Lake Huleh, Israel. Bull. Res. Counc. Isr., 8G(4), p. 177-199.
Hooijer, D. A., 1960. A Stegodon from Israel. Bull. Res. Counc. Isr., 9G(2-3), p. 104-108.
Horowitz, A., 1971. Climatic and vegetational developments in northeastern Israel during upper Pleistocene-Holocene times. Pollen et Spores, 13(3), p. 255-278.
Horowitz, A., 1973. Development of the Hula Basin, Israel. Isr. J. Earth Sci., 22(2), p. 107-139.
Horowitz, A., 1974. The late Cenozoic stratigraphy and paleogeography of Israel: 184 p. Inst. Archaeol., Tel Aviv Univ.
Horowitz, A., 1975b. Late Pleistocene clastic dykes and rates of erosion in the Galilee, Israel. Tel Aviv 2(3), p. 93-96.
Horowitz, A., 1979. The Quaternary of Israel: 394 p. New York: Academic Press.
Horowitz, A., 1987a. Subsurface palynostratigraphy and paleoclimates of the Quaternary Jordan Rift Valley fill, Israel. Isr. J. Earth Sci., 36(1-2), p. 31-44.
Horowitz, A., 1987b. Travertines of the arid regions, oxygen isotope stages, and late Quaternary climates of Israel. Quat. Res. 27(1), p. 103-105.
Horowitz, A., 1987c. Palynological evidence for the age and rate of sedimentation along the Dead Sea Rift, and structural implications. Tectonophysics 141(1-3), p. 107-115.
Horowitz, A., 1988. Synthese de la stratigraphie et des paleoclimats quaternaires du rift de la Mer Morte, Israel. L'Anthropologie, 92(3), p. 753-767.
Horowitz, A., 1989a. Prehistoric cultures of Israel: correlation with the oxygen isotope scale. In: O. Bar Yosef and B. Vandermeersch (eds), Investigations in South Levantine prehistory, p. 5-17. Oxford: BAR Intl. Ser., 497.
Horowitz, A., 1989b. Palynological evidence for the Quaternary rates of accumulation along the Dead Sea Rift, and structural implications. Tectonophysics 164(1). p. 63-71.
Horowitz, A., 1989c. Continuous pollen diagrams for the last 3.5 M.Y. from Israel: vegetation, climate and correlation with the oxygen isotope record. Palaeogeogr. Palaeoclimatol. Palaeoecol. 72(1-2), p. 63-78.
Horowitz, A., 1992a. Palynology of arid lands. Elsevier, Amsterdam, 546 p.
Horowitz, A., 1992b. AP factors and late prehistoric settlement patterns of the Levant. Aix-en-Provence: Abst., 8th Intl. Palynol. Cong., 67.
Horowitz, A., 1996. Palynostratigraphy of Sedom Deep 1 borehole and the late Cenozoic climate of Israel. Houston: Abst., IX Intl. Palynol. Cong., 67.
Horowitz, A., 1997. Palynostratigraphy and subsidence of the Dead Sea Rift fill. The 13th GIF Meeting on the Dead Sea Rift as a Unique Global Site, February 23-27, 1997, Dead Sea. Schriften der Alfred-Wegener Stiftung, Terra Nostra 4/97 (no page numbers).
Horowitz, A., 2001. The Jordan Rift Valley. A. A. Balkema Publishers, Lisse-Abingdon-Exton-Tokyo, 73 p.
Horowitz, A., and Horowitz, M., 1985. Subsurface late Cenozoic palynostratigraphy of the Hula Basin, Israel. Pollen et Spores, 27(3-4), p. 365-390.
Horowitz, A., and Horowitz, M., 1990. Neogene-Recent paleogeography of the southern Dead Sea. Tel Aviv: Israel National Oil Co. Rep., 153 p. (unpubl.).
Horowitz, A., Siedner, G., and Bar-Yosef, O., 1973. Radiometric dating of the Ubeidiya Formation, Jordan Valley, Israel. Nature 242(5394), p. 186-187.
Huckriede, R., 1966. Das Quartär des arabischen Jordan-Tales and Beobachtungen über "Pebble Culture" and "Prä-Aurignac". Eiszeitalter u. Gegenw., 17, p. 211-212.
Hull, E., 1885. On the origin of fishes of the Sea of Galilee. Brit. Assoc. Adv. Sci., 55th Meet., Rep., p. 1066-1068.
Hull, E., 1886. The Survey of Western Palestine. Memoir on the Geology and Geography of Arabia Petraea, Palestine and adjoining Districts, with ppecial reference to the mode of formation of the Jordan - Arabah Depression and the Dead Sea. London, Richard Bentley & Son, 154 p., Maps.
Ionides, M. G., and Blake, G. S., 1940. Report on the water resources of Transjordan and their development: 372 p. London: Crown Agents.
Issar, A., 1961. The Plio Pleistocene geology of the Ashdod area. Isr. Res. Counc., Bull., 10G(1-4), p. 173-182.
Issar, A., 1968. Geology of the central Coastal Plain of Israel. Isr. J. Earth Sci., 17(1), p. 16-29.
Kafri, U., and Heimann, A., 1994. Reversal of the paleodrainage system in the Sea of Galilee area as an indicator of the formation timing of the Dead Sea Rift Valley base level in northern Israel. Palaeogeogr Palaeoclimatol. Palaeoecol., 109(1), p. 101-109.
Kansou, M., 1961. Decouverte de vertebras pontiens au Liban, dans la plaine de la Bekaa. Bull. Scient. (Yugoslavia), 6(3), p. 65.
Kaufman, A., 1971. U-series dating of Dead Sea Basin carbonates. Geochim. Cosmochim. Acta, 35(12), p. 1269-1281.
Kolodny, Y., Schulman, N., and Gross, S., 1973. Hazeva Formation sediments affected by Mottled Zone Event. Isr. J. Earth Sci., 22(3), p. 185-193.
Kronfeld, J., Vogel, J. C., Rosenthal, E., and Weinstein-Evron, M., 1988. Age and paleoclimatic implications of the Bet She'an travertines. Quat. Res., 30(3), p. 298-303.
Langotzky, Y., 1960. The petrography and geochemistry of the Lisan Formation. Unpubl. M.Sc. Thesis, Dept. Geol., Hebrew University Jerusalem, 54 p. (In Hebrew).
Langotzky, Y., 1966. Clastic deposition in the Dead Sea Graben., Semi Annual Progress Report.
Lartet, L., 1869. Essai sur la géologie de la Palestine et des contrées avoisinantes, telles que l'Égypte et l'Arabie, comprenant les observations recueillies dans le cour de l'Expédition du Duc de Luynes a la Mer Morte: 292 p. Paris: Masson.
Levin, N., and Horowitz, A., 1987. Palynostratigraphy of the early Pleistocene QI Palynozone. Isr. J. Earth Sci., 36(1-2), p. 45-58.
Livnat, A., and Kronfeld, J., 1985. Paleoclimatic implications of U-series dates for lake sediments and travertines in the Arava rift valley, Israel. Quat. Res., 24(2),

p. 164-172.
Livnat, A., and Kronfeld, J., 1990. Pleistocene lakes in the Arava Rift of Israel (Sayif Formation): facies and paleoenvironmental setting. J. Afr. Earth Sci., 10(3), p. 409-420.
Loewengart, S., 1928. Zur Geologie der Kustenebene Palästinas. Cbl. Fur Mineral. 9B, p. 498-519.
Lorch, J., 1966. A Pleistocene florule from the central Jordan Valley. Isr. J. Botany 15(1), p. 31-34.
Marcus, E., and Slager, J., 1985. The sedimentary-magmatic sequence of the Zemah 1 well (Dead Sea Rift, Israel) and its emplacement in time and space. Isr. J. Earth Sci., 34(1), p. 1-10.
Matthews, A., and Nathan, Y., 1977. The decarbonation of carbonate-fluorapatite (francolite). Amer. Mineralogist, 62(5-6), p. 565-573.
Mor, D., 1986. The volcanism of the Golan Heights. Jerusalem: Geol. Surv. Israel Rep. GSI/5/86, 159 p. (In Hebrew, English summary).
Mor, D., and Steinitz, G., 1985. The history of the Yarmouk River based on K-Ar dating and its implication on the development of the Jordan Rift. Jerusalem: Geol. Surv. Israel Rep. GSI/40/85, 18 p.
Moshkovitz, S., 1963. The Mollusca in the upper part of the Sakie Beds (Upper Neogene-Lower Pleistocene) in the central Coastal Plain of Israel. Isr. J. Earth Sci., 12(3), p. 97-146.
Moshkovitz, S., 1968. The Mollusca in the marine Pliocene and Pleistocene sediments of the south-eastern Mediterranean Basin (Cyprus-Israel). Ph.D. Thesis, Hebrew University Jerusalem, 157 p., Plates. (In Hebrew; English Abstract).
Neev, D., 1967. The late Holocene fluviatile history of the Kinneret (Tiberias) and Bet She'an Basins. Isr. J. Earth Sci., 16(1), p. 50.
Neev, D., and Emery, K. O., 1967. The Dead Sea. Bull. Geol. Surv. Israel, 41, p. 1-147.
Picard, L., 1928. Zur Geologie der Kischon Ebene. Zeitschr. Deutsch. Pal□t. Ver., 51(1), p. 5-72, 2 Maps.
Picard, L., 1929. Zur Geologie der Besan-Ebene. Zeitschr. Deutsch. Paläst. Ver. 52, p. 24-90.
Picard, L., 1931, Geological researches in the Judea Desert, Jerusalem, 108 p.
Picard, L., 1932. Zur Geologie des mittleren Jordantales. Zeitschr. Deutsch. Paläst. Ver. 55, p. 169-236.
Picard, L., 1937. Inferences on the problem of the Pleistocene climate of Palestine and Syria. Proc. Prehist. Soc. Cambridge 5, p. 58-70.
Picard, L., 1938. Synopsis of stratigraphic terms in Palestinian geology. Bull. Geol. Dept. Hebrew Univ. Jerusalem 2(2), p. 1-24.
Picard, L., 1943. Structure and evolution of Palestine, with comparative notes on neighboring countries. Bull. Geol. Dept. Hebrew. Univ. Jerusalem, 4(2-4), 134 p.
Picard, L., 1952. The Pleistocene peat of Lake Hula. Bull. Res. Counc. Isr., II(2), p. 147-156.
Picard, L., 1955. Geological map of Palestine, 1:100,000, Sheet 9: Ramle. Isr. Geol. Surv., 1 Map.
Picard, L., 1959. Geology and oil exploration of Israel. Bull. Res. Counc. Isr., 8G(1), p. 1-30.
Picard, L., 1963. The Quaternary in the northern Jordan Valley. Proc. Israel Acad. Sci. Hum., 1(4), p. 1-34.
Picard, L., 1965. The geological evolution of the Quaternary in the central-northern Jordan Graben, Israel. Geol. Soc. Am., Spec. Pap. 84, p. 337-366.
Picard, L., and Baida, U., 1966a. Stratigraphic position of the Ubeidiya Formation. Proc. Israel Acad. Sci. Hum. 4, p. 1-8.
Picard, L., and Baida, U., 1966b. Geological report on the lower Pleistocene deposits of the Ubeidiya excavations: 39 p. Jerusalem: Israel Acad. Sci. Hum.
Picard, L., and Solomonica, P., 1936. On the geology of the Gaza-Be'er Sheva district. J. Palestine Oriental Soc. 16, p. 180-223.
Reiss, Z., 1964. Range charts of Israel foraminifera. Isr. Geol. Surv., Rep. Pal/6/64, 9 p., Plates.
Reiss, Z., and Issar, A., 1961. Subsurface Quaternary correlations in the Tel Aviv region. Isr. Geol. Surv., Bull. 32, p. 10-26.
Roded, R., Zilberman, E., and Buchbinder, B., 1993. The Red Unit: a pedogenic flood plain facies of the Ahuzam Formation in the eastern part of the Beer Sheva Valley. Isr. Geol. Surv., Current Res., Vol. 8, p. 65-68.
Ronen, A., 1996. The earliest hominids in Israel. In: Beinhauer, K. W., Kraatz, R., and Wagner, A., (eds), Homo erectus heidelbergensis von Mauer, Heidelberg: Jan Thorbecke Sigmaringen, p. 99-102.
Rosenfeld, A., Honigstein, A. and Scarpa, D., 2002. Pliocene-Pleistocene Lakes in Southern Israel - Ostracods and Hominids. GSI, Current Res., 13, p. 86-93.
Rosenfeld, A., Segev, A., and Halbersberg, E., 1981. Ostracode species and paleosalinities of the Pliocene Bira and Geshor formations (northwestern Jordan Valley). Isr. J. Earth Sci., 30(4), p. 113-119.
Rosenfeld, A., and Vesper, B., 1977. The variability of the sieve pores in recent and fossil species of *Cyprideis torosa* (Jones, 1850) as an indicator for salinity and palaeo-salinity. (Israel - Lisan Formation). 6th Int. Ostracod Symp., Saalfelden, p. 55-67.
Rosenthal, E., 1980. Hydrogeology and hydrogeochemistry of the Bet She'an, Harod and Mehola Valleys. Unpubl. Ph.D. Thesis, Dept. Geol., Hebrew University Jerusalem, 244 p. (In Hebrew, English Summary).
Rossignol, M., 1969a. Sedimentation palynologique récente dans la Mer Morte. Pollen et Spores, 11(1), p. 17-38.
Rossignol, M., 1969b. Une sequence climatique du Pleistocene dans la region de la Mer Morte (Israel). Pollen et Spores, 11(3), p. 603-614.
Schramm, A., Stein, M., and Goldstein, S. L., 1997. ^{14}C time-scale calibration and relation to global paleoclimate: evidence from U-series and ^{14}C dating of Lake Lisan (paleo-Dead Sea sediments. The 13th GIF Meeting on the Dead Sea Rift as a Unique Global Site, February 23-27, 1997, Dead Sea. Schriften der Alfred-Wegener Stiftung, Terra Nostra 4/97 (no page numbers).
Schulman, N., 1959. The geology of the central Jordan Valley. Bull. Res. Counc. Isr., 8G(2-3), p. 63-90.
Schulman, N., 1962. The geology of the central Jordan Valley. Unpubl. PhD Thesis, Dept. Geol., Hebrew University Jerusalem, 103 p. (In Hebrew, English Summary).
Schulman, N., 1967. Remarks on the Quaternary in the northern Jordan Valley. Isr. J. Earth Sci., 16(2), p. 104-106.
Schütt, H., and Ortal, R., 1993. A preliminary correlation between the Plio-Pleistocene malacofaunas of the Jordan Valley (Israel) and the Orontes Valley (Syria). Zool. Middle East 8, p. 69-111.
Schwarcz, H. P., Blackwell, B., Goldberg, P., and Marks, A. E., 1979. Uranium series dating of travertine from archaeological sites, Nahal Zin, Israel. Nature 277(5697), p. 558-560.
Schwarcz, H. P., Goldberg, P. D., and Blackwell, B., 1980. Uranium series dating of archaeological sites in Israel. Isr. J. Earth Sci., 29(1-2). p. 157-165.
Shachnai, E., 1967. The geology and hydrogeology of the western Besor region. Unpubl. M.Sc. Thesis, Hebrew University Jerusalem, 64 p., Maps. (In Hebrew).
Shaliv, G., Mimran, Y., and Hatzor, Y., 1991. The sedimentary and structural history of the Bet She'an area and its regional implications. Isr. J. Earth Sci., 40(1-4), p. 161-179.
Shaw, S. H., 1948. The geology and mineral resources of Palestine. Bull. Imper. Inst. 46(1), p. 87-103.
Siedner, G., and Horowitz, A., 1974. Radiometric ages of late Cainozoic basalts from northern Israel: chronostratigraphic implications. Nature, 250(5461), p. 23-26.
Sneh, A., 1982. Quaternary of the northwestern Arava, Israel. Isr. J. Earth Sci., 31(1), p. 9-16.
Sneh, A. and Langotzky, Y., 1966. Semi Annual Progress Report, 10 p. 3 Figs.
Sneh, A., 1996. The Dead Sea Rift: Lateral displacement and downfaulting phases. Tectonophysics, 263(1-4), p. 277-292.
Solomonica, P., 1948. Some stratigraphical inferences. J. Palestine Orient. Soc. 21, p. 97.
Stein, M., Starinsky, A., Katz, A., Goldstein, S. L., Machlus, M., and Schramm, A., 1997. Sr isotopic, chemical and sedimentological evidence for the evolution of Lake Lisan and the Dead Sea. The 13th GIF Meeting on the Dead Sea Rift as a Unique Global Site, February 23-27, 1997, Dead Sea. Schriften der Alfred-Wegener Stiftung, Terra Nostra 4/97 (no page numbers).
Stekelis, M., 1948. Rephaim-Baq'a: A paleolithic station in the vicinity of Jerusalem. J. Palest. Orient. Soc., 21, p. 80-96.
Stekelis, M., 1960. The Paleolithic deposits of Jisr Banat Yaqub. Bull. Res. Counc. Isr., 9G(2-3), p. 61-87.
Stekelis, M., 1960/1961. La necropolis megalitica de Ala-Safat, Transjordania. Ampurias XXII-XXIV, p. 49-128.
Stekelis, M., 1966a. The Yarmoukian culture. Museum of Prehistory, Sha'ar Hagolan

(Israel), 65 p., 76 plates. (In Hebrew).
Stekelis, M., 1966b. Archaeological excavations at Ubeidiya, 1960-1963. Israel Acad. Sci. Hum., Jerusalem, 32 p., 37 plates.
Stekelis, M., and Gilead, D., 1966. Ma'ayan Baruch: an early Stone Age site at the upper Galilee. MiTekufat Ha'Even 8, p. 1-24. (In Hebrew).
Stekelis, M., Picard, L., and Bate, D. M. A., 1937. Jisr Banat-Yaqub. Quart. Dept. Antiquities Palestine, 6(3-4), p. 214-215.
Stekelis, M., Picard, L., Schulman, N., and Haas, G., 1960. Villafranchian deposits near Ubeidiya in the central Jordan Valley (preliminary report). Bull. Res. Counc. Isr., 9G(4), p. 175-183.
Tchernov, E., 1973. On the Pleistocene mollusks of the Jordan Valley. Israel Acad. Sci. Hum., Jerusalem, 46 p.
Tchernov, E., 1975. The early Pleistocene mollusks of Erk el Ahmar. Israel Acad. Sci. Hum., Jerusalem, 36 p.
Tchernov, E., 1979. Quaternary fauna. In A. Horowitz (ed.), The Quaternary of Israel. Academic Press, New York, p. 260-292.
Tchernov, E., 1980. The biostratigraphy of the Middle East. Préhistoire du Levant, 598, p. 67-97.
Tchernov, E., 1996. Rodent faunas, chronostratigraphy and paleobiogeography of the southern Levant during the Quaternary. Acta Zool., Cracov, 39(1), p. 513-530.
Tobias, P. V., 1966. A member of the genus Homo from Ubeidiya. Israel Acad. Sci. Hum., Jerusalem, 12 p., 3 plates.
Valladas, H., Joron, J. L., Valladas, G., Arensburg, B., Bar Yosef, O., Belfer-Cohen, A., Goldberg, P. D., Laville, H., Meignen, L., Rak, Y., Tchernov, E., Tillier, A. M., and Vandermeersch, B., 1987. Thermoluminescence dates for the Neanderthal burial site at Kebara in Israel. Nature, 330(6144), p. 159-160.
Verosub, K. L., and Tchernov, E., 1991. Resultats préliminaires de l'étude magnetostratigraphique d'une sequence sedimentaire à industrie humaine en Israel. Les Premiers Europeens. Proc., 114th Natl. Congr. Of Learned Soc., Paris, p. 237-242.
Vita-Finzi, C., 1966. The Hasa Formation: an alluvial deposition in Jordan. Man 1(3), p. 384-390.
Weinstein-Evron, M., 1987. Palynology of Pleistocene travertines from the Arava Valley, Israel. Quat. Res. 27(1), p. 82-88.
Wetzel, R., and Morton, D. M., 1959. Contribution a la géologie de la Tranjordanie. Notes et Mém. Moyen Orient VII, p. 95-191.
Zak, I., 1967. The geology of Mount Sedom. Unpubl. Ph.D. Thesis, Dept. Geol., Hebrew University Jerusalem, 207 p. (In Hebrew, English Summary).



Memories of a bygone era.
The cover of one of the early issues of the Research Council of Israel, Section G, Geo-Sciences. This publication, published by the Weizmann Science Press of Israel in Jerusalem, later became the Israel Journal of the Earth-Sciences. Many important papers on the geology of Israel graced its pages in the early days of the country.

Chapter 18J

Strike-slip Faulting West of the Dead Sea Escarpment

Arie Gilat
Geological Survey of Israel, 30 Malchei Israel St. Jerusalem 95501, Israel

ABSTRACT

Geological, geomorphological and geochemical mapping of the strike-slip faulting in the southern Judea Mountains-Judea Desert areas has delineated structural and morphological features of the main strike-slip and oblique-slip faults belonging to the Syrian Arc and the Dead Sea systems west of the Dead Sea escarpment. Major conclusions are:

a) Numerous strike-slip faults, associated with the Dead Sea Transform, are superimposed on and cut through the structures of the Syrian Arc in Judea;

b) At least some of the main monoclines of the Syrian Arc belt are bordered by and caused by oblique-slip faults;

c) The 'Sinai-Levant micro-plate' has been broken into smaller blocks by dominantly horizontal dislocations, probably since the Mesozoic Era. Some of these strike-slips are still active and landscape-forming; they also operate as good conductors for magmatic intrusions and circulating solutions, thus the 'micro-plate' can be evaluated as a potentially metallogenic province.

INTRODUCTION

Begin (1973), Gilat (1985, 1987, 1998), and Gilat and Agnon (1981) mapped strike-slip faults and shear zones west of the Dead Sea. Some of these faults are of regional scale, part of the generally N-S oriented, ~30 to ~90 km wide transform shear-zone. Contrary to most parts of this zone, its southern part is not camouflaged by Phanerozoic sediments, and is clearly visible on satellite images and on the geological map (Bartov, 1994). Further north and west of the Dead Sea, in the Judean Desert, the total thickness of the Phanerozoic sedimentary cover reaches 3-4 km, and the appearance of strike-slip movements on the surface is inferior to that in the eastern Sinai. Some of the strike-slip faults border asymmetric anticlines of different trends. Gilat (1994) described morphological and geochemical features of these structures. The latter included anomalies of the trace and noble elements. Numerous metallic mineralizations, associated with different lineaments, were also described by Ilani (1989), and others (references can be found in Gilat, 1994).

Gorodnitsky and Gilat (2000) analyzed the change from stress in the Dead Sea Transform in the Pliocene-Pleistocene towards the back of the Syrian Arc, to tension accompanied by the development of grabens, salt diapirism, and volcanic activity. They suggested possible back-arc spreading along the Dead Sea Transform, much the same way as in the northern Pacific back-arc stress-modification model.

STRIKE-SLIP FAULT-RELATED STRUCTURES

Judean Desert

The western region of the Judean Desert is a large structural terrace formed since the earliest Santonian (Flexer et al., 1989). It is comprised of different N-S and NE-SW trending anticlinal flexures, belonging to the Syrian Arc system, which are deformed by a well-developed and still active system of faults related to the Dead Sea Transform (Gilat, 1998). In conjunction with activated faults of the northeastern trend, these faults form the structural framework (**Fig. 18J.1**), which reflects the northward movements of the blocks.

The largest among the strike-slip faults of the Judean Desert is the Qana'im wrench fault zone, conceived sometime in the Late Turonian. Its main N-S trending Pre-Santonian fault transects the prevailingly NE Syrian Arc meso-structures 8 to 10 km west of the Dead Sea cliffs (Fig. 18J.1), and subdivides the southern part of the Judean Desert into two different geological regions, which have a different Late Cretaceous-Neogene geological history. These are reflected in the Late Santonian-Early Campanian 'Double-Chert' sequence, and the development of numerous circular dolomite bodies during the Miocene-Pliocene, both phenomena occurring only in the eastern region (Gilat and Honigstein, 1982; Gilat et al., 1978). In some of the fault segments, which comprise the main fault and its branches, the limestone and even the chalky rock sequences have been massively dolomitized in the faults' vicinity by hydrothermal-metasomatic processes, probably during the Pliocene, following the formation of the circular dolomite bodies (Gilat, 1994).

The main Qana'im wrench fault runs parallel to the major western Dead Sea fault, from the area of Hamakhtesh Haqatan in the south to Biq'at Hureqanya and farther to the north, where it sinistrally displaces and is dextrally displaced by the Samia fault; farther north it passes along the Auja monocline (Gilat, 1998). Its NNW trending branches are 3-15 (or more) km long, crossing the entire Judean Desert and parts of the horst-anticlines of the Judean and Shomeron Mountains (Fig. 18J.1). These faults show alternating faces with both normal and thrust throws. They also form flexures, V-shaped synclines, and shear zones with horizontal slickensides. Vertical displacements of up to 0.3 km and sinistral offsets of 0.1-1.3 km were observed, and an experiment in their reconstruction was made (*ibid*). Many fault segments are superposed on pre-existing structures: in the Adasha Valley the younger (Plio-Pleistocene) fault is about 100 m west and parallel to the pre-Santonian fault; near Mt. Holed it passes through a long and narrow graben, above which the Senonian sequence is much thinner, suggesting a horst

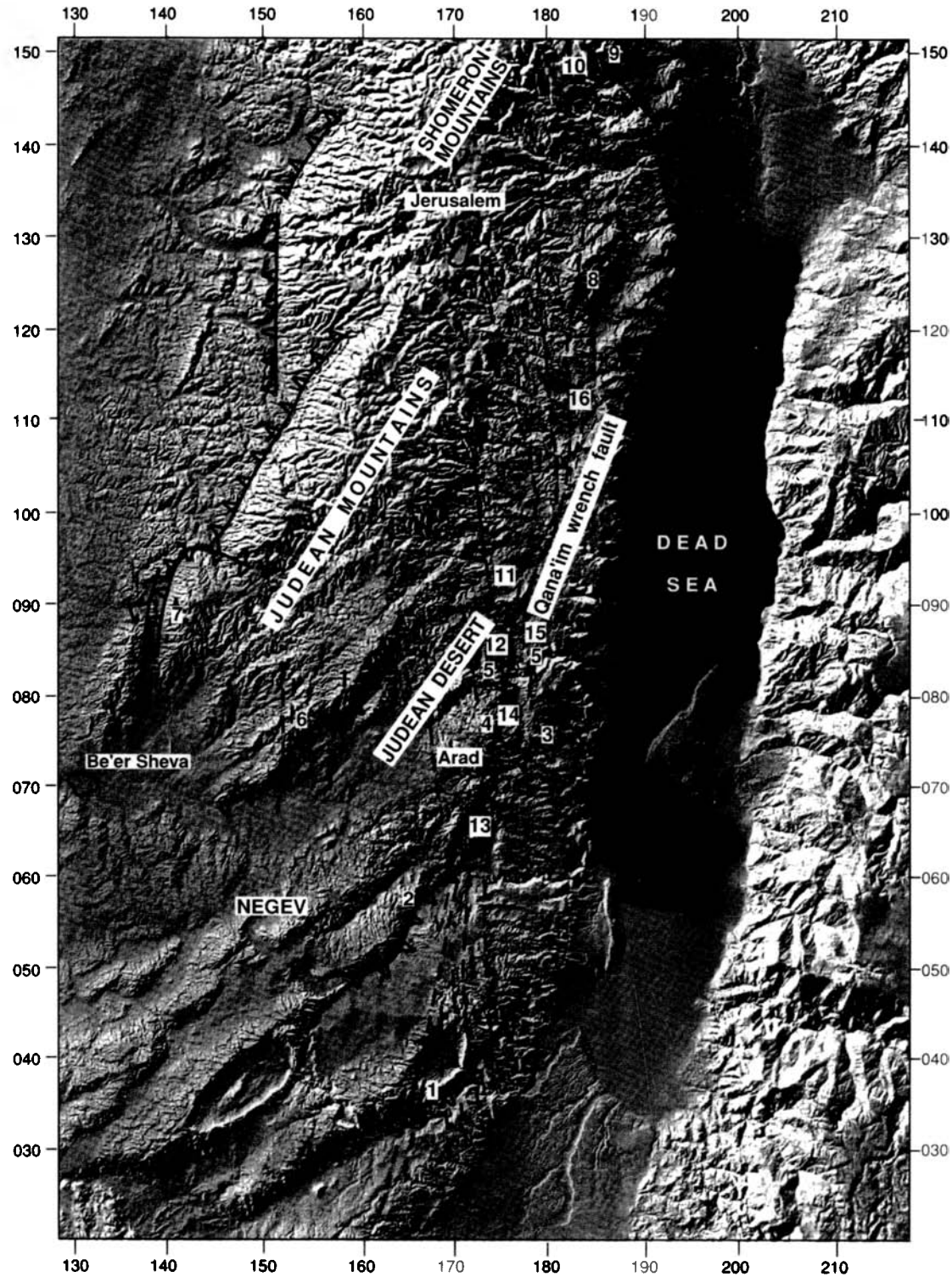


Figure 18J.1. Location map of the Qana'im wrench fault shown on the digital shaded-relief map of Israel and environs (Hall, 1997). Continuous lines denote strike-slip fault; dashed are strike-slip faults, locality inferred; Line with arrowheads are flexures, arrows indicate down-dip. Numbers on the map show the localities of flexures: 1 - Makhtesh Hazera; 2 - Dimona - Zohar; 3 - N. Rahaf; 4 - Biq'at Qana'im; 5 - N. Ze'elim; 6 - eastern flexure of the Judean Mts.; 7 - western flexure of the Judean Mts.; 8 - Biq'at Hureqanya; 9 - Auja; 10 - Samia fault strip; Additional localities: 11 - Mt. Holed; 12 - N. Adasha; 13 - Hatrurim basin; 14 - Har - Menahem; 15 - HarNamer; 16 - N. Darga. (After Gilat, 1998, Fig. 1).

development during that period (Gilat and Honigstein, 1982). The strike-slip movement on the Qana'im fault occurred in two-stages, in the Pliocene (a period of massive dolomitization) and in the Lower Pleistocene (as indicated by Acheulean tools found buried in the base of a displaced river terrace).

Between the main fault of the Qana'im zone and the main Dead Sea cliff there are at least three more N-S trending sinistral strike-slip faults of more than 20 km length, and a system of E-W trending dextral strike-slip shear zones up to 1.5 km wide, solely responsible for the development of enormous U-shaped box canyons in the easternmost Judean Desert area. Present-day structures in the area illustrate the idealized scheme of sinistral faults causing counterclockwise rotation of domains nested between sub-perpendicular dextral faults. Even the triangular gaps (crumbled sections, Gilat, 1992, Fig. 2) along domain boundaries are well-preserved, and arc systems of tensional fractures, separating southeastern block-edges that protrude (as a result of rotation) into the few km deep Dead Sea graben, are even clearly visible on aerial photographs (Gilat, 1992, Fig. 4).

Block-rotation and development of oversized canyons (a result of intensive shearing, caused by repeated reversals in the sense of rotation of adjacent domains, which dramatically increased sheet-erosion and mass-wasting of valley slopes, multiplying valley bed-load), occurred in the Late Pliocene-early Late Pleistocene following massive dolomitization (Gilat, 1994), and preceded the Lisan Lake sedimentation (about 100,000 BP).

Comparatively small N to NW-striking faults that branch from the Qana'im main fault produce parallel fracturing (shearing), steps, and local secondary flexures on the western flexure of the Qana'im Valley, and cross the southern and eastern parts of the Judean Desert (Fig. 18J.1). These faults change their throw direction, with vertical displacement on some reaching 60 m. Among the geomorphological forms they produce are all the major combinations characteristic of the main Qana'im faults, including graben-like (ramp) structures, horsts, vertically displaced V-synclines, and flexures opposite up-lifted blocks; horizontal slickensides can be found locally. In places they follow older Turonian-Senonian faults, which appear as normal, but were formed as compressional and not tensional features. Additional NNW-striking faults can be traced on the satellite maps, branching off from the main Qana'im fault north of Nahal Ze'elim, Nahal Dragot and Nahal Darga (Gilat, 1987).

Most of the branch faults are sinistral, but some of them displaced older structures dextrally by 50 to 300 m (near Old Israel Coord. 173.0E/083.3N and 173.6E/083.3N, *ibid*). Some of them caused temporal closure of the Ze'elim, Adasha, and Harduf Valleys and accumulation of alluvial material in terraces up to 18 m high at the base of N. Adasha, where flint tools of probably Acheulean culture were found (Gilat, 1994).

Judean Mountains

Numerous NNW, NNE, and E-W trending shear zones cross the Judean Mountains structures, displacing valleys and producing typical sharp bends in the valley course ('dog-leg bends') that are clearly visible on the 1:50,000 scale topographic maps. Shear zones are densest in the corridor between major twin NNW trending lineaments, which dextrally offset the southern block of the Hebron horst-anticline (Gilat, 1985). The southern segment of its western flexure is opposed by an uplifted block, which indicates strike-slip displacement. Its eastern flexure is displaced by at least seven minor shear zones with N and NNW trends. Some of these are branch faults of the Qana'im fault. Within the main structure, NE trending lineaments include the well-pronounced Luzifar-Mizpe Shalem lineament; part of its segment excavated near Luzifar displayed a shear zone containing several small strike-slip faults and a large scale metasomatic type alteration (*ibid*). On the structural maps (Gilat, 1977, 1987) these shear zones can be traced as very narrow synclines and secondary anticlines. Two large lineaments cross the main structure latitudinally, the southernmost was identified as a large south-dipping flexure, whose Turonian rocks are strongly dolomitized (Gilat, 1985). Many additional lineaments can be seen on satellite images and on aerial photographs. The field survey found them to be traceable on the ground, where they displayed intense jointing, minor faulting and folding, epigenetic variations, and sometimes horizontal slickensides (*ibid*).

Morphology of strike-slip faults in the Judean Mountains-Judean Desert

Large scale lineaments crossing the Negev, the Judean Desert, and the Judean and Shomeron mountain areas of Israel are seen on satellite images and on the digital shaded relief map (Fig. 18J.1). Flexures with NNE SSW and NE-SW trends which belong to the Syrian Arc system are clearly seen. The western flexure of the Judean Mountains is dextrally displaced; its eastern flexure is deformed by numerous lineaments with N-S and NNW trends. Some of these are branch faults, which belong to the Qana'im fault system (Fig. 18J.1). In the Qana'im Fault zone, four main morphological forms of fault profiles, which recur so often, may typify strike-slip faults (**Fig. 18J.2**). These are:

a) V-syncline (flexure opposite flexure);
b) V-syncline vertically displaced;
c) Shear zone;
d) Straightening monocline or flexure.

Usually on a typical cross-section it was possible to find not one, but a few sub-vertical faults (probably flower-structure). With the exception of type (d) above, which is also typical for reverse faults, all the other types can result only from strike-slip movements.

Strike-slip faults younger than the hydrographic network displace valleys and produce typical sharp bends in the valley course ('dog-leg bends'). These, together with dome and 'half-dome' structures, and short brachy-synclines along the lineaments, give sufficient indications for determining the nature of a given lineament even though more hard evidence is absent.

THE NATURE AND EVOLUTION OF THE SYRIAN ARC BELT

The field-data described herein confirms the widespread notion

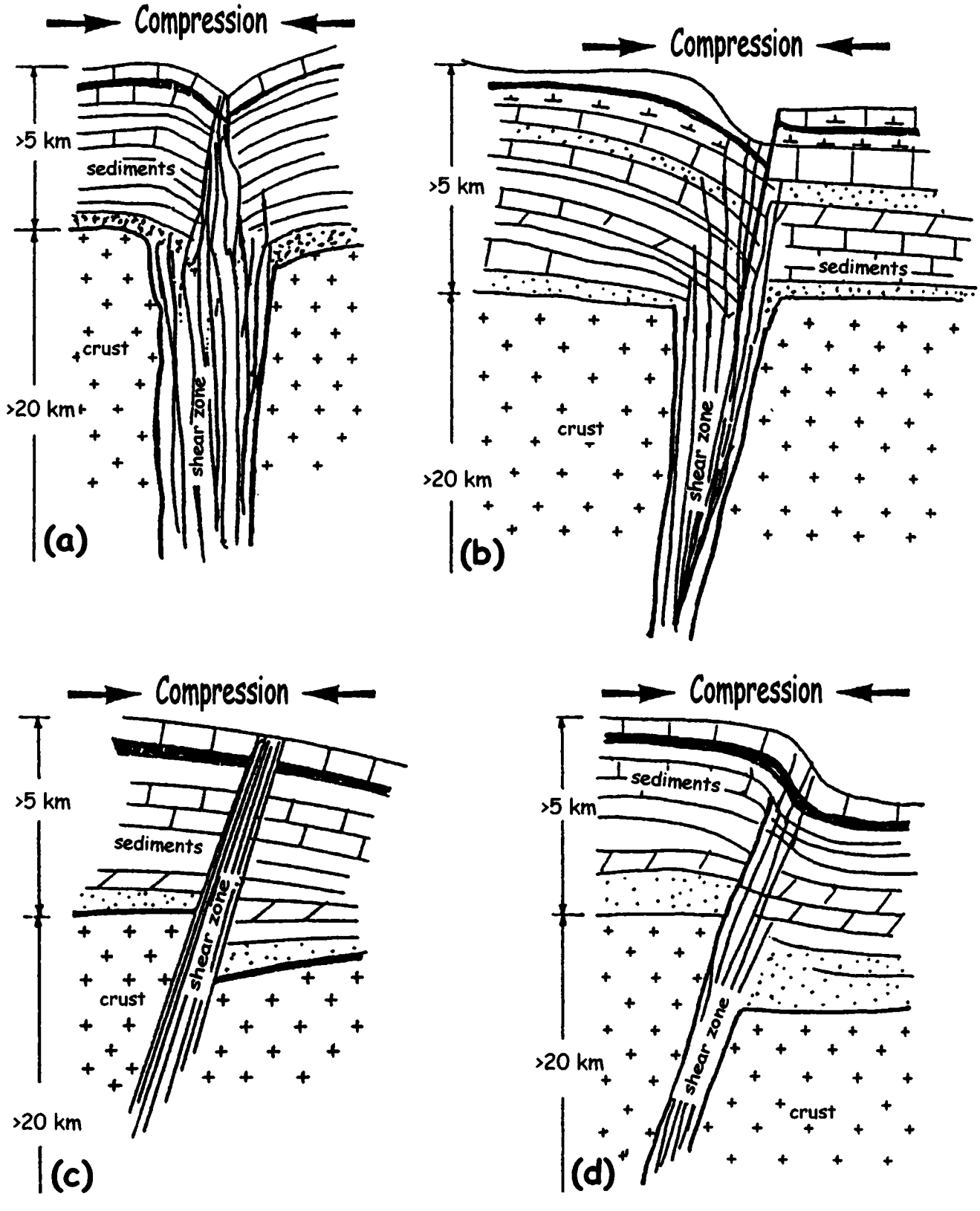


Figure 18J.2. Strike-slip faulting in Judea, typical sections across converging slice-blocks: (a) V-syncline (flexure opposite flexure); (b) Uplifted block opposite flexure (V-syncline vertically displaced); (c) shear zone; (d) straightening flexure.

of the northward movement of the Levantine 'micro-plate' against the background of the larger scale differential northward movement of the Arabian Plate with respect to the African. In addition, this data indicates a very complicated character of the strike-slip displacements in the region of the 'micro-plate', which is usually viewed as whole and 'rigid'. According to our data, the whole area west of the Dead Sea Transform (the central part of the Syrian Arc) is a deeply faulted zone, where blocks of the earth's crust are displaced horizontally or obliquely, rather than simply thrusted.

The mechanics of the long-time NW-SE pressure that is called-upon nowadays to explain the steep thrusting of the Syrian Arc, and the use of the terms 'plate', or the 'micro-plate' for the Syrian Arc belt, are difficult to accept, because their structural features are inconsistent with the following concepts:

1) Normally typical for large scale thrusting are: regularity of steep reverse faulting, and broad monoclinal features from the NW-SE directed 'thrusting' in Israel, and lack of low-angle reverse faults, and symmetrical or complex and allochtonous folds.

2) Repeated magmatic-intrusive activity along the faults of the Syrian Arc belt before and since pre-Cretaceous time, which includes the National Park Volcanics of Neogene age. Such activity is very unusual for a transpressional fold-belt of any plate or sub-plate - though very common in the wide transpressional mobile belts of the San-Andreas type; accompanied by *en-echelon* folding, also typical for the Levant (Fig. 18J.1). Only the faulting which 'breaks' crystalline crusts and generates pull-aparts or other forms of stretching can bring intrusions to the surface.

3) Monoclines of the Syrian Arc have different trends, and are superimposed: the Plio-Pleistocene structures on the Miocene (*i.e.* dextral E-W-trending oblique thrust displacing the southwestern monocline of Hebron's horst-anticline, Fig. 18J.1), or the Tertiary on the Upper Cretaceous (superposition of the NNE-trending flexures on the N-S-trending flexures); to create those features, a more complicated mechanism than one-directional stress is needed. Some of those features as well as stress-direction rotation were characteristic of the Syrian Arc folds already in the 'embrionic stage' of transpressional activity in the Senonian period (Steinitz, 1981).

4) Maps of historic and instrumental seismicity (*e.g.* Bartov, 1994; Kawar, 1996) suggest a close relationship between the spatial distribution of earthquakes and the tectonic lines (part of them belonging to the Syrian Arc structure). This relationship extends to scales much finer than expected in the classical 'rigid plate' model.

5) It is difficult to imagine a tectonic model of the region in which the deeply faulted structure of the Syrian Arc, bounded on the west and east by the global scale Pelusium and Dead Sea shear zones, behaves as a rigid plate in which the smaller blocks comprising it would not participate in differential lateral movements.

Some reverse faults were found during oil drilling and seismic investigations in the Negev (Aharoni, 1976). Others were deduced from mechanical and tectonic modelling (*e.g.* Reches et al., 1981). Numerous strike-slip faults and strike-slip shear zones, recognized during geologic mapping in Judea (Begin, 1973; Gilat, 1985; 1987; Gilat and Agnon, 1981), exhibit geomorphological forms indicative of strike-slip faulting, which include steep reverse faults (on two-dimensional cross-sections) and the large flexures related to them.

Two major conclusions can be drawn:

1) The Syrian Arc structures of Judea, that constitute the 'Backbone of Israel', are cut through by numerous strike-slip faults, related in time and kinematics to the Dead Sea Transform mega-shear zone;

2) Some of the major monoclines of the Syrian Arc belt must have been produced between bounding strike-slip faults.

Morphological expressions of the strike-slip faults, which were studied in numerous cross-sections, indicate four basic forms of relationship between blocks (Fig. 18J.2):

a) V-syncline (flexure opposite flexure);
b) V-syncline vertically displaced;
c) Shear zone;
d) Straightening flexure.

With the exception of type (d) above, which is also typical for reverse faults, all the other types can result only from strike-slip (or oblique-slip) movements. Form (a) is very common in the Judean Desert. It is also found on the eastern flexure of the southern Judean Mountains mega-block (Fig. 18J.1), and on some other major faults belonging to the Syrian Arc (Gilat, 1994). Form (b), also common in the Judean Desert and in the northern Negev (*e.g.* Mizpe Zohar, *ibid*), is also found on the western flexure of the southern Judean Mountains (Fig. 18J.1).

To explain the V-syncline morphology which is typical for strike-slip, one must take into account the process known to reduce vertical displacements of faults in the chalky-marly sequence (Mimran and Michaeli, 1986). Thus, an additional sedimentary cover of a few hundred meters in the Qana'im area would reduce the vertical displacements on a strike-slip fault cross-section to near zero, at the same time retaining flexures produced by compression on both sides of the fault.

It has been noted that folds form at an oblique angle to the strike-slip fault in an *en-echelon* pattern, though if transpression is dominant, the folds are rotated so that they are nearly parallel to the strike-slip fault (Harland, 1971). Reading (1980, p. 16) noted, that "*en-echelon* folds are ... important indicators in plastic cover rocks of strike-slip in more rigid basement rocks at depth".

This field study suggests that the Syrian Arc mega-structure may be a mobile belt with dominantly lateral displacements, active also in the pre-Dead Sea Transform (pre-Miocene) period.

DISCUSSION OF PROPOSED MOBILE BELT

The proposed mobile belt model is discussed with reference to **Fig. 18J.3**, in which the approximately 100 km of sinistral movement along the Dead Sea Transform is reconstructed.

The proposed belt is bordered on the southeast by the ENE-trending dextral strike-slip faults of the central and southern Negev-Sinai and their continuation into Transjordan. The western boundary of the belt probably coincides with the present-day Pelusium shear-zone, subparallel to the Mediterranean shoreline (Neev, 1977).

Formation of the Syrian Arc belt may have begun as a trans-tensional phase during Triassic-Jurassic times. This is consistent

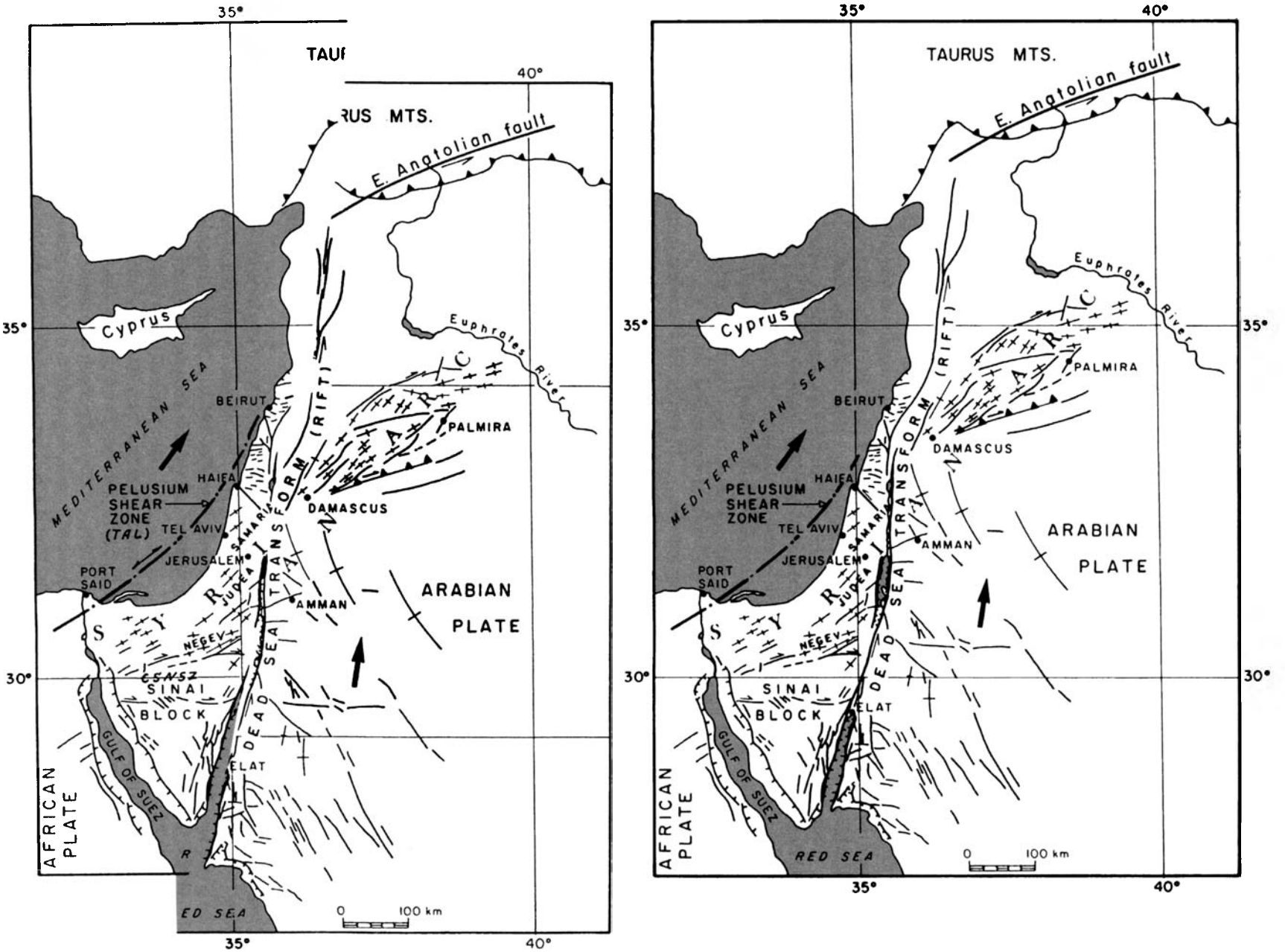


Figure 18J.3. Schematic structural map of the Levant upon which the 100 km sinistral movement along the Dead Sea Transform is reconstructed TAL - Trans-African Lineament..

with the model proposed by Freund et al. (1975) of the Permian to Turonian strike-parallel normal faults of appreciable magnitude, which subsequently reversed their movement. During the latter phase, the basin in central Israel was filled by a Triassic-Jurassic sequence more than 6 km thick.

Reviewing the structural reversal model of Freund et al. (1975), Druckman (1981) compared Paleozoic and Tertiary structures and Upper Triassic sections across reverse faults of the Negev folds, and came to the conclusion that Early Mesozoic and Tertiary structures are genetically and geometrically unrelated. The dissimilarity of these structures and sections can be easily explained by taking into account the third, strike-slip, dimension of faulting movement.

The trans-tensional phase culminated with Early Cretaceous igneous activity, possibly associated with many of the strike-slip faults (*e.g.* Ramon and Dimona-Zohar faults). It has been commonly observed that a trans-tensional phase, preceding the transpressional one, with igneous activity in between, is a normal process in the development of an ancient strike-slip mobile belt (Reading, 1980, p. 19).

The major transformation in the main trend of the Syrian Arc is traceable during the transpressional phase of its development. Among the oldest trends of the Syrian Arc, recognized on the surface in Judea (and Samaria), are the north-south trends of the intra Turonian-Santonian faults and those of the Santonian-Early Paleogene main monoclines (Fig. 18J.1). Their ages are evidenced by ostracode biostratigraphy (Flexer et al., 1989). The trends of countless small syn-silicified *en-echelon* folds of Campanian Age point to an additional shift in the main trend to NE (20° to 80° of the lower chert folds) and then to the NNE (0° to 40° of the main chert, Steinitz, 1981). The main monoclines were probably deformed in the Late Paleogene-Early Miocene by dominantly dextral NNE trending faults (Fig. 18J.1). Indirect evidence of strike-slip faulting during these stages is the formation of smaller brachy-syncline or brachy-anticline (dome) structures (at least one of which, the Har Holed dome, was developed during the Senonian Period - Gilat and Honigstein, 1982).

Since the Early Miocene, numerous strike-slips associated with the Dead Sea Transform were superimposed on and cut into the structures of the Syrian Arc, at least in Judea. Megalineaments visible on satellite images largely reflect the Late Miocene-Pliocene stage of the structural development of the southern Judean Mountains, and are often accompanied by dolomitization (Gilat, 1985). Smaller shear zones, visible on aerial photographs, reflect later tectonic stages, and are often associated with secondary calcitization and recrystallization with textural changes of the country rock (*ibid*). Metallic mineralizations follow massive dolomitization (Gilat, 1994).

The main conclusion from the tectonic analysis is that the 'Levantine micro-plate' is a long-lived, still active, mobile belt on the boundary of the Afro-Arabian plate ('Syrian Arc' belt), cut by Mio-Pleistocene secondary strike-slip faults associated with the Dead Sea Transform. As such, it is a potential conductor for magmatic intrusions because of the characteristic changes from compression to tension along the strike-slip faults, *i.e.* local 'pull-apart' basins, chasms, or other structures produced by stretching. As its movements were accompanied by hydrothermal-metasomatic processes (*ibid*), it can be evaluated as a potentially metallogenic province.

REFERENCES CITED

Aharony, E., 1976. The surface and subsurface structure of southern Judean Desert, Israel. Unpubl. Ph.D. thesis, Hebrew University Jerusalem, 2 vol., 6 maps (In Hebrew, English Abstract 6 p.).

Bartov, Y., 1994. Geological photomap and seismicity of Israel and adjacent areas, 1:750,000 scale. 2nd Ed. Isr. Geol. Surv.. 1 sheet.

Begin, Z. B., 1974. The Geological Map of Israel, 1:50,000, Sheet 9-III: Jericho, Isr. Geol. Surv., 2 maps with explanatory notes, 11 p.

Druckman, Y., 1981. Comments on the structural reversal model as a factor of the geological evolution of Israel. Isr. J. Earth Sci., 30(1), p. 44-48.

Flexer, A., Gilat, A., Hirsch, F., Honigstein, A., Rosenfeld, A. and Rueffer, T., 1989. Cretaceous evolution of the Judean Mountains as indicated by ostracods. Terra Nova, 1(4), p. 349-358.

Freund, R., Goldberg, M., Weissbrod, T., Druckman, Y., and Derin, B., 1975. The Triassic-Jurassic structure of Israel and its relation to the origin of the eastern Mediterranean. Geol. Surv. Isr. Bull., 65, 26 p.

Gilat, A., 1977. The Geological Map of Israel, 1:50,000, Sheet 15-1: Eshtemoa', Geol. Surv. Isr., 2 maps.

Gilat, A., 1985. Lineaments as indicators of Tertiary-Quaternary tectonics, southwestern Judean Mountains. Isr. Geol. Surv., Current Res., Vol. 5, p. 50-56.

Gilat, A., 1987. The Geological Map of Israel, 1:50,000, Sheet 15-II: Har Hezron, Revised Edition, Isr. Geol. Surv., 2 maps.

Gilat, A., 1992. Oversized U-shaped canyons development at the edge of rotating blocks due to wrench faulting on margins of the Dead Sea graben. Terra Nova, 3(6), p. 638-647.

Gilat, A., 1994. Tectonics and associated mineralization activity, southern Judea, Israel. Unpubl. Ph.D. thesis, Ben-Gurion Univ. of the Negev, 280 p., 7 maps, Appendices. (In Hebrew, English Abstract, 26 p.). Also published as Isr. Geol. Surv., Rep. GSI/19/94, 280 p. (In Hebrew).

Gilat, A., 1998. Strike-slip fault morphology and reconstruction of offsets along the Qana'im fault zone, Judean Desert. Isr. Geol. Surv., Current Res., Vol. 11, p. 33-41.

Gilat, A., and Agnon, A., 1981. Geological map 1:20,000 scale of the `En Boqeq-Mezada area, Explanatory notes. Geol. Surv. Isr. Rept. No. MM/2/81, 20 p. 1 map.

Gilat, A., and Honigstein, A., 1982. The polyphase history of the Qana'im Valley fault zone. Isr. Geol. Surv. Current Research 1981, p. 63-69.

Gilat, A., Mimran, Y., Bogoch, R., and Roth, I., 1978. Circular and tabular (discordant) dolomite bodies in the south Judean Desert, Israel. J. Sed. Petrol., 48(4), p. 1159-1166.

Gorodnitsky, A. M., and Gilat, A., 2000. Geophysical field structures, geochemical anomalies and tectonic evolution of the eastern Mediterranean and the Levant subplate. Scientific Israel-Technological Advantages, 2(3-4), p. 53-59.

Hall, J. K., 1997. Landforms of Israel and adjacent areas, 1:500,000 scale. Isr. Geol. Surv., 1 map.

Harland, W. B., 1971. Tectonic transpression in Caledonian Spitzebergen. Geol. Mag., 108(1), p. 27-42.

Ilani, S., 1989. Epigenetic metallic mineralization along tectonic elements in Israel. Ph.D. Thesis, Tel-Aviv University, 221 p., Appendices. (In Hebrew, English Abstract, 3 p.). Also published as Isr. Geol. Surv., Rep. GSI/12/89, 221 p.

Kawar, R. S., 1996. The Dead Sea Transform fault system: An integrated

geophysical study. Ph.D thesis, University of Newcastle upon Tyne, 196 p., Maps, Appendices.

Mimran, Y., and Michaeli, L., 1986. The transition of a major fault into secondary faults in chalk and its effects on the mechanics of the host rock. Isr. J. Earth Sci., 35(2), p. 114-123.

Neev, D., 1977. The Pelusium Line-a major transcontinental shear. Tectonophysics, 38(3-4), p. Tl-T8.

Reading, H. G., 1980. Characteristics and recognition of strike-slip fault systems. Spec. Publ., Int. Assoc. Sediment., 4, p. 7-26.

Reches, Z., Hoexter, D. F., and Hirsch, F., 1981. The structure of a monocline in the Syrian Arc system, Middle East - surface and subsurface analysis. J. Petrol. Geol., 3(4), p. 413-425.

Steinitz, G., 1981. Enigmatic chert structures in the Senonian cherts of Israel. Geol. Surv. Isr. Bull., 75, 46 p.



Pictorial map of the Levant on the eve of World War One.

Pictorial map in perspective by the noted illustrator G. F. Morrell, provided courtesy of Aharon (Ronni) Sade, source unknown. The map shows the Turkish Hedjaz Railway system on the eve of World War One. It is interesting to note the dominance of the steep topography along the rift, and the paucity of information available for the desert areas farther east.

Chapter 18K

Tectonic Evolution of Israel

Akiva Flexer
Department of Geophysics and Planetary Sciences, Tel-Aviv University, Tel-Aviv 69 978, Israel
Francis Hirsch, and John K. Hall
Geological Survey of Israel, 30 Malchei Israel Street, Jerusalem 95 501, Israel

INTRODUCTION

The tectonic setting of the Eastern Mediterranean and the Levant consists of the triple junction of the African, Arabian, and Anatolian Plates, bounded by the Cyprian Arc, the Peri-Arabian Ophiolitic crescent, and the Dead Sea Transform.

Israel is located along the northwestern margins of the Arabian-Nubian continental craton that is a part of the African-Arabian Plates; rigid blocks composed of a complex assemblage of Precambrian igneous, metamorphic, and sedimentary rocks. During Cambrian to Holocene time, regional geologic conditions were dominated by interactions between this rigid continental mass and the oceanic areas to the north and northwest that produced the stratigraphic sequences that have so far been observed in the surface and subsurface geological record of Israel and surrounding areas. This interaction between the Arabian Craton and adjacent oceanic areas is controlled by:

1) Alternating advance and retreat of shallow epicontinental seas on the Arabian Craton, in response to cratonic subsidence/ emergence and eustatic sea level changes.

2) Opening and closing of the Neotethys, accompanied by faulting and volcanism.

3) Convergence and development of an alpidic folding system: the Levantid folds or the Senonian-Eocene Syrian Arc stress field.

4) Regional uplift and fracturing of the Arabian Craton margin as a part of the dismantling of the Arabian-African Plate, isostatic readjustments, and Dead-Sea stress field activity since Oligocene, the opening of the Red Sea, the Dead Sea Transform, and Palmyrid thrusting and folding.

Israel subdivides into a number of tectonic provinces. These provinces are defined in the geological sense as zones having common geophysical, seismological, structural, and sedimentary characteristics. In most cases a tectonic province is expressed by a typical morphological character. The Sinai-Levant Plate can be divided, largely in the sense of the five classical morpho-tectonic units of the Middle East of Picard (1937). **(Figure 18K.1).**

1) The Arabian-Nubian Massif, consisting of Precambrian terrain devoid of sedimentary cover;

2) The Tabular zone, consisting of a thin sedimentary cover on a relatively thick continental crust that has been relatively stable during and since the Paleozoic. It has only been subjected to slow, epeirogenic, long wave-length oscillations that brought about rhythmic advances and retreats of the sea over its margins. During the Paleozoic and the greater part of the Mesozoic, these generated a typical platform sedimentary cover of mature clastics (primarily sandstones) on a flat continental landscape, or carbonate-shale sequences in shallow epeiric seas. An accentuation of earth movements took place in the Late Triassic and in Late Jurassic-Early Cretaceous times. The rate of historical seismicity in this tectonic province appears to have been very low.

3) The simple folding zone consists of the Levantid Fold Belt or folds of the 'Syrian Arc'. It is a flat S-shaped band of folds that extends from northwestern Sinai, through Israel and Lebanon, into Syria. The common characteristic of this tectonic province is the presence of generally normal concentric folds developed in the sedimentary cover. Most of the folds are strongly asymmetric, a feature generally attributed today to the presence of reverse faults at depth.

4) The Alpine mobile Belt, thrusted over the African-Arabian Plates.

The Levantid folding belt is a segment of the Peri-Arabian foreland folding-arc, extending from the Pelusium transform in the west to the Euphrates Graben in the east. **(Figure 18K.2)**. This Levantid belt is split into the segments of the Negev-Folds and of the Palmyrids by the Dead-Sea Transform, giving it an apparent S-shape. These folding arcs share NE trending axes, asymmetry due to the presence of basement controlled reverse faults, and a multiphase history of deformation. The Senonian-Early Miocene W-WNW trend is actually referred to as the 'Syrian Arc' stress field, followed by

5) The Miocene-Pleistocene 'Dead Sea' stress field (Eyal and Reches, 1983).

Starting in the Coniacian, the Levantid compression decomposes into transversal faulting with strike slip components and vertical displacements, and in reverse faulting with asymmetric folding. These compressional pulses reoccurred until the Early Miocene. Post-Oligocene deformation decomposes into folding and sinistral strike slip movements, possibly both in combination. In the Hermon, the compressional deformation, though present from the Senonian, reached its peak only after the Oligocene, as in the Palmyrides (Chaimov et al., 1990).

A WNW-trending fault system is discerned in central and northern Israel by fieldwork, air photos, and geophysical methods.

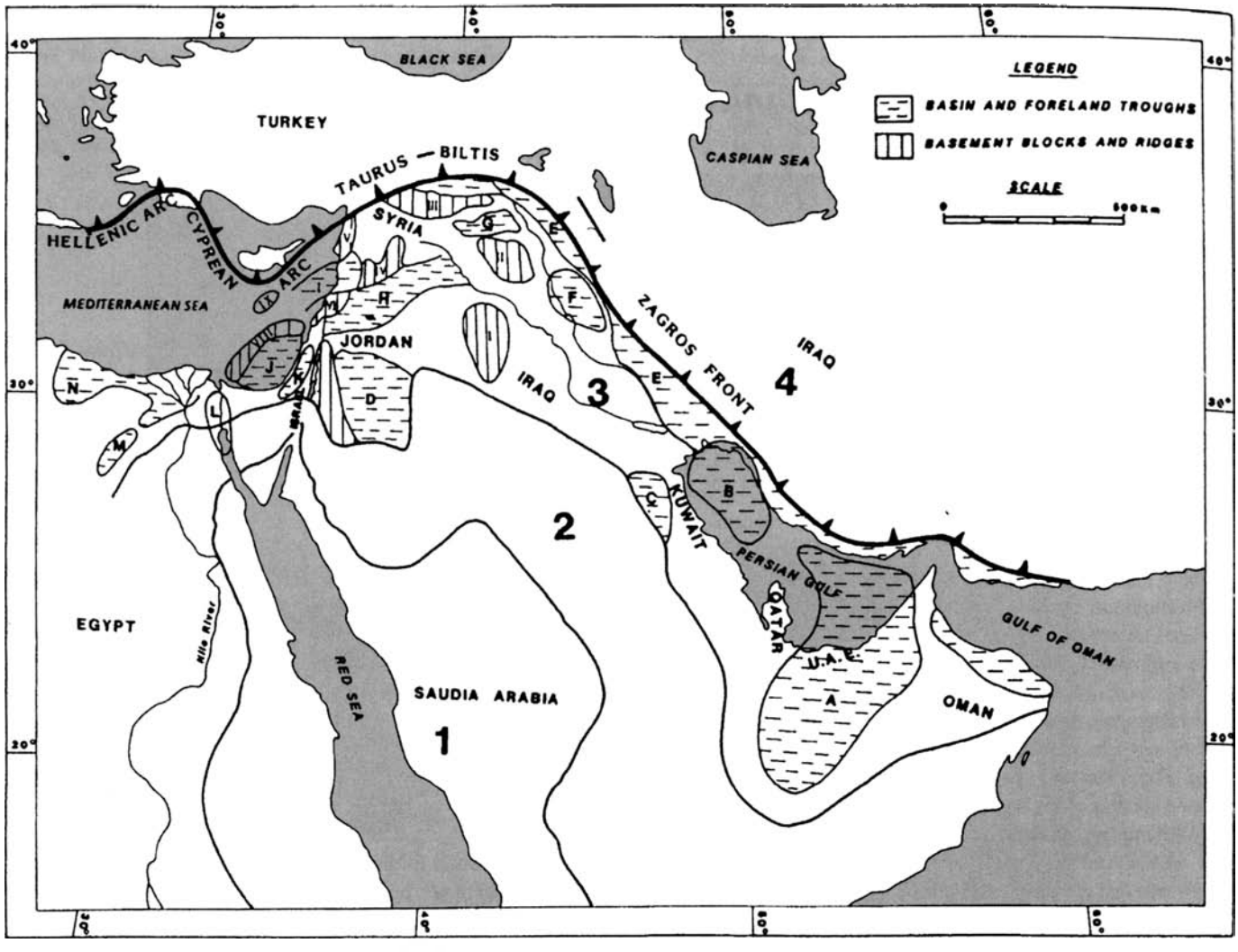


Figure 18K.1: Middle East tectono-sedimentary framework. 1. Arabo-Nubian Shield; 2. Stable Shelf (continental beds and thin marine intercalations); 3. Unstable Shelf (mainly marine sediments); 4. Mobile Belt - the Alpine thrust zone.

Basins and Foreland Troughs. A. Rub al Khali; B. North Persian Gulf; C. Dibbdibba; D. Sirhan -Turajf; E. Oman and Zagros Mountains forelands; F. Kirkuk; G. Sinjar; H. Palmyra; I. Phoenician; J. Pleshet; K. Judea; L. Suez; M. Western Desert; N. Matruh and Natrun.

Basement Blocks and Ridges: I. Rutbah; II. Khleisia; III. Mardin; IV. Haleb; V. Amanos; VI. Beirut; VII. Jordan; VIII. Pleshet Western Flank; IX. Eratosthenes.

From Cohen, Z., Flexer, A., and Kapstan, V., 1988, which is modified after Picard (1937), Henson (1951), Said (1962), Powers et al. (1966), Ponikarov et al. (1967), Salem (1976), Druckman et al. (1982), Alsharhan and Nairn (1986), and Ben-Avraham and Ginzburg (1986).

Nature and structure of our crust

The crustal structure is an important factor affecting the tectonic processes discerned in the sedimentary epidermis. Ginzburg et al. (1979) point out that the relatively thick cratonic continental crust beneath southern and central Israel becomes thinner towards the Mediterranean Sea, as well as to the north, across an E-W zone in central Israel. These zones of crustal thinning have been interpreted as ancient margins of the Arabian Craton, now buried beneath a Phanerozoic sedimentary cover that thickens to the west (Ginzburg and Gvirtzman, 1978; Ginzburg and Folkman, 1980).

In the present day Mediterranean shelf of Israel the crust underlying the sedimentary prism might represent a transition zone to oceanic type crust (Ginzburg and Gvirtzman, 1979).

A thinning of the crust also takes place under the rift valley to a distance of 20 km west of the rift. Ginzburg et al. (1981) interpret this as a zone of upwelling where upper mantle material is intruded into the lower crust along a narrow active zone. This process probably began in the south close to the geodynamically active area of the Red Sea, and gradually proceeded to the north.

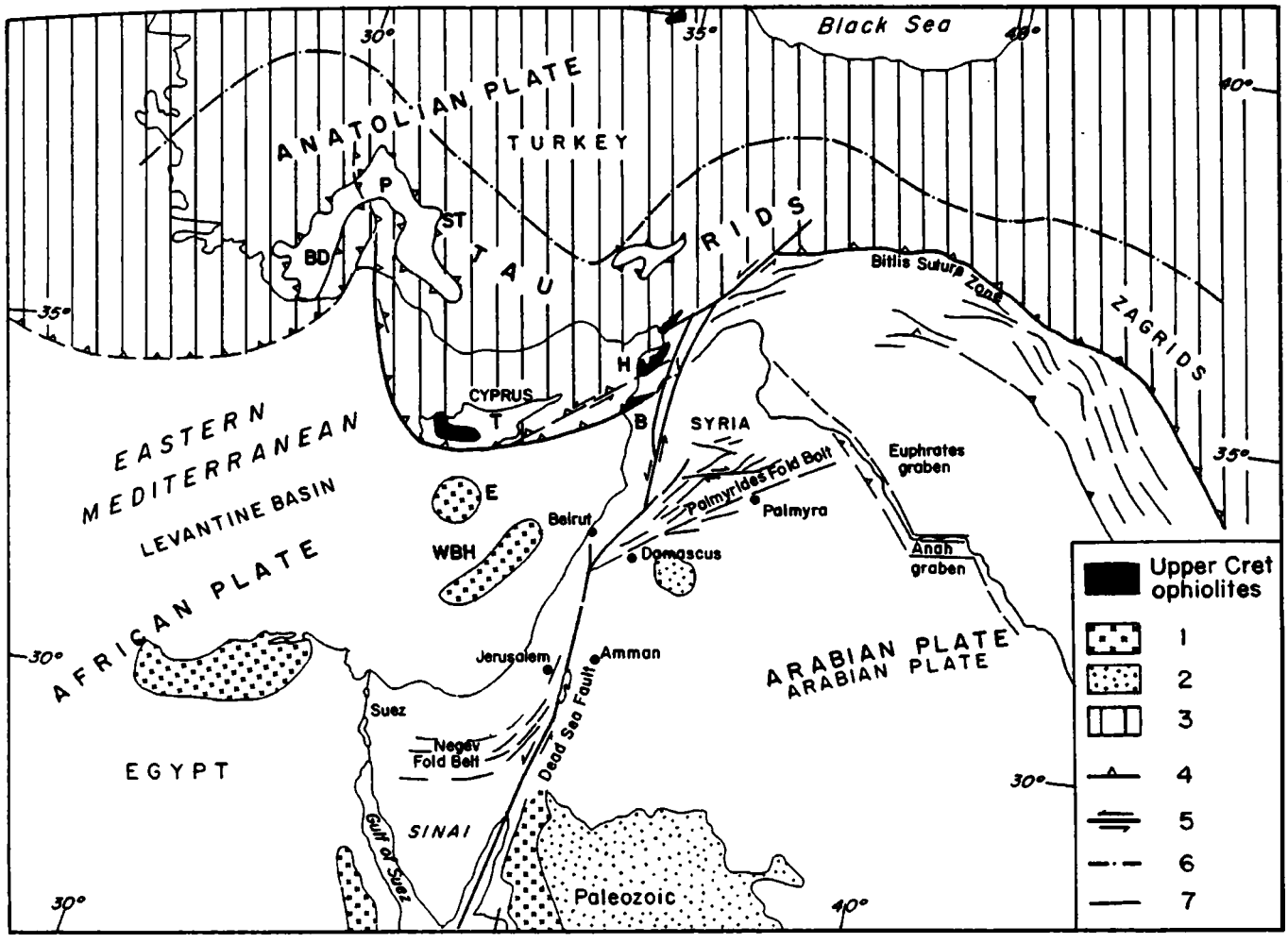


Figure 18K.2: Plate tectonic pattern of the eastern Mediterranean Levant with main Levantid features (modified after Hirsch et al., 1995; Searle, 1994). Gondwanian elements: African and Arabian Plates in white; **[1]** Precambrian basement exposed or geophysically signaled; **[2]** Paleozoic sediments; **BD** Bey Daglari; **P** Pisidia; **ST** Seydisehir-Tarasci; **E** Eratosthenes; **WBH** Western Basement High; **PB** Pleshet Paleobasin. Neotethyan elements: **[3]** Anatolian Plate. Ophiolites in black: **B** Baer -Bassit; **H** Hatay; **T** Troodos. Boundaries: **[4]** Tauro-Zagrid thrust front; **[5]** Dead Sea transform; **[6]** Neotethyan suture; **[7]** present coastlines.

More recently, Ben Avraham and Ginzburg (1990) have interpreted the region in terms of terranes. Typical structure sections are given for the Negev, Judea-Samaria, Galilee-Lebanon, the Levantine Basin, Eratosthenes and Cyprus (**Figure 18K.3**).

We thus can subdivide the region of Israel into four crustal provinces:

1) Southern - Central Israel with a thick continental crust;

2) Northern Israel with thinned continental crust;

3) The Dead Sea Rift with a thin continental crust and possible mantle upwelling;

4) The Eastern Mediterranean Levantine basin, paved by a thinned ancient crust, and filled by thick Phanerozoic sediments of epicontinental nature.

Geophysical and geological data suggest that paleotectonic structures cross the present Levant coast, and that a number of highs and paleo-landmasses encircle the Mesozoic Pleshet aulacogen, a basin extending from the present Mediterranean offshore to the coastal plain subsurface and into the Judean Embayement.

Plates and Plate Boundaries

The Middle Eastern portion of the African-Arabian Plate can be subdivided into the Arabian sub-plate, comprising Saudi Arabia, Jordan, Iraq, and parts of Syria; the Sinai-Levant sub-plate comprising the Sinai Peninsula, Israel, Lebanon, and parts of Syria; and the eastern Mediterranean sub-plate comprising the Levantine Basin.

The Arava-Dead Sea-Jordan Rift Valley is the plate boundary separating the Arabian sub-plate from the African Plate. It should

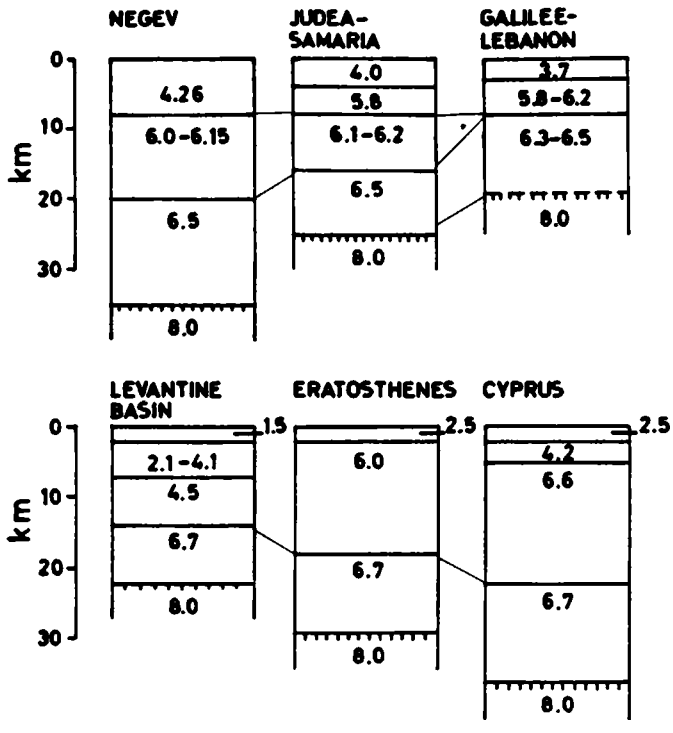


Figure 18K.3. Typical crustal sections in the Levant (from Ben-Avraham and Ginzburg, 1990, Tectonics, 9(4), p. 615, Fig. 3). Typical structure sections at selected locations from seismic refraction measurements (after Ginzburg and Ben-Avraham, 1987; Ginzburg and Folkman, 1980; Makris et al., 1983). The depth to the Moho in Galilee is gravimetrically derived. Velocities are shown in km/s.

be pointed out that this boundary has developed since Miocene time as a major left-lateral transform fault zone in response to the culmination of a major collision of the African-Arabian and Eurasian Plates. During most of the Phanerozoic era the African-Arabian Plate consisted of the Arabian-Nubian Massif or Craton.

The boundary separating the Sinai Levant Plate from the Levantine Basin has been defined in different ways by various authors. For Neev et al. (1976), the zone is a plate boundary, characterized by geophysical discontinuities and sedimentary facies and thickness change, which they named Pelusium Line. Ben-Avraham et al. (1978) interprets the zone as a transition of continental crust to an oceanic-type crust and the present-day toe of the continental slope.

Interplay and collision of African-Arabian Plates

The strongly interwoven geological and tectonic history of the Levant is punctuated by periods of subsidence and uplift, subdivided into phases:

1) The early geological history of the Levant is Gondwanian. A basement of accreted terranes, consisting of plutonics, volcanics, ophiolites, and metasediments was consolidated by the Late Precambrian Pan-African orogeny, including the Menderes, Eratosthenes, and Arabian-Nubian massifs, prior to regional peneplanisation.

2) The Paleozoic history of the Levant is one of domal uplifts: End-Devonian, Permian, and post Permian that resulted in the erosion of much of the Paleozoic deposits. Hardly anything is left of the Ordovician-Devonian sedimentation and the earliest Triassic is missing. A paleo-geological subcrop map of the Near East **(Figure 18K.4)** suggests that the post-Devonian high encompasses a large area of the Eastern Mediterranean.

3) The Early Triassic opening of Neotethys across Gondwana was echoed by Mesozoic epicontinental sedimentary cycles of Ramon (Olenekian-Rhaetian), Arad (Pliensbachian-Tithonian), Kurnub (Berriassian-Albian), Galilee (Barremian-Early Albian) and Judea (Albian-Coniacian). The Mesozoic depocenters **(Figure 18K.5)** are Neotethyan: the Triassic Galilee (Devorah) and the Jurassic Judea Embayements, both merging into the Palmyra depocenter. The cycles are paced by intracratonic rifting, uplifts, volcanics and/or eustatic sea level changes, possibly echoing the neotethyan island arc and mid-oceanic volcanism and spreading. From the Early Cretaceous a new basin configuration appeared by the opening of the Gevar'Am trough, which developed into the Cretaceous Pleshet Paleobasin, echoed to the East by the Judea Basin (Figure 18K.1).

4) Echoing the Alpidic Eurasian-Gondwana collision, the Levantid deformation of the Negev-Palmyrid belts is the result of the inversion of Early Mesozoic faults, producing the asymmetrical folds of the S-shaped Syrian Arc. These extend from Northern Sinai to the Palmyrids. The Syrian Arc shaped a paleogeography of basins and highs (sometimes islands), that controlled the carbonatic and siliceous sedimentation of the Senonian-Paleocene Mount Scopus Group and of the Eocene Avedat Group. The Oligocene lower part of the Saqiye Group represents the last period of this phase. Sediments of this age were widely destroyed by the regional uplift that started the next phase, leaving only a few marine outcrops in the northern Negev, the Coastal Plain and Golan Heights.

5) A possible mid-Oligocene tectonic rebound coincides with a sea-level drop, enhancing regional regression, emersion and erosion. Since Late Oligocene, the Red Sea opening split the Gondwanian foreland into separate African and Arabian Plates. The continued underthrusting below the neotethyan Anatolian Plate, at different speeds, generated the Dead Sea transform, resulting in the Miocene deformation of the Palmyrid belt, and absorbing a part of the pressure. The sinistral strike-slip also opened a chain of rhomb-shaped grabens along the Jordan-Gulf of Aqaba line, accompanied by basalt eruptions at its northern end. Pliocene isostatic readjustments produced the downwarp of the eastern Mediterranean basin, echoed by the differential uplift of portions of the African, Levantine and Arabian sub-plates.

The Levantid Folding Belt

The Arabian-Nubian Massive is a classical cratonic nucleus surrounded by concentric morpho-tectonic sedimentary belts. The picture shown by many authors (Picard, 1937; Henson, 1951) includes four geologic provinces:

1) The Arabian-Nubian Massif;

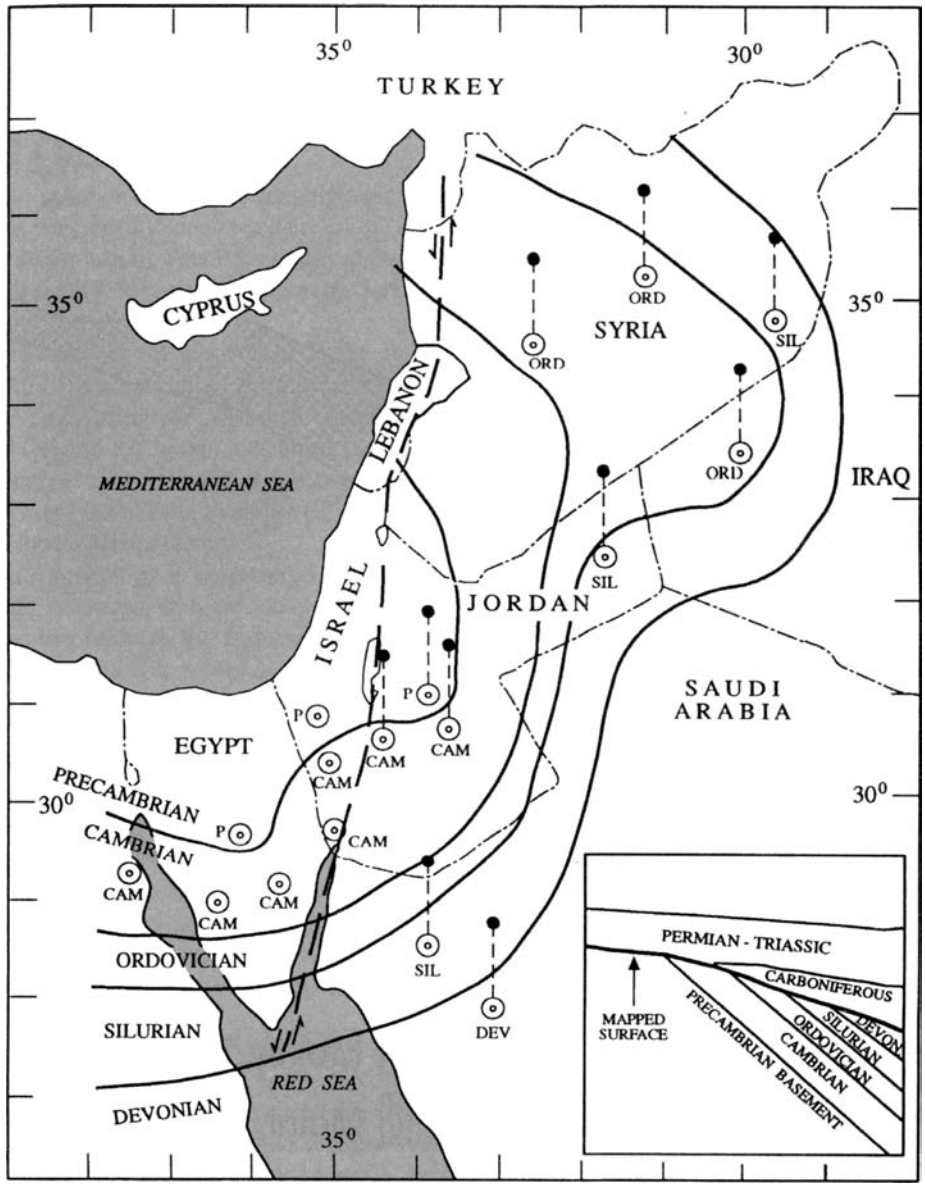


Figure 18K.4: Post-Devonian subcrop map (after Zaslawskaya et al., 1995, Fig. 3, p. 66). Paleo-geological (Carboniferous) subcrop map of the Near East showing Precambrian-Devonian exposures, subsequent to the Devono-Carboniferous uplift and erosion (from Gvirtzman and Weissbrod, 1984). The map shows the location (circles) of Precambrian (**P**), Cambrian (**CAM**), Ordovician (**ORD**), Silurian (**SIL**) and Devonian (**DEV**) stations. Stations east of the Cenozoic Dead Sea transform (interrupted line) were displaced northward (black dots).

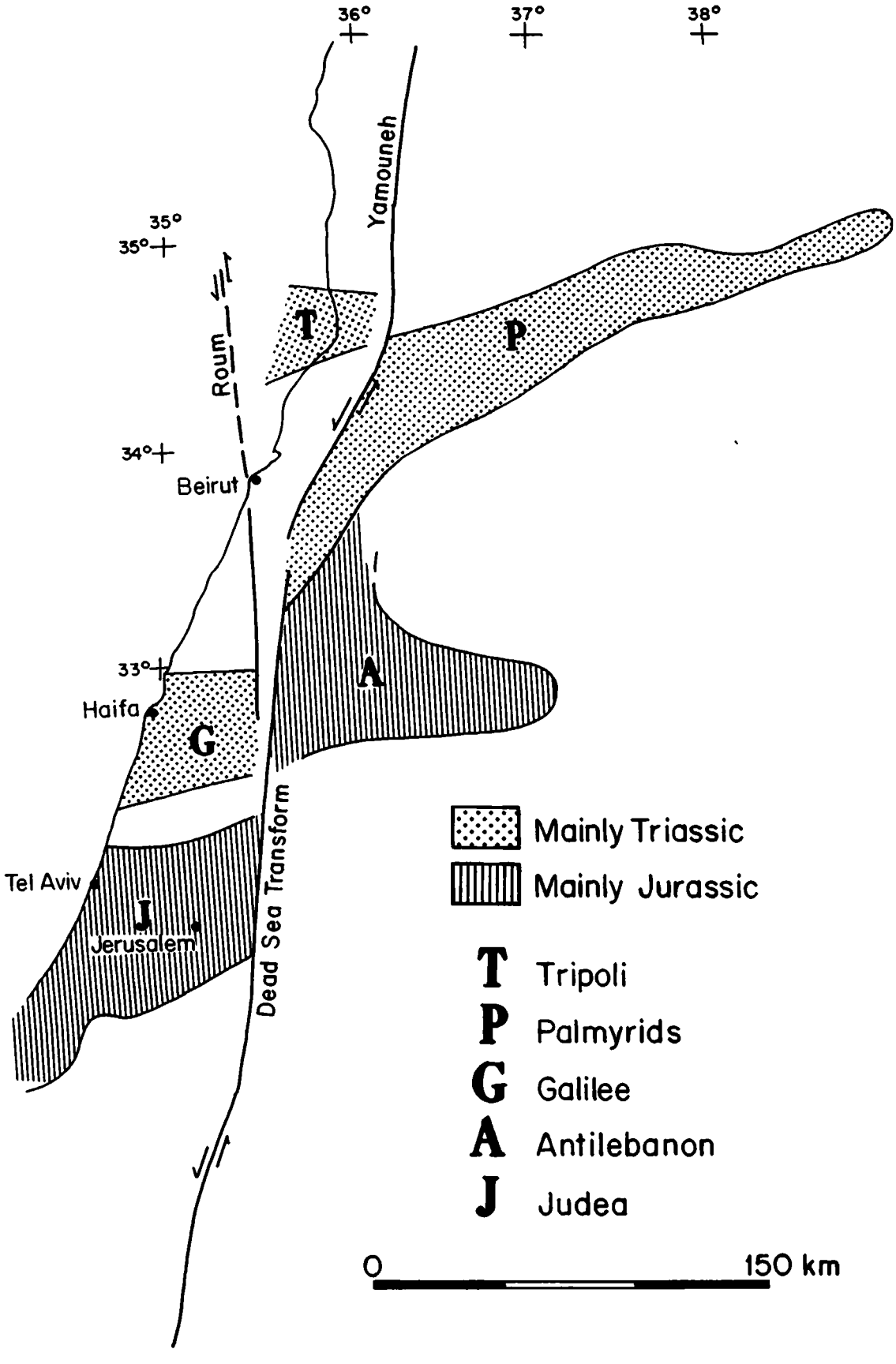
2) The stable shelf;

3) The unstable shelf including a series of Paleozoic, Mesozoic and Tertiary lows and highs having a complex inversed tectonic history, the last of which is known as the **Levantid fold belt** (Picard, 1959) or Krenkel's (1924) **Syrian Arc (Figure 18K.6)**; and

4) The mobile belt of the Alpine thrust zone, with its nappes of ophiolites, in the Taurus and Cyprean Arcs (Figure 18K.1). It appears that these belts are still seismically active (Rotstein and Ben Avraham, 1986), and also the Dead Sea transform. Southwards from the thrust zone the degree of tectonism decreases, through the fairly simple folded zone of the Syrian Arc extending from Sinai (Egypt) through Israel, to Jordan and Palmyrides in Syria, as well as to the eastern Mediterranean Sea, under which a number of folds are buried beneath Neogene and Quaternary sediments.

The Syrian Arc Stress Field Folding

The Syrian Arc crosses northern Sinai, Israel and Jordan into Syria. It consists of a series of surface and subsurface anticlines


36°
37°
38°
35°
35°
34°
33°
Yamouneh
Roum
Beirut
Haifa
Tel Aviv
Jerusalem
Dead Sea Transform
T
P
G
A
J
Mainly Triassic
Mainly Jurassic
T Tripoli
P Palmyrids
G Galilee
A Antilebanon
J Judea
0
150 km

which strike mostly in an ENE, NE and NNE direction portraying a flat and huge S-shaped form. This folding system comprises a segment with a broader belt of folds, which continue eastwards to Iraq and the northeastern parts of Saudi Arabia (Figure 18K.2).

The belt is located mainly on the unstable shelf between the Arabian Craton and the Zagros-Taurus thrust zone.

Different tectonic interpretations and descriptive terms have been proposed for the belt of folded mountains of the lands bordering the eastern Mediterranean. Krenkel introduced the term 'Syrian Arc' in 1924. Picard (1959) replaced the term by 'Levantid Fold Belt'.

Folds are well preserved in the Negev and in the Judean upland and, due to Plio-Pleistocene uplift, form broad upwarps of anticlinorial style, culminating in Makhtesh Ramon (R), HaMakhtesh HaGadol (N) and the Judean anticlines (J). **(Figure 18K.6).** To these are attached the synclinoria or downwarps: in the west, the Halutza (NW) and the Shefela foothills (CP) and in the east the Paran-Zin and Judean Desert region.

A 'Jura' type fold morphology is characteristic of most of the Negev-Judean desert landscape, with erosion cirques (Picard, 1951), cluses, ruzes and hog-backs on the frequently steep flanks of the asymmetric anticlines, and with mesas and tabular features in the synclines.

The fold morphology is less noticeable in the western Judean Mountains in Samaria and Galilee, most likely due to the effect of faulting and the influence of the semi-arid, semi-humid climate with its caliche crust and terra rossa soil cover on the rocks.

The folds of the Central and Northern Negev Highlands are all strongly asymmetric with a steep flank to the southeast. Other structures, such as the Hebron anticline are strongly asymmetric to the west. Still other structures, such as Fari'a, are roughly symmetric or of the box-fold type with steeply dipping flanks on both sides.

This feature was substantiated by several deep oil wells discovering strata repetitions, by many seismic profiles revealing at depth the reverse faults and by theoretical geometrical calculations (Reches et al., 1981), a feature generally attributed today to the presence of reverse faults in depth, as first suggested by De Sitter (1962). The folds are often described as concentric or parallel, *i.e.* not changing their bed thickness as a result of the compressive stress-thickness changes inherited from the sedimentological pattern. Superimposed domal structures are common, mainly in the anticlines of the Northern Negev Highlands and in the Ramon structure (Eran, 1982).

The folding phase started in Late Coniacian, and the folds received their final shape before the Eocene. They became uplifted and block-faulted, during the Neogene and still more so during the Pleistocene (Picard and Eliezri, 1964).

The study of the Levantid fold belt, roughly parallel with the frontal zone of the Zagro-Taurid-Cyprian and Hellenic Arcs thrusts, at the northern edge of the Arabian and African Plates, has gained considerable new impetus with the advent of plate tectonics. The collision course of the relative and differential northward movement of the African and Arabian Plates towards the Eurasian Plate generated the accompanying features of southward obduction of Neotethyan terrane elements, now forming the Anatolian and Persian Plates, instead of underthrusting the Eurasian Plate (Scott, 1981). A complex relationship exists between the old structural unit of the Arabian-Nubian Massif, forming the nucleus of the Arabian and African Plates, and united from Precambrian to Neogene times, and the surrounding Levantid folding belt.

The large S-shaped Syrian Arc is a segment of the peri-Arabian foreland arc which encircles the Arabian Craton. It is characterized by consistent shelf-type carbonate sedimentation exceeding several thousands of meters, deposited during Mesozoic and Early Tertiary times.

The southern part of the belt by the stable zone underwent primarily epeirogenic and only mild horizontal movements.

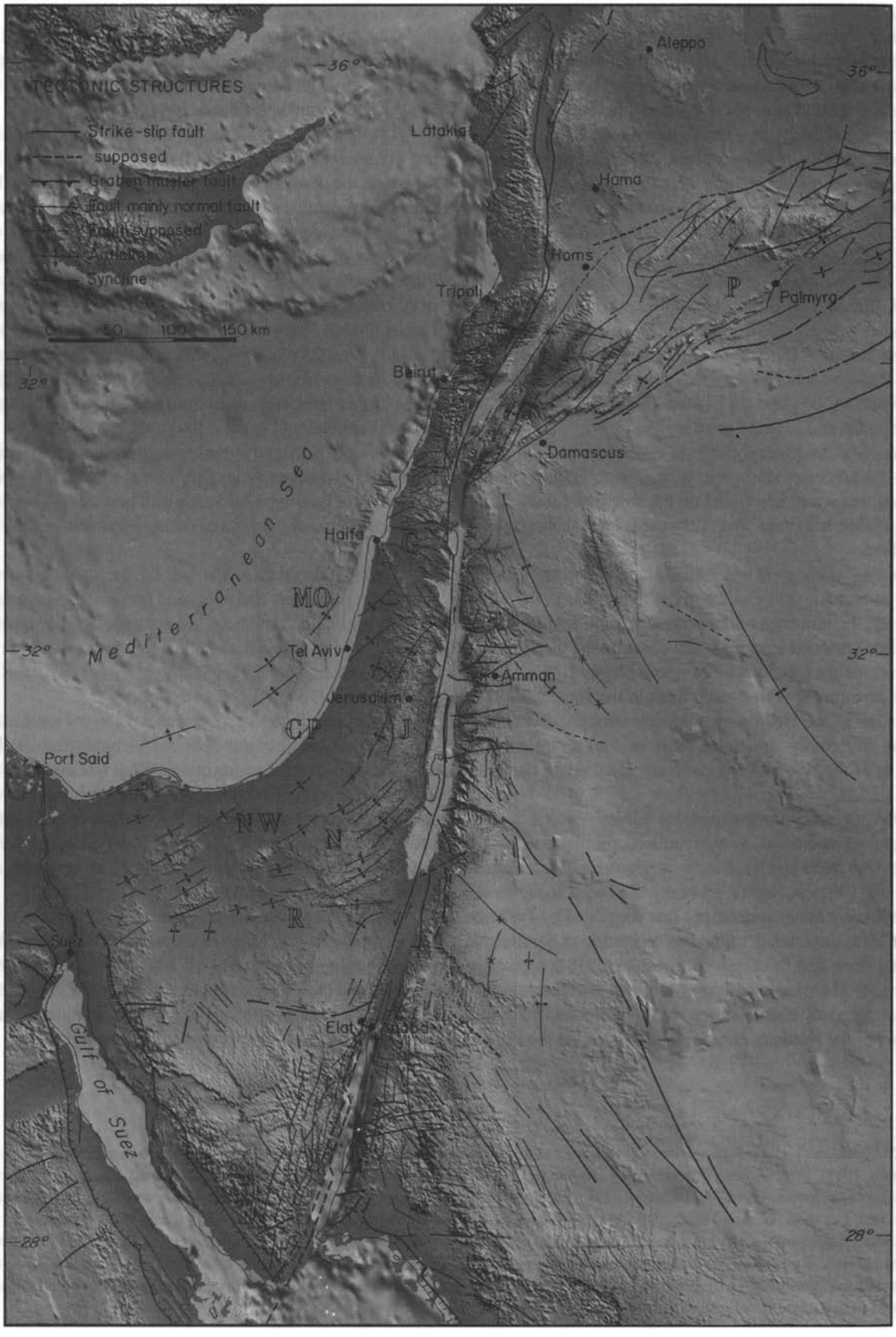
The strong deformations are accompanied by unconformities and facies changes, differentiating the anticlinal from synclinal features, affecting the sedimentation of the Mt. Scopus (Coniacian-Paleocene) and Avdat (Eocene) cycles.

Since Late Oligocene, differential pacing of subduction within the Gondwanian foreland split the African-Arabian Plate into separate units, each plunging at a different rate under the Anatolian Plate. The resulting Red Sea chasm, with sinistral relative motion along the Dead-Sea transform, and continued collision with the neotethyan Anatolian Plate, generated the Miocene deformation, decomposed into the sinistral strike slip movements along the Dead Sea and renewed folding of the Palmyrid belt.

The ultimate Levantid deformation is related to Late Neogene-Quaternary rifting, arching and volcanism. The Levantid belt is thus presently split by the Dead-Sea Jordan Rift into the Negev-folds to the west, and the Palmyra structure to the east. They both share NE trending axes and asymmetry of the folds, a feature mainly due to the presence of basement-controlled reverse faults.



Figure 18K.5: Mesozoic (Triassic-Jurassic) depocenters, prior to the Dead-Sea Transform (modified from Triassic isopach map of the Levant, in Beydoun and Habib, 1995). Presently one observes: The Triassic Galilee (Devorah) embayement at 33°N (**G**) and the Jurassic Judean Embayement (**J**) at 32°N, west of the Roum - Dead-Sea Transform; The Triassic Tripoli embayement (**T**) at 34°-30'N, between Roum and Yammouneh transforms; The Jurassic Anti-Lebanon (Hermon) aulacogen (**A**) at 33°N and the Triassic Palmyra aulacogen (**P**) at 34°-30'N, east of the Yammouneh - Dead Sea Transforms); Restoration of 105 km along the Dead Sea transform allows the fitting of the Triassic Palmyra and, Galilee - and of the Jurassic Judea and Anti-Lebanon deeps. The Triassic Tripoli deep is either part of the Galilee-Palmyrid embayement (main transform along either Roum fault) or it represents an additional feature further north (main displacement along the Yammouneh fault). The Miocene folding of the Palmyrids, as a result of absorption of part of the transform, would support the latter hypothesis.


TECTONIC STRUCTURES
Strike-slip fault
supposed
Graben master fault
Fault mainly normal fault
Fault supposed
Anticline
Syncline
0 50 100 150 km
36°
32°
28°
Aleppo
Latakia
Hama
Homs
Tripoli
Palmyra
Beirut
Damascus
Haifa
Mediterranean Sea
Tel Aviv
Amman
Jerusalem
Port Said
Suez
Elat
Aqaba
Gulf of Suez
MO
NW
N
R
P

Unraveling and timing the multiphase history of deformation of the Levantid compressional folding is dependant upon many field and seismic sections. Quantitative analysis of burial history and tectonic subsidence curves carried out from various boreholes clearly shows the initiation time, peak and attenuation of the folding phase. Models for sedimentation, erosional events and non-deposition were delineated.

Starting in the Coniacian, compressional pulses continuously recurred until the Early Miocene.

The compressional deformation extends from the central Negev into the Eastern Mediterranean. The Coniacian-Eocene folding is the main folding of the Negev folding arc. The Palmyra arc was deformed by the Senonian-Paleogene folding phase, though deformation during the Neogene, as a the result of the Dead Sea transformational compression, accounts for the bulk of the presently observable deformation.

Although generally simple folds are common in the sedimentary cover, the belts are, however, not uniform. Some of the folds are basement controlled through deep-seated reverse fault and some are rootless, more superficial epidermal folds. The general understanding is that the folding of the Levantid fold belt roughly coincides with the main Alpine orogeny, associated with the Senonian-Paleogene collision of the Gondwanian and Eurasian Plates (Syrian Arc stress field) and the differential plunging of the African-Arabian Plates under the Anatolian Plate since the Oligocene (Dead Sea transform stress field) (Eyal and Reches, 1983).

Magnetic and gravimetric anomaly lineaments accompany many of the structures. The magnetic anomalies represent either an elongated escarpment (fault or flexure) at the top of the crystalline basement or an elongated vertical boundary separating two crystalline rock types with different magnetic properties (Domzalski, 1967). The gravity anomalies reflect both basement features and mostly the steep flexures of the top of the thick carbonate sequence of the Judea Group **(Figure 18K.7)**.

Geological and geophysical analysis shows (with a high degree of confidence) that there is a genetic relationship between:

a) Magnetic anomalies;

b) The assumed deep-seated reverse faults, which penetrate the sedimentary cover and are expressed in seismic profiles; and

c) The external epidermal folds associated with gravimetric and morphometric anomalies (Flexer, 1987).

Many authors proposed ages of the folding and they range from Early Turonian or Senonian to post-Middle Eocene and Neogene (Picard, 1943, 1959; Bentor and Vroman, 1960; Flexer, 1971; Eyal and Reches, 1983).

Apparently the folding took place in several stages. Activity and intensity were different in time and space (Figure 18K.5). The evidence for the tectonic activity comes usually from angular unconformities between Turonian, Senonian and Eocene strata, thickness variations in Senonian rocks, or diastems. Stratigraphic condensation of the Senonian succession marks the crest of the anticlines, whereas thick full sections characterize the synclines (Bentor and Vroman, 1960; Flexer, 1971; Bartov and Steinitz, 1977).

Gvirtzman (1979) distinguishes, on the basis of studies carried out in the Shefela, Coastal Plain and Be'er Sheva regions, two phases of folding. During the first phase, from the Senonian to the Middle Eocene, broad, long wavelength (30-40 km) and long (70-80 km) structures came into being. On these, many narrow (5 km) and shorter (25 km) anticlines and synclines were superimposed during a second phase, lasting from upper Eocene to lower Miocene.

Bartov et al. (1980), in a detailed study of the Areif-en Naqa structure, found that asymmetric folding took place in the Early Coniacian, and accompanied by faulting, persisted through the Late Campanian-Maastrichtian. Post-Eocene folding formed the present-day symmetric component of the structure. Eyal and Reches (1983) found that a W to WNW trending compressional stress field was responsible, in Late Cretaceous through Early Neogene times, for the folds west of the Dead Sea rift, identified by them as the 'Syrian Arc stress'. These authors distinguish another stress field, active in Neogene-Recent times, with dominating horizontal extension, and trending E to ENE, in all rocks inside the rift and 'proximal' thereto.

Mimran, (1984) investigating the Fari'a structure in Samaria concluded that the structural interpretation of folding development in this structure does not conform to the model of folding migration suggested by Freund and Zak (1973). He found significant folding after Late Turonian times, in the Early Eocene, between Middle Eocene and Pliocene, and a fourth post Pliocene phase. Honigstein et al. (1988) analyzed some of the Negev and Judean Desert structures using ostracode biozones. They found that Late Turonian-Early Santonian times are distinguished by one of the main folding phases of this belt, forming angular unconformities by onlap position of the sediments and local faulting. Recurrent and continuous movements during the Santonian and Campanian are responsible for the thickness variations, caused by condensed sections on high structures, and extended sequences in low areas, as well as by faults (Flexer et al., 1989).

The cores of the Levantid structures expose in general Triassic to Turonian strata, whereas Senonian to Paleocene rocks are associated with the flanks. Eocene strata are generally restricted to the synclines. It should be noted that the Qeren-Rogem and Givat



Figure 18K.6: The Aqaba-Levant Structure and the Levantides Fold belt with provinces of folding and *en echelon* arrangement (modified after Bayer, 1985). Central Negev or Ramon area **[R]**, northern Negev **[N]**, northwestern Negev lowland province (where most of the structures are buried in the subsurface except the Qeren-Rogem structure) **[NW]**, the Judea-Samaria anticlinorial areas (including Mt. Carmel and Umm El Fahm) **[J]**, the coastal plain province (totally in subsurface with Sadot and Helez the leading structures) **[CP]**, the Mediterranean offshore structures **[MO]**, the Galilee structures **[G]**, and the Palmyra Fold Belt **[P]**.

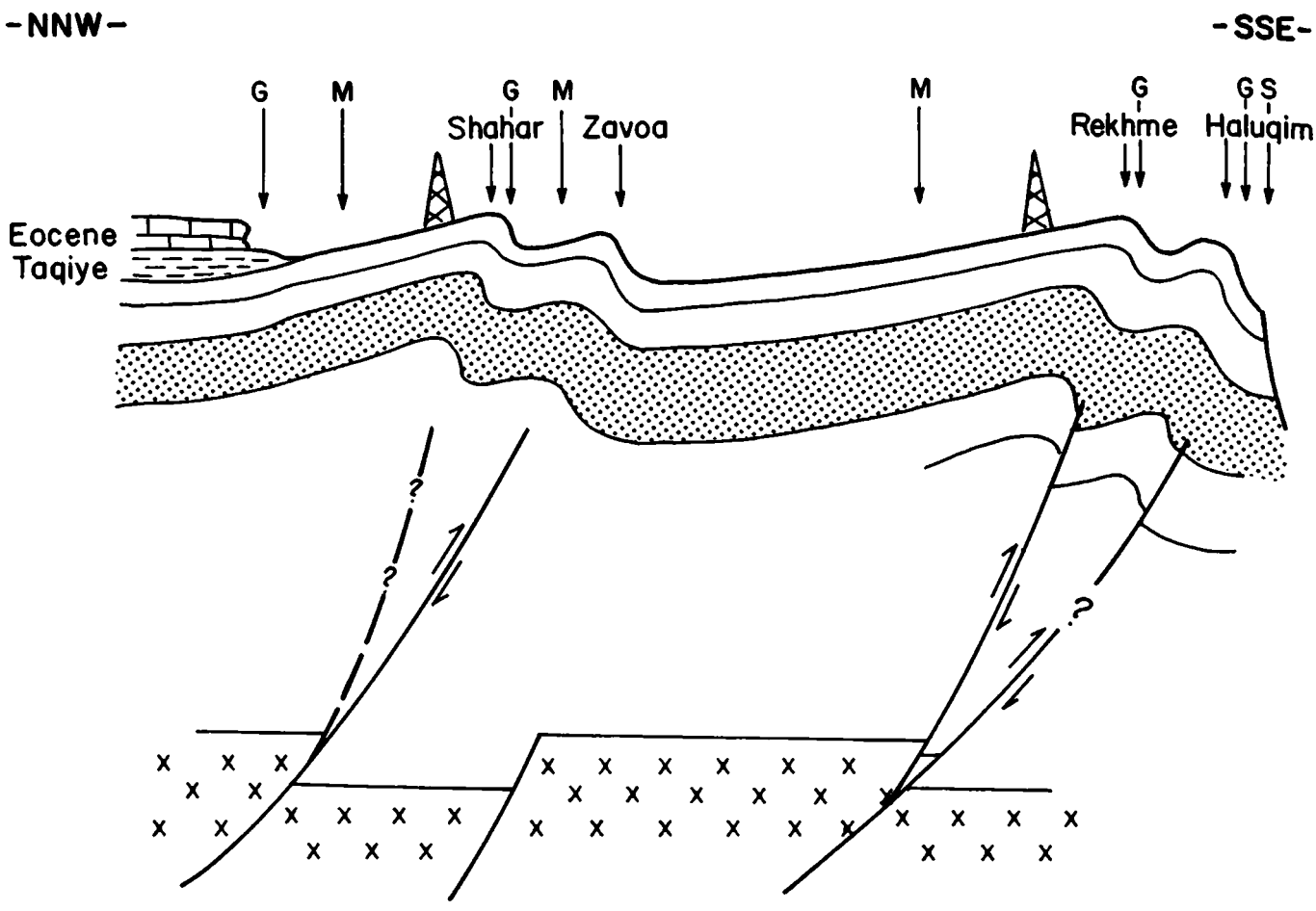


Figure 18K.7: Schematic cross-section in the Negev anticlines showing the genetic association between basement faults, magnetic anomalies (M), gravimetric anomalies (G) and surface structures (After Flexer et al., 1987).

Hayil structures are the only exposed structures in Israel where Paleocene (Taqiye Formation) or Eocene (Adulam Formation) rocks comprise the core of the anticline. Deep subsurface analysis suggests a basement participation controlling shape, tectonic style, and amplitude of the anticlines.

Some calculations of the relationship between the mean throws of the reverse faults in the anticlines, and their amplitude as reflected by the top of the Judea Group, show the ratio of 1:6-1:8 (Flexer, 1987). As an example of this development, the Qeren-Rogem structure and its associated deep-seated reverse fault are considered a typical Levantid representative exhibiting Late Cretaceous and post Eocene tectonic activity.

Initially part of a shelf ramp sedimentary basin, a more restricted depocenter may have been generated by a graben, probably since the Triassic, with reactivations in Late Jurassic and Early Cretaceous times, as can be derived from the thickness relations of the Mesozoic sediments. The Late Turonian eustatic emersion was followed by the Early Senonian NW-SE compressional activation of the Qeren normal fault into a reverse fault, resulting in the folding and subsequent emersion of the anticlinal structure. Further activity took place during Senonian times, as can be deduced from the sharp thickness variations of the Santonian-Campanian Menuha and Campanian Mishash Formations across the Qeren structure.

Mimran and Begin (1984) calculated a Senonian deformation rate for the Qeren structure of 0.017 mm/year, reaching an accentuated rate of 0.034 mm/year during the Campanian.

The folded Early to Middle Eocene formations suggest a post Middle Eocene end of compressional deformation, the Neogene and Pleistocene deformations (Zilberman, 1986) being of a different nature.

The displacement of the Qeren reverse fault, affecting the top Judea reflector, reaches 100 m.

The seismic profiles show that the Mt. Scopus and Avedat Groups onlap the top of the Judea Group, proving the existence of a post Turonian Qeren-Rogem anticline as an elevated (subaerial) structure. With an amplitude of folding of 650-800 m on top of the Judea Group, the relation of folding to faulting is 1:6 to 1:8. The amplitude of folding on the top of the Taqiye Formation is on the

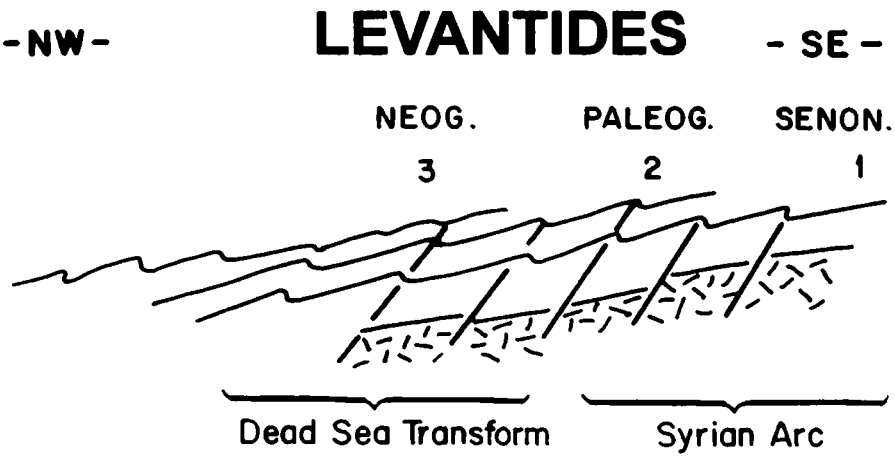


Figure 18K.8: Hypothetical sketch of Levantid folding in space and time. Syrian Arc stress field: [1] Senonian folding phase and [2] Paleogene folding phase. Dead Sea transform stress field: [3] Neogene folding phase.

order of 200 m to 250 m and that on the Eocene marker (Arkin et al., 1972) only 140 m, suggesting that the maximum tectonic activity occurred in Early Senonian time. The decay of the Qeren Fault and anticlinal amplitude in the successive stratigraphic levels suggests that the folding apparently ceased during Oligocene times. Post Pliocene tectonic rejuvenation generated geomorphic anomalies on the Plio-Pleistocene Pleshet-Ahuzam terraces (Zilberman, 1986).

The Dead-Sea Stress Field

In his study on the Arabian Plate boundary interactions, Hempton (1987) suggests that the Palmyrid fold belt began in Mid-Miocene as the result of a 65 km northward displacement of the Arabian Plate along the Dead Sea Fault relative to the African Plate. Both plates move northward at different rates, resulting in the Red Sea opening. Walley (1988) assumes 100-110 km sinistral displacement on the Dead Sea Fault, transmitted northwards in a braided strike-slip fault complex, consisting in the Roum, Yammouneh, Hasbayah, Rachaya, Serrhaya and south Palmyrid faults. The movement is suggested to have started around 30 Ma (Styles and Hall, 1980), lasting until ~14 Ma in its first phase, resuming around 4.5 Ma in its second phase.

The more detailed study of Chaimov et al. (1990) on the crustal shortening in the Palmyrid fold belt, caught between the Aleppo Plateau to the north and the Rutbah Uplift to the south, suggests that most of it took place after the Late Oligocene, the amount of which is ~20 km., including folding and thrusting on reverse faults. This figure, added to the estimated 25 km of slip along the northern segment of the Dead Sea transform may represent the Syrian Arc stress field compressional shortening.

The remaining 60 km of the assumed 105 km total displacement along the Dead Sea Fault are possibly distributed along a braided pattern in northern Syria or along the Roum Fault in Lebanon.

This mostly 'Dead Sea' stress field is supported by paleomagnetic data (Zijderveld and Van der Voo, 1973).

Ultimately for Searle (1994), while the folding of the intraplate Palmyride fold Belt began during the Late Cretaceous, most deformation was clearly post-Oligocene, resulting from a phase of NW-SE compression, followed by Neogene-Recent dextral transpression. This author emphasizes the importance of dextral shearing and transpressive folding along the Palmyrides, conjugate with the main sinistral strike-slip movement along the Dead Sea Fault, superimposed on earlier folds resulting from inversion of the Mesozoic Palmyrid aulacogen. The total thickness of the Phanerozoic sediments in this basin reaches over 10 km. (See Volume I, Part II, Chapter 8, Tectonics of Syria).

Transversal Faults (Figure 18K.6)

Two generations of transversal faults crossing the Sinai-Levant Plate are observed:

1) The ancient basement faults (Najd trend) that were rejuvenated on several occasions. These bound the Carmel Mount and the Yizre'el Valley, including the Carmel-Gilboa fault, forming the boundary between the Galilee and Judea structural areas. Further south, the Beersheva Valley, forming the boundary between the Negev and Judean Mountains, corresponds to this same ancient trend. At a smaller scale, a large number of small faults of N~290°E trend, the so called 'Senonian patio' fractures, are visible over the entire country, as they affect mostly the Santonian-Campanian sediments.

2) The Central Sinai-Negev Shear Zone, that in the south of the country consists of a series of east-west trending tectonic lineaments that transverse the Sinai Plate and extend from the Thamad fault northwards to the Paran fault, the Ramon-Arif fault system, and the Zin Line. Each lineament consists of a system of faults accompanied by many small folds and fault-controlled depressions that form a conspicuous morphotectonic belt. Collectively, this series of east-west trending lines are referred to as the Central Sinai-Negev Shear Zone.

STRUCTURAL EVOLUTION

Different authors have speculated on the mechanisms generating the Levantides. Today, most authors seem to agree that the Negev structures are the result of reverse faults in depth.

Such faults have by now been identified in six deep wells, located on five anticlines in the Northern Negev. Freund et al. (1975) assume that every monocline in Israel is underlain by a reverse fault which originated as a Mesozoic normal fault; such an assumption would explain why the anticlines are asymmetric to one side or the other, or sometimes box-shaped as well as the varying outline of several monoclines, interpreted as the surface expression of the zigzag-shaped subsurface outline of the Mesozoic normal faults.

If the concept of structural inversion of Freund et al. (1975) is commonly accepted, not every present-day anticline was previously a graben. Sometimes the concept fits a province of several associated chains of folds. Druckman (1981), examining the Negev structures, concludes that contrary to Freund et al. (1975), the Early Mesozoic and Tertiary structures are genetically and geometrically unrelated. He prefers interference between broad and shallow Mesozoic basins and narrow, high amplitude Tertiary folds as an explanation for the existing fold pattern.

Neev et al. (1982) relate the formation of the folds of the 'Syrian Arc' to a compression resulting from an oblique collision of 'slices' of the crust due to a 'systematic northward counter-clockwise conveyance movement of the slices between the sinistral' (NNE-trending) shears.

It rather appears that the tensional regime that prevailed from the Triassic to the Early Cretaceous changed during the Late Cretaceous to a compressional regime. Arbenz (1984), summarizes that during the formation of a collisional thrust belt, due to the northward migration of the Afro-Arabian Plate into a subduction zone along the Iranian-Turkish microcontinent, a broad belt of the Israeli-Lebanese-Syrian continental foreland underwent mild 'thick skin' (*i.e.* basement included) compressional deformation, resulting in the early state of the 'Syrian Arc'. This author states that the geodynamic cause for this foreland or 'cratonic type' deformation is not properly understood.

The intensive tectonic activity, that occurred during the Senonian in Cyprus, Turkey and Syria (Robertson, 1978; Biju-Duval et al., 1976), is expressed in a lower intensity in the anticlines of the Syrian Arc and fault structures, discerned by lateral thickness variations of the sections between zero and a few hundred meters (Bentor and Vroman, 1960; Freund, 1965; Flexer, 1971; Bartov and Steinitz, 1977).

These thickness variations are related to the tectonic evolution of the paleostructures, during the Senonian and Paleogene (Figure 18K.6).

Thickness changes in low amplitude and long wavelength structures are, in general, difficult to interpret, because of poorly exposed lateral continuity of the sediments and hiatuses (Ilani et al., 1984).

In the homogenous Senonian chalks of the northern Negev and the Judean Desert, fine biostratigraphy (*e.g.* ostracods) has been used to monitor thickness variations over short distances. Its resolution and interpretation allowed identification of different types of tectonic mechanisms (Honigstein et al., 1988). This study can discern three basic types of thickness reductions within the Late Coniacian-Campanian interval:

1) An onlap relationship, in which horizontal strata were deposited progressively against initially inclined surfaces. Here, the tectonic event predated the deposition of the beds.

2) Condensed successions, containing all litho- and biostratigraphic units, against nearby extended sequences. Such cases indicate simultaneous and continuous or repeated tectonic activity during the deposition of the sediments.

3) Biostratigraphically controlled thickness variations of both sides of a fault determine the age and movement of that fault. Such analysis exhibits a multiple history of folding, uplift and faulting, resulting in thickness variations, due to onlap relationships and stratigraphic condensation. The main tectonic phase took place in the interval of the Late Coniacian and Early Santonian, and faulting activity occurred during the middle part of the Campanian, though continued stratigraphic condensation during Santonian and Campanian times indicates continuous activity during the whole period.

A Late Turonian and syn-Senonian activity of the Syrian Arc folding belt has been postulated before (*e.g.*, Bentor and Vroman, 1960; Freund, 1965; Flexer et al., 1970; Flexer, 1971; Bartov et al., 1972; Bartov and Steinitz, 1977; Braun et al., 1987; Mart, 1994).

However Hirsch (1984), Flexer et al. (1989) and Lewy (1990) make a distinction between the Late Turonian erosion phase, due to a global sea-level drop, and the pre-Late Coniacian start of the tectonic activity of the Syrian Arc.

The early Senonian phase described herein represents only one stage in the evolution of the Levantid folding system, which continued into the Neogene (*e.g.*, Picard, 1943; Eyal and Reches, 1983), or even into the Quaternary.

A younging of the folding process can be postulated as one moves away from the craton. In other terms, the completion of the folding of the internal Negev can be derived from the Paleocene and Eocene onlap outside the Hathira anticline, whereas at the NW edge of the Negev, strata of this age are still involved in the Qeren anticline. The analysis of seismic profiles off the shores of Israel may eventually suggest a similar interpretation **(Figure 18K.8)**.

The age of the latest folding activity, related to the formation of the Levantid folding belt, varies. Though Freund (1965, p. 192) infers a post Pliocene differential continuation of the upheaval of the Negev Mountains from the altitude of the Hazeva Formation in the Northern Negev, Roded (1982) points only to a broad-wavelength uplift of the mountainous backbone of the Negev. Evidence for post-Miocene tilting, timing the last phase of deformation in the southern Hebron Mountains, is indicated by the inclination of the strata of the Middle Miocene Ziqlag Formation that onlap the steeper strata of the Turonian Bina Formation (Gilat, 1977; Gilat and Arkin, 1978).

Mimran (1984) finds a 'post Neogene' age for the latest folding phase in the Fari'a anticline (NE Samaria).

However, it appears that the Levantid compressional folding is best analyzed following Eyal and Reches (1983), who recognized two stress fields within the Levantid folding belt. The Senonian-Early Neogene 'Syrian arc' stress field and the Miocene-Pleistocene 'Dead Sea' stress field.

Neotectonics

The question remains whether the pattern of the youngest activity developed independently from the mechanism that brought about the formation of the Rift system (the Red Sea, Suez and Dead Sea), or whether it was a reaction to, or part of, the stresses and motions that formed the rift system.

Neo-tectonic isostatic readjustments reshaped the Eastern Mediterranean and the Levant. The eastern Mediterranean portion of the African Plate underwent deepening of its basins, echoed by the differential uplift of the adjacent Levant-Sinai portion of the African Plate, which was dissected into Negev, Judean and Galilee blocks. The continuous sinking of the Dead Sea Rift and uplift of the Transjordan portion of the Arabian Plate generated a totally new orography, affecting the mountainous backbone of the Sinai-Levant sub-plate.

These neo-tectonic events were accompanied by the volcanism of the Bashan Group, characterized by the basalt, scoria and tuff eruptions on the Golan Heights and Eastern Galilee, filling also parts of the Yizre'el Valley and the Jordan-Dead Sea-Arava Rift.

The sinistral strike-slip along the Jordan-Gulf of Aqaba line is a 105 km northward displacement of the East bank, the continuous graben-deepening being echoed by the deposition of the Dead Sea Group. Presumably Tortonian marine ingressions in the Yizre'el Valley found their way into the young Rift, filling with thick evaporites the freshly formed rhombs south of the Sea of Galilee and in the Dead Sea area, prior to the Messinian evaporites in the Mediterranean. The Pleistocene Lake Lisan filled parts of the Jordan and Arava Valleys, preceding the Holocene-Present Dead Sea.

SUMMARY AND CONCLUSIONS

The geological history of the eastern Mediterranean and of the Levant is strongly interwoven.

A large part of the present eastern Mediterranean, together with the Nubian Craton, was part of the Gondwanian African-Arabian Plate until approximately the end of the Oligocene, when it was separated from the Arabian Plate by the Syrian-African sinistral transform, and more recently by the Dead Sea Rift. The Arabian Plate comprises the Arabian Craton. Both the African and Arabian Plates plunge beneath the Anatolian Plate, which is made up of obducted Tethyan elements. The Mediterranean portion of the African Plate plunges under the Cyprian Arc and reappears in the Bey Daglari, Akseki, and Pisidian Taurus windows. The Arabian Plate plunges under the Tauro-Zagrid alpine thrusts. The Anatolian elements are characterized by Early and Late Mesozoic ophiolites, the former being part of the Triassic-Early Cretaceous Mammonia complex and equivalents, the latter forming the Turonian Troodos, and related Peri-Arabian ophiolites.

The triple junction of the African, Arabian, and Anatolian Plates characterizes the nature of the tectonics in the eastern Mediterranean Levantine region (Figure 18K.1).

The tectonic history of the Levant subdivides into phases:

1) The Late Precambrian pan-African orogeny consolidated the Gondwanian eastern Mediterranean and Arabian-Nubian basement by accretion of terranes, consisting of plutonics, volcanics, ophiolites, and metasediments, prior to regional peneplanization.

2) The early Phanerozoic times subdivide into a Cambrian-Devonian period of sedimentation and subsidence, ended by pre-Carboniferous uplift and erosion, followed by sedimentation and subsidence and recurrent uplifts and denudations in Late Carboniferous-Early Permian and Early Triassic times. End-Devonian, Permian, and Permo-Triassic uplifts resulted in the erosion of much of the Paleozoic deposits.

3) Mesozoic depocenters are Neotethyan. The Early Triassic opening of Neotethys was echoed by Olenekian-Rhaetian, Pliensbachian-Tithonian, and Berriasian-Coniacian sedimentary cycles, interrupted by rifting and volcanism. Paleogeograpically one can distinguish the Triassic Galilee (Devorah) Embayement; the Jurassic Judea Embayement, and the Cretaceous Pleshet Paleobasin, prior to Alpine-Levantinid deformation and subsequent syntectonic deposition.

4) The Alpine orogeny was echoed by the Levantid inversion of Early Mesozoic faults, producing the asymmetrical folds of a S-shaped Syrian Arc, that extends from northern Sinai to the Palmyrids. The Syrian Arc shaped a paleogeography of basins and highs (sometimes islands), that controlled the carbonatic and siliceous sedimentation of the Senonian-Paleocene Mount Scopus Group, the Lower-Middle Eocene Avedat Group, and the Late Eocene-Oligocene lower part of the Saqiye Group.

5) The mid-Oligocene emersion and regional uplift widely destroyed the youngest of the foregoing sediments, leaving only a few marine outcrops in the northern Negev, the Coastal Plain, and Golan Heights. Since the Late Oligocene or Early Miocene a sinistral strike-slip along the Jordan-Gulf of Aqaba line opened a chain of rhomb-shaped grabens, accompanied by basalt eruptions.

6) Finally the isostatic readjustments of the Plio-Pleistocene produced the downwarp of the eastern Mediterranean Basin, echoed by the differential uplift of portions of the African, Levantine, and Arabian sub-plates. This was followed by the Late Pleistocene Lake Lisan, filling parts of the Jordan and Arava Valleys, of which the Sea of Galilee and the Dead Sea are Holocene – Recent remnants.

The term 'Levantid folding belt' designates a tectonic province in the Levantine area, characterized by a huge S-shaped belt of folds. The fold belt was built and shaped by two main stress fields, the Syrian Arc stress field and the Dead Sea Transform fault stress field. The term 'Syrian Arc Stress Field' relates to pre-middle Miocene compressional folding that coincides with the Alpine orogeny and reflects the collision between Gondwanian and Eurasian Plates, whereas the term 'Dead Sea Transform Stress Field' is restricted to the differential plunge since the end of the Oligocene of the African and Arabian Plates under the Anatolian Plate. The Levantid arc is a segment of a larger arc that

encompasses the foreland folds bordering the Arabian Craton, from the Pelusium transform system in the west, including parts of Egypt, the Mediterranean, Israel, Jordan, Lebanon, and Syria, to the Euphrates-Graben in the east.

The two segments of the Levantid arc, the Negev and Palmyrid fold belts, split by the Dead Sea Rift and Transform system, have many common geological characteristics. These include their common NE trend, asymmetry due to the presence of basement controlled reverse faults, and multiphase history of deformation. Ages of folding range from Coniacian to Neogene, though in the Palmyrids, compressional deformation reached its peak during the Miocene (Chaimov et al., 1990).

REFERENCES CITED

Alsharhan, A. S., and Nairn, A. E. M., 1986. A review of the Cretaceous formations in the Arabian Peninsula and Gulf, Part 1, Lower Cretaceous (Thamama Group) stratigraphy and paleogeography. J. Petrol. Geol., 9(4), p. 365-392.

Arbenz, J. K., 1984. Oil potential of the Dead Sea area. Report 84/111, 44 p., Seismica Oil Exploration, Tel Aviv.

Arkin, Y., Nathan, Y. and Starinsky, A., 1972. Paleocene-early Eocene environments of deposition in the northern Negev (southern Israel). Isr. Geol. Surv., Bull. 56, 17 p.

Bartov, Y., Eyal, Y., Garfunkel, Z., and Steinitz, G., 1972. Late Cretaceous and Tertiary stratigraphy and paleogeography of Southern Israel. Isr. J. Earth Sci., 21(2), p. 69-97.

Bartov, Y., and Steinitz, G., 1977a. Senonian tectonics of the Sinai and Negev as reflected in the Sayyarim Formation and equivalent units. Isr. Geol. Soc., Annu. Meet., Abstr., p. 40-41.

Bartov, Y., and Steinitz, G., 1977b. The geology of Gebel E Risha, eastern Sinai. Isr. Geol. Surv., Rep. MM/3/77, 11 p.

Bartov, Y., and Steinitz, G., 1977c. The Judea and Mount Scopus Groups in the Negev and Sinai with trend surface analysis of the thickness data. Isr. J. Earth Sci., 26(3-4), p. 119-148.

Bartov, Y., Steinitz, G., Eyal, M., and Eyal, Y., 1980. Sinistral movement along the Gulf of Aqaba - Its age and relation to the opening of the Red Sea. Nature, 285(5762), p. 220-221.

Bayer, H., 1985. Kollisions- und Kompressionstektonik am Ostsaum des Golfes von Aqaba. Geologische Rundschau, 74(3), p. 599-610.

Ben-Avraham, Z., 1978. The structure and tectonic setting of the Levant continental margin - eastern Mediterranean. Tectonophysics, 46(3/4), p. 313-331.

Ben-Avraham, Z., and Ginzburg, A., 1986. Magnetic anomalies over the central Levant continental margin. Mar. Petrol. Geol., 3(3), p. 220-233.

Ben-Avraham, Z., and Ginzburg, A., 1990. *Displaced terranes and crustal evolution of the Levant and the eastern Mediterranean.* Tectonics, 9(4), p. 613-622.

Bentor, Y. K., and Vroman, A. J., 1960. Geological Map Of Israel, 1:100,000, Sheet 16: Mount Sdom. Isr. Geol. Surv., 117 p., Figs., Separate Folder With 19 Encl. (Hebrew & Engl. Editions). 1st Edition - 1954; 2nd Edition - 1960.

Beydoun, Z. R., and. Habib, J. G., 1995. Lebanon revisited: new insights into Triassic hydrocarbon prospects. J. Petrol. Geol., 18(1), p. 75-90.

Biju-Duval, B., Dercourt, J., and Le Pichon, X., 1976. From the Tethys Ocean to the Mediterranean Seas: A plate tectonic model for the evolution of the western Alpine System. In: B. Biju-Duval and L. Montadert (eds.), Structural History of the Mediterranean Basins. Proceedings of the International Symposium held 25-29 October 1976 in Split, Yugoslavia, XXV Congres-Assemblee Pleniere de la C.I.E.S.M., Editions Technip, Paris, p. 143-164.

Braun, M., Flexer, A., Honigstein, A., Rosenfeld, A., and Baida, U., 1987. Sedimentary setting of the Turonian, mainly Nezer Formation in the Northern Negev (Israel) structures - A precursor of the Syrian Arc folding phase. Newsl. Stratigr., 17(2), p. 57-70.

Chaimov, T. A., Barazangi, M., Al-Saad, D., Sawaf, T., and Gebran, A., 1990, Crustal shortening in the Palmyride Fold Belt, Syria, and implications for movement along the Dead Sea Fault System. Tectonics, 9(6), p. 1369-1386.

Cohen, Z., Flexer, A., and Kapstan, V., 1988. The Pleshet Basin: a newly-discovered link in the peripheral chain of basins of the Arabian Craton. J. Petrol. Geol., 11(4), p. 403-414.

De Sitter, L., 1962. Structural development of the Arabian Shield in Palestine. Geologie en Mijnbouw, 41(3), p. 116-124.

Domzalski, W., 1967. Aeromagnetic survey of Israel: Interpretation. Inst. Petrol. Res. Geophys., Rep. SMA/ 482/67, 66 p.

Druckman, Y., 1981. Comments on the structural reversal model as a factor of the geological evolution of Israel. Isr. J. Earth-Sci., 30(1), p. 44-48.

Druckman, Y., Hirsch, F., and Weissbrod, T., 1982. The Triassic of the southern margin of the Tethys in the Levant and its correlation across the Jordan rift valley. Geol. Runds., 71(3), p. 919-936.

Eran, G., 1982. Geometrics of the monoclines in the Negev. M.Sc. thesis, Hebrew Univ. Jerusalem, 89 p. (In Hebrew with English abstract).

Eyal, Y., and Reches, Z., 1983. Tectonic analysis of the Dead Sea Rift region since the Late Cretaceous based on mesostructures. Tectonics, 2(2), p. 167-185.

Flexer, A., 1971. Late Cretaceous Paleogeography of Northern Israel and its significance for the Levant Geology. Palaeogeogr. Palaeoclimatol. Palaeoecol., 10(4), p. 293-316.

Flexer, A., 1987.The Syrian Arc folding system (In Israel). Tel Aviv, Oil Exploration {Investments}, Rep. 87/22, 29 p.

Flexer, A., Freund, R., Reiss, Z., and Buchbinder, B., 1970. Santonian paleostructure of the Galilee. Isr. J. Earth Sci., 19(3-4), p. 141-146.

Flexer, A., Gilat, A., Hirsch, F., Honigstein, A., Rosenfeld, A., Rueffer, T., 1989. Late Cretaceous evolution of the Judean Mountains as indicated by Ostracodes. Terra Nova, 1(4?), p. 349-358.

Flexer, A., Honigstein, A., and Gerry, E., 1987. Late Permian-Triassic Ostracoda; Final Report. Report submitted to the Minist. of Energy & Infrastructure, 5 p., 1 tab.

Freund, R., 1965. A model of the structural development of Israel and adjacent areas since Upper Cretaceous times. Geol. Mag., 102(3), p. 189-205. 3 references

Freund, R., Goldberg, M., Weissbrod, T., Druckman, Y., and Derin, B., 1975. The Triassic-Jurassic structure of Israel and its relation to the origin of the eastern Mediterranean. Isr. Geol. Surv., Bull. 65, 26 p.

Freund, R., and Zak, I., 1973. Shifting of folding and faulting along geological structures. (In Hebrew). Teva Va'aretz, 15(6), p. 264-270.

Gilat, A., 1977. The Geological Map of Israel, 1:50,000, Sheet 15-I: Esthtemoa, Geol. Surv. Isr.

Gilat, A., and Arkin, Y., 1978. Geotechnical map, Eshtamoa sheet 1:50,000. Geological data for regional planning and preservation of the environment. Isr. Geol. Surv., Rep. MM/6/78, 17 p., map.

Ginzburg, A., and Folkman, Y., 1980. The crustal structure between the Dead Sea Rift and the Mediterranean Sea. Earth Planet. Sci. Lett., 51(1), p. 181-188.

Ginzburg, A., and Gvirtzman, G., 1979. Changes in the crust and in the sedimentary cover across the transition from the Arabian platform to the Mediterranean basin: evidence from refraction and sedimentary studies in Israel and in Sinai. Sediment. Geol., 23(1-4), p. 19-26.

Ginzburg, A., Makris, J., Fuchs, K., Prodehl, C., Kaminski W., and Amitai, U., 1978. Seismic study of the crust and upper mantle of the Jordan-Dead Sea Rift and their transition towards the Mediterranean Sea. IPRG Rep., Hamburg Univ. and Karlsrhue Univ.

Ginzburg, A., Makris, J., Fuchs, K., and Prodehl, C., 1981. The structure of the crust and upper mantle in the Dead Sea Rift. Tectonophysics, 80(1-4), p. 109-119.

Gvirtzman, G., 1979. Geology and geomorphology of the Be'er Sheva Valley. The Beer Sheva Book, Y. Grados and A Shtern (eds.), Sde Boqer, Ben Gurion Univ. and Ben Gurion Inst., p. 333-354, (In Hebrew).

.Gvirtzman, G., and Weissbrod, T., 1984. The Hercynian Geanticline of Helez and the late Palaeozoic history of the Levant. In: J. E. Dixon and A. H. F. Robertson, (eds.). The Geological Evolution of the Eastern Mediterranean. Geol. Soc. Spec. Publ. No. 17, Blackwell, Oxford, p. 177-186.

Hempton, M., 1987. Constraints on Arabian Plate motion and extensional history of the Red Sea. Tectonics, 6(6), p. 687-705.

Henson, F. R. S., 1951. Observations on the geology and petroleum occurrences of the Middle East. Proc. Third World Petroleum Congress, The Hague.Section 1, p. 118-140.

Hirsch, F., 1984. The Arabian sub-plate during the Mesozoic. In: J. E. Dixon and A. H. F. Robertson, (eds.). The Geological Evolution of the Eastern Mediterranean. Geol. Soc. Spec. Publ. No. 17, Blackwell, Oxford, p. 669-676.

Hirsch, F., Flexer, A., Rosenfeld, A., and Yellin-Dror, A., 1995. Palinspastic and crustal studies of the Eastern Mediterranean. J. Petrol. Geol. 18(2), p. 149-170.

Honigstein, A., Flexer, A. and Rosenfeld, A., 1988. Tectonic activity in the Syrian Arc in Israel, as indicated by Senonian ostracodes. N. Jb. Geol. Palaeontol., Monats., 1988(3), p. 173-183.

Ilani, S., Shiloni, Y., and Gilat, A., 1984. Indications of Senonian activities across the Ramon fault. Isr. Geol. Soc. Ann. Meet., Abst., Arad, April 1984, p. 50-51.

Krenkel, E., 1924. Der Syrische Bogen. Central. Mineral. Geol. Palaeont. Abh. B. 9, p. 274-281, 10, p. 301-313.

Lewy, Z., 1990. Transgressions, regressions and relative sea level changes on the Cretaceous shelf of Israel and adjacent countries. A critical evaluation of Cretaceous global sea level correlations. Paleoceanography, 5(4), p. 619-637.

Mart, Y., 1994. Ptolomaïs basin: The tectonic origin of a Senonian marine basin underneath the southeastern Mediterranean Sea. Tectonophysics, 234(1-2), p. 5-17.

Mimran, Y., 1984. Unconformities on the eastern flank of the Fari'a Anticline, and their implications on the structural evolution of Samaria (central Israel). Isr. J. Earth Sci., 33(1-2), p. 1-11.

Mimran, Y., and Begin, Z. B., 1984. Unpublished report on the Qeren anticline prepared for the I.A.E.C.

Neev, D., Almagor, G., Arad, A., Ginzburg, A., Hall, J. K., 1976. The geology of the southeastern Mediterranean Sea. (Including a note on seismicity by E. Arieh). Isr. Geol. Surv., Bull. 68, 51 p.

Neev, D., and Hall, J. K., 1982. A global system of spiraling geosutures. J. Geophys. Res., 87(B13), p. 10,689-10,708.

Picard, L., 1937. On the structure of the Arabian Peninsula. Heb. Univ. Jerusalem, Geol. Dept., Bull. 3, 12 p.

Picard, L., 1943. Structure and evolution of Palestine; with comparative notes on neighbouring countries. Heb. Univ. Jerusalem, Geol. Dept., Bull., 4(2-3-4), 187 p.

Picard, L., 1951. Geomorphology of Israel. Part 1 - The Negev. Geol. Surv. Isr. Bull. 1, 28 p.

Picard, L., 1959. Geology and oil exploration of Israel. Isr. Res. Counc., Bull., 8G(1), p. 1-30. Also World Petrol. Congr., 5th, New York; Proc., Sect. 1, p. 311-336.

Picard, L., and Eliezri, I., 1964. Oil exploration in Israel. Beolam Hadelek, No. 9-10, p. 77-104.

Ponikarov, V. P., Kazmin, V. G., Dolginov, Ye. A., Sulidi-Kondrat'yev, Ye. D., 1967. The character of the contact between the Arabian Platform and the Alpine geosynclinal region. Sovietskaya Geologiya, Vol. 2, p. 54-66. [In Russian].

Powers, R. W., Ramirez, L. F., Redmond, C. D., and Elberg, E. L. Jr., 1966. Geology of the Arabian Peninsula - Sedimentary geology of Saudi Arabia. USGS, Prof. Pap., No. 560-D, 147 p.

Reches, Z., Hoexter, D. F., and Hirsch, F., 1981. The structure of a monocline in the Syrian Arc system, Middle East; surface and subsurface analysis. J. Petrol. Geol., 3(4), p. 413-425.

Robertson, A. H. F., 1978. The sedimentary evolution of the Troodos Ocean: an excursion guide to the sedimentary geology of southern Cyrus. 75 p.

Roded, R., 1982. On the age of the folding of the Efe anticline (northern Negev, Israel). Isr. Geol. Surv. Rep. S/3/ 82, 21 p.

Rotstein, Y. and Ben-Avraham, Z., 1986. Active tectonics in the eastern Mediterranean: the role of oceanic plateaus and accreted terranes Isr. J. Earth Sci. 35(1), p. 23-39

Said, R., 1962. The geology of Egypt. Elsevier, Amsterdam-New York, 377 p.

Salem, R., 1976. Evolution of Eocene-Miocene sedimentation patterns in parts of northern Egypt. Am. Assoc. Petrol. Geol. Bull., 60(1), p. 34-64.

Scott, B., 1981. The Eurasian-Arabian and African contnental margin from Iran to Greece. J. Geol. Soc. Lond., 138(6), p. 719-733.

Searle, M. P., 1994. Structure of the Intraplate Eastern Palmyride Fold Belt, Syria. Geol. Soc. Am. Bull., 106(10), p. 1332-1350.

Styles, P., and Hall, S. A., 1980. A comparison of the seafloor spreading histories of the western Gulf of Aden and the central Red Sea. In: Geodynamic Evolution of the Afro-Arabian Rift System, Accad. Naz. Lincei, Rome, p. 587-606.

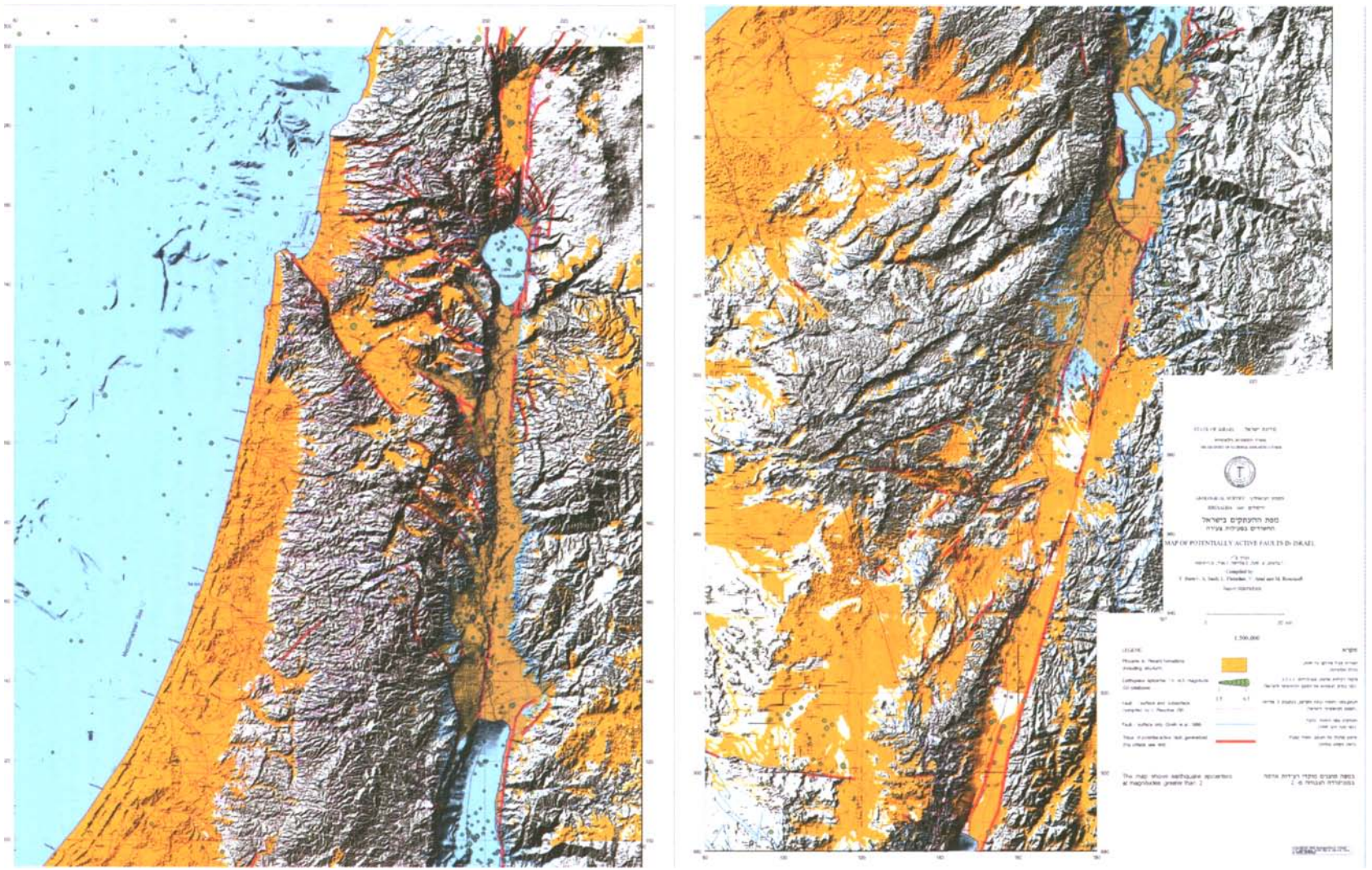
Walley, C. D., 1988. A braided strike-slip model for the northern continuation of the Dead Sea Fault and its implications for Levantine tectonics. Tectonophysics, 145(1-2), p. 63-72.

Zaslavskaya, N., Eshet, Y., Hirsch, F., Weissbrod, T., and Gvirtzman, G., 1995. Recycled Lower Paleozoic microfossils (Chitinozoa) in the Carboniferous of Sinai (Egypt) and Permo-Triassic of the Negev (Israel): Paleogeographic considerations. Newsl. Stratign, 32(1), p. 57-72.

Zijderveld, J. D. A., and Van Der Voo, R., 1973. Paleomagnetism in the Mediterranean area. In: D. H. Tarling and S. K. Runcorn, (eds.), Implications of Continental Drift in the Earth Sciences, Vol. 1, Academic Press, London, p. 133-161.

Zilberman, E., 1986. Pliocene-Early Pleistocene surfaces in the northwestern Negev: paleogeography and tectonic implications. Isr. Geol. Surv., Rep. GSI/26/86, 52 p.

Map of potentially active faults in Israel. Compiled by Y. Bartov, A. Sneh, L. Fleischer, V. Arad, and M. Rosensaft. Geol. Surv. Israel Report GSI/23/2000. Hill shading by Global Mapper® from the DTM of Israel, 100 m grid spacing; sun illumination from N315°E and 45° elevation. Vertical exaggeration 20x, 31 m pixels, blue shading added below Mediterranean sealevel. Green circles are epicenters between Richter magnitude 2 and 6.5. Orange shading for Pliocene to recent formations. Reproduced with permission, courtesy of the Geological Survey of Israel.



Chapter 19

Bouguer Gravity Map of the Levant – A New Compilation

Michael Rybakov
Geophysical Institute of Israel, 6 Baal-Shem Tov Street, P.O. Box 182, Lod 71100, Israel
Abdallah Al-Zoubi
Research and Studies Dept., Faculty of Graduate and Scientific Research, Al-Balqa' Applied University, Al-Salt 19117, Jordan

INTRODUCTION

Over the last decade a gravity database has been established for the Levant area (Rybakov et al., 1997). It includes the eastern Mediterranean, the Dead Sea Rift, Israel, and its surrounding countries (**Fig. 19.1**). The database consists of earlier marine reconnaissance measurements supplemented by data from the following sources:

1) Jordanian gravity network. Within the framework of the peace treaty between Jordan and Israel a cooperative project was initiated entailing a joint study of the gravity field (ten Brink et al, 1998, 1999, 2002) of the Dead Sea Rift and surrounding areas in Jordan and Israel.

2) Marine gravity measurements of the northeastern part of the Mediterranean Sea south and west of Cyprus (V. Toulin, this book).

3) The results of marine gravity surveys in the Israeli offshore produced by Horizon (Seismic Geocode Ltd., 1984), Belco Petroleum of Israel Ltd. (1968), and Teledyne Exploration (1975). All their maps were digitized and the values obtained recalculated using a density of 2,670 kg/m^3. Large discrepancies (more than 10-15 mGal) were found in some places between the results of these studies, and were corrected.

4) The regional gravity values derived from the Cornell Syria Database allowed us to supplement the regional gravity coverage and to fill in gaps in our database for the northeastern part of Saudi Arabia and the western part of Iraq (M. Barazangi and his team at the Institute for the Study of the Continents at Cornell University; website at: http://atlas.geo.cornell.edu/).

THE NEW BOUGUER GRAVITY ANOMALY MAP

The new compilation of the regional scale gravity map of the Levant is only based on Bouguer values, and not on recalculation of Free Air gravity measurements through the use of height data. This is due to the Bouguer gravity coverage which was directly digitized from the published Bouguer maps of Syria, Egypt etc.

The gravity network contains all the available data and consists of approximately 127,000 data points. The Bouguer gravity values were compiled using the 1967 reference ellipsoid and formula and a density of 2,670 kg/m^3 for all land data. Sea level was taken as the reference datum and the same density (2,670 kg/m^3) was attributed to the water body. All the gravity data sets have been incorporated and were interpolated to a grid with 2.5 km cell size by a kriging algorithm (**Fig. 19.2**).

The new Bouguer gravity map should be the most reliable gravity map of the Levant area, as it mainly shows the first order tectonic features.

CONCLUSIONS

The gravity pattern in the Bouguer gravity map allows some conclusions to be drawn:

1) The regional gravity anomalies most likely reflect the crustal type.

2) The negative gravity values of the African and Arabian plates are typical for continental crust. In the Red Sea and eastern Mediterranean (Levantine Basin) positive values are associated with oceanic crust.

3) A pronounced elongated gravity high characterizes much of Cyprus, where oceanic ophiolites are documented. This anomaly, coinciding with the Cyprian arc, is bounded on the south by a chain of gravity lows, probably corresponding to the trench of the subduction zone.

4) High values extend eastward on land to the Dead Sea Transform (DST), suggesting a relatively thin basaltic crust under northern Israel and Lebanon. We assume that the density difference existed before initiation of the DST motion.

5) The development of the DST used the eastern boundary of the dense block of the Sinai and Levant Sub-plates as a zone of weakness. On the other hand, the DST has broken up the crust and made it easier to uplift the low-density eastern block.

6) One of the pronounced gravity features is a string of intense gravity lows along the DST fault system.

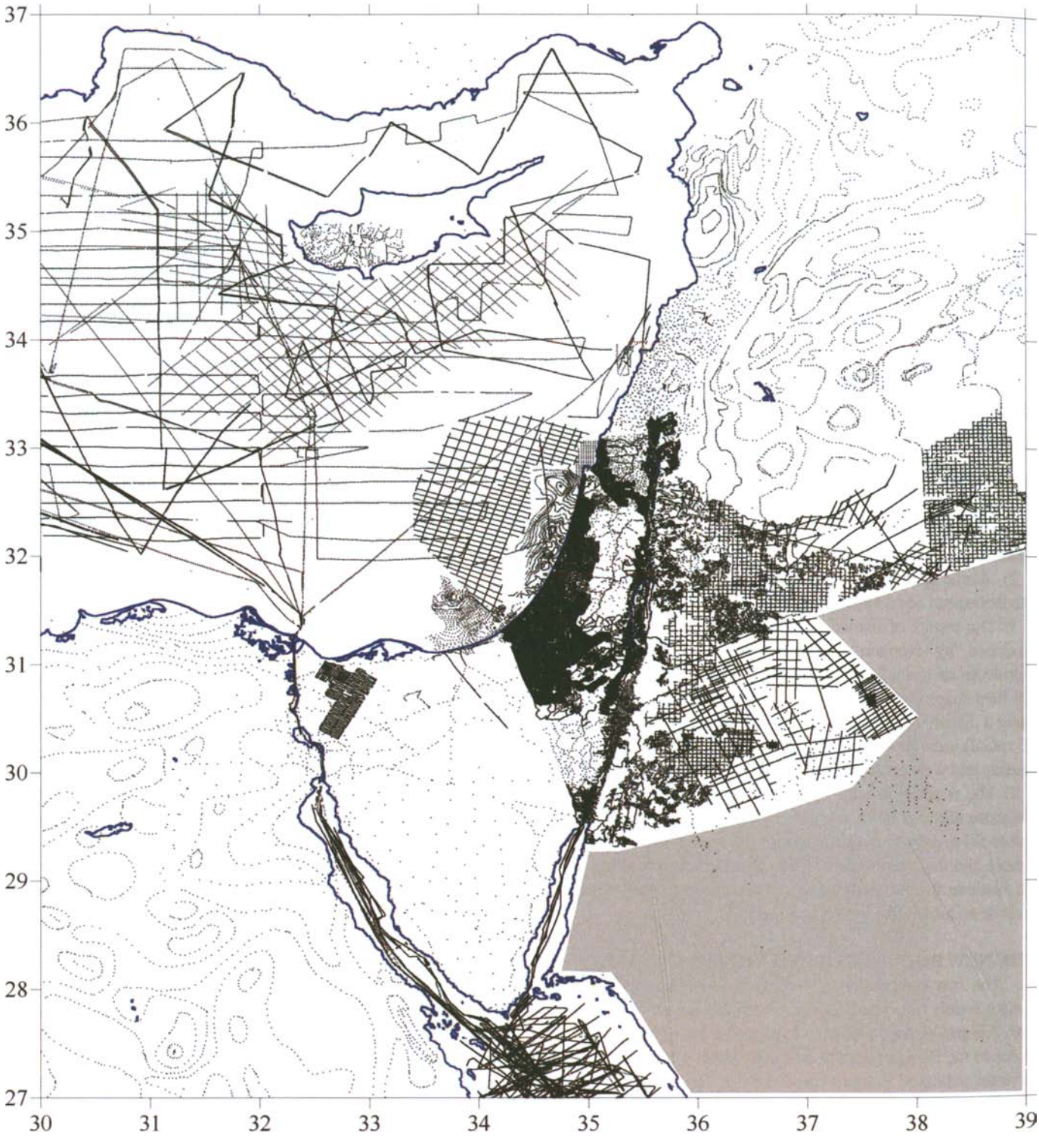


Figure 19.1. Levant. Gravity coverage map. See text for explanation.

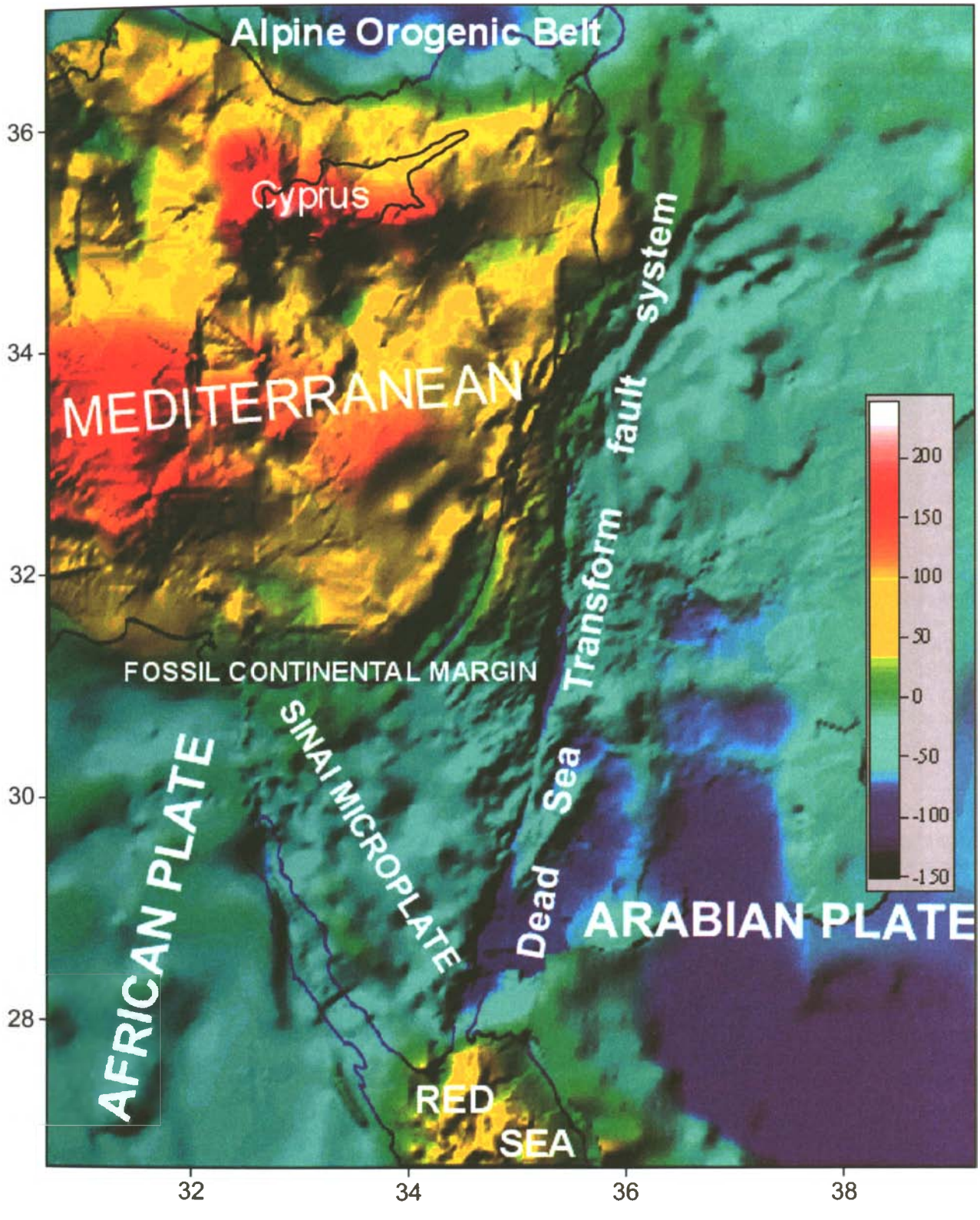


Figure 19.2. Levant. Color shaded Bouguer Gravity map superimposed on the main tectonic features.

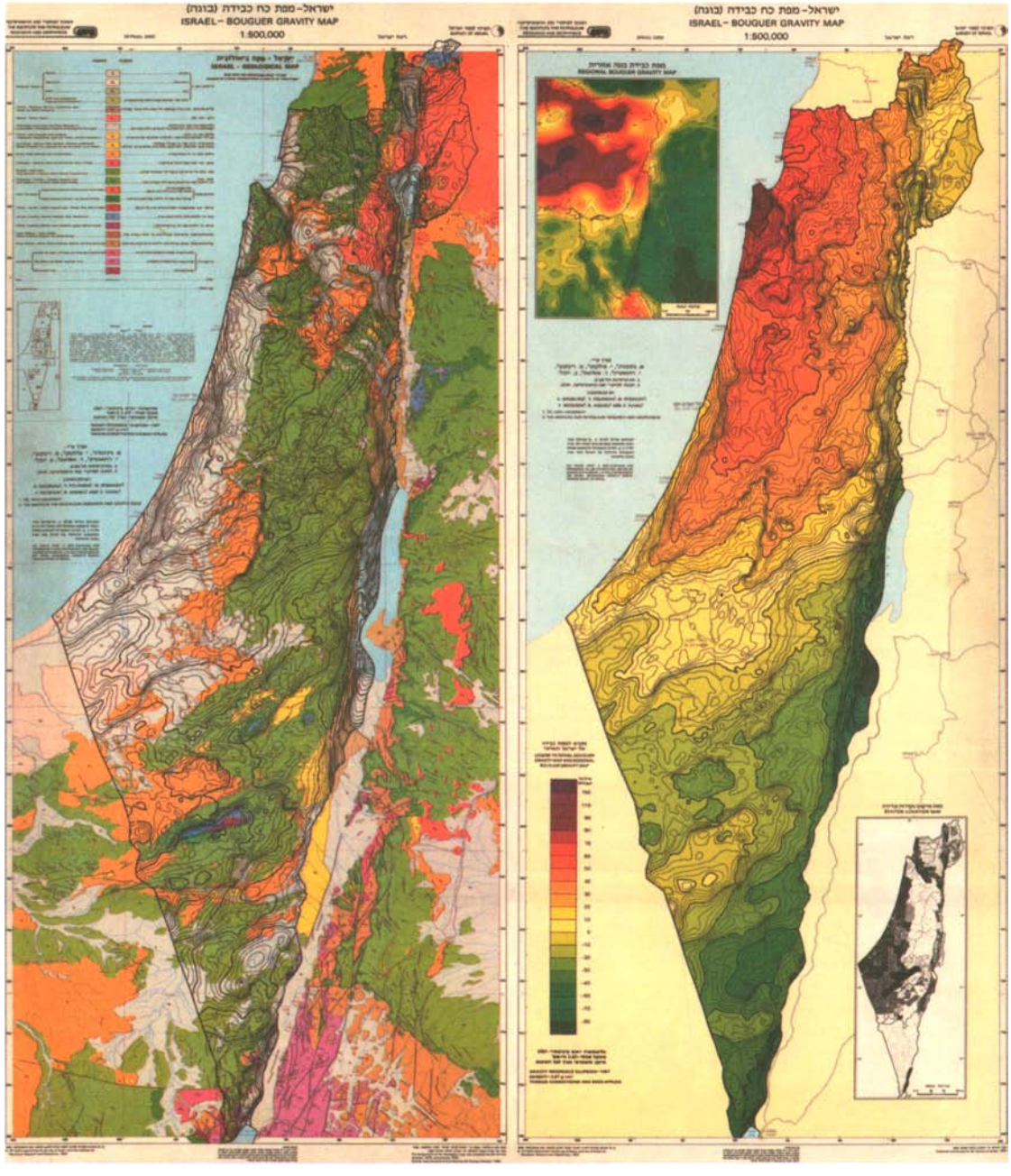
REFERENCES

Rybakov, M., Goldshmidt, V. and Rotstein, Y., 1997. A new compilation of gravity and magnetic data from the Levant and their preliminary interpretation, Geophysical Research Letters, 24(1), p. 33-36.

ten Brink, U., Rybakov, M., Al-Zoubi, A., Hassouneh, M., Batayneh, A., Frieslander, U., Goldschmit, V., Daoud, M., and Rotstein, Y., 1998. Bouguer gravity anomaly map of the Dead Sea fault system, Jordan and Israel. September, 1998. Poster 1 sheet.

ten Brink, U., Rybakov, M., Al-Zoubi, A., Hassouneh, M., Frieslander, U., Batayneh, A., Goldshmidt, V., Daoud, M., Rotstein, Y. and Hall, J. K., 1999. The anatomy of the Dead Sea plate boundary: does it reflect continuous changes in plate motion? Geology, 27(10), p. 887-890.

ten-Brink, U., Al-Zoubi, A. and Rybakov, M., 2002. Bouguer gravity anomaly map of the Dead Sea fault system, Jordan and Israel. Open file report 01-216, online publication, USGS, Woods Hole Field Center.



Bouguer Gravity Map of Israel circa 1993.
Reduction of poster published in 1993 by the Israel Institute for Petroleum Research and Geophysics (IPRG – now GII) showing the Bouguer gravity anomalies in Israel contoured at 2 mGal intervals on the cultural map of Israel (right), and also superimposed on the Geological Map of Israel (left), prepared in 1979 by Dr. Y. Bartov for the Atlas of Israel. Bouguer gravity map compiled by A. Ginzburg, Y. Folkman, M. Rybakov, Y. Rotstein, R. Assael, and Z. Yuval. The reduction was accomplished using the DTM of Israel.

Chapter 20

Depth to Crystalline Basement in the Middle East with Emphasis on Israel and Jordan

Michael Rybakov
Geophysical Institute of Israel, 6 Baal-Shem Tov Street, P.O.B. 182, Lod 71100, Israel
Amit Segev
Geological Survey of Israel, 30 Malchei Israel Street, Jerusalem 95501, Israel

INTRODUCTION

The basement of the continental areas surrounding the Eastern Mediterranean area (**Fig. 20.1**) belongs to the northern part of the Arabian Nubian Shield (ANS), which formed during the Neoproterozoic (Pan-African) orogenic cycle (Bentor, 1985; Stern, 1994; Stein and Goldstein, 1996) and ended in the Early Cambrian ca. 532 Ma (Segev, 1987; Beyth and Heimann, 1999; Mushkin et al., 1999). At that time the study area was located in the northern part of Gondwana, which later on, during the Variscan (Hercynian) orogeny, collided with Laurussia, and since then was broken up several times into continental fragments (Şengör et al., 1984; Segev, 2000a, 2002; Stampfli, 2000). Detailed information about the geology, stratigraphy, tectonism, and magmatism of this area is presented by several authors in this book.

The relief of the top crystalline basement in the Middle East was therefore produced mainly during the Phanerozoic Era. The Cenozoic structural elements are relatively well-preserved, whereas the older structures are preserved depending upon their relations with the younger ones.

The study of the crystalline basement depth in the subsurface of central Israel is based on the Helez Deep-1A and Gevim-1 boreholes, seismic reflection profiles, structural data (Trachtman et al., 1990), and 3-D gravity and magnetic analyses. Rybakov et al. (1999a) previously prepared a small schematic map of the top crystalline basement.

The team at the Institute for the Study of the Continents in Cornell University (Barazangi, Isacks, Brew, Seber, Gomez, Sandvol, Steer, Vallve, Orgren, Fielding and others) compiled a regional map of the top crystalline basement. They collected a considerable amount of geophysical and geological data for the Middle East and organized it into a comprehensive GIS database.

In the framework of studying the lithospheric structure of the Levant area and its continental margins, Segev et al. (2003, Fig. 1) constructed a map of the top crystalline basement at better resolution in their study area.

In the present compilation of a regional scale map of the top crystalline basement, we used published data from Israel, Jordan and adjacent regions. Our new map reflects the overall geological processes that produced or significantly affected the basement topography of the study area.

SOURCES AND METHODS

Several recently published studies concerning basement data for Israel and adjacent areas (see sources in **Fig. 20.2**) produced detailed and accurate maps. These maps, and the various types of source data that were used, are described below.

Deep Boreholes

The most reliable data is from deep boreholes (El Beialy, 1988; Abu Ollo and El Kholy, 1992; Alfy et al, 1992; Abu Saad and Andrews, 1993; Abdel Aal et al., 1994; Rybakov et al, 1999b; Folkman, personal communication). A few deep boreholes (Helez Deep-1A, Bessor-1 and Gevim-1 in Israel, Abu Hamth-1 in the Sinai peninsula, and Adjlun-1, Safra-1, and Jaffr-1 in Jordan) penetrated the whole sedimentary succession and thus provided direct measurement of its total thickness. The other deep boreholes were used as constraints in estimating the minimal basement depth, and to allow stratigraphic extrapolations.

The density logs for the oil and water boreholes were used for interpreting sedimentary basins and for calculating a general depth-density function (*e.g.* Rybakov et al., 1999b).

Seismic Profiles

Four seismic refraction profiles located in northern and central Israel (Ginzburg and Folkman, 1979, Fig. 1) provided additional information on the depth to basement. These data were reanalyzed using the results of a commercial seismic reflection survey carried out recently in northern Israel (Lutzkin, personal communication). This survey showed a few deep seismic reflectors corresponding to Mesozoic strata as well as the basement surface (two-way travel times are 3 s and 4.5 s). Taking into account the high velocity of the mainly carbonate Mesozoic sequence, the depths of the crystalline basement are estimated at ~2 km deeper than previous estimates. For the areas of Israel, Jordan, and the Sinai Peninsula (yellow polygons on the source map, Fig. 20.1), we digitized the available structural and isopach maps (Croatero, personal communication; Eyal et al., 1987; Ryan, 1978; Andrews, 1991; Andrews, 1992a, b).

Recently, Ben-Avraham et al. (2002) reported on a seismic refraction/wide-angle reflection experiment along two lines crossing the continental shelf of Israel (Fig. 20.1). The results of this study (location and crustal structure) were digitized and

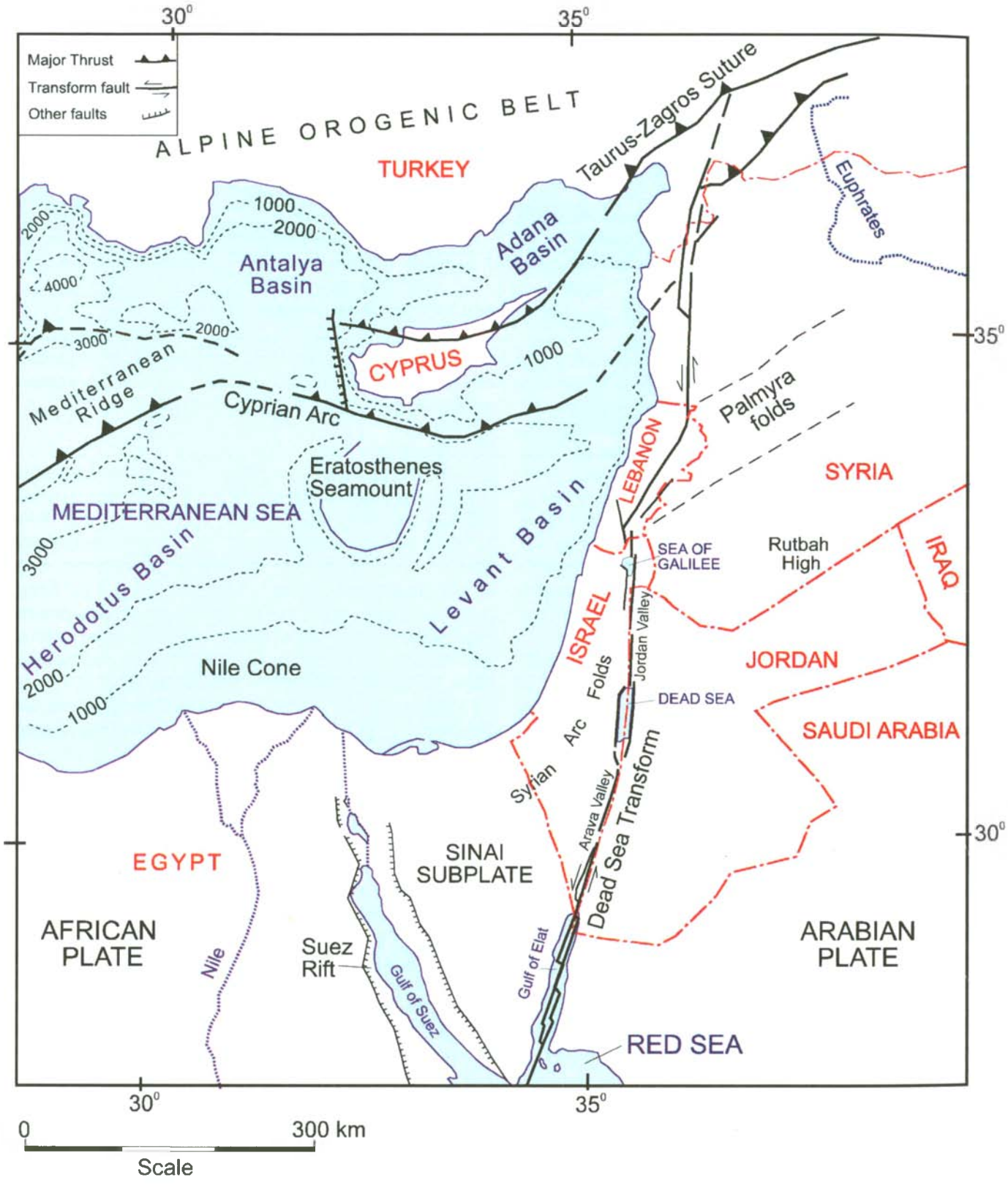


Fig. 20.1: Location map.

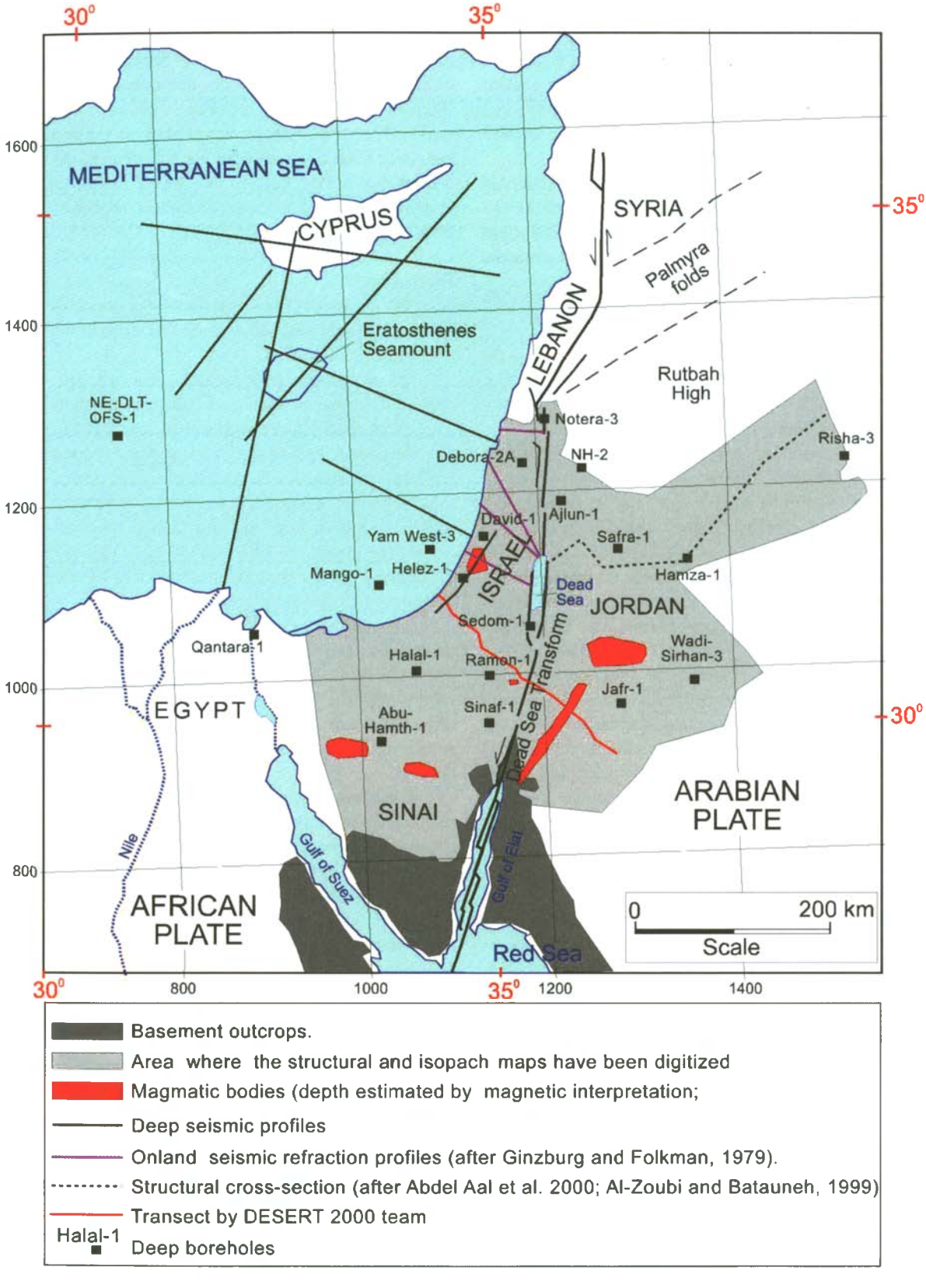


Fig. 20.2: Source map.

added to this dataset. The scheme of sedimentary thickness for the Eastern Mediterranean (Malovitsky et al., 1975) is also included in the present compilation. For the westernmost part of the region, the results of deep seismic soundings on the Herodotus abyssal plain (profile between Egypt and Rhodes from Makris and Wang, 1995) were taken into account even though they are located beyond our study area

Structural cross-sections, based on seismic profiles (Abdel Aal et al., 2000 - western profile, and Al-Zoubi and Batayneh, 1999 - Eastern profile), were also taking into account. The last profile was correlated with boreholes and thus, provides information about the sedimentary sequence in northern Jordan.

Gravity Data

Gravity data were used for estimating the sedimentary fill within the tectonic basins. Detailed information about the gravity network is presented in the previous Chapter 19 'Bouguer Gravity Map of the Levant – A New Compilation'.

Depths to the crystalline basement along the Dead Sea Transform (DST) have been adjusted using the results of the 3-D interpretation of the gravity data. The gravity anomalies, with magnitudes up to 140 mGal relative to the surrounding mountains, are caused by young low-density sedimentary rocks resting on top of older and denser rocks. Starting from the north, the gravity lows are found in continental basins corresponding to the Ghab, Bekka-Lebanon, Hula, Kinneret, Damia, Dead Sea, Timna, and Elat-Aqaba grabens respectively (ten Brink et al., 1999). These gravity lows were inverted to estimate the thickness of young sediments using the method developed by Jachens and Moring (1990). The sedimentary basin parameters obtained from the automatic inversion were used as initial conditions for the 3-D forward modeling. The density logs of the deep oil and water wells provided important information for the interpretation. Recently Rybakov et al. (2003) described in detail the methodology used in the 3-D gravity interpretation.

Magnetic Data

Comparison of the geological and aeromagnetic data for the exposed crystalline basement in southern Sinai, the Eastern Desert of Egypt, and Saudi Arabia, shows that Precambrian basic magmatics cause intensive magnetic anomalies (Folkman and Assael, 1980). Similar magmatics, covered by Phanerosoic sediments, should be identified by their low frequency magnetic anomalies. Interpretation of the aeromagnetic data could therefore be used to provide additional information about the basement depth and its composition. In the framework of the present study we have interpreted a few reliably identified low frequency magnetic anomalies as being caused by Precambrian magmatic bodies.

Since any result obtained from the analysis of potential field data is inherently ambiguous, several approaches to determine the causative body parameters were utilized in this study. The interpretation began by using an automatic inversion program by Troshkov and Groznova (Rybakov et al., 2000) and the widely known Werner deconvolution technique (the USGS package of Phillips, 1997). The features interpreted by both techniques generally coincide, however those obtained by the Werner deconvolution technique yielded slightly shallower results. The parameters of the magnetic bodies calculated by the automatic inversion programs were used as initial conditions for 3-D magnetic modeling, which helped to verify the confidence intervals of the calculated parameters (Rybakov et al., 2000, 2002).

Discussion

The compiled map of depth to the crystalline basement is shown in **Figure 20.3** as a shaded relief map with hypsometric tints related to depth.

All the direct and indirect measurements of depth to crystalline basement were used as data points in the total data set. These were then gridded with a node spacing of 2.5 km using the 'inverse distance to a power' method. The file containing digitized fault traces was used in the gridding process. The two-dimensional fault file defines a line acting as a barrier to information flow when gridding. Data on one side of a fault is not directly used when calculating grid node values on the other side of the fault. Only the largest faults crossing the crust (such as the DST fault system) were thus included in the gridding process.

It should be noted that a large discrepancy in the basement depth values (about 2 km) was noted between the Cornell database and the present compilation along the Syria-Jordan border. Based on the Adjlun-1 well, which penetrated the crystalline basement (Abu Saad and Andrews, 1993), the basement depth values in southernmost Syria were gradually aligned with the Jordanian data set.

In regions where crystalline rocks outcrop at the surface, the relief elevations derived from the GTOPO30 data set were used in generating the basement surface. In the central part of Israel, the current model of the crystalline basement topography is based on the recently published grid from Rybakov et al. (1999a).

THE MAIN FEATURES OF THE CRYSTALLINE BASEMENT MAP

Figure 20.4 shows the study area divided into seven different terrains (A through G), based on features in the top crystalline basement map. Each terrain has certain attributes related to the underlying geology.

We begin with the younger and better-known Terrain A. Both Terrains A in the south, and G in the north, delimit the Levant area. Terrain G is an uplifted Cenozoic region north of the Cyprus Trench and the Palmyrides, on both sides of the DST. It represents the margins of the Alpine Orogenic Belt, a consequence of the collision of the African and Arabian plates with the Anatolian sub-plate. The geological characteristics of this terrain are beyond the scope of this work.

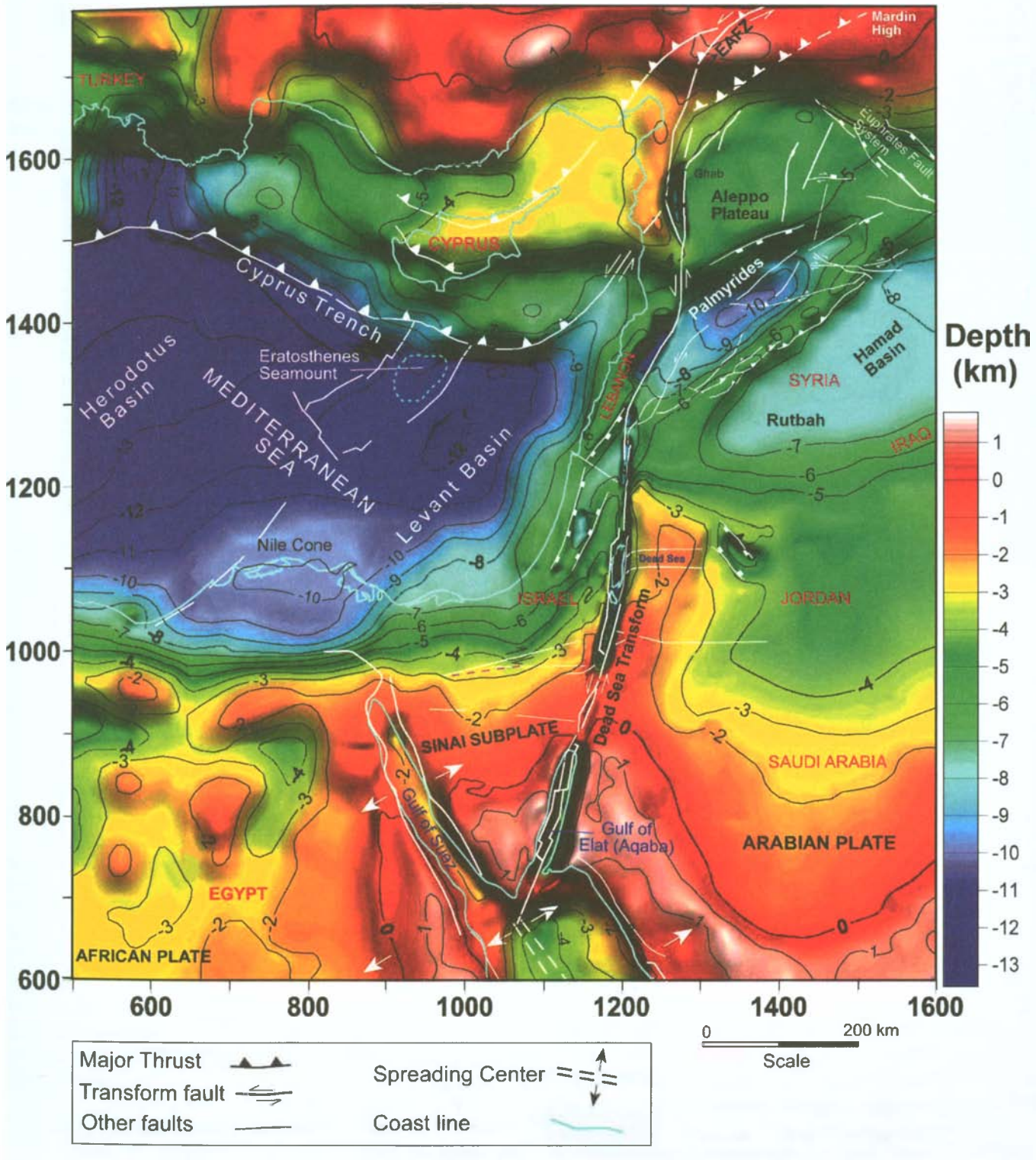


Fig. 20.3: Top basement map (main faults after: Garfunkel and Bartov, 1977; Garfunkel, 1981; Ben-Avraham, 1985; Brew et al. 1999; Abdel Aal et al., 2000; facies change after Druckman et al., 1975; Klitzsch, 1991; Hirsch et al., 1998; Al-Husseini, 1997).

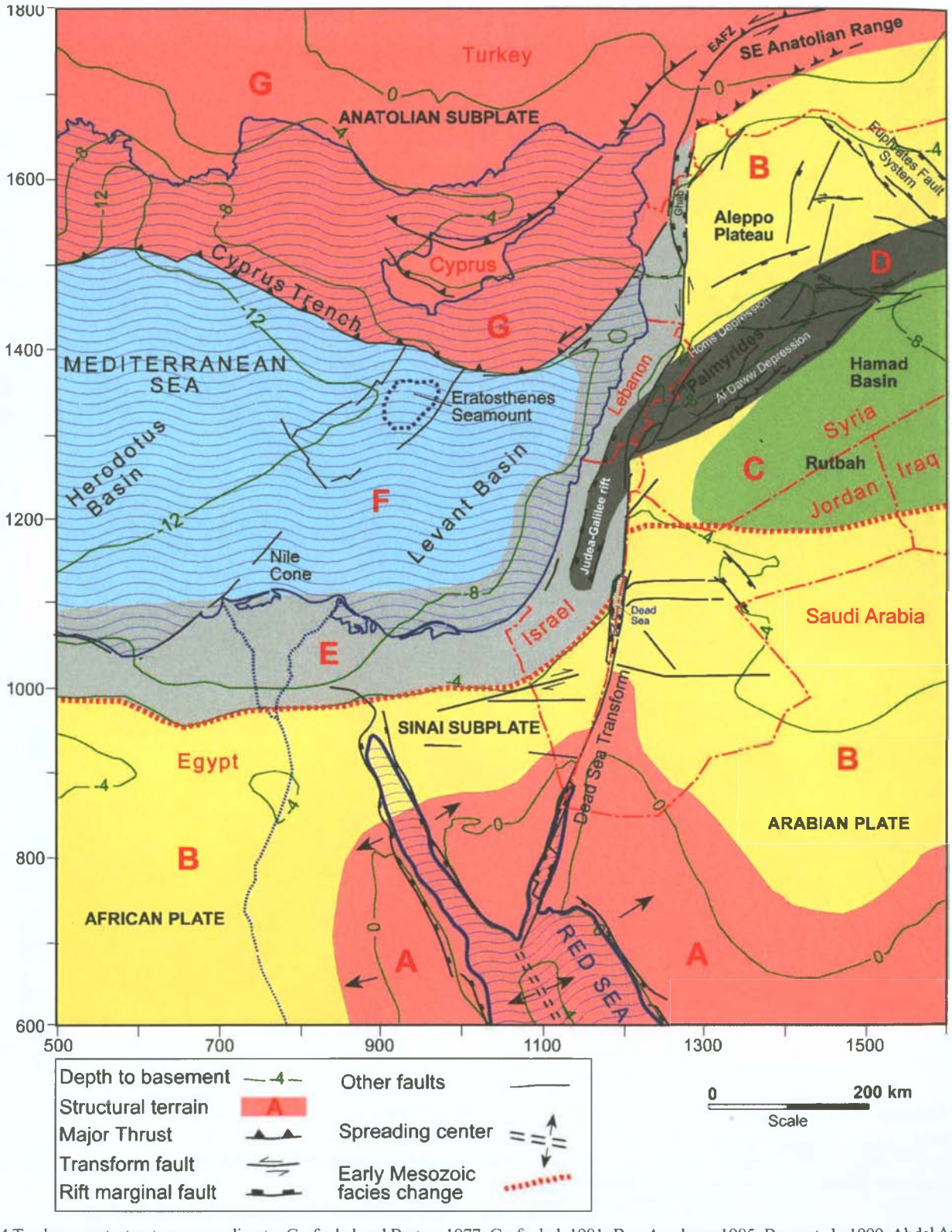


Fig. 20.4 Top basement, structures according to: Garfunkel and Bartov, 1977; Garfunkel, 1981; Ben-Avraham, 1985; Brew et al., 1999; Abdel Aal et al., 2000). Of these lithofacies, the sandy one in the south typifies the shallow platform part of the Arabian Shield, and the carbonate one in the north follows the Mesozoic shallow continental margins (Druckman et al., 1975; Klitzsch, 1991; Hirsch et al., 1998; Al-Husseini, 1997).

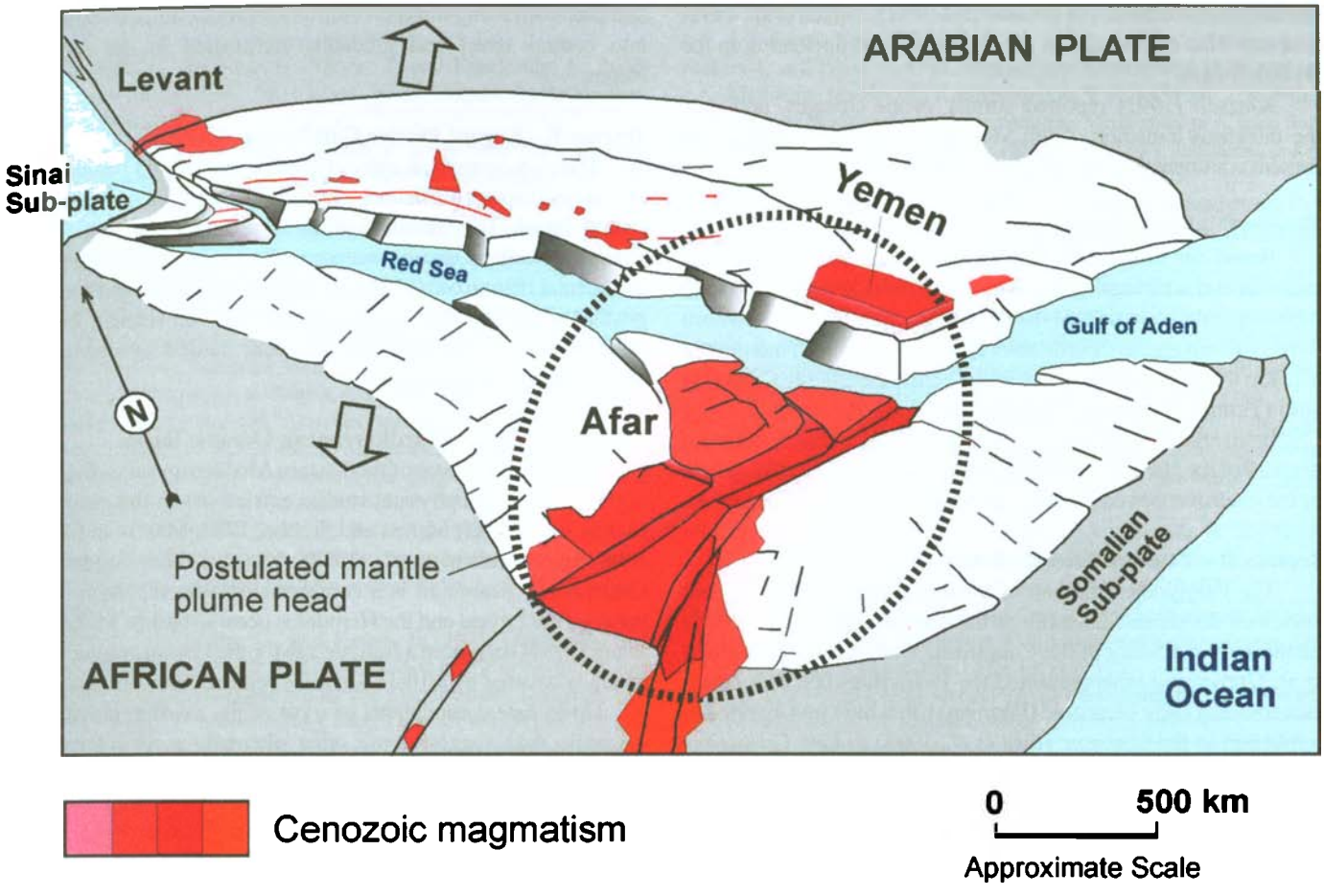


Fig. 20.5: The Tertiary-Recent Afro-Arabia or the Afar dome (from Segev, 2000b) caused by the Afar plume activity.

Terrain A – Northern Afar Dome

Regions of Cenozoic uplift surround the Red Sea, Gulf of Elat (Aqaba), and the Gulf of Suez in the southeastern part of the study area where Precambrian crystalline basement rocks are exposed. This regional geological feature belongs to the northernmost part of the Afar dome structure (**Fig. 20.5**), which is a result of the Afar plume activity, initiated during the Eocene (Segev, Chapter 21 in this volume). This activity produced vast amounts of volcanic rock (mainly the Afar-Yemen trap volcanics and the Arabian Harrats) that extend from Kenya to Turkey. The entire area of the Afar province was uplifted and later breached by the onset of the Red Sea spreading center.

Terrain B – Arabian/African Continental Platform

Terrain B comprises the elevated platform terrain of the Arabian Nubian Shield, which is covered by intermittent Paleozoic to Cenozoic sedimentary successions consisting mainly of clastic units with several carbonate marine intercalations. In this terrain various sedimentary rock units, overlying diverse types of Precambrian crystalline basement, reveal some discrepancies in the definition of the top basement interface. The main problem is probably due to the presence or absence of the volcano-sedimentary Saramuj or Zenifim Formations of Precambrian-Early Cambrian age. This arkosic sequence, associated with conglomerates and igneous rocks (mainly of dolerite and rhyo-dacite composition, reviewed by Weissbrod and Sneh, 2002), may have very similar petrophysical properties to those of the Late Precambrian alkaline volcanic suites. In southern and central Jordan, and southern Israel, the clastic sediments of these units accumulated within tectonic basins (Weissbrod and Sneh, 2002), which formed during the Late Precambrian-Early Cambrian post-Pan African orogenic basin-and-range tectonic regime (Stern, 1994; Segev et al., 1999). In northeastern Jordan and further north, the thickness of Saramuj/ Zenifim Formation increases (Hamad basin, Terrain C, see below). Therefore the transition between Terrains B and C is mainly caused by the thickening of this Precambrian volcano-sedimentary unit.

The change in the Mesozoic facies belts, from relatively thin continental clastics in the south to thicker shallow marine

carbonates in the north (Druckman et al., 1975; Hirsch et al., 1998) probably also contributed to the fast northward thickening in the Rutbah region.

Klitzsch (1991) reported similar facies changes, and thus the thickness transition of the Mesozoic rock units parallels the present continental margins of Sinai and Egypt.

Terrain C – Hamad Basin

Based on integration of results from several geophysical methods and well logs, Seber et al. (1993) and Brew et al. (1997) have suggested a basement depth of more than 8 km in southern Syria (Rutbah region). Furthermore, Brew et al. (1997) interpreted a ~3 km thick sedimentary succession below the Middle Cambrian Burj (Timna) Formation. Therefore, this Late Precambrian-Early Cambrian arkosic succession, as noted above, is probably the main deep fill of the Hamad Basin. This interpretation may explain some of the controversies concerning the basement depth in this terrain.

Terrain D – Palmyra Tectonic Belt

The Palmyrides fold belt of Syria is a tectonic belt that has been well-documented, mainly by the team at Cornell University's Institute for the Study of the Continents. Best et al. (1993), Brew et al. (2001), and others reported the Palmyrides belt as a north-east-trending early Mesozoic (Permian) rift, which was inverted to a fold belt in the Cenozoic (Best et al., 1993) or Late Cretaceous (Brew et al., 1999). The deep basement (up to ~10 km) and thick sedimentary succession of this terrain is mainly due to the fact that its long rifting activity preserved the Paleozoic and the Early Mesozoic successions, which were only partially eroded during the Pre-Early Permian and the Early Cretaceous regional uplifts. Both uplifts and denudations were part of the Permian and the Cretaceous plume activities (Segev, 2000b; Segev, 2002; Segev, Chapter 21 in this volume).

Many of the studies (*e.g.* Brew et al., 1999) dealing with the Palmyrides fold belt delineated its southwestward continuation, after restoration of the DST, to the Levant oceanic basin. However, the basement high (Fig. 20.3) along Lebanon and western Israel is sealing off the trend of the Palmyrides rift. It is therefore possible that part of the long duration Palmyrides rifting turned southward into central Israel and gradually terminated in the northern Negev.

Terrain E – Levant Passive Continental Margin

The N-S continental margin along Lebanon and Israel shows two steps displaced offshore opposite the Carmel structure and central Israel. The transition from continental to oceanic crust along the northern step is steeper and closer to shore. The E-W continental margin of NE Africa and Sinai originally had a similar gradual slope like that along the southern step (Israel), but the Pliocene-Recent loading of the Nile cone caused subsidence and thus a much steeper margin.

Terrain F – Eastern Mediterranean Oceanic Basin

The oceanic nature of the Eastern Mediterranean is discussed in many of the geophysical studies carried out in this area (*e.g.*, Makris et al., 1983; Makris and Stobbe, 1984; Makris and Wang, 1994; Ben-Avraham et al., 2002). These authors suggest that Eratosthenes Seamount is a continental crustal stumbling block between the Levant and the Herodotus oceanic basins. Makris and Wang (1994) suggested a Jurassic age for the Levant oceanic crust, which is covered by a 10-14 km thick sedimentary succession.

Up-to-date compilations of most of the existing gravity and magnetic data suggest some other alternatives for interpreting the origin and structure of Eratosthenes Seamount, but these are beyond the scope of this paper.

Terrain G – North of the Collisional Zones

The continental and marine areas in Terrain G are beyond the limits of our specific area of interest and will not be considered here.

ACKNOWLEDGEMENTS

The authors express their thanks to L. Fleischer, Z. Ben-Avraham, Z. Garfunkel V. Goldshmidt, Y. Rotstein, G. Shamir, and U. ten Brink for fruitful discussions.

REFERENCES CITED

Abdel Aal, A., El Barkooky, A., Gerrits, M., Meyer, H., Schwander, M., and Zaki, H., 2000. Tectonic evolution of the Eastern Mediterranean basin and its significance for hydrocarbon prospectivity in the ultra deep water of the Nile Delta. The Leading Edge, 19(10), p. 1086-1102.

Abdel Aal, A., Price, R. J., Vaitl, J. D., and Shrallow, J. A., 1994. Tectonic evolution of the Nile delta, its impact on sedimentation and hydrocarbon potential. 12th EPGC Conference, Cairo, p. 1-6.

Abu Ollo, S., and El Kholy, H., 1992. West Abu Qir discovery, its exploration, significance and case history as a part of the Nile delta exploration tasks. 11th EPGC Conference, Cairo, p. 514-543

Abu Saad, L., and Andrews, I. J., 1993. A database of stratigraphic information from deep boreholes in Jordan. Natural Resources Authority, Jordan, Subsurface Geol. Bull.. 6, 182 p.

Alfy, M., Polo, F., and Shash, M., 1992. The geology of Abu-Madi gas field. 11th EPGC Conference, Cairo, p. 485-513.

Al-Zoubi, A. S., and Batayneh, A. T., 1999. Two main play concepts identified in Jordan's basins. Oil & Gas Journal 97(26), p. 86-89.

Andrews, I. J., 1991. Palaeozoic lithostratigraphy in the subsurface of Jordan. Natural Resources Authority, Jordan, Subsurface Geol. Bull. 2.

Andrews, I. J., 1992a. Permian, Triassic and Jurassic lithostratigraphy in the subsurface of Jordan. Natural Resources Authority, Jordan, Subsurface Geol. Bull.. 4, 60 p.

Andrews, I. J., 1992b. Cretaceous and Paleogene lithostratigraphy in the subsurface of Jordan, Natural Resources Authority, Jordan, Bulletin 5.

Ben-Abraham, Z., 1985. Structural framework of the Gulf of Elat (Aqaba), northern Red Sea. J. Geophys. Res. 90(B1), 703-726.

Ben-Avraham, Z., Ginzburg, A., Makris, J., and Eppelbaum, L., 2002. Crustal structure of the Levant Basin, eastern Mediterranean. Tectonophysics. *346(1-2), p. 23-43.*

Bentor, Y. K., 1985. The crustal evolution of the Arabian-Nubian Massif with special reference to the Sinai Peninsula. Precambrian Research, 28(1), p. 1-74.

Best, J. A., Barazangi, M., Al-Saad, D., Sawaf, T., and Gebran, A., 1993. Continental margin evolution of the northern Arabian platform in Syria. Am. Assoc. Petrol. Geol. Bull., 77(2), p. 173-193.

Beyth, M., and Heimann, A., 1999. The youngest igneous event in the crystalline basement of the Arabian-Nubian shield, Timna Igneous Complex. Isr. J. Earth Sci. 48(2), p. 113-120.

Brew, G. E., Barazangi, M., Al-Maleh, A. K., and Sawaf, T., 2001. Tectonic and geologic evolution of Syria. GeoArabia, 6(4), p. 573-616.

Brew, G. E., Litak, R. K., Barazangi, M., Sawaf, T., and Zaza, T., 1999. Tectonic evolution of northeast Syria: Regional implications and hydrocarbon prospects. GeoArabia, 4(3), p. 289-318.

Brew, G. E., Litak, R. K., Seber, D., Barazangi, M., Al-Imam, A., and Sawaf, T., 1997. Basement depth and sedimentary velocity structure in the northern Arabian platform, eastern Syria. Geophys. J. Intern., 128(3), p. 617-631.

Druckman, Y., Gvirtzman, G., and Kashai, E., 1975. Distribution and environment of deposition of upper Triassic on the northern margins of the Arabian Shield and around the Mediterranean Sea. Proc. IXth Intern. Cong. of Sedimentology, Nice, Theme 5, v. 1, p. 183-192.

El Beialy, S. Y., 1988. Palynology, palaeoecology and dynocyst stratigraphy of the Oligocene trough Pliocene in the Qantara 1 well, eastern Nile delta, Egypt. J. Afr. Earth Sci., 11(3-4), p. 291-307.

Eyal, M., Bartov, Y., Shimron, A., and Bentor, Y., 1987. The geology of Sinai – explanatory notes on the geological photomap. In: Gvirtzman, G., Shoueli, A., Gardos, Y., Ben-Arie and Harel, M. (eds.), Tel-Aviv University, Ministry of Defense, (in Hebrew).

Folkman, Y., and Assael, R., 1980. Aeromagnetic map - Sinai Peninsula. Holon, IPRG, Rep. AM/575/79.

Garfunkel, Z., 1981. Internal structure of the Dead Sea leaky transform (rift) in relation to plate kinematics. Tectonophysics, 80(1-4), p. 81-108.

Garfunkel, Z., and Bartov, Y., 1977. The tectonics of the Suez rift. Isr. Geol. Surv. Bull. 71, 44 p.

Ginzburg, A., and Folkman, Y., 1979. Seismic refraction investigation of the crystalline basement under central and northern Israel, IPRG, Rep. Ref/518/79.

Hirsch, F., Bassoullet, J. P., Cariou, E., Conway, B. H., Feldman, H. R., Grossowicz, L., Honigstein, A., Owen, E. F. and Rosenfeld, A., 1998. The Jurassic of the southern Levant. Biostratigraphy, palaeogeography and cyclic events. In: S. Crasquin-Soleau and E. Barrier (eds), Peri-Tethys Memoir 4: epicratonic basins of Peri-Tethyan platforms. Mém. Mus. natn. Hist. Nat. 179, p. 213-235.

Jachens, R. C., and Moring, B.C., 1990. Maps of the thickness of Cenozoic deposits and the isostatic residual gravity over basement for Nevada. U.S. Geol. Surv. Open-File Rep., 90-404, 11 p.

Klitzsch, E., 1991. Geological observations from Nubia and their structural interpretation. In: Salem, M. J., Busrewil, M. T. and Ashour, A. M. (eds), The Geology of Libya VII, p. 101-105.

Makris, J., and Stobbe, C., 1984. Physical properties and state of the crust and upper mantle of the eastern Mediterranean Sea deduced from geophysical data. Marine Geology, 55(3-4), p. 347-363.

Makris, J., Ben-Abraham, Z., Behle, A., Ginzburg, A., Giese, A., Steinmetz, I., Whitmarsh, R. B., and Eleftheriou, S., 1983. Seismic refraction profiles between Cyprus and Israel and their interpretation. Geophys. J. R. Astron. Soc. 75(3), p. 575-591.

Makris, J., and Wang, J., 1994. Bouguer gravity anomalies of the eastern Mediterranean Sea. In: Krasheninnikov, V. A. and Hall, J. K. (eds.) Geological structure of the northeastern Mediterranean (Cruise 5 of the research vessel 'Akademik Nikolaj Strakhov'), Jerusalem, p. 87-98.

Makris, J., and Wang, J., 1995. Geophysical study and geodynamics of the eastern Mediterranean Sea, Institut für Geophysik, Universität Hamburg, Aktenzeichen Ma 719/48-1, 135 p.

Makris, J., Wang, J., Odintsov, S. D., and Udintsev, G. B., 1994. The magnetic field of the eastern Mediterranean Sea. In: Krasheninnikov, V. A. and Hall, J. K. (eds.) Geological structure of the northeastern Mediterranean (Cruise 5 of the research vessel 'Akademik Nikolaj Strakhov'), Jerusalem, p. 75-85.

Malovitsky, Ya. P., Esina, A., Kazakov, O. V., Moskalenko, V. N., and Osipov, G. V., 1975. Basic features of the deep bottom structure of the Mediterranean sea floor. Rapp. Comm. int. Mer Medit., 23(4a), p. 125.

Mushkin, A., Navon, O., Halicz, L., Heimann, A., Woerner, G., and Stein, M., 1999. Geology and geochronology of the Amram Massif, southern Negev Desert, Israel. Isr. J. Earth Sci., 48(3-4), p. 179-193.

Phillips, J., D., 1997. Potential-Field Geophysical Software for the PC, Version 2.2. Open-File Report, U.S. Geological Survey Report; OF 97-0725, U. S. Department of the Interior, 34 p.

Ryan, W. B. F., 1978. Messinian badlands on the southeastern margin of the Mediterranean Sea. Marine Geology, 27(3-4), p. 349-363.

Rybakov, M., Goldshmidt, V., Fleischer, L., and Ben-Gai, Y., 2000. 3-D gravity and magnetic interpretation for the Haifa Bay area (Israel). J. Appl. Geophys., 44(4), p. 353-367.

Rybakov, M., Goldshmidt, V., Fleischer, L., and Rotstein, Y., 1999a. Crystalline basement in central Israel derived from gravity and magnetic data. Isr. J. Earth Sci., 48(2), p. 101-111.

Rybakov, M., Goldshmidt, V., Rotstein, Y, Fleischer, L., and Goldberg, I., 1999b. Petrophysical constraints on gravity/magnetic interpretation in Israel. The Leading Edge, 18(2), p. 269-272.

Rybakov, M., Fleischer, L., Reznikov, M., and Segev, A. 2002. Study of the crystalline basement in Israel and adjacent areas (continuation). GII Rep. No. 840/199/01, — p.

Rybakov, M., Fleischer, L., and ten Brink, U., 2003. Structure of base fill in the Hula basin inferred from gravity data. Isr. J. Earth Sci (Submitted)

Seber, D., Barazangi, M., Chaimov, T. A., Al-Saad, D., Sawaf, T., and Khaddour, M., 1993. Upper crustal velocity structure and basement morphology beneath the intracontinental Palmyride fold-thrust belt and north Arabian platform in Syria. Geophys. J. Int., 113(3), p. 752-766.

Segev, A., 1987. The age of the latest Precambrian volcanism in southern Israel, northeastern Sinai and southwestern Jordan - a re-evaluation. Precambrian Res., 36(3-4), p. 277-285.

Segev, A., 2000a. Synchronous magmatic cycles during the fragmentation of Gondwana: radiometric ages from the Levant and other provinces. Tectonophysics, 325(3-4), p. 257-277.

Segev, A., 2000b. The principal Phanerozoic tectono-magmatic periods in the Levant and their stratigraphic record. Geol. Surv. Isr. Current. Res., 12, p. 115-124.

Segev, A., 2002. Flood basalts, continental breakup and the dispersal of Gondwana: evidence for periodic migration of upwelling mantle flows (plumes). Europ. Geosci. Uni., Stephan Mueller Spec. Publ. Ser. 2, p. 171-191.

Segev, A., Goldshmidt, V., and Rybakov, M., 1999. Late Precambrian-

Cambrian tectonic setting of the crystalline basement in the northern Arabian-Nubian Shield as derived from gravity and magnetic data: basin-and-range characteristics. Isr. J. Earth Sci., 48(3-4), p. 159-178.

Segev, A., Rybakov, M., Lyakhovsky, V., Hofstetter, A., Tibor, G., and Ben-Abraham, Z., 2003. The Levant and southeastern Mediterranean lithospheric structure and isostatic compensation since the Pliocene times. EGS-AGU-EUG Joint Assembly, Nice, v. 5.

Şengör, A. M., Yilmaz, Y., and Süngürlu, O., 1984. Tectonics of the Mediterranean Cimmerides: nature and evolution of the western termination of Palaeo-Tethys. In: Dixon, J. E., and Robertson, A. H. F. (eds.), The Geological Evolution of the Eastern Mediterranean. Geol. Soc. London, Spec. Publ., 17, p. 77-112.

Stampfli, G. M., 2000. Tethyan oceans. In: Bozkurt, E., Winchester, J. A., and Piper, J.D.A. (eds.), Tectonic and Magmatism in Turkey and the Surrounding Area. Geol. Soc. London, Spec. Publ., 173, p. 1-23.

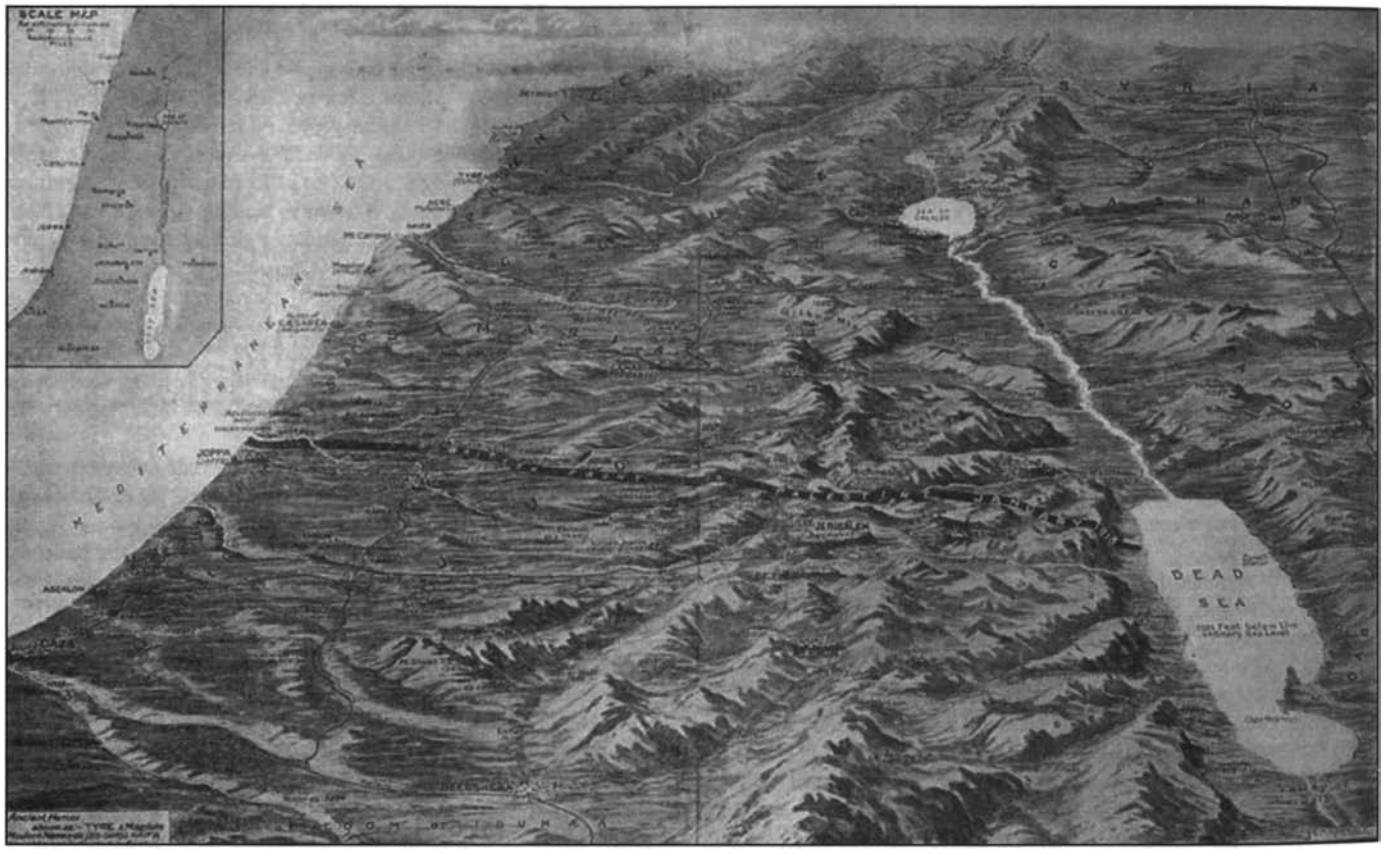
Stein, M., and Goldstein, S. L., 1996. From plume head to continental lithosphere in the Arabian-Nubian shield. Nature, 382(6594), p. 773-778.

Stern, R. J., 1994. Arc assembly and continental collision in the Neoproterozoic East African Orogen: Implication for the consolidation of Gondwanaland. Ann. Rev. Earth Planet. Sci., 22, p. 319-351.

ten Brink, U., Rybakov, M., Al-Zoubi, A., Hassouneh, M., Frieslander, U., Batayneh, A., Goldshmidt, V., Daoud, M., Rotstein, Y., and Hall, J. K., 1999. The anatomy of the Dead Sea plate boundary: does it reflect continuous changes in plate motion? Geology, 27(10), p. 887-890.

Trachtman, P., Rotstein, Y., and Frieslander, U., 1990. Deep crustal reflections in the coastal plane of Israel, IPRG Report 894/415/90, 4 p.

Weissbrod, T., and Sneh, A., 2002. Sedimentology and paleogeography of the Late Precambrian-Early Cambrian arkosic and conglomeratic facies in the northern margins of the Arabo-Nubian Shield. Isr. Geol. Surv. Bull., 87, 44 p.



Perspective of Central Israel looking north – the wresting of Palestine from the Ottoman Empire.
Pictorial map in perspective by the noted illustrator G. F. Morrell, provided courtesy of Aharon (Ronnie) Sade, source unknown. Morrell provided detailed map sketches to various British illustrated publications from early in the 20th century through World War II. The black line across the center of the map from the Mediterranean to the Dead Sea shows the British Front in Palestine as of January 1918. Advancing from the south, British and Colonial forces had taken Beersheba by the end of October 1917, Gaza at the beginning of November, and Jerusalem by the 9th of December. Many biblical areas are denoted, *viz.* Bashan, Galilee, Phenicea, Land of the Philistines, Gilead, Samaria.

Chapter 21

Phanerozoic Magmatic Activity Associated with Vertical Motions in Israel and the Adjacent Countries

Amit Segev
Geological Survey of Israel, 30 Malchei Israel Street, Jerusalem 95 501, Israel

INTRODUCTION

The Middle East is located on the northern part of the Arabian Nubian Shield, which formed during the Neoproterozoic orogenic (Pan-African) cycle (*e.g.* Stern, 1994; Stein and Goldstein, 1996). The final post-orogenic stage, which is typified by alkaline granite, monzonite, quartz monzonite, rhyolites and dolerite dikes, started at ~600 Ma (Bentor, 1985; Beyth et al., 1994; Stein and Goldstein, 1996) and ended in the Early Cambrian at ~532 Ma (Segev, 1987; Beyth and Heimann, 1999; Mushkin et al., 1999). The A-type granites and equivalent volcanics of this phase (Beyth et al., 1994; Kessel et al., 1998; Mushkin et al., 1999) put them in the field of intra-plate, post-orogenic, mantle derived magmas (Eby, 1992) associated with extension and crustal thinning. The regional tectonic setting, the presence of large dike swarms, and the geochemical affinity of this magmatism, point to mantle plume activity during the last tectono-magmatic stage of the Arabian Nubian Shield (Segev et al., 1999). The result of this intensive extensional tectonics was collapse and disintegration of the Pan-African orogenic belt and the formation of tectonically controlled basins filled by volcano-sedimentary series (*e.g.* Zenifim Formation in Israel and Saramuj Formation in Jordan). Intensive erosion during this post-orogenic or transitional stage lowered the relief of the Pan-African orogenic belt and in the end, when the area was stabilized, produced a vast low-relief landscape and extensive drainage systems. The stabilization and cooling of the northern Arabian Nubian Shield, which belongs to the Gondwana lithosphere, was accompanied by its subsidence toward the north and the beginning of the platformal stage.

MANTLE PLUMES

Large (~1000 km in diameter or more) mantle plumes ascending from a thermal layer just above the core-mantle boundary are a result of lower mantle upwelling (Olson et al., 1990; Griffiths and Campbell, 1990). The penetration of a plume head into the upper mantle is presumed to cause major stirring in upper mantle convective cells (Griffiths and Campbell, 1990), and thereby causes antithetical circulation in the upper mantle. Subsequently, the adjustment of this contradictory convection will produce divergent environments (Segev 2000a, Fig. 5) of upper mantle convection cells that lead to continental extension, heating the base of the lithosphere, regional domal uplift, rifting and breakup of the continental lithosphere, massive igneous activity (flood volcanics), spreading, and drifting. When the plume head is capped by the lithosphere it commonly spreads out along a specific trend controlled by its geodynamic evolution (Segev, 2000c, 2001).

The geochemical characteristics of the primary, mantle-derived mafic magmas, ranging from silica-undersaturated alkaline magmas (nephelinites, basanites, alkali basalts) through transitional basalts to subalkaline continental tholeiites, reflect varying degrees of partial melting of both asthenospheric and lithospheric mantle sources. Any of these parental magmas may then differentiate at crustal levels to produce a diverse range of more silica-rich magmas (Wilson, 1989, 1993a, b).

THE BREAKUP OF GONDWANA

Generally, after the termination of the Carboniferous Hercynian orogeny, a long process of breakup and dispersal began in which Pangea, and later Gondwana, were reduced to smaller continental fragments. These processes were associated with vast magmatic activities belonging to four super igneous provinces (**Figure 21.1**; Segev, 2000a, 2001): (a) Tethyan; (b) Atlantic; (c) Indian; (d) southeast Gondwana. Among these the Tethyan super province includes the Mesozoic igneous provinces (Western Tethyan and Levant-Nubian) that operated in our region, and the Indian super province that is responsible for our Cenozoic magmatic activity (the Afar province). All these igneous provinces are related to mantle plume activities accompanied by continental breakup and drifting (White and McKenzie, 1989, 1995; Storey, 1995; Wilson and Guiraud, 1998; Segev, 2000a, 2001).

The Levant region was dramatically affected by four periods of plume activity. A brief description of them follows:

1) Permo-Triassic

The regional stress field over the Carboniferous Variscan (Hercynian) orogen reorganized from compression to post-convergent extension at about 305 Ma (Ziegler, 1990; Burg et al., 1994), or even earlier at about 320 Ma when the associated magmatism began (see review by Henk, 1999). Henk (1999) suggests that this reorganization resulted from tensile forces, possibly by the internal (buoyancy) force produced by an active mantle plume.

The post-convergent extension is typified by crustal thinning, low viscosity of the lower crust, significant uplift, formation of numerous sedimentary basins (basin-and-range type, Lorenz and Nicholls, 1984; Ménard and Molnar, 1988) and widespread alkaline/subalkaline magmatism. It started in the Moldanubian

Zone and spread outward toward the forelands between ~320 and 240 Ma. The magmas derived from partial melting of lower crustal rocks as well as mantle-derived melts (Lorenz and Nicholls, 1984).

2) Jurassic

During this time major lithospheric extension, associated with breakup processes of the Gondwana super continent, took place in four synchronous plume provinces (Fig. 21.1, and Segev, 2000a):

a) The Karoo plume (southern Gondwana) caused the opening between eastern and western Gondwana (Fig. 21.1) along the Weddel Sea-Somali proto-oceanic rift (*e.g.* Storey, 1995; Duncan et al., 1997).

b) The central Atlantic plume (western Gondwana) caused the opening of the Central Atlantic rift (*e.g.* White and McKenzie, 1989; McHone, 1996; Wilson, 1997).

c) The western Tethys plume (northern Gondwana) caused the opening of the Mediterranean rift (*e.g.* Keeley and Wallis, 1991; Segev, 2000a). During this time, the Mesotethys, or the present eastern Mediterranean area (Herodotus basin), began to open.

d) The northwest Australia plume (western Gondwana), which produced mainly oceanic plateaus (Rowley Terrace - Scott and the Exmouth), caused the initial opening of the Indian Ocean (*e.g.* Mutter et al., 1988, 1989; White and McKenzie, 1989; Hopper et al., 1992; Crawford and von Rad, 1994).

3) Cretaceous

Lithospheric extension accompanied by domal uplift, Continental Flood Volcanics, and breakup processes, as a result of mantle plume activities, continued during the Cretaceous period in all parts of Gondwana (Fig. 21.1):

a) The equatorial Atlantic and the South Atlantic plumes in western Gondwana caused the opening between Africa and South America (*e.g.* White and McKenzie, 1989; Turner et al., 1994; Gibson et al., 1995; Wilson and Guiraud, 1998).

b) The Rajmahal-Kerguelen plume (eastern Gondwana) caused the opening between India and Antarctica (*e.g.* Kent, 1991; Crawford and von Rad, 1994) and shortly thereafter the nearby Madagascar plume caused the opening of the Mascarene Ridge between Madagascar and India – the Seychelles (White and McKenzie, 1989; Kent et al., 1992; Coffin and Eldholm, 1994; Storey, 1995).

c) The Marie Bird Land plume (southeast Gondwana) caused the opening of the Tasman Sea between Antarctica-Australia and New Zealand and the Lord Howe Rise (Weaver et al., 1994; Davey and Wood, 1994; Mortimer and Parkinson, 1996; Storey et al., 1999).

d) The Levant-Nubia plume (northern Gondwana) caused rifting in the Palmyrides (Stein and Hofmann, 1992, 1994).

4) Tertiary to Recent

The plume activities within the lithospheric fragments of Gondwana continued in three areas (Fig. 21.1):

a) The Balleny plume (southeast Gondwana; Vogt and Johnson, 1973; LeMasurier and Rex, 1991; Behrendt et al., 1992; Lanyon et al., 1993) caused the cessation of spreading on the Tasman Ridge and the onset of the southeast Indian Ridge between southern Australia and Antarctica.

b) The Deccan plume (*e.g.* White and McKenzie, 1989; Storey, 1995; Courtillot et al., 1999) continued migrating along the Indian path (Segev, 2001) and caused the opening between the Seychelles and India.

c) The Afar plume impinged upon the base of the African lithosphere below Kenya and southern Ethiopia (Figs. 21.1 and 21.8) in the Eocene and the initial volcanic event lasted between ~40 and 34 Ma (Ebinger et al., 1993; George et al., 1998). After some northward propagation, the dominant trap volcanism in Ethiopia and Yemen lasted between 31 and 21 Ma (Sebai et al., 1991; Baker et al., 1996; Hofmann et al., 1997) and led to the opening of the Red Sea and the Gulf of Aden.

RADIOMETRIC AGES

Most of the cited radiometric ages from Israel are reliable $^{40}Ar/^{39}Ar$ step-heating measurements of whole-rock basaltic rocks. The various sources for this radiometric data and the evaluation of their results have been published in Segev (2000a). K/Ar dates were cited only in cases where $^{40}Ar/^{39}Ar$ step-heating ages were lacking. It is important to note, however, that whole rock K/Ar dates for basaltic rocks in Israel and elsewhere are often uncertain and they actually show wide variations in time. This behavior is a result of natural Ar loss or gain by post crystallization thermal or other events that open the isotopic systematic, as well as analytical errors.

Well-defined Rb/Sr isochron ages, mainly for acid igneous rocks, were considered to represent reliable ages when the dated minerals were completely homogenized and the samples remained closed to Rb and Sr. Part of the cited reliable radiometric ages from igneous provinces over Gondwana were obtained by the U/Pb method, mainly for zircon minerals.

Now, internally published reliable $^{40}Ar/^{39}Ar$ step-heating ages (Weissbrod, et al., 2001; Segev, 2002 and unpublished results) have been added to the previous data set from Israel and are discussed herein.

OBJECTIVES

The present chapter summarizes geological, geochemical and geochronological evidence for subsurface and exposed magmatic rocks belonging to 13 magmatic events, as well as to one thermo-tectonic event in Israel in the course of the last half a billion years after the stabilization and cooling of the region. All these events were characterized by vertical motions of varying intensities. The above-mentioned information for the exposed magmatic rocks in Israel is generally sufficient and reliable, but information on the subsurface magmatic rocks is scarce and insufficient.

Regional correlations with coexisting magmatic events in adjacent countries still suffer from a lack of reliable geochronological data.

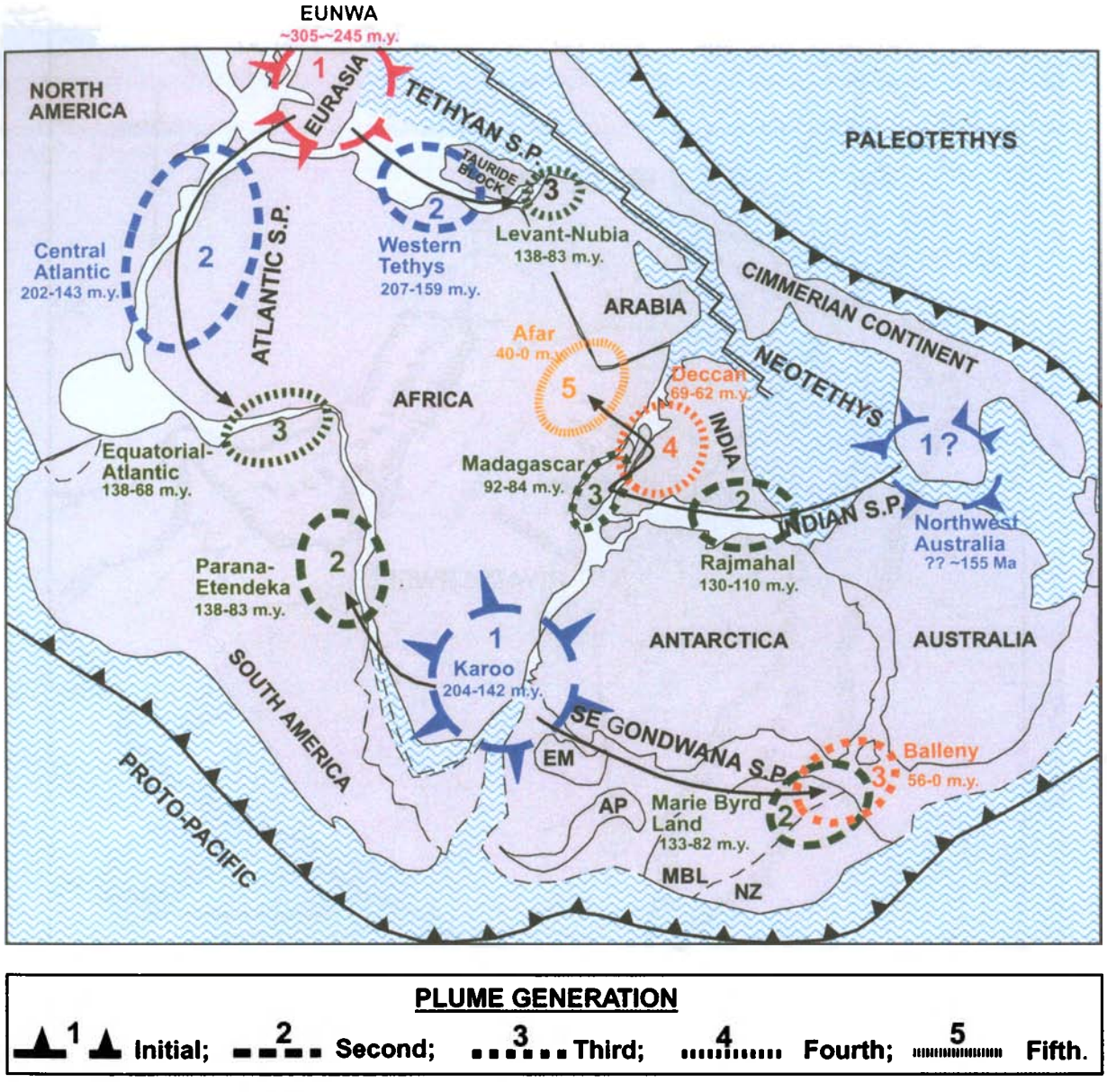


Fig. 21.1. Plume provinces throughout the Gondwana super continent (Gondwana reconstruction modified mainly after Lawver et al., 1992 and Wilson et al., 1996). The different lines and the numbers mark the various plume generations (from Segev, 2001) and the various colors represent different geological periods: purple – Permo-Triassic; blue – Jurassic; green – Cretaceous; ocher - Tertiary. EM - Ellsworth Mountains; AP - Antarctic Peninsula; MD - Madagascar; SR - Sri Lanka; SEY - Seychelles; MBL - Marie Byrd Land; NZ - New Zealand.

Middle-Late Devonian thermo-tectonic event

Since Early Cambrian time (circa 525 Ma), and during ~145 Ma, the northern part of Gondwana was stable and subsided, allowing the accumulation of several thousand meters of alternating continental and marine sediments (*e.g.* Weissbrod, 1981; Weissbrod and Gvirtzman, 1988).

A thermo-tectonic event, starting in Middle-Late Devonian time (Kohn et al., 1984, 1992; Segev et al., 1985, 1995), marks the cessation of accumulation of sedimentary rocks and the beginning of regional uplift and denudation. A regional analysis of stratigraphic evidence led Gvirtzman and Weissbrod (1984) and Weissbrod and Gvirtzman (1988, 1989) to suggest two regional Late Devonian swells (Heletz and Riyadh) over the present Arabian plate (**Figure 21.2**). They also point to the NE African Sirt basin of Libya as a similar feature: all are dome forming structures associated with crustal thinning and a parallel increase in heat flow.

This thermal event in Israel, which to various degrees affected different isotopic systematics and different minerals, was traced by

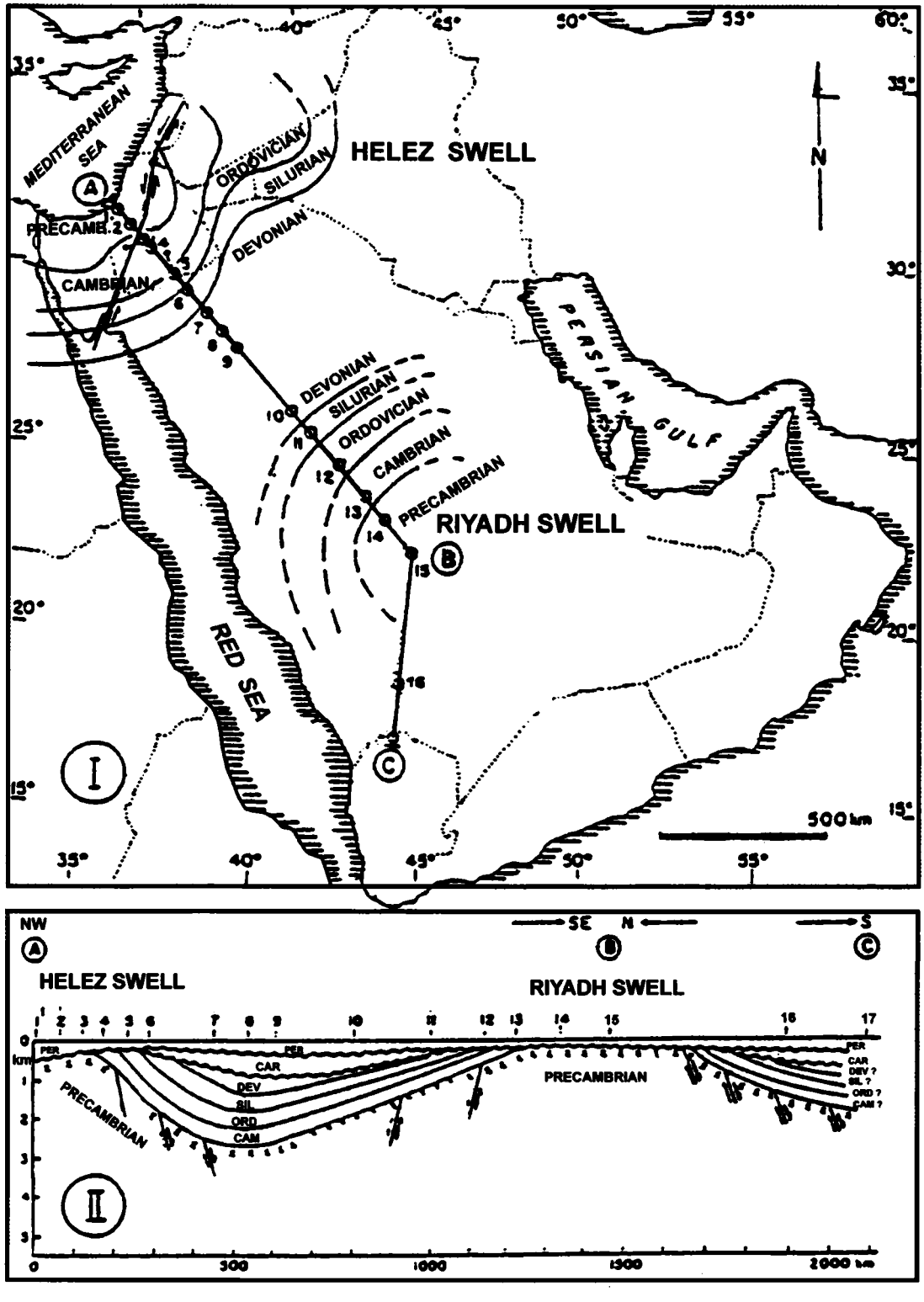


Fig. 21.2. I) Schematic outline of the Heletz and Riyadh swells on the reconstructed sub-Permian erosion surface (from Weissbrod and Gvirtzman, 1989). II) Schematic stratigraphic section across the Heletz and Riyadh swells (data points are projected).

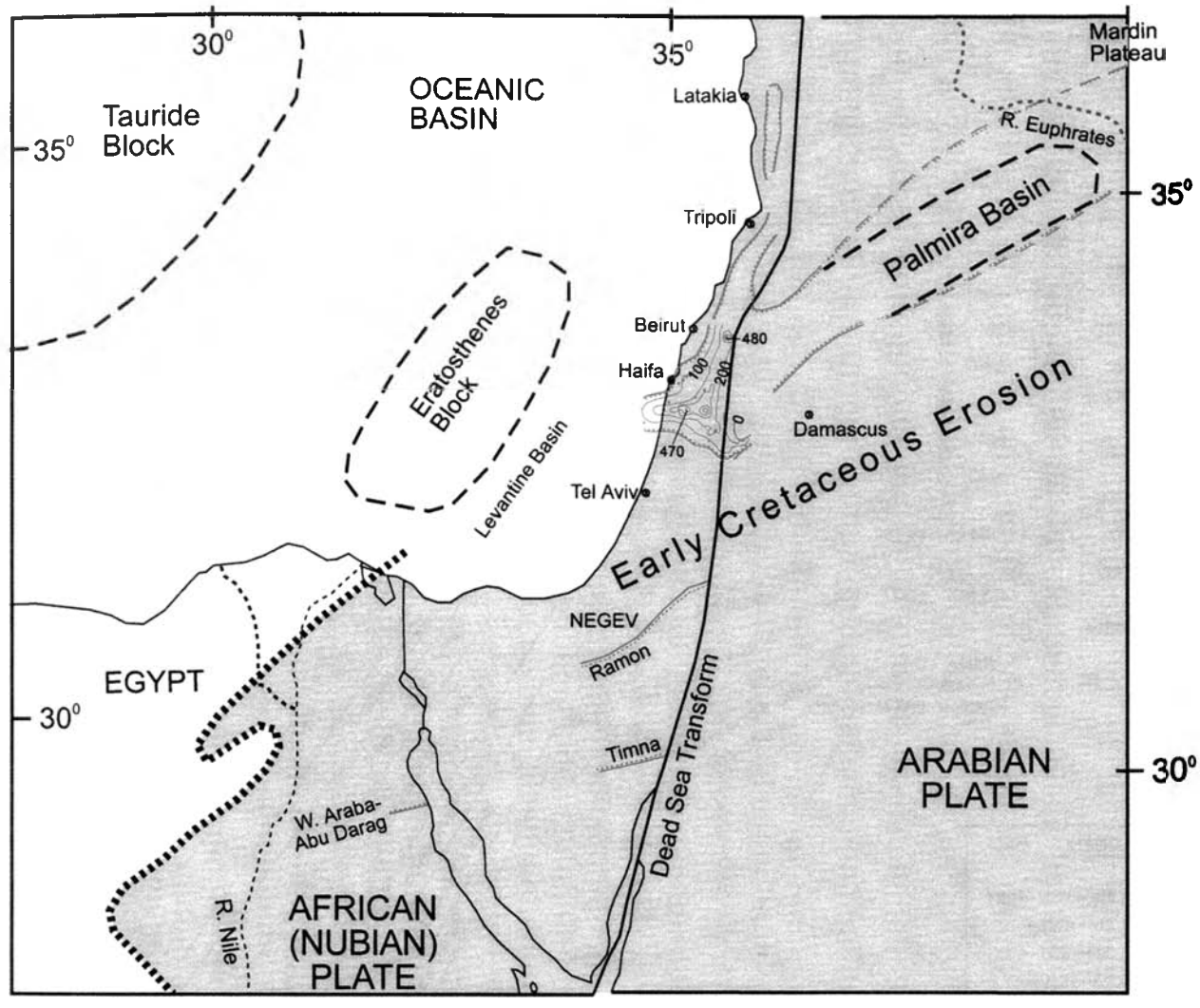


Fig. 21.3. Location map of the Early Cretaceous magmatic rocks in the Levant after restoration of the Arabian Plate to its pre-strike-slip location. The isopach map of Tayasir volcanics is after Katz and Eppelbaum (1999). Information about Lebanon from Mouty et al. (1992), and about Israel from Garfunkel (1989). The Early Cretaceous erosion in Egypt is after Said (1990).

several researchers:

a) Segev (1986) and Segev et al. (1985, 1995) dated illite clays hosted by the Early-Middle Cambrian Timna Formation to 365-381 Ma, using K/Ar and Rb/Sr methods. They suggested thermal resetting of both isotope systematics at their maximal burial depth;

b) Kohn et al. (1992) measured fission-tracks on zircons from Late Precambrian-Cambrian host formations and suggested an age range of 330-375 Ma;

c) Heimann et al. (1995) dated biotites from Precambrian schistose dikes by the $^{40}Ar/^{39}Ar$ method. Three plateau ages yielded an average age of 378 Ma, which they interpreted as a reset age during hydrothermal conditions below, but close to, the biotite closure temperature.

Although in Israel this event caused only updoming and high heat flow, in NE Africa a few magmatic complexes were dated, but these results must be taken with reservation. Microgranite dikes (363-343 Ma) are described from north and central Libya (Massa, 1988). An alkaline complex in the southern Eastern Desert of Egypt is K/Ar dated to 351±7 Ma (Serencsits et al., 1981). The Rb/Sr age of alkaline complexes from Sabaloka in Sudan varies between 357 and 339 Ma (Cavanagh, 1979; Harris et al., 1983) and a ring complex from the Bayuda Desert in Sudan is Rb/Sr dated to 332±34 Ma (Barth et al., 1983). On the Arabian plate dolerites and ignimbrites are described from western Oman (~350 and 340 Ma; Qidwai et al., 1988).

The Late Devonian event, which is represented by a few regional swells over the Arabian and North African plates, is contemporaneous with the Variscan (Hercynian) orogeny at

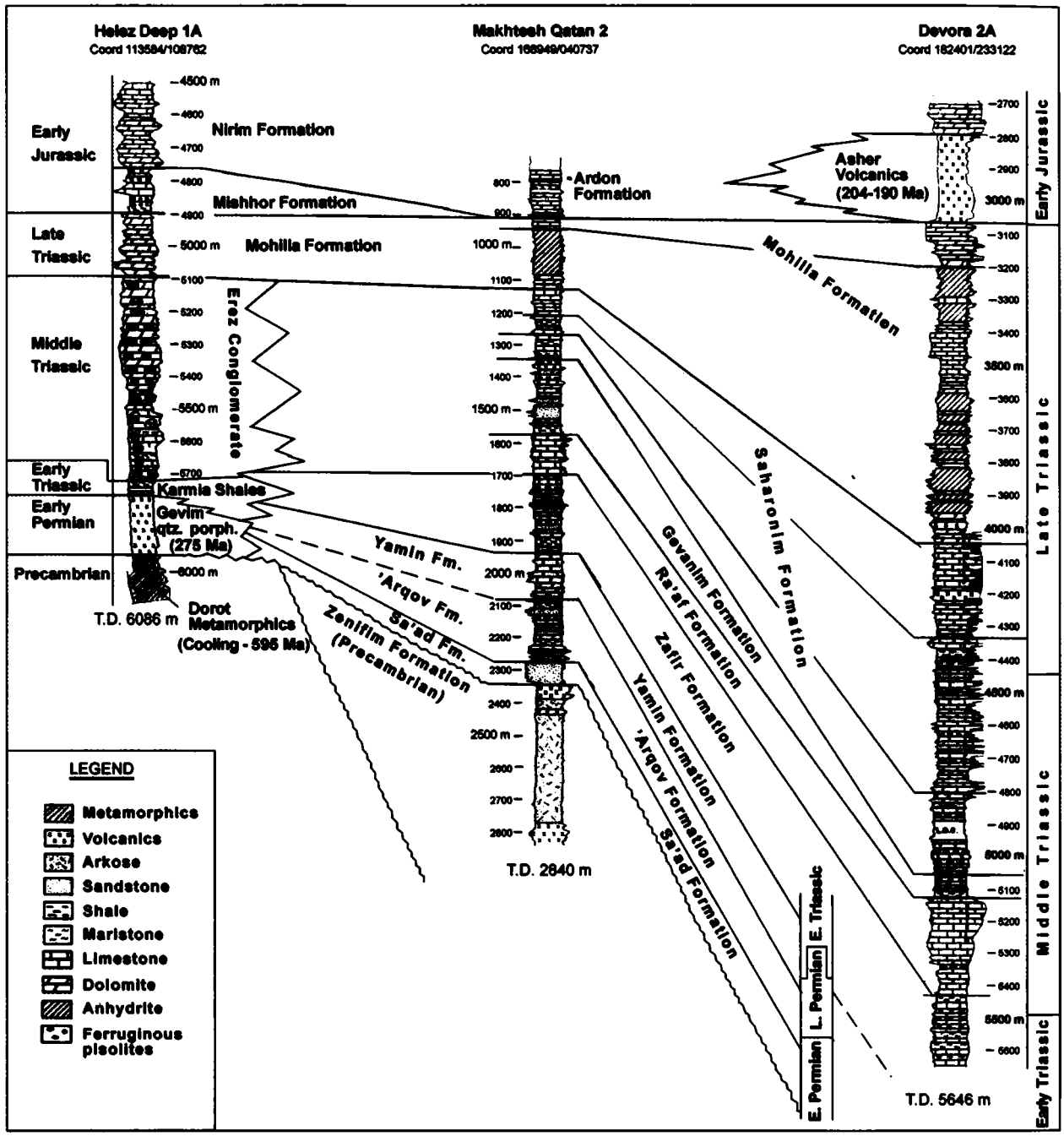


Fig. 21.4. Stratigraphic correlation of typical pre-Jurassic sections in southern and northern Israel (after Druckman and Kashai, 1981). Note the 600 m thick Erez Conglomerate of Early Middle Triassic age and the underlying ~200 m thick Gevim quartz porphyry.

the time of welding between Gondwana and Laurasia and the formation of the Pangea super continent. These Paleozoic swells are thermal updomings as a result of weak and relatively small mantle plumes that did not reach the stages of trap volcanism, rifting, and continental breakup (Segev, 2000a).

Permo-Triassic magmatism

Doblas et al. (1998) reviewed the Permo-Triassic igneous activity in Europe and enlarged this province toward northwest Africa (European - northwest African province - EUNWA). By suggesting super-plume activity in this province, the latter authors followed

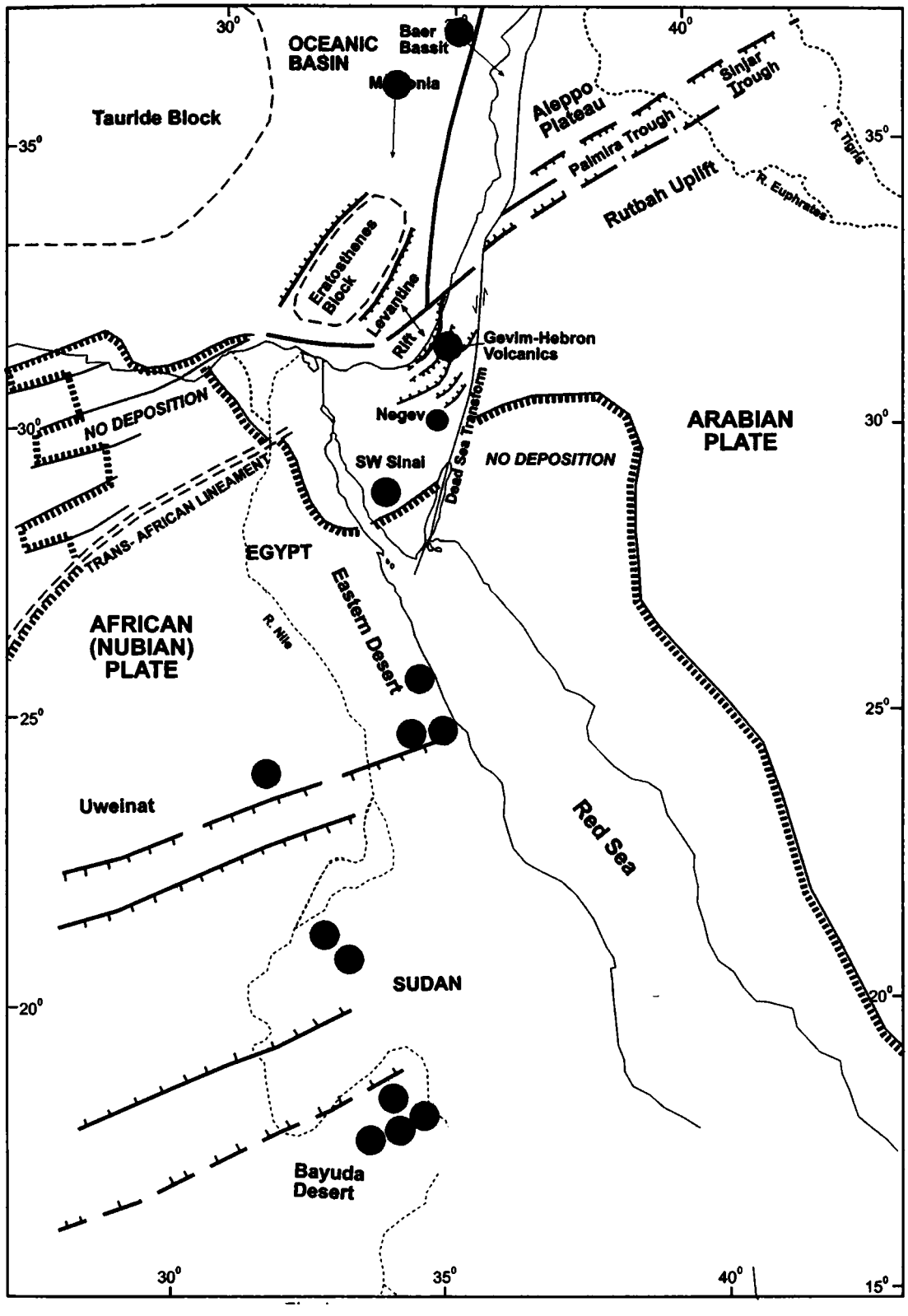


Fig. 21.5. Location map of magmatic rocks, main structures and general paleogeography in the Permo-Triassic times (sources: Keeley and Massoud, 1998; Garfunkel, 1998; Brew et al., 2000; Segev 2000b). Location of allochthonous complexes shown schematically (thin arrows indicate their present position).

the mantle uprising hypotheses of Lorenz and Nicholls (1976) and Ziegler (1990). Segev (2000b) suggested the continuation of this province toward the southeast, including the Levant and NE Africa areas. Major uplifting, rifting and magmatism affected this area, which is situated at the southeast edge of the EUNWA province. The main extensional process in this direction caused northward drifting of the Cimmeride micro-continent (Şengör et al., 1984; Guiraud, 1998) by the opening of the Permo-Triassic Neotethys. During this period, the Levant and the western Eratosthenes and Tauride blocks were affected by uplift, rifting, and magmatism, and the eastern side of Arabia was rifted and developed as a new passive margin (see review by Garfunkel, 1998).

In most parts of Israel, the stratigraphic sequence starts with the Early Permian rocks, which indicates pre-Early Permian major events of uplift and erosion (Weissbrod, 1981). The rock units from this period are mainly known from the subsurface but the extent of magmatism from this period is unknown. The Hebron magnetic anomaly, which is the largest in central Israel, has been interpreted as representing a large (extending ~150 km in an E-W direction) basic magmatic body penetrating the Permian and Triassic formations at a depth of ~3.5-4 km below sea level in this area (Rybakov et al., 1995). The previous alternative model (Folkman and Bein, 1978) suggested that the crystalline basement is elevated to the same depth as the magnetic causative body and has more or less similar magnetic properties. According to Rybakov et al. (1995) the structural maps, seismic reflection lines and oil-well data show a gradual northward thickening of the Jurassic and Triassic strata without any evidence of an existing basement high in the area. Moreover, the Hebron causative body has high magnetic susceptibility (about 0.005 cgs) and low average density (about 2.55 g/cm^3) which is in accord with basic volcanic rocks (Rybakov et al., 1995), mainly tuff. The latter authors suggested an Early Jurassic volcanic causative body, similar to the Asher volcanics in the Carmel, northern Israel, although their best-fit model (**Figure 21.3**) shows a complete Jurassic sequence and a magnetic body within Triassic and Paleozoic strata. It is therefore suggested to accept the best-fit model of Rybakov, Fleisher and Goldshmidt (1995), which shows that these volcanics are at the same elevation ('penetrating') as the Permian and Triassic formations (~3.5-4 km below sea level). However, it is suggested that these basic volcanics belong to a Permo-Triassic volcanic event contemporaneous to its host formations.

West of the Hebron magnetic body, in the Heletz Deep-1A borehole, a ~200 m quartz porphyry unit (Gevim Volcanics) overlies the Precambrian Dorot schist (Druckman, 1984) (**Figure 21.4**). Rb/Sr age determination of the Gevim volcanic rocks yielded a three point isochron age of 275±47 Ma (Segev and Eshet, 2004, after Steinitz, 1980). The overlying Karmia Shale, which is related by palynomorphs to an Early Triassic (Scythian) age (Segev and Eshet, 2004), supports this Rb/Sr age.

Several unreliable K/Ar measurements of mafic rocks from wells in the Negev yielded dates between 250 to 288 Ma (Recanati et al., 1989). A few unpublished $^{40}Ar/^{39}Ar$ dates of exposed basaltic sills within a Carboniferous clastic succession from southwestern Sinai show a wide range of mainly Permian ages (274±4, 266±4 and 240±4 Ma; Steinitz et al., 1992). Coeval and younger (245-215 Ma) regional heating of the lithosphere is suggested by fission track ages of apatites and sphenes within Precambrian basement rocks (Kohn and Eyal, 1981). Geochemical investigation of these Permo-Triassic igneous rocks in Israel has not been done yet.

In the northern Levant general geological evidence also indicates Triassic magmatism. At the Palmyrides (**Figure 21.5**) Searle (1994) reported the occurrence of a thin early Carnian volcanic horizon. The Mamonia Complex in SW Cyprus contains Triassic lavas (Robertson and Xenophontos, 1993), and probably similar rocks are exposed in the allochthonous Baer-Bassit in NW Syria (*e.g.* Robertson, 1990). More than 80% of the Mamonia volcanic rocks are mid-ocean ridge basalt (MORB)-like tholeiitic pillow lavas. The remaining volcanics are mainly alkaline basalts, which may have formed as oceanic island basalt. This extension-related volcanism in small ocean basins northeast of the Levant may represent the initial stages of opening of the Neo-Tethys ocean (Stampfli, 1996).

Farther to the southwest of the Levant area, in NE Africa, intraplate alkaline complexes associated with local and regional uplifts developed over large areas. Cahen et al. (1984) and Massa and Delort (1984) reported granite dated at 256 Ma, granodiorite at 230 Ma from the Uaddan horst, and basalts (251 Ma) and microsyenite sills (245 Ma) from the Amal horst, both in northern Libya. Meneisy (1990) reported basalts dated at 235±5 Ma (K/Ar date) in the Uweinat region, and Franz et al. (1987) reported volcanism at 233±5 Ma in the nearby Gebel Kamil area. In the central and southern Eastern Desert of Egypt Sayyah et al. (1978, in Meneisy, 1990) dated magmatic bodies at 290±15 Ma (an average Rb/Sr isochron age); 273±15 and 245±15 Ma (Rb/Sr isochron ages, reviewed by Meneisy, 1990). In the Bayuda Desert of northeastern Sudan Barth et al. (1983) and Höhndorf et al. (1994) reported intrusive activity at 240-236 Ma (Rb/Sr ages), and in the Nubian Desert of Sudan at 257-250 Ma. In the Nuba Mountains of central Sudan the magmatic activity was at 251-238 Ma (Rb/Sr ages; Curtis and Lenz, 1985), and in the Darfur province of western Sudan 243±10 Ma (K/Ar date, Vail and Rex, 1971). On the basis of these Rb/Sr isochron ages Höhndorf et al. (1994) concluded that the peak of magmatic activity in NE Africa was between 270 and 220 Ma.

The wide spread of the radiometric (Rb/Sr and K/Ar) dates, as well as insufficient spatial information, enable only a general estimation of the Permo-Triassic igneous activity in the Levant area, which had a very important influence on the initial architecture of the Levantine continental margin and its sedimentary cover.

JURASSIC MAGMATIC PERIOD

Early Jurassic (J_1) magmatic event (Hettangian- Pliensbachian – Asher Volcanics)

Regional erosion of upper Triassic units and the absence of Early Jurassic sedimentary rocks in Israel, Sinai, Egypt, and Libya (Conway, 1990; Keeley and Massoud, 1998) indicate major uplift

and denudation of the Arabian-Nubian area (**Figure 21.6**). Similar evidence was also reported from the Tauride block (*e.g.* Monod and Akay, 1984). Furthermore, Lower Jurassic faulting (Garfunkel and Derin, 1984) accompanied by alkaline magmatism (Bonen, 1980; Kohn et al., 1993) is known mainly from northern Israel boreholes.

Bonen (1980) reviewed and summarized the distribution of these basal Jurassic volcanics, from their 60 m thickness in the southern Mount Hermon (Arna crater, after Dubertret, 1955; Razvalyaev, 1966; Mouty, 2000), to 272 m thickness in the Devorah-2A borehole; +200 m in the Asher-2/Yagur-1 borehole; to 2499 m thickness in the Atlit-1 borehole. Gvirtzman et al. (1990) interpreted magnetic and gravity data, and proposed that the Asher Volcanics form a large buried shield volcano below Mount Carmel. Northeast of the Carmel the basalts erupted in shallow lagoonal environments (Bonen, 1980), and partially sub-marine in places (Mt. Hermon, after Razvalyaev, 1966). The alkali olivine basalts of this volcanism fall within the broad normative tholeiitic category and have trace-element patterns of transitional types with typical enrichment of incompatible elements and an enriched LREE pattern (Bonen, 1980).

In the Negev area (En Saharonim, eastern Makhtesh Ramon, coord. 1441/0022), small shallow basaltic sills (Saharonim basalts) intrude gypsum layers of the Late Triassic Mohilla Formation ~30 m below its top. Segev et al. (1996) interpreted magnetic and gravity data, and suggested that a coexisting shallow mafic intrusion (5×6 km horizontal dimensions) lies ~500 m below these sills.

The Saharonim basaltic sills were $^{40}Ar/^{39}Ar$ dated by Baer et al. (1995) to 210±2 Ma and recently reinterpreted by Segev and Lang (unpublished data) to 204±2 Ma, which represents the age of the initial basal (Asher) Jurassic igneous activity. Less reliable $^{40}Ar/^{39}Ar$ ages for the Atlit-1 borehole yielded 206±4 Ma (Kohn, et al., 1993). Three correlative samples from 200 m thick alkali olivine basalts at the bottom of the Yagur-1 borehole yielded a similar K/Ar average age of 200±5 Ma. A slightly younger phase in the Atlit-1 borehole yielded 190±3 Ma (Segev, 2000a, after Kohn, et al., 1993).

Late Jurassic (J_2) magmatic event (Callovian-Oxfordian – Devorah-Bhannes volcanics)

Less intensive and less defined is the Late Jurassic (Callovian-Oxfordian) volcanic activity in the subsurface of northern Israel (Devorah volcanics), and outcrops in northern Lebanon (Bhannes volcanic complex, Dubertret, 1975). Dubertret (1975) described a 180 m thick volcanic sequence consisting of basaltic flows and weathered pillows, volcanic tuff and cinerites (volcanic ash deposited in an aqueous environment) interfingered by marl, limestone and lignitiferous rocks.

In the Devorah-1 and Devorah-2A boreholes, which are 130 m apart, a different complicated volcanic sequence is open to controversial interpretations. The upper ~200 m of volcanic tuffs with minor basalts and sandstone intercalations are of Early Cretaceous age (Bonen, 1980) and are discussed below. The lower volcanic interval (between 965 and 1190 m) is less certain but, based on petrographic evidence, Bonen (1980) proposed a single Early Cretaceous diatreme that hosted Jurassic limestone xenoliths. Low quality K/Ar dates and chemical determinations for these volcanic intervals, as well as correlation with the Atlit-1 borehole, led Lang and Steinitz (1987) to suggest a magmatic phase between 160 and 150 Ma. These magmatic rocks consist of high-alkali (Na-rich) small intrusives with petrochemical features different from those of the older (Early Jurassic) and younger (Early Cretaceous) basalts. The correlative spillitized (comprising mainly albite) quartz keratophyre (Dvorkin and Kohn, 1989) from the Atlit-1 borehole yielded a $^{40}Ar/^{39}Ar$ reset age of 161.0±2.2 Ma (Segev, 2000a, after Kohn et al., 1993).

In the offshore Delta-1 borehole northwest of Caesarea, volcanic fragments are interbedded with Oxfordian pebbles derived from the shelf edge and transported by turbidity currents (Friedman et al., 1971). These poorly studied volcanics also support the existence of a Late Jurassic volcanic event in the Levant area.

In northern Libya, basalt dated at 164 Ma, and rhyolite (161 Ma) and microsyenite (159 Ma) magmatism are known from the Uaddan and Amal horsts, and are coeval with rhyolite (160 Ma) from the Zelten horst (Cahen et al., 1984; Massa and Delort, 1984). Correlative basic magmatic rocks (~165 Ma) have also been found in boreholes in the northern part of the Western Desert of Egypt (Keeley and Wallis, 1991).

Bonen (1980) as well as Laws and Wilson (1997) grouped together the Callovian-Oxfordian Devorah-Bhannes volcanics and the Early Cretaceous Tayasir Volcanics. It is herein suggested that these two magmatic events be defined separately.

CRETACEOUS MAGMATIC

Early Cretaceous (C_1) magmatic event (Valanginian – Tayasir volcanics)

Many deep boreholes in northern Israel (Hula-2; Rosh Pinna-1; Hazon-1; Devorah-1, 2A; Sarid-1; Carmel-1; Asher-1; Haifa Bay-1; Delta-1; Har Amir-1 and Caesarea-1) penetrated volcanic rocks located between the marine Jurassic units and the continental early Cretaceous rocks (Mimran, 1972; Bonen, 1980). Only two outcrops of these volcanics are known in Israel, one in the Mount Hermon area (Shimron and Pelz, 1993; Shimron, 1998) and the other near Wadi El Malih, in northeast Samaria (Mimran, 1972).

The thickness of the Tayasir volcanics, which are mainly extrusive and effusive sequences, varies between a few meters and 480 m (Mimran, 1972). Katz and Eppelbaum (1999) constructed an isopach map for the Tayasir volcanics from Natanya to southern Lebanon (~70 km long, Fig. 21.3). Within Lebanon these volcanics extended over ~150 km (Dubertret, 1963; Roberts, 1971; Mouty et al., 1992).

Early Cretaceous basalt flows cover a wide area in the Mardin Plateau and Palmyrides of Syria, and within the margins of the Euphrates graben in Iraq (Wilson and Guiraud, 1998).

In central Israel fresh tuffaceous (~30%) sandstone is reported from the Heletz area at the base of the Valanginian Heletz Formation ('Kochav B sand') (Shenhav, 1971).

In southern Israel, in Makhtesh Ramon, exposed intrusive bodies, such as the complex gabbroic laccolith within a Triassic gypsum unit and the Nahal Ardon dikes within Triassic and Jurassic sedimentary rocks, represent this event (Garfunkel, 1989; Teutsch et al., 1996). The source of the latter dikes, ranging from olivine basalt to trachyte, is probably the subsurface Hare Govay intrusion (Baer, 1989; Segev et al., 1996) south of eastern Makhtesh Ramon.

Magmatism is reported from two localities in the northern Eastern Desert of Egypt (reviewed by Meneisy, 1990). In Wadi Araba mainly nepheline-bearing dikes and plugs and pyroclastic rocks cut the upper Paleozoic sedimentary succession. In the Abu Darag area olivine basalt, andesitic basalt and rhyolite were found at several localities. The wide range of two K/Ar minimum dates (126±4 - 116±3 Ma, Meneisy and Kreuzer, 1974) may indicate that some of these volcanics could have been active since the first Early Cretaceous magmatism. In some of the Libyan Sirt troughs and rift shoulders Cahen et al. (1984), Massa (1988) and Rossi et al. (1992) have reported granite intrusions (152-122 Ma) and basic-intermediate volcanic rocks (148-127 Ma).

Early Cretaceous extrusive and intrusive rocks exposed in Israel and the adjacent countries stimulated several detailed geochemical studies. In Israel these rocks are mainly sub-alkaline to alkaline basalts together with nephelinites, basanites and micro-gabbros (Bonen, 1980; Stein and Hofmann, 1992; Laws and Wilson, 1997). All these rocks are enriched in incompatible elements (*e.g.* LREE) and are related to hot spots (Garfunkel, 1989) or to a mantle plume (Stein and Hofmann, 1992, 1994). The presence of lower crustal and lithospheric mantle xenoliths in these volcanics (Stein and Katz, 1989; Sharkov et al., 1994) suggests rapid ascent of the magmas from their mantle source with minimal residence times in the upper crust (Laws and Wilson, 1997). They also mentioned that the Sr-Nd isotopic compositions are similar to HIMU (high $^{238}U/^{204}Pb$ [μ] end member, which is thought to be derived from ancient recycled subducted basaltic oceanic crust) Oceanic Island Basalts. The limited Pb isotope data available also have a HIMU composition (Stein and Hofmann, 1992). This composition, suggesting an enriched mantle source, results from a plume (Stein and Hofmann, 1992; Laws and Wilson, 1997).

Limited reliable $^{40}Ar/^{39}Ar$ ages for the beginning of this magmatic event were obtained for the Nahal Ardon dikes (137.7±0.2 Ma, Teutsch et al., 1996), and for the Ramon laccolith in southern Israel (139.2±5.7 Ma; reinterpretation of data from Lang and Steinitz, 1994). A similar age (137 Ma) has been reported for correlative volcanic rocks from Mount Hermon or Lebanon (Laws and Rex unpubl. data, in Laws and Wilson, 1997). The upper lava flow at Mount Hermon has been recently $^{40}Ar/^{39}Ar$ dated to 133±1 Ma (Segev, 2002). An additional $^{40}Ar/^{39}Ar$ reset (cooling) age of whole rock basalt affected by prehenite-pumpelyte metamorphic facies in Atlit-1 borehole, Carmel area, yielded an age of 132.0±1.9 Ma (Segev, 2000a, after Kohn et al., 1993). More reliable ages are needed to determine the final age of the C_1 event.

A regional updoming, several hundreds of kilometers wide, occurred from Lebanon and Syria to eastern Egypt and Sudan (Garfunkel, 1989; Said, 1990; Reynolds et al., 1997). At this initial stage the maximum uplift probably took place in northern Israel and nearby areas, where the Tayasir volcanics erupted. Later on, deep erosion (about 1 km) toward the east and the south truncated the upper Jurassic and older formations (Garfunkel and Derin, 1988; Garfunkel, 1989).

Early Cretaceous (C_2) magmatic event (Barremian – Shen Ramon magmatism)

Reliable radiometric ages made it possible to define this event. Segev (2000a) suggested that the exposed Shen Ramon and Gavnunim complex syenitic-trachytic intrusions represent this event in southern Israel. He obtained two identical best-estimate $^{40}Ar/^{39}Ar$ ages from Lang and Steinitz (1994):

a) whole rock quartz syenite from Gavnunim yielded an age of 124.4±1.3 Ma; and

b) whole rock trachytic dike cutting the laccolith yielded an age of 124.9±1.2 Ma. In addition, two Rb-Sr isochrons (from Lang et al., 1988) yielded similar ages of 123±9 Ma (for the Har Arif intrusion) and 124±13 Ma (for Gavnunim). One reliable K/Ar isochron of six adularia separates from metallic veins cutting the Gavnunim body (Itamar and Steinitz, 1988) yielded a similar age of 125±2 Ma. All these close radiometric measurements suggest that the time interval of phase C_2, namely 125-123 Ma, is accurate.

The Gavnunim bodies were interpreted by Segev et al. (1996) as representing a transition from shallow subvolcanic to subaerial conditions. Similarly, Itamar et al. (1998) described multi-phase activity in the Shen Ramon body, from emplacement of quartz syenite intrusion through propyllitic and argillitic alteration up to explosions along fissures and vents. Garfunkel and Katz (1967) suggested a few vents of trachy-basalt and pyroclastics with quartz-syenite xenoliths that erupted before most of the erosion took place. Therefore it should belong to this post emplacement stage of the quartz-syenite bodies.

The several hundred meters thick Early Cretaceous volcanic succession in northern Israel (Fig. 21.3) has not yet been dated; it is possible that it comprises a continuity of both, the first (C_1) and the second (C_2) magmatic events.

In the Coastal Range of Lebanon, near Bloudance and in Wadi Al Karn in the Anti-Lebanon, Mouty et al., (1992; Fig. 21.4) described and dated ~30 m of volcanics overlying ~40 m of mainly sandstone. The samples from Bloudance yielded K/Ar dates of 124.0±2.6, 125.0±2.7, 127.5±2.9 Ma; those from Machta près de Kafroun 126.2±2.7 Ma, and from Massiaf, 125.0±3.1 Ma. Barremian-Aptian limestones overlie these volcanic units (Mouty et al., 1992). The presence of Early Cretaceous sedimentary rocks below these volcanics, as well as the K/Ar dates averaging 125±2.8 Ma, strongly suggest that these volcanics belong to the C_2 magmatic event.

Twenty three volcanic pipes filled by kimberlitic rocks within Jurassic limestones were found on the Coastal Ridge (Jebel Ansariye) of Syria and K/Ar dated by Sharkov et al. (1989). Five of six samples yielded dates between 127±3 and 120±5 Ma; one sample yielded 113±4.5 Ma.

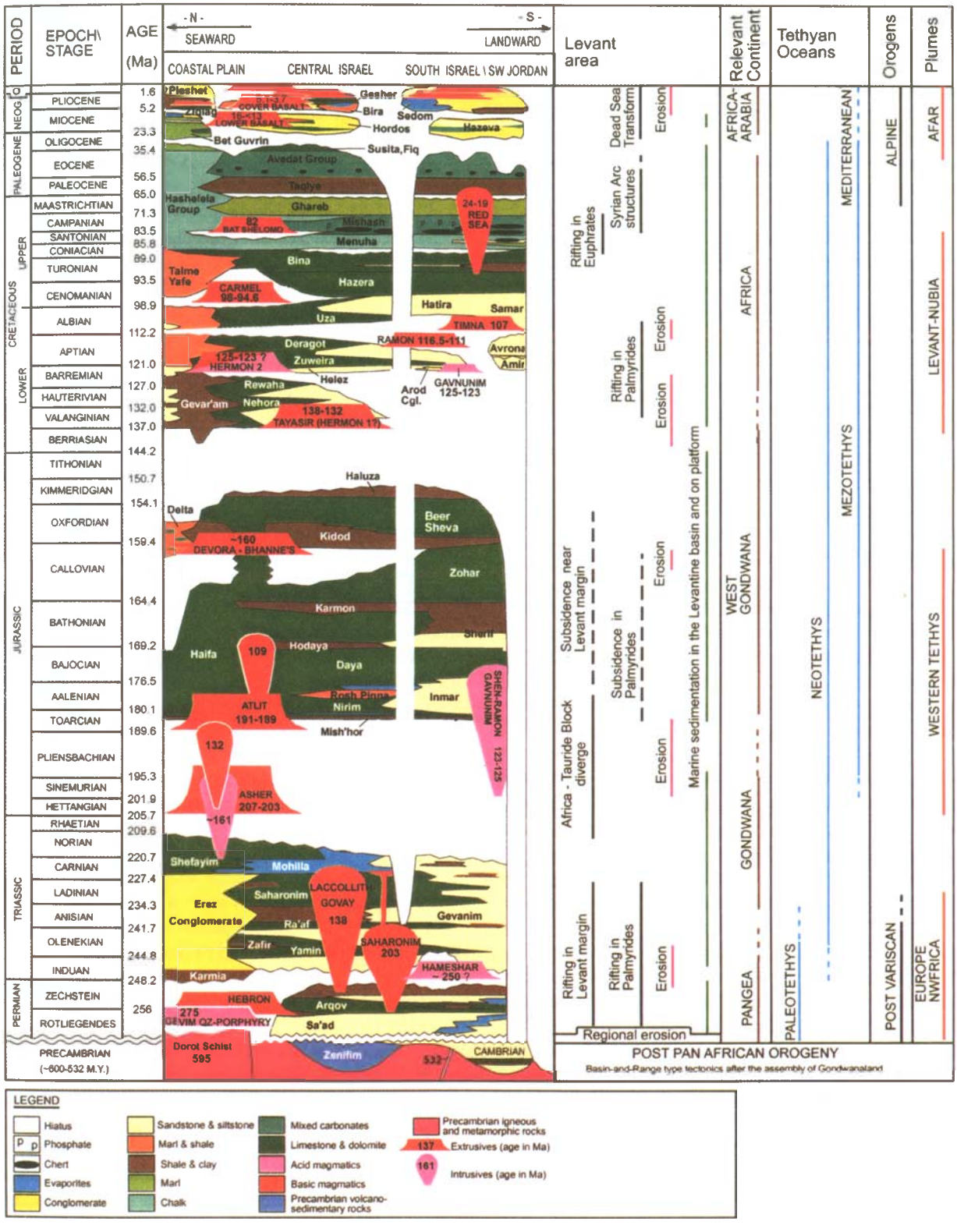


Fig. 21.6. Generalized chronostratigraphic chart of Israel showing the cycles of sedimentation, erosion and magmatism (the reliable radiometric ages reviewed in Segev, 2000a), alongside summary chart showing the evolution of geological events in the Levant region, over Gondwana and the Tethyan oceans.

The regional uplifting of the Levant, which started during the C_1 magmatic event, continued along with this magmatic event, probably through local swells such as the Arif-Meshar swell in the central Negev (Gvirtzman and Garfunkel, 1998). Segev et al. (1994) reported the presence of C_2 (122-83 Ma, minimum K/Ar dates) trachytic and gabbroic pebbles within the sediments of the Arod Conglomerate, which is situated on the regional erosional unconformity and marks the subsidence and the beginning of Early Cretaceous sedimentation at about 118 Ma.

Early Cretaceous (C_3) magmatic event (Aptian-Albian – Ramon-Timna volcanics)

The most extensive exposures of volcanic rocks in the Negev are those in Makhtesh Ramon which have been thoroughly studied (*e.g.* Bentor, 1952; Garfunkel and Katz, 1967; Bonen, 1980; Lang et al., 1988; Ron and Baer, 1988; Garfunkel, 1989; Lang and Steinitz, 1989; Eyal et al., 1996; Segev et al., 1996). Volcanics of this phase are also exposed in Har Arif and Arif en-Naqa in a similar stratigraphic position.

The volcanic sequence in the western Makhtesh Ramon area, which overlies 55 m of Aptian sediments (Gvirtzman et al., 1996), reachs its maximal thickness of ~200 m there (Garfunkel and Katz, 1967). At Ma'ale Ramon the volcanics are 37 m thick and disappear in the easternmost part of Makhtesh Ramon.

Segev et al. (1996) interpreted gravity and magnetic data and suggested an elongated WSW-ENE trending 14×4 km intrusion at the western part of the erosion cirque (Arod), <500 m below the surface, and about 2 km thick. As a result of their volcanological study of Mount Arod, Eyal et al. (1996) described the dome structure around this volcano and suggested that it resulted from sub-volcanic intrusions during the late stage of the volcanic activity.

The Qarne Ramon hills and the basal flow at Har Arod consist of tephrite-basanite lava flows, whereas basanitic-nephelenitic lava flows and tuff deposits (in places, containing large kaersutite crystals), stocks, dikes and a diatreme form the upper part of the Har Arod volcano (Eyal et al., 1996). The latter authors interpret the Qarne Ramon lava flows as representing pre-Arod volcanic activity.

The reliable age of the basal basanitic flow of Qarne Ramon (116.5±1.5 Ma) defines the initiation of the basanitic volcanism in the western part of Makhtesh Ramon (Segev and Lang, unpublished data). The age of the upper basanite flow in Qarne Ramon, which contains the large kaersutite megacrysts, is interpreted from similar weighted average K/Ar ages of 14 kaersutite megacrysts as 113±1 Ma.

The Har Arod volcano (110.7±0.4 Ma; Segev and Lang, unpublished data after Lang and Steinitz, 1996) represents the youngest volcanic eruptions in western Makhtesh Ramon.

Farther to the south, Beyth and Segev (1983) described a small basaltic plug, intruded within Cambrian rocks in the northern Timna Valley (Fig. 21.3). Later, Weissbrod et al. (1990) described volcaniclastic sequences within Cambrian and Lower Cretaceous formations at four sites in the same area, interpreting them as phreatomagmatic phenomena, all associated with the same Lower Cretaceous intrusion. Segev et al. (1995) suggested the existence of an elongated (15 by 2 km), shallow, E-W trending, gabbroic intrusion (Har Mikhrot) at ~600 m depth and a second, parallel intrusion that may lie north of it. Three biotite xenocrysts from the volcaniclastic unit at northwestern Timna Valley (Tamar site) yielded similar well-defined reliable plateau ages with a weighted average of 107.5±07 Ma (Weissbrod et al., 2001; Segev and Lang, unpublished data).

The recent reliable geochronological evidence for the Ramon-Timna volcanism in southern Israel clearly defines a relatively long magmatic event between 116.5 Ma and 107.5 Ma. In northern Israel, a quartz keratophyre sample from a depth of 5057-5060 m in the Atlit-1 borehole yielded a best estimate $^{40}Ar/^{39}Ar$ age of 109.2±1.6 Ma (Segev, 2000a after data from Kohn et al., 1993). The spectrum of this sample (Kohn et al., 1993) and another quartz keratophyre sample represents thermal resetting of Early Jurassic rocks. This evidence points to a high heating event in northern Israel during the late Aptian to early Albian C_3 magmatic event.

In Wadi Natash, about 125 km E-NE of Aswan, 600 km^2 of volcanic rocks are exposed along the boundary between the Nubian sandstones and the Precambrian basement. El Ramly et al. (1971) report that this volcanic sequence started with olivine basalts followed by trachybasalts, latites, and trachytes. Hashad and El Reedy (1979) obtained a Rb/Sr age of 104±7 Ma. Because many of the Rb/Sr and K/Ar dates suffered from later alteration or heating, we should consider these dates as minimum ages. Therefore the Wadi Natash volcanics probably belong to the C_3 magmatic event. One olivine basalt from Wadi Abu Darag, in the northern Eastern Desert of Egypt (Fig. 21.3), yielded a K/Ar date of 116±3 Ma (Meneisy and Kreuzer, 1974), also supporting the possibility of volcanic activity during the C_3 event in this area. The trace element characteristics of these rocks led Moghazi et al. (1997) to suggest a pattern very similar to those of oceanic island basalts, in which the asthenosphere is the main source of these rocks and their compositional variation can be attributed to limited crystal fractionation. They also suggest that the less evolved trachytic magma represents the product of 60-70% fractional crystallization of an alkali olivine basaltic parent by a separation of olivine, clinopyroxene, plagioclase, and Fe-Ti-oxides.

Late Cretaceous (C_4) magmatic event (Cenomanian – Carmel volcanics)

The Late Cretaceous volcanic activity in Israel took place in the Mount Carmel-Umm El Fahm area. The dominant volcanic rocks are pyroclastics of basic composition, which in places contain basic and ultrabasic xenoliths and xenocrysts (or megacrysts) (Sass, 1980). Lava flows played a minor role in this volcanic activity. **Figure 21.7** (modified by Segev et al., 2002, from Sass and Bein, 1978) demonstrates the complex lithostratigraphic relationships of the Upper Cretaceous Judea and Talme Yafe host-groups in the Carmel area with correlation to the Umm el Fahm area. This volcanism took place in a shallow marine environment (Sass, 1980), with intimate contact with marine sediments containing

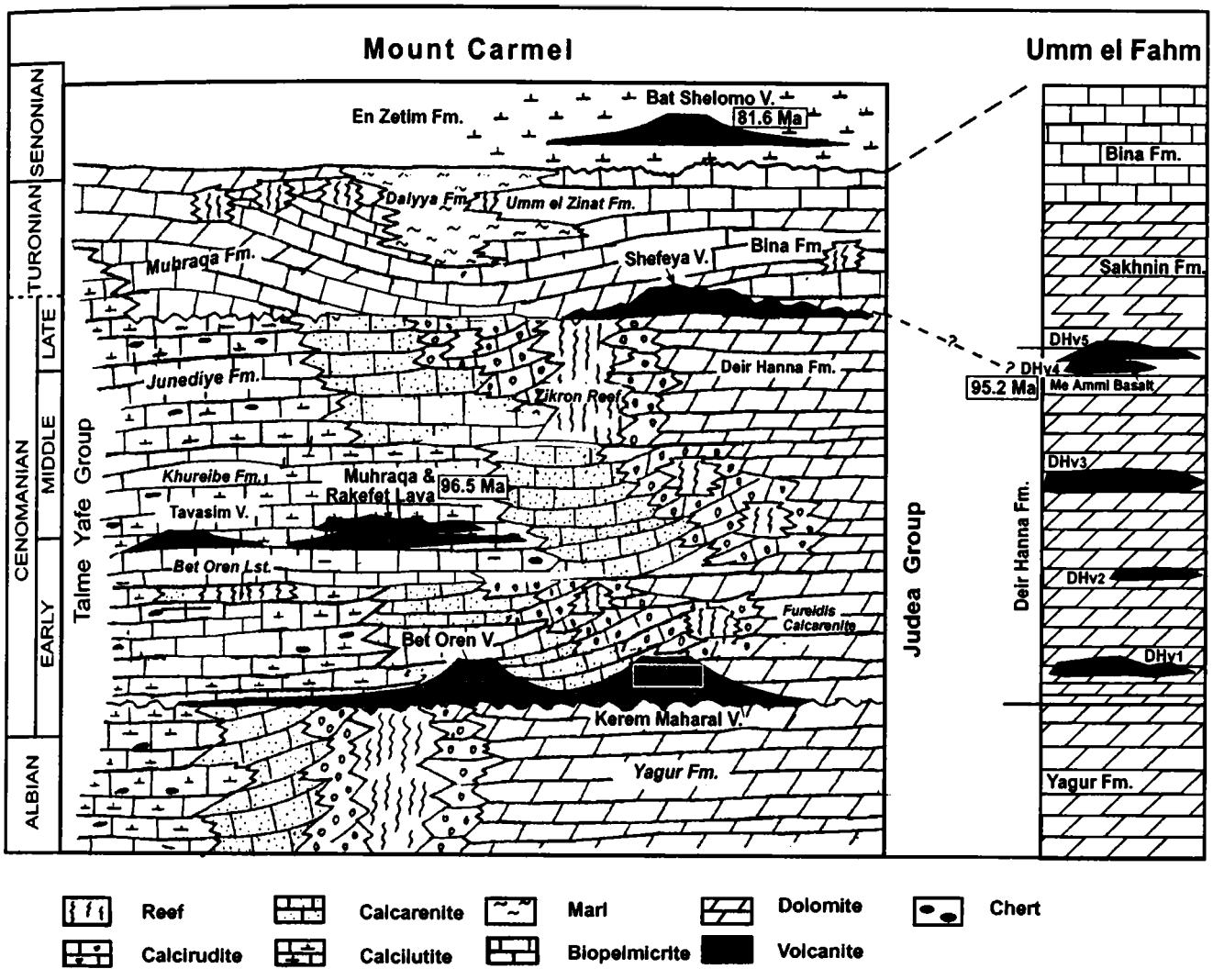


Fig. 21.7. Lithostratigraphic relationships of the Judea and Talme Yafe groups in the Carmel and Umm el Fahm regions (the Carmel modified after Bein and Sass, 1978; Cenomanian subdivision after Lipson-Benitah et al., 1997).

rich assemblages of fossils.

Several outcrops of black and variegated pyroclastics occur in isolated areas west of Kerem Maharal. These pyroclastics overly the Yagur Formation of Albian (see Bein, 1974; Rosenfeld and Raab, 1974; Lewy and Raab, 1978) to earliest Cenomanian age (Lewy, 1996) and represent the first volcanic eruption in the area. The pyroclastics contain xenoliths of garnet-bearing clino-pyroxenite, one of the rarest types of ultramafic inclusions associated with alkali basalts, and rare peridotite and olivine gabbro. Xenocrysts of augite, garnet, kaersutite, biotite and spinel are common and seem to have resulted from the disintegration of the xenoliths (Sass, 1980). Gottlieb (1980) classified the xenoliths as: (a) garnet clinopyroxenite; (b) garnet-plagioclase clino-pyroxenite; and (c) kaersutite-phlogopite clinopyroxenite. The latter author suggested that both garnet and garnet-plagioclase clinopyroxenite may have formed under pressures of 13 to 15 kb, at temperatures of 700°C for the plagioclase-bearing samples and 860°C for the plagioclase-free samples, at a depth of 40 km in the upper mantle. According to Segev et al., (2002) the $^{40}Ar/^{39}Ar$ age of the Kerem Maharal volcano, which represents the beginning of the C_4 event, is 96.9±0.6 Ma.

The Raqefet volcano includes three volcanic phases: the two older phases consist of pyroclastics while the youngest is represented by massive olivine basaltic flows totaling ~25 m thick (Sass, 1980). This unit was sampled and $^{40}Ar/^{39}Ar$ dated by Kolodny and Ron to 96.7±2.5 Ma (see Segev et al., 2002). The nearby Muhraqa lavas (~4 km east of Nahal Raqefet) represent a correlative unit of porphyritic olivine basalt. This unit was also

$^{40}Ar/^{39}Ar$ dated by Kolodny and Ron to 96.2±2.5 Ma (see Segev et al., 2002). The weighted average age of these two samples is 96.5±0.4 Ma.

The Me Ammi lava flow in the Umm El Fahm area (south of Mount Carmel) represents the upper volcanic unit (DHv4 of Sass, 1968) emplaced within the upper Deir Hanna Formation. One whole rock basalt from this flow (95.3±0.3 Ma) and two plagioclase fractions (93.9±2.2 and 95.0±2.0 Ma) yielded similar $^{40}Ar/^{39}Ar$ ages with weighted average age of 95.2±0.4 Ma for all these samples (Segev et al., 2002).

According to Bonen (1980) the petrological diversity of this magmatic event varies from olivine tholeiites through transitional basalt to alkali olivine basalt, and it is characterized by its marked explosive nature. The lack of Upper Cenomanian rock units in the Mount Carmel area (Lipson-Benitah et al., 1997) indicates local uplift of this area

Correlative volcanism is known from northern Lebanon and in the central Syrian Coastal Range, covering about 50 km^2 between Qadmous in the north and Marmarita in the south (Mouty et al., 1992). In the central Syrian Coastal Range the lava flow, which has a maximum thickness of 50 m, is an augite bearing basalt interbedded in a neritic limestone with an Upper Albian microfauna (Mouty and Saint-Marc, 1982). Eastwards it gradually thins out, and is replaced by volcano-detritic layers.

A few alkali ring complexes in the southern Eastern Desert of Egypt were K/Ar dated to Late Cretaceous. Meneisy and Kreuzer (1974a) K/Ar dated the nepheline syenites from Gabal Abu Khrug and Gabal el Naga at ~95 Ma, whereas Serencsits et al., (1981) obtained a minimum date of 90±2 Ma for Gabal Abu Khrug. Seven K/Ar measurements for umptekite and nepheline syenites from El Kahfa yielded a range of dates between 96±2 and 88±2 Ma (Serencsits et al., 1981), indicating an emplacement age around 96 Ma. These two ring complexes fall along a northwesterly trending lineament, implying tectonic control for their emplacement. El Shazly et al. (1973) report Rb/Sr ages around 90 Ma for granite bodies from the Abu Sawyel area.

Late Cretaceous (C_5) magmatic event (Senonian – Bat Shelomo volcanics)

The small Bat Shelomo (Mount Carmel) volcanic vent located close to the contact between the Menuha (Santonian-Lower Campanian) and Mishash (Campanian) Formations (Sass, 1980; Lewy, pers. comm. 1999) represents the last Cretaceous magmatic event in Israel. Sass (1980) described dark pyroclastic rocks, 30 m thick, containing ejecta of sedimentary blocks, volcanic bombs, xenoliths, and xenocrysts of hornblende. Segev et al. (2002) recently dated this volcano by $^{40}Ar/^{39}Ar$ at 81.6±0.8 Ma.

One $^{40}Ar/^{39}Ar$ best-estimate age of K-feldspar from a highly altered dike in Nahal Ardon, Makhtesh Ramon (Teutsch et al. 1996), yielded a similar age (83±1 Ma) that probably represents hydrothermal activity. A further indication for high heating that affected central Israel at the same time can be deduced from K-Ar dates for authigenic K-feldspars and illites from the Kokhav oil wells ranging from 94 to 77 Ma (Calvo, 1993).

Several K/Ar measurements for nepheline syenites from Gabal Abu Khrug and Gabal el Naga, southern Eastern Desert of Egypt, yielded ages around 83 Ma. In the Uweinat area, southern Western Desert K/Ar dates for olivine basalts from the Darb el-Arbain area are between 83±2 and 78±2 Ma (Meneisy and Kreuzer, 1974b). Although the K/Ar dates are not definitive they do point to a magmatic or thermal event that probably took place in NE Africa around 83 Ma.

SUMMARY

Although the timing of the Cretaceous magmatic cycles in the Levant are well constrained, the geodynamic processes are less known. According to the plume evolution scenario, we would expect to find evidence for a rift/drift zone that might have opened during this period. Such evidence has not yet been found, and explanations for the geodynamic processes in the Levant during the mid-Cretaceous may have derived from the major change of the plate tectonic regime when Africa and Eurasia began to converge. Even though the initiation of subduction in the Mesotethys is constrained by the 90-92 Ma age of the Troodos complex (Garfunkel, 1998), the decay of the lithospheric stretching probably began in the Early Cretaceous. Therefore, the coexisting thermal plume caused thinning of the lithosphere, regional uplift, melting within the crust, and rise of magmas to the surface, without successful rifting. The decay of the Cretaceous plume in northern Gondwana marks the end of the lower mantle upwelling along the Tethyan super-province (Fig. 21.1 and Segev, 2001).

Tertiary to Recent magmatic period

In the Levant area, which is located some 2000 km north of the Afar plume head, the magmatic activity was initiated during the Late Oligocene (~24 Ma, Sebai et al., 1991; Ilani et al., 2001). The Oligocene to Recent stratigraphy of Israel (Fig. 21.6) may represent a typical transitional zone between a deep sea (Levant basin) and a continental environment of deposition along the margins of an active igneous province caused by plume activity. The main characteristics for such a period are a deep hiatus, as a result of major uplift and denudation, followed by cycles of continental clastic (Hazeva, Hordos, Arava formations) and evaporite sedimentation (Sedom and Bira formations), alternating with volcanic rocks (Miocene, and Pliocene to Recent volcanism) coeval with the hiatus intervals. The marine sequences generally thicken northwestward, responding to cycles of mainly vertical movements, according to their position relative to local swells and basins, and depending on magmatic and fracturing episodes.

In the Levant area three magmatic events can be distinguished within the Tertiary and Quaternary time span.

Tertiary (T_1) magmatic event (Oligocene-Early Miocene – Red Sea magmatism)

Basaltic dikes and volcanic fields trending mainly northwest along the Red Sea and the Suez rift (**Figure 21.8**, *e.g.* Said, 1962; Blank, 1977; Garfunkel and Bartov, 1977; Eyal et al.,

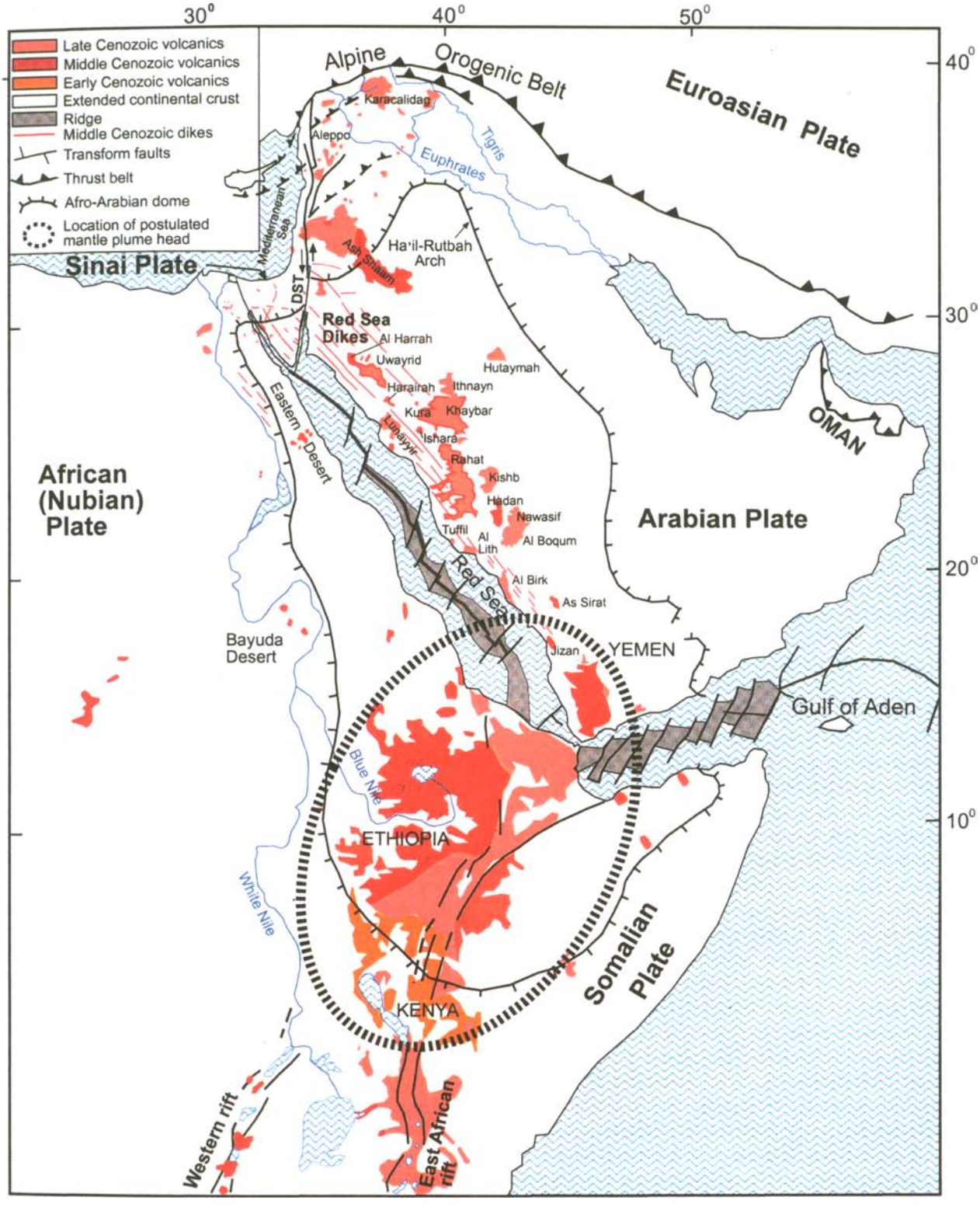


Fig. 21.8. Location of Early, Middle and Late Cenozoic volcanics of the Afar igneous province over the Afro-Arabian plates (after: Coleman et al., 1983; Giannerini et al., 1988; Garfunkel, 1989; Baldridge et al. 1991; Sebai et al., 1991; Camp and Roobol, 1992; Davison et al., 1994; Zumbo et al., 1995; Baker et al., 1996; Tarawneh et al., 2000), the area of the Afro-Arabian dome (hatched line, after Almond, 1986; Camp and Roobol, 1992) and the Afar mantle plume (*e.g.* Zeyen et al., 1997; Ebinger and Sleep, 1998).

1981; Garfunkel, 1989) extended on both sides of the Red Sea, but dominantly on the Arabian plate along its western margin (asymmetric magmatism), in a belt several hundred kilometers wide. From the El Birk area in the south to the Sinai in the north, a system of 10-100 m thick basic dikes follows the eastern coast of the Red Sea over ~1700 km. Some of them may be followed continuously over several tens of kilometers (Coleman et al., 1983). According to Coleman et al. (1983), in Saudi Arabia this magmatic activity produced:

a) alkali basalt volcanic fields (Harrats);

b) tholeiitic to transitional intrusive complexes (dense dike swarms and plutons); and

c) thick gabbroic dikes of tholeiitic affinity.

In southern and southeastern Sinai these dikes crop out in the Precambrian domain and in central and northern Sinai they are emplaced in a Phanerozoic domain, where they are associated with linear grabens and crypto-volcanic features (Baldrige et al., 1991). This magmatic system, which is represented in the Negev only by the Nahal Ashosh plug, dies out in the central Negev-central Sinai shear zone (Bartov, 1974). In southeast Sinai these dikes are offset by the left-lateral motion along the Dead Sea transform (Eyal et al., 1981), which shows that this motion lasted ~24 Ma or more.

The magmatic rocks are mainly tholeiitic to transitional lavas, and minor granophyres are also present (Camp and Roobol, 1992). Baldrige et al. (1991) infers that the basaltic dikes in Sinai equilibrate at a depth of 35-50 km, possibly within an enriched mantle.

According to reliable $^{40}Ar/^{39}Ar$ dating of mineral separates and whole rock samples from the Harrat Hadan lava flows and dikes, Sebai et al. (1991) determined early activity at 28-27 Ma and main activity during the younger (24-21 Ma) tholeiitic phase. They suggested that the dikes are the feeders of the lava flows.

The Harrat Ash Shaam volcanic field, the largest on the Arabian plate, covers ~50,000 km^2 in Saudi Arabia, Jordan, Syria and Israel (its northwestern edge ~1,500 km^2). Conventional K/Ar dating of whole rock basalts from this volcanic field in Jordan yielded a wider range of dates between 26 and 22 Ma (Ilani et al., 2001). This volcanism can be related to the 24-21 Ma phase, as obtained by the above-mentioned $^{40}Ar/^{39}Ar$ method for volcanic fields in Saudi Arabia. The northern part of the Harrat Ash Shaam volcanic field (Syrian area) is less eroded and thus exposes mostly younger volcanic units (Garfunkel, 1989). Five lava flows from western Syria (at Jebel-El-Kalb, Menkat-El-Khatab and 10 and 15 km south of Damascus) yielded K/Ar dates of 19.9±0.5 – 20.9±0.5 Ma (Sharkov et al., 1994). Several outcrops in the northwestern Syrian Coastal Range yielded K/Ar dates between 23.5±0.7 and 14.6±1.2 Ma (Mouty et al., 1992). This similar range of dates therefore indicates that the T_1 volcanism extended over the whole Harrat Ash Shaam volcanic field and even northwestward.

The southern Israel Nahal Ashosh plug, in the western Arava Valley, and central Sinai (Gebel Iktapa, Raqabat e Na'ame and Themed) doleritic dikes, sills and plugs intrude rocks of up to Middle Eocene age (Steinitz et al., 1978). Using conventional K/Ar dates Steinitz et al. (1978) obtained $^{40}Ar/^{36}Ar$ vs. $^{40}K/^{36}Ar$ isochron dates of: 20.7±2.2 Ma (N. Ashosh plug), 24.8±1.5 (Raqabat e Na'ame), and 20.3±0.7 (Gebel Iktapa), all in the range of the younger Red Sea magmatism between 24 and 21 Ma. Steen (1982) reported a similar range of conventional K/Ar dates for other dikes in Sinai: Gebel Araba (31±2 and 18±1 Ma), Wadi Nukhul (22±1 Ma), and Wadi Tayiba (21 Ma). Conventional K/Ar dating of basalts from the Western Desert, Red Sea area, and the Bahariya Oasis in Egypt also yielded a similar wide range of dates, mainly between 24 and 18 Ma (reviewed by Meneisy, 1990).

Based on fission-track dating, Omar and Steckler (1995) suggested two distinct pulses of uplift and rifting along the entire length of the Red Sea: the first between 35 and 30 Ma, and the second between 25 and 20 Ma. The uplift pulses caused the Eocene marine regression from most of the Arabian and African plates and the development of regional erosional conditions. The Oligocene and Early Miocene sequence in Israel (Fig. 21.6) is characterized by a sedimentary hiatus followed by cycles of continental clastic deposits (Hordos and Hazeva Formations), whereas the marine sequences generally thicken northwestward.

Both dating methods, radiometric and fission-track, indicate two tectono-magmatic episodes of uplift, rifting and magmatism along the Red Sea region, whereas seafloor spreading and MORB production along the Red Sea axial trough began at ~5 Ma (*e.g.* Coleman and McGuire, 1988; Altherr et al., 1990).

Tertiary (T_2) magmatic event (Middle Miocene – Lower Basalt volcanism)

The Middle Miocene volcanism (Lower Basalt Formation; after Schulman, 1962) in the Lower Galilee and the Yizre'el Valley (**Figure 21.9**) was studied by Bentor (1957), Oppenheim (1962), Schulman (1962), Shaliv and Steinitz (1988), Shaliv (1991), Shaliv et al. (1991) and Weinstein (1998).

Volcanic rocks of this event extended mainly in the southeastern Lower Galilee and the Yizre'el Valley, mainly within a northwest-trending morphotectonic extensional continental trough (rift), with E-W normal faults in its northern part (*e.g.* Matmon, 2000). Outcrops of these volcanics and small intrusions are distributed in a triangle between Mount Gilbo'a in the southeast, Qiryat Tiv'on in the northwest, and Teverya (Tiberias) in the northeast. Only a few lava flows occur east of the Dead Sea Transform, within the lower Hordos Formation, southwestern Golan area (Michelson, 1972; Shaliv, 1991). Shaliv (1991) calculated the present volume (~200 km^3) and an estimated original volume (~300 km^3) of basalts produced in this event, with a maximum thickness of 630 m (Gid'on-5 borehole) and ~650 m (Kokhav Hayarden outcrop and its nearby Belvoir-1 borehole) in the main volcanic centers.

On a regional scale, the SE-NW trending Yizre'el rift system is the northwestern continuation of the T_1 Harrat Ash Shaam tectono-magmatic system, as one of its rifts running from the Wadi Sirhan depression toward the Mediterranean Sea, displaced by the left-lateral motion along the Dead Sea Transform (Shaliv, 1991). This SE-NW direction is parallel to many Tertiary dikes, volcanic features, rifts and faults on the Arabian plate, dictated by the northeast horizontal extension stress field, which caused the opening of the Red Sea and the sinistral displacement along the Dead Sea

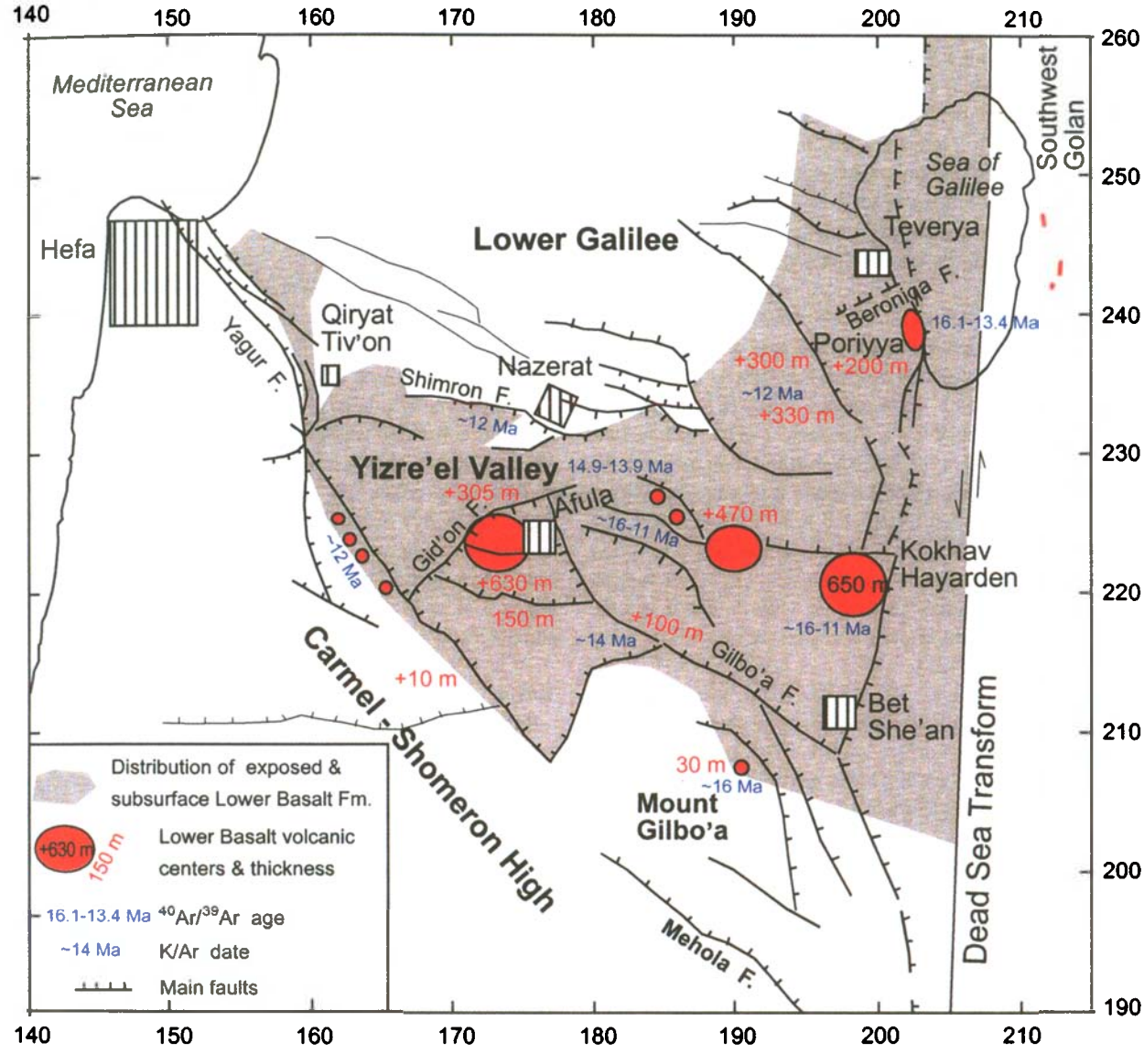


Fig. 21.9. Location of Early to Middle Miocene Lower Basalt volcanics in the Yizre'el Valley and the Lower Galilee, northern Israel. Distribution and thickness of the exposed and subsurface volcanic rocks is after Shaliv (1991). Ages after Shaliv (1991) and McWilliams and Ron in Segev (2000a).

Transform (Giannérini et al., 1988; Eyal, 1996). In the Tavor River vent the dikes show two semi-perpendicular sets, trending NW and NE, controlled by the regional stress field, in which σ_1 (maximum compressive stress) is vertical and σ_3 (minimum compressive stress) trends NE-SW (Baer and Agnon, 1995; Aharon, 1997).

The T_2 basalts are typified in their outcrops by their weathered appearance, whereas calcite and zeolite amygdules, as well as chlorite and limonite are common (Schulman, 1962). However, fresh basaltic flows are also found. Pyroclastic rocks within the Lower Basalt Formation have a limited distribution close to the eruptive centers in Poriyya (Bentor, 1946), Kokhav Hayarden (Schulman, 1962; Shaliv, 1991), Giv'at Hamore (Dicker, 1969) and the Tavor River (Aharon, 1997). Preliminary volcanological study of the Umm Sabune Formation clastics, which overlies the Lower Basalt Formation, led Shirav (Schwartz) et al. (1995) to suggest that this formation is a sequence in which intervals of volcanic debris flows are interbedded with normal fluvial sediments. Such volcaniclastic units are defined as typical syn-eruption sequences. Therefore the T_2 event terminated post deposition of the Umm Sabune Formation (Shirav (Schwartz) et al., 1995).

Weinstein (1998) studied in detail and established a comprehensive geochemical database for the Tertiary-Recent

volcanics of northern Israel. Beside the well-defined alkali-olivine-basalts (Oppenheim, 1962; Brenner, 1979) in the eastern Galilee he determined highly alkaline basanites and nephelinites in the Yizre'el Valley and Giv'at Hamore, which he interpreted to be younger. In his geochemical data processing Weinstein (1998) grouped together all the Neogene-Quaternary mafic rocks from Israel and compared them to equivalent rocks produced by the Afar plume. He found most of the samples to be relatively primary (Mg > 0.55), indicating fractionation of olivine and clinopyroxene. He suggested that the Israeli basalts are lithosphere-derived, having two principal sources:

a) amphibole-rich peridotite (N), which occurred during the Late Proterozoic when slab-derived fluids infiltrated and equilibrated with the recently created Arabian-Nubian lithosphere; and

b) amphibole-garnet-rich pyroxenitic veins (E) within the peridotitic source, produced by a Paleozoic (~370 Ma) within-lithosphere partial melting event. In the Neogene-Quaternary basalts from NE Jordan, Weinstein (1998) defined a mixing line with a Nb-depleted source (N_2) and interpreted it as a result of melting at a shallower lithospheric level. Further comparison with other Arabian and East African basalts led Weinstein (1998) to suggest two more lithospheric sources that mixed with N. These are the EM_1/EM_2 (Enriched Mantle, high Sr isotopes) and the HIMU (very radiogenic Pb: $^{206}Pb/^{204}Pb$ ~21).

Reliable $^{40}Ar/^{39}Ar$ ages of whole rock basalt samples (McWilliams and Ron, in Segev, 2000a) were obtained for five volcanic flows along the Poriyya section. The basal lava flow yielded a reliable age of 16.05±0.07 Ma, representing the initiation of the T_2 event. The second (15.61±0.10 Ma), the third (15.34±0.05 Ma), and the upper flow (13.31±0.06 Ma) represent the lower part of the T_2 event. There isn't yet a reliable $^{40}Ar/^{39}Ar$ age for the final volcanic activity, but a group of conventional K/Ar isochron dates: Midrach Oz - 10.9±0.2 Ma, Migdal HaEmeq - 10.7±0.4 Ma, Mishmar HaEmeq - 12.3±0.6 Ma, Hirbet Lid - 10.2±1.7, as well as several point K/Ar dates (Shaliv, 1991) in the same range, strongly indicate that the T_2 event was terminated close to 11±1 Ma. All the relatively young conventional point K/Ar dates from basalt bodies within the Umm Sabune and Bira formations in the Kokhav Hayarden section and Belvoir-1 borehole (8.4-7.0 Ma) are apparent, uncertain dates.

Two reliable $^{40}Ar/^{39}Ar$ ages were obtained for basalts east of Afula (Etgar Camp; 14.9±0.1 and 13.9±0.1 Ma; McWilliams and Ron, in Segev, 2000a).

Beside the Poriyya volcano, basalts from the initial volcanic activity were also found in Kokhav Hayarden, Giv'at Hamore, and Mount Gilboa, as well as in southwestern Golan (Shaliv, 1991). This distribution points to the possibility that the volcanism started in the Yizre'el rift margins and later migrated toward the downfaulted blocks of the rift. The main basaltic outpouring in this area probably lasted between 14 and 12 Ma. Only reliable $^{40}Ar/^{39}Ar$ ages will improve the conventional K/Ar dates of Shaliv (1991) and accurately constrain the various T_2 volcanic units.

The southeastern continuation of the T_2 event, toward the Harrat Ash Shaam volcanic field, was partially dated recently by the conventional K/Ar method. The dating obtained a volcanic episode between 13 and 8 Ma (Ilani et al., 2001), which means that the younger part of the T_2 event (probably up to about 11 Ma) is widespread in Jordan. Six basaltic flows in western Syria (Mazraet Adham, Tahunet-El-Vashie, and Aivar) yielded a similar range (17.3±0.6 – 12.8±0.6 Ma) of K/Ar dates (Sharkov et al., 1994). Further accurate $^{40}Ar/^{39}Ar$ age determinations for the Harrat Ash Shaam volcanic field (in Syria, Jordan, and Saudi Arabia) are necessary to establish the exact timing of the T_2 event in these areas.

The Lower Basalt Formation locally interfingers with the coarse fluviatile and lacustrine sediments of the Hordos Formation (Schulman, 1962; Shaliv, 1991). Near the Poriyya (Teverya) volcanic center, some 350 m of the Hordos Formation underlies the basal lava flow, dated to 16.05±0.07 Ma, whereas the upper 300 m of this formation is interbedded with the overlying flows (up to 13.31±0.06 Ma). Farther south and west, in the Kokhav Hayarden and Yavne'el areas, the Lower Basalt Formation (600 and 300 m, respectively) overlies a pre-Neogene formation without any interbedded sediments (Shaliv, 1991). This evidence led Garfunkel (1989) to suggest a local fault-controlled depression near Teverya, which is close to the intersection of the initial Dead Sea transform and the Yizre'el rift, shortly before the T_2 volcanism.

Tertiary-Recent (T_3) magmatic event (Pliocene-Quaternary – Bashan volcanism)

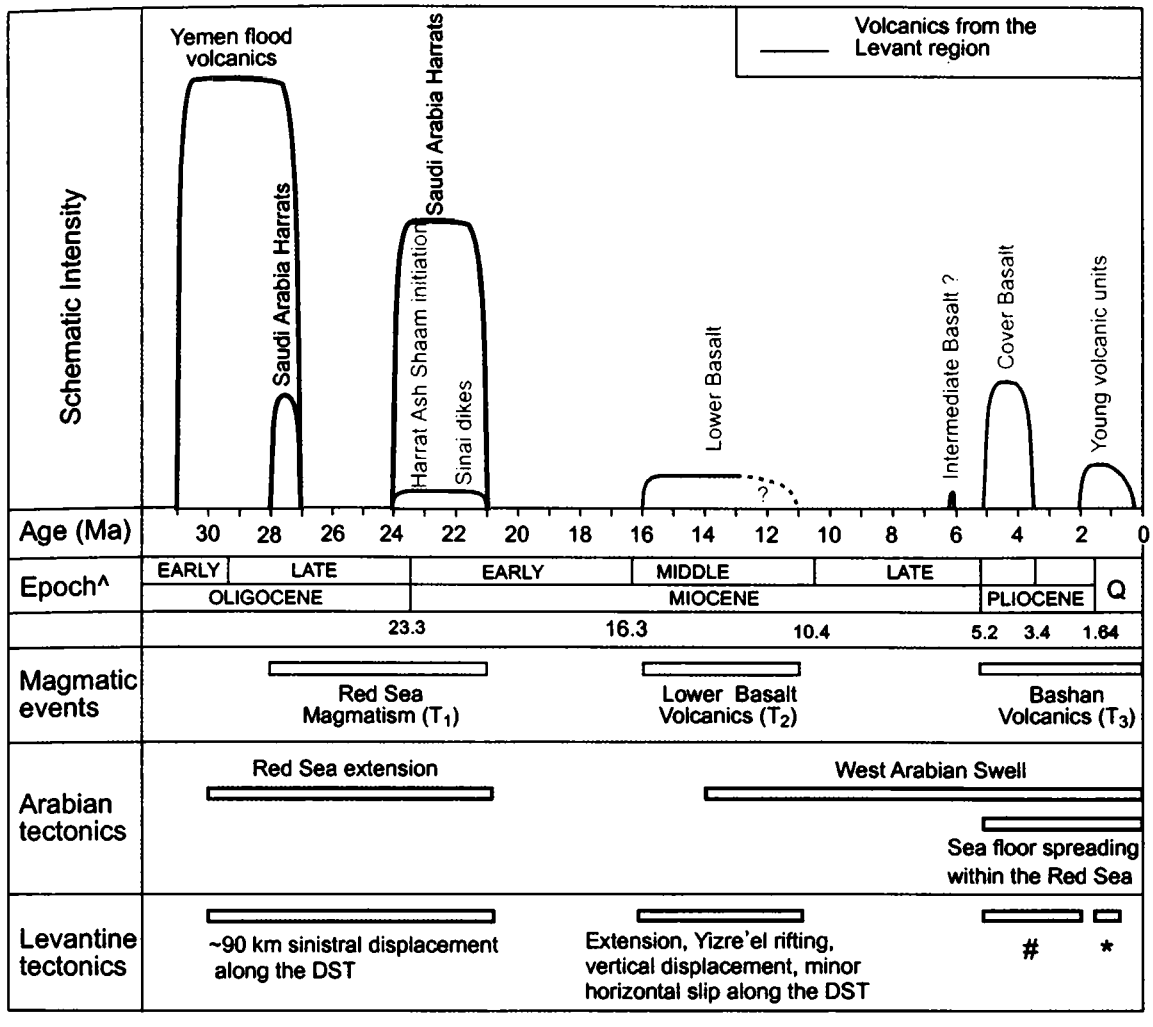
According to the wide spread in the conventional K/Ar apparent dates, some of the upper T_2 volcanic units, as well as several basaltic units (Intermediate Basalts of Schulman, 1962) within the Pliocene marly Bira Formation yielded Late Miocene apparent dates between about 9 and 6 Ma. Until reliable $^{40}Ar/^{39}Ar$ age determinations, as well as detailed field relationships, prove the existence of volcanic products in this time interval, it is suggested that it be considered as a volcanic break.

The intensive volcanism of the Bashan event generally produced more than 100 m of fresh basaltic pile on top of the various Upper Cretaceous-Neogene rock units in northern Israel; its outcrops are well-preserved and commonly cover large areas in the Lower Galilee and most of the Golan area.

The Bashan Group (Mor, 1986) is comprised of five volcanic units: the Cover Basalt (Schulman, 1962); the Eitar Basalt (Mor et al., 1997); the Ortal Formation; the Golan Formation; and the youngest (<0.1 Ma) Leja Formation (the last three units after Mor, 1986). The Fejjas Tuff (Schulman, 1962), a local volcanic unit west of the Sea of Galilee and the northern Jordan Valley, interfingers with the base of the Cover Basalt and the Pliocene Gesher Formation (Schulman, 1962; Shaliv, 1991).

The Cover Basalt (55-175 m thick) extended over most of the Lower Galilee, the Golan, southern Syria and northern Jordan. Heimann et al. (1996) estimated a minimum volume of the Cover Basalt in these countries at about 1500 km^3, which is the largest among the Neogene basalts.

Less intensive volcanic activity typifies the Pleistocene in which ~13 volcanic units were defined mainly on the Golan Heights



* Folding and faulting, compressional regime.

\# Asymmetric uplift of DST margins, minor horizontal slip along the DST.

^ Time-Scale of Harland et al. (1990).

Fig. 21.10. Generalized chart showing the cycles of magmatism over the Arabian plate and the main Arabian and Levantine tectonic events (see sources in text).

(summarized by Mor et al., 1997).

The geochemistry of the Bashan volcanics is similar to that of the earlier Miocene volcanics and is summarized above. Brenner (1979) and Weinstein (1998) identified most of the Cover Basalt as alkali basalt with olivine and olivine-augite phenocrysts. The younger volcanic units are mainly basanites; at Dalton in the Galilee, it has lower silica and a higher La/Nb ratio, whereas on the Golan it has higher silica and a lower La/Nb ratio (Weinstein, 1998). Weinstein (1998) suggested that the geochemical variability of these basalts is a result of mixing between hydrated peridotite and hydrated pyroxenite veins produced by previous within-lithosphere partial melting of hydrated peridotite.

Reliable $^{40}Ar/^{39}Ar$ age determinations of Cover Basalts from the Lower Galilee and the Golan yielded ages between 5.1±0.1 Ma and 3.5±0.1 (Heimann et al., 1996). Therefore all the lava flows of the Cover Basalt accumulated within about 1.6 Ma during the Early Pliocene. The conventional K/Ar radiometric dates for the Late Pliocene and Pleistocene volcanics are more problematic because of the much higher analytical errors. Only a few reliable $^{40}Ar/^{39}Ar$ ages were obtained for the volcanic units above the Cover Basalt. These are as follows:

a) within Dead Sea rift valley: Hula depression – 2.16±0.28, 1.87±0.09 and 0.95±0.03 Ma, Ayyelet Hashahar – 1.46±0.28 Ma (Heimann, 1990, with modifications in Segev, 2000a);

b) lava flow that descended westward to the rift valley along the gorge of the Yarmouk River (Yarmouk Basalt) – 0.66±0.09 Ma (Heimann and Braun, 2000);

c) on the Golan: Keramim Basalt in the margins of Berekhat Ram – 0.233±0.003 (Féraud et al., 1983), and the youngest volcanic unit (Leja Basalts) is estimated to be younger than 0.1 Ma (Heimann et al., 1993).

Basalts of the T_3 event are known from boreholes (Bat Yam-1, National Park-1 and others) in the coastal plain of Israel (Gvirtzman, 1970) and small exposed bodies in the foothills (Livnat, 1974). In the latter boreholes the basalts and the pyroclastic rocks, which have a total thickness of 207 m and 468 m respectively, occur between Late Miocene and Pliocene marine sediments (Gvirtzman, 1970; Derin and Reiss, 1973). Conventional K/Ar measurements for the subsurface rocks yielded mainly Pliocene dates (6.1-3.5 Ma after Lang and Steinitz, 1987; and 5.5- 4.4 Ma, after Heimann et al., 1996) in the range of the Cover Basalt Formation. Similarly the Shukba dike (Shomeron foothills) yielded a K/Ar date of 4.7±1.7 Ma, and the Hulda (Nahal Hashlosha) volcanics, 6.8±0.8 Ma (Steinitz et al., 1978).

In southern Israel the En Yahav dike (Bentor and Vroman, 1957), on the western margin of the Dead Sea rift, is associated with a pyroclastic deposit within a small caldera (Levitte, 1966; Eidelman, 1979). Two reliable $^{40}Ar/^{39}Ar$ ages for whole rock basalt samples yielded similar 'marginal plateaus' (Baksi, 1999) of 6.3±0.3 and 6.2±0.4 Ma (Steinitz et al., 2000). These reliable ages are in the range of K/Ar dates for basaltic flows on the eastern margin of the Dead Sea rift in the same area. These are: Wadi Mujib (Shihan plateau) - 6.0±0.5 Ma (Barberi et al., 1980) and 6.1±0.2 Ma (Duffield et al., 1988); Wadi Dana - 9.3-5.1 Ma (Steinitz and Bartov, 1991). Sharkov et al. (1994) obtained two similar K/Ar dates for basaltic flows in Western Syria. Therefore, the latest Miocene age of 6.2±0.4 Ma may represent this basaltic volcanism on the Dead Sea rift margins, about one million years before the appearance of the Cover Basalt in northern Israel. Some of the basaltic flows within the Bira Formation and equivalents, which are defined as the Intermediate Basalt (Schulman, 1962; Shaliv, 1991), may belong to this phase.

Although reliable $^{40}Ar/^{39}Ar$ ages around 6.2 Ma from Harrat Ash Shaam and other volcanic fields in the Arabian plate are scarce, there is a small peak of conventional K/Ar dates around this age (Camp and Roobol, 1992; Ilani et al., 2001) that indicate much wider volcanic activity at this time.

To sum up: the opening of the Red Sea and the formation of the Dead Sea Transform, as a partial tectonic consequence of the Afar plume activity, were contemporaneous with the magmatism **(Figure 21.10)**.

The Dead Sea Transform is one of the still-active plate boundaries, between the Arabian and the Sinai plates. The left-lateral motion of ~100 km along the Dead Sea Transform, affecting Eocene and earlier rock units, seems to be widely accepted. Sneh (1996) reviewed and discussed in detail the stratigraphic and structural evidence on both side of the Dead Sea Transform, including the available information on its internal basins. He suggested that approximately 100 km of left-lateral displacement took place between the late Early Oligocene and the early Middle Miocene (~30-16 Ma, biostratigraphic age). Therefore, most of the northward lateral motion of the Arabian plate relative to the Sinai plate coexisted with the NW-SE trending Red Sea magmatism (T_1) and ended about 21 Ma. During this event the Harrat Ash Shaam field was activated over the Arabian plate with insignificant dikes crossing the Dead Sea Transform along deep fractures. The Red Sea extension, breakup and magmatism, which started at about 31 Ma, developed during the most extensive magmatic event of the Afar plume (*e.g.* Camp and Roobol, 1992).

Sneh (1996) also proposed that the time interval between the Middle Miocene and Early Pleistocene is characterized by extensional processes, downfaulting and maybe minor horizontal slip on the Dead Sea Transform. The NW-SE trending rifting, associated with intensive volcanism, was initiated in the northern Sinai plate (Yizre'el rift) at about 16 Ma. According to Camp and Roobol (1992) and Ilani et al. (2001) this time falls within a magmatic and tectonic quiescence interval between ~22 and ~13 Ma. The available reliable radiometric ages support a magmatic quiescence of no longer than 5 Ma, between 21 and 16 Ma (Segev, 2001). Moreover, the interval of ~5 Ma repeatedly typifies also the duration of the Lower Basalt (T_2) event, the following quiescence and the Bashan (T_3) event (Fig. 21.10).

During the Oligocene and the Miocene both sides of the Dead Sea Transform were part of a continuous low-relief landscape, which drained towards the Mediterranean (*e.g.* Picard, 1951; Garfunkel and Horowitz, 1966; Garfunkel, 1981; Zilberman, 1992). These authors and others suggested that the major change in the morphology, or the establishment of the Dead Sea Transform drainage system and the deposition of fluvial-lacustrine sediments within the narrow rift valley occurred only in the Early Pliocene (~5-4 Ma). At this T_3 time the Harrat Ash Shaam flood basalts covered large parts of Jordan and Syria with a small extension toward northern Israel. When this event crossed the Dead Sea Transform it also produced volcanic rocks and magmatic intrusions (found in the Notera-3 and Zemah-1 boreholes) within the rift's downfaulted blocks. This intra-rift magmatism has an abundance similar to that on the rift margins suggesting deep-seated closure of the Dead Sea Transform system.

The uplift and tilting of the present-day morphotectonic blocks in northern Israel postdated the Cover Basalt Formation (<3.5 Ma) and developed up to ~2 Ma (Matmon et al., 2000).

REFERENCES CITED

Aharon, L., 1997. A shallow magmatic system of Miocene age, The Tavor River volcanic vent. Isr. Geol. Surv. Rep. GSI/13/97, 91 p. (In Hebrew, English abstract).

Almond, D. C., 1986. Geological evolution of the Afro-Arabian dome. Tectonophysics, 131(3-4), p. 301-332.

Altherr, R., Henjes-Kunst, F., and Baumann, A., 1990. Asthenosphere versus lithosphere as possible source for basaltic magmas erupted during formation of the Red Sea: constraints from Sr, Pb, and Nd. Earth Planet. Sci. Lett., 96(3-4), p. 269-286.

Baer, G., 1989. Igneous intrusions in Makhtesh Ramon, Israel: mechanics of emplacement and structural implication. Isr. Geol. Surv. Rep. GSI/48/89, 88 p. (In Hebrew, English abstract).

Baer, G., and Agnon, A., 1995. The Tavor River vent. In: A. Heimann and G. Baer, (eds.) Dykes in Israel and their Tectonic and Magmatic Setting. 3rd Int. Dyke Conf. Excur. Guid., p. 22-31.

Baer, G., Heimann, A., Eshet, Y., Weinberger, R., Mussett, A., and Sherwood, G., 1995. The Saharonim basalt: a Late Triassic - Early Jurassic intrusion in southeastern Makhtesh Ramon, Israel. Isr. J. Earth Sci., 44(1), p. 1-10.

Baker, J., Snee, L., and Menzies, M., 1996. A brief Oligocene period of flood volcanism in Yemen: Implication for the duration and rate of continental flood volcanism at the Afro-Arabian triple junction. Earth Planet. Sci. Lett., 138(1-4), p. 39-55.

Baksi, A. K., 1999. Reevaluation of plate motion models based on hotspot tracks in the Atlantic and Indian oceans. J. Geol., 107(1), p. 13-26.

Baldridge, W. S., Eyal, Y., Bartov, Y., Steinitz, G., and Eyal, M., 1991. Miocene magmatism of Sinai related to the opening of the Red Sea. Tectonophysics, 197(2-4), p. 181-201.

Barberi, F., Capaldi, G., Gasparini, P., Marinelli, G., Santacroce, R., Scandone, R., Treuil, M., and Varet, J., 1980. Recent basaltic volcanism of Jordan and its implications on the geodynamic history of the Dead Sea shear zone. In: Geodynamics and Evolution of the Afro-Arabia Rift System. Academia Nazionale dei Lincei, Rome, p. 667-683.

Barth, H., C. Besang, H. Lenz, and K. D. Meinhold, 1983. Results of petrological investigations and Rb/Sr age determinations on the non-orogenic igneous ring- complexes in the Bayuda desert, Sudan. Geol. Jb. B51, p. 3-34.

Bartov, Y., 1974. A structural and paleogeographic study of the central Sinai faults and domes. Unpublished Ph.D. thesis, Hebrew Univ. Jerusalem, 143 p. (In Hebrew, English abstract).

Behrendt, J. C., LeMasurier, W. E., and Cooper, A. K., 1992. The West Antarctic rift system–a propagating rift 'captured' by mantle plume. In: Y. Yoshida, K. Kaminuma, and K. Shirashi, (eds.), Recent Progress in Antarctic Earth Science. Terra Scientific Publishing Comp. (TERRAPUB), Tokyo, p. 315-322.

Bein, A., 1974. Reef development in the Judea Group from the coastal plain and the Carmel. Unpublished Ph.D. thesis, Hebrew Univ. Jerusalem, 193 p. (In Hebrew, English abstract).

Bein, A., and Sass, E., 1978. Platform carbonates and reef in the Judean Hills, Carmel and Galilee. 10th Inter. Cong. Sediment., Guidebook, p. 241-274.

Bentor, Y. K., 1946. The hydrological conditions of the area Tiberias – Kinneret – Yavneel – Hadata – Kefar Kama – Lubiya. Palest. Water Co., Unpubl. Rep., 76 p.

Bentor, Y. K., 1952. Magmatic intrusions and lava sheets in the Ramon area of the Negev. Geol. Mag., 89(2), p. 129-140.

Bentor, Y. K., 1957. Cenozoic volcanism of Israel. Int. Geol. Cong. 20th, Mexico, Sec. 1, p. 121-136.

Bentor, Y. K., 1985. The crustal evolution of the Arabian-Nubian Massif with special reference to the Sinai Peninsula. Precambr. Res., 28(1), p. 1-74.

Bentor, Y. K., and Vroman, A., 1957. The geological map of Israel 1:100,000, Sheet 19, Arava Valley (with explanatory notes). Jerusalem: The Government Printer.

Bentor, Y. K., Vroman, A., and Zak, I., 1965. The geologic map of Israel, scale 1:250,000, southern sheet. Isr. Surv.

Beyth, M., and Heimann, A., 1999. The youngest igneous event in the crystalline basement of the Arabian-Nubian shield, Timna Igneous Complex. Isr. J. Earth Sci., 48(2), p. 113-120.

Beyth, M., and Segev, A., 1983. Lower Cretaceous basaltic plug in Timna Valley Israel. Isr. J. Earth Sci., 32(4), p. 165-166.

Beyth, M., Stern, J. R., Altherr, R., and Kroner, A., 1994. The Late Precambrian Timna igneous complex, southern Israel: Evidence for comagmatic-type sanukitoid monzodiorite and alkali granite magma. Lithos, 31(3-4), p. 103-124.

Blank, H. R., Jr., 1977. Aeromagnetic and geologic study of Tertiary dikes and related structures on the Arabian margin of the Red sea. In: Red Sea Research 1970-1975. Saudi Arabia, Dir. Gen. Miner. Resour. Bull. 22, p. G1-G18.

Bonen, D., 1980. The Mesozoic basalts of Israel. Unpublished Ph.D. Thesis, Hebrew Univ. Jerus., 158 p. (In Hebrew, English abstract).

Brenner, I. B., 1979. The geochimical relation and evolution of the Tertiary-Quaternary volcanic rocks in northern Israel. Unpublished Ph.D. thesis, Hebrew Univ. Jerusalem, 202 p.

Brew, G., Barazangi, M., Sawaf, T., and Al-Maleh, K., 2000. Tectonic map and geologic evolution of Syria: The role of GIS. The Leading Edge, 19(2), p. 176-182.

Burg, J. P., van den Driessche, J., and Brun, J. P., 1994. Syn- to post-thickening extension in the Variscan Belt of Western Europe: Modes and structural consequences. Geol. Fr. 3, p. 33-51.

Cahen, L., Snelling, N. J., Delhal, J., Bonhomme, M., and Ledent, D., 1984. The Geochronology and Evolution of Africa. Clarendon Press, Oxford, 512 p.

Calvo, R., 1993. The diagenetic history of Helez Formation and the timing of hydrocarbons accumulation in the Helez-Kokhav oil field. Isr. Geol. Surv. Rep. GSI/1/93. (In Hebrew, English abstract).

Camp, V. E. and Roobol, M. J., 1992. Upwelling asthenosphere beneath western Arabia and its regional implications. J. Geophys. Res., 97(B11), p. 15,255-15,271.

Cavanagh, B J., 1979. Rb/Sr geochronology of some pre-Nubian igneous complexes of central and northeastern Sudan. Unpubl. Ph.D. thesis, Univ. Leeds.

Coffin, M. F., and Eldholm, O., 1994. Large igneous provinces: Crustal structure, dimensions, and external consequences: Rev. Geophys., 32, p. 1-36.

Coleman, R. G., Gregory, R. T., and Brown, G. F., 1983. Cenozoic volcanic rocks of Saudi Arabia. U.S. Geol. Surv. Open File Rep. OF-03-93.

Coleman, R. G., and McGuire, A. V., 1988. Magma systems related to the Red Sea opening. Tectonophysics, 150(1-2), p. 77-100.

Conway, B., 1990. Paleozoic-Mesozoic palinology of Israel. II. Palinostratigraphy of the Jurassic succession in the subsurface of Israel. Isr. Geol. Surv. Bull. 82, 39 p.

Courtillot, V., Jaupart, C., Manighetti, I., Tapponnier, P., and Besse, J., 1999. On the causal links between flood basalts and continental breakup. Earth Planet. Sci. Lett., 166(3-4), p. 177-195.

Crawford, A. J., and von Rad, U., 1994. The petrology, geochemistry and implication of basalts dredged from the Rowley Terrace-Scott Plateau and Exmouth Plateau margins, northwestern Australia. AGSO J. Austr. Geol. and Geophysics, 15(1), p. 43-54.

Curtis, P., and Lenz, H., 1985. Geological and geochronological investigations of selected alkali igneous complexes in the Nuba Mountains, southern Kordofan, Sudan. Geol. Jb. D69, p. 3-24.

Davey, B., and Wood, R., 1994. Gravity modelling of the Hikurangi Plateau. Marine Geol., 118(1-2), p. 139-151.

Davison, I., Al-Kadasi, M., Al-Khirbash, S., Al-Subbary, A. -K., Baker, J., Blakey, S., Bosence, D., Dart, C., Heaton, R., McClay, K., Menzies, M., Nichols, G., Owen, L., and Yelland, A., 1994. Geological evolution of the south-eastern Red Sea rift margin, Republic of Yemen. Bull. Geol. Soc. Am. 106(11), p. 1474-1493.

Derin, B., and Reiss, Z., 1973. Revision of marine Neogene stratigraphy in Israel. Isr. J. Earth Sci., 22(4), p. 199-210.

Dicker, T., 1969. Geology of central Yizre'el Valley. Isr. J. Earth Sci., 18(1), p. 39-66.

Doblas, M., Oyarzun, R., López-Ruiz, J., Cebriá, J. M., Youbi, N., Mahecha, V., Lago, M., Pocovi, A., and Cabanis, B., 1998. Permo-Carboniferous volcanism in Europe and northwest Africa: a superplume exhaust valve in the center of Pangaea. J. Afr. Earth Sci., 26(1), p. 89-99.

Druckman, Y., 1984. Evidence for Early-Middle Triassic faulting and possible

rifting from the Helez Deep borehole in the coastal plain of Israel. In: J. E. Dixon and A. H. F. Robertson, (eds.), The Geological Evolution of the Eastern Mediterranean. Geol. Soc. London, Spec. Publ. 17, p. 203-212.

Druckman, Y., and Kashai, E., 1981. The Helez Deep and Devora 2A boreholes and their implication for oil prospects in pre-Jurassic strata in Israel. Isr. Geol. Surv. Rep. OD/1/81, 23 p.

Dubertret, L., 1955. Carte géologique du Liban au 1:200,000, avec notice explicative. Beirut: Ministry of Public Works, 74 p.

Dubertret, L., 1963. Liban. In: Lexique stratigraphique international, V, III (Asie), Paris: CNRS, p. 1-55.

Dubertret, L., 1975. Introduction à la géologique à 1/50,000 du Liban. Notes et Mémoires sur le Moyen-Orient 13, p. 345-403.

Duffield, W. A., McKee, E. H., el Salem, F., and Feimeh, M., 1988. K-Ar ages, chemical composition and geothermal significance of Cenozoic basalt near the Jordan Rift. Geothermics, 17(4), p. 635-644.

Duncan, R. A., Hooper, P. R., Rehacek, J., Marsh, J. S., and Duncan, A. R., 1997. The timing and duration of the Karoo igneous event, southern Gondwana. J. Geophys. Res., 102(B8), p. 18,127-18,138.

Dvorkin, A., and Kohn, B., 1989. The Asher Volcanics, northern Israel: Petrography, mineralogy, and alteration. Isr. J. Earth Sci., 38(2-4), p. 105-123.

Ebinger, C. J., and Sleep, N. H., 1998. Cenozoic magmatism throughout east africa resulting from impact of a single plume. Nature, 395(6704), p. 788-791.

Ebinger, C. J., Yemane, T., WoldeGabriel, G., Aronson, J. L., and Walter, R. C., 1993. Late Eocene-Recent volcanism and faulting in the southern main Ethiopian rift. J. Geol. Soc. London, 150(1), p. 99-108.

Eby, N. G., 1992. Chemical subdivision of the A-type granitoids: Petrogenetic and tectonic implications. Geology, 20(7), p. 641-644.

Eidelman, A., 1979. The geology of the Arava Rift margin in the En Yahav – Ramat Zofar region. M.Sc. thesis, Hebrew Univ. Jerusalem, Isr. Geol. Surv. Rep. MM/10/79, 66 p. (In Hebrew).

El Ramly, M. F., Budanov, V. I., and Hussein, A. A., 1971. The alkaline rocks of South Eastern Desert. Geol. Surv. Egypt, Rep. 35, 111 p.

Eyal, M., Becker, A., and Samoylov, V., 1996. Mt. Arod; An Early Cretaceous basanitic volcano with a fossil lava lake. Isr. J. Earth Sci., 45(1), p. 31-38.

Eyal, M., Eyal, Y., Bartov, Y., and Steinitz, G., 1981. The tectonic development of the western margin of the Gulf of Elat (Aqaba) rift. Tectonophysics, 80(1-4), p. 39-66.

Eyal, Y., 1996. Stress field fluctuations along the Dead Sea rift since the middle Miocene. Tectonics, 15(1), p. 157-170.

Féraud, G., York, D., Hall, C. M., Goren, N., and Schwarcz, H. P., 1983. $^{40}Ar/^{39}Ar$ age limit for an Acheulian site in Israel. Nature, 304(5923), p. 263-265.

Folkman, Y., and Bein, A., 1978. Geophysical evidence for a pre-Late Jurassic fossil continental margin oriented east-west under central Israel. Earth Planet. Sci. Lett., 39(3), p. 335-340.

Franz, G., Puchelt, H., and Pasteels, P., 1987. Petrology, geochemistry and age relations of Triassic and Tertiary volcanic rocks from SW Egypt and NW Sudan. J. Afr. Earth Sci., 6(3), p. 335-352.

Freidman, G., Barzel, A., and Derin, B., 1971. Paleoenvironments of the Jurassic in the central coastal belt of northern and central Israel and their significance in the search for petroleum reservoirs. Isr. Geol. Surv. Rep. OD/1/71, p. 1-26.

Garfunkel, Z., 1981. Internal structure of the Dead Sea leaky transform (rift) in relation to plate kinematics. Tectonophysics, 80(1-4), p. 81-108.

Garfunkel, Z., 1989. Tectonic setting of Phaneorozoic magmatism in Israel. Isr. J. Earth Sci., 38(2-4), p. 51-74.

Garfunkel, Z., 1998. Constraints on the origin and history of the Eastern Mediterranean basin. Tectonophysics, 298(1-3), p. 5-35.

Garfunkel, Z., and Bartov, Y., 1977. The tectonics of the Suez Rift. Isr. Geol. Surv. Bull. 71, 44 p.

Garfunkel, Z., and Derin, B., 1984. Permian-Early Mesozoic tectonism and continental margin formation in Israel and its implication for the history of the eastern Mediterranean. In: J. E. Dixon. and A. H. F. Robertson, (eds.), The Geological Evolution of the Eastern Mediterranean. Geol. Soc. London, Spec. Publ., 17, p. 187-201.

Garfunkel, Z., and Horowitz, A., 1966. The upper Tertiary and the Quaternary morphology of the Negev. Isr. J. Earth Sci., 15(3), p. 101-117.

Garfunkel, Z., and Katz, A., 1967. New magmatic features in Makhtesh Ramon, southern Israel. Geol. Mag., 104(6), p. 608-629.

George R., Rogers N., and Kelley, S., 1998. Earliest magmatism in Ethiopia: Evidence for two mantle plumes in one flood basalts province. Geology, 26(10), p. 923-926.

Giannérini, G., Campredon, R., Féraud, G., and Abou Zakhem, B., 1988. Déformations intraplaques et volcanisme associé: example de la bordure NW de la plaque Arabique au Cénozoïque. Bull. Soc. géol. France, Ser., 8(IV), p. 937-947.

Gibson, S. A., Thompson, R. N., Leonardos, O. H., Dickin, A. P., and Mitchell, J. G., 1995. The Late Cretaceous impact of the Trindade mantle plume: evidence from large-volume, mafic, potassic magmatism in SE Brazil. J. Petrology, 36(1), p. 189-229.

Gottlieb, S., 1980. The petrography and mineral chemistry of a suit of ultramafic xenoliths from the Carmel area (Kerem Maharal volcano), Israel. Unpublished M.Sc. thesis, Hebrew Univ. Jerusalem, 72 p.

Griffiths, R. W., and Campbell, I. H., 1990. Stirring and structure in mantle starting plumes. Earth Planet Sci. Lett., 99(1-2), p. 66-78.

Guiraud, R., 1998. Mesozoic rifting and basin inversion along the northern African Tethyan margin: an overview. In: D. S. MacGregor, R. T. J. Moody, and D. D. Clark-Lowes, (eds.), Petroleum Geology of North Africa. Geol. Soc. London, Spec. Publ. 132, p. 217-229.

Gvirtzman, G., 1970. The Saqiye Group (Late Eocene to Early Pleistocene) in the coastal plain and HaShephela regions, Israel. Isr. Geol. Surv. Rep. OD/5/67, 180 p. (In Hebrew, Engl. Abstr.).

Gvirtzman, G., Klang, A., and Rotstein, Y., 1990. Early Jurassic shield volcano below Mount Carmel: new interpretation of the magnetic and gravity anomalies and implication for Early Jurassic rifting. Isr. J. Earth Sci., 39(2), p. 149-159.

Gvirtzman, G., and Weissbrod, T., 1984. The Hercynian geanticline of Helez and the Late Paleozoic history of the Levant. In: J. E. Dixon, and A. H. F. Robertson, (eds.), The Geological Evolution of the Eastern Mediterranean. Geol. Soc. London, Spec. Publ. 17, p. 177-186.

Gvirtzman, G., Weissbrod, T., Baer, G., and Brenner, J., 1996. The age of the Aptian stage and its magnetic events: new Ar-Ar ages and palaeomagnetic data from the Negev, Israel. Cretaceous Res., 17(3), p. 293-310.

Gvirtzman, Z., and Garfunkel, Z., 1998. The transformation of southern Israel from a swell to a basin: stratigraphic and geodynamic implications for intracontinental tectonics. Earth Planet. Sci. Lett., 163(1-4), p. 275-290.

Harland, W. B., Armstrong, R. L., Cox, A. V., Craig, L. E., Smith, A. G., and Smith, D. G., 1990. A Geologic Time Scale 1989. Cambridge Univ. Press, Cambridge.

Harris, N. B. W., Duyverman, H. J., and Almond, D. C., 1983. The trace element and isotope geochemistry of the Sabaloka igneous complex, Sudan. J. Geol. Soc Lond., 140, p. 245-256.

Hashad, A. H. and El Reedy, M. W. M., 1979. Geochronology of some alkalic rocks, south Eastern Desert, Egypt. Ann. Geol. Surv. Egyp. 9, p. 81-101.

Heimann, A., 1990. The development of the Dead Sea Rift and its margins in northern Israel during the Pliocene and the Pleistocene. Isr. Geol. Surv. Rep. GSI/28/90, 114 p. (In Hebrew, English abstract).

Heimann, A., and Braun, D., 2000. Quaternary stratigraphy of the Kinnarot Basin, Dead Sea Transform, northeastern Israel. Isr. J. Earth Sci., 49(1), p. 31-44.

Heimann, A., Eyal, Y., Eyal, M., and Foland, K. A., 1995. Thermal events and low temperature alteration in the Precambrian schistose dykes and their host rocks in the Elat area, southern Israel: $^{40}Ar/^{39}Ar$ geochronology. In: G. Baer, and A. Heimann, (eds.) Physics and Chemistry of Dykes, Balkema, Rotterdam, p. 281-292.

Heimann, A., Mor, D., Stein, M., and Foland, K.A., 1993. $^{40}Ar/^{39}Ar$ dating of Prehistoric basalts in southwest Syria. Geol. Soc. Isr. Annu. Meet., Arad, p. 60 (abstract).

Heimann, A., Steinitz, G., Mor, D., and Shaliv, G., 1996. The Cover Basalt Formation, its age and its regional and tectonic setting: Implication from K-Ar and $^{40}Ar/^{39}Ar$ geochronology. Isr. J. Earth Sci., 45(2), p. 55-71.

Henk, A., 1999. Did the Variscides collapse or were they torn apart?: A quantitative evaluation of the driving forces for postconvergent extension in central Europe. Tectonics, 18(5), p. 774-792.

Hofmann, C., Courtillot, V., Féraud, G., Rochette, P., Yirgu, G., Ketefo, E., and Pik, R., 1997. Timing of the Ethiopian flood basalts event and implications for plume birth and global change. Nature, 389(6653), p. 838-841.

Höhndorf, A., Meinhold, K. -D., and Vail, J. R., 1994. Geochronology of anorogenic

igneous complexes in the Sudan: isotopic investigations in North Kordofan, the Nubian Desert and the Red Sea Hills. J. Afr. Earth Sci., 19(1-2), p. 3-15.

Hopper, J. R., Mutter, J. C., Larson, R. L., Mutter, C. Z., and the Northwest Australia Study Group, 1992. Magmatism and rifted margin evolution: evidence from NW Australia. Geology, 20(9), 853-857.

Ilani, S., Harlavan, Y., Tarawneh, K., Rabba, I., Weinberger, R., Ibrahim, K., Peltz, S., and Steinitz, G., 2001. New K-Ar ages of basalts from the Harrat Ash Shaam volcanic field in Jordan: Implications for the span and duration of the upper-mantle upwelling beneath the western Arabian plate. Geology, 29(2), p. 171-174.

Itamar, A., Segev, A., and Peltz, S., 1998. The acid magmatic bodies associated with volcanism, hydrothermal alteration and mineralization in southern Makhtesh Ramon. Isr. Geol. Soc. Annu. Meet. Field Trip 7, p. 3-E - 19-E.

Itamar, A., and Steinitz, G., 1988. Potassium-Argon ages of polymetallic mineralization in the Gavnunim Valley, Makhtesh Ramon, Israel. Isr. J. Earth Sci., 37(2-3), p. 83-89.

Katz, Y., and Eppelbaum, L., 1999. Preliminary results of basin mapping of the Lower Cretaceous traps in northern Israel. Isr. Geol. Soc. Annu. Meet, p. 40 (abstract).

Keeley, M. L., and Massoud, M. S., 1998. Tectonic controls on the petroleum geology of NE Africa. In: D. S. MacGregor, R. T. J. Moody, and D. D. Clark-Lowes, (eds.), Petroleum Geology of North Africa. Geol. Soc. London, Spec. Publ. 132, p. 265-281.

Keeley, M. L., and Wallis, R. J., 1991. The Jurassic system in northern Egypt: II. Depositional and tectonic regimes. J. Petrol. Geol., 14(1), p. 49-64.

Kent, R. W., Storey, M., and Saunders, A. D., 1992. Large igneous provinces: Sites of plume impact or plume incubation? Geology, 20(10), p. 891-894.

Kessel, R., Stein, M., and Navon, O., 1998. Petrogenesis of late Neoproterozoic dikes in the northern Arabian-Nubian shield implications for the origin of A-type granites. Precambr. Res., 92(2), p. 195-213.

Kohn, B. P., and Eyal, M., 1981. Late Paleozoic-Late Tertiary evolution of the Sinai crystalline basement: Evidence from fission tracks dating of apatites and sphenes. Abs. ECOG VIII, Jerusalem.

Kohn, B. P., Eyal, M., and Feinstein, S., 1984. Early Carboniferous fission-track ages from southern Israel and Sinai: evidence for major uplift and erosion of thick Lower Paleozoic section. Isr. Geol. Soc. Annu. Meet., p. 56 (abst.).

Kohn, B. P., Eyal, M., and Feinstein, S., 1992. A major Late Devonian-Early Carboniferous (Hercynian) thermotectonic event at the NW margin of the Arabian-Nubian Shield: evidence from zircon fission track dating. Tectonics, 11(5), p. 1018-1027.

Kohn, B. P., Lang, B., and Steinitz, G., 1993. $^{40}Ar/^{39}Ar$ dating of the Atlit-1 volcanic sequence, northern Israel. Isr. J. Earth Sci., 42(1), p. 17-28.

Lang, B., Hebeda, E. H., and Priem, H. N. A., 1988. K-Ar and Rb-Sr ages of Early Cretaceous magmatic rocks from Makhtesh Ramon, southern Israel. Isr. J. Earth Sci., 37(2-3), p. 65-72.

Lang, B., and Steinitz, G., 1987. K-Ar dating of subsurface Mesozoic and Cenozoic magmatic rocks in Israel. Isr. Geol. Surv. Rep. GSI/8/87, 52 p.

Lang, B., and Steinitz, G., 1989. K-Ar dating of Mesozoic magmatic rocks in Israel: A review. Isr. J. Earth Sci., 38(2-4), p. 89-103.

Lang, B., and Steinitz, G., 1994. New $^{40}Ar/^{39}Ar$ dating of Early Cretaceous intrusive magmatics in Makhtesh Ramon: Geol. Surv. Isr. Curr. Res. 9, p. 37-40.

Lang, B., and Steinitz, G., 1996. $^{40}Ar/^{39}Ar$ dating of Early Cretaceous basalts in Har Arod, Makhtesh Ramon. Isr. Geol. Surv. Curr. Res. 10, p. 106-110.

Lanyon, R., Varne, R., and Crawford, A. J., 1993. Tasmanian Tertiary basalts, the Balleny plume, and opening of the Tasman Sea (Southwest Pacific Ocean). Geology, 21(6), p. 555-558.

Laws, E. D. and Wilson, M., 1997. Tectonics and magmatism associated with Mesozoic passive continental margin development in the Middle East. J. Geol. Soc. London, 154, p. 459-464.

Lawver, L. A., Gahagan, L. M., and Coffin, M. F., 1992. The development of Palaeo seaways around Antarctica. Antarc. Res. Ser. 56, p. 7-30.

LeMasurier, W. E., and Rex, D. C., 1991. The Marie Byrd Land volcanic province and its relation to the Cenozoic West Antarctic rift system. In: Tingey, R.J. (ed.), The Geology of Antarctica. Clarendon Press, Oxford, p. 249-284.

Levitte, D., 1966. The magmatic features of the Arava. M.Sc. thesis, Hebrew Univ. Jerusalem, 50 p. (In Hebrew).

Lewy, Z., 1996. Raw materials for the building industry: Hefa and Atlit Sheets. Isr. Geol. Surv. Rep. GSI/22/95, 13 p. + 2 maps (In Hebrew).

Lewy, Z., and Raab, M., 1978. Mid-Cretaceous stratigraphy of the Middle East. Annals du Museum d' Histoire Naturelle de Nice 4 (for 1976), p. 32.1-32.20.

Lipson-Benitah, S., Almogi-Labin, A., and Sass, E., 1997. Cenomanian biostratigraphy and palaeoenvironments in the northwest Carmel region, northern Israel. Cretaceous Res., 18(3), p. 469-491.

Livnat, A., 1974. Geology of the northwestern slopes of the Judean Hills (the Abud-Qibya-Rantis area). Isr. J. Earth Sci., 34(1), p. 11-29.

Lorenz, V., and I. A. Nicholls, 1984. Plate and intraplate processes of Hercynian Europe during the Late Paleozoic. Tectonophysics, 107(1-2), p. 25-56.

Massa, D., 1988. Paleozoique de Libye occidentale. Stratigraphie et paleogeographie I, II. Ph.D. thesis, Univ. Nice.

Massa, D., and Delort, T., 1984. Evolution du bassin de Syrte (Libye) du Cambriene au Crétacé basal. Bulletine de la Société géologique de France XXVI(6), p. 1087-1096.

Matmon, A., 2000. The Lower Galilee – A continental rift!? Isr. Geol. Soc. Annu. Meet. (Ma'a lot) p. 87 (abstract).

Matmon, A., Zilberman, E., and Enzel, Y., 2000. The development of the landscape and the tectonics of Beit HaKerem Valley. Geol. Soc. Isr. Annu. Meet., Field Trips Guidebook, p. 23-54.

McHone, J. G., 1996. Broad-terrene Jurassic flood basalts across northeastern North America. Geology, 24(4), p. 319-322.

Ménard, G., and Molnar, P., 1988. Collapse of a Hercynian Tibetan Plateau into a late Palaeozoic European Basin and Range province. Nature, 334(6179), p. 235-237.

Meneisy, M. Y., 1990. Vulcanicity. In: Said, R. (ed.) The Geology of Egypt, Balkema, Rotterdam, Netherlands, p. 157-172.

Meneisy, M. Y., and Kreuzer, H., 1974a. Potassium-Argon ages of Nepheline syenite ring complexes in Egypt. Geol. Jb., D9, p. 33-39.

Meneisy, M. Y,. and Kreuzer, H., 1974b. Potassium-Argon ages of Egyptian basaltic rocks. Geol. Jb., D9, p. 21-31.

Michelson, H., 1972. The hydrogeology of southern Golan Heights. TAHAL Rep. HR/72/037 (In Hebrew).

Mimran, Y., 1972. The Tayasir volcanics. Isr. Geol. Surv. Bulletin 52, 9 p.

Moghazi, A. M., Hassanen, M. A., and Mohamed, F. H., 1997. Source and evolution history of some Mesozoic alkaline volcanics in the Eastern Desert of Egypt: inference from petrology and geochemistry. J. Afr. Earth Sci., 24(1-2), p. 11-28.

Monod, O., and Akay, E., 1984. Evidence for a Late Triassic Early Jurassic orogenic event in the Taurides. In: J. E. Dixon, and A. H. F. Robertson, (eds.), The Geological Evolution of the Eastern Mediterranean. Geol. Soc. London, Spec. Publ. 17, p. 113-122.

Mor, D., 1986. The volcanism of the Golan Heights. Isr. Geol. Surv. Rep. GSI/5/86, 159 p. (In Hebrew, English abstract).

Mor, D., Michelson, H., Druckman, Y., Mimran, Y., Heimann, A., Goldberg, M., and Sneh, A., 1997. Notes on the geology of the Golan Heights (based on the 1:50,000 geological maps of Har Odem and Qazrin sheets by D. Mor and Gamla sheet by H. Michelson and D. Mor). Isr. Geol. Surv. Rep GSI/15/97, 38 p.

Mortimer, N., and Parkinson, D., 1996. Hikurangi Plateau: a Cretaceous large igneous province in the southwest Pacific Ocean. J. Geophys. Res., 101(B1), p. 687-696.

Mouty, M., 2000. The Jurassic in Syria: an overview. Lithostratigraphic and biostratigraphic correlations with adjacent areas. In: Crasquin-Soleau, S. and Barrier, E. (eds.) Peri-Tethys Memoir 5: New Data on Peri-Tethyan Sedimentary Basins. Mém. Mus. Natn. Hist. Nat., 182, p. 159-168.

Mouty, M., Delaloye, M., Fontignie, D., Piskin, O., and Wagner, J. J., 1992. The volcanic activity in Syria and Lebanon between Jurassic and actual. Schweiz. Mineral. Petrogr. Mitt., 72(1), p. 91-105.

Mouty, M., and Saint-Marc, P., 1982. Le Crétacé moyen du Massif Alaouite (Nwde la Syrie). Cahiers de micropal., CNRS, Paris, 3, p. 55-69.

Mushkin, A., Navon, O., Halicz, L., Heimann, A., Woerner, G., and Stein, M., 1999. Geology and Geochronology of the Amram massif, southern Negev Desert, Israel. Isr. J. Earth Sci., 48(3-4), p. 179-193.

Mutter, J. C., Buck, W. R., and Zehnder, C. M., 1988. Convective partial melting. 1. A model for the formation of thick basaltic sequences during the initiation of spreading. J. Geophys. Res., 93(B2), p. 1031-1048.

Mutter, J. C., Larson, R. L., and the Northwest Australia Study Group. 1989. Extension of the Exmouth plateau, offshore northwest Australia: deep seismic reflection/refraction evidence for simple and pure shear mechanism. Geology, 17(1), p. 15-18.

Olson, P., Silver, P. G., and Carlson, R. W., 1990. The large-scale structure of convection in the Earth's mantle. Nature, 344(6263), p. 209-215.

Omar, G. I., and Steckler, M. S., 1995. Fission track evidence on the initial rifting of the Red Sea: two pulses, no propagation. Science, 270(5240), p. 1341-1344.

Oppenheim, M. J., 1962. The geology of the southeastern Galilee lava fields. Bull. Res. Counc. Isr., 11G(2), p. 58-84.

Picard, L., 1951. Geomorphogeny of Israel, 1, The Negev. Res. Counc. Bull. 8G, p. 1-30.

Qidwai, H. A., Khalifa, M. I., and Ba-Mkhalif, K. A., 1988. Evidence of Permo-Carboniferous glaciation in the basal Murbat Sandstone formation, southern region, Sultanate of Oman. J. Petrol. Geol., 11(1), p. 81-88.

Razvalyaev, A. V., 1966. Explanatory notes to the Geological map of Syria 1:200,000. Syrian Arab Report of the Ministry of Industry, Depart. Geol. Mineral Res., Damascus, p. 1-122.

Recanati, P., Steinitz, G., Platzner, I., and Starinsky, A., 1989. Early Cretaceous igneous activity in the northern Negev: evidence from K-Ar dating of subsurface cores. Isr. J. Earth Sci., 38(2-4), p. 155-162.

Reynolds, P. Schandelmeier, O., H., and Semtner, A. K., 1997. The early Cretaceous (Valanginian, ~138 Ma). In: H. Schandelmeier, and P. O. Reynolds, (eds.), Palaeogeographic Palaeotectonic Atlas of Northeastern Africa, Arabia, and Adjacent Areas. Balkema, Rotterdam, Netherlands, p. 65-71.

Roberts, J. L., 1971. Some features of the Mesozoic volcanicity in the Lebanon. Geol. Mag., 108(2), p. 115-118.

Robertson, A. H. F., 1990. Tectonic evolution of Cyprus. In: J. Malpas, E. M. Moores, A. Panayiotou, and C. Xenophontos, (eds.), Ophiolites, Oceanic Crustal Analogues. Geol. Surv. Depart. Nicosia, p. 235-249.

Robertson, A. H. F., and Xenophontos, C., 1993. Development of concepts concerning the Troodos ophiolite and adjacent units in Cyprus. In: H. M. Prichard, T. Alabaster, N. B. Harris, and C. R. Neary, (eds.), Magmatic Processes and Plate Tectonics. Geol. Soc. London, Spec. Publ. 76, p. 85-119.

Ron, H., and Baer, G., 1988. Paleomagnetism of Early Cretaceous rocks from southern Israel. Isr. J. Earth Sci., 37(2-3), p. 73-82.

Rosenfeld, A., and Raab, M., 1974. Cenomanian–Turonian ostracodes from the Judea Group in Israel. Isr. Geol. Surv. Bull. 62, p. 1-64.

Rossi, M. E., Tonna, M., and Larbash, M., 1992. Latest Jurassic-Early Cretaceous deposits in the subsurface of the eastern Sirt basin (Libya): facies and relationships with tectonics and sea-level changes. In: N. J. Salem, A. M. Sbeta, and M. R. Bakbak, (eds.) The Geology of Libya, Vol. 6. Elsevier, Amsterdam, p. 2212-2225.

Rybakov, M., Fleisher, L., and Goldshmidt, V., 1995. A new look at the Hebron magmatic anomaly. Isr. J. Earth Sci., 44(1), p. 41-49.

Said, R., 1962. The geology of Egypt. Amsterdam: Elsevier, 377 p.

Said, R., 1990. Cretaceous paleogeographic maps. In: R. Said, (ed.), The Geology of Egypt, Balkema, Rotterdam, Netherlands, p. 439-449.

Sass, E., 1968. Geology of the Umm El Fahm area, northern Israel. Isr. J. Earth Sci., 17(3), p. 115-130.

Sass, E., 1980. Late Cretaceous volcanism in Mount Carmel, Israel. Isr. J. Earth Sci., 29(1-2), p. 8-24.

Sass, E., and Bein, A., 1978. Platform carbonates and reefs in the Judean Hills, Carmel and Galilee. Inter. Assoc. Sediment. 10th Inter. Cong. Sediment. Guidebook, Part II, p. 239-274.

Schulman, N., 1962. The Geology of the central Jordan Valley. Ph.D. Thesis, Hebrew Univ. Jerusalem, 103 p. (In Hebrew, English abstract).

Searle, M. P., 1994. Structure of the intraplate eastern Palmyride fold belt, Syria. Geol. Soc. Am. Bull., 106(10), p. 1332-1350.

Sebai, A., Zumbo, V., Féraud, G., Bertrand, H., Hussain, A. G., Giannérini, G., and Campredon, R., 1991. $^{40}Ar/^{39}Ar$ dating of alkaline and tholeiitic magmatism of Saudi Arabia related to the early Red Sea rifting. Earth Planet. Sci. Lett., 104(2-4), p. 473-487.

Segev, A., 1986. Lithofacies relations and mineralization occurrences in the Timna Formation, Timna Valley. Unpublished Ph.D. Thesis, Hebrew Univ. Jerusalem, 118 p. (In Hebrew, English abstract).

Segev, A., 1987. The age of the latest Precambrian volcanism in southern Israel, northeastern Sinai and southwestern Jordan - a re-evaluation. Precambr. Res., 36(3-4), p. 277-285.

Segev, A., 2000a. Synchronous magmatic cycles during the fragmentation of Gondwana: radiometric ages from the Levant and other provinces. Tectonophysics, 325(3-4), p. 257-277.

Segev, A., 2000b. The principal Phanerozoic tectono-magmatic periods in the Levant and their stratigraphic record. Isr. Geol. Surv. Curr. Res. 12, p. 115-124.

Segev, A., 2000c. Continental breakup and the dispersal of Gondwana: evidence for temporal plume migration. The 1th Stephan Mueller Con., Eur. Geophys. Soc., p. 11 (abst.).

Segev, A., 2002. Flood basalts, continental breakup and the dispersal of Gondwana: evidence for periodic migration of upwelling mantle flows (plumes). Europ. Geophys. Soc. Spec. Publ., Series, Vol. 2, p. 171-191.

Segev, A., and Eshet, Y., 2004. Significance of Rb/Sr age of Early Permian volcanics, Helez Deep 1A borehole, central Israel. Africa Geoscience Review, 10(4), p. 333-346.

Segev, A., and Lang, B., 2002. $^{40}Ar/^{39}Ar$ dating of the upper Tayasir volcanics in the Mount Hermon area, northern Israel. Isr. Geol. Surv. Curr. Res. 13, p. 100-104.

Segev, A., Goldshmidt, V., Itamar, A., and Rybakov, M., 1996. Effects of Mesozoic magmatism on composition, structure and metallic mineralization in the Ramon area (southern Israel): Magnetometric and gravimetric evidence. Isr. J. Earth Sci., 45(2), p. 89-112.

Segev, A., Goldshmidt, V., and Rybakov, M., 1999. Late Precambrian-Cambrian tectonic setting of the crystalline basement in the northern Arabian-Nubian shield as derived from gravity and magnetic data: basin-and-range characteristic. Isr. J. Earth Sci., 48(3-4), p. 159-178.

Segev, A., Halicz, L., Steinitz, G., and Lang, B., 1995. Post-depositional processes on a buried Cambrian sequence in southern Israel, north Arabian Massif: evidence from new K-Ar dating of Mn-nodules. Geol. Mag. 132(4), p. 375-385.

Segev, A., Itamar, A., and Peltz, S., 1994. The age of the Arod Conglomerate by K-Ar dating of igneous pebbles, Makhtesh Ramon, southern Israel. Isr. Geol. Surv. Curr. Res. 9, p. 33-36.

Segev, A., Itamar, A., and Peltz, S., 1996. The Early Cretaceous Gavnunim magmatic history. Isr. Geol. Surv. Curr. Res. 10, p. 103-105.

Segev, A., Sass, E., Ron, H., Lang, B., Kolodny, Y. and McWilliams, M. 2002. Stratigraphic, geochronologic and paleomagnetic constraints on Late Cretaceous volcanism in northern Israel. Isr. J. Earth Sci., 51(3-4), p. 297-309.

Segev, A., Steinitz, G., Platzner, I., and Starinsky, A., 1985. An Upper Devonian thermal event in southern Israel based on Rb-Sr and K-Ar ages of illites <2μ from Cambrian rocks. Isr. Geol. Soc. Annu. Meet., p. 87-88 (abstract).

Şengör, A. M., Yilmaz, Y., and Süngürlu, O., 1984. Tectonics of the Mediterranean Cimmerides: nature and evolution of the western termination of Palaeo-Tethys. In: J. E. Dixon, and A. H. F. Robertson, (eds.), The Geological Evolution of the Eastern Mediterranean. Geol. Soc. London, Spec. Publ. 17, p. 77-112.

Serencsits, C. McC., El Ramly, M. F., Faul, H., Foland, K. A., Hussein, A. A., and Lutz, T. M., 1981. Alkaline ring complexes in Egypt: their ages and relationship in time. J. Geophys. Res., 86(B4), p. 3009-3013.

Shaliv, G., 1991. Stages in the tectonic and volcanic history of the Neogene basin in the Lower Galilee and the valleys. Isr. Geol. Surv. Rep. GSI/11/91, Ph.D. Thesis, Hebrew Univ. Jerusalem, 94 p. (In Hebrew, English abstract).

Shaliv, G., Mimran, Y., and Hatzor, Y., 1991. The sedimentary and structural history of the Bet She'an area and its regional implications. Isr. J. Earth Sci., 40(1-4), p. 161-179.

Shaliv, G., and Steinitz, G., 1988. K-Ar ages of Lower Basalt, Intermediate Basalt and base of Cover Basalt in northern Israel. Isr. Geol. Surv. Curr. Res., 6, p. 22-28.

Sharkov, E. V., Chernyshev, I. V., Devyatkin, E. V., Dodonov, A. E., Ivanenko, V. V., Karpenko, M. I., Leonov, Yu. G., Novikov, V. M., Hanna, S., and Khatib, K., 1994. Geochronology of Late Cenozoic basalts in Western Syria. Petrology, 2(4), p. 385-394.

Sharkov, E. V., Jermakani, E., Hanna, S., and Bagdasaryan, G. P., 1989. First K-Ar dates for kimberlitic rock diatremes in the coastal part of Syria. Doklady, 301(4), p. 132-135.

Shenhav, H., 1971. Lower Cretaceous sandstone reservoirs, Israel: petrography,

porosity, and permeability. Bull. Am. Assoc. Petrol. Geol., 55(12), p. 2194-2224.

Shimron, A., 1998. Tectonic evolution of southern Mount Hermon. Isr. Geol. Surv. Rep. GSI/10/98, 138 p.

Shimron, A., and Peltz, S., 1993. Early Cretaceous pyroclastic volcanism on the Hermon range. Isr. Geol. Surv. Bull. 84, 43 p.

Shirav (Schwartz), M., Peltz, S., Baer, G., Aharon, L., and Agnon, A., 1995. The Umm Sabune section revisited. Isr. Geol. Soc. Meet., Zikhron Ya'aqov, p. 105 (abstract).

Sneh, A., 1996. The Dead Sea Rift: lateral displacement and downfaulting phases. Tectonophysics, 263(1-4), p. 277-292.

Stampfli, G. M., 1996. The Intra-Alpine terrain: a Paleotethyan remnant in the Alpine Variscides. Eclog. Geol. Helv., 89, p. 13-42.

Steen, G., 1982. Radiometric age dating and tectonic significance of some Gulf of Suez igneous rocks. 6th Petrol. Explor. Seminar, p. 24, EGPC, Cairo.

Stein, M., and Goldstein, S. L., 1996. From plume head to continental lithosphere in the Arabian-Nubian Shield. Nature, 382(6594), p. 773-778.

Stein, M., and Hofmann, A. W., 1992. Fossil plume head beneath the Arabian lithosphere?. Earth Planet. Sci. Lett., 114(1), p. 193-209.

Stein, M., and Hofmann, A. W., 1994. Mantle plumes and episodic crustal growth. Nature, 372(6501), p. 63-68.

Stein, M., and Katz, A., 1989. The composition of the subcontinental lithosphere beneath Israel: Inferences from peridotitic xenoliths. Isr. J. Earth Sci., 38(2-4), p. 75-87.

Steinitz, G., 1980. Rb-Sr age determination on basement rocks from Heletz Deep 1A well. Isr. Geol. Surv. Rep. MM/1/80, 10 p.

Steinitz, G., and Bartov, Y., 1991. The Miocene-Pliocene history of the Dead Sea segment of the rift in light of K-Ar ages of basalts. Isr. J. Earth Sci., 40(1-4), p. 199-208.

Steinitz, G., Bartov, Y., and Eyal, M., 1992. K-Ar and Ar-Ar dating of Permo-Triassic magmatism in Sinai and Israel - initial results. Isr. Geol. Soc. Annu. Meet., p. 147-148.

Steinitz, G., Bartov, Y., and Hunziker, J. C., 1978. K-Ar determination of some Miocene- Pliocene basalts in Israel: their significance to the tectonics of the Rift Valley. Geol. Mag., 115(5), p. 329-340.

Steinitz, G., Calvo, R., and Bartov, Y., 2000. New $^{40}Ar/^{39}Ar$ age for the En Yahav dike and its implications for the age of the Hazeva Formation. Isr. Geol. Surv. Curr. Res. 12, p. 206-208.

Stern, R. J., 1994. Arc assembly and continental collision in the Neoproterozoic east African orogen: Implications for the consolidation of Gondwanaland. Ann. Rev. Earth Planet. Sci., 22, p. 319-351.

Storey, B. C., 1995. The role of mantle plumes in continental breakup: case histories from Gondwanaland. Nature, 377(6547), p. 301-308.

Storey, B. C., Leat, P. T., Weaver, S. D., Pankhurst, R. J., Bradshaw, J. D., and Kelley, S., 1999. Mantle plumes and Antarctica-New Zealand rifting: evidence from mid-Cretaceous mafic dykes. J. Geol. Soc. London, 156, p. 659-671.

Tarawneh, K., Ilani, S., Rabba, I., Harlavan, Y., Peltz, S., Ibrahim, K., Weinberger, R., and Steinitz, G., 2000. Dating the Harrat Ash Shaam basalts northeast Jordan (Phase I). Isr. Geol. Surv. Rep. GSI/2/2000, 58 p.

Teutsch, N., Ayalon, A., and Kolodny, Y., 1996. Late Cretaceous exposure and paleoweathering of a basaltic dike, Makhtesh Ramon, Israel: Geochemical and stable isotope studies. Isr. J. Earth Sci., 45(1), p. 19-30.

Turner, S., Regelous, M., Kelley, S., Hawkesworth, C., and Mantovani, M., 1994. Magmatism and continental break-up in the South Atlantic: High precision ^{40}Ar-^{39}Ar geochronology. Earth Planet. Sci. Lett., 121(3-4), p. 333-348.

Vail, J. R., and Rex, D. C., 1971. Potassium-argon age measurements on pre-Nubian basement complex rocks from Sudan. Proc. Geol. Soc. London, 1664, p. 205-214.

Vogt, P. R., and Johnson, G. L., 1973. A longitudinal seismic reflection profile of the Reykjanes Ridge: Part II–Implication for the mantle hotspot hypotethis. Earth Planet. Sci. Lett., 18(1), p. 49-58.

Weaver, S. D., Storey, B. C., Pankhurst, R. J., Mukasa, S. B., DiVenere, V. J., and Bradshaw, J. D., 1994. Antarctica - New Zealand rifting and Marie Byrd Land lithospheric magmatism linked to ridge subduction and mantle plume activity. Geology, 22(9), p. 811-814.

Weinstein, Y. S., 1998. Mechanisms of generation of intra-continental alkali-basalts in northeastern Israel. Ph.D. Thesis, Hebrew Univ. Jerusalem, 101 p.

Weissbrod, T., 1981. The Paleozoic of Israel and adjacent countries (lithostratigraphic study. Isr. Geol. Surv. Rep. MP 600/81, 276 p. (In Hebrew, English abstract).

Weissbrod, T., and Gvirtzman, G., 1988. The Late Devonian event in the Near East. Cour. Fosch. Int. Senckenberg, 100, p. 221-233.

Weissbrod, T, and Gvirtzman, G., 1989. Crustal thinning possibly related to Late Paleozoic updoming: evidence from two Near Eastern megastructures. Bull. Soc. Belge Géol. 98-2, p. 235-237.

Weissbrod, T., Segev, A., and Beyth, M., 1990. Lower Cretaceous volcaniclastic and crater-lake deposits within Paleo-Mesozoic sandstones at Timna Valley, southern Israel. Intern. Volcanol. Cong. IAVCEI.

Weissbrod, T., Segev, A., and Kapusta, Y., 2001. $^{40}Ar/^{39}Ar$ dating of the Early Cretaceous volcanic event in the Timna Valley. Isr. Geol. Surv. Rep. GSI/16/01, 16 p.

White, R. S., and McKenzie, D., 1989. Magmatism at rift zones: The generation of volcanic continental margins and flood basalts. J. Geophys. Res., 94(6), p. 7685-7729.

White, R. S., and McKenzie, D., 1995. Mantle plumes and flood basalts. J. Geophys. Res., 100(B9), p. 17,543-17,585.

Wilson, J. T., Grunow, A. M., and Hanson, R. E.,1996. Gondwana assembly: The view from southern Africa and east Gondwana. J. Geodynam., 23(3-4), p. 263-286.

Wilson, M., 1989. Igneous Petrogenesis: a Global Tectonic Approach. Chapman and Hall, London, — p.

Wilson, M., 1993a. Magmatism and the geodynamics of basin formation. Sediment. Geol., 86(1-2), p. 5-29.

Wilson, M., 1993b. Geochemical signature of continental and oceanic basalts: a key to mantle dynamics? J. Geol. Soc. London, 150(5), p. 977-990.

Wilson, M., 1997. Thermal evolution of the Central Atlantic passive margins: continental break-up above a Mesozoic super-plume. J. Geol. Soc. London, 154(3), p. 491-495.

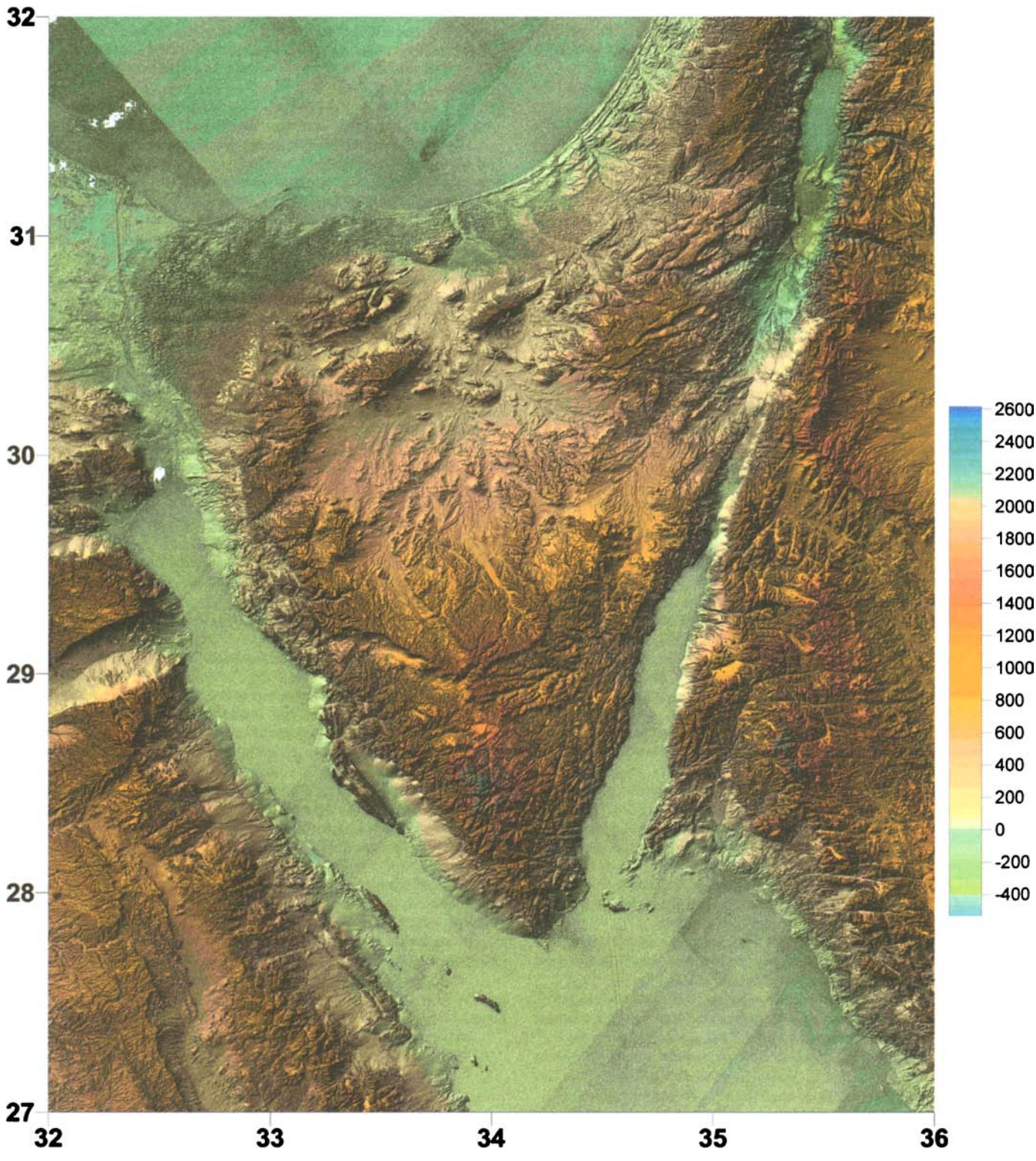
Wilson, M., and Guiraud, R., 1998. Late Permian to Recent magmatic activity on the African-Arabian margin of Tethys. In; D. S. MacGregor, R. T. J. Moody, and D. D. Clark-Lowes, (eds.), Petroleum Geology of North Africa. Geol. Soc. London, Spec. Publ. 132, p. 231-263.

Zeyen, H., Volker, F., Wehrle, V., Fuchs, K., Sobolev, S. V., and Altherr, R., 1997. Styles of continental rifting: Crust-mantle detachment and mantle plumes. Tectonophysics, 278(1-4), p. 329-352.

Ziegler, P. A., 1990. Geological Atlas of Western and Central Europe. Shell Int. Pet. Maatschappij, The Hague, 239 p.

Zilberman, E., 1992. Remnants of Miocene landscape in the central and northern Negev and their paleogeographic implications. Isr. Geol. Surv. Bull., 83, p. 1-54.

Zumbo, V., Féraud, G., Bertrand, H., and Chazot, G., 1995. $^{40}Ar/^{39}Ar$ chronology of Tertiary magmatic activity in Southern Yemen during the early Red Sea-Aden rifting. J. Volcan. Geotherm. Res., 65(3), p. 265-279.



Hypsometrically colored shaded relief of the Sinai Peninsula and environs. This image is based upon the 90 m (0.05') topographic data obtained from the Shuttle Radar Topographic Mission (SRTM) flown by the space shuttle Endeavour in February 2000 on mission STS-99. Global Mapper® was used to read in the compressed 1° by 1° tiles available to the public on the internet. Because of holes in the dataset due to layover of the synthetic aperture radar returns, this was overlain on the complete SRTM 30" (≤900 m) dataset, and then reinterpolated to a binary grid file for Surfer® 8, which then generated the image. This type of representation clearly shows the multiplicity of structures in the area. Projection is Geographic.

Chapter 22

Whole Mantle Convection as the Cause of the Spiraling Global System of Lithospheric Geosutures: With Special Attention to the Central Plate (Between the Pelusium Line and the Lut Vortex).

David Neev and John K. Hall
Geological Survey of Israel, Marine Geology, Mapping & Tectonics Division, 30 Malchei Israel Street, Jerusalem 95501, Israel

I: INTRODUCTION

The purpose of our study is to interpret tectonic processes across our globe by incorporating external and internal aspects (*i.e.* the combination of a bird's-eye view and down-to-earth methods). This was carried out by the use of data recovered by satellites as well as results of published geological-geophysical studies.

The existence of a global system of spiraling geosutures (**Fig. 22.1**), the 'eye' of which is located within the Alpine-Himalayan orogenic belt, was described by Neev and Hall (1982, Figs. 1, 2). Nevertheless, one important interpretational concept had to be omitted from the manuscript before its publication, following one reviewer's objection. It concerned the process that generated the discussed global system, which involves the convection of the whole mantle as the chief driving mechanism for the occurrence of tectonic movements across the lithosphere. It seems that this last point is not stressed enough in many of the relevant papers.

The bulk of our text (Sections V-XII) includes our subjective interpretation of structural patterns and geological histories of relevant regional features, which are focused on their genetic relationship (their agreement or disagreement as well as their relevance) to the discussed Global System of Geosutures.

We have defined the following four points, which are inferred from the text below, to serve as leads and limits in the procedure of our evaluations:

i) The smooth extension of the oceanic fracture zones toward and under the continents to form a global pattern.

ii) The continued tectonic activities extended along the fracture zones (or across our Global System of Geosutures) since Precambrian times.

iii) The functioning of the whole mantle convection process, combined with the effect of the Earth's spin, serves as the chief driving mechanism that generates the lithosphere plates and tectonic patterns, as well as the system of global spiraling geosutures.

iv) Our own interpretation of the distribution pattern and differential movements of the Laurentian and Gondwanian super-continents.

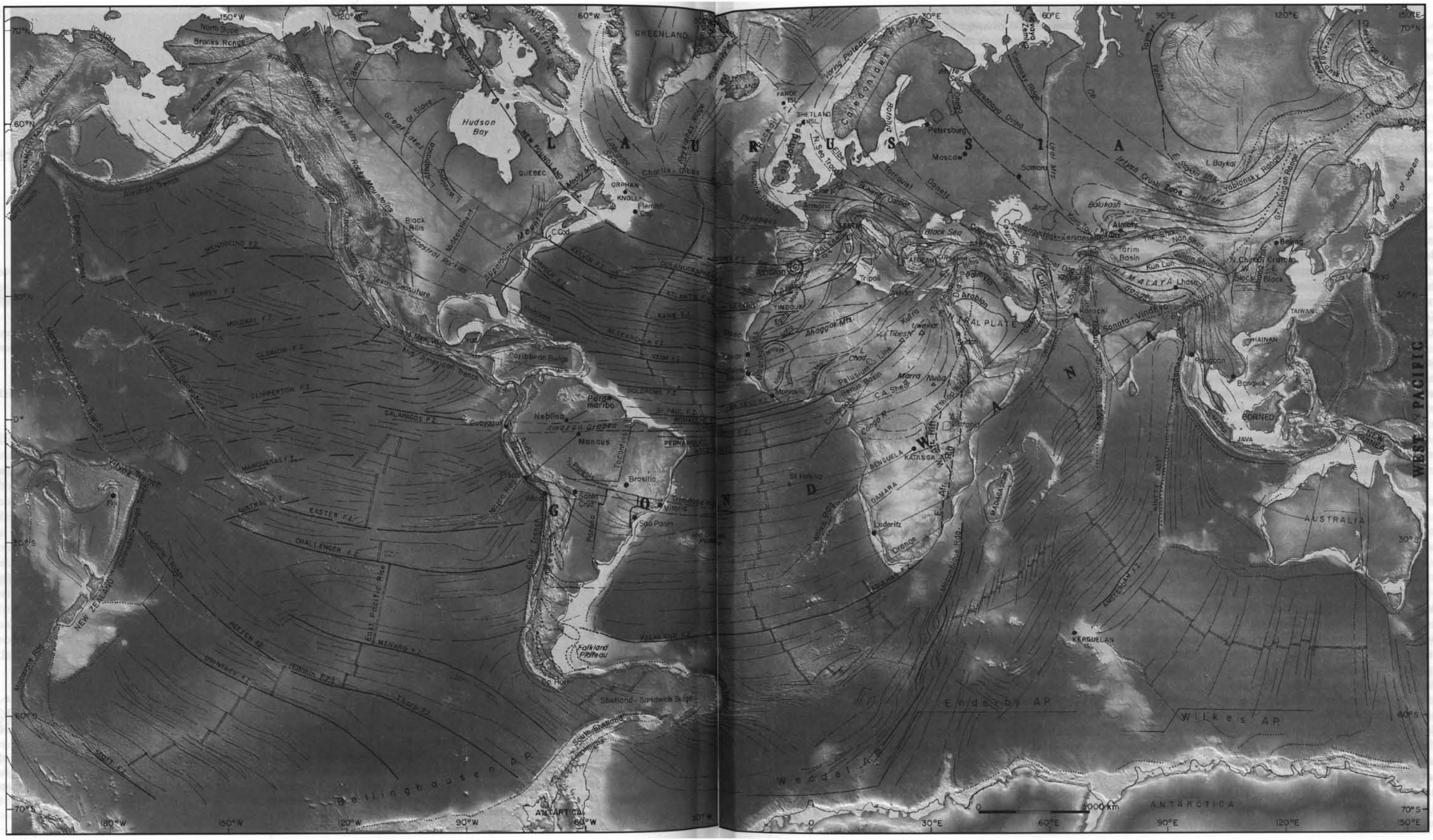
II: PRELIMINARY REMARKS REGARDING THE FOLLOWING FOUR SUBJECTS:

1) The age of the Mediterranean Sea:

We infer from the data studied (see below) and from our relevant interpretations, that the continents of northern Gondwana (*i.e.* the African/Arabian merged continent, and the Indian sub-plate) have continuously drifted northward to collide with Eurasia, since even before early Phanerozoic time. If that model is correct, then its implication should be projected on the mode of origin of both the Alpine-Himalayan Orogenic belt, as well as the associated foreland troughs. Most of these paleotroughs were originally floored by oceanic crust on both the north and south (the present-day basins such as the western Gobi-desert, the Tarim, the Peri-Caspian, and the Black-Sea Basins) and southwest (the NW Pakistan, Mesopotamian, and the Mediterranean Basins). We believe that all these basins should be of similar origin, *i.e.* formed by mechanisms that are analogous to a ramp-valley model (a compressional graben, bordered by wrench faults - Gary et al., 1974).



Figure 22.1. The Global Distribution Pattern of (i) Counterclockwise Curving and Converging Geosutures, and (ii) Volcanoes and Earthquakes: All geosutures distributed south of and between the Sea of Labrador-Pyrenees on the west, and the Indonesian-Burma-Kunlun on the southeast, are approaching the Alpine-Himalayan eye of the global system from the south in a head-on collision mode. All the rest are approaching it from the north in a tangential mode. Approximate locations of the four superplumes rising beneath the SW and NW Pacific as well as the southern fringes of the Atlantic and Pacific Oceans are stippled. Sources: Morphology of ocean's floor - after Heezen and Tharp (1977); Gravity field of the World's Oceans - Haxby (1987) and others; The Global Distribution of Volcanoes and Earthquakes (Simkin et al., 1994); Morphologic onshore data - Different Geological-Topographic maps, satellite images, and geological publications.
Background is ETOPO2 global 2' elevations/depths. Projection is Mercator, with central meridian 25°W.


GREENLAND
Hudson Bay
QUEBEC
ORPHAN KNOLL
Flemish Cap
Black Hills
Ancestral Rockies
Appalachian Mountains
C. Cod
Caribbean Bulge
Barbados Ridge
Trench
Para maribo
Nebilna
Amazon Graben
Mangus
Brasilia
Santa Cruz
São Paulo
Trindade I.
Vitoria
Folkland Plateau
Falkland Is.
Shetland - Sandwich Bulge
South Shetland Trench
Bellingshausen A.P.
ANTARCTICA
Alaskan Trench
Aleutian Trench
Brooks Range
North Slope
Mackenzie Mts.
Rocky Mountains
Great Slave
Great Bear
Great Lakes
Labrador Sea
Baffin Is.
Charlie-Gibbs
Mendocino F.Z.
Murray F.Z.
Molokai F.Z.
Clarion F.Z.
Clipperton F.Z.
Galapagos F.Z.
Marquesas F.Z.
Austral
Easter F.Z.
Challenger F.Z.
East Pacific Rise
Menard F.Z.
Hero F.Z.
Tharp F.Z.
Udintsev F.Z.
Eltanin F.Z.
Pitcairn
Tuamotu Trough
Kermadec Trough
New Zealand
Macquarie Ridge
Scott F.Z.
Iceland
Faroe Is.
Shetland Is.
N. Sea Trough
Caledonides
Rockall
Petersburg
Moscow
Samara
Ural Mts.
Siberian Platform
Taymyr
Yenisey
Lena
Verkhoyansk Mts.
Cherskiy Mts.
Kolyma
Okhotsk
Kamchatka
Irtysh Crush Zone
Altai Mts.
L. Baykal
Yablonovy Range
Gr. Khingan Range
Sea of Japan
Aral
Caspian Sea
Black Sea
Armoric
Torquist
Donetz
Hercynides
Tripoli
Athens
Aegean
Cyprus
Palestine
Suez Canal
Red Sea
Bitter Lakes
Nile Delta
Tarim Basin
Kun Lun
Qaidam Basin
Himalaya
Lhasa
Karachi
Ganges
Sonata-Vindhyan
Arabian Plate
Ahaggar Mts.
Tibesti
Chad
Kufra
Sirte
Murzuk
Ghadames
Pelusium
Benue Basin
Marra
Nuba
Monrovia
Congo R.
Cameroon
Ethiopian Rift
Victoria
Benguela
Katanga
Damara
Lüderitz
Orange
St. Helena
Walvis Ridge
Mozambique Ridge
Madagascar
Agulhas F.Z.
Amsterdam F.Z.
Kerguelan Is.
Ninetyeast Ridge
Chagos-Laccadive Ridge
Bengal
N. China Craton
Taiwan
Hainan
Bangkok
Borneo
Java
New Guinea
Australia
Enderby A.P.
Wilkes A.P.
Wedell A.P.
Indian Ocean
Pacific
0 3000 km

That interpretation is not in agreement with the widely accepted concept of three large stages (or episodes) of back and forth movements of Gondwana (more specifically Africa, Arabia, and India). According to Konert et al. (2001) their chronology is as follows: Proterozoic to Ordovician (southward translation); Silurian to Carboniferous (clockwise rotation, but without N-S translation movement); and Permian to Recent (rapid northward translation). It should be expected therefore that the first and second episodes were associated with an extensional tectonic regimen along the northern fringes of Gondwana, whereas during the third one (Permian to Recent episode) a compressional regimen would prevail.

A somewhat different interpretation is expressed by Livermore and Smith (1984), Robertson and Dixon (1984), Robertson et al. (1996), and Garfunkel (1998). These authors postulate that extensional-rifting processes dominated the Eastern Mediterranean Basin during early Permian to late Jurassic times. These tectonic widening processes were associated with upward mantle intrusions throughout the crust. Although we concur with the northward movement of Africa during the third episode, as suggested by Konert et al. (2001) (see above), we do not agree with both of these concepts.

It is widely accepted that the initial age of the Mediterranean Sea (at least of its eastern basin) should be closely identical to the age of the oldest marine (Tethyan) sediments deposited at its bottom. It is also agreed that the answer to this problem should only be given by the drill-bit, (*i.e.* very deep boreholes through the seafloor). Nevertheless the performance of such an option is, for the time being, unrealistic, first because of the lack of sufficient technical capabilities, and second because of the magnitude of financial investments involved.

We consider the following two pieces of information to be relevant to the age problem of the Eastern Mediterranean basin:

i) The maximal total thickness of the entire Phanerozoic sedimentary sequence across the trough of that basin is 12 to 15 km;

ii) Only the upper part (3-5 km) of that sequence is reliably correlated with the Messinian (Miocene to Pliocene ages), much of which consists of rock-salt sediments. The latter is overlain by the even younger stratigraphic units of Pliocene to Recent age.

The joint Arabian and Sinai sub-plate of the Central Plate (see below) is suggested to be moving northward at a faster rate than its neighbor to the west (the Eastern Mediterranean basin, and the Western Desert), as well as on its east (the Iranian sub-plate). That process of differential horizontal movements has been maintained at least since early to mid-Cambrian times. It is therefore considered likely that the depositional troughs stretched along both the NW and SE flanks of the joint Sinai and Arabian Plate. Marine Paleozoic sediments accumulated within these two basins. The above conclusions are based on subsurface geological and geophysical information (see the relevant section below). We therefore suggest that:

i) The lower part of the Phanerozoic sedimentary sequence within the Eastern Mediterranean basin may include Early Paleozoic units, a supposition also borne in mind by Hirsch et al. (1995) when assuming a Pan-African age for the Eastern Mediterranean;

ii) The present-day tectonic regime and pattern which dominate the Eastern Mediterranean and the Central Plate have functioned at least since Early Paleozoic time.

We also believe that the probability that the above hypothesis is close to the real geological history scenario is not lower than for those hypotheses expressed by Livermore and Smith (1985), Robertson et al. (1991, 1996), Garfunkel (1998), and Abdel Aal et al. (2000, 2001). These authors suggest that:

i) The Eastern Mediterranean basin was rifted not earlier than Late Permian, and;

ii) Its sedimentary fill sequence is floored by Early Jurassic oceanic crust.

Robertson and Dixon (1984), as well as Robertson et al. (1996), also infer the continuous existence of a single Tethyan Ocean in the Eastern Mediterranean region, at least from the Late Paleozoic through the Mesozoic into the Tertiary, under the influence of northward subduction of Tethyan oceanic crust beneath Eurasia and the northward drift of Gondwanian continental fragments toward Eurasia. This last interpretation is closer to ours (see above).

Considering the above limitations, all of the hitherto published suggestions dealing with the age and evolution of the Mediterranean Sea (including, of course, our present one) should be considered as mere working hypotheses. They include, among others, Malovitskiy et al. (1975), Neev (1975), Robertson and Dixon (1984), Livermore and Smith (1985), Garfunkel (1998), and Abdel Aal et al. (2000, 2001).

2) Paleomagnetism

Although the technical aspects of paleomagnetic and dating measurements, upon which the polar wandering theory is based, are reliable, the theories explaining the origin of the magnetic changes are still ambiguous. The problems begin, however, with the interpretation of the true meaning of these results. Umbgrove (1947) does not agree with Vening Meinesz's hypothesis (1943), which implies that the origin of the earth's lineament system could only be explained by large polar displacements, which occurred during and following early Precambrian times. Umbgrove's reservation is based on the assumption that the rotating earth is analogous to a spinning top or gyroscope, which has powerful tendency to keep its relative position of rotation axis constant. He suggests that any drastic alteration of the pole's locations would cause worldwide tectonic disturbances of unprecedented magnitude. The fact that nothing of the kind has been identified in the global record, implies that the theory of Vening Meinesz is unsatisfactory. The same rationale may also be relevant to other aspects of the Polar Wandering concepts.

Another dilemma resulting from the same problem is whether the entire continent of Gondwana actually moved (or drifted) together with the pole of rotation (as well as the magnetic poles) or whether they move independently. The terms of 'apparent' versus 'true' polar wandering (Van der Voo, 1988, p. 322) are related to

that subject.

Recent seismological studies made by Glatzmaier and Roberts (1995) on geomagnetism and the core of the globe, have opened new horizons for the understanding of the relevant processes. They developed a three-dimensional self-consistent numerical geodynamic model that generates the Earth's magnetic field. They were followed by Song and Richards (1996) whose seismological records provided evidence that the Earth's inner core spins independently, although in the same direction, as the rest of the planet, but about 2/3 of a second per day faster. The Earth as a dynamo may thus be explained by this mechanism.

The process of slow cooling of the pristine Earth's liquid iron core has led to the formation and growth of the solid inner core. The hexagonal, closely packed structure of the newly formed iron crystals makes the inner core anisotropic (faster propagation of seismic energy along certain crystallographic directions) with a cylindrical symmetry about an axis aligned approximately with the Earth's north-south spin axis. The exothermal energy, produced by the iron crystallization process within the inner core, provides heat to the low viscosity liquidous outer core. This energy is thought to drive convection and turbulence in the outer core (our **Fig. 22.2**, after Kumazawa and Maruyama, 1994, Fig. 7). That process drives the inner core to rotate in an eastward direction at a very high rate which is about 1° per year faster than the daily rotation of the mantle and crust (*i.e.* independently rotated in the same direction but at a higher angular speed).

The numerical model of the earth's magnetic field of Glatzmaier and Roberts (1995) describes a reversal of the dipole magnetic axis as well as several excursions, or aborted reversals, to have occurred, during the last 9000-year interval of the simulation. They have also determined through their model the changing geographic locations of the virtual magnetic pole as well as those of the true magnetic pole (their Fig. 5). The tracks of these changes, although beginning close to the south rotational pole and ending close to the northern one, do not follow straight lines. In fact, they could be compared with the magnetic polar wandering tracks of Van der Voo (1988, Tables 1, 2, and Fig. 6). Moreover, these results are in agreement with Umbgrove's postulation (1947, see above) regarding the mechanical stability of the rotational axis of the earth.

3). Paleoclimatology

The polar wandering theory is based on knowledge of paleogeography, paleomagnetism, paleoclimatology and biogeography, acquired mostly during the 20th century. Each of these subdisciplines has its drawbacks, uncertainties, and controversies. The key paleoclimatological problem is to understand comprehensively all the factors which have caused climatic changes in our globe. Van der Voo (1988, p. 312) states, "What is needed is a model that 'translates' dry or wet conditions (combined with warm- or cold-temperature indicators) into latitudinal position". Nevertheless, even if that procedure were accomplished, the solution would not be simple, as important additional uncertainties would arise when the paleomagnetic data are added to the polar wandering model (see above).

Hoffman et al. (1998), Hoffman and Schrag (2000), and Evans (2000) recently came to an important new understanding of the paleoclimatic sub-discipline. Thereby the snow-ball model and theory was developed, based on a thorough compilation of Neoproterozoic glacial deposits, as compared with those of the Phanerozoic. The climatic-glacial distribution patterns of these two periods paradoxically differ from each other. The Neoproterozoic glacial archetype has dominated mostly the low latitude zones both south and north of the Equator, but more moderately the mid-latitude zones. Not a single deposit in the high-paleolatitudinal zone (poleward of 60°) has hitherto been convincingly documented. On the other hand, the archetype of Phanerozoic glaciation occurs within both the north and south polar latitudes.

Hoffman and Schrag (2000) quoted both W. B. Harland (Cambridge Univ.) and M. Budyko (Leningrad Geophysical Observatory) regarding their models in which the necessary conditions are specified for the accumulation of the Neoproterozoic glaciers and their long periods of survival so close to the tropical zone. One of these situations is the clustering together of continents as islands along the Equator, prior to the Great Infra-Cambrian Glaciation. The mathematical model developed by Budyko explains that if and when ice is being formed at latitudinal belts less than 30° from the Equator, the direct sunlight would be striking a large surface area per degree of latitude. Therefore the surface albedo there should be rising at a faster rate than elsewhere on the planet. The more the planet reflects back radiation, the cooler its temperature. Budyko's climatic simulations also revealed that such a feedback might become sufficiently vigorous to run completely out of control. Under such circumstances the surface temperatures could plummet to a point that the entire planet would freeze over to become the Snowball Earth.

Although tropical glaciations are known to have occurred since 550 Ma, it does not seem possible that the origin of at least some of the Paleozoic glaciations known to have occurred across Africa, Arabia, and India in Cambrian to Permian times (Semtner and Klitzsh, 1994; Ziegler, 2001; Johnson et al., 1997) could have been associated with processes similar to those which occurred during the Late Proterozoic.

The transition from the Neoproterozoic archetype to the early Phanerozoic type should have occurred rather rapidly near the beginning of Cambrian time. Although a relevant conceptual genetic model has been suggested to account for the widespread low latitude Neoproterozoic glaciation (Hoffman and Schrag, 2000), a comprehensive conclusion has not yet been reached. Perhaps it is significant that neither Hoffman and Schrag (2000) nor Evans (2000), have referenced papers regarding the effect of the geographic and paleomagnetic polar wandering concepts on the Neoproterozoic climate changes.

4) Paleogeography (the actual geographic displacements) of the North Gondwana Margin

The east and west fragments of Gondwana were merged along the Pan-African Mozambique Belt during the Neoproterozoic,

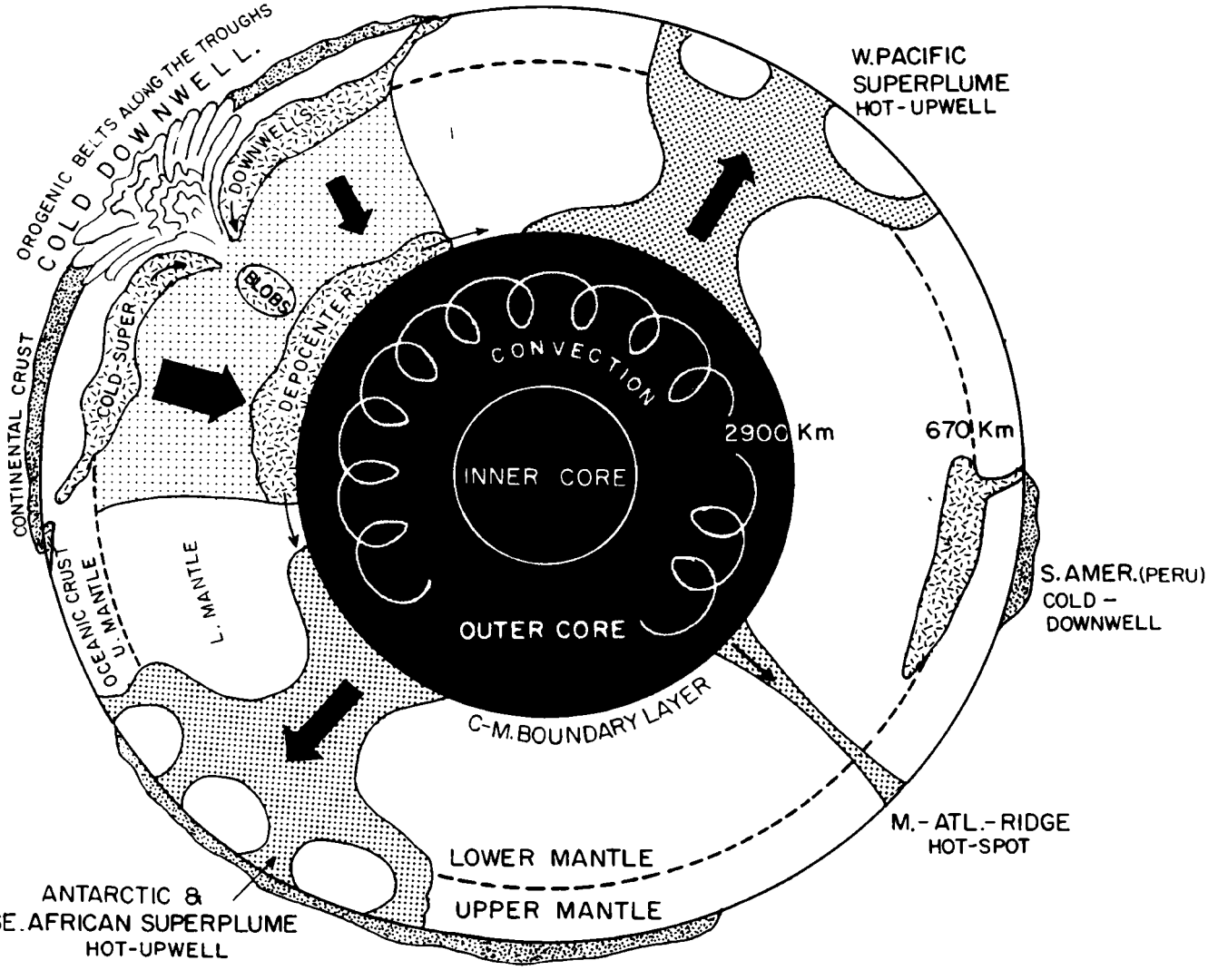


Figure 22.2. A cross-section through the Earth: Schematic illustration showing the mechanisms responsible for the Whole Mantle Convection process (after Fukao et al., 1994, Fig. 12; Kumazawa and Maruyama, 1994, Fig. 7). Orogenic belts and geosynclines are formed along the belts where the upper mantle and lithospheric cold materials are approaching each other from opposite directions, thereby converging, colliding, and sinking downward along the trough. Upon reaching a critical mass they downwell as blobs toward the Core-Mantle Boundary (C.M.B.) layer to accumulate there at depocenters. At the surface of the converging zone lighter crustal material is being crumpled upward because of the crustal shortening and compressional processes, thereby forming the highlands of the orogenic belt (after Holmes, 1955, Fig. 199).

On its way downward the heavier mantle material is being heated by compression. Another type of heating process occurs at the depocenters by upward diffusion and outburst of the heated fluidic Upper Core material. The energized mantle material then flows sideways and convects upward, thereby generating superplumes whose tracks are affected by the spin of the earth. Upon reaching the bottom of the lithosphere the resulting convectional flows are dragging the former with them, thereby generating the counterclockwise converging and spiraling pattern of the global system of geosutures. Linear mid-ocean ridges and hotspots are generated by the rise of heated lower mantle material through long deep fractures or other types of weak spots.

about 1000 Ma. ago. The northern extension of that belt is situated along the western side of the Arabian-Nubian shield. That structural-linear contact is expressed by the combination of ophiolitic intrusion and inland arcs and named as the East African Rift (EAR) (Stern, 1994). Between early Cambrian and Cretaceous times the northeast African-Arabian shield has gradually subsided to be transgressed and covered by a thick continental and marine sedimentary sequence. The North African flank of that belt is traced from Morocco in the west through Algeria-Libya and Egypt, continuing across Sinai-Arabia and S. Iran, and terminating at the

Punjab (North Pakistan) in the East (Semtner and Klitzsch. 1994; Husseini, 2000). The southern flank of that belt extends from Mauritania in the west through Niger, Chad, and Sudan on the Red Sea.

During Late Proterozoic (Precambrian) to the end of Early Paleozoic (late Silurian) times the northern margin of Gondwana experienced extreme climatic conditions. These events could be associated with sea level fluctuations caused by epeirogenic up and down movements, such as those that occurred during the Caledonian orogenic phase. They could have triggered the repeated accumulation and melting process on top of ice caps at the high inland massifs, along the northern flanks of the North Africa, Arabia, and the Indian continents (such as the Ahaggar, Tibesti, and the Arabo-Nubian massifs). Semtner and Klitzsch (1994) reported indications of northward advances and southward retreats of glaciers away and toward these massifs. During ice ages coastlines were regressed northward and sea levels dropped. Occasionally, large masses of seawater were trapped within internal basins situated across the newly exposed terrains of the north Gondwanian margins. Such a sequence of events could explain the origin and mechanism responsible for the great extent and thickness (up to thousands of meters) of the rock-salt precipitates accumulated across South Arabia, Iran, and the Punjab. On the other hand, inter-glacials occurred at about the same time periods (Late Proterozoic to Mid-Paleozoic), when global sea levels went appreciably higher due to the melting of the ice caps, layers of rich organic shale up to hundreds of meters thick (potential source rocks) were deposited within the same basins.

When carefully analyzed, the presence of both rock salt and 'hot' shale deposits may serve as reliable indicators for past occurrences of both structural and climatic processes.

The occurrences of the interglacial climatic phases were associated with the following processes:

i) The eustatic rise of sea level;

ii) The dilution of the sea;

iii) The global warming of the ocean's upper water masses. Consequently the physical structure of the entire water column (*i.e.* stratification) was stabilized so that overturning could not destroy it, and the lower water masses within the semi-closed and closed basins became euxinic. At the same time, concentrations of suspended organic particles gradually sank downward to reach the bottom, because of the gravitational settling process. Eventually, when the organically rich suspended matter reached the 'kitchen' at the sub-bottom, it became the regionally distributed 'hot' source rocks. A sequence of these source rocks hundreds of meters thick has been identified under the sand-seas of the Rub-al-Khali in the southern Arabian Peninsula (Konert et al. 2001).

The above could be the model for the distribution pattern of the Silurian source rocks all over the Middle East from Diyarbakir in Southern Turkey through Wadi Sirhan in S. Jordan, Oman, Qatar and the oilfields of Saudi-Arabia (Konert et al. *ibid,* fig. 17d, p. 502). A small quantity of oil has recently been sampled within a carbonate rock sequence of Triassic-Jurassic age penetrated at the Meged-2 wildcat (central coastal plain of Israel). The source rock of that oil sample is of Silurian-Devonian age, as indicated by a biomarker analysis carried out by the Geo Mark Research Inc. in Houston, Texas (Mr. Tuvia Luskin, Director, Givat Olam Oil Exploration Co. Ltd., Jerusalem, Israel - pers. comm.). Apparently the same geochemical parameters were also found in the oil fields of North Africa (the black shales of the Tanezrouft Formation), Turkey, and the Arabian Peninsula (Selley, 1997, p. 9-10).

Repeated Advance and Retreat Process of Glaciers across North Africa

The origin of the late Carboniferous to Early Permian glaciation at the Jebel Uweinat-Abu Ras region (the Wadi Malik Formation of SW Egypt and NW Sudan) is considered by Klitzsch (1990) to have been related to a regional structural uplifting movement that was associated with the global Hercynian orogenic phase. By that time, the regional drainage system across the discussed region was trending southward (*i.e.* flowing from the north, southward and southwestward). That pattern was maintained until early Jurassic times. A similar tectonic-climatic event also took place across the southern half of the Arabian Peninsula (Oman, Yemen, and Southern Saudi Arabia) between the late Carboniferous and early Permian times (Ziegler, 2001), as indicated by the occurrence of glacial sediments deposited there.

These late Paleozoic glacial sediments, together with those of NW Sudan, are forming an E-W trending belt, whose width extends both southward and northward between 14°N and 24°N, *i.e.* a total of more than one thousand km.

An analogous and parallel belt of glacial deposits also existed farther north in Early Paleozoic times, extending from Morocco in the west to the Punjab (N. Pakistan) in the east (see above). In that respect, the proximity of these two belts, and the fact that their trends parallel one another, as well as the present-day equator, could also be of significance. These facts argue against the occurrence of large scale rotational crustal movements that could have affected the mutual climatic-geographic conditions established within these three belts since their times of origin.

Yet Semtner and Klitzsch (1994) also mention another model for the origin of the climatic change into the extreme conditions experienced in Northern Gondwana during the Early Paleozoic. They postulate a large-scale southward and counterclockwise rotational movement of that continent during the Cambrian and Early Ordovician. That movement caused the Northern Gondwana margin to shift from inter-tropical to southern polar latitudes (60°). Moreover, between Ordovician and Middle Devonian times the paleo-south pole was shifted eastward from a point offshore Africa to approximately southwest Libya. Although such a scenario of west to east shifting could be in agreement with the counterclockwise rotational movement (see above), it doesn't match so well with the description of the glacial cycle of events: Three glacial periods are inferred to have prevailed across North Gondwana (from Morocco in the west to Saudi Arabia in the east) between the Neo-Proterozoic and the Early Silurian. These climatic changes were characterized by fluctuations with repeated glacial advance and retreat movements (Semtner and Klitzsch, *ibid,* Figs. 1-4). The dominant direction of

these glacial movements coincides with the NNE axial trend of the Arabo-Nubian Massif (or the 'Median Geosuture' of the Central Plate – see above, and Fig. 22.21 below).

The purpose of the Preliminary Remarks is to put all of the above concepts and arguments into a somewhat wider perspective. We are therefore freely quoting below a few relevant sentences following Miller (1985, p 143): "Pangea was not the first super continent. The plates may have been on the move since at least half of earth's 4.5 billion years; the recorded history of plate tectonics had actively started about 2 billion years ago. Considering the present average rate of drifting of the continents, they could have circled the globe at least four times. During this journey, two or three predecessors to Pangea may have formed. Repeated joining and fracturing as well as wrench faulting have actively occurred along many of the same sutures."

"Ample evidences are found for possible occurrences of extraordinary continental wanderings: ancient orientation of Africa and North America to the magnetic poles indicate them to have been 6000 miles apart 450 million years ago (in Cambro-Ordovician times), when the Sahara was under the great dome of ice that covered the south pole and when North America straddled the equator. Yet 250 million years later the two continents were locked tightly together as parts of Pangea, and they would eventually drift thousands of miles apart again".

Some aspects of the first half of the above free quotation corroborate our interpretation regarding the very old age of the global system of geosutures (especially those crossing the Americas as well as Europe and Africa via the Atlantic Ocean - see below). If this is accepted then the reliability of the large scale N-S drifting of the same continents (perhaps synchronously with the opening and closing of the Atlantic ocean) should be questioned. Nevertheless all of us should remember the quotation of Donald Forsyth (of Brown University [Miller, *ibid*]) that all assumptions about the driving mechanism are "completely unrestrained by observation of what is going on underneath the plates".

III: THE GLOBAL PATTERN OF GEOSUTURES - THE RESULT (OR EFFECT):

Earlier attempts to portray different patterns of global distributions of geosutures and lineaments as well as their origins, were discussed by Neev and Hall (1982, p. 10,692). In that respect, it seems worthwhile to add the essence of the following relevant observations and conclusions made by Umbgrove, (1947, p. 294-320):

i) The presence of a unique and relatively simple fracture pattern is common to a large portion of the earth's outer shell (quoting Hobbs, 1911);

ii) A pattern of structural lineaments predominates on the Earth's surface across the continents as well as across the deep ocean basins in trends that often diagonally bisect the meridians. The same trends are recognized in the different continents. These are structural-geological features dated from Precambrian times, perhaps from the earth's primeval days, hence their planetary significance, some of which have been repeatedly rejuvenated.

The existence of the global pattern of geosutures was noticed following the identification of the track and nature of the Pelusium Megashear across Africa (Neev et al. 1982) beginning at the 'border zone' between East and West Anatolia (Turkey), extending southward subparallel to the eastern Mediterranean coastline, and continuing southwestward across Africa between the Nile and Niger deltas. It further extends westward along and in *en-echelon* with the Atlantic equatorial fracture zones and along the Amazon Basin to emerge into the Pacific Ocean and to terminate upon approaching the Aleutian Trench. The magnitude of the Pelusium Megashear and its pattern are portrayed by similar geological features all over the globe, thereby suggesting a concerted action involved in the origin and maintainence of the global system of geosutures. These are corroborated by their uninterrupted mode of extension, where they are crossing both ocean basins, continents and plate boundaries, as well as by their smooth courses, which gradually curve counterclockwise to terminate as vortices upon approaching the global eye. The surface expressions of these geosutures may change along their tracks from deep shears, that apparently reach the base of the lithosphere, to 'linear' long fold belts, as well as by linear patterns of intrusives or of volcanic centers. Occasionally their surficial expressions are only marked by feeble linear morphological features.

Lithospheric slices that are bounded on both of their flanks by geosutures are approaching the Alpine-Himalayan system from the south and north. They are colliding with each other in a 'head-on' mode, where they form the eye of that global spiraling system. On their course toward the E-W elongate eye these geosutures are counterclockwise curving; those of the southern group are segregated into eight sub-groups that eventually form the following eight vortices (**Fig. 22.1**):

1) Alboran Vortex;
2) Sestri Vortex;
3) Aegean-Crete-Menderes Vortex;
4) Kirşehir-Cyprus Vortex;
5) Ararat Vortex (The Central Plate or Middle East and East Anatolia);
6) Lut Vortex (East Iran and Kopet Dag);
7) Pamir Vortex;
8) Brahmaputra Vortex.

The northern group of geosutures and slices are also curving counterclockwise but are approaching the E-W trending eye of the global system in a tangential mode (with respect to the axis of the global eye).

The criteria for the identification of these geosutures, and for segregating them from other nearby tectonic features, is their:

i) Smooth extension along their length, and

ii) Their harmonious fit into the unified geometric pattern of the global spiraling system.

A bird's eye view of the coherent global spiraling pattern of geosutures (Fig. 22.1) may intuitively lead one to suggest that these lithospheric features are expressing Results, or Effects, induced by a unified motive force or Cause such as the energy stored in the whole mantle convection process. Such a mechanism could

drive the lithosphere by dragging it from beneath to move in agreement with the global pattern of the whole mantle convection. That concerted mantle movement would produce the imitated and unified lithospheric global system of spiraling geosutures. Moreover, the dominant tendency of these geosutures to curve and converge counterclockwise suggests a genetic relationship between the discussed process and the eastward spin direction of our globe (which is a pattern common to most members of our solar system).

It is therefore possible that the functioning of both the spiraling geosutures and whole mantle convection are motivated by processes maintained since pristine times, perhaps inherited from primordial stages of our globe when it was totally molten and the viscosity of its magma appreciably lower than it is today. Apparently, by that time it was more intensely convecting and affected by the spin of the earth. Perhaps later on, for different reasons, this type of activity could have become cyclic, *i.e.* being repetitively decayed and rejuvenated several times.

The oceanic segments of the global pattern of geosutures (Neev and Hall, 1982, Fig 2) were portrayed mostly after Heezen and Tharp (1977), where the fracture zones are well represented. Swarms of linear gravity anomalies distributed across the oceans' floors were delineated from SEASAT, GEOSAT, and ERS radar altimeter measurements of the shape of the ocean surface (Haxby, 1987; Gahagan et al., 1988; Sandwell and Smith, 1995; Knudsen and Andersen, 1995). The results of these four independent studies were very similar to each other, indicating the reliability of the highly sophisticated methods used. It is even more astonishing how similar are the interpretations of Heezen and Tharp (1977) as well as ours (*op cit,* 1982, Fig. 2) to the latter four patterns.

Haxby and Weissel (1986) interpret the origin of the linear gravity anomaly swarm patterns across the ocean floor to be associated with horizontal flow of the magma at the top of the asthenosphere. A similar idea is expressed by McKenzie (1978, p. 250-251), who suggests that the surface motions in wide zones of continental deformation may reflect the convective motions in the mantle below. He also adds that these lithospheric movements are often poorly explained by plate tectonics. Sleep (1996, 1997) describes the upslope flows of mantle material that, upon reaching the base of the lithosphere, continue as lateral flows. All of these features are associated with upside-down (*i.e.* inverted) drainage-like patterns, or even levees. Apparently these close to horizontal linear flow patterns are preferentially occurring beneath patterns of the linear gravity anomalies.

We consider that the movement of the lithospheric slices toward the global eye is and was influenced by the dragging effect of the discussed horizontal flow caused by the whole mantle convection. Upon reaching the 'eye', each of the eight clusters of lithospheric geosutures gradually obtained the structural pattern of a counterclockwise curving and spiraling vortex. The main zone of convergence, where most of the upper mantle flow is downwelling, is suggested to be situated beneath the global eye. Upon reaching the core-mantle boundary (C.M.B.), that flow is moving horizontally toward the eastern periphery of the Siberian-Tibetan-Chinese-Vietnam-Indonesia zone.

Although the concept of the whole mantle convection, and the origin of the global pattern of the spiraling geosutures, differs from the theory of Plate Tectonics, these two concepts should not necessarily contradict one another and may even be complementary. Some of the differences are:

i) Until a few years ago, the mantle was considered to be practically immobile (except for the 200 km thick asthenosphere, which separates the lithosphere from the mantle, and is plastic and mobile). It is now agreed, however (see below), that the whole mantle convection process does exist. It should also imply, therefore, that horizontal flows of great magnitude do occur within the mantle, in addition to the vertical ones.

ii) Many scientists are postulating that the present phase of convergence within the Mediterranean Sea was initiated in early Jurassic time, and its origin is related to the process of sea floor spreading. Moreover its spreading history is correlated with that of the Atlantic Ocean (*i.e.* Livermore and Smith, 1985). Apparently such a concept cannot work, at least within the Levantine (eastern) Mediterranean basin, because based on recently recovered marine geophysical and drill-hole data from the continental slope off Israel, it is now suggested that the Jurassic sequence there is underlain by a several km thick sequence of older (Triassic to Early Paleozoic?) sediments. The total thickness of that Phanerozoic sequence which overlies the oceanic basement is 12 to 15 km (Neev, Greenfield and Hall, 1985; Ben-Avraham et al., 2002; Makris and Wang, 1994, p. 95, 96; see below).

iii) The global dimensions and the gently curving nature of the geosutures that smoothly extend across oceanic basins and continents, which belong to different plates, does not seem compatible with the 'orthodox' definitions of transform faults and fracture zones. An example is found along the eastern extensions of the equatorial Atlantic St. Paul and Romanche fracture zones. According to Francheteau and Le Pichon (1972, Figs. 2,3), these extensions should fit into the framework of 'small circles'. Consequently they show them curving northward and further extending along that trend across NW Africa. Indeed a few secondary faults do branch off northward, away from the St. Paul F.Z. and across the northern coastline of the Gulf of Guinea. These northward extensions are relatively short, and terminate by curving clockwise (*i.e.* to the NE), to merge with the other geosutures that are subparallel to the Pelusium Line on its north.

Nevertheless, based on the available geological data from that region, we interpret these E-W trending equatorial fracture zones to smoothly continue on the same trend into Africa along the Benue Basin and Lake Chad, where they gradually curve northeastward across NE Africa, to reach the eastern limit of the Nile Delta. That geosuture, named by us the 'Pelusium Line', continues northward along and parallel to the Eastern Mediterranean coastline to terminate at the borderline between East and West Anatolia (Neev 1975; Neev et al. 1982, Fig. 1; Neev and Hall, 1982, Fig. 2). A similar feature was described across Africa by Nagy et al. (1976) and named the 'Trans-African Lineament'.

Existing models interpret the origin of the sea floor spreading

and mid-oceanic ridge processes to be associated with leaks from the deep mantle through major lithospheric cracks. We suggest the origin of the above two features, as well as of the discussed global pattern of geosutures, is associated with the whole mantle convection processes as well. It is also reasonable to assume that the mid-ocean ridges could be a secondary feature, somehow superimposed on and related to the whole mantle convection. Such a concept could be compatible with the Wilson Cycle process, which suggests the repeated opening and closing of the Atlantic Ocean since Precambrian times (Wilson 1965, 1966; Maruyama, 1994). Accordingly, some of the Atlantic fracture zones, including their eastern and western landward extensions, could have functioned already during Precambrian and Paleozoic times (see below).

Following that approach we suggest that features such as the Amazon-Pelusium geosutures or the Labrador-Biscay-Sestri one, did exist across the Iapetus (the proto-Atlantic) Ocean at least since Infra-Cambrian times and were rejuvenated as active tectonic ones all through its cyclic history (see below). That interpretation is based upon data presented by Emery and Uchupi (1984, Figs. 105, 112, and 381).

IV: WHOLE MANTLE CONVECTION – THE CAUSE (Fig. 22.2):

Until a decade or two ago it was widely accepted that the viscosity of mantle material (especially the lower mantle) is too high to allow its convection. It was also considered that the value of the Reynolds number's upper bound for the lower mantle, which is close to 10^{-10}, precludes any significant influence of rotational forces on it. That number is a dimensionless index characterizing the type of flow or the ratio of inertial forces to viscous forces (Gary et al., 1974). However, as the viscosity of the lower mantle is not really known, the relevant Reynolds number should also be unknown. Nevertheless the structure of convection is governed principally by viscosity, not density (Loper, 1985, p. 1810-11, 1816-19, and 1828). It should also be remembered that, under different temperature and pressure conditions the mantle may behave both as brittle solid and as plastic fluid (analogous to rock salt or asphalt).

A remarkable breakthrough in the understanding of whole mantle convection processes occurred during the last decade (see below, as well as Grand, 1994 and Richards, 1999). That progress has resulted from the imaging techniques of seismic velocity tomography developed by the study of variations in the speed of earthquake waves. This newly acquired understanding made obsolete the previous postulations regarding the inability of the mantle to convect.

At one time many researchers believed that the 660 km deep discontinuity marked a compositional change between the upper and lower mantle that divided the mantle into two separate flow regimes, with large scale topography on the interface. It is now widely recognized that such topography and phase changes are unlikely to prevent whole mantle convection. Similar analyses invalidated hypothetical discontinuities at other depths as well, such as those at 300 km, 410, 900, 1000, and 1600 km. It also seems that many of the observations could represent the same interface at different depths and therefore uncorrelated at global scales (Shearer, 2000).

It could be implied from Figure 22.1 that the global pattern of the geosutures begins close to the western margins of the Pacific Ocean and extends eastwards by curving and converging counterclockwise. Most of these geosutures approach the Alpine-Himalayan orogenic belt from the south and terminate in a spiral mode. Those situated within the northwestern part of the pattern sequentially approach that orogenic belt in a tangential mode. If that entire surficial pattern reflects and imitates movements within the underlying system of the whole mantle convection, then the Alpine-Himalayan belt is an expression of a collision between these two oppositely trending and converging (or down-welling) currents of magma within the mantle flow pattern. The following items corroborate the above concept.

The schematic eastward sequence of N-S seismic velocity cross section of the Tethyan domain (Fukao et al., 1994, Fig. 6) indicates a systematic eastward increase in size and depth of high velocity (cold and heavy) subducted slabs, along a route that extends rather continuously from the Western Alps in the west through the Himalayas and terminating close to the contact of Eurasia with the West Pacific Ocean. Upon reaching its easternmost limit, the spatial dimension of this body of cold and dense material (high-velocity anomaly) expands and deviates both northward along the East Siberian margin and southward along the Indonesian archipelago. On their downward way, the subducted slabs are being delayed and accumulate at different levels within the upper and middle mantle until a critical mass is attained, when they sink (as blobs) downward (Stein and Hofmann, 1994), being heated as they go, to spread and reside at depocenters just on top of the C.M.B. At that boundary this dense material gains more heat by being pierced by super-heated upward convecting material derived from the upper core. These depocenters are stretched at the C.M.B. along a belt that underlies East Asia. It extends from Indonesia in the south through Vietnam, eastern China, Manchuria-Japan, and East Siberia in the north (Fukao et al., 1994; p. 9-11, Table 1, Fig. 9 - bottom). This seems to be the largest accumulation of dense material (high velocity anomaly) detected hitherto on top of the C.M.B. Another similar depocenter of high velocity material, perhaps of smaller dimension, underlies Antarctica. This depocenter is more speculative, since the resolution of seismic tomography in this region is poor (*ibid*, p. 11, Fig. 5 - right image, bottom).

Massive upwelling movements of hot (low velocity) magnetic bodies are rising as superplumes from the depocenter at the C.M.B. toward the upper mantle. The causative-genetic relationship between the downwelling process of cold (subducted) plumes, that settle on the C.M.B., and the upwelling one of the hot superplumes, is schematically expressed in our Fig. 22.2 (after Maruyama, 1994, Figs. 1, 10; Fukao et al., 1994, Fig. 12).

Two main hot upwelling superplumes have hitherto been detected (Fig. 22.1) (Fukao et al., 1994). The first is situated in the West Pacific (close to and north of the French Polynesian region) and the other is reaching beneath the northern limits of Antarctica and is

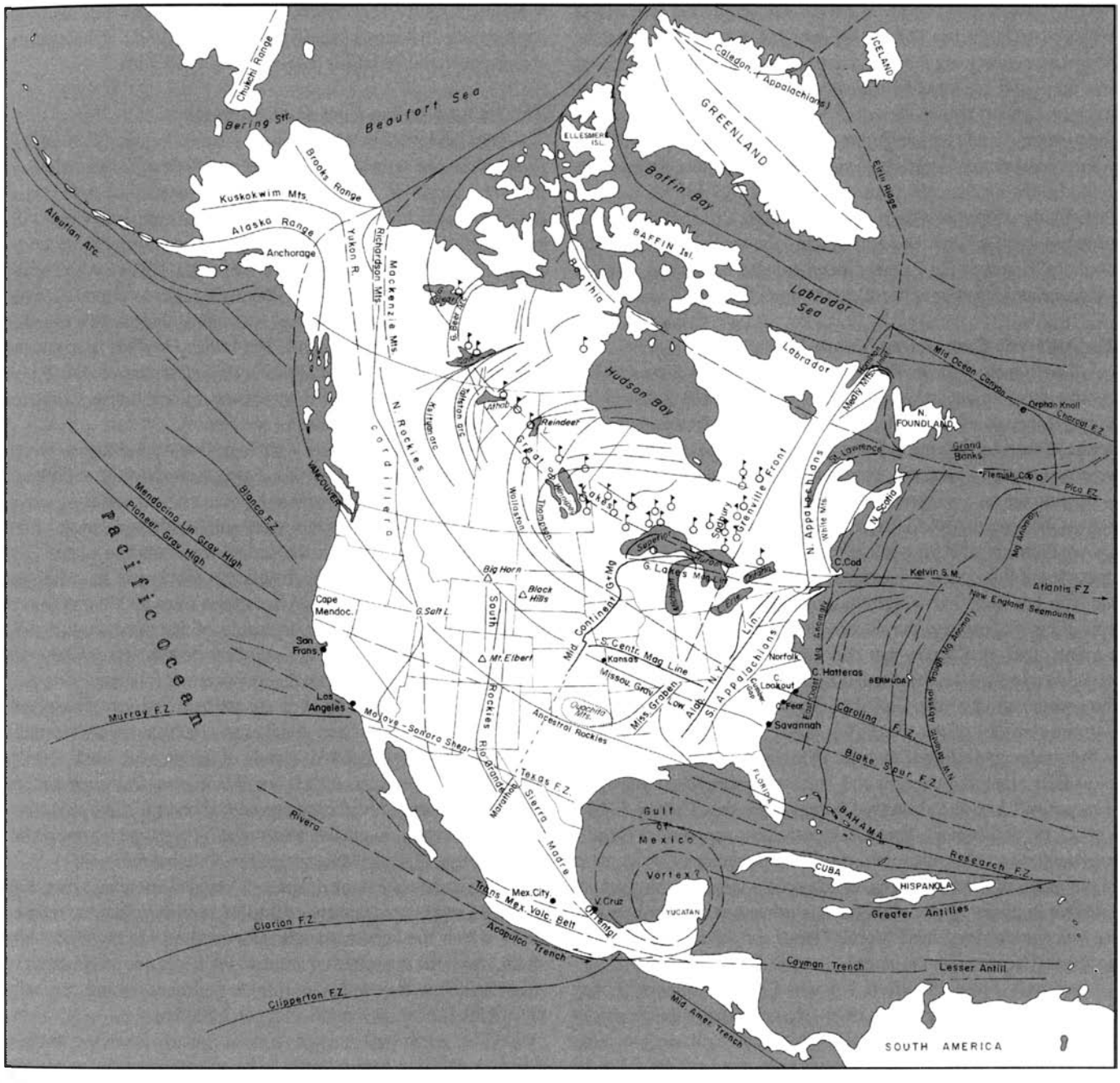


Figure 22.3. Pattern of Geosutures across North America: The general trend of the Global Pattern of Geosutures is latitudinal across the central and eastern areas. Further on to the west they curve northward to become meridional. Another group of geosutures, which attain a meridional trend all across North America, are the linear Magnetic Anomalies off and parallel to the Atlantic coastline, the Appalachians, the Mid-Continent, and the Cordillera. In the central and eastern areas these are usually crossing the latitudinal ones, but sometimes merge with one another (*i.e.* the North Rockies). Note the structural common denominator of the sharply curving (concave eastward) magnetic, gravity, and structural lineaments associated with the northeastern segment of the Great Lake Geosuture and its offshore extension as well as with the Grand Banks-Azores Fracture Zone. The distribution pattern of Deep Gold Mines along the Great Lakes geosuture is also shown. This pattern is interpreted as a geochemical indicator for its origin as pristine, residual fluids associated with formation of the Earth's crust, and their rise along deep cracks of the lithosphere since early Precambrian times. The best example is the distribution pattern of economically important ore deposits along the Great Lakes geosuture of North America.

flowing toward South and East Africa. Apparently the former was triggered (Figs. 22.1 to **22.3**) by the cumulative pressures within the depocenter underlying the East Asian cold plume, whereas the latter (*i.e.* the S. African) was by a similar mechanism occurring under western Antarctica (see above). It is assumed that additional hot superplumes would be found in the Northwest and North Pacific as well as beneath the Alaska-Arctic Ocean region. Those depocenters could be fed by the cold slabs accumulated beneath NE Eurasia. Perhaps the extreme activity and the unique distribution pattern of the volcano-seismic belt surrounding the southwest, west, and northern fringes of the Pacific Ocean are also associated with the existence and location of the relevant superplumes.

The Antarctic-East African Mantle Flows:

The 'Great African Plume', as described by Kerr (1999), quoting the opinions of several geophysicists who took part in the Spring Meeting of the AGU in Boston, clearly demonstrates the nature of that superplume. A large rising flow of hot and light (slow seismic velocities) material, several thousand km wide at its base, is flowing upward and northeastward, away from its source at the C.M.B. beneath the Weddell A.P., toward the upper mantle beneath the southern tip of Africa. Along that course it narrows and rises through the lithosphere beneath the East African Rift System and the Afar hot spot. The pattern described there seems to track the upwelling magma and the counterclockwise curving convective currents that rise from the depocenter beneath West-Central Antarctica toward South Africa. It is in rather good agreement with the configuration of the Global Pattern of Geosutures across the relevant territory of the globe (Fig. 22.1). Such an interpretation is even more appealing if the vast volcanic fields of the Red Sea, as well as along the western and northern Arabian sub-plate, are incorporated into the discussed pattern (see the 'Central Plate', Fig. 22.19, and below). That mechanism also supplies an elegant explanation as to the cause of the specific counterclockwise increase in curvature of the geosutures, which occurs upon reaching a N-S line that extends across central and northeastern Africa between the volcanic fields of Jebel Marra, Tibesti and Jebel Sawda (in the north) and Katanga (in the south).

Norman Sleep (Stanford U.) and Cynthia Ebinger (U. of London), as quoted by Kerr (1999), describe that superplume as having hit the African Plate beneath Ethiopia 45 to 30 million years ago. That flow of mantle then spreads across at least 5000 km of the underside of the lithospheric plate, and is being channeled along pre-existing 'inverted ruts'. Such a description corroborates the perception of Haxby and Weissel (1986), as well as ours, regarding the origin of the swarms of gravity lineaments (as expressed on the map of Haxby, 1983), as an upward imprint on the underside of the overlying lithosphere, left as tracks of the horizontal flowing segments of the convective currents. As it spread that plume would have raised East Africa "and fired up hot spots from Cameroun on the west coast to the Comoro Islands off Madagascar on the east" (Kerr, *ibid*).

The continuous northward drifting of Africa between Proterozoic and Early Jurassic times could have been caused by the same mechanism. This conclusion is inferred from the structural-stratigraphic histories of the Karoo (South Africa) and Owambo (Northern Namibia) basins (see below, Section VId).

The Tethyan-Indian-Eurasian Convergence:

Other relevant results of new seismic tomographic studies deal with subducted mantle materials of different seismic velocities that were identified in N-S cross sections under East Asia. These data seem to us to lend additional support to our perception of the whole mantle convection. The first indication comes from under India and Northern Tibet (Van der Voo et al., 1999a), whereas the second one is from under East Siberia (Van der Voo et al., 1999b; Richards, 1999). The following summarizes their results together with our relevant interpretations. The Indian Plate has been rotated counterclockwise by some 20-30°, (being pinned at the Pamir Vortex in the northwestward protrusion of the Indian Peninsula during its collision with Eurasia - see below).

Several subducted slabs with high P-wave velocities, which are separated from each other like cusps, were detected at different depths along their way downward across slanted surfaces, which are oppositely dipping (southward and northward) away from the collision zone between the Indian and Eurasian plates. The evolutionary stages, associated with the process of that Tethyan subduction zone, are expressed in cartoon form by Van der Voo et al. (1999a, Fig. 7) based upon the results of that tomographic study (their Figs. 4 and 5). From our point of view the most important conclusions to be drawn from that paper are as follows:

i) The pre-collisional stage of the relevant Tethyan lithospheric pattern (between India and Asia) was associated with the three relatively small and isolated islands of continental crust, namely India, Lhasa, and Asia, which are floating on and separated by appreciably longer stretches of segmented oceanic (Tethyan) crust. Such a description is suitable to serve as a prototype for our model on the 'origin of the Mediterranean Sea' (see below).

ii) The southward slanted surface (Van der Voo et al., *ibid*, Fig. 4) should represent a density controlled contact within the mantle, along which the subducted lithospheric slabs are gravitationally sliding from the uppermost mantle, to the lower one at the depth of about 2100 km. Below that level these blobs are sinking vertically toward the C.M.B. at a depth of about 2,700 km.

iii) The northward slanted surface (away from the Indian-Eurasian collision zone) seems to be shorter than the southward dipping one (see above), although well expressed and apparently of similar origin ("...this same slab shows a roll-over structure with the deeper portion overturned and dipping southward...", Van der Voo, *ibid*, p. 7 and Fig. 7). According to that figure Eurasia is over-riding India, therefore suppressing the discussed slab and bending it beneath it.

iv) Close to the Yunnan-Burma zone, the trends of the tomographic P-wave anomalies across the mantle are sharply changing from E-W (in the upper mantle under the Alpine-Himalayan belt) and NE-SW (in the deeper mantle further on to the east) to N-S trending anomalies across the mantle that underlies the zone of Burma-Sumatra-Indochina and Yunnan (eastern China)

(Van der Voo et al., 1999a, Fig. 5c-h). That same change, although inferred from different indicators, is discussed below (our Figs. 22.21-22.23).

v) Much (if not most) of the subducted materials that descend to the C.M.B. Layer beneath the Himalayan and Burma-Indonesia subduction zones, reach the depocenters of super-heated (although heavy) material beneath the West Pacific Ocean, from where the super plumes are rising.

There is a rationale for the changes in the flow directions of the mantle. These occur both from south to north (across and downward beneath the Alpine-Himalayan belt) as well as from the west eastward along the C.M.B. to reach the upwelling points beneath the West Pacific Ocean, where the super-plumes are rising:

i) The downwelling mantle is both colder and denser (being horizontally compressed beneath the lithosphere from both north and south); and

ii) Upon reaching the C.M.B. their eastward flow is affected both by the spin of the globe and because there is less resistance in that direction (the active downwelling beneath the Alpine-Himalayan is increasing the pressure upon approaching the C.M.B.).

The East Siberian–West Pacific Convergence:

The following is our interpretation of the processes occurring within the discussed zone as inferred from Van der Voo et al. (1999b) and Richards (1999): Two NNE to NE trending oceanic belts that parallel each other exist there. The western belt stretches from the NE corner of Mongolia along the East Siberian coastline as far as Okhotsk, to terminate at the sites of Kular-Gora, south of the Novosibirsk Islands and the SE coastline of the Arctic Ocean. That belt forms a westward concave arc, which is roughly accompanied by the Yablonovy and the Verkhoyansk-Cherski Ridges (Figs. 22.1 and 22.23). The eastern belt stretches along the western limits of the Pacific Ocean, which is subducted westward beneath the Kamchatka-Kurile-Japan geosuture. The subduction process of both the western and eastern oceanic belts has been maintained at least since Jurassic times.

An E-W trending and close to 4,500 km long seismic tomography cross-section through both the discussed belts extending from the Japan Trench (between the islands of Honshu and Hokkaido) in the east through Lake Baikal to terminate at E. Kazakhstan (midway between the Baikal and the Caspian Sea), is presented and discussed by Van der Voo (*ibid*, Figs. 2, 3). The discussed cross-section clearly displays the downward tracks of the two subduction zones (both the eastern and western ones) which slant westward from the surface to a depth of about 1,400 km. From that level the two descending flows of cold-dense mantle material are being swallowed down vertically to reach the C.M.B. Layer, where they accumulate to form a huge 'graveyard' which is common to both of these subduction zones, at a depth of about 2,800 km. At that level they gain heat, caused both by the pressure effect and by upward erupting material from the turbulent upper core. The resulting super-heated material then crawls eastward to reach the depocenters along the C.M.B. layer where the hot super plumes are beginning their upward rising tracks that initiate the global cycle of the whole mantle convection process (our Figs. 22.1 and 22.2).

The East Siberian suture zone that extends from the SW-NE trending W. Sayan Range (SW Baikal) through Okhotsk and along the Verhoyansk eastward concave range, displays a 'Z' shaped feature in map view. That same 'Z' shaped feature is still recognized along the westward sloping subducted surface, which is expressed by the high-velocity anomalies all the way down to a depth of 2,300 km (Van der Voo, 1999b, Figs. 2 and 4), without changing much its 'Z' shaped affinity (Richards, 1999).

There are, however, a few points of difference between the interpretation of Van der Voo et al. (1999a, b) and our approach. Two of these are as follows:

i) Neev and Hall (1982) consider the Verkhoyansk arcuate orogenic geosutures to be the easternmost member of the system of geosutures that extends to the east of the Tornquist and Elbe ones. The map tracks of those geosutures are concave eastward and are associated with dextral strike-slip shifts. Apparently the Elbe-Verkhoyansk system of geosutures could have been activated since and through the Baikalian (Proterozoic), Variscan (Late Paleozoic) and Alpine orogenic phases (Mstislavski et al., 1980). Van der Voo et al. (1999b) consider however the age of the Mongol-Okhotsk-Verkhoyansk sector to be a Jurassic one.

ii) Most members of the Elbe-Verkhoyansk system of geosutures are tangentially approaching the Alpine-Himalayan eye of the Global Spiral System on its north. Nevertheless, the overall orientation of those members situated to the east of the Onega-Kara Tau-Tien Shan geosutures (and including the Timansky-Irtysh-Altai, the Yenisey and the Verkhoyansk geosutures), is being gradually deviated northeastward. We suggest that this systematic deflection is imitating a similar change within the flow of the upper mantle. It is assumed that upon approaching the periphery of the Mongol-Okhotsk zone, as well as the NE to SW trending West Pacific coastal suture (adjacent to the West Pacific Superplume), the eastward flow of the upper mantle is being diverted to the left (*i.e.* northeastward), thereby shaping the folded-faulted crustal structures. As a result of that change a convergence (or an oblique collision) occurs between the eastward rising upper mantle and the underlying middle and lower mantle materials which are crawling downward and westward beneath the slanted plain (as explained above). The East Siberian orogenic belts (to the east of the line between the Yenisey River and the Altai Mountains) were therefore appreciably folded and uplifted (Fig. 22.2). Such a process is well known from other converging-orogenic belts (*e.g.* Holmes, 1951, Figs. 198, 199, 204).

Concluding Remarks:

i) Our model is attempting to explain the origin and mechanism of the whole mantle convection as the driving force for generating the global system of geosutures. By incorporating into it the concept of the Wilson Cycle (Wilson, 1966), the consistency of our model is indicated back at least to Proterozoic-Early Paleozoic times. We consider the activity of the whole mantle convection to

be the major mechanism responsible for the transport of hot magma from the C.M.B. through the upper mantle, to the lithosphere. It is possible that their activities are synchronized with the hotspot activity which is responsible for the cyclic opening and closing process of the Atlantic Ocean. These two mechanisms could somehow be synchronized.

ii) Although there is some agreement between the N-S trend outlined by the Ural Orogenic Belt and the general trend of the Northern Group of geosutures, the former does not seem to be genetically affiliated to the latter. We do not yet have a satisfactory explanation for that exception.

V: RELEVANT SYSTEMS OF GEOSUTURES ACROSS DIFFERENT REGIONAL PROVINCES:

Va: The North American-Greenland Geosuture (Figs. 22.3, 22.4a, and 22.4b):

Our interpretations regarding the landward extensions of North Atlantic fracture zones across the U.S., as well as those that parallel the Atlantic coastline (Neev and Hall, 1982), are substantially corroborated by data recovered from North America. Good examples are the identification of major linear geological features, as expressed by the Magnetic Anomaly Map of the Appalachian Orogeny (Zietz et al., 1980), and by the Digital Magnetic Anomaly Map of Central United States (inserted as Fig. 1 of Hildenbrand, Kucks, and Sweeney, 1983). We consider these features to be segments of the proposed geosutures. Four of these megalineaments are interpreted by Hildenbrand et al. (*ibid*) to be associated with major crustal discontinuities that were formed during Archean time when the crust was thinner and weaker. The first two examples (out of the four) are trending NE-SW, *i.e.* paralleling the eastern coastline of North America. These are:

1) The mid-continent Gravity and Magnetic High that extends to the southwest for nearly 1000 km from Lake Superior to southern Kansas (Jachens et al., 1989; Kane and Godson, 1989).

2) The New York-Alabama lineament and magnetic terrain, that extends along 1600 km and represents the southeast edge of a stable crustal block that acted as a barrier to the strong deformation of the N. Appalachian foldbelt.

The other two linear geological-magnetic features are the NW-SE trending anomalies that extend the Atlantic Ocean's fracture zones. On their northwestern extension they curve clockwise to intersect the former two (the northeastward trending). These are:

3) The Great Lakes Magnetic Lineament (see below).

4) The South-Central Magnetic Lineament, which parallels the Pelusium Line and was named 'The Missouri Gravity Low' by Arvidson et al. (1982).

Altogether these four features form a close to regmatic pattern of strike-slip displacements.

The Great Lakes Geosuture (Figs. 22.1, 22.3, 22.4a and b):

An uninterrupted counterclockwise curving linear magnetic anomaly extends landward (*i.e.* westward) from the eastern limit of the New England Seamounts (1500 km east of the coastline) to Lake Winnipeg in the NW (Hinze and Hood, 1989, Plate I (B)). It is still recognized beyond that point, but in a less prominent way. This problem is referred to by Neev and Hall (1982, Fig. 2), regarding the northwestward extension of the segment between Lake Winnipeg and Great Bear Lake. Although the definition of that segment as a geosuture of tectonic origin is based upon indirect arguments, the fact remains that its integration with the other segments forms a remarkably solid and smooth curvilinear feature. It stretches westward from the Anti-Atlas Geosuture (see below), crossing the Eastern Atlantic coastline, and continuing along the E-W trending Canary chain of islands to merge with the Atlantis Fracture Zone. Thereafter it follows the New England chain of seamounts and Kelvin Seamount to continue along the eastward extension of the Great Lakes geosuture. That last connecting segment coincides with the eastward convergence pattern of the otherwise NNE-SSW trending Southern and Northern Appalachian ranges (which takes place between Philadelphia and Cape Cod).

The study of a different type of geological-geophysical information indicates the existence of a sequence of curvilinear magnetic (as well as gravimetric) anomalies along the on-land northwestern segment of the Great Lakes geosutures (Hildenbrand et al., 1983; Hanna et al., 1984; Hinze and Hood, 1989, Plate I (A and B); our Fig. 22.3). Each of these features is concave southeastward, enveloping (mostly on their NW) the Superior, Winnipeg, Reindeer, Athabasca, Great Slave, and Great Bear Lakes. The 'finger-prints' of these features resemble the configurations and distribution pattern of Early Proterozoic (2.0 to 1.8 Ga) collisional curvilinear orogenic belts, across which the seven provinces of the Laurentian proto-craton were aggregated and welded together during post Late Archean times (Hoffman, 1989, p. 465 and Figs. 3, 13, 17, 20, and 47). Many of the individual features within these two patterns could be correlated. The above data corroborate our interpretation on the tectonic origin of the Great Lakes geosuture as well as its old age.

Both the Southern and Northern Appalachians curve eastward to merge with the E-W trending geosuture of the Nantucket Island-New England (Kelvin) Seamounts. Beyond that point the merged geosuture extends further eastward along the Atlantis-Canary Islands F.Z. to cross the coastline into NW Africa along the South Atlas Geosuture.

The same pattern of eastward kinking is repeatedly noted in the offshore, across additional northeastward trending (coast-parallel) geosutures associated with linear magnetic anomalies. These kinks occur at the crossing points of the northeastward trending and coast-perpendicular geosutures. The former are recognized in the offshore, to a distance of almost 1500 km, as prominent magnetic anomalies which parallel the shelf edge off the East Coast of North America between the Florida-Bahamas and the east coast of the Labrador Sea, as well as across the trough of the NW Atlantic Abyssal Plain.

The most important WNW-ESE trending geosutures, which are perpendicularly crossing the Atlantic coastline of North America, are:

i) The Lincoln Sea-Baffin Bay-Davis Strait-Labrador Sea (eastern coastline)-Charcot-Biscay-Pyrenees geosuture.

ii) The Great Lakes-New England (Kelvin) Seamounts-Atlantis F.Z-Canary Islands-South Atlas geosuture.

iii) The geosuture running via Franklin Bay (SE Beaufort Sea)-Vancouver Island, across the Rocky Mts., along the 'Ancestral Rockies'-Ouachita-Florida-Bahamas and the Nares Abyssal Plain, to Cape Verde-Dakar, and across Africa south of the Ahaggar Massif, along the eastern flank of Jebel Akhdar, and across the Eastern Mediterranean Sea (along the Strabo-Herodotus geosuture and Antalya), to merge with the E. Menderes Massif (the Aegean Vortex) (Fig. 22.1, 22.3 to **22.5**; Bally, 1989, Plate I (A and B); Emery and Uchupi, 1984, Chart I; Behrendt and Grim, 1983, Maps A, B, and C).

Returning to the origin of the entire length of the Great Lakes Geosuture, another type of information should also be considered. Frape and Fritz (1987, Fig. 1) describe a linearly distributed pattern of gold (and other ore minerals) mines penetrating 1000 to 3000 m into the Archean plutons of the Canadian Shield (Fig. 22.3). The hypothesis of both the tectonic origin and antiquity of that linear feature is corroborated by the unique linear pattern formed by these mines, that exactly corresponds with the Great Lakes lineament, and the inferred history of these ores' depositional processes until reaching the deep seated veins (*i.e.* the separation of residual magmatic liquids which migrated along faults to be precipitated during Precambrian time). Moreover, the presence of another linear chain (although relatively short) of numerous similar ore mines which are distributed along a NNE perpendicularly trending pattern, between Sudbury (NE corner of Lake Huron) and Matagami (SE of Hudson Bay), suggest an analogous history. The NNE trend of that feature raises the possibility that originally it was unified with a southwestward extension of the Midcontinent Gravity and Magnetic Highs (see Fig. 22.3 above). It is therefore possible that sometime in the past a right-lateral shift of close to 600 km occurred across this NNE trending linear geological feature and along the Great Lakes Geosuture (Figs. 22.1, 22.3). The same sense of movement was also marked by Neev and Hall (1982, Fig. 2) along the eastern segments of that geosuture, namely the South Atlas and the New England (Kelvin) Seamounts-Long Island-Great Lakes.

The Gulf of Mexico Geosutures:
Post Late Precambrian geosutures across the Southeast Margin of North America (Figs. 22.1, 22.3, 22.4a and b).

The existence of the Guinea Bissau (W. Africa)-Bahamas-Florida-Ouachita-Ancestral Rocky Mountains (Oklahoma) geosuture, was discussed by Neev and Hall (1982). As expressed in Sections II and III, we believe that the entire global system of geosutures has functioned since Precambrian time. That interpretation is corroborated by a crustal study on the structure and evolution of the southeastern margin of North America (made by Buffler and Thomas, 1994, text and Figs. 2, 3, 6, 7, 15). The crust within the discussed region was and is disturbed since Late Precambrian time along the following two different linear tectonic trends, which cross one another:

i) the WNW-ESE trending Texas Transform, Alabama-Oklahoma (=our Bahamas-Florida-Ouachita-Ancestral Rockies); and the Virginia-Tennessee (=our Cape Lookout – Cumberland Gap-Wollaston-Reindeer Lake Geosuture);

ii) the NNE-SSW rifts (associated with magmatic intrusions); The Marathon-Mid Continent positive anomalies; The Mississippi Graben-Grenville Front; And the thrusted foldbelts of the Appalachian Geosuture, *i.e.* the Pine Mountain-Birmingham-Blue Ridge; The Mid-Iapetus Ridge (= our East Coast Magnetic Anomaly). A similar approach is also inferred from Ortega-Gutierrez et al. (1994, Figs. 6, 8, 9, 10).

Although the discussed movements along both of these trends of geosutures took place continuously all through their geological history, the nature of the regional tectonics appreciably changed with time. It occurred in three phases, mostly across the NE-SW trending rifts: Phase A (Late Precambrian-Early Paleozoic time) was dominated by crustal divergence. Phase B (Late Paleozoic) was characterized by converging-compressional activities along present-day NE-SW trending geosutures. During Phase C, diverging activity was renewed in the Early Mesozoic and is still going on. Nevertheless, some activities were maintained along orogenic features such as the Appalachians, during all three phases. The same also applies to movements across the WNW-ESE trending transforms (geosutures) that have maintained their horizontal differential (strike-slip) movements.

The first indication for the subsidence of the Gulf of Mexico is known from early Middle-Jurassic time (Phase C). It occurred because of the accumulation of the heavier oceanic crust at its center, due to the crustal stretching across NE-SW trending pre-existing rifts. It was associated with strike slip and vertical movements along Mesozoic-transform systems. Essentially these movements have rejuvenated earlier activities along the early Paleozoic transform system. The factors causing the subsidence of the Gulfs are explained by Buffler and Thomas (1994, p. 219, Fig. 1) and Ortega-Gutierrez et al. (1994, Fig. 13, 17, 19) as having been associated with:

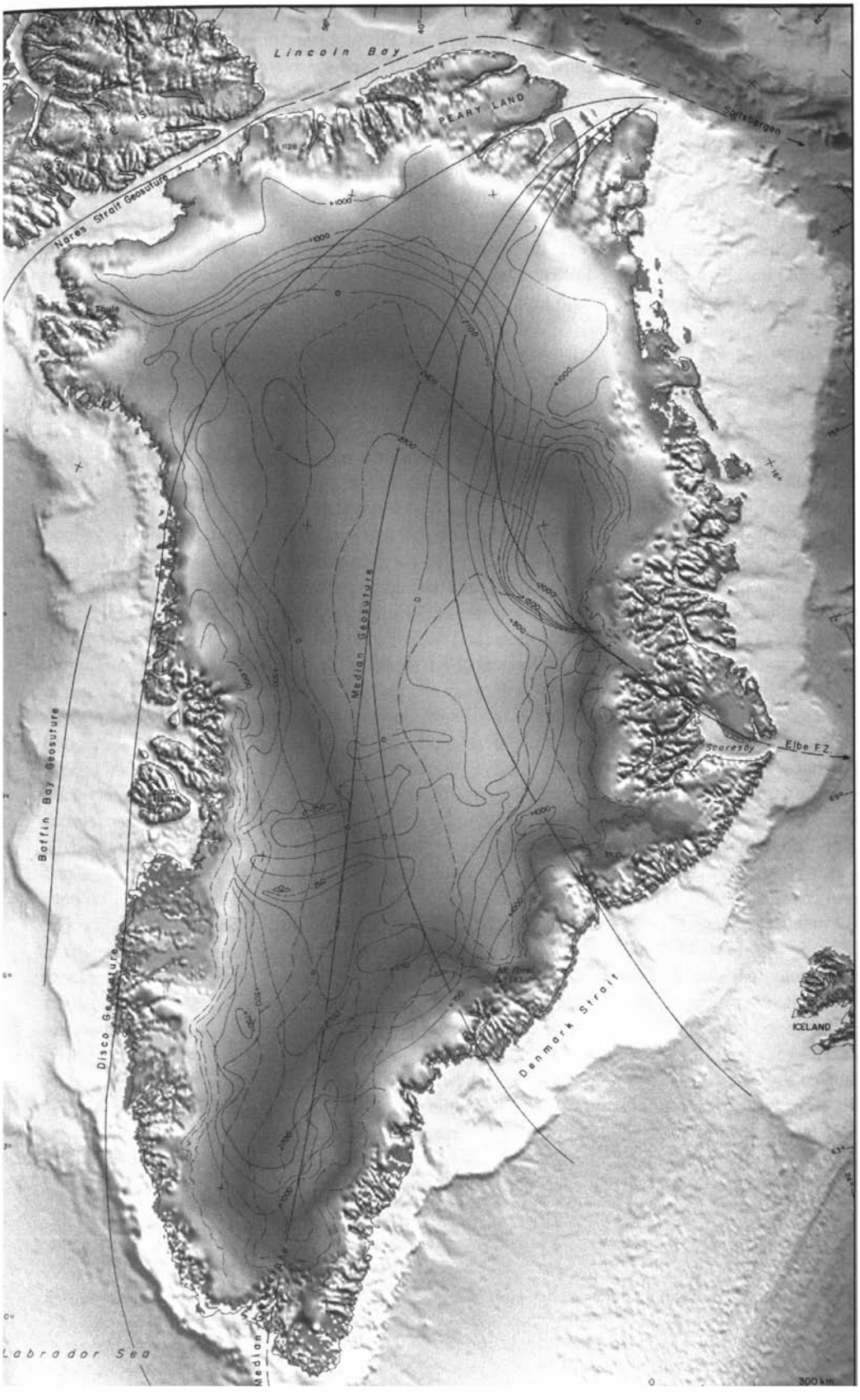
i) The separation of the North and South Americas (breakup of Pangea); and

ii) The thermal cooling of the new crust.

We infer from both Ortega-Gutierrez et al. (*ibid*, Figs. 2, 3, 5) and from Buffler and Thomas (*ibid*, Figs. 1, 14) that the oceanic crust under the Mexican Gulf attains a circular shape: On its west it is limited by the southern extension of the Rocky Mountains and the Pacific Ocean, on its south by the trans-Mexican Volcanic belt, and in the east by the Yucatan Peninsula. The circle is completed in the north along the E-W trending submarine limit of the continental crust of the southeastern U.S. It seems plausible to assume that the oceanic crust beneath the Gulf is subsiding gravitationally or even being sucked downward (instead of an upward piercing mechanism).

Considering the whole mantle convection process, and the associated global counter-clockwise flow pattern of the upper mantle, the southeastward flowing upper mantle on its route from the Pacific Ocean toward the Gulf of Mexico, and through the gap between the continental shields of the Americas, could converge


GREENLAND
Shelf
Barents Sea
Baffin Bay
Norwegian Sea
ICELAND
Greenland Basin
Reykjanes R.
Greenland Fracture Zone
Jan Mayen
Iceland Basin
Rockall
Scotland
Moscow
Black Sea
Caspian Sea
Tripoli
Ghadames
Erg Oriental
Erg Occid.
Atlas Mts.
Atlantic Ocean
Kane
Kelvin
Vema
Quaternary
Atlantis
Bermuda
Azores
C.Cod
3rd Bank
Grand Banks
Newfoundland
Labrador Sea
Sea of Labrador
Davis Strait
Baffin Island
Hudson Bay
Hudson Strait
Ungava Peninsula
Ungava Bay
Labrador
Nain
Hopedale
Makkovik
Cape Harrison
Cape Chidley
Resolution I.
Belle Isle
Strait of Belle Isle
Anticosti I.
Gulf of St. Lawrence
Gaspe Peninsula
Gaspe
Quebec
Montreal
Ottawa
Toronto
Lake Ontario
Lake Erie
Lake Michigan
Lake Huron
Lake Superior
Lake Winnipeg
Lake Manitoba
Lake Athabasca
Great Slave Lake
Great Bear Lake
Mackenzie R.
Mackenzie Mts.
Yukon
Alaska
Aleutian Trench
Aleutian Islands
Kodiak I.
Gulf of Alaska
Vancouver I.
Vancouver
Seattle
Portland
San Francisco
Los Angeles
San Diego
Mexico City
Gulf of Mexico
Yucatan
Cuba
Havana
Jamaica
Haiti
Puerto Rico
Trinidad
Caribbean Sea
Venezuela Basin
Colombia Basin
Panama
Panama Canal
Maracaibo
Caracas
Barbados
Guyana
Suriname
French Guiana
Cayenne
Paramaribo
Georgetown
Manaus
Amazon
Amazon Cone
Para
Belem
Fortaleza
Natal
Recife
Salvador
Brasilia
Mato Grosso
Goias
Minas Gerais
Vitoria
Rio de Janeiro
S. Paulo
Santos
Parana
Rio Grande
Montevideo
Uruguay
Buenos Aires
Argentina
Rio Grande Rise
Argentine Rise
Falkland Plateau
Falkland Is.
Malvinas Basin
Magellan Basin
Tierra del Fuego
Cape Horn
S. Georgia
Scotia Sea
Drake Passage
Antarctic Peninsula
Weddell Sea
Ronne Ice Shelf
Filchner Ice Shelf
Antarctica
Dakar
Cape Verde
Bissau
Bamako
Niger R.
Niamey
Benue
Lake Chad
Tibesti
Ahaggar
Sudan
Khartoum
Nile R.
Libya
Egypt
Cairo
Suez Canal
Red Sea
Arabian Peninsula
Persian Gulf
Iran
Iraq
Turkey
Ankara
Istanbul
Black Sea
Caspian Sea
Aral Sea
Kazakhstan
Urals
Moscow
Volga R.
Caspian Depression
Barents Sea
Novaya Zemlya
Kara Sea
Taimyr Peninsula
Lena R.
Yakutsk
Verkhoyansk Mts.
Kolyma Mts.
Chukchi Sea
Bering Sea
Bering Strait
Wrangel I.
Beaufort Sea
Prudhoe Bay
Point Barrow
Arctic Ocean
Canada Basin
Alpha Ridge
Lomonosov Ridge
Nansen Basin
Franz Josef Land
Spitsbergen
Greenland Sea
Jan Mayen
Iceland
Faroe Islands
Faroe Ridge
Rockall
Scotland
Ireland
Dublin
Belfast
Irish Sea
Wales
Cardiff
London
Paris
Seine R.
Rhine R.
Rhine Graben
Black Forest
Alps
Geneva
Lyon
Rhone R.
Marseille
Corsica
Sardinia
Balearic Islands
Madrid
Spain
Portugal
Lisbon
Tagus R.
Gibraltar
Strait of Gibraltar
Alboran Sea
Algeria
Algiers
Tunisia
Tunis
Sicily
Malta
Italy
Rome
Naples
Po R.
Venice
Adriatic Sea
Greece
Athens
Crete
Aegean Sea
Dardanelles
Sea of Marmara
Bosporus
Ukraine
Kiev
Dnieper R.
Volga R.
Don R.
Sea of Azov
Crimea
Sevastopol
Odessa
Romania
Bucharest
Hungary
Budapest
Danube R.
Poland
Warsaw
Vistula R.
Baltic Sea
Gulf of Bothnia
Gulf of Finland
Helsinki
Stockholm
Sweden
Norway
Oslo
Oslo Graben
Skagerrak
Kattegat
Denmark
Copenhagen
North Sea
Dogger Bank
Hebrides
Orkney Islands
Shetland Islands
Faroe-Shetland Channel
Rockall Trough
Porcupine Seabight
Celtic Sea
English Channel
Bay of Biscay
Brittany
Normandy
Netherlands
Amsterdam
Belgium
Brussels
Luxembourg
Switzerland
Zurich
Austria
Vienna
Czechoslovakia
Prague
Germany
Berlin
Hamburg
Munich
Frankfurt
Cologne
Ruhr
Elbe R.
Weser R.
Oder R.
Vistula R.
Pripet Marshes
Belarus
Minsk
Lithuania
Latvia
Estonia
Riga
Tallinn
Finland
Helsinki
Gulf of Bothnia
Lapland
Kola Peninsula
Murmansk
White Sea
Arkhangelsk
Novaya Zemlya
Kara Sea
Taimyr Peninsula
Severnaya Zemlya
New Siberian Islands



Background for 22.4a is from ETOPO2 at 2' grid spacing, Mercator projection. Basemap for Figure 22.4b of Greenland is from National Geographic Atlas Plate 30. Background is ETOPO2 2' grid spacing, Azimuthal Equidistant projection, central meridian 90°W and central parallel 90°N.

and generate a vortical pattern. Magmatic vortices, similarly to hydraulic ones, are expected to occur where the velocities of the currents involved are being choked, upon approaching bottlenecks or points of convergence with other currents, where friction increases. It is not impossible therefore that the origin of the Mexican Gulf was associated with a vortical mechanism.

Vb: The Pelusium Line (Neev, 1975; Neev, 1977; Neev, Hall and Saul, 1982; our Fig. 22.1, 22.4, and 22.5):
On the antiquity (pre-Early Paleozoic) of the Pelusium Line along the Benue-Amazon troughs (Fig. 22.1) and its landward extensions across and beyond both the eastern and western limits of the Atlantic Ocean.

Wilson (1965, p. 345, Fig. 7) postulates that the apparent offsets across the Mid-Atlantic ridge are inherited from the shape of the break that first formed between the coasts of Africa and the Americas. The above is in agreement with Heezen's postulation (1962, p. 247) of more than 3,000 km of left-lateral displacement of the Mid-Atlantic Ridge along the *en-echelon* sinistral system of the Equatorial Fracture Zone extending between the Chain and Vema-Bahamas fracture zones (between 2°S and 15°N respectively).

Its track should be headed into the Atlantic Ocean near Accra (Ghana-W. Africa) and emerge westward at Sao Luis (NE Brazil) exactly where predicted by Miller (1985 after Hurley, 1968). According to Francheteau and Le Pichon (1972, Figs. 4, 5, and p. 996) the Chain F.Z. parallels the E-W trending southern limit of the Apodi basin (NE Brazil close to 37°-55'W) "which would be the homolog of the Benue Trough".

Following DeLoczy (1970), Gansser (1973) and Ladd (1976) the Atlantic equatorial fracture zones can be connected via the E-W trending Amazon sinistral transcurrent zone to the Carnegie-Galapagos Ridge in the Pacific. The above is also in the agreement with the concept of the sinistral differential movements of the Guayana and Brazilian shields as well as with respect to the southernmost limits of the North American continent. These movements occur along the Amazon, Orinoco, the Trans-Mexico Neovolcanic Belt (deCaerna, 1989, Fig. 5; our Fig. 22.1 and 22.3) and the Texas shears as well as the Guinea-Bissau-Florida left-lateral F.Z. It is also in agreement with the overall respective sinistral movement postulated to have functioned between North and South America (Neev and Hall, 1982, and our Fig. 22.1).

Grabert (1976, 1983, Fig. 1) postulates the Amazon graben, with its Early Paleozoic sedimentary fill, to be a huge geofracture that extends from Guayaquil in the west (at the Pacific coast of Ecuador) through the equatorial fracture zones of the Atlantic, via the Benue graben (Gulf of Guinea) to terminate at Lake Chad (Central Africa). We also agree with his conclusion that this linear feature originated in Precambrian times, although differential movements have rejuvenated it several times since then (Neev and Hall, 1982). That consideration is based upon subsurface data – mostly stratigraphic isopaching and facial aspects – from the Amazon graben (Grabert, 1976, Figs. 1, 2-4). Based on these data it is also suggested that the discussed trough subsided in stages at least since Ordovician times.

Vc: The North Atlantic Basin and its western and eastern limits: The Appalachian-Mauritanian Fold Belts (Figs. 22.4, 22.5 and 22.6):

Le Pichon and Fox (1971) and Le Pichon et al. (1971, 1977) suggested the following four fracture zones to bridge between the North American and West African coastlines across the Atlantic Ocean: (1) the Bahamas-Guinea Bissau; (2) Cape Fear-Cape Verde; (3) Norfolk-Cape Blanc; (4) Cape Cod-Canary Islands-Tarfaya-South Atlas. We adopt their postulate, but consider these fracture zones to be segments within geosutures which are incorporated within the proposed global system. The following discussion is not limited to these four but expanded to those crossing the Atlantic Ocean farther to the north even into the Arctic. It deals with both the antiquity and the unique affinities of these Atlantic crossing geosutures, as well as the adjacent continents (including the Appalachian and Mauritanide NE-SW trending orogenic belts).

The overall NE trend of the Appalachian belt is changing its course systematically and rather abruptly both to the ENE and to the NNE in an alternating dogleg mode of kinks. Some of these kinks are correlated with similar features such as those found across the NE trending Mid-Continental Gravity and Magnetic Anomaly (Fig. 22.3). Identification of the bridging segments across the Atlantic Ocean and the Appalachians are sometimes problematic, as explained by Le Pichon et al. (1977, p. 183): "the continentward extensions of the Cape Fear and Cape Blanc flow-lines mark major changes in trends and structures of both the Appalachian and Mauritanides Late Paleozoic fold belts. The landward (westward) extensions of the Norfolk fracture zone strikes the Blue Ridge in the middle of one of the straightest stretches in the northern Virginia segment. It lies about 150 km to the north of the major Roanoke recess which marks a major change in the trend of the Appalachian fold belt. The lack of coincidence between the new oceanic fracture zone and the zone of major changes in the adjacent continental fold belts, may be explained by the fact that both structures are conditioned by older structures". Such an interpretation corroborates our postulation regarding the antiquity of the geosutures, as well as their crossing both continents and

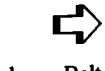
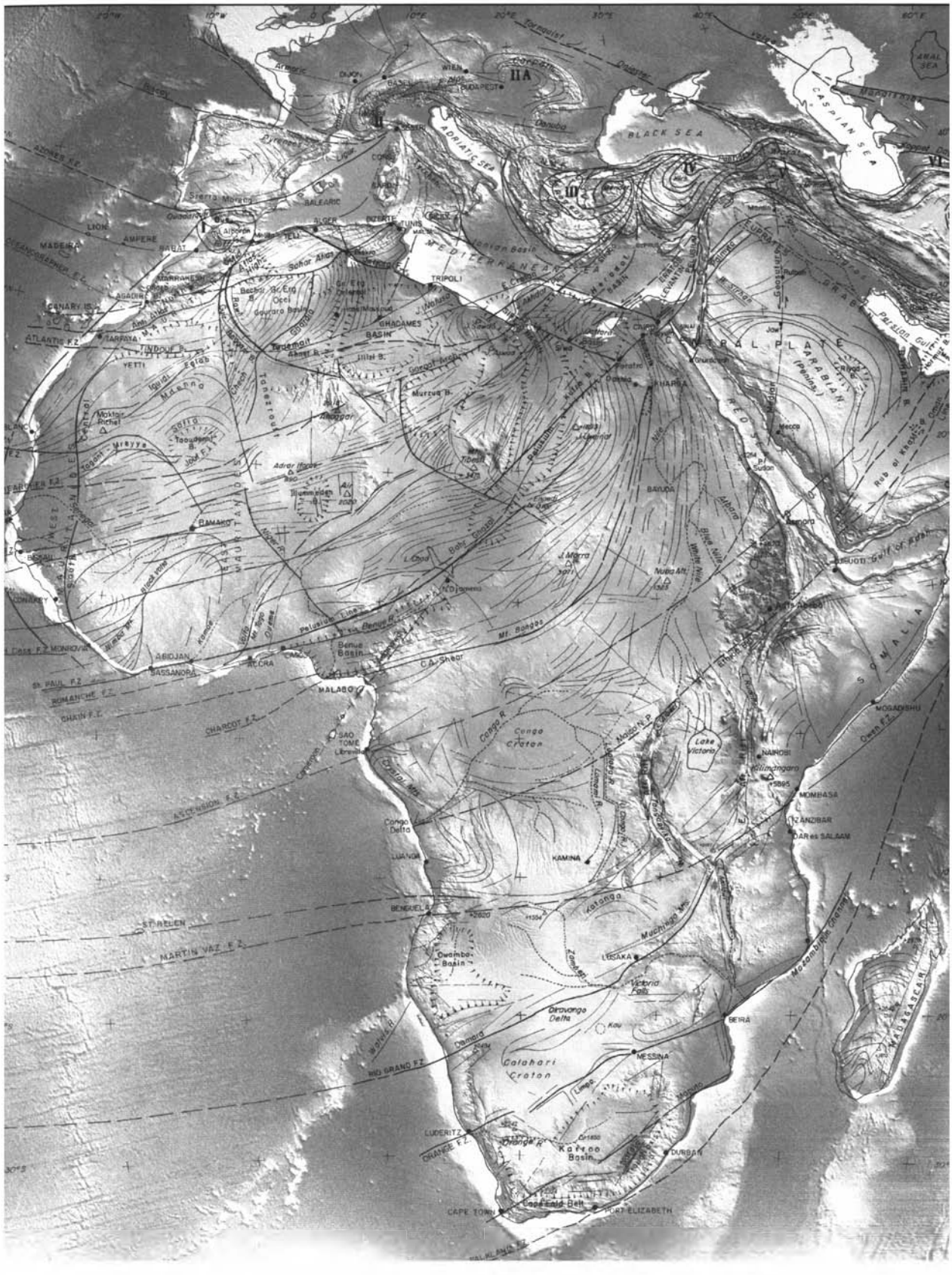
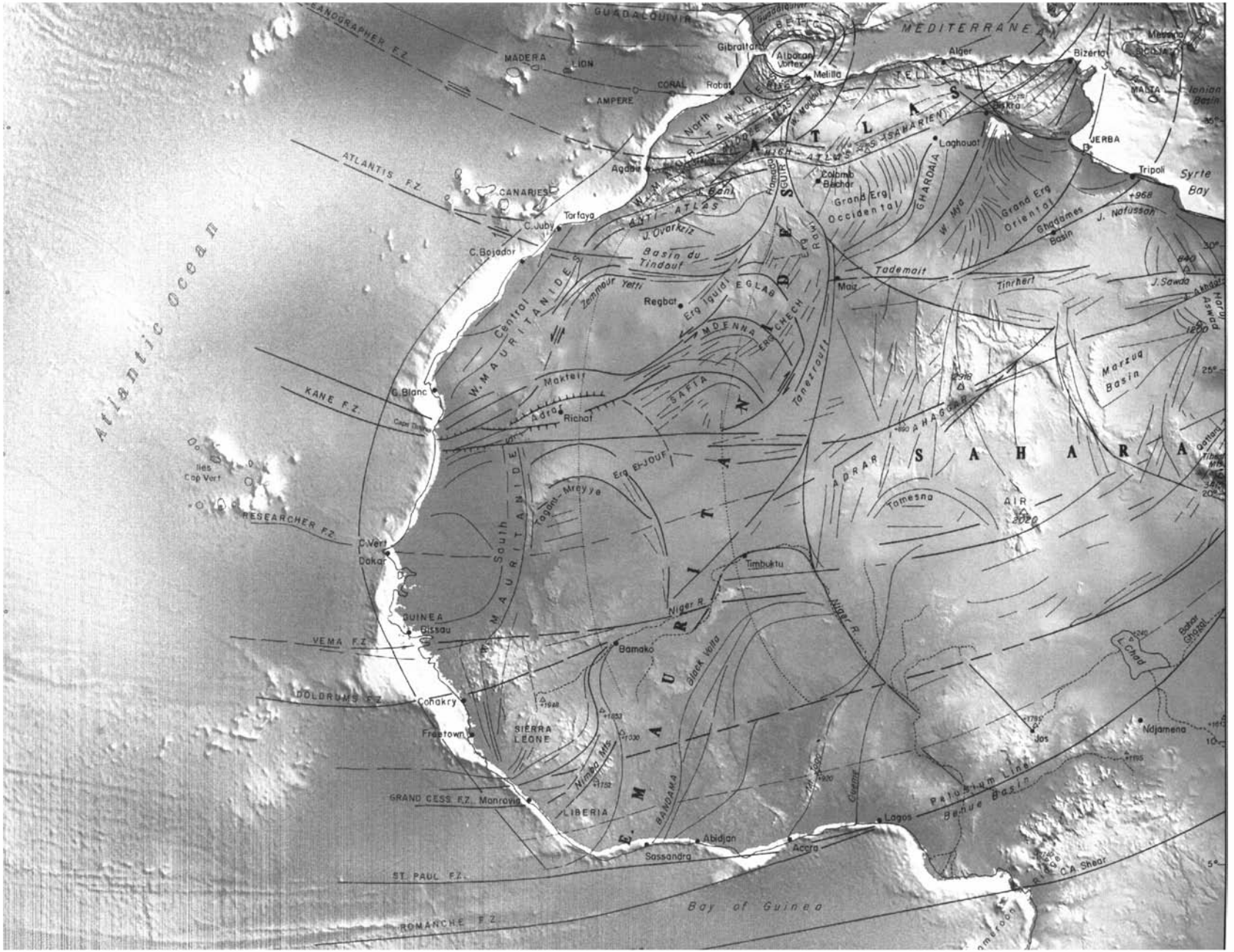


Figure 22.5. The African Continent and the Arabian Peninsula: Six of the eight vortices along the Global Eye (which is the Alpine-Himalayan Belt - see the text) are marked in this figure by Roman Numerals. The major geosutures of the Global System are marked by thicker lines. Secondary geosutures, situated between the major ones, are traced by thinner lines. Major basins are encircled by virtual lines of small wedges. Elevations of major mountain peaks are indicated by triangles with the altitude in meters. Rivers are indicated by dashed lines. Basemap is National Geographic Atlas Plate 109, ETOPO2 global 2' elevations/depths. Azimuthal Equidistant projection, central meridian 20°E and central parallel 10°S.


BLACK SEA
CASPIAN SEA
ARAL SEA
MEDITERRANEAN SEA
ADRIATIC SEA
ARABIAN PLATE
SOMALIA
Congo Craton
Kalahari Craton
Karroo Basin
Owambo Basin
Okavango Delta
Congo Delta
Lake Victoria
Benue Trough
Red Sea
Gulf of Aden
Persian Gulf
Mediterranean Ridge
Nile R.
Congo R.
Zambezi R.
Orange R.
Limpopo R.
Niger R.
Senegal R.
Volta R.
Benue R.
Tibesti Mts.
Hoggar Mts.
Air Mts.
Ahaggar
Darfur
Kordofan
Ethiopian Plateau
Nubia Mt.
Kilimanjaro
Mt. Bongo
Mt. Cameroon
Mt. Elgon
Mt. Kenya
Mt. Meru
Mt. Margherita
Mt. Stanley
Mt. Kilimanjaro
Mt. Mulanje
Mt. Moramba
Mt. Gamsberg
Mt. Brandberg
Mt. Erongo
Mt. Waterberg
Mt. Soutpansberg
Mt. Drakensberg
Mt. Lebombo
Mt. Chimanimani
Mt. Nyanga
Mt. Inyangani


Atlantic Ocean
MEDITERRANEAN
GUADALQUIVIR
Gibraltar
Alboran Vortex
Melilla
Alger
Bizerta
Messina
SICILY
MALTA
Ionian Basin
MADERA
LION
CORAL
AMPERE
Rabat
ATLANTIS F.Z.
CANARIES
Agadir
Laghouat
JERBA
Tripoli
Syrte Bay
Tarfaya
C. Juby
C. Bojador
Colomb Bechar
Grand Erg Occidental
GHARDAIA
Ghadames Basin
J. Nafussah
Basin du Tindouf
Tademait
Maiz
Tinrhert
Regbat
Erg Iguidi
EGLAB
Zemmour
Yetti
MOENNA
Erg CHECH
Tanezrouft
Marzuq Basin
J. Sawda
Harud Aswad
KANE F.Z.
G. Blanc
Cape Timiris
Makteir
Adra
Richat
SAFFA
AHAGGAR
ADRAR
SAHARA
Tamesna
AIR
2020
Iles Cap Vert
RESEARCHER F.Z.
C. Vert
Dakar
Erg Er-JOUF
Tagant-Mreyye
Timbuktu
Niger R.
GUINEA
Bissau
VEMA F.Z.
Bamako
Black Volta
DOLDRUMS F.Z.
Conakry
Freetown
SIERRA LEONE
Nimba Mts.
GRAND CESS F.Z.
Monrovia
LIBERIA
BANDAMA
Abidjan
Sassandra
Accra
Lagos
Benue Trough
Pati Sham Line
Jos
Ndjamena
L. Chad
Baker Chotal
C.A. Shear
ST. PAUL F.Z.
ROMANCHE F.Z.
Bay of Guinea

oceans in a perpetually rejuvenating process on a global scale. It is also in agreement with the concept of Wilson (1966) on the cyclic nature of the ocean floor opening and closing process (although we cannot yet explain its origin).

Another aspect of that subject deals with the antiquity of the dogleg feature, occurring where the Appalachians are crossed by a segment of the Great Lakes-Long Island-Cape Cod- New England (Kelvin) Seamount-Canary Island and the Tarfaya-South Atlas geosuture (Figs. 22.3 and 22.5). Le Pichon et al. (1977) quotes Drake and Woodward (1963) who proposed that the change of the Appalachian axis from NNE to almost E-W along a 350 km segment between Altoona (Pennsylvania) and New York City is a "...right-lateral strike slip fault with an offset of 140km, *[which]* lies beneath the Triassic basin... That offset reflects angular irregularities in the Early Paleozoic edge of the North American continent formed in Late Precambrian." The right-lateral sense of movement seems to us to have been maintained along that geosuture across the Mid-Atlantic Ridge as far as the South Atlas and beyond. Drake and Woodward (1963) also postulate that the Kelvin seamount chain lies in the prolongation of the 40° discontinuity.

The term Mauritanides was coined by Sougy (1962) for the Paleozoic orogenic belt formed all along the Atlantic coastline of NW Africa from Liberia in the south to Tanger-Melilla (Mediterranean coast of Morocco) in the north – a length of more than 3000 km (Figs. 22.1, 22.4a, 22.5, 22.6 and **22.7**). West to east trending geosutures, which emerge from the Atlantic coast of NW Africa and extend inland for very long distances, are recognized by Sougy (1962) to cause transverse deflections across the Mauritanides, such as the Tindouf Basin with its thick sedimentary fill. The latter is also identified along an inland extension of the Atlantis F.Z.-Canary Island-Tarfaya (Cape Juby) that runs along the southern limits of the Atlas ranges. A number of structural curvilinear features branch off to the NE to reach further to the north from the E-W trending landward extensions of the fracture zones (or geosutures) of the Atlantic Ocean. These are aggregated into four sub-groups:

i) The Middle Atlas, which curves northward from the Tarfaya-Agadir coastal zone and terminates in a vortical mode at the Alboran (Gibraltar) basin;

ii) The entire complex of the ENE-WSW trending Atlas orogenic system (namely the Tell, High, and Saharan Atlas ranges), which are gradually curving northward and are crossing the Mediterranean coastline close to Bizerte and Tunis;

iii) Some of the counterclockwise curving geosutures are merging with the Western Mauritanides while others merge with the Eastern Mauritanides. The Western Mauritanides bound the two northward trending sequences of southward concave structures, which are paralleling one another, namely the Mreyye-Yetti, as well as the Safia-Mdennah-Eglab-Rawi northward trending sequences. The Adrar (Richat) ENE trending canoe-shaped structure, with the circular granite plug at its top, has developed along one of the counterclockwise curving geosutures. It branches off of the Kane F.Z. and curves counterclockwise around the Richat and Makteir southward concave arcs;

iv) The geosutures of the Monrovia-Nimba Mts.-Bamako-uppermost Niger River and the Sassandra-Bandama-Black Volta Rivers branch off gradually toward the NNE from the Grand Cess and St. Paul Fracture Zones respectively (Behrendt and Grim, 1983; Behrendt et al., 1974). These two geosutures are bounding the Eastern Mauritanides along both its flanks.

Each of the three southward concave arcs (namely the Safia-Mdennah-Eglab within sub-group iv above) is branching off counterclockwise from their original linear N-S trending geosuture. We believe that this sequence of southward concave structure, together with similar and parallel ones, are forming the Eastern Mauritanide ranges (which are subparallel to the western ones). These two ranges are approaching each other from the south northward to merge in the north at the Alboran vortex (between Rabat and Melilla) (Figs. 22.5 and 22.6). East of Dakar, their combined width is close to 1000 km, whereas in the north between Rabat and Wadi Moulouya, it is just 300 km.

Alternation of older and younger E-W trending zones across the close to N-S trending Western Mauritanides belt indicate the splitting of the latter into tectonically subsiding and uplifted transversal zones developed along the landward extensions of the oceanic geosutures. Excessive deposition of younger sediments (of Cretaceous, Tertiary, and Quaternary age) occurs along the structurally negative zones, whereas excessive erosion of Mesozoic, Paleozoic, and Precambrian rocks occurs across the structurally positive areas.

The great N-S trending orogenic belt of the Mauritanides could have extended farther northward along the western flank of the Iberian Peninsula to join the Caledonides of Ireland, Scotland, and Norway.



Figure 22.6. Northwest Africa (rotated): Major E-W trending geosutures are crossing the Atlantic coastline into NW Africa and mapped as photo-lineaments Often linear dunes are deposited along the faults and the tectonic troughs, thereby emphasizing their structure-related nature rather than just an eolian mechanism. The close to latitudinally trending geosutures are crossing through the close to meridionally-trending West African coastline and the double belt of the western and eastern Mauritanides (that converge northward). Counterclockwise branching-off patterns away from the latitudinal geosutures are often noted. A few of those branching-off geosutures are crossing the Mediterranean Basin (Figs. 22.10a, b) northward, thereby forming sills which divide it into the following secondary basins: Alboran, Balaeric, Tyrhennian, Ionian, western Levantine (Herodotus), and eastern Levantine (see Fig. 22.11 below). The basic pattern is inferred after the International Bathymetric Chart of the Mediterranean (IOC, 1981) and the National Geographic Atlas (1995, Maps 90-92). Symbols are the same as in Figs. 22.4 and 22.5. Basemap is National Geographic Atlas Plate 109, ETOPO2 global 2' elevations/depths. Azimuthal Equidistant projection, central meridian 15°E and central parallel 15°S.

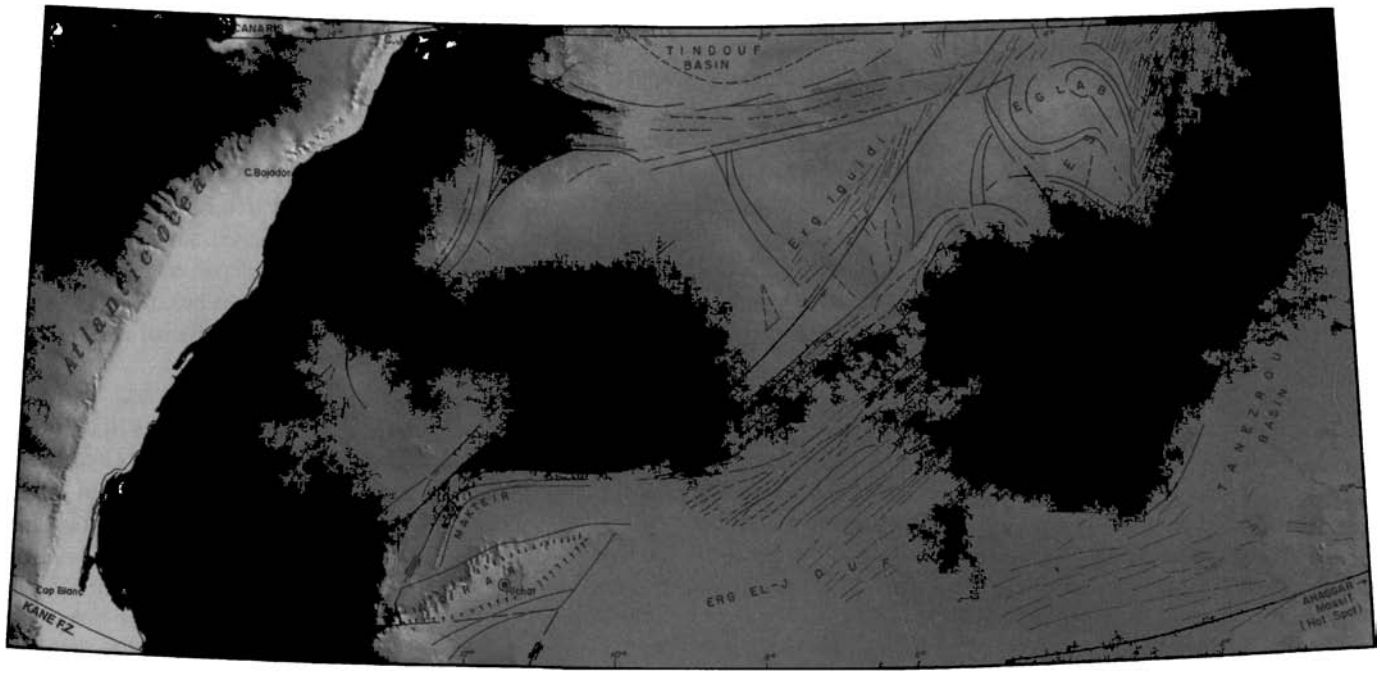


Figure 22.7. The Western Sahara: Structural relations between two almost orthogonal groups: 1) The more or less Meridional Group of the (N-S to NE-SW) trending and converging ranges of the West and East Mauritanides. Apparently the NNE-SSW trending twin ridges of the Mdenna and Eglab arcs on the east, and the analogous southward concave system of the Tagant-Mreyye (south of the figure), Adrar-Richat, and Makteir and Zemour-Yetti on the west also belong to the Meridional Group. 2) The second Latitudinal Group is composed of latitudinally trending geosutures that cross the Atlantic coastline eastward to form (i) the Atlantic F.Z.-Tindouf-Tademait Plateau (Algeria)-Jebel Sawda (Libya) in the north, and (ii) the Kane F.Z.-Richat (Adrar)-Ahaggar (Algeria)-Jebel Akhdar (Libya) in the south (see Fig. 22.6).
Legend:
i) Relatively thick lines – major tectonic geosutures.
ii) Thin lines (±dashes) are swarms of tectonic lineaments, emphasized by the entrapped eolian sands within the weathered furrows.
iii) Relatively short, linear diorite dikes are marked by thick alternating black and white segments. The correspondence of the trends of these dikes with those of the major structural features (both folds and faults) and with the dominating swarms of linear dunes, corroborates the involvement of the tectonic factor in the origin of the dunes.
Background is ACE satellite altimetry at 0.5' overlain on the GEBCO GDA global 1' grid of elavations and depths. Transverse Mercator projection, center meridian 9°W.

If our interpretation on the extended lengths of both the Appalachian (including the Caledonides of NE Greenland) and Mauritanides (including the NW European Caledonide orogenic belts) is correct, then the great similarity between these two systems (each close to 6000 km long) as well as the cumulative weight of other factors (see below), suggest a genetic relationship between the two. Such a connection between the British Caledonian and the Mauritanide (Western Sahara) orogenic belts appealed to Holmes (1951, p. 498), although, at that time, he did not find it adequately substantiated. We also concur with the interpretations of Wilson (1966, Figs. 1, 2, 3) and Umbgrove (1947, Plate 1) who consider the Caledonide range of NE Greenland to be the northernmost segment of the Appalachian orogenic belt. Following the Wilson Cycle concept (*ibid*) the Mauritanides-Caledonians and Appalachian ridges could have been formed as a continuous and joint system, perhaps repetitively activated during closure events of earlier cycles of the pre-rifting Iapetus (proto-Atlantic) Ocean.

Other aspects of the same subject are:

i) The similar ages of the orogenic phases along these two belts of the Appalachians and the Mauritanides, beginning with the youngest Precambrian Grenville orogen, are based on data from southern Sweden to southern Mexico (Hoffman, 1989, p. 496 and Figs. 13, 47). The rest of the phase came on in a sequence which ended in the Carboniferous (or even early Permian times) (Hartz et al., 1997; Haller, 1981);

ii) The Silurian-Carboniferous closing phase that followed the late Proterozoic-early Paleozoic Iapetus Ocean, was marked by westward thrusting and napping across East Greenland and North America, as well as eastward ones across Scandinavia and NW Africa (*i.e.* Haller, 1981; Hoffman, 1989, Fig. 13);

iii) The absence of Caledonides and Grenville rocks along the southeastern coastal ranges of Greenland and the presence of the latter (Grenvillian rocks) in core holes along the crest of the Rockall plateau (to the west of the Ireland-Scotland Caledonides) bothered many authors (*i.e.* Roberts et al., 1973; Van der Linden and Srivastava, 1975). We are not sure if Holmes (1951, p. 496,

Fig. 258) was correct in his suggestion regarding the route of the Caledonian-Hercynian (Appalachian) Front, that deviates along an S-shaped swell (or a broad rise) extending from Newfoundland-Labrador to traverse the ocean, thereby linking Greenland to Britain by way of Iceland and the Faroes;

iv) Prior to the beginning of the Jurassic phased sea-floor spreading, the Rockall Plateau existed as a transverse independent E-W trending block that was a part of the Greenland-Scotland Ridge (Emery and Uchupi, 1984, p. 654, Fig. 381, Chart XII). The southern limit of that ridge was marked by the joint suture along the Sea of Labrador and the Bay of Biscay (*ibid*, see below). We suggest the northern limit of that transverse rise which is marked by a northwestward extension of the Elbe Geosuture (Figs. 22.1, 22.7) (just north of Iceland) to enter Greenland through Scoresby Fjord.

The NW extension of the Elbe Geosuture separates the belt of NE Greenland (together with its Caledonides as well as Scandinavia and most of East Europe) and the southwestern half of Greenland (together with Western Europe), which is situated to the south and southwest of the Scoresby-Elbe geosuture. The southern limit of that southern belt is marked by the E-W trending coastline along the Pyrenees-Biscay geosuture.

Vd: The Sea of Labrador-Bay of Biscay Geosuture (Our Figs. 22.3 and 22.4):

As implied from the paleographic reconstruction of the North Atlantic region, the pre-rifting history of the above two features (Laughton, 1970, Figs. 10, 12, 14, 16-19), indicate them to be genetically related. The same holds true with regard to the reconstruction made by Le Pichon et al. (1977, Figs. 9, 10). In both of them the earlier (Paleozoic) phase of intensive seafloor closure is well expressed (Wilson, 1966). During that early phase the tectonic pattern, along which the subsequent opening process was carried out, had existed already. Accordingly a single (unified) zone of weakness seems to have preexisted along the troughs of the Bay of Biscay and the Labrador Sea joint feature, along which tectonic activities rejuvenated through geological time.

Arthaud and Matte (1977, Fig. 1) consider the Biscay-North Pyrenean Fault to separate the Iberian micro-plate from the rest of the West European continent. We interpret that geosuture to begin at the Sestri (Gulf of Genoa), extending westward across the Atlantic Ocean as a submarine anomaly (Le Pichon et al., 1977, Fig. 11). This same linear feature is also expressed as an almost continuous gravity anomaly, curving smoothly (concave northward) and crossing the Mid-Atlantic Ridge at a right angle. It curves gently again to the NW before entering the Labrador Sea, just north of Orphan Knoll, where it truncates and terminates the westernmost end of the E-W trending Charlie-Gibbs F.Z. (Haxby, 1987; Knudsen and Anderson, 1995; Smith and Sandwell, 1997a). It further continues northwestward along the shelf break off the NE coastline of Labrador, as inferred from the bathymetric, gravity, magnetic and seismic reflection data (Van der Linden and Srivastava, 1975, Figs. 1-7).

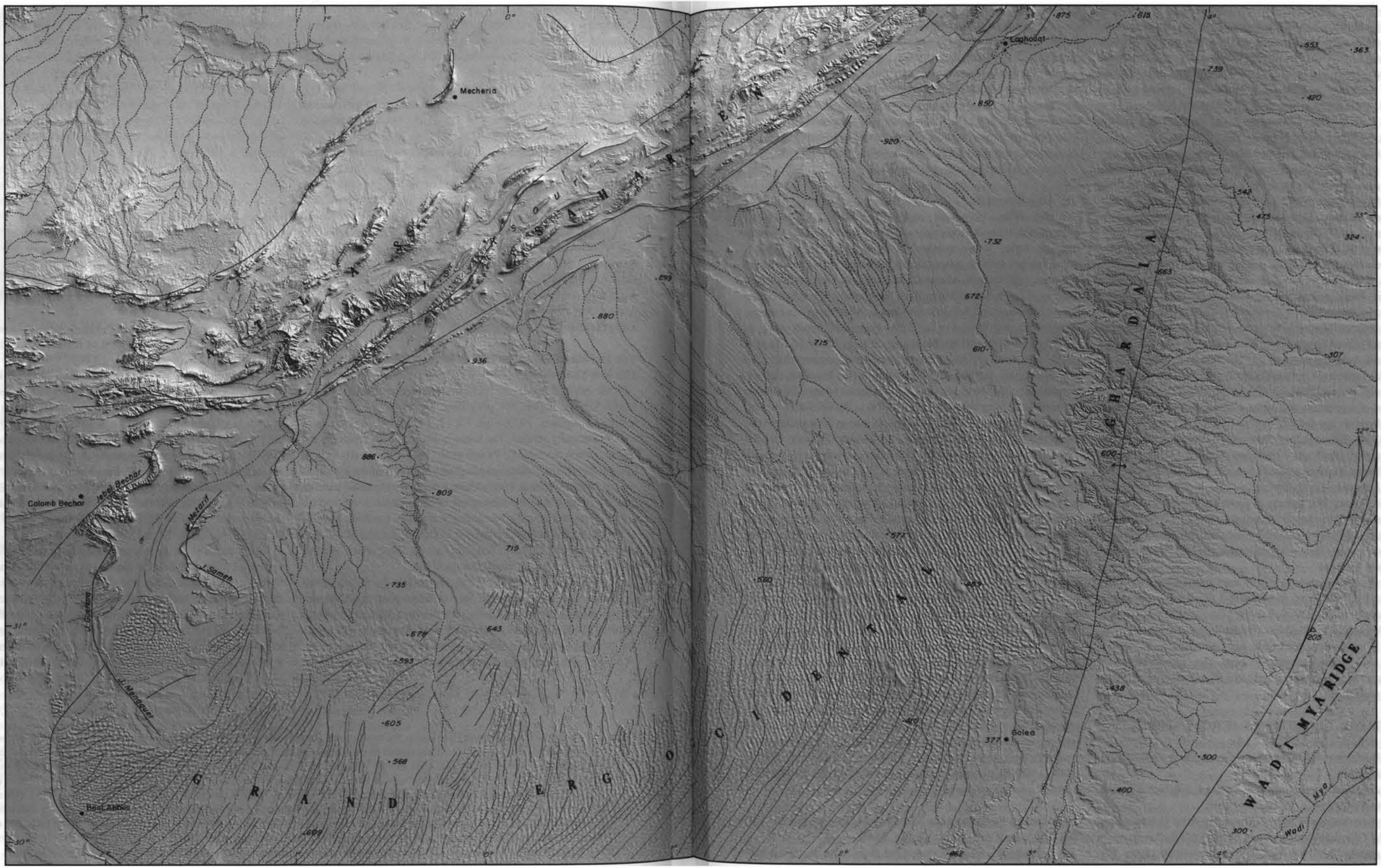
The Charlie-Gibbs transform fault is a 650 km long and 35 km wide linear ridge, resulting from the initial westward offset of the Northwest European sub-plate (British Isles, Armoric Massif and north of the Western Alps) and its continental margin (see above). It was forcibly intruded by ultrabasic magma through the tholeitic crust. We interpret the south boundary limit of that sub-plate to be related to a left-lateral offset of the region extending from the southeastern margin of the Labrador Sea, across the Mid-Atlantic Ridge and farther eastward along the Biscay and the Pyrenees faults. Its northern limit extends along a system of eastward trending right-lateral shifts, from Scoresby Sound in East Greenland, along the northern limit of Iceland, to continue along the Elbe geosuture (Fig. 22.4a).

The presence of very narrow and deep (6 to 20 km depths to the basement) trenches (or fosses) is noticed to underlie the bottom of the continental slope along the Atlantic Ocean coastlines of both North and South America as well as along both flanks of the Labrador Sea and the western coastlines of Europe and Africa. Very similar features are also extensively noticed elsewhere within the Atlantic Ocean, such as the Equatorial Fracture Zones (or the Pelusium Line between the Amazon and the Benue Basins), as well as the multiple occurrences of N-S trending features across the western Gulf of Mexico and the Caribbean Sea (Emery and Uchupi, 1984, Charts 5A and 5B).

Left-lateral shifts are recognized along the faults following the southern border fault and the median trough of the Labrador Sea, as well as the Charlie-Gibbs transform, upon their crossing of both the different segments of the Mid-Atlantic Ridge and the associated sets of N-S trending magnetic anomalies along its flanks. We therefore consider both of these faults to constitute an interrelated tectonic system along which the sub-plate of Northwestern Europe, together with south Greenland, had been left-laterally shifted



Figure 22.8. Grand Erg Occidental: For location, see north-central quadrant of Fig. 22.6. Sketch map of the pattern of hydraulically eroded system of drywash-rivers (dotted lines) and the linear system of sand dunes (marked by continuous thin lines) across the Western Grand Erg of the Northern Sahara (situated between the Saharan Atlas and the Tademait and Ghardaia features – see Fig. 22.6). That joined pattern of two erosional and tectonic systems suggests their generation by a coherent and unified factor. It is gradually curving clockwise from the north, in spite of the fact that it was generated by two agents (mechanisms) that genetically differ from one another (hydraulic erosion versus eolian deposition). That observation deserves an explanation that could be provided by a pre-existing, but still functioning, systematic fracturing process carried out across the relatively young sedimentary fill of that basin. That process seems to be associated with a torsional factor produced by the differential horizontal movements between the Saharan Atlas mountain ranges and the adjacent inter-mountain troughs.
Background is SRTM elevations on a 90 m grid, Transverse Mercator projection. Shading by Global Mapper®.


Mecheria
Laghouat
Colomb Bechar
Jebel Bechar
J. Metarfi
J. Sameh
J. Bechna
J. Mechaguer
Beat Abbes
Golea
ANTI-ATLAS
SOUTH ATLAS
ATLAS
GRAND ERG OCCIDENTAL
WADI MYA RIDGE
Wadi Mya
0°
1°
2°
3°
4°
29°
30°
31°
32°
33°
875
618
553
363
739
420
850
920
543
475
324
732
663
672
715
610
307
600
899
880
936
886
809
719
735
643
678
593
605
568
609
577
560
549
438
410
377
300
400
205

relative to that of Labrador-Newfoundland and Iberia across the Baffin Bay-Labrador Sea-Charcot geosuture. On the other hand the Caledonides of north Greenland and Norway are right-laterally shifted with respect to the British Caledonides and the North Appalachians-Grenville-Labrador belt. The pre-drift reconstruction pattern of Archean and Late Precambrian rocks across southern Greenland, the Labrador Sea, and SE Labrador (Quebec), is in agreement with the above interpretation of Precambrian sinistral shift along the trough of the Labrador Sea.

A Late Precambrian tectonic phase has produced a major system of grabens and horsts across the East Arctic archipelago, including also Baffin Bay, and the Labrador Sea. The resulting system of depressions allowed a seaway between the Iapetus (Proto-Atlantic) and the Arctic Ocean to function since those ancient times (Pelletier et al., 1975; Grant, 1975).

Parson et al. (1984) describe a randomly distributed pattern of limestone mounds at depths ranging between 1600 and 2300 m along a northwesterly trending submarine belt that parallels a bathymetric break across the present-day southern continental slope of the Labrador Sea. Orphan Knoll (Fig. 22.4a) is one of these mounds, which are interpreted to be depositional peaks consisting of resistant reef-related limestones of Late Paleozoic (Devonian) age. Nevertheless, a dredge rammed into the side of a pinnacle rising from the flat surface of Orphan Knoll recovered a rock sample, the standard palynological analysis of which yields a rich and varied assemblage of Acritarche and some Chitinozoans which indicate a Late Ordovician age for that mound (instead of Late Devonian) (Legault, 1982). Although that result and its inferred conclusion are still being argued (Ruffman, 1989), they should not be dismissed as they corroborate the above postulation regarding the Precambrian age of the Labrador-Biscay feature.

A close to regmatic pattern of geosutures is exhibited across most of the North American continent and the North Atlantic Basin on its west, as well as across North Africa and Western Europe, by territories on its east. These close to meridional trending geosutures (from west to east) are:

i) The cordillera (accompanied by the Coastal-Cascades-Sierra Nevada-Baja California on the west and the Rocky Mountains-Sierra Madre on its east), as well as the Mid-Continent Anomaly;

ii) The Appalachians; the Mid-Atlantic Ridge;

iii) The Mauritanides-Caledonide; and perhaps also

iv) The Ural Mountains orogenic belts. The close to latitudinal geosutures are more numerous, and more densely distributed (Figs. 22.1, 22.3 and 22.4).

VI: TECTONIC GEOSUTURES ACROSS AFRICA (Figs. 22.4a and b, 22.5, 22.6, 22.7 and 22.8):

VIa: North African (Mediterranean) Coastal Belt – A Regional-Structural Divide:

The structural-morphological attitude of this belt is clearly divided into the following two different units:

1) A western one, the WSW-ENE trending Atlas Belt (confined between the Gibraltar-Tunis segment of the SW Mediterranean in the north, and the Tarfaya-Jerba Island segment in the south - Fig. 22.6);

2) An eastern one, the WNW-ESE Libyan-Western Desert Belt (confined between the Tunis-Cairo Line in the north and the Jerba Island-Farafra Oasis on the Pelusium Line on the south - Fig. 22.5). Apparently that division is also responsible for the division of the Mediterranean Sea into its eastern and western basins.

Although we do not yet have a comprehensive or satisfactory explanation for this belt, it seems somehow to be related to the following enveloping vortices: The Alboran and Sestri Vortices in the western segment; and the Aegean (Menderes) and the Kirşehir Vortices in the eastern one - see Fig. 22.5).

The Atlas Geosuture

The Atlas Geosuture forms the landward (eastward) continuation of the Oceanographer-Madeira and the Atlantis-Canary Fracture Zones. It is comprised of three ENE trending folded-faulted ranges that are subparallel to each other. The southern one is named Anti Atlas (in Morocco) and Saharan Atlas (in Algeria); the central one is named High Atlas; the northern one is named the Rif (in Morocco) and Tell Atlas in Algeria. All of these three ranges converge toward Tunisia in the ENE, where their trends swing to the left (northeastward) in a branching off style. Based on Klemme (1958, Figs. 6 and 7) the Atlas geosuture curves counterclockwise and is plunging into the Mediterranean in two branches that are crossing the coastline at two sites; the westernmost one is branching off northward away from the Tellian Atlas at the Gulf of Bejaia (to the east of the port of Alger). It gradually curves counterclockwise along the troughs of the Algerian, the Sardino-Balearic and the Corso-Sardinian abyssal plains. The other one submerges beneath the Mediterranean Sea at Bizerte, which is the northernmost promontory of Tunisia. These two seem to extend northward along both flanks of the Sardinian-Corsican geosuture that forms the sill separating between the Balearic and Tyrrhenian basins (Fig. 22.5). These two branching off features follow along both bases of the eastern and western continental slopes of the two islands (although more prominently along the eastern one) and continue northward as far as Sestri (Vanney and Gennesseaux, 1985, Figs. 1.7; 1.11).

Klemme (1958) presents isopach and lithofacies evidence for the occurrences of three main stages of folding activities within the Atlas Province that correspond with the Caledonian, Hercynian and Alpine orogenic periods. According to Zizi (1996), an extensional tectonic regime affected the Precambrian basement of Morocco between Early Paleozoic and the end of Early Mesozoic times. Consequently, deep elongate basins (grabens) were formed along the present-day trends of both the High and Middle Atlas mountain ranges. That regime was inverted to a compressional-folding one during Late Cretaceous to Recent times, when the Mesozoic basement faults were reactivated. We interpret the tectonic regime of the entire Phanerozoic period (*i.e.* including the Paleozoic to Early Mesozoic) to have been a compressional one.

The Alboran Vortex and the Middle Atlas Ranges (*i.e.* the Rif-Tell, High, and Anti-Atlas - see Fig. 22.6):

Although the ENE trending three main Atlas ranges are sub-

parallel to each other, a few kinks are noticed along their long axes. There seems to be some correspondence between the locations and trends (NNE) of these kinks across the three main Atlas ranges, and the sites where the counterclockwise branching-off features are diagonally crossing them. The most prominent north-northeastward trending and branching-off feature within the Atlas orogenic belt corresponds with the Middle Atlas Mountains which coincides with the northward extension of the Mauritanide folded range trend (Klemme, 1958).

The SW end of the Middle Atlas merges with the SW segment of the High Atlas, at a point situated between Agadir on the Atlantic coast and a point some 100 km east of Marrakesh. From there on the Middle Atlas branches off to the left (*i.e.* attaining a NNE trend) to terminate at the northward promontory of Melilla along the Mediterranean coast (the northeastern end of the Rif mountain range). However, the southwestern segment of the Middle Atlas may further extend to the SSW to merge with the westernmost SSW trending segment of the Anti-Atlas. The latter, however, is comprised mostly of Precambrian to Early Paleozoic rocks. If this interpretation is correct, then the branching-off of the Middle Atlas from the E-W trending Atlantis (Canary Islands) F.Z. should be genetically associated with the NNE trending Mauritanides. It is therefore possible that a similar architecture may also occur within the other fracture zones of the Atlantic, which are diagonally crossing the Atlantic coastline.

NW Africa close to Agadir:

A prominent similarity is found between the geological age, facies and structural-architectural affinities of the rock sequences that are cropping out at the Rif and Betic zones. These two zones, situated in the Rif of northern Morocco and the Betic of southern Spain (Gibraltar-Guadalquivir) respectively, look like a mirror image of each other or like two halves of a natural amphitheater. A genetic explanation is therefore called for. Klemme (1958) and Flinch (1997) note that each of these two zones subdivides into Internal and External domains. Internal nappes include sequences of crystalline Precambrian and Variscan (or Hercynian) metamorphics, and a sedimentary sequence of Paleozoic to Mesozoic rocks in the external nappes. These have been thrusted and shifted southward in the Rif and northward in the Betic area as well as westward across the continental slope of the Atlantic. These shifted masses have their roots in the now submerged western Mediterranean (or Alboran Sea). Flinch (1997) considers them to be the northern and southern parts of the same circular structure.

The similar changes of the stratigraphic (facies) and structural affinities that have occurred simultaneously across these domains in both the Spanish and Moroccan provinces suggest therefore that this common and same zonal pattern prevailed since Early Mesozoic or even earlier times. Perhaps a combined operation of a downward sucking mantle vorticing mechanism, and an increasing pressure-process which is associated with the collision of the African-European plates, is responsible for both the subsidence of the Alboran basin and for the outward thrusting of crustal material. The same process could explain the peripheral negative magnetic anomaly values in the Betic and Rif coastal areas as well as in the Alboran Sea between them, as compared with the positive ones that characterize the western Mediterranean. The configuration of bathymetric contours within the Alboran Sea (Choubert and Faure-Muret, 1976) suggests it to be an almost closed basin, separated by two sills from both the Balearic and Atlantic basins.

Klemme (1958) suggested the existence of a genetic connection between the interruption caused by the northward projection of the Middle Atlas and the tight arcs of the Betic-Rif. The existence of a circularly distributed pattern of earthquake epicenters noticed across the discussed area on the maps of Jackson and McKenzie (1988, for the period 1961-1983) and of Goter (1988, for the period 1979-1988), corroborates Klemme's opinion. It is therefore suggested that the combined pattern of the Middle Atlas and the Betic-Rif zones exhibit a vortex system which is still functioning. It resembles the Hellenic-Menderes vortex system (see below).

If our interpretation on the development of the Alboran (Betic-Rif) vortex is correct, at least since early Mesozoic times, then it may raise some doubt as to the validity of the hypothesis on the simultaneous occurrence of differential sinistral movements of appreciable magnitude between NW Africa and SW Europe (Carey, 1976, p.257; Neev et al., 1982, p.1025). It is therefore possible that during all that long time period the straits of Gibraltar functioned both as a pivot on which Africa moved counterclockwise toward Eurasia, and as a sill which separated and also often acted as a land bridge between these two continents. In the following pages we attempt to define a common denominator for some of the (1) physiographic-structural characteristics of the Atlas Orogenic Belt (mostly counterclock-wise curving and branching-off features) and (2) of those noticed across the joint African-Arabian continent (Neev et al. 1982, Fig. 1; Neev and Hall, 1992, Fig. 1).

A bird's-eye view of the physiographic characteristics across the African-Arabian continents (considered as a unified feature) reveals a pronounced difference between its northern and southern halves (the National Geographic Atlas of the World, 6th Edition 1995, and the 7th Edition 1999, which include different mosaic maps of false-color satellite scenes), as well as our Fig. 22.5. One of these differences is the obvious greater coverage of linear dunes, deposited in sand-seas ('ergs'), across the Saharan-Arabian territories, as compared with that found at the southern half (Kalahari-Namibia). Nevertheless, the reason for the difference does not seem to be in the availability of source rocks which eroded to produce loose sands which were imported, nor in the regional distribution pattern of climatic belts; As stressed by Neev et al. (1982, Fig. 1) and Neev and Hall (1982, Fig. 2; 1992, Figs. 1-6), the origin of the linear dunes as well as yardangs, could be mostly related to the more intensive tectonic activity across the tectonic lineament patterns to the north of the Equator, as compared with the areas on its south (Fig. 22.5), and not only to climatic factors. In other words it was mostly affected by the bulk intensity of the linear tectonic patterns across Africa, which is gradually increasing from the south across the equator and northward, *i.e.* upon approaching the territories in which the geosutures of the global eye are converging and spiraling

counterclockwise more intensively.

The new mosaic maps of satellite scenes of Africa enabled us now to trace the southern segments of the very long N-S trending lineaments that gently curve and converge counter-clockwise and northward. We have now identified those segments of different geosutures which, although subparallel to each other, extend southward from the lower Nile River, as well as the Median Geosuture of the Central Plate (along the Arabian Peninsula – see below Fig. 22.21) through the Marra and Nuba mountains as well as through Port Sudan to curve counterclockwise across the equatorial-tropical belt, to merge with the Chain and the Ascension Equatorial fracture zones of the Atlantic Ocean (Fig. 22.5). It seems that the origin of at least these lineaments, that cross through the entire width of the tropical belt (which is and was wet and heavily vegetated for a very long time), should not be related entirely to changes in the recent and sub-recent meteorological processes that induce the erosion and deposition of dune sands. An additional tectonic basis is thereby requested.

The Central African shear zone of Bermingham et al (1983, Figs. 1, 4), Browne and Fairhead (1983, Fig. 10) and Browne et al (1985, Fig. 6) is interpreted by Katz (1987, Fig. 1) to be a transform-type lineament which is one member within a system of nine across Africa. In the second and third papers these authors express their doubts regarding the northeastward extension of that shear zone beyond a point SE of Jebel Marra at the NW top of the Bagarra Basin (close to 11°N, 26°E). As an alternative they propose an hypothetical lineament along which the C.A. Shear should be extended as a straight line to the NE, through the Baiyuda Volcanic Line (18°N 32°E) and beyond, as far as the Red Sea coastline close to 23.5°N. That line diagonally divides the African basement into a northern territory, where NE-SW to N-S trending faults dominate, and a southern one where NW-SE trending faults predominate. We suggest a different version, a group of northwestward concave geosutures, which seems to agree better with a more specific and consistent photogeological marking (Fig. 22.5). The Pelusium Line is the most prominent member within that group of geosutures, that extend southwestward as a swarm of smooth and gently curving photogeological tectonic lineaments which begin in the northeast close to the Mediterranean coastline (between the Nile Delta and the Qattara Depression). On its western periphery this huge concave northwestward swarm of tectonic lineaments (such as the Dead Sea) parallels the Pelusium Line. The width of that swarm at the latitude of Jebel Uweinat exceeds 1000 km. From there on it diverges southwestward with its width increasing. The eastern edge of that swarm extends from Cairo southward (sub-parallel to the Red Sea) through Mount Nuba and merges with the Ascension F.Z. (the southern member of the Equatorial F.Z. - Fig. 22.5).

We consider the Chaine de Bongo to be one of the features defining the Central African Shear, which according to Browne et al. (1985, Fig. 6 - insert), is crossing the Atlantic coastline to merge with the Chain F.Z. (our Fig. 22.6). According to Browne and Fairhead (1983, Fig. 10) the NNE trending Adamawa Ridge could be a segment of the C.A. Shear. We do not concur with that possibility, because in the discussed region where these two linear features intersect, the C.A. Shear is trending ENE; whereas the Adamawa volcanic ridge trends NE-SW. The Adamawa Ridge is the tectonic prolongation of the SW-NE trending offshore geosuture of the Cameroon volcanic islands (Sao Tome to Molaba islands within the Gulf of Guinea - The National Geographic Atlas of the World, 1995, Maps 90-92; Knudsen and Andersen, 1995; Neev et al, 1982, Fig. 1). On-land that geosuture further extends northeastward at least as far as the city of N'Djamena (south of Lake Chad) where it merges diagonally with the NE trending geosuture of the Pelusium Line. It is doubtful, therefore, whether a genetic relationship exists between the Cameroon-Adamawa-N'Djamena ridge and the Pelusium Line or with the entire global system of geosutures (see the description of the Ascension-Port Sudan-Ararat geosuture below in the section on the Ararat Vortex).

The northwestern half of Africa is dominated by the N-1 Slice which is limited on its north by the right-lateral South Atlas geosuture and on its south by the left-lateral Pelusium System (Neev and Hall, 1982, Figs. 1, 2). Nevertheless, the distribution patterns of the geosutures and swarms of tectonic lineaments that occur across both the N1 and its adjacent S-1 slice (south of the Pelusium Line), are very similar to each other (Neev et al, 1982, Fig. 1). The S-1 slice could have also been involved in the tectonic processes that are and were producing the system of geosutures across Africa. It is therefore suggested to expand the use of the term 'Pelusium System' from the easternmost Mediterranean to Africa, so that it would include both the N-1 and S-1 slices (Neev and Hall, 1982, Fig. 2). This implies that most of the Arabian Peninsula (or sub-plate) should be incorporated within the Pelusium System. The southeastern and eastern limits of the latter would therefore be along the Oman Line and the West Lut Geosuture (see below), as suggested by Neev et al, (1985, Fig. 12.11) and Neev and Hall, (1992, Fig. 4).

In a map view the configuration of the counterclockwise curving and converging patterns of lineament swarms across both Africa and the Arabian Peninsula suggest the existence of two semi-circular features of huge dimensions across the area under discussion. Both of these features are bulging to the east: The western one is centered at the Tibesti-Uweinat massifs of northeastern Africa (Neev et al., 1982, Fig. 1; Neev and Hall, 1982). The eastern feature is centered on the western limit of the Arabian Shield, at the east-central segment of the Red Sea coastline (Neev and Hall, 1992; Fig. 1; our Figs. 22.1 and 22.21). Both of these two semi-circular physiographic features are abruptly terminated along their western flanks by the major geosutures of the Pelusium Line and the Red Sea. Their origin is suggested to be induced by the counterclockwise horizontal underflows within the upper mantle (see above and Neev and Hall, 1984). The difference between these two features is recognized by the nature of their western limits: Whereas a major left-lateral movement functions across the Pelusium Line, an expansion-rifting process is the dominant tectonic affinity of the Red Sea which is the western limit of the Arabian massif.

The occurrences of a few additional counterclockwise curving and converging swarms of linear features were suggested by Neev

et al. (1982) to exist just to the south of the Atlas Geosuture. This is based mostly on the maps in the 1975 Times Atlas of the World (Times of London, 1975), the UNESCO 1:10,000,000 Geological Map of Africa (Choubert and Faure-Muret, 1976), and the atlases of the National Geographic Society (1995, 1999). These swarms are situated at the eastern and western Grand Ergs of northwestern Sahara, as well as at the Jouf and Chech ergs (sand seas) of Western Sahara (Figs. 22.5 to 22.8). These features are associated both with geosutures of the Global System and with much smaller patterns of counterclockwise curving and converging fractures. They are expressed by swarms of linear sand dunes and other landforms.

Only recently we had the opportunity to study those landforms through their physiographic features as expressed in the Geological Map of Algeria at 1:500,000 (Batier, 1951-52) for the western and eastern Grand Ergs and from the Geological Map of Western Sahara 1:2,000,000 (Gevin and Sougy, 1952) for the Ergs of Chech, Jouf, and Iguidi. Sheet Nos. 1 and 2 of the Geological Map of Northwest Africa (*ibid*, scale 1:2,000,000, - Morocco-W. Algeria and Algerian-Tunisia respectively) describe the entire scope of the Atlas Mountains and Grand Erg Occidental as well as the Grand Erg Oriental. These maps describe in some detail the Recent distribution patterns of both linear eolian and hydraulically eroded landforms as well as the relevant geologic background of the underlying more consolidated rocks. Our interpretations and conclusions regarding the origin of the linear sand-dunes across the great ergs, as deduced from these maps, are presented below (Section VIb) and in Neev et al. (1982).

The Atlantis, Kane, Researcher, and Vema F.Z.s across the Atlantic Ocean:

Four additional eastward trending geosutures of less prominent, adjacent, and in-between character are diagonally crossing the Atlantic coastline of NW Africa close to Cape Juby-Tarfaya, at Cape Boujdour, south of Cap Blanc at Cape Vert-Dakar, and at Guinea-Bissau respectively. Further inland these four geosutures moderately and gradually curve counterclockwise to form the boundaries of a few basins, as well as the Ahaggar and Air massifs. They converge northward upon crossing Cyrenaica close to Jebel Akhdar, Wadi Farigh, and the Gulf of Salum where they attain a NNW trend and plunge into the Mediterranean Sea. They also form the sills that separate the different basins within the Mediterranean Sea (see below).

The main landward extension of the Atlantis F.Z. emerges eastward into Africa at Tarfaya (Cape Juby) (Fig. 22.7) and continues as a geosuture eastward along the southern limit of the Tindouf Basin and then abuts tangentially along the northern limit of the northward protruding elongated Safia-Mdennah-Eglab structure of the Eastern Mauritanides (Figs. 22.5, 22.6, 22.7 and 22.8). From that point this structural axis extends further north as a geosuture to merge both with the northeastward curving and branching-off geosuture of the Middle Atlas and the linear-structural trend of Erg Iguidi and Hamada de Guir (Gevin and Sougy, *ibid*; National Geographic Society, 7th edition, 1999, Map 113) which are curving to the northwest. The merged geosuture continues to the NNE along Wadi Moulouya and sub-parallel to the Middle Atlas, to terminate at Melilla where the Middle Atlas is plunging northward into the Alboran Sea. At that point the geosuture of the Alboran Vortex is curving counterclockwise to be enveloped by the Rif and Betic mountain ranges.

This northward branching-off feature could begin even farther on to the south of the point where the Kane F.Z. is crossing the African coast of Mauritania, (close to 20°S and south of Cap Blanc). This southern member of the first continental counterclockwise curving segment of the Kane geosuture extends along the canoe-shaped Adrar ENE trending structure, at whose apex the circular granitic plug of Richat is situated. It then continues, with a gradually increasing degree of counterclockwise curvature, northward along the western rim of the huge N-S trending complex of southward concave sequential system of arched structures, *i.e.* Safia, Mdennah, and Eglab (see below and Figs. 22.6 and 22.7). The members of that sequence of arcs are superimposed one ahead of the other toward the north. An additional and similar north-south trending sequence of structures whose length is close to 1500 km exists parallel and west of the Safiya-Eglab sequence, coinciding with much of the Western Mauritanides. This consists (from N to S) of the Jebel Bani (Anti-Atlas), Yetti, Richat-Adrar-Makteir (Tagant), and the Tagant-El Mreyya arc (after Choubert and Faure-Muret, 1978, Sheet 9; National Geographic Society, 1999, Maps 109, 113), all of which are expressing southward concave structures.

The joined pattern of these twin S-N trending sequences, each of them consisting of southward concave structures, forms a rather broad positive belt which is bounded on its west by the Atlantic Ocean coastline (and the Western Mauritanides) and on its east by the eastern limit of the Eglab-Safia sequence of the Eastern Mauritanides (that follows the southward flowing segment of the Niger River as far as its junction with the Benue River). This joint S to N trending structure forms a westward concave feature and has a broad basin on its south (extending from Bissau on the west and Bamako on the Niger River junction in the east). It appreciably narrows northward toward the Alboran Vortex. The eastern limit of that northward trending large scale slice extends as far as the northern termination of the Middle Atlas to terminate at the Alboran Vortex on the Mediterranean coastline (36°N 3°W). The total length of that feature should be close to 3000 km.

To the east the contact between the Atlantis F.Z.-Jebel Akhdar geosuture and the apex of the Eglab arch is of a tangential nature. The former is branching off again in a counterclockwise curving mode at El-Maiz (close to the 0° meridian and the 28°N parallel). That curvilinear secondary geosuture then extends to the northeast and north along the western limit of the Ghardaia structure, which is 800 km long and 80 km wide (Figs. 22.5 and 22.6). The Ghardaia structure forms a physiographic divide between the Grand Western and Eastern Ergs (or sand seas). It is also expressed as a NE-SW trending structural positive element along which Cretaceous rocks are cropping out. On its north it merges with and terminates at the foothills of the Saharan Atlas east of Laghuat (about 34°N and 3°W).

The next northeastward branching-off feature away from the

Atlantis-Jebel Akhdar main geosuture occurs about 100 km farther on to the east, along the secondary geosuture of Wadi Mya (water in Arabic), which is subparallel to the Ghardaia secondary geosuture. Each of these last two linear tectonic features are more than 800 km long. Nevertheless the Ghardaia feature forms a structurally positive feature, whereas Wadi Mya (the more eastern one) forms a fault-controlled structurally negative (topographically low) element, filled with Quaternary sediments. Rainwater draining toward the latter accumulates in sabkhas along the trough of the Wadi Mya curvilinear feature that marks the western limit of the Grand Erg Oriental. It terminates on its north at the site of Biskra along the SE foot of the Saharan Atlas. The elongated Ghardaia structure separating these two structural elements attains the shape of a flat wedge which becomes somewhat wider towards the north. Its average structural elevation is intermediate between those that dominate across the Ghardaia and Wadi Mya features.

Another counterclockwise branching off geosuture is recognized along the northeastward extension of the Atlantis-Tademait geosuture close to Ft. Flatters (28°-01'N, 6°-08'E). It follows the southeastern limit of the Grand Erg Oriental and continues along the contact of the latter and the Late Cretaceous plateau of Hamada el Hamra, where it crosses the site of Ghadames and follows the NE trending long dimension of Jebel Naffusah before plunging into the Mediterranean Sea just east of Tripoli. It then continues along the N-S trending submarine Malta escarpment and through the Straits of Messina (Sicily), beyond which it follows the NW trending steep submarine contact of the West Italian continental slope and the abyssal plain of the Tyrrhenian Sea through Elba to continue as far as the eye of the Sestri Vortex.

The Kane F.Z. (Geosuture) of the Atlantic Ocean crosses the coastline just south of Cape Blanc and continues landward across the NE-SW trending geosutures of the East and West Mauritanides Ridges. At its western on-land segment it subparallels the ENE trending canoe-shaped, close to 100 km long, basement structure of Richat, most of which is covered by Infracambrian sedimentary rocks. At the apex of that very large dome the circular Infracambrian gabbro structure of Richat (about 21°-01'N 11°-20'W) is plugged up. Close to its westward plunge this elongate and high structural feature is truncated and left-laterally shifted close to 70 km by a wrench fault that extends along (*i.e.* parallel to) the Mauritanide geosuture (Figs. 22.5, 22.6, and 22.7). Perhaps these movements along the Mauritanides are related to the repeated phases of the Late Paleozoic opening-closing-opening process of the Iapetus-Atlantic Oceans, during which the Appalachian-Mauritanides orogens cyclically collided and separated (Wilson, 1966; Hatcher, 1978; Ziegler and Roure, 1996).

The large structurally positive feature of Safia-Mdennah-Eglab consists of a S-N trending sequence of three concave arches which are open to the south (one nestling another) that extend along the long median axis of that mega-structure. It gradually curves counterclockwise and changes its course from a NE trend at its southwest, to north at its northern termination. The two northern arches are being enveloped by sedimentary rocks, most of which are of Infracambrian to Middle Paleozoic ages. The southernmost (Safi) arc encompasses younger rocks of Late Paleozoic to Middle Mesozoic age. As the age of the rocks within each of these archs is getting younger in a southward direction along the median axis, it seems possible that the composite pattern of axes within this N-S trending feature represents an elongated continuously subsiding trough or synclinal structure, developed within the larger positive (mega) feature of Safia-Eglab.

The N-S trending counterclockwise curving and southward concave Safia-Mdennah-Eglab sequence of arched structures is analogous and similar to other branching-off features within the Alpine-Himalayan eye, such as the Oman-Lut (eastern Iran) elongated vortex along the eastern limit of the Arabian sub-plate (Neev and Hall, 1992; and below), as well as the anomalous Pamir (NW India) one. Their common denominator is the northward sequence of secondary branching-off and southward concaved arched structural features.

A different type of belt, where Precambrian granitic and Infracambrian sedimentary rocks are cropping out, is abutting both the N-S trending Safia-Eglab positive feature on its east, and the Western Mauritanides Range on its west. The southward limit of that belt is at the E-W trending Makteir twin basin and range features. These last two are relatively narrow, intensely folded, and mostly composed of Infracambrian rocks. Much younger rocks (Cretaceous to Tertiary sedimentary rocks overlain by Recent dunes) are extensively exposed along the counterclockwise curving and northward trending Tanezrouft basin, which marks the eastern and southeastern boundaries of the above Safia-Eglab positive feature. It is situated to the west of the Ahaggar massif. The Tanezrouft basin, together with the NW trending tensional graben feature of Hamada du Guir on its north, are forming a negative tectonic feature (Figs. 22.5, and 22.7) where Cretaceous and Tertiary rocks are extensively exposed.

VIb: A genetic relationship between the linear tectonic fracturing pattern and the swarms of linear dunes across the Western Sahara and the Grand Erg (Figs. 22.5, 22.6, 22.7 and 22.8):

The huge elongated structurally positive feature of Safia-Eglab is surrounded and partly covered by three major Ergs (sand-seas): Iguidi in the NW; Chech in the NE; and Jouf in the south. These Ergs are dominated by NE to NNE trending very long linear sand dune ridges. Occasionally, these large swarms of dunes are very moderately changing their courses (or curving) perhaps in agreement with the configurations of the neighboring and underlying large positive morphological features.

There is a discrepancy between our approach and that of many other scientists who interpret the formation of linear eolian sand dunes to be controlled only by the regional atmospheric circulation (Dubief, 1952; Mainguet, 1968; Wilson, 1971; Warren, 1972; Cooke and Warren, 1973; Vail, 1978; El-Baz et al., 1979). Our interpretation, as expressed below and by Neev et al. (1982) and Neev and Hall (1992), is at least partly different. We attribute the triggering mechanism for the formation of the long linear sand dunes (seifs) to the deposition (or trapping) of drifting sand within the

pre-existing corrugated erosional surfaces associated with 'swarm' patterns of long linear tectonic-fractures. That interpretation is based on data recovered from the geological maps of NW Sahara (see our Figs. 22.6 and 22.7). We believe that the additional results of the following new studies will lend support to the above hypothesis (especially with respect to the Grand Erg Occidental).

We also refer to the results of new regional meteorological studies carried out by Ganor (1991) and Alpert and Ganor (1993), who prepared a trajectory map of dust-carrying storms across North Africa and Arabia, the Mediterranean Sea, and neighboring southern Europe. Based on their interpretation of satellite imagery obtained over the past 30 years, as well as their analyses of airborne clay-minerals, these authors reveal a dynamically changing pattern of a northward dust transport process from the Sahara and the Arabian Peninsula to Europe over a distance of more than 2400 km. These data, together with their analyses of the distribution of the relative humidity and wind direction, plus its intensity within the atmospheric column above the study areas, revealed a system of cyclones forming above the Mediterranean Sea and southern Europe, where the dry desert air mass from Sahara is confronted with the more moist Mediterranean and European air masses. No indications were found, however, in the Ganor and Alpert (*ibid*) data, to corroborate or contradict our suggestions regarding the relationship between these atmospheric processes and the landforms described by us (see above - the counterclockwise converging and curving patterns as exhibited by the extensive swarms of sand dune lineaments across the Sahara-North Africa region).

The following gives the essence of two instructive case-histories inferred from the geological maps of Northwest Africa: The first one refers to the distribution pattern of sand-dunes across Western Sahara as described in the Geological Map of Western Sahara at scale 1:2,000,000 (Gevin and Sougy, 1952). It is therefore suggested that the origin of the Saharan sand dunes is in the eroded relatively high landforms abundantly scattered all across the northern half of Africa. The dominance of sand dunes in the Sahara was therefore determined by dry climatic conditions. An apparent origin in the west, beyond the Atlantic coastline (such as that of Mauritania) does not seem to be plausible. The distribution pattern of these very long linear dunes, which terminate at the coastline, and the well-based fact that the dominating transporting agent is the wind, as well as other observations (see below), suggest that structural-physiographic factors (both mega- and minor ones), as well as a new understanding of the depositional mechanisms of linear dunes, are vital tools for proper analyses.

The composite LANDSAT image of the entire African continent (ASPRS, 2000) clearly shows the massive sand deposition within areas of troughs and sinks which are tectonically controlled. Even in such small scale figures the genetic relationship between linearly-trending tectonically fractured patterns and linear dunes is indicated. One of the areas that we paid attention to is the Erg Chech, which partly overlies the Infracambrian to Early Paleozoic coverage of the Safia-Eglab positive feature. The two most prominent structural features that characterize that old massif are:

i) The dominant northeastward strike of the cuesta-like northwestward tilted major stratigraphic contacts along its western flank, and

ii) The abundant long strike-parallel linear fracture and dike systems, most of which were filled by intrusive doleritic magma in later times. That fracturing activity produced swarms of similar linear fractures, most of them were apparently not intruded by doleritic magma. During the Quaternary the entire region (including the discussed massif) was covered by the young sand dunes of the Ergs of Chech and Iguidi. Most of these sands were trapped by, and have continued to move along the linear fractures. The long axes of all of these features have acquired the same trends as those of the underlying ancient linear fractures and dikes. (Figs. 22.6 to 22.8).

The above data are in agreement with our earlier interpretation on the mechanism of linear sand-dunes deposition. (Neev et al., 1982; Neev and Hall, 1992). The rationale of the hypothesis is summarized as follows: Initial deposition of sand occurs along linear shallow grooves formed by the joint effect of the differential weathering of the linear systems of fractures and dikes formed throughout much of the geological history across the hard rock surfaces as well as by the differential accumulation of the deposited eolian dust-soil blanket on top of these wave-like surfaces. The low and flat sand waves, that are the first to be accumulated along the troughs of those wavy surfaces are named 'Zibars'. The first sand grains deposited within the troughs are trapping additional eolian drifted sands more efficiently than the smooth and barren weathered rock surfaces as well as the pebble-strewn 'Hammada'. Thereby the vertical dimension of the initial linear sand dunes is preferentially growing higher. The trends and locations of the linear dunes are therefore predetermined because of the increasing friction of the wind upon crossing the linear fractures and dikes.

Our (unpublished) field observations, made in western Sinai in 1974, as well as those of Tsoar (1974), indicate that wind direction *per se* has very little to do with determining the trends of linear dunes. When a wind approaches a linear sand dune, either perpendicularly or diagonally, it carries the sand grains upslope with it in the wind direction as far as the dune's crest. From there on, the grains fall freely along the leeward steep slip face, where they gain speed. Because of the potential energy acquired, this same windfall reachs the base of the dune to occasionally erode it. It then rises again in a helicoidal flow pattern hugging the slip face, and advancing close to the brink of the dune along and parallel to the crest, but on its leeward side. The direction of that horizontal helicoidal flow (right or left) is determined by the direction of the obtuse angle formed between the trends of the regional wind and of that specific dune crest.

During that process sand grains would be deposited within and behind local saddles, which are dynamically formed along the crest of the linear dunes. The wind sweeps into these relatively low points because of the absence of a barrier (*i.e.* a reduced pressure zone: where the wind speed dissipates and the tangential-helicoidal flows are losing part of their energy). At these crestal saddles, where the wind energies are reduced, the longitudinal horizontal helicoidal flows are diverted to the relatively empty space formed by the micromorphology of the dune's crest. That way linear dunes

are growing mostly along their long axes and not perpendicular to them along the regional trend of the winds. If and when the trend of the prevailing wind coincides with that of the long axes of the seif dunes, the latter configuration should attain a symmetrically dipping shape across the crests (*i.e.* steeply dipping toward both the lee and windward sides. The first landform produced by drifted sands in a newly formed erg (sand sea) should produce a barchan (crescent)-shaped dune. That would advance along the regional wind direction. Eventually however one of its two horns should develop into a perpendicularly trending linear dune.

The joint pattern of curving and converging counterclockwise linear dunes, noted across the three ergs (Iguidi, Jouf, and Chech) that surround the ancient feature of Safia-Eglab, extends northeastward into the Grand Western Erg through a bottle-neck, or a strait-like zone situated across the linear NW trending Hamada du Guir tensional feature, between Erg er Raoui in the NE, and Plateau du Tademait in the SW (Figs. 22.4 to 22.7).

The eastern limits of both the Chech and Grand Western Ergs are marked by a very long, practically unified, structurally and physiographically positive feature which is relatively clean of sands. This flat, low, and relatively narrow feature mostly consists of Cretaceous rocks, which occasionally crop out across it. It is comprised of the following three segments:

1) The southern one stretches along the contact of the Tanezrouft plain and the Erg-e-Chech.

2) The intermediate segment consists of the Plateau du Tademait, which branches northeastward to form the northern segment, which is the flat Ghardaia ridge separating the West and East Grand Ergs.

3) The 'S' shaped, relatively narrow 'strait' formed by the narrow Rawi-Guir NW trending feature, could be functioning as a physiographic 'gate', through which the sands are being transferred from the southwestern Chech and Iguidi ergs into the Western Grand Erg in the northeast.

The section below presents the second case history for understanding the origin of the linear sand dunes as inferred from data across the Western Grand Erg (Fig. 22.8). That study is based on data from the 1:500,000 scale Geological Map of Algeria (Batier, 1951-52) and the 1:5,000,000 scale International Tectonic Map of Africa (Choubert, 1968). The conclusions of that study corroborate our earlier impression that a hydraulic erosional mechanism was responsible for the generation of the northern (upper) segments of the linear landforms generated across that part of the erg (Neev et al. 1982), whereas the southwestern extensions of these same landforms were produced solely by a wind-energy mechanism (*i.e.* they consist of linear eolian sand dunes).

The northern segments of these linear landforms consist of a relatively dense pattern (or swarm) of consequent wadis (*i.e.* trending NW-SE or perpendicular to the front-range of the Saharan Atlas and parallel to the regional physiographic slope across the northern half of the Western Grand Erg). These wadis are entrenched into the sedimentary fill underlying the extensive floodplain that spreads out away from the northeastward trending range of the Saharan Atlas.

Upon approaching the outlets of the wadis from the Saharan Atlas mountain ranges, many of the large mountainous wadis sharply change their course by 90° to the left (*i.e.* from a NE-SW trend that follows wrench faults which parallel the foothills range of the Saharan Atlas, to a SE-NW one across the flood-plain). Such an abrupt change could suggest a sub-recent renewed activity of the right-lateral (dextral) shift of that range relative to the adjacent flood-plain of the Western Grand Erg across the South Saharan Atlas fault line. This possibility is in agreement with the postulations of Arthaud and Matte (1977 p. 1305) and Manspeizer et al (1978, p. 915) regarding late Paleozoic dextral movements along the South Atlas fracture zone.

On their way across the northern zone of the Grand Western Erg (*i.e.* the 'Flood-Plain' zone) most of these wadis do not merge with one another but maintain their straight southeastward courses, which parallel each other for relatively long distances (close to 100 km). Beyond that segment they gradually but systematically change their courses by curving to the south and then southwestward. Although they maintain their nature of a linear swarm of parallel wadis, they are gradually being transformed into linear dunes: the latter continue along the same curving tracks toward the southwest. Along their southwesternmost (last) segment, all members of that swarm are at first sub-parallel and then parallel to the northwestward and north facing edges of the Tademait Plateau as well as the southwestern flank of the Ghardaia flat ridge.

The above data suggest that a common factor dictates the same trends and stream-line continuity of these two linear systems of swarms of sand dunes and of flood-eroded wadis, which are theoretically (genetically) very different from each other. A common denominator should therefore be sought. It is hard to believe that such a smooth way of imitating each other, as well as their occasional interfingering and merging (that suggest contemporaneity of their formation or at least their coexistence) could have resulted from a mere coincidence. We therefore suggest that a cyclically renewed tectonic activity along the underlying swarm of tectonic linear fractures could be the enigmatic factor which determines both the trends and locations where the discussed joint swarms of linear (eolian) sand dunes, and the hydrographic drainage pattern of wadis, have been produced. The relevant mechanism is discussed above.

The pattern of dune swarms within the Grand Erg Oriental (Figs. 22.5 and 22.6) differs from those within the western one in the following aspects: The shape of the western erg is closer to that of a saucer. The lineaments across it form a systematic counterclockwise curving and northward converging pattern, and are also composed of a combination of linear dunes and wadis. On the other hand, the Grand Erg Oriental attains an elongate NE curving shape. The lineaments across it form two separate swarms, a southern and a northern one. The contact between the two swarms is about midway along the Wadi Mya structural limit. Unlike the case in the Grand Erg Occidental, the lineaments of both swarms in the eastern erg are composed just of sand dunes (*i.e.* the wadis do not participate as segments of the lineament swarms). The lineaments of the southern swarm are denser on the west, and they curve and converge counterclockwise (toward the NW) and terminate along

Wadi Maya. On the other hand, the linear dunes of the northern one are curving clockwise (*i.e.* its members are getting closer to each other and converging toward the north). These linear dunes terminate rather sharply along an E-W trending structural trough on their north. That ESE-WNW trending trough extends between the Isle of Jerba and Gabes (Tunisian Mediterranean coastline) on its east, and extends westward along the northern limit of Chott Jerid and through a series of other Chotts (sabkhas), to terminate at the Chott Mellhir on its west. The clockwise curving pattern of that northern swarm seems to envelop the southwestern quarter of a circular structural feature. The other three quarters of that circular feature are concealed.

The different trends of curving of the two swarms within the Eastern Grand Erg is another indication that the origin of the NW African linear dune systems should not be associated just with an eolian process. Moreover, the general trend and the converging pattern of the linear dunes within the northern swarm seem to correspond with or extend into the northwestward trending and converging pattern of structural lineaments as mapped across the northeasternmost segment of the Atlas orogenic belt. That section of the Atlas ranges is limited between the Biskra-Bizerta tectonic lineament on its northwest, the N-S trending Tunisian Mediterranean coastline on its east, and the Jerba-Biskra structural trough on its south (Fig. 22.6).

VIc: Geosutures across the joint African-Arabian Shield (which are indirectly related to the Sestri Vortex):

Three main geosutures of the global system are crossing the South Atlantic to penetrate the West African coastline south of the Equator. From there they gradually curve counterclockwise and cross that continent from west to east.

As specified in Section IVa above (Fig. 22.4), the northernmost one extends from Southern Brazil (the Vitroia-San Paulo Zone) along Colombia Seamount, the Martin Vaz F.Z., and the St. Helena Island zone as far east as the Bay of Benguela across the South Angola coastline. The distribution pattern of the Angolan and Brazilian diapiric salt fields (E. S. W. Simpson, 1971 and pers. comm.) corroborate the correlation between S. America and W. Africa across these two fields as well as the delineation of that geosuture across both coastlines along the opposite sides of the Atlantic. The tectonic style of both the Brazilian and Angolan evaporitic basins during the Aptian (Early Cretaceous) was one of continental crustal attenuation (Emery and Uchupi, 1984, p. 581).

East of Benguela that geosuture extends inland where it is very gradually curving counterclockwise along the watershed that separates the Congo and Zambesi drainage systems, as far as the Katanga Plateau. That ENE trending divide is also marked by a linear topographic high feature. The trend of that segment is also in agreement with the general regional trend of the isogals, as exhibited on the Bouguer anomaly map. Apparently, both of these trends, in spite of their different nature, also reflect the southward transition of physical-lithologic (facies) characteristics that occur between the Congo Craton in the north through the Damara orogenic belt, to the Kalahari Craton in the south (Deane, 1995; Choubert, 1968, Maps 5, 6, and 7). That presumed segment of tectonic lineament may therefore extend eastward from the northern reach of the Katanga Plateau, where the sources of the Lomami and Lualaba (Upper Congo) Rivers are found at (8°-30'S, 25°E) to gradually curve counterclockwise and continue further on between Lake Malawi (on the south) and Lake Tanganyika (on the NW). It then crosses the coastline of the Indian Ocean (between Mombasa and Zanzibar), to merge with the Owen F.Z. (see below).

The Lomami River is turning rather sharply northward from the ENE trend of the Benguela-Mombasa geosuture and extends in that direction to a distance of about 1000 km before joining the Congo River (some 150 km to the WNW of Kisangani (Stanleyville), just north of the Equator. The tectonic origin of the discussed segment of the curvilinear Lomami river gorge (Fig. 22.5) is inferred from the sharply linear distribution of patchy outcrops of Triassic sediments which stretch along and parallel to the eastern bank of that gorge as far as about 700 km downstream (or northwards). That segment is marked as a fault-line on the Geological Map of Sectors of Gondwana (De Wit et al., 1988) as well. From that point onward that geosuture curves moderately clockwise (to the NE) to diagonally cross the Upper Congo (Lualaba) River. It then continues northeastward over a distance of about 400 km between the Maiko National Park and the southwestern tip of Lake Albert.

The geosuture of the Upper Congo (or the Lualaba) River extends along and parallel to the Lomami River close to 1300 km, from its sources as far as the Boyama Falls (some 100 km SE of Kisangani-Stanleyville) from whence it becomes the main Congo River. The course of the Lualaba River is diagonally but sharply shifted some 100 km to the NW in a dogleg mode at a point some 800 km downstream. From that point it continues downstream (northward) in an *en-echelon* way as a straight lineament.

The origin of these three linear features, *i.e.* the Lomami and Lualaba (Upper Congo) Rivers as well as the West African Rift (between the middle part of Lake Tanganyika and Lake Albert), that parallel each other, is considered to be tectonic (Choubert and Faure-Muret, 1976, Maps Nos. 7, 8; Nat. Geographic Atlas, 1995, Map Nos. 83, 90, 94). At their northern segments they gradually and smoothly curve clockwise to merge with each other, forming the NE trending geosuture (or tectonic trough) of Lake Albert. That feature further extends in the same direction, as a straight lineament and a unified geosuture along the Ethiopian Rift Valley as far as Djibouti, close to the eastern tip of the Horn of Africa (McConnell, 1972).

McConnell (1972) noticed some indications for an early Precambrian dextral displacement along the northwestern flank of the Lake Albert rift lineament. He also considers that the unified Lake Albert-Ethiopian Rift feature marks the northern limit of the East African Rift System. Toward the northeast the Lake Albert-Djibouti geosuture (Katz, 1987) further extends across Bab Al Mandab and beyond, paralleling the southeastern limit of the Arabian Peninsula on its north. It crosses the Rub Al Khali desert as a geosuture and is prolonged along the northeastern coastline of the Oman Peninsula. Its further northward extension across the Hormuz Straits into Iran, marks the western limit of the Lut Vortex

(eastern Iran) (see Fig. 22.21 of the Central Plate below, and Neev and Hall, 1982, 1992). The dextral (right-lateral) sense of movement along the Oman Line (*ibid*) within that segment is in agreement with our interpretations regarding the sense of movements across other segments of the same geosuture. An analogous indication is our morpho-tectonic interpretation of the Bay of Benguela (the site where the discussed geosuture is crossing the Atlantic coastline): We therefore suggest an E-W trending dextral fault-line to control the indentation pronounced by the Atlantic coastline at the southern flank of the bay of Benguela.

The Benguela-Katanga-Mombasa dextral fault system is situated along the E-W water divide close to 11°S, where the sources of the Lomami and Upper Congo (Lualaba) rivers are found (Geological Map of Sectors of Gondwana, De Wit et al., 1988).

Another South African geosuture is the Damara-Zanzibar-Mombasa Geosuture that extends northeastward from Walvis Bay along the Atlantic coastline. Its westernmost segment is the NE trending Damara orogenic belt that extends for a distance of about 1000 km as far eastward as the inland delta of Okavango. New geophysical (magnetometric) surveys indicate that the Damara segment extends even farther on to the northeast where it is camouflaged by the overlying young sediments of the Kalahari Desert. That 400 km wide (N-S) orogenic belt was active since Proterozoic times and is separating between the Congo and Kalahari cratons (Deane, 1995; Eberle et al., 1995). Its next segment further extends northeastward from the Okavango inland delta across Victoria Falls (on the Zambezi) to continue along Lake Kariba and the Luangwa River (that parallels the Muchinga mountain-range on its south) as far as the northern segment of Lake Malawi, where it merges with the Benguela-Mombasa geosuture, and further extends in the offshore along the northeastward trending coastline of the Horn of Africa. That interpretation was corroborated by the observations of J. W. Verwoerd (1979, pers. comm.), McConnell (1972), and Katz (1987).

The Owen F.Z. crosses the Indian Ocean in a NNE direction, parallel to the eastern coast of Somalia (the Horn of Africa) on the south, and the easternmost corner of Oman (SE Arabian Peninsula-**Fig. 22.21** see below) on the north. The Ascension-Asmara-Rub Al Khali and the Martin Vaz-Owen geosutures are counterclockwise curving and converging along both the northern and southern flanks of the Oman Peninsula and Abyssal Plain as well as the Lut Vortex (Figs. 22.5, 22.21). East of the Oman Peninsula (off Ras Al Hadd) the Owen F.Z. bifurcates: The western branch extends as a dextral fault northward along the eastern limit of the Lut Vortex (the Zabul Harirud-Kopet Dag geosuture). The eastern branch curves counterclockwise along the Murray Ridge and extends northward along the Indus River, the Quetta-Chaman ridges, and the *en-echelon* complex of N-S trending ranges of the Sulaiman-Hindu Kush ranges, which together are forming the northwestern flank of the Pamir Vortex (see below).

In one of our earlier papers we have erroneously named the Damara-Zanzibar (Mombasa) segment of geosuture across Africa, as the Luderitz-Mombasa geosuture (Neev and Hall, 1982). The port of Luderitz is sited along the Atlantic coastline much closer to the outlet of the Orange River than to Walvis Bay, where the southwestern termination of the Damara Orogen is located. Katz (1987) described the Luderitz-Lindi NE trending lineament where a minor sinistral offset occurs on its intersection with the east African coastline.

The Orange River Delta-Messina-Beira-Mozambique Channel-Owen F.Z. Geosuture is marked as a dashed line on our Fig. 22.4 (or Fig. 2 of Neev and Hall, 1982). It is probably the landward extension of the Tristan-Da-Cunha Fracture zone across the Atlantic and the associated marine gravity anomaly lineament (Heezen and Tharp, 1977; Haxby, 1987). On land it further extends to the ENE as the nearly 400 km long NE trending segment of a tectonically disturbed lineament. The next inland segment occurs along the same trend where it is crossing the southern limit of the Kalahari Desert, as marked by the tracks of the Molopo dry-wash. The latter one sharply curves to the SE, thereby connecting the previous two segments in an *en-echelon*-dogleg way to the last segment on-land, which stretches over a distance of 1200 km.

It consists of two sub-segments: The southwestern one follows the upper (western) segment of the Limpopo River along a NE-SW trend across the city of Messina (still on the Limpopo River). It continues along the same trend to terminate at the port of Beira (Mozambique), from whence it further extends across the coastline into the Indian Ocean to merge with the Owen F.Z. east of the tip of the horn of Africa.

Support for some of our conclusions could be drawn from the interpretation of the gravity measurements across Africa made by Brown and Girdler (1980). Corroboration regarding the existence of most of the discussed geosutures is deduced from the Bouguer anomaly maps, as well as from the varying degrees of lithospheric thinning and the seismicity map of Africa (their Figs. 2, 9, 11 and 12). Special attention should be drawn to a sharp change of course (90° to the south), which is recognized as a kink in a belt of minimal thinning. It stretches eastward from Western Sahara and occurs across the Pelusium Line, close to where the Tibesti Massif is located. Two other conclusions of these authors are: (i) the state of tension affecting the African lithosphere that causes its fracturing, induced by uprising mantle convection; and (ii) the fact that lithospheric thinning across Africa is increasing from south to north.

VId: Continuous Northward Drift of Africa since Late Proterozoic Time:

The discussed movement is inferred mostly from the stratigraphic-structural histories of several basins, which are distributed across the entire length (S-N) of the African continent from the Karoo Basin in the south to the Tindouf-Ghadames-Qattara basin in the north (Fig. 22.5).

The Karoo and Owambo Basins.

The most convincing indicators are known from two basins in south and southwestern Africa, namely (i) the Foreland Karoo Basin of South Africa (after Johnson et al., 1997, Figs. 1, 2 3, and

24), and (ii) the Owambo Basin, situated parallel to the Atlantic coastline of northwestern Namibia and Angola (Miller, 1983, Figs. 1, 2, and 4).

The southern limits of both of these two basins are marked by the intensely folded and E-W trending orogenic belts of the Southern Cape and Damaraland respectively. Eight to ten km thick sedimentary sequences accumulated between Late Proterozoic and Early Jurassic times within both of these basins just north of the above two orogenic belts. Both of these sequences are gradually thinning northward to wedge out at the respective limits of the basins.

The origin of the Karoo Basin could be inferred from the description of its tectonic setting (Johnson et al., 1997, p. 305). The basin constitutes a retro-arc foreland, situated behind a magmatic arc and is associated with an E-W trending linear fold-thrust belt, produced by the northward subduction movement of the oceanic lithosphere, which is located south of the arc. That denser oceanic basalt was thrusted northward under the continental margin during the Late Proterozoic. The eastern limit of the Karoo Basin is marked by the NNE trending Drakensberg Ridge, that parallels the Indian Ocean coastline. A northward shift of the Karoo Trough, and a westward shift of the Natal Trough (or the Drakensberg Ridge), occurred between early Paleozoic and Permian times.

A similar tectonic setting and history could also be inferred for the Owambo Basin (Miller, 1983, p. 266). Unlike the former, the eastern limit of the Owambo Basin is not marked by any (N-S trending) structural high. Its western limit, however, is bounded by a pre-Pan-African NNW trending folded belt that parallels the Atlantic coastline (Fig. 22.5).

Based on the above data it is suggested that the southern half of the African continent went through a northward drifting process since mid- or late Proterozoic, that was maintained at least until Early Jurassic time. That process could still be active.

The Karoo Basin is bordered on its south by the geosutures of the Falkland-Agulhas-Mozambique Channel. The limits of the Owambo Basin are marked by the Martin Vaz F.Z. on its north and by the Rio Grande F.Z.-Walvis Ridge on its south. Both of these geosutures merge together close to the point where the Tanganyika and Malawi grabens are being shifted away from each other. The merged geosuture extends farther northeastward along the Owen F.Z. (Fig. 22.5).

North Africa (Figs. 22.4, 22.5, and 22.6):

Three E-W trending structural belts extend across North Africa (northwest of the Pelusium Line). They are, from south to north:

1) The Precambrian basement that is gently dipping toward the Mediterranean Sea;

2) The Sahara Platform;

3) The Atlas Fold Belt(only in NW Africa).

The following four basement structural trends are recognized there:

i) The northward regional dip (see above);

ii) The NE-SW geosutures (*i.e.* the Pelusium Line-Tibesti Massif):

iii) ENE-WSW fold and fault belts (the Atlas Mountains and its Mediterranean coastline in Morocco and Libya):

iv) The E-W and ESE-WNW (mostly in Cyrenaica and the Western Desert) coastal and inland faults (our Figs. 22.5 and 22.6; Hantar, 1990).

The Tethyan Ocean cyclically transgressed North Africa southward and regressed northward in early Cambrian to Miocene times. The isopach trends were influenced by the configuration of the above-mentioned structural features.

According to Selley (1997) the greatest thickness of Phanerozoic sediments deposited in NW Africa, whose ages range from Infra-Cambrian to Cretaceous (or even Tertiary considering the existence of Messinian evaporites in the mountains of eastern Tunisia), was attained within the Atlas geosyncline. Although the dextral shift of the South Atlas Ranges (relative to the continental territory of Africa) is not doubted, it seems reasonable to interpret the Atlas geosyncline to be genetically related both to the West Mediterranean Trough and to the NW African foredeep (see above).

A system of North African basins, distributed along a belt whose general trend is east-west, extends from the Tindouf Basin in the west (Tarafya on the Atlantic coast) to the Kufra Basin (situated along the Pelusium Line, close to the Tibesti Massif) in the east. The structural fabric of these basins was inherited from the Late Proterozoic and was reactivated many times since (based on Keeley, 1994; Selley, 1997; Fekirine and Abdallah, 1998).

The east-west trending, 700 km long Tindouf Basin has a history comparable to that of many other Saharan basins (Selley, *ibid*). Its cross-section is asymmetric, having a steeper limb on its south flank. It is filled by a nearly eight km thick sedimentary sequence, ranging in age from Early Cambrian to Carboniferous.

The above data suggests that the northern half of Africa has undergone a geological history of northward drifting and compression in its collision with Eurasia, that is very similar to that of the southern half of Africa (see above).

Several secondary geosutures are branching-off the Atlantis F.Z. in a counterclockwise mode. The most prominent one extends to the ENE from the Canary Islands along the Anti and Saharan Atlas toward Bizerte (North Tunisia) and terminates at the Sestri Vortex. An analogous example is the geosuture that extends from the Researcher F.Z., through the Ahaggar Hotspot and the Herodotus Basin, to merge within the Aegean-Menderes Vortex.

VII: THE ALPINE OROGENIC SYSTEM:

VIIa: General Characteristics of the Alpine-Himalayan Vortices (Figs. 22.1, 22.9, 22.10a, and 22.10b):

The following is a more elaborated version of our concept (Neev and Hall, 1982, 1984) on the origin of the vortices produced by the counterclockwise curving pattern of faults and fold ranges *i.e.* sequentially branching-off away from E-W trending geosutures which are crossing the Atlantic Ocean. Each of them is generating a vortical feature along the Alpine-Himalayan system. Five of these eight vortices have been developed into symmetric-circular patterns of counterclockwise curving vortices. These are

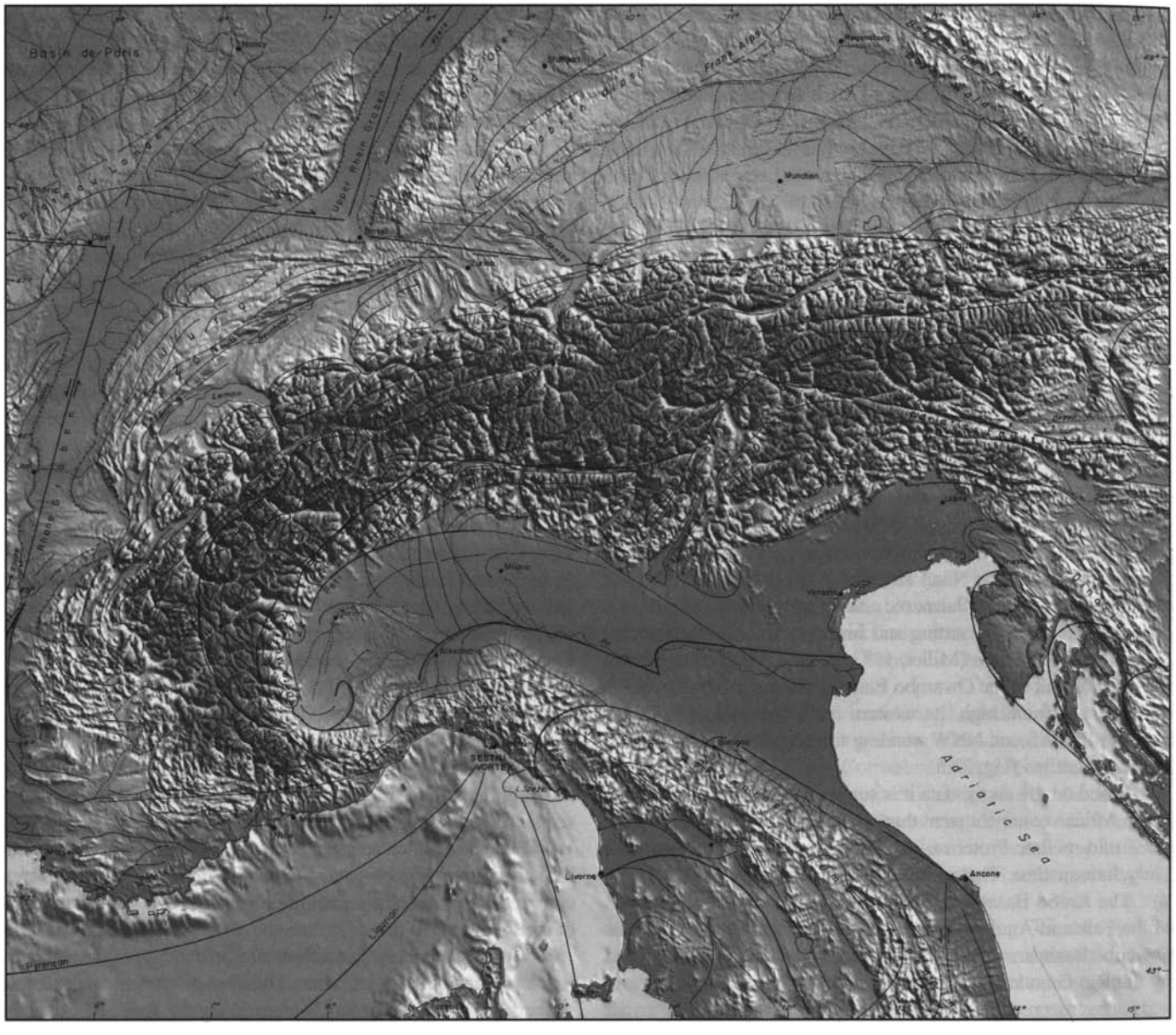


Figure 22.9. The Western Alpine System – The 'Eye' of the Sestri Vortex: Although interpreted, that sketch-map is compiled and based on published results of many geological studies carried out by generations of geologists who devoted their efforts to decipher the origin and history of this feature.

The resulting counterclockwise horizontal vorticing movement seems to be obvious. The tectonic process associated with the inferred evolution of the western Alpine system are being maintained at least since late Paleozoic times.

Legend: xxx External Precambrian Massifs. vvv Internal Precambrian Massifs.

Background shaded relief is IBCM bathymetry at 0.25', together with the ACE 0.5' land grid. Universal Transverse Mercator projection.

the Alboran (or Rif-Betic), the Sestri, Aegean, Kirşehir, and the Brahmaputra Vortices. The other three are the Ararat, Lut, and Pamir Vortices (Figs. 22.1 and 22.10a, b).

Considerable differences exist however between the two groups of vortices. The first five are recognized by an equal width to length ratio (*i.e.* a close to perfect spiral-circular shape). The second group of three is characterized by a repeated sequence of northward counterclockwise curving and branching-off pattern of arcs, which are often asymmetric to the west. The most impressive characteristic of the second group is the elongate and northward pointing, finger-like shape, which suggests a horizontal northward piercing (or bulging) through the E-W trending Alpine-Himalayan collisional belt. The geosutures which approach the global eye from the north (see Section III above) are tangentially



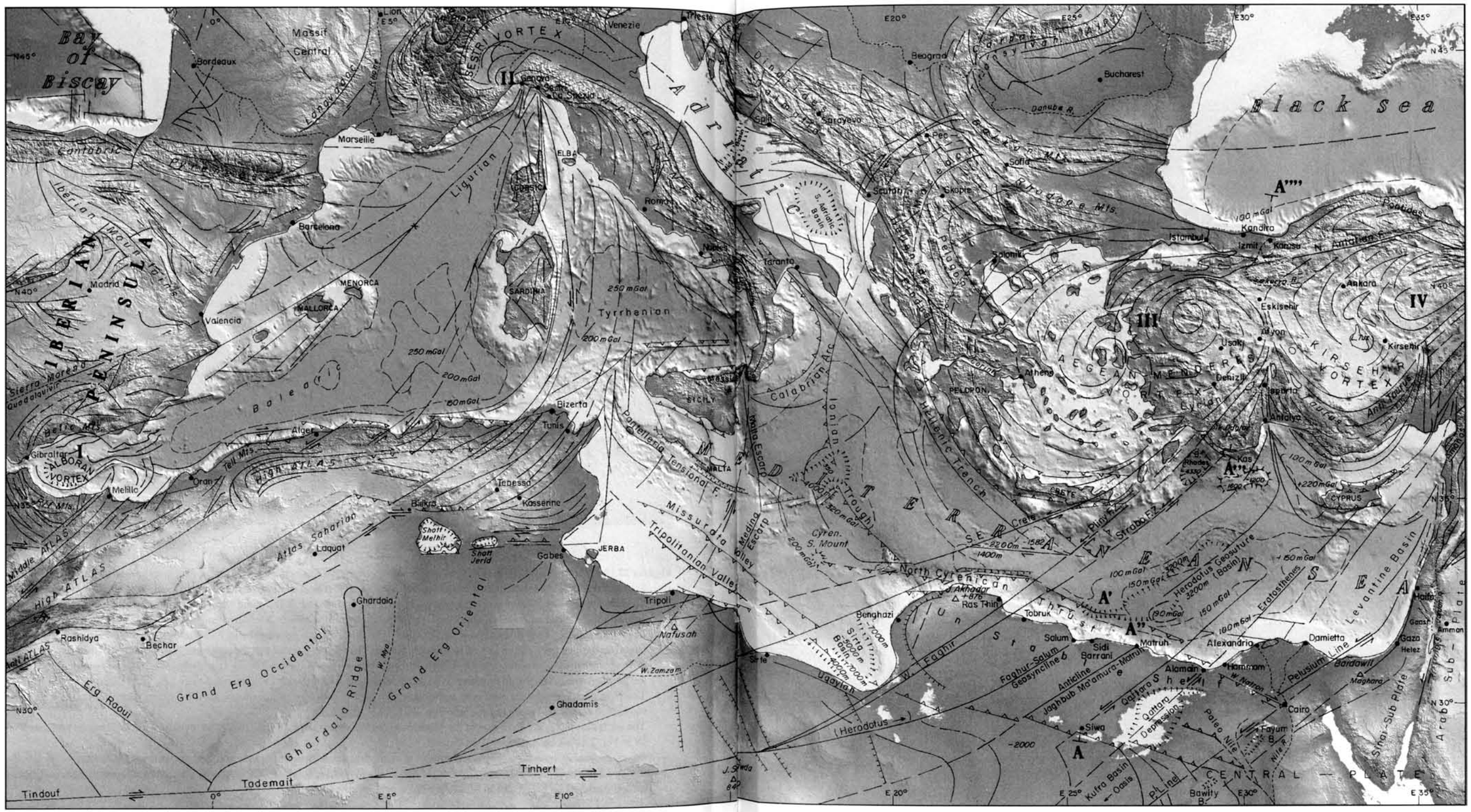
Figures 22.10a (overleaf), **b** (above). **The Mediterranean Sea and the Central Plate:** Based on stratigraphic data for the Central Plate, as well as from the Levantine Basin of the Mediterranean Sea, it is suggested that both of these territories were continuously drifting northward at least since pre-Mesozoic times. The following conclusions could therefore be inferred: i) The same history could also be implied for the rest of the Mediterranean Basins; ii) The mode of origin of the oceanic crust that underlies the eastern Mediterranean does not have to be by bulging up of magma from the Upper Mantle since early to mid-Phanerozoic times. It should have been associated with N-S tensional movements (*i.e.* the southward drift of Africa). Based on the data from Africa as well as from the Central Plate it is suggested that the continental crust of North Africa has maintained its northward drifting and thrusting process over the Mediterranean (Tethyan) Sea perhaps since the Late Proterozoic. The occurrence of oceanic basement under the Mediterranean Sea should therefore to be interpreted as an Alpine parallel belt inherited since very early times.

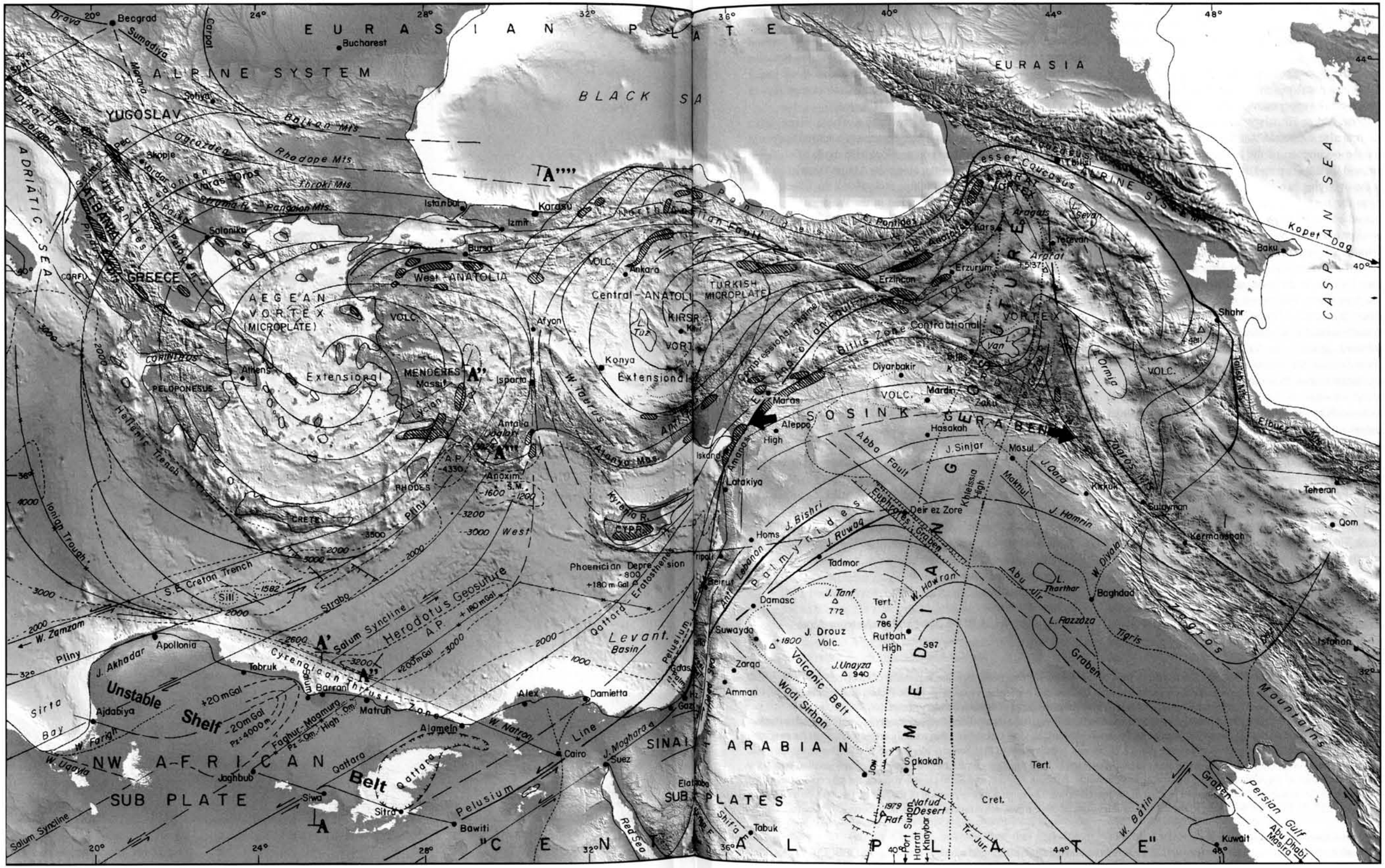
The mild counterclockwise rotational movement of Africa is therefore in agreement with the above interpretation as well as with the sinistral movement across the Pelusium Line (see Figs. 22.1, 22.5, and 22.22).

The six basins along the E-W axis of the Mediterranean Sea (see caption of Fig. 22.6), and the four vortices along its northern flanks (marked I to IV in Fig. 22.10a), have thereby been formed.

Figure 22.10a background is IBCM bathymetry at 0.25', together with the ACE 0.5' land grid. Projection is Mercator.

Figure 22.10b basemap is National Geographic Atlas Plate 69. Background is ETOPO2 global 2' elevations/depths. Azimuthal Equidistant projection, central meridian 23°E and central parallel 52°N.


Bay of Biscay
Massif Central
Bordeaux
Lyon
Marseille
Venezie
Trieste
Beograd
Bucharest
Black Sea
Sarajevo
Split
Pec
Sofia
Skopje
Istanbul
Izmit
Kandira
Barcelona
Madrid
Valencia
MENORCA
MALLORCA
Ligurian
Tyrrhenian
ELBA
Corsica
Roma
Napoli
Taranto
SARDINIA
Adriatic
Ionian
Aegean
Athens
PELOPONNESUS
Rhodes
Crete
Eskisehir
Ankara
Usaki
Afyon
Denizli
Isparta
Antalya
Kirsehir
Kas
CYPRUS
Bizerta
Tunis
Alger
Oran
Melilla
Gibraltar
Tebessa
Kasserine
Sfax
Gabes
JERBA
Tripoli
Benghazi
Tobruk
Ras Thin
Natusah
Ghadamis
Ghardaia
Rashidya
Bechar
Laquat
Salum
Sidi Barrani
Matruh
Alexandria
Damietta
Gaza
Helez
Amman
Malta
Siwa
Cairo
Fayum
Alaman
Hammam
Baridawil
Pelusium Line
Levantine Basin
Arabian Sub-Plate
Sinai Sub-Plate
Nile R.
Danube R.
Sakarya R.
Euphrates R.
Tigris R.
Orontes R.
Jordan R.
Dinarides
Hellenic Trench
Calabrian Arc
Ionian Trough
Cyren. S. Mount
North Cyrenican Thrust
Faghur-Salum Geosyncline
Herodotus Geosuture
Eratosthenes
Qattara Depression
Qattara Sheet
Paleo Nile
Kufra Basin
Oasis
Bawity
Pliny
Strabo FZ
Tripolitanian Valley
Missurata
Medina Escarp
Sirte Basin
Ugeylah
Tinhert
Tademait
Tindouf
Grand Erg Occidental
Grand Erg Oriental
Erg Raoui
Ghardaia Ridge
Hamada
Atlas Saharian
Middle ATLAS
High ATLAS
Anti Taurides
Bitlis
Zagros
Caspian Sea
Iranian Plateau
Kopet Dag
Elburz Mts.
Caucasus
Black Sea
Anatolian Plateau
Eastern Pontides
Kura R.
Caspian Basin
Apsheron Sill
Kura Basin
Lesser Caucasus
Greater Caucasus
Kuban R.
Rostov
Volgograd
Saratov
Samara
Orenburg
Aktyubinsk
Caspian Depression
Ural Mts.
Ural R.
Emba R.
Mangyshlak
Ustyurt Plateau
Aral Sea
Aral Basin
Kara Kum
Kara Kum Canal
Amu Darya
Kyzyl Kum
Syr Darya
Tashkent
Fergana Basin
Fergana Valley
Kopet Dag
Turkmenbashi
Krasnovodsk
Ashkhabad
Mary
Chardzhou
Bukhara
Kermine
Navoi
Samarkand
Dushanbe
Kulyab
Kurgan-Tyube
Termez
Amu Darya
Afghanistan
Kabul
Kandahar
Herat
Helmand
Quetta
Pakistan
Zhob
Sibi
Kalat
Chaman
Khyber Pass
Peshawar
Indus R.
Indus Basin
Indus Delta
Karachi
Hyderabad
Thatta
Jacobabad
Sukkur
Rohri
Multan
Lahore
Amritsar
Jammu
Srinagar
Kashmir
Himalayas
Nanga Parbat
Rawalpindi
Islamabad
Jhelum R.
Chenab R.
Ravi R.
Sutlej R.
Beas R.
Jullundur
Ludhiana
Ambala
Simla
Delhi
Agra
Jaipur
Ajmer
Jodhpur
Bikaner
Thar Desert
Rann of Kutch
Kutch
Gulf of Kutch
Gulf of Cambay
Ahmedabad
Baroda
Surat
Bombay
Nasik
Aurangabad
Ahmednagar
Poona
Sholapur
Hyderabad
Bidar
Gulbarga
Raichur
Bijapur
Belgaum
Goa
Panaji
Mangalore
Karwar
Hubli
Dharwar
Bellary
Kolar
Bangalore
Mysore
Cochin
Trivandrum
Madras
Pondicherry
Cuddalore
Tiruchirapalli
Madurai
Tuticorin
Salem
Coimbatore
Erode
Ootacamund
Cape Comorin
Palk Strait
Gulf of Mannar
Palk Bay
Ceylon
Colombo
Kandy
Jaffna
Trincomalee
Batticaloa
Hambantota
Galle
Ratnapura
Nuwara Eliya
Anuradhapura
Polonnaruwa
Vavuniya
Mannar
Puttalam
Negombo
Kalutara
Matara
Ratnapura
Kurunegala
Badulla
Monaragala
Ampara
Kegalla
Gampaha
Chilaw
Mullaitivu
Kilinochchi
Point Pedro
Elephant Pass
Adam's Bridge
Gulf of Manaar
Bay of Bengal
Andaman Sea
Andaman Islands
Nicobar Islands
Port Blair
Car Nicobar
Great Nicobar
Little Andaman
Middle Andaman
North Andaman
Ritchie's Archipelago
Diamond Island
Cinque Islands
Barren Island
Narcondam Island
Preparis Island
Cocos Islands
Coco Channel
Landfall Island
Interview Island
Rutland Island
Long Island
Tavoy
Mergui
Victoria Point
Kawthaung
Tenasserim
Tenasserim R.
Moulmein
Martaban
Gulf of Martaban
Thailand
Bangkok
Chao Phraya R.
Chao Phraya Basin
Phitsanulok
Nakhon Sawan
Ayutthaya
Lopburi
Saraburi
Nakhon Ratchasima
Khorat Plateau
Khon Kaen
Udon Thani
Nong Khai
Mekong R.
Vientiane
Laos
Luang Prabang
Phongsali
Sam Neua
Xieng Khouang
Thakhek
Savannakhet
Pakse
Cambodia
Phnom Penh
Tonle Sap
Tonle Sap Lake
Mekong Delta
Gulf of Thailand
Ko Samui
Ko Pha Ngan
Ko Tao
Surat Thani
Phuket
Phang Nga
Krabi
Trang
Songkhla
Hat Yai
Pattani
Yala
Narathiwat
Kota Bharu
Kuala Lumpur
Malacca
Malacca Strait
Singapore
Singapore Island
Johore Bahru
Kuantan
Mersing
Pahang
Pahang R.
Endau R.
Tioman Island
Anambas Islands
Natuna Islands
Natuna Sea
Natuna Basin
Natuna Arch
Natuna Trough
Natuna Ridge
Natuna Plateau
Natuna Fracture Zone
Natuna Fault
Natuna Transform
Natuna Rift
Natuna Graben
Natuna Horst
Natuna Block
Natuna Platform
Natuna Shelf
Natuna Slope
Natuna Rise
Natuna Abyssal Plain
Natuna Deep
Natuna Trench
Natuna Subduction Zone
Natuna Accretionary Prism
Natuna Forearc Basin
Natuna Backarc Basin
Natuna Volcanic Arc
Natuna Island Arc
Natuna Ridge
Natuna Plateau
Natuna Fracture Zone
Natuna Fault
Natuna Transform
Natuna Rift
Natuna Graben
Natuna Horst
Natuna Block
Natuna Platform
Natuna Shelf
Natuna Slope
Natuna Rise
Natuna Abyssal Plain
Natuna Deep
Natuna Trench
Natuna Subduction Zone
Natuna Accretionary Prism
Natuna Forearc Basin
Natuna Backarc Basin
Natuna Volcanic Arc
Natuna Island Arc
I
II
III
IV
A
A'
A''
A'''
A''''
A'''''
A''''''
A'''''''
A''''''''
A'''''''''
A''''''''''
A'''''''''''
A''''''''''''
A'''''''''''''
A''''''''''''''
A'''''''''''''''
A''''''''''''''''
A'''''''''''''''''
A''''''''''''''''''
A'''''''''''''''''''
A''''''''''''''''''''
A'''''''''''''''''''''
A''''''''''''''''''''''
A'''''''''''''''''''''''
A''''''''''''''''''''''''
A'''''''''''''''''''''''''
A''''''''''''''''''''''''''
A'''''''''''''''''''''''''''
A''''''''''''''''''''''''''''
A'''''''''''''''''''''''''''''
A''''''''''''''''''''''''''''''
A'''''''''''''''''''''''''''''''
A''''''''''''''''''''''''''''''''
A'''''''''''''''''''''''''''''''''
A''''''''''''''''''''''''''''''''''
A'''''''''''''''''''''''''''''''''''
A''''''''''''''''''''''''''''''''''''
A'''''''''''''''''''''''''''''''''''''
A''''''''''''''''''''''''''''''''''''''
A'''''''''''''''''''''''''''''''''''''''
A''
A'''
A''
A'''
A''
A'''
A''
A'''
A''
A'''
A''
A'''
A''
A'''
A''
A'''
A''
A'''
A''
A'''
A''
A'''
A''
A'''
A''
A'''
A''
A'''
A''
A'''
A''
A'''
A''
A'''
A''
A'''
A''
A'''
A''
A'''
A''
A'''
A''
A'''
A''
A'''
A''
A'''
A''
A'''
A''
A'''
A''
A'''
A''
A'''
A''
A'''
A''
A'''
A''
A'''
A''
A'''
A''
A'''
A''
A'''
A''
A'''
A''
A'''
A''
A'''
A''
A'''
A''
A'''
A''
A'''
A''
A'''
A''
A'''
A''
A'''
A''
A'''
A''
A'''
A''
A'''
A''
A'''
A''
A'''
A''
A'''
A''
A'''
A''
A'''
A''
A'''
A''
A'''
A''
A'''
A''
A'''
A''
A'''
A''
A'''
A''
A'''
A''
A'''
A''
A'''
A''
A'''
A''
A'''
A''
A'''
A''
A'''
A''
A'''
A''
A'''
A''
A'''
A''
A'''
A''
A'''
A''
A'''
A''
A'''
A''
A'''
A''
A'''
A''
A'''
A''
A'''
A''
A'''
A''
A'''
A''
A'''
A''
A'''
A''
A'''
A''
A'''
A''
A'''
A''
A'''
A''
A'''
A''
A'''
A''
A'''
A''
A'''
A''
A'''
A''
A'''
A''
A'''
A''
A'''


EURASIAN PLATE
EURASIA
ALPINE SYSTEM
BLACK SEA
CASPIAN SEA
ADRIATIC SEA
Ionian Trough
Hellenic Trench
S.E. Cretan Trench
Sill
Pliny
Strabo
Ptolemy
Herodotus Geosuture
Eratosthenes Seamount
Phoenician Depression
Levant Basin
Qattara Ridge
Pelusium Line
Salum Syncline
Cyrenaican Thrust Zone
Unstable Shelf
Sirte Bay
Faghur-Maqmura High
NW AFRICAN SUB PLATE
ARABIAN SUB PLATE
AEGEAN VORTEX (MICROPLATE)
TURKISH MICROPLATE
SOSINK
Anatolian Fault
Bitlis Zone Contractional
Dead Sea Transform Fault
Palmyrides
Euphrates Graben
Abu Jir
Tigris Graben
Persian Gulf
Red Sea
Aqaba
Suez
Cairo
Alexandria
Damietta
Beirut
Damascus
Amman
Jerusalem
Tel Aviv
Gaza
Latakia
Aleppo
Homs
Tripoli
Tadmor
Deir ez Zore
Hasakah
Mosul
Kirkuk
Sulaymaniyah
Baghdad
Kermanshah
Tehran
Qom
Isfahan
Shahr
Baku
Kopet Dag
Tabriz
Elburz Mts.
Zagros Mts.
Mountains
Kuwait
Abu Dhabi
Masira
Diyarbakir
Mardin
Batman
Siirt
Bitlis
Van
Lake Van
Lake Urmia
Erzurum
Erzincan
Kars
Yerevan
Ararat
Sevan
Tbilisi
Lesser Caucasus
Pontides
Anatolides
Taurides
Menderes Massif
Isparta
Afyon
Konya
Ankara
Kirsir
Kalir
Tuz
Izmir
Karasu
Bursa
Istanbul
Edirne
Thrace
Rhodope Mts.
Balkan Mts.
Pangaion Mts.
Strouma R.
Vardar
Axios
Skopje
Sofia
Belgrade
Bucharest
Drava
Sumadija
Morava
Carpat
Dinarides
Hellenides
Pindus Mts.
Corfu
Peloponesus
Corinthos
Athens
Rhodes
Crete
Cyprus
Kyrenia R.
Antalya
Aksu
Ataturk Dam
Euphrates R.
Tigris R.
Jordan R.
Nile Delta
Aswan
Sinai
Tabuk
Nafud Desert
Port Sudan
Harrat Khaybar
Raf
Jafurah Basin
Tert.
Cret.
Tr.-Jur.
Plio-Pleist.
Volc.
Volcanic Belt
Wadi Sirhan
Rutbah High
J. Drouz Volc.
J. Unayza
J. Tanf
J. Sinjar
J. Bishri
J. Homrin
J. Qara
J. Akhdar
J. Moghara
Makhul
Abbas Fault
Khleissia High
Ormia
Zagros
Graben
Line
Fault
High
Basin
Mts.
Sea
Gulf
Trough
Trench
Ridge
Plate
Belt
Shelf
Syncline
Geosuture
Vortex
Extensional
Compressional
Contractional
Transform
Thrust
Zone
Massif
Graben
Basin
Ridge
Fault
Line
Sea
Gulf
Trough
Trench

trending with respect to the Alpine-Himalayan belt. The above characteristics of the Alpine-Himalayan orogenic belt are unique, as no similar features are known to exist across other orogenic belts of our globe.

It is reasonable to assume that the driving force which generates the above crustal pattern is composed of oppositely trending counterclockwise upper mantle currents that converge and collided beneath the Alpine-Himalayan orogenic belt to generate the global eye. It is also suggested that the two currents are also responsible for the occurrence of the collision between Eurasia and Gondwana, and for the sharp and linear nature of their contact. Consequently the overlying two 'hitch-hiking' lithospheric plates (the Eurasian on the north and the African-South Asian on the south), together with their relevant geosutures, should also collide along the equivalent overlying linear contact. There are however, a few specific features which accentuate different characteristics.

The limits of the Western and Central Alps are clearly defined along the Rhone Graben on the west, and by the Basel-Salzburg tectonic line on their north. That vortex is being enveloped on its northern periphery by a chain of three large arcuate structures that could be genetically related to the discussed feature. These are:

i) The southward concave arc (or secondary vortex) of the Carpathian-Transylvanian Mountains on its northeast, limited by the Drava River lineament on its south;

ii) The second structure is the Bohemian Massif, which is surrounded on its north by the southward concave arc of the Sudet and Ore mountain ranges, and by the Bohemian Forest and the Danube River (Linz to Bratislava segment) on its south;

iii) The third structure also forms a southward concave and westward thrusted arc which is composed on its northern limits by the Thuringian-Harz, and Eifel-Ardennes mountain ranges (or Forests) (World Sat International Inc., 1994). Its southern limit is marked by the right-laterally shifted Somme-Luxembourg-Vienna geosuture. That geosuture should belong to the tangentially approaching northern system of geosutures. It is truncating the northward plunging noses of the Vosges and Black Forest twin mountain ranges, and then further extends eastward along the uppermost segment of the Danube River. It also extends westward from Luxembourg through the West Somme River and along the trough of the English Channel to curve clockwise along the northward trending bathymetric-tectonic deep trough, situated between Porcupine Bank and the western coastline of Ireland (Emery and Uchupi, 1984, Charts IA and 5A), as well as between the Faroe and Shetland Islands. All of the above three major structures are characterized by distinct counterclockwise (*i.e.* to the west or southwest) asymmetries.

Analogous interpretations are made where large scale horizontal shifting of crustal masses repetitively occurred as a result of, and in agreement with, a counterclockwise mode of vorticing of the underlying upper mantle, along the Alpine-Himalayan fold ranges (Neev and Hall, 1984; Phillipe et al., 1996). Such horizontal-lateral movements have also occurred in the Western Alps along with, or oblique to, the horizontal dimensions of the arcuated fold axes (Figs. 22.1, 22.4a and 22.9). This can be seen by observing the Western Alps sheet (No. D-01E/EU-S1) of the Global Satellite Image Map at scale 1:1,000,000 (Geospace, 1998), where the axes of the subaerial members of the Sestri Vortex systematically curve horizontally and counterclockwise to converge as recumbent folds and thrust faults. In other words, they are moving sideways and not frontally. That mode also refers to the Appenines of Umbria-Tuscana and the Alpi-Apuane (east of La Spezia), to the Maritime, Dauphine and Jura Mountains of the Western Alps, as well as to other similar features.

VIIb: The Sestri Vortex: (Figs. 22.4, 22.5, 22.9, 22.10a, b and 22.11):

The Sestri Vortex (close to Genoa, Neev and Hall, 1984) is composed of the following geosutures (from Sestri southward and clockwise):

1) Messina-Tripoli-Ghadamis-Tindouf-Atlantis F.Z.;
2) Tyrrhenian-Jerba-Tindouf-Atlantis F.Z.;
3) Ligurian-E. Sardinia-Corsica-S. Atlas-Oceanographer F.Z.;
4) W. Sardinia-Corsica-Alger-Rabat;
5) Balaeric-Guadalquivir-Azores;
6) Pyrenees-Charcot F.Z.;
7) Marseille-Biscay;
8) Monaco-Rhone;
9) Argentera-Mont Blanc-Aar-North Calcareous Alps;



Figure 22.11. The Eastern Mediterranean Sea and the northern part of the 'Central Plate': The distribution patterns of epicenters, geosutures, and other topographic-physiographic-geological features are described after Jackson and McKenzie (1988, Fig. 7), Le Pichon and Angelier (1979, Fig. 4), as well as other sources. Note the Aegean and Kirşehir (Pelusium) Vortices as well as the Ararat secondary vortex.

Legend: Coastlines - fine line; bathymetric contours - fine dashed lines; tectonic lineaments - heavy lines. Positive gravity anomalies are often marked in the offshore; The N-S trending double dotted line represents the newly-defined 'Median Geosuture', that roughly corresponds with the structural axis of the 'Central Plate' (or the Arabian sub-plate) (see Fig. 22.21 below). It extends from Port Sudan – along the SW coastline of the Red Sea, to the Ararat Secondary Vortex (east Anatolia). Intrusions of ophiolites (mostly E-W trending ellipsoidal bodies with diagonal striation which are sub-parallel to the contours of the Alpine Belt) are marked across the Ararat, Kirşehir, Aegean, and Sestri crustal Vortices, thereby corroborate their genetic relationship to the underlying N-S collisional process of the mantle flows. The more northern position of the Ararat, Lut, and Pamir Vortices (Fig. 22.1, 22.21, 22.24, 22.25) could be related to the increasing intensities of these flows, as compared with the neighboring vortices (both to the west and east).

Legend: numbers - elevations or depths; Δ peaks.

Background shaded relief is ACE satellite altimetry at 0.5', superimposed on the IBCM 0.25' grid which is overlying the GEBCO GDA 1' global grid. Mercator projection.

10) Dora Maria- Arbia-Carnic Alps;
11) Peri-Adriatic-Dinarides;
12) Ligure-Appenines-Reggio (Calabria);

Their surficial and subsurface expressions are the best suited for an attempt to understand their origin and their mode of formation as vortices. Features of counterclockwise curving and asymmetric secondary vortices, such as the Carpathians and Jura features, are superimposed on the Sestri Vortex.

Figure 22.9 shows a map of the main structural limits of the different tectonic units mapped in the Western and Central Alpine system. If we imagine this map to be a vertical structural cross-section instead of a map, it could be interpreted as expressing a large recumbent fold, across which many reverse (thrust) faults and overturned folds are identified. Such features may indicate large-scale horizontal shifting of crustal masses to have occurred along it, which emphasizes its vortical structure as well. Similar features are assumed to be repetitively occurring as a byproduct of, and in agreement with, a counterclockwise mode of flow of the underlying upper mantle, along the Alpine-Himalayan fold ranges (Neev and Hall, 1984; Phillipe et al., 1996). Such horizontal-lateral movements could have occurred in the Western Alps along with, or oblique to, the horizontal dimensions of arcuated fold axes (Figs. 22.1 and 22.9). This can be sensed by observing the Western Alps sheet (No. D-01E/EU-S1) of the Global Satellite Image Map 1:1,000,000 (Geospace, 1998) where the axes of the subaerial members of the Sestri Vortex systematically curve counterclockwise and horizontally converge as recumbent folds and thrust faults, which are moving sideways and not frontally. That mode is expressed vividly in maps and LANDSAT imagery of the Western Alps (including the Maritime, Dauphine and Jura Mountains), as well as the Apennines of Umbria-Tuscana and the Apuane Alps. The northeastern limit of the Apuane Alps extends northwestward from Firenze to further curve southwestward and terminate at Genova-Sestri.

Some notion on the mode of origin of that unique pattern could be deduced from geophysical and geological studies carried out by Wunderlich (1964, p. 73) across the western Alps and close to the Sestri vortex. He states that "... these frontal zones of active deformation rotate counter-clockwise around a centre situated at the junction of the Alps and northern Appennines; a process that seems to be very much like atmospheric cyclones". Wunderlich (1966) excluded gravitational sliding as the cause for the orogenic shortening process of the western Alps. Based on results of deep crustal studies carried out by the use of seismic explosion in the same province, Giese et al. (1982, Fig. 11) produced a structural contour map of the crust-mantle boundary. The pattern exhibited by this map is in agreement with that portrayed by the surface distribution of the geosuture that composes the Sestri Vortex (Neev and Hall, 1984, Figs. 1, 2, 3, 4). Moreover, cross-sections made by Giese et al. (1982, Figs. 5, 6, 9, 10, 12, 19, 21) that are outlined perpendicular to the long axes of the Alps, Apennines, Hellenids, and Pyrenees as well as Corsica, indicate that the underlying lithospheric/mantle contacts form asymmetrically tilted planes that are striking parallel to the trends of these geosutures, and are dipping away from the eye of the Sestri Vortex. These data suggest that a flow of mantle material is involved with the crustal movements that generated the Sestri Vortex. Counterclockwise mass movements of the crust occur in association with that process as well (see above).

Most authors who studied the geological evolution and history of the Alpine orogenic era consider the ages of its events to be restricted to between the Jurassic and the end of the Tertiary (Gary et al., 1974), and apparently also being maintained even today (authors).

Philippe et al. (1996, p. 255) conclude that "the development of the Jura fold-and-thrust belt is governed by the distribution (pattern) of Triassic evaporites...". They also show the overlapping similarity between the configuration and areal distribution patterns of the Triassic basin (isopach maps of the evaporites) and the structural and stress-axes maps of the overlying Jura fold-and-thrust belt, (see their Figures 6 and 10, 11, and 12 respectively). It is therefore suggested that the tectonic factors, responsible for the development of the present-day architecture of the Alpine Belt, could have been active since Variscan (Late Paleozoic times), or perhaps even earlier. Both Philippe et al. (1996) and Ziegler and Roure (1996) suggest that oblique collisions and lateral mass movements, were involved in the processes that occurred within the Alpine orogenic belt during its formative phase.

In more recent papers edited and published in monographs by Ziegler and Horvath (1996), Grecula et al. (1997), and Frey et al. (1999), it is suggested that the embryionic stages of the Alpine geosyncline could have first occurred during much earlier ages than hitherto considered, such as Early Paleozoic, or even Late Precambrian. One example is inferred from the geochemical studies made by Hovorka and Meres (1997) on the Early Paleozoic metamorphic rocks of the Western Carpathians. These authors found evidence for the involvement of a Caledonian thermal event in the processes that led to the formation of the Carpathian secondary vortex. Metavolcanics as well as basic volcanoclastics are interbedded there within a sedimentary sequence of (black) shales and carbonate rocks. They consider that complex to reflect a back-arc environment that could have prevailed in that same site ever since and even before the occurrence of the discussed thermal event. From the point of view of age, environments and geological history, the discussed rock unit is identical with the metavolcanics and volcanoclastics of the Graywacke Zone of the Eastern Alps as well as of the Southern Alps, where the radiometric ages are between 400 and 500 Ma. Different metamorphic patterns and histories from the West Alpine External Massif are described by von Raumer et al. (1999). These are interpreted as having been generated through intrusive depositional and reworking processes that occurred between Gondwana and Eurasia during Precambrian to Ordovician subduction and collisional cycles. These processes are not restricted to the External Massif. According to the Map of Pre-Alpine Metamorphism (Frey et al., 1999) as well as their Introduction attached to the special volume of relevant papers, and Desmons et al. (1999), similar processes have occurred during about the same time span, within many of the Internal Massifs which are rather abundant all along the west, central, and East

Alpine ranges.

Frey et al. (1999) also cast doubt on some of the younger ages measured within the Internal Basement massifs. Intrusions of Late Variscan granitoids may have altered the isotopic ratios within their country rocks. That same approach should also be applied regarding the important study of Tricart et al. (2001) on the history of tectonic dynamics of the Western Alps since the Miocene.

VIIc: Other Features Along and North of the Alpine Orogenic System (Figs. 22.9 and 22.10b):

It is reasonable to assume that the E-W trending collisional contact between the two groups of oppositely trending counterclockwise upper mantle currents, that together generate and compose the global eye, would be sharp and linear. Nevertheless that expectation is not always fulfilled. The following examples illustrate the existence of deviations from, and irregularities within, the model.

VIIc(1): The Carpathian Secondary Vortex:

In outline the northward protruding, loop-shaped feature of the Carpathian chain of mountains is close to 1000 km long (E-W) and 700 km wide (N-S). It is separated from the Fennoscandian (Russian) Platform by the Tiessseyere-Tornquist geosuture. The Western Carpathians are divided into three belts:

1) The Outer one welds the Alpine and Carpathian mountains into a coherent orogenic system.

2) The Central, which is an immediate extension of the Austroalpine system.

3) The Inner Carpathians which encompass Paleozoic and Mesozoic carbonates, and link them to the South Alpine and Dinaridic belts (Plasienka et al., 1997).

The Carpathian fold belt forms a peculiar (northward protruding and asymmetric) shape away from the West Alpine-Himalayan Orogen (Figs. 22.1, 22.5, 22.9, and 22.10b), which is superimposed on the otherwise nearly linear feature. The discussed Alpine-Himalayan orogenic belt resulted from the convergence and collisional processes that occurred between Laurasia and Gondwana along the Prototethys at least since the transition between Precambrian and Early Phanerozoic (see above).

Four orogenic phases of diachronous southward migrating processes occurred across the Carpathian-Fenoscandian collisional contact. The first started sometime prior to ~480 Ma and terminated close to 400 Ma (Plasienka et al., 1997, Fig. 6). It climaxed in the late Devonian. The second orogenic cycle was the Variscan, that lasted from Early Carboniferous to Late Permian. The third orogenic phase took place during Mesozoic time, when paleotectonic evolution of the Carpathian area occurred through the following four different periods extending from Late Permian (245 Ma) to Maestrichtian (Late Cretaceous - 70 Ma):

1) A platform stage (Early to Mid-Triassic). Carbonate shelf facies dominated to the north of the Maliatic collisional geosuture and the sandstone facies to its south.

2) Rifting - extensional and crustal thinning regime (Middle Triassic - Mid-Jurassic).

3) Compressional and crustal-thickening regime (Late Jurassic - Late Cretaceous).

4) Transpressional - transtensional regime and partial disintegration of the stacked crust (Late Cretaceous-Late Tertiary). The southward migration of the collisional front that dominated the West Carpathians during the Paleozoic was switched over to a northward one during the Mesozoic (*ibid*, 1997, Figs. 6, 7).

The fourth orogenic phase is the Cenozoic tectonic evolution (Oligocene - 30 Ma to Pliocene - 5 Ma - *ibid*, 1997, Fig. 8): Following the Late Cretaceous subsidence, a flexure and roll-back effects were formed along the outer margins of the Alpine orogeny, possibly by subcrustal erosion, trench suction, and subduction. Further compression during the Miocene increased the rate of Molasse sedimentation in the foredeep. Oblique collisional processes led to changes in the directions of movement, counterclockwise rotation, and uplift of rigid basement blocks, together with thrust and wrench faulting. That process created more mountains along the inclined crustal detachment zone. More than 60° of Miocene counterclockwise rotation of the Eastern Alpine - Western Carpathian - Pannonian lithosphere fragment is documented by paleomagnetic results (Kovac et al, 1997, p. 60, Fig. 12).

Lithospheric thinning, high heat flow, and high density values across the internides of the Carpathian domain (West and East Carpathians), together with the Pannonian basin physiography between them, as well as the regional distribution of the Neogene volcanics, indicate extensive asthenospheric upheaval there, associated with lithospheric extensional features. On the other hand, contemporaneous crustal thickening and high rate of deposition within the foredeep belts (*i.e.* compressional features) are found across the peripheral zones (Kovac et al. 1997).

Lithostratigraphic information recovered from the geological map of Rumania (Sandulescu et al., 1978) and Dr. S. Peltz (personal communication), regarding the Apuseni Massif (located between the Pannonian and the Transylvanian Basins at the central point 46°-30'N, 23°E), indicate that the massif consists of a mosaic of igneous rocks. The igneous components are of both crystalline and volcanic rocks of different ages, indicating the occurrence of different magmatic events in the nearby areas during the Permian, Jurassic, Cretaceous, Eocene, and Neogene.

The origin of the Carpathian northward asymmetric bulge (or apophysis) is therefore suggested to have been associated with the consistent process of mantle flows, which generate the vortical movement of the mantle and their northward protrusions (see above). That process could have functioned since the early Paleozoic and even earlier. In other words, that counterclockwise rotational movement is a secondary vorticing process which is associated with the mantle subduction and superimposed on the Sestri Vortex. As a vortex it shares many of the characteristics of the Sestri, as well as with the Alboran, the Aegean, and the Kirşehir Vortices.

VIIc(2): The Northern Flank of the Alpine Orogenic Belt:

The independent functioning of the geosutures of the northern

group is indicated if and when they are being crossed (or breached) by the vortices (the origin of which is related just to the southern group). The WNW trending promontory of the Armoric Massif of Brittany is bordered and crossed by a WNW dextrally-shifted system of strike-slip faults that were tectonically active during the Hercynian Orogen. That massif is situated at the western tip at the Atlantic coastline (NW France, between 5°W and 0°W). Along its eastward extension it is being onlapped by the Early Jurassic to Neogene sediments accumulated within the Paris Basin (Figs. 22.4a, 22.9 and 22.10b). These old faults extend further in the sub-surface, beneath the younger sequence of sediments, to be exposed again east of the limit of that basin. It further extends eastward through Dijon and Basel to right-laterally shift the Rhine Graben (together with its adjacent mountain chains of the Vosges and Black Forest on its west and east). Therefore the Rhone-Saone graben, together with the Languedoc and Jura-Dauphine chains of mountains on its west and east, are shifted to the west. Beyond Basel the Armoric-Dijon dextral fault extends further eastward toward Budapest.

On the other hand, the Carnic Alps, together with their two southwestward curving geosutures, which extend along the Dravas-Sava River, as well as the Dinarides Ranges, are considered to be genuine components of the Sestri Vortex. The Taurean Alps, together with the Dolomites, make up the Eastern Alps, which are separated from the Western Alps across the sinistral NNE-SSW trending Trentino Fault. The architecture of these individual provinces (including the Dinarides) expresses secondary vortical efforts, which (together with the Western and Southern Alps) are well incorporated and orchestrated within the entire complex of the Sestri Vortex.

The above secondary vortices developed across the Western, Central, and Eastern Alps. They do not extend to the west of the Rhone Basin and to the north of the Basel-Salzburg line. Their external limits, however, are enveloped by a belt of three large structures that seem to be less intensively folded and uplifted, as compared with the Western Alps. Nevertheless they seem to be genetically related to the discussed Alps (Figs. 22.9 and 22.10b). These are:

i) The ear-shaped Carpathian-Transylvanian chain of mountains that is concave southward, westward, and northeastward. Its southwestern limit is marked by the lineament of the Sava-Drava River (see above);

ii) The second peripheral structure is the Bohemian Massif, which is surrounded on its north by the southward concave arc of the Sudet and Ore mountain ranges, whereas on its south it is limited by the tectonic lineament composed of the Bohemian Forest and the Danube River (Linz to Bratislava segment);

iii) The northern limits of the third structure are composed of several tectonic lineaments which are merging together toward the northwest, thereby forming a northwestward pointing acute angle. These are the NW-SE trending lineaments of the Bohemian-Thuringian forest and the Harz mountains on the east and the NE-SW trending lineaments of the Eifel-Ardennes mountain ranges on its east (National Geographic Atlas, 7th Ed., Plates 67, 69; World Sat International Inc., 1994).

That arrowhead, formed by the Harz-Thuringian-Ardennes (Fig. 22.10b) is suggested to be the northeastward extension of the Vienna-Bohemian Forest geosuture. It further extends along the trough of the North Sea and gently curves clockwise along the Viking Bank and the eastern flank of the Norwegian Sea, paralleling the Elbe Geosuture.

Although no unequivocal indications are found, it seems justified to speculate that the Viking-Vienna geosuture extends eastward along the southern limit of the Carpathian Basin (through Budapest and the Apuseni Mountain), across the Danube Delta and the Black Sea (south of the Crimean Peninsula), to continue eastward between the Lesser Caucasus and the Caucasus mountain range. The latter is a segment of the Tornquist-Dniestre-Caucasus-Kopet Dag-Harirud-Paropamisus-Khyber Pass geo-suture (Figs. 22.1 and 22.10b, as well as Choubert and Faure-Muret, 1976, Sheet 9). The same geosutures of Sochi and the Danube Delta bifurcate at Vienna and extend westward through Luxembourg and Le Havre toward the English Channel, where it curves clockwise between Porcupine Bank and the western coastline of Ireland (Figs. 22.1, 22.4a and 22.10b; Emery and Uchupi, 1984, Chart I), as well as between the Faroe and Shetland Islands.

Toward the east that geosuture truncates the northward plunging noses of the Vosges and Black Forest twin mountain ranges, and then further extends along the uppermost segment of the Danube River.

Each of the above three major southward arcuate structures is characterized by distinct counterclockwise (*i.e.* to the west or southwest) asymmetry. Both of these westward and northwestward bifurcating geosutures belong to the tangentially approaching, right-laterally shifted system of geosutures that approaches the global eye from the northwest.

VIId: On the Age and Origin of the Alpine Orogenic Belt

There are two possible scenarios regarding this subject. As long as the definition of the initial age and mode of formation of the Eastern Mediterranean is not unanimously agreed upon, that dilemma will have to remain undecided. Similarly, the initial age and mode of formation of the Alpine orogenic belt is still also being argued.

The platform of the first scenario is predicated on assuming relatively young ages for both the Alpine orogen (initial folding took place between the Jurassic and Late Cretaceous) and the Mediterranean Sea (initial rifting either in the Permian or Middle Jurassic). The second scenario (ours) is associated with older ages (late Precambrian or very early Phanerozoic) for both the continuous process of northward drift and the collision of Gondwana with Eurasia. That concept also includes the pre-existence of a sequence of latitudinally alternating oceanic and continental crustal belts that separated these two continents. Some of these belts had already been consumed or had merged as a result of the converging process across the pre-Alpine orogenic zone situated between Gondwana and Eurasia. The Mediterranean Basin, together with similar ones which existed to the north of the Arabian and Indian sub-plates,

have formed such a belt on the southern side of the collision zone. The Black Sea, together with the peri-Caspian Sea and the Tarim and western Gobi basins have formed an analogous belt along the northern flank of the collision zone (see below).

If the first scenario is correct, then the age of the initial rifting of the trough of the Mediterranean Sea had to be associated with the initial folding of the Alpine orogeny. Therefore the rifting event should really have occurred between early Permian and Middle Jurassic time, prior to the complete disintegration of Pangea (Robertson et al., 1991, 1996; Garfunkel, 1998). The extensive accretion of the Pan-African continental crust to the Eurasian continent should have happened prior to the discussed Jurassic rifting. Micro-continents were detached from northern Gondwanaland (both Africa and Arabia) and drifted northward to collide with Eurasia in Late Paleozoic to Late Triassic times to produce the Triassic to Late Jurassic Kimmerian orogeny (Şengör et al., 1984; Robertson et al., 1996). Metamorphic and crystalline rocks identified within the cores of the Western and Central Alpine Massifs indicate their origin should be 'older than Variscan'. Some of these units of continental crust are of Pan-African affinities. They were amalgamated to both the Internal and External massifs of the Western and Central Alps (Frey et al., 1999).

On the other hand, according to the second scenario, the Mediterranean Sea has existed as a trough since the Precambrian. That E-W trending belt was situated north of and parallel to the northern margin of the African continent. Both processes of the northward drift of the Afro-Arabian continent, and the narrowing of the Mediterranean Sea, were associated with the northward flow of the mantle. The subsidence of the oceanic crust that underlies the Mediterranean trough was maintained probably because of (i) the weight of the oceanic basement, and (ii) because of the gradual and persistently increasing N-S lateral compressions caused by northward drift and collision of Afro-Arabia occurring across the Alpine geosuture (a ramp-valley mechanism). Such a scenario does not support a southward drifting process of northern Gondwana during the same time period (Late Paleozoic to Late Jurassic).

The basic concept of that model follows Van der Voo et al. (1999, Figures 1, 3, 4, 5 and 7), who describe the evolution of Mesozoic to Late Tertiary north-south convergence of India and Asia and the associated collisional process. Their study is based on the results of tomographic imaging of P-wave velocity anomalies, as figured out for eight different depths, ranging from 320 km to 2100 km. The results reveal several depth zones of alternating relative high and low P-wave velocities. These are interpreted to reflect a chain of alternating E-W trending crustal zones composed of continental and oceanic crustal materials. That process is assumed to have occurred between the Late Jurassic to Late Tertiary period through five evolutionary stages of 'subduction' process. We adhere to that idea, as it offers a simple and more coherent hypothetical model to explain the available data and the origin of the tectonic movements between Afro-Arabia and Eurasia. That concept of evolutionary scenario was borrowed by Van der Voo et al. (*ibid*) from Claude Allegre (1988).

More arguments in favor of our second scenario are to be found in Sections VIII and IX below dealing with the origin and history of the Eastern Mediterranean Sea and the Middle East (The Central Plate).

VIII: THE MEDITERRANEAN SEA (Figs. 22.10a, b, 22.11, and 22.12).

VIIIa: The Six Main Basins:

The Mediterranean Sea is segmented into six basins, which are separated from each other by longitudinally (N to NE) trending sills. The configuration of the basins is mostly controlled by the northward curving and branching off extensions of the E-W trending Atlantic Ocean and North African geosutures. These basins are distributed from the west eastwards as follows:

i) On land the Alboran Sea (or Vortex) is surrounded by a mountainous ring of ridges that is separated into two arcs, the Rif Arc on its south, and the Betic Arc on its north. Each of these two arcs is composed of internal and external zones (*i.e.* secondary arcs). At least during Eocene and Oligocene times the African and European plates converged inward, causing the external zones of the Betic and Rif arcs to overthrust their internal zones. The western limits of both the Rif and Betic arcs are curving northwestward and southwestward respectively. A similar mode is also inferred on its east, as expressed by the bathymetric contours (Choubert and Faure-Muret, 1976; IOC-IBCM, 1987). The northwestward thrusting of the Middle Atlas-Wadi Moulouya-Mellilia geosuture is further extended by the westward concave submarine morphological feature, thereby completing the circle. The maximal water depth inside the circle is more than 1500 m.

We interpret the origin of the Alboran Vortex to be related to sub-lithospheric northward mantle flow beneath and along the Mauritanide-Middle Atlas geosutures, which attains a vortical mode under the ring (see Section VI above).

ii) The Balaeric Sea is bordered on its south by the High and the Tell Atlas mountain chains. On its west it is bordered by the east coast of the Iberian Peninsula. On its east it is closed by the sill-forming belt, whose two geosutures are branching off northward from the northeastern Atlas at Alger and Bizerta (N. Tunisia) respectively, to continue along both flanks of the islands of Sardinia and Corsica as far as Sestri. The Balaeric Sea is diagonally crossed northeastward by the geosuture of the Grand Banks-Azores-Guadalquivir-Balaeric Islands which runs along the trough of the Ligurian Sea, and terminates at the Sestri vortex (Gulf of Genova - Neev and Hall, 1984).

iii-iv) The Tyrrhenian and Ionian Basins respectively are separated from each other by the island of Sicily and the sill of Malta-Pantelleria (the Strait of Sicily). The latter is bordered on its east by the Malta Escarpment, along which the Atlantis-Tindouf-Ghadamis-Tripoli geosuture extends northward through the Strait of Messina and beyond along the Tyrrhenian-West Italy coastline as far as Sestri.

v) The West Levantine or Herodotus Basin is separated from the Ionian Sea by an E-W trending sill stretching across the Mediterranean between Jabel Akhdar (northwestern promontory of Cyrenaica) and E. Crete (**Figs. 22.10a, b, 22.11, and 22.12**).

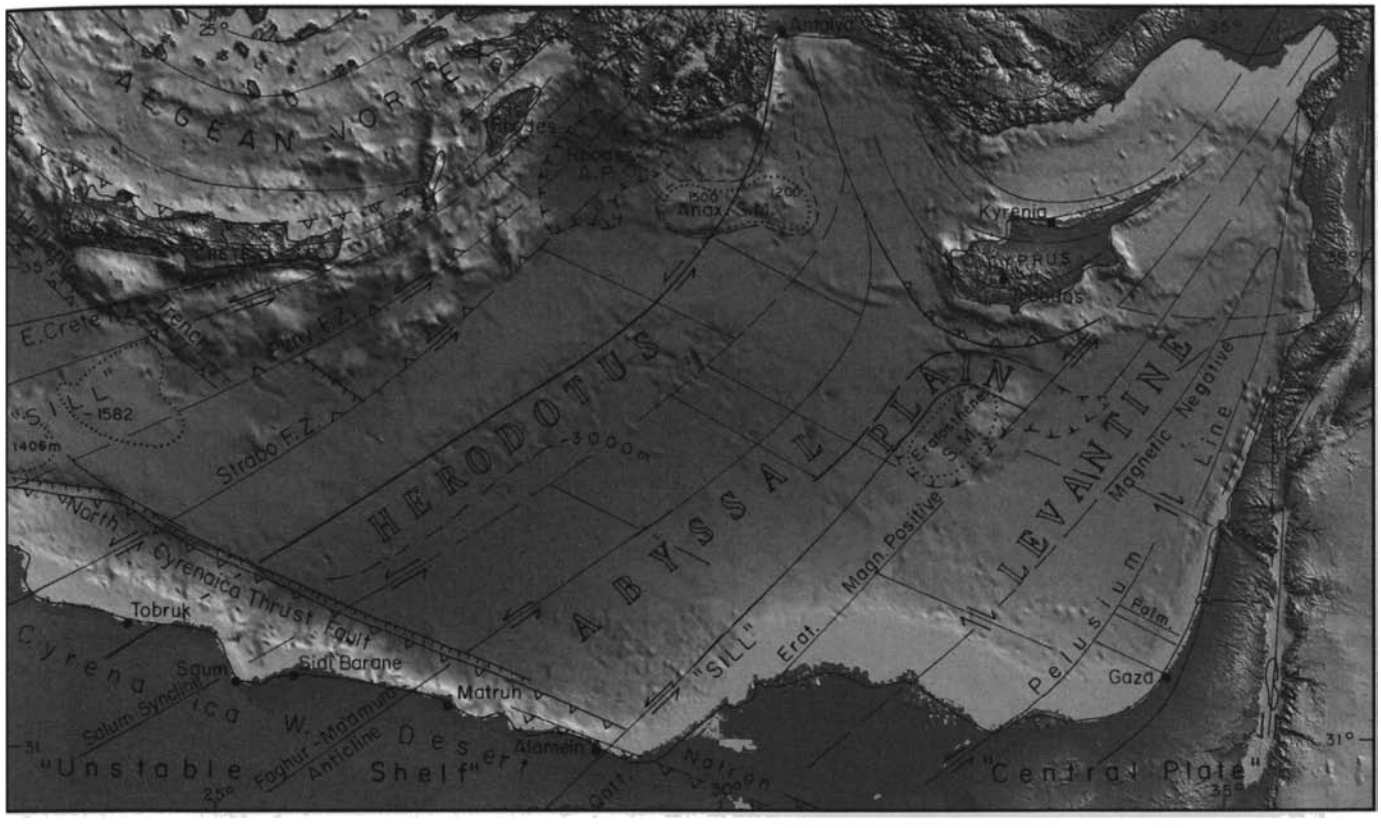


Figure 22.12. Tectonic Elements Across the Eastern Mediterranean Basin. Note the dominance of sinistral movements along the NE-SW trending and counterclockwise curving geosutures across most of the Levantine (Eastern Mediterranean) Basin (from the E. Cretan Fracture Zone in the west to the Dead Sea in the east). The North Cyrenaican Fault is interpreted as an expression of a major - and old - thrust movement of Africa over the southern Mediterranean Basin.
Background shaded relief is ACE satellite altimetry at 0.5' overlying the IBCM 0.25' grid. Mercator projection.

The shallowest depth on that sill is 1298 m, situated close to its northwestern limit (IOC-IBCM, 1987). That sill extends northward along the NNE trending Pliny-Strabo trenches where it defines the eastern limit of the Aegean Vortex.

vi) The East Levantine Basin is separated from the western one by a NE trending sill along the Qattara-Eratosthenes geosuture that extends northeastward from the eastern edge of the Qattara Depression (Western Desert) toward Eratosthenes Seamount, NE Cyprus, and the northern tip of Iskenderun Bay (Figs. 22.12, and 22.15).

The greatest water depths over the rather flat-bottomed East Levantine Basin trough are ~2200 m. The trough of that abyssal plain attains a NNE trend and drops from a depth of about 1000 m (close to the base of the continental rise), along both its eastern and southern flanks, as well as at its northern flank (at the southern limit of the Latakia Basin, south of the E-W trending sill that extends between Cape Greco in eastern Cyprus and Banias on the Mediterranean coastline of Syria). The East Levantine Basin is being crossed latitudinally by the E-W trending tectonic trough of the Phoenician Basin whose maximal depth is 2700 m. Its north and south limits are situated between Limasol (S. Cyprus) in the north and the northward plunge of Eratosthenes Seamount in the south, That basin extends westward to merge with the NE-SW trending Herodotus Basin (3200 m maximum depth) (Hall, 1994).

Data and arguments supporting the old age (Precambrian) estimated for the Levantine Basin and its continuous tectonic subsidence process since then, are discussed by Neev (1975), Neev et al. (1985), and below.

VIIIb: The Aegean-Menderes-Crete Vortex

The unique circular structural ring-shaped outline of the Aegean Microplate (McKenzie, 1970; Le Pichon and Angelier, 1979; our Figs. 22.10a, b, 22.12, **22.13**) is best expressed by the distribution pattern of earthquake epicenters for the period 1904-1989 (Espinosa et al., 1981; Goter, 1989; IOC, 1990; Jackson and McKenzie, 1984, 1988; Simkin et al., 1994). That pattern surrounds the Aegean Sea together with the westernmost Anatolian (Menderes) area on its east. That same impression is emphasized by the presence of several secondary, inner rings encompassed by the main outer one. The integration of the entire pattern suggests

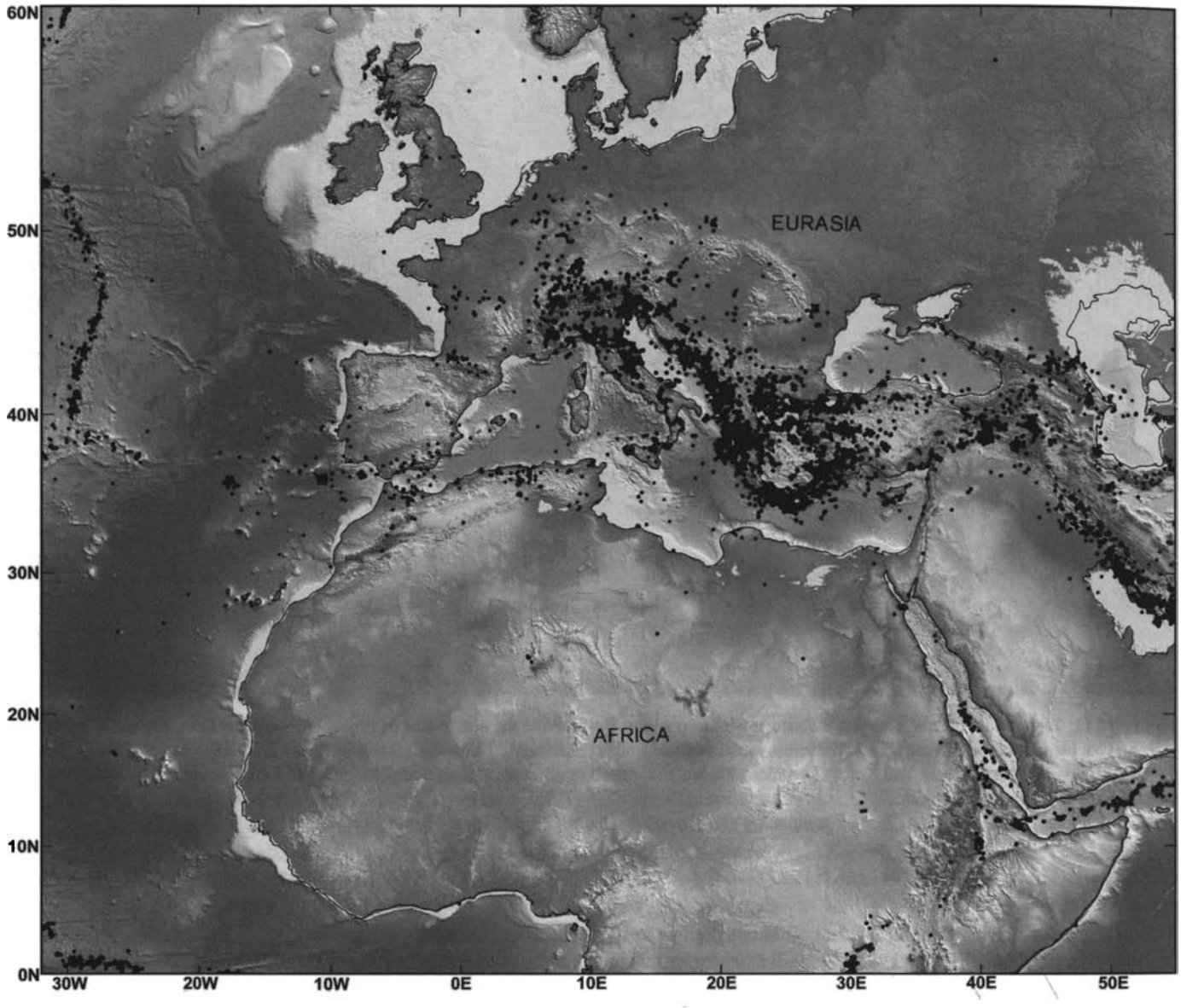


Figure 22.13. Distribution Pattern of Earthquake Epicenters along and across the North Mediterranean-Alpine Orogenic System: Shows epicenters reported between 1961 and 1983 extending from the Caspian-Persian Gulf in the east to the Pyrenees in the west. After Jackson and McKenzie (1984, Fig. 1; 1988, Fig. 7). Background shaded relief is from the GEBCO GDA 1' global grid. Mercator projection.

the involvement of a counterclockwise converging spiral pattern, or a vortical mechanism which is associated with its origin.

The presence of that pattern of earthquakes suggests the existence of a genetic relationship between the Sestri and the Aegean-Menderes, as well as the Kirşehir Vortices. The significance of each of these three is in their specific locations along the Alpine-Himalayan Global Eye: whereas the northern limit of the Sestri Vortex is abutting the Armoric-Basel geosuture, the Aegean and Kirşehir Vortices are abutting the North Anatolian Fault Zone. The architectural shaping of that unique crustal tectonic framework which is common to these three features suggests the massive involvement of underlying mantle vorticing activity in their origin.

In spite of the elegant ring-shaped configuration exhibited by the pattern of the recorded epicenters, it does not seem to exactly imitate the tectonic features as expressed by the surface geological maps. Still we consider that the epicentral pattern represents more reliably the deeper structure, which is the core of the problem, as it should be more closely associated with the 'cause', or vortical mechanism produced by the upper mantle's horizontal flow.

Superficially it could be inferred from the distribution pattern of the epicenters (Fig. 22.13) that the Dinarides and Hellenides are smoothly extending each other. Yet the NW trending Dinaride

ranges, which parallel the East Adriatic coastline, sharply change their trend in a dog-leg fashion (although at an obtuse angle) into a NNW one beyond the point of merging with the northern Hellenides. That change occurs along the SW-NE trending Scutari-Pec transverse fault (Pamic, 1983, Fig. 1), or transform fault (Robertson and Dixon, 1984, Fig. 1). That fault line begins at the Adriatic coastline and continues as a gradually eastward curving geosuture along the Albanian-Montenegro border-line where it marks the rather sharp boundary between Lherzolite and Harzburgite subprovinces, which is situated within the ophiolite belt along the Hellenides-Dinarides. The above suggestion is in agreement with a relevant remark of Robertson and Dixon (*ibid*, p. 22) that "some major hitherto undiscovered oceanic suture must exist to the northeast, presumably within the Serbo Macedonian zone". Apparently that structural line extends further along the same general NE trend although slightly curving clockwise to merge with the west to east trending segment of the Rhodope Mountains geosuture. The latter continues eastward to cross the Black Sea (Fig. 22.10b). Two additional NE trending transverse faults that are paralleling the Scutari-Pec lines, also exist farther on to the north across the Dinarides (Pamic, 1983, Fig. 1). The southern fault (out of these two) extends between Sarajevo and Beograd (thereby separating between the Lherzolite ophiolitic subprovince in the NE and the Harzburgite one in the SW). It may also extend to the west as far as Split. On its east it may extend further to curve and merge with the EW segment of the Transylvanian Alps, in a similar way as the Scutari-Pec transform is merging with the E-W trending Rhodope and Balkan mountain ranges. The third member of these three NE trending transverse faults is marked (Pamic, *ibid*) north of Zagreb. It parallels and coincides with (from west to east) the Zumberacka Ridge, the Karpina and Bednja rivers, Lake Balaton, Bakony Ridge, and the Tatra Mountains, to terminate against the northeastern Carpathian Mountains.

We suggest the following different groups of tectonic trends to have simultaneously functioned across the northern and western flanks of the Aegean Vortex:

i) The ophiolite-orogenic geosutures of the Dinarides and Hellenides ranges that trend NW and NNW. The first one (the Dinarides) is affiliated with the Sestri Vortex of the Alpine orogenic system (Neev and Hall, 1984), whereas the second one is an essential member of the Aegean Vortex (the concave southward segment of the northernmost arc).

ii) An E-W trending dextrally shifted strike-slip group of faults, which is limited in the south by the North Anatolian Fault, and in the north by the Caucasus-Dneister (Tornquist) Fault. At their western flanks, upon approaching the 25°E meridian, that group splits and each of its faults gradually curves either to the northwest (Subgroup ii), or to the southwest (Subgroup iii). The E-W trending segments of the Balkan, Rhodope, and Vardar-Thraki ranges, as well as the faults along the Sea of Marmara, are the most important members of that combined group.

iii) All of the discussed northwestward curving elements are merging with different members of the Dinaride geosuture. The latter one alone is merging with the Carnic-Rhaetian-Maritime Alpine geosuture within the Sestri Vortex (*ibid* and Figs. 22.4a, 22.9, 22.10a, b, and 22.11).

iv) The southwestward curving extensions of the E-W geosutures, to the north of the Aegean and Kirşehir (Central Anatolia - see below) Vortices, seem to be in better agreement with the circular pattern of epicenters across the relevant territory, than with the highly faulted basins and ranges pattern of the Hellenides. As stressed earlier, we believe that the Aegean epicenteral pattern better expresses the most important asthenospheric mechanism which is producing the Aegean Vortex.

The interaction between these tectonic trends have shaped the northern and western segments of the Aegean vortical geosutures. Moreover, the discussed interpretation regarding the counterclockwise rotations is corroborated by recent GPS measurements.

Le Pichon and Angelier (1979, Figs. 2, 3; our Fig. 22.11) defined the existence of a sequence of two concave northward arcs within the south-central part of the Aegean Sea, representing two different isodepth zones of intermediate seismic events which were recorded beneath them. The northern arc represents their occurrence at depths of 150 km and extends from Aegina Island in the northwest (situated southeast of the Korinthian Canal) through the islands of Milos and Thera (Santorini) along the central part of the arc to terminate at Nisyros and Kos Islands close to the coastline of southwestern Anatolia. As these five islands are the most prominent active volcanic centers within the Aegean Sea, the discussed arc represents both the 150 km isodepth of seismic events and the locations of most intensive volcanic activity within the Aegean Sea. Simkin et al. (1994) mark on their map the existence of a large Holocene volcano in western Anatolia, that could be correlated with the +1555 m high Umurbaba Dagi (mountain) at approximately 38°25'N 28°40'E (National Geographic Atlas of the World, 1995, Map 66; our Fig. 22.11). As this volcanic center is the only one in western Anatolia marked on that map to the west of the northwest segment of the Taurus Range, and as its site fits perfectly with the northeastern extension of the discussed arc, we suggest that it is genetically related to that arc.

The southern arc of Le Pichon and Angelier (1979, Fig. 3) marks the depth distribution of epicenters at depths of 100 km. It extends along the median line of the Peloponessus (along the river Evrocas), curving southeastward (counterclockwise) across the Kythira Island and along the deep arcuate submarine trough situated just north of Crete. The latter parallels its northern and northwestern coastlines, as well as those of the islands of Karpathos and Rhodes to terminate inland within W. Anatolia (between Umurbaba Dagi and Afyun - see above). It is implied from different bathymetric data of the Aegean Sea (*i.e.* Le Pichon and Angelier, 1979, Fig. 4; National Geographic Society, 1995, Map 66) that analogous arc structures also dominate across the northern half of the Aegean Sea (in other words across the entire N-S length of that sea). While those arcs (situated in the southern domain) are concave northward, additional arcs that are concave southward do exist across the northern part of the Aegean Sea.

The peripheries of the two outermost arcs around the

(external) Aegean Vortex, are more clearly exhibiting the specific bathymetric as well as the structural-geological expressions of these arcuated features: The Hellenic and South Cretan trenches, which parallel each other, are concave northward. They further extend northeastward along the SE Cretan and Pliny trenches to cross W. Anatolia through the Menderes Massif (where they also cross other E-W trending structural features). On their western and northern flanks, these arcs are abutting and crossing the Ionian coastline close to the southern island of Corfu, and gradually curve to the northeast and east along the Macedonian Ranges (in the break between the NW trend of the Dinarides and the NNW trend of the Pindus ranges, along the Voras and Belsica ranges), and then merge with the close to E-W trending segment of the Rhodope Mountains.

The dominant idea about the geodynamics of the Aegean Sea and the surrounding lands, is that of McKenzie (1970) who considered the Turkish Microplate to be moving westward whereas the Aegean Microplate is being displaced southwestward by the Turkish one. Both of these two microplates are being laterally driven to the west relative to Eurasia along the dextral North Anatolian Fault, because of the northward movement of the Arabian microplate (McKenzie, 1970, 1972, 1978; Neev, 1975; Le Pichon and Angelier, 1979; Dewey and Şengör, 1979; Makris, 1976; Kenyon et al., 1982; Gripp and Gordon, 1990; Makris and Wang, 1994; Makris et al., 1994; Kiratzi and Papazachos, 1995; Limonov et al., 1996; Fusi and Kenyon, 1996).

Rotstein (1984, 1985) considers that both the Aegean and Turkish microplates are rotating counterclockwise. We concur with that suggestion, but consider the discussed rotations to be associated with the northward flows of the upper mantle, which generate both the Aegean-Menderes and the Kirşehir Vortices (see above). We do not dismiss, however, the westward compressional vector exerted by the northward wedging-in movement of the Central Plate (East Anatolia and the Arabian and Sinai Sub-plates - see below). That same mechanism generates the southeastward asymmetric NE-SW trending fold system of the western Levant (Israel and Sinai).

Extensional crustal movements are dominant across the entire Aegean province (Şengör et al., 1985): beginning at northernmost Greece, southernmost Albania, Yugoslavia, and Bulgaria in the north, through western Anatolia in the east (as far as Antalya which is the northward trending limit between the Aegean and Turkish microplates of McKenzie (1978), and reaching southward as far as the northern fringe of Crete. The sharp transition from the extensional processes within the Aegean Vortex to compressional-consumption processes, occurs close to the Ionian-Cretan trenches and the Pliny-Strabo trenches.

We concur with Le Pichon and Angelier's (1979) conclusion regarding the northward oblique collision and underthrusting of Africa across the NW-SE trending Ionian trench, whereas the E-W trending island of Crete (which is subparallel to the nearby African coastline), is being perpendicularly underthrusted from the south. At the same time the Aegean Microplate is underthrusting Crete from the opposite side, *i.e.* from the northeast, north, and northwest.

The group of three linear NE-SW trending submarine trenches, namely the SE Cretan, Pliny, and Strabo (Figs. 22.10a, b, 22.11, 22.12, 22.13 and 22.14) are subparallel to each other and are obliquely approaching E. Crete from the southwest. They form an angle of 110° between their NE trend and the E-W trend of the island of Crete (Le Pichon and Angelier, 1979). Their tectonic origin and a left-lateral mode of motion are implied by their specific *en-echelon* setup as well as the configuration of the bathymetric and Bouguer gravity anomaly contours, and the distribution of the earthquake epicenters (*ibid*, their Figs. 1, 4; McKenzie, 1978, Fig. 18; and the IOC-IHO 1:5,000,000 scale IBCM – IOC, 1981; IBCM-G – IOC, 1989; and IBCM-S – IOC, 1990 compilations).

At its northeasternmost segments the Strabo Pliny-SE Cretan trenches appear to converge into a joint pattern that is moderately curving counterclockwise toward the trough of the Rhodes Abyssal Plain (~4300 m) to continue inland along the NNE trending fjord-like system of features (embayements, ridges, and rivers, such as the Dalaman-Kirennis River).

The northern segment of the Strabo Trench seems however to split into two branches:

1) A northward curving branch that merges with the Pliny and SE Crete trenches to extend along the trough of the Rhodes Abyssal Plain (see above).

2) A northeastward one that extends along its original trend through the submarine western flanks of the Anaximander Seamount to breach the Mediterranean coastline of the western Antalya Peninsula at Kas. It then gradually curves northward on-land along a N-S trending ridge that parallels the western coastline of the Bay of Antalya, to continue inland along N-S trending ridges, through Isparta and beyond as far as Afyun, from where it gradually curves counterclockwise.

Upon approaching Afyun (Central Anatolia around 28°30'N 30°-30'E) from the south, the Strabo-W. Anaximander-Antalya-Isparta lineament is merging again with the joint Pliny-Dalaman-Egridir lineament. The merged geosutures then gradually curve counterclockwise to the northwest and west along the Turkmen and the +2540 m high Olympus (Ulu Dag) mountain ranges (Fig. 22.11). It then joins the complex of E-W trending North Anatolian Fault lines to reach the NE Aegean coastline just north of the isle of Lesvos. Beyond that point the latter one is merging with one of the southwestward concave arc systems of the N. Aegean Sea.

We agree with the concept that "... the geological identity of Aegean, including the Aegean Sea and western Anatolia, is actually inherited from a much earlier geological evolution in which the Antalya bend may have played quite a significant role" (Le Pichon and Angelier, 1979, p. 32, quoting Biju-Duval et al., 1977). That opinion is in agreement with the presence of a Cambrian to Carbonifierous sequence of sediments (with a greater development of marine carbonates during Devonian to Carboniferous times) overlying the basement north of Antalya and elsewhere across the Tauride block (*i.e.* Gutnic et al., 1979; Dean and Monod, 1990; Garfunkel, 1998).

The Menderes metamorphic massif may represent the eastern half of the eye of the Aegean Vortex. The western half could have

been assimilated in the rising mantle material during the vortical process. That massif acquired an onion-shaped structure, with a 'gneiss core' at the base, which is covered by a 'schist envelope', both being overlain by a 'marble envelope'. Thereby metamorphism increased with time when the first episode of intense deformation and metamorphism occurred during the Precambrian Baikalian or Pan African orogenic phases which terminated prior to 500 MaBP. It was followed by a very long phase of relative tectonic stability, as indicated by the close to continuous marine depositional regime across the Menderes Massif, which began in the Devonian (about 400 MaBP) and continued through Carboniferous, Permian, Triassic, Jurassic, Cretaceous, and Eocene times. This close to 400 Ma long phase was interrupted by several important events of metamorphism that took place mainly during Late Triassic and Late Cretaceous times. Another major event of tectonism and metamorphism took place between Late Eocene and Early Oligocene (close to 35 Ma), following a phase of collisional activity across the Tethys. It was associated with vertical tectonism (the MMM or the Main Menderes Metamorphism) that was followed by a low-grade metamorphic event which began during Tortonian (Middle Miocene, 11.5 Ma) and extended to the end of the Mio-Pliocene (Messinian - 5 Ma). It was related to the extensional deformation activity in the Aegean and western Turkey (Şengör, Satir and Akkok, 1984, Figs. 1-3; Şengör and Yilmaz, 1981, Figs. 2 and 3).

VIIIc: The Kirşehir-Cyprus Vortex (The 'Turkish Microplate', McKenzie, 1970), Figs. 22.10a, b, and 22.11:

The center of the Kirşehir Vortex is at the gneiss and granite core of the Kirşehir Massif, some 100 km southeast of Ankara, at the northeastern limit of the Central Anatolian Volcanic field, and at the center of the elevated Central Anatolian Plateau (Şengör and Yilmaz, 1981, Fig. 2; Yalcin et al., 1998, Fig. 10, 12a, 12b). Unlike the Aegean Vortex, the Kirşehir one has a more asymmetric, pear-shaped configuration, expressed by the southward elongate pattern of concentric structural belts. Perhaps that pattern results from lateral compressions that this vortex went through during the long period of northward wedging-in movements of the Central Plate (the Ararat Vortex in NE Anatolia across the Pelusium Line - see below) on its east, and of the Aegean Vortex on its west.

Close to Afyun is the zone where the easternmost arc of the Aegean Microplate (or the Aegean-Menderes Vortex) is tangentially approaching the westernmost arc of the Turkish microplate (or the Kirşehir Vortex - Neev and Hall, 1984). The southern limit of the Kirşehir Massif (or the 'Turkish Microplate') is very well pronounced by the northward concave configuration of the arcs. The effect of lateral compressions in forming the southward pointing obtuse angle between the NW-SE trending Anamas-Taurus ranges and the SW trending Anti-Taurus mountain ranges cannot be ignored. Nevertheless the northward counterclockwise flow of the upper mantle should be the dominant factor in the production of the lithospheric vortices.

On their northern parts many of the arcs of the Kirşehir Vortex are branching off southwestward from the North Anatolian Fault to curve moderately and form a close to regular pattern of sequentially southwestward concave arcs (see more about the analogy in the section on the Pamir Vortex below). The northernmost one is composed of the Pontide-Kuzei-Anadolu ranges along the Black Sea. The innermost one is practically enveloping the Kirşehir Massif itself, extending from Ankara on the west, along the northeastward curving Yozgat-Erzincan suture, through Merzifon to terminate at the North Anatolian Fault (Tuysuz et al., 1995; Andrieux et al., 1995). Exactly the same pattern is found across the northern half of the Aegean-Menderes Vortex. Southwestward curving geosutures are branching off from the E-W trending western extension of the North Anatolian Fault between Izmit (easternmost reach of the Sea of Marmara) and the island of Thassos (or Saloniki) along the northern coastline of the Aegean Sea.

It is possible that at present the Kirşehir Massif is being in a relatively inactive vortical situation (as suggested by the relative absence of earthquake epicenters across it as compared with that of the neighboring Aegean Vortex - Figs. 22.10a, b and 22.11). Nevertheless, considering the earthquake epicenter distribution pattern across these two features (Fig. 22.13) the interpretation on the existence of the discussed vortex is corroborated. The fault plane solutions presented in that figure corroborate Rotstein's interpretation regarding the counterclockwise rotation of the Kirşehir Vortex, and its separate entity as related to the Aegean Vortex (Rotstein, 1984, Fig. 4), which is situated between Isparta and Afyun (see our Figs. 22.10a, b).

The above conclusion is further supported by the asymmetric configuration of the two southern Cyprean Arcs: upon reaching their northwestern ends their curvature appreciably increases so that both the Limassol-Cape Arnauti and the Kyrenia Ridges are converging southwestward to parallel the western Taurus Ranges. A similar conclusion is also inferred from the Digital Shaded Relief Map of the Island of Cyprus (Hall, 1998a, b); The three E-W trending and northward concave geosutures, *i.e.* the northern, central, and southern ones, that are crossing the elevated ophiolitic terrains of the Troodos Massif (South Cyprus), are curving rather sharply toward Antalya in the NW, to parallel the extension of the Kyrenia Ridge. A similar interpretation is also expressed by Mutlu and Gulec (1998, Fig. 1). The role of Cyprus, as the southern segment of the outermost concentric (although asymmetric) belt of the Kirşehir Vortex, is analogous to the role of the island of Crete with respect to the Aegean Vortex. The counterclockwise rotation of the Kirşehir Vortex, as deduced by Rotstein (*ibid* - see above) is in agreement with the interpretation of Moores and Vine (1971) on the 90° counterclockwise rotation of the Troodos massif (Cyprus) in post-Cretaceous times, as well as with our perception of all the vortices along the Alpine-Himalayan vortices and the sense of movements of the underlying mantle flows.

Rotstein (1985) considers the Aegean block (plus W. Anatolia) and the Central Anatolian one, to behave as separate entities, although both are rotating counterclockwise and exhibit extensional processes away from their centers. They are both moving to the west however, with respect to Eurasia along the dextral (right lateral) North Anatolian strike-slip fault. We believe that, in spite

of their different patterns of deformation, both these two vortices were formed and are still functioning within the same pattern of the upper mantle flows which are converging counterclockwise as a result of the global whole mantle convection mechanism which is driving the subduction of Africa beneath Eurasia (within the relevant sector of the Eastern Mediterranean).

VIIId: Processes within the Aegean and Kirşehir Vortices:

The following points are agreed to by many, regarding the tectonic processes associated with the Aegean Sea:

i) The westward movement of the 'Turkish microplate' (the Kirşehir Massif) and the southwestward movement of the Aegean microplate (together with westernmost Anatolia) along the dextral North Anatolian Fault.

ii) The dominance of extensional southeastward crustal movements across most of the Aegean province, extending from northernmost Greece, southernmost Albania, Yugoslavia, and Bulgaria as well as westernmost Anatolia (as far as Antalya and the northward trending limit between the Aegean and Turkish microplates).

iii) The sharp transition from the extensional processes to compressional consumption ones along the Ionian-Cretan trenches and the Pliny-Strabo trenches (*i.e.* McKenzie, 1970, 1972, 1978; Le Pichon and Angelier, 1979; Kiratzi and Papazachos, 1995).

Beyond these points all authors have faced difficulties in explaining situations where lithospheric compressional and tensional regional movements appear to occur (almost) simultaneously within the same arena (such as within the limits of the Aegean Sea). This is a critical example where a new approach should be sought to help in solving such a problem. Because of the limiting conditions of timing and arena, an alternating regime mechanism was proposed by Le Pichon and Angelier (1979, p. 27-28) regarding the paleo-deformation processes within the Aegean Sea. In addition, the need to diminish the westward offset along the North Anatolian Fault was expressed by McKenzie (1978). The somewhat constrained solutions offered are not easy to accept. Perhaps because of these difficulties, McKenzie (1978, p. 251) states that within the Aegean microplate "Lithosphere consisting of thin (25 km) continental crust overlying mantle material (that) appears to be more easily deformed than oceanic lithosphere and hence the surface motions reflect more closely the convective motions below than they do in true oceanic regions". Moreover McKenzie (*ibid*) also states that "Except where asiesmic regions exist, the motions are poorly described by plate tectonics". Dewey and Şengör (1979) had similar difficulties. We concur in these thoughts, and suggest that the whole mantle convection process could be considered as the cause (or the motive force) that drives the lithospheric (plate) movements (the result, see above).

Makris (1976) considers the deformation which occurred within the Aegean region to be the surface expression of a mantle plume. Basically such a model is rather close to our hypothesis. He compiled gravity and seismic data from Greece and adjacent areas to reveal that:

i) A large 'plume' of hot upper-mantle material is rising below the Aegean region thereby causing strong attenuation of the crust, and the high heat-flow.

ii) The specific (ring-shape) distribution of earthquake epicenters. Such a pattern calls for a model in which a cylindrical plug of mantle material was forced to rise thereby causing the adjacent areas of the Aegean region to sink.

iii) These processes have been initiated by the relative movement of Africa and Europe.

In our opinion, the relevant mechanism is a whole mantle convection which generated a vortex beneath the Aegean province. It is one of the eight vortices along the Alpine-Himalayan orogenic belt (Neev and Hall, 1984).

Perhaps the following quotation of McKenzie (1978, p. 250-251) may help the reader to consider unorthodox ideas as reasonable possbilities: "arguments concerned with stresses and with the driving mechanism are always more speculative than those concerned with kinematics and thermal structure... There is a suggestion that the surface motions in wide zones of continental deformation may directly reflect motions in the mantle below... These ideas are strikingly similar to those proposed by the few tectonic geologists who accepted continental drift early this century (Argand, 1924; Holmes, 1951)."

The essence of our concept regarding the Aegean Vortex is as follows: The involvement of eight vortical flowing systems in the upper mantle magma is the mechanism that generates the fracturing and folding process within the overlying lithosphere, thereby attaining the spiral crustal structures along the Alpine Himalayan belt (one of which is the Sestri Vortex in the Western Alps).

The development of vortical movements within the magma of the upper mantle is suggested to occur as a result of collision between different mantle currents, which are flowing in almost opposite directions. Although most of these currents are coming from the southwest and flowing toward the Alpine belt, another group of mantle currents are flowing from the NW and north toward the global eye, and approach it in a tangential way. Both the northward and southeastward flowing mantle currents are curving and converging counterclockwise and therefore are related to the same system of whole mantle convection.

The Aegean Vortex was produced as a result of the collision between the northeastward flowing mantle beneath central and northeast Africa, and the southeastward mantle flows beneath the northern and eastern parts of Europe (east of the Armoric and Tornquist Geosuture). That collision occurs between the northward mantle flows beneath the East Levantine Basin and the Central Plate (see below), and the southeastward flows under easternmost Europe. Its surficial expression is to be found along the North Anatolian Fault.

We consider the SE Cretan, the Pliny, and Strabo linear furrow-structures to be geosutures that reflect the mantle flow which generates and drives the Aegean Vortex. The vortical sense is both upward and counterclockwise. The same holds true regarding the mantle flows beneath the Levantine and Anatolian sub-plates that produce the mechanism responsible for the Turkish (Kirşehir) Vortex. We are not able yet to suggest a detailed explanation for

the prominent differences noted in the seismic activities occurring within these two vortices.

VIIIe: The Herodotus Basin and its Southern Limit (Western Desert and Cyrenaica, Figs. 22.10a, b and 22.11).

The Herodotus Abyssal Plain makes up the most dominating feature of the East Mediterranean Basin. The configuration of that basin attains a shape of a parallelogram which is limited by the following geosutures:

i) The three NE-SW trending East Cretan, Pliny, and Strabo Trenches that parallel one another on its west.

ii) The NE-SW trending Qattara-Eratosthenes geosuture, which separates the Herodotus and Levantine Basins, on its east.

iii) The WNW-ESE trending linear contact between the continental slope off and parallel to the southern Mediterranean coastline off the Western Desert and Cyrenaica (between El Alamein and Jebel Akhdar) and the eastern Mediterranean Basin.

iv) The linear WNW trending northern limit of the Eastern Mediterranean abyssal plain that extends between the Isle of Karpathos (between Rhodes and East Crete) and the northward plunge of Eratosthenes Seamount. It is best expressed in the Bouguer gravity anomaly contours of Makris and Wang (1994, Fig. 4.3c) and our Figs. 22.10a and 22.11. The areal dimensions of that abyssal plain are about 300 by 550 km. It lies between the 3200 to 2600 m depth contours and between the +190 and +100 mGal Bouguer gravity anomaly contours, which practically coincide with each other and which define the interior of the parallelogram. The same lineaments (marked by the configuration of the gravity anomalies) also express the existence of two strike-slip faults, stretching along different trends. The first one trends WNW-ESE, paralleling the Cyrenaican-Western Desert coastline. The second one trends NE-SW (after Makris and Wang, 1994, Figs. 4.2, 4.3; and our Figs. 22.10a and 22.11).

VIIIf: The Southern Limit of the Herodotus and Levantine Basins -A Northward Thrusting Fault.

That southern limit is made up of a belt along the continental margin (shelf and slope). It is close to 600 km long and extends from off Ras at-Tin (the northeasternmost point of the northward protruding Jebel (mountain) Akhdar block of Western Cyrenaica - close to 23°E) in the west, to El Alamein (the western fringe of the Nile Delta, close to 29°E) in the east. The N-S width of that belt is about 80 km on its west (off Tobruk), and some 30 km on its east (between El Alamein and Matruh - Fig. 22.10a). On the other hand, the 30 km wide segment of the continental shelf off Tobruk is narrowing eastward to become just a few km off Matruh. Correspondingly, the steepness of the continental slope is increasing appreciably eastward from less than 5° in the west to close to 15° in the east. The break between the continental slope and the abyssal plain is both abrupt (sharp) and linear all along the discussed belt. That line is also expressed as a Bouguer gravity anomaly high, at least from off Jebel Akhdar to off El Alamein (IOC-IHO, 1987; Makris and Wang, 1994, Figs. 3.4a, 3.4b, 4.2a-c).

We interpret that belt to express the northward thrusting of North Africa over the Mediterranean Basin. A similar linear feature further extends to the ESE in an *en-echelon* way (*i.e.* more remote to the north) from El-Hammam (the western limit of the Nile Delta) through the Wadi Natron depression as far as Cairo, where it abruptly terminates). That South Delta ESE-WNW trending fault line could have been left-laterally shifted to the NE across the NE-SW trending Qattara-Eratosthenes geosuture. It further extends along Wadi Natron (forming a linear trough a few tens of meters below sea level) as far as Cairo, (at its crossing point with the Pelsuium Line). Note that in Arabic El-Hammam means Hot Springs and Natron means Hydrous sodium carbonate "occurring in nature only in solution, as in the soda lakes of Egypt" (Ford, 1951, p. 530), as well as in volcanoes such as Vesuvius, and especially those of East Africa.

The most prominent geological feature within the Herodotus Basin is its NE-SW trending bathymetric trough (3397 m at its deepest point), which is associated with high Bouguer gravity anomaly values (the highest is +190 mGal - Makris and Wang, 1994, Figs. 4.3a-c).

One of the most significant tectonic features within that basin is the linear WNW-ESE trending narrow and more than 3000 m deep furrow (or trench) mapped along the base of the continental slope off Cyrenaica and the Western Desert. Maximal depths are found within a few coast-parallel closed basins. The deepest of these basins is situated 90 km off Tobruk, where its depth is 3382 m. The next basin is situated some 150 km farther to the east at the junction of the furrow at the base of the continental slope with a large southwest-trending submarine canyon. This canyon is reaching updip (*i.e.* to the SSW) as far as the head of the canyon at the Bay of Salum (Fig. 22.10a). The deepest point of the Salum offshore basin is 3260 m, where it attains a coast-parallel furrow that further extends to the ESE a few tens of km. Beyond that point its northern wall is losing its identity, apparently because the ESE-WNW trending furrow abuts (and merges with) the SW corner of the very broad (more than 100 km wide) and flat trough of the NE-SW trending Herodotus Abyssal Plain. The steepness of the adjacent continental slope even increases farther away to the ESE from off Sidi Barrani, and maintains its straight linearity as well as the nature of its sharp contact with the abyssal plain on its north.

The entrenchment of submarine canyons across the steep continental slope escarpments around the Mediterranean Sea especially occurs where they are associated with perpendicularly-trending furrows (or narrow troughs, see above; Vanney and Gennesseaux, 1985, Figs. 1, 2, 3, 5, 7, 12; Finetti, 1985, Figs. 10.1, 12; IOC-IHO, 1987). The existence of closed, long, and deep furrows along the bottom of the continental slope off the Western Desert and Cyrenaica, more than 1000 m beneath the flat bottom of the Eastern Mediterranean basins on their north, suggests that the rate of subsidence of these furrows is faster than that of the flat bottom over the rest of the basin. A continuous subsidence process of the oceanic crust that underlies the Eastern Mediterranean basins occurs because of its being depressed by the northward thrusting (or over-riding) of the Northeast African continental crust over it.

The type locality of these furrows is found between Cyrenaica

Seamount (33°-30'N, 20°E) and off Sidi-Barrani in the east (30°E). At a point north of Tobruk the discussed furrow sharply changes its course from WNW-ESE to E-W along which an E-W trending furrow is situated between the northern face of Jebel Akhdar and the Herodotus Rise (the 'Sill' separating between Crete and Jebel Akhdar). That furrow is heading toward Cyrenaica Seamount (already within the Ionian Basin at 18°E). That change of trend occurs off Ras et Tin, where the discussed furrow is crossed by the southwestward extension of the Strabo Geosuture (see our interpreted pattern of tectonic elements - Figs. 22.10a and 22.11).

We therefore consider that the straight, linear, furrow-like narrow and deep trenches, which are found along the limits of the Herodotus and Ionian Basins, are associated with an active process of subsidence and with thrust faulting of compressional (not tensional) tectonic origin, such as the consistent collision of Africa and Europe.

VIIIg: The Westward Extension of the Cyrenaican Thrust Faults into the Ionian Basin.

The sill which separates Jebel Akhdar (the northward promontory of Cyrenaica) from the island of Crete (Figs. 22.10a, 22.11) is described by Le Pichon and Angelier (1979, Fig. 4), Makris and Wang (1994, Figs. 4.2a-c), Makris et al. (1995, Fig. 3.4), Fusi and Kenyon (1996, Fig. 1), as well as Loubrieu, Satra, and Cagna (2001) as a high bathymetric feature, whose outline is enclosed by the 2000 m isobath and whose two tops lie at depths of 1172 and 1298 m. It forms an E-W trending quadrangle, with a northward protrusion at its northeastern corner. Its western and eastern faces are diagonally truncated by the southwestward extensions of the East Cretan, Pliny, and Strabo geosutures. These three sinistrally-shifted ENE-WSW trending wrench faults (after Vanney and Gennesseaux, 1985, Fig. 5) are crossing the Libyan coastline at Wadi Zamzam, Ras et Tin, and Tobruk.

Three linear E-W trending dextral wrench faults are shaping the northern and southern faces of the sill. The southern face of the Sill is separated from Jebel Akhdar by an E-W trending narrow and deep (-2795 m) trench. A change in trend is noticed along the North Cyrenaican Thrust Fault from WNW along the Cyrenaican and Western Deserts to an E-W trend that occurs where it is crossed by the southwestward extensions of the Strabo and Pliny geosutures. Three E-W trending wrench faults are shaping the northern and southern faces of the island of Crete as well.

The western segment of the North Cyrenaican Thrust Fault further extends westward (into the Ionian Basin) at least as far as the Cyrenaican Seamount (close to 17°E). Beyond that point it ceases to form a furrow and gradually curves northwestward to merge with the NNW trending Sicily-Malta submarine escarpment.

A system of at least three NW-SE trending lineaments are paralleling one another and the southern coastline of the Tripolitanian Bay (extending from Gabes-Jerba in the west through Tripoli and Sirte to Uqaylah (the southeast corner of the Bay of Sirte) in the east. The southern two (the submarine valleys and troughs of Misurata and Tripolitania - Fig. 22.10a) are analogous to furrows and seem to merge toward the South Cyrenaican Thrust Fault (the southern face of the Qattara Depression). These two, as well as the Pantelleria and Malta furrows, have been dextrally shifted across the geosutures of Ghadames-Medina and Malta Escarpments through Messina toward the Sestri Vortex eye.

The southwest face of Sicily is interpreted to be the fourth member within the group of WNW-ESE trending linear faults across the Sill of Malta and Tripolitania (which also covers the Tunisian Plateau and the Bay of Sirte). The southwestern face of Sicily, like the southern faces of Crete and Cyprus, is interpreted to be a northward thrusted fault.

Another (northward) branching-off geosuture is suggested to curve gradually northward from off Jebel Akhdar (NW Cyrenaica) along the trough of the Ionian Basin to continue tangentially to the eastern limit of the Calabrian Fore-Arc (continental slope), across the Strait of Taranto, the Apulian Plateau, and to follow the NNE trending west Albanian coastline, and join the dextrally shifted Scutari-Pec fault (Pamic, 1983; Robertson and Dixon, 1984). It is then merging with eastward-trending segment of the Balkan Mountains as far as the Bay of Burgas on the Black Sea (our Fig. 22.11).

We agree with the interpretation of Finetti (1985, Figs. 10.1 and 12) regarding the northeastward underthrusting of the eastern flank of the Ionian Abyssal Basin beneath the Hellenic Arc, as well as with the eastward continuation of the northward underthrusting fault beneath the southern face of Crete. We disagree however, with a model where the northward facing cliff of the E-W trending Cyrenaican uplifted block is underthrusting the subsiding Mediterranean deep sea floor; as implied from the same figures of Finetti (*ibid*).

VIIIh: The Western Desert - Northwest Cyrenaican Belt.

Information was gathered from deep drillings and regional geophysical modeling across the northwestern desert, mostly drawn from Hantar (1990), Klitzsch (1990), and Kerdany and Cherif (1990).

The distribution pattern and lithologic-paleontologic characteristics within the Phanerozoic sequence across the Western and Libyan Deserts indicate the occurrence of repeated back and forth marine transgressions from the north southward. One of these indications is inferred from lithologic correlation of the same guide-horizon of Carboniferous age identified within the sedimentary sequences of eleven wells located SE of Sidi Barrani (Cyrenaican coastline). The facies there change gradually from marine carbonates and light-colored shales as well as sandstones in the north into continental red brick shales and coarse-grained sandstones in the south. These changes occur across the relatively narrow WNW-ESE trending zone of the 'unstable shelf', north of which the paleo- as well as the present-day continental slope is steeply dipping toward the north. The southern limit of the unstable shelf extends some 300 km to the south of the present Mediterranean coastline as far as its ESE trending limit as a straight line stretched between Ajdabiya (eastern corner of the Bay of Sirte) and the SW tip of the Qattara Depression (Figs. 22.10a and 22.11).

The existence of the NE-SW trending folded structural high

of Jaghbub-Faghur Ma'amura is best expressed in the isopach map of the total Paleozoic sequence (Hantar, 1990, Fig. 15.3; Kerdany and Cherif, 1990, Fig. 22.1, Table 22.3). On top of that structure the entire Paleozoic sequence was almost completely truncated, whereas toward the west and northwest that same sequence gradually thickens to more than 4000 m, thereby forming a syncline that parallels the Jaghbub-Faghur-Ma'amura-Matruh structural high. That syncline was developed through the Paleozoic and maintained its subsidence until at least the Early Cretaceous (Kerdany and Cherif, *ibid*). At their northernmost reach on land, both of the discussed 'high' and 'low' NE trending axes of structural features are faulted upon crossing the present-day coastline. That segment of coastal fault line extends between Matruh in the east (27°E) and Tobruk in the west (25°E). Both the discussed structurally high and low features extend southwestward from the coastline at least as far as Jaghbub (close to 30°N 25°E and the Egyptian-Libyan border). We suggest however, that the discussed geosuture of twin high and low structures further extends and gradually curves to the southwest to continue across the Ahaggar Massif and the igneous plug of Richat to cross the Atlantic coastline between Cape Blanc and Cape Timiris and merge with the Missouri or Kane F.Z. (Figs. 22.3 and 22.6).

The following is our interpretation of the relevant information on the magnetic field and the Bouguer gravity anomalies obtained from the southernmost fringe belt of the eastern Mediterranean (Makris et al., 1994; Makris and Wang, 1994). The structural conclusions are implied from the geophysical data from the onshore and offshore coastal belt, as well as on the configuration of the isopachs on land.

Relatively long and narrow coast-parallel Bouguer gravity highs (close to +100 mGal) practically coincide with the coast-parallel bathymetric trench grooved along the base of the continental slope between Tobruk (24°E) and Matruh (27°E), *i.e.* a large segment of the interpreted track of the North Cyrenaican Thrust Fault (our Fig. 22.11; Makris and Wang, 1994, Fig. 4.3b). The pattern of the same structural feature, as expressed in the configuration of the magnetic intensity values of the Eastern Mediterranean Sea (Makris et al., 1994, Fig. 3.2b) is both similar to the Bouguer gravity high (see above) and different. It is similar in that the general configuration of the iso-intensity values portrays a linear coast-parallel feature that follows the North Cyrenaican Thrust Fault (as far as about 100 km off the coastline - from the 'Sill' in the west off El Alamein). It is different in that the values over its western half are negative (as low as -150 nT).

It seems therefore that the magnetic field data from the offshore zone of the North Cyrenaican Thrust Fault indicate the existence of a significantly different crustal composition between the eastern and western segments. That change occurs on land along the NE-SW trending axis of the Salum geosyncline. It probably also extends into the offshore along the same trend at least as far as the negative magnetic field values along the northwestern flank of the Herodotus Basin (-100 nT at 34°N 30°E).

The Bouguer gravity anomaly values (Makris and Wang, 1994, Figs. 4.3a, b) indicate the existence of a NE-SW trending on-land low gravity anomaly (from +50 mGals off Tobruk to -20 mGal at 31°N, 23°E about 100 km landward - to the southwest). This anomaly represents the northeastern edge of the Salum geosyncline axis (Figs. 22.10a and 22.11). Its northeastward extension is probably responsible for the formation of the saddle across the linear Bouguer gravity anomaly features (at 32°30'N, 25°E), as well as NE-SW trending gravity anomaly trough extending along the northwestern face of the Herodotus Basin from 33°-30'N, 27°E to 34°-30'N, 29°E. Apparently the Bay of Salum is also associated somehow with that gravity feature.

VIIIi: The Inter-Related Histories of the Cyrenaican-Western Desert Belt and the Herodotus Abyssal Plain (Figs. 22.10a, 22.11).

It is difficult to dismiss the genetic association between the on-land NE-SW axes of the twin structures *i.e.* the Salum geosyncline together with its adjacent anticlines (on its SE) of Jahbub-Ma'amura-Matruh, and its offshore extension expressed by the large, prominent NE-SW trending bathymetric trough together with the Bouguer gravity positive anomaly (as high as +190 mGal) that dominates the Herudotus Abyssal Plain of the Eastern Mediterranean Sea. The above notion is based on the following considerations:

i) The northeastward offshore axial extensions of the Bouguer high, and the structural trends as well as the zero-isopach configuration of the Paleozoic sequence, which exactly coincide with and extend each other across the coastline segment between Sidi Barrani and Matruh. The same holds true with respect to the low Bouguer values and the more than 4000 m thick Paleozoic sequence (that juxtapose the structural high on its east) across the coastline between Sidi Barrani and Tobruk, thereby suggesting the existence of a Salum-West Herodotus geosyncline.

ii) The northeastward breaching of the Cyrenaican coastline along the morphological-structural axis of Salum Bay. It is interpreted to be a northeastward trending geosuture along which the coastal belt has been left-laterally shifted. This is inferred mainly from the Pole-reduced total magnetic intensity maps of the Mediterranean Sea (Makris et al., 1994, Figs. 3.2 and 3.3) as well as from the configurations of the bathymetric as well as iso-Gal contours of the Eastern Mediterranean Bouguer gravity anomaly map (Makris and Wang, 1994, Figs. 4.2 and 4.3). It belongs, however, to the group of geosutures crossing the Eastern Mediterranean Sea (or the eastern flank of the Central Plate - see below) such as the sinistrally-shifted Dead Sea, Pelusium, Eratosthenes, Herodotus (the Matruh high and the Salum geosyncline), and East Cretan-Wadi Zamzam (midway between Wadi Uqaylah and Tripoli across the coastline of the Bay of Sirte), and finally the Strabo and Pliny faults.

Substantial support for the systematic sinistral shifts occurring across all the members of the above NE trending group of geosutures within the Eastern Mediterranean Sea could be inferred from our interpretation of satellite maps (NGS, 1999; ASPRS, 2000). The southern limit of the Unstable Belt (Cyrenaica and Western Desert) is very prominently expressed as an ESE-WNW trending photogeological lineament, extending between Sirte

(where it is crossed by the East Cretan-Wadi Zamzam geosuture) and the southern limit of the Fayum Basin along the Pelusium Line.

The Bouguer gravity anomaly contours across the Herodotus Basin portray a parallelogram frame where ESE-WNW and NE-SW trends dominate its faces (in a plan view) (Figs. 22.10a and 22.11). The genetic relationships to faulting between the gravity and tectonic features are discussed above. Sinistral movements dominate the latter ones. It is not clear whether lateral movements occurred across the ESE-WNW trending faces. We did not find indications for the occurrence of dextral movements across the North Cyrenaican Thrust Fault (assuming that its vertical landward extension would have crossed the sinistral faults of the Dead Sea, East Mediterranean, and the Pelusium Line).

(iii) Judging from the oldest ages of the tectonic activity across the Salum and the Matruh structures (see above) the initial age of the entire system should be very old (perhaps Late Proterozoic). Therefore the chances for the functioning of the North Cyrenaican Thrust Fault also as a wrench fault are very slim. This is inferred from the straight linear northeastward extension of the on-land twin structures of the Faghur-Ma'amura anticlines and the Salum syncline. Considering the very old age of origin of the discussed twin structures on-land (Late Proterozoic to Early Paleozoic) the age of the joint onshore and offshore system could also be that old (the same as that of the Pelusium system).

Thrust faulting should therefore be considered as the preferred mechanism for the functioning of ESE-WNW faults across the eastern Mediterranean, which is perpendicular to the main collisional vector of North Africa and Southern Europe (Fig. 22.14). The origin of the NE-SW trending sinistral wrench faults, such as the Pelusium Line as well as the Pliny-Strabo Trenches (Vanney and Gennesseaux, 1985, Fig. 1.5) is related to the counterclockwise mantle flow, associated with the Aegean and Kirşehir Vortices.

As indicated by Finetti (1985, Figs. 10.1, 10.12), the eastern limit of the Ionian Abyssal Plain attains an eastward concave shape, extending via Cyrenaican Seamount in the south (33°-30'N, 20°E) and the NNE trending Kefallinia Fault to terminate as a dextral fault crossing the coastline of Epirus in Greece at about 39°-10'N, 20°-30'E. The oceanic crust of the Ionian Abyssal Plain is underthrusting eastward the Mediterranean Ridge. The Hellenic arc was thereby shifted away from the discussed eastern limit of the Ionian Abyssal Plain. The discussed limit continues to the south, toward the Cyrenaican Seamount along the 1000 m deep N-S trending bathymetric contour, toward the western flank of Jebel Akhdar, as far as Uqaylah in the SW corner of the Gulf of Sidra.

The E-W trending fault along the northern coastline of Jebel Akhdar is marked by a northward thrusted fault. It is hard to agree with that interpretation for the segment off Jebel Akhdar, as well as its eastward extension along the entire length of the Cyrenaican-Western Desert Thrust Fault, as it is not reasonable to assume that the low density continental crust of North Africa would underthrust the denser oceanic crust of the eastern Mediterranean on its north (Makris and Wang, 1994, Figs. 4.3a, b, and c), no matter how powerful the northward dragging effect exerted by the underlying mantle flow.

Considering the above reservation, our N-S trending ramp-valley model, functioning since early Paleozoic time, may better explain the origin of the eastern Mediterranean (at least for the Herodotus and Levantine Basins). The presence of a less than 100 km wide and more than +200 m high belt that parallels the Mediterranean coastline of Cyrenaica and the Western Desert could be another expression of the tectonic rise (and not a northward underthrusting) of that belt. It is reasonable to assume that the discussed fault line has resulted from the overthrusting of the northern African plate on the depressed southern Mediterranean plate on its north. Toward the south that belt of continental crust is terminated along the WNW-ESE trending tectonic lineament which extends from the depressions of Wadi Uqaylah in the west (the SE corner of the Sirte Basin) through the oases of Siwa, and Sitra, at the southern limit of the Qattara depression.

That segmented tectonic line also marks the southern limit of the Unstable Shelf belt. Mega-basement structures and major faults across that belt are described by the isopach (thickness distribution) maps of the different sedimentary formations deposited between Early Paleozoic and Tertiary (Miocene) times (Hantar, 1990, text and Figs. 15.1 to 15.16). The first two figures (Nos. 15.1 and 15.2) express the distribution pattern of mega-basement features with E-W trends. Figures 15.3 and 15.4 mostly describe the NE-SW trending structures of Jaghbub-Matruh and Alamein-Qattara by the isopachs of pre-Permian and pre-Triassic sediments. Figures 15.5 to 15.16 are isopach maps of sediments of different ages ranging from Early Jurassic to Middle Tertiary. The dominant trend of the structures is E-W, *i.e.* parallel to the southern Mediterranean coastline (or to the North Cyrenaican Thrust Fault), although activity along the ancient NE-SW trend is also still noticed. The depocenter trends and locations along the E-W trending newer structures are fluctuating northward and southward, thereby justifying the name Unstable Shelf given to that belt.

VIIIj: The Age and Origin of the Eastern Mediterranean (Herodotus and Levantine Basins) (Fig. 22.14).

The hitherto dominant concept on the age and origin of the Mediterranean Sea says that basins were formed both on its east and west, by rifting northward and southward due to tensional processes. Thereby oceanic crust formed the floor of the basins in pre-Middle Jurassic times. That formative phase occurred contemporaneously with the opening of the Atlantic Ocean between the Americas and Africa (Livermore and Smith, 1985), together with Europe. It is difficult to adopt such a scenario because of the inferred simultaneous occurrence of the E-W rifting process across the Atlantic, and a similar but N-S trending process across the Mediterranean basin (if both events were affiliated with the same tectonic system). Comparison of hotspot tracks for Europe and Africa shows that between 66 and 48 MaBP the northward migrations of these two plates are similar to each other, resulting in very little convergence between them. Yet these authors consider that the Mediterranean will probably be completely closed within the coming 30-40 Ma (*ibid*).

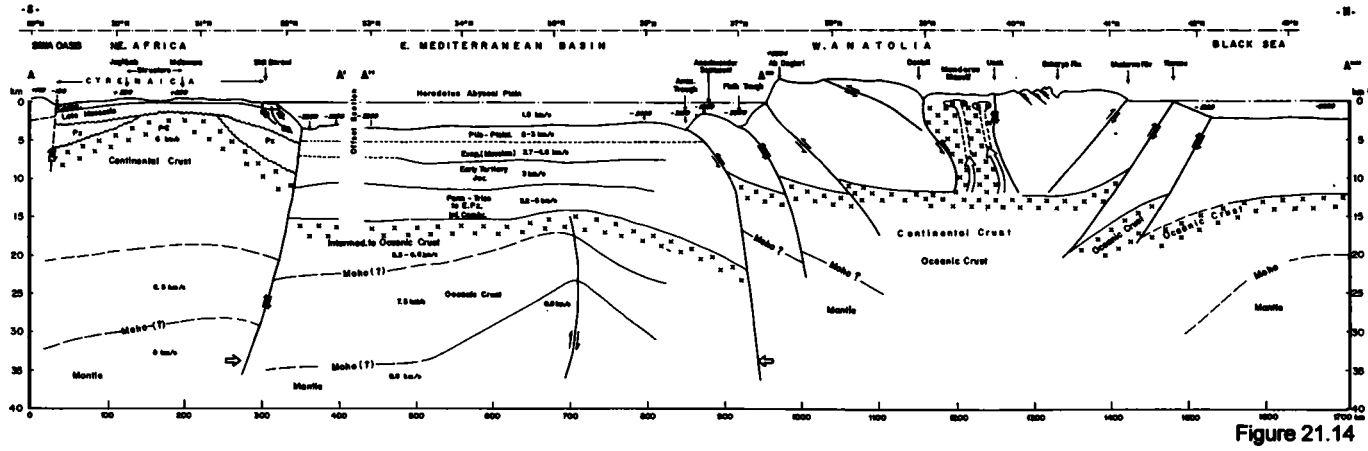


Figure 22.14. A S-N Geological Cross-Section between North Africa (Cyrenaica) and the Black Sea: The eastern Mediterranean Sea (across the Herodotus Basin) is interpreted to be a 'Ramp Valley' suppressed between the northward moving African continent and its collisional front with Eurasia across the West Anatolian-Mediterranean fault-line. The resistance to any further northward crustal movement is exhibited by the subduction process across the Alpine compressional belt (the West Anatolian zone is its southern member).

Perhaps the dominant present-day concept in the geological literature regarding the Middle Jurassic age of the Mediterranean rifting and the associated mechanism of extensive rise of the oceanic magma and the formation of a new basement at the bottom of the Mediterranean Sea (or the Neotethys), should be opened to reconsideration. In view of our limited factual knowledge regarding the identity and nature of the pre-Messinian sedimentary sequence within the eastern Mediterranean basin (Livermore and Smith, 1985; Garfunkel, 1998), and considering the necessity to acquire essential information by indirect methods, a more skeptical approach on one hand, and a much more tolerant one on the other, should be adopted.

Our approach to the age of the eastern Mediterranean (Levantine and Herodotus) basins is based on the following assumptions:

i) Both of these basins are underlain by a 6 km thick oceanic or semi-oceanic type crust;

ii) Both are overlain by a close to 15 km thick sequence of phanerozoic sediments (Makris et al., 1983; Makris and Wang, 1994);

iii) The base Messinian reflector within the above two basins is found some 3 km beneath the seafloor;

iv) Between 12 and 8.5 km out of these 15 km are of pre-Messinian ages (after Garfunkel, 1998; de Voogd et al., 1992; Abdel Aal et al., 2000);

v) The total thickness of sediments overlying the bottom of the Middle Jurassic sequence along the eastern flank of the Levantine Basin's paleo-trough is close to 5.5 km;

vi) The vertical trend of the thickening-thinning curve for the post-Middle Jurassic sedimentation sequence within the eastern Mediterranean Sea points to an increased rate of sedimentation with decreasing age. It is reasonable to expect that the same trend also prevailed during the lower (or older) half of the entire relevant sedimentary sequence. It is therefore assumed that the same regimen of excessive rate of sedimentary accumulation (as compared with the equivalent ones across the nearby lands) has prevailed within the Levantine and Herodotus troughs since the Early Paleozoic, or even Late Proterozoic time (Neev et al., 1985).

The above paleogeological analysis and assumptions are being corroborated by three analogies of similar basins situated along the northeastern periphery of the Alpine-Himalayan orogenic system:

i) The Tarim;

ii) The Peri-Caspian; and

iii) The Black Sea basins. Almost complete marine (Tethyan) sedimentary sequences have been accumulated within these three basins since early Phanerozoic (or Eocambrian) times.

VIIIk: The Paleozoic Tethys.

The thick sequence of continental Old Red Sandstone, intercalated with marine and lagoonal facies (shales and sandstones), was the first Phanerozoic sediments deposited across the broad boundary zone between SE Britain, the Baltics, and NW Europe (the Ardennes, Rhenish, Harz, Thuringia and Bohemian regions). That process of cyclically alternating southward marine transgressions and northward regressions dominated these areas between the Late Caledonian (the Silurian through Early Devonian) to terminate in the Late Carboniferous. That broad belt (or continent) of Old Red Sandstone extended eastward as far as Lake Ladoga-Onega and the White Sea. A comparable facies change also occurred in North Africa where the transition from continental red to the purple Lalun Sandstone in the south, alternating with marine facies of light-colored carbonates and marl in the north, is found along a west to east trending belt extending from southern Morocco across to the northern Sahara, Libya, and Western Desert, as far east as Mesopotamia (Gignoux, 1954; see also Hantar, 1990).

Sonnenfeld (1981) corroborates and complements the above

by describing the extension of the Lalun purple to red Sandstone (see above) from Transcaucasia to eastern and central Iran and into the Zagros Mountains, over an additional distance of about one thousand km. According to that the external belt of continental red sediments completes a circle which surrounds the marine sediments of the Tethys Ocean. Gignoux (1954) described the regional distribution of the Mediterranean marine facies; which include deep water shales and cephalopod limestone that were deposited continuously from the Devonian to the Carboniferous across the Pyrenees, Sardinia and Morocco in the south, through the Massif Central, the Vosges, and the Carnic Alps in the north. These areas are encompassing the marine territories, which practically represent the present-day Alpine orogenic system, coinciding with the 'eye' (or central basin) of the Paleozoic Ocean that was encircled by the Old Red and Lalun purple-red Sandstone formations.

A similar process of 7 to 8 major repetitive cycles of facies changes from shallow to deep marine sediments (mostly evaporites and carbonates), separated by major unconformities, occurred through the stratigraphic sequence of the Salt Range province of northern Pakistan (the Indian Sub-Plate) beginning with the Eocambrian (some 600 MaBP) through the Early Permian, Early Triassic, Early Jurassic, Early Cretaceous, Paleocene, Oligocene, and Late Pliocene (some 4 MaBP) (Gee, 1989).

Red gypsiferous dolomite, marls, rock-salt, maroon fine sandstone, purple and blood red shales, light green to olive green carbonates, and sandstones, alternate through that sequence. Cycling occurrences of a similar spectrum of rock types occur again with the Miocene.

Perhaps the Indian segment is a link that connects the two large arcs to become the global ring, which is encompassing the Old Red northern and southern continents. Perhaps the red sandstone formations found along the belt, which later on was folded to become the Appalachian orogeny along the northeastern coastline of North America and East Greenland between the Late Silurian and the Permian, could have formed the western segment of the above ring (Ziegler, 1989, Plates 1-12).

IX - THE CENTRAL PLATE – A: THE SINAI SUB-PLATE

IXa: Regional Background.

According to our model, the merged lithospheric slices of the northern Central Plate (*i.e.* the Sinai-Arabo-Nubian and the Iranian sub-plates) are still being dragged northward along a curved counterclockwise track by the underlying northward flowing mantle. That process has been going on at least since late Proterozoic times. On their north the discussed geosutures and slices are converging and colliding with the Eurasian continent along the Alpine-Himalayan orogenic system. The main tectonic elements which are associated with that process are discussed below.

The western limit of the Central Plate coincides with the Pelusium Line and with the continental margin of the eastern Mediterranean. Its southern and eastern limits are marked by the joint geosuture of the Agulhas, Mozambique, Somali and Owen F.Z. that extend farther northeastward along the eastern limit of the Lut Block (which is marked by the Harirud-Zabul Fault - Fig. 22.24). Its northern limit is marked by the two vortices of Ararat and Lut (Fig. 22.23), as well as by the Black Sea and the Caspian depressions. The areal dimensions of the Central Plate are measured out by its length of about 3200 km, between Aden in the south (15°-30'N, 45°E), and Mount Ararat in the north (Tibilisi - 42°N, 45°E). Its width is about 3500 km, between the Pelusium Line in the west (at the Kufra Basin just east of the Tibesti Massif - 25°N, 25°E) and Ras Al Hadd in the southeast (22°N, 58°E) (Fig. 22.21).

During Late Precambrian and Early Paleozoic times the northern periphery of Gondwanaland was bordered by the Paleo-Tethys. Its collision with the Eurasian continent had also occurred during the Late Precambrian, as inferred from the presence of the Precambrian massifs, whose rock-type is indicative of their Pan-African origin.

A similar collisional event between the Eurasian and Gondwanaland had occurred during the Hercynian Orogeny (Late Paleozoic), as indicated by the consumption of the oceanic crust of the paleo-Tethys. The South Caspian depression and the tectonically uplifted Alburz Range are the relicts of the Paleo-Tethys (Stocklin, 1974), resulting from the southward drift of the Baltic Shield to collide with the Iranian and Arabian forelands.

The dextrally-shifted Tornquist Fault (Arthaud and Matte, 1977) is interpreted by Mosar (1999) to be genetically related to the southward drift of the Baltic Shield (including the East European craton) that occurred during early Paleozoic to early Mesozoic times. It is the prototype of the 'school' of concave northeastward geosutures that approach the 'Global Eye' from the north (Neev and Hall, 1982). That 'school' extends from the Voring-Rockall-Armoric geosuture in the west to the Yenisey in the east (our Fig. 22.1).

The 'Global Eye' is defined by the seven (out of eight) vortices along it: Sestri, Aegean, Kirşehir, Ararat, Lut, and Brahmaputra (the Alboran is, perhaps, a secondary vortex). The northward protrusion of the central Plate (headed by the Ararat and Lut Vortices) splits the 'Global Eye' into two main *en-echelon* segments: the Alpine and Himalayan ones.

The architectural crustal features of the Mediterranean, Black, and Caspian Seas, have some basic similarities to each other (Ross, 1974, quoting Neprochnov et al., 1964). The most pronounced ones are the large Bouguer gravity anomalies, the positive magnetic anomalies, as well as the large-scale boundary faults which are mostly paralleling the Alpine orogenic system, and their great thicknesses of sedimentary fill. Estimates of the age of origin of these three basins vary between Precambrian (to which we concur) to Late Mesozoic. Wider agreement is reached regarding the mechanism of origin, which is associated with the convergence of the Eurasian and African Plates (Erickson and Simmons, 1974 for the Black Sea, as quoted by Ross, 1974).

Until a decade or two ago, age interpretation of borehole stratigraphy and seismic data suggested the sequence of the Peri-Caspian depression to include just Devonian and younger sediments. Nevertheless more recent deep seismic data indicate the presence of an older 5-7 km thick sequence of Riphean

(Infracambrian) to Early Paleozoic ages to underlie the Middle Paleozoic sediments of the Peri-Caspian Basin and the Karpinsky Swell (with its 15 km thick sedimentary column) on its north. That swell is thrusted southward over the lower Permian strata of the Peri-Caspian Basin. The results of deep seismic refraction surveys in the same area display the collisional process between the East European craton in the north and the Arabian-Iranian sub-plate (or the Scythian Plate, as defined by Kostyuchenko, 1999) in the south.

Ross (1974, quoting Neprochnov et al., 1964) suggests that the processes of basinal subsidence and accumulation of sediments within the Caspian and Black Seas began as early as the Paleozoic. Ross (*ibid*, p. 678 and Fig. 10) suggests that the E-W alignment of the offshore narrow strip of alternating positive and negative magnetic anomalies parallels the southern coastline of the Black Sea, as well as the structural trend of the Caucasus and Pontic ranges, indicating "that during the Mesozoic and Cenozoic the Black Sea area was a zone of north-south compression". That postulation is in agreement with the regional interpretations of Stocklin (1974), Erickson and Simmons (1974), and Kostyuchenko (1999).

IXb: The Precambrian Basement of the Sinai Peninsula.

The discussed sub-plate (of the African-Arabian Plate) was rifted away since the Oligocene. Nevertheless, its earlier existence as an embryonic rift or shallow depression, cannot be ruled out. That possibility is inferred from:

i) The Cambrian fossils found near Abu-Durba (about the middle of the present-day northeast coastline of the Gulf of Suez);

ii) The relatively thick sequence of Carboniferous marine sediments along the southwestern flank of the Gulf (after Garfunkel and Bartov, 1977, p. 4 and 14).

Vertical crustal oscillations of a long wavelength nature characterized the tectonic regimen of that region in pre-Rift (pre-Neogene) times. The first large scale vigorous vertical oscillatory movement of the Sinai Peninsula (an uplift of about 4 km) took place in mid-Miocene times. The indications for these vertical changes are the highest and lowest present-day elevations of the outcrops of Eocene carbonates (with flint concretions) to Nubian sandstones on the Tih Plateau on the east, and the outcroppings as well as deeply buried sedimentary and crystalline rocks within the Rift.

Lacustrine sediments of alternating high and low water energies were deposited along three separate E-W trending segments stretching along the river bed of Wadi Feiran and its upstream extension, the Wadi-el-Sheikh, as far as the Watia Pass (28°-10'N, 34°E), some 20 km north of Mount St. Katherine (Issar and Eckstein, 1969; Awad, 1953). These authors suggest the sequence below to represent separate lakes at different levels:

i) The lowest (westernmost) reach of the Feiran Lake is at an elevation of close to +600 m m.s.l., whereas its eastern limit is close to +750 m and its length is about 10 km.

ii) The length of the next segment to the east is 14 km long, stretching along Wadi-el-Sheik between altitudes of +800 and +875 m;

iii) The third (upstream) segment is trending E-W from an elevation of +1150 m to +1250 m beyond (east of) Watia Pass. It is merging there with the N-S trending relics of a more regional lake (25 by 10 km in size). The relics are distributed in patches along the water divide. Present-day evaluation of these flat-bottomed relics are from about +1600 m in the south to close to +1360 m in the north (Ghor el Ajram).

This Water Divide of Mount Sinai forms an extremely straight N-S trending linear feature extending from about 20 km north of the Watia Pass (about 28°-52'N, 34°E) through Mount St. Katherine at +2642 m, which is the highest peak of Sinai, to Jebel Hanchur al Ghatti (+796 m, 28°-03'N, 34°E).

The southernmost segment of the Mount Sinai Water Divide extends northward from Jebel Hanchur al Ghatti some 110 km, as far as 29°-03'N, 34°E at the head of the E-W trending Wadi el Biar (where the dividing ranges are at elevations of close to +1600 m). At that point the water divide is shifted some 30 km eastward in a dogleg fashion as far as 29°-01'N, 34°-16'E. The Water Divide continues along a NNE trend from Sinai, abutting the southwestern corner of the Ramon Anticline, then along the western flank of the Hatira Anticline across Hebron and Jerusalem, and terminates in northern Lebanon. The northward trending water divide repeatedly occurs from the latitude of Wadi el Biar (29°-03'N) at least to Beirut (33°-50'N) and Tripoli (34°-30'N) along major E-W trending linear disturbances such as the Thammad-Abu-Alaliq, the Paran, Zin, and Beersheba Faults. Acco, Rosh Haniqra, the Litani River, and Beirut are all dextrally shifted along these E-W features.

The extent (30-40 km W-E) and the vertical distribution pattern (range of elevations from +600 to +1250 m) as well as the loosely cemented nature of the lake sediments within and along the gorge of Wadi Feiran - Wadi-el-Sheikh - Watia Pass puzzled the scientists who studied its geological history (*i.e.* Issar and Eckstein, 1969; Awad, 1953). To make the problem more acute, the results of several radiocarbon analyses made on samples of different depth horizons, and elevations (*i.e.* from all of the three lakes), indicated the age of deposition of all of these lake deposits to be within the range of the last glacial period of the Pleistocene (*i.e.* 20,000 to 40,000 yBP., Issar, pers. comm.).

The solution to that dilemma is in the decrease in the potential energy along the course of that river by dividing the 700 m of elevation differences between Wadi Feiran and the Watia Pass that occurs over the course of that river (a horizontal distance of about 40 km), into three segments. Awad (1953) suggests the damming elements at the downstream end of each segment (lake) to have been formed by an un-equal thickness pattern of the accumulated thick alluvial fan deposits. Issar and Eckstein (1969) however suggest the changes in the damming efficiency factor to have been the more erosional resistant efficiency of the magmatic dikes (which are abundantly present). Both of these solutions could have temporarily functioned, but an additional factor should also be sought, such as the tectonic activity.

The present-day morphology is mostly the product of vertical tectonic (± oscillatory movements) as well as local and global changes of aquatic base levels. The relevant data on the changing

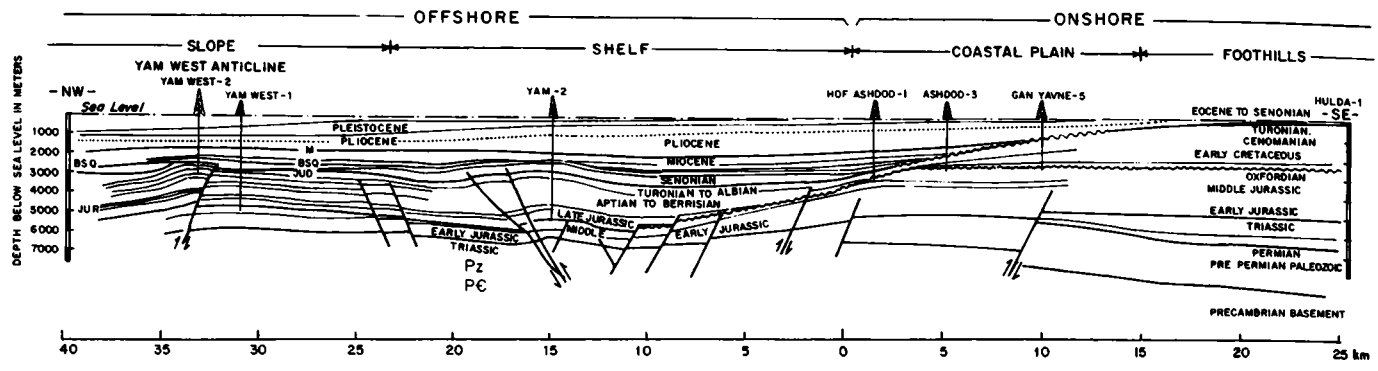


Figure 22.16. Hulda to Yam-West: A 65 km long coast-perpendicular (ESE-WNW trending) geological cross-section based on geophysical and oil exploration data (deep wells) (courtesy of Dr. Y. Folkman and the ISRAMCO Oil Exploration Ltd.). It begins at the Hulda-1 well in the east, crosses the westward truncated Early Paleozoic to Early Cretaceous coast-parallel fold structure, continues westward through the Late Jurassic to Pliocene coast-parallel and mid-shelf inverted syncline, and terminates just west of the eastward thrusted Jurassic to Base Neogene fold structure (the Yam-West Anticline) at the Continental Slope.

Late Pleistocene lake levels preserved along the water divide north of Mount St. Katherine were interpreted by integrating their elevations (mostly gravelly beds) distributed across a 10 km wide and 20 km long segment of the N-S trending water divide. The elevations of that Late Pleistocene (Würm) lake are changing from close to +1600 m in the south (at the northern foot of St. Katherine's Monastery) to about +1400 m just east of the Watia Pass, to +1200 m at its northern end (28°-47'N, 34°E). We interpret that 400 m northward drop in elevation across the depositional plain as an expression of the effect of a northward tilt of the water divide, caused by the vigorous rate of additional young uplift of the peak of the Mount Sinai Massif. Similar types of data were also found along the westward flowing gorges of the Sinai Massif.

They also indicate rather abrupt westward changes of river gradients, suggesting the occurrence of recent tectonic uplift movements across the western (NW-SE trending) as well as along the N-S trending water divide (or structural backbone).

Although we agree that the origin of the Red Sea (including the Gulf of Suez) is associated with tensional movements, it seems more plausible that these two indications from the Sinai Peninsula were associated with compressional tectonism. The Sinai Peninsula is an integral part of the Central Plate, the northward wedging-in movement of which is generating increasing rates of lateral compression. The continuous tectonic uplift (although in phases) of the Sinai Massif since Miocene times could be the product of that tectonic compressional regimen. We admit that we do not yet have all the necessary components of the puzzle needed to decipher the detailed mechanism of the above process, but we are convinced that the above suggestion should not be dismissed.

IXc: The Israel-Lebanon Slice and the adjacent easternmost Mediterranean Sea (Figs. 22.15a, b, 22.16).

The counterclockwise converging and northeastward curving system of left-lateral shears, which belong to the global pattern of spiraling geosutures, have played a major role in shaping the structure of the eastern Mediterranean and the Levant. That system is composed of the Dead Sea, the Pelusium Line, and the Qattara-Eratosthenes shears (Neev, 1975, 1977; Neev and Hall, 1982, 1992; Neev et al., 1976, 1982, 1985). Several other geosutures of secondary importance, such as the coastline and Foot-Hill faults of Israel, are also marked (Neev et al., 1985, Figs. 12-2, 12-3, and 12-4; Figs. 22.15a and 22.15b below).

Depositional basins were formed between geosutures along axes of lithospheric slices during most of Phanerozoic times, for example, along the axis of the easternmost on-land basin within the discussed system. It extends N-S along the Structural Backbone of Israel (Neev, 1960) between the Dead Sea and the Pelusium Line geosutures. Its sedimentary fill thickens rapidly to the west of the Dead Sea geosuture to reach an estimated total thickness of close to 10 km along the trough. Excessive rates of sedimentation are assumed to have taken place in these troughs since Early Paleozoic (or even Infracambrian) times (Neev et al., 1985, Fig. 14-4 upper part).

The trough along the Structural Backbone was gradually subjected with time to an increasing process of lateral compression due to the northward counterclockwise convergence of this system of geosutures, as well as the *en-echelon* (eastward) order of more advanced northward positions reached by the in-between slices (Neev et al., 1985, Fig. 12-11). That process has caused the entire sedimentary fill across the Backbone Trough to thicken as well as to be squeezed both laterally and upward. We do not know how much of the Phanerozoic sedimentary sequence was therefore eroded or had never been deposited

The same lateral compressional mechanism (see above) also generated the southeastward asymmetric folding of the northeastward trending anticlines within the Syrian Arc (between the Pelusium Line and the Dead Sea geosutures). In fact we have identified similar asymmetric fold structures also in the offshore to

the west of the Pelusium Line.

A number of vigorous tectonic vertical-differential cycles of oscillatory uplift-subsidence types of movement are inferred to have repeatedly occurred across and to the east of the Mediterranean coastal zone of Israel. The earliest known age of the beginning of the first cycle of vertical oscillatory tectonic movements is Hercynian (Permo-Triassic) time. That interpretation is inferred mostly from the stratigraphic data derived from the Heletz Deep Borehole situated on top of the Heletz structure, a few km east of the southern Mediterranean coastline of Israel NE of Gaza (Druckman, 1985, Figs. 2, 7, 8; Garfunkel, 1998, Figs. 2A, 2B, 5, 7).

Following a long period of uplifting, non-deposition and erosion, a 43 m thick unit of dark gray calcareous shales, intercalated by quartzitic sandstone lenses (the Karmia Shale), was deposited on top of the Precambrian basement rocks at the peak of the Heletz structure. The beginning of the downwarping-depositional phase of that cycle is therefore inferred.

The more than 600 m thick polymictic Erez Conglomerates unit is overlying the Karmia Shale. It consists of up to 0.5 m size boulders (mostly carbonate fragments), interbedded by a few horizons of dolomitized carbonate and megafauna debris as well as several 7-10 m thick horizons of reddish brown silty shales. A shallow marine to sub-aerial environment of deposition and a tectonic regime of subsidence are therefore suggested. Age analyses were performed on palynomorphs obtained from (i) within the underlying Karmia Shale, (ii) fragments of the conglomerate, (iii) the matrix of the latter, and (iv) the dolomitized muds of the overlying Mohilla Formation (Carnian, or early Late Triassic age). It is therefore suggested that prior to deposition of the Erez Conglomerate the Heletz area went through an uplifting and erosional phase sometime in Late Permian (some 250 MaBP). That cycle ended with a post-conglomerate tectonic subsidence mud deposition that ended in Middle Triassic time (Anisian, or some 230 MaBP).

The above interpretation assumes that the coastal zone of Israel and the Heletz Structure along it were breached during the Late Permian erosional phase following the regional uplift movement. Therefore it could be implied that the folding process of the Heletz Structure has occurred during an earlier time.

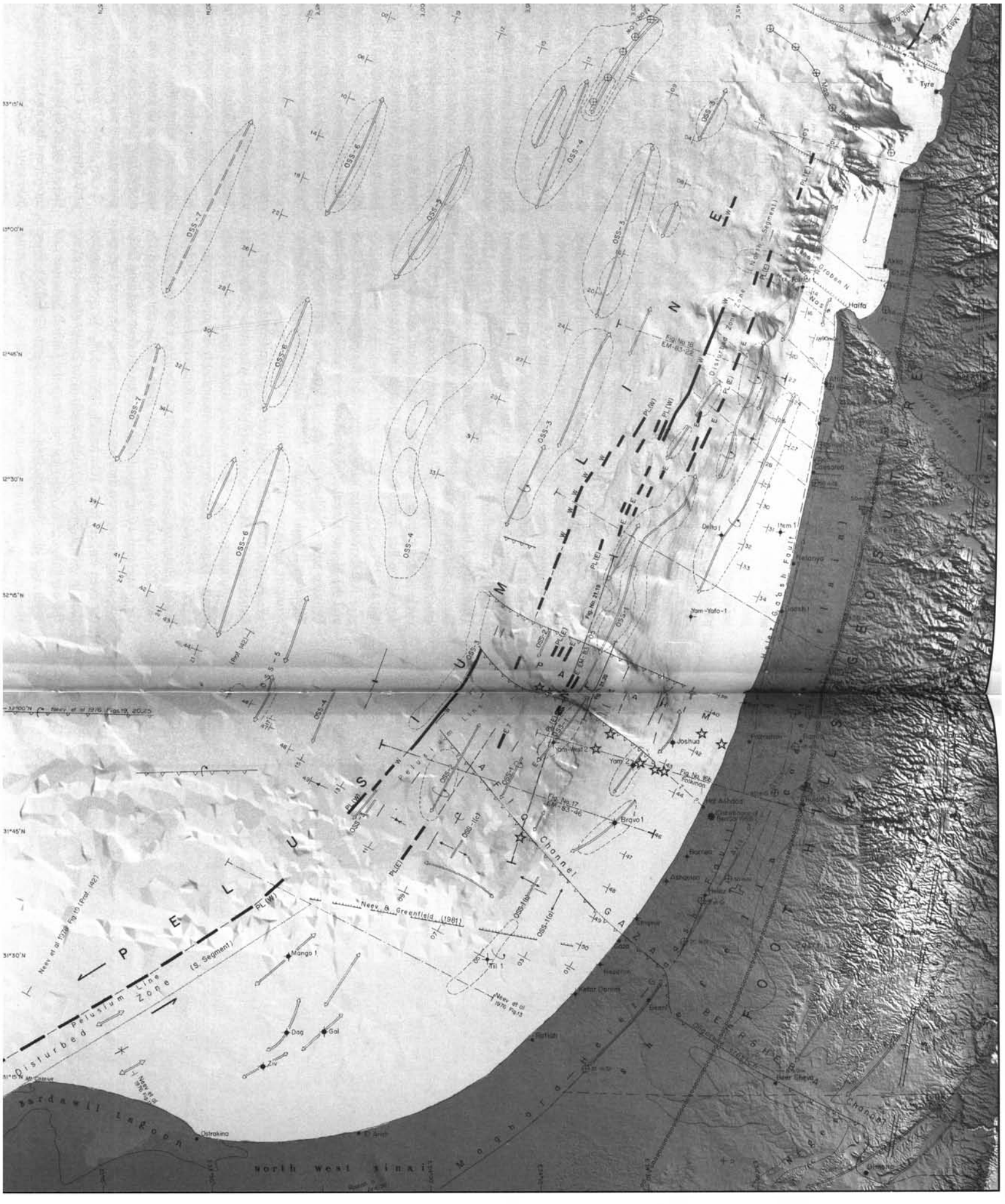
A somewhat different interpretation is preferred, however, by Druckman (1985) and Garfunkel (1998), who consider the Heletz Conglomerate to have been accumulated at the base of a coast-parallel Heletz fault escarpment. Accordingly the involvement of repetitive cycles of tectonic phases of re-emergence of the Heletz-Ga'ash Structure, its re-erosion and re-subsidence (as suggested by Neev, 1975; Neev et al., 1976; Neev et al., 1982) is not needed. On the other hand we agree with the presence of a deep and long fault-line along the western flank of the Heletz Structure since Permian (or even earlier) times (Garfunkel, 1998, *ibid*). We consider that fault to extend farther on to the north in an *en-echelon* way along the coastal zone (on its west) as far as the Ga'ash Structure and wildcat (at the Mediterranean coastline, about 32°-20'N). From there it continues along the littoral zone as far as off Mt. Carmel and beyond. It also continues to the south of Heletz, but gradually deviates away from the Mediterranean coastline to abut along the western flank of the NE-SW trending Risan Aneiza and Jebel Mughara chain of structures in western Sinai, and then continuing south of Cairo, *en-echelon* with the Pelusium Line, and across the Kufra Basin (Fig. 22.15).

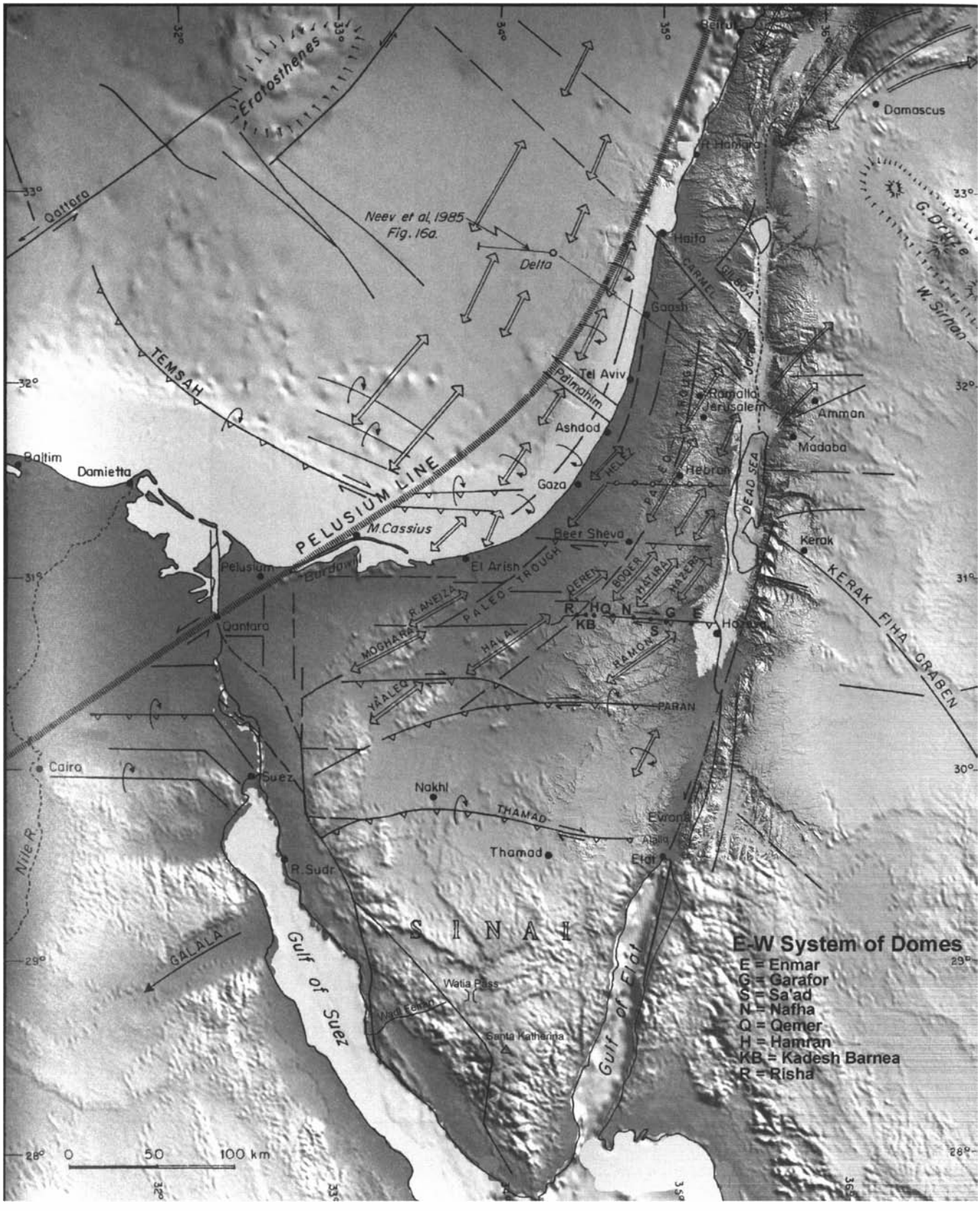
Chains of structures and faults sub-parallel to the coast are most abundant offshore of Israel, across the shelf, slope, and the Eastern Levantine Basin. Data recovered from multi-channel seismic profiles to depths of 7 seconds, across the area as far as the Pelusium Line (Fig. 231.15b), indicate the presence of several coast-parallel eastward asymmetrical folded chains of pre-Cretaceous structures which are associated with thrust faults (Neev and Greenfield, 1981; Neev et al., 1985, Figs. 12.3 to 12.9).

The Heletz-Ga'ash coast-parallel chain of structures was repeatedly folded, uplifted, and again subsided, several times at least since Permian times. This is indicated by the truncation of its axial zone and the thinning-thickening pattern. These vertical oscillatory movements are documented as having occurred during the transition periods since at least the Permo-Triassic (Neev et al., 1976, 1985). The thick sequence of Permian to Tertiary sediments, accumulated to the east, along the N-S trending paleo-syncline that underlies the Beersheba-Jerusalem-Ramallah-Nazareth Arch, thins again eastward toward the Dead Sea-Jordan geosuture. In post-Cretaceous times that N-S trending paleo-geosyncline went through inversion to become the 'Structural Backbone' of Israel (our Figs. 22.15a, 22.16; Neev, 1975, p., 683; Neev et al., 1985, Fig. 12.4; and Garfunkel, 1998, Figs. 2A, 2B). The Phanerozoic sedimentary sequence within that syncline has subsided about 10 km along its troughs which underlie and parallel the N-S trending present-day structural ridge (the 'Structural Backbone' of Israel). That conclusion is solidly based on the analyses of data recovered from the 5 km deep well of the Ramallah #1 drill hole (which bottomed in Triassic rocks). The pattern of reflections recovered from a west to east oriented multichannel seismic profile extending inland to a distance of 10 km east of that Ga'ash well buttresses this interpretation. These seismic reflection data were tied to and correlated with the stratigraphic and seismic velocity data yielded by studies and measurements in that well.

It is inferred from our regional studies that the Heletz-Ga'ash chain of structures went through much earlier cycles of uplifting, truncation, and subsidence than those of the Permo-Triassic. The Triassic-aged Heletz Conglomerate should have been deposited during the secondary tectonic cycle, or a phase of subsidence that followed an earlier phase of differential vertical uplifting movement when entrenchment of transverse rivers occurred. The westward transportation of gravels and the deposition of the conglomerates could have taken place both within the known segment of the channel and west of it along the foot of the down-thrown block.

A similar, although younger, oscillatory tectonic event was detected by Cohen (1976) across the same structure of the Heletz oil field. It was also associated with a differential vertical movement that took place during the transition from the Jurassic to the Early Cretaceous periods. The 1 km deep Gevaram Canyon was entrenched across the Heletz structure as well as the present-day


Tyre
Haifa
Akko
Caesarea
Dalia 1
Item 1
Yam-Yafo-1
Joshua
Yam-West 2
Yam 2
Bravo 1
Mango 1
Dag
Gal
Ziv
Ostrakina
Delta
Kelanya
Gaash
Barnea
Ashqelon
Beer Sheva
Dimona
Neev & Greenfield (1981)
Neev et al 1976 Fig 13
Neev et al 1978 Fig 15 (Prof. 142)
Fig. No. 17 EM-83-46
Fig. No. 16b Eskimon
Fig. No. 15 EM-83-22
Fig. No. 21b
Fig. No. 21a
Pelusium Line Zone (S. Segment)
Disturbed
PELUSIUM
PL(W)
PL(E)
Coast-Line Channel
Coast-Line Geosuture
Foot-Hills Geosuture
Gaash Fault
Negev Basin
Negev Basin Margin
Negev Basin Flexure
Negev Basin Hinge Line
Negev Basin Boundary
Negev Basin Channel
Negev Basin Ridge
Negev Basin Trough
Negev Basin Terrace
Negev Basin Plateau
Negev Basin Escarpment
Negev Basin Valley
Negev Basin Canyon
Negev Basin Gully
Negev Basin Ravine
Negev Basin Gorge
Negev Basin Cliff
Negev Basin Slope
Negev Basin Rise
Negev Basin Abyssal Plain
Negev Basin Abyssal Hill
Negev Basin Seamount
Negev Basin Guyot
Negev Basin Atoll
Negev Basin Reef
Negev Basin Lagoon
Negev Basin Island
Negev Basin Peninsula
Negev Basin Cape
Negev Basin Bay
Negev Basin Gulf
Negev Basin Strait
Negev Basin Isthmus
Negev Basin Delta
Negev Basin Estuary
Negev Basin Fjord


Eratosthenes
Qattera
Neev et al. 1985
Fig. 16a.
Delta
TEMSAH
PELUSIUM LINE
M.Cassius
Baltim
Damietta
Pelusium
Burdawil
El Arish
PALEO TROUGH
Qantara
Beirut
Damascus
R. Hamara
Haifa
CARMEL
Gilboa
G. Druze
W. Sirhan
Gaash
Tel Aviv
Palmahim
Ashdod
Gaza
Jordan
Ramalla
Jerusalem
Amman
Madaba
Hebron
HELEZ
PAZ
DEAD SEA
Beer Sheva
Kerak
AEREN
BOQER
HATIRA
NAZEREA
KERAK FIHA GRABEN
RANEIZA
MOGHARA
HALAL
RAMON
YAALEQ
PARAN
Eilat
Caira
Suez
Nakhl
THAMAD
Thamad
Evrona
Ataiqa
R.Sudr
Nile R.
GALALA
SINAI
Gulf of Suez
Gulf of Eilat
Watia Pass
Wadi Feiran
Santa Katharina
E-W System of Domes
E = Enmar
G = Garafor
S = Sa'ad
N = Nafha
Q = Qemer
H = Hamran
KB = Kadesh Barnea
R = Risha
0 50 100 km

coastline. It was mapped along a 16 km long west to east trending segment where its width attained 7 km (NE-SW). That canyon was entrenched into Middle Jurassic limestones, the detritus of which were deposited along its trough, and was unconformably overlain by the dark gray shales with some sandy beds of the Early Cretaceous Gevar'Am Formation. Its generation should have been associated with the tectonic cycle of differential vertical movements as described above.

The third cycle of oscillatory vertical movements is evidenced on land and offshore by subsurface geological-geophysical as well as drill hole studies (Neev, 1960; Neev and Emery, 1967; Neev et al., 1976; Gvirtzman and Buchbinder, 1978; Druckman et al., 1995). Neev (1960, 1979) described the Afiq Channel as being a nearly 120 km long riverbed which transversely drained much of the Sinai Sub-plate. It extended from the Jordanian Highlands through the subsiding Dead Sea Basin along the Rift Valley (when the rates of deposition exceeded the rates of subsidence) and Beersheba (north-central Negev) to cross the Mediterranean coastline and terminate close to Gaza. It was initially incised in Pre-Neogene (*i.e.* Oligocene) time when its depth (beneath the channel's shoulders) increased westward from a few tens of meters (across the dense limestone anticlines of the NE Negev), to 250 m across the Beersheba anticline (Eocene to Late Cretaceous chalks), to 1100 m at the Afiq-1 borehole. There the channel crosses the NNE trending axes of the Heletz chain of structures (where the channel fill bottoms in shales and marls with some sands and pebbles of Early Oligocene age, that are unconformably overlying the Early Cretaceous dense dolomites). A coast-parallel NNE trending subsurface lineament, situated some 4 km inland from the coastline, is marking the western limit of the Beeri-Heletz-Negba chain of structures across which a facies divide occurred in Early Cretaceous times. It is equivalent to the Heletz deep-seated fault (see above). It is also expressed by the crowding of the post-Messinian isopachs.

Significant morphological changes are noted in a compilation of relevant data from Neev (1960) and Druckman et al. (1995, p. 170, Figs. 3, 5-10) describing the three segments along the bottom of the Afiq Canyon between Beersheba and its outlet to the Mediterranean Sea (Fig. 22.15a). These are:

i) The Upstream (Eastern) segment;

ii) The Central segment (across the Heletz-Beeri structures); and

iii) The northwestern coastline-crossing segment.

The three segments are described as follows:

i) The upstream segment is close to 30 km long and trends WNW-ESE. Its track is rather linear and wide (up to 4 km rim to rim), having an average westward slope of 0.7°. It extends between Beersheba in the east and the Shoqeda-2 drill hole close to the eastern flank of the Heletz-Beeri chain of structures.

ii) The 17 km long central segment extends between the Shoqeda-2 and the Nahal Oz-1 holes where its course is sharply changing from WNW to NNW. Depth values along the trough of that segment (where Oligocene marls are overlying Early Cretaceous dolomite and shales) are increasing from -600 m m.s.l. (at Shoqeda) to -1700 m m.s.l. at the Nahal Oz hole at its northern limits *i.e.* an average slope of 4-5°. Transverse seismic-stratigraphic profiles cross the canyon both on shore (Druckman et al, 1995, Fig. 5, across the Heletz-Beeri chain of structures) and offshore (*op cit.* Figs. 6, 7). Their Figure 5 indicates both the V shaped morphology and the fault-controlled origin of that transverse cross-section; relatively steep NNE dips are exhibited by strong reflectors between 0.4 and 2 second depths between the Beeri-2 and Afiq-1 (at the trough) holes. That fault appears to extend northwestward, as suggested by the linear trending configuration of the Yafo Formation isopach contours both on and offshore (Druckman et al., 1995). That fault is limiting the northwestward nosing Nezarim feature as well as the southwestern rim of the offshore box-shaped extension of the Gaza Channel (Druckman et al., *ibid*, Fig. 3).

iii) Upon approaching its third segment (*i.e.* westward or seaward from the Heletz-Beeri structure) the canyon appreciably changes both its trend (from NNW to NW) and morphology (from a narrow V shaped gorge with a downstream dip of 4-5° into a 15 km wide, flat-bottomed and box-shaped valley with an average downstream dip of 1.8°). Most of that western segment is recognized in the offshore as a sub-bottom feature (seen in the isopach map of the post-Messinian Pliocene Yafo Formation) at least as far as the present-day shelf edge (Druckman et al., *ibid*, Fig. 3).

Druckman et al. (*ibid*, p. 182) consider that box-shaped valley to have originated as a failure of the slope which gradually developed through mass movement processes of sediments, where the Afiq Canyon reaches its maximum relief at the paleo-shelf break (their Figs. 1-3), in an analogous way to those proposed by Farre et al. (1983) for the Oceanographer and Baltimore Canyons on the Atlantic coast of North America. Apparently that conclusion served as the basis for the sweeping conclusion of those authors that the Afiq Channel (at least between Beersheba and the shelf edge) was incised as a canyon by submarine hydraulic processes.

Although we do not totally dismiss the above interpretation on the submarine origin of the Afiq Canyon, we do not accept it either (at least not for the on-land segment). The main point of disagreement is the involvement of large-scale oscillatory vertical tectonic movements in the process of its entrenchment. Beyond the

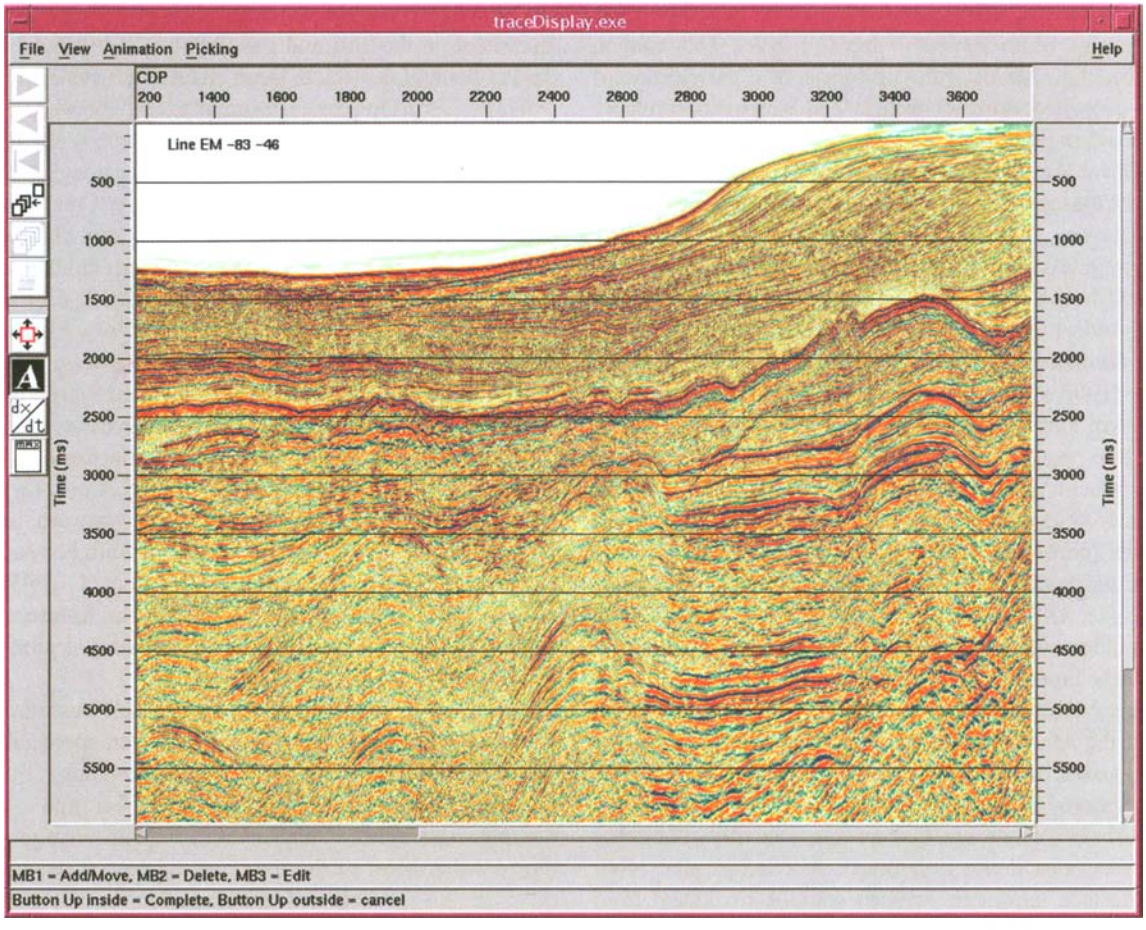


Figure 22.15b. Major Structural Elements across the Easternmost Mediterranean Sea and the Sinai Peninsula + the territories of Israel and Jordan:

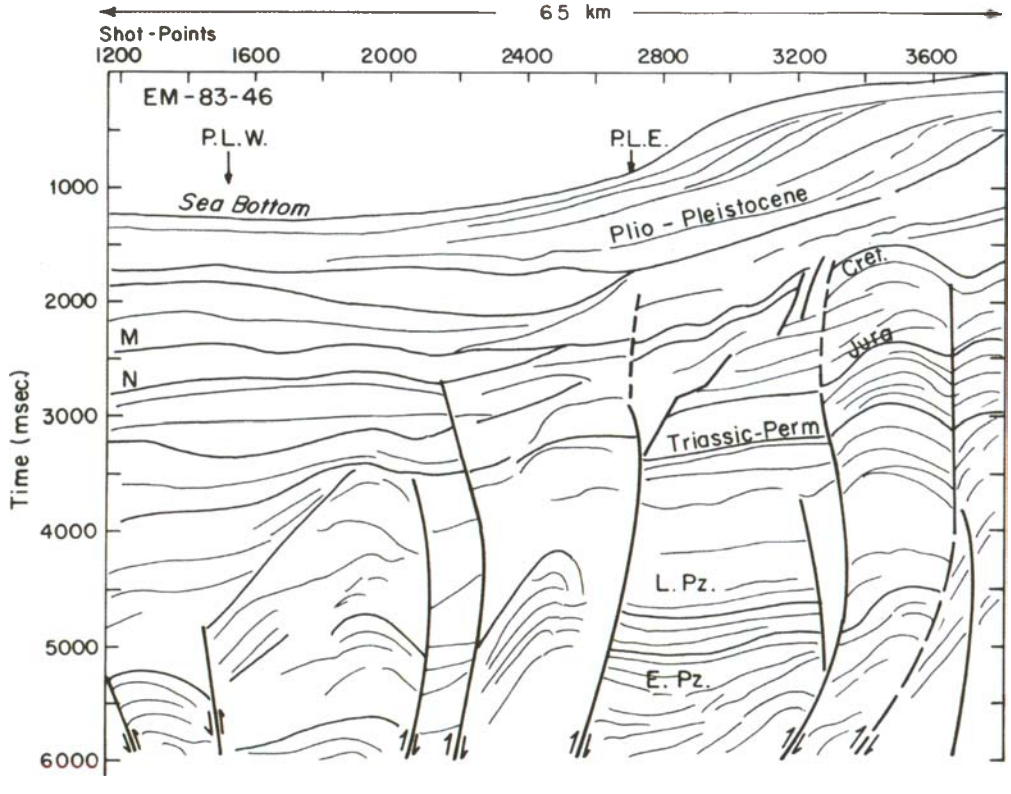
Figure is after Neev, 1975, Fig. 1, and Neev et al., 1976, Fig. 25.

Background shaded relief is the gridded bathymetric chart of the Eastern Mediterranean (Hall, 1994) with the 90 m DTM of Israel, 30 m ASTER data for southern Lebanon, and ACE satellite altimetry at 0.5' for northern Sinai. Mercator projection.

(a)


traceDisplay.exe
File View Animation Picking Help
CDP
200 1400 1600 1800 2000 2200 2400 2600 2800 3000 3200 3400 3600
Line EM -83 -46
Time (ms)
500 1000 1500 2000 2500 3000 3500 4000 4500 5000 5500
MB1 = Add/Move, MB2 = Delete, MB3 = Edit
Button Up inside = Complete, Button Up outside = cancel

(b)


65 km
Shot-Points
1200 1600 2000 2400 2800 3200 3600
EM-83-46
P.L.W.
P.L.E.
Sea Bottom
Plio-Pleistocene
Cret.
Jura
M
N
Triassic-Perm
L. Pz.
E. Pz.
Time (msec.)
1000 2000 3000 4000 5000 6000

data and arguments both for and against presented by Neev (1960) and Druckman et al., (1995), we mention herewith the following two new aspects:

i) Four analogous cases of large-scale vertical oscillatory tectonic movements are reported at the end of this sub-chapter. The first two concern Eratosthenes Seamount and the Mount Sinai Massif-Suez Graben (which are associated with the Pelusium System of Geosutures). The other two are from the Ionian Basin and adjacent mountains (Tunisia; Calabria-Sicily), as well as from the Equatorial Fracture Zones of the Atlantic Ocean.

ii) The approximately 100 km long on-land part of the Afiq Channel stretches between the Edom Mountains (east of the Arava Valley) in the SE, and the Mediterranean coastline (Gaza) in the NE (Figs. 22.15 and 22.21). On its track it is breaching through at least five chains of structures (Hazera, Hatira, Boqer, Beersheva, and the Beeri-Heletz one). The breaching of each of these structures had to involve both hydraulic milling of the very dense carbonate rock members within the Early to Middle Cretaceous age sequence, and formation of a much narrower V shaped canyon, as well as by a chemical dissolution process of that thick (100 m) to very thick (1000 m) sequence (Druckman et al., 1995, Figs. 1, 2, 3, and 10; Neev, 1960). The thalwegs of these entrenched segments are always forming large-scale meanders, thereby indicating a decrease in hydraulic velocities (and therefore also of the milling output). Chemical dissolution may take part in the process only if meteoric water is involved. Under such circumstances the probability of a submarine breaching process is appreciably reduced.

The sub-bottom configuration of the offshore segment of the Afiq Canyon is inferred from the study of the contours of the Yafo Formation's (Pliocene to Early Pleistocene) isopachs (isochrons). The information appears in two seismic profiles, one of which extends along the coastline, whereas the other one stretches diagonally northward from the coastline. Both of them are trending close to right angles to the channel (Druckman et al., 1995, Figs. 3 to 7). The integration of the isopachs and reflection data expresses the pattern of a rectangular box-shaped valley entrenched due to repetitive cut and fill processes. These features were incised through the offshore post-Oligocene to Pliocene sedimentary sequence apparently composed of soft (less cohesive) deposits. The width of the offshore segment of the Afiq Canyon (following Druckman, *ibid*) increases from close to 10 km along the coastline (north of Gaza) to about 15 km, some 20 km offshore.

A coast-parallel (SSW-NNE) spark-array seismic profile (#90A in Fig. 12 of Neev et al., 1976), running approximately along the 450 m isobath, revealed a system of gaps or scars formed by down-slope gravitational sliding of the uppermost 50 m (or less) sedimentary layer (representing the Holocene and perhaps the uppermost Pleistocene sedimentary sequence). Only one coast-perpendicular trending fault line (whose throw is not more than 20 m) was indicated to have crossed the close to 40 km long profile. Our interpretation then and now is that the present-day shelf-break off the coast of Israel is a new hinge line formed because of a rejuvenated phase of subsidence of the eastern Mediterranean Basin. That interpretation is similar to ones arrived at by Finetti and Morelli (1972) and Stanley et al. (1974).

A system of eastward asymmetric small-scale folds are often noticed across the shelf-edge and somewhat west of it (**Figs. 22.17** and **22.18**; Neev et al., 1976, Fig. 12, Profile #40; Almagor and Garfunkel, 1979, Fig. 7, Profile Teledyne-44). We interpret these small asymmetric folds to result from the recent to sub-recent westward warping of the more compacted underlying layers. The latter are being pulled downward and westward (seaward) because of the bending of the shelf (see above). That westward dragging effect on the overlying semi-consolidated sediments is decreasing away from the contact between these two layers (*i.e.* upward).

Box-shaped valleys are also generated on land in subaerial environments (although by hydraulic mechanisms such as those acting between the sharp lateral limits of the actual erosional gorge along the Jordan River). It is being entrenched into the flat, fragile, and well-stratified sedimentary sequence of the Late Pleistocene Lake Lisan. That process occurred following the shrinkage of that lake from the level of the Sea of Galilee (-150 to -200 m m.s.l.) to the level of the Dead Sea (-400 m to more than -700 m m.s.l.) during the Early Holocene.

Based on the configuration of reflection time contours from mean sea level to Horizon M (Messinian or Late Miocene), we consider the total length of the Afiq Canyon's offshore segment to be close to 50 km (Almagor, 1980, Fig. 9). It extends from the Nahal Oz well - 5 km east of the coastline - in the SE, to the Pelusium Line in the NW. The thickness of the Yafo Formation (Plio-Pleistocene) and the Kurkar Group (Plio-Pleistocene) along the canyon trough is close to 1100 m at Nahal Oz and increases to 2200 m in the present-

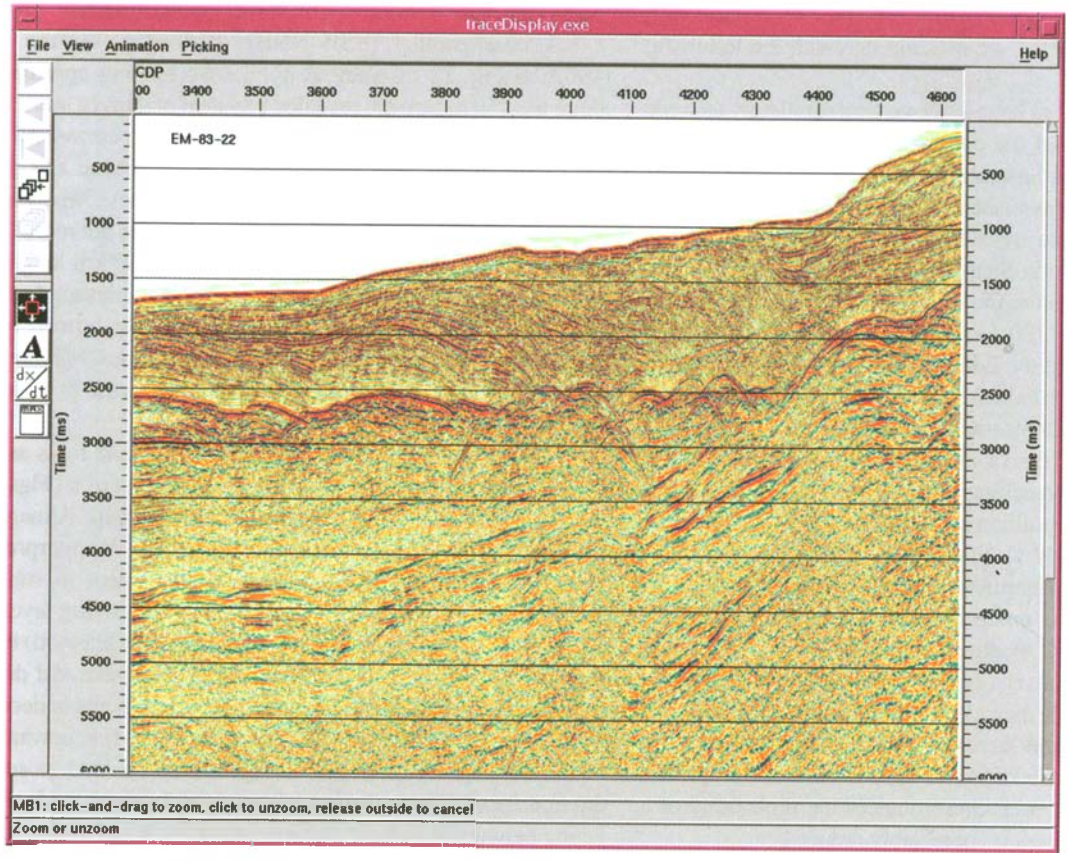


Figures 22.17a and b. CDP Profile EM-83-46: Coast-perpendicular seismic reflection profile off southern Israel, with its geological interpretation (Fig. 22.17b). See Fig. 22.15a for location. Most of the Phanerozoic sedimentary sequence is expressed by the recovered reflectors. Two rather abrupt thickness as well as facies changes are noticed across that seismic profile. One is at the lower Continental Slope (below SP2800 where the P.L.E. - Pelusium Line East is marked) and the second is beneath SP3600 within the Mid to Outer Shelf zone. These sharp changes suggest a genetic association of the tectonic phases and the pre-Neogene coast-parallel subsidence of the offshore basin. The involvement of sinistral shifting (*i.e.* a more intensive northward movement of the Central Plate), could also occur.

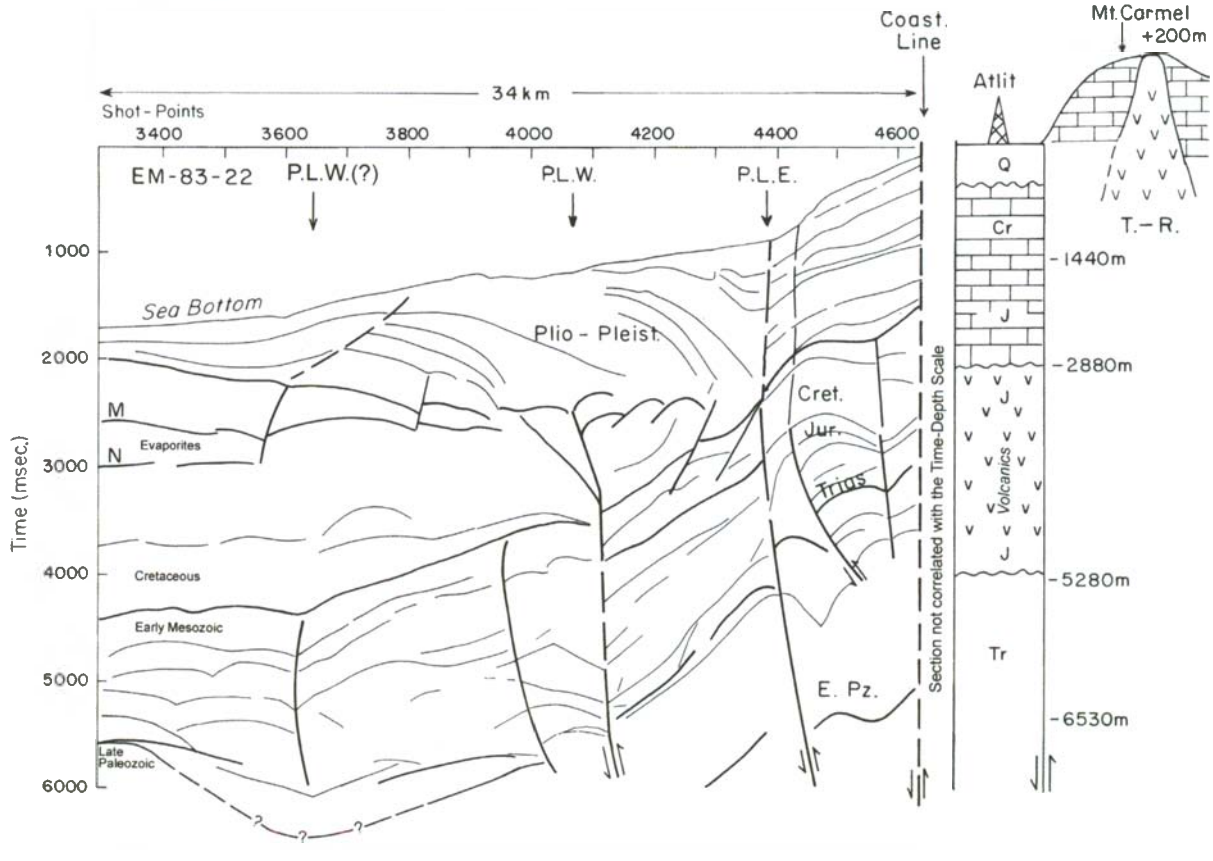
It is also implied from the configuration of the post-M (Mio-Pliocene) reflectors, as well as from the data of Fig. 22.16 (see above), that the tectonic subsidence of the eastern Mediterranean Basin, as well as the eastward tectonic rise of the Central Plate, occurred during the following three phases: Late Jurassic, Top Turonian, and Early Oligocene.

The Offshore Structure #1 is situated beneath the Shelf Break (~SP3500). Profile provided courtesy of the Israel Ministry of National Infrastructures, and the Geophysical Institute of Israel.

(a)


traceDisplay.exe
File View Animation Picking Help
CDP
3400 3500 3600 3700 3800 3900 4000 4100 4200 4300 4400 4500 4600
EM-83-22
Time (ms)
500 1000 1500 2000 2500 3000 3500 4000 4500 5000 5500
MB1: click-and-drag to zoom, click to unzoom, release outside to cancel
Zoom or unzoom

(b)


Coast Line
Mt.Carmel
+200m
Atlit
34 km
Shot-Points
3400 3600 3800 4000 4200 4400 4600
EM-83-22
P.L.W.(?)
P.L.W.
P.L.E.
Sea Bottom
Plio-Pleist.
M
N
Evaporites
Cretaceous
Early Mesozoic
Late Paleozoic
Cret.
Jur.
Trias
E. Pz.
Time (msec.)
1000 2000 3000 4000 5000 6000
Section not correlated with the Time-Depth Scale
Q
Cr
J
Volcanics
Tr
T.-R.
-1440m
-2880m
-5280m
-6530m

day shelf-break (Druckman et al., 1995, Figs. 2 and 3) which may increase to more than 2500 m across the Pelusium Line in the northwest. The stratigraphy of the canyon's fill indicates the pre- or early Oligocene age of the first erosional phase which eroded that canyon in the offshore (Neev, 1960; Druckman et al., 1995, Figs. 4, 6, and 7). Since then large quantities of coarse to fine detritus were transported to the abyssal plain to be deposited along a linear NNE trending trough, formed along the Pelusium Line, which is sub-parallel to the Jebel Moghara-Heletz-Ga'ash chain of structures. It also marks the contact between the continental and oceanic types of crust, as well as between the continental rise and the abyssal plain.

The trend of the offshore segment of the Afiq Channel is, however, NW-SE, which coincides with the Afiq-1-Gaza-1 wells,. It also parallels the NE dipping flanks of the Nezarim offshore northwestward nosing structure (Druckman et al., 1995, Fig. 3). This feature could express a northwestward trending thrust-fault that extends (perhaps in an *en-echelon* way) a northward thrusted fault line interpreted by a deep seismic-reflection survey between the Beeri structure and the NW-SE trending segment of the Afiq Canyon (L. L. Greenfield, pers. comm.). We therefore suggest that the entire offshore segment of the Afiq Canyon is fault-controlled. The outer half of the discussed offshore segment seems to curve slightly to the north, *i.e.* parallel to the trend of the Pelusium Line - (indicated by the slight but systematic kinking of bathymetric contours, thereby forming a slightly curving depressed belt some 15 km wide across the continental slope) (Almagor, 1980, Figs. 2 and 9).

It should be stressed that the NW trending Palmahim Disturbance (or Graben), whose width is the same order of magnitude as the offshore segment of the Afiq Channel, is also a depressed belt. Neev (1975) and Neev et al. (1976) interpreted the Palmahim Disturbance to be a tectonic depression similar in origin to the NW trending Red Sea, Wadi Sirhan, and Mt. Carmel-Wadi Faria tensional features. Nevertheless, following a newly processed version of the EM-83-05 (**Figs. 22.19** and **22.20**) coast parallel seismic-reflection profile (see Fig. 22.15 for location), it is now suggested that both NW-SE trending border faults of the Palmahim Disturbance are high-angle northward thrusted faults and not gravity-normal faults. Garfunkel et al., (1979, Fig. 5) considered that the coast perpendicular Palmahim, Afiq (Gaza), and Dor disturbances were formed during the Late Eocene-Oligocene upheaval period, and their origin is associated with large slumps triggered by halokinetic movements of the Late Miocene rock-salt deposits (or 'rootless' structures). They also note that "deeply rooted Neogene-Quaternary faulting was not identified south of the Carmel Nose". We do not agree with the above conclusions, as we think that both the slices of the Sinai-Israel-Lebanon and their adjacent Continental Margin, were subjected to a compressional regime at least since early Mesozoic and probably even since the Late Percambrian.

We prefer to discuss the three on-land segments of the Afiq Canyon as one single 120 km long river, extending from the western outlet of the canyon (away from the Beeri-Heletz breach at the Nahal Oz well) through Beersheba, as far east as the Jordanian



Figures 22.18. CDP profile EM-83-22. A similar interpretation to that of Fig. 22.17 is presented herewith for another coast-perpendicular seismic reflection profile situated farther to the north, off Atlit adjacent to Mount Carmel. See Fig. 22.15a for location. The Pelusium Line West (P.L.W.) could in fact be situated farther on to the west (marked P.L.W.(?), between SP3600 and SP3700).

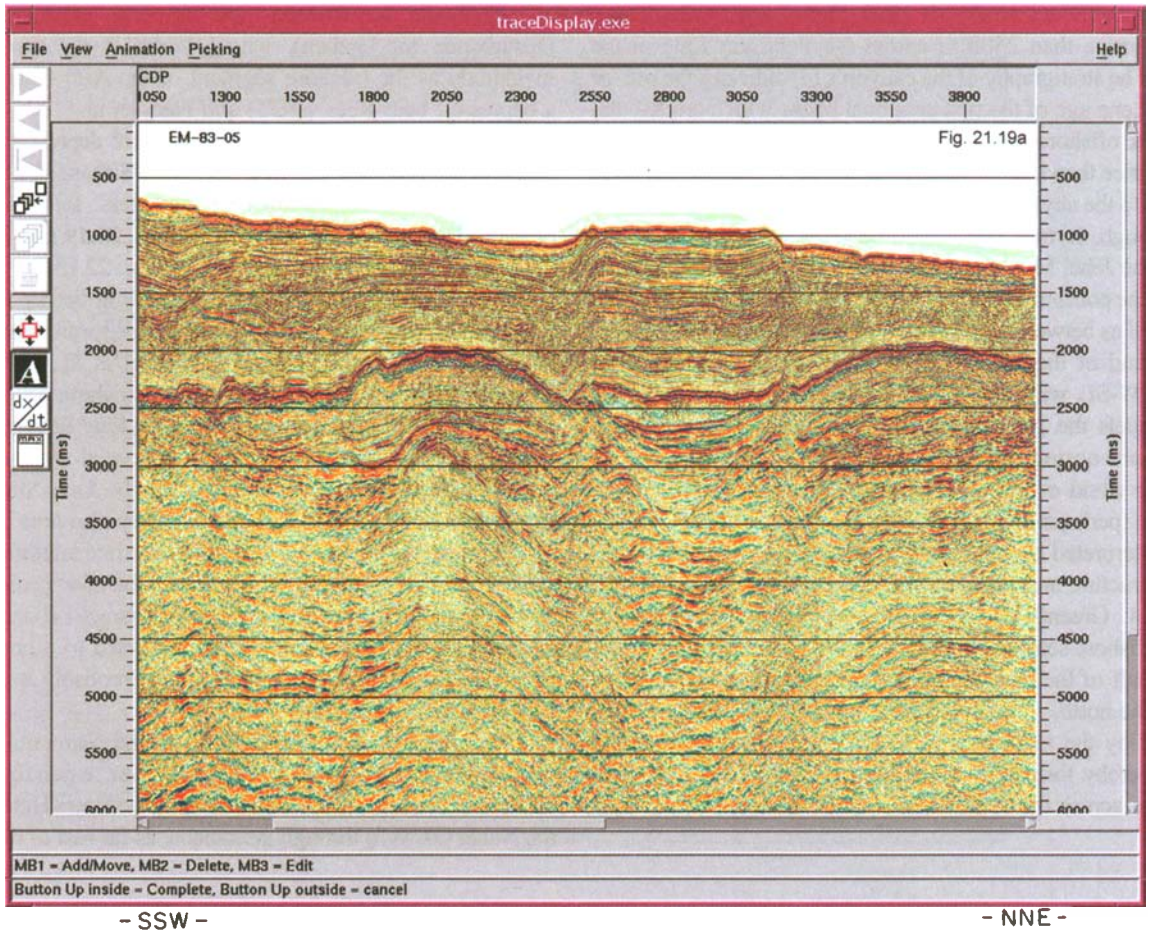
The westward tilted Cretaceous-Early Mesozoic contact abruptly attains a horizontal orientation at SP3600 at a depth of 4400 msec. An even deeper structural trough is indicated below that point, which is a broad coast-parallel syncline. The deepest reflectors identified across that trough are at time (depth) values of more than 6 sec.

The same trough also seems to exist along the seismic profile off southern Israel (Fig. 22.17 between SP1200 and SP2600). However there is an important difference between the above two structural set-ups in the south and north. In the south the entire sedimentary sequence beneath the top Cretaceous belt had subsided at about the same rate all across a relevant segment beginning in the mid-shelf and westward to the end of that profile (Fig. 22.17 – see also Neev et al., 1976, Fig. 3 that covers the shelf from the littoral to the upper slope). However, in the north (Fig. 22.18) the Earth's crust has gradually been tilted westward at least from the upper 'slope' as far as the trough of the syncline SP3600). The implied westward thickening process of the entire pre-'M' sedimentary sequence has been maintained perhaps since early Phanerozoic time.

Profile provided courtesy of the Israel Ministry of National Infrastructures, and the Geophysical Institute of Israel.

Figures 22.19 and 22.20. North-South CDP Profiles across the Palmachim Disturbance: The south to north compressional effort seems to be the chief factor in creating the Palmachim Disturbance. The second factor could be the apparent pre-existence of two transverse faults across the shelf and slope. The main effect is the wedge-like subsidence of the block bound between the two transverse faults. The result is a compressional graben. The bulging up of the stratigraphic sequence above the 'M' Reflector could be associated with both an excessive accumulation of evaporites within the Palmachim Graben, as well as the flowing property (or tendency) under pressure of these sediments. Figure 22.20 is an enlarged part of the N-S seismic reflection profile across a more southerly part of the Palmachim Disturbance. It enables the reader to analyze the upper part of the latter more conveniently (see also Neev et al., 1976, Fig. 14 - three successive coast-parallel seismic profiles across the Palmachim Disturbance).

Profiles provided courtesy of the Israel Ministry of National Infrastructures, the Geophysical Institute of Israel, and Dr. Y. Folkman, ISRAMCO Oil Exploration Ltd.


traceDisplay.exe
File View Animation Picking Help
CDP
1050 1300 1550 1800 2050 2300 2550 2800 3050 3300 3550 3800
EM-83-05
Fig. 21.19a
Time (ms)
500 1000 1500 2000 2500 3000 3500 4000 4500 5000 5500 6000
MB1 = Add/Move, MB2 = Delete, MB3 = Edit
Button Up inside = Complete, Button Up outside = cancel

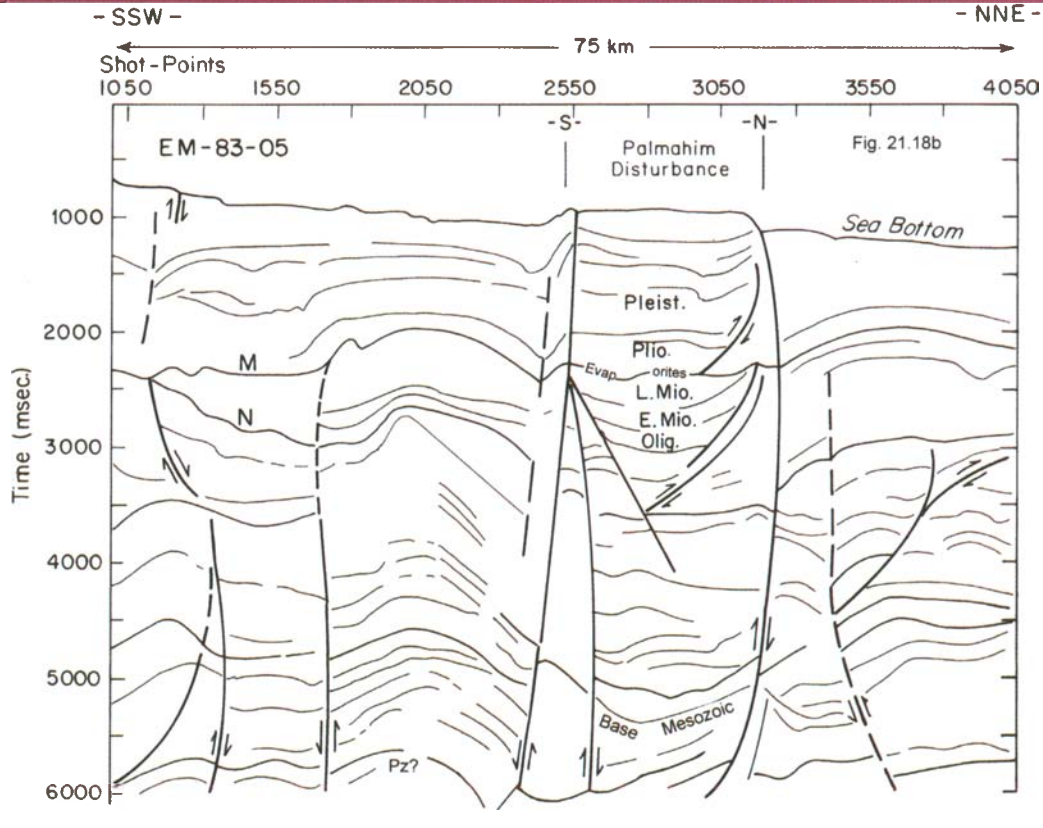

- SSW -
- NNE -
75 km
Shot-Points
1050 1550 2050 2550 3050 3550 4050
-S-
-N-
EM-83-05
Palmahim Disturbance
Fig. 21.18b
Sea Bottom
Pleist.
Plio.
Evap.
orites
L. Mio.
E. Mio.
Olig.
M
N
Base Mesozoic
Pz?
Time (msec.)
1000 2000 3000 4000 5000 6000

Fig. 22.19.

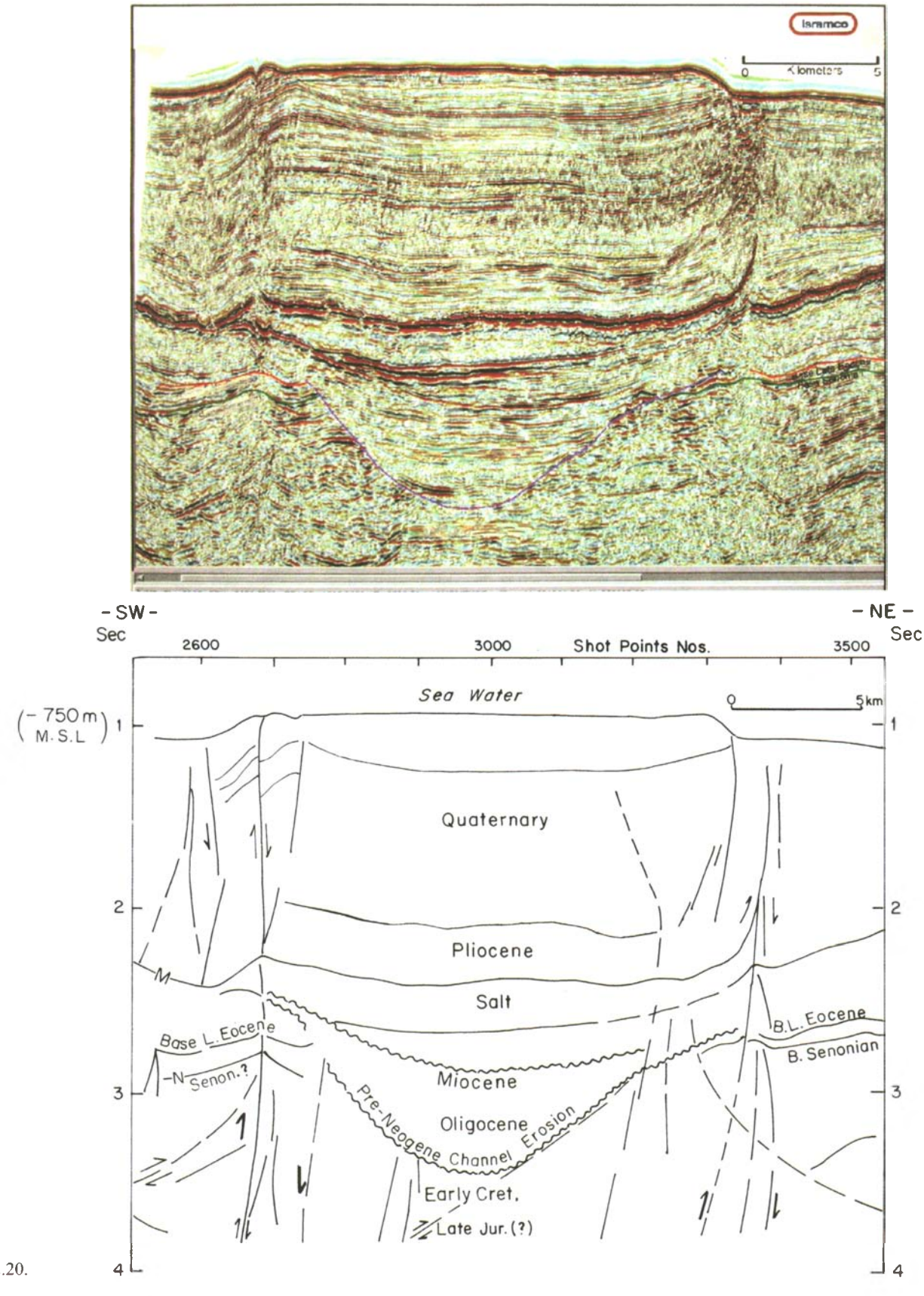

Isramco
0 Kilometers 5
- SW -
Sec
- NE -
Sec
2600
3000
Shot Points Nos.
3500
Sea Water
0 5km
(- 750m M.S.L)
1
2
3
4
Quaternary
Pliocene
Salt
Base L. Eocene
-N-Senon.?
Miocene
Oligocene
Pre-Neogene Channel Erosion
Early Cret.
Late Jur. (?)
B.L. Eocene
B. Senonian

Fig. 22.20.

(Moab) Plateau. Along the easternmost 40 km sub-segment the pattern is changing in the following way: A narrow V shaped gorge is found where the river breached the dense Cretaceous dolomite anticlines. Further west, across the synclines, the river widened to a few km both southward and northward, occasionally forming intermediate lakes more than 10 km long. Fresh water sediments and megafauna, including relics of hippopotamuses and horses of Middle Miocene age were deposited within the Rotem Basin (between the Hatira and Hazera anticlines - Fig. 22.15b) at the present-day elevation of +350 m to +400 m (Neev, 1960). In the next basin to the west (the Yerouham Basin) a marine intercalation is indicated by the presence of a Crassostrea bed of Middle Miocene age within marls and chalks, interbedded by continental reddish sands up to elevations of +500 to +570 m (*ibid*). As that elevation is much above the +100 to +150 m level (as indicated by the eustatic curve of Fig. 4 of Druckman et al., 1995) it is implied that its present-day high elevation is due to tectonic compressional uplift movements which were induced due to the northward differential *en-echelon* movements across the Levant and Eastern Mediterranean (the western flanks of the Central Plate) and occurred sometime in post-Miocene time.

Early Pleistocene mammalian fauna (including hippopotamuses) are present near Bethlehem (80 km north of the Rotem Basin and less than 10 km south of Jerusalem) at the present-day elevation of close to +800 m m.s.l. That faunal assemblage is of an aquatic (swamp) environment, thereby suggesting a very low relief and an elevation that is close to mean sea level at the time of deposition. These data suggest a differential tectonic uplifting movement that lifted up the Structural Backbone of Israel (close to Jerusalem) by about 800 m since the early Pleistocene. The Crassostrea bed of the Yerouham Basin could also have been uplifted during the same tectonic 'Phase D' (Neev, 1960, p. 19, and the 'Additional Note', p. 21).

An E-W trending multi-channel seismic profiles (Neev et al., 1985, Fig. 12.5, DS-618), extends westward from the Ga'ash #1 well on the coastline to a distance of 10 km. A pronounced eastward diverging pattern is exhibited by the different reflectors; the uppermost one is the Neogene-Cretaceous angular unconformity. On land the Neogene beds are close to horizontal and wedging out sequentially eastward toward the westward-dipping unconformable surface of the Cretaceous-Eocene complex. The Cretaceous-Jurassic and Jurassic-Triassic reflectors are still dipping to the west but the relevant westward angles are decreasing downward. The base Triassic- (or Late Permian)-Late Precambrian basement (or the top of the Infracambrian sedimentary sequence) contact (at a depth of 3 seconds beneath the Ga'ash #1) is pronounced by a seismic reflector which is more prominent than those recognized above it (up to the Top Triassic reflector). The dips of the in-between reflectors are gradually decreasing downward. The 'Base Triassic' reflector under Ga'ash #1 (at the Mediterranean coastline) is already dipping eastward. A sequence of eastward dipping sub-parallel reflectors is recognized down to a depth of 4 seconds at the eastern end of that seismic profile. These differences in time values could be numerically tripled when translated into thicknesses (*i.e.* up to a few km of eastward thickening).

Weissbrod (1969) as well as Gvirtzman and Weissbrod (1984) interpreted the unconformable long hiatus contact identified at Heletz between the Late Permian and the Precambrian basement as extending eastward and southeastward as such, as far as the Ramon #1 deep hole in the Central Negev, where it overlies the Infracambrian arkosic-detrital Zenifim Formation. This in turn overlies the Precambrian basement at the bottom of that well. These authors consider the above unconformity to represent a regional event of non-deposition that took place over most of the Levant due to large-scale phase of tectonic uplift.

We do not agree with the above interpretation because of the significant indications for the existence of an ancient N-S (or NNE-SSW) trending paleo-geosynclinal axis that underlies the Shekhem-Ramallah-Hebron Arch. Based on the stratigraphic data from the Ramallah #1 well and the seismic data recovered from profiles east of Ga'ash #1, as well as the deep N-S trending seismic reflection profiles carried out along the Coastal Plain of Israel to the east of the Heletz-Ga'ash uplift, our interpretation is given below.

Even if the Permian to Early Paleozoic sedimentary sequence had not been deposited along the southern extension of the Paleo-Trough (*i.e.* across that area of the northern Negev, situated to the south of the E-W trending Hebron positive magnetic anomaly - as suggested by Gvirtzman and Weissbrod, *ibid*), there are data suggesting the discussed segment to have functioned as a tectonically subsiding trough during Early Mesozoic (Triassic-Jurassic) time.

Druckman et al. (1995b) have studied the subsurface geology and the structural evolution of the northwestern Negev (southern Israel) by correlating the detailed stratigraphy (mostly from ten deep boreholes) with the interpreted 2000 km cumulative length of seismic reflection profiles. We imply from their figures, especially the structural map on Top Turonian and the isopach maps of the Triassic, Jurassic, and Early Cretaceous (Figs. 3 to 10), the following points regarding the geological history of the studied 2200 km² area (a rectangle 40 km long by 55 km wide south and southwest of Beersheva):

i) The isopach maps of the Triassic and Jurassic formations indicate continuous functioning of basically the same tectonic processes that have produced elongated compressional ridge and basin features along which differential rates of deposition took place. Along that paleo (Triassic-Jurassic) NE-SW trending system of anticlines and synclines of the 'Syrian Arc', alternating sequences of respective thinning and thickening processes have occurred.

ii) Comparison of the Top Turonian structural map across the discussed study area with the Triassic-Jurassic map, indicates that the structural pattern of that same area was inverted during the Levantine (Senonian-Eocene) folding phase. The message of that inversion process is that the pattern of anticlinal axes was already formed during Triassic-Jurassic time but were inverted into synclinal ones during the Senonian-Eocene and younger folding phase. It is therefore implied that the basic regional tectonic pattern was maintained since Early Triassic time and perhaps even earlier.

The above conclusions, based on good and sufficient stratigraphic and seismic reflection control, substantiate the inversion model presented by Freund et al. (1975).

Freund et al. (1975, after Picard, 1959; Grader, 1960; Weissbrod, 1969; Goldberg, 1970; Gvirtzman and Klang, 1972; Goldberg and Friedman, 1974; Derin, 1974; Druckman, 1974; Cohen, 1979; and a pers. comm. by E. Aharoni, 1967) showed that the dominant tectonic features along the present-day mountain ranges of Samaria and Judea (*i.e.* the 'Structural Backbone of Israel' - D. Neev, 1960) are the rapid subsidence and the accumulation of a few km thick sequence of sediments. That deep trough extended northward into the Galilee and Lebanon, as well as southwestward along the Qeren-Halutza depression and perhaps even farther away along an ancient axis (a trough situated between the present-day Moghara-Anieza and Yaaleq-Hillal structures). In their map of the Late Jurassic distribution pattern of 'lows' and 'highs' (Freund et al., *ibid*, Fig. 1) they show the Heletz-Ga'ash structural high (their Nirim-Beer Ya'aqov-Carmel 'horst') separating the East Mediterranean large basin from the El Khabra-Qeren-Halutza (-Judea-Samaria-Galilee) depression. Freund et al. (*ibid*, p. 20) also adopted the interpretations of Picard (1959) and of Gvirtzman and Klang (1972) regarding the definition of the coast-parallel boundary between the Nirim (Heletz)-Beer Ya'akov-Carmel coastline horst and the East Mediterranean large basins, as a large and deep-seated fault zone (the western fault of the Heletz structure).

Freund et al. (*ibid*) and Druckman et al. (1995) consider the origin of the early Mesozoic subsidence along the Ramallah-Hebron-North Central Negev trough to be related to a regional extensional tectonic process. However, they relate the tectonic inversion, and the associated Senonian-Eocene folding phase of the Syrian Arc, to a regional compressional phase. They relate the Extensional Phase to regional rifting associated with the opening of the Neotethys, and the inversion process and the compressional phase to the collision of Africa and Eurasia. Druckman et al. (*ibid*), quoting Best et al. (1993) and Chaimov et al. (1993), note that their two phase model also applies to the SW Palmyride fold belt of southern Syria.

We have the following remarks concerning the above data and interpretation (based on Druckman et al., 1995b):

i) The different isopach and structural maps and cross-sections presented (Figs. 4 to 14) show the dominance and consistancy of NE-SW trending structural features across the study area during the entire period of time since the Triassic.

ii) The earliest indications for the initiation of the structural inversion process from the interpreted NW-SE trending seismic reflection profiles EM-7726 (and EM-7728) as well as the cross-section B-B' (Fig. 14) are the Early Cretaceous (Figs. 11 and 14). It is possible, however, that an even earlier indication is offered by the change in the thickening pattern from an eastward direction during the Triassic (Fig. 4) to a westward or NW one during the Early Jurassic (Fig. 5).

iii) We have tried, but failed, to find field evidence (from the literature) to justify the authors' postulation regarding the southward drift of the joined African-Arabian continent during Jurassic time (except for paleomagnetic measurements, the interpretation of which we have argued against - see above).

iv) On the other hand we have found indications from the Mediterranean offshore and coastal zone of Israel suggesting the origin and mechanism of the tectonic instability across the contact between the Central Plate (the Sinai sub-plate) and the eastern Mediterranean basin. Examples are the eastward asymmetric folding and thrust faulting of the anticlines there, such as in the Heletz-Ga'ash structural high, as well as their association with the oscillatory down and up large-scale tectonic movements across it.

v) There are indications for the functioning of the Sosink Graben (SE Turkey) as a tectonically subsiding N-S zone which extended southward as far as central Jordan, since early or mid-Cambrian times (see below).

Interpretation of a new multi-channel S-N seismic profile that parallels the Mediterranean coastline of Israel some 10 km east of the Heletz-Ga'ash structural high feature (location marked as DS-3589 on our Fig. 22.15a), indicates the occurrence of a significant northward thickening of all the pre-Cretaceous sedimentary sequence. The pre-Permian sequence, which is close to 2.5 seconds thick at the northern end of the profile, is wedging out completely toward the southern half of that profile. It begins close to the Huldah #1 well (some 30 km NE of Heletz #1, Fig. 22.15a) and extends to the NNE as far as a point a few km to the SE of Caesarea.

We infer from the integration of all the above data that:

i) The axial zone of the Paleo-Trough extends from northwestern Sinai at least as far as the Yizre'el (Jezreel) Graben in the north. Deepening occurred, as well as thickening of the entire Paleozoic sequence beyond (and northward of) the E-W trending positive Hebron Magnetic Anomaly (Fig. 22.15a);

ii) That structural-stratigraphic pattern has functioned at least since Early Paleozoic time.

The E-W and SE-NW trending Transverse Faults of the Negev and Sinai (Fig. 22.15b - see above).

For a proper interpretation of the tectonic oscillations across the Sinai sub-plate it is important to bear in mind the mutual influence of the following two systems of folds and faults (which are close to perpendicular trending to each other):

i) The NNE-SSW trending system of geosutures situated between the Pelusium Line on the west and the Dead Sea Transform on the east;

ii) The E-W trending faults.

These same two systems also occur across the Jordanian territories (or at least its western half – Y. Bartov, pers. comm.).

The latter system includes the following five members, and five main E-W trending, northward thrusting and dextrally shifted faults, often associated with folding, as described below:

1) The large Hebron-Gaza positive magnetic anomaly (Rybakov et al., 1994) extends westward from the Dead Sea (west coast of the northern basin) through Hebron as far as the Mediterranean coastline east of Gaza. The highest value of that anomaly is +289 nT (nanoTesla, or gammas), situated a few km southwest of Hebron. The significance of that E-W trending magnetic anomaly

is in two points. First it reflects a change in basement composition from acidic in the southern part of the Sinai Sub-plate to more basic in the north. Second, the N-S trending paleo-trough is becoming deeper north of it, therefore enabling a thicker sequence of marine Paleozoic sediments to accumulate and be preserved within that basin (although absent south of it — Folkman, 1971, and pers. comm.).

2) The Arad-Beersheva-Rafah E-W trending morphologic-tectonic trough is characterized by the extremely straight linear east-west trending contours of magnetic intensities (between -50 and -100 nT — Rybakov et al., 1994). That same disturbed feature is also expressed as a large E-W trending kink across the NE-SW trending Bouguer gravity contours (Ginsburg et al., 1993):

3) The E-W trending boundary between the large blocks of the Hatira and Hazera anticlines in the north, and the Ramon anticline in the south, is forming a 20 to 30 km wide belt which is limited by two E-W tectonic lines on its north (3a) and south (3b); the Nahal Zin and the Sa'ad-Nafha-Jebel Halal E-W trending faults –after Eyal et al. (1980, 1985, Fig. 9);

3a) It extends between the Hazeva-Arava Rift in the east to Romani-Suez in the west. It is composed of segments of faults, each of which is systematically shifted northward with respect to its neighbor to the east. The discussed E-W fault zone is composed of individual small elongated domes. The easternmost limit is at Ein-Hazeva (northeast corner of the Arava valley), passing through the NE plunging noses of the Hazera, Hatira, Boqer, and Qeren anticlines, to jump southwestward in a dog-leg fashion. It continues along the E-W tectonic lineament of Nahal Lavan-Wadi Azariq Harreidin-Bir-Lakhfan, straight westward along the NE plunge of the Risan Aneiza anticline as far as Romani (close to the western tip of the Bardawil Lagoon and 33 km east of the Suez Canal, 31°-00'N, 32°-40'E), where it terminates at its junction with the Pelusium Line.

3b) The northern boundary of the Ramon anticline is marked by an E-W trending depressed belt across which south to north compressional movements took place. A linear system of separate structural domes is situated along that depression. It begins at the Marzeva Dome, within the Arava Graben in the east, and continues through the domes of Enmar, Geraphon, Sa'ad, Nafha, Qemer, Hamran, Qadesh-Barnea, and Jebel Er Risha, then along the northern plunge of the Jebel Halal anticline, separating Risan Aneiza from the large NE-SW trending Jebel Moghara anticlines in the west;

4) The Nahal Paran-Be'er Menuha fault begins at the Dead Sea Rift Valley in the east to continue westward and alternate with Nahal (Wadi) Karkom north of Jebel Araif En Naqa as far as Jebel Burqa (30°-25'N, 34°-20'E). At that point the Paran transverse fault bifurcates into two branches: A WNW trending branch along the narrow ridges of Sherif, El-Bidan, El-Mitmatni, and El-Abeiriq which terminates at the tectonic trough separating the NE-SW trending major anticlinal blocks of the Jebel Hallal and Jebel Ya'alaq; The second branch curves southwestward along Wadi El-Bouruq and Wadi Sudr (between Ras El Jundie in the NE and the outlet of that wadi into the NW-SE trending Suez Graben).

5) An E-W trending fault from Evrona (South Arava at 29°-40'N, 35°E) to Wadi Sudr (Gulf of Suez 29°-40'N, 32°-50'E) is the southernmost member of the discussed transverse fault system. It extends westward from the large N-S trending western border fault escarpment of the Arava-Dead Sea Rift along the E-W trending Wadi Alaliq fault line that sharply separates the acidic Precambrian volcanic field in the south from the Cretaceous dolomites and chalks in the north. It was named the Thamad Fault by Garfunkel and Bartov (1977). That fault further extends westward by curving mildly west-northwestward as far as 29°-50'N, 33°-40'E (just south of Nakhl), from whence the curvature gradually changes to WSW to terminate at the outlet of Wadi Sudr into the northwest trending eastern Suez Gulf. On its way the westernmost segment (between Nakhl and Ras Sudr) is crossing through the NW-SE trending mountain ridge of Raha-Sumar which separates the Sinai Peninsula from the Gulf of Suez.

The following three points summarize the characteristics of the above five transverse features:

1) Dextral movements took place across all of the members of the E-W trending system of compressional transverse faults and folds studied in the Negev and North Sinai by Neev et al. (1976) and Eyal et al. (1980).

2) The segmented *en-echelon* style of progressive northward positions (from E to W) as well as their northward structural asymmetry, which are maintained along the same course, suggest an origin associated with deep northward flow movements of the underlying upper mantle. The source of energy for such a process does not seem to be found within the lithosphere.

3) The discussed system across Sinai is analogous to that of the transverse E-W faults mapped west of the Suez Canal as well as across the Galilee (in northern Israel). It is not clearly expressed however across Judea (north of Hebron) and southern Samaria (as far as Shchem-Nablus).

IXd: Analogous Occurrences of Large-Scale Vertical Tectonic Movements Associated with Linear Geosutures Across the Mediterranean Sea and the Equatorial Fracture Zones.

IXd$_1$: Eratosthenes Seamount:

Eratosthenes Seamount is a NW-SE trending, 120 by 80 km elliptical feature whose morphological relief exceeds 2000 m (measured from its summit at a water depth -690 m to the abyssal plain to the west at -2700 m). It stretches along the Qattara-Eratosthenes Geosuture (Neev et al., 1985) and is located some 100 km south of Cyprus (Mart and Robertson, 1998). Krasheninnikov et al., (1994) described the results of dredging operations across the western slope of the seamount by the NES Strakhov. Emeis et al. (1996) reported on the drilling of a transect of four holes along its north-south access by ODP Leg 160. The significance of their results, which are relevant to our subject (after Mart and Robertson, 1998; Robertson, 1998), is inferred from the granite rock sample recovered by the Strakhov's dredge. It represents an outcrop of the northward drifting African-Gondwanian Precambrian basement rock at the base of the seamount that could have reached the present-day sea floor as a result of an upward crustal piercing event

associated with destructive deformations (Krasheninnikov et al., 1994, p. 128).

IXd$_2$: The Messinian Event across the Mediterranean.

The Messinian Event took place during Late Miocene to Early Pliocene times, when the Mediterranean sea water was totally evaporated. It was studied by the Deep Sea Drilling Project (DSDP, Leg 42, April-May 1975), and the Initial Reports were edited and published by R. B. Kidd and P. J. Worstell (1978) on behalf of the National Science Foundation. Anhydrite (plus gypsum) and halite deposits of Messinian age were sampled at very different elevations both in the depths of the Mediterranean as well as on-land, and "... the maximum amplitude of the vertical displacement is about ±3.5 km" (Sonnenfeld, 1975, 1981, 1985, Fig. 16.5). But even this value is too small to explain the presence of a Messinian gypsum and anhydrite bed at an elevation of 3000 m in Tunisia (Burollet, 1971, as quoted by Sonnenfeld, 1985).

Messinian brine deposits (rock salts and potassium bearing 'bitterns') are reported by Decima and Wezel (1971) and Ruggieri (1985) in the offshore within the Messina Abssal Plain at the center of the Ionian Basin (35°-50.87'N, 18°-11.78'E) at DSDP Site 374, where the water depth is 4,088 m. The recovery from Core No. 22 that represents the Upper Evaporites was only 4.5 m (see Ruggieri, *ibid*), whereas Core Nos. 23 and 24 were empty. Nevertheless "drilling rates suggest that these intervals also represented penetration through salts". The lower part of Core 22 contains translucent halite crystals in association with polyhalite and kainite, sulphobarite, sylvite, and bischofite minerals (which contain potassium, magnesium, and calcium chloride and sulfide compounds). These characteristics of offshore endbrine deposits are similar to those of the primary potash salts precipitated on-land at Sicily and Calabria: The average bromine content in the halite (320 ppm) and kainite (830 ppm) crystals recovered from DSDP Site 374 are comparable to those found in Caltanissetta, Sicily and Calabria, suggesting all of them to have been precipitated from evaporated seawater.

Although the 'water' depth of the brines during the precipitation process of the above salts was relatively shallow, they were sampled at Site 374 at a present depth of 4,500 m. Considering the average present-day elevation of (i) the endbrine deposits in Sicily and Calabria (which is close to +500 m) and (ii) the 4,500 depth where the similar deposit was found at Site 374 in the offshore, it is estimated that the amplitude of the maximal post-Messinian vertical tectonic movement across these sites should be close to 5000 m.

The large-scale vertical oscillatory movements across the coast-parallel fault of the Heletz-Ga'ash geosuture (along the eastern Mediterranean coast of Israel) as well as those across the Qattara-Eratosthenes geosuture, should be analogous to the ones associated with Sicily, ODP Site 374 and Calabria, which are situated on opposite sides of the Ghadames-Tripoli (Libya)-Messina-Sestri geosuture. The order of magnitude of these other vertical oscillatory movements in the Mediterranean region (see above) is the same.

IXd$_3$: The Equatorial Fracture Zones of the Atlantic Ocean.

Large-scale up and down oscillatory tectonic movements, the amplitudes of which are on the order of 2 to 3 km, occur across the Equatorial Fracture Zones of the Atlantic Ocean at least since Miocene times (Bonatti, 1973, 1978, 1990; Bonatti et al., 1977; and Bonatti and Chermak, 1981).

The history of vertical movements, as documented at the Romanche Fracture Zone, may represent similar events of vertical tectonism, known to have also occurred along other large oceanic fracture zones. The Romanche F.Z. was initiated across the Mid-Atlantic Ridge at about 25°W, when its depth was close to 3 km below sea-level, as estimated according to the Sclater et al. (1971) age/depth curve (Bonatti et al., 1977). Since Miocene time the study area along the Romanche F. Z. has drifted eastward and simultaneously also moved upward. As inferred from the results of sedimentological-paleontological analysis of dredged samples, it had risen close to sea level by 5 MaBP.

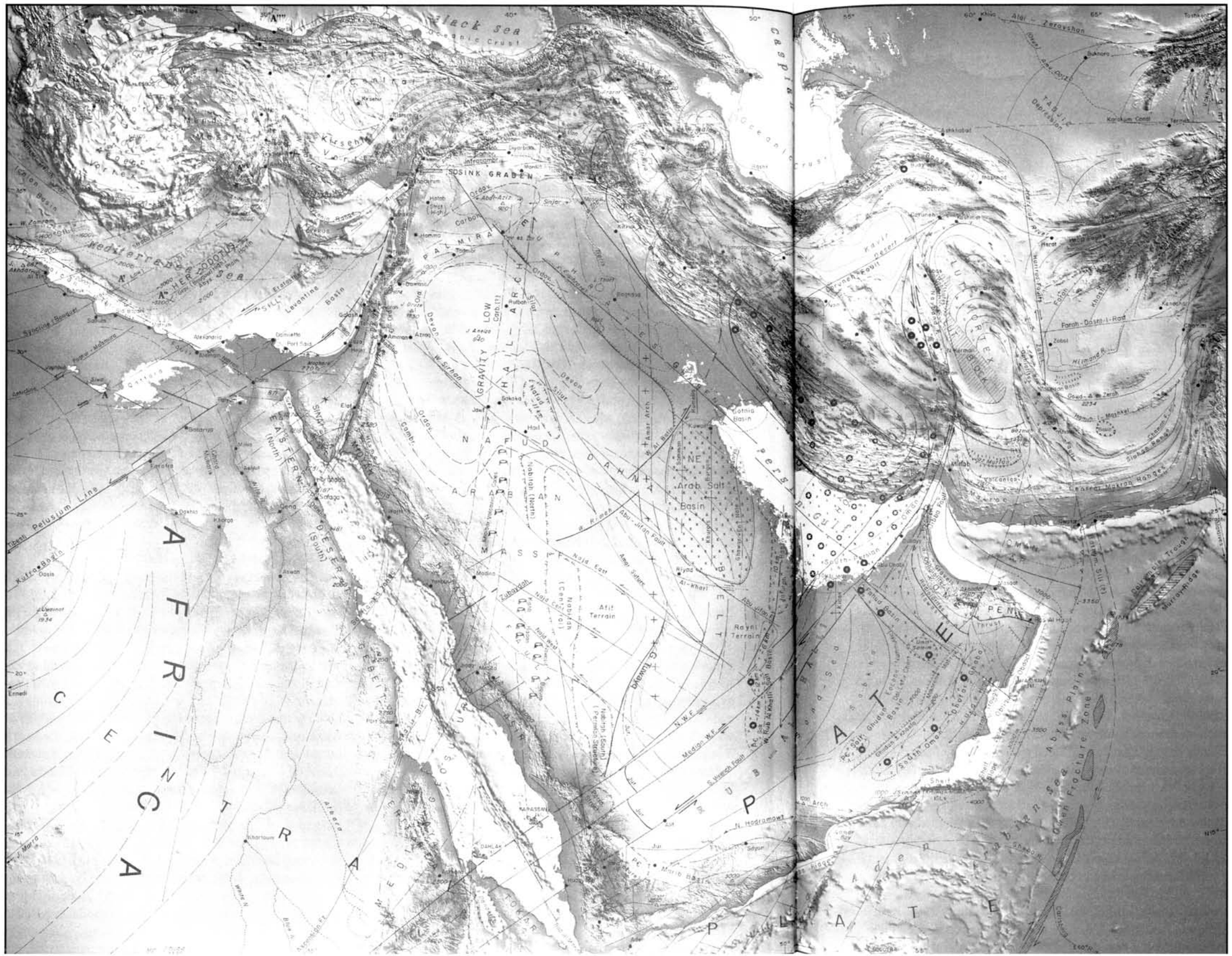
During the past 5 Ma that study area continued drifting eastward as far as its present location which is close to 900 km farther eastward, away from its point of origin at the axis of the Mid-Atlantic Ridge. During the same 5 Ma period that study area also subsided from the Mio-Pliocene ocean-level to the water depth of 950 to 1300 m below present sea level, at an average rate of more than one order of magnitude faster than oceanic crust of an equivalent age, which is subsiding only because of thermal contraction processes. The discussed type of fracture zone subsidence tectonism is assumed to have been caused by the effect of large-scale horizontal offsets occurring along the transforms, and not as the result of mantle-plume tectonism or excess volcanism (Bonatti and Chermak, 1981; Bonatti and Crane, 1982).

X: THE CENTRAL PLATE B:

Xa: The Ararat Vortex and the Median Geosuture: (Figs. 22.21 to 22.24).

The Sinai-Arabian Sub-plate and the concept of the Pelusium System of geosutures (that generated the Kirşehir Vortex) has gradually evolved since 1973 (the first draft of Neev et al., 1976). The following is an updated summary of relevant data conclusions regarding tectonic elements and structural history of the discussed pattern.

The Pelusium System is a pattern of NE to NNW trending counterclockwise converging geosutures. It is limited on its west by the Qattara-Eratosthenes geosuture, followed eastward by the Pelusium Line and the Dead Sea left-lateral strike-slip faults, and terminates at the Kirşehir Vortex of Central Anatolia. It is also defined as the Sinai Sub-Plate. Together with the Arabian and the NE African sub-plates, these two territories are called by Neev (1975, Fig. 2) the 'Central Plate', which is situated in a more advanced northward position relative to both the Afghan+Indian sub-plates on its east and to the Aegean+West Anatolian microplates (see above), together with the Ionian and West Levantine Mediterranean basins, on its west. The general trends of the discussed patterns of geosutures are in agreement with our concept on the origin of the global system of geosutures which is associated with the upper


AFRICA
ARABIA
PLATE
Black Sea
Caspian Sea
Mediterranean Sea
Red Sea
Gulf of Aden
Gulf of Suez
Gulf of Aqaba
Gulf of Oman
Persian Gulf
Arabian Sea
Nile Delta
Sinai
Levantine Basin
Eratosthenes Seamount
Cyprus
Crete
Anatolian Plate
Kirsehir
Ararat
Zagros
Pelusium Line
Rub-Al-Khali-Oman Line
Owen F.Z.
Dead Sea Transform
Palmyra Fold Belt
Euphrates Graben
Sinjar
Rutbah
Jawf
Hail
Qatrana Basin
Arab Salt Basin
Najd
Afif Terrain
Ayn Dhuruma
Ghawar
Median W.F.
S. Wasia Fault
N. Hagrama W.F.
Mecca
Medina
Riyadh
Jubbah
Tabuk
Nafud
Dahna
Rub-Al-Khali
Hadramaut Arch
Masirah Graben
Masirah Island
Owen Fracture Zone
Abyssal Plain
Murray Ridge
Indus Fan
Makran
Kopet Dag
Lut Block
Helmand R.
Farah - Dasht-i-Rud
Herat
Kandahar
Zabol
Nayband
Kerman
Bam
Jiroft
Bandar Abbas
Qeshm
Hormuz
Khuzestan
Dezful Embayment
Zagros Thrust
Main Recent Fault
Main Zagros Reverse Fault
Oligocene Fold Belt
Miocene Fold Belt
Pliocene Fold Belt
Quaternary Fold Belt
Gravity Low
Oceanic Crust
Continental Crust
Transitional Crust
Suez Canal
Aswan
Khartoum
Port Sudan
Asmara
Addis Ababa
Assab
Djibouti
Aden
Muscat
Salalah
Socotra
Kuwait
Basra
Abadan
Bushehr
Shiraz
Isfahan
Tehran
Mashhad
Tabriz
Ashkhabad
Krasnovodsk
Karakum Canal
Turan Depression
Kavir Desert
Dasht-e-Lut
Sistan Basin
Sistan Range
Chagai Hills
Quetta
Kirthar Range
Indus Plain
Indus R.
Jaisalmer
Barmer
Jodhpur
Ahmadabad
Surat
Bombay
Goa
Mangalore
Cochin
Trivandrum
Colombo
Madras
Hyderabad
Nagpur
Bhopal
Indore
Kanpur
Lucknow
Allahabad
Varanasi
Patna
Calcutta
Dhaka
Chittagong
Andaman Islands
Nicobar Islands
Sumatra
Malacca Strait
Bay of Bengal
Andaman Sea
Irrawaddy R.
Mandalay
Rangoon
Andaman Trough
Sagaing Fault
Shan Plateau
Khorat Plateau
Mekong R.
Vientiane
Bangkok
Gulf of Thailand
Malay Peninsula
Kra Isthmus
Phuket
Penang
Singapore
Java
Java Trench
Timor
Timor Trough
Banda Sea
Arafura Sea
Australia
Darwin
Alice Springs
Perth
Great Victoria Desert
Great Sandy Desert
Gibson Desert
Nullarbor Plain
Eucla Basin
Carnarvon Basin
Canning Basin
Officer Basin
Amadeus Basin
Musgrave Block
Gawler Craton
Flinders Ranges
Lake Eyre
Murray Basin
Murray R.
Adelaide
Melbourne
Tasmania
Hobart
Great Australian Bight
Tasman Sea
Lord Howe Rise
New Caledonia
Norfolk Ridge
Coral Sea
Great Barrier Reef
Queensland Plateau
Brisbane
Sydney
Canberra
New Zealand
Wellington
Auckland
Christchurch
Chatham Rise
Campbell Plateau
Macquarie Ridge
Antarctica
Ross Sea
Ross Ice Shelf
Marie Byrd Land
Amundsen Sea
Pine Island Glacier
Thwaites Glacier
Antarctic Peninsula
Weddell Sea
Filchner Ice Shelf
Ronne Ice Shelf
Transantarctic Mountains
Victoria Land
Ellsworth Land
Ellsworth Mountains
Vinson Massif
Pelagic Sediments
Terrigenous Sediments
Carbonate Sediments
Evaporites
Volcanics
Volcanic Islands
Ice Shelves
Sea Ice
Pack Ice
Icebergs
Glaciers
Ice Sheets
Ice Caps
Ice Streams
Ice Rises
Ice Tongues
Ice Fronts
Ice Edges
Ice Shelf Edges
Ice Sheet Edges
Ice Cap Edges
Ice Stream Edges
Ice Rise Edges
Ice Tongue Edges
Ice Front Edges
Ice Edge Edges
Ice Shelf Edge Edges
Ice Sheet Edge Edges
Ice Cap Edge Edges
Ice Stream Edge Edges
Ice Rise Edge Edges
Ice Tongue Edge Edges
Ice Front Edge Edges
Ice Edge Edge Edges
Ice Shelf Edge Edge Edges
Ice Sheet Edge Edge Edges
Ice Cap Edge Edge Edges
Ice Stream Edge Edge Edges
Ice Rise Edge Edge Edges
Ice Tongue Edge Edge Edges
Ice Front Edge Edge Edges
Ice Edge Edge Edge Edges
Ice Shelf Edge Edge Edge Edges
Ice Sheet Edge Edge Edge Edges
Ice Cap Edge Edge Edge Edges
Ice Stream Edge Edge Edge Edges
Ice Rise Edge Edge Edge Edges
Ice Tongue Edge Edge Edge Edges
Ice Front Edge Edge Edge Edges
Ice Edge Edge Edge Edge Edges
Ice Shelf Edge Edge Edge Edge Edges
Ice Sheet Edge Edge Edge Edge Edges
Ice Cap Edge Edge Edge Edge Edges
Ice Stream Edge Edge Edge Edge Edges
Ice Rise Edge Edge Edge Edge Edges
Ice Tongue Edge Edge Edge Edge Edges
Ice Front Edge Edge Edge Edge Edges
Ice Edge Edge Edge Edge Edge Edges
Ice Shelf Edge Edge Edge Edge Edge Edges
Ice Sheet Edge Edge Edge Edge Edge Edges
Ice Cap Edge Edge Edge Edge Edge Edges
Ice Stream Edge Edge Edge Edge Edge Edges
Ice Rise Edge Edge Edge Edge Edge Edges
Ice Tongue Edge Edge Edge Edge Edge Edges
Ice Front Edge Edge Edge Edge Edge Edges
Ice Edge Edge Edge Edge Edge Edge Edges
Ice Shelf Edge Edge Edge Edge Edge Edge Edges
Ice Sheet Edge Edge Edge Edge Edge Edge Edges
Ice Cap Edge Edge Edge Edge Edge Edge Edges
Ice Stream Edge Edge Edge Edge Edge Edge Edges
Ice Rise Edge Edge Edge Edge Edge Edge Edges
Ice Tongue Edge Edge Edge Edge Edge Edge Edges
Ice Front Edge Edge Edge Edge Edge Edge Edges
Ice Edge Edge Edge Edge Edge Edge Edge Edges
Ice Shelf Edge Edge Edge Edge Edge Edge Edge Edges
Ice Sheet Edge Edge Edge Edge Edge Edge Edge Edges
Ice Cap Edge Edge Edge Edge Edge Edge Edge Edges
Ice Stream Edge Edge Edge Edge Edge Edge Edge Edges
Ice Rise Edge Edge Edge Edge Edge Edge Edge Edges
Ice Tongue Edge Edge Edge Edge Edge Edge Edge Edges
Ice Front Edge Edge Edge Edge Edge Edge Edge Edges
Ice Edge Edge Edge Edge Edge Edge Edge Edge Edges
Ice Shelf Edge Edge Edge Edge Edge Edge Edge Edge Edges
Ice Sheet Edge Edge Edge Edge Edge Edge Edge Edge Edges
Ice Cap Edge Edge Edge Edge Edge Edge Edge Edge Edges
Ice Stream Edge Edge Edge Edge Edge Edge Edge Edge Edges
Ice Rise Edge Edge Edge Edge Edge Edge Edge Edge Edges
Ice Tongue Edge Edge Edge Edge Edge Edge Edge Edge Edges
Ice Front Edge Edge Edge Edge Edge Edge Edge Edge Edges
Ice Edge Edge Edge Edge Edge Edge Edge Edge Edge Edges
Ice Shelf Edge Edge Edge Edge Edge Edge Edge Edge Edge Edges
Ice Sheet Edge Edge Edge Edge Edge Edge Edge Edge Edge Edges
Ice Cap Edge Edge Edge Edge Edge Edge Edge Edge Edge Edges
Ice Stream Edge Edge Edge Edge Edge Edge Edge Edge Edge Edges
Ice Rise Edge Edge Edge Edge Edge Edge Edge Edge Edge Edges
Ice Tongue Edge Edge Edge Edge Edge Edge Edge Edge Edge Edges
Ice Front Edge Edge Edge Edge Edge Edge Edge Edge Edge Edges
Ice Edge Edge Edge Edge Edge Edge Edge Edge Edge Edge Edges
Ice Shelf Edge Edge Edge Edge Edge Edge Edge Edge Edge Edge Edges
Ice Sheet Edge Edge Edge Edge Edge Edge Edge Edge Edge Edge Edges
Ice Cap Edge Edge Edge Edge Edge Edge Edge Edge Edge Edge Edges
Ice Stream Edge Edge Edge Edge Edge Edge Edge Edge Edge Edge Edges
Ice Rise Edge Edge Edge Edge Edge Edge Edge Edge Edge Edge Edges
Ice Tongue Edge Edge Edge Edge Edge Edge Edge Edge Edge Edge Edges
Ice Front Edge Edge Edge Edge Edge Edge Edge Edge Edge Edge Edges
Ice Edge Edge Edge Edge Edge Edge Edge Edge Edge Edge Edge Edges
Ice Shelf Edge Edge Edge Edge Edge Edge Edge Edge Edge Edge Edge Edges
Ice Sheet Edge Edge Edge Edge Edge Edge Edge Edge Edge Edge Edge Edges
Ice Cap Edge Edge Edge Edge Edge Edge Edge Edge Edge Edge Edge Edges
Ice Stream Edge Edge Edge Edge Edge Edge Edge Edge Edge Edge Edge Edges
Ice Rise Edge Edge Edge Edge Edge Edge Edge Edge Edge Edge Edge Edges
Ice Tongue Edge Edge Edge Edge Edge Edge Edge Edge Edge Edge Edge Edges
Ice Front Edge Edge Edge Edge Edge Edge Edge Edge Edge Edge Edge Edges
Ice Edge Edge Edge Edge Edge Edge Edge Edge Edge Edge Edge Edge Edges
Ice Shelf Edge Edge Edge Edge Edge Edge Edge Edge Edge Edge Edge Edge Edges
Ice Sheet Edge Edge Edge Edge Edge Edge Edge Edge Edge Edge Edge Edge Edges
Ice Cap Edge Edge Edge Edge Edge Edge Edge Edge Edge Edge Edge Edge Edges
Ice Stream Edge Edge Edge Edge Edge Edge Edge Edge Edge Edge Edge Edge Edges
Ice Rise Edge Edge Edge Edge Edge Edge Edge Edge Edge Edge Edge Edge Edges
Ice Tongue Edge Edge Edge Edge Edge Edge Edge Edge Edge Edge Edge Edge Edges
Ice Front Edge Edge Edge Edge Edge Edge Edge Edge Edge Edge Edge Edge Edges
Ice Edge Edge Edge Edge Edge Edge Edge Edge Edge Edge Edge Edge Edge Edges
Ice Shelf Edge Edge Edge Edge Edge Edge Edge Edge Edge Edge Edge Edge Edge Edges
Ice Sheet Edge Edge Edge Edge Edge Edge Edge Edge Edge Edge Edge Edge Edge Edges
Ice Cap Edge Edge Edge Edge Edge Edge Edge Edge Edge Edge Edge Edge Edge Edges
Ice Stream Edge Edge Edge Edge Edge Edge Edge Edge Edge Edge Edge Edge Edge Edges
Ice Rise Edge Edge Edge Edge Edge Edge Edge Edge Edge Edge Edge Edge Edge Edges
Ice Tongue Edge Edge Edge Edge Edge Edge Edge Edge Edge Edge Edge Edge Edge Edges
Ice Front Edge Edge Edge Edge Edge Edge Edge Edge Edge Edge Edge Edge Edge Edges
Ice Edge Edge Edge Edge Edge Edge Edge Edge Edge Edge Edge Edge Edge Edge Edges
Ice Shelf Edge Edge Edge Edge Edge Edge Edge Edge Edge Edge Edge Edge Edge Edge Edges
Ice Sheet Edge Edge Edge Edge Edge Edge Edge Edge Edge Edge Edge Edge Edge Edge Edges
Ice Cap Edge Edge Edge Edge Edge Edge Edge Edge Edge Edge Edge Edge Edge Edge Edges
Ice Stream Edge Edge Edge Edge Edge Edge Edge Edge Edge Edge Edge Edge Edge Edge Edges
Ice Rise Edge Edge Edge Edge Edge Edge Edge Edge Edge Edge Edge Edge Edge Edge Edges
Ice Tongue Edge Edge Edge Edge Edge Edge Edge Edge Edge Edge Edge Edge Edge Edge Edges
Ice Front Edge Edge Edge Edge Edge Edge Edge Edge Edge Edge Edge Edge Edge Edge Edges
Ice Edge Edge Edge Edge Edge Edge Edge Edge Edge Edge Edge Edge Edge Edge Edge Edges
Ice Shelf Edge Edge Edge Edge Edge Edge Edge Edge Edge Edge Edge Edge Edge Edge Edge Edges
Ice Sheet Edge Edge Edge Edge Edge Edge Edge Edge Edge Edge Edge Edge Edge Edge Edge Edges
Ice Cap Edge Edge Edge Edge Edge Edge Edge Edge Edge Edge Edge Edge Edge Edge Edge Edges
Ice Stream Edge Edge Edge Edge Edge Edge Edge Edge Edge Edge Edge Edge Edge Edge Edge Edges
Ice Rise Edge Edge Edge Edge Edge Edge Edge Edge Edge Edge Edge Edge Edge Edge Edge Edges
Ice Tongue Edge Edge Edge Edge Edge Edge Edge Edge Edge Edge Edge Edge Edge Edge Edge Edges
Ice Front Edge Edge Edge Edge Edge Edge Edge Edge Edge Edge Edge Edge Edge Edge Edge Edges
Ice Edge Edge Edge Edge Edge Edge Edge Edge Edge Edge Edge Edge Edge Edge Edge Edge Edges
Ice Shelf Edge Edge Edge Edge Edge Edge Edge Edge Edge Edge Edge Edge Edge Edge Edge Edge Edges
Ice Sheet Edge Edge Edge Edge Edge Edge Edge Edge Edge Edge Edge Edge Edge Edge Edge Edge Edges
Ice Cap Edge Edge Edge Edge Edge Edge Edge Edge Edge Edge Edge Edge Edge Edge Edge Edge Edges
Ice Stream Edge Edge Edge Edge Edge Edge Edge Edge Edge Edge Edge Edge Edge Edge Edge Edge Edges
Ice Rise Edge Edge Edge Edge Edge Edge Edge Edge Edge Edge Edge Edge Edge Edge Edge Edge Edges
Ice Tongue Edge Edge Edge Edge Edge Edge Edge Edge Edge Edge Edge Edge Edge Edge Edge Edge Edges
Ice Front Edge Edge Edge Edge Edge Edge Edge Edge Edge Edge Edge Edge Edge Edge Edge Edge Edges
Ice Edge Edge Edge Edge Edge Edge Edge Edge Edge Edge Edge Edge Edge Edge Edge Edge Edge Edges
Ice Shelf Edge Edge Edge Edge Edge Edge Edge Edge Edge Edge Edge Edge Edge Edge Edge Edge Edge Edges
Ice Sheet Edge Edge Edge Edge Edge Edge Edge Edge Edge Edge Edge Edge Edge Edge Edge Edge Edge Edges
Ice Cap Edge Edge Edge Edge Edge Edge Edge Edge Edge Edge Edge Edge Edge Edge Edge Edge Edge Edges
Ice Stream Edge Edge Edge Edge Edge Edge Edge Edge Edge Edge Edge Edge Edge Edge Edge Edge Edge Edges
Ice Rise Edge Edge Edge Edge Edge Edge Edge Edge Edge Edge Edge Edge Edge Edge Edge Edge Edge Edges
Ice Tongue Edge Edge Edge Edge Edge Edge Edge Edge Edge Edge Edge Edge Edge Edge Edge Edge Edge Edges
Ice Front Edge Edge Edge Edge Edge Edge Edge Edge Edge Edge Edge Edge Edge Edge Edge Edge Edge Edges
Ice Edge Edge Edge Edge Edge Edge Edge Edge Edge Edge Edge Edge Edge Edge Edge Edge Edge Edge Edges
Ice Shelf Edge Edge Edge Edge Edge Edge Edge Edge Edge Edge Edge Edge Edge Edge Edge Edge Edge Edge Edges
Ice Sheet Edge Edge Edge Edge Edge Edge Edge Edge Edge Edge Edge Edge Edge Edge Edge Edge Edge Edge Edges
Ice Cap Edge Edge Edge Edge Edge Edge Edge Edge Edge Edge Edge Edge Edge Edge Edge Edge Edge Edge Edges
Ice Stream Edge Edge Edge Edge Edge Edge Edge Edge Edge Edge Edge Edge Edge Edge Edge Edge Edge Edge Edges
Ice Rise Edge Edge Edge Edge Edge Edge Edge Edge Edge Edge Edge Edge Edge Edge Edge Edge Edge Edge Edges
Ice Tongue Edge Edge Edge Edge Edge Edge Edge Edge Edge Edge Edge Edge Edge Edge Edge Edge Edge Edge Edges
Ice Front Edge Edge Edge Edge Edge Edge Edge Edge Edge Edge Edge Edge Edge Edge Edge Edge Edge Edge Edges
Ice Edge Edge Edge Edge Edge Edge Edge Edge Edge Edge Edge Edge Edge Edge Edge Edge Edge Edge Edge Edges
Ice Shelf Edge Edge Edge Edge Edge Edge Edge Edge Edge Edge Edge Edge Edge Edge Edge Edge Edge Edge Edge Edges
Ice Sheet Edge Edge Edge Edge Edge Edge Edge Edge Edge Edge Edge Edge Edge Edge Edge Edge Edge Edge Edge Edges
Ice Cap Edge Edge Edge Edge Edge Edge Edge Edge Edge Edge Edge Edge Edge Edge Edge Edge Edge Edge Edge Edges
Ice Stream Edge Edge Edge Edge Edge Edge Edge Edge Edge Edge Edge Edge Edge Edge Edge Edge Edge Edge Edge Edges
Ice Rise Edge Edge Edge Edge Edge Edge Edge Edge Edge Edge Edge Edge Edge Edge Edge Edge Edge Edge Edge Edges
Ice Tongue Edge Edge Edge Edge Edge Edge Edge Edge Edge Edge Edge Edge Edge Edge Edge Edge Edge Edge Edge Edges
Ice Front Edge

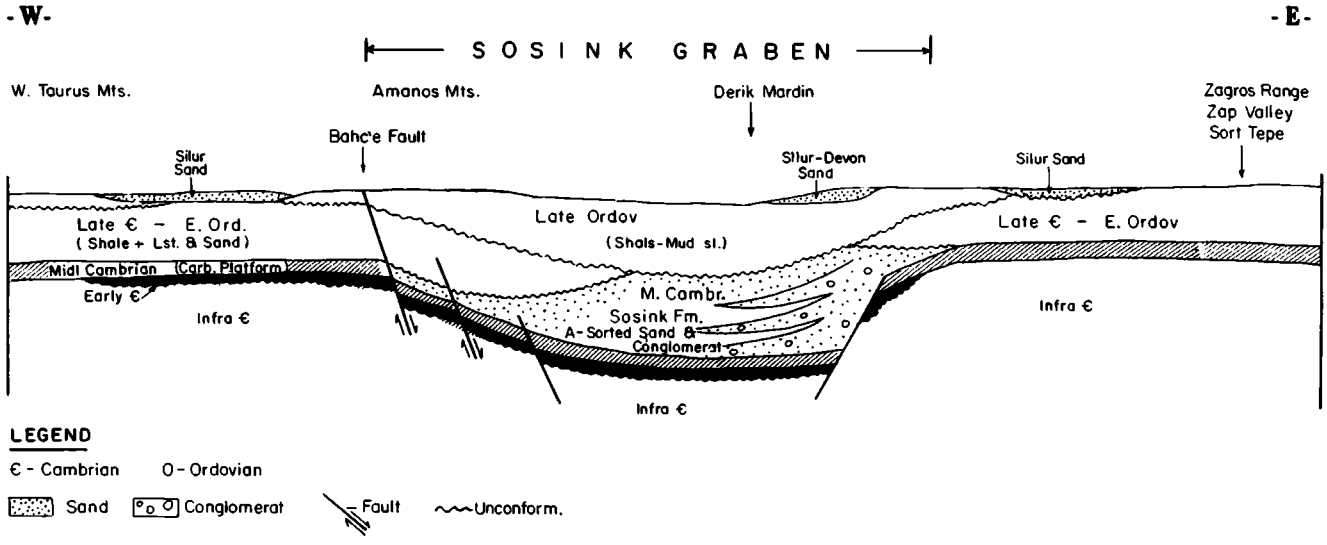


Figure 22.22 (see 22.23 for location). Geological Cross-Section of the Sosink Graben: The deposition of Early and Middle Cambrian sediments of the Sosink Formation (assorted and conglomerates) as well as of the Late Ordovician shales and mudstones is limited to the Sosink Graben (situated between the Amanos Mountains in the west and a point east of Mardin in the east). It is therefore suggested that the initial age of formation of this Graben is that old. (Cross-section after Dean and Monod, 1990, Fig. 6).

mantle's flow patterns (see above).

In other words the 'Central Plate' is moving northward at a faster rate than its two adjacent plates and is wedged-in between them. It is frontally colliding with Eurasia by piercing through East Anatolia like a spear-head. The northern limit of that protrusion is sharply marked by the tangentially approaching Elbe-Dniestre geosuture from the northwest. On its west the 'Central Plate' is obliquely colliding with the Herodotus (or West Levantine) Basin along the sinistral Pelusium and Eratosthenes transcurrent faults. On its east the Central Plate is obliquely colliding with the Afghan Sub-Plate along the Harirud Fault and the northern extension of the Owen F.Z. (along the western limit of the Lut Vortex – Figs. 22.21 and 22.23).

The discussed northward wedging-in process generates oblique collisions along both its eastern and western flanks, resulting in compressional landward asymmetric fold ranges which parallel both the NW, N, and E flanks of the Central Plate. The wedging-in process of the Central Plate also explains the westward drift of the Turkish microplate (see above and McKenzie 1970; Dewey and Şengör, 1979). Stocklin (1968, 1974), Neev (1975), as well as Lovelock (1984), and Brew et al. (2000) agree that repeated reactivation of old tectonic patterns (geosutures or other types of zones and lineaments) are relict products of the Pan African accretion event, which formed the Arabian Plate. In other words they have been continuously rejuvenated by the same style of tectonic activity.

The existence of the S-N trending structural backbone along the Sinai-Arabian wedge (or the Central Plate) is marked on Figs. 22.11, 22.21, and 22.23 as the 'Median Geosuture' (or the Hail-Jawf Structure) as indicated by the isopach contour pattern of the Phanerozoic sedimentary cover based on Neev (1975, Fig. 2, after Choubert, 1968).

The most prominent segment of that backbone is the N-S trending 120 by 50 km structure, which is composed of Paleozoic-Mesozoic sandstones of the Sakakah Formation (USGS, 1963), situated at the northwestern corner of the Nafud Desert (or sand-sea). The western limit of that structure extends between Jebel Raf in the south (29°10'N, 39°55'E) and Al-Jawf in the north (29°45'N, 30°50'E). Al-Jawf is situated at the southeastern termination of Wadi Sirhan's NW-SE trending graben. The N-S trending Al-Jawf structure is plunging beneath the Late Cretaceous chalks and marls of the Aruma Formation, some 30 km north of Sakakah (30°N, 40°15'E). That same structure further extends to the north as the broad mildly folded structure of the Rutbah High (33°00'N, 40°00'E; Lovelock, 1984, Fig. 1; Brew et al., 2000, Fig. 1). The northward extension of the Rutbah High is well recognized on the satellite map of the northern Levant (Hall, 2000), along the same trend as a chain of structures. This chain crosses the Euphrates River at Mari and the Khleissia High, and continues as far as the eastern plunge of the E-W trending Jebel Singar. From that point northward it mildly curves counterclockwise along Lake Van and Mount Ararat to terminate at the westwardly asymmetric apex of the Lesser Caucasus mountain range (41°-55'N, 42°40'E).

The structural backbone (or the Median Geosuture – Figs. 22.11, 22.21, and 22.23) of the Central Plate appears to extend southward beyond the Sakakah-Jawf-Jebel Raf Paleozoic-Early Mesozoic structure. Although the first part of that additional southern part is covered by the dunes of the recent sand sea of the

Nafud Desert, it emerges beyond the southern limit of the latter, along the narrow linear N-S trending structure of Jibal al Misma. The sharp linear nature of the western limit of that structure could reflect a sinistral wrench fault across the Median Geosuture. To the east of that structure an E-W trending belt of Cambro-Ordovician sandstone (the UmSahm and Ram formations) extensively crop out, whereas the Nafud sand-sea is on its west. Beyond that point it further extends southward (*i.e.* along exactly the same trend) as a 550 km long and 50 to 100 km wide belt of Quaternary-Tertiary volcanic cones (basalt and andesite rocks) which comprise a chain of the following three volcanic fields: Hutaym, Khaybar, and Rahat (between 27°N and 22°N). An elongated linearly distributed pattern of a few tens of volcanic cones is noticed all along the physiographic crests of that ridge (USGS, 1963), thereby indicating their relationship to the presence of an underlying, major linear tectonic (extensional) fracture.

The Median Geosuture diagonally crosses a N-S trending segment of the eastern coastline of the Red Sea between Ras Mastura in the north (at 23°N) and south of Jiddah (at 20°-15'N), which is mostly composed of Precambrian rocks (greenstone, granite, gneiss and granodiorite formations and some Quaternary-Tertiary basalts). A system of NE-SW trending faults slices the coastal segment, dividing it into long and narrow parallel trending strips, thus attaining the shape of a northward tilted parallelogram. Both of the NE-SW trending limits of that parallelogram are extending into the Red Sea along two of the few NE-SW trending fracture zones (or transverse faults), which divide the axial trough of the Red Sea and consequently also shape the adjacent coastlines, into alternating NW and N-S (and sometimes NNW) trending segments (or fault lines).

A third NE-SW trending transverse fault extends from Jiddah (eastern shoreline 21°30'N, 39°10'E) and terminates south of Port Sudan (19°-15'N, 37°20'E) along the west coast.

We suggest the extension of the Median Geosuture (which marks the tectonic backbone along the Central Plate) to extend northward from Port Sudan to Lake Van. It marks the tectonic divide between the Kirşehir and Ararat Vortices. In spite of a few important points of difference, it seems that all the geosutures situated between the Qattara-Eratosthenes in the west and the Zagros in the east, are forming a harmonious pattern by their trends and configurations.

The southern limit of the Dead Sea geosuture is close to the northwestern end of the Red Sea at Hurghada (Jezirat Gafatin) (26°45'N, 34°00'E). From that point it gently curves along the NNE to N trending transform along which the linear troughs of the Gulf of Aqaba-Elat, and the Arava, Jordan, Beq'a, and Orontes Valleys are stretched. On their west and north these linear troughs are being followed by a system of ridges that extend from eastern Sinai through the 'Structural Backbone' of Israel and Lebanon, which is merging with the southward concave arc of the NE Taurus-Amanos-NE Anatolia and Armenia ridges. The peak of that eastward asymmetric arc is at the Ararat Vortex (close to Yerovan in Armenia).

That geosuture also very much resembles the Pelusium Line, with which it finally merges. These three are therefore members of the Pelusium system of geosutures, which are merging at the apex of the Lesser Caucasus mountain range (Fig. 22.21; NATO, 1964). Occasionally these three demonstrate extensional characteristics along their southern segments (where basalts are extruded) and compressional characteristics along the northern segments (where the Central Plate is wedging into the Alpine orogenic belt). Unlike the Zagros dextrally shifted geosuture, the rest of the 'Central Plate's' geosutures, which belong to the Pelusium System, (*i.e.* the 'backbone', Dead Sea, 'Pelusium', and 'Qattara-Eratosthenes'), are sinistrally shifted (that conclusion, regarding the geosuture of the 'Central Plate', is inferred from data of the N-S trending Jibal al Misma - see above).

Two tectonic troughs that extend along the East Anatolian foredeep are delineated in the isopachs of the Phanerozoic sedimentary sequence (Neev, 1975, Fig. 2, after Choubert, 1968). The northern trough is situated between Lake Van and Diyarbakir to the Mardin High. The maximal thickness of the Phanerozoic sequence is about 7,000 m. The second (southern) trough coincides with the Sinjar Trough.

The maximal thickness of the sedimentary sequence along the Zagros foredeep (the Mesopotamian Basin) is 12,000 m (Neev, 1975, Fig. 2). An analogous order of magnitude of thickness occurs across the trough of the East Levantine Basin (limited by the Qattara-Eratosthenes and the Pelusium Geosutures). According to Makris and Wang (1994) it is even greater (close to 15 km).

A second system of lineaments, which is composed of NW-SE trending tensional fractures, was formed across the Central Plate (or the Sinai-Arabian+NE African sub-plates). Their southernmost member is the Red Sea-Gulf of Suez geosuture, along the trough of which Upper Mantle material is upwelling. The Najd and Hisma Fault systems extend adjacent and sub-parallel to the northeastern coastline of the Red Sea, but they diverge from one another southeastward. The most prominent of these faults is the Hisma Fault, extending between Aqaba and Medina, through which Quaternary-Tertiary basalt was extruded.

The next four members of the NW trending system of tensional elements are situated to the north of the Arabian and Sinai Peninsulas. These four different features (although with the same trend - Fig. 22.21) are:

i) The Palmahim Graben (50 by 14 km filled with marly sands and some basalts), which extends off the Mediterranean coastline as far to the NW as the Pelusium Line;

ii) The NE-SW trending tectonic features of Mount Carmel, and the grabens of Yizre'el and Beit Shean. All three are bordered on their SW by the two *en-echelon* Carmel and Gilboa Ridges (80 by 25 km). The ridges consist of Mesozoic carbonates which are occasionally intruded by basalts, at least since the Jurassic. They extend southeastward from the shelf-edge off Haifa to the junction of the Beit Shean Valley with the Dead Sea Rift. The Yizre'el and Beit Shean Valleys (grabens) are filled with alternating marine and terrestrial sediments as well as with basalt flows.

iii) The Wadi Sirhan graben is a 300 km long and 25 km wide feature, filled with marls, limestones, and sands, at least since Late

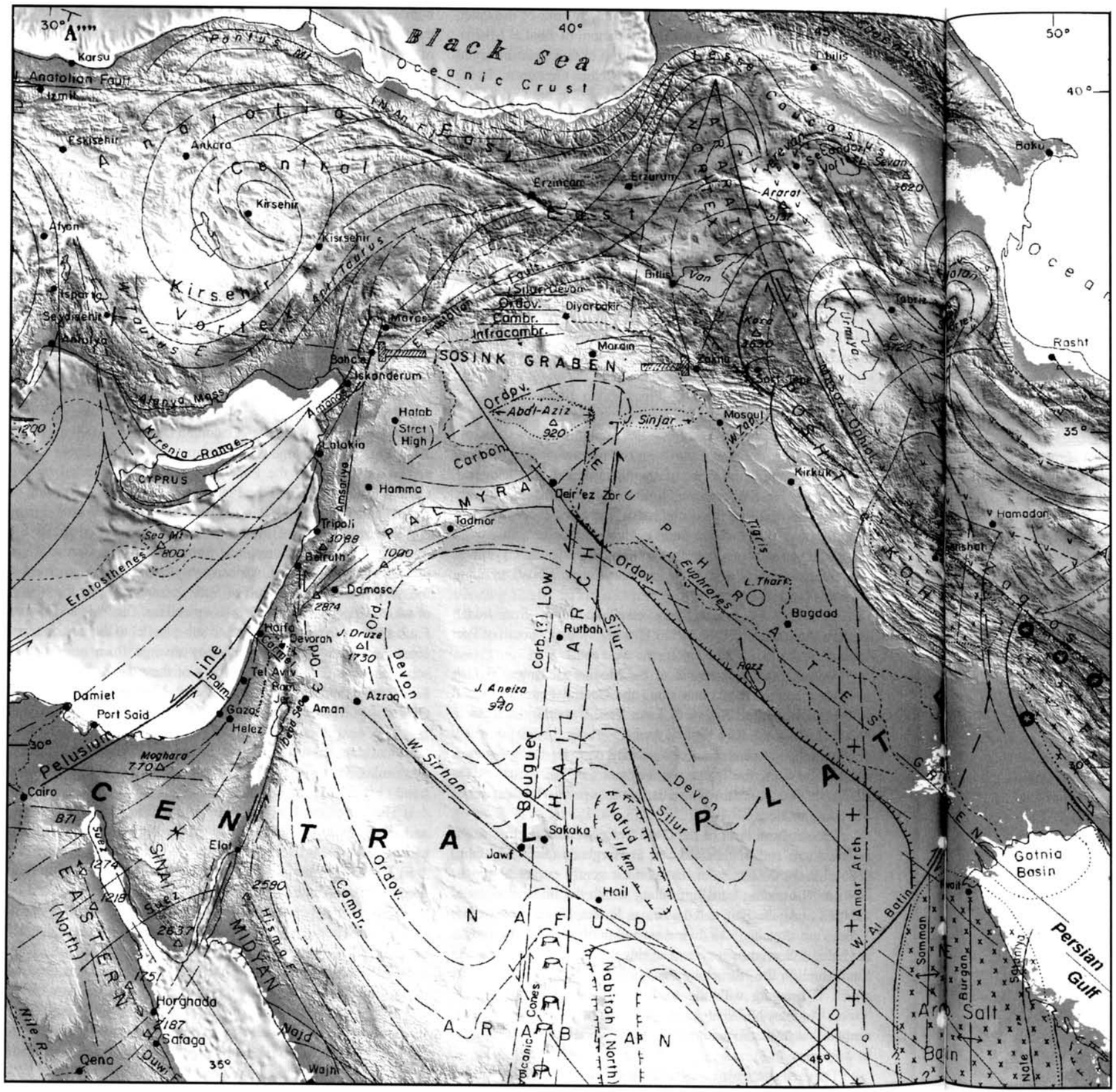


Figure 22.23. See Fig. 22.21 for reference.

Tertiary. It extends from Qasr al Asraq in the NW (31°-50'N, 36°-50'E, about 80 km east of Amman) to Al Jawf in the SE (29°-25'N, 39°-50'E). Wadi Sirhan extends parallel and adjacent to the NW trending volcanic belt about 550 km long and 100 km wide of Damascus-Jebel Drouze, along which volcanic cones and basalt flows (extruded at least since Late Tertiary times) are abundantly scattered.

It is not impossible that these three NW trending tensional features, which are *en-echelon* to one another (Fig. 22.21) were originally formed as segments of the same tensional-structural pattern, that was later disrupted and its three members shifted by left-lateral movements along the Pelusium, Mediterranean Coastline, and Dead Sea faults (see Neev, 1975 and Neev et al., 1985 for the suggested regional mechanism). Apparently that separation process should have been rejuvenated in different phases since very ancient times. Similar NW trending tectonic features were not hitherto identified across the Eastern Mediterranean basin to the west of the Pelusium Line. It should also be stressed that until now no reliable data, which could indicate the northwestward extension of the Suez Gulf into the E. Mediterranean basin, are known to exist.

iv) The next NW-SE trending linear tectonic element within the above extensional system of the Red Sea is the integrated ancient depression along the Euphrates Graben and the Persian Gulf. It was formed in Pre-Cretaceous (perhaps even much earlier) time as a tensional feature in response to north-south compression exerted by the collision between the Central Plate and Eurasia (Lovelock, 1984; our Fig. 22.20). The same mechanism was inferred by Neev (1975) for the origin of all the NW trending tensional elements across the 'Central Plate': the compressional forces were also exerted by oblique collisions along both the eastern and western flanks of that Plate.

The general trend of the Zagros orogenic belt suggests that feature to be also related to the NW tensional features across the Central Plate. Nevertheless its dextral strike-slip fault affinity, as well as the associated prominent compressional features noticed across the contact between the Arabian and Iranian sub-plates, suggest a long period of oblique collision between them (Wellman, 1966; Gidon et al., 1974; Neev, 1975). An analogous (close to mirror image) situation occurs along the Pelusium Line across the contact of the western flank of the Sinai-Arabian sub-plate and that of the Levantine Basin.

The NW trending Zagros fold belt is limited on its NE and SW by two dextral wrench faults. To the north of Kirkuk and Sulaymaniyah they both curve slightly clockwise and cross between Lake Van and Lake Ormia, to continue along both flanks of Mount Ararat (and the Ararat Vortex) until they terminate at the Lesser Caucasus fold range.

The Kurdistan Ranges (Fig. 22.11) are branching off to the left from the Zagros geosuture (fold range) at Mt. Kara (37°-30'N, 44°-00'E, 3630 m elevation), in a counterclockwise mode, and extend as a concave southward arcuate belt between Zaku and the Bitlis Zone to merge with the East Anatolian Fault and the N-S trending Amanos Range. Similar southward concave arcs appear to exist farther on to the south, between Mari (on the Euphrates River) and

the Palmyra Arc (central Syria) which marks the northern flanks of the Arabian Shield (Neev and Hall, 1992, Figs. 1, 4). These features are analogous to the sequences of southward concave structural arcs noticed along the Eastern Mauritanides (the Safia-Mdennah-Eglab arcs (Figs. 22.6 and 22.7 and Section VIa below), as well as along the Lut Vortex (Section IXh above, and Neev and Hall, 1992, Fig. 5) and along the Pamir Vortex (Section Xb below).

The origin of all of these arcs should be associated with the collision of the underlying northward flow of the upper mantle with the tangential (southeastward) flow beneath the Eurasian Plate. The westward asymmetry recognized along all of the northern arcs of the Sinai-Arabian sub-plate are in agreement with the counterclockwise movement of the Arabian sub-plate (away from the Red Sea), as well as with the sense of curving of all the six vortices identified along the Alpine-Himalayan 'eye' of the global pattern of geosutures. This interpretation is also in agreement with that of McKenzie (1970) on the westward movement of the Turkish microplate (see the exact quotation in Section VIIIc-d above). The configuration of the geosutures associated with the northern extension of the Zagros fold belt suggests that the Sava Vortex is a secondary feature adhering to the Ararat Vortex with its asymmetric northward protrusion. Its architecture is very similar to those of the Lut and Indus-Pamir vortices (Figs. 22.1, 22.20 to 22.24; Neev and Hall, 1992).

Xb: The Joint Arabian and Iranian Sub-Plate:

Xb_1: General.

It is inferred by Stocklin (1968, 1974) that in late Percambrian and Paleozoic times Iran was merged with and functioned as an extension of the Arabian continental platform. In the same publications that author also concludes that the Alpine to present-day fundamental tectonic framework of these two sub-plates were inherited from Precambrian times.

A similar approach was also expressed by Husseini (1989, p. 119), who considered that during late Precambrian time the Iranian terrain (from its westernmost reaches to the Lut Block in the east) was merged with the Arabian Sub-plate. He also suggested (quoting Stoeser and Camp, 1985) that until 715 MaBP the west Arabian terrains of Midyan, Hijaz, and Asir, were still merged with the Nubian terrain of the NE African massif, onto the northeastern margin of the African Plate. Husseini (2000, p. 530) concludes that the "Sinai Triple Junction - matches three active Precambrian-Cambrian rift branches..".

Stern (1994) considers that the super-continent of Gondwanaland had been formed by seafloor spreading and accretion of island arc processes, which occurred during Meso- and Neoproterozoic times, prior to 1.1 Ga ago. Although ~200 Ma long cycles of rifting and compression did occur across the East African Orogen, it seems that the overall disintegration process, and the northward drifting of most of the components of that supercontinent, are being maintained during the past 900 Ma (see below). The Arabian and Nubian massifs remained integrated as a part of east Gondwanaland until Tertiary time.

It is inferred from Husseini (2000) and Stocklin (1968, 1974) that during Proterozoic to Permo-Triassic times the Iranian and Arabian sub-plates as well as the African Plate were merged together.

At 715-680 MaBP the westernmost belt of the Arabian Shield was composed of a linear sequence of three terrains (along the eastern coastline of the Red Sea), namely Midyan, Hijaz, and Asir. Each of these terrains has its southwestward lithologically equivalent extension into NE Africa across the present-day western coastline of the Red Sea (the terrains of the Eastern desert, Gaba, Haya, and Tokar - after Stern, 1994, Fig. 4; Husseini, 2000, Figs. 1 and 2 and our Fig. 22.21). The boundaries between the terrrains on both sides of the Red Sea are marked by the following NE-SW trending faults:

i) The Qena (on the Nile) - Elat-Dead Sea Transform;

ii) The Sol Hamad-Yanbu;

iii) The Nakasir (Port Sudan) - Bir Umq (Jidda);

iv) The Lake Tana-Dahlak-Farasan Islands (Husseini, 1989, Fig. 2; our Fig. 22.21).

Until 620 MaBP the central zone of the Arabian Shield (the Afif and Rayan terrains as well as the Nabita Belt) collided westward and were consumed under the western zone, as a result of the activity across the East African Orogen (Stern, 1994, Fig. 3). That E-W compressional process was functioning also across the N-S trending Amar Suture, which bisects the Arabian Peninsula, dividing it into eastern and western provinces.

That same collisional process also caused the fracturing of the northeastern part of the Arabian sub-plate into a system of N-S trending linear blocks, each of which is associated with a westerly directed thrust fault. The southern limit of that system is at the NW-SE trending Abu Jifan Fault, which could be a southeastward extension of the Wadi Sirhan tensional feature. Across the eastern flank the major oil fields in the Arabian Peninsula could have been developed along and on top of N-S trending fault blocks, such as (from west to east),

i) The Jebel Tuwaya-Dibdibah;

ii) The Khuraysan-Burgan-Zubair;

iii) The Summan-Ghawar-Nala-Safaniya;

iv) The Qatar Peninsula.

Other N-S trending linear structural elements are also found across the Arabian-Iranian Craton. Examples are the Gulf of Elat (Aqaba), the Dead Sea Transform, the Mecca-Medina-Jawf-Hail-Rutbah-Mardin-Median Geosuture, which marks the axis of the Sosink Graben (between the Central Anatolian and the Ararat Vortices - Fig. 22.22), and the Lut Structure. The latter is limited by the Oman Line on its west and the Harirud Fault on its east (see Neev and Hall, 1994, and below), and perhaps also the Ninety East-Maldives-Khambhat-Pamir (see below). Each of these last five features is incorporated, however, with one of the geosutures in the counterclockwise curving global system.

An extensional tectonic phase followed the compressional one across the Arabo-Nubian Shield between 620 and 530 Ma. It culminated in the development of a complementary (*i.e.* tensional) system of elongated pull-apart rift basins, that separate the N-S trending system of linear horst structures. Within these extensional

rifts were accumulated Late Precambrian rhyolites, ophiolites, and calcalkaline volcanics, overlain by conglomerates of pebbles to sands and shale clastic layers, and topped by banks of limestones and evaporites of the Infracambrian Hormuz Formation.

The above system of N-S anticlines was bounded by the following two strike-slip fault systems which are orthogonally stretching and interacting with each other: the NE trending (Wadi Al-Batin fault) and the NW trending i) Abu Jifan-Wadi Sirhan Fault; ii) Najd Fault system; iii) Zagros-Euphrates.

The Rayan anticlines were strongly reactivated later during the following major regional tectonic episodes:

i) The Najd Rift system;

ii) The Hercynian Orogeny;

iii) The Permo-Triassic Zagros Rift; and

iv) The Late Cretaceous Cyprus-Taurus-Zagros-Oman subduction.

Xb:The Extensional Collapse (620-530 Ma),

Intrusions of granites and extrusions of rhyolites that occurred across the Arabo-Nubian Shield following the Amar Collision (~620 Ma) indicate a change in the tectonic regime from that of orogenic compression into one of extensional collapse (Husseini, 2000).

The age of the NW-SE Najd faults is 680-630 Ma (Nehlig et al., 2001). These sub-parallel faults are sinistrally dislocated by 250-300 km (of cumulative movement) across the much older NNW-SSE trending Nabita Suture. The width of the Najd system is 300 km and its exposed length is 1100 km (Fig. 22.21).

The Jubaylah Group of NW Arabia covers unconformities - the 581-565 Ma old Shammar Rhyolite. It consists of conglomerates and other clastics overlain by calcalkaline volcanics and topped by a limestone and shale sequence. That group is unconformably overlain by the Siq sandstone and the Bud Formations. The first age-diagnostic fossils (across the Arabian Peninsula) were found within the Bud Formation, dating it to late Early to early Middle Cambrian age (or about 520 Ma).

The post-collisional extensional collapse of the Arabian-Nubian Shield (600-530 Ma) is attributed to crustal gravitational instability, associated with lithospheric over-thickening during the collisional phases. These extensional processes culminated in the development of elongated complementary pull-apart rift basins between the N-S trending structures to the east of the Amar Arc (The Arab Salt Basin – Fig. 22.21).

Below are four remarks concerning the paleotectonic implications of the distribution pattern of the above Infracambrian evaporitic basins across the Arabian Peninsula, Iran, and North Pakistan. They are based on the study of seismic reflection imaging as well as outcrops and results of deep drilling. The presence of eight distinct areas of salt deposition is indicated during Infracambrian and Cambrian times (Stocklin, 1968, 1974; Zharkov, 1984; Neev and Hall, 1992; Husseini, 2000). These are as follows:

i) North Kerman;

ii) Hormuz (SW-NE of Bandar Abbas);

iii) Shiraz;

iv) South Persian Gulf;

v) Fahud;

vi) South Oman;

vii) NE Saudia (Ghawar-Burgan); and

viii) Kuwait.

The four remarks are as follows:

1) The northeastward trending Oman Line (our Fig. 22.21; Gansser, 1955; Neev and Hall, 1982, 1992) or the Dibba Fault (Husseini, 2000, Fig. 1) gradually curve counterclockwise along the north Kerman and west flank of the Lut Vortex and N-S trending block.

2) We interpret the Hormuz and South Persian Gulf areas to have functioned as a unified basin. The latter was bisected, however, by the southeastward extension of the Euphrates Graben, that was inherited from a Late-Proterozoic accretion phase of the Arabian Plate (Brew et al., 1997).

3) The northeastward concave NW-SE trending Fahud Basin parallels the Oman Mountains and the Hawasina thrust and is limiting them on the southwest.

4) The Ghaba-Dhofar and South Oman NNE trending structures, as well as the linear and narrow chain of basins (700 by 100 km), are bounded on their east by the sinusoidal SW-NE coastline of the Indian Ocean and the in-between narrow Huqf High. The Ghaba-South Oman chain of basins is bounded on its west by the *en-echelon* set of NE-SW trending narrow and linear anticlines of Ghudun-Khasfah, Ahzauz-Rudhwan and Makaran-Mabrouk (Fig. 22.21). The latter were intensively folded during the Early Cambrian compressive tectonic phase. These three anticlines are bounded along their northwestern flank by major normal faults which are downthrown to the NW as much as 5 km. Apparently this is the Oman Rift, mentioned by Husseini (2000, Fig. 5), that should mark the southeastern structural limit of the Rub Al Khali (Fig. 22.21).

Xc: The Southern Periphery of the Arabian Peninsula.

Sedimentation within the South Oman-Ghaba basin began in Late Proterozoic time (some 570 Ma ago) with the Abu Mahara Super-Group, which consists predominantly of clastic sediments with glacial deposits at their base. That supergroup terminates with the two groups of the Ara evaporites and the Nimr clastics, whose ages are considered to be the lower part of the Early Cambrian (Husseini, 2000, Fig. 5).

It is reasonable to assume that rock-salt sediments of Infracambrian and Early Cambrian ages, situated across Eastern and Southern Arabia (Husseini, 2000), as well as in Eastern Iran (Stocklin, 1968, 1974; Zharkov, 1984), and the Salt Range of Northern Pakistan (Gee, 1989), were deposited rather synchronically. The close genetic association between the deposition of oil-bearing source rocks and evaporitic environments is therefore corroborated: the proximity of ages (Late Proterozoic, Cambrian, and Lower Ordovician) of the source rocks that were found within the same (Tarim) basin, to the initial ages of its tectonic subsidence, suggests that the oil pools found there within the different reservoir rocks were generated, migrated, and stored within that same basin.

The above conclusion is not in agreement, however, with results of studies on the age of the first extensive generation and storage of hydrocarbons across North Africa and the Arabian Peninsula (and therefore also across southwestern Iran). Although most major structural features across the Saharan Platform were formed before the Paleozoic, their first major tectonic rejuvenation took place in the Caledonian phase (Silurian-Devonian) (Fekirine and Abdallah, 1998). Boote et al. (1998, p. 16) state that the Early Silurian black radioactive shales of the Lower Tanezzuft Formation, were the initial marine sediments of Phanerozoic times, deposited across much of the North African and Arabian Platforms during a postglacial flooding event. They also state that these sediments are the source of 80-90% of the Paleozoic-aged hydrocarbons of North Africa (with a further 10% from the Upper Devonian Frasnian shales), both charging a number of Intra-Paleozoic and basal Triassic reservoirs.

The most important tectonic systems across the Central Plate should be associated with the northward movements of both the lithosphere and its underlying mantle. The resulting tectonic processes along both the eastern and western flanks of the Plate were associated with oblique collisions and sinistral as well as dextral strike-slip movements. Large-scale vertical movements were also involved across these faults, such as across the normal faults of the coastline of Israel (stretching from beyond Jebel Moghara in the southwest, through Heletz and Ga'ash to Mount Carmel).

The following are tectonic elements and case histories initiated in Precambrian times, which are still functioning now. These are situated across (and along the boundaries of) the joint Arabo-Nubian-Iranian paleo-craton and are segregated according to their dominant trends (Neev, 1975; Neev et al., 1985; Neev and Hall, 1994).

Xd: The N-S alternating compressional-tensional phases (most dominant across the central territories of the Arabian Sub-Plate).

Three different categories of linear tectonic features are thereby generated: NW-SE, NE-SW, and the counterclockwise curving geosutures. As segments of some geosutures occasionally fit into the NE-SW category, the differentiation between these three is not always clear cut.

The NW-SE trending elements which are mostly tensional features are associated with basic volcanism but also with strike-slip movements. These elements (from the east westward) are characterized by:

i) The Red Sea;

ii) The Najd System, which is composed of three faults which are sub-parallel to each other. Husseini (2000) considers the age of that system to be 570-530 Ma, but data presented by Nehlig et al. (2001) suggest a considerably older age (close to 680 Ma). The length of that system across the Arabian Shield from Elat-Aqaba in the north (29°-30'N, 34°E) to the NW corner of the Rub Al Khali (20°N, 45°E) is between 1100 and 1400 km, whereas its width is close to 200 km in the NW (east of the Gulf of Elat-Aqaba) and some 300 km in the SW.

iii) The Palmahim Disturbance (see above) (Neev, 1975; Neev et al., 1976, 1985);

iv) The Mount Carmel-Yizre'el Valley (functioning at least since the Jurassic;

v) The Abu-Jifan Fault (Husseini, 2000);

vi) The Wadi Sirhan-Jebel Druze (see above);

vii) The Euphrates Graben and Persian Gulf.

Xe: The Mesopotamian Basin and the Zagros Geosyncline (After Stocklin (1968, 1974); Zharkov (1994); Neev and Hall (1982, 1992); Husseini (2000); and our Fig. 22.20).

The following remarks, on a few key areas in Iran, suggest that their present-day fundamental tectonic frameworks were inherited from Precambrian times. Brew et al. (1997) suggested that the Euphrates Graben extends further southeastward as a linear feature, off the southwestern shoreline of the Persian Gulf, whence it emerges on land in Abu Dhabi. It could continue along the same track to parallel the axis of the Fahud Basin (see below), or tangential to the southwestward convex configuration of the Hawasina Arc that parallels the Oman Peninsula. That last segment should have therefore been shifted dextrally, relative to the rest of this last geosuture. The Euphrates Graben should therefore terminate at the southwestern plunge of Mesira Island, along the coastline of the Indian Ocean.

The joint Zagros-Oman Tethyan Geosyncline zone, is marked by intrusions of ophiolites and deposits of radiolarites. It did subside and was filled up with sediments during Late Precambrian times (Stocklin, 1968, 1974; Stern, 1994). Feeble indications for compressional activity are evident from that early stage along the northeastern fringe of the Arabian Sub-Plate. That zone remained tectonically quiet during early Phanerozoic and up to Permo-Triassic times, when it was reactivated together with the juvenation of ophiolitic intrusions, that were associated with the deposition of radiolarites. The latter are overlain by Triassic and younger carbonates and shales that later on went through the Alpine Orogenic phase (Late Jurassic to the present).

The Main Zagros Thrust (MZT) is a conspicuous feature because of its straight NW-SE trending linearity, which extends from Neyriz in the SE (NNE of Bandar Abbas at the Straits of Hormuz) to Kermanshah and Sulaymaniye in the NW. From that last point it gradually curves to the NNE along the coastline of Lake Orumiyeh and then curves counterclockwise (to the west) around Mount Ararat to portray the southward concave shape of the Ararat Vortex. It is also branching off northward to generate the two secondary vortices of Savalan and Yerevan (Fig. 22.23). The lithospheric block of Central Iran is being shifted dextrally with respect to the Crush Zone and the Arabian Sub-Plate across the MZT by at least 40 km.

Unlike the straight-linearity of the MZT, the Crush Zone on its southwest is divided into the following three southwestward convex arcuate segments:

i) The Kermanshah (Bakhtaran) Arc in the north;

ii) The central Neyriz (or Fars) Arc; and

iii) The Oman Peninsula Arc.

All of these three are characterized by arcuate folds and faults which limit the ophiolitic and radiolaritic outcrops. We interpret the break between each of these three arcs to have been determined by the presence of nearly perpendicular trending (NE-SW) faults. These are assumed to be segments of geosutures, which are affiliated with the global system. The boundary between the Kermanshah and the Neyriz Arc is marked by the Dez River Fault (Fig. 22.11 - which is a dextrally-shifted strike-slip fault between Dezful and Arak). This tectonic line extends northeastward toward Qom. Toward the southwest it seems to be genetically related by extension through the subsurface and across the Mesopotamian Trough to merge in an *en-echelon* way with the Wadi Al Batin and with Wadi al Rimah. These two are forming a NE-SW trending fault (or tectonic line), which is crossing the entire width of the Arabian Sub-Plate (Figs. 22.21 and 22.23). We believe that this tectonic line further extends across the Red Sea to merge with the Median Geosuture at Port Sudan.

The boundary between the Neyriz and Oman Arcs is marked by the NE-SW trending Oman Line (Gansser, 1955; Stocklin, 1958; Neev and Hall, 1982), or the Dibba fault (Husseini, 2000). As in the case of the Dez Fault, dextral movements have also occurred along the Oman Line, which is curving counterclockwise to mark the northward trending western limits of the Lut Block (Neev and Hall, 1982). Its southwestward extension is across the Persian Gulf as a straight line between Bandar Abbas through the island of Dhalmah and along the northwestern limits of the Rub Al Khali to cross the Red Sea between the islands of Farasan and Dahlak, and Asmara (Fig. 22.21). Beyond that point (to the SW) it is merging with the Port Sudan-Ascension geosuture (Fig. 22.5) close to the Massif de Bongo. Its Precambrian age is inferred from the presence of the Infracambrian Hormuz rock salt formation deposits accumulated within ancient depressions along it.

It is widely agreed that the down-buckling, rifting, faulting, and thrusting movements across the Zagros and Oman Troughs were produced in Late Triassic time by the reactivation of a much older rift. As discussed above (the sections on North Syria and the Arabian Sub-Plate), the NW-SE trending Euphrates Graben is a shear zone possibly inherited from the Late Proterozoic accretion stage of the Arabian Plate (Brew et al., 1997). In our analysis of the 'Tectonic Evolution of the Middle East' (Neev, 1975), we suggested that the Euphrates Graben is affiliated with the pattern of northwest trending tensional faults, namely the Red Sea, Wadi Sirhan, Mount Carmel-Yizre'el Valley, and the Palmahim Depression. We now consider the Euphrates Graben to extend southeastward along the axis of the Persian Gulf, as far as Abu Dhabi. The origin of the discussed system of tensional elements could be associated with the northward wedging-in movement of the Central Plate and with the involved oblique collisions associated with the Ararat vorticing process.

Xf: The role of the Hormuz evaporitic sequence as an indicator for deciphering the structural history of Iran and the Southern Arabian Peninsula.

Stocklin (1975, p. 876-7 and Figs. 1-3) as well as Zharkov (1984, Fig. 17) clearly define the distribution and facies variation patterns of the Infracambrian to Early Cambrian Hormuz Formation. These evaporitic deposits (rock salt, gypsum, and dolomites) are rather abundant across Iran, as well as the southeastern half of the Arabian Peninsula. They are considered to be reliable indicators for portraying the fundamental tectonic framework of the Baikalian (Late Precambrian) orogeny across the basement of these territories. The discussed sediments are being precipitated from marine water-bodies rather late in the evaporitic cycle, and their distribution pattern therefore marks the limits of these paleobasin troughs, whereas their absence suggests the existence of paleohighs. The presence of rock salt basins should not necessarily indicate the occurrence of a tectonic extensional phase, as suggested by Husseini (1988, 1989, 2000) and Oterdoom et al. (1999), as orogenic folding is genetically associated with nearby parallel-trending basins, where evaporites are often being accumulated and preserved.

Sharp linear transitions are also noticed between provinces of densely populated Hormuz salt plugs and of basement outcrops. They indicate the presence of the several large troughs inherited from Precambrian time, whose locations are as follows (Figs. 22.21 and 22.23):

i) Close to Kopet Dag at the external southward concave geosuture of the Binalud Range;

ii) At the North Kerman field of Hormuz salt domes along the western limit's fault of the Lut Block between Kerman and Tabas;

iii) The sharp southwestward linear limits formed by the Oman Line across Bandar Abbas and Abu Dhabi, which separates the south Persian Gulf field of Hormuz salt domes from the Oman Peninsula;

iv) The Infracambrian Hormuz field of salt domes along the NE-SW trending Fahud Basin, southwest of the Hawasina Thrust fault and the Oman Peninsula;

v) The presence of Infracambrian aged (Hormuz Formation) rock salt deposits are found at great depth beneath the surface of the central western part of the Rub Al Khali (north of 20°N, 48°E), as inferred from the results of seismic, gravity, and magnetic surveys (Husseini, 1988, 1989, 2000; Faqira and Al-Hawuag, 1998). Similar deposits, associated with an oil field, are also found farther south (the Ghudun Basin), still within the limits of the Rub Al Khali (Husseini, 2000; Oterdoom et al., 1999).

Konert et al., (2001, Fig. 2) describe the configuration of the depths to basement (in km below sea level) during Paleozoic time. That map reflects three different linear trends each of which is also of different affinity:

i) A N-S trending belt composed of a system of long, narrow, and deep (each up to 14 km wide) rifts and horsts that dominates the southeastern part of the Arabian Peninsula (between the 45°E to 50°E meridians), or between the Ma'rib Basin (in the southwest of the peninsula) and Kuwait in the north;

ii) NW-SE trending major graben features, such as the Red Sea, the trough of the Euphrates-Persian Gulf trough and the Fahud Basins (plus the Gulf of Oman) as well as the shorter ones of Wadi Sirhan, Palmahim, Valley of Yizre'el (Mount Carmel), and the Rutbah Deep (12 km) basins. The NW-SE axis of the Zagros

geosyncline is the deepest (more than 14 km along the trough);

iii) The NE-SW trending belt of the Rub Al Khali and the Owen F.Z. that are gradually curving northward along both the eastern and western flanks of the Lut Block, to terminate at the Lut-Kopet Dag Vortex.

The same very deep seated NW-SE trending rock salt structure which is described by Husseini (2000, Fig. 1) from the western periphery of the Rub Al Khali, is interpreted by Konert et al. (2001, Figs. 1 and 2) as a N-S trending rift, more than 300 km long and close to 50 km wide. The down-thrown block across that Precambrian relief is reaching a maximum depth of more than 12 km. That long rift is segmented into two parts, apparently by three NE-SW trending dextral wrench faults that parallel each other, as well as the southeastern coastline of the Arabian Peninsula.

The southernmost one of these three wrench faults is crossing the N-S trending rift at about 18°N, 48°E, and extends gradually northeastward to curve counterclockwise across the eastern segment of the Rub Al Khali desert. The southwestward extension of that dextral wrench fault is crossing along the Alif oil field, separating between the northwestern Jurassic lobe. The southeastern one follows a NW-SE structural high feature that further extends toward the Red Sea close to San'a and across the Hudaydah, to continue southwestward along the southern limit of the Danakil Depression (NE Ethiopia). The northeastward extension of the dextral fault line is very gradually curving counterclockwise to continue along the Dibba (or Daba) fault (along the eastern face of the Oman Peninsula's northward protrusion).

Some 200 km inland (north) of the Strait of Hormuz the southern Northern Rub Al Khali wrench fault and the Dibba wrench faults are merging to continue northward as the dextrally shifted Oman Line (Gansser, 1955; Neev and Hall, 1992, Fig. 5). That merged fault further extends northward as the Nayband Fault that bounds the Lut Block (and Vortex) on its west. The trace of the Nayband wrench fault separates the North Kerman Infracambrian (Hormuz Formation) salt basin in the west, and the ophiolites - colored melange of the Kashmar-Subzevar-Bojnurd at the northern apex of the Lut-Kopet Dag Vortex (Arvin and Shokri, 1997).

Another important feature to be noted across the northern flank of the Rub Al Khali is the counterclockwise curving of three different tectonic facies belts. Each of these three suggests however a different tectonic connotation, which are: The Jebel Tuwayq-Amar arc; The Arab Salt Basin; and the Bahariya Trough. All three are branching northward from the linear NW edge of the Rub Al Khali's sand sea and away from the northward concave bay of the Persian Gulf between the Nafud-Dahna-Qatar Peninsula and Abu Dhabi.

The dominant pattern across the Rub Al Khali sand sea itself consists of the recent very long and linear dunes (see above, Neev and Hall, 1982; Neev and Hall, 1992). These swarms of seif dune are very gradually curving counterclockwise in agreement with the general configuration of the Rub Al Khali belt as well as with the belt of Paleozoic through Tertiary to Quaternary sedimentary sequences which are wrapping around the Arabian Massif on its southeast and east.

Two other belts stretch southeast of the Rub Al Khali. These are the northeastward trending 'Sabkha' and Gudun basins. The surfaces of both are characterized by swarms of alternating, stripe-forming, recent to sub-recent low sand dunes, as well as flat lying evaporites, and mud deposits. The latter are underlain by Early to Middle Eocene deposits of *in situ* shallow water dolomitic limestone with nummulitic chert of the Dammam Formation. Farther to the southwest, toward Hadramawt, Ma'rib, and Yemen (Aden), the ages of the underlying rock formations are older, including metamorphic and magmatic rocks of Precambrian age, as well as Quaternary basalts. Strips of recent eolian sands were trapped within the morphologic-depositional 'lows', thereby emphasizing the striped pattern. The lithologies (environments of deposition) within these two belts are very different, but the lineation trends are rather uniform within each of them; their patterns are consistent and very similar to each other, suggesting a common architecture of their infrastructures. It could be inferred that the undulating patterns of the linear low ridges and shallow troughs predated the eolian sand depositional process. If true the origin of these patterns may not have been associated with eolian processes.

The existence of the two north-northeastward extensions of the Southern and Median Wrench Faults is clearly expressed along both the western and eastern flanks of the Oman northward promontory: the Oman Line (Gansser, 1955; Neev and Hall, 1992) and the Dibba Fault (Husseini, 2000).

The NW-SE trending Euphrates Graben (Figs. 22.21 and 22.23) is marked from close to the western limit of the Sosink Graben (Central Syria) in the northwest along the geometric axis of the Persian Gulf, almost to the southeastern end of the Persian Gulf (off Abu Dhabi and Dubayy – USGS-ARAMCO, 1963), where it is crossed by the Northern Wrench Fault of the Rub Al Khali system. It is dextrally shifted some 100 km along that wrench fault. The Fahud Basin was shifted dextrally away from the Persian Gulf along the northwestern faults of the Rub Al Khali and tangentially along the concave northeastward arc of the Oman Peninsula to terminate off the coastline of the Arabian Sea.

Xg: The Owen F.Z. and the SE Face of the Arabian Peninsula: (Fig. 22.22; U.S.G.S.-ARAMCO, 1963; Beauchamp et al., 1995; Oterdoom et al., 1999; Al-Husseini, 2000; Faqira and Al-Hawaug, 1998; Konert et al., 2001).

Two chains of SW-NNE trending structural highs which parallel each other, are stretched between the southeastern limit of the Rub Al Khali and the relevant segment of the Arabian Peninsula's coastline. There are:

i) The NE trending chain of structural highs of the Ghudun-Khashfah-Auzauz-Rudhwan and Makarem-Mabrouk anticlines that were intensely folded during the tectonic phase of the Early Cambrian. That chain of structures is bounded on the northwest by major normal faults with throws to the northwest of as much as 5 km (the Ghudun and the Western Rub Al Khali Infracambrian Salt Basins).

ii) The Huqf Uplift that extends from 18°N 56°E (north of the Kuria Muria Island) to 22°N 60°E (Jebel Ja'alan or Ras Al Hadd).

The core of that structure is made of Precambrian basement rocks which are overlain by Infracambrian Cambro-Ordovician and Late Carboniferous to early Permian sequences (each separated from the other by unconformities); Jurassic to late Cretaceous, to terminate unconformably in the Tertiary formations.

The South Oman and Dhofar-Ghaba 600 km long Infracambrian salt basin (the Ara Formation) extends between and parallel to the above two linear structures. These sediments, together with Cambro-Ordovician sandstones, are thrusted southeastward over the Huqf Uplift. The South Oman-Dhofar-Ghaba Salt Basin and the Fahud Salt Basin are trending perpendicular to each other, being separated by the Makarem-Mabrouk NE-SW trending anticline. Taken as a whole, the Rub Al Khali-Oman and the Persian Gulf-Euphrates troughs, together with the Masirah Graben (see below), are expressing a coherent (although broken in a dogleg fashion) system of very old grabens across the Central Plate and its southern limit.

The coast-parallel Masirah Graben is situated between the Huqf Anticline and Masirah Island (built of Late Cretaceous to Tertiary ophiolites, which are similar to the Batain-Hawasina ophiolites) along the coast of the Oman Peninsula Mountains. The Masirah Graben was filled up with a sequence of Infracambrian to late Cretaceous sediments which is similar to the one accumulated on the Huqf Uplift, although somewhat thicker. That graben-sequence is topped by the up to 3 seconds (two way travel time) thick ophiolite unit which is thrusted northwestward onto the Huqf-Jebel Ja'alan anticlinal axis. The Huqf Uplift was initiated as a large southeastward thrusted anticlinal structure, thereby forming the eastern margin of the South Oman salt basins since Infracambrian to Ordovician time (Beauchamp et al., 1995, Figs. 3, 6, 7, 8, and 12). Husseini (2000) considers the contact between the northern flanks of the Ghudun-Khasfah-Makarem-Mabrouk anticlines and the Rub Al Khali to be bounded to the northwest by major normal faults with throws of as much as 5 km. Beauchamp et al. (*ibid*) consider the Late Cretaceous to Mid-Tertiary sequence of ophiolites within the Masirah Graben to be thrusted northwestward. On the other hand, the underlying sequence of rocks (Middle Cretaceous to Infracambrian plus basement) within the same basin were subjected, in earlier times, to an extensional tectonic regime (normal faults).

The discussed co-occurrence of extensional and collisional processes, or their frequent alternation, seems to create difficult problems. An example from a nearby territory is expressed by Husseini (2000, p. 533) who remarked that "... collisional models are incompatible with the regional extensional collapse of the Arabian-Nubian Shield during the Late Precambrian and Early Cambrian". It is reasonable to assume that the Owen F.Z. is (i) a right-lateral strike-slip fault, and (ii) that it marks a segment of the Arabian-Indian plate boundary (Gordon and DeMets, 1989). Our model suggests that the lithospheric slice, limited between the geosutures of the Rub Al Khali and the Owen F.Z., is moving consistently counterclockwise to terminate with the Lut Vortex to the north. The Owen F.Z. and the offshore fault line along the northeastern limit of the Arabian Peninsula, are converging counterclockwise toward the Zabul-Harirud fault system, which are limiting the Lut (Block) Vortex on its east. Perhaps the above model could help to explain the discussed enigma.

Beauchamp et al. (*ibid*, Fig. 13), as well as Oterdoom et al. (1999, Fig. 1) consider the eastern limit of the Masirah Graben to be subducted or underthrusted eastward. This is inferred from the two outcropping Tertiary ophiolite sites on Masirah Island and at the coastal point of Ras Madrakah (19°N, 57°-45'E). It is described by Oterdoom et al. (*ibid*) as 'The Limit of Sinistral Obduction (thrusting)'.

Nevertheless, the more prominent expression of the limit between the continental crust of the Arabian Peninsula and the oceanic crust of the Arabian Sea is farther on to the east, somewhere between the straight-linear and sharp NNE-SSW trending shelf break (at -200 m) and the bottom of the continental slope at -3000 m, more than 60 km south of the shelf-break (and parallel to the latter). Both of these linear features are sharply curving eastward off the southeastern corner of the Arabian Peninsula (Ras Al Hadd) to shape the northwestward tongue-like configuration of the Gulf of Oman.

The E-W trending (Abd al Kuri) lineament, which parallels the Khuriya-Muria feature, extends to the west of the island of Sucotra (12°N, 51°E) at least as far as 12°N, 50°E where it is traversed by a SW-NE trending very deep furrow (where depths of 3600 and 4500 m are recorded) (USGS, 1963). That furrow terminates at the Al-Qamar Bay along the SW coastline of the Arabian Peninsula (Fig. 22.20).

The Simahan-West Socotra-Horn of Africa NNE-SSW trending fault is only one of a system of transforms across the Gulf of Aden and the Sheba Ridge. The latter is segmented and the resulting slices are left-laterally shifted across the discussed transform faults, as inferred from their associated expression of their Free-Air gravity anomalies (Knudsen and Andersen, 1995) as well as the distribution pattern of earthquakes (Gordon and DeMets, 1989, Fig. 1). One of these 'transforms' (extending between the Bay of Qamar in the NE and the western face of the Horn of Africa at 12°N, 51°E) attains a shape of an exceptionally narrow and deep (-4500 m) furrow (our Fig. 22.20).

We interpreted the discussed pattern of mildly counterclockwise curving fault system to extend between the Owen F.Z. in the east and the three northwestern Rub Al Khali faults on the northwest. The dominant trend of linear structures (both folds and faults), mapped between these two limiting geosutures (see above and our Fig. 22.21) is parallel (or sub-parallel) to these two, such as:

i) The Ghudun Salt Basin (along the SE limit of the Rub Al Khali) and the South Oman-Dhofar-Ghaba Salt Basins, as well as the fault line (down-thrown 5000 m to the west);

ii) The Ghudun-Kasfah-Makarem-Mabrouk chain of structures;

iii) The Hufq and Masirah Uplifts and the in-between Masirah Graben;

iv) The Shelf Break (at -200 m) and Slope-Abyssal Plain Break (-3000 m);

v) The 'transform' fault across the Gulf of Aden.

Dextral movements are marked across the three NE-SW trending faults that are paralleling each other along the NW limit of

the Rub Al Khali Basin (see above). Dextral movements also occur across the Owen F.Z. as inferred by Gordon and DeMets (1989) based on earthquake slip movements. These authors also consider the rate of counterclockwise northeastward movement across the Owen F.Z. to be the slowest known on Earth. All of the linear faults paralleling the Owen and Rub Al Khali faults, or situated between them, are dextrally shifted. The integrated connotations of the above data seem to corroborate our regional interpretation regarding both the counterclockwise movement of the entire slice of the Rub Al Khali-Owen and the Lut Block (and vortex) as compared with the rest of the Arabian-Iranian sub-plates on its north and with the Arabian Sea-Indian sub-plate on its east, as well as with the antiquity, consistency and the slow rate of that process.

The entire scope of our hypothesis and the connecting link between the Owen F.Z. and the Harirud-Zabul-Khash (eastern fault of the Lut Block) across the eastern flank of the Oman Abyssal Plain are based on the following points:

i) The straight northward linear extension of the Owen F.Z. crosses the Makran E-W coastal ridge of Pakistan, *i.e.* the NE trending Dalrymple/Murray trough and ridge is sharply deviating more than 45° eastward away from the 350° trend of the discussed trough and ridge extension of the Owen F.Z (Heezen and Tharp, 1976);

ii) Both Haxby (1987) and Knudsen and Andersen (1995) show a strong negative gravity anomaly to directly extend the Owen F.Z. northward as far as and through the Makran E-W trending coastal ridge;

iii) Seismicity events since 1910 shown along the Owen F.Z. as well as the Dalrymple trough (Gordon and DeMets, 1989, Figs. 1 and 7) suggest the quite crowded concentrations of tectonic events along their northern and northwestward extensions (respectively) including the occurrences of at least one exceptionally high magnitude event on each of them;

iv) Changes of both photogeological features (curving of lineaments from coast parallel to oblique ones) and distribution pattern and types of sedimentary and volcanic rock units, are noticed on EarthSat (2001) satellite imagery and in the Geological Map across the E-W trending Makran Ridge.

Husseini (1988, Fig. 1 and p. 95) extrapolates the NW-SE trending exposed segment of the Najd faults system southeastward (*i.e.* beyond the limits of the Arabian Shield proper), across the western flank of the Rub Al Khali ("based on data from gravity and magnetic surveys as well as satellite images"). He also interprets the NW-SE fault lines across Yemen (extending from close to Sa'dah in the NW to the bay of Al-Ayn on the coastline of the Gulf of Aden, in the SE at 48°E) to belong (genetically) to the Najd Fault System. If correct, then that fault line could have been dextrally shifted across the northwestern fault line of the Rub Al Khali (between Dahlak-Jizan Island, in the southern Red Sea, to the Oman Line-Bandar Abbas). No other NW-SE fault lines are noticed across the Hadramawt-Huqf mountainous ridge (between the Bay of Al-Ayn and Masirah Island) along the SE coastline of the Arabian Peninsula.

XI: THE LUT BLOCK (VORTEX) - A Regional Divide (Figs. 22.21 and 22.24).

The Owen F.Z. and the eastern faults along the Lut Block (or Vortex) are forming the eastern limit of the Central Plate. In a similar perspective the Lut Block was discussed by Neev and Hall (1982, 1992), based mostly on the National Iranian Oil Company (N.I.O.C., 1957) Geological Map of Iran, Gansser (1955), Stocklin (1968, 1975), and Wellman (1965). The essence of the relevant geological history is that:

i) The N-S trending Lut Block represents an old Precambrian horst covered by a reduced sedimentary sequence of Paleozoic, Mesozoic, and Tertiary age. The sharp limitation of the Infracambrian N-S trending Kerman Salt Basin by the western face of the Lut Block corroborates its old age.

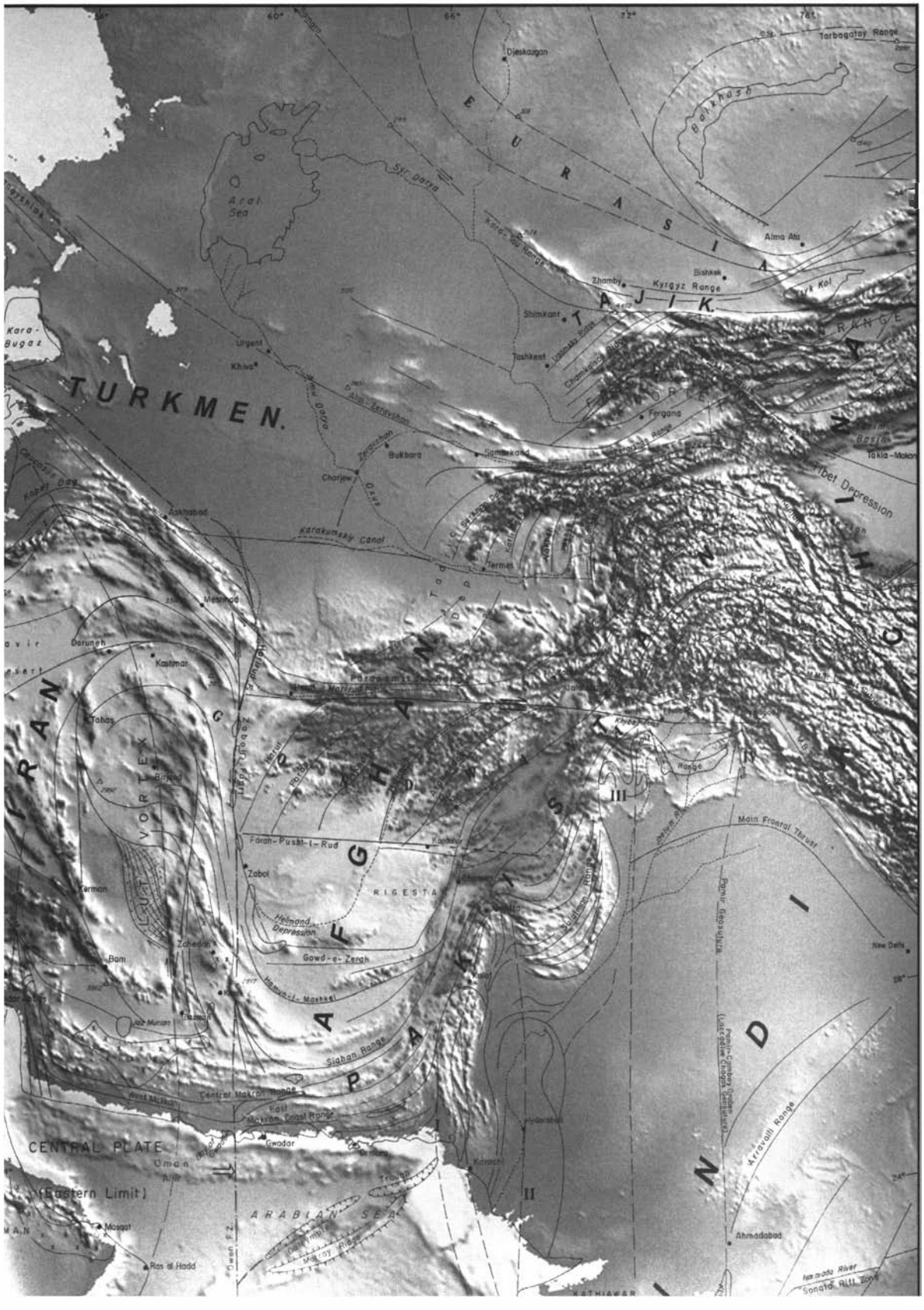
ii) Examination of the facies distribution of the Jurassic and lower Cretaceous deposits on its western side with those found along its northern and NE segments as well as the metamorphic and 'ophiolite ring' along the Lut Block, suggest a substantial difference between the north Afghan and Iranian territories across the Harirud Fault. It is also suggested that the Kopet Dag and Binalud southward concave ranges are the northernmost members of asymmetric arcs that are composing the Lut Vortex. Their folds and ophiolite belt

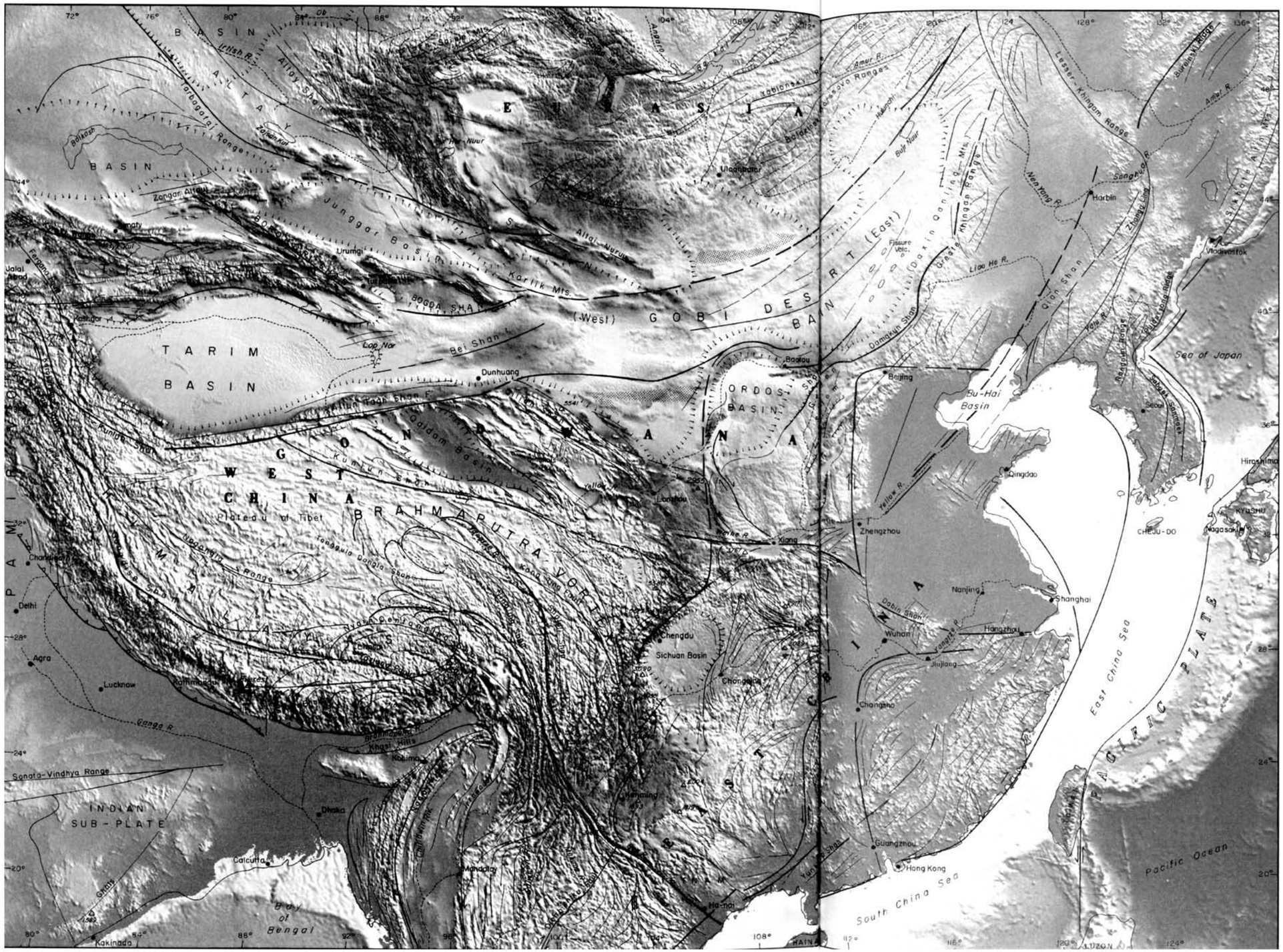


Figure 22.24. The Afghanistan Intermediate Slice, separating between the Lut and the Indus-Pamir Vortices: The territory of Afghanistan is separating between the merged territories of the Iranian, Arabian, and African Sub-plates on the west, and the Indian Sub-plate on the east. The separating elements are: (i) The N-S trending geosuture of the Owen F.Z. and its northward extension along the western flank of the Lut Block (*i.e.* the Zabol Fault, and; (ii) The western limit of the Indian Sub-plate (expressed by the SW Indian Ocean Ridge - Figs. 22.26 and 22.27 - and its northward extension along the Quetta-Kabul + Jalalabad-Pamir *en-echelon* set of geosutures in the east.

Five prominent E-W trending geosutures are recognized across the Afghan territory: From north to south the Karakum, Paropamissus, Pusht i Rud-Kandahar, Gowd-e-Zerah and the W-E trending northern coastlines of the Arabian Sea (between the head of the Oman Gulf and a point northwest of Karachi). These five could be relics of a northern group of geosutures, which are approaching the Global Eye from the northwest. These segments were preserved because the discussed sectors incidentally remained relatively undisturbed following the northward piercing effect of the Lut-Kopet Dag and the Pamir Vortices.

Basemap is National Geographic Atlas Plate 91, which is Two-point Equidistant projection. Shaded relief is ETOPO2 2' global elevation/depth grid. Two-point Equidistant (Equidistant Conic B) projection. First standard parallel 30°N, second standard parallel 50°N, central meridian 90°E, origin latitude 90°N.


EURASIA
TURKMEN.
TAJIK.
Aral Sea
Kara-Bugaz
Syr Darya
Amu Darya
Kara-Kum Canal
Karakumskiy Canal
Tarbagatay Range
Dieskazgan
Balkhash
Alma Ata
Bishkek
Zhambyl
Kyrgyz Range
Issyk Kol
Shimkent
Tashkent
Urgent
Khiva
Fergana
Bukhara
Samarkand
Chorjew
Askhabad
Termez
Mesched
Derunch
Kashmar
Tabas
Birjand
Zahedan
Bam
Zabol
Farah-Pushti-i-Rud
Helmand Depression
Gowd-e-Zerah
Hamun-i-Mashkel
Jaz Murian
Sistan
Kandahar
Quetta
Sibhan Range
Central Makran Range
East Makran Coast Range
Gwadar
Karachi
Hyderabad
CENTRAL PLATE
(Eastern Limit)
Oman
Arab
ARABIAN SEA
Masqat
Ras al Hadd
Owen F.Z.
Murray Ridge
Indus
Tibet Depression
Takla-Makan
Basin
Kunlun Range
Tarim
Turfan Depression
Lop Nor
Altyn-Tagh
Kopeh Dagh
Elburz
Range
Main Frontal Thrust
Pamir Front
Panjab Plain
New Delhi
Aravalli Range
Ahmadabad
Narmada River
Sonata Rift Zone
KATHIAWAR
I
II
III
IV
V
VORTEX


BASIN
ALTAY
Irtish R.
Altay Shan
Tarbagatai Range
Balkash
Zaysan Kol
Zhungar Basin
Zhungar Altau
Urumqi
Karlik Mts.
BOGDA SHAN
Altai-Nuruu
Hovd
Uvs Nuur
Ulaanbaatar
EURASIA
Selenga R.
Baikal
Yablonsky Range
Sayan Mts.
Krasnoyarsk
Angara R.
Lake Baikal
Kodar Mts.
Stanovoy Range
Amur R.
Lesser Khingan Range
Buryatsky Ridge
Vladivostok
Sikhote Alin Mts.
Sea of Japan
Nen Yang R.
Harbin
Zhangwu Ling
Liao He R.
Qian Shan
Yalu R.
Taebaek Sanmaek
Seoul
Bu-Hai Basin
Beijing
Hirosima
Kyushu
Nagasaki
CHEJU-DO
Qingdao
Yellow R.
Zhengzhou
Nanjing
Shanghai
Dabie Shan
Wuhan
Yangtze R.
Hangzhou
Jiujiang
Changsha
East China Sea
PACIFIC PLATES
Pacific Ocean
South China Sea
Guangzhou
Hong Kong
LUZON
Hainan
Ha-noi
Mandalay
Bay of Bengal
Calcutta
Kakinada
Dhaka
INDIAN SUB-PLATE
Sonata-Vindhya Range
Ganga R.
Lucknow
Agra
Delhi
Kathmandu
Chomolungma
Kosimba
Khasi Hills
Brahmaputra R.
Namche Barwa
Chengdu
Sichuan Basin
Chongqing
Xiang
Lanzhou
Yellow R.
Kunlun Shan
Qaidam Basin
Kunlun Shan
Plateau of Tibet
BRAHMAPUTRA-YORTZANGBO
Indus R.
Tsangpo Gangla Shan
Himalaya Range
Yadong
Gyangze
Lhasa
Tsangpo R.
Karakoram Range
Tarim Basin
Loop Nur
Bei Shan
Dunhuang
Baotou
ORDOS BASIN
Qilian Shan
Altai-Nuruu
Gobi Desert (West)
Gobi Desert (East)
Daxin Qanling Mts.
Khingan Range
Buir Nuur
Halhgol
Fissure Volc.
Jalal Abad
Fergana Valley
Kashgar
Turfan
Hami
Gobi Altai
Gobi Altai Range
Bogda Shan
Karlik Mts.
Qilian Shan
Altyn Tagh Shan
Kunlun Shan
Qaidam Basin
Kumun Shan
Yellow R.
Lanzhou
Xiang
Chengdu
Sichuan Basin
Chongqing
Changsha
Nanjing
Shanghai
Wuhan
Hangzhou
Jiujiang
Zhengzhou
Qingdao
Beijing
Harbin
Vladivostok
Seoul
Hirosima
Nagasaki
Kyushu
Cheju-do
Lake Baikal
Ulaanbaatar
Irtish R.
Ob
Angara
Yablonsky Range
Sayan Mts.
Krasnoyarsk
Amur R.
Lesser Khingan Range
Buryatsky Ridge
Stanovoy Range
Sikhote Alin Mts.
Nen Yang R.
Songhua R.
Zhangwu Ling
Liao He R.
Qian Shan
Yalu R.
Taebaek Sanmaek
Bu-Hai Basin
Sea of Japan
Yellow R.
Dabie Shan
Yangtze R.
Jiujiang
Changsha
East China Sea
PACIFIC PLATES
Pacific Ocean
South China Sea
Guangzhou
Hong Kong
Luzon
Hainan
Ha-noi
Mandalay
Bay of Bengal
Calcutta
Kakinada
Dhaka
Sonata-Vindhya Range
Ganga R.
Lucknow
Agra
Delhi
Kathmandu
Chomolungma
Kosimba
Khasi Hills
Brahmaputra R.
Namche Barwa
Chengdu
Sichuan Basin
Chongqing
Xiang
Lanzhou
Yellow R.
Kunlun Shan
Qaidam Basin
Kum


SIBERIAN PLATEAU
MOUNTAIN RANGES
EAST
GOBI
TARIM
Tarim Basin
Shanghai
Yellow Sea
Caspian Sea
Black Sea
N. SEA
RIYAD
Riyad
Red Sea
Aden Ridge
Owen Fracture Zone
Carlsberg Ridge
Mid-Indian Ridge
Chagos-Laccadive Ridge
Ninety East Ridge
Broken Ridge
Amirante Ridge
Madagascar Ridge
Mascarene Basin
Crozet Basin
Somali Basin
Mozambique Basin
Natal Valley
Agulhas Basin
Agulhas Fracture Zone
Prince Edward Fracture Zone
Conrad Rise
Del Cano Rise
Kerguelen Plateau
Nazca Plate
Antarctic Plate
Pacific Plate
Philippine Plate
Eurasian Plate
African Plate
Indian Plate
Australian Plate
North American Plate
South American Plate
Arabian Plate
Somalian Plate
Nubian Plate
Caribbean Plate
Scotia Plate
Juan de Fuca Plate
Cocos Plate
Rivera Plate
Gorda Plate
Explorer Plate
Juan Fernandez Plate
Easter Plate
Galapagos Plate
Bismarck Plate
Solomon Plate
Woodlark Plate
Fiji Plate
Tonga Plate
Kermadec Plate
Macquarie Plate
Balleny Plate
Sandwich Plate
Shetland Plate
Aegean Sea Plate
Anatolian Plate
Iranian Plate
Afghan Block
Pamir
Hindu Kush
Himalayas
Tibetan Plateau
Qaidam Basin
Junggar Basin
Tien Shan
Kunlun Mts.
Altyn Tagh
Qilian Shan
Nan Shan
Hoang Ho
Yangtze Kiang
Mekong
Irrawaddy
Salween
Brahmaputra
Ganges
Indus
Narmada
Godavari
Krishna
Kaveri
Deccan Plateau
Western Ghats
Eastern Ghats
Sri Lanka
Maldive Islands
Laccadive Islands
Andaman Islands
Nicobar Islands
Sumatra
Java
Borneo
Celebes
Timor
New Guinea
Australia
Great Dividing Range
Great Australian Bight
Tasmania
New Zealand
South Island
North Island
Alps
Pyrenees
Apennines
Balkans
Carpathians
Caucasus
Urals
Scandinavian Mts.
Iceland
Greenland
Baffin Island
Hudson Bay
Labrador Sea
Davis Strait
Grand Banks
Newfoundland
Gulf of St. Lawrence
Great Lakes
Rocky Mts.
Sierra Nevada
Cascade Range
Aleutian Trench
Kuril Trench
Japan Trench
Ryukyu Trench
Philippine Trench
Mariana Trench
Tonga Trench
Kermadec Trench
Peru-Chile Trench
Middle America Trench
Puerto Rico Trench
Java Trench
Sunda Trench
Aleutian Islands
Kuril Islands
Japan
Taiwan
Hawaiian Islands
Fiji Islands
Samoa
Tonga
Galapagos Islands
Easter Island
Juan Fernandez Islands
Azores
Canary Islands
Cape Verde Islands
Madeira
Bermuda
Falkland Islands
South Georgia
South Sandwich Islands
South Orkney Islands
South Shetland Islands
Bouvet Island
Prince Edward Islands
Kerguelen Islands
Heard Island
Macquarie Island
Balleny Islands
Scott Island
Peter I Island
Ross Sea
Ross Ice Shelf
Weddell Sea
Filchner Ice Shelf
Ronne Ice Shelf
Antarctic Peninsula
Graham Land
Palmer Land
Ellsworth Land
Marie Byrd Land
Victoria Land
Transantarctic Mts.
Queen Maud Land
Enderby Land
Kemp Land
Mac. Robertson Land
Princess Elizabeth Land
Wilkes Land
Adelie Land
George V Land
Oates Land
Knox Land
Budd Coast
Sabrina Coast
Banzare Coast
Amery Ice Shelf
Lambert Glacier
Prydz Bay
Shackleton Ice Shelf
Totten Glacier
Vostok
Amundsen Sea
Bellingshausen Sea
Pine Island Glacier
Thwaites Glacier
Getz Ice Shelf
Siple Coast
Ross Ice Shelf
Beaufort Sea
Chukchi Sea
East Siberian Sea
Laptev Sea
Kara Sea
Barents Sea
White Sea
Baltic Sea
Gulf of Bothnia
Gulf of Finland
Gulf of Riga
Gulf of Bothnia
Gulf of Finland
Gulf of Riga
Gulf of Bothnia
Gulf of Finland
Gulf of Riga

fan out westward against the South Caspian Block along a flexure in the Turan plate. It is therefore considered that this N-S trending block is an old feature.

The occurrence of a Hormuz salt plug of Infracambrian age at 37°N 56°E (Stocklin, 1974, Fig. 2), within an outcrop of undifferentiated Paleozoic rocks along the concave southward facing Binalud Arc (the N.I.O.C., 1957), suggest that the northward piercing of the Lut Vortex reached at least that far north during such an early time. The results of a photo-geological study of Iran, Afghanistan, and Pakistan (Wellman, 1965, Figs. 1, 3) are expressed in a map of the major faults and main lineations across these territories. He figured out the 'Maximal Horizontal Shortening' (M.H.S.) directions from the integrated pattern of fault displacements and from the topography. The tracks of nine major active wrench faults across the above territories were also plotted. Wellman (*ibid*, Fig. 3 and p. 731-733) infers from his data that the 'Lut Centre' (in the Dasht-i-Lut region) is both:

i) A relatively low-morphologic closure expressing a downward vertically moving cylinder of crustal material;

ii) The close to circular 'eye' of that feature is centered around the M.H.S., as well as the elongate pattern of high ridges and intervening troughs. They are both spiraling out over the whole of eastern Iran. We herewith apologize for not being aware of Wellman's (1955) paper until after our 1992 paper had been published. Wellman (*ibid*) also notes that similar cases of linear "tectonic features which spiral out probably occur at many other places". One of these sites is close to the west end of the Po Valley in northern Italy (apparently identical with our Sestri Vortex).

The NIOC Geological Map of Iran (1957) clearly indicates the eastern limits of the Lut Vortex (or 'Block') to be expressed by two sets of N-S trending faults that parallel each other (Fig. 22.21).

The western one extends northward from the Bazman (ultrabasic) Volcanic Cone (+3490 m at 28°N, 60°E) through Neh, to Mashhad where it is merging with the southward concave arc (the Binalud Range).

Its southward extension is crossing the Gulf of Oman north coastline at Cha-Bahar Bay along the 60°E meridian where a N-S group of mud volcanoes are situated and where the axial bathymetric contours show some irregularities. It further extends along the bottom of the continental slope (~3000 m depth) off Ras Al Hadd (the easternmost point of the Arabian Peninsula). From that point it practically parallels the Owen F.Z. on its west to bisect the southwestward concave Sheba Ridge (Gordon and DeMets, 1989), which is also expressed as a curved gravity high feature associated with a slim gravity low 'string' along its backbone (Knudsen and Andersen, 1995). It further extends to the east of the Socotra Island, to follow the eastern continental slope of Somalia (the Horn of Africa).

The eastern set of faults along the Lut Block begins at Gwatar Bay at the northern coastline of the Gulf of Oman, along the 60°E meridian, through Kash and along the Zabol-Harirud N-S trending faults, to curve northwestward as far as the Caspian Sea.

Its southward extension is suggested to extend southward across the E-W trending Makran Ranges belt and the Gulf of Oman, to merge with the Owen F.Z. some 250 km east of Ras Al Hadd (close to 21°N, 62°E).

The mode of southward crossing through the Makran Belt of both the Zabol-Gwatar eastern set of faults as well as the Bazman-Cha-Bahar western one, without inflicting a major offset across the Makran, is surprising. An analogous problem is why the crossing of the Oman Line-Dibba Fault (or the northwestern geosutures of the Rub Al Khali – see above), through the Zagros-Makran geosynclines and along the western flank of the Lut Block, did inflict a major dextral shift on these two.

The northward extension of the Owen F.Z. from off Ras Al Hadd toward Gwatar is suggested based on the following two arguments:

i) A NNE trending belt of low gravity anomalies extends between the edge of the continental shelf at the SE coastline of the Arabian Peninsula (which is marked by a narrow strip of positive free-air gravity anomalies).

ii) A similar linear belt of high values is found along the Owen F.Z. itself. The belt is recognized from off Qamar Bay through Ras Al Hadd and beyond to the center of the Gulf of Oman and is slightly curving counterclockwise to the trough of the Gulf of Oman. A similar linear gravity high belt also extends along the linear western flank of the Owen F.Z. (Knudsen and Andersen, 1995).

The mode of northward piercing and the geological history of the Lut Vortex are similar to those of the Ararat (see above) and Pamir (see below) Vortices. Most of the joined counterclockwise northward lithospheric movements of the Rub Al Khali-Oman Peninsula, together with the Lut Block, should have been accomplished prior to Phanerozoic time (see above). An underlying upper mantle flow, which is being maintained along the same route even today, is the suggested mechanism for the present-day tectonic activities across the northernmost segments of all these eight discussed vortices of the global eye. Therefore our interpretation may not be in agreement with that expressed by the interpretation of Al-Husseini (1988, Figs. 3 and 4; 1989, Figs. 2, 5, 6, 10, and 11; 2000, Fig. 6) regarding the structural history and processes through which the Lut Block, the Afghan and Indian Plates (with the Oman and Punjab rifts between them, respectively) could have reached their present-day positions.

XIa: The (Lut,) Pamir, and Brahmaputra Vortices. China and the Tarim Basin (Figs. 22.1, 22.24, 22.25, 22.26, and 22.27).

The Lut and Pamir Vortices, as well as the Ararat Vortex, differ from the other five vortices by their elongate finger-like configurations. These three consist of a northward sequence of southward concave arcs, each of which is curving counterclockwise and are often open to the west. Their width (E-W) dimension at their tops is close to that of their southward extensions (the 'fingers'). The crustal shapes of the other five vortices (Alboran, Sestri, Aegean, Kirşehir, and to a certain extent also the Brahamputra) are closer to that of perfect circles, which are produced by counterclockwise spiraling geosutures.

The origin of the entire group of eight vortices seems to be related to a northward flow pattern of the upper mantle in which


Arctic Ocean
Bering Sea
Pacific Ocean
SAKHALIN
Okhotsk
AUSTRALIA
Indian ocean
Ninety East
Mid Indian ridge
Chagos ridge
Owen ridge
Sir Thomas ridge
Kerguelen Plateau
Broken Ridge
Naturaliste Plateau
Wallaby Plateau
Diamantina Zone
Perth Basin
Cuvier Basin
Gascoyne Abyssal Plain
Argo Abyssal Plain
Cape Basin
Agulhas Plateau
Agulhas Basin
Mozambique Ridge
Mozambique Basin
Natal Valley
Crozet Basin
Crozet Plateau
Prince Edward Islands
Del Cano Rise
Conrad Rise
Kerguelen Islands
Heard Island
Macquarie Island
Tasmania
Lord Howe Rise
Norfolk Ridge
Tasman Basin
Tasman Sea
Coral Sea
Fiji Basin
Lau Basin
Hikurangi Plateau
Chatham Rise
Campbell Plateau
Bounty Trough
Antipodes Islands
Auckland Islands
Macquarie Ridge
Emerald Basin
Bounty Basin
Aleutian Basin
Aleutian Trench
Kamchatka Basin
Kamchatka Trench
Kuril Basin
Kuril Trench
Japan Trench
Japan Basin
Shatsky Rise
Hess Rise
Emperor Seamounts
Hawaiian Ridge
Hawaiian Swell
Mid-Pacific Mountains
Line Islands
Marshall Islands
Wake Seamounts
Wake Guyot
Marcus Guyot
Magellan Seamounts
Nauru Basin
Caroline Basin
Caroline Ridge
Caroline Islands
Mariana Trench
Mariana Islands
Philippine Sea
Philippine Trench
Parece Vela Basin
Shikoku Basin
Ryukyu Trench
Ryukyu Islands
Okinawa Trough
Taiwan
Luzon
Luzon Trough
Sulu Sea
Celebes Sea
Celebes Basin
Celebes Trench
Sangihe Islands
Halmahera Islands
Halmahera Basin
Halmahera Trench
Molucca Sea
Molucca Basin
Molucca Trough
Sulawesi
Banda Sea
Banda Basin
Banda Arc
Timor Trough
Timor
Aru Trough
Aru Islands
Arafura Sea
Arafura Basin
Arafura Shelf
Gulf of Carpentaria
Gulf of Papua
Coral Sea Basin
Coral Sea Plateau
Queensland Plateau
Queensland Trough
Great Barrier Reef
Great Australian Bight
Great Australian Bight Basin
Eucla Basin
Eucla Platform
Ceduna Terrace
Ceduna Basin
Duntroon Basin
Otway Basin
Otway Ridge
Otway Basin
Bass Basin
Bass Strait
Flinders Island
Flinders Ridge
Flinders Trough
Lord Howe Rise
Norfolk Ridge
Norfolk Basin
Norfolk Islands
Lord Howe Islands
Lord Howe Basin
Lord Howe Trough
Middleton Basin
Middleton Ridge
Middleton Trough
Gascoyne Abyssal Plain
Cuvier Basin
Cuvier Abyssal Plain
Perth Basin
Naturaliste Plateau
Naturaliste Trough
Wallaby Plateau
Wallaby Trough
Diamantina Zone
Diamantina Trough
Broken Ridge
Broken Basin
Kerguelen Plateau
Kerguelen Trough
Kerguelen Islands
Heard Island
McDonald Islands
Ninety East Ridge
Ninety East Trough
Mid Indian Ridge
Chagos Ridge
Chagos Trough
Owen Ridge
Owen Trough
Sir Thomas Ridge
Sir Thomas Trough
Mascarene Basin
Mascarene Plateau
Mascarene Trough
Madagascar
Madagascar Basin
Madagascar Ridge
Madagascar Trough
Somali Basin
Somali Ridge
Somali Trough
Arabian Basin
Arabian Ridge
Arabian Trough
Arabian Sea
Arabian Plateau
Arabian Trough
Arabian Basin
Arabian Ridge
Arabian Trough
Arabian Basin
Arabian Ridge
Arabian Trough
Arabian Basin
Arabian Ridge

counterclockwise curving eddies are involved. The collisional pattern of Eurasia and Africa-India across the Alpine-Himalayan belt differ not only by the tangential mode along the northern zone and the head-on mode of vorticing along the southern zone. The northward finger-like mantle flows under and along the Ararat, Lut, and Pamir (as well as the Brahmaputra) elongate vortices seem to penetrate northward and breach through the contact zone into Eurasia appreciably farther away than the other four.

The architecture of these elongate patterns is especially instructive along the Pamir and Brahmaputra Vortices (as outlined in Figs. 22.24, 22.25 and 22.26). The bounding north-south trending geosutures are approaching the Indian sub-plate from the southern Indian Ocean. They continue on-land along its western flank (as far as the Pamir) and along the eastern one (as far as the Brahmaputra). We compare these geosutures to railroad tracks along which the upper mantle was flowing northward and converging beneath the present-day location of the Himalayas, long before India started to move to the north from Gondwana to collide with Eurasia along the Himalayas. The western geosuture begins NE of Antarctica along the Southwest Indian Ridge to very gradually curve counterclockwise and extend along the Chagos-Laccadive Ridge to penetrate the Indian sub-continent through the Khambhat Gulf and the Cambay Graben, and farther northward across the Salt Range and the N-S trending median axis of the Pamir Vortex as far northward as the northward concave Tien Shan belt of ranges. The eastern geosuture begins north of Antarctica at Kerguelen Island and continues northward along the Amsterdam F.Z. and the Ninety-East Ridge, to merge with the Andaman Islands and Western Burma, and terminate along the counterclockwise curving Brahmaputra Vortex (Heezen and Tharp, 1977).

The E-W trending Makran Range, that parallels the south Iran (Pakistan) coastline of the Arabian Sea, gradually curves counterclockwise to become drag-folds that merge with the N-S trending Quetta-Chaman Ranges along the western flank of the Indian peninsula. Another system of drag-folds, although clockwise curving, is found along the eastern flank of the peninsula as well, thereby forming a mirror image of the former. These two systems of drag-folds ('railroad') along both flanks of the Indian sub-plate, are associated with major strike-slip faults; sinistral on the west and dextral on its east. Although the upper (northern) segments of the Pamir and Brahmaputra geosutures are slightly curving in opposite directions on their way northward (NW and NE respectively), both of them are spiraling counterclockwise and terminate at their respective vortices. By that the westward asymmetries of the vortices are emphasized. A secondary geosuture is leading toward the Pamir Vortex, beginning north of Antarctica at the Enderby Abyssal Plain, extending north along the Mozambique Channel, the Seychelles, and merging with the Owen F.Z. The NE-SW trending Dalrymple Trough and Murray Ridge, which are diverging from the Owen F.Z., are curving counterclockwise, to penetrate Pakistan at Ras Ormara (some 200 km west of Karachi) and merge with the Quetta-Chaman and Hindu Kush ranges along the western face of the Pamir Vortex.

The northward elongate Pamir feature (Fig. 22.24) seems to belong to the same category of vortices as the Lut (Figs. 22.1, 22.21, and 22.24), the Ararat (Figs. 22.21 and 22.23) and the Safia-Eglab (Eastern Mauritanides Figs. 22.6 and 22.7) Vortices. The Pamir Vortex is unique, however, because of two different features: Its pattern consists of four northward-trending and protruding, finger-like, narrow and long structures, which are *en-echelon* and, parallel to one another, and marking the western limit (or flank) of the Indian Peninsula. Each of these fingers is reaching farther northward as compared with its neighbor on the west. They are separated from each other by sinistral faults (Figs. 22.21 and 22.24). Each of these crustal fingers, as is the case for all the other vortices, is being dragged northward and curved counterclockwise by the underlying mantle currents and energized by mechanisms similar to that described in an earlier section (Whole Mantle Convection), regarding the 'Great African Plume' (Kerr, 1999, see above).

The first finger of the Pamir Vortex on its west terminates at Chaman in the north. The second finger (farther on to its east), is marked by a N-S structural high situated between the Karachi and the Hyderabad structural low. It extends northward along the flood plain of the lower Indus River, from its delta just to a point east of Kalat (Figs. 22.21 and 22.24) and terminates at the 32°N parallel. The third *en-echelon* finger is the structural high of the Sulaiman Range, that begins close to the 28°N parallel and terminates at the Khyber Pass (east of Kabul, between Jalalabad and Peshawar, where the eastern end of the Harirud-Paropamisos E-W trending transverse fault is situated). The latter is a member of the tangential system of geosutures. It could have been dextrally shifted by the Harirud-Zabul geosuture, *i.e.* it once was the extension of the Caucasus-Dneister-Tornquist geosuture (Fig. 22.1).

The fourth finger virtually begins at Islamabad (east of the Khyber Pass). It is the longest member within the discussed pattern (close to 1000 km) as it is the northward extension of the Chagos-Laccadive-Cambay Graben geosuture (the western member of the 'railroad' along which most of the Indian sub-plate moved



Figure 22.27 . A Relief Map of East Asia (rotated): It expresses the configuration and nature of the elevated-crumpled territories extending from the western Himalayas both eastward (W. China), northeastward (across the Baikal, Verkhoyansk and NE Siberia), and southeastward (along the Burma-Indochina-Indonesian ranges). These trends resulted from the collisional processes of Eurasia with Africa-India on the one hand, and the long, N-S trending compressional contact of East Asia with the West Pacific plate on the other (see Figs. 22.2 and 22.26 for the mechanism associated with the formation of the orogenic-downwelling belt). Plate motion vectors after Gripp and Gordon, 1990.
Figure 22.27. Shaded relief is ETOPO2 global 2' elevations/depths. Mercator projection.


EURASIA
SCANDINAVIA
Gulf Both
White Sea
Kola Penins.
Viking – Elbe
Norwegian Basin
Mohns Ridge
Greenland Sea
Jan Mayen
Kolbeinsey Ridge
ICELAND
Reykjanes
GREENLAND
BARENTS SEA
BARENTS SHELF
BASIN
FRANZ JOSEF LAND
NORTH LAND
Lomonosov Ridge
North Pole
Marvin Alpha
Mendeleyev Ridge
ARCTIC BASIN
CANADA BASIN
NORTH SIBERIAN SHELF
EAST SIBERIAN SHELF
Shelf Slope
Wrangel Isl.
Beaufort Sea
NORTH SLOPE
Brooks Range
Fairbanks
Yukon R.
Kolyma R.
Verkhoyansk Range
Lena
Yana Range
Baffin Bay
Davis Strait
Baffin Island
Foxe Basin
Foxe Channel
Hudson Strait
Southampton Island
Melville Peninsula
Boothia
Victoria Island
Great Slave L.
Great Bear L.
Mackenzie R.
Mackenzie Mts.
Richardson Mts.
Porcupine R.
Brooks Range
ALASKA
CANADA

northward across the Indian Ocean and Pakistan). That N-S trending submarine geosuture crosses the coastline at the Gulf of Khambhat and continues northward as the concealed Cambay-Islamabad segment of the Cambay-Pamir geosuture (Fig. 22.21).

We suggest the upper mantle flow beneath the Pamir geosuture to have protruded northward as far as the point where its southward concave arc abuts upon the more moderate northward concave arcs (or geosuture) formed by the southward plunging Ural-Kara Tau geosutures. It is therefore assumed that the geographic point of 40°N 70°E represents:

i) The contact-zone between the two global systems of geosutures: The northern one is where the southeastward curving geosutures are tangentially approaching the global eye;

ii) The southern one, whose members are vorticing counter-clockwise upon colliding head-on with the northern system.

XIIb: A system of E-W trending belts (or segments of geosutures) does exist across Afghanistan.

Subsystems of southwestward curving ridges are branching off from the E-W trending segments of geosutures which are limiting each of these belts on its north (Figs. 22.1, 22.21, and 22.24).

i) The northernmost set across the Pamir Vortex is bound on the north by the geosuture crossing through the Lake Onega-Samara-Kara Tau-Kyrgyz and the West Tien Shan ranges and by the Mangyshlak-Alai-Zeravsham geosutures in the south. The southwestward trending Ugomsky, Chamkalsko, and other secondary ridges are however linear, and not curved (Fig. 22.24).

ii) The next set to the south is composed of southeastward concave (and southwestward curving) secondary ridges. That set is limited on its south by the E-W trending geosuture that begins at Ashkabad in the west and extends eastward along the Karakum Canal, Thermes, and Feyzabad to terminate at the N-S trending faulted flank of the Pamir Vortex.

iii) The third belt is bordered on its south by the E-W trending Paropamisus range, which crosses Jalalabad and terminates at the Khyber Pass. No obvious southwestward curving secondary ridges are noticed across that belt.

iv) The fourth belt is limited on its south by the E-W trending geosuture which extends from Lake Saberi on the west (along the N-S trending Zabol Fault at 31°-30'N, 61°E, which is the eastern limit of the Lut Block), across Kandahar to terminate at the northern tip of the first (westernmost) 'finger' of the Pamir Vortex (north of Quetta and Chaman – see above, Fig. 22.24). The southwestward curving secondary ridges across that belt are strongly pronounced by the configurations of these ridges as well as by the intervening system of rivers.

Additional E-W segments of geosutures are noticed further on to the south. These are: (i) the Helmand Depression; (ii) the Gowd-e-Zerah; (iii) the Hamian-I-Mashkal; and (iv) the Siahan Range. However these southern belts are shorter, as compared with the latter four, mostly because of the space occupied by the N-S trending Karachi-Kalat-Quetta structural 'finger' (see above).

Two examples of very similar diagonal fault patterns (although of smaller dimension) are found in NW Turkey, associated with the southern flank of the North Anatolian dextral Fault Zone of the Kirşehir and Aegean Vortices (40°N, 27°E and 33°E; Neugebauer, 1995, Fig. 6, and Yilmaz et al., 1995, Fig. 7, as well as Rotstein, 1984, p. 77 and Fig. 5 - after Şengör and Yilmaz, 1981). The last example represents a system of counterclockwise curving dextral faults which are branching off from the N. Anatolian Fault, and extend to the west of Erzincan. These southeastward concave arcuate faults are of larger dimensions as compared with those of the second example, which is from northwestern Anatolia. The origin of those from the first example is associated with the tight counterclockwise rotation of Central Anatolia (Rotstein, 1984, p. 88; our Figs. 22.21 and 22.23).

We suggest that these patterns of diagonally trending faults could also have been generated because of dextral relative movements of the terrritories north and south of the E-W transverse faults, like those found across Afghanistan and the Pamir Vortex. (Figs. 22.21 and 22.26).

Based on the above, it is assumed that the E-W trending collisional front (or contact) was formed along the global eye, separating between the northward and the southeastward flow patterns of the upper mantle. That front is being breached by occasional northward protrusions along some of the vortices. The intensity and the depth (or length) of the protrusions are changing along the 'eye', being the highest at the Indus-Pamir vortex (and perhaps also along the Andaman-Brahmaputra one). The mantle's northward flows beneath both of these two easternmost vortices appear to extend over long distances. The long axis of the Bhramaputra Vortex is gradually curving to the NE toward the East Siberian Ranges, whereas the other six do not. The route of the Pamir's vortex extension may occur through the Sayan, Baikal, and Skalistyy features, This northeastward curvature of the Brahmaputra vortex seems to extend smoothly into the funnel-shaped continental 'strait' which is situated between the Yablonskyy Range (and its parallels) and the Great Kingan Range. Both extensions seem to merge toward the Kolyma Range (Figs. 22.1, 22.25, 22.26, 22.27, and 22.28).

The stratigraphic sequence of the northern half of Pakistan was studied by Gee (1989), based on data from the Salt Range region.



Figure 22.28. Extension of the spiraling geosutures into the Arctic: Although not discussed in the text, the poleward extensions of the various geosutures converge around the Arctic Ocean. Discussion can be found in Neev and Hall (1982, Fig. 4), and Hall (1990). Note the merger of the North American geosutures along the relatively straight margin north of Canada and Greenland (the Queen Charlotte – Beaufort Sea geosuture).
Shaded relief is IBCAO bathymetry, ArcInfo format on a 2.5 km grid at 75°N. Polar Stereographic projection.

His results indicate the occurrence of eight important unconformities across the Indian continent through its geological history. Among these the following five are considered to be the major ones:

i) between the Precambrian basement and the Eocambrian Salt Range Formation;

ii) between Middle Cambrian and Early Permian;

iii) between Early Cretaceous and the Paleocene;

iv) between Middle Eocene and Early Miocene;

v) between the Pliocene and the Pleistocene.

The physical nature that prevailed during these periods of unconformities, as well as during the in-between phases (the 'Type of Formations' column of Gee's Table 1), reflect the alternating occurrences of both vigorous vertical tectonic movements and extreme climatic changes (evaporitic to humid and vice versa). The relevant description of the Early Cretaceous and Mid-Eocene to Miocene periods (130 Ma to 30 Ma) across the Indian Peninsula, indicate even less extreme conditions to have prevailed then, as compared with the other periods. On the other hand the first (Precambrian to Eocambrian) and second (Ordovician to Early Permian) seem to reflect the most extreme changes which occurred during longer phases, as compared with the other six periods of unconformities.

Burtman and Molner (1993, p. 1 and 48-9, Figs. 2-4, 8, 14, 23-25, 38) describe "A Paleozoic suture between Eurasia and continental fragments originally from Gondwanaland [which] crosses northern Afghanistan and follows the Kunlun in northern Tibet". That late Paleozoic belt includes middle to late Paleozoic volcanic and ultramafic rocks, which are now wrapping around the Northern Pamir from northern Afghanistan into the Western Kunlun. "Although the rocks of Pamir have been assembled by collisions in late Paleozoic and in Mesozoic time, deformation of Cretaceous and Tertiary rocks attests to Cenozoic crustal shortening. In some cases klippen allow estimates of minimum 300 km of shortening within the Pamir implying that the southern edge of the Pamir has moved northward 600 km or more with respect to the area further north". The E-W trending Tadjik Depression was filled with 10-15 km thick Mesozoic-Cenozoic sequences of detrital and carbonate sediments that went through abrupt truncations and were dragged northward along the westward edge of the Pamir Wedge. A close to mirror image pattern also exists along the eastern limit of the Pamir. The configurations and geographic positions of these two belts (which include the Karakoram and the Indus-Tsapona ranges) are expressing a counterclockwise asymmetric (westward) pattern of counterclockwise rotational movements across these southward concave arcuate geosutures.

The configuration, strength and other crustal characteristics of the Indian basement across the North Pakistan territories are inferred from the results of topographic and gravimetric surveys, as well as seismic reflection and drilling data (Duroy et al., 1989).

The load of the Himalayan Mountains, together with the northward underthrusting of the Indian Plate, are generating a northward sequence of E-W trending elongate crustal bulges and troughs (*i.e.* trending perpendicular to the northward movement of the West Indian plate, or the Pamir Wedge). These are (from north to south):

i) The Himalayan foredeep, filled mostly by eroded sediments and extending between the Pamirs and the Main Karakoram Thrust (M.K.T.);

ii) The Kohistan Area, extending , between the M.K.T. and the Main Mantle Thrust, where more positive gravity values, which are associated with a flexural bulging feature, occur and from where the values of negative Bouguer gravity anomalies are doubling northward (from -200 to -400 mGal). Both of these important changes occur because this is where the crustal underthrusting beneath the crust of Kohistan (Duroy et al., *ibid*, Figs. 2, 3, 9, 11) is taking place;

iii) A mass deficit underlies a broad area extending from southern Kohistan through the Peshawar Basin. The Potwar Plateau and the Salt Range terminate at the northern fringe of the Sargodha High (about 300 km north of Peshawar). The top of the basement surface is dropping northward about 2° from sea level elevation at the Sargodha High to a depth of more than 11 km below sea level at the boundary between Peshwar and Kohistan, where the E-W trending and northward dipping Main Mantle Thrust is found. The MOHO dramatically drops northward at that point, reaching a depth of 65 km beneath the North Kohistan Arc. The crust across that belt is doubling its thickness due to its northward underthrusting (*ibid*, Fig. 3).

The overall upward convexity of the basement surface between the Pamir and the Sargodha suggest that it was generated by a lithospheric flexuring (or a ramp-like mechanism) along the N-S axis of the West Indian sub-continent-Pamir, which is a wedge-like geosuture. Analogous to the case of the Arabian-Ararat wedge (see above), the faster northward rate of movement of the Pamir-West Indian wedge, as compared with its Afghan and East-Indian neighbors, is associated with oblique collisions (as indicated by the asymmetric drag folds and wrench faults which are generated along its western flanks).

Duroy et al. (*ibid*) developed an elastic flexural model that shows the changes in the stress-compression-densities (or gravity) values as a result of the depth-crustal thickness changing conditions. That model enables the prediction of the extension and contractional changes (and therefore also its facial characteristics such as more basic-oceanized or continental types of crust). It may therefore explain not only the origin of the south to north changes within the sequence of E-W trending facial-structural belts along the north Pakistan-Pamir wedge during and because of the northward motion of the Indian plate; it may also offer a genetic explanation to the origin of the northward changing sequence of perpendicularly trending facies-structural belts along the Arabian-Ararat wedge. It may also supply an alternative explanation to the origin and tectonic processes across the East Mediterranean basin.

CAVEATS

This paper has evolved through many drafts over the past eight years. Each draft refined and amplified earlier versions, while adding new regions to the synthesis. For inclusion in this book, which focuses on the Levant, we have primarily concentrated on

the areas of the Mediterranean and the Central Plate. Many of the figures for these areas have additional details only briefly discussed in the text. A number of other figures showed the extension of the geosutures over the rest of the world. For the sake of completeness we have added them too.

The study of these ancient first-order features is still in its very early stages. Our experience has been that as new data appears, some implications may become improbable, while others are corroborated or subject to modification. We would hope that the reader would gain something from our efforts.

With her physiography, Mother Earth is trying to tell us something. Only by looking at the big picture can we hope to gain an understanding of the devil in the details. Fortunately, some of these details may be almost upon us with the continuing release of the spectacular land topography from the STS-99 Shuttle Radar Topography Mission (SRTM) of the Endeavour in February 2000. This data, at a 3" grid spacing (≤90 m), is already showing impressive features.

ACKNOWLEDGEMENTS

This work was carried out under the aegis of Project 20743 with the Geological Survey of Israel (GSI), Israel Ministry of National Infrastructures. The opinions expressed by the authors are their own and do not necessarily reflect those of the GSI or our colleagues. We gratefully acknowledge Francis Hirsch for his interest, encouragement, and critical comments. Petter Grossman drafted the figures through their many evolutions. Early manuscripts were typed by Eva Daniels and Rivka Bachmann.

The senior author is especially indebted to the GSI for allowing him to maintain 'emeritus' status far in excess of the legal norms. The GSI Documentation Center was essential for copying articles, and the source of much useful reference material. Additional assistance was given by Ms. Zelda Colodner and Ms. Debby Magen at the Earth Sciences Library of the Hebrew University in Givat Ram.

We are also indebted to our wives and children for their forebearance over the many years that this work was in progress: Tamar Neev, who put up with a room that must never be reordered, and Yuval, Yossi, and Ofer Neev for their moral support and understanding that this project had a life of its own; Ruti Hall who got used to calls and trips at odd hours, and twins Naomi and Daniel Hall who had to share their father far too often.

REFERENCES CITED

Abdel Aal, A., El Barkooky, A., Gerrits, M., Meyer, H., Schwander, M., and Zaki, H., 2000. Tectonic evolution of the Eastern Mediterranean Basin and its significance for hydrocarbon prospecting in the ultra deepwater of the Nile Delta. The Leading Edge, October 2000, p. 1086-1101.

Abdel Aal, A., El Barkooky, A., Gerrits, M., Meyer, H., Schwander, M., and Zaki, H., 2001. Tectonic evolution and prospectivity of the Nile Delta Deepwater Area. GeoArabia, 6(3), Gulf Petrolink, Bahrain, p. 363-383(?).

Al-Husseini, Moujahed I., (Gulf PetroLink), 2000. Origin of the Arabian Plate structures: Amar Collision and Najd Rift. GeoArabia, 5(4), p. 527-542/t.

Allegre, Claude, 1988. The behavior of the Earth, Harvard University Press, Cambridge, MA, USA, 272 p.

Almagor, G., 1980. Halokinetic deep-seated slumping on the Mediterranean slope of Northern Sinai and Southern Israel. Marine Geology, 4(1), p. 83-105.

Almagor, G., and Garfunkel, Z., 1979. Submarine slumping in continental margin of Israel and Southern Sinai. Am. Assoc. Petrol. Geol. Bull., 63(3), p. 324-340.

Alpert, P., and Ganor, E., 1993. A jet-stream associated heavy dust storm in the Western Mediterranean, J. geophys. Res., 98(4D), p. 7339-7349.

ASPRS, 2000. Landsat imaging of the African Continent (Color). In: Am. Soc. Photogramm. Rem. Sens. J., 66(9), front cover. Based on the GeoCover OrthoTM Landsat TM Mosaic, 540 m pixels, by Earth Satellite Corporation, Rockville, MD, 2001.

Andrieux, J. J., Over, S., Poisson, A., and Bellier, O., 1995. The North Anatolian Fault Zone: distributed Neogene deformation in its northward convex part. Tectonophysics, 243(1-2), p. 135-154.

Argand, E., 1924. La tectonique d'Asie. C. R. Congr. Géol. Intern, 13e, 1922, Liege, p. 169-371.

Arthaud, R., and Matte, Ph., 1977. Late Paleozoic strike-slip faulting in southern Europe and northern Africa: Result of a right-lateral shear zone between the Appalachians and the Urals. Geol. Soc. Am. Bull., 88(9), p. 1305-1320.

Arvidson, R. E., Guiness, E. A., Strebeck, J. W., Davies, G. F., and Schulz, K. J., 1982. Image processing applied to gravity and topographic data covering the continental U.S., Eos Trans. AGU, 63(18), p. 261-265.

Arvin, M., and Shokri, B., 1997. Genesis and eruptive environment of basalts from the Gogher Ophiolitic Melange, SW of Kerman, Iran. Ofioliti, 22(2), p. 175-182.

Awad, H., 1951. La montagne du Sinai central. Publ. Soc. Geogr. Egypte, Caire, 247 p.

Awad, H., 1953. Signification Morphologique des Depots Lacsutres de la Montagne du Sinai Central. Bull. Soc. Roy. Geogr. Egypte, XXV, p. 23-28.

Bally, A. W., 1989. Phanerozoic Basins of North America. In: Bally, A. W., and Palmer, A. R., (eds.), The Geology of North America, DNAG Volume A, Geol. Soc. Am., 619 p.

Batier, M. G. (Editor), 1951-52. Geological Map of Algeria, Second Edition. Scale 1:500,000. Service Géologique, Gouvernment Général de Algeria.

Beauchamp, W. H., Barazangi, M., Demnat, A., and El Algi, M., 1996. Intracontinental rifting and inversion. Missour Basin and Atlas Mountains, Morocco. Am. Assoc. Petrol. Geol. Bull., 80(9), p. 1459-1482.

Beauchamp, W. H., Ries, A. C., Coward, M. P., and Miles, J. A., 1995. Masirah Graben, Oman: A Hidden Cretaceous Rift Basin? Am. Assoc. Petrol. Geol. Bull., 79(6), p. 864-879.

Behrendt, J. C., and Grim, M. S., 1983. Structural elements of the U. S. Atlantic Margin delineated by second vertical derivative of aeromagnetic data. 3 maps, 1:2,500,000, Map GP-956, U.S.G.S. Federal Center, Denver, CO 80225.

Behrendt, J. C., Schlee, J. Robb, J. M., and Silverstein, M. K., 1974. Structure of the continental margin of Liberia, West Africa. Geol. Soc. Am. Bull., 85(7), p. 1143-1158.

Ben-Avraham, Z., Ginzburg, A., Makris, J., and Eppelbaum, L., 2002. Crustal structure of the Levant Basin, eastern Mediterranean. Tectonophysics, 346(1-2), p. 23-43.

Ben-Avraham, Z., Nur, A., and Cello, G., 1987. Active transcurrent fault system along the north African passive margin. Tectonophysics, 141, p. 249-260.

Ben-Gai, Y., and Shamir, G., 1997. The evolution and seismicity of the Palmahim Disturbance (Southeast Mediterranean Continental Margin). Final Report – Phase I. Report No. 631/9/96, Geophysical Institute of Israel, 6 p, 1 table, 7 figs.

Bermingham, P. M., Fairhead, J. D., and Stuart, G. W., 1983. Gravity study of the Central African Rift System: a model of continental disruption. 2. The Dafur domal uplift and associated Cainozoic volcanism. In: P. Morgan and B. H. Baker (eds.), Processes of Continental Rifting, Tectonophysics, 94(1-4), p. 205-222.

Berry, P. A. M., Hilton, R. D., and Johnson, C. P. D., 2002. ACE: first full release of the new 30" GDEM incorporating satellite altimeter derived heights. European Geophysical Assembly, Nice France, April 2002. Also see: http://www.cse.dmu.ac.uk/geomatics/ace/ACE_report.pdf.

Best, J. A., Barazangi, M., Al-Saad, D., Sawaf, T., and Gabran, A., 1993. Continental margin evolution of the northern Arabian platform in Syria. Am. Assoc. Petrol. Geol. Bull., 77(--), p. 173-193.

Biju-Duval, B., Dercourt, J., and Le Pichon, X., 1977. From the Tethys Ocean to the Mediterranean seas: a plate tectonic model of the evolution of the Western Alpine system. In: Biju-Duval, B., and L. Montadert (eds.), Structural history of the Mediterranean Basins, p. 143-164. Proceedings of the International Symposium held 25-29 October 1976 in Split, Yugoslavia, XXV^e Congrès-Assemblée Plénière de la C.I.E.S.M., Éditions technip, Paris, 448 p.

Biju-Duval, B., Letouzey, J., Montadert, L., Courrier, P., Mugniot, J. F., and Sancho, J., 1974. Geology of the Mediterranean Sea Basins. In: C. A. Burk and C. L. Drake (eds.), The Geology of Continental Margins, Springer Verlag, Berlin, p. 695-721.

Bonatti, E., 1973. Origin of offsets of the Mid-Atlantic Ridge in fracture zones. J. Geol., 81(--), p. 144-156.

Bonatti, E., 1978. Vertical tectonism in oceanic fracture zones. Earth Planet. Sci. Lett., 37(3), p. 364-379.

Bonatti, E., 1990. Subcontinental mantle exposed in the Atlantic Ocean on St. Peter-Paul islets. Nature, 345(6278), p. 800-802.

Bonatti, E., and Chermak, A., 1981. Formerly emerging crustal blocks in Equatorial Atlantic. Tectonophysics, 72(1-4), p. 165-180.

Bonatti, E., and Crane, K., 1982. Oscillatory spreading explanation of anomalously old uplifted crust near oceanic transforms. Nature, 300(5890), p. 343-345.

Bonatti, E., Sarnthein, M., Boersma. A., Gorini, M., and Honnorez, J., 1977. Neogene crustal emersion and subsidence at the Romanche Fracture Zone, Equatorial Atlantic. Earth Planet. Sci. Lett., 35(3), p. 369-383.

Boote, D. R. D., Clark-Lowes, D. D., Traut, M. W., 1998. Palaeozoic petroleum systems of North Africa. In: D. S. Macgregor, R. Moody, and D. D. Clark-Lowes (eds.), Petroleum Geology of North Africa. Geol. Soc. London, Spec. Pap. 132, p. 7-68.

Bottomley, D. J., Katz, A., Chan, L. H., Starinsky, A., Douglas, M., Clark, I. D., and Raven, K. G., 1999. The origin and evolution of Canadian Shield brines: evaporation or freezing of seawater? New lithium isotope and geochemical evidence from the Slave craton. Chem. Geol., 155(3-4), p. 295-320.

Brew, G., Barazangi, M., Sawaf, T., Al-Maleh, K., 2000. Tectonic map and geologic evolution of Syria: The role of GIS. The Leading Edge, 19(2), p. 176-182.

Brew, G., Litak, R. K., Barazangi, M., and Sawaf, T., 1999. Tectonic evolution of Northeast Syria: Regional implications of hydrocarbon prospects. GeoArabia, 4(3), p. 289-318.

Brew, G., Litak, R. K., Seber, D., Barazangi, M., Al-Imam, A., and Sawaf, T., 1997. Basement depth and sedimentary velocity structures in the North Arabian Platform, eastern Syria. Geophys. J. Intl., 128(--), p. 617-631.

Brown, G. F., 1972. Tectonic map of the Arabian Peninsula. Saudi Arabian Directorate General of Mineral Resources, Arabian Peninsula Map AP-2.

Brown, C., and Girdler, R. W., 1980. Interpretation of African gravity and its implication for the breakup of the continents. J. Geophys. Res., 85(B11), p. 6443-6455.

Brown, G. F., and Jackson, R. O., 1960. The Arabian Shield. 21st Int. Geol. Congr., Copenhagen, 9, p. 69-77.

Browne, S. E., and Fairhead, J. D., 1983. Gravity study of the Central African Rift System: a model of continental disruption. 1. The Ngaoundere and Abu Gabra Rifts. In: P. Morgan and B. H. Baker (eds.), Processes of Continental Rifting, Tectonophysics, 94(1-4), p. 187-203.

Browne, S. E., Fairhead, J. D., and Mohamed, I. I., 1985. Gravity study of the White Nile Rift, Sudan, and its regional tectonic setting. Tectonophysics, 113(1/2), p. 123-137.

Buffler, R. T., and Thomas, W. A., 1994. Crustal structure and evolution of the southeastern margin of North America and the Gulf of Mexico basin. Chapter 4, p. 219-264. In: R. L. Speed (ed.), Phanerozoic Evaluation of North American Continent-Ocean Transitions, DNAG Continent-Ocean Transect, Summary Volume, Geol. Soc. Am., 504 p.

Burollet, P. F., 1971. Remarques geodynamiques sur le Nord-East de la Tunisie. C. R. Soc. Geol., France, Somm., 8, p. 411-413.

Burtman, V. S., and Molnar, P., 1993. Geological and geophysical evidence for deep subduction of continental crust beneath the Pamirs. Geol. Soc. Am., Spec. Pap. 281, p. 1-76.

Chaimov, T. A., Barazangi, M., Al-Saad, T., Sawaf, T., and Khaddour, M., 1993. Seismic fabric and 3-D upper crustal structure of the southwestern intracontinental Palmyride fold belt, Syria. Am. Assoc. Petrol. Geol. Bull., 77(12), p. 2032-2047.

Choubert, G., 1968. International Tectonic Map of Africa 1: 5,000,000. Paris, UNESCO, Sheets 2, 3, 4, 5, 6, and 7.

Choubert, G., and Faure-Muret, A., 1976. Geological World Atlas, 1:10,000,000, Sheets 5-9. UNESCO and Commission for the Geological Map of the World, 7 Place de Fontenoy, Paris.

Cohen, A., 1983. The North-Caspian Depression - a knot of ancient subduction zones. In: R. H. Gabrielsen, I. B. Ramberg, D. Roberts, and O. D. Steinlein (eds.), Proceedings of the 4th International Conference of Basement Tectonics, Oslo, Norway, Aug. 10-14, 1981, International Basement Tectonics Association, Publication No. 4, Salt Lake City, Utah 84111, p. 87-101.

Cohen, Z., 1976. Early Cretaceous buried canyon: Influence on accumulation of hydrous in Heletz Oil Field, Israel. Am. Assoc. Petrol. Geol. Bull., 60(1), p. 108-114.

Cohen, Z., 1979. The subsurface geology of the southern Coastal Plain and petroleum research. Unpubl. Ph.D. thesis. The Hebrew University, Jerusalem, 69 p. (In Hebrew, English summary).

Cooke, R. U., and Warren, A., 1973. Geomorphology in deserts. B. T. Batsford Ltd., London, 394 p.

Creer, K. M., 1964. A reconstruction of the continents for the upper Palaeozoic from palaeomagnetic data. Nature, 203(4950), p. 1115-1120.

Deane, J. D., 1995. The structural evolution of the Kombat deposits, Otavi Mountainland, Namibia. Communications, Geol. Survey of Namibia, 10, p. 99-107.

Dean, W. T., and Monod, O., 1990. Revised stratigraphy and relationships of Lower Paleozoic rocks, eastern Taurus Mountains, south central Turkey. Geol. Mag., 127(4), p. 333-347.

deCaerna, Z., 1989. An outline of the geology of Mexico. In: A. W. Bally and A. R. Palmer (eds.), The Geology of North America, DNAG Volume A, Geol. Soc. Am., p. 233-264.

Decima, A., and Wezel, F. C., 1971. Osservazioni sulle evaporiti Messiane della Sicilia xentromeridionalle. Riv. Min. Sicil., 22(130-132), p. 170-187.

DeLoczy, L., 1970. Tectonismo transversal na América do Sul e suas relações genéticas com as zonas de fratura das Cadeias Meio-Oceânicas, An. Acad. Bras. Ciênc., 42, p. 185-205.

Dercourt, J., Zonenshain, L. P., Ricou, L. E., Kazmin, V. G., Le Pichon, X., Knipper, A. L., Grandjacquet, C., Sbortshikov, I. M., Geyssant, J., Lepvrier, C., Pechersky, D. H., Boulin, J., Sibuet, J. C., Savostin, L. A., Sorokhtin, O., Westphal, M., Baznerinov, M. L., Lauer, J. P., and Biju-Duval, B., 1986. Geological evolution of the Tethys Belt from the Atlantic to the Pamirs since the Lias. Tectonophysics, 123(1-4), p. 241-315, 10 plates. (In: J. Aubouin, X. Le Pichon, and A. S. Monin, (eds.).

Derin, B., 1974. The Jurassic of Central and Northern Israel. Unpubl. Ph.D. thesis, Hebrew University, Jerusalem, 152 p. 10 pls. plus vi. (In Hebrew, 5 p. English abstract).

Desheng, Li, Digang, Liang, Chengzao, Jia, Gang, Wang, Wu, Qizhi, and He, Dengfa, 1996. Hydrocarbon accumulations in the Tarim Basin, China. Am. Assoc. Petrol. Geol. Bull., 80(10), p. 1587-1603.

Desmons, J., Companoni, R., Cortesogno, L., Frey, M., and Gaggero, L., 1999. Peri-Alpine metamorphism of the Eastern Alps. Swiss. Bull. Mineralogy and Petrology, Band 79, haft 1, p. 23-39.

Dewey, J. F., and Şengör Celal, A. M., 1979. Aegean and surrounding regions: Complex multiplate and continuum tectonics in a convergent zone. Geol. Soc. Am. Bull., Pt. 1, 90(1), p. 84-92.

De Wit, M., Jeffrey, M., Bergh, H., and Nicolaysen, L., 1988. Geological Map of Sectors of Gondwana, reconstructed to their disposition at about 150 Ma.

Scale 1:10,000,000. Tulsa, OK, Am. Assoc. Petrol. Geol., and Johannesburg, So. Africa, Univ. Witwatersrand.

Dixon, J. E., and Robertson, A. H. F., (eds.), 1985. The geological evolution of the Eastern Mediterranean. Geological Society of London, Spec. Publ. No. 7, Blackwell Scientific Publications, Oxford, UK, 848 p.

Drake, C. L., and Woodward, H. P., 1963. Appalachian curvature, wrench faulting and offshore structures. Trans. New York Acad. Sci., Ser. 11, 26, p. 48-63.

Druckman, Y., 1974. The stratigraphy of the Triassic sequence in Southern Israel. Geol. Surv. Israel Bull. 64, 92 p.

Druckman, Y., 1985. Evidence for Early-Middle Triassic faulting and possible rifting from the heletz Deep Borehole in the coastal plain of Israel. In: J. E. Dixon and A. H. F. Robertson (eds.), The Geological Evolution of the Eastern Mediterranean, Geological Societ of London, Spec. Publ. No. 7, Blackwell Scientific Publications, Oxford, UK, p. 203-212.

Druckman, Y., Buchbinder, B. Martinotti, G. M., Simantov, R., and Aharon, P., 1995a. The buried Afiq Canyon (eastern Mediterranean, Israel): a case study of a Tertiary submarine canyon exposed in late Messinian times. Marine Geology, 123(--), p. 167-185.

Druckman, Y., Gill, D., Fleischer, L., Gelberman, E., and Wolff, O., 1995b. Subsurface geology and structural evolution of the Northwestern Negev, Southern Israel. Isr. J. Earth-Sci., 44(1), p. 115-135, 15 figs.

Dubief, J., 1952. Le vent et le deplacement du sable au Sahara, Trav. Inst. Rech. Sahar., 8, 123-162.

Duroy, Y., Farah, A., and Lillie, R. J., 1989. Subsurface densities and lithospheric flexure of the Himalaya foreland in Pakistan. In: L. M. Malinconico Jr. and R. J. Lillie, (eds.), Tectonics of the Western Himalayas, Geol. Soc. Am. Spec. Pap. 232, p. 217-236.

Eberle, D., Andritzky, G., and Wackerle, R., 1995. The new magnetic data set of Namibia: Its contribution to the understanding of crustal evolution and regional distribution of mineralization. Communications, Geol. Survey of Namibia, 10, p. 141-150.

El-Baz, F., C. S. Breed, M. J. Grolier, and J. F. McCauley, 1979. Eolian features in the Western Desert of Egypt and some applications to Mars, J. Geophys. Res., 84, p. 8205-8221.

Emeis, K. -C., Robertson, A. H. F., Richter, C., et al., (Eds.), 1996. Proceedings of the Ocean Drilling Program, Initial Reports, U. S. Govt. Printing Office, Washington, DC, Vol. 160, 972 p.

Emery, K. O., and Uchupi, E., 1984. The geology of the Atlantic Ocean. Springer-Verlag, New York, Berlin, Heidelberg, Tokyo, 1050 p., 12 charts.

Erickson, A., and Simmons, G., 1974. Environmental and geophysical interpretation of heat-flow measurements in Black Sea. In: Degens, E. T., and Ross, D. A. (eds.), The Black Sea – Geology, Chemistry, and Biology. Am. Assoc. Petrol. Geol., Mem. 20, p. 50-62.

Espinosa, A. F., Rinehart, W., and Tharp, M., 1981. Seismicity of the Earth, 1960-1980. Ocean shaded relief basemap, scale 1:46,460,000, U. S. Geological Survey, 1982.

Evans, D. A. D., 2000. Stratigraphic, geochronological, and paleomagnetic constraints upon the Neoproterozoic climate paradox. Am. J. Science, 300(5), p. 347-433.

Eyal, M., Bartov, Y., Shimron, A. E., and Bentor, Y. K., 1980. Geological Map of Sinai, Scale 1:500,000. Geol. Surv. Israel.

Eyal, M., Bartov, Y., Shimron, A. E., and Bentor, Y. K., 1985. The Geology of Sinai. Explanatory Notes to the 1980 Geological and Geological Photomap, scale 1:500,000Map of Sinai. Isr. Geol. Surv. Rept. GSI/1/85, 81 p., 10 Figs. (In Hebrew).

Faqira Mohammad, I., and Al-Hawuag Ali, Y., 1998. Infracambrian salt basin in the Western Rub Al Khali, Saudi Arabia. GeoArabia, Abstracts, 3(1), p. 93.

Farah, A., and DeJong. K. A., Editors, 1979. Geodynamics of Pakistan. Geological Survey of Pakistan, Quetta, 361 p.

Farre, J. A., McGregor, B. E., Ryan, W. B. F., and Robb, J. M., 1983. Breaching the shelfbreak: Passage from youthful to mature phase in submarine canyon evolution. SEPM Special Publication No. 33, p. 25-39.

Fekirine, B., and Abdallah, H., 1998. Paleozoic lithofacies correlation and sequence stratigraphy of the Saharan Platform, Alegria. In: D. S. Macgregor, R. T. J. Moody, and D. D. Clark-Lowes, (eds.), Petroleum Geology of North Africa. Geological Society of London, Spec. Publ. 132, p. 97-108.

Finetti, I., 1985. Structure and evolution of the central Mediterranean (Pelagonian and Ionian Seas). Chapter 10 in: D. J. Stanley and F. -C. Wezel (eds.), Geological Evolution of the Mediterranean Basin, Springer-Verlag, New York, p. 215-230.

Flinch, J. F., 1997. Accretion and extensional collapse of the external Western Rif (North Morocco). In: P. A. Ziegler and F. Horvath (eds.), Structure and Prospects of Alpine Basins and Forelands, Mém. Mus. Nat. d'Hist. Natur., Vol. 170, 2 vols., 552 p., Atlas, 31 foldouts, CGMW Peri-Tethys Memoir 2, p. 61-86.

Folkman, Y., 1971. Aeromagnetic survey of the areas of the Golan, Shomron, Judea, and Gaza offshore. Institute for Petroleum Researrch and Geophysics, Report SMA/760/70, 34 p.

Folkman, Y., 1999. A Tertiary submarine canyon: The key to understanding the "Palmachim Disturbance" under the continental slope of Israel. In: S. Ilani, Y. Harlavan, M. Shirav (eds.), The Annual Meeting of the Israel Geological Society, Dead Sea, 8-10 March 1999, p. 22.

Ford, W. E., 1951. Dana's Textbook of Mineralogy Fourth Edition, 851 p.

Francheteau, J., and Le Pichon, X., 1972. Marginal fracture zones as structural framework of continental margins in the South Atlantic Ocean. Am. Assoc. Petrol. Geol. Bull., 56(6), p. 991-1007.

Frape, S. K., and Fritz, P., 1987. Geochemical trends for groundwaters from the Canadian Shield: In: P. Fritz and S. K. Frape (eds.), Saline water and ages in crystalline rocks. Geological Association of Canada Special Paper 33, p. 19-38.

Freund, R., Goldberg, M., Weissbrod, T., Druckman, Y., and Derin, B., 1975. The Triassic-Jurassic structure of Israel and its relation to the origin of the eastern Mediterranean. Geol. Surv. Israel., Bull. 65, 26 p.

Frey, M., Desmons, J., and Neubaur, F., 1999. Editors of the new metamorphic map of the Alps. Includes: (i) Map of Pre-Alpine Metamorphism, 1:1,000,000. (ii) Map of Alpine Metamorphism, 1:500,000, (iii) Special volume (230 p.) that contains 12 relevant articles and an introduction (by the editors) p. 1-4. Swiss Bull. of Minerology and Petrology, Band 79, Heft 1, Staubli Verlag AG, Zurich.

Fukao, Y., Maruyama, S., Obayashi, M., and Inoue, H., 1994. Geologic implication of the whole mantle Pwave tomography. J. Geol. Soc. Japan, 100(1), p. 4-23.

Fusi, N., and Kenyon, N. H., 1996. Distribution of mud diapirism and other geological structures from long-range sidescan sonar (GLORIA) data, in the Eastern Mediterranean Sea. Mar. Geol. 132(1), p. 21-38.

Gaertner, H. -R., Walther, H. W., 1971-1972. Carte Géologique de l'Europe et des regions riveraines de la Méditerranée, 1:5,000,000. Eastern sheet. BGR, Hannover and UNESCO, Paris.

Gahagan, L. M., Scotese, C. R., Royer, J. Y., Sandwell, D. T., Winn, J. K., Tomlins, R. L., Ross, M. I., Newman, J. S., Mueller, R. D., Mayes, C. L., Lawver, L. A., Huebeck, C. E., 1988. Tectonic fabric map of the ocean basins from satellite altimetry data. In: C. R. Scotese and W. W. Sager (eds.), Mesozoic and Cenozoic plate reconstructions, Tectonophysics, 155(1-4), p. 1-26.

Ganor, E., 1991. The composition of clay minerals transported to Israel as indicators of Saharan dust emission. Atmospheric Environment, 25A(12), p. 2657-2664.

Gansser, A., 1955. New aspects of the geology in Central Iran. 4th World Petrol. Congress, Proc., Rome, Sect. IA/5, Paper 2, p. 279-300.

Gansser, A., 1964. Geology of the Himalayas. John Wiley & Sons, Interscience Publishers, London and New York, 289 p.

Gansser, A., 1973. Facts and theories on the Andes. J. Geol. Soc. London, 129, p. 93-131.

Garfunkel, Z., 1998. Constraints in the origin and history of the Eastern Mediterranean basin. Tectonophysics, 298(1-3), p. 5-35.

Garfunkel, Z., Arad, A., and Almagor, G., 1979. The Palmahim Disturbance and its regional setting. Geological Survey of Israel, Bull., No. 72, 58 p.

Garfunkel, Z., and Bartov, Y., 1977. The tectonics of the Suez Rift. Geol. Surv. Israel, Bull. 71, p. 1-44, 12 figs., 2 tables.

Gary, M., McAfee, R. Jr., and Wolf, C. L., 1974. Glossary of Geology. American Geological Institute, Washington, D.C., 805+52 p.

GEBCO, 2003. Centenary Edition of the GEBCO Digital Atlas (GDA), produced on a 1' grid at the British Oceanographic Data Centre, Birkenhead, UK, from data compiled by the working groups of the General Bathymetric Chart of the Oceans of IOC and IHO. See: http://www.bodc.ac.uk/cgi-bin/framer? http://www.bodc.ac.uk/projects/gebco/ for general information, and

http://jules.unavco.org/GMT/gebco_2003/gridhelp.pdf for the User Guide to the Centenary Edition.

Gee, E. R., 1989. Overview of the geology and structure of the Salt Range, with observation on related areas of northern Pakistan. In: L. M. Malinconico Jr. and R. J. Lillie (eds.), Tectonics of the Western Himalayas, Geol. Soc. Am., Spec. Pap. 232, p. 95-112.

Geospace, 1998. Global Satellite Image Map 1:1,000,000, The Alps. Sheet No. D-0IE/Eu-51. Geospace, Vienna.

Gevin, P., and Sougy, J., 1952. Carte géologique du nord-ouest de l'Afrique: Sahara occidental au 1:2,000,000, Congrés Géologique International, Alger, 1952, 1 sheet.

Gevin, M. P., Alia Medina, M., Blaise, J., Cornet, A., Fabre, J., Jacquet, F., Karpoff, R., Lameyre, J., de la Vina, J., Menchikoff, N., de Meyendorf, A., Monod, T., Muñoz Cabezon, C., Ten Dam, A., Bourgeois, M., Durozoy, G., Bois, C., Claracq, P., Hindermeyer, J., Jacqmin, A., Mollier, M., Poulet, M., and Sallé, C., 1962. Carte géologique du nord-ouest de l'Afrique: Sahara occidental au 1:2,000,000, 2nd Edition, C.N.R.S., 1 sheet.

Gidon, M., Berthier, F., Brilliant, J. P., Halbronn, B., and Maurizot, P., 1974. Character and amplitude of strike-slip of the "main fault" in the Borudjerd-Dorud region (eastern Zagros, Iran). Acad. Sci. Comptes Rendus, ser. D, v. 278, p. 701-704. (In French).

Giese, P. K., Reutter, K. J., Jakobshagen, V., and Nicolich, R., 1982. Explosion-seismic crustal studies in the Alpine-Mediterranean region and their implications to tectonic processes. In: Berckhemer H., and Hsü, K. (eds.), Alpine Mediterranean Geodynamics, AGU Geodynam. Ser., 7, Am. Geophys. Un., Washington, DC, p. 34-74.

Gignoux, Maurice, 1954. Stratigraphic Geology. W. H. Freeman Publishers, San Francisco, CA, 682 p.

Ginzburg, A., Folkman, Y., Rybakov, M., Rotstein, Y., Assael, R., and Yuval, Z., 1993. Israel – Bouguer Gravity Map 1:500,000. Holon, Inst. Petrol. Res. Geophys. and Survey of Israel, 1 map, 2 mGal contours, terrain corrected using 25 m DTM of Israel.

Glatzmaier, G. A., and Roberts, P. H., 1995. A three-dimensional self-consistent computer simulation of a geomagnetic field reversal. Nature, 377(6546), p. 203-209.

Goldberg, M., 1970. The lithostratigraphy of Arad Group (Jurassic) in the northern Negev. Unpubl. Ph.D. thesis, Hebrew University, Jerusalem, 137 p. (In Hebrew, English abstract).

Goldberg, M., and Friedman, G. M., 1974. Paleo-environments and paleogeographic evolution of the Jurassic system in southern Israel. Geol. Surv. Israel, Bull. 61, 44 p.

Gordon, R. G., and DeMets, C., 1989. Present-day motion along the Owen Fracture Zone and Dalrymple Trough in the Arabian Sea. J. Geophys. Res., 94(B5), p. 5560-5570.

Goter, S. K., 1989. World Seismicity 1979-1982 (map). National Earthquake Information Center. U.S.G.S. Fed. Center-Denver, M.S. 967, CO 80225.

Grabert, H., 1976. Das Amazonas-Schersystem. N. Jb. Geol. Plaont. Mh. H. 1, p. 1-20.

Grabert, H., 1983. The Amazon Shearing System. Tectonophysics, 95(3/4), p. 329-336.

Grader, P., 1960. Geological history of the Heletz-Brur area, Israel: Lower Cretaceous. Geol. Surv. Israel, Bull. 31, p. 1-50.

Grand, S. P., 1994. Mantle shear structure beneath the Americas and surrounding oceans. J. Geophys. Res., 99(B6), p. 11,591-11,621.

Grant, A. C., 1975. Structural modes of the western margin of the Labrador Sea. In: Willem J. M. Van der Linden and J. A. Wade, (eds.), Offshore Geology of Eastern Canada, Vol. 2 - Regional Geology, Geol. Surv. Canada, Geological Paper 74-30, p. 217-231.

Grecula, P., Horovka, D., and Putis, M. (Editors), 1997. Geological evolution of the West Carpathians. IUGS/UNESCO, IGCP Project No. 276. Geol. Surv. Slovak Republic, Mineralia Slovaca Corporation, Bratislava, 370 p.

Gripp, A. E., and Gordon, R. G., 1990. Current plate motions relative to the hotspots incorporating the NUVEL-1 plate motion model. Geophys. Res. Lett., 17(8), p. 1109-1112.

Gurnis, M., 2001. Sculpting the Earth from the Inside Out. Scientific American, 284(3), p. 34-41.

Gutnic, M., Monod, O., Poisson, A., and Dumont, J. F., 1979. Geologie des Taurides occidental (Turquie). Mem. Soc. Geol. Fr., 58, 112 p.

Gvirtzman, G., and Buchbinder, B., 1978. The Tertiary history of the coastal plain and continental shelf of Israel, and its bearing on the history of the Eastern Mediterranean. Initial Rept. D.S.D.P., Vol. 42B, p. 1195-1222.

Gvirtzman, G., and Klang, E., 1972. A structural and depositional hinge line along the Coastal Plain of Israel, evidence from magneto-tellurics. Geol. Surv. Israel, Bull. 55, p. 1-18.

Gvirtzman, G., and Weissbrod, T., 1984. The Hercynian anticline of helez and the Late Paleozoic history of the Levant. In: J. E. Dixon and A. H. F. Robertson (eds.), The Geological Evolution of the Eastern Mediterranean, Geological Society of London, Spec. Publ. No. 7, Blackwell Scientific Publications, Oxford, UK, p. 177-186.

Hall, J. K., 1990. Chukchi Borderland. Chapter 19 In: A. Grantz, G. L. Johnson and J. F. Sweeney (eds.), The Arctic Ocean Region, Geology of North America, DNAG Volume L,. Geological Society of America, Boulder, CO, p. 337-350.

Hall, J. K., 1994. Bathymetric Chart of the Eastern Mediterranean Sea, Scale 1:625,000. 1 Map sheet (Plate I, Fig. 1.13) accompanying Hall, J. K., Udintsev, G. B. and Odinokov, Yu. Yu., (1994). The bottom relief of the Levantine Sea. In: Krasheninnikov, V., and Hall, J. K. (eds.), Geological structure of the North-eastern Mediterranean (Cruise 5 of the Research Vessel 'Akademik Nikolaj Strakhov'), p. 5-31. Historical Productions-Hall, Jerusalem, April 1994.

Hall, J. K., 1998a. Digital Shaded Relief Map of the Island of Cyprus, scale 1:250,000. Geological Survey of Israel, Jerusalem, 1 sheet.

Hall, J. K. 1998b. Digital terrain model (DTM) of the island of Cyprus. In: T. Weissbrod, (ed.), Geol. Surv. Isr. Current Research, Vol. 11, p. 47-52.

Hall, J. K., 2000. Satellite map of the northern Levant. Geol. Surv. Isr., Rept. GSU19/2000, March 2000. 1 sheet, LANDSAT TM imagery, UTM projection, scale 1:1,039,500.

Haller, J., 1981. The East Greenland Caledonides - Reviewed. Terra cognita, 1(1), p. 49-50.

Hamilton, W., 1970. The Uralides and the motion of the Russian and Siberian platforms. Geol. Soc. Am. Bull., 81(9), p. 2553-2576.

Hanna, W. F., Sweeney, R. E., Hildenbrand, T. G., Tanner, J. G., McConnell, R. K., and Godson, R. H., 1984. The Gravity Anomaly Map of North America p. 17-28 and Plate 1(A), Chapter 2, In: A. W. Bally, and A. R. Palmer (eds.), The Geology of North America, DNAG, Geol. Soc. Am., 619 p.

Hantar, G., 1990. North Western Desert. Chapter 15 in Rushdi Said, (ed.), The Geology of Egypt, A. A. Balkema (Publishers), Rotterdam, Netherlands, and Brookfield, VT, USA, p. 293-319.

Hartz, E. H., Torvik, T. A., and Andersen, A., 1997. Carboniferous age for the East Greenland "Devonian" basin: Paleomagnetic and isotopic constraints on age, stratigraphy and plate reconstructions. Geology, 25(8), p. 675-678.

Hatcher, R. D. Jr., 1978. Tectonics of the western Piedmont and Blue Ridge, southern Appalachians: review and speculation. Am. J. Science, 278(3), p. 276-304.

Haxby, W. F., 1983. 'The Gravity Field of the Worlds Oceans Recovered from SEASAT Altimeter Data.' Color map at 1:46,460,000. Published as a figure in Olson (1983).

Haxby, W. F., 1987. Gravity Field of the World's Oceans. World Data Center A for Marine Geology and Geophysics Report MGG-3. Published for ONR by NGDC, NOAA. 1 sheet, Mercator projection, scale approx. 1:40,000,000 at the Equator, with shaded hypsometry map of the Sea Surface, and of SEASAT Tracks.

Haxby, W. F., and Weissel, J. K., 1986. Evidence for small-scale mantle convection from Seasat altimeter data. J. Geophys. Res., 91(B3), p. 3507-3520.

Heezen, B. C., 1962. The deep sea floor. In: S. K. Runcorn (ed.), Continental Drift, Academic Press, New York, p. 235-288.

Heezen, B. C., and Tharp, M., 1977. World ocean floor, Mercator panoramic chart, scale 1:23,230,300, U.S. Navy, Washington, D.C., 1 sheet.

Hildenbrand, T. G., Kucks, R. P., and Sweeney, R. E., 1983. Digital magnetic-anomaly map of central United States: description of major features. Geophysical Investigations Map, plus text and references, MAP GP-955, U. S. Geol. Surv., Reston, Va., 1 sheet at 1:2,500,000 scale.

Hinze, W. J., and Hood, P. J., 1989. The Magnetic Anomaly Map of North America; A new tool for regional geological mapping. p. 29-38 and Plate 1(B), Chapter 3, In: A. W. Bally, and A. R. Palmer (eds.), The Geology of North America,

DNAG, Geol. Soc. Am., 619 p.

Hirsch, F., Flexer, A., Rosenfeld, A., and Yellin-Dror, A., 1995. Palinspastic and crustal setting of the Eastern Mediterranean. J. Petrol. Geol., 18, p. 149-170.

Hobbs, W. H., 1911. Repeating pattens in the relief and in the structure of the land. Bull. Geol. Soc. Am., 22(1), p. 123-176.

Hoffman, P. F., 1989. Precambrian geology and tectonic history of North America. In: A. W. Bally and A. R. Palmer (Editors), The Geology of North America, DNAG Volume A, Geol. Soc. Am., p. 447-512.

Hoffman, P. F., Kaufman, A. F., Halverson, G. P., and Schrag, D. P., 1998. A Neoproterozoic Snowball Earth. Science, 281(5381), p. 1342-1346.

Hoffman, P. F., and Schrag, D. P., 2000. Snowball Earth. Scientific American, 282(1), p. 68-75.

Holmes A., 1951. Principles of Physical Geology. Thomas Nelson,and Son Ltd., London, 532 p.

Hovorka, D., and Meres, S., 1997. Geochemistry of the Early Paleozoic felsic metavolcanics of the Gemeric Unit (Western Carpathians). In: Grecula, P., Hovorka, D., and Putiš, M., (eds.), Geological evolution of the Western Carpathians, Mineralia Slovaca Corporation, Bratislava, Geol. Survey of Slovak Republic, Bratislava, Monograph, p. 289-300.

Hsü, K. J., 1978. Messina Abyssal Plain. In: R. B. Kidd and P. J. Worstell (eds.), Initial Reports of the D.S.D.P. (JOIDES), Vol. 42 (Leg 42A). Part II-5 - Shipboard Studies, NSF - Univ. Cal. Scripps Inst. of Oceanography, La Jolla, CA. p. 175-218.

Hurley, P. M., 1968. The confirmation of Continental Drift. Scientific American, April 1968.

Husseini, Moujahed I., 1988. The Arabian Infracambrian extensional system. Tectonophysics, 148(1/2), p. 93-103.

Husseini, Moujahed I., 1989. Tectonic and deposition model of Late Precambrian-Cambrian Arabian and adjoining plates. Am. Assoc. Petrol. Geol. Bull., 73(9), p. 1117-1131.

Husseini, Moujahed I., (Gulf PetroLink), 2000. Origin of the Arabian Plate structures: Amar Collision and Najd Rift. GeoArabia, 5(4), p. 527-542/t.

Intergovernmental Oceanographic Commission (IOC), 1981. International Bathymetric Chart of the Mediterranean, Mercator projection, scale 1:1,000,000 at 38°N latitude, 10 sheets with 200 m contour interval published by the Head Department of Navigation and Oceanography, Ministry of Defence, Leningrad, USSR, under the authority of IOC (UNESCO), Ist Edition. Republished 1987 as a single sheet at 1:5,000,000 scale.

Intergovernmental Oceanographic Commission (IOC), 1990. Seismicity (Instrumental) (IBCM-S). IBCM Geological-Geophysical Series, Mercator projection, scale 1:1,000,000 at 38°N latitude, 10 sheets with approximately 20,000 instrumentally determined earthquake epicenters, heights and depths in meters, hypsometric tints for shallow and deep marine areas, published by the Head Department of Navigation and Oceanography, Ministry of Defence, Leningrad, USSR, under the authority of IOC (UNESCO), Preliminary Edition, 1988, Final edition 1990.

Intergovernmental Oceanographic Commission (IOC), 1987. International Bathymetric Chart of the Mediterranean. Mercator projection, scale 1:5,000,000 at 38°N latitude, published by the Head Department of Navigation and Oceanography, Ministry of Defence, Leningrad, USSR, under the authority of IOC (UNESCO), 1st Edition.

Intergovernmental Oceanographic Commission (IOC), 1989. Bouguer Gravity Anomalies (IBCM-G). IBCM Geological-Geophysical Series, Mercator projection, scale 1:1,000,000 at 38°N latitude, 10 sheets with terrain corrected Bouguer anomalies and 10 mgal contours, heights and depths in meters, published by the Head Department of Navigation and Oceanography, Ministry of Defence, Leningrad, USSR, under the authority of IOC (UNESCO). Final Edition, 1989.

Intergovernmental Oceanographic Commission (IOC) 1989. Bouguer Gravity Anomalies (IBCM-G). IBCM Geological-Geophysical Series. Mercator projection, scale 1:5,000,000 at 38°N latitude, 1 sheet with terrain corrected Bouguer anomalies and 10 mgal contours, heights and depths in meters, published by the Head Department of Navigation and Oceanography, Ministry of Defence, Leningrad, USSR, under the authority of IOC (UNESCO). Final Edition, 1989.

Intergovernmental Oceanographic Commission (IOC), 1989. Unconsolidated bottom surface sediments of the Mediterranean and Black Seas (Layer 0-5 cm) (IBCM-U). IBCM Geological-Geophysical Series, Mercator projection, scale 1:5,000,000 at 38°N latitude, 1 sheet with 21 sedimentological symbols and 6 generic tints based upon a compilation of all sedimentological data, heights and depths in meters, published by the Head Department of Navigation and Oceanography, Ministry of Defence, Leningrad, USSR, under the authority of IOC (UNESCO), Preliminary Version December 1989.

Intergovernmental Oceanographic Commission (IOC), 1989. Plio-Quaternary Isopach map (IBCM-PQ). IBCM Geological-Geophysical Series, Mercator projection, scale 1:1,000,000 at 38°N latitude, 10 sheets with 200 m isopach contours borehole designations, and structural interpretations, prepared by Profs. Burollet and Gennesseaux under the authority of IOC (UNESCO), Preliminary Version, December 1989.

Intergovernmental Oceanographic Commission (IOC), 1990. Seismicity (Instrumental) (IBCM-S). IBCM Geological-Geophysical Series, Mercator projection, scale 1:1,000,000 at 38°N latitude, 10 sheets with approximately 20,000 instrumentally determined earthquake epicenters, heights and depths in meters, hypsometric tints for shallow and deep marine areas, published by the Head Department of Navigation and Oceanography, Ministry of Defence, Leningrad, USSR, under the authority of IOC (UNESCO), Preliminary Edition, 1988, Final edition 1990.

Issar, A., and Eckstein, Y., 1969. The Lacustrine Beds of Wadi Feiran, Sinai. Isr. J. Earth-Sci., 18(1), p. 18-27.

Jachens, R. C., Simpson, R. W., Blakely, R. J., and Saltus, W. R., 1989. Isostatic residual gravity and crustal geology of the United States. Plates 1 & 2, Chapter 19, p. 405-524, In: L. C. Pakiser, and W. D. Mooney (eds.), Geophysical Framework of the United States, Geol. Soc. Am., Memoir 172, 826 p.

Jackson, J. A., and McKenzie, D. P., 1984. Active tectonics of the Alpine-Himalayan Belt between western Turkey and Pakistan. Geophys. J. R. astr. Soc., 77(1), p. 185-264.

Jackson, J. A., and McKenzie, D. P., 1988. The relationship between plate motions and seismic moment tensors, and the rates of active deformation in the Mediterranean and Middle East. Geophys. J., 93(1), p. 45-73.

Jakobsson, M., Cherkis, N. Z., Woodward, J., Macnab, R., and Coakley. B., 2000. New grid of Arctic bathymetry aids scientists and mapmakers; Eos,Transactions, American Geophysical Union, 81(9), p. 89, 93, and 96.

Jaswal, T. M., Lillie, R. J., and Lawrence, R. D., 1997. Structure and evolution of the Northern Potwar Deformed Zone, Pakistan. Am. Assoc. Petrol. Geol. Bull., 81(2), p. 308-222.

Johnson, M. R., Van Vouren, C. J., Visser, J. N. S., Cole, D. I., Wickens, H. deV., Christie, A. D. M., and Roberts, D. L., 1997. The Foreland Karoo Basin, South Africa. Part 3, Chapter 12, p. 269-317. In: Selley, R. C. (ed.), African Basins, Elsevier, Amsterdam, 394 p.

Kane, M. F., and Godson, R. H., 1989. A crust/mantle structural framework of the conterminous United States based on gravity and magnetic trends, Chapter 18, p. 383-404, In: L. C. Pakiser and W. D. Mooney (eds.), 1989. Geophysical Framework of the United States. Geol. Soc. Am. Mem. 172, 826 p.

Katz, M. B., 1987. East African rift and NE lineaments: Continental spreading – transform system? J. Afr. Earth-Sci., 6(1), p. 103-107.

Keeley, M. I., 1994. Phanerozoic evolution of the basins of Northern Egypt and adjacent areas. Geol. Rundschau, 83(4), p. 728-742.

Keen, C. E., Keen, M. J., Ross, D. I., and Lack, M., 1974. Baffin Bay: Small ocean basin formed by sea floor spreading. Am. Assoc. Geol. Bull., 58(6, Part II of II), p. 1089-1108.

Keming, Yang, Gouyou, Xu, and Ping, Jiang, 1993. Paleozoic structures and oil exploration prospects in the eastern Turim Basin, NW China. J. Petroleum Geology, 16(3), p. 323-334.

Kenyon, N. H., Belderson, R. H., and Stride, A. H., 1982. Detailed tectonic trends on the central part of the Hellenic Outer Ridge and in the Hellenic Trench System. In: J. K. Leggett (ed.), Trench-Forearc Geology, Spec. Publ. 10, Geol. Soc. (Lond.), p. 335-343.

Kerdany, M. T., and Cherif, O. H., 1990. Mesozoic. Chapter 22 in Rushdi Said, (ed.), The Geology of Egypt, A. A. Balkema (Publishers), Rotterdam (Netherlands), and Brookfield, VT, USA, p. 407-438.

Kerr, R. A., 1999. The great African plume emerges as a tectonic player. Science, 285(5425), 9 July 1999, p. 187-188.

Khattri, K. N., Rogers, A. M., Perkins, D. M., and Algermissen, S. T., 1984. A Seismic Hazard Map of India and Adjacent Areas. Tectonophysics, 108(1/2),

p. 93-134.
Kidd, R. B., and Worstell, P. J., (Editors), 1978. Initial Reports of the D.S.D.P. (JOIDES), Vol. 42 (Leg 42A). NSF - Univ. Cal. Scripps Inst. of Oceanography, La Jolla, CA, 1225 p. (plus appendices).
Kiratzi, A. A., and Papazachos, C. B., 1995. Active crustal deformation from the Azores triple junction to the Middle East. Tectonophysics, 243(1-2), p. 1-24.
Klemme, H. D., 1958. Regional Geology of Circum-Mediterranean Region. Am. Assoc. Petrol. Geol. Bull., 42(3), Pt. 1, p. 477-512.
Klitzsch, E., 1990. Paleozoic. Chapter 21 in Rushdi Said, (ed.), The Geology of Egypt, A. A. Balkema (Publishers), Rotterdam, Netherlands, and Brookfield, VT, USA, p. 393-406.
Knudsen, P., and Andersen, O. B., 1995. Free Air Gravity anomalies from ERS-1 Geodetic Mission altimetry. Kort & Matrikelstyrelson, Copenhagen, Denmark, Poster, November 1995.
Konert, G., Afifi, A. M., Al-Hajri, S. A., de Groot, K., Al Naim, A. A., and Droste, H. J., 2001. Paleozoic stratigraphy and hydrocarbon habitat of the Arabian Plate. In: M. W. Downey, J. C. Threet, and W. A. Morgan (eds.), Petroleum provinces of the twenty-first century. Am. Assoc. Petrol. Geol. Mem. 74, p. 483-515.
Korotaev, M. V., Nikishin, A. M., Ershov, A. V., and Brunet, M. F., 1999. The Black Sea Basin: Tectonic history and modelling (Abstract). G-O-5, Europrobe Georift Project Workshop, 5 Oct. 1999. Romanian J. Tectonics and Regional Geology, V. 77, Suppl. 1, p. 81.
Kostyuchenko, S. L., 1999. Geologic environments and geodynamics of the southern margin of East European Craton (Abstract). G-O-6, Europrobe Georift Project Workshop, 5 Oct. 1999. Romanian J. Tectonics and Regional Geology, V. 77, Suppl. 1, p. 81-82.
Kovac, M., Biefc, M., Lexa, J., Pereszlenyi, M., Sefara, J., Tunyi, I., and Vass, D., 1997. The Western Carpathians intramontane basins. In: P. Grecula, D. Horovka, and M. Putis (eds.), Geological evolution of the West Carpathians. IUGS/UNESCO IGCP Project No. 276. Geol. Surv. Slovak Republic, Mineralia Slovaca Corporation, Bratislava, p. 43-64.
Krasheninnikov, V. A., Udintsev, G. B., Mouraviou, V., and Hall, J. K., 1994. Geological structure of the Eratsothenes Seamount. In: V. A. Krashenninikov and J. K. Hall (eds.), Geological Structure of the North-Eastern Mediterranean (Cruise 5 of the Research Vessel 'Akademik Nikolaj Strakhov'), Historical Productions-Hall, Jerusalem, p. 113-130.
Kravchenko, K. N., 1979. Tectonic evolution of the Tien Shan, Pamir and Karakorum. In: Abed Farah and. Kees A. DeJong. (eds.), Geodynamics of Pakistan. Geological Survey of Pakistan, Quetta, p. 25-27.
Kuehen, R., and Hsu, K. J., 1978. Chemistry of halite and potash salt cores, DSDP Sites 374 and 376, Leg 42A, Mediterranean Sea. In: R. B. Kidd and P. J. Worstell (eds.), Initial Reports of the D.S.D.P. (JOIDES), Vol. 42 (Leg 42A). Part III - Post Cruise Studies, Section 4 (Studies of Evaporites). NSF - Univ. Cal. Scripps Inst. of Oceanography, LaJolla, CA, p. 613-620.
Kumazawa, M., and Maruyama, S., 1994. Whole Earth Tectonics. Jour. Geol. Soc. Japan, 100(1), p. 81102.
Ladd, J. W., 1976. Relative motion of South America with respect to North America and Caribbean tectonics. Geol. Soc. Am. Bull., 87(7), p. 969-976.
Laughton, A. S., 1970. The southern Labrador Sea - A key to the Mesozoic and Early Tertiary evolution of the North Atlantic. In: A. S. Laughton, W. A. Berggren et al., (eds.), Vol. XII, Initial Reports of the Deep Sea Drilling Project, U. S. Govt. Printing Office, p. 1155-1179.
Lear, C. H., Elderfield, H., Wilson, P. A., 2000. Cenozoic deep-sea temperatures and global ice volumes from Mg/Ca in benthic foraminiferal calcite. Science, 287(5451), p. 269-272.
Le blanc, D., and Olivier, Ph., 1984. Role of strike-slip faults in the Betic-Rifean Orogeny. Tectonophysics, 101(3/4), p. 345-355.
Legault, J. A., 1982. First report of Ordovician (Caradoc-Ashgill) palynomorphs from Orphan Knoll, Labrador Sea. Can. J. Earth Sci., 19(9), p. 1851-1856.
Le Pichon, X., and Angelier, J., 1979. The Hellenic arc and trench system: A key to the neotectonic evolution of the eastern Mediterranean area. Tectonophysics, 60(1/2), p. 1-42.
Le Pichon, X., and Fox, P. J., 1971. Marginal offsets, fracture zones, and the early opening of the North Atlantic. J. Geophys. Res., 76(26), p., 6294-6308.
Le Pichon, X., Hyndman, R. D., and Pautot, G., 1971. Geophysical study of the Opening of the Labrador Sea. J. Geophys. Res., 76(20), p. 4724-4743.
Le Pichon, X., Sibuet, J-C., and Francheteau, J., 1977. The fit of the continents around the North Atlantic Ocean. Tectonophysics, 38(3/4), p. 169-209.
Li, Maowen, Xiaoa, Zongyao, Snowdon, Lloyd, Lin, Reweir, Wang, Pairong, Hou, Dujie, Zhan Linye, Zhang, Shuichang, and Liang, Digang, 2000. Migrated hydrocarbons in outcrop samples; revised petroleum exploration directions in the Tarim Basin. Organic Geochemistry, 31(6), p. 594-603.
Limonov, A. F., Woodside, J. M., Cita, M. B., and Ivanov, M. K., 1996. The Mediterranean Ridge and related mud diapirism: a background. Mar. Geol., 132(1), p. 7-19.
Livermore, R. A., and Smith, A. G., 1985. Some boundary conditions for the evolution of the Mediterranean region. Chapter 5 in: D. J. Stanley and F. -C. Wezel (eds.), Geological Evolution of the Mediterranean Basin (Raimondo Selli Commemorative Volume), Springer-Verlag, New York, NY, p. 83-98.
Loper, D. E., 1985, A simple model of whole-mantle convection. J. Geophys. Res., 90(B2), p. 1809-1836.
Loubrieu, B., Satra, C., and Cagna, R., 2001. Morpho-bathymetry of the Mediterranean Ridge and surrounding areas. Acoustic image of the Mediterranean Ridge and surrounding areas. Two sheets, Mercator Projection, at scale 1:1,500,000 at 35°N, Ifremer, Plouzane.
Lovelock, F. E. R., 1984. A review of the tectonics of the northern Middle East region. Geol. Mag., 121(G), p. 577-587.
Macgregor, D. S., Moody, R. T. J., and Clark-Lowes, D. D. (editors), 1998. Petroleum Geology of North Africa. Geological Society of London, Spec. Publ. 132, 442 p.
Madin, I. P., Lawrence, R. D., and Ur-Rehman, S., 1989. The northwestern Nangat ParbatHaramosh Massif; Evidence for crustal uplift at the northwestern corner of the Indian Craton. In: L. L. Malinconico Jr. and R. J. Lillie, (eds.), Tectonics of the Western Himalayas, Geol. Soc. Am. Spec. Paper 232, p. 109-122.
Mainguet, M., 1968. Le Borkou, aspect d'une modelé eolien. Ann. Geogr., 77, p. 296-322.
Makris, J., 1976. A dynamical model of the Hellenic Arc deduced from geophysical data. Tectonophysics, 36(4), p. 339-346.
Makris, J., Ben-Avraham, Z., Behle, A., Ginzburg, A., Giese, P., Steinmetz, L., Whitmarsh, R. B., and Eleftheriou, S., 1983. Seismic refraction profiles between Cyprus and Israel and their interpretation. Geophys. J., Roy. Astron. Soc., 75(3), p. 575-591.
Makris, J., Wang. J., Odintsov, S. D., and Udintsev, G. B., 1994. The magnetic field of the eastern Mediterranean Sea. In: V. A. Krashenninikov and J. K. Hall (eds.), Geological Structure of the NorthEastern Mediterranean (Cruise 5 of the Research Vessel 'Akademik Nikolaj Strakhov'), Historical Productions-Hall, Jerusalem, p. 75-85.
Makris, J., and Wang, J., 1994. Bouguer gravity anomalies of the eastern Mediterranean Sea. In: V. A. Krashenninikov and J. K. Hall (eds.), Geological Structure of the North-Eastern Mediterranean (Cruise 5 of the Research Vessel 'Akademik Nikolaj Strakhov'), Historical Productions-Hall, Jerusalem, p. 87-98.
Malovitskiy, Y. P., Emelyanov, E. M., Kazakov, O. V., Moskalenko, V. N., Osipov, G. V., Shimkus, K. M., and Chumakov, I. S., 1975. Geological structure of the Mediterranean sea floor (based on geological-geophysical data). Marine Geology, 18(4), p. 231-261.
Manspeizer, W. R., Puffer, J. H., and Cousminer, H. L., 1978. Separation of Morocco and eastern North America: A Triassic-Liassic stratigraphic record. Geol. Soc. Am. Bull., 89(6), p. 901-920.
Mart, Y., and Robertson, A. H. F., 1998. Eratosthenes Seamount: An oceanographic yardstick recording the Late Mesozoic-Tertiary geological history of the Eastern Mediterranean. Article 52 in: A. H. F. Robertson, K. -C. Emais, C. Richter, and A. Camerlenghi (eds.), Proceedings of the Ocean Drilling Program, Scientific Results, Vol. 160, p. 701-708.
Maruyama, S., 1994. Plume tectonics. Jour. Geol. Soc. Japan, 100(1), p. 24-49.
McClusky, S., Balassarian, S., Barka, A., Demir, C., Ergintav, S., Georgiev, I., Gurkan, O., Hamburger, M., Hurst, K., Kahle, H., Kastens, K., Kekelidze, G., King, R., Kotzev, V., Lenk, O., Mahmoud, S., Mishin, A., Nadariya, M., Ouzounis, A., Paradissis, D., Peter, Y., Prilepin, M., Reilinger, R, Sanli, I., Seeger, H., Tealeb, A., Toksöz, M. N., and Veis, G, 2000. Global Positioning System constraints on plate kinematics and dynamics in the eastern Mediterranean and Caucasus. J. Geophys. Res., 105(B3), p. 5,695-5,719.
McConnell, R. B., 1972. The geological development of the Rift System of Eastern

Africa. Geol. Soc. Am. Bull., 83(9), p. 2549-2572.McKenzie, D. P., 1970. Plate tectonics in the Mediterranean region. Nature, 226(5242), p. 239-243.

McKenzie, D. P., 1972. Active tectonics of the Mediterranean region. Geophys. J. Roy. Astr. Soc., 30(1), p. 109-185.

McKenzie, D. P., 1978. Active tectonics of the Alpine-Himalayan belt: the Aegean Sea and surrounding regions. Geophys. J. Roy. astr. Soc., 55(1), p. 217-254.

McQuilken, J., 2001. Petroleum geochemistry and basin modelling: offshore Levant Basin, Israel. (Abstract). In: Z. Gvirtzman and R. Amit (eds.), Abstracts of the Israel Geological Society, Elat, p. 79.

Miller, R., 1983 (revised 1985). Planet Earth - Continents in Collision. Time-Life Books, Alexandria VA, USA, 176 p.

Moores, E. M., and Vine, F. J., 1971. The Troodos Massif, Cyprus, and other ophiolites as oceanic crust: Evolution and implications. Roy. Soc. London, Phil. Trans., Ser. A, Vol. 268,. 443-466.

Morelli, C., 1985. Geophysical contribution to the knowledge of the Mediterranean crust. In: D. J. Stanley and F. -C. Wezel (eds.), Geological Evolution of the Mediterranean Basin (Raimondo Selli Commemorative Volume), Springer-Verlag, New York, NY, p. 65-82.

Mosar, J., 1999. Paleozoic Circum-Baltica Plate Tectonics (Abstract). G-O-1 , Europrobe Georift Project Workshop, 5 Oct. 1999. Romanian J. Tectonics and Regional Geology, V. 77, Suppl. 1, p. 79.

Moshkowitz, S., 1971. Biostratigraphy of the genus *Nannoconus* in the Lower Certaceous sediments of the subsurface; Ashkelon-Helez area, Central Israel. Isr. J. Earth-Sci., 21(1), p. 1-28.

Mstislavski, M. M., Mezentzev, A. M., and Olofinsky, L. V., 1980. Tectonic zonation of the Pre-Jurassic basement of the Mangishlak uplift zone. Geotectonics, 2, p. 63-77.

Musky, T. M., Li, Jiang-Hai, and Tucker, R. D., 2001. The Archean Dongwanzi Ophiolite Complex, North China Craton: 2.505 billion-year-old ocean crust and mantle. Science (Reports), 292(5519), p. 1142-1145.

Mutlu, H., and Gulec, N., 1998. Hydrogeological outline of thermal waters and geothermometry applications in Anatolia (Turkey). J. Volcanology and Geothermal Research, 85(--), p. 495-515.

Nadin, P. A., 2001. Crustal structure of the Levant continental passive margin: An analysis using quantitative 2-D structural/stratigraphic modelling (Abstract). In: Z. Gvirtzman and R. Amit (eds.), Abstracts of the Israel Geological Society, Elat, p. 86.

Nagy, R. M., Ghuma, A., and Rogers, J. J. W., 1976. A crustal suture and lineament in North Africa. Tectonophysics, 31(1/2), p. 67-72.

National Geographic Society, 1995. National Geographic Atlas of the World, 2nd Revision, Sixth Edition. National Geographic Society, Washington, DC, 270 p.

National Geographic Society, 1999. National Geographic Atlas of the World, Seventh Edition. National Geographic Society, Washington, DC, v+137 double page maps+134 p. index.

National Iranian Oil Company, 1957. Geological Map of Iran, scale 1:2,500,000. The Iran Oil Company, Tehran, Iran, 1 sheet.

NATO Research Centre, LaSpezia, 1964. Red Sea Bathymetric Chart, Scale 1:2,300,000, contour interval 100 fathoms.

Neev, 1960. A pre-Neogene erosian channel in the southern coastal plain of Israel. Geol. Surv. Isr., Bull. 25, 20 p.

Neev, D., 1975. Tectonic evolution of the Middle East and the Levantine Basin (easternmost Mediterranean). Geology, 3(12), p. 683-686.

Neev, D., 1977. The Pelusium Line - a major transcontinental shear. Tectonophysics, 38(3/4), p. T1-T8.

Neev, D., 1979. Deep water gypsum deposits as indicated by the Neogene geological history of the central coastal plain of Israel. Sedimentary Geology, 23(1-4), p. 127-132.

Neev, D., Almagor, G., Arad, A., Ginzburg, A., and Hall, J. K., 1976. The geology of the southeastern Mediterranean Sea; Geol. Surv. Israel Bull. 68, Jerusalem, 51 p.

Neev, D., and Emery, K. O., 1967. The Dead Sea, depositional processes and environments of evaporites. State of Israel, Ministry of Development, Geological Survey, Bull. 41, Jerusalem, 147 p.

Neev, D., and Greenfield, L. L., 1981. Oil possibilities of the continental margin off Israel, based on seismic interpretation. Oil Exploration (Investments) Ltd., Israel, Rept. No. 81/54, 23 p., 17 figs.

Neev, D., Greenfield, L. L., and Hall, J. K., 1985. Slice tectonics in the Eastern Mediterranean basin. Chapter 12 in: D. J. Stanley and F. -C. Wezel (eds.), Geological Evolution of the Mediterranean Basin (Raimondo Selli Commemorative Volume), Springer-Verlag, New York, NY, p. 249-269.

Neev, D. and Hall, J. K., 1982. A Global System of spiraling geosutures; J. Geophys. Res., 87(B13), p. 10,689-10,709.

Neev, D., and Hall, J. K., 1984. Mantle-produced counterclockwise vortices along the northern Mediterranean Belt (A genetic hypothesis for the Alpine System). Mitt. Geol.-Palaont. Inst. Univ. Hamburg, Festband Georg Knetsch, Heft 56, p. 111-127.

Neev, D., and Hall, J. K., 1992. Counterclockwise converging basement fracturing patterns across the Arabian Peninsula and Eastern Iran. In: R. Mason (ed.), Basement Tectonics, 7, p. 13-31.

Neev, D., Hall, J. K., and Saul, J. M., 1982. The Pelusium Megashear System across Africa and associated lineament swarms; J. Geophys. Res., 87(B2), p. 1015-1030.

Nehlig, P., Asfirane, F. Genna, A., Guerrot, C., Nicol, N., Salpeteur, I, Shanti, M., and Thiéblemont, D., 2001. Aeromagnetic map constrains cratonization of the Arabian Shield. Terra Nova, Blackwell Science Ltd., 13(5),p. 347-353.

Neprochnov, Yu. P., Neprochnova, A. F., Zverev, S. M., Mironova, V. I., Bokuni, R. A., Chekunov, A. V., 1964. New data on the structure of the Black Sea crust south of the Crimea. Akad. Nauk SSSR Dokl., 156(3), p. 561-564.

Neugebauer, J., 1995. Structures and kinematics of the North Anatolian Fault zone, Adapazari-Bolu region, northwest Turkey. Tectonophysics, 243(1-2), p. 119-134.

Nikishin, A. M., Ziegler, P. A., Panov, D. I., Nazarevich, B. P., Brunet, M. F., Stephenson, R. A., Bolotov, S. N., Korotaev, M. V., and Tikhomirov, P., 1999. Mesozoic and Cenozoic evolution of the Scythian Platform - Black Sea-Caucasus Domain (Abstract). G-O-5, Europrobe Georift Project Workshop, 5 Oct. 1999. Romanian J. Tectonics and Regional Geology, V. 77, Suppl., 1, p. 79-80.

Olson, S. 1983. 'The contours below.' Science 83, 4(6), p. 38-41. (Contains color map of W. F. Haxby's 'Gravity Field of the Worlds Oceans Recovered from SEASAT Altimeter Data').

Ortega-Gutierrez, F., Sedlock, R. L., and Speed, R. C., 1994. Phanerozoic tectonic evolution of Mexico. In: R. C. Speed (ed.), Phanerozoic evolution of North American Continent-Ocean Transitions, DNAG Continent-Ocean Transect, Summary Volume, Geol. Soc. Am., 504 p

Oterdoom, W. H., Worthing, M. A., and Partington, M., 1999. Petrological and tectonostratigraphic evidence for a Mid-Ordovician Rift Pulse on the Arabian Peninsula. GeoArabia, 4(4), p. 467-500.

Pakiser, L. C., and Mooney, W. D., (eds.), 1989. Geophysical Framework of the United States. Geol. Soc. Am. Mem. 172, 826 p.

Pamic, J., 1983. Considerations on the boundary between Lherzolite and Harzburgite sub-provinces in the Dinarides and Northern Hellenides. Ofioliti, 8(l), p. 153-164.

Parson, L. M., Masson, D. G., and Rothwell, R. G., 1984. Remnants of a submerged pre-Jurassic (Devonian?) landscape on Orphan Knoll, offshore eastern Canada. Can. J. Earth Sci., 21(1), p. 61-66.

Pelletier, B. R., Ross, D. I., Keen, C. E., and Keen, M. J., 1975. Geology and geophysics of Baffin Bay. In: Willem J. M. Van der Linden and J. A. Wade, (eds.), Offshore Geology of Eastern Canada, Vol. 2 - Regional Geology, Geol. Surv. Canada, Geological Paper 74-30, p. 247-257.

Philippe, Y., Colletta, B., Deville, E., and Mascle, A. 1996. The Jura fold and thrust belt: a kinematic model based on map-balancing. In: Ziegler, P. A. and Horvath, F. (Eds.), 1996., Peri-Tethys Memoir 2: Structure and Prospects of Alpine Basins and Forelands. Mem. Mus. nat., 170, p. 235-261 + Encl. 1-2. Paris, ISBN: 2-85653-507-0.

Picard, L., 1959. Geology and oil exploration of Israel. Bull. Res. Council of Israel, Vol. G.8, No. 1, p. 1-30, 10 figs., 1 map.

Picard, L., and Solomonica, P., 1936. On the geology of the Gaza-Beersheba District. Bull. Geol. Dept. Hebrew Univ., Jerusalem, V. 1, No. 2, p. 1-44. (Reprint from the Palestine Oriental Society Vol. XVI, 1936, p. 180-223). Includes: Solomonica, P., Geological Sketch-Map of the Gaza-Beersheba District (under the direction of L. Picard).

Plasienka, D., Grecula P., Putis, M., Kovac, M., and Hovorka, D., 1997. Evolution and structure of the Western Carpathians: an overview. In: P. Grecula, D.

Horovka, and M. Putis (eds.), Geological evolution of the West Carpathians. IUGS/UNESCO IGCP Project No. 276. Geol. Surv. Slovak Republic, Mineralia Slovaca Corporation, Bratislava, p. 1-24.

Powell, McA. C., 1979. A speculative tectonic history of Pakistan and surroundings: some constraints from the Indian Ocean. In: Abed Farah and Kees A. DeJong. (eds.), Geodynamics of Pakistan, Geological Survey of Pakistan, Quetta, p. 5-24.

Richards, M. A., 1999. Prospecting for Jurassic slabs. Nature, 21 Jan. 1999, 397(6716), p. 203-204.

Roberts, D. G., Ardus, D. A., and Dearnley, R., 1973. Precambrian rocks drilled on Rockall Bank. Nature Phys. Sci., 244(132), July 9, 1973, p. 21-23.

Robertson, A. H. F., 1998. Tectonic significance of the Eratosthenes Seamount: a continental fragment in the process of collision with a subduction zone in the eastern Mediterranean (Ocean Drilling Program Leg 160). Tectonophysics, 298(1-3), p. 63-82.

Robertson, A. H. F., Clift, P. D. Degnan, P. J., and Jones, G., 1991. Paleogeographic and paleotectonic evolution of the Eastern Mediterranean Neotethys. Paleogeography, Paleoclimatology, Paleoecology, 87(1-4), p. 289-343.

Robertson, A. H. F., and Dixon, J. E., 1984. Introduction: Aspects of the geological evolution of the Eastern Mediterranean. In: J. E. Dixon and A. H. F. Robertson (eds.), The Geological Evolution of the Eastern Mediterranean, Geological Society of London, Spec. Publ. No. 7, Blackwell Scientific Publications, Oxford, UK, p. 1-74.

Robertson, A. H. F., Dixon, J. E., Brown, S., Collins, A., Morris, A., Pickett, E., Sharp, I, and Ustaomer, T, 1996. Alternative tectonic models for the Late Palaeozoic-Early Tertiary development of the Eastern Mediterranean. In: A. Morris and D. H. Tarling (eds.), Palaeomagnetism and Tectonics of the Mediterranean Region, Geol. Soc. Spec. Publ. 105, p. 239-263.

Ross, D. A., 1974. The Black Sea. In: C. A. Burk and C. L. Drake (eds.), The Geology of Continental Margins. Springer-Verlag, Berlin, Heidelberg, New York, p. 669-681.

Rotstein, Y., 1984. Counterclockwise rotation of the Anatolian Block. Tectonophysics, 108(1/2), p. 71-91.

Rotstein, Y., 1985. Tectonics of the Aegean Block: Rotation, side arc collision and crustal extension. Tectonophysics, 117(1/2), p. 117-137.

Ruffman, A., 1989. First report of Ordovician (Caradoc-Ashgill) palynomorphs from Orphan Knoll, Labrador Sea: Discussion. Can. J. Earth Sci., 26(12), p. 2749-2751.

Ruggieri, G., 1985. NATO-ARI Field Excursion - A short trip across the geology of Sicily. Appendix in: D. J. Stanley and F. -C. Wezel (eds.), Geological Evolution of the Mediterranean Basin (Raimondo Selli Commemorative Volume), Springer-Verlag, New York, NY, p. 573-579.

Rybakov, M., Goldschmidt, V., Folkman, Y., Rotstein, Y., Ben-Avraham, Z., and Hall, J. K., 1994. Israel Magnetic Anomaly Map, 1:500,000. Prepared by the Institute for Petroleum Research and Geophysics, Lod, Israel, 1 sheet.

Sander, N. S., 1970. Structural evolution of the Mediterranean region during the Mesozoic Era. Reprinted from p. 43-132 of Geology and History of Sicily. Annual Field Conference No. 12, W. Alvarez and K. O. Gohrbandt (eds.), Petrol. Explor. Soc. Libya, 1970. In Peter Sonnenfeld (ed.), 1981

Sandulescu, M., Krautner, H. G., Borcos, M., et al., 1978. Geological Map of Romania, 1:1,000,000. Institute of Geology and Geophysics, Bucharest, Romania.

Sandwell, D. T., and Smith, W. H. F., 1995. Marine gravity anomaly from satellite altimetry. Geological Data Center, Scripps Institute of Oceanography, La Jolla, CA, poster, 34" x 53", Mercator projection, scale 1:31,270,000.

Sclater, J. G., Anderson, R. N., and Bell, M. L., 1971. Elevation of ridges and evolution of the central eastern Pacific. J. Geophys. Res., 76(32), p. 7,888-7,915.

Selley, R. C., 1997. The Basins of NW Africa: Structural Evolution. Part I, Chapter 2, p. 17-26, In: R. C. Selley (ed.), African Basins, Elsevier, Amsterdam, 394 p.

Semtner, A. –K., and Klitzsch, E., 1994. Early Paleozoic paleogeography of the Northern Gondwana margin: new evidence for Ordovician and Silurian glaciation. Geol. Rundsch., 83(4), p. 743-751.

Şengör, A. M. C., Gurur, N., Saroglu, F., 1985. Strike-slip faulting and related basin formation in zones of tectonic escape: Turkey as a case study. In: T. R. Biddle and N. Christie-Blick, (eds.), Strike-slip deformation, basin formation and sedimentation. Soc. Econ. Paleontol. and Mineralogy Spec. Publ. 37, p. 227-264.

Şengör, A. M. C., Satir, M., and Akkok, R., 1984. Timing of tectonic events in the Menderes Massif, Western Turkey: Implications for tectonic evolution and evidence for pan-African basement in Turkey. Tectonics, 3(7), p. 693-707.

Şengör, A. M. C., and Yilmaz, Y., 1981. Tethyan evolution of Turkey: a plate tectonic approach. Tectonophysics, 75(3/4), p. 181-241.

Shearer, P. M., 2000. Upper Mantle seismic discontinuities. In: S. Kasato, A. Firte, R. Lieberman, G. Masters, and L. Stirrude (eds.), Earth's Deep Interior, Mineral Physics and Tomography from Atomic to Global Scale. Am. geophys. Un., Geophys. Monogr. 117, p. 115-131.

Simkin, T., Unger, J. D., Tilling, R. I., Vogt, P. R., and Spall, H, 1994. This Dynamic Planet, World map of volcanoes, earthquakes, impact craters and plate tectonics. Scale (at the Equator) 1:30,000,000, Smithsonian Institution, U.S.G.S. and U.S. Naval Research Lab., 1 sheet.

Simpson, E. S. W., 1971. The geology of the south-west African continental margin: a review. In: F. M. Delaney, (ed.), The geology of the East Atlantic continental margin. Inst. Geol. Sci., London, Rept. 70/16, p. 153-170.

Sleep, N. H., 1996. Lateral flow of hot plume material ponded at sublithospheric depths. J. Geophys. Res., 102(B12), p. 28,065-28,083.

Sleep, N. H., 1997. Lateral flow and ponding of starting plume material. J. Geophys. Res., 102(B5), p. 10,001-10,012.

Smith, W. H. F., and Sandwell, D. T., 1997a. Measured and estimated seafloor topography (version 4.2), World Data Center A for Marine Geology and Geophysics, research publication RP-1, poster, 34" x 53", Mercator projection, scale 1:31,270,000, January 1997.

Smith, W. H. F., and Sandwell, D. T., 1997b. Global sea floor topography from satellite altimetry and ship depth soundings, Science, 277(5334), p. 1956-1962.

Song, X., and Richards, P. G., 1996. Seismological evidence for differential rotation of the Earth's inner core. Nature, 382(6588), p. 221-224.

Sonnenfeld, P., 1975. The significance of Upper Miocene (Messinian) evaporites in the Mediterranean Sea. J. Geol., 83(3), p. 287-311.

Sonnenfeld, P., 1981. The Phanerozoic Tethys Sea. p. 18-53, In: P. Sonnenfeld (ed.), Tethys - The Ancestral Mediterranean, Benchmark Papers in Geology, Vol. 53 Hutchinson-Ross Publishing Co., Stroudsburg, PA, USA, 333 p.

Sonnenfeld, P., 1985. Models of Upper Miocene evaporite genesis in the Mediterranean Sea. In: D. J. Stanley and F. -C. Wezel (eds.), Geological Evolution of the Mediterranean Basin, Springer-Verlag, New York, p. 323-346.

Sougy, J., 1962. West African fold belt. Geol. Soc. Am. Bull., 73(7), p. 871-876.

Stein, M., and Hofmann, A. W., 1994. Mantle plumes and episodic crustal growth. Nature, 372(6501), p. 63-68.

Stern, R. J., 1985. The Najd Fault System, Saudia Arabia and Egypt: A Late Precambrian rift-related transform system. Tectonics, 4(5), p. 493-511.

Stern, R. J., 1994. Arc assembly and continental collision in the Neoproterozoic East African orogen: Implications for the consolidation of Gondwanaland. Earth and Planetary Science , Annual Reviews Inc., Vol. 22, p. 319-351.

Stocklin, J., 1968. Structural history and tectonics of Iran: A review. Am. Assoc. Petrol. Geol. Bull., 52(7), p. 1229-1258.

Stocklin, J., 1974. Possible ancient continental margins in Iran. In: C. A. Burk and C. L. Drake (eds.), The Geology of Continental Margins. Springer, Berlin, Heidelberg, New York, p. 873-887.

Stoeser, D. B., and Camp, V. E., 1985. Pan-African microplate accretion of the Arabian Shield. Bull. Geol. Soc. Am., 96(7), p. 817-826.

Suess, Edward, 1893. Are great ocean depths permanent? Natural Sci. 2, p. 180-187. In: P. Sonnenfeld (ed.), Tethys - The Ancestral Mediterranean, Benchmark Papers in Geology, Vol. 53, Hutchinson-Ross Publishing Co., Stroudsburg, PA, USA, p. 4-11.

Tchernov, E. L., Ginsburg, P., Tassy, N. F., and Goldsmith, N., 1987. Miocene mammals of the Negev. J. Vertebrate Paleontology, V. 7, p. 284-310.

Times of London, 1975. Times Atlas of the World, 5th ed., prepared in collaboration with John Bartholomew & Son, Ltd., Edinburgh, 120 Maps.

Tricart, P, Schwartz, S., Sue, C., Poupeau, G., and Lardeaux, J. M., 2001. The tectonic denudation of the a Ultradauphine Zone and the inversion of the Brianconnais frontal thrust to the southeast of the Pelvoux Massif (western Alps): a Miocene to present-day dynamics. Bull. Soc. Géol. France, 172(1),

p. 49-58.

Tsoar, H., 1974. Desert dunes morphology and dynamics, El Arish (Northern Sinai). Zeit. Geomorphology, Suppl., 20, p. 40-61.

Tuysuz, O., Dellaloglu, A. A., and Terzioglu, N., 1995. A magmatic belt within the Neo-Tethyan suture zone and its role in the tectonic evolution of northern Turkey. Tectonophysics, 243(1-2), p. 173-191.

Umbgrove, J. H. F., 1947. The pulse of the Earth. 2nd edition. M. Nijhoff, The Hague, 232 p.

UNESCO, 1976. Geological World Atlas, scale 1:10,000,000. Sheet 6: West Africa; Sheet 7: Sub-Equatroial Africa; Sheet 8: East Africa. UNESCO Publishing/ Commission for the Geological Map of the World, Paris.

U.S.G.S.-ARAMCO, 1963. Geologic Map of the Arabian Peninsula, 1:2,000,000. Miscellaneous Geologic Investigations, Map 1-270A, Interior-Geological Survey, Washington, DC 10049.

Vail, J. R., 1978. Outline of the geology and mineral deposits of the Democratic Republic of the Sudan and adjacent areas, Overseas Geol. Miner. Resour., 49.

Van der Linden, W. J. M., and Srivastava, S. P., 1975. The crustal structure and the continental margin off Central Labrador; Offshore Geology of Eastern Canada. Geol. Surv. Canada, Paper 74-30, Vol. 2, p. 233-245.

Van der Voo, R., 1988. Paleozoic paleogeography of North America, Gondwana, and intervening displaced terranes: Comparisons of paleomagnetism with paleoclimatology and biogeographical patterns. Geol. Soc. Am. Bull., 100(3), p. 311-324.

Van der Voo, R., Spakman, W., and Bijwaard, H., 1999a. Tethyan subducted slabs under India. Earth Planet. Sci. Lett., 171(1), p. 7-20.

Van der Voo, R., Spakman, W., and Bijwaard, H., 1999b. Mesozoic subducted slabs under Siberia. Nature, 21 January 1999, 397(6716), p. 246-249.

Vanney, J. R., and Gennesseaux, M., 1985. Mediterranean seafloor features: overview and assessment. In: D. J. Stanley and F. -C. Wezel (eds.), Geological Evolution of the Mediterranean Basin, Springer Verlag, New York, p. 3-32.

Vening Meinesz, F. A., 1943. Spanningen in de aardkorst ten gevolge van poolverschuivingen [Stresses in the earth's crust due to plate motions]. Verslag van de gewone vergadering der Afdeeling Natuurkunde, Koninklijke Nederlandsche Akademie van Wetenschappen to Amsterdam [Report to the Royal Academy of Science] 52, p. 185-196. (In Dutch). In: Umbgrove (1947, Ref. List for Chap XI).

von Raumer, J., Abrecht, J., Bussy, F., Lombardo, B., Menot, R P., and Schaltegger, U., 1999. The Paleozoic metamorphic evolution of the Alpine External Massifs. In: M. Frey, J. Desmons, and F. Neubaur (eds.), The New Metamorphic Map of the Alps. p. 5-22. Swiss Bull. of Minerology and Petrology, Band 79, Heft 1,Special Volume, Stauble Verlog AG, Zurich.

de Voogd, B., Truffert, C., Chamot-Rooke, N., Huchon, P., Lallemant, S., and Le Pichon, X., 1992. Two ship deep seismic sounding in the basins of the Eastern Mediterranean Sea (Pasiphae Cruise). Geophys. J. Intl., 109(3), p. 536-552.

Warren, A., 1972. Observations on dunes and bimodal sands in the Tenere Desert, Sedimentology, 19(1), p. 37-44.

Weissbrod, T., 1969a. The Paleozoic of Israel and adjacent countries, Part I. Geol. Surv. Israel, Bull. 47, 34 p.

Weissbrod, T., 1969b. The Paleozoic of Israel and adjacent countries, Part II. The Paleozoic outcrops in southwestern Sinai and their correlation with those of southern Israel. Geol. Surv. Israel, Bull. 48, 32 p.

Wellman, H. W., 1965. Active wrench faults of Iran, Afghanistan and Pakistan. Geol. Rundschau, Band 53, Heft 3, p. 716-735.

Wilson, I. G., 1971.Desert sandflow basins and a model for the development of ergs, Geogr. J., 137(2), p.180-199.

Wilson, J. T., 1965. A new class of faults and their bearing on continental drift. Nature, 207(4995), p. 343-347.

Wilson, J. T., 1966. Did the Atlantic close and then re-open? Nature, 211(5050), p. 676-681.

World Sat International Inc. 1994. Europe, North Africa and the Middle East - A new satellite image, enhanced shaded relief, Scale 1:10,600,000 at the Equator, Canada, Ontario, 1 sheet.

Wunderlich, H. G., 1964. Gebirgsbildung im Alpen – Nordappenin-Oroen. Tectonophysics, 1(1), p. 73-84.

Wunderlich, H. G., 1966. Mass Ablauf und Ursachen Orogenen Einengung am Beispiel der Westalpen und des Nordappinen. Geol. Rundschau, 55(3), p. 699-715.

Yalcin, H., Gundogdu, M. N., Gourgaud, A., Vidal, P., and Ucurum, A., 1998. Geochemical characteristics of Yamadagi volcanics in central east Anatolia: an example from collision-zone volcanism. J. Volcanology and Geothermal Research, 85(1-4), p. 303-326.

Yilmaz, Y., Genc., S. C., Yigitbas, E., Bozcu, M., and Yilmaz, K., 1995. Geological evolution of the late Mesozoic continental margin of Northwestern Anatolia. Tectonophysics, 243(1-2), p. 155-171.

Zeigler, A. M., Scotese, C. R., McKerrow, W. S., Johnson, M. E., and Bambach, R. K., 1977. Paleozoic biogeography of continents bordering the Iapetus (Pre-Caledonian) and Rheic (Pre-Hercynian) oceans. In: R. M. West (ed.), Paleontology and plate tectonics with special reference to the history of the Atlantic Ocean. Milwaukee Public Museum, Spec. Publ. in Biology and Geology, no. 2, p.1-22.

Zeigler, A. M., Scotese, C. R., McKerrow, W. S., Johnson, M. E., and Bambach, R. K., 1979. Paleozoic paleogeography. Earth Planet. Sci. Lett., Ann. Rev., v. 7, p. 473-502.

Zharkov, M. V., 1984. Paleozoic salt bearing formations of the World. p. 45-54. Chapter II In: Iran-Pakistan Basin, Springer-Verlag, Berlin, Heidelberg, New York, Tokyo, 427 p.

Ziegler, M. A., 2001. Late Permian to Holocene paleofacies evolution of the Arabian Plate and its hydrocarbon occurrences. Geo-Arabia, 6(3), p. 445-497.

Ziegler, P. A., 1989. Evolution of Laurussia. A study in Late Paleozoic plate tectonics. Kluwer Academic Publishers, Dordrecht, Boston, London, 77 p., 14 plates.

Ziegler, P. A., and Horvath, F. (Editors), 1996. Peri-Tethys Memoir 2 - Structure and Prospects of Alpine Basins and Foreland. Mémoires du Museum National d'Histoire Naturelle, Édition du Museum, Paris, Tome 170 - Géologie, 560 p.

Ziegler, P. A., and Roure, F., 1996. Architecture and petroleum systems of the Alpine orogen and associated basins. In: P. A. Ziegler and F. Horvath (eds.), Peri-Tethys Memoir 2 - Structure and Prospects of Alpine Basins and Foreland. Memoires du Museum National d'Histoire Naturelle, Edition du Museum, Paris, Tome 170 - Geologie, p.15-46.

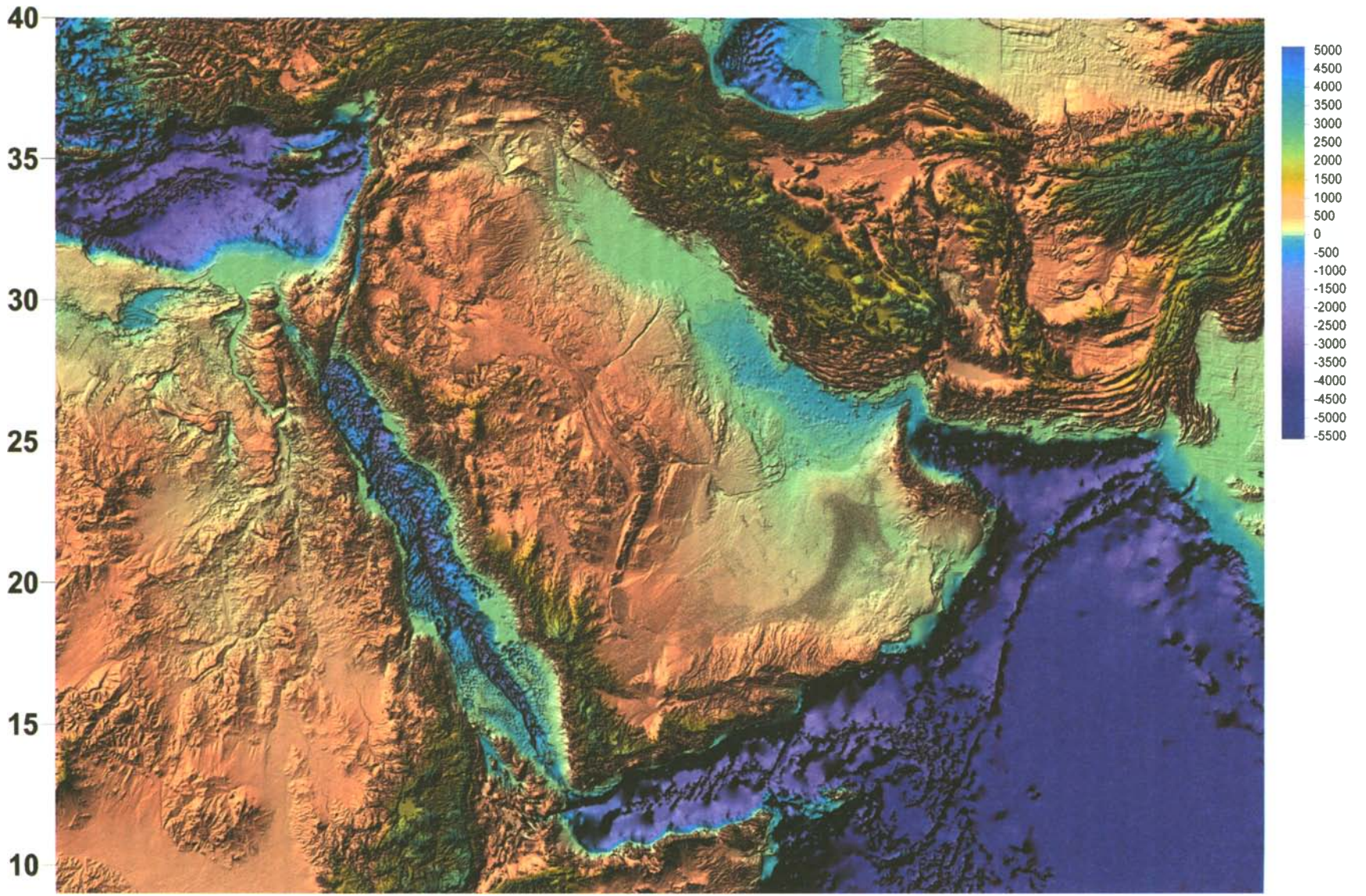
Zietz, I., Harwarth, R. T., Williams, H., and Daniels, D. L., 1980. Magnetic anomaly map of the Appalachian Orogeny. 1:1,000,000 scale. Maps 1(S) and 2(N), USGS Contribution No. 65 to the IGCP Project No. 27, the Appalachian-Caledonian Orogeny.

Zizi, M., 1996. Triassic-Jurassic extension and Alpine inversion in Northern Morocco. In: P. A. Ziegler and F. Horvath (eds.), Peri-Tethys Memoir 2 - Structure and Prospects of Alpine Basins and Foreland. Mémoires du Museum National d'Histoire Naturelle, Édition du Museum, Paris, Tome 170 - Géologie, p. 87-102.

Shaded relief of the Arabian Plate and environs.

New datasets for the Middle East clearly show the opening of the Red Sea, the surrounding oceanic basins, and the fabric of the adjacent continents. Topography is from the 0.5' Shuttle Radar Topographic Mission (SRTM) dataset, overlain by Global Mapper® on the 1' GEBCO Digital Atlas dataset, and presented as shaded relief using Surfer® 8. Sun illumination is at an elevation of 45° from the NW (N315°E). Geographic projection. Additional bathymetry for the southern Caspian Sea added from the compilation by Hall (2003).

Reference: Hall, J. K., 2003. Bathymetry of the seas around Israel: The Black and Caspian Seas. In: R. Bogoch (ed.), Geol. Surv. Isr. Current Res., Vol. 13, p. 105-108.



Chapter 23

New Look at the Region of Eratosthenes Seamount as Revealed by Gravity and Magnetic Data

Michael Rybakov, Michael A. Gardosh
Geophysical Institute of Israel, 6 Baal-Shem Tov Street, P.O. Box 182, Lod 71100, Israel
Zvi Ben-Avraham
Department of Geophysics and Planetary Sciences, Faculty of Exact Sciences, Tel Aviv University, Ramat Aviv 69978, Israel

ABSTRACT

We present the results of the interpretation of gravity and magnetic data in the area around Eratosthenes Seamount (ESM). The updated datasets clearly show two partially superimposed magnetic dipoles, which also correspond well to disturbances in the gravity field. The pronounced Eratosthenes magnetic anomaly (EMA) is only the positive part of the southeastern dipole. There is no large gravity anomaly here, however the specific gravity pattern corresponds to the magnetic body. The northwestern magnetic dipole coincides with a prominent gravity high. This combination allowed us to interpret the anomalies as being caused by a hitherto unknown dense and magnetic body which we have named the Niklas structure.

The parameters of both bodies were calculated by inverse programs and forward modeling using the seismic refraction and reflection constraints. The reliability of the final model was verified using forward modeling. The magnetic data were interpreted by assuming an induced magnetization as the main magnetizing factor. The final model consists of two large compact bodies oriented NE-SW and located south of the Cyprean arc.

The results help us to gain a better understanding of the present crustal structure and the tectonic evolution of the Eastern Mediterranean. This study is also a methodological example of how improved understanding of subsurface geology can be obtained using integrated interpretations in other complicated geological regions.

INTRODUCTION

The Eratosthenes Seamount (ESM) and Eratosthenes magnetic anomaly (EMA) are the most prominent features of the bathymetry and magnetic field of the Eastern Mediterranean (**Figures 23.1 and 23.2**). A number of multidisciplinary studies were devoted to this unique area (*e.g.* Ben-Avraham et al., 2002 and the references therein). The most recent gravity and magnetic interpretation was carried out by Ben-Avraham et al. (*ibid.*). Using the constraints of seismic refraction these authors suggested that the EMA is caused by a normal magnetized high susceptibility (2000 mA/m) block with a density of 2.75 g/cm^3. This thick (~10 km) body is located at the depth of about of 5 km.

All the researches studying the ESM and EMA noted that the seamount occupies a relatively small part of the complicated magnetic anomaly. And only the positive magnetic anomaly has been described as the EMA. To the best of our knowledge, no study of the positive part of the magnetic dipole of EMA was ever done. While the vector of the total magnetic field has an inclination of ~45° at the latitude of the study area, the normally magnetized body has to produce both the positive and negative anomalies (**Fig. 23.3**). The aim of the present study was to reinterpret the magnetic data. Doing this we used not only the magnetic grid data (Rybakov et al, 1997) but also the raw magnetic observations along the lines of marine surveys. That allowed better delineation of the magnetic gradients and gave more reliable and accurate depth estimations.

A significant free air gravity high (60 mGal) corresponds to the ESM (Makris and Wang, 1994). This anomaly is clearly seen even on the satellite gravity. At the same time no pronounced Bouguer gravity anomaly was mapped that corresponds to the ESM and EMA (**Fig. 23.4**). In 1990 the area south and west of Cyprus was again covered by a marine gravity survey (Toulin, Chapter 14 in this volume). The dense gravity measurements, confirming the general gravity features established by previous surveys, allowed detailing of the pattern of the gravity anomalies in the study area. A high-density block was first reported northwest of the ESM (Toulin, Chapter 14 in this volume). A petrophysical crustal model of the ESM region was developed by Makris and Stobbe (1984) by evaluating the results of some seismic refraction lines and interpreting the potential field data. Ben-Avraham et al. (2002) reconfirmed this model. In general, the model shows that the crust of the study region appears to be as follows: low magnetic sediments beneath the sea floor (thickness about 10 km, density 2.42 g/cm^3) cover oceanic crust (density ~2.9 g/cm^3) with an estimated thickness on the order of 10 km. The density of the mantle was reported to be around 3.3 g/cm^3. We used these parameters as initial constraints interpreting the potential filed data.

The present work concentrates mainly on the problems of 3-D integrated interpretation of potential fields to provide a reliable subsurface model for future tectonic compilations.

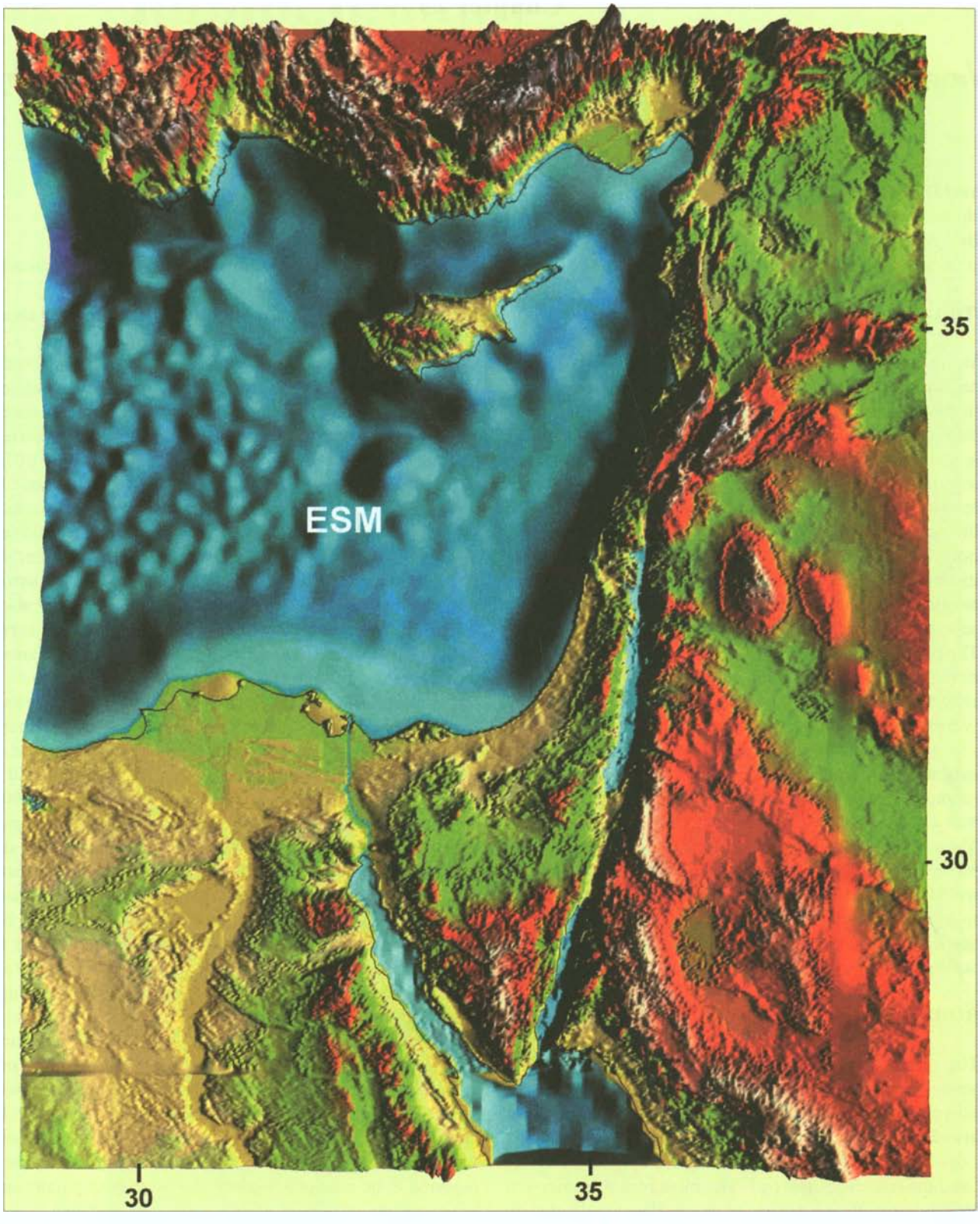


Fig. 23.1. Topography and bathymetry of the Levant simplified after Hall (pers. comm.). ESM – Eratosthenes Seamount.

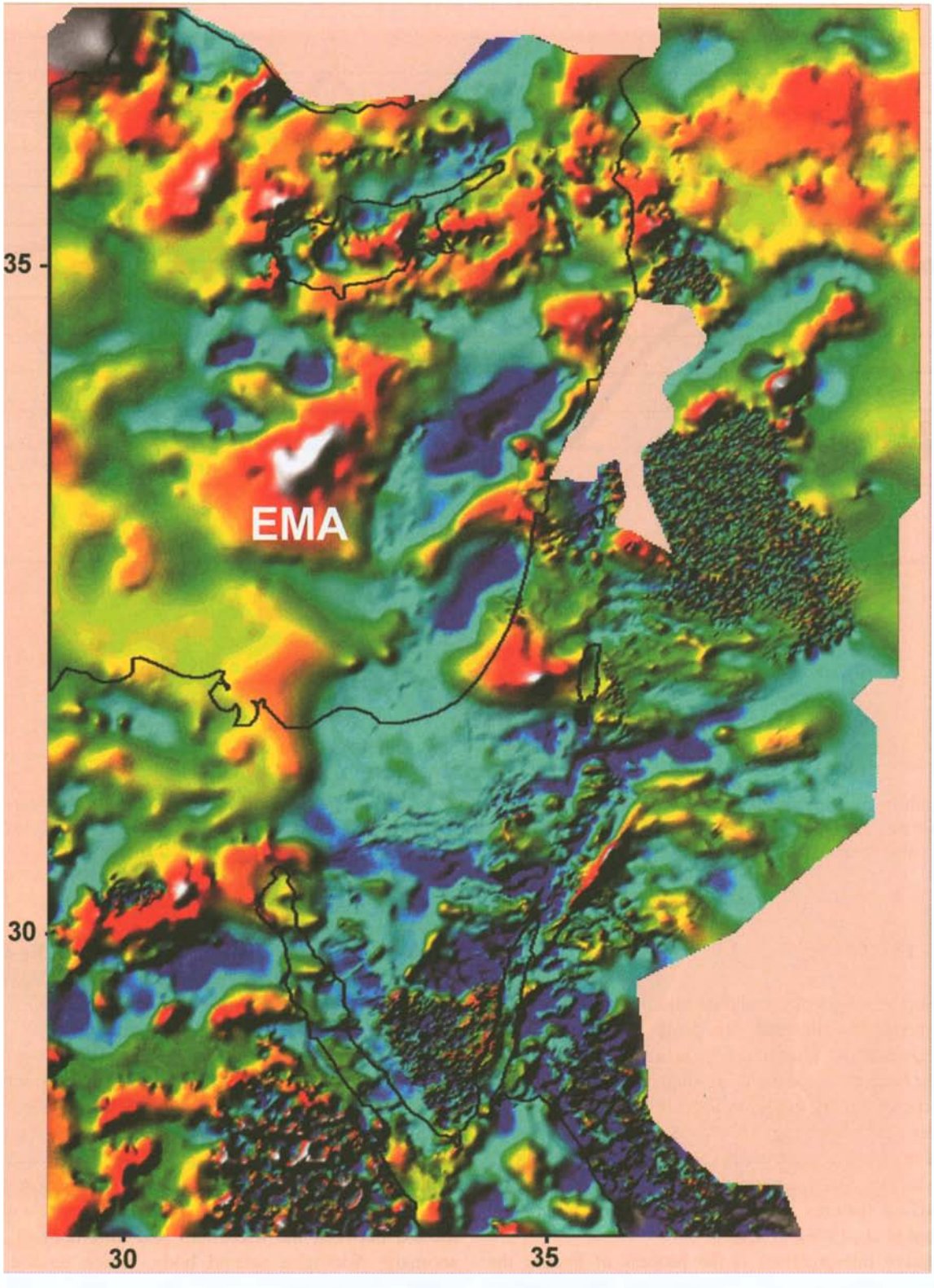


Fig. 23.2. Magnetic anomaly map of the Levant after Rybakov et al. (1997). EMA – Eratosthenes Magnetic Anomaly.

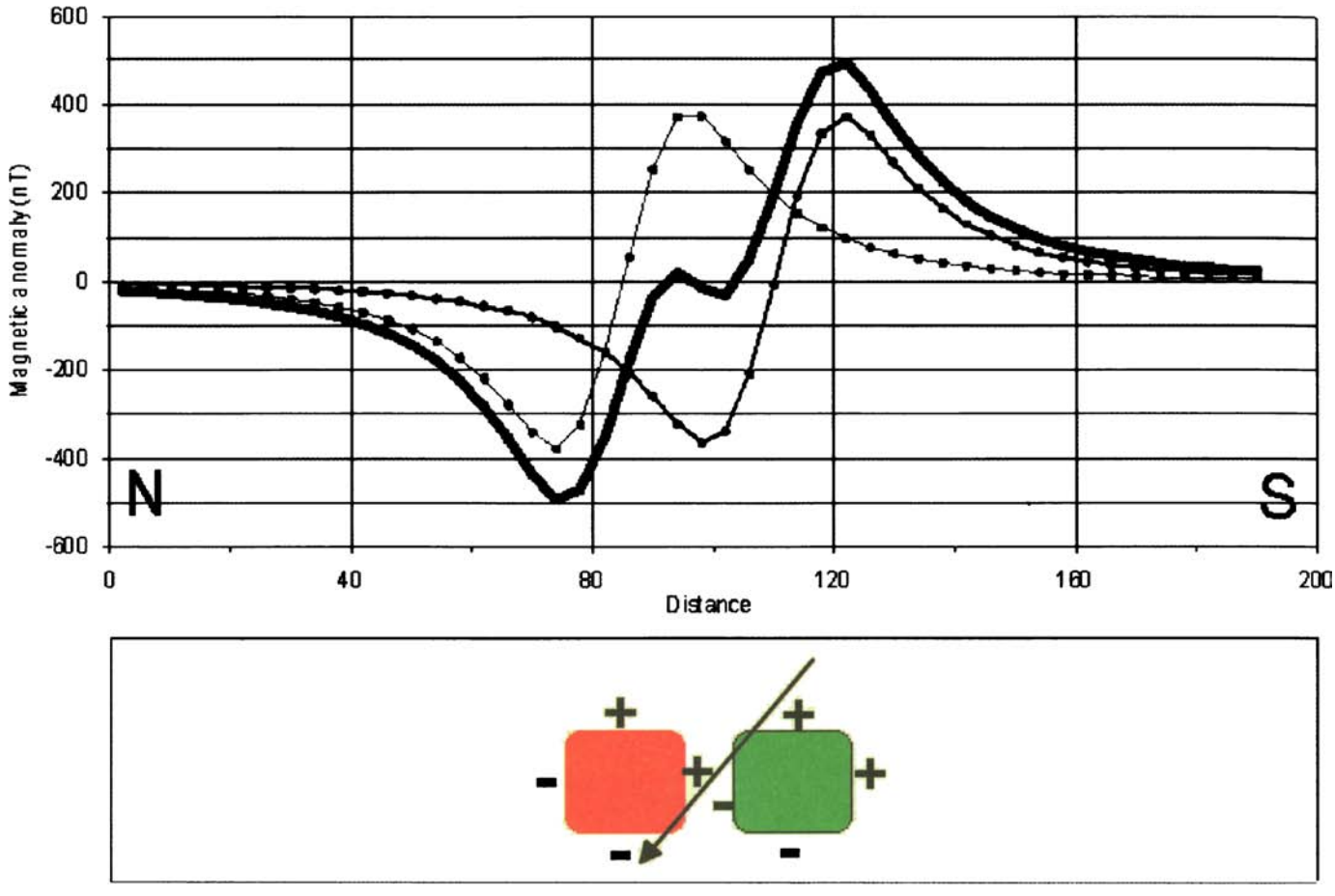


Fig. 23.3. Synthetic magnetic anomaly pattern. Green graph corresponds to the green body, red graph to the red body, and the blue graph is the composite magnetic anomaly. This model shows the following: total maximum has grown a little; minimum corresponding to the southern body has almost vanished; the anomaly of the northern body appears as a small disturbance of the total field.

INTERPRETATION

The objective of geophysical data interpretation is usually to locate anomalous material, its depth, dimensions, and properties. Qualitative interpretation is a process revealing characteristic features of the materials under study, their spatial location, and preliminary geological identification. Qualitative interpretation "is something of a fine art; the interpreter experienced in magnetics can usually see a geological structure merely by looking at a magnetic map, much as one can visualize surface features from the contour of a topographic map" (Telford et al., 1976).

Quantitative interpretation is the process of finding the depth, and geometrical and petrophysical characteristics of geological bodies, locally revealed in plan and initially identified as a result of the qualitative interpretation. This stage also includes estimation of the accuracy and reliability of the results. Success in the interpretation strongly depends on the quality of the initial model while "any wrong efforts on the way will just multiply mistakes".

Qualitative interpretation

We analyzed the pattern of the magnetic anomalies on the ESM and its vicinity by starting with a synthetic magnetic anomaly caused by a buried susceptible body that had been magnetized by the Earth's magnetic field at the typical inclination and declination of the study area (Fig. 23.3). The body has a distinctive magnetic dipole signature with the body located between the maximum and minimum of the dipole anomaly. Adding a second body, which caused the same dipole anomaly, we have the total anomaly, which is not so simple (Fig. 23.3). While the main maximum grew a little, the anomaly minimum corresponding to the southern body almost vanished. The anomaly of the northern body appeared as a small

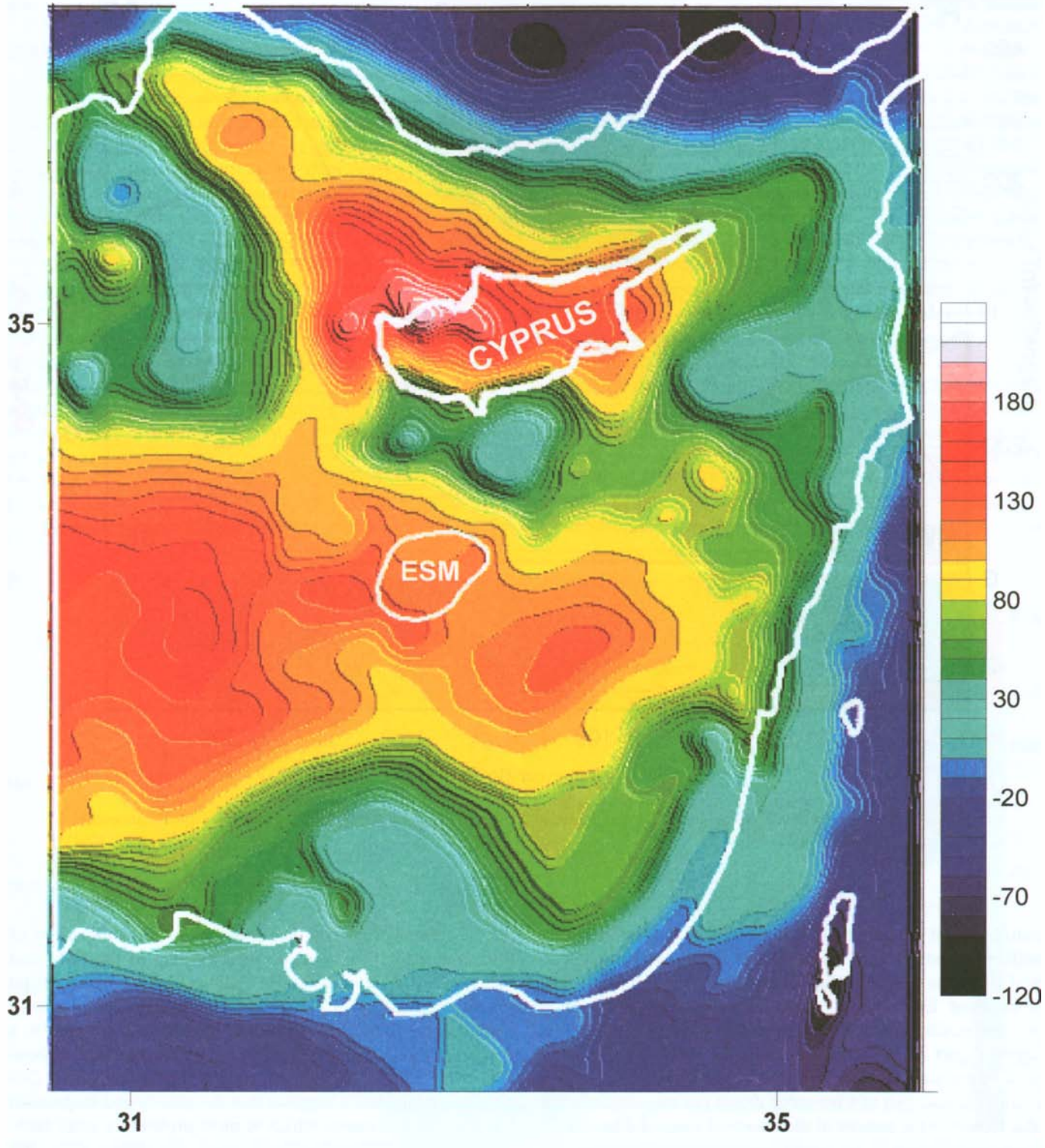


Fig. 23.4. Bouguer gravity map of the Levant after Rybakov et al. (1997).

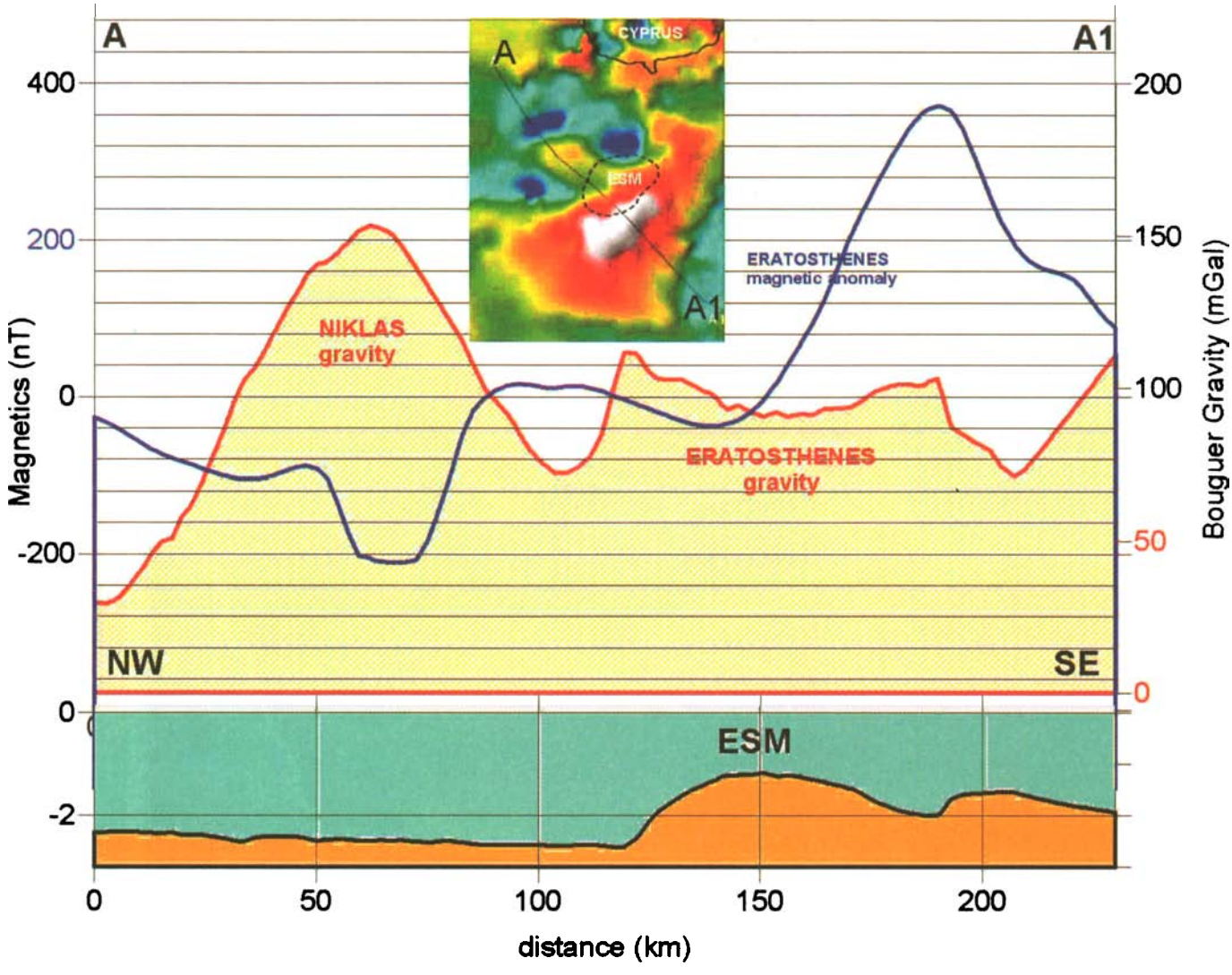


Fig. 23.5. Bathymetry (black), magnetic (blue), and gravity (red) profiles along the line A-A1. Inset – magnetic anomaly map of the ESM and vicinity.

disturbance of the total field. Comparison of the pattern of the synthetic anomaly with the pattern of the observed magnetic field (the blue graph in **Fig. 23.5**) suggests a similarity. The pronounced Eratosthenes magnetic anomaly (~450 nT) is only the positive part of a complicated magnetic dipole. The negative part of the dipole is partially masked by another positive anomaly located northwest of the ESM. This positive anomaly is also part of a magnetic dipole (its magnitude is 100 nT). However the pattern of the observed magnetic anomalies is essentially more complicated than the theoretical one. The insert in Fig. 23.5 shows that the relatively simple positive part of the EMA is accompanied in the northwest by a magnetic high and a few magnetic lows. These can be explained by the presence of at least two separated deep-seated bodies.

The detailed gravity data provides good confirmation of this assumption. The Bouguer gravity map of the ESM and vicinity (**Fig. 23.6**, after Toulin, Chapter 14 in this volume) and gravity profile (Fig. 23.5) suggests that the complicated gravity pattern of the Eratosthenes structure appears to correspond to a seamount. The prominent gravity high with magnitude of about 100 mGal coincides with the magnetic dipole (magnitude 200 nT). The coincidence suggests that the gravity and magnetism have a common cause, which is most probably a large basic or ultramafic intrusive body or block of oceanic crust. We have named this body the Niklas structure. It is located 120 km southwest of Cyprus and about 100 km northwest of the ESM. It became clear that the gravity low obviously separates the Niklas gravity high from the specific pattern of the ESM,

confirming the assumption of two bodies based on the magnetic data.

Quantitative interpretation

The aim at this stage was to define the parameters of the targets delineated above. Inverse solutions and forward modeling were used to help locate the anomalous bodies and determine their shape and properties. There are many different techniques to estimate source depth from potential field data. All automated and semi-automated methods derive depth from curvature of the field with reference to the curvature produced by a reference model of idealized geometric shape.

Based on our past experience (Rybakov et al., 2000) the Werner deconvolution technique was chosen to calculate the depth of the causative bodies. **Fig. 23.7** illustrates the 2-D inversion of the gravity and magnetic data. The clusters of dots, highlighted by blue (magnetic) and red (gravity) ellipses, are indicative of a strong solution. These clusters appeared to be useful for compiling an initial iteration for the 3-D modeling. Iterative methods involve calculating the field which a model would produce, comparing it with the observed field, and then iterations of model changes until a satisfactory degree of fit is achieved between the model field and the observed field.

Iterative 3-D modeling (MAGPOLY and GRAVPOLY programs, Cordell et al., 1992) allowed us to compile a general 3-D model of the subsurface. Two horizontal planes and a series of intersecting vertical planes bound the elements of these models. The effect of an assemblage of polygonal prisms is calculated for all locations of the field observations and is then compared with the observed values. In our case the prism assemblage included two compact bodies (Eratosthenes and Niklas). We combined the MAGPOLY and GRAVPOLY programs with interactive PC programs that permit digitization of polygon corners as well as imaging, analysis, and comparison of the observed and calculated fields. The programs allow determination of the best density contrast and the best magnetic susceptibility for the assemblage of polygonal prisms by a least-squares comparison between the observed and calculated values. To interpret the magnetic data we assumed that the total magnetization vector coincides with the vector of the Earth's total magnetic field.

The resulting 3-D models were obtained after some trials. The iterative modeling process was stopped when the main features, such as amplitudes and gradients of the calculated anomaly, had been adjusted to fit the observations. The 3-D modeling showed that the gravity and magnetic anomalies are caused by concealed bodies located inside as well as outside the investigated area. At the next stage the parameters of the

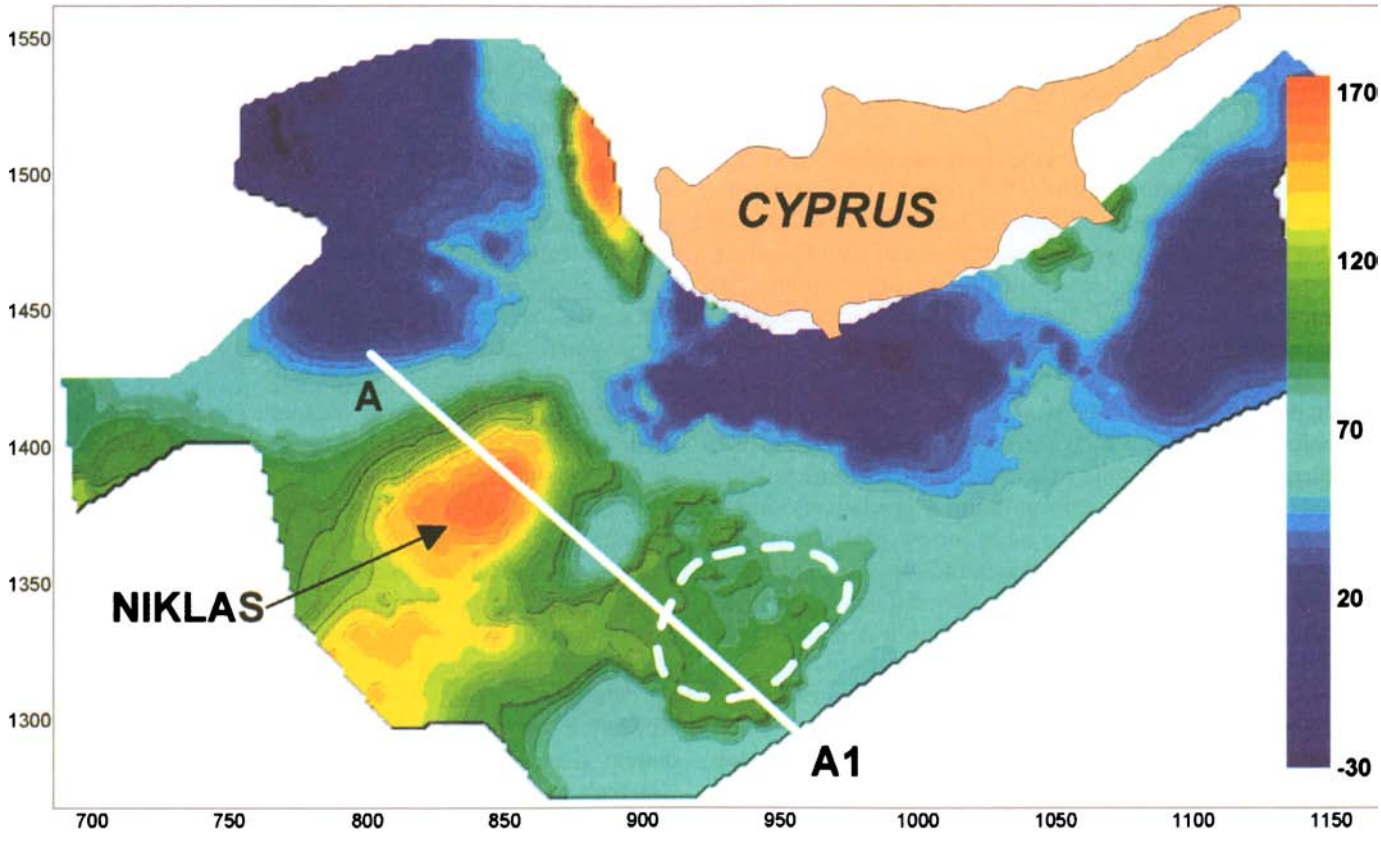


Fig. 23.6. Detailed Bouguer gravity map of the ESM and vicinity (after Toulin, Chapter 14 in this volume). A-A1 is the location of the gravity profile shown in Fig. 23.5. The ESM is denoted by a white dashed line.

Table 23.1. Figures 23.8 and 23.9 illustrate the plane view and vertical cross-sections of the Eratosthenes and Niklas bodies.

	Eratosthenes			Niklas	
	Seamount	**Magnetic body**	**Gravity target**	**Magnetic body**	**Gravity target**
Magnitude of anomaly	1.2 km	500 nT	25 mGal	200 nT	100 mGal
Distance from Cyprus	110 km south	135 km south	110 km south	95 km southwest	95 km southwest
Length	100 km	160 km	135 km	75 km	100 km
Width	75 km	60 km	100 km	35 km	75 km
Top	-0.8 km	7 ± 2 km	5 ± 2 km	8 ± 3 km	6 ± 2 km
Bottom	-2 km	16 ± 4 km	15 ± 3 km	15 ± 5 km	14 ± 5 km
Density or Magnetic susceptibility	—	$7 \cdot 10^{-2}$ SI	2.75 g/cm^3	$7 \cdot 10^{-2}$ SI	3.0 g/cm^3

subsurface model were developed using the 2.5-D and 3-D packages. Interactive modifications of the model parameters (geometry, rock density and susceptibility) enabled us to design the model as realistically as possible and to estimate the confidence intervals of the model parameters. In interpreting the data we followed a principle akin to Occam's razor – "The simpler the model, the better it is". The parameters providing the best fit for the gravity and magnetic anomalies observed in the area are given below.

RESULTS AND DISCUSSION

Analyzing the subsurface model one has to remember that the results obtained from potential field data are inherently non-unique. The present interpretation should also be considered a member of the class of possible solutions that could produce magnetic and gravity patterns matching the observations. The accuracy and reliability of such model parameters as top and bottom and density contrast and magnetic properties is strongly dependant on the correctness of the initial model and constraints. The appraised values of the density, magnetic susceptibility, and calculated depths should be regarded as rough estimates. The plane projections of the causative bodies are more reliably defined than their upper and lower limits. The relatively simple geometry can be altered using a more complicated assemblage of polygonal prisms (such as a pyramid), which could lead to bodies with smoother slopes. The difference between the anomalies from the simple and complicated models is negligible.

Discussing the final model we will describe the results according to their reliability. The most important result is that there are two bodies – Eratosthenes and Niklas - disturbing the gravity and magnetic fields in the study area. The bodies are located south and southwest of Cyprus and south of the plate boundary (**Fig. 23.8**). All the subsurface targets are elliptical in shape and are oriented northeast-southwest. Both bodies appear to be located approximately at the same depth, however the magnetic and gravity sources only partially coincide (**Fig. 23.9**).

Study of the EMA and ESM has a long history that does not include the Niklas structure. Its existence is reported here for the first time and therefore it was important to verify its crustal heterogeneity. Fortunately the Deep Seismic Sounding Profile VI (**Fig. 23.10**) surveyed southwest of Cyprus by the Geological Survey of Cyprus (simplified in Fig. 23.8 after Makris and Wang, 1995) shows a high-velocity cone-shaped block that coincides with the Niklas body. The depths to the top and bottom of this block are 7 and 13 km respectively, corresponding well to the results of the interpretation of the potential fields (Fig. 23.9 and **Table 23.1**). Analyzing the location of the seismic profile with respect to the gravity and magnetic patterns, one can see that the seismic line doesn't cross the main features causing the potential fields (Fig. 23.10, upper insets). Nevertheless the seismic refraction clearly indicates a block which appears to coincide with the body responsible for the magnetic dipole (magnitude ~200 nT) and the prominent (~100m Gal) positive gravity anomaly.

Analyzing the gravity and magnetic patterns of the Eastern Mediterranean, we suggest that the combination of the Niklas strong gravity high and magnetic dipole is unique for the region, and only the ophiolites of the Troodos Massif display the same character (**Fig. 23.11**). However the magnitude of the anomalies caused by the deep-seated Niklas body are less than the anomalies of the outcropping Troodos and the horizontal gradients of the gravity and magnetic anomalies of the Niklas are obviously smoothed.

The Eratosthenes structure is considered to embody a volcanic block, broken off from the Afro-Arabia continental margin during the early Mesozoic rifting of this margin (Garfunkel and Derin, 1984; Kempler, 1998). The gravity and magnetic data suggests that the strongest EMA isn't associated with a significant gravity high. The same combinations were described for the largest onshore Hebron magnetic anomaly and for the Carmel magnetic anomaly (Rybakov et al., 1995;

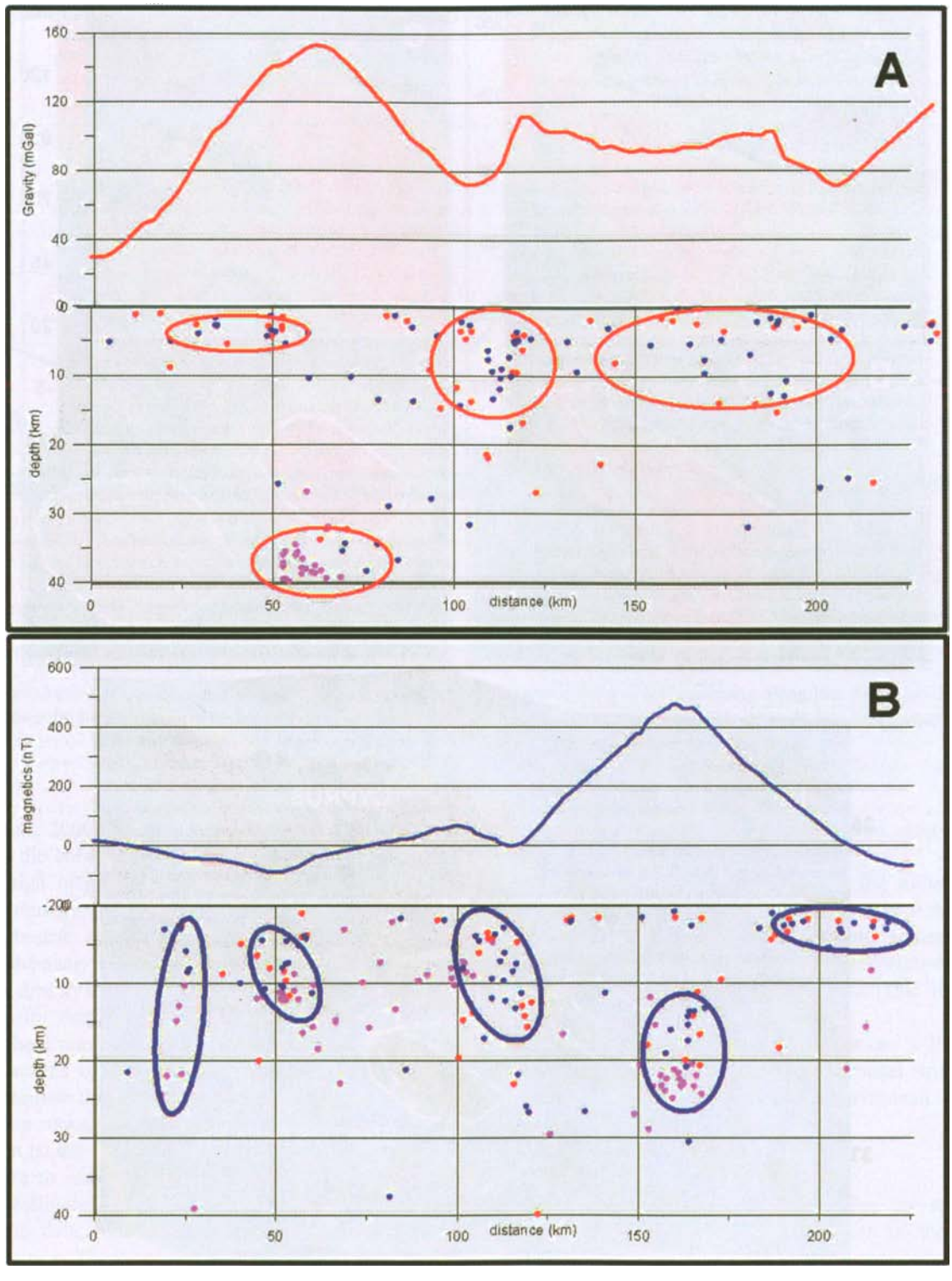


Fig. 23.7. Preliminary 2-D depth solution derived by the Werner deconvolution method (Cordell et al., 1992). A - gravity and B - magnetic inversions. Dots obtained with different degrees of interference polynomial (n=0, 2 and 5) are shown by pink, blue, and red colors respectively. The visually determined clusters of plotted dots (indicative of a strong solution) are highlighted by blue (magnetic) and red (gravity) ellipses.

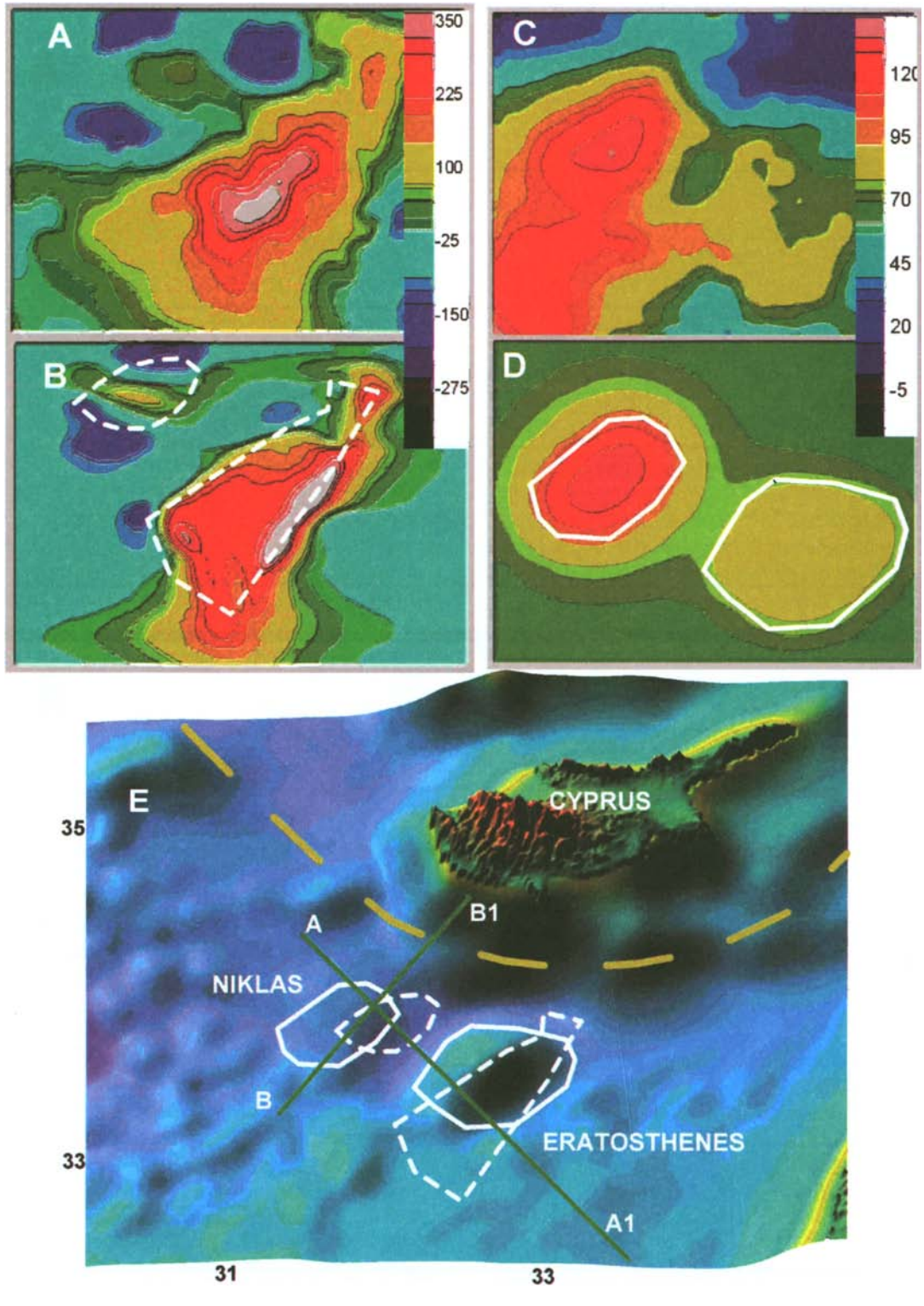


Fig. 23.8. Best fit of the 3-D magnetic (A-observed, B-calculated) and gravity (C-observed, D-calculated) MAGPOLY and GRAVPOLY forward modeling programs (Cordell et al., 1992). E – plan view of the prism assemblages. White solid and dashed polygons denote the gravity and magnetic targets respectively. The Eratosthenes and Niklas bodies are located south of the plate boundary (yellow dashed line). Green lines A-A1 and B-B1 show the locations of the interpreted profile (Fig. 23.9) and the seismic refraction profile (Fig. 23.10).

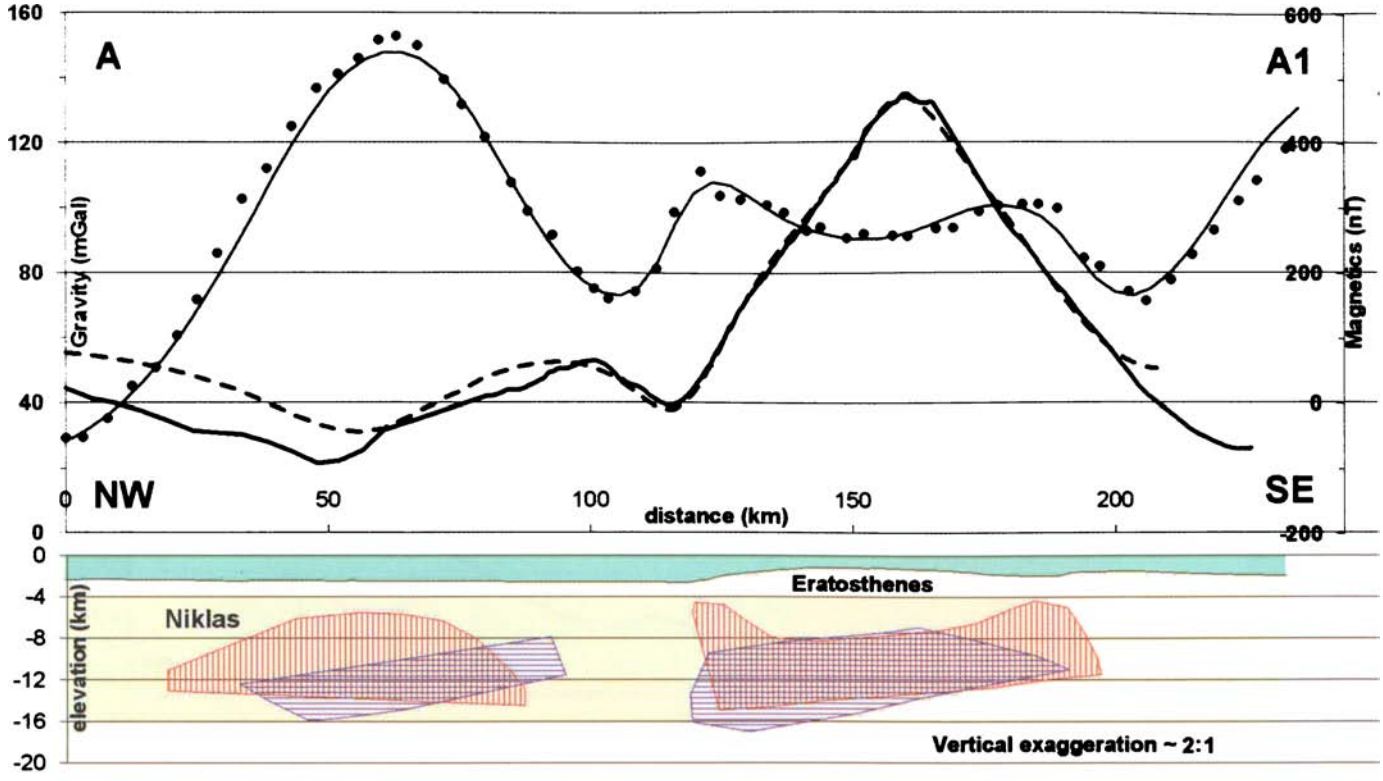


Fig. 23.9. Final depth solution derived by 2.5-D gravity (red color) and magnetic (blue color) modeling along line A-A1 (see location in Fig. 23.5). The solid lines show observed data. Calculated values are shown by red dots (gravity) and a blue dashed line (magnetics).

Rybakov et al., 2000). They interpreted such a combination to result from the Jurassic Asher Volcanics Formation (mainly tuffs with high magnetic properties and with average rock-percentage density equal or even less than the density of country carbonate rocks – about 2.65 g/cm^3). The marine sediments (the shaly lithofacies) surrounding the Eratosthenes body have a density of 2.4-2.5 g/cm^3 (Makris and Wang, 1995). Such a density contrast would explain the specific gravity pattern of the Eratosthenes body. Based on the gravity and magnetic patterns of the Eratosthenes, Carmel, and Hebron areas we speculate that the Eratosthenes structure is associated with volcanic rocks, possibly similar to the Asher Volcanics Formation in Israel.

We have to note that the contrast in the petrophysical properties, estimated from the interpretation of the gravity and magnetic data, more or less reliably suggests only the rock composition. There are no direct geological observations allowing us to define the age and origin of the Eratosthenes and Niklas bodies.

CONCLUSIONS

As a result of the gravity and magnetic interpretation, it became clear that two deep-seated bodies exist in the region of the ESM.

Both bodies – Eratosthenes and the hitherto unknown Niklas – appear to be located approximately at the same depth and they both appear to have the same estimated order of magnitude in size and magnetic properties. However the Niklas body seems to be denser (~3.0 g/cm^3) than that of Eratosthenes (~2.75 g/cm^3).

We believe that these new observations will contribute to a better understanding of the present crustal structure and the tectonic evolution of the Eastern Mediterranean.

ACKNOWLEDGEMENTS

The authors gratefully acknowledge the support of the Earth Sciences Research Administration of the Ministry of National Infrastructures. We thank our colleagues Profs. A. Ginzburg, Z. Garfunkel, and V. Goldshmidt, and Drs. A. Agnon, Y. Ben-Gay, A. Hofstetter, Y. Folkman, A. Segev, and G. Shamir for useful discussions.

The authors also wish to thank Dr. J. K. Hall for extensive editing of this chapter, and his assistance in using the DTM of Israel and adjacent areas.

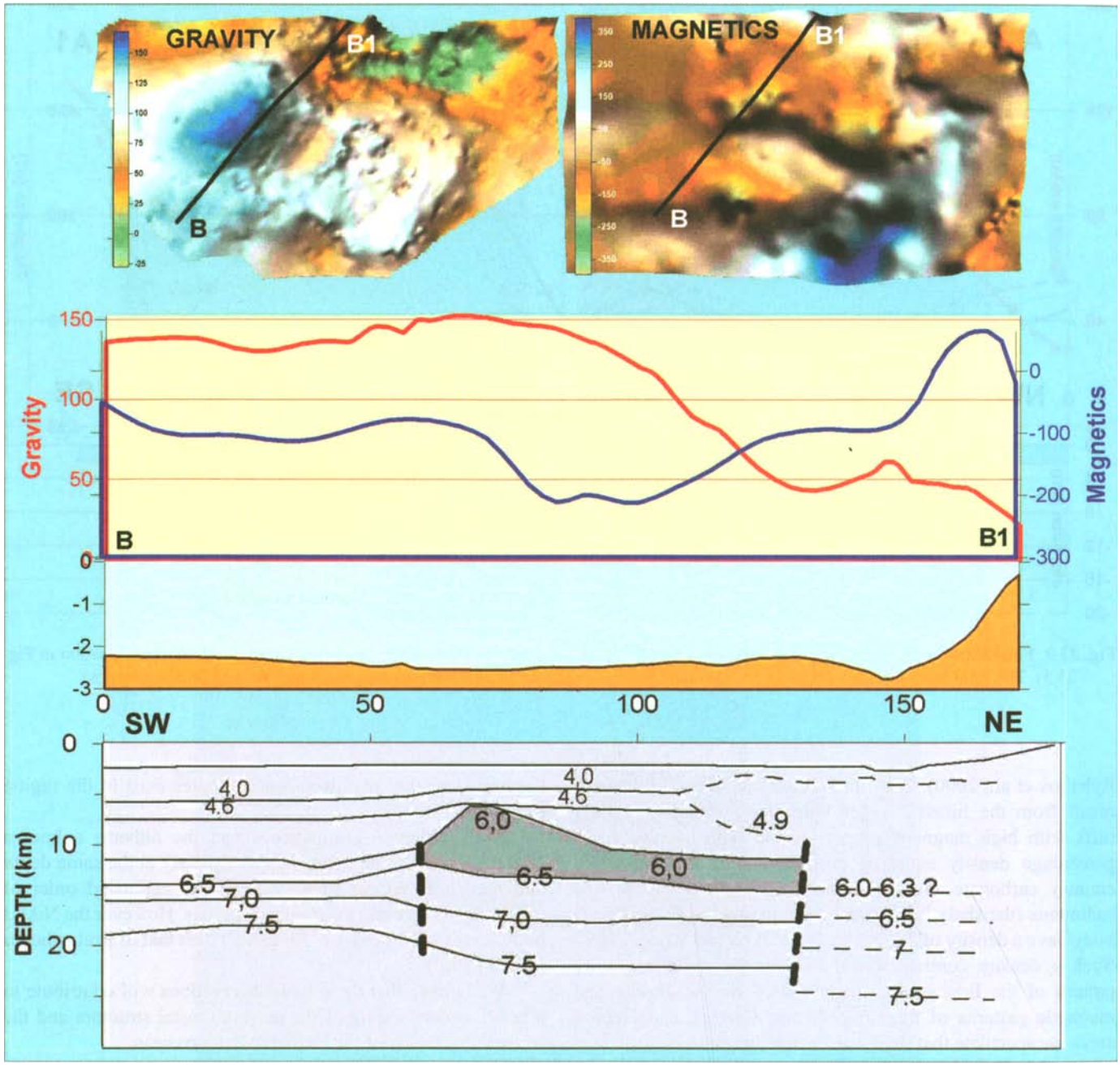


Fig. 23.10. Deep Seismic Sounding Profile VI surveyed by the Geological Survey of Cyprus (simplified after Makris and Wang, 1995). The depth-velocity model (see location in Fig. 23.8), accompanied by gravity and magnetic data, shows a thick high-velocity cone-shaped block that coincides with the Niklas body. Analyzing the location of the seismic profile with respect to the gravity and magnetic patterns, one can see that the seismic line doesn't cross the highest features of the potential fields (upper insets). Despite this the block, derived from seismic refraction, appears to coincide with the magnetic dipole and local positive gravity anomaly.

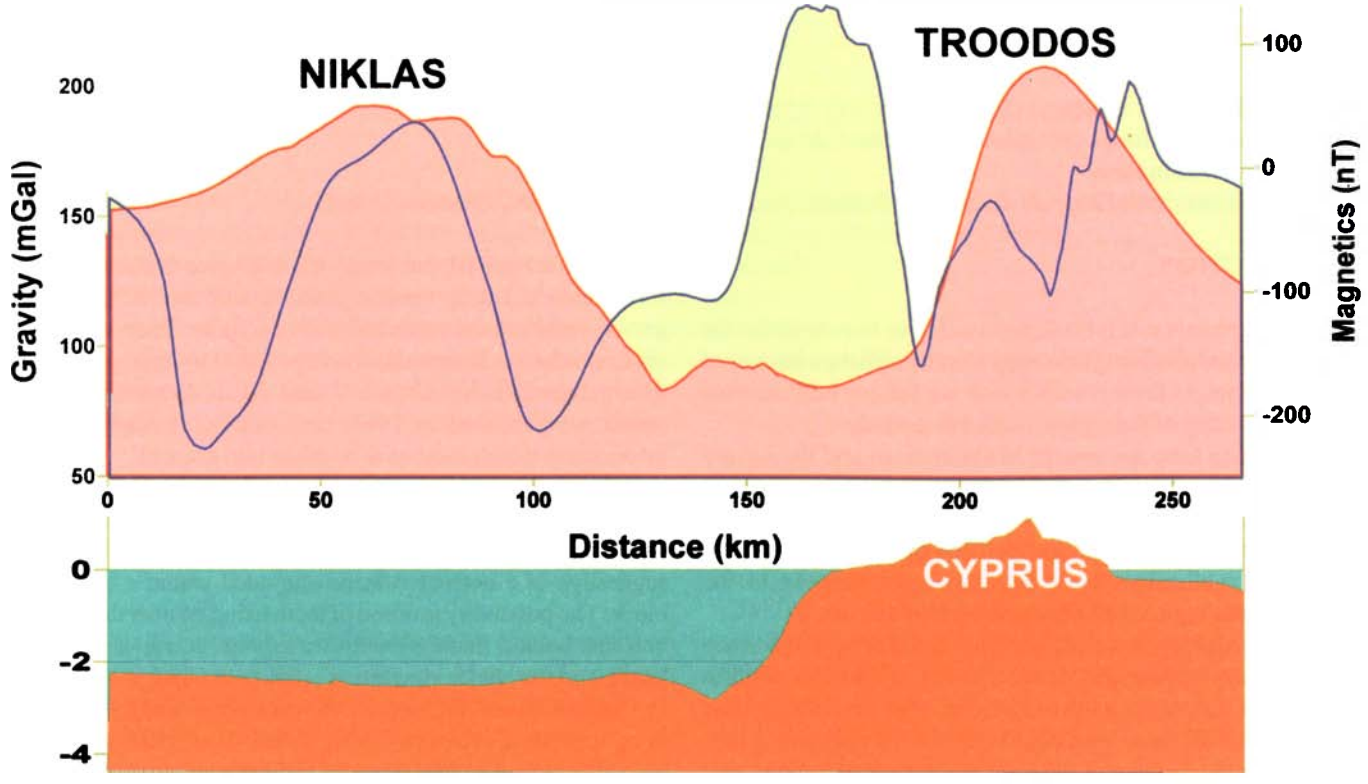


Fig. 23.11. Comparison of the potential field patterns of the Troodos Massif and the Niklas body. The positive gravity anomaly reaches 200 mGal inland and the magnitude of the magnetic anomalies is 300 nT. High horizontal gradients of the gravity and magnetic anomalies are typical onshore. The potential field pattern of the Niklas feature appears to be similar, however the anomaly range is less and the horizontal gradients are obviously smoothed.

REFERENCES CITED

Ben-Avraham, Z., Ginzburg, A., Makris, J., and Eppelbaum, L., 2002. Crustal structure of the Levant Basin, eastern Mediterranean. Tectonophysics, 346(1-2), p. 23-43.

Cordell, L. E., Phillips, J. D. and Godson, R. H., 1992. U. S. Geological Survey potential-field geophysical software; version 2.0. Open-File Report - U. S. Geological Survey, Report OF 92-0018-A through G, 16 p. and diskettes.

Garfunkel, Z., and Derin, B., 1984. Permian-early Mesozoic tectonism and continental margin formation in Israel and its implications for the history of the Eastern Mediterranean. In J. E. Dixon and A. H. F. Robertson, (eds.), The Geological Evolution of the Eastern Mediterranean. Geol. Soc. Spec. Publ. 17, London, p. 187-201.

Kempler, D., 1998. Eratosthenes seamount: the possible spearhead of incipient continental collision in the eastern Mediterranean. In: A. H. F. Robertson, K. -C. Emeis, C. Richter, and A. Camerlenghi and others (eds.), Proceedings of the Ocean Drilling Program, Scientific Results, Vol. 160, p. 709-721.

Makris, J., and Stobbe, C., 1984. Physical properties and state of the crust and upper mantle of the Eastern Mediterranean Sea deduced from geophysical data. Marine Geology, 55(3-4), p. 345-361.

Makris, J., and Wang, J., 1994. Bouguer gravity anomalies of the eastern Mediterranean Sea. In: V. A. Krasheninnikov and J. K. Hall (eds.), Geological Structure of the North-Eastern Mediterranean, Historical Productions-Hall, Jerusalem, p. 87-99.

Makris, J. and Wang, J., 1995. Geophysical study and geodynamics of the eastern Mediterranean Sea. Universität Hamburg, Institut für Geophysik, Ma 719/48-1, 135 p.

Rybakov, M., Fleischer, L., and Goldshmidt, V., 1995. A new look at the Hebron magnetic anomaly. Israel J. Earth Sci., 44(1), p. 41-49.

Rybakov, M., Goldshmidt, V., Fleischer, L., and Ben-Gai, Y., 2000. 3-D gravity and magnetic interpretation for the Haifa Bay area (Israel), J. Applied Geophysics, 44(4), p. 353-367

Rybakov, M., Goldshmidt, V., and Rotstein, Y. 1997. A new compilation of gravity and magnetic data from the Levant and their preliminary interpretation, Geophysical Research Letters, 24(1), p. 33-36.

Telford, W. M., Geldart, L. P., Sheriff R. E., and Keys, D. A. 1976. Applied Geophysics. Cambridge University Press, 860 p.

Toulin, V. A., 2005. Gravity field of the northeastern part of the Mediterranean Sea (South and West of Cyprus). Chapter 14, In: J. K. Hall, V. A. Krasheninnikov, F. Hirsch, C. Benjamini, and A. Flexer (eds.), Geological Framework of the Levant, Volume II, Historical Productions-Hall, Jerusalem, p. 123-130.

Epilogue

John K. Hall, Francis Hirsch,
Geological Survey of Israel, 30 Malchei Israel Street, Jerusalem 95501, Israel
Valery A. Krasheninnikov
Geological Institute of the Russian Academy of Sciences, Pyzhevskiy pereulok 7, 109017 Moscow, Russia

INTRODUCTION

As an epilogue to this book, we would like to summarize the highlights of the preceding detailed accounts with their masses of data, and to assess those results which we believe best describe the characteristics of the region studied as a whole.

For a long time the eastern Mediterranean and the Levant have attracted the attention of scientists as it is a relatively small area where the principal problems of regional (and global) geology can be confronted and perhaps even solved. A great number of publications have therefore been devoted to the geology of this region, and this book adds to that list.

With one exception, our tome does not deal with the entire eastern Mediterranean and Levant. Often our results confirm the findings of previous investigations, thus increasing their reliability. But in other cases our results have introduced new insights into the geology of the area, raising new questions, and sometimes answering old questions.

The book has two volumes, each with two parts. Volume I describes the results of the Russian investigations dealing with:

Part I: The Island of Cyprus.

Part II: Syria, located mainly to the east of the Dead Sea Transform.

Volume II deals with the more southerly portions of the Near East. They are:

Part III: The Levantine Basin in the easternmost part of the Mediterranean, and its topography and that of Cyprus, as well as the recent cover of the Mediterranean Sea.

Part IV: Israel, to the west of the Dead Sea Transform.

In Parts I and III, our study of SW Cyprus is combined with some reworked deep seismic profiles, and new refraction and gravity results to the south and east of Cyprus. Deep-sea drilling on Eratosthenes Seamount, made possible in large part by the data gathered during Cruises 5 and 10 of Akademik Strakov which we published in 1994, has contributed important new information which must now be taken into account.

Cyprus confronts us with the events from before and after the Alpine collision, while Eratosthenes Seamount on the sunken part of the African Plate beneath the eastern Mediterranean is suggestive of a hotspot volcano shrouded within a continental block. The possibility is raised of there being another three buried volcanic bodies, under Mount Carmel, the 'Jonah' structure off Israel, and the Niklas structure west of Eratosthenes.

In Parts II and IV, much of the geology of the Levant is seen to be a result of events occurring in and around the Palmyrides. Indeed, a period of 200 Ma, the sediment cover of the Levant passive platform margin ultimately appears to reflect the activity of this complex fracture system. From the Late Paleozoic until Early Cenozoic times, this Palmyrid furrow attempted and ultimately failed to turn the 'northern-most' tip of the Levant into a micro-continent. After Late Paleozoic opening and Mesozoic deepening of the Tethys, Late Cretaceous-Cenozoic emplacement of the Tethyan seafloor as ophiolites was the result of the Alpine collision. Thereafter followed the Neogene opening of the Red Sea and the rifting and separation of Arabia from Africa, which produced further shortening and thrusting within the Palmyrides aulacogen, which was once the centerpiece of Levant geology.

Parts I & III

From South-Western Cyprus to Eratosthenes

V. A. Krasheninnikov[1], J. K. Hall[2], N. Bragin[1], D. Klaeschen[3], A. Kopf[4], S. Silantyev[5], N. Vidal[6], R. von Huene[3], and S. Zverev[7]
[1]*Geological Institute of the Russian Academy of Sciences, Pyzhevskiy pereulok 7, 109017 Moscow, Russia*
[2]*Geological Survey of Israel, 30 Malchei Israel Street, Jerusalem 95501, Israel*
[3]*GEOMAR Research Centre, Wischofstrasse 1-3, D-24148 Kiel, Germany*
[4]*Geosciences Azur, B. P. 48, 06230 Villefranche-sur-Mer Cedex, France*
[5]*Vernadsky Institute of Geochemistry and Analytical Chemistry of the Russian Academy of Sciences, Kosygin Str. 19, 117975 Moscow, Russia*
[6]*Escola Universitaria Salesiana de Sarria, Rafael Battle 7, 08017 Barcelona, Spain*
[7]*Institute of Physics of the Earth of the Russian Academy of Sciences, Bolshaya Grusinskaya Str. 10, 123810 Moscow, Russia*

1. TROODOS, MAMONIA AND THE NEOAUTOCHTHON

1.1. Petrology and geochemistry of igneous and metamorphic rocks

The data on the petrology and geochemistry of the igneous and metamorphic rocks from the Troodos and Mamonia Complexes provide the necessary base for the reconstruction of the main stages of the magmatic and metamorphic history of SW Cyprus.

Judging from their geochemical peculiarities, these magmatic and metamorphic episodes occurred in two different geodynamic settings. The first exhibits a suprasubduction style of magmatism and definite features of ophiolite (or oceanic) metamorphism. The second episode produced igneous and sedimentary rocks within a *passive continental margin* with possible initial oceanic rifting events. In contrast to ideas previously put out, there are no features that are characteristic of a mature oceanic basin.

The high grade metamorphic rocks of the Mamonia Complex represent an intermediate link between the two main episodes mentioned above, as their protholith has clear geochemical signatures of passive continental margin origin. This protholith was further subjected to high pressure metamorphism in a shallow subduction zone.

The principle conclusions regarding the petrology and geochemistry of the Troodos and Mamonia Complexes are as follows:

1) Existing data on the compositional characteristics of the Troodos Ophiolite Complex rocks allow us to recognize two main broadly defined magmatic rock assemblages of suprasubductional affinity. The first one is composed of the lower cumulative sequences of the plutonic complex, the sheeted dyke complex, and the lower pillow lavas. This assemblage belongs to the first stage of formation of the Troodos Complex and must be related to the consequent extension in a supra-subduction setting. These rocks originated from island arc tholeiitic magmas, which are characteristic for intra-arc and back-arc basins of the transitional zones. The second magmatic assemblage consists of the upper portion of the cumulative sequence, and includes the latest mafic dykes, as well as the upper pillow lavas. This assemblage belongs to the second stage of magmatic evolution of the Troodos Complex, and represents the products of transformed bonitite-type magmas, which are characteristic of the entire basement of intra-oceanic island arcs.

2) The mineralogy and geochemistry of spinel lherzolite recently discovered in the core of the Troodos Ophiolite Complex (Sobolev and Batanova, 1995), as compared with the associated strong depleted dunite-harzburgite suite, allow us to refer all these peridotites to a single suprasubduction ultramaphic assemblage formed in the same subduction zone.

3) Geochemical data provide evidence supporting a concept in which the Dhiarizos lavas were formed in a marginal part of the initially rifted oceanic basin which resembles the present Red Sea area. This similarity between the volcanic rocks of the Dhiarizos group and those of the Red Sea region is buttressed by the chemical variability of the Red Sea basalts, which include both analogues of depleted oceanic tholeiites and the alkali basalts of the Dhiarizos lava complex.

4) The harzburgite from the Mamonia Complex may have been formed in a geodynamic setting similar to that of the Troodos harzburgites and could represent a product of mantle melting above a subduction zone. On other hand, the most primitive lherzolites of the Mamonia Complex closely resemble the most primitive lherzolites of mid-ocean ridges and may have formed in a geodynamic setting representing a transitional stage from continental to oceanic rifting. In contrast to the Mamonia lherzolites, the Troodos spinel lherzolites described by Sobolev and Batanova (1995) display a significantly greater degree of partial melting as compared with the Mamonia lherzolites. High temperature amphibolization, characteristic of some varieties of the Mamonia lherzolites, does not occur in the Troodos lherzolites. It is possible that this amphibolization occurred after melt extraction when lherzolites were elevated and emplaced into the overlying crustal horizons composed of volcanics which resemble the Dhiarizos group lavas, as did the known peridotites of passive continental margins. An alternative explanation of such amphibolization may be related to the penetration of water into the deep levels of subducted passive margin lithospheric slabs during formation of normal tension fractures, compression of lithospheric mantle, and accompanying hydration of the lherzolites with their

subsequent extrusion into upper crust levels.

5) Most gabbroids and associated diabases of the Mamonia Complex in SW Cyprus belong to the boninite series. The rocks of boninite-type in the Mamonia Complex are juxtaposed with gabbroids, most of which are identical to those of the late-stage magmatic assemblage from the Troodos Complex. These gabbros are associated with geochemically similar diabases and pillow lavas belonging to the same magmatic series. Therefore the main part of the Mamonia gabbroids was probably formed in the same geodynamic setting as the plutonic complex of Troodos, or, at least, of its late-stage boninitic rocks. A distinct kind of gabbroic rock, which has no analogue among the gabbroids of the Troodos ophiolite, is only present in the Xeros Potamos River valley. These gabbros, with their distinctive alkaline specificity, are considered to be plutonic derivatives of the Dhiarizos Group magmatic complex, and consist mainly of pillow lavas having alkali basaltic, trachybasaltic, and trachytic compositions.

6) Metamorphic blocks within the Mamonia Complex are similar in lithology and textural fabric to specific ophiolite-related metamorphics associated with the so-called 'sub-ophiolitic soles', but differ from the metamorphic products of various igneous rocks belonging to the ophiolite sequence, in both P-T conditions and structural features. In contrast to the 'ophiolite-type' metamorphics, diverse sedimentary rocks metamorphosed in isofacial conditions (together with their associated igneous rocks), widely occur among the sub-ophiolitic high-pressure complexes and high-grade metamorphic rocks of the Mamonia Complex.

Therefore the model for the metamorphism of the Mamonia amphibolites proposed by Spray and Roddick (1981) has become untenable in light of the data given above, which clearly indicate non-oceanic conditions. Geochemistry suggests the presence of typical protoliths ranging from marginal oceanic basins to passive continental margins. The tectonic scenario for the Mamonia metamorphics thus implies that the geodynamic setting differs from that of modern oceanic basins, including transform faults.

All high grade metamorphic complexes associated with the Mediterranean ophiolites are characterized by the similarity in P-T conditions and the geochemical features of their protholiths (Alavi-Tehrani, 1980; Pamic and Adib, 1982; Silantyev, 1993; Ghent and Stout, 1981). These sub-ophiolitic metamorphic complexes share one notable common trait: both the high-pressure metamorphics formed under non-oceanic conditions and the low-pressure oceanic (or ophiolitic) metamorphics have the same or very similar ages (Silantyev, 1993). This coincidence in age of metamorphism of the two contrasting pressure types of metamorphism, now occurring in tectonically juxtaposed complexes, is evidence for their formation within different geodynamic settings.

Most sub-ophiolitic high-pressure metamorphics in the eastern Mediterranean, including the Mamonia Complex, may have been formed by progressive obduction of ophiolite masses onto the continental margin (volcano-sedimentary successions) (Silantyev, 1993). However, the pure obduction model of formation of high grade amphibolites has some contradictions. This model needs a certain thickness for the ophiolite succession to realize the required pressure, as well as similar ages for the low temperature hydrothermal metamorphism in both the Troodos igneous sequence and the high grade metamorphic rocks of the Mamonia Complex.

We assumed that the P-T conditions corresponding to the shallow subduction zone, where warm lithosphere slabs are sinking, could be suitable for the formation of the Mamonia Complex metamorphics. A similar geodynamic model has been proposed by Hacker (1991) who, in the case of the Semail ophiolite, suggests that the metamorphic sole must coincide with ridge subduction. According to Shervais (2001), formation of high grade metamorphic rocks from sub-ophiolitic soles belongs to a stage of 'resurrection' in the evolution of Tethyan subtype ophiolites such as Troodos and Oman; this resurrection accompanied the emplacement of ophiolite on a passive continental margin.

All the geochemical and petrological signatures listed above in the igneous and metamorphic rocks from SW Cyprus can be used to indicate the geodynamic style of their formation and to match the data on lithology, stratigraphy, and geophysics in this volume.

1.2. Mesozoic Stratigraphy and Sedimentology of the Troodos and Mamonia Complexes

The lithology and stratigraphic succession of the Mesozoic deposits of the Troodos and Mamonia Complexes illustrate nearly 150 million years of the geological history of SW Cyprus.

1) The Cretaceous sedimentary cover of the Troodos Ophiolite Complex consists of two units: the Perapedhi Formation and Kannaviou Formation.

The Perapedhi Formation is composed of metalliferous sediments (umbers) and directly overlies the Upper Pillow Lavas and is associated with volcaniclastic breccias. The sediments of this unit are the oldest paleontologically-dated deposits in Cyprus. They were deposited just after the formation of the Troodos Ophiolite Complex, and prior to the emplacement of the allochthonous Mamonia Complex. Abundant radiolarians in the shuffled succession give various ages for the top of the Turonian-Lower Campanian interval at different places in SW Cyprus. Nevertheless the development of the Troodos Ophiolite Complex was apparently completed before the end of the Santonian or at the beginning of the Campanian.

The Upper Cretaceous umbers of Cyprus have much in common with the recent hydrothermal sediments of the mid-oceanic ridges.

The overlying Kannaviou Formation is made up of bentonite clays with abundant radiolarians of Campanian-Lower Maastrichtian age (the *Amphipyndax pseudoconulus* and *Amphipyndax tylotus* Zones). Both the Perapedhi and Kannaviou Formations have a normal stratigraphic relationship.

2) The sedimentary rocks of the allochthonous Mamonia Complex belong to two tectono-stratigraphic units: the Ayios Photios Group and the Dhiarizos Group.

The Ayos Photios Group consists mainly of Upper Triassic to Middle Cretaceous sedimentary rocks and is subdivided into two formations. The Vlambouros Formation is Upper Triassic in age.

It is mainly represented by proximal to distal clastic turbidites and calciturbidites with abundant redeposited material of shallow-water origin and beds of background sediments (micritic limestones). It is characterized by pelecypods and conodonts of Carnian to Early Norian age. Upward in the section, cherts yield Late Norian to Rhaetian radiolarians. The deposits of the Vlambouros Formation can be interpreted as rift-related sediments formed on the southern passive margin of the Tethys.

The Episkopi Formation (Middle Jurassic-Cenomanian) is composed of radiolarian cherts, cherty mudstones, and clays, with subordinate calciturbidites and sandstones. A nearly continuous succession of abundant Callovian, Oxfordian, Kimmeridgian-Tithonian, Valanginian-Hauterivian and Albian-Cenomanian radiolarian assemblages is present in this formation. Lower Jurassic deposits have not been identified. The sediments of the Episkopi Formation originated in a marginal sea or immature ocean type basin. During Callovian-Oxfordian times eupelagic biogenic (siliceous) deposition with a low sedimentation rate was prevalent. Later on, it became hemipelagic with a decrease in the amount of cherts and an increase in clastics.

The Dhiarizos Group is represented by various volcanics; sedimentary rocks are present as lenses, interbeds and inclusions of limestones and cherts. It is subdivided into three formations: Phasoula, Petra tou Romiou and Loutra tis Aphroditis.

The Phasoula Formation is widely distributed throughout the Mamonia Complex. Its lower part (volcanics, micritic limestones and subordinate cherts) is characterized by Upper Carnian to Lower Norian conodonts and radiolarians. The upper part of this formation (cherts and cherty mudstones) has a tectonic contact with the underlying strata and yields radiolarians of the Upper Norian to Middle Jurassic.

The Petra tou Romiou Formation is characterized by numerous blocks of shallow-water reefal limestones mixed with volcanics and incorporated into a mélange with clayey matrix. Limestones yield corals and bivalves of the Upper Triassic.

The Loutra tis Aphroditis Formation is only present in the Akamas Peninsula (Western Cyprus). This formation consists of volcanic breccia and lava flows with interbeds of micrites and cherts containing abundant radiolarians of Early Jurassic age (probably the Late Sinemurian to Pliensbachian).

Some blocks of recrystallized limestones and cherts contain radiolarians of the late Middle Jurassic (Nea Choletria) and Early Cretaceous (in the vicinity of Ayia Varvara) but their relation to the Dhiarizos Group remains unclear.

1.3. Late Campanian/Cenozoic Stratigraphy and Sedimentology of the Neoautochthon

After the 'mise en place', Mamonia and Troodos formed the backbone of Cyprus, and the latter became the new basement (or 'para-autochthon') underlying the neoautochtonous Late Campanian-Cenozoic sedimentation.

The deposits of the neoautochthon of SW Cyprus represent the long interval from the Upper Campanian/Lower Maastrichtian to the Quaternary. A continuous succession is observed in the depression of the Kouris and Kryos rivers, where the standard subglobal (tropical-subtropical) planktonic foraminiferal and radiolarian zones of the Paleogene, and the planktonic foraminifera and nannoplankton zones of the Neogene are found. In the adjacent elevated areas of Mamonia and the Limassol Forest, the sections are incomplete with several unconformities and depositional gaps. In SW Cyprus the following succession is observed:

1) Maastrichtian-Lower Eocene calcareous clays and marls;

2) A thick uppermost Lower Eocene (P9 Zone) and the basal part of the Middle Eocene (P10 and P11 Zones) consisting of a pile of alternating brown and black flints and limestones;

3) Middle-Upper Eocene pelagic chalk;

4) Oligocene limestones and marls with significant addition of calcareous clays;

5) Lower Miocene to basal Middle Miocene chalky limestones;

6) Middle and Upper Miocene (Tortonian) calcareous clays, sandstones and marls;

7) Upper Miocene (Messinian) evaporites; and

8) Pliocene clays and marls.

The peculiarities of these rock units derive from some global and regional (Mediterranean) events, and similar successions of the same rock units have been found in Syria, Israel and Egypt.

Local events influenced the general paleo-environmental conditions, generating special facies types, whose distribution complicated the overall picture:

- In the Kouris-Kryos depression of SW Cyprus, a stable deep water regime of sedimentation prevailed;
- The Upper Campanian-Lower Maastrichtian is composed of radiolarian oozes, precipitated under greater bathyal depths, well below the CCD; and
- The upper Maastrichtian oozes were formed below the lysocline of the planktonic foraminifera but above the lysocline of the calcareous benthic foraminifera;
- The Danian oozes were laid down near the lysocline of planktonic foraminifera, but all their shells were dissolved and replaced by silica;
- The Upper Paleocene-Upper Eocene sequence is represented by radiolarian/foraminiferal and foraminiferal/radiolarian oozes;
- The Oligocene is characterized by the appearance of terrigenous (clayey) material;
- The Lower Miocene and the basal Middle Miocene are represented by pure calcareous pelagic foraminiferal oozes;
- The Middle and Upper Miocene (Tortonian) are characterized by neritic calcareous-terrigenous sedimentation;
- The Upper Miocene (Messinian) deposits indicate restricted environments;
- The Pliocene calcareous silty-clay sediments are typical for the outer shelf;
- Marine Quaternary shelf sediments, which for the first time contain debris of ophiolites, point to the beginning of denudation of the Troodos and Mamonia complexes.

The above features of the neoautochton allow us to outline its important properties as follows:

1) The environmental and bathymetric stability of deep water radiolarian and foraminiferal/ radiolarian oozes in sediments of the Upper Campanian-Upper Eocene is a unique feature of the Cyprus stratigraphy. Such facies are absent in the contemporaneous deposits of Eratosthenes Seamount, the Near Eastern countries, and Egypt.

2) As a result of the secondary processes of redistribution of silicious matter, the Paleocene-Eocene sediments contain thin lenses and nodules of silicious rocks at various stratigraphic levels. However their main concentration belongs to the dark flints of the Lower Eocene P9 Zone and to the silicified limestones of the Middle Eocene P10-P11 Zones. Such concentrations are typical for other areas of the eastern Mediterranean. On account of the redistribution of siliceous matter, soft unbedded chalk was converted into hard cryptocrystalline limestone.

3) The difference between the Eocene foraminiferal oozes of Eratosthenes Seamount and the radiolarian-foraminiferal oozes in the Kouris-Kryos depression of SW Cyprus permits us to suggest that in Eocene time, these two regions were still widely separated.

4) A clear distinction exists between the deep water facies of the Kouris-Kryos depression and the shallower facies of the Mamonia cover. The former is characterized by up to 1.3 km of slow rate pelagic deposition, whereas the latter consists of much faster sedimentation, but due to several erosional gaps, its composite thickness only amounts to 0.7 km. These differences in facies and thickness are a function the dissected relief of the underwater southern slope of the Troodos Massif.

5) In the Upper Campanian-Quaternary sequence of the Kryos-Kouris depression one can observe the change in major sedimentary types, from abyssal and lower bathyal non-carbonate radiolarian oozes to carbonate terrigenous and evaporitic neritic and littoral facies. The same trend, with minor differences, can also be discerned in the Upper Mesozoic-Cenozoic succession of the Mamonia Massif. This aspect of the geological development of Cyprus was previously mentioned by several scientists. The geodynamic nature of such positive movements, whether from subduction of the African plate, horizontal push generated by the Troodos Massif, or isostatic motion, is still poorly understood.

6) In addition to positive tectonic movements, there are well-documented global sealevel changes expressed in the sedimentary sequence of SW Cyprus, such as:

- the transgressive character of the Paleocene, Lower Eocene and lower half of the Middle Eocene;
- the first signs of regression, which appeared in the second half of the Middle Eocene and are evidenced by the restricted occurrence of the Upper Eocene;
- maximum regression coincides with the Oligocene, when sediments of this age were identified only in the depression;
- transgression in the Lower-Middle Miocene;
- regression, starting in the Upper Miocene (Tortonian) and culminating in the Messinian;
- the Pliocene transgression of limited geographic extent.

A parallel evolution can be observed throughout most of the Levant.

1.4 The structural evolution of SW Cyprus

A thorough investigation of the inter-relationships between the petrological, lithological, and structural features of the ophiolites of the Troodos subautochton, the Mamonia allochtonous complex, the various melanges, and the Neo-autochton, suggests a specific scenario for the crustal evolution of SW Cyprus.

This process spans the Late Triassic to the Cenozoic, and can be subdivided into ten stages.

1) Late Triassic break-up of the continental African margin: spreading resulted in the formation of lherzolites with subsequent high-temperature amphibolization that gave rise to interplate mafic rocks and depleted ultramafites (harzburgites included). On the surface this led to the formation of volcanic piles and volcanism with intraplate as well as spreading affinities. Simultaneously a well-defined continental slope developed, accompanied by gradual subsidence and deepening of the entire basin. Turbidites accumulated at the base of the slope and, prior to the Rhaetian, red radiolarites in the deeper depression of the basin were already below the CCD.

2) The onset of the Jurassic in the southern part of the Tethys was manifested by further sagging of the basin. In the Early Jurassic, which is preserved in the Amanus Peninsula, vigorous bottom currents hampered deposition. Magmatism consisted of oceanic basalts and deformation began with the appearance of the 'pre-Troodos' ophiolitic olistostromes.

3) During the Middle Jurassic, bottom current activity waned and deep-sea silicious sedimentation below the CCD became the norm for the entire basin.

4) During the Late Middle-Late Jurassic (Callovian-Tithonian) eupelagic organogenic siliceous as well as hemipelagic sedimentation occurred. Reactivation of differential block-movements generated calciturbidites. Consequently this deep-water basin had the character of a small young ocean with rugged topography.

5) In the Neocomian, the basin was invaded by the Amanus sandstone, and cherts disappeared from the Ayios Photios Group, pointing to a regressive cycle. In the inner part of the basin, however, pelagic sedimentation with cherts persisted until the Albian-Cenomanian.

6) The Albian-Cenomanian interval corresponds to the Austrian orogenic phase, generating a major rearrangement of the entire Tethys. In the Cyprus Basin, development of the Mamonia composite terranes ceased and a subduction zone was initiated.

7) The Cenomanian-Turonian spreading process over the newly formed subduction zone consisted of the latitudinal opening of the Troodos Basin. Its frontal part experienced compression while its rear part underwent extension. In front of the Cyprean subduction zone, accretion proceeded with underthrusting of oceanic fragments beneath the continental rise. This accretion embraced various crustal levels. The deeper portions of oceanic lithosphere, involved in the accretion, produced the peculiar ophiolitic assemblages of the Mamonia complex. The peridotites of this complex were tectonized and recrystallized under upper greenshist to amphibolite facies

conditions (450-600°C), and the lherzolites became tectonically juxtaposed with the harzburgites.

8) In the Campanian, the frontal part of the spreading zone acquired the shape of an uplift with a complex thrust-related structure like that of the Mamonia terrane. The emplacement of the metamorphic rocks and enriched lherzolites into the upper crustal horizons must have occurred rapidly as evidenced by the lack of retrograde recrystallization in both of these rock groups. These movements produced various serpentine melanges. Ultramafic diapirism resulted in the tectonic disintegration of the thermal aureole in the subduction zone and transportation of its fragments to the the surface, where they were incorporated into unmetamorphosed continental margin deposits and the Troodos ophiolites.

9) In the Late Campanian-Early Maastrichtian the last significant change in plate motions took place. Active spreading in the Troodos basin ceased but it retained its deep water character, as witnessed by the radiolarian oozes of the Perapedhi and Kannaviou Formations. Terrigenous and submarine slump materials accumulated, derived from the incipient Mamonia rise. The rugged topography favored formation of the terrigenous mélange of the Kathikas Formation, consisting of fine debris along with huge olistoliths reaching up to 1.5 km in size. The Troodos plate experienced a 90° rotation and the Mamonia composite terrane was thrust back onto the southwestern edge of the Troodos. The oceanic Troodos rocks underwent tectonic disintegration and serpentinization, generating the unnamed monomictic serpentinite mélanges of Troodos fragments. Finally, the newly formed structures were covered by the neoautochthon deposition.

10) The Late Maastrichtian-Cenozoic history of the neoautochthon, described above in this Epilogue, can now be briefly summarized. A thick series of Neoautochthon sediments was laid down in a depocenter on rugged submarine relief inherited from the tectonic evolution of SW Cyprus. This depocenter, the Krios-Kouris trough, is bound on the north by the Troodos, on the west by Mamonia, and on the east by Limassol Forest. Continuous slow pelagic sedimentation at the center of the Krios-Kouris basin has accumulated a pile 1.3 km thick, whereas on the edges of the basin the thickness is nearly half of this because the sedimentation in shallower water was characterized by fast deposition, but interrupted by numerous gaps,. From the Maastrichtian upwards, the facies evolved from bathyal to neritic, due to vertical motion of the substratum, though the nature of the tectonic source is debatable. Sea level changes are evident in the sedimentary sequence as the elevations of similar rock-units are compared around the eastern Mediterranean. Quaternary sediments are characterized by the first appearance of ophiolitic debris, the result of denudation of the Troodos and Mamonia complexes.

2. STRUCTURAL EVOLUTION OF THE CYPREAN ARC AND ERATOSTHENES SEAMOUNT (LEVANTINE BASIN)

The investigation of the Levantine Basin consists of analysis of both seismic reflection and refraction profiles as well as marine gravity measurements and swath bathymetry.

2.1. Offshore Reflection

Approximately 1700 km of multichannel deep seismic data recorded in the eastern Mediterranean Sea between the southwestern offshore of Cyprus and the Syrian coast were reprocessed (**Fig. E.1**). These data, acquired during Cruise 5 of the Research Vessel 'Akademik Nikolaj Strakhov', illustrate the deeper structures and the deformational pattern of the area.

The data required careful reprocessing, including individual deconvolution operators to remove the effects of ghost and bubble inherited from streamer and airgun configurations, and to improve temporal resolution. The primary reflections were covered by multiple energy from the seafloor and the uppermost sedimentary layers which required f-κ and wave-equation demultiple procedures. Prestack depth migration provides a first insight into both subsurface and deep velocity information for the area, which reveals a complex pattern of crustal blocks and sedimentary-tectonic units, reflecting various stages of incipient collision between Africa and Eurasia from west to east.

The geometry and precise location of the plate boundary between Africa and Eurasia in the eastern Mediterranean Sea has been a matter of debate, and its evolution is still unclear (*e.g.* Kempler, 1994; Woodside et al., 1997). Seismicity, high resolution bathymetry, gravity, and magnetics, as well as several shallow seismic and some wide-angle data indicate that there are different tectonic segments (Hall et al., 1994; Makris and Wang, 1994; Makris et al., 1994; Udintsev et al., 1994; Makris et al., 1983).

The multichannel seismic data acquired during Cruise 5 of the R/V 'Akademik Nikolaj Strakhov' depict the deeper structures and the deformational pattern of the area. A set of profiles from south east of Cyprus to the coast of Syria are oriented subparallel to the presumed direction of plate convergence and are tied by a crosscutting, SW-NE-striking line (Fig. E.1). The most prominent topographic high in the area, Eratosthenes Seamount to the south of Cyprus, is cut by two crossing profiles (Profiles 8 and 10). Another topographic high, the Florence Rise to the west of Cyprus, is cut by Profile 9. The three seismic lines in the west allow a comparative study of the deformational patterns caused by the collision of tectonic fragments in a convergent regime (both from the north and the south), and their influence on the vertical tectonics of Cyprus.

Collision Zone SE of Cyprus

The tectonic patterns along the plate boundary between Africa and Eurasia are found to be highly variable along the Cyprean Arc. From the southern extension of the island of Cyprus (*i.e.* the Hecataeus Rise) towards the east, a series of WSW-ENE-trending sutures and ridges can be observed on the bathymetric chart (Profiles 1 and 2, **Figs. E.2 and E.3**). Especially along Profiles 3 and 4, these ridges can be shown to represent thrust faults,

indicating an outward migration of the deformation front towards the south (**Figs. E.4 and E.5**). Although this process does not exactly match the classical 'trench roll back' (*e.g.* Thomson et al., 1998), the principle as well as the driving force are similar at most. Further east (Profiles 5 and 6), close to the area where the SW-NE-trending East Anatolian Fault Zone and the roughly N-S-trending Dead Sea Fault Zone meet, the subduction system disappears (**Figs. E.6 and E.7**). In this easternmost area the obliqueness between the directions of the East Anatolian Fault Zone, and the plate convergence vector, play a crucial role in the asymmetry of the plate boundary along strike. The observed faulting and its implications for the regional tectonism are discussed below. A summary of the area southeast of Cyprus is found in Vidal et al. (Chapter 10, this volume).

Collision zone SW of Cyprus

Unlike the area to the east, the western part of the Strakhov Cruise 5 study area is characterized by two topographic highs, the Florence Rise and Eratosthenes Seamount. As has been proved by deep marine drilling (ODP Sites 965-968; Emeis et al., 1996), the initial collision of the seamount occurred in the early Pliocene, which is reflected in the vertical tectonics of Cyprus. Eratosthenes Seamount is presently located in a depression SSE of Cyprus, and is in the process of being underthrust beneath the NW-SE-striking Giermann Trench (or graben). The seamount is assumed to represent a detached fragment of the North African shelf. Its base is rooted deeply in the subducting plate, and can be traced to depths greater than 12 km on seismic Profiles 8 and 10 (Klaeschen et al., Chapter 9, and Kopf et al., Chapter 11, this volume).

Eratosthenes Seamount is also broken up internally, most prominently by a NW-SE-trending reverse fault which can be followed to ~9 km depth. Consequently, it is inferred that, as in the area further east (see previous section), the deformation front is in the process of migrating southward. The faulting and outward migration of Eratosthenes Seamount is most likely due to the hindered subduction on its northern flank, where the island of Cyprus is acting as a mechanical abutment. Another consequence of the blocked fragment is seen at its southern flank. Here, Eratosthenes Seamount is over-ridden by the northward-moving sedimentary cover of the converging African plate (*i.e.* the Levantine basin fill), structurally representing 'backthrusting'.

The Florence Rise northwest of Eratosthenes Seamount also suffers incipient fragmentation and imbrication (Profile 9). It probably represents a continental fragment derived from the Taurides (southern Turkey), which was moving southward along active shear zones. Along Profile 9, an entire series of reverse and thrust faults provides evidence for tectonic shortening here at the Africa-Eurasia plate boundary. Like the Florence Rise itself, the majority of these thrust faults strike NW-SE. As discussed below, the plate boundary exhibits a considerably shallower dip than further east. A summary of the area southwest of Cyprus can be found in Vidal et al. (Chapter 10, this volume).

Discussion

While it is evident that in the east, a complex pattern of reverse and transform (or strike-slip) faults exists, the southern part of the study area by the Hecataeus Rise mainly exhibits flower structures (*i.e.* strike-slip faulting; *e.g.* Harding, 1985). The predominantly steep to vertically oriented fault traces separate the Hecataeus Rise from the sediments of the Levantine Basin (Profiles 1 and 2; Vidal et al., Chapter 10, this volume). The evaporite-bearing deposits are dragged upward and undergo micro-scale folding and faulting.

The approximately vertical fault representing the plate boundary south of Hecataeus Rise flattens considerably (and almost continuously) towards the east. Near the Syrian shelf, dip angles of ~40° are observed (Profile 6). However, it should be noted that these estimates are the apparent dip of the down-going plate because the orientation of the profile is oblique to the direction of plate convergence. Along Profile 10, acquired somewhat orthogonal to Profiles 1-6, the numerous faults seen on Profiles 1-6 can be found as well, although with shallower apparent dips (**Fig. E.8**). The observed ridges and topographic elevations on Profile 10 most likely result from reverse faulting perpendicular to the direction of plate convergence (*i.e.* the dip-slip component being the dominant force in the displacement).

The orientation and geometry of the different faults is predominantly controlled by the sinistral shear zones in the east (the prolongation of the Dead Sea Fault Zone) and to the north (the East Anatolian Fault Zone), and their interaction with the converging African Plate. A second controlling parameter of the subduction zone is the impact of Eratosthenes Seamount on the Cyprean Arc. The collision and ongoing subduction of Eratosthenes Seamount has caused a variety of processes, like the uplift of the island of Cyprus (and the accompanying dragging of sediment, *i.e.* seismic reflectors) and the initiation of reverse and strike-slip fault systems. Nevertheless, in the west where subduction is only slightly oblique, the well-known thrusting and imbrication is found (Profile 9, the Florence Rise).

In all, four main tectonic trends appear to cause the complex pattern of fault scars on the bathymetric chart, and the highly variable geometry of the plate boundary at depth (*i.e.* on seismic profiles). From east to west, these are:

1) NW-SE trending structures: Florence Rise, Giermann Trench;

2) ENE-WSW trending structures: southernmost margin of Cyprus, faults cross-cutting the Eratosthenes seamount; strike-slip faulting along Profile 10 (mainly the eastern part), thrust/reverse faults on Profiles 3-6;

3) SW-NE trending features: East Anatolian Fault Zone, Larnaca Ridge, Latakia Ridge, and the basins between these ridges; and

4) roughly N-S-oriented structures: Dead Sea Fault Zone, and its prolongation to the north.

This rather simplistic net of structural lineaments (Fig. E.1, the tectonic interpretation overlain on bathymetry) takes into account all the information gained from reprocessed MCS data, and can therefore be considered to be the least complicated model proposed for the easternmost Mediterranean. The two sets of

shears which are oriented perpendicular to each other (red lines) within the postulated shear zone (dashed heavy red lines) follow the mechanical principles from which brittle failure is predicted to occur at angles of 45° relative to the boundary of the shear zone. The red lines shown are located where faults and shears are observed on seismic profiles, however, they can be envisaged as being representative of numerous others in between the lines.

The model is rather schematic, but as already mentioned, it neither violates any mechanical principles nor is it in contradiction to any of main tectonic observations (trends 1-4, as the Florence Rise in the west appears unaffected in any way by the shear zone). However, here it should be noted that the model may not accommodate the complex tectonic movements due to plate rotations affecting the shear zone with time (namely the interplay between the East Anatolian, Dead Sea, and the North Anatolian Fault Zones). In the model, the influence of shear movement, and especially the sinistral forces related to the East Anatolian Fault Zone and its effects, are hindered (or even stopped) by Eratosthenes Seamount in the west of the study area.

2.2. Offshore Refraction.

Seismic refraction allows us to investigate the velocity within the rocks and the layer thicknesses, revealing their structure as well as their shape, and hinting at their composition. A network of profiles in the eastern Mediterranean obtained refracted arrivals down to depths of nearly 20 km. It revealed new information about deep structures, important for tectonic interpretation. These data are of complicated and variable nature. They were converted into seismic models and deep sections for the Eratosthenes Seamount region.

The seismic refraction sections show that Eratosthenes Seamount is not a uniform geological structure. The southern part of the seamount is covered by layers of high seismic velocity (6 km/s), coming close to the surface. Alternating high and low velocity interlayers occur further down at depth. We found 7.0 km/s layers at the depth of 7-8 km. The zone of high seismic velocity layers coincides nicely with the known large positive magnetic anomaly observed above the southern slope of the seamount. We suppose that this 7.0 km/s layer probably represents a highly magnetized magmatic body. The northern part of the seamount is covered by a pile of thick dense sediments, which apparently seem to be sinking down over several kilometers along a significant fault, which cuts the northern side of the seamount and which is probably related to the influence of the nearby subduction zone. Comparison of seismic data with the bottom relief, gravity, and magnetic fields suggests that Eratosthenes Seamount is an ancient great volcanic edifice, broken by a large fault. In addition the seismic velocities suggest that this edifice might have been constructed on continental crust.

The seismic wave properties were studied along all the available seismic profiles, and the influence of the bottom and subbottom topography on them used to weigh the possible tectonic implications. The most prominent common features are as follows:

Values of velocities and depths were combined in order to create the final sections shown on **Figs. E.9 and E.10**. They show the distribution of velocities after 2-D modeling (Fig. E.9)' and their generalization (Fig. E.10). One can see significantly different internal structures for the separate blocks, *i.e.* the internal peculiarities of the sediments and basement. These two sections show:

1) the presence of 4.5 km/sec material (salt) in the northern block;

2) a large thickness of sediments below the Hecateus Ridge;

3) a rise in the basement towards the Cyprus basin;

4) a sharp change in the structure of the northern side of Eratosthenes Seamount; and

5) the boundaries with velocities 6.2 and 7.0 km/s coincide well with the top of layers K3 and K4 described in the text. We can assume that the K5 surface can be attributed to the 7.0 km/sec boundary in the depression between Eratosthenes Seamount and the Hecateous Ridge.

The seismic basement velocities are extremely high - often 7.0 km/s, sometimes 7.5 km/s south of Cyprus (Fig. E.9). The surface of the basement is usually broken into several blocks.

Narrow zones were found, where dense Messinean layers are distorted and replaced by soft low velocity sediments which extend downwards. These zones are observed on three profiles located at the base of the submerged slopes of Hecataeus Ridge and Cyprus. Here also, large basement faults and a rise of basement layers toward the island have been identified.

It is suggested that such peculiarities can be attributed to tectonic features such as subduction, obduction, tension, and accretion, which have been taking place in this complicated convergence zone.

The behavior of the seismic waves from the deep structures is closely related to some major local blocks, which are clearly identified in the bottom relief. In our region the main blocks are Eratosthenes Seamount and the Hecataeus Ridge. They are separated by the Cyprean depression and the flat plains of the northern Cyprean depression. Sharp boundaries, *i.e.* deep faults, divide these blocks (Fig. E.10).

The deep structure of the region is extremely complicated and cannot reliably be attributed to any main type of crust, either oceanic or continental. The conversion of the observed seismic wave fields into adequately detailed deep sections remains difficult, due to the very simplified interpretational models which are commonly used in seismic refraction studies.

2.3. Gravity

A good quality gravity survey was carried out during the marine expedition of 1990. A dense network was laid out and the high accuracy of the gravity measurements, accompanied by precise echo soundings, provided a better coherence of the gravity data with the deep geological structure than was available on previous gravity maps. A close correlation between seismic and gravity data

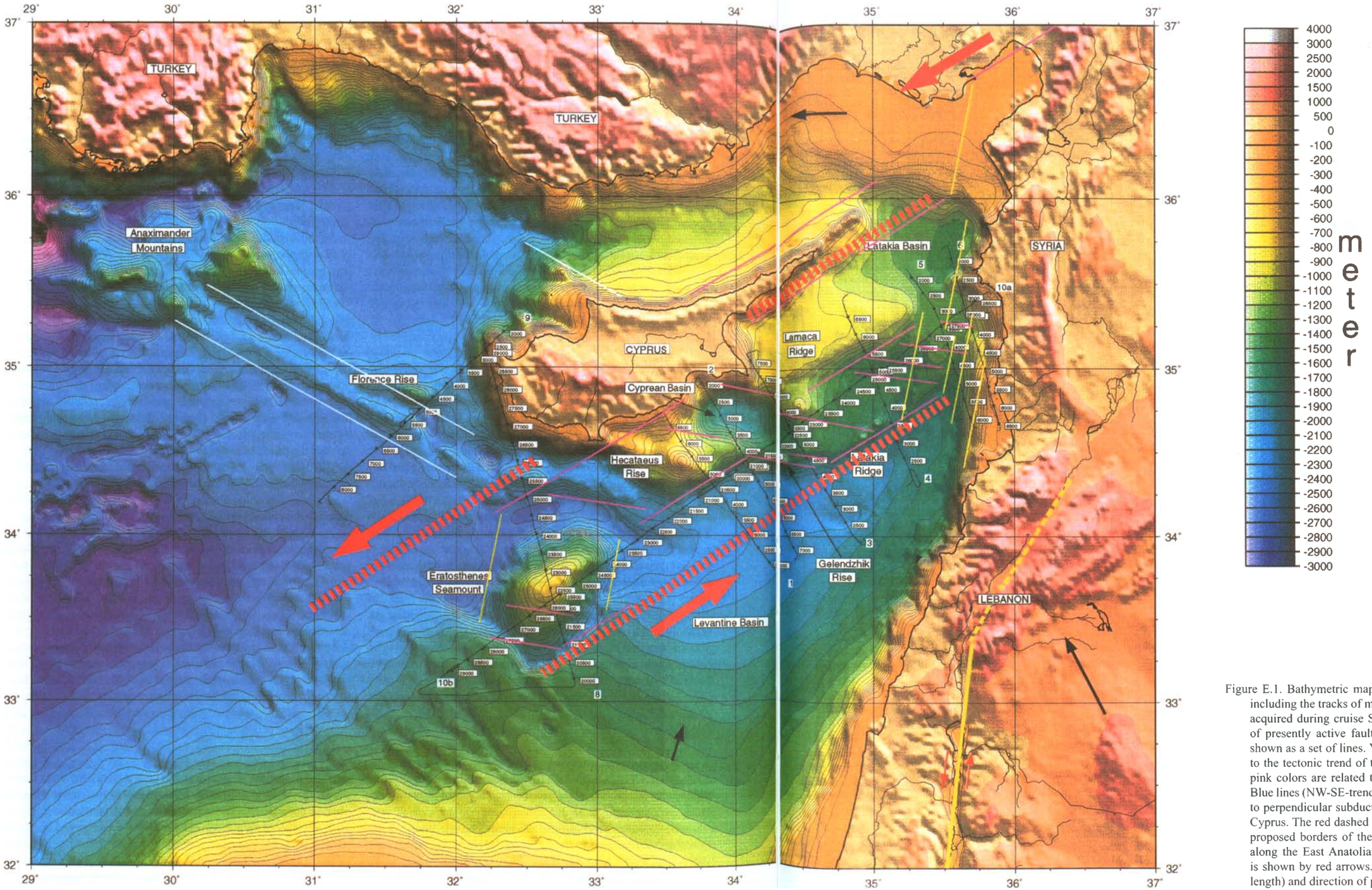


Figure E.1. Bathymetric map of the Eastern Mediterranean Sea including the tracks of multi-channel (MCS) seismic profiles acquired during cruise Strakhov 5. The presumed locations of presently active faults outcropping on the sea floor are shown as a set of lines. Yellow colors reflect faulting related to the tectonic trend of the Dead Sea Transform fault while pink colors are related to the East Anatolian fracture zone. Blue lines (NW-SE-trending) indicate the plate boundary due to perpendicular subduction along the Florence Rise east of Cyprus. The red dashed double line is meant to illustrate the proposed borders of the area affected by shear movements along the East Anatolian fracture zone; the sense of shear is shown by red arrows. Black arrows refer to the rate (*i.e.* length) and direction of plate convergence.

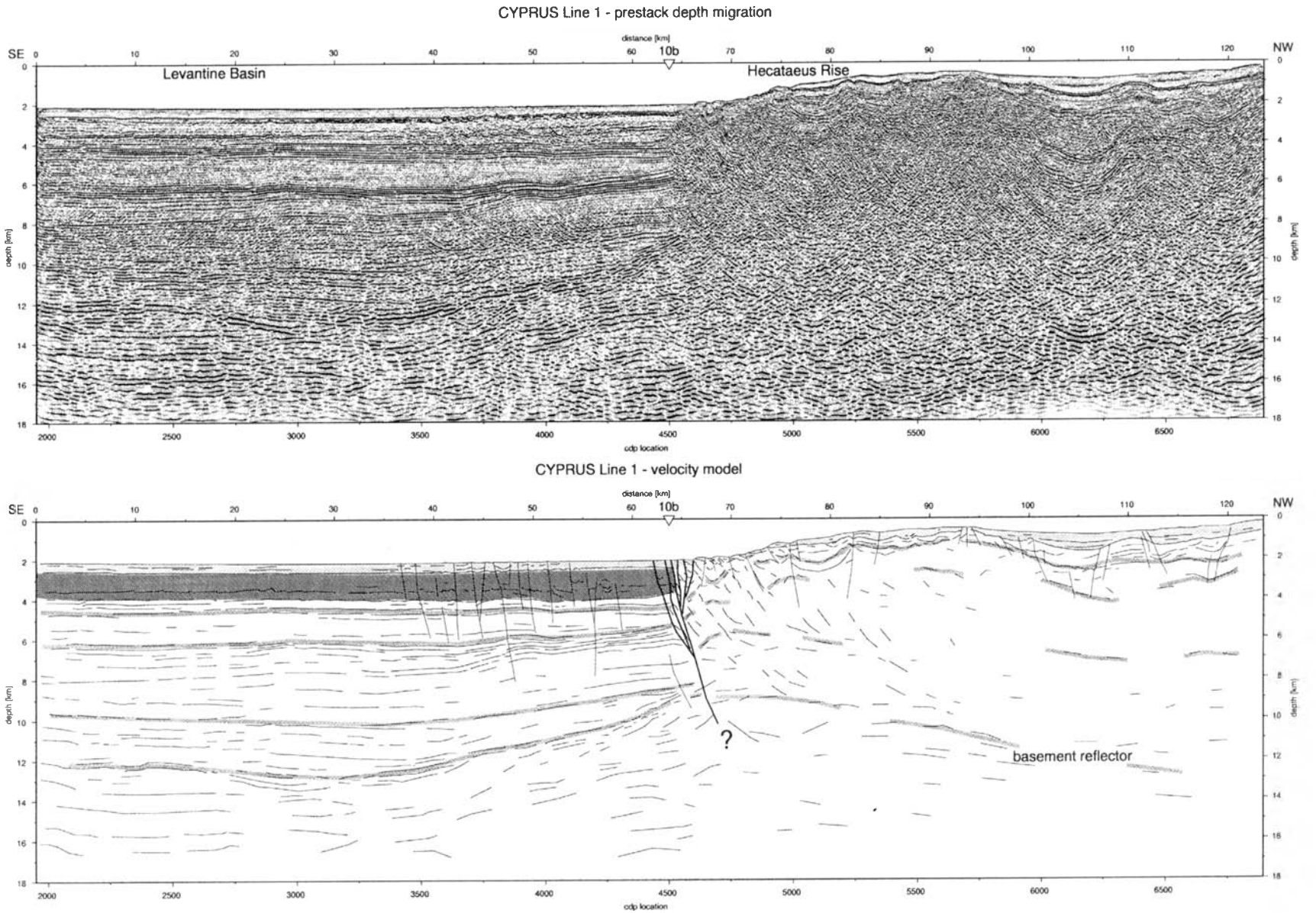


Figure E.2. Pre-stack depth migration (top) and interpreted line drawing underlain by the interpreted tectono-stratigraphic units (bottom) for MCS Profile 1. Plio-Quaternary sediments show light gray shading; Messinian evaporites are dark gray. Prominent reflectors are underlain by gray colors. See Figure E.1 for location.

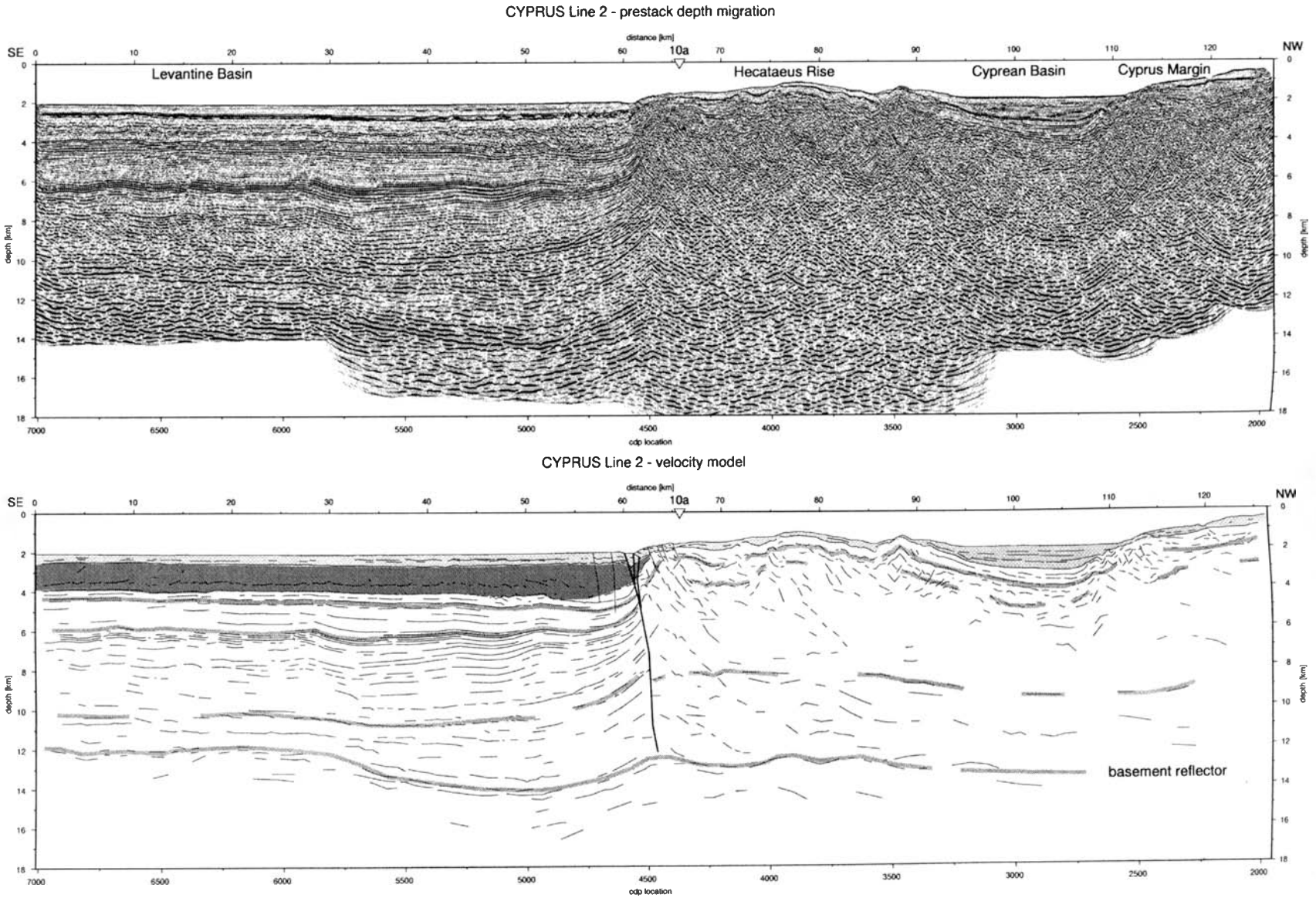


Figure E.3. Pre-stack depth migration (top) and interpreted line drawing underlain by the interpreted tectono-stratigraphic units (bottom) for MCS Profile 2. Plio-Quaternary sediments show light gray shading; Messinian evaporites are dark gray. Prominent reflectors are underlain by gray colors. See Figure E.1 for location.

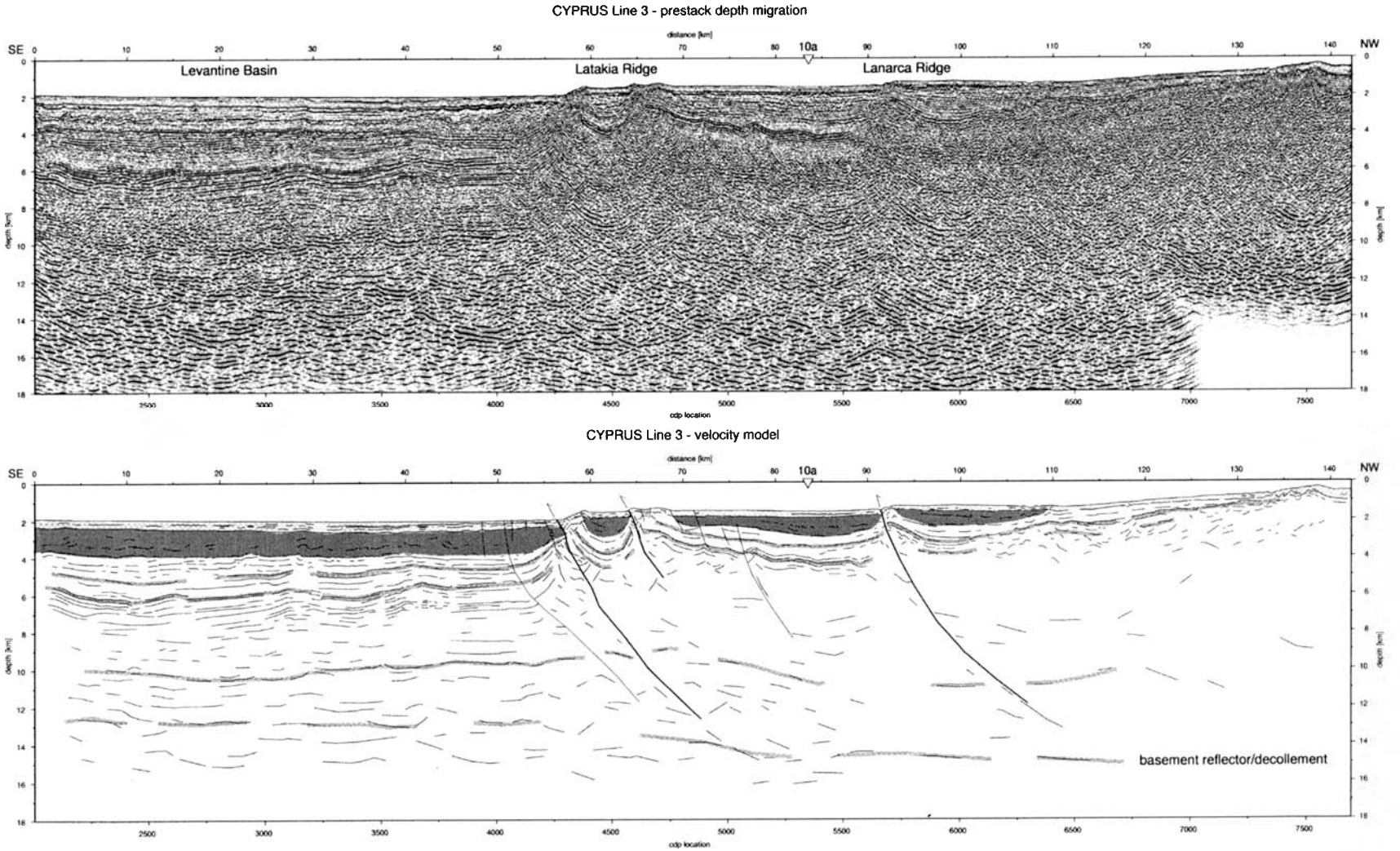


Figure E.4. Pre-stack depth migration (top) and interpreted line drawing underlain by the interpreted tectono-stratigraphic units (bottom) for MCS Profile 3. Plio-Quaternary sediments show light gray shading; Messinian evaporites are dark gray. Prominent reflectors are underlain by gray colors. See Figure E.1 for location.

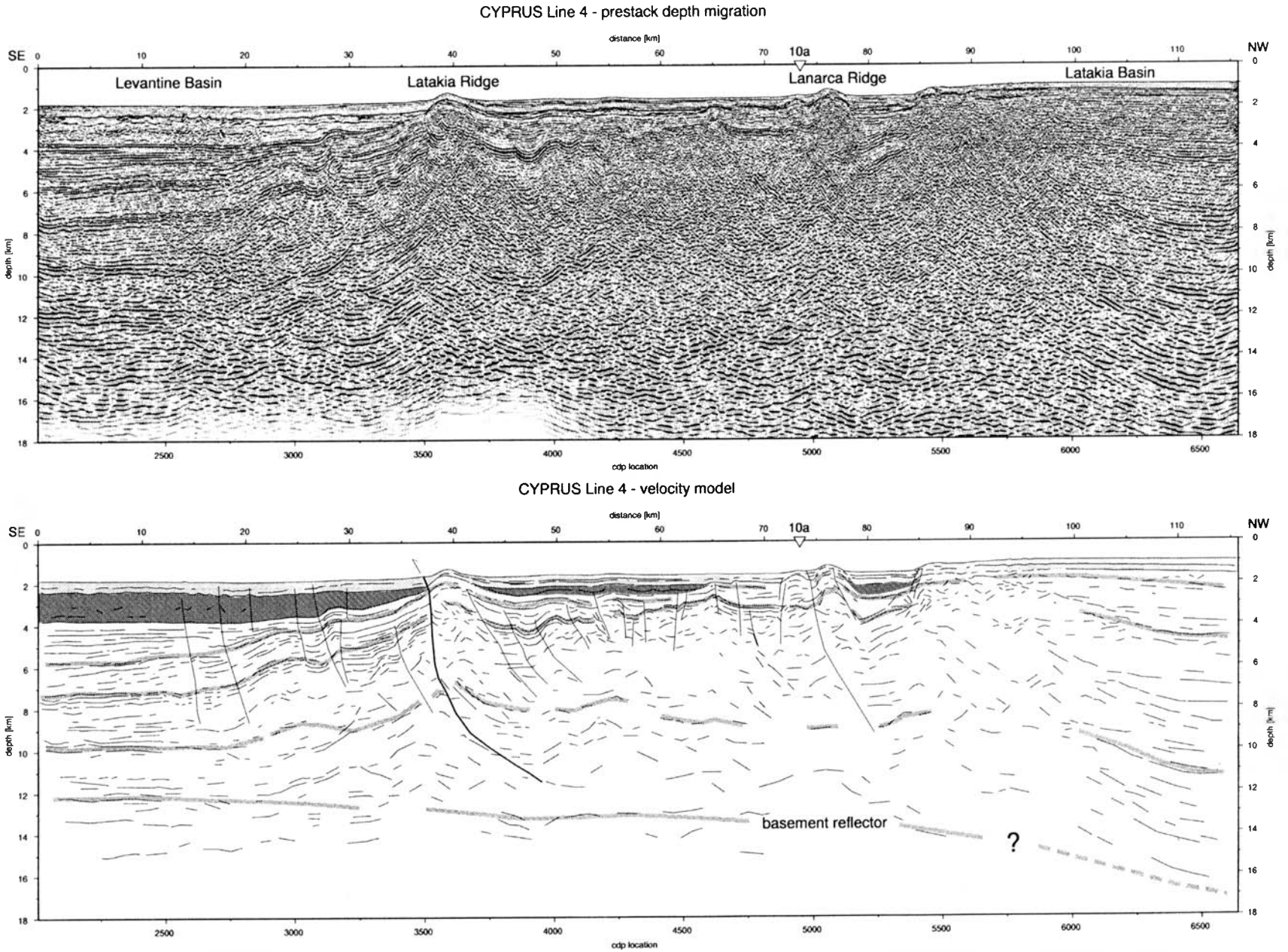


Figure E.5. Pre-stack depth migration (top) and interpreted line drawing underlain by the interpreted tectono-stratigraphic units (bottom) for MCS Profile 4. Plio-Quaternary sediments show light gray shading; Messinian evaporites are dark gray. Prominent reflectors are underlain by gray colors. See Figure E.1 for location.

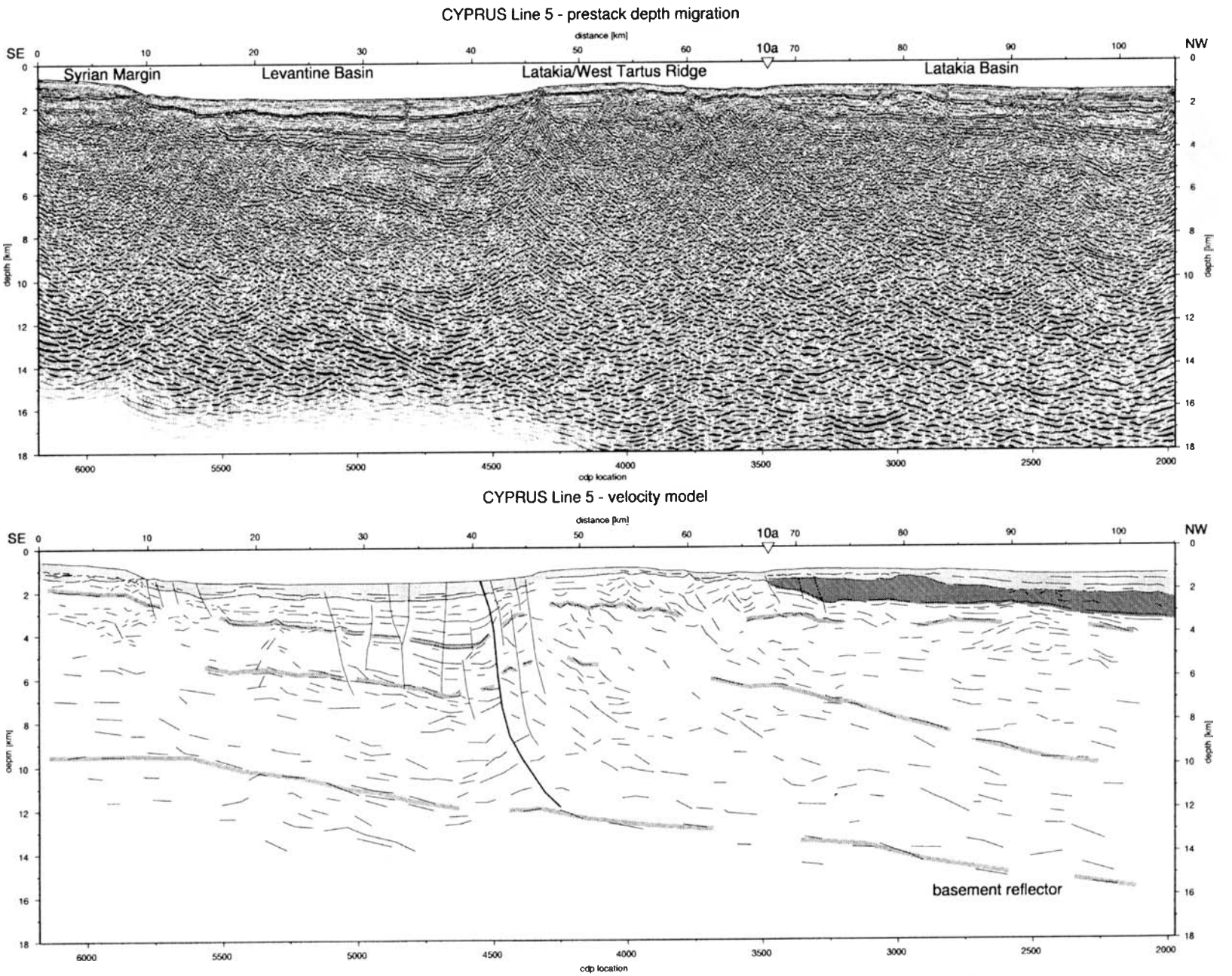


Figure E.6. Pre-stack depth migration (top) and interpreted line drawing underlain by the interpreted tectono-stratigraphic units (bottom) for MCS Profile 5. Plio-Quaternary sediments show light gray shading; Messinian evaporites are dark gray. Prominent reflectors are underlain by gray colors. See Figure E.1 for location.

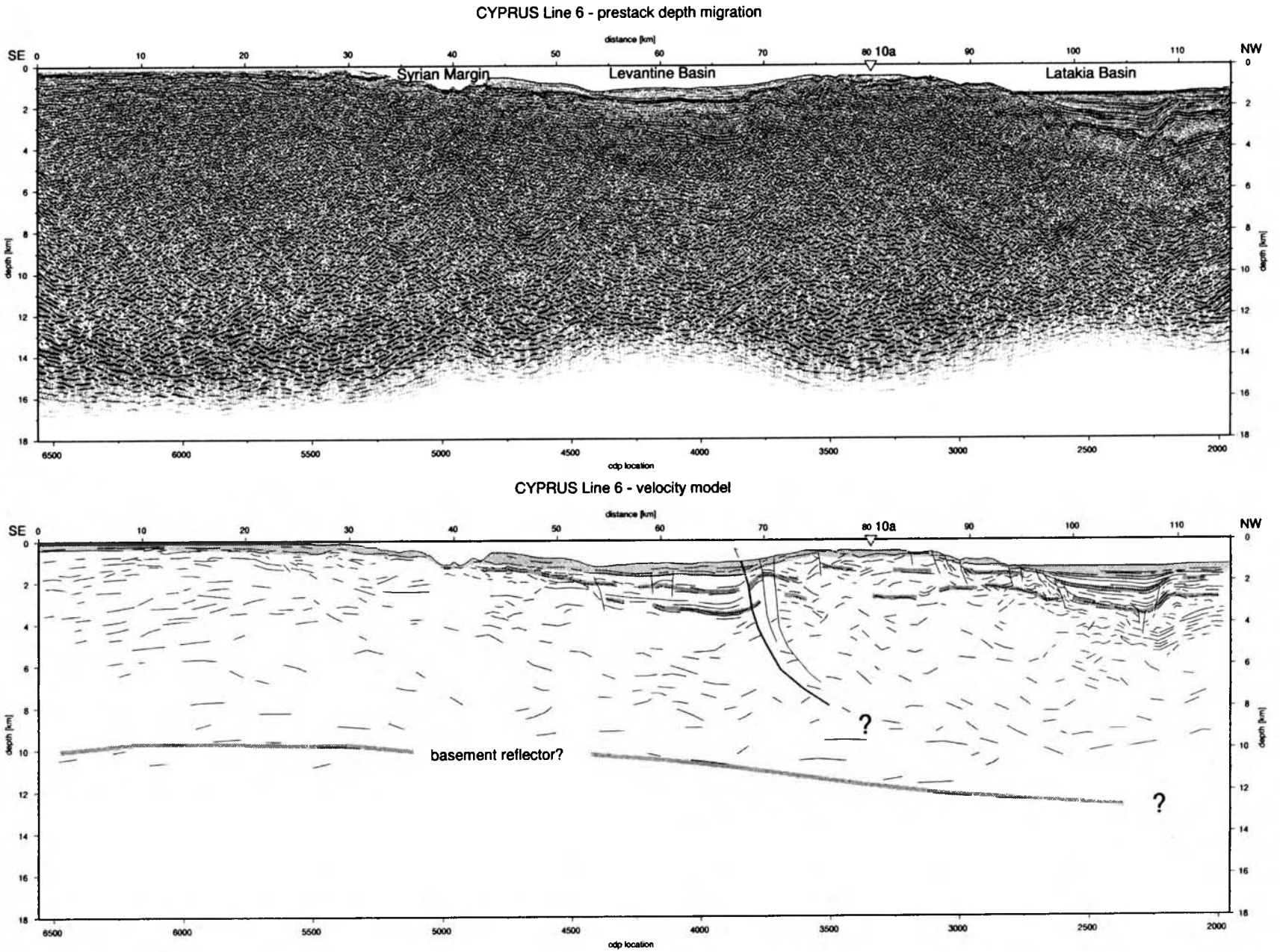


Figure E.7. Pre-stack depth migration (top) and interpreted line drawing underlain by the interpreted tectono-stratigraphic units (bottom) for MCS Profile 6. Plio-Quaternary sediments show light gray shading; Messinian evaporites are dark gray. Prominent reflectors are underlain by gray colors. See Figure E.1 for location.

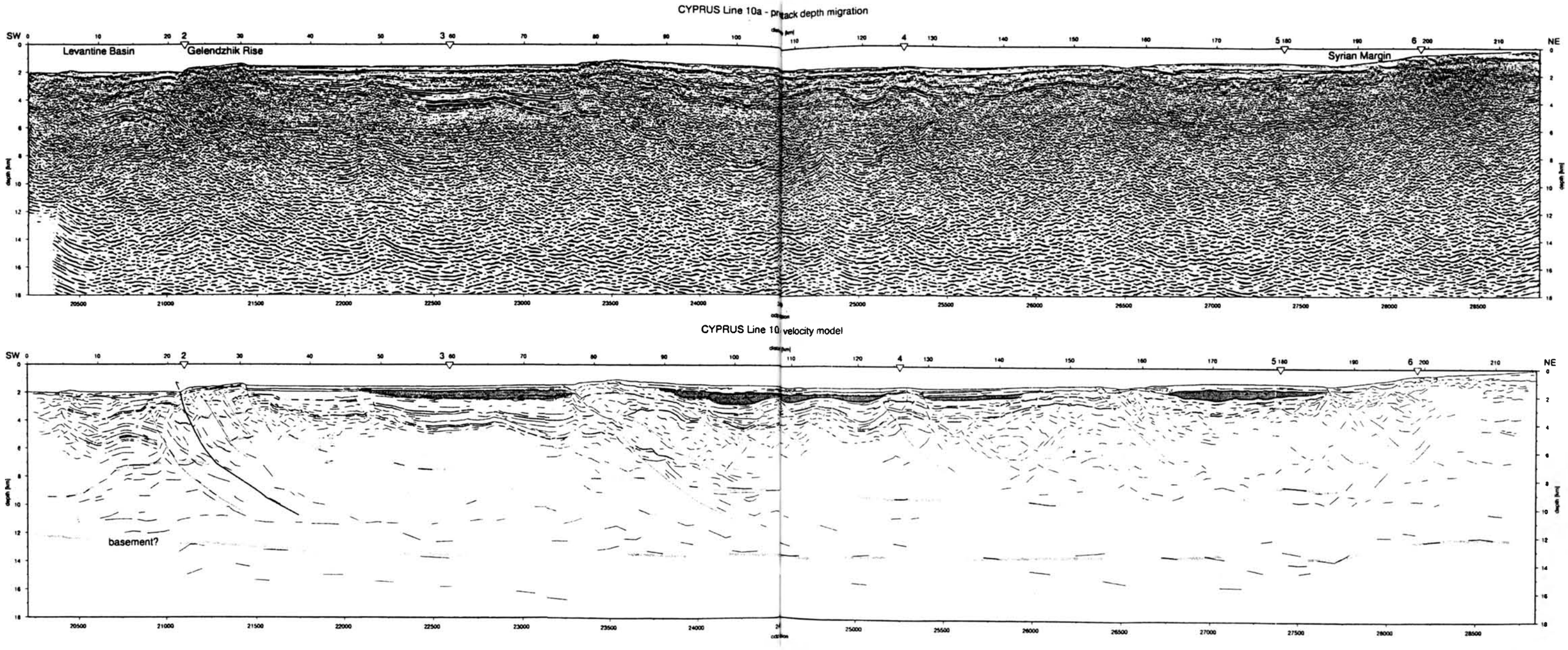


Figure E.8. Pre-stack depth migration (top) and interpreted line drawing underlain by the interpreted tectono-stratigraphic units (bottom) for MCS Profile 10a. Plio-Quaternary sediments show light gray shading; Messinian evaporites are dark gray. Prominent reflectors are underlain by gray colors. See Figure E.1 for location.

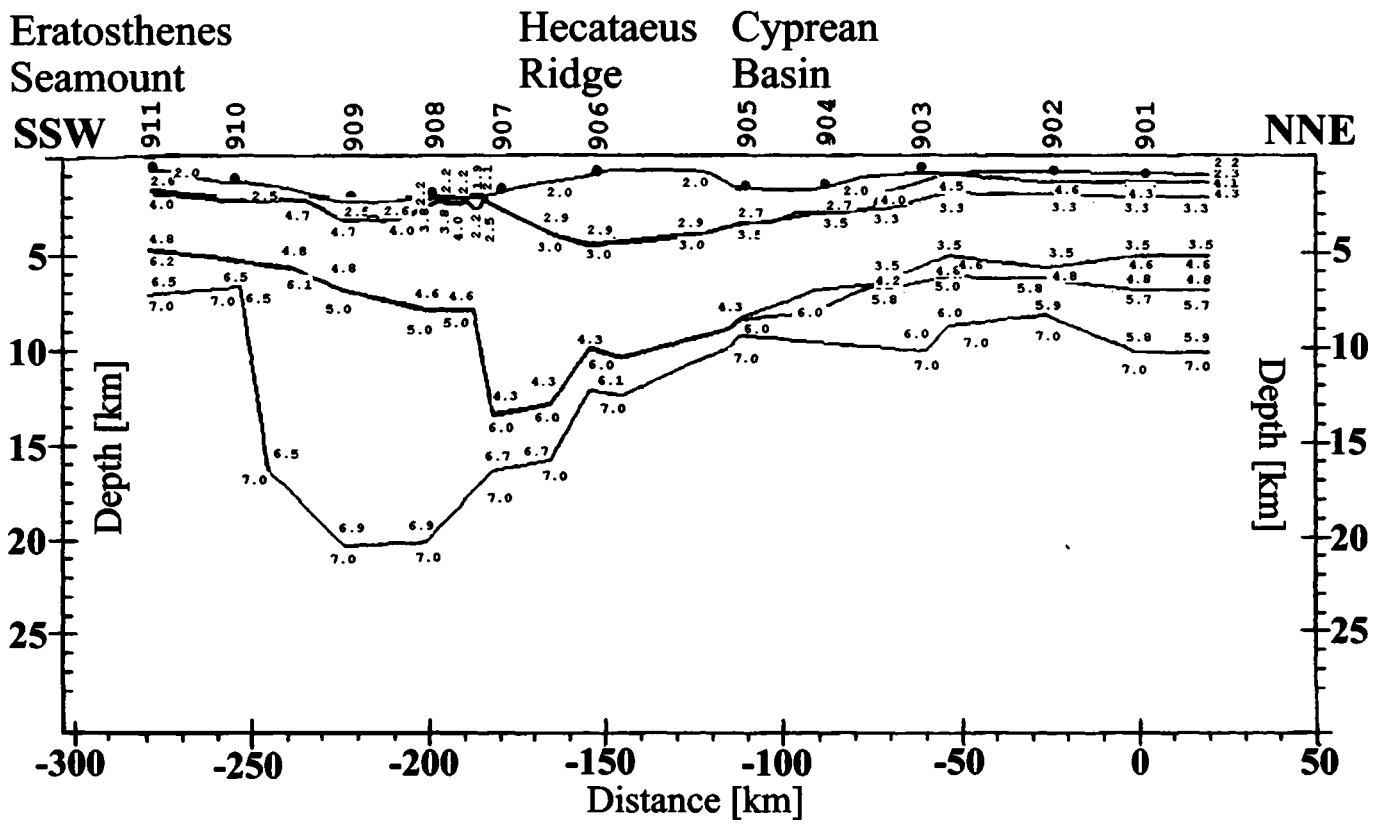


Figure E.9. Deep seismic section along profile No. 9, running across Eratosthenes Seamount toward NNE near Cyprus Island shore (See Chapters 12 and 13). Sea bottom relief, OBS locations and positions of seismic boundaries are shown. Numbers above and below boundaries indicate seismic velocities, taken after 2-D modeling procedure.

can be seen, with different relationships for different blocks.

2.4. Land Topography of Cyprus

In 1994-1995 J. K. Hall prepared a digtal terrain model (DTM) of Cyprus from the 1:50,000 topographic contour maps of the island. This DTM, requiring some 3,000 hours of interactive computer work, was on a 25 m grid, and has been used extensively for local scientific studies.

A 1:250,000 shaded relief poster (Hall, 1998b) of the island was prepared for distribution at the ICGEM-3 Third International Conference on the Geology of the Eastern Mediterranean held in Nicosia in September 1998. This was accompanied by a brief article in the annual Current Research publication of the Geological Survey of Israel (Hall, 1998a).

Publication of this book has spurred the unification of the land topography with some 183,000 soundings digitized from British hydrographic surveys at 1:50,000 scale done around Cyprus in the 1930s and 1950s, and offered an opportunity to reprint the combined dataset as a colored shaded relief representation (Plate X).

This compilation shows the immense value of the natural topography and bathymetry in telegraphing the geological and tectonic secrets that Nature generally conceals in the subsurface. It is fervently hoped that this compilation will aid others in continuing their investigations of this enchanting island.

2.5. Bathymetry

New survey results from French multibeam swath mapping (Loubrieu et al., 2001) show some additional details beyond what was available on the chart published by Hall et al. (1994). The primary difference is the pronounced rectangular moat around Eratosthenes Seamount.

The new compilations for the areas around Cyprus and along the coasts of Syria and Lebanon are based upon sounding data collected mostly between the 1860s and the 1950s in British hydrographic surveys and digitized from their hydrographic fairsheets and navigational charts. Data from a 1982 Israeli survey off southern Lebanon (Hall et al., 1983) is included for the first time. Extensive use has also been made of soundings from Russian nautical charts and from Russian topographical maps of the adjacent land areas.

Recently the French multibeam surveys of Loubrieu et al.

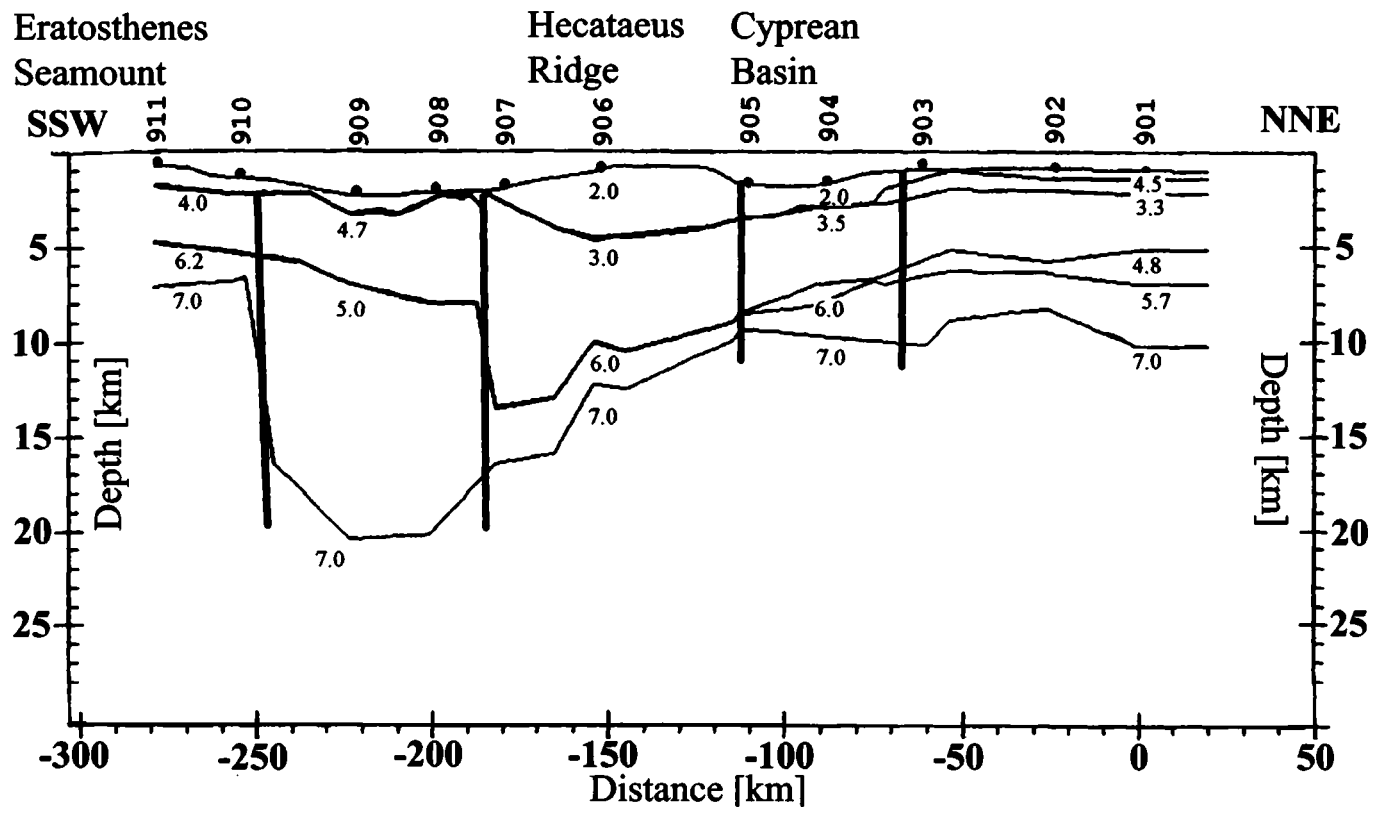


Figure E.10. Deep seismic section, which shows the dominant seismic velocities and main fault zones, dividing blocks, corresponding to sea bottom structures.

(2001) were extended into the generally unmapped reaches of the easternmost Mediterranean off Syria and Lebanon (Le Suroît Cruises Shalimar and Blac in October and November 2003), and additional work was done off the Nile Cone. Reconnaissance Hydrosweep surveys by the F/S METEOR adjacent to Israel in 2002 have shown the complete inadequacy of the existing single-beam compilations, and brought home the need to undertake this task as soon as possible. Hence efforts are underway to locate and charter a vessel with a broad deep-sea swath capability. Inshore, the Israeli research vessel Etziona has been making detailed multibeam surveys of the Israel continental margin to depths of 1000 m since 2001.

2.6. Recent Sediments

The surficial sediments of the Mediterranean and Black Seas were compiled as one of the six overlays of the International Bathymetric Chart of the Mediterranean (IBCM). A chart at one million scale in ten sheets was published by Emelyanov, Shimkus and Kuprin (2000). This chapter represents the explanatory notes to this compilation, along with the printed map at reduced scale of 1:5,000,000.

The map shows the respective distributions and compositions of these sediments throughout these two seas. Several lithologies can be grouped into four main genetic categories: terrigenous, biogenic carbonates, volcanic, and chemical. The main features reflect the tectonic and morphological structures, climate, water exchange with the ocean, hydrology, chemistry and hydrodynamics.

The principal differences between the Mediterranean and Black Sea sedimentation are outlined. The Mediterranean is characterized by its variety of provinces, whereas the Black Sea is dominated by the hydrogen sulfide contamination of its sapropelic abyssal sediments.

Certainly much of the data connected with this section and its map are outside the relatively narrow purview of this book - the eastern Mediterranean and the Near East. However, it does impinge upon our area in defining the special features of the Recent sedimentation in the Levantine Basin.

Parts II & IV
The Levant
Phanerozoic History and Tectono-Environmental Evolution In and Around The Palmyra Embayment

Valery A. Krasheninnikov
Geological Institute of the Russian Academy of Sciences, Pyzhevskiy pereulok 7, 109017 Moscow, Russia
Vladimir G. Kazmin, and
P. P. Shirshov Institute of Oceanology of the Russian Academy of Sciences, Nakhimovsky Prospect 36, 117851 Moscow, Russia
Francis Hirsch
Geological Survey of Israel, 30 Malchei Israel Street, Jerusalem 95501, Israel

Structurally, the Levant is part of the Gondwanian, pan-African, African-Arabian basement. Dominant lineament swarms determine a set of primarily pan-African fracture systems, probably related to ancient accretionary sutures. One, the so-called 'Najd' trend, strikes NNW (N290-320°E azimuth) and is expressed by important faults and intra-cratonic rifts, *e.g.* Al Furat, Sirhan, and Yizre'el. In contrast, another is the NNE striking trend of the Sinjar-Palmyrides – Judea-N. Sinai fracture system. It may express another direction of fracturing in the basement, reactivated during Mesozoic times, as suggested by Best et al. (1993[1]), prior to its Senonian-Eocene inversion, that generated the Levantid Syrian Arc, and is sub-parallel to Tethys.

Finally the Dead Sea Transform added the N-S component of differential subduction and Neogene opening of the Red Sea, further deforming the eastern branch of the Palmyrides system.

1. STRATIGRAPHY

1.1. The Precambrian-Paleozoic Framework of the Levant

Precambrian

Late Precambrian rocks west of Mardin in southern Turkey, consist of the volcano-sedimentary Tebelsmi Formation, exceeding 1000 m in thickness. In Israel, the volcano-sedimentary Zenifim Formation is over 2014 m thick, and the basement was not reached.

This suggests Late Riphean (Vendian) terrigenic-volcanic graben fills within the crystalline basement. These deposits are analogues to Upper Riphean so-called 'Infracambrian' fillings of the Arabian-Nubian and Aden-Somalian shields. Slightly deformed and metamorphosed during the Pan-African orogenic stage, they may correspond to the so-called 'Baikal structures' which are a part of the basement of the Arabian Platform. Later uplifts and erosional episodes resulted in the destruction of Vendian deposits on vast areas of the platform, preserved in the deepest tectonic depressions (Dolginov, Kazmin and Ponikarov, 1969). The blanket of post-pan-African sediments is as follows:

LOWER PALEOZOIC

The Lower Paleozoic stratigraphy of the area covered by the book is taken from the geological literature of southern Turkey, the Syrian subsurface, and from sporadic outcrops along the Dead Sea and southern Arava.

Cambrian

In Syria Cambrian deposits have been penetrated in the southern part of the Aleppo Plateau. They comprise red quartz sandstones, salt, and basic volcanic tuffs of the Zabuk Formation; dolomites and limestones of the Burj Formation; and the red sandstones of the the Sosink Formation. Similar Cambrian sections are found in Jordan and in Turkey west of Mardin (Rigassi, 1971). The Cambrian deposits of Syria are also similar to the southern Israel Timna sections, which comprise the red conglomerates and subarkosic sandstones of Amudei Shelomo (Pillars of Solomon), the dolomitic limestones of Timna with trilobites of Lower Cambrian age, the white subarkoses of Shehoret, and the Netafim quartzites.

Cambrian sediments are thus distributed over wide areas and may reach a considerable thickness. Seismic and gravimetric data in Syria, Jordan, Israel, Turkey, and Saudi Arabia allow us to suggest that a 400-2000 m thick Late Precambrian-Lower Cambrian sequence of volcanic sediments evidently fills grabens in the crystalline basement. The carbonate Burj Formation corresponds to the Koruk Formation of Turkey, the Tabuk Formation of Saudi Arabia, and the Timna Formation of Israel, all ranging up to 150-200 m. They reflect a quiet tectonic situation of shallow-water calcareous sedimentation, which prevailed over the Arabian Plate

[1] In a summary of the tectonic evolution of the northern Arabian Platform in Syria these authors conceive that after the Proterozoic suturing of the three major crustal blocks (Aleppo, Rutbah, Rawda), Syria became part of an Early Paleozoic epicontinental region of the east-facing Gondwanaland margin and that the Late Paleozoic development of a depocenter in central Syria was the possible precursor to later Mesozoic rifting. They envision an Early Mesozoic development of the Levantine margin and the Palmyride rift, prior to the Late Mesozoic development of the Euphrates Depression.

during the Early-Middle Cambrian time and was replaced by terrigenous sedimentation in the Late Cambrian.

Ordovician

Ordovician deposits are widely distributed in Syria. Up to 2500 m of terrigenous rocks, with rare intercalations of limestone and anhydrite were penetrated, mainly on the northern slope of the Rutbah Uplift as well as south of the Aleppo Uplift. They overlie the Cambrian unconformably, starting at the base with up to 500 m of the sandstone Khanasser Formation, followed by 500-900 m of the predominantly shaly Swab Formation, and topped by over 1000 m of alternating sands and clays of the Afendi Formation. The presence of Ordovician strata in Israel has been postulated in the past, but deposits of that age were probably removed by the post-Devonian and post-Carboniferous denudation processes, related to the Helez Uplift mentioned below.

Silurian

Silurian deposits are restricted to the southern and central regions of Syria. Evidently, a considerable part of the Silurian was removed by subsequent erosion. One can suggest that the most complete sections of Silurian were preserved within the limits of the Euphrates and Sinjar paleo-depressions. The Silurian is represented by the 400 m thick Tanf Formation, a monotonous sequence of shales, siltstones, and sandstones. It overlies the underlying Ordovician rocks with a gap corresponding to the Ashgill and locally Caradoc deposits. To the west the Silurian deposits are clearly missing, as Ordovician strata are directly overlain by the Late Paleozoic or the Mesozoic. In Israel, no Silurian deposits were found.

Devonian

Devonian marine deposits are missing in Syria and only a few continental remnants are preserved in a few small depressions. Intensive processes of erosion also resulted in the destruction of a significant part of the underlying Silurian deposits. In Israel, Devonian deposits are completely absent.

Summing up, the 1500-5000 m thick terrigenous sandy and clayey deposits of the Lower Paleozoic depositional cycle begins with the Cambrian transgression, when deposition of evaporites and marine, shallow-water platform limestones and dolomites took place. The transgression reached its maximum during the Ordovician and Lower Silurian, and is characterized by shales with graptolites, acritarchs, and chitinozoans. The end of the cycle, with intensive Devonian regression and denudation processes, corresponds with the uplift of the huge Helez dome, affecting Lower Paleozoic sediments over a radius of several hundred kilometers. All these events occurred prior to the development of a Palmyrides Trough.

UPPER PALEOZOIC

Upper Paleozoic deposits transgressively overlie the eroded surface of Ordovician and Silurian rocks. In rare cases they are underlain by continental sandstones barren of organic remains and conventionally referred to the Devonian.

Carboniferous

Carboniferous deposits were widely penetrated in Syria, in the slopes of the Rutbah Uplift, the northeastern part of the Palmyrides trough, the south of the Aleppo Uplift, the Euphrates depression, the northern slope of the Rawda Uplift and the Sinjar depression.

The Latest Tournaisian-Early Visean Markada Formation reaches 1100 m in the Rutbah Uplift, where it rests on an eroded Lower Silurian surface. It mostly consists of terrigenous sediments, with some limestone in its upper half, topped by sandstone, siltstone, and shale. In the Palmyrides depression (Dola-1 and Doubayyat-1 bore-holes) Middle and Upper Carboniferous are developed, in contrast to the situation on the Rutbah Uplift. In northeastern Syria (Euphrates depression, the northern slope of the Rawda Uplift, and the Sinjar depression) Tournaisian, Visean, Namurian, Westphalian, and (?)Stephanian are also found represented by sandy-clayey rock units with subordinated limestone members.

Rootless exotic blocks of limestones, shales and sandstones with diverse groups of the Lower Carboniferous (Upper Tournaisian-Lower Visean) fauna, exposed in the core of Jebel Abd El-Aziz, are considered as an olistostrome which appeared as a result of horizontal shifting in the Late Cretaceous from the Taurus Zone towards the Arabian platform.

Permian

The Permian deposits of Syria are predominantly represented by continental red-colored sediments; marine intercalations are found only in northeastern Syria. The Amanus Formation consists of soft sandstone and clays of mixed continental and shallow-marine origin, with brown coal and conglomerates. In the western part of the Palmyrides, red clays and limestone are developed. On the NW flank of the Rawda Uplift (Markada-101 Hole) the Amanus Formation consists of red and green quartz and graywacke sandstones and gray mudstones. The thickness of the Amanus Formation is usually 250-350 m, but in the Palmyrides it reaches 650 m. It overlies Carboniferous to Upper Ordovician rocks. In the extreme northeast of Syria the Amanus Formation consists of 85 m of Lower Permian sandstones followed by 568 m of mostly marine Upper Permian shales with sandstone and limestone intercalations which yield brachiopods, corals, and crinoids (Ponikarov et al., 1967; Bebeshev et al., 1988). In the southwestern Palmyrides, below the Triassic Kurachine s.l. (*sensu lato* = in the broad sense) Formation, the 1200 m thick terrigenous sequence of the Qaryatein Formation, whose relation to the Amanus Formation is still unclear, may include Late Carboniferous to Early Triassic strata.

The depositional patterns and main events of the Israeli Permian were restricted to a relatively narrow marine belt crossing Israel along a NE-SW axis, which borders the Arabian-Nubian landmass.

The Permian deposits overlie the pre-Permian unconformity, which was the result of uplift of the so-called Helez dome, causing a large part of the Paleozoic sediment to be eroded from the Levant

(Gvirtzman and Weissbrod, 1984). The possible extension of this dome into the present eastern Mediterranean has been mentioned before. The Permian-Triassic boundary is para-conformable; it is marked by a late Paleozoic algal spike, followed by the hiatus at the base of the Lower Triassic (Induan stage), as witnessed by reworked Early Paleozoic microfossils (Hirsch, 1990; Eshet, 1990).

The Permian in Israel consists of the Middle-Late Permian Sa'ad Formation (=Um Irna in Jordan) and Late Permian Arq'ov Formation (=Khuff in Saudia Arabia). This sequence, up to 250 m thick, consists of continental deposits, sea marginal flats, and shallow marine fusulinid-limestone. These are well developed in boreholes of the Coastal Plain (Gevim, Pleshet), where the Late Permian Midian, Dzhulfian, and Dorashamian stages were identified (Orlova and Hirsch, Chapter 18C this volume). The isopach-map of the Arq'ov Formation indicates an axis extending across the Gulf of Suez into the central part of the Sinai Peninsula and in the direction of Wadi Araba, where the Permian Aheimar Formation occurs (Abdallah and El-Adindani, 1965).

The distribution of Permian sediments in Syria creates the impression that in the south the Permian is represented by red and mottled sandy-clayey rocks of continental origin. In northeastern Syria, which occupies the marginal part of the Arabian platform, continental sediments were replaced by marine terrigenous sediments with intercalations of fossiliferous limestones, which are especially typical for the Upper Permian.

Leonov et al. (1989) and Kopp and Leonov (2000) showed that the thickness of the Paleozoic deposits in Syria increases from north to south, from 3-3.5 km in the Aleppo Uplift to 5-7 km in the Rutbah Uplift; the highest Paleozoic rate of sedimentation being centered within the Rutbah Uplift. Though a mosaic pattern and absence of contrasting features generally characterize the distribution of the Paleozoic deposits, they do not display linear structures typical to the Mesozoic and Cenozoic. In the Paleozoic, the Palmyrides basin containing 3-6 km of Paleozoic deposits, the Euphrates, and the Drouze basins did not have the appearance of independent structures, and the Rutbah and Rawda Uplifts were not separated from one another (Krasheninnikov, Chapter 6, in Volume I). Therefore, the ancient Paleozoic origin for the main structural elements of Syria as postulated by Ponikarov et al. (1966, 1967, 1969) should be reconsidered, as these events took place in the Late Paleozoic and especially in the Mesozoic.

Consequently, during the Paleozoic Era as a whole, Syria was the site of intensive platform terrigenous sedimentation in which carbonates were definitely subordinate in importance. A very thick succession, up to 5000 m of sandy-clayey rocks was laid down during the Cambrian and Ordovician, as well as in the Early Silurian. The predominantly marine environment was replaced by a continental one in the Late Silurian (Wenlock, Ludlow Stages) and in the Devonian. Deposits of this age are either absent or occupy limited areas.

The next cycle of sedimentation occurred during the Carboniferous and Permian interval. It commences with the widespread transgression of the Early Carboniferous, when a thick succession of sandy-clayey rocks with subordinate intercalations of limestones accumulated. In the Middle-Late Carboniferous and Permian, marine sedimentation was localized in Mesopotamia, the marginal part of the platform, and in the Palmyrides in the most depressed structure of central Syria. In the upper part of the Carboniferous and the Upper Permian there was facies differentiation between the southern Syrian continental redbeds with rare marine limestone intercalations and the northern Syrian gray sandy-clays with marine intercalations. This occurred in parallel with the embryonic development of a fracture-system that comprises the Sinjar Trough, the Euphrates depression, and the Palmyrides trough, which with time received increasing amounts of Upper Paleozoic deposits. Simultaneously, the Palaeo-Tethys was closing, accompanied by the splitting off of micro-continents from the Gondwana-superplate, *e.g.* Anatolia and Iran. (Dercourt et al., 2000, Paleogeographic Map 3 Wordian - end of Permian).

1.2. The Mesozoic Interplay of Neotethys and Intra-cratonic fracture systems

Triassic

The Induan stage is absent and occupies a hiatus above the Permian/Triassic boundary, which in the Negev subsurface is marked by a late Paleozoic algal spike and reworked Early Paleozoic microfossils. Elsewhere in the Near East the Triassic is represented by:

1) A Werfen-like shallow, clastic marine facies prevails from the Olenekian to earliest Anisian, dated in Israel and Jordan by conodonts and in Israel and Syria by the *Densoisporites neiburgii* - *Lunatisporites pellucidus* palynomorphs. These rocks are known in Israel as the Yamin and Zafir Formations, which apparently correspond to the Amanus Shale Formation in Syria.

2) The Late Anisian to Early Carnian carbonates in the Sephardic biofacies of the Ra'af and Saharonim Formations, intercalated in the Negev and Jordan by the terrigenous Gevanim Formation, correspond to the Kurachine s.l. and Butmah Formations in Syria. The Middle Triassic Kurachine s.l. Formation, found in Syria east of the Al Furat River (Markada 101 Hole), contains conodonts of more Tethyan affinity. It is interesting to note that the minor Ladinian evaporites within the middle and upper parts of the Saharonim Formation in Israel are replaced in the Mesopotamian Basin of Syria by the very thick Kurachine Anhydrite Formation.

3) The Carnian evaporite event of the Saharan Salinity Crisis is strongly developed in the Mohilla Formation of Israel and in the Hadayah and Alan Formations in Syria. A clear regression is noticeable in the narrowing of the marine passage between the Aleppo and Rutba Massifs.

4) In Israel and western Syria, the Late Carnian to Rhaetian restoration of shelf and offshore marine conditions is apparent in the deposits of the Mohilla Formation and Shefayim Formations of Israel and in the Rimeh Formation of the Anti-Lebanon as well as the Muss and Serjelu Formations of the Mesopotamian Basin.

5) The Triassic sequence is truncated sharply by Early Jurassic volcanics and laterites, both in Israel and Syria (the Anti-Lebanon and Palmyrides).

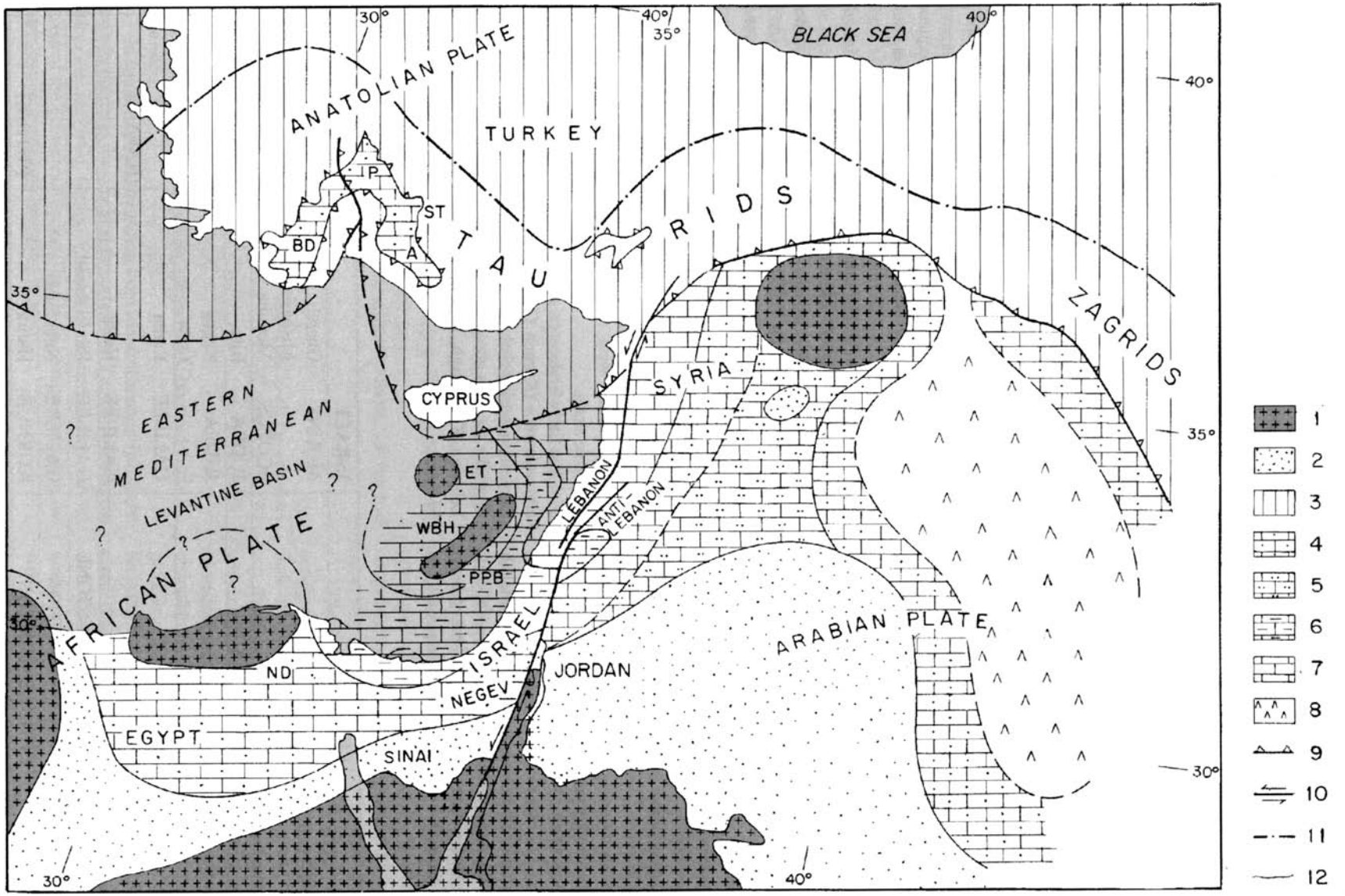


Figure E.11. Schematic Jurassic paleogeographic map of the Levant and adjacent areas.

Legend: 1 - Precambrian basement; 2 - Predominantly sandstone; 3 - Tauro-Zagrid Tethyan terranes; 4 - Carbonatic Negev type facies; 5 - Semi-clastic facies of the Syrian promontory; 6 - Shales and carbonate facies of Delta and Judean Embayment; 7 - Bank and reef carbonate facies of Haifa and Lebanon type; 8- Evaporites; 9 - Alpine thrust front; 10 - Dead Sea Transform; 11 - Approximate northern limit of African-Arabian Plates; 12 - Present coastlines; BD - Bey Daglari; ST - Seydisehir-Tarasci; ET - Eratosthenes Seamount; WBH - Western Basement High; PPB - Pleshet Paleo Basin; ND - Nile Delta.

The facies belts follow the contours of the Arabian-Nubian Massif. The Galilee-Palmyrides Embayment in the west and the Sinjar zone to the east separate the Aleppo-Mardin swell in the north from the Rutbah Uplift in the south.

Jurassic

The nature of the Triassic-Jurassic unconformity is tectonic as well as regressional.

The process which generated an angular unconformity also caused a progressive erosional truncation and karstification of the underlying Triassic substratum. The event was accompanied by volcanics, the Asher Formation in the Galilee and the Aarne Formation in the adjacent Anti-Lebanon. Large parts of the Arabian platform were affected by regression, producing a Hettangian-Sinemurian regional exposure, evidenced by formation of lateritic soils (the Mishhor Formation in Israel and the Zubeideh Formation in Syria). They filled deep karstic pockets within the Upper Triassic substratum with laterites (kaolinite, bauxite) and alunite.

The Jurassic sequence in Israel is characterized by:

1) Three volcanic events: Asher (at the Triassic/Jurassic boundary); Devorah/Bahnnes (Oxfordian); Tayasir (Tithonian-Berriassian);

2) Six major Pre-Toarcian, Aalenian, Late Bajocian, Middle Bathonian, Callovian-Oxfordian and Kimmeridgian transgressive cycles, affected by the Early Liassic uplift;

3) A pre-Oxfordian tectonic event; and

4) Tithonian tilting and uplift.

The Jurassic paleogeography of the southern Levant (**Fig. E.11**) consists of the following:

1) The up to 1500 m thick Negev-type facies around the Arabian-Nubian craton. This belt is highly differentiated into the formations of the Arad Group, representing alternating clastic and carbonatic deposition;

2) The 100 to 3000 m thick Judean Embayment (Helez-Ramallah-Hermon-Palmyra). In the west it consists of Liassic-Callovian carbonates, Oxfordian shales, Kimmeridgian reef limestone, or bedded limestones. In the Anti-Lebanon these correspond to the Liassic-Callovian dominantly carbonate rocks, the Oxfordian shales, and the Kimmeridgian limestones. Further east in the Palmyrides, the Middle Jurassic is strongly reduced in thickness and is represented by a sequence with a strong resemblance to the Negev shallow-water facies;

3) Above the Triassic/Jurassic boundary volcanic, the ~700 to 2000 m thick Galilee-Lebanon-Coastal Syria sequence consists of massif Liassic-Oxfordian carbonates, Oxfordian volcanics, and Kimmeridgian limestones, to which some Tithonian strata can be added in Lebanon. In northwestern Syria this sequence corresponds to the monotonous Dolaa Group and in the coastal An Nusseiriyeh Range a diversified sequence consists predominantly of carbonates with minor clastics;

4) The isthmus of the Syrian promontory: the Rutbah-Mardin sequence is characterized by much reduced Jurassic deposition;

5) The Late Jurassic Arabian evaporite basin;

6) The 3000 m thick northern Sinai Maghara basin sequence strongly resembles the adjacent Negev sequence, but is much thicker;

7) A postulated Mediterranean paleo-land, from which the clastics found in offshore drillings were possibly derived;

8) The Delta-Akkuyu trough: an extension of the drilled offshore Jurassic of Israel into the Pisidian Taurus.

Thus it seems that during Jurassic times the E-W connection across the Palmyrides fracture system was extremely reduced.

Cretaceous

The Jurassic-Cretaceous boundary is again characterized by an angular unconformity, accompanied by erosional hiatus and volcanics in the west, truncating the underlying Mesozoic and Paleozoic strata.

The Early Cretaceous consists primarily of continental clastics and volcanics (Kurnub Group), passing laterally into Tithonian-Barremian marine shales in the Coastal Plain (Gevar'Am Group). A similar facies is observed in various parts of Syria *e.g.* the Anti-Lebanon, Kurd-Dagh, Palmyrides, and Mesopotamia (Jebel Abd El-Aziz).

Table E.1:

	LEBANON	**ISRAEL**		**SYRIA**
Maastrichtian Campanian Santonian	CHEKKA	MOUNT SCOPUS	Ghareb Mishash Menuha	SHIRANISH SOUKHNE
Turonian	MAAMELTAIN	JUDEA	Bina	JUDEA
Cenomanian Late Albian	SANNINE	JUDEA	Negba Yagur	JUDEA
Couches à Knemiceras Banc de Zumoffen C. à Orbitolines	HAMMANA	GALILEE GALILEE	Rama Hidra	HAYANE
Falaise de Blanche	MDAIREJ LIMESTONE	GALILEE	Ein El Assad	
Couches à gastéropodes	ABEIH FORMATION	GALILEE	Nabi Said	
Grès de Base	CHOUF SANDSTONE	KURNUB	Hatira	RUTBAH

Platform-carbonates of the Aptian-Albian (Galilee Group) and the Albian-Cenomanian-Turonian-Early Coniacian (Judea Group) extend progressively from Lebanon and the Galilee to the Elat region and the Sinai Peninsula, passing laterally westwards into the basinal facies of the Coastal Plain (Talme Yafe Group). Eastwards into Jordan, the Negev facies still dominates in Jordan's Ajlun Series. These carbonates are very well-developed in Syria – limestones predominate in the western areas, dolomites in the eastern.

The facies of northern Israel and Lebanon can easily be compared with the Cretaceous of the Syrian Anti-Lebanon. Within the Palmyrides there is a strong resemblance with the Negev facies, though the Maastrichtian Shiranish chalks are much thicker.

1.3. The Senonian-Paleogene Inversion of the Syrian Arc Orogeny

The Alpine orogeny was echoed in the Levantid inversion of Early Mesozoic faults, producing the asymmetrical folds of the S-shaped Syrian Arc. These extend from northern Sinai to the Negev, the southern Coastal Plain of Israel, and Judea and the Galilee. They defined a palaeogeographic configuration of basins and islands that controlled the Senonian carbonaceous and siliceous sediments (Mount Scopus Group) and the Syrian Palmyrides farther to the east. For the southern facies the correlation into Syria is probably best via Jordan and for the northern and eastern Syria via Lebanon. As the deepening progressed there was a growing similarity between the pelagic facies of the onland Levantine sequences with the offshore Mediterranean and to some extent with Cyprus.

Senonian

Certain facies types are extremely typical for the Senonian interval. They are:

1) white soft chalk for the whole eastern Mediterranean;

2) black and brown flints for the Upper Campanian of Egypt, Israel, Jordan, and Syria;

3) phosphatic deposits of the Upper Campanian-Lower Maastrichtian of Syria, Israel and Egypt; and

4) black oil shales of the Maastrichtian in Syria, Jordan and Israel.

Paleogene

The Paleogene deposits occupy vast areas in all the countries of the Levant.

Paleocene

The paleogeography of this period was inherited from the Senonian.

In Israel, a gradual transition from Maastrichtian to Paleocene deposits occurs in the synclinal facies (*e.g.* the Zin valley), whereas along the anticlinal flanks, Paleogene deposits onlap various levels of the Cretaceous rocks. The Danian Stage starts with the *Parvularugoglobigerina eugubina* Zone.

In Syria, as a rule, this zone is missing; a short hiatus at the base of the Danian Stage is indicated by an erosional surface with traces of mud-eaters and a glauconite horizon, but the character of the sediments below and above this unconformity is the same. On some anticlinal structures of the Palmyrides and the Anti-Lebanon the hiatus between the Maastrichtian and Paleocene deposits is longer, indicating syngenetic folding. The hiatus is especially pronounced on the horst structure of Jebel An-Nusseiriyeh (near Jisr Esh-Shoughur), where the Senonian chalk is overlain by shallow-water organogic limestones with abundant Upper Maastrichtian orbitoids followed by nummulitic limestones of the Middle Eocene. The lithological composition of the Paleocene deposits is identical with that of the Esna Shale of Egypt, which passes into the Taqiye shales of Israel. The calcareous clays, marls and clayey limestones of the Danian, Selandian and Thanetian Stages of Syria correspond to the similar gray marls and marly limestones (sometimes with flint nodules) of the same stratigraphic interval in Cyprus belonging to the basal part of the Lefkara Group. Along the right bank of the Nahr El-Yarmouk River in Syria, a continuous sequence of black oil shales continues up into Paleocene limestones, although a decreasing organic matter content lowers them to the rank of kerogen limestones.

Eocene

The Eocene (Avedat Group) in Israel consists of calcareous and silicious sediments. The Levantid folding (Syrian Arc) controls the thickness of the Eocene. In the Negev area of Avedat, it is around 250 m, although the individual facies-controlled formations vary greatly in thickness. Elsewhere, as in the Shefela, it reaches over 400 m and the maximum thickness of the Eocene strata is less than 1000 m.

The Ypresian-Lutetian sequence is composed of calcareous shale, pelagic chalks, limestone, and partly silicified limestone, often containing flint beds and flint concretions in the basin facies, and nummulitic limestone of 'conglomeratic' appearance in the reef facies. The soft chalks and shales are partly glauconitic, limonitic, and slightly phosphatic. Subsurface deposits are sometimes bituminous and pyritic. A major unconformity occurs within the upper part of the Middle Eocene (Lutetian), marked by a base conglomerate. The Late Lutetian-Early Priabonian marine strata occur only in the Negev and in the subsurface of the Hashefela.

The Eocene strata in Israel span the P6-P12 and P14-P15 zones. Strata of P12 age and younger are poorly represented in most of the Negev and appear to be mostly pelagic.

The Eocene sequence starts with Ypresian pelagic foraminiferal white chalk with chert bands and nodules, with limestone interbeds increasing upward, often distorted by slump structures and angular unconformities. Continuing upward Lutetian white pelagic globigerinid chalks devoid of chert make up the basin facies, limestones with large Nummulites, Dyscocyclina and calcareous algae characterize the shallow-water facies. Laterally the latest Ypresian-Middle Lutetian bedded chalky limestones may contain quartz sand, passing laterally and vertically into conglomerate with chalk matrix. Above the hiatus, marked by a conglomerate, follow Late Lutetian-Priabonian pelagic chalk and marl with intercalated

banks of Nummulites. Indurated chalk and massive coral reef limestones occur at the top. The Bet Guvrin Formation of the Late Eocene starts in a boulder conglomerate. This type of rock is also encountered in the Oligocene.

Numerous unconformities indicate that in the later Middle Eocene the regions of the Negev (pelagic sediments with nummulitic intercalations) and Samaria became decoupled.

The depo-centers of the Shehem syncline and the Paran basin strike approximately northeast and are affected by the Levantide structure. The Shehem basin may extend to the offshore Pleshet basin, whereas the Paran basin may be one of a string of basins, extending from Sinai in Egypt to the Jordan Valley and opposite the Dead Sea Transform into the Yarmuk Valley in Jordan. Maps 17 and 18 of Dercourt et al. (2000) show that Levantide structural ridges separate the basins. These ridges do not show Eocene deposits, but some may have been covered by Eocene sediments before their removal in pre-Latest Lutetian and certainly in Oligocene times. Relicts of Eocene chalk within karstic sinkholes in the northeastern Negev bear witness to the presence of Eocene sediments on the flanks and possibly on top of the anticlines of the Levantides prior to erosion.

While sedimentation was continuous from the Late Eocene into the Oligocene in some of the subsurface basins in western Israel, in other places there strata of Oligocene (or later) age rest unconformably (often with conglomerates) on Eocene deposits.

In Syria the Eocene deposits can be subdivided into four rock units resembling those in Israel. The first two units are practically identical to those of Israel.

The lower unit is composed of soft marls and clayey limestones of the Lower Eocene (the Ypresian Stage, from the *Morozovella subbotinae* Zone, P6 up to the *Morozovella aragonensis* Zone, P8). These sediments are closely connected with those of the Paleocene and with them constitute one mapping unit. The transition from the Paleocene to the Eocene deposits is gradual, and the quantity of clayey material in the Lower Eocene rocks drops although the boundary itself is indistinct.

The second unit consists of frequent alternating layers, lenses, and nodules of brown and black flints and limestones and refers to the uppermost Lower Eocene (the *Acarinina pentacamerata* Zone, P9); its thickness varies from 42 m to 500 m. These deposits determine the character of the landscape in many areas of Syria and belong to a very distinct mapping unit. In the southern regions of Syria (Rutbah) the deposits of this age are characterized by rich accumulations of phosphorites and this belt stretches all the way to Iraq. In Cyprus the *Acarinina pentacamerata* Zone is also made up of alternating flints and hard limestones.

The third unit is represented by a facies of classical white, soft, thick-bedded chalk (basinal facies of planktonic foraminifera oozes) which is replaced in the Anti-Lebanon, Jebel An-Nusseiriyeh, and some ridges of northwestern Syria by thick piles of nummulitic limestones. In contrast to Israel, the transition from the Lutetian to Bartonian is gradual. Nevertheless, along the northern rim of the Palmyrides, deposits of the *Morozovella lehneri* Zone – P12, are absent and sediments of the next *Orbulinoides beckmanni* Zone – P13 unconformably overlie Lutetian sediments at Bir Hasseiye, Bir Qdeir, Talaat Ismir, and Jebel Dilaa. Above all, the distribution of shallow-water nummulitic limestones in the Bartonian is noticably increased.

The fourth unit has a rather complicated composition. It consists partly of chalk similar to that of the Middle Eocene and partly of hard limestones typical of the Oligocene. In some northwestern areas of Syria as well as in adjacent areas in Lebanon, the Upper Eocene deposits were not encountered. Consequently in Syria, as in Israel, the distribution of Upper Eocene sediments indicates the beginning of regression. In Syria the limestones of the Middle and Upper Eocene are shown on geological maps as a single mapping unit. In SW Cyprus the Upper Eocene is represented by limestones of the upper part of the Lefkara Group.

Oligocene

The Oligocene regression resulted in regional emersion and erosion. Open-ocean marine chalky marls and fine-grained chalky limestone of the Bet Guvrin Formation occur to the west. Shallow equivalents are the Lakhish Formation in the Shefelah, consisting of reworked chalky boulders and of *in situ* hard biosparites and biomicrites. The Early Oligocene Fiq and Sussita Formations, east of the Sea of Galilee, are made of marl, limestone, dolomite, and sandy limestones. To the east these marine strata interfinger with the mainly fluviatile and lacustrine Late Oligocene-Early Miocene deposits.

The Oligocene uplift was also felt to the west, where a 350-600 m thick unit of conglomerates and sands, embedded in marl or chalk, wedge into the Bet Guvrin Formation near Ashdod and Gaza, filling the canyons. One such canyon reaches as far inland as Beersheva.

The Oligocene regression is well-expressed in Syria. In the western and northwestern areas, Jebel An-Nusseiriyeh, Jebel Az-Zawiyeh, the Al-Latheqiyeh area, Jebel Dwele, and Jebel Baricha, Oligocene sediments are absent or exposed as isolated outcrops as seen near Aafrine. In the Anti-Lebanon, the Palmyrides, and the Rutbah Uplift the Oligocene is represented by shallow-water limestones of the following varieties: very hard thick-bedded recrystallized (cemented calcareous sands), nummulitic (in the Lower Oligocene), lepidocyclinid (in the Upper Oligocene), algal-coral reefal, and organogenous detrital. In sections of the eastern Palmyrides and Rutbah Uplift members of yellow-greenish clays and sands appear; they are especially typical for the Upper Oligocene. In those regions of the Palmyrides and the Rutbah Uplift where the uppermost layers of the Oligocene were preserved, they are made up of sandy limestones with vertical holes filled by siliceous matter (nodules) of irregular shape. Evidently they are remnants of roots of plants and rocks themselves and should be treated as sediments of lagoons and bogs of a formerly marine basin. Pelagic sedimentation was only preserved in the northern area of the Aleppo Plateau and in the Mesopotamian Basin where sediments of this age are represented by light-gray and yellowish chalky limestones and marls with abundant planktonic foraminifera. Due to the continuing subsidence the thickness of the

Oligocene chalk reaches 150-170 m.

The total thickness of the Paleogene in Syria in the continuous section at Maaloula in the Anti-Lebanon reaches 1400 m.

Regressive marly-clayey sediments of the Oligocene in Cyprus are restricted to the Kryos-Kouris depression and are usually included in the Lefkara Group in the regional stratigraphy.

1.4. The Neogene Opening of the Red Sea and its Implications

In Israel, from the beginning of the Neogene, an ever-sharper differentiation occurs between deposition west and east of the Dead Sea Transform.

West of the Dead Sea Transform, the marine Neogene in the Coastal Plain of Israel interfingers with continental deposits from the east. Beginning in the Miocene, a sinistral strike-slip along the Jordan Valley-Gulf of Aqaba line opened a series of rhomb-shaped grabens. Isostatic neo-tectonic readjustments produced the sinking of the eastern Mediterranean basin and the differential uplift of portions of the African, Levantine, and Arabian sub-plates. These orogenic events generated a new relief *e.g.* the Yizre'el Graben and the Jordan - Dead Sea - Arava Rift, accompanied by basalts that extend from the Golan Plateau to the eastern Galilee, filling large parts of the rift. Marine ingressions in the Yizre'el Valley reached the rift, leaving thick evaporites.

A very complicated paleogeographic setting characterizes the Neogene of Syria. To the west of the Dead Sea Transform, on the Mediterranean coast, and in the Nahr El-Kabir and Aafrine grabens, the entire Neogene is represented by marine sediments. East of the Dead Sea Transform, in northern Syria, the Aleppo Plateau saw marine Lower and Middle Miocene sedimentation, whereas the inland areas of southern Syria, such as the Anti-Lebanon, the Homs depression, and the Palmyrides, saw only continental Neogene deposition.

The Mesopotamian Basin represents the main Neogene depocenter of marine and continental sediments.

Miocene

In the Coastal Plain and adjacent embayments in Israel, the Lower Miocene-basal Middle Miocene open marine facies of the Bet Guvrin Formation (the *Globigerinoides primordius-Globorotalia kugleri* Zone, N4 – *Orbulina suturalis-Globorotalia peripheroronda* Zone, N9) predominates. In its upper part it is replaced by the shallow marine reef limestones of the Ziqlag Formation (the *Praeorbulina glomerosa* Zone, N8 – *Orbulina suturalis-Globorotalia peripheroronda* Zone, N9). Near Gaza and Ashqelon, sands and conglomerates bear witness to the edge of the platform.

The Middle-Upper Miocene open marine facies consists of the Ziqim Formation which corresponds to the interval of the *Globorotalia peripheroacuta* Zone, N10 – *Globigerina nepenthes* Zone, N14 and the *Globorotalia acostaensis* Zone, N16 – and *Globorotalia plesiotumida* Zone, N17. It penetrates into the Beersheva embayment, where it interfingers with shallower deposits. The latest Miocene (Messinian) evaporites of the Mavqi'im Formation are covered by fluvio/lacustrine conglomerates, with sandstone and shale on top. The Late Miocene-Pliocene (4.6-8.4 Ma) National Park Volcanics wedge between the Mavqi'im and Yafo Formations.

The Miocene deposits express sealevel and eustatic changes. An elevated surface 400-500 m above the present Mediterranean represents the highest occurrence of the Middle Miocene Ziqlag reefs, which form an important morphological landmark. A lower surface, at 120-150 m above sealevel, is made up of the Late Miocene Pattish reefs (N16-N17 Zones).

Canyons, formed during the main Oligocene regression, were then invaded by marine sediments, like the *Crassostrea gingensis* bank, which is found nearly 100 km inland from the present Mediterranean coast. Presumably it may represent a Ziqlag equivalent (the N8-N9 Zones). To the east the Early and Middle Miocene interfingers with the continental deposits of the Late Oligocene-Middle Miocene Hordos and Hazeva Formations. These include up to 300 m and 1000 m respectively of fluviatile sandstones, conglomerates, and lacustrine limestones with cherts. The Hordos Formation wedges into and is covered by the Lower Basalt (9-17.5 Ma). The Hazeva deposition is underlain by volcanics (23-21 Ma).

Miocene neo-tectonic isostatic readjustments reshaped the eastern Mediterranean and the Levant. The eastern Mediterranean part of the African Plate underwent a deepening of its basins, mirroring the differential uplift of the adjacent Levant-Sinai part of the African Plate. The sinking of the Dead Sea Rift was echoed by the uplift of the Jordan High and generated a new relief, producing the mountainous backbone of the Sinai-Levant subplate.

Subsequent to the opening of the Dead Sea Rift, the Late Miocene filling of the Beersheva Canyon consisted of thick marls and some conglomerates, equivalent to the Pattish (N16-N17 Zones) rhodoliths and poritid corals. A Tortonian marine ingression penetrated into the Yizre'el Valley, from where it inundated the newly formed Dead Sea Graben. Conglomerates, sands and shale with evaporites and huge salt masses (the southern end of the Sea of Galilee) filled the graben, interbedded with basalt flows (at 8.4 Ma, 7.3, and 6.2 Ma.).

All over Syria, a very sharp unconformity separates the Miocene from the underlying deposits.

In the Mediterranean area, the Miocene is transgressive. Different lithologies and stratigraphic ranges are found in the Nahr El-Kabir and Aafrine grabens.

In the Nahr El-Kabir, a continuous Aquitanian-Messinian succession about 800 m thick is developed. It mainly consists of Lower Miocene and basal Middle Miocene chalky soft limestones and marls, followed by Middle and Upper Miocene (Tortonian) alternating limestones, marls, calcareous sands, clays and conglomerates, with terrigenous admixture increasing upwards. The section is terminated by Messinian gypsum with interlayers of clays and stromatolite limestones.

In the Aafrine graben terrigenous deposits predominate. The Lower-Middle Miocene is composed of alternating limestones, clays, marls, sands, and conglomerates, with sediments of the

Upper Miocene being absent.

The Aleppo Plateau is occupied by transgressive hard and massive shallow-water cryptocrystalline and organogenic detrital limestones, which correspond to the Mediterranean pelagic facies of the *Praeorbulina glomerosa* Zone, N8, and *Globigerina nepenthes* Zone, N14. Thus, no deposition of Early Miocene sediments took place here.

The intracontinental depressions of the inner areas of Syria, such as the Damascus, Homs, Ad-Daww, and Faidate depressions, are characterized by various types of alluvial, proluvial, and lacustrine continental deposits; quartz sands, conglomerates, siltstones, clays etc.

In the Mesopotamian depression, the Miocene succession consists of four formations:

1) the regressive Dibbane Formation – marls and clays with subordinate intercalations of limestones and gypsum. The very impoverished planktonic foraminifera indicate a restricted environment and determine the age as the interval of the *Globigerinoides primordius-Globorotalia kugleri* Zone, N4b, and the *Globigerinatella insueta-Globigerinoides trilobus* Zone, N7 (Lower Miocene);

2) the transgressive Jeribe Formation consists of predominently shallow-water fine-grained and organogenic limestones with molluscs and benthic foraminifera of normal salinity. Very often these rocks are leached and cavernous. Correlation with the Mediterranean Miocene sequence of northwestern Syria reveals an exact correspondance to the interval from the *Praeorbulina glomerosa* Zone, N8, to the *Globigerina nepenthes* Zone, N14 (uppermost Lower Miocene-Middle Miocene). In adjacent Iraq these cavernous limestones contain huge accumulations of oil;

3) the regressive Lower Fars Formation consists of alternating marls and limestones with thick and numerous layers of gypsum and sometimes salt. Faunas of molluscs, ostracods, and benthic foraminifera are evidence of restricted environmental conditions (with abnormal salinity). Correlation with the Mediterranian Miocene sequence of Syria allows us to refer the Lower Fars Formation to the Tortonian (Upper Miocene). These deposits form the cap-rock of the oil fields in nearby Iraq;

4) the most regressive Upper Fars Formation consists of alternating gray and red-colored continental siltstones and claystones with thin intercalations of sandstones. A direct correlation with the Mediterranean Miocene of Syria is impossible but the paleogeographic reconstruction suggests that the Upper Fars Formation belongs to the Messinian (Upper Miocene).

In the Syrian part of the Mesopotamian Basin, the boundaries between the Dibbane, Jeribe, and the Lower Fars Formations were determined by fauna and can be considered isochronous within the studied area. In this sense, they correspond to the term 'suite' of the Russian stratigraphic nomenclature. These lithostratigraphic subdivisions are widely used in Iraq and Iran but may differ in age in those countries.

The Miocene deposits of the Mediterranean, Mesopotamian, and inner areas of Syria describe the main stages in the geological development of this area:

1) Lower Miocene transgression of limited extent in the Nahr El-Kabir and Aafrine grabens. It resulted in restricted links between the open sea and the Mesopotamian Basin, as well as the appearance of continental quartz sands overlying the erosional surface of Oligocene limestone in the inner regions of Syria;

2) Widespread Latest Lower Miocene (Lower Langhian)-Middle Miocene (N8-N14 Zones) transgression, covering the Mediterranean area, the Aleppo Plateau, and the Mesopotamian Basin, freely communicating from west to east, while in the inner continental regions the sandy-silty sedimentation was replaced by a red-colored clayey-silty one.

3) Tortonian isolation of the Mediterranean from the Mesopotamian Basin, with its evaporitic Lower Fars Formation deposits. These basins were separated by the 'land-bridge' of the Aleppo Plateau. Nevertheless the presence of an impoverished marine fauna in the Mesopotamia Basin indicates the possible existence of restricted links.

4) A maximum of the Miocene regression in the Messinian.

Comparison of the evolution of the Miocene in Syria and Israel shows similarities for the main events, although in the details their respective geological evolution was rather different, due to their complicated paleogeographies.

Pliocene

In Israel, the Pliocene strata of the Saqiye Group consist of the marine Yafo Formation, which in the Coastal Plain includes 1000 m of gray pyritic marls. In the Jordan Valley, limestones with conglomerates and evaporites are sealed by the so-called Cover Basalt (5.3-4.9 Ma). After the opening of the Dead Sea Rift, the Mediterranean-Dead Sea water divide generated a new hydrologic system draining the Negev into the Dead Sea. It comprises fluviatile polimictic rounded boulder conglomerates and lacustrine limestones and chalks, interfingered by the Sedom salt plugs (Dead Sea) resulting from Pliocene marine penetration into the Rift.

The late Pliocene global sealevel drop terminated the marine flooding of the Jordan Valley and its surrounding areas, where lagoons, lakes, and rivers deposited a suite of Pliocene formations. The base level was lowered with the regression, causing a westward channeling toward the retreating sea, accompanied by slight structural disturbances and volcanism.

In Syria transgressive marine Pliocene deposits occupy limited areas of the coastal belt. Near Al-Latheqiyeh they are represented by monotonous calcareous clays with subordinate intercalations of fine-grained sandstones and clayey limestones up to 500 m thick.

All other areas of Syria are characterized by the continental Pliocene.

In the Damascus, Homs, and Ad-Daww Basins it consists of two units:

1) The lower unit is composed of conglomerates and sandstones. They rest unconformably on a paleorelief that reflects tectonic deformations at the Mio-Pliocene boundary;

2) The upper unit is made up of lacustrine limestones, marls and calcareous clays. Fresh-water lacustrine sediments predominate in the El-Ghab depression.

In the Mesopotamian depression, the Pliocene is transgressive and unconformably overlies older deposits. It is more widespread than the Upper Fars Formation (Upper Miocene). As in western Syria, the Pliocene succession can be subdivided into two units. However, as compared with the Damascus, Homs, and Ad-Daww Basins, the order is reversed, indicating different tectono-environmental conditions:

1) The lower unit includes clays, sandy marls and siltstones with subordinate interlayers of sandstones and conglomerates;

2) The upper unit is characterized by rough conglomerates, gravelites, and sandstones with rare intercalations of clays and fresh-water limestones, similar to the Bachtiari Formation in Iraq.

Pleistocene

The Mediterranean units in the Coastal Plain of Israel consist of the so-called 'Kurkar', a littoral carbonate cemented quartz and calcareous pebbly sandstone. These 'Mediterranean' deposits of the Coastal Plain reflect the isostatic movements of the Levant platform and the oscillations of the Mediterranean Sea prior to and during the glacial periods.

The early Pleistocene Calabrian and Sicilian transgressions raised sealevel to approximately 120 and 90 meters respectively, as compared to the present day. These rises only deposited marine sediments on the Mediterranean coastal plain, as they could not even come close to reaching the Jordan Valley region (Horowitz 1979). However the higher erosion base levels caused silting up of the drainage systems, leaving predominantly fluviatile sediments behind, with several intermediate lakes occupying basins within the slowly subsiding Jordan Rift Valley (Levin and Horowitz, 1987).

In-rift formations consist of fluvial terraces and lake deposits, conglomerates, sands, marls, and travertines. Volcanism is active on the Golan Plateau and in eastern Galilee.

The coastal plain of Syria displays the same set of marine terraces as in Israel and Lebanon. They are as follows:

I – 2 to 4 m, Recent;
II – 10 to 20 m, Upper Pleistocene;
III – 30 to 40 m, Middle Pleistocene;
IV – 60 to 80 m, Lower-Middle Pleistocene and
V – 90 to 120 m, Lower Pleistocene.

The greater part of Syria is covered by Quaternary continental deposits belonging to various facies types – alluvial, proluvial, eluvial, and lacustrine. The alluvial river terraces of the Al-Furat, Orontes, Nahr El-Kabir, and Tigris are of great anthropological/ archeological importance since they contain flint tools of the Abbevillian, and Lower, Middle, and Upper Acheulean cultures. Rich Upper Paleolithic remnants, namely the Levallois and Mousterian cultures, were discovered in caves near Palmyra, Aafrine, Damascus, and Dmeir, and along the banks of the Orontes River.

2. VOLCANICS

The Levant region was dramatically affected by the activity of the Levant-Nubia plume of northern Gondwana, which was related to Mesozoic-Cenozoic Palmyrian rifting.

The volcanism of the earlier epochs accompanied the origin of the Neo-Tethys and the development of the eastern Mediterranean Mesogea.

The Neogene-Quaternary volcanism is connected to the opening of the Red Sea rift and to movements along the system of Levantine faults.

Some events were only of local significance, whereas others were regional:

1) **Permian**: The Gevim volcanics of Helez in the Israel Coastal Plain (275 Ma);

2) **Late Triassic-Early Jurassic**: The Asher and Aarne Volcanics in a belt extending from the Carmel region to Galilee, and in the southwest of Syria in the Hermon Massif. They form a stratified body between Norian-Rhaetian and Pliensbachian-Toarcian limestones. These basalts are effusive (pillow lavas), definitely formed under submarine conditions.

3) **Late Jurassic**: Pyroclastics have been found in northwestern Syria in the axial part of Jebel An-Nusseiriyeh, deposited on Oxfordian and, perhaps Lower Kimmerigian sediments. The explosive character of the volcanics of the Jebel An-Nusseiriyeh eruptions is similar to the Bhannes basaltic tuff in Lebanon and the Galilee (Devorah Volcanics).

4) **Lower Cretaceous**: The Lower Cretaceous basalts, as compared to those of the Jurassic, are spread much wider. They are exposed in Syria, Lebanon, and Israel. In Syria they occur in the Anti-Lebanon, the Golan, Jebel An-Nusseiriyeh, the southeastern side of the Kurd-Dagh, as well as in the Palmyrides (Jebel Rmah). In Israel, they are exposed in the Negev (Makhtesh Ramon) and in Samaria (Tayasir Volcanics) as well as in the subsurface of the Galilee.

5) **Upper Cretaceous**: Two horizons of Upper Cretaceous basalts have been found in the southwestern part of Jebel An-Nusseiriyeh. They lie at the base and in the lower part of the Cenomanian sediments. The basalts are characterized by pillow lavas, attesting to underwater eruption. Such rocks are frequent in the Cenomanian and Santonain of the Carmel region and might be compared with the Eratosthenes volcanics.

6) **Eocene**: Basalts and tuffs of Early Eocene age are only known in the northwest of Syria, not far away from the Kurd Dagh, north of the town of Aafrine.

7) **Neogene-Quaternary**: The large basaltic fields are the Jebel Drouze and Hauran basaltic flows, which largely spilled across the Dead Sea Rift and into the Galilee.

This Neogene-Quaternary volcanism is connected to the opening of the Red Sea Rift and to movements along the system of Levantine faults. Five periods of volcanic activity can be differentiated:

1) Oligocene-Early Miocene (Red Sea magmatism) (28-15 Ma);
2) Middle Miocene (11-15 Ma);
3) Late Miocene-Early Pliocene (4.5-11 Ma);
4) Late Pliocene-Pleistocene (0.3-1.95 Ma); and
5) Holocene.

The Neogene-Quaternary volcanics of Syria had a tendency to

change over time from a tholeiitic to sub-alkaline and even alkaline composition and belong to the single Afro-Arabian alkaline olivine basalt province. The changes in the petrochemical composition to a higher or lower alkalinity were dictated by the depth of magma formation and the grade of melting of the mantle matter.

Further basalts of this time span are connected to different plumes, such as those found in the Mesopotamian Basin and in the southwest margin of the Aleppo Plateau.

3. TECTONICS

The tectonic setting of the eastern Mediterranean and the Levant consists of the triple junction of the African, Arabian, and Anatolian Plates, bound by the Cyprian (Cyprean) Arc, Peri-Arabian Ophiolitic Crescent, and the Dead Sea Transform.

The most prominent tectonic line appears to be the Dead Sea Transform that separates the Levant into eastern and western sections. The tectonics of these sections are represented separately in our Syria and Israel chapters.

3.1. East of the Dead-Sea Transform

1) The Syrian basement was supposedly formed by amalgamation of three terranes (Rutbah, Aleppo, and Khleissia) in the Late Precambrian. Since then this area has belonged to the Gondwana passive margin. Accumulation of the platform cover started in the Middle Cambrian and was interrupted in the Late Silurian-Early Devonian, presumably due to thermal uplift related to rifting and opening of the Paleo-Tethys.

2) From the latest Paleozoic to Senonian time its evolution was dominated by several phases of extension and rifting. As a result the orthogonal rifts (the Palmyrides, Sinjar, Euphrates, and Drouz) developed concurrently and were filled with thick sequences (up to 8-10 km) of marine sediments.

3) The major rifting episodes occurred in the Late Carboniferous-Permian, the Middle-Late Triassic, and at the end of the Early Cretaceous. None of these episodes shows a clear connection with plume activity. The first episode correlates with the rifting of several microcontinents from the Gondwana passive margin, and the origin of Neotethyan spreading centers. It is speculated that this happened when the Paleo-Tethyan ridge was subducted and the slab-pull was directly transmitted from the active margin to Gondwana. The Triassic episode (probably two stages) was related to rifting and the transition to spreading in Mesogea. Early Cretaceous rifting coincided with formation of the south-facing Peri-Arabian trench system. Possibly slab-pull was again the source of extension.

4) Collision of the Arabian passive margin with the trench system and immature island arcs culminated in obduction of the Baer-Bassit ophiolites in the Campanian-Early Maastrichtian. This event correlates with the first phase of inversion in the North Arabian and North Sinai rift basins (*i.e.* formation of the Syrian Arc). Later stages of inversion correlate with the African-Eurasian and Arabian-Eurasian collisions. Compressional deformation reached its maximum in Late Miocene-Quaternary time. Fault-related anticlines and their corresponding ridges developed in the deepest trough of the Southern Palmyrides while the broad anticlinorium of the Northern Palmyrides formed an extension of the Anti-Lebanon. Deformation of the Palmyrides was enhanced by the effect of the restraining bend of the Yammuneh strike-slip fault in Lebanon, and by clockwise rotation of the Rutbah block. East of the El-Furat transcurrent fault compressional deformation was weak: the Sinjar Trough was converted into a broad and flat antiform (rampart).

5) In northwestern Syria the asymmetric anticlinorium of Jebel An-Nusseiriyeh, the Al-Ghab depression, and the Jebel Az-Zawieh Uplift (a deformed margin of the Aleppo High) evolved under a transpressional regime and are closely related to the displacement along the Al-Ghab fault (which is the northern extension of the Levantine fault system). About 10 km of displacement since the Late Pliocene is registered along this fault; its bend to the east creates a 'restraining effect'. Generally speaking, the compression in northwestern Syria probably resulted from non-parallelism of the Arabian and Sinai plate motions relative to Eurasia.

6) The indentation of Arabia into the Alpine fold belt led to the westward expulsion of several blocks, including Anatolia and Cyprus. The Al-Latheqiyeh fault (a former front of the early Alpine nappe) was activated as a sinistral strike-slip fault. Seismic surveys have traced this fault and the Amanos fault in southeast Turkey to Cyprus. Thus they constitute the southeastern boundary of the Cyprus subplate as it moved to the west relative to Africa.

3.2. West of the Dead Sea Transform

1) The early geological history of the Levant is Gondwanian. A basement of accreted terranes, consisting of plutonics, volcanics, ophiolites, and metasediments was consolidated by Late Precambrian Pan-African orogeny, including the Menderes, Eratosthenes, and Arabian-Nubian Massifs, prior to regional peneplanation.

2) The Paleozoic history of the Levant is one of domal uplifts: Latest-Devonian, Permian, and post-Permian, that resulted in the erosion of much of the Paleozoic deposits. Hardly anything is left of the Ordovician-Devonian sedimentation and the earliest Triassic is missing. A paleo-geological subcrop map of the Near East suggests that the post-Devonian high encompasses a large area of the eastern Mediterranean.

3) The Early Triassic opening of the Neotethys across Gondwana was echoed by Mesozoic epicontinental sedimentary cycles such as Ramon (Olenekian-Rhaetian), Arad (Pliensbachian-Tithonian), Galilee (Berriassian-Aptian) and Judea (Albian-Coniacian), well-developed in the depo-centers of the Galilee, Palmyrides, and Judea embayments respectively. These cycles are punctuated by interruptions: intracratonic rifting, uplifts, volcanics, and/or eustatic sealevel changes, possibly echoing the Neo-Tethyan island arc and mid-oceanic volcanism and spreading.

4) Echoing the Alpidic Neo-Tethys-Gondwana collision, the Levantid deformation of the Negev-Palmyrides belts is the result of the inversion of Early Mesozoic faults, producing the asymmetrical folds of the S-shaped Syrian Arc. These extend from northern Sinai to the Palmyrides. Folds in the Negev and Judea are typically asymmetric. The Syrian Arc shaped a palaeogeography of basins

and heights, sometimes islands, that controlled the calcareous and siliceous sedimentation of the Senonian-Paleocene Mount Scopus Group and of the Eocene Avedat Group. The lower part (Oligocene) of the Saqiye Group represents the last period of this phase. Sediments of this age were widely destroyed by the regional uplift that started the next phase, leaving only a few marine outcrops in the northern Negev, the Coastal Plain and the Golan Heights.

5) A possible mid-Oligocene tectonic rebound coincides with a drop in sealevel, enhancing regional regression, emersion, and erosion. Since the Late Oligocene, the Red Sea opening split the Gondwanian foreland into separate African and Arabian plates. The continued collision with the Neo-Tethyan Anatolian plate at different speeds, generating the Dead Sea Transform, also resulted in the Miocene deformation of the Palmyrides belt, absorbing a part of the pressure. The sinistral strike-slip also opened a series of rhomb-shaped grabens along the Jordan Valley-Gulf of Aqaba line, accompanied by basalt eruptions at its northern end. Pliocene isostatic readjustments produced the downwarp of the eastern Mediterranean basin, echoed by the differential uplift of portions of the African, Levantine, and Arabian sub-plates.

ACKNOWLEDGEMENTS

Delays of over three years in getting this book into print have enabled the inclusion of a number of new topographical and imagery datasets, as well as their use by ever-improving computer programs. The authors wish to express their gratitude to:

a) The compilers of the HYDRO1K, GTOPO30, ETOPO2, ACE, and the GEBCO GDA topographic datasets, which enabled us to first see the 'forests and the trees';

b) The fathers who sired the Shuttle Radar Topographic Mission (SRTM) of February 2000, which finally gave free and accurate digital terrain models (DTMs) on a 90 m grid for the areas under study. These fathers were NIMA (the National Imagery and Mapping Agency, now the National Geospatial-Intelligence Agency - NGA), NASA and the STS-99 astronauts, JPL (the Jet Propulsion Laboratory), and the U. S. Geological Survey (USGS);

c) The people at Golden Software whose Surfer® 8 opened the door to fascinating 3-D imagery of topography and other three dimensional datasets;

d) The people at Global Mapper Software LLC who constantly expanded the capabilities of Global Mapper® so that it could digest and convert all of the spatial formats, projections, and datums, and render imagery that was easy to use and candy for the eyes.

e) The people at NGA-NIMA, the USGS, and EarthSat who provided free wall to wall coverage at high resolution of LANDSAT satellite imagery for the world.

To you all a great debt of thanks. [J.K.H.].

REFERENCES CITED

Abdallah, A. M., and El-Adindani, A., 1965. Stratigraphy of Upper Paleozoic rocks, western side of the Gulf of Suez. United Arab Republic, Geological Survey, Paper No. 25, 18 p., 7 figs., 5 pl.

Alavi-Tehrani, N., 1980. The distribution of ophiolites in Iran and their significance. Ofioliti, Vol. 2, Special Issue on Tethyan ophiolites, p. 315-334.

Bebeshev, I. I., Dzhalilov, Yu. M., Portnyagina, L. A., Yudin, G. T., Mualla, A, Zaza, T., and Yussef, A., 1988. The Triassic deposits of Syria. Trans. of the USSR Acad. Sci., Ser. Geol., N 11, p. 43 53. (In Russian).

Best, J. A., Barazangi, M., Al-Saad, D., Sawaf, T., and Gebran, A., 1993. Continental margin evolution of the northern Arabian platform in Syria. Am. Assoc. Petrol. Geol. Bull., 77(2), p. 173 193.

Dercourt, J., Gaetani, M., Vrielynck, B., Barrier, E., Biju-Duval, B., Brunet, M. F., Cadet, J. P., Crasquin, S., and Sandulescu, M., (Eds.), 2000. Atlas Peri-Tethys: Paleogeographical Maps, Comm. for the Geological Map of the World, Paris, 268+xx p.

Dolginov, E. A., Kazmin, V. G., and Ponikarov, V. P., 1969. Structure of the Upper Precambrian sections and Precambrian history of development of the Arabian Platform and its marginal folded zones. Bull. Moscow Soc. of Testers of Nature, Ser. Geol., Vol. XLIV, No. 6, p. 61-76. (In Russian).

Emeis, K. -C., and Shipboard Scientific Party (1996). Proceedings ODP, Initial Reports, 160, College Station, TX (Ocean Drilling Program), 972 p.

Eshet, Y., 1990. The palynostratigraphy of the Permian-Triassic boundary in Israel: Two approaches to biostratigraphy. Isr. J. Earth Sci., 39(1), p. 1-15.

Ghent, E. D., and Stout, M. Z., 1981. Metamorphism at the Base of the Samail Ophiolite, Southeastern Oman Mountains. J. Geophys. Res., 86(B4), p. 2557-2571.

Gvirztman, G., and Weissbrod, T., 1984. The Hercynian geanticline of Helez and the Late Palaeozoic history of the Levant. In: Dixon, J. E. and Robertson, A. H. F. (eds.), The Geological Evolution of the Eastern Mediterranean, Geol. Soc. London, Spec. Pub. 17, p. 177-186.

Hacker, B. A., 1991. The role of deformation in the formation of metamorphic gradients: Ridge subduction beneath the Oman ophiolite. Tectonics, 10(2), p. 455-473.

Hall, J. K., 1998a. Digital terrain model (DTM) of the island of Cyprus. In: T. Weissbrod (ed.), Geol. Surv. Isr. Current Research, Vol. 11, Jerusalem, p. 47-52.

Hall, J. K., 1998b. Digital shaded relief map of the Island of Cyprus. Geological Survey of Israel and Republic of Cyprus Geological Survey Department, Laminated grayscale analytic hill-shading on modified UTM projection at 1:250,000 scale, Jerusalem, one sheet. Prepared for the ICGEM-3, Third International Conference on the Geology of the Eastern Mediterranean, Nicosia, Cyprus, Sept. 23-26, 1998.

Hall, J. K., Ben-Avraham, Z., and Shamai, E., 1983. A marine geophysical survey off Southern Lebanon. In: A. Ehrlich and B. Katz (eds)., Geol. Surv. Isr. Current Research, 1982, p. 88-89.

Hall, J. K., Udintsev, G. B., and Odinokov, Y. Y., 1994. The bottom relief of the Levantine Sea. In: V. A. Krasheninnikov and J. K. Hall (eds.), Geological Structure of the North-Eastern Mediterranean (Cruise 5 of R/V Akademik Nikolaj Strakhov). Historical Productions-Hall Ltd., Jerusalem, Israel, p. 5-28.

Harding, T. P., (1985). Seismic characteristics and identification of negative flower structures, positive flower structures, and positive structural inversion. Am. Assoc. Petrol. Geol. Bull., 69(4), p. 582-600.

Hirsch, F., 1990. Aperçu de l'histoire phanérozoique d'Israël. J. Afr. Earth Sci., 11(1-2), p. 177-196.

Horowitz, A., 1979. The Quaternary of Israel. Academic Press, New York, 394 p.

Kempler, D., 1994. Tectonic patterns in the easternmost Mediterranean. Unpubl. Ph.D. thesis, Hebrew University Jerusalem, 137 p.

Kopp, M. L., and Leonov, Yu. G. 2000. Tectonics. In: Outline of geology of Syria, Trans. of the Geol. Inst of the Russian Acad. Sci., Vol. 526, p. 7-104. (In Russian).

Leonov, Yu. G., Sigachev, S. P., Otri, M., Yusef, A., Zaza, T., and Sawaf, T., 1989. New data on the Paleozoic complex of the platform cover of Syria. Geotectonics, 23(6), p. 538-542.

Levin, N., and A. Horowitz, 1987. Palynostratigraphy of the early Pleistocene QI Palynozone. Isr. J. Earth Sci., 36(1-2), p. 45-58.

Loubrieu, B., Satra, C., and Cagna, R., 2001. Cartographie par sondeur multifasceaux de la Ride Méditeranéenne et des domaines voisins: Morpho-Bathymetry and Acoustic Image of the Mediterranean Ridge and surrounding areas. Scale

1:500,000 at 35°N. Ifremer, Brest.

Makris, J., Ben-Avraham, Z., Behle, A., Ginzburg, A., Gieze, P., Steinmetz, L., Whitmarsh, R. B., and Eleftheriou, S., 1983. Seismic refraction profiles between Cyprus and Israel and their interpretation. Geophys. J. R. Astron. Soc., 75(3), p. 575-591.

Makris, J., and Wang, J., 1994. Bouguer gravity anomalies in the eastern Mediterranean Sea. In: V. A. Krashenninikov and J. K. Hall (eds.), Geological structure of the northeastern Mediterranean (Cruise 5 of R/V Akademik Nikolaj Strakhov). Historical Productions-Hall, Jerusalem, Israel, p. 87-98.

Makris, J., Wang, J., Odintsov, S. D., and Udintsev, G. B., 1994. The magnetic field of the Eastern Mediterranean Sea. In: Krashenninikov, V. A., and Hall, J. K. (eds.), Geological structure of the northeastern Mediterranean (Cruise 5 of R/V Akademik Nikolaj Strakhov). Historical Productions-Hall, Jerusalem, Israel, p. 75-86.

Pamic, J., and Adib, D., 1982. High grade amphibolites and granulites at the base of the Neiriz Peridotites in Southern Iran. N. Jb. Miner. Abh., B.143, No 2, p. 113-121.

Ponikarov, V. P., Kazmin, V. G., Kozlov, V. V., Krasheninnikov, V. A., Mikhailov, I. A., Razvalyaev, A. V., Soulidi-Kondratiyev, E. D., Oufland, A. K., and Faradzhev, V. A., 1969. Geology and mineral resources of foreign countries. Syria. Scientific Laborat. of geology of foreign countries, Vol. 18, Publ. Off. "Nedra", Leningrad, 216 p. (In Russian).

Ponomarev, B. Ya., 1966. The Geological map of Syria. Scale 1:200,000. Sheet J-37-IV (Tuwal El-Aba). Explanatory Notes. Technoexport, USSR, 47 p.

Ponomarev, B. Ya. and Bivshev, A. S., 1966. The Geological map of Syria. Scale 1:200,000. Sheets J-37-V, XI (Al-Hasakeh). Explanatory Notes. Technoexport, USSR, 67 p.

Rigassi, F., 1971. Petroleum geology of Turkey. In: A. S. Campbell (ed.), Geology and History of Turkey. Petroleum Exploration Society of Libya, Tripoli, p. 453-482.

Shervais, J. W., 2001 (January 31). Birth, death, and resurrection: The life cycle of suprasubduction zone ophiolite. - Geochemistry Geophysics Geosystem (G3), An Electronic Journal of the Earth Sciences, Vol. 2, Paper number 2000GC000080.

Silantyev, S. A., 1993. Metamorphic Complexes of the Eastern Mediterranean: Metamorphic Conditions, Protoliths, and Geodynamic Environment. Petrology, 1(4), p. 395-416.

Sobolev, A. V., and Batanova, V. G., 1995. Mantle lherzolites of the Troodos ophiolite complex, Cyprus: Clinopyroxene geochemistry. Petrology, 3(5), p. 440-448.

Spray, J. G., and Roddick, J. C., 1981. Evidence for Upper Cretaceous transform fault metamorphism in West Cyprus. Earth Planet. Sci. Lett., 55(2), p. 273-291.

Thomson, S. N., Stöckhert, B., and Brix, M. R., 1998. Thermochronology of the high-pressure metamorphic rocks of Crete, Greece: Implications for the speed of tectonic processes. Geology, 26(3), p. 259-262.

Udintsev, G. B., Zverev, A. S., Odinokov, Y. Y., Efremov, V. N., Eleftheriou, S., and Hall, J. K., 1994. Structure of the Post-Messinian Sedimentary Cover in the Eastern Part of the Mediterranean Sea. In: V. A. Krasheninnikov and J. K. Hall, (eds.), Geological Structure of the North-Eastern Mediterranean, Historical Productions-Hall Ltd., Jerusalem, Israel, p. 33-73.

Woodside, J. M., 1977. Tectonic elements and crust of the Eastern Mediterranean Sea. Mar. Geophys. Res., 3(3), p. 317-354.



Figure E.12. Official STS-99 Crew Portrait (NASA photograph). An international crew assigned to STS-99 takes a break from training to pose for the traditional crew portrait at NASA's Johnson Space Center (JSC). In front are international astronauts Mamoru Mori and Gerhard P. J. Thiele, both mission specialists. In back are astronauts Janice Voss, mission specialist; Kevin R. Kregel, mission commander; Dominic L. Gorie, pilot; and Janet L. Kavandi, mission specialist. Mohri represents Japan's National Space Development Agency (NASDA) and Thiele represents the European Space Agency (ESA).
The 90 m DTM resulting from the STS-99 mission was an important factor in improving the figures in these volumes.

Appendix A

Regional Bibliographies on CD-ROM: Geology, Geophysics, Oceanology, and Related Subjects

John K. Hall
Geological Survey of Israel, Marine Geology, Mapping & Tectonics Division, 30 Malchei Israel Street, Jerusalem 95 501, Israel

INTRODUCTION

The bibliography that was included in our last book on Cruise 5 of the NES Nikolaj Strakhov was printed out (Hall, 1994) on some 86 pages, or over 20% of the book. With the several-fold expansion in the area under consideration, digitization of journal back-issues, more rapid and expanded scientific publication, this bibliography has grown significantly. Luckily in the interim the introduction of superior OCR and OS software, faster computers, better scanners, and the Internet has provided tools for dealing with this proliferation. Now, rather than printing an update, files in Microsoft® Word 2000 for Windows 2000 have been prepared and are available separately on CD-ROM, with other materials described in these appendices.

The methodology used was essentially that described by Hall (1994), and therefore this section of the old bibliography is reproduced with minor changes below.

BACKGROUND

This bibliography is the outcome of three factors, brought together by the IBCM Project of the IOC (Intergovernmental Oceanographic Commission of UNESCO) and the IHO (International Hydrographic Organization) for producing the International Bathymetric Chart of the Mediterranean (IBCM) and its Geological/Geophysical Overlay Sheets. The first factor is my good fortune in having devoted most of my professional life to studies of the Arctic and the Eastern Mediterranean. These areas are surprisingly similar in their geological complexity, their enigmatic and apparently lengthy histories, and their continuing resistance to elucidation by a model of origin fitting all the available data which invites professional consensus. The second factor is my personal conviction that these areas will only be understood by a rigorous program combining brave leaps of the imagination with a painstaking compilation of all the geological and geophysical material at common scales. Implicit in this, of course, is a thorough compilation of all work published to date. The third factor has been the lack of such a bibliographic compilation, due in large part to the fact that:

i) The Eastern Mediterranean touches a number of different landmasses with different cultures, languages, histories, and political systems,

ii) The scientific literature for the Eastern Mediterranean is similarly divided among a large number of single and multi-disciplinary journals, books, reports and other publications,

iii) In the past the marine scientists have been neither cognizant nor conversant with the detailed findings of their land-based colleagues, and especially vice versa,

iv) The literature is written in a number of unrelated and alphabetically disparate languages, and

v) It is often concerned with purely regional aspects because of the historical, commercial, and political sectoring of the area.

The IBCM Project thus provided the catalyst for preparing a computerized geological and geophysical bibliography on the Eastern Mediterranean, beginning primarily with the basic data sets. In the future, regionally specialized groups such as IBCM will be a likely source of such compilations. The present compilation uses methods which I developed previously for a compilation on the Arctic Ocean under the D-NAG Project of the Geological Society of America (Hall, 1986, 1990). Other bibliographies are being prepared for all the Mediterranean Sea (within the framework of the IBCM for inclusion in the final IBCM Supporting Volume as well as a complement to the digital variants of the graphical compilations), and for the Red Sea (Hall, 1984ff) as part of the Israeli REDMAP Project.

SCOPE AND COMPREHENSIVENESS

The Eastern Mediterranean has historically been the most poorly mapped part of the Mediterranean. The reasons for this have been political, geographical, and sociological. However, coincident with the detailed work of the R/V Akademik Nikolaj Strakhov there has been renewed interest in this sediment-filled end of the Mediterranean whose genesis, age, and geological and tectonic framework continue to invite, incite, or excite much speculation.

The primary objective of this compilation has therefore been to concentrate on referencing all the articles, reports, books, abstracts, theses, and other sources of original data, as well as analyses, and conclusions drawn from them, for the area within the bathymetric chart of the Eastern Mediterranean which is reproduced here. Because the original bibliography was prepared to assist in the bathymetric, geological and geophysical data compilations of the IBCM Project, the references dealing with data sources are quite complete. These also include a number of appended comments regarding the specifics of hard data.

The secondary objective has been to tie in all the geological and geophysical material from the adjacent landmasses, so that information will be available for studies of the nature and history of the entire area. In this respect the coverage is definitely uneven.

In some cases the detailed geological literature for the landmasses has been voluminous, and references for the most part have been chosen that will cast light on subjects which may be important for understanding the whole. Because the Eastern Mediterranean is located in a very complex junction of belts, rifts, faults, shears, fronts, platforms, basins and seas, additional references which deal with these factors, even hundreds if not a thousand kilometers away, have been added. Hence, the overall area includes all the Mediterranean Sea, the northern Red Sea, and the continental rim including southern Turkey and western Syria (and sometimes extending as far east as the Palmyrides), Cyprus, Lebanon, Jordan by the Dead Sea rift, Israel, and northern Egypt including Sinai.

Material from related fields (oceanology, meteorology, marine biology, remote sensing, and modeling) is included if these studies provided an opportunity for simultaneous geophysical work, or if the subject matter would provide a better understanding of the geology and geophysics of the area. A few distantly related references are given to give the user a starting point into these fields. Almost every type of written, graphic, and even digital material which might assist students of the area, including maps, program abstracts, theses, and unpublished technical reports is included. Often these references are second- or third-hand, and thus fragmentary and incomplete. However, this approach is necessary to ensure the survival of much work which was never properly published, and will be worthwhile if it provides the initial clues for locating a crucial piece of the puzzle.

Hence the scope reflects my own concept of what an investigator should be aware of in order to properly approach the puzzle. In this I was aided by the compilational method (described below), which strongly depends upon material which other investigators considered sufficiently important to reference.

This compilation is as comprehensive as the available time and library resources would allow. Beyond my own third-century collection of material, augmented by contributions from colleagues who knew about the bibliographies, I have benefited from the excellent Documentation Center at the Geological Survey of Israel, and from the detailed knowledge and contributions of my co-editor, V. A. Krasheninnikov. Within the 3596 references found in this bibliography, I have singled out forty-three which are themselves bibliographies. These are cited separately below for the reader's convenience, with updates since 1994.

For the future, improvements will likely come from the concentrated focus of the next Mediterranean Phase of the Ocean Drilling Program, the eventual conclusion of the IBCM Project, and an anticipated D-NAG-like effort to produce an international compilation on the geology of the Levant (*this book – ed.*).

METHODOLOGY AND ORGANIZATION

An unorthodox methodology was used in compiling this bibliography. Starting with a simple listing of materials gathered as the first offshore compilations were prepared at the Geological Survey of Israel (GSI), additional bibliographic citations were added from reprints, theses, journals and books within my own library, and that of the original Marine Geology Division library under the supervision of the late Mrs. Rachel Gill. Thus, by perusing the widening circle of references, the bibliography steadily grew.

The references were originally kept on the DEC VAX11/750 computer at the GSI in Jerusalem. The references are cited as completely as possible, with missing information noted by dashes. This system was transferred to an IBM PCAT in 1985, and at present, for the purposes of this monograph, whole bibliographies from more recent compendiums were scanned directly into the computer using optical character recognition technology (HP ScanJet IIc with Caere OmniPage Professional™ software), and then typeset using the local Israeli Dagesh™ for Windows (Latin-Hebrew-Cyrillic) desk-top publishing software. The various Dagesh files were merged and sorted using simple FORTRAN programs, and then output on a 600 dpi HP LaserJet 4 printer.

Because of the 'third hand' nature of many of these references, considerable effort was devoted to correcting the many obvious errors. Names, which appeared in a number of variants, have been given uniform spellings. Author's initials are given as fully and consistently as possible, including Jr., III, etc. Ambiguities were resolved whenever possible by consulting the original references. Despite this, there remain many small and probably even some grave errors, and for these I apologize in advance. In addition, Murphy's Law assures that this compilation will overlook the works of some deserving authors whose publications should have been included, and will include every scribbling of others. For this too, my sincere apologies.

ORGANIZATION OF BIBLIOGRAPHIES ON CD-ROM

The bibliographies are available as Microsoft® Word 2000 for Windows 2000 .doc files on the CD-ROM. With tools such as Word 2000, it is now a simple matter to search the files for specific authors, keywords or any words, journals etc. In many cases this should be simpler than using somewhat more rigid database programs, with the added benefit of being able to copy references to other files, resorting groups of references, changing reference formats etc.

1) GSI Current Research Volumes 1 through 13 (1975-2002). These are given as 13 separate files, each with the references to the articles within, their references, and then the accumulated references for articles and abstracts published by the personnel at the GSI. Close to 9000 references are given, some of which are of course repeated. These references primarily cover the work of the approximately 100 scientists at the GSI, working on many aspects of the geology, geochemistry, and geophysics of Israel and its environs.

2) The Original 1994 bibliography. This includes the 3596 references originally printed.

3) Bibliographies of the various chapters in the present two volumes.

4) Bibliography of the Red Sea. This is an ongoing rag-tag collection that has been underway since the early 1980s, which will hopefully assist in a compilation of references pertinent to geological and geophysical compilations of the Red Sea and its adjacent margins.

5) Bibliography of geological maps of Israel and the countries around Israel on file at the GSI Documentation Center. Most of these are also to be found printed in Appendix D.

6) Bibliography of all M.Sc. and Ph.D. theses on file at the GSI Documentation Center.

CAVEATS

While a considerable effort has been put into the preparation of these bibliographies, and while a very large number of errors, blunders, misspellings, and incongruities have been rectified or ameliorated, these files are not without mistakes etc. It is my hope that the material within will be helpful to users, as I know the last bibliography was. However it is not perfect and acknowledging human frailty, it never will be.

Unlike the first volume, the present two volumes on the Geological Framework of the Levant have adopted the reference format of giving the authors' initials *after* the name. This has been done in recognition of the fact that digital sorting puts less emphasis on the initials. Both systems are liable to be found in the digital files due to the labor intensive nature of this change.

ACKNOWLEDGEMENTS

This work would not have been possible without the time and facilities made available to me by the Geological Survey of Israel, Ministry of National Infrastructures. The GSI's traditionally liberal approach is gratefully acknowledged. Library support came from the late Mrs. Rachel Gill of the Marine Geology Division, and Varda Arad and Oksana Zaripov of the Documentation Center at the Geological Survey of Israel, Deborah Magen and Zelda Colodner of the Geology Library at the Hebrew University of Jerusalem, and Ruth Paldi at the Israel National Oceanographic Institute in Haifa. Many of the early references were entered by Mrs. Dina Ashkenazi. Ya'akov Nir provided a number of rare documents from his personal library, and John Woodside kindly sent the latest references to works resulting from the UNESCO\ TREDMAR Training through Research program aboard the R/V Gelendzhik.

REFERENCES CITED

Hall, J. K., 1984ff. The REDMAP Geophysical Bibliography of the (northern) Red Sea and adjacent areas. Unpublished 120 p. manuscript with 1800+ references and a digital file.

Hall, J. K., 1986. Arctic Ocean Bibliography: Marine Geology, Geophysics, Oceanography, Acoustics, and Related Subjects. 4407 references, including introduction, and author and subject indices. Geol. Surv. Israel Rep. GSI/1/86, Jerusalem, February 1986, 194 p.

Hall, l. K., 1990. Arctic Ocean Bibliography: Marine Geology, Geophysics, Oceanography, Acoustics, and Related Subjects. 4407 references, including introduction, and author and subject indices. Two Microfiches, In: A. Grantz, L. Johnson, and J. F. Sweeney, (eds.), The Arctic Ocean region, Geological Society of America, Boulder, CO, The Geology of North America, Volume L.

Hall, J. K., 1994. Eastern Mediterranean regional bibliography: Geology, Geophysics, Oceanology, and related subjects. Chapter 18 In: V. A. Krashinninikov and J. K. Hall (eds.), Geological Structure of the North-Eastern Mediterranean (Cruise 5 of the Research Vessel 'Academik Nikolaj Strakhov'), Historical Productions-Hall, Jerusalem, p. 307-394.

EXISTING MEDITERRANEAN BIBLIOGRAPHIES

American University, Beirut, Economic Research Institute, 1967. A selected and annotated bibliography of economic literature on the Arab countries of the Middle East, 1953-1965, Beirut, 458 p. [Jordan - p. 72-99; Lebanon - p. 117-189; Syria - p. 301-349].

Anonymous, 1975. Marine geology and geophysics of the Mediterranean region; Bibliography 1973-1974 (In French). Rapp. Comm. int. Mer Medit., 23(46), 450 p.

Arad, V., and Bartov, Y., 1981. Geological Research in Sinai: Bibliography. Geol. Surv. Israel, Special Publication No. 2, Jerusalem, 110 p., 1969 refs.

Arad, V., and Bartov, Y., 1988. Golan Heights and Mt. Hermon; Bibliography of Geological Research. Isr. Geol. Surv. Rep. GSI/12/85, June 1985, Jerusalem, 43 p., 449 refs.

Arad, V., Beyth, M., and Bartov, Y., 1984. The Dead Sea and its Surroundings: Bibliography. Isr. Geol. Surv., Special Publication No. 3, Jerusalem, April 1984, 111 p., 1326 refs.

Arad, V., Beyth, M. and Vardi, J., 1990. Mediterranean-Dead Sea project: Bibliography. Isr. Geol. Surv., Rep. GSI/9/90, 50 p.

Arad, V., and Ehrlich, A., 1985. The Geology of Lebanon; Bibliography 1772-1984. Isr. Geol. Surv. Rep. GSI/12/85, June 1985, Jerusalem, 74 p.

Arad, V., Ehrlich, A., and Bartov, Y., 1991. The Geology of Iraq; Bibliography.Isr. Geol. Surv. Rep. GSI/1/91, January 1991, Jerusalem, 189 p., 2256 refs.

Arad, V., Ehrlich, A., and Bartov, Y., 1993. The Geology of Iraq; Bibliography.2nd Updated Edition. Isr. Geol. Surv. Rep. GSI/5/93, January 1993, Jerusalem, 204 p., 2403 refs.

Arad, V., Ehrlich, A., and Nathan, Y., 1985. The Geology of Syria; Bibliography. Isr. Geol. Surv. Rep. GSI/39/85, 107 p., 1274 refs.

Arad, V., and Rosenthal, E., 1985. Water in Israel, 1970-1982; Selected Bibliography. National Council for Research and Development, Report 85-4, 149 p., 1836 refs.

Arad, V., Weissbrod, T., and Bartov, Y., 1990. The Cretaceous of Israel and Adjacent Countries; Bibliography. Isr. Geol. Surv. Rep. GSI/43/90, September 1990, Jerusalem, 218 p., 2437 refs.

Atiyeh, G. N., 1975. The contemporary Middle East, 1948-1973. A selective and annotated bibliography, G. K. Hall, Boston, 664 p.

Avnimelech, M., 1965. Bibliography of Levant Geology, Volume I., Israel Program for Scientific Translations, Jerusalem, 192 p.

Avnimelech, M., 1969. Bibliography of Levant Geology, Volume II., Israel Program for Scientific Translations, Jerusalem, 194 p.

Barazangi, M., 1983. Selected bibliography of the Arab region and surrounding areas. In: K. Cidlinsky and B. M. Rouhban (eds.), Assessment and mitigation of earthquake risk in the Arab region, Volume prepared by UNESCO for the Arab Fund for Economic and Social Development and Islamic Development Bank, UNESCO, p. 59-77.

Bartov, Y., and Arad, V., 1987. Makhtesh Ramon: Bibliography of Geological Research. Isr. Geol. Surv. Rep. GSI/34/87, November 1987, Jerusalem, 37 p., 410 refs.

Bartov, Y., and Arad, V., 1988. Carmel and Carmel Coast; Bibliography of Geological Research. Isr. Geol. Surv. Rep. GSI/8/88, March 1988, Jerusalem, 52 p., 584 refs.

Bartov, Y., Arad, V., and Arad, A., 1992. The Geology of Jordan; Bibliography.2nd Updated Edition. Isr. Geol. Surv. Rep. GSI/12/92, June 1992, Jerusalem, 182 p., 2086 refs.

Bartov, Y., and Arad, V., 1989. Arava and Elat Region; Bibliography of Geological Research. Isr. Geol. Surv. Israel, Rep. GSI/15/89, February 1989, Jerusalem, 92 p., 1118 refs.

Bartov, Y., and Arad, V., 1991. Southern Coastal Plain; Bibliography of Geological

Research. Isr. Geol. Surv. Rep. GSI/33/91, November 1991, Jerusalem, 160 p., 1887 refs.

Bartov, Y., and Arad, V., 1992. Judean Desert; Bibliography of Geological Research. Isr. Geol. Surv. Rep. GSI/11/92, April 1992, Jerusalem, 68 p., 747 refs.

Bartov, Y., Arad, V., and Z. Kukal, 1992. The Geology of Kuwait; Bibliography. Isr. Geol. Surv. Rep. GSI/25/92, December 1992, Jerusalem, 67 p., 733 refs.

Begin, Z. B., and Arieh, V., 1983. Bibliography of geological contributions relevant to the siting of nuclear power plants in the NW Negev and southern Shephela, Israel. Preliminary Environmental Geology Division Report, 433 references with keywords, 63 p.

Bellan-Santini, D., et al., 1985. [Benthos of the Mediterranean Sea. Reports of the International Commission for the Scientific Exploration of the Mediterranean Sea.] Rapp. Proc. Verb. Reun. Commn. Int. Explor. Scient. Met Medit., 29(5), p. 9-361. 81 papers (French and English). Includes two bibliographies, one covering the Red Sea.

Closs, H., and Glashoff, H., 1975. Documentation of earth-scientific literature for the Mediterranean area, 1973-1974. Rapp. Comm. int. Mer Medit., 23(46), 350 p.

Closs, H., Burollet, p. F., and Glashoff, H., (eds.), 1973. Documentation of earth-scientific literature for the Mediterranean area, 1969-1972. Rapp. Comm. int. Mer Medit., 22(2a), 215 p.

Glashoff, H. (Editor), 1977. Documentation of earth-scientific literature for the Mediterranean area. 1975-1976. Rapp. Comm. int. Mer Medit., 24(76), 525 p.

Glenn, C. R., and Denman, J. M., 1980. Geologic literature on Egypt, 1933 to 1978. U. S. Geol. Surv. Open-file Rept. 89-930, 221 p.

Inbar, M., Bartov, Y., and Arad, V., 1989. Hula Valley and Korazim Region; Bibliography of Geological Research. Isr. Geol. Surv. Rep. GSI/40/89, July 1989, Jerusalem, 66 p., 761 refs.

Keldani, E. H., 1941, A bibliography of geology and related sciences concerning Egypt up to the end of 1939, Geol. Surv., Cairo.

Kerambrun, p. (coordinator), et al., 1986. Coastal lagoons along the southern Mediterranean coast. (Algeria, Egypt, Libya, Morocco, Tunisia) description and bibliography. UNESCO Repts. Mar. Sci., 34, 184 p.

Krasheninnikov, V. A., 1971. Stratigraphy of the Miocene deposits of the Mediterranean on the base of Foraminifera. Trans. of the Geol. Inst., Acad. Sci., USSR, v. 220, Nauka, Moscow, 230 p. Contains bibliography of Mediterranean Neogene with 353 references.

Masson, p., 1919. Element d'une Bibliographie Française de la Syrie, (Geographie). Typ. Barlatier, Marseille, 528 p.

Mediterranean Basin Program, 1993. Nile delta project database listings. Washington, D.C., U.S. National Museum of Natural History Records, 547 p.

Nowak, J., and G. Niedermeier, 1981. Documentation of earth-scientific literature for the Mediterranean area, 1977-1978. Rapp. Comm. int. Met Medit., 27(8bis), 725 p.

Patai, R., 1957. Jordan, Lebanon and Syria: An annotated bibliography. Hraf Press, New Haven, CT, 289 p.

Said, R., Mikhail, M. F., Mansour, A. O., and Elias, A. N., 1975. Bibliography of geology and related sciences concerning Egypt for the period 1965-1973. Geol. Surv. Egypt and Mining Authority, Cairo,, UAR Ministry of Industry and Mineral Wealth, 192 p.

Tharp, M., 1980. Bibliography of the Mediterranean Region. Off-line search list of 2,908 citations generated by ORBIT IV, S.D.C.'s international search service on GEOREF, September 15, 1980, 3 Xeroxed listing notebooks, 1057 p.

UNEP/FAO/Unesco/WHO/WMQ/IOC/IAEA, 1981. Selected bibliography on the pollution of the Mediterranean Sea. UNEF Reaional Seas Directories and Bibliographies. Geneva, UNEP, 130 p. (out of print).

UNEP/FAO, 1985. Bibliography of the marine environment in Mediterranean, 1978-1984. UNEP Regional Seas Directories and Bibliographies. 2nd ed. Rome, FAO, 151 p.

U. S. Department of Commerce, 1991. Meteorology and Oceanography of the Middle East. NOAA-NESDIS-NODC, March 1991. 494 refs and data distribution plots.

Weiner, D., Bartov, Y., and Arad, V., 1989. Northern Negev; Bibliography of Geological Research. Isr. Geol. Surv. Rep. GSI/36/89, July 1989, Jerusalem, 115 p., 1430 refs.

Weiner, D., Bartov, Y., and Arad, V., 1990. Beer-Sheva Valley and Western Foothills; Bibliography of Geological Research. Isr. Geol. Surv. Rep. GSI/10/90, April 1990, Jerusalem, 72 p., 776 refs.

Wolfart, R., 1967. Geologie von Syrien und dem Libanon. Gebrueder Borntraeger, Berlin, 326 p., maps.

NEW BIBLIOGRAPHIES SINCE 1994

Abu Jassar, W., Abu Azzam, H., Rosenfeld, A., Honigstein, A., Bartov, Y., Arad, V., 1999. Paleontology in Israel and Jordan; Bibliography. Jordan, Nat. Resour. Authority & Isr. Geol. Surv., Rep. GSI/7/99, 258 p.

Arad, V., 1994. Current Bibliography of Middle East Geology. Afr. Geosci. Rev., Vol. 1, No. 4, p. 579-592.

Arad, V., 1995. Current Bibliography of Middle East Geology. Afr. Geosci. Rev., Vol. 2, No. 1, p. 179-188.

Arad, V., 1995. Current Bibliography of Middle East Geology. Afr. Geosci. Rev., Vol. 2, No. 2, p. 311-321.

Arad, V., 1995. Current Bibliography of Middle East Geology. Afr. Geosci. Rev., Vol. 2, No. 3-4, p. 615-626.

Arad, V., 1995. Current Bibliography of Middle East Geology. Afr. Geosci. Rev., Vol. 2, No. 3-4, p. 627-639.

Arad, V., 1996. Current Bibliography of Middle East Geology. Afr. Geosci. Rev., Vol. 3, No. 2, p. 343-354.

Arad, V., 1996. Current Bibliography of Middle East Geology. Afr. Geosci. Rev., Vol. 3, No. 3-4, p. 537-549.

Arad, V., 1996. Current Bibliography of Middle East Geology. Afr. Geosci. Rev., Vol. 3, No. 1, p. 83-96.

Arad, V., 1996. Current Bibliography of Middle East Geology. Afr. Geosci. Rev., Vol. 3, No. 3-4, p. 525-535.

Arad, V., 1997. Current Bibliography of Middle East Geology. Afr. Geosci. Rev., Vol. 4, No. 1, p. 139-151.

Arad, V., 1997. Current Bibliography of Middle East Geology. Afr. Geosci. Rev., Vol. 4, No. 2, p. 285-296.

Arad, V., 1997. Current Bibliography of Middle East Geology. Afr. Geosci. Rev., Vol. 4, No. 3-4, p. 417-430.

Arad, V., 1997. Current Bibliography of Middle East Geology. Afr. Geosci. Rev., Vol. 4, No. 3-4, p. 525-536.

Arad, V., 1998. Current Bibliography of Middle East Geology. Afr. Geosci. Rev., Vol. 5, No. 1-2, p. 219-232.

Arad, V., 1998. The Documentation Center of the Geological Survey - Migration of the software. Isr. Geol. Surv., Rep. TR-GS1/15/98, 2 p. (In Hebrew).

Arad, V., 1998. Current Bibliography of Middle East Geology. Afr. Geosci. Rev., Vol. 5, No. 4, p. 575-587.

Arad, V., 1999. Current Bibliography of Middle East Geology. Afr. Geosci. Rev., Vol. 6, No. 1-2, p. 105-120.

Arad, V., 1999. Current Bibliography of Middle East Geology. Afr. Geosci. Rev., Vol. 6, No. 1-2, p. 197-211.

Arad, V., 1999. Current Bibliography of Middle East Geology. Afr. Geosci. Rev., Vol. 6, No. 4, p. 397-409.

Arad, V., 1999. Current Bibliography of Middle East Geology. Afr. Geosci. Rev., Vol. 6, No. 3, p. 301-314.

Arad, V., 2000. Current Bibliography of Middle East Geology. Afr. Geosci. Rev., Vol. 7, No. 1, p. 101-113.

Arad, V., and Bartov, Y., 1994. Arava Region - Israel and Jordan; Bibliography of Geological Research. Isr. Geol. Surv., Rep. GSI/15/94, 86 p.

Arad, V., and Bartov, Y., 1996. Oil and Gas Wells Drilled in Israel, 1953-1995; Bibliography. Isr. Geol. Surv., Rep. GSI/23/96 & Minist. of National Infrastructures, Oil & Gas Unit, Rep. OG/3/96, 274 p.

Arad, V., and Bartov, Y., 1996. Samaria (Shomeron) Area - Geology and Water Resources; Bibliography. Isr. Geol. Surv., Rep. GSI/4/96, 54 p.

Arad, V., and Bartov, Y., 1998. Northern Negev and Judean Desert: Geological and Related Subjects; Bibliography. Isr. Geol. Surv., Rep. GSI/13/98, 144 p.

Arad, V., and Bartov, Y., 2001. Middle East Database: List of Keywords. Isr. Geol. Syrv., Rep. TR-GSI/1/2001, 227 p., Figs.

Arad, V., Bartov, Y., and Colodner, Z., 1995. Greater Jerusalem; Bibliography of Geological Research. Isr. Geol. Surv., Rep. GSI/36/95, 47 p.

Arad, V., Bartov, Y., and Colodner, Z., 1996. Judean Mountains: Geology and Water Resources; Bibliography. Isr. Geol. Surv., Rep. GSI/31/96, 112 p.

Arad, V., Bartov, Y., and Hambright, K.D., 1998. Lake Kinneret Research; Bibliography. Isr. Geol. Surv., Rep. GSI/20/98 & Isr. Oceanogr. Limnol. Res., 154 p.

Arad, V., Bartov, Y., and Horowitz, A., 1997. The Lower Jordan Valley (Lake Kinneret - Dead Sea) - Geology and Water Resources; Bibliography. Isr. Geol. Surv., Rep. GSI/8/97, 121 p.

Arad, V., Bartov, Y., and Weiler, Y., 1998. Seismicity and Earthquakes in Israel; Bibliography. Isr. Geol. Surv., Rep. GSI/16/98, 94 p.

Arad, V., Beyth, M., Bartov, Y., and Gavrieli, I., 1998. The Dead Sea and Its Surroundings: Geological and Limnological Research; Bibliography. 2nd Ed. Isr. Geol. Surv., Rep. GSI/2/98, 277 p.

Bartov, Y., Sneh, A., Fleischer, L., Arad, V., and Rosensaft, M., 2000. Map and Catalogue of Young Faults in Israel. (In Hebrew). Isr. Geol. Surv., Rep. GSI/23/2000, 6 p., Appen., Map.

Bartov, Y., Sneh, A., Fleischer, L., Arad, V., and Rosensaft, M., 2002. Potentially Active Faults in Israel; Stage B. (In Hebrew; Appen. in Engl.). Isr.Geol. Surv., Rep. GSI/29/2002, 8 p., Appen., Maps.

Battikhi, A., 1995. Abstracts of M.A. Theses, First Semester 94-95. Amman, Univ. of Jordan, 305 p.

Cornell University and Syrian Petroleum Company (SPC) Syria Project, 1996. Hosted at http://www.geo.cornell.edu/me_na/report/bibliography.html. Has about 750 references, primarily in geophysics.

Hall, J. K., 1994. Eastern Mediterranean Regional Bibliography: Geology, Geophysics, Oceanology, and Related Subjects. In: V. A. Krasheninnikov and J. K. Hall, (eds.), Geological Structure of The North Eastern Mediterranean (Cruise 5 of The Research Vessel Akademik Nikolaj Strakhov), Historical Production-Hall Ltd., Jerusalem, p. 307-394.

Holubeshen, M., and Amery, H. A., 1995. Annotated Bibliography of Water in the Middle East. Toronto Univ., Centre for Int. Stud., 129 p.

Inbar, M., Bartov, Y., and Arad, V., 1994. Yizreel and Harod Valleys; Bibliography of Geological Research. Isr. Geol. Surv., Rep. GSI/20/94, 49 p.

Ingrosso, P., Abu Jabal, M., and Oddo, B., 1997. Groundwater in Israel, Palestine and Sinai; Selected Bibliography (1985-1996). Gaza City, Water Res. Cent., Al Azhar Univ., & Ciss, Italy, 192 p.

Israel Geological Survey, 1997. Israel: Mediterranean Shore & Offshore Bibliography. Isr. Geol. Surv., Rep., 125 p. (Published also in the Dutch-Israeli Steering Committee Tech. Rep., Phase I, Vol. III).

Israel Geological Survey, 1997. Kurkar & Kurkar Group, Coastal Plain and Offshore Israel; Bibliography. Isr. Geol. Surv., Rep., 41 p. (Published also in the Dutch - Israeli Steering Committee Tech. Rep., Phase I, Vol. III).

Israel Geological Survey, 1997. Mediterranean - Israel Offshore Oil Wells: Bibliography. Isr. Geol. Surv., Rep., 12 p.

Manser, W., and Batchelor, D.A.F., 1995. Earth Sciences Data Sources, Sultanate of Oman; An Annotated Bibliography and Indices of The Geology, Geophysics, and Mineral Resources (Including Petroleum and Water) of The Sultanate of Oman. Muscat, Sultanate of Oman, Minist. of Petroleum & Minerals, Dir. Gen. of Minerals, 417 p.

Ortal, R., and Nemtzov, S. C., 1997. Israeli National Report on Nature Conservation and the Coral Reef Ecosystem in the Israeli Part of the Gulf of Aqaba. Report of the Middle East Seas Regional Strategy Workshop, Aqaba, Sept. 1997, 56 p.

Otto, I., Schmidt- and Dumont, M., 1995. Die Wasserfrage im Nahen und Mittleren Osten: Literatur Seit 1985; Eineauswahlbibliographie. Hamburg, Deutsche Ubersee Inst., Ubersee Dokumentation, Referat Vorderer Orient, 162 p.

Qummou, S., Abu Jassar, W., Arad, V., and Bartov, Y., 1997. Bibliography of Middle East Geology. Part 1: Jordan. Jordan, Nat. Resour. Authority & Isr. Geol. Surv., Rep. GSI/27/97, 315 p.

Romi, R., 1998. Arab Shipping & Ports - Bibliography. Haifa Univ., Wydra Inst. of Shipping & Aviation Res., Info. Center, 41 p.

Stanley, D. J., Schepis, K., Arad, V., and Bartov, Y., 1997. Aswan High Dam: Geological and Environmental Research; Bibliography. Isr. Geol. Surv., Rep. GSI/21/97 & Natl. Mus. Nat. Hist., Smithsonian Inst., 65 p.

Zaripov, O., 2000. Current Bibliography of Middle East Geology. Afr. Geosci. Rev., Vol. 7, No. 4, p. 401-413.

Zaripov, O., 2001. Current Bibliography of Middle East Geology. Afr. Geosci. Rev., Vol. 8, No. 1-2, p. 257-269.

Zaripov, O., 2001. Current Bibliography of Middle East Geology. Afr. Geosci. Rev., Vol. 8, No. 4, p. 437-450.

Zaripov, O., 2001. Current Bibliography of Middle East Geology. Afr. Geosci. Rev., Vol. 8, No. 3, p. 351-364.

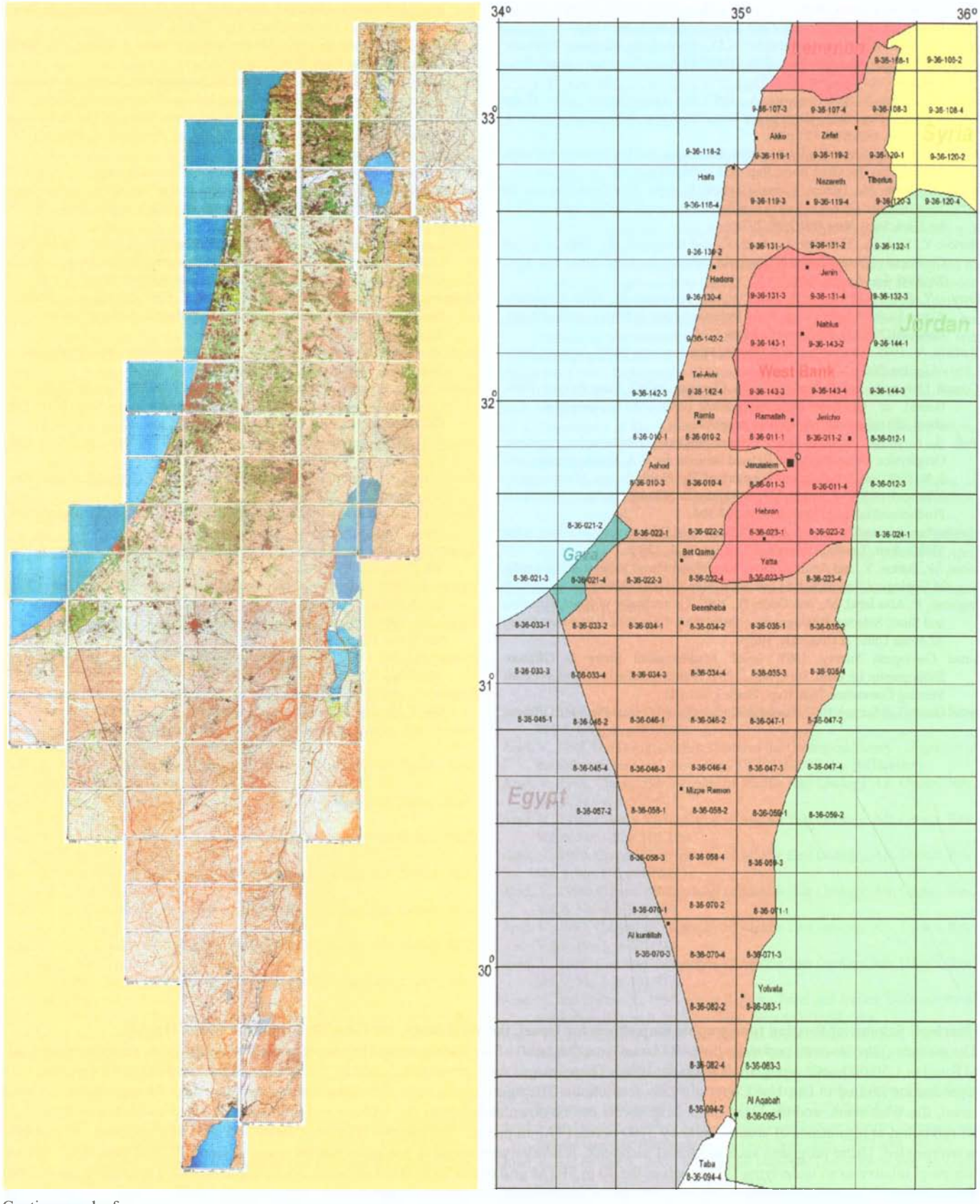
Zaripov, O., 2002. Current Bibliography of Middle East Geology. Afr. Geosci. Rev., Vol. 9, No. 1-2, p. 93-105.

Zaripov, O., 2002. Current Bibliography of Middle East Geology. Afr. Geosci. Rev., Vol. 9, No. 1-2, p. 183-197.

Zaripov, O., 2002. Current Bibliography of Middle East Geology. Afr. Geosci. Rev., Vol. 9, No. 3, p. 265-278.

Zaripov, O., 2002. Current Bibliography of Middle East Geology. Afr. Geosci. Rev., Vol. 9, No. 4, p. 433-447.

Overleaf: Scheme of Russian topographic map sheets for Israel, the West Bank, the Gaza Strip and the Golan Heights.
The website (http://www.lib.berkeley.edu/EART/israel/israel50k.html) of the library at the University of California Berkeley provides downloads of Russian 1:50,000 scale topographic maps for Israel. These images are copyrighted ©2003 by the Regents of the University of California, with reproduction limited to Fair Use Copyright Law restrictions. The figure on the right shows the naming scheme of the 99 map sheets covering Israel, the West Bank, and the Gaza Strip. Map sheets can be downloaded from this website and are available either as JPEGs or Tiffs in 24 bit rgb color, at resolutions of around 2600 by 3700 pixels (~7.5 m pixels). The contour interval is 10 m, and a UTM grid (Zone 36) graticule is overprinted. Using programs such as Global Mapper®, it is relatively trivial to geo-reference the maps to GeoTiffs, and then to do 'texture mapping' relative to an underlying DTM such as the 90 m SRTM grid or the 25 m DTM of Israel. An example of such a procedure can be seen in the figure on page vi of Volume I. The left side of the figure shows the result of making all the maps into GeoTiffs and then joining them in Global Mapper®.



Caption overleaf.

Appendix B

The NES Akademik Nikolaj Strakhov and its Eastern Mediterranean Multi-Beam Swath Sounding Data on CD-ROM

John K. Hall

Geological Survey of Israel, Marine Geology, Mapping & Tectonics Division, 30 Malchei Israel Street, Jerusalem 95 501, Israel

INTRODUCTION

This Appendix describes the multibeam sounding data obtained during Cruises 5 and 10 of the Academik Nikolaj Strakhov in the eastern Mediterranean Sea. This data is available on CD-ROM from the author, or from the Documentation Center of the Geological Survey of Israel, (+972-2-531-4266). The text below is taken with minor changes and additions from an Appendix to Chapter 1 (Hall, Udintsev and Odinokov, 1994) of our last book on the Geological Structure of the North-Eastern Mediterranean (Cruise 5 of the Research Vessel 'Akademik Nikolaj Strakhov').

The author expresses his deep gratitude to Academician Andrei L. Knipper for his decision in 1987 to make the digital multibeam sounding data from Cruise 5 available to the international community. This decision initiated the close collaboration which has resulted in publication of this book. The material below is included for the benefit of readers who are interested in the physical plant of the R/V Akademik Nikolaj Strakhov, and the structure and format of the data from the Strakhov's Hollming EKHOS II Narrow Beam/Multibeam Echosounder system.

Finally this section describes the specific data from Cruises 5 and 10, and the steps that were undertaken to make it available for use in this book and in the future.

THE R/V AKADEMIK NIKOLAJ STRAKHOV

Details on the Strakhov and its sister-ships are given in a 12 page color descriptive brochure in Russian and English (Hollming, 1984) which is abstracted in greater detail below.

The three ships in the series were built in Finland for the USSR Academy of Sciences by the Hollming Ltd. Shipyard (Yard Nos. 0251- 0253) on the order of V/O Sudoimport. The Strakhov's sister ships are the 'Akademik Boris Petrov' and the 'Akademik M. A. Lavrentyev'. The Strakhov was launched in Finland in February 1984.

The ships have a deadweight and gross displacement of 860 and 2600 tons respectively. The length over all is 75.5 m (248'), beam of 14.7 m (48'), and design draft of 4.5 m (15'). The maximum speed at design draft is 15.2 kt. The reported cost of each of the ships was $34 million, paid for in barter of timber.

The vessels are designed and built for sampling, analyzing and measuring of the atmosphere, sea water and sea bottom.

The Ocean Systems Department of the Shipyard has developed and assembled the integration of the research equipment. This integrated scientific system consists of computers, measuring and analyzing equipment and the system software.

The ships have been designed and built in conformity with the class requirements for unrestricted service of the USSR Register of Shipping to have a class notation: KM⊛L_1⊡A_2 (research vessel).

During construction special attention was paid to vibration and noise reduction and to designing the hull for good sea-keeping characteristics.

The design of the ships was done together by the shipyard's Design Department and Ocean Systems Department in co-operation with several USSR organizations, *e.g.* the Department of the Marine Expedition.

Workers and Institutes of the Academy of Sciences of the USSR, Leningrad Central Design Bureau and Inspectorates of the USSR Register of Shipping, collaborated in order to agree upon the plans of the project.

The hull of the vessel was assembled on the building berth from sections which had been fitted with piping, the foundations of machinery, cable layers, windows, etc. prior to their lifting onto the berth. The majority of the systems onboard were prefabricated to modules which were lifted into the hull sections. The construction project was completed by an extensive testing and trial program.

In connection with this project Hollming Ltd. Ocean Systems Department has brought a new idea into the automation and integration of onboard research systems, called NETOS 625 which is an application of a special local area network (LAN) for ship-borne use.

The main components of the scientific system connected to the NETOS 625 are the main computers and the sub-system consisting of laboratory computers, the CAMAC-system., laboratory analyzers, echo sounders, navigation system, seismic system, automatic weather station and other measuring equipment.

The main computer centre is on the between-deck in the centre of the vessel which is minimally affected by the ships' movements on the seaway. The laboratory computers are located in each laboratory.

In addition to the standard system and utility software of the computers, the software of the scientific complex consists of networking software for the LAN, integrated scientific system software (including automatic data acquisition and archiving programs) and scientific program packages for measurement data post-processing.

Laboratories in the aft part of the main deck have a seismic data

acquisition system connected to the main computers.

The laboratory area on the forepart of the main deck includes two laboratories and a wet room, which are equipped mainly for hydrological purposes, *e.g.* a hydrosond with its water sampling bottles and CTD measuring unit and control unit, salinometer, ionanalyzer, CAMAC-system and repeater display for the deep-sea echo sounder.

The laboratory area on the wheelhouse deck is intended for navigation, echo sounding and weather observations.

The echo sounding equipment consists of a multi-beam echo sounder and a deep water narrow beam research echo sounder. The multi-beam sounder is a 15 beam Hollming EKHOS II system. In 2002 the NES Boris Petrov was upgraded to an Atlas DS-2 Hydrosweep system.

Weather observations are carried out by an automatic weather station connected to the LAN as well.

The sensors of the weather station are installed on the ship's masts and on a bow boom specially made for this purpose.

To comply with the standards set for the navigation of a research vessel, a NAVOS 625 integrated navigation system is installed using the onboard navigation equipment. The system continuously determines the vessel's position and automatically steers the vessel along the desired research lines. As a part of the integrated scientific system, the NAVOS 625 provides the navigational data as well as the control for some of the measurement systems, such as the seismic system.

Reliable research winches are essential to research vessels. In these vessels there are a total of seven hydraulic research winches, one of which has three drums.

On the main deck aft there is the biggest winch of the vessel: a 100 kN pull winch for 12 km of wire. This winch is designed to be used together with the A-frame, making use of the trawler stern of the vessel. The other winches vary from 8 kN to 24 kN pull and are also to be used with cables.

The radio station is built mainly of Soviet-made equipment having transceivers and receivers for both normal and emergency traffic, VHF radio telephones and a telex station.

The ship is powered by a medium speed diesel engine coupled through a reduction gear to a controllable pitch propeller (CPP) running in a steerable nozzle. Stable and good maneuverability is improved still further by a bow thruster.

The electrical power onboard is produced by three diesel generators and one shaft generator. A special 'no-break' system is provided to ensure a stable and continuous supply of power to the laboratory equipment and computers. An efficient monitoring and alarm system has been provided for all the machinery plant.

The navigation system is completed by ordinary ship navigational instruments: two radars, speed log, echo sounder, RDF and navigator, etc.

Each vessel accommodates 74 persons. Onboard the vessel there are a total of 42 cabins, consisting of 3 apartments, 13 single bed cabins (of which 6 are with additional 'Pullman-bed') and 26 twin bed cabins.

Two mess rooms are arranged to seat a total of 52 persons; the mess rooms can be separated or combined by means of a sliding wall. Also a conference room for 8 persons can be combined with the officers' mess. The galley is located just below the mess rooms and is close to the provision stores.

MULTIBEAM SOUNDING DATA FORMAT

In a shallow sea such as the Eastern Mediterranean the 15 beam Hollming EKHOS II system records a sweep of the seafloor topography at right angles to the direction of the ship at intervals of about 10 seconds. The geometry of the beam is such that the sweep width is nearly 80% of the water depth. The soundings go sequentially from left (port) to right (starboard). The records are processed by a DEC-PDP-like computer (of Hungarian origin) and are stored on ½″ magnetic tape as ASCII files, each with 1168 sounding sweeps. Each file is given a sequential number, of the form MBxxxx. The file size is 307852 bytes, and consists of a header and 1168 sweeps of 221 bytes each, with time, position, speed, course, and 15 depths and its corresponding offsets from the center of the ship. The original depths are all based upon an assumed sound velocity of 1500 m/sec. The position and course/speed data are from the ship's DR (deduced reckoning) navigational computer. These position data show jumps after acquisition of new fixes from the TRANSIT satellite navigation system, a process which occurs at varying intervals up to 10-12 times per day. The TRANSIT fixes take up to 20 minutes to acquire, and have absolute accuracies of 120-600 m depending upon the amount of maneuvering during the fix, and whether the equipment has dual receiving frequencies to remove the ionospheric refraction errors.

THE SCOPE OF THE DIGITAL DATA

The MB files for Cruise 5 were originally received on magnetic tape, and later were augmented (while the author participated on Cruise 11 in the Atlantic) by PC diskettes downloaded from the ship's computer along with the data from Cruise 10. During preparation of the book, an additional 16 files which were originally missing were found and added to the database.

For the purpose of reducing the size of these files, the headers were removed, along with certain unnecessary data in the message. These smaller renditions were called MBxxxx.DMB files, and they are each 205568 bytes in length. The Cruise 5 data are found on files MB0653-MB0841 and those of Cruise 10 on MB 1647-MB 1726.

CORRECTION OF THE DATASET

As noted above, the original data files have navigation that is not corrected for the set and drift of currents between fixes, or errors in the deduced reckoning (DR) track, as well as other errors. In addition, they have all kinds of errors in acquisition of sounding information. Before they can be used for detailed compilations, it was necessary to find and correct or remove these errors. The correction of the navigation and sounding data proceeded as follows:

1) The first stage in correcting the data was to prepare a master file for each cruise which contained the times, positions, courses and speeds, and center beam depths. Initially it was assumed that it

would a simple process to work up the navigation and bathymetry. However, when the navigation from this master file was plotted as an overlay to the master track chart produced by the Head Department of Navigation and Oceanography (HDNO or GUNIO) for the Geological Institute, large differences of up to 5-10 km were noted. However, the HDNO chart was useful in that it showed portions of the track which were missing, as well as the details of some of the maneuvering at the ends of profiles. Luckily, from all this data, only 2 files are missing. These are:

File 712 (4.6.1987 - 18:08:45 to 21:52:00) is a repeat of File 702, and almost 4 hours of data are missing and presumed lost.

File 762 (from sometime between 1030 on 21.6.1987 and 1630 on 28.6.1987) should contain about 3.5 hours of data.

2) To provide a basis for checking the digital data, the HDNO track chart was digitized at all annotated times and also during unannotated maneuvers, with times being interpolated afterwards assuming a constant speed along the track. Crossover checks at the 219 crossing points showed significant errors in the corresponding depths.

3) The Cruise 5 and 10 master files of time, navigation, and center beam data, corrected for the variation of sound velocity in the Eastern Mediterranean (Carter, 1980), were then checked for time continuity. The end of File 668, all of 669, and the beginning of 670 were 'frozen' in time, navigation, and course/speed. Depths were okay. This portion was several hours between profiles on the south coast of Cyprus. This group of 2791 depths were given artificial times every 10-11 seconds, and assigned navigation, courses, and speeds using interpolated positions from the HDNO chart.

4) A total of twenty-six places where time went backward were found and corrected. Most were from jumps in the Julian day number, beginning at about 0030 and lasting until 0130; others were repeats of blocks of 1 to about 15 fixes. In File 0653 a group of 54 fixes which were off by some 17h 50m were corrected. A total of 7981 repeated times were found, most of them occurring singly; times were reassigned by interpolation.

5) The navigation was found to have a number of logging errors. A few records had 9999s in the coordinates, course, and speed, and usually followed repeats of the apparently authentic fixes, courses and speeds, as if the system was stuck. These were smoothly interpolated. Once the file had been corrected so that there were no time backtracks or repeats, it was broken up into a number of continuous data blocks with no breaks in time. In block 7 some 20 fixes were found where the degrees and minutes figure of 3359 appeared as 3399 before or after passing through 3400 degrees. These were manually corrected.

6) Following all these manipulations, the data were corrected for jumps occurring after the acquisition of a new TRANSIT satellite navigation fix. Several programs were written which could plot out up to 4000 fixes, showing the hours in different colors, and indicating where the instantaneous speeds exceeded the maximum speed of the vessel. In some programs it was also possible to interactively investigate the time behavior of the latitude and longitude, and to locate specific fixes exhibiting strange behavior. After it was found that sudden speeds of 20 kts or more were indicative of fix updates, an automatic program was written to correct all the fixes by applying a linear correction with time, as if all the navigational error was a result of currents with constant set and drift. These were then replotted, again interactively to allow checking of all changes, and stored in corrected block files. Within block 8, all the data for the detailed survey of 30 June - 2 July 1987 over the crest of Eratosthenes Seamount was found to have the strange jumps every 8th fix which Alexander Ioffe had once written me about. A detailed analysis of these jumps indicated that they were probably valid corrections of the navigation and that the other seven fixes needed to be corrected. The times of all the excursions related to fixes were digitized, a total of more than a hundred, and another interactive program was written to apply these corrections.

7) When all the continuous blocks had been corrected, a program was written to plot out the detailed navigation using Postscript language on a LaserJet 4 printer. The many DMB files were then rewritten as MBxxxx.DMC files with the corrected navigation, times, and speeds for future detailed analysis of the multibeam bathymetry. The ship's course in most cases was left untouched, for the reason that it gives the best estimate of the instantaneous azimuth of the beams.

8) The center beam sounding data was then plotted out on the LaserJet 4 as depth versus time with a separate Postscript file for each day. This clearly showed all erroneous soundings resulting from inability to track the bottom, side echoes, scattering layer, and other problems. Using these plots, the bad soundings were then cancelled by entering a negative sign before the latitude in the respective MBxxxx.DMC files. Far less than 1% of the sounding data were thus invalidated.

USE OF THE MULTIBEAM DATA

To date, the multibeam data have not been used with the corrected navigation to produce detailed bathymetric maps. During Cruise 11, the data were plotted out on a HP PaintJet color printer as overlays to the maps of Hall (1980, 1981). Hypsometric color schemes for 200 and 50 m depth intervals were used, with data from all beams being printed. These indicated that in general the data were good, but no further analysis was done. While multibeam data was used to produce the color maps of Eratosthenes Seamount in the 1994 book, no rigorous navigation corrections were then applied.

For Cruise 5, some 217,541 sounding sweeps and positions were recorded. For Cruise 10 there are an additional 92,418, giving a total of 309,959 for the two cruises. Taking into account that each sweep is 15 separate soundings, this gives a total of nearly 4.65 million soundings. Considering that since 1970 my MEDMAP project has succeeded in acquiring less than one million soundings from all sources, this is indeed a significant contribution to our understanding of the Eastern Mediterranean.

For the future, this dataset will be very useful for defining the detailed bathymetry in the survey area. The first expected use will probably be for the IBCM Project, which is planning to produce a Second Edition of the International Bathymetric Chart of the Mediterranean (IOC, 1981/1987) in the next few years, based upon a DTM to be compiled on a grid of 0.25 minute of arc (about 450

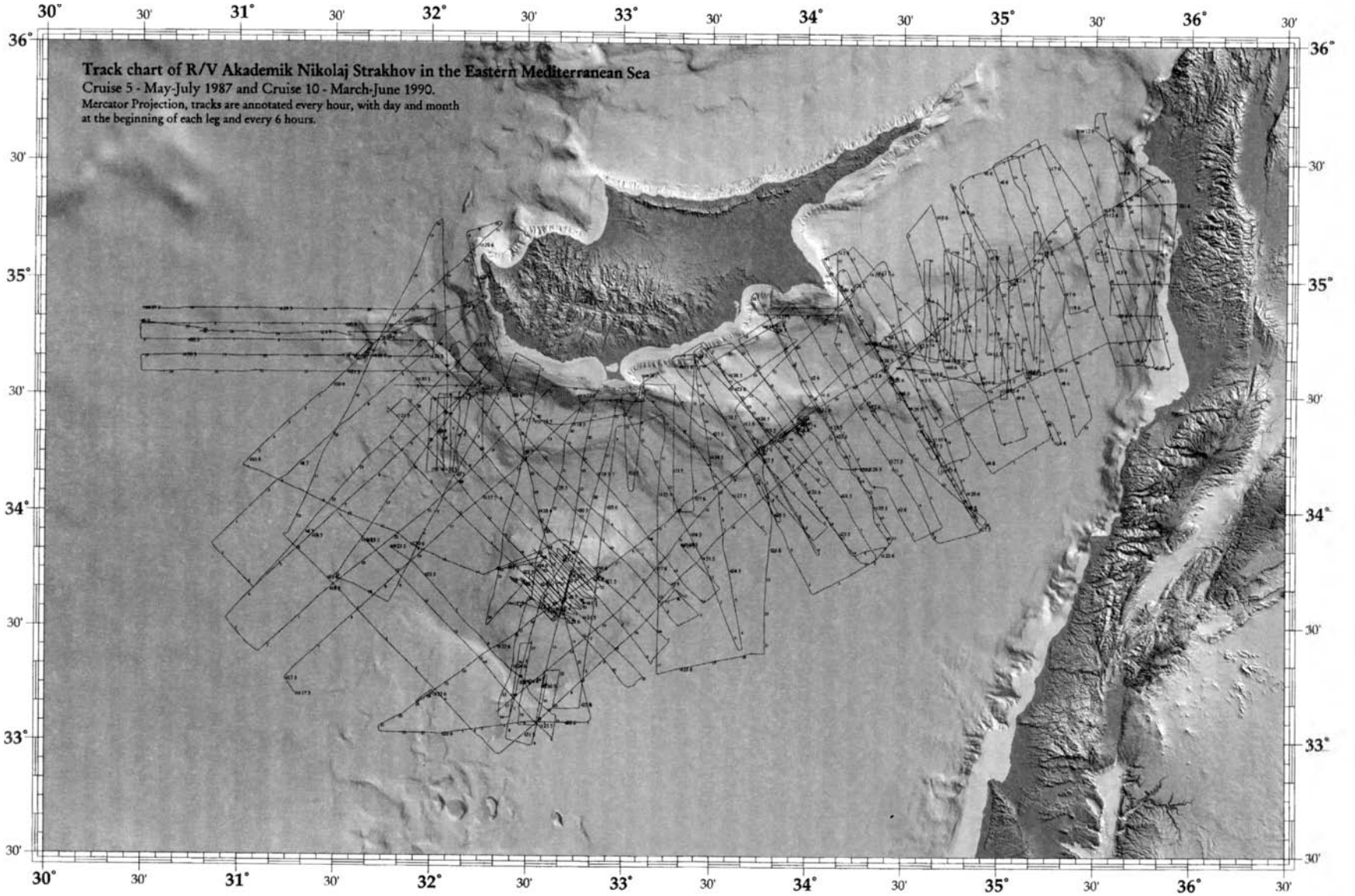


Figure AppB.1. Track chart of the R/V Akademik Nikolaj Strakhov in the Eastern Mediterranean Sea during Cruise 5, May-July 1987 and Cruise 10, March-June 1990. Mercator projection. The tracks are annotated every hour, with day and month at the beginning of each line and every 6 hours. Adapted from the frontispiece of Krashenninikov and Hall (1994). The background consists of bathymetry from the 2' ETOPO2 dataset, overlain by the 0.25' gridded bathymetry from the digitized Hall (1994) chart at 1:625,000, plus 50 m topography for Cyprus, together with the 50 m interpolation of the UKHO bathymetry around Cyprus (Chapter 15), and the 90 m SRTM data for Israel, Lebanon, and Syria.

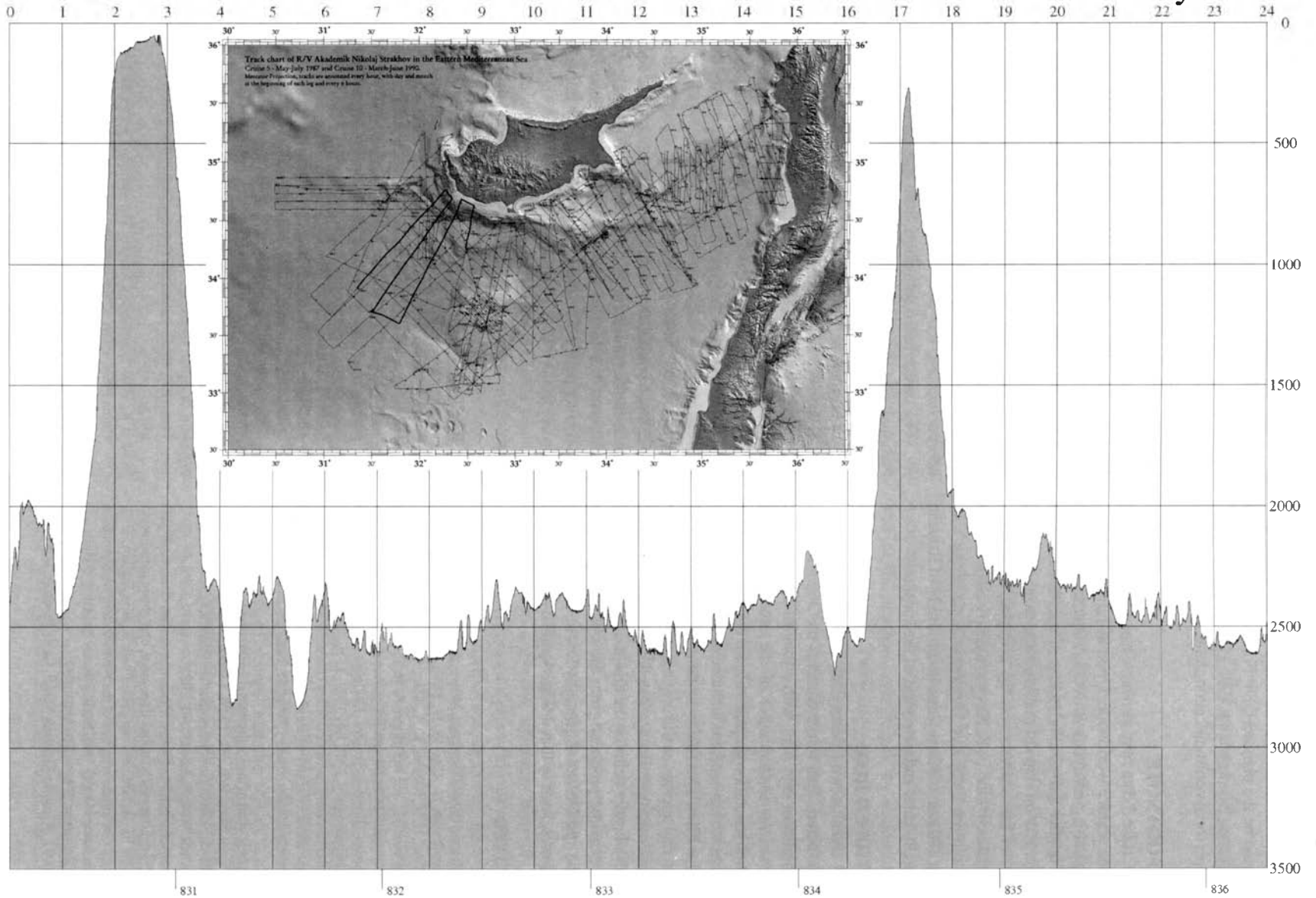


Figure AppB.2. Example of the daily Center Beam Profile for 3 July 1987. The horizontal axis is time, from 0000 to 2400 hours GMT, while the vertical axis is corrected depth in meters. Each of the 62 days surveyed during Strakhov Cruises 5 and 10 is stored as a JPEG (.jpg) and Encapsulated Postscript file on the CD-ROM. The numbers below the figure show the beginning times of the 268 DMC multibeam data files. The inset shows the location of the day's observations as a heavier line on the tracks to the southwest of Cyprus. The 50-100 m of topography in the deep waters offshore appears as a definite texture to the seafloor on the more recent French Prismed II multibeam survey.

m). The Second Edition is expected to be available as a shaded hypsometric map as well as a gridded data set. Another impetus to use of this data should be the planned ODP Phase One of Shallow Drilling on Eratosthenes Seamount in 1995 (Camerlenghi et al., 1992; D. Kempler, personal communication, January 1994).

A HISTORICAL FOOTNOTE

The Strakhov Cruise 5 data may also have had a very fortunate side effect for marine science worldwide. Upon its release in 1987, the data was analyzed by scientists at NOAA in the USA who determined that its quality was similar to that of data collected by the multibeam equipment on ships of the American academic fleet. One apparent result of this analysis was the dropping (Anderson, 1989) of a 1985 initiative by the U. S. Navy to classify all American multibeam data within the Exclusive Economic Zone of the U.S. (the band extending 200 nmi offshore), due to the ability of Russian research ships to legally enter and map most of these waters.

CONTENTS OF THE CD-ROM

The CD-ROM contains two folders. These are:

1) **MB-Files Corrected**. This folder contains the 268 MBxxxx. DMC corrected multibeam data files, with a total of 52.5 Mbytes. A track map overlaid on shaded relief of the area is given in **Fig. AppB.1**. The high resolution graphics file for this figure and for the track map without background are included on the CD-ROM.

2) **Daily Postscript Files**. This folder contains 186 files for the 62 days of survey. Each day appears as the original FORTRAN written Postscript file (.ps extension), its Encapsulated Postscript equivalent (.eps extension) with a header defining the title and the plot size, and a JPEG file (.jpg extension) produced from the .eps file by Adobe Photoshop® 5.5. The .jpg files are at generally low resolution. Much higher resolution figures, such as that in **Fig. AppB.2** may be made with conversion programs such as GSview v. 4.6 from Ghostgum Software Pty Ltd. in Australia. This folder occupies 22.1 Mbytes. Altogether the CD-ROM has about 83.9 Mbytes.

NOTES ADDED IN 2004

Great changes have occurred since Cruises 5 and 10 of the NES Akademik Nikolaj Strakhov and the publication in 1994 of our first volume, the Geological Structure of the North-Eastern Mediterranean (Cruise 5 of the Research Vessel 'Akademik Nikolaj Strakhov').

A transect was indeed drilled across Eratosthenes Seamount by the JOIDES Resolution during ODP Leg 160. The results were summarized in the book by Robertson, Emeis, Richter and Camerlenghi (1998). The transect comprised Holes 965, 966, 967, and 968. All the drilling results are available at http://www-odp.tamu.edu/publications/160_SR/TOC_PPG.HTM.

The center beam soundings from this survey were sent to the National Geophysical Data Center in Boulder CO, USA. These soundings, later supplemented by all 15 of the beams, were used by Robert Sarmast to 'pinpoint' the location of Atlantis with the help of 3-D visualizations produced by Patrick H. Lowry of the Scotia Group, an oil and gas services firm in Dallas, TX. According to Sarmast's analysis, Atlantis should be found at a depth of some 1500 m in the vicinity of 35°N, 35°E. As the book was going to press Mr. Sarmast had concluded a more detailed survey of the area with sidescan sonar.

The 0.25' IBCM-II compilation quickly evolved into a 0.1' effort, made possible by the steady progression of far more detailed French multibeam surveys with the N/O L'Atalante and N/O Le Suroît, and the release of the 0.05' Shuttle Radar Topographic Mission topography acquired by the Endeavour during STS-99 in February 2000.

REFERENCES CITED

Anderson, Alun, 1989. Release of sea-floor maps. Nature, 338, p. 448.

Camerlenghi, A., Chamot-Rooke, N., Cita, M. B., Della Vedova, B., Kempler, D., Hieke, W., Hirschleber, H. B., Kastens, K. A., Mart, Y., McCoy, F. W., Mirabile, L., Polonia, A., Rebesco M., and Robertson, A. H. F., 1992. Time progressive continental collision: the Mediterranean Ridge Accretionary Complex in the Eastern Mediterranean (Phase-1 Shallow Drilling). ODP Drilling Proposal (new version former proposal N. 330), July 1992, 31 p.

Carter, D. J. T., 1980. Echo-sounding correction tables (formerly Matthews' Tables). Hydrographic Department, Ministry of Defence, Taunton, Publ. NP-139, 3rd Edition, 150 p. Eastern Mediterranean - Table 45, Northern Red Sea - Table 75.

Hall, J. K., 1980. Bathymetric chart of the southeastern Mediterranean Sea, 1:625,000 scale at 46°N. Isr. Geol. Surv., Rep. MG/13/80, 1 sheet.

Hall, J. K., 1981. Bathymetric chart of the northeastern Mediterranean Sea, 1:625,000 scale at 46°N. Isr. Geol. Surv., Rep. MG/2/81, 1981.

Hall, J. K., 1994. Bathymetric Chart of the Eastern Mediterranean Sea. Scale 1:625,000 at Latitude 46°N, 50 m corrected contours, three color, blue shade hypsometric gradations every 200 m. Included in map packet with Krasheninnikov, V. A. and Hall, J. K. (eds.), Geological structure of the North-eastern Mediterranean (Cruise 5 of the Research Vessel 'Akademik Nikolaj Strakhov'), Historical Productions-Hall, Jerusalem, 396 + vii p, April 1994.

Hollming Ltd., 1984. 2600T Scientific Research Vessel. Color brochure in Russian and English, 12 p.

Hall, J. K., Udintsev, G. B., and Odinokov, Yu. Yu., 1994. The bottom relief of the Levantine Sea. In: V. A. Krasheninnikov and J. K. Hall (eds.), The Geological Structure of the North-Eastern Mediterranean (Cruise 5 of the 'Akademik Nikolaj Strakhov'), Historical Productions-Hall, Jerusalem, p. 5-31.

Intergovernmental Oceanographic Commission, 1981/1987. International Bathymetric Chart of the Mediterranean. Series established under the Cooperative Investigations in the Mediterranean (C.I.M.), Mercator projection. Scale 1:1,000,000 at 38°N latitude. 10 sheets with heights and depths in meters, published by the Head Department of Navigation and Oceanography, Ministry of Defence, Leningrad, USSR, under the authority of IOC (UNESCO), 1st Edition, June 1981. Single sheet at 1:5,000,000 scale published in 1987.

Krasheninnikov, V. A., and Hall, J. K., (Editors.), 1994. The Geological Structure of the North-Eastern Mediterranean (Cruise 5 of the Akademik Nikolaj Strakhov), Historical Productions-Hall, Jerusalem, 396+vii p.

Robertson, A. H. F., Emeis, K.-C., Richter, C., and Camerlenghi, A. (Eds.), 1998. Proc. ODP, Sci. Results, 160: College Station, TX (Ocean Drilling Program), 817 p.

Sarmast, R., 2003. Discovery of Atlantis: The Startling Case for the Island of Cyprus. Origin Press, 190 p. 67 illustrations.

Udintsev, G. B., Odinokov, Yu. Yu., and Golod, V. M., 1987. Multibeam echo sounding: experience and prospects for use in marine geomorphology. Oceanology, 27(3), p. 370-376.

Appendix C

Top Judea Group – Digital Structural Map of Israel

Lorian Fleischer and Rina Gafsou
Geophysical Institute of Israel, 6 Baal-Shem Tov Street, P.O. Box 182, Lod 71 100, Israel

PREFACE

New 1:200,000 and 1:500,000 structural maps of Israel on the Top Judea Group have been prepared by the Geophysical Institute of Israel (GII) as a project sponsored by the Earth Sciences Research Administration of the Israel Ministry of National Infrastructures. The structural maps are based on available outcrop data as well as selected seismic reflection interpretation maps calibrated by oil, structure hole, and water well data. They are also available at scales of 1:50,000 and 1:100,000 with a contour interval of 50 m. The digital data set is stored by GII and available for future updates and/or the next tectonic study.

The mapped area covers the country from the north to south: the Galilee, Emeq Yizre'el and Emeq Bet She'an, Har Carmel, Hasharon, the Shomeron, Coastal Plain, Hashefela, Har Yehuda, Judean Desert, and the northern, central, and southern Negev.

Detailed geological and geophysical mapping has been carried out in Israel for several decades. Publication of a digital version of the geological map, revised by the Geological Survey of Israel (GSI), has appeared as an elementary step in preserving the available data and also facilitating easy revision in the future. Tectonic data from areas previously mapped on the exposures and in the subsurface can be found, in general, as hard copy at various scales and as contour maps of different stratigraphic levels. The aim of the current project is to produce a single digital structural contour map to be used in conjunction with the existing geological maps of the same areas. The key horizon selected for this structural map is the boundary between the Senonian Mt. Scopus chalk and marl and the Turonian-Cenomanian Judea limestone and dolomite which is easily recognizable almost everywhere. The first, and preliminary, version of a 1:250,000 structural contour map on top Turonian was prepared by Bentor and Vroman (1954). This map was later enlarged and updated by Greenberg (Gilboa) (1959), by Marcus and Kaptzan (1978), and by Kashai and OE(I)L exploration staff (1988). Owing to their small scale, these maps could mostly be used only as a general tectonic framework.

In addition, detailed structural maps on the top Judea Group covering the northern and central Coastal Plain at 1:50,000 scale were prepared by Mimran et al. (1980a, b) based only on borehole data, and by Klang and Gvirtzman (1983, 1987) using seismic and well data. A preliminary structural map on Top Judea and Top Talme Yafe (1:100,000) of the southern Coastal Plain and Hashefela areas was prepared by Klang and Gvirtzman (1988). Preliminary hard copies were also prepared for the Arad-Be'er Sheva and the Yizre'el Valley-Bet She'an areas at 1:50,000 by Klang and Gvirtzman (1990a, b).

A regional seismic interpretation, part of a comprehensive basin analysis, was carried out during 1986-1989 by OE(I)L and the results were used in the Top Judea Group structural map (at 1: 100,000 scale) of Gelbermann and Grossowicz (1990). A revised and updated version of the Top Judea Group map, using 6,000 km of seismic data and 650 boreholes, was compiled by Fleischer et al. (1993) and later appeared in partially digitized form in Gelbermann (1995). A revised seismic interpretation was carried out in the northwestern Negev by Gelbermann and Fleischer (Druckman et al., 1994) using outcrops and oil and water wells. A new seismic interpretation was carried out in the western margin of the Arava Valley by Fleischer and Frieslander (Fleischer et al., 1996, 1997a, b), using outcrops and water well data, to prepare a structural map of the Top Judea Group. In the deeper part of the Arava-Dead Sea Graben, the Top Judea Group boundary is difficult to identify. In such areas, a Base Neogene fill map was presented in order to elucidate the tectonic pattern of the area (Fleischer and Gafsou, 1998a).

A major problem related to such a study arises from the fact that Late Cretaceous strata of the Judea and Mt. Scopus Groups were affected by erosion, especially in highly elevated structures. In such cases, a reconstruction of the Top Judea key level was carried out based on deeper structural mapped data, by adding the respective thickness intervals as known for the area. Such a reconstruction could cast some doubt on the general configuration of the restored structures. As well as in the Coastal Plain, the Judea Group rocks are deeply truncated by the Base Saqiye unconformity along some channels trending toward the present Mediterranean Sea. Successive parts of the Saqiye rocks were unconformably deposited on this composite erosional relief of channels and interfluves; therefore, the map in this area presents only an erosional relief at the boundary between the Judea and Saqiye Groups and will be treated accordingly.

The geological development of Israel is characterized by superposition of several tectonic phases (Garfunkel, 1988). In order to investigate the relationship between the present and older structures, detailed key maps are required. The structural map of Top Judea Group could be used as one of the most important key horizons for the next study of the tectonic development of Israel, and will be useful in the reassessment of the hydrocarbon or water potential of the area.

The sources of information on which the structural map is based comprise a large number of Geological Survey of Israel maps, published and unpublished, academic works (M.Sc. and Ph.D. theses), and oil company reports supplemented by seismic

reflection data interpreted by Oil Exploration (Investments) Ltd. and GII over the past ten years (for details see the annexed Top Judea Key Map and sources of information, also reproduced at reduced size in **Fig. AppC.1**).

BRIEF DISCUSSION

Israel is located in the western and northern margins of the Arabian Shield. The Israeli block is separated from the Jordan-Arabian Shield block by the major Dead Sea Transform fault system with a cumulative left-lateral movement of about 105 km (Freund et al., 1970). The structural features and fault pattern of the Israeli block are cratonic in character, as represented by a series of asymmetric, monoclinic structures, most typical in the northern Negev, Judea and Samaria, less pronounced in the Coastal Plain and Hasharon areas, and disappearing completely in the Galilee. This structural pattern could have been produced by a tilting of the Basement accompanied by advance warping of the Mesozoic strata over the deep-seated Basement faults (Ball and Ball, 1953). Later on this pattern was deformed by faulting and block rotation as a predominant effect of the Dead Sea Transform movement (Garfunkel, 1981; Ron and Eyal, 1985).

Tectonically, based on the present map of the Top Judea Group, the country can be divided into eight geological provinces:

1) The Galilee.
2) Qishon-Emeq Yizre'el-Bet She'an.
3) The Carmel and Umm El Fahm.
4) Judea and Samaria.
5) The southern Coastal Plain and northern Negev.
6) The central Negev.
7) The southern Negev.
8) The Dead Sea rift system.

1. THE GALILEE

The Galilee, as with the other regions of Israel, has also been affected by the Syrian Arc folding system, but the present structural pattern appears completely different. The Galilee has been intensively deformed by three sets of faults accompanied by some anticlockwise rotation of the faulted blocks, and some strike-slip displacement along their boundaries (Ron, 1984; Ron and Eyal, 1985). The principal fault set, trending E-W, has a considerable throw of several hundred meters displacing the pre-existing structure in a large number of horsts and grabens and/or tilted blocks as developed specifically in the western Galilee. Two additional sets of faults, such as a right-lateral set trending NE and a left-lateral conjugate trending NW, are superimposed on the previous E-W set. As a result of these deformation processes, a large anticlinorium trending N-S occurred in the central part of the Galilee highlands and another half-faulted anticline is present in the Naftali Mountains in front of the Hula Graben. These two structures are separated by the very symmetrical Alma Syncline.

In the southern Galilee, in front of the Emeq Yizre'el Graben, a half-faulted Devora-Nazareth anticline, trending NE-SW (Weiler, 1968), is the only Galilee structure with an axis orientation similar to the opposing Umm El Fahm or Carmel structures.

2. THE QISHON-EMEQ YIZRE'EL-BET-SHE'AN

These deep throws are developed north of the Carmel and Gilboa main border faults. The Carmel-Tirtza fault system is one of the most prominent tectonically active elements in Israel. Three distinct segments of the Carmel fault trend can be seen as follows:

i) in a NW-SE direction in front of the Qishon Graben,
ii) N-S in front of the Tivon Hills and
iii) NW-SE in front of the Yizre'el Valley (Achmon, 1986; Rotstein et al., 1993). A maximum throw of more than 2,000 m is observed in the area of the Qishon Graben (Gvirtzman et al., 1986), but diminishes to a few hundred meters on the eastern side of the Yizre'el Valley. Interpretation of high resolution seismic data (Rotstein et al., 1993) suggests left-lateral motion of a few hundred meters along the fault in the eastern segment and about 3-4 km offset in the western segment.

The Gilboa Fault cuts the northern margin of the highly uplifted Gilboa block and the plunge of the Fari'a anticline. The fault system forms a zigzag pattern of an *en-echelon* normal fault trending WNW-ESE. The maximum throw is about 750 m, while in some subordinate faults the throw decreases to 100 m (Hatzor and Reches, 1990).

The Qishon Graben is an asymmetric rift unit, dipping to the south, comprised of a series of south dipping, tilted blocks. This system of narrow elongated step blocks accumulates a down-thrown drop of about 2,000 m from the Afeq Horst, where the Top Judea datum is at sea level (Gvirtzman et al., 1986).

The Yizre'el Valley throw is separated from the Qishon Graben by the elevated area of the Tivon Hills. A dense and complicated fault pattern dissects the area into a large number of individual blocks which generally deepen toward the main border Carmel-Yagur Fault. A pronounced uplifted nose develops in a NE-SW direction in the Sarid-Megido area. This narrow, oblique alignment separates the Yizre'el throw from the Ta'anah-Jenin throw.

The Bet She'an throw, located north of the Gilboa Fault, gradually deepens toward the Jordan Valley and is probably transected by the Dead Sea Transform fault.

3. THE CARMEL AND UMM EL FAHM

These two anticlinal trends are separated by the deep asymmetrical syncline of the Ramot Menashe-Hadera area. The Carmel anticline is the most westerly located structure in the northern Coastal Plain. The subordinate structures of the Zikhron and Zinat anticlines trend in a NE-SW direction with an asymmetrical, steep flexure on their southeastern flank. The most elevated area of the Carmel structure, the 'Isfiya Horst' (Kashai, 1966b) is faulted in front of the Qishon Graben and Yizre'el Valley by the main border Carmel Fault with a throw of approximately 1,000 m (Achmon, 1986) and a possible component of strike-slip movement. A dense pattern of faults breaks the structure in a curved or diagonal trend in a mostly NW-SE direction, forming a series of step blocks downthrown to the east.

The Umm El Fahm anticline is situated between the Ramot

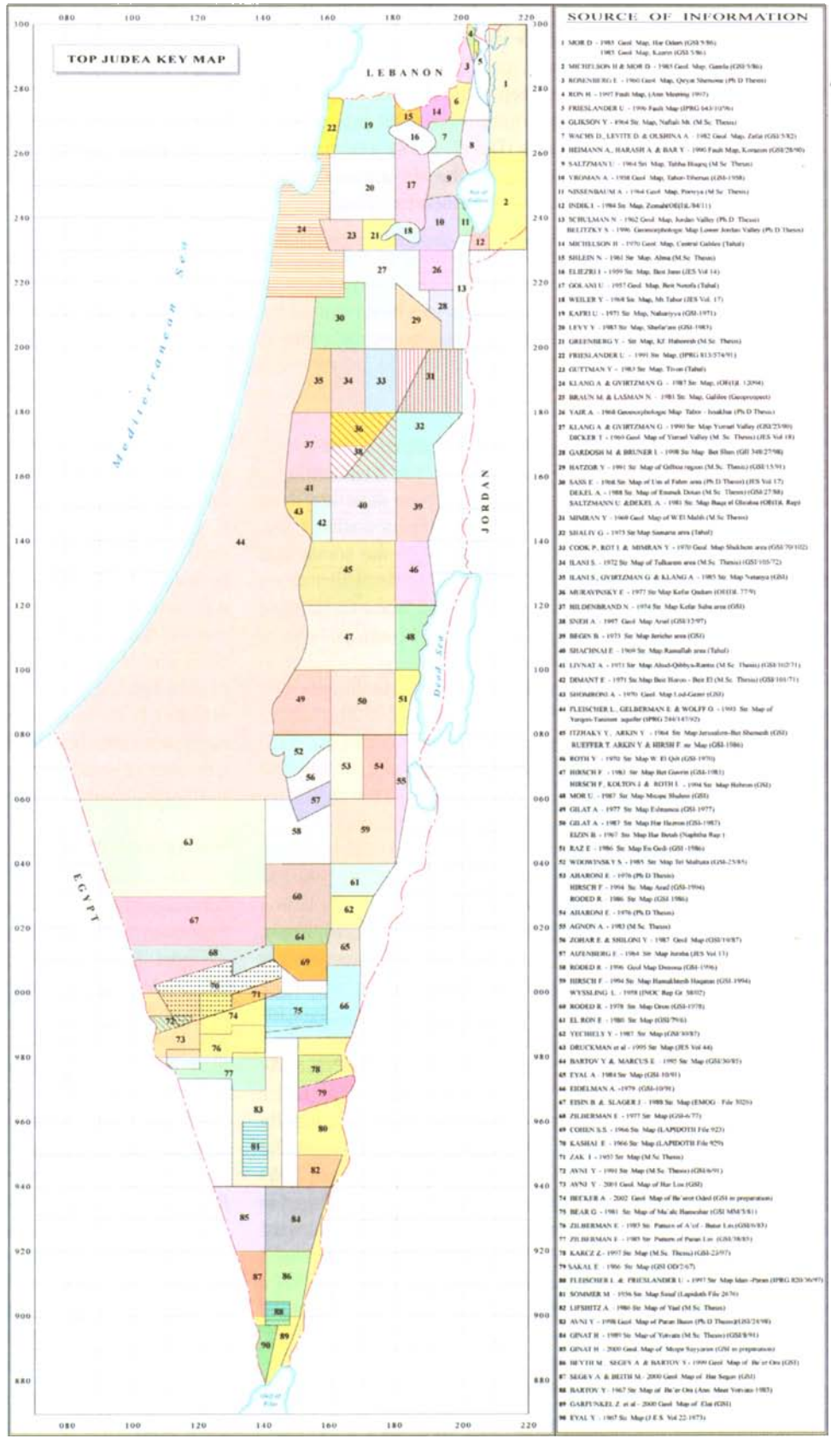


Figure AppC.1. Key Map for the digital structural map of the Top Judea Group. This is a reduction of the full size key map which is printed with the accompanying plates.

Menashe syncline to the north and the Shekhem syncline in the southeast. The crest of the structure is 10 km long, trending NE-SW subparallel to the other Syrian Arc folds of Central Israel. The structure is asymmetrical with a steep, narrow northwestern flank dipping 25-35° (Sass, 1968) and a southeastern flank dipping 8-15° to the Yabed and Emeq Dotan area (Dekel, 1988). The structural plunge in a southwestern direction toward the Ma'anit area is quite moderate (3° dip) in comparison to the northeastern plunge (7-11° dip).

In front of the Yizre'el Graben the plunge of the structure is down-thrown faulted (1,000 m throw). The Umm El Fahm structure is traversed by several faults, most of which occur in the vicinity of the crest, running almost E-W, having variable throws from 150 to 400 m.

4. JUDEA AND SAMARIA

Three NNE trending Hebron, Ramallah and Fari'a monoclines represent the prominent backbone between the Mediterranean Sea and the Dead Sea Rift system. The Hebron structure is an elongated, doubly plunging, NNE-SSW trending monocline about 35 km long with some subordinate branches to the south. The structure has a very steep (up to 50° dip) monoclinal flexure on its western flank which continues in the subsurface as a possible high-angle reverse fault (Reches et al., 1981). The eastern flank of the structure has a broad, moderate eastern dip.

The Ramallah anticline is the highest structure in the area with a reconstructed Top Judea level at an elevation of 1500 m above sea level. The Ramallah structure is *en-echelon*, located west of the Hebron monocline, and trends NNE-SSW for about 50 km. The western flank of the structure from Bet Shemesh to Sha'ar HaGay and further to Bet Horon is steeply inclined with dips of 14-40° (Itzhaky and Arkin, 1964; Dimant, 1971) and trends mostly north-south except in the north where the flank is oriented NE-SW. The slope of the western flank is reduced abruptly north of Bet Horon to a 3-6° dip. The eastern flank of the 'Judean Arch' (Picard, 1943), expressed by the Auja monocline in a generally N-S direction, has an eastern inclination of about 30° (Begin, 1975). The Ramallah structure is bisected by numerous normal faults, generally east-west oriented with a relatively small vertical displacement.

The Fari'a structure, about 25 km long, has a NNE-SSW trending axis similar to the Ramallah structure. The Fari'a anticline appears symmetrically developed with flanks normally inclined to the northwest (Shekhem syncline) and to the southeast (Jordan Valley). The structure is bisected by a dense set of NW-SE oriented faults which form a series of tilted blocks arranged in bilateral symmetry from the central graben (Nahal Tirza) toward both plunges of the structure (Weiler, 1982). Several horizontal movements of a few km produced a dextral offset of the Fari'a structure from the Ramallah structure along a NW-SE running fault (Begin, 1975).

5. THE SOUTHERN COASTAL PLAIN AND NORTHERN NEGEV

This province is characterized by a series of subparallel, asymmetric monoclines generally trending NE-SW. A broad and very gentle NW flank is supported by a narrow but very steep SE flank, which is more like an abrupt flexure. In the deep-seated part of the structure this flexure could be underlain by a low angle, reverse fault (de Sitter, 1962; Coates et al., 1963; Aharoni, 1976; Gelbermann, 1995). The monoclines are separated by sharp, almost horizontal, unbroken synclines.

The culmination of the Top Judea is located in the Makhtesh Hatira at about 1300 m above sea level, descending westward to about 100 m below sea level in the Helez-Kokhav area.

6. THE CENTRAL NEGEV

This province is dominated by the effects of the continuation of the central Sinai shear belts into the Negev as expressed by the Ramon lineament and by the Afir and Sa'ad-Nafha subordinate lineaments.

The generally ENE-WSW oriented Ramon structure is the major anticlinal feature in the area. The culmination of the reconstructed Top Judea is about 1800 m above sea level, and it descends gradually northwards. The southern flank of the structure is crossed by a longitudinal strike-slip fault complicated by some half-domal undulations (Garfunkel, 1988). The structure was active from Late Cretaceous to Cenozoic times. A large erosive valley incised the anticlinal crest, producing very steep cliffs and large outcrops of the Cretaceous, Early Jurassic, and Middle Triassic rocks. The Hamran-Nafha-Sa'ad lineament of E-W orientation is situated between the Avedat Plateau to the north and the Ramon anticline to the south. The structure is characterized by a number of small, asymmetrical domal features, accompanied by E-W segmented transcurrent strike-slip faults (Zilberman, 1977).

7. THE SOUTHERN NEGEV

This province is again dominated by the effects of the continuation of the central Sinai shear belts into the Negev as expressed by the 'Arif-Batur and the Paran and Reches Menuha - Kippat 'Eshet and Thamed lineaments, and by the Biq'at Uvda and Biq'at Sayarim subordinate lineaments of the Arava Valley main graben..

The 'Arif-Batur lineament is situated south of the Ramon fault. The lineament, which trends E-W in central Sinai, changes direction to the NE in the Negev, subparallel to the Ramon fault. The lineament is marked by a continuous fault system accompanied by a few small elongated structures (Zilberman, 1983).

The Paran lineament, situated to the south of the above lineament, has an E-W orientation and is also the eastern continuation of the main shear zone of the central Sinai.

The Karkom Graben splits the lineament into two tectonic elements: the western Paran segment and the eastern Reches Menuha - Kippat 'Eshet segment (Zilberman, 1985). Traces of the lineaments are marked by a continuous fault system accompanied by small elongated fold structures. The dextral strike-slip offsets of a few hundred meters measured in central Sinai on dikes and half domes (Bartov, 1974) are plainly evident on these Negev segments.

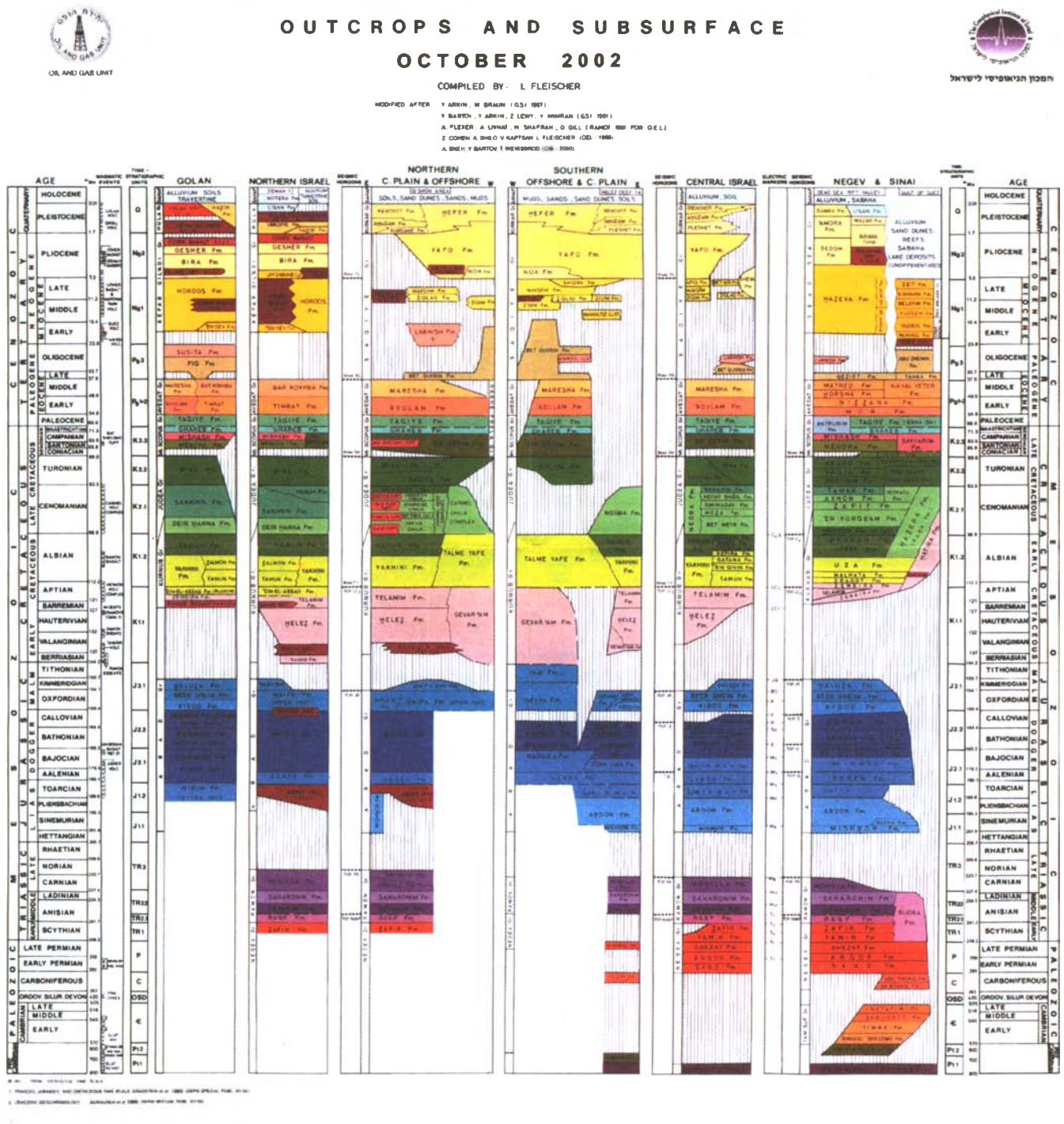


Figure AppC.2. Stratigraphic Table of Israel: Outcrops and Subsurface, compiled by L. Fleischer, October 2002. The table is modified after Y. Arkin and M. Braun (G.S.I. 1967), Y. Bartov, Y. Arkin, Z. Lewy, and Y. Mimran (G.S.I. 1981), A. Flexer, A. Livnat, N. Shafran, and D. Gill (Ramot 1981 for O.E.(I.)L), Z. Cohen, A. Shilo, V. Kapstan, and L. Fleischer (O.E.(I.)L, 1986), and A. Sneh, Y. Bartov, and T. Weissbrod (G.S.I. 2000). The Triassic, Jurassic, and Cretaceous time scale is from Gradstein et al. (1995), and the Cenozoic geochronology from Berggren et al. (1995), both in S.E.P.M. Special Publication 54.

The original black and white table has been given the stratigraphic colors of the 1:200,000 scale geological maps of the GSI (Sneh, Bartov and Weissbrod, 2000). Addition of color was done by Hanna Cohen-Netzer of the GSI Graphics Department. The coloring of stratigraphic units that are not exposed at the surface has been slightly altered in consultation with Dr. Zeev Lewy. The full-size table is printed with the separate plates.

The Karkom Graben is the major depression situated between the western Paran segment and the eastern Reches Menuha segment of the Paran lineament. Tectonically, the Karkom depression is a rhomb-shaped graben, about 17 km long and approximately 8 km wide. Its long axis is oriented E-W. The graben is filled with a very thick series (over 1000 m) of clastic sediments of the Hazeva Formation and the Arava Conglomerate. The sediments are generally subhorizontal, deepening gently to the northwest (Calvo et al., 1998).

Har Zenifim (Sinaf anticline) is the major anticlinal structure in the southern Negev area. The Sinaf structure is an elongated, doubly plunging, NNE-SSW trending anticline, about 20 km long. The structure is asymmetrical with gentle (5-10°) dips on the western flank and a very steep (dips up to 50°) eastern flank accompanied by a reverse fault (Avni, 1998). The structure is extensively faulted. Most of the NW-SE oriented faults affecting the structure are transversal, with insignificant displacement or throw.

Har Timna, the major anticlinal structure or fault block in the area, is generally oriented ENE-WSW. The culmination of the reconstructed Top Judea is at about 1100 m above sea level, descending gradually northwards. The southern flank of the structure is crossed by a large number of faults complicated by some half-domal undulations. The structure was active from Late Cretaceous to Cenozoic time. A large erosive cirque incised the anticlinal crest, producing very steep cliffs and large outcrops of the Cretaceous, Early Paleozoic, and Precambrian basement rocks.

The E-W trending Thamed lineament is situated between the Central Sinai shear zone on the west and the Arava Valley. The structure is characterized by a number of small, asymmetrical domal features, accompanied by dextral shifts of 0.3 to 0.5 km that are observed in the Central Sinai (Bartov, 1967).

Three structural elements are distinguished in the Elat area: the Elat block, the Shelomo-Roded block, and the Gishron block, composed of Precambrian Basement complex rocks and separated by the two narrow Yotam and Shelomo sedimentary grabens (Eyal, 1973). These grabens are generally oriented north-south, subparallel to the main Arava-Dead Sea tectonic graben.

The preserved sedimentary section in these grabens contains Paleozoic to Early Cretaceous colored sandstones, Late Cretaceous carbonates (Judea Group), Senonin chalky marls with chert beds (Mt. Scopus Group), and some Middle Eocene limestones (Avedat Group).

The area is intensely folded and faulted with a large number of strike-slip movement and block rotation effects. Two phases of faulting occurred in the Elat region: the first took place between the Middle Eocene and the deposition of the Miocene Raham Conglomerate (Garfunkel et al., 1973), and the second probably occurred after the deposition of the Conglomerate.

8. THE DEAD SEA RIFT SYSTEM

The last, most prominent, structural deformation probably started in Middle Miocene time with the approximately 105 km of sinistral slip between the Sinai-Israeli sub-plate and the Arabian Shield (Quennell, 1959; Freund et al., 1970; Quennell, 1984; Heimann, 1990). This N-S tectonic disturbance produced three major basins, the Arava-Dead Sea, the Bet She'an-Kinneret, and the Hula Valley, commonly interpreted as pull-apart basins (Freund et al., 1970; Garfunkel, 1981). They are separated by high barriers such as the Paran, Buqei'a, and Korazim elevated blocks (Garfunkel, 1981). The high rate of sedimentation in the deep basins produced a reactivation of pre-existing faults, an uplift of the high elevated structure in Judea and Samaria, and the generation of N-S oriented normal border and listric faults. Some are conjugated in small scale normal faults, developed diagonally across the graben (Kashai and Croker, 1987).

The compressional regime related to the Dead Sea transform system probably produced some compressional features, salt halokinesis, and, finally strong volcanic activity in the Zemah area.

DESCRIPTION OF THE PLATES

The Top Judea Group digital structural map of Israel has been printed in color and appears on separate plates. Two plates present the coverage for Israel at a scale of 1:200,000, as a North Sheet and a South Sheet. On one side they are printed as color shaded relief, and on the reverse side as contours. A third plate presents the same at 1:500,000 scale. A fourth plate presents the Stratigraphic Table of Israel (Fleischer, 2002), which is also reproduced at reduced size in **Fig. AppC.2**.

The stratigraphic table was prepared at the Oil and Gas Unit of the Geophysical Institute of Israel in October 2002. Although the original was not colored, permission was obtained to color it according to the stratigraphic colors of the 1:200,000 scale geological maps of the GSI (Sneh, Bartov and Weissbrod, 2000). Addition of color was done by Hanna Cohen-Netzer of the GSI Graphics Department. The coloring of stratigraphic units that are not exposed at the surface has been slightly altered in consultation with Dr. Zeev Lewy. The Triassic, Jurassic, and Cretaceous time scale is taken from Gradstein et al. (1995) and the Cenozoic geochronology from Berggren et al. (1995).

ACKNOWLEDGEMENTS

The authors are grateful to the Earth Sciences Research Administration of the Israel Ministry of National Infrastructures for permission to use the most recently acquired geological, geophysical, and well data from the Israel area, and for their sponsorship of this study.

Our thanks are also extended to I. Celinski for drafting some of the illustrations, and to D. Artzi for editing and typing the manuscript.

REFERENCES AND SOURCES OF INFORMATION

Achmon, M., 1986. The Carmel border fault between Yoqneam and Nesher. Unpubl. M.Sc. Thesis, Hebrew University of Jerusalem, 54 p.

Agnon, A., 1983. The geology of the Neve Zohar and Sdom areas. Unpubl. M.Sc. Thesis, Hebrew University of Jerusalem, 61 p. (In Hebrew).

Aharoni, E., 1976. The surface and subsurface structure of the southern Judean desert, Israel, 2 Vols. (In Hebrew; Engl. Abstr.). Hebrew Univ. of Jerusalem, 100 p., Appen., Figs., Maps.

Aizenberg, E., 1964. Unconformities in the northern Juraba area north eastern Negev, Israel. Isr. J. Earth Sci., 13(3-4), p. 150-157.

Arad, A., 1965. Geological outline of the Ramot Menashe region (northern Israel), Isr. J. Earth Sci, 14(1), p. 18-32.

Arkin, Y., and Braun, M., 1965. Type sections of Upper Cretaceous formations in the northern Negev, Southern Israel. Isr. Geol. Surv., Stratigr. Sec. 2a, 19 p.

Arkin, Y., Braun, M., and Itzhaki, Y., 1967. Cenomanian mapping units and their correlation in the Negev. Isr. Geol. Surv., Bull. 43, p. 15-21, Plates.

Avni, Y., 1991. The geology, paleogerography and landscape evaluation in the central Negev Highlands and the Western Ramon Structure. M.Sc. Thesis, Hebrew University of Jerusalem, GSI/6/1991, 153 p. (This is the 1989 M.Sc thesis).

Avni, Y., 1998. Paleogeography and Tectonics of the central Negev and the Dead Sea Rift western margins during the Late Neogene and Quaternary. Ph.D. Thesis, Hebrew University of Jerusalem, GSI/24/1998, 238 p. (In Hebrew, English abstract).

Avni, Y., 2001. Geological map of Har Loz (Sheet 21-III), 1:50,000, GSI-2001.

Baer, G., 1981. The geology of the 'Arif-Batur Lineament, Ma'ale Hameshar area, Geological Survey of Israel Report GSI/MM/5/81, 56 p.

Ball, M. W., and Ball, D., 1953. Oil prospects of Israel, Am. Assoc. Petrol. Geol. Bull., 37(1), p. 1-113.

Bartov, Y., 1967. The geology of the Beer-Ora area. Unpubl. M.Sc. Thesis, Hebrew University of Jerusalem, 39 p.

Bartov, Y., 1974. A structural and paleogeographical study of the central Sinai faults and domes. Unpubl. Ph.D. Thesis, Hebrew University of Jerusalem, 143 p.

Bartov, Y., 1985. The geological map of Har Ardon (Sheet 11-I), 1:50,000, Geological Survey of Israel, unpublished.

Bartov, Y., Arkin, Y., Lewy, Z., and Mimran, Y., 1981. Regional stratigraphy of Israel; A guide for Geological Mapping. Isr. Geol. Surv., 1 Colored Chart.

Bartov, Y., and Hirsch, F., 1985. Structural map on Top Judea Group in Har Ardon area, 1:50,000, Geological Survey of Israel Report GSI/30/85.

Bartov, Y., and Steinitz, G., 1997. The geology of Gebel E Risha area, Eastern Sinai, Geological Survey of Israel Report MM/77/3.

Becker, A., 2002. Geological map of Be'erot Od'ed (Sheet 21-IV), 1:50,000 (GSI, in preparation).

Begin, Z., 1975. Jericho geological map of Israel, 1:50,000, explanatory notes, Geological Survey of Israel Bulletin, No. 67.

Belitzky, S., 1996. Tectonic geomorphology of the Lower Jordan Valley. Unpubl. Ph.D. Thesis, Hebrew University of Jerusalem, 98 p.

Bentor, Y. K., and Vroman, A. J., 1954. A structural contour map of Israel (1:250,000) with remarks on its dynamic interpretation, Bull. Research Council of Israel, IV(2), p. 125-135.

Berggren, W. A., Kent, D. V., Swisher, C. C., III, Aubry, M. -P., 1995. A revised Cenozoic geochronology and chronostratigraphy. In: W. A. Berggren, D. V. Kent, M. -P. Aubry, and J. Hardenbol, (eds.), Geochronology, time scales and global stratigraphic correlation. SEPM (Society for Sedimentary Geology), Special Publication 54, p.129-212.

Beyth, M., Segev, A., and Bartov, Y., 1999. Geological map of Beer-Ora (Sheet 25-IV), 1:50,000, GSI-1999.

Braun, M., and Lasman, N., 1981. Explanatory notes to the structural maps of Galilee, Geoprospect Ltd. Report.

Bruner, I., 1991. Investigation of the subsurface in the northern Negev, Israel, using seismic reflection techniques. Ph.D. Thesis, Tel-Aviv University, 105 p.

Bruner, I., Weiner, D., Goldman, M., Calvo, R., and Bartov, Y., 1999. Geophysical research in the Mishor Yamin area, GII Report 641/170/96 and Geological Survey of Israel Report GSI/10/99.

Calvo, R., Bartov, Y., Avni, Y., Garfunkel, Z., and Frieslander, U., 1998. Field trip in the Karkom graben, Israel Geol. Soc. Annual Meeting, Field Trips Guidebook, 47-62.

Coates, J., Gottesman, E., Jacob, M., and Rosenberg, E., 1963. Gas discoveries in the western Dead Sea region, 6th World Petroleum Congress, Frankfurt, Section I, Paper 26, 15 p.

Cohen, S., 1966. The geological and structural maps of the Marzeva Permit, Lapidoth Report.

Cook, P., 2000. Geological map of Shekhem (Sheet 5-IV), 1:50,000, Geological Survey of Israel.

Cook, P., Rot, I., and Mimran, Y., 1970. Geological map of Shechem syncline, Geological Survey of Israel Report 2/70.

de Sitter, L.U., 1962. Structural development of the Arabian Shield in Palestine, Geol. Mijnbow, 41(3), p. 116-124.

Dekel, A., 1988. The geology of the Emeq Dotan area. M.Sc. Thesis, Tel Aviv University, 57 p., and Geological Survey of Israel Report GSI/27/88. (In Hebrew).

Dicker, T., 1969. Geology of central Yizre'el Valley. Isr. J. Earth Sci., 18(2), p. 39-69.

Dimant, E., 1971. The geology of the Bet Horon area and the eastern flanks of the Bet El anticline. M.Sc. Thesis, 79 p., and Geological Survey of Israel Report MM/101/71.

Druckman, Y., Gill, D., Fleischer, L., Gelbermann, E., and Wolff, O., 1994. Subsurface stratigraphy and structure of the northwestern Negev, IPRG Report 502/344/93 and GSI Report GSI/21/94, 24 p.

Eidelman, A., 1979. The geology of the Arava Rift margin in the 'En Yahav – Ramat Zofar region. M.Sc. Thesis, Hebrew Unversity of Jerusalem, 66 p. (In Hebrew and English Abstract). Geological Survey of Israel Report MM/10/79, 66 p.

Eisin, B., 1967. Har Betakh structural map on Top Turonian, 1:20,000, Naphtha Report.

Eisin, B., and Slager, J., 1988. Structural map on Top Judea Group in the central Negev, EMOG Report.

Eliezri, I. Z., 1965. The geology of the Bein Jann region (Galilee, Israel), Isr. J. Earth Sci., 14(2), p. 51-66.

Elron, E., 1980. The geology of the Nahal Zin area (northern Hazeva Sheet). M.Sc. Thesis, Hebrew University of Jerusalem, 54 p. (In Hebrew, English Abstract). Geological Survey of Israel Report MM/6/79.

Eyal, A., 1984. The geology of the northern Arava and its western margins in the 'En Yahav-Hazeva region. M.Sc. Thesis, Hebrew University of Jerusalem, 63 p. (In Hebrew, English Abstract). Geological Survey of Israel Report GSI/10/1991, 63 p.

Eyal, Y., 1973. The tectonics of the Shelomo and Yotam grabens, Elat, Israel, Isr. J. Earth Sci., 22(3), p. 165-184.

Fleischer, L., 2002. Stratigraphic Table of Israel: Outcrops and Subsurface. Compiled by L. Fleischer, Geophysical Institute of Israel, Oil and Gas Unit, original not colored, 1 sheet.

Fleischer, L., Gelbermann, E., and Wolff, O., 1993. A geological-geophysical reassessment of the Judea Group, IPRG Report 244/247/92, 91 p.

Fleisher, E., Fleischer, L., and Frieslander, U., 1996. The Arava ground water potential in the Ya'alon-Yotvata area, IPRG Report 820/56/96, 16 p.

Fleisher, E., Fleischer, L., and Frieslander, U., 1997a. The hydrology of the Idan-Ein Yahav area, GII Report 820/147/96, 10 p.

Fleisher, E., Fleischer, L., and Frieslander, U., 1997b. The hydrology of the Zofar-Paran area, GII Report 820/36/97, 13 p.

Fleischer, L., and Gafsou, R., 1998a. Top Judea Group – digital structural map of Israel, Arava Valley and the Galilee (Phase I), GII Report 873/90/97.

Fleischer, L., and Gafsou, R., 1998b. Top Judea Group - digital structural map of Israel, Central Israel (Phase II), GII Report 873/68/98.

Fleischer, L., and Gafsou, R., 2000. Top Judea Group – digital structural map of Israel, Central Israel (Phase III), GII Report 873/55/99.

Fleischer, L., and Gafsou, R., 2001. Top Judea Group – digital structural map of Israel, Negev and Northern Galilee (Phase IV), GII Report 875/96/01.

Fleischer, L., and Gafsou, R., 2002. Top Judea Group – digital structural map of Israel, Har Timna' and Biq'at 'Uvda (Phase V), GII Report 875/170/02.

Fleischer, L., and Gafsou, R., 2003. Top Judea Group – digital structural map of Israel, Har Ramon to Biq'at Shizzafon (Phase VI), GII Report 753/306/03.

Freund, R., 1970. The geometry of faulting in the Galilee, Isr. J. Earth Sci., 19(3-4), p. 117-140.

Freund, R., Garfunkel, Z., Zak, I., Goldberg, M., Weissbrod, T., and Derin, B., 1970. The shear along the Dead Sea rift, Phil. Trans. Royal Soc. London, A267, p. 107-130.

Frieslander, U., 1991. Subsurface mapping of the Western Galilee area, GII Report 813/574/91.

Frieslander, U., 1996. Seismic reflection survey, Kfar Yuval-Kfar Giladi area, GII Report 643/100/96.

Frieslander, U., 2000. The structure of the Dead Sea transform emphasizing the Arava using new geophysical data. Ph.D. Thesis, Hebrew University of Jerusalem, 101 p.

Gardosh, M., and Bruner, I., 1998. Seismic survey in the Bet Shean area, GII Report 348/27/98.

Garfunkel, Z., 1981, Internal structure of the Dead Sea leaky transform and its relation to plate kinematics, Tectonophysics, 80(1-4), p. 81-108.

Garfunkel, Z., 1988. Structural development and subsurface structure of Israel, superimposed tectonics in the Negev, Prepared for OE(I)L, 41 p.

Garfunkel, Z., Bartov, Y., Eyal, Y., and Steinitz, G., 1974. Raham Conglomerate - New evidence for Neogene tectonism in the southern part of the Dead Sea Rift. Geol. Mag., 111(1), p. 55-64.

Garfunkel, Z., Eyal, Y., Eyal, M., Weissbrod, T., Bakler, N., Shimron, E. A., Pettz, S., Gutkin, V., Bartov, Y., Druckman, Y., Rosensaft, M., and Sneh, A., 2000. Geological map of the northern gulf of Elat area, 1:100,000 (Sheet 26), Geological Survey of Israel.

Gelbermann, E., and Grossowicz, Y. (Eds.), 1990. Seismic structural and isopach maps of central, southern and offshore Israel, PIC (IPRG) Report 201/89-90, 12 p.

Gelbermann, E., 1995. Revised seismic structural and isopach maps of central and southern Israel, IPRG Report 201/22/89-94, 32 p.

Gilat, A., 1977. The geological and structural mps of Eshtemoa' area (Sheet 15-I), 1: 50,000, Geological Survey of Israel.

Gilat, A., 1987. The geological and structural maps of Har Hezron (Sheet 15-II), 1: 50,000, Geological Survey of Israel.

Gilat, A., and Agnon, A., 1981. The geological map of 'En Boqeq-Mezada area, 1: 20,000, Geological Survey of Israel Report GSI/MM/2/81.

Ginat, H., 1991. The geology and geomorphology of the Yotvata area, Geological Survey of Israel Report GSI/8/1991, 75 p.

Ginat, H., 2001. Geological map of Mizpe Sayyarim (Sheet 25I), 1:50,000 (GSI, in preparation).

Glikson, Y., 1964. The geology of Nahal Dishon. M.Sc. Thesis, Hebrew University of Jerusalem, 52 p. (In Hebrew).

Golani, U., 1959. The geology of Biqa'at Bet Netofa, Tahal Report.

Gradstein, F. M., Agterberg, F. P., Ogg, J. G., Hardenbol, J., van Veen, P., Thierry, J., Huang, Z., 1995. A Triassic, Jurassic and Cretaceous time scale. In: W. A. Berggren, D. V. Kent, M. -P. Aubry, and J. Hardenbol, (eds.), Geochronology, time scales and global stratigraphic correlation. SEPM (Society for Sedimentary Geology), Special Publication 54, p. 95-126.

Greenberg (Gilboa), Y., 1959. Top Turonian - a structural contour map of Israel (1: 250,000), prepared for INOC (map only).

Greenberg, Y., 1964. The Eocene of Kefar Hahoresh-Illut region and its correlation with the Eocene of northern Israel, Isr. J. Earth Sci., 12(3), p. 147-158.

Guttman, Y., 1983. Geological mapping of trhe Tiv'on-Nazareth area, Tahal Report 04/83/44.

Gvirtzman, G., Klang, A., Buchbinder, B., Marionotti, G., and Moshkovitz, S., 1986. Structure and evolution of the Kishon rift, Geological Society of Israel, Annual Meeting, Abstracts, 60-61.

Hatzor, Y., 2000. Geological map of Bet She'an (Sheet 6 I, II), 1:50,000, Geological Survey of Israel.

Hatzor, Y., and Reches, Z., 1990. Structure and paleostresses in the Gilboa region, western margins of the Central Dead Sea rift, Tectonophysics, 180(1), p. 87-100.

Heimann, A., 1990. The development of the Dead Sea Rift and its margins in northern Israel during the Pliocene and Pleistocene. Ph.D. Thesis, Hebrew University of Jerusalem, 110 p. (In Hebrew, English Abstract). Geological Survey of Israel Report GSI/28/90, 83 p.

Hildebrand, N., 1974, 1993. Geological and structural maps of Kefar Sava (Sheet 8 I), 1:50,000, Geological Survey of Israel.

Hirsch, F., 1983. Geological and structural maps of Bet Guvrin area (Sheet 11 III), 1: 50,000, Geological Survey of Israel.

Hirsch, F., 1994. Structural map on Top Turonian in the Arad area (Sheet 15-IV), 1: 50,000, Geological Survey of Israel (unpublished).

Hirsch, F., 1995. The geological and structural maps of Hamakhtesh Haqatan (Sheet 19-II), 1:50,000, Geological Survey of Israel.

Hirsch, F., Kolton, J., and Roth, I., 1994. Geological and structural maps of Hebron (Sheet 11-IV), 1:50,000, Geological Survey of Israel (unpublished).

Ilani, S., 1972. The geology of Tulkarem area. M.Sc. Thesis, Hebrew University of Jerusalem, Geological Survey of Israel Report MM/105/72, 71 p.

Ilani, S., Gvirtzman, G., and Klang, A., 1985. Geological and structural maps of Netanya (Sheet 5 III), 1:50,000, Geological Survey of Israel.

Itzhaky, Y., and Arkin, Y., 1964. Jerusalem-Bet Shemesh geological and structural map, 1:50,000, GSI.

Kafri, U., 1971. Nahariyya geological and structural map (Sheet I-IV), 1:50,000, Geological Survey of Israel.

Karcz, Z., 1997. The geology of the North Paran region. M.Sc. Thesis, Hebrew University of Jerusalem, 99 p. (In Hebrew, English Abstract). Geological Survey of Israel Report GSI/23/1997, 99 p.

Kashai, E., 1966a. Structural map on Lower Cretaceous of Makhtesh Ramon area, Lapidoth Report.

Kashai, E., 1966b. The geology of the eastern and southwestern Carmel. Ph.D. Thesis, Hebrew University of Jerusalem, 115 p. (In Hebrew, English Abstract).

Kashai, E., and Crocker, P., 1987. Structural geometry and evolution of the Dead Sea-Jordan rift system as deduced from new subsurface data. Tectonophysics, 141(1-3), p. 33-60.

Kashai, E., and OE(I)L exploration staff, 1988. A structural map of Israel on Base Senonian. In: Hydrocarbon Potential of Israel, Highlights of Basin Analysis, OE(I)L, 148 p.

Klang, A., and Gvirtzman, G., 1983. Preliminary structural analysis of the Sharon area and its continental shelf, OE(I)L Report 83/30, 47 p.

Klang, A., and Gvirtzman, G., 1987. Structural contour map of Top Judea or Talme Yafe in western Galilee and Mt. Carmel coastal plain and continental shelf, Prepared for OE(I)L (map only).

Klang, A., and Gvirtzman, G., 1988. Structural map of the Top Judea Group and Talme Yafe formation in the southern Coastal Plain and the Shefela region, Israel (draft), GSI/47/88, 40 p.

Klang, A., and Gvirtzman, G., 1990a. Structural contour map of the top of the Judea Group in the valleys of Be'er Sheva and Arad (draft), Geological Survey of Israel Report GSI/22/90, 8 p.

Klang, A., and Gvirtzman, G., 1990b. Structural contour map of the top of the Judea Group in the valleys of Yizre'el, Harod and Bet She'an (draft), Geological Survey of Israel Report GSI/23/90, 7 p.

Levitte, D., 2001. Geological map of Zefat (Sheet 2-III), 1:50,000, Geological Survey of Israel.

Levy, Y., 1983. Shefar'am geological and structural map (Sheet 3-II), 1:50,000, Geological Survey of Israel.

Lifshitz, A., 1986. The geology of Nahal Ya'alon area. M.Sc. Thesis, Tel-Aviv University, 135 p. (In Hebrew).

Livnat, A., 1971. The geology of the north western slopes of the Judean Hills ('Abud-Qibya-Rantis area). M.Sc. Thesis, Hebrew University of Jerusalem. (In Hebrew). Geological Survey of Israel Report GSI/MM/71/102, 60 p.

Marcus, E., and Kaptzan, V., 1978. A structural contour map of Israel (1:250,000) datum horizons: Top Turonian and Top Jurassic, prepared for OE(I)L (map only).

Mimran, Y., 1969. The geology of the Wadi Malih region. M.Sc. Thesis, Hebrew University of Jerusalem, 68 p. (In Hebrew).

Mimran, Y., Buchbinder, B., and Gvirtzman, G., 1980a. Preliminary geological survey for siting of nuclear power plants in the Besor area, GSI Report MM/ 7/80, 108 p.

Mor, D., 1986. The volcanism of the Golan Heights. Ph.D. Thesis, Hebrew University of Jerusalem, Geological Survey of Israel Report GSI/5/86, 159 p.

Mor, U., 1987. The geology of the Judean Desert in the Nahal Darga region. M.Sc. Thesis, Hebrew University of Jerusalem, 112 p. (In Hebrew, English Abstract). Geological Survey of Israel Report GSI/21/87.

Mor, U., and Burg, A., 2000. The geological map of Mizpe Shalem (Sheet 12-III), 1: 50,000, Geological Survey of Israel.

Muravinsky, E., 1977. Possibilities of oil and gas exploration on the south Shekhem

and Kfar Qadum, OE(I)L Report 77/09.

Nissenbaum, A., 1964. The egochemistry and petrography of the Poriyya and Deganiya Formations in the escarpment of Poriyya. M.Sc. Thesis, 73 p. Hebrew University of Jerusalem. (In Hebrew).

Picard, L., 1943. Structure and evolution of Palestine with comparative notes on neighboring countries. Hebrew University of Jerusalem, Geology Department, Bulletin 4(3-4), p. 1-184.

Quennell, A. M., 1959. Tectonics of the Dead Sea rift, 20th International Geol. Congress, Session 20, 1956, Mexico, Asoc. Serv. Geol. Africanos, p. 385-405.

Quennell, A. M., 1984. The Western Arabia rift system, in: J. E. Dixon and A. H. F. Robertson (Eds.) Symposium on the East Mediterranean, Blackwell, Oxford, p. 775-789.

Raz, E., 1983. The geology of the Judean Desert ('En Gedi area). M.Sc. Thesis, Hebrew University of Jerusalem, 110 p. (In Hebrew). Geological Survey of Israel Report GSI/S/3/83, 110 p.

Raz, E., 1986. The geological and structural maps of 'En Gedi area (Sheet 16-I), 1: 50,000, Geological Survey of Israel.

Reches, Z., Hoexter, D., and Hirsch, F., 1981. The structure of a monocline in the Syrian Arc system, Middle East surface and subsurface analysis, J. Petrol. Geol., 3(4), p. 413-425.

Roded, R., 1978. The geological and structural maps of Oron (Sheet 19-III), 1:50,000, Geological Survey of Israel.

Roded, R., 1986. Structural map on Top Turonian-Negev area, Geological Survey of Israel.

Roded, R., 1996. The geological map of Dimona (Sheet 19-I), 1:50,000, Geological Survey of Israel.

Rofe & Raffety Consulting Eng., 1965. Nablus District water resources survey. Geological and Hydrological Report. London, Report for Jordan Govt., Central Water Authority, 120 p., Appen., Maps.

Ron, H., 1984. Paleomagnetic investigation of the fault structure of the Galilee, northern Israel. Ph.D. Thesis, Hebrew University of Jerusalem, 102 p. (In Hebrew).

Ron, H., and Eyal, Y., 1985. Intraplate deformation by block rotation and mesostructures along the Dead Sea transform, northern Israel, Tectonics, 4(1), p. 85-105.

Ron, H., Shamir, G., and Eyal, Y., 1997. The deformation in the Misgav Am-Margaliyot block, Geological Survey of Israel, Annual Meeting, Field Trips Guidebook, 33-45.

Rosenberg, E., 1960. Geologische Untersuchungen in den Naftalibergen, (Am Rande des Noerdlichsten Teiles der Jordansenke, Israel). Ph.D. Thesis, University of Zurich, Mitt. Geol. Inst. Eidg. Tech. Hochsch., Ser. C, No. 80, 107 p. (In German).

Roth, I., 1970. Geological and structural maps of Wadi el Qilt (Sheet 12 I), 1:50,000, Geological Survey of Israel.

Rotstein, Y., Bruner, I., and Kafri, U., 1993. High-resolution seismic imaging of the Carmel fault and its implications for the structure of Mt. Carmel, Isr. J. Earth Sci., 42(2), p. 55-69.

Rueffer, T., Arkin, Y., and Hirsch, F., 1986. Top Judea Group structural map, 1: 50,000, Geological Survey of Israel.

Sakal, E., 1967. The geology of the Reches Menuha area. M.Sc. Thesis, Hebrew University of Jerusalem, 80 p. (In Hebrew). Geological Survey of Israel Report GSI/OD/2/67. (Engl. Translation, 1968, 96 p., Figs.).

Saltzman, U., 1964. The geology of the Tabgha-Huqoq-Migdal area. M.Sc. Thesis, Hebrew University of Jerusalem, 55 p. (In Hebrew).

Saltzman, V., and Dekel, A., 1981. The structure of Baqa el Gharabiya area, Report for OE(I)L.

Sass, E., 1968, Geology of the Umm El Fahm area, northern Israel. Isr. J. Earth Sci., 17(3), p. 115-30.

Schlein, N., 1961. The geology of the Alma region. M.Sc. Thesis, Hebrew University of Jerusalem, 49 p. (In Hebrew).

Segev, A., and Beyth, M., 2000. Geological map of Har Seguv (Sheet 25-III), 1: 50,000 (GSI-2000).

Shachnai, E., 1969, 2000. Geological and structural maps of Ramallah area (Sheet I IV), 1:50,000, Geological Survey of Israel.

Shaliv, G., 1972. The hydrogeology of Wadi Faria region. Part I: Geology; Part II: Hydrology. (In Hebrew). Tel Aviv, Tahal, 81 and 91 p., Appen. (M.Sc. Thesis, Hebrew University of Jerusalem) {Hr/72/097}.

Shaliv, G., 1973. Top Turonian structural map of Samaria area, Tahal.

Shomrony, A., 1970. Geological map of the Lod-Gezer area (Sheet 8-III), 1:50,000.

Shulman, N., 1962. The geology of the central Jordan Valley. Ph.D. Thesis, Hebrew University of Jerusalem, 103 p. (In Hebrew, English Abstract). Also Bull. Research Council of Israel, Vol. 8G(2-3), p. 63-90.

Sneh, A. (ed.), 1997. Geological map of Ari'el (Sheet 8-II), 1:50,000, Geological Survey of Israel.

Sneh, A. (ed.), 1997. Geological map of Ma'ale Efrayim (Sheet 9-I), 1:50,000, Geological Survey of Israel.

Sneh, A., Bartov, Y., and Weissbrod, T., 2000. Stratigraphic chart of exposed rock units in Israel. In: R. Bogoch (ed.), GSI Current Research, Vol. 12, Jerusalem, July 2000, p. 257-262.

Sommer, M., and Biro, Ph., 1956. Geological survey of the Sinaf Anticline, Lapidoth (Rep. 1956).

Vroman, A. J., 1958. Geological map of Israel Tabor-Tiberias, 1:50,000, Geological Survey of Israel.

Wachs, D., Levitte, D., and Olshina, A., 1982. Land map Zefat area (1:50,000), Geological Survey of Israel Report 5/82.

Wdowinski, S., 1985. The geology of the southern Hebron Mountains. M.Sc. Thesis, Hebrew University of Jerusalem, 68 p. (In Hebrew, English Abstract). Geological Survey of Israel Report GSI/25/85, 68 p.

Weiler, Y., 1968. Geology of Nazareth Hills and Mount Tabor (southern Galilee, Israel). Isr. J. Earth Sci., 17(2), p. 63-82.

Weiler, Y., 1982. Ro'i-1 recommendation for drilling, OE(I)L Report 82/11, 21 p.

Wyssling, L., and Drzewiecki, J., 1958. The geological report of the Makhtesh Katan area, Israel National Oil Co. Report GR/58/02.

Yair, A., 1968. Phenomenes géomorphologiques dans le valées d'Issakhar et de Tabor. Ph.D. Thesis, Hebrew University of Jerusalem. 185 p. (In Hebrew, French Abstract).

Yechieli, Y., 1987. The geology of the northern Arava Valley and Mahmal Anticline, Hazeva region. M.Sc. Thesis, Hebrew University of Jerusalem, 94 p. (In Hebrew, English Abstract). Geological Survey of Israel Report GSI/30/87, 94 p.

Yechieli, Y., 1997. Geological map of Lod (Sheet 8-III), 1:50,000, Geological Survey of Israel.

Yechieli, Y., Elron, E., and Sneh, A., 1994. The geological map of Neot Hakikar (Sheet 19-IV, 20-III), 1:50,000, Geological Survey of Israel.

Zak, I., 1957. The Triassic stratigraphy in Makhtesh Ramon. M.Sc. Thesis, Hebrew University of Jerusalem, 84 p. (In Hebrew).

Zilberman, E., 1977. The geology of the Sa'ad-Nafha lineament Avedat Plateau. M.Sc. Thesis, Hebrew University of Jerusalem, 70 p. (In Hebrew, English Abstract). Geological Survey of Israel Report MM/6/77, 81 p.

Zilberman, E., 1981. The geology of the central Sinai-Negev shear zone, Part A: The Sa'ad-Nafha Lineament, Geological Survey of Israel Report GSI/HYDRO/1/ 81.

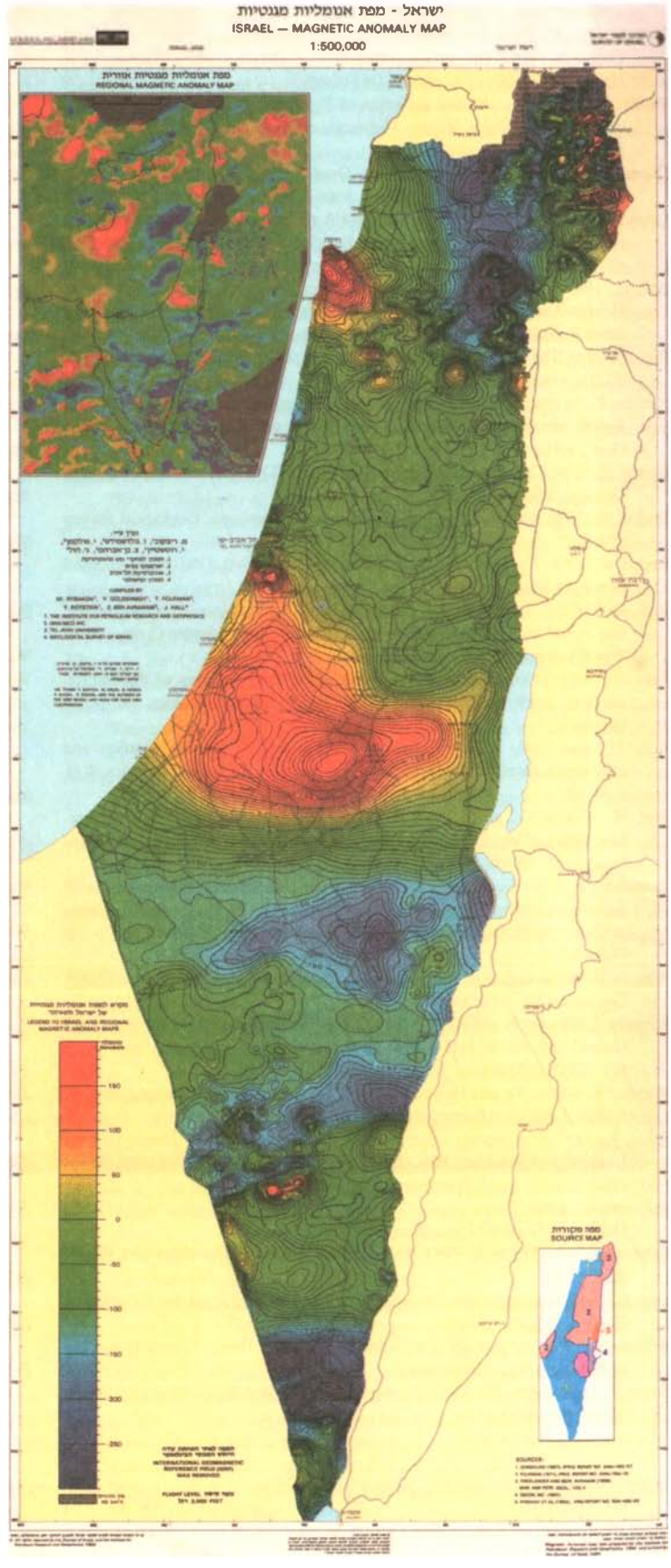
Zilberman, E., 1982. The geology of the Qeren-Haluza area, Geological Survey of Israel Report GSI/EG/4/82, 33 p.

Zilberman, E., 1983. The geology of the Central Sinai-Negev Shear zone, Part B., the 'Arif-Batur Lineament, Geological Survey of Israel Report GSI/EG/6/83, 58 p.

Zilberman, E., 1985. The geology of the Central Sinai-Negev Shear zone, Part C, the Paran Lineament, Geological Survey of Israel Report GSI/38/85, 53 p.

Zilberman, E., 2001. The geological map of Nizzana (Sheet 17-IV), 1:50,000, Geological Survey of Israel.

Zohar, E., and Shiloni, Y., 1987. The geological map of the Arad Basin, Geological Survey of Israel Report GSI/19/87.



Israel Magnetic Anomaly Map.
Compilation by M. Rybakov, V. Goldshmidt, Y. Folkman, Y. Rotstein, Z. Ben Avraham, and J. K. Hall. Prepared in 1994 by the Institute for Petroleum Research and Geophysics (IPRG) and printed by the Survey of Israel. Primarily based upon an aeromagnetic survey by Domzalski (1967 – IPRG Rept. SMA/482/67) at a flight level of 3,000 ft, with the addition of smaller later surveys. IGRF removed, contour interval 10 γ (nT).

Appendix D

Geological Map Inventory for some Middle Eastern Countries (Israel, Jordan, Syria, and Lebanon)

Rani Calvo *

Geological Survey of Israel, Mapping Division, 30 Malchei Israel Street, Jerusalem 95501, Israel

John K. Hall

Geological Survey of Israel, Marine Geology, Mapping & Tectonics Division, 30 Malchei Israel Street, Jerusalem 95501, Israel

INTRODUCTION

Geological mapping of the Middle East started in the late 19th century (Hudleston, 1885; Noetling, 1887). Since then more accurate geological maps at much larger scales were prepared and printed. For each country, a series of geological map sheets was laid out in such a way as to accommodate the whole country at a given scale. The purpose of this appendix is to give a list of these map sheets and their references for some of the Middle Eastern countries (Israel, Jordan, Syria, and Lebanon). This summary is based on the data inventory of the Documentation Center at the Geological Survey of Israel.

All figures in this appendix were prepared with the ESRI ArcGIS (Geographic Information System) program. A CD-ROM is available in SHP (shapefile) format, containing the schemes of the map sheet coverage as illustrated in the figures.

REGIONAL MAP SHEETS

Regional and small scale geological map mosaics (≤1:500,000 scale) of Middle Eastern countries were produced by combining the larger scale map sheets of Bender (1967, 1975), Bartov (1975), Dubertret (1966), Ponikarov et al. (1966), and Toloczyki and Trumit, 1998. These are shown in **Fig. AppD.1**. Some of these small scale geological maps and mosaics are reproduced as foldouts in Appendix E, which describes the digital files in geo-referenced MrSID file format that are available on a CD-ROM upon request from the Geological Survey of Israel.

COUNTRY SCALE MAP SHEETS

Fig. AppD.2 shows the small-scale geological map coverage for Israel. The two older map sheets in the 1:250,000 series (Fig. AppD.2A) are based on the 1:100,000 scale Israel/Palestine series, and older versions of the 1:250,000 series (Blake, 1939; Shaw, 1947). The four map sheets in the new 1:200,000 scale series (Fig. AppD.2B) are based mainly on the 1:50,000 scale sheets of Israel and were produced using an Intergraph GIS. These maps are available either as digital images or in digital vector formats (Sneh et al., 2001).

Fig. AppD.3 shows the layout scheme for the large scale geological maps of Israel. Only 16 of the 24 map sheets were published in the original 1:100,000 series (Fig. AppD.3A). New 1:100,000 scale maps were recently printed from the new 1:200,000 scale digital series (Sneh, et al., 1996a-g; Sneh et al., 1997). Only 42 of the 84 1:50,000 scale map sheets were published (Fig. AppD.3B). Some of these 1:50,000 maps were produced using older GIS software (*i.e.* Begin, 1997; Hilderbrand-Mittlefeldt, 1997). These map sheets are referenced below according to their mapping scale. All these map sheets are available in hardcopy form the Documentation Center of the Geological Survey of Israel (library@gsi.gov.il).

Fig. AppD.4 shows the scheme for the five map sheets for Jordan in the 1:250,000 series prepared by the German Geological Mission for Jordan (Bender, 1968). These maps are also based on the mapping of Quennell (1956). **Fig. AppD.5** shows the scheme for the 1:100,000 series, of which 14 map sheets were completed. **Fig. AppD.6** shows the scheme for the 1:50,000 series, following that of the Defense Mapping Agency K737 Series of topographic maps of the 1960s. At least 58 out of the 170 map sheets appear to have been published - our knowledge about the Jordanian mapping is current to 2001. Most of the 1:50,000 scale map sheets were prepared in the last two decades by Jordanian geologists from the National Resources Authority (NRA) in Amman. These map sheets are referenced below according to their mapping scale. All maps are available in the NRA library.

Fig. AppD.7 shows the scheme for the 20 map sheets covering Syria in the 1:200,000 scale series of the Russian mapping mission (Ponikarov, 1962; Ponikarov and Compilers, 1964). Several 1:50,000 series map sheets are listed in the references and are also presented in Figure AppD.7.

Fig. AppD.8 shows the scheme for the 1:50,000 scale geological map sheets in Lebanon. Louis Dubertret (1904-1979) and his colleagues published 18 sheets at 1:50,000, and 2 sheets of the 1:250,000 scale series.

AVAILIBILITY AND USAGE

The usefulness of these geological map series is limited by several factors. These series are up to 50 years in age, out of print or in very limited supply, often incomplete, and restricted to use in a limited number of libraries or archives.

Appendix E describes the method that was used to establish a geo-referenced digital form of some of these maps.

* For correspondence: rani.calvo@gsi.gov.il

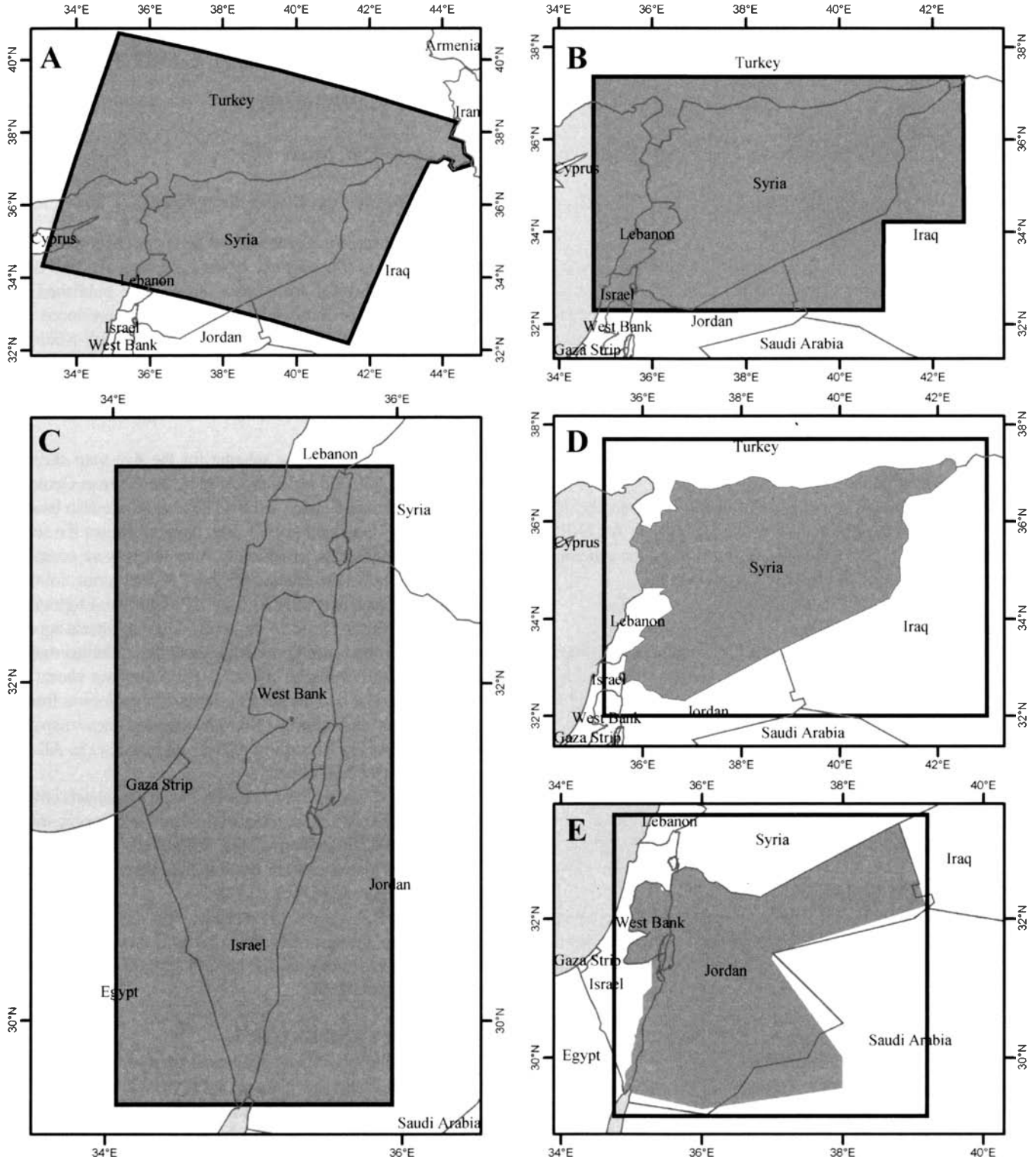


Figure AppD.1. Scheme of regional and small scale geological map sheets of the Middle East countries. (A) International geological map of Europe and the Mediterranean region (1:1,500,000; Toloczyki and Trurnit, 1998); (B) Liban-Syrie (1:1,000,000; Dubertret, 1966); (C) Israel (1:500,000; Bartov, 1979); (D) Syria (1:1,000,000; Ponikarov et al., 1966); (E) Jordan (1:750,000 and 1:500,000; Bender, 1967).

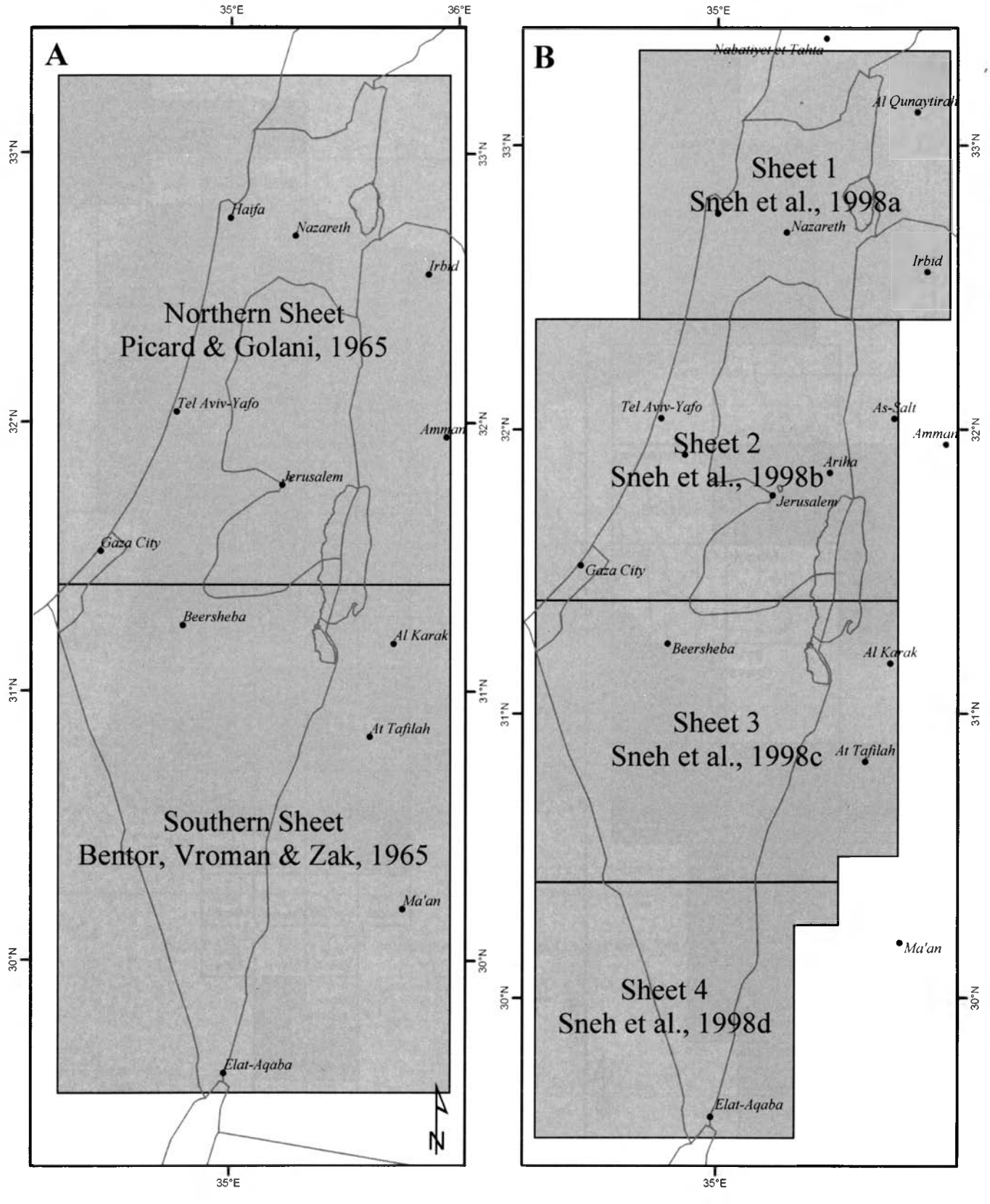


Figure AppD.2: Scheme of geological map sheets of Israel at scale (A) 1:250,000 and (B) 1:200,000.

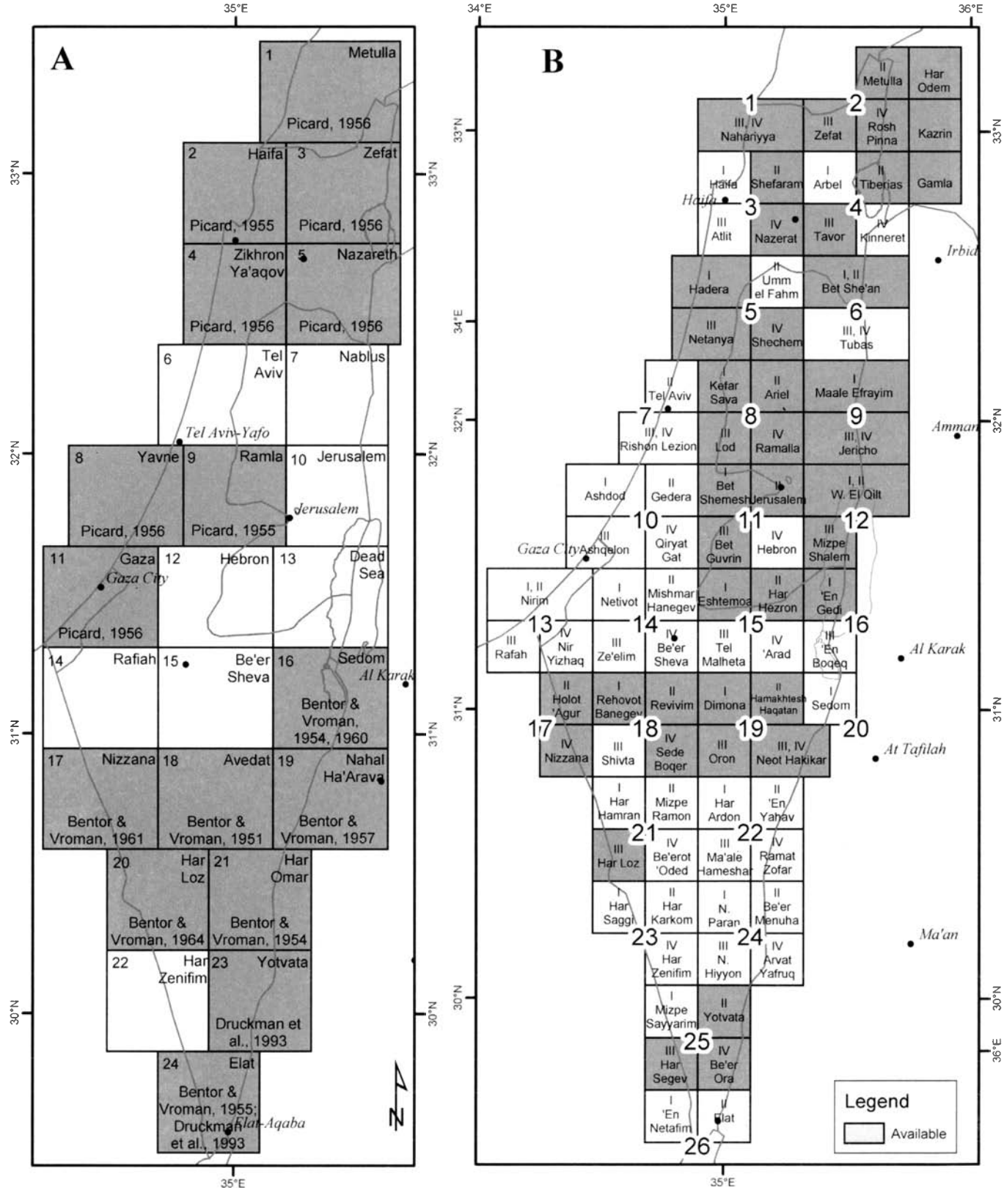


Figure AppD.3. Scheme of geological map sheets of Israel at scale (A) 1:100,000 and (B) 1:50,000 (see the references for the authors of each map sheet).

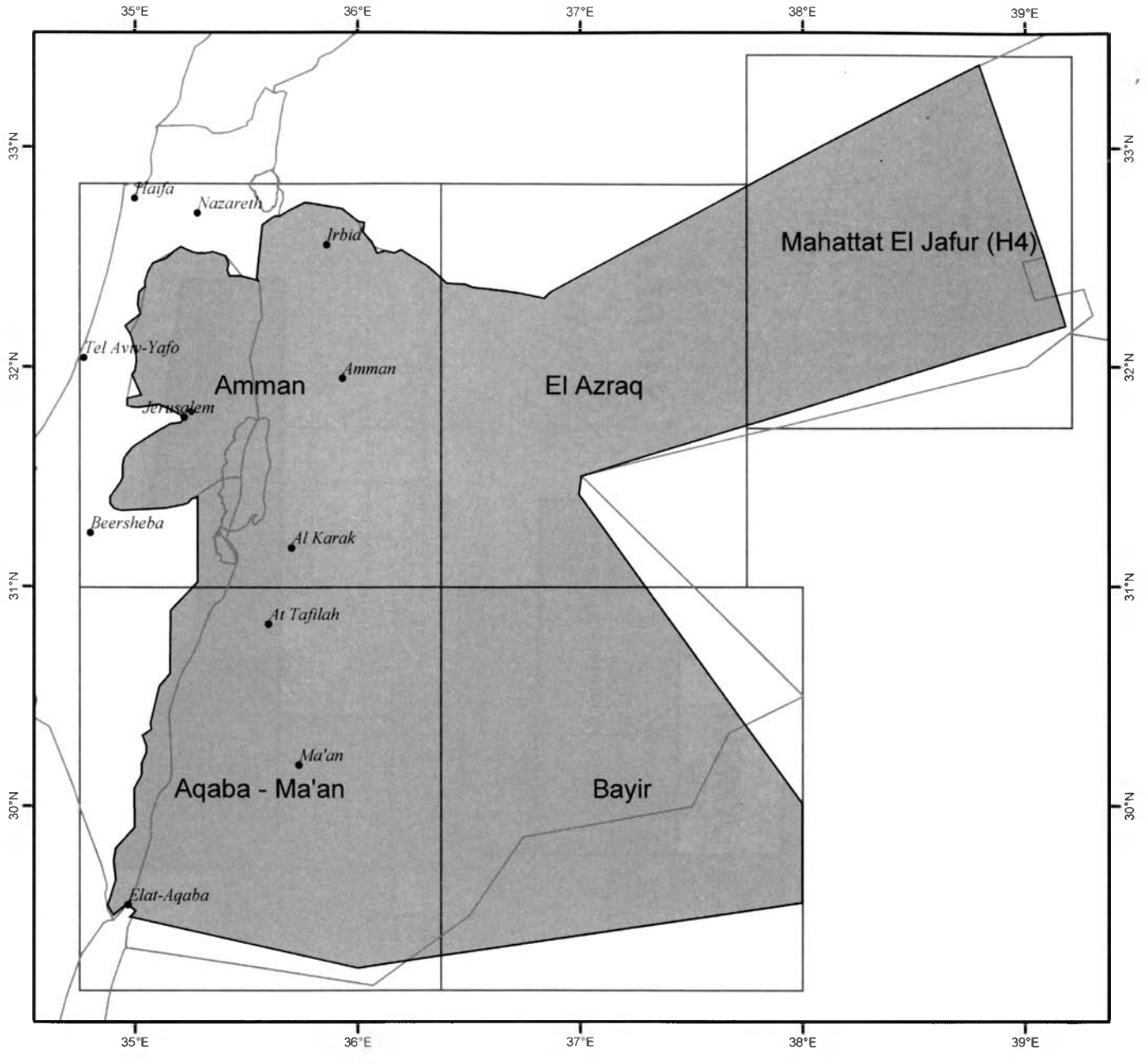


Figure AppD.4: Scheme of geological map sheets of Jordan at scale 1:250,000 (Bender, 1968).

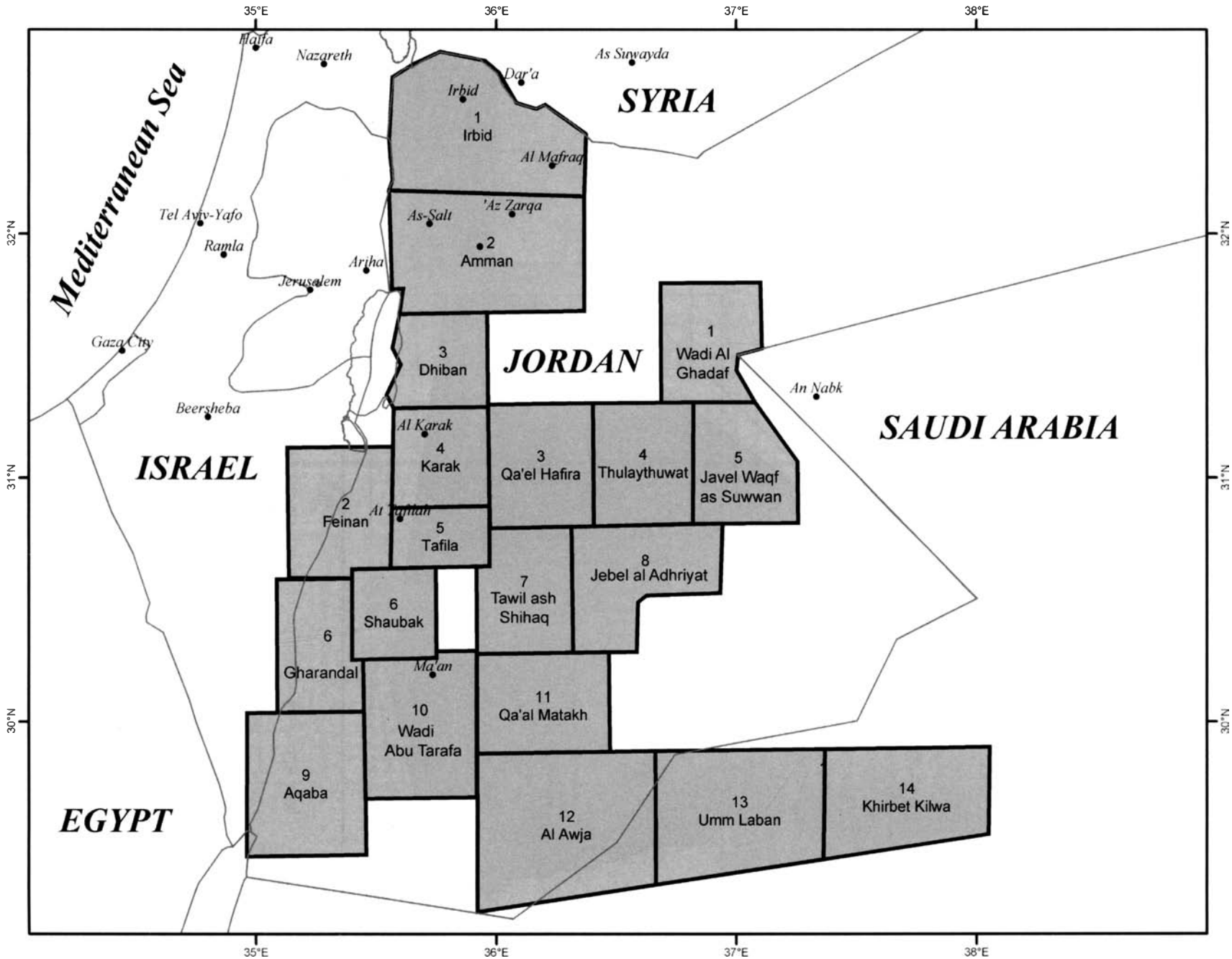


Figure AppD.5. Scheme of geological map sheets of Jordan at scale 1:100,000 (McDonald and Comp., 1965; Bender et al., 1970; Bender, 1974).

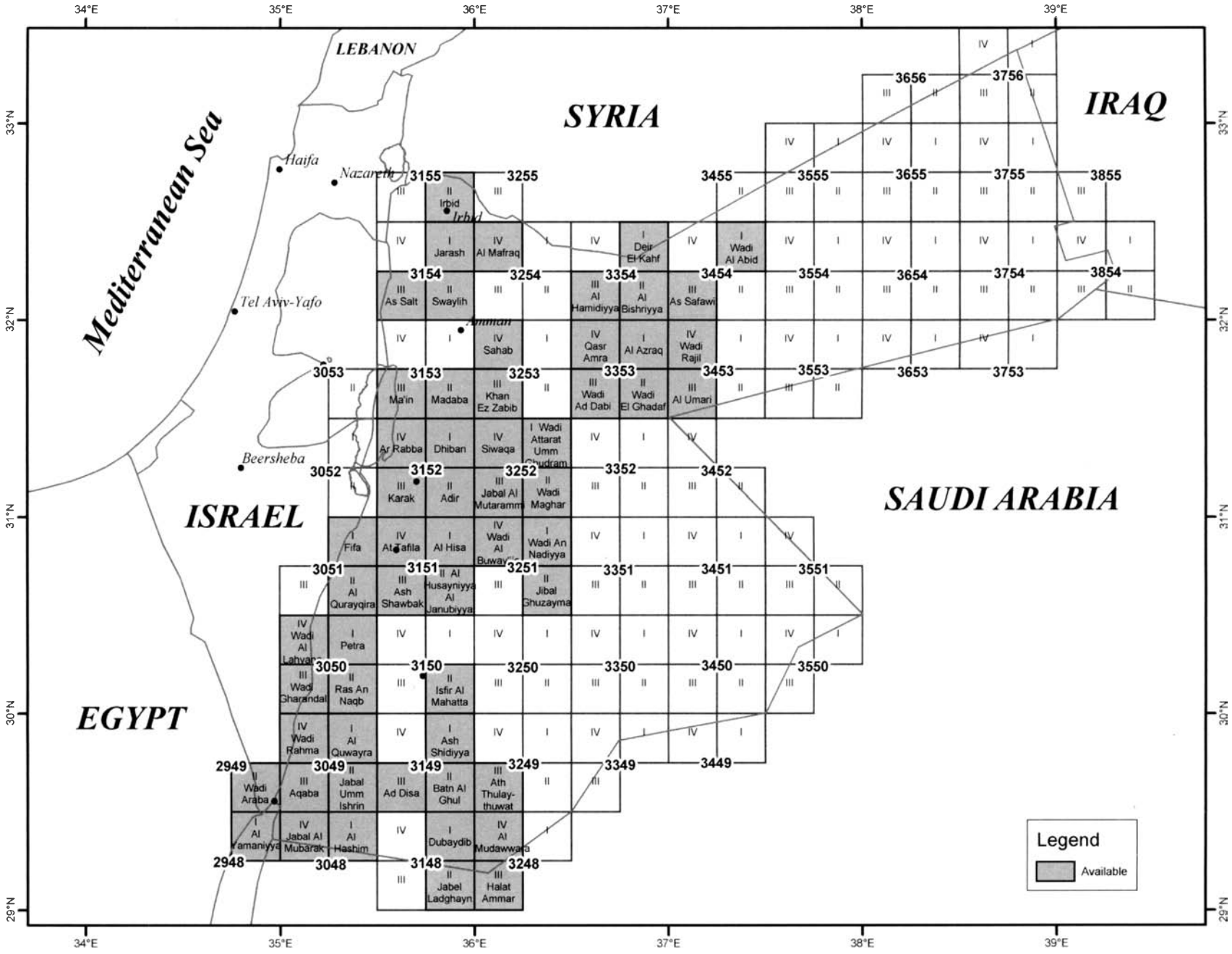


Figure AppD.6. Scheme of geological map sheets of Jordan at scale 1:50,000 (see the references for the authors of each map sheet).

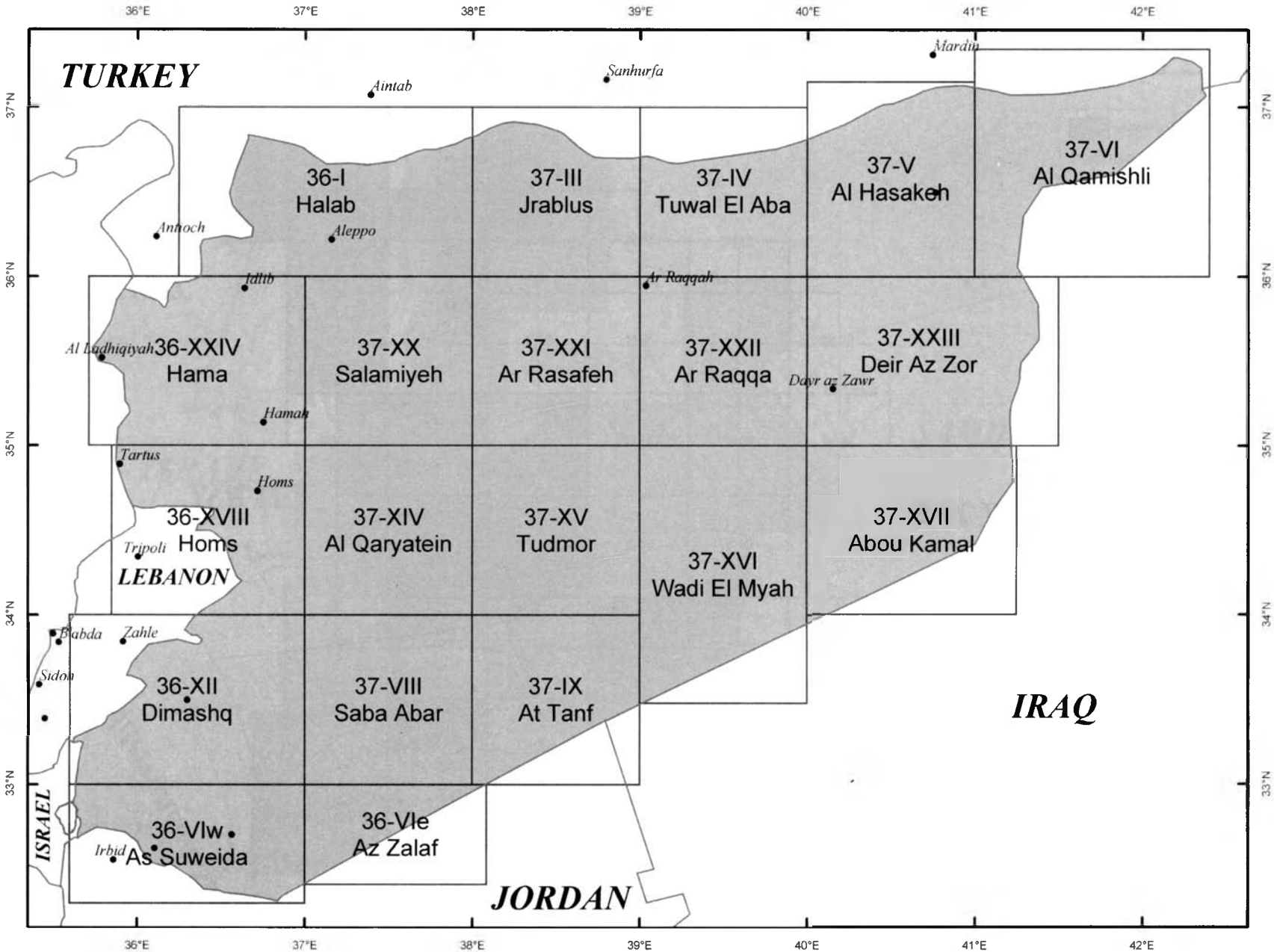


Figure AppD.7. Scheme of geological map sheets of Syria at scale 1:200,000 (Ponikarov and Comp., 1964), and 1:50,000 (see the references for the authors of each map sheet).

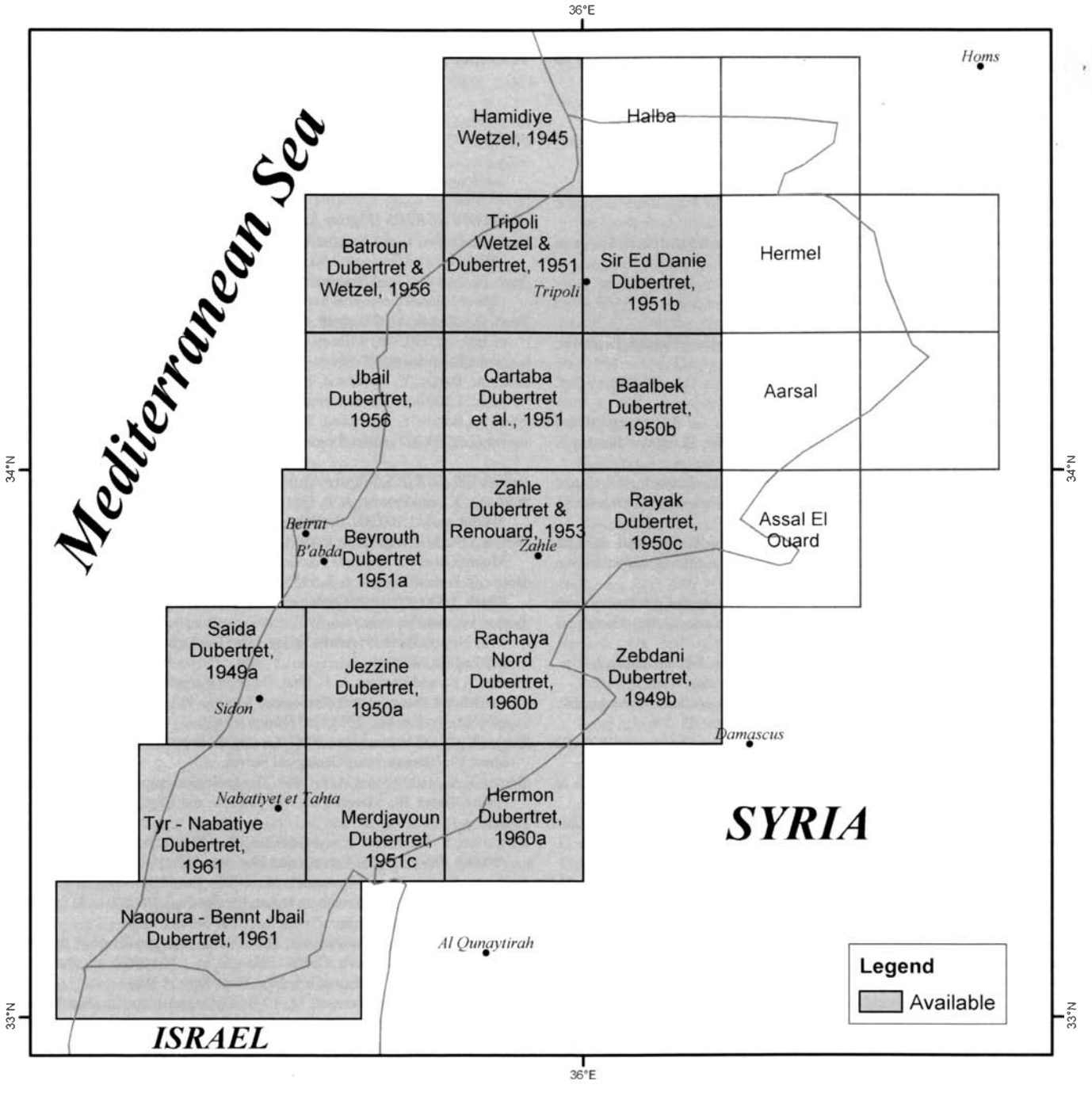


Figure AppD.8. Scheme of geological map sheets of Lebanon at scale 1:50,000.

ACKNOWLEDGEMENTS

We are most grateful to Mrs. Varda Arad of the Documentation Center of the Geological Survey of Israel for giving us access to the extensive GSI map collection, and for providing many of the references below.

REFERENCES CITED

Note: the geological map sheet references are sorted by country and by mapping scale.

General reference and regional small scale maps

Bartov, Y., 1990. Geological photomap of Israel and adjacent areas. Israel Geological Survey, 1 map, scale 1:750,000.

Bartov, Y., 1995. Geological map of Israel 1:700,000. New Atlas of Israel, Survey of Israel and Heb. Univ. Jerusalem, p. 20-22.

Bartov, Y., 1979. Israel geological map, 1:500,000. Tel Aviv, Survey of Israel.

Bartov, Y., and Arkin, Y., 1975. The geological photomap of Israel, 1:500,000. Israel Geological Survey.

Bender, F., 1967. Geological report on oil and gas prospects in Jordan. Hannover, Bundes. F. Boden. Rep., 98 p., 1 geol. map 1:750,000.

Bender, F., 1975. Geology of the Arabian Peninsula: Jordan. U.S. Geol. Surv., Prof. Pap. 560-I, 36 p., 1 geol. map 1:500,000.

Boom, G. Van Den, and Suwwan, O., 1966. Report on the geological and petrological studies of the plateau basalt in NE Jordan. Hannover, Bundes. F. Boden. Rep., 42 p, 1 geol. map 1:500,000.

Choubert, G., Faure-Muret, A., and Comp., 1985, International Geological Map of Africa scale 1:5,000,000. Commission for the Geological Map of the World, Sheet 3. UNESCO

Dubertret, L., 1966. Liban, Syrie et bordure des pays voisins. Tableau stratigraphique avec carte géologique au millionieme. Notes et memoires sur le Moyen Orient, Vol. 8, p. 251-358, geol. map, 1:1,000,000.

Ginzburg, D., Ecker, A., and Rosensaft, M., 1998, Computerized database of earth sciences maps from Israel and neighboring countries. Israel Geological Survey, Current Research, v. 11, p. 51-52.

Hudleston, W. H., 1885. The Geology of Palestine. London. Edward Stanford, 76 p., 1 map. (reprinted from: Geol. Assoc. London; Proc., Vol. 8 and 9).

Noetling, F., 1887. Der Jura am Hermon; eine geognostische monographie. Stuttgart, 46 p., 1 map 1:25,000.

Picard, L., 1959. Geological map of Israel and adjoining territories, 1:500,000. Tel Aviv, Survey of Israel.

Picard, L., 1970. Geological map, 1:500,000.; geological cross-sections. Atlas of Israel. Tel Aviv, Survey of Israel and Amsterdam, Elsevier, 2nd Ed.

Ponikarov, V. P., and Compilers, 1964. Geological map of Syria, 1:1,000,000. (compiled on the basis of geological survey 1:200,000). Moscow, V. O. Technoexport, Contract No. 944, 1 map.

Ponikarov, V. P., Kazmin, V. G., Mikhailov, I. A., Razvalyayev, A. V., Krasheninnikov, V. A., Kozlov, V. V., Sulidi-Kondratev, E. D., and Faradzhev, V. A., 1966. The geological map of Syria, scale 1:1,000,000. Explanatory notes. (translated by T. F. Lokhova). Damascus, Ministry of Industry, Dept. Geol. and Miner. Res., 111 p. (prepared for the Ministry of Industry S.A.R. under contract No. 944 By "Technoexport", Ministry Geol. USSR).

Quennell, A.M., 1951. The geology and mineral resources of (former) Trans-Jordan. Colonial Geol. Min. Resour. Lond., Vol. 2, No. 2, p. 85-115, map 1:500,000.

Sneh, A., Bartov, Y., Weissbrod, T., Rosensaft, M., and Hall, J. K., 2000. Geological shaded-relief map of Israel and environs. Israel Geological Survey.

Toloczyki, M., and Trumit, P., 1998. Carte géologique internationale de l'Europe et des regions Mediterraneennes, 1:1,500,000: Sheet F6: Halab. Hannover, Bundes. F. Geowis. U. Rohstoffe and UNESCO, 1\geol. map.

ISRAEL

***1:250,000 SERIES* (Figure AppD.2a)**

Blake, G. S., 1939. Geological map of Palestine, scale 1:250,000 (**North Sheet**). Jerusalem, Survey of Palestine.

Bentor, Y. K., Vroman, A. J., and Zak, I., 1965. The geological map of Israel, scale 1:250,000, **Southern Sheet**. Tel Aviv, Survey of Israel.

Picard, L., and Golani, U., 1965. The geological map of Israel, scale 1:250,000, **Northern Sheet**. Tel Aviv, Survey of Israel.

Shaw, S. H., 1947. **Southern Palestine** geological map on a scale of 1:250,000 with explanatory notes. Palestine, Govt. Printer, 42 p.

***1:200,000 SERIES* (Figure AppD.2b)**

Sneh, A., Bartov, Y., and Rosensaft, M., 1998a. Geological map of Israel, 1:200,000 - **Sheet 1**. Israel Geological Survey.

Sneh, A., Bartov, Y., and Rosensaft, M., 1998b. Geological map of Israel, 1:200,000 - **Sheet 2**. Israel Geological Survey.

Sneh, A., Bartov, Y., Rosensaft, M., and Weissbrod, T., 2001. Geological map of Israel, 1:200,000, 4 Sheets. Israel Geological Survey., Rep. GSI/8/2001, 4 geological maps on PC format, Version 1.0.

Sneh, A., Bartov, Y., Weissbrod, T., and Rosensaft, M., 1998c. Geological map of Israel, 1:200,000 - **Sheet 3**. Israel Geological Survey.

Sneh, A., Bartov, Y., Weissbrod, T., and Rosensaft, M., 1998d. Geological map of Israel, 1:200,000 - **Sheet 4**. Israel Geological Survey.

***1:100,000 SERIES* (Figure AppD.3a)**

Bentor, Y. K., and Vroman, A. J., 1951. The geological map of the Negev, **Sheet 18: Avedat**, scale 1:100,000. (In Hebrew). Israeli Army, Sci. Sect., 98 p.

Bentor, Y. K., and Vroman, A. J., 1954. The geological map of the Negev, **Sheet 21: Mount Omer**. Isr. Defence Forces, Scale 1:100,000.

Bentor, Y. K., and Vroman, A. J., 1955. The geological map of the Negev. **Sheet 24: Eilath**, 1:100,000. Israel Geological Survey.

Bentor, Y.K., and Vroman, A. J., 1957. Geological map of Israel, 1:100,000, Series A - The Negev. **Sheet 19: Arava Valley**. Israel Geological Survey., 66 p., (Hebrew and English editions).

Bentor, Y. K., and Vroman, A. J., 1960. Geological map of Israel, 1:100,000, **Sheet 16: Mount Sdom**. Israel Geological Survey., 117 p., (Hebrew and English editions). 1st Edition - 1954; 2nd Edition - 1960.

Bentor, Y. K., and Vroman, A. J., 1961. Geological map of Israel, Ser. A: The Negev, **Sheet 17: Nitsana**. Israel Geological Survey.

Bentor, Y. K., and Vroman, A. J., 1964. The geological map of Israel, Ser. A - The Negev. **Sheet 20: Mount Lots**. (In Hebrew and English). Israel Geological Survey.

Druckman, Y., Weissbrod, T., and Garfunkel, Z., 1993. Geological map of Israel, 1: 100,000. **Sheets 25, 26: Yotvata and Elat**. Israel Geological Survey.

Sneh, A., Bartov, Y., and Rosensaft, M., 1996a. Geological map of the **Lower Galilee, Carmel** and southern Golan. Enlarged to 1:100,000 scale from the 1: 200,000 geological map of Israel. Isr. Geol. Surv., 1 Map.

Sneh, A., Bartov, Y., and Rosensaft, M., 1996b. Geological map of the **Upper Galilee and Northern Golan**. Enlarged to 1:100,000 scale from the 1: 200,000 geological map of Israel. Isr. Geol. Surv., 1 Map.

Sneh, A., Bartov, Y., and Rosensaft, M., 1996c. Geological map of the **Northwestern Negev**. Enlarged to 1:100,000 scale from the 1:200,000 geological map of Israel. Isr. Geol. Surv., 1 Map.

Sneh, A., Bartov, Y., and Rosensaft, M., 1996d. Geological map of the **Southern Pleshet**. Enlarged to 1:100,000 scale from the 1:200,000 geological map of Israel. Isr. Geol. Surv., 1 Map.

Sneh, A., Bartov, Y., and Rosensaft, M., 1996e. Geological map of the **Northern Pleshet**. Enlarged to 1:100,000 scale from the 1:200,000 geological map of Israel. Isr. Geol. Surv., 1 Map.

Sneh, A., Bartov, Y., and Rosensaft, M., 1996f. Geological map of the **Southern Shomeron**. Enlarged to 1:100,000 scale from the 1:200,000 geological map of Israel. Isr. Geol. Surv., 1 Map.

Sneh, A., Bartov, Y., and Rosensaft, M., 1996g. Geological map of the **Northern Shomeron**. Enlarged to 1:100,000 scale from the 1:200,000 geological map of Israel. Isr. Geol. Surv., 1 Map.

Sneh, A., Bartov, Y., Rosensaft, M., Avni, Y., Baer, G., Becker, A., Soudry, D., and Zilberman, E., 1997. Geological map of **Makhtesh Ramon** and vicinity,

Israel. (sheets 21, 22). Isr. Geol. Surv., 1 Geol. Map, Scale 1:100,000.

Sneh, A., and Rosensaft, M., 1994. Geological map (1:100,000) of the Coastal Plain of Israel: **Netanya, Tel Aviv - Yafo, Ashqelon** and **Nirim** sheets. Isr. Geol. Surv., Rep. GSI/29/94, 4 p., 4 maps.

Picard, L., 1955. Geological map of Israel, 1:100,000. **Sheet 2: Haifa**. Israel Geological Survey.

Picard, L., 1955. Geological map of Palestine, 1:100,000, **Sheet 9: Ramle**. Israel Geological Survey.

Picard, L., 1956. Geological map of Israel 1:100,000. **Sheet 4: Zikhron Yaaqov**. Israel Geological Survey.

Picard, L., 1956. The geological map of Israel, 1:100,000. **Sheet 3: Safad**. Israel Geological Survey.

Picard, L., 1956. The geological map of Israel, 1:100,000. **Sheet 1: Metulla**. Israel Geological Survey.

Picard, L., 1956. The geological map of Israel, 1:100,000. **Sheet 5: Nazareth**. Israel Geological Survey.

Picard, L., 1956. The geological map of Palestine, 1:100,000. **Sheet 8: Yibna**. Israel Geological Survey.

Picard, L., 1956. The geological map of Palestine, 1:100,000. **Sheet 11: Gaza**. Israel Geological Survey.

1:50,000 SERIES (Figure AppD.3b)

Arkin, Y., 1984. Geological map of Israel, 1:50,000: **Sheet 18-IV Sede Boqer** (preliminary edition). Israel Geological Survey

Arkin, Y., Braun, M., Buchbinder, B., Diamant, E., Itzhaki, Y., Lasman, N., Rot, I., and Shachnai, E., 1976. Geological map of Israel, 1:50,000: **Sheet 11-II Jerusalem and Vicinity**. Israel Geological Survey.

Avni, Y., 2001. Geological map of Israel, 1:50,000: **Sheet 21-III: Har Loz**. Israel Geological Survey.

Begin, Z. B., 1974. The geological map of Israel, 1:50,000: **Jericho**. Israel Geological Survey, 15 p. (explanatory notes in English and Hebrew).

Begin, Z. B., 1997. Geological Map, 1:50,000: **Sheet 9-III, Jericho** (preliminary computerized edition). Israel Geological Survey, Rep. GSI/12/97.

Beyth, M., Segev, A., and Bartov, Y., 1999. Geological map of Israel, 1:50,000: **Beer Ora**. Israel Geological Survey.

Cook, P., 1991. Geological map of Israel, 1:50,000: **Sheet 5-IV: Shekhem** (preliminary edition). Geological survey - by P. Cook, 1971-72; Digital processing and editing by M. Rosensaft and A. Sneh, 1991. Israel Geological Survey.

Gilat, A., 1977. Geological map of Israel, 1:50,000: **Sheet 15-I Eshtemoa**. Israel Geological Survey.

Gilat, A., 1983. Geological map of Israel, 1:50,000: **Sheet 15-II Har Hezron** (preliminary edition). Israel Geological Survey.

Gilat, A., 1987. Geological map of Israel, 1:50,000: **Sheet 15-II Har Hezron**. Israel Geological Survey.

Ginat, H., 1994. Geological map of Israel, 1:50,000: **Sheet 25-II Yotvata**. Israel Geological Survey.

Hatzor, Y., 2000. Geological map of Israel, 1:50,000: **Sheets 6-I, 6-II: Bet Shean**. Israel Geological Survey.

Hildebrand-Mittlefehldt, N., 1993. Geological map of Israel, 1:50,000: **Sheet 8-I Kefar Sava**. Israel Geological Survey.

Hildebrand-Mittlefehldt, N., 1997. Geological map, 1:50,000: **Sheet 8-I Kefar Sava**. Updated computerized edition. Israel Geological Survey, Rep. GSI/12/97, Edited by M. Rosensaft and A. Sneh.

Hirsch, F., 1983. Geological map of Israel, 1:50,000: **Sheet 11-III Bet Guvrin**. Israel Geological Survey. (explanatory notes, 16 p. in English; 10 p. in Hebrew).

Hirsch, F., 1995. Geological map of Israel, 1:50,000: **Sheet 19-II Hamakhtesh Haqatan**. Israel Geological Survey.

Ilani, S., 1985. Geological map of Israel, 1:50,000: **Sheet 5-III Netanya**. Israel Geological Survey.

Itzhaki, Y., Arkin, Y., Braun, M., and Lasman, N., 1964. **Jerusalem - Bet Shemesh**: geological map, 1:50,000. Israel Geological Survey.

Kafri, U., 1972. Geological map of Israel, 1:50,000: **Sheet 1-III, 1-IV Nahariyya**, with explanatory notes. (In Hebrew and English). Israel Geological Survey.

Levitte, D., 2001. Geological map of Israel, 1:50,000: **Sheet 2-III: Zefat**. Israel Geological Survey.

Levy, Y., 1983. Geological map of Israel, 1:50,000: **Sheet 3-II Shefaram**. Israel Geological Survey.

Michelson, H., and Mor, D., 1985. Geological map of Israel, 1:50,000: **Gamla**. (preliminary edition). Israel Geological Survey.

Mor, D., 1987. Geological map of Israel, 1:50,000: **Har Odem**. Israel Geological Survey.

Mor, D., 1987. Geological map of Israel, 1:50,000: **Kazrin**. Israel Geological Survey.

Mor, U., 1996. Geological map of Israel, 1:50,000: **Sheet 12-III Mizpe Shalem** (preliminary map and summary of explanation notes, in Hebrew). Israel Geological Survey, Rep. GSI/1/96, 6 p.

Mor, U., and Burg, A., 2000. Geological map of Israel, 1:50,000: **Sheet 12-III: Mizpe Shalem**. Israel Geological Survey.

Raz, E., 1983. Geological map of Israel, 1:50,000: **Sheet 16-I 'En Gedi** (preliminary map). Israel Geological Survey.

Raz, E., 1986. Geological map of Israel, 1:50,000: **Sheet 16-I 'En Gedi**. Israel Geological Survey.

Roded, R., 1978. Geological map of Israel, 1:50,000: **Sheet 19-III Oron**. Israel Geological Survey.

Roded, R., 1996. Geological map of Israel, 1:50,000: **Sheet 19-I Dimona**. Israel Geological Survey.

Roth, I., 1970. Geological map of Israel, 1:50,000: **Wadi El Qilt** Israel Geological Survey.

Segev, A., and Beyth, M., 2000. Geological map of Israel, 1:50,000 - **Har Seguv** Sheet. Israel Geological Survey.

Shachnai, E., 1997. Geological map, 1:50,000: **Sheet 8-IV Ramallah** (preliminary computerized map). Israel Geological Survey, Rep. GSI/12/97, Edited by M. Rosensaft and A. Sneh

Shachnai, E., 2000. Geological map of Israel, 1:50,000: **Sheet 8-IV: Ramallah**. Israel Geological Survey.

Sneh, A., Ed., 1997. Geological map, 1:50,000: **Sheet 9-I Maale Efrayim** (preliminary computerized edition). Israel Geological Survey, Rep. GSI/12/97, Edited by M. Rosensaft and A. Sneh.

Sneh, A., Ed., 1997. Geological map, 1:50,000: **Sheet 8-II Ariel** (preliminary computerized edition). Israel Geological Survey, Rep. GSI/12/97, Edited by M. Rosensaft and A. Sneh.

Sneh, A., Sass, E., Bein, A., Arad, A., and Rosensaft, M., 1998. Geological map of Israel 1:50,000: **Sheet 5-I Hadera**. Israel Geological Survey.

Sneh, A., and Weinberger, R., 2003, The geological mapping of 1:50,000 **Metulla** quadrangle - implications for the stratigraphic division and fault pattern around the Hula Valley, Israel. Israel Geological Survey. Rep. GSI/7/03 27 p. (In Hebrew).

Starinsky, A., Zilberman, E., and Braun, M., 1984. **Sheet 18-II Revivim**; geological map, 1:50,000 (preliminary edition). Israel Geological Survey.

Vroman, A. J., 1958. The geological map of Israel, 1:50,000. Serie 1: Galilee. Israel Geological Survey, 6 Maps. (Sheet 1: **Tarshiha**; 2-W: **Safad**; 2-E: **Hula**; 3-E: **Nazareth**; 4-W: **Tabor**; 4-E: **Tiberias**).

Yechieli, Y., 1997. Geological map, 1:50,000, **Sheet 8-III, Lod** (preliminary computerized edition). Israel Geological Survey, Rep. GSI/12/97, Edited by M. Rosensaft and A. Sneh.

Yechieli, Y., Elron, E., and Sneh, A., 1994. Geological map of Israel, 1:50,000: **Sheet 19-IV, 20-III Neot Hakikar**. Israel Geological Survey.

Zilberman, E., 2001. Geological map of Israel, 1:50,000: **Sheet 17-IV Nizzana**. Israel Geological Survey.

Zilberman, E., 2002. Geological map of Israel, 1:50,000: **Sheet 17-II Holot Agur**. Israel Geological Survey.

Zilberman, E., 2002. Geological map of Israel, 1:50,000: **Sheet 21-IV Rehovot Banegev**. Israel Geological Survey.

JORDAN

1:250,000 SERIES (Figure AppD.4)

Bender, F., and Comp., 1968. Geological map of Jordan, 1:250,000. Sheets: **Amman; El Azraq; Mahattat El Jufur (H4); Aqaba - Maan; Bayir**. Hannover, Bundes. F. Boden., 5 maps.

Quennell, A. M., 1948. Geological map of Trans-Jordan on a 1:250,000 scale. The Hashemite Kingdom of Jordan.

Quennell, A. M., 1956. Geological map of Jordan (East of the Rift Valley), 1: 250,000. Sheets: **Amman, Kerak, Ma'an**. Jordan, Dept. Lands and Surveys.

1:100,000 SERIES (Figure AppD.5)

Bender, F., Heimbach, W., Khdeir, M. K., and Wiesemann, G., 1970. Geological map of Jordan (Draft Map), Scale 1:100,000. **Sheets: 1, 3, 4, 5, 7, 8, 10, 11, 12, 13, 14.** Hannover, Bundes. F. Boden.

Bender, F., 1974. Explanatory notes on the geological map of the Wadi Araba, Jordan. (Scale 1:100,000, 3 Sheets). Geol. Jahrb., Reihe B, No. 10, 62 p.

1:50, 000 SERIES (Figure AppD.6)

Abdelhamid, G., 1990. The geology of the **Jabal Umm Ishrin** area (Wadi Ram), map sheet No. **3049-II**. Jordan, Nat. Resour. Authority, Bull. 14, 76 p., map 1: 50,000.

Abdelhamid, G., 1995. The geology of **Jarash** area, map sheet **3154-I**. Jordan, Nat. Resour. Authority, Bull. 30, 51 p., Map 1:50,000.

Abdelhamid, G., 1997. Geological map of **Wadi Rajil 3453-IV**. Jordan, Nat. Resour. Authority, Geol. Mapping Div., 1 geol. map 1:50,000, with brief description on the geology. In English and Arabic.

Abdelhamid, G., Ibrahim, K. M., and Mortimer, C., 1994. The geology of **Ayn Al Hashim**, **Jabal Al Mubarak** and **Al Yamaniyya**, map sheets No. **3048-I**, **3048-IV** and **2948-I**. Jordan, Nat. Resour. Authority, Bull. 27, 57 p., 2 maps, 1: 50,000.

Abu Hammour, H., 1998. Geological map of **Wadi Maghar 3252-II**. Jordan, Nat. Resour. Authority, Geol. Mapping Div., 1 geol. map 1:50,000, with brief description on the geology. In English and Arabic.

Abu Lihie, O., 1985. Geological map of **Wadi An Nadiyya**, **3251-I**. Jordan, Nat. Resour. Authority, Geol. Mapping Div., 1 geol. map 1:50,000, with brief description on the geology. In English and Arabic.

Abu Lihie, O., 1986. The geology of **Wadi An Na'diya** map sheet No. **3251-I**. Jordan, Nat. Resour. Authority, Bull. 2, 27 p., map 1:50,000.

Abu Lihie, O., 1988. Geologic map of **Jabal Ladghayn 3148-II** and **Dubaydib 3148-I**. Amman, Nat. Resour. Authority, Geol. Mapping Div., 1 geol. map 1: 50,000, with brief description on the geology. In English and Arabic.

Abu Qudaira, M., 1997. Geological map of **Qasr Amra 3353-IV**. Jordan, Nat. Resour. Authority, Geol. Mapping Div., 1 geol. map 1:50,000, with brief description on the geology. In English and Arabic.

Abu Qudaira, M. A., 1996. The geology of the **Wadi Attarat Umm Ghudran** area, map sheet No. **3252-I**. Jordan, Nat. Resour. Authority, Bull. 33, 31 p., map 1: 50,000.

Al Hunjul, N. G., 1995. The geology of **Madaba** area, map sheet No. **3153-II**. Jordan, Nat. Resour. Authority, Bull. 31, 65 p., map 1:50,000.

Al Khatib, F., 1987. Geologic map of **Al Yamaniyya - 2948-I** and **Jabal Al Mubarak - 3048-IV**. Amman, Nat. Resour. Authority, Geol. Mapping Div., 1 geol. map 1:50,000, with brief description of the geology. In English and Arabic.

Al Nawasreh, M. K., 1994. Geological map of **As Safawi** (Al Hafif) **3454-III**. Jordan, Nat. Resour. Authority, Geol. Mapping Div., 1 geol. map 1:50,000, with brief description on the geology. In English and Arabic.

Barakat, H., 1986. Geologic map of **Ayn Al Hashim 3048-I**. Jordan, Nat. Resour. Authority, Geol. Mapping Div., 1 geol. map 1:50,000, with brief description on the geology. In English and Arabic.

Barjous, M. O., 1986. The geology of **Siwaqa**, map sheet No. **3252-IV**. Jordan, Nat. Resour. Authority, Bull. 4, 70 p., map 1:50,000.

Barjous, M. O., 1988. Geologic map of **Ash Shawbak 3151-III**. Amman, Nat. Resour. Authority, Geol. Mapping Div., 1 geol. map 1:50,000, with brief description on the geology. In English and Arabic.

Barjous, M. O., 1992. The geology of the **Ash Shawbak** area, map sheet No. **3151-III**. Jordan, Nat. Resour. Authority, Bull. 19, 79 p., map 1:50,000.

Barjous, M. O., 1995. **Petra** and **Wadi Al Lahyana** (**3050-I** and **3050-IV**). Amman, Nat. Resour. Authority, 1 map, 1:50,000 with explanatory notes on the back.

Faddah, E. H., 1989. Geologic map of **Sahab 3253-IV**. Jordan, Nat. Resour. Authority, Geol. Mapping Div., 1 geol. map 1:50,000, with brief description on the geology. In English and Arabic.

Faddah, E. H., 1991. The geology of the **Sahab** area, map sheet No. **3253-IV**. Jordan, Nat. Resour. Authority, Bull. 17, 31 p., map 1:50,000.

Faddah, E. H., 1996. The geology of **Wadi El Ghadaf** area, map sheet **3353-II**. Jordan, Nat. Resour. Authority, Bull. 34, 26 p., map 1:50,000.

Faddah, E. H., 1997. Geological map of **Wadi Ad Dabi 3353-III**. Jordan, Nat. Resour. Authority, Geol. Mapping Div., 1 geol. map 1:50,000, with brief description on the geology. In English and Arabic.

Halasa, W., 1996. Geological map of **Ash Shidiyya** (Fassua) **3149-I**. Jordan, Nat. Resour. Authority, Geol. Mapping Div., 1 geol. map 1:50,000, with brief description on the geology. In English and Arabic.

Halaseh, W., 1997. Geological map of **Isfir Al Mahatta 3150-II**. Jordan, Nat. Resour. Authority, Geol. Mapping Div., 1 geol. map 1:50,000, with brief description on the geology. In English and Arabic.

Ibrahim, K., 1993. The geology of the **Wadi Gharandal** area, map sheet No. **3050-II**. Jordan, Nat. Resour. Authority, Bull. 24, map 1:50,000.

Ibrahim, K. M., 1989. Geologic map of **Wadi Rahma 3049-IV**. Jordan, Nat. Resour. Authority, Geol. Mapping Div., Bull. 15, 122 p., 1 geol. map 1:50,000, with brief description on the geology. In English and Arabic.

Ibrahim, K. M., 1990. Geologic map of **Wadi Gharandal 3050-III**. Jordan, Nat. Resour. Authority, Geol. Mapping Div., 1 geol. map 1:50,000, with brief description on the geology. In English and Arabic.

Ibrahim, K. M., 1993. Geologic map of **Al Azraq 3353-I**. Jordan, Nat. Resour. Authority, Geol. Mapping Div., 1 geol. map 1:50,000, with brief description on the geology. In English and Arabic.

Ibrahim, K. M., 1996. Geological map of **Al Bishriyya** (Al Aritayn) **3354-II**. Jordan, Nat. Resour. Authority, Geol. Mapping Div., 1 geol. map 1:50,000, with brief description on the geology. In English and Arabic.

Jaser, D., 1986. The geology of **Khan Ez Zabib**, map sheet No. **3253-III**. Jordan, Nat. Resour. Authority, Bull. 3, 47 p., map 1:50,000.

Khalil, B., 1992. The geology of the **Ar Rabba** area, map sheet No. **3152-IV**. Jordan, Nat. Resour. Authority, Bull. 22, 105 p., map 1:50,000.

Khalil, B., 1994. The geology of **Ad Disa** area (Qannassiya), map sheet No. **3149-III**. Jordan, Nat. Resour. Authority, Bull. 26, 56 p., geol. map, 1:50,000.

Kherfan, A., 1987. The geology of **Jibal Ghuzayma**, map sheet No. **3251-II**. Jordan, Nat. Resour. Authority, Bull. 6, 26 p., map 1:50,000.

Ma'an, A., 1985. Geological map of **Jabal Al Mutarammil** (sheet No. **3252-III**). Jordan, Nat. Resour. Authority, geol. map 1:50,000.

Masri, A., 1988. The geology of **Halat Ammar** and **Al Mudawwara**, map sheet Nos. **3248-III**, **3248-IV**. Jordan, Nat. Resour. Authority, Bull. 13, 60 p., map 1: 50,000.

Masri, A., 1992. The geology of the **Ath Thulaythuwat** area, map sheet No. **3249-III**. Jordan, Nat. Resour. Authority, Bull. 23, 31 p., map 1:50,000.

Masri, A., 1996. Geological map of **Dhiban** (Wadi Al Mujib) **3152-I**. Jordan, Nat. Resour. Authority, Geol. Mapping Div., 1 geol. map 1:50,000, with brief description on the geology. In English and Arabic.

Masri, A., 1998. Geological map of **Batn Al Ghul** (Jabal Al Harad) **3149-II**. Jordan, Nat. Resour. Authority, Geol. Mapping Div., 1 geol. map 1:50,000, with brief description on the geology. In Eng. and Arabic.

Mohd, B. K., 1986. The geology of **Wadi Al Buway'ija**, map sheet No. **3251-IV**. Jordan, Nat. Resour. Authority, Bull. 5, 47 p., map 1:50,000.

Mohd, B. K., 1989. Geologic map of **Ar Rabba 3152-IV**. Jordan, Nat. Resour. Authority, Geol. Mapping Div., 1 geol. map 1:50,000, with brief description on the geology. In English and Arabic.

Mohd, B. K., 1989. Geological map of **Ad Disa** (Jabal Al Qannasiyya) **3149-III**. Jordan, Nat. Resour. Authority, Geol. Mapping Div., 1 geol. map 1:50,000, with brief description on the geology. In English and Arabic.

Mohd, B. K., 1997. Geological map of **Irbid 3155-II**. Jordan, Nat. Resour. Authority, Geol. Mapping Div., 1 geol. map 1:50,000, with brief description on the geology. In English and Arabic.

Moumani, K. A., 1996. Geological map of **Al Husayniyya Al Janubiyya** (Jurf Ad Darawish) **3151-II**. Jordan, Nat. Resour. Authority, Geol. Mapping Div., 1 geol. map 1:50,000, with brief description on the geology. In English and Arabic.

Muneizel, S., and Khalil, B., 1993. Geological map of **As Salt 3154-III**. Jordan, Nat. Resour. Authority, Geol. Mapping Div., 1 geol. map 1:50,000, with brief description on the geology. In English and Arabic.

Nawasra, M. K., 1997. Geological map of **Deir El Kahf** (Jibal Abu El Idham) **3354-I**. Jordan, Nat. Resour. Authority, Geol. Mapping Div., 1 geol. map 1:50,000, with brief description on the geology. In English and Arabic.

Powell, J. H., 1988. The geology of the **Karak** area, map sheet No. **3152-III**. Jordan, Nat. Resour. Authority, Bull. 8, 172 p., map 1:50,000.

Rabba, I., 1994. The geology of the **Al Qurayqira** (Jabal Hamra Faddan), map sheet No. **3051-II**. Jordan, Nat. Resour. Authority, Bull. 28, 60 p., map 1:50,000.

Rabba, I., 1997. Geological map of **Al Umari** (Abar Al Hazim) **3453-III**. Jordan,

Nat. Resour. Authority, Geol. Mapping Div., 1 geol. map 1:50,000, with brief description on the geology. In English and Arabic.

Rabba, I. A., 1988. Geologic map of **Al Quwayra 3049-I**. Jordan, Nat. Resour. Authority, Geol. Mapping Div., 1 geol. map 1:50,000, with brief description on the geology. In English and Arabic.

Rabba, I. A., 1991. The geology of the **Al Quwayra** area, map sheet No. **3049-I**. Jordan, Nat. Resour. Authority, Bull. 16, 50 p., map 1:50,000.

Rashdan, M., 1988. The regional geology of the **Aqaba - Wadi Araba** area, map sheets **3049-III**, **2949-II**. Jordan, Nat. Resour. Authority, Bull. 7, 87 p., map 1: 50,000.

Sawariah, A., and Barjous, M. O., 1993. Geological map of **Swaylih 3154-II**. Jordan, Nat. Resour. Authority, Geol. Mapping Div., 1 geol. map 1:50,000, with brief description on the geology. In English and Arabic.

Shawabkeh, K., 1991. The geology of the **Adir** area, map sheet No. **3152-II**. North Jordan. Jordan, Nat. Resour. Authority, Bull. 18, 32 p., map 1:50,000.

Shawabkeh, K., 1996. Geological map of **Main 3153-III**. Jordan, Nat. Resour. Authority, Geol. Mapping Div., 1 geol. map 1:50,000, with brief description on the geology. In English and Arabic.

Smadi, A. A., 1997. Geological map of **Al Mafraq 3254-IV**. Jordan, Nat. Resour. Authority, Geol. Mapping Div., 1 geol. map 1:50,000, with brief description on the geology. In English and Arabic.

Tarawneh, B., 1988. The geology of **At Tafila**, map sheet No. **3151-IV**. Jordan, Nat. Resour. Authority, Bull. 12, 55 p., map 1:50,000.

Tarawneh, B., 1992. The geology of the **Fifa** area. map sheet No. **3051**. Jordan, Nat. Resour. Authority, Bull. 20, 46 p., map, 1:50.000.

Tarawneh, B., 1996. Geological map of **Al Hisa** (Al Ina) **3151-I**. Jordan, Nat. Resour. Authority, Geol. Mapping Div., 1 geol. map 1:50,000, with brief description on the geology. In English and Arabic.

Tarawneh, K., 1996. The geology of the **Al Hamidiyya** (Al Hababiyya) area. map sheet No. **3354-III**. Jordan, Nat. Resour. Authority, Bull. 35, 33 p., map 1: 50,000.

Tarawneh, K., 1999. Geological map of **Wadi Al Abid** (sheet No. **3454-I**). Jordan, Nat. Resour. Authority, geol. map 1:50,000.

SYRIA

1:200,000 SERIES (Figure AppD.7)

Dubertret, L., 1955. Géologie de roches vertes du Nord Quest de la Syrie et du Hatay (Turquie). Nôtes et mémoires sur le Moyen Orient, Vol. 6, p. 1-179, maps.

Ponikarov, V. P., 1962. Brief report on geological map of Syrian Arab Republic in a scale 1:200,000, Compiled by Soviet geologists under the contract No. 944. Damascus, 24 p.

Ponikarov, V. P., and Comp., 1964. Geological map of Syria, 1:200,000. Moscow, V.O. Technoexport, **20 Sheets** with geological cross sections and explanatory notes. (prepared for the Ministry of Industry, S.A.R. under contract No. 944. Translated from Russian).

1:50,000 SERIES

Jack, A., and Algamal, N. E., 1983. Geological survey of **Kalat Alhosell** area, scale 1:50,000. Damascus, Gen. Establ. Geol. Mineral. Resour.

Kazmin, V. G., Kulakov, V. V., and Compilers, 1968. The geological map of Syria 1:50,000 (**western Syria - Turkey border**); Explanatory notes. Syria, Ministry Pet. Electricity and Execution of Industrial Projects. Dept. of Geological and Mineral Research, 124 p.

Kurbanov, N. K., Narjanov, Y., and Compilers, 1968. The geological map of Syria 1:50,000 (**Zebdani; Rayak**); Explanatory notes. Syria, Ministry Pet. Electricity and Execution of Industrial Projects. Dept. of Geological and Mineral Research, 120 p.

Kurbanov, N. K., and Zarjanov, Y. P., 1962. Geological map of Syria, scale 1: 50,000, Sheets I-37-VII-3a, I-37-VII-3c. Report on geological operations carried out in 1958-1959 on the territory previously mapped by the French geologists (L. Dubertret, Etc.) on 1:50,000 scale. Moscow.

Ponikarov, V. P., 1962. Geological map of Syria, 1:50,000, Sheet I-36-XXIV-4b, d; I-37-XIX-3c. Moscow, V.O. Technoexport, 2 Maps.

Ponikarov, V. P., 1962. Geological map of Syria, 1:50,000, Sheet J-37-I-4 a, b, c, d. Moscow, V.O. Technoexport, 1 Map. (chief geologist: V. Ponikarov; Compiled By L. Protasevich and V. Kurbanov).

Ponikarov, V. P., 1968. Geological map of Syria, 1:50,000, Sheet I-37-VII-3a, c. Moscow, V.O. Technoexport, 1 Map. (Chief Geologist: V. Ponikarov; Compiled By N. Kurbanov and Y. Zarjanov, 1962; printed in USSR, 1968).

Ponikarov, V. P., 1968. The geological map of Syria, 1:50,000 (**Lattaquie**). Explanatory notes. Damascus, Ministry of Pet., Dept. Geol. Miner. Res., 124 p., 1 map.

Protasevich, L. T., Kurbatov, V. P., and Compilers, 1968. The geological map of Syria, 1:50,000 (**Radjou; Aafrine; Meidane Ekbez; Bulbul**); Explanatory notes. Syria, Ministry Pet. Electricity and Execution of Industrial Projects. Dept. of Geological and Mineral Research, 83 p.

Ruske, R., 1978. Geological map of Syria 1:50,000, Sheet **Qerdaha**, N-I-37-S-1-C; Explanatory notes. Syria, Ministry Pet. Miner. Resour., General Establishment of Geology and Mineral Resources, 36 p.

Ruske, R., and Sanlaville, P., 1978. Geological map of Syria, Scale 1:50,000, Sheet **Jableh**, Explanatory notes. Damascus.

Youssef, S., 1979. Geological map of Syria 1:50,000, Sheet **Haffeh**, Ni 37-S-3-A; Explanatory notes. Syria, Ministry Pet. Miner. Resour., General Establishment of Geology and Mineral Resources, 35 p.

LEBANON

1:200,000 SERIES

Dubertret, L., and Wetzel, R., 1949. Carte géologique au 200,000, feuille de Tripoli. Beirut, Ministère des Travaux Publics, 64 p.

1:50,000 SERIES (Figure AppD.8)

Dubertret, L., 1949a. Carte géologique au 50,000, feuille de **Saida**. Beirut, Ministère des Travaux Publics, 46 p.

Dubertret, L., 1949b. Carte géologique au 50,000, feuille de **Zebdani**. Damas, Ministère des Travaux Publics, 62 p.

Dubertret, L., 1950a. Notice explicative de la carte géologique de **Jezzine** au 50,000. Beirut, Ministère des Travaux Publics, 80 p.

Dubertret, L., 1950b. Carte géologique au 50,000, feuille de **Baalbek**. Beirut, Ministère des Travaux Publics, 52 p.

Dubertret, L., 1950c. Carte géologique au 50,000, feuille de **Rayak**. Beirut, Ministère des Travaux Publics, 48 p.

Dubertret, L., 1951a. Carte géologique au 50,000, feuille de **Beyrouth**. Beirut, Ministère des Travaux Publics, 66 p. (map published in 1945).

Dubertret, L., 1951b. Carte géologique au 50,000, feuille de **Sir Ed Danie**. Beirut, Ministère des Travaux Publics, 51 p.

Dubertret, L., 1951c. Notice explicative de la carte géologique de **Merdjayoun**. Beirut, Ministère des Travaux Publics, 64 p., map scale 1:50,000.

Dubertret, L., 1956. Feuille de **Jbail** au 50,000; notice explicative. Beirut, Ministère des Travaux Publics, 34 p. (map published in 1945).

Dubertret, L., 1960. Carte géologique au 1:50,000 feuille **Hermon (Rachaya Sud)**. Beirut, Ministère des Travaux Publics, 46 p. (map published in 1957).

Dubertret, L., 1960. Carte géologique au 50,000, feuille de **Rachaya Nord**. Beirut, Ministère des Travaux Publiques, 46 p. (map published by L. Dubertret and H. Vautrin in 1950).

Dubertret, L., 1961. Carte géologique au 1:50,000 - feuilles de **Tyr - Nabatiye** et **Naqoura - Bennt Jbail**. Beyrouth, Ministère des Travaux Publics.

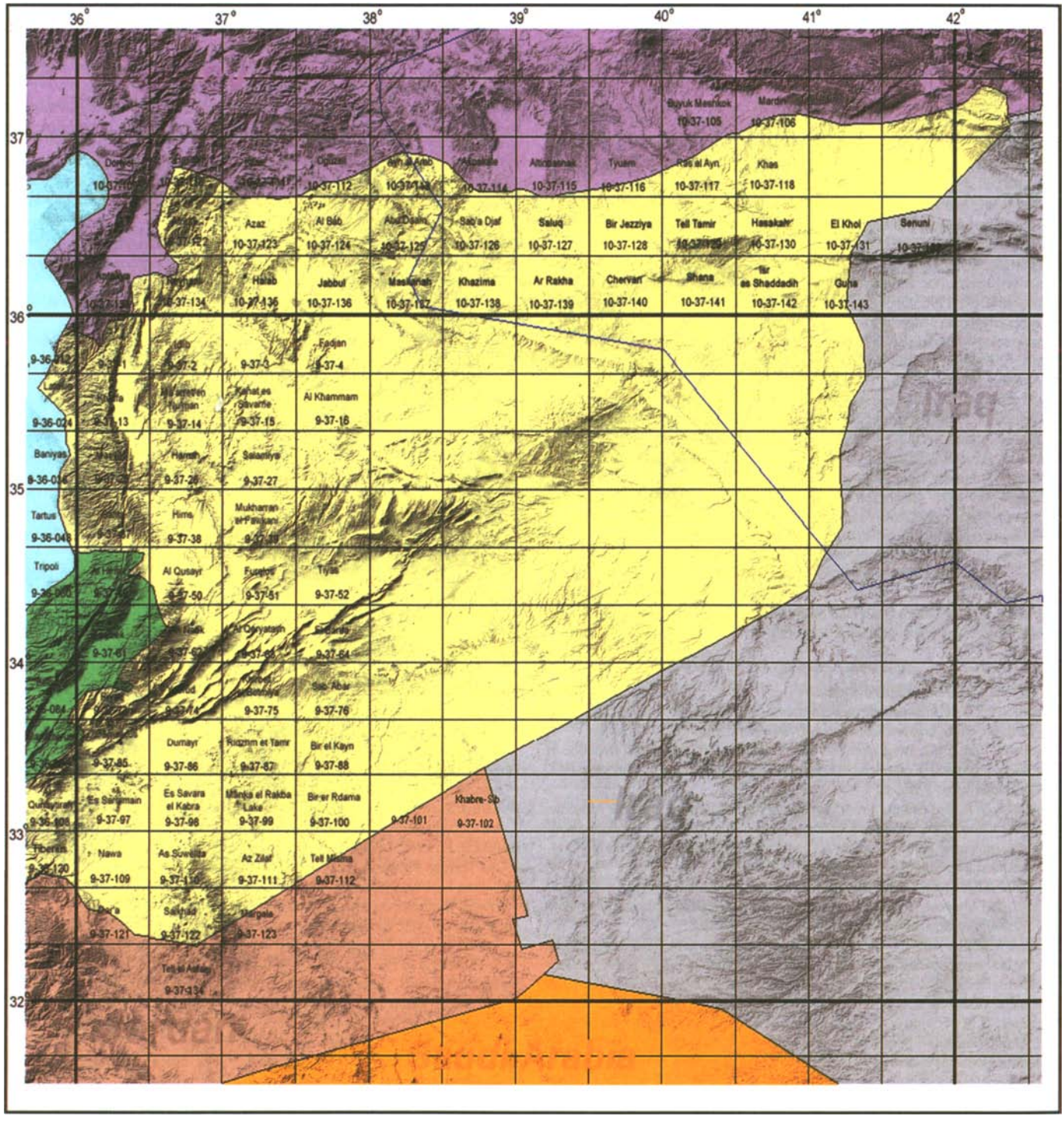
Dubertret, L., and Renouard, G., 1953. Carte géologique au 50,000, feuille de **Zahle**. Beirut, Ministère des Travaux Publics, 64 p.

Dubertret, L., Renouard, G., and Wetzel, R., 1951. Carte géologique au 50,000, feuille de **Qartaba**. Beirut, Ministère des Travaux Publics, 56 p. (map published in 1945).

Dubertret, L., and Wetzel, R., 1956. Carte géologique au 50,000, feuille de **Batroun**. Beirut, Ministère des Travaux Publics, 33 p. (map published in 1945).

Wetzel, R., 1945. Carte géologique au 50,000 du Liban, feuille de **Hamidiye**. Beyrouth, Ministère des Travaux Publics.

Wetzel, R., and Dubertret, L., 1951. Carte géologique au 1:50,000, feuille de **Tripoli**. Beirut, Ministère des Travaux Publics, 62 p.



Scheme of Russian 1:100,000 scale topographic map sheets for Syria.
The website (http://www.lib.berkeley.edu/EART/syria/syria100k.html) of the library at the University of California Berkeley provides downloads of Russian 1:100,000 scale topographic maps for Syria. These images are copyrighted ©2003 by the Regents of the University of California, with reproduction limited to Fair Use Copyright Law restrictions. Using Global Mapper®, the scheme has been geo-referenced, 'texture mapped' with the 90 m SRTM DTM of Syria and environs (which in binary format occupies 476 Mbyte), and then converted to Mercator projection. The figure shows the naming scheme of the 88 map sheets covering Syria. Map sheets can be downloaded from this website and are available either as JPEGs or Tiffs in 24 bit rgb color, at resolutions of around 2600 by 3700 pixels (~15 m pixels). The contour interval is 20 m, and a UTM grid (Zone 37N) graticule is overprinted. The two shaded relief map sheets on page vi of Volume I come from the northwest corner of this figure.

Appendix E

Geo-referenced and Mosaicked Geological Map Sets of Syria, Jordan, Lebanon Israel, and Cyprus

Rani Calvo *
Geological Survey of Israel, Mapping Division, 30 Malchei Israel Street, Jerusalem 95501, Israel
John K. Hall
Geological Survey of Israel, Marine Geology, Mapping & Tectonics Division, 30 Malchei Israel Street, Jerusalem 95501, Israel

INTRODUCTION

Geological maps are traditionally printed on paper at various scales. This hard-copy format suffers from several disadvantages. Most of the geological maps of Israel, Syria, Lebanon, and Jordan are up to 50 years old, out of print, or in very limited supply. They are often incomplete, restricted to use in a limited number of libraries or archives, folded in various ways, and torn or unreadable. And in common with all such sets, they are usually subdivided so that areas of interest are to be found on several sheets. For use in a GIS (Geographic Information System) and for other computer manipulations, a digital format of the maps is needed.

Our first goal was to digitally scan every small scale map (1:200,000 and smaller, *i.e.* less details) available in the archives of the Documentation Center of the Geological Survey of Israel. In the near future we also intend to do all the available larger scale map sheets (*i.e.* with more details). By doing so, these images can now be viewed on-screen, printed at various scales, or be compatible to other computer manipulations, such as are described below.

Since each map sheet represents real geographical areas, printed in various projections, our second goal was to geo-reference each map sheet according to its original projection. After this stage, images could be correctly placed when used by GIS programs and re-projected ('on the fly' or permanently) to any other projection.

Our third goal was to make country-scale mosaics of all 1:200,000 to 1:250,000 map sheets for Israel, Jordan, and Syria.

To address these goals, and to add value to this source book, it was decided in 2000 to scan the complete map sheets sets available in the GSI Documentation Center, and to use the relatively new methods of geo-referencing maps, and mosaicking them, to produce a highly compressed digital file which would be available on a CD-ROM.

METHODOLOGY USED

The original map sheets (some more than 1 m by 1 m in size) were scanned in Jerusalem on commercial scanners in color (RGB) at 300 dpi, as uncompressed TIFF files (*.tif). At this stage, map sheet files were >200 Megabytes each.

All the scanned images were imported into ESRI's ArcGIS software and registered in geographic space, using the built-in 'Georeferencing Tool' in the ArcMap module. The first step was to establish the projection of the map sheet. In the second step all points with known coordinates were used as control points to register/adjust the scanned map sheet. Several maps had only 4 points (4 corners of the sheet), while most of them had ~40 points, and others had as many as 200 points on an overprinted coordinate grid or graticule. A second or third order polynomial transformation was then used to correct all scan problems (scanning orientation, folds in the paper, paper stretch, *i.e.* rubber-sheeting). The Root Mean Square (RMS) error was always better than 50 m (real world distance). Each map sheet image was stored in two ways:

a) As the original TIF image with its auxiliary file (.aux) file. The AUX file accompanies the raster image and stores any auxiliary information that cannot be stored in the raster file itself, such as coordinate system, transformation coefficients, and projection information.

b) As a newly rectified image with its WORLD file, which is a text file (with the extension .wld; *e.g.*, .tfw, .sdw, .jpw) containing the coordinates of the image corners and its resolution (the ratio of an image pixel to the corresponding area in the real world).

All map sheets for a single country (Israel – 4 maps, Jordan, – 5 maps, and Syria – 20 maps) were merged together as one mosaic, using the ERDAS Imagine program. Using the ArcGIS MrSID encoder, the files were compressed and saved as a MrSID (Multi-Resolution Seamless Image Database) file with their world file (.sdw). All original MrSID files are available on the CD-ROM, together with the mosaic files.

The MrSID compression format from LizardTech Inc. uses techniques developed at the Los Alamos National Laboratory to compress 3 band digital image files by up to 22 times. The technique was originally for compressing grayscale finger-print scans. The compression method is based upon transformation of the raster image into wavelet space using Discrete Wavelet Transformations (DWT), and then quantizing and encoding the wavelet space images. Two competing firms, LizardTech Inc. (MrSID) and ER Mapper (ECW), employ this method. Although ER Mapper's ECW is today perhaps more user-friendly and with a

* For correspondence: rani.calvo@gsi.gov.il

DWT specifically designed for color imagery, the original decision to go with the MrSID format was taken before the latest ECW was available. For ECW *aficionados*, the MrSID files can be converted into ECW files by first producing a giant GEOTIFF file and then using the free ECW compressor available for download on the web (www.ermapper.com); a copy is included on the CD-ROM.

IMAGES OF THE MOSAICKED MAP SETS

Several of the mosaicked geological maps are printed here as centerfolds. The mosaicked map sets were printed together with the 2-D black and white shaded relief images derived from the highest resolution DTMs (Digital Terrain Models) available for each area. The DTM used on the figures are: for Israel, 25 m (Hall, 1996, 1997), for Cyprus, 25 m (Hall, 1998a, b), and for Jordan and Syria, 90 m from the SRTM datesets. Each map is printed twice, once with the geological map alone, and once with the shaded-relief as described above.

The map figures are as follows:

Figure AppE.1: Location map.

Figure AppE.2: (a) International Geological Map of Africa (**IGMA**) (Choubert et al., 1985), and (b) with shaded-relief background.

Figure AppE.3: (a) International Geological Map of Europe (**IGME**) (Toloczyki and Trumit, 1998), and (b) with shaded-relief background.

Figure AppE.4: (a) Geological map of Lebanon-Syria (**Liban-Syrie**) (Dubertret, 1966), and (b) with shaded-relief background.

Figure AppE.5: (a) Geological map of **Israel** (Sneh et al., 2001), and (b) with shaded-relief background.

Figure AppE.6: (a) Geological map of **Jordan** (Bender and Comp., 1968), and (b) with shaded-relief background.

Figure AppE.7: (a) Geological map of **Syria** (Ponikarov and Comp., 1964), and (b) with shaded-relief background.

Figure AppE.8: (a) Geological map of **Cyprus** (Constantinou, 1995), and (b) with shaded-relief background.

Table App E.1: List of files in the CD-ROM

Name of file	Description
Israel	
Israel.SID + .SDW	Israel mosaic, from 1:200,000 map sheets
map 1	Map 1 - 1:200,000 map sheet
map 2	Map 2 - 1:200,000 map sheet
map 3	Map 3 - 1:200,000 map sheet
map 4	Map 4 - 1:200,000 map sheet
Israel_legend_ 1.JPG	Legend of Israel map sheets - **alphabetic**
Israel_legend_ 2.JPG	Legend of Israel map sheets - **chronologic**
north_color	Northern sheet of the stractural map of Top Judea Gr. - **color ramp**
south_color	Southern sheet of the stractural map of Top Judea Gr. - **color ramp**
Top_judea_color.SID + .SDW	Stractural map of top Judea Gr. in Israel - **color ramp**, lower resolution
color_legend.JPG	Legend of structural map of top Judea Gr. - **color ramp**
north_line	Northern sheet of the stractural map of Top Judea Gr. - **contour**
south_line	Southern sheet of the stractural map of Top Judea Gr. - **contour**
Top_judea_line.SID + .SDW	Stractural map of top Judea Gr. in Israel - **contour**, lower resolution
line_legend.JPG	Legend of structural map of top Judea Gr. - **contour**
isr_ 50 k	Vector layer of the 1:50 k maps of Israel
isr_ 100 k	Vector layer of the 1:100 k maps of Israel
isr_ 200 k	Vector layer of the 1:200 k maps of Israel
isr_ 250 k	Vector layer of the 1:250 k maps of Israel
isr_ 500 k	Vector layer of the 1:500 k map of Israel

Name of file	Description
Jordan	
Amman .SID + .SDW	Amman 1:250,000 map sheet
Aqaba .SID + .SDW	Aqaba 1:250,000 map sheet
Bayir .SID + .SDW	Bayir 1:250,000 map sheet
Elazraq .SID + .SDW	El Azraq 1:250,000 map sheet
Mahattat .SID + .SDW	Mahattat 1:250,000 map sheet
Jordan .SID + .SDW	Jordan mosaic, from 1:250,000 map sheets, lower resolution
Jordan_legend.JPG	Legend of Jordan map sheets
Jordan_CS.JPG	Geological cross-sections from the map sheets
jord_ 50 k	Vector layer of the 1:50 k maps of Jordan
jord_ 100 k	Vector layer of the 1:100 k maps of Jordan
jord_ 250 k	Vector layer of the 1:250 k maps of Jordan
Syria	
36 - I	Halab 1:200,000 map sheet
36 - VIe	Az Zalaf 1:200,000 map sheet
36 - VIw	As Suweida 1:200,000 map sheet
36 - XII	Dimashq 1:200,000 map sheet
36 - XVIII	Homs 1:200,000 map sheet
36 - XXIV	Hama 1:200,000 map sheet
37 - III	Jrablus 1:200,000 map sheet
37 - IV	Tuwal El Aba 1:200,000 map sheet
37 - V	Al Hasakeh 1:200,000 map sheet
37 - VI	Al Qamishli 1:200,000 map sheet
37 - VIII	Saba Abar 1:200,000 map sheet
37 - IX	At Tanf 1:200,000 map sheet

Table App E.1: Continued

Name of file	Description
37 - XIV	Al Qaryatein 1:200,000 map sheet
37 - XV	Tudmor 1:200,000 map sheet
37 - XVI	Wadi El Myah 1:200,000 map sheet
37 - XVII	Abou Kamal 1:200,000 map sheet
37 - XX	Salamiyeh 1:200,000 map sheet
37 - XXI	Ar Rasafeh 1:200,000 map sheet
37 - XXII	Ar Raqqa 1:200,000 map sheet
37 - XXIII	Deir Az Zor 1:200,000 map sheet
Syria.SID + .SDW	Syria mosaic, from 1:200,000 map sheets, lower resolution
Syria_legend.JPG	Legend of Syria map sheets
syr_ 200 k	Vector layer of the 1:200 k maps of Syria
Cyprus	
Cyprus.SID + .SDW	Cyprus map sheet, scale 1:250,000
Cyprus_legend.TIF	Legend of Cyprus map sheets
cyp_ 250 k	Vector layer of the 1:250 k map of Cyprus
Lebanon	
lbn_ 50 k	Vector layer of the 1:50 k maps of Lebanon
Liban_Syrie	
Liban-Syrie.SID + .SDW	Lebanon - Syria map sheet, scale 1:1,000,000
Liban-Syrie_legend.JPG	Legend of Lebanon-Syria map sheet
lbn_syr_ 1000 k	Vector layer of the 1:1000 k map of Liban and Syrie
IGME	
IGME.SID + .SDW	Int. Geol. Map of Europe map sheet, scale 1:1,500,000
IGME_legend.JPG	Legend of Int. Geol. Map of Europe map sheet
imge_ 1500 k	Vector layer of the 1:1500 k map of IMGE
IGMA	
IGMA.SID + .SDW	Int. Geol. Map of Africa map sheet, scale 1:5,000,000
IGMA_legend.JPG	Legend of Int. Geol. Map of Africa map sheet
imga_ 5000 k	Vector layer of the 1:5000 k map of IMGA
Med_Sea	
Mediter_tectono.SID + .SDW	Tectonic map of the Mediterranean Sea
Mediter_tectono_legend.JPG	Legend of tectonic map of the Mediterranean Sea map sheet
Other	
Strat_table.JPG	Stratigraphic table of Israel
Programs	
MrSID Viewer	MrSID Viewer installation program
ECW compressor	ECW compressor installation program

USES OF THE RESULTING SEAMLESS MAPS

The geological mosaic map sheets can be viewed with the MrSID viewer. A free viewer is available for download on the web (www.lizardtech.com/download) a copy is included with the MrSID files on the CD-ROM. With this viewer it is possible to view the seamless geological map images at any resolution, and to write a TIFF graphics file of any part of the data at the desired resolution.

The images can be imported into a GIS project, used as reference background, or converted into a vector form, using on screen direct digitization or one of the many 'raster to vector' programs (*viz.* ArcScan, R2V etc.).

The images can be draped on a DEM for 3-D visualization. The geological contacts, topographic heights, and coordinates can be extracted from a DEM, and geological cross-sections can be constructed.

AVAILABILITY OF THE CD-ROM

The CD-ROM is available upon request from the Geological Survey of Israel or from the authors. It contains the files listed below in Table AppE.1:

ACKNOWLEDGEMENTS

We are indebted to our colleague Adi Bin-Nun from the GIS Laboratory of the Hebrew University of Jerusalem for useful help in GIS and image analysis of the scanned maps. The invaluable assistance of Ms. Varda Arad from the Documentation Center of the Geological Survey of Israel is gratefully acknowledged, for library services, and for allowing us to borrow very precious original map sheets for scanning purposes.

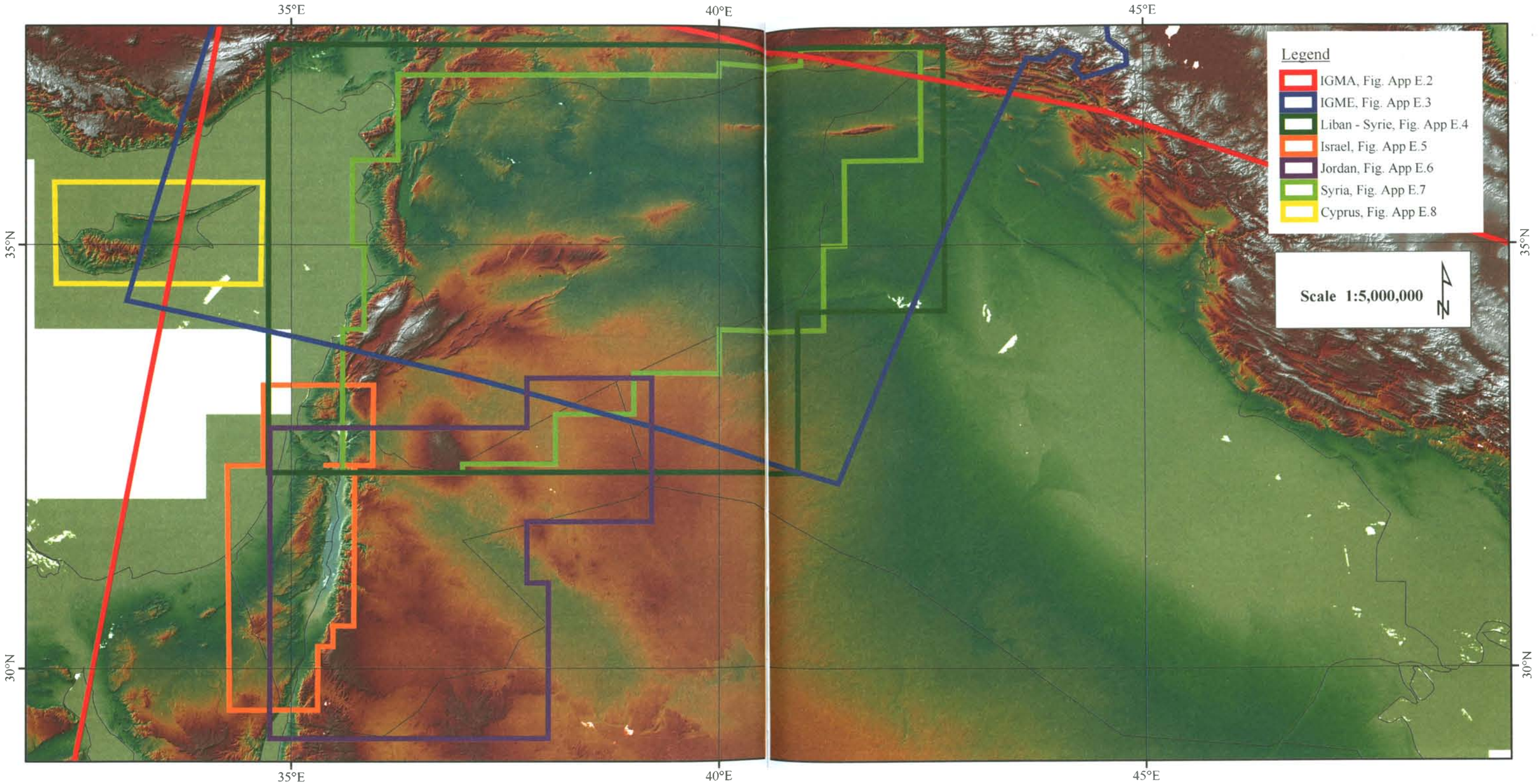


Figure App F. 1: Location map of figures AppF.2 to AppE.8.

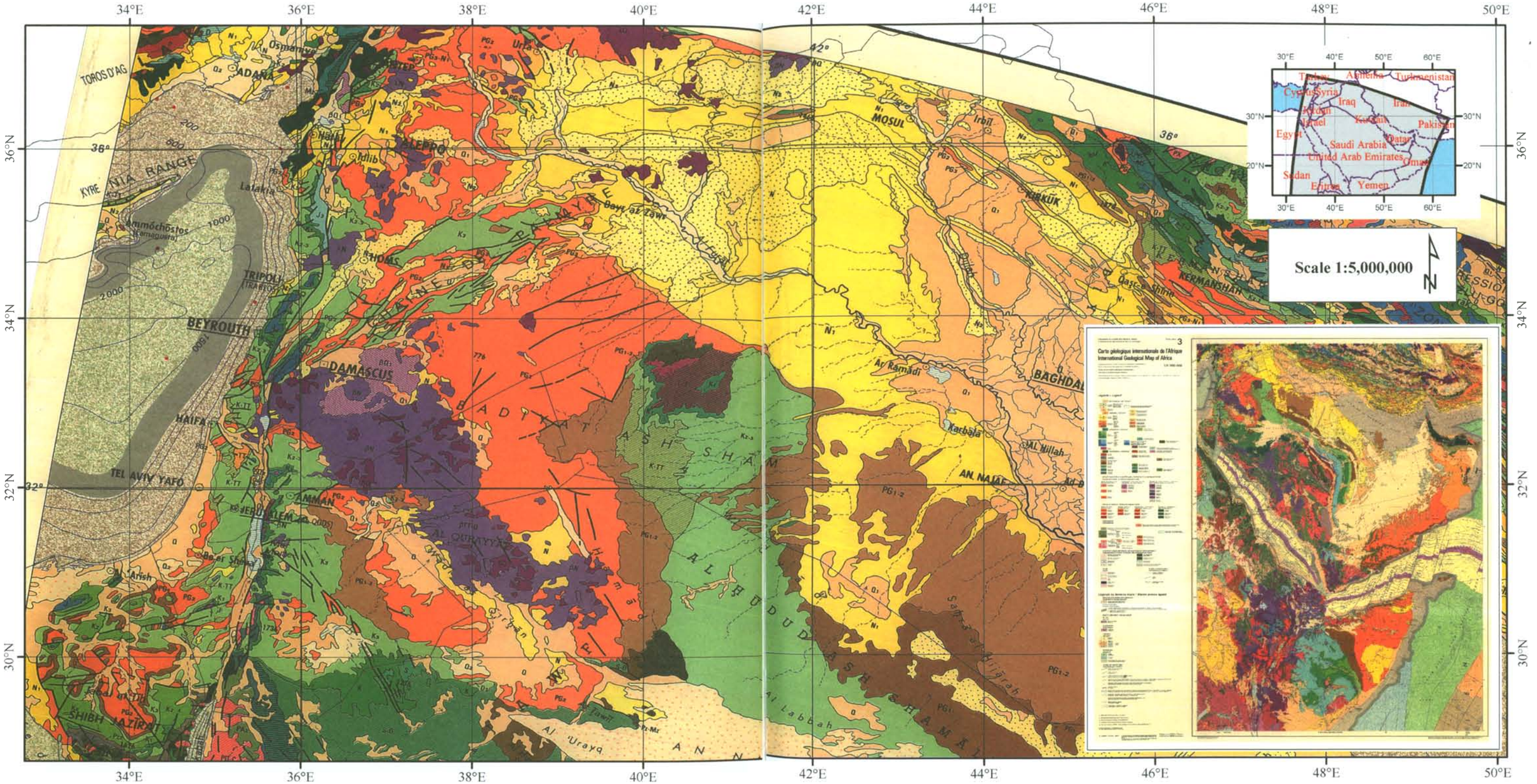


Figure App E.2a: International geological map of Africa (Chouheil et al., 1995). Original hard-copy scale is 1:5,000,000. The scanned image was geo-referenced and it is projected here in WGS1984 geographic system.

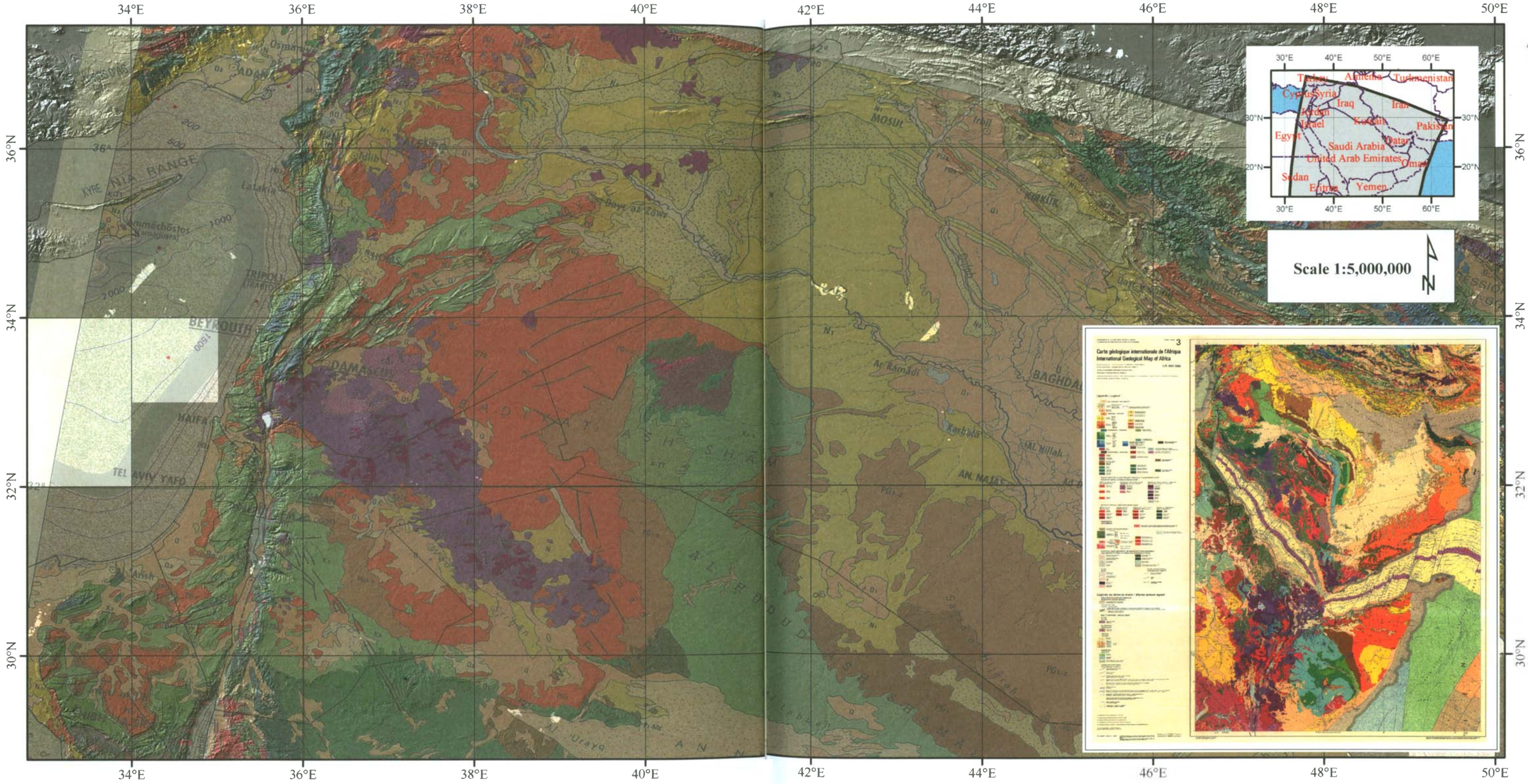


Figure App E.2b: International geological map of Africa (Choubert et al., 1985) overlain with the shaded relief build from the SRTM data.

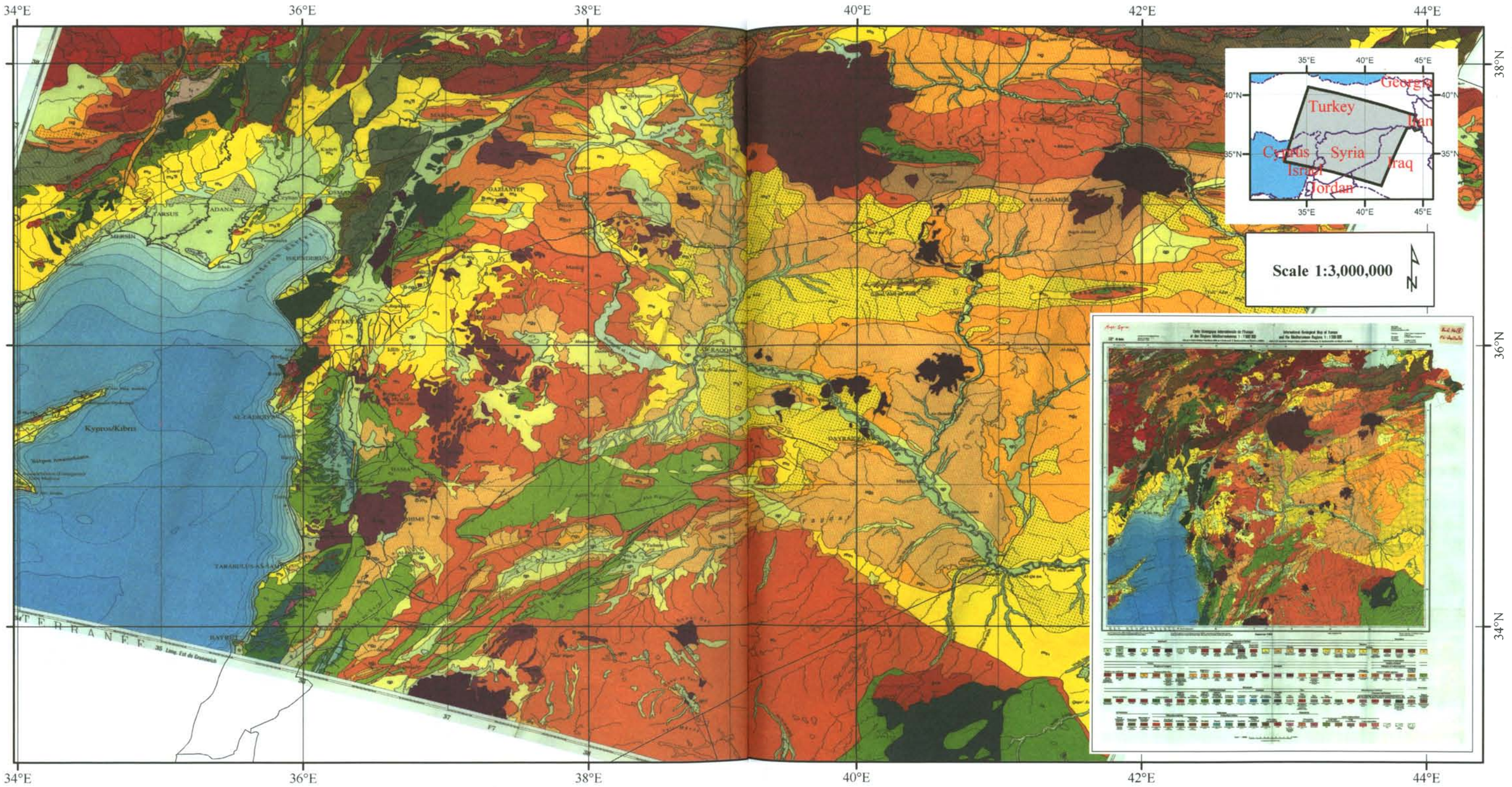


Figure App E.3a: International geological map of Europe and the Mediterranean region (Tolozyki and Trurnit, 1998). Original hard-copy scale is 1:1,500,000. The scanned image was geo-referenced and it is projected here in WGS1984 geographic system.

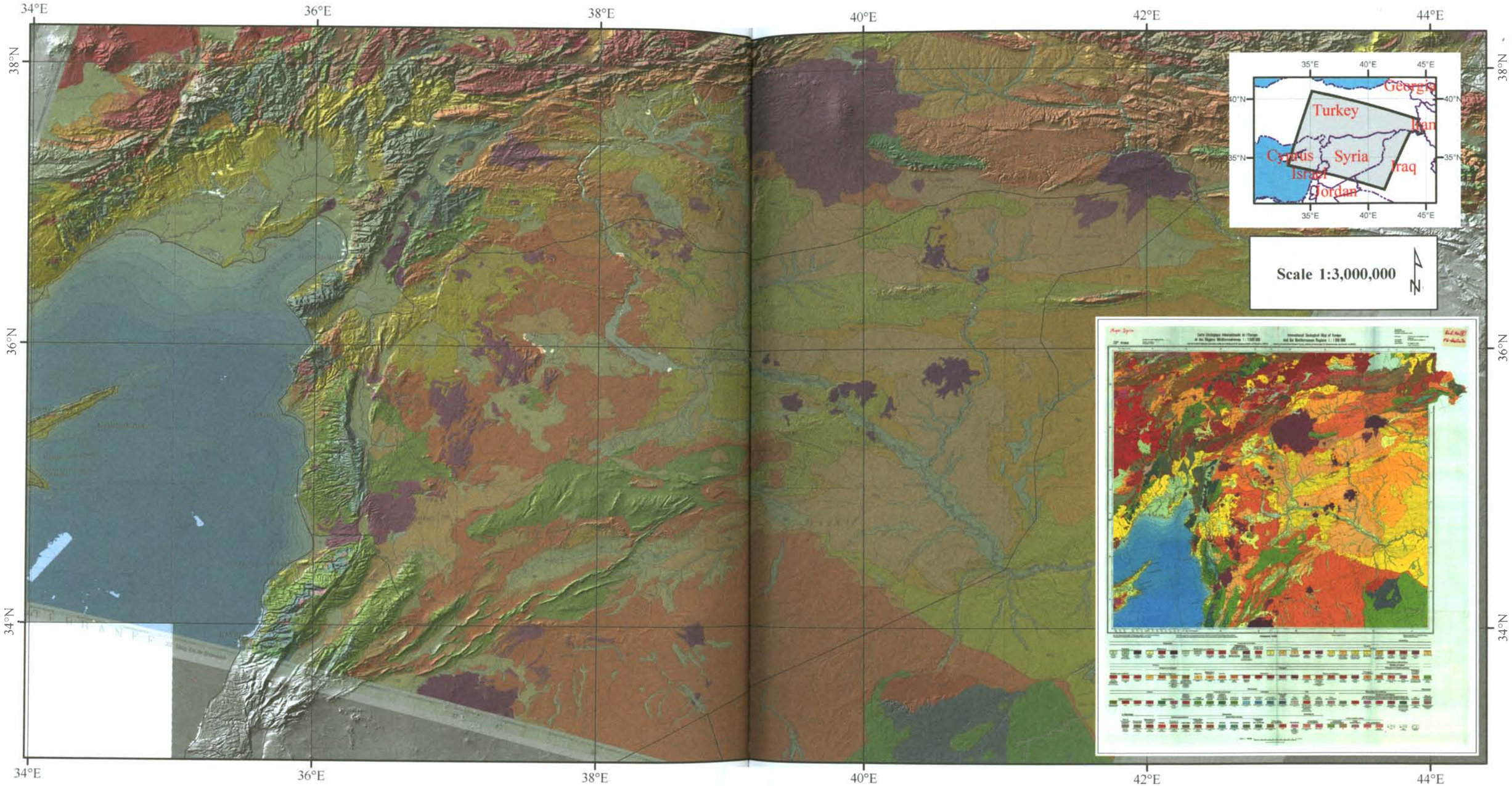


Figure App E.3b: International geological map of Europe and the Mediterranean region (Tolozyki and Trurnit, 1998) overlain with the shaded relief image build from the SRTM data.

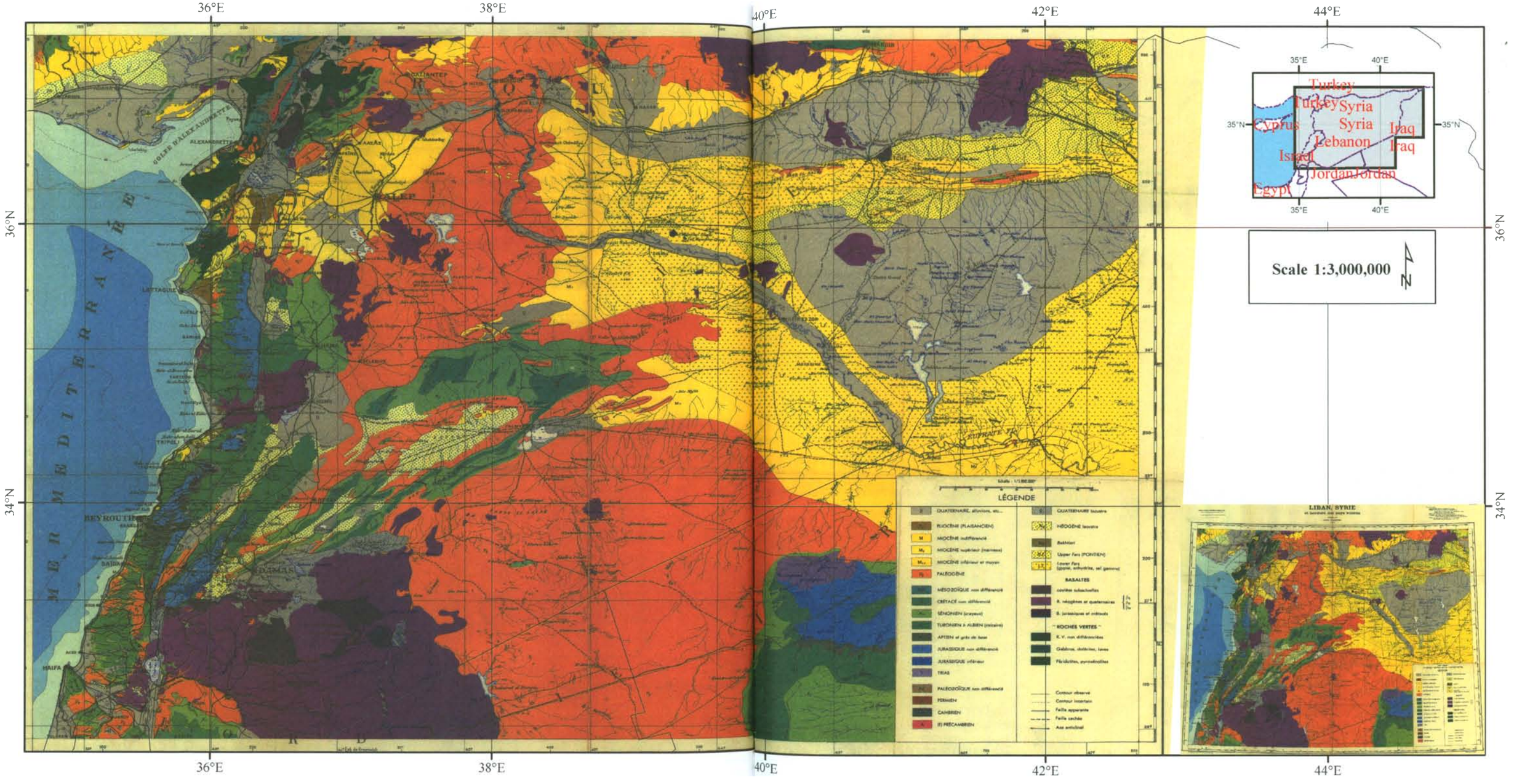


Figure App E.4a: Liban - Syrie (Durbertret, 1966). Original hard-copy scale is 1:1,000,000. The scanned image was geo-referenced and it is projected here in WGS1984 geographic system.

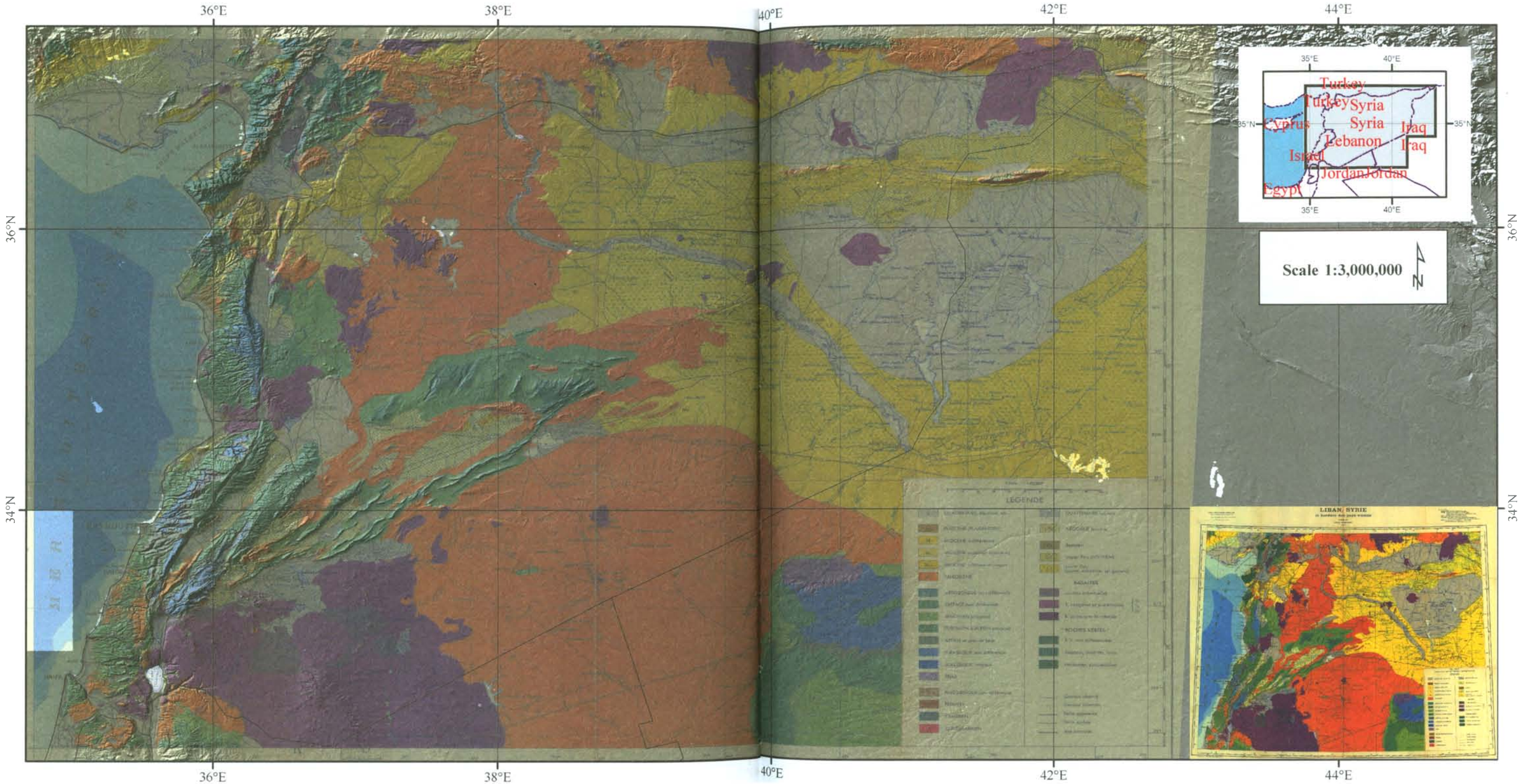


Figure App E.4b: Liban - Syrie (Durbertret, 1966) overlain with the shaded relief image build from the SRTM data.

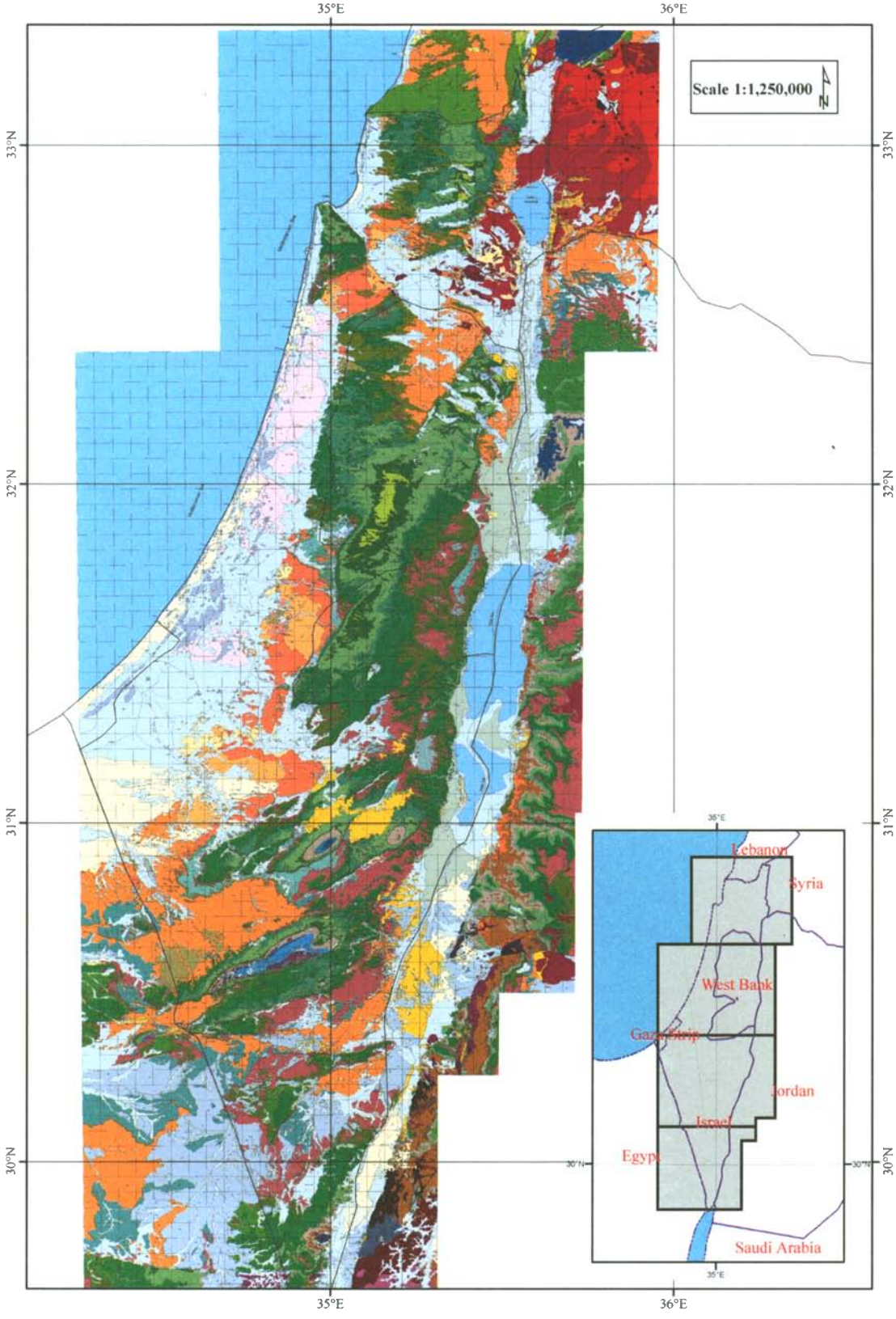


Figure App E.5a: Israel (Sneh et al., 1998a, b, c, d). Original hard-copy scale is 1:200,000. The scanned image was geo-referenced and it is projected here in WGS1984 geographic system.

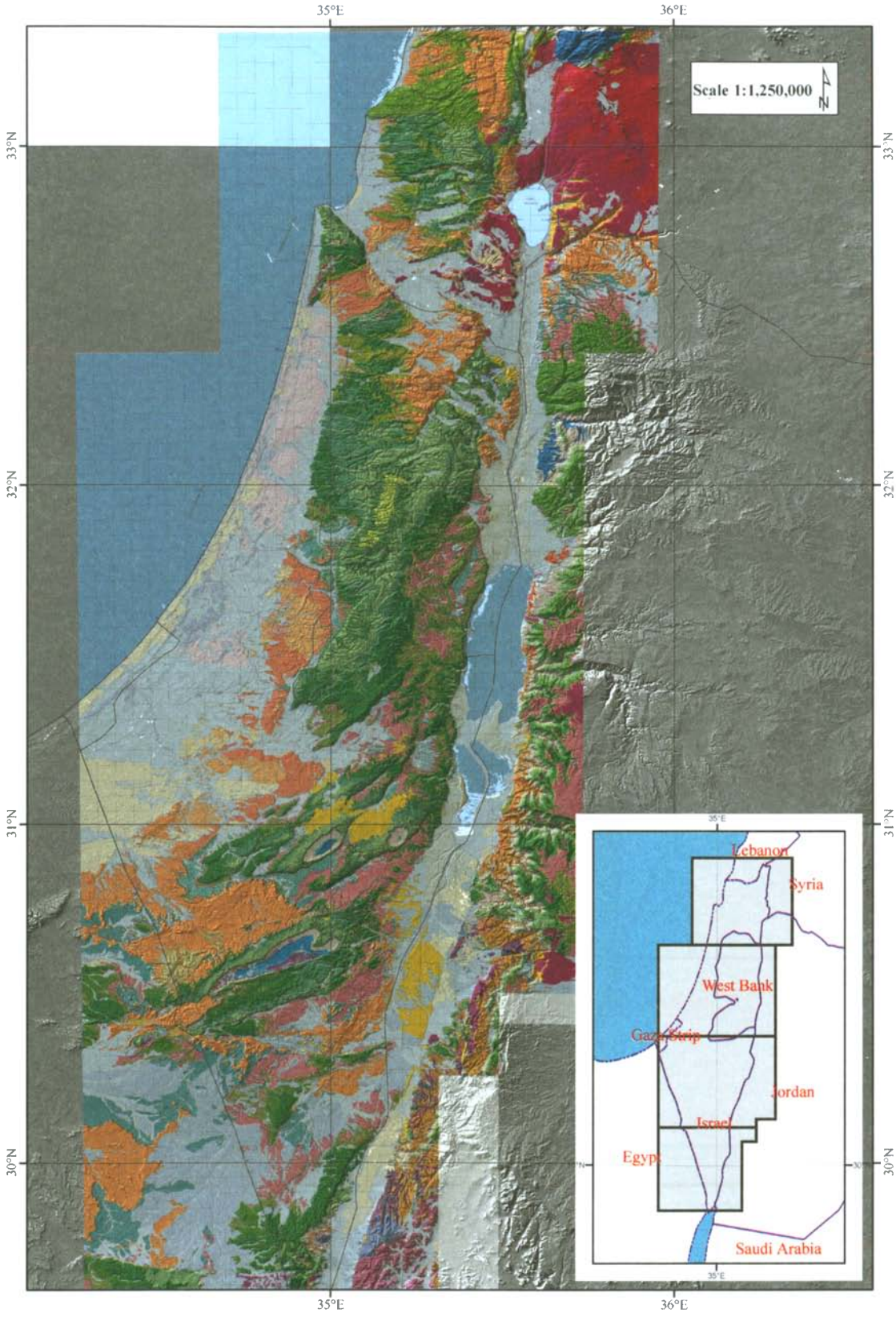


Figure App E.5b: Israel (Sneh et al., 1998a, b, c, d) overlain with the shaded relief image build from SRTM data.

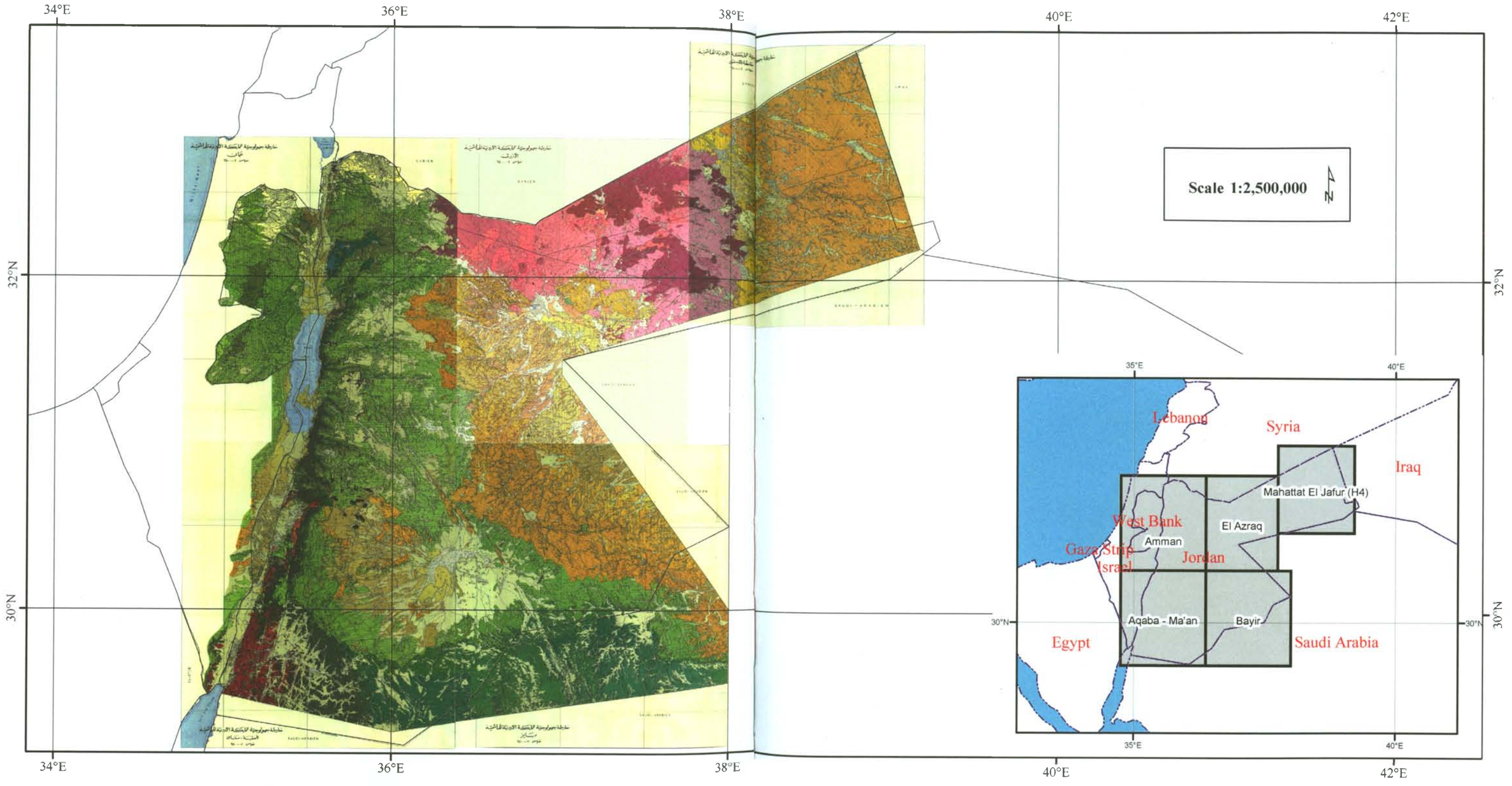


Figure App E.6a: Jordan (Bender an comp., 1968). Original hard-copy scale is 1:250,000. The scanned image was geo-referenced and it is projected here in WGS1984 geographic system.

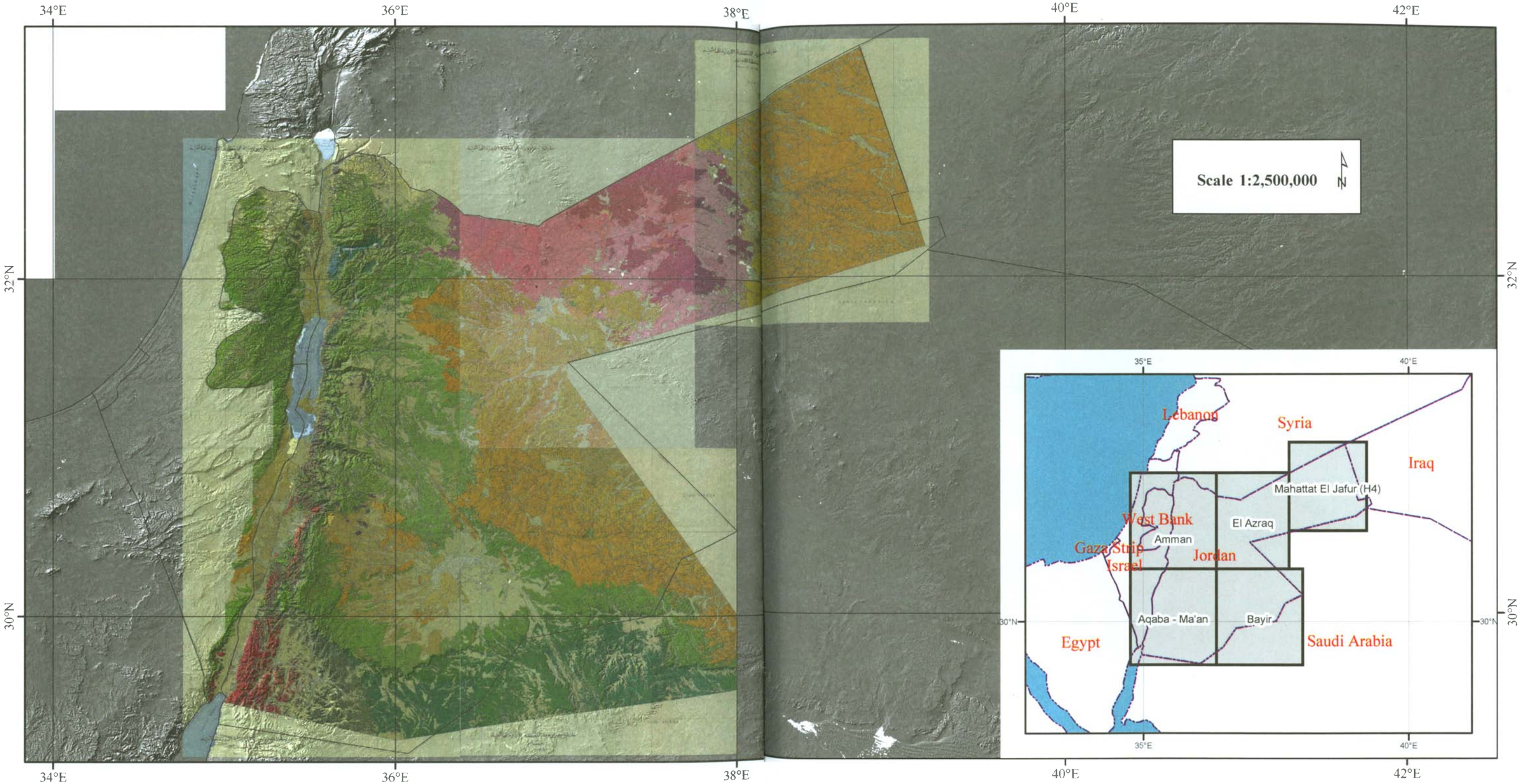


Figure App E.6b: Jordan (Bender and comp., 1968) overlain with the shaded relief image build from the SRTM data.

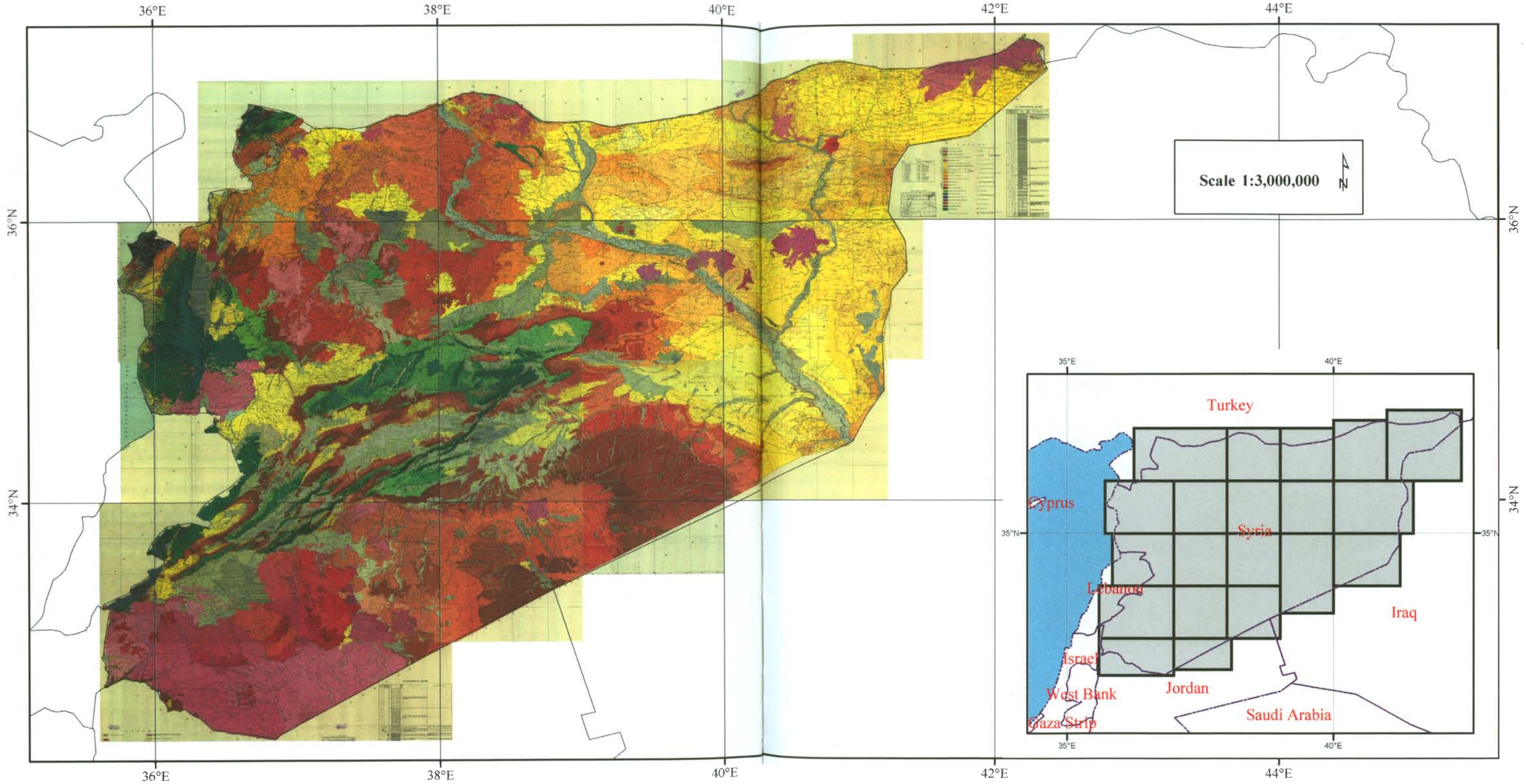


Figure App E.7a: Syria (Ponikarov and Comp., 1964). Original hard-copy scale is 1:200,000. The scanned image was geo-referenced and it is projected here in WGS1984 geographic system.

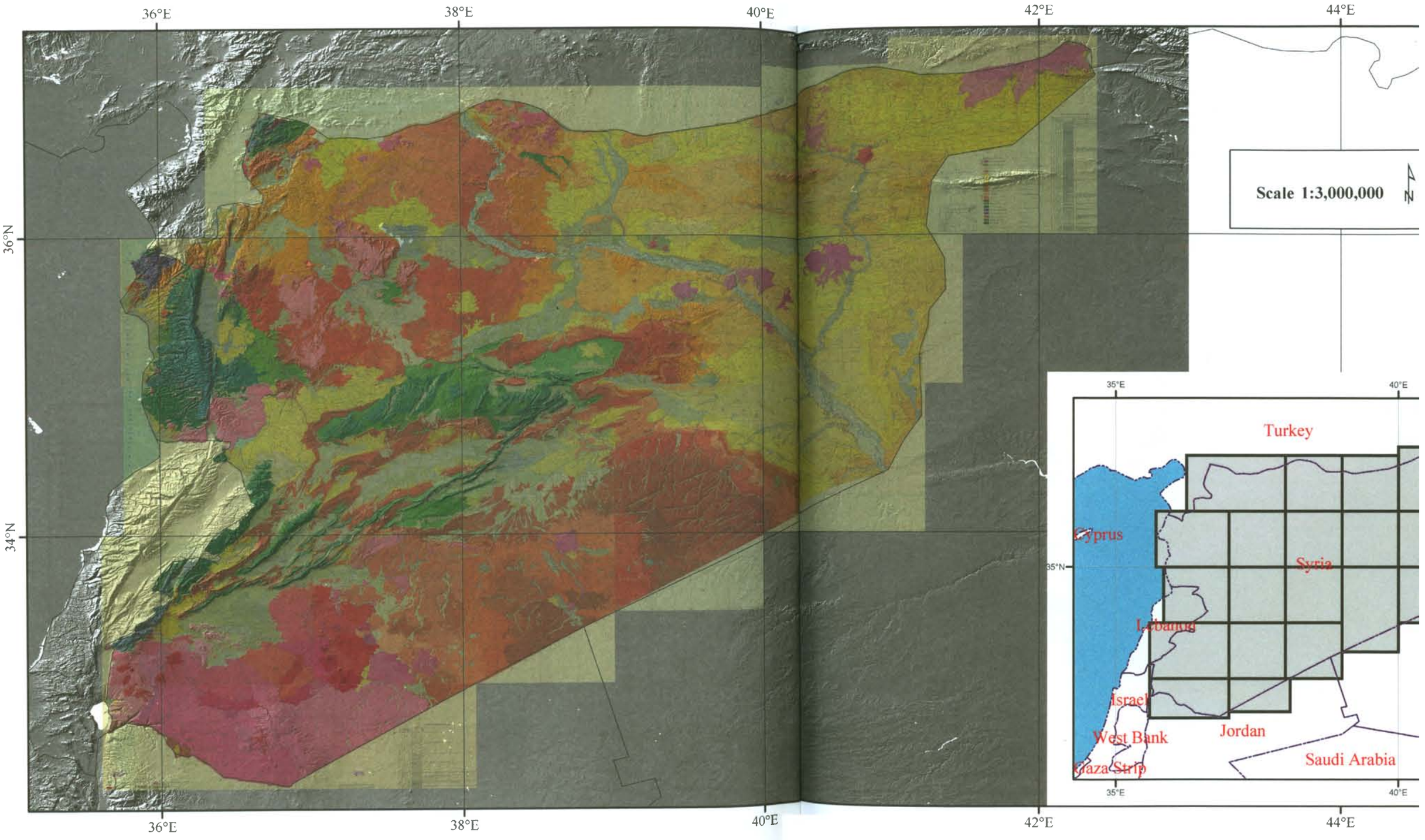


Figure App E.7b: Syria (Ponilarov and Comp., 1964) overlain with the shaded relief image build from the SRTM data.

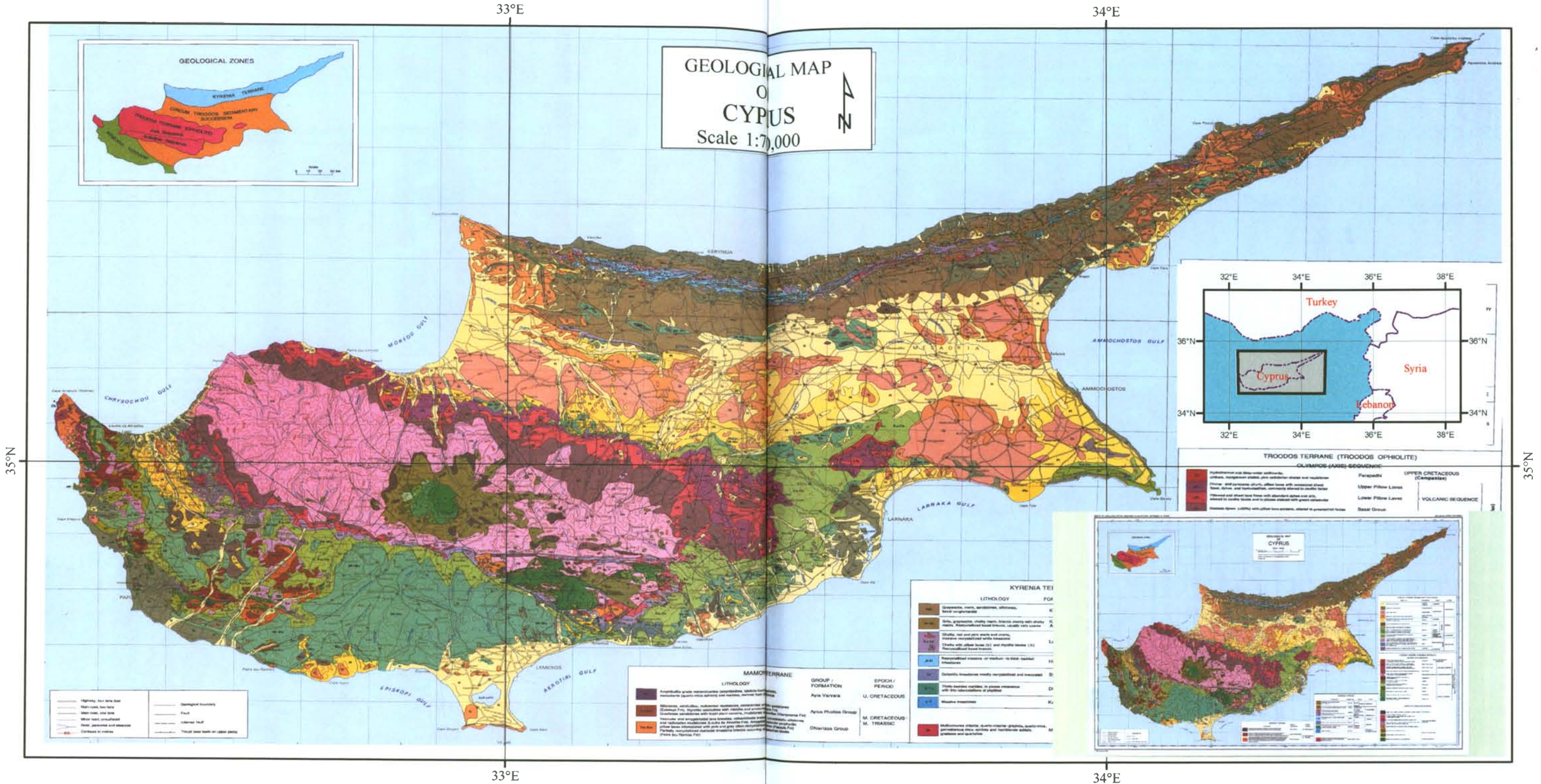


Figure App E.8a: Geological map of Cyprus (Constantinou, 1995). Original hard-copy scale is 1:250,000. The scanned image was geo-referenced and it is projected here in WGS1984 geographic system.



Figure App E.8b: Geological map of Cyprus (Constantinou, 1995) overlain with the shaded relief image (Hall, 1998).

REFERENCES

Bender, F., and Comp., 1968. Geological map of Jordan, 1:250,000. Sheets: Amman; El Azraq; Mahattat El Jufur (H4); Aqaba - Maan; Bayir. Hannover, Bundes. F. Boden., 5 maps.

Bogdanov, N. A., Koronosky, N. V., Lomize, M. G., Chekhovich, V. D., and Yutsis, V. V., 1994, Tectonic map of Mediterranean Sea. Institute of Lithosphere of the Academy of Sciences of Russia.

Choubert, G., Faure-Muret, A., and Comp., 1985, International Geological Map of Africa scale 1:5,000,000. Commission for the Geological Map of the World, Sheet 3. UNESCO

Constantinou, G., 1995, Geological map of Cyprus, scale 1:250,000. Ministry of Agriculture, Natural Resources and Environment, Government of Cyprus. 1 geol. map.

Dubertret, L., 1966. Liban, Syrie et bordure des pays voisins. Tableau stratigraphique avec carte geologique au millionieme. Notes et memoires sur le Moyen Orient, Vol. 8, pp. 251-358, geol. map, 1:1,000,000.

Fleisher, L., 2003, Stratigraphic table of Israel outcrops and subsurface. The Geophysical Institute of Israel, Oil and Gas Unit.

Fleisher, L., 2003, Structural map on top Judea Group, scale 1:200,000 (2 sheets). The Geophysical Institute of Israel.

Hall, J. K., 1996. Topography and bathymetry of the Dead Sea depression. Tectonophysics. 266(1-4): 177-185.

Hall, J. K., 1997, Landforms of Israel and adjacent areas, 1:500,000 scale. Geological Survey of Israel.

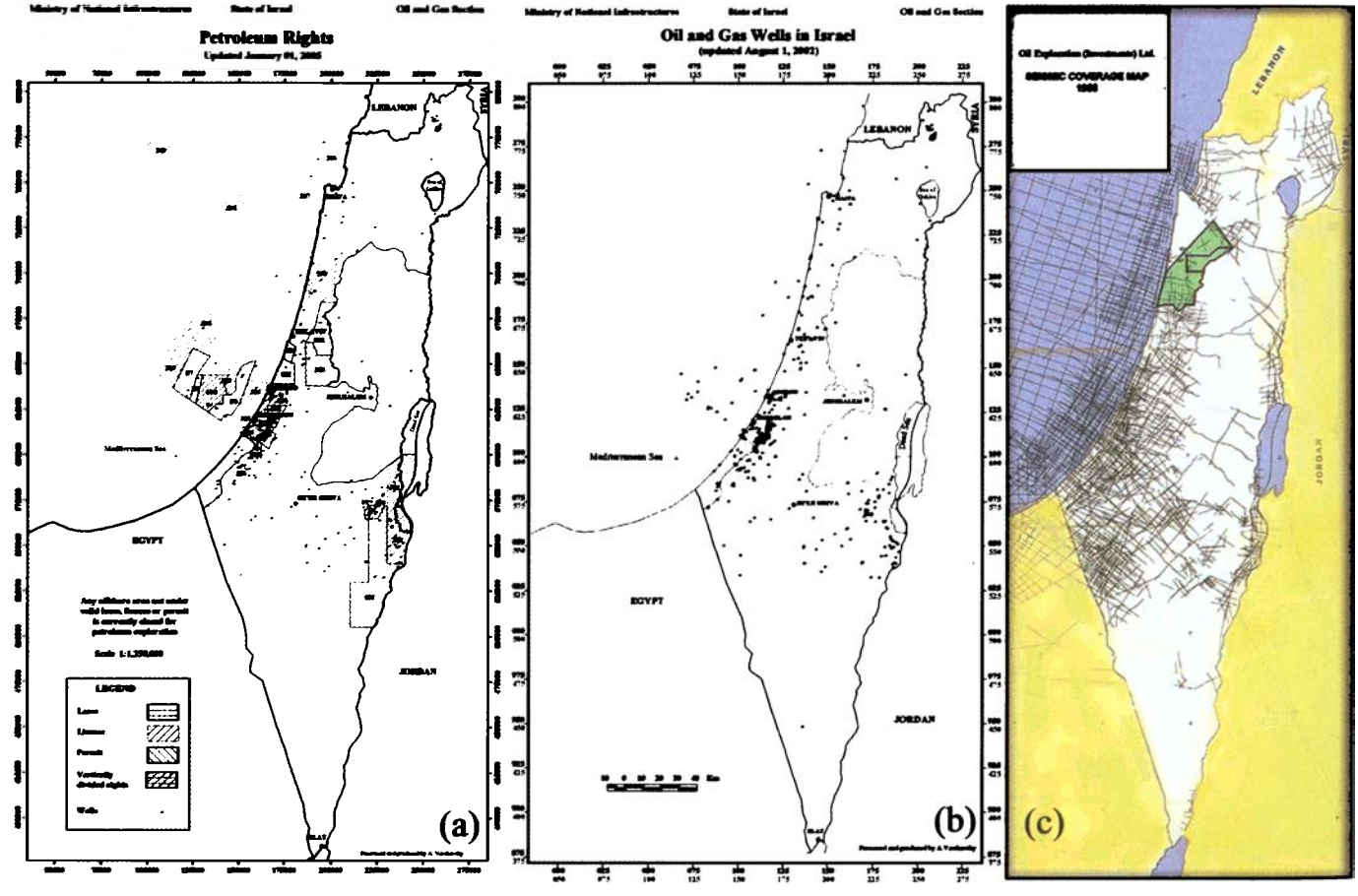
Hall, J. K., 1998a. Digital terrain model (DTM) of the island of Cyprus. In: Geol. Surv. Isr. Current Research, Volume 11. (T. Weissbrod, ed.). pp. 47-52. Jerusalem.

Hall, J. K., 1998b. Three-dimensional map of the Island of Cyprus. Grayscale sheet of land topography at 1:250,000 scale, Geological Survey of Israel and Cyprus, Jerusalem, one sheet. Sheet prepared for ICGEM-3, Third International Conference on the Geology of the Eastern Mediterranean, Nicosia, Cyprus, September 23-26, 1998.

Ponikarov, V. P., and Comp., 1964. Geological map of Syria, 1:200,000. Moscow, V.O. Technoexport, 20 Sheets with geological cross sections and explanatory notes. (prepared for the Minist. of Industry, S.A.R. under contract No. 944. Translated from Russian).

Sneh, A., Bartov, Y., Rosensaft, M., and Weissbrod, T., 2001. Geological map of Israel, 1:200,000, 4 Sheets. Israel Geological Survey., Rep. GSI/8/2001, 4 geological maps on PC format, Version 1.0.

Toloczyki, M., and Trumit, P., 1998. Carte geologique internationale de l'Europe et des regions Mediterraneennes, 1:1,500,000: Sheet F6: Halab. Hannover, Bundes. F. Geowis. U. Rohstoffe and Unesco, 1 geol. map.



Oil Exploration in Israel - Pickings from the Internet.

Three plots downloaded from the Internet give an indication of the oil exploration activity in Israel and the amount of drilling and seismic data involved. Maps (a) and (b) are from the website of the Ministry of National Infrastructures (www.mni.gov.il). Map (a) shows the various areas for which petroleum rights have been granted. The index is available on the website. Map (b) shows the oil and gas wells drilled up to August 2002. These plots were prepared by A. Varshavsky. Map (c), taken from the website of www.zionoil.org, reproduces the distribution of seismic lines run in Israel, as compiled in 1988 by Oil Exploration (Investments) Ltd. (O.E.I.L.). Many additional seismic lines have since been obtained both on land and in the Mediterranean and Dead Sea.

Appendix F

RAS Marine Gravity Data from the Levantine Basin

Vladimir A. Toulin
Institute of Physics of the Earth of the Russian Academy of Sciences, Bolshaya Grusinskaya Str. 10, 123810 Moscow, Russia
John K. Hall
Geological Survey of Israel, Marine Geology, 30 Malchei Israel Street, Jerusalem 95 501, Israel

INTRODUCTION

The gravity data presented in Chapter 14 of this volume constitutes an important new data set for future compilations of the gravity field of the eastern Mediterranean (*viz.* Chapters 19 and 23). For this reason a request was made to the World Data Center B (Moscow) for the digital data set. In due time it was provided for inclusion in the data CD-ROM, which is available upon request from the Documentation Centre of the Geological Survey of Israel (library@mail.gsi.gov.il). The sections below are excerpted from Chapter 14, in order to discuss the methods behind the observations in the file.

Gravity field investigations in the eastern Mediterranean (to the south and west of Cyprus) were carried out by scientists of the Schmidt Institute of Physics of the Earth (IPhE) of the Russian Academy of Sciences during Cruise 12 of R/V 'Akademik Boris Petrov' (1989) and Cruise 10 of R/V 'Akademik Nikolaj Strakhov' (1990).

The observations of 1989 only followed the lines of deep seismic sounding (DSS), but the limited reconnaissance data which were collected were used for planning the network for 1990. The gravity observation program for 1990 aimed to investigate in detail the gravity field in those areas to the south and west of Cyprus where the deep seismic sounding lines were situated.

Equipment and treatment procedure

Observations were made with AMG broad band gravimeters, developed by the IPhE for global oceanic investigations (Toulin and Osinskaya, 1970). The gravimeters were installed on a passive type of gyroscopic stabilizer, developed by the IPhE and the Tula Polytechnic Institute (Kireev et al., 1978). As is the usual practice in Russia, several identical gravimeters were used aboard the vessel to carry out simultaneous measurements. This allows a check on the data collected, to identify malfunctions, and it increases the measurement accuracy. Four instruments were used aboard each vessel, three in operation and one kept as a spare.

Prior to each cruise, the gravimeters passed laboratory tests on land, including calibration, and trials on a platform for imitating the accelerations aboard ship. The most important step is adjusting the stabilization to minimize errors generated by the ship's vertical and horizontal accelerations. Some numerical corrections should be including after trials, and accelerometers are mounted for this purpose on one of the stabilizer sets. Cross-coupling errors are low for the AMG due to the use of a pair of oppositely oriented pendulums in the sensor of a gravimeter, and its influence is negligible.

The AMG's measurement counts are recorded on a magnetic tape. The scanning frequency is 10 cps, 30 adjoining counts are averaged and written on the tape. Original data are thus presented as a sequence of averaged data at 3 sec intervals. The tapes are read into a computer at the end of measurement intervals of up to 12 hours duration. The analysis showed that no corrections for horizontal accelerations were necessary.

Shipboard analysis included calculation of average counts for standard time intervals (usually 5 min), including accuracy estimation from the redundant gravimeters counts, and without making corrections for zero-point deviation, and Eötvös-effect. This was sufficient to guarantee proper performance and control of the observations.

The 3 sec measuring interval and the average of the last 5 min of observations were available for cleaning the gravity signal by filtering out the influence of vertical accelerations. The last analysis procedure is the calculation of weighted averages by Cosine weighting techniques, applied to the ends of the averaging interval. Such a simple method is very effective, reducing the remaining errors to less than 0.1 mGal.

Computing Equipment on the Ship

The ship's main computer was of the ES-1011 type, connected to the basic ship's equipment. An additional KAMAK computer was used for inserting the gravity data into it, with the results of the shipboard treatment then stored on floppy disks.

Positioning and Navigational Coordinates

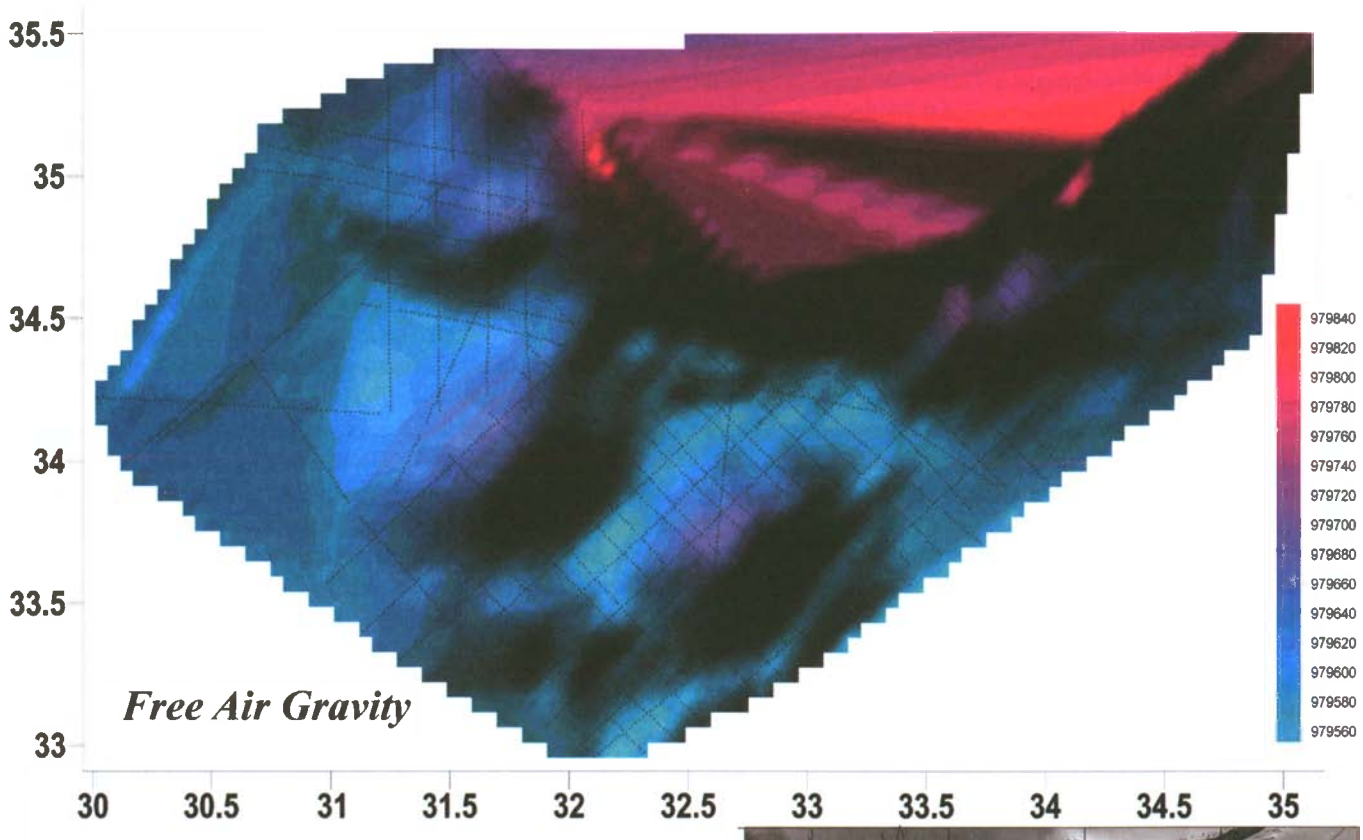
Position fixing for the cruises was carried out with an U. S. Navy TRANSIT satellite Doppler navigation system. The time interval between observations was usually 40-60 minutes, but sometimes increased to 2 hours. Observational data from a MAGNAVOX navigation receiver were operated on by the KOKOS navigation survey program (Boyarsky and Afanasieva, 1992) for navigating the profiles and repetition of the measurements if necessary.

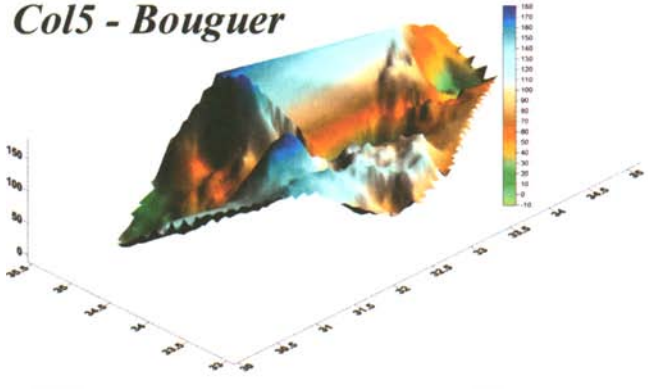
This program operates on the principle that the real track of a ship on a profile is not a series of lines (as shown by linear interpolation between fix points), but by some smooth curve, resulting from the influence of winds and currents on the ship. A search of the best fitting curve was made by using bicubic spline interpolation. Experiments show that such a technique

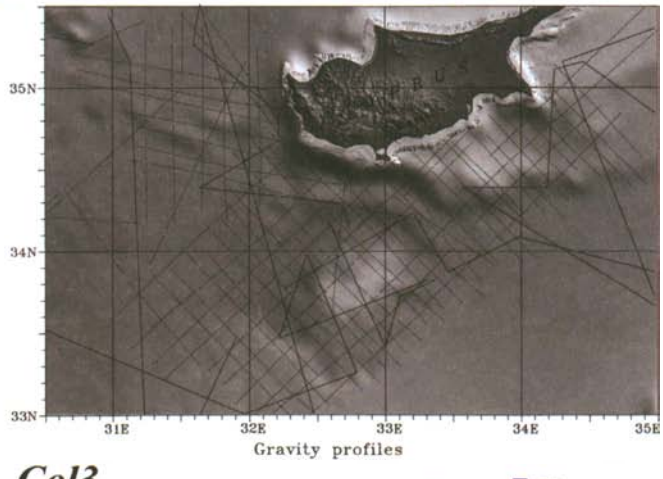
```
1        MVF78              51511910722STRAKH106 INST. PHYSICS EARTH ACAD        01
USSR                AKADEMIK STRAKHOV    1SHIP CHIEF GRAVITY TULIN V.A.        02
AST1 10                                                                       03
900318 SEVASTOPOL,USSR                    900701 KALININGRAD,USSR             04
MAGNAVOX/RADAR                            SATELLITE (WITH SPLINE-SMOOTHING)   05
GEL-3, ELAC-ENIF WITH REC. TO LADOGA      IOAN, ANALOG. RECORDS               06
                                                                              07
4*AMG (IFZ AN USSR)              10111213 IFZ AN (MAGNETIC TAPE)              08
AUTONOM.BOTM.SEISMOGR.                    IOAN (MAGN.TAPE)                    09
AI1,I5,I4,I1,I2,I3,I2,I4,I2,I3,I2,I4,I2,F4.1,I2,I1,I2,I3,2I1,I2,4I1,I2,F      10
BI1,I4,4I2,I3,F5.3,I4,F5.3,F5.1,F6.1,F7.1,F5.1,I1,F5.1,I1                     11
050             1500000                                                       12
                                                                              13
050002 INTERNAT 1930   3IGSN-71          13GMT       DRIFT,  TARE (N 11)     14
9797917 LIMASOL, CYPRUS                                                       15
 1 3303 9999                                                                  16
                                                                              17
                                                                              18
                                                                              19
         THIS CATALOGUE WAS CREATED  UNDER PROGRAM PACKET "MAGELLAN"          20
         (IFZ AN SSSR,                                                        21
         THE AUTHORS: BOYARSKY E.A., AFANASYEVA L.V., NIKIFOROVA O.D.)        22
         ANY QUESTIONS:  MOSCOW, 123810, BOL. GRUZINSKAYA, 10, IFZ AN SSSR    23
                                                                              24
312101   531 0 3434   3453 3508   3415 10812 75   543735554
0   1 1 1 05 1426  34 33.915   34 53.173  -434  1547.5 9796304  -784.2   27.7 0 -786 -778 -781 -791
0   2 1 1 05 1431  34 34.592   34 52.453  -434  1543.5 9796294  -804.2   25.4 0 -804 -800 -800 -812
0   3 1 1 05 1436  34 35.268   34 51.734  -434  1525.5 9796295  -812.2   23.3 0 -802 -803 -810 -834
0   4 1 1 05 1441  34 35.944   34 51.014  -434  1528.0 9796293  -824.2   22.3 0 -821 -828 -827 -820
0   5 1 1 05 1446  34 36.621   34 50.294  -434  1532.5 9796301  -825.2   22.5 0 -828 -825 -828 -819
                   Day Month Hour Minute Lat Deg Lat Min Long Deg Long Min Col-1 Col-2 Depth Col-3 Free Air Gravity Col-4 Col-5 Bouguer Anomaly
```

Figure AppF.1. Printout of the AST10 file header. The meaning of some of the columns, whose FORTRAN formats are given in Line 11, are indicated below. There are some 5149 measurements. The positions of assumed decimal points are also indicated.

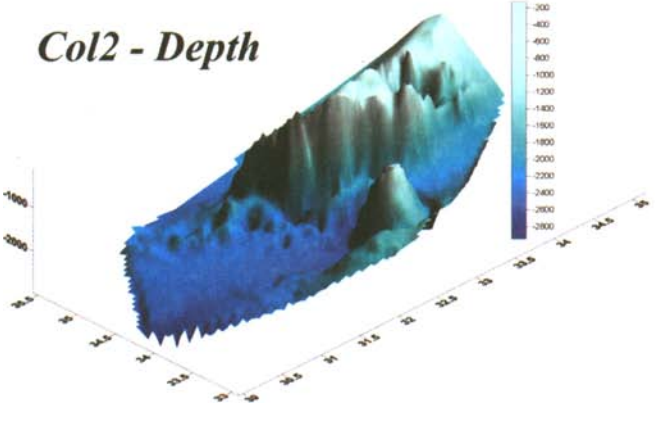
Figure AppF.2. Plot of the data distribution relative to Cyprus, as well as 3-D Surfer®8 plots of the Depth in COL2, the Free Air gravity anomalies in COL3, and the Bouguer anomalies in COL5. The grid files were made using TIN interpolation of the respective COL2.xyz, COL3.xyz, and COL5.xyz files. Note the large anomaly west of Eratosthenes Seamount, which has a much pronounced Bouguer anomaly relative to that of Eratosthenes.

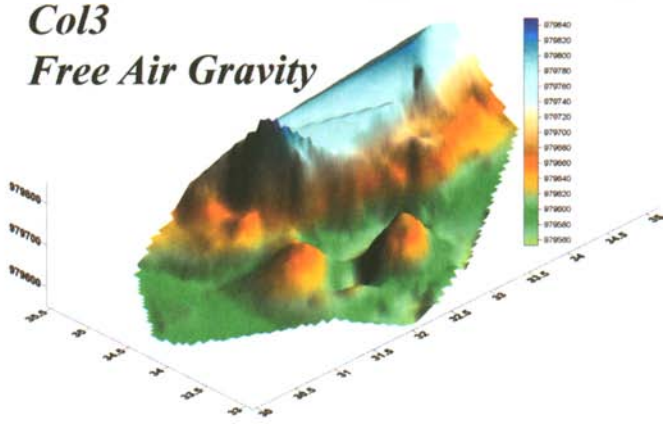






Gravity profiles





increases the accuracy of the gravity measurements. A good computer and some effort is necessary to carry out this procedure, but the navigation data can be post-processed at home. The final 'smoothed' coordinates probably lie within 0.1 miles of the correct position. On gravity tracks we used 'coursographics' for defining the course changes between tracks.

Depths

The two ships were equipped with Hollming multibeam (15 beams) swath echosounders. According to the instructions issued for gravity survey we used only the depths directly under the ship as determined by the center beam.

The depths collected for the gravity reductions are different from those used for geomorphological observations. When traditional and approximate methods are used, the various methods for processing navigational information can give variations in the ship's position of up to 1 mile at the very same time. Thus in the bathymetric mapping of areas of complicated relief some mistakes can occur. This is the reason that the bathymetric maps drawn by our methods can differ in details from the traditional maps. These errors are probably negligible in geological-geophysical interpretation, but are very important to the accuracy evaluation by track crossings in a gravity survey. The depths are thus used as a very well determined third coordinate and any misties at the crossing points are an indication of positional error.

Depths were digitally recorded on magnetic tape on the ES-1011 computer, and for backup insurance in analog form on echograms. Depths were sampled every minute, and the average value was calculated from 5 adjacent samples. The resulting depth is associated with the center of the gravity observation interval, which is also the gravity value. To control errors these were plotted out, and echograms were used if necessary. In practice, depth data was always available.

Gravity Base Station Observations

The gravity observations at sea were tied to the world gravity base network in Limassol Harbor. The base network on the island of Cyprus was set up in 1958 by the British Geological Survey (Gass and Masson-Smith, 1960). Two points from the 46 in the base network are located in Limassol, but, unfortunately, we had no possibility of reaching these points. At our request, Dr. C. Xenophontos of the Geological Survey of Cyprus made the connection between the Malounda base point and a local site in the harbor. We then tied the gravity value from this place to the ship's position. The ships measured several positions for Limassol Harbor, with the main position data as follows: g=979,791.7 mGal, latitude 34°39'35"N, longitude 33°01'03"E. These coordinates were taken from the TRANSIT satellite observations (which were based on the WGS-72 datum).

Some doubts exist about the magnitude of the errors for basic gravity determinations. The random error for ties is estimated at around 0.10-0.15 mGal, but we do not know the accuracy of the base point in Nicosia, from which the Cyprus base network evolved. According to the last recommendation of Gass and Masson-Smith (1960) we have to take into account a value for systematic error of -11.1 mGal. This contradicts the widely known correction to the IGSN-71system of 14.0 mGal.

However, this uncertainty in the base value does not distort the results of our sea survey, as the primary and final ties were occupied at the same point. Only a small variation (2-3 mGal) in the general level of the results is possible.

Gravity Observations at Sea

The gravimeters were mounted in the place closest to the pitch/roll center of each ship. The instruments (including the stabilizer) were switched on some days before observations began and were not switched off until the end of the survey. The survey was made along tracks planned in advance, and its positioning was checked by the gravity men on duty. The course and speed of the ships were held constant (on log and gyrocompass), and in the case of changes appropriate remarks were made in an observation log, which was later used for reduction of the navigational data.

The work at sea lasted a total of 23 days, and took place over three periods of time:

1) 1.5 days prior to initial arrival in Limassol;

2) 18.5 days between Limassol-2 berthing and Limassol-3 berthing;

3) 3 days after departure from Limassol.

The 1st and 3rd periods were not closed by gravity tie calibrations, but we do not expect significant errors due to the null-point extrapolation, so the time interval for them was very close to the basic observations.

Ninety-nine gravity tracks were run, but two of them were useless due to stormy weather. The 97 good tracks covered a total length of 4839 nautical miles, and 5149 gravity points were determined. The spacing between tracks was around 7 miles. The survey was made on a grid of orthogonal tracks, and controlled by the values at the crossing points. The positions of the tracks are shown on **Fig. AppF.1**. The tracks are marked by the locations of the gravity observations. The total area surveyed is about 53,000 km^2.

The main aim of the survey was a more precise observation, depending not only on the gravimeter measurement accuracy, but also on the ship displacement, instrument mounting place, an area of study, and sea state. The survey errors depended equally on gravimeters and on the quality of the navigation. In the process of planning sea work more attention should be given to the arrangement of precise (inside and outside) measurement control.

Final treatment of data

The Magellan-PC software package (Boyarsky and Afanasieva, 1992) was used to analyze the data. The package contains (as of December 1990) 14 programs for treatment of laboratory and marine gravity measurements at catalog level in the Russian MVF-77 format (which practically coincides with the international MGD-77 format), including accuracy of estimation. The package provides the possibility of using the Golden Software Inc. GRAPHER® programs to visualize the results.

The error of measurement for one point was estimated from its similarity to mutual results of the group of gravimeters, and totals 1.01 mGal. The overall error, estimated by the misties at 318 crossing points, is equal to 1.98 mGal. This allows us to draw gravity maps with contours of 5 mGal. The accuracy of the data in our cruises depended not only on errors from longitude smoothing (Eötvös correction calculation) but also from latitude smoothing, because there are large areas with high gravity gradients in the region studied.

The new Global Positioning System (GPS) would give the best navigational results in a gravity survey. The GPS system permits continuous observations with insignificant errors. As a result, the level of navigation mistakes can be lowered to below 1 mGal.

THE DATA FILE FROM WORLD DATA CENTER B (MOSCOW)

The header from the data file ast10.org is shown in **Figure AppF.1**. Line 11 of the header gives the FORTRAN format of the 5149 gravity measurements. As indicated below the figure, the first columns give the date, time, latitude and longitude of the measurements. The positions are in degrees and decimal minutes. To better facilitate understanding of the data, files were prepared in *x,y,z* format with the position and the values in columns 1 through 5 (noted beneath the header). These are on the CD-ROM as COL1.XYZ through COL5.XYZ, along with the Surfer® 8 TIN interpolated grid files. COL2 appears to be depths, which were made negative. COL3 is measured Free Air gravity, and COL5 appears to be the Bouguer anomaly as it is set to 999.9 when the depth is missing. Missing values denoted by 999.9 were removed.

The file ast10.xyz gives a listing of just the data with the positions in decimal degrees.

Figure AppF.2 shows various 3-D and shaded relief plots of the depths, data distribution, and Free Air and Bouguer anomalies. Note the size of the Free Air anomaly and the large Bouguer anomaly associated with the buried Niklas structure (Chapter 23 of this volume) as compared with those of Eratosthenes Seamount.

ACKNOWLEDGEMENTS

The preparation of the equipment, the carrying out of the measurements at sea, and the analysis of the data were made by the author with the able assistance of L. V. Afanasieva, C. M. Baranova, E. A. Bojarsky, A. A. Efremov, D. A. Illinsky, O. D. Nikiforova, T. K. Nikiforov, and V. A. Juzvenko.

The authors thank the World Data Center B (Moscow) for providing the gravity file for digital distribution.

REFERENCES CITED

Boyarsky, E. A., and L. V. Afanasieva, 1992. The software for treatment of gravity measurements. In: International science-technical conference "Marine Gravimetry-92", St. Petersburg, p. 26-27. (In Russian).

Gass I. G., and D. Masson-Smith, 1960. The geology and gravity anomalies of the Troodos massif, Cyprus. Phil. Trans. of the Royal Society of London, ser. A., N 1060, v. 255, p. 417-467.

Kireev, K. N., V. S. Koutepov, L. V. Poushina, V. A. Toulin, and V. G. Cheremisin, 1978. Stabilization of the marine gravimeter. Moscow, "Nauka", 79 p. (In Russian.

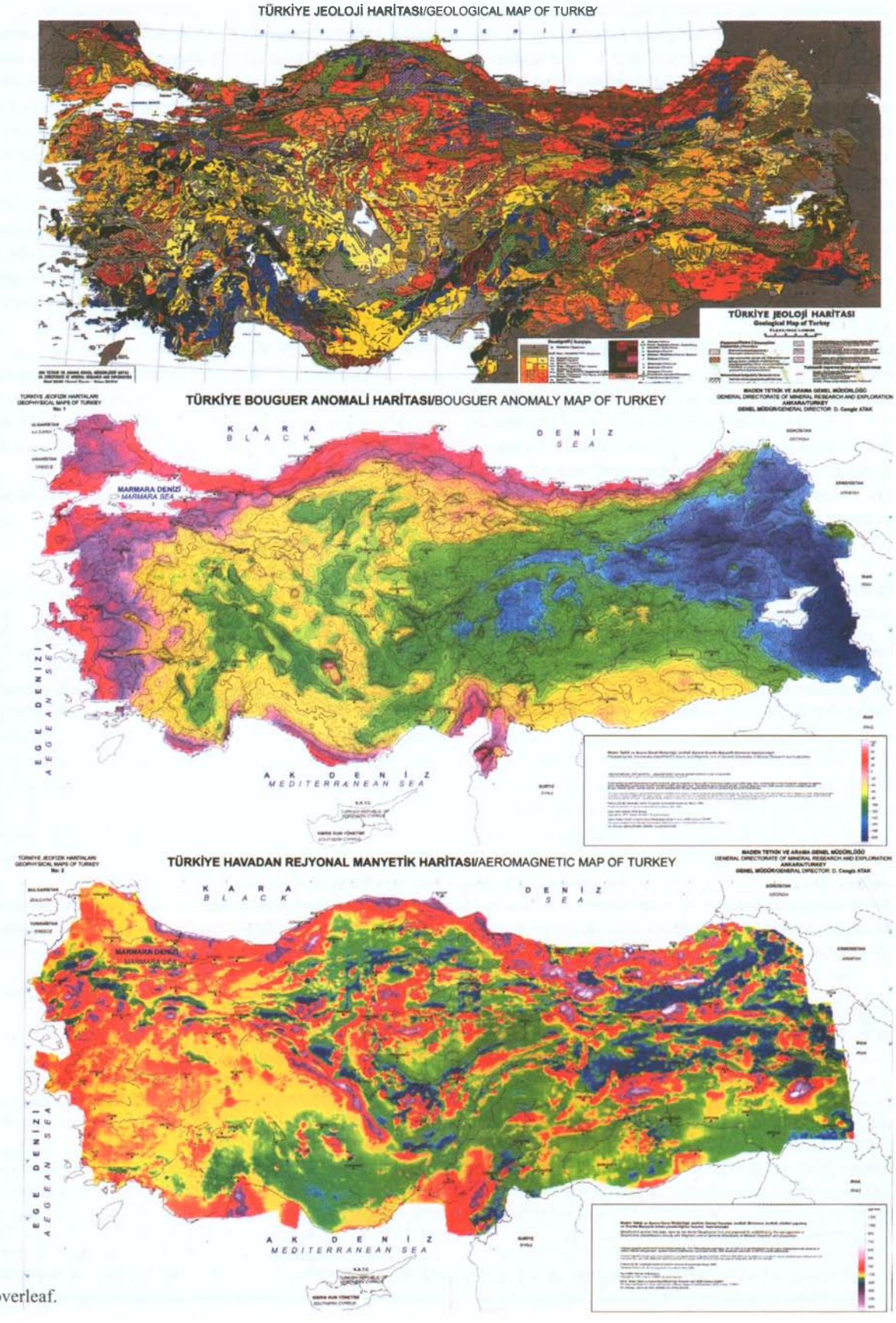
Toulin, V. A. and S. V. Osinskaya, 1970. Marine gravimeter with automatic counting. In: Equipment and methods of counting of gravity figures at sea, Moscow, "Nauka", p. 93-101. (In Russian)

Overleaf: Geology, Bouguer Gravity, and Aeromagnetics of Turkey - Pickings from the Internet.

The website (www.mta.gov.tr/english/harita/harita.asp) of the Turkish General Directorate of Mineral Research and Exploration (MTA) in Ankara gives information on ordering various geological, geophysical, and mineral maps of Turkey. These maps are also available for download at intermediate resolution. Downloads of the 1:2,000,000 scale geological, Bouguer gravity, and aeromagnetic maps are reproduced overleaf for reference.

The Bouguer gravity anomaly map, prepared by the Geophysics Department's Gravity and Magnetic Unit, is based upon a density of 2.67 g/cm^{3}and topographically corrected out to 5.5 km. The base map was drawn in the Lambert Projection transformation system. Gravity values are connected to the MTA and General Command of Mapping base networking system according to Potsdam (982,274,.00 mGal, latitude corrections have been done by the International Gravity Formula (1967). The elevations are from sea level. The anomaly values are mGals (0.001 cm/sec^2) and the contour interval is 5 mGal. The Bouguer gravity anomaly contours are drawn by gridding at 5 km intervals by using gravity station values. Map produced by Surfer® 5.0 software, and printed in May 1999 by Petkom Ltd. Copyright MTA Ankara, Turkey, all rights reserved. The map is available at MTA, e-mail bdt@mta.gov.tr, address is MTA Gn. Md. BDT D.Bşk.Basın ve Halkla İlişkiler Servisi 06520-ANKARA Tel: +90-312-287 34 30; Fax: +90-312-285 99 82. Maps are printed in English and Turkish.

The Aeromagnetic Map of Turkey, compiled by the Aerial Geophysics Unit and prepared for publishing by the management of the Geophysics Department's Gravity and Magnetic Unit is based upon airborne magnetic surveys accomplished on overlapping areas in the years between 1975 and 1989. Data from each survey was corrected for diurnal variation and heading errors, and reduced to the June 1982 epoch. Flights were done at 2,000 feet on average. IGRF corrections have been applied and the data gridded at 2 x 2 km intervals. The map was produced by Surfer® 6.0 software, and printed in May 1999 by Petkom Ltd. Copyright MTA Ankara, Turkey, all rights reserved. The map is available at MTA, e-mail bdt@mta.gov.tr, address is MTA Gn. Md. BDT D.Bşk.Basın ve Halkla İlişkiler Servisi 06520-ANKARA Tel: +90-312-287 34 30/287 87 00; Fax: +90-312-285 99 82. Maps are printed in English and Turkish.



Caption overleaf.

Appendix G

Shaded Relief Images of the IBCM Bathymetry and Geological-Geophysical Overlays

John K. Hall
Geological Survey of Israel, Marine Geology, 30 Malchei Israel Street, Jerusalem 95 501, Israel

INTRODUCTION

The International Bathymetric Chart of the Mediterranean (IBCM) and its five Geological-Geophysical Overlay Series have been described in some detail in the Introduction to Part III and Chapters 16 and 17 of this volume. In the final stages of preparation of these volumes, during the author's 2003-2004 sabbatical at the University of New Hampshire's Center for Coastal and Ocean Mapping (CCOM), the opportunity arose to scan all the 66 sheets produced by the IBCM project on a commercial grade 54" scanner donated to the Nippon Foundation/GEBCO Training Project at the university. The scans were at 400 dpi in rgb color. For five of these map sets (the exception being IBCM-S Seismicity – which had a generalized 1:5 million reduction with the epicenters emphasized), the individual scans of the ten sheets at 1:1 million scale were joined together to produce a single digital file for the entire Mediterranean, with the Black Sea at 1:2 million scale in the northeast corner. Merging the 1' gridded worldwide bathymetric compilation of the new GEBCO Digital Atlas (GDA) (BODC, 2003) together with the 0.5' SRTM land topography, a file was prepared at 0.5' with the bathymetry and topography underlying the IBCM compilations (**Fig. AppG.1**). Global Mapper® software was then used to georeference each overlay image as a GeoTiff, to 'texture map' it with the shaded relief of the land topography and marine bathymetry, and output it as a high resolution (254 m pixels) JPEG file.

As an added aid to visualization of these valuable compilations, this appendix reproduces as centerfolds the six IBCM compilations at an approximate scale of 1:10 million for the Mediterranean and 1:20 million for the Black Sea (**Figs. AppG.2**-7). These digital files will eventually be made available via the Internet. The original printed sheets are available for purchase from Geopubs, 4 Glebe Crescent, Minehead, Somerset, TA24 5SN, England (Tel: +44-1643-709001; Fax: +44-1643-709002.

Geopubs' e-mail is accounts@geopubs.co.uk and the website is http//www.geopubs.co.uk/.

THE SIX COMPILATIONS

IBCM - Bathymetry - Figure AppG.2

The IBCM bathymetric chart was published in 1981 by the Charts Division of the Head Department of Navigation and Oceanography of the Russian Navy in Leningrad, under the authority of the Intergovernmental Oceanographic Commission (IOC) of UNESCO. Originally compiled from ninety 1:250,000 scale British Admiralty Mercator plotting sheets for oceanic soundings, it presents the bathymetry and land topography as 200 m contours with supplemental 20 m, 50 m, and 100 m contours at sea. Several versions are available; a 10 sheet set (each 74 x 90 cm) at 1:1,000,000 scale at 38°N, and a reduction to 1:5,000,000 scale. An inset map shows the geographic subdivisions of the seven regional seas within the Mediterranean. This chart, with an inset of the entire Black sea at 1:2 million scale, is also the basemap for the series of five IBCM Geological/Geophysical Overlays. Digital scans and both printed and digital (pdf format) explanatory brochures for these series are available. The digitized marine contours are available on CD-ROM as part of the British Oceanographic Data Centre's GEBCO GDA (BODC, 2003).

IBCM-G - Bouguer Gravity Anomalies - Figure AppG.3

The IBCM-G Bouguer gravity anomaly map was compiled by Prof. Jannis Makris of the Institut für Geophysik in Hamburg, and Prof. Carlo Morelli of the Istituto di Miniere e Geofisica Applicata in Trieste. It was published in 1988 by the Charts Division of the Head Department of Navigation and Oceanography in Leningrad under the authority of the Intergovernmental Oceanographic Commission (IOC) of UNESCO. The primary data are from over 114,000 nm of marine survey carried out in 1965-1972 by OGS in Trieste, and in 1973-1974 by the Dept. of Geodesy and Geophysics of Cambridge University, together with land compilations. It presents the anomalies in milligals, based upon the 1967 normal gravity formula, a 2.67 g/cm^3 Bouguer density, and topographic corrections to 167 km for the land area in the easternmost four sheets. Contours are every 10 mGal with changes in tint every 50 mGal. Red tints are positive. The bathymetry is from the 200 m contours of the original IBCM with supplemental 20 m, 50 m, and 100 m contours at sea. An inset map shows the geographic subdivisions of the seven regional seas within the Mediterranean. Two versions are available; a 10 sheet set (each 74 x 90 cm) at 1:1,000,000 scale at 38°N, and a reduction to 1:5,000,000 scale. An article describing the compilation and the map was published by Makris et al. (1998).

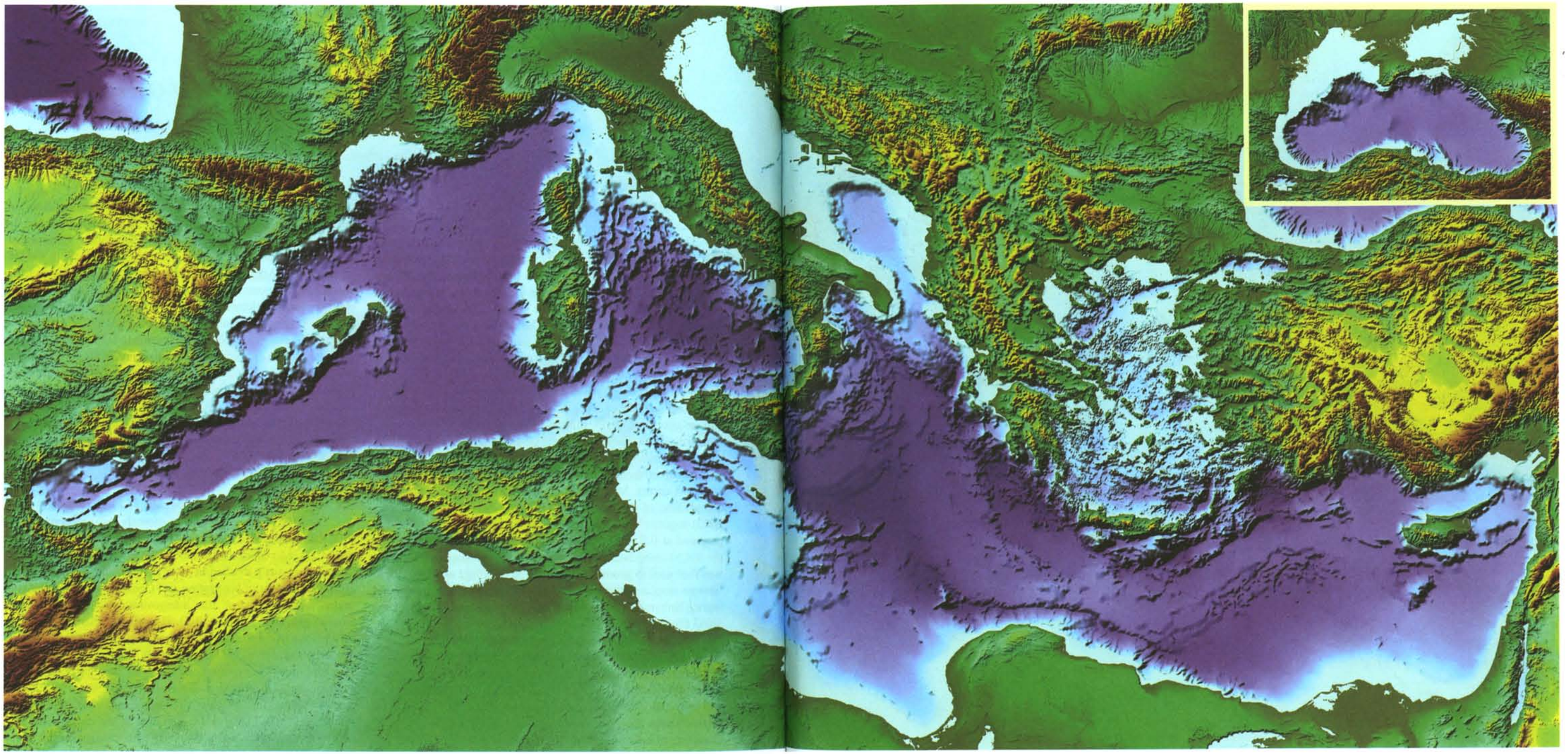


Figure AppG.1. IBCM – Basemap grid for texture mapping the IBCM compilations. Land data is 0.5' SRTM together with GEBCO GDA at sea.



Figure AppG.2. IBCM – The Bathymetric Chart of the Mediterranean.

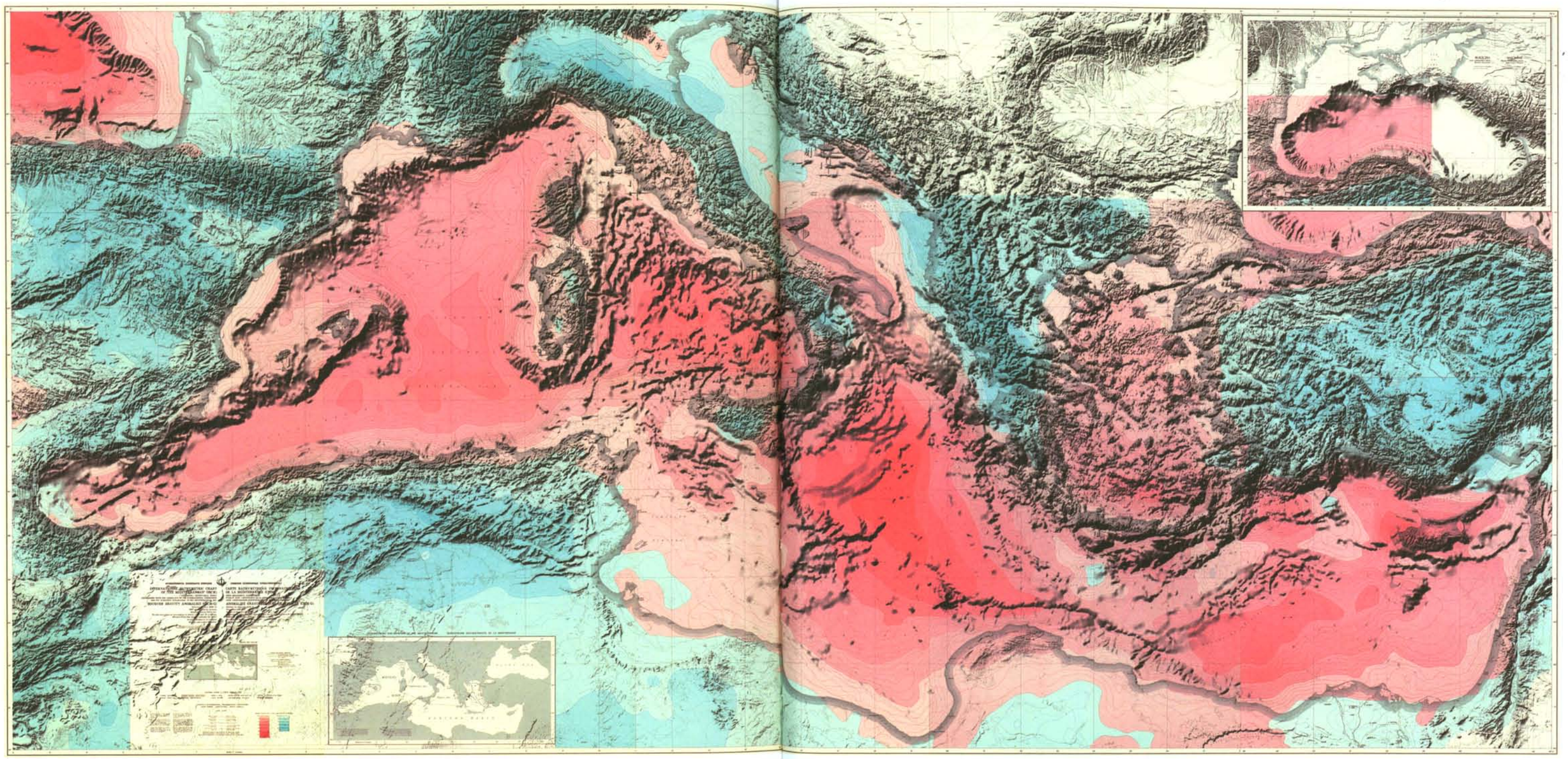


Figure AppG.3. IBCM-G. Bouguer Gravity Anomaly Map of the Mediterranean and Black Seas.

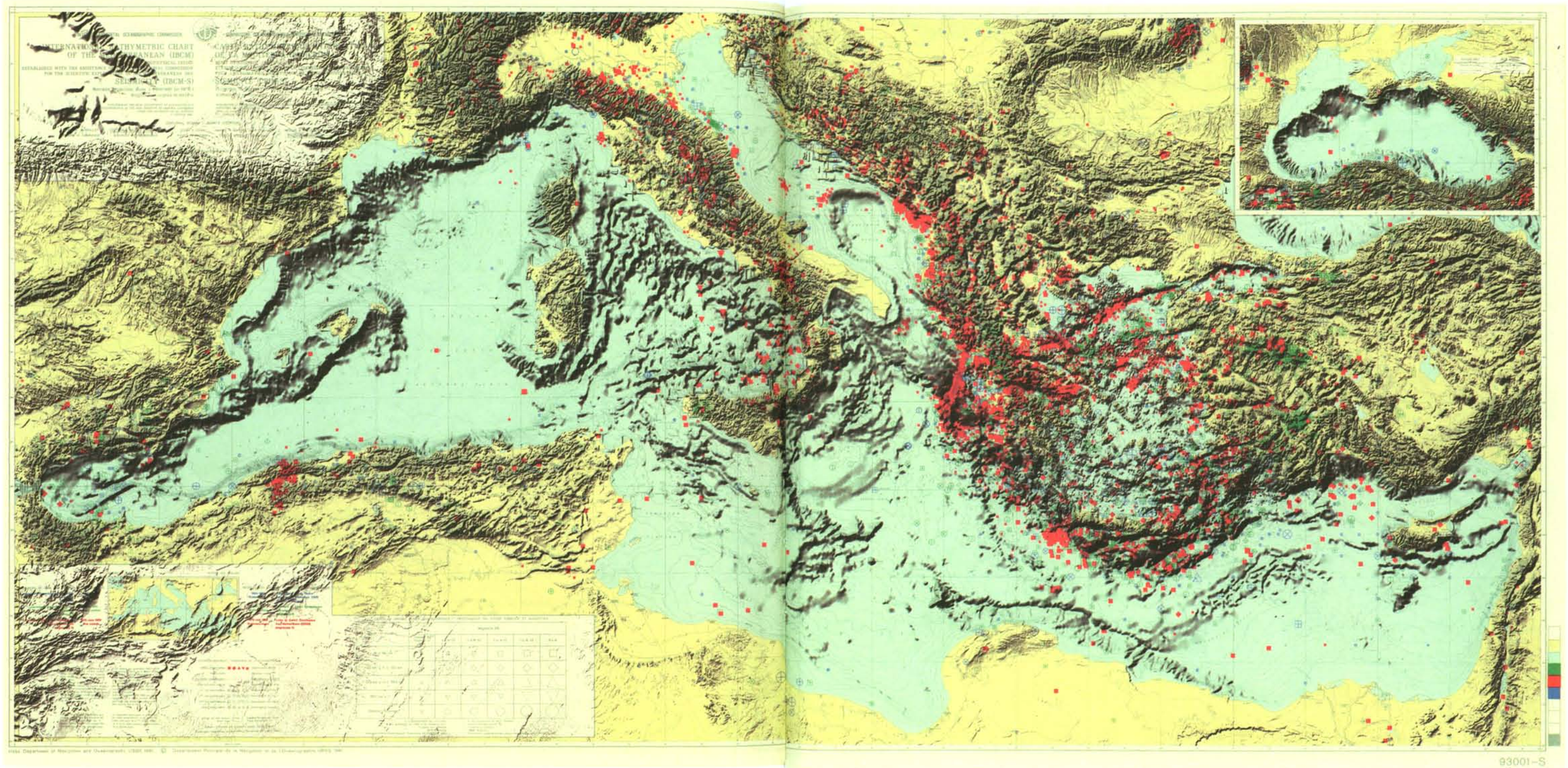


Figure AppG.4. IBCM-S. Seismicity Map of the Mediterranean and Black Seas.

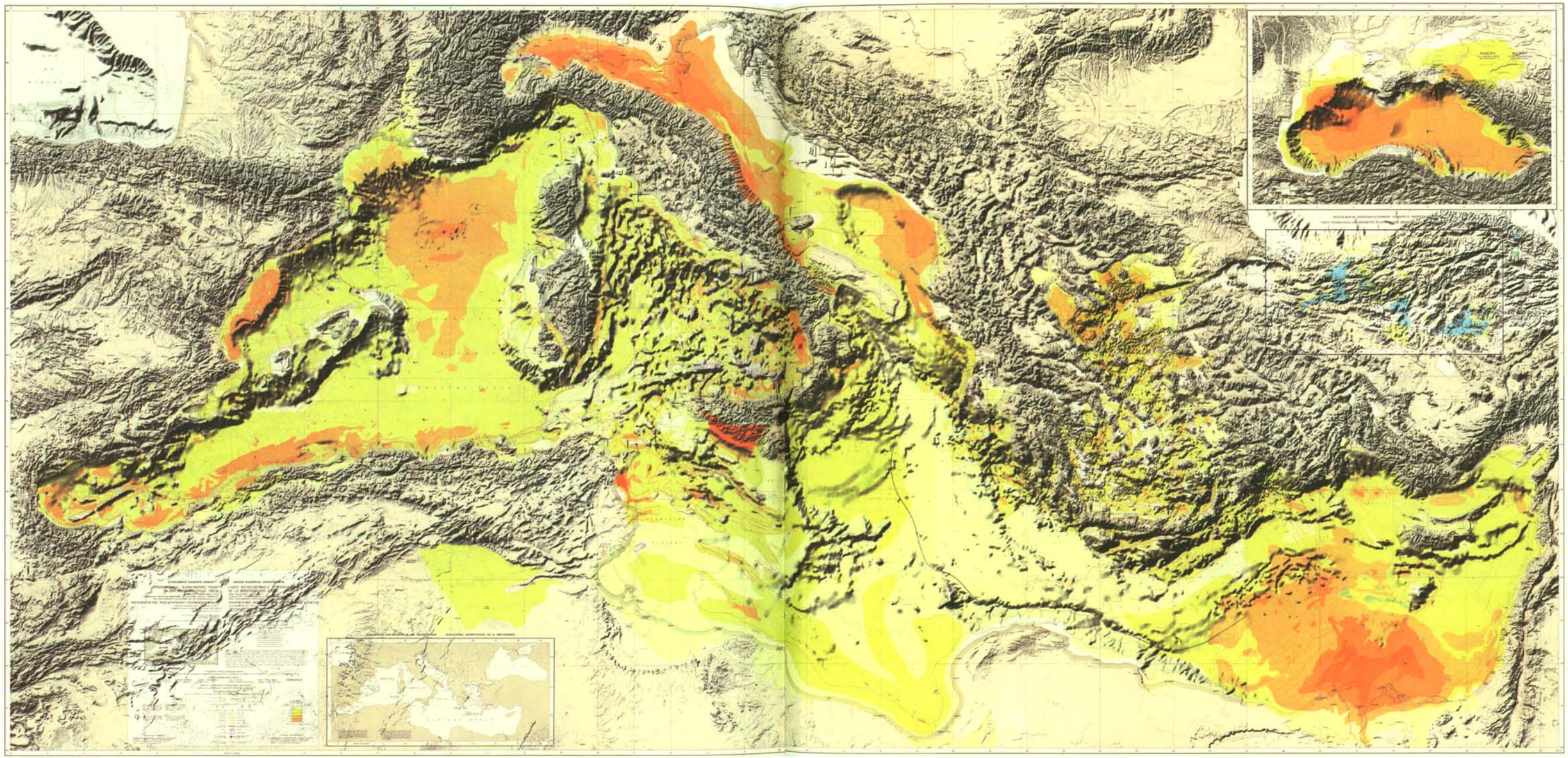


Figure AppG.5. IBCM-PQ. Plio-Quaternary Sediment Thickness Map of the Mediterranean and Black Seas.

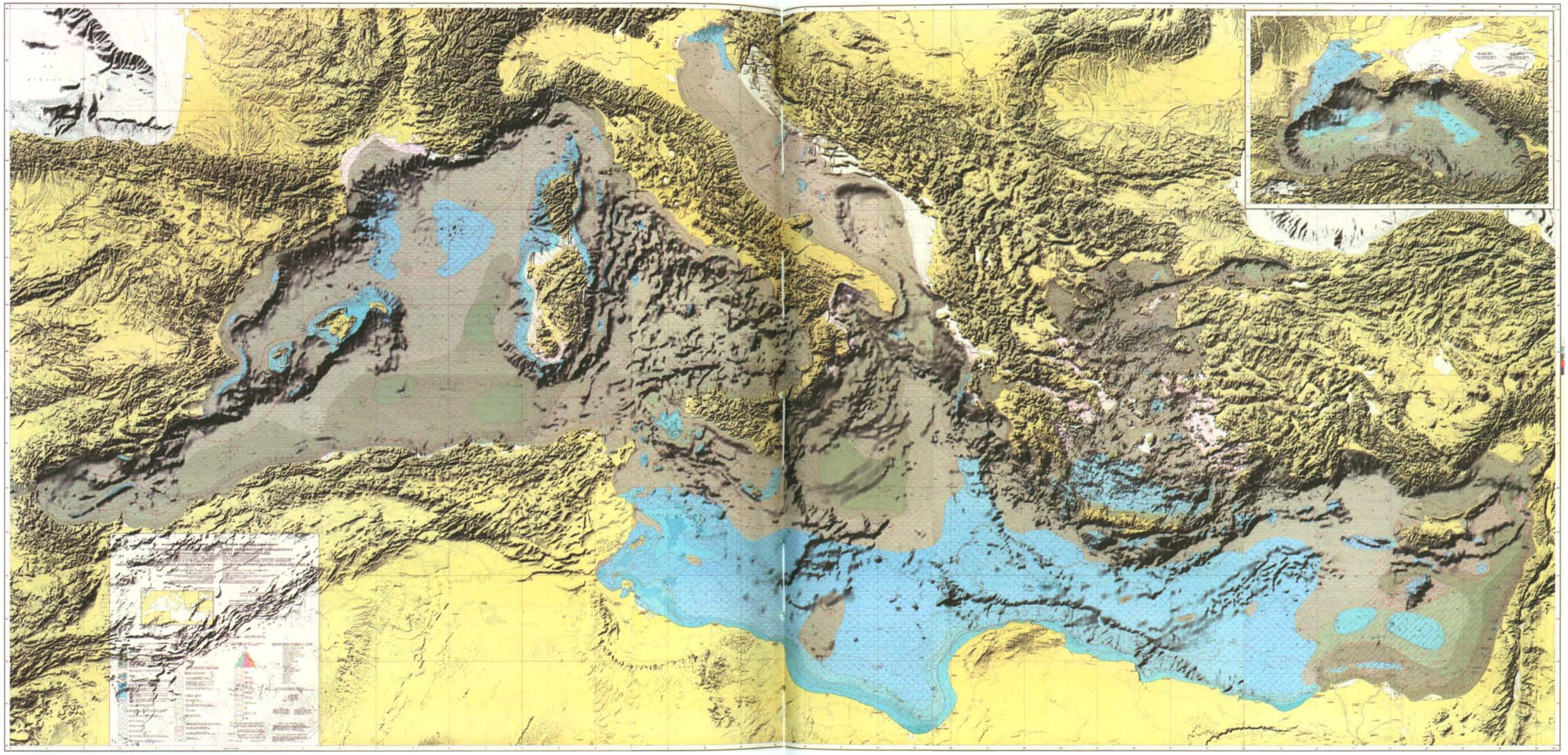


Figure AppG.6. IBCM-SED. Unconsolidated Bottom Surface Sediment Map of the Mediterranean and Black Seas.

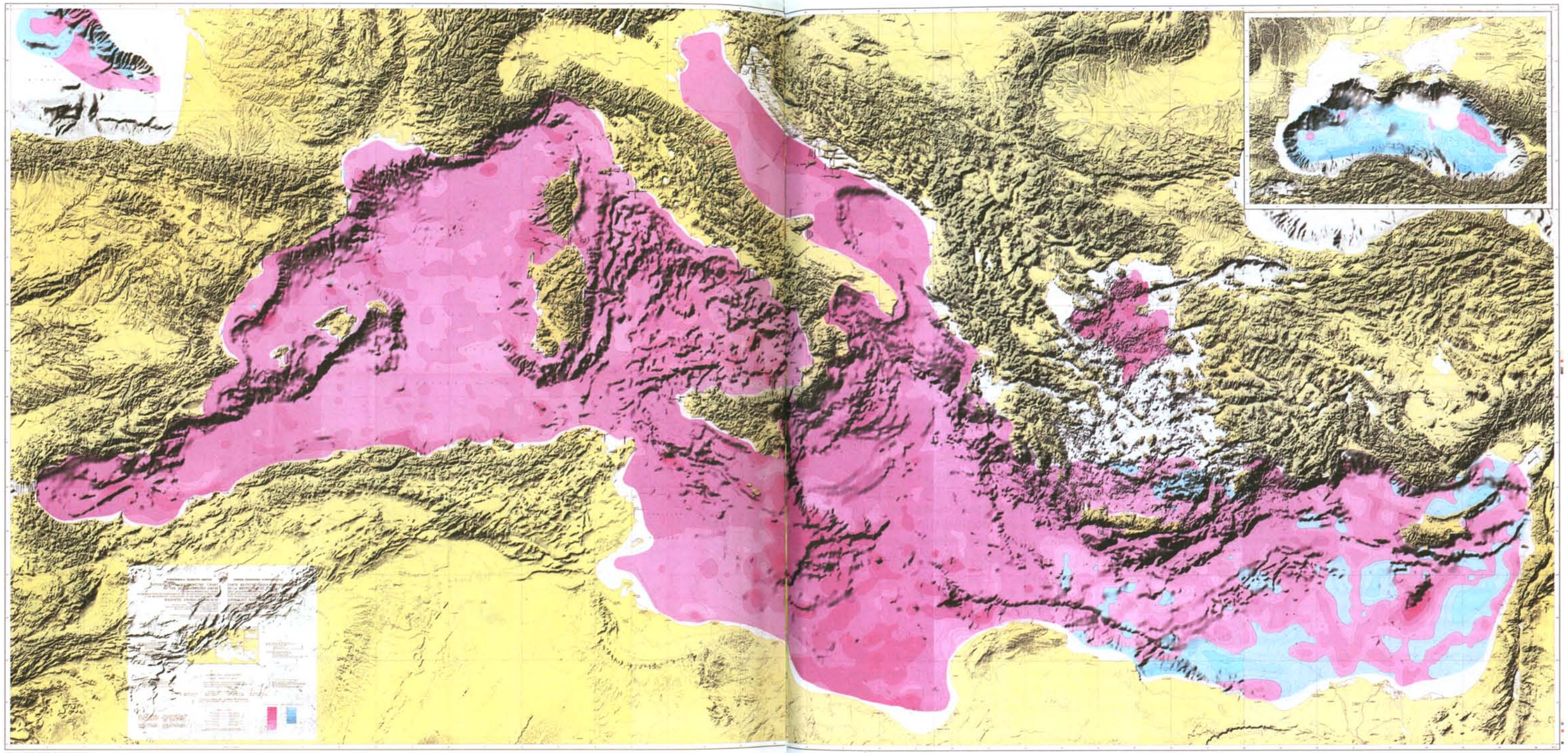


Figure AppG.7. IBCM-M. Marine Magnetic Anomaly Map of the Mediterranean and Black Seas.

IBCM-S – Instrumental Seismicity - Figure AppG.4

The IBCM-S Mediterranean seismicity map was compiled by Yvette Legros and Prof. Jean Bonnin under the scientific coordination of Prof. Bonnin of the European-Mediterranean Seismological Centre (EMSC) in Strasbourg, France. It was published in 1991 by the Charts Division of the Head Department of Navigation and Oceanography in Russia under the authority of the Intergovernmental Oceanographic Commission (IOC) of UNESCO. Some 33,000 separate seismic earthquake epicenters in the Mediterranean region were recalculated and are plotted as colored symbols, with shape denoting depth of focus, size reflecting magnitude, and color (blue, green, red) showing the historical catalog (1904-1963; 1964-1975; 1976-1988) from which the events are taken. Explanations are in English and French. The bathymetry is from the 200 m contours of the original IBCM with supplemental 2 m, 50 m, and 100 m contours at sea. Two versions are available; a 10 sheet set (each 74 x 90 cm) at 1:1,000,000 scale at 38°N, and a photo reduction to 1:5,000,000 scale. An expanded explanatory brochure and printed earthquake catalog were published by Legros and Bonnin (1996, 1999).

IBCM-PQ - Plio-Quaternary Isopachs - Figure AppG.5

The IBCM-PQ Plio-Quaternary sediment thickness map was compiled under the direction of Profs. P. Burollet, M. Gennesseaux, P. Kuprin, E. Tzotzolakis, and É. Winnock. It was published in 1993 by the Charts Division of the Head Department of Navigation and Oceanography in Saint Petersburg under the authority of the Intergovernmental Oceanographic Commission (IOC) of UNESCO. The primary data derive from numerous marine seismic surveys of the depth to the top of the Messinian salt layer, together with land compilations. Contours are in increments of 0.2 sec two-way travel time, with changes in tint at 0.2, 1.0, 2.0, and >30 sec. The bathymetry is from the 200 m contours of the original IBCM with supplemental 20 m, 50 m, and 100 m contours at sea. Explanations are in English and French, and tectonic, diapiric, and volcanic features are indicated. Insets show a sketch map of the Messinian evaporate deposits in the Mediterranean, as well as the geographic subdivisions of the seven regional seas within the Mediterranean. Two versions are available; a 10 sheet set (each 74 x 90 cm) at 1:1,000,000 scale at 38°N, and a photo reduction to 1:5,000,000 scale. An article describing the compilation was published by Gennesseaux et al. (1999).

IBCM-SED – Unconsolidated Bottom Sediments - Figure AppG.6

The IBCM-SED map of the Unconsolidated Sediments of the Mediterranean and Black Seas was compiled by Profs. E. M. Emelyanov and K. M. Shimkus of the Atlantic Branch of the P. P. Shirshov Institute of Oceanology in Kaliningrad, Russia, and Prof. P. N. Kuprin of the Moscow State University, with numerous contributions from regional scientists. It was published in 1996 by the Charts Division of the Head Department of Navigation and Oceanography in Russia under the authority of the Intergovernmental Oceanographic Commission (IOC) of UNESCO. The sediments are displayed both genetically and according to grain size, using both colors and hachure patterns. The background bathymetry is from the 200 m contours of the original IBCM with supplemental 20 m, 50 m, and 100 m contours at sea. Explanations are in English and French. Two versions are available; a 10 sheet set (each 74 x 90 cm) at 1:1,000,000 scale at 38°N, and a photo reduction to 1:5,000,000 scale. A description of the compilational process and discussion of the results by Emelyanov et al. (2005) appears in Chapter 17.

IBCM-M - Marine Magnetic Anomalies - Figure AppG.7

The IBCM-M Magnetic Anomalies map was compiled by Prof. Claudio Zanolla of the Osservatorio Sperimentale (OGS), and Profs. Carlo Morelli and Iginio Marson of the Department of Naval Architecture, Marine and Environmental Engineering of the University of Trieste. It was published in 2000 by the Charts Division of the Head Department of Navigation and Oceanography in Saint Petersburg, Russia under the authority of the Intergovernmental Oceanographic Commission (IOC) of UNESCO. The anomalies are contoured at intervals of 50 nT, with an accuracy of 10 nT. Positive anomalies are red and negative anomalies are blue, with tint changes every 100 nT. The bathymetry is from the 200 m contours of the original IBCM with supplemental 20 m, 50 m, and 100 m contours at sea. Explanations are in English and French. To date the map is only available as a 10 sheet set (each 74 x 90 cm) at 1:1,000,000 scale at 38°N. A description of the compilational process and discussion of the results appears in publications by Zanolla et al. (1998, 2000).

ACKNOWLEDGEMENTS

I gratefully acknowledge the support of the IBCM Chairman, Prof. Carlo Morelli, and the other members of the IBCM Editorial Board, as well as the former GEBCO Permanent Secretaries, Despond P. D. Scott, and Brian Harper. The new 54" Ideal Magnum XL color scanner, was a contribution to the Nippon Foundation/GEBCO Training Project at UNH-CCOM from the Margaret Kendrick Blodgett Foundation.

This scanner, with 1200 dpi resolution, 32 bit color capability, and extensive raster to vector conversion software, is available for making archival digital scans of analog bathymetric charts and other sounding data.

The assistance of Nathan Paquin from CCOM in the setting up and operation of the scanner is gratefully acknowledged.

REFERENCES CITED

British Oceanographic Data Centre, 2003. Centenary Edition of the IHO/IOC General Bathymetric Chart of the Oceans. 2 CDROMs and brief printed explanation.

Emelyanov, E. M., Shimkus, K. M., and Kuprin, P. N., 2005. Explanatory Notes to the IBCM-SED Map Series Unconsolidated Sediments of the Mediterranean Sea (Scale 1:1,000,000) and the Black Sea (Scale 1:2,000,000). In: V. A. Krasheninnikov, J. K. Hall, F. Hirsch, C. Benjamini, and A. Flexer (eds.), The Geological Framework of the Levant, Volume II, The Levantine Basin and Israel, Historical Productions-Hall Ltd., Jerusalem, p. 179-210.

Gennesseaux, M. Burollet P. and Winnock E., 1999. Thickness of the Plio-Quaternary sediments (IBCM-PQ). Boll. Geof. Teor. ed Appl., 39(4), p. 243-284.

Intergovernmental Oceanographic Commission, 1981/1987. International Bathymetric Chart of the Mediterranean. Series established under the Cooperative Investigations in the Mediterranean (C.I.M.), Mercator projection. Scale 1:1,000,000 at 38°N latitude. 10 sheets with heights and depths in meters, published by the Head Department of Navigation and Oceanography, Ministry of Defence, Leningrad, USSR, under the authority of IOC (UNESCO), 1st Edition, June 1981. Single sheet at 1:5,000,000 scale published in 1987.

Intergovernmental Oceanographic Commission, 1988/1989. Bouguer Gravity Anomalies (IBCM-G). International Bathymetric Chart of the Mediterranean, Geological-Geophysical Series established with the assistance of the International Commission for the Scientific Exploration of the Mediterranean Sea. Mercator projection. Scale 1:1,000,000 at 38°N latitude. 10 sheets with Bouguer anomalies in 10 mGal contours, 50 mGal tints, 1967 normal gravity formula, 2.67 g/cm3 Bouguer density, and terrain corrections for land stations in Sheets 4, 5, 9 and 10 to 167 km. Heights and depths in meters. Published by the Head Department of Navigation and Oceanography, Ministry of Defence, Leningrad, USSR, under the authority of IOC (UNESCO), Preliminary Edition, 1988, Published 1989. Single sheet at 1:5,000,000 published in April 1989.

Intergovernmental Oceanographic Commission, 1991. Seismicity (IBCM-S). International Bathymetric Chart of the Mediterranean, Geological-Geophysical Series established with the assistance of the International Commission for the Scientific Exploration of the Mediterranean Sea. Mercator projection. Scale 1:1,000,000 at 38°N latitude. 10 sheets compiled by Yvette Legros and Jean Bonnin, with relocated earthquake epicenters. Heights and depths in meters. Published by the Head Department of Navigation and Oceanography, Ministry of Defence, Leningrad, USSR, under the authority of IOC (UNESCO). Single sheet at 1:5,000,000 also published in 1991.

Intergovernmental Oceanographic Commission, 1993. Thickness of the Plio-Quaternary sediments (IBCM-PQ). International Bathymetric Chart of the Mediterranean, Geological-Geophysical Series established with the assistance of the International Commission for the Scientific Exploration of the Mediterranean Sea. Mercator projection. Scale 1:1,000,000 at 38°N latitude. 10 sheets compiled under the scientific coordination of P. Burollet, M. Gennesseaux, P. Kuprin, E. Tzotzolakia, and E. Winnock. Heights and depths in meters. Published by the Head Department of Navigation and Oceanography, Ministry of Defence, St. Petersburg, Russia, under the authority of IOC (UNESCO). Single sheet at 1:5,000,000 published in 1993.

Legros, Y., and Bonnin, J., 1996. Seismicity (IBCM-S) Explanatory booklet. European-Mediterranean Seismological Centre, International Bathymetric Chart of the Meditarranean (IBCM). 52 p.

Legros, Y., and Bonnin, J., 1999. Investigating instrumental seismicity data sources for the Mediterranean Region (IBCM-S). Boll. Geof. Teor. ed Appl., 40(2), p. 79-146.

Makris J., Morelli C., and Zanolla C., 1998. The Bouguer gravity map of the Mediterranean Sea (IBCM-G). Boll. Geof. Teor. ed Appl., 39(1), p. 79-98.

Morelli, C., and Val'chuk, S., 1988. The International Bathymetric Chart of the Mediterranean (I.B.C.M.) published under the authority of the Intergovernmental Oceanographic Commission of UNESCO. In: J. K. Hall (ed.), Preprint of Chapter 1 in the IBCM Supporting Volume, Jerusalem, Israel, 10 p.

Zanolla, C., Morelli, C., and Marson, I.; 1998. The magnetic anomalies of the Mediterranean Sea (IBCM-M). Boll. Geof. Teor. ed Appl., 39(1), p. 1-36.

Zanolla, C., Morelli, C., and Marson, I., 2000. The magnetic anomalies of the Eastern Mediterranean revisited and the Black Sea ones presented. Boll. Geof. Teor. ed Appl., 41(1), p. 79-83.

Charts series should be referenced as follows:

Emelyanov, E. M., Shimkus, K. M., and Kuprin, P. N., 1996. Unconsolidated Bottom Surface Sediments of the Mediterranean and Black Seas. Intergovernmental Oceanographic Commission (UNESCO), IBCM Geological-Geophysical Series, Scale 1:1,000,000, 10 sheets, St. Petersburg, Russia.

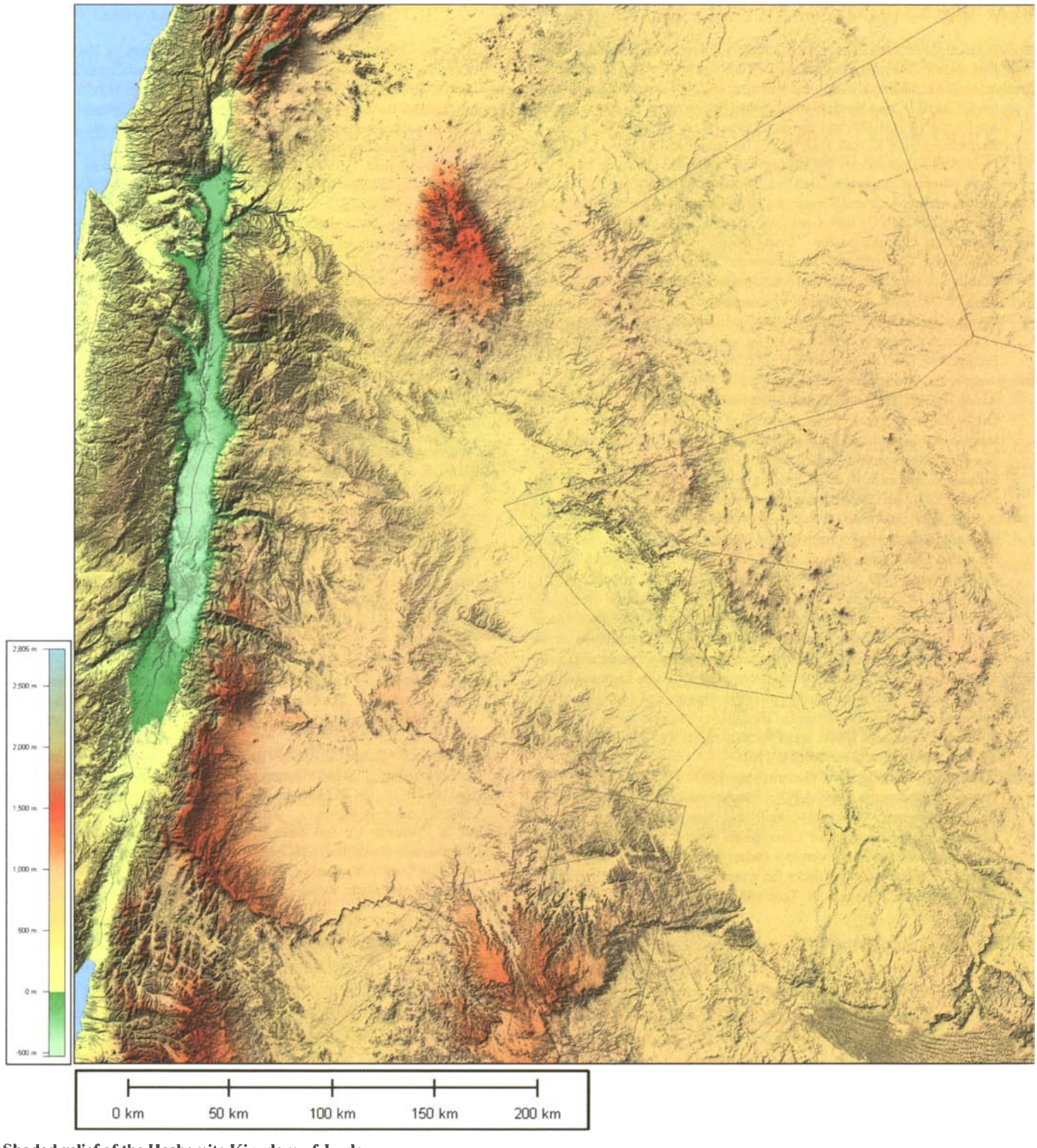
Gennesseaux, M., and Winnock, E., 1993. Thickness of Mediterranean Plio-Quaternary Sediments. Intergovernmental Oceanographic Commission (UNESCO), IBCM Geological-Geophysical Series, Scale 1:1,000,000, 10 sheets, St. Petersburg, Russia.

Legros, Y., and Bonnin, J., 1989. IBCM Seismicity. Intergovernmental Oceanographic Commission (of UNESCO), IBCM Geological-Geophysical Series, Scale 1:1,000,000, 10 sheets, Leningrad, Russia.

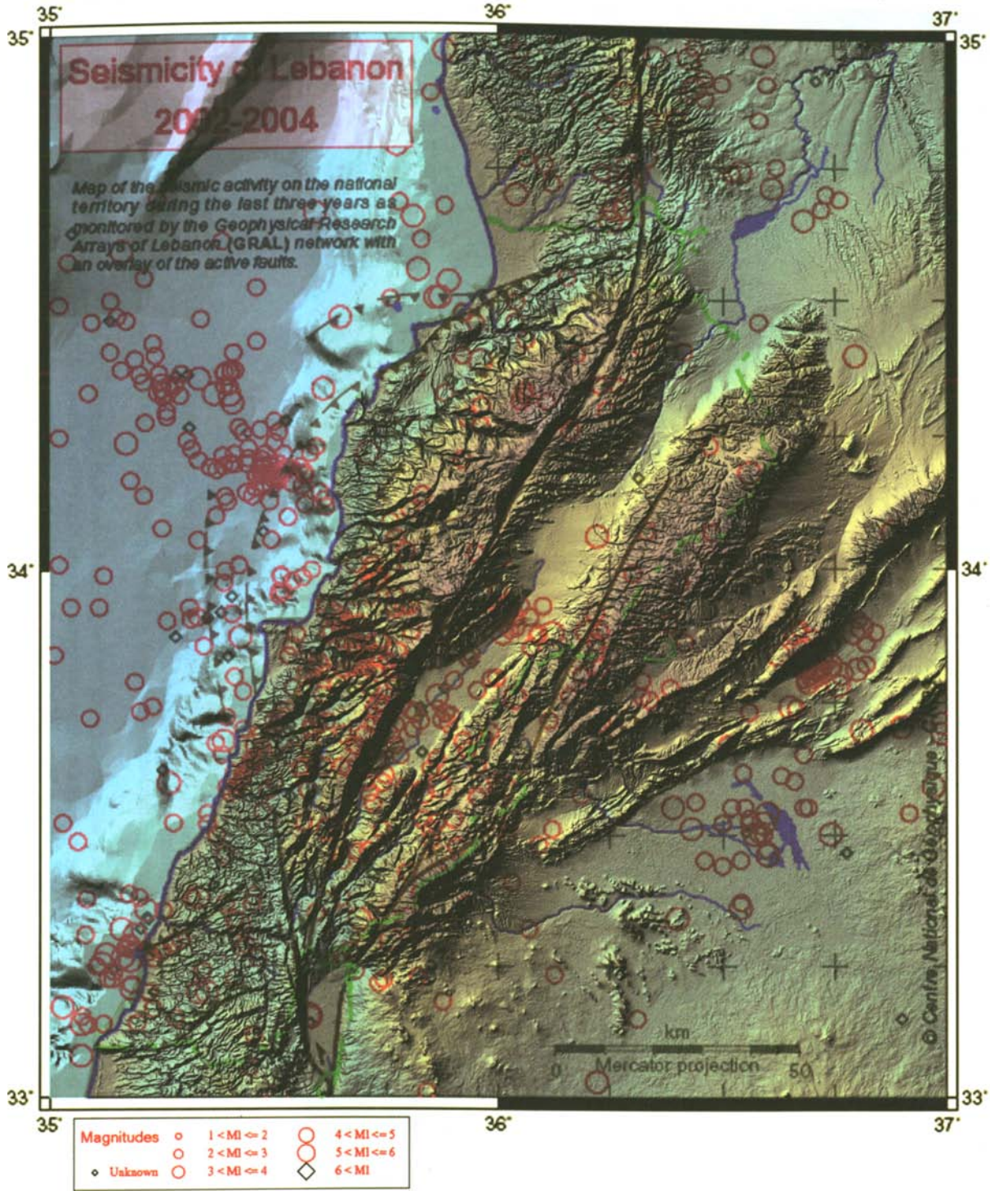
Makris, J., Morelli, C., and Sarrailh, M., 1989. Bouguer Gravity Anomalies. Intergovernmental Oceanographic Commission (of UNESCO), IBCM Geological-Geophysical Series, Scale 1:1,000,000, 10 sheets, Leningrad, Russia.

Morelli, C., and Val'chuk, S., 1981. The International Bathymetric Chart of the Mediterranean (I.B.C.M.). Intergovernmental Oceanographic Commission (of UNESCO), IBCM Geological-Geophysical Series, Scale 1:1,000,000, 10 sheets, Leningrad, Russia.

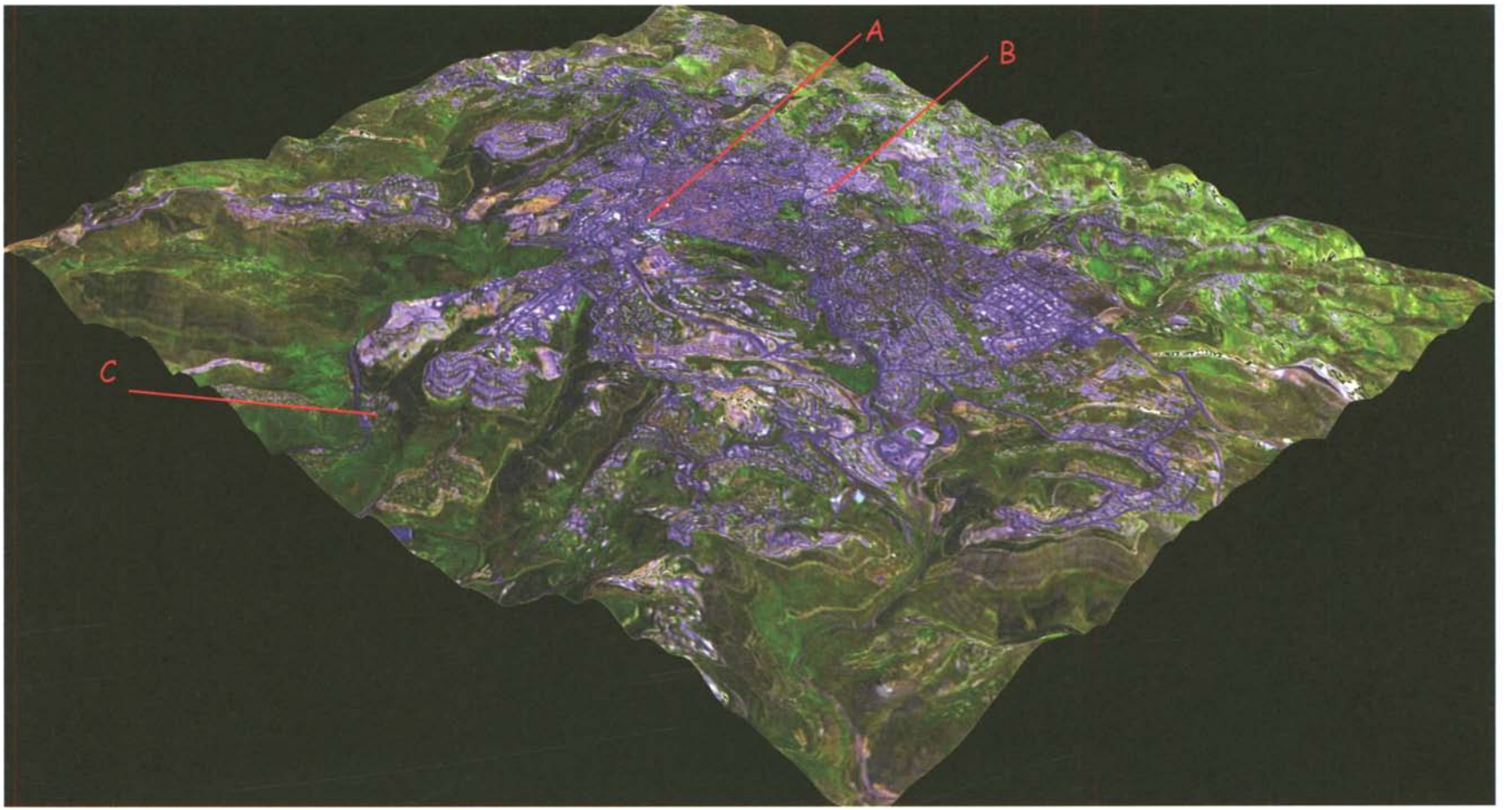
Zanolla, C., Morelli, C., and Marson, I., 2000. Magnetic anomalies of the Mediterranean and Black Seas. Intergovernmental Oceanographic Commission (UNESCO), IBCM Geological-Geophysical Series, Scale 1:1,000,000, 10 sheets, St. Petersburg, Russia.



Shaded relief of the Hashemite Kingdom of Jordan.
Topography is from the 90 m Shuttle Radar Topographic Mission (SRTM) dataset, overlain in Global Mapper® on the 900 m SRTM30 dataset in order to fill holes. Vertical exaggeration is 20 times and sun illumination is at an elevation of 45°from the NW (N315°E). The limits of the image are 29.1°N to 33.6°N, and 34.9°E to 39.6°E. The projection is Mercator.
Coastline and country boundaries are taken from the NOAA Coastline Extractor - **http://rimmer.ngdc.noaa.gov/mgg/coast/getcoast.html.** Boundaries are approximate, for reference only. The three available Aster 30 m DTMs shown in this volume in Figure 16.10 (pages 170-171) are outlined in the south central areas.



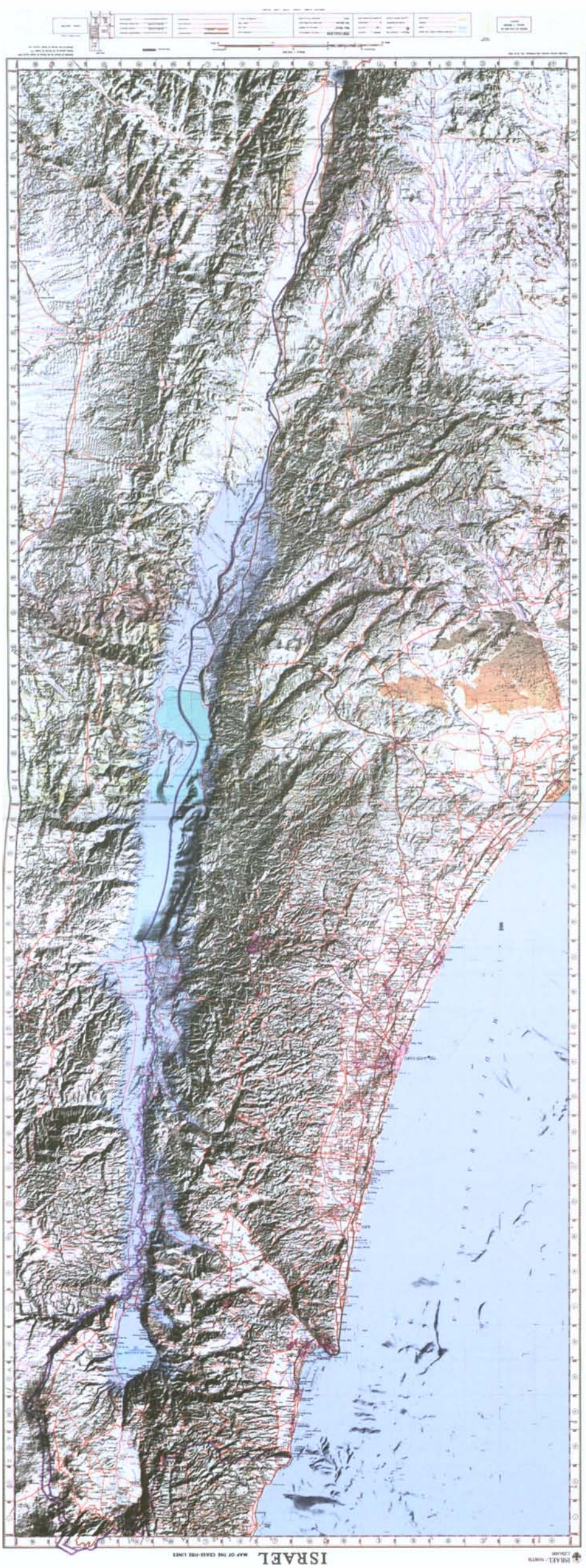
Seismicity of Lebanon for the years 2002-2004.
Map of the seismic activity on the national territory of Lebanon during the three years 2002-2004, as monitored by the Geophysical Research Arrays of Lebanon (GRAL) network. Faults considered as active are overlain. This image, ©Centre National de Geophysique (CNRS), was downloaded from the internet at www.cnrs.edu.lb/download/pdf/bul0412.pdf. The image is shown draped on a 75 m DTM of topography for the land and sea obtained from the DTM of Israel, ASTER DEMs, and the 90 m SRTM. Global Mapper® v.6.07 was used to texture map the two, producing this hypsometrically tinted shaded relief image. Vertical exaggeration is 5.4x, sun illumination from the northwest at 45° elevation, Global Shader palette, 60% translucency. Mercator projection. Borders in light green, epicenters in red with diameter proportional to instrumental magnitude.

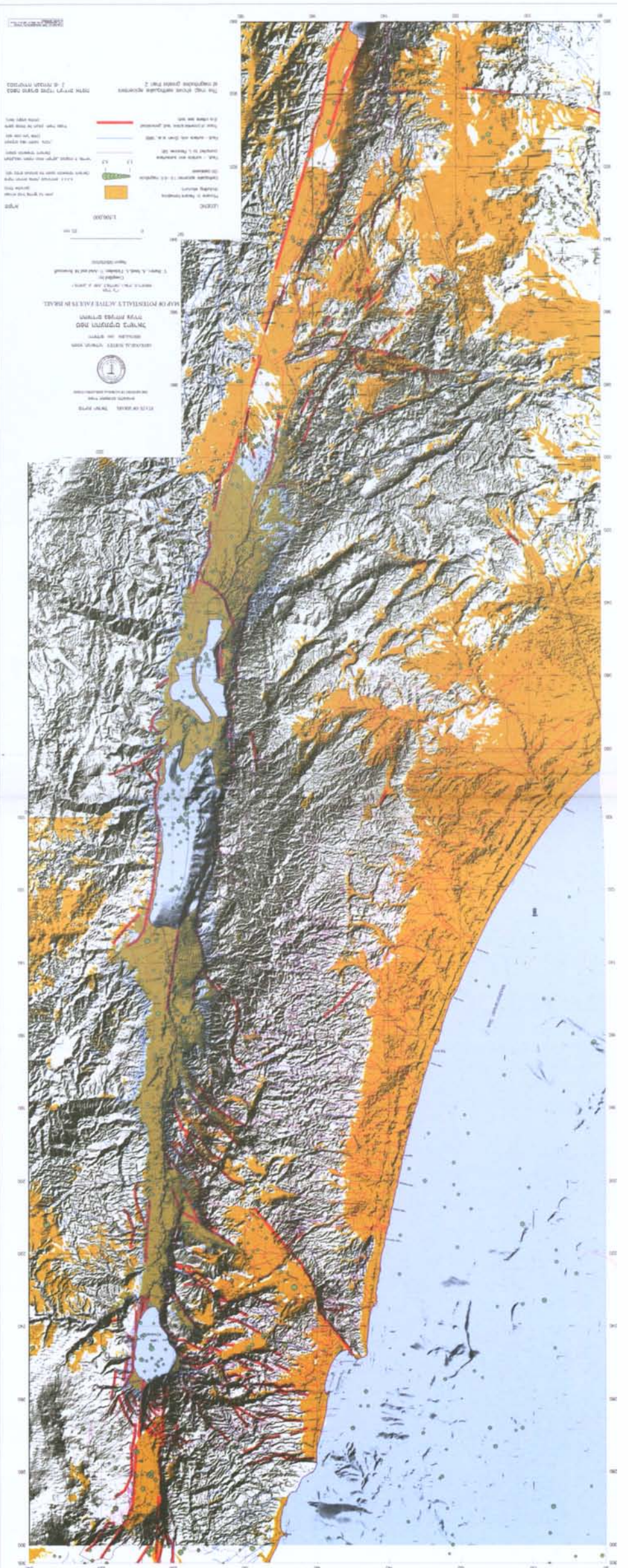


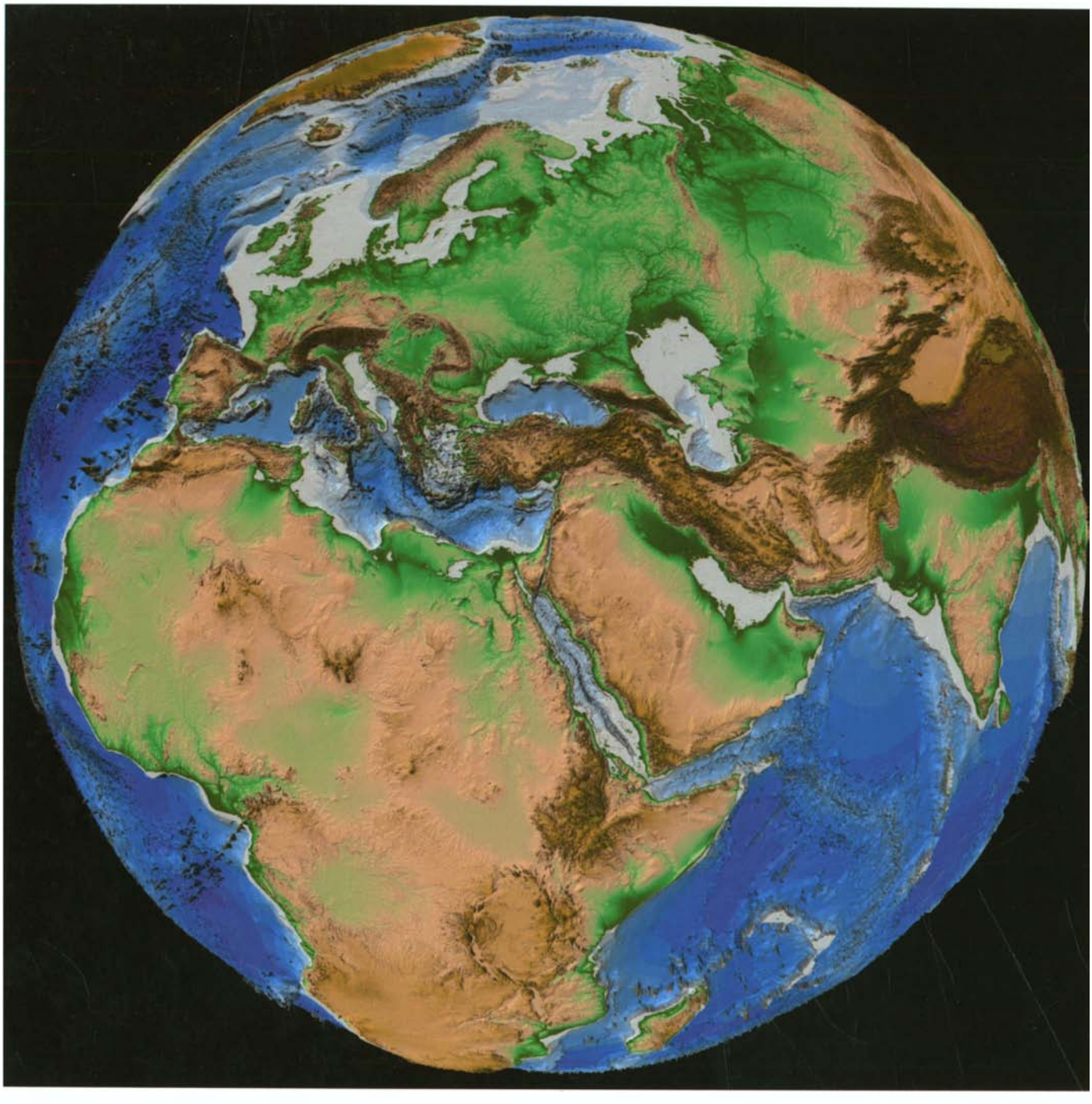
Jerusalem from space in 3-D

This ASTER (Advanced Spaceborne Thermal Emission and Reflection Radiometer) 15 m resolution sub-image was acquired on April 3, 2000 and covers an area of 10.5 x 12 km centered on Jerusalem. The data were processed to create a simulated natural color image, with green vegetation and orange tile roofs. The old city is the lighter blue area in the right center of the image, surrounded by a 400-year-old wall built by the Ottoman Turks. Easily visible are the Dome of the Rock and the Al Aksa Mosque on the eastern side of the old city. Jerusalem is the source of three major religions - Judaism, Christianity, and Islam - and is considered holy by all three. Image courtesy of NASA/GSFC/METI/ERSDAC/JAROS, and the U.S./Japan ASTER Science Team. It is available on the internet at http://asterweb.jpl.nasa.gov/gallery/gallery.htm?name=Jerusalem.

The 3-D image was rendered by increasing the resolution by 5 times, and georeferencing the image with Global Mapper® using the 1:50,000 scale Russian UTM topo map for ИЕРУСАЛИМ (H-36-11-B) available from the library at USC Berkeley. Then the image was draped over the 30 m DTM of Israel in UTM projection using IVS Fledermaus®, with 2.5 times vertical exaggeration. The view is looking northeast. The Geological Survey of Israel is located at point A in Mea Shearim, the walled Old City is at Point B, and the house of Volume II editor J. K. Hall is at Point C in Ramat Motza, above the main Jerusalem Tel Aviv highway.


ISRAEL
MAP OF THE CEASE-FIRE LINES





ISBN 965-7297-03-6



Ben Gurion University of the Negev
Department of Geological & Environmental Sciences



Tel Aviv University
Department of Geophysics and Planetary Sciences

Geological Framework of the Levant

Volume I: Cyprus and Syria

V. A. Krasheninnikov, J. K. Hall, F. Hirsch, C. Benjamini, and A. Flexer (Eds.)
ISBN 965-7297-02-8
Jerusalem, April 2005

Volume II: The Levantine Basin and Israel

J. K. Hall, V. A. Krasheninnikov, F. Hirsch, C. Benjamini, and A. Flexer (Eds.)
ISBN 965-7297-03-6
Jerusalem, April 2005

Plates

Plate I:
Geomorphological Map of Syria (1963) – Scale 1:1,000,000. (Kazmin, Chapter 8).

Plate II:
Tectonic Units of Syria (Kazmin, Chapter 8).

Plate III:
Structural Map of Syria (Kazmin, Chapter 8).

Plate IV:
IBCM-SED Unconsolidated Bottom Surface Sediments of the Mediterranean and Black Seas. (Emelyanov, Shimkus, and Kuprin, Chapter 17).

From Appendix C: Fleischer, L., and Gafsou, R.

Plate V:
Structural Map on Top Judea Group – Northern Israel – Scale 1:200,000
Front – Colored contour map, 100 m contours
Back – Contour map – 50 m contours

Plate VI:
Structural Map on Top Judea Group – Southern Israel – Scale 1:200,000
Front – Colored contour map, 100 m contours
Back – Contour map – 50 m contours

Plate VII:
Structural Map on Top Judea Group - Scale 1:500,000

Plate VIII:
Stratigraphic Table of Israel – L. Fleischer (2002)

Plate IX:
Tectonic Map of the Mediterranean Sea – Scale 1:5 million (Bogdonov et al., 1994).

Plate X:
Digital Shaded Relief Maps of the Island of Cyprus (Hall, Chapter 15).

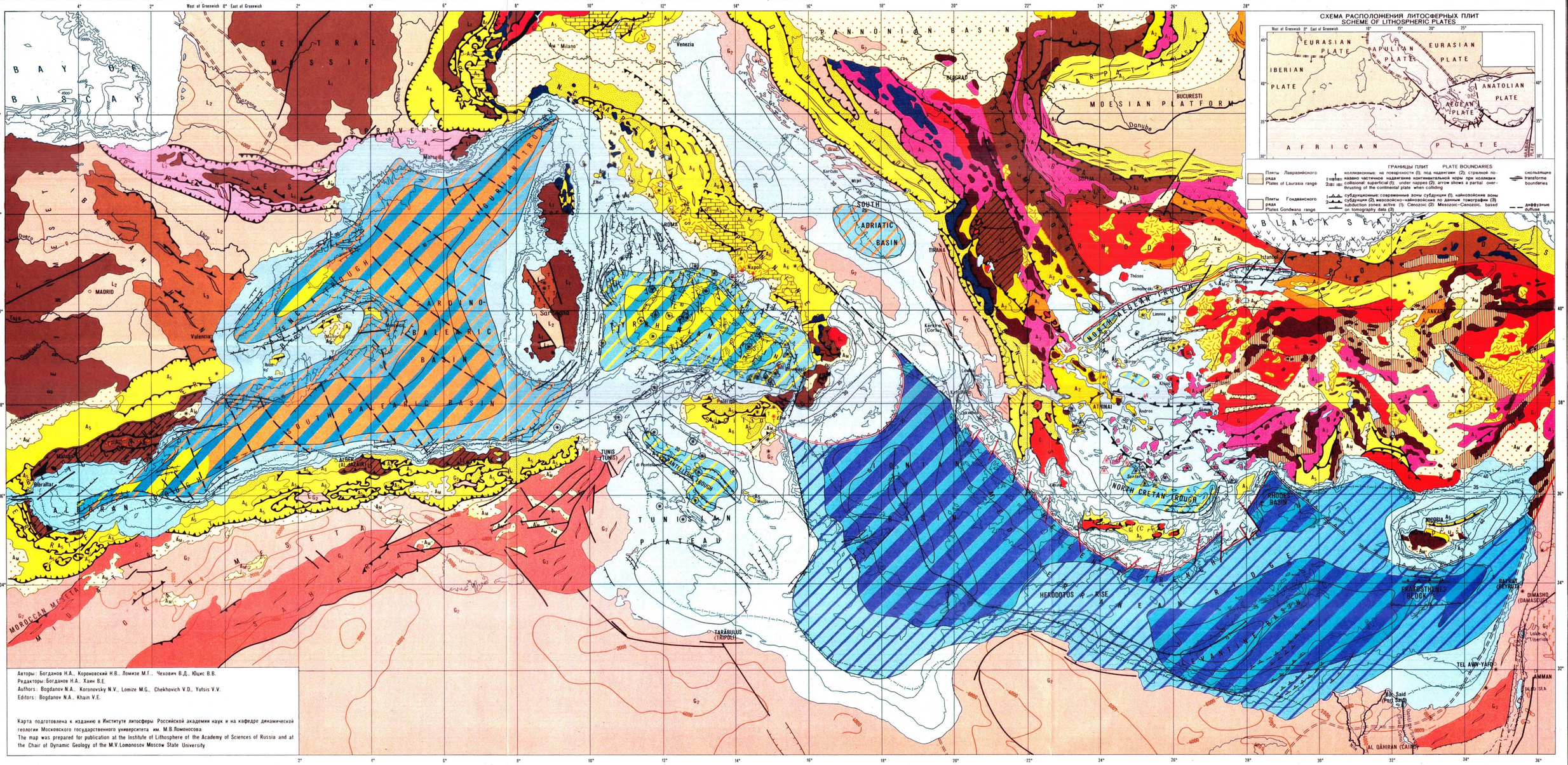
Plate XI:
Landforms of Israel, Digital Shaded Relief Maps (Part IV Introduction).

© 2005 Historical Productions-Hall Ltd. All rights reserved. Printed and bound in Israel

PLATES - Geological Framework of the Levant
Volume I: Cyprus and Syria, and Volume II: The Levantine Basin and Israel
V. A. Krasheninnikov, J. K. Hall, F. Hirsch, C. Benjamini, and A. Flexer (Editors)

ТЕКТОНИЧЕСКАЯ КАРТА СРЕДИЗЕМНОГО МОРЯ

TECTONIC MAP OF MEDITERRANEAN SEA



Авторы: Богданов Н.А., Короновский Н.В., Ломизе М.Г., Чехович В.Д., Юцис В.В.
Редакторы: Богданов Н.А., Хаин В.Е.
Authors: Bogdanov N.A., Koronovsky N.V., Lomize M.G., Chekhovich V.D., Yutsis V.V.
Editors: Bogdanov N.A., Khain V.E.

Карта подготовлена к изданию в Институте литосферы Российской академии наук и на кафедре динамической геологии Московского государственного университета им. М.В.Ломоносова
The map was prepared for publication at the Institute of Lithosphere of the Academy of Sciences of Russia and at the Chair of Dynamic Geology of the M.V.Lomonosov Moscow State University

СХЕМА РАСПОЛОЖЕНИЯ ЛИТОСФЕРНЫХ ПЛИТ
SCHEME OF LITHOSPHERIC PLATES

ГРАНИЦЫ ПЛИТ PLATE BOUNDARIES

Плиты Лавразийского ряда Plates of Laurasia range

Плиты Гондванского ряда Plates Gondwana range

коллизионные: на поверхности (1), под надвигами (2), стрелкой показано частичное надвигание континентальной коры при коллизии
collisional: superficial (1), under nappes (2), arrow shows a partial overthrusting of the continental plate when colliding

субдукционные: современные зоны субдукции (1), чайнозойские зоны субдукции (2), мезозойско-чайнозойские по данным томографии (3)
subduction zones: active (1), Cenozoic (2), Mesozoic–Cenozoic, based on tomography data (3)

скользящие transforme boundaries

диффузные diffuse

L E G E N D

КОНТИНЕНТАЛЬНЫЕ ЕДИНИЦЫ
CONTINENTAL UNITS

Лавразийского ряда: а) без осадочного чехла, штриховка указывает аллохтонное положение, b) перекрытые осадочным чехлом, с) зоны альпийских складчатых деформаций
Of Laurasia range:(a) without sedimentary cover, hatching identifies an allochthon;(b) with sedimentary cover; (c) zones of Alpine fold deformations

Гондванского ряда: а) без осадочного чехла, b) перекрытые осадочным чехлом, с) зоны альпийских складчатых деформаций
Of Gondwana range: (a) without sedimentary cover; (b) with sedimentary cover;(c) zones of Alpine fold deformations

Локальные выходы пород континентальной мантии
Local exposures of continental mantle rocks

АЛЬПИЙСКИЕ СКЛАДЧАТЫЕ КОМПЛЕКСЫ
ALPINE FOLD COMPLEXES

A_1 Киммерийские (юра–неоком)
Kimmeridgian (Jurassic–Neocomian)

A_2 Австрийские (постнеокомские–сеноманские) 130m.y. (M–10)
Austrian (post–Neocomian–Cenomanian)

A_3 Субгерцинские и ларамийские (сенон–ранний эоцен) 95m.y. (KM0Z)
Sub–Hercynian and Laramian (Senonian–early Eocene)

A_4 Пиренейские (поздний эоцен) 53m.y. (24m.a.)
Pyrenean (late Eocene)

$A_{5,6}$ Позднеальпийские (A_5–поздний эоцен–миоцен; A_6–конец миоцена–плейстоцен) 43m.y. (18m.a.)
Late Alpine (A_5–late Eocene–Miocene; A_6–the latest Miocene–Pleistocene) 20–25m.y. (6m.a.)

A_M Постскладчатые комплексы передовых и межгорных прогибов
Post–folded complexes of foredeep and intermontane troughs

Перестройки спрединга в Индийском и Атлантическом океанах m.a.–миллионы лет
Rearrangements of spreading in Indian and Atlantic oceans m.a.–magnetic anomalies m.y.–million years

ГЕОДИНАМИЧЕСКИЕ КОМПЛЕКСЫ И ФОРМАЦИИ
GEODYNAMIC COMPLEXES AND FORMATIONS

Альпийские офиолиты в тектонических покровах: а) океанические, b) островодужные, с) предполагаемое их размещение
Alpine ophiolites in nappes: (a) oceanic, (b) island arc, (c) their supposed location

Осадочные комплексы океанского происхождения
Oceanic sedimentary complexes

Субдукционные вулканоплутонические пояса: а) окраинно–континентальные, b) островодужные
Subduction volcanic belts: (a) of continental margins, (b) of island arcs

Коллизионные вулканиты: a,b) миоценовые, c,d) плиоцен–четвертичные, в том числе вне масштаба (b,d)
Collisional volcanics: (a,b) Miocene, (c,d) Pliocene–Quaternary, including those "not to scale" (b,d)

Кайнозойские рифтогенные вулканиты
Cenozoic rift volcanics

Флиш
Flysch

Моласса
Molasse

Комплексы карбонатных „платформ"
Complexes of carbonate "platforms"

МОРСКИЕ БАССЕЙНЫ
MARINE BASINS

Области с корой континентального типа
Areas with continental crusts

Области с утоненной континентальной корой (переходной): а) доранненелового возраста, b) досреднемиоценового возраста, с) доплиоценового возраста
Areas with thinned continental crust (transitional): (a) pre–Early Cretaceous age, (b) pre–mid–Miocene age, (c) pre–Pliocene age

Области с корой океанического типа: а) доранненелового возраста, b) досреднемиоценового возраста, с) доплиоценового возраста
Areas with oceanic crust: (a) pre–Early Cretaceous age, (b) pre–mid–Miocene age, (c) pre–Pliocene age

Акватории за пределами Средиземного моря
Aquatoria outside the Mediterranean Sea

Изолинии мощностей земной коры в км
Contours of the Earth's crust thickness in km

Граница распространения мессинских эвапоритов
Boundary of Messinian evaporites

СТРУКТУРНЫЕ ОБОЗНАЧЕНИЯ
STRUCTURES

Зоны субдукции: а) активные, b) реликтовые
Subduction zones: (a) active, (b) relics

Разломы, главным образом сдвиги
Fractures, mainly strike–slip faults

Линейные зоны сейсмичности
Linear zones of seismicity

Коллизионные сутуры
Collision sutures

То же, выраженное надвигами
Idem expressed by overthrusts

Трансформные разломы
Transform faults

Крутоориентированные разломы, в том числе сдвиги (а), сбросы (b) и взбросы (с)
Steep faults, including strike–slip faults (a), normal faults (b), and reversed faults (c)

Надвиги: а) установленные, b) предполагаемые
Overthrusts: (a) identified, (b) supposed

Внешние границы альпийских покровов: а) установленные, b) предполагаемые
Outer limits of Alpine nappes: (a) identified, (b) supposed

Активные границы литосферных плит и микроплит
Active boundaries of lithospheric plates and microplates

Разломы фундамента, отраженные в осадочном чехле
Faults in basement echoed in sedimentary cover

Простирание складчатости
Strike of folding

Южная граница Средиземноморского хребта
South limits of the Mediterranean Ridge

Вулканические постройки: а) активные, b) неактивные; в случаях подводных вулканов и построек вне вулканических полей: 1–коллизионные, 2–субдукционные 3–связанные с растяжением
Volcanoes: (a) active, (b) inactive; in case of submarine volcanoes and volcanoes outside volcanics field: 1–collisional, 2–subductional, 3–extension related

Направление шарьирования альпийских офиолитов
Direction of napping of Alpine ophiolites

Изолинии глубин фундамента в м
Depth contours of the basement in m

Условные границы
Conventional boundaries

В качестве географической основы использована:
As a geographical base was used:
"International Bathymetric Chart of the Mediterranean, 1987. 1st. Edition. Series established under the cooperative investigations in the Mediterranean. Published by the Head Department of Navigation and Oceanography, Ministry of Defence, Leningrad, USSR. Under the authority of IOC (UNESCO). Scale 1:5,000,000."

Проекция Меркатора. Масштаб 1:5 000 000 по параллели 38°
Mercator Projection– Scale 1:5,000,000 at latitude 38°

ИСПОЛЬЗОВАННЫЕ ИСТОЧНИКИ REFERENCES

Bigi, G., and others, sci. coord. and ed., 1990. Structural model of Italy and gravity map. Consiglio Nazionale dell Ricerche. Progetto finalizzato geodinamica. Prepared and printed by S.E.L.CA., Florence, Italy. Scale 1:500,000.

Bocaletti, M., and others, 1984. Tectonic map of the Western Mediterranean area. Printing LAC, Florence, Italy.

Bogdanoff, A.A., Khain, V.E., coordonnateurs généraux, 1981. Carte tectonique internationale de l'Europe et des régions avoisinantes (2e edition). Congrès géologique international, Comission de la carte géologique du monde, Sous–Comission de la carte tectonique du monde. Direction Générale de Géodésie et de Cartographie auprès du Conseil des Ministres de l'U.R.S.S. Moscou. Echelle 1:2,500,000.

Bouguer Gravity Anomalies (IBCM–G), 1989, 1st. Edition. International Bathymetric Chart of the Mediterranean (IBCM). Geological–Geophysical Series established with the Assistance of the International Comission for the scientific Exploration of the Mediterranean Sea. Published by the Head Department of Navigation and Oceanography Ministry of Defence, Leningrad, USSR. Under the authority of IOC (UNESCO). Scale 1:5,000,000.

Dietrich, V.J., 1979. Ophiolitic belts of the Central Mediterranean. IGCP Project «Ophiolites». Published by the Geological Society of America, Penrose Place Boulder, Colorado. Scale 1:2,500,000.

ФЕДЕРАЛЬНАЯ СЛУЖБА ГЕОДЕЗИИ И КАРТОГРАФИИ РОССИИ
МОСКВА 1994

Карта подготовлена к печати и отпечатана Производственным картосоставительским объединением «Картография» в 1994 г. 109 125 г. Москва, Волгоградский проспект,45
Редактор Д.М.Мень
Технический редактор А.И.Тимофеенко
Подписана к печати 29.12.94 г.

Формат бумаги 60×84
Бумага картографическая
Тираж 1500 экз. Заказ № 689
Печ.л. 1 Усл.печ.л. 0,93
Ч–48
5301000000–76
071(02)–95 без объяв.

© Институт литосферы РАН
© Роскартография

RUSSIAN ACADEMY OF SCIENCES

Explanatory Notes For The Tectonic Map of the Mediterranean Sea Scale 1:5,000,000

compiled by

N. A. Bogdanov, V. E. Khain, V. D. Chekhovich,
Institute of the Lithosphere, Russian Academy of Sciences, 22, Staromonetny per., Moscow 109180, Russia
N. V. Koronovsky, M. G. Lomize
Geological Department, Moscow State University, Leninskie gory, Moscow 119899, Russia

ABSTRACT

The Tectonic Map of the Mediterranean Sea (scale 1:5,000,000) represents a synthesis of new data on the structure of the sea floor and adjacing fold belts. The Mediterranean basins are interpreted as remnants of the Tethyan ocean, which in the Cretaceous period being of crucial importance. The basin borderland is also heterogeneous in the northern and western parts it comprises the Alpine orogen fold belts, whereas the southern and eastern parts are represented by the northern slope of the African Archean paleoplatform. Structural analysis of the lithospheric plates of the region allows several important stages of evolution to be distinguished. Moreover, when East Mediterranean basins formed Mid-Tertiary, when West Mediterranean basins originated, and Late Tertiary, when the Aegean, Valencia troughs, as well as troughs of Central Mediterranean came into existence. The Explanatory Notes to the Map consist of a brief outline of the continental framework, their position in the ophiolite structure, as well as the Cenozoic volcanism.

INTRODUCTION

The Tectonic Map of the Mediterranean Sea is a synthesis of the recent recent data on the structure of its sea floor and adjacent fold belts. It was conceived to summarize the results of marine geological studies by the Soviet Geological Survey and interpretation of the plate tectonics of this important region. The Bathymetric Map of the Mediterranean Sea, Scale 1:5,000,000, is compiled by the Department of Navigation and Oceanography, Ministry of Defense of Russia, to order of the IOC and UNESCO, has served as a topographic base. When considering the tectonic structure of the region have used the latest maps available of individual continental areas and marine basins.

The authors do not intend to show in detail the tectonics of the Peri-Mediterra- Eurasian and African continental plates contiguous with the Mediterranean belt. The structures directly related to the sea floor origin are mostly represented on the map, and in so doing, some details were omitted in order to show the main trends in the structure of the Mediterranean Sea.

The Map was compiled by collaborators from the institute of the Lithosphere of the Russian Academy of Sciences and the Department of Marine Geology of the Geological Faculty, Moscow State University. Besides the principal collaborators, Dr. V. Yatsiv, as well as N. G. Tsvetanova-I. A. Trotchyanu and L. B. Makarova contributed much when compiling the Map and preparing the manuscript of the Explanatory Notes. *Mrs. D. I. Petv* carried out the map editing. The work was done under the sponsorship of the State Program "The World Ocean" of the Ministry of Science and Technical Policy.

ACKNOWLEDGMENTS

We wish cordially to thank Prof. A. H. F. Robertson from University of Edinburgh, United Kingdom, for his efforts in editing the English version of the Explanatory Notes. We also express our gratitude to professors F. Mauffe from Laboratoire Geodynamique Sous-Marine, Villefranche-sur-Mer, France, J. Woodside from Vrije Universiteit, Amsterdam, the Netherlands, as well as A. F. Limonov and M. K. Ivanov from Moscow State University, Russia, for their valuable remarks during preliminary work to the map publishing.

1. Geological structure of the Mediterranean region

The Mediterranean basin is distinguished by an irregular configuration, with a complex inner structure indicating a long and complicated history of formation, to which the Late Cenozoic tectonics was of crucial importance. The setting of the Mediterranean basin is a result of interaction between the Eurasian and African plates, which suppe structures to the north and west, and by the northern slope of the African- Arabian paleoplatform to the south and east.

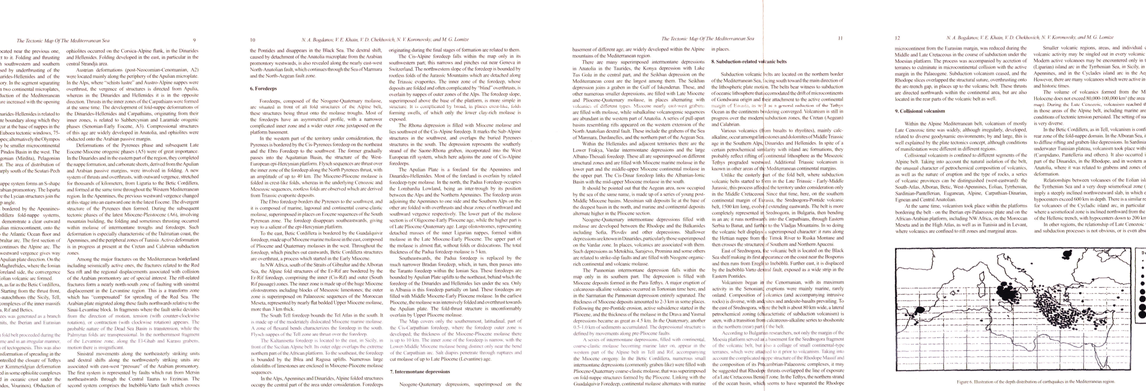


Figure 1. Principal structures of the Mediterranean region
1 – Alpine-Himalayan fold belts; 2 – Caledonian and Hercynian folds; 3 – Cretaceous-Paleogene orogenic belts; 4 – Mesozoic-Cenozoic platforms; 5 – Archean cratons; 6 – Oman Mts.; 7 – Arabian Shield; 8 – Nubian Shield; 9 – Somalian Plateau; 10 – diffusive; 11 – boundaries of basins with oceanic crust.
Arrows indicate the direction of movement of lithospheric plates and their sections relative to Africa: 12 – to Eurasia; from 13 – to Eurasian basins; 14 – to Eurasian and African basins.

Linking the Atlantic Ocean in the west through the narrow Gibraltar Strait formed in the Pliocene, the Mediterranean basin began with the small Alboran Sea, underlain by thinned continental crust (**Figure 1**). The Alboran Sea is bordered by the Alpine fold-nappe system of the Betic Cordillera to the north and by a similar system, that of the Er-Rif and western Tell-Atlas to the south. In between, the Betic and Rif-Tell systems are connected by the Gibraltar arcuate platform, shortly adjoins the coastal area. To the east, the Alboran Sea opens up into the wider and deeper South Balearic Basin (trending east-northeastward), like the Alboran one, but being more elongate and representing the southern end of the largest, Sardinia-Balearic Basin in the Western Mediterranean. This basin is underlain by the oceanic crust. To the east, via the deep area between the Balearic Archipelago and Sardinia, the South Balearic basin joins the Balearic, Provence, and Ligurian basins, representing the northern part of the Sardinia-Balearic Basin. The North-Balearic Basin proper, called also the Valencia trough, is separated from the Provence basin by a sill, which is shallow alternate with subbasement rocks and are well distinguished on seismic profiles. Although the building of sediments is flat in some regions, note the low, sub-linear arcuate ridges, which form the part of the basin, near the Algerian coast. The thickness of the Messinian sequence is 1 km. The lower sequence – subsalt deposits comprising both calcareous ooze and terrigenous deposits – is also of significant thickness, up to 2 km or more. The thickness of the sedimentary cover decreases noticeably near the Algerian continental slope. French researchers believe that the sedimentary cover was subducted under the steep scarp of the African continent. This seems also to be true for a trench that existed in the southern part of the basin.

As a whole, the South Balearic Basin was probably formed as a result of extension along a narrow spreading zone situated parallel to the northern coast of Africa. It is not accompanied simultaneously by compression in the Provence basin, which is filled with Miocene boundary (about 23 Ma ago). These tectonic movements clearly manifested themselves as E-Rif. In its outer zone, or Un-Rif, a thick sedimentary sequence started to form in the Miocene. In the inner zones, the main deformation and nappe formation occurred in the Middle Miocene, whereas in t o E-Rif in the latest Miocene-Early Pliocen. Rift fault movements were replaced by recent arching and block uplift. Therefore, the continental setting of the South-Balearic Basin was accompanied by active folding throughout the Miocene. The folding involved tectonic stacking, nappe formation and uplift which might have compensated for the simultaneous subsidence of the basin floor. Deep-sea Tell-Fallaux beds served as a boundary (to an accretionary prism).

In the eastern part of the Western Mediterranean, two basins are situated, that of the Tyrrhenian Sea and of the Tunisian Plateau; these are separated from the Sardinia-Balearic and South Balearic Basins by Corsica and Sardinia and the Sicily-Maghreb Swell. It seems more reasonable to single out this region as an independent central part of the Mediterranean as it differs both from the western

Figure 1. Principal structures of the Mediterranean region
1 – Alpine-Himalayan fold belts; 2 – Caledonian and Hercynian folds; 3 – Cretaceous-Paleogene orogenic belts; 4 – Mesozoic-Cenozoic platforms; 5 – Archean cratons; 6 – Oman Mts.; 7 – Arabian Shield; 8 – Nubian Shield; 9 – Somalian Plateau; 10 – diffusive; 11 – boundaries of basins with oceanic crust.
Arrows indicate the direction of movement of lithospheric plates and their sections relative to Africa: 12 – to Eurasia; from 13 – to Eurasian basins; 14 – to Eurasian and African basins.

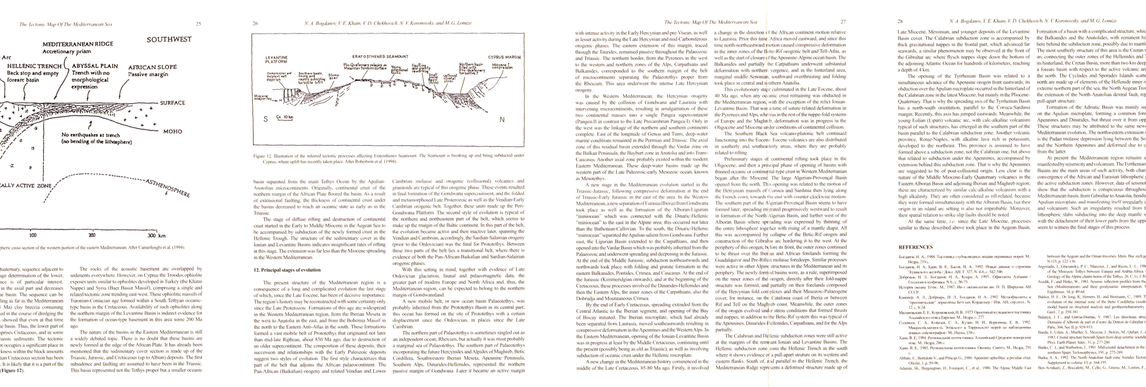


Figure 1. Principal structures of the Mediterranean region
1 – Alpine-Himalayan fold belts; 2 – Caledonian and Hercynian folds; 3 – Cretaceous-Paleogene orogenic belts; 4 – Mesozoic-Cenozoic platforms; 5 – Archean cratons; 6 – Oman Mts.; 7 – Arabian Shield; 8 – Nubian Shield; 9 – Somalian Plateau; 10 – diffusive; 11 – boundaries of basins with oceanic crust.
Arrows indicate the direction of movement of lithospheric plates and their sections relative to Africa: 12 – to Eurasia; from 13 – to Eurasian basins; 14 – to Eurasian and African basins.

Figure 1. Principal structures of the Mediterranean region
1 – Alpine-Himalayan fold belts; 2 – Caledonian and Hercynian folds; 3 – Cretaceous-Paleogene orogenic belts; 4 – Mesozoic-Cenozoic platforms; 5 – Archean cratons; 6 – Oman Mts.; 7 – Arabian Shield; 8 – Nubian Shield; 9 – Somalian Plateau; 10 – diffusive; 11 – boundaries of basins with oceanic crust.
Arrows indicate the direction of movement of lithospheric plates and their sections relative to Africa: 12 – to Eurasia; from 13 – to Eurasian basins; 14 – to Eurasian and African basins.

Figure 1. Principal structures of the Mediterranean region
1 – Alpine-Himalayan fold belts; 2 – Caledonian and Hercynian folds; 3 – Cretaceous-Paleogene orogenic belts; 4 – Mesozoic-Cenozoic platforms; 5 – Archean cratons; 6 – Oman Mts.; 7 – Arabian Shield; 8 – Nubian Shield; 9 – Somalian Plateau; 10 – diffusive; 11 – boundaries of basins with oceanic crust.
Arrows indicate the direction of movement of lithospheric plates and their sections relative to Africa: 12 – to Eurasia; from 13 – to Eurasian basins; 14 – to Eurasian and African basins.

Figure 1. Principal structures of the Mediterranean region
1 – Alpine-Himalayan fold belts; 2 – Caledonian and Hercynian folds; 3 – Cretaceous-Paleogene orogenic belts; 4 – Mesozoic-Cenozoic platforms; 5 – Archean cratons; 6 – Oman Mts.; 7 – Arabian Shield; 8 – Nubian Shield; 9 – Somalian Plateau; 10 – diffusive; 11 – boundaries of basins with oceanic crust.
Arrows indicate the direction of movement of lithospheric plates and their sections relative to Africa: 12 – to Eurasia; from 13 – to Eurasian basins; 14 – to Eurasian and African basins.

Figure 1. Principal structures of the Mediterranean region
1 – Alpine-Himalayan fold belts; 2 – Caledonian and Hercynian folds; 3 – Cretaceous-Paleogene orogenic belts; 4 – Mesozoic-Cenozoic platforms; 5 – Archean cratons; 6 – Oman Mts.; 7 – Arabian Shield; 8 – Nubian Shield; 9 – Somalian Plateau; 10 – diffusive; 11 – boundaries of basins with oceanic crust.
Arrows indicate the direction of movement of lithospheric plates and their sections relative to Africa: 12 – to Eurasia; from 13 – to Eurasian basins; 14 – to Eurasian and African basins.

Figure 1. Principal structures of the Mediterranean region
1 – Alpine-Himalayan fold belts; 2 – Caledonian and Hercynian folds; 3 – Cretaceous-Paleogene orogenic belts; 4 – Mesozoic-Cenozoic platforms; 5 – Archean cratons; 6 – Oman Mts.; 7 – Arabian Shield; 8 – Nubian Shield; 9 – Somalian Plateau; 10 – diffusive; 11 – boundaries of basins with oceanic crust.
Arrows indicate the direction of movement of lithospheric plates and their sections relative to Africa: 12 – to Eurasia; from 13 – to Eurasian basins; 14 – to Eurasian and African basins.

Figure 1. Principal structures of the Mediterranean region
1 – Alpine-Himalayan fold belts; 2 – Caledonian and Hercynian folds; 3 – Cretaceous-Paleogene orogenic belts; 4 – Mesozoic-Cenozoic platforms; 5 – Archean cratons; 6 – Oman Mts.; 7 – Arabian Shield; 8 – Nubian Shield; 9 – Somalian Plateau; 10 – diffusive; 11 – boundaries of basins with oceanic crust.
Arrows indicate the direction of movement of lithospheric plates and their sections relative to Africa: 12 – to Eurasia; from 13 – to Eurasian basins; 14 – to Eurasian and African basins.

Figure 1. Principal structures of the Mediterranean region
1 – Alpine-Himalayan fold belts; 2 – Caledonian and Hercynian folds; 3 – Cretaceous-Paleogene orogenic belts; 4 – Mesozoic-Cenozoic platforms; 5 – Archean cratons; 6 – Oman Mts.; 7 – Arabian Shield; 8 – Nubian Shield; 9 – Somalian Plateau; 10 – diffusive; 11 – boundaries of basins with oceanic crust.
Arrows indicate the direction of movement of lithospheric plates and their sections relative to Africa: 12 – to Eurasia; from 13 – to Eurasian basins; 14 – to Eurasian and African basins.

Figure 1. Principal structures of the Mediterranean region
1 – Alpine-Himalayan fold belts; 2 – Caledonian and Hercynian folds; 3 – Cretaceous-Paleogene orogenic belts; 4 – Mesozoic-Cenozoic platforms; 5 – Archean cratons; 6 – Oman Mts.; 7 – Arabian Shield; 8 – Nubian Shield; 9 – Somalian Plateau; 10 – diffusive; 11 – boundaries of basins with oceanic crust.
Arrows indicate the direction of movement of lithospheric plates and their sections relative to Africa: 12 – to Eurasia; from 13 – to Eurasian basins; 14 – to Eurasian and African basins.

Figure 1. Principal structures of the Mediterranean region
1 – Alpine-Himalayan fold belts; 2 – Caledonian and Hercynian folds; 3 – Cretaceous-Paleogene orogenic belts; 4 – Mesozoic-Cenozoic platforms; 5 – Archean cratons; 6 – Oman Mts.; 7 – Arabian Shield; 8 – Nubian Shield; 9 – Somalian Plateau; 10 – diffusive; 11 – boundaries of basins with oceanic crust.
Arrows indicate the direction of movement of lithospheric plates and their sections relative to Africa: 12 – to Eurasia; from 13 – to Eurasian basins; 14 – to Eurasian and African basins.

Figure 1. Principal structures of the Mediterranean region
1 – Alpine-Himalayan fold belts; 2 – Caledonian and Hercynian folds; 3 – Cretaceous-Paleogene orogenic belts; 4 – Mesozoic-Cenozoic platforms; 5 – Archean cratons; 6 – Oman Mts.; 7 – Arabian Shield; 8 – Nubian Shield; 9 – Somalian Plateau; 10 – diffusive; 11 – boundaries of basins with oceanic crust.
Arrows indicate the direction of movement of lithospheric plates and their sections relative to Africa: 12 – to Eurasia; from 13 – to Eurasian basins; 14 – to Eurasian and African basins.

Figure 1. Principal structures of the Mediterranean region
1 – Alpine-Himalayan fold belts; 2 – Caledonian and Hercynian folds; 3 – Cretaceous-Paleogene orogenic belts; 4 – Mesozoic-Cenozoic platforms; 5 – Archean cratons; 6 – Oman Mts.; 7 – Arabian Shield; 8 – Nubian Shield; 9 – Somalian Plateau; 10 – diffusive; 11 – boundaries of basins with oceanic crust.
Arrows indicate the direction of movement of lithospheric plates and their sections relative to Africa: 12 – to Eurasia; from 13 – to Eurasian basins; 14 – to Eurasian and African basins.

Figure 1. Principal structures of the Mediterranean region
1 – Alpine-Himalayan fold belts; 2 – Caledonian and Hercynian folds; 3 – Cretaceous-Paleogene orogenic belts; 4 – Mesozoic-Cenozoic platforms; 5 – Archean cratons; 6 – Oman Mts.; 7 – Arabian Shield; 8 – Nubian Shield; 9 – Somalian Plateau; 10 – diffusive; 11 – boundaries of basins with oceanic crust.
Arrows indicate the direction of movement of lithospheric plates and their sections relative to Africa: 12 – to Eurasia; from 13 – to Eurasian basins; 14 – to Eurasian and African basins.

Figure 1. Principal structures of the Mediterranean region
1 – Alpine-Himalayan fold belts; 2 – Caledonian and Hercynian folds; 3 – Cretaceous-Paleogene orogenic belts; 4 – Mesozoic-Cenozoic platforms; 5 – Archean cratons; 6 – Oman Mts.; 7 – Arabian Shield; 8 – Nubian Shield; 9 – Somalian Plateau; 10 – diffusive; 11 – boundaries of basins with oceanic crust.
Arrows indicate the direction of movement of lithospheric plates and their sections relative to Africa: 12 – to Eurasia; from 13 – to Eurasian basins; 14 – to Eurasian and African basins.

Figure 1. Principal structures of the Mediterranean region
1 – Alpine-Himalayan fold belts; 2 – Caledonian and Hercynian folds; 3 – Cretaceous-Paleogene orogenic belts; 4 – Mesozoic-Cenozoic platforms; 5 – Archean cratons; 6 – Oman Mts.; 7 – Arabian Shield; 8 – Nubian Shield; 9 – Somalian Plateau; 10 – diffusive; 11 – boundaries of basins with oceanic crust.
Arrows indicate the direction of movement of lithospheric plates and their sections relative to Africa: 12 – to Eurasia; from 13 – to Eurasian basins; 14 – to Eurasian and African basins.

Figure 1. Principal structures of the Mediterranean region
1 – Alpine-Himalayan fold belts; 2 – Caledonian and Hercynian folds; 3 – Cretaceous-Paleogene orogenic belts; 4 – Mesozoic-Cenozoic platforms; 5 – Archean cratons; 6 – Oman Mts.; 7 – Arabian Shield; 8 – Nubian Shield; 9 – Somalian Plateau; 10 – diffusive; 11 – boundaries of basins with oceanic crust.
Arrows indicate the direction of movement of lithospheric plates and their sections relative to Africa: 12 – to Eurasia; from 13 – to Eurasian basins; 14 – to Eurasian and African basins.

Figure 1. Principal structures of the Mediterranean region
1 – Alpine-Himalayan fold belts; 2 – Caledonian and Hercynian folds; 3 – Cretaceous-Paleogene orogenic belts; 4 – Mesozoic-Cenozoic platforms; 5 – Archean cratons; 6 – Oman Mts.; 7 – Arabian Shield; 8 – Nubian Shield; 9 – Somalian Plateau; 10 – diffusive; 11 – boundaries of basins with oceanic crust.
Arrows indicate the direction of movement of lithospheric plates and their sections relative to Africa: 12 – to Eurasia; from 13 – to Eurasian basins; 14 – to Eurasian and African basins.

Figure 1. Principal structures of the Mediterranean region
1 – Alpine-Himalayan fold belts; 2 – Caledonian and Hercynian folds; 3 – Cretaceous-Paleogene orogenic belts; 4 – Mesozoic-Cenozoic platforms; 5 – Archean cratons; 6 – Oman Mts.; 7 – Arabian Shield; 8 – Nubian Shield; 9 – Somalian Plateau; 10 – diffusive; 11 – boundaries of basins with oceanic crust.
Arrows indicate the direction of movement of lithospheric plates and their sections relative to Africa: 12 – to Eurasia; from 13 – to Eurasian basins; 14 – to Eurasian and African basins.

Figure 1. Principal structures of the Mediterranean region
1 – Alpine-Himalayan fold belts; 2 – Caledonian and Hercynian folds; 3 – Cretaceous-Paleogene orogenic belts; 4 – Mesozoic-Cenozoic platforms; 5 – Archean cratons; 6 – Oman Mts.; 7 – Arabian Shield; 8 – Nubian Shield; 9 – Somalian Plateau; 10 – diffusive; 11 – boundaries of basins with oceanic crust.
Arrows indicate the direction of movement of lithospheric plates and their sections relative to Africa: 12 – to Eurasia; from 13 – to Eurasian basins; 14 – to Eurasian and African basins.

Figure 1. Principal structures of the Mediterranean region
1 – Alpine-Himalayan fold belts; 2 – Caledonian and Hercynian folds; 3 – Cretaceous-Paleogene orogenic belts; 4 – Mesozoic-Cenozoic platforms; 5 – Archean cratons; 6 – Oman Mts.; 7 – Arabian Shield; 8 – Nubian Shield; 9 – Somalian Plateau; 10 – diffusive; 11 – boundaries of basins with oceanic crust.
Arrows indicate the direction of movement of lithospheric plates and their sections relative to Africa: 12 – to Eurasia; from 13 – to Eurasian basins; 14 – to Eurasian and African basins.

Figure 1. Principal structures of the Mediterranean region
1 – Alpine-Himalayan fold belts; 2 – Caledonian and Hercynian folds; 3 – Cretaceous-Paleogene orogenic belts; 4 – Mesozoic-Cenozoic platforms; 5 – Archean cratons; 6 – Oman Mts.; 7 – Arabian Shield; 8 – Nubian Shield; 9 – Somalian Plateau; 10 – diffusive; 11 – boundaries of basins with oceanic crust.
Arrows indicate the direction of movement of lithospheric plates and their sections relative to Africa: 12 – to Eurasia; from 13 – to Eurasian basins; 14 – to Eurasian and African basins.

Figure 1. Principal structures of the Mediterranean region
1 – Alpine-Himalayan fold belts; 2 – Caledonian and Hercynian folds; 3 – Cretaceous-Paleogene orogenic belts; 4 – Mesozoic-Cenozoic platforms; 5 – Archean cratons; 6 – Oman Mts.; 7 – Arabian Shield; 8 – Nubian Shield; 9 – Somalian Plateau; 10 – diffusive; 11 – boundaries of basins with oceanic crust.
Arrows indicate the direction of movement of lithospheric plates and their sections relative to Africa: 12 – to Eurasia; from 13 – to Eurasian basins; 14 – to Eurasian and African basins.

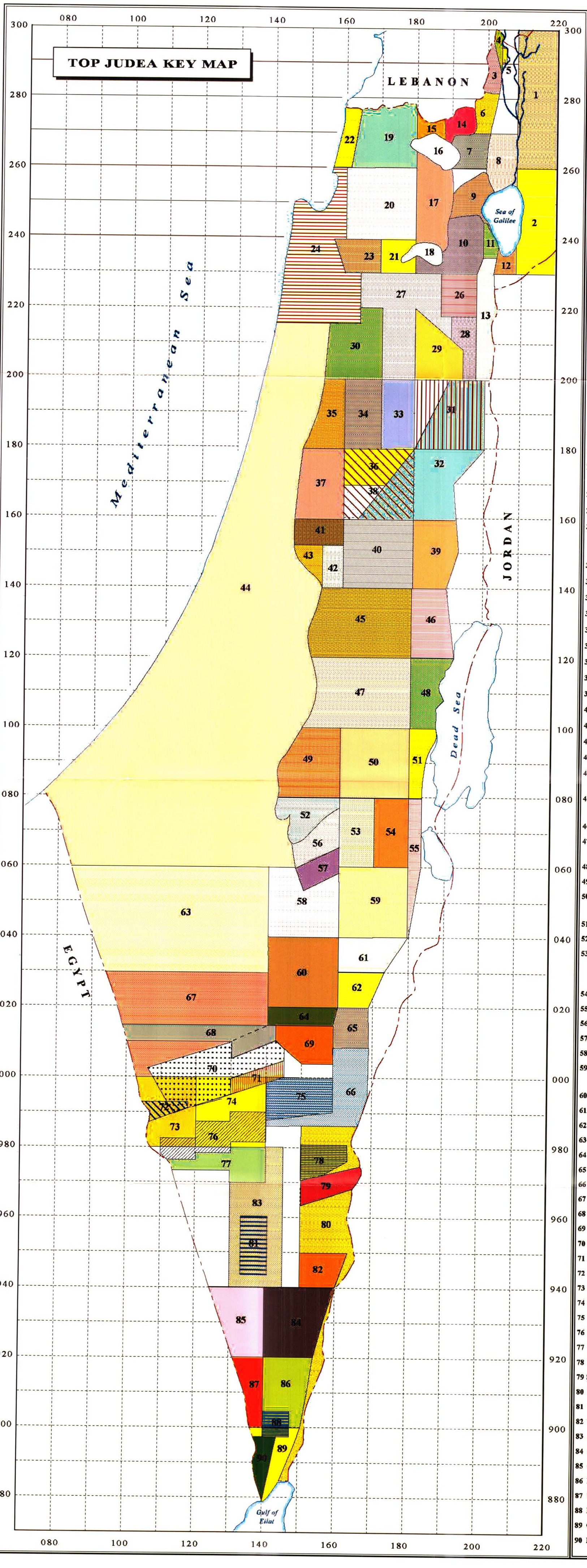
Figure 1. Principal structures of the Mediterranean region
1 – Alpine-Himalayan fold belts; 2 – Caledonian and Hercynian folds; 3 – Cretaceous-Paleogene orogenic belts; 4 – Mesozoic-Cenozoic platforms; 5 – Archean cratons; 6 – Oman Mts.; 7 – Arabian Shield; 8 – Nubian Shield; 9 – Somalian Plateau; 10 – diffusive; 11 – boundaries of basins with oceanic crust.
Arrows indicate the direction of movement of lithospheric plates and their sections relative to Africa: 12 – to Eurasia; from 13 – to Eurasian basins; 14 – to Eurasian and African basins.

Figure 1. Principal structures of the Mediterranean region
1 – Alpine-Himalayan fold belts; 2 – Caledonian and Hercynian folds; 3 – Cretaceous-Paleogene orogenic belts; 4 – Mesozoic-Cenozoic platforms; 5 – Archean cratons; 6 – Oman Mts.; 7 – Arabian Shield; 8 – Nubian Shield; 9 – Somalian Plateau; 10 – diffusive; 11 – boundaries of basins with oceanic crust.
Arrows indicate the direction of movement of lithospheric plates and their sections relative to Africa: 12 – to Eurasia; from 13 – to Eurasian basins; 14 – to Eurasian and African basins.

Figure 1. Principal structures of the Mediterranean region
1 – Alpine-Himalayan fold belts; 2 – Caledonian and Hercynian folds; 3 – Cretaceous-Paleogene orogenic belts; 4 – Mesozoic-Cenozoic platforms; 5 – Archean cratons; 6 – Oman Mts.; 7 – Arabian Shield; 8 – Nubian Shield; 9 – Somalian Plateau; 10 – diffusive; 11 – boundaries of basins with oceanic crust.
Arrows indicate the direction of movement of lithospheric plates and their sections relative to Africa: 12 – to Eurasia; from 13 – to Eurasian basins; 14 – to Eurasian and African basins.

Figure 1. Principal structures of the Mediterranean region
1 – Alpine-Himalayan fold belts; 2 – Caledonian and Hercynian folds; 3 – Cretaceous-Paleogene orogenic belts; 4 – Mesozoic-Cenozoic platforms; 5 – Archean cratons; 6 – Oman Mts.; 7 – Arabian Shield; 8 – Nubian Shield; 9 – Somalian Plateau; 10 – diffusive; 11 – boundaries of basins with oceanic crust.
Arrows indicate the direction of movement of lithospheric plates and their sections relative to Africa: 12 – to Eurasia; from 13 – to Eurasian basins; 14 – to E

TOP JUDEA KEY MAP



SOURCE OF INFORMATION

1 MOR D. - 1985 Geol. Map, Har Odem (GSI/5/86)
1985 Geol. Map, Kazrin (GSI/5/86)

2 MICHELSON H.& MOR D. - 1985 Geol. Map, Gamla (GSI/5/86)

3 ROSENBERG E. - 1960 Geol. Map, Qiryat Shemone (Ph.D Thesis)

4 RON H. - 1997 Fault Map, (Ann Meeting 1997)

5 FRIESLANDER U. - 1996 Fault Map (IPRG 643/10/96)

6 GLIKSON Y. - 1964 Str. Map, Naftali Mt. (M.Sc. Thesis)

7 WACHS D., LEVITE D. & OLSHINA A. - 1982 Geol. Map, Zefat (GSI/5/82)

8 HEIMANN A., HARASH A. & BAR Y. - 1990 Fault Map, Korazim (GSI/28/90)

9 SALTZMAN U. - 1964 Srt. Map, Tabha-Huqoq (M.Sc. Thesis)

10 VROMAN A. - 1958 Geol. Map, Tabor-Tiberias (GSI-1958)

11 NISSENBAUM A. - 1964 Geol. Map, Poriyya (M.Sc. Thesis)

12 INDIK I. - 1984 Str. Map, Zemah(OE(I)L/84/11)

13 SCHULMAN N. - 1962 Geol. Map, Jordan Valley (Ph.D. Thesis)
BELITZKY S. - 1996 Geomorphologic Map Lower Jordan Valley (Ph.D.Thesis)

14 MICHELSON H. - 1970 Geol. Map, Central Galilee (Tahal)

15 SHLEIN N. - 1961 Str. Map, Alma (M.Sc. Thesis)

16 ELIEZRI I. - 1959 Str. Map, Beit Jann (JES Vol.14)

17 GOLANI U. - 1957 Geol. Map, Beit Netofa (Tahal)

18 WEILER Y. - 1968 Str. Map, Mt.Tabor (JES Vol. 17)

19 KAFRI U. - 1971 Str. Map, Nahariyya (GSI-1971)

20 LEVY Y. - 1983 Str. Map, Shefar'am (GSI-1983)

21 GREENBERG Y. - Str. Map, Kf. Hahoresh (M.Sc. Thesis)

22 FRIESLANDER U. - 1991 Str. Map, (IPRG 813/574/91)

23 GUTTMAN Y. - 1983 Str. Map, Tivon (Tahal)

24 KLANG A. & GVIRTZMAN G. - 1987 Str. Map, (OE(I)L 12094)

25 BRAUN M. & LASMAN N. - 1981 Str. Map, Galilee (Geoprospect)

26 YAIR A. - 1968 Geomorphologic Map Tabor - Issakhar (Ph.D Thesis)

27 KLANG A. & GVIRTZMAN G. - 1990 Str. Map Yizrael Valley (GSI/23/90)
DICKER T. - 1969 Geol. Map of Yizrael Valley (M. Sc. Thesis) (JES Vol.18)

28 GARDOSH M. & BRUNER I. - 1998 Str Map Bet Shen (GII 348/27/98)

29 HATZOR Y. - 1991 Str. Map of Gilboa region (M.Sc. Thesis) (GSI/15/91)

30 SASS E. - 1968 Str. Map of Um el Fahm area (Ph.D.Thesis) (JES Vol.17)
DEKEL A. - 1988 Str. Map of Emmek Dotan (M.Sc. Thesis) (GSI/27/88)
SALTZMANN U. &DEKEL A. - 1981 Str. Map Baqa el Ghrabia (OE(I)L Rep)

31 MIMRAN Y. - 1969 Geol. Map of W.El.Malih (M.Sc.Thesis)

32 SHALIV G. - 1973 Str.Map Samaria area (Tahal)

33 COOK P., ROT I. & MIMRAN Y. - 1970 Geol. Map Shekhem area (GSI/70/102)

34 ILANI S. - 1972 Str. Map of Tulkarem area (M.Sc. Thesis) (GSI/105/72)

35 ILANI S., GVIRTZMAN G. & KLANG A. - 1985 Str. Map Netanya (GSI)

36 MURAVINSKY E. - 1977 Str.Map Kefar Qadum (OE(I)L 77/9)

37 HILDENBRAND N. - 1974 Str. Map Kefar Saba area (GSI)

38 SNEH A. - 1997 Geol. Map Ariel (GSI/12/97)

39 BEGIN B. - 1973 Str. Map Jericho area (GSI)

40 SHACHNAI E. - 1969 Str. Map Ramallah area (Tahal)

41 LIVNAT A. - 1971 Str. Map Abud-Qibbya-Rantis (M.Sc. Thesis) (GSI/102/71)

42 DIMANT E. - 1971 Str.Map Beit Horon - Beit El (M.Sc. Thesis) (GSI/101/71)

43 SHOMRONI A. - 1970 Geol. Map Lod-Gezer (GSI)

44 FLEISCHER L., GELBERMAN E. & WOLFF O. - 1993 Str. Map of Yarqon-Taninim aquifer (IPRG 244/147/92)

45 ITZHAKY Y., ARKIN Y. - 1964 Str. Map Jerusalem-Bet Shemesh (GSI)
RUEFFER T. ARKIN Y. & HIRSH F. str. Map (GSI-1986)

46 ROTH Y. - 1970 Str. Map W. El Qilt (GSI-1970)

47 HIRSCH F. - 1983 Str. Map Bet Guvrin (GSI-1983)
HIRSCH F., KOLTON J. & ROTH I. - 1994 Str. Map Hebron (GSI)

48 MOR U. - 1987 Str. Map Mitzpe Shalem (GSI)

49 GILAT A. - 1977 Str. Map Eshtamoa (GSI-1977)

50 GILAT A. - 1987 Str. Map Har Hezron (GSI-1987)
EIZIN B. - 1967 Str. Map Har Betah (Naphtha Rep.)

51 RAZ E. - 1986 Str. Map En Gedi (GSI -1986)

52 WDOWINSKY S. - 1985 Str. Map Tel Malhata (GSI-25/85)

53 AHARONI E. - 1976 (Ph.D Thesis)
HIRSCH F. - 1994 Str. Map Arad (GSI-1994)
RODED R. - 1986 Str. Map (GSI-1986)

54 AHARONI E. - 1976 (Ph.D Thesis)

55 AGNON A. - 1983 (M.Sc. Thesis)

56 ZOHAR E. & SHILONI Y. - 1987 Geol. Map (GSI/19/87)

57 AIZENBERG E. - 1964 Str. Map Juraba (JES Vol.13)

58 RODED R. - 1996 Geol Map Dimona (GSI-1996)

59 HIRSCH F. - 1994 Str. Map Hamakhtesh Haqatan (GSI-1994)
WYSSLING L. - 1958 (INOC Rep Gr. 58/02)

60 RODED R. - 1978 Str. Map Oron (GSI-1978)

61 EL RON E. - 1980 Str. Map (GSI/79/6)

62 YECHIELY Y. - 1987 Str. Map (GSI/30/87)

63 DRUCKMAN et al - 1995 Str. Map (JES Vol.44)

64 BARTOV Y. &. MARCUS E. - 1995 Str. Map (GSI/30/85)

65 EYAL A.- 1984 Str. Map (GSI-10/91)

66 EIDELMAN A. -1979 (GSI-10/91)

67 EISIN B. & SLAGER J. - 1988 Str. Map (EMOG - File 3026)

68 ZILBERMAN E. - 1977 Str. Map (GSI-6/77)

69 COHEN S.S. - 1966 Str. Map (LAPIDOTH File 923)

70 KASHAI E. - 1966 Str. Map (LAPIDOTH File 929)

71 ZAK I. - 1957 Str. Map (M.Sc.Thesis)

72 AVNI Y. - 1991 Str. Map (M.Sc. Thesis) (GSI/6/91)

73 AVNI Y. - 2001 Geol. Map of Har Loz (GSI)

74 BECKER A. - 2002 Geol. Map of Be'erot Oded (GSI in preparation)

75 BEAR G. - 1981 Str. Map of Ma'ale Hameshar (GSI MM/5/81)

76 ZILBERMAN E. - 1983 Str. Pattern of A'rif - Batur Lin.(GSI/6/83)

77 ZILBERMAN E. - 1985 Str. Pattern of Paran Lin. (GSI/38/85)

78 KARCZ Z.- 1997 Str. Map (M.Sc. Thesis) (GSI-23/97)

79 SAKAL E. - 1966 Str. Map (GSI OD/2/67)

80 FLEISCHER L. &. FRIESLANDER U. - 1997 Str. Map Idan -Paran (IPRG 820/36/97)

81 SOMMER M. - 1956 Str. Map Sinaf (Lapidoth File 2676)

82 LIFSHITZ A. - 1986 Str. Map of Yael (M.Sc. Thesis)

83 AVNI Y. - 1998 Geol. Map of Paran Basin (Ph.D Thesis)(GSI/24/98)

84 GINAT H. - 1989 Str. Map of Yotvata (M.Sc. Thesis) (GSI/8/91)

85 GINAT H. - 2000 Geol. Map of Mizpe Sayyarim (GSI in preparation)

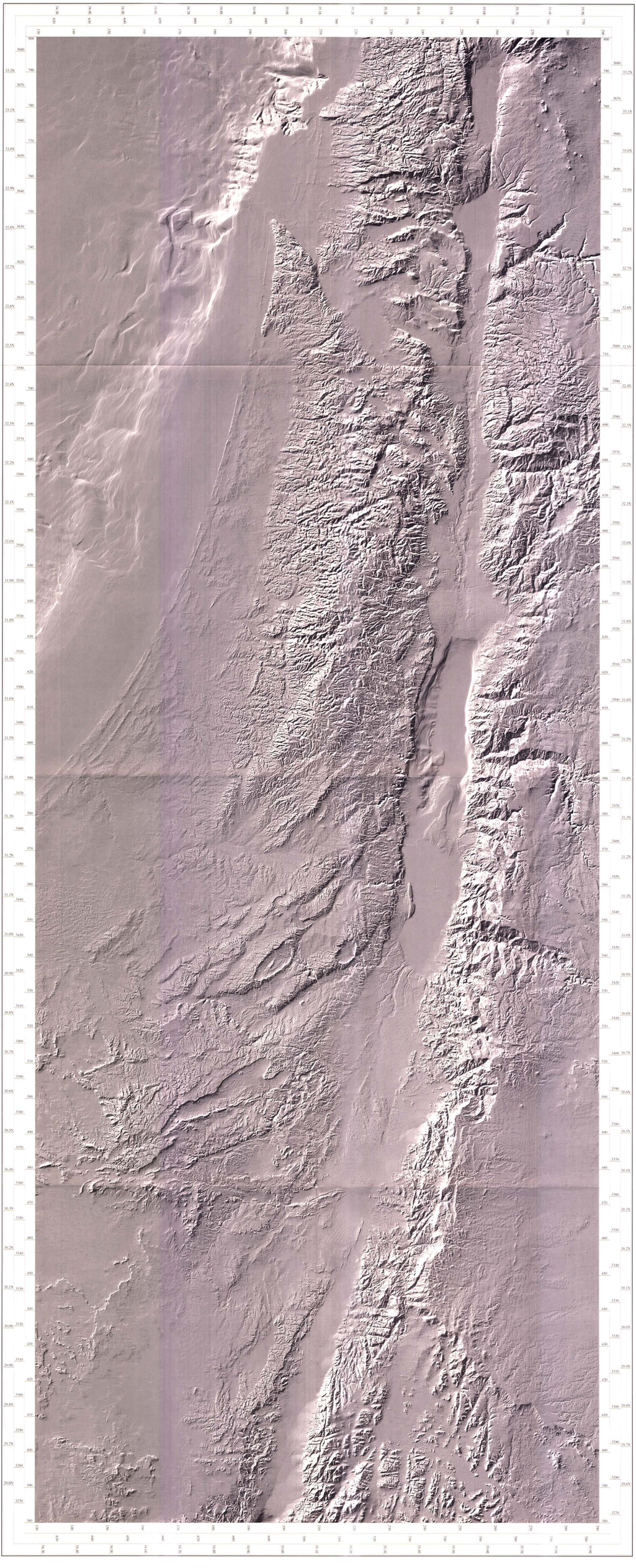
86 BEYTH M., SEGEV A. & BARTOV Y.- 1999 Geol. Map of Be'er Ora (GSI)

87 SEGEV A. & BEITH M.- 2000 Geol. Map of Har Seguv (GSI)

88 BARTOV Y.- 1967 Str. Map of Be'er Ora (Ann. Meet Yotvata-1983)

89 GARFUNKEL Z. et al - 2000 Geol. Map of Elat (GSI)

90 EYAL Y. - 1967 Str. Map (J.E.S. Vol.22-1973)



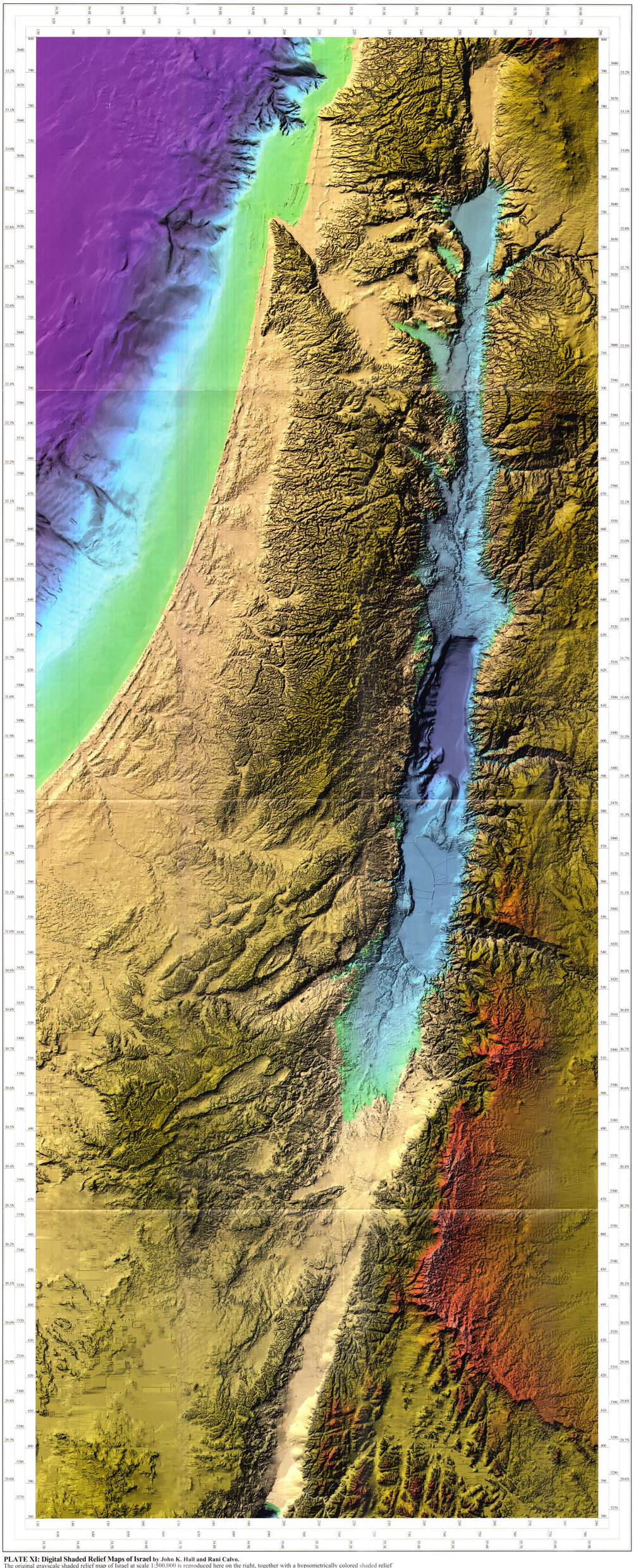


PLATE XI: Digital Shaded Relief Maps of Israel by John K. Hall and Rani Calvo.
The original grayscale shaded relief map of Israel at scale 1:500,000 is reproduced here on the right, together with a hypsometrically colored shaded relief map. The maps are based upon the 25 m Digital Terrain Model (DTM) of Israel, prepared from the 1:50,000 scale topographic maps of the Survey of Israel, the U. S. Defense Mapping Agency, and bathymetric compilations by the Geological Survey of Israel. The map graticules show the three projections commonly used in Israel. The inner one is the New Israel Grid in kilometers, the center one is the Univeral Transverse Mercator (UTM – Zone 36) also in km, and the outer one is geographic coordinates (latitudes and longitudes) in decimal degrees. The UTM and Geographic coordinates are on the WGS84 datum (World Geodetic System, 1984), the datum of the positions obtained by the Global Positioning System (GPS).

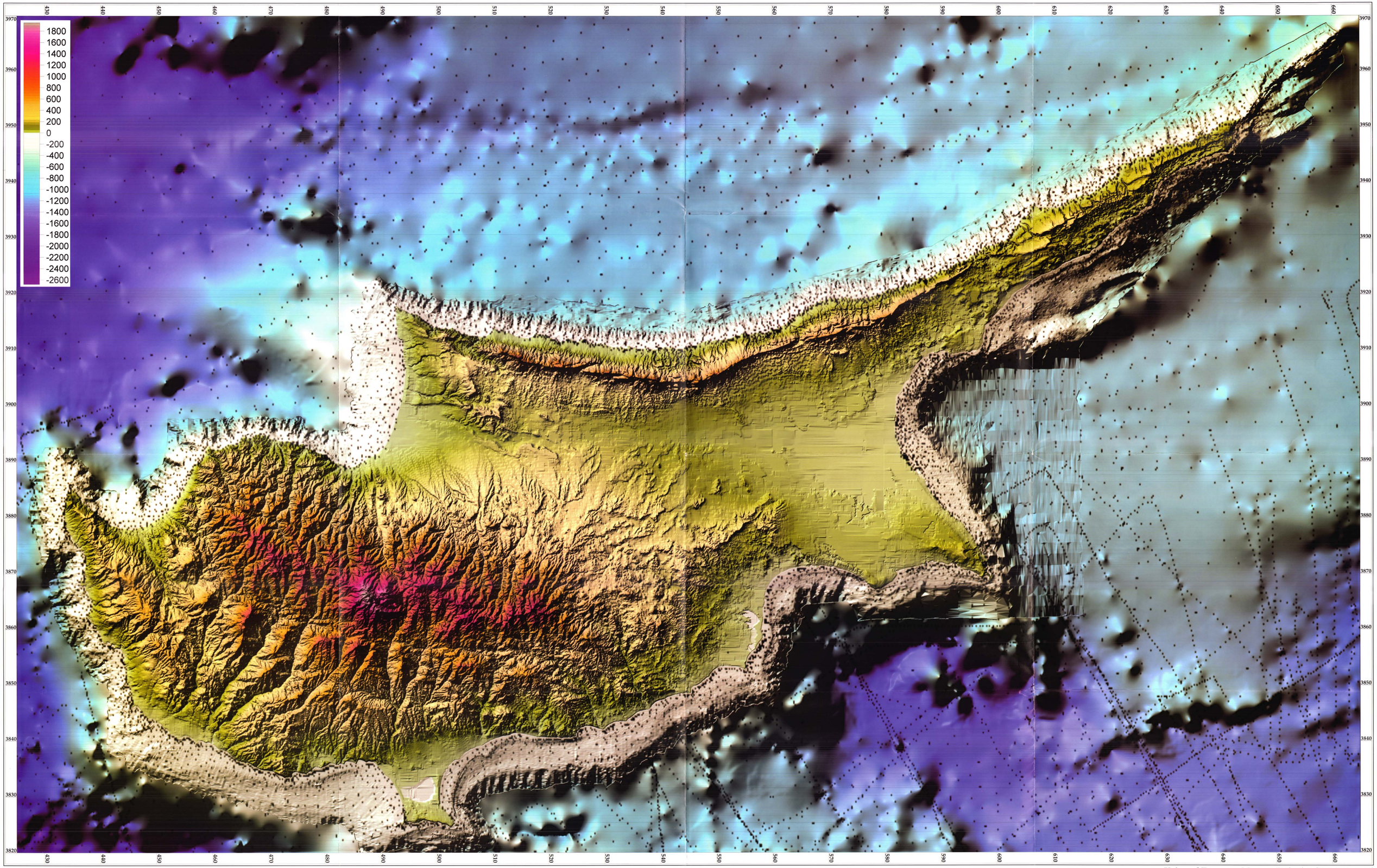


PLATE X: Topography and Bathymetry of the Island of Cyprus.
This image is a composite of the 25 m DTM of Cyprus, together with the 181,748 soundings from the UKHD/UKHO hydrographic surveys interpolated to 25 m, plus every 20th center beam sounding from NES Strakhov Cruises 5 and 10, and depth soundings digitized from the navigational charts of the Head Department of Navigation and Oceanography of the Russian Federation. Black dots show the locations of the depth soundings in these last two datasets. The deeper bathymetry was interpolated to a 100 m grid, using multiquadric surfaces, and overlain by the land topography and nearshore bathymetry reduced to 50 m. These datasets are described in Volume II, Chapter 15, p. 135-148. The resulting grid file, produced by Global Mapper® v. 6.09 in Universal Transverse Mercator (UTM) projection in Zone 36, was then plotted out as hypsometrically colored shaded relief by Surfer® 8. The graticule is in kilometers. This compilation shows some similarities and a number of differences with Figure 15.8 (Volume II, page 145) where the land and nearshore bathymetry are overlaid on the 50 m contours of the 1:625,000 scale Mercator chart of the Eastern Mediterranean (Hall, 1994). A few of the isolated peaks are probably from unreliable spot soundings. The need for seamless multibeam coverage is evidenced by the hints of structure in the widely dispersed sounding coverage.

Universal Transverse Mercator Projection (UTM - Zone 36)
Scale 1:250,000
0 5 10 15 20 25 Km

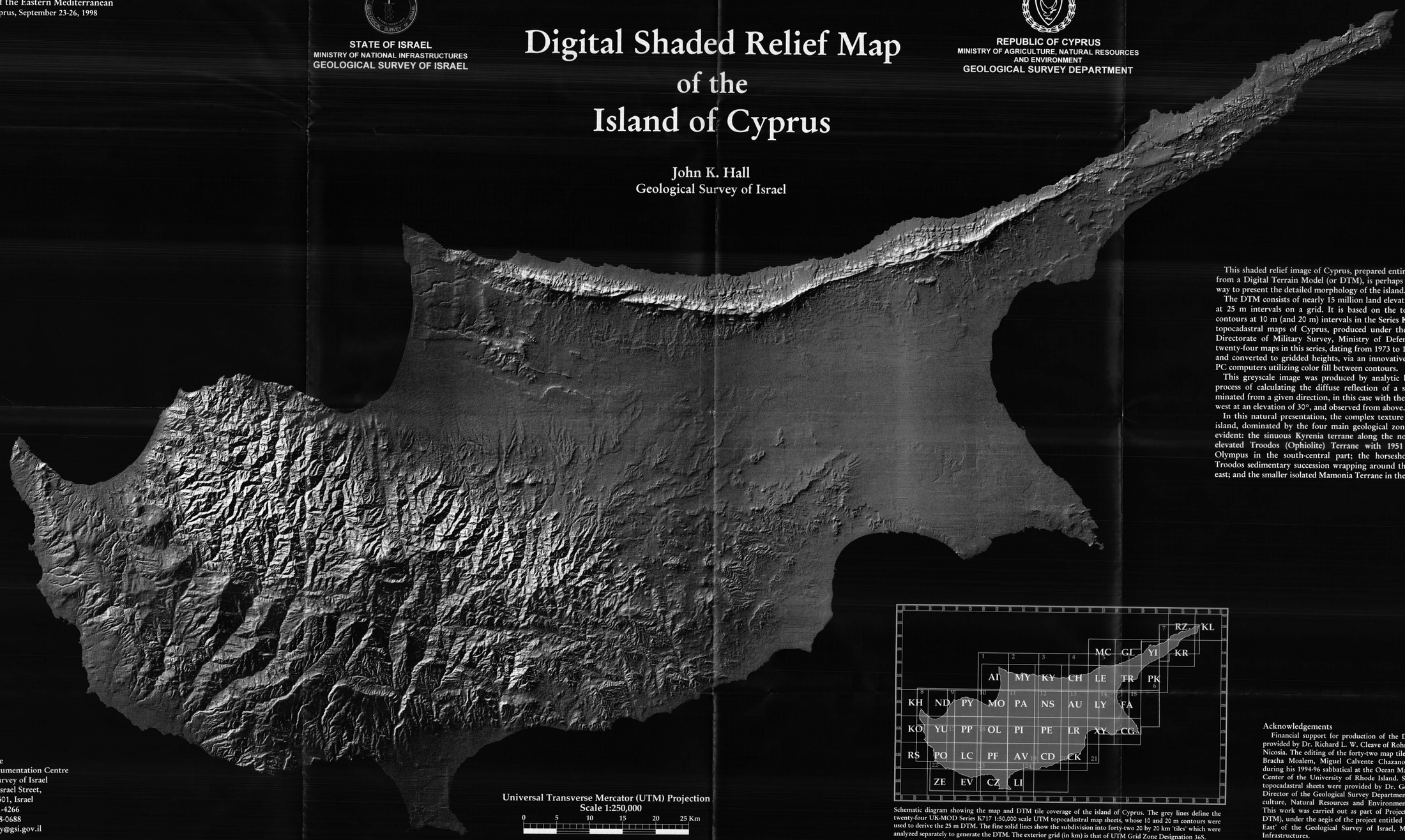
Prepared for ICGEM-3,
Third International Conference on the
Geology of the Eastern Mediterranean
Nicosia, Cyprus, September 23-26, 1998

STATE OF ISRAEL
MINISTRY OF NATIONAL INFRASTRUCTURES
GEOLOGICAL SURVEY OF ISRAEL

Digital Shaded Relief Map of the Island of Cyprus

John K. Hall
Geological Survey of Israel

REPUBLIC OF CYPRUS
MINISTRY OF AGRICULTURE, NATURAL RESOURCES AND ENVIRONMENT
GEOLOGICAL SURVEY DEPARTMENT



This shaded relief image of Cyprus, prepared entirely by a computer from a Digital Terrain Model (or DTM), is perhaps the most effective way to present the detailed morphology of the island.

The DTM consists of nearly 15 million land elevations evenly spaced at 25 m intervals on a grid. It is based on the topographic height contours at 10 m (and 20 m) intervals in the Series K717 1:50,000 scale topocadastral maps of Cyprus, produced under the direction of the Directorate of Military Survey, Ministry of Defence, London. The twenty-four maps in this series, dating from 1973 to 1988, were scanned and converted to gridded heights, via an innovative process on small PC computers utilizing color fill between contours.

This greyscale image was produced by analytic hill shading - the process of calculating the diffuse reflection of a surface when illuminated from a given direction, in this case with the sun in the northwest at an elevation of 30°, and observed from above.

In this natural presentation, the complex texture and fabric of the island, dominated by the four main geological zones of Cyprus, are evident: the sinuous Kyrenia terrane along the northern coast; the elevated Troodos (Ophiolite) Terrane with 1951 m high Mount Olympus in the south-central part; the horseshoe-shaped circum-Troodos sedimentary succession wrapping around the Troodos on the east; and the smaller isolated Mamonia Terrane in the southwest.

For sale at the
Library - Documentation Centre
Geological Survey of Israel
30 Malkhe Yisrael Street,
Jerusalem 95501, Israel
Tel: 972-2-531-4266
Fax: 972-2-538-0688
E-mail: library@gsi.gov.il

Universal Transverse Mercator (UTM) Projection
Scale 1:250,000
0 5 10 15 20 25 Km

Schematic diagram showing the map and DTM tile coverage of the island of Cyprus. The grey lines define the twenty-four UK-MOD Series K717 1:50,000 scale UTM topocadastral map sheets, whose 10 and 20 m contours were used to derive the 25 m DTM. The fine solid lines show the subdivision into forty-two 20 by 20 km 'tiles' which were analyzed separately to generate the DTM. The exterior grid (in km) is that of UTM Grid Zone Designation 36S.

Acknowledgements

Financial support for production of the DTM of Cyprus was provided by Dr. Richard L. W. Cleave of Rohr Productions Inc. in Nicosia. The editing of the forty-two map tiles was carried out by Bracha Moalem, Miguel Calvente Chazanoff, and the author during his 1994-96 sabbatical at the Ocean Mapping Development Center of the University of Rhode Island. Some of the original topocadastral sheets were provided by Dr. George Constantinou, Director of the Geological Survey Department, Ministry of Agriculture, Natural Resources and Environment, Nicosia, Cyprus. This work was carried out as part of Project 2743 (MEDMAP-DTM), under the aegis of the project entitled 'DTM of the Middle East' of the Geological Survey of Israel, Ministry of National Infrastructures.

STRATIGRAPHIC TABLE OF ISRAEL

OUTCROPS AND SUBSURFACE

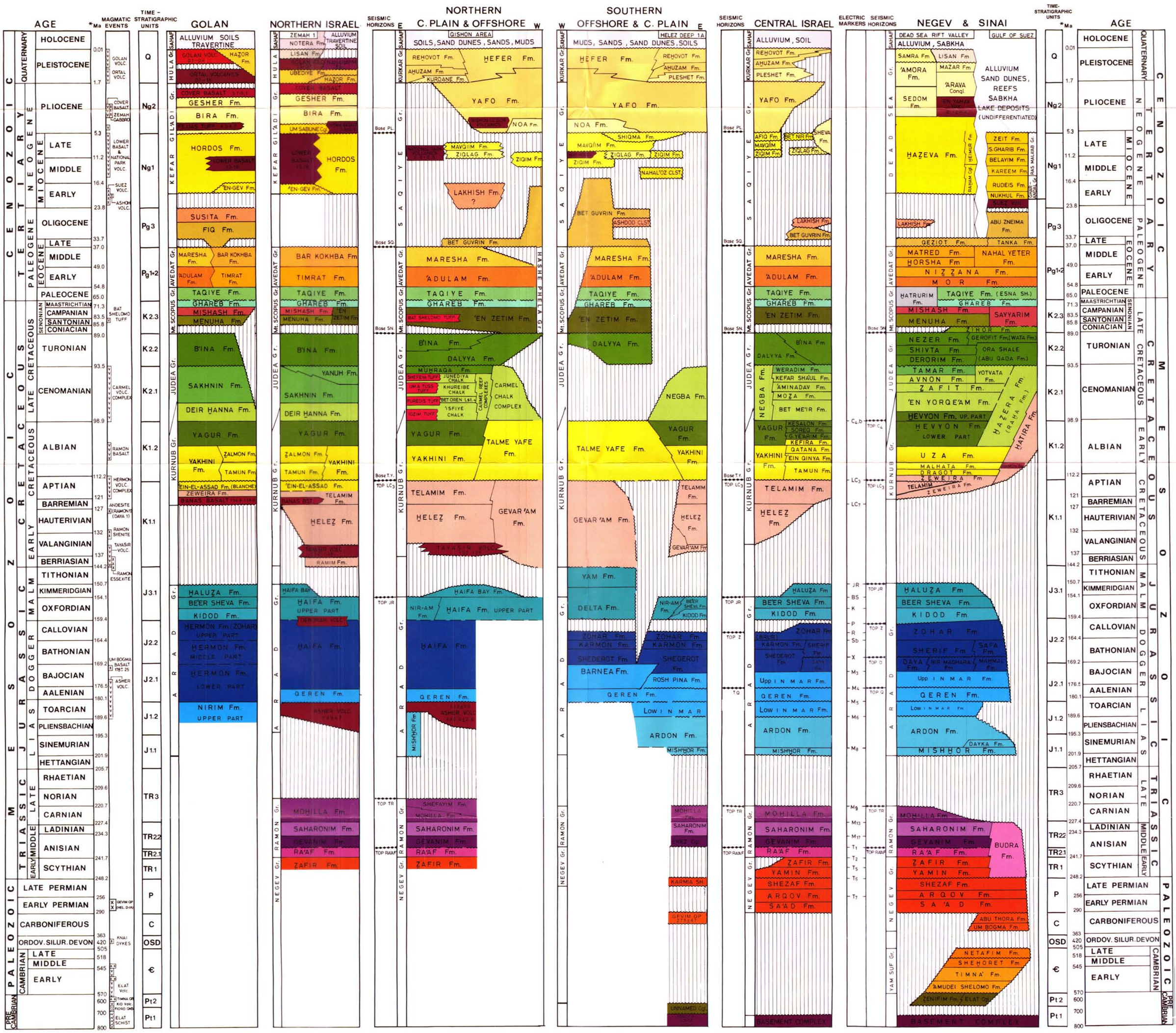
OCTOBER 2002

OIL AND GAS UNIT

המכון הגיאופיסי לישראל

COMPILED BY: L. FLEISCHER

MODIFIED AFTER: Y. ARKIN, M. BRAUN (G.S.I. 1967)
Y. BARTOV, Y. ARKIN, Z. LEWY, Y. MIMRAN (G.S.I. 1981)
A. FLEXER, A. LIVNAT, N. SHAFRAN, D. GILL (RAMOT 1981 FOR O.E.L.)
Z. COHEN, A. SHILO, V. KAPTSAN, L. FLEISCHER (OEL - 1986)
A. SNEH, Y. BARTOV, T. WEISSBROD (GSI - 2000)



* Ma. FROM "GEOLOGICAL TIME SCALE"

① TRIASSIC, JURASSIC, AND CRETACEDUS TIME SCALE: GRADSTEIN et al 1995 (SEPM SPECIAL PUBL. NY.54)

② CENOZOIC GEOCHRONOLOGY.....BERGGREN et al 1995 (SEPM SPECIAL PUBL. NY.54)

Stratigraphic Table of Israel: Outcrops and subsurface. By Lorian Fleischer, Geophysical Institute of Israel, with stratigraphic colors according to the 1:200,000 scale geological maps of the Geological Survey of Israel, published in Sneh, Bartov, and Weissbrod (2000). Coloring of the non-colored original by Hanna Cohen-Netzer. The coloring of the units that are not exposed has been slightly altered in consultation with Dr. Zeev Lewy. The Triassic, Jurassic, and Cretaceous time scale is taken from Gradstein et al. (1995) and the Cenozoic geochronology from Berggren et al. (1995).

PLATE VIII from THE GEOLOGICAL FRAMEWORK of the LEVANT

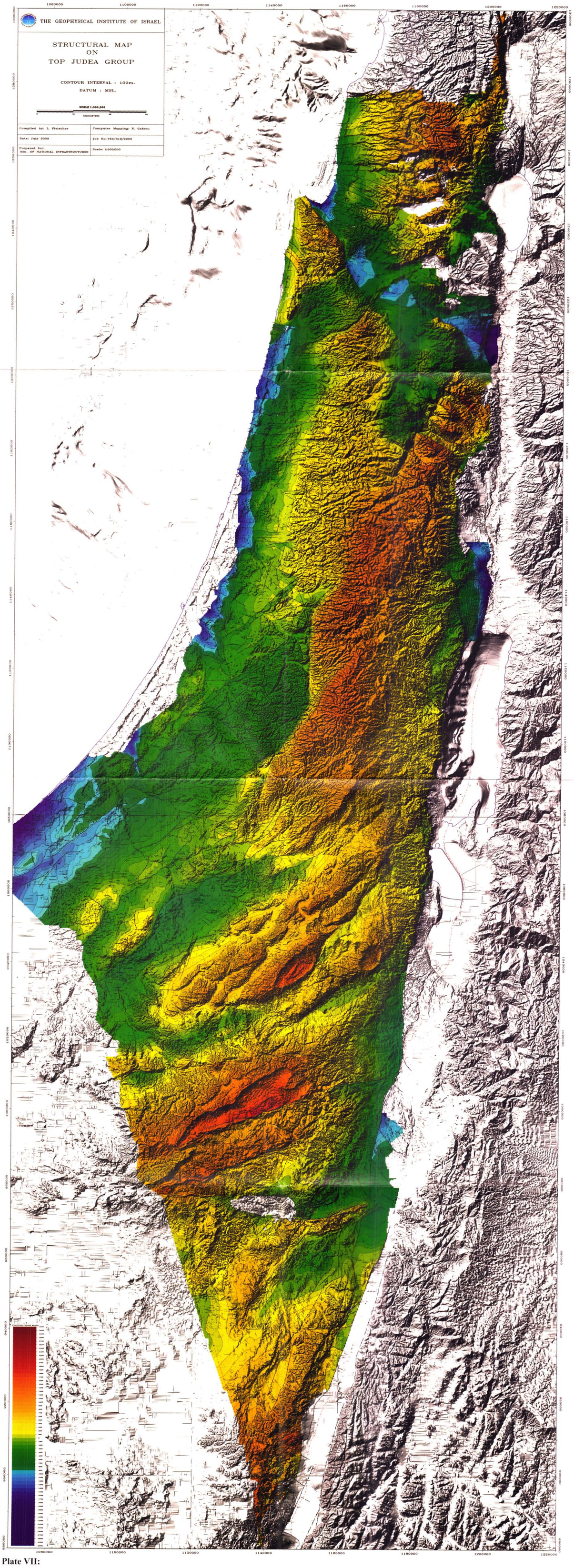
Volume I: Cyprus and Syria: V. A. Krasheninnikov, J. K. Hall, F. Hirsch, C. Benjamini, and A. Flexer (Eds.)

Volume II: The Levantine Basin and Israel: J. K. Hall, V. A. Krasheninnikov, F. Hirsch, C. Benjamini, and A. Flexer (Eds.)

Berggren, W. A., Kent, D. V., Swisher, C. C., III, Aubry, M. -P., 1995. A revised Cenozoic geochronology and chronostratigraphy. In: W. A. Berggren, D. V. Kent, M. -P. Aubry, and J. Hardenbol, (eds.), Geochronology, time scales and global stratigraphic correlation. SEPM (Society for Sedimentary Geology), Special Publication 54, p.129-212.

Gradstein, F. M., Agterberg, F. P., Ogg, J. G., Hardenbol, J., van Veen, P., Thierry, J., Huang, Z., 1995. A Triassic, Jurassic and Cretaceous time scale. In: W. A. Berggren, D. V. Kent, M. -P. Aubry, and J. Hardenbol, (eds.), Geochronology, time scales and global stratigraphic correlation. SEPM (Society for Sedimentary Geology), Special Publication 54, p. 95-126.

Sneh, A., Bartov, Y., and Weissbrod, T., 2000. Stratigraphic chart of exposed rock units in Israel. In: R. Bogoch (ed.), GSI Current Research, Vol. 12, Jerusalem, July 2000, p. 257-262.


THE GEOPHYSICAL INSTITUTE OF ISRAEL
STRUCTURAL MAP
ON
TOP JUDEA GROUP
CONTOUR INTERVAL : 100m.
DATUM : MSL.
SCALE 1:500,000
KILOMETERS
Compiled by: L. Fleischer
Computer Mapping: R. Gafsou
Date: July 2003
Job No: 753/312/2003
Prepared for:
Min. OF NATIONAL INFRASTRUCTURES
Scale: 1:500,000
1080000
1100000
1120000
1140000
1160000
1180000
1200000
1220000

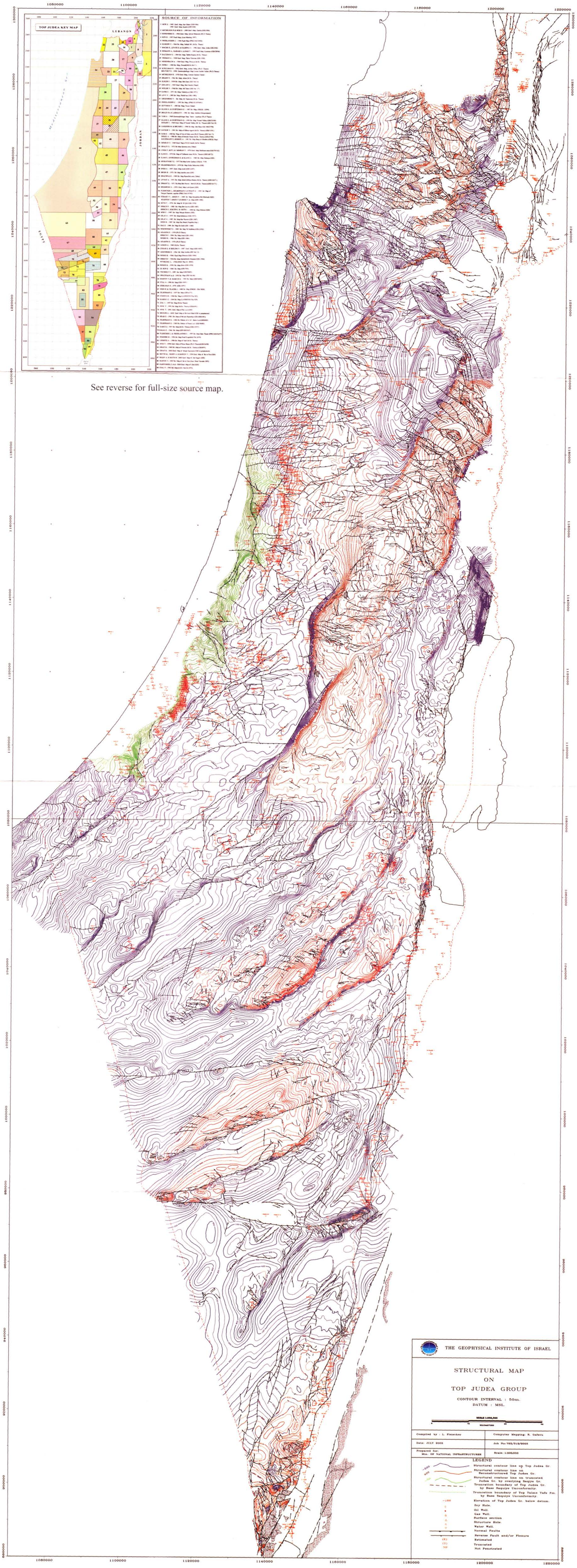
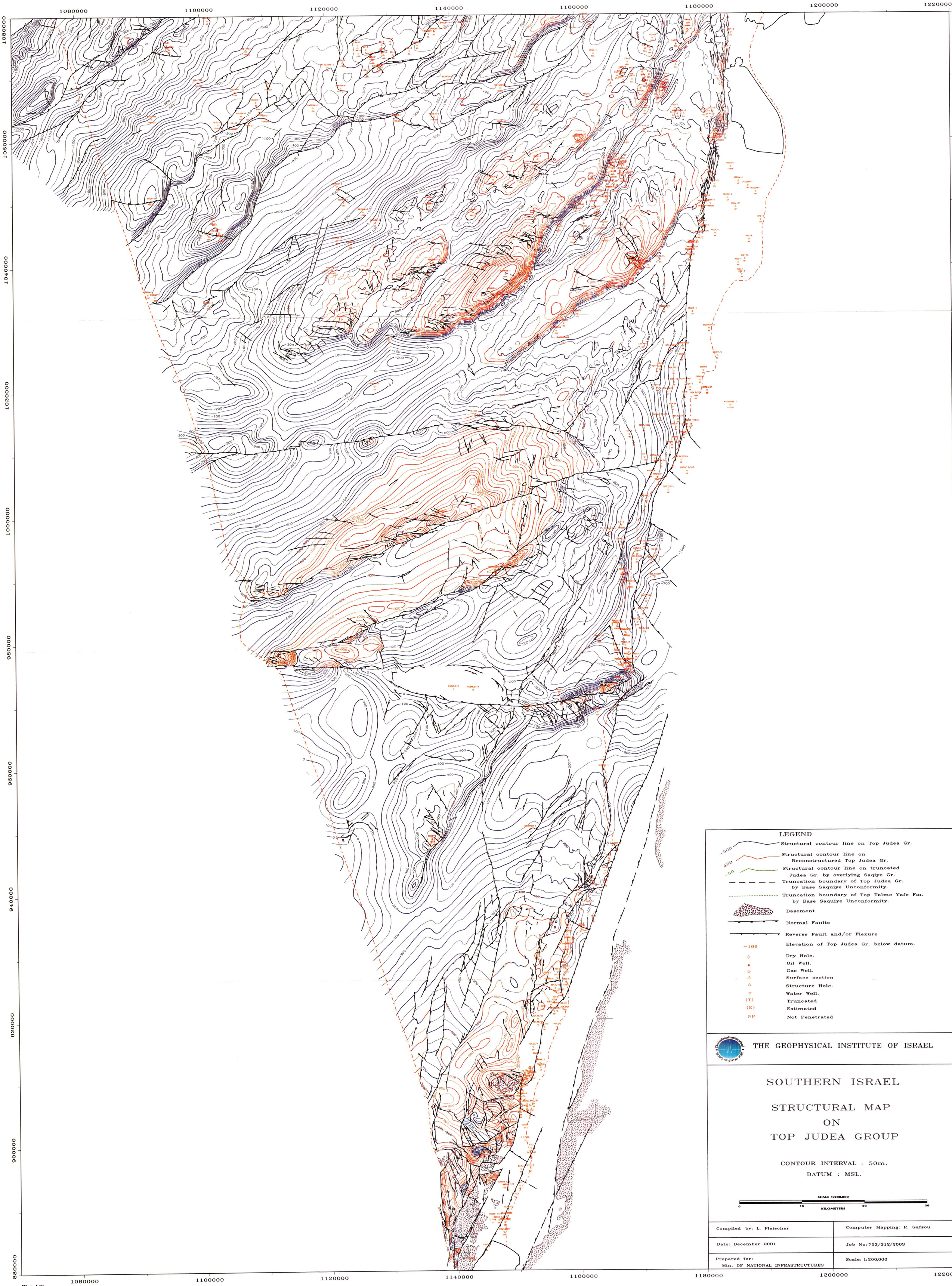

TOP JUDEA KEY MAP
LEBANON
JORDAN
SOURCE OF INFORMATION
See reverse for full-size source map.
THE GEOPHYSICAL INSTITUTE OF ISRAEL
STRUCTURAL MAP
ON
TOP JUDEA GROUP
CONTOUR INTERVAL : 50m.
DATUM : MSL.
SCALE 1:500,000
KILOMETERS
Compiled by : L. Fleischer
Computer Mapping: R. Gafsou
Date: JULY 2003
Job No: 753/312/2003
Prepared for:
Min. OF NATIONAL INFRASTRUCTURES
Scale: 1:500,000
LEGEND
Structural contour line on Top Judea Gr.
Structural contour line on Reconstructured Top Judea Gr.
Structural contour line on truncated Judea Gr. by overlying Saqiye Gr.
Truncation boundary of Top Judea Gr. by Base Saqiye Unconformity.
Truncation boundary of Top Talme Yafe Fm. by Base Saqiye Unconformity.
Elevation of Top Judea Gr. below datum.
Dry Hole.
Oil Well.
Gas Well.
Surface section
Structure Hole.
Water Well.
Normal Faults
Reverse Fault and/or Flexure
Estimated
Truncated
Not Penetrated
1080000
1100000
1120000
1140000
1160000
1180000
1200000
1220000

Plate VII:

1080000 1100000 1120000 1140000 1160000 1180000 1200000 1220000

1080000 1060000 1040000 1020000 1000000 980000 960000 940000 920000 900000 880000



LEGEND

- Structural contour line on Top Judea Gr.
- Structural contour line on Reconstructured Top Judea Gr.
- Structural contour line on truncated Judea Gr. by overlying Saqiye Gr.
- Truncation boundary of Top Judea Gr. by Base Saquiye Unconformity.
- Truncation boundary of Top Talme Yafe Fm. by Base Saquiye Unconformity.
- Basement
- Normal Faults
- Reverse Fault and/or Flexure
- −166 Elevation of Top Judea Gr. below datum.
- Dry Hole.
- Oil Well.
- Gas Well.
- Surface section
- Structure Hole.
- Water Well.
- (T) Truncated
- (E) Estimated
- NP Not Penetrated

THE GEOPHYSICAL INSTITUTE OF ISRAEL

SOUTHERN ISRAEL

STRUCTURAL MAP ON TOP JUDEA GROUP

CONTOUR INTERVAL : 50m.

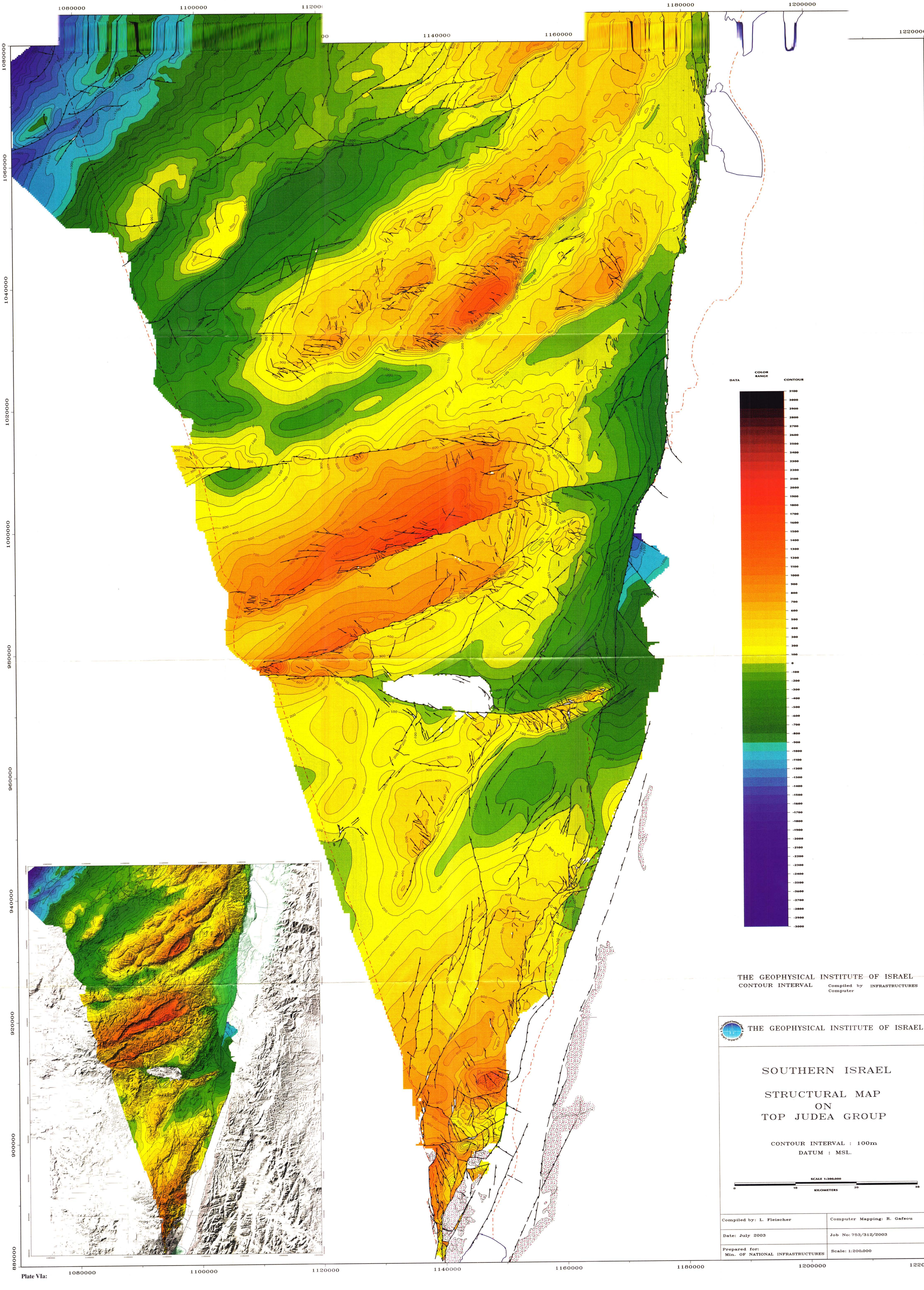
DATUM : MSL.

SCALE 1:200,000

0 10 20 30 KILOMETERS

Compiled by: L. Fleischer	Computer Mapping: R. Gafsou
Date: December 2001	Job No: 753/312/2003
Prepared for: Min. OF NATIONAL INFRASTRUCTURES	Scale: 1:200.000

Plate VIb:



THE GEOPHYSICAL INSTITUTE OF ISRAEL
CONTOUR INTERVAL — Compiled by INFRASTRUCTURES Computer

THE GEOPHYSICAL INSTITUTE OF ISRAEL

SOUTHERN ISRAEL

STRUCTURAL MAP ON TOP JUDEA GROUP

CONTOUR INTERVAL : 100m
DATUM : MSL.

SCALE 1:200.000
0 10 20 30
KILOMETERS

Compiled by: L. Fleischer	Computer Mapping: R. Gafsou
Date: July 2003	Job No: 753/312/2003
Prepared for: Min. OF NATIONAL INFRASTRUCTURES	Scale: 1:200.000

Plate VIa:

THE GEOPHYSICAL INSTITUTE OF ISRAEL

NORTHERN ISRAEL

STRUCTURAL MAP

ON

TOP JUDEA GROUP

CONTOUR INTERVAL : 50m.

DATUM : MSL.

SCALE 1:200,000

0 10 20 30

KILOMETERS

Compiled by : L. Fleischer	Computer Mapping: R. Gafsou
Date: JULY 2003	Job No: 753/312/2003
Prepared for: Min. OF NATIONAL INFRASTRUCTURES	Scale: 1:200,000

LEGEND

−500	Structural contour line on Top Judea Gr.
400	Structural contour line on Reconstructured Top Judea Gr.
−50	Structural contour line on truncated Judea Gr. by overlying Saqiye Gr.
	Truncation boundary of Top Judea Gr. by Base Saquiye Unconformity.
	Truncation boundary of Top Talme Yafe Fm. by Base Saquiye Unconformity.
−166	Elevation of Top Judea Gr. below datum.
	Dry Hole.
	Oil Well.
	Gas Well.
	Surface section
	Structure Hole.
	Water Well.
	Normal Faults
	Reverse Fault and/or Flexure
(E)	Estimated
(T)	Truncated
NP	Not Penetrated

Plate Vb:

THE GEOPHYSICAL INSTITUTE OF ISRAEL

NORTHERN ISRAEL

STRUCTURAL MAP ON TOP JUDEA GROUP

CONTOUR INTERVAL : 100m.

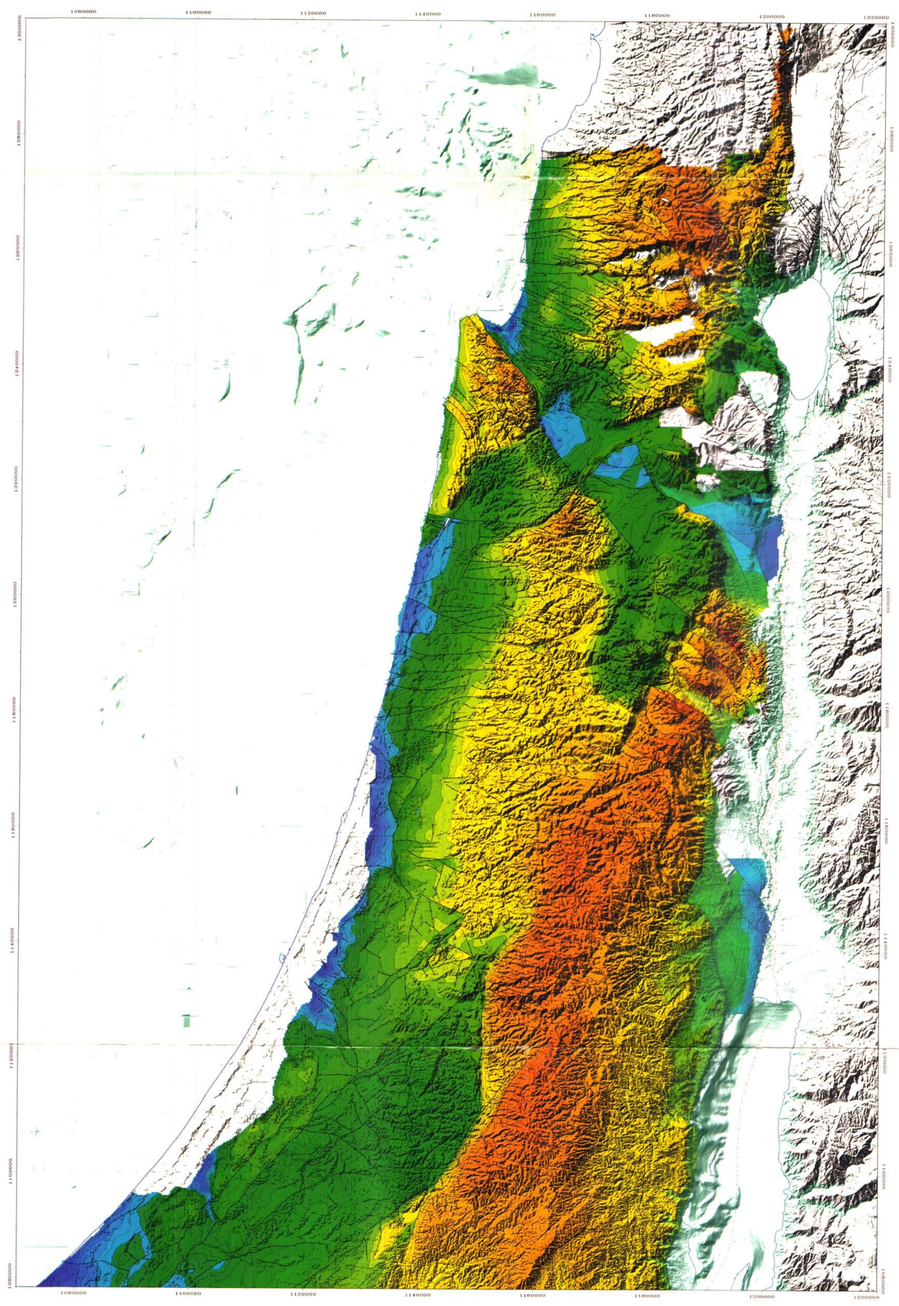
DATUM : MSL.

SCALE 1:200000

0 10 20 30

KILOMETERS

Compiled by: L. Fleischer	Computer Mapping: R. Gafsou
Date: July 2003	Job No: 753/312/2003
Prepared for: Min. OF NATIONAL INFRASTRUCTURES	Scale: 1:200.000



COLOR RANGE

DATA CONTOUR

3100 3000 2900 2800 2700 2600 2500 2400 2300 2200 2100 2000 1900 1800 1700 1600 1500 1400 1300 1200 1100 1000 900 800 700 600 500 400 300 200 100 0 -100 -200 -300 -400 -500 -600 -700 -800 -900 -1000 -1100 -1200 -1300 -1400 -1500 -1600 -1700 -1800 -1900 -2000 -2100 -2200 -2300 -2400 -2500 -2600 -2700 -2800 -2900 -3000

1080000 1100000 1120000 1140000 1160000 1180000 1200000 1220000

1300000 1280000 1260000 1240000 1220000 1200000 1180000 1160000 1140000 1120000 1100000 1080000

Plate Va:

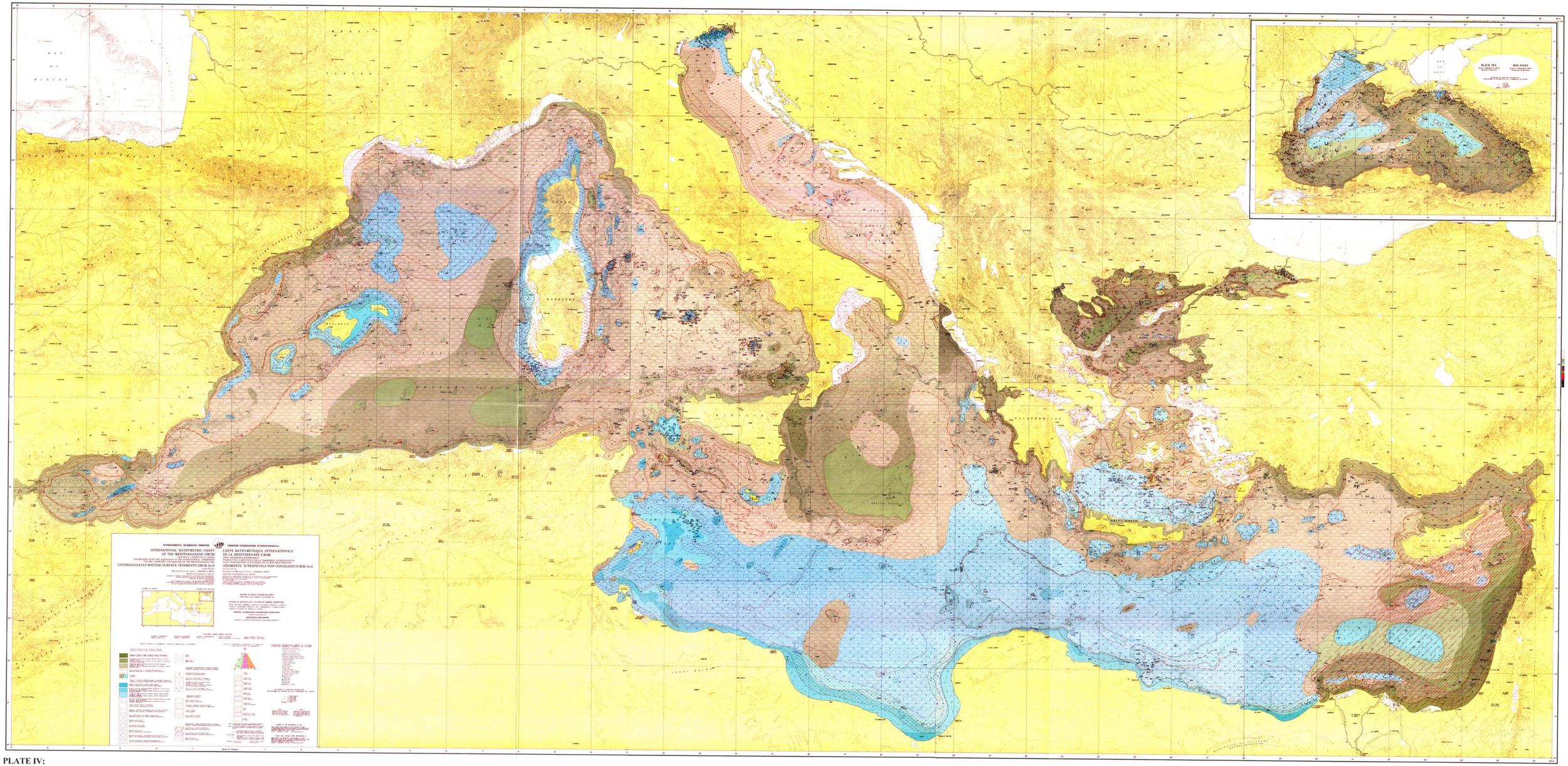


PLATE IV:
Unconsolidated Bottom Surface Sediments of the Mediterranean and Black Seas, IBCM-SED.
Composite of the ten 1:1,000,000 scale sheets, reproduced here at scale 1:5,000,000. The description of the chart is given in Volume II, Chapter 17, p. 183-214.

This IBCM-SED Chart Series to be referred to as:
Emelyanov, E. M., Shimkus, K. M., and Kuprin, P. N., 1996. Unconsolidated Bottom Surface Sediments of the Mediterranean and Black Seas. Intergovernmental Oceanographic Commission (UNESCO). IBCM Geol.-Geoph. Series. Scale 1:1,000,000, 10 sheets. St. Petersburg, Russia.

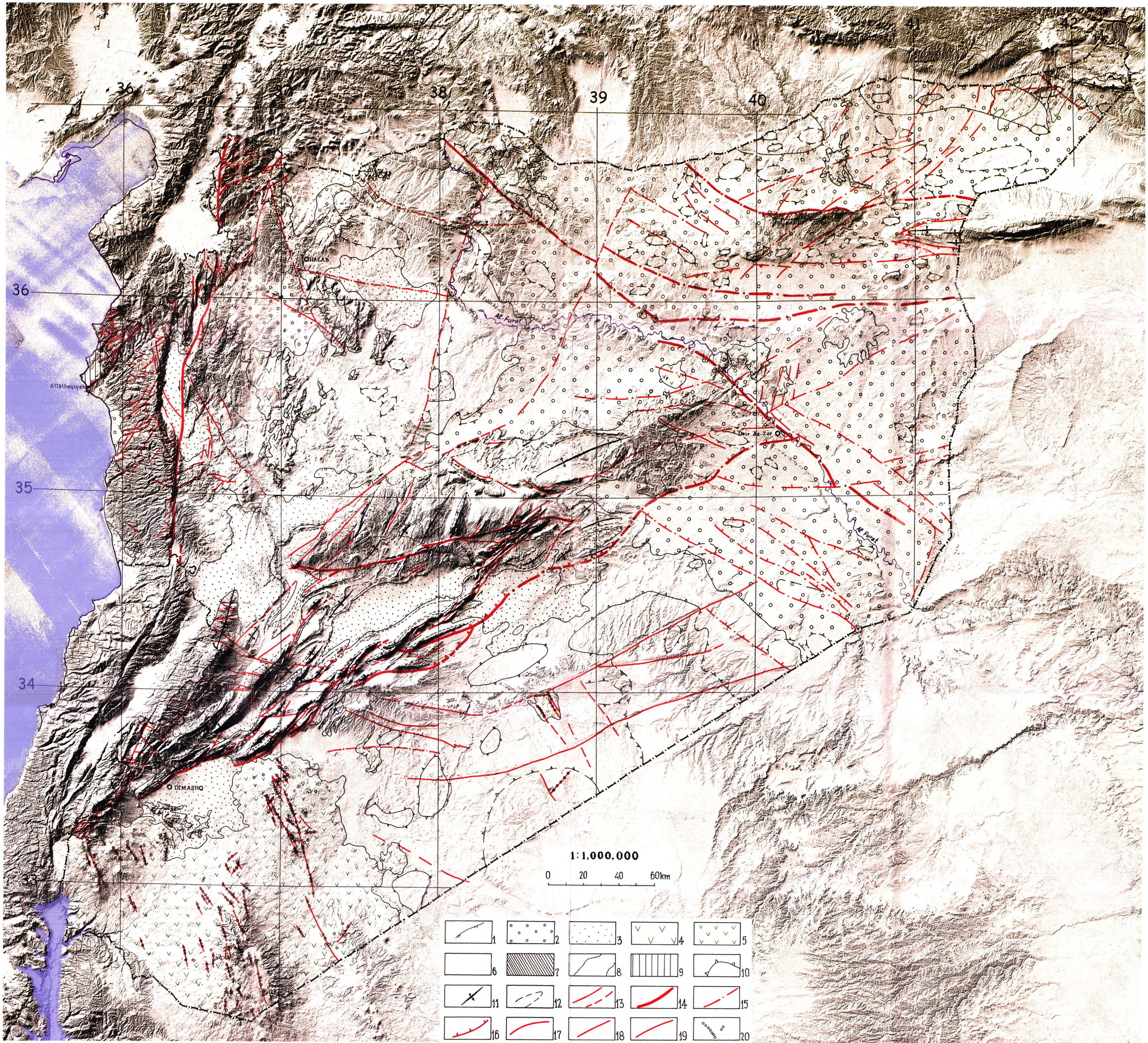


PLATE III: Structural Map of Syria by Vladimir G. Kazmin (Volume I, Fig. 8.2, p. 466).
Structural Map of Syria at a scale of 1:1,000,000. Using Global Mapper® (ver. 6.08) the map has been georeferenced (Mercator projection, Pulkovo 1942 datum), and then 'texturized' with the 90 m topography of Syria and environs from the Shuttle Radar Topographic Mission.

Legend: **1** – outer margin of the pre-Neogene outcrops; **2** – Miocene-Quaternary cover; **3** – Pliocene depressions; **4** – Upper Miocene basalts; **5** – Pliocene basalts; **6** – outcrops of pre-Neogene platform sediments; **7-8** – allochthonous complexes; **7** – Ophiolite nappe; **8** – Tamima nappe; **9** – neoautochthone; **10** – limits of domal uplifts and brachyanticlines; **11** – linear folds; **12** – structural line; **13** – mapped faults (a) certain; (b) uncertain); **14** – major faults; **15** – faults revealed by geophysical methods; **16** – normal faults; **17** – nappes, thrusts; **18** – strike-slip faults; **19** – flexures; **20** – volcanic cones.

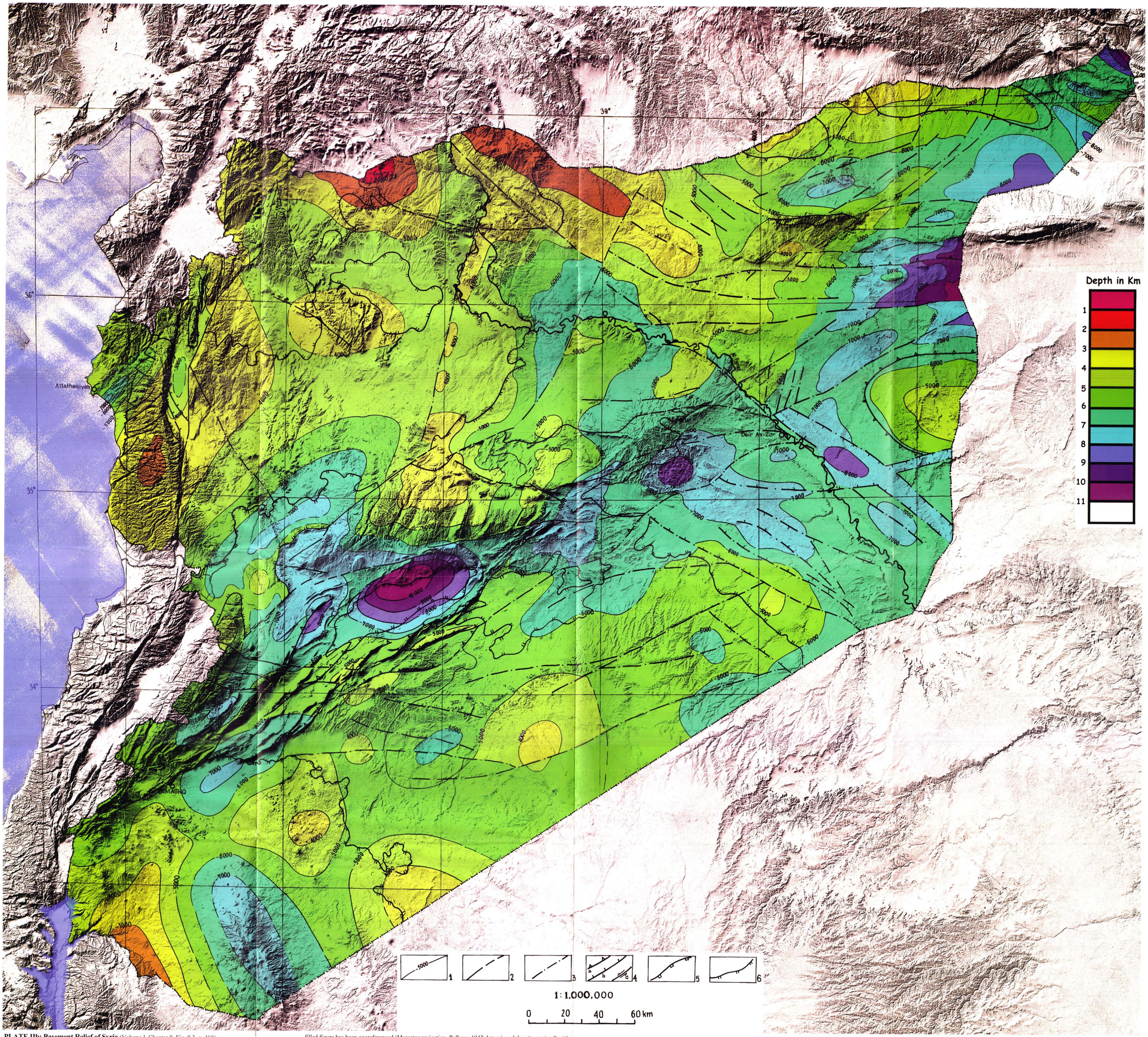


PLATE IIb: Basement Relief of Syria (Volume I, Chapter 8, Fig. 8.3, p. 468).
Map of the basement relief at 1:1,000,000 scale with structural contours relative to sealevel at 1000 m intervals. This map is based on the 'Depth Scheme Map of Crystalline Basement at scale 1:500,000', compiled in 1986 by T. Sawaf, Syrian Petroleum Company. Small changes added by V. Kazmin, and coloring by J. K. Hall, who noted some slight topological difficulties. Using Global Mapper® (ver. 6.08) the color-filled figure has been georeferenced (Mercator projection, Pulkovo 1942 datum), and then 'texturized' with the 90 m topography from the Shuttle Radar Topographic Mission.
Legend: 1 - Isolines of basement surface, depth in meters; **Faults: 2** - traced on the surface; **3** – revealed by geophysical methods; **4** – (a) thrust, (b) normal fault; (c) strike-slip fault; **5** – flexure; **6** – limit of the uplifted block (contact with the Neogene cover).

PLATE IIa: Tectonic Units of Syria by Vladimir G. Kazmin, (Volume I, Fig. 8.1, p. 464).
Map of tectonic units at 1:1,000,000 scale. Using Global Mapper® (v. 6.08) the colored figure has been georeferenced (Mercator projection, Pulkovo 1942 datum), and then 'texturized' with the 90 m topography from the Shuttle Radar Topographic Mission.

Legend:
Tectonic units of Syria: **1-3**: uplifts of the platform basement. **1** – Southern block; **2** – Northern block; 3 – uplifted blocks buried by the Neogene-Quaternary sediments; **4** – Mesozoic rifts below the Neogene-Quaternary cover; **5-9** – zones of the Neogene-Quaternary deformation. **5-6** – Palmyra fold belt; **5a** – South Palmyra zone; **5b** – North Palmyra zone; **6** – buried extension of the Palmyra belt; **7** – Sinjar zone; **8** – folded foreland (extension of the Zagros fold belt); **9** – structures related to the Levant fault system; **10** – frontal zone of the Alpine fold belt; **11** – early-late Alpine foredeep; **12** – Neogene-Quaternary platform cover; **13** – deepest part of the Al-Ghab depression; **14** – (a) limits of the Neogene-Quaternary basins; (b) limits of domal uplifts; 15 – mapped faults: (a) traced; (b) inferred; **16** – faults revealed by geophysical methods; **17** – flexures; **18** – types of faults: (a) thrusts; (b) normal faults; (c) strike-slip faults; **19** – position of restored cross-sections with shortening measured.

Structures: **1** – Baer-Bassit block; **2** – Kurd-Dagh block; **3** – Nahr El-Kebir foredeep; **4** – Aafrine foredeep; **5** – Jebel An-Nusseiriyeh uplift; **6** – Jebel Az-Zawieh uplift; **7** – Al-Ghab depression; **7a** – Asharneh depression; **8** – Karasu depression; **9** – Jebel Wastani anticline; **10** – Aafrine depression; **11** – Homs depression; **12** – Al Daww depression; **13** – Anti-Lebanon anticline; **14** – Drouz depression; **15** – Al-Furat depression; **16** – slope of the Rutbah Uplift; **16a** – Tanf domal uplift; **16b** – El Murabbaa domal uplift; **17** – Rawda Uplift; **18** – El-Balas block; **19** – Bishri anticline; **20** – Albaida-Derro zone; **21** – Jebel Abd El-Aziz anticline; **22** – Qamishli and **22a** – Ras El-Ein swells (eastern termination of the Mardin uplift); **23** – Aleppo High; **23a** – Jrablus block; **24** – Qarashouk anticline; **25** – slope of the Mardine-Qamishli uplift; **26** – buried extension of the Aleppo High.
Faults: **27** – Al-Latheqiyeh-Kilis; **28** – Yammuneh; **29** – Al-Ghab; **30** – South Palmyra; **31** – Sawwaneta-Heil; **32** – Jhar; **33** – Al-Furat transcurrent zone; **34** – El Madabe fault step; **35** – Maksar; **36** – Hama; **37** – Sheikh Barakat; **38** – Serrhaya.

V.O. TECHNOEXPORT
MOSCOW USSR
CONTRACT №944

GEOMORPHOLOGICAL MAP OF SYRIA

Compiled by K. MIRZAYEV from the data obtained by the Soviet geologists of V/O Technoexport (Contract № 944)

Scale 1 : 1,000,000

1963

LEGEND

A. BLOCK TYPE MOUNTAINS

a_1 MOUNTAINS FORMED BY BLOCKS

Medium – height mountains (1,000 metres or higher).

1. Medium – height mountains with sharp divides and steep precipitous slopes confined to highly elevated horsts (N_2-Q_3)

Low mountains (500 to 1,000 metres)

2. Low mountains with flattened divides, partly of the table type, and deeply cut valleys (N_2-Q_3)

3. Low mountains with ridge – like divides separated by broad valleys (N_2-Q_3)

a_2 FRONT ELEVATIONS FORMED BY MONOCLINAL HORSTS

4. Gently undulating elevations (N_2-Q_3)

a_3 LOW AREAS ASSOCIATED WITH GRABENS

5 Undulating plains slightly cut by erosion (Q_2)

6. Swampy lowlands with relict lakes (Q_3-Q_4)

B. FOLDED MOUNTAINS

b_1 MOUNTAINS FORMED BY LARGE BOX-SHAPED ANTICLINES

7. Medium – height mountains with flattened divides and steep abrupt slopes (N_2-Q_3)

8. Low mountains with small and low ridges

b_2 MOUNTAINS FORMED BY LINEAR ANTICLINES

9. Medium – height mountains with narrow divides and longitudinal valleys (N_2-Q_3)

10. Low mountains with undulating hilly relief (Q_3)

b_3 MOUNTAINS FORMED BY LARGE GENTLE BRACHY-ANTICLINES

11. Low mountains with highly dissected, low-ridge – like relief (Q_3-Q_4)

12. Medium – height mountains with flat broad divides separated by V-shaped valleys (N_2-Q_3)

13. Low mountains with conform and – cuesta-hilly relief (N_2-Q_3)

14. Low mountains with flattened divides and low – dipping slopes (N_2-Q_3)

b_4 LARGE INTERMONTANE AREAS AND BASINS

15. Slightly dipping alluvial – proluvial undulating plains (Q_3)

16. Slightly sloping undulating plains (Q_3)

C. BLOCK – FOLDED MOUNTAINS

c_1 MOUNTAINS FORMED BY HIGHLY DISLOCATED MESOZOIC AND CENOZOIC SEDIMENTS

17. Medium – height mountains with narrow flat divides and steep dissected slopes (N_2-Q_3)

18. Low mountains with flattened divides and V-shaped valleys, complicated by faults (N_2-Q_3)

c_2 INTERMONTANE VALLEYS FORMED IN HIGHLY DISLOCATED CENOZOIC SEDIMENTS

19. Sloping plains with small terraces (Q_3)

D. PLATEAUS AND PLAINS FORMED BY FLAT LAYERS

d_1 PLATEAU

20. Plateau with flattened gently rolling surface, slightly dissected in places (N_2)

d_2 PLATEAU-SHAPED PLAINS

21. Gently undulating plains (Q_1)

22. Sloping plains with ravines (Q_2-Q_3)

23. Slightly undulating plains with desert-type weathered outliers and a network of dry wadis (Q_2)

24. Flat, slightly undulating plains with depressions in places (Q_1)

d_3 AGGRADATION PLAINS

d_{3a} CONTINENTAL AGGRADATION PLAINS

25. Sloping piedmont plains with distinct erosion cut (Q_2)

26. Undulating proluvial and alluvial-proluvial plains with shallow erosion valleys (Q_2)

27. Flat saline plains (Q_2)

d_{3b} MARINE AGGRADATION PLAINS

28. Undulating, slightly – terraced, abrasion-aggradation, sloping plain with a thin proluvial cover (Q_3)

d_4 DRAINLESS BASINS

29. Sloping, valley-side plains passing into flat lake floors (Q_2-Q_3)

d_5 HILLS FORMED BY LOCAL ANTICLINES

30. Rolling hills with distinctly recognizable individual ridges, locally highly dissected by erosion (Q_2-Q_3)

E. VOLCANIC MOUNTAINS, PLATEAUS AND PLAINS

e_1 VOLCANIC MOUNTAINS

31. Medium – height mountains with plateau – like divides and canyon-shaped valleys between them (N_2-Q_3)

e_2 RELICT VOLCANIC MOUNTAINS

32. Low mountains with flat divides and steep slopes (N_2-Q_3)

e_3 VOLCANIC PLATEAUS AND PLAINS

33. Gently undulating lava plateaus with strongly dissected slopes (N_2)

34. Lava plateaus and plains with small hills and depression (Q_4)

35. Similar plateaus and plains partly covered by alluvial – proluvial mantle with well – defined erosion cut (Q_1)

36. Slightly dissected lava plateaus (Q_1-Q_2)

EROSION RELIEF FORMS:

- Places of intense stream cut
- Scarps
- Outliers
- Cusps of aggradation terraces
- Cusps of compound terraces
- Cusps of erosion terraces
- Finely-terraced valleys
- Wadis

KARST FORMS:

- Funnels
- Karsted places
- Corries (crags)
- Corrie fields
- Caves and niches

VOLCANIC FORMS:

- Volcanoes (extinct)
- Calderas
- Lava flows
- Necks

DENUDATION STRUCTURAL FORMS:

- Longitudinal ribbing on slopes due to rock bedding
- Monoclinal ridges
- Cuesta escarpments
- Troughs on anticlinal structures
- Individual anticlinal folds recognized in the relief as positive forms
- Desert weathering outliers
- Big escarpments

DESERT AGGRADATION FORMS:

- Takyrs
- Coarse ripples on loamy and sandy floors of dry valleys

EROSION-DENUDATION FORMS:

- Small table – lands

GRAVITATIONAL FORMS:

- Landslide

WATER- AGGRADATION FORMS:

- Dry deltas
- Recent alluvial fans
- Upper Quaternary and recent alluvial fans
- Middle Quaternary alluvial fans
- Flood plain
- First terrace above the flood-plain (recent)
- Second terrace above the flood plain (Upper Quaternary)
- Third terrace above the flood plain (Middle Quaternary)
- Fourth terrace above the flood plain (Lower Quaternary)

WIND-BORNE FORMS:

- Barchans

THALASSOGENIC FORMS:

- Erosion scarps

BIOGENIC FORMS:

- Peat bogs

ANTHROPOGENIC FORMS:

- Tells

TECTONIC FORMS:

- Faults recognizable in the relief as scarps
- Faults recognizable in the relief as low areas

OTHER FORMS:

- Places of flint tool findings

SCHEME OF DISPOSITION OF SHEETS

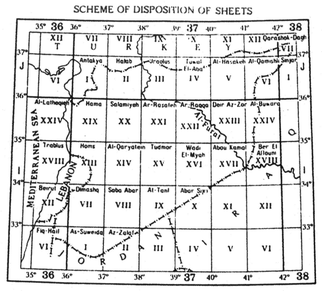


PLATE I: Geomorphological Map of Syria. Compiled by K. Mirzayev from the data obtained by the Soviet geologists V/O Technoexport (Contract No. 944). This map, dated 1963, was printed in the USSR in 1964. The printed copies were sent to Syria, and several decades later could not be located. This personal copy of V. A. Krasheninnikov has been scanned and is reproduced above.

Made in USSR 1964